

MECHANICAL ENGINEERS' HANDBOOK

Volume
Energy and Power » 4

MYER KUTZ EDITOR

FOURTH EDITION

WILEY

Mechanical Engineers' Handbook

Mechanical Engineers' Handbook
Fourth Edition

Energy and Power

Edited by
Myer Kutz

WILEY

Cover Design: Wiley
Cover Image: © denisovd / Thinkstock

This book is printed on acid-free paper.
Copyright © 2014 by John Wiley & Sons, Inc. All rights reserved

Published by John Wiley & Sons, Inc., Hoboken, New Jersey
Published simultaneously in Canada

No part of this publication may be reproduced, stored in a retrieval system, or transmitted in any form or by any means, electronic, mechanical, photocopying, recording, scanning, or otherwise, except as permitted under Section 107 or 108 of the 1976 United States Copyright Act, without either the prior written permission of the Publisher, or authorization through payment of the appropriate per-copy fee to the Copyright Clearance Center, 222 Rosewood Drive, Danvers, MA 01923, (978) 750-8400, fax (978) 646-8600, or on the web at www.copyright.com. Requests to the Publisher for permission should be addressed to the Permissions Department, John Wiley & Sons, Inc., 111 River Street, Hoboken, NJ 07030, (201) 748-6011, fax (201) 748-6008, or online at www.wiley.com/go/permissions.

Limit of Liability/Disclaimer of Warranty: While the publisher and author have used their best efforts in preparing this book, they make no representations or warranties with the respect to the accuracy or completeness of the contents of this book and specifically disclaim any implied warranties of merchantability or fitness for a particular purpose. No warranty may be created or extended by sales representatives or written sales materials. The advice and strategies contained herein may not be suitable for your situation. You should consult with a professional where appropriate. Neither the publisher nor the author shall be liable for damages arising herefrom.

For general information about our other products and services, please contact our Customer Care Department within the United States at (800) 762-2974, outside the United States at (317) 572-3993 or fax (317) 572-4002.

Wiley publishes in a variety of print and electronic formats and by print-on-demand. Some material included with standard print versions of this book may not be included in e-books or in print-on-demand. If this book refers to media such as a CD or DVD that is not included in the version you purchased, you may download this material at <http://booksupport.wiley.com>. For more information about Wiley products, visit www.wiley.com.

Library of Congress Cataloging-in-Publication Data:

Mechanical engineers handbook : energy and power / edited by Myer Kutz. – Fourth edition.

1 online resource.

Includes index.

Description based on print version record and CIP data provided by publisher; resource not viewed.

ISBN 978-1-118-95636-6 (ePub) – ISBN 978-1-118-95637-3 (Adobe PDF) –

ISBN 978-1-118-11899-3 (4-volume set) – ISBN 978-1-118-11285-4 (cloth : volume 4 : acid-free paper)

1. Mechanical engineering—Handbooks, manuals, etc. I. Kutz, Myer, editor of compilation.

TJ151

621—dc23

2014005952

Printed in the United States of America

10 9 8 7 6 5 4 3 2 1

To Arthur and Bess, Tony and Mary-Ann, for all the good times

Contents

Preface	ix
Vision for the Fourth Edition	xi
Contributors	xiii

PART 1 ENERGY

1

1. Thermophysical Properties of Fluids	3
<i>Peter E. Liley</i>	
2. Mechanics of Incompressible Fluids	41
<i>Egemen Ol Ogretim and Wade W. Huebsch</i>	
3. Thermodynamics Fundamentals	135
<i>Adrian Bejan</i>	
4. Exergy Analysis, Entropy Generation Minimization, and the Constructal Law	157
<i>Adrian Bejan</i>	
5. Heat Transfer Fundamentals	183
<i>G. P. Peterson</i>	
6. Temperature Measurement	247
<i>Peter R. N. Childs</i>	
7. Heat Flux Measurement	285
<i>T. E. Diller</i>	
8. Furnaces	313
<i>Carroll Cone</i>	
9. Heat Exchangers, Vaporizers, and Condensers	375
<i>Joseph W. Palen</i>	
10. Heat Pipes	415
<i>Hongbin Ma</i>	
11. Air Heating	443
<i>Richard J. Reed</i>	
12. Cooling Electric Equipment	451
<i>Allan Kraus, Avram Bar-Cohen, and Abhay A. Wative</i>	
13. Refrigeration	499
<i>Dennis L. O'Neal</i>	
14. Cryogenic Engineering	543
<i>J. G. Weisend II</i>	
15. Indoor Environmental Control	577
<i>Jelena Srebric</i>	
16. Thermal Systems Optimization	599
<i>Vikrant C. Aute</i>	

PART 2 POWER**633**

-
17. Combustion 635
Eric G. Eddings
 18. Gaseous Fuels 673
Richard J. Reed
 19. Liquid Fossil Fuels from Petroleum 683
Richard J. Reed
 20. Coals, Lignite, and Peat 703
James G. Keppeler
 21. Clean Power Generation from Coal 719
James W. Butler and Prabir Basu
 22. Biofuels for Transportation 767
Aaron Smith, Cesar Granda, and Mark Holtzaple
 23. Solar Energy Measurements 805
Tariq Muneer and Yieng Wei Tham
 24. Geothermal Resources and Technology: Introduction 839
Peter D. Blair
 25. Pumps, Fans, Blowers, and Compressors 857
Keith Marchildon and David Mody
 26. Gas Turbines 901
Harold E. Miller and Todd S. Nemeç
 27. Wind Power Generation 955
Todd S. Nemeç
 28. Cogeneration 963
Jerald A. Caton
 29. Hydrogen Energy 991
E. K. Stefanakos, D. Y. Goswami, and S. S. Srinivasan
 30. Steam Turbines 1029
William W. Peng
 31. Fuel Cells 1055
Matthew M. Mench and Feng-Yuan Zhang
 32. Fluid Power Systems 1089
Andrew Alleyne
- Index 1123

Preface

The fourth volume of the fourth edition of the *Mechanical Engineers' Handbook* comprises 32 chapters divided into two parts, the first on energy and the second on power. Part 1 begins with a chapter on thermophysical properties of fluids, then proceeds to cover fundamentals of mechanics of incompressible fluids, thermodynamics (including a chapter on exergy and entropy generation minimization), heat transfer, and temperature and heat flux measurements. Additional heat transfer topics in this volume include heat exchangers, heat pipes, air heating, and electronic equipment cooling. There are chapters on refrigeration and cryogenic engineering. One chapter deals with environmental issues: indoor environmental control. A chapter on thermal systems optimization rounds out this part of this volume.

Part 2 opens with a chapter on combustion. This part also includes chapters on conventional energy sources—gaseous and liquid fuels and coal (one chapter on properties of coals, lignite, and peat and a second chapter on clean power generation from coal)—and alternative energy sources—biofuels, solar, geothermal and fuel cells. There are, in addition, chapters on cogeneration and hydrogen energy. There are six chapters on power machinery: one on fans, blowers, compressors, and pumps; one each on gas, wind, and steam turbines; one on internal combustion engines and one on fluid power.

Two chapters—on cryogenic engineering and steam turbines—replace the old versions of the chapters on these important topics. To provide greater emphasis on sustainability than in earlier editions, I have included four chapters—on clean power generation from coal, wind power generation, cogeneration, and hydrogen energy—from my book, *Environmentally Conscious Alternative Energy Production* (chapters updated as contributors found necessary) and one chapter on biofuels from *Environmentally Conscious Transportation*. I have also included three chapters—on temperature, heat flux, and solar energy measurements—from my *Handbook of Measurement in Science and Engineering* and one on mechanics of incompressible fluids from the current edition of *Eshbach's Handbook of Engineering Fundamentals*, which I edited. Inclusion of these chapters enriches this handbook. All told, more than half the chapters in this volume contain material new to this handbook.

Vision for the Fourth Edition

Basic engineering disciplines are not static, no matter how old and well established they are. The field of mechanical engineering is no exception. Movement within this broadly based discipline is multidimensional. Even the classic subjects, on which the discipline was founded, such as mechanics of materials and heat transfer, keep evolving. Mechanical engineers continue to be heavily involved with disciplines allied to mechanical engineering, such as industrial and manufacturing engineering, which are also constantly evolving. Advances in other major disciplines, such as electrical and electronics engineering, have significant impact on the work of mechanical engineers. New subject areas, such as neural networks, suddenly become all the rage.

In response to this exciting, dynamic atmosphere, the Mechanical Engineers' Handbook expanded dramatically, from one to four volumes for the third edition, published in November 2005. It not only incorporated updates and revisions to chapters in the second edition, published seven years earlier, but also added 24 chapters on entirely new subjects, with updates and revisions to chapters in the Handbook of Materials Selection, published in 2002, as well as to chapters in Instrumentation and Control, edited by Chester Nachtigal and published in 1990, but never updated by him.

The fourth edition retains the four-volume format, but there are several additional major changes. The second part of Volume I is now devoted entirely to topics in engineering mechanics, with the addition of five practical chapters on measurements from the Handbook of Measurement in Science and Engineering, published in 2013, and a chapter from the fifth edition of Eshbach's Handbook of Engineering Fundamentals, published in 2009. Chapters on mechanical design have been moved from Volume I to Volumes II and III. They have been augmented with four chapters (updated as needed) from Environmentally Conscious Mechanical Design, published in 2007. These chapters, together with five chapters (updated as needed, three from Environmentally Conscious Manufacturing, published in 2007, and two from Environmentally Conscious Materials Handling, published in 2009) in the beefed-up manufacturing section of Volume III, give the handbook greater and practical emphasis on the vital issue of sustainability.

Prefaces to the handbook's individual volumes provide further details on chapter additions, updates and replacements. The four volumes of the fourth edition are arranged as follows:

Volume 1: Materials and Engineering Mechanics—27 chapters

Part 1. Materials—15 chapters

Part 2. Engineering Mechanics—12 chapters

Volume 2: Design, Instrumentation and Controls—25 chapters

Part 1. Mechanical Design—14 chapters

Part 2. Instrumentation, Systems, Controls, and MEMS —11 chapters

Volume 3: Manufacturing and Management—28 chapters

Part 1. Manufacturing—16 chapters

Part 2. Management, Finance, Quality, Law, and Research—12 chapters

Volume 4: Energy and Power—35 chapters

Part 1: Energy—16 chapters

Part 2: Power—19 chapters

The mechanical engineering literature is extensive and has been so for a considerable period of time. Many textbooks, reference works, and manuals as well as a substantial number of journals exist. Numerous commercial publishers and professional societies, particularly in the United States and Europe, distribute these materials. The literature grows continuously, as applied mechanical engineering research finds new ways of designing, controlling, measuring, making, and maintaining things, as well as monitoring and evaluating technologies, infrastructures, and systems.

Most professional-level mechanical engineering publications tend to be specialized, directed to the specific needs of particular groups of practitioners. Overall, however, the mechanical engineering audience is broad and multidisciplinary. Practitioners work in a variety of organizations, including institutions of higher learning, design, manufacturing, and consulting firms, as well as federal, state, and local government agencies. A rationale for a general mechanical engineering handbook is that every practitioner, researcher, and bureaucrat cannot be an expert on every topic, especially in so broad and multidisciplinary a field, and may need an authoritative professional summary of a subject with which he or she is not intimately familiar.

Starting with the first edition, published in 1986, my intention has always been that the Mechanical Engineers' Handbook stand at the intersection of textbooks, research papers, and design manuals. For example, I want the handbook to help young engineers move from the college classroom to the professional office and laboratory where they may have to deal with issues and problems in areas they have not studied extensively in school.

With this fourth edition, I have continued to produce a practical reference for the mechanical engineer who is seeking to answer a question, solve a problem, reduce a cost, or improve a system or facility. The handbook is not a research monograph. Its chapters offer design techniques, illustrate successful applications, or provide guidelines to improving performance, life expectancy, effectiveness, or usefulness of parts, assemblies, and systems. The purpose is to show readers what options are available in a particular situation and which option they might choose to solve problems at hand.

The aim of this handbook is to serve as a source of practical advice to readers. I hope that the handbook will be the first information resource a practicing engineer consults when faced with a new problem or opportunity—even before turning to other print sources, even officially sanctioned ones, or to sites on the Internet. In each chapter, the reader should feel that he or she is in the hands of an experienced consultant who is providing sensible advice that can lead to beneficial action and results.

Can a single handbook, even spread out over four volumes, cover this broad, interdisciplinary field? I have designed the Mechanical Engineers' Handbook as if it were serving as a core for an Internet-based information source. Many chapters in the handbook point readers to information sources on the Web dealing with the subjects addressed. Furthermore, where appropriate, enough analytical techniques and data are provided to allow the reader to employ a preliminary approach to solving problems.

The contributors have written, to the extent their backgrounds and capabilities make possible, in a style that reflects practical discussion informed by real-world experience. I would like readers to feel that they are in the presence of experienced teachers and consultants who know about the multiplicity of technical issues that impinge on any topic within mechanical engineering. At the same time, the level is such that students and recent graduates can find the handbook as accessible as experienced engineers.

Contributors

Andrew Alleyne
University of Illinois, Urbana–Champaign
Urbana, Illinois

Avram Bar-Cohen
University of Maryland
College Park, Maryland

Prabir Basu
Dalhousie University
Halifax, Nova Scotia

Adrian Bejan
Duke University
Durham, North Carolina

Peter D. Blair
National Academy of Sciences
Washington, DC

James W. Butler
Dalhousie University
Halifax, Nova Scotia

Jerald A. Caton
Texas A&M University
College Station, Texas

Peter R. N. Childs
Imperial College
London, England

Carroll Cone
Toledo, Ohio

T. E. Diller
Virginia Polytechnic Institute and State
University
Blacksburg, Virginia

Eric G. Eddings
University of Utah
Salt Lake City, Utah

D. Y. Goswami
University of South Florida
Tampa, Florida

Cesar Granda
Texas A&M University
College Station, Texas

Mark Holtzapple
Texas A&M University
College Station, Texas

Wade W. Huebsch
West Virginia University
Morgantown, West Virginia

James G. Keppeler
Progress Materials, Inc.
St. Petersburg, Florida

Allan Kraus
Beachwood, Ohio

Peter E. Liley
Purdue University
West Lafayette, Indiana

Hongbin Ma
University of Missouri
Columbia, Missouri

Keith Marchildon
Queen's University
Kingston, Ontario, Canada

Matthew M. Mench
University of Tennessee
Knoxville, Tennessee
and
Oak Ridge National Lab
Oak Ridge, Tennessee

Harold E. Miller
G.E. Energy
Schenectady, New York

David Mody
Queen's University
Kingston, Ontario, Canada

Tariq Muneer
Edinburgh Napier University
Edinburgh, Scotland

Todd S. Nemece
GE Energy
Schenectady, New York

Dennis L. O'Neal
Texas A&M University
College Station, Texas

Egemen Ol Ogetim
West Virginia University
Morgantown, West Virginia

Joseph W. Palen
Eugene, Oregon

William W. Peng
California State University
Fresno, California

G. P. Peterson
Georgia Institute of Technology
Atlanta, GA

Reinhard Radermacher
University of Maryland
College Park, Maryland

Richard J. Reed
North American Manufacturing Company
Cleveland, Ohio

Aaron Smith
Heat Transfer Research, Inc.
Navasota, TX

Jelena Srebric
University of Maryland
College Park, MD

S. S. Srinivasan
Florida Polytechnic University
Lakeland, FL

E. K. Stefanakos
University of South Florida
Tampa, Florida

Abhay A. Wative
Intel Corp.
Chandler, Arizona

Yieng Wei Tham
Edinburgh Napier University
Edinburgh, Scotland

J. G. Weisend II
European Spallation Source
Lund, Sweden

Feng-Yuan Zhang
University of Tennessee Space Institute
Tullahoma, Tennessee

PART 1

ENERGY

CHAPTER 1

THERMOPHYSICAL PROPERTIES OF FLUIDS

Peter E. Liley
Purdue University
West Lafayette, Indiana

Table 1 Conversion Factors

Table 2 Phase Transition Data for Elements

Table 3 Phase Transition Data for Compounds

Table 4 Thermodynamic Properties of Liquid and Saturated Vapor Air

Table 5 Ideal Gas Thermophysical Properties of Air

Table 6 Thermophysical Properties U.S. Standard Atmosphere

Table 7 Thermophysical Properties of Condensed and Saturated Vapor Carbon Dioxide from 200 K to Critical Point

Table 8 Thermophysical Properties of Gaseous Carbon Dioxide at 1 Bar Pressure

Figure 1 Enthalpy–Log Pressure Diagram for Carbon Dioxide

Table 9 Thermodynamic Properties of Saturated Mercury

Figure 2 Enthalpy–Log Pressure Diagram for Mercury

Table 10 Thermodynamic Properties of Saturated Methane

Table 11 Thermophysical Properties of Methane at Atmospheric Pressure

Table 12 Thermophysical Properties of Saturated Refrigerant 22

Table 13 Thermophysical Properties of Refrigerant 22 at Atmospheric Pressure

Figure 3 Enthalpy–log Pressure Diagram for Refrigerant 22

Table 14 Thermodynamic Properties of Saturated Refrigerant 134a

Table 15 Thermophysical Properties of Refrigerant 134a

Figure 4 Compressibility Factor of Refrigerant 134a

Figure 5 Enthalpy–Log Pressure Diagram for Refrigerant 134a

Table 16 Thermodynamic Properties of Saturated Sodium

Table 17 Thermodynamic Properties of Ice/Water

Table 18 Thermodynamic Properties of Saturated Steam/Water

Table 19 Thermophysical Properties of Miscellaneous Substances at Atmospheric Pressure

Table 20 Physical Properties of Numbered Refrigerants

Table 21 Specific Heat (kJ/kg · K) at Constant Pressure of Saturated Liquids

Table 22 Ratio of Principal Specific Heats, c_p/c_v , for Liquids and Gases at Atmospheric Pressure

Table 23 Surface Tension (N/m) of Liquids

Table 24 Thermal Conductivity (W/m · K) of Saturated Liquids

Table 25 Viscosity (10^{-4} Pa · s) of Saturated Liquids

Table 26 Thermochemical Properties at 1.013 Bars, 298.15 K

Table 27 Ideal Gas Sensible Enthalpies (kJ/kg · mol) of Common Products of Combustion

Figure 6 Psychometric Chart

4 Thermophysical Properties of Fluids

In this chapter, information is usually presented in the System International des Unités, called in English the International System of Units and abbreviated SI. Various tables of conversion factors from other unit systems into the SI system and vice versa are available. The following table is intended to enable rapid conversion to be made with moderate, that is, five significant figure, accuracy, usually acceptable in most engineering calculations. The references listed should be consulted for more exact conversions and definitions.

Table 1 Conversion Factors

Density: $1 \text{ kg/m}^3 = 0.06243 \text{ lb}_m/\text{ft}^3 = 0.01002 \text{ lb}_m/\text{U.K. gallon} = 8.3454 \times 10^{-3} \text{ lb}_m/\text{U.S. gallon} = 1.9403 \times 10^{-3} \text{ slug/ft}^3 = 10^{-3} \text{ g/cm}^3$

Energy: $1 \text{ kJ} = 737.56 \text{ ft} \cdot \text{lb}_f = 239.01 \text{ cal}_{\text{th}} = 0.94783 \text{ Btu} = 3.7251 \times 10^{-4} \text{ hp h} = 2.7778 \times 10^{-4} \text{ kWh}$

Specific energy: $1 \text{ kJ/kg} = 334.54 \text{ ft} \cdot \text{lb}_f/\text{lb}_m = 0.4299 \text{ Btu}/\text{lb}_m = 0.2388 \text{ cal/g}$

Specific energy per degree: $1 \text{ kJ/kg} \cdot \text{K} = 0.23901 \text{ Btu}_{\text{th}}/\text{lb} \cdot ^\circ\text{F} = 0.23901 \text{ cal}_{\text{th}}/\text{g} \cdot ^\circ\text{C}$

Mass: $1 \text{ kg} = 2.20462 \text{ lb}_m = 0.06852 \text{ slug} = 1.1023 \times 10^{-3} \text{ U.S. ton} = 10^{-3} \text{ tonne} = 9.8421 \times 10^{-4} \text{ U.K. ton}$

Pressure: $1 \text{ bar} = 10^5 \text{ N/m}^2 = 10^5 \text{ Pa} = 750.06 \text{ mm Hg at } 0^\circ\text{C} = 401.47 \text{ in. H}_2\text{O at } 32^\circ\text{F} = 29.530 \text{ in. Hg at } 0^\circ\text{C} = 14.504 \text{ lb/in.}^2 = 14.504 \text{ psia} = 1.01972 \text{ kg/cm}^2 = 0.98692 \text{ atm} = 0.1 \text{ MPa}$

Temperature: $T(\text{K}) = T(^{\circ}\text{C}) + 273.15 = [T(^{\circ}\text{F}) + 459.69]/1.8 = T(^{\circ}\text{R})/1.8$

Temperature difference: $\Delta T(\text{K}) = \Delta T(^{\circ}\text{C}) = \Delta T(^{\circ}\text{F})/1.8 = \Delta T(^{\circ}\text{R})/1.8$

Thermal conductivity: $1 \text{ W/m} \cdot \text{K} = 0.8604 \text{ kcal/m} \cdot \text{h} \cdot ^\circ\text{C} = 0.5782 \text{ Btu}/\text{ft} \cdot \text{h} \cdot ^\circ\text{F} = 0.01 \text{ W/cm} \cdot \text{K} = 2.390 \times 10^{-3} \text{ cal/cm} \cdot \text{s} \cdot ^\circ\text{C}$

Thermal diffusivity: $1 \text{ m}^2/\text{s} = 38,750 \text{ ft}^2/\text{h} = 3600 \text{ m}^2/\text{h} = 10.764 \text{ ft}^2/\text{s}$

Viscosity, dynamic: $1 \text{ N} \cdot \text{s}/\text{m}^2 = 1 \text{ Pa} \cdot \text{s} = 10^7 \mu\text{P} = 2419.1 \text{ lb}_m/\text{ft} \cdot \text{h} = 10^3 \text{ cP} = 75.188 \text{ slug}/\text{ft} \cdot \text{h} = 10 \text{ P} = 0.6720 \text{ lb}_m/\text{ft} \cdot \text{s} = 0.02089 \text{ lb}_f \cdot \text{s}/\text{ft}^2$

Viscosity, kinematic (*see* thermal diffusivity)

Source: E. Lange, L. F. Sokol, and V. Antoine, *Information on the Metric System and Related Fields*, 6th ed., G. C. Marshall Space Flight Center, AL (exhaustive bibliography); B. N. Taylor, *The International System of Units*, NBS S.P. 330, Washington, D.C., 2001; E. A. Mechtly, *The International System of Units. Physical Constants and Conversion Factors*, NASA S.P. 9012, 1973. numerous revisions periodically appear: see, for example, *Pure Appl. Chem.*, **51**, 1–41 (1979) and later issues.

Table 2 Phase Transition Data for Elements^a

Name	Symbol	Formula Weight	T_m (K)	Δh_{fus} (kJ/kg)	T_b (K)	T_c (K)
Actinium	Ac	227.028	1323	63	3,475	
Aluminum	Al	26.9815	933.5	398	2,750	7,850
Antimony	Sb	121.75	903.9	163	1,905	5,700
Argon	Ar	39.948	83	30	87.2	151
Arsenic	As	74.9216	885	—	—	2,100
Barium	Ba	137.33	1,002	55.8	—	4,450
Beryllium	Be	9.01218	1,560	1,355	2,750	6,200
Bismuth	Bi	208.980	544.6	54.0	1,838	4,450
Boron	B	10.81	2,320	1,933	4,000	3,300
Bromine	Br	159.808	266	66.0	332	584
Cadmium	Cd	112.41	594	55.1	1,040	2,690
Calcium	Ca	40.08	1,112	213.1	1,763	4,300
Carbon	C	12.011	3,810	—	4,275	7,200
Cerium	Ce	140.12	1,072	390	—	9,750
Cesium	Cs	132.905	301.8	16.4	951	2,015
Chlorine	Cl ₂	70.906	172	180.7	239	417

Table 2 (Continued)

Name	Symbol	Formula Weight	T_m (K)	Δh_{fus} (kJ/kg)	T_b (K)	T_c (K)
Chromium	Cr	51.996	2,133	325.6	2,950	5,500
Cobalt	Co	58.9332	1,766	274.7	3,185	6,300
Copper	Cu	63.546	1,357	206.8	2,845	8,280
Dysprosium	Dy	162.50	1,670	68.1	2,855	6,925
Erbium	Er	167.26	1,795	119.1	3,135	7,250
Europium	Eu	151.96	1,092	60.6	1,850	4,350
Fluorine	F ₂	37.997	53.5	13.4	85.0	144
Gadolinium	Gd	157.25	1,585	63.8	3,540	8,670
Gallium	Ga	69.72	303	80.1	2,500	7,125
Germanium	Ge	72.59	1,211	508.9	3,110	8,900
Gold	Au	196.967	1,337	62.8	3,130	7,250
Hafnium	Hf	178.49	2,485	134.8	4,885	10,400
Helium	He	4.00260	3.5	2.1	4.22	5.2
Holmium	Ho	164.930	1,744	73.8	2,968	7,575
Hydrogen	H ₂	2.0159	14.0	—	20.4	—
Indium	In	114.82	430	28.5	2,346	6,150
Iodine	I ₂	253.809	387	125.0	457	785
Iridium	Ir	192.22	2,718	13.7	4,740	7,800
Iron	Fe	55.847	1,811	247.3	3,136	8,500
Krypton	Kr	83.80	115.8	19.6	119.8	209.4
Lanthanum	La	138.906	1,194	44.6	3,715	10,500
Lead	Pb	207.2	601	23.2	2,025	5,500
Lithium	Li	6.941	454	432.2	1,607	3,700
Lutetium	Lu	174.967	1,937	106.6	3,668	—
Magnesium	Mg	24.305	922	368.4	1,364	3,850
Manganese	Mn	54.9380	1,518	219.3	2,334	4,325
Mercury	Hg	200.59	234.6	11.4	630	1,720
Molybdenum	Mo	95.94	2,892	290.0	4,900	1,450
Neodymium	Nd	144.24	1,290	49.6	3,341	7,900
Neon	Ne	20.179	24.5	16.4	27.1	44.5
Neptunium	Np	237.048	910	—	4,160	12,000
Nickel	Ni	58.70	1,728	297.6	3,190	8,000
Niobium	Nb	92.9064	2,740	283.7	5,020	12,500
Nitrogen	N ₂	28.013	63.2	25.7	77.3	126.2
Osmium	Os	190.2	3,310	150.0	5,300	12,700
Oxygen	O ₂	31.9988	54.4	13.8	90.2	154.8
Palladium	Pd	106.4	1,826	165.0	3,240	7,700
Phosphorus	P	30.9738	317	—	553	995
Platinum	Pt	195.09	2,045	101	4,100	10,700
Plutonium	Pu	244	913	11.7	3,505	10,500
Potassium	K	39.0983	336.4	60.1	1,032	2,210
Praseodymium	Pr	140.908	1,205	49	3,785	8,900
Promethium	Pm	145	1,353	—	2,730	—
Protactinium	Pa	231	1,500	64.8	4,300	—
Radium	Ra	226.025	973	—	1,900	—
Radon	Rn	222	202	12.3	211	377
Rhenium	Re	186.207	3,453	177.8	5,920	18,900
Rhodium	Rh	102.906	2,236	209.4	3,980	7,000
Rubidium	Rb	85.4678	312.6	26.4	964	2,070
Ruthenium	Ru	101.07	2,525	256.3	4,430	9,600
Samarium	Sm	150.4	1,345	57.3	2,064	5,050
Scandium	Sc	44.9559	1,813	313.6	3,550	6,410

(continued)

6 Thermophysical Properties of Fluids

Table 2 (Continued)

Name	Symbol	Formula Weight	T_m (K)	Δh_{fus} (kJ/kg)	T_b (K)	T_c (K)
Selenium	Se	78.96	494	66.2	958	1,810
Silicon	Si	28.0855	1,684	1802	3,540	5,160
Silver	Ag	107.868	1,234	104.8	2,435	6,400
Sodium	Na	22.9898	371	113.1	1,155	2,500
Strontium	Sr	87.62	1,043	1042	1,650	4,275
Sulfur	S	32.06	388	53.4	718	1,210
Tantalum	Ta	180.948	3,252	173.5	5,640	16,500
Technetium	Tc	98	2,447	232	4,550	11,500
Tellurium	Te	127.60	723	137.1	1,261	2,330
Terbium	Tb	158.925	1,631	67.9	3,500	8,470
Thallium	Tl	204.37	577	20.1	1,745	4,550
Thorium	Th	232.038	2,028	69.4	5,067	14,400
Thulium	Tm	168.934	1,819	99.6	2,220	6,450
Tin	Sn	118.69	505	58.9	2,890	7,700
Titanium	Ti	47.90	1,943	323.6	3,565	5,850
Tungsten	W	183.85	3,660	192.5	5,890	15,500
Uranium	U	238.029	1,406	35.8	4,422	12,500
Vanadium	V	50.9415	2,191	410.7	3,680	11,300
Xenon	Xe	131.30	161.3	17.5	164.9	290
Ytterbium	Yb	173.04	1,098	44.2	1,467	4,080
Yttrium	Y	88.9059	1,775	128.2	3,610	8,950
Zinc	Zn	65.38	692.7	113.0	1,182	
Zirconium	Zr	91.22	2125	185.3	4,681	10,500

^a T_m = normal melting point; Δh_{fus} = enthalpy of fusion; T_b = normal boiling point; T_c = critical temperature.

Table 3 Phase Transition Data for Compounds^a

Substance	T_m (K)	Δh_m (kJ/kg)	T_b (K)	Δh_v (kJ/kg)	T_c (K)	P_c (bars)
Acetaldehyde	149.7	73.2	293.4	584	461	55.4
Acetic acid	289.9	195.3	391.7	405	594	57.9
Acetone	178.6	98	329.5	501	508	47
Acetylene	—	96.4	189.2	687	309	61.3
Air	60	—	—	—	133	37.7
Ammonia	195.4	331.9	239.7	1368	405.6	112.8
Aniline	267.2	113.3	457.6	485	699	53.1
Benzene	267.7	125.9	353.3	394	562	49
<i>n</i> -Butane	134.8	80.2	261.5	366	425.2	38
Butanol	188	125.2	391.2	593	563	44.1
Carbon dioxide	216.6	184	194.7	573	304.2	73.8
Carbon disulfide	161	57.7	319.6	352	552	79
Carbon monoxide	68.1	29.8	81.6	215	133	35
Carbon tetrachloride	250.3	173.9	349.9	195	556	45.6
Carbon tetrafluoride	89.5	—	145.2	138	227.9	37.4
Chlorobenzene	228	—	405	325	632.4	45.2
Chloroform	210	77.1	334.4	249	536.6	54.7
<i>m</i> -Cresol	285.1	—	475.9	421	705	45.5
Cyclohexane	279.6	31.7	356	357	554.2	40.7
Cyclopropane	145.5	129.4	240.3	477	397.8	54.9
<i>n</i> -Decane	243.2	202.1	447.3	276	617	21
Ethane	89.9	94.3	184.6	488	305.4	48.8

Table 3 (Continued)

Substance	T_m (K)	Δh_m (kJ/kg)	T_b (K)	Δh_v (kJ/kg)	T_c (K)	P_c (bars)
Ethanol	158.6	109	351.5	840	516	63.8
Ethyl acetate	190.8	119	350.2	366	523.3	38.3
Ethylene	104	119.5	169.5	480	283.1	51.2
Ethylene oxide	161.5	117.6	283.9	580	469	71.9
Formic acid	281.4	246.4	373.9	502	576	34.6
Heptane	182.6	140.2	371.6	316	540	27.4
Hexane	177.8	151.2	341.9	335	507	29.7
Hydrazine	274.7	395	386.7	1207	653	147
Hydrogen peroxide	271.2	310	431	1263	—	—
Isobutane	113.6	78.1	272.7	386	408.1	36.5
Methane	90.7	58.7	111.5	512	191.1	46.4
Methanol	175.4	99.2	337.7	1104	513.2	79.5
Methyl acetate	174.8	—	330.2	410	507	46.9
Methyl bromide	180	62.9	277.7	252	464	71.2
Methyl chloride	178.5	127.4	249.3	429	416.3	66.8
Methyl formate	173.4	125.5	305	481	487.2	60
Methylene chloride	176.4	54.4	312.7	328	510.2	60.8
Naphthalene	353.2	148.1	491	341	747	39.5
Nitric oxide	111	76.6	121.4	460	180.3	65.5
Octane	216.4	180.6	398.9	303	569.4	25
Pentane	143.7	116.6	309.2	357	469.8	33.7
Propane	86	80	231.1	426	370	42.5
Propanol	147	86.5	370.4	696	537	51.7
Propylene	87.9	71.4	225.5	438	365	46.2
Refrigerant 12	115	34.3	243.4	165	385	41.2
Refrigerant 13	92	—	191.8	148	302.1	38.7
Refrigerant 13B1	105.4	—	215.4	119	340	39.6
Refrigerant 21	138	—	282.1	242	451.7	51.7
Refrigerant 22	113	47.6	232.4	234	369	49.8
Steam/water	273.2	334	373.2	2257	647.3	221.2
Sulfuric acid	283.7	100.7	v	v	v	v
Sulfur dioxide	197.7	115.5	268.4	386	430.7	78.8
Toluene	178.2	—	383.8	339	594	41

^a v = variable; T_m = normal melting point; Δh_m = enthalpy of fusion; T_b = normal boiling point; Δh_v = enthalpy of vaporization; T_c = critical temperature; P_c = critical pressure.

Table 4 Thermodynamic Properties of Liquid and Saturated Vapor Air^a

T (K)	P_f (MPa)	P_g (MPa)	v_f (m ³ /kg)	v_g (m ³ /kg)	h_f (kJ/kg)	h_g (kJ/kg)	s_f (kJ/kg · K)	s_g (kJ/kg · K)
60	0.0066	0.0025	0.001027	6.876	-144.9	59.7	2.726	6.315
65	0.0159	0.0077	0.001078	2.415	-144.8	64.5	2.727	6.070
70	0.0340	0.0195	0.001103	1.021	-144.0	69.1	2.798	5.875
75	0.0658	0.0424	0.001130	0.4966	-132.8	73.5	2.896	5.714
80	0.1172	0.0826	0.001160	0.2685	-124.4	77.5	3.004	5.580
85	0.1954	0.1469	0.001193	0.1574	-115.2	81.0	3.114	5.464
90	0.3079	0.2434	0.001229	0.0983	-105.5	84.1	3.223	5.363
95	0.4629	0.3805	0.001269	0.0644	-95.4	86.5	3.331	5.272
100	0.6687	0.5675	0.001315	0.0439	-84.8	88.2	3.436	5.189

(continued)

8 Thermophysical Properties of Fluids

Table 4 (Continued)

T (K)	P_f (MPa)	P_g (MPa)	v_f (m ³ /kg)	v_g (m ³ /kg)	h_f (kJ/kg)	h_g (kJ/kg)	s_f (kJ/kg · K)	s_g (kJ/kg · K)
105	0.9334	0.8139	0.001368	0.0308	-73.8	89.1	3.540	5.110
110	1.2651	1.1293	0.001432	0.0220	-62.2	89.1	3.644	5.033
115	1.6714	1.5238	0.001512	0.0160	-49.7	87.7	3.750	4.955
120	2.1596	2.0081	0.001619	0.0116	-35.9	84.5	3.861	4.872
125	2.743	2.614	0.001760	0.0081	-19.7	78.0	3.985	4.770
132.5 ^b	3.770	3.770	0.00309	0.0031	33.6	33.6	4.38	4.38

^a v = specific volume; h = specific enthalpy; s = specific entropy; f = saturated liquid; g = saturated vapor. 1 MPa = 10 bars.

^bApproximate critical point. Air is a multicomponent mixture.

Table 5 Ideal Gas Thermophysical Properties of Air^a

T (K)	v (m ³ /kg)	h (kJ/kg)	s (kJ/kg · K)	c_p (kJ/kg · K)	γ	\bar{v}_s (m/s)	η (N · s/m ²)	λ (W/m · K)	Pr
200	0.5666	-103.0	6.4591	1.008	1.398	283.3	1.33,-5 ^b	0.0183	0.734
210	0.5949	-92.9	6.5082	1.007	1.399	290.4	1.39,-5	0.0191	0.732
220	0.6232	-82.8	6.5550	1.006	1.399	297.3	1.44,-5	0.0199	0.730
230	0.6516	-72.8	6.5998	1.006	1.400	304.0	1.50,-5	0.0207	0.728
240	0.6799	-62.7	6.6425	1.005	1.400	310.5	1.55,-5	0.0215	0.726
250	0.7082	-52.7	6.6836	1.005	1.400	317.0	1.60,-5	0.0222	0.725
260	0.7366	-42.6	6.7230	1.005	1.400	323.3	1.65,-5	0.0230	0.723
270	0.7649	-32.6	6.7609	1.004	1.400	329.4	1.70,-5	0.0237	0.722
280	0.7932	-22.5	6.7974	1.004	1.400	335.5	1.75,-5	0.0245	0.721
290	0.8216	-12.5	6.8326	1.005	1.400	341.4	1.80,-5	0.0252	0.720
300	0.8499	-2.4	6.8667	1.005	1.400	347.2	1.85,-5	0.0259	0.719
310	0.8782	7.6	6.8997	1.005	1.400	352.9	1.90,-5	0.0265	0.719
320	0.9065	17.7	6.9316	1.006	1.399	358.5	1.94,-5	0.0272	0.719
330	0.9348	27.7	6.9625	1.006	1.399	364.0	1.99,-5	0.0279	0.719
340	0.9632	37.8	6.9926	1.007	1.399	369.5	2.04,-5	0.0285	0.719
350	0.9916	47.9	7.0218	1.008	1.398	374.8	2.08,-5	0.0292	0.719
360	1.0199	57.9	7.0502	1.009	1.398	380.0	2.12,-5	0.0298	0.719
370	1.0482	68.0	7.0778	1.010	1.397	385.2	2.17,-5	0.0304	0.719
380	1.0765	78.1	7.1048	1.011	1.397	390.3	2.21,-5	0.0311	0.719
390	1.1049	88.3	7.1311	1.012	1.396	395.3	2.25,-5	0.0317	0.719
400	1.1332	98.4	7.1567	1.013	1.395	400.3	2.29,-5	0.0323	0.719
410	1.1615	108.5	7.1817	1.015	1.395	405.1	2.34,-5	0.0330	0.719
420	1.1898	118.7	7.2062	1.016	1.394	409.9	2.38,-5	0.0336	0.719
430	1.2181	128.8	7.2301	1.018	1.393	414.6	2.42,-5	0.0342	0.718
440	1.2465	139.0	7.2535	1.019	1.392	419.3	2.46,-5	0.0348	0.718
450	1.2748	149.2	7.2765	1.021	1.391	423.9	2.50,-5	0.0355	0.718
460	1.3032	159.4	7.2989	1.022	1.390	428.3	2.53,-5	0.0361	0.718
470	1.3315	169.7	7.3209	1.024	1.389	433.0	2.57,-5	0.0367	0.718
480	1.3598	179.9	7.3425	1.026	1.389	437.4	2.61,-5	0.0373	0.718
490	1.3882	190.2	7.3637	1.028	1.388	441.8	2.65,-5	0.0379	0.718
500	1.4165	200.5	7.3845	1.030	1.387	446.1	2.69,-5	0.0385	0.718
520	1.473	221.1	7.4249	1.034	1.385	454.6	2.76,-5	0.0398	0.718
540	1.530	241.8	7.4640	1.038	1.382	462.9	2.83,-5	0.0410	0.718
560	1.586	262.6	7.5018	1.042	1.380	471.0	2.91,-5	0.0422	0.718
580	1.643	283.5	7.5385	1.047	1.378	479.0	2.98,-5	0.0434	0.718
600	1.700	304.5	7.5740	1.051	1.376	486.8	3.04,-5	0.0446	0.718
620	1.756	325.6	7.6086	1.056	1.374	494.4	3.11,-5	0.0458	0.718
640	1.813	346.7	7.6422	1.060	1.371	501.9	3.18,-5	0.0470	0.718
660	1.870	368.0	7.6749	1.065	1.369	509.3	3.25,-5	0.0482	0.717

Table 5 (Continued)

T (K)	v (m ³ /kg)	h (kJ/kg)	s (kJ/kg · K)	c_p (kJ/kg · K)	γ	\bar{v}_s (m/s)	η (N · s/m ²)	λ (W/m · K)	Pr
680	1.926	389.3	7.7067	1.070	1.367	516.5	3.32.-5	0.0495	0.717
700	1.983	410.8	7.7378	1.075	1.364	523.6	3.38.-5	0.0507	0.717
720	2.040	432.3	7.7682	1.080	1.362	530.6	3.45.-5	0.0519	0.716
740	2.096	453.9	7.7978	1.084	1.360	537.5	3.51.-5	0.0531	0.716
760	2.153	475.7	7.8268	1.089	1.358	544.3	3.57.-5	0.0544	0.716
780	2.210	497.5	7.8551	1.094	1.356	551.0	3.64.-5	0.0556	0.716
800	2.266	519.4	7.8829	1.099	1.354	557.6	3.70.-5	0.0568	0.716
820	2.323	541.5	7.9101	1.103	1.352	564.1	3.76.-5	0.0580	0.715
840	2.380	563.6	7.9367	1.108	1.350	570.6	3.82.-5	0.0592	0.715
860	2.436	585.8	7.9628	1.112	1.348	576.8	3.88.-5	0.0603	0.715
880	2.493	608.1	7.9885	1.117	1.346	583.1	3.94.-5	0.0615	0.715
900	2.550	630.4	8.0136	1.121	1.344	589.3	4.00.-5	0.0627	0.715
920	2.606	652.9	8.0383	1.125	1.342	595.4	4.05.-5	0.0639	0.715
940	2.663	675.5	8.0625	1.129	1.341	601.5	4.11.-5	0.0650	0.714
960	2.720	698.1	8.0864	1.133	1.339	607.5	4.17.-5	0.0662	0.714
980	2.776	720.8	8.1098	1.137	1.338	613.4	4.23.-5	0.0673	0.714
1000	2.833	743.6	8.1328	1.141	1.336	619.3	4.28.-5	0.0684	0.714
1050	2.975	800.8	8.1887	1.150	1.333	633.8	4.42.-5	0.0711	0.714
1100	3.116	858.5	8.2423	1.158	1.330	648.0	4.55.-5	0.0738	0.715
1150	3.258	916.6	8.2939	1.165	1.327	661.8	4.68.-5	0.0764	0.715
1200	3.400	975.0	8.3437	1.173	1.324	675.4	4.81.-5	0.0789	0.715
1250	3.541	1033.8	8.3917	1.180	1.322	688.6	4.94.-5	0.0814	0.716
1300	3.683	1093.0	8.4381	1.186	1.319	701.6	5.06.-5	0.0839	0.716
1350	3.825	1152.3	8.4830	1.193	1.317	714.4	5.19.-5	0.0863	0.717
1400	3.966	1212.2	8.5265	1.199	1.315	726.9	5.31.-5	0.0887	0.717
1450	4.108	1272.3	8.5686	1.204	1.313	739.2	5.42.-5	0.0911	0.717
1500	4.249	1332.7	8.6096	1.210	1.311	751.3	5.54.-5	0.0934	0.718
1550	4.391	1393.3	8.6493	1.215	1.309	763.2	5.66.-5	0.0958	0.718
1600	4.533	1454.2	8.6880	1.220	1.308	775.0	5.77.-5	0.0981	0.717
1650	4.674	1515.3	8.7256	1.225	1.306	786.5	5.88.-5	0.1004	0.717
1700	4.816	1576.7	8.7622	1.229	1.305	797.9	5.99.-5	0.1027	0.717
1750	4.958	1638.2	8.7979	1.233	1.303	809.1	6.10.-5	0.1050	0.717
1800	5.099	1700.0	8.8327	1.237	1.302	820.2	6.21.-5	0.1072	0.717
1850	5.241	1762.0	8.8667	1.241	1.301	831.1	6.32.-5	0.1094	0.717
1900	5.383	1824.1	8.8998	1.245	1.300	841.9	6.43.-5	0.1116	0.717
1950	5.524	1886.4	8.9322	1.248	1.299	852.6	6.53.-5	0.1138	0.717
2000	5.666	1948.9	8.9638	1.252	1.298	863.1	6.64.-5	0.1159	0.717
2050	5.808	2011.6	8.9948	1.255	1.297	873.5	6.74.-5	0.1180	0.717
2100	5.949	2074.4	9.0251	1.258	1.296	883.8	6.84.-5	0.1200	0.717
2150	6.091	2137.3	9.0547	1.260	1.295	894.0	6.95.-5	0.1220	0.717
2200	6.232	2200.4	9.0837	1.263	1.294	904.0	7.05.-5	0.1240	0.718
2250	6.374	2263.6	9.1121	1.265	1.293	914.0	7.15.-5	0.1260	0.718
2300	6.516	2327.0	9.1399	1.268	1.293	923.8	7.25.-5	0.1279	0.718
2350	6.657	2390.5	9.1672	1.270	1.292	933.5	7.35.-5	0.1298	0.719
2400	6.800	2454.0	9.1940	1.273	1.291	943.2	7.44.-5	0.1317	0.719
2450	6.940	2517.7	9.2203	1.275	1.291	952.7	7.54.-5	0.1336	0.720
2500	7.082	2581.5	9.2460	1.277	1.290	962.2	7.64.-5	0.1354	0.720

^a v = specific volume; h = specific enthalpy; s = specific entropy; c_p = specific heat at constant pressure; γ = specific heat ratio, c_p/c_v (dimensionless); \bar{v}_s = velocity of sound; η = dynamic viscosity; λ = thermal conductivity; Pr = Prandtl number (dimensionless). Condensed from S. Gordon, *Thermodynamic and Transport Combustion Properties of Hydrocarbons with Air*, NASA Technical Paper 1906, 1982, Vol. 1. These properties are based on constant gaseous composition. The reader is reminded that at the higher temperatures the influence of pressure can affect the composition and the thermodynamic properties.

^bThe notation 1.33.-5 signifies 1.33×10^{-5} .

Table 6 Thermophysical Properties of U.S. Standard Atmosphere^a

Z (m)	H (m)	T (K)	P (bars)	ρ (kg/m ³)	g (m/s ²)	\bar{v}_s (m/s)
0	0	288.15	1.0133	1.2250	9.8067	340.3
1,000	1,000	281.65	0.8988	1.1117	9.8036	336.4
2,000	1,999	275.15	0.7950	1.0066	9.8005	332.5
3,000	2,999	268.66	0.7012	0.9093	9.7974	328.6
4,000	3,997	262.17	0.6166	0.8194	9.7943	324.6
5,000	4,996	255.68	0.5405	0.7364	9.7912	320.6
6,000	5,994	249.19	0.4722	0.6601	9.7882	316.5
7,000	6,992	242.70	0.4111	0.5900	9.7851	312.3
8,000	7,990	236.22	0.3565	0.5258	9.7820	308.1
9,000	8,987	229.73	0.3080	0.4671	9.7789	303.9
10,000	9,984	223.25	0.2650	0.4135	9.7759	299.5
11,000	10,981	216.77	0.2270	0.3648	9.7728	295.2
12,000	11,977	216.65	0.1940	0.3119	9.7697	295.1
13,000	12,973	216.65	0.1658	0.2667	9.7667	295.1
14,000	13,969	216.65	0.1417	0.2279	9.7636	295.1
15,000	14,965	216.65	0.1211	0.1948	9.7605	295.1
16,000	15,960	216.65	0.1035	0.1665	9.7575	295.1
17,000	16,954	216.65	0.0885	0.1423	9.7544	295.1
18,000	17,949	216.65	0.0756	0.1217	9.7513	295.1
19,000	18,943	216.65	0.0647	0.1040	9.7483	295.1
20,000	19,937	216.65	0.0553	0.0889	9.7452	295.1
22,000	21,924	218.57	0.0405	0.0645	9.7391	296.4
24,000	23,910	220.56	0.0297	0.0469	9.7330	297.7
26,000	25,894	222.54	0.0219	0.0343	9.7269	299.1
28,000	27,877	224.53	0.0162	0.0251	9.7208	300.4
30,000	29,859	226.51	0.0120	0.0184	9.7147	301.7
32,000	31,840	228.49	0.00889	0.01356	9.7087	303.0
34,000	33,819	233.74	0.00663	0.00989	9.7026	306.5
36,000	35,797	239.28	0.00499	0.00726	9.6965	310.1
38,000	37,774	244.82	0.00377	0.00537	9.6904	313.7
40,000	39,750	250.35	0.00287	0.00400	9.6844	317.2
42,000	41,724	255.88	0.00220	0.00299	9.6783	320.7
44,000	43,698	261.40	0.00169	0.00259	9.6723	324.1
46,000	45,669	266.93	0.00131	0.00171	9.6662	327.5
48,000	47,640	270.65	0.00102	0.00132	9.6602	329.8
50,000	49,610	270.65	0.00080	0.00103	9.6542	329.8

^aZ = geometric altitude; H = geopotential altitude; ρ = density; g = acceleration of gravity; \bar{v}_s = velocity of sound. Condensed and in some cases converted from *U.S. Standard Atmosphere 1976*, National Oceanic and Atmospheric Administration and National Aeronautics and Space Administration, Washington, DC. Also available as NOAA-S/T 76-1562 and Government Printing Office Stock No. 003-017-00323-0.

Table 7 Thermophysical Properties of Condensed and Saturated Vapor Carbon Dioxide from 200 K to Critical Point^a

T (K)	P (bars)	Specific Volume		Specific Enthalpy		Specific Entropy		Specific Heat (c_p)		Thermal Conductivity		Viscosity		Prandtl Number	
		Condensed ^b	Vapor	Condensed ^b	Vapor	Condensed ^b	Vapor	Condensed ^b	Vapor	Liquid	Vapor	Liquid	Vapor	Liquid	Vapor
200	1.544	0.000644	0.2362	164.8	728.3	1.620	4.439								
205	2.277	0.000649	0.1622	171.5	730.0	1.652	4.379								
210	3.280	0.000654	0.1135	178.2	730.9	1.682	4.319								
215	4.658	0.000659	0.0804	185.0	731.3	1.721	4.264								
216.6	5.180	0.000661	0.0718	187.2	731.5	1.736	4.250								
216.6	5.180	0.000848	0.0718	386.3	731.5	2.656	4.250	1.707	0.958	0.182	0.011	2.10	0.116	1.96	0.96
220	5.996	0.000857	0.0624	392.6	733.1	2.684	4.232	1.761	0.985	0.178	0.012	1.86	0.118	1.93	0.97
225	7.357	0.000871	0.0515	401.8	735.1	2.723	4.204	1.820	1.02	0.171	0.012	1.75	0.120	1.87	0.98
230	8.935	0.000886	0.0428	411.1	736.7	2.763	4.178	1.879	1.06	0.164	0.013	1.64	0.122	1.84	0.99
235	10.75	0.000901	0.0357	420.5	737.9	2.802	4.152	1.906	1.10	0.160	0.013	1.54	0.125	1.82	1.01
240	12.83	0.000918	0.0300	430.2	738.9	2.842	4.128	1.933	1.15	0.156	0.014	1.45	0.128	1.80	1.02
245	15.19	0.000936	0.0253	440.1	739.4	2.882	4.103	1.959	1.20	0.148	0.015	1.36	0.131	1.80	1.04
250	17.86	0.000955	0.0214	450.3	739.6	2.923	4.079	1.992	1.26	0.140	0.016	1.28	0.134	1.82	1.06
255	20.85	0.000977	0.0182	460.8	739.4	2.964	4.056	2.038	1.34	0.134	0.017	1.21	0.137	1.84	1.08
260	24.19	0.001000	0.0155	471.6	738.7	3.005	4.032	2.125	1.43	0.128	0.018	1.14	0.140	1.89	1.12
265	27.89	0.001026	0.0132	482.8	737.4	3.047	4.007	2.237	1.54	0.122	0.019	1.08	0.144	1.98	1.17
270	32.03	0.001056	0.0113	494.4	735.6	3.089	3.981	2.410	1.66	0.116	0.020	1.02	0.150	2.12	1.23
275	36.59	0.001091	0.0097	506.5	732.8	3.132	3.954	2.634	1.81	0.109	0.022	0.96	0.157	2.32	1.32
280	41.60	0.001130	0.0082	519.2	729.1	3.176	3.925	2.887	2.06	0.102	0.024	0.91	0.167	2.57	1.44
285	47.10	0.001176	0.0070	532.7	723.5	3.220	3.891	3.203	2.40	0.095	0.028	0.86	0.178	2.90	1.56
290	53.15	0.001241	0.0058	547.6	716.9	3.271	3.854	3.724	2.90	0.088	0.033	0.79	0.191	3.35	1.68
295	59.83	0.001322	0.0047	562.9	706.3	3.317	3.803	4.68	—	0.081	0.042	0.71	0.207	4.1	1.8
300	67.10	0.001470	0.0037	585.4	690.2	3.393	3.742	—	—	0.074	0.065	0.60	0.226	—	—
304.2 ^c	73.83	0.002145	0.0021	636.6	636.6	3.558	3.558	—	—	—	—	—	—	—	—

^aSpecific volume, m³/kg; specific enthalpy, kJ/kg; specific entropy, kJ/kg · K; specific heat at constant pressure, kJ/kg · K; thermal conductivity, W/m · K; viscosity, 10⁻⁴ Pa · s. Thus, at 250 K the viscosity of the saturated liquid is 1.28 × 10⁻⁴ N · s/m² = 0.000128 Pa · s. The Prandtl number is dimensionless.

^bAbove the solid line the condensed phase is solid; below the line, it is liquid.

^cCritical point.

Table 8 Thermophysical Properties of Gaseous Carbon Dioxide at 1 Bar Pressure^a

	T (K)														
	300	350	400	450	500	550	600	650	700	750	800	850	900	950	1000
v (m ³ /kg)	0.5639	0.6595	0.7543	0.8494	0.9439	1.039	1.133	1.228	1.332	1.417	1.512	1.606	1.701	1.795	1.889
h (kJ/kg)	809.3	853.1	899.1	947.1	997.0	1049	1102	1156	1212	1269	1327	1386	1445	1506	1567
s (kJ/kg·K)	4.860	4.996	5.118	5.231	5.337	5.435	5.527	5.615	5.697	5.775	5.850	5.922	5.990	6.055	6.120
c_p (kJ/kg·K)	0.852	0.898	0.941	0.980	1.014	1.046	1.075	1.102	1.126	1.148	1.168	1.187	1.205	1.220	1.234
λ (W/m·K)	0.0166	0.0204	0.0243	0.0283	0.0325	0.0364	0.0407	0.0445	0.0481	0.0517	0.0551	0.0585	0.0618	0.0650	0.0682
M (10 ⁻⁴ Pa·s)	0.151	0.175	0.198	0.220	0.242	0.261	0.281	0.299	0.317	0.334	0.350	0.366	0.381	0.396	0.410
Pr	0.778	0.770	0.767	0.762	0.755	0.750	0.742	0.742	0.742	0.742	0.742	0.742	0.742	0.743	0.743

^a v = specific volume; h = enthalpy; s = entropy; c_p = specific heat at constant pressure; λ = thermal conductivity; η = viscosity (at 300 K the gas viscosity is 0.0000151 N·s/m² = 0.0000151 Pa·s); Pr = Prandtl number.

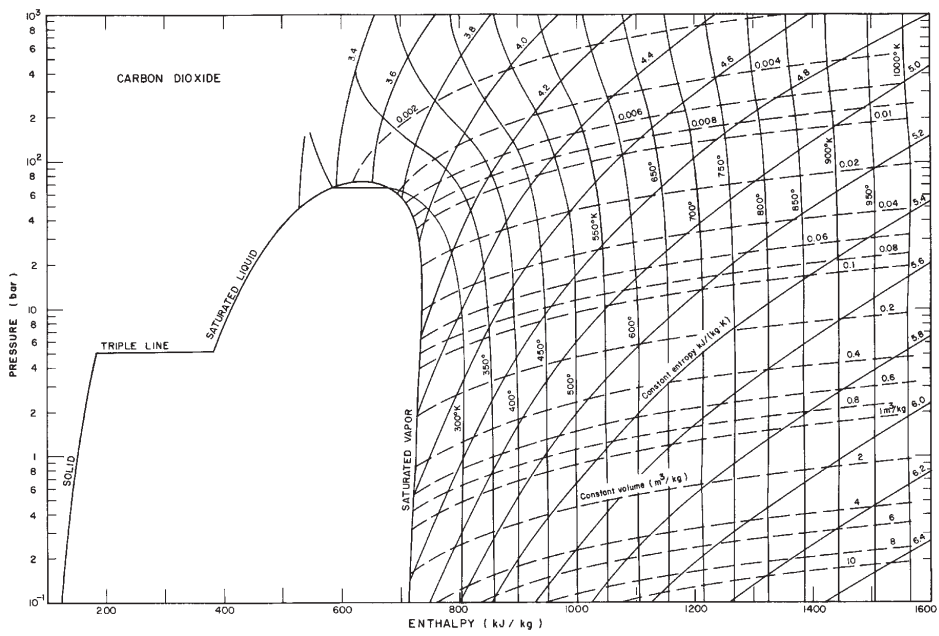


Figure 1 Enthalpy–log pressure diagram for carbon dioxide.

Table 9 Thermodynamic Properties of Saturated Mercury^a

T (K)	P (bars)	v (m ³ /kg)	h (kJ/kg)	s (kJ/kg · K)	c_p (kJ/kg · K)
0		6.873. ⁻⁵ ^b	0	0	0
20		6.875. ⁻⁵	0.466	0.0380	0.0513
40		6.884. ⁻⁵	1.918	0.0868	0.0894
60		6.897. ⁻⁵	3.897	0.1267	0.1067
80		6.911. ⁻⁵	6.129	0.1588	0.1156
100		6.926. ⁻⁵	8.497	0.1852	0.1209
120		6.942. ⁻⁵	10.956	0.2076	0.1248
140		6.958. ⁻⁵	13.482	0.2270	0.1278
160		6.975. ⁻⁵	16.063	0.2443	0.1304
180		6.993. ⁻⁵	18.697	0.2598	0.1330
200		7.013. ⁻⁵	21.386	0.2739	0.1360
220		7.034. ⁻⁵	24.139	0.2870	0.1394
234.3	7.330.-10	7.050. ⁻⁵	26.148	0.2959	0.1420
234.3	7.330.-10	7.304. ⁻⁵	37.585	0.3447	0.1422
240	1.668.-9	7.311. ⁻⁵	38.395	0.3481	0.1420
260	6.925.-8	7.339. ⁻⁵	41.224	0.3595	0.1409
280	5.296.-7	7.365. ⁻⁵	44.034	0.3699	0.1401
300	3.075.-6	7.387. ⁻⁵	46.829	0.3795	0.1393
320	1.428.-5	7.413. ⁻⁵	49.609	0.3885	0.1386
340	5.516.-5	7.439. ⁻⁵	52.375	0.3969	0.1380
360	1.829.-4	7.472. ⁻⁵	55.130	0.4048	0.1375
380	5.289.-4	7.499. ⁻⁵	57.874	0.4122	0.1370
400	1.394.-3	7.526. ⁻⁵	60.609	0.4192	0.1366
450	0.01053	7.595. ⁻⁵	67.414	0.4352	0.1357
500	0.05261	7.664. ⁻⁵	74.188	0.4495	0.1353
550	0.1949	7.735. ⁻⁵	80.949	0.4624	0.1352
600	0.5776	7.807. ⁻⁵	87.716	0.4742	0.1356
650	1.4425	7.881. ⁻⁵	94.508	0.4850	0.1360
700	3.153	7.957. ⁻⁵	101.343	0.4951	0.1372
750	6.197	8.036. ⁻⁵	108.242	0.5046	0.1382
800	11.181	8.118. ⁻⁵	115.23	0.5136	0.1398
850	18.816	8.203. ⁻⁵	122.31	0.5221	0.1416
900	29.88	8.292. ⁻⁵	129.53	0.5302	0.1439
950	45.23	8.385. ⁻⁵	137.16	0.5381	0.1464
1000	65.74	8.482. ⁻⁵	144.41	0.5456	0.1492

^a v = specific volume; h = specific enthalpy; s = specific entropy, c_p = specific heat at constant pressure. Properties above the solid line are for the solid; below they are for the liquid. Condensed, converted, and interpolated from the tables of M. P. Vukalovich, A. I. Ivanov, L. R. Fokin, and A. T. Yakovlev, *Thermophysical Properties of Mercury*, Standartov, Moscow, USSR, 1971.

^bThe notation 6.873.⁻⁵ signifies 6.873×10^{-5} .

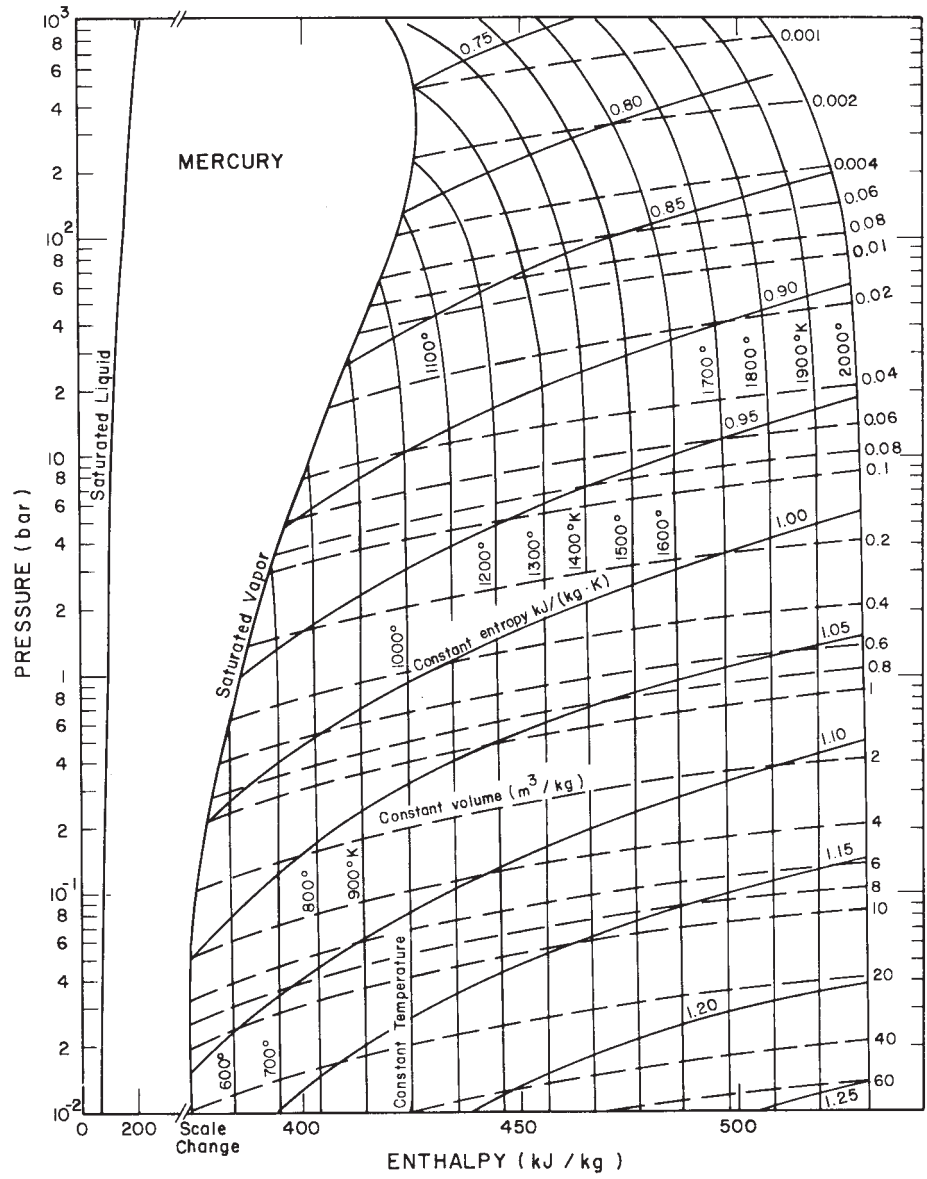


Figure 2 Enthalpy-log pressure diagram for mercury.

Table 10 Thermodynamic Properties of Saturated Methane^a

T (K)	P (bars)	v_f (m ³ /kg)	v_g (m ³ /kg)	h_f (kJ/kg)	h_g (kJ/kg)	s_f (kJ/kg · K)	S_g (kJ/kg · K)	c_{pf} (kJ/kg · K)	\bar{v}_s (m/s)
90.68	0.117	2.215.–3 ^b	3.976	216.4	759.9	4.231	10.225	3.288	1576
92	0.139	2.226.–3	3.410	220.6	762.4	4.279	10.168	3.294	1564
96	0.223	2.250.–3	2.203	233.2	769.5	4.419	10.006	3.326	1523
100	0.345	2.278.–3	1.479	246.3	776.9	4.556	9.862	3.369	1480
104	0.515	2.307.–3	1.026	259.6	784.0	4.689	9.731	3.415	1437
108	0.743	2.337.–3	0.732	273.2	791.0	4.818	9.612	3.458	1393
112	1.044	2.369.–3	0.536	287.0	797.7	4.944	9.504	3.497	1351
116	1.431	2.403.–3	0.401	301.1	804.2	5.068	9.405	3.534	1308
120	1.919	2.438.–3	0.306	315.3	810.8	5.187	9.313	3.570	1266
124	2.523	2.475.–3	0.238	329.7	816.2	5.305	9.228	3.609	1224
128	3.258	2.515.–3	0.187	344.3	821.6	5.419	9.148	3.654	1181
132	4.142	2.558.–3	0.150	359.1	826.5	5.531	9.072	3.708	1138
136	5.191	2.603.–3	0.121	374.2	831.0	5.642	9.001	3.772	1093
140	6.422	2.652.–3	0.0984	389.5	834.8	5.751	8.931	3.849	1047
144	7.853	2.704.–3	0.0809	405.2	838.0	5.858	8.864	3.939	999
148	9.502	2.761.–3	0.0670	421.3	840.6	5.965	8.798	4.044	951
152	11.387	2.824.–3	0.0558	437.7	842.2	6.072	8.733	4.164	902
156	13.526	2.893.–3	0.0467	454.7	843.2	6.177	8.667	4.303	852
160	15.939	2.971.–3	0.0392	472.1	843.0	6.283	8.601	4.470	802
164	18.647	3.059.–3	0.0326	490.1	841.6	6.390	8.533	4.684	749
168	21.671	3.160.–3	0.0278	508.9	839.0	6.497	8.462	4.968	695
172	25.034	3.281.–3	0.0234	528.6	834.6	6.606	8.385	5.390	637
176	28.761	3.428.–3	0.0196	549.7	827.9	6.720	8.301	6.091	570
180	32.863	3.619.–3	0.0162	572.9	818.1	6.843	8.205	7.275	500
184	37.435	3.890.–3	0.0131	599.7	802.9	6.980	8.084	9.831	421
188	42.471	4.361.–3	0.0101	634.0	776.4	7.154	7.912	19.66	327
190.56	45.988	6.233.–3	0.0062	704.4	704.4	7.516	7.516		

^a v = specific volume; h = specific enthalpy; s = specific entropy; c_p = specific heat at constant pressure; \bar{v}_s = velocity of sound; f = saturated liquid; g = saturated vapor. Condensed and converted from R. D. Goodwin, N.B.S. Technical Note 653, 1974.

^bThe notation 2.215.–3 signifies 2.215×10^{-3} .

Table 11 Thermophysical Properties of Methane at Atmospheric Pressure^a

	Temperature (K)									
	250	300	350	400	450	500	550	600	650	700
v	1.275	1.532	1.789	2.045	2.301	2.557	2.813	3.068	3.324	3.580
h	1090	1200	1315	1437	1569	1709	1857	2016	2183	2359
s	11.22	11.62	11.98	12.30	12.61	12.91	13.19	13.46	13.73	14.00
c_p	2.04	2.13	2.26	2.43	2.60	2.78	2.96	3.16	3.35	3.51
Z	0.997	0.998	0.999	1.000	1.000	1.000	1.000	1.000	1.000	1.000
\bar{v}_s	413	450	482	511	537	562	585	607	629	650
λ	0.0276	0.0342	0.0417	0.0486	0.0571	0.0675	0.0768	0.0863	0.0956	0.1052
η	0.095	0.112	0.126	0.141	0.154	0.168	0.180	0.192	0.202	0.214
Pr	0.701	0.696	0.683	0.687	0.690	0.693	0.696	0.700	0.706	0.714

^a v = specific volume (m³/kg); h = specific enthalpy (kJ/kg); s = specific entropy (kJ/kg · K); c_p = specific heat at constant pressure (kJ/kg · K); Z = compressibility factor = Pv/RT ; \bar{v}_s = velocity of sound (m/s); λ = thermal conductivity (W/m · K); η = viscosity 10^{-4} N · s/m² (thus, at 250 K the viscosity is 0.095×10^{-4} N · s/m² = 0.0000095 Pa · s); Pr = Prandtl number.

Table 12 Thermophysical Properties of Saturated Refrigerant 22^a

T (K)	P (bars)	v (m ³ /kg)		h (kJ/kg)		s (kJ/kg · K)		c _p (Liquid)	η (Liquid)	λ (Liquid)	τ (Liquid)
		Liquid	Vapor	Liquid	Vapor	Liquid	Vapor				
150	0.0017	6.209.—4 ^b	83.40	268.2	547.3	3.355	5.215	1.059		0.161	
160	0.0054	6.293.—4	28.20	278.2	552.1	3.430	5.141	1.058		0.156	
170	0.0150	6.381.—4	10.85	288.3	557.0	3.494	5.075	1.057	0.770	0.151	
180	0.0369	6.474.—4	4.673	298.7	561.9	3.551	5.013	1.058	0.647	0.146	
190	0.0821	6.573.—4	2.225	308.6	566.8	3.605	4.963	1.060	0.554	0.141	
200	0.1662	6.680.—4	1.145	318.8	571.6	3.657	4.921	1.065	0.481	0.136	0.024
210	0.3116	6.794.—4	0.6370	329.1	576.5	3.707	4.885	1.071	0.424	0.131	0.022
220	0.5470	6.917.—4	0.3772	339.7	581.2	3.756	4.854	1.080	0.378	0.126	0.021
230	0.9076	7.050.—4	0.2352	350.6	585.9	3.804	4.828	1.091	0.340	0.121	0.019
240	1.4346	7.195.—4	0.1532	361.7	590.5	3.852	4.805	1.105	0.309	0.117	0.0172
250	2.174	7.351.—4	0.1037	373.0	594.9	3.898	4.785	1.122	0.282	0.112	0.0155
260	3.177	7.523.—4	0.07237	384.5	599.0	3.942	4.768	1.143	0.260	0.107	0.0138
270	4.497	7.733.—4	0.05187	396.3	603.0	3.986	4.752	1.169	0.241	0.102	0.0121
280	6.192	7.923.—4	0.03803	408.2	606.6	4.029	4.738	1.193	0.225	0.097	0.0104
290	8.324	8.158.—4	0.02838	420.4	610.0	4.071	4.725	1.220	0.211	0.092	0.0087
300	10.956	8.426.—4	0.02148	432.7	612.8	4.113	4.713	1.257	0.198	0.087	0.0071
310	14.17	8.734.—4	0.01643	445.5	615.1	4.153	4.701	1.305	0.186	0.082	0.0055
320	18.02	9.096.—4	0.01265	458.6	616.7	4.194	4.688	1.372	0.176	0.077	0.0040
330	22.61	9.535.—4	9.753.—3	472.4	617.3	4.235	4.674	1.460	0.167	0.072	0.0026
340	28.03	1.010.—3	7.479.—3	487.2	616.5	4.278	4.658	1.573	0.151	0.067	0.0014
350	34.41	1.086.—3	5.613.—3	503.7	613.3	4.324	4.637	1.718	0.130	0.062	0.0008
360	41.86	1.212.—3	4.036.—3	523.7	605.5	4.378	4.605	1.897	0.106	—	—
369.3	49.89	2.015.—3	2.015.—3	570.0	570.0	4.501	4.501	∞	—	—	0

^ac_p in units of kJ/kg · K; η = viscosity (10⁻⁴ Pa · s); λ = thermal conductivity (W/m · K); T = surface tension (N/m). Sources: P, v, T, h, s interpolated and extrapolated from I. I. Perelshteyn, *Tables and Diagrams of the Thermodynamic Properties of Freons 12, 13, 22*, Moscow, USSR, 1971. c_p, η, λ interpolated and converted from *Thermophysical Properties of Refrigerants*, ASHRAE, New York, 1976. T calculated from V. A. Gruzdev et al., *Fluid Mech. Sov. Res.*, **3**, 172 (1974).

^bThe notation 6.209.—4 signifies 6.209 × 10⁻⁴.

Table 13 Thermophysical Properties of Refrigerant 22 at Atmospheric Pressure^a

	Temperature (K)					
	250	300	350	400	450	500
v	0.2315	0.2802	0.3289	0.3773	0.4252	0.4723
h	597.8	630.0	664.5	702.5	740.8	782.3
s	4.8671	4.9840	5.0905	5.1892	5.2782	5.3562
c _p	0.587	0.647	0.704	0.757	0.806	0.848
Z	0.976	0.984	0.990	0.994	0.995	0.996
\bar{v}_s	166.4	182.2	196.2	209.4	220.0	233.6
λ	0.0080	0.0110	0.0140	0.0170	0.0200	0.0230
η	0.109	0.130	0.151	0.171	0.190	0.209
Pr	0.800	0.765	0.759	0.761	0.766	0.771

^av = specific volume (m³/kg); h = specific enthalpy (kJ/kg); s = specific entropy (kJ/kg · K); c_p = specific heat at constant pressure (kJ/kg · K); Z = compressibility factor = Pv/RT; \bar{v}_s = velocity of sound (m/s); λ = thermal conductivity (W/m · K); η = viscosity 10⁻⁴ N · s/m² (thus, at 250 K the viscosity is 0.109 × 10⁻⁴ N · s/m² = 0.0000109 Pa · s); Pr = Prandtl number.

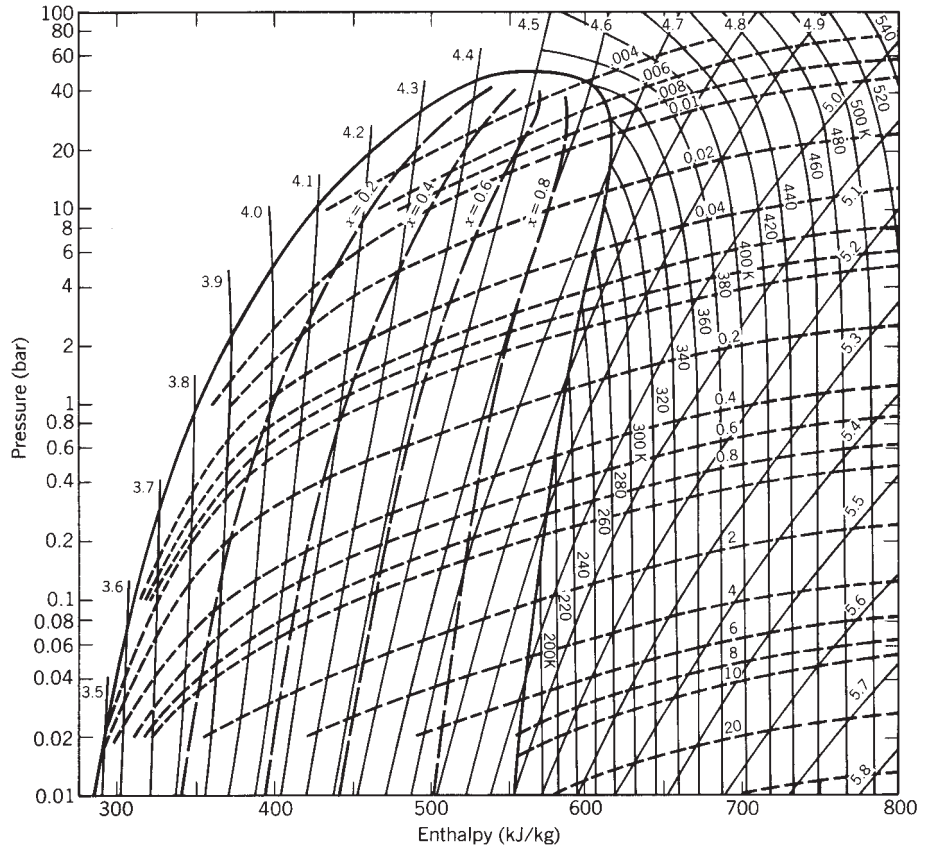


Figure 3 Enthalpy–log pressure diagram for Refrigerant 22.

Table 14 Thermodynamic Properties of Saturated Refrigerant 134a^a

P (bars)	t (°C)	v_f (m ³ /kg)	v_g (m ³ /kg)	h_f (kJ/kg)	h_g (kJ/kg)	s_f (kJ/kg · K)	s_g (kJ/kg · K)	c_{pf} (kJ/kg · K)	c_{pg} (kJ/kg · K)
0.5	-40.69	0.000707	0.3690	-0.9	225.5	-0.0036	0.9698	1.2538	0.7476
0.6	-36.94	0.000712	0.3109	3.3	227.5	0.0165	0.9645	1.2600	0.7584
0.7	-33.93	0.000716	0.2692	7.7	229.4	0.0324	0.9607	1.2654	0.7680
0.8	-31.12	0.000720	0.2375	11.2	231.2	0.0472	0.9572	1.2707	0.7771
0.9	-28.65	0.000724	0.2126	14.4	233.0	0.0601	0.9545	1.2755	0.7854
1	-26.52	0.000729	0.1926	16.8	234.2	0.0720	0.9519	1.2799	0.7931
1.5	-17.26	0.000742	0.1314	28.6	240.0	0.1194	0.9455	1.2992	0.8264
2	-10.18	0.000754	0.1001	37.8	243.6	0.1547	0.9379	1.3153	0.8540
2.5	-4.38	0.000764	0.0809	45.5	247.3	0.1834	0.9340	1.3297	0.8782
3	0.59	0.000774	0.0679	52.1	250.1	0.2077	0.9312	1.3428	0.9002
4	8.86	0.000791	0.0514	63.3	254.9	0.2478	0.9270	1.3670	0.9400
5	15.68	0.000806	0.0413	72.8	258.8	0.2804	0.9241	1.3894	0.9761
6	21.54	0.000820	0.0344	81.0	262.1	0.3082	0.9219	1.4108	0.9914
8	31.35	0.000846	0.0257	95.0	267.1	0.3542	0.9185	1.4526	1.0750
10	39.41	0.000871	0.0204	106.9	270.9	0.3921	0.9157	1.4948	1.1391
12	46.36	0.000894	0.01672	117.5	273.9	0.4246	0.9132	1.539	1.205
14	52.48	0.000918	0.01411	127.0	276.2	0.4533	0.9107	1.586	1.276
16	57.96	0.000941	0.01258	135.7	277.9	0.4794	0.9081	1.637	1.353
18	62.94	0.000965	0.01056	143.9	279.3	0.5031	0.9052	1.695	1.439
20	67.52	0.000990	0.00929	151.4	280.1	0.5254	0.9021	1.761	1.539
22.5	72.74	0.001023	0.00800	160.9	280.8	0.5512	0.8976	1.859	1.800
25	77.63	0.001058	0.00694	169.8	280.8	0.5756	0.8925	1.983	1.883
27.5	82.04	0.001096	0.00605	178.2	280.3	0.5989	0.8865	2.151	2.149
30	86.20	0.001141	0.00528	186.5	279.4	0.6216	0.8812	2.388	2.527
35	93.72	0.001263	0.00397	203.7	274.1	0.6671	0.8589	3.484	4.292
40	100.34	0.001580	0.00256	227.4	257.2	0.7292	0.8090	26.33	37.63
40.59	101.06	0.001953	0.00195	241.5	241.5	0.7665	0.7665		

^aConverted and reproduced from R. Tillner-Roth and H. D. Baehr, *J. Phys. Chem. Ref. Data*, **23** (5), 657–730 (1994). $h_f = s_f = 0$ at 233.15 K = -40°C.

20 Thermophysical Properties of Fluids

Table 15 Thermophysical Properties of Refrigerant 134a

<i>t</i> (°C)	Property	<i>P</i> (bars)							Sat. Vapor
		1	2.5	5	7.5	10	12.5	15	
0	c_p (kJ/kg·K)	0.8197	0.8740						0.8975
	μ (10^{-6} Pa·s)	11.00	10.95						10.94
	k (W/m·K)	0.0119	0.0120						0.0120
	Pr	0.763	0.798						0.809
10	c_p (kJ/kg·K)	0.8324	0.8815						0.9408
	μ (10^{-6} Pa·s)	11.38	11.42						11.42
	k (W/m·K)	0.0126	0.0127						0.0129
	Pr	0.753	0.786						0.821
20	c_p (kJ/kg·K)	0.8458	0.8726	0.9642					0.9864
	μ (10^{-6} Pa·s)	11.78	11.83	11.91					11.93
	k (W/m·K)	0.0134	0.0135	0.0138					0.0139
	Pr	0.747	0.774	0.830					0.838
30	c_p (kJ/kg·K)	0.8602	0.8900	0.9587	1.044				1.048
	μ (10^{-6} Pa·s)	12.27	12.28	12.29	12.36				12.37
	k (W/m·K)	0.0141	0.0143	0.0145	0.0150				0.0150
	Pr	0.743	0.764	0.805	0.857				0.859
40	c_p (kJ/kg·K)	0.8747	0.8998	0.9547	1.027	1.134			1.145
	μ (10^{-6} Pa·s)	12.57	12.61	12.66	12.75	12.88			12.89
	k (W/m·K)	0.0148	0.0150	0.0153	0.0156	0.0161			0.0161
	Pr	0.740	0.757	0.789	0.839	0.907			0.916
50	c_p (kJ/kg·K)	0.8891	0.9112	0.9555	1.017	1.120	1.213		1.246
	μ (10^{-6} Pa·s)	12.96	13.00	13.05	13.14	13.23	13.33		13.47
	k (W/m·K)	0.0156	0.0158	0.0160	0.0163	0.0167	0.0171		0.0173
	Pr	0.739	0.752	0.778	0.820	0.887	0.946		0.960
60	c_p (kJ/kg·K)	0.9045	0.9230	0.9589	1.003	1.060	1.151	1.248	1.387
	μ (10^{-6} Pa·s)	13.35	13.39	13.44	13.51	13.60	13.75	13.96	14.16
	k (W/m·K)	0.0164	0.0165	0.0167	0.0170	0.0173	0.0178	0.0184	0.0185
	Pr	0.739	0.750	0.772	0.801	0.829	0.889	0.935	1.059
70	c_p (kJ/kg·K)	0.9201	0.9359	0.9652	0.9972	1.046	1.100	1.175	1.606
	μ (10^{-6} Pa·s)	13.74	13.77	13.82	13.89	13.97	14.10	14.27	15.04
	k (W/m·K)	0.0171	0.0172	0.0174	0.0176	0.0179	0.0183	0.0189	0.0197
	Pr	0.739	0.750	0.759	0.787	0.813	0.848	0.886	1.226
80	c_p (kJ/kg·K)	0.9359	0.9520	0.9715	0.9992	1.038	1.222	1.313	2.026
	μ (10^{-6} Pa·s)	14.11	14.14	14.19	14.25	14.33	14.43	14.59	16.31
	k (W/m·K)	0.0178	0.0179	0.0180	0.0182	0.0185	0.0188	0.0193	0.0205
	Pr	0.741	0.752	0.757	0.782	0.804	0.938	0.993	1.612
Sat. vapor	c_p (kJ/kg·K)	0.7931	0.8782	0.9761	1.059	1.139	1.223	1.314	
	μ (10^{-6} Pa·s)	—	—	11.72	12.34	12.86	13.34	13.81	
	k (W/m·K)	—	—	0.0136	0.0149	0.0161	0.0173	0.0184	
	Pr	—	—	0.841	0.877	0.910	0.943	0.986	

^aNote: At 0° C, 1 bar the viscosity is 11×10^{-6} Pa·s.; Pr = Prandtl number.

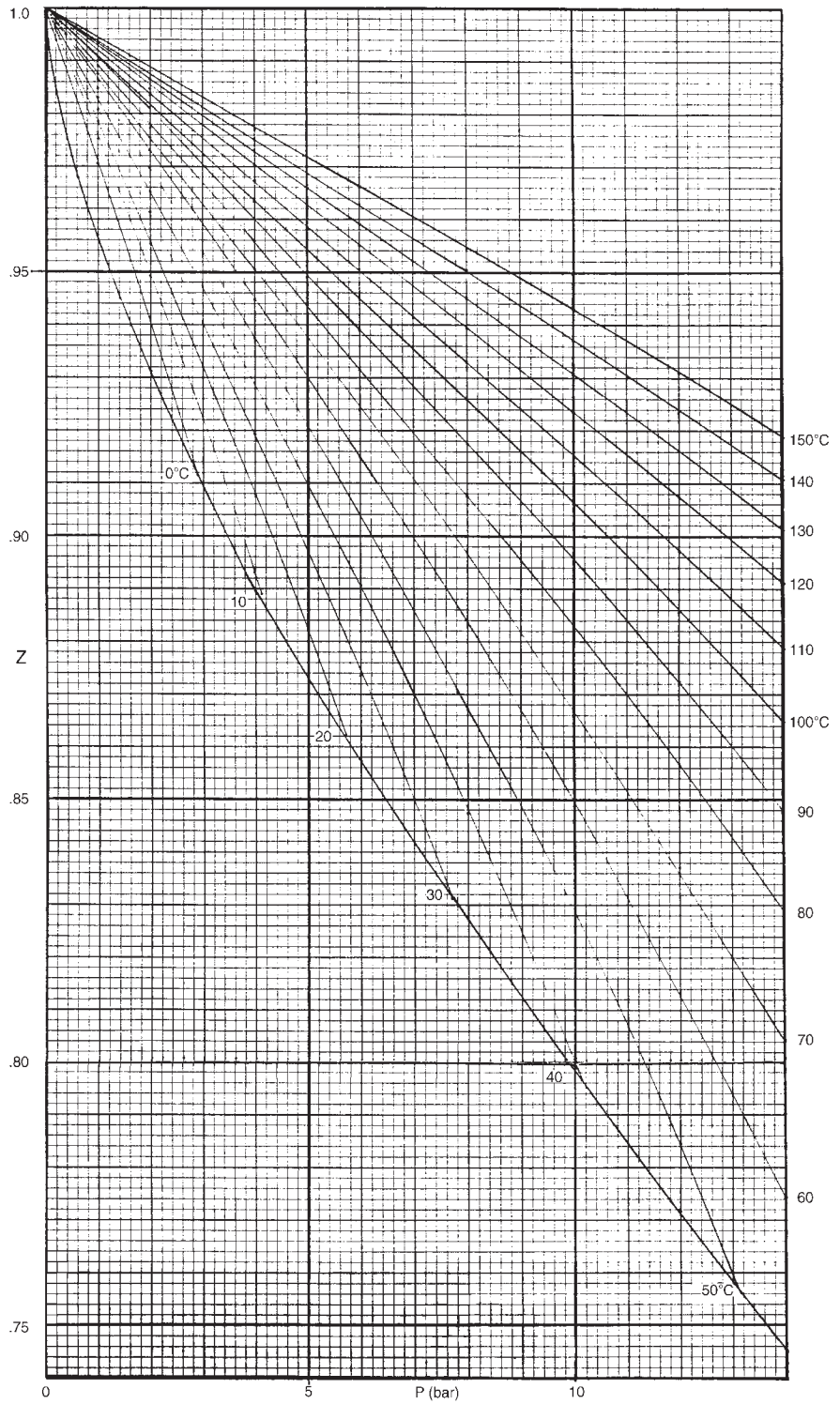


Figure 4 Compressibility factor of Refrigerant 134a.

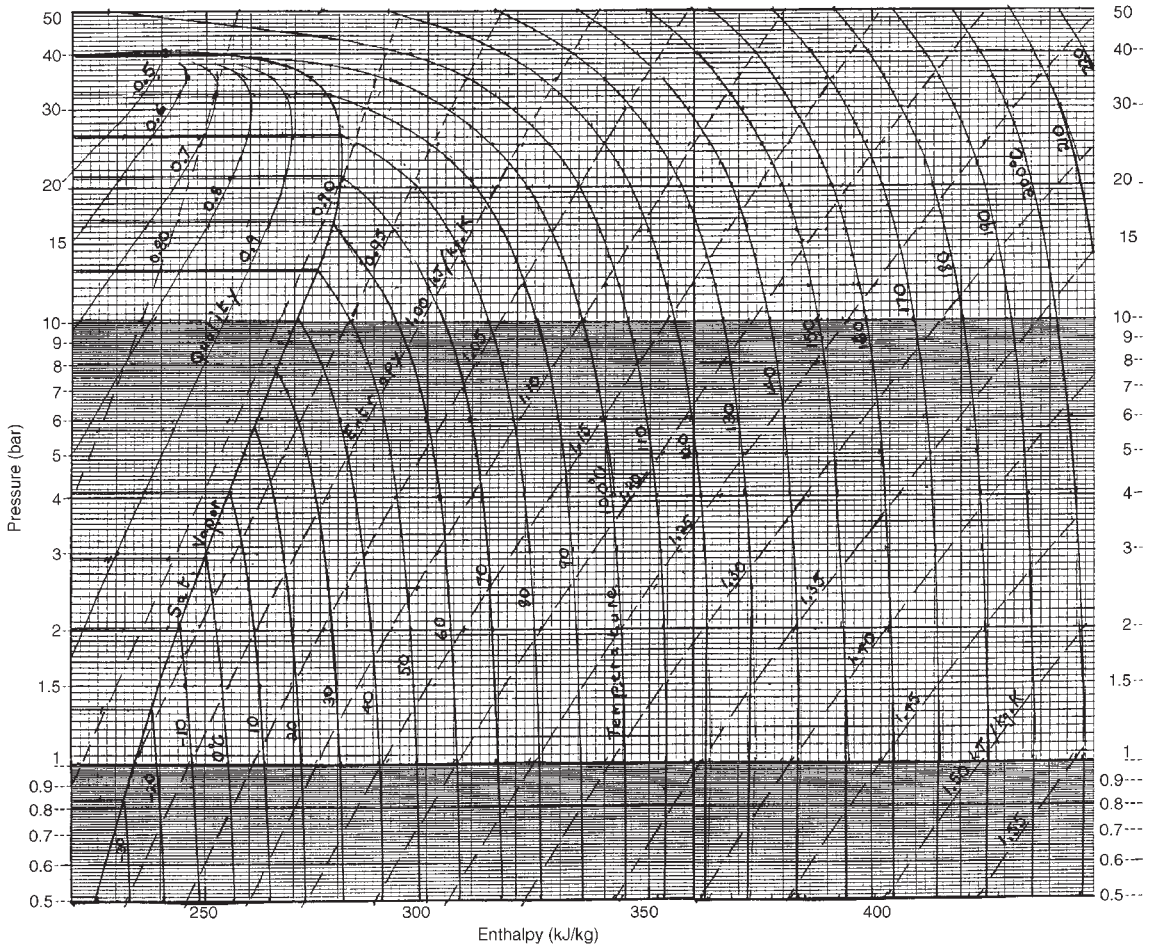


Figure 5 Enthalpy–log pressure diagram for Refrigerant 134a.

Table 16 Thermodynamic Properties of Saturated Sodium^a

$T(K)$	P (bars)	v_f	v_g	h_f	h_g	s_f	s_g	C_{pf}	c_{pg}
380	2.55.-10 ^b	1.081.-3	5.277.+9	0.219	4.723	2.853	14.705	1.384	0.988
400	1.36.-9	1.086.-3	2.173.+9	0.247	4.740	2.924	14.158	1.374	1.023
420	6.16.-9	1.092.-3	2.410.+8	0.274	4.757	2.991	13.665	1.364	1.066
440	2.43.-8	1.097.-3	6.398.+7	0.301	4.773	3.054	13.219	1.355	1.117
460	8.49.-8	1.103.-3	1.912.+7	0.328	4.790	3.114	12.814	1.346	1.176
480	2.67.-7	1.109.-3	6.341.+6	0.355	4.806	3.171	12.443	1.338	1.243
500	7.64.-7	1.114.-3	2.304.+6	0.382	4.820	3.226	12.104	1.330	1.317
550	7.54.-6	1.129.-3	2.558.+5	0.448	4.856	3.352	11.367	1.313	1.523
600	5.05.-5	1.145.-3	41511	0.513	4.887	3.465	10.756	1.299	1.745
650	2.51.-4	1.160.-3	9001	0.578	4.915	3.569	10.241	1.287	1.963
700	9.87.-4	1.177.-3	2449	0.642	4.939	3.664	9.802	1.278	2.160
750	0.00322	1.194.-3	794	0.705	4.959	3.752	9.424	1.270	2.325
800	0.00904	1.211.-3	301	0.769	4.978	3.834	9.095	1.264	2.452
850	0.02241	1.229.-3	128.1	0.832	4.995	3.910	8.808	1.260	2.542
900	0.05010	1.247.-3	60.17	0.895	5.011	3.982	8.556	1.258	2.597
1000	0.1955	1.289.-3	16.84	1.021	5.043	4.115	8.137	1.259	2.624
1200	1.482	1.372.-3	2.571	1.274	5.109	4.346	7.542	1.281	2.515
1400	6.203	1.469.-3	0.688	1.535	5.175	4.546	7.146	1.330	2.391
1600	17.98	1.581.-3	0.258	1.809	5.225	4.728	6.863	1.406	2.301
1800	40.87	1.709.-3	0.120	2.102	5.255	4.898	6.649	1.516	2.261
2000	78.51	1.864.-3	0.0634	2.422	5.256	5.064	6.480	1.702	2.482
2200	133.5	2.076.-3	0.0362	2.794	5.207	5.235	6.332	2.101	3.307
2400	207.6	2.480.-3	0.0196	3.299	5.025	5.447	6.166	3.686	8.476
2500	251.9	3.323.-3	0.0100	3.850	4.633	5.666	5.980		

^a v = specific volume (m³/kg); h = specific enthalpy (MJ/kg); s = specific entropy (kJ/kg · K); c_p = specific heat at constant pressure (kJ/kg · K); f = saturated liquid; g = saturated vapor. Converted from the tables of J. K. Fink, Argonne Nat. Lab. rept. ANL-CEN-RSD-82-4, 1982.

^bThe notation 2.55.-10 signifies 2.55×10^{-10} .

Table 17 Thermodynamic Properties of Ice/Water^a

$T(K)$	P (bars)	v (m ³ /kg)	h (kJ/kg)	s (kJ/kg · K)	c_p (kJ/kg · K)
150	6.30.-11 ^b	0.001073	94.7	1.328	1.224
160	7.72.-10	0.001074	107.3	1.409	1.291
170	7.29.-9	0.001076	120.6	1.489	1.357
180	5.38.-8	0.001077	134.5	1.569	1.426
190	3.23.-7	0.001078	149.1	1.648	1.495
200	1.62.-6	0.001079	164.4	1.726	1.566
210	7.01.-6	0.001081	180.4	1.805	1.638
220	2.65.-5	0.001082	197.1	1.882	1.711
230	8.91.-5	0.001084	214.6	1.960	1.785
240	2.73.-4	0.001085	232.8	2.038	1.860
250	7.59.-4	0.001087	251.8	2.115	1.936
260	0.00196	0.001088	271.5	2.192	2.013
270	0.00469	0.001090	292.0	2.270	2.091
273.15	0.00611	0.001091	298.7	2.294	2.116
273.15	0.00611	0.001000	632.2	3.515	4.217
280	0.00990	0.001000	661.0	3.619	4.198
290	0.01917	0.001001	702.9	3.766	4.184
300	0.03531	0.001003	744.7	3.908	4.179

^a v = specific volume; h = specific enthalpy; s = specific entropy; c_p = specific heat at constant pressure. Properties above the solid line are for the solid; below they are for the liquid. Ice values ($T \leq 273.15$ K) converted and rounded off from S. Gordon, NASA Tech. Paper 1906, 1982.

^bThe notation 6.30.-11 signifies 6.30×10^{-11} .

24 Thermophysical Properties of Fluids

Table 18 Thermophysical Properties of Saturated Steam/Water^a

P (bars)	T (K)	v_f	v_g	h_f	h_g	η_g	λ_f	λ_g	Pr_f	Pr_g
1.0	372.78	1.0434.-3 ^b	1.6937	417.5	2675.4	0.1202	0.6805	0.0244	1.735	1.009
1.5	384.52	1.0530.-3	1.1590	467.1	2693.4	0.1247	0.6847	0.0259	1.538	1.000
2.0	393.38	1.0608.-3	0.8854	504.7	2706.3	0.1280	0.6866	0.0268	1.419	1.013
2.5	400.58	1.0676.-3	0.7184	535.3	2716.4	0.1307	0.6876	0.0275	1.335	1.027
3.0	406.69	1.0735.-3	0.6056	561.4	2724.7	0.1329	0.6879	0.0281	1.273	1.040
3.5	412.02	1.0789.-3	0.5240	584.3	2731.6	0.1349	0.6878	0.0287	1.224	1.050
4.0	416.77	1.0839.-3	0.4622	604.7	2737.6	0.1367	0.6875	0.0293	1.185	1.057
4.5	421.07	1.0885.-3	0.4138	623.2	2742.9	0.1382	0.6869	0.0298	1.152	1.066
5	424.99	1.0928.-3	0.3747	640.1	2747.5	0.1396	0.6863	0.0303	1.124	1.073
6	432.00	1.1009.-3	0.3155	670.4	2755.5	0.1421	0.6847	0.0311	1.079	1.091
7	438.11	1.1082.-3	0.2727	697.1	2762.0	0.1443	0.6828	0.0319	1.044	1.105
8	445.57	1.1150.-3	0.2403	720.9	2767.5	0.1462	0.6809	0.0327	1.016	1.115
9	448.51	1.1214.-3	0.2148	742.6	2772.1	0.1479	0.6788	0.0334	0.992	1.127
10	453.03	1.1274.-3	0.1943	762.6	2776.1	0.1495	0.6767	0.0341	0.973	1.137
12	461.11	1.1386.-3	0.1632	798.4	2782.7	0.1523	0.6723	0.0354	0.943	1.156
14	468.19	1.1489.-3	0.1407	830.1	2787.8	0.1548	0.6680	0.0366	0.920	1.175
16	474.52	1.1586.-3	0.1237	858.6	2791.8	0.1569	0.6636	0.0377	0.902	1.191
18	480.26	1.1678.-3	0.1103	884.6	2794.8	0.1589	0.6593	0.0388	0.889	1.206
20	485.53	1.1766.-3	0.0995	908.6	2797.2	0.1608	0.6550	0.0399	0.877	1.229
25	497.09	1.1972.-3	0.0799	962.0	2800.9	0.1648	0.6447	0.0424	0.859	1.251
30	506.99	1.2163.-3	0.0666	1008.4	2802.3	0.1684	0.6347	0.0449	0.849	1.278
35	515.69	1.2345.-3	0.0570	1049.8	2802.0	0.1716	0.6250	0.0472	0.845	1.306
40	523.48	1.2521.-3	0.0497	1087.4	2800.3	0.1746	0.6158	0.0496	0.845	1.331
45	530.56	1.2691.-3	0.0440	1122.1	2797.7	0.1775	0.6068	0.0519	0.849	1.358
50	537.06	1.2858.-3	0.0394	1154.5	2794.2	0.1802	0.5981	0.0542	0.855	1.386
60	548.70	1.3187.-3	0.0324	1213.7	2785.0	0.1854	0.5813	0.0589	0.874	1.442
70	558.94	1.3515.-3	0.0274	1267.4	2773.5	0.1904	0.5653	0.0638	0.901	1.503
80	568.12	1.3843.-3	0.0235	1317.1	2759.9	0.1954	0.5499	0.0688	0.936	1.573
90	576.46	1.4179.-3	0.0205	1363.7	2744.6	0.2005	0.5352	0.0741	0.978	1.651
100	584.11	1.4526.-3	0.0180	1408.0	2727.7	0.2057	0.5209	0.0798	1.029	1.737
110	591.20	1.4887.-3	0.0160	1450.6	2709.3	0.2110	0.5071	0.0859	1.090	1.837
120	597.80	1.5268.-3	0.0143	1491.8	2689.2	0.2166	0.4936	0.0925	1.163	1.963
130	603.98	1.5672.-3	0.0128	1532.0	2667.0	0.2224	0.4806	0.0998	1.252	2.126
140	609.79	1.6106.-3	0.0115	1571.6	2642.4	0.2286	0.4678	0.1080	1.362	2.343
150	615.28	1.6579.-3	0.0103	1611.0	2615.0	0.2373	0.4554	0.1172	1.502	2.571
160	620.48	1.7103.-3	0.0093	1650.5	2584.9	0.2497	0.4433	0.1280	1.688	3.041
170	625.41	1.7696.-3	0.0084	1691.7	2551.6	0.2627	0.4315	0.1404	2.098	3.344
180	630.11	1.8399.-3	0.0075	1734.8	2513.9	0.2766	0.4200	0.1557	2.360	3.807
190	634.58	1.9260.-3	0.0067	1778.7	2470.6	0.2920	0.4087	0.1749	2.951	8.021
200	638.85	2.0370.-3	0.0059	1826.5	2410.4	0.3094	0.3976	0.2007	4.202	12.16

Table 18 (Continued)

P (bars)	s_f	s_g	c_{pf}	c_{pg}	η_f	γ'_f	γ_g	\bar{v}'_{sf}	\bar{v}'_{sg}	τ
1.0	1.3027	7.3598	4.222	2.048	2.801	1.136	1.321	438.74	472.98	0.0589
1.5	1.4336	7.2234	4.231	2.077	2.490	1.139	1.318	445.05	478.73	0.0566
2.0	1.5301	7.1268	4.245	2.121	2.295	1.141	1.316	449.51	482.78	0.0548
2.5	1.6071	7.0520	4.258	2.161	2.156	1.142	1.314	452.92	485.88	0.0534
3.0	1.6716	6.9909	4.271	2.198	2.051	1.143	1.313	455.65	488.36	0.0521
3.5	1.7273	6.9392	4.282	2.233	1.966	1.143	1.311	457.91	490.43	0.0510
4.0	1.7764	6.8943	4.294	2.266	1.897	1.144	1.310	459.82	492.18	0.0500
4.5	1.8204	6.8547	4.305	2.298	1.838	1.144	1.309	461.46	493.69	0.0491
5	1.8604	6.8192	4.315	2.329	1.787	1.144	1.308	462.88	495.01	0.0483
6	1.9308	6.7575	4.335	2.387	1.704	1.144	1.306	465.23	497.22	0.0468
7	1.9918	6.7052	4.354	2.442	1.637	1.143	1.304	467.08	498.99	0.0455
8	2.0457	6.6596	4.372	2.495	1.581	1.142	1.303	468.57	500.55	0.0444
9	2.0941	6.6192	4.390	2.546	1.534	1.142	1.302	469.78	501.64	0.0433
10	2.1382	6.5821	4.407	2.594	1.494	1.141	1.300	470.76	502.64	0.0423
12	2.2161	6.5194	4.440	2.688	1.427	1.139	1.298	472.23	504.21	0.0405
14	2.2837	6.4651	4.472	2.777	1.373	1.137	1.296	473.18	505.33	0.0389
16	2.3436	6.4175	4.504	2.862	1.329	1.134	1.294	473.78	506.12	0.0375
18	2.3976	6.3751	4.534	2.944	1.291	1.132	1.293	474.09	506.65	0.0362
20	2.4469	6.3367	4.564	3.025	1.259	1.129	1.291	474.18	506.98	0.0350
25	2.5543	6.2536	4.640	3.219	1.193	1.123	1.288	473.71	507.16	0.0323
30	2.6455	6.1837	4.716	3.407	1.143	1.117	1.284	472.51	506.65	0.0300
35	2.7253	6.1229	4.792	3.593	1.102	1.111	1.281	470.80	505.66	0.0280
40	2.7965	6.0685	4.870	3.781	1.069	1.104	1.278	468.72	504.29	0.0261
45	2.8612	6.0191	4.951	3.972	1.040	1.097	1.275	466.31	502.68	0.0244
50	2.9206	5.9735	5.034	4.168	1.016	1.091	1.272	463.67	500.73	0.0229
60	3.0273	5.8908	5.211	4.582	0.975	1.077	1.266	457.77	496.33	0.0201
70	3.1219	5.8162	5.405	5.035	0.942	1.063	1.260	451.21	491.31	0.0177
80	3.2076	5.7471	5.621	5.588	0.915	1.048	1.254	444.12	485.80	0.0156
90	3.2867	5.6820	5.865	6.100	0.892	1.033	1.249	436.50	479.90	0.0136
100	3.3606	5.6198	6.142	6.738	0.872	1.016	1.244	428.24	473.67	0.0119
110	3.4304	5.5595	6.463	7.480	0.855	0.998	1.239	419.20	467.13	0.0103
120	3.4972	5.5002	6.838	8.384	0.840	0.978	1.236	409.38	460.25	0.0089
130	3.5616	5.4408	7.286	9.539	0.826	0.956	1.234	398.90	453.00	0.0076
140	3.6243	5.3803	7.834	11.07	0.813	0.935	1.232	388.00	445.34	0.0064
150	3.6859	5.3178	8.529	13.06	0.802	0.916	1.233	377.00	437.29	0.0053
160	3.7471	5.2531	9.456	15.59	0.792	0.901	1.235	366.24	428.89	0.0043
170	3.8197	5.1855	11.30	17.87	0.782	0.867	1.240	351.19	420.07	0.0034
180	3.8765	5.1128	12.82	21.43	0.773	0.838	1.248	336.35	410.39	0.0026
190	3.9429	5.0332	15.76	27.47	0.765	0.808	1.260	320.20	399.87	0.0018
200	4.0149	4.9412	22.05	39.31	0.758	0.756	1.280	298.10	387.81	0.0011

$^a v$ = specific volume (m^3/kg); h = specific enthalpy (kJ/kg); s = specific entropy ($\text{kJ}/\text{kg} \cdot \text{K}$); c_p = specific heat at constant pressure ($\text{kJ}/\text{kg} \cdot \text{K}$); η = viscosity ($10^{-4} \text{ Pa} \cdot \text{s}$); λ = thermal conductivity ($\text{W}/\text{m} \cdot \text{K}$); Pr = Prandtl number; $\gamma = c_p/c_v$ ratio; \bar{v}_s = velocity of sound (m/s); T = surface tension (N/m); f' = wet saturated vapor; g = saturated vapor. Rounded off from values of C. M. Tseng, T. A. Hamp, and E. O. Moeck, Atomic Energy of Canada Report AECL-5910, 1977.

b The notation 1.0434.-3 signifies 1.0434×10^{-3} .

Table 19 Thermophysical Properties of Miscellaneous Substances at Atmospheric Pressure^a

	Temperature (K)					
	250	300	350	400	450	500
<i>n-Butane</i>						
v	0.0016	0.411	0.485	0.558	0.630	0.701
h	236.6	718.9	810.7	913.1	1026	1149
s	3.564	5.334	5.616	5.889	6.155	6.414
c_p	2.21	1.73	1.94	2.15	2.36	2.56
Z	0.005	0.969	0.982	0.988	0.992	0.993
\bar{v}_s	1161	211	229	245	259	273
λ	0.0979	0.0161	0.0220	0.0270	0.0327	0.0390
η	2.545	0.076	0.088	0.101	0.111	0.124
Pr	5.75	0.84	0.82	0.81	0.80	0.80
<i>Ethane</i>						
v	0.672	0.812	0.950	1.088	1.225	1.362
h	948.7	1068	1162	1265	1380	1505
s	7.330	7.634	7.854	8.198	8.467	8.730
c_p	1.58	1.76	1.97	2.18	2.39	2.60
Z	0.986	0.992	0.995	0.997	0.998	0.998
\bar{v}_s	287	312	334	355	374	392
λ	0.0103	0.0157	0.0219	0.0288	0.0361	0.0438
η	0.079	0.094	0.109	0.123	0.135	0.148
Pr	1.214	1.056	0.978	0.932	0.900	0.878
<i>Ethylene</i>						
v	0.734	0.884	1.034	1.183	1.332	1.482
h	966.8	1039	1122	1215	1316	1415
s	7.556	7.832	8.085	8.331	8.568	8.800
c_p	1.40	1.57	1.75	1.93	2.10	2.26
Z	0.991	0.994	0.997	0.998	0.999	1.000
\bar{v}_s	306	330	353	374	394	403
λ	0.0149	0.0206	0.0271	0.0344	0.0425	0.0506
η	0.087	0.103	0.119	0.134	0.148	0.162
Pr	0.816	0.785	0.767	0.751	0.735	0.721
<i>n-Hydrogen</i>						
v	10.183	12.218	14.253	16.289	18.324	20.359
h	3517	4227	4945	5669	6393	7118
s	67.98	70.58	72.79	74.72	76.43	77.96
c_p	14.04	14.31	14.43	14.48	14.50	14.51
Z	1.000	1.000	1.000	1.000	1.000	1.000
\bar{v}_s	1209	1319	1423	1520	1611	1698
λ	0.162	0.187	0.210	0.230	0.250	0.269
η	0.079	0.089	0.099	0.109	0.118	0.127
Pr	0.685	0.685	0.685	0.684	0.684	0.684
<i>Nitrogen</i>						
v	0.7317	0.8786	1.025	1.171	1.319	1.465
h	259.1	311.2	363.3	415.4	467.8	520.4
s	6.650	6.840	7.001	7.140	7.263	7.374
c_p	1.042	1.041	1.042	1.045	1.050	1.056
Z	0.9992	0.9998	0.9998	0.9999	1.0000	1.0002
\bar{v}_s	322	353	382	407	432	455
λ	0.0223	0.0259	0.0292	0.0324	0.0366	0.0386
η	0.155	0.178	0.200	0.220	0.240	0.258
Pr	0.724	0.715	0.713	0.710	0.708	0.706

Table 19 (Continued)

	Temperature (K)					
	250	300	350	400	450	500
<i>Oxygen</i>						
v	0.6402	0.7688	0.9790	1.025	1.154	1.282
h	226.9	272.7	318.9	365.7	413.1	461.3
s	6.247	6.414	6.557	6.682	6.793	6.895
c_p	0.915	0.920	0.929	0.942	0.956	0.972
Z	0.9987	0.9994	0.9996	0.9998	1.0000	1.0000
\bar{v}_s	301	330	356	379	401	421
λ	0.0226	0.0266	0.0305	0.0343	0.0380	0.0416
η	0.179	0.207	0.234	0.258	0.281	0.303
Pr	0.725	0.716	0.713	0.710	0.708	0.707
<i>Propane</i>						
v	0.451	0.548	0.644	0.738	0.832	0.926
h	877.2	957.0	1048	1149	1261	1384
s	5.840	6.131	6.409	6.680	6.944	7.202
c_p	1.50	1.70	1.96	2.14	2.35	2.55
Z	0.970	0.982	0.988	0.992	0.994	0.996
\bar{v}_s	227	248	268	285	302	317
λ	0.0128	0.0182	0.0247	0.0296	0.0362	0.0423
η	0.070	0.082	0.096	0.108	0.119	0.131
Pr	0.820	0.772	0.761	0.765	0.773	0.793
<i>Propylene</i>						
v	0.482	0.585	0.686	0.786	0.884	0.972
h	891.8	957.6	1040	1131	1235	1338
s	6.074	6.354	6.606	6.851	7.095	7.338
c_p	1.44	1.55	1.73	1.91	2.09	2.27
Z	0.976	0.987	0.992	0.994	0.995	0.996
\bar{v}_s	247	257	278	298	315	333
λ	0.0127	0.0177	0.0233	0.0296	0.0363	0.0438
η	0.072	0.087	0.101	0.115	0.128	0.141
Pr	0.814	0.769	0.754	0.742	0.731	0.728

^a v = specific volume (m^3/kg); h = specific enthalpy (kJ/kg); s = specific entropy ($\text{kJ}/\text{kg} \cdot \text{K}$); c_p = specific heat at constant pressure ($\text{kJ}/\text{kg} \cdot \text{K}$); Z = compressibility factor = Pv/RT ; \bar{v}_s = velocity of sound (m/s); λ = thermal conductivity ($\text{W}/\text{m} \cdot \text{K}$); η = viscosity (10^{-4})($\text{N} \cdot \text{s}/\text{m}^2$) (thus, at 250 K for *n*-butane the viscosity is $2.545 \times 10^{-4} \text{ N} \cdot \text{s}/\text{m}^2 = 0.0002545 \text{ Pa} \cdot \text{s}$); Pr = Prandtl number.

Table 20 Physical Properties of Numbered Refrigerants^a

Number	Formula, Composition, Synonym	Molecular Weight	n.b.p. ($^{\circ}\text{C}$)	Crit. P (bar)	Crit. T ($^{\circ}\text{C}$)
4	R-32/125/134a/143a (10/33/21/36)	94.50	-49.4	40.1	77.5
10	CCl_4 (carbon tetrachloride)	153.8	76.8	45.6	283.2
CFC-11	CCl_3F	137.37	23.8	44.1	198.0
11B1	CBrCl_2F	181.82	52		
11B2	CBr_2ClF	226.27	80		
11B3	CBr_3F	270.72	107		
CFC-12	CCl_2F_2	120.91	-29.8	41.1	112.0

(continued)

Table 20 (Continued)

Number	Formula, Composition, Synonym	Molecular Weight	n.b.p. (°C)	Crit. <i>P</i> (bar)	Crit. <i>T</i> (°C)
12B1	CBrClF ₂	165.36	-2.5	42.5	153.0
12B2	CF ₂ Br ₂	209.81	24.5	40.7	204.9
CFC-13	CClF ₃	104.46	-81.4	38.7	28.8
BFC-13B1	CBrF ₃ (Halon 1301)	148.91	-57.8	39.6	67.0
FC-14	CF ₄ (carbon tetrafluoride)	88.00	-127.9	37.5	-45.7
20	CHCl ₃ (chloroform)	119.38	61.2	54.5	263.4
21	CHCl ₂ F	102.92	8.9	51.7	178.5
HCFC-22	CHClF ₂	86.47	-40.8	49.9	96.2
HFC-23	CHF ₃	70.01	-82.1	48.7	26.3
HCC-30	CH ₂ Cl ₂ (methylene chloride)	84.93	40.2	60.8	237.0
31	CH ₂ ClF	68.47	-9.1	56.2	153.8
HFC-32	CH ₂ F ₂	52.02	-51.7	58.0	78.2
33	R-22/124/152a (40/43/17)	96.62	-28.8		
40	CH ₃ Cl (methyl chloride)	50.49	-12.4	66.7	143.1
FX-40	R-32/125/143a (10/45/45)	90.70	-48.4	40.5	72.0
HFC-41	CH ₃ F (methyl fluoride)	34.03	-78.4	58.8	44.3
50	CH ₄ (methane)	16.04	-161.5	46.4	-82.5
FX-57	R-22/124/142b (65/25/10)	96.70	-35.2	47.0	105.0
110	CCl ₃ CCl ₃	236.8	185	33.4	401.8
111	CCl ₃ CCl ₂ F	220.2	137		
112	CCl ₂ FCCl ₂ F	203.8	92.8	33.4	278
CFC-113	CClF ₂ CCl ₂ F	187.38	47.6	34.4	214.1
113a	CCl ₃ CF ₃	187.36	47.5		
CFC-114	CClF ₂ CClF ₂	170.92	3.8	32.5	145.7
114a	CF ₃ CCl ₂ F	170.92	3.0	33.0	145.5
CFC-115	CClF ₂ CF ₃	154.47	-39.1	31.5	79.9
FC-116	CF ₃ CF ₃ (perfluoroethane)	138.01	-78.2	30.4	19.9
120	CHCl ₂ CCl ₃	202.3	162	34.8	373
121	CHCl ₂ CCl ₂ F	185.84	116.6		
122	CClF ₂ CHCl ₂	131.39	72.0		
HCFC-123	CHCl ₂ CF ₃	152.93	27.9	36.7	183.7
HCFC-123a	CHClFCClF ₂	152.93	28.0	44.7	188.5
HCFC-124	CHClFCF ₃	136.48	-12.0	36.4	122.5
E-125	CHF ₂ OCF ₂	136.02	-41.9	33.3	80.4
HFC-125	CHF ₂ CF ₃	120.02	-48.1	36.3	66.3
131	CHCl ₂ CHClF	151.4	102.5		
132	CHClFCHClF	134.93	58.5		
133	CHClFCHF ₂	118.5	17.0		
E-134	CHF ₂ OCHF ₂	118.03	6.2	42.3	153.5
HFC-134	CHF ₂ CHF ₂	102.03	-23.0	46.2	118.7
HFC-134a	CH ₂ FCF ₃	102.03	-26.1	40.6	101.1
141	CH ₂ ClCHClF	116.95	76		
141a	CHCl ₂ CH ₂ F	116.95			
HCFC-141b	CH ₃ CCl ₂ F	116.95	32.2	42.5	204.4
142	CHF ₂ CH ₂ Cl	100.49	35.1		
142a	CHClFCH ₂ F	100.49			
HCFC-142b	CH ₃ CClF ₂	100.50	-9.8	41.2	137.2
143	CHF ₂ CH ₂ F	84.04	5.		
E-143a	CH ₃ OCF ₃	100.04	-24.1	35.9	104.9
HFC-143a	CH ₃ CF ₃	84.04	-47.4	38.3	73.6

Table 20 (Continued)

Number	Formula, Composition, Synonym	Molecular Weight	n.b.p. (°C)	Crit. <i>P</i> (bar)	Crit. <i>T</i> (°C)
151	CH ₂ FCH ₂ Cl	82.50	53.2		
152	CH ₂ FCH ₂ F	66.05	10.5	43.4	171.8
HFC-152a	CH ₃ CHF ₂	66.05	-24.0	45.2	113.3
HCC-160	CH ₃ CH ₂ Cl	64.51	12.4	52.4	186.6
HFC-161	CH ₃ CH ₂ F	48.06	-37.1	47.0	102.2
E-170	CH ₃ OCH ₃ (dimethyl ether)	46.07	-24.8	53.2	128.8
HC-170	CH ₃ CH ₃ (ethane)	30.07	-88.8	48.9	32.2
216	C ₃ Cl ₂ F ₆	220.93	35.7	27.5	180.0
FC-218	CF ₃ CF ₂ CF ₃	188.02	-36.7	26.8	71.9
HFC-227ca	CHF ₂ CF ₂ CF ₃	170.03	-17.0	28.7	106.3
HFC-227ea	CF ₃ CHF ₂ CF ₃	170.03	-18.3	29.5	103.5
234da	CF ₃ CHClCHClF	114.03	70.1		
235ca	CF ₃ CF ₂ CH ₂ Cl	156.46	28.1		
HFC-236ca	CHF ₂ CF ₂ CHF ₂	152.04	5.1	34.1	153.2
HFC-236cb	CH ₂ FCF ₂ CF ₃	152.04	-1.4	31.2	130.2
HFC-236ea	CHF ₂ CHFCF ₃	152.04	6.6	35.3	141.2
HFC-235fa	CF ₃ CH ₂ CF ₃	152.04	-1.1	31.8	130.7
HFC-245ca	CH ₂ FCF ₂ CHF ₂	134.05	25.5	38.6	178.5
E-245cb	CHF ₂ OCH ₂ CF ₃	150.05	34.0		185.2
HFC-245cb	CH ₃ CF ₂ CF ₃	134.05	-18.3	32.6	108.5
E-245fa	CHF ₂ OCH ₂ CF ₃	150.05	29.2	37.3	170.9
HFC-245fa	CHF ₂ CH ₂ CF ₃	134.05	15.3	36.4	157.6
HFC-254cb	CH ₃ CF ₂ CHF ₂	116.06	-0.8	37.5	146.2
HC-290	CH ₃ CH ₂ CH ₃ (propane)	44.10	-42.1	42.5	96.8
RC-318	cyclo-CF ₂ CF ₂ CF ₂ CF ₂	200.04	-5.8	27.8	115.4
400	R-12/114				
R-401a	R-22/124/152a (53/34/13)	94.44	-33.1	46.0	108.0
R-401b	R-22/124/152a (61/28/11)	92.84	-34.7	46.8	106.1
R-401c	R-22/124/152a (33/52/15)	101.04	-28.4	43.7	112.7
R-402a	R-22/125/290 (38/60/2)	101.55	-49.2	41.3	75.5
R-402b	R-22/125/290 (60/38/2)	94.71	-47.4	44.5	82.6
R-403a	R-22/218/290 (75/20/5)	91.06	-50.0	50.8	93.3
R-403b	R-22/218/290 (56/39/5)	102.06	-49.5	50.9	90.0
R-404a	R-125/134a/143a (44/4/52)	97.60	-46.5	37.3	72.1
R-405a	R-22/142b/152a/C318 (45/5/ 7/43)	116.00	-27.3	42.6	106.1
R-406a	R-22/142b/600a (55/41/4)	89.85	-30.0	47.4	123.0
R-407a	R-32/125/134a (20/40/40)	90.10	-45.5	45.4	82.8
R-407b	R-32/125/134a (10/70/20)	102.94	-47.3	41.6	75.8
R-407c	R-32/125/134a (23/25/52)	86.20	-43.6	46.2	86.7
R-408a	R-22/125/143a (47/7/46)	87.02	-43.5	43.4	83.5
R-409a	R-22/124/142b (60/25/15)	97.45	-34.2	45.0	107.0
R-410a	R-32/125 (50/50)	72.56	-50.5	49.6	72.5
R-410b	R-32/125 (45/55)				
R-411a	R-22/152a/1270 (88/11/2)				
R-411b	R-22/152a/1270 (94/3/3)				
R-412a	R-22/142b/218 (70/25/5)				
R-500	R-12/152a (74/26)	99.31	-33.5	44.2	105.5
R-501	R-12/22 (25/75)				
R-502	R-22/115 (49/51)	111.64	-45.4	40.8	82.2
R-503	R-13/23 (60/40)	87.28	-87.8	43.6	19.5

(continued)

Table 20 (Continued)

Number	Formula, Composition, Synonym	Molecular Weight	n.b.p. (°C)	Crit. <i>P</i> (bar)	Crit. <i>T</i> (°C)
R-504	R-32/115 (48/52)	79.2	-57.2	47.6	66.4
R-505	R-12/31 (78/22)	103.5	-30		
R-506	R-31/114 (55/45)	93.7	-12		
R-507	R-125/143a (50/50)	98.90	-46.7	37.9	70.9
R-508	R-23/116 (39/61)	100.10	-85.7		23.1
R-509	R-22/218 (44/56)	124.0	-47		
R-600	CH ₃ CH ₂ CH ₂ CH ₃ (butane)	58.13	-0.4	38.0	152.0
R-600a	CH ₃ CH ₂ CH ₂ CH ₃ (isobutane)	58.13	-11.7	36.5	135.0
R-610	C ₄ H ₁₀ O (ethyl ether)	74.12	-116.3	36.0	194.0
R-611	C ₂ H ₄ O ₂ (methyl formate)	60.05	31.8	59.9	204
630	CH ₃ NH (methyl amine)	31.06	-6.7	74.6	156.9
631	C ₂ H ₅ NH ₂ (ethyl amine)	45.08	16.6	56.2	183.0
702	H ₂ (hydrogen)	2.016	-252.8	13.2	-239.9
702p	Parahydrogen	2.016	-252.9	12.9	-240.2
704	He (helium)	4.003	-268.9	2.3	-267.9
717	NH ₃ (ammonia)	17.03	-33.3	114.2	133.0
718	H ₂ O (water)	18.02	100.0	221.0	374.2
720	Ne (neon)	20.18	-246.1	34.0	-228.7
728	N ₂ (nitrogen)	28.01	-198.8	34.0	-146.9
728a	CO (carbon monoxide)	28.01	-191.6	35.0	-140.3
729	— (air)	28.97	-194.3	37.6	-140.6
732	O ₂ (oxygen)	32.00	-182.9	50.8	-118.4
740	A (argon)	39.95	-185.9	49.0	-122.3
744	CO ₂ (carbon dioxide)	44.01	-78.4	73.7	31.1
744a	N ₂ O (nitrous oxide)	44.02	-89.5	72.2	36.5
R-764	SO ₂ (sulfur dioxide)	64.07	-10.0	78.8	157.5
1113	C ₂ ClF ₃	116.47	-27.9	40.5	106
1114	C ₂ F ₄	100.02	-76.0	39.4	33.3
1120	CHClCCl ₂	131.39	87.2	50.2	271.1
1130	CHClCHCl	96.95	47.8	54.8	243.3
1132a	C ₂ H ₂ F ₂	64.03	-85.7	44.6	29.7
1141	C ₂ H ₃ F (vinyl fluoride)	46.04	-72.2	52.4	54.7
1150	C ₂ H ₄ (ethylene)	28.05	-103.7	51.1	9.3
1270	C ₃ H ₆ (propylene)	42.09	-185	46.2	91.8
R-7146	SF ₆ (sulfur hexafluoride)	146.05	-63.8	37.6	45.6

^aRefrigerant numbers in some cases are tentative and subject to revision. Compositions rounded to nearest weight percent. Based on data supplied by M. O. McLinden, NIST, Boulder, CO, PCR Chemicals, Gainesville, FL, G. H. Thomson, DIPPR, Bartlesville, OK, and literature sources.

Table 21 Specific Heat (kJ/kg · K) at Constant Pressure of Saturated Liquids

Substance	Temperature (K)															
	250	260	270	280	290	300	310	320	330	340	350	360	370	380	390	400
Acetic acid	— ^a	—	—	—	2.03	2.06	2.09	2.12	2.16	2.19	2.23	2.26	2.29	2.33	2.36	2.39
Acetone	2.05	2.07	2.10	2.13	2.16	2.19	2.22	2.26	2.30	2.35	2.40	—	—	—	—	—
Ammonia	4.48	4.54	4.60	4.66	4.73	4.82	4.91	5.02	5.17	5.37	5.64	6.04	6.68	7.80	10.3	21
Aniline	—	—	2.03	2.04	2.05	2.07	2.10	2.13	2.16	2.19	2.22	2.26	2.31	2.38	2.47	2.58
Benzene	—	—	—	1.69	1.71	1.73	1.75	1.78	1.81	1.84	1.87	1.91	1.94	1.98	2.03	2.09
<i>n</i> -Butane	2.19	2.23	2.27	2.32	2.37	2.43	2.50	2.58	2.67	2.76	2.86	2.97	3.08	—	—	—
Butanol	2.13	2.17	2.22	2.27	2.33	2.38	2.44	2.51	2.58	2.65	2.73	2.82	2.93	3.06	3.20	3.36
Carbon tetrachloride	0.833	0.838	0.843	0.848	0.853	0.858	0.864	0.870	0.879	0.891	0.912	0.941	0.975	—	—	—
Chlorobenzene	1.29	1.31	1.32	1.32	1.33	1.33	1.34	1.36	1.38	1.40	1.42	1.44	1.46	1.47	1.49	1.51
<i>m</i> -Cresol	—	—	—	—	2.04	2.07	2.11	2.14	2.18	2.21	2.24	2.27	2.30	2.32	2.35	2.38
Ethane	2.97	3.20	3.50	4.00	5.09	9.92	—	—	—	—	—	—	—	—	—	—
Ethanol	—	2.24	2.28	2.33	2.38	2.45	2.54	2.64	2.75	2.86	2.99	3.12	3.26	3.41	3.56	3.72
Ethyl acetate	—	—	—	1.89	1.92	1.94	1.97	2.00	2.03	2.06	2.09	2.13	2.16	2.20	2.24	2.28
Ethyl sulfide	1.96	1.97	1.97	1.98	2.00	2.01	2.02	2.03	—	—	—	—	—	—	—	—
Ethylene	3.25	3.78	5.0	—	—	—	—	—	—	—	—	—	—	—	—	—
Formic acid	—	—	—	—	2.15	2.16	2.17	2.18	2.20	2.22	2.24	2.26	2.28	2.30	2.33	2.36
Heptane	2.08	2.10	2.13	2.17	2.20	2.24	2.28	2.32	2.36	2.41	2.45	2.49	2.54	2.59	2.64	2.70
Hexane	2.09	2.12	2.15	2.19	2.22	2.26	2.31	2.36	2.41	2.46	2.51	2.56	2.62	2.69	2.76	2.83
Methanol	2.31	2.34	2.37	2.41	2.46	2.52	2.58	2.65	2.73	2.82	2.91	3.01	3.12	3.24	3.36	3.49
Methyl formate	—	—	—	—	2.16	2.16	—	—	—	—	—	—	—	—	—	—
Octane	2.07	2.10	2.13	2.16	2.19	2.22	2.26	2.31	2.35	2.39	2.43	2.47	2.52	2.57	2.62	2.69
Oil, linseed	1.58	1.61	1.65	1.69	1.73	1.78	1.82	1.87	1.91	1.95	1.99	2.03	2.08	2.13	2.17	2.21
Oil, olive	1.90	1.92	1.95	1.98	2.01	2.05	2.09	2.13	2.16	2.20	2.24	2.28	2.32	2.37	2.41	2.46
Pentane	1.96	2.02	2.08	2.14	2.21	2.28	2.35	2.42	2.49	2.56	2.63	2.70	2.77	2.84	2.91	2.98
Propane	2.35	2.41	2.48	2.56	2.65	2.76	2.89	3.06	3.28	3.62	4.23	5.98	—	—	—	—
Propanol	2.04	2.10	2.16	2.24	2.32	2.41	2.51	2.62	2.74	2.86	2.99	3.12	3.26	3.40	3.55	3.71
Propylene	2.22	2.27	2.34	2.43	2.55	2.69	2.87	3.12	3.44	3.92	4.75	6.75	—	—	—	—
Sulfuric acid	—	—	—	—	1.39	1.41	1.43	1.45	1.46	1.48	1.50	1.51	1.53	1.54	1.56	1.57
Sulfur dioxide	1.31	1.32	1.33	1.34	1.36	1.39	1.42	1.46	1.50	1.55	1.61	1.68	1.76	1.85	1.99	2.14
Turpentine	1.60	1.65	1.70	1.75	1.80	1.85	1.90	1.95	2.00	2.05	2.10	2.15	2.20	2.25	2.30	2.35

^aDashes indicate inaccessible states.

Table 23 Surface Tension (N/m) of Liquids

Substance	Temperature (K)															
	250	260	270	280	290	300	310	320	330	340	350	360	370	380	390	400
Acetone	0.0291	0.0279	0.0266	0.0253	0.0240	0.0228	0.0214	0.0201	0.0187	0.0174	0.0162	0.0150	0.0139	0.0128	0.0117	0.0106
Ammonia	0.0317	0.0294	0.0271	0.0248	0.0226	0.0203	0.0181	0.0159	0.0138	0.0117	0.0099	0.0080	0.0059	0.0040	0.0021	0.0003
Benzene	0.0177	0.0165	0.0153	0.0141	0.0129	0.0116	0.0104	0.0092	0.0080	0.0069	0.0059	0.0049	0.0040	0.0031	0.0167	0.0155
Butane	0.0092	0.0071	0.0051	0.0032	0.0016	0.0003	—	—	—	—	—	—	—	—	—	—
CO ₂	0.0244	0.0228	0.0213	0.0198	0.0183	0.0168	0.0153	0.0138	0.0123	0.0108	0.0094	0.0080	0.0066	0.0052	0.0044	0.0037
Chlorine	0.0059	0.0047	0.0035	0.0024	0.0013	0.0005	—	—	—	—	—	—	—	—	—	—
Ethane	0.0271	0.0261	0.0251	0.0242	0.0232	0.0223	0.0214	0.0205	0.0196	0.0186	0.0177	0.0167	0.0158	0.0148	0.0137	0.0126
Ethanol	0.0032	0.0019	0.0009	0.0002	—	—	—	—	—	—	—	—	—	—	—	—
Ethylene	0.0244	0.0234	0.0224	0.0214	0.0205	0.0195	0.0185	0.0176	0.0166	0.0156	0.0147	0.0137	0.0127	0.0118	0.0109	0.0099
Heptane	0.0229	0.0218	0.0207	0.0197	0.0186	0.0175	0.0165	0.0154	0.0145	0.0135	0.0125	0.0115	0.0106	0.0096	0.0086	0.0076
Hexane	0.474	0.472	0.470	0.468	0.466	0.464	0.462	0.460	0.458	0.456	0.454	0.452	0.450	0.448	0.446	0.444
Mercury	0.0251	0.0243	0.0234	0.0225	0.0216	0.0207	0.0197	0.0188	0.0179	0.0170	0.0161	0.0152	0.0143	0.0135	0.0127	0.0120
Methanol	0.0132	0.0118	0.0104	0.0091	0.0079	0.0067	0.0056	0.0046	0.0037	0.0028	0.0018	0.0009	—	—	—	—
Octane	0.0133	0.0120	0.0106	0.0091	0.0078	0.0065	0.0053	0.0042	0.0032	0.0023	0.0014	0.0006	—	—	—	—
Propane	0.0148	0.0135	0.0122	0.0109	0.0096	0.0083	0.0070	0.0058	0.0047	0.0036	0.0027	0.0018	0.0010	0.0003	—	—
Propylene	0.0057	0.0042	0.0029	0.0018	0.0009	0.0003	—	—	—	—	—	—	—	—	—	—
R-12	0.0342	0.0327	0.0312	0.0298	0.0285	0.0272	0.0260	0.0249	0.0236	0.0225	0.0214	0.0203	0.0193	0.0183	0.0173	0.0163
R-13	—	—	—	0.0746	0.0732	0.0716	0.0699	0.0684	0.0666	0.0650	0.0636	0.0614	0.0595	0.0575	0.0555	0.0535
Toluene	—	—	—	—	—	—	—	—	—	—	—	—	—	—	—	—
Water	—	—	—	—	—	—	—	—	—	—	—	—	—	—	—	—

Table 25 Viscosity (10^{-4} Pa · s) of Saturated Liquids

Substance	Temperature (K)															
	250	260	270	280	290	300	310	320	330	340	350	360	370	380	390	400
Acetic acid	—	—	—	—	13.1	11.3	9.77	8.49	7.40	6.48	5.70	5.03	4.45	3.95	3.52	3.15
Acetone	5.27	4.63	4.11	3.68	3.32	3.01	2.73	2.49	2.28	2.10	1.94	—	—	—	—	—
Ammonia	2.20	1.94	1.74	1.58	1.44	1.31	1.20	1.08	0.98	0.88	0.78	0.70	0.64	0.58	0.53	0.48
Aniline	—	—	96.9	71.6	53.5	40.3	30.7	23.6	18.2	14.2	11.2	8.84	7.03	5.63	4.54	3.68
Benzene	—	—	—	8.08	6.80	5.84	5.13	4.52	4.05	3.60	3.29	2.98	2.70	2.45	2.24	2.04
Butane	2.63	2.37	2.15	1.95	1.77	1.61	1.56	1.33	1.21	1.10	1.00	0.90	0.81	0.73	0.66	0.60
Butanol	94.2	70.9	53.9	41.4	32.1	25.1	19.8	15.7	12.6	10.1	8.22	6.71	5.50	4.53	3.75	3.13
Carbon tetrachloride	—	—	14.0	11.9	10.2	8.78	7.70	6.81	6.06	5.43	4.89	4.41	4.00	3.65	3.34	3.07
Chlorobenzene	13.9	12.2	10.7	9.50	8.44	7.53	6.74	6.05	5.46	4.93	4.47	4.07	3.70	3.39	3.10	2.85
<i>m</i> -Cresol	—	—	—	—	261	136	72.0	39.0	21.5	12.1	6.90	—	—	—	—	—
Ethane	0.81	0.70	0.60	0.51	0.42	0.35	—	—	—	—	—	—	—	—	—	—
Ethanol	—	23.3	18.9	15.5	12.8	10.6	8.81	7.39	6.24	5.29	4.51	3.86	3.31	2.86	2.48	2.15
Ethyl acetate	7.21	6.53	5.86	5.28	4.78	4.33	3.95	3.60	3.30	3.03	2.79	2.57	2.38	2.20	2.04	1.90
Ethyl sulfide	7.69	6.68	5.86	5.19	4.64	4.18	3.78	3.45	3.16	2.92	2.70	2.51	2.34	2.20	2.06	1.95
Ethylene	0.582	0.505	0.418	0.31	—	—	—	—	—	—	—	—	—	—	—	—
Formic acid	48.3	37.4	29.5	23.6	19.2	15.9	13.3	11.2	9.56	8.24	7.16	6.27	5.53	4.91	4.39	3.94
Heptane	7.25	6.25	5.46	4.82	4.28	3.83	3.45	3.14	2.87	2.62	2.39	2.20	2.03	1.87	1.72	1.59
Hexane	5.03	4.46	3.97	3.57	3.22	2.93	2.68	2.45	2.24	2.07	1.92	1.78	1.63	1.50	1.38	1.26
Methanol	12.3	10.1	8.43	7.15	6.14	5.32	4.60	4.09	3.60	3.19	2.84	2.53	2.28	2.06	1.85	1.65
Methyl formate	5.71	5.04	4.50	4.04	3.66	3.34	3.06	2.82	2.61	2.43	2.27	2.13	2.01	1.89	1.79	1.70
Octane	10.5	8.80	7.49	6.45	5.66	5.01	4.48	4.03	3.65	3.33	3.05	2.80	2.58	2.38	2.18	2.02
Oil, linseed	2300	1500	1000	700	490	356	263	198	152	118	93.5	74.8	60.6	49.6	41.1	34.3
Oil, olive	8350	4600	2600	1600	1000	630	410	278	193	136	98.3	72.2	54.0	40.9	31.0	24.6
Pentane	3.50	3.16	2.87	2.62	2.39	2.20	2.03	1.87	1.73	1.59	1.46	1.34	1.22	1.11	1.01	0.92
Propane	1.71	1.53	1.37	1.23	1.10	0.98	0.87	0.76	0.66	0.58	0.51	0.45	—	—	—	—
Propanol	67.8	50.0	37.7	29.0	22.7	18.0	14.6	11.9	9.87	8.27	6.99	5.97	5.14	4.46	3.90	3.44
Propylene	1.41	1.27	1.16	1.05	0.94	0.84	0.75	0.67	0.60	0.53	0.47	0.42	—	—	—	—
Sulfuric acid	—	—	363	259	189	141	107	82.6	64.7	51.4	41.4	33.7	27.7	23.1	19.4	19.4
Sulfur dioxide	5.32	4.53	3.90	3.39	2.85	2.42	2.09	1.83	1.62	1.45	1.30	1.16	1.02	0.89	0.77	0.66
Turpentine	36.3	28.8	23.3	19.1	15.9	13.4	11.4	9.80	8.50	7.44	6.56	5.83	5.21	4.68	4.23	3.85

Table 26 Thermochemical Properties at 1.013 Bars, 298.15 K

Substance	Formula	ΔH_f° (kJ/kg · mol)	ΔG_f° (kJ/kg · mol)	S° (kJ/kg · mol · K)
Acetaldehyde	C ₂ H ₄ O(g)	-166,000	-132,900	265.2
Acetic acid	C ₂ H ₄ O ₂ (g)	-436,200	+315,500	282.5
Acetone	C ₃ H ₆ O(l)	-248,000	-155,300	200.2
Acetylene	C ₂ H ₂ (g)	+266,740	+209,190	200.8
Ammonia	NH ₃ (g)	-46,190	-16,590	192.6
Aniline	C ₆ H ₇ N(l)	+35,300	+153,200	191.6
Benzene	C ₆ H ₆ (l)	+49,030	+117,000	172.8
Butanol	C ₄ H ₁₀ O(l)	-332,400	-168,300	227.6
<i>n</i> -Butane	C ₄ H ₁₀ (l)	-105,900		
<i>n</i> -Butane	C ₄ H ₁₀ (g)	-126,200	-17,100	310.1
Carbon dioxide	CO ₂ (g)	-393,510	-394,390	213.7
Carbon disulfide	CS ₂ (g)	-109,200		237.8
Carbon monoxide	CO(g)	-110,520	-137,160	197.6
Carbon tetrachloride	CCl ₄ (g)	-103,000	-66,100	311.3
Carbon tetrafluoride	CF ₄ (g)	-921,300	-878,200	261.5
Chloroform	CHCl ₃ (g)	-104,000	-70,500	295.6
Cyclohexane	C ₆ H ₁₂ (g)	-123,100	+31,800	298.2
Cyclopropane	C ₃ H ₆ (g)	+53,300	+104,300	237.7
<i>n</i> -Decane	C ₁₀ H ₂₂ (l)	-332,600	-17,500	425.5
Diphenyl	C ₁₂ H ₁₀ (g)	-172,800	-283,900	348.5
Ethane	C ₂ H ₆ (g)	-84,670	-32,900	229.5
Ethanol	C ₂ H ₆ O(g)	-235,200	-168,700	282.7
Ethanol	C ₂ H ₆ O(l)	-277,600	-174,600	160.7
Ethyl acetate	C ₄ H ₈ O ₂ (g)	-432,700	-325,800	376.8
Ethyl chloride	C ₂ H ₅ Cl(g)	-107,600	-55,500	274.8
Ethyl ether	C ₄ H ₁₀ O(g)	-250,800	-118,400	352.5
Ethylene	C ₂ H ₄ (g)	+52,280	+68,130	219.4
Ethylene oxide	C ₂ H ₄ O(g)	-38,500	-11,600	242.9
Heptane	C ₇ H ₁₆ (g)	-187,800	-427,800	166.0
Hexane	C ₆ H ₁₈ (g)	-208,400	16,500	270.7
Hydrazine	N ₂ H ₄ (l)	-50,600	-149,200	121.2
Hydrazine	N ₂ H ₄ (g)	+95,400	+159,300	238.4
Hydrogen peroxide	H ₂ O ₂ (l)	-187,500	-120,400	109.6
Isobutane	C ₄ H ₁₀ (g)	-134,500	-20,900	294.6
Isopentane	C ₅ H ₁₂ (g)	-154,500	-14,600	343.6
Methane	CH ₄ (g)	-74,840	-50,790	186.2
Methanol	CH ₄ O(l)	-238,600	-126,800	81.8
Methanol	CH ₄ O(g)	-200,900	-162,100	247.9
Methyl acetate	C ₃ H ₆ O ₂ (l)	-444,300		
Methyl bromide	CH ₃ Br(g)	-36,200	-25,900	246.1
Methyl chloride	CH ₃ Cl(g)	-86,300	-63,000	234.2
Methyl formate	C ₂ H ₄ O ₂ (g)	-335,100	-301,000	292.8
Methylene chloride	CH ₂ Cl ₂ (g)	-94,000	-67,000	270.2
Naphthalene	C ₁₀ H ₈ (g)	-151,500	-224,200	336.5
Nitric oxide	NO(g)	+90,300	86,600	210.6
Nitrogen peroxide	NO ₂ (g)	+33,300		240.0
Nitrous oxide	N ₂ O(g)	+82,000	+104,000	219.9
Octane	C ₈ H ₁₈ (l)	-250,000	6,610	360.8

Table 26 (Continued)

Substance	Formula	ΔH_f° (kJ/kg · mol)	ΔG_f° (kJ/kg · mol)	S° (kJ/kg · mol · K)
Octane	$C_8H_{18}(g)$	-208,400	16,500	466.7
<i>n</i> -Pentane	$C_5H_{12}(g)$	-146,400	-8,370	348.9
Propane	$C_3H_8O(g)$	-103,800	-107,200	269.9
Propanol	$C_3H_8(g)$	-258,800	-164,100	322.6
Propylene	$C_3H_6(g)$	+20,400	+62,700	267.0
R11	$CFCl_3(g)$	-284,500	-238,000	309.8
R12	$CCl_2F_2(g)$	-468,600	-439,300	300.9
R13	$CClF_3(g)$	-715,500	-674,900	285.6
R13B1	$CF_3Br(g)$	-642,700	-616,300	297.6
R23	$CHF_3(g)$	-682,000	-654,900	259.6
Sulfur dioxide	$SO_2(g)$	-296,900	-300,200	248.1
Sulfur hexafluoride	$SF_6(g)$	-1,207,900	-1,105,000	291.7
Toluene	$C_7H_8(g)$	-50,000	-122,300	320.2
Water	$H_2O(l)$	-285,830	-237,210	70.0
Water	$H_2O(g)$	-241,820	-228,600	188.7

Table 27 Ideal Gas Sensible Enthalpies (kJ/kg · mol) of Common Products of Combustion^{a,b}

<i>T</i> (K)	Substance							
	CO	CO ₂	H ₂ O(g)	NO	NO ₂	N ₂	O ₂	SO ₂
200	-2,858	-3,414	-3,280	-2,950	-3,494	-2,855	-2,860	-3,736
220	-2,276	-2,757	-2,613	-2,345	-2,803	-2,270	-2,279	-3,008
240	-1,692	-2,080	-1,945	-1,749	-2,102	-1,685	-1,698	-2,266
260	-1,110	-1,384	-1,277	-1,148	-1,390	-1,105	-1,113	-1,508
280	-529	-667	-608	-547	-668	-525	-529	-719
300	54	67	63	54	67	55	60	75
320	638	822	736	652	813	636	650	882
340	1,221	1,594	1,411	1,248	1,573	1,217	1,238	1,702
360	1,805	2,383	2,088	1,847	2,344	1,800	1,832	2,541
380	2,389	3,187	2,768	2,444	3,130	2,383	2,429	3,387
400	2,975	4,008	3,452	3,042	3,929	2,967	3,029	4,251
420	3,562	4,841	4,138	3,641	4,739	3,554	3,633	5,123
440	4,152	5,689	4,828	4,247	5,560	4,147	4,241	6,014
460	4,642	6,550	5,522	4,849	6,395	4,737	4,853	6,923
480	5,334	7,424	6,221	5,054	7,243	5,329	5,468	7,827
500	5,929	8,314	6,920	6,058	8,100	5,921	6,088	8,749
550	7,427	10,580	8,695	7,589	10,295	7,401	7,655	11,180
600	8,941	12,915	10,500	9,146	12,555	8,902	9,247	13,545
650	10,475	15,310	12,325	10,720	14,875	10,415	10,865	16,015
700	12,020	17,760	14,185	12,310	17,250	11,945	12,500	18,550
750	13,590	20,270	16,075	13,890	19,675	13,490	14,160	21,150
800	15,175	22,820	17,990	15,550	22,140	15,050	15,840	23,720
850	16,780	25,410	19,945	17,200	24,640	16,630	17,535	26,390

(continued)

Table 27 (Continued)

T (K)	Substance							
	CO	CO ₂	H ₂ O(g)	NO	NO ₂	N ₂	O ₂	SO ₂
900	18,400	28,040	21,920	18,860	27,180	18,220	19,245	29,020
950	20030	30,700	23,940	20,540	29,740	19,835	20,970	31,700
1,000	21,690	33,410	25,980	22,230	32,340	21,460	22,710	34,430
1,050	23,350	36,140	28,060	23,940	34,950	23,100	24,460	37,180
1,100	25,030	38,890	30,170	25,650	37,610	24,750	26,180	39,920
1150	26,720	41,680	32,310	27,380	40,260	26,430	27,990	42,690
1200	28,430	44,480	34,480	29,120	42,950	28,110	29,770	45,460
1250	30,140	47,130	36,680	30,870	45,650	29,810	31,560	48,270
1300	31,870	50,160	38,900	32,630	48,350	31,510	33,350	51,070
1350	33,600	53,030	41,130	34,400	51,090	33,220	35,160	53,900
1400	35,340	55,910	43,450	36,170	53,810	34,940	36,970	56,720
1450	37,090	58,810	45,770	37,950	56,560	36,670	38,790	59,560
1500	38,850	61,710	48,100	39,730	59,310	38,410	40,610	62,400
1550	40,610	64,800	50,460	41,520	62,070	40,160	42,440	65,260
1,600	42,380	67,580	52,840	43,320	64,850	41,910	44,280	68,120
1,650	44,156	70,530	55,240	45,120	67,640	43,670	46,120	71,000
1,700	45,940	73,490	57,680	46,930	70,420	45,440	47,970	73,870
1,750	47,727	76,460	60130	48,740	73,220	47,210	49,830	76,760
1,800	49,520	79,440	62,610	50,560	76,010	49,000	51,690	79,640
1,850	51,320	82,430	65,100	52,380	78,810	50,780	53,560	82,540
1,900	53,120	85,430	67,610	54,200	81,630	52,570	55,440	85,440
1,950	54,930	88,440	70,140	56,020	84,450	54,370	57,310	88,350
2,000	56,740	91,450	72,690	57,860	87,260	56,160	59,200	91,250
2,100	60,380	97,500	77,830	61,530	92,910	59,760	62,990	97,080
2,200	64,020	103,570	83,040	65,220	98,580	63,380	66,800	102,930
2,300	67,680	109,670	88,290	68,910	104,260	67,010	70,630	108,790
2,400	71,350	115,790	93,600	72,610	109,950	70,660	74,490	114,670
2,500	75,020	121,930	98,960	76,320	115,650	74,320	78,370	120,560
2,600	78,710	128,080	104,370	80,040	121,360	77,990	82,270	126,460
2,700	82,410	134,260	109,810	83,760	127,080	81,660	86,200	132,380
2,800	86,120	140,440	115,290	87,490	132,800	85,360	90,140	138,300
2,900	89,830	146,650	120,810	91,230	138,540	89,050	94,110	144,240
3,000	93,540	152,860	126,360	94,980	144,270	92,750	98,100	150,180

^aConverted and usually rounded off from *JANAF Thermochemical Tables*, NSRDS-NBS-37, 1971.

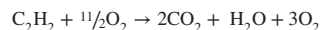
^bTo illustrate the term *sensible enthalpy*, which is the difference between the actual enthalpy and the enthalpy at the reference temperature, 298.15 K (=25°C = 77°F = 537°R), the magnitude of the heat transfer, in kJ/kg · mol fuel and in kJ/kg fuel, will be calculated for the steady-state combustion of acetylene in excess oxygen, the reactants entering at 298.15 K and the products leaving at 2000 K. All substances are in the gaseous phase.

The basic equation is

$$Q + W = \sum_P n_i (\Delta h_f^\circ + \Delta h_s)_i - \sum_R n_i (\Delta h_f^\circ + \Delta h_s)_i$$

where P signifies products and R reactants, Δh_s signifies sensible enthalpy, and the Δh_s are looked up in the table for the appropriate temperatures.

If the actual reaction was



then $W=0$ and $Q=2(-393,510 + 91,450) + 1(-241,810 + 72,690) + 3(0 + 59,200) - (226,740 + 0) - \frac{1}{2}(0 + 0) = -604,120 + (-169,120) + 177,600 - 226,740 = -822,380$ kJ/mg mol. $\text{C}_2\text{H}_2 = -31,584$ kJ/kg C_2H_2 . Had the fuel been burnt in air one would write the equation with an additional 3.76(5.5) N_2 on each side of the equation. In the above, the enthalpy of formation of the stable elements at 298.15 K has been set equal to zero. For further information, most undergraduate engineering thermodynamics texts may be consulted.

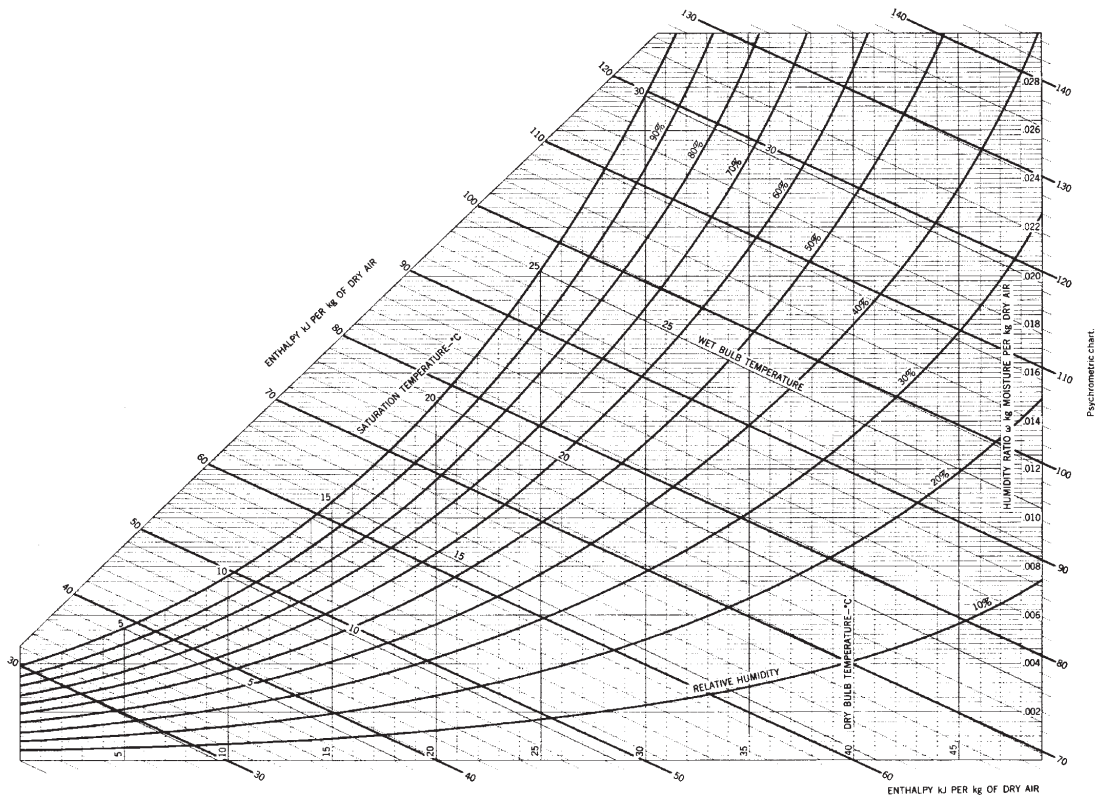


Figure 6 Psychrometric chart. (ASHRAE chart No. 1, 1981. Prepared at the Center for Applied Thermodynamic Studies, University of Idaho, Moscow, ID. Republished with permission of ASHRAE, from *The ASHRAE Fundamentals Handbook* 1981; permission conveyed through Copyright Clearance Center, Inc.)

CHAPTER 2

MECHANICS OF INCOMPRESSIBLE FLUIDS

Egemen OI Ogretim and Wade W. Huebsch
West Virginia University
Morgantown, West Virginia

1 INTRODUCTION	41	6 SIMILITUDE AND	79
1.1 Definition of a Fluid	42	DIMENSIONAL ANALYSIS	
1.2 System of Units and Dimension	42	6.1 Similitude	79
2 FLUID PROPERTIES	42	6.2 Dimensional Analysis	81
2.1 Density, Specific Weight, and Specific Gravity	42	7 FLOW IN CLOSED	82
2.2 Compressibility	44	CONDUITS	
2.3 Viscosity	48	7.1 Velocity Distribution	83
2.4 Surface Tension and Capillarity	49	7.2 Pipe Friction	87
2.5 Vapor Pressure	50	7.3 Minor Losses	92
3 FLUID STATICS	51	7.4 Steady-State Pipeline Analysis	95
3.1 Pressure Variation in a Fluid at Rest	51	7.5 Pipe Network Analysis	99
3.2 Basic Pressure-Measuring Devices	52	7.6 Unsteady Flow in Pipe Systems	102
3.3 Fluid Forces on Plane Surfaces	53	8 FLOW IN OPEN CHANNELS	108
3.4 Fluid Forces on Curved Surfaces	54	8.1 Uniform Flow	108
3.5 Buoyancy and Stability	56	8.2 Steady, Nonuniform Flow	112
3.6 Accelerated Fluid Masses without Relative Motion	57	8.3 Unsteady, Nonuniform Flow	113
4 IDEAL (INVISCID) FLUID	58	9 FLOW ABOUT IMMERSED	115
DYNAMICS		OBJECTS	
4.1 One-Dimensional Flow	59	9.1 Flat-Plate Boundary Layer	116
4.2 Two- and Three-Dimensional Flow	62	9.2 Drag on Immersed Objects	117
5 VISCOUS FLUID DYNAMICS	71	9.3 Lift	118
5.1 Internal Flows	72	10 FLUID MEASUREMENTS	118
5.2 External Flows	73	10.1 Fluid Property Measurement	118
5.3 Navier–Stokes Equations	73	10.2 Pressure Measurement	121
		10.3 Velocity Measurement	122
		10.4 Flow Rate Measurement	126
		REFERENCES	133
		BIBLIOGRAPHY	133

1 INTRODUCTION

We experience and interact with fluids, such as air, water, oil, and gas, in many aspects of our daily life. These fluids can be categorized in different ways depending on the level of analysis required. An obvious first categorization is that they can be viewed as liquid or gas; but they

can be classified depending on their behavior in a particular application as well. Some common fluid classifications are viscous or inviscid, compressible or incompressible, laminar or turbulent, Newtonian or non-Newtonian, and steady or unsteady. These classifications are sometimes idealizations (approximations) and sometimes exact descriptions. Overall, they offer information on fluid properties and characteristics, the state of the flow field, and how to approach an engineering solution to the relevant flow problem. This chapter will cover the basics on many of these classifications but will primarily restrict a bulk of the discussion to the category of Newtonian incompressible fluids.

All substances are compressible to some extent and fluids are no exception. However, in many cases, fluids may be treated as incompressible without introducing unacceptable inaccuracies in either computations or measurements. In the case of liquids, the vast majority of problems may be addressed as incompressible flow problems. Even in situations where pressure changes are significant enough to cause small changes in density (water hammer), incompressible flow techniques are applied to solve problems. For gases where flow velocities are low compared to the local speed of sound (low Mach number) or where density changes in the system are small, incompressible flow theory may be used to good approximation.

1.1 Definition of a Fluid

A *fluid*, which can be a liquid or gas, is defined as a collection of molecules of a substance (or several substances) that cannot support a shearing stress of any size (magnitude) without undergoing permanent and continual angular deformation. Even though the fluid is a collection of molecules, it is generally considered to be a continuous substance without voids, referred to as a continuum (typical liquid has on the order of 10^{21} molecules/mm³). Newtonian fluids are those whose rate of angular deformation is linear with respect to the magnitude of the deforming shear stress. Most common liquids and gases are Newtonian fluids (e.g., air, water, oil). Non-Newtonian fluids are those whose rate of angular deformation bears a nonlinear relationship to the applied shear stress. Examples of non-Newtonian fluids are blood, paints, and suspensions.

1.2 System of Units and Dimension

The scientific world is in the midst of a conversion from various systems of units to SI (Système International d'Unités) units. However, the English FSS (foot–slug–second) system is still in widespread use throughout the United States. Hence, this work will use both the English system of units as well as the SI equivalent in the text, tables, and numerical examples. Table 1 provides the units used to identify the basic dimensional quantities in each system, and Table 2 gives a conversion table for fluid properties and other commonly used quantities.

2 FLUID PROPERTIES

Properties of fluids generally encountered in engineering practice are presented in tables and figures in this section. Included are the commonly used properties of density, specific gravity, bulk modulus (compressibility), viscosity, surface tension, and vapor pressure.

2.1 Density, Specific Weight, and Specific Gravity

Density is defined as the mass per unit volume ρ . Table 3 provides values for a selection of liquids at standard atmospheric pressure (14.7 lb/in.² or 101,325 Pa), and Table 4 provides properties of some common gases. Density varies with temperature and pressure, but for liquids,

Table 1 Basic Dimensions and Abbreviations in English and SI Units

Abbreviations		
BTU = British thermal unit	m = meter (SI) = mile (FSS)	
cfs = cubic feet per second	mb = millibar = 10^{-3} bar	
fps; ft/s = feet per second	mm = millimeter = 10^{-3} meter	
ft = foot	mm ² = square millimeter	
gpm = gallons per minute	mph = miles per hour	
hp = horsepower	mps; m/s = meters per second	
h = hour	N = newton	
Hz = hertz	Pa = pascal = N/m ²	
in. = inch	psi = pounds per square inch	
J = joule = N-m	sec s = second	
kg = kilogram = 10^3 grams	W = watt = J/s	
lb = pound force		
Units		
Quantity	SI Unit Name (Symbol)	FSS Unit Name (Symbol)
<i>Basic Units</i>		
Length	Meter (m)	Foot (ft)
Mass	Kilogram (kg)	Slug (slug)
Time	Second (s)	Second (sec)
Temperature	Kelvin (K)	Rankine (°R)
	Celsius (°C)	Fahrenheit (°F)
<i>Derived Units</i>		
Energy	Joule (J)	Foot-pound (ft-lb)
Force	Newton (N)	Pound (lb)
Frequency	Hertz (Hz)	Hertz (Hz)
Power	Watt (W)	Horsepower (hp)
Pressure	Pascal (Pa)	—

Source: From Ref. 1.

variation with pressure is generally negligible. Also included in these tables are the specific weight γ , which is the density multiplied by the gravitational acceleration, which produces a measure of weight per unit volume (pounds per cubic feet or newtons per cubic meter).

For a gas, the density depends heavily on the pressure and temperature. Most gases closely follow the ideal gas equation of state

$$\rho = \frac{p}{RT} \quad (1)$$

where p is the absolute pressure, T is the absolute temperature, and R is the specific gas constant. This equation should be used with discretion under conditions of very high temperature or very low pressure or when the gas approaches a liquid. Because all gases at the same temperature and pressure contain the same number of molecules per unit volume (Avogadro's law), the specific gas constant can be calculated to good accuracy by dividing the universal gas constant, 8314 J/mol-K, by the molecular weight of the gas. For example, oxygen has the molecular weight of 32 kg/mol. The specific gas constant of oxygen is calculated as $R = 8314/32 = 258$ J/kg-K (compare with Table 4).

Another widely used fluid property is the specific gravity, SG, which is defined as the ratio of the fluid density to the density of water at a specified temperature (typically 32°F, or 4°C,

44 Mechanics of Incompressible Fluids

Table 2 Conversion Factors for English FSS and SI Units

Absolute viscosity: 1 slug/ft-s = 1 lb-s/ft ² = 47.88 N-s/m ² = 47.88 kg/m-s = 478.8 P	
Acceleration due to gravity: 32.174 ft/s ² = 80665 m/s ²	
Area: 1 ft ² = 0.0929 m ²	
1 in. ² = 645.2 mm ²	
Density: 1 slug/ft ³ = 515.4 kg/m ³	
Energy: 1 ft-lb = 1.356 J = 1.356 Nm = 3.77 × 10 ⁻⁷ kWh	
1 Btu = 778.2 ft-lb = 1055 J = 2.93 × 10 ⁻⁴ kWh	
Flow rate: 1 ft ³ /s = 0.02832 m ³ /s = 28.32 liters/s	
1 mgd = 1.55 cfs = 0.0438 m ³ /s = 43.8 liters/s	
Force: 1 lb = 4.448 N	
Frequency: 1 cycle/s = 1 Hz	
Kinematic viscosity: 1 ft ² /s = 0.0929 m ² /s = 929 stokes	
Length: 1 in. = 25.4 mm	
1 ft = 0.3048 m	
1 mile = 1.609 km	
Mass: 1 slug = 14.59 kg	
Power: 1 ft-lb/s = 1.356 W = 1.356 J/s	
1 hp = 550 ft-lb/s = 745.7 W	
Pressure: 1 psi = 6895 N/m ² = 6895 Pa	1 atm = 14.70 psi (1)
1 in. Hg = 25.4 mm Hg = 3386 N/m ²	= 29.92 in. Hg = 760 mm Hg (2)
1 in. H ₂ O = 249.1 N/m ²	= 101.325 kN/m ² (3)
1 lb/ft ² = 47.88 N/m ² = 47.88 Pa = 0.4788 mb	1 bar = 14.504 psi (4)
	= 10 ⁵ N/m ² = 100 kN/m ²
Specific heat, engineering gas constant: 1 ft-lb/slug °R = 0.1672 Nm/kg K	
Specific weight: 1 lb/ft ³ = 157.1 N/m ³	
Temperature: 1°C = 1 K = 1.8°F = 1.8°R	
Velocity: 1 fps = 0.3048 mps = 0.3048 m/s	
1 mph = 1.609 km/h = 0.447 m/s	
1 knot = 1.152 mph = 1.689 fps = 0.5155 m/s	
Volume: 1 ft ³ = 0.02832 m ³	
1 U.S. gallon = 0.1337 ft ³ = 0.003785 m ³ = 3.785 liters	

Source: From Ref. 1.

which gives a density of water as 1.94 slugs/ft³ or 1000 kg/m³). So the specific gravity can be found from

$$SG = \frac{\rho}{\rho_{\text{water}}} \quad (2)$$

This provides a direct measure of whether the fluid is less dense or more dense than water and by what degree; for example, the specific gravity of mercury is 13.6, so it is 13.6 times denser than water.

2.2 Compressibility

The *compressibility* of fluids is confined to their behavior in the mode of compression. The definition of the bulk modulus of elasticity stems from the relative change in volume and provides a measure of the compressibility of a fluid:

$$E_v = -\frac{\Delta p}{\Delta V/V} \quad (3)$$

Table 3 Approximate Physical Properties of Some Common Liquids

British Gravitational Units									
Liquid	Temperature (°F)	Density, ρ (slugs/ft ³)	Specific Weight, γ (lb/ft ³)	Dynamic Viscosity, μ (lb - s/ft ²)	Kinematic Viscosity, ν (ft ² /s)	Surface Tension, ^a σ (lb/ft)	Vapor Pressure, ρ_v [lb/in. ² (abs)]	Bulk Modulus, E_v (lb/in. ²)	
Carbon tetrachloride	68	3.09	95	2.00×10^{-5}	6.47×10^{-6}	1.84×10^{-3}	1.9	1.91×10^5	
Ethyl alcohol	68	1.53	43	2.49×10^{-5}	1.63×10^{-5}	1.56×10^{-3}	0.85×10^{-1}	1.54×10^5	
Gasoline ^c	60	1.32	42.5	6.5×10^{-6}	4.9×10^{-6}	1.5×10^{-3}	8.0	1.9×10^5	
Glycerin	68	2.44	78.6	3.13×10^{-2}	1.28×10^{-2}	4.34×10^{-3}	2.0×10^{-6}	6.56×10^5	
Mercury	68	26.3	847	3.28×10^{-5}	1.25×10^{-6}	3.19×10^{-2}	2.3×10^{-5}	4.14×10^6	
SAE 30 oil ^c	60	1.77	57.0	8.0×10^{-3}	4.5×10^{-3}	2.5×10^{-3}	—	2.2×10^5	
Seawater	60	1.99	64.0	2.51×10^{-5}	1.26×10^{-5}	5.03×10^{-3}	0.226	3.39×10^5	
Water	60	1.94	62.4	2.34×10^{-5}	1.21×10^{-5}	5.03×10^{-3}	0.226	3.12×10^5	

SI Units									
Liquid	Temperature (°C)	Density, ρ (kg/m ³)	Specific Weight, γ (kN/m ³)	Dynamic Viscosity, μ (N - s/m ²)	Kinematic Viscosity, ν (m ² /s)	Surface Tension, ^a σ (N/m)	Vapor Pressure, ρ_v [N/m ² (abs)]	Bulk Modulus, E_v (N/m ²)	
Carbon tetrachloride	20	1,590	15.6	58×10^{-4}	6.03×10^{-7}	2.69×10^{-2}	1.3×10^4	1.31×10^9	
Ethyl alcohol	20	789	7.74	1.19×10^{-3}	1.51×10^{-6}	2.28×10^{-2}	5.9×10^3	1.06×10^9	
Gasoline ^c	15.6	680	6.67	3.1×10^{-4}	4.6×10^{-7}	2.2×10^{-2}	5.5×10^4	1.3×10^9	
Glycerin	20	1,260	12.4	1.50	1.19×10^{-3}	6.33×10^{-2}	1.4×10^{-2}	4.52×10^9	
Mercury	20	13,600	133	1.57×10^{-3}	1.15×10^{-7}	0.466	0.16	2.85×10^{10}	
SAE 30 oil ^c	15.6	912	8.95	0.38	4.2×10^{-4}	3.6×10^{-2}	—	1.5×10^9	
Seawater	15.6	1,030	10.1	1.20×10^{-3}	1.17×10^{-6}	7.34×10^{-2}	$1.77 \times 10^{+3}$	2.34×10^9	
Water	15.6	999	80	1.12×10^{-3}	1.12×10^{-6}	7.34×10^{-2}	$1.77 \times 10^{+3}$	2.15×10^9	

^aIn contact with air.

^bIsentropic bulk modulus calculated from speed of sound.

^cTypical values. Properties of petroleum products vary.

Source: From Ref. 2.

Table 4 Approximate Physical Properties of Some Common Gases at Standard Atmospheric Pressure

British Gravitational (BG) Units							
Gas	Temperature (°F)	Density, ρ (slugs/ft ³)	Specific Weight, γ (lb/ft ³)	Dynamic Viscosity, μ (lb - s/ft ²)	Kinematic Viscosity, ν (ft ² /s)	Gas Constant, ^a R (ft-lb/slug)	Specific Heat Ratio, ^b k
Air (standard)	59	2.38×10^{-3}	7.65×10^{-2}	3.74×10^{-7}	1.57×10^{-4}	1.716×10^3	1.40
Carbon dioxide	68	3.55×10^{-3}	0.114	3.07×10^{-7}	8.65×10^{-5}	1.130×10^3	1.30
Helium	68	3.23×10^{-4}	1.04×10^{-2}	4.09×10^{-7}	1.27×10^{-3}	1.242×10^4	1.66
Hydrogen	68	1.63×10^{-4}	5.25×10^{-3}	1.85×10^{-7}	1.13×10^{-3}	2.466×10^4	1.41
Methane (natural gas)	68	1.29×10^{-3}	4.15×10^{-2}	2.29×10^{-7}	1.78×10^{-4}	3.099×10^3	1.31
Nitrogen	68	2.26×10^{-3}	7.28×10^{-2}	3.68×10^{-7}	1.63×10^{-4}	1.775×10^3	1.40
Oxygen	68	2.58×10^{-3}	8.31×10^{-2}	4.25×10^{-7}	1.65×10^{-4}	1.554×10^3	1.40

SI Units							
Gas	Temperature (°C)	Density, ρ (kg/m ³)	Specific Weight, γ (N/m ³)	Dynamic Viscosity, μ (N - s/m ²)	Kinematic Viscosity, ν (m ² /s)	Gas Constant, ^a R (J/kg-K)	Specific Heat Ratio, ^b k
Air (standard)	15	1.23	12	1.79×10^{-5}	1.46×10^{-5}	2.869×10^2	1.40
Carbon dioxide	20	1.83	18	1.47×10^{-5}	8.03×10^{-6}	1.889×10^2	1.30
Helium	20	0.166	1.63	1.94×10^{-5}	1.15×10^{-4}	2.077×10^3	1.66
Hydrogen	20	0.0838	0.822	8.84×10^{-6}	1.05×10^{-4}	4.124×10^3	1.41
Methane (natural gas)	20	0.667	6.54	1.10×10^{-5}	1.65×10^{-5}	5.183×10^2	1.31
Nitrogen	20	1.16	0.114	1.76×10^{-5}	1.52×10^{-5}	2.968×10^2	1.40
Oxygen	20	1.33	13	2.04×10^{-5}	1.53×10^{-5}	2.598×10^2	1.40

^aValues of the gas constant are independent of temperature.^bValues of the specific heat ratio depend only slightly on temperature.
Source: From Ref. 2.

where Δp is the pressure increment that causes a relative decrease in volume, $\Delta V/V$. The E_v value has the dimensions of pressure, and it depends on the pressure and temperature of a liquid. For a gas, the E_v value depends on the thermodynamic process governing the change in volume resulting from the pressure increment. For example, if the process is isentropic, $E_v = kp$, where k is the ratio of the specific heats given in Table 4. If the process is isothermal, $E_v = p$. Values of E_v for a variety of liquids at standard temperature and pressure are given in Table 3.

As expected, the values of E_v for liquids are large, which indicates the fluid can be considered incompressible. Figure 1 is provided to demonstrate the variation of E_v with pressure for pure water. Entrained gas in a liquid can drastically affect the E_v value; Fig. 2 illustrates the effect of entrained air on the compressibility of water for relatively small amounts of air.

One of the common applications of the property of fluid compressibility is in the computation of the acoustic wave speed (speed of sound) in a fluid. The equation applicable to both liquids and gases is

$$a = \sqrt{\frac{E_v}{\rho}} \quad (4)$$

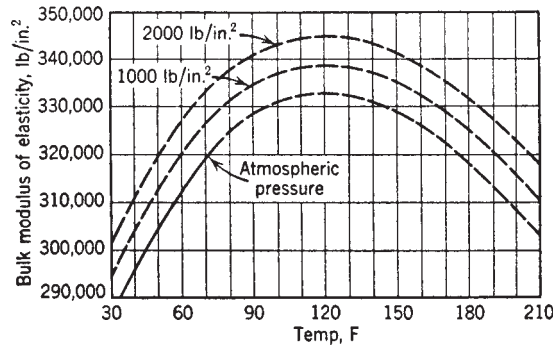


Figure 1 Bulk modulus of elasticity for pure water as function of temperature and pressure. *Source:* By permission from H. Rouse, *Fluid Mechanics for Hydraulic Engineers*, McGraw-Hill, New York, 1938. © McGraw-Hill Education.

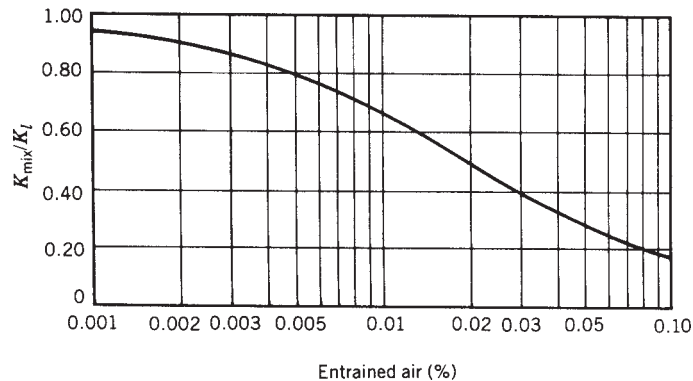


Figure 2 Effect of entrained air on elasticity of water. © McGraw Hill-Education.

where a is the acoustic wave speed. The value of E_v is obtained from a table (e.g., Table 3) or, in the case of gases, computed using the isentropic thermodynamic process. For reference, the speed of sound is much higher in water than in air.

2.3 Viscosity

Viscosity is a fluid's resistance to angular deformation under action of a shearing stress. It is a measure of how easy or difficult a fluid "flows." For example, pancake syrup has a higher viscosity than water. Viscosity is a property that changes according to the thermodynamic conditions; thus, it strongly depends on temperature but is relatively unaffected by pressure.

In liquids, viscosity depends on the strength of cohesive forces between fluid molecules; hence an increase in temperature results in a decrease in viscosity. For gases, viscosity depends on the momentum exchange between layers of gas moving at different velocities. An increase in temperature provides an increase in molecular activity and an increase in viscosity.

All real fluids have some level of viscosity. However, for certain types of flows or specific regions of the flow field, it is sometimes reasonable to assume that the effects of viscosity are negligible. In these cases, the flow is classified as inviscid and the viscosity is set to zero. If the flow cannot be assumed inviscid, then you must account for the effects of viscosity.

A fundamental device for measuring fluid viscosity leads to the definition of viscosity. Figure 3 illustrates the flow situation occurring when a moving plate, under the action of a shearing force, slides over a fixed plate separated by a fluid. If the movement is sufficiently slow so that the flow between the plates is laminar, the shear stress is related to the velocity difference by the equation

$$\tau = \mu \frac{du}{dy} \quad (5)$$

where τ is the shear stress, du/dy is the velocity gradient (or rate of angular strain), and μ is the coefficient of viscosity.

In a more precise sense, μ is known as the absolute (or dynamic) viscosity and has the units pound-seconds per foot squared in the English FSS system. The values of μ for various fluids are listed in Tables 3 and 4. Because the viscosity shows up in many instances divided by the density, the ratio $\nu = \mu/\rho$ is defined as the kinematic viscosity with the English FSS units square feet per second. In the metric system, absolute viscosity is commonly given in poises (dyne-second per square centimeter) where $1 \text{ lb} - \text{s}/\text{ft}^2 = 478.8 \text{ P}$. The metric equivalent of kinematic viscosity is the stoke (square centimeters per second) where $1 \text{ ft}^2/\text{s} = 929 \text{ stokes}$. Figures 4 and 5 give absolute and kinematic viscosities for a wide range of liquids and gases. The English FSS values may be converted to the SI values using the conversions

$$\begin{aligned} \mu &= 1 \text{ lb} - \text{s}/\text{ft}^2 = 47.88 \text{ N} - \text{s}/\text{m}^2 \\ \nu &= 1 \text{ ft}^2/\text{s} = 0.0929 \text{ m}^2/\text{s} \end{aligned}$$

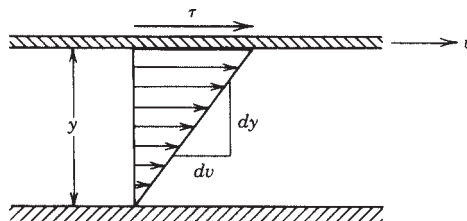


Figure 3 Definition sketch for absolute viscosity.

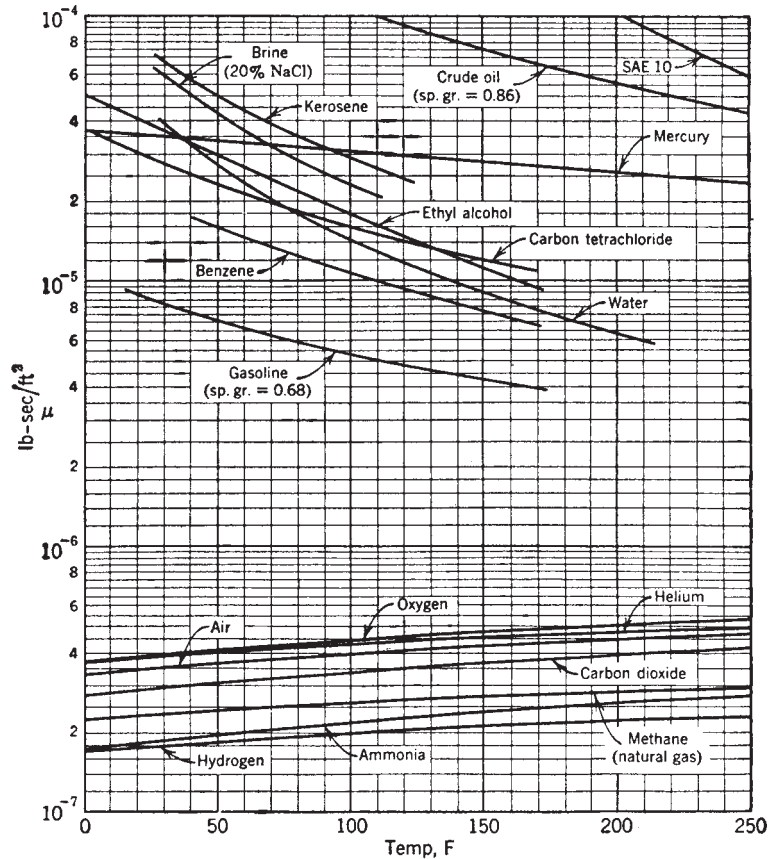


Figure 4 Dynamic viscosity versus temperature for common gases and liquids. (Courtesy of Hunter Rouse, State University of Iowa, Iowa City.)

2.4 Surface Tension and Capillarity

Molecules of a liquid exert a mutual cohesive force that causes those molecules in the interior of a liquid to be in a balanced state of cohesive forces that is attracted equally in all directions. However, liquid molecules at a surface are attracted by the interior molecules but experience no balancing attraction from above the surface. This imbalance of forces causes the liquid surface to behave as though it were covered with an elastic membrane, hence the term *surface tension*. This phenomenon is also apparent at the interface between immiscible liquids. This is why surface tension values for a liquid must always specify what fluid lies across the interface. As a result of its dependence on molecular cohesion, surface tension σ (in pounds per foot or newtons per meter) decreases with increasing temperature. Table 3 gives values for a variety of liquids.

Surface tension manifests itself in free liquid jets, bubbles, small waves, and capillary action in small conduits. At the interface between two fluids, surface tension can sustain a pressure discontinuity across the interface. The magnitude of the pressure difference is a function of the surface curvature with the higher pressure on the concave side of the interface.

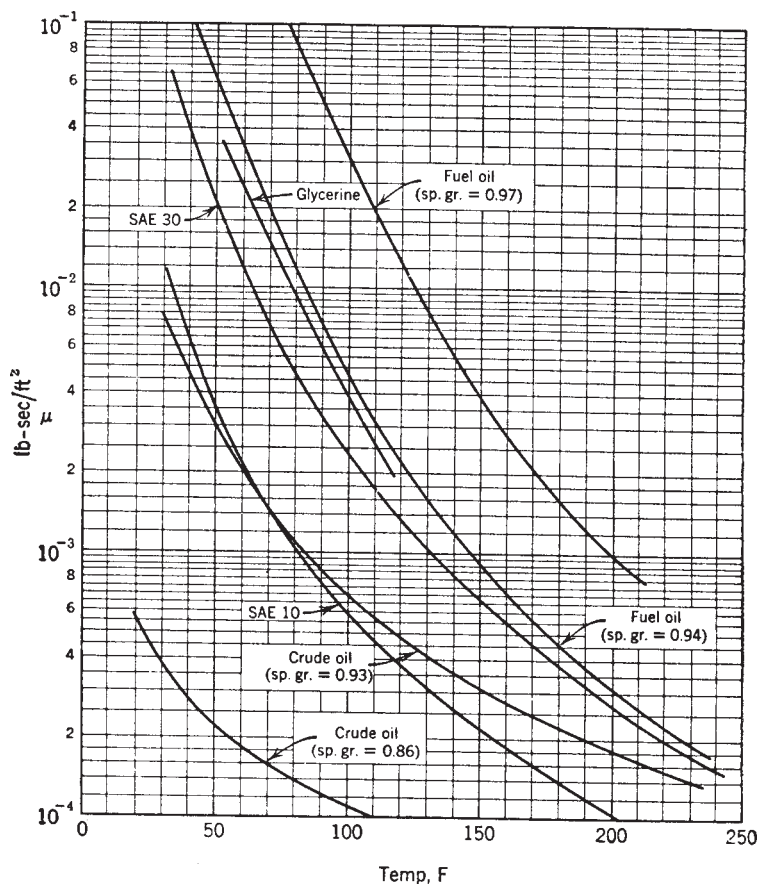


Figure 5 Dynamic viscosity versus temperature for typical grades of oil. (Courtesy of Hunter Rouse, State University of Iowa, Iowa City.)

Capillary rise in a circular tube is an important application of surface tension (Fig. 6). The equation for capillary rise h is

$$h = \frac{2\sigma\cos\theta}{\gamma r} \quad (6)$$

The value of h depends heavily on the contact angle Θ , which in turn depends strongly on the liquid and the tube material as well as the cleanliness of the tube surface. This equation should not be used unless the capillary tube is small enough that the liquid surface is approximately spherical in shape (constant curvature).

2.5 Vapor Pressure

A liquid exhibiting a free surface is continually ejecting and absorbing molecules of the liquid across the free surface. Some of the molecules at the surface have enough energy due to local collisions that they can break free of the intermolecular cohesive forces. If more molecules leave than return, the liquid is said to be evaporating. In an equilibrium situation, the number of molecules expelled equals the number returning. The molecules of the liquid in the overlying

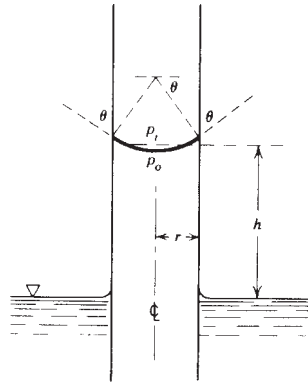


Figure 6 Capillary rise in a small circular tube. *Source:* By permission from J. K. Vennard and R. L. Street, *Elementary Fluid Mechanics*, 5th ed., Wiley, New York, 1975.

gaseous fluid exert a force on the liquid surface, in conjunction with the other gas molecules bombarding the surface, to make up the total surface pressure. That portion of the surface pressure generated by the vapor molecules from the liquid is called the partial pressure, or *vapor pressure*, p_v , of the liquid. An alternative view is if you started with a completely liquid-filled container. You were then able to move one end of the container outward, which increased the volume, but did not allow air to enter the container. The free space between the liquid and the movable end would become filled with a vapor from the liquid and impose a pressure on the liquid surface equal to the vapor pressure of the liquid. Table 3 provides values of the vapor pressure p_v for a variety of liquids.

The higher the liquid temperature, the more vigorous the molecular activity and the larger the fraction of the total pressure contributed by the liquid vapor. When the liquid temperature is elevated to a level where the vapor pressure is equal to the total pressure, boiling occurs (formation of vapor bubbles in liquid). Boiling is also experienced when the total pressure is reduced to the liquid vapor pressure, for example, in liquid cavitation in pumps, valves, and propellers. Therefore, boiling can occur by either raising the temperature to increase the vapor pressure to meet the local pressure or reducing the local pressure to meet the vapor pressure at the current temperature. In fluid mechanics, the latter is the most common phenomenon; flow conditions and geometry contribute to a significant reduction in local pressure. If the pressure is low enough to reach the vapor pressure of the liquid, vapor bubbles will form. In some instances, these vapor bubbles travel downstream and suddenly collapse due to higher pressure regions, which causes cavitation to occur. Cavitation can have enough intensity to cause structural damage to the system.

3 FLUID STATICS

3.1 Pressure Variation in a Fluid at Rest

By definition, a Newtonian fluid at rest has no internal shear stresses, only normal stresses. As a consequence, pressure does not vary horizontally in a homogeneous fluid, only vertically. The equation describing the vertical variation in pressure is

$$\frac{dp}{dz} = -\rho g = -\gamma \quad (7)$$

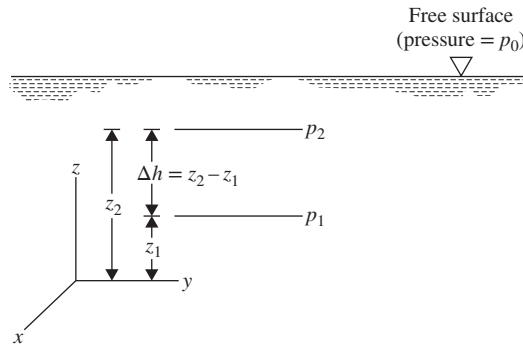


Figure 7 Notation for pressure variation in a fluid at rest. (From Ref. 2.)

where z is measured vertically upward as shown in Fig. 7. If a fluid has variable density, this expression must be integrated to determine differences in pressure. However, for an incompressible fluid (i.e., constant density), the commonly used form of this equation is the hydrostatic pressure variation equation

$$\Delta p = \gamma \Delta h \quad (8)$$

where Δh is the difference in elevation between two points and Δp is the corresponding pressure difference. Note that the pressure is increased linearly with increasing depth; the fluid at a lower level needs to support all the fluid above it so the pressure is higher.

3.2 Basic Pressure-Measuring Devices

Pressure is generally measured from one of two data locations—absolute zero or the surrounding environment (gauge). Pressures measured above absolute zero, for example, barometric pressure, are known as absolute pressure. Those measured above the local atmospheric pressure are known as gauge pressures. Absolute pressure always equals gauge pressure plus atmospheric pressure:

$$P_{\text{absolute}} = P_{\text{gauge}} + P_{\text{atmospheric}} \quad (9)$$

It is possible to have negative gauge pressure since it is measured with respect to a datum. But, it is impossible to have negative absolute pressure since the minimum you can achieve is a perfect vacuum, which is zero absolute pressure.

A fundamental pressure-measuring device, which is based on the hydrostatic pressure variation equation, is the manometer (Fig. 8). Because one end of this manometer is open to the atmosphere, it is known as an open-end manometer. By making use of the fact that pressure

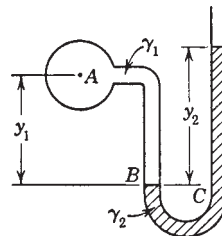


Figure 8 Simple manometer.

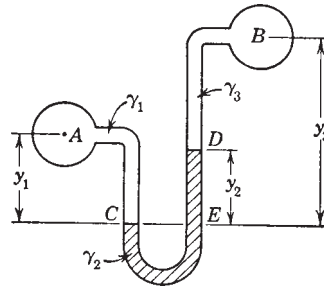


Figure 9 Differential manometer.

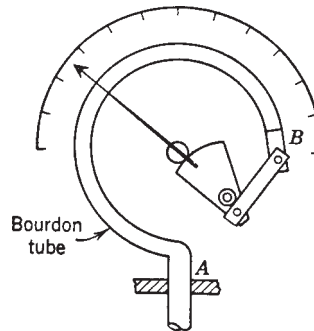


Figure 10 Essential features of Bourdon gauge.

does not vary in the horizontal direction for a fluid at rest and making use of the hydrostatic pressure equation at various points, the gauge pressure at A is calculated as

$$p_A = \gamma_2 y_2 - \gamma_1 y_1 \quad (10)$$

Figure 9 illustrates a differential manometer. The difference in pressure between A and B is calculated as

$$p_B - p_A = \gamma_1 y_1 - \gamma_2 y_2 - \gamma_3 (y_3 - y_2) \quad (11)$$

Another commonly used mechanical device for measuring both gauge pressure and absolute pressure is the Bourdon-type gauge (Fig. 10).

3.3 Fluid Forces on Plane Surfaces

The magnitude of the total fluid force exerted on a plane (flat) surface can be calculated with the equation (refer to Fig. 11)

$$F_R = p_c A \quad (12)$$

where p_c is the pressure at the centroid of the surface and A is the total area of the surface. Note that pressure always acts normal to the surface.

If the fluid is a liquid with a free surface open to the atmosphere,

$$p_c = \gamma h_c \quad (13)$$

where h_c is the distance the centroid lies below the free surface. Locations of centroids of variously shaped areas are shown in Table 5.

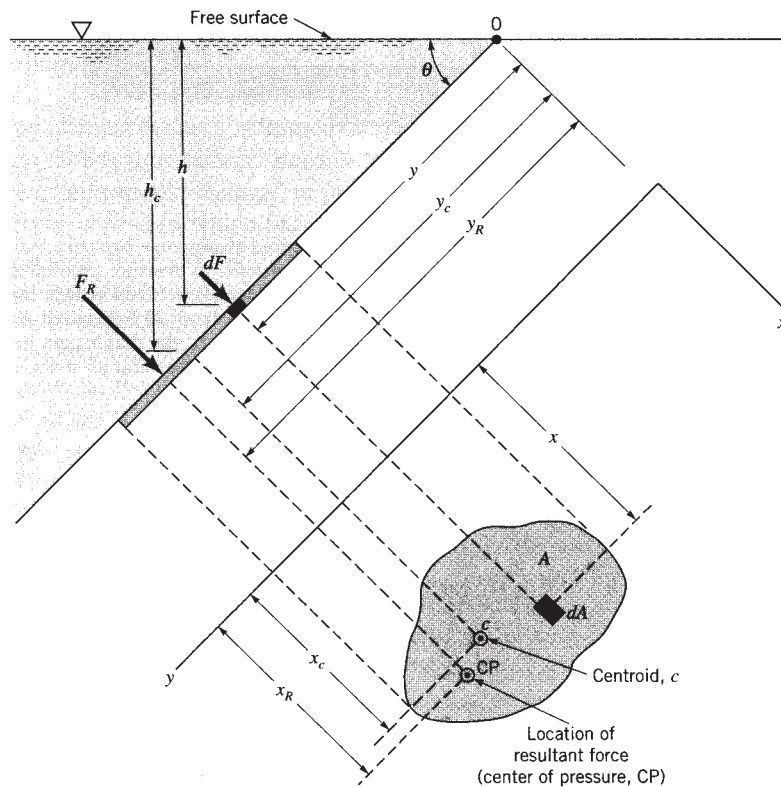


Figure 11 Notation for pressure force calculation on submerged plane of arbitrary shape. (From Ref. 2.)

The location of the resultant of the pressure forces acting on a plane area is known as the center of pressure. For a plane area lying below a liquid surface, the center-of-pressure location is computed with the equation

$$y_R - y_c = \frac{I_c}{y_c A} \quad (14)$$

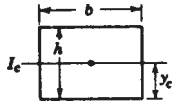
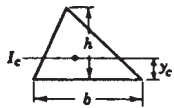
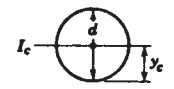
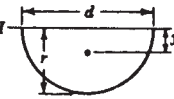
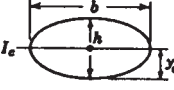
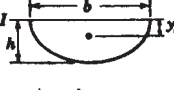





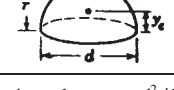
where y_R is measured in the plane of the area (slant distance) from the free surface to the center of pressure, y_c is the distance (in the same plane) from the free surface to the centroid of the area, and I_c is the second moment of the area about a horizontal axis through the centroid and in the plane of the area. Values of I_c for common geometric shapes are given in Table 5.

Two special cases of this application are the horizontal-plane and the vertical-plane cases. For a horizontal plane ($\theta = 0^\circ$ of inclination), the centroid of the surface and the center of pressure coincide since the pressure distribution over the entire surface area is uniform. For the vertical case ($\theta = 90^\circ$ of inclination), the center of pressure will always be below the centroid of the surface since the pressure acting on the surface increases with depth. Note that for deeply submerged plane areas, the center of pressure approaches the centroid of the area regardless of the angle of inclination.

3.4 Fluid Forces on Curved Surfaces

Pressure forces exerted on curved surfaces vary in direction and must usually be divided into horizontal and vertical components to facilitate calculation. The resultants of the horizontal and

Table 5 Properties of Areas and Volumes

	Sketch	Area or Volume	Location of Centroid	I or I_c
Rectangle		bh	$y_c = \frac{h}{2}$	$I_c = \frac{bh^2}{12}$
Triangle		$\frac{bh}{2}$	$y_c = \frac{h}{3}$	$I_c = \frac{bh^2}{36}$
Circle		$\frac{\pi d^2}{4}$	$y_c = \frac{d}{2}$	$I_c = \frac{\pi d^4}{64}$
Semicircle ^a		$\frac{\pi d^2}{8}$	$y_c = \frac{4r}{3\pi}$	$I = \frac{\pi d^4}{128}$
Ellipse		$\frac{\pi bh}{4}$	$y_c = \frac{h}{2}$	$I_c = \frac{\pi bh^2}{64}$
Semiellipse		$\frac{\pi bh}{4}$	$y_c = \frac{4h}{3\pi}$	$I = \frac{\pi bh^2}{16}$
Parabola		$\frac{2}{3}bh$	$y_c = \frac{3h}{5}$ $x_c = \frac{3b}{8}$	$I = \frac{2bh^2}{7}$
Cylinder		$\frac{\pi d^2 h}{4}$	$y_c = \frac{h}{2}$	
Cone		$\frac{1}{3} \left(\frac{\pi d^2 h}{4} \right)$	$y_c = \frac{h}{4}$	
Paraboloid of revolution		$\frac{1}{2} \left(\frac{\pi d^2 h}{4} \right)$	$y_c = \frac{h}{3}$	
Sphere		$\frac{\pi d^2}{6}$	$y_c = \frac{d}{2}$	
Hemisphere		$\frac{\pi d^2}{12}$	$y_c = \frac{3r}{8}$	

^aFor the quarter-circle, the respective values are $\pi d^2/16$, $4r/3\pi$, and $\pi d^4/256$.

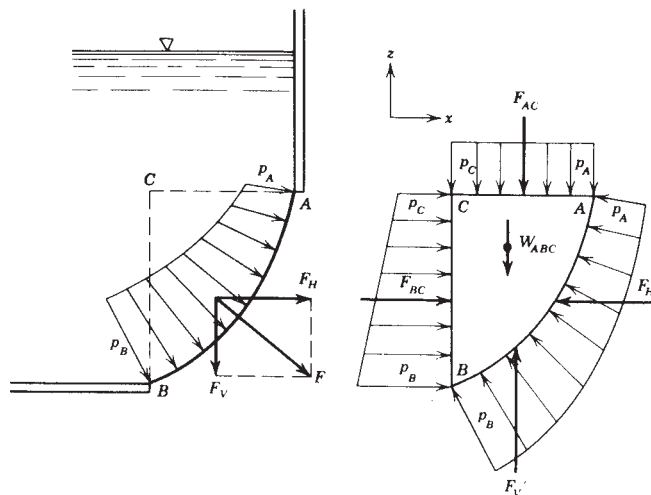


Figure 12 Forces acting on curved surface. *Source:* By permission from J. K. Vennard and R. L. Street, *Elementary Fluid Mechanics*, 5th ed., Wiley, New York, 1975.

vertical components of the pressure forces are determined with assistance from the equations developed for plane surfaces. Figure 12 illustrates a common situation. The fluid mass ABC is in equilibrium under the action of pressure forces; hence the vertical component of the resultant of the pressure forces is equal to the weight of the fluid mass plus the force F_{AC} exerted on the upper surface of the fluid mass by the overlying fluid. The horizontal component of the resultant of the pressure forces is equal to the force on a vertical projection of the curved surface. The line of action and point of application (center of pressure) for the resultant force is determined by taking moments of the contributing forces about an axis of convenience. The force F_{BC} is located using the formula for plane surfaces. The weight W_{ABC} is concentrated at the centroid of the area ABC (see Table 5).

3.5 Buoyancy and Stability

An object floating or submerged in a fluid at rest experiences pressure forces from the surrounding fluid. Consider a square block of material that is submerged in a liquid; due to hydrostatic pressure variation with depth, the pressure on the bottom surface will be greater than on the top surface (pressure on the two sides is equal and opposite). The resultant of these pressure forces is known as the buoyant force, which acts in the upward direction, and is equal in magnitude to the weight of the displaced fluid. The line of action of the buoyant force is vertical through the centroid of the volume of displaced fluid (center of buoyancy). The magnitude of the buoyant force can be found from the following equation:

$$F_B = \gamma V \quad (15)$$

where V is the volume of the displaced fluid. If the object is totally submerged in the fluid, then the volume of the displaced fluid equals the volume of the object; otherwise, the displaced volume equals only the volume of the submerged portion of the object.

The overturning stability (Fig. 13) of a floating or submerged body is affected by the relative position of the center of gravity (CG) of the body and the center of buoyancy. When the

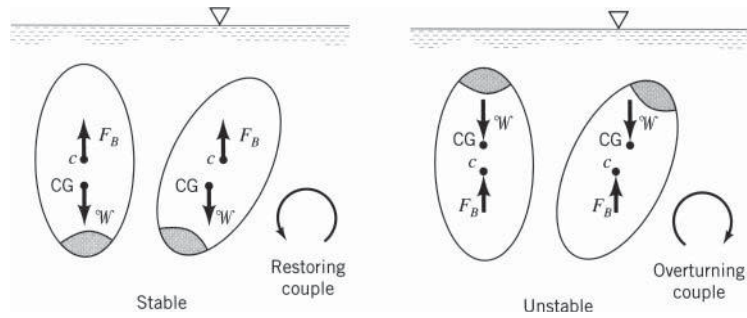


Figure 13 Stable and unstable settings for totally submerged body. (From Ref. 2.)

center of gravity lies below the center of buoyancy, the body is always *stable*. If the center of buoyancy is below the center of gravity, the body may or may not be stable in terms of overturning. If the geometric shape of the body is such that a rocking motion results in a shift of the buoyancy center that in turn causes a righting action, the body is stable. For example, a 2×4 board floating on its side would be stable. However, the same board floating on its edge would be unstable.

3.6 Accelerated Fluid Masses without Relative Motion

There are situations when a fluid body is accelerated with no relative motion among fluid particles (zero-shear stress). This is true only for constant accelerations. As in a fluid at rest, the pressure will still vary linearly with elevation, but the pressure gradient will generally not equal the specific weight. Further, there will be a variation in pressure in the horizontal plane in this situation.

For horizontal acceleration of a container of liquid (Fig. 14), the free surface will tilt just enough to provide the unbalanced hydrostatic force on the opposite sides of the container required to impart a constant acceleration to the fluid mass. As shown in the figure, this will produce lines of constant pressure that are parallel to the tilted free surface. Under these conditions the slope of the free surface is given as

$$\text{Slope} = \frac{a_x}{g} \quad (16)$$

where a_x is the constant horizontal acceleration.

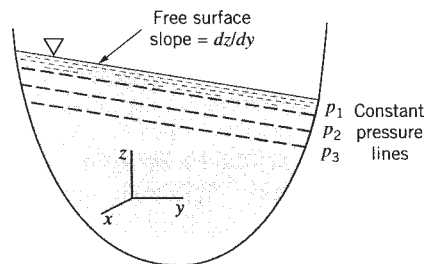


Figure 14 Horizontal acceleration of liquid with free surface. (From Ref. 2.)

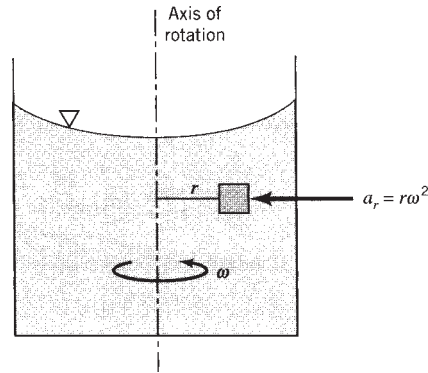


Figure 15 Rotation of tank filled with liquid. (From Ref. 2.)

For vertical acceleration, the free surface remains horizontal, but the pressure variation with depth is given by the equation

$$\frac{dp}{dz} = -\gamma \left(1 + \frac{a_z}{g} \right) \quad (17)$$

Note that if $a_z = -g$ (free fall), the pressure gradient throughout the fluid is zero.

Another situation occurs for a container of liquid undergoing a constant rotational angular velocity (Fig. 15). When the relative motion between fluid particles ceases, the free surface forms the shape of a parabola described by the equation

$$z = \frac{\omega^2}{2g} r^2 \quad (18)$$

where z is the elevation of the free surface at radius r above that at the center of rotation and ω is the angular velocity of rotation of the container. Pressure in the fluid varies parabolically with radius,

$$p = p_o + \frac{\gamma\omega^2}{2g} r^2 \quad (19)$$

where p is the pressure at radius r in a horizontal plane and p_o is the pressure at the center of rotation in the same horizontal plane. Because there is no vertical acceleration, pressure variation in the vertical direction is the same as if the fluid were at rest.

4 IDEAL (INVISCID) FLUID DYNAMICS

An *ideal fluid* is a hypothetical substance exhibiting all the characteristics of a real fluid except that it is a continuum (no molecular spaces), it has no viscosity (frictionless) or inviscid, and it can accept pressures down to negative infinity. These characteristics greatly simplify the mathematical treatment of fluid flow and, in many cases, give acceptable engineering results for real fluid situations where viscous effects are not significant.

Although not restricted to ideal fluid flow, some definitions are common to all flow situations. Steady flow occurs when all conditions in the flow at any point do not change with time. In turbulent flows, this definition is extended to include temporal mean values of all conditions. Uniform flow is defined as the condition where the velocity is everywhere the same at a given time. For one-dimensional flow, this definition refers to the average velocity at any cross section of the flow. In nonuniform flow, the velocity varies with position in the flow domain at any given time.

Qualitative aspects of a fluid flow situation can be illustrated effectively through the use of streamlines. For steady flow, *streamlines* are tracks of fluid particles that are everywhere tangent to fluid velocity vectors. As a consequence, flow cannot occur across streamlines; so a collection of streamlines defining a closed surface (a stream tube) would act like a conduit within the flow. Further, regions of flow where streamlines are close together represent locally high velocities (and low pressures). Regions where the streamlines are straight and parallel identify situations where there is no acceleration normal to the flow; therefore, the pressure variation normal to the flow is hydrostatic.

4.1 One-Dimensional Flow

Most real flows are three dimensional in nature. However, in order to simplify the analysis and obtain solutions to engineering problems, some assumptions can be made. Some types of flows have a dominant flow direction, with the remaining two spatial directions only contributing secondary effects. Therefore, making the assumption that the flow is one dimensional can simplify the analysis and provide reasonable results under certain conditions. The introduction of the various conservation laws (mass, momentum, and energy) for fluid flow is also simplified by using a one-dimensional analysis, which is given below.

Conservation of Mass (Continuity)

Conservation of mass is an analog of the conservation of energy. It states that in a fluid flow accumulation of mass within a control volume (a volume whose boundaries are specified) is equal to the difference of the net inflow and the net outflow of mass. For steady state, the accumulation, by definition, is zero. Consequently, conservation of mass simplifies to a balance of net inflow and net outflow of mass.

For one-dimensional flow, the control volume is generated by the cross-sectional area of the conduit at two specified locations, where the streamlines are essentially straight and parallel to each other and normal to the cross-sectional area, and the walls of the conduit between these two locations (see Fig. 16).

For steady flow, the mass flow rate \dot{m} (slugs per second or kilograms per second) is a constant along the conduit and is written

$$\dot{m} = \rho AV = \rho Q = \text{const} \quad (20)$$

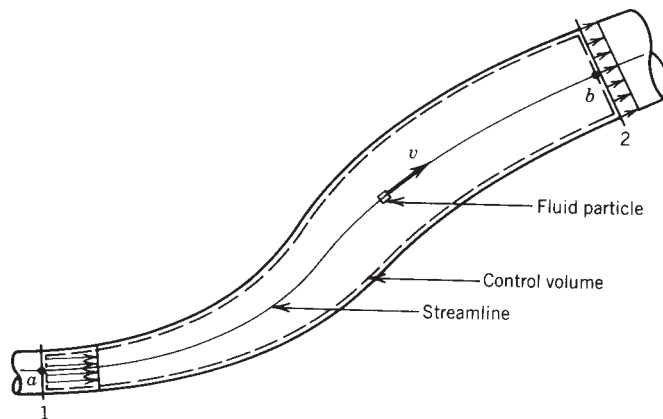


Figure 16 One-dimensional inviscid flow.

where Q is the volume flow rate (cubic feet per second), A is the cross-sectional area of the conduit, and V is the average velocity, Q/A . In cases where the flow enters the control volume at section 1 and leaves at section 2 (see Fig. 16), conservation of mass states that the mass inflow rate equals mass outflow rate, or

$$\rho_1 A_1 V_1 = \rho_1 A_2 V_2 \quad (21)$$

In the case of incompressible flow, the density will not vary and therefore will drop from the above expression, yielding constant volume flow rate:

$$Q_1 = Q_2 \quad (22)$$

Euler's Equations

Application of Newton's second law to a fluid particle gives Euler's equations of motion, assuming inviscid flow. Along a streamline (see Fig. 16)

$$\frac{dp}{\gamma} + \frac{v}{g} dv + dz = 0 \quad (23)$$

where v is the local velocity. Normal to the streamline,

$$\frac{dp}{\gamma} - \frac{v^2}{gr} dr + dz = 0 \quad (24)$$

where r is the local radius of curvature of the streamline along which the fluid particle is moving.

Bernoulli Equation

Integration of the Euler equation along a streamline for constant density yields the Bernoulli equation

$$\frac{p}{\gamma} + \frac{v^2}{2g} + z = \text{const} \quad (25)$$

If the integration is performed along a streamline between points a and b (Fig. 16), the Bernoulli equation takes the form

$$z_a + \frac{P_a}{\gamma} + \frac{v_a^2}{2g} = z_b + \frac{P_b}{\gamma} + \frac{v_b^2}{2g} \quad (26)$$

Multiplying through by the specific weight, the Bernoulli equation can also be written as

$$p_a + 1/2 \rho v_a^2 + \gamma z_a = p_b + 1/2 \rho v_b^2 + \gamma z_b \quad (27)$$

This states that the combination of these three terms remains constant everywhere along the streamline.

The Bernoulli equation can be "expanded" to apply to a full-sized one-dimensional flow (as opposed to a single streamline) if the sections at 1 and 2 (Fig. 16) are regions where the streamlines are essentially straight and parallel and the velocity profile uniform (irrotational flow),

$$p_1 + 1/2 \rho V_1^2 + \gamma z_1 = p_2 + 1/2 \rho V_2^2 + \gamma z_2 \quad (28)$$

where V is the average velocity. This is true because at a section where the streamlines are straight and parallel the velocity is constant over the cross section and the pressure variation is hydrostatic ($z + p/\gamma = \text{const}$). Hence the sum of the three terms on each side of the equation is a constant regardless of the streamline selected. Because 1 and 2 are sections and not points, the quantities z and p/γ (or γz and P) are usually evaluated at some arbitrary point in the cross section, for example, at the centerline for a cylindrical pipe.

A further conclusion extends from the uniform-flow section concept. If the sum of the three terms is the same for all streamlines at the special cross section, the sum is everywhere constant throughout the flow:

$$p_1 + 1/2 \rho V_1^2 + \gamma z_1 = \text{const throughout flow field for irrotational flow} \quad (29)$$

Work–Energy Equation

An equation similar to the Bernoulli equation can be derived from work–energy principles. However, the work–energy equation has broader application because it can include thermal energy and heat transfer. Utilizing the principle that the work done on a fluid system is equal to the change in energy of the system and applying this principle to the fluid in the control volume of Fig. 16,

$$z_1 + \frac{p_1}{\gamma} + \frac{V_1^2}{2g} = z_2 + \frac{p_2}{\gamma} + \frac{V_2^2}{2g} \quad (30)$$

This equation is identical to the Bernoulli equation; however, we have not considered other energies beyond mechanical energies. Further, the terms in the work–energy equation have the following meanings:

z = potential energy per pound of fluid flowing

$V^2/(2g)$ = kinetic energy per pound of fluid flowing

p/γ = “flow work” done on fluid in control volume per pound of fluid flowing (also known as “pressure energy”)

Based on the fact that we can obtain the Bernoulli equation from both Newton’s second law and the conservation of energy, we can conclude that it is a very powerful equation, which is also witnessed by its numerous applications in nature.

Momentum Equation

Linear Momentum. Newton’s second law was applied to a fluid particle moving along a streamline to produce the Euler equations. If the second law is applied to a finite fluid mass within a control volume (e.g., Fig. 16), another set of useful equations are derived. All internal forces cancel so that only external forces due to pressure, shear (for real fluids), and gravity need be considered. The resulting linear momentum equations are vector equations and are written as

$$\sum \mathbf{F}_{\text{ext}} = \sum (Q\rho\mathbf{V})_{\text{out}} - \sum (Q\rho\mathbf{V})_{\text{in}}$$

where \mathbf{F}_{ext} is the external forces acting on the fluid in the control volume and summations are used if there are multiple inlets and outlets. Again, the control volume is generally selected in such a way that the sections where the momentum enters and leaves the control volume are regions where the streamlines are straight and parallel.

In applying the linear momentum equations to a problem, it is customary to use the vector component equations with the orthogonal axes chosen in a convenient orientation. For example, the scalar equation in the x direction would be

$$\sum (F_x)_{\text{ext}} = \sum (Q\rho V_x)_{\text{out}} - \sum (Q\rho V_x)_{\text{in}} \quad (32)$$

It should be noted that this equation can be used to determine the resultant force but not the distribution of that force. Also note that in the calculation of Q the velocity that is normal to the cross section is used [also see explanation for Eq. 20], whereas the V_x term only refers

to the component of that velocity in the x direction. Therefore, when dealing with the y and z component of this equation, the Q term is always calculated with the velocity that is normal to the cross section, and the V_y or V_z is calculated by considering the respective component of velocity in those directions. When considering the component magnitudes, it is also important to pay attention to the sign of the magnitudes as (+) or (-).

Moment of Momentum. In problems involving fluid flow through a conduit, the linear momentum equation provides the necessary force information. However, for some problems the moment of a force, or the torque, is important; for example, fluid flow through a rotary water sprinkler. In these cases, a moment-of-momentum equation is needed that relates torque to angular momentum.

For the derivation of this equation, a similar approach to that which resulted in the linear momentum equation is used; but this time, the moments of the vectors are used instead. The resultant moment-of-momentum equation is

$$\sum (\mathbf{r} \times \mathbf{F})_{\text{ext}} = \sum [Q\rho(\mathbf{r} \times \mathbf{V})]_{\text{out}} - \sum [Q\rho(\mathbf{r} \times \mathbf{V})]_{\text{in}} \quad (33)$$

where the terms in parentheses are vector cross products.

A more directly usable form of the equation is that applicable in two dimensions,

$$\sum (M_o)_{\text{ext}} = \sum (Q\rho r V_t)_{\text{out}} - \sum (Q\rho r V_t)_{\text{in}} \quad (34)$$

where M_o is the moments of the external forces about an axis through o and V_t is the value of the velocity normal to a vector \mathbf{r} extending from the moment center o to the location of the V_t . This equation is vastly used in the design of turbomachinery such as pumps and turbines.

4.2 Two- and Three-Dimensional Flow*

The equations describing two- and three-dimensional ideal fluid flow are derived using a small cubic fluid element or control volume of sides dx , dy , and dz .

Conservation of Mass (Continuity)

The continuity equation for an ideal fluid states that under steady-state conditions the net flow rate into any small volume must be zero. In equation form

$$\frac{\partial u}{\partial x} + \frac{\partial v}{\partial y} + \frac{\partial w}{\partial z} = 0 \quad (35)$$

or in vector notation

$$\nabla \cdot \mathbf{V} = 0 \quad (36)$$

that is, the divergence of the velocity vector \mathbf{V} is everywhere zero.

Euler's Equation of Motion

Consideration of body and pressure forces on a fluid element and neglecting the viscous contributions lead to the Euler equations:

$$X - \frac{1}{\rho} \frac{\partial p}{\partial x} = u \frac{\partial u}{\partial x} + v \frac{\partial u}{\partial y} + w \frac{\partial u}{\partial z} + \frac{\partial u}{\partial t} \quad (37)$$

$$Y - \frac{1}{\rho} \frac{\partial p}{\partial y} = u \frac{\partial v}{\partial x} + v \frac{\partial v}{\partial y} + w \frac{\partial v}{\partial z} + \frac{\partial v}{\partial t} \quad (38)$$

* Illustrations and material all or in part from *Eshbach's Handbook of Engineering Fundamentals* (Hoboken, NJ: Wiley).

$$Z - \frac{1}{\rho} \frac{\partial p}{\partial z} = u \frac{\partial w}{\partial x} + v \frac{\partial w}{\partial y} + w \frac{\partial w}{\partial z} + \frac{\partial w}{\partial t} \quad (39)$$

where X, Y, Z are the components of the body (extraneous) forces per unit mass in the xyz directions, respectively; ρ is the mass density; p is the pressure at a point (independent of direction); and u, v, w are velocity components in the xyz directions at any point x, y, z . The terms on the right-hand side of the equations are acceleration components, the first three of which are known as the *convective* acceleration (account for fluid convecting in space) and the fourth as the *local* acceleration (accounts for local unsteadiness).

Boundary Conditions

A kinematic boundary condition must be satisfied at every solid boundary. For real fluids (i.e., with viscosity), the widely known “no-slip” condition states that the fluid particles adjacent to a solid boundary move with the same velocity as the boundary. Therefore, in the case of wind over a stationary flat plate, for example, the air particles adjacent to the plate will not move, while their fellow particles that are further into the air will move with the wind. Therefore, both u and v components of the velocity at the solid boundary are zero according to the no-slip condition for real fluids. However, the Euler equations are derived for inviscid cases, and so, for Euler solutions to flow problems, there will be a slip velocity tangent to the solid boundary. Therefore, the u component of the velocity, in the case of wind over a flat plate, will be equal to the free-stream velocity, whereas the normal component of the velocity, v , of the air particles at the solid boundary will be zero (since there is no suction or blowing from the surface and it is not a porous surface).

Irrotational Flow-Velocity Potential

Rotation of a fluid element may be represented by a vector that has a length proportional to the magnitude of the rotation (radians per second) and in a direction parallel to the instantaneous axis of rotation. The right-handed rule is adopted; that is, the positive direction of the vector is the direction a right-handed screw would progress when rotating in the same sense as the element. In vector notation the *curl* of the velocity vector is twice the rotation vector, which is called vorticity (Ω):

$$\nabla \times \mathbf{V} = 2\omega = \Omega \quad (40)$$

Scalar components of the rotation vector $\omega_x, \omega_y, \omega_z$ in the directions of the xyz axes may be used in place of the vector itself. Defining a rotation component of an element about an axis as the average angular velocity of two infinitesimal line segments through the point, mutually perpendicular to themselves and the axis,

$$\omega_x = \frac{1}{2} \left(\frac{\partial w}{\partial y} - \frac{\partial v}{\partial z} \right) \quad (41)$$

$$\omega_y = \frac{1}{2} \left(\frac{\partial u}{\partial z} - \frac{\partial w}{\partial x} \right) \quad (42)$$

$$\omega_z = \frac{1}{2} \left(\frac{\partial v}{\partial x} - \frac{\partial u}{\partial y} \right) \quad (43)$$

For an irrotational flow, each of these rotational components must be zero, or

$$\nabla \times \mathbf{V} = 0 \quad (44)$$

Then,

$$\frac{\partial w}{\partial y} = \frac{\partial v}{\partial z} \frac{\partial u}{\partial z} = \frac{\partial w}{\partial x} \frac{\partial v}{\partial x} = \frac{\partial u}{\partial y} \quad (45)$$

A visual concept of irrotational flow may be obtained by considering as a free body a small element of fluid in the form of a sphere. As the fluid is frictionless, no tangential stresses or forces may be applied to its surface. The pressure forces act normal to its surface and hence through its center. Extraneous, or body, forces act through its mass center, which is also its geometric center for constant density. Hence, it is evident that no torque may be applied about any diameter of the sphere. The angular acceleration of the sphere must always be zero. If the sphere is initially at rest, it cannot be set in rotation by any means whatsoever; if it is initially in rotation, there is no means of changing its rotation. As this applies to every point in the fluid, one may visualize the fluid elements as being pushed around by boundary movements but not being rotated if initially at rest. Rotation or lack of rotation of the fluid particles is a property of the fluid itself and not its position in space.

The velocity potential Φ is a scalar function of space such that its rate of change with respect to any direction is the velocity component in that direction. In vector notation

$$\mathbf{V} = \nabla\Phi \quad (46)$$

or in terms of Cartesian coordinates

$$u = \frac{\partial\Phi}{\partial x}, v = \frac{\partial\Phi}{\partial y}, w = \frac{\partial\Phi}{\partial z} \quad (47)$$

The assumption of irrotational flow is equivalent to the assumption of a velocity potential.

Laplace Equation

The Laplace equation results when the continuity equation is written in terms of the velocity potential. By using Eqs. 36 and 46, we get

$$\nabla \cdot \mathbf{V} = \nabla \cdot (\nabla\Phi) = \nabla^2\Phi = 0 \quad (48)$$

$$\frac{\partial^2\Phi}{\partial x^2} + \frac{\partial^2\Phi}{\partial y^2} + \frac{\partial^2\Phi}{\partial z^2} = 0 \quad (49)$$

For plane polar coordinates (r, θ)

$$\frac{\partial\Phi}{\partial r} + r \frac{\partial^2\Phi}{\partial r^2} + \frac{1}{r} \frac{\partial^2\Phi}{\partial \theta^2} = 0 \quad (50)$$

For spherical polar coordinates (r, θ, γ) , where r is the distance from the origin, θ is the polar angle and γ is the meridian angle,

$$\frac{\partial}{\partial r} \left(r^2 \frac{\partial\Phi}{\partial r} \right) + \frac{1}{\sin\theta} \frac{\partial}{\partial \theta} \left(\sin\theta \frac{\partial\Phi}{\partial \theta} \right) + \frac{1}{\sin^2\theta} \frac{\partial^2\Phi}{\partial \gamma^2} = 0 \quad (51)$$

Once the velocity field is found by use of the potential function, the pressure distribution may be found by the Bernoulli equation.

Two-Dimensional Flow

In two-dimensional flow all lines of motion are parallel to a fixed plane, say the xy plane, and the flow patterns are identical in all planes to this plane. Application of this assumption to the Laplace equation in Cartesian coordinates gives

$$\nabla^2\Phi = \frac{\partial^2\Phi}{\partial x^2} + \frac{\partial^2\Phi}{\partial y^2} = 0 \quad (52)$$

In addition to streamlines as a means of visualizing the flow, equipotential lines are also useful in two dimensions. Equipotential lines are defined as the lines connecting the points in the flow domain where the value of the potential function Φ remains constant. Both the streamlines and the equipotential lines are utilized in the following sections of this chapter.

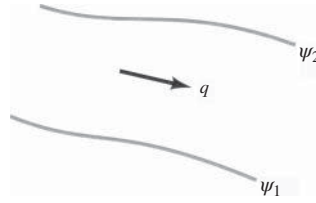


Figure 17 Flow between two streamlines. (From Ref. 2).

Stream Function. A streamline is a continuous line drawn through the fluid in such a way that at every point it is tangent to the velocity vector; therefore, there is no flow across a streamline. The stream function ψ is a scalar function of space whose value remains constant along a streamline. The volume rate of flow between two streamlines is given by the difference in values of the stream function along these streamlines, as shown in Fig. 17. So,

$$\psi_2 - \psi_1 = q \quad (53)$$

This notion of the stream function suggests that for the no-slip condition in real fluids the value of the stream function is zero at the stationary solid boundary; as for Euler solutions where viscous effects are neglected, the stream function will have a nonzero value proportional to the slip velocity tangent to the solid boundary. However, the important point is not the actual value used for the stream function at the surface but rather the difference in stream function values between two streamlines, indicating the flow rate at that location.

The velocity components u, v in the x and y directions, respectively, can be expressed in terms of stream function ψ as

$$u = \frac{\partial \psi}{\partial y}, v = -\frac{\partial \psi}{\partial x} \quad (54)$$

From the definition of the stream function, it is subject to addition of an arbitrary constant. Substituting these values of u and v into the continuity equation for two-dimensional flow,

$$\frac{\partial u}{\partial x} + \frac{\partial v}{\partial y} = \frac{\partial}{\partial x} \left(\frac{\partial \psi}{\partial y} \right) + \frac{\partial v}{\partial y} \left(-\frac{\partial \psi}{\partial x} \right) = 0 \quad (55)$$

which exactly satisfies the conservation of mass.

Application of Complex Variables to Irrotational Flow. The idea of combining the stream function and the velocity potential function into a single variable can be realized through the use of complex variables. This method of expression provides simplicity in the formulations.

Let $z = x + iy$ be a complex variable where x and y are real and $i = \sqrt{-1}$. Any function of z

$$w = f(z) = f(x + iy) = \phi + i\psi \quad (56)$$

that is defined throughout a region and that has a derivative throughout the region gives rise to two possible irrotational flow cases since it may be shown that

$$\nabla^2 w = \nabla^2 \phi + i\nabla^2 \psi = 0 \quad (57)$$

and hence $\nabla^2 \phi = 0$ and $\nabla^2 \psi = 0$. Here, w is termed the complex potential, ϕ is the real part of w , and ψ is the pure imaginary part of w . The complex velocity

$$\frac{dw}{dz} = -u + iv \quad (58)$$

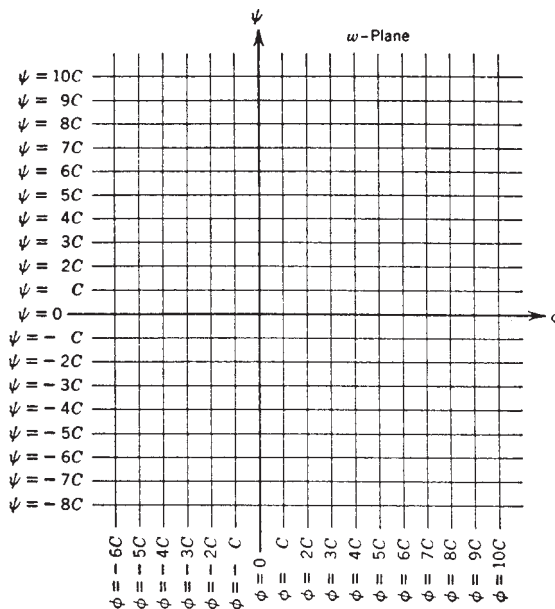


Figure 18 Flow net in w plane.

provides a simple method of finding velocity components from the complex potential. Stagnation points occur at those points in the flow where the velocity is zero, that is,

$$\frac{dw}{dz} = 0 \tag{59}$$

Conformal Mapping. Each of the two complex variables w and z introduced in the preceding paragraphs may be represented by plotting on a graph. The w plane is a graph having ϕ as abscissa and ψ as ordinate, showing values of $\phi = \pm nc$, $\psi = \pm nc$, where n is every integer and c is a constant. Figure 18 is a flow net of the simplest form showing equipotential and streamlines as series of parallel straight lines. The z plane is a plot of the equipotential and streamlines of the w plane, with x as abscissa and y as ordinate. The particular flow net in the z plane depends entirely on the functional relation between w and z , that is, $w = f(z)$. Since

$$w = f(z) = \phi + i\psi z = x + iy \tag{60}$$

where ϕ, ψ, x, y are real,

$$\phi = \phi(x, y) \quad \psi = \psi(x, y) \tag{61}$$

The values of $\phi = \text{const}$ and $\psi = \text{const}$ can be plotted on the z plane from the functional relations of ϕ and ψ with x, y .

Examples of Two-Dimensional Flow. Since the Laplace equation is linear in ϕ , the sum of two solutions is also a solution, and the product of a solution by a constant is a solution. Several of the important solutions are given.

RECTILINEAR FLOW. Uniform straight-line flow is given by

$$w = Uz - iVz\phi = Ux + Vy\psi = -Vx + Uy \tag{62}$$

where the character of flow is easily seen from the complex velocity

$$\frac{dw}{dz} = u + iv = U + iVu = Uv = V \quad (63)$$

and U, V are the x, y components of the velocity, respectively.

SOURCE OR SINK. A source in two-dimensional flow is a point from which fluid flows outward uniformly in all directions. A sink is a negative source; that is, the flow is into the point:

$$\phi = -\mu \ln r \quad \psi = -\theta \quad (64)$$

where $2\pi\mu$ is the outward flow from the line per unit length, known as the *strength*, with r and θ shown in Fig. 19. In this figure, streamlines are the radial lines and equipotential lines are the concentric circles. When μ is negative, the equations become those for a sink.

VORTEX. A vortex defines a rotation around a point. The relevant equations for a vortex are

$$\phi = -\mu\theta \quad \psi = \mu \ln r \quad (65)$$

Figure 20 is the flow net for a vortex with the radial lines now equipotential lines and the concentric circles streamlines. The vortex causes circulation about itself. Circulation about any closed curve is defined as the line integral of the velocity around the curve. The circulation

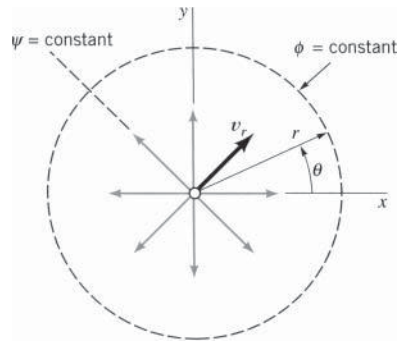


Figure 19 Streamline pattern for source (or sink). (From Ref. 2.)

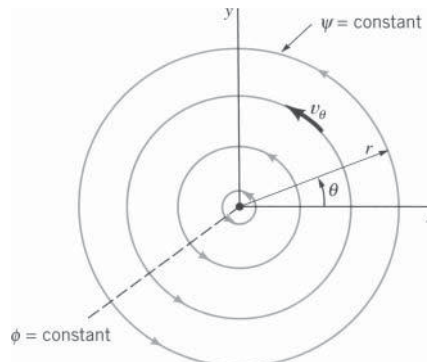


Figure 20 Flow net for vortex. (From Ref. 2.)

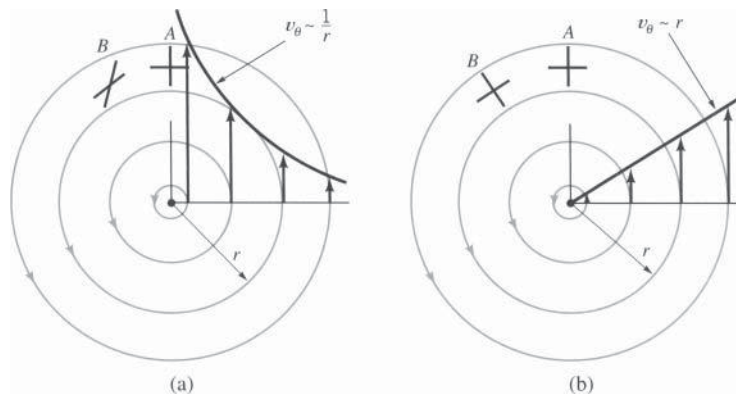


Figure 21 Depiction for (a) free vortex and (b) forced vortex. (From Ref. 2.)

about the vortex is $\kappa = 2\pi\mu$, considered positive in the counterclockwise direction around the vortex.

Based on the radial variation of the strength of the rotation, two major types of vortices are assumed: forced vortex and free vortex (Fig. 21). In the forced vortex, which is also known as solid-body rotation, the angular velocity is the same at all points, and the tangential velocity increases linearly with distance from the center of the vortex. In the free vortex, however, both the angular velocity and the tangential velocity decay with distance from the vortex center.

Doublet

The doublet is defined as the limiting case of a source and a sink of equal strength that approach each other such that the product of the strength by the distance between them remains a constant. The constant μ is called the strength of the doublet:

$$\phi = \frac{\mu x}{x^2 + y^2} \quad \psi = \frac{\mu y}{x^2 + y^2} \quad (66)$$

Figure 22 shows the flow net. The axis of the doublet is in the direction from sink to source and is parallel to the $+x$ axis as given here. The equipotential lines are circles having their centers on the x axis; the streamlines are circles having centers on the y axis.

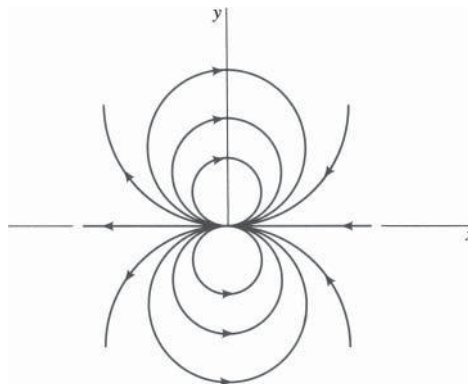


Figure 22 Streamlines for doublet. (From Ref. 2.)

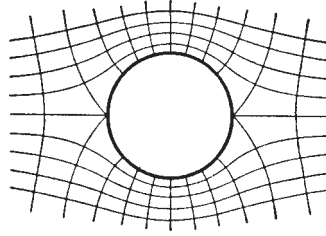


Figure 23 Flow pattern for uniform flow around circular cylinder without circulation.

Flow around a Circular Cylinder

The superposition of a uniform flow in the $-x$ direction on a doublet with axis in the $+x$ direction results in flow around a circular cylinder. Adding the two flows, taking $\mu = Ua^2$, where a is the radius of the cylinder,

$$\phi = U \left(r + \frac{a^2}{r} \right) \cos \theta \psi = U \left(r - \frac{a^2}{r} \right) \sin \theta \quad (67)$$

The streamline $\psi = 0$ is given by $\Theta = 0, \pi$ and by $r = a$; hence the circle $r = a$ may be taken as a solid boundary and the flow pattern of Fig. 23 is obtained.

Three-Dimensional Flow

Three-dimensional flows in general are more difficult to handle than those in two dimensions, primarily owing to a lack of methods comparable to the use of complex variables and conformal mapping. A velocity potential must be found that satisfies the Laplace equation and the boundary conditions. When the velocity potential is *single valued*, it may be shown that the solution is unique. For a body moving through an infinite fluid, otherwise at rest, a necessary condition is that the solution be such that the fluid at infinity remains at rest. Flow cases are usually found by investigating solutions of the Laplace equation to determine the particular boundary conditions that they satisfy.

Stokes's Stream Function. The Stokes stream function is defined only for those three-dimensional flow cases that have axial symmetry, that is, where the flow is in a series of planes passing through a given line and where the flow pattern is identical in each of these planes. The intersection of these planes is the axis of symmetry.

In any one of these planes through the axis of symmetry select two points A, P such that A is fixed and P is variable. Draw a line connecting AP . The flow through the surface generated by rotating AP about the axis of symmetry is a function of the position of P . Let this function be $2\pi\psi$, x the axis the axis of symmetry, r the distance from the origin, and Θ the angle the radius vector makes with the x axis. The meridian angle is not needed because of axial symmetry. Then

$$v_r = -\frac{1}{r^2 \sin \theta} \frac{\partial \psi}{\partial \theta} v_\theta = \frac{1}{r \sin \theta} \frac{\partial \psi}{\partial r} \quad (68)$$

and

$$\frac{1}{\sin \theta} \frac{\partial \psi}{\partial \theta} = r^2 \frac{\partial \phi}{\partial r} \frac{\partial \psi}{\partial r} = -\sin \theta \frac{\partial \phi}{\partial \theta} \quad (69)$$

The surfaces $\psi = \text{const}$ are stream surfaces. Since A is an arbitrary point, the stream function is always subject to the addition of an arbitrary constant. These equations are useful in dealing with flow about spheres, ellipsoids, and disks and through apertures. Stokes's stream function has the dimensions *volume per unit time*.

Examples of Three-Dimensional Flow. Two examples of three-dimensional flow with axial symmetry follow.

SOURCE IN A UNIFORM STREAM. A point source is a point from which fluid issues at a uniform rate in all directions. Its strength m is the flow rate from the point, and the velocity potential and stream function for a source at the origin are

$$\phi = \frac{m}{4\pi r} \quad \psi = \frac{Ur^2}{2} \sin^2 \theta \quad (70)$$

The flow net is shown in Fig. 24. Superposing a uniform flow on a point source results in a *half-body*, with the flow equations

$$\phi = \frac{m}{4\pi r} + U r \cos \theta \quad \psi = \frac{m}{4\pi} \cos \theta + \frac{Ur^2}{2} \sin^2 \theta \quad (71)$$

The resulting flow net is shown in Fig. 25. The body extends to infinity in the downstream direction and has the asymptotic cylinder whose radius is

$$R_{\text{asympt}} = \sqrt{\frac{m}{\pi U}} \quad (72)$$

The equation of the half-body is

$$r = \frac{1}{2} \sqrt{\frac{m}{\pi U}} \sec \frac{\theta}{2} \quad (73)$$

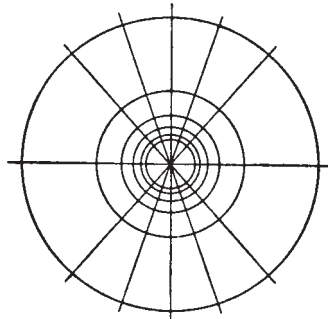


Figure 24 Streamlines and equipotential lines for source.

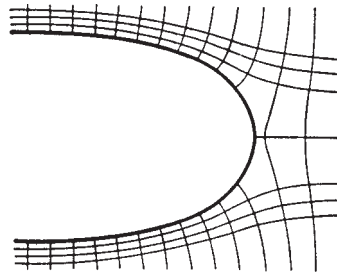


Figure 25 Streamlines and equipotential lines for half-body.

The pressure on the half-body is given by

$$p = \frac{\rho}{2} U^2 \left(\frac{3m^2}{16\pi^2 r^4 U^2} - \frac{m}{2\pi r^2 U} \right) \quad (74)$$

showing that the dynamic pressure drops to zero at great distances downstream along the body.

FLOW AROUND A SPHERE. A doublet is defined as the limiting case as a source and sink approach each other such that the product of their strength by the distance between them remains a constant. The doublet has directional properties. Its axis is positive from the sink toward the source. For a doublet at the origin with axis in the $+x$ direction

$$\phi = \frac{\mu}{r^2} \cos \theta \quad \psi = -\frac{\mu}{r} \sin^2 \theta \quad (75)$$

where μ is the strength of the doublet.

Superposing a uniform flow, $u = -U$, on the doublet results in flow around a sphere:

$$\begin{aligned} \phi &= \frac{Ua^3}{2r^2} \cos \theta + Ur \cos \theta \\ \psi &= -\frac{Ua^3}{2r} \sin^2 \theta + \frac{Ur^2}{2} \sin^2 \theta \end{aligned} \quad (76)$$

where $\mu = Ua^3/2$. This is shown to be the case since the streamline $\psi = 0$ is satisfied by $\Theta = 0, \pi$ and $r = a$.

The flow net is shown in Fig. 26.

5 VISCOUS FLUID DYNAMICS

The additional consideration of viscosity in the flow of fluids greatly complicates analysis and understanding of flow situations. In the fundamental sense, viscosity only introduces the possibility of shear stress into the flow process. However, the effects are far-reaching and for many years have caused researchers and designers to rely heavily on experimental techniques. In recent years the wide availability of supercomputers has led to an increasing use of numerical analysis to predict the behavior of fluid flows (known as computational fluid dynamics, or CFD).

Viscous flows are typically classified as laminar or turbulent, although in any given flow there may be regions of both laminar and turbulent flow. In laminar flow, fluid particles slide smoothly over one another with no mixing except that which normally occurs as a result of molecular activity. Shear stress τ in laminar flow depends directly on the local velocity gradient and the fluid viscosity,

$$\tau = \mu \frac{du}{dy} \quad (77)$$

Shear stress is not affected by boundary roughness in laminar flow so long as the boundary roughness is small in comparison to the flow cross section.

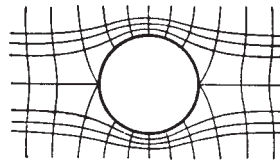


Figure 26 Streamlines and equipotential lines for uniform flow about sphere at rest.

In turbulent flow, a great deal of mixing occurs with random motion of fluid masses of various sizes occurring. Shear stress in turbulent flow depends strongly on the momentum exchange occurring as the result of turbulent mixing. An equivalent expression for shear stress in turbulent flow is

$$\tau = \varepsilon \frac{du}{dy} \quad (78)$$

where ε is the eddy viscosity, which is a function of both fluid viscosity and the local structure of the turbulent flow. This expression was unsatisfactory because it was impossible to quantify ε . An analysis of the turbulent momentum exchange process by Reynolds yielded a shear stress equation directly related to the flow turbulence:

$$\tau = -\rho \overline{u'v'} \quad (79)$$

where u', v' are the turbulent velocity fluctuations about the mean values and $\overline{u'v'}$ is the time average of the product of the fluctuations in the x and y directions. This expression is also not very useful in a practical sense. Research eventually led to the Prandtl–von Karman equation for shear stress:

$$\tau = \rho \kappa^2 \frac{(dv/dy)^4}{(d^2v/dy^2)^2} \quad (80)$$

where κ is a dimensionless turbulence constant. This practical form of the shear stress equation can be integrated to generate velocity profiles.

5.1 Internal Flows

Flow in pipes and ducts under the action of viscosity requires some changes in basic concepts as well as in the equations for one-dimensional flow. Specifically, the velocity is no longer uniform in the cross section where the streamlines are straight and parallel. The velocity will be zero at the wall due to the no-slip condition and increase to a maximum near the center of the conduit. This nonuniform velocity profile requires correction coefficients in the work–energy and momentum equations.

In addition to the need for compensating for the nonuniform velocity profile in one-dimensional flow, it is necessary to account for the energy converted to heat through the frictional processes caused by viscosity. If heat transfer is of no interest or concern, then energy conversion to heat is considered a loss in usable energy. The amount of useful energy converted to heat per pound of fluid flowing is designated by h_L , or the head loss. The one-dimensional work–energy equation now has the form

$$\frac{P_2}{\gamma} + \alpha_2 \frac{\overline{V}_2^2}{2g} + z_2 = \frac{P_1}{\gamma} + \alpha_1 \frac{\overline{V}_1^2}{2g} + z_1 - h_{L_{1-2}} \quad (81)$$

where α_1, α_2 are the correction factors for a nonuniform velocity profile ($\alpha \geq 1$ with $\alpha = 1$ for uniform profile) and \overline{V} is an average velocity. Looking at Fig. 16, this equation states that the frictional effects reduce the amount of incoming available energy [i.e., $P_1/\gamma + \alpha_1 \overline{V}_1^2/(2g) + z_1$] by an amount h_L , resulting in a reduced amount of available energy in the fluid leaving the control volume. In actuality, the h_L term reveals itself in an increase in internal energy (temperature) of the fluid or a heat transfer from the fluid. It should be noted that the Bernoulli equation (same as above except for the h_L term) is a statement that the amount of incoming and outgoing available energy are equal since a primary assumption is inviscid flow, or no frictional losses.

Another phenomenon stemming directly from the effect of friction is flow separation. Separation occurs when the fluid is forced to decelerate too rapidly or change direction too quickly.

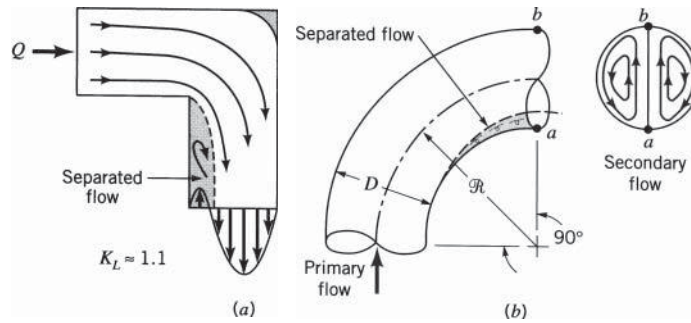


Figure 27 Character of flow in 90° -turn elbow and subsequent viscous phenomena: (a) separated flow and (b) secondary flow. (From Ref. 2.)

The result is regions of reversed flow, formation of wakes and eddies, poor pressure recovery, and excessive friction losses (see Fig. 27a).

The nonuniform velocity profile occurring in viscous flow also causes vortices and cross currents to occur at certain locations. Vortices form in corners and at abrupt changes in cross section or flow direction. Cross currents or secondary flows occur at bends in the conduit. These secondary flows are the consequence of equal pressure gradients in the bend acting on fluid particles moving at different speeds in the flow cross section. The result is a spiral flow(s) superposed on the main flow (Fig. 27b). Both vortices and secondary flows generate additional head losses and may cause some additional problems in hydraulic machinery

5.2 External Flows

External flows are generally associated with lift and drag on solid bodies in a fluid of large extent. Although for ideal fluids there is no drag, this is not the case for real fluids. Frictional effects on the surface of the body create skin friction drag. That is, the no-slip fluid condition at the body surface creates a velocity profile and the resulting shear stress at the surface to occur. The frictional effects are confined to the “boundary layer” near the body where the flow may be laminar, turbulent, or both. Theoretical analysis of skin friction drag has been relatively successful. Some specifics on lift and drag are presented in a subsequent section.

Separation in external flows is also caused by “adverse” pressure gradients that are forcing the flow to decelerate faster than it can and still remain “attached” to the boundary. Separation manifests itself as a turbulent wake behind the body (see Fig. 28), which creates considerable drag on the body largely resulting from the pressure difference between the front and rear. Smooth bodies with gradually changed form tend to generate less separation and lower drag than blunt or sharp-cornered objects.

5.3 Navier–Stokes Equations*

Application of Newton’s second law to an incompressible small fluid particle of dimension dx , dy , dz yields a set of equations comparable to the Euler equation previously derived, but now

* Illustrations and material all or in part from *Eshbach’s Handbook of Engineering Fundamentals* (Hoboken, NJ: Wiley).

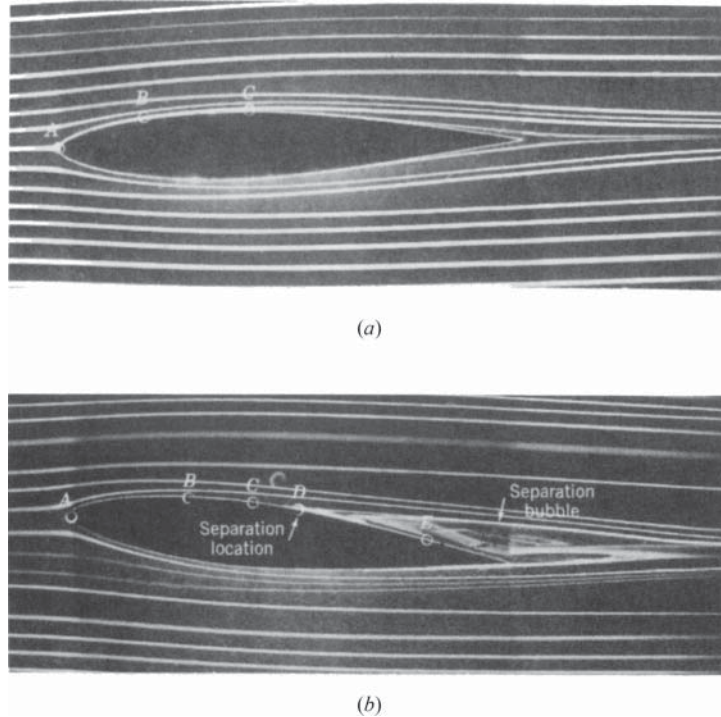


Figure 28 Flow visualization past an airfoil at (a) 0° angle of attack with no flow separation and (b) 5° angle of attack with flow separation. (From Ref. 2.)

viscous effects are included. The equations are referred to as the Navier–Stokes equations, and they take the following form for laminar flow:

$$X - \frac{1}{\rho} \frac{\partial p}{\partial x} + \nu \left(\frac{\partial^2 u}{\partial x^2} + \frac{\partial^2 u}{\partial y^2} + \frac{\partial^2 u}{\partial z^2} \right) = u \frac{\partial u}{\partial x} + v \frac{\partial u}{\partial y} + w \frac{\partial u}{\partial z} + \frac{\partial u}{\partial t} \quad (82)$$

$$Y - \frac{1}{\rho} \frac{\partial p}{\partial y} + \nu \left(\frac{\partial^2 v}{\partial x^2} + \frac{\partial^2 v}{\partial y^2} + \frac{\partial^2 v}{\partial z^2} \right) = u \frac{\partial v}{\partial x} + v \frac{\partial v}{\partial y} + w \frac{\partial v}{\partial z} + \frac{\partial v}{\partial t} \quad (83)$$

$$Z - \frac{1}{\rho} \frac{\partial p}{\partial z} + \nu \left(\frac{\partial^2 w}{\partial x^2} + \frac{\partial^2 w}{\partial y^2} + \frac{\partial^2 w}{\partial z^2} \right) = u \frac{\partial w}{\partial x} + v \frac{\partial w}{\partial y} + w \frac{\partial w}{\partial z} + \frac{\partial w}{\partial t} \quad (84)$$

where X , Y , Z are external force components per unit mass in the xyz directions, respectively; ρ is the mass density, considered constant for incompressible flow; p is the average pressure at a point; ν is the kinematic viscosity; and u , v , w are the velocity components in the xyz directions.

These simultaneous, nonlinear, differential equations cannot be integrated except for extremely simple flow cases where many of the terms are neglected. They contain the basic assumption that the stresses on a particle may be expressed as the most general linear function of the velocity gradients.

Boundary Conditions

A real fluid in contact with a solid boundary must have a velocity exactly equal to the velocity of the boundary; this is much more restrictive than for an inviscid fluid, where no restrictions are placed on tangential velocity components at a boundary.

When two fluids are flowing side by side, a dynamical boundary condition arises at the interface. Applying the equation of motion to a thin layer of fluid enclosing a small portion of the interface shows that the terms containing mass are of higher order of smallness than the surface stress intensities and hence that the stresses must be continuous through the surface.

In general, the viscous boundary conditions at a solid surface give rise to rotational flow. Although the Navier–Stokes equations are satisfied by a velocity potential, since the viscous terms drop out, the viscous boundary conditions cannot be satisfied.

Continuity

The continuity equation must hold, as in the case of inviscid flow. It is

$$\frac{\partial u}{\partial x} + \frac{\partial v}{\partial y} + \frac{\partial w}{\partial z} = 0 \quad (85)$$

Several examples of flow at low Reynolds numbers are given. It is assumed that in each case any turbulent fluctuations are completely damped out by viscous action, and the dominant flow is one dimensional with incompressible conditions.

Flow between Parallel Boundaries: Pressure-Driven Flow. For steady flow between fixed parallel boundaries at low Reynolds numbers, the Navier–Stokes equations can be greatly reduced. Taking the coordinates as shown in Fig. 29 and assuming a pressure gradient exists in the x direction that drives the flow, the differential equations reduce to

$$\frac{\partial}{\partial x}(p + \gamma h) = \mu \frac{\partial^2 u}{\partial z^2} \quad (86)$$

where h is measured vertically upward and γ is the specific weight of the fluid.

Integrating and introducing the boundary conditions $u = 0$ for $z = \pm b$, which are the no-slip conditions for this pressure-driven flow,

$$u = \frac{z^2 - b^2}{2\mu} \frac{\partial}{\partial x}(p + \gamma h) \quad (87)$$

As the z^2 term implies, and as is shown in Fig. 29, such a velocity profile is a parabolic one. It has the maximum value at the center of the pipe—hence maximum velocity. Given a linear pressure gradient, which is an acceptable assumption for such a laminar flow, the derivative term becomes a constant, and the velocity profile becomes only a function of radial distance from the center; thus it remains the same along the length of the pipe (assuming the pipe does not change in direction, diameter, or makeup). Keep in mind that the sustainability of laminar flow in a pipe is subject to various conditions. Therefore, once the flow characteristics change (e.g., transition to turbulence, development of secondary flows), this formula is no longer applicable.

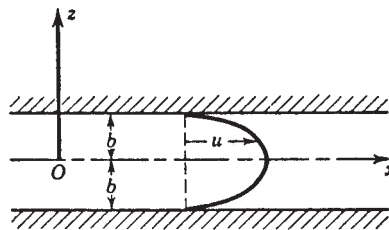


Figure 29 Viscous flow between fixed parallel boundaries.

Although the velocity potential function is essentially for irrotational flows (i.e., inviscid cases), for this special case, it is possible to express the parabolic velocity profile in terms of a velocity potential

$$u = \frac{z^2 - b^2}{2\mu} \frac{\partial}{\partial x}(p + \gamma h) = \frac{\partial}{\partial x} \left[(p + \gamma h) \left(\frac{z^2 - b^2}{2\mu} \right) \right] = \frac{\partial \phi}{\partial x} \quad (88)$$

where ϕ , the velocity potential, is the quantity in brackets.

Flow between Parallel Boundaries: Shear-Driven Flow. A similar approach can be used for flow between parallel plates, one of which is moving with a constant speed U in the x direction. In this case, the motion of the fluid is due to the viscous force between the moving plate and the adjacent fluid layer. Thus, despite the absence of a pressure gradient, there will be a flow. Without the pressure gradient, the simplified version of the Navier–Stokes equations further simplifies to

$$\frac{d^2 u}{dz^2} = 0 \quad (89)$$

The relevant boundary conditions for this case are $u = 0$ for $z = -b$ and $u = U$ for $z = +b$. Again integrating and using the boundary conditions, the velocity profile becomes

$$u = \frac{U}{2} \left(1 + \frac{z}{b} \right) \quad (90)$$

This results in a linear velocity profile between the plates.

Flow between Parallel Boundaries: Combined Effects of Pressure Gradient and Shear. One can also have the effect of both pressure gradient and shear for flow between parallel plates. For that case, the simplified version of the Navier–Stokes equations is the same as that for the pressure-driven flow, but the boundary conditions are those for the shear-driven flow. The resultant velocity profile is

$$u = \frac{U}{2} \left(1 + \frac{z}{b} \right) + \frac{z^2 - b^2}{2\mu} \frac{\partial}{\partial x}(p + \gamma h) \quad (91)$$

This is still a parabolic velocity profile, but now the maximum velocity has been displaced from the middle plane.

Theory of Lubrication

The equations for two-dimensional viscous flow are applicable to the case of a slider bearing and can be applied to journal bearings. The simple case of a bearing of unit width is developed here, under the assumption that there is no flow out of the sides of the block, that is, normal to the plane of Fig. 30, where the clearance b is shown to a greatly exaggerated scale. The motion of a

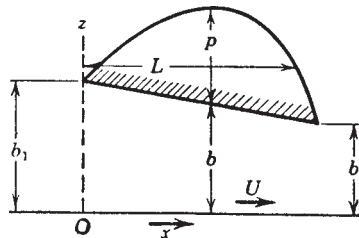


Figure 30 Free-body diagram of cylinder of fluid in steady laminar flow through circular pipe. (From Ref. 2.)

bearing block sliding over a plane surface, inclined slightly so that fluid is crowded between the two surfaces, develops large supporting forces normal to the surfaces. The angle of inclination is very small; therefore, the differential equations of the preceding example apply. Since elevation changes also are very small and flow is in the x direction only, the equations reduce to

$$\frac{\partial p}{\partial x} = \mu \frac{\partial^2 u}{\partial z^2} = 0 \quad (92)$$

Considering the inclined block stationary and the plane surface in motion and taking the pressure at the two ends of the block as zero, the boundary conditions become $x = 0$, $x = L$, $p = 0$; $z = 0$, $u = U$; and $z = b$, $u = 0$. Integrating the equations and considering unit width normal to the figure, the discharge Q and pressure distribution are determined:

$$Q = \frac{U b_1 b_2}{b_1 + b_2} p = \frac{6 \mu U x (b - b_2)}{b^2 (b_1 + b_2)} \quad (93)$$

The last relation shows that b must be greater than b_2 for positive pressure buildup in the bearing. The point of maximum pressure and its value are

$$x|_{p_{\max}} = \frac{b_1 L}{b_1 + b_2} p_{\max} = \frac{3 \mu U L}{2 b_1 b_2} \frac{b_1 - b_2}{b_1 + b_2} \quad (94)$$

The force P that the bearing will sustain is

$$P = \int_0^L p \, dx = \frac{6 \mu U L^2}{b_2^2 (k - 1)^2} \left[\ln k - \frac{2(k - 1)}{k + 1} \right] \quad (95)$$

The maximum bearing load is obtained for $k = 2.2$, yielding

$$P = 0.16 \mu \frac{U L^2}{b_2^2} D = 0.75 \mu \frac{U L}{b_2} \quad (96)$$

The ratio

$$\frac{P}{D} = 0.21 \frac{L}{b_2} \quad (97)$$

can be made very large since b_2 is small. For $k = 2.2$, the line of action of the bearing load is at $x = 0.58L$. In general the line of action is given by

$$\bar{x} = \frac{L}{2} \left[\frac{2k}{k - 1} - \frac{k^2 - 1 - 2k \ln k}{(k^2 - 1) \ln k - 2(k - 1)^2} \right] \quad (98)$$

Journal bearings are computed in an analogous manner. In general the clearances are so small compared with the radius of curvature of the bearing surface that the equations for plane motion can be applied.

Flow through Circular Tubes

For steady flow through circular tubes with values of the Reynolds number, $UD\rho/\mu$, less than 2000, the motion is laminar. Equilibrium conditions on a cylindrical element concentric with the tube axis (Fig. 31) show that the shear stress varies linearly from zero at the pipe axis to a

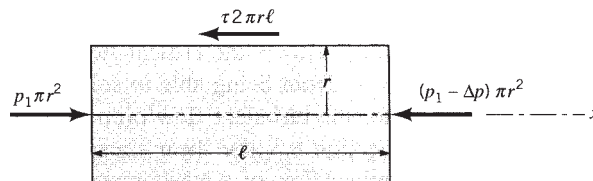


Figure 31 Slider bearing.

maximum $\Delta p r_0/2\Delta L$ at the wall, where $\Delta p/\Delta L$ is the drop in pressure per unit length of tube. In one-dimensional laminar flow the relation between shear stress and the velocity gradient is given by Newton's law of viscosity,

$$\tau = -\mu \frac{du}{dr} \quad (99)$$

Using this relation for the value of shear stress, the velocity distribution is found to be

$$u = \frac{\Delta p}{\Delta L} \frac{r_0^2 - r^2}{4\mu} \quad (100)$$

where r is the distance from the tube axis. The maximum velocity is at the axis:

$$u_{\max} = \frac{\Delta p}{\Delta L} \frac{r_0^2}{4\mu} \quad (101)$$

The average velocity is half the maximum velocity:

$$V = \left(\frac{\Delta p}{\Delta L} \right) \left(\frac{r_0^2}{8\mu} \right) \quad (102)$$

The discharge, obtained by multiplying average velocity by cross-sectional area, is

$$Q = \left(\frac{\Delta p}{\Delta L} \right) \left(\frac{\pi D^4}{128\mu} \right) \quad (103)$$

which is the *Hagen–Poiseuille* law. The preceding equations are independent of the surface condition in the tube, and they therefore hold for either rough or smooth tubes as long as the flow is laminar.

Viscous Flow around a Sphere: Stokes's Law

The flow of an infinite viscous fluid around a sphere at very low Reynolds numbers ($Re \ll 1$, which states that viscous forces are dominant compared to inertial forces) has been solved by Stokes.³ The Navier–Stokes equations with the acceleration terms omitted must be satisfied, as well as continuity and the boundary condition that the velocity vanish at the surface of the sphere. Stokes's solution is

$$u = U \left[\frac{3}{4} \frac{ax^3}{r^3} \left(\frac{a^2}{r^2} - 1 \right) + 1 - \frac{1}{4} \frac{a}{r} \left(3 + \frac{a^2}{r^2} \right) \right] \quad (104)$$

$$v = U \frac{3}{4} \frac{axy}{r^3} \left(\frac{a^2}{r^2} - 1 \right) \quad (105)$$

$$w = U \frac{3}{4} \frac{axz}{r^3} \left(\frac{a^2}{r^2} - 1 \right) \quad (106)$$

$$p = -\frac{3}{2} \frac{\mu U a x}{r^3} \quad (107)$$

The radius of a sphere is a ; the undisturbed velocity is in the x direction, $u = U$; and p is the average dynamic pressure at a point. The drag on a sphere is made up from the pressure difference over the surface of the sphere and from the shear stress. The viscous drag due to shear stress is twice as great as that due to the pressure difference. The total drag is

$$D = 6\pi a\mu U \quad (108)$$

This is known as *Stokes's law*.

The settling velocity of small spheres may be obtained by writing the equation for drag, weight of particle, and buoyant force. Solving for the settling velocity,

$$U = \frac{2}{9} \frac{a^2}{\mu} (\gamma_s - \gamma) \quad (109)$$

where γ_s is the specific weight of the solid particle. Stokes's law has been found by experiment to hold for Reynolds numbers below 1, that is,

$$\frac{2apU}{\mu} < 1 \quad (110)$$

6 SIMILITUDE AND DIMENSIONAL ANALYSIS

Similitude and dimensional analysis are inextricably tied to experimental testing and the analysis of experimental data. Principles of similitude permit the prediction of prototype behavior based on the performance of models. Techniques of dimensional analysis permit the efficient and logical presentation of test data in dimensionless form. Even in recent times when CFD techniques are supplementing laboratory work at an increasing pace (note: CFD will never totally replace experiments), many flow phenomena are so complex as to warrant experimental investigation.

6.1 Similitude

For complete similitude the model and the prototype must be geometrically, kinematically, and dynamically similar. In this context, the prototype is the physical system for which you are trying to predict the behavior, while the model (typically a scaled version of the prototype) is the device used for testing in the laboratory. Geometric similarity exists when the model is a photographic reduction (or enlargement) of the prototype. Kinematic similarity occurs when the streamline pattern in the model is a photographic reduction (or enlargement) of that of the prototype. Also ratios of velocity vectors at corresponding points are constant. Dynamic similarity requires that the ratios of similar forces at all corresponding points in the flow be constant. In general, if geometric similarity and dynamic similarity exist, then kinematic similarity is guaranteed.

Quantitative relationships for dynamic similarity are obtained by considering the contributing forces acting on a fluid particle. Potential contributing forces include viscosity (shear), pressure, gravity, elasticity, and surface tension. These forces all contribute to the acceleration of the fluid particle in the prototype flow:

$$\mathbf{F}_v + \mathbf{F}_p + \mathbf{F}_g + \mathbf{F}_e + \mathbf{F}_s = m\mathbf{a} = -\mathbf{F}_I \quad (\text{inertial force}) \quad (111)$$

Dividing by the inertial force and considering the prototype (P),

$$\left(\frac{\mathbf{F}_v}{\mathbf{F}_I}\right)_P + \left(\frac{\mathbf{F}_p}{\mathbf{F}_I}\right)_P + \left(\frac{\mathbf{F}_g}{\mathbf{F}_I}\right)_P + \left(\frac{\mathbf{F}_e}{\mathbf{F}_I}\right)_P + \left(\frac{\mathbf{F}_s}{\mathbf{F}_I}\right)_P = -1 \quad (112a)$$

If the same process is followed in the model (m),

$$\left(\frac{\mathbf{F}_v}{\mathbf{F}_I}\right)_m + \left(\frac{\mathbf{F}_p}{\mathbf{F}_I}\right)_m + \left(\frac{\mathbf{F}_g}{\mathbf{F}_I}\right)_m + \left(\frac{\mathbf{F}_e}{\mathbf{F}_I}\right)_m + \left(\frac{\mathbf{F}_s}{\mathbf{F}_I}\right)_m = -1 \quad (112b)$$

This scaling procedure renders the force polygons at the corresponding points in the model and prototype as congruent provided the force ratios for each source of force are the same in

the model and prototype. In fact, the scaled polygons are congruent if *all but one* of the force ratios are equal. This relationship can be summarized as follows:

Viscous Forces:

$$\left(\frac{\rho V l}{\mu}\right)_m = \left(\frac{\rho V l}{\mu}\right)_p \quad (113)$$

where $\rho V l / \mu$ is the Reynolds number, Re is the inertia force/viscous force.

Pressure Forces:

$$\left(\frac{P}{\rho V^2}\right)_m = \left(\frac{P}{\rho V^2}\right)_p \quad (114)$$

where $P / \rho V^2$ is the Euler number, and E is the pressure force/inertia force.

Gravity Forces:

$$\left(\frac{V^2}{g l}\right)_m = \left(\frac{V^2}{g l}\right)_p \quad (115)$$

where $V / \sqrt{g l}$ is the Froude number, and F is the inertia force/gravitational force.

Elastic Forces:

$$\left(\frac{V}{a}\right)_m = \left(\frac{V}{a}\right)_p \quad (116)$$

where a is the speed of sound, V/a is the Mach number, and M is the inertia force/compression force.

Surface Tension Forces:

$$\left(\frac{\rho V^2 l}{\sigma}\right)_m = \left(\frac{\rho V^2 l}{\sigma}\right)_p \quad (117)$$

where $\rho V^2 l / \sigma$ is the Weber number, and W is the inertia force/surface tension force.

In most fluid problems, some of these forces are negligible and can be ignored in model–prototype relationships. For example, if there is no free surface and flows are well below the sonic velocity, then only viscous and pressure forces are important. In this case, equality of Reynolds numbers would guarantee similarity. Typically, pressure forces are always in existence, and the Euler number is the force ratio omitted in specifying similarity (as noted earlier).

Example 1

Model testing of a new submarine is to be conducted in a wind tunnel using standard air at sea level conditions. Due to the limitations on the test section size, the model needs to be a one-twentieth-scale version of the prototype. If the actual submarine will have a velocity of $V_p = 0.5$ ft/s in seawater at 20°C, what must the air velocity be in the wind tunnel for the model to achieve dynamic similarity?

For dynamic similarity, $Re_p = Re_m$, or $(\rho V l / \mu)_m = (\rho V l / \mu)_p$. Solving for model velocity V_m yields

$$V_m = \frac{l_p}{l_m} \frac{\rho_p}{\rho_m} \frac{\mu_m}{\mu_p} V_p$$

The necessary values are found as follows:

$$\begin{aligned} \rho_m &= 0.00238 \text{ slug/ft}^3 & \mu_m &= 3.74 \times 10^{-7} \text{ lb-s/ft}^2 \\ \rho_p &= 2.0 \text{ slugs/ft}^3 & \mu_p &= 2.23 \times 10^{-5} \text{ lb-s/ft}^2 \end{aligned}$$

So, the required wind tunnel velocity is found from

$$V_m = \left(\frac{20}{1}\right) \left(\frac{2.0}{0.00238}\right) \left(\frac{3.74 \times 10^{-7}}{2.23 \times 10^{-5}}\right) (0.5)$$

$$= 141 \text{ ft/s}$$

There are situations where complete similarity cannot be practically achieved. For example, in the modeling of ship hulls, if water is used as the modeling fluid, the model must be as large as the prototype. This is true because viscous and gravity forces predominate and both Reynolds and Froude numbers must be equal to guarantee similarity. In this case, to get around the problem, the model–prototype relation is determined by the Froude number equality and the viscous effects on hull drag are determined through other means. This situation is known as incomplete similarity or distorted model.

In other flow situations such as rivers and harbors, the lateral dimensions are so large compared to the vertical dimensions that geometric scaling would make the model so shallow as to be under strong surface tension effects. Also the boundary roughness would be reduced to supersmoothness. In these situations, two different model scales are used: one for horizontal dimensions, another for vertical dimensions. These models generally have to be adjusted for “scale effects” by employing artificial roughness to properly represent prototype behavior.

6.2 Dimensional Analysis

Dimensional analysis is based on the principle that meaningful physical relationships between quantities must be dimensionally homogeneous; that is, both sides of an equation must have the same dimensions. The four basic dimensions used in fluid mechanics are force (F), mass (M), length (L), and time (T). In fact, the dimension of force is related to the dimensions of mass, length, and time through Newton’s second law:

$$F = M \frac{L}{T^2} \quad (118)$$

The units of force are said to be *equivalent* to the units of mass \times length/time squared.

The principle of dimensional homogeneity can be used to develop a formal procedure for establishing relations between physical quantities and, most importantly, dimensionless groups. Dimensionless groups of quantities are extremely valuable in the analysis and presentation of experimental data. Their use permits large amounts of data to be presented on simple graphs, graphs with parametric relationships, or in some more complex cases multicorrelational graphs.

For example, consider the case of the drag force on a sphere falling at constant velocity in a very viscous liquid. Drag (D) is a function of velocity (V), size (d), and viscosity (μ):

$$D = f(V, d, \mu)$$

In basic dimensions,

$$F = f' \left(\frac{L}{T}, L, \frac{FT}{L^2} \right)$$

The only combination of quantities on the right-hand side that will make the relationship dimensionally correct is

$$D = KVd\mu \quad (119)$$

where K is a dimensionless constant. Thus, by dimensional reasoning alone, Stokes’s law has been deduced. Sometimes the relationship does not fall out so easily, quantities may need to have positive or negative exponents to create a combination that is dimensionally correct.

However, formal dimensional analysis does not always offer a unique approach to generating the desired dimensionless groups. A more modern and intuitive method, called

the Buckingham Π theorem, is more useful. This theorem informs the user as to how many dimensionless groups may be formed and leaves the configuration of each group up to the user. This freedom, coupled with knowledge of the important similarity principles, permits the user to make a good choice of the proper groups.

According to the Buckingham Π theorem, a problem described by k variables can be expressed in terms of $k - r$ nondimensional Π terms, where r is the minimum number of reference dimensions involved in the problem. For example, when establishing the quantities affecting the drag on a ship's hull, the list includes

$$D(\text{drag}) = f(l, V, \mu, \rho, g) \quad (120)$$

or

$$f'(D, l, V, \mu, \rho, g) = 0 \quad (121)$$

The Π theorem allows the formation of three dimensionless groups ($k - r = 6 - 3$). Knowing that viscous and gravitational effects are most significant in affecting drag, the dimensionless groups of Reynolds number and Froude number are selected. Then the drag force D is combined into a third group. The final relationship states that the nondimensional drag (i.e., drag coefficient) is a function of the Reynolds and Froude numbers:

$$\frac{D}{\rho l^2 V^2} = \phi \left(\frac{\rho V l}{\mu}, \frac{V^2}{g l} \right) \quad (122)$$

or

$$C_D = \phi(\text{Re}, F^2) \quad (123)$$

The use of this kind of nondimensional expression allows the experimenter to make use of scale-size models and can perform experiments more easily and affordably by reducing the number of parameters that need to be varied. Once the experiments are performed on the model, the experimenter can plot all data on one graph using the nondimensional values; for example, $D/\rho l^2 V^2$ as the ordinate, Re as the abscissa, and F as the parametric variable.

7 FLOW IN CLOSED CONDUITS

Flow through a conduit may be steady or unsteady, uniform or nonuniform, and laminar or turbulent. Steady flow refers to flow at constant rate, uniform flow to prismatic sections of conduit, and laminar flow to those cases where viscous forces predominate and the losses are a linear function of the velocity, whereas for turbulent flow the losses vary as the velocity to some power (1.7–2.0), depending in part upon the Reynolds number.

The classical methods of hydrodynamics applying to an ideal fluid are of little value in solving flow problems in conduits, although they are extremely useful in connection with flow around immersed bodies (see Section 9). The nature of turbulent flow, on the other hand, is not sufficiently well understood to permit computation of the energy losses for given boundary conditions and rates of flow, and hence recourse must generally be taken to experimentation.

The work–energy equation is of first importance in solving flow problems. Momentum relationships are of use in certain cases in which the forces acting on the fluid are known or are desired. In special situations where both the energy and momentum equations are applicable, the energy loss may be computed without recourse to experimentation. The continuity equation in steady flow usually states that the flow past every cross section is the same. When the fluid is compressible, this is a statement of mass or weight flow, but for liquids it is sufficient to deal with volume rates only. The three types of equations (energy, momentum, and continuity), together with the experimentally determined loss relationships, provide the general framework for solving closed-conduit problems.

7.1 Velocity Distribution*

The velocity distribution for established laminar flow through round tubes and between parallel plates has been discussed under laminar fluid motion in Section 5.

Development of Flow

The velocity distribution for fully developed uniform flow in a closed conduit is determined by the relationship between the radial velocity gradient and the shear stress. In turbulent flow the velocity distribution cannot be derived exactly, although much has been accomplished in recent years in the analytical approach to rational velocity–distribution equations.

Downstream from any change m cross section or direction, there is a length over which the velocity distribution regains its characteristic form (entrance region), depending on the shape of cross section, the wall roughness, and the Reynolds number. For example (follow the description from Fig. 32), when the flow passes from a reservoir through a rounded entrance into a conduit, the velocity is practically constant over the section at the upstream end of the conduit. Such flow during the initial stages is therefore practically irrotational since the boundary layer is very thin. The effect of boundary resistance, however, is to retard the fluid in the wall vicinity, resulting, through lateral transmission of shear, in a continuous growth of the boundary layer with distance from the inlet. Since the mean velocity must nevertheless remain constant, the central portion of the fluid is simultaneously accelerated until the forces of shear and pressure gradient reach equilibrium as the velocity distribution of uniform flow becomes fully developed some distance downstream. If the flow experiences a change in cross section or direction, it will undergo another developing flow region until fully developed flow is once again achieved (see Fig. 32).

For laminar flow, experiments by Nikuradse give the entrance length l for development of flow as

$$\frac{l_e}{D} = 0.06 \text{ Re} \quad (124)$$

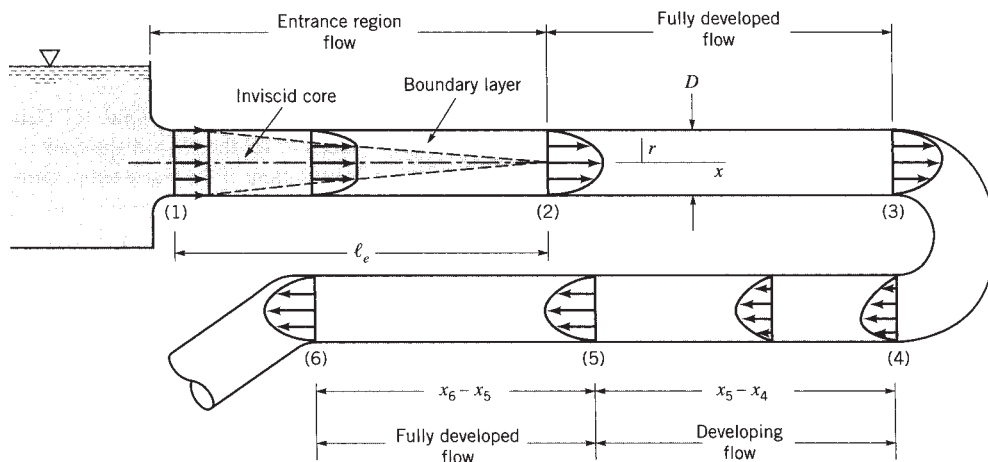


Figure 32 Entrance region, developing flow, and fully developed flow in pipe system. (From Ref. 2.)

* Illustrations and material all or in part from *Eshbach's Handbook of Engineering Fundamentals* (Hoboken, NJ: Wiley).

where D is the pipe diameter and the Reynolds number is based on average velocity and diameter.

In turbulent flow, the transition to the established velocity distribution is affected in a much shorter reach because of the pronounced mixing action that then prevails. Nikuradse's experiments indicate that a distance of 25–40 diameters is sufficient and that the length is not so dependent on the Reynolds number.

Rational Formulas for Fully Developed Turbulent Flow

In turbulent flow, the ratio of shear stress to velocity gradient depends not only on the physical properties of the fluid but also on the characteristics of the flow.

Stanton first stated that the turbulent velocity distribution in the central portions of a conduit has a form that is independent of the wall roughness and viscous effects provided that the wall shear remains the same. In equation form

$$\frac{v_{\max} - v}{\sqrt{\tau_o/\rho}} = F\left(\frac{r}{r_o}\right) \tag{125}$$

where v_{\max} is the velocity at the pipe axis, v is the velocity at the distance r from the axis, r_o is the pipe radius, τ_o is the wall shear, ρ is the mass density of fluid, and F is an unknown function. The proof is evident by an inspection of the Nikuradse data on smooth and sand-roughened pipes, given in Fig. 33; k is the diameter of sand grains cemented to the pipe walls.

Based on the preceding, von Karman⁴ obtained the formula for smooth pipes:

$$\frac{v}{\sqrt{\tau_o/\rho}} = C_1 + \frac{1}{\kappa} \ln\left(\sqrt{\frac{\tau_o y}{\rho \nu}}\right) \tag{126}$$

where κ is a universal constant having the value 0.40 and ν is the kinematic viscosity. Figure 34, based on Nikuradse's tests, shows the value of C_1 to be 5.5 for best agreement with the data.

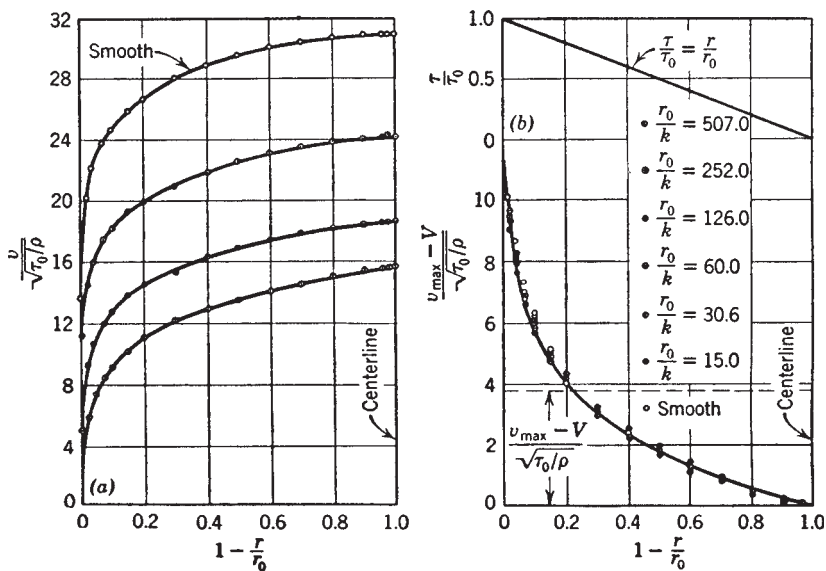


Figure 33 Generalized plot of velocity distribution for smooth and rough pipes.

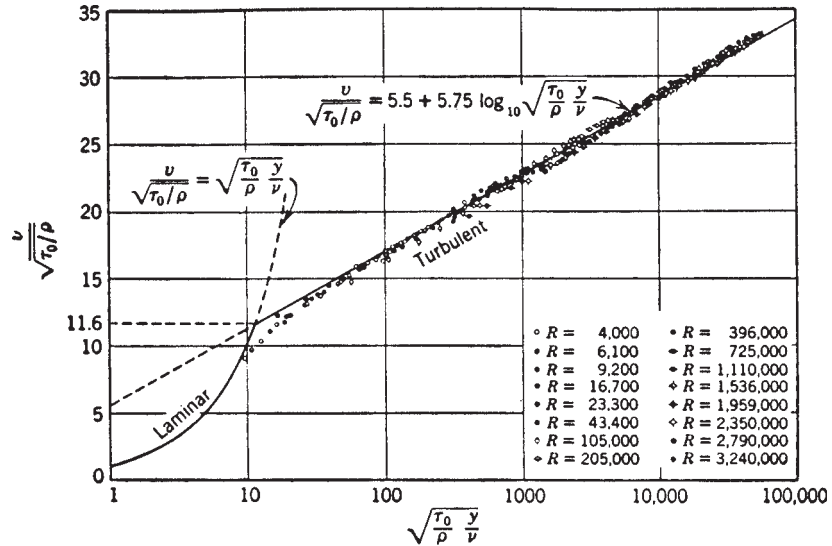


Figure 34 Universal velocity distribution for smooth pipes.

In the immediate vicinity of the pipe wall, through a film called the *laminar sublayer*, the velocity is given closely by $v = y\tau_o/\mu$. This may be written as

$$\frac{v}{\sqrt{\tau_o/\rho}} = \sqrt{\frac{\tau_o}{\rho}} \frac{y}{\nu} \quad (127)$$

and is plotted in Fig. 34. The intersection of the two curves may be taken arbitrarily as the border between the two types of flow, although actually there is a transition phase from the laminar to the turbulent zone. From the figure, the laminar film has the thickness

$$\delta = \frac{11.6\nu}{\sqrt{\tau_o/\rho}} \quad (128)$$

For rough pipes von Karman obtained the formula

$$\frac{v}{\sqrt{\tau_o/\rho}} = C_2 + \frac{1}{\kappa} \ln\left(\frac{y}{\kappa}\right) \quad (129)$$

Figure 35 shows the Nikuradse sand-roughened pipe tests. From these data, $C_2 = 8.5$.

The two logarithmic equations do not give a zero slope of the velocity distribution curve at the centerline. This is a defect in the formulas that, nevertheless, has little significance from a practical viewpoint. The equations actually portray the true velocity distribution in the central region of the flow very well, although they were derived for the region near the wall.

Energy and Momentum Correction Factors

In writing the work-energy equation between two cross sections of a conduit, it is usually satisfactory to express the mean kinetic energy per unit weight simply as $V^2/2g$, where V is the average velocity at a section. As discussed earlier, however, this is strictly true only when the velocity is constant over both cross sections. For laminar flow, the correction α by which $V^2/2g$ must be multiplied to give the true mean value is 2.0, and for sections where there is back flow, the factor may be even larger. Values of α and β based on Prandtl-Karman turbulent velocity distribution equations are given in Fig. 36.

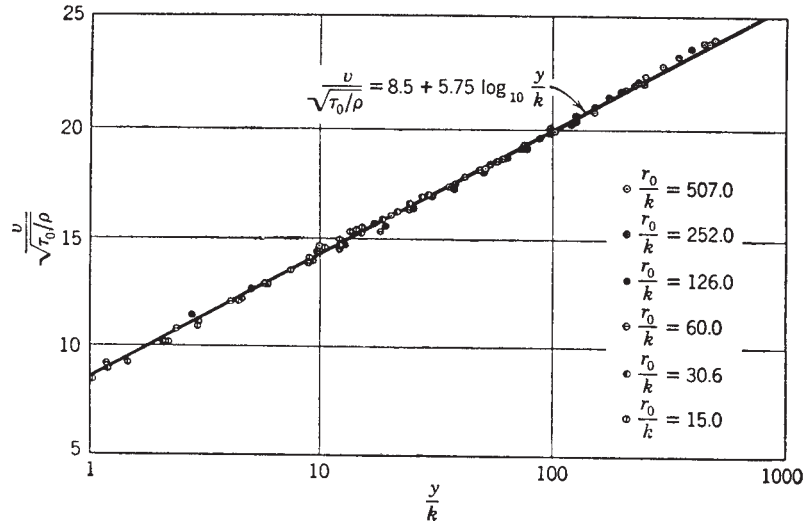


Figure 35 Universal velocity distribution for rough pipes.

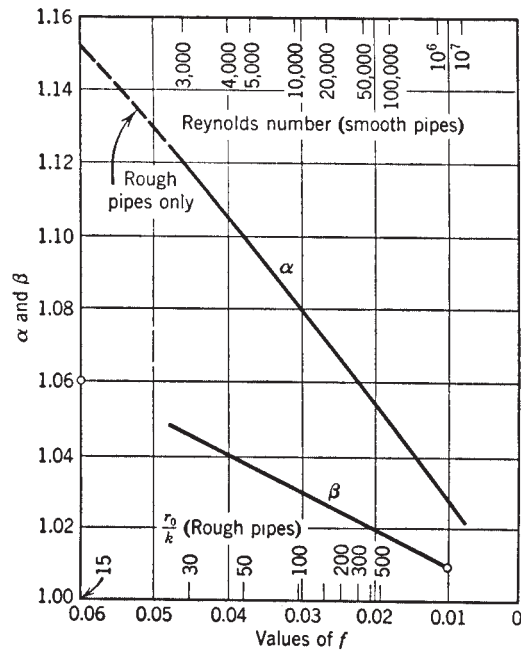


Figure 36 Energy and momentum correction factors for smooth and rough pipes.

7.2 Pipe Friction*

A general equation for solving one-dimensional pipe flow problems is the work–energy equation

$$\frac{P_1}{\gamma} + \alpha_1 \frac{V_1^2}{2g} + z_1 = \frac{P_2}{\gamma} + \alpha_2 \frac{V_2^2}{2g} + z_2 + \sum h_{L_{1-2}} \quad (130)$$

where $\sum h_{L_{1-2}}$ is the total of all the friction losses between cross sections 1 and 2. These losses can be divided into two general categories: pipe friction and minor losses. Pipe friction losses are those caused by the continuing viscous action along the conduit. Minor losses are the result of the additional friction losses over and above the pipe friction. These losses are caused by flow separation, eddies, and wakes that are generated by changes in flow direction or cross section and pipe components such as a valve. This section deals with pipe friction.

Pipe friction losses for circular cylindrical pipes depend on the flow velocity, pipe size, fluid viscosity, and wall roughness. In regard to wall roughness, friction loss specifically depends on *relative* roughness, that is, the *absolute* roughness compared with the pipe diameter. The various formulas for pipe friction loss differ in how they incorporate wall roughness into the head loss equation. The formulas in most common use today are the following:

$$h_f = f \frac{L}{D} \frac{V^2}{2g} \quad (\text{Darcy–Weisbach}) \quad (131)$$

$$V = 0.55CD^{0.63}S^{0.54} \quad (\text{Hazen–Williams}) \quad (132)$$

$$V = \frac{0.59}{n} D^{2/3} S^{1/2} \quad (\text{Manning}) \quad (133)$$

where f , C , n are friction coefficients; S is head loss per unit length of pipe, D is inside pipe diameter, and L is pipe length. The Darcy–Weisbach formula, commonly referred to as the Darcy formula, is the most general in application. It can be used for a variety of liquids and gases, for laminar and turbulent flow, and for rough or smooth pipes. Its main disadvantage is the fact that the friction factor f is often dependent on one of the design unknowns (pipe diameter or discharge) and an iterative solution results. However, engineers are increasingly using this formula because of its breadth of application.

The Hazen–Williams formula was developed for the computation of friction losses for water flowing in distribution system pipes. It works well for moderately smooth pipes (such as cast iron), but it is not accurate for rough pipes, small pipes, or laminar flow.

The main task is to find the friction factor f . The value depends on two parameters: Reynolds number and relative roughness. The Reynolds number measures the effect of viscosity on f and is defined as

$$\text{Re} = \frac{VD}{\nu} \quad (134)$$

where ν is the kinematic viscosity of the fluid. The relative roughness measures the roughness of the pipe wall relative to the pipe diameter and is expressed as k/D , where k is a measure of pipe wall roughness.

For convenience, Table 6 was compiled from several sources to provide assistance in selecting roughness values for various pipe materials. It should be noted that, typically, there are several inconsistencies between the roughness values given in Table 6 for the different formulas and those generated using the following equations.

The Reynolds number and the relative roughness are used in conjunction with the Moody diagram (Fig. 37) to find the f value. The use of the Moody diagram can best be shown by example.

* Material and illustrations used by permission from G. Z. Watters, *Analysis and Control of Unsteady Flow in Pipelines*, Butterworth, Stoneham, MA, 1984.

Table 6 Roughness Values for Commercial Pipes

Pipe Material	k (in.)	C (Hazen-Williams)	n (Manning)
Riveted steel	0.036–0.36	110	0.013–0.017
Concrete	0.012–0.12	120–140	0.011–0.014
Cast iron (new)	0.010	130	0.013
Cast iron (old)	—	100	0.015–0.035
Galvanized iron	0.0060	—	0.016
Asphalted iron	0.0048	—	0.013
Welded steel	0.0018	120	0.012
Asbestos cement	—	140	0.011
Copper, aluminum tube	Smooth	150	0.010
PVC, plastic	Smooth	150	0.009

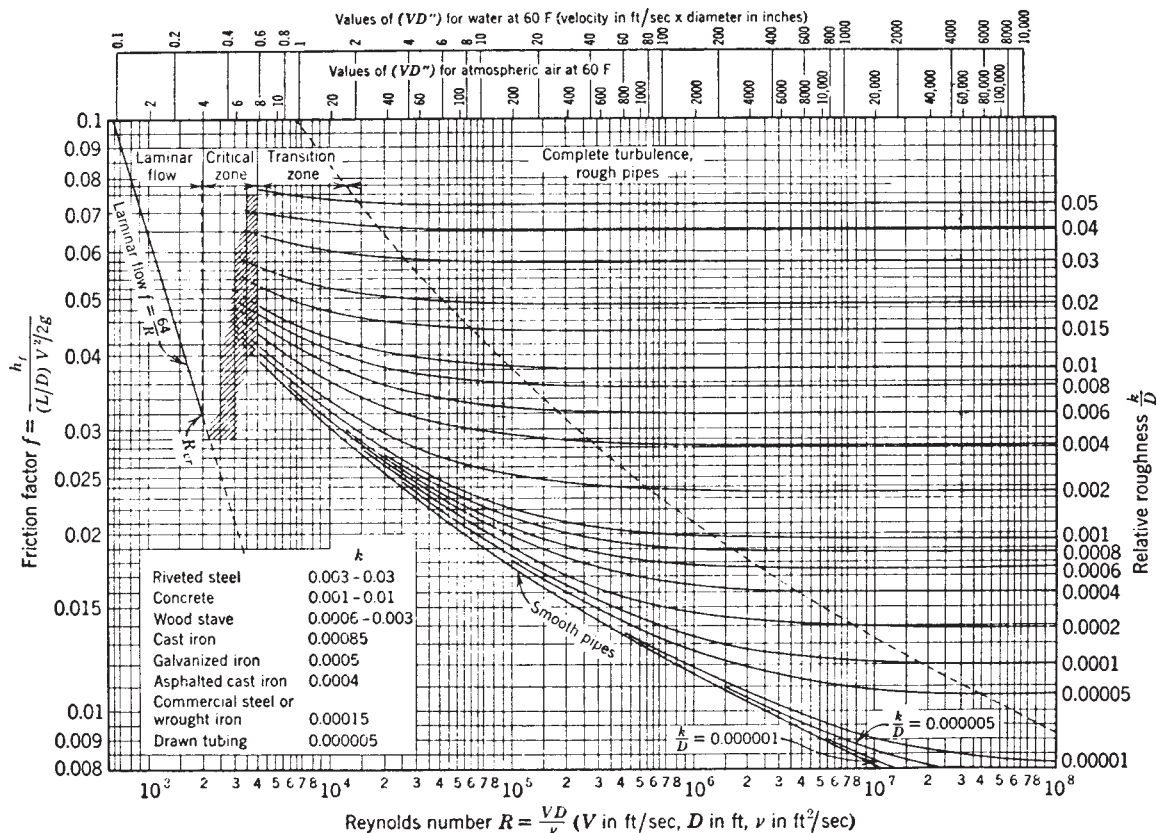


Figure 37 Resistance diagram. *Source:* Reproduced with permission from L. F. Moodes, "Friction Factor for Pipe Flow," *Transactions ASME*, November 1944, Princeton, NJ.

Example 2

Compute the friction factor f for the flow of 1500 gpm of water at normal temperature in a 10-in. cast-iron pipe.

$$\begin{aligned} V &= \frac{1500}{449(\pi/4)(10/12)^2} \\ &= 6.13 \text{ ft/s} \end{aligned}$$

From Table 6

$$\frac{k}{D} = \frac{0.01}{10} = 0.001$$

Using $\nu = 1.22 \times 10^{-5} \text{ ft}^2/\text{s}$, from Eq. 133

$$\begin{aligned} \text{Re} &= \frac{6.13 \times (10/12)}{1.22 \times 10^{-5}} \\ &= 418,000 \end{aligned}$$

From Fig. 37, $f = 0.020$.

Both the Hazen–Williams and Manning formulas can be manipulated into the same form as the Darcy formula. The resulting f expressions may be compared with the Darcy f value to deduce the situations where these formulas may be confidently applied:

$$h_f = \left(\frac{1090}{C^{1.85} \text{Re}^{0.15}} \right) \frac{L}{D} \frac{V^2}{2g} \quad (\text{Hazen–Williams}) \quad (135)$$

$$h_f = \left(\frac{185n^2}{D^{1/3}} \right) \frac{L}{D} \frac{V^2}{2g} \quad (\text{Manning}) \quad (136)$$

Both C and n are roughness values that can be obtained from tables such as Table 6. For additional information on C values see Davis and Sorensen⁵; for n values see Chow.⁶

The areas of applicability of the three head loss formulas can be deduced. It is clear that the Manning formula is indeed a rough pipe formula because the Reynolds number does not appear. On the other hand, the Hazen–Williams formula is a relatively smooth pipe formula because the head loss varies with discharge in the same manner as smooth pipes. Their use should be strictly limited to these specific hydraulic conditions. However, in actual design use of the formulas, the results are not quite so dramatic. Consider the following example.

Example 3

Select a pipe to convey $20 \text{ ft}^3/\text{s}$ of water between two reservoirs 5 miles apart and 200 ft different in elevation. Use welded steel pipe.

Hazen–Williams: From Table 6, $C = 120$. From Eq. 131,

$$r/Q = AV = \frac{1}{4} \pi D^2 \times 0.55 C D^{0.63} S^{0.54}$$

$$20 = \frac{1}{4} \pi D^2 \times 0.55 \times 120$$

$$\times D^{0.63} \left(\frac{200}{5 \times 5280} \right)^{0.54}$$

$$D = 1.90 \text{ ft or } 22.8 \text{ in.} \quad \text{Design } D = 24 \text{ in.}$$

Equivalent f value = 0.019

Manning: From Table 6, $n = 0.012$. From Eq. 132,

$$rIQ = AV = \frac{1}{4}\pi D^2 \times \frac{0.59}{n} D^{2/3} S^{1/2}$$

$$20 = \frac{1}{4}\pi D^2 \times \frac{0.59}{0.012} D^{2/3} \left(\frac{200}{5 \times 5280} \right)^{1/2}$$

$$D = 1.95 \text{ ft or } 23.4 \text{ in.} \quad \text{Design } D = 24 \text{ in.}$$

$$\text{Equivalent } f \text{ value} = 0.021$$

Darcy–Weisbach: This is an iterative solution because the Reynolds number and relative roughness cannot be found unless the diameter is known. Because we know roughly what the diameter is from the previous solution, we will use that as an estimate. From an estimated $D \approx 24$ in., from Table 6, $k/D = 0.000075$. Then

$$V = \frac{20}{(\pi/4)D^2} = 6.4 \text{ ft/s}$$

$$\text{Re} = \frac{6.4 \times 2}{1.2 \times 10^{-5}} = 1.07 \times 10^6$$

From Fig. 37,

$$f = 0.0135$$

$$D = 1.85 \text{ ft or } 22 \text{ in.} \quad \text{Design } D = 22 \text{ in.}$$

Even though there is a rather dramatic variance in the f value (variation of almost 50%), the resulting effect on the design pipe diameter is quite a lot less. This is a consequence of the fact that diameter varies at about the $\frac{1}{5}$ power of the f value; so, dramatic differences in f value have greatly reduced impact.

For purposes of computer application, it is advantageous to express the information on the Moody diagram in algebraic form. This is most commonly done with the equations of Colebrook⁷:

$$\frac{1}{\sqrt{f}} = -2 \log_{10} \left(\frac{2.51}{\text{Re} \sqrt{f}} \right) \quad (\text{smooth}) \quad (137)$$

$$\frac{1}{\sqrt{f}} = 1.74 - 2 \log_{10} \left(2 \frac{k}{D} + \frac{18.7}{\text{Re} \sqrt{f}} \right) \quad (\text{transition}) \quad (138)$$

$$\frac{1}{\sqrt{f}} = -2 \log_{10} \left(0.266 \frac{k}{D} \right) \quad (\text{rough}) \quad (139)$$

These equations can then be solved iteratively by computer to determine f for a given Re value and k/D value.

Effects of Aging*

The values of k given for the various pipe materials of Fig. 37 and Table 6 are for new, clean pipes. In general, pipes become increasingly rough with age, owing to deposition or corrosion. Colebrook and White have determined an approximately linear increase in absolute roughness with time, which may be expressed as

$$k = k_0 + \alpha t \quad (140)$$

* Illustrations and material all or in part from *Eshbach's Handbook of Engineering Fundamentals* (Hoboken, NJ: Wiley).

where k_0 is the absolute roughness of the new material, α is a constant, and k is the absolute roughness at time t .

Example 4

After 10 years of service, a 10-in cast-iron pipeline in water service has a drop of 3.13 psi per 1000 ft for a flow of 1000 gpm. What is the estimated pressure drop for 1200 gpm after 20 years of service?

$$V = \frac{1000}{7.48 \times 60 (\pi/4) (5/6)^2} = 4.1 \text{ ft/s} \quad \frac{V^2}{2g} = 0.262 \text{ ft}$$

$$h_f = \frac{3.13 \times 144}{62.4} = f \frac{1000}{5/6} 0.262 f = 0.023$$

Taking $\nu = 1.2 \times 10^{-5} \text{ ft}^2/\text{s}$,

$$\text{Re} = \frac{4.1 \times 5}{6 \times 1.2 \times 10^{-5}} = 285,000$$

From Fig. 37, for the above calculated values of f and Re , we get $k/D = 0.0017$ and $k = 0.00142 \text{ ft}$. For new cast iron take $k_0 = 0.001 \text{ ft}$; hence for 10 years,

$$0.00142 = 0.001 + 10\alpha = 0.000042 \text{ ft/yr}$$

and for 20 years,

$$k = 0.001 + 20 \times 0.000042 = 0.00184 \text{ ft}$$

$$\frac{k}{D} = 0.0022V = \frac{1200}{1000} \times 4.1 = 4.92 \text{ ft/s}$$

$$\text{Re} = \frac{4.92}{4.1} \times 285,000 = 342,000$$

From Fig. 37, $f = 0.025$; then

$$h_f = 0.025 \times \frac{1000}{5/6} \frac{4.92^2}{64.4} = 11.3 \text{ ft}$$

$$\Delta p = \frac{11.3 \times 62.4}{144} = 4.9 \text{ psi}$$

Conduits of Noncircular Cross Section

The Darcy–Weisbach equation may also be applied to noncircular conduits if the diameter D is replaced by some equivalent linear measure of the cross section. The hydraulic radius R , widely used in open-channel equations, can be related to D for the circular cross section; this relationship is usually assumed to be a valid replacement of D in the pipe formula. The hydraulic radius is defined as the ratio of the cross-sectional area to the wetted perimeter. For a circular cross section

$$R = \frac{\pi D^2/4}{\pi D} = \frac{D}{4} \quad (141)$$

Hence the diameter may be replaced by four times the hydraulic radius in the Reynolds number, the relative roughness, and the resistance equation; the resistance equation becomes

$$h_f = f \frac{L}{4R} \frac{V^2}{2g} \quad (142)$$

Although satisfactory for conduits that are reasonably comparable to pipes in cross-sectional form, this equation cannot be expected to give accurate results for cross sections that are at great variance therefrom.

Example 5

Find the head loss per 1000 ft for a flow of 200 gpm of water through a clear cast-iron conduit of rectangular cross section 3 in. by 6 in.

$$R = \frac{3 \times 6}{12 + 6} = 1 \text{ in.} = \frac{1}{2} \text{ ft}$$

$$Q = \frac{200}{7.48 \times 60} = 0.446 \text{ ft}^3/\text{s}$$

$$V = \frac{0.446}{18} \times 144 = 3.57 \text{ ft/s}$$

Taking $\nu = 1.2 \times 10^{-5} \text{ ft}^2/\text{s}$

$$\text{Re} = \frac{V4R}{\nu} \approx 99,000$$

$$\frac{k}{D} = \frac{k}{4R} = \frac{0.00085}{4/12} = 0.00255$$

From Fig. 37, $f = 0.025$; hence

$$h_f = f \frac{L}{4R} \frac{V^2}{2g} = \frac{0.025 \times 1000}{4 \times \frac{1}{12}} \frac{3.57^2}{64.4} = 14.88 \text{ ft}$$

7.3 Minor Losses

Minor losses are the second type of friction losses and are caused by flow separation, eddies, and excessive turbulence beyond that occurring as a result of normal pipe friction. While the losses occur over a finite length of pipe, they are usually assumed to be concentrated at the location of the causative valve, fitting, and so on. This definition is depicted in Fig. 38.

The formula for minor losses of all kinds is generally of the form

$$h_m = K_L \frac{V^2}{2g} \quad (143)$$

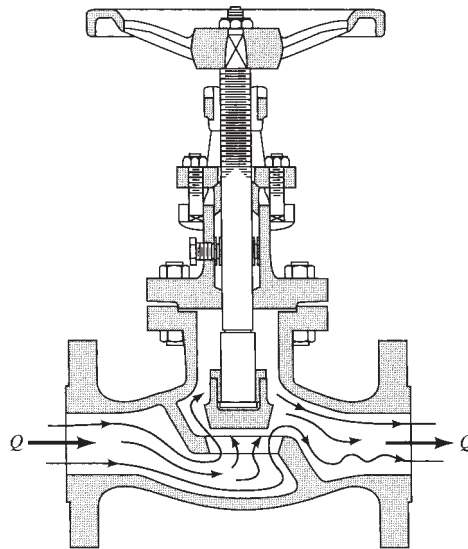


Figure 38 Depiction of flow through valve illustrating causes of minor losses. (From Ref. 2.)

Table 7 Loss Coefficients for Enlargements and Contractions Based on Velocity in Small Pipe

Diameter Ratio	0	0.1	0.2	0.3	0.4	0.5	0.6	0.7	0.8	0.9	1.0
Contraction K_L	0.5	0.48	0.45	0.42	0.38	0.34	0.29	0.22	0.12	0.04	0.0
Enlargement K_L	1.0	0.98	0.92	0.83	0.70	0.57	0.40	0.26	0.12	0.04	0.0

Source: Courtesy of Crane Company.⁸

Table 8 Selected Minor Loss Coefficients

Minor Loss Device	K_L	Minor Loss Device	K_L
Pipe entrances		Valves	
Inward projecting	0.78	Globe	$340f^a$
Sharp edged	0.50	Angle	$145f$
Slightly rounded	0.23	Ball or plug	$3f$
Well rounded	0.04	Butterfly	$40f$
Pipe exits (all types)	1.00	Gate (fully open)	$13f$
Bends		(75% open)	$35f$
90° miter bends	$58f^a$	(50% open)	$160f$
45° miter bends	$15f$	(25% open)	$900f$
Fittings			
90° standard elbow	$30f^{17}$		
45° standard elbow	$16f$		

^a f is friction factor for pipe.

Source: Courtesy of Crane Company.⁸

where h_m is the minor head loss, K_L is the loss coefficient whose value depends on the device causing the loss, and V is the velocity of flow in the smaller pipe. Virtually all hydraulics or fluid mechanics textbooks have tables of loss coefficients for various types of devices. In addition, Davis and Sorensen⁵ list several tables of K_L values. The reference book published by the Crane Company⁸ is also a good source for loss coefficients, and a selection of K_L values for common situations has been presented in Tables 7 and 8. For an exhaustive collection of loss coefficients, see Idelchik.⁹

To demonstrate the use of the tables and a complete friction loss situation in pipeline analysis, the following example is presented.

Example 6

A series of pipes connecting two reservoirs composed of 150-ft-long 12-in. pipeline and 8-ft-long 6-in. pipeline conveys water at 50°F between two reservoirs. The pipes are asphalted cast iron and the entrance to the pipe is sharp edged. Compute the discharge in the pipeline.

Before starting the solution to the problem, it is useful to classify the various losses that are going to be acting on the flow:

$$h_{m_{en}} = \text{minor loss at sharp - edged entry to pipeline}$$

$$h_{f_{12}} = \text{friction loss in 12 - in. pipe}$$

$$h_{m_c} = \text{minor loss at connection between 12 - and 6 - in. pipes}$$

$$h_{f_6} = \text{friction loss in 6 - in. pipe}$$

$$h_{m_{ex}} = \text{minor loss at exit from pipeline}$$

When the discharge is unknown, a flow velocity must be estimated to permit calculating Re and finding an f value.

Assume the velocity in the 12-in. pipe is 7 ft/s. From Table 6

$$v = 1.41 \times 10^{-5} \text{ft}^2/\text{s}$$

$$Re_{12} = \frac{VD}{\nu} = \frac{7 \times 1.0}{1.41 \times 10^{-5}} = 496,000$$

$$Re_6 = \frac{28 \times 0.5}{1.41 \times 10^{-5}} = 993,000$$

From Table 6

$$k = 0.0048 \text{ in.}$$

$$\left(\frac{k}{D}\right)_{12} = \frac{0.0048}{12} = 0.0004$$

$$\left(\frac{k}{D}\right)_6 = \frac{0.0048}{6} = 0.0008$$

From Fig. 36

$$f_{12} = 0.017f_6 = 0.019$$

From the work–energy equation

$$z_1 + \frac{p_1}{\gamma} + \frac{V_1^2}{2g} = z_2 + \frac{p_2}{\gamma} + \frac{V_2^2}{2g} + \sum h_{L_{1-2}}$$

$$4230 + 0 + 0 = 4200 + 0 + 0 + \sum h_{L_{1-2}}$$

$$\sum h_{L_{1-2}} = 30$$

Summarizing frictional head losses,

$$\sum h_{L_{1-2}} = h_{m_{en}} + h_{f_{12}} + h_{m_c} + h_{f_6} + h_{m_{ex}}$$

From Table 7

$$h_{m_{en}} = 0.5 \frac{V_{12}^2}{2g} h_{m_r} = 0.34 \frac{V_6^2}{2g}$$

$$h_{m_{ex}} = 1.0 \frac{V_6^2}{2g}$$

$$\sum h_{L_{1-2}} = 0.5 \frac{V_{12}^2}{2g} + 0.017 \times \frac{150}{1.0} \frac{V_{12}^2}{2g} + 0.34 \frac{V_6^2}{2g}$$

$$+ 0.019 \times \frac{8}{6/12} \frac{V_6^2}{2g} + 1.0 \frac{V_6^2}{2g}$$

From continuity considerations

$$V_6 = 4V_{12}$$

$$\sum h_{L_{1-2}} = (0.5 + 2.55 + 5.44 + 4.86 + 16.0) \frac{V_{12}^2}{2g}$$

Solving for V_{12} ,

$$29.35 \frac{V_{12}^2}{2g} = 30$$

$$V_{12} = 8.11 \text{ fps} \quad V_6 = 32.45 \text{ fps} \quad Q = 6.37 \text{ cfs}$$

Now a check must be made on the accuracy of the initial assumption used to find the f values:

$$r/Re_{12} = 575,000f_{12} = 0.0169$$

$$Re_6 = 1,150,000f_6 = 0.0190$$

Because these values are as close to the initial estimates as one could reasonably expect, we will consider the first estimates as the final values.

Another form of expressing minor losses is often used by the manufacturers of valves. This formula is

$$Q = C_v \sqrt{\Delta p} \quad (144)$$

where C_v is the flow coefficient for the valve in question and Δp and Q are expressed in psi (pounds per square inch) and gpm (gallons per minute), respectively. Of course, C_v and K_L measure the same thing. They are approximately related by the equation

$$K_L = \frac{890}{C_v^2} D^4 \quad (145)$$

for the units already described with diameter expressed in inches.

Transitions are sections of conduit that connect one prismatic portion to another by a gradual change in cross section. Since, owing to the inherent stability of accelerated flow, losses are small in gradual contractions, transition design is usually determined by factors other than energy loss. For example, it is often important that the pressure decrease continuously to that of the reduced section, so that the sections will be both *separation proof* and *cavitation proof*.

In expanding transitions or diffusers, wherein kinetic energy is converted into potential energy, it is even more essential that separation be avoided. The slowly moving fluid near the wall, which is retarded by surface resistance, is also retarded by the adverse pressure gradient due to the flow expansion. If the adverse pressure gradient acts over a sufficient length, it is certain to result in boundary layer separation. Once separation occurs, with the backflow and eddies that accompany it, the losses become high. A series of experiments was conducted by Gibson¹⁰ on conical diffusers, the results of which are shown in Fig. 39.

7.4 Steady-State Pipeline Analysis

The design situation in pipelines is generally that of selecting a pipe diameter that will convey a prescribed amount of discharge between two locations of known elevation with specified reservoir surface elevations or pressure requirements. The attractiveness of the Hazen–Williams and Manning formulas is immediately clear because, if minor losses are neglected, both formulas

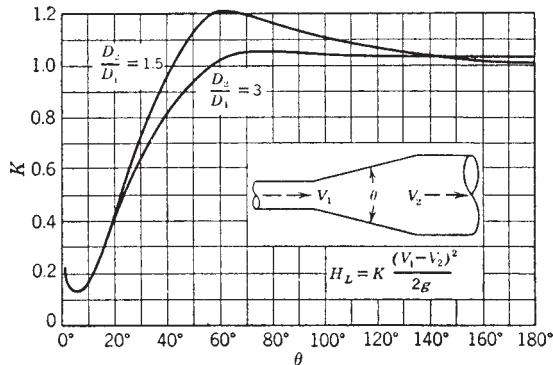


Figure 39 Loss coefficients for conical diffusers.

lead to direct solutions for the required diameter. Use of the Darcy formula requires several iterations beginning with an assumed diameter and ending with a final check on f , Re , and k/D to ensure all are consistent in the final solution. Techniques and skills can be developed to streamline this Darcy equation to determine head loss in a variety of systems with the purpose of refamiliarizing the reader with the techniques.

Single Pipelines

Single-pipeline problems are solved by applying the work–energy equation between two points of known energy levels. An example best illustrates the procedure.

Example 7

An 18-in. welded steel pipeline 1200 ft long connects two reservoirs differing in elevation by 20 ft (see Fig. 40). The pipe has a sharp-edged entrance and a wide-open globe valve at the downstream end near the location where it enters the lower reservoir. Find the flow rate in the pipe. From the work–energy equation,

$$z_1 + \frac{p_1}{\gamma} + \frac{V_1^2}{2g} = z_2 + \frac{p_2}{\gamma} + \frac{V_2^2}{2g} + \sum h_{L_{1-2}}$$

Using the lower reservoir surface as a datum,

$$20 + 0 + 0 = 0 + 0 + 0 + \sum h_{L_{1-2}}$$

where $\sum h_{L_{1-2}}$ = (entrance + friction + valve + exit) losses. From Tables 7 and 8,

$$\begin{aligned} \sum h_{L_{1-2}} &= 0.5 \frac{V^2}{2g} + f \frac{L}{D} \frac{V^2}{2g} + 340f \frac{V^2}{2g} + \frac{V^2}{2g} \\ &= \left(0.5 + f \frac{L}{D} + 340f + 1.0 \right) \frac{V^2}{2g} \end{aligned}$$

From Table 6

$$k = 0.0018 \frac{k}{D} = 0.0001$$

From Table 3

$$V \approx 8 \text{ ft/s} \quad Re = \frac{8 \times 1.5}{1.2 \times 10^{-5}} = 1 \times 10^6$$

From Fig. 36, $f = 0.0135$. Substituting into the preceding work–energy equation,

$$\begin{aligned} 20 &= 0 + \left(0.5 + 0.0135 \times \frac{1200}{1.5} + 340 \times 0.0135 + 1.0 \right) \frac{V^2}{2g} \\ &= (0.5 + 10.8 + 4.6 + 1.0) \frac{V^2}{2g} \\ &= 16.9 \frac{V^2}{2g} \\ V &= 8.73 \text{ ft/s} \end{aligned}$$

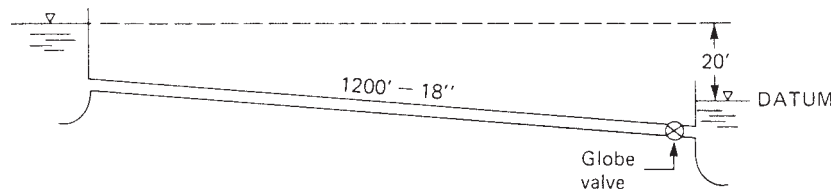


Figure 40 Diagram for Example 7. Source: By permission from G. Z. Watters, *Analysis and Control of Unsteady Flow in Pipelines*, Stoneham, MA, 1984.

Checking on initial assumptions,

$$\text{Re} = \frac{8.73 \times 1.5}{1.2 \times 10^{-5}} = 1.1 \times 10^6$$

$$f = 0.0135 \quad (\text{so solution is acceptable})$$

$$Q = AV = 0.7854 \times 1.5^2 \times 8.73$$

$$Q = 15.4 \text{ ft}^3/\text{s} \text{ or } 6927 \text{ gpm}$$

Series pipelines, that is, pipelines of different diameters connected end to end, are handled in a manner similar to the previous example. It is only required that the single-pipe friction term be replaced by a summation of the pipe friction losses in each of the pipes, including the additional minor losses between pipes.

Single Pipelines with Pumps

The pumped pipeline is a common design situation with which engineers are confronted. Pumps occur at the upstream end of pipelines (source pumps) and at intermediate locations in the pipeline (booster pumps). In each case, the discharge through the pump and the head increase across the pump are affected by the pipe system in which the pump is installed.

To analyze pumped pipelines, the work-energy equation must be modified to include the energy added by the pump:

$$z_1 + \frac{p_1}{\gamma} + \frac{V_1^2}{2g} + H_p = z_2 + \frac{p_2}{\gamma} + \frac{V_2^2}{2g} + \sum h_{L_{1-2}} \quad (146)$$

where H_p is the energy added to each pound of liquid passing through the pump. In the case of series or multistaged pumps, H_p is the sum of the head increases across each pump or stage.

The head increase across a pump is a function of discharge through the pump and is determined experimentally by the manufacturer. The information is presented graphically on a diagram known as the characteristic diagram. Information on the power requirements and pump efficiencies at varying discharges is also included. An example of a typical pump characteristic diagram is shown in Fig. 41.

Because power requirements for a pumping situation are of interest, it is important to establish the relation between energy added (H_p) and brake horsepower required. The power added to the liquid by the pump can be expressed as

$$\text{WHP} = \frac{Q\gamma H_p}{550} \quad (147)$$

where WHP is the horsepower added to the water. Of course, a greater amount of power must be added to the pump shaft because of friction and other losses in the pumping process. The power that must be supplied to a pump shaft (brake horsepower, BHP) in order to provide a given WHP is related to the hydraulic parameters by the equation

$$\text{BHP} = \frac{Q\gamma H_p}{550\eta} \quad (148)$$

where η is the overall pump efficiency. Both overall pump efficiency and brake horsepower are displayed on the pump characteristic diagram in Fig. 41.

Two examples follow that demonstrate the use of the characteristic diagrams in pipeline analysis.

Example 8

A single-stage pump with the characteristics shown in Fig. 41 (curve A) is used to pump water from a reservoir of elevation 1350 ft to another reservoir at elevation 1400 ft. The line is 6000 ft long and 24 in. in diameter with an f value of 0.021.

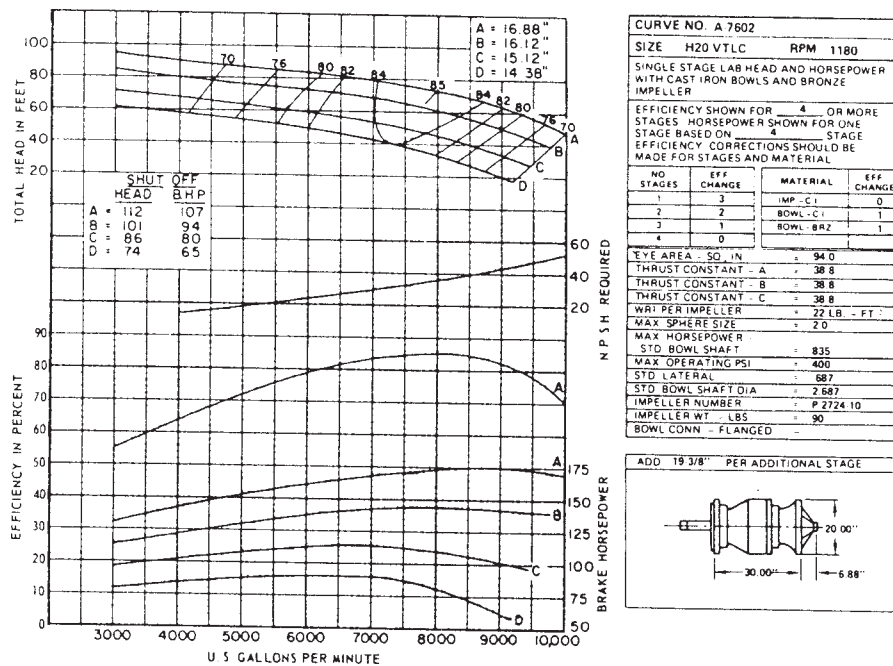


Figure 41 Typical pump characteristics diagram for vertical turbine pump. (Courtesy of Allis-Chalmers.)
 Source: By permission from G. Z. Waters, *Analysis and Control of Unsteady Flow in Pipelines*, Butterworth, Stoneham, MA, 1984.

Neglecting minor losses, compute the discharge in the pipeline. From the work-energy equation

$$z_1 + \frac{p_1}{\gamma} + \frac{V_1^2}{2g} + H_p = z_2 + \frac{p_2}{\gamma} + \frac{V_2^2}{2g} + \sum h_{L_{1-2}}$$

$$1350 + 0 + 0 + H_p = 1400 + 0 + 0 + f \frac{L}{D} \frac{V^2}{2g}$$

$$H_p = 50 + 0.021 \times \frac{6000}{2} \frac{V^2}{2g}$$

$$= 50 + 63.0 \frac{V^2}{2g}$$

This equation must be solved by trial in conjunction with the head-versus-discharge characteristic for the pump given in Fig. 41. In the solution process we neglect losses in the pump discharge column and head, which would normally be included in an analysis.

The solution is best approached using a trial solution table:

Assume Q (gpm)	V (ft/s)	$\frac{V^2}{2g}$	$63 \frac{V^2}{2g}$	RHS ^a	H_p (ft) ^a
8000	5.67	0.50	31.5	81.5	73
7000	4.96	0.38	24.1	74.1	79
7500	5.32	0.44	27.7	77.7	76
7400	5.25	0.43	26.9	76.9	77

^aRight-hand side $(50 + 63.0V^2/2g)$.

The solution is $Q = 7400$ gpm.

Example 9

Solve the problem of Example 8 if two three-stage parallel pumps with curve C characteristics were employed.

The pipeline analysis would remain the same:

$$H_p = 50 + 63.0 \frac{V^2}{2g}$$

However, H_p is now the total head put out by the three stages in each pump. Also the pipeline discharge must be halved to obtain the amount passing through each pump.

The resulting trial solution table is as follows:

Assume Pump Q (gpm)	Q_{pipe}	V (ft/s)	$\frac{V^2}{2g}$	RHS	H_p /stage	H_p (ft)
7000	14,000	93	1.53	146	54	159
7500	15,000	10.63	1.76	161	50	150
7250	14,500	10.28	1.64	153	51	153

The solution is $Q = 7250$ gpm.

7.5 Pipe Network Analysis

The steady-state analysis of flows in pipe networks can be a very complex problem. Devices such as pressure-reducing valves, minor losses, booster pumps, and supply pumps, as well as reservoirs, all serve to complicate the analysis. The subject is covered comprehensively by Jeppson,¹¹ and the reader is referred to that text for detailed information. The presentation here will be introductory and will apply only to relatively simple systems. However, we shall discuss all three of the most popular analysis methods—the Hardy Cross method, the linear theory method, and the Newton—Raphson method. In addition, a good summary of the application of these three methods is given by Wood and Rayes.¹²

Hardy Cross Method

Because of its simplicity of application, its easily understood theory, and its amenability to hand calculation, the Hardy Cross method has enjoyed (and still enjoys) considerable popularity among practicing engineers.

The first step is to estimate flow rates in all the pipes in a network so that continuity is satisfied at each junction (node). Of course, it is unlikely that the energy line (EL) and hydraulic grade line (HGL) are continuous throughout the network because the original estimates of the flow rates are always erroneous to some degree. This method assumes that there can be found a unique flow rate adjustment that can be applied to each loop in the network that will cause the EL–HGL to be continuous around each loop. In hydraulic terms this continuity is expressed as

$$\sum_{i=1}^N h_{L_i} = 0 \quad (149)$$

around each loop where i is the pipe number and N is the number of pipes in the loop. Assuming that the head loss can be written in the form

$$h_{L_i} = K_i Q_i^n \quad (150)$$

and assuming a correction ΔQ is being added to each pipe flow in the loop to satisfy the requirement that the sum of the head loss equals zero, this equation becomes

$$\sum_{i=1}^N K_i (Q_i + \Delta Q)^n = 0 \quad (151)$$

where Q_i is the most recent estimate for the discharge in each pipe in the loop. It remains only to solve for ΔQ .

Because n is generally a noninteger, the preceding is generally expanded by the binomial theorem to yield an equation for ΔQ . Retaining only the first two terms of the binomial expansion, the following equation for ΔQ is derived:

$$\Delta Q = \frac{\sum_{i=1}^N K_i Q_i^n}{-n \sum_{i=1}^N K_i Q_i^{n-1}} \quad (152)$$

To produce the proper sign on ΔQ , the denominator is kept negative and the terms in the summation in the numerator are positive or negative, depending on whether one moves with or against the flow while proceeding clockwise around the loop.

Once the ΔQ is computed for each loop, it is added (or subtracted) from the flow rates in each member of the loop to get a better estimate of the true flow rate. Because the decomposition of $(Q_i + \Delta Q)^n$ with the binomial theorem was not exact and because pipes that are common to more than one loop have multiple ΔQ corrections, the calculated ΔQ 's will not be correct. Therefore, the process is iterative and must be continued until the error is acceptably small (or no convergence to a solution occurs).

Although this numerical method is not so sophisticated as the other methods, the results are just as valid, provided convergence is obtained. Actually, a more careful investigation would reveal that Hardy Cross analysis is a decoupled Newton–Raphson analysis.

Linear Theory Method

The linear theory method is a technique for solving a set of network equations, some of which are nonlinear, for the unknown flow rates in the pipes. The equations are generated by writing continuity equations for flow into and out of each junction and by specifying that the algebraic sum of the head losses around each loop is zero. Solving a set of nonlinear equations is an iterative process and there are many techniques for doing this. In the linear theory approach the nonlinear equations for the sum of the head losses around each loop are linearized. Then the complete set of linear equations (the continuity equations are already linear) is solved.

To understand how the procedure works, look at the equations involved. For each loop in the network the following equation is valid:

$$\sum_{i=1}^N h_{L_i} = \sum_{i=1}^N K_i Q_i^n = 0 \quad (153)$$

where N is the number of pipes in the loop. To linearize this equation, Q_i^n is decomposed into two parts so that this equation becomes

$$\sum_{i=1}^N (K_i Q_i^{n-1}) Q_i = \sum_{i=1}^N K'_i Q_i = 0 \quad (154)$$

Of course K'_i is now a function of Q_i , so the process is still iterative.

As the set of linear-plus-linearized equations is successively solved, the estimate of K'_i is revised after each solution. After several iterations the values of Q_i and K'_i should converge to their final values. The mathematical form of the iteration equation is

$$\sum_{i=1}^N K_i [Q_i^{(j-1)}]^{n-1} Q_i^j = 0 \quad (155)$$

where j is the iteration number. For example, if we are making the eighth iteration ($j = 8$), then we would calculate K'_i 's from the results of the seventh iteration.

Experience with the linear theory has shown that the numerical solution tends to oscillate around the final values. To damp out this numerical oscillation, the iteration equation is altered to include the last two iterations for Q_i in computing K'_i :

$$\sum_{i=1}^N K_i \left[\frac{Q_i^{(j-1)} + Q_i^{(j-2)}}{2} \right]^{n-1} Q_i^{(j)} = 0 \quad (156)$$

When starting an analysis, only the direction of flow (not the quantity) has to be specified. This is a substantial savings in effort over the Hardy Cross approach. For the first iteration $K'_i^{(1)}$ is assumed to be equal to K_i . For the second iteration $K'_i^{(2)}$ will equal $K_i [Q_i^{(1)}]^{n-1}$. Thereafter, Eq. 156 will be used for each loop.

Newton–Raphson Method

The Newton–Raphson technique has the same conceptual basis as the Hardy Cross method. Flow rates in each pipe are assumed that satisfy continuity, and these flow rates are corrected so that the sum of the head losses around each loop approaches zero. In the Hardy Cross method the flow rates in each pipe are corrected after each ΔQ computation. In the Newton–Raphson method the equations containing ΔQ are written for each loop; then this nonlinear set of equations is solved successively for the final value of ΔQ in each loop. When the solution is complete, only then are the initial flow rates in each pipe adjusted to their final value.

The method gets its name from the technique used to solve the nonlinear set of equations. The Newton–Raphson technique is a frequently used, powerful method of numerical analysis. In operation, it adjusts successive approximations to the solution by computing the way the solution is moving with respect to each variable and then, based on that computation, calculates new trial values for the unknowns.

The Newton–Raphson technique in two or more dimensions (two or more equations with two or more unknowns) is most conveniently expressed in matrix form,

$$\{F^{(j-1)}\} + [\mathbf{J}^{(j-1)}]\{x^{(j)} - x^{(j-1)}\} = \{0\} \quad (157)$$

where \mathbf{J} is a $K \times K$ matrix of $\partial F^{(j-1)} / \partial x_k$ known as the Jacobian. Converting this to another form,

$$\{x^{(j)}\} = \{x^{(j-1)}\} - [\mathbf{J}^{(j-1)}]^{-1} \{F^{(j-1)}\} \quad (158)$$

Because all the F_k can be differentiated, the Jacobian can be evaluated at each new approximation for x_i and the inverse computed. However, this is a very large computational task for large systems of equations; hence, a slightly different approach is employed when working with hydraulic networks.

In hydraulic networks,

$$F_k = \sum_{i=1}^N K_i Q_i^n = 0 \quad (159)$$

However, because the Q_i 's are unknown, a value in each pipe must be estimated and a search for ΔQ 's, which will correct the Q_0 's to the proper value, must be made. The loop equations now are of the form

$$F_k = \sum_{i=1}^N K_{L_i} \left[Q_{0_i} + \sum_{l=1}^K \Delta Q_l \right]^n = 0 \quad k = 1, K \quad (160)$$

because any pipe in a given loop may be a member of other loops and their ΔQ 's must be included. Then, in general,

$$F_k(\Delta Q_1, \Delta Q_2, \dots, \Delta Q_k) = 0 \quad k = 1, K \quad (161)$$

If $\Delta Q^{(j)} - \Delta Q^{(j-1)}$ is now represented as $\delta Q^{(j)}$ in each loop, then

$$[\mathbf{J}^{(j-1)}]\{\delta Q^{(j)}\} = -\{F^{(j-1)}\} \quad (162)$$

This equation is now solved for $\{\delta Q^{(j)}\}$ and

$$\{\Delta Q^{(j)}\} = \{\Delta Q^{(j-1)}\} + \{\delta Q^{(j)}\} \quad (163)$$

after each iteration. When the δQ 's become small enough, an acceptable solution has been obtained.

It should be noted here that this method only requires the solution to a set of equations equal in number to the number of loops. The linear theory must solve a set of equations equal in number to the number of unknown flow rates. Consequently, the Newton–Raphson technique may require substantially less storage space for solution.

7.6 Unsteady Flow in Pipe Systems

Unsteady flow in pipe systems is important because it can result in serious problems. Some of these are:

1. Pipe rupture
2. Pipe collapse
3. Vibration
4. Excessive pipe displacements
5. Pipe fitting and support deformation or failure
6. Vapor cavity formation (cavitation, column separation)

Some of the primary causes of unsteady flow are:

1. Valve closure (or opening)
2. Flow demand changes
3. Pump shutdown (or power failure to the pump)
4. Pump startup
5. Air venting from lines
6. Failure of flow or pressure regulators
7. Pipe rupture

Unsteady flow analysis in pipe systems is generally divided into two categories:

1. Rigid water column theory (surge theory) where the fluid and pipe are inelastic, pressure changes propagate instantaneously, and the differential equation of motion is “ordinary”
2. Elastic theory (water hammer) where the elasticity of fluid and pipe affect pressure changes, pressure changes propagate with wave speed a (1000–4700 ft/s), and the differential equations of motion are partial and nonlinear

A simple problem is used to demonstrate phenomena and introduce concepts. A steady flow situation is shown in Fig. 42 where velocity V is caused by head H in reservoir. Friction is neglected and the EL and HGL are coincident because water hammer pressures are large compared to velocity head.

The valve is closed suddenly causing a pressure head to propagate upstream at speed a . The sequence of events shown in Fig. 42 are as follows:

1. Pressure head increase ΔH reaches reservoir at L/a seconds. Velocity = 0 and pressure head = $H + \Delta H$ throughout pipe. Pipe is stretched. Water is compressed.

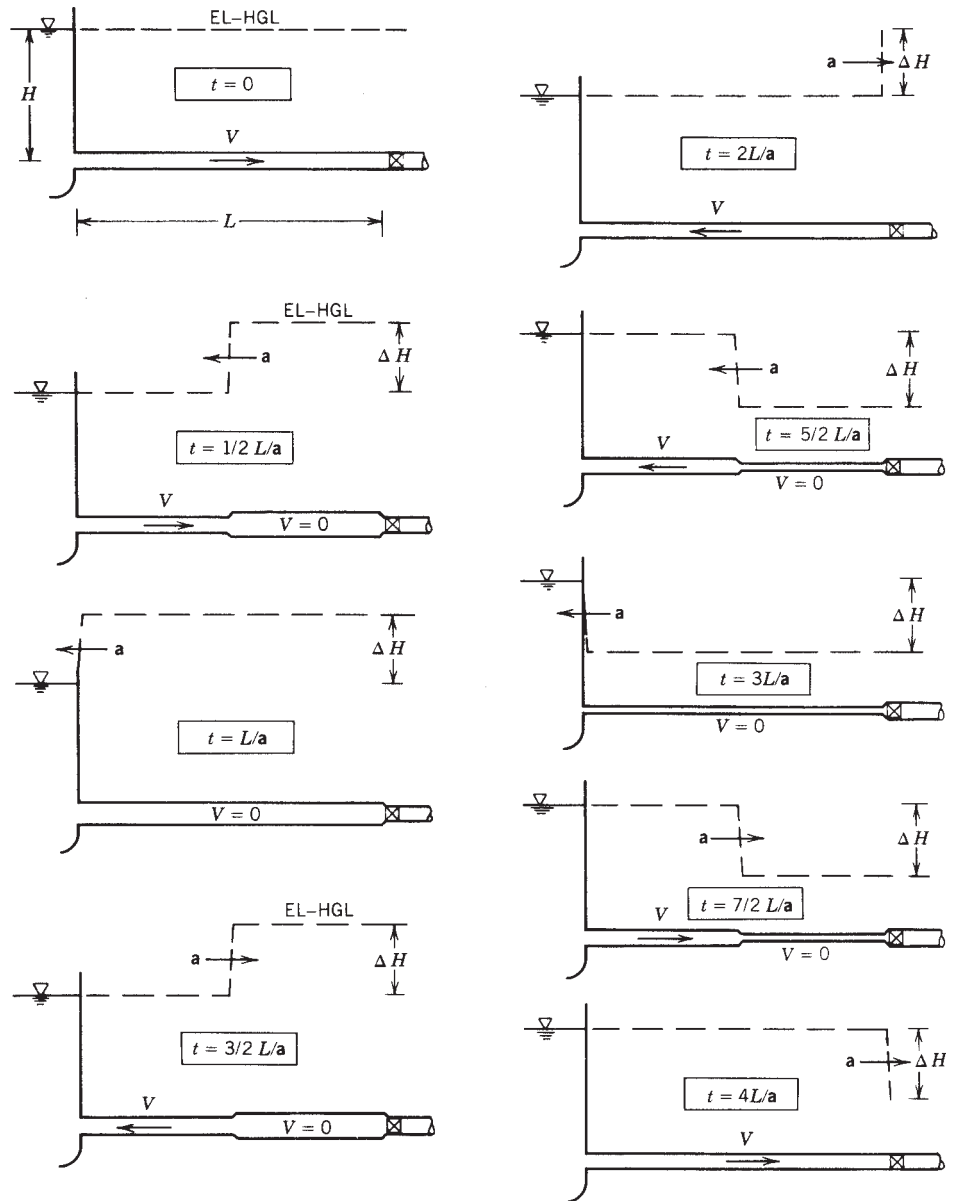


Figure 42 Pressure wave propagation in simple pipe system. *Source:* By permission from G. Z. Watters, *Analysis and Control of Unsteady Flow in Pipelines*, Butterworth, Stoneham, MA, 1984.

2. High pressure in pipe ejects water into reservoir. At $2L/a$ seconds, velocity = $-V$, pressure head = H throughout pipe.
3. Upstream flow suddenly stopped at valve. Negative wave propagates upstream. At $3L/a$ seconds, velocity = 0 , pressure head = $H - \Delta H$ throughout pipe.
4. High pressure in reservoir forces water into pipe giving downstream flow. At $4L/a$, velocity = V , pressure = H , and wave period is complete.

5. As long as valve remains closed, these cycles repeat. Any friction in system would cause damping of ΔH until it eventually disappears.

The following are important ideas:

1. L/a is an important time parameter in water hammer situations.
2. Pressure head at the valve reaches its maximum if the valve is closed in any time less than $2L/a$ seconds. Valve need not be suddenly closed to create maximum water hammer pressures.

Column Separation

When pressure change is severe enough to drop pressure in the pipe to the vapor pressure of water, "column separation" occurs. Dissolved gases come out of solution, water vapor cavities occur, and liquid columns "separate." Eventually cavity closure causes water hammer pressure "shocks" of a magnitude difficult to calculate and potentially destructive.

Column separation could be caused by simple valve closure. In Fig. 42, if ΔH were large enough, column separation would occur on both sides of the valve, although at different times.

Rigid Water Column Theory

This analysis uses Newton's second law, $F = ma$. For unsteady flow the equation is

$$\frac{P_1}{\gamma} - \frac{P_2}{\gamma} - \frac{fL}{2gD} V^2 = \frac{L}{g} \frac{dV}{dt} \quad (164)$$

where

- p = pressure
- f = Darcy–Weisbach friction factor
- L = pipe length
- γ = specific weight of water
- D = pipe diameter
- V = flow velocity
- g = acceleration of gravity
- dV/dt = liquid acceleration

Example 10

Flow establishment in a pipe. The physical situation is shown in Fig. 43 with free discharge at the valve.

The equation applied to this problem is

$$H_0 - \frac{fL}{2gD} V^2 = \frac{L}{g} \frac{dV}{dt}$$

This expression can be integrated in closed form. The time to reach steady flow is infinite. To reach 99% of V ,

$$t_{99} = 2.65 \frac{LV_0}{gH_0}$$

Pipe systems may not be single, constant-diameter pipes. The equivalent pipe technique may be used to reduce complex pipe systems to single pipes. Criteria for equivalence is friction loss equality and similar dynamic behavior. For series pipes

$$\left[\frac{fL}{D^5} \right]_{\text{eq}} = \sum_{i=1}^N \left[\frac{F_i L_i}{D_i^5} \right] \quad (165)$$

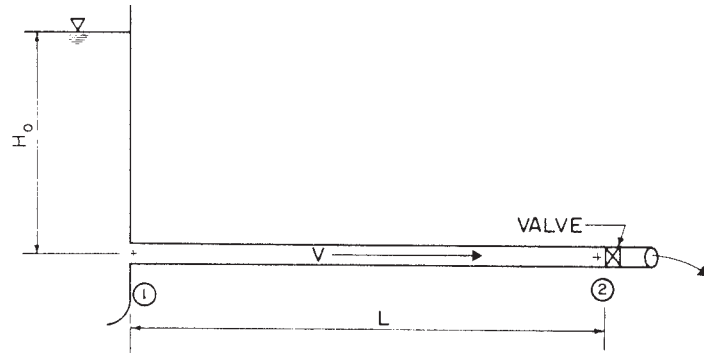


Figure 43 Simple system for applying rigid water column theory. *Source:* By permission from G. Z. Watters, *Analysis and Control of Unsteady Flow in Pipelines*, Butterworth, Stoneham, MA, 1984.

$$\left[\frac{L}{D^2} \right]_{\text{eq}} = \sum_{i=1}^N \left[\frac{L_i}{D_i^2} \right] \quad (166)$$

For parallel pipes

$$\left[\frac{D_{\text{eq}}^5}{F_{\text{eq}} L_{\text{eq}}} \right]^{1/2} = \sum_{i=1}^N \left[\frac{D_i^5}{f_i L_i} \right]^{1/2} \quad (167)$$

$$\left[\frac{D_{\text{eq}}^2}{L_{\text{eq}}} \right] = \sum_{i=1}^N \left[\frac{D_i^2}{L_i} \right] \quad (168)$$

Example 11

A three-unit pumped storage facility is shown in Fig. 44. Flow through the turbines is shut down so that penstock velocities decrease from 60 ft/s to zero linearly in 30 s. Compute p_{max} if the f value is the same for all pipes.

Using the parallel-pipe equations,

$$\frac{D_{\text{eq}}^2}{L_{\text{eq}}} = 3 \left(\frac{8^2}{800} \right) = 0.240 \left(\frac{D_{\text{eq}}^5}{L_{\text{eq}}} \right)^{1/2} = 3 \left(\frac{8^5}{800} \right)^{1/2} = 19.20$$

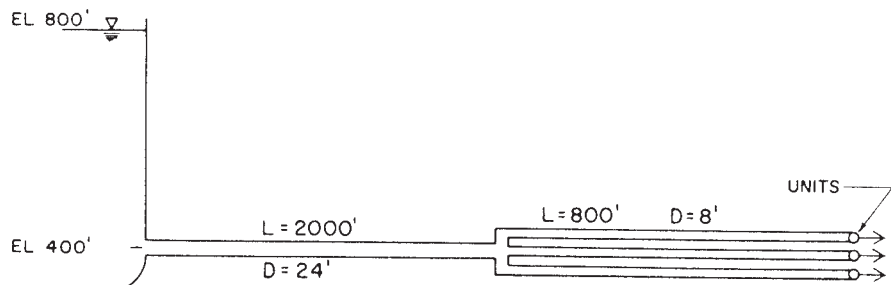


Figure 44 Schematic sketch of a pumped storage facility. *Source:* By permission from G. Z. Watters, *Analysis and Control of Unsteady Flow in Pipelines*, Butterworth, Stoneham, Mass., 1984.

The parallel pipes can be replaced by a single pipe $D = 11.54$ ft and $L = 555$ ft. Using the series-pipe equation,

$$\frac{L_{\text{eq}}}{D_{\text{eq}}^2} = \frac{2000}{24^2} + \frac{555}{11.54^2} = 7.64$$

$$\frac{L_{\text{eq}}}{D_{\text{eq}}^5} = \frac{2000}{24^5} + \frac{555}{11.54^5} = 0.00296$$

This series pipe is replaced by the single pipe $D = 13.71$ ft and $L = 1437$ ft. Steady flow velocity in the equivalent pipe is

$$V_{\text{eq}} = \frac{Q}{A_{\text{eq}}} = 61.3 \text{ ft/s}$$

From the unsteady flow equation,

$$400 - \frac{p_2}{\gamma} - \frac{fLV^2}{2gD} = \left(\frac{1437}{32.2} \right) \frac{0 - 61.3}{30}$$

$$\frac{p_2}{\gamma} = 400 + 91.2 - \frac{fLV^2}{2gD}$$

A maximum pressure head of 491 ft occurs at the instant the valve is completely closed.

Elastic Theory

Elastic theory includes the effect of water and pipe elasticity on pressures and velocities. The impulse–momentum equation and the conservation-of-mass equation are used.

The impulse–momentum equation is used to develop the equation for ΔH . The x component of the equation is

$$\left(\sum \mathbf{F}_{\text{ext}} \right)_x = Q\rho(V_{\text{out}} - V_{\text{in}}) \quad (169)$$

where the x direction is along the pipe, F_x are forces in the x direction, and Q is discharge.

To make the unsteady case steady, the coordinate system is moved along the pipe at the wave speed so the wave appears to be standing still. The resulting analysis gives

$$\Delta H = \frac{\mathbf{a}}{g} \Delta V \quad (170)$$

It is clear that ΔH depends on the wave speed \mathbf{a} . Conservation of mass is used to find an equation for wave speed. The result for thin-walled pipes is

$$\mathbf{a} = \frac{(K/\rho)^{1/2}}{[1 + (K/E)(D/e)(C)]^{1/2}} \quad (171)$$

where

K = bulk modulus of elasticity of liquid

E = modulus of elasticity of pipe

D = pipe diameter

e = pipe wall thickness

C = restraint coefficient

$C = \frac{5}{4} - \mu$ if pipe is free to stretch in longitudinal direction as a pressure vessel.

$C = 1 - \mu^2$ if no longitudinal stretching occurs.

$C = 1.0$ if functioning expansion joints occur, where μ is Poisson's ratio

Thin-walled pipes have D/e greater than about 40. Suggested values of E and μ are shown in Table 9.

Table 9 E and μ Values for Common Pipe Materials

Steel	$E = 30 \times 10^6 \text{ psi}$	$\mu \approx 0.30$
Ductile cast iron	$E = 24 \times 10^6 \text{ psi}$	$\mu \approx 0.28$
Copper	$E = 16 \times 10^6 \text{ psi}$	$\mu \approx 0.36$
Brass	$E = 15 \times 10^6 \text{ psi}$	$\mu \approx 0.34$
Aluminum	$E = 10.5 \times 10^6 \text{ psi}$	$\mu \approx 0.33$
Polyvinyl chloride	$E = 4 \times 10^5 \text{ psi}$	$\mu \approx 0.45$
Fiberglass-reinforced plastic (FRP)	$E_2 = 4.0 \times 10^6 \text{ psi}$ $E_1 = 1.3 \times 10^6 \text{ psi}$	$\mu_2 = 0.27 - 0.30$ $\mu_1 = 0.20 - 0.24$
Asbestos cement	$E \approx 3.4 \times 10^6 \text{ psi}$	$\mu \approx 0.30$
Concrete	$E = 57,000 \sqrt{f'_c}$ ^a	$\mu \approx 0.24$ (dynamically)

^aWhere f'_c = 28-day strength.

For water $(K/\rho)^{1/2} = 4720 \text{ ft/s}$. Most buried-pipe situations are close to $C = 1 - \mu^2$; however, for $\mu \approx 0.3$, the result is about the same regardless of restraint.

Example 12

A 10,000-ft pipe has $V = 10 \text{ ft/s}$ and a wave speed of 3220 ft/s. Compute head increase at a valve for sudden valve closure:

$$\Delta H = \frac{\mathbf{a}}{g} \Delta V = \frac{3220}{32.2} 10 = 1000 \text{ or } 433 \text{ psi}$$

Note that $L/\mathbf{a} = 3.1 \text{ s}$. If the valve is closed in less than 6 s, full water hammer pressure is developed.

The previous C values for thin-walled pipes must be modified when D/e is less than 40. For homogeneous pipes,

$$\text{Case (a): } C = \frac{1}{1 + e/D} \left[\left(\frac{5}{4} - \mu \right) + 2 \frac{e}{D} (1 + \mu) \left(1 + \frac{e}{D} \right) \right] \quad (172)$$

$$\text{Case (b): } C = \frac{1}{1 + e/D} \left[(1 - \mu^2) + 2 \frac{e}{D} (1 + \mu) \left(1 + \frac{e}{D} \right) \right] \quad (173)$$

$$\text{Case (c): } C = \frac{1}{1 + e/D} \times \left[1 + 2 \frac{e}{D} (1 + \mu) \left(1 + \frac{e}{D} \right) \right] \quad (174)$$

These C values are used in the wave speed equation to compute wave speed.

When air or other dissolved gases come out of solution and form small bubbles, wave speed is affected dramatically. This occurs because:

1. Low pressure at pipeline summit allows air release.
2. Pump sump is aerated by improper inflow design.

If the fraction of the air volume is known, the wave speed can be estimated from the following equation:

$$\mathbf{a} = \frac{\sqrt{K_l/\rho_{\text{ave}}}}{\sqrt{1 + (K_l/E)(D/e)C + (\text{void fraction})(K_l/K_a)}} \quad (175)$$

Amounts of air as low as 0.5% can reduce wave velocity to 25% of its unaerated value.

The previous approach permits calculation of pressure head increase at a point where velocity changes suddenly. Generally, it is necessary to find head H and velocity V at any section of pipe system at any time t .

To accomplish this Newton's second law and conservation of mass are applied to a differential length of pipe through which the water hammer wave is passing. The result is two partial differential equations,

$$\frac{dV}{dt} + g \frac{\partial H}{\partial s} + \frac{1}{2} \frac{f}{D} V|V| = 0 \quad (176)$$

$$\frac{a^2}{g} \frac{\partial V}{\partial s} + V \left[\frac{\partial H}{\partial s} - \frac{\partial z}{\partial s} \right] + \frac{\partial H}{\partial t} = 0 \quad (177)$$

where s is the location along pipe and z is the elevation above datum.

This type of equation can be solved using the "method of characteristics." First, the equations are simplified by replacing dV/dt with $\partial V/\partial t$ and deleting $\partial H/\partial s$ in Eqs. 176 and 177. This approximation had been shown to have negligible effects on accuracy. If independent variables s and t follow certain relationship in Eqs. 176 and 177, namely

$$\frac{ds}{dt} = \pm a \quad (178)$$

then *partial* differential equations can be written as *total* differential equations:

$$C^+ : \frac{dV}{dt} + \frac{g}{a} \frac{dH}{dt} + \frac{f}{2D} V|V| = 0 \quad (179)$$

if

$$\frac{ds}{dt} = a \quad (180)$$

and

$$C^- : \frac{dV}{dt} = \frac{g}{a} \frac{dH}{dt} + \frac{f}{2D} V|V| = 0 \quad (181)$$

if

$$\frac{ds}{dt} = -a \quad (182)$$

Equations 180 and 182 are called the characteristics of the C^+ and C^- equations, respectively.

The physical meaning of C^+ , C^- and characteristic equations is that changes in pressure caused by disturbances (valve closing) propagate at wave speeds upstream and downstream in the pipe ($ds/dt = \pm a$). If this rule is followed, the partial differential equations become total differential equations. The equations are solved numerically as described in Watters,¹³ Wylie and Streeter,¹⁴ and Chaudhry.¹⁵

8 FLOW IN OPEN CHANNELS*

Flow in open channels is similar to that in pipes in that flow can be laminar or turbulent, can have smooth or rough boundaries, and be uniform or nonuniform. Open-channel flow has the one unique characteristic that the pressure is zero on the free surface. Laminar flow is quite rare and will not be addressed here. This work will consider primarily uniform and nonuniform flow in the turbulent rough boundary mode.

8.1 Uniform Flow

In steady uniform flow, the slope for channel bottom, free surface (hydraulic grade line), and energy grade line are the same ($\tan \theta$, Fig. 45). For very wide channels, the shear stress varies

* Illustrations and material all or in part from *Eshbach's Handbook of Engineering Fundamentals* (Hoboken, NJ: Wiley).

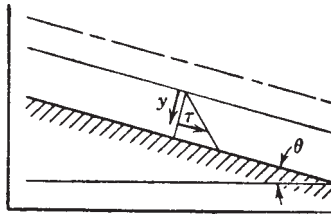


Figure 45 Uniform flow.

linearly with distance from the free surface y , given by $\tau = y\gamma \sin \theta$. For other channels, the average shear stress τ_0 at the solid boundary is $\tau_0 = \gamma R \sin \theta$, where R is the hydraulic radius, which is defined as the ratio of area of cross section A to wetted perimeter P . The liquid velocity at the solid boundary is zero; it increases generally with distance from a boundary. The maximum velocity is usually below the free surface.

The *Manning formula* is the most commonly used open-channel formula,

$$V = \frac{1.49}{n} R^{2/3} S^{1/2} \quad (183)$$

where V is the average velocity, R is the hydraulic radius, $S = \sin \theta$ (Fig. 45), and n is an absolute roughness factor, having the dimensions $L^{1/6}$, whose values for different surfaces are determined experimentally. Table 10 lists many of these values. Since the constant in the Manning formula is not dimensionless, it is necessary to use the foot–pound–second system of units.

Multiplying the formula by A ,

$$Q = \frac{1.49}{n} A R^{2/3} S^{1/2} \quad (184)$$

When the cross section is known, the equation may be solved directly for any one of the other quantities that is unknown. For determination of depth of flow in a given section, with Q , n , S given, the solution is affected by trial.

Example 13

Find the depth of flow in a trapezoidal channel of roughness 0.012, bottom width 10 ft, and side slopes 1:1 for 650 ft³/s. The channel slope is 0.000.

Writing

$$A R^{2/3} = \frac{A^{5/3}}{P^{2/3}}$$

from the Manning formula

$$\frac{Qn}{1.49S^{1/2}} = \frac{A^{5/3}}{P^{2/3}} = \frac{650 \times 0.012}{1.49 \times 0.03} = 174.7$$

$$A = 10D + D^2 \quad P = 10 + 2\sqrt{2}D$$

hence

$$f(D) = \frac{(100 + D^2)^{5/3}}{(10 + 2\sqrt{2}D)^{2/3}} = 174.7$$

Trying $D = 5$, $f(D) = 160$; hence D must be larger. Trying $D = 5.5$, $f(D) = 191$. By straight-line interpolation, $D = 5.24$, $f(D) = 174$, which is a satisfactory check. Hence $D = 5.24$ ft is the answer sought.

Table 10 Average Manning n Values for Selected Boundaries

Closed Conduits Flowing Partially Full	
Welded steel	0.012
Coated cast iron	0.013
Uncoated cast iron	0.014
Corrugated metal storm drain	0.024
Cement mortar	0.013
Concrete culvert	0.011
Finished concrete	0.012
Unfinished concrete (smooth wood form)	0.014
Vitrified sewer pipe	0.014
Lined open channels	
Painted steel	0.013
Cement mortar	0.013
Planed, untreated wood	0.012
Unfinished concrete	0.017
Gunite concrete (good)	0.019
Glazed brick	0.013
Cemented rubble	0.025
Smooth asphalt	0.013
Excavated channels	
Earth, straight, uniform and clean	0.018
Gravel, straight, uniform and clean	0.025
Earth with short grass and a few weeds	0.027
Dredged channel	0.028
Smooth rock cuts	0.035
Jagged rock cuts	0.040

Source: V. T. Chow, *Open Channel Hydraulics*, McGraw-Hill, New York, 1959.

The cross section having the least perimeter for given conditions is called the *most efficient* cross section. The semicircular section is the most efficient of all cross sections since it has the least perimeter for a given area. The most efficient *rectangular* channel has a bottom width twice the depth. The most efficient *trapezoidal* channel is half of a hexagon.

Specific Energy—Critical Depth

The mechanical energy per unit weight, with elevation datum taken as the bottom of the channel, is called *specific energy*. It is simply the sum of depth of flow and velocity head. In steady uniform flow, when all cross sections are identical, the specific energy is constant along the channel.

Referring to Fig. 46, the specific energy is

$$E = y + \frac{V^2}{2g} \quad (185)$$

assuming uniform distribution of velocity over the cross section. For a given discharge Q , the specific energy varies with the depth of flow. Substituting $V = Q/A$, where A is the

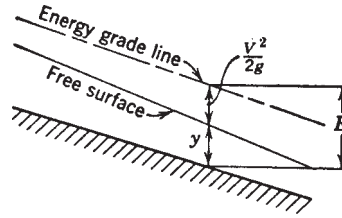


Figure 46 Specific energy.

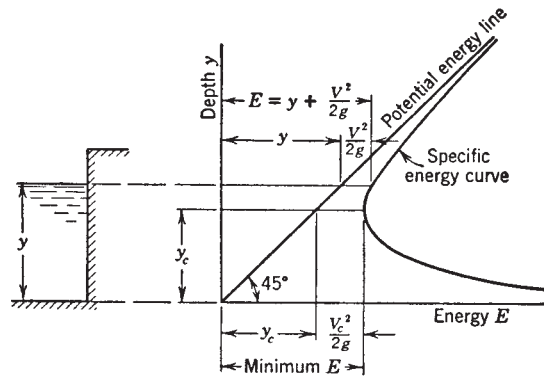


Figure 47 Specific energy diagram. (Courtesy of R. A. Dodge, University of Michigan, Ann Arbor.)

cross-sectional area and a function of y ,

$$E = y + \frac{Q^2}{2gA^2} \quad (186)$$

For a unit width of rectangular channel, with q the discharge per unit width,

$$E = y + \frac{q^2}{2gy^2} \quad (187)$$

A plot of specific energy against depth, Fig. 47, for a constant q , reveals that a certain minimum specific energy is required for the flow, found by setting $dE/dy = 0$. Calling this depth y_c the *critical depth*, we have

$$y_c = \left(\frac{q^2}{g} \right)^{1/3} \quad (188)$$

In terms of the velocity, $V_c = \sqrt{gy_c}$. Hence the critical depth is the depth at which the velocity of flow V_c is just equal to the velocity of an elementary wave \sqrt{gy} in still liquid. Greater specific energy is required for both greater and lesser depths of flow. It is obvious from Fig. 47 that there are two depths at which the flow has the same specific energy.

For nonrectangular channels the critical depth occurs when

$$\frac{Q^2}{g} = \frac{A^3}{b} \quad (189)$$

where b is the top width of the cross section at the liquid surface.

8.2 Steady, Nonuniform Flow

Gradually varied channel flow is steady flow in which changes in depth, section, slope, and roughness with respect to length along the channel are small. By assuming that the energy loss at any section is the same as in uniform flow at the same discharge and the same depth, a differential equation for change in depth as a function of distance along the channel can be developed:

$$\frac{dy}{dl} = \frac{S_0 - n^2 Q^2 / [(1.49)^2 A^2 R^{4/3}]}{1 - Q^2 b / (g A^3)} \tag{190}$$

where y is the depth, l the distance along the channel, S_0 the angle the bottom makes with the horizontal, n the Manning roughness factor, Q the discharge, A the cross-sectional area, R the hydraulic radius, and b the width of cross section at the liquid surface. Solving for l ,

$$l = \int \frac{1 - Q^2 b / (g A^3)}{S_0 - n^2 Q^2 / [(1.49)^2 A^2 R^{4/3}]} dy \tag{191}$$

For constant S_0 and n , the integrand is a function of y only, and l may be determined as a function of y , usually by numerical integration. When the integrand is zero, $Q^2 b / g A^3 = 1$, which is the condition for critical depth. Hence for a change in depth there is no change in l ; that is, neglecting the effects of the curvature of streamlines and the nonhydrostatic pressure distribution, the liquid surface is vertical as the flow goes through critical. When the denominator is zero, uniform flow occurs, and there is no change in depth along the channel.

The various possible free-surface profiles given by the preceding equation are shown in Fig. 48. In each case the flow is from left to right. Here, y_0 is the normal depth, that is, the depth given by the Manning uniform flow equation; y_c is the critical depth. When the normal depth is greater than the critical depth, the slope of the channel is *mild*; when normal depth equals critical depth, the slope is *critical*; when normal depth is less than critical depth, the slope is *steep*. The two other cases are *horizontal* and *adverse*.

The determination of surface profiles from the equation is affected by starting the numerical integration at a *control* section. When the flow is above critical depth, the control is always

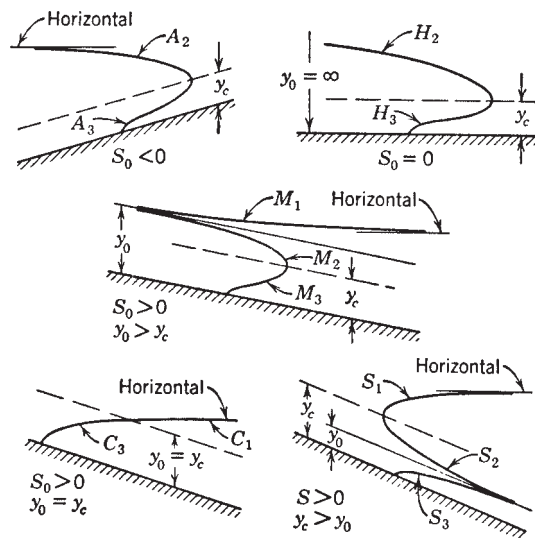


Figure 48 Surface profiles on adverse, horizontal, mild, critical, and steep slopes. (Courtesy of Hunter Rouse, State University of Iowa, Iowa City.)

downstream, and the depth is evaluated first for the control section, and then use is made of the gradually varied flow equation. Writing the equation in the form

$$l = \int F(y) dy$$

a plot of $F(y)$ as ordinate against y as abscissa is made, starting with the control depth and varying y in the direction indicated by the characteristic curves. This plot (Fig. 49) gives the value of l from the control section to the new depth y as the area under the curve between the values of y . In this manner the whole profile may be worked out.

When the depth of flow is less than critical, the control section is upstream (i.e., flow is out from under a gate), and the integration is handled in a similar fashion for determination of the profile downstream from the control.

A phenomenon known as the *hydraulic jump* occurs under certain conditions in channel flow. The flow prior to the jump must always be below the critical depth, and when the downstream depth is such that the momentum equation is satisfied for the liquid contained in the jump, the hydraulic jump will occur. The momentum equation applied to the liquid between sections 1 and 2 of Fig. 50 for a rectangular channel yields the relation between depths

$$D_2 = -\frac{D_1}{2} + \sqrt{\frac{2D_1V_1^2}{g} + \frac{D_1^2}{4}} \quad (192)$$

Examples of occurrence of the surface profiles, including situations where the jump results, are given in Fig. 51.

8.3 Unsteady, Nonuniform Flow

Any change in discharge in an open channel results in an unsteady nonuniform flow. The changes in flow result in gravity waves moving through the system. In certain cases, waves of fixed form propagate along the channel. The most common is the surge wave depicted in Fig. 52. In a rectangular channel, the celerity of the surge can be computed by the equation

$$c = \sqrt{gy_1} \left[\frac{1}{2} \frac{y_2}{y_1} \left(\frac{y_2}{y_1} + 1 \right) \right]^{1/2} \quad (193)$$

where c is the surge celerity relative to the undisturbed fluid velocity V_1 .

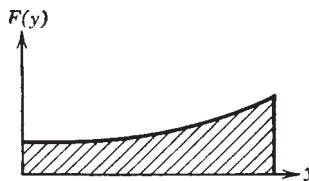


Figure 49 Plot for determination of liquid surface profile.

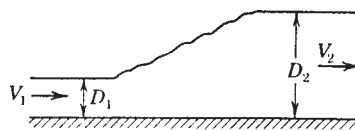


Figure 50 Hydraulic jump.

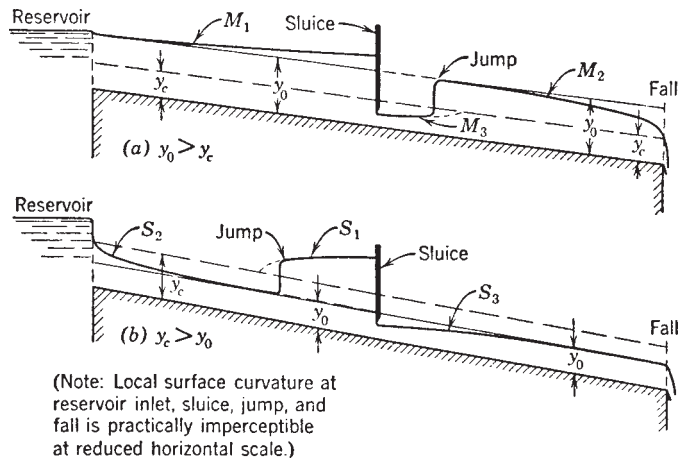


Figure 51 Examples of surface profiles. (Courtesy of Hunter Rouse, State University of Iowa, Iowa City.)

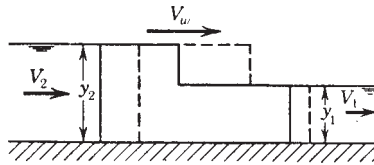


Figure 52 Surge wave.

There are other waves of fixed form, including the monoclinal rising flood wave, the solitary wave, and roll waves. All of these are the result of special flow or channel conditions and can be found in the literature.

The most general approach to open-channel unsteady flow is through a procedure similar to that used in pipe flow. The principles of continuity and momentum are employed to develop a pair of nonlinear partial differential equations:

$$\frac{\partial A}{\partial t} + V \frac{\partial A}{\partial x} + A \frac{\partial V}{\partial x} = q \tag{194}$$

$$g \frac{\partial y}{\partial x} + \frac{\partial V}{\partial t} + V \frac{\partial V}{\partial x} = g(S_0 - S_f) - \frac{V}{A} q \tag{195}$$

where

A = cross-sectional area

V = velocity of flow

y = depth of flow

S = slope of energy gradient

q = lateral inflow per unit length

In a manner similar to that in pipe flow these two equations can be transformed into ordinary differential equations so that

$$\frac{dV}{dt} + \frac{g}{c} \frac{dy}{dt} + g(S - S_0) + \frac{q}{A} (V + c) = 0 \tag{196}$$

if

$$\frac{dx}{dt} = V + c \quad (197)$$

and

$$\frac{dV}{dt} - \frac{g}{c} \frac{dy}{dt} + g(S - S_0) + \frac{q}{A}(V - c) = 0 \quad (198)$$

if

$$\frac{dx}{dt} = V - c \quad (199)$$

where c is $\sqrt{gA/b}$ and b is the surface width of the channel.

The equations can now be solved numerically by finite-difference methods. This application of the method of characteristics requires that considerable care be exercised to guarantee that the Courant condition-relating time step, length step, and wave celerity,

$$\Delta t \leq \frac{\Delta x}{|V| + c} \quad (200)$$

be satisfied. The work of Wylie and Streeter¹⁴ detail this general approach to the analysis of unsteady flow in open channels.

9 FLOW ABOUT IMMERSED OBJECTS

Flow about immersed objects has been discussed in Section 4 for the case of an ideal (frictionless) fluid. This section considers the effects of viscosity.

When a viscous fluid flows past an object, the fluid exerts a shear stress on the surface of the object as well as a normal pressure force. If the components of the surface shear and pressure in the direction of the flow are summed, the resulting force is known as the *drag*. The drag consists of a contribution from shear (skin friction drag) and pressure (form drag). In the case of well-formed bodies, the skin friction drag is the most significant. For blunt bodies, form drag dominates.

If the components of shear and pressure forces normal to the oncoming flow are summed, the *lift* on the body results. Typically, shear forces play a minor *direct* role on lift. Pressure is the dominant contributor. However, viscous forces can have a considerable indirect effect on lift and drag by causing boundary layer separation. It is common to represent lift L and drag D in terms of lift and drag coefficients:

$$D = C_D \frac{1}{2} \rho A V_o^2 \quad (201)$$

$$L = C_L \frac{1}{2} \rho A V_o^2 \quad (202)$$

where

C_D , C_L = drag and lift coefficients, respectively

ρ = fluid density

A = frontal area of object

V_o = free-stream velocity

In 1904 Prandtl developed the concept of the boundary layer and thus forged the link between ideal fluid mechanics and viscous flow. For fluids of relatively small viscosity, the effects of fluid friction are confined to a thin layer of fluid adjacent to the boundary known as the boundary layer. The flow outside the boundary layer can be determined with the tools of ideal fluid flow analysis. It is important to note that the boundary layer is thin and there is little normal acceleration; hence, the pressure variation along the body is determined, for all practical purposes, by the ideal fluid flow. This revelation led to the first analytical approach to the calculation of drag.

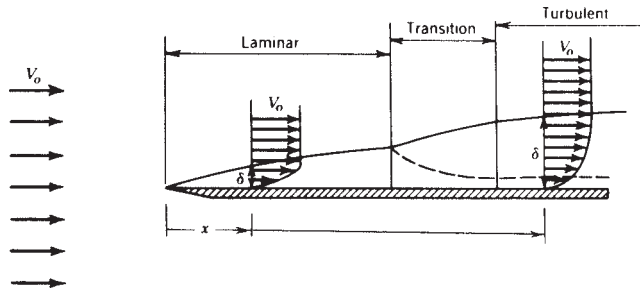


Figure 53 Boundary layers on flat plate. *Source:* By permission from J. K. Vennard and R. L. Street, *Elementary Fluid Mechanics*, 5th ed., Wiley, New York, 1975.

9.1 Flat-Plate Boundary Layer

Flow across a flat plate parallel to the flow direction is subject to boundary layer growth. The forward portion of the plate develops a laminar boundary layer. The laminar boundary layer then “breaks down,” forming a turbulent boundary layer that continues downstream indefinitely (see Fig. 53). The laminar boundary layer exists until a Reynolds number of 3900 occurs:

$$\text{Re} = \frac{V\delta}{\nu} \quad (203)$$

where δ is the boundary layer thickness. Note that if the approaching flow is turbulent or the leading edge of the plate is rough, the laminar boundary layer may be considerably shorter.

Analysis of the flow on a flat plate provides the following values of shear stress and drag for the laminar flow portion:

$$\tau_o = c_f \frac{1}{2} \rho V_o^2 \quad (204)$$

where

$$c_f = \sqrt{\frac{8}{15\text{Re}_x}} \quad \text{and} \quad \text{Re}_x = \frac{V_o x}{\nu} \quad (205)$$

where x is the distance from forward edge of the plate. The total drag force D is given by

$$D = C_f \frac{1}{2} A \rho V_o^2 \quad (206)$$

where

$$C_f = \sqrt{\frac{32}{15\text{Re}_x}} \quad (207)$$

These formulas are valid for Reynolds numbers based on Re_x up to 500,000 where

$$\text{Re}_x = \frac{Vx}{\nu} \quad (208)$$

If the flow over the flat plate is largely turbulent, then the drag coefficient C_f can be expressed as

$$\frac{1}{\sqrt{C_f}} = 4.13 \log C_f \text{Re}_x \quad (209)$$

In general the C_f values in Fig. 54 can be used in the drag force equation to compute total drag on a smooth flat plate.

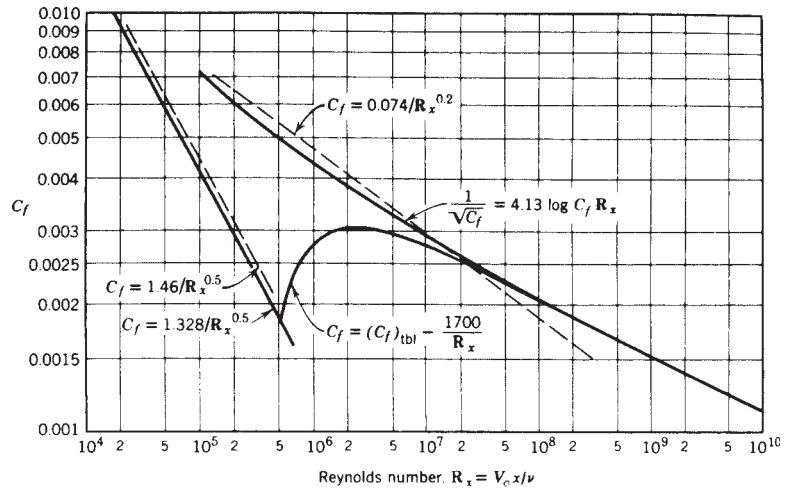


Figure 54 Drag coefficients for smooth, flat plates. *Source:* By permission from J. K. Vennard and R. L. Street, *Elementary Fluid Mechanics*, 5th ed., Wiley, New York, 1975.

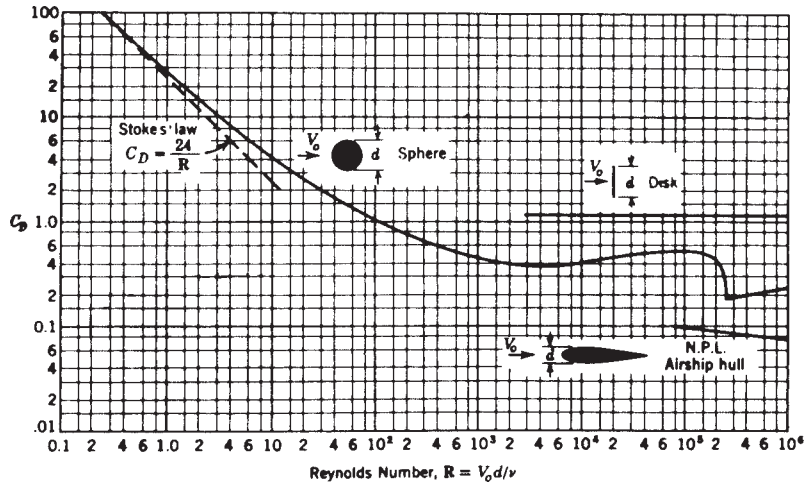


Figure 55 Drag coefficients for sphere, disk, and streamlined body. *Source:* By permission from J. K. Vennard and R. L. Street, *Elementary Fluid Mechanics*, 5th ed., Wiley, New York, 1975.

9.2 Drag on Immersed Objects

The total drag on an immersed object may be dominated by skin friction or form drag but, in any case, is generally obtained by experiment. The data are presented as drag coefficients and plotted as C_D versus Reynolds number. The total drag force can then be calculated from Eq. 201. Data on drag coefficients for common objects are presented in Figs. 55 and 56.

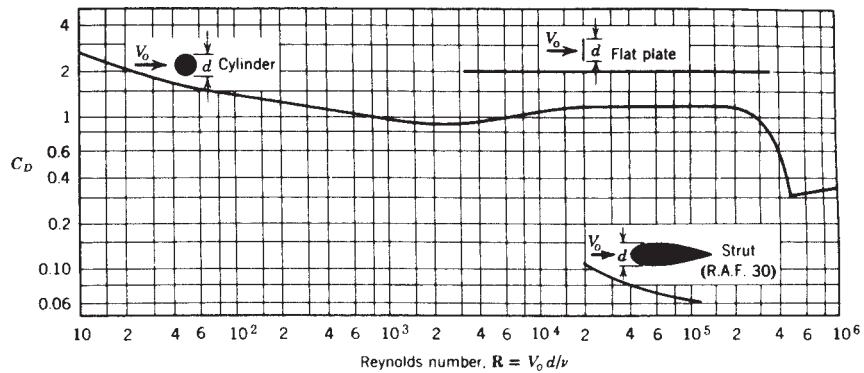


Figure 56 Drag coefficients for circular cylinders, flat plates, and streamlined struts of infinite length. *Source:* By permission from J. K. Vennard and R. L. Street, *Elementary Fluid Mechanics*, 5th ed., Wiley, New York, 1975

9.3 Lift

Lift is also presented through graphs of C_L .

10 FLUID MEASUREMENTS*

In spite of the advances in numerical analysis, analytical techniques, and computer power in recent years, the complex phenomena of fluid flow must still be addressed empirically. The measurement of pressure, shear, discharge, velocity, and so forth remain necessary skills to the serious fluid mechanician. Many techniques and devices remain relatively unchanged over the years. Others, particularly in velocity measurement, reflect the recent advances in technology. This section presents an abbreviated review of the range of devices available.

10.1 Fluid Property Measurement

Specific Weight or Density

Measurement of the specific weight of a liquid relies on fundamental concepts and devices that generally need no calibration. Figure 57 illustrates three methods that depend on buoyancy calculations and one (Fig. 57d) that utilizes hydrostatics. Probably the simplest method is not illustrated—simply weighing a known volume of liquid. The device or method selected depends on the availability of the required equipment.

Figure 57a utilizes the submerged weight of a known volume of liquid. Figure 57b, in a somewhat reversed approach, submerges a known weight and volume into the unknown liquid. Figure 57c uses calibrated hydrometers.

Viscosity Measurement

Viscosity-measuring devices (viscometers) generally employ one of three approaches to measuring viscosity—the falling sphere, the flowing tube, or the rotating cylinder. All the devices require that laminar flow be maintained throughout the measurement period.

* This section follows closely the treatment in J. K. Vennard and R. L. Street, *Elementary Fluid Mechanics*, 5th ed., Wiley, New York, 1975.

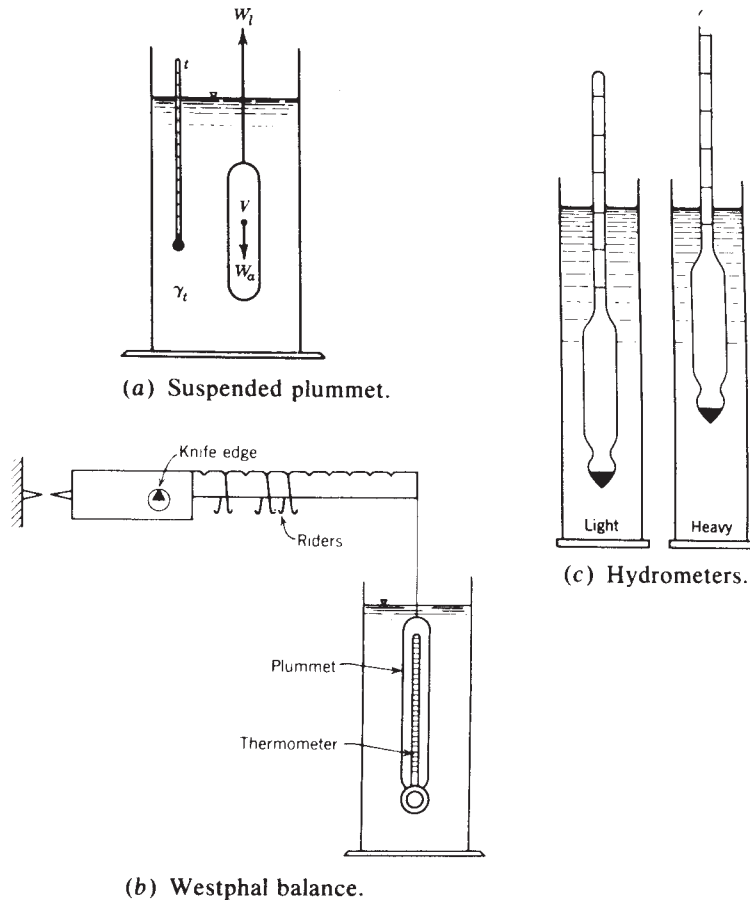


Figure 57 Devices for density measurement. *Source:* By permission from J. K. Vennard and R. L. Street, *Elementary Fluid Mechanics*, 5th ed., Wiley, New York, 1975.

The falling-sphere device is illustrated in Fig. 58. Stokes's law for a sphere falling in a viscous liquid is employed. The time required for a sphere of known size and weight to fall a specified distance is measured. The absolute viscosity can be calculated from the equation

$$\mu = \frac{d^2(\gamma_s - \gamma_l)}{18V} \quad (210)$$

where

- d = sphere diameter
- V = sphere velocity
- γ_s, γ_l = specific weight of sphere and liquid, respectively

The flowing-tube devices (Ostwald, Saybolt, Bingham, Redwood, and Engler viscometers) are typified by the Ostwald and Saybolt devices in Fig. 59. All these devices depend on the laminar unsteady flow of a liquid. The time required for a given volume of liquid to flow through a small tube is measured, and an empirical formula based on laminar flow principles is used

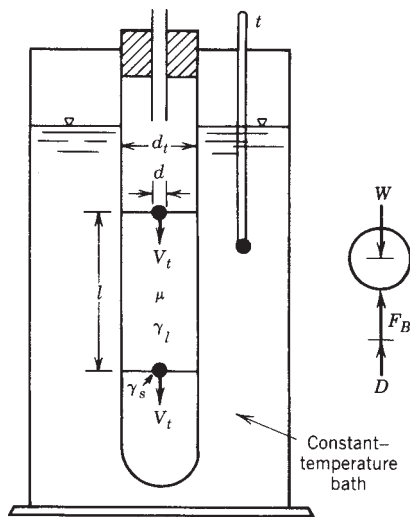


Figure 58 Falling-sphere viscometer. *Source:* By permission from J. K. Vennard and R. L. Street, *Elementary Fluid Mechanics*, 5th ed., Wiley, New York, 1975.

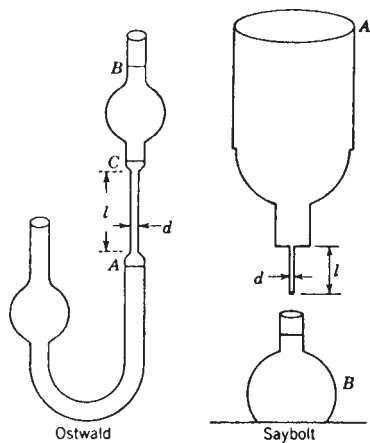


Figure 59 Tube viscometers. *Source:* By permission from J. K. Vennard and R. L. Street, *Elementary Fluid Mechanics*, 5th ed., Wiley, New York, 1975.

to calculate kinematic viscosity. For example, in the Saybolt device, the time required for the liquid level to drop from level B to C is recorded. The kinematic viscosity is calculated from the equation

$$v \text{ (ft}^2\text{/s)} = 0.000002365t - \frac{0.001935}{t} \tag{211}$$

where t is time in seconds required for liquid level to drop.

The other devices will not be discussed here as the principles are similar and instructions and calibrated equations are supplied with the devices.

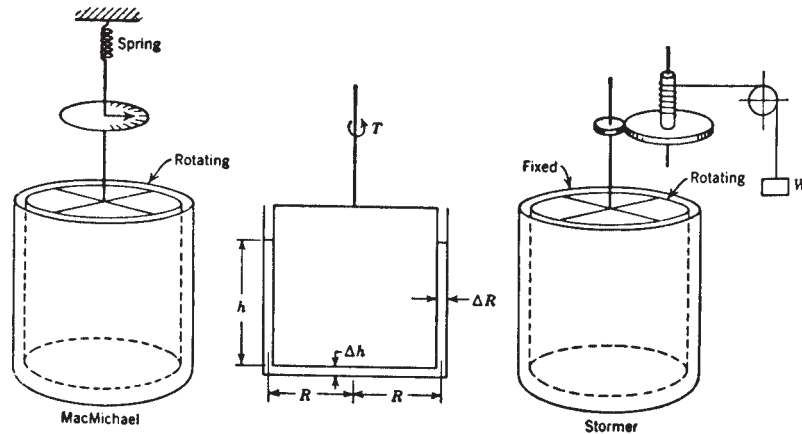


Figure 60 Rotational viscometers (schematic). *Source:* By permission from J. K. Vennard and R. L. Street, *Elementary Fluid Mechanics*, 5th ed., Wiley, New York, 1975.

The rotating-cylinder devices (Stormer, MacMichael, Brookfield) generally employ a fixed cylindrical container and a rotating inner cylinder (see Fig. 60). The space between the two cylinders and the speed of rotation is purposely kept small enough to maintain laminar flow. Measurement of the time required to complete a given number of revolutions under a constant torque leads to a calculation of absolute viscosity. The fundamental equation used is

$$T = \frac{2\pi R^2 h \mu V}{\Delta R} + \frac{\pi R^3 \mu V}{2\Delta h}$$

10.2 Pressure Measurement

Pressure measurement in a fluid at rest is relatively easy to accomplish. The manometers and Bourdon gauges discussed in Section 3 are common devices used for this purpose. If the fluid is moving, pressure measurement is more difficult.

Of primary concern is the pressure-sensing connection between the fluid and the pressure-measuring system. In measuring *static* pressure (pressure unaffected by the velocity of flow), an opening is made in the conduit wall or the pressure probe, such as a pitot-static tube (see Fig. 61), so that the pressure in the flow at the surface may be conducted to the pressure-measuring device. The surface opening must be small (less than 1 mm) and well finished (square edged, no burr) so that the flow is not disturbed. In the case of a probe, the device must be small enough to not disturb the flow and alter the pressure situation and properly oriented to produce the true static pressure.

The pressure-measuring devices used in fluid flows may be manometers or gauges. However, for electronic recording as well as measurement of fluctuating pressures, a pressure transducer is commonly used. A typical pressure transducer is a small diaphragm to which is attached a strain gauge to measure deflection of the diaphragm. The gauge is part of a Wheatstone bridge circuit and is calibrated to an electrical output that can be processed to produce a plot, directed to a computer for further analysis, or simply stored on some electronic device.

Piezoelectric transducers are also used wherein the sensing device is a piezoelectric crystal that produces an electric field when deformed. Care must be taken to install the sensors in a shock-free environment as they are very sensitive to any vibration of the facility hardware.

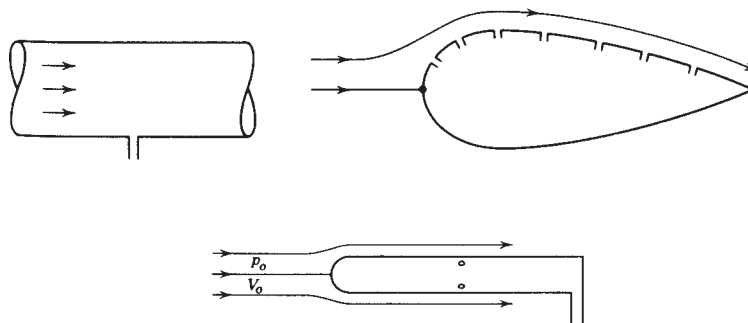


Figure 61 Static tube. *Source:* By permission from J. K. Vennard and R. L. Street, *Elementary Fluid Mechanics*, 5th ed., Wiley, New York, 1975.

Pressure-sensitive paint (PSP) is a special paint material that adjusts its color based on the local pressure acting on the paint. Due to its nature, PSP provides nonintrusive, global surface pressure measurements. Therefore, PSP can be applied to the model surface being tested, and through special imaging equipment, a quantitative picture of surface pressure values can be produced. Although PSP technology was initially developed in the 1970s, its use for flow visualization was first proposed in 1980. Since then, many different chemical formulations have been developed and have been used in all fields of aerodynamics, including low subsonic, high subsonic, transonic, and supersonic.

The working mechanism of PSP is simple but it is not reflected in its name. Actually, the paint is sensitive not to the local pressure but to the local partial pressure of oxygen. If the fluid that is used in the experiment is air and at constant composition (nonreacting), then the partial pressure of oxygen is directly proportional with the pressure of the air. Therefore, the higher the air pressure, the higher the “quenching effect.” As a result of this quenching effect, the energy of the fluorescent light coming from the PSP decreases, which translates to an increase in the wavelength of the fluorescent light. Modified wavelength leads to variable color based on the magnitude of the quenching, and hence the local pressure. Once calibrated for different wavelength–pressure correspondence, PSP can be used on the model object.

A PSP system consists of a light source to excite the paint for luminescence, the model painted with the PSP, a high-definition camera, and a processing unit for matching the light intensity values to the pressure values. As in all other measurement devices, PSPs also have their own error sources and they require a calibration for different operating conditions.

10.3 Velocity Measurement

One of the commonest and simplest devices for the measurement of velocity is a pitot-static tube (see Fig. 62). The device senses the difference in pressure between the tip of the pitot-static tube and the side of the tube. This pressure difference can be used to calculate the velocity from the equation

$$V_o = \sqrt{\frac{2(p_s - p_o)}{\rho}} = \sqrt{\frac{2g(p_s - p_o)}{\gamma}} \quad (213)$$

where $p_s - p_o$ is the aforementioned difference in pressure.

In very low velocity flows, the anemometer or current meter is often used (see Fig. 63). These are calibrated devices that relate flow velocity to the number of revolutions per minute of the rotating element in the meter. Anemometers are typically used to measure wind speeds, and current meters are employed to measure water velocities in rivers.

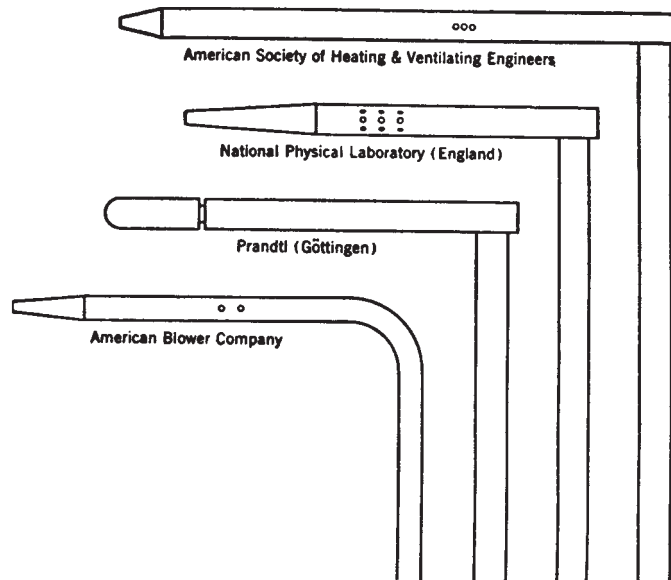


Figure 62 Pitot-static tubes (to scale). *Source:* By permission from J. K. Vennard and R. L. Street, *Elementary Fluid Mechanics*, 5th ed., Wiley, New York, 1975.

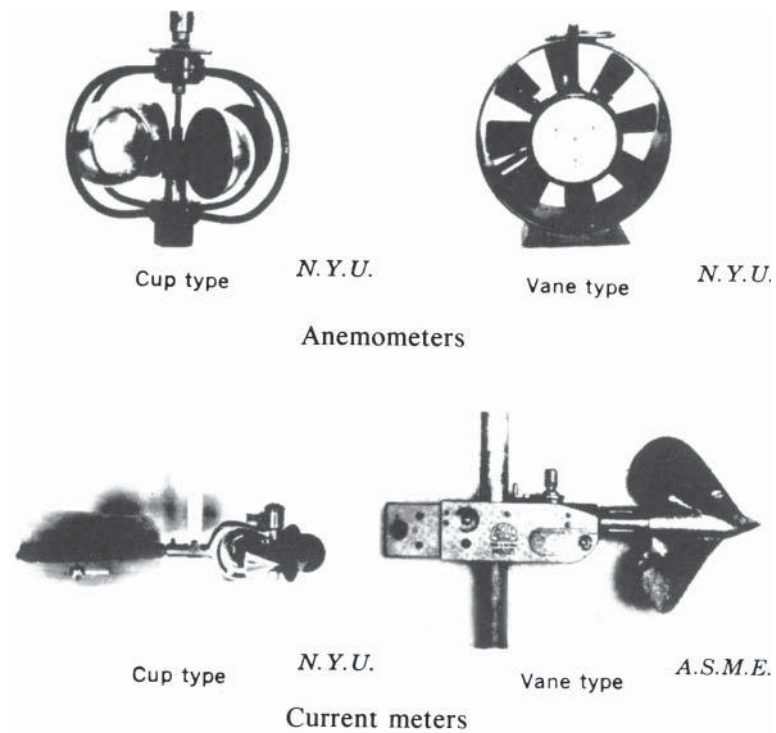
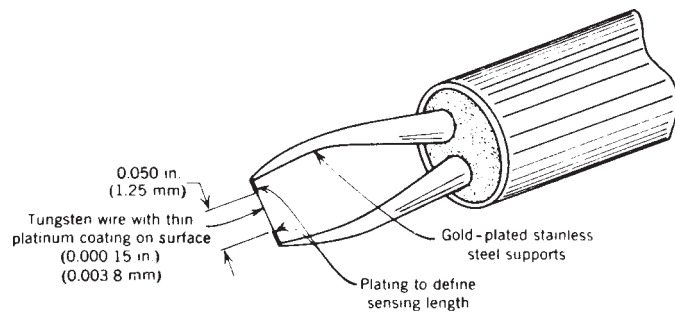
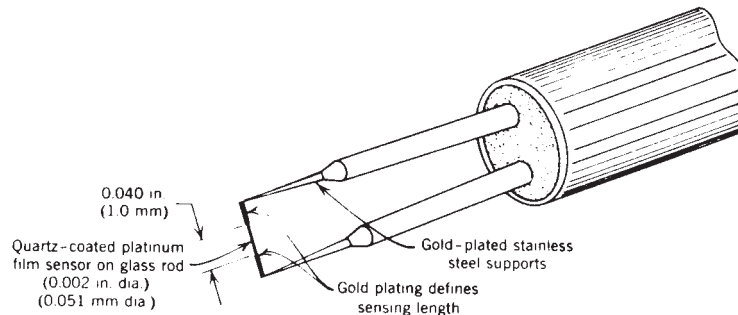


Figure 63 Examples of anemometers and current meters. *Source:* By permission from J. K. Vennard and R. L. Street, *Elementary Fluid Mechanics*, 5th ed., Wiley, New York, 1975.



(a) Hot-wire sensor and support needles.



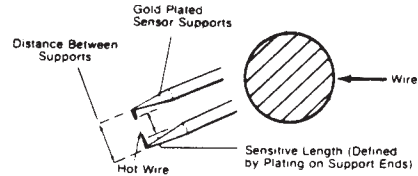
(b) Hot-film sensor and support needles.

Figure 64 Anemometer sensors: (a) Hot wire and (b) hot film sensors and support needles. *Source:* Reproduced from TB5, Thermo-Systems, Inc., 2500 Cleveland Ave. North, St. Paul, Minnesota, 55113. By permission from J. K. Vennard and R. L. Street, *Elementary Fluid Mechanics*, 5th ed., Wiley, New York, 1975.

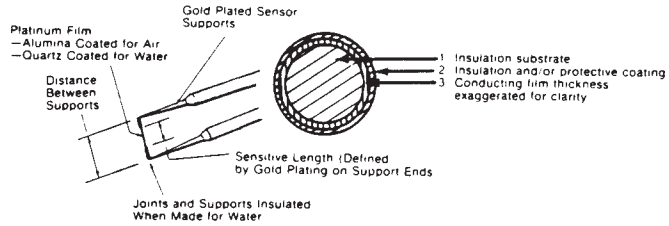
Measurement of rapidly fluctuating velocities in air and water require devices that can respond quickly to changes in velocity. The hot-wire anemometer is commonly used to measure velocity fluctuations in air. A thin wire connected between two supports passes an electric current that heats the wire (see Fig. 64a). Air moving perpendicular to the wire cools the wire in proportion to the flow velocity. The electronics of the system measures the increased voltage necessary to keep the wire temperature constant and relates that voltage to the flow velocity. In some devices the current flowing through the probe is kept constant and the voltage change required for this to occur is related to the flow velocity. However, the constant-temperature device is by far the most popular.

A variation on the hot-wire anemometer is the hot-film anemometer. The hot-film device is similar to the hot wire except the wire is coated to protect it from contaminated environments. In addition to coated wires, hot-film anemometry employs probes of other shapes that are sturdier and less likely to trap impurities in the flow (lint, small pieces of organic material, etc.). Figure 65 illustrates a few of these different types of probes. Hot-film devices are commonly used in liquid flows. Both these devices are capable of measuring velocity fluctuation frequencies of better than 300 kHz.

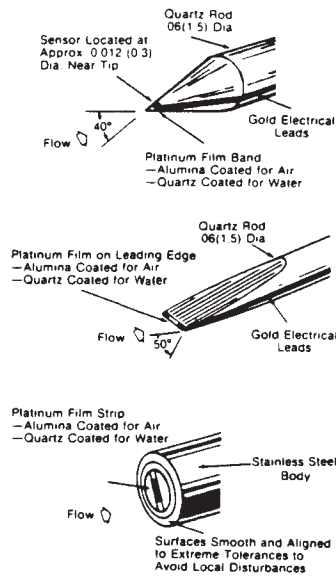
Another technique for measuring velocities is laser-Doppler velocimetry (LDV). The fundamental basis for the technique is the Doppler shift of light that is scattered from extremely



(a) CROSS SECTION OF HOT-WIRE SENSOR



(b) CROSS SECTION OF HOT-FILM SENSOR



(c)

Figure 65 Thermal sensor configuration. *Source:* By permission from R. J. Goldstein, *Fluid Mechanics Measurements*, Hemisphere, New York, 1983.

small particles in a moving fluid. One valuable attribute of LDV is that it is nonintrusive, that is, the sensing device is not in the flow. It only needs visual access to the flow for the required light beams. Refer to Goldstein¹⁶ for a thorough treatment of the subject. One of the most recent advances in measuring fluid velocities is particle image velocimetry (PIV), which also makes use of the laser and seed particles but works with a planar laser light sheet. This provides the advantage of measuring an entire two-dimensional plane of the flow field simultaneously, as compared to LDV, which only offers a point measurement. For more details on PIV, see Raffel et al.¹⁷

10.4 Flow Rate Measurement

Methods of measuring flow rate or discharge can generally be categorized into total quantity measurements, pressure drop or pressure difference measuring devices, tracer transport techniques, and devices that induce critical flow conditions or simply changes in water surface depth in open channels. Another indirect approach is the measurement of velocity at several points and a numerical integration of velocity times area to calculate discharge.

Total Quantity Methods

The success of these methods depends on the availability of a means to collect and measure (or weigh) the amount of liquid captured in the container in a given time period. Advantages are the lack of any need to calibrate a device. This approach is often used to calibrate other flow-rate-measuring devices.

Pressure Difference Methods

All the devices that create pressure differences in a fluid flow to permit calculation of flow rate also create friction losses in the flow. One of the devices that has the lowest friction loss is the venturi meter (see Fig. 66). In the venturi meter the Bernoulli effect is used to generate a pressure difference between the entrance and the throat of the device. This pressure difference is related to the flow rate through the equation

$$Q = \frac{C_v A_2}{\sqrt{1 - (A_2/A_1)^2}} \sqrt{2g[(p_1/\gamma) + z_1 - (p_2/\gamma) - z_2]} \quad (214)$$

where A is the cross-sectional area of the meter and C_v is a calibration coefficient shown in Fig. 66. Venturi meters are relatively expensive but produce very little friction loss and are quite accurate.

A device based on a similar technique to the venturi meter is the flow nozzle. This device resembles the upstream portion of a venturi meter (see Fig. 67). Pressure recovery experienced in the downstream section of the venturi meter is not realized here so the flow nozzle creates a larger friction loss than the venturi meter. The calculation for discharge is made with the same equation used for the venturi meter with the C_v value taken from Fig. 67.

One further step in the direction of simplicity (and lower cost) is the orifice meter (see Fig. 68). This device is simply a circular plate with a hole cut out of its center and installed in a pipe, generally in a flanged connection. The orifice meter creates considerably more friction loss than the venturi meter or flow nozzle, but its low cost makes it attractive in many instances. Flow rates through an orifice meter may be calculated with the equation

$$Q = CA \sqrt{2g[(p_1/\gamma) + z_1 - (p_2/\gamma) - z_2]} \quad (215)$$

The value of C for a given flow rate is found from Fig. 69.

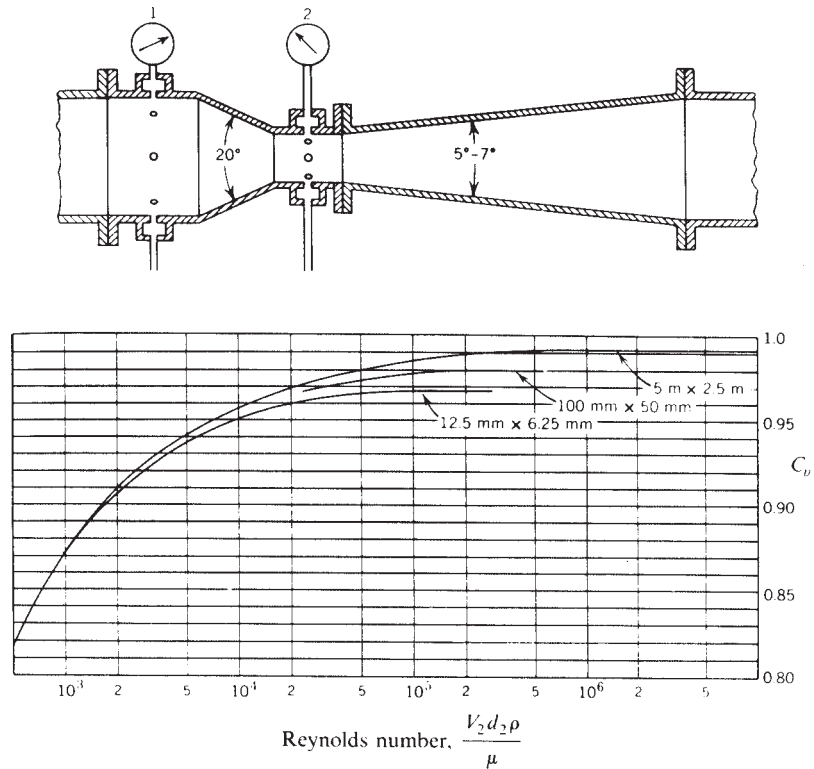


Figure 66 Venturi meter and coefficients. *Source:* By permission from J. K. Vennard and R. L. Street, *Elementary Fluid Mechanics*, 5th ed., Wiley, New York, 1975.

There are certain special cases of “orifice meters” shown in Fig. 70 where discharges through the orifice can be related to liquid levels on one (or two) side(s) of the opening. The equations used to compute the discharge are

$$Q = A_2 V_2 = C_c C_v A \sqrt{2g(h_1 - h_2)} = CA \sqrt{2g(h_1 - h_2)} \quad (216)$$

$$= C_c C_v A \sqrt{2gh} = CA \sqrt{2gh} \quad (217)$$

All the C values for various types of orifices can be found in Fig. 71. More precise data for C values of sharp-edged orifices over a large range of heads are given in Fig. 72.

Probably the most inexpensive technique for calculating flow rate by the pressure difference method is the elbow meter (see Fig. 73). The only requirements are two pressure taps on the inner and outer portions of the elbow. The flow rate is calculated from the equation

$$Q = CA \sqrt{2g[(P_o/\gamma) + z_o - (p_i/\gamma) - z_i]} \quad (218)$$

Because the value of C depends strongly on the elbow geometry, it must generally be determined through a calibration procedure.

Tracer Transport Techniques

This technique is based on the premise that the discharge in a conduit can be measured by the time of travel of the average concentration of a tracer between two points. The tracer could be

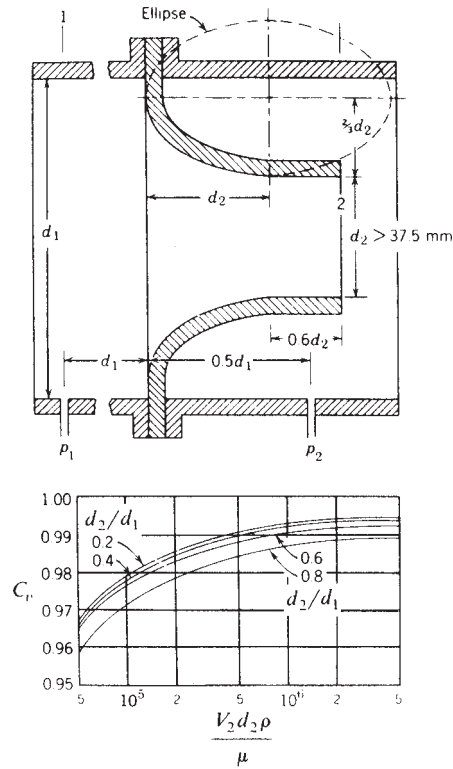


Figure 67 ASME flow nozzle and coefficients. *Source:* By permission from J. K. Vennard and R. L. Street, *Elementary Fluid Mechanics*, 5th ed., Wiley, New York, 1975.

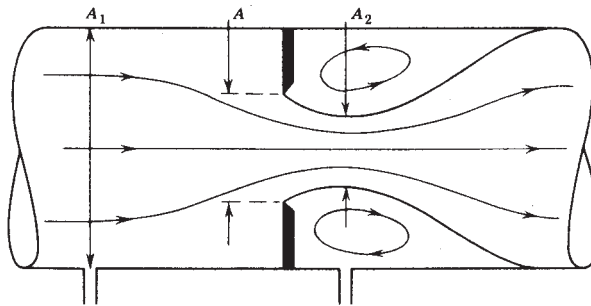


Figure 68 Definition sketch for orifice meter. *Source:* By permission from J. K. Vennard and R. L. Street, *Elementary Fluid Mechanics*, 5th ed., Wiley, New York, 1975.

as simple as salt where concentration is measured via conductivity instruments (see Fig. 74), although any other tracer may be employed. Fluorescent dyes are commonly used because they have little effect on water quality and are detectable in minute quantities. From Fig. 74, the average velocity is computed from dividing the length l between sensors by the time t required for the centroid of the concentration curve to travel over the distance. This approach

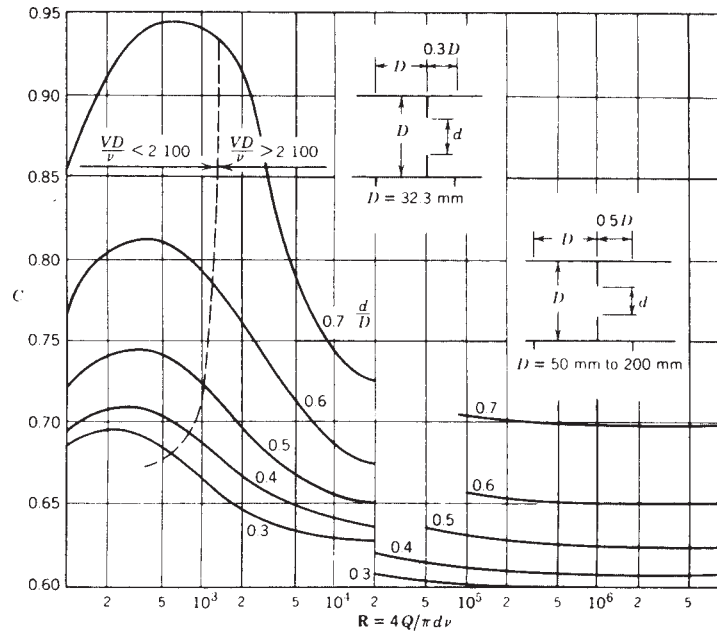


Figure 69 Orifice meter coefficients. *Source:* By permission from J. K. Vennard and R. L. Street, *Elementary Fluid Mechanics*, 5th ed., Wiley, New York, 1975.

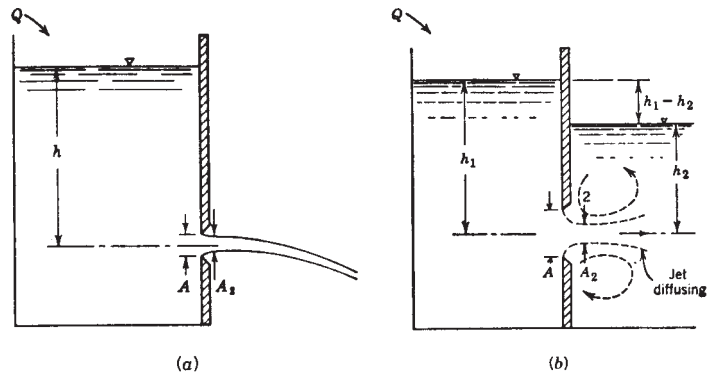


Figure 70 (a) Orifice discharging freely and (b) submerged orifice. *Source:* By permission from J. K. Vennard and R. L. Street, *Elementary Fluid Mechanics*, 5th ed., Wiley, New York, 1975.

is particularly useful in open channels of relatively constant cross section and conduits where, for one reason or another, other techniques cannot be used.

Open-Channel Flow-Measuring Devices

In free-surface flows, the common techniques for flow measurement center on either (a) constricting the flow to create differences in water surface elevations that can be related to flow rate or (b) creating critical flow conditions (see Section 8) that provide a strong analytical connection to discharge calculation.

Orifices and their Nominal Coefficients				
	Sharp edged	Rounded	Short tube	Borda
C	0.61	0.98	0.80	0.51
C_c	0.62	1.00	1.00	0.52
C_v	0.98	0.98	0.80	0.98

Figure 71 C values for various types of orifices. *Source:* By permission from J. K. Vennard and R. L. Street, *Elementary Fluid Mechanics*, 5th ed., Wiley, New York, 1975.

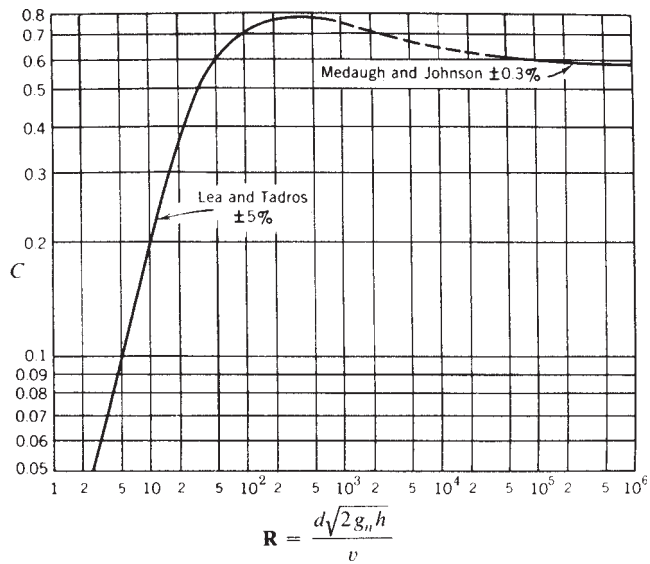


Figure 72 Coefficient for sharp-edged orifices under static head ($h/d > 5$). *Source:* By permission from J. K. Vennard and R. L. Street, *Elementary Fluid Mechanics*, 5th ed., Wiley, New York, 1975.

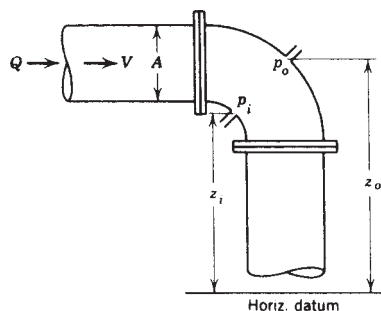


Figure 73 Elbow meter. *Source:* By permission from J. K. Vennard and R. L. Street, *Elementary Fluid Mechanics*, 5th ed., Wiley, New York, 1975.

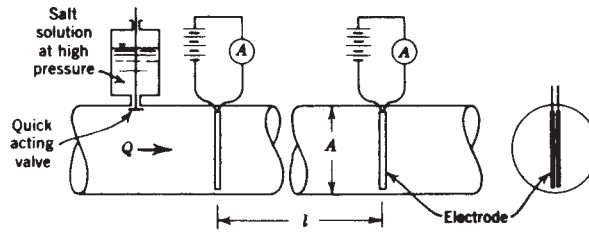


Figure 74 Measurement of Salt dilution discharge. *Source:* By permission from J. K. Vennard and R. L. Street, *Elementary Fluid Mechanics*, 5th ed., Wiley, New York, 1975.

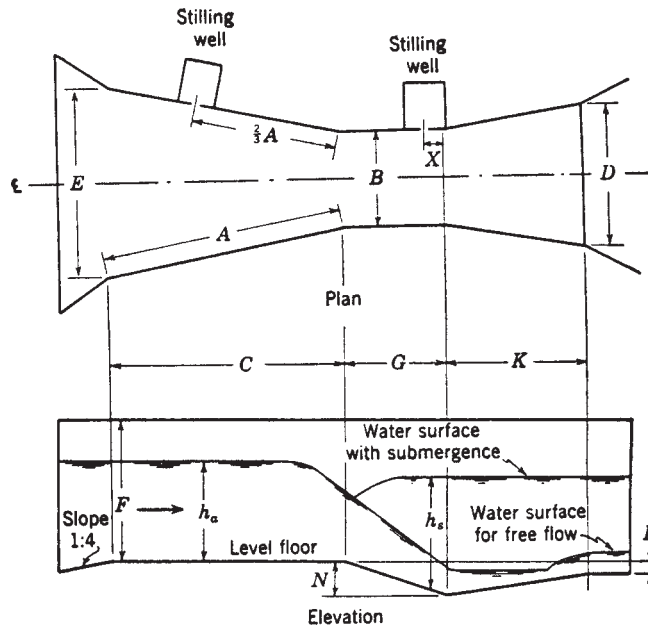


Figure 75 Parshall measuring flume. *Source:* From R. K. Linsley and J. B. Franzini, *Elements of Hydraulic Engineering*, McGraw-Hill, New York, 1955. Copyright 1955 McGraw-Hill. Reprinted by permission.

The simplest devices are venturi flumes, which are the open-channel version of venturi meters. The drop in water surface in the flume throat is measured and related to the flow rate. Although not extremely accurate, this approach does not create large friction losses.

A simpler version similar to the flow nozzle in closed conduits is the cutthroat flume where the diverging recovery section is not present.

A somewhat more complicated version of the venturi flume, which causes critical or near-critical flow to occur, is the Parshall flume (see Fig. 75). This device has been commonly used in irrigation systems for well over 70 years. The discharge is calculated from the equation

$$Q = 4Bh_a^{1.522B^{0.26}} \quad (219)$$

Another category of open-channel flow-measuring devices is weirs. These devices generally generate more friction loss than the previously described devices, but they are relatively simple

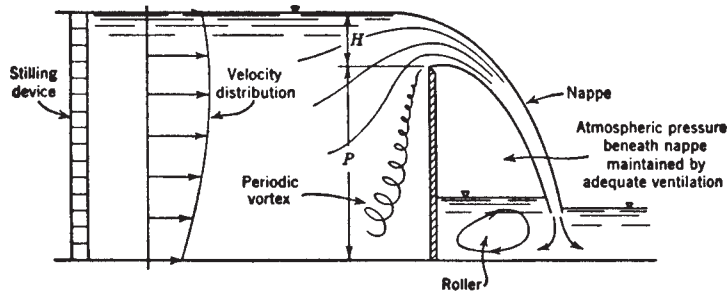


Figure 76 Weir flow (actual). *Source:* By permission from J. K. Vennard and R. L. Street, *Elementary Fluid Mechanics*, 5th ed., Wiley, New York, 1975.

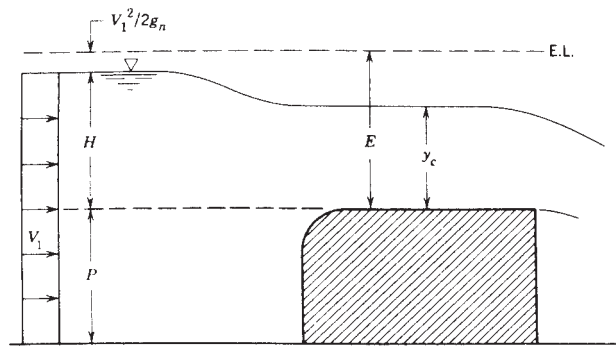


Figure 77 Broad-crested weir. *Source:* By permission from J. K. Vennard and R. L. Street, *Elementary Fluid Mechanics*, 5th ed., Wiley, New York, 1975.

and accurate. A typical sharp-crested rectangular weir is shown in Fig. 76. The other types of weirs are broad crested (Fig. 77) and triangular (Fig. 78). The general form of the discharge equation per foot of width for weirs with two-dimensional flow is

$$q = C_w \frac{2}{3} \sqrt{2g} H^{3/2} \tag{220}$$

where H is defined in Figs. 76 and 77 as the head on the weir. The value of C_w for sharp-crested well-ventilated weirs (Fig. 76) is given by the equation

$$C_w = 0.605 + 0.08 \frac{H}{P} + \frac{1}{305H} \tag{221}$$

For broad-crested weirs (Fig. 77), the flow rate per foot of width is given by

$$q = \sqrt{g \left(\frac{2E}{3} \right)^3} = \left(\frac{2}{3} \right)^{3/2} \sqrt{g} E^{3/2} \tag{222}$$

or Eq. 219 where

$$C_w = \frac{1}{\sqrt{3}} \left(\frac{E}{H} \right)^{3/2} \tag{223}$$

where E is defined in Fig. 77.

For triangular notch weirs (Fig. 78) the equation for computing discharge is

$$Q = C_w \frac{8}{15} \tan \alpha \sqrt{2g} H^{5/2}$$

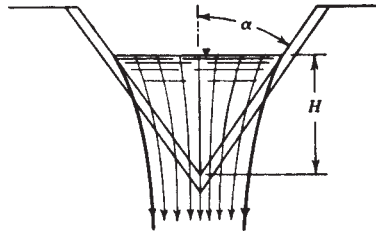


Figure 78 Triangular weir. *Source:* By permission from J. K. Vennard and R. L. Street, *Elementary Fluid Mechanics*, 5th ed., Wiley, New York, 1975.

where C_w depends on the notch angle α . For $\alpha = 90^\circ$,

$$C_w = 0.56 + \frac{0.70}{R^{0.165} W^{0.170}}$$

REFERENCES

1. J. K. Vennard, and R. L. Street, *Elementary Fluid Mechanics*, 5th ed., Wiley, New York, 1975.
2. B. R. Munson, D. F. Young, and T. H. Okiishi, *Fundamentals of Fluid Mechanics*, 5th ed., Wiley, Hoboken, NJ, 2006.
3. G. Stokes, *Trans. Cambridge Phil. Soc.*, **8**, 1845, and 9, 1851.
4. Th. von Kármán, "Turbulence and Skin Friction," *J. Aeronaut. Sci.*, **1**(1), 1, 1934.
5. C. V. Davis, and K. E. Sorenson, *Handbook of Applied Hydraulics*, 3rd ed., McGraw-Hill, New York, 1969.
6. V. T. Chow, *Open Channel Hydraulics*, McGraw-Hill, New York, 1959.
7. C. F. Colebrook, "Turbulent Flow in Pipes, with Particular Reference to the Transition Region between the Smooth and Rough Pipe Laws," *J. Inst. Civil Eng. London*, **11**, 1938–1939.
8. Crane Company, *Flow of Fluids through Valves, Fittings and Pipe*, Tech. Paper No. 410, Crane Co., New York, 1969.
9. J. E. Idelchik, *Handbook of Hydraulic Resistance*, 2nd ed., Hemisphere Publishing, New York, 1986.
10. A. H. Gibson, *Hydraulics and Its Applications*, Constable, London, 1912.
11. R. W. Jeppson, *Analysis of Flow in Pipe Networks*, Ann Arbor Science, Ann Arbor, MI, 1976.
12. D. J. Wood, and A. G. Rayes, "Reliability of Algorithms for Pipe Network Analysis," *J. Hydraulics Div.*, ASCE, **107**(10), 1981.
13. G. Z. Watters, *Analysis and Control of Unsteady Flow in Pipelines*, Butterworth, Stoneham, MA, 1984.
14. E. B. Wylie, and V. L. Streeter, *Fluid Transients*, McGraw-Hill, New York, 1978.
15. M. H. Chaudhry, *Applied Hydraulic Transients*, Van Nostrand Reinhold, New York, 1979.
16. R. J. Goldstein, *Fluid Mechanics Measurements*, Hemisphere Publishing, New York, 1983.
17. M. Raffel, C. Wifferk, and J. Kompenhans, *Particle Image Velocimetry: A Practical Guide*, Springer, Berlin, 1998.

BIBLIOGRAPHY

- R. K. Linsley, and J. B. Franzini, *Elements of Hydraulic Engineering*, McGraw-Hill, New York, 1955.
 L. F. Moody, "Friction Factors for Pipe Flow," *Trans. ASME*, **66**, 1944.
 H. Rouse, *Fluid Mechanics for Hydraulic Engineers*, McGraw-Hill, New York, 1938.
 V. L. Streeter, *Fluid Dynamics*, 3rd ed., McGraw-Hill, New York, 1962.
 J. K. Vennard, *Elementary Fluid Mechanics*, 4th ed., Wiley, New York, 1961.

CHAPTER 3

THERMODYNAMICS FUNDAMENTALS

Adrian Bejan
Duke University
Durham, North Carolina

1	INTRODUCTION	135	5	LAWS OF THERMODYNAMICS FOR OPEN SYSTEMS	143
2	FIRST LAW OF THERMODYNAMICS FOR CLOSED SYSTEMS	138	6	RELATIONS AMONG THERMODYNAMIC PROPERTIES	144
3	SECOND LAW OF THERMODYNAMICS FOR CLOSED SYSTEMS	140	7	ANALYSIS OF ENGINEERING SYSTEM COMPONENTS	153
4	ENERGY MINIMUM PRINCIPLE	142		REFERENCES	156

1 INTRODUCTION

Thermodynamics describes the relationship between work, heat, and other forms of energy. There are two aspects of contemporary thermodynamics that must be stressed in a review such as this. The first is the equivalence of *work* and *heat* as two possible forms of energy exchange. This is expressed by the first law of thermodynamics. The second aspect is the one-way character, or irreversibility, of all processes (changes) that occur in nature. As expressed by the second law of thermodynamics, irreversibility or entropy generation is what prevents us from extracting the most possible work from various sources; it is also what prevents us from doing the most with the work that is already at our disposal. The objective of this chapter is to review the first and second laws of thermodynamics and their implications in mechanical engineering, particularly with respect to such issues as energy conversion and conservation. The analytical aspects (the formulas) of engineering thermodynamics are reviewed primarily in terms of the behavior of a pure substance, as would be the case of the working fluid in a heat engine or in a refrigeration machine. In the next chapter we review in greater detail the newer field of entropy generation minimization (thermodynamic optimization) and the generation of system configuration (the constructal law).

Symbols and Units.

c	specific heat of incompressible substance, J/(kg · K)
c_p	specific heat at constant pressure, J/(kg · K)
c_T	constant temperature coefficient, m ³ /kg
c_v	specific heat at constant volume, J/(kg · K)
COP	coefficient of performance
E	energy, J
f	specific Helmholtz free energy ($u-Ts$), J/kg

\vec{F}	force vector, N
g	gravitational acceleration, m/s^2
g	specific Gibbs free energy ($h-Ts$), J/kg
h	specific enthalpy ($u + Pv$), J/kg
K	isothermal compressibility, m^2/N
m	mass of closed system, kg
\dot{m}	mass flow rate, kg/s
m_i	mass of component in a mixture, kg
M	mass inventory of control volume, kg
M	molar mass, g/mol or kg/kmol
n	number of moles, mol
N_0	Avogadro's constant
P	pressure
δQ	infinitesimal heat interaction, J
\dot{Q}	heat transfer rate, W
\vec{r}	position vector, m
R	ideal gas constant, J/(kg · K)
s	specific entropy, J/(kg · K)
S	entropy, J/K
S_{gen}	entropy generation, J/K
\dot{S}_{gen}	entropy generation rate, W/K
T	absolute temperature, K
u	specific internal energy, J/kg
U	internal energy, J
v	specific volume, m^3/kg
\bar{v}	specific volume of incompressible substance, m^3/kg
V	volume, m^3
V	velocity, m/s
δW	infinitesimal work interaction, J
\dot{W}_{lost}	rate of lost available work, W
\dot{W}_{sh}	rate of shaft (shear) work transfer, W
x	linear coordinate, m
x	quality of liquid and vapor mixture
Z	vertical coordinate, m
β	coefficient of thermal expansion, 1/K
γ	ratio of specific heats, c_p/c_v
η	“efficiency” ratio
η_I	first-law efficiency
η_{II}	second-law efficiency
θ	relative temperature, °C

Subscripts.

$()_f$	saturated liquid state (f = “fluid”)
$()_g$	saturated vapor state (g = “gas”)
$()_s$	saturated solid state (s = “solid”)
$()_{\text{in}}$	inlet port
$()_{\text{out}}$	outlet port
$()_{\text{rev}}$	reversible path
$()_H$	high-temperature reservoir
$()_L$	low-temperature reservoir

$()_{\max}$	maximum
$()_T$	turbine
$()_C$	compressor
$()_N$	nozzle
$()_D$	diffuser
$()_0$	reference state
$()_1$	initial state
$()_2$	final state
$()_*$	moderately compressed liquid state
$()_+$	slightly superheated vapor state

Definitions

Boundary is the real or imaginary surface delineating the thermodynamic system. The boundary separates the system from its environment. The boundary is an unambiguously defined surface. The boundary has zero thickness and zero volume.

Closed system is the thermodynamic system the boundary of which is not crossed by mass flow.

Cycle is the special process in which the final state coincides with the initial state.

Environment is the thermodynamic system external to the thermodynamic system.

Extensive properties are properties the values of which depend on the size of the system (e.g., mass, volume, energy, enthalpy, entropy).

Intensive properties are properties the values of which do not depend on the system size (e.g., pressure, temperature). The collection of all intensive properties constitutes the *intensive state*.

Open system, or flow system, is the thermodynamic system the boundary of which is permeable to mass flow. Open systems have their own nomenclature: the thermodynamic system is usually referred to as the *control volume*, the boundary of the open system is the *control surface*, and the particular regions of the boundary that are crossed by mass flows are the *inlet* and *outlet ports*.

Phase is the collection of all system elements that have the same intensive state (e.g., the liquid droplets dispersed in a liquid–vapor mixture have the same intensive state, that is, the same pressure, temperature, specific volume, specific entropy, etc.).

Process is the change of state from one initial state to a final state. In addition to the end states, knowledge of the process implies knowledge of the *interactions* experienced by the system while in communication with its environment (e.g., work transfer, heat transfer, mass transfer, and entropy transfer). To know the process also means to know the *path* (the history or the succession of states) followed by the system from the initial to the final state.

State is the condition (the being) of a thermodynamic system at a particular point in time, as described by an ensemble of quantities called *thermodynamic properties* (e.g., pressure, volume, temperature, energy, enthalpy, entropy). Thermodynamic properties are only those quantities that depend solely on the instantaneous state of the system. Thermodynamic properties do not depend on the “history” of the system between two different states. Quantities that depend on the system evolution (path) between states are not thermodynamic properties (examples of nonproperties are the work, heat, and mass transfer; the entropy transfer; the entropy generation; and the destroyed exergy—see also the definition of *process*).

Thermodynamic system is the region or the collection of matter in space selected for analysis.

2 FIRST LAW OF THERMODYNAMICS FOR CLOSED SYSTEMS

The first law of thermodynamics is the statement that brings together three concepts in thermodynamics: work transfer, heat transfer, and energy change. Of these concepts, only energy change (or, simply, energy) is a thermodynamic property. We begin with a review¹ of the concepts of work transfer, heat transfer, and energy change.

Consider the force F_x experienced by a system at a point on its boundary. The infinitesimal *work transfer* between system and environment is

$$\delta W = -F_x dx$$

where the boundary displacement dx is defined as positive in the direction of the force F_x . When the force \bar{F} and the displacement of its point of application $d\bar{r}$ are not collinear, the general definition of infinitesimal work transfer is

$$\delta W = -\bar{F} \cdot d\bar{r}$$

The work transfer interaction is considered positive when the system does work on its environment—in other words, when \bar{F} and $d\bar{r}$ are oriented in opposite directions. This sign convention has its origin in heat engine engineering because the purpose of heat engines as thermodynamic systems is to deliver work while receiving heat.

In order for a system to experience work transfer, two things must occur: (1) a force must be present on the boundary and (2) the point of application of this force (hence, the boundary) must move. The presence of forces on the boundary, without the displacement or the deformation of the boundary, does not mean work transfer. Likewise, the presence of boundary displacement without a force opposing or driving this motion does not mean work transfer. For example, in the free expansion of a gas into an evacuated space, the gas system does not experience work transfer because throughout the expansion the pressure at the imaginary system–environment interface is zero.

If a closed system can interact with its environment only via work transfer (i.e., in the absence of heat transfer δQ , discussed later), then measurements show that the work transfer during a change of state from state 1 to state 2 is the same for all processes linking states 1 and 2:

$$-\left(\int_1^2 \delta W\right)_{\delta Q=0} = E_2 - E_1$$

In this special case the work transfer interaction $(W_{1-2})_{\delta Q=0}$ is a property of the system because its value depends solely on the end states. This thermodynamic property is the *energy change* of the system, $E_2 - E_1$. The statement that preceded the last equation is the first law of thermodynamics for closed systems that do not experience heat transfer.

Heat transfer is, like work transfer, an energy interaction that can take place between a system and its environment. The distinction between δQ and δW is made by the second law of thermodynamics discussed in the next section: Heat transfer is the energy interaction accompanied by entropy transfer, whereas work transfer is the energy interaction taking place in the absence of entropy transfer. The transfer of heat is driven by the *temperature difference* established between the system and its environment.^{2,3} The system temperature is measured by placing the system in thermal communication with a test system called *thermometer*. The result of this measurement is the *relative temperature* θ expressed in degrees Celsius, $\theta(^{\circ}\text{C})$, or Fahrenheit, $\theta(^{\circ}\text{F})$; these alternative temperature readings are related through the conversion formulas

$$\theta(^{\circ}\text{C}) = 5/9[\theta(^{\circ}\text{F}) - 32]$$

$$\theta(^{\circ}\text{F}) = 5/9\theta(^{\circ}\text{C}) + 32$$

$$1^{\circ}\text{F} = 5/9^{\circ}\text{C}$$

The boundary that prevents the transfer of heat, regardless of the magnitude of the system–environment temperature difference, is *adiabatic*. Conversely, the boundary that is

crossed by heat even in the limit of a vanishingly small system–environment temperature difference is *diathermal*.

Measurements also show that a closed system undergoing a change of state $1 \rightarrow 2$ in the absence of work transfer experiences a heat interaction whose magnitude depends solely on the end states:

$$\left(\int_1^2 \delta Q \right)_{\delta W=0} = E_2 - E_1$$

In the special case of zero work transfer, the heat transfer interaction is a thermodynamic property of the system, which is by definition equal to the energy change experienced by the system in going from state 1 to state 2. The last equation is the first law of thermodynamics for closed systems incapable of experiencing work transfer. Note that, unlike work transfer, the heat transfer is considered positive when it increases the energy of the system.

Most thermodynamic systems do not manifest purely mechanical ($\delta Q = 0$) or purely thermal ($\delta W = 0$) behavior. Most systems manifest a *coupled* mechanical and thermal behavior. The preceding first-law statements can be used to show that the first law of thermodynamics for a process executed by a closed system experiencing both work transfer and heat transfer is

$$\underbrace{\int_1^2 \delta Q}_{\text{heat transfer}} - \underbrace{\int_1^2 \delta W}_{\text{work transfer}} = \underbrace{E_2 - E_1}_{\text{energy change}}$$

energy interactions (nonproperties)
(property)

The first law means that the net heat transfer into the system equals the work done by the system on the environment, plus the increase in the energy of the system. The first law of thermodynamics for a cycle or for an integral number of cycles executed by a closed system is

$$\oint \delta Q = \oint \delta W = 0$$

Note that the net change in the thermodynamic property energy is zero during a cycle or an integral number of cycles.

The energy change term $E_2 - E_1$ appearing on the right-hand side of the first law can be replaced by a more general notation that distinguishes between macroscopically identifiable forms of energy storage (kinetic, gravitational) and energy stored internally,

$$E_2 - E_1 = \underbrace{U_2 - U_1}_{\text{internal energy change}} + \underbrace{\frac{mV_2^2}{2} - \frac{mV_1^2}{2}}_{\text{kinetic energy change}} + \underbrace{mgZ_2 - mgZ_1}_{\text{gravitational energy change}}$$

If the closed system expands or contracts *quasi-statically* (i.e., slowly enough, in mechanical equilibrium internally and with the environment) so that at every point in time the pressure P is uniform throughout the system, then the work transfer term can be calculated as being equal to the work done by all the boundary pressure forces as they move with their respective points of application,

$$\int_1^2 \delta W = \int_1^2 P dV$$

The work transfer integral can be evaluated provided the path of the quasi-static process, $P(V)$, is known; this is another reminder that the work transfer is path dependent (i.e., not a thermodynamic property).

3 SECOND LAW OF THERMODYNAMICS FOR CLOSED SYSTEMS

A *temperature reservoir* is a thermodynamic system that experiences only heat transfer and whose temperature remains constant during such interactions. Consider first a closed system executing a cycle or an integral number of cycles *while in thermal communication with no more than one temperature reservoir*. To state the second law for this case is to observe that the net work transfer during each cycle cannot be positive:

$$\oint \delta W = 0$$

In other words, a closed system cannot deliver work during one cycle, while in communication with one temperature reservoir or with no temperature reservoir at all. Examples of cyclic operation are the vibration of a spring–mass system or a ball bouncing on the pavement: In order for these systems to return to their respective initial heights, that is, in order for them to execute cycles, the environment (e.g., humans) must perform work on them. The limiting case of frictionless cyclic operation is termed *reversible* because in this limit the system returns to its initial state without intervention (work transfer) from the environment. Therefore, the distinction between reversible and irreversible cycles executed by closed systems in communication with no more than one temperature reservoir is

$$\oint \delta W = 0 \quad (\text{reversible})$$

$$\oint \delta W < 0 \quad (\text{irreversible})$$

To summarize, the first and second laws for closed systems operating cyclically in contact with no more than one temperature reservoir are (Fig. 1)

$$\oint \delta W = \oint \delta Q \leq 0$$

This statement of the second law can be used to show¹ that in the case of a closed system executing one or an integral number of cycles *while in communication with two temperature reservoirs*, the following inequality holds (Fig. 1):

$$\frac{Q_H}{T_H} + \frac{Q_L}{T_L} \leq 0$$

where *H* and *L* denote the high-temperature and the low-temperature reservoirs, respectively. Symbols Q_H and Q_L stand for the value of the cyclic integral $\oint \delta Q$, where δQ is in one case exchanged only with the T_H reservoir and in the other with the T_L reservoir. In the reversible limit, the second law reduces to $T_H/T_L = -Q_H/Q_L$, which serves as definition for the absolute *thermodynamic temperature* scale denoted by symbol T . Absolute temperatures are expressed either in degrees Kelvin, $T(\text{K})$, or in degrees Rankine, $T(^{\circ}\text{R})$; the relationships between absolute and relative temperatures are

$$T(\text{K}) = \theta(^{\circ}\text{C}) + 273.15 \text{ K} \quad T(^{\circ}\text{R}) = \theta(^{\circ}\text{F}) + 459.67^{\circ}\text{R}$$

$$1 \text{ K} = 1^{\circ}\text{C}$$

$$1 \text{ R} = 1^{\circ}\text{F}$$

A *heat engine* is a special case of a closed system operating cyclically while in thermal communication with two temperature reservoirs, a system that during each cycle receives heat and delivers work:

$$\oint \delta W = \oint \delta Q = Q_H + Q_L > 0$$

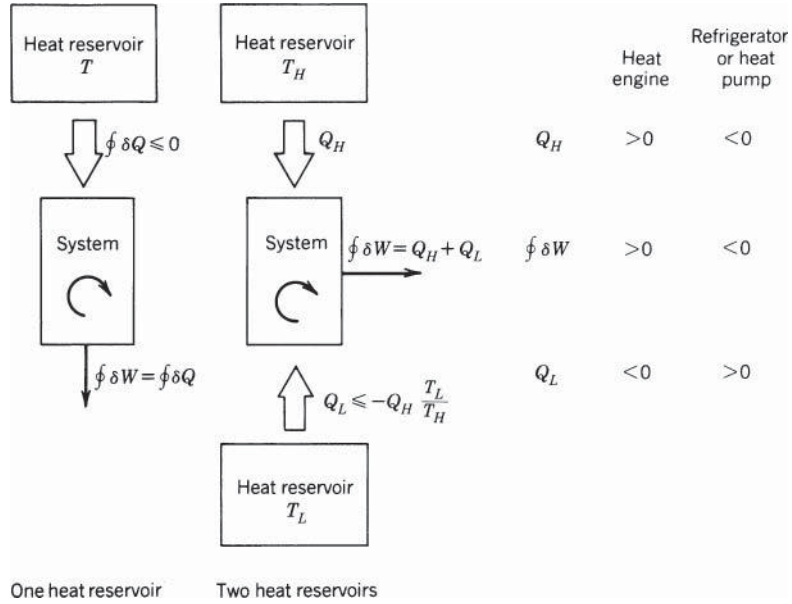


Figure 1 First and second laws of thermodynamics for a closed system operating cyclically while in communication with one or two heat reservoirs.

The goodness of the heat engine can be described in terms of the heat engine efficiency or the first-law efficiency:

$$\eta = \frac{\oint \delta W}{Q_H} \leq 1 - \frac{T_L}{T_H}$$

Alternatively, the second-law efficiency of the heat engine is defined as^{1,4,5}

$$\eta_{II} = \frac{\oint \delta W}{\left(\oint \delta W \right)_{\text{maximum}}} = \frac{\eta_I}{1 - T_L/T_H}$$

where “maximum” refers to the reversible case. A *refrigerating machine* or a *heat pump* operates cyclically between two temperature reservoirs in such a way that during each cycle it receives work and delivers net heat to the environment:

$$\oint \delta W = \oint \delta Q = Q_H + Q_L < 0$$

The goodness of such machines can be expressed in terms of a coefficient of performance (COP):

$$\text{COP}_{\text{refrigerator}} = \frac{Q_L}{-\oint \delta W} \leq \frac{1}{T_H/T_L - 1}$$

$$\text{COP}_{\text{heat pump}} = \frac{-Q_H}{-\oint \delta W} \leq \frac{1}{1 - T_L/T_H}$$

Generalizing the second law for closed systems operating cyclically, one can show that if during each cycle the system experiences any number of heat interactions Q_i with any number of temperature reservoirs whose respective absolute temperatures are T_i , then

$$\sum_i \frac{Q_i}{T_i} \leq 0$$

Note that T_i is the absolute temperature of the boundary region crossed by Q_i . Another way to write the second law in this case is

$$\oint \frac{\delta Q}{T} \leq 0$$

where, again, T is the temperature of the boundary pierced by δQ . Of special interest is the reversible cycle limit, for which the second law states $(\oint \delta Q/T)_{\text{rev}} = 0$. According to the definition of thermodynamic property, the second law implies that during a reversible process the quantity $\delta Q/T$ is the infinitesimal change in a property of the system: by definition, that property is the *entropy change*:

$$dS = \left(\frac{\delta Q}{T} \right)_{\text{rev}} \quad \text{or} \quad S_2 - S_1 = \left(\int_1^2 \frac{\delta Q}{T} \right)_{\text{rev}}$$

Combining this definition with the second law for a cycle, $\oint \delta Q/T \leq 0$, yields the second law of thermodynamics for *any process* executed by a closed system:

$$\underbrace{S_2 - S_1}_{\substack{\text{entropy} \\ \text{change} \\ \text{(property)}}} - \underbrace{\int_1^2 \frac{\delta Q}{T}}_{\substack{\text{entropy} \\ \text{transfer} \\ \text{(nonproperty)}}} \geq 0$$

The entire left-hand side in this inequality is by definition the *entropy generated* by the process:

$$S_{\text{gen}} = S_2 - S_1 - \int_1^2 \frac{\delta Q}{T}$$

The second law states that S_{gen} cannot be negative. The entropy generation is a measure of the inequality sign in the second law and hence a measure of the irreversibility of the process. As shown in Chapter 4, the entropy generation is proportional to the useful work destroyed during the process.^{1,4,5} Any heat interaction (δQ) is accompanied by entropy transfer ($\delta Q/T$), whereas the work transfer δW is not.

4 ENERGY MINIMUM PRINCIPLE

Consider now a closed system that executes an infinitesimally small change of state, which means that its state changes from (U, S, \dots) to $(U + dU, S + dS, \dots)$. The first law and the second law statements are

$$\begin{aligned} \delta Q - \delta W &= dU \\ dS - \frac{\delta Q}{T} &\geq 0 \end{aligned}$$

If the system is *isolated* from its environment, then $\delta W = 0$ and $\delta Q = 0$, and the two laws dictate that during any such process the energy inventory is constant ($dU = 0$), and entropy inventory cannot decrease,

$$dS \geq 0$$

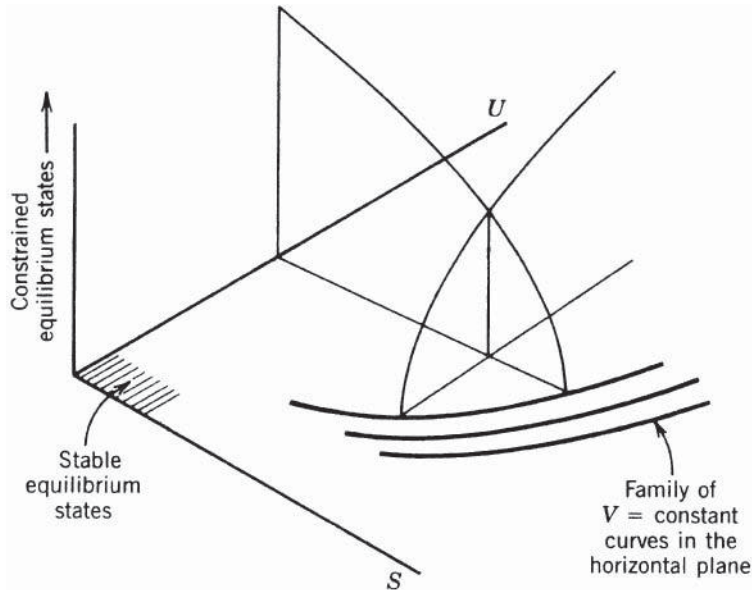


Figure 2 Energy minimum principle, or the entropy maximum principle.

Isolated systems undergo processes when they experience internal changes that do not require intervention from the outside, e.g., the removal of one or more of the *internal constraints* plotted qualitatively in the vertical direction in Fig. 2. When all the constraints are removed, changes cease; and according to $dS \geq 0$, the entropy inventory reaches its highest possible level. This *entropy maximum principle* is a consequence of the first and second laws combined. When all the internal constraints have disappeared, the system has reached the *unconstrained equilibrium state*.

Alternatively, if changes occur in the absence of work transfer and at constant S , the first law and the second law require respectively, $dU = \delta Q$ and $\delta Q \leq 0$, hence

$$dU \leq 0$$

The energy inventory cannot increase, and when the unconstrained equilibrium state is reached the system energy inventory is minimum. This *energy minimum principle* is also a consequence of the first and second laws for closed systems.

The interest in this classical formulation of the laws (e.g., Fig. 2) has been renewed by the emergence of the constructal law as a first-principle that governs the phenomenon of generation and evolution of flow configuration⁶⁻⁸ (see Chapter 4.)

5 LAWS OF THERMODYNAMICS FOR OPEN SYSTEMS

If \dot{m} represents the mass flow rate through a port in the control surface, the principle of *mass conservation* in the control volume is

$$\underbrace{\sum_{\text{in}} \dot{m} - \sum_{\text{out}} \dot{m}}_{\text{mass transfer}} = \underbrace{\frac{\partial M}{\partial t}}_{\text{mass change}}$$

Subscripts in and out refer to summation over all the inlet and outlet ports, respectively, while M stands for the instantaneous mass inventory of the control volume.

The *first law of thermodynamics* is more general than the statement encountered earlier for closed systems because this time we must account for the flow of energy associated with the \dot{m} streams:

$$\underbrace{\sum_{\text{in}} \dot{m} \left(h + \frac{V^2}{2} + gZ \right) - \sum_{\text{out}} \dot{m} \left(h + \frac{V^2}{2} + gZ \right) + \sum_i \dot{Q}_i - \dot{W}}_{\text{energy transfer}} = \underbrace{\frac{\partial E}{\partial t}}_{\text{energy change}}$$

On the left-hand side we have the energy interactions: heat, work, and the energy transfer associated with mass flow across the control surface. The specific enthalpy h , fluid velocity V , and height Z are evaluated right at the boundary. On the right-hand side, E is the instantaneous system energy integrated over the control volume.

The *second law of thermodynamics* for an open system assumes the form

$$\underbrace{\sum_{\text{in}} \dot{m}s - \sum_{\text{out}} \dot{m}s + \sum_i \frac{\dot{Q}_i}{T_i}}_{\text{entropy transfer}} \leq \underbrace{\frac{\partial S}{\partial t}}_{\text{entropy change}}$$

The specific entropy s is representative of the thermodynamic state of each stream right at the system boundary. The *entropy generation rate* is defined by

$$\dot{S}_{\text{gen}} = \frac{\partial S}{\partial t} + \sum_{\text{out}} \dot{m}s - \sum_{\text{in}} \dot{m}s - \sum_i \frac{\dot{Q}_i}{T_i}$$

and is a measure of the irreversibility of open system operation. The engineering importance of \dot{S}_{gen} stems from its proportionality to the rate of destruction of available work. If the following parameters are fixed—all the mass flows (\dot{m}), the peripheral conditions (h, s, V, Z), and the heat interactions (\dot{Q}_i, T_i) except (\dot{Q}_0, T_0)—then one can use the first law and the second law to show that the work transfer rate cannot exceed a theoretical maximum^{1,4,5}

$$\dot{W} \leq \sum_{\text{in}} \dot{m} \left(h + \frac{V^2}{2} + gZ - T_0 s \right) - \sum_{\text{out}} \dot{m} \left(h + \frac{V^2}{2} + gZ - T_0 s \right) - \frac{\partial}{\partial t} (E - T_0 S)$$

The right-hand side in this inequality is the maximum work transfer rate $\dot{W}_{\text{sh,max}}$, which would exist only in the ideal limit of reversible operation. The rate of *lost work*, or the rate of exergy (availability) destruction, is defined as

$$\dot{W}_{\text{lost}} = \dot{W}_{\text{max}} - \dot{W}$$

Again, using both laws, one can show that lost work is directly proportional to entropy generation,

$$\dot{W}_{\text{lost}} = T_0 \dot{S}_{\text{gen}}$$

This result is known as the Gouy–Stodola theorem.^{1,4,5} Conservation of useful work (exergy) in thermodynamic systems can only be achieved based on the systematic minimization of entropy generation in all the components of the system. Engineering applications of entropy generation minimization as a design optimization philosophy may be found in Refs. 1, 4, and 5 and in Chapter 4.

6 RELATIONS AMONG THERMODYNAMIC PROPERTIES

The analytical forms of the first and second laws of thermodynamics contain properties such as internal energy, enthalpy, and entropy, which cannot be measured directly. The values of

these properties are derived from measurements that can be carried out in the laboratory (e.g., pressure, volume, temperature, specific heat); the formulas connecting the derived properties to the measurable properties are reviewed in this section. Consider an infinitesimal change of state experienced by a closed system. If kinetic and gravitational energy changes can be neglected, the first law reads

$$\delta Q_{\text{any path}} - \delta W_{\text{any path}} = dU$$

which emphasizes that dU is path independent. In particular, for a reversible path (rev), the same dU is given by

$$\delta Q_{\text{rev}} - \delta W_{\text{rev}} = dU$$

Note that from the second law for closed systems we have $\delta Q_{\text{rev}} = T dS$. Reversibility (or zero entropy generation) also requires internal mechanical equilibrium at each stage during the process; hence, $\delta W_{\text{rev}} = P dV$, as for a quasistatic change in volume. The infinitesimal change experienced by U is therefore

$$T dS - P dV = dU$$

Note that this formula holds for an infinitesimal change of state along any path (because dU is path independent); however, $T dS$ matches δQ and $P dV$ matches δW only if the path is reversible. In general, $\delta Q < T dS$ and $\delta W < P dV$. The formula derived above for dU can be written for a unit mass: $T ds - P dv = du$. Additional identities implied by this relation are

$$T = \left(\frac{\partial u}{\partial s} \right)_v \quad -P = \left(\frac{\partial u}{\partial v} \right)_s$$

$$\frac{\partial^2 u}{\partial s \partial v} = \left(\frac{\partial T}{\partial v} \right)_s = - \left(\frac{\partial P}{\partial s} \right)_v$$

where the subscript indicates which variable is held constant during partial differentiation. Similar relations and partial derivative identities exist in conjunction with other derived functions such as enthalpy, Gibbs free energy, and Helmholtz free energy:

- Enthalpy (defined as $h = u + Pv$)

$$dh = T ds + v dP$$

$$T = \left(\frac{\partial h}{\partial s} \right)_P \quad v = \left(\frac{\partial h}{\partial P} \right)_s$$

$$\frac{\partial^2 h}{\partial s \partial P} = \left(\frac{\partial T}{\partial P} \right)_s = \left(\frac{\partial v}{\partial s} \right)_P$$

- Gibbs free energy (defined as $g = h - Ts$)

$$dg = -s dT + v dP$$

$$-s = \left(\frac{\partial g}{\partial T} \right)_P \quad v = \left(\frac{\partial g}{\partial P} \right)_T$$

$$\frac{\partial^2 g}{\partial T \partial P} = - \left(\frac{\partial s}{\partial P} \right)_T = \left(\frac{\partial v}{\partial T} \right)_P$$

- Helmholtz free energy (defined as $f = u - Ts$)

$$df = -s dT - P dv$$

$$-s = \left(\frac{\partial f}{\partial T} \right)_v \quad -P = \left(\frac{\partial f}{\partial v} \right)_T$$

$$\frac{\partial^2 f}{\partial T \partial v} = - \left(\frac{\partial s}{\partial v} \right)_T = - \left(\frac{\partial P}{\partial T} \right)_v$$

In addition to the (P, v, T) surface, which can be determined based on measurements (Fig. 3), the following partial derivatives are furnished by special experiments¹:

- The specific heat at constant volume, $c_v = (\partial u / \partial T)_v$, follows directly from the constant volume ($\partial W = 0$) heating of a unit mass of pure substance.
- The specific heat at constant pressure, $c_p = (\partial h / \partial T)_p$, is determined during the constant-pressure heating of a unit mass of pure substance.
- The Joule–Thomson coefficient, $\mu = (\partial T / \partial P)_h$, is measured during a throttling process, that is, during the flow of a stream through an adiabatic duct with friction (see the first law for an open system in the steady state).
- The coefficient of thermal expansion, $\beta = (1/v)(\partial v / \partial T)_p$.
- The isothermal compressibility, $K = (-1/v)(\partial v / \partial P)_T$.
- The constant temperature coefficient, $c_T = (\partial h / \partial P)_T$.

Two noteworthy relationships between some of the partial-derivative measurements are

$$c_p - c_v = \frac{Tv\beta^2}{K}$$

$$\mu = \frac{1}{c_p} \left[T \left(\frac{\partial v}{\partial T} \right)_p - v \right]$$

The general equations relating the derived properties (u, h, s) to measurable quantities are

$$du = c_v dT + \left[T \left(\frac{\partial P}{\partial T} \right)_v - P \right] dv$$

$$dh = c_p dT + \left[-T \left(\frac{\partial v}{\partial T} \right)_p + v \right] dP$$

$$ds = \frac{c_v}{T} dT + \left(\frac{\partial v}{\partial T} \right)_v dv \quad \text{or} \quad ds = \frac{c_p}{T} dT - \left(\frac{\partial v}{\partial T} \right)_p dP$$

These relations also suggest the following identities:

$$\left(\frac{\partial u}{\partial T} \right)_v = T \left(\frac{\partial s}{\partial T} \right)_v = c_v \quad \left(\frac{\partial h}{\partial T} \right)_p = T \left(\frac{\partial s}{\partial T} \right)_p = c_p$$

The relationships between thermodynamic properties and the analyses associated with applying the laws of thermodynamics are simplified considerably in cases where the pure substance exhibits *ideal gas* behavior. As shown in Fig. 3, this behavior prevails at sufficiently high temperatures and low pressures where the (P, v, T) surface is fitted closely by the simple expression

$$\frac{Pv}{T} = R \text{ (constant)}$$

where R is the ideal gas constant of the substance of interest (Table 1). The formulas for internal energy, enthalpy, and entropy, which concluded the preceding section, assume the following form in the ideal gas limit:

$$du = c_v dT \quad c_v = c_v(T)$$

$$dh = c_p dT \quad c_p = c_p(T) = c_v + R$$

$$ds = \frac{c_v}{T} dT + \frac{R}{v} dv \quad \text{or} \quad ds = \frac{c_p}{T} dT - \frac{R}{P} dP \quad \text{or} \quad ds = \frac{c_v}{P} dP + \frac{c_p}{v} dv$$

If the coefficients c_v and c_p are constant in the temperature domain of interest, then the *changes* in specific internal energy, enthalpy, and entropy relative to a reference state $()_0$ are

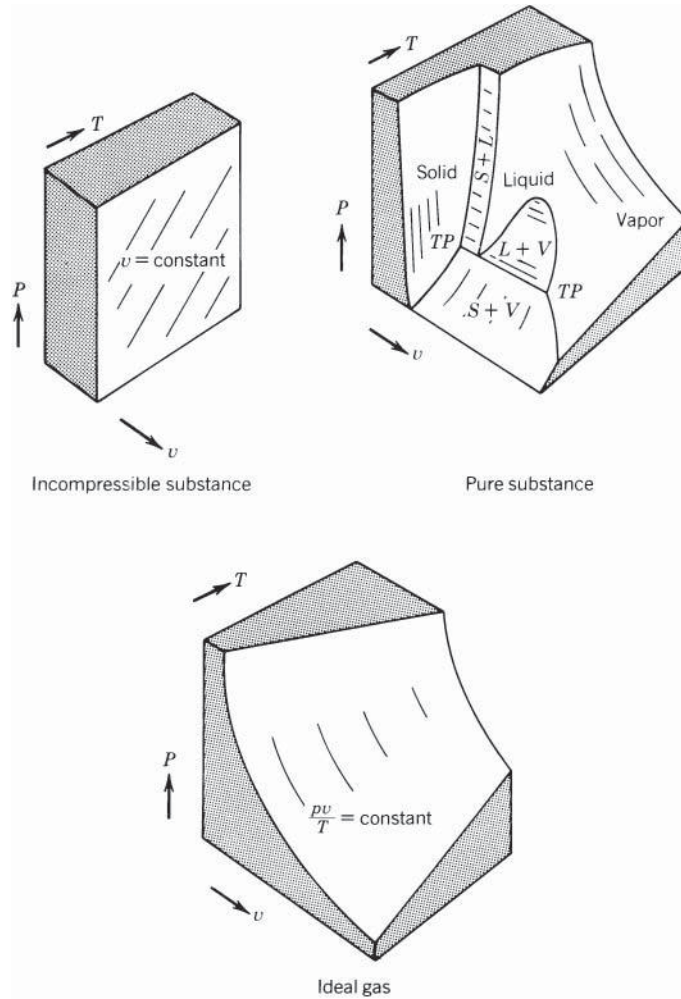


Figure 3 The (P, v, T) surface for a pure substance that contracts upon freezing, showing regions of ideal gas and incompressible fluid behavior. (In this figure, S = solid, V = vapor, L = liquid, TP = triple point.)

given by the formulas

$$u - u_0 = c_v(T - T_0)$$

$$h - h_0 = c_p(T - T_0) \quad (\text{where } h_0 = u_0 + RT_0)$$

$$s - s_0 = c_v \ln \frac{T}{T_0} + R \ln \frac{v}{v_0}$$

$$s - s_0 = c_p \ln \frac{T}{T_0} - R \ln \frac{P}{P_0}$$

$$s - s_0 = c_v \ln \frac{P}{P_0} + c_p \ln \frac{v}{v_0}$$

Table 1 Values of Ideal Gas Constant and Specific Heat at Constant Volume for Gases Encountered in Mechanical Engineering

Ideal Gas	$R \left(\frac{\text{J}}{\text{kg} \cdot \text{K}} \right)$	$c_p \left(\frac{\text{J}}{\text{kg} \cdot \text{K}} \right)$
Air	286.8	715.9
Argon, Ar	208.1	316.5
Butane, C ₄ H ₁₀	143.2	1595.2
Carbon dioxide, CO ₂	188.8	661.5
Carbon monoxide, CO	296.8	745.3
Ethane, C ₂ H ₆	276.3	1511.4
Ethylene, C ₂ H ₄	296.4	1423.5
Helium, He ₂	2076.7	3152.7
Hydrogen, H	4123.6	10216.0
Methane, CH ₄	518.3	1687.3
Neon, Ne	412.0	618.4
Nitrogen, N ₂	296.8	741.1
Octane, C ₈ H ₁₈	72.85	1641.2
Oxygen, O ₂	259.6	657.3
Propane, C ₃ H ₈	188.4	1515.6
Steam, H ₂ O	461.4	1402.6

Source: From Ref. 1.

The ideal gas model rests on two empirical constants, c_v and c_p , or c_v and R , or c_p and R . The ideal gas limit is also characterized by

$$\mu = 0 \quad \beta = \frac{1}{P} \quad K = \frac{1}{P} \quad c_T = 0$$

The extent to which a thermodynamic system destroys available work is intimately tied to the system's entropy generation, that is, to the system's departure from the theoretical limit of reversible operation. Idealized processes that can be modeled as reversible occupy a central role in engineering thermodynamics because they can serve as standard in assessing the goodness of real processes. Two benchmark reversible processes executed by closed ideal gas systems are particularly simple and useful. A *quasi-static adiabatic process* $1 \rightarrow 2$ executed by a closed ideal gas system has the following characteristics:

$$\int_1^2 \delta Q = 0$$

$$\int_1^2 \delta W = \frac{P_2 V_2}{\gamma - 1} \left[\left(\frac{V_2}{V_1} \right)^{\gamma - 1} - 1 \right]$$

where $\gamma = c_p/c_v$

- Path

$$PV^\gamma = P_1 V_1^\gamma = P_2 V_2^\gamma \text{ (constant)}$$

- Entropy change

$$S_2 - S_1 = 0$$

hence the name *isoentropic* or *isentropic* for this process.

- Entropy generation

$$S_{gen_{1 \rightarrow 2}} = S_2 - S_1 - \int_1^2 \frac{\delta Q}{T} = 0 \text{ (reversible)}$$

A *quasi-static isothermal process* 1 → 2 executed by a closed ideal gas system in communication with a single temperature reservoir T is characterized by

- Energy interactions

$$\int_1^2 \delta Q = \int_1^2 \delta W = mRT \ln \frac{V_2}{V_1}$$

- Path

$$T = T_1 = T_2(\text{constant}) \quad \text{or} \quad PV = P_1V_1 = P_2V_2(\text{constant})$$

- Entropy change

$$S_2 - S_1 = mR \ln \frac{V_2}{V_1}$$

- Entropy generation

$$S_{gen_{1 \rightarrow 2}} = S_2 - S_1 - \int_1^2 \frac{\delta Q}{T} = 0 \quad (\text{reversible})$$

Mixtures of ideal gases also behave as ideal gases in the high-temperature, low-pressure limit. If a certain mixture of mass m contains ideal gases mixed in mass proportions m_i , and if the ideal gas constants of each component are (c_{vi} , c_{pi} , R_i), then the equivalent ideal gas constants of the mixture are

$$c_v = \frac{1}{m} \sum_i m_i c_{vi}$$

$$c_p = \frac{1}{m} \sum_i m_i c_{pi}$$

$$R = \frac{1}{m} \sum_i m_i R_i$$

where $m = \sum_i m_i$.

One mole is the amount of substance of a system that contains as many elementary entities (e.g., molecules) as there are in 12 g of carbon 12; the number of such entities is Avogadro's constant, $N_0 \cong 6.022 \times 10^{23}$. The mole is not a mass unit because the mass of 1 mol is not the same for all substances. The *molar mass* M of a given molecular species is the mass of 1 mol of that species, so that the total mass m is equal to M times the number of moles n :

$$m = nM$$

Thus, the ideal gas equation of state can be written as

$$PV = nMRT$$

where the product MR is the *universal gas constant*

$$\bar{R} = MR = 8.314 \frac{\text{J}}{\text{mol} \cdot \text{K}}$$

The equivalent molar mass of a mixture of ideal gases with individual molar masses M_i is

$$M = \frac{1}{n} \sum_i n_i M_i$$

where $n = \sum_i n_i$. The molar mass of air, as a mixture of nitrogen, oxygen, and traces of other gases, is 28.966 g/mol (or 28.966 kg/kmol). A more useful model of the air–gas mixture relies on only nitrogen and oxygen as constituents, in the proportion 3.76 mol of nitrogen to every mole of oxygen; this simple model is used frequently in the field of combustion.¹

At the opposite end of the spectrum is the *incompressible substance* model. At sufficiently high pressures and low temperatures in Fig. 3, solids and liquids behave so that their density

or specific volume is practically constant. In this limit the (P, v, T) surface is adequately represented by the equation

$$v = \bar{v} \quad (\text{constant})$$

The formulas for calculating changes in internal energy, enthalpy, and entropy become (see the end of this section)

$$du = c dT$$

$$dh = c dT + \bar{v} dP$$

$$ds = \frac{c}{T} dT$$

where c is the sole specific heat of the incompressible substance,

$$c = c_v = c_p$$

The specific heat c is a function of temperature only. In a sufficiently narrow temperature range where c can be regarded as constant, the finite changes in internal energy, enthalpy, and entropy relative to a reference state denoted by $()_0$ are

$$u - u_0 = c(T - T_0)$$

$$h - h_0 = c(T - T_0) + \bar{v}(P - P_0) \quad (\text{where } h_0 = u_0 + P_0 \bar{v})$$

$$s - s_0 = c \ln \frac{T}{T_0}$$

The incompressible substance model rests on two empirical constants, c and \bar{v} .

As shown in Fig. 3, the domains in which the pure substance behaves either as an ideal gas or as an incompressible substance intersect over regions where the substance exists as a mixture of two phases, liquid and vapor, solid and liquid, or solid and vapor. The two-phase regions themselves intersect along the *triple point* line labeled TP–TP on the middle sketch of Fig. 3. In engineering cycle calculations, more useful are the projections of the (P, v, T) surface on the P - v plane or, through the relations reviewed earlier, on the T - s plane. The terminology associated with two-phase equilibrium states is defined on the P - v diagram of Fig. 4a, where we imagine the isothermal compression of a unit mass of substance (a closed system). As the specific volume v decreases, the substance ceases to be a pure vapor at state g , where the first droplets of liquid are formed. State g is a *saturated vapor state*. Isothermal compression beyond g proceeds at constant pressure up to state f , where the last bubble (immersed in liquid) is suppressed. State f is a *saturated liquid state*. Isothermal compression beyond f is accompanied by a steep rise in pressure, depending on the compressibility of the liquid phase. The *critical state* is the intersection of the locus of saturated vapor states with the locus of saturated liquid states (Fig. 4a). The temperature and pressure corresponding to the critical state are the *critical temperature* and *critical pressure*. Table 2 contains a compilation of critical-state properties of some of the more common substances.

Figure 4b shows the projection of the liquid and vapor domain on the T - s plane. On the same drawing is shown the relative positioning (the relative slopes) of the traces of various constant-property cuts through the three-dimensional surface on which all the equilibrium states are positioned. In the two-phase region, the temperature is a unique function of pressure. This one-to-one relationship is indicated also by the *Clapeyron* relation

$$\left(\frac{dP}{dT} \right)_{\text{sat}} = \frac{h_g - h_f}{T(v_g - v_f)} = \frac{s_g - s_f}{v_g - v_f}$$

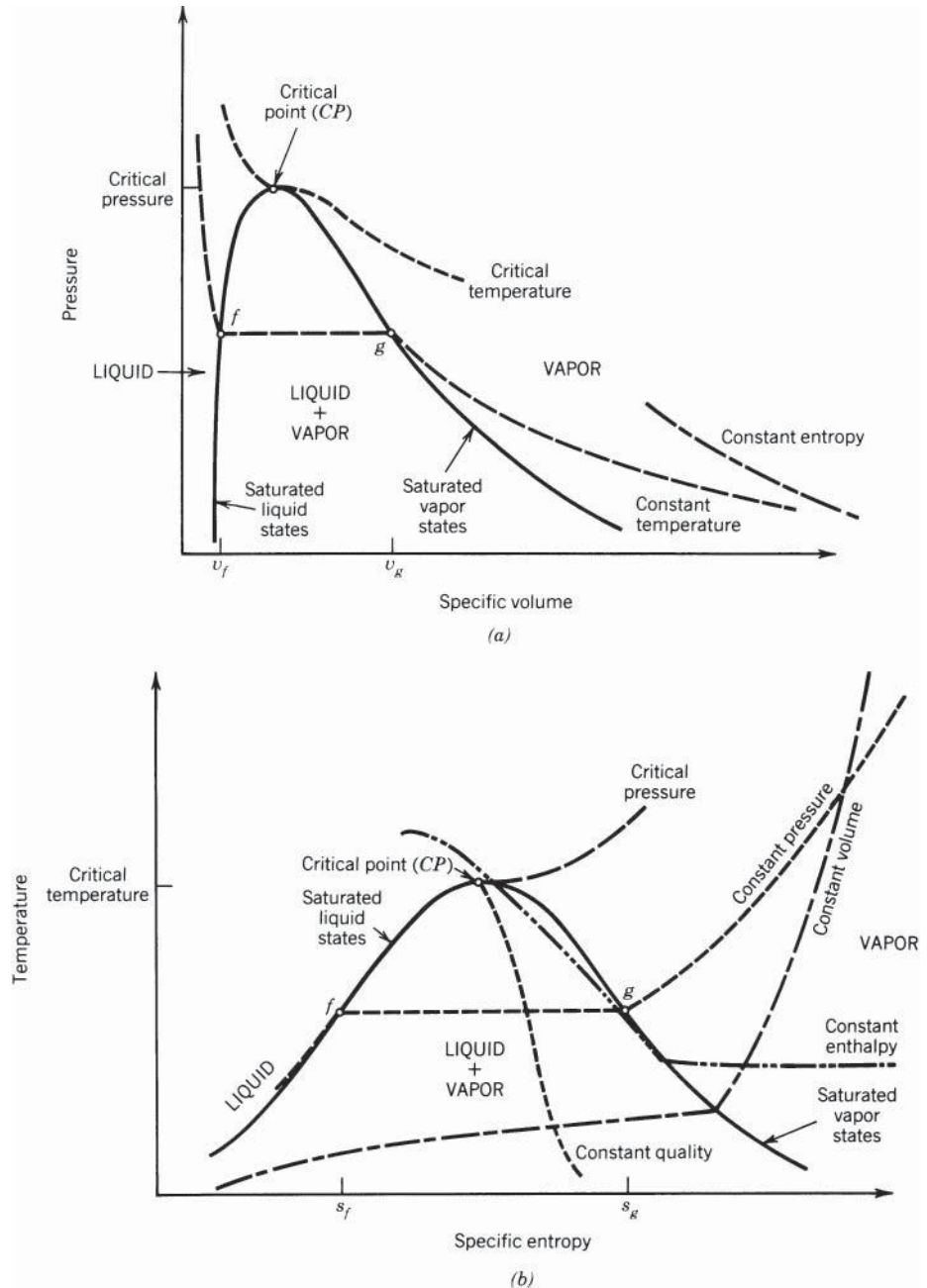


Figure 4 Locus of two-phase (liquid and vapor) states, projected on (a) the P - v plane and (b) the T - s plane.

Table 2 Critical-State Properties

Fluid	Critical Temperature		Critical pressure		Critical Specific Volume (cm ³ /g)
	[K]	[°C]	[MPa]	[atm]	
Air	133.2	(−140)	3.77	(37.2)	2.9
Alcohol (methyl)	513.2	(240)	7.98	(78.7)	3.7
Alcohol (ethyl)	516.5	(243.3)	6.39	(63.1)	3.6
Ammonia	405.4	(132.2)	11.3	(111.6)	4.25
Argon	150.9	(−122.2)	4.86	(48)	1.88
Butane	425.9	(152.8)	3.65	(36)	4.4
Carbon dioxide	304.3	(31.1)	7.4	(73)	2.2
Carbon monoxide	134.3	(−138.9)	3.54	(35)	3.2
Carbon tetrachloride	555.9	(282.8)	4.56	(45)	1.81
Chlorine	417	(143.9)	7.72	(76.14)	1.75
Ethane	305.4	(32.2)	4.94	(48.8)	4.75
Ethylene	282.6	(9.4)	5.85	(57.7)	4.6
Helium	5.2	(−268)	0.228	(2.25)	14.4
Hexane	508.2	(235)	2.99	(29.5)	4.25
Hydrogen	33.2	(−240)	1.30	(12.79)	32.3
Methane	190.9	(−82.2)	4.64	(45.8)	6.2
Methyl chloride	416.5	(143.3)	6.67	(65.8)	2.7
Neon	44.2	(−288.9)	2.7	(26.6)	2.1
Nitric oxide	179.2	(−93.9)	6.58	(65)	1.94
Nitrogen	125.9	(−147.2)	3.39	(33.5)	3.25
Octane	569.3	(296.1)	2.5	(24.63)	4.25
Oxygen	154.3	(−118.9)	5.03	(49.7)	2.3
Propane	368.7	(95.6)	4.36	(43)	4.4
Sulfur dioxide	430.4	(157.2)	7.87	(77.7)	1.94
Water	647	(373.9)	22.1	(218.2)	3.1

Source: From Ref. 1.

where the subscript sat is a reminder that the relation holds for saturated states (such as g and f) and for mixtures of two saturated phases. Subscripts g and f indicate properties corresponding to the saturated vapor and liquid states found at temperature T_{sat} (and pressure P_{sat}). Built into the last equation is the identity

$$h_g - h_f = T(s_g - s_f)$$

which is equivalent to the statement that the Gibbs free energy is the same for the saturated states and their mixtures found at the same temperature, $g_g = g_f$.

The properties of a two-phase mixture depend on the proportion in which saturated vapor, m_g , and saturated liquid, m_f , enter the mixture. The composition of the mixture is described by the property called *quality*:

$$x = \frac{m_g}{m_f + m_g}$$

The quality varies between 0 at state f and 1 at state g . Other properties of the mixture can be calculated in terms of the properties of the saturated states found at the same temperature:

$$\begin{aligned} u &= u_f + xu_{fg} & s &= s_f + xs_{fg} \\ h &= h_f + xh_{fg} & v &= v_f + xv_{fg} \end{aligned}$$

with the notation $(\)_{fg} = (\)_g - (\)_f$. Similar relations can be used to calculate the properties of two-phase states other than liquid and vapor, namely, solid and vapor or solid and liquid.

For example, the enthalpy of a solid and liquid mixture is given by $h = h_s + xh_{sf}$, where subscript s stands for the *saturated solid state* found at the same temperature as for the two-phase state, and where h_{sf} is the latent heat of melting or solidification.

In general, the states situated immediately outside the two-phase dome sketched in Figs. 3 and 4 do not follow very well the limiting models discussed earlier in this section (ideal gas, incompressible substance). Because the properties of closely neighboring states are usually not available in tabular form, the following approximate calculation proves useful. For a *moderately compressed liquid state*, which is indicated by the subscript $(*)_*$, that is, for a state situated close to the left of the dome in Fig. 4, the properties may be calculated as slight deviations from those of the saturated liquid state found at the same temperature as the compressed liquid state of interest:

$$h_* \cong (h_f)_{T_*} + (v_f)_{T_*} [P_* - (P_f)_{T_*}]$$

$$s \cong (s_f)_{T_*}$$

For a *slightly superheated vapor state*, that is, a state situated close to the right of the dome in Fig. 4, the properties may be estimated in terms of those of the saturated vapor state found at the same temperature:

$$h_+ \cong (h_g)_{T_+}$$

$$s_+ \cong (s_g)_{T_+} + \left(\frac{P_g v_g}{T_g} \right)_{T_+} \ln \frac{(P_g)_{T_+}}{P_+}$$

In these expressions, subscript $(*)_+$ indicates the properties of the slightly superheated vapor state.

7 ANALYSIS OF ENGINEERING SYSTEM COMPONENTS

This section contains a summary¹ of the equations obtained by applying the first and second laws of thermodynamics to the components encountered in most engineering systems, such as power cycles and refrigeration cycles. It is assumed that each component operates in *steady flow*.

- *Valve* (throttle) or adiabatic duct with friction (Fig. 5a):

$$\text{First law} \quad h_1 = h_2$$

$$\text{Second law} \quad \dot{S}_{\text{gen}} = \dot{m}(s_2 - s_1) > 0$$

- *Expander* or *turbine* with negligible heat transfer to the ambient (Fig. 5b):

$$\text{First law} \quad \dot{W}_T = \dot{m}(h_1 - h_2)$$

$$\text{Second law} \quad \dot{S}_{\text{gen}} = \dot{m}(s_2 - s_1) \geq 0$$

$$\text{Efficiency} \quad \eta_T = \frac{h_1 - h_2}{h_1 - h_{2,\text{rev}}} \leq 1$$

- *Compressor* or *pump* with negligible heat transfer to the ambient (Fig. 5c):

$$\text{First law} \quad \dot{W}_C = \dot{m}(h_2 - h_1)$$

$$\text{Second law} \quad \dot{S}_{\text{gen}} = \dot{m}(s_2 - s_1) \geq 0$$

$$\text{Efficiency} \quad \eta_C = \frac{h_{2,\text{rev}} - h_1}{h_2 - h_1} \leq 1$$

- *Nozzle* with negligible heat transfer to the ambient (Fig. 5d):

First law $\frac{1}{2} (V_2^2 - V_1^2) = h_1 - h_2$

Second law $\dot{S}_{\text{gen}} = \dot{m}(s_2 - s_1) \geq 0$

Efficiency $\eta_N = \frac{V_2^2 - V_1^2}{V_{2,\text{rev}}^2 - V_1^2} \leq 1$

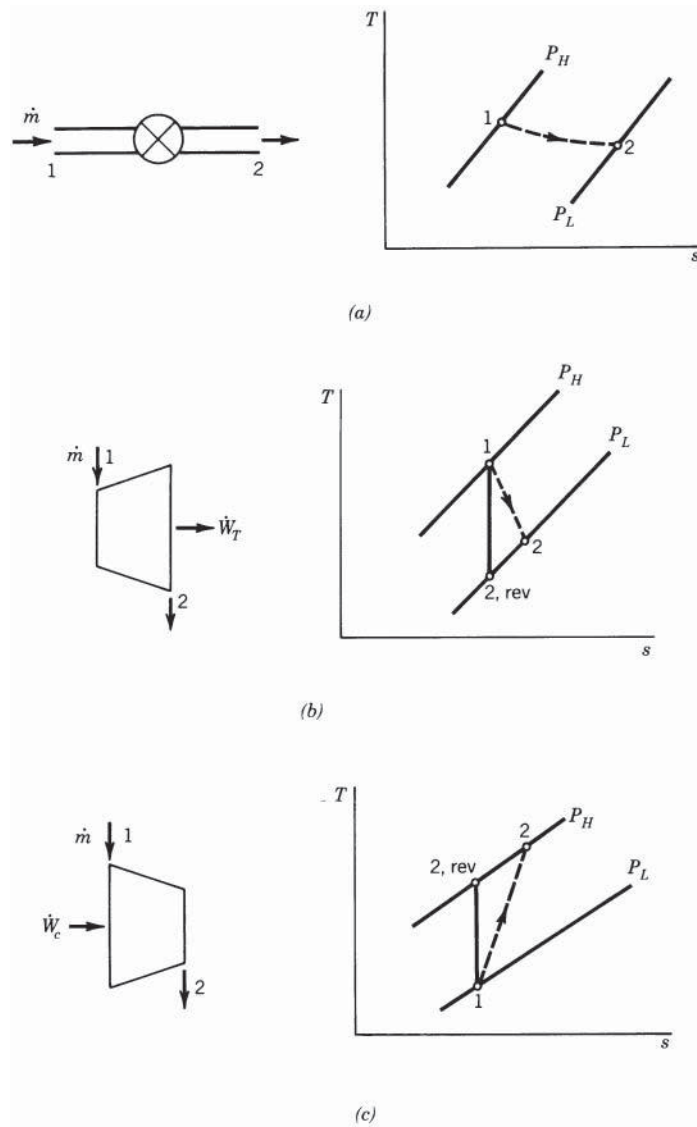
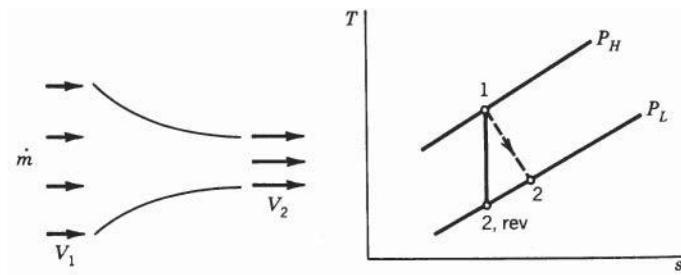
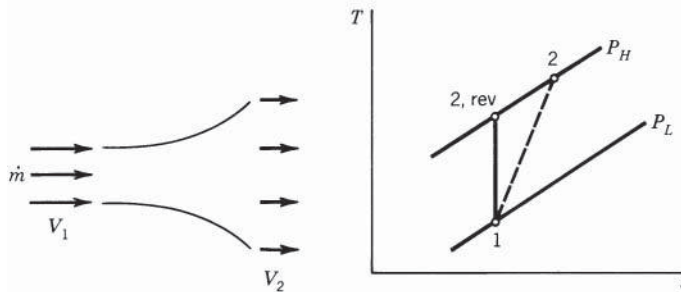


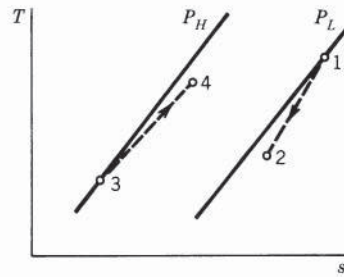
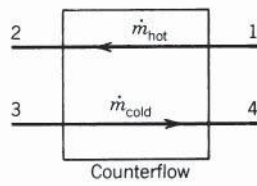
Figure 5 Engineering system components and their inlet and outlet states on the T - s plane, (P_H = high pressure; P_L = low pressure).



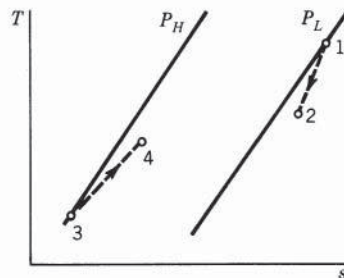
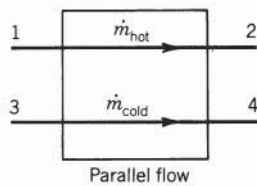
(d)



(e)



(f)



(g)

Figure 5 (continued)

- *Diffuser* with negligible heat transfer to the ambient (Fig. 5e):

$$\text{First law} \quad h_2 - h_1 = \frac{1}{2} (V_1^2 - V_2^2)$$

$$\text{Second law} \quad \dot{S}_{\text{gen}} = \dot{m}(s_2 - s_1) \geq 0$$

$$\text{Efficiency} \quad \eta_D = \frac{h_{2,\text{rev}} - h_1}{h_2 - h_1} \leq 1$$

- *Heat exchangers* with negligible heat transfer to the ambient (Figs. 5f and 5g):

$$\text{First law} \quad \dot{m}_{\text{hot}}(h_1 - h_2) = \dot{m}_{\text{cold}}(h_4 - h_3)$$

$$\text{Second law} \quad \dot{S}_{\text{gen}} = \dot{m}_{\text{hot}}(s_2 - s_1) + \dot{m}_{\text{cold}}(s_4 - s_3) \geq 0$$

Figures 5f and 5g show that a pressure drop always occurs in the direction of flow, in any heat exchanger flow passage.

REFERENCES

1. A. Bejan, *Advanced Engineering Thermodynamics*, 3rd ed., Wiley, Hoboken, NJ, 2006.
2. A. Bejan, *Heat Transfer*, Wiley, New York, 1993.
3. A. Bejan, *Convection Heat Transfer*, 4th ed., Wiley, Hoboken, NJ, 2013.
4. A. Bejan, *Entropy Generation through Heat and Fluid Flow*, Wiley, New York, 1982.
5. A. Bejan, *Entropy Generation Minimization*, CRC Press, Boca Raton, FL, 1996.
6. A. Bejan and S. Lorente, "The Constructal Law and the Thermodynamics of Flow Systems with Configuration," *Int. J. Heat Mass Transfer* **47**, 3203–3214, 2004.
7. A. Bejan and S. Lorente, *Design with Constructal Theory*, Wiley, Hoboken, NJ, 2008.
8. A. Bejan and J. P. Zane, *Design in Nature*, Doubleday, New York, 2012.

CHAPTER 4

EXERGY ANALYSIS, ENTROPY GENERATION MINIMIZATION, AND THE CONSTRUCTAL LAW

Adrian Bejan
Duke University
Durham, North Carolina

1	INTRODUCTION	157	6	STORAGE SYSTEMS	168
2	EXERGY ANALYSIS	160	7	SOLAR ENERGY CONVERSION	169
3	ENTROPY GENERATION MINIMIZATION	164	8	POWER PLANTS	170
4	CRYOGENICS	165	9	CONSTRUCTAL LAW	173
5	HEAT TRANSFER	166		REFERENCES	182

1 INTRODUCTION

In this chapter, we review three methods that account for much of the newer work in engineering thermodynamics and thermal design and optimization. The method of *exergy analysis* rests on thermodynamics alone. The first law, the second law, and the environment are used simultaneously in order to determine (i) the theoretical operating conditions of the system in the reversible limit and (ii) the entropy generated (or exergy destroyed) by the actual system, that is, the departure from the reversible limit. The focus is on *analysis*. Applied to the system components individually, exergy analysis shows us quantitatively how much each component contributes to the overall irreversibility of the system.^{1,2}

Entropy generation minimization (EGM) is a method of *modeling* and *optimization*. The entropy generated by the system is first developed as a function of the physical characteristics of the system (dimensions, materials, shapes, constraints). An important preliminary step is the construction of a system model that incorporates not only the traditional building blocks of engineering thermodynamics (systems, laws, cycles, processes, interactions) but also the fundamental principles of fluid mechanics, heat transfer, mass transfer, and other transport phenomena. This combination makes the model “realistic” by accounting for the inherent irreversibility of the actual device. Finally, the minimum entropy generation design ($S_{\text{gen,min}}$) is determined for the model, and the approach of any other design (S_{gen}) to the limit of realistic ideality represented by $S_{\text{gen,min}}$ is monitored in terms of the entropy generation number $N_S = S_{\text{gen}}/S_{\text{gen,min}} > 1$.

In order to calculate S_{gen} and minimize it, the analyst does not need to rely on the concept of exergy. The EGM method represents an important step beyond thermodynamics. It is a self-standing method³ that combines thermodynamics, heat transfer, and fluid mechanics into

a powerful technique for modeling and optimizing real systems and processes. The use of the EGM method has expanded greatly.⁴

The most recent development in thermodynamic optimization is the focus on the generation of flow system configuration (architecture, shape, structure).^{1,5-7} Flow systems are thermodynamically imperfect because of resistances for fluid, heat, electricity, etc. Resistances cannot be eliminated. At best, they can be distributed (balanced) such that their combined effect is minimum. Distribution means configuration, drawing, design. The search for design is being pursued on the basis of principle—the *constructal law*, which is the statement that as configurations change on the designer's table the ones that survive are those that offer greater access (less resistance) to currents. The numerous observations that the flow configurations generated by constructal design (e.g., tree networks) and that also occur in nature have led to *constructal theory*,^{1,5-7} which is the idea that natural flow structures can be predicted based on the same principle. The constructal law is a first principle in physics. It bridges the gap between engineered and natural flow systems and elevates “design” to the rank of physics concept and scientific method. Moreover, the evolutionary search for the best design can be summarized in terms analogous to the classical energy minimum principle, as shown in the concluding section of this chapter.

Symbols and Units

a	specific nonflow availability, J/kg
A	nonflow availability, J
A	area, m ²
b	specific flow availability, J/kg
B	flow availability, J
B	duty parameter for plate and cylinder
B_s	duty parameter for sphere
B_0	duty parameter for tube
Be	Bejan number, $\dot{S}_{gen,\Delta T}''' / (\dot{S}_{gen,\Delta T}''' + \dot{S}_{gen,\Delta P}''')$
c_p	specific heat at constant pressure, J/(kg · K)
C	specific heat of incompressible substance, J/(kg · K)
C	heat leak thermal conductance, W/K
C^*	time constraint constant, s/kg
D	diameter, m
e	specific energy, J/kg
E	energy, J
\bar{e}_{ch}	specific flow chemical exergy, J/kmol
\bar{e}_t	specific total flow exergy, J/kmol
e_x	specific flow exergy, J/kg
\bar{e}_x	specific flow exergy, J/kmol
E_Q	exergy transfer via heat transfer, J
\dot{E}_w	exergy transfer rate, W
E_x	flow exergy, J
EGM	method of entropy generation minimization
f	friction factor
F_D	drag force, N
g	gravitational acceleration, m/s ²
G	mass velocity, kg/(s · m ²)
h	specific enthalpy, J/kg

h	heat transfer coefficient, W/(m ² K)
h°	total specific enthalpy, J/kg
H°	total enthalpy, J
k	thermal conductivity, W/(m K)
L	length, m
m	mass, kg
\dot{m}	mass flow rate, kg/s
M	mass, kg
N	mole number, kmol
\dot{N}	molal flow rate, kmol/s
N_S	entropy generation number, $S_{\text{gen}}/S_{\text{gen,min}}$
Nu	Nusselt number
N_{tu}	number of heat transfer units
P	pressure, N/m ²
Pr	Prandtl number
q'	heat transfer rate per unit length, W/m
Q	heat transfer, J
\dot{Q}	heat transfer rate, W
r	dimensionless insulation resistance
R	ratio of thermal conductances
Re _D	Reynolds number
s	specific entropy, J/(kg · K)
S	entropy, J/K
S_{gen}	entropy generation, J/K
\dot{S}_{gen}	entropy generation rate, W/K
\dot{S}'_{gen}	entropy generation rate per unit length, W/(m · K)
\dot{S}'''_{gen}	entropy generation rate per unit volume, W/(m ³ K)
t	time, s
t_c	time constraint, s
T	temperature, K
U	overall heat transfer coefficient, W/(m ² K)
U_∞	free-stream velocity, m/s
v	specific volume, m ³ /kg
V	volume, m ³
V	velocity, m/s
\dot{W}	power, W
x	longitudinal coordinate, m
z	elevation, m
ΔP	pressure drop, N/m ²
ΔT	temperature difference, K
η	first law efficiency
η_{II}	second law efficiency
θ	dimensionless time
μ	viscosity, kg/(sec · m)
μ_i^*	chemical potentials at the restricted dead state, J/kmol
$\mu_{0,i}$	chemical potentials at the dead state, J/kmol

ν	kinematic viscosity, m^2/s
ξ	specific nonflow exergy, J/kg
Ξ	nonflow exergy, J
Ξ_{ch}	nonflow chemical exergy, J
Ξ_t	nonflow total exergy, J
ρ	density, kg/m^3

Subscripts

$()_B$	base
$()_C$	collector
$()_C$	Carnot
$()_H$	high
$()_L$	low
$()_m$	melting
$()_{max}$	maximum
$()_{min}$	minimum
$()_{opt}$	optimal
$()_p$	pump
$()_{rev}$	reversible
$()_t$	turbine
$()_0$	environment
$()_\infty$	free stream

2 EXERGY ANALYSIS

Figure 1 shows the general features of an open thermodynamic system that can interact thermally (\dot{Q}_0) and mechanically ($P_0 dV/dt$) with the atmospheric temperature and pressure reservoir (T_0, P_0). The system may have any number of inlet and outlet ports, even though only two such ports are illustrated. At a certain point in time, the system may be in communication with

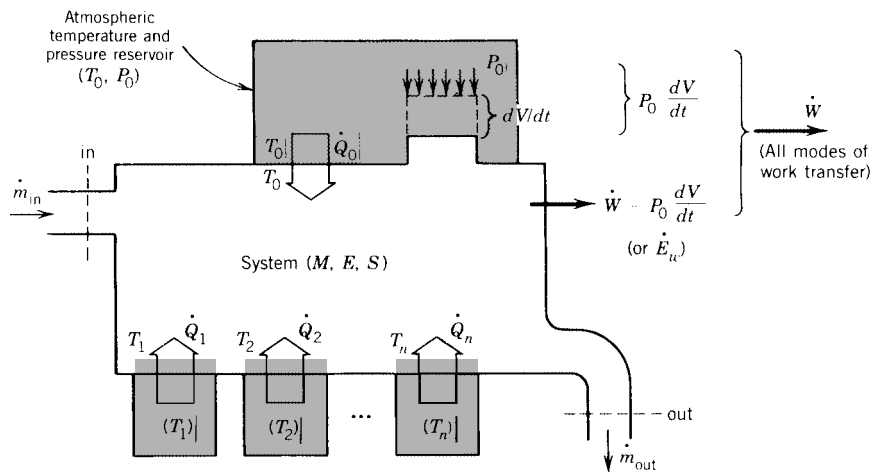


Figure 1 Open system in thermal and mechanical communication with the ambient. (From A. Bejan, *Advanced Engineering Thermodynamics*. © 1997 John Wiley & Sons, Inc. Reprinted by permission.)

any number of additional temperature reservoirs (T_1, \dots, T_n), experiencing the instantaneous heat interactions, $\dot{Q}_1, \dots, \dot{Q}_n$. The work transfer rate \dot{W} represents all the possible modes of work transfer: the work done on the atmosphere ($P_0 dV/dt$) and the remaining (useful, deliverable) portions such as $P dV/dt$, shaft work, shear work, electrical work, and magnetic work. The useful part is known as available work (or simply exergy) or, on a unit time basis,

$$\dot{E}_w = \dot{W} - P_0 \frac{dV}{dt}$$

The first law and the second law of thermodynamics can be combined to show that the available work transfer rate from the system of Fig. 1 is given by the equation¹:

$$\begin{aligned} \dot{E}_w = & \underbrace{-\frac{d}{dt}(E - T_0 S + P_0 V)}_{\text{Accumulation of nonflow exergy}} + \underbrace{\sum_{i=1}^n \left(1 - \frac{T_0}{T_i}\right) \dot{Q}_i}_{\text{Exergy transfer via heat transfer}} \\ & + \underbrace{\sum_{\text{in}} \dot{m}(h^\circ - T_0 s)}_{\text{Intake of flow exergy via mass flow}} - \underbrace{\sum_{\text{out}} \dot{m}(h^\circ - T_0 s)}_{\text{Release of flow exergy via mass flow}} - \underbrace{T_0 \dot{S}_{\text{gen}}}_{\text{Destruction of exergy}} \end{aligned}$$

where E , V , and S are the instantaneous energy, volume, and entropy of the system, and h° is shorthand for the specific enthalpy plus the kinetic and potential energies of each stream, $h^\circ = h + 1/2 V^2 + gz$. The first four terms on the right-hand side of the \dot{E}_w equation represent the exergy rate delivered as useful power (to an external user) in the limit of reversible operation ($\dot{E}_{w,\text{rev}}, \dot{S}_{\text{gen}} = 0$). The \dot{E}_w equation is a restatement of the Gouy–Stodola theorem (see Section 5 in the preceding chapter), which is the proportionality between the rate of exergy destruction and the rate of entropy generation

$$\dot{E}_{w,\text{rev}} - \dot{E}_w = T_0 \dot{S}_{\text{gen}}$$

A special exergy nomenclature has been devised for the terms formed on the right side of the \dot{E}_w equation. The exergy content associated with a heat transfer interaction (Q_i , T_i) and the environment (T_0) is the *exergy of heat transfer*,

$$E_{Q_i} = Q_i \left(1 - \frac{T_0}{T_i}\right)$$

This means that the heat transfer with the environment (Q_0 , T_0) carries zero exergy.

Associated with the system extensive properties (E , S , V) and the two specified intensive properties of the environment (T_0 , P_0) is a new extensive property: the thermomechanical or physical *nonflow availability*,

$$A = E - T_0 S + P_0 V$$

$$a = e - T_0 s + P_0 v$$

where A_0 represents the nonflow availability when the system is at the *restricted dead state* (T_0 , P_0), that is, in thermal and mechanical equilibrium with the environment, $A_0 = E_0 - T_0 S_0 + P_0 V_0$. The difference between the nonflow availability of the system in a given state and its nonflow availability in the restricted dead state is the thermomechanical (or physical) *nonflow exergy*,

$$\Xi = A - A_0 = E - E_0 - T_0(S - S_0) + P_0(V - V_0)$$

$$\xi = a - a_0 = e - e_0 - T_0(s - s_0) + P_0(v - v_0)$$

The nonflow exergy represents the most work that would become available if the system were to reach its restricted dead state reversibly, while communicating thermally only with the environment. In other words, the nonflow exergy represents the exergy content of a given closed system relative to the environment.

Associated with each of the streams entering or exiting an open system is the thermomechanical (or physical) *flow availability*,

$$B = H^\circ - T_0 S$$

$$b = h^\circ - T_0 s$$

At the restricted dead state, the nonflow availability of the stream is $B_0 = H_0^\circ - T_0 S_0$. The difference $B - B_0$ is the thermomechanical (or physical) *flow exergy* of the stream

$$E_x = B - B_0 = H^\circ - H_0^\circ - T_0(S - S_0)$$

$$e_x = b - b_0 = h^\circ - h_0^\circ - T_0(s - s_0)$$

The flow exergy represents the available work content of the stream relative to the restricted dead state (T_0, P_0). This work could be extracted from a system that operates reversibly in thermal communication only with the environment (T_0), while receiving the given stream (\dot{m}, h°, s) and discharging the same stream at the environmental pressure and temperature (\dot{m}, h_0°, s_0).

In summary, *exergy analysis* means that the \dot{E}_w equation can be rewritten more simply as

$$\dot{E}_w = -\frac{d\Xi}{dt} + \sum_{i=1}^n \dot{E}_{Q_i} + \sum_{\text{in}} \dot{m} e_x - \sum_{\text{out}} \dot{m} e_x - T_0 \dot{S}_{\text{gen}}$$

Examples of how these exergy concepts are used in the course of analyzing component by component the performance of complex systems can be found in Refs. 1–4. Figure 2 shows one such example.¹ The upper part of the drawing shows the traditional description of the four components of a simple Rankine cycle. The lower part shows the exergy streams that enter and exit each component, with the important feature that the heater, the turbine, and the cooler destroy significant portions (shaded, fading away) of the entering exergy streams. The numerical application of the \dot{E}_w equation to each component tells the analyst the exact widths of the exergy streams to be drawn in Fig. 2. In graphical or numerical terms, the “exergy wheel” diagram¹ shows not only *how much* exergy is being destroyed but also *where*. It tells the designer how to rank order the components as candidates for optimization according to the method of *entropy generation minimization* (Sections 3–8).

To complement the traditional (first law) energy conversion efficiency, $\eta = (\dot{W}_t - \dot{W}_p) / \dot{Q}_H$ in Fig. 2, exergy analysis recommends as the figure of merit the *second law efficiency*:

$$\eta_{II} = \frac{\dot{W}_t - \dot{W}_p}{\dot{E}_{Q_H}}$$

where $\dot{W}_t - \dot{W}_p$ is the net power output (i.e., \dot{E}_w earlier in this section). The second law efficiency can have values between 0 and 1, where 1 corresponds to the reversible limit. Because of this limit, η_{II} describes very well the fundamental difference between the method of exergy analysis and the method of EGM because in EGM the system always operates *irreversibly*. The question in EGM is how to change the system such that its \dot{S}_{gen} value (always finite) becomes smaller, while the system constraints are respected.

Consider next a nonflow system that can experience heat, work, and mass transfer in communication with the environment. The environment is represented by T_0, P_0 , and the n chemical potentials $\mu_{0,i}$ of the environmental constituents that are also present in the system. Taken together, the $n + 2$ intensive properties of the environment ($T_0, P_0, \mu_{0,i}$) are known as the *dead state*.

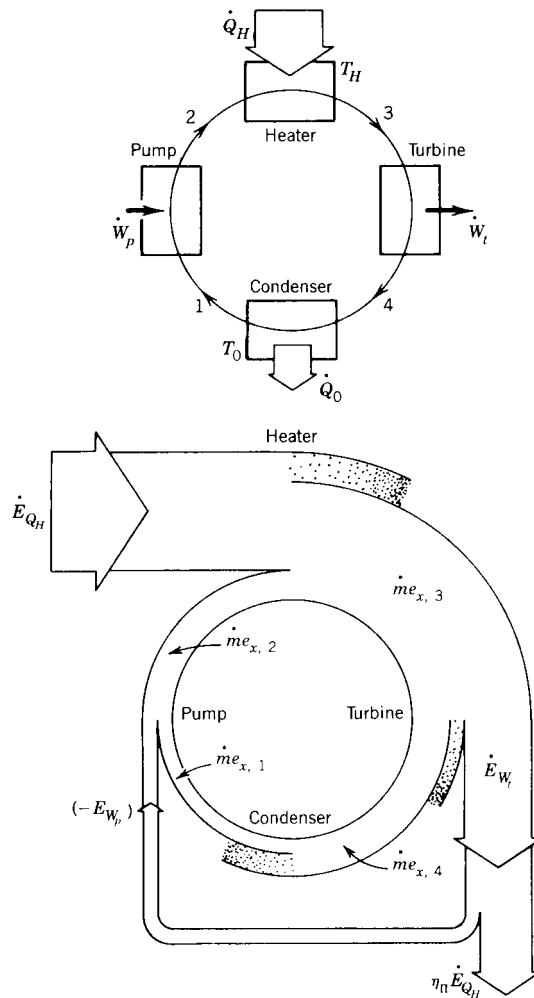


Figure 2 Exergy wheel diagram of a simple Rankine cycle. (Top) The traditional notation and energy interactions. (Bottom) The exergy flows and the definition of the second law efficiency. (From A. Bejan, *Advanced Engineering Thermodynamics*. © 1997 John Wiley & Sons, Inc. Reprinted by permission.)

Reading Fig. 3 from left to right, we see the system in its initial state represented by E , S , V and its composition (mole numbers N_1, \dots, N_n), and by its $n + 2$ intensities (T , P , μ_i). The system can reach its dead state in two steps. In the first, it reaches only thermal and mechanical equilibrium with the environment (T_0 , P_0), and delivers the nonflow exergy Ξ defined in the preceding section. At the end of this first step, the chemical potentials of the constituents have changed to μ_i^* ($i = 1, \dots, n$). During the second step, mass transfer (in addition to heat and work transfer), and, in the end, the system reaches chemical equilibrium with the environment, in addition to thermal and mechanical equilibrium. The work made available during this second step is known as *chemical exergy*¹:

$$\Xi_{\text{ch}} = \sum_{i=1}^n (\mu_i^* - \mu_{0,i}) N_i$$

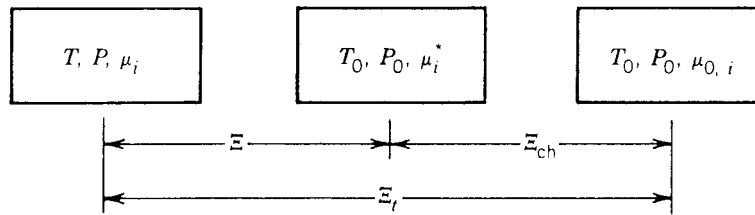


Figure 3 Relationship between the nonflow total (Ξ_t), physical (Ξ), and chemical (Ξ_{ch}) exergies. (From A. Bejan, *Advanced Engineering Thermodynamics*. © 1997 John Wiley & Sons, Inc. Reprinted by permission.)

The total exergy content of the original nonflow system (E, S, V, N_i) relative to the environmental dead state ($T_0, P_0, \mu_{0,i}$) represents the *total nonflow exergy*:

$$\Xi_t = \Xi + \Xi_{ch}$$

The *total flow exergy* of a mixture stream of total molal flow rate \dot{N} (composed of n species, with flow rates \dot{N}_i) and intensities T, P , and $\mu_i (i = 1, \dots, n)$ is, on a mole of mixture basis,

$$\bar{e}_t = \bar{e}_x + \bar{e}_{ch}$$

where the physical flow exergy \bar{e}_x was defined above, and \bar{e}_{ch} is the *chemical exergy* per mole of mixture,

$$\bar{e}_{ch} = \sum_{i=1}^n (\mu_i^* - \mu_{0,i}) \frac{\dot{N}_i}{\dot{N}}$$

In the \bar{e}_{ch} expression $\mu_i^* (i = 1, \dots, n)$ are the chemical potentials of the stream constituents at the restricted dead state (T_0, P_0). The chemical exergy is the additional work that could be extracted as the stream evolves reversibly from the restricted dead state to the dead state ($T_0, P_0, \mu_{0,i}$) while in thermal, mechanical, and chemical communication with the environment.

3 ENTROPY GENERATION MINIMIZATION

The EGM method^{3,4} is distinct from exergy analysis because in exergy analysis the analyst needs only the first law, the second law, and a convention regarding the values of the intensive properties of the environment. The critically new aspects of the EGM method are: the modeling of the system, the development of S_{gen} as a function of the physical parameters of the model, and the *minimization* of the calculated entropy generation rate. To minimize the irreversibility of a proposed design, one must use the relations between temperature differences and heat transfer rates and between pressure differences and mass flow rates. One must relate the degree of thermodynamic nonideality of the design to the physical characteristics of the system, namely, to finite dimensions, shapes, materials, finite speeds, and finite-time intervals of operation. For this, the modeler must rely on heat transfer and fluid mechanics principles, in addition to thermodynamics. Only by varying one or more of the physical characteristics of the system can the modeler bring the design closer to the operation characterized by minimum entropy generation subject to finite size and finite time constraints.

The modeling and optimization progress made in EGM is illustrated by some of the simplest and most fundamental results of the method, which are reviewed in the following sections. The structure of the EGM field is summarized in Fig. 4 by showing on the vertical the expanding list of applications. On the horizontal, we see the two modeling approaches that are being used. One approach is to focus from the start on the total system, to divide the system into

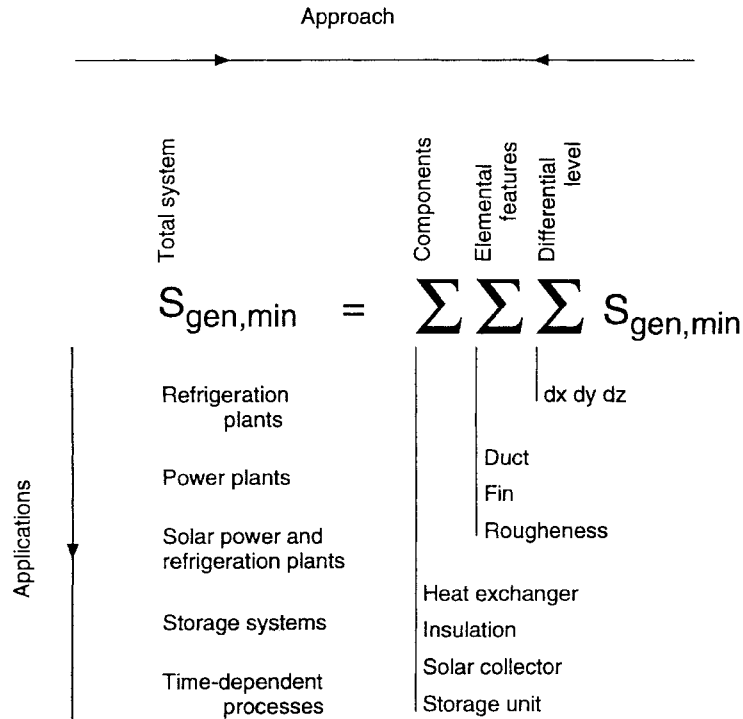


Figure 4 Approaches and applications of the method of entropy generation minimization (EGM). (Reprinted by permission from A. Bejan, *Entropy Generation Minimization*. Copyright CRC Press, Boca Raton, Florida. © 1996.)

compartments that account for one or more of the irreversibility mechanisms, and to declare the rest of the system irreversibility free. In this approach, success depends on the modeler's intuition because the assumed compartments do not always correspond to the pieces of hardware of the real system.

In the alternative approach (from the right in Fig. 4), modeling begins with dividing the system into its real components, and recognizing that each component may contain large numbers of one or more elemental features. The approach is to minimize S_{gen} in a fundamental way at each level, starting from the simple and proceeding toward the complex. When a component or elemental feature is imagined separately from the larger system, the quantities assumed specified at the points of separation act as constraints on the optimization of the smaller system. The principle of thermodynamic isolation (Ref. 4, p. 125) must be kept in mind during the later stages of the optimization procedure, when the optimized elements and components are integrated into the total system, which itself is optimized for *minimum cost* in the final stage.²

4 CRYOGENICS

The field of low-temperature refrigeration was the first where EGM was developed and became an established method of modeling and optimization.³ Consider a path for heat leak (\dot{Q}) from room temperature (T_H) to the cold end (T_L) of a low-temperature refrigerator or liquefier. Examples of such paths are mechanical supports, insulation layers without or with radiation

shields, counterflow heat exchangers, and electrical cables. The total rate of entropy generation associated with the heat leak path is

$$\dot{S}_{\text{gen}} = \int_{T_L}^{T_H} \frac{\dot{Q}}{T^2} dT$$

where \dot{Q} is in general a function of the local temperature T . The proportionality between the heat leak and the local temperature gradient along its path, $\dot{Q} = kA (dT/dx)$, and the finite size of the path [length L , cross section A , material thermal conductivity $k(T)$] are accounted for by the integral constraint:

$$\int_{T_L}^{T_H} \frac{k(T)}{\dot{Q}(T)} dT = \frac{L}{A} \quad (\text{constant})$$

The optimal heat leak distribution that minimizes \dot{S}_{gen} subject to the finite-size constraint is^{3,4}

$$\dot{Q}_{\text{opt}}(T) = \left(\frac{A}{L} \int_{T_L}^{T_H} \frac{k^{1/2}}{T} dT \right) k^{1/2} T$$

$$\dot{S}_{\text{gen, min}} = \frac{A}{L} \left(\int_{T_L}^{T_H} \frac{k^{1/2}}{T} dT \right)^2$$

The technological applications of the variable heat leak optimization principle are numerous and important. In the case of a mechanical support, the optimal design is approximated in practice by placing a stream of cold helium gas in counterflow (and in thermal contact) with the conduction path. The heat leak varies as $d\dot{Q}/dT = \dot{m}c_p$, where $\dot{m}c_p$ is the capacity flow rate of the stream. The practical value of the EGM method is that it pinpoints the optimal flow rate for minimum entropy generation. To illustrate, if the support conductivity is temperature independent, then the optimal flow rate is $\dot{m}_{\text{opt}} = (Ak/Lc_p) \ln(T_H/T_L)$. In reality, the conductivity of cryogenic structural materials varies strongly with the temperature, and the single-stream intermediate cooling technique can approach $\dot{S}_{\text{gen, min}}$ only approximately.

Other applications include the optimal cooling (e.g., optimal flow rate of boil-off helium) for cryogenic current leads, and the optimal temperatures of cryogenic radiation shields. The main counterflow heat exchanger of a low-temperature refrigeration machine is another important path for heat leak in the end-to-end direction ($T_H \rightarrow T_L$). In this case, the optimal variable heat leak principle translates into^{3,4}

$$\left(\frac{\Delta T}{T} \right)_{\text{opt}} = \frac{\dot{m}c_p}{UA} \ln \frac{T_H}{T_L}, \quad (\text{constant})$$

where ΔT is the local stream-to-stream temperature difference of the counterflow, $\dot{m}c_p$ is the capacity flow rate through one branch of the counterflow, and UA is the fixed size (total thermal conductance) of the heat exchanger.

5 HEAT TRANSFER

The field of heat transfer adopted the techniques developed in cryogenic engineering and applied them to a vast selection of devices for facilitating heat transfer. The EGM method was applied to complete components (e.g., heat exchangers) and elemental features (e.g., ducts, fins). For example, consider the flow of a single-phase stream (\dot{m}) through a heat exchanger tube of internal diameter D . The heat transfer rate per unit of tube length q' is given. The entropy generation rate per unit of tube length is

$$\dot{S}'_{\text{gen}} = \frac{q'^2}{\pi k T^2 \text{Nu}} + \frac{32 \dot{m}^3 f}{\pi^2 \rho^2 T D^5}$$

where Nu and f are the Nusselt number and the friction factor, $Nu = hD/k$ and $f = (-dP/dx)\rho D/(2G^2)$ with $G = \dot{m}/(\pi D^2/4)$. The \dot{S}'_{gen} expression has two terms: the irreversibility contributions made by heat transfer and fluid friction. These terms compete against one another such that there is an optimal tube diameter for minimum entropy generation rate^{3,4}:

$$Re_{D,opt} \cong 2B_0^{0.36} Pr^{-0.07}$$

$$B_0 = \frac{q' \dot{m} \rho}{(kT)^{1/2} \mu^{5/2}}$$

where $Re_D = VD/\nu$ and $V = \dot{m}/(\rho\pi D^2/4)$. This result is valid in the range $2500 < Re_D < 10^6$ and $Pr > 0.5$. The corresponding entropy generation number is

$$N_S = \frac{\dot{S}'_{gen}}{\dot{S}'_{gen,min}} = 0.856 \left(\frac{Re_D}{Re_{D,opt}} \right)^{-0.8} + 0.144 \left(\frac{Re_D}{Re_{D,opt}} \right)^{4.8}$$

where $Re_D/Re_{D,opt} = D_{opt}/D$ because the mass flow rate is fixed. The N_S criterion is being used extensively in the literature to monitor the approach of actual designs to the optimal irreversible designs conceived subject to the same constraints. This work is reviewed in Refs. 3 and 4.

The EGM of elemental features was extended to augmentation techniques such as extended surfaces (fins), roughened walls, spiral tubes, twisted tape inserts, and full-size heat exchangers that have such features. For example, the entropy generation rate of a body with heat transfer and drag in an external stream (U_∞, T_∞) is

$$\dot{S}'_{gen} = \frac{\dot{Q}_B(T_B - T_\infty)}{T_B T_\infty} + \frac{F_D U_\infty}{T_\infty}$$

where \dot{Q}_B , T_B and F_D are the heat transfer rate, body temperature, and drag force. The relation between \dot{Q}_B and temperature difference ($T_B - T_\infty$) depends on body shape and external fluid and flow and is provided by the field of convective heat transfer.⁸ The relation between F_D , U_∞ , geometry and fluid type comes from fluid mechanics.⁸ The \dot{S}'_{gen} expression has the expected two-term structure, which leads to an optimal body size for minimum entropy generation rate.

The simplest example is the selection of the swept length L of a plate immersed in a parallel stream (Fig. 5 inset). The results for $Re_{L,opt} = U_\infty L_{opt}/\nu$ are shown in Fig. 5 where B is a constraint (a duty parameter):

$$B = \frac{\dot{Q}_B/W}{U_\infty (k\mu T_\infty Pr^{1/3})^{1/2}}$$

and W is the plate dimension perpendicular to the figure. The same figure shows the corresponding results for the optimal diameter of a cylinder in cross flow, where $Re_{D,opt} = U_\infty D_{opt}/\nu$ and B is given by the same expression as for the plate. The optimal diameter of the sphere is referenced to the sphere duty parameter defined by

$$B_s = \frac{\dot{Q}_B}{\nu (k\mu T_\infty Pr^{1/3})^{1/2}}$$

The fins built on the surfaces of heat exchangers act as bodies with heat transfer in external flow. The size of a fin of given shape can be optimized by accounting for the internal heat transfer characteristics (longitudinal conduction) of the fin, in addition to the two terms (convective heat and fluid flow) shown in the last \dot{S}'_{gen} formula. The EGM method has also been applied to complete heat exchangers and heat exchanger networks. This vast literature is reviewed in Refs. 1 and 4. One technological benefit of EGM is that it shows how to select certain dimensions of a device so that the device destroys minimum power while performing its assigned heat and fluid flow duty.

Several computational heat and fluid flow studies recommended that future commercial CFD packages have the capability of displaying entropy generation rate fields (maps) for both

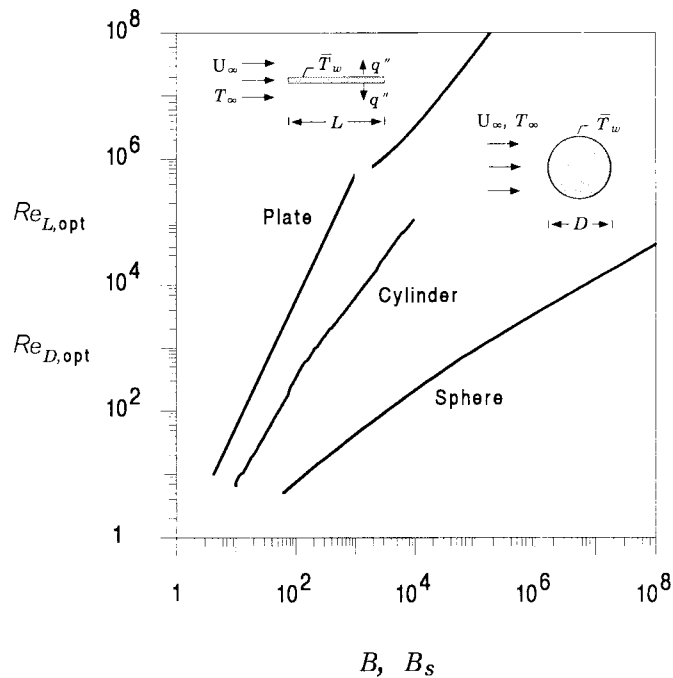


Figure 5 Optimal size of a plate, cylinder, and sphere for minimum entropy generation. (From Ref. 2. © 1996 John Wiley & Sons, Inc. Reprinted by permission.)

laminar and turbulent flows. For example, Paoletti et al.⁹ recommend the plotting of contour lines for constant values of the dimensionless group $Be = \dot{S}_{gen,\Delta T}''' / (\dot{S}_{gen,\Delta T}''' + \dot{S}_{gen,\Delta P}''')$, which they termed the Bejan number, where \dot{S}_{gen}''' means local (volumetric) entropy generation rate, and ΔT and ΔP refer to the heat transfer and fluid flow irreversibilities, respectively. This dimensionless group should not be confused with the dimensionless pressure drop that governs the optimization of spacings in heat transfer assemblies with forced convection.^{7,8}

6 STORAGE SYSTEMS

In the design of time-dependent heating or cooling processes, the search is for ways of executing the processes optimally in time. Consider the sensible heating of an amount of incompressible substance (mass M , specific heat C), by circulating a stream of hot ideal gas through it (\dot{m} , c_p , T_∞) (Fig. 6). Initially, the storage material is at the ambient temperature T_0 . The thermal conductance of the heat exchanger placed between the storage material and the gas stream is UA and the pressure drop is negligible. After flowing through the heat exchanger, the gas stream is discharged into the atmosphere. The entropy generated from $t = 0$ until a time t reaches a minimum when t is of the order of $MC/(\dot{m}c_p)$. Charts for calculating the optimal heating (storage) time interval are available in Refs. 3 and 4. For example, when $(T_\infty - T_0)$, the optimal heating time is given by $\theta_{opt} = 1.256/[1 - \exp(-N_{tu})]$, where $\theta_{opt} = t_{opt} \dot{m} c_p / (MC)$ and $N_{tu} = UA/(\dot{m} c_p)$.

Another example is the design of the sensible-heat cooling process subject to an overall time constraint. Consider the cooling of an amount of incompressible substance (M , C) from

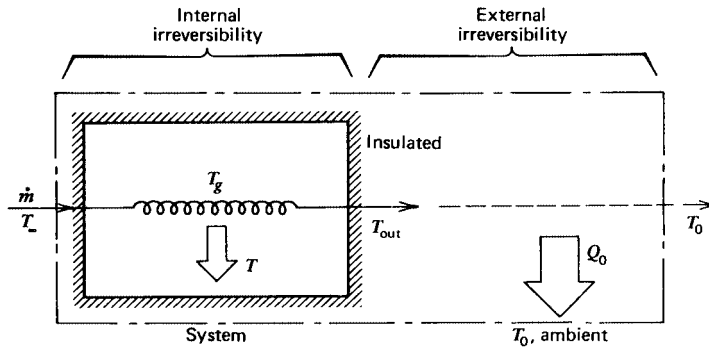


Figure 6 Entropy generation during sensible-heat storage.³

a given initial temperature to a given final temperature, during a prescribed time interval t_c . The coolant is a stream of cold ideal gas with flow rate \dot{m} and specific heat $c_p(T)$. The thermal conductance of the heat exchanger is UA ; however, the overall heat transfer coefficient generally depends on the instantaneous temperature, $U(T)$. The cooling process requires a minimum amount of coolant m (or minimum refrigerator work for producing the cryogen m),

$$m = \int_0^{t_c} \dot{m}(t) dt$$

when the gas flow rate has the optimal history^{3,4}

$$\dot{m}_{\text{opt}}(t) = \left[\frac{U(T)A}{C * c_p(T)} \right]^{1/2}$$

In this expression, $T(t)$ is the corresponding optimal temperature history of the object that is being cooled, and $C *$ is a constant that can be evaluated based on the time constraint, as shown in Refs. 3 and 4. The flow rate history (\dot{m}_{opt}) tells the operator that at temperatures where U is small the flow rate should be decreased. Furthermore, because during cooldown the gas c_p increases, the flow rate should decrease as the end of the process nears.

In the case of energy storage by melting there is an optimal melting temperature (i.e., optimal type of storage material) for minimum entropy generation during storage. If T_∞ and T_0 are the temperatures of the heat source and the ambient, the optimal melting temperature of the storage material has the value $T_{m,\text{opt}} = (T_\infty T_0)^{1/2}$.

7 SOLAR ENERGY CONVERSION

The generation of power and refrigeration based on energy from the sun has been the subject of some of the oldest EGM studies, which now cover a wide territory. A characteristic of these EGM models is that they account for the irreversibility due to heat transfer in the two temperature gaps (sun–collector and collector–ambient) and that they reveal an optimal *coupling* between the collector and the rest of the plant.

Consider the steady operation of a power plant driven by a solar collector with convective heat leak to the ambient, $\dot{Q}_0 = (UA)_c(T_c - T_0)$, where $(UA)_c$ is the collector–ambient thermal conductance and T_c is the collector temperature (Fig. 7). Similarly, there is a finite size heat exchanger $(UA)_i$ between the collector and the hot end of the power cycle (T), such that the heat input provided by the collector is $\dot{Q} = (UA)_i(T_c - T)$. The power cycle is assumed

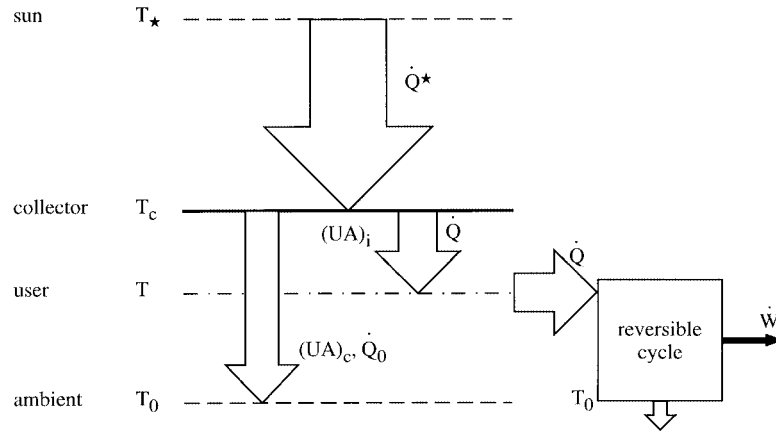


Figure 7 Solar power plant model with collector–ambient heat loss and collector–engine heat exchanger.³

reversible. The power output $\dot{W} = \dot{Q}(1 - T_0/T)$ is maximum, or the total entropy generation rate is minimum, when the collector has the temperature^{3,4}

$$\frac{T_{c,\text{opt}}}{T_0} = \frac{\theta_{\text{max}}^{1/2} + R\theta_{\text{max}}}{1 + R}$$

where $R = (UA)_c/(UA)_i$, $\theta_{\text{max}} = T_{c,\text{max}}/T_0$, and $T_{c,\text{max}}$ is the maximum (stagnation) temperature of the collector.

Another design feature is discovered when the overall size of the installation is fixed. For example, in an extraterrestrial power plant with collector area A_H and radiator area A_L , if the total area is constrained¹

$$A_H + A_L = A \text{ (constant)}$$

the optimal way to allocate the area is $A_{H,\text{opt}} = 0.35A$ and $A_{L,\text{opt}} = 0.65A$. Other examples of optimal allocation of hardware between various components subject to overall size constraints are given in Ref. 4.

8 POWER PLANTS

There are several EGM models and optima of power plants that have fundamental implications. The loss of heat from the hot end of a power plant can be modeled by using a thermal resistance in parallel with an irreversibility-free compartment that accounts for the power output \dot{W} of the actual power plant (Fig. 8). The hot-end temperature of the working fluid cycle T_H can vary. The heat input \dot{Q}_H is fixed. The bypass heat leak is proportional to the temperature difference, $\dot{Q}_C = C(T_H - T_L)$, where C is the thermal conductance of the power plant insulation. The power output is maximum (and \dot{S}_{gen} is minimum) when the hot-end temperature reaches the level^{3,10}

$$T_{H,\text{opt}} = T_L \left(1 + \frac{\dot{Q}_H}{CT_L} \right)^{1/2}$$

The corresponding efficiency ($\dot{W}_{\text{max}}/\dot{Q}_H$) is

$$\eta = \frac{(1+r)^{1/2} - 1}{(1+r)^{1/2} + 1}$$

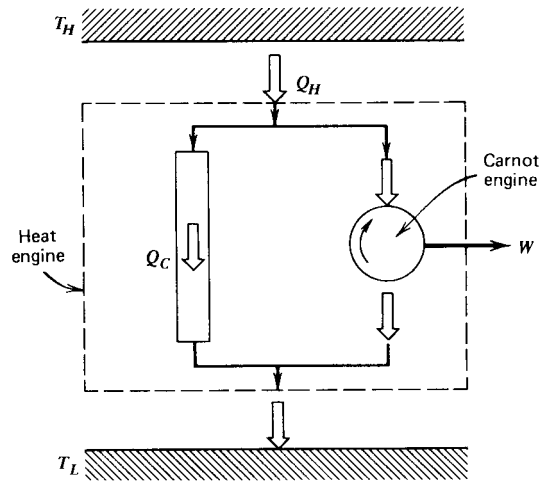


Figure 8 Power plant model with bypass heat leak.^{3,10}

where $r = \dot{Q}_H / (CT_L)$ is the dimensionless size (thermal resistance) of the power plant. An optimal T_H value exists because when $T_H < T_{H,opt}$, the Carnot efficiency of the power producing compartment is too low, while when $T_H > T_{H,opt}$, too much of the unit heat input \dot{Q}_H bypasses the power compartment.

Another optimal hot-end temperature is revealed by the power plant model shown in Fig. 9. The power plant is driven by a stream of hot single-phase fluid of inlet temperature T_H and constant specific heat c_p . The model has two compartments. The one sandwiched between the heat exchanger surface (T_{HC}) and the ambient (T_L) operates reversibly. The other is a heat exchanger: For simplicity, the area of the T_{HC} surface is assumed sufficiently large that the stream outlet temperature is equal to T_{HC} . The stream is discharged into the ambient. The optimal hot-end

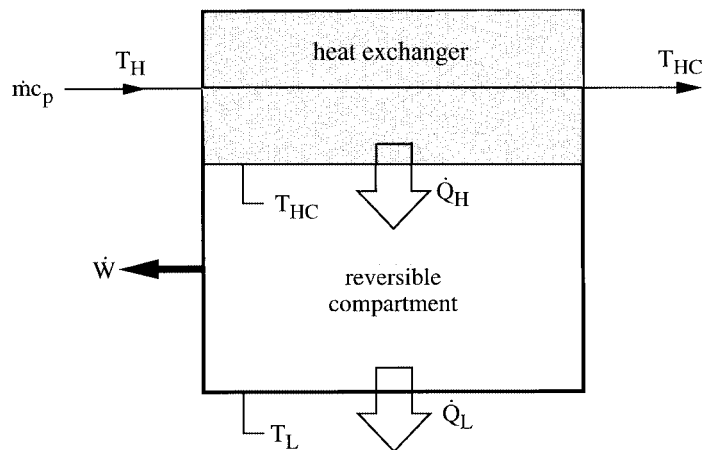


Figure 9 Power plant driven by a stream of hot single-phase fluid.^{1,4}

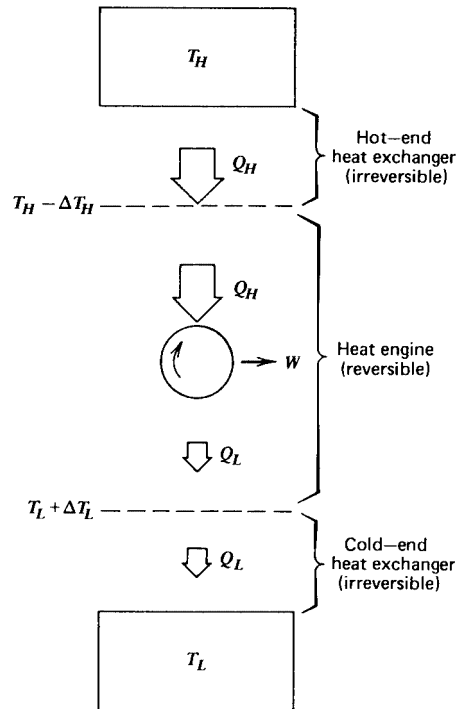


Figure 10 Power plant with two finite-size heat exchangers.³

temperature for maximum \dot{W} (or minimum \dot{S}_{gen}) is^{1,4} $T_{\text{HC,opt}} = (T_H T_L)^{1/2}$. The corresponding first-law efficiency, $\eta = \dot{W}_{\text{max}}/\dot{Q}_H$, is $\eta = 1 - (T_L/T_H)^{1/2}$.

The optimal allocation of a finite heat exchanger inventory between the hot end and the cold end of a power plant is illustrated by the model with two heat exchangers proposed in Ref. 3 and Fig. 10. The heat transfer rates are proportional to the respective temperature differences, $\dot{Q}_H = (UA)_H \Delta T_H$ and $\dot{Q}_L = (UA)_L \Delta T_L$, where the thermal conductances $(UA)_H$ and $(UA)_L$ account for the sizes of the heat exchangers. The heat input \dot{Q}_H is *fixed* (e.g., the optimization is carried out for one unit of fuel burnt). The role of overall heat exchanger inventory constraint is played by

$$(UA)_H + (UA)_L = UA \quad (\text{constant})$$

where UA is the total thermal conductance available. The power output is maximized, and the entropy generation rate is minimized, when UA is allocated according to the rule

$$(UA)_{H,\text{opt}} = (UA)_{L,\text{opt}} = 1/2 UA$$

The corresponding maximum efficiency is, as expected, lower than the Carnot efficiency:

$$\eta = 1 - \frac{T_L}{T_H} \left(1 - \frac{4\dot{Q}_H}{T_H UA} \right)^{-1}$$

The EGM modeling and optimization progress on power plants is extensive, and is reviewed in Ref. 4. Similar models have also been used in the field of refrigeration, as we saw already in Section 4. For example, in a steady-state refrigeration plant with two

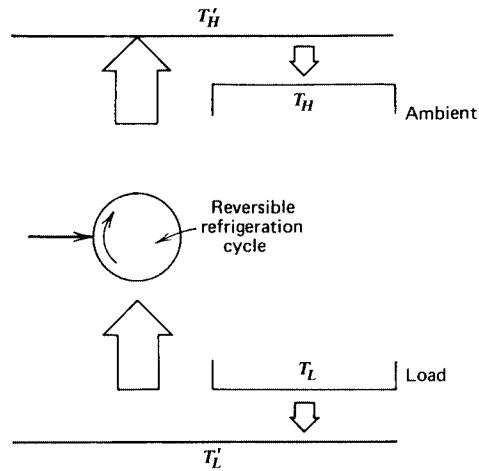


Figure 11 Refrigerator model with two finite-size heat exchangers.³

heat exchangers (Fig. 11) subjected to the total UA constraint listed above, the refrigerator power input is minimum when UA is divided equally among the two heat exchangers, $(UA)_{H,opt} = 1/2 UA = (UA)_{L,opt}$.

9 CONSTRUCTAL LAW

Flow systems are imperfect thermodynamically because of the many kinds of resistances that their flows must overcome. Depending on system purpose and complexity, the currents may carry fluids, heat, electricity, and chemical species. The resistances are an integral and unavoidable presence because of the finite-size constraints that define the flow system. For example, the resistance to the flow of heat between two streams in a balanced counterflow heat exchanger can be made vanishingly small if the heat transfer surface can be made infinitely large. In reality, the surface size is fixed, and this means that the heat current is destined to encounter a thermal resistance. The current flows irreversibly, and this feature has a negative effect on global thermodynamic performance. The flow system is destined to be imperfect.

When the flow system is complex, the currents and resistances are many and diverse. The route to higher global performance consists of balancing each resistance against the rest. The distributing and redistributing of imperfection through the complex flow system is accomplished by making changes in the flow architecture, i.e., by *evolving* the design. A prerequisite then is for the flow system to be free to change its configuration—free to morph. The morphing of structure is the result of the competition between the global objective and the global constraints. The generation flow architecture is the means by which the flow system achieves its global objective under the constraints.

In recent years, this activity of selection of flow configuration has become more focused on the process of generation of the architecture of the flow system.^{1,5,7} This is particularly evident in modern computational heat and fluid flow, where large numbers of flow configurations can be simulated, compared, and optimized. The generation of flow architecture is a phenomenon everywhere, not only in engineered flow systems but also in natural flow systems (animate and inanimate). The universality of this phenomenon was expressed in a compact statement (the constructal law) that proclaims a natural tendency in time: In order for a finite-size flow

system to persist in time (to live), it must evolve such that it provides easier and greater access to its currents.^{1,6} The thought that this principle can be used to rationalize the occurrence of optimized flow structures in nature (e.g., tree networks, round tubes) was named constructal theory.

In this section the constructal law is formulated in analytical and graphical terms that are analogous to terms employed in thermodynamics.⁶ This formulation makes the universality of the constructal law more evident.

A flow system, or nonequilibrium thermodynamic system, is characterized by “properties” (constraints), such as total volume, total volume occupied by all the ducts, etc. A flow system is also characterized by “performance” (function, objective) and “flow structure” (configuration, layout, geometry, architecture). Unlike the black box of classical thermodynamics, which represents a system at equilibrium, a flow system has performance and especially configuration. Each flow system has a *drawing* (a design).

Consider one of the simplest examples of how the collision between global objective and global constraints generates the complete architecture of the flow system: the flow between two points (Fig. 12), where “simple” are only the optimal and near-optimal architectures. This makes the example easy to present graphically. The rest of the design process is conceptually as vast and complicated as in any other example. When the flow architecture is free to morph, the design space is infinite. There is an infinity of flow architectures that can be chosen to guide a fluid stream (\dot{m}) from one point to another point.

Constructal theory begins with the global objective(s) and the global constraint(s) of the flow system, and the fact that in the beginning geometry is the unknown. In Fig. 12 the objective is to force the single-phase fluid stream \dot{m} to flow from one point to another, while using less pumping power. When \dot{m} is fixed, this objective is the same as seeking flow architectures with lower pressure overall difference (ΔP), smaller flow resistance (R), or smaller rate of entropy generation by fluid friction.

There are two global constraints, one external and the other internal. The external constraint is the “system size,” which is represented by the distance between the two points, L . The internal global constraint is the “amount” invested in making the flow architecture. In Fig. 12 that amount is the total volume (V) of all the ducts of the flow structure. Without such an investment there is no flow—not even a drawing that would show the flow. A flow must be guided. Flow means direction and architecture, in addition to flow rate.

There are many reasons why there is an infinity of eligible flow architectures that meet the global objective and global constraints recognized above, i.e., many thoughts in the direction of which the number of possible architectures increases without bounds: (i) The flow pattern may be two dimensional (in the plane of Fig. 12) or three dimensional: (ii) Any number of ducts may be connected in parallel between the two points: (iii) A duct may have any number of branches or tributaries at any location between the two points: (iv) A single duct may have any length: (v) The cross-sectional shape may vary along the duct: (vi) A duct may have any cross-sectional shape.

How do we identify the geometric features that bring a flow architecture to the highest level of global performance? There are many lessons of this type throughout engineering, and, if remembered, they constitute *strategy*—they shorten dramatically the search for the geometry in which all the features are “useful” in serving the global objective. Constructal theory is about strategy, about compact lessons of optimal shape and structure, which are fundamental and universally applicable. They are geometric relatives of truths such as the universal observation that all things flow naturally from high to low (the second law of thermodynamics).

Here are the classical lessons that abbreviate the search through the broad categories listed as (i)–(vi). Assume that ducts are slender, and the flows are slow so that in each cross section the regime is laminar and fully developed. Each lesson is identified by the symbol of the geometric feature that it addresses: (i)–(iii) A single duct with large cross section offers a smaller flow

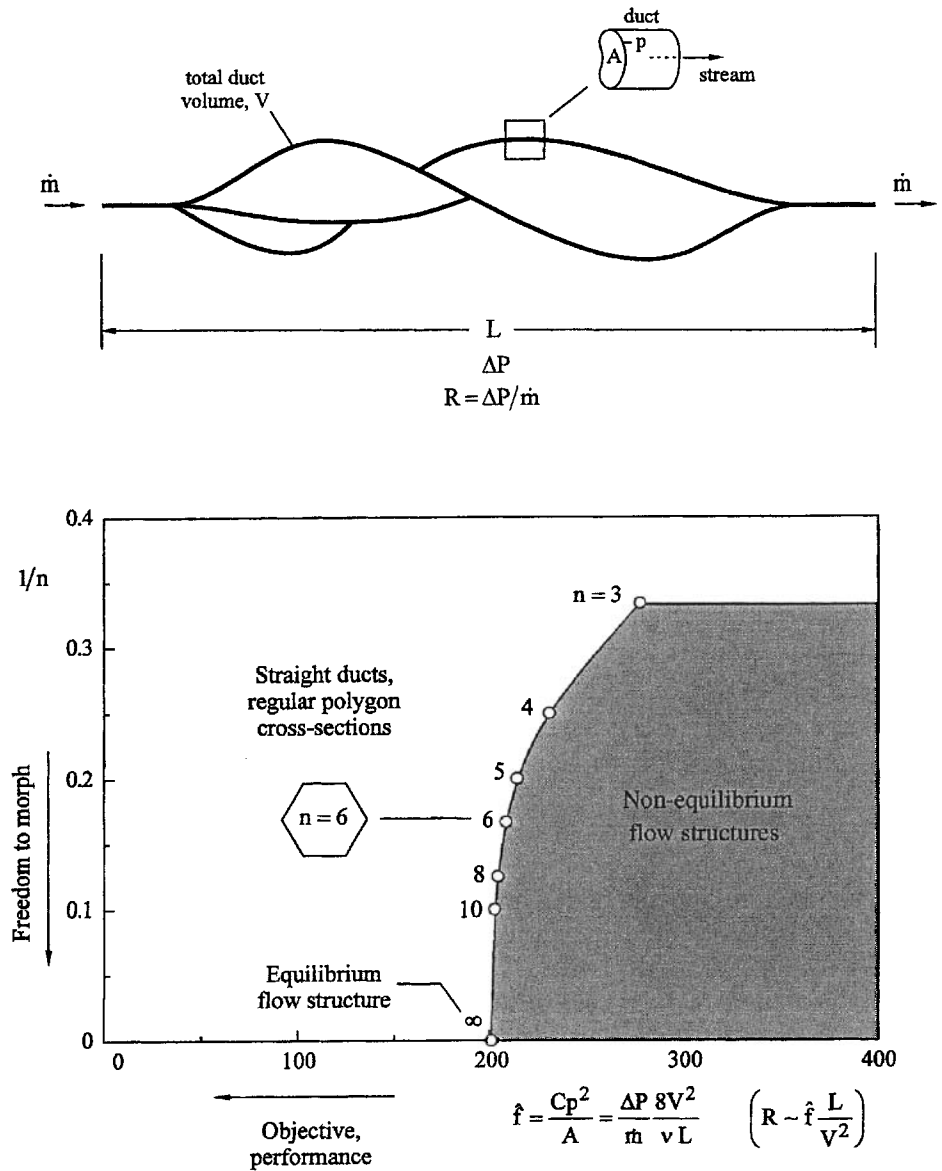


Figure 12 General flow architecture for guiding a stream from one point to another point, and the approach to the minimal global flow resistance when the number of sides of the regular-polygon cross section (n) increases (data from Table 1).⁶

resistance than two ducts with smaller cross sections connected in parallel. (iv) The lowest resistance belongs to the shortest duct, i.e., the straight duct between the two points: (v) The duct with cross-sectional geometry that does not vary longitudinally has a lower resistance than the duct with variable cross section.

Summing up, out of the infinity of designs represented by (i)–(v) we have selected a single straight duct with a cross-sectional shape that does not vary from one end of the duct to the

other. According to (vi), however, there is still an infinite number of possible cross-section shapes: symmetric vs. asymmetric, smooth vs. polygonal, etc. Which impedes the flow the least? The answer becomes visible if we assume cross sections with polygonal shapes. Start with an arbitrary cross section shaped as a triangle. The area of the cross section A is fixed because the total duct volume V and the duct length L are fixed, namely $A = V/L$. Triangular cross sections constrict the flow when one of the angles is much smaller than the other two.

The least resistance is offered by the most “open” triangular cross section, which is shaped as an equilateral triangle. Once again, if one very small angle and two larger ones represent a nonuniform distribution of geometric features of imperfection (i.e., features that impede the flow), then the equilateral triangle represents the constructal architecture, i.e., the one with “optimal distribution of imperfection.”

The same holds for any other polygonal shape. The least resistance is offered by a cross section shaped as a regular polygon. In conclusion, out of the infinity of flow architectures recognized in class (vi) we have selected an infinite number of candidates. They are ordered according to the number of sides (n) of the regular polygon, from the equilateral triangle ($n = 3$) to the circle ($n = \infty$). The flow resistance for Hagen–Poiseuille flow through a straight duct with polygonal cross section can be written as^{1,6}

$$\frac{\Delta P}{\dot{m}} = \frac{\nu L}{8V^2} \frac{Cp^2}{A}$$

where p is the perimeter of the cross section. As shown in Table 1, the dimensionless perimeter $p/A^{1/2}$ is only a function of n . The same is true about C , which appears in the solution for friction factor in Hagen–Poiseuille flow,

$$f = \frac{C}{\text{Re}}$$

where $\text{Re} = \bar{U} D_h/\nu$, $D_h = 4A/p$, and $\bar{U} = \dot{m}/(\rho A)$. In conclusion, the group Cp^2/A depends only on n , and accounts for how this last geometric degree of freedom influences global performance. The group Cp^2/A is the dimensionless global flow resistance of the flow system. The smallest Cp^2/A value is the best, and the best is the round cross section.

Figure 12 shows a plot of the flow resistance data of Table 1. The flow structure with minimal global resistance is approached gradually (with diminishing decrements) as n increases. The polygonal cross section with $n = 10$ performs nearly as well as the round cross section ($n = \infty$). The “evolution” of the cross-sectional shape stops when the number of features (n) has become infinite, i.e., when the structure has become the most free. This configuration where changes in global performance have stopped is the *equilibrium flow architecture*.

The curve plotted in Fig. 12 was generated by calculations for regular-polygon cross sections. The curve is in reality a sequence of discrete points, one point for each n value.

Table 1 Laminar Flow Resistances of Straight Ducts with Regular Polygonal Cross Sections with n Sides⁶

N	C	$p/A^{1/2}$	Cp^2/A
3	40/3	4.559	277.1
4	14.23	4	227.6
5	14.74	3.812	214.1
6	15.054	3.722	208.6
8	15.412	3.641	204.3
10	15.60	3.605	202.7
∞	16	$2\pi^{1/2}$	201.1

Source: From Ref. 6.

We drew a continuous line through these points in order to stress an additional idea. Regardless of n , the regular polygon and straight duct with constant cross section is already the “winner” from an infinitely larger group of competing architectures. This means that the global flow resistances of all the designs that are not covered by Table 1 fall to the right of the curve plotted in Fig. 12.

In sum, the immensely large world of possible designs occupies only a portion of the two-dimensional domain illustrated in Fig. 12. This two-dimensional domain can be described as “performance versus freedom,” when global properties such as L and V are specified. The boundary of the domain is formed by a string of the better flow structures. The better ones are achieved by putting more freedom in the geometry of the flow structure (e.g., a larger n). The best performance belongs to the structure that was most free to morph—the equilibrium configuration. In its immediate vicinity, however, we find many configurations that are different (they have finite n values) but have practically the same global performance level. These are *near-equilibrium* flow structures.

The evolution of flow configuration illustrated in Figs. 1 and 2 for point-to-point flows is a universal phenomenon, which manifests itself during any search for constructal flow architectures. Additional examples are given in Ref. 6. Some of the more complex architectures that have been developed recently are the flow structures that connect one point (source or sink) with an infinity of points (line, area, or volume). According to constructal theory, the best flow path that makes such a connection is shaped as a tree.^{1,5,7} The tree is for point-area flows and the straight duct is for point–point flows.

All the possible configurations inhabit the hyperspace suggested in Fig. 13a. All the constant- L flow configurations that are possible inhabit the volume visualized by the constant- V and constant- R cuts. Fig. 13b shows the view of all the possible flow structures, projected on the base plane. Plotted on the R axis is the global resistance of the flow system, namely $R = \Delta P/\dot{m}$ in the preceding examples. The abscissa accounts for the total volume occupied by the ducts (V): This is a global measure of how “porous” or “permeable” the flow system is. The constant- V plane that cuts through Fig. 13a is the same as the plane of Fig. 12.

The constructal law is the statement that summarizes the common observation that flow structures that survive are those that morph in one direction in time: toward configurations that make it easier for currents to flow. This holds for natural and engineered flow structures. The first such statement was^{1,5,7} “for a finite-size system to persist in time (to live), it must evolve in such a way that it provides easier access to the imposed currents that flow through it.”

If the flow structures are free to change (free to approach the base plane in Fig. 13a), they will move at constant L and constant V in the direction of progressively smaller R . If the initial configuration is represented by point 1 in Fig. 13b, then a more recent configuration is represented by point 2. The relation between the two configurations is $R_2 \leq R_1$ (constant L, V). If freedom to morph persists, then the flow structure will continue toward smaller R values. Any such change is characterized by

$$dR \leq 0 \quad (\text{constant } L, V)$$

The end of this migration is the equilibrium flow structure (point e), where the geometry of the flow enjoys total freedom. Equilibrium is characterized by minimal R at constant L and V . In the vicinity of the equilibrium point we have

$$dR = 0 \quad \text{and} \quad d^2R > 0 \quad (\text{constant } L, V)$$

The $R(V)$ curve shown in Fig. 13b is the edge of the cloud of possible flow architectures with the same global size L . The curve has negative slope because of the physics of flow: The flow resistance always decreases when the flow channels open up, $(\partial R/\partial V)_L < 0$.

The constant- R cut through the configuration space shows another way of expressing the constructal law. If free to morph, the flow system will evolve from point 1 to point 2' at constant

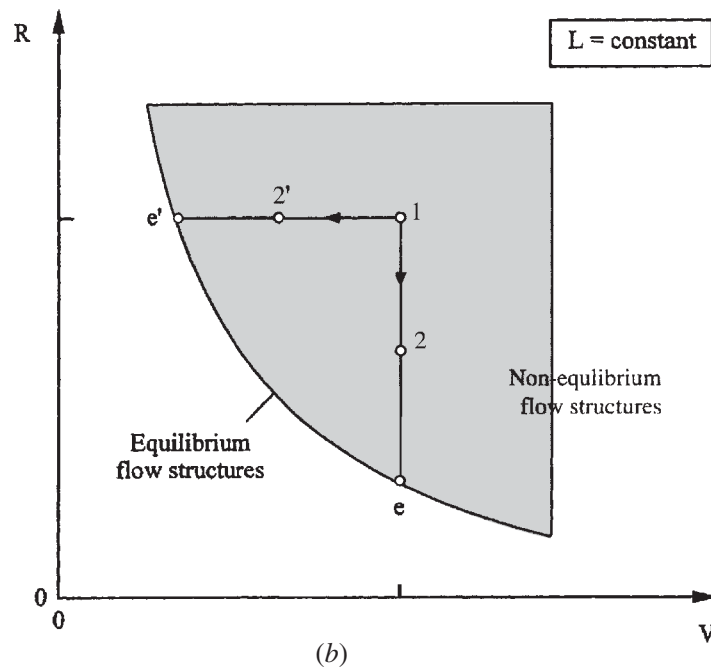
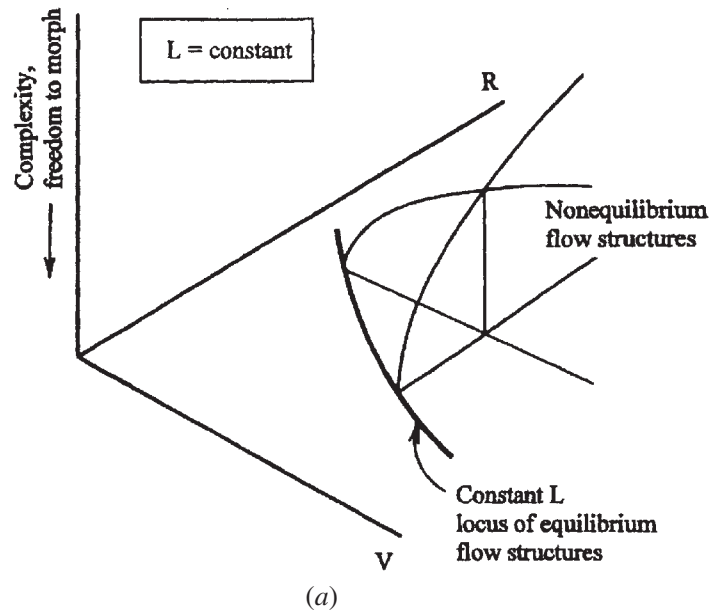


Figure 13 Space occupied by all the flow architectures when the global external size (L) is fixed.⁶

L and R . In the limit of total freedom, the geometry will reach another equilibrium configuration, which is represented by point e' . The alternative analytical statement of the constructal law is

$$dV \leq 0 \quad (\text{constant } L, R)$$

For changes in structure in the immediate vicinity of the equilibrium structure, we note

$$dV = 0 \quad \text{and} \quad d^2V > 0 \quad (\text{constant } L, R)$$

Paraphrasing the original statement of the constructal law, we may describe processes of type 1 – 2' – e' as follows: For a system with fixed global size and global performance to persist in time (to live), it must evolve in such a way that its flow structure occupies a smaller fraction of the available space.

The constant- V alternative to Fig. 13 is shown in Fig. 14. The lower drawing is the projection of the space of possible flow architectures on the base plane $R - L$. The continuous line is the locus of equilibrium flow structures at constant V , namely the curve $R(V)$ where $(\partial R/\partial L)_V > 0$. The fact that the slope is positive is flow physics: The flow resistance always increases as the distance that must be overcome by the flow increases.

The constructal law statement can be read off Fig. 14*b* in two ways. One is the original statement^{1,5,7}: at constant V and L , the evolution is from a suboptimal structure (point 1) to one that has a lower global resistance (point 2). If the flow geometry continues to morph freely, the structure approaches the equilibrium configuration (point e).

The alternative is when structural changes are made such that R remains constant while V is also fixed. Then the evolution in Fig. 14*b* is from point 1 to point 2''. Such changes mean that

$$dL \geq 0 \quad (\text{constant } R, V)$$

and that the constructal law statement becomes: In order for a flow system with fixed global resistance (R) and internal size (V) to persist in time, the architecture must evolve in such a way that it covers a progressively larger territory.

Equilibrium is reached at point e'' . The changes in flow structures in the immediate vicinity of the equilibrium structure are such that the global external dimension at equilibrium is maximal,

$$dL = 0 \quad d^2L < 0 \quad (\text{constant } R, V)$$

Accordingly, the constructal law states that the ultimate flow structure with specified global resistance (R) and internal size (V) is the largest. A flow architecture with specified R and V has a maximum size, and this global size belongs to the equilibrium architecture. A flow structure larger than this does not exist. This formulation of the constructal law has implications in natural design, for example, in the S-curve phenomena of the spreading of species and river deltas without access to the sea¹¹ and the spreading of ideas.¹²

The original statement of the constructal law was about the maximization of flow access under global size constraints (external L , internal V). This behavior is illustrated by the structural changes 1 – 2 – e in Figs. 13*b* and 14*b*. This means survival by increasing efficiency—survival of the fittest. The physics principle behind Darwin's observations is the constructal law, and it governs not only the animate natural flow systems but also the inanimate natural flow systems and the engineered flow systems. Engineered systems are diverse species of "human + machine" beings, evolving every day.

The alternative shown by the changes 1 – 2'' – e'' in Fig. 14*b* is survival by spreading: growth as the mechanism for being able to persist in time. The limit to growth is set by the specified constraints, in this case the fixed global flow resistance R and the global internal size V . A given living species (river delta, animal population) will spread over a certain, maximal territory.

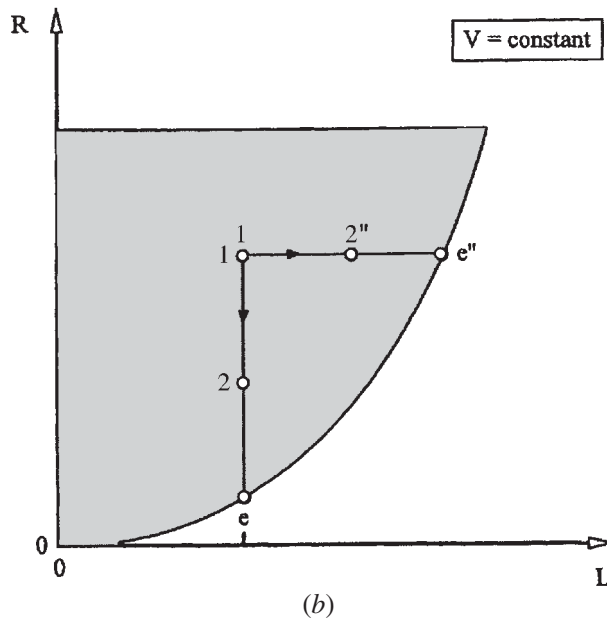
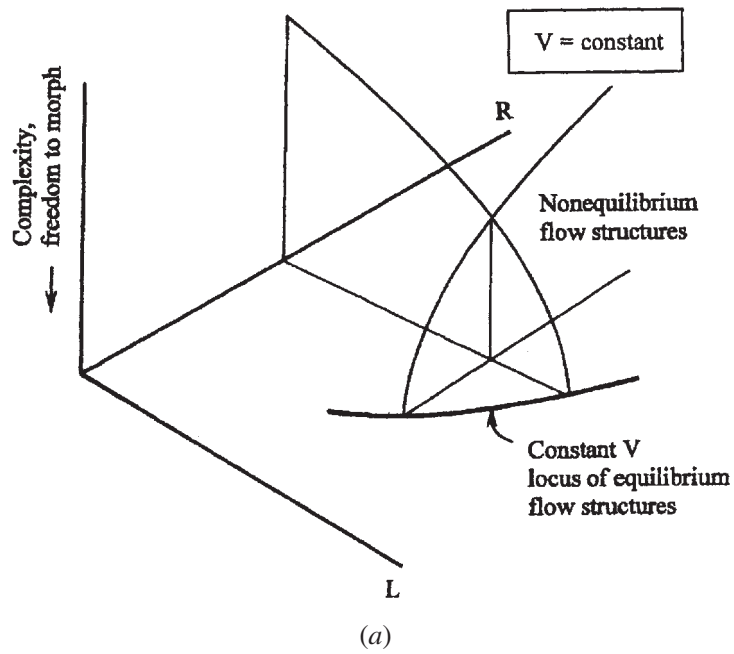


Figure 14 Space occupied by all the flow architectures when the global internal size (total duct volume V) is fixed.⁶

An equivalent interpretation of the constructal principle is based on processes of type 1–2'–e', Fig. 13*b*. Flow architectures with the same performance (R) and size (L) evolve toward compactness—smaller volumes dedicated to the internal ducts, i.e., larger volumes dedicated to the working volume elements, which are the interstices. This is survival based on the maximization of the use of the available space.

In summary, changes in performance (R) can be achieved through changes of three types:

- (i) Flow configuration
- (ii) Global external size, or covered territory, L
- (iii) Global internal size, or duct volume, V

The examples discussed so far showed that changes may occur in one category or, simultaneously, in two or three. The simplest illustration is possible for the case of equilibrium flow architectures. For them the solid curves shown in Figs. 13*b* and 14*b* proclaim the existence of the fundamental relation $R(L, V)$, the differential of which is

$$dR = Y_L dL + Y_V dV \quad (\text{equilibrium})$$

Physics requires that the first partial derivatives of R have opposite signs, $Y_L > 0$ and $Y_V < 0$, as noted earlier in this section. In general, when the flow architecture has not reached equilibrium, R can be decreased by means I, II, and III. Then the general version of the last equation is

$$dR \leq Y_L dL + Y_V dV$$

where the inequality sign refers to the time arrow of structural changes in a flow configuration that, at least initially, was not of the equilibrium type. This inequality is a concise statement of the three analytical formulations of the constructal law that we discussed so far:

- R minimum at constant L and V
- V minimum at constant R and L
- L maximum at constant V and R

Another way to summarize the analytical formulation that we have just constructed is by recognizing the analogy between the analytical constructal law and the analytical formulation of classical thermodynamics (cf. chapter 3 in this handbook). The analogy is presented in Table 2. It is stressed further by Fig. 2 of chapter 3, which is from present-day thermodynamics¹ and expresses the energy minimum principle, which states that as the internal constraints of a closed system are removed at constant volume and entropy, the energy approaches a minimal value. Figure 2 of chapter 3 is analogous to Fig. 14*a*.

The analytical formulation of the constructal law presented in this section expresses a universal phenomenon: Figures such as Fig. 12 characterize the evolution toward equilibrium configuration in any flow system with global objective, global constraints, and freedom to morph. In Ref. 6, this was demonstrated through examples from three wide classes of flow architectures: flow between two points, flow between a circle and its center, and flow between one point and an area. Many other examples can be contemplated, and they will all reveal the image of Fig. 12 on the road to equilibrium flow architectures.

At equilibrium the flow configuration achieves the most that its freedom to morph has to offer. Equilibrium does not mean that the flow architecture (structure, geometry, configuration) stops changing. On the contrary, it is here at equilibrium that the flow geometry enjoys most freedom to change. Equilibrium means that the global performance does not change when changes occur in the flow architecture.

Table 2 Concepts and Principles of Classical Thermodynamics and Constructal Theory

Thermodynamics	Constructal Theory
State	Flow architecture (geometry, configuration, structure)
Process, removal of internal constraints	Morphing, change in flow configuration
Properties (U , S , Vol, ...)	Global objective and global constraints (R , L , V , ...)
Equilibrium state	Equilibrium flow architecture
Fundamental relation, $U(S, \text{Vol}, \dots)$	Fundamental relation, $R(L, V, \dots)$
Constrained equilibrium states	Nonequilibrium flow architectures
Removal of constraints	Increased freedom to morph
Energy minimum principle:	Constructal principle:
U minimum at constant S and Vol	R minimum at constant L and V
Vol minimum at constant F and T	V minimum at constant R and L
S maximum at constant U and Vol	L maximum at constant V and R

REFERENCES

1. A. Bejan, *Advanced Engineering Thermodynamics*, 3rd ed., Wiley, Hoboken, NJ, 2006.
2. A. Bejan, G. Tsatsaronis, and M. Moran, *Thermal Design and Optimization*, Wiley, New York, 1996.
3. A. Bejan, *Entropy Generation through Heat and Fluid Flow*, Wiley, New York, 1982.
4. A. Bejan, *Entropy Generation Minimization*, CRC Press, Boca Raton, FL, 1996.
5. A. Bejan, *Shape and Structure, from Engineering to Nature*, Cambridge University Press, Cambridge, UK, 2000.
6. A. Bejan and S. Lorente, "The Constructal Law and the Thermodynamics of Flow Systems with Configuration", *Int. J. Heat Mass Transfer*, **47**, 3203–3214, 2004.
7. A. Bejan and S. Lorente, *Design with Constructal Theory*, Wiley, Hoboken, NJ, 2008.
8. A. Bejan, *Convection Heat Transfer*, 4th ed., Wiley, Hoboken, NJ, 2013.
9. S. Paoletti, F. Rispoli, and E. Sciubba, "Calculation of Exergetic Losses in Compact Heat Exchanger Passages", *AES* **10**(2), 21–29 (1989).
10. A. Bejan, *Solved Problems in Thermodynamics*, Massachusetts Institute of Technology, Department of Mechanical Engineering, 1976, Problem VII-D.
11. A. Bejan and S. Lorente, "The Constructal Law Origin of the Logistics S Curve", *J. Appl. Phys.*, **110**, 024901, 2011.
12. A. Bejan and S. Lorente, "The Physics of Spreading Ideas", *Int. J. Heat Mass Transfer*, **55**, 802–807, 2012.

CHAPTER 5

HEAT TRANSFER FUNDAMENTALS

G. P. Peterson
Georgia Institute of Technology
Atlanta, GA

1 CONDUCTION HEAT TRANSFER	185	2.4 The Log-Mean Temperature Difference	214
1.1 Thermal Conductivity	186	3 RADIATION HEAT TRANSFER	214
1.2 One-Dimensional Steady-State Heat Conduction	187	3.1 Blackbody Radiation	216
1.3 Two-Dimensional Steady-State Heat Conduction	193	3.2 Radiation Properties	218
1.4 Heat Conduction with Convection Heat Transfer on the Boundaries	194	3.3 Configuration Factor	223
1.5 Transient Heat Conduction	198	3.4 Radiative Exchange among Diffuse Gray Surfaces in an Enclosure	228
1.6 Conduction at the Microscale	199	3.5 Thermal Radiation Properties of Gases	229
2 CONVECTION HEAT TRANSFER	204	4 BOILING AND CONDENSATION HEAT TRANSFER	234
2.1 Forced Convection—Internal Flow	205	4.1 Boiling	234
2.2 Forced Convection—External Flow	207	4.2 Condensation	237
2.3 Free Convection	211	4.3 Heat Pipes	239
		REFERENCES	244
		BIBLIOGRAPHY	246

Symbols and Units

A	area of heat transfer
Bi	Biot Number, hL/k , dimensionless
C	circumference, m, constant defined in text
C_p	specific heat under constant pressure, $J/kg \cdot K$
D	diameter, m
e	emissive power, W/m^2
f	drag coefficient, dimensionless
F	cross-flow correction factor, dimensionless
F_{i-j}	configuration factor from surface i to surface j , dimensionless
Fo	Fourier number, atA^2/V^2 , dimensionless
$F_{o-\lambda T}$	radiation function, dimensionless
G	irradiation, W/m^2 ; mass velocity, $kg/m^2 \cdot s$
g	local gravitational acceleration, $9.8 m/s^2$
g_c	proportionality constant, $1 kg \cdot m/N \cdot s^2$
Gr	Grashof number, $gL^3\beta \Delta T/\nu^2$ dimensionless
h	convection heat transfer coefficient, equals $q/A \Delta T$, $W/m^2 \cdot K$

Symbols and Units

h_{fg}	heat of vaporization, J/kg
J	radiosity, W/m ²
k	thermal conductivity, W/m · K
K	wick permeability, m ²
L	length, m
Ma	Mach number, dimensionless
N	screen mesh number, m ⁻¹
Nu	Nusselt number, $Nu_L = hL/k$, $Nu_D = hD/k$, dimensionless
\overline{Nu}	Nusselt number averaged over length, dimensionless
P	pressure, N/m ² , perimeter, m
Pe	Peclet number, $RePr$, dimensionless
Pr	Prandtl number, $C_p\mu/k$, dimensionless
q	rate of heat transfer, W
q''	rate of heat transfer per unit area, W/m ²
R	distance, m; thermal resistance, K/W
r	radial coordinate, m; recovery factor, dimensionless
Ra	Rayleigh number, $GrPr$; $Ra_L = Gr_LPr$, dimensionless
Re	Reynolds Number, $Re_L = \rho VL/\mu$, $Re_D = \rho VD/\mu$, dimensionless
S	conduction shape factor, m
T	temperature, K or °C
t	time, s
T_{as}	adiabatic surface temperature, K
T_{sat}	saturation temperature, K
T_b	fluid bulk temperature or base temperature of fins, K
T_e	excessive temperature, $T_s - T_{sat}$, K or °C
T_f	film temperature, $(T_\infty + T_s)/2$, K
T_i	initial temperature; at $t = 0$, K
T_0	stagnation temperature, K
T_s	surface temperature, K
T_∞	free-stream fluid temperature, K
U	overall heat transfer coefficient, W/m ² · K
V	fluid velocity, m/s; volume, m ³
w	groove width, m; or wire spacing, m
We	Weber number, dimensionless
x	one of the axes of Cartesian reference frame, m

Greek Symbols

α	thermal diffusivity, $k/\rho C_p$, m ² /s; absorptivity, dimensionless
β	coefficient of volume expansion, 1/K
Γ	mass flow rate of condensate per unit width, kg/m · s
γ	specific heat ratio, dimensionless
ΔT	temperature difference, K
δ	thickness of cavity space, groove depth, m
ϵ	emissivity, dimensionless
ε	wick porosity, dimensionless
λ	wavelength, μm
η_f	fin efficiency, dimensionless

Greek Symbols

μ	viscosity, $\text{kg}/\text{m} \cdot \text{s}$
ν	kinematic viscosity, m^2/s
ρ	reflectivity, dimensionless; density, kg/m^3
σ	surface tension, N/m ; Stefan–Boltzmann constant, $5.729 \times 10^{-8} \text{W}/\text{m}^2 \cdot \text{K}^4$
τ	transmissivity, dimensionless, shear stress, N/m^2
Ψ	angle of inclination, degrees or radians

Subscripts

a	adiabatic section, air
b	boiling, blackbody
c	convection, capillary, capillary limitation, condenser
e	entrainment, evaporator section
eff	effective
f	fin
i	inner
l	liquid
m	mean, maximum
n	nucleation
o	outer
O	stagnation condition
p	pipe
r	radiation
s	surface, sonic or sphere
w	wire spacing, wick
v	vapor
λ	spectral
∞	free stream
–	axial hydrostatic pressure
+	normal hydrostatic pressure

Transport phenomena represents the overall field of study and encompasses a number of sub-fields. One of these is heat transfer, which focuses primarily on the energy transfer occurring as a result of an energy gradient that manifests itself as a temperature difference. This form of energy transfer can occur as a result of a number of different mechanisms, including *conduction*, which focuses on the transfer of energy through the direct impact of molecules; *convection*, which results from the energy transferred through the motion of a fluid; and *radiation*, which focuses on the transmission of energy through electromagnetic waves. In the following review, as is the case with most texts on heat transfer, *phase change heat transfer*, i.e., *boiling* and *condensation*, will be treated as a subset of convection heat transfer.

1 CONDUCTION HEAT TRANSFER

The exchange of energy or heat resulting from the kinetic energy transferred through the direct impact of molecules is referred to as *conduction* and takes place from a region of high energy (or temperature) to a region of lower energy (or temperature). The fundamental relationship that governs this form of heat transfer is *Fourier's law of heat conduction*, which states that

in a one-dimensional system with no fluid motion, the rate of heat flow in a given direction is proportional to the product of the temperature gradient in that direction and the area normal to the direction of heat flow. For conduction heat transfer in the x direction this expression takes the form

$$q_x = -kA \frac{\partial T}{\partial x}$$

where q_x is the heat transfer in the x direction, A is the area normal to the heat flow, $\partial T/\partial x$ is the temperature gradient, and k is the thermal conductivity of the substance.

Writing an energy balance for a three-dimensional body and utilizing Fourier's law of heat conduction yields an expression for the transient diffusion occurring within a body or substance:

$$\frac{\partial}{\partial x} \left(k \frac{\partial T}{\partial x} \right) + \frac{\partial}{\partial y} \left(k \frac{\partial T}{\partial y} \right) + \frac{\partial}{\partial z} \left(k \frac{\partial T}{\partial z} \right) + \dot{q} = \rho c_p \frac{\partial}{\partial x} \frac{\partial T}{\partial t}$$

This expression, usually referred to as the *heat diffusion equation* or heat equation, provides a basis for most types of heat conduction analyses. Specialized cases of this equation can be used to solve many steady-state or transient problems. Some of these specialized cases follow:

Thermal conductivity is a constant:

$$\frac{\partial^2 T}{\partial x^2} + \frac{\partial^2 T}{\partial y^2} + \frac{\partial^2 T}{\partial z^2} + \frac{\dot{q}}{k} = \frac{\rho c_p}{k} \frac{\partial T}{\partial t}$$

Steady-state with heat generation:

$$\frac{\partial}{\partial x} \left(k \frac{\partial T}{\partial x} \right) + \frac{\partial}{\partial y} \left(k \frac{\partial T}{\partial y} \right) + \frac{\partial}{\partial z} \left(k \frac{\partial T}{\partial z} \right) + \dot{q} = 0$$

Steady-state, one-dimensional heat transfer with no heat sink (i.e., a fin):

$$\frac{\partial}{\partial x} \left(\frac{\partial T}{\partial x} \right) + \frac{\dot{q}}{k} = 0$$

One-dimensional heat transfer with no internal heat generation:

$$\frac{\partial}{\partial x} \left(\frac{\partial T}{\partial x} \right) = \frac{\rho c_p}{k} \frac{\partial T}{\partial t}$$

In the following sections, the heat diffusion equation will be utilized for several specific cases. However, in general, for a three-dimensional body of constant thermal properties without heat generation under steady-state heat conduction the temperature field satisfies the expression

$$\nabla^2 T = 0$$

1.1 Thermal Conductivity

The ability of a substance to transfer heat through conduction can be represented by the constant of proportionality, k , referred to as the thermal conductivity. Figure 1 illustrates the characteristics of the thermal conductivity as a function of temperature for several solids, liquids, and gases. As shown, the thermal conductivity of solids is higher than liquids, and liquids higher than gases. Metals typically have higher thermal conductivities than nonmetals, with pure metals having thermal conductivities that decrease with increasing temperature, while the thermal conductivity of nonmetallic solids generally increases with increasing temperature and density. The addition of other metals to create alloys, or the presence of impurities, usually decreases the thermal conductivity of a pure metal.

In general, the thermal conductivity of liquids decreases with increasing temperature. Alternatively, the thermal conductivity of gases and vapors, while lower, increases with increasing temperature and decreases with increasing molecular weight. The thermal conductivities

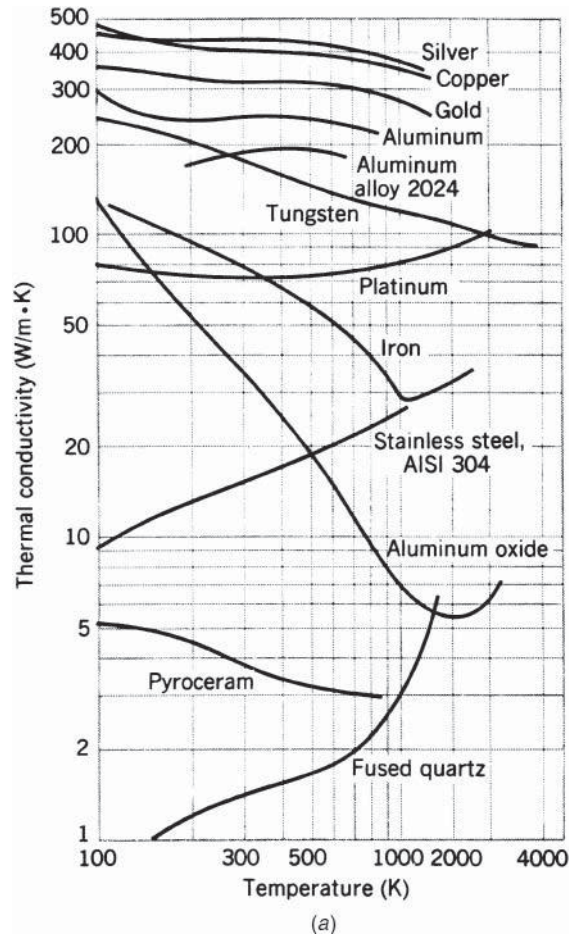


Figure 1(a) The temperature dependence of the thermal conductivity of selected solids.¹

of a number of commonly used metals and nonmetals are tabulated in Tables 1 and 2, respectively. Insulating materials, which are used to prevent or reduce the transfer of heat between two substances or a substance and the surroundings, are listed in Tables 3 and 4, along with the thermal properties. The thermal conductivities for liquids, molten metals, and gases are given in Tables 5, 6, and 7, respectively.

1.2 One-Dimensional Steady-State Heat Conduction

The steady-state rate of heat transfer resulting from heat conduction through a homogeneous material can be expressed in terms of the rate of heat transfer, q , or $q = \Delta T/R$, where ΔT is the temperature difference and R is the *thermal resistance*. This thermal resistance is the reciprocal of the *thermal conductance* ($C = 1/R$) and is related to the thermal conductivity by the cross-sectional area. Expressions for the thermal resistance, the temperature distribution,

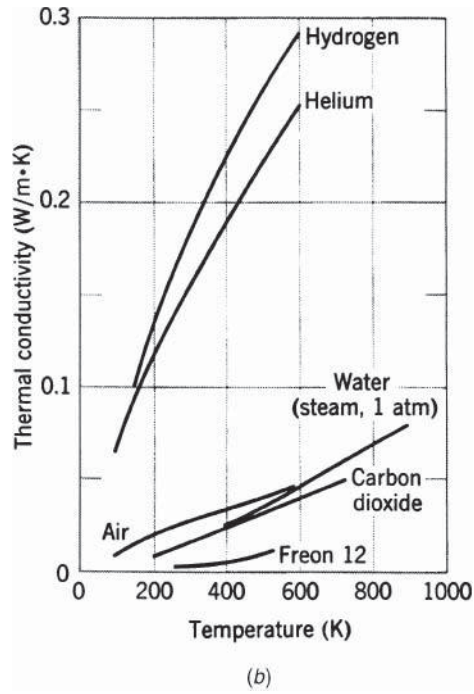


Figure 1(b) The temperature dependence of the thermal conductivity of selected nonmetallic liquids under saturated conditions.¹

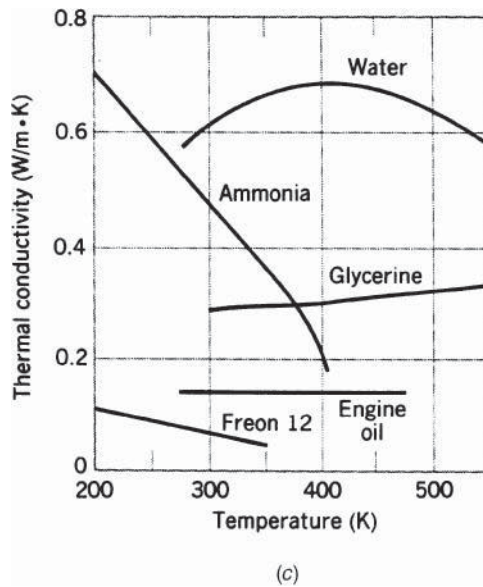


Figure 1(c) The temperature dependence of the thermal conductivity of selected gases at normal pressures.¹

Table 1 Thermal Properties of Metallic Solids

Composition	Melting Point (K)	Properties at 300 K				Properties at Various Temperatures (K)		
		ρ (kg/m ³)	C_p (J/kg · K)	k (W/m · K)	$\alpha \times 10^6$ (m ² /s)	k (W/m · K); C_p (J/kg · K)		
						100	600	1200
Aluminum	933	2,702	903	237	97.1	302; 482	231; 1033	
Copper	1,358	8,933	385	401	117	482; 252	379; 417	339; 480
Gold	1,336	19,300	129	317	127	327; 109	298; 135	255; 155
Iron	1,810	7,870	447	80.2	23.1	134; 216	54.7; 574	28.3; 609
Lead	601	11,340	129	35.3	24.1	39.7; 118	31.4; 142	
Magnesium	923	1,740	1,024	156	87.6	169; 649	149; 1170	
Molybdenum	2,894	10,240	251	138	53.7	179; 141	126; 275	105; 308
Nickel	1,728	8,900	444	90.7	23.0	164; 232	65.6; 592	76.2; 594
Platinum	2,045	21,450	133	71.6	25.1	77.5; 100	73.2; 141	82.6; 157
Silicon	1,685	2,330	712	148	89.2	884; 259	61.9; 867	25.7; 967
Silver	1,235	10,500	235	429	174	444; 187	412; 250	361; 292
Tin	505	7,310	227	66.6	40.1	85.2; 188		
Titanium	1,953	4,500	522	21.9	9.32	30.5; 300	19.4; 591	22.0; 620
Tungsten	3,660	19,300	132	174	68.3	208; 87	137; 142	113; 152
Zinc	693	7,140	389	116	41.8	117; 297	103; 436	

Source: Adapted from Ref. 1.

Table 2 Thermal Properties of Nonmetals

Description/ Composition	Temperature (K)	Density, ρ (kg/m ³)	Thermal Conductivity, k (W/m · K)	Specific Heat, C_p (J/kg · K)	$\alpha \times 10^6$ (m ² /s)
Bakelite	300	1300	0.232	1465	0.122
Brick, refractory					
Carborundum	872	—	18.5	—	—
Chrome-brick	473	3010	2.32	835	0.915
Fire clay brick	478	2645	1.0	960	0.394
Clay	300	1460	1.3	880	1.01
Coal, anthracite	300	1350	0.26	1260	0.153
Concrete (stone mix)	300	2300	1.4	880	0.692
Cotton	300	80	0.059	1300	0.567
Glass, window	300	2700	0.78	840	0.344
Rock, limestone	300	2320	2.15	810	1.14
Rubber, hard	300	1190	0.160	—	—
Soil, dry	300	2050	0.52	1840	0.138
Teflon	300	2200	0.35	—	—
	400	—	0.45	—	—

Table 3 Thermal Properties of Building and Insulating Materials (at 300 K)

Description/Composition	Density, $\rho(\text{kg/m}^3)$	Thermal Conductivity, $k(\text{W/m} \cdot \text{K})$	Specific Heat, $C_p(\text{J/kg} \cdot \text{K})$	$\alpha \times 10^6$ (m^2/s)
Building boards				
Plywood	545	0.12	1215	0.181
Acoustic tile	290	0.058	1340	0.149
Hardboard, siding	640	0.094	1170	0.126
Woods				
Hardwoods (oak, maple)	720	0.16	1255	0.177
Softwoods (fir, pine)	510	0.12	1380	0.171
Masonry materials				
Cement mortar	1860	0.72	780	0.496
Brick, common	1920	0.72	835	0.449
Plastering materials				
Cement plaster, sand aggregate	1860	0.72	—	—
Gypsum plaster, sand aggregate	1680	0.22	1085	0.121
Blanket and batt				
Glass fiber, paper faced	16	0.046	—	—
Glass fiber, coated; duct liner	32	0.038	835	1.422
Board and slab				
Cellular glass	145	0.058	1000	0.400
Wood, shredded/cemented	350	0.087	1590	0.156
Cork	120	0.039	1800	0.181
Loose fill				
Glass fiber, poured or blown	16	0.043	835	3.219
Vermiculite, flakes	80	0.068	835	1.018

Source: Adapted from Ref. 1.

and the rate of heat transfer are given in Table 8 for a plane wall, a cylinder, and a sphere. For a plane wall, the heat transfer is typically assumed to be one dimensional (i.e., heat is conducted in only the x direction), and for a cylinder and sphere, only in the radial direction.

Aside from the heat transfer in these simple geometric configurations, other common problems encountered in practical applications is that of heat transfer through layers or composite walls consisting of N layers, where the thickness of each layer is represented by Δx_n and the thermal conductivity by k_n for $n = 1, 2, \dots, N$. Assuming that the interfacial resistance is negligible (i.e., there is no thermal resistance at the contacting surfaces), the overall thermal resistance can be expressed as

$$R = \sum_{n=1}^N \frac{\Delta x_n}{k_n A}$$

Similarly, for conduction heat transfer in the radial direction through a number of N concentric cylinders with negligible interfacial resistance, the overall thermal resistance can be expressed as

$$R = \sum_{n=1}^N \frac{\ln(r_{n+1}/r_n)}{2\pi k_n L}$$

where r_1 is the inner radius, and r_{N+1} is the outer radius.

Table 4 Thermal Conductivities for Some Industrial Insulating Materials

Description/Composition	Maximum Service Temperature (K)	Typical Density (kg/m ³)	Typical Thermal Conductivity, k (W/m · K), at Various Temperatures (K)			
			200	300	420	645
Blankets						
Blanket, mineral fiber, glass; fine fiber	450	10	0.048			
organic bonded		48	0.033			
Blanket, alumina-silica fiber	1530	48	0.105			
Felt, semirigid; organic bonded	480	50–125	0.038		0.063	
Felt, laminated; no binder	920	120			0.051	
Blocks, boards, and pipe insulations						
Asbestos paper, laminated and corrugated, 4-ply	420	190	0.078			
Calcium silicate	920	190			0.063	
Polystyrene, rigid						
Extruded (R-12)	350	56	0.023	0.027		
Molded beads	350	16	0.026	0.040		
Rubber, rigid foamed	340	70	0.032			
Insulating cement						
Mineral fiber (rock, slag, or glass)						
With clay binder	1255	430			0.088	
With hydraulic setting binder	922	560			0.123	
Loose fill						
Cellulose, wood, or paper pulp	—	45			0.039	
Perlite, expanded	—	105	0.036	0.053		
Vermiculite, expanded	—	122	0.068			

Source: Adapted from Ref. 1.

Table 5 Thermal Properties of Saturated Liquids^a

Liquid	T (K)	ρ (kg/m ³)	C_p (kJ/kg · K)	$\nu \times 10^6$ (m ² /s)	$k \times 10^3$ (W/m · K)	$\alpha \times 10^7$ (m ² /s)	Pr	$\beta \times 10^3$ (K ⁻¹)
Ammonia, NH ₃	223	703.7	4.463	0.435	547	1.742	2.60	2.45
	323	564.3	5.116	0.330	476	1.654	1.99	2.45
Carbon dioxide, CO ₂	223	1156.3	1.84	0.119	85.5	0.402	2.96	14.0
	303	597.8	36.4	0.080	70.3	0.028	28.7	14.0
Engine oil (unused)	273	899.1	1.796	4280	147	0.910	47,000	0.70
	430	806.5	2.471	5.83	132	0.662	88	0.70
Ethylene glycol, C ₂ H ₄ (OH) ₂	273	1130.8	2.294	57.6	242	0.933	617.0	0.65
	373	1058.5	2.742	2.03	263	0.906	22.4	0.65
Glycerin, C ₃ H ₅ (OH) ₃	273	1276.0	2.261	8310	282	0.977	85,000	0.47
	320	1247.2	2.564	168	287	0.897	1,870	0.50
Freon (Refrigerant-12), CCl ₂ F ₂	230	1528.4	0.8816	0.299	68	0.505	5.9	1.85
	320	1228.6	1.0155	0.190	68	0.545	3.5	3.50

^aSee Table 23 for H₂O.

Source: Adapted from Ref. 2.6

Table 6 Thermal Properties of Liquid Metals

Composition	Melting		$\rho(\text{kg/m}^3)$	C_p (kJ/kg · K)	$\nu \times 10^7$ (m ² /s)	k (W/m · K)	$\alpha \times 10^5$ (m ² /s)	Pr
	Point (K)	T (K)						
Bismuth	544	589	10,011	0.1444	1.617	16.4	0.138	0.0142
		1033	9,467	0.1645	0.8343	15.6	1.001	0.0083
Lead	600	644	10,540	0.159	2.276	16.1	1.084	0.024
		755	10,412	0.155	1.849	15.6	1.223	0.017
Mercury	234	273	13,595	0.140	1.240	8.180	0.429	0.0290
		600	12,809	0.136	0.711	11.95	0.688	0.0103
Potassium	337	422	807.3	0.80	4.608	45.0	6.99	0.0066
		977	674.4	0.75	1.905	33.1	6.55	0.0029
Sodium	371	366	929.1	1.38	7.516	86.2	6.71	0.011
		977	778.5	1.26	2.285	59.7	6.12	0.0037
NaK (56%/44%)	292	366	887.4	1.130	6.522	25.6	2.55	0.026
		977	740.1	1.043	2.174	28.9	3.74	0.0058
PbBi (44.5%/55.5%)	398	422	10,524	0.147	—	9.05	0.586	—
		644	10,236	0.147	1.496	11.86	0.790	0.189

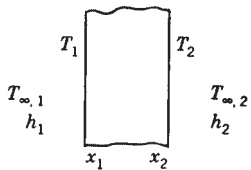
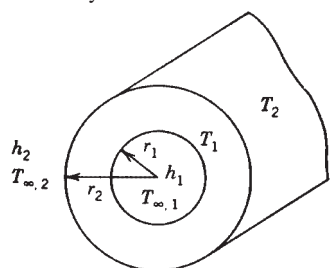
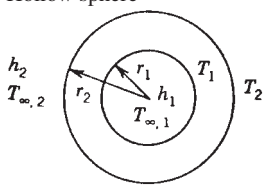
Source: Adapted from *Liquid Metals Handbook*, The Atomic Energy Commission, Department of the Navy, Washington, DC, 1952.

Table 7 Thermal Properties of Gases at Atmospheric Pressure

Gas	T (K)	$\rho(\text{kg/m}^3)$	C_p (kJ/kg · K)	$\nu \times 10^6$ (m ² /s)	k (W/m · K)	$\alpha \times 10^4$ (m ² /s)	Pr
	300	1.1774	1.0057	16.84	0.02624	0.2216	0.708
	2500	0.1394	1.688	543.0	0.175	7.437	0.730
Ammonia, NH ₃	220	0.3828	2.198	19.0	0.0171	0.2054	0.93
	473	0.4405	2.395	37.4	0.0467	0.4421	0.84
Carbon dioxide	220	2.4733	0.783	4.490	0.01081	0.0592	0.818
	600	0.8938	1.076	30.02	0.04311	0.4483	0.668
Carbon monoxide	220	1.5536	1.0429	8.903	0.01906	0.1176	0.758
	600	0.5685	1.0877	52.06	0.04446	0.7190	0.724
Helium	33	1.4657	5.200	3.42	0.0353	0.04625	0.74
	900	0.05286	5.200	781.3	0.298	10.834	0.72
Hydrogen	30	0.8472	10.840	1.895	0.0228	0.02493	0.759
	300	0.0819	14.314	109.5	0.182	1.554	0.706
	1000	0.0819	14.314	109.5	0.182	1.554	0.706
Nitrogen	100	3.4808	1.0722	1.971	0.009450	0.02531	0.786
	300	1.1421	1.0408	15.63	0.0262	0.204	0.713
	1200	0.2851	1.2037	156.1	0.07184	2.0932	0.748
Oxygen	100	3.9918	0.9479	1.946	0.00903	0.02388	0.815
	300	1.3007	0.9203	15.86	0.02676	0.2235	0.709
	600	0.6504	1.0044	52.15	0.04832	0.7399	0.704
Steam (H ₂ O vapor)	380	0.5863	2.060	21.6	0.0246	0.2036	1.060
	850	0.2579	2.186	115.2	0.0637	1.130	1.019

Source: Adapted from Ref. 2.

Table 8 One-Dimensional Heat Conduction

Geometry	Heat Transfer Rate and Temperature Distribution	Heat Transfer Rate and Overall Heat Transfer Coefficient with Convection at the Boundaries
Plane wall 	$q = \frac{T_1 - T_2}{(x_2 - x_1)/kA}$ $T = T_1 + \frac{T_2 - T_1}{x_2 - x_1}(x - x_1)$ $R = \frac{x_2 - x_1}{kA}$	$q = UA(T_{\infty,1} - T_{\infty,2})$ $U = \frac{1}{\frac{1}{h_1} + \frac{x_2 - x_1}{k} + \frac{1}{h_2}}$
Hollow cylinder 	$q = \frac{T_1 - T_2}{[\ln(r_2/r_1)]/2\pi kL}$ $T = \frac{T_2 - T_1}{\ln(r_2/r_1)} \ln \frac{r}{r_1}$ $R = \frac{\ln(r_2/r_1)}{2\pi kL}$	$q = 2\pi r_1 L U_1 (T_{\infty,1} - T_{\infty,2})$ $= 2\pi r_1 L U_2 (T_{\infty,1} - T_{\infty,2})$ $U_1 = \frac{1}{\frac{1}{h_1} + \frac{r_1 \ln(r_2/r_1)}{k} + \frac{r_1}{r_2} \frac{1}{h_2}}$ $U_2 = \frac{1}{\left(\frac{r_2}{r_1}\right) \frac{1}{h_1} + \frac{r_2 \ln(r_2/r_1)}{k} + \frac{1}{h_2}}$
Hollow sphere 	$q = \frac{T_1 - T_2}{\left(\frac{1}{r_1} - \frac{1}{r_2}\right)/4\pi k}$ $T = \frac{1}{\left(1 - \frac{r_1}{r_2}\right)} \left[\frac{r_1}{r} (T_1 - T_2) + \left(T_2 - T_1 \frac{r_1}{r_2}\right) \right]$ $R = \left(\frac{1}{r_1} - \frac{1}{r_2}\right)/4\pi k$	$q = 4\pi r_1^2 U_1 (T_{\infty,1} - T_{\infty,2})$ $= 4\pi r_2^2 U_2 (T_{\infty,1} - T_{\infty,2})$ $U_1 = \frac{1}{\frac{1}{h_1} + r_1^2 \left(\frac{1}{r_1} - \frac{1}{r_2}\right)/k + \left(\frac{r_1}{r_2}\right)^2 \frac{1}{h_2}}$ $U_2 = \frac{1}{\left(\frac{r_1}{r_2}\right)^2 \frac{1}{h_1} + r_2^2 \left(\frac{1}{r_1} - \frac{1}{r_2}\right)/k + \frac{1}{h_2}}$

For N concentric spheres with negligible interfacial resistance, the thermal resistance can be expressed as

$$R = \sum_{n=1}^N \left(\frac{1}{r_n} - \frac{1}{r_{n+1}} \right) / 4\pi k$$

where r_1 is the inner radius, and r_{N+1} is the outer radius.

1.3 Two-Dimensional Steady-State Heat Conduction

Two-dimensional heat transfer in an isotropic, homogeneous material with no internal heat generation requires solution of the heat diffusion equation of the form $\partial^2 T / \partial X^2 + \partial T / \partial y^2 = 0$, referred to as the *Laplace equation*. For certain geometries and a limited number of fairly simple combinations of boundary conditions, exact solutions can be obtained analytically. However, for anything but simple geometries or for simple geometries with complicated

boundary conditions, development of an appropriate analytical solution can be difficult and other methods are usually employed. Among these are solution procedures involving the use of *graphical* or *numerical* approaches. In the first of these, the rate of heat transfer between two isotherms, T_1 and T_2 , is expressed in terms of the conduction shape factor, defined by

$$q = kS(T_1 - T_2)$$

Table 9 illustrates the shape factor for a number of common geometric configurations. By combining these shape factors, the heat transfer characteristics for a wide variety of geometric configurations can be obtained.

Prior to the development of high-speed digital computers, shape factor and analytical methods were the most prevalent methods utilized for evaluating steady-state and transient conduction problems. However, more recently, solution procedures for problems involving complicated geometries or boundary conditions utilize the finite-difference method (FDM). Using this approach, the solid object is divided into a number of distinct or discrete regions, referred to as *nodes*, each with a specified boundary condition. An energy balance is then written for each nodal region and these equations are solved simultaneously. For interior nodes in a two-dimensional system with no internal heat generation, the energy equation takes the form of the Laplace equation discussed earlier. However, because the system is characterized in terms of a nodal network, a finite-difference approximation must be used. This approximation is derived by substituting the following equation for the x -direction rate of change expression:

$$\left. \frac{\partial^2 T}{\partial x^2} \right|_{m,n} \approx \frac{T_{m+1,n} + T_{m-1,n} - 2T_{m,n}}{(\Delta x)^2}$$

and for the y -direction rate of change expression:

$$\left. \frac{\partial^2 T}{\partial y^2} \right|_{m,n} \approx \frac{T_{m,n+1} + T_{m,n-1} + T_{m,n}}{(\Delta y)^2}$$

Assuming $\Delta x = \Delta y$ and substituting into the Laplace equation results in the following expression:

$$T_{m,n+1} + T_{m,n-1} + T_{m+1,n} + T_{m-1,n} - 4T_{m,n} = 0$$

which reduces the exact difference to an approximate algebraic expression.

Combining this temperature difference with Fourier's law yields an expression for each internal node

$$T_{m,n+1} + T_{m,n-1} + T_{m+1,n} + T_{m-1,n} + \frac{\dot{q}\Delta x \Delta y l}{k} - 4T_{m,n} = 0$$

Similar equations for other geometries (i.e., corners) and boundary conditions (i.e., convection) and combinations of the two are listed in Table 10. These equations must then be solved using some form of matrix inversion technique, Gauss-Seidel iteration method, or other method for solving large numbers of simultaneous equations.

1.4 Heat Conduction with Convection Heat Transfer on the Boundaries

In physical situations where a solid is immersed in a fluid, or a portion of the surface is exposed to a liquid or gas, heat transfer will occur by convection (or when there is a large temperature difference, through some combination of convection and/or radiation). In these situations, the heat transfer is governed by *Newton's law of cooling*, which is expressed as

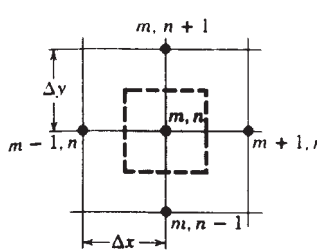
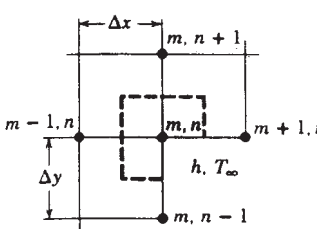
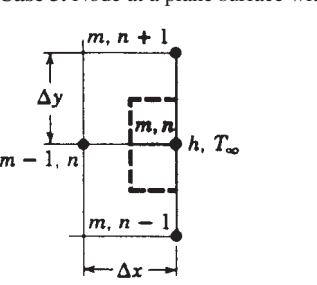
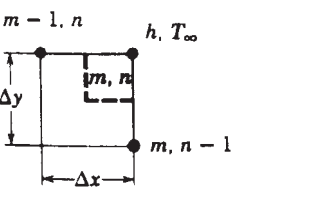
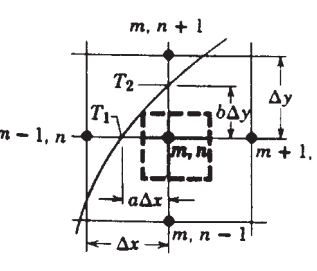
$$q = hA \Delta T$$

where h is the *convection heat transfer coefficient* (Section 2), ΔT is the temperature difference between the solid surface and the fluid, and A is the surface area in contact with the fluid.

Table 9 Conduction Shape Factors

System	Schematic	Restrictions	Shape Factor
Isothermal sphere buried in a semi-infinite medium having isothermal surface		$z > D/2$	$\frac{2\pi D}{1 - D/4z}$
Horizontal isothermal cylinder of length L buried in a semi-infinite medium having isothermal surface		$\left. \begin{aligned} L &\gg D \\ L &\gg D \\ z &> 3D/2 \end{aligned} \right\}$	$\frac{2\pi L}{\cosh^{-1}(2z/D)} \frac{2\pi L}{\ln(4z/D)}$
The cylinder of length L with eccentric bore		$L \gg D_1, D_2$	$\frac{2\pi L}{\cosh^{-1}\left(\frac{D_1^2 + D_2^2 - 4e^2}{2D_1D_2}\right)}$
Conduction between two cylinders of length L in infinite medium		$L \gg D_1, D_2$	$\frac{2\pi L}{\cosh^{-1}\left(\frac{4W^2 - D_1^2 - D_2^2}{2D_1D_2}\right)}$
Circular cylinder of length L in a square solid		$\left. \begin{aligned} L &\gg W \\ w &> D \end{aligned} \right\}$	$\frac{2\pi L}{\ln(1.08 w/D)}$
Conduction through the edge of adjoining walls		$D > L/5$	$0.54D$
Conduction through corner of three walls with inside and outside temperature, respectively, at T_1 and T_2		$L \ll \text{length and width of wall}$	$0.15L$

Table 10 Summary of Nodal Finite-Difference Equations

Configuration	Finite-Difference Equation for $\Delta x = \Delta y$
<p>Case 1. Interior node</p> 	$T_{m,n+1} + T_{m,n-1} + T_{m-1,n} - 4T_{m,n} = 0$
<p>Case 2. Node at an internal corner with convection</p> 	$2(T_{m-1,n} + T_{m,n+1}) + (T_{m+1,n} + T_{m,n-1}) + 2\frac{h\Delta x}{k}T_{\infty} - 2\left(3 + \frac{h\Delta x}{k}\right)T_{m,n} = 0$
<p>Case 3. Node at a plane surface with convection</p> 	$(2T_{m-1,n} + T_{m,n+1} + T_{m,n-1}) + \frac{2h\Delta x}{k}T_{\infty} - 2\left(\frac{h\Delta x}{k} + 2\right)T_{m,n} = 0$
<p>Case 4. Node at an external corner with convection</p> 	$(T_{m,n-1} + T_{m-1,n}) + 2\frac{h\Delta x}{k}T_{\infty} - 2\left(\frac{h\Delta x}{k} + 1\right)T_{m,n} = 0$
<p>Case 5. Node near a curved surface maintained at a nonuniform temperature</p> 	$\frac{2}{a+1}T_{m+1,n} + \frac{2}{b+1}T_{m,n-1} + \frac{2}{a(a+1)}T_1 + \frac{2}{b(b+1)}T_2 - \left(\frac{2}{a} + \frac{2}{b}\right)T_{m,n} = 0$

The resistance occurring at the surface abounding the solid and fluid is referred to as the *thermal resistance* and is given by $1/hA$, i.e., the *convection resistance*. Combining this resistance term with the appropriate conduction resistance yields an *overall heat transfer coefficient* U . Usage of this term allows the overall heat transfer to be defined as $q = UA \Delta T$.

Table 8 shows the overall heat transfer coefficients for some simple geometries. Note that U may be based either on the inner surface (U_1) or on the outer surface (U_2) for the cylinders and spheres.

Critical Radius of Insulation for Cylinders

A large number of practical applications involve the use of insulation materials to reduce the transfer of heat into or out of cylindrical surfaces. This is particularly true of steam or hot water pipes where concentric cylinders of insulation are typically added to the outside of the pipes to reduce the heat loss. Beyond a certain thickness, however, the continued addition of insulation may not result in continued reductions in the heat loss. To optimize the thickness of insulation required for these types of applications, a value typically referred to as the critical radius, defined as $r_{cr} = k/h$, is used. If the outer radius of the object to be insulated is less than r_{cr} , then the addition of insulation will increase the heat loss, while for cases where the outer radii is greater than r_{cr} any additional increases in insulation thickness will result in a decrease in heat loss.

Extended Surfaces

In examining Newton's law of cooling, it is clear that the rate of heat transfer between a solid and the surrounding ambient fluid may be increased by increasing the surface area of the solid that is exposed to the fluid. This is typically done through the addition of extended surfaces or fins to the primary surface. Numerous examples often exist, including the cooling fins on air-cooled engines, i.e., motorcycles or lawn mowers or the fins attached to automobile radiators.

Figure 2 illustrates a common uniform cross-section extended surface, fin, with a constant base temperature, T_b , a constant cross-sectional area, A , a circumference of $C = 2W + 2t$, and

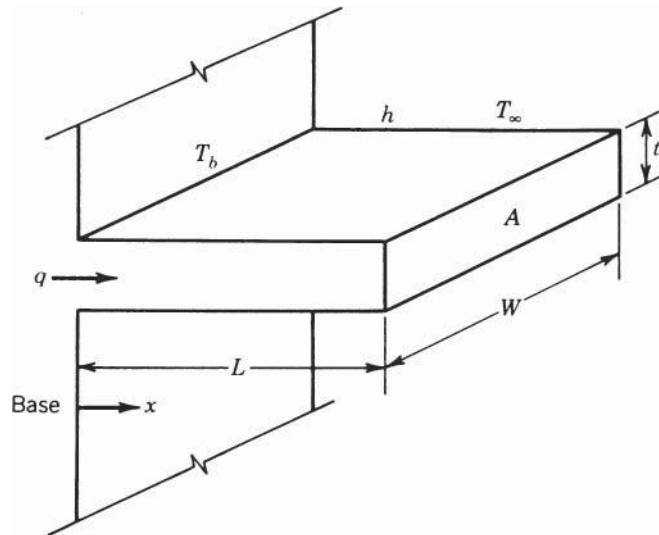


Figure 2 Heat transfer by extended surfaces.

Table 11 Temperature Distribution and Heat Transfer Rate at the Fin Base ($m = \sqrt{hc/kA}$)

Condition at $x = L$	$\frac{T - T_\infty}{T_b - T_\infty}$	Heat Transfer Rate $q/mkA (T_b - T_\infty)$
$h(T_{x=L} - T_\infty) = -k\left(\frac{dT}{dx}\right)_{x=L}$ (convection)	$\frac{\cosh m(L-x) + \frac{h}{mk} \sinh m(L-x)}{\cosh mL + \frac{h}{mk} \sinh mL}$	$\frac{\sinh mL + \frac{h}{mk} \cosh mL}{\cosh mL + \frac{h}{mk} \sinh mL}$
$\left(\frac{dT}{dx}\right)_{x=L} = 0$ (insulated)	$\frac{\cosh m(L-x)}{\cosh mL}$	$\tanh mL$
$T_{x=L} = T_L$ (prescribed temperature)	$\frac{(T_L - T_\infty)/(T_b - T_\infty) \sinh mx + \sinh m(L-x)}{\sinh mL}$	$\frac{\cosh mL - (T_L - T_\infty)/(T_b - T_\infty)}{\sinh mL}$
$T_{x=L} = T_\infty$ (infinitely long fin, $L \rightarrow \infty$)	e^{-mx}	1

a length, L , which is much larger than the thickness, t . For these conditions, the temperature distribution in the fin must satisfy the following expression:

$$\frac{d^2T}{dx^2} - \frac{hC}{kA}(T - T_\infty) = 0$$

The solution of this equation depends on the boundary conditions existing at the tip, i.e., at $x = L$. Table 11 shows the temperature distribution and heat transfer rate for fins of uniform cross section subjected to a number of different tip conditions, assuming a constant value for the heat transfer coefficient, h .

Two terms are used to evaluate fins and their usefulness. The first of these is the *fin effectiveness*, defined as the ratio of the heat transfer rate with the fin to the heat transfer rate that would exist if the fin were not used. For most practical applications, the use of a fin is justified only when the fin effectiveness is significantly greater than 2. A second term used to evaluate the usefulness of a fin is the *fin efficiency*, η_f . This term represents the ratio of actual heat-transfer rate from a fin to the heat-transfer rate that would occur if the entire fin surface could be maintained at a uniform temperature equal to the temperature of the base of the fin. For this case, Newton’s law of cooling can be written as

$$q = \eta_f h A_f (T_b - T_\infty)$$

where A_f is the total surface area of the fin and T_b is the temperature of the fin at the base. The application of fins for heat removal can be applied to either forced or natural convection of gases, and while some advantages can be gained in terms of increasing the liquid–solid or solid–vapor surface area, fins as such are not normally utilized for situations involving phase change heat transfer, such as boiling or condensation.

1.5 Transient Heat Conduction

Given a solid body, at a uniform temperature, T_∞ , immersed in a fluid of different temperature T_∞ , the surface of the solid body will be subject to heat losses (or gains) through convection from the surface to the fluid. In this situation, the heat lost (or gained) at the surface results from the conduction of heat from inside the body. To determine the significance of these two heat transfer modes, a dimensionless parameter referred to as the *Biot number* is used. This dimensionless number is defined as $Bi = hL/k$, where $L = V/A$ or the ratio of the volume of the solid to the surface area of the solid, and really represents a comparative relationship of the importance of convections from the outer surface to the conduction occurring inside. When this value is less than 0.1, the temperature of the solid may be assumed uniform and dependent on

time alone. When this value is greater than 0.1, there is some spatial temperature variation that will affect the solution procedure.

For the first case, $Bi < 0.1$, an approximation referred to as the *lumped heat capacity* method may be used. In this method, the temperature of the solid is given by

$$\frac{T - T_\infty}{T_i - T_\infty} = \exp\left(\frac{-t}{\tau_t}\right) = \exp(-BiFo)$$

where τ_t is the *time constant* and is equal to $\rho C_p V/hA$. Increasing the value of the time constant, τ_t , will result in a decrease in the thermal response of the solid to the environment and, hence, will increase the time required for it to reach thermal equilibrium (i.e., $T = T_\infty$). In this expression, Fo represents the dimensionless time and is called the *Fourier number*, the value of which is equal to atA^2/V^2 . The Fourier number, along with the Biot number, can be used to characterize transient heat conduction problems. The total heat flow through the surface of the solid over the time interval from $t = 0$ to time t can be expressed as

$$Q = \rho V C_p (T_i - T_\infty) \left[1 - \exp\left(-\frac{t}{\tau_t}\right) \right]$$

Transient Heat Transfer for Infinite Plate, Infinite Cylinder, and Sphere Subjected to Surface Convection

Generalized analytical solutions to transient heat transfer problems involving infinite plates, cylinders, and finite diameter spheres subjected to surface convection have been developed. These solutions can be presented in graphical form through the use of the *Heisler charts*,³ illustrated in Figs. 3–11 for plane walls, cylinders, and spheres. In this procedure, the solid is assumed to be at a uniform temperature, T_i , at time $t = 0$ and then is suddenly subjected to or immersed in a fluid at a uniform temperature T_∞ . The convection heat transfer coefficient, h , is assumed to be constant, as is the temperature of the fluid. Combining Figs. 3 and 4 for plane walls, Figs. 6 and 7 for cylinders, and Figs. 9 and 10 for spheres allows the resulting time-dependent temperature of any point within the solid to be found. The total amount of energy, Q , transferred to or from the solid surface from time $t = 0$ to time t can be found from Figs. 5, 8, and 11.

1.6 Conduction at the Microscale

The mean free path of electrons and the size of the volume involved has long been recognized as having a pronounced effect on electron transport phenomena. This is particularly true in applications involving thin metallic films or wires where the characteristic length may be close to the same order of magnitude as the scattering mean free path of the electrons.⁵ The first notable work in this area was performed by Tien et al.⁶ where the thermal conductivity of thin metallic films and wires were calculated at cryogenic temperatures. Because the length of the mean free path in these types of applications is shortened near the surface, due to termination at the boundary, a reduction in transport coefficients, such as electrical and thermal conductivities, was observed. Tests at cryogenic temperatures were first performed because the electron mean free path increases as temperature decreases, and the size effects were expected to become especially significant in this range. The primary purpose of this investigation was to outline in a systematic manner a method by which the thermal conductivity of such films and wires at cryogenic temperatures could be determined. The results indicated that, particularly in the case of thin metallic films, size effects may become an increasingly important part of the design and analysis required for application. Due to the increased use of thin films in optical components and solid-state devices and systems, there has been an increasing interest in the effect of decreasing size on the transport properties of thin solid films and wires.

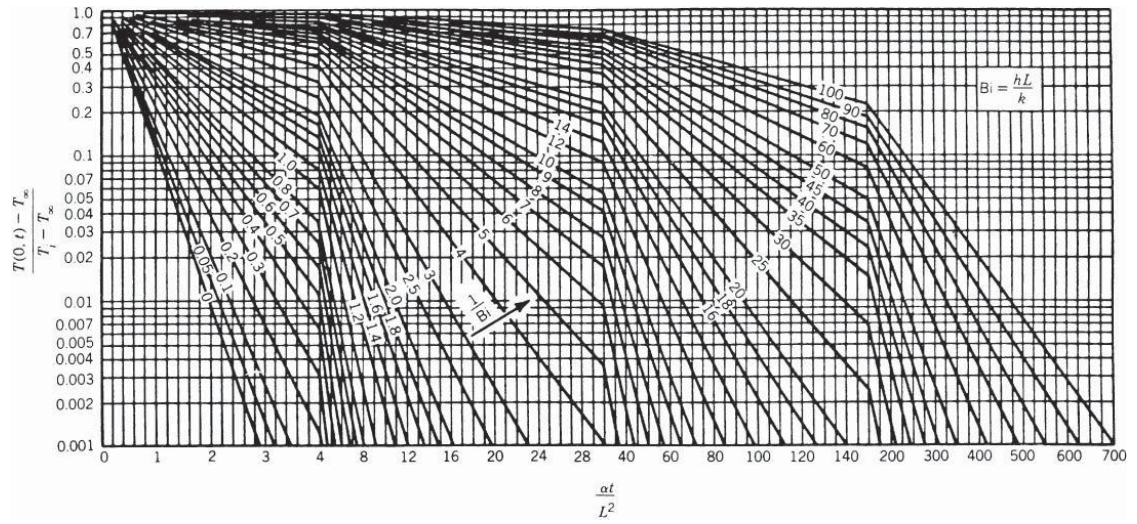


Figure 3 Midplane temperature as a function of time for a plane wall of thickness $2L$. (Adapted from Heisler.³)

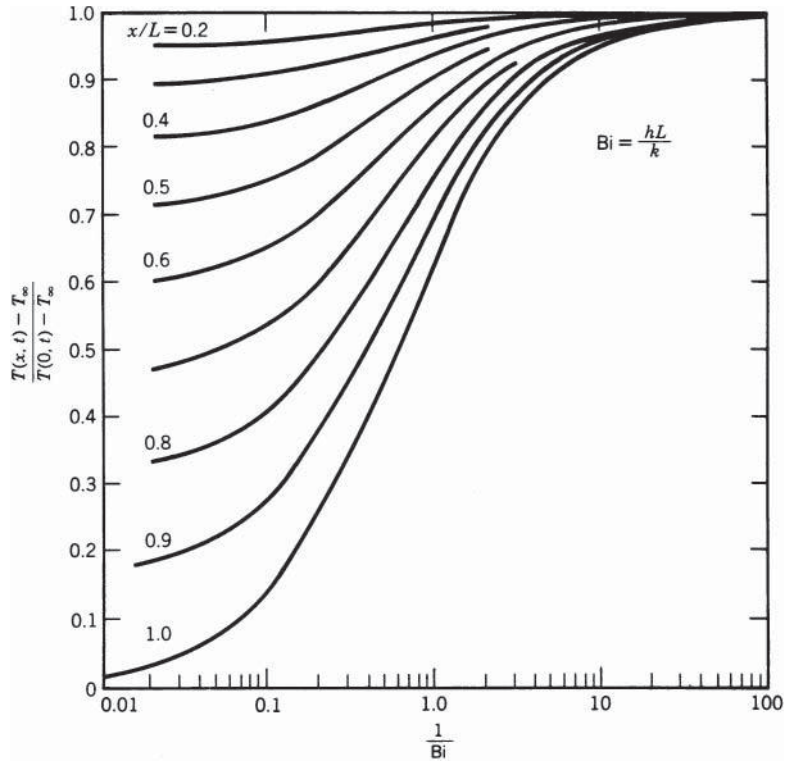


Figure 4 Temperature distribution in a plane wall of thickness $2L$. (Adapted from Heisler.³)

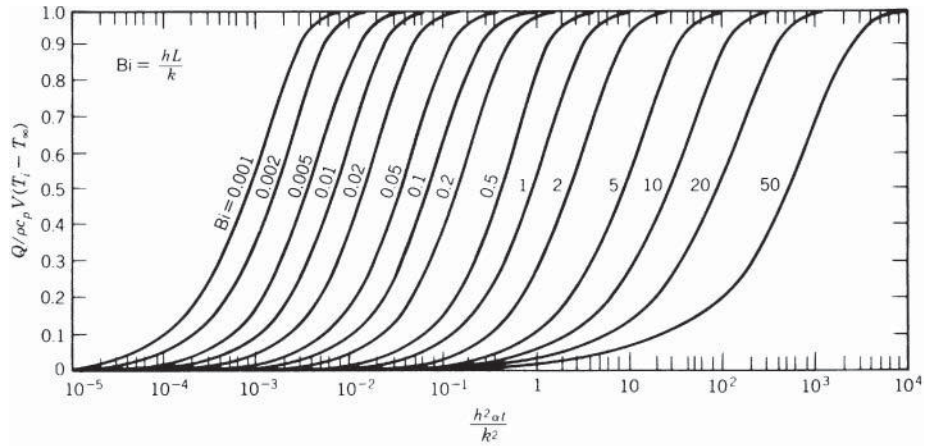


Figure 5 Internal energy change as a function of time for a plane wall of thickness $2L$.⁴ (Used with the permission of McGraw-Hill Book Company.)

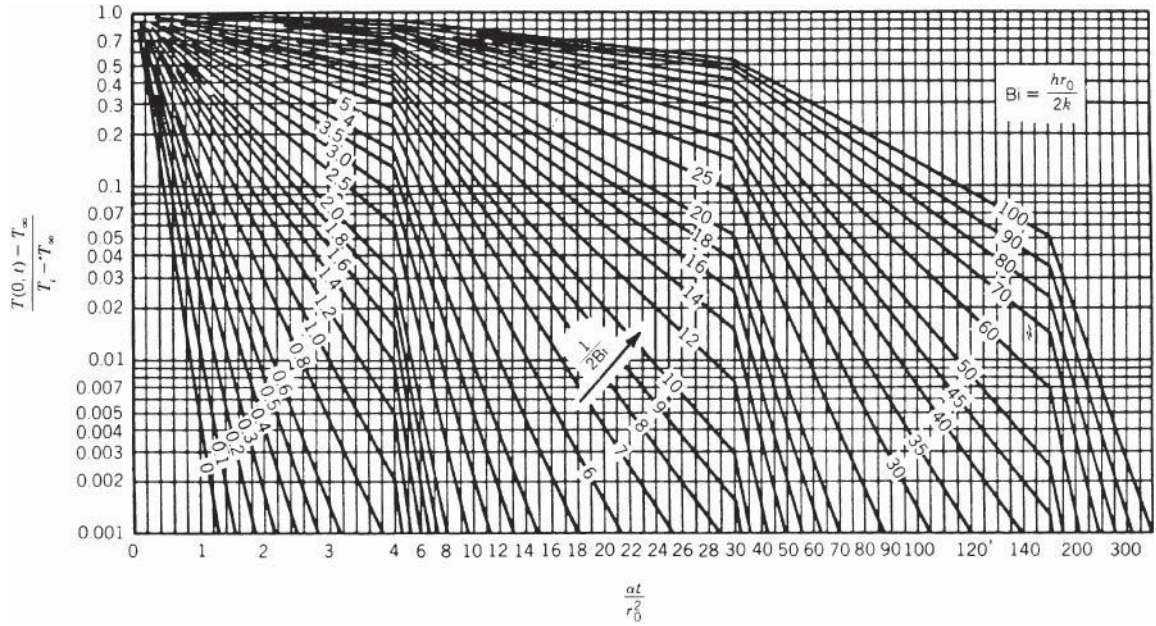


Figure 6 Centerline temperature as a function of time for an infinite cylinder of radius r_0 . (Adapted from Heisler.³)

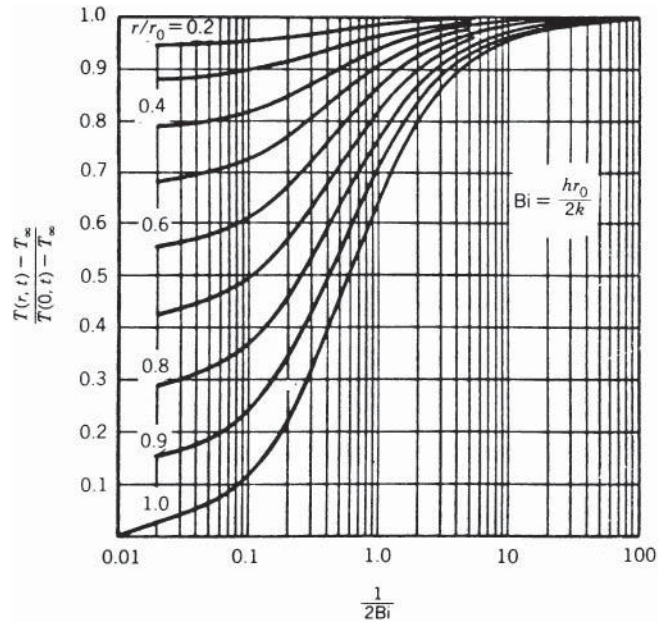


Figure 7 Temperature distribution in an infinite cylinder of radius r_0 . (Adapted from Heisler.³)

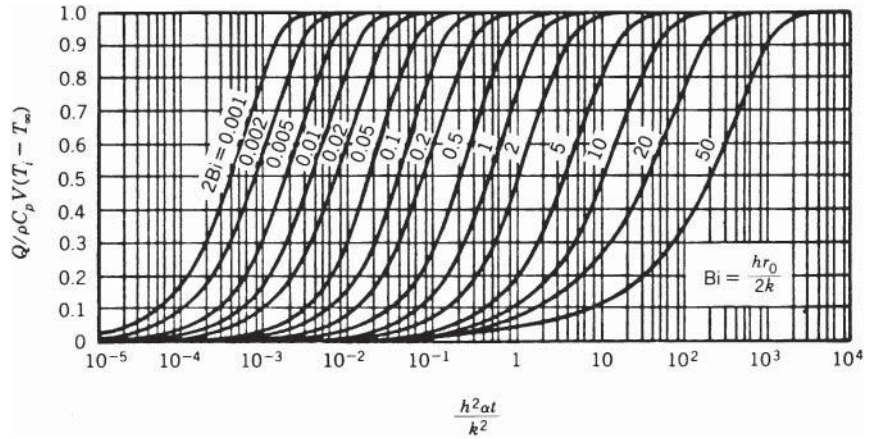


Figure 8 Internal energy change as a function of time for an infinite cylinder of radius r_0 .⁴ (Used with the permission of McGraw-Hill Book Company.)

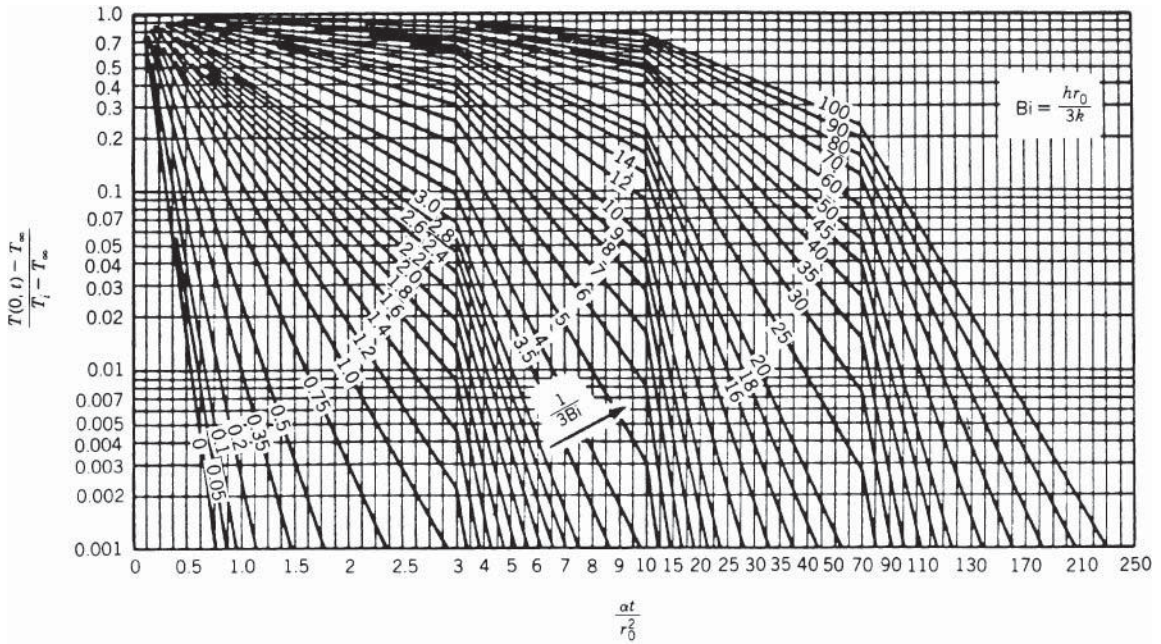


Figure 9 Center temperature as a function of time in a sphere of radius r_0 . (Adapted from Heisler.³)

The most common method for calculating the thermal conductivities in thin films and wires consists of three essential steps:

1. Identifying the appropriate expression for the electrical conductivity size effect
2. Determining the mean free path for electrical conductivity, which is essential in calculations of all electron transport properties
3. Applying the electrical–thermal transport analogy for calculating the thermal conductivity size effect⁵

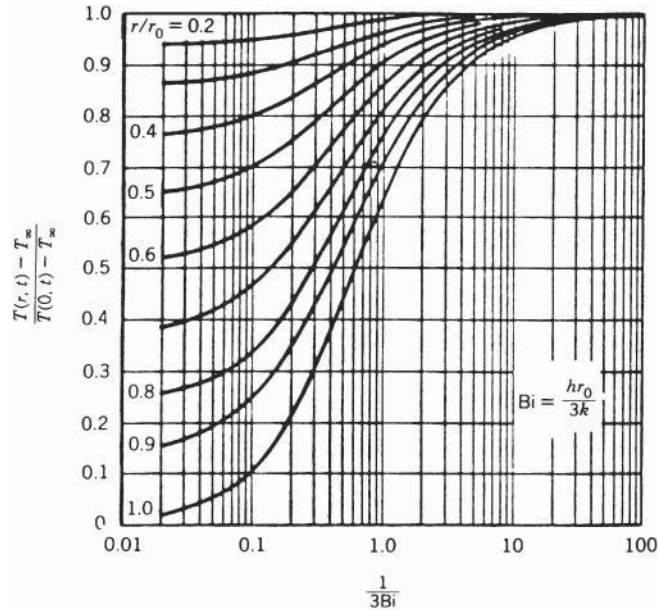


Figure 10 Temperature distribution in a sphere of radius r_o . (Adapted from Heisler.³)

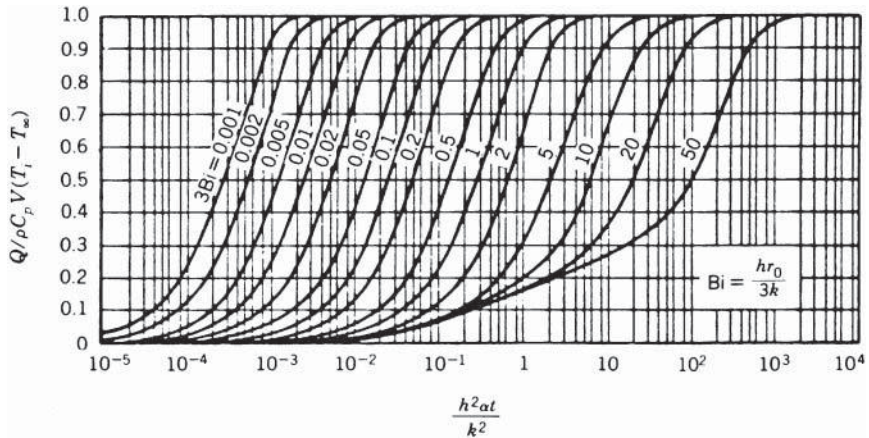


Figure 11 Internal energy change as a function of time for a sphere of radius r_o .⁴ (Used with the permission of McGraw-Hill Book Company.)

For domain thicknesses on the order of the carrier mean free path, jump boundary conditions significantly affect the solution of the conduction problem. This problem can be resolved through the solution of the hyperbolic heat-equation-based analysis, which is generally justifiable engineering applications.⁷

2 CONVECTION HEAT TRANSFER

As discussed earlier, convection heat transfer is the mode of energy transport in which the energy is transferred by means of fluid motion. This transfer can be the result of the random molecular motion or bulk motion of the fluid. If the fluid motion is caused by external forces,

the energy transfer is called *forced convection*. If the fluid motion arises from a buoyancy effect caused by density differences, the energy transfer is called *free convection* or *natural convection*. For either case, the heat transfer rate, q , can be expressed in terms of the surface area, A , and the temperature difference, ΔT , by Newton's law of cooling:

$$q = hA \Delta T$$

In this expression, h is referred to as the convection heat transfer coefficient or film coefficient and a function of the velocity and physical properties of the fluid, and the shape and nature of the surface. The nondimensional heat transfer coefficient $\text{Nu} = hL/k$ is called the *Nusselt number*, where L is a characteristic length and k is the thermal conductivity of the fluid.

2.1 Forced Convection—Internal Flow

For internal flow in a tube or pipe, the convection heat transfer coefficient is typically defined as a function of the temperature difference existing between the temperature at the surface of the tube and the *bulk* or *mixing-cup temperature*, T_b , i.e., $\Delta T = T_s - T_b$ can be defined as

$$T_b = \frac{\int C_p T \, d\dot{m}}{\int C_p \, d\dot{m}}$$

where \dot{m} is the axial flow rate. Using this value, heat transfer between the tube and the fluid can be written as $q = hA(T_s - T_b)$.

In the entrance region of a tube or pipe, the flow is quite different from that occurring downstream from the entrance. The rate of heat transfer differs significantly, depending on whether the flow is *laminar* or *turbulent*. From fluid mechanics, the flow is considered to be turbulent when $\text{Re}_D = V_m D/\nu > 2300$ for a smooth tube. This transition from laminar to turbulent, however, also depends on the roughness of tube wall and other factors. The generally accepted range for transition is $200 < \text{Re}_D < 4000$.

Laminar Fully Developed Flow

For situations where both the thermal and velocity profiles are fully developed, the Nusselt number is constant and depends only on the thermal boundary conditions. For *circular tubes* with $\text{Pr} \geq 0.6$, and $x/D \text{Re}_D \text{Pr} > 0.05$, the Nusselt numbers have been shown to be $\text{Nu}_D = 3.66$ and 4.36, for constant temperature and constant heat flux conditions, respectively. Here, the fluid properties are based on the mean bulk temperature.

For *noncircular tubes*, the hydraulic diameter, $D_h = 4 \times$ the flow cross-sectional area/wetted perimeter, is used to define the Nusselt number Nu_D and the Reynolds number Re_D . Table 12 shows the Nusselt numbers based on hydraulic diameter for various cross-sectional shapes.

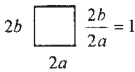
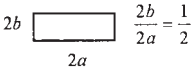
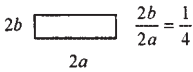
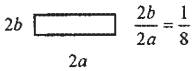
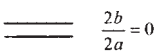


Laminar Flow for Short Tubes

At the entrance of a tube, the Nusselt number is infinite, and decreases asymptotically to the value for fully developed flow as the flow progresses down the tube. The Sieder–Tate equation⁸ gives good correlation for the combined entry length, i.e., that region where the thermal and velocity profiles are both developing or for short tubes:

$$\frac{\overline{\text{Nu}}_D = \bar{h}D}{k} = 1.86(\text{Re } D \text{ Pr})^{1/3} \left(\frac{D}{L}\right)^{1/3} \left(\frac{\mu}{\mu_s}\right)^{0.14}$$

for $T_s = \text{constant}$, $0.48 < \text{Pr} < 16,700$, $0.0044 < \mu/\mu_s < 9.75$, and $(\text{Re}_D \text{Pr} D/L)^{1/3} (\mu/\mu_s)^{0.14} > 2$.

Table 12 Nusselt Numbers for Fully Developed Laminar Flow for Tubes of Various Cross Sections^a

Geometry ($L/DH > 100$)	Nu_{H1}	Nu_{H2}	Nu_r
	3.608	3.091	2.976
	4.123	3.017	3.391
	5.099	4.35	3.66
	6.490	2.904	5.597
	8.235	8.235	7.541
	5.385	—	4.861
	4.364	4.364	3.657

^a Nu_{H1} = average Nusselt number for uniform heat flux in flow direction and uniform wall temperature at particular flow cross section.
 Nu_{H2} = average Nusselt number for uniform heat flux both in flow direction and around periphery.
 Nu_{Hr} = average Nusselt number for uniform wall temperature.

In this expression, all of the fluid properties are evaluated at the mean bulk temperature except for μ_s , which is evaluated at the wall surface temperature. The average convection heat transfer coefficient \bar{h} is based on the arithmetic average of the inlet and outlet temperature differences.

Turbulent Flow in Circular Tubes

In turbulent flow, the velocity and thermal entry lengths are much shorter than for a laminar flow. As a result, with the exception of short tubes, the fully developed flow values of the Nusselt number are frequently used directly in the calculation of the heat transfer. In general, the Nusselt number obtained for the constant heat flux case is greater than the Nusselt number obtained for the constant temperature case. The one exception to this is the case of liquid metals, where the difference is smaller than for laminar flow and becomes negligible for $Pr > 1.0$. The Dittus–Boelter equation⁹ is typically used if the difference between the pipe surface temperature and the bulk fluid temperature is less than 6°C (10°F) for liquids or 56°C (100°F) for gases:

$$Nu_D = 0.023 Re_D^{0.8} Pr^n$$

for $0.7 \leq Pr \leq 160$, $Re_D \geq 10,000$, and $L/D \geq 60$, where

$$n = 0.4 \text{ for heating, } T_s > T_b$$

$$= 0.3 \text{ for cooling, } T_s < T_b$$

For temperature differences greater than specified above, use⁸

$$\text{Nu}_D = 0.027 \text{Re}_D^{0.8} \text{Pr}^{1/3} \left(\frac{\mu}{\mu_s} \right)^{0.14}$$

for $0.7 \leq \text{Pr} \leq 16,700$, $\text{Re}_D \geq 10,000$, and $L/D \geq 60$. In this expression, the properties are all evaluated at the mean bulk fluid temperature with the exception of μ_s , which is again evaluated at the tube surface temperature.

For *concentric tube annuli*, the hydraulic diameter $D_h = D_o - D_i$ (outer diameter – inner diameter) must be used for Nu_D and Re_D , and the coefficient h at either surface of the annulus must be evaluated from the Dittus–Boelter equation. Here, it should be noted that the foregoing equations apply for smooth surfaces and that the heat transfer rate will be larger for rough surfaces and are not applicable to liquid metals.

Fully Developed Turbulent Flow of Liquid Metals in Circular Tubes

Because the Prandtl number for liquid metals is on the order of 0.01, the Nusselt number is primarily dependent on a dimensionless parameter number referred to as the *Peclet number*, which in general is defined as $\text{Pe} = \text{RePr}$:

$$\text{Nu}_D = 5.0 + 0.025 \text{Pe}_D^{0.8}$$

which is valid for situations where $T_s = \text{a constant}$ and $\text{Pe}_D > 100$ and $L/D > 60$.

For $q'' = \text{constant}$ and $3.6 \times 10^3 < \text{Re}_D < 9.05 \times 10^5$, $10^2 < \text{Pe}_D < 10^4$, and $L/D > 60$, the Nusselt number can be expressed as

$$\text{Nu}_D = 4.8 + 0.0185 \text{Pe}_D^{0.827}$$

2.2 Forced Convection—External Flow

In forced convection heat transfer, the heat transfer coefficient, h , is based on the temperature difference between the wall surface temperature and the fluid temperature in the free stream outside the thermal boundary layer. The total heat transfer rate from the wall to the fluid is given by $q = hA(T_s - T_\infty)$. The Reynolds numbers are based on the free-stream velocity. The fluid properties are evaluated either at the free-stream temperature T_∞ or at the film temperature $T_f = (T_s + T_\infty)/2$.

Laminar Flow on a Flat Plate

When the flow velocity along a constant temperature semi-infinite plate is uniform, the boundary layer originates from the leading edge and is laminar and the flow remains laminar until the local Reynolds number $\text{Re}_x = U_\infty x / \nu$ reaches the *critical Reynolds number*, Re_c . When the surface is smooth, the Reynolds number is generally assumed to be $\text{Re}_c = 5 \times 10^5$, but the value will depend on several parameters, including the surface roughness.

For a given distance x from the leading edge, the *local Nusselt number* and the *average Nusselt number* between $x = 0$ and $x = L$ are given below (Re_x and $\text{Re}_L \leq 5 \times 10^5$):

$$\left. \begin{aligned} \text{Nu}_x &= \frac{hx}{k} = 0.332 \text{Re}_x^{0.5} \text{Pr}^{1/3} \\ \overline{\text{Nu}}_L &= \frac{\overline{h}L}{k} = 0.664 \text{Re}_L^{0.5} \text{Pr}^{1/3} \end{aligned} \right\} \text{for } \text{Pr} \geq 0.6$$

$$\left. \begin{aligned} \text{Nu}_x &= 0.565 (\text{Re}_x \text{Pr})^{0.5} \\ \overline{\text{Nu}}_L &= 1.13 (\text{Re}_L \text{Pr})^{0.5} \end{aligned} \right\} \text{for } \text{Pr} \leq 0.6$$

Here, all of the fluid properties are evaluated at the mean or average film temperature.

Turbulent Flow on a Flat Plate

When the flow over a flat plate is turbulent from the leading edge, expressions for the *local Nusselt number* can be written as

$$\begin{aligned} \text{Nu}_x &= 0.0292 \text{Re}_x^{0.8} \text{Pr}^{1/3} \\ \overline{\text{Nu}}_L &= 0.036 \text{Re}_L^{0.8} \text{Pr}^{1/3} \end{aligned}$$

where the fluid properties are all based on the mean film temperature and $5 \times 10^5 \leq \text{Re}_x$ and $\text{Re}_L \leq 10^8$ and $0.6 \leq \text{Pr} \leq 60$.

The Average Nusselt Number between $x = 0$ and $x = L$ with Transition

For situations where transition occurs immediately once the critical Reynolds number Re_c has been reached¹⁰

$$\overline{\text{Nu}}_L = 0.036 \text{Pr}^{1/3} [\text{Re}_L^{0.8} - \text{Re}_c^{0.8} + 18.44 \text{Re}_c^{0.5}]$$

provided that $5 \times 10^5 \leq \text{Re}_L \leq 10^8$ and $0.6 \leq \text{Pr} \leq 60$. Specialized cases exist for this situation i.e.,

$$\overline{\text{Nu}}_L = 0.036 \text{Pr}^{1/3} (\text{Re}_L^{0.8} - 18,700)$$

for $\text{Re}_c = 4 \times 10^5$, or

$$\overline{\text{Nu}}_L = 0.036 \text{Pr}^{1/3} (\text{Re}_L^{0.8} - 23,000)$$

for $\text{Re}_c = 5 \times 10^5$. Again, all fluid properties are evaluated at the mean film temperature.

Circular Cylinders in Cross Flow

For circular cylinders in cross flow, the Nusselt number is based upon the diameter and can be expressed as

$$\overline{\text{Nu}}_D = (0.4 \text{Re}_D^{0.5} + 0.06 \text{Re}_D^{2/3}) \text{Pr}^{0.4} \left(\frac{\mu_\infty}{\mu_s} \right)^{0.25}$$

for $0.67 < \text{Pr} < 300$, $10 < \text{Re}_D < 10^5$, and $0.25 < \mu_\infty/\mu_s < 5.2$. Here, the fluid properties are evaluated at the free-stream temperature except μ_s , which is evaluated at the surface temperature.¹¹

Cylinders of Noncircular Cross Section in Cross Flow of Gases

For noncircular cylinders in cross flow, the Nusselt number is again based on the diameter, but is expressed as

$$\overline{\text{Nu}}_D = C(\text{Re}_D)^m \text{Pr}^{1/3}$$

where C and m are listed in Table 13, and the fluid properties are evaluated at the mean film temperature.¹²

Flow past a Sphere

For flow over a sphere, the Nusselt number is based on the sphere diameter and can be expressed as

$$\overline{\text{Nu}}_D = 2 + (0.4 \text{Re}_D^{0.5} + 0.06 \text{Re}_D^{2/3}) \text{Pr}^{0.4} (\mu_\infty/\mu_s)^{0.25}$$

for the case of $3.5 < \text{Re}_D < 8 \times 10^4$, $0.7 < \text{Pr} < 380$, and $1.0 < \mu_\infty/\mu_s < 3.2$. The fluid properties are calculated at the free stream temperature except μ_s , which is evaluated at the surface temperature.¹¹

Table 13 Constants and m for Noncircular Cylinders in Cross-Flow

Geometry	Re_D	C	m
Square			
$V \rightarrow \diamond \begin{matrix} \overline{\downarrow} D \\ \overline{\uparrow} \end{matrix}$	$5 \times 10^3 - 10^5$	0.246	0.588
$V \rightarrow \square \begin{matrix} \overline{D} \\ \overline{\uparrow} \end{matrix}$	$5 \times 10^3 - 10^5$	0.102	0.675
Hexagon			
$V \rightarrow \begin{matrix} \overline{\downarrow} D \\ \overline{\uparrow} \end{matrix}$	$5 \times 10^3 - 1.95 \times 10^4$	0.160	0.538
$V \rightarrow \begin{matrix} \overline{D} \\ \overline{\uparrow} \end{matrix}$	$1.95 \times 10^4 - 10^5$	0.0385	0.782
	$5 \times 10^3 - 10^5$	0.153	0.638
Vertical plate			
$V \rightarrow \begin{matrix} \overline{\downarrow} D \\ \overline{\uparrow} \end{matrix}$	$4 \times 10^3 - 1.5 \times 10^4$	0.228	0.731

Flow across Banks of Tubes

For banks of tubes, the tube arrangement may be either *staggered* or *aligned* (Fig. 12), and the heat transfer coefficient for the first row is approximately equal to that for a single tube. In turbulent flow, the heat transfer coefficient for tubes in the first row is smaller than that of the subsequent rows. However, beyond the fourth or fifth row, the heat transfer coefficient becomes approximately constant. For tube banks with more than 20 rows, $0.7 < Pr < 500$, and $1000 < Re_{D,max} < 2 \times 10^6$, the average Nusselt number for the entire tube bundle can be expressed as¹³

$$\overline{Nu}_D = C(Re_{D,max})^m Pr^{0.36} \left(\frac{Pr_\infty}{Pr_s} \right)^{0.25}$$

where all fluid properties are evaluated at T_∞ except Pr_s , which is evaluated at the surface temperature. The constants C and m used in this expression are listed in Table 14, and the Reynolds

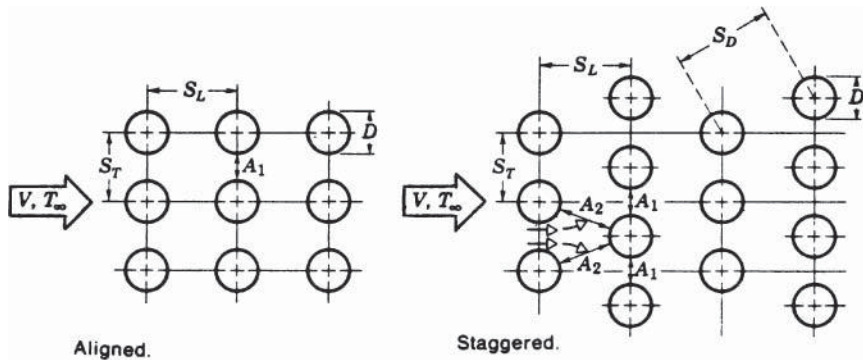


Figure 12 Tube arrangement.

Table 14 Constants C and m of Heat Transfer Coefficient for the Banks in Cross Flow

Configuration	$Re_{D,\max}$	C	m
Aligned	$10^3 - 2 \times 10^5$	0.27	0.63
Staggered ($S_T/S_L < 2$)	$10^3 - 2 \times 10^5$	$0.35(S_T/S_L)^{1/5}$	0.60
Staggered ($S_G/S_L > 2$)	$10^3 - 2 \times 10^5$	0.40	0.60
Aligned	$2 \times 10^5 - 2 \times 10^6$	0.21	0.84
Staggered	$2 \times 10^5 - 2 \times 10^6$	0.022	0.84

number is based on the maximum fluid velocity occurring at the minimum free flow area available for the fluid. Using the nomenclature shown in Fig. 12, the maximum fluid velocity can be determined by

$$V_{\max} = \frac{S_T}{S_T - D} V$$

for the aligned or staggered configuration provided

$$\sqrt{S_L^2 + (S_T/2)^2} > \frac{S_T + D}{2}$$

or as

$$V_{\max} = \frac{S_T}{\sqrt{S_L^2 + (S_T/2)^2}} V$$

for staggered if

$$\sqrt{S_L^2 + (S_T/2)^2} < \frac{S_T + D}{2}$$

Liquid Metals in Cross Flow over Banks of Tubes

The average Nusselt number for tubes in the inner rows can be expressed as

$$\overline{Nu}_D = 4.03 + 0.228(Re_{D,\max} Pr)^{0.67}$$

which is valid for $2 \times 10^4 < Re_{D,\max} < 8 \times 10^4$ and $Pr < 0.03$ and the fluid properties are evaluated at the mean film temperature.¹⁴

High-Speed Flow over a Flat Plate

When the free-stream velocity is very high, the effects of viscous dissipation and fluid compressibility must be considered in the determination of the convection heat transfer. For these types of situations, the convection heat transfer can be described as $q = hA(T_s - T_{as})$, where T_{as} is the *adiabatic surface temperature* or *recovery temperature*, and is related to the *recovery factor* by $r = (T_{as} - T_\infty)/(T_0 - T_\infty)$. The value of the *stagnation temperature*, T_0 , is related to the free-stream static temperature, T_∞ , by the expression

$$\frac{T_0}{T_\infty} = 1 + \frac{\gamma - 1}{2} M_\infty^2$$

where γ is the specific heat ratio of the fluid and M_∞ is the ratio of the free-stream velocity and the acoustic velocity. For the case where $0.6 < Pr < 15$,

$$r = Pr^{1/2} \quad \text{for laminar flow } (Re_x < 5 \times 10^5)$$

$$r = Pr^{1/3} \quad \text{for turbulent flow } (Re_x > 5 \times 10^5)$$

Here, all of the fluid properties are evaluated at the reference temperature $T_{\text{ref}} = T_{\infty} + 0.5(T_s - T_{\infty}) + 0.22(T_{as} - T_{\infty})$. Expressions for the local heat transfer coefficients at a given distance x from the leading edge are given as²

$$\text{Nu}_x = 0.332 \text{Re}_x^{0.5} \text{Pr}^{1/3} \quad \text{for } \text{Re}_x < 5 \times 10^5$$

$$\text{Nu}_x = 0.0292 \text{Re}_x^{0.8} \text{Pr}^{1/3} \quad \text{for } 5 \times 10^5 < \text{Re}_x < 10^7$$

$$\text{Nu}_x = 0.185 \text{Re}_x (\log \text{Re}_x)^{-2.584} \quad \text{for } 10^7 < \text{Re}_x < 10^9$$

In the case of gaseous fluids flowing at very high free-stream velocities, dissociation of the gas may occur and will cause large variations in the properties within the boundary layer. For these cases, the heat transfer coefficient must be defined in terms of the enthalpy difference, i.e., $q = hA(i_s - i_{as})$, and the recovery factor will be given by $r = (i_s - i_{as})/(i_0 - i_{\infty})$, where i_{as} represents the enthalpy at the adiabatic wall conditions. Similar expressions to those shown above for Nu_x can be used by substituting the properties evaluated at a reference enthalpy defined as $i_{\text{ref}} = i_{\infty} + 0.5(i_s - i_{\infty}) + 0.22(i_{as} - i_{\infty})$.

High-Speed Gas Flow Past Cones

For the case of high-speed gaseous flows over conical shaped objects, the following expressions can be used:

$$\text{Nu}_x = 0.575 \text{Re}_x^{0.5} \text{Pr}^{1/3} \quad \text{for } \text{Re}_x < 10^5$$

$$\text{Nu}_x = 0.0292 \text{Re}_x^{0.8} \text{Pr}^{1/3} \quad \text{for } \text{Re}_x > 10^5$$

where the fluid properties are evaluated at T_{ref} as in the plate.¹⁵

Stagnation Point Heating for Gases

When the conditions are such that the flow can be assumed to behave as *incompressible*, the Reynolds number is based on the free-stream velocity and \bar{h} is defined as $q = \bar{h}A(T_s - T_{\infty})$.¹⁶ Estimations of the Nusselt can be made using the following relationship:

$$\text{Nu}_D = C \text{Re}_D^{0.5} \text{Pr}^{0.4}$$

where $C = 1.14$ for cylinders and 1.32 for spheres, and the fluid properties are evaluated at the mean film temperature. When the flow becomes *supersonic*, a bow shock wave will occur just off the front of the body. In this situation, the fluid properties must be evaluated at the stagnation state occurring behind the bow shock and the Nusselt number can be written as

$$\bar{\text{Nu}}_D = C \text{Re}_D^{0.5} \text{Pr}^{0.4} \left(\frac{\rho_{\infty}}{\rho_0} \right)^{0.25}$$

where $C = 0.95$ for cylinders and 1.28 for spheres; ρ_{∞} is the free-stream gas density and ρ_0 is the stagnation density of stream behind the bow shock. The heat transfer rate for this case is given by $q = \bar{h}A(T_s - T_0)$.

2.3 Free Convection

In free convection the fluid motion is caused by the buoyant force resulting from the density difference near the body surface, which is at a temperature different from that of the free fluid far removed from the surface where velocity is zero. In all free convection correlations, except for the enclosed cavities, the fluid properties are usually evaluated at the mean film temperature $T_f = (T_1 + T_{\infty})/2$. The thermal expansion coefficient β , however, is evaluated at the free fluid temperature T_{∞} . The convection heat transfer coefficient h is based on the temperature difference between the surface and the free fluid.

Free Convection from Flat Plates and Cylinders

For free convection from flat plates and cylinders, the average Nusselt number \overline{Nu}_L can be expressed as⁴

$$\overline{Nu}_L = C(Gr_L Pr)^m$$

where the constants C and m are given as shown in Table 15. The *Grashof Prandtl number* product ($Gr_L Pr$) is called the *Rayleigh number* (Ra_L) and for certain ranges of this value, Figs. 13 and 14 are used instead of the above equation. Reasonable approximations for other types of *three-dimensional shapes*, such as short cylinders and blocks, can be made for $10^4 < Ra_L < 10^9$, by using this expression and $C = 0.6, m = 1/4$, provided that the characteristic length, L , is determined from $1/L = 1/L_{hor} + 1/L_{ver}$, where L_{ver} is the height and L_{hor} is the horizontal dimension of the object in question.

Table 15 Constants for Free Convection from Flat Plates and Cylinders

Geometry	$Gr_L Pr$	C	m	L
Vertical flat plates and cylinders	$10^{-1} - 10^4$	Use Fig. 12	Use Fig. 12	Height of plates and cylinders; restricted to $D/L \geq 35/Gr_L^{1/4}$ for cylinders
	$10^4 - 10^9$	0.59	$1/4$	
	$10^9 - 10^{13}$	0.10	$1/3$	
Horizontal cylinders	$0 - 10^{-5}$	0.4	0	Diameter D
	$10^{-5} - 10^4$	Use Fig.13	Use Fig.13	
	$10^4 - 10^9$	0.53	$1/4$	
Upper surface of heated plates or lower surface of cooled plates	$2 \times 10^4 - 8 \times 10^6$	0.54	$1/4$	Length of a side for square plates, the average length of the two sides for rectangular plates
	$8 \times 10^6 - 10^{11}$	0.15	$1\ 1/3$	
Lower surface of heated plates or upper surface of cooled plates	$10^5 - 10^{11}$	0.58	$1/5$	0.9D for circular disks

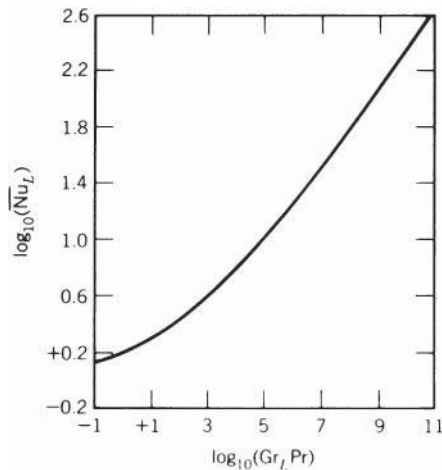


Figure 13 Free convection heat-transfer correlation for heated vertical plates and cylinders. (Adapted from Ref. 17. Used with permission of McGraw-Hill Book Company.)

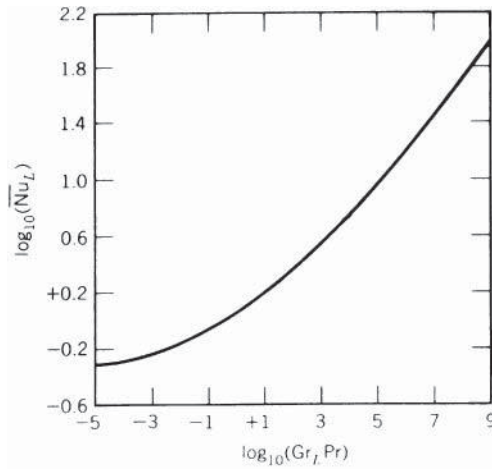


Figure 14 Free convection heat transfer correlation from heated horizontal cylinders. (Adapted from Ref. 17. © McGraw-Hill Education.)

For *unsymmetrical horizontal* square, rectangular, or circular surfaces, the characteristic length L can be calculated from the expression $L = A/P$, where A is the area and P is the wetted perimeter of the surface.

Free Convection from Spheres

For free convection from spheres, the following correlation has been developed:

$$\overline{Nu}_D = 2 + 0.43(Gr_D Pr)^{0.25} \quad \text{for } 1 < Gr_D < 10^5$$

Although this expression was designed primarily for gases, $Pr \approx 1$, it may be used to approximate the values for liquids as well.¹⁸

Free Convection in Enclosed Spaces

Heat transfer in an enclosure occurs in a number of different situations and with a variety of configurations. When a temperature difference is imposed on two opposing walls that enclose a space filled with a fluid, convective heat transfer will occur. For small values of the Rayleigh number, the heat transfer may be dominated by conduction, but as the Rayleigh number increases, the contribution made by free convection will increase. Following are a number of correlations, each designed for a specific geometry. For all of these, the fluid properties are evaluated at the average temperature of the two walls.

Cavities between Two Horizontal Walls at Temperatures T_1 and T_2 Separated by Distance δ (T_1 for Lower Wall, $T_1 > T_2$)

$$\begin{aligned} q'' &= \bar{h}(T_1 - T_2) \\ \overline{Nu}_\delta &= 0.069 Ra_\delta^{1/3} Pr^{0.074} \quad \text{for } 3 \times 10^5 < Ra_\delta < 7 \times 10^9 \\ &= 1.0 f \quad \text{or } Ra_\delta < 1700 \end{aligned}$$

where $Ra_\delta = g\beta(T_1 - T_2)\delta^3/\alpha\nu$; δ is the thickness of the space.¹⁹

Cavities between Two Vertical Walls of Height H at Temperatures by Distance T_1 and T_2 Separated by Distance δ ^{20,21}

$$q'' = \bar{h}(T_1 - T_2)$$

$$\overline{Nu}_\delta = 0.22 \left(\frac{Pr}{0.2 + Pr} Ra_\delta \right)^{0.28} \left(\frac{\delta}{H} \right)^{0.25}$$

for $2 < H/\delta < 10$, $Pr < 10^5$, $Ra_\delta < 10^{10}$;

$$\overline{Nu}_\delta = 0.18 \left(\frac{Pr}{0.2 + Pr} Ra_\delta \right)^{0.29}$$

for $1 < H/\delta < 2$, $10^3 < Pr < 10^5$, and $10^3 < Ra_\delta Pr/(0.2 + Pr)$; and

$$\overline{Nu}_\delta = 0.42 Ra_\delta^{0.25} Pr^{0.012} \left(\frac{\delta}{H} \right)^{0.3}$$

for $10 < H/\delta < 40$, $1 < Pr < 2 \times 10^4$, and $10^4 < Ra_\delta < 10^7$.

2.4 The Log-Mean Temperature Difference

The simplest and most common type of heat exchanger is the *double-pipe heat exchanger* illustrated in Fig. 15. For this type of heat exchanger, the heat transfer between the two fluids can be found by assuming a constant overall heat transfer coefficient found from Table 8 and a constant fluid specific heat. For this type, the heat transfer is given by

$$q = UA \Delta T_m$$

where

$$\Delta T_m = \frac{\Delta T_2 - \Delta T_1}{\ln(\Delta T_2/\Delta T_1)}$$

In this expression, the temperature difference, ΔT_m , is referred to as the *log-mean temperature difference* (LMTD); ΔT_1 represents the temperature difference between the two fluids at one end and ΔT_2 at the other end. For the case where the ratio $\Delta T_2/\Delta T_1$ is less than two, the *arithmetic mean temperature difference*, $(\Delta T_2 + \Delta T_1)/2$, may be used to calculate heat transfer rate without introducing any significant error. As shown in Fig. 15,

$$\Delta T_1 = T_{h,i} - T_{c,i} \quad \Delta T_2 = T_{h,o} - T_{c,o} \quad \text{for parallel flow}$$

$$\Delta T_1 = T_{h,i} - T_{c,o} \quad \Delta T_2 = T_{h,o} - T_{c,i} \quad \text{for counterflow}$$

Cross-Flow Coefficient

In other types of heat exchangers, where the values of the overall heat transfer coefficient, U , may vary over the area of the surface, the LMTD may not be representative of the actual average temperature difference. In these cases, it is necessary to utilize a correction factor such that the heat transfer, q , can be determined by

$$q = UAF \Delta T_m$$

Here the value of ΔT_m is computed assuming counterflow conditions, i.e., $\Delta T_1 = T_{h,i} - T_{c,i}$ and $\Delta T_2 = T_{h,o} - T_{c,o}$. Figures 16 and 17 illustrate some examples of the *correction factor F* for various multiple-pass heat exchangers.

3 RADIATION HEAT TRANSFER

Heat transfer can occur in the absence of a participating medium through the transmission of energy by electromagnetic waves, characterized by a wavelength, λ , and frequency, ν , which

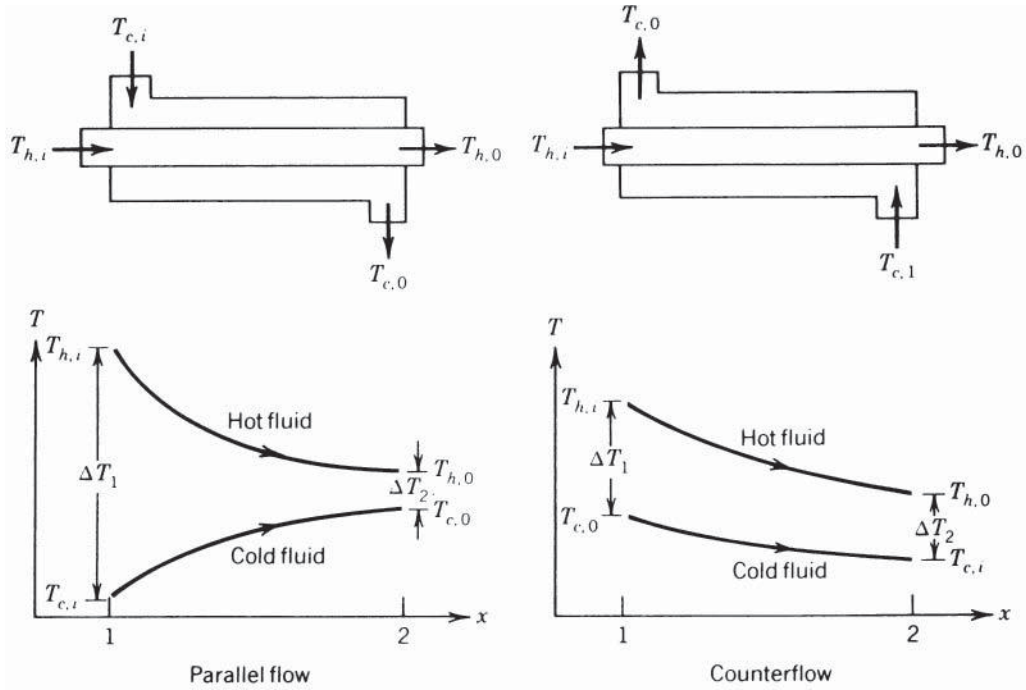


Figure 15 Temperature profiles for parallel flow and counterflow in double-pipe heat exchanger.

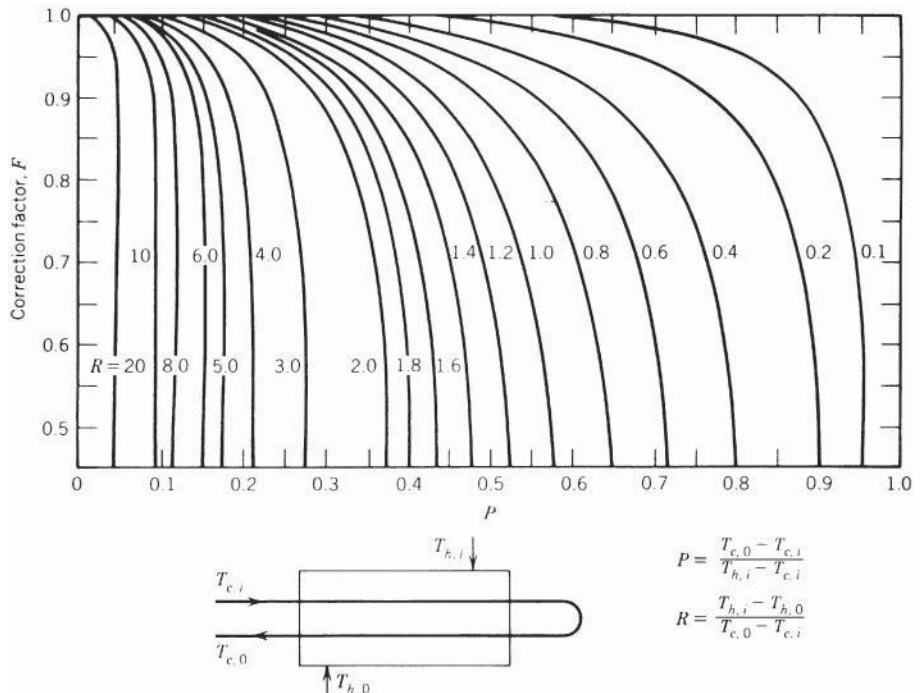


Figure 16 Correction factor for a shell-and-tube heat exchanger with one shell and any multiple of two tube passes (two, four, etc., tube passes).

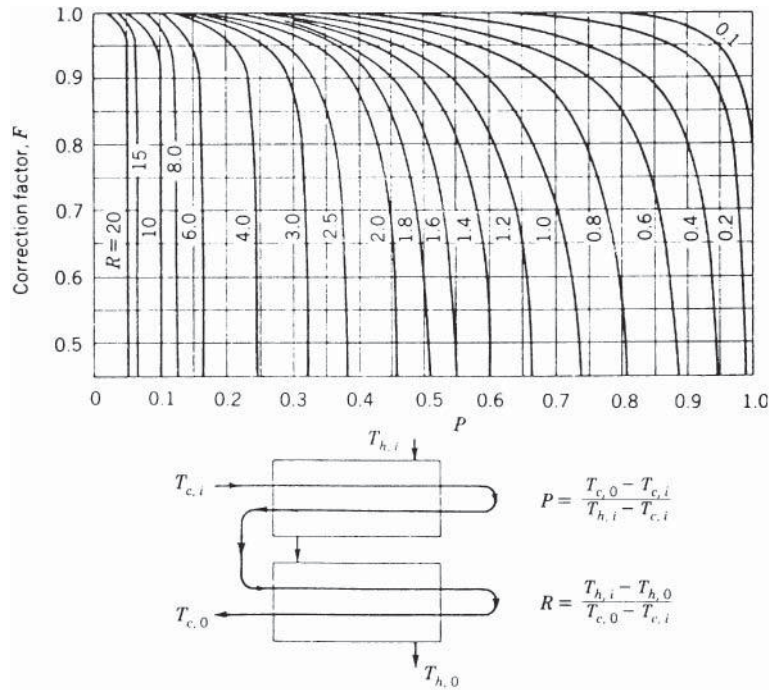


Figure 17 Correction factor for a shell-and-tube heat exchanger with two shell passes and any multiple of four tubes passes (four, eight, etc., tube passes).

are related by $c = \lambda v$. The parameter c represents the velocity of light, which in a vacuum is $c_o = 2.9979 \times 10^8 \text{m/s}$. Energy transmitted in this fashion is referred to as *radiant energy* and the heat transfer process that occurs is called radiation heat transfer or simply *radiation*. In this mode of heat transfer, the energy is transferred through electromagnetic waves or through photons, with the energy of a photon being given by $h\nu$, where h represents Planck's constant.

In nature, every substance has a characteristic wave velocity that is smaller than that occurring in a vacuum. These velocities can be related to c_o by $c = c_o/n$, where n indicates the refractive index. The value of the refractive index, n , for air is approximately equal to 1. The wavelength of the energy given or for the radiation that comes from a surface depends on the nature of the source and various wavelengths sensed in different ways. For example, as shown in Fig. 18, the electromagnetic spectrum consists of a number of different types of radiation. Radiation in the visible spectrum occurs in the range $\lambda = 0.4 - 0.74 \mu\text{m}$, while radiation in the wavelength range $0.1 - 100 \mu\text{m}$ is classified as *thermal radiation* and is sensed as heat. For radiant energy in this range, the amount of energy given off is governed by the temperature of the emitting body.

3.1 Blackbody Radiation

All objects in space are continuously being bombarded by radiant energy of one form or another and all of this energy is either absorbed, reflected, or transmitted. An ideal body that absorbs all the radiant energy falling upon it, regardless of the wavelength and direction, is referred to as a *blackbody*. Such a body emits maximum energy for a prescribed temperature and wavelength. Radiation from a blackbody is independent of direction and is referred to as a *diffuse emitter*.

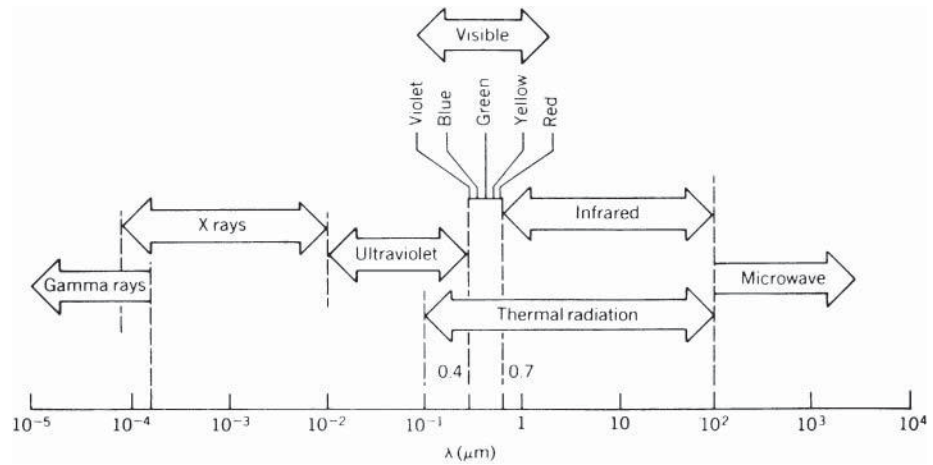


Figure 18 Electromagnetic radiation spectrum.

The Stefan–Boltzmann Law

The Stefan–Boltzmann law describes the rate at which energy is radiated from a blackbody and states that this radiation is proportional to the fourth power of the absolute temperature of the body,

$$e_b = \sigma T^4$$

where e_b is the *total emissive power* and σ is the Stefan–Boltzmann constant, which has the value $5.729 \times 10^{-8} \text{ W/m}^2 \cdot \text{K}^4$ ($0.173 \times 10^{-8} \text{ Btu/h} \cdot \text{ft}^2 \cdot \text{°R}^4$).

Planck's Distribution Law

The temperature amount of energy leaving a blackbody is described as the *spectral emissive power*, $e_{\lambda b}$, and is a function of wavelength. This function, which was derived from quantum theory by Planck, is

$$e_{\lambda b} = \frac{2\pi C_1}{\lambda^5 [\exp(C_2/\lambda T) - 1]}$$

where $e_{\lambda b}$ has a unit $\text{W/m}^2 \cdot \mu\text{m}$ ($\text{Btu/h} \cdot \text{ft}^2 \cdot \mu\text{m}$).

Values of the constants C_1 and C_2 are $0.59544 \times 10^{-16} \text{ W} \cdot \text{m}^2$ ($0.18892 \times 10^8 \text{ Btu} \cdot \mu\text{m}^4/\text{h ft}^2$) and $14,388 \mu\text{m} \cdot \text{K}$ ($25,898 \mu\text{m} \cdot \text{°R}$), respectively. The distribution of the spectral emissive power from a blackbody at various temperatures is shown in Fig. 19, which shows that the energy emitted at all wavelengths increases as the temperature increases. The maximum or peak values of the constant temperature curves illustrated in Fig. 20 shift to the left for shorter wavelengths as the temperatures increase.

The fraction of the emissive power of a blackbody at a given temperature and in the wavelength interval between λ_1 and λ_2 can be described by

$$F_{\lambda_1 T - \lambda_2 T} = \frac{1}{\sigma T^4} \left(\int_0^{\lambda_1} e_{\lambda b} d\lambda - \int_0^{\lambda_2} e_{\lambda b} d\lambda \right) = F_{0-\lambda_1 T} - F_{0-\lambda_2 T}$$

where the function $F_{0-\lambda T} = (1/\sigma T^4) \int_0^{\lambda} e_{\lambda b} d\lambda$ is given in Table 16. This function is useful for the evaluation of total properties involving integration on the wavelength in which the spectral properties are piecewise constant.

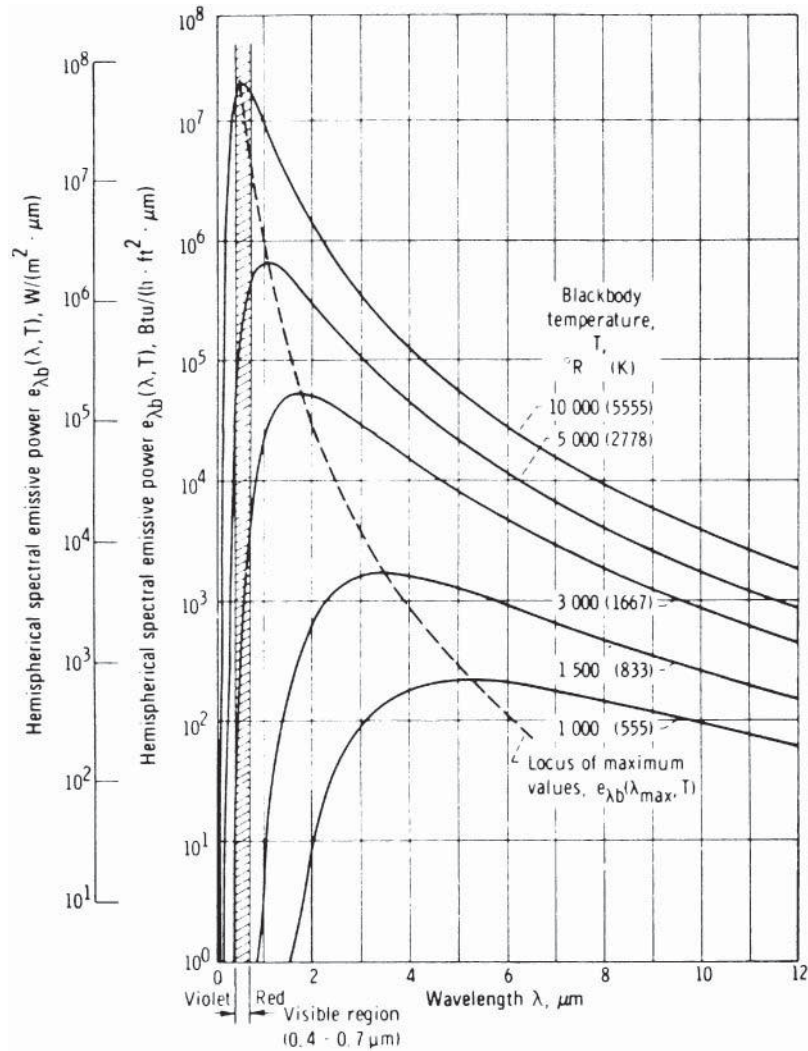


Figure 19 Hemispherical spectral emissive power of a blackbody for various temperatures.

Wien’s Displacement Law

The relationship between these peak or maximum temperatures can be described by *Wien’s displacement law*:

$$\lambda_{\text{max}} T = 2897.8 \mu\text{m} \cdot \text{K}$$

or

$$\lambda_{\text{max}} T = 5216.0 \mu\text{m} \cdot ^{\circ}\text{R}$$

3.2 Radiation Properties

While to some degree, all surfaces follow the general trends described by the Stefan–Boltzmann and Planck laws, the behavior of real surfaces deviates somewhat from these. In fact, because

$$dA_i dF_{d_i-d_j} = dA_j dF_{d_j-d_i}$$

$$dA_i F_{d_i-j} = A_j dF_{j-d_i}$$

$$A_i F_{i-j} = A_j F_{j-i}$$

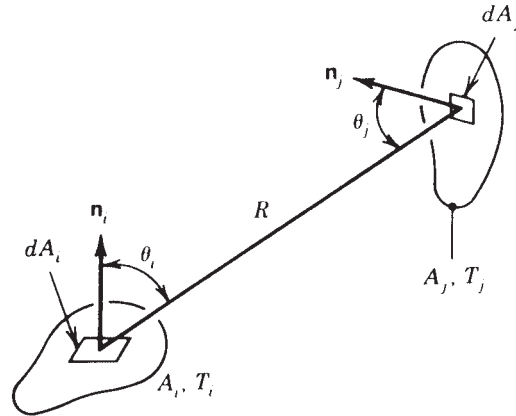


Figure 20 Configuration factor for radiation exchange between surfaces of area dA_i and dA_j .

blackbodies are ideal, all real surfaces emit and absorb less radiant energy than a blackbody. The amount of energy a body emits can be described in terms of the emissivity and is, in general, a function of the type of material, the temperature, and the surface conditions, such as roughness, oxide layer thickness, and chemical contamination. The emissivity is, in fact, a measure of how well a real body radiates energy as compared with a blackbody of the same temperature. The radiant energy emitted into the entire hemispherical space above a real surface element, including all wavelengths is given by $e = \epsilon \sigma T^4$, where ϵ is less than 1.0 and is called the *hemispherical emissivity* (or *total hemispherical emissivity* to indicate averaging over the total wavelength spectrum). For a given wavelength the *spectral hemispherical emissivity* ϵ_λ of a real surface is defined as

$$\epsilon_\lambda = \frac{e_\lambda}{e_{\lambda b}}$$

where e_λ is the hemispherical emissive power of the real surface and $e_{\lambda b}$ is that of a blackbody at the same temperature.

Spectral irradiation, G_λ , ($\text{W}/\text{m}^2 \cdot \mu\text{m}$), is defined as the rate at which radiation is incident upon a surface per unit area of the surface, per unit wavelength about the wavelength λ , and encompasses the incident radiation from all directions.

Spectral hemispherical reflectivity, ρ_λ , is defined as the radiant energy reflected per unit time, per unit area of the surface, per unit wavelength/ G_λ .

Spectral hemispherical absorptivity, α_λ , is defined as the radiant energy absorbed per unit area of the surface, per unit wavelength about the wavelength/ G_λ .

Spectral hemispherical transmissivity is defined as the radiant energy transmitted per unit area of the surface, per unit wavelength about the wavelength/ G_λ .

For any surface, the sum of the reflectivity, absorptivity, and transmissivity must equal unity, i.e.,

$$\alpha_\lambda + \rho_\lambda \tau_\lambda = 1$$

Table 16 Radiation Function $F_{o-\lambda T}$

λT			λT			λT		
$\mu\text{m} \cdot \text{K}$	$\mu\text{m} \cdot ^\circ\text{R}$	$F_{o-\lambda T}$	$\mu\text{m} \cdot \text{K}$	$\mu\text{m} \cdot ^\circ\text{R}$	$F_{o-\lambda T}$	$\mu\text{m} \cdot \text{K}$	$\mu\text{m} \cdot ^\circ\text{R}$	$F_{o-\lambda T}$
400	720	0.1864×10^{-11}	3400	6120	0.3617	6400	11,520	0.7692
500	900	0.1298×10^{-8}	3500	6300	0.3829	6500	11,700	0.7763
600	1080	0.9290×10^{-7}	3600	6480	0.4036	6600	11,880	0.7832
700	1260	0.1838×10^{-5}	3700	6660	0.4238	6800	12,240	0.7961
800	1440	0.1643×10^{-4}	3800	6840	0.4434	7000	12,600	0.8081
900	1620	0.8701×10^{-4}	3900	7020	0.4624	7200	12,960	0.8192
1000	1800	0.3207×10^{-3}	4000	7200	0.4809	7400	13,320	0.8295
1100	1980	0.9111×10^{-3}	4100	7380	0.4987	7600	13,680	0.8391
1200	2160	0.2134×10^{-2}	4200	7560	0.5160	7800	14,040	0.8480
1300	2340	0.4316×10^{-2}	4300	7740	0.5327	8000	14,400	0.8562
1400	2520	0.7789×10^{-2}	4400	7920	0.5488	8200	14,760	0.8640
1500	2700	0.1285×10^{-1}	4500	8100	0.5643	8400	15,120	0.8712
1600	2880	0.1972×10^{-1}	4600	8280	0.5793	8600	15,480	0.8779
1700	3060	0.2853×10^{-1}	4700	8460	0.5937	8800	15,840	0.8841
1800	3240	0.3934×10^{-1}	4800	8640	0.6075	9000	16,200	0.8900
1900	3420	0.5210×10^{-1}	4900	8820	0.6209	10,000	18,000	0.9142
2000	3600	0.6673×10^{-1}	5000	9000	0.6337	11,000	19,800	0.9318
2100	3780	0.8305×10^{-1}	5100	9180	0.6461	12,000	21,600	0.9451
2200	3960	0.1009	5200	9360	0.6579	13,000	23,400	0.9551
2300	4140	0.1200	5300	9540	0.6694	14,000	25,200	0.9628
2400	4320	0.1402	5400	9720	0.6803	15,000	27,000	0.9689
2500	4500	0.1613	5500	9900	0.6909	20,000	36,000	0.9856
2600	4680	0.1831	5600	10,080	0.7010	25,000	45,000	0.9922
2700	4860	0.2053	5700	10,260	0.7108	30,000	54,000	0.9953
2800	5040	0.2279	5800	10,440	0.7201	35,000	63,000	0.9970
2900	5220	0.2505	5900	10,620	0.7291	40,000	72,000	0.9979
3000	5400	0.2732	6000	10,800	0.7378	45,000	81,000	0.9985
3100	5580	0.2958	6100	10,980	0.7461	50,000	90,000	0.9989
3200	5760	0.3181	6200	11,160	0.7541	55,000	99,000	0.9992
3300	5940	0.3401	6300	11,340	0.7618	60,000	108,000	0.9994

When these values are averaged over the entire wavelength from $\lambda = 0$ to ∞ , they are referred to as *total* values. Hence, the *total hemispherical reflectivity*, *total hemispherical absorptivity*, and *total hemispherical transmissivity* can be written as

$$\rho = \int_0^\infty \frac{\rho_\lambda G_\lambda d\lambda}{G}$$

$$\alpha = \int_0^\infty \frac{\alpha_\lambda G_\lambda d\lambda}{G}$$

and

$$\tau = \int_0^\infty \frac{\tau_\lambda G_\lambda d\lambda}{G}$$

respectively, where

$$G = \int_0^\infty G_\lambda d\lambda$$

As was the case for the wavelength-dependent parameters, the sum of the total reflectivity, total absorptivity, and total transmissivity must be equal to unity, i.e.,

$$\alpha + \rho + \tau = 1$$

It is important to note that while the emissivity is a function of the material, temperature, and surface conditions, the absorptivity and reflectivity depend on both the surface characteristics and the nature of the incident radiation.

The terms *reflectance*, *absorptance*, and *transmittance* are used by some authors for the real surfaces and the terms reflectivity, absorptivity, and transmissivity are reserved for the properties of the ideal surfaces (i.e., those optically smooth and pure substances perfectly uncontaminated). Surfaces that allow no radiation to pass through are referred to as *opaque*, i.e., $\tau_\lambda = 0$, and all of the incident energy will be either reflected or absorbed. For such a surface,

$$\alpha_\lambda + \rho_\lambda = 1 \text{ and } \alpha + \rho = 1$$

Light rays reflected from a surface can be reflected in such a manner that the incident and reflected rays are symmetric with respect to the surface normal at the point of incidence. This type of radiation is referred to as *specular*. The radiation is referred to as *diffuse* if the intensity of the reflected radiation is uniform over all angles of reflection and is independent of the incident direction, and the surface is called a *diffuse surface* if the radiation properties are independent of the direction. If they are independent of the wavelength, the surface is called a *gray surface*, and a *diffuse gray surface* absorbs a fixed fraction of incident radiation from any direction and at any wavelength, and $\alpha_\lambda = \varepsilon_\lambda = \alpha = \varepsilon$.

Kirchhoff's Law of Radiation

The directional characteristics can be specified by the addition of a prime to the value; for example, the spectral emissivity for radiation in a particular direction would be denoted by α'_λ . For radiation in a particular direction, the spectral emissivity is equal to the directional spectral absorptivity for the surface irradiated by a blackbody at the same temperature. The most general form of this expression states that $\alpha'_\lambda = \varepsilon'_\lambda$. If the incident radiation is independent of angle or if the surface is diffuse, then $\alpha_\lambda = \varepsilon_\lambda$ for the hemispherical properties. This relationship can have various conditions imposed on it, depending on whether spectral, total, directional, or hemispherical quantities are being considered.²²

Emissivity of Metallic Surfaces

The properties of pure smooth metallic surfaces are often characterized by low emissivity and absorptivity values and high values of reflectivity. The spectral emissivity of metals tends to increase with decreasing wavelength, and exhibits a peak near the visible region. At wavelengths $\lambda > \sim 5\mu\text{m}$ the spectral emissivity increases with increasing temperature, but this trend reverses at shorter wavelengths ($\lambda < \sim 1.27\mu\text{m}$). Surface roughness has a pronounced effect on both the hemispherical emissivity and absorptivity, and large *optical roughnesses*, defined as the mean square roughness of the surface divided by the wavelength, will increase the hemispherical emissivity. For cases where the optical roughness is small, the directional properties will approach the values obtained for smooth surfaces. The presence of impurities, such as oxides or other nonmetallic contaminants, will change the properties significantly and increase the emissivity of an otherwise pure metallic body. A summary of the normal total emissivities for metals are given in Table 17. It should be noted that the hemispherical emissivity for metals is typically 10–30% higher than the values normally encountered for normal emissivity.

Table 17 Normal Total Emissivity of Metals

Materials	Surface Temperature (K)	Normal Total Emissivity
Aluminum		
Highly polished plate	480–870	0.038–0.06
Polished plate	373	0.095
Heavily oxidized	370–810	0.20–0.33
Bismuth, bright	350	0.34
Chromium, polished	310–1370	0.08–0.40
Copper		
Highly polished	310	0.02
Slightly polished	310	0.15
Black oxidized	310	0.78
Gold, highly polished	370–870	0.018–0.035
Iron		
Highly polished, electrolytic	310–530	0.05–0.07
Polished	700–760	0.14–0.38
Wrought iron, polished	310–530	0.28
Cast iron, rough, strongly oxidized	310–530	0.95
Lead		
Polished	310–530	0.06–0.08
Rough unoxidized	310	0.43
Mercury, unoxidized	280–370	0.09–0.12
Molybdenum, polished	310–3030	0.05–0.29
Nickel		
Electrolytic	310–530	0.04–0.06
Electroplated on iron, not polished	293	0.11
Nickel oxide	920–1530	0.59–0.86
Platinum, electrolytic	530–810	0.06–0.10
Silver, polished	310–810	0.01–0.03
Steel		
Polished sheet	90–420	0.07–0.14
Mild steel, polished	530–920	0.27–0.31
Sheet with rough oxide layer	295	0.81
Tin, polished sheet	310	0.05
Tungsten, clean	310–810	0.03–0.08
Zinc		
Polished	310–810	0.02–0.05
Gray oxidized	295	0.23–0.28

Source: Adapted from Ref. 22.

Emissivity of Nonmetallic Materials

Large values of total hemispherical emissivity and absorptivity are typical for nonmetallic surfaces at moderate temperatures and, as shown in Table 18, which lists the normal total emissivity of some nonmetals, the temperature dependence is small.

Absorptivity for Solar Incident Radiation

The spectral distribution of solar radiation can be approximated by blackbody radiation at a temperature of approximately 5800 K (10,000°R) and yields an average solar irradiation at the outer limit of the atmosphere of approximately 1353 W/m² (429 Btu/ft² · h). This solar

Table 18 Normal Total Emissivity of Nonmetals

Materials	Surface Temperature (K)	Normal Total Emissivity
Asbestos, board	310	0.96
Brick		
White refractory	1370	0.29
Rough Red	310	0.93
Carbon, lampsoot	310	0.95
Concrete, rough	310	0.94
Ice, smooth	273	0.966
Magnesium oxide, refractory	420–760	0.69–0.55
Paint		
Oil, all colors	373	0.92–0.96
Lacquer, flat black	310–370	0.96–0.98
Paper, white	310	0.95
Plaster	310	0.91
Porcelain, glazed	295	0.92
Rubber, hard	293	0.92
Sandstone	310–530	0.83–0.90
Silicon carbide	420–920	0.83–0.96
Snow	270	0.82
Water, deep	273–373	0.96
Wood, sawdust	310	0.75

Source: Adapted from Ref. 22.

irradiation is called the *solar constant* and is greater than the solar irradiation received at the surface of the earth, due to the radiation scattering by air molecules, water vapor, and dust, and the absorption by O_3 , H_2O , and CO_2 in the atmosphere. The absorptivity of a substance depends not only on the surface properties but also on the sources of incident radiation. Since solar radiation is concentrated at a shorter wavelength, due to the high source temperature, the absorptivity for certain materials when exposed to solar radiation may be quite different from that which occurs for low-temperature radiation, where the radiation is concentrated in the longer-wavelength range. A comparison of absorptivities for a number of different materials is given in Table 19 for both solar and low-temperature radiation.

3.3 Configuration Factor

The magnitude of the radiant energy exchanged between any two given surfaces is a function of the emissivity, absorptivity, and transmissivity. In addition, the energy exchange is a strong function of how one surface is viewed from the other. This aspect can be defined in terms of the *configuration factor* (sometimes called the *radiation shape factor*, *view factor*, *angle factor*, or *interception factor*). As shown in Fig. 20, the configuration factor, $F_{i \rightarrow j}$, is defined as that fraction of the radiation leaving a black surface, i , that is intercepted by a black or gray surface, j , and is based on the relative geometry, position, and shape of the two surfaces. The configuration factor can also be expressed in terms of the differential fraction of the energy or $dF_{i \rightarrow dj}$, which indicates the differential fraction of energy from a finite area A_i that is intercepted by an infinitesimal area dA_j . Expressions for a number of different cases are given below for several common geometries.

Table 19 Comparison of Absorptivities of Various Surfaces to Solar and Low Temperature Thermal Radiation

Surface	Absorptivity	
	For Solar Radiation	For Low-Temperature Radiation (~300 K)
Aluminum, highly polished	0.15	0.04
Copper, highly polished	0.18	0.03
Tarnished	0.65	0.75
Cast iron	0.94	0.21
Stainless steel, No. 301, polished	0.37	0.60
White marble	0.46	0.95
Asphalt	0.90	0.90
Brick, red	0.75	0.93
Gravel	0.29	0.85
Flat black lacquer	0.96	0.95
White paints, various types of pigments	0.12–0.16	0.90–0.95

Source: Adapted from Refs. 23 and 24.

Infinitesimal area dA_j to infinitesimal area dA_j :

$$dF_{di-dj} = \frac{\cos \theta_i \cos \theta_j}{\pi R^2} dA_j$$

Infinitesimal area dA_j to finite area A_j :

$$F_{di-j} = \int_{A_j} \frac{\cos \theta_i \cos \theta_j}{\pi R^2} dA_j$$

Finite area A_i to finite area A_j :

$$F_{i-j} = \frac{1}{A_i} \int_{A_j} \int_{A_j} \frac{\cos \theta_i \cos \theta_j}{\pi R^2} dA_i dA_j$$

Analytical expressions of other configuration factors have been found for a wide variety of simple geometries and a number of these are presented in Figs. 21–24 for surfaces that emit and reflect diffusely.

Reciprocity Relations

The configuration factors can be combined and manipulated using algebraic rules referred to as configuration factor geometry. These expressions take several forms, one of which is the reciprocal properties between different configuration factors, which allow one configuration factor to be determined from knowledge of the others:

$$dA_i dF_{di-dj} = dA_j dF_{dj-di}$$

$$dA_i dF_{di-j} = A_j dF_{j-di}$$

$$A_i F_{i-j} = A_j F_{j-i}$$

These relationships can be combined with other basic rules to allow the determination of the configuration of an infinite number of complex shapes and geometries from a few select, known geometries. These are summarized in the following sections.

	<p>Area dA_1 of differential width and any length, to infinitely long strip dA_2 of differential width and with parallel generating line to dA_1:</p>
	$dF_{d1-d2} = \frac{\cos \varphi}{2} d\varphi = \frac{1}{2} d(\sin \varphi)$
	<p>Two infinitely long plates of unequal widths h and w, having one common edge, and at an angle of 90° to each other:</p>
	$H = \frac{h}{w}$ $F_{1-2} = \frac{1}{2}(1 + H - \sqrt{1 + H^2})$
	<p>Two infinitely long, directly opposed parallel plates of the same finite width:</p>
	$H = \frac{h}{w}$ $F_{1-2} = F_{2-1} = \sqrt{1 + H^2} - H$
	<p>Infinitely long enclosure formed by three plane areas:</p>
	$F_{1-2} = \frac{A_1 + A_2 - A_3}{2A_1}$
	<p>Concentric cylinders of infinite length:</p>
	$F_{1-2} = 1$ $F_{2-1} = \frac{r_1}{r_2}$ $F_{2-2} = 1 - \frac{r_1}{r_2}$
	<p>Concentric spheres:</p>
	$F_{1-2} = 1$ $F_{2-1} = \left(\frac{r_1}{r_2}\right)^2$ $F_{2-2} = 1 - \left(\frac{r_1}{r_2}\right)^2$
	<p>Differential or finite areas on the inside of a spherical cavity:</p>
	$dF_{d1-d2} = dF_{1-d2} = \frac{dA_2}{4\pi r^2}$ $F_{d1-2} = F_{1-2} = \frac{A_2}{4\pi r^2}$

Figure 21 Configuration factors for some simple geometries.²² © McGraw-Hill Education.

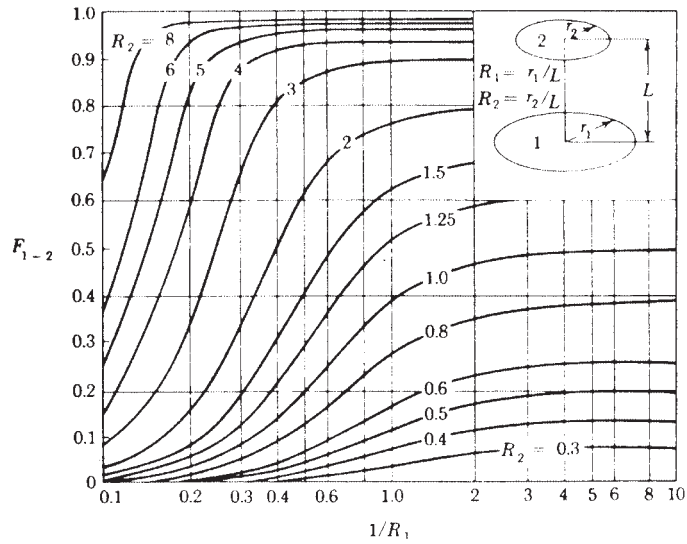


Figure 22 Configuration factor for coaxial parallel circular disks.

$$A_i F_{i-j} = \sum_{n=1}^N \sum_{m=1}^M A_{in} F_{in-jm}$$

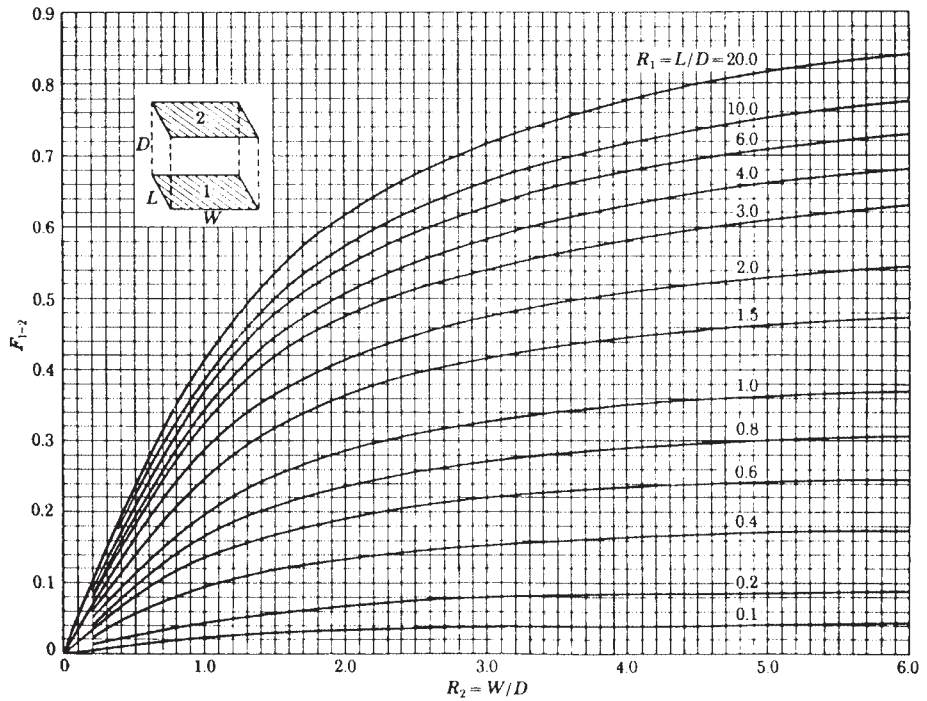


Figure 23 Configuration factor for aligned parallel rectangles.

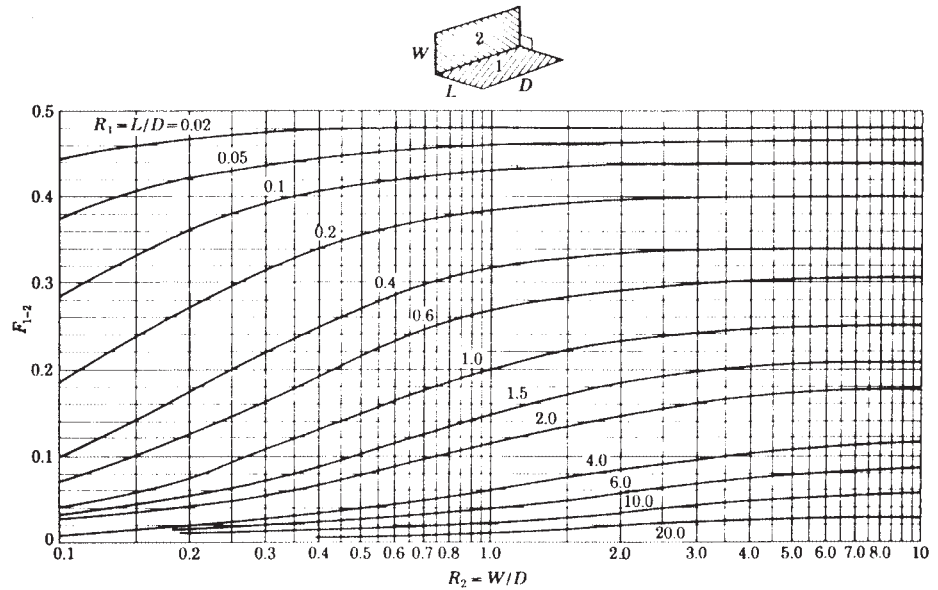


Figure 24 Configuration factor for rectangles with common edge.

The Additive Property

For a surface A_i subdivided into N parts ($A_{i_1}, A_{i_2}, \dots, A_{i_N}$) and a surface A_j subdivided into M parts ($A_{j_1}, A_{j_2}, \dots, A_{j_M}$),

$$A_i F_{i-j} = \sum_{n=1}^N \sum_{m=1}^M A_{i_n} F_{i_n-j_m}$$

Relation in an Enclosure

When a surface is completely enclosed, the surface can be subdivided into N parts having areas A_1, A_2, \dots, A_N , respectively, and

$$\sum_{j=1}^N F_{i-j} = 1$$

Blackbody Radiation Exchange

For black surfaces A_i and A_j at temperatures T_i and T_j , respectively, the net radiative exchange, q_{ij} , can be expressed as

$$q_{ij} = A_i F_{i-j} \sigma (T_i^4 - T_j^4)$$

and for a surface completely enclosed and subdivided into N surfaces maintained at temperatures T_1, T_2, \dots, T_N , the net radiative heat transfer, q_i , to surface area A_i is

$$q_i = \sum_{j=1}^N A_i F_{i-j} \sigma (T_i^4 - T_j^4) = \sum_{j=1}^N q_{ij}$$

3.4 Radiative Exchange among Diffuse Gray Surfaces in an Enclosure

One method for solving for the radiation exchange between a number of surfaces or bodies is through the use of the *radiosity*, J , defined as the total radiation that leaves a surface per unit time and per unit area. For an opaque surface, this term is defined as

$$J = \epsilon \sigma T^4 + (1 - \epsilon)G$$

For an enclosure consisting of N surfaces, the irradiation on a given surface i can be expressed as

$$G_i = \sum_{j=1}^N J_j F_{i-j}$$

and the net radiative heat transfer rate at given surface i is

$$q_i = A_i(J_i - G_i) = \frac{\epsilon_i A_i}{1 - \epsilon_i} (\sigma T_i^4 - J_i)$$

For every surface in the enclosure, a uniform temperature or a constant heat transfer rate can be specified. If the surface temperature is given, the heat transfer rate can be determined for that surface and vice versa. Shown below are several specific cases that are commonly encountered.

Two Diffuse Gray Surfaces Forming an Enclosure

The net radiative exchange, q_{12} , for two diffuse gray surfaces forming an enclosure are shown in Table 20 for several simple geometries.

Radiation Shields

Often in practice, it is desirable to reduce the radiation heat transfer between two surfaces. This can be accomplished by placing a highly reflective surface between the two surfaces. For this

Table 20 Net Radiative Exchange between Two Surfaces Forming an Enclosure

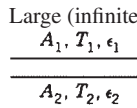
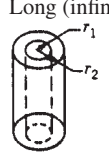

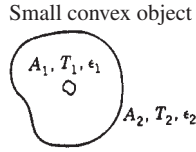
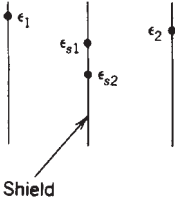
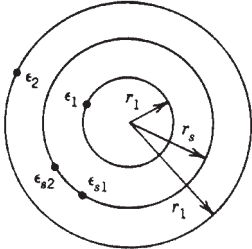
<p>Large (infinite) parallel planes</p> 	$A_1 = A_2 = A$	$q_{12} = \frac{A\sigma(T_1^4 - T_2^4)}{\frac{1}{\epsilon_1} + \frac{1}{\epsilon_2} - 1}$
<p>Long (infinite) concentric cylinders</p> 	$\frac{A_1}{A_2} = \frac{r_1}{r_2}$	$q_{12} = \frac{\sigma A_1 (T_1^4 - T_2^4)}{\frac{1}{\epsilon_1} + \frac{1 - \epsilon_2}{\epsilon_2} \left(\frac{r_1}{r_2}\right)}$
<p>Concentric sphere</p> 	$\frac{A_1}{A_2} = \frac{r_1^2}{r_2^2}$	$q_{12} = \frac{\sigma A_1 (T_1^4 - T_2^4)}{\frac{1}{\epsilon_1} + \frac{1 - \epsilon_2}{\epsilon_2} \left(\frac{r_1}{r_2}\right)^2}$
<p>Small convex object in a large cavity</p> 	$\frac{A_1}{A_2} \approx 0$	$q_{12} = \sigma A_1 \epsilon_1 (T_1^4 - T_2^4)$

Table 21 Values of X for Radiative Shields

Geometry	X
	$\frac{\frac{1}{\epsilon_{s1}} + \frac{1}{\epsilon_{s2}} - 1}{\frac{1}{\epsilon_1} + \frac{1}{\epsilon_2} - 1}$
	$\frac{\left(\frac{r_1}{r_2}\right)^2 \left(\frac{1}{\epsilon_{s1}} + \frac{1}{\epsilon_{s2}} - 1\right)}{\frac{1}{\epsilon_1} + \left(\frac{1}{\epsilon_2} - 1\right) \left(\frac{r_1}{r_2}\right)^2}$ <p>$n = 1$ for infinitely long concentric cylinders $n = 2$ for concentric spheres</p>

configuration, the ratio of the net radiative exchange with the shield to that without the shield can be expressed by the relationship

$$\frac{q_{12} \text{ with shield}}{q_{12} \text{ without shield}} = \frac{1}{1 + \chi}$$

Values for this ratio, χ , for shields between parallel plates, concentric cylinders, and concentric spheres are summarized in Table 21. For the special case of parallel plates involving more than one or N shields, where all of the emissivities are equal, the value of χ equals N .

Radiation Heat Transfer Coefficient

The rate at which radiation heat transfer occurs can be expressed in a form similar to Fourier's law or Newton's law of cooling, by expressing it in terms of the temperature difference $T_1 - T_2$, or as

$$q = h_r A (T_1 - T_2)$$

where h_r is the radiation heat transfer coefficient or *radiation film coefficient*. For the case of radiation between two large parallel plates with emissivities, respectively, of ϵ_1 and ϵ_2 ,

$$h_r = \frac{\sigma(T_1^4 - T_2^4)}{T_1 - T_2(1/\epsilon_1 + 1/\epsilon_2 - 1)}$$

3.5 Thermal Radiation Properties of Gases

All of the previous expressions assumed that the medium present between the surfaces did not affect the radiation exchange. In reality, gases such as air, oxygen (O_2), hydrogen (H_2), and nitrogen (N_2) have a symmetrical molecular structure and neither emit nor absorb radiation at low to moderate temperatures. Hence, for most engineering applications, such *nonparticipating gases* can be ignored. However, polyatomic gases such as water vapor (H_2O), carbon dioxide (CO_2), carbon monoxide (CO), sulfur dioxide (SO_2), and various hydrocarbons emit

and absorb significant amounts of radiation. These *participating gases* absorb and emit radiation in limited spectral ranges, referred to as *spectral bands*. In calculating the emitted or absorbed radiation for a gas layer, its thickness, shape, surface area, pressure, and temperature distribution must be considered. Although a precise method for calculating the effect of these participating media is quite complex, an approximate method developed by Hottel²⁵ will yield results that are reasonably accurate.

The effective total emissivities of carbon dioxide and water vapor are a function of the temperature and the product of the partial pressure and the mean beam length of the substance as indicated in Figs. 25 and 26, respectively. The *mean beam length*, L_e , is the characteristic length that corresponds to the radius of a hemisphere of gas, such that the energy flux radiated to the center of the base is equal to the average flux radiated to the area of interest by the actual gas volume. Table 22 lists the mean beam lengths of several simple shapes. For a geometry for which L_e has not been determined, it is generally approximated by $L_e = 3.6V/A$ for an entire gas volume V radiating to its entire boundary surface A . The data in Figs. 25 and 26 were obtained for a total pressure of 1 atm and zero partial pressure of the water vapor. For other total and partial pressures the emissivities are corrected by multiplying C_{CO_2} (Fig. 27) and $C_{\text{H}_2\text{O}}$ (Fig. 28), respectively, to ϵ_{CO_2} and $\epsilon_{\text{H}_2\text{O}}$, which are found from Figs. 25 and 26.

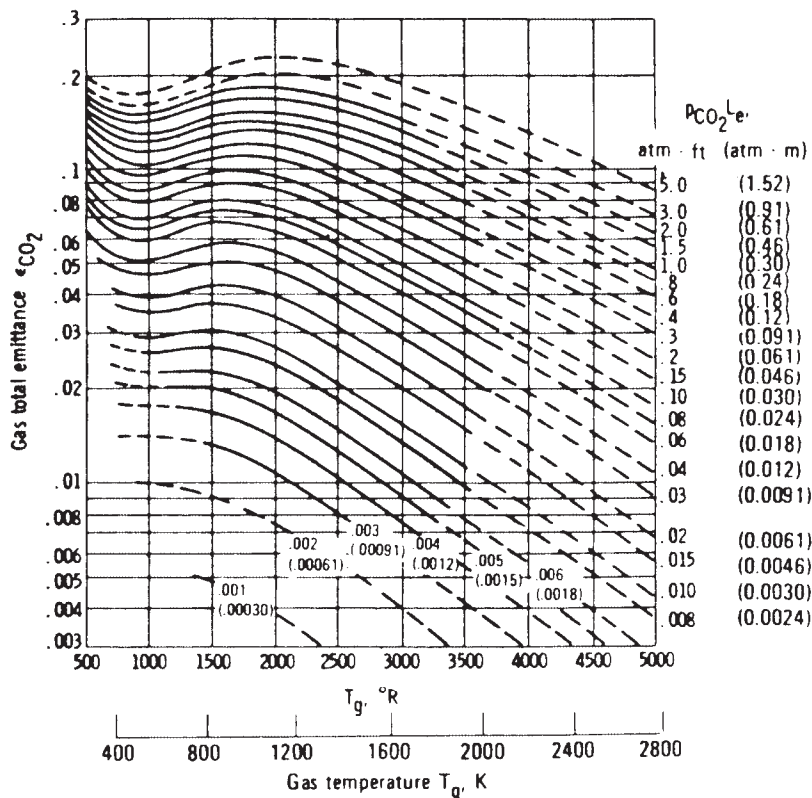


Figure 25 Total emissivity of CO_2 in a mixture having a total pressure of 1 atm. (From Ref. 25. © McGraw-Hill Education.)

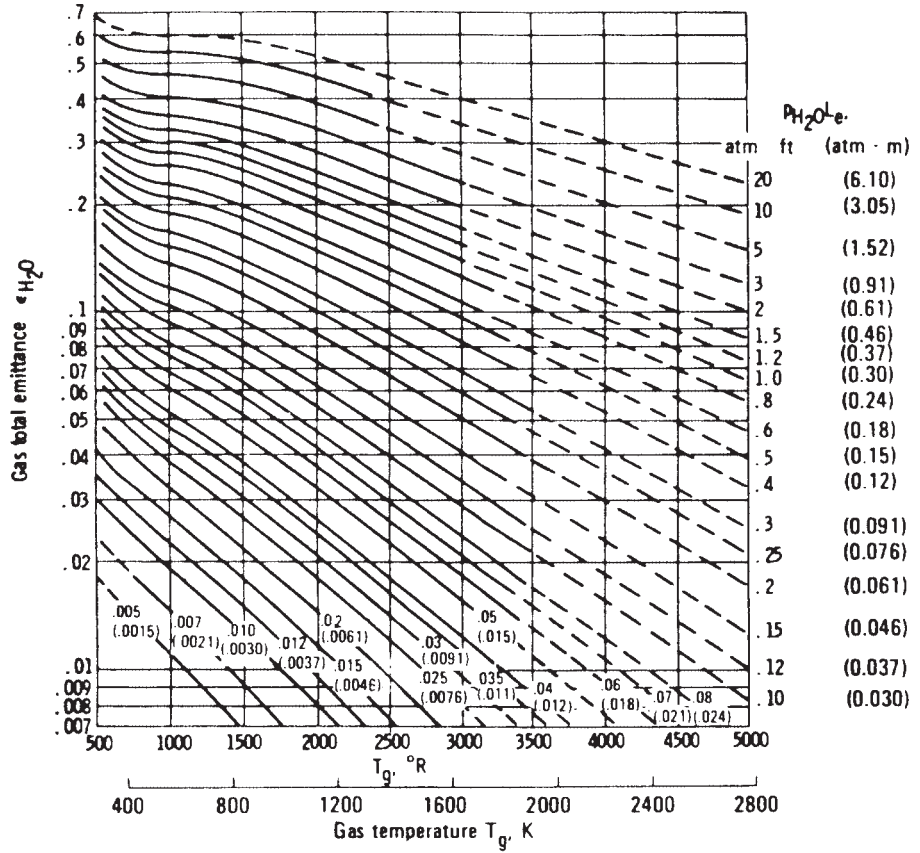


Figure 26 Total emissivity of H₂O at 1 atm total pressure and zero partial pressure. (From Ref. 25. © McGraw-Hill Education.)

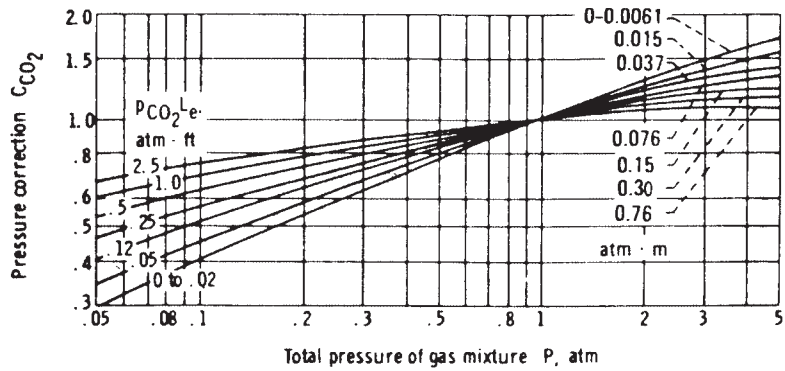


Figure 27 Pressure correction for CO₂ total emissivity for values of P other than 1 atm. (Adapted from Ref. 25. © McGraw-Hill Education.)

Table 22 Mean Beam Length

Geometry of Gas Volume	Characteristic Length	L_e
Hemisphere radiating to element at center of base	Radius R	R
Sphere radiating to its surface	Diameter D	$0.65D$
Circular cylinder of infinite height radiating to concave bounding surface	Diameter D	$0.95D$
Circular cylinder of semi-infinite height radiating to:		
Element at center of base	Diameter D	$0.90D$
Entire base	Diameter D	$0.65D$
Circular cylinder of height equal to diameter radiating to:		
Element at center of base	Diameter D	$0.71D$
Entire surface	Diameter D	$0.60D$
Circular cylinder of height equal to two diameters radiating to:		
Plane end	Diameter D	$0.60D$
Concave surface	Diameter D	$0.76D$
Entire surface	Diameter D	$0.73D$
Infinite slab of gas radiating to:		
Element on one face	Slab thickness D	$1.8D$
Both bounding planes	Slab thickness D	$1.8D$
Cube radiating to a face	Edge X	$0.6X$
Gas volume surrounding an infinite tube bundle and radiating to a single tube:		
Equilateral triangular array:		
$S = 2D$	Tube diameter D and spacing	$3.0(S-D)$
$S = 3D$	between tube centers, S	$3.8(S-D)$
Square array:		
$S = 2D$		$3.5(S-D)$

Source: Adapted from Ref. 22.

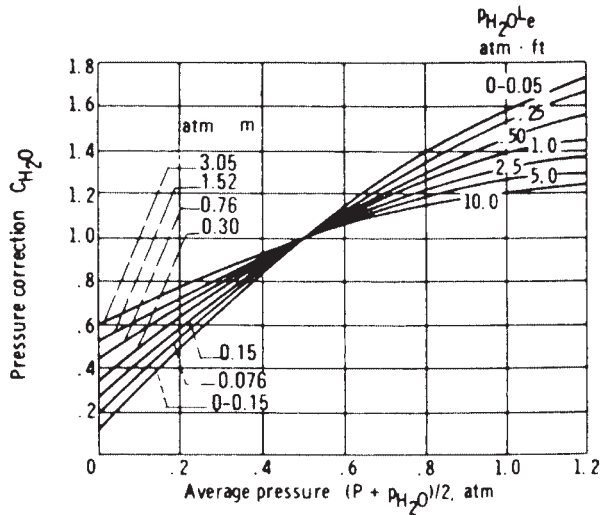


Figure 28 Pressure correction for water vapor total emissivity for values of P_{H_2O} and P other than 0 and 1 atm. (Adapted from Ref. 25. © McGraw-Hill Education.)

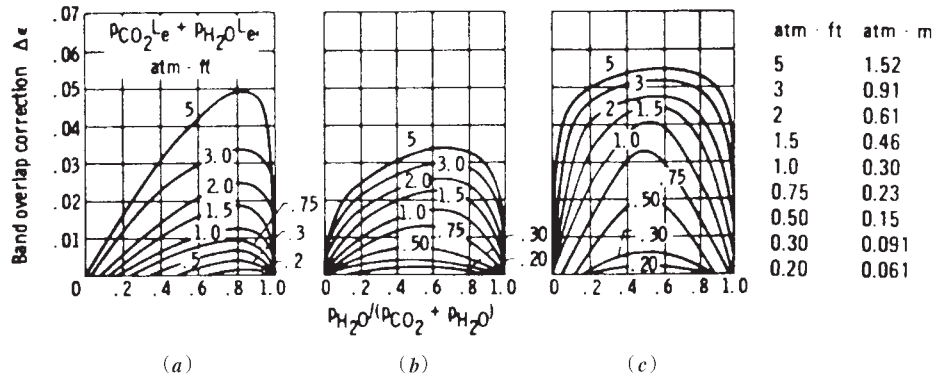


Figure 29 Correction on total emissivity for band overlap when both CO₂ and water vapor are present: (a) gas temperature $T_g = 400$ K (720°R), (b) gas temperature $T_g = 810$ K (1460°R), and (c) gas temperature $T_g = 1200$ K (2160°R). (Adapted from Ref. 25. © McGraw-Hill Education.)

These results can be applied when water vapor or carbon dioxide appear separately or in a mixture with other nonparticipating gases. For mixtures of CO₂ and water vapor in a nonparticipating gas, the total emissivity of the mixture, ϵ_g , can be estimated from the expression

$$\epsilon_g = C_{CO_2}\epsilon_{CO_2} + C_{H_2O}\epsilon_{H_2O} - \Delta\epsilon$$

where $\Delta\epsilon$ is a correction factor given in Fig. 29.

Radiative Exchange between Gas Volume and Black Enclosure of Uniform Temperature

When radiative energy is exchanged between a gas volume and a black enclosure, the exchange per unit area, q'' , for a gas volume at uniform temperature, T_g , and a uniform wall temperature, T_w , is given by

$$q'' = \epsilon_g(T_g)\sigma T_g^4 - \alpha_g(T_w)\sigma T_w^4$$

where $\epsilon_g(T_g)$ is the gas emissivity at a temperature T_g and $\alpha_g(T_w)$ is the absorptivity of gas for the radiation from the black enclosure at T_w . As a result of the nature of the band structure of the gas, the absorptivity, α_g , for black radiation at a temperature T_w is different from the emissivity, ϵ_g , at a gas temperature of T_g . When a mixture of carbon dioxide and water vapor is present, the empirical expression for α_g is

$$\alpha_g = \alpha_{CO_2} + \alpha_{H_2O} - \Delta\alpha$$

where

$$\alpha_{CO_2} = C_{CO_2}\epsilon'_{CO_2} \left(\frac{T_g}{T_w}\right)^{0.65}$$

$$\alpha_{H_2O} = C_{H_2O}\epsilon'_{H_2O} \left(\frac{T_g}{T_w}\right)^{0.45}$$

where $\Delta\alpha = \Delta\epsilon$ and all properties are evaluated at T_w .

In this expression, the values of ϵ'_{CO_2} and ϵ'_{H_2O} can be found from Figs. 25 and 26 using an abscissa of T_w , but substituting the parameters $p_{CO_2}L_eT_w/T_g$ and $p_{H_2O}L_eT_w/T_g$ for $p_{CO_2}L_e$ and $p_{H_2O}L_e$, respectively.

Radiative Exchange between a Gray Enclosure and a Gas Volume

When the emissivity of the enclosure, ϵ_w , is larger than 0.8, the rate of heat transfer may be approximated by

$$q_{\text{gray}} = \left(\frac{\epsilon_w + 1}{2} \right) q_{\text{black}}$$

where q_{gray} is the heat transfer rate for gray enclosure and q_{black} is that for black enclosure. For values of $\epsilon_w < 0.8$, the band structures of the participating gas must be taken into account for heat transfer calculations.

4 BOILING AND CONDENSATION HEAT TRANSFER

Boiling and condensation are both forms of convection in which the fluid medium is undergoing a change of phase. When a liquid comes into contact with a solid surface maintained at a temperature above the saturation temperature of the liquid, the liquid may vaporize, resulting in boiling. This process is always accompanied by a change of phase, from the liquid to the vapor state, and results in large rates of heat transfer from the solid surface, due to the latent heat of vaporization of the liquid. The process of condensation is usually accomplished by allowing the vapor to come into contact with a surface at a temperature below the saturation temperature of the vapor, in which case the liquid undergoes a change in state from the vapor state to the liquid state, giving up the latent heat of vaporization.

The heat transfer coefficients for condensation and boiling are generally larger than that for convection without phase change, sometimes by as much as several orders of magnitude. Application of boiling and condensation heat transfer may be seen in a closed-loop power cycle or in a device referred to as a *heat pipe*, which will be discussed in the following section. In power cycles, the liquid is vaporized in a boiler at high pressure and temperature. After producing work by means of expansion through a turbine, the vapor is condensed to the liquid state in a condenser, and then returned to the boiler where the cycle is repeated.

4.1 Boiling

The formation of vapor bubbles on a hot surface in contact with a quiescent liquid without external agitation; it is called *pool boiling*. This differs from *forced-convection boiling* in which forced convection occurs simultaneously with boiling. When the temperature of the liquid is below the saturation temperature, the process is referred to as *subcooled boiling*. When the liquid temperature is maintained or exceeds the saturation temperature, the process is referred to as *saturated or saturation boiling*. Figure 30 depicts the surface heat flux, q'' , as a function of the excess temperature, $\Delta T_e = T_s - T_{\text{sat}}$, for typical pool boiling of water using an electrically heated wire. In the region $0 < \Delta T_e < \Delta T_{e,A}$ bubbles occur only on selected spots of the heating surface, and the heat transfer occurs primarily through free convection. This process is called *free convection boiling*. When $\Delta T_{e,A} < \Delta T_e < \Delta T_{e,C}$, the heated surface is densely populated with bubbles, and the bubble separation and eventual rise due to buoyancy induce a considerable stirring action in the fluid near the surface. This stirring action substantially increases the heat transfer from the solid surface. This process or region of the curve is referred to as *nucleate boiling*. When the excess temperature is raised to $\Delta T_{e,C}$, the heat flux reaches a maximum value, and further increases in the temperature will result in a decrease in the heat flux. The point at which the heat flux is at a maximum value, is called the *critical heat flux*.

Film boiling occurs in the region where $\Delta T_e > \Delta T_{e,D}$, and the entire heating surface is covered by a vapor film. In this region the heat transfer to the liquid is caused by conduction and radiation through the vapor. Between points *C* and *D*, the heat flux decreases with

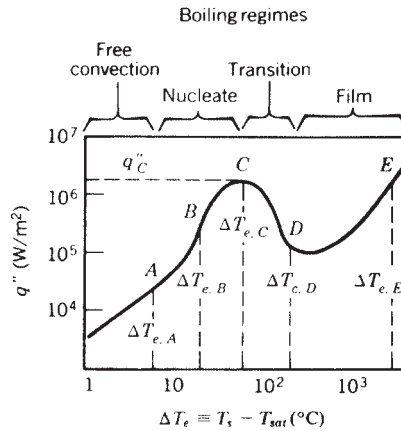


Figure 30 Typical boiling curve for a wire in a pool of water at atmospheric pressure.

increasing ΔT_e . In this region, part of the surface is covered by bubbles and part by a film. The vaporization in this region is called *transition boiling* or *partial film boiling*. The point of maximum heat flux, point *C*, is called the *burnout point* or the *Lindenfrost point*. Although it is desirable to operate the vapor generators at heat fluxes close to q''_C , to permit the maximum use of the surface area, in most engineering applications it is necessary to control the heat flux and great care is taken to avoid reaching this point. The primary reason for this is that, as illustrated, when the heat flux is increased gradually, the temperature rises steadily until point *C* is reached. Any increase of heat flux beyond the value of q''_C , however, will dramatically change the surface temperature to $T_s = T_{sat} + T_{e,E}$, typically exceeding the solid melting point and leading to failure of the material in which the liquid is held or from which the heater is fabricated.

Nucleate Pool Boiling

The heat flux data are best correlated by²⁶

$$q'' = \mu_l h_{fg} \left[\frac{g(\rho_l - \rho_v)}{g_c \sigma} \right]^{1/2} \left(\frac{c_{p,l} \Delta T_e}{Ch_{fg} Pr_l^{1.7}} \right)^3$$

where the subscripts *l* and *v* denote saturated liquid and vapor, respectively. The surface tension of the liquid is σ (N/m). The quantity g_c is the proportionality constant equal to $1 \text{ kg} \cdot \text{m}/\text{N} \cdot \text{s}^2$. The quantity g is the local gravitational acceleration in m/s^2 . The values of *C* are given in Table 23. The above equation may be applied to different geometries, such as plates, wire, or cylinders.

Table 23 Values of the Constant *C* for Various Liquid–Surface Combinations

Fluid–Heating Surface Combinations	<i>C</i>
Water with polished copper, platinum, or mechanically polished stainless steel	0.0130
Water with brass or nickel	0.006
Water with ground and polished stainless steel	0.008
Water with Teflon-plated stainless steel	0.008

The *critical heat flux* (point *C* of Fig. 30) is given by²⁷

$$q_c'' = \frac{\pi}{24} h_{fg} \rho_v \left[\frac{\sigma g g_c (\rho_l - \rho_v)}{\rho_v^2} \right]^{0.25} \left(1 + \frac{\rho_v}{\rho_l} \right)^{0.5}$$

For a water–steel combination, $q_c'' \approx 1290 \text{ kW/m}^2$ and $\Delta T_{e,c} \approx 30^\circ\text{C}$. For water–chrome-plated copper, $q_c'' \approx 940 - 1260 \text{ kW/m}^2$ and $\Delta T_{e,c} \approx 23 - 28^\circ\text{C}$.

Film Pool Boiling

The heat transfer from the surface to the liquid is due to both convection and radiation. A total heat transfer coefficient is defined by the combination of convection and radiation heat transfer coefficients of the following form²⁸ for the outside surfaces of horizontal tubes:

$$h^{4/3} = h_c^{4/3} + h_r h^{1/3}$$

where

$$h_c = 0.62 \left[\frac{k_v^3 \rho_v (\rho_l - \rho_v) g (h_{fg} + 0.4 c_{p,v} \Delta T_e)}{\mu_v D \Delta T_e} \right]^{1/4}$$

and

$$h_r = \frac{5.73 \times 10^{-8} \varepsilon (T_s^4 - T_{\text{sat}}^r)}{T_s - T_{\text{sat}}}$$

The vapor properties are evaluated at the film temperature $T_f = (T_s + T_{\text{sat}})/2$. The temperatures T_s and T_{sat} are in kelvins for the evaluation of h_r . The emissivity of the metallic solids can be found from Table 17. Note that $q = hA (T_s - T_{\text{sat}})$.

Nucleate Boiling in Forced Convection

The total heat transfer rate can be obtained by simply superimposing the heat transfer due to nucleate boiling and forced convection:

$$q'' = q''_{\text{boiling}} + q''_{\text{forced convection}}$$

For forced convection, it is recommended that the coefficient 0.023 be replaced by 0.014 in the Dittus–Boelter equation (Section 2.1). The above equation is generally applicable to forced convection where the bulk liquid temperature is subcooled (*local forced convection boiling*).

Simplified Relations for Boiling in Water

For nucleate boiling,²⁹

$$h = C(\Delta T_e)^n \left(\frac{p}{p_a} \right)^{0.4}$$

where p and p_a are, respectively, the system pressure and standard atmospheric pressure. The constants C and n are listed in Table 24.

Table 24 Values of C and n for Simplified Relations for Boiling in Water

Surface	q'' (kW/m ²)	C	n
Horizontal	$q'' < 16$	1042	$\frac{1}{3}$
	$16 < q'' < 240$	5.56	$\frac{3}{4}$
Vertical	$q'' < 3$	5.7	$\frac{1}{7}$
	$3 < q'' < 63$	7.96	$\frac{3}{4}$

For *local forced convection boiling inside vertical tubes*, valid over a pressure range of 5–170 atm,³⁰

$$h = 2.54(\Delta T_e)^3 e^{p/1.551}$$

where h has the unit $\text{W}/\text{m}^2 \cdot ^\circ\text{C}$, ΔT_e is in $^\circ\text{C}$, and p is the pressure in $10^6 \text{ N}/\text{m}^3$.

4.2 Condensation

Depending on the surface conditions, the condensation may be a *film condensation* or a *dropwise condensation*. Film condensation usually occurs when a vapor, relatively free of impurities, is allowed to condense on a clean, uncontaminated surface. Dropwise condensation occurs on highly polished surfaces or on surfaces coated with substances that inhibit wetting. The condensate provides a resistance to heat transfer between the vapor and the surface. Therefore, it is desirable to use short vertical surfaces or horizontal cylinders to prevent the condensate from growing too thick. The heat transfer rate for dropwise condensation is usually an order of magnitude larger than that for film condensation under similar conditions. Silicones, Teflon, and certain fatty acids can be used to coat the surfaces to promote dropwise condensation. However, such coatings may lose their effectiveness owing to oxidation or outright removal. Thus, except under carefully controlled conditions, film condensation may be expected to occur in most instances, and the condenser design calculations are often based on the assumption of film condensation.

For condensation on surface at temperature T_s the total heat transfer rate to the surface is given by $q = \bar{h}_L A (T_{\text{sat}} - T_s)$, where T_{sat} is the saturation temperature of the vapor. The mass flow rate is determined by $\dot{m} = q/h_{fg}$; h_{fg} is the latent heat of vaporization of the fluid (see Table 25 for saturated water). Correlations are based on the evaluation of liquid properties at $T_f = (T_s + T_{\text{sat}})/2$, except h_{fg} , which is to be taken at T_{sat} .

Film Condensation on a Vertical Plate

The Reynolds number for *condensate flow* is defined by $\text{Re}_\Gamma = \rho_l V_m D_h / \mu_l$, where ρ_l and μ_l are the density and viscosity of the liquid, V_m is the average velocity of condensate, and D_h is the hydraulic diameter defined by $D_h = 4 \times$ condensate film cross-sectional area/wetted perimeter. For the condensation on a vertical plate $\text{Re}_\Gamma = 4\Gamma/\mu_l$, where Γ is the mass flow rate of condensate per unit width evaluated at the lowest point on the condensing surface. The condensate flow is generally considered to be laminar for $\text{Re}_\Gamma < 1800$, and turbulent for $\text{Re}_\Gamma > 1800$. The average Nusselt number is given by³¹

$$\begin{aligned} \bar{\text{Nu}}_L &= 1.13 \left[\frac{g\rho_l(\rho_l - \rho_v)h_{fg}L^3}{\mu_l k_l (T_{\text{sat}} - T_s)} \right]^{0.25} && \text{for } \text{Re}_\Gamma < 1800 \\ \bar{\text{Nu}}_L &= 0.0077 \left[\frac{g\rho_l(\rho_l - \rho_v)L^3}{\mu_l^2} \right]^{1/3} \text{Re}_\Gamma^{0.4} && \text{for } \text{Re}_\Gamma > 1800 \end{aligned}$$

Film Condensation on the Outside of Horizontal Tubes and Tube Banks

$$\bar{\text{Nu}}_D = 0.725 \left[\frac{g\rho_l(\rho_l - \rho_v)h_{fg}D^3}{N\mu_l k_l (T_{\text{sat}} - T_s)} \right]^{0.25}$$

where N is the number of horizontal tubes placed one above the other; $N = 1$ for a single tube.³²

Table 25 Thermophysical Properties of Saturated Water

Temperature, T (K)	Pressure, P (bar) ^a	Specific Volume (m ³ /kg)		Heat of Vaporization, h_{fg} (kJ/kg)	Specific Heat (kJ/kg · K)		Viscosity (N · sec/m ²)	Thermal Conductivity (W/m · K)		Prandtl Number	Surface Tension $\sigma_l \times 10^3$ (N/m)	Expansion Coefficient, $\beta_l \times 10^6$ (K ⁻¹)	
		$v_f \times 10^3$	v_u		$C_{p,l}$	$C_{p,u}$		$k_l \times 10^3$	$k_v \times 10^3$				Pr_l
273.15	0.00611	1.000	206.3	2502	4.217	1.854	1750	659	18.2	12.99	0.815	75.5	-68.05
300	0.03531	1.003	39.13	2438	4.179	1.872	855	613	19.6	5.83	0.857	71.7	276.1
320	0.1053	1.011	13.98	2390	4.180	1.895	577	640	21.0	3.77	0.894	68.3	436.7
340	0.2713	1.021	5.74	2342	4.188	1.930	420	660	22.3	2.66	0.925	64.9	566.0
360	0.6209	1.034	2.645	2291	4.203	1.983	324	674	23.7	2.02	0.960	61.4	697.9
380	1.2869	1.049	1.337	2239	4.226	2.057	260	683	25.4	1.61	0.999	57.6	788
400	2.455	1.067	0.731	2183	4.256	2.158	217	688	27.2	1.34	1.033	63.6	896
450	9.319	1.123	0.208	2024	4.40	2.56	152	678	33.1	0.99	1.14	42.9	
500	26.40	1.203	0.0766	1825	4.66	3.27	118	642	42.3	0.86	1.28	31.6	
550	61.19	1.323	0.0317	1564	5.24	4.64	97	580	58.3	0.87	1.47	19.7	
600	123.5	1.541	0.0137	1176	7.00	8.75	81	497	92.9	1.14	2.15	8.4	
647.3	221.2	3.170	0.0032	0	∞	∞	45	238	238	∞	∞	0.0	

Film Condensation Inside Horizontal Tubes

For low vapor velocities such that Re_D based on the vapor velocities at the pipe inlet is less than 3500³³

$$\overline{Nu}_D = 0.555 \left[\frac{g\rho_l(\rho_l - \rho_v)h'_{fg}D^3}{\mu_l k_l (T_{sat} - T_s)} \right]^{0.25}$$

where $h'_{fg} + \frac{3}{8}C_{p,l}(T_{sat} - T_s)$. For higher flow rate,³⁴ $Re_G > 5 \times 10^4$,

$$\overline{Nu}_D = 0.0265 Re_G^{0.8} Pr^{1/3}$$

where the Reynolds number $Re_G = GD/\mu_l$ is based on the equivalent mass velocity $G = G_l + G_v(\rho_l/\rho_v)^{0.5}$. The mass velocity for the liquid G_l and that for vapor G_v are calculated as if each occupied the entire flow area.

The Effect of Noncondensable Gases

If noncondensable gas such as air is present in a vapor, even in a small amount, the heat transfer coefficient for condensation may be greatly reduced. It has been found that the presence of a few percent of air by volume in steam reduces the coefficient by 50% or more. Therefore, it is desirable in the condenser design to vent the noncondensable gases as much as possible.

4.3 Heat Pipes

Heat pipes are two-phase heat transfer devices that operate on a closed two-phase cycle³⁵ and come in a wide variety of sizes and shapes.^{36,37} As shown in Fig. 31, they typically consist of three distinct regions, the evaporator or heat addition region, the condenser or heat rejection region, and the adiabatic or isothermal region. Heat added to the evaporator region of the container causes the working fluid in the evaporator wicking structure to be vaporized. The high temperature and corresponding high pressure in this region result in flow of the vapor to

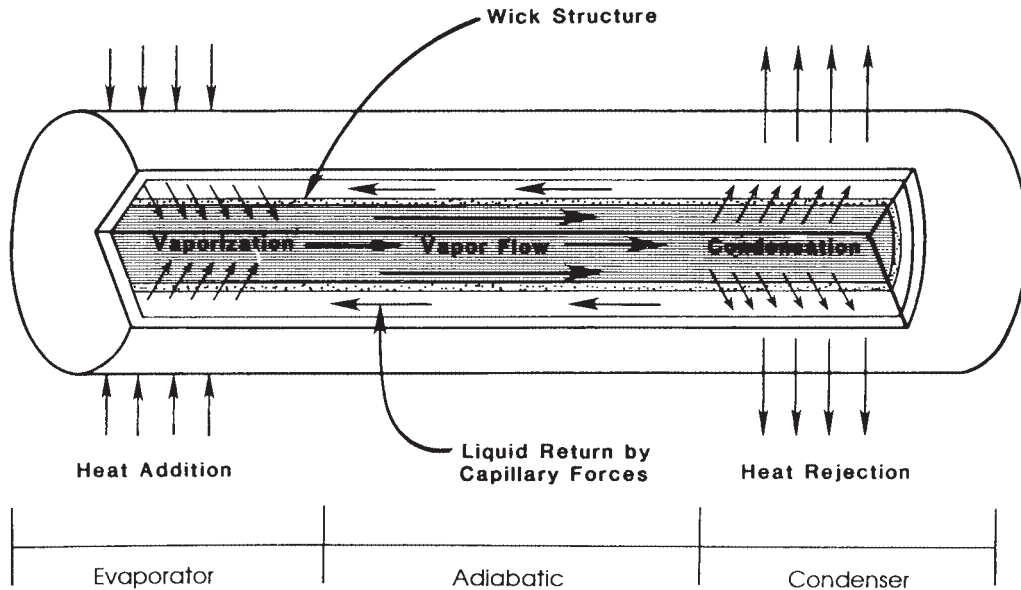


Figure 31 Typical heat pipe construction and operation.³⁸ From "Effective Thermal Conductivity of Sintered Heat Pipe Wicks," by G.P. Peterson and L.S. Fletcher; reprinted by permission of the American Institute of Aeronautics and Astronautics, Inc.

the other, cooler end of the container where the vapor condenses, giving up its latent heat of vaporization. The capillary forces existing in the wicking structure then pump the liquid back to the evaporator section. Other similar devices, referred to as two-phase thermosyphons, have no wick and utilize gravitational forces to provide the liquid return. Thus, the heat pipe functions as a nearly isothermal device, adjusting the evaporation rate to accommodate a wide range of power inputs, while maintaining a relatively constant source temperature.

Transport Limitations

The transport capacity of a heat pipe is limited by several important mechanisms. Among these are the capillary wicking limit, viscous limit, sonic limit, entrainment, and boiling limits. The capillary wicking limit and viscous limits deal with the pressure drops occurring in the liquid and vapor phases, respectively. The sonic limit results from the occurrence of choked flow in the vapor passage, while the entrainment limit is due to the high liquid vapor shear forces developed when the vapor passes in counterflow over the liquid saturated wick. The boiling limit is reached when the heat flux applied in the evaporator portion is high enough that nucleate boiling occurs in the evaporator wick, creating vapor bubbles that partially block the return of fluid.

To function properly, the net capillary pressure difference between the condenser and the evaporator in a heat pipe must be greater than the pressure losses throughout the liquid and vapor flow paths. This relationship can be expressed as

$$\Delta P_c \geq \Delta P_+ + \Delta P_- + \Delta P_l + \Delta P_v$$

where

- ΔP_c = net capillary pressure difference
- ΔP_+ = normal hydrostatic pressure drop
- ΔP_- = axial hydrostatic pressure drop
- ΔP_l = viscous pressure drop occurring in the liquid phase
- ΔP_v = viscous pressure drop occurring in the vapor phase

If these conditions are not met, the heat pipe is said to have reached the *capillary limitation*.

Expressions for each of these terms have been developed for steady-state operation, and are summarized below.

$$\text{Capillary pressure } \Delta P_{c,m} = \left(\frac{2\sigma}{r_{c,e}} \right)$$

Values for the effective capillary radius, r_c , can be found theoretically for simple geometries or experimentally for pores or structures of more complex geometry. Table 26 gives values for some common wicking structures.

Table 26 Expressions for the Effective Capillary Radius for Several Wick Structures

Structure	r_c	Data
Circular cylinder (artery or tunnel wick)	r	r = radius of liquid flow passage
Rectangular groove	ω	ω = groove width
Triangular groove	$\omega / \cos \beta$	ω = groove width β = half-included angle
Parallel wires	ω	ω = wire spacing
Wire screens	$(\omega + d_\omega) / 2 = \frac{1}{2}N$	d = wire diameter N = screen mesh number
		ω = wire spacing
Packed spheres	$0.41r_s$	r_s = sphere radius

Table 27 Wick Permeability for Several Wick Structures

Structure	K	Data
Circular cylinder (artery or tunnel wick)	$r^2/8$	r = radius of liquid flow passage
Open rectangular grooves	$2\varepsilon(r_{h,l})^2/(f_l Re_l) = \omega/s$	ε = wick porosity ω = groove width s = groove pitch δ = groove depth $(r_{h,l}) = 2\omega\delta/(\omega + 2\delta)$
Circular annular wick	$2(r_{h,l})^2/(f_l Re_l)$	$(r_{h,l}) = r_1 - r_2$
Wrapped screen wick	$1/122d_\omega^2\varepsilon^3/(1 - \varepsilon)^2$	d_ω = wire diameter $\varepsilon = 1 - (1.05\pi N d_\omega/4)$ N = mesh number
Packed sphere	$1/37.5r_s^2\varepsilon^3/(1 - \varepsilon)^2$	r_s = sphere radius ε = porosity (dependent on packing mode)

Normal and axial hydrostatic pressure drop $\Delta P_+ = \rho_l g d_v \cos \psi$

$$\Delta P_- = \rho_l g L \sin \psi$$

In a gravitational environment, the axial hydrostatic pressure term may either assist or hinder the capillary pumping process, depending on whether the tilt of the heat pipe promotes or hinders the flow of liquid back to the evaporator (i.e., the evaporator lies either below or above the condenser). In a zero- g environment, both this term and the normal hydrostatic pressure drop term can be neglected because of the absence of body forces:

$$\text{Liquid pressure drop } \Delta P_l = \left(\frac{\mu_l}{KA_w h_{fg} \rho_l} \right) L_{\text{eff}} q$$

where L_{eff} is the effective heat pipe length defined as

$$L_{\text{eff}} = 0.5L_e + L_a + 0.5L_c$$

and K is the liquid permeability as shown in Table 27.

$$\text{Vapor pressure drop } \Delta P_v = \left(\frac{C (f_v Re_v) \mu_v}{2(r_{h,v})^2 A_v \rho_v h_{fg}} \right) L_{\text{eff}} q$$

Although during steady-state operation the liquid flow regime is always laminar, the vapor flow may be either laminar or turbulent. It is therefore necessary to determine the vapor flow regime as a function of the heat flux. This can be accomplished by evaluating the local axial Reynolds and Mach numbers and substituting the values as shown below:

$$Re_v < 2300, \quad Ma_v < 0.2$$

$$(f_v Re_v) = 16$$

$$C = 1.00$$

$$Re_v < 2300, \quad Ma_v > 0.2$$

$$(f_v Re_v) = 16$$

$$C = \left[1 + \left(\frac{\gamma_v - 1}{2} \right) Ma_v^2 \right]^{1/2}$$

$$Re_v > 2300, \quad Ma_v < 0.2$$

$$(f_v \text{Re}_v) = 0.038 \left[\frac{2(r_{h,v})q}{A_v \mu_v h_{fg}} \right]^{3/4}$$

$$C = 1.00$$

$$\text{Re}_v > 2300, \quad \text{Ma}_v > 0.2$$

$$(f_v \text{Re}_v) = 0.038 \left[\frac{2(r_{h,v})q}{A_v \mu_v h_{fg}} \right]^{3/4}$$

$$C = \left[1 + \left(\frac{\gamma_v - 1}{2} \right) \text{Ma}_v^2 \right]^{-1/2}$$

Since the equations used to evaluate both the Reynolds number and the Mach number are functions of the heat transport capacity, it is necessary to first assume the conditions of the vapor flow. Using these assumptions, the maximum heat capacity, $q_{c,m}$, can be determined by substituting the values of the individual pressure drops into Eq. (1) and solving for $q_{c,m}$. Once the value of $q_{c,m}$ is known, it can then be substituted into the expressions for the vapor Reynolds number and Mach number to determine the accuracy of the original assumption. Using this iterative approach, accurate values for the capillary limitation as a function of the operating temperature can be determined in units of $\text{W} \cdot \text{m}$ or watts for $(qL)_{c,m}$ and $q_{c,m}$, respectively.

The *viscous limitation* in heat pipes occurs when the viscous forces within the vapor region are dominant and limit the heat pipe operation:

$$\frac{\Delta P_v}{P_v} < 0.1$$

for determining when this limit might be of a concern. Due to the operating temperature range, this limitation will normally be of little consequence in the design of heat pipes for use in the thermal control of electronic components and devices.

The *sonic limitation* in heat pipes is analogous to the sonic limitation in a converging–diverging nozzle and can be determined from

$$q_{s,m} = A_v \rho_v h_{fg} \left[\frac{\gamma_v R_v T_v}{2(\gamma_v + 1)} \right]^{1/2}$$

where T_v is the mean vapor temperature within the heat pipe.

Since the liquid and vapor flow in opposite directions in a heat pipe, at high enough vapor velocities, liquid droplets may be picked up or entrained in the vapor flow. This entrainment results in excess liquid accumulation in the condenser and, hence, dryout of the evaporator wick. Using the Weber number, We , defined as the ratio of the viscous shear force to the force resulting from the liquid surface tension, an expression for the *entrainment limit* can be found as

$$q_{e,m} = A_v h_{fg} \left[\frac{\sigma \rho_v}{2(r_{h,w})} \right]^{1/2}$$

where $(r_{h,w})$ is the hydraulic radius of the wick structure, defined as twice the area of the wick pore at the wick–vapor interface divided by the wetted perimeter at the wick–vapor interface.

The *boiling limit* occurs when the input heat flux is so high that nucleate boiling occurs in the wicking structure and bubbles may become trapped in the wick, blocking the liquid return and resulting in evaporator dryout. This phenomenon, referred to as the boiling limit, differs from the other limitations previously discussed in that it depends on the evaporator heat flux as

opposed to the axial heat flux. This expression, which is a function of the fluid properties, can be written as

$$q_{b,m} = \left[\frac{2\pi L_{\text{eff}} k_{\text{eff}} T_v}{h_{fg} \rho_v \ln(r_i/r_n)} \right] \left(\frac{2\sigma}{r_n} - \Delta P_{c,m} \right)$$

where k_{eff} is the effective thermal conductivity of the liquid–wick combination, given in Table 28, r_i is the inner radius of the heat pipe wall, and r_n is the nucleation site radius. After the power level associated with each of the four limitations is established, determination of the maximum heat transport capacity is only a matter of selecting the lowest limitation for any given operating temperature.

Heat Pipe Thermal Resistance

The *heat pipe thermal resistance* can be found using an analogous electrothermal network. Figure 32 illustrates the electrothermal analog for the heat pipe illustrated in Fig. 31.

Table 28 Effective Thermal Conductivity for Liquid-Saturated Wick Structures

Wick Structures	k_{eff}
Wick and liquid in series	$\frac{k_l k_w}{\epsilon k_w + k_l(1 - \epsilon)}$
Wick and liquid in parallel	$\epsilon k_l + k_w(1 - \epsilon)$
Wrapped screen	$\frac{k_l[(k_l + k_w) - (1 - \epsilon)(k_l - k_w)]}{(k_l + k_w) + (1 - \epsilon)(k_l - k_w)}$
Packed spheres	$\frac{k_l[(2k_l + k_w) - 2(1 - \epsilon)(k_l - k_w)]}{(2k_l + k_w) + (1 - \epsilon)(k_l - k_w)}$
Rectangular grooves	$\frac{(w_f k_f k_w \delta) + w k_l (0.185 w_f k_w + \delta k_l)}{(w + w_f)(0.185 w_f k_f + \delta k_l)}$

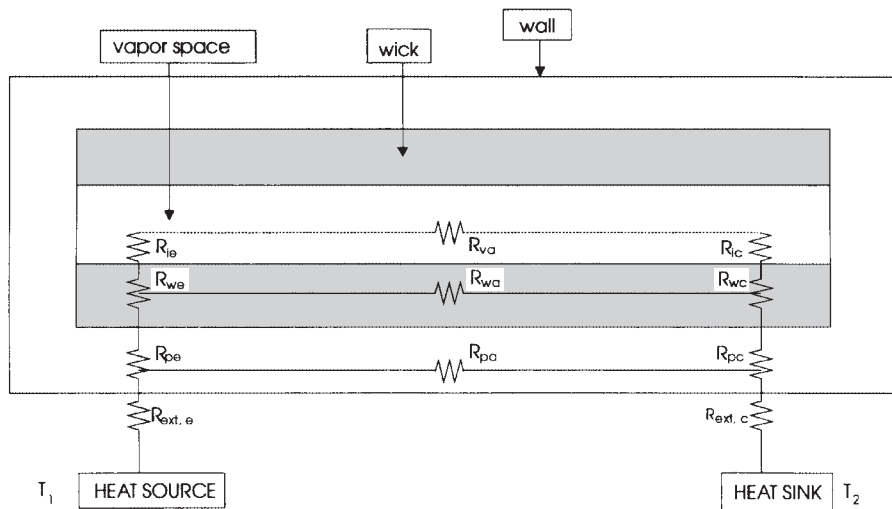


Figure 32 Equivalent thermal resistance of a heat pipe.

As shown, the overall thermal resistance is composed of nine different resistances arranged in a series/parallel combination, which can be summarized as follows:

R_{pe}	The radial resistance of the pipe wall at the evaporator
R_{we}	The resistance of the liquid–wick combination at the evaporator
R_{ie}	The resistance of the liquid–vapor interface at the evaporator
R_{ya}	The resistance of the adiabatic vapor section
R_{pa}	The axial resistance of the pipe wall
R_{wa}	The axial resistance of the liquid–wick combination
R_{ic}	The resistance of the liquid–vapor interface at the condenser
R_{wc}	The resistance of the liquid–wick combination at the condenser
R_{pc}	The radial resistance of the pipe wall at the condenser

Because of the comparative magnitudes of the resistance of the vapor space and the axial resistances of the pipe wall and liquid–wick combinations, the axial resistance of both the pipe wall and the liquid–wick combination may be treated as open circuits and neglected. Also, because of the comparative resistances, the liquid–vapor interface resistances and the axial vapor resistance can, in most situations, be assumed to be negligible. This leaves only the pipe wall radial resistances and the liquid–wick resistances at both the evaporator and condenser. The radial resistances at the pipe wall can be computed from Fourier’s law as

$$R_{pe} = \frac{\delta}{k_p A_e}$$

for flat plates, where δ is the plate thickness and A_e is the evaporator area, or

$$R_{pe} = \frac{\ln(D_o/D_i)}{2\pi L_e k_p}$$

for cylindrical pipes, where L_e is the evaporator length. An expression for the equivalent thermal resistance of the liquid–wick combination in circular pipes is

$$R_{we} = \frac{\ln(D_o/D_i)}{2\pi L_e k_{\text{eff}}}$$

where values for the effective conductivity, k_{eff} , can be found in Table 28. The adiabatic vapor resistance, although usually negligible, can be found as

$$R_{va} = \frac{T_v(P_{v,e} - P_{v,c})}{\rho_v h_{fg} q}$$

where $P_{v,e}$ and $P_{v,c}$ are the vapor pressures at the evaporator and condenser. Combining these individual resistances provides a mechanism by which the overall thermal resistance can be computed and hence the temperature drop associated with various axial heat fluxes can be computed.

REFERENCES

1. F. P. Incropera and D. P. Dewitt, *Fundamentals of Heat Transfer*, Wiley, New York, 1981.
2. E. R. G. Eckert and R. M. Drake, Jr., *Analysis of Heat and Mass Transfer*, McGraw-Hill, New York, 1972.
3. M. P. Heisler, “Temperature Charts for Induction and Constant Temperature Heating,” *Trans. ASME*, **69**, 227, 1947.
4. H. Grober and S. Erk, *Fundamentals of Heat Transfer*, McGraw-Hill, New York, 1961.
5. A. B. Duncan, and G. P. Peterson, “A Review of Microscale Heat Transfer,” Invited Review Article, *Appl. Mech. Rev.*, **47**(9), 397–428, 1994.

6. C. L. Tien, B. F. Armaly, and P. S. Jagannathan, "Thermal Conductivity of Thin Metallic Films," Proc. 8th Conference on Thermal Conductivity, October 7–10, 1968.
7. C. Bai and A. S. Lavine, "Thermal Boundary Conditions for Hyperbolic Heat Conduction," *ASME HTD*, **253**, 37–44, 1993.
8. E. N. Sieder and C. E. Tate, "Heat Transfer and Pressure Drop of Liquids in Tubes," *Ind. Eng. Chem.*, **28**, 1429, 1936.
9. F. W. Dittus and L. M. K. Baelter, *Univ. Calif., Berkeley, Pub. Eng.*, **2**, 443, 1930.
10. A. J. Chapman, *Heat Transfer*, Macmillan, New York, 1974.
11. S. Whitaker, *AIChE J.*, **18**, 361, 1972.
12. M. Jakob, *Heat Transfer*, Vol. 1, Wiley, New York, 1949.
13. A. Zhukauska, "Heat Transfer from Tubes in Cross Flow," in J. P. Hartnett and T. F. Irvine, Jr. (Eds.), *Advances in Heat Transfer*, Vol. 8, Academic, New York, 1972.
14. F. Kreith, *Principles of Heat Transfer*, Harper & Row, New York, 1973.
15. H. A. Johnson and M. W. Rubesin, "Aerodynamic Heating and Convective Heat Transfer," *Trans. ASME*, **71**, 447, 1949.
16. C. C. Lin (Ed.), *Turbulent Flows and Heat Transfer, High Speed Aerodynamics and Jet Propulsion*, Vol. V, Princeton University Press, Princeton, NJ, 1959.
17. W. H. McAdams, *Heat Transmission*, McGraw-Hill, New York, 1954.
18. T. Yuge, "Experiments on Heat Transfer from Spheres Including Combined Natural and Forced Convection," *J. Heat Transfer*, **82**, 214, 1960.
19. S. Globe and D. Dropkin, "Natural Convection Heat Transfer in Liquids Confined between Two Horizontal Plates," *J. Heat Transfer*, **81C**, 24, 1959.
20. I. Catton, "Natural Convection in Enclosures," Proc. 6th International Heat Transfer Conference, 6, Toronto, Canada, 1978.
21. R. K. MacGregor and A. P. Emery, "Free Convection through Vertical Plane Layers: Moderate and High Prandtl Number Fluids," *J. Heat Transfer*, **91**, 391, 1969.
22. R. Siegel and J. R. Howell, *Thermal Radiation Heat Transfer*, McGraw-Hill, New York, 1981.
23. G. G. Gubareff, J. E. Janssen, and R. H. Torborg, *Thermal Radiation Properties Survey*, 2nd ed., Minneapolis Honeywell Regulator Co., Minneapolis, MN, 1960.
24. J. P. Holman, *Heat Transfer*, McGraw-Hill, New York, 1981.
25. H. C. Hottel, in *Heat Transmission*, W. C. McAdams (Ed.), McGraw-Hill, New York, 1954, Chapter. 2.
26. W. M. Rohsenow, "A Method of Correlating Heat Transfer Data for Surface Boiling Liquids," *Trans. ASME*, **74**, 969, 1952.
27. N. Zuber, "On the Stability of Boiling Heat Transfer," *Trans. ASME*, **80**, 711, 1958.
28. L. A. Bromley, "Heat Transfer in Stable Film Boiling," *Chem. Eng. Prog.*, **46**, 221, 1950.
29. M. Jakob and G. A. Hawkins, *Elements of Heat Transfer*, Wiley, New York, 1957.
30. M. Jakob, *Heat Transfer*, Vol. 2, Wiley, New York, 1957, p. 584.
31. W. H. McAdams, *Heat Transmission*, 3rd ed., McGraw-Hill, New York, 1954.
32. W. M. Rohsenow, "Film Condensation" in W. M. Rohsenow and J. P. Hartnett (Eds.), *Handbook of Heat Transfer*, McGraw-Hill, New York, 1973.
33. J. C. Chato, "Laminar Condensation inside Horizontal and Inclined Tubes," *ASHRAE J.*, **4**, 52, 1962.
34. W. W. Akers, H. A. Deans, and O. K. Crosser, "Condensing Heat Transfer within Horizontal Tubes," *Chem. Eng. Prog., Sym. Ser.*, **55**(29), 171, 1958.
35. G. P. Peterson, *An Introduction to Heat Pipes: Modeling, Testing and Applications*, Wiley, New York, 1994.
36. G. P. Peterson, A. B. Duncan, and M. H. Weichold, "Experimental Investigation of Micro Heat Pipes Fabricated in Silicon Wafers," *ASME J. Heat Transfer*, **115**, 3, 751, 1993.
37. G. P. Peterson, "Capillary Priming Characteristics of a High Capacity Dual Passage Heat Pipe," *Chem. Eng. Commun.*, **27**, 1, 119, 1984.
38. G. P. Peterson and L. S. Fletcher, "Effective Thermal Conductivity of Sintered Heat Pipe Wicks," *AIAA J. Thermophys. Heat Transfer*, **1**(3), 36, 1987.

BIBLIOGRAPHY

- American Society of Heating, Refrigerating and Air Conditioning Engineering, *ASHRAE Handbook of Fundamentals*, ASHRAE, Atlanta, GA, 1972.
- V. S. Arpaci, *Conduction Heat Transfer*, Addison-Wesley, Reading, MA, 1966.
- H. S. Carslaw and J. C. Jager, *Conduction of Heat in Solid*, Oxford University Press, London, 1959.
- S. W. Chi, *Heat Pipe Theory and Practice*, McGraw-Hill, New York, 1976.
- J. A. Duffie and W. A. Beckman, *Solar Engineering of Thermal Process*, Wiley, New York, 1980.
- P. D. Dunn and D. A. Reay, *Heat Pipes*, 3rd ed., Pergamon Press, New York, 1983.
- B. Gebhart, *Heat Transfer*, McGraw-Hill, New York, 1971.
- H. C. Hottel and A. F. Saroffin, *Radiative Transfer*, McGraw-Hill, New York, 1967.
- W. M. Kays, *Convective Heat and Mass Transfer*, McGraw-Hill, New York, 1966.
- J. G. Knudsen and D. L. Katz, *Fluid Dynamics and Heat Transfer*, McGraw-Hill, New York, 1958.
- M. N. Ozisik, *Radiative Transfer and Interaction with Conduction and Convection*, Wiley, New York, 1973.
- M. N. Ozisik, *Heat Conduction*, Wiley, New York, 1980.
- G. P. Peterson, *An Introduction to Heat Pipes: Modeling, Testing and Applications*, Wiley, New York, 1994.
- M. Planck, *The Theory of Heat Radiation*, Dover, New York, 1959.
- W. M. Rohsenow and H. Y. Choi, *Heat, Mass, and Momentum Transfer*, Prentice-Hall, Englewood Cliffs, NJ, 1961.
- W. M. Rohsenow and J. P. Hartnett, *Handbook of Heat Transfer*, McGraw-Hill, New York, 1973.
- H. Schlichting, *Boundary-Layer Theory*, McGraw-Hill, New York, 1979.
- P. J. Schneider, *Conduction Heat Transfer*, Addison-Wesley, Reading, MA, 1955.
- E. M. Sparrow and R. D. Cess, *Radiation Heat Transfer*, Wadsworth, Belmont, CA, 1966.
- C. L. Tien, "Fluid Mechanics of Heat Pipes," *Annu. Rev. Fluid Mech.*, **167**, 1975.
- W. C. Turner and J. F. Malloy, *Thermal Insulation Handbook*, McGraw-Hill, New York, 1981.
- N. B. Vargafik, *Table of Thermophysical Properties of Liquids and Gases*, Hemisphere, Washington, DC, 1975.
- J. A. Wiebelt, *Engineering Radiation Heat Transfer*, Holt, Rinehart & Winston, New York, 1966.

CHAPTER 6

TEMPERATURE MEASUREMENT

Peter R. N. Childs
Imperial College
London, United Kingdom

1 INTRODUCTION	247	4 SEMI-INVASIVE METHODS	272
1.1 Measurement Process	248	4.1 Peak-Temperature-Indicating Devices	272
1.2 Calibration	249	4.2 Temperature-Sensitive Paints	273
2 SELECTION	250	4.3 Thermographic Phosphors	273
3 INVASIVE TEMPERATURE MEASUREMENT	251	4.4 Thermochromic Liquid Crystals	274
3.1 Liquid-in-Glass Thermometers	252	5 NONINVASIVE METHODS	275
3.2 Manometric Thermometry	253	5.1 Infrared Thermometry	275
3.3 Bimetallic Thermometers	254	5.2 Thermal Imaging	278
3.4 Thermocouples	255	6 CONCLUSIONS	279
3.5 Resistance Temperature Devices	267	REFERENCES	281
3.6 Semiconductor Devices	270		
3.7 Diode Thermometers	271		
3.8 Noise Thermometry	271		
3.9 Pyrometric Cones	271		

1 INTRODUCTION

Temperature can be defined qualitatively as a measure of hotness of a body. Temperature is the property that determines whether a system is in thermal equilibrium with other systems. If the temperature of two bodies in thermal contact with each other is the same, then there will be no net transfer of thermal energy. Quantitatively temperature can be defined from the second law of thermodynamics in terms of the rate of change of entropy with energy.

To allow the assignment of numerical values to bodies at different temperatures, some form of temperature scale is necessary. The SI unit of the thermodynamic temperature scale is Kelvin, with symbol K. This is defined in terms of the interval between absolute zero, 0 K, and the triple point of pure water, 273.16 K. Kelvin is defined as the fraction 1/273.16 of the temperature of a system exhibiting the triple point of water. Other temperature units are also in common use, including the Celsius, Fahrenheit, and Rankine temperature scales. Conversion equations for these are given as

$$t = T - 273.15 \quad (1)$$

$$T_{\circ_F} = 1.8t + 32 \quad (2)$$

$$T_{\circ_R} = T_{\circ_F} + 459.67 \quad (3)$$

where t = temperature in degrees Celsius ($^{\circ}\text{C}$)
 T = absolute temperature (K)
 T_{F} = temperature in degrees Fahrenheit ($^{\circ}\text{F}$)
 T_{R} = temperature in the Rankine scale ($^{\circ}\text{R}$)

The thermodynamic temperature scale is defined by means of theoretically perfect heat engines. These are not practically realizable, and the International Temperature Scale of 1990 (see Ref. 1), denoted by ITS-90, was developed as a practical best approximation using available technologies to the thermodynamic temperature scale. Its range of application extends from 0.65 K up to the highest temperature practically measurable using Planck's law of thermal radiation. The ITS-90 is believed to represent thermodynamic temperature to within ± 2 mK from 2 to 273 K, ± 3.5 mK at 730 K, and ± 7 mK at 900 K (one standard deviation limit; see Ref. 2). The ITS-90 is constructed using a number of overlapping temperature ranges. This leads to some ambiguity, albeit small, in the true value of a temperature across an overlapping region but allows greater flexibility in the use of the scale. The ranges are defined between repeatable conditions using a variety of specified materials at their melting, freezing, and triple points. The ITS-90 was developed under the auspices of the Metric Treaty and the associated consultative committees, BIPM (Bureau International des Poids et Mesures), CIPM (Comité International des Poids et Mesures), and CCT (Comité Consultatif de Thermométrie) and was adopted by the International Committee of Weights and Measures in 1989.

The principal role of the ITS-90 in practical measurement is to allow a means of traceability between the measurement that is actually made and the temperature scale defined by the ITS-90. Thermometers or systems used in defining the ITS-90 are unlikely to be used to measure the temperature of a system of interest. Instead a thermometer can be used that has been calibrated against another device calibrated using guidelines specified in ITS-90. Calibration is the process of relating the output value from a measurement system to a known input value. The schematic given in Fig. 1 illustrates this process whereby there is a transfer of calibration between practical and specialist devices. The chain between the thermometer in use and the ITS-90 may in practice have more links than those shown in the diagram, each link tending to increase the uncertainty associated with the measurement.

1.1 Measurement Process

A measurement provides information about a property and gives magnitude to that property. Temperature can be measured by observing physical phenomena that are temperature dependent. This may involve inserting a probe containing a transducer into the medium of interest and relating the observed effect on the transducer to temperature. A measurement

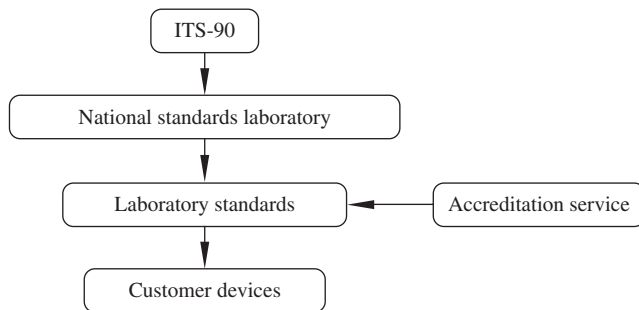


Figure 1 Traceability between customer devices and ITS-90.

system may comprise a transducer to convert a temperature-dependent phenomenon into a signal that is a function of that temperature, a method to transmit the signal from the transducer, some form of signal processing, and a display and method of recording the data. In a given application some of these functions such as data recording may be undertaken by the sensor system itself or by a human operator. A calibration is used to convert the measured quantity into a value of temperature. The significance of temperature can then be considered. The related subject of heat flux measurement is reviewed by Childs et al.³

Whenever a measurement is made, it is unlikely that the measured value will equal the true value, the actual or exact value of the measured variable. The difference between the measured value and the true value is the error. There are a number of reasons why a measured value will not equal the true value, and many of these can be inferred by considering the measurement process. The insertion of a transducer, or sometimes even thermal interactions between a remote sensor and an application, will result in disturbance to the temperature distribution in an application. The magnitude of this disturbance will depend on the heat transfer processes involved. Natural instabilities associated with the transducer and signal-measuring devices also contribute to a deviation between the true and measured values. Further deviations between the measured and true values are due to the processing of the signal and data and uncertainties arising from the calibration process.

1.2 Calibration

Calibration can be achieved in a number of ways. The sensor to be calibrated can be placed in an environment at a known temperature such as one of the fixed points, for example, the triple point of water. The output from the sensor can be recorded and, within the uncertainties associated with the temperature of the fixed point, taken as an indication of that temperature. The sensor can then be exposed to a different temperature using a different fixed point, for example, the melting point of gallium, and the process repeated. For intermediate values of temperature between the fixed points, the special interpolation equations documented in the ITS-90 can be used. The process described so far is appropriate for producing a sensor with very low uncertainty capability. This, however, is an expensive undertaking and is rarely necessary for the majority of scientific and industrial applications. Instead, a sensor that has been calibrated in this way and is stable is used to calibrate another sensor by comparison. The calibrated and uncalibrated sensors are placed in thermal contact in an enclosure such as a bath of liquid or in a specially constructed heating block or furnace. The medium is heated and the output of both the calibrated and the uncalibrated sensor is recorded. The output from the uncalibrated sensor can then be related to the temperature indicated by the calibrated sensor. In this way a transfer between values of temperatures set up in the ITS-90 and sensors used in practice can be achieved as illustrated schematically in Fig. 1. It is normally recommended that there should be no more than three or four links between a practical measurement and the ITS-90. The details of the calibration process depend partly on the type of sensor concerned typically involving established procedures for record keeping, inspection and conditioning of the sensor, generic checks, intercomparison either with another sensor or with a medium at a known temperature, analysis of the data, quantification of uncertainties, and completion of records.

Traceability involves ensuring that appropriate procedures have been followed, and in the current industrial setting, this is typically associated with quality standards. Two approaches can be adopted. The first involves following a set of standards and obtaining the appropriate approval and registration certificates for that quality system. The second approach is to accept the principles of the process commended within quality standards and to follow them closely to be able to state that the spirit of the standard has been followed. This latter approach negates the need for registration to a standards system but does require a level of trust.

The difference between a measurement and the true value of temperature is known as the error. The term *uncertainty* can be used to quantify confidence in the measurement indicated by a sensor. For instance, a sensor may be supplied with a 95% confidence interval uncertainty of $\pm 1.5^\circ\text{C}$. This means that, provided the device does not disturb the temperature distribution in the medium of interest, measurements made will be within 1.5°C of the true value for 95% of the measurements made. The term uncertainty is used in preference to *accuracy* as the latter should generally be reserved for qualitative use. The subject of measurement uncertainty is addressed comprehensively by Figliola and Beasley.⁴

2 SELECTION

The selection of a specific sensor or system for temperature measurement can require consideration of a number of aspects, including:

- Uncertainty
- Temperature range
- Thermal disturbance
- Level of contact
- Size of the sensor
- Transient response
- Sensor protection
- Availability
- Cost

For many applications there is often more than one method that will provide an adequate determination of temperature. A key consideration is application, whether the measurement is of a liquid, gas, solid body, or surface.

The measurement of temperature of a solid material can be achieved in several ways. A transducer can be embedded in the material by forming a hole, inserting the device, and, in the case of an electrically based transducer, feeding the wires out through the drill hole. This method can also be used for liquid-in-glass or bimetallic thermometers where the stem of a device is inserted to a specific depth bringing the transducer into thermal contact with the region of interest. In the case of a liquid-in-glass thermometer the device may have to be removed from the application in order to reveal the scale to enable the temperature to be read against the scale. It is important that the transducer is in good thermal contact with the solid body in order to ensure that the transducer takes up the local temperature. Thermal contact can be improved in some cases by filling the hole or pocket with high-thermal-conductivity oil or other liquid, which will provide a much better conduction path than if a gas is filling the space between the probe and the hole walls. Errors arising from the effects of unwanted heat conduction along the connecting wires or the presence of the probe should be minimized, subject to the requirements of the measurement.

Surface temperatures can be measured by attaching a sensor to the surface, drilling or forming a channel on the underside of the surface and attaching a sensor, applying a temperature-sensitive paint to the surface, or observing the surface remotely using, say, an infrared thermometer. For approximate assessment of surface temperature, bimetallic thermometers are available with flat bases, spring clips, and permanent magnets. However, if a substantial temperature difference exists between the surface and the immediate surroundings, uncertainties can arise. Thermocouples, platinum resistance thermometers, or thermistors equipped with flat or suitably formed pads can also be considered. To obtain the

best uncertainty with applied probes it is usually advantageous if they are small and perhaps also recessed in shallow grooves. An alternative method of surface temperature measurement is the noninvasive techniques of infrared radiation or thermal imaging. These techniques may be more expensive to implement. At the other end of the scale there is frequently a need to obtain a quick and uncomplicated way of checking the temperature of a surface. Temperature-indicating paints can be applied very readily to provide an indication of the temperatures that are being encountered. The measurement of the temperature of a surface that is in thermal contact with a gas and also exchanging thermal radiation with its surroundings is subject to a series of processes that could contribute to deviations between the measured temperature and that of the undisturbed object.

The measurement of liquid temperatures usually involves using a transducer that is immersed in the liquid. If a simple visual indication is required, a liquid-in-glass thermometer can be considered. Extremely low uncertainty is possible with an appropriate, calibrated instrument. If a larger indicator is required, a bimetallic thermometer might be suitable. Bimetallic thermometers are robust and self-contained. However, in many cases an electrical signal is required for processing, recording, or controlling purposes. Electrically based devices include thermocouples and resistance thermometers. The actual device will be dependent on the temperature range and the precision required. If the temperatures are changing with time, the response characteristics of the sensor and system must be adequate. Thermocouples or resistance temperature detectors will probably be the best choice if a particularly rapid response is needed. Infrared thermometers can be used to measure the surface temperature of molten materials such as metals and glass.

Many of the considerations that influence the measurement of liquid temperatures also apply to measuring the temperature of a body of gas. If the gas is moving, then there is potential for heat transfer due to conduction along the sensing probe, connection wires, and supports, which can lead to significant errors, unless accounted for. In addition, if the gas is at a different temperature to the surrounding surfaces, then thermal radiation exchanges will occur between the sensor and surfaces, again leading to a deviation between the indicated temperature and the gas temperature unless accounted for. High gas velocities can give rise to dynamic heating with an immersed sensor and due allowance must be made for this effect. For simple, isolated measurements, liquid-in-glass or bimetallic thermometers may well be suitable. If electrical signals are required, the choice again lies between thermocouples, platinum resistance thermometers, thermistors, or transistor instruments. If protection has to be added, the increase in thermal mass and thermal resistance will tend to degrade the response of the sensor more seriously in a gas than in a liquid. For some gas temperature measurements, generally associated with combustion processes, it may be undesirable or impossible to use conventional sensors and cooled devices or a noninvasive technique may be suitable.

An indication of the temperature range of a variety of methods is given in Table 1.

3 INVASIVE TEMPERATURE MEASUREMENT

One option for measuring temperature is to locate the sensor in the medium of interest or on its surface. The sensor will, due to its presence, alter the distribution of temperature within the medium. This is due to differences in the thermal conductivity and heat capacity of the sensing device and the medium of interest. As a result, the installation of a sensor in or on a solid or fluid can be classified as invasive. A wide range of invasive sensors are available, including liquid-in-glass thermometers, manometric thermometers, bimetallic thermometers, thermocouples, resistance temperature devices such as platinum resistance thermometers (PRTs) and thermistors, noise thermometers, and pyrometric cones. These are described in Sections 3.1–3.7.

Table 1 Approximate Temperature Measurement Range Capabilities for Different Methods

Method	Minimum Temperature (°C)	Maximum Temperature (°C)
Gas thermometer	about -269	700
Liquid-in-glass thermometer	-200	600
Bimetallic thermometer	-73	540
Thermocouple	-270	2300
Electrical resistance device	-260	1064
Thermistors	-100	700
Semiconductor devices	-272	300
Fiber-optic probes	-200	2000
Capacitance	-272	-170
Noise	-273	1500
Thermochromic liquid crystals	-40	283
Thermographic phosphors	-250	2000
Heat-sensitive paints	300	1300
Infrared thermometer	-40	2000
Schlieren	0	2000
Shadowgraph	0	2000
Interferometry	0	2000
Line reversal	727	2527
Absorption spectroscopy	20	2500
Emission spectroscopy	20	2700
Rayleigh scattering	20	2500
Raman scattering	20	2227
CARS	20	2000
LIF	0	2700
Acoustic thermography	-26.9	2000

3.1 Liquid-in-Glass Thermometers

Liquid-in-glass thermometers exploit the higher volumetric expansion of liquids with temperature in comparison with that of solids. A liquid-in-glass thermometer typically consists of a reservoir and capillary tube containing a thermometric liquid, supported in a stem with a temperature-indicating scale. On heating, the volume of the liquid increases relative to that of the container and the liquid expands up the capillary tube. Liquid-in-glass thermometers can be used from approximately -196°C to 650°C , although no single instrument is capable of measuring temperature across the whole range because of the limitations of the thermometric liquids. Liquid-in-glass thermometers do not require an external power supply and can be relatively inexpensive. As glass is generally chemically stable, these thermometers can be used in a wide variety of chemical environments. Their disadvantages include fragility and the lack of remote logging capability.

In the case of a solid stem thermometer the bulb reservoir is usually a thin glass container with 0.35–0.45-mm-thick walls holding a thermometric liquid such as mercury, ethanol, pentane, toluene, or xylene. The choice of the liquid depends on the desired temperature range:

- Mercury, -35 – 510°C
- Ethanol, -80 – 60°C
- Pentane, -200 – 30°C

- Toluene, -80 – 100°C
- Xylene, -80 – 50°C

The space above the thermometric liquid can be evacuated or filled with an inert gas. As the temperature of the liquid in the bulb rises, the liquid will expand and some of it will be forced up the capillary. The temperature of the bulb is indicated by the position of the top of the meniscus, in the case of a mercury thermometer, against markings engraved on the stem.

Liquid-in-glass thermometers can be calibrated at a number of fixed points and a scale subsequently applied to the stem supporting the capillary tube to indicate the value of the temperature. The uncertainty of industrial glass thermometers depends on the device concerned with values ranging from ± 0.01 to $\pm 4^{\circ}\text{C}$ (see, e.g., BS 1041⁵). The use of liquid-in-glass thermometers is reviewed by Ween,⁶ Wise,⁷ Nicholas and White,⁸ Nicholas,⁹ and Childs.^{10,11}

Mercury-in-glass thermometers are increasingly being replaced by resistance-based temperature devices, which have cost and environmental advantages, and by infrared devices and noninvasive measurement or by thermally sensitive paint devices, which give a visible color-based indication of temperature.

3.2 Manometric Thermometry

Methods of temperature measurement based on the measurement of pressure are known as manometric thermometry. There are two principal categories: gas thermometry and vapor pressure thermometry.

Gas thermometry is based on the ideal gas law:

$$pV = n\mathcal{R}T \quad (4)$$

where p = pressure (N/m^2)
 V = volume (m^3)
 n = number of moles of gas [$n = m/M$ (m = mass, M = molar mass)]
 \mathcal{R} = universal gas constant (8.314510 J/mol K ^{12,13})
 T = temperature (K)

By assuming values for the quantity of mass and for the gas constant, the temperature is obtained by measuring pressure and/or volume. The basic components of a gas thermometer are enclosures to hold the gas sample of interest under carefully controlled conditions and a flow circuit to allow the pressure to be measured. Gas thermometers can be used for applications from a few Kelvin to 1000 K. The principal application has been in cryogenics, and the gas enclosure, commonly known as the bulb, is usually located within a cryostat. Figure 2 illustrates the principal components of a constant-volume gas thermometer. Gas thermometry tends to be a specialist activity and is usually confined to standards laboratories and cryogenic applications.

Direct use of Eq. 4 requires knowledge of the gas constant. To reduce uncertainty arising from uncertainty in the gas constant, a number of methods have been devised that eliminate the need for knowing the gas constant, operating on the principle of maintaining either constant pressure, constant volume, and/or constant bulb temperature. Such techniques include:

- Absolute pressure volume (PV) isotherm thermometry
- Constant-volume gas thermometry
- Constant-pressure gas thermometry
- Constant-bulb- temperature gas thermometry
- Two-bulb gas thermometry

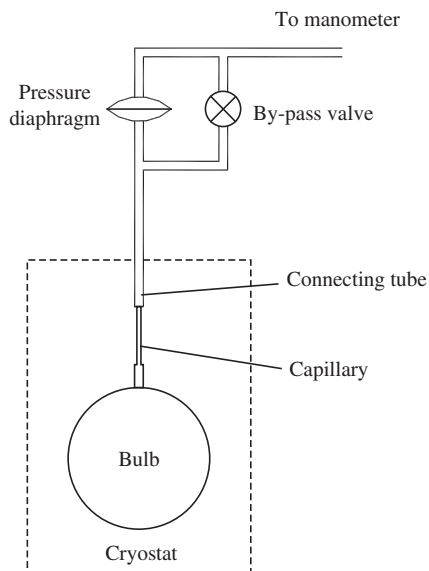


Figure 2 Principal constant-volume gas thermometer components.

Uncertainty in the measurement of temperature using gas thermometry is a function of the care taken and the temperature range. Pavese and Steur,¹⁴ for example, report an uncertainty of 0.5 mK for the temperature range 0.5–30 K.

Real gases do not behave exactly according to the ideal gas equation and the nonideal nature of real gases can be modeled using the virial equation

$$p = \left(\frac{\mathfrak{R}T}{V} + \frac{B(T)}{V^2} + \frac{C(T)}{V^3} + \frac{D(T)}{V^4} + \dots \dots \right) \quad (5)$$

where $B(T)$, $C(T)$, $D(T)$, etc., are the second, third, fourth virial coefficients, and so on.

The saturation vapor of a pure substance above its liquid phase varies with temperature and is known with low uncertainty for a number of cryogenic liquids such as helium 3 and 4, hydrogen, neon, nitrogen, oxygen, argon, methane, and carbon dioxide. Measurement of the vapor pressure can therefore be used to determine the temperature, and this technique provides a method with good sensitivity and requires relatively simple equipment. Equations quantifying the relationship between pressure and temperature for a variety of cryogenic liquids are given by Pavese,¹⁵ and vapor pressure thermometry is described in detail by Pavese and Molinar.¹⁶

3.3 Bimetallic Thermometers

A bimetallic thermometer consists of two strips of materials, typically two different types of metal that are bonded together. When heated, the assembly will deform due to a mismatch of the coefficient of linear expansion between the two materials. If one end is fixed, then a needle mounted on the other end can be used to indicate the temperature against a calibrated scale. To maximize the bending of the assembly and hence the sensitivity of the device, materials with significantly different coefficients of expansion can be used. Table 2 lists some of the materials typically used in bimetallic thermometers.

A bimetallic strip can be coiled in a spiral or helical configuration in order to provide increased sensitivity for a given volume and this form is commonly used in dial thermometers.

Table 2 Properties of Selected Materials Used in Bimetallic Elements

Material	Density (kg/m ³)	Young's Modulus (GPa)	Heat Capacity (J/kg K)	Coefficient of Thermal Expansion (10 ⁻⁶ K)	Thermal Conductivity (W/m K)
Al	2,700	61–71	896	24	237
Brass	8,500	110.6	820	19	106
Cu	8,954	129.8	383.1	17	386
Cr	7,100	279	518	6.5	94
Au	19,300	78.5	129	14.1	318
Fe	7,870	211.4	444	12.1	80.4
Ni	8,906	199.5	446	13.3	90
Ag	10,524	82.7	234.0	19.1	419
Sn	7,304	49.9	226.5	23.5	64
Ti	4,500	120.2	523	8.9	21.9
W	19,350	411	134.4	4.5	163
Invar (Fe64/Ni36)	8,000	140–150	480	1.7–2.0	13

Dial bimetallic thermometers tend to be reasonable rugged devices and have the advantage that they do not need an independent power supply. A variety of options are typically available for attaching the instrument to an application, including magnetic bases and clips.

The uncertainty of typical commercial bimetallic thermometers is 1–2% of the full-scale deflection with an operating range of -70 – 600°C . The theoretical limit of operation however is from about -270°C to the elastic limit of available materials.

The general equations for defining the curvature of a bimetallic strip are developed by Timoshenko¹⁷ and Childs.^{10,11} An advanced design device with a sensitivity of $0.0035^{\circ}\text{C}/\text{mm}$ and a repeatability of 0.027°C was demonstrated by Huston.¹⁸ The merits of bimetallic thermometers include that they can be easily read, can be used as an indicator of temperature or as an actuator, are relatively inexpensive, and do not require an independent power supply. Their disadvantages include that they are subject to drift, the measurements are usually relatively uncertain in comparison to, say, thermocouples and industrial PRTs, and they cannot provide a remote indication of temperature.

3.4 Thermocouples

In its simplest practical form a thermocouple can consist of two dissimilar wires connected together at one end with a voltage measurement device across the free ends, as indicated in Fig. 3. A net electromotive force (emf) due to the Seebeck effect will be indicated by the voltmeter, which is a function of the temperature difference between the joint and the voltmeter connections. Thermocouples are widely used in industry and research with applications from -272 to 2000°C . The merits of thermocouples are their relatively low cost, small size, rugged nature, versatility, reasonable stability, reproducibility, reasonable uncertainty, and fast speed of response. Although PRTs are more accurate and stable and thermistors are more sensitive, thermocouples are often a more economical solution than PRTs and their temperature range is greater than thermistors. The main disadvantage of thermocouples is their relatively weak signal, which makes the reading sensitive to electrical noise. For example, the output is about 4.1 mV at 100°C for a type K thermocouple. Other disadvantages include a nonlinear output

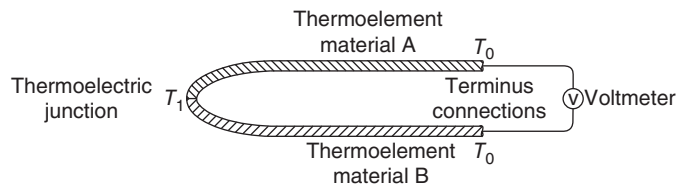


Figure 3 Simple practical thermocouple circuit: T_1 = temperature at thermoelectric junction; T_0 = temperature at terminus connections.^{10,11}

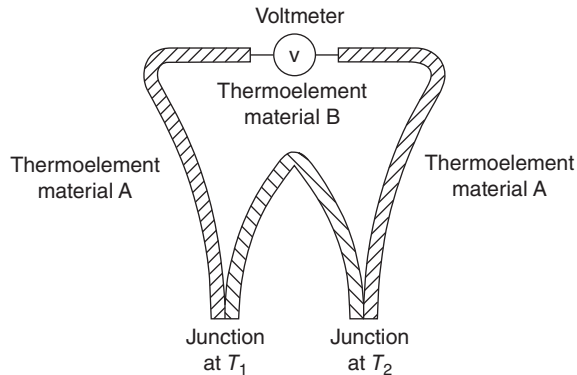


Figure 4 A current will flow through the above circuit that is proportional to the temperature difference between the two junctions.^{10,11}

that requires amplification, and calibrations can vary with contamination of the thermocouple materials, cold working, and temperature gradients.

The fundamental physical phenomenon exploited in thermocouples, discovered by Johann Seebeck, is that heat flowing in a conductor produces a movement of electrons and thus an emf. Seebeck demonstrated that a small current flowed through the circuit shown in Fig. 4 when the temperature of the two junctions was different (Seebeck, 1823). The emf produced is proportional to the temperature difference and is called the Seebeck emf or thermoelectric potential. As well as being a function of the net temperature difference, the magnitude of the emf produced is also a function of the materials used.

Thermocouple Analysis

Thermocouple circuits can consist of the simple forms illustrated in Figs. 3 and 4 or much more complex systems resulting from considerations of data logging and long distances between the point of interest and emf measurement. In this case the use of thermocouple wire for the whole length may be prohibitively expensive and alternative materials, known as extension and compensation cable, can be used to convey the emf. In order to ensure correct assessment of the signal produced, the circuit must be analyzed. Analysis of a given thermocouple circuit can be undertaken using fundamental physical relationships (see, e.g., Refs. 19–23). Alternatively, thermocouple behavior can be modeled in most applications using a number of laws or an algebraic technique. The thermocouple laws allow a quick commonsense approach to be taken to practical temperature measurement and have been developed by a number of authors (e.g., Refs. 10, 11, and 24–26).

Law of Interior Temperatures

The thermal emf of a thermocouple with the junction at T_1 and terminus connections at T_0 is unaffected by temperature elsewhere in the circuit provided the properties of the two thermoelements used are homogenous. This requirement means that the physical properties of the wires must be constant with length. If the wire is stretched or strained in a region or the chemical makeup of the wire varies along its length, this will affect the thermoelectric output and could invalidate the law. The law of interior temperatures is illustrated in Fig. 5. Provided the wire is uniform and homogenous on both sides of the hot spot, no net emf is generated by the hot spot. The thermocouple will respond only to the temperature difference between the thermoelectric junction and the terminus connections. This result is particularly useful as it means that the emf from a thermocouple is not dependent on intermediate temperatures along a thermoelement.

Law of Inserted Materials

If a third homogenous material C is inserted into either thermoelement A or B, then, as long as the two new thermoelectric junctions are at the same temperature, the net emf of the circuit is unchanged irrespective of the temperature in material C away from the thermoelectric junctions. This law is illustrated in Fig. 6, where a third material is inserted into the thermoelement A and then heated locally. Provided the thermoelectric junctions between C and A are both at the same temperature, the net emf of the thermocouple is unaffected by the presence of the inserted material and any local hot spot as the emf excursion between 2 and 3 is canceled by that between 3 and 4.

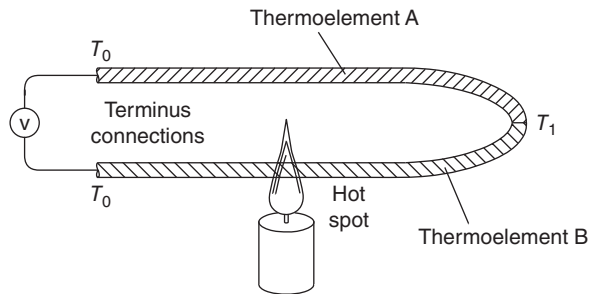


Figure 5 Illustration of law of interior temperatures. The thermocouple is unaffected by hot spots along the thermoelement, and the reading is only a function of T_1 and T_0 .^{10,11}

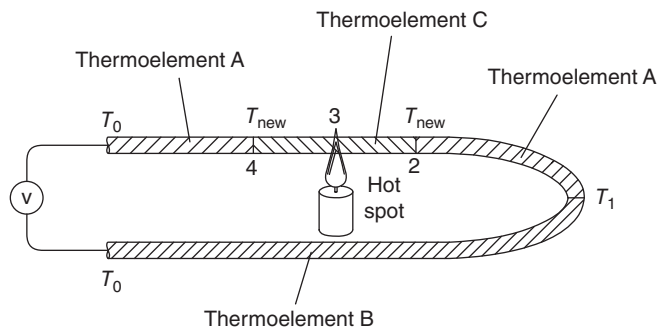


Figure 6 Illustration of law of inserted materials. The thermocouple is unaffected by the presence of the inserted material and any local hot spot.

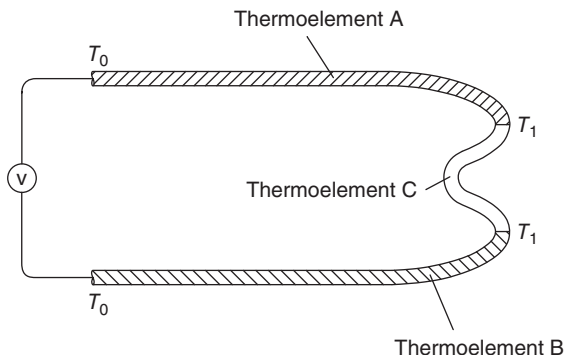


Figure 7 Illustration of law of intermediate materials. As there is no thermal gradient across the new thermoelectric junctions, the presence of the inserted material does not contribute to the net emf produced by the thermocouple.

Law of Intermediate Materials

If material C is inserted between A and B, the temperature of C at any point away from the junctions A–C and B–C is not significant. This law is illustrated in Fig. 7. Here an intermediate thermoelectric material is inserted between the two thermoelements. As there is no thermal gradient across the new thermoelectric junctions, the presence of the inserted material does not contribute to the net emf produced by the thermocouple. This law is of great practical significance as it allows us to model the implications of manufacturing techniques used to form thermoelectric junctions. Provided there is no thermal gradient across the thermoelectric junction, it does not matter if the thermoelements are joined by a third material such as solder or if local thermoelectric properties are changed at the junction by, for instance, welding.

Modeling Fundamental Thermoelectric Phenomena

An assessment of the fundamental thermoelectric phenomena can be made. These are the Seebeck, Peltier, and Thompson effects, but in practical thermocouple circuits the contribution of the Peltier and Thompson effects is insignificant. The Seebeck effect is the generation of emf in a conductor whenever there is heat transfer and is a consequence of electron movements when heat transfer occurs. An emf will be generated in a material whenever there is a temperature difference in the material and its magnitude will be a function of the temperature difference and the type of material. The Seebeck coefficient is a measure of how the electrons are coupled to the metal lattice and grain structure. It is sensitive to changes in the chemical and physical structure of the solid and will alter if the material is contaminated, oxidized, strained, or heat treated. Data for thermocouple materials normally use the relative Seebeck coefficient, stating the Seebeck coefficient relative to platinum.

The Seebeck coefficient is defined by Eq. 6 and is a transport property of all electrically conducting materials:

$$S(T) = \lim_{\Delta T \rightarrow 0} \frac{\Delta E}{\Delta T} = \frac{dE}{dT} \quad (6)$$

where S = Seebeck coefficient ($\mu\text{V}/\text{K}$)
 ΔT = temperature difference across a segment of the conductor (K)
 ΔE = absolute Seebeck emf (μV)

The Seebeck coefficient cannot be measured directly. Instead it must be determined by measuring the Thomson coefficient and using a thermodynamic relationship. The Seebeck coefficient varies with temperature so it must be mathematically defined by the gradient dE/dT at a specific temperature.

Rearranging Eq. 6 allows modeling of the net thermoelectric emf generated by a practical thermocouple circuit:

$$dE = S(T)dT \quad (7)$$

If the circuit comprises two materials, A and B, then

$$E = \int_{T_1}^{T_2} S_A dT - \int_{T_1}^{T_2} S_B dT = \int_{T_1}^{T_2} (S_A - S_B) dT \quad (8)$$

where E = thermoelectric emf (μV)

S_A = Seebeck coefficient for material A ($\mu\text{V/K}$)

S_B = Seebeck coefficient for material B ($\mu\text{V/K}$)

In Eq. 8 a difference in the Seebeck coefficients in the two thermoelements appears. It is this difference that is of practical interest in thermocouple thermometry, and it is called the relative Seebeck coefficient. The relative Seebeck coefficient is normally determined with respect to a reference material such as platinum:

$$S_{APt} = S_A - S_{Pt} \quad (9)$$

$$S_{BPt} = S_B - S_{Pt} \quad (10)$$

$$S_{AB} = S_A - S_B = S_{APt} - S_{BPt} \quad (11)$$

where S_{APt} = Seebeck coefficient for material A relative to platinum ($\mu\text{V/K}$)

S_{BPt} = Seebeck coefficient for material B relative to platinum ($\mu\text{V/K}$)

Values for the Seebeck coefficient relative to platinum are listed in Table 3 for a variety of materials.

Substituting for S_A and S_B in Eq. 11 gives

$$E = \int_{T_1}^{T_2} S_{AB} dT \quad (12)$$

and if the relative Seebeck coefficient can be taken as constant over the temperature range, then

$$E = S_{AB}(T_2 - T_1) \quad (13)$$

Equation 13 is particularly useful as it allows the analysis of a wide range of circuits. This can be achieved using loop analysis. In loop analysis the contribution of emf due to the thermal gradient across each element is summed together to produce the total emf that would be indicated by a voltage-measuring device.

The influence of connection leads shown in Fig. 8 on the output can be analyzed using Eq. 13. If identical conductors are used, then by using loop analysis

$$E = S_C(T_1 - T_0) + S_A(T_2 - T_1) + S_B(T_1 - T_2) + S_C(T_0 - T_1) \quad (14)$$

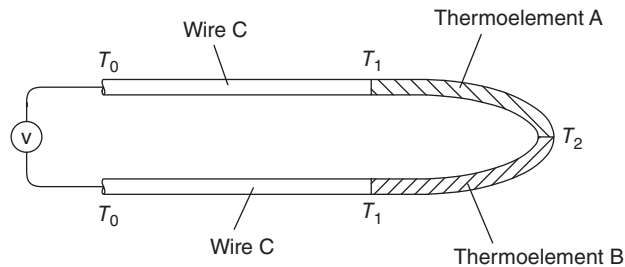
This simplifies to

$$E = S_{AB}(T_2 - T_1) \quad (15)$$

Table 3 Seebeck Coefficients for Various Materials

Material	20°C	1000°C
Chromel	22.2	9.4
Fe	13.3	-7
Nicrosil	11.8	8.8
Au	2.0	4
Cu	1.9	7
Ag	1.7	
W	1.3	20.3
Pt	4.7	21.4
Nisil	-14.8	-29.8
Alumel	-18.2	-29.6
Ni	-19.5	-35.4
Constantan	-38.3	-65.6

Source: After Ref. 27.

**Figure 8** Use of connection leads for a thermocouple.

The output emf is therefore dependent only on the temperature difference between the thermoelement junction and the terminus junctions. In other words, the temperature of the connections at the multimeter or data logger does not contribute to the emf produced by the thermocouple circuit. In effect the reference temperature T_1 has been moved from the data logger to the terminus connections.

Use of the circuit illustrated in Fig. 8 requires the temperature T_1 to be known. This can be achieved by using an alternative method of temperature measurement at this junction such as a thermistor or PRT. Alternatively, the terminus connections can be submerged in an ice bath. The temperature at T_1 will then be known and at 0°C .

In practical use it is uncommon to need values for the Seebeck coefficients. Instead the emf temperature characteristics of certain selected thermocouples have been identified under controlled conditions and standardized and these data can be used. If, however, you are involved in the design of a new type of thermocouple or some unusual application, data for Seebeck coefficients of a wide range of materials are tabulated by Pollock¹⁹ and Mott and Jones.²³

Thermocouple Types

There are hundreds of types of thermocouples that have been developed. In principle almost any dissimilar metals and even semiconductors can be used to form thermocouples. The wide scope of alloys indicates the range possible. Kinzie,²⁸ for example, lists more than 300 combinations

of materials for thermocouples. A series of international and national standards are however available for thermocouples listing just eight combinations of materials that are widely used. Stringent guidelines are provided for these thermocouples to ensure that devices that are manufactured to be compatible with the specific standard concerned from one company perform in a similar fashion to those manufactured by another company.

The eight standardized thermocouples fall into three general categories:

- Rare metal thermocouples (types B, R, and S)
- Nickel-based thermocouples (types K and N)
- Constantan negative thermocouples (types E, J, and T)

In the rare metal group, types B, R, and S are based on platinum and its alloys with rhodium. These are the most stable of the standard thermocouples and can be used at high temperatures (up to 1750°C) but are generally more expensive and sensitive to contamination. In nickel-based thermocouples, types N and K are commonly used for applications not requiring the elevated temperature range of the rare metal thermocouples. In constantan negative leg thermocouples, types E, J, and T have high emf outputs as constantan has a strong negative Seebeck coefficient.

The criteria for thermocouple selection include cost, maximum and minimum operating temperatures, chemical stability, material compatibility, atmospheric protection, mechanical limitations, duration of exposure, sensor lifetime, sensitivity, and output emf.

Standards organizations throughout the world have specified allowable tolerances for the deviation of the thermocouple output from standardized tables. Many of the standards are based on the results and research at national laboratories and there is similarity between the magnitude of tolerances in the standards from one country to another. Tables 4 and 5 give the manufacturing tolerances for American Society for Testing and Materials (ASTM) and British Standard (BS) thermocouples. Many countries use the term Class 1 for special tolerance and Class 2 for standard tolerance.

The data for thermoelectric emf versus temperature for two of the standardized thermocouples, types K and T, according to International Electrotechnical Commission (IEC) 584.1: 1995³⁰ and BS EN 60584.1: 1996³¹ is reproduced in Tables 6 and 7 and for all the standardized thermocouples plotted in Fig. 9. In the tables just part of the data available are presented in 10°C steps. Complete data sets, with listings in 1°C steps, are available in the standards and have also been reproduced in many manufacturers' catalogs.

Table 4 Manufacturing Tolerances for ASTM Thermocouples

Type	Temperature Range (°C)	Standard Tolerance (°C)	Special Tolerance (°C)
B	870–1700	±0.5%	±0.25%
E	0–870	±1.7 or ±0.5%	±1.0 or ±0.4%
J	0–760	±2.2 or ±0.75%	±1.1 or ±0.4%
K	0–1260	±2.2 or ±0.75%	±1.1 or ±0.4%
N	0–1260	±2.2 or ±0.75%	±1.1 or ±0.4%
R	0–1480	±1.5 or ±0.25%	±0.6 or ±0.1%
S	0–1480	±1.5 or ±0.25%	±0.6 or ±0.1%
T	0–370	±1.0 or ±0.75%	±0.5 or ±0.4%
E	–200 to 0	±1.7 or ±1.0%	
K	–200 to 0	±2.2 or ±2.0%	
T	–200 to 0	±1.0 or ±1.5%	

Source: ASTM E 230-98 (Ref. 29).

Table 5 Manufacturing Tolerances for Thermocouples

Type	Tolerance Class 1	Tolerance Class 2
B	—	±0.25% (600–1700°C)
E	±1.5°C (–40–375°C) ±0.4% (375–800°C)	±2.5°C (–40–333°C) ±0.75% (333–900°C)
J	±1.5°C (–40–375°C) ±0.4% (375–750°C)	±2.5°C (–40–333°C) ±0.75% (333–750°C)
K	±1.5°C (–40–375°C) ±0.4% (375–1000°C)	±2.5°C (–40–333°C) ±0.75% (333–1200°C)
N	±1.5°C (–40–375°C) ±0.4% (375–1000°C)	±2.5°C (–40–333°C) ±0.75% (333–1200°C)
R	±1.0°C (0–1100°C) ±[1+0.003(t – 1100)] (1100–1600°C)	±1.5°C (0–600°C) ±0.25% (600–1600°C)
S	±1.0°C (0–1100°C) ±[1+0.003(t – 1100)] (1100°C–1600°C)	±1.5°C (0–600°C) ±0.25% (600–1600°C)
T	±0.5°C (–40°C to 125°C) ±0.4% (125°C–350°C)	±1.0°C (–40–133°C) ±0.75% (133–350°C)

Source: BS EN 60584.2 (Ref. 31).

Table 6 Standard Reference Data to IEC 584.1:1995 and BS EN 60584.1 Part 4: 1996 for Type K Nickel–Chromium/Nickel–Aluminum Thermocouples Giving Thermocouple emf (μV) for Various Tip Temperatures Assuming Cold Junction at 0°C

°C	Type K											
	0	10	20	30	40	50	60	70	80	90	100	
–200	–5,891	–6,035	–6,158	–6,262	–6,344	–6,404	–6,441	–6,458				
–100	–3,554	–3,852	–4,138	–4,411	–4,669	–4,913	–5,141	–5,354	–5,550	–5,730	–5,891	
0	0	–392	–778	–1,156	–1,527	–1,889	–2,243	–2,587	–2,920	–3,243	–3,554	
100	4,096	4,509	4,920	5,328	5,735	6,138	6,540	6,941	7,340	7,739	8,138	
200	8,138	8,539	8,940	9,343	9,747	10,153	10,561	10,971	11,382	11,795	12,209	
300	12,209	12,624	13,040	13,457	13,874	14,293	14,713	15,133	15,554	15,975	16,397	
400	16,397	16,820	17,243	17,667	18,091	18,516	18,941	19,366	19,792	20,218	20,644	
500	20,644	21,071	21,497	21,924	22,350	22,776	23,203	23,629	24,055	24,480	24,905	
600	24,905	25,330	25,755	26,179	26,602	27,025	27,447	27,869	28,289	28,710	29,129	
700	29,129	29,548	29,965	30,382	30,798	31,213	31,628	32,041	32,453	32,865	33,275	
800	33,275	33,685	34,093	34,501	34,908	35,313	35,718	36,121	36,524	36,925	37,326	
900	37,326	37,725	38,124	38,522	38,918	39,314	39,708	40,101	40,494	40,885	41,276	
1000	41,276	41,665	42,053	42,440	42,826	43,211	43,595	43,978	44,359	44,740	45,119	
1100	45,119	45,497	45,873	46,249	46,623	46,995	47,367	47,737	48,105	48,473	48,838	
1200	48,838	49,202	49,565	49,926	50,286	50,644	51,000	51,355	51,708	52,060	52,410	
1300	52,410	52,759	53,106	53,451	53,795	54,138	54,479	54,819				

Thermocouple Assemblies and Installation

Temperature measurement can rarely be undertaken using a bare thermocouple wire. Often the thermocouple wires must be electrically isolated from the application and protected from the environment. When measuring the temperature of a moving fluid, it may also be necessary to locate the thermocouple within a specialized assembly to produce a measurement that can be

Table 7 Standard Reference Data to IEC 584.1:1995 and BS EN 60584.1 Part 5: 1996 for Type T Copper/Copper–Nickel Thermocouples giving Thermocouple emf (μV) for Various Tip Temperatures Assuming Cold Junction at 0°C

		Type T										
$^\circ\text{C}$	0	10	20	30	40	50	60	70	80	90	100	
-200	-5,603	-5,753	-5,888	-6,007	-6,105	-6,180	-6,232	-6,258				
-100	-3,379	-3,657	-3,923	-4,177	-4,419	-4,648	-4,865	-5,070	-5,261	-5,439	-5,603	
0	0	-383	-757	-1121	-1,475	-1,819	-2,153	-2,476	-2,788	-3,089	-3,379	
0	0	391	790	1,196	1,612	2,036	2,468	2,909	3,358	3,814	4,279	
100	4,279	4,750	5,228	5,714	6,206	6,704	7,209	7,720	8,237	8,759	9,288	
200	9,288	9,822	10,362	10,907	11,458	12,013	12,574	13,139	13,709	14,283	14,862	
300	14,862	15,445	16,032	16,624	17,219	17,819	18,422	19,030	19,641	20,255	20,872	
400	20,872											

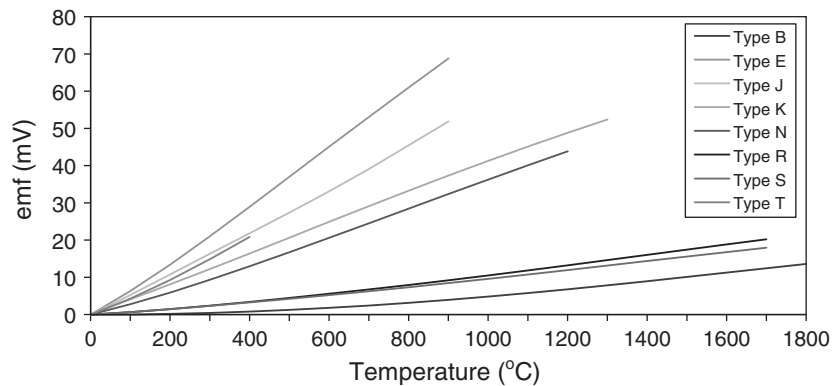


Figure 9 emf versus temperature characteristics for standard thermocouples.

related to the temperature of the flow. A thermocouple assembly therefore involves consideration of joining the wires at the tip to form the thermoelectric junction, electrical isolation of the wires, protection of the wires, installation of the assembly into the application, and connection of the thermocouple to the voltage-measuring device.

As indicated by the law of intermediate materials, the precise form of connection of the two thermoelements does not significantly affect the output provided the temperature of the bead formed is relatively uniform. Thermocouple beads can therefore be formed by twisting a few millimeters of the wire end together at the tip, which provides only limited strength, crimping, or welding, as illustrated in Fig. 10. The choice of connection depends upon the requirements of the application such as the need for strength or high speed of response. For applications requiring high strength of the bead or resistance to vibration, a welded bead may be most appropriate. The vast majority of commercial thermocouples are welded during manufacture, and this need not be a concern for the bulk of users. If, however, thermocouples are being assembled from wire, then the bead can be formed by using a discharge-welding machine.

Many applications require the thermocouple wires to be electrically or chemically isolated from the environment or medium of interest. Examples of insulation materials include PVC (polyvinyl chloride) for temperatures from -30 to 105°C , Teflon from -273 to $+250^\circ\text{C}$, glass

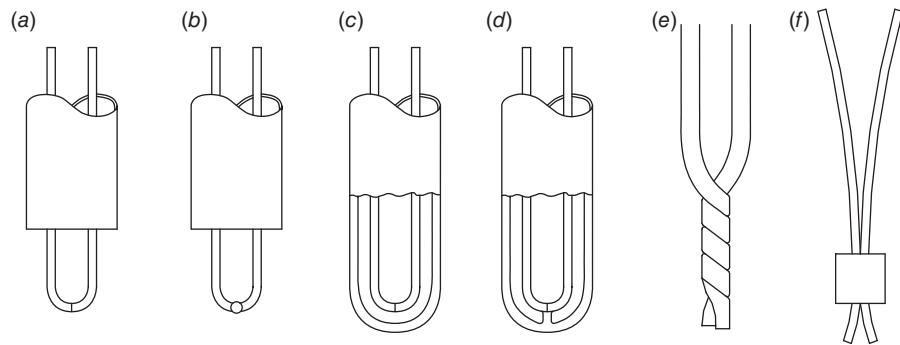


Figure 10 Bead formation options: (a) butt welded, (b) welded bead, (c) butt welded and sheathed, (d) grounded and sheathed, (e) twisted wires, and (f) crimped.

fiber from -50 to -400°C , and polyimide from -269 to 400°C . Higher temperatures can be achieved using ceramic sheaths. The requirements of electrical or chemical isolation and good thermal contact are often in conflict, giving rise to thermal disturbance errors.

In addition to the need to electrically isolate the thermocouple, it is also necessary in some applications to protect the thermocouple from exposure to the local environment that could otherwise impair the function of the measurement device. An example is the immersion of a thermocouple into a corrosive fluid. Levels of protection can be achieved by use of a protection tube or sheath around the insulation. An example of a thermocouple assembly with a protecting tube and head is illustrated in Fig. 11. These tubes and connectors are commercially available. Choice of the insulator and sheath materials depends on the application. The ASTM manual³² on the use of thermocouples in temperature measurement lists a wide range of protecting tube materials for different applications. The mineral insulated metal sheathed (MIMS) thermocouple attempts to combine high-temperature capability and protection from the environment in a single assembly. In these devices a mineral such as magnesium oxide is compacted around the thermocouple wires to electrically isolate and support them and this assembly is encapsulated within a metal sheath (Fig. 12). MIMS thermocouples can be used for the range -200 – 1250°C .

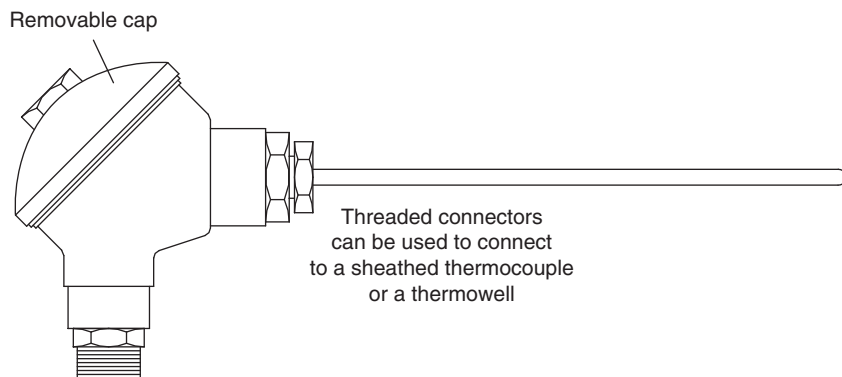


Figure 11 Protection tube and connector designs.

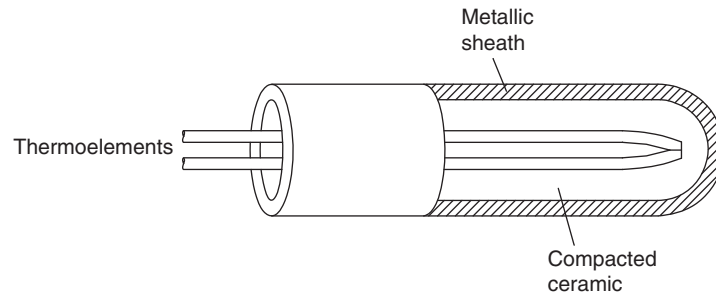


Figure 12 MIMS thermocouple for high-temperature capability and protection from local environment.

Thermocouples are useful for determining the temperature for a wide range of applications from surfaces and solid bodies to stationary and flowing fluids. As a thermocouple consists simply of the thermoelectric wires it is usually necessary to insulate the wires and sometimes encapsulate the wires in a protective sheath. In addition, in order to avoid errors caused by heat transfer, it may be necessary to install the thermocouple within a specialized assembly to ensure appropriate measurement of the parameter of interest.

The temperature of a solid surface can be measured using a thermocouple by a variety of means depending on the type of surface and uncertainty desired. Typically the choice is limited to surface mounting or installing the thermocouple in a hole or recess. In the case of surface mounting, an adhesive or shims may be used to secure the thermoelement wires to the surface and to improve thermal contact between the surface of interest and the thermocouple bead. An example of the use of shims for a gas turbine application is shown in Fig. 13.

Solid temperatures and the temperature of a liquid flowing in a pipe are sometimes measured with the thermocouple immersed in a thermowell. A thermowell is a protecting tube to

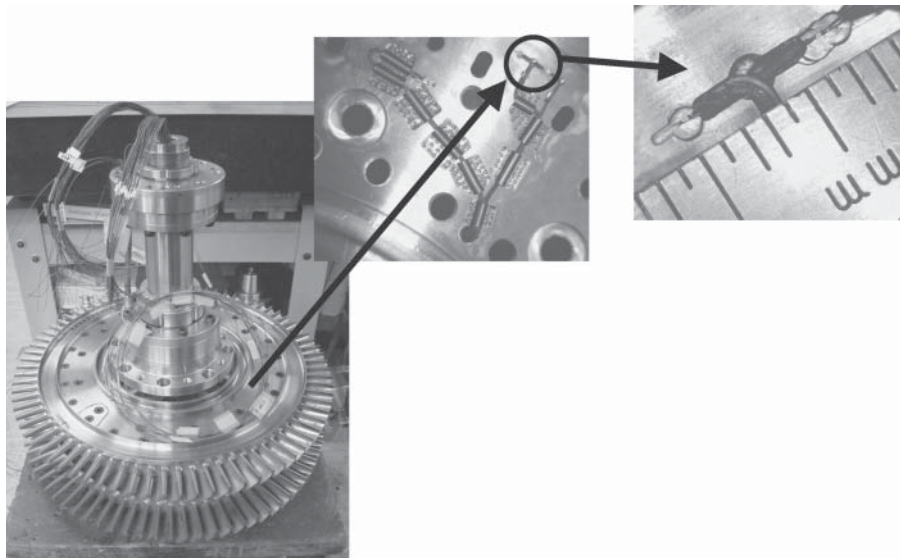


Figure 13 Thermocouple installation.³³

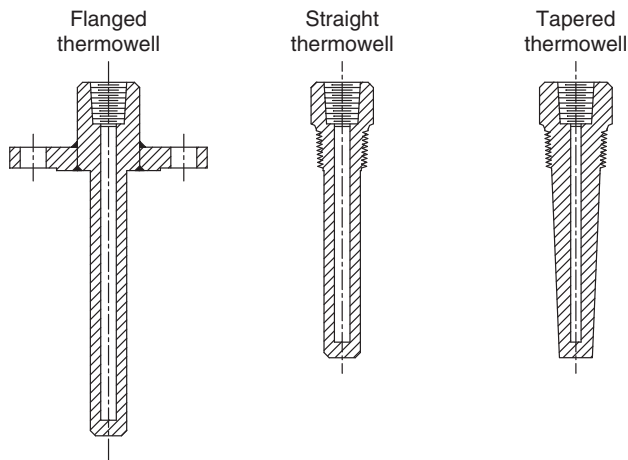


Figure 14 Thermowells.³² Reprinted with permission from Manual on the Use of Thermocouples in Temperature Measurement, 4th Edition. Copyright ASTM International, 100 Barr Harbor Drive, West Conshohocken, PA 19428.

prevent or minimize damage from harmful atmospheres, corrosive fluids, or mechanical damage and common commercial forms are illustrated in Fig. 14. As a general rule of thumb a thermowell should be immersed in the liquid to a depth of 10 times the diameter. Material property requirements for thermowells are documented in American Society of Mechanical Engineers (ASME) PTC 19.3.³⁴

A thermocouple placed in a gas environment will experience heat transfer by conduction along its wires and support, convective heat transfer with the surrounding gas both at the tip and along the length of the wires and support, and radiative heat exchange with the surroundings. The contribution due to conduction is usually relatively small in comparison to convection. Radiative heat transfer tends to be a function of the fourth power of the absolute temperature and can therefore be significant if the temperature of the gas is distinctly different to the temperature of the enclosure. Because of these exchanges of heat, the measurement of gas temperature needs to be carefully thought through and undertaken (see Refs. 10 and 11).

Extension Leads and Compensation Cable

In some applications the measurement location and readout instrumentation are separated by a considerable length. An example is the measurement of temperatures of various different components in an engine on test, for example, a hundred thermocouples all connected to a data acquisition system some 30 m away. In most applications the thermal gradient and resultant emf is most significant in the first few meters of the wire. The remaining wire length serves the purpose of transmitting the emf to the data acquisition system. The thermoelectric properties of this length of wire are less critical than the part in the region of large thermal gradient. The drive for economy can make the use of a lower specification and hence cheaper wire for this region of wire attractive, and these lengths of wire are known as extension leads or extension wires. There are two types of extension wire: those with similar physical composition to the thermocouple wire itself but manufactured to a less stringent specification and those manufactured using a different material altogether. Some people use the term extension leads for wires manufactured using the same material as the thermocouple and the term compensation lead for wires manufactured using different materials. However, this terminology is not universal and the terms extension and compensation lead, wire, and cable are used interchangeably. The use of extension leads in a thermocouple circuit is illustrated in Fig. 15.

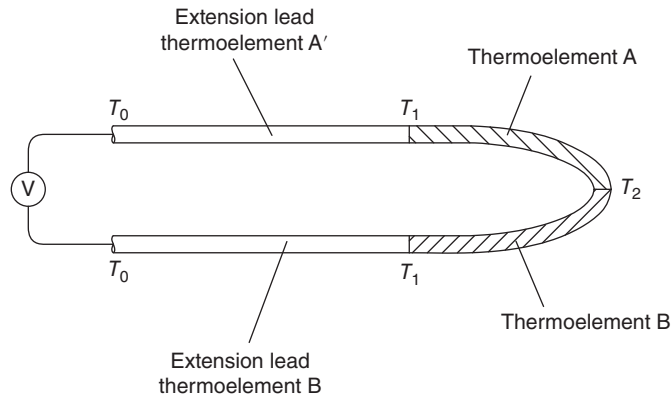


Figure 15 Use of extension leads in thermocouple circuit.^{10,11}

For the configuration shown in Fig. 15 loop analysis can again be used to analyze the output. If the Seebeck coefficients of the extension leads are S_A and S_B , respectively, then

$$E = S_{A'}(T_1 - T_0) + S_A(T_2 - T_1) + S_B(T_1 - T_2) + S_{B'}(T_0 - T_1) \quad (16)$$

This simplifies to

$$E = S_{A'B'}(T_1 - T_0) + S_{AB}(T_2 - T_1) \quad (17)$$

If the wire pair $A'B'$ is selected so that it has approximately the same relative Seebeck coefficient as AB , then

$$S_{A'B'} \approx S_{AB} \quad (18)$$

and

$$E \approx S_{AB}(T_2 - T_0) \quad (19)$$

So the reference junction is effectively located at the connections between the voltmeter or the data logger and the extension leads.

3.5 Resistance Temperature Devices

The electrical resistance of a material is a function of temperature, and this phenomenon is exploited by the class of instruments called *resistance temperature detectors* (RTDs). Types of RTDs include *platinum resistance thermometers*, thermistors, and a variety of semiconductor-based instruments. RTDs are used in a wide range of applications. Some types such as PRTs can have very low uncertainty, better than 0.002 K,² and are used in the definition of the ITS-90, and others such as thermistors and some semiconductor-based devices can be inexpensive in comparison to, say, thermocouples.

In an RTD the measurement of resistance is made across the length of material. This is usually a metal, although germanium and carbon are used in some cryogenic (<273 K) applications. Any metal could in principle be used, but stability considerations normally limit the choice to platinum, copper, and nickel. Copper and nickel are useful over the range of 212 to 350°C,³⁵ and are cheap in comparison to platinum. Platinum is more chemically stable and tends to be the preferred material for the majority of metal-based RTDs where low uncertainty is required or a message of quality is important in branding. PRTs are used to define part of the ITS-90.

Platinum Resistance Thermometers

Platinum resistance thermometers consist of a length of platinum, connection wires, and an instrument to measure the resistance. Platinum resistance thermometers fall into a number of broad categories:

- *Standard platinum resistance thermometers* (SPRTs) which are used for low uncertainty measurements
- *Industrial platinum resistance thermometers* (IPRTs) which are used for practical laboratory and industrial use
- Secondary SPRTs which are designed for laboratory environments and limited temperature ranges while still providing low uncertainty measurements

The relationship between resistance and temperature can be approximated by

$$R_t = R_0(t + \alpha t) \quad (20)$$

where R_0 = resistance at 0°C (Ω)
 R_t = resistance at temperature t (Ω)
 α = temperature coefficient of resistance ($^{\circ}\text{C}^{-1}$)
 t = temperature ($^{\circ}\text{C}$)

The temperature coefficient of resistance, α , is calculated from

$$\alpha = \frac{R_{100} - R_0}{100^{\circ}\text{C} \times R_0} \quad (21)$$

where R_{100} = resistance at 100°C (Ω)

Much of the original work on resistance thermometry was undertaken by Siemens³⁶ and Callendar.³⁷⁻³⁹ Callendar found that the resistance of platinum could fairly accurately be described by a quadratic in the form

$$R_t = R_0(1 + At + Bt^2) \quad (22)$$

where A and B are constants.

This equation has traditionally been written in the form given in Eq. 23, known as Callendar's equation, which simplifies the calculations necessary to determine the calibration constants α and δ :

$$R_t = R_0 \left[1 + \alpha t + \alpha \delta \left(\frac{t}{100} \right) \left(1 - \frac{t}{100} \right) \right] \quad (23)$$

where δ is a constant.

For temperatures below 0°C, additional terms are needed and the temperature resistance characteristic is relatively accurately defined by the Callendar–Van Dusen equation 24, which was the basis of the now superseded International Practical Temperature Scales of 1927, 1948, and 1968.

$$R_t = R_0(1 + At + Bt^2 + C(t - 100)t^3) \quad (24)$$

Here C = a constant and is zero above 0°C. Typical values for the coefficients in Eq. 24 for a standard PRT and an industrial PRT are listed in Table 8.

The resistance element may be a coil of fine wire or a track of platinum deposited on a surface. The design of the resistance element depends on the requirements of the thermometer (see Ref. 40). Most materials tend to expand and contract with temperature and this induces strain in a material. This can affect the PRT in a number of ways. Expansion of a track of platinum can alter the cross-sectional area available for conduction and therefore alter the resistance. In addition, repetitive strain cycling can modify the microscopic structure of the platinum and therefore

Table 8 Typical Values for Constants in Callendar–Van Dusen Equation for SPRT and IPRT

Constant	SPRT	IPRT
<i>A</i>	$3.985 \times 10^{-3}/^{\circ}\text{C}$	$3.908 \times 10^{-3}/^{\circ}\text{C}$
<i>B</i>	$-5.85 \times 10^{-7}/^{\circ}\text{C}^2$	$-5.80 \times 10^{-7}/^{\circ}\text{C}^2$
<i>C</i>	$-4.27 \times 10^{-12}/^{\circ}\text{C}^4$	$-4.27 \times 10^{-12}/^{\circ}\text{C}^4$
α	$3.927 \times 10^{-3}/^{\circ}\text{C}$	$3.85 \times 10^{-3}/^{\circ}\text{C}$

Source: From Ref. 8.

the resistance. A further compounding effect is any variation in the electrical properties of the insulation and connection wires.

Standards (BS 1041: Part 3⁴¹; ASTM E1137⁴²; BS EN 60751⁴³) have been produced for PRTs. Values for resistance and the corresponding temperature can be readily interpolated in order to determine a given reading. Two classes of uncertainty are defined for IPRTs: Class A devices where the uncertainty is within $\pm(0.15+0.002|t|)$ and Class B devices, with an uncertainty $\pm(0.3+0.005|t|)$.

The delicate strain-free designs of an SPRT would not survive the shock and vibration encountered in some industrial environments. The IPRT typically comprises a platinum wire encapsulated within a ceramic housing or a thick film sensor coated onto a ceramic surface. The actual sensing element of an IPRT can be further protected from the environment by a metal sheath. In the design of an IPRT the constraint for mounting the platinum wire so that strain is minimized is relaxed in favor of producing a robust device. Most designs have just two wires sealed within the sensor body as this reduces the risk of short circuits and makes the device more robust. The ceramic encapsulation used should be selected so that its thermal coefficient of expansion closely matches that of platinum and the former over the temperature range of the PRT. The ceramic material used for encapsulation can include compounds and impurities that react with the platinum and change the transducer's temperature coefficient. The uncertainty achievable for an IPRT is generally of the order of $\pm 0.01^{\circ}\text{C}$ to $\pm 0.2^{\circ}\text{C}$ over the range 0–300°C (see Ref. 44).

The platinum-sensing element can also be deposited as a thin or thick film on an insulating substrate such as alumina. For a thick-film sensor, the surface area can be of the order of 25 mm² with an active area of 5 mm². They are mass produced with each sensor individually trimmed to produce the desired resistance. The thick-film structure produces a device that is robust and capable of operating in applications experiencing minor shock or vibration. They are noninductive and therefore insensitive to stray electrical fields. Thick-film PRTs are normally designated to Class B of IEC-751.⁴⁵ An innovative form of temperature measurement is the application of thin-film PRTs to polyamide sheet.⁴⁶ Massed arrays of PRTs can be formed on a polyamide sheet substrate by evaporating or sputtering platinum followed by depositing gold leads using a magnetron. The resulting sheet is flexible and can be glued to the geometry of interest.

In order to obtain a measure of temperature using an RTD, the resistance must be measured. Simplistically this can be achieved by passing a current through the sensing resistor and measuring the potential across it. If the current is known, then the ratio of potential to current provides the measurement of the resistance from Ohm's law, and the temperature can be determined from the resistance temperature characteristic. However, even if an uncertainty of only 1°C is desired, the resistance must be measured to better than 0.4% and as a result must be undertaken with care.⁸ There are two basic methods for measuring resistance commonly used in platinum resistance thermometry, potentiometric methods, and bridge methods, and these are reviewed by Nicholas and White,⁸ Connolly,⁴⁷ and Wolfendale et al.⁴⁸

Rhodium Iron, Doped Germanium, and Carbon Resistors

A number of types of RTDs are suitable for cryogenic applications including platinum, rhodium iron, doped germanium, and carbon. Although used to define the ITS-90 between 1234.93 K and 13.81 K, the sensitivity of platinum falls off below about 20 K. Rhodium iron alloy has a similar resistance temperature characteristic to platinum at temperatures above 30 K. Below 30 K the sensitivity drops to a minimum between 25 K and 15 K and then rises again giving a RTD with good sensitivity at low temperatures (see Refs. 49 and 50). Doped germanium resistors are available with a relatively wide temperature range for cryogenic applications, from 0.05 to 325 K, and typically comprise the semiconductor encapsulated in a 3-mm-diameter, 8.5-mm-long cylinder (example cited is the GR-200A from Lakeshore Cryotronics www.lakeshore.com). Certain carbon resistors produce stable RTDs.

Thermistors

Thermistors use the variation in resistance with temperature of ceramic semiconductor. Modern thermistors are usually mixtures of oxides of chromium, nickel, manganese, iron, copper, cobalt, titanium, other metals, and doped ceramics. Thermistors can have either a *positive temperature coefficient* or a *negative temperature coefficient*. A typical resistance temperature characteristic is $1 \Omega/0.01^\circ\text{C}$. The temperature can be determined approximately from the relationship given in the equation⁵¹

$$R_T = R_0 \exp \left[1 - B \left(\frac{1}{T} - \frac{1}{T_0} \right) \right] \quad (25)$$

where R_0 is the resistance at T_0 and B is a constant for the particular thermistor material.

The resistance characteristic of a thermistor expressed by Eq. 25 is negative and nonlinear. This can be offset if desired using two or more matched thermistors packaged in a single device so that the nonlinearities of each device negate each other (see Refs. 52–54). Thermistors are usually designated by their resistance at 25°C , with common resistances ranging from 470 Ω to 100 k Ω . The high resistivity of thermistors normally negates the need for a four-wire bridge circuit.

In order to produce a lower uncertainty fit for the resistance temperature characteristic of a thermistor, a polynomial can be used with the degree used depending on the temperature range and the type of thermistor. Equation 26 is adequate for most systems:

$$\ln R_T = A_0 + \frac{A_1}{T} + \frac{A_2}{T^2} + \frac{A_3}{T^3} \quad (26)$$

Here A_0 , A_1 , A_2 , and A_3 are constants.

Alternatively Eq. 27 can be used where the second-order term has been neglected:

$$\frac{1}{T} = b_0 + b_1 R_T + b_3 (\ln R_T)^3 \quad (27)$$

where b_0 , b_1 , and b_3 are constants.

3.6 Semiconductor Devices

A forward voltage across a transducer junction can be used to generate a temperature-sensing output proportional to absolute temperature. Temperature sensors based on simple transistor circuits can be readily incorporated as a part of an integrated circuit to provide on-board diagnostic or control capability. The majority of semiconductor junction sensors use a diode connected bipolar transistor. If the base of the transistor is shorted to the collector, then a constant current flowing in the remaining p – n junction (base to emitter) produces a forward voltage that

is proportional to absolute temperature. This can be modeled by Eq. 28 and in practice has a temperature coefficient of approximately $-2 \text{ mV}/^\circ\text{C}$:

$$V_F = \left(\frac{kT}{q} \right) \ln \left(\frac{I_F}{I_S} \right) \quad (28)$$

where k = Boltzmann's constant ($1.38 \times 10^{-23} \text{ J/K}$)
 T = temperature (K)
 q = charge of electron ($1.6 \times 10^{-19} \text{ C}$)
 I_F = forward current (A)
 I_S = junction's reverse saturation current (A)

3.7 Diode Thermometers

The forward voltage drop across a p - n junction increases with decreasing temperature. For certain semiconductors the relationship between voltage and temperature is almost linear and in silicon this occurs between 400 and 25 K with a sensitivity of approximately 2.5 mV/K . Commonly used semiconductors for thermometry are Si and GaAs with the addition of certain elements for stability. The merits of diode thermometers include price, simple voltage-temperature relationship, relatively large temperature range (1–400 K), no need for a reference junction, relatively high sensitivity, uncertainty lower than $\pm 50 \text{ mK}$,⁵⁵ and simplicity of operation with a constant current source and a digital voltmeter.

3.8 Noise Thermometry

The thermal motion of atoms and molecules and charge carriers within an electrical conductor generates broadband electrical noise.^{56,57} The noise power generated is called Johnson noise and is related to temperature by

$$\text{Power} = 4kT \Delta f \quad (29)$$

where k = Boltzmann's constant (J/K)
 T = absolute temperature (K)
 Δf = frequency band (Hz)

In noise thermometry the thermal noise is measured across a resistor. The thermal noise power generated in a resistor is usually very small and sensitive instrumentation is therefore necessary. In principle the temperature range of application is from a few mK to over 2500°C . The circuitry used depends on the temperature range and has been reviewed by Kamper,⁵⁸ Blalock and Shepard,⁵⁹ and White et al.⁶⁰

3.9 Pyrometric Cones

A number of deforming temperature- and heat-rate-indicating devices have been developed, known as pyrometric cones, thermoscope bars, and Bullers rings, for use in kilns and furnaces. Pyrometric cones, also known as Harrison, Seger, or Orton cones, are slender trihedral pyramids manufactured from mixtures of various mineral oxides.⁶¹ On heating the effects of gravity cause the inclined cone to progressively bend as the material softens; see Fig. 16. Pyrometric cones do not provide a precise indication of temperature as their deformation is a function of both



Figure 16 Pyrometric cones.

the rate of heating and the temperature cycle. They tend to be used to provide an indication of process completion such as completion of firing.

Cones vary in shape, size, and method of use according to the manufacturer. They are an economic means of identifying firing completion and can be distributed at a number of locations in a kiln to indicate local conditions. An alternative is the use of thermocouples, RTDs, or infrared thermometers, but these have a higher initial cost. One manufacturer, Orton Ceramics, provides cones suitable for temperatures in the range 590–2015°C. Determination of performance equivalents between different manufacturers is standardized in ANSI/ASTM C24-79 and reported by Fairchild and Peters⁶² and Beerman.⁶³ The practical use of pyrometric cones is described by McGee⁶⁴ and Childs,^{10,11} and in manufacturers' guidelines. Thermoscope bars comprise a rod of material mounted on a stand. The bars soften and deform with temperature, and the deformation can be measured and compared with a look-up table supplied by the manufacturer to provide an indication of temperature. Bullers rings are dust pressed rings that shrink linearly with temperature rise. Use of thermoscope bars and Bullers rings is outlined in BS 1041, Part 7.⁶⁵

4 SEMI-INVASIVE METHODS

Some temperature measurement scenarios permit the modification of a surface of interest with a thermally sensitive material that can be observed remotely. These techniques can be classed as semi-invasive and include heat-sensitive paints, thermographic phosphors, thermochromic liquid crystals, and a variety of crayons and labels. Some of the materials available provide a means of continuously monitoring temperature while others merely provide a means of identifying that a certain temperature has been reached or exceeded. The latter are known as peak-temperature indicators.

4.1 Peak-Temperature-Indicating Devices

A number of products are available that provide an indication that a particular temperature has been attained or exceeded. On heating above some critical temperature the material used for the indicator melts, fuses, or changes composition providing a permanent record that a

given temperature has been reached or more likely exceeded. Commercially available products include heat-sensitive crayons, pellets, labels, and paints.

Fuseable material can be applied to a surface by means of a crayon. Applications include identifying temperatures in metal treatment and welding. Self-adhesive labels consisting of a temperature-sensitive indicator sealed under a transparent window are also available. These provide a convenient means of identifying whether a component such as an electronics package has experienced an excessive temperature or in medical applications to validate that a process temperature has been attained. The indicating material permanently changes color from say a light gray to black at the rated temperature, which is printed on the label. Some labels include multiple indicators, sensitive to a range of temperatures, to enable greater resolution of the peak temperature.

4.2 Temperature-Sensitive Paints

The same kind of fusible material as used in the peak-temperature-indicating crayons is available in paint form. Thermally sensitive paint has also been developed for high-temperature applications in order to indicate the peak temperatures on turbine blades (1989). Early work on turbines involved the use of proprietary paints from Thermindex, Faber Castel, and Tempil. The development of a range of multichange paints is reported by Bird et al.⁶⁶ Some paint formulations are available that provide a reversible indication of peak temperature. One principle exploited is to drive water off a colorful salt, thus changing its color. On cooling, the salt can reabsorb water vapor from the atmosphere and revert to its initial color state.

Parameter-sensitive paints are sensitive to a number of physical parameters including pressure and temperature. The paints comprise luminescent molecules and a polymer binder material that can be dissolved in a solvent. Temperature-sensitive paint (TSP) can be applied by brush or spray, and as the paint dries, the solvent evaporates to leave luminescent molecules embedded in a polymer matrix. The principle exploited by TSPs is photoluminescence where a probe molecule is promoted to an excited state by the absorption of a photon of appropriate energy in a fashion comparable to thermographic phosphors. The difference is that the intensity of the luminescence is related to temperature by photophysical processes known as thermal and oxygen quenching⁶⁷ and the intensity of luminescence is inversely proportional to the temperature.

4.3 Thermographic Phosphors

The luminescent properties of materials, known as thermographic phosphors, such as the lanthanide doped ceramics YAG:Tb, YAG:Dy, or Y₂O₃:Eu, are temperature dependent. In order to measure the temperature of a surface temperature, a thin layer of luminescent materials can be applied, illuminated with UV light, typically from a laser, and the subsequent luminescence observed and analyzed. Thermographic phosphors can be used to indicate temperatures from cryogenic levels to about 2000°C. A phosphor-based thermometry system will generally consist of a source of excitation energy, a method of delivery of energy to the target, a fluorescing medium bonded to the target, optical, detector and data acquisition, and analysis systems. Before excitation phosphor's electronic levels are populated in their ground state. They can be excited by the absorption of energy by, for instance, electromagnetic radiation such as visible or UV light, X- or γ -rays, particle beams, or an electric field. After absorption of energy the atomic configuration of the material may not remain excited but may return to its initial or some intermediate state. The intensity of emitted light is an inverse function of temperature. In the case of europium-based phosphors experiencing continuous illumination, it is given by the equation⁶⁸

$$I_T = [a_j + a_j A e^{-\Delta E/kT}]^{-1} \quad (30)$$

where I_T = intensity
 a_j = probability rate
 A = factor related to a_j
 E = energy (J)
 T = temperature (K)
 k = Boltzmann's constant (J/K)

Sensitivities of 0.05°C and an uncertainty of 0.1–5% of the Celsius temperature reading are possible.⁶⁹ Most thermographic phosphors are ceramics and therefore relatively inert. Bonding of the phosphor to the application can be achieved by mixing the phosphor slurry with epoxy, paint, or glue and then applying the mixture onto the surface by brushing or spraying. For harsh environments subject to, for example, high mechanical shock or large thermal gradients, chemical bonding by vapor deposition, RF sputtering, and laser ablation can also be considered. Thermographic phosphors are reviewed by Heyes,^{70,71} and the development of a thermal barrier coating for turbomachinery components capable of both sustaining a high thermal gradient and indicating temperature is described by Feist et al.^{72,73}

4.4 Thermochromic Liquid Crystals

Thermochromic liquid crystals are a class of materials that display significant changes in color over discrete temperature bands. As the temperature rises, a thermochromic liquid crystal mixture will change from colorless, black against a blackened background and pass through the visible spectrum of colors, red to orange to yellow to green to blue to violet, before turning colorless again. The process of color change is reversible with cooling. The colors displayed can be related to temperature by a calibration process. The sensitivity to temperature arises from the structure within the thermochromic liquid crystal with transition between solid and liquid states. In the liquid crystal phase, molecules lose positional order, becoming fluid, but retain orientation order and the optical properties of crystalline solids.⁷⁴ When a thermochromic liquid crystal is illuminated with white light, it will selectively reflect monochromatic light with wavelength equal to the pitch of the helical molecular structure. The wavelength of the reflected light decreases as the temperature increases and the color observed will therefore change from red through the visible spectrum to blue.

Pure crystals deteriorate rapidly with age and exposure to ultraviolet light but their life can be extended by encapsulation of the crystals within a polymer coating. Thermochromic crystals are commercially available in the form of water-based slurry. This can be sprayed onto a dark or blackened surface using an airbrush (see, e.g., Refs. 74–76 for practical guidance). They are also available as a preformed layer on a blackened substrate of mylar or paper.

The temperature at which a liquid crystal formulation begins to display color is called its red-start temperature. The range of temperature over which the crystals display color is often referred to as the color play bandwidth or the temperature event range. The range of temperature over which a liquid crystal displays a single color is called the isochrome bandwidth and this can be as little as 0.1°C. For narrow-band thermochromic liquid crystals the color changes over a range of about 1°C and these can be used to determine surface temperature with an uncertainty of about 0.1°C. Wide-band thermochromic liquid crystals are typically active across a range of 5–20°C and can be used to determine the distribution of surface temperature. The value of the red-start temperature and the color play bandwidth can be controlled by selecting appropriate cholesteric esters and their proportions.

A number of approaches have been adopted in determining the value of temperature from color in the use of thermochromic crystals. For instance, in the use of forehead clinical thermometers, human eyesight and judgment are used comparing the displayed color to a look-up

table or identifying the most significant illumination in a panel. A CCD camera can also be used to capture the images produced by liquid crystals and the resulting RGB image processed to hue and a calibration used to convert this to a corresponding temperature (see Refs. 74 and 77).

Applications of thermochromic liquid crystals have included forehead and fish-tank thermometers, novelty stickers, turbine heat transfer experiments (e.g., Refs. 78 and 79, jet engine nacelles, and vehicle interiors.⁸⁰

5 NONINVASIVE METHODS

A number of temperature-dependent phenomena such as the emission of radiation, scattering, and luminescence can be observed remotely, thereby providing the possibility of measuring temperature without disturbing the medium of interest. Remote observation can under certain circumstances be classed as noninvasive to the medium of interest or target. It should however be noted that optical techniques, particularly for methods requiring use of a laser system, can involve use of bulky and complicated equipment, and while this may not require machining or installation of a measurement device on the surface of interest or location of a sensor in a fluid, the equipment may nevertheless be bulky and will likely require optical access through, say, special windows. Noninvasive methods are potentially attractive for a variety of reasons and applications, including:

- Targets in motion
- Fragile targets
- Remote targets
- Unsteady temperature applications
- Harsh environments
- Temperature distribution required

Noninvasive methods of temperature measurement have developed with the advances in semiconductor fabrication technology and the availability of lasers as a source of excitation. Use of infrared thermometers is now commonplace for inspection in industry and retail. Temperature measurement techniques based on infrared radiation are reviewed in Sections 5.1 and 5.2.

A series of sophisticated methods for noninvasive measurement of gas temperature are available, such as index of refraction, absorption and emission spectroscopy, line reversal, scattering, laser-induced fluorescence, light polarization, speed of sound, and speckle methods. Some of the techniques, such as laser-induced fluorescence, are highly specialized and expensive, requiring extensive expertise and high-cost capital equipment. This type of method is not available off the shelf and its use should be carefully justified in terms of the value of the data it would produce. These methods are reviewed in ESDU⁸¹ and Childs.^{10,11}

5.1 Infrared Thermometry

Infrared thermometers measure the thermal radiation emitted by a body due to its temperature and have found applications from cryogenic temperatures to over 6000 K. Infrared thermometers are widely available with examples used in industry and retail where the cost is the same order of magnitude as, for example, a thermocouple indicator to highly sophisticated traceable devices for high-temperature gas or surface measurement, suitable for laboratory and research use. Anybody will emit energy in the form of thermal radiation due to its temperature with the quantity of radiation rising with increasing temperature. The energy emitted over the electromagnetic spectrum due to temperature by a blackbody is modeled by Planck's law [Eq. 31]. The

energy radiated reduces with temperature but the wavelength distribution shifts toward those with longer wavelengths:

$$E_{\lambda,b} = \frac{C_1}{\lambda^5 [\exp(C_2/\lambda T) - 1]} \quad (31)$$

where $E_{\lambda,b}$ = spectral emissive power for a blackbody (W/m³)
 C_1 = first radiation constant ($3.7417749 \times 10^{-16}$ W m², Ref. 12)
 λ = wavelength (m)
 C_2 = second radiation constant (0.01438769 m K, Ref. 12)
 T = absolute temperature (K)

Integration of Eq. 31 over all wavelengths gives the total thermal radiation emitted by the blackbody equation

$$E_b = \sigma T^4 \quad (32)$$

where σ is the Stefan–Boltzmann constant.

$$\sigma = 5.67051 \times 10^{-8} \text{ W/m}^2 \text{ K}^4 \text{ (Ref. 12)}$$

An infrared system consists of three basic elements, the source, propagation medium, and measuring device. The infrared-measuring device may comprise an optical system, a detector, processing circuit, and display. The purpose of the optical system is to focus the energy emitted by the target onto the sensitive surface of the infrared detector, which usually converts the energy into an electrical signal. There are a number of types of infrared thermometers depending on whether the device is sensitive to all or a specific band of wavelengths. Those sensitive to all wavelengths are classed as total radiation or broadband thermometers. Those sensitive to radiation in a specific band of wavelengths are classed as spectral band thermometers, ratio thermometers, and thermal imagers.

The radiation emitted by real targets does not match the ideal simplification of Eqs. 31 and 32. Radiation emitted by real bodies is a function of both the surface temperature and surface properties. The surface property limiting the quantity of radiation is called the emissivity, ϵ , and is the ratio of the electromagnetic flux that is emitted from a surface to that emitted from a blackbody at the same temperature. Emissivity is a function of the dielectric constant and subsequently its refractive index and is generally wavelength dependent. Quantification and accounting for the effects of emissivity in undertaking a temperature measurement using an infrared thermometer are usually necessary. Target surfaces can be classified into three categories:

- Blackbodies
- Graybodies
- Nongraybodies

Information about the emissivity of a wide range of materials is documented in the reference texts edited by Touloukian et al.^{82–84} and also tends to be available from infrared thermometer suppliers.

The medium across which the radiation is transmitted can attenuate the radiation due to absorption, scattering, and turbulence with absorption and emission dependent on the energy structure of the constituent molecules. As well as nitrogen and oxygen, air typically contains a proportion of water vapor and CO₂ along with a number of trace molecules. The strong dipole moment and light hydrogen atoms in water vapor result in strong and broad absorption bands. In addition, water vapor is an asymmetric top and this gives an irregular absorption spectrum. The properties of water vapor and CO₂ along with those of other trace substances in air act to absorb a proportion of the radiation emitted from a target at specific wavelengths and even make air

opaque at some frequencies. This means that using Eq. 31 without modification to account for the radiation not transmitted would lead to an error. Information concerning the transmissive properties of air, which varies with distance and local composition, has been published by Yates and Taylor⁸⁵ and is also modeled in a number of software packages, such as LOWTRAN,^{86–89} MODTRAN, HITRAN, and FASCODE. These codes represent long-running research and development and are reviewed in Smith⁹⁰ and are available elsewhere (see, e.g., Ref. 91). When dealing with other transmission mediums or specific particulates such as smoke, the transmission characteristics for the system concerned must be identified in order to allow for the temperature reading to be correctly interpreted.

An approach to negate the impact of nontransmission of thermal radiation is to use spectrally sensitive detectors. These operate across a specific wave band only and a detector can be selected to match the characteristics of a given application. For example, there are a number of wavelengths, known as windows, near 0.65, 0.9, 1.05, 1.35, 1.6, 2.2, 4, and 10 μm , where the transmittance is high and air is effectively transparent to thermal radiation. A large number of detectors have now been identified that are sensitive to thermal radiation such as PbS, PbSe, InSb, HgCdTe, and PbSnTe (for further data see, e.g., Ref. 92). As a general rule instruments used for measuring hot targets operate at shorter wavelengths (e.g., 0.9–1.1 μm) and those for cooler objects operate at longer wavelengths (3–5 or 8–14 μm). A further issue arises from the use of optical devices and windows between the target and the detector as materials used for lenses and windows also have their own spectral characteristics and only transmit a proportion of the incident radiation at specific wavelengths. An infrared sensor should only be operated when the spectral range over which a target and the media transmit and over which the detector is sensitive all overlap.

A compounding problem affecting a temperature measurement using an infrared thermometer is background radiation. An infrared thermometer will read any radiation incident on the detector whether it is emitted, transmitted, or reflected from a target. If a surface is not a perfect absorber of incident radiation, then a proportion of the incident radiation can be reflected, and this can distort the indicated temperature. If, for example, a target surface is at a temperature, say 300 K, but is in close proximity to a hotter object, then it is possible for an infrared thermometer to read the radiation emitted from both the surface and a proportion of radiation from the hotter object that is reflected off the surface of the target. The temperature indicated for the target will be artificially high, without appropriate offsetting. A number of strategies are available to minimize such effects involving repositioning the detector or using screens. The practical use of infrared thermometers is described by Kaplan.⁹³

When an infrared thermometer is aimed at a target it collects energy within a collecting beam, or zone, whose shape is determined by the optical system and detector and is typically conical. The cross section of the collecting beam is called the field of view and this determines the spot size, the area on the target over which a temperature measurement is made.

In principle it is possible to side step the requirement of knowing the surface emissivity by using ratio thermometers. These measure the radiation emitted from a surface around two fixed wavelengths. The ratio of the radiation emitted is given by

$$R = \frac{\varepsilon(\lambda_1)\lambda_2^5(e^{C_2/\lambda_2 T} - 1)}{\varepsilon(\lambda_2)\lambda_1^5(e^{C_2/\lambda_1 T} - 1)} \quad (33)$$

If the emissivity is not spectrally sensitive and is near unity, the emissivities will cancel, and provided the target temperature is low, then

$$T = \frac{C_2(\lambda_1 - \lambda_2)/\lambda_1\lambda_2}{\ln \left[R \left(\frac{\lambda_1}{\lambda_2} \right)^5 \right]} \quad (34)$$

An optical fiber can be used to convey thermal radiation into a narrow wavelength band from a location of interest or a convenient viewing point to a detector. This enables the detector to be remote from the target and is particularly useful in monitoring very hot applications such as combustion processes. Optical fiber-based devices are useful for temperatures in the range 100–4000°C. The use of this technique is reported by Dils,⁹⁴ Saaski and Hartl,⁹⁵ Sun,⁹⁶ Ewan,⁹⁷ Zhang et al.,⁹⁸ Grattan and Zhang,⁹⁹ and Krohn.¹⁰⁰

5.2 Thermal Imaging

Infrared radiation principles can be used to measure the spatial distribution of temperature on a target surface and this is known as thermal imaging or thermography. Applications of thermal imaging are extensive, ranging from plant condition monitoring, diagnostics, materials testing, process control, energy auditing for structures, and surveillance. The developments in semiconductor technology have resulted in the wider availability of thermal imaging devices, including reasonably priced items for process control. Thermal imagers typically comprise an optical system, a detector, processing electronics, and a display and are extensions of infrared thermometer technologies combined with some form of scanning optics. Thermal imagers do not require any form of additional illumination in order to operate, and this makes them highly attractive in surveillance applications. It should be noted that military and surveillance thermal imagers tend to be configured to produce an image rather than quantitative information on the distribution of temperatures.

It is possible to make use of a single detector with some form of scanner to transmit the radiation signal from specific regions of the optical system to enable a two-dimensional image of the temperature distribution to be built up. The disadvantage of single-detector scanners is the trade-off between the speed of response of the instrument and the signal-to-noise ratio of the detector. The detector typically needs to be cooled and operated at performance limits in order to achieve the desired time response. Multidetector scanners comprising a linear detector array or a two-dimensional array of detectors, known as a staring array, enable the temporal-to-spatial burden to be reduced. Cooling of the detectors can be achieved in a number of ways such as use of liquid nitrogen, Peltier coolers, or a miniature Sterling engine.

The optimum wave band for a thermal imager as for most other infrared thermometers is dictated by the wavelength distribution of the emitted radiation, the transmission characteristics of the atmospheric environment between the imager and the target, and the characteristics of the available detector technology. The following optical bands for air are defined:

- Short-wavelength infrared imaging band (SWIR), 1.1–2.5 μm
- Medium-wavelength infrared imaging band (MWIR), 2.5–7 μm , with a notch at 4.2 μm due to CO_2 absorption
- Long-wavelength imaging band (LWIR), 5–15 μm
- Further bands beyond 15 μm classed as far infrared (FIR) and very long wave infrared (VLWIR)

The emissivity of most naturally occurring objects and organic paints is high in the long-wave infrared but is lower and more variable in the medium-wave infrared. Metallic surfaces tend to have lower emissivity in either band. As such, the use of a thermal imager to provide quantitative information for the temperature distribution, particularly for a surface comprising different materials, has to be carefully managed. Without correction for local emissivity values the thermal imager will assume a default value and apply this to the whole image. However, basing the choice of thermal imager on emissivity alone ignores attenuation in the transmission medium. Fog particles, for example, attenuate radiation by scattering with the magnitude dependent on the particulate size. If moderately sized particulates are present,

scattering affects the MWIR region more than the LWIR, and a LWIR system can generally provide better range performance.

A number of performance parameters can be used for thermal imagers, allowing different systems to be compared (see also Refs. 101–103):

- Thermal sensitivity [noise equivalent differential temperature (NEDT)] refers to the smallest temperature differential that can be detected and depends on the optical system, the responsivity of the detector, and the noise of the system.
- Spatial resolution defines the smallest quantity that can be discerned and is often quantified by Airy disc size.
- Minimum resolvable temperature (MRT).
- Minimum detectable temperature (MDT).

The price of a thermal imager usually reflects the performance, ruggedness, and image processing capability. Some compact imagers can be readily hand held while other systems are designed to be mounted on a platform weighing as much as 100 kg. The availability of uncooled and Sterling engine-cooled detector arrays has made battery-powered portable devices viable. The uncertainty associated with the temperature measurement is specific to the device, but typical figures are ± 2 K or $\pm 2\%$ full-scale output. Modern thermal imagers can be particularly easy to use needing simply to be aimed at the target of interest and the image captured by pressing a button.

6 CONCLUSIONS

A wide variety of methods are available for measuring temperature. Despite the many types of temperature-measuring systems, the choice for a given application is typically limited by a number of factors, including uncertainty, temperature range, thermal disturbance, level of contact, size of the sensor, transient response, sensor protection, availability, and cost. This chapter has provided a review of a range of invasive, semi-invasive, and noninvasive instrumentation along with an introduction to the measurement process, calibration, and traceability. Some applications permit the installation of a sensor on or within the medium of interest. Alternatively it may be desirable to observe the target remotely using an infrared pyrometer, a thermal imager, or other form of noninvasive method.

Nomenclature.

a_{CTS}	Charge transfer state rate
a_j	Probability rate
$B(T)$	Second virial coefficient (cm^3/mol)
$C(T)$	Third virial coefficient (cm^6/mol^2)
C_1	First radiation constant ($3.7417749 \times 10^{-16} \text{ W}\cdot\text{m}^2$, Ref. 12)
C_2	Second radiation constant (0.01438769 m.K, Ref. 12)
$D(T)$	Fourth virial coefficient (cm^9/mol^3)
E	Thermoelectric emf (μV); energy (J)
$E_{\lambda,b}$	Spectral emissive power for a blackbody (W/m^3)
E_b	Emissive power for a blackbody (W/m^2)
I_F	Forward current (A)
I_S	Junction reverse saturation current (A)
I_T	Intensity
k	Boltzmann's constant ($1.380658 \times 10^{-23} \text{ J/K}$, Ref. 12)

n	Number of moles of the gas
p	Pressure (N/m ²)
q	Charge of electron (1.6×10^{-19} C)
\mathcal{R}	Universal gas constant (8.314510 J/mol K, Ref. 12)
R_0	Resistance at 0°C (Ω)
R_t	Resistance at temperature t (Ω)
R_T	Resistance at temperature T (Ω)
R_{100}	Resistance at 100°C (Ω)
S	Seebeck coefficient ($\mu\text{V/K}$)
S_A	Seebeck coefficient for material A ($\mu\text{V/K}$)
S_B	Seebeck coefficient for material B ($\mu\text{V/K}$)
S_{AB}	Relative Seebeck coefficient ($\mu\text{V/K}$)
S_{APt}	Seebeck coefficient for material A relative to platinum ($\mu\text{V/K}$)
S_{BPt}	Seebeck coefficient for material B relative to platinum ($\mu\text{V/K}$)
t	Temperature (°C)
T	Temperature (K)
$T_{\text{°F}}$	Temperature in degrees Fahrenheit (°F)
$T_{\text{°R}}$	Rankine temperature (°R)
T_0	Temperature at a reference condition (K)
V	Volume (m ³)
V_F	Forward voltage (V)
α	Temperature coefficient of resistance ($\Omega\Omega^{-1}\text{°C}^{-1}$ or °C^{-1})
δ	Constant
ϵ	Emissivity
λ	wavelength (m)
σ	Stefan–Boltzmann constant equal to $5.67051 \times 10^{-8}\text{W/m}^2 \text{K}^4$ (Ref. 12)
ΔE	Absolute Seebeck emf (μV)
Δf	Frequency interval (Hz)
ΔT	Temperature difference across segment of conductor (K)
ANSI	American National Standards Institute
ASTM	American Society for Testing and Materials
BS	British Standard
FIR	Far infrared
IPRT	Industrial platinum resistance thermometer
IR	Infrared
ITS-90	International Temperature Scale of 1990
MDT	Minimum detectable temperature
MRT	Minimum resolvable temperature
MWIR	Medium-wavelength infrared
NEDT	Noise equivalent differential temperature
NTC	Negative temperature coefficient
PRT	Platinum resistance thermometer
PSP	Parameter-sensitive paint
PTC	Positive temperature coefficient
RTD	Resistance temperature detector
SPRT	Standard platinum resistance thermometer
SWIR	Short-wavelength infrared
TSP	Temperature-sensitive paints
UV	Ultraviolet
VLWIR	Very long wave infrared

REFERENCES

1. H. Preston-Thomas, "The International Temperature Scale of 1990 (ITS-90)," *Metrologia*, **27**, 3–10, 1990.
2. B. W. Mangum and G. T. Furukawa, "Guidelines for Realizing the ITS-90," Technical Note 1265, National Institute of Standards and Technology, Gaithersburg, MD, 1990.
3. P. R. N Childs, J. R. Greenwood, and C. A. Long, "Heat Flux Measurement Techniques," *J. Mech. Eng. Sci.*, **213**, 655–677, 1999.
4. R. S. Figliola and D. E. Beasley, *Theory and Design for Mechanical Measurements*, 4th ed., Wiley, Hoboken, NJ, 2005.
5. British Standard (BS), "Section 2.1: British Standard Temperature Measurement. Part 2: Expansion Thermometers. Section 14.2.1: Guide to Selection and Use of Liquid-in-Glass Thermometers," BS 1041, 1985.
6. S. Ween, "Care and Use of Liquid-in-Glass Thermometers," *ISA Trans.*, **7**, 94, 1968.
7. J. A. Wise, "Liquid in Glass Thermometry," *NBS Monograph*, **150**, 1976.
8. J. V. Nicholas and D. R. White, *Traceable Temperatures, An Introduction to Temperature Measurement and Calibration*, Wiley, New York, 1994.
9. J. V. Nicholas, "Liquid-in-Glass Thermometers. Section 32.8," in J. G. Webster (Ed.), *The Measurement Instrumentation and Sensors Handbook*, CRC Press, Boca Raton, FL, 1999.
10. P. R. N. Childs, *Practical Temperature Measurement*, Butterworth-Heinemann, Oxford, 2001.
11. P. R. N. Childs, "Advances in Temperature Measurement," *Adv. Heat Transfer*, **36**, 111–181, 2001.
12. E. R. Cohen and B. N. Taylor, "The 1986 Adjustment of the Fundamental Physical Constants," *Rev. Modern Phys.*, **59**, 1121, 1987.
13. E. R. Cohen and B. N. Taylor, "The Fundamental Physical Constants," *Phys. Today*, **52**, pp. BG5–BG9, 1999.
14. F. Pavese and P. P. M. Steur, "³He Constant-Volume Gas Thermometry: Calculations for a Temperature Scale between 0.8 K and 25 K," *J. Low Temp. Phys.*, **69**, 91–117, 1987.
15. F. Pavese, "Manometric Thermometers. Section 32.9," in J. G. Webster (Ed.), *The Measurement Instrumentation and Sensors Handbook*, CRC Press, Boca Raton, FL, 1999.
16. F. Pavese and G. Molinar, *Modern Gas-Based Temperature and Pressure Measurements*, Plenum, New York, 1992.
17. S. P. Timoshenko, *The Collected Papers*, McGraw Hill, New York, 1953.
18. W. D. Huston, "The Accuracy and Reliability of Bimetallic Temperature Measuring Elements," in C. H. Herzfeld (Ed.), *Temperature: Its Measurement and Control in Science and Industry*, Vol. **3**, Reinhold, New York, 1962, pp. 949–957.
19. D. D. Pollock, *Thermocouples: Theory and Properties*, CRC Press, Boca Raton, FL, 1991.
20. R. D. Barnard, *Thermoelectricity in Metals and Alloys*, Taylor and Francis, London, 1972.
21. F. J. Blatt, P. A. Schroeder, C. L. Foiles, and D. Greig, *Thermoelectric Power in Metals*, Plenum, New York, 1976.
22. R. R. Bourassa S. Y. Wang, and B. Lengeler, "Energy Dependence of the Fermi Surface and Thermoelectric Power of the Noble Metals," *Phys. Rev. B*, **18**, 1533–1536, 1978.
23. N. F. Mott and H. Jones, *Theory and Properties of Metals and Alloys*, Dover, New York, 1958.
24. W. F. Roeser, "Thermoelectric Thermometry," *J. Appl. Phys.*, **11**, 388–407, 1940.
25. E. O. Doebelin, *Measurement Systems: Application and Design*, 4th ed., McGraw Hill, New York, 1990.
26. ESDU, "Temperature Measurement. Thermocouples," ESDU 06018, ESDU Heat Transfer Series Vol. 4 ("Insulation and Temperature Measurement"), 2007.
27. R. E. Bentley, *Handbook of Temperature Measurement*, Vol. 3, *Theory and Practice of Thermoelectric Thermometry*, Springer, Singapore, 1998.
28. P. A. Kinzie, *Thermocouple Temperature Measurement*, Wiley-Interscience, New York, 1973.
29. American Society for Testing and Materials (ASTM), "Standard Specification and Temperature-Electromotive Force (emf) Tables for Standardized Thermocouples," ASTM, E230-98, ASTM, West Conshohocken, PA, 1999.

30. International Electrotechnical Commission (IEC), "International Standard. Thermocouples—Part 1: Reference Tables," 2nd ed. 1995-09, IEC 584-1, IEC, Geneva, 1995.
31. British Standard (BS), "Thermocouples. Part 1: Reference Tables. Part 2: Tolerances," BS EN 60584, 1996.
32. American Society for Testing and Materials (ASTM), *Manual on the Use of Thermocouples in Temperature Measurement*, 4th ed., ASTM PCN 28-012093-04, ASTM, West Conshohocken, PA, 1993.
33. D. Coren, J. Turner, D. Eastwood, S. Davies, N. Atkins, P. R. N. Childs, J. Dixon, and T. Scanlon, "An Advanced Multi-Configuration Turbine Stator Well Cooling Test Facility," Paper GT2010-23450, ASME, New York, 2010.
34. American Society of Mechanical Engineers (ASME), "Performance Test Codes Supplement on Instruments and Apparatus Part 3 Temperature Measurement," ASME PTC 19.3, ASME New York, 1974.
35. T. J. Claggett, R. W. Worrall, and B. G. Liptak, "Thermocouples," in B. G. Liptak (Ed.), *Instrument Engineers' Handbook Process Measurement and Analysis*, 3rd ed., Chilton, 1995.
36. W. H. Siemens, "On the Increase of Electrical Resistance in Conductors with Rise of Temperature and Its Application to the Measure of Ordinary and Furnace Temperatures; Also on a Simple Method of Measuring Electrical Resistances," *Proc. Roy. Soc. Lond.*, **19**, 443, 1871.
37. H. L. Callendar, "Notes on Platinum Thermometry," *Philos. Mag.*, **47**:191, 1899.
38. H. L. Callendar, "On Construction of platinum Thermometers," *Philos. Mag.*, **34**, p. 104, 1891.
39. H. L. Callendar, "On the Practical Measurement of Temperature. Experiments Made at the Cavendish Laboratory, Cambridge," *Philos. Trans. Roy. Soc. Lond.*, **178**, 161, 1887.
40. ESDU, "Temperature Measurement: Resistance Thermometry," ESDU 06019, ESDU Heat Transfer Series Vol. 4 ("Insulation and Temperature Measurement"), 2007.
41. British Standard (BS), "Part 3: Temperature Measurement: Guide to the Selection and Use of Industrial Resistance Thermometers," BS 1041, 1989.
42. American Society for Testing and Materials (ASTM), "Standard Specification for Industrial Platinum Resistance Thermometers," ASTM E1137, ASTM, West Conshohocken, PA, 1997.
43. British Standard (BS), "Industrial Platinum Resistance Thermometer Sensors," BS EN 60751, 1996.
44. H. M. Hashemian and K. M. Petersen, "Achievable Accuracy and Stability of Industrial RTDs," in J. F. Schooley (Ed.), *Temperature: Its Measurement and Control in Science and Industry*, Vol. **6**, American Institute of Physics, Melville, NY, 1992, pp. 427–432.
45. International Electrotechnical Commission (IEC), "Standard for Industrial Resistance Thermometers," IEC-751, IEC, Geneva, 1983.
46. T. V. Jones, "The Thin Film Heat Transfer Gauge—A History and New Developments," in *Proceedings 4th UK Conference on Heat Transfer*, IMechE Conference Transactions, Paper C510/150/95, 1995, pp. 1–12.
47. J. J. Connolly, "Resistance Thermometer Measurement," in R. E. Bentley (Ed.), *Handbook of Temperature Measurement*, Vol. 2, *Resistance and Liquid in Glass Thermometry*, Springer, New York, 1998.
48. P. C. F. Wolfendale, J. D. Yewen, and C. I. Daykin, "A New Range of High Precision Resistance Bridges for Resistance Thermometry," in J. F. Schooley (Ed.), *Temperature. Its Measurement and Control in Science and Industry*, Vol. **5**(2), American Institute of Physics, New York, 1982, pp. 729–732.
49. R. L. Rusby, "The Rhodium–Iron Resistance Thermometer: Ten Years On," in J. F. Schooley (Ed.), *Temperature. Its Measurement and Control in Science and Industry*, Vol. **5**(2), American Institute of Physics, New York, 1982, pp. 829–834.
50. G. Schuster, "Temperature Measurement with Rhodium–Iron Resistors below 0.5K," in J. F. Schooley (Ed.), *Temperature. Its Measurement and Control in Science and Industry*, Vol. **6**(1), American Institute of Physics, New York, 1992, pp. 449–452.
51. S. D. Wood, B. W. Mangum, J. J. Filliben, and S. B. Tillett, "An Investigation of the Stability of Thermistors," *J. Res. NBS*, Vol **83**, 247–263, 1978.
52. W. R. Beakley, "The Design of Thermistor Thermometers with Linear Calibration," *J. Sci. Instrum.*, **28**, 176–179, 1951.
53. M. Sapoff and R. M. Oppenheim, "Theory and Application of Self-Heated Thermistors," *Proc. IEEE*, **51**, 1292, 1964.
54. M. Sapoff, "Thermistors: Part 4, Optimum Linearity Techniques," *Measur. Control*, **14**, pp. 112–119, 1980.

55. J. K. Krause and B. C. Dodrill, "Measurement System Induced Errors in Diode Thermometry," *Rev. Soc. Econ.*, **57**, 661–665, 1986.
56. J. B. Johnson, "Thermal Agitation of Electricity in Conductors," *Phys. Rev.*, **32**, 97–109, 1928.
57. H. Nyquist, "Thermal Agitation of Electric Charge in Conductors," *Phys. Rev.*, **32**, 110–113, 1928.
58. R. A. Kamper, "Survey of Noise Thermometry," in H.H. Plumb (Ed.), *Temperature. Its Measurement and Control in Science and Industry*, **4**(1), Instrument Society of America, Pittsburgh, 1972, pp. 349–354.
59. T. V. Blalock and R. L. Shepard, "A Decade of Progress in High Temperature Johnson Noise Thermometry," in J. F. Schooley (Ed.), *Temperature. Its Measurement and Control in Science and Industry*, Vol. **5**(2), American Institute of Physics, New York, 1982, pp. 1219–1223.
60. D. R. White, R. Galleano, A. Actis, H. Brixy, M. DeGroot, J. Dumbledam, A. L. Reesink, F. Elder, H. Sakurai, R. L. Shepard, and J. C. Gallop, "The Status of Johnson Noise Thermometry," *Metrologia*, **33**, 325–335, 1996.
61. H. Seger, *Thorindustrie Zeitung*, 1886, pp. 135, 229.
62. C. O. Fairchild and M. F. Peters, "Characteristics of Pyrometric Cones," *J. Am. Ceram. Soc.*, **9**, 701–743, 1926.
63. H. P. Beerman, "Calibration of Pyrometric Cones," *J. Am. Ceram. Soc.*, **39**, 47–54, 1956.
64. T. D. McGee, *Principles and Methods of Temperature Measurement*, Wiley, New York, 1988.
65. British Standard (BS), "Part 7: Temperature Measurement. Guide to the Selection and Use of Temperature/Time Indicators," BS 1041, 1988.
66. C. Bird, J. E. Mutton, R. Shepherd, M. D. W. Smith, and H. M. L. Watson, "Surface Temperature Measurement in Turbines," in AGARD CP 598, Advisory Group for Aerospace Research and Development, 1998, pp. 21-1–21-10.
67. J. Gallery, M. Gouterman, J. Callis, G. Khalil, B. McLachlan, and J. Bell, "Luminescent Thermometry for Aerodynamic Measurements," *Rev. Sci. Instrum.*, **65**, 712–720, 1994.
68. W. H. Fonger and C. W. Struck, "Eu₃D Resonance Quenching to the Charge-Transfer States in Y₂O₂S, La₂O₂S and LaOCl," *J. Chem. Phys.*, **52**, 6364–6372, 1970.
69. S. W. Allison and G. T. Gillies, "Remote Thermometry with Thermographic Phosphors: Instrumentation and Applications," *Rev. Sci. Instrum.*, **68**, 2615–2650, 1997.
70. A. L. Heyes, "Thermographic Phosphor Thermometry for Gas Turbines," in C. H. Sieverding and J. F. Brouckaert (Eds.), *Advanced Measurement Techniques for Aero and Stationary Gas Turbines*, VKI LS 2004-04, Von Karman Institute, 2004.
71. A. L. Heyes, "On the Design of Phosphors for High Temperature Thermometry," *J. Luminesc.*, **129**, 2004–2009, 2009.
72. J. P. Feist, A. L. Heyes, and J. R. Nicholls, "Phosphor Thermometry in an EBPVD Produced TBC Doped with Dysprosium," *Proc. Instrum. Mech. Eng.*, **215**: Part G, 333–341, 2001.
73. J. P. Feist, A. L. Heyes, K. L. Choy, and J. R. Nicholls, "Thermographic Phosphor Thermometry: Recent Development for Applications in Gas Turbines," in C. Greated, J. Cosgrove, and J. M. Buick, (Eds.), *Optical Methods for Data Processing in Heat and Fluid Flow*, Professional Engineering Publishing, Bury St Edmunds, 2002.
74. V. U. Kakade, G. D. Lock, M. Wilson, J. M. Owen, and J. E. Mayhew, "Accurate Heat Transfer Measurements Using Thermochromic Liquid Crystal. Part 1: Calibration and Characteristics of Crystals," *Int. J. Heat Fluid Flow*, **30**, 939–949, 2009.
75. J. W. Baughn, Review—liquid crystal methods for studying turbulent heat transfer. *Int. J. Heat Fluid Flow*, **16**:365–375, 1995.
76. G. T. Roberts and R. A. East, "Liquid Crystal Thermography for Heat Transfer Measurement in Hypersonic Flows: A Review," *J. Spacecraft and Rockets*, **33**, 761–768, 1996.
77. V. U. Kakade, G. D. Lock, M. Wilson, J. M. Owen, and J. E. Mayhew, "Accurate Heat Transfer Measurements Using Thermochromic Liquid Crystal. Part 2: Application to a Rotating Disc," *Int. J. Heat Fluid Flow*, **30**, 950–959, 2009.
78. R. P. Campbell and M. J. Molezzi, "Applications of Advanced Liquid Crystal Video Thermography to Turbine Cooling Passage Heat Transfer Measurement," Paper 96-GT-225, ASME, New York, 1996.
79. S. Ou, R. Rivir, M. Meininger, F. Soechting, and M. Tabbita, "Transient Liquid Crystal Measurement of Leading Edge Film Cooling Effectiveness and Heat Transfer with High Free Stream Turbulence," Paper 2000-GT-0245, American Society of Mechanical Engineers, New York, 2000.
80. S. J. Lee and J. H. Yoon, "Temperature Field Measurement of Heated Ventilation Flow in a Vehicle Interior," *Int. J. Vehicle Design*, **19**, 228–243, 1998.

81. ESDU, "Temperature Measurement: Techniques," ESDU 02006, ESDU Heat Transfer Series Vol. 4 ("Insulation and Temperature Measurement"), 2002.
82. Y. S. Touloukian and D. P. DeWitt, *Thermophysical Properties of Matter*, Vol. 7, *Thermal Radiative Properties. Metallic Elements and Alloys*, IFI/Plenum, New York, 1970.
83. Y. S. Touloukian and D. P. DeWitt, *Thermophysical Properties of Matter*, Vol. 8, *Thermal Radiative Properties. Nonmetallic Solids*, IFI/Plenum, New York, 1972.
84. Y. S. Touloukian, D. P. DeWitt, and R. S. Hemicz, *Thermophysical Properties of Matter*, Vol. 9, *Thermal Radiative Properties. Coatings*, IFI/Plenum, New York, 1972.
85. H. W. Yates and J. H. Taylor, Infrared transmission of the atmosphere. NRL Report 5453, U.S. Naval Research Laboratory, Washington, DC, 1960.
86. J. E. A. Selby and R. A. McClatchey, "Atmospheric Transmittance from 0.25 to 28.5 μm : Computer Code LOWTRAN 2," Report AFCRL-72-0745, Air Force Cambridge Research Laboratory, 1972.
87. J. E. A. Selby and R. A. McClatchey, "Atmospheric Transmittance from 0.25 to 28.5 μm : Computer Code LOWTRAN 3," Report AFCRL-75-0255, Air Force Cambridge Research Laboratory, 1975.
88. J. E. A. Selby and R. A. McClatchey, "Atmospheric Transmittance from 0.25 to 28.5 μm : Computer Code LOWTRAN 3B," Report AFCRL-TR-76-0258, Air Force Cambridge Research Laboratory, 1976.
89. J. E. A. Selby, F. X. Kneizys, J. H. Chetwynd, and R. A. McClatchey, "Atmospheric Transmittance from 0.25 to 28.5 μm : Computer Code LOWTRAN 4," Report AFGL-TR-78-0053, Air Force Cambridge Research Laboratory, 1978.
90. F. G. Smith (Ed.), "*The Infrared and Electro-Optical Systems Handbook*," Vol. 2, *Atmospheric Propagation of Radiation*, MI and SPIE Press, Ann Arbor, Michigan, 1993.
91. HITRAN, available: <http://www.cfa.harvard.edu/hitrان>, accessed June 25, 2010.
92. W. D. Rogatto (Ed.), *The Infrared and Electro-Optical Systems Handbook*, Vol. 3, *Electro-Optical Components*, MI and SPIE Press, Ann Arbor, Michigan, 1993.
93. H. Kaplan, *Practical Applications of Infrared Thermal Sensing and Imaging Equipment*, 2nd ed, Vol. TT34, SPIE Press, 1999.
94. R. R. Dils, "High Temperature Optical Fiber Thermometer," *J. Appl. Phys.*, **54**, 1198–1201, 1983.
95. E. W. Saaski and J. C. Hartl, "Thin-Film Fabry Perot Temperature Sensors," in J. F. Schooley (Ed.), *Temperature: Its Measurement and Control in Science and Industry*, Vol. 6(2), American Institute of Physics, New York, 1992, pp. 731–734.
96. M. Sun, "Fibreoptic Thermometry Based on Photoluminescent Decay Times," in J. F. Schooley (Ed.), *Temperature: Its Measurement and Control in Science and Industry*, Vol. 6, American Institute of Physics, New York, 1992, pp. 715–719.
97. B. C. R. Ewan, "A Study of Two Optical Fiber Probe Designs for Use in High Temperature Combustion Gases," *Measur. Sci. Technol.*, **9**, 1330–1335, 1998.
98. Z. Zhang, K. T. V. Grattan, and A. W. Palmer, "Fibre Optic High Temperature Sensor Based on the Fluorescence Lifetime Of Alexandrite," *Rev. Sci. Instrum.*, **63**, 3869–3873, 1992.
99. K. T. V. Grattan and Z. Y. Zhang, *Fibre Optic Fluorescence Thermometry*, Chapman & Hall, London, New York, 1995.
100. D. A. Krohn, *Fiber Optic Sensors*, ISA, New York, 2000.
101. G. C. Holst, *Electro-Optical Imaging System Performance*, JCD Publishing, Winter Park, FL, 1995.
102. G. C. Holst, *Common Sense Approach to Thermal Imaging*, JCD Publishing/SPIE Press, Bellingham, Washington, USA, 2000.
103. H. M. Runciman, "Thermal Imaging. Section 35.1," in J. G. Webster (Ed.), *The Measurement, Instrumentation and Sensors Handbook*, CRC Press, Boca Raton, FL, 1999.

CHAPTER 7

HEAT FLUX MEASUREMENT

T. E. Diller

Virginia Polytechnic Institute and State University
Blacksburg, Virginia

1 INTRODUCTION	285	4.2 Transient Optical Methods	299
2 IMPORTANT ISSUES	286	4.3 Coaxial Thermocouple	300
2.1 Heat Sink	287	4.4 Null-point Calorimeter	300
2.2 Potential Disruption of Surface-Mounted Gauges	287	4.5 Slug Calorimeter	301
2.3 Potential Disruption of Insert Gauges	288	4.6 Differential Flame Thermometer	302
3 GAUGES BASED ON SPATIAL TEMPERATURE DIFFERENCE	289	5 GAUGES BASED ON ACTIVE HEATING METHODS	302
3.1 One-Dimensional Planar Gauges	289	5.1 Constant Heat Flux	302
3.2 Insert Heat Flux Gauges	294	5.2 Constant Surface Temperature	303
3.3 Radiometers	297	6 CALIBRATION AND ERRORS	306
4 GAUGES BASED ON TEMPERATURE CHANGE WITH TIME	297	6.1 Heat Flux Gauge Calibration	306
4.1 Thin-film Methods	298	6.2 Error Estimates	307
		REFERENCES	307

1 INTRODUCTION

As the cost of energy increases, the importance of predicting and controlling its movement is of increasing concern. For many years the calculation of heat transfer has been considered a fundamental part of the engineering design of any thermal system. Whether for building environments, power production, or manufacturing processes, temperature control is often of paramount concern for physical comfort and the production of industrial materials and products. To effectively control temperature requires that energy be transferred in a known and controlled manner. It is understood that good temperature measurements are essential, and many companies offer extensive lines of temperature sensors for almost any environment. But it is equally important to know the details of the energy transfer itself.

Temperature is a fundamental property of a material and accurate measurement and calibration standards are readily available. The measurement of heat transfer, however, is a very different situation. First, it is much more challenging because heat transfer is the movement of thermal energy through a material and is not a property. Consequently, establishing measurement standards and calibration methods is much more challenging. Second, the whole concept of heat flux or thermal energy transfer per area is not as well understood by the general

population. Even many engineers do not have a good physical understanding of a W/m^2 or a $Btu/ft^2\cdot h$. Heat flux gauge sales are a minuscule fraction of the thermal measurement market. Hopefully this chapter will encourage researchers and practitioners to use this important technology. Part of an engineer's or scientist's education should be the experience of using heat flux gauges and measuring heat transfer.

Previous reviews have covered the history of heat flux instrumentation. The most comprehensive was done in 1993.¹ Combustion applications were covered by Arai et al.,² focusing on radiation heat transfer measurement. An emphasis on electronic cooling was given by Keltner.³ Heat transfer measurements in buildings was presented by Flanders.⁴ Childs et al.⁵ covered the broad range of sensors used for convection measurements, while Han et al.⁶ focused more specifically on gas turbine applications. A compilation of heat flux gauge manufacturers with details of the available gauges is also available.⁷

The focus of the present review is the most useful current heat flux instrumentation, particularly heat flux gauges. Although some heat flux gauges are available commercially and may even be standard stock items, others are currently limited to research laboratories. The latter may be the commercial gauges of the future. Optical methods are discussed briefly, but these are generally research methods that require sophisticated equipment and data processing techniques. General principles for the proper use of heat flux gauges are discussed first, followed by the details of specific gauges along with some of their typical applications. Three classifications of gauges are considered based on measured temperature difference over space, the temperature change with time, and the power dissipated at a maintained temperature. In all of these cases it is important to understand the pathways of heat in and around the sensor, which means that how gauges are mounted on or in materials can consequently be crucial. The measurement methods are also categorized according to the type of temperature measurement. The three common techniques are thermocouples (either individually or differentially), resistance temperature devices (RTDs), and optical (liquid crystals, infrared, or thermographic phosphors). Calibration of heat flux gauges is then discussed along with error analysis. Obtaining a signal from a heat flux gauge is easy; properly interpreting the measurements is the challenge.

2 IMPORTANT ISSUES

There are a number of styles of gauges commercially available, made by several companies in the United States and Europe. While many of these gauges are easy to install and read the output, it is often crucial that a gauge with the correct style and range is selected to give meaningful results for a specific application. For example, it is desirable to use different types of gauges to measure the low heat fluxes typical of buildings and natural convection, the moderate heat fluxes of radiation from fires and forced convection in fluids, and the high heat fluxes of high-speed combustion and hypersonic flow.

As explained in this section, there are a number of problems and complications that should be taken into account while planning for any heat flux measurements. The most important issue is maintaining the proper heat flow and corresponding temperature distributions while making the measurements. The presence of a heat flux gauge on or in a surface will necessarily alter the temperature field and heat flux to some extent. For considering this effect the gauges can be categorized as either surface mounted or insert. The surface-mounted gauges are flat and are attached to the surface with some type of glue or paste. The insert gauges are usually cylindrical and are pressed into a hole flush with the surface. An additional issue that is sometimes neglected is where the heat goes, or the heat sink. This will be considered first, followed by the potential heat flow disruption. If these issues are not properly considered, even the most accurate heat flux gauge will give erroneous results.

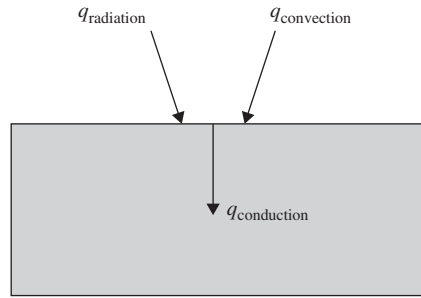


Figure 1 Surface heat balance.

2.1 Heat Sink

For the transfer of thermal energy to occur there must be a heat source and there must be a heat sink. Heat flux gauges are designed to measure the net heat transfer between the heat source and the heat sink, usually normal to a surface between them. For example, if a heat flux gauge is mounted to a surface that does not provide a good heat source or sink, it will usually measure no heat flux at steady-state conditions, irregardless of the surrounding temperatures.

Figure 1 illustrates the usual condition at the surface of a material. Conduction occurs through the material to the heat sink or source with convection and/or radiation exchange at the surface. If the material is low thermal conductivity, the heat flux at steady-state conditions will be very small. Therefore, high conductivity metals are usually desired for the material. Also, it is usually difficult to arrange conditions at the surface that provide only convection or radiation. There is usually always some of both at least to some extent. The surface heat balance is then expressed as

$$q_{\text{conduction}} = q_{\text{convection}} + q_{\text{radiation}} \quad (1)$$

Alternatively, another material may be placed against the surface to provide conduction in place of the convection and radiation.

2.2 Potential Disruption of Surface-Mounted Gauges

The measured heat flux at the surface of the material on which the gauge is mounted is assumed to be one dimensional. Because of the thermal disruption caused by the placement of the gauge on the surface, this may not be true, however. Wesley⁸ and Baba et al.⁹ have analyzed the thermal effects of a flat gauge mounted on the surface of the material. They determined that the one-dimensional assumption is valid when

$$\left(\frac{k}{k_s}\right)\left(\frac{\delta}{R}\right) \gg 1 \quad (2)$$

where k_s is the thermal conductivity of the substrate, R is the radius of the gauge, and δ and k are the effective thickness and thermal conductivity of the gauge and adhesive.

Measurements of convective heat flux are particularly sensitive to disturbances of the temperature of the surface. Convection is often expressed in terms of a heat transfer coefficient (h) and the fluid and surfaced temperatures:

$$q''_{\text{convection}} = h(T_{\text{fluid}} - T_{\text{surface}}) \quad (3)$$

Because the heat transfer coefficient in a boundary layer is increased locally by any surface temperature change, the effect of a small temperature change with location is further amplified at the

gauge location, as explained by Diller.¹ Therefore, any surface temperature disruptions caused by the gauge should be kept much smaller than the surface-to-environment temperature difference causing the heat flux. For gauges with one-dimensional heat transfer according to Eq. (2), the corresponding criterion for surface disruption of temperature (5% of the fluid-to-surface temperature difference) is

$$h \frac{\delta}{k} \leq 0.05 \quad (4)$$

where h is the heat transfer coefficient between the fluid and surface. The important parameter is the ratio of the gauge thickness (δ) to the gauge thermal conductivity (k). As this ratio increases, the sensitivity of the gauge increases, but the disruption caused by the gauge also increases according to Eq. (4). An optimum value for the particular application must be determined. If the gauge material uniformly covers the entire surface, however, the value of $h\delta/k$ can be up to an order of magnitude larger because there are no local disruptions of the surface temperature. Independent measures of the substrate surface temperature and the gauge surface temperature are advantageous in defining a value of the heat transfer coefficient and ensuring that the sensor does indeed provide a small thermal disruption.

Measurements of radiation heat transfer *from* the surface have similar sensitivities to surface temperature disturbances as convection. This is not true for radiation *to* the surface, however. This asymmetry of disturbance effects is due to the radiation heat flux being proportional to the fourth power of the absolute temperature. Consequently, a high-temperature heat source dominates the transfer exchange over the low-temperature heat sink. The surface coating properties of the gauge (absorptivity, transmissivity, reflectivity, and emissivity), however, should be matched with those of the surrounding surface for either case with radiation present. If the coating is nearly black, a match of emissivity is usually sufficient.

2.3 Potential Disruption of Insert Gauges

Insert heat flux gauges appear to cause less disruption of the surface because they can be mounted flush with the surface. This does not ensure a good temperature match with the surrounding surface, however. The local temperature and heat flux in the vicinity of the sensor is disturbed whenever the thermal properties and heat sink of the gauge are different than those of the surrounding surface. Gifford et al.¹⁰ have modeled the two effects as

$$\frac{q''_g}{q''_p} = \frac{1}{(h_p/h_g) + h_p R''} \quad (5)$$

where the heat flux measured by the gauge (q''_g) is compared to that of the surrounding undisturbed surface (q''_p). The thermal resistance of the gauge is represented by R'' , which causes a lower apparent heat flux from the gauge. It also decreases the apparent heat transfer coefficient over the gauge h_g relative to the surrounding undisturbed surface h_p . The effect has been demonstrated for laminar flow¹ and calculated for turbulent boundary layer flow.¹¹ Moffat et al.¹² have shown experimentally that this effect is larger than originally anticipated for turbulent boundary layers. It is counterintuitive that this effect actually becomes larger as the gauge size becomes smaller. Therefore, surface temperature disruptions caused by the gauge should be kept much smaller than the surface-to-environment temperature difference causing the heat flux.

If the gauge is not water cooled, it relies on the surrounding material to conduct away the heat it receives. Therefore, it must have a good thermal path to the surface into which it is mounted. It should also have good physical contact ensured by a tight fit in the hole or threads with a method to tighten the gauge into the surface. For steady-state measurements the gauge should have an effective thermal conductivity as high or higher than the surrounding material because all of the heat must be dissipated into the surrounding surface. For unsteady

heat transfer conditions, however, the gauge properties should match those of the surrounding material to ensure the same thermal transients. If the gauge is water cooled, the surrounding substrate can still affect the readings whenever forced or natural convection is present.¹³ In either case, independent measures of the substrate and the gauge surface temperatures are advantageous in defining a value of the heat transfer coefficient and for ensuring that the gauge does indeed match the surface temperature.

3 GAUGES BASED ON SPATIAL TEMPERATURE DIFFERENCE

These heat flux gauges operate by measuring a temperature difference over a spatial distance. There are several different geometries and temperature measurement methods. Because these gauges measure continuously, the heat flux through the gauge can be measured as long as the signal is monitored. They can be attached on the surface or inserted into the material. The different styles are discussed in separate subsections.

3.1 One-Dimensional Planar Gauges

The simplest concept for heat flux measurement is the layered gauge as illustrated in Fig. 2. The temperature is measured on either side of a thermal resistance layer in the direction normal to the surface. The two most common methods of measuring the temperature difference are RTDs and thermocouples. A new American Society for Testing and Materials (ASTM) standard is devoted to these heat flux gauges.¹⁴

The voltage output of the heat flux gauge illustrated in Fig. 2 is not only a function of the temperature difference but also the thickness and thermal conductivity of the thermal resistance material, δ and k . At steady state the one-dimensional conduction equation reduces to

$$q'' = \frac{k}{\delta} (T_1 - T_2) \quad (6)$$

The transient response of the gauge is a function of the thermal resistance layer thickness and the thermal diffusivity of the material. Hager¹⁵ has analyzed the one-dimensional transient response when mounted on a perfect heat sink and gives the time required for 98% response as

$$t = \frac{1.5\delta^2}{\alpha} \quad (7)$$

where α is the gauge thermal diffusivity. It should be noted that the sensitivity increases linearly with the thermal resistance layer thickness, but the response time increases as the square of the thickness. Consequently, sensitivity versus time response is one of the major tradeoffs in the design of these gauges.

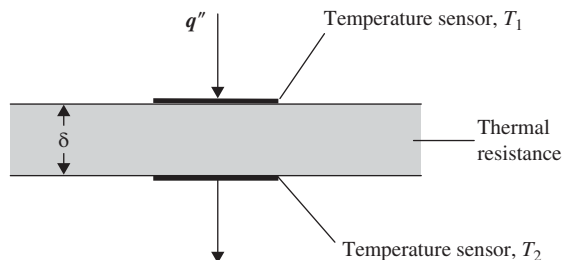


Figure 2 Layered heat flux gauge.

Surface-Mounted Gauges Using RTD Sensors

Any material that is an electrical conductor and changes electrical resistance with temperature can in theory be used as an RTD. The temperature sensitivity for most metals is nearly constant over a wide temperature range, but is small (a fraction of a percent change in resistance per °C). The advantage of an RTD is that it usually has a higher precision in measuring temperature than a thermocouple and it gives absolute temperature. It must be supplied with a small constant current, however, for measurements. Another disadvantage is that its resistance is also sensitive to strain and other factors, such as aging.

Epstein et al.¹⁶ produced a heat flux gauge for turbomachinery research using a 25- μm -thick sheet of polyimide (Kapton) with nickel RTDs deposited on either side. The nickel resistance element (1.0 mm by 1.3 mm) is immediately contacted to gold leads to isolate the voltage drop of the measurement at the sensor location. The leads from the bottom element are brought through the polyimide sheet so that all four leads can be taken to the edge of the sheet together. The nickel elements are either vacuum deposited with direct-current (dc) sputtering or electroless plated. Up to frequencies of about 20 Hz the gauge responds directly to the heat flux, as indicated in Eq. (6). For frequencies above 1 kHz the polyimide resistance layer appears infinitely thick, and the top resistance element (T_1) responds like a transient heat flux gauge described in Section 4.1. To cover the entire range from dc to 100 kHz a numerical data reduction technique is used to reconstruct the heat flux signal. One of the advantages of these gauges is that they can be wrapped onto curved surfaces, although the temperature calibrations change during this process, which may necessitate in situ calibration.

The heat flux gauge developed by Piccini et al.¹⁷ is made by sputtering platinum RTDs onto one side of a 50- μm -thick sheet of Upilex to measure T_1 . A thermocouple is mounted into the metal substrate onto which the sheet is glued for the second temperature measurement, T_2 . The heat flux at steady state is calculated from the temperature difference between the RTD and the thermocouple as shown in Eq. (6). The thickness and thermal conductivity of the Upilex and the glue layer are determined from direct calibration. Analytical solutions of the unsteady heat transfer equations are used to determine the unsteady heat flux up to frequencies of 100 kHz, similar to the method used by Epstein et al.¹⁶

For higher temperature applications, Talib et al.¹⁸ painted platinum films onto an enameled piece of 2-mm-thick Inconel. This was mounted onto a surface with embedded thermocouples to create a heat flux gauge of the same functionality as Piccini et al.¹⁷ This was used in a propane burner for fire testing. Fralick and Wrbanek¹⁹ have demonstrated a heat flux gauge with platinum RTDs printed on both sides of a 1-mm-thick slice of alumina for high-temperature applications. This double-sided arrangement keeps both temperature measurements on the gauge itself, which avoids the required in situ calibration of the previous two methods.

Surface-Mounted Gauges Using Thermocouple Sensors

The temperature sensitivity of different combinations of materials for thermocouples is indicated by the Seebeck coefficient, S_T . Excluding the semiconductor materials, the maximum sensitivity for any of the possible pairs is 50–100 $\mu\text{V}/^\circ\text{C}$. Kinzie²⁰ lists details of many non-standard thermocouple pairs. Although a reference temperature is required for measuring absolute temperature, thermocouples generate an electrical output without the excitation current required of RTDs. For measuring temperature difference, however, a reference temperature is not needed. This is illustrated in Fig. 3 where the output voltage E is

$$E = S_T (T_1 - T_2) \quad (8)$$

If a number of these units are connected together in series, the result is a thermopile that increases the voltage output for a given temperature difference. An example of such a thermopile heat flux gauge is illustrated in Fig. 4. Figure 4 shows three and one-half pairs of thermocouples combined in series across the thermal resistance layer. Each produces an output

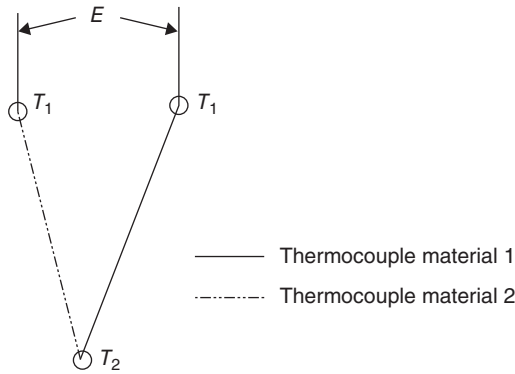


Figure 3 Thermocouple measurement of temperature difference.

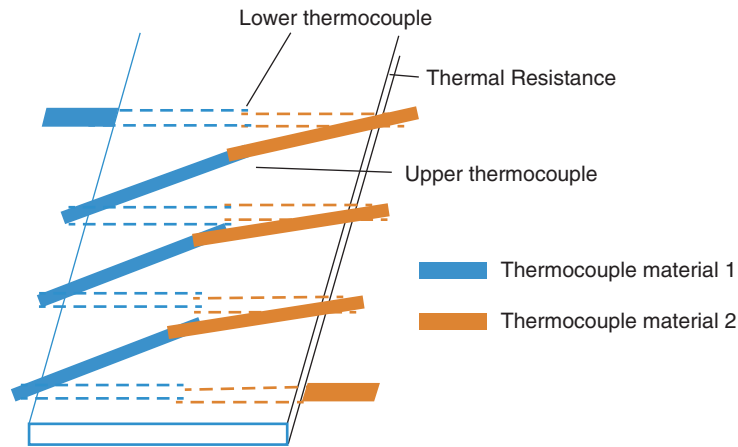


Figure 4 Thermopile heat flux gauge.

voltage that is proportional to the temperature difference, $T_1 - T_2$. The total output voltage is then proportional to the number of thermocouple pairs, N , and the Seebeck coefficient for the thermocouple pair, S_T :

$$E = NS_T(T_1 - T_2) \quad (9)$$

Using a thermopile, therefore, can easily overcome the greater sensitivity of individual RTDs. Thermocouples are also insensitive to strain and most other factors besides temperature. Moreover, only two leads are required for a heat flux measurement, versus four for two RTDs. The corresponding heat flux sensitivity of the ideal layered gauge is therefore

$$S_q = \frac{E}{q''} = \frac{NS_T\delta}{k} \quad (10)$$

To minimize the temperature disruption of the gauge, the thickness, δ , should be kept as small as possible, particularly if there is a large convection coefficient on the surface, as shown in Eq. (4).

The values of δ used in different gauges vary widely depending on the range of heat fluxes to be measured. Thermal resistance layers with thicknesses of 1 mm or more have generally

been used for heat fluxes less than 1 kW/m^2 . The time response is on the order of a second or more. Applications are typically conduction heat flux in building structures or insulation and natural convection. Bales et al.²¹ have published a book of articles discussing the design, calibration, and use of heat flux gauges for building applications. One design uses welded wire to form the thermopile across a sensor about 1 mm thick with an upper temperature limit of 300°C . These are manufactured in a range of sizes by International Thermal Instrument Co. Applications include heat transfer in buildings and physiology. Sensors with higher sensitivity are made with semiconductor thermocouple materials for geothermal applications.

For heat fluxes of up to 100 kW/m^2 thermal resistance thicknesses of $25\text{--}100 \mu\text{m}$ have been used. The corresponding time response is as low as 50 ms. Some improvement in the frequency response is possible with appropriate signal conditioning.²² To measure the temperature difference, $T_1 - T_2$, Ortolano and Hines²³ used a thermopile constructed of thin metal foils built around a Mylar or Kapton sheet. It is very versatile because it easily conforms to most surface shapes. Applications have included many types of conduction, convection, and radiation. These gauges are manufactured by the RdF Corp. and sold by several distributors. One effective method of eliminating the problem of the thermal and physical disruption from gluing the gauge onto the surface during forced convection measurements is to mask the entire surface with an equivalent thickness of the gauge material. The same approach was used by Hubble and Diller²⁴ to produce an array of heat flux sensors on a Kapton sheet. Instead of connecting the differential thermocouples in series, they were isolated individually as single pairs that gave 10 heat flux readings on each sheet. With appropriate data processing a 95% time response of 36 ms was obtained.

Thick-film technology was used by Van Dorth et al.²⁵ to put over 500 thermocouple pairs on a heat flux sensor that was 15 by 30 mm in size. Platinum and platinum–gold conductors were printed over and under a thermal resistance layer of glasslike material. This gave good sensitivity for demonstrated heat fluxes up to 200 kW/m^2 and temperatures up to 500°C .

A smaller, but similar sensor design has been made with screen printing techniques of conductive inks.²⁶ A copper–nickel thermocouple pair was used with a dielectric ink for the thermal resistance layer. The inks were printed onto anodized aluminum sheets for the substrate. Although the entire package is $350 \mu\text{m}$ thick, the thermal resistance is low because of the high thermal conductivity of all of the materials. Sensitivities are sufficient to measure heat fluxes as low as 0.1 kW/m^2 . The thermal time constant is about 1 s, and the upper temperature limit is approximately 150°C . The aluminum base provides some limited conformance to a surface.

Printed circuit techniques were previously used by Vatel Corp. to produce a heat flux gauge by plating two thermocouple materials on either side of a 0.2-mm-thick printed circuit board. The thermocouples were connected in series by holes drilled and plated through the board, forming many thermocouple pairs to give good sensitivity. The time constant for transient response was approximately 1 s.

An array of heat flux sensors was made with thermal vapor deposition by Ewing et al.²⁷ Thermocouple pairs were formed on both sides of a $50\text{-}\mu\text{m}$ -thick sheet of Kapton individually wired to give a separate heat flux and temperature output for each pair. There are a number of fabrication tricks to make a reliable sensor, including fluxless soldering of lead wires, vacuum depositing through holes in the sheet, and sealing the entire sensor to prevent oxidation with time.

A robust high-temperature heat flux gauge (HTHFS) was designed and fabricated by Gifford et al.²⁸ by welding Chromel and Alumel strips as illustrated in Fig. 5. The thermal resistance between the top and bottom thermocouples is formed by the elements themselves. The ceramic (ZTA) strips are included to provide electrical insulation between elements. An additional thermocouple wire welded to the top of the gauge provides the surface temperature, which is useful for interpreting the heat flux signal. Long time operation and cycling to 1000°C was

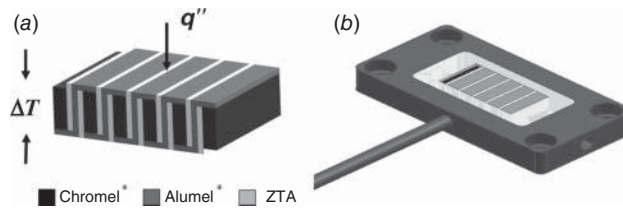


Figure 5 HTHFS, schematic of the measuring element on the left, complete sensor on the right.

demonstrated. The time constant was less than 1 s. The measurement chip can also be mounted in an insert-type housing that can be air or water cooled for gauge temperature control.

Hubble and Diller²⁹ developed a simple data processing method to extend the operation of the HTHFS so that it could be used on any substrate material. All of the sensors in this section are designed for the heat to go through the sensor into the material on which they are mounted as described in Section 2. The calorimeters described in Section 4 actually absorb the heat into the sensor itself, using the rate of temperature rise as the measure of heat transfer. The HTHFS can operate in both modes simultaneously—as a differential sensor and a calorimeter. Combining the heat transfer at the surface gives what is termed the “hybrid heat flux”:

$$q'' = q''_{\text{differential}} + 1/2 q''_{\text{calorimeter}} \quad (11)$$

This gives the correct heat flux whether the gauge is mounted on a good heat sink (high-conductivity material) or a good insulator (low-conductivity material). It also increases the time response of the gauge by about an order of magnitude. The differential heat flux is proportional to the usual temperature difference measured across the gauge and the calorimeter heat flux is proportional to the time rate of temperature change of the gauge.

A thin-film version of a high-temperature heat flux gauge has been developed by Meso-Scribe Technologies, Inc. that can be deposited directly onto test surfaces using a direct write thermal spray process.³⁰ Eighty thermocouple pairs (type K or N) are scribed around a layer of dielectric serving as the thermal resistance for the heat flux signal and a separate thermocouple gives the surface temperature. A layer of yttria-stabilized zirconia is first deposited on a metal surface to provide electrical isolation. It can also be deposited over the gauge to encapsulate it for better durability. All of the layers are on the order of 0.1 mm thick, which gives a good output signal.

An anisotropic thermoelement has been used by Mityakov et al.³¹ to produce a heat flux gauge with ten to one hundred times the voltage output of the usual thermopile gauges. This is attributed to the transverse Seebeck effect which is experienced in single crystal bismuth strips. The strips are wired in series and mounted on a mica base. The output voltage is generated at the surface of the material, which can be as thin as 0.1 mm.

Surface-Mounted Wire-Wound Gauges

The wire-wound gauge is similar to the thermopile layered gauges except for the method of producing the thermocouple junctions around the thermal resistance layer. A fine wire of one of the thermocouple materials, for example, constantan, is wrapped around the thermal resistance layer N number of turns. One-half of the wire is then electroplated with the other thermocouple material, for example, copper. The result is a set of thermocouple junctions where the electroplating stops on the top and bottom of the thermal resistance layer. It is different from the thermopile gauges of Section 3.1.2, however, because one of the wires is continuous all around the sensor. This forms a thermopile with the wire on one side and the wire and plating in series

on the other side. There are N pairs of thermocouple junctions corresponding to the N windings. The theoretical output is therefore less than a true thermopile gauge and is a function of the plating thickness in addition to the overall geometry and thermoelectric output of the materials.

A major use of these gauges is low heat flux measurements on the surface of equipment to measure heat losses and insulation effectiveness. A summary of the theory is given by Hauser³² and a review of the applications by van der Graaf.³³ Thicknesses of the thermal resistance layer vary from 0.5 to 3.0 mm, with time constants from 1 to 30 s. Some of the sensors are flexible for wrapping around pipes and curved surfaces. Applications include building structures, insulation, geothermal, and medicine, with heat fluxes generally less than 1 kW/m^2 . Concept Engineering offers this type of gauge commercially.

3.2 Insert Heat Flux Gauges

These heat flux gauges are mounted through a hole in the material flush with the surface. The heat sink is provided either by the material in which it is mounted or by water cooling through channels in the gauge. A new ASTM standard is devoted to these heat flux gauges.³⁴

Insert Gauges Using Thin-Film Thermocouple Sensors

A differential thermopile as illustrated in Fig. 4 can be deposited directly onto a substrate to give design and manufacturing flexibility. Such a thin-film device has been described in detail by Diller and Onishi³⁵ and was first produced by Hager et al.^{36,37} using sputtering techniques. Microfabrication methods are used to deposit hundreds of thermocouple pairs around a silicon monoxide layer to create the differential thermopile. Either photolithography or stencil masks can be used to define the patterns. The resulting physical and thermal disruption of the surface due to the presence of the sensor is extremely small.

While the original version of this heat flux microsensor (HFM) placed the temperature sensors almost directly over top of each other across a single thermal resistance layer as illustrated in Fig. 4, it is not a requirement. The bottom temperature sensors simply need to be at a uniform temperature, and the top temperature sensors need to be at a temperature dictated by the heat flux perpendicular to the surface. This can be accomplished on a high conductivity substrate (aluminum nitride) by separate thermal resistance pads ($1 \mu\text{m}$ layer of silicon monoxide) underneath the top thermocouples. The pattern is illustrated in Fig. 6.³⁸ The bottom temperature

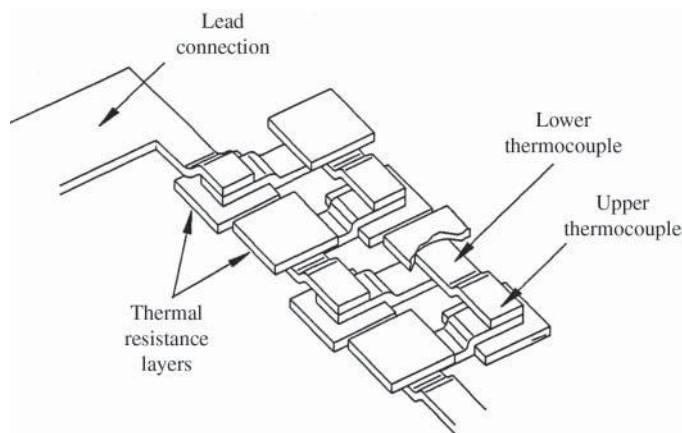


Figure 6 Heat flux microsensor pattern.³⁸

sensors can then be placed directly on the substrate with or without thermal resistance pads on top. Leads are taken down the side and attached to wires on the side or behind the sensor substrate, which is then press fit into a high conductivity metal housing typically with an outside diameter of about 6 mm. A thin-film RTD or thermocouple is also deposited on the surface for independent temperature measurement of the sensor surface. The applicable range for heat flux measurement is from 1 kW/m^2 to over 10 MW/m^2 . Because the sensor is so thin, the thermal response time is less than $10 \mu\text{s}$,³⁸ giving a good frequency response well above 10 kHz .

Note that the opposite arrangement does not work. If all of the temperature sensors are placed on the substrate with thermal pads over one-half of them, the resulting signal cannot be easily related to the surface heat flux. Instead it measures a pattern of lateral temperature gradients in the substrate with very different time constants.

Insert Wire-Wound Gauges

The Schmidt–Boelter version of the wire-wound gauge is described by Kidd and Nelson³⁹ with details of the theoretical output compared with actual gauge sensitivities. The gauge geometry is illustrated in Fig. 7. It is meant as a gauge to be inserted through a hole in the material, mounted flush with the surface for measuring moderate to high heat fluxes ($10\text{--}1000 \text{ kW/m}^2$). Consequently, the thermal resistance layer (wafer) is usually made of a high thermal conductivity material, for example, anodized aluminum ($\sim 0.5 \text{ mm}$ thick). The nonconductive coating is necessary to provide electrical insulation with the bare wire of the thermopile. The entire wafer is placed in contact with a heat sink and surrounded by potting material to give a smooth surface to the top of the gauge. The wire is usually constantan with copper plating on one side of the wires top and bottom. This forms a type of differential thermopile, but the segmented plating on the wire gives an output less than for a true thermopile.

Schmidt–Boelter gauges are manufactured by Medtherm Corp. in a range of sizes down to 1.5 mm diameter. One advantage of the Schmidt–Boelter gauge is that it can be contoured to a curved surface. One of the drawbacks is that one-dimensional heat transfer is not really maintained. Two-dimensional effects can be significant and the potting material affects the gauge sensitivity. The transient response is typically $25\text{--}50 \text{ ms}$ but is usually not first order. Techniques for improving and correcting the time response are presented by Kidd and Adams⁴⁰ for making time-resolved measurements. A Schmidt–Boelter design having a first-order response has been patented.⁴¹

An alternative design was produced by Long et al.⁴² by winding constantan wire onto an annular disk of Macor. Copper plating of the outer radius of the wire produced a circular thermopile for use in turbomachinery research. Epoxy resin was used to cover the wires and appeared to substantially increase the thermal resistance of the gauge.

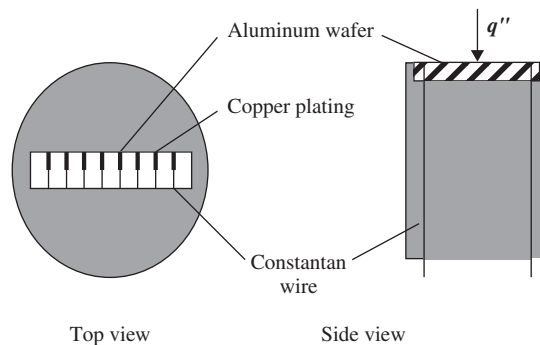


Figure 7 Schematic of an insert wire-wound heat flux gauge.

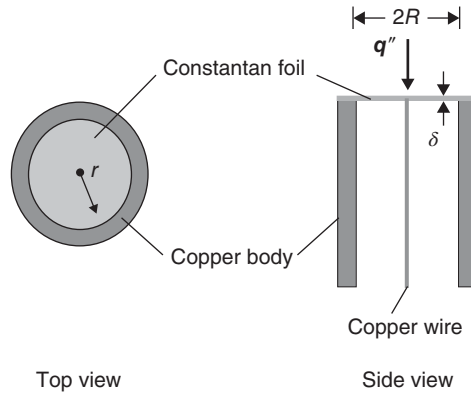


Figure 8 Schematic of a circular foil gauge.

Circular Foil Gauge (Gardon)

The circular foil gauge was originated by Robert Gardon⁴³ and consequently is often called a Gardon gauge. A sketch of the circular foil gauge is shown in Fig. 8. Constantan is usually used for the disk material and is attached to a hollow copper body. A copper wire is attached to the center of the foil to create a differential thermocouple between the center and edge of the disk. Unlike the previous gauges discussed, however, the heat transfer in the gauge is not in the direction that it enters the surface. The thermal energy is collected by the disk and transported laterally to the heat sink connected to the edge of the disk. The recorded temperature difference is, therefore, a function of the total heat transfer to the disk but also is a function of the distribution of heat flux over the disk surface. Analytical models of circular foil gauges have been presented in the literature including these nonlinear effects.^{1,44–46}

The usual application for Gardon gauges is radiation to a water-cooled gauge. Because there is negligible radiation from the gauge, the heat flux is uniform and the temperature distribution across the foil is parabolic

$$T - T_w = \frac{q''}{4k\delta}(R^2 - r^2) \quad (12)$$

where R is the foil outer radius, r is the radial coordinate, and T_w is the temperature of the wall, which is assumed equal to the temperature at the outer edge of the foil. When convection is present, however, the convective heat transfer is proportional to the difference in temperature between the fluid and the gauge. Because of the temperature distribution radially across the gauge, the heat flux is no longer uniform. For the same total heat transfer, therefore, the gauge will give less output than for radiation. If the convection heat transfer coefficient is uniform over the gauge, the analytical correction of the heat flux for convection is approximately⁴⁷

$$\frac{q''_{\text{corrected}}}{q''_{\text{uncorrected}}} = \frac{1}{1 - (3/4)(S_q h/S_T)} \quad (13)$$

where S_q is the sensitivity of the gauge as calibrated by radiation, h is the convection heat transfer coefficient, and S_T is the thermoelectric constant for the thermocouple pair. The correction is proportional to the gauge sensitivity and the heat transfer coefficient. Consequently, the sensitivity of the gauge should be kept low to limit the size of the correction and associated uncertainties. A general rule for specifying copper constantan gauges is

$$\frac{q''_{\text{convection}}}{q''_{\text{fullscale}}} \leq \frac{T_{\text{fluid}} - T_w}{3200^\circ\text{C}} \quad (14)$$

where the full-scale heat flux is that corresponding to an output of 10 mV. The measurement error becomes even larger if the heat transfer coefficient is nonuniform over the gauge surface, as can occur in strong shear flows. In addition, the surface temperature disruption caused by the presence of a circular foil gauge affects the local thermal boundary layer and changes the local heat transfer coefficient, as discussed in Section 2.3.

These corrections are all based on the assumption that the gauge makes perfect contact with the wall. Because the gauge is normally slip fit into place, there may be an additional temperature drop between the heat sink of the gauge and the wall. This would cause an additional drop in gauge output and would require an additional correction of the results.

Most Gardon gauges are made with a water cooling jacket as part of the sensor to keep it from overheating when in high heat flux environments. Water cooling should never be used when convection is being measured. The problem is that this causes a local “cold spot” and results in an erroneously high heat flux measurement, the opposite of the foil temperature disruption effect just discussed.

Circular foil gauges are manufactured and sold by Medtherm Corp. and Vatel Corp. Most are used for radiation measurements and are water cooled. The ASTM standard⁴⁸ for these gauges provides a good summary of the best practice for their use.

3.3 Radiometers

With the proper surface coating any heat flux gauge can be used to measure radiation, although specialized radiometers have been developed to increase the accuracy of radiation heat flux measurements.⁴⁹ One example is the Kendall radiometer,⁵⁰ which is a blackbody cavity with thermopile and an installed electric heater. This allows the electric power measurement to serve as the standard to provide a self-calibrated device for total irradiance. Several models are available from Medtherm Corp.

To eliminate the effects of convection, a transparent window or lens is often placed over the end of the gauge to transmit only the desired radiation transfer. The reduced angular view of the gauge with a window must be included in the calibration, along with the transmissivity of the window. Without a window the effects of natural convection are particularly a problem at low heat flux levels (less than 15 kW/m²).¹³ An additional problem in dirty environments is deposits on the window that reduce the transmissivity. One solution is to blow air past the window. Another possibility is the transpiration radiometer, which blows air through a porous plug that composes the exposed surface of the gauge. This not only blows off the fluid boundary layer with any contaminants but the air is heated as it passes through the plug. The measured radiation is then related to the temperature change of the air as it passes through the plug.^{51,52}

Brajuskovic et al.⁵³ have developed a slightly different version to operate in boilers. Instead of going through the plug, the air is directed through slots around a solid plug. The airflow keeps particles from reaching the heat flux element and it takes away the thermal energy. The path of the heat transfer is radial through the plug, however, as in a circular foil gauge. The heat flux is proportional to the temperature difference between the center and edge of the plug.

4 GAUGES BASED ON TEMPERATURE CHANGE WITH TIME

With the correct thermal model a single temperature measurement of a material can be used to infer the heat flux based on the time–temperature history. This involves solving the conduction heat transfer problem in the gauge and the wall material. Because the solution starts with the measured temperature as a function of time and calculates backward to find the needed heat flux boundary condition, it is in the form of an inverse heat transfer problem. The type of solution needed differs according to the gauge used and the corresponding assumptions.

4.1 Thin-film Methods

The operating principle of the thin-film gauges is to measure the surface temperature of a semi-infinite material (substrate) in response to the applied surface heat flux. The requisite transient conduction solutions for the one-dimensional semi-infinite model are given numerous references and explained in detail for this application by Schultz and Jones.⁵⁴ The starting point is the solution of the one-dimensional heat diffusion equation for a step change in surface temperature from a uniform initial temperature:

$$q'' = \frac{\sqrt{k \rho C}}{\sqrt{\beta t}} (T_w - T_0) \quad (15)$$

The material properties of the substrate enter as the square root of the product of $k\rho C$ (thermal conductivity, density, specific heat). A number of data reduction schemes have been developed based on variations of this solution to determine the heat flux from the surface temperature history, represented by measured temperatures at specified times. One common method is given by

$$q''(t_n) = \frac{2\sqrt{k\rho C}}{\sqrt{\beta}} \sum_{i=1}^n \frac{T_i - T_{i-1}}{\sqrt{t_n - t_i} + \sqrt{t_n - t_{i-1}}} \quad (16)$$

The summation for the heat flux at each given time is based on the current and all previous temperatures. One limitation of this equation is that constant thermal properties have been assumed for the substrate. A more serious problem, however, is the inherent instability of using a temperature record to infer the heat flux. This is akin to taking the derivative of the temperature signal, which greatly amplifies any noise present in the signal and is particularly important when making detailed measurements of time-resolved heat flux. To increase sensitivity and solution stability, a variety of inverse heat conduction techniques have been developed.^{55,56}

The advancement of thin-film deposition techniques has made the fabrication of large numbers of resistance elements for temperature measurement on the surface of models much simpler. All that is required is the application of a thin temperature measuring layer (usually an RTD) on the model with appropriate lead connections. The most popular methods have been to apply a thin layer of platinum paint or to directly sputter onto an electrically insulated substrate. With a typical thickness of 0.1 μm the response of the RTDs is of the order of 0.01 μs . This causes negligible effect on the heat flux measurements for times greater than a few microseconds. Therefore, results that are properly processed are essentially instantaneous even for high-speed flows. There is a limit on the length of the useful test data, however, due to the semi-infinite substrate assumption used in the modeling. The upper time limit for a 1% error in the heat flux at the surface is

$$t = 0.3 \frac{\delta^2}{\alpha} \quad (17)$$

For a typical insulating substrate (Macor) of $\delta = 1$ mm thickness the corresponding maximum time is nearly 400 ms. This makes the technique useful for many types of short-duration flows, such as shock tubes or high-speed blowdown facilities.

To measure the resistance of the RTD to determine the transient temperature history, a small current is used to drive a bridge circuit. The constant current source must be large enough to provide a measurable output voltage, but small enough to keep the self-heating effects negligible. This optimization is made easier if the sensor resistance is a high value. For a resistance of at least 100 Ω , a current of 1–2 mA provides good results. One of the advantages of vacuum-deposited resistance films is that the value of resistance is easier to control during fabrication.

Calibration of the sensors for heat flux measurements requires two steps. First, the resistance versus temperature relationship must be determined for each sensor. This can simply be done by putting the model in an oven and monitoring the resistance of each gauge over a set temperature range. The second part of the calibration is to determine the thermal properties

of the substrate. The most popular method is to measure the response of the sensor to a pulse of energy provided by an electrical discharge through the resistance film or a pulsed radiation source to the surface. It is important to measure the value of $k\rho C$ for each model because properties can vary significantly for many of the substrate materials between batches.

A group at Oxford has developed a technique to apply the thin-film gauges to metal substrates using a vitreous enamel coating to provide electrical insulation.⁵⁷ Although this gives much greater flexibility for experimental application of the method, it also complicates the data analysis. One method is to use an analog circuit plus digital processing of the signals, including filters and a frequency boosting circuit.⁵⁸ The calibration is also more complicated because of the multiple layers making up the substrate. A further refinement has been to place multiple RTDs on a single polyimide sheet that is then glued to the metal surface.⁵⁹

Another group has developed round Pyrex inserts that are placed in metal surfaces for measuring time-resolved heat flux in short duration turbine research test facilities. The data reduction includes both analog circuits and digital data processing, including Fourier transforms to optimize the frequency response and accuracy of the time-resolved results.⁶⁰ Concern over the thermal disruption caused by the Pyrex inserts was investigated and reported to be insignificant for the short 20- to 25-ms test times of the experiments.⁶¹ Moffat et al.¹² have investigated the more general case of longer times when the temperature rise of the insert becomes substantially more than the surrounding metal material.

4.2 Transient Optical Methods

A number of optical methods have been developed to measure the transient surface temperature for determination of heat flux. These include liquid crystals, infrared radiation measurement, temperature-sensitive paints, and thermographic phosphors. The advantage is that cameras can be used to give full coverage of the surface, although the results are usually limited to steady-state convection. The usual method involves a flow facility where either the model is injected into the flow at a different temperature or the flow is suddenly initiated with the model at a different initial temperature.

Infrared cameras offer the most potential measurement capability. Once the surface emissivity is calibrated, the data processing is relatively easy.⁶² High-speed versions are currently available that allow time-dependent measurements of heat flux from the transient temperature signals.⁶³ Proper surface coatings should be used. Viewing angles are important along with reflections from other surfaces.

Thermographic phosphors emit radiation in the visible spectrum when illuminated with ultraviolet light, which can be related to temperature at specific wavelengths.⁶⁴ Their main advantage is that they offer the possibility to operate in elevated temperature environments.⁶⁵ A charge-coupled device (CCD) camera is required to record the optical images and the data processing and calibration are challenging.⁶⁶

The temperature-sensitive paint method uses an europium complex as the luminophore with a mercury–xenon arc lamp for illumination.⁶⁷ A CCD camera is used to collect the images as a function of time. Because the paint layer has a low thermal conductivity, a two-layer model to relate the measured surface temperature to the heat flux is usually required.

Liquid crystals are chiral-nematic molecules that reversibly change color as a function of temperature. They are limited to a temperature range of about 25–40°C and are available commercially from Hallcrest in a convenient microencapsulated form. A hue capturing technique is used with a temperature calibration to reduce the data to temperatures as a function of time.⁶⁸ The liquid crystal method is used almost exclusively with convection testing in air to obtain the distribution of heat transfer coefficients as defined in Eq. (3).^{69,70} Multiple steps in the air temperature can even be used to obtain additional information, such as adiabatic wall temperatures.⁷¹

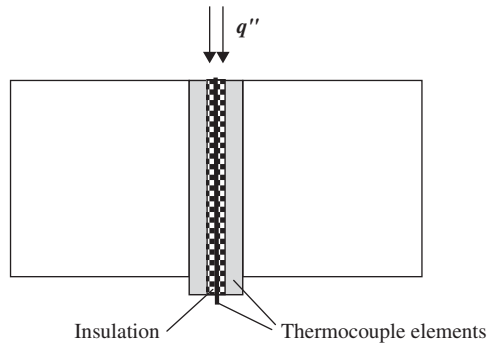


Figure 9 Schematic of a coaxial thermocouple.

4.3 Coaxial Thermocouple

Coaxial thermocouples are rugged sensors designed to be inserted through a material to measure the surface temperature of the model wall as a function of time, the same as thin-film gauges. Consequently, the same equations can be used to determine the corresponding heat flux. The physical concept is simple,⁷² as illustrated in Fig. 9. One thermocouple material forms the center wire, which is surrounded by an electrical insulator. The second thermocouple material forms a sheath around these two layers. The final assembly is often then drawn down to a smaller diameter. A second insulating material is sometimes placed around the assembly to isolate the thermocouple electrically from a metal substrate, which can affect the reading. The completed unit is press fit into the model. The actual thermocouple junction is formed at the very end by plating a thin layer of one of the materials, vacuum deposition, or by simply lightly sanding to mix the two materials together and bridge the thin insulating layer. Because the thickness of the top junction layer can be on the order of $10\ \mu\text{m}$, the initial response time can be much less than 1 ms. Smith et al.⁷³ include a second thermocouple with the use of a parameter estimation method to reduce the temperature data to heat flux.

The most important parameter in specifying the coaxial thermocouple gauges is to match the material thermal properties with those of the wall. As seen from Eq. (16), the property of importance is the product $k\rho C$, which for the coaxial thermocouple is taken as the average of all the layers. Usually this can be matched quite well by judicious choice of the thermocouple pair and the thickness ratios.

4.4 Null-point Calorimeter

In very high heat flux environments gauges that measure surface temperature cannot physically survive for long. One solution is to make the gauge body from high conductivity copper and move the thermocouple back away from the surface, as illustrated in Fig. 10. The goal of the design is to produce the same temperature history at the null point (thermocouple location) as would occur on the surface of a semi-infinite slab of the model if the gauge were not present. Consequently, the gauge is called a null-point calorimeter. The proper placement of the thermocouple relative to the surface and the size and depth of the hole in the gauge behind it are based on analytical modeling. An ASTM standard⁷⁴ gives the design details and guidelines on its proper use. The typical value for the useful measurement time for a copper body is between 1 and 300 ms. The usual thermocouple pair is chromel/alumel. Its attachment to the gauge is one of the major fabrication difficulties. To accomplish a test within the recommended test time, the

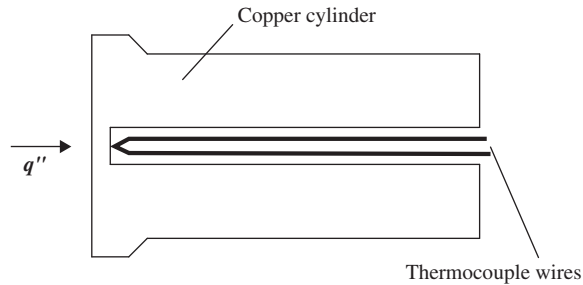


Figure 10 Null-point calorimeter schematic.

model is often swept through the flow. This also minimizes the time that the model and gauges are exposed in high heat flux environments and extends their useful life. Because the null-point temperature on the back of the gauge is designed to match the undisturbed wall temperature, the front side of the gauge is necessarily hotter. Although this creates a “hot spot” effect, these gauges are often used at the stagnation point of models where the effect is small.⁷⁵

4.5 Slug Calorimeter

A calorimeter is a device used for measuring the quantity of absorbed thermal energy as a function of time. In all of the other sensors in this section the temperature distribution as a function of time is used for a specific solid shape and size. A slug calorimeter uses one temperature measurement on the back surface to represent the entire mass of the slug, which is assumed to be at a uniform temperature. This corresponds to a negligible internal thermal resistance, which implies a large thermal conductivity for the material. If a control volume is taken around the slug, application of energy conservation yields

$$q = m C \frac{dT}{dt} + q_{\text{losses}} \quad (18)$$

where q is the heat transfer at the gauge surface and mC is the thermal mass of the slug. The losses are minimized by insulating all of the surfaces other than the front surface. If the losses can be neglected and the heat flux is constant with time, the gauge temperature increases linearly with time:

$$T = T_0 + \frac{q'' A}{m C} t \quad (19)$$

The result is a straight line on a temperature versus time plot, with the slope of the line giving the desired heat flux. The ASTM standard⁷⁶ also recommends calculating the slope for the cooling process after the heat source is removed as an indication of the losses during heating. To neglect losses, the rate of cooling should be less than 5% of the rate of heating. A method for accounting for losses, however, has been demonstrated,⁷⁷ which allows for accurate measurements when larger losses are present.

There are several inherent problems in using slug calorimeters. Because the thermocouple is mounted on the back of the slug, the temperature measurement is not the average temperature of the slug. The material of the gauge should be the same as the wall to minimize nonuniform temperature effects. The heat losses are usually hard to control in models with high heat flux conditions. Although slug calorimeters are rarely used currently, they can provide an important standard in the calibration process.

4.6 Differential Flame Thermometer

The differential flame thermometer⁷⁸ consists of two Inconel plates separated by a layer of insulation with a thermocouple mounted on each plate. The plates are 120 mm by 120 mm and the insulation is 19 mm thick. The resulting time constant for the system is about 90 s. The application is in a radiation-dominated furnace or combustor to measure the heat flux and steady-state temperature. Inverse heat transfer methods are used to convert the two temperature records into heat flux. It should be noted that this device is different from a standard heat flux gauge because it is suspended in the furnace or environment and does not have a heat sink.

5 GAUGES BASED ON ACTIVE HEATING METHODS

Because electric power dissipation can be easily and accurately measured, it is attractive to incorporate electric resistance heating into the measurement of heat transfer. At steady-state conditions the electric power supplied to the system must equal the heat transfer from the surface plus the heat losses. One drawback is that the transfer is always *from* the surface. Consequently, this method is most useful in well-controlled laboratory experiments. Because of the time constraints and power limitations, it is not used in high heat flux or high-temperature situations. This eliminates most high-speed flows. In addition, it is difficult to maintain truly steady-state conditions. Because the thermal capacitance of the surface material is usually large, very small time rates of temperature change may cause large errors in the measured heat transfer and it may take a long time to achieve steady-state conditions under which the temperature is no longer changing.

The techniques used can be grouped according to the two boundary conditions that normally result, constant heat flux and constant wall temperature. In constant heat flux cases the experiment usually runs until a steady-state temperature distribution is achieved. For constant wall temperature, manual or active control of the power is required to stabilize the system at the prescribed constant temperature.

5.1 Constant Heat Flux

Measurements of convective heat transfer coefficients with electrically heated constant heat flux surfaces have been done for many years. The most common method is to use a heater with uniform resistance, insulate the back surface, and minimize lateral conduction by the design. A thin metal sheet is often used as the heater to provide uniformity of resistance (and heat flux) and to minimize the lateral conduction. Several centimeters of good insulation as the backing material usually ensures acceptable heat loss from the back surface. Unfortunately, the response time for this arrangement is typically very long, depending on the surface convection and substrate properties. With a surface heat transfer coefficient of $100 \text{ W/m}^2 \cdot \text{K}$ and a good substrate insulator, the time from a cold start to reach steady-state conditions (within 2%) is typically over one hour. The time limitation is the result of transient heat transfer into the insulation backing layer.

Surface temperature measurements are not needed to determine the heat flux, but they are required to quantify the conditions under which the heat flux occurs. Temperature is particularly necessary for the determination of the heat transfer coefficient. Although any of the methods for measuring temperature are possible candidates, only thermocouples, resistance temperature devices, infrared cameras, and liquid crystals are commonly used. Their use is discussed in that order.

When thermocouples are used to measure the surface temperature, their attachment and layout is important because of the potential problems caused by heat transfer through the wires. Because the wires have a much larger thermal conductivity than the insulation, the measured

temperature can be significantly lowered. Running the wires parallel to the surface for a distance and using small-diameter wire can minimize the effect.

If the temperature is measured with an RTD, it may also be used for supplying the electrical power. A thin-film resistance element sputtered onto quartz was used by Samant et al.⁷⁹ for boiling studies of refrigerant 113. Because the surface of the heated film was only 0.25 mm by 2.0 mm, significant heat was transferred laterally through the quartz substrate, giving the heater a larger effective surface area by an estimated 12–15%. Normally, the edge effect is much larger, but the high heat fluxes in boiling kept it to a minimum.

Infrared optical techniques have been used extensively with large heater foils to measure the temperature distributions on constant heat flux surfaces to infer the convective heat transfer coefficients.⁸⁰ Images are taken with an infrared camera, which is calibrated for the surface emissivity using surface thermocouples.⁸¹

Praisner and Smith⁸² used liquid crystals to record the instantaneous heat transfer distributions for water flow over a surface. A stainless steel foil was painted black and heated electrically. The liquid crystals were applied to the underside of the test plate where the temperature distributions were read with a thermal imaging system. The frequency response of the system for determining the surface heat transfer coefficients was greater than 100 Hz. Heating can also be supplied by an infrared source to a thin sheet with the liquid crystals applied to the other side with the appropriate thermal imaging camera.⁸³

5.2 Constant Surface Temperature

The design and operation of constant surface temperature experiments are substantially different than those for constant heat flux. Instead of measuring the temperature that results from an imposed heat flux, the electrical power is measured that is required to maintain a set temperature. This typically requires a control system to maintain the temperature constant spatially and/or temporally, depending if steady or unsteady measurements are desired. Although electric resistance heating is almost exclusively used, providing heat transfer *from* the surface, a device capable of providing a measured heat transfer in either direction has been constructed using Peltier devices.⁸⁴

Many time-averaged measurements of spatial distributions of heat transfer have been made using segmented plates and heaters. If the plates are made of a thick, high-conductivity material, the surface will be nearly isothermal, even if the heat transfer coefficient has large spatial variations. Some thermal isolation is required between segments, often provided by insulation strips. Usually the individual heaters are adjusted manually to achieve a uniform temperature, although a good set of proportional-integral derivative (PID) automatic temperature controllers can speed the stabilization process by an order of magnitude. On-off type controllers are generally not adequate to maintain a steady-state condition.

Figure 11 illustrates the typical geometry for segmented plate heaters. The measured heat flux occurs from the top surface of the plates that have a thickness of d . The bottom side of the plate is well insulated. The heat loss from the edges usually causes the major errors. The two modes of heat loss⁸⁵ are shown as q'_1 , the loss per unit width through the insulation and by convection from the insulation surface, and q'_2 , the loss per unit width by conduction through the insulation to the adjoining plates. The reason for having the insulation is to thermally isolate the plates to allow individual heat transfer measurements from each. The potential error represented by q'_2 arises from conduction between the plates when the temperatures are not perfectly matched. It was demonstrated that the one-dimensional conduction solution

$$q'_2 = \Delta T \frac{kd}{w} \quad (20)$$

is almost always sufficient to represent this measurement uncertainty. The thermal conductivity of the insulation is k , the thickness of the insulation is w , and the temperature offset between

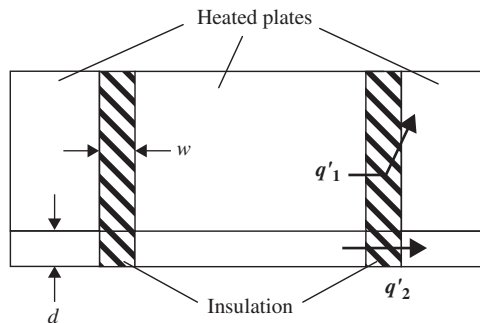


Figure 11 Segmented-plate constant wall temperature system.

any two plates is represented by ΔT . As expected, the conduction error decreases as the insulation width w increases. Conversely, the correction for the convection loss q'_1 increases with increasing w , and the centerline temperature of the insulation is further depressed below the wall temperature of the plates. The optimal design is where these competing effects are minimized.

Most experiments are designed with an insulation thickness much larger than needed for negligible conduction effects. The convection loss through the insulation and temperature disruption of the surface over the insulation, therefore, are much larger than necessary. In addition, there is a limit to how small the errors can be made for heater plates of any given size. As the measurement plate becomes smaller, the area of the edges increases relative to the surface area of the plate. Consequently, the errors become larger relative to the measured heat transfer as the plate area decreases, which limits the theoretical resolution of the method. Furthermore, if guard plates are not used on all edges, the measurement accuracy is even more limited. Only if the measurement plate is large and the heat transfer coefficient high is the relative convection loss through the insulation on the sides small.

One of the most detailed descriptions of the use of the segmented constant temperature plate method is the review of the turbulent boundary layer experiments at Stanford by Moffat and Kays.⁸⁶ The method was used in a well-regulated wind tunnel and continually refined for over 25 years. To achieve the quoted accuracy of $\pm 2\%$ required meticulous detail to experimental procedure and refinement of the data reduction programs. The latter is a lengthy process to eliminate any small errors and to build up an experience base to include all of the small corrections needed.

Small gauges for local heat flux measurements have been produced to actively match the surrounding wall temperatures while measuring power dissipated at the surface. Kraabel et al.⁸⁷ used a cone-shaped copper plug to minimize the gap at the surface while still minimizing the thermal interaction with the housing. A differential thermocouple was used to control the power input to a thermistor heater. The design concept is illustrated in Fig. 12. The experimental uncertainty for steady-state measurements was given as 2%. It should be noted that this low uncertainty is only possible with the very small gap at the surface, cone shape for the sensor and differential thermocouple for the control. Such experiments, however, are very time consuming to perform. Baughn et al.⁸⁸ used a nichrome ribbon in place of the copper plug.

To measure time-resolved heat flux, active control of the power is required. Thin-film gauges deposited on a low conductivity substrate are used to minimize the system time response. A thin-film resistance element can serve as both the heater and temperature measurement device. There are three important issues that must be addressed for accurate time-resolved heat flux measurements. The first is that the thin-film gauge temperature must

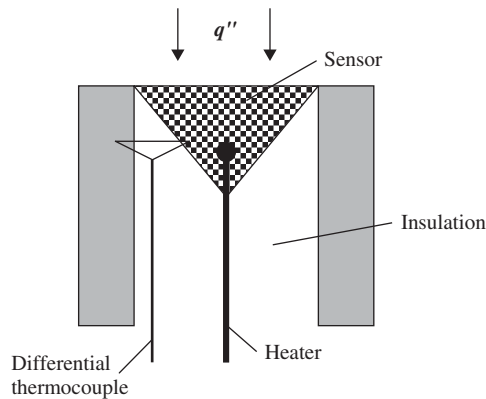


Figure 12 Heated gauge concept.

match the temperature of the surrounding surface. Temperature controllers usually have a small temperature drop. To match the temperature increases the instability of the system, which requires careful tuning of the system. The third problem is the consequent attenuation of the frequency response because of the thermal capacitance of the substrate material, even if it is a good thermal insulator. Higher frequencies may still be seen in the signal, but the amplitude is much smaller than the actual value. A good test of the system is to use a chopped heat input over a range of frequencies from high to a simple on–off. The measured magnitude should be the same independent of the frequency.

To overcome these problems and experimentally observe the temperature of the heater film, Campbell et al.⁸⁹ embedded a thermocouple made with 76- μm wire at the surface of the substrate underneath the sensor film. The low-conductivity sensor was mounted flush with the surrounding aluminum surface. The heated thin film was actively powered with a modified hot-wire bridge. To match the sensor and surrounding surface temperatures, a second matched thermocouple was embedded in the surrounding surface to form a differential thermocouple. A slow response differential controller was used to match the temperatures by driving the differential to zero. Consequently, the hot-wire bridge controlled the power to the sensor during fast surface heat flux transients, and the second controller matched temperatures over long times by adjusting the power to the surrounding material. This system was capable of maintaining the temperature match within $\pm 0.1^\circ\text{C}$. The compensation tuning of the bridge had to be adjusted very close to the instability point for proper response and no measurable temperature change of the surface. The resulting heat flux uncertainty was estimated to be $\pm 5\%$.

Dinu et al.⁹⁰ performed a numerical solution of the transient response of their actively heated thin film. There are three components to these probes: the heated thin film, the substrate on which it is deposited, and a protective coating layer on top. The sensor was assumed to be mounted into an isothermal plate, which defined all of the boundary conditions except the surface. The results of their model clearly indicated the importance of precise control over the sensor temperature. With only a 0.5°C higher temperature the heat flux was 20% higher. Even larger errors were seen in the amplitude of a sinusoidal heat flux.

Lee et al.⁹¹ created an array of actively heated gauges consisting of 96 individual thin-film elements, each 270 μm by 270 μm . The entire assembly is only 2.7 mm on a side. It was used for measuring time-dependent boiling events. Because of the very high heat flux associated with boiling, the losses are relatively small and the controller stability is not as crucial as the gauges used in air convection.

6 CALIBRATION AND ERRORS

There are two basic approaches to calibration of heat flux sensors. The first is to use a system that provides a comparison with a primary standard. The second uses another heat flux sensor as a secondary standard for the comparison. If the gauge temperature will be outside the normal room temperature range, the sensitivity should be measured over the range of gauge temperatures for the intended use because it may be temperature dependent. In addition, the mode of heat transfer can be important to the heat flux sensor response. Therefore, identification and separation of convection from radiation is an issue to address. Errors can be separated into the measurement uncertainty and the bias error of the calibration.

6.1 Heat Flux Gauge Calibration

There are three methods for absolute radiation calibration of heat flux sensors as illustrated in the facilities at National Institute of Standards and Technology (NIST).⁹² They are all designed for water-cooled sensors that are kept at room temperature for the calibration. One uses an electrical substitution radiometer as the primary standard⁹³ in a narrow-angle facility. The second is a spherical cavity that uses the temperature of the wall as the standard along with the Stefan–Boltzmann law for the blackbody radiation to the sensor.⁹⁴

$$q''_{\text{inc}} = \sigma T^4 \quad (21)$$

The heat flux sensor should be located at the bottom of the sphere or the sphere should be in a vacuum to minimize the effects of convection. The third method is insertion into a graphite tube blackbody cavity with a pyrometer on the opposite side of the center partition for the primary standard. This method has been tested both experimentally and analytically.^{95–97} It also has some convection effects and is dependent on the sensor placement in the cavity and time response of the temperature controller of the blackbody during its insertion.

The narrow-angle facility has minimal convection effects because the sensor is located outside of the blackbody high-temperature source. However, because of the narrow-angle radiation beam that heats the sensor, the maximum heat flux is relatively low (50 kW/m^2) and it has shorter wavelength (higher required source temperature) than the other methods. In addition, most coatings have some angular dependence of the absorptivity.⁹⁸ The result is a small, but consistent, difference in calibration results between the narrow-angle and wide-angle facilities.⁹⁶

For all three cases the resulting calibration for the gauge sensitivity S_{rad} is based on the incident radiation to the gauge surface, q''_{inc} :

$$S_{\text{rad}} = \frac{E}{q''_{\text{inc}}} \quad (22)$$

The emissivity of the surface ε is required to calculate the absorbed radiation:

$$q''_{\text{abs}} = \varepsilon q''_{\text{inc}} \quad (23)$$

The gauge surface is assumed to be gray with the absorptivity equal to the emissivity, ε , and both values constant with angle and wavelength for the conditions of use. The gauges are kept at room temperature, using water cooling if necessary. This minimizes any emission from the gauge surface, which is neglected.

Once the secondary standard gauge has been calibrated, it is used to calibrate other gauges by comparison under the same incident heat flux. One method is with simultaneous measurements on either side of an electrically heated flat plate. The other common method is using sequential substitution under a quartz lamp or bank of lamps. In all cases the size and range of the two gauges should be matched to minimize the differences in the radiation experienced.

If the gauges are to be used at elevated temperatures, the calibrations are more difficult. First, the gauge will experience substantial convection. Second, the emitted energy from the gauge will become important. These require corrections and raise the uncertainty of the calibration. Pullins and Diller⁹⁸ have minimized these problems by designing an enclosure that mounts the gauge to be calibrated on the hot surface and the secondary standard in a water-cooled cold plate. Convection is minimized by putting the cold plate horizontal and beneath the hot plate. Because the enclosure is insulated, essentially all of the energy from the hot plate necessarily goes to the cold plate, as measured by the secondary standard. Corrections are needed only for the small nonuniformities of temperature of the hot and cold surfaces.

Convection calibrations are more difficult but have been done to heat flux levels of about 5 kW/m² using electrical power measurement as the standard.^{47,100} The gauge sensitivity is based on the convective heat flux, q''_{conv} , provided by a wind tunnel¹⁰⁰ or a large stagnating air jet⁴⁷

$$S_{\text{conv}} = \frac{E}{q''_{\text{conv}}} \quad (24)$$

The standard is the electrical power input into a constant temperature plate with guard heaters on all sides and operating at steady-state conditions, as discussed in Section 5.2. The resulting sensitivity corresponds to the absorbed radiation. Consequently, the usual incident radiation calibration must be adjusted to correspond to the convection sensitivity by the emissivity of the original surface coating.

$$S_{\text{conv}} = \frac{S_{\text{inc}}}{\epsilon} \quad (25)$$

Conduction calibrations are time consuming for the thin flat gauges because of the time required to reach steady-state conditions. Guarded hot plate calibration systems are commercially available and can be traced to standards at NIST. An ASTM standard covers the calibration method.¹⁰¹

$$S_{\text{cond}} = \frac{E}{q''_{\text{cond}}} \quad (26)$$

6.2 Error Estimates

Heat flux gauge calibrations usually are repeatable to within 2–3%. The bias error introduced into the measurement uncertainty will be larger depending on how close the measurement conditions are to the calibration conditions. The precision uncertainty is usually dominated by the voltage measurement uncertainty. This can be minimized by properly specifying the heat flux range of the gauge and using quality amplifiers and/or data acquisition units. For radiation the coating properties may contribute a substantial uncertainty. Taken together the combined uncertainty for heat flux gauge measurements that are performed carefully is often between 5 and 10%.

REFERENCES

1. T. E. Diller, "Advances in Heat Flux Measurement," in J. P. Hartnett, et al. (Eds.), *Advances in Heat Transfer*, Vol. 23, Academic, Boston, pp. 279–368, 1993.
2. N. Arai, A. Matsunami, and S. W. Churchill, "A Review of Measurements of Heat Flux Density Applicable to the Field of Combustion," *Exp. Thermal and Fluid Sci.*, **12**, 452–460, 1996.
3. N. R. Keltner, "Heat Flux Measurements: Theory and Applications," in K. Azar (Ed.), *Thermal Measurements in Electronics Cooling*, CRC Press, Boca Raton, FL, pp. 173–320, 1997.
4. S. N. Flanders, "Heat Flux Transducers Measure "in-situ" Building Thermal Performance," *J. Thermal Insul. and Building Envs.*, **18**, 28–52, 1994.
5. P. R. N. Childs, J. R. Greenwood, and C.A. Long, "Heat Flux Measurement Techniques," *Proc. Inst. Mech. Engrs.*, **213C**, 655–677, 1999.

6. J.-C. Han, S. Dutta, and S. Ekkad, *Gas Turbine Heat Transfer and Cooling Technology*, Taylor and Francis, New York, 2001.
7. T. E. Diller, "Heat Flux," in J. G. Webster (Ed.), *The Measurement, Instrumentation and Sensors Handbook*, Ch. 34, CRC Press, Boca Raton, FL, pp. 34.1–15, 1999.
8. D. A. Wesley, "Thin Disk on a Convectively Cooled Plate—Application to Heat Flux Measurement Errors," *ASME J. Heat Transfer*, **101**, 346–352, 1979.
9. T. Baba, A. Ono, and S. Hattori, "Analysis of the Operational Error of Heat Flux Transducers Placed on Wall Surfaces," *Rev. Sci. Instrum.*, **56**, 1399–1401, 1985.
10. A. Gifford, A. Hoffie, T. Diller, and S. Huxtable, "Convection Calibration of Schmidt–Boelter Heat Flux Gages in Stagnation and Shear Air Flow," *ASME J. Heat Transfer*, **132**, 031601, 2010.
11. M. Kandular, and G. Haddad, "Two-Dimensional Thermal Boundary Layer Corrections for Convective Heat Flux Gauges," *J. Thermophys. Heat Transfer*, **21**, 543–547, 2007.
12. R. J. Moffat, J. K. Eaton, & D. Mukerji, "A General Method for Calculating the Heat Island Correction and Uncertainties for Button Gauges," *Meas. Sci. Technol.*, **11**, 920–932, 2000.
13. A. F. Robertson, and T. J. Ohlemiller, "Low Heat-Flux Measurements: Some Precautions," *Fire Safety J.*, **25**, 109–124, 1995.
14. ASTM E2684-09, "Standard Test Method for Measuring Heat Flux Using Surface-Mounted One-Dimensional Flat Gauges," *Ann. Book ASTM Standards*, 15.03, 2009.
15. N. E. Hager, Jr., "Thin Foil Heat Meter," *Rev. Sci. Instrum.*, **36**, 1564–1570, 1965.
16. A. H. Epstein, G. R. Guenette, R. J. Norton, and Y. Cao, "High-Frequency Response Heat-Flux Gauge," *Rev. Sci. Instrum.*, **57**, 639–649, 1986.
17. E. Piccini, S. M. Guo, and T. V. Jones, "The Development of a New Direct-Heat-Flux Gauge for Heat-Transfer Facilities," *Meas. Sci. Technol.*, **11**, 342–349, 2000.
18. A. R. A. Talib, A. J. Neely, P. T. Ireland, and A. J. Mullender, "Detailed Investigation of Heat Flux Measurements Made in a Standard Propane-Air-Fire-Certification Burner Compared to Levels Derived from a Low-Temperature Analog Burner," *J. Eng. Gas Turbines Power*, **127**, 249–256, 2005.
19. G. Fralick, and J. Wrbacnek, *Thin Film Heat Flux Sensor of Improved Design*, NASA TM-2002–211566.
20. P. A. Kinzie, *Thermocouple Temperature Measurement*, Wiley, New York, 1973.
21. E. Bales, M. Bomberg, and G. E. Courville, *Building Applications of Heat Flux Transducers*, ASTM, Philadelphia, 1985.
22. W. D. Bauer, and J. B. Heywood, "Transfer Function of Thin-Film Heat Flux Sensor," *Exp. Heat Transfer*, **10**, 181–190, 1997.
23. D. J. Ortolano, and F. F. Hines, "A Simplified Approach to Heat Flow Measurement," *Adv. Instrum.*, **38**(II), 1449–1456, 1983.
24. D. O. Hubble, and T. E. Diller, "Development and Evaluation of the Time-Resolved Heat and Temperature Array," *J. Thermal Sci. Eng. Appl.*, **2**, 031003, 2010.
25. A. C. Van Dorth, "Thick Film Heat Flux Sensor," *Sensors Actuators*, **4**, 323–331, 1983.
26. L. Langley, A. Barnes, G. Matijasevic, and P. Gandhi, "High Sensitivity, Surface-Attached Heat Flux Sensors," *Microelectr. J.*, **30**, 1163–1168, 1999.
27. J. Ewing, A. Gifford, D. Hubble, P. Vlachos, A. Wicks, and T. Diller, "A Direct-Measurement Thin-Film Heat Flux Sensor Array," *Measur. Sci. Tech.*, **21**, 105201, 2010.
28. A. R. Gifford, D. O. Hubble, C. A. Pullins, S. T. Huxtable, and T. E. Diller, "A Durable Heat Flux Sensor for Extreme Temperature and Heat Flux Environments," *J. Thermophys. Heat Transfer*, **24**, 69–76, 2010.
29. D. O. Hubble, and T. E. Diller, "A Hybrid Method for Measuring Heat Flux," *J. Heat Transfer*, **132**, 031602, 2010.
30. J. R. Trelewicz, C. Gouldstone, and J. Longtin, "Direct Write Sensors for Scramjet Engines and Sounding Rockets," Proc. JANNAF Joint Propulsion Meeting, Colorado Springs, CO, 3–4 May, 2010.
31. A. V. Mityakov, V. Yu. Mityakov, S. Z. Sapozhnikov, and Yu. S. Chumakov, "Application of the Transverse Seebeck Effect to Measurement of Instantaneous Values of a Heat Flux on a Vertical

- Heated Surface under Conditions of Free-Convection Heat Transfer," *High Temp.*, **40**, 620–625, 2002.
32. R. L. Hauser, "Construction and Performance of in Situ Heat Flux Transducers," in E. Bales et al. (Eds.), *Building Applications of Heat Flux Transducers*, ASTM STP 885, 1985, pp. 172–183.
 33. F. Van der Graaf, "Heat Flux Sensors," in W. Gopel et al., (Eds.), *Sensors*, Vol. **4**, VCH, New York, 1989, pp. 295–322.
 34. ASTM E2683-09, Standard Test Method for Measuring Heat Flux Using Flush-Mounted Insert Temperature-Gradient Gages, *Ann. Book ASTM Standards*, Vol. 15.03, ASTM, West Conshohocken, PA, 2009.
 35. T. E. Diller, and S. Onishi, Heat Flux Gage, U.S. Patent No. 4,779,994, issued 25 October, 1988.
 36. J. M. Hager, S. Simmons, D. Smith, S. Onishi, L. W. Langley, and T. E. Diller, "Experimental Performance of a Heat Flux Microsensor," *J. Eng. Gas Turbines Power*, **113**, 246–250, 1991.
 37. J. M. Hager, S. Onishi, L. W. Langley, and T. E. Diller, "High Temperature Heat Flux Measurements," *AIAA J. Thermophys. Heat Transfer*, 531–534, 1993.
 38. D. G. Holmberg, and T. E. Diller, "High-Frequency Heat Flux Sensor Calibration and Modeling," *ASME J. Fluids Eng.*, **117**, 659–664, 1995.
 39. C. T. Kidd, and C. G. Nelson, "How the Schmidt-Boelter Gage Really Works," Proceedings of the 41st International Instrumentation Symposium, ISA, Research Triangle Park, pp. 347–368, 1995.
 40. C. T. Kidd and J. C. Adams, Jr., "Fast-Response Heat-Flux Sensor for Measurement Commonality in Hypersonic Wind Tunnels," *J. Spacecraft Rockets*, **38**, 719–729, 2001.
 41. S. Hevey, and L. Langley, Schmidt-Boelter Gage, U.S. Patent No. 6,186,661, issued 13 February, 2001.
 42. C. A. Long, P. R. N. Childs, J. R. Greenwood, and K. M. Tham, "Manufacture and Calibration of Robust Heat Flux Sensors for Rotating Turbomachinery," *Exp. Heat Transfer*, **17**, 181–197, 2004.
 43. R. Gardon, "An Instrument for the Direct Measurement of Intense Thermal Radiation," *Rev. Sci. Instrum.*, **24**, 366–370, 1953.
 44. C. H. Kuo, and A. K. Kulkarni, "Analysis of Heat Flux Measurement by Circular Foil Gages in a Mixed Convection/Radiation Environment," *J. Heat Transfer*, **113**, 1037–1040, 1991.
 45. B.C. Liechty, M. M. Clark, M. R. Jones, R. S. Larson, and B. L. Woolford, "Nonlinear Thermal Model of Circular Foil Heat Flux Gauges," *J. Thermophys. Heat Transfer*, **21**, 468–474, 2007.
 46. A. M. Agnone, "Solution of the Nonlinear Heat Equation for Circular-Foil Heat Flux Gauges," *J. Thermophys. Heat Transfer*, **23**, 33–40, 2009.
 47. G. J. Borell, and T. E. Diller, "A Convection Calibration Method for Local Heat Flux Gages," *J. Heat Transfer*, **109**, 83–89, 1987.
 48. ASTM E511-07, Measurement of Heat Flux Using a Copper-Constantan Circular Foil Heat-Flux Gage, *Ann. Book ASTM Standards*, Vol. 15.03, ASTM, West Conshohocken, PA, 2009.
 49. A. V. Murthy, I. Wetterlund, and D. P. DeWitt, "Characterization of an Ellipsoidal Radiometer," *J. Res. NIST*, **108**, 115–124, 2003.
 50. J.M. Kendall, and C. M. Berdahl, "Two Blackbody Radiometers of High Accuracy," *Appl. Opt.*, **9**, 1082–1091, 1970.
 51. N. Martins, M. G. Carvalho, N. Afgan, and A. I. Leontiev, "A Radiation and Convection Fluxmeter for High Temperature Applications," *Exp. Thermal Fluid Sci.*, **22**, 365–373, 2000.
 52. N. Martins, H. Calisto, N. Afgan, and A. I. Leontiev, "The Transient Transpiration Heat Flux Meter," *Appl. Thermal Eng.*, **26**, 1152–1155, 2006.
 53. B. Brajuskovic, and N. Afgan, "A Heat Flux Meter for Ash Deposit Monitoring Systems – II. Clean Heat Flux-Meter Characteristics," *Int. J. Heat Mass Transfer*, **34**, 2303–2315, 1991.
 54. D. L. Schultz, and T. V. Jones, "Heat Transfer Measurements in Short Duration Hypersonic Facilities," *AGARDograph* 165, 1973.
 55. G. Walker, and E.P. Scott, "Evaluation of Estimation Methods for High Unsteady Heat Fluxes from Surface Measurements," *J. Thermophys. Heat Transfer*, **12**, 543–551, 1997.
 56. M. L. G. Oldfield, "Impulse Response Processing of Transient Heat Transfer Gauge Signals," *J. Turbomach.*, **130**, 021023, 2008.
 57. J. E. Doorly, and M. L. G. Oldfield, "New Heat Transfer Gages for Use on Multilayered Substrates," *ASME J. Turbomach.*, **108**, 153–160, 1986.

58. R. W. Ainsworth, J. L. Allen, M. R. D. Davies, J.E. Doorly, C. J. P. Forth, M. A. Hilditch, M. L. G. Oldfield, and A. G. Sheard, "Developments in Instrumentation and Processing of Transient Heat Transfer Measurements in a Full-Stage Model Turbine." *ASME J. Turbomach.*, **111**, 20–27, 1989.
59. S. M. Guo, C. C. Lai, T. V. Jones, M. L. G. Oldfield, G. D. Lock, and A. J. Rawlinson, "The Application of Thin-Film Technology to Measure Turbine-Vane Heat Transfer and Effectiveness in a Film-Cooled, Engine-Simulated Environment," *Int. J. Heat Fluid Flow*, **19**, 594–600, 1998.
60. M. G. Dunn, W. K. George, W. J. Rae, S. H. Woodward, J. C. Moller, and P. J. Seymour, "Heat-Flux Measurements for a Full-Stage Turbine: Part II – Description of Analysis Technique and Typical Time-Resolved Measurements," *ASME J. Turbomach.*, **108**, 98–107, 1986.
61. M.G. Dunn, J. Kim and W. J. Rae, "Investigation of the Heat-Island Effect for Heat-Flux Measurements in Short-Duration Facilities," *J. Turbomach.*, **119**, 753–760, 1997.
62. S. V. Ekkad, S. Ou, and R. B. Rivir, "A Transient Thermography Method for Simultaneous Film Effectiveness and Heat Transfer Coefficient Measurements from a Single Test," *J. Turbomach.*, **126**, 597–603, 2004.
63. J.-W. Ahn, R. Maingi, D. Mastrovito, and A. L. Roquemore, "High Speed Infrared Camera Diagnostic for Heat Flux Measurement in NSTX," *Rev. Sci. Instrum.*, **81**, 023501, 2010.
64. A. H. Khalid, and K. Kontis, "Thermographic Phosphors for High Temperature Measurements: Principles, Current State of the Art and Recent Applications," *Sensors*, **8**, 5673–5744, 2008.
65. D. J. Bizzak, and M. K. Chyu, "Use of Laser-Induced Fluorescence Thermal Imaging System for Local Jet Impingement Heat Transfer Measurement," *Int. J. Heat Mass Transfer*, **38**, 267–274, 1995.
66. D. G. Walker, "Heat Flux Determination from Measured Heating Rates Using Thermographic Phosphors," *J. HeatTransfer*, **127**, 560–570, 2005.
67. I. Kurits, and M. J. Lewis, "Global Temperature-Sensitive Paint System for Heat Transfer Measurements in Long-Duration Hypersonic Flows," *J. Thermophys. Heat Transfer*, **23**, 256–266, 2009.
68. P. T. Ireland, and T. V. Jones, "Liquid Crystal Measurements of Heat Transfer and Surface Shear Stress," *Meas. Sci. Technol.*, **11**, 969–986, 2000.
69. G. Wagner, M. Kotulla, P. Ott, B. Wegand, and J. von Wolfersdorf, "The Transient Liquid Crystal Technique: Influence of Surface Curvature and Finite Wall Thickness," *J. Turbomach.*, **127**, 175–182, 2005.
70. M. K. Das, A. Tariq, P. K. Phanigrahi, and K. Muralidhar, "Estimation of Convective Heat Transfer Coefficient from Transient Liquid Crystal Data Using an Inverse Technique," *Inverse Prob. Sci. Eng.*, **13**, 133–155, 2005.
71. A. R. A. Talib, A. J. Neely, P. T. Ireland, and A. J. Mullender, "A Novel Liquid Crystal Image Processing Technique Using Multiple Gas Temperature Steps to Determine Heat Transfer Coefficient Distribution and Adiabatic Wall Temperature," *J. Turbomach.*, **126**, 587–596, 2004.
72. C. T. Kidd, "Coaxial Surface Thermocouples: Analytical and Experimental Considerations for Aerothermal Heat-Flux Measurement Applications," Proc. 36th International Instrumentation Symposium, ISA, Research Triangle Park, pp. 203–211, 1990.
73. T. B. Smith, J. A. Schetz, and D. G. Walker, "Development and Ground Testing of Heat Flux Gages for High Enthalpy Supersonic Flight Tests," AIAA Paper No. 2002–3133, 2002.
74. ASTM E598-08, Standard Test Method for Measuring Extreme Heat-Transfer Rates from High-Energy Environments Using a Transient, Null-Point Calorimeter, *Ann. Book ASTM Standards*, Vol. 15.03, ASTM, West Conshohocken, PA, 2009.
75. C. T. Kidd, High Heat Flux Measurements and Experimental Calibrations/Characteristics, NASA CP3161, pp. 31–50, 1992.
76. ASTM E547-08, Standard Test Method for Measuring Heat-Transfer Rate Using a Thermal Capacitance (Slug) Calorimeter, *Ann. Book ASTM Standards*, Vol. 15.03, ASTM, West Conshohocken, PA, 2009.
77. T. M. Hightower, and R. A. Olivares, "Thermal Capacitance (Slug) Calorimeter Theory Including Heat Losses and Other Decaying Processes," NASA/TM-2008-215364, 2008.
78. N. R. Keltner, J. V. Beck, and J. T. Nakos, "Using Directional Flame Thermometers for Measuring Thermal Exposure," *J. ASTM Int.*, **7**, 102280, 2010.
79. K. R. Samant, T. W. Simon, and R. V. Stuart, "Using Thin-Film Technology to Fabricate a Small-Patch Boiling Heat Transfer Test Section," in O. C. Jones and N. M. Farukhi (Eds.), *New Experimental Techniques in Heat Transfer*, ASME, New York, pp. 33–38, 1984.

80. J. M. Buchlin, "Convective Heat Transfer and Infrared Thermography (IRTH)," *J. Appl. Fluid Mech.*, Vol. 3, 55–62, 2010.
81. W. Colban, A. Gratton, K. A. Thole, and M. Haendler, "Heat Transfer and Film-Cooling Measurements on a Stator Vane With Fan-Shaped Cooling Holes," *J. Turbomach.*, **128**, 53–61, 2006.
82. T. J. Praisner, and C. R. Smith, "The Dynamics of the Horseshoe Vortex and Associated Endwall Heat Transfer-Part 1: Temporal Behavior," *J. Turbomach.*, **128**, 747–754, 2006.
83. A. D. Ochoa, J. W. Baughn, and A. R. Byerley, "A New Technique for Dynamic Heat Transfer Measurements and Flow Visualization Using Liquid Crystal Thermography," *Int. J. Heat Fluid Flow*, **26**, 264–275, 2005.
84. E. C. Shewen, K. G. T. Holland, and G. D. Raithby, "The Measurement of Surface Heat Flux Using the Peltier Effect," *ASME J. Heat Transfer*, **111**, 798–803, 1989.
85. T. VandenBerghe, and T. E. Diller, "Analysis and Design of Experimental Systems for Heat Transfer Measurement from Constant Temperature Surfaces," *Exp. Thermal Fluid Sci.*, **2**, 236–246, 1989.
86. R. J. Moffat, and W. M. Kays, "A Review of Turbulent-Boundary-Layer Heat Transfer Research at Stanford 1948–1983," *Adv. Heat Transfer*, **16**, 241–365, 1984.
87. J. S. Kraabel, J. W. Baughn, and A. A. McKillop, "An Instrument for the Measurement of Heat Flux from a Surface with Uniform Temperature," *J. Heat Transfer*, **102**, 576–578, 1980.
88. J. W. Baughn, M. A. Hoffman, B. E. Launder, D. Lee, and C. Yap, "Heat Transfer, Temperature, and Velocity Measurements Downstream of an Abrupt Expansion in a Circular Tube at a Uniform Wall Temperature," *ASME J. Heat Transfer*, **111**, 870–876, 1989.
89. D. S. Campbell, M. Gundappa, and T. E. Diller, "Design and Calibration of a Local Heat-Flux Measurement System for Unsteady Flows," *ASME J. of Heat Transfer*, **111**, 552–557, 1989.
90. C. Dinu, D. E. Beasley, and R. S. Figliola, "Frequency Response Characteristics of an Active Heat Flux Gage," *ASME J. Heat Transfer*, **120**, 577–582, 1998.
91. J. Lee, J. Kim, and K. T. Kiger, "Time and Space Resolved Heat Transfer Characteristics of Single Droplet Cooling Using Microscale Heater Arrays," *Int. J. Heat Fluid Flow*, **22**, 188–200, 2001.
92. A. V. Murthy, B. K. Tsai, and R. D. Saunders, "Radiative Calibration of Heat-Flux Sensors at NIST: Facilities and Techniques," *J. Res. Natl. Inst. Stand. Tech.*, **105**, 293–305, 2000.
93. A. V. Murthy, B. K. Tsai, and R. D. Saunders, "Transfer Calibration Validation Tests on a Heat Flux Sensor in the 51 mm High-Temperature Blackbody," *J. Res. Nat. Inst. Stand. Tech.*, **106**, 823–831, 2001.
94. ISO/DIS 14934, *Fire Tests—Calibration and Use of Heat Flux Meters*, ISO, Geneva, 2009.
95. A. N. Abdelmessih, and T. J. Horn, "Experimental and Computational Characterization of High Heat Fluxes During Transient Blackbody Calibrations," *J. Heat Transfer*, **132**, 023304, 2010.
96. A. V. Murthy, F. T. Fraser, and D. P. DeWitt, "Experimental In-Cavity Radiative Calibration of High-Heat-Flux Meters," *J. Thermophys. Heat Transfer*, **20**, 327–335, 2006.
97. A. V. Murthy, A. V. Prokhorov, and D. P. DeWitt, "High Heat-Flux Sensor Calibration: A Monte Carlo Modeling," *J. Thermophys. Heat Transfer*, **18**, 333–341, 2004.
98. R. L. Alpert, L. Orloff, and J. L. de Ris, "Angular Sensitivity of Heat Flux Gages," in ASTM STP 1427, pp. 67–80, ASTM, West Conshohocken, PA, 2003.
99. C. A. Pullins, and T. E. Diller, "In situ High Temperature Heat Flux Sensor Calibration," *Int. J. Heat Mass Transfer*, **53**, 3429–3438, 2010.
100. D. G. Holmberg, and C. A. Womeldorf, "Design and Uncertainty Analysis of a Second-Generation Convective Heat Flux Calibration Facility," *HTD*, 364–4, ASME, New York, 65–70, 1999.
101. ASTM C1130-07, Standard Practice for Calibrating Thin Heat Flux Transducers, *Ann. Book ASTM Standards*, Vol. 4.06, ASTM, West Conshohocken, PA, 2009.

CHAPTER 8

FURNACES

Carroll Cone
Toledo Ohio

1 SCOPE AND INTENT	314	9 FLUID FLOW	354
2 STANDARD CONDITIONS	314	9.1 Preferred Velocities	355
2.1 Probable Errors	314	9.2 Centrifugal Fan Characteristics	358
3 FURNACE TYPES	314	9.3 Laminar and Turbulent Flows	360
4 FURNACE CONSTRUCTION	318	10 BURNER AND CONTROL EQUIPMENT	361
5 FUELS AND COMBUSTION	319	10.1 Burner Types	362
6 OXYGEN ENRICHMENT OF COMBUSTION AIR	325	10.2 Burner Ports	364
7 THERMAL PROPERTIES OF MATERIALS	325	10.3 Combustion Control Equipment	365
8 HEAT TRANSFER	330	10.4 Air Pollution Control	367
8.1 Solid-State Radiation	331	11 WASTE HEAT RECOVERY SYSTEMS	367
8.2 Emissivity–Absorptivity	331	11.1 Regenerative Air Preheating	368
8.3 Radiation Charts	332	11.2 Recuperator Systems	369
8.4 View Factors for Solid-State Radiation	332	11.3 Recuperator Combinations	370
8.5 Gas Radiation	336	12 FURNACE COMPONENTS IN COMPLEX THERMAL PROCESSES	371
8.6 Evaluation of Mean Emissivity–Absorptivity	338	13 FURNACE CAPACITY	371
8.7 Combined Radiation Factors	339	14 FURNACE TEMPERATURE PROFILES	372
8.8 Steady-State Conduction	340	15 REPRESENTATIVE HEATING RATES	372
8.9 Non–Steady-State Conduction	341	16 SELECTING NUMBER OF FURNACE MODULES	373
8.10 Heat Transfer with Negligible Load Thermal Resistance	345	17 FURNACE ECONOMICS	373
8.11 Newman Method	345	17.1 Operating Schedule	374
8.12 Furnace Temperature Profiles	346	17.2 Investment in Fuel-Saving Improvements	374
8.13 Equivalent Furnace Temperature Profiles	347	REFERENCE	374
8.14 Convection Heat Transfer	350		
8.15 Fluidized-Bed Heat Transfer	351		
8.16 Combined Heat Transfer Coefficients	352		

1 SCOPE AND INTENT

This chapter has been prepared for the use of engineers with access to an electronic calculator and to standard engineering reference books but not necessarily to a computer terminal. The intent is to provide information needed for the solution of furnace engineering problems in areas of design, performance analysis, construction and operating cost estimates, and improvement programs.

In selecting charts and formulas for problem solutions, some allowance has been made for probable error, where errors in calculations will be minor compared with errors in the assumptions on which calculations are based. Conscientious engineers are inclined to carry calculations to a far greater degree of accuracy than can be justified by probable errors in data assumed. Approximations have accordingly been allowed to save time and effort without adding to probable margins for error. The symbols and abbreviations used in this chapter are given in Table 1.

2 STANDARD CONDITIONS

Assuming that the user will be using English rather than metric units, calculations have been based on pounds, feet, Btus, and degrees Fahrenheit, with conversion to metric units provided in the following text (see Table 2).

Assumed standard conditions include ambient temperature for initial temperature of loads for heat losses from furnace walls or open cooling of furnace loads—70°F. Condition of air entering system for combustion or convection cooling: temperature, 70°F; absolute pressure, 14.7 psia; relative humidity, 60% at 70°F, for a water vapor content of about 1.4% by volume.

2.1 Probable Errors

Conscientious furnace engineers are inclined to carry calculations to a far greater degree of accuracy than can be justified by uncertainties in basic assumptions such as thermal properties of materials, system temperatures and pressures, radiation view factors, and convection coefficients. Calculation procedures recommended in this chapter will, accordingly, include some approximations, identified in the text, that will result in probable errors much smaller than those introduced by basic assumptions, where such approximations will expedite problem solutions.

3 FURNACE TYPES

Furnaces may be grouped into two general types:

1. As a source of energy to be used elsewhere, as in firing steam boilers to supply process steam, or steam for electric power generation, or for space heating of buildings or open space
2. As a source of energy for industrial processes, other than for electric power

The primary concern of this chapter is the design, operation, and economics of industrial furnaces, which may be classified in several ways:

By function:

Heating for forming in solid state (rolling, forging)

Melting metals or glass

Heat treatment to improve physical properties

Table 1 Symbols and Abbreviations

<i>A</i>	area in ft ²
<i>a</i>	absorptivity for radiation, as fraction of blackbody factor for receiver temperature: <i>a_g</i> combustion gases <i>a_w</i> furnace walls <i>a_s</i> load surface <i>a_m</i> combined emissivity-absorptivity factor for source and receiver
<i>C</i>	specific heat in Btu/lb·°F or cal/g·°C
cfm	cubic feet per minute
<i>D</i>	diameter in ft or thermal diffusivity (<i>k/dC</i>)
<i>d</i>	density in lb/ft ³
<i>e</i>	emissivity for radiation as fraction of blackbody factor for source temperature, with subscripts as for <i>a</i> above
<i>F</i>	factor in equations as defined in text
fpm	velocity in ft/min
<i>G</i>	mass velocity in lb/ft ² ·h
<i>g</i>	acceleration by gravity (32.16 ft/s ²)
<i>H</i>	heat-transfer coefficient (Btu/h·ft ² ·°F) <i>H_r</i> for radiation <i>H_c</i> for convection <i>H_t</i> for combined <i>H_r</i> + <i>H_c</i>
HHV	higher heating value of fuel
<i>h</i>	pressure head in units as defined
<i>k</i>	thermal conductivity (Btu/h·ft·°F)
<i>L</i>	length in ft, as in effective beam length for radiation, decimal rather than feet and inches
LHV	lower heating value of fuel
ln	logarithm to base <i>e</i>
MTD	log mean temperature difference
<i>N</i>	a constant as defined in text
psi	pressure in lb/in ² . psig, pressure above atmospheric psia, absolute pressure
Pr	Prandtl number (<i>μC/k</i>)
<i>Q</i>	heat flux in Btu/h
<i>R</i>	thermal resistance (<i>r/k</i>) or ratio of external to internal thermal resistance (<i>k/rH</i>)
Re	Reynolds number (<i>DG/μ</i>)
<i>r</i>	radius or depth of heat penetration in ft
<i>T</i>	temperature in °F, except for radiation calculations where °S = (°F + 460)/100 <i>T_g</i> , combustion gas temperature <i>T_w</i> , furnace wall temperature <i>T_s</i> , heated load surface <i>T_c</i> , core or unheated surface of load
<i>t</i>	time in h
<i>μ</i>	viscosity in lb/h·ft
WC	inches of water column as a measure of pressure
<i>V</i>	volume in ft ³
<i>v</i>	velocity in ft/s
<i>W</i>	weight in lb
<i>X</i>	time factor for nonsteady heat transfer (<i>tD/r²</i>)
<i>x</i>	horizontal coordinate
<i>y</i>	vertical coordinate
<i>z</i>	coordinate perpendicular to plane <i>xy</i>

Table 2 Conversion of Metric to English Units

Length	1 m = 3.281 ft 1 cm = 0.394 in.
Area	1 m ² = 10.765 ft ²
Volume	1 m ³ = 35.32 ft ³
Weight	1 kg = 2.205 lb
Density	1 g/cm ³ = 62.43 lb/ft ³
Pressure	1 g/cm ² = 2.048 lb/ft ² = 0.0142 psi
Heat	1 kcal = 3.968 Btu 1 kWh = 3413 Btu
Heat content	1 cal/g = 1.8 Btu/lb 1 kcal/m ² = 0.1123 Btu/ft ²
Heat flux	1 W/cm ² = 3170 Btu/h · ft ²
Thermal conductivity	$\frac{1 \text{ cal}}{\text{s} \cdot \text{cm} \cdot ^\circ\text{C}} = \frac{242 \text{ Btu}}{\text{h} \cdot \text{ft} \cdot ^\circ\text{F}}$
Heat transfer	$\frac{1 \text{ cal}}{\text{s} \cdot \text{cm}^2 \cdot ^\circ\text{C}} = \frac{7373 \text{ Btu}}{\text{h} \cdot \text{ft}^2 \cdot ^\circ\text{F}}$
Thermal diffusivity	$\frac{1 \text{ cal/s} \cdot \text{cm} \cdot ^\circ\text{C}}{\text{C} \cdot \text{g/cm}^3} = \frac{3.874 \text{ Btu/h} \cdot \text{ft} \cdot ^\circ\text{F}}{\text{C} \cdot \text{lb/ft}^3}$

Preheating for high-temperature coating processes, galvanizing, vitreous enameling, other coatings

Smelting for reduction of metallic ores

Firing of ceramic materials

Incineration

By method of load handling:

Batch furnaces for cyclic heating, including forge furnaces arranged to heat one end of a bar or billet inserted through a wall opening, side door, stationary-hearth-type car bottom designs

Continuous furnaces with loads pushed through or carried by a conveyor

Tilting-type furnace

To avoid the problem of door warpage or leakage in large batch-type furnaces, the furnace can be a refractory-lined box with an associated firing system, mounted above a stationary hearth, and arranged to be tilted around one edge of the hearth for loading and unloading by manual handling, forklift trucks, or overhead crane manipulators.

For handling heavy loads by overhead crane, without door problems, the furnace can be a portable cover unit with integral firing and temperature control. Consider a cover-type furnace for annealing steel strip coils in a controlled atmosphere. The load is a stack of coils with a common vertical axis, surrounded by a protective inner cover and an external heating cover. To improve heat transfer parallel to coil laminations, they are loaded with open coil separators between them, with heat transferred from the inner cover to coil ends by a recirculating fan. To start the cooling cycle, the heating cover is removed by an overhead crane, while atmosphere circulation by the base fan continues. Cooling may be enhanced by air blast cooling of the inner cover surface.

For heating heavy loads of other types, such as weldments, castings, or forgings, car bottom furnaces may be used with some associated door maintenance problems. The furnace hearth is a movable car to allow load handling by an overhead traveling crane. In one type of furnace, the door is suspended from a lifting mechanism. To avoid interference with an overhead crane and to achieve some economy in construction, the door may be mounted on one end of the car

and opened as the car is withdrawn. This arrangement may impose some handicaps in access for loading and unloading.

Loads such as steel ingots can be heated in pit-type furnaces, preferably with units of load separated to allow radiating heating from all sides except the bottom. Such a furnace would have a cover displaced by a mechanical carriage and would have a compound metal and refractory recuperator arrangement. Loads are handled by overhead crane equipped with suitable gripping tongs.

Continuous-Type Furnaces

The simplest type of continuous furnace is the hearth-type pusher furnace. Pieces of rectangular cross section are loaded side by side on a charge table and pushed through the furnace by an external mechanism. In the design shown, the furnace is fired from one end, counterflow to load travel, and is discharged through a side door by an auxiliary pusher lined up by the operator.

Furnace length is limited by thickness of the load and alignment of abutting edges to avoid buckling up from the hearth. A more complex design would provide multiple zone firing above and below the hearth, with recuperative air preheating.

Long loads can be conveyed in the direction of their length in a roller-hearth-type furnace. Loads can be bars, tubes, or plates of limited width, heated by direct firing, by radiant tubes, or by electric-resistor-controlled atmosphere, and conveyed at uniform speed or at alternating high and low speeds for quenching in line.

Sequential heat treatment can be accomplished with a series of chain or belt conveyors. Small parts can be loaded through an atmosphere seal, heated in a controlled atmosphere on a chain belt conveyor, discharged into an oil quench, and conveyed through a washer and tempering furnace by a series of mesh belts without intermediate handling.

Except for pusher-type furnaces, continuous furnaces can be self-emptying. To secure the same advantage in heating slabs or billets for rolling and to avoid scale loss during interrupted operation, loads can be conveyed by a walking-beam mechanism. Such a walking-beam-type slab heating furnace would have loads supported on water-cooled rails for over- and underfiring and would have an overhead recuperator.

Thin strip materials, joined in continuous strand form, can be conveyed horizontally or the strands can be conveyed in a series of vertical passes by driven support rolls. Furnaces of this type can be incorporated in continuous galvanizing lines.

Unit loads can be individually suspended from an overhead conveyor, through a slot in the furnace roof, and can be quenched in line by lowering a section of the conveyor.

Small parts or bulk materials can be conveyed by a moving hearth, as in the rotary hearth-type or tunnel kiln furnace. For roasting or incineration of bulk materials, the shaft-type furnace provides a simple and efficient system. Loads are charged through the open top of the shaft and descend by gravity to a discharge feeder at the bottom. Combustion air can be introduced at the bottom of the furnace and preheated by contact with the descending load before entering the combustion zone, where fuel is introduced through sidewalls. Combustion gases are then cooled by contact with the descending load, above the combustion zone, to preheat the charge and reduce flue gas temperature.

With loads that tend to agglomerate under heat and pressure, as in some ore-roasting operations, the rotary kiln may be preferable to the shaft-type furnace. The load is advanced by rolling inside an inclined cylinder. Rotary kilns are in general use for sintering ceramic materials.

Classification by Source of Heat

The classification of furnaces by source of heat is as follows:

- Direct firing with gas or oil fuels

- Combustion of material in process, as by incineration with or without supplemental fuel

Internal heating by electrical resistance or induction in conductors or dielectric heating of nonconductors

Radiation from electric resistors or radiant tubes in controlled atmospheres or under vacuum

4 FURNACE CONSTRUCTION

The modern industrial furnace design has evolved from a rectangular or cylindrical enclosure, built up of refractory shapes and held together by a structural steel binding. Combustion air was drawn in through wall openings by furnace draft, and fuel was introduced through the same openings without control of fuel/air ratios except by the judgment of the furnace operator. Flue gases were exhausted through an adjacent stack to provide the required furnace draft.

To reduce air infiltration or outward leakage of combustion gases, steel plate casings have been added. Fuel economy has been improved by burner designs providing some control of fuel/air ratios, and automatic controls have been added for furnace temperature and furnace pressure. Completely sealed furnace enclosures may be required for controlled atmosphere operation or where outward leakage of carbon monoxide could be an operating hazard.

With the steadily increasing costs of heat energy, wall structures are being improved to reduce heat losses or heat demands for cyclic heating. The selection of furnace designs and materials should be aimed at a minimum overall cost of construction, maintenance, and fuel or power over a projected service life. Heat losses in existing furnaces can be reduced by adding external insulation or rebuilding walls with materials of lower thermal conductivity. To reduce losses from intermittent operation, the existing wall structure can be lined with a material of low heat storage and low conductivity to substantially reduce mean wall temperatures for steady operation and cooling rates after interrupted firing.

Thermal expansion of furnace structures must be considered in design. Furnace walls have been traditionally built up of prefired refractory shapes with bonded mortar joints. Except for small furnaces, expansion joints will be required to accommodate thermal expansion. In sprung arches, lateral expansion can be accommodated by vertical displacement, with longitudinal expansion taken care of by lateral slots at intervals in the length of the furnace. Where expansion slots in furnace floors could be filled by scale, slag, or other debris, they can be packed with a ceramic fiber that will remain resilient after repeated heating.

Differential expansion of hotter and colder wall surfaces can cause an inward-bulging effect. For stability in self-supporting walls, thickness must not be less than a critical fraction of height.

Because of these and economic factors, cast or rammed refractories are replacing prefired shapes for lining many types of large, high-temperature furnaces. Walls can be retained by spaced refractory shapes anchored to the furnace casing, permitting reduced thickness as compared to brick construction. Furnace roofs can be suspended by hanger tile at closer spacing, allowing unlimited widths.

Cast or rammed refractories, fired in place, will develop discontinuities during initial shrinkage that can provide for expansion from subsequent heating to eliminate the need for expansion joints.

As an alternative to cast or rammed construction, insulating refractory linings can be gunned in place by jets of compressed air and retained by spaced metal anchors, a construction increasingly popular for stacks and flues.

Thermal expansion of steel furnace casings and bindings must also be considered. Where the furnace casing is constructed in sections, with overlapping expansion joints, individual sections can be separately anchored to building floors or foundations. For gas-tight casings, as required for controlled atmosphere heating, the steel structure can be anchored at one point

and left free to expand elsewhere. In a continuous galvanizing line, for example, the atmosphere furnace and cooling zone can be anchored to the foundation near the casting pot and allowed to expand toward the charge end.

5 FUELS AND COMBUSTION

Heat is supplied to industrial furnaces by combustion of fuels or by electrical power. Fuels now used are principally fuel oil and fuel gas. Because possible savings through improved design and operation are much greater for these fuels than for electric heating or solid fuel firing, they are given primary consideration in this section.

Heat supply and demand may be expressed in units of British thermal units or kilocalories or as gallons or barrels of fuel oil, tons of coal, or kilowatt-hours of electric power. For the large quantities considered for national or world energy loads, a preferred unit is the "quad," one quadrillion or 10^{15} Btu. Conversion factors are

$$\begin{aligned} 1 \text{ quad} &= 10^{15} \text{ Btu} \\ &= 172 \times 10^6 \text{ barrels of fuel oil} \\ &= 44.34 \times 10^6 \text{ tons of coal} \\ &= 10^{12} \text{ ft}^3 \text{ of natural gas} \\ &= 2.93 \times 10^{11} \text{ kWh electric power} \end{aligned}$$

At 30% generating efficiency, the fuel required to produce 1 quad of electrical energy is 3.33 quads. One quad of fuel is accordingly equivalent to 0.879×10^{11} kWh net power.

Fuel demand in the United States during recent years has been about 75 quads per year from the following sources:

Coal	15 quads
Fuel oil	
Domestic	18 quads
Imported	16 quads
Natural gas	23 quads
Other, including nuclear	3 quads

Hydroelectric power contributes about 1 quad net additional. Combustion of waste products has not been included but will be an increasing fraction of the total in the future.

Distribution of fuel demand by use is estimated at:

Power generation	20 quads
Space heating	11 quads
Transportation	16 quads
Industrial, other than power	25 quads
Other	4 quads

Net demand for industrial furnace heating has been about 6%, or 4.56 quads, primarily from gas and oil fuels.

The rate at which we are consuming our fossil fuel assets may be calculated as (annual demand)/(estimated reserves). This rate is presently highest for natural gas, because, besides

being available at the wellhead for immediate use, it can be transported readily by pipeline and burned with the simplest type of combustion system and without air pollution problems. It has also been delivered at bargain prices under federal rate controls.

As reserves of natural gas and fuel oil decrease, with a corresponding increase in market prices, there will be an increasing demand for alternative fuels such as synthetic fuel gas and fuel oil, waste materials, lignite, and coal.

Synthetic fuel gas and fuel oil are now available from operating pilot plants, but at costs not yet competitive.

As an industrial fuel, coal is primarily used for electric power generation. In the form of metallurgical coke, it is the source of heat and the reductant in the blast furnace process for iron ore reduction and as fuel for cupola furnaces used to melt foundry iron. Powdered coal is also being used as fuel and reductant in some new processes for solid-state reduction of iron ore pellets to make synthetic scrap for steel production.

Since the estimated life of coal reserves, particularly in North America, is so much greater than for other fossil fuels, processes for conversion of coal to fuel gas and fuel oil have been developed almost to the commercial cost level and will be available whenever they become economical. Processes for coal gasification, now being tried in pilot plants, include the following:

1. *Producer Gas.* Bituminous coal has been commercially converted to fuel gas of low heating value (LHV), around 110 Btu/scf LHV, by reacting with insufficient air for combustion and steam as a source of hydrogen. Old producers delivered a gas containing sulfur, tar volatiles, and suspended ash and have been replaced by cheap natural gas. By reacting coal with a mixture of oxygen and steam and removing excess carbon dioxide, sulfur gases, and tar, a clean fuel gas of about 300 Btu/scf LHV can be supplied. Burned with air preheated to 1000°F and with a flue gas temperature of 2000°F, the available heat is about 0.69 high heating value (HHV), about the same as for natural gas.

2. *Synthetic Natural Gas.* As a supplement to dwindling natural gas supplies, a synthetic fuel gas of similar burning characteristics can be manufactured by adding a fraction of hydrogen to the product of the steam–oxygen gas producer and reacting with carbon monoxide at high temperature and pressure to produce methane. Several processes are operating successfully on a pilot plant scale, but with a product costing much more than market prices for natural gas. The process may yet be practical for extending available natural gas supplies by a fraction to maintain present market demands. For gas mixtures or synthetic gas supplies to be interchangeable with present gas fuels, without readjustment of fuel/air ratio controls, they must fit the Wobbe index:

$$\frac{\text{HHV Btu/scf}}{(\text{specific gravity})^{0.5}}$$

The fuel gas industry was originally developed to supply fuel gas for municipal and commercial lighting systems. Steam was passed through incandescent coal or coke, and fuel oil vapors were added to provide a luminous flame. The product had a heating value of around 500 HHV and a high carbon monoxide content and was replaced as natural gas or coke oven gas became available. Coke oven gas is a by-product of the manufacture of metallurgical coke that can be treated to remove sulfur compounds and volatile tar compounds to provide a fuel suitable for pipeline distribution. Blast furnace gas can be used as an industrial or steam-generating fuel, usually after enrichment with coke oven gas. Gas will be made from replaceable sources such as agricultural and municipal wastes, cereal grains, and wood as market economics for such products improve.

Heating values for fuels containing hydrogen can be calculated in two ways:

1. Higher heating value is the total heat developed by burning with standard air in a ratio to supply 110% of net combustion air, cooling products to ambient temperature, and condensing all water vapor from the combustion of hydrogen.
2. Lower heating value is equal to HHV less heat from the condensation of water vapor. It provides a more realistic comparison between different fuels, since flue gases leave most industrial processes well above condensation temperatures.

HHV factors are in more general use in the United States, while LHV values are more popular in most foreign countries. For example, the HHV value for hydrogen as fuel is 319.4 Btu/scf, compared to a LHV of 270.2.

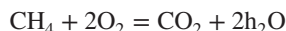
The combustion characteristics for common fuels are tabulated in Table 3 for combustion with 110% standard air. Weights in pounds per 10° Btu HHV are shown, rather than corresponding volumes, to expedite calculations based on mass flow. Corrections for flue gas and air temperatures other than ambient are given in charts to follow.

The heat released in a combustion reaction is given as

Total heats of formation of combustion products – total heats of formation of reactants

Heats of formation can be conveniently expressed in terms of Btu per pound mol, with the pound mol for any substance equal to a weight in pounds equal to its molecular weight. The heat of formation for elemental materials is zero. For compounds involved in common combustion reactions, values are shown in Table 4.

Data in Table 4 can be used to calculate the higher and lower heating values of fuels. For methane:



HHV

$$\begin{aligned} 169,20 + (2 \times 122,976) - 32,000 \\ = 383,042\text{Btu/lb} \cdot \text{mol} \\ 383,042/385 = 995 \text{ Btu/scf} \end{aligned}$$

Table 3 Combustion Characteristics of Common Fuels

Fuel	Btu/scf	Weight in lb/10 ⁶ Btu		
		Fuel	Air	Flue Gas
Natural gas (SW U.S)	1073	42	795	837
Coke oven gas	539	57	740	707
Blast furnace gas	92	821	625	1446
Mixed blast furnace and coke oven gas:				
Ratio CO/BF 1/1	316	439	683	1122
1/3	204	630	654	1284
1/10	133	752	635	1387
Hydrogen	319	16	626	642
	Btu/lb			
No. 2 fuel oil	19,500	51	810	861
No. 6 fuel oil	18,300	55	814	
With air atomization				869
With steam atomization at 3 lb/gal				889
Carbon	14,107	71	910	981

Table 4 Heats of Formation

Material	Formula	Molecular Weight	Heats of Formation (Btu/lb · mol ^a)
Methane	CH ₄	16	32,200
Ethane	C ₂ H ₆	30	36,425
Propane	C ₃ H ₈	44	44,676
Butane	C ₄ H ₁₀	58	53,662
Carbon monoxide	CO	28	47,556
Carbon dioxide	CO ₂	44	169,290
Water vapor	H ₂ O	18	104,040
Liquid water			122,976

^aThe volume 1 lb mol, for any gas, is 385 scf.

LHV

$$\begin{aligned}
 &169,290 + (2 \times 104,040) - 32,200 \\
 &= 345,170 \text{ Btu/lb} \cdot \text{mol} \\
 &345,170/385 = 897 \text{ Btu/scf}
 \end{aligned}$$

Available heats from combustion of fuels as a function of flue gas and preheated air temperatures can be calculated as a fraction of the HHV. The net ratio is 1 plus the fraction added by preheated air less the fraction lost as sensible heat and latent heat of water vapor from combustion of hydrogen in flue gas leaving the system.

Available heats can be shown in chart form, as in the Figures 1–5 for common fuels. On each chart, the curve on the right is the fraction of HHV available for combustion with 110% cold air, while the curve on the left is the fraction added by preheated air, as functions of air or flue gas temperatures. For example, the available heat fraction for methane burned with 110% air preheated to 1000°F, and with flue gas out at 2000°F, is shown in Fig. 1 : 0.41 + 0.18 – 0.59 HHV. Values for other fuels are shown in as follows:

Fig. 2, fuel oils with air or steam atomization

Fig. 3, by-product coke oven gas

Fig. 4, blast furnace gas

Fig. 5, methane

For combustion with other than 110% of net air demand, the corrected available heat can be calculated as follows. For methane with preheated air at 1000°F and flue gas out at 2000°F and 150% net air supply:

$$\begin{aligned}
 &\text{Available heat from Fig. 1 : } 0.59 \\
 &\text{Add excess air } + 0.18 (1.5 - 1.1) = 0.072 \\
 &\quad \quad \quad -0.41 (1.5-1.1) = \underline{-0.164} \\
 &\text{Net total at 150\% } 0.498
 \end{aligned}$$

Available heats for fuel gas mixtures can be calculated by adding the fractions for either fuel and dividing by the combined volume. For example, a mixture of one-quarter coke oven gas and three-quarters blast furnace gas is burned with 110% combustion air preheated to 1000°F and with flue gas out at 2000°F. Using data from Table 3 and Figs. 3 and 4,

$$\begin{aligned}
 &\text{CO } (539 \times 0.25 = 134.75) (0.49 + 0.17) = 88.93 \text{ BF } (92 \times 0.75 = 69.00) (0.21 + 0.144) \\
 &= 24.43
 \end{aligned}$$

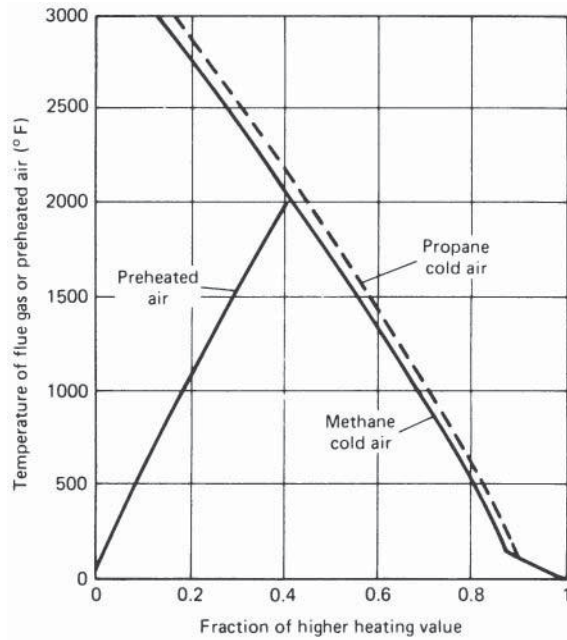


Figure 1 Available heat for methane and propane combustion. Approximate high and low limits for commercial natural gas.^a

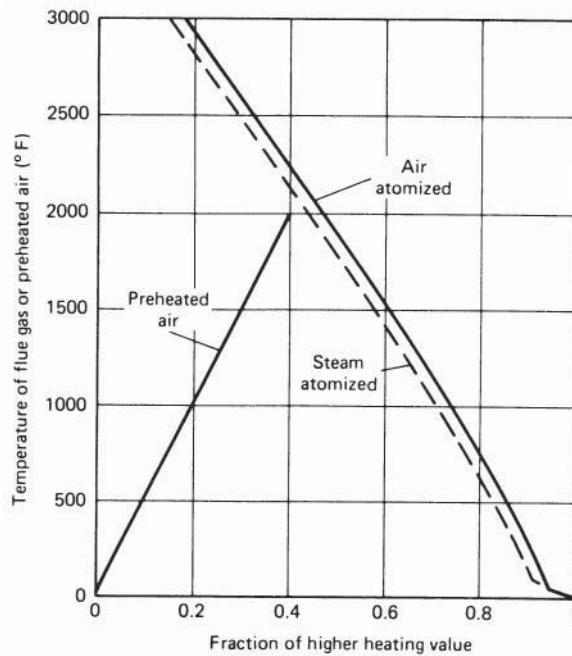


Figure 2 Available heat ratios for fuel oils with air or steam atomization.^a

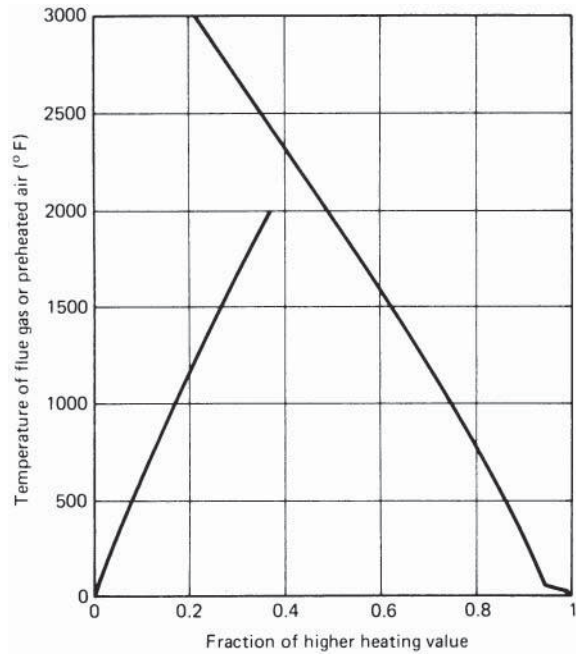


Figure 3 Available heat ratios for by-product coke oven gas.^a

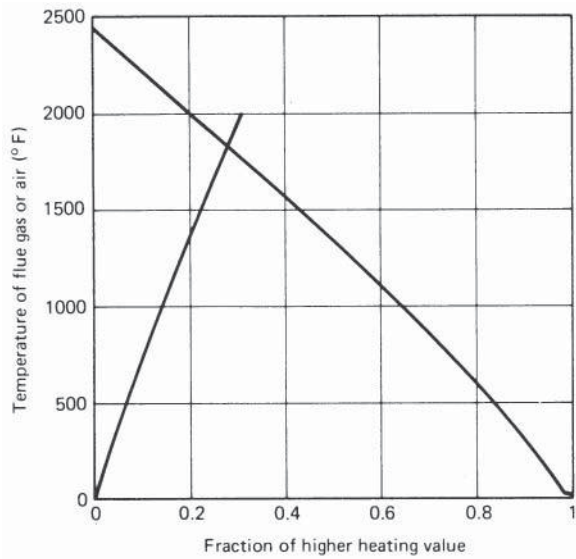


Figure 4 Available heat ratios for blast furnace gas.^a

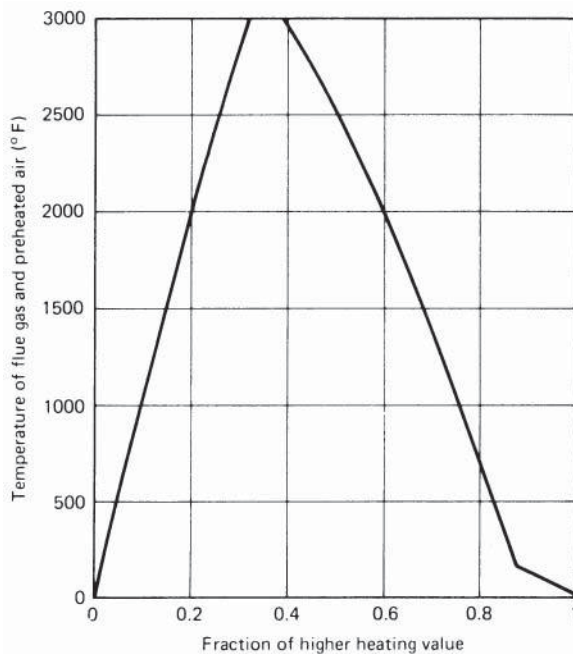


Figure 5 Available heat ratios for combustion of methane with 110% air containing 35% O₂.^a

$$\text{HHV } 203.75 \quad \text{Available} = 113.36$$

$$\text{Net} : 113.36/203.75 = 0.556 \text{ combined HHV}$$

6 OXYGEN ENRICHMENT OF COMBUSTION AIR

The available heats of furnace fuels can be improved by adding oxygen to combustion air. Some studies have been based on a total oxygen content of 35%, which can be obtained by adding 21.5 scf pure oxygen or 25.45 scf of 90% oxygen per 100 scf of dry air. The available heat ratios are shown in Fig. 5.

At present market prices, the power needed to concentrate pure oxygen for enrichment to 35% will cost more than the fuel saved, even with metallurgical oxygen from an in-plant source. As plants are developed for economical concentration of oxygen to around 90%, the cost balance may become favorable for very high temperature furnaces.

In addition to fuel savings by improvement of available heat ratios, there will be additional savings in recuperative furnaces by increasing preheated air temperature at the same net heat demand, depending on the ratio of heat transfer by convection to that by gas radiation in the furnace and recuperator.

7 THERMAL PROPERTIES OF MATERIALS

The heat content of some materials heated in furnaces or used in furnace construction is shown in Fig. 6 in units of Btus per pounds. Vertical lines in curves represent latent heats of melting

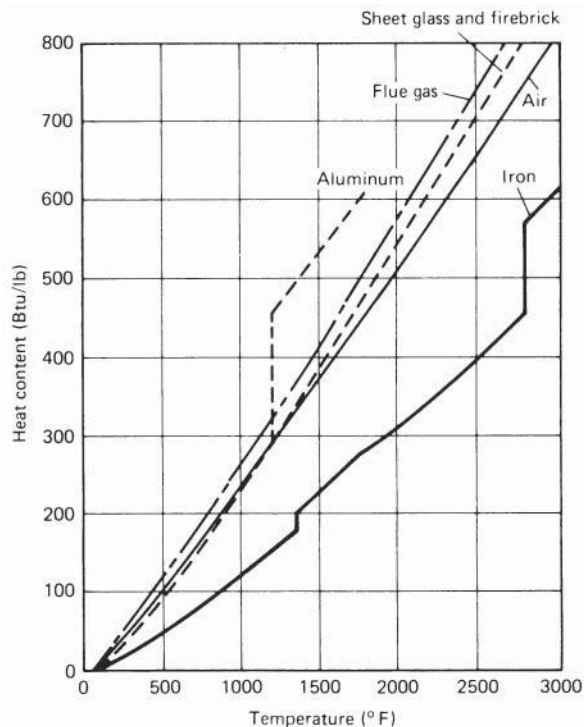


Figure 6 Heat content of materials at temperature.^a

or other phase transformations. The latent heat of evaporation for water in flue gas has been omitted from the chart. The specific heat of liquid water is, of course, about 1.

Thermal conductivities in English units are given in reference publications as $[\text{Btu}/(\text{ft}^2 \cdot \text{h})]/(^\circ\text{F}/\text{in.})$ or as $[\text{Btu}/(\text{ft}^2 \cdot \text{h})]/(^\circ\text{F}/\text{ft})$. To keep dimensions consistent, the latter term, abbreviated to $k = \text{Btu}/\text{ft} \cdot \text{h} \cdot ^\circ\text{F}$ will be used here. Values will be 1/12th of those in terms of $^\circ\text{F}/\text{in.}$

Thermal conductivities vary with temperature, usually inversely for iron, steel, and some alloys and conversely for common refractories. At usual temperatures of use, average values of k in $\text{Btu}/(\text{ft} \cdot \text{h} \cdot ^\circ\text{F})$ are given in Table 5.

To expedite calculations for nonsteady conduction of heat, it is convenient to use the factor for "thermal diffusivity," defined as

$$D = \frac{k}{DC} = \frac{\text{thermal conductivity}}{\text{density} \times \text{specific heat}}$$

in consistent units. Values for common furnace loads over the usual range of temperatures for heating are:

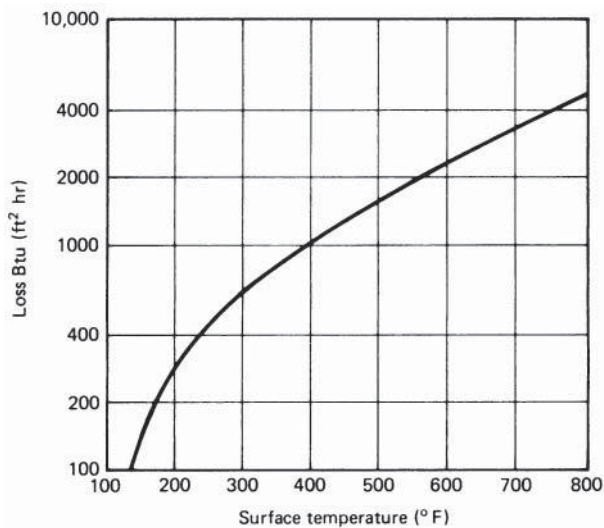
Carbon steels, 70–1650°F	0.32
70–2300°F	0.25
Low-alloy steels, 70–2000°F	0.23
Stainless steels, 70–2000°F	
300 type	0.15
400 type	0.20
Aluminum, 70–1000°F	3.00
Brass, 70/30, 70–1500°F	1.20

Table 5 Average Values of k (Btu/ft · h · °F)

	Mean Temperature (°F)				2500
	100	1000	1500	2000	
Steel, SAE 1010	33	23	17	17	
Type HH HRA	8	11	14	16	
Aluminum	127	133			
Copper	220	207	200		
Brass, 70/30	61	70			
Firebrick	0.81	0.82	0.85	0.89	0.93
Silicon carbide	11	10	9	8	6
Insulating firebrick	0.12	0.17	0.20	0.24	

In calculating heat losses through furnace walls with multiple layers of materials with different thermal conductivities, it is convenient to add thermal resistance $R = r/k$, where r is thickness in feet. For example:

	r	k	r/k
9 in. firebrick	0.75	0.9	0.833
4½ in. insulating firebrick	0.375	0.20	1.875
	0.208	0.15	<u>1.387</u>
2¼ in. block insulation	Total R for wall materials		4.095

**Figure 7** Furnace wall losses as function of surface temperature.^a

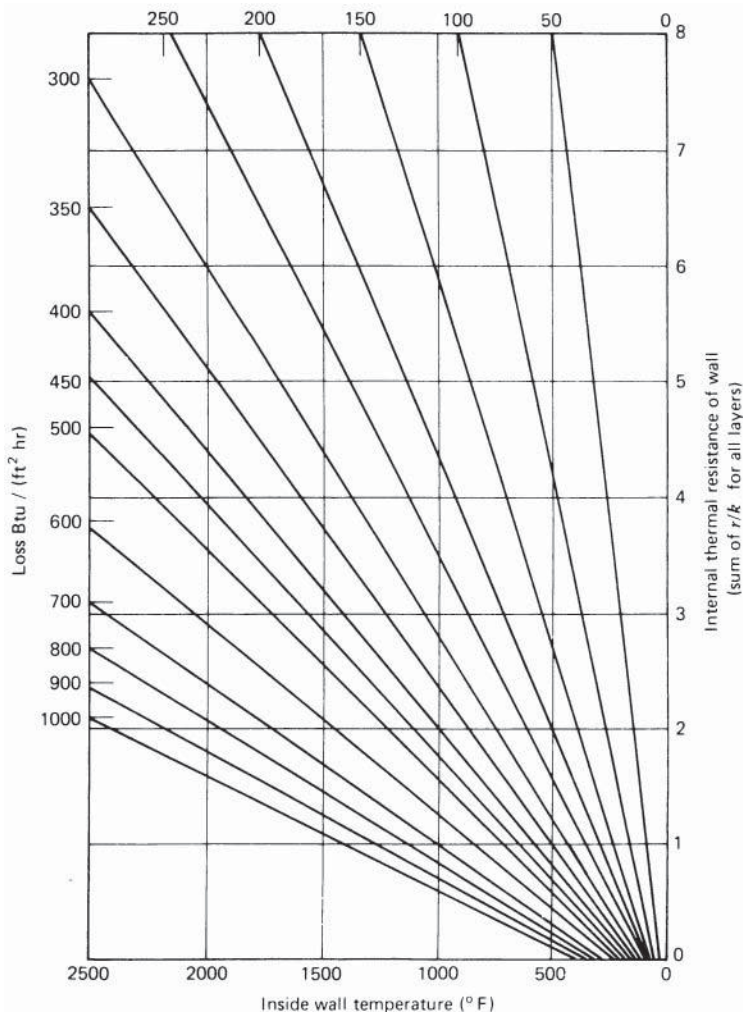


Figure 8 Furnace wall losses as function of composite thermal resistance.^a

Overall thermal resistance will include the factor for combined radiation and convection from the outside of the furnace wall to ambient temperature. Wall losses as a function of wall surface temperature for vertical surfaces in still air are shown in Fig. 7 and are included in the overall heat loss data for furnace walls shown in Fig. 8.

Figure 9 shows the thermodynamic properties of air and flue gas over the usual range of temperatures for use in heat transfer and fluid flow problems. Data for other gases, in formula form, are available in standard references.

Linear coefficients of thermal expansion are the fractional changes in length per degrees Fahrenheit change in temperature. Coefficients in terms of $10^6 \times$ net values are listed below for materials used in furnace construction and for the usual range of temperatures:

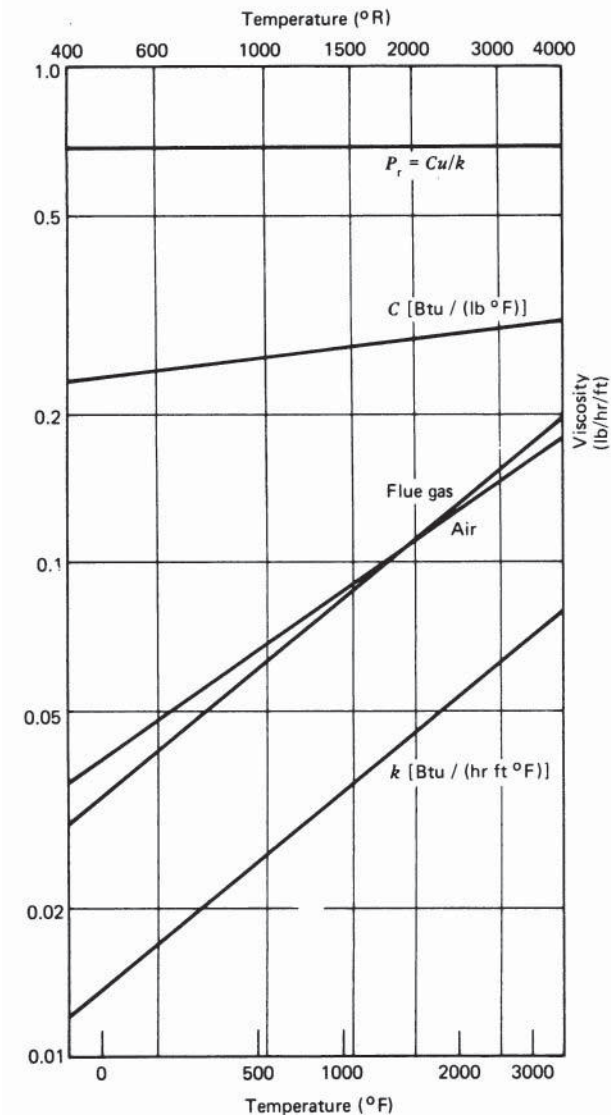


Figure 9 Thermodynamic properties of air and flue gas.^a

Carbon steel	9
Cast heat-resistant alloys (HRA)	10.5
Aluminum	15.6
Brass	11.5
Firebrick, silicon carbide	3.4
Silica brick	3.4

Coefficients for cubical expansion of solids are about $3 \times$ linear coefficients. The cubical coefficient for liquid water is about 185×10^{-6} .

8 HEAT TRANSFER

Heat may be transmitted in industrial furnaces by radiation—gas radiation from combustion gases to furnace walls or direct to load and solid-state radiation from walls, radiant tubes, or electric heating elements to load—or by convection—from combustion gases to walls or load. Heat may be generated inside the load by electrical resistance to an externally applied voltage or by induction, with the load serving as the secondary circuit in an alternating current transformer. Nonconducting materials may be heated by dielectric heating from a high-frequency source.

Heat transfer in the furnace structure or in solid furnace loads will be by conduction. If the temperature profile is constant with time, the process is defined as “steady-state conduction.” If temperatures change during a heating cycle, it is termed “non-steady-state conduction.”

Heat flow is a function of temperature differentials, usually expressed as the “log-mean temperature difference” with the symbol MTD. MTD is a function of maximum and minimum

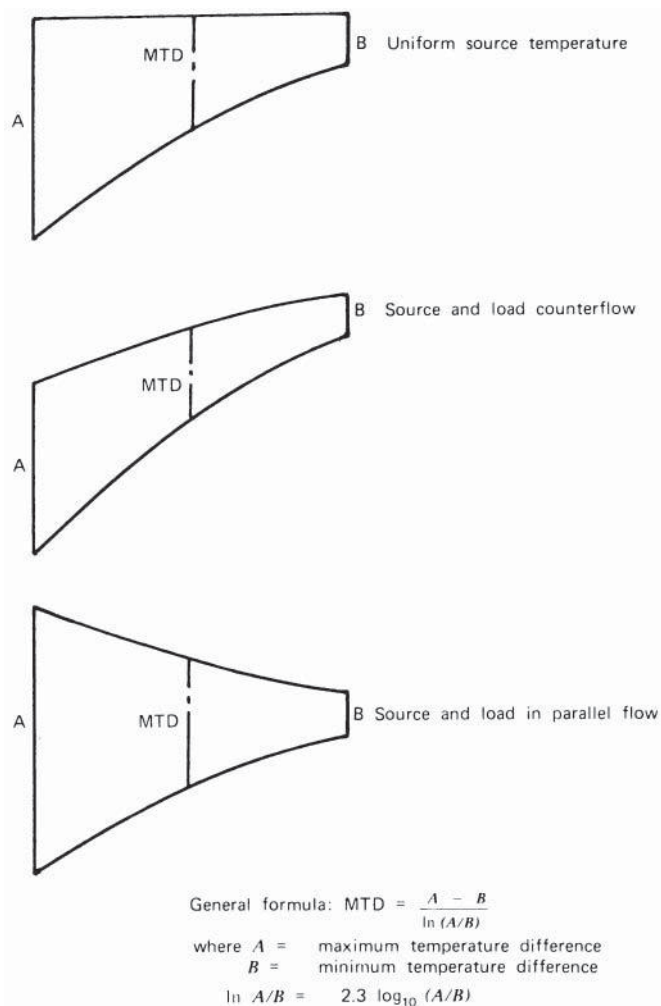


Figure 10 Diagrams of log-MTD.^a

temperature differences that can vary with position or time. Three cases encountered in furnace design are illustrated in Fig. 10. If the maximum differential, in any system of units, is designated as A and the minimum is designated by B :

$$MTD = \frac{A - B}{\ln(A/B)}$$

8.1 Solid-State Radiation

“Blackbody” surfaces are those that absorb all radiation received, with zero reflection, and exist only as limits approached by actual sources or receivers of solid radiation. Radiation between blackbodies is expressed by the Stefan–Boltzmann equation:

$$Q/A = N(T^4 - T_0^4) \text{Btu/h} \cdot \text{ft}^2$$

where N is the Stefan–Boltzmann constant, now set at about 0.1713×10^{-8} for T and T_0 , source and receiver temperatures, in degrees Rankine. Because the fourth powers of numbers representing temperatures in degrees Rankine are large and unwieldy, it is more convenient to express temperatures in °S, equivalent to $(°F + 460)/100$. The constant N is then reduced to 0.1713.

With source and receiver temperatures identified as T_s and T_r in °S, and with allowance for emissivity and view factors, the complete equation becomes

$$\frac{Q}{A} = 0.1713 \times \text{em} \times \text{Fr}(T_s^4 - T_r^4) \text{Btu/h} \cdot \text{ft}^2$$

at the receiving surface,

where em = combined emissivity and absorptivity factors for source and receiving surfaces

Fr = net radiation view factor for receiving surface

T_s and T_r = source and receiving temperature in °S

The factor em will be somewhat less than e for the source or a for the receiving surface and can be calculated as

$$\text{em} = 1 / \left(\frac{1}{a} + \frac{A_r}{A_s} \left(\frac{1}{e} - 1 \right) \right)$$

where a = receiver absorptivity at T_r

A_r/A_s = area ratio, receiver/source

e = source emissivity at T_s

8.2 Emissivity–Absorptivity

While emissivity and absorptivity values for solid materials vary with temperature, values for materials commonly used as furnace walls or loads, in the usual range of temperatures, are:

Refractory walls	0.80–0.90
Heavily oxidized steel	0.85–0.95
Bright steel strip	0.25–0.35
Brass cake	0.55–0.60
Bright aluminum strip	0.05–0.10
Hot-rolled aluminum plate	0.10–0.20
Cast heat-resisting alloy	0.75–0.85

For materials such as sheet glass, transparent in the visible light range, radiation is reflected at both surfaces at about 4% of incident value, with the balance absorbed or

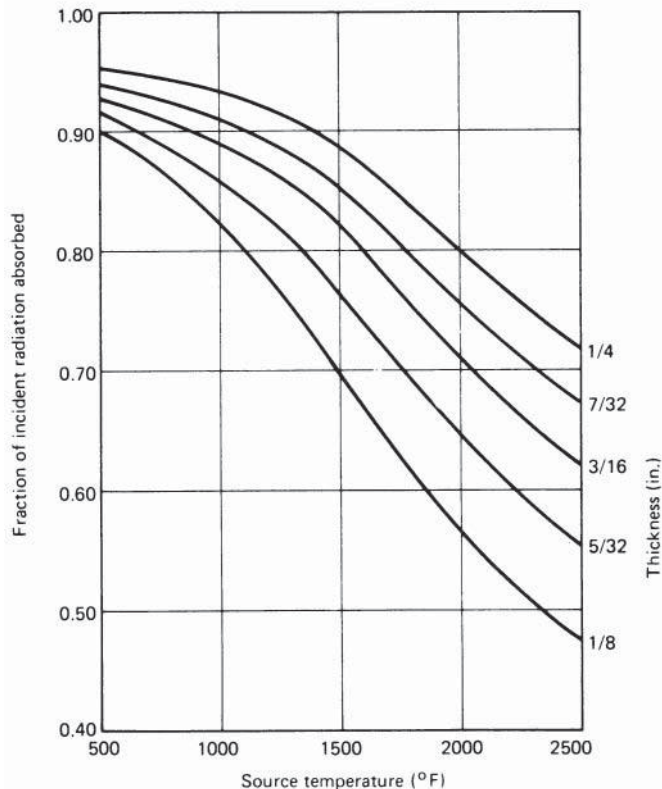


Figure 11 Radiation absorptivity of sheet glass with surface reflection deducted.^a

transmitted. Absorptivity decreases with temperature, as shown in Fig. 11. The absorptivity of liquid water is about 0.96.

8.3 Radiation Charts

For convenience in preliminary calculations, blackbody radiation as a function of temperature in degrees Fahrenheit is given in Fig. 12. The value for the receiver surface is subtracted from that of the source to find net interchange for blackbody conditions, and the result is corrected for emissivity and view factors. Where heat is transmitted by a combination of solid-state radiation and convection, a blackbody coefficient, in $\text{Btu/h} \cdot ^\circ\text{F}$, is shown in Fig. 13. This can be added to the convection coefficient for the same temperature interval, after correcting for emissivity and view factor, to provide an overall coefficient (H) for use in the formula

$$Q/A = H(T - T_r)$$

8.4 View Factors for Solid-State Radiation

For a receiving surface completely enclosed by the source of radiation or for a flat surface under a hemispherical radiating surface, the view factor is unity. Factors for a wide range of geometric

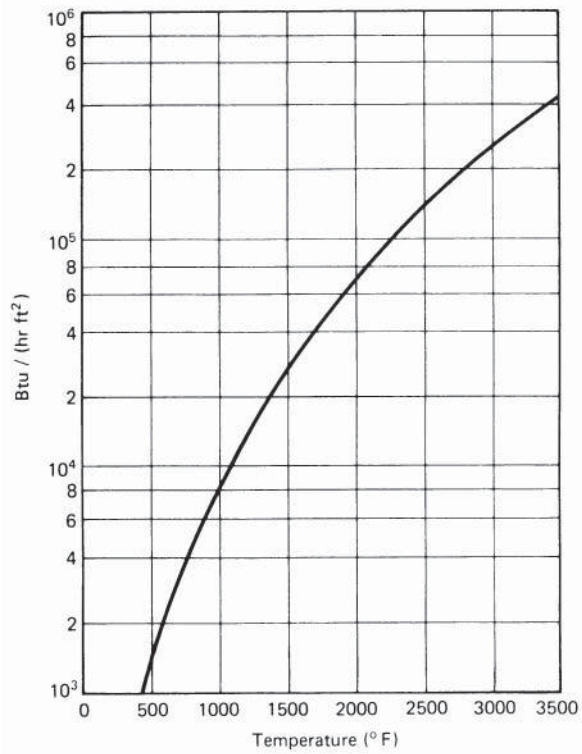


Figure 12 Blackbody radiation as function of load surface temperature.

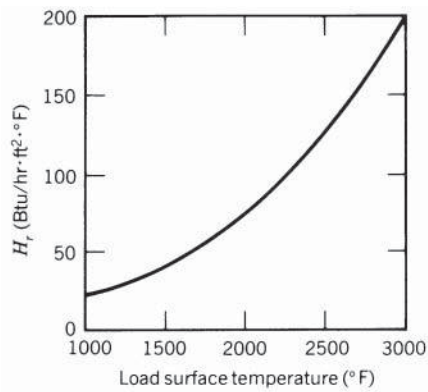


Figure 13 Blackbody radiation coefficient for source temperature uniform at 50–105° above final load surface temperature.

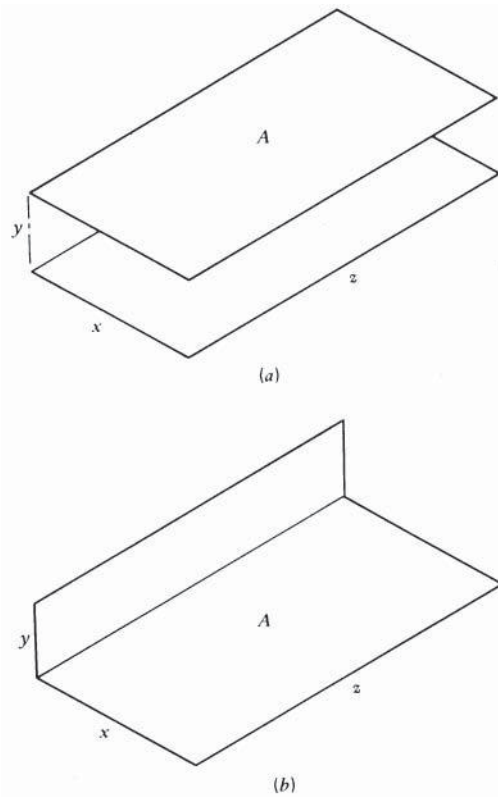


Figure 14 Diagram of radiation view factors for parallel and perpendicular planes.^a

configurations are given in available references. For cases commonly involved in furnace heat transfer calculations, factors are shown in Figs. 14–19.

For two parallel planes with edges in alignment as shown in Fig. 14a, view factors are given in Fig. 15 in terms of ratios of x , y , and z . For two surfaces intersecting at angle of 90° at a common edge, the view factor is shown in Fig. 16. If surfaces do not extend to a common intersection, the view factor for the missing areas can be calculated and deducted from that with surfaces extended as in the figure to find the net value for the remaining areas.

For spaced cylinders parallel to a furnace wall, as shown in Fig. 17, the view factor is shown in terms of diameter and spacing, including wall reradiation. For tubes exposed on both sides to source or receiver radiation, as in some vertical strip furnaces, the following factors apply if sidewall reradiation is neglected:

Ratio C/D	1.0	1.5	2.0	2.5	3.0
Factor	0.67	0.793	0.839	0.872	0.894

For ribbon-type electric heating elements, mounted on a back-up wall as shown in Fig. 18, exposure factors for projected wall area and for total element surface area are shown as a function of the (element spacing)/(element width) ratio. Wall reradiation is included, but heat loss

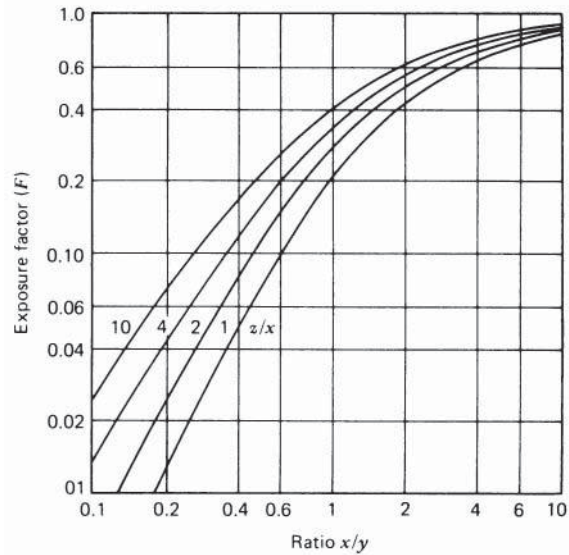


Figure 15 Radiation view factors for parallel planes.^a

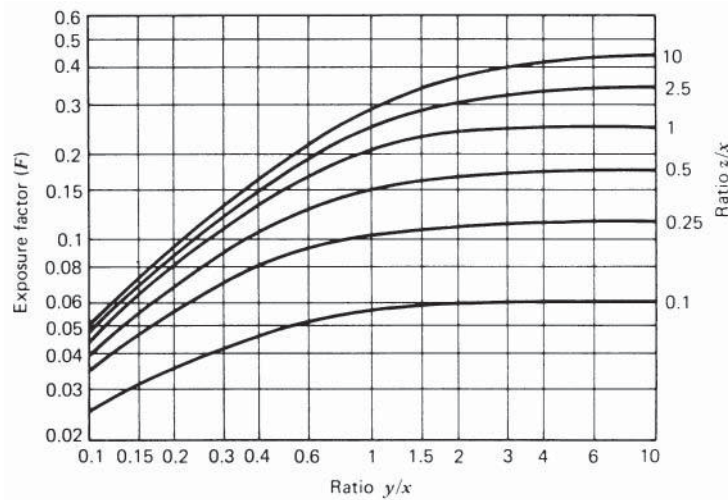


Figure 16 Radiation view factors for perpendicular planes.^a

through the backup wall is not considered. The emission rate from the resistor surface will be $W/\text{in.}^2 = Q/491A$, where

$$\frac{Q}{A} = \frac{\text{Btu/h}}{\text{ft}^2}$$

For parallel planes of equal area, as shown in Fig. 14, connected by reradiating walls on four sides, the exposure factor is increased as shown in Fig. 19. Only two curves, for $z/x = 1$ and $z/x = 10$, have been plotted for comparison with Fig. 13.

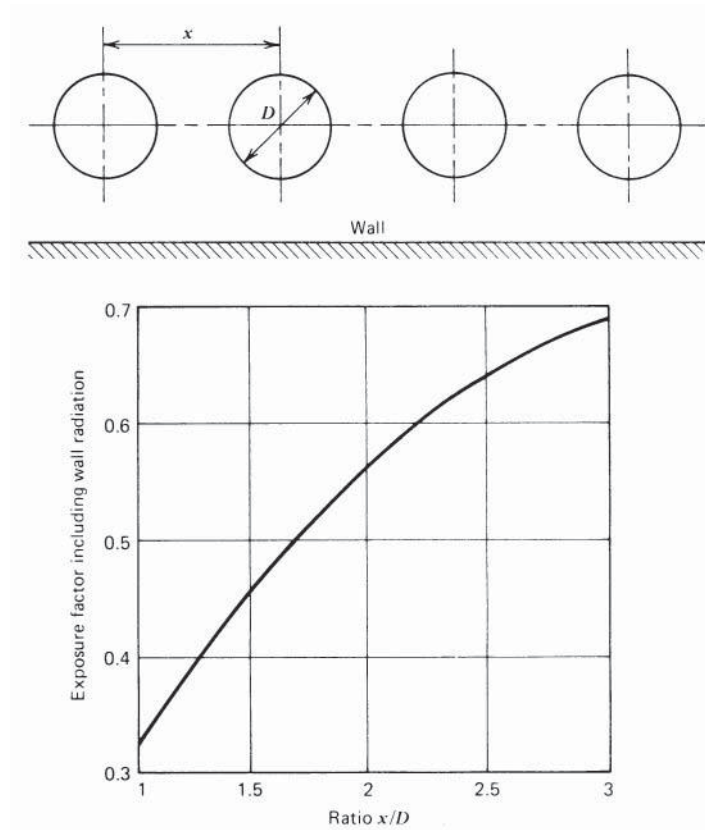


Figure 17 View factors for spaced cylinders with backup wall.^a

8.5 Gas Radiation

Radiation from combustion gases to walls and load can be from luminous flames or from nonluminous products of combustion. Flame luminosity results from suspended solids in combustion gases, either incandescent carbon particles or ash residues, and the resulting radiation is in a continuous spectrum corresponding to that from solid-state radiation at the same source temperature. Radiation from nonluminous gases is in characteristic bands of wavelengths, with intensity depending on depth and density of the radiating gas layer, its chemical composition, and its temperature.

For combustion of hydrocarbon gases, flame luminosity is from carbon particles formed by cracking of unburned fuel during partial combustion and is increased by delayed mixing of fuel and air in the combustion chamber. With fuel and air thoroughly premixed before ignition, products of combustion will be nonluminous in the range of visible light but can radiate strongly in other wavelength bands for some products of combustion including carbon dioxide and water vapor. Published data on emissivities of these gases show intensity of radiation as a function of temperature, partial pressure, and beam length. The combined emissivity for mixtures of carbon dioxide and water vapor requires a correction factor for mutual absorption. To expedite calculations, a chart has been prepared for the overall emissivity of some typical flue gases, including these correction factors. The chart in Fig. 20 has been calculated for products of

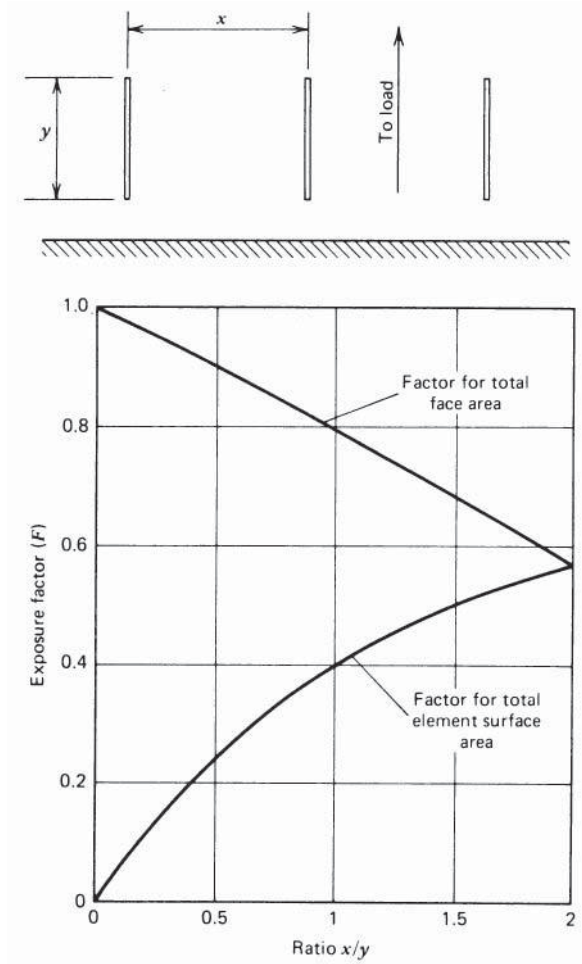


Figure 18 View factors for ribbon-type electric heating elements mounted on backup wall.^a

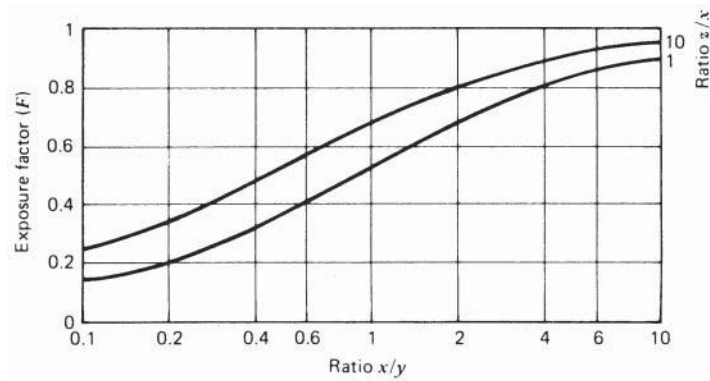


Figure 19 View factors for parallel planes connected by reradiating sidewalls.^a

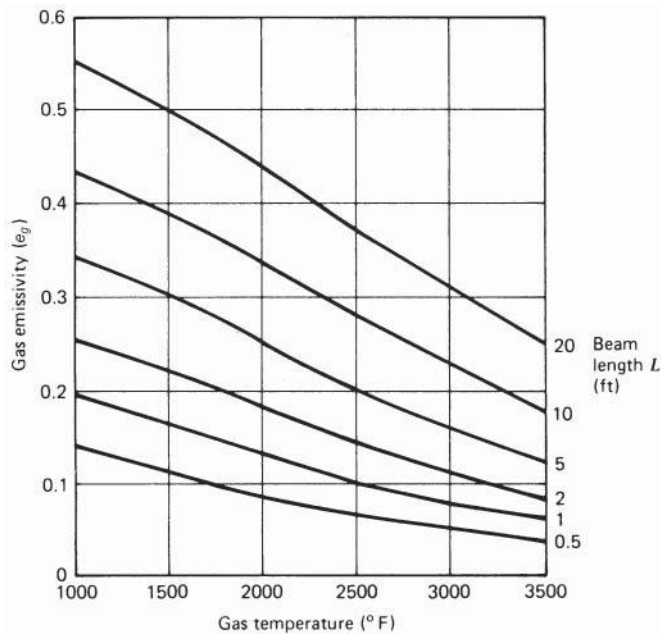


Figure 20 Gas emissivity for products of combustion of methane burned with 110% air. Approximate for fuel oils and coke oven gas.^a

combustion of methane with 110% of net air demand and is approximately correct for other hydrocarbon fuels of high heating value, including coke oven gas and fuel oils. Emissivities for producer gas and blast furnace gas will be lower because of dilution of radiating gases by nitrogen.

The emissivity of a layer of combustion gases does not increase directly with thickness or density, because of partial absorption during transmission through the depth of the layer. Figure 20 provides several curves for a range of values of L , the effective beam length in feet, at a total pressure of 1 atm. For other pressures, the effective beam length will vary directly with gas density.

Beam lengths for average gas densities will be somewhat less than for very low density because of partial absorption. For some geometric configurations, average beam lengths are:

Between two large parallel planes, $1.8\times$ spacing

Inside long cylinder, about $0.85\times$ diameter in feet

For rectangular combustion chambers, $3.4V/A$ where V is volume in cubic feet and A is total wall area in square feet

Transverse radiation to tube banks, with tubes of D outside diameter spaced at x centers:

L/D ranges from 1.48 for staggered tubes at $x/D = 1.5$ to 10.46 for tubes in line and $x/D = 3$ in both directions.

8.6 Evaluation of Mean Emissivity–Absorptivity

For a gas with emissivity e_g radiating to a solid surface at a temperature of T_s °F, the absorptivity a_g will be less than e_g at T_s because the density of the gas is still determined by T_g . The effective

power level PL becomes $T_s/T_g \times \text{PL}$ at T_s . Accurate calculation of the combined absorptivity for carbon dioxide and water vapor requires a determination of ag for either gas and a correction factor for the total. For the range of temperatures and PL factors encountered in industrial heat transfer, the net heat transfer can be approximated by using a factor e_{gm} somewhat less than e_g at T_g in the formula

$$Q/A = 0.173e_{gm}F(T_g^4 - T_s^4)$$

where T_g is an average of gas temperatures in various parts of the combustion chamber; the effective emissivity will be about $e_{gm} = 0.9e_g$ at T_g and can be used with Fig. 20 to approximate net values.

8.7 Combined Radiation Factors

For a complete calculation of heat transfer from combustion gases to furnace loads, the following factors will need to be evaluated in terms of the equivalent fraction of blackbody radiation per unit area of the exposed receiving surface:

F_{gs} = coefficient for gas direct to load plus radiation reflected from walls to load

F_{gw} = coefficient for gas radiation absorbed by walls

F_{ws} = coefficient for solid-state radiation from walls to load

Convection heat transfer from gases to walls and load is also involved but can be eliminated from calculations by assuming that gas-to-wall convection is balanced by wall losses and that gas-to-load convection is equivalent to a slight increase in load surface absorptivity. Mean effective gas temperature is usually difficult to measure but can be calculated if other factors are known. For example, carbon steel slabs are being heated to rolling temperature in a fuel-fired continuous furnace. At any point in the furnace, neglecting convection,

$$F_{gw}(T_g^4 - T_w^4) = F_{ws}(T_w^4 - T_s^4)$$

where T_g , T_w , and T_s are gas, wall, and load surface temperatures in °S. For a ratio of 2.5 for exposed wall and load surfaces and a value of 0.17 for gas-to-wall emissivity, $F = 2.5 \times 0.17 = 0.425$. With wall-to-load emissivity equal to $F = 0.89$, wall temperature constant at 2350°F (28.1°S), and load temperature increasing from 70 to 2300°F at the heated surface ($T_s = 5.3\text{--}27.6^\circ\text{S}$), the mean value of gas temperature (T_g) can be determined:

$$\text{MTD, walls to load} = \frac{2280 - 50}{\ln(2280/50)} = 584^\circ\text{F}$$

$$\text{Mean load surface temperature } T_{sm} = 2350 - 584 = 1766^\circ\text{F} (22.26^\circ\text{S})$$

Q/A per unit of load surface, for reradiation:

$$\begin{aligned} 0.425 \times 0.1713T_g^4 - 28.12 &= 0.89 \times 0.171328.14 - 22.264 \\ &= 57,622 \text{ Btu h} \cdot \text{ft}^2 \end{aligned}$$

$$T_g = 34.49^\circ\text{S} (2989^\circ\text{F})$$

With a net wall emissivity of 0.85, 15% of gas radiation will be reflected to the load, with the balance being absorbed and reradiated. Direct radiation from gas to load is then

$$1.15 \times 0.17 \times 0.1713(34.49^4 - 22.26^4) = 47,389 \text{ Btu/h} \cdot \text{ft}^2$$

$$\text{Total radiation : } 57,622 + 47,389 = 105,011 \text{ Btu/h} \cdot \text{ft}^2$$

For comparison, blackbody radiation from walls to load, without gas radiation, would be 64,743 Btu/h·ft² or 62% of the combined total.

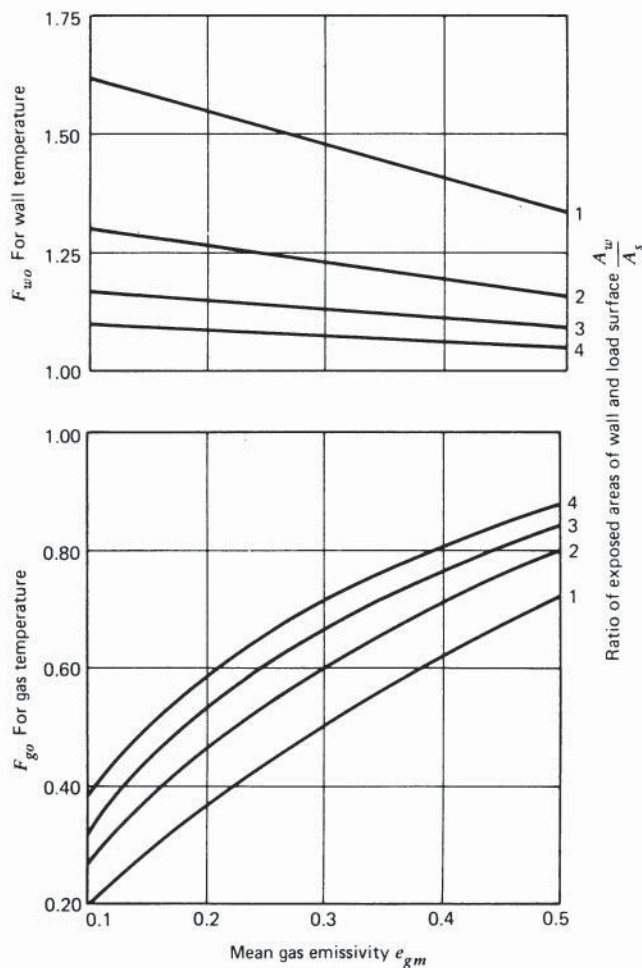


Figure 21 Overall heat transfer coefficients for gas and solid radiation as function of gas emissivity and wall-to-load area ratio for uniform gas or wall temperature compared to blackbody radiation.^a

With practical furnace temperature profiles, in a counterflow, direct-fired continuous furnace, gas and wall temperatures will be depressed at the load entry end to reduce flue gas temperature and stack loss. The resulting net heating rates will be considered in Section 8.12.

Overall heat transfer coefficients have been calculated for constant wall temperature in the upper chart in Fig. 21 or for constant gas temperature in the lower chart. Coefficients vary with mean gas emissivity and with A_w/A_s , the ratio of exposed surface for walls and load, and are always less than unity for overall radiation from gas to load or greater than unity for wall-to-load radiation. Curves can be used to find gas, wall, or mean load temperatures when the other two are known.

8.8 Steady-State Conduction

Heat transfer through opaque solids and motionless layers of liquids or gases is by conduction. For constant-temperature conditions, heat flow is by “steady-state” conduction and does not

vary with time. For objects being heated or cooled, with a continuous change in internal temperature gradients, conduction is termed “non–steady state.”

Thermal conduction in some solid materials is a combination of heat flow through the material, radiation across the internal space resulting from porosity, and convection within individual pores or through the thickness of porous layers.

Conductivities of refractory and insulating materials tend to increase with temperature, because of porosity effects. Values for most metals decrease with temperature, partly because of reduced density. Conductivity coefficients for some materials used in furnace construction or heated in furnaces are listed in Table 5. A familiar problem in steady-state conduction is the calculation of heat losses through furnace walls made up of multiple layers of materials of different thermal conductivities. A convenient method of finding overall conductance is to find the thermal resistance ($r/k = \text{thickness}/\text{conductivity}$ in consistent units) and add the total for all layers. Because conductivities vary with temperature, mean temperatures for each layer can be estimated from a preliminary temperature profile for the composite wall. Overall resistance will include the effects of radiation and conduction between the outer wall surface and its surroundings.

Figure 7 shows heat loss from walls to ambient surrounding at 70°F, combining radiation and convection for vertical walls. The corresponding thermal resistance is included in the overall heat transfer coefficient shown in Fig. 8 as a function of net thermal resistance of the wall structure and inside face temperature.

As an example of application, assume a furnace wall constructed as follows:

Material	r	k	r/k
9 in. firebrick	0.75	0.83	0.90
4 1/2 in. 2000°F insulation	0.375	0.13	2.88
2 1/2 in. ceramic fiber block	0.208	0.067	<u>3.10</u>
	Total R for solid wall		<u>6.88</u>

With an inside surface temperature of 2000°F, the heat loss from Fig. 7 is about 265 Btu/ft · h². The corresponding surface temperature from Fig. 8 is about 200°F, assuming an ambient temperature of 70°F.

Although not a factor affecting wall heat transfer, the possibility of vapor condensation in the wall structure must be considered by the furnace designer, particularly if the furnace is fired with a sulfur-bearing fuel. As the sulfur dioxide content of fuel gases is increased, condensation temperatures increase to what may exceed the temperature of the steel furnace casing in normal operation. Resulting condensation at the outer wall can result in rapid corrosion of the steel structure.

Condensation problems can be avoided by providing a continuous membrane of aluminum or stainless steel between layers of the wall structure at a point where operating temperatures will always exceed condensation temperatures.

8.9 Non–Steady-State Conduction

Heat transfer in furnace loads during heating or cooling is by transient or non–steady-state conduction, with temperature profiles within loads varying with time. With loads of low internal

thermal resistance, heating time can be calculated for the desired load surface temperature and a selected time–temperature profile for furnace temperature. With loads of appreciable thermal resistance from surface to center or from hot to colder sides, heating time will usually be determined by a specified final load temperature differential and a selected furnace temperature profile for the heating cycle.

For the case of a slab-type load being heated on a furnace hearth, with only one side exposed, and with the load entering the furnace at ambient temperature, the initial gradient from the heated to the unheated surface will be zero. The heated surface will heat more rapidly until the opposite surface starts to heat, after which the temperature differential between surfaces will taper off with time until the desired final differential is achieved.

In Fig. 22 the temperatures of heated and unheated surface or core temperature are shown as a function of time. In the lower chart temperatures are plotted directly as a function of time. In the upper chart the logarithm of the temperature ratio ($Y = \text{load temperature} / \text{source temperature}$) is plotted as a function of time for a constant source temperature. After a short initial heating time, during which the unheated surface or core temperature reaches its maximum rate of increase, the two curves in the upper diagram become parallel straight lines.

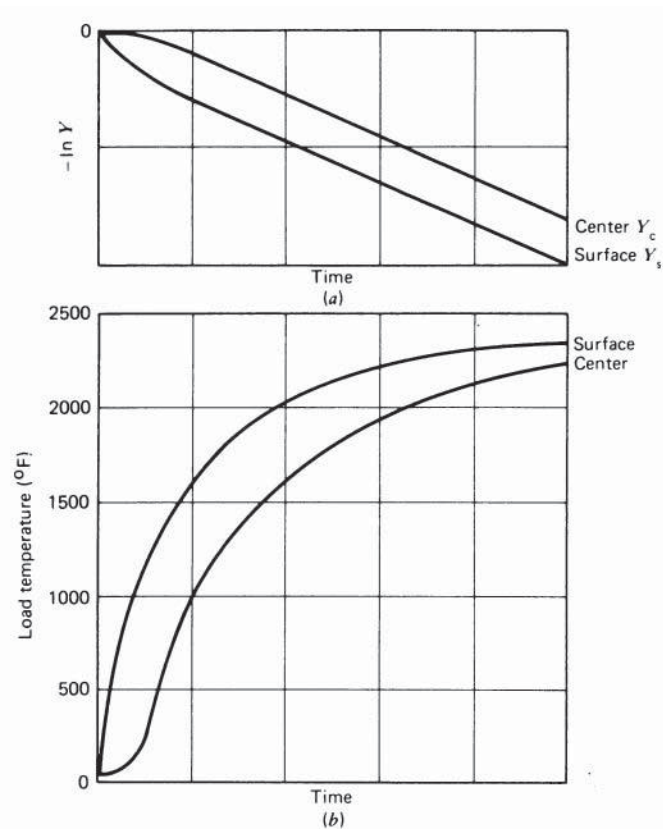


Figure 22 Maximum and minimum load temperatures and $-\ln Y_s$ or $-\ln Y_c$ as a function of heating time with constant source temperature.^a

Table 6 Non-steady-State Conduction Factors and Symbols

T_f	= Furnace temperature, gas or wall as defined
T_s	= Load surface temperature
T_c	= Temperature at core or unheated side of load
T_0	= Initial load temperature with all temperatures in units of $(^{\circ}\text{F} - 460)/100$ or $^{\circ}\text{S}$
Y_s	$= \frac{T_f - T_s}{T_f - T_0}$
Y_c	$= \frac{T_f - T_c}{T_f - T_0}$
R	= External/internal thermal resistance ratio = k/rH
X	= Time factor = tD/r^2
D	= Diffusivity as defined in Section 45.7
r	= Depth of heat penetration in feet
k	= Thermal conductivity of load (Btu/ft · h · $^{\circ}\text{F}$)
H	= External heat transfer coefficient (Btu/ft ² · h · $^{\circ}\text{F}$)

Factors considered in non-steady-state conduction and their identifying symbols are listed in Table 6.

Charts have been prepared by Gurney-Lurie, Heisler, Hottel, and others showing values for Y_s and Y_c for various R factors as a function of X . Separate charts are provided for Y_s and Y_c , with a series of curves representing a series of values of R . These curves are straight lines for most of their length, curving to intersect at $Y = 1$ and $X = 0$. If straight lines are extended to $Y = 1$, the curves for Y_c at all values of R converge at a point near $X = 0.1$ on the line for $Y_c = 1$. It is accordingly possible to prepare a single line chart for $-\ln Y_c/(X - 0.1)$ to fit selected geometrical shapes. This has been done in Fig. 23 for slabs, long cylinders, and spheres. Values of Y_c determined with this chart correspond closely with those from conventional charts for $X - 0.1$ greater than 0.2.

Because the ratio Y_s/Y_c remains constant as a function of R after initial heating, it can be shown in chart form, as in Fig. 24, to allow Y_s to be determined after Y_c has been found.

By way of illustration, a carbon steel slab 8 in. thick is being heated from cold to $T_s = 2350^{\circ}\text{F}$ in a furnace with a constant wall temperature of 2400°F , with a view factor of 1 and a mean emissivity-absorptivity factor of 0.80. The desired final temperature of the unheated surface is 2300°F , making the Y_c factor

$$Y_c = \frac{2400 - 2300}{2400 - 70} = 0.0429$$

From Fig. 23, $H_r = 114 \times 0.80 = 91$; $r = 8/12 = 0.67$; R is assumed at 17. The required heating time is determined from Fig. 24:

$$R = \frac{17}{0.67 \times 91} = 0.279$$

$$\frac{-\ln Y_c}{X - 0.1} = 1.7$$

and

$$X = \frac{-\ln 0.0429}{1.7} + 0.1 = 1.95 = tD/r^2$$

With $D = 0.25$, from Section 7,

$$t = \frac{Xr^2}{D} = \frac{1.95 \times 0.67^2}{0.25} = 3.50 \text{ h}$$

Slabs or plates heated from two sides are usually supported in the furnace in a horizontal position on spaced conveyor rolls or rails. Support members may be uncooled, in which case

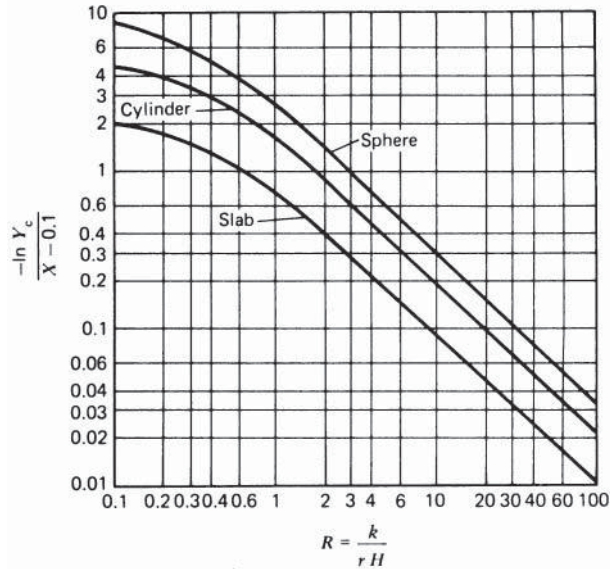


Figure 23 A plot of $-\ln Y_c / (X - 0.1)$ as a function of R^a

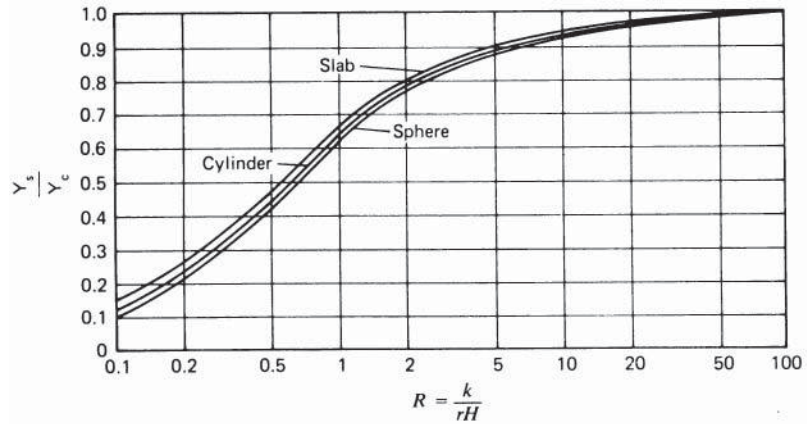


Figure 24 The ratio Y_s / Y_c plotted as a function of R^a

radiation to the bottom surface will be reduced by the net view factor. If supports are water cooled, the additional heat input needed to balance heat loss from load to supports can be balanced by a higher furnace temperature on the bottom side. In either case, heating times will be greater than for a uniform input from both sides.

Furnace temperatures are normally limited to a fraction above final load temperatures to avoid local overheating during operating delays. Without losses to water cooling, top and bottom furnace temperature will accordingly be about equal.

8.10 Heat Transfer with Negligible Load Thermal Resistance

When heating thin plates or small-diameter rods, with internal thermal resistance low enough to allow heating rates unlimited by specified final temperature differential, the non-steady state-conduction limits on heating rates can be neglected. Heating time then becomes

$$t = \frac{W \times C \times (T_s - T_0)}{A \times H \times MTD}$$

The heat transfer coefficient for radiation heating can be approximated from the chart in Fig. 13 or calculated as follows:

$$H_r = \frac{0.1713 e_m F_s [T_f^4 - MTD]^4}{MTD \times A_s}$$

As an illustration, find the time required to heat a steel plate to 2350°F in a furnace at a uniform temperature of 2400°F. The plate is 0.25 in. thick with a unit weight of 10.2 lb/ft² and is to be heated from one side. Overall emissivity-absorptivity is $e_m = 0.80$. Specific heat is 0.165. The view factor is $F_s = 1$. MTD is

$$\begin{aligned} \frac{(2400 - 70) - (2400 - 2350)}{\ln(2400 - 70)/(2400 - 2350)} &= 588^\circ\text{F} \\ H_r &= \frac{0.1713 \times 80 \times 1 [28.6^4 - 5.88^4]}{588} = 93.8 \\ t &= \frac{10.2 \times 0.165 \times (2350 - 70)}{1 \times 93.8 \times 588} = 0.069 \text{ h} \end{aligned}$$

8.11 Newman Method

For loads heated from two or more perpendicular sides, final maximum temperatures will be at exposed corners, with minimum temperatures at the center of mass for heating from all sides, or at the center of the face in contact with the hearth for hearth-supported loads heated equally from the remaining sides. For surfaces not fully exposed to radiation, the corrected H factor must be used.

The Newman method can be used to determine final load temperatures with a given heating time t . To find time required to reach specified maximum and minimum final load temperatures, trial calculations with several values of t will be needed.

For a selected heating time t , the factors Y_s and Y_c can be found from charts in Figs. 23 and 24 for the appropriate values of the other variables— T_s , T_c , H , k , and r —for each of the heat flow paths involved— r_x , r_y , and r_z . If one of these paths is much longer than the others, it can be omitted from calculations:

$$\begin{aligned} Y_c &= Y_{cx} \times Y_{cy} \times Y_{cz} \\ Y_s &= Y_{sx} \times Y_{sy} \times Y_{sz} \end{aligned}$$

For two opposite sides with equal exposure only one is considered. With T_c known, T_s and T_f (furnace temperature, T_g or T_w) can be calculated.

As an example, consider a carbon steel ingot, with dimensions 2 ft × 4 ft × 6 ft, being heated in a direct-fired furnace. The load is supported with one 2 ft × 4 ft face in contact with the refractory hearth and other faces fully exposed to gas and wall radiation. Maximum final temperature will be at an upper corner, with minimum temperature at the center of the 2 ft × 4 ft bottom surface. Assuming that the load is a somewhat brittle steel alloy, the initial

heating rate should be suppressed and heating with a constant gas temperature will be assumed. Heat transfer factors are then as follows:

Flow paths $r_x = 1$ ft and $r_y = 2$ ft, the contribution of vertical heat flow, on axis r_z , will be small enough to be neglected.

Desired final temperatures: $T_c = 2250^\circ\text{F}$ and T_s (to be found) about 2300°F , with trial factor $t = 9$ h.

H from gas to load = 50.

k mean value for load = 20 and $D = 0.25$.

Radial Heat Flow Path	r_x	r_y
r	1	2
$X = tD/r^2$	2.25	0.5625
$R = k/H_r$	0.4	0.2
$-\ln Y_c/(X-0.1)$ from Fig. 23	1.3	1.7
Y_s/Y_c from Fig. 24	0.41	0.26
Y_c	0.0611	0.455
Y_s	0.025	0.119

Combined factors:

$$Y_c = 0.0611 \times 0.455 = 0.0278 = \frac{T_g - T_c}{T_g - 70}$$

$$Y_s = 0.025 \times 0.119 = 0.003 = \frac{T_g - T_s}{T_g - 70}$$

For $T_c = 2250^\circ\text{F}$,

$$T_g = 2316^\circ\text{F}$$

$$T_s = 2309^\circ\text{F}$$

This is close enough to the desired $T_s = 2300^\circ\text{F}$.

The time required to heat steel slabs to rolling temperature as a function of the thickness heated from one side and the final load temperature differential is shown in Fig. 25. Relative heating times for various hearth loading arrangements for square billets are shown in Fig. 26. These have been calculated by the Newman method, which can also be used to evaluate other loading patterns and cross sections.

8.12 Furnace Temperature Profiles

To predict heating rates and final load temperatures in either batch or continuous furnaces, it is convenient to assume that source temperatures, gas (T_g) or furnace wall (T_w), will be constant in time. Neither condition is achieved with contemporary furnace and control system designs. With constant gas temperature, effective heating rates are unnecessarily limited, and the furnace temperature control system is dependent on measurement and control of gas temperatures, a difficult requirement. With uniform wall temperatures, the discharge temperature of flue gases at the beginning of the heating cycle will be higher than desirable. Three types of furnace temperature profiles, constant T_g , constant T_w , and an arbitrary pattern with both variables, are shown in Fig. 27.

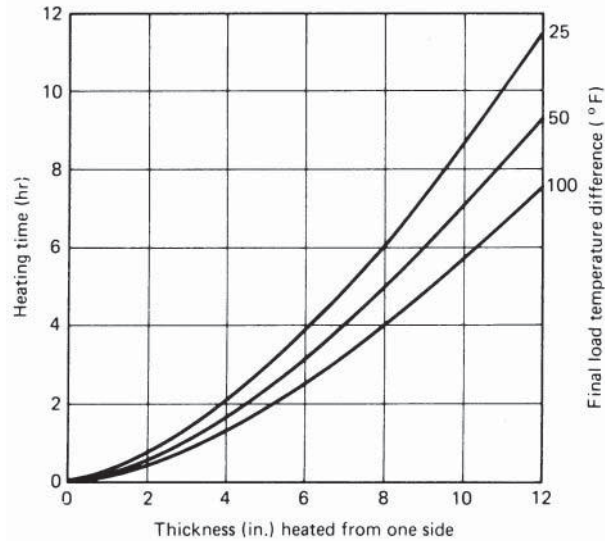


Figure 25 Relative heating time for square billets as function of loading pattern.^a

Contemporary designs of continuous furnaces provide for furnace temperature profiles of the third type illustrated to secure improved capacity without sacrificing fuel efficiency. The firing system comprises three zones of length: a preheat zone that can be operated to maintain minimum flue gas temperatures in a counterflow firing arrangement, a firing zone with a maximum temperature and firing rate consistent with furnace maintenance requirements and limits imposed by the need to avoid overheating of the load during operating delays, and a final or soak zone to balance furnace temperature with maximum and minimum load temperature specifications. In some designs, the preheat zone is unheated except by flue gases from the firing zone, with the resulting loss of furnace capacity offset by operating the firing zone at the maximum practical limit.

8.13 Equivalent Furnace Temperature Profiles

Furnace heating capacities are readily calculated on the assumption that furnace temperature, either combustion gases or radiating walls, is constant as a function of position or time. Neither condition is realized in practice, and to secure improved capacity with reduced fuel demand in a continuous furnace, contemporary designs are based on operation with a variable temperature profile from end to end, with furnace wall temperature reduced at the load charge and flue gas discharge end, to improve available heat of fuel, and at the load discharge end, to balance the desired maximum and minimum load temperatures. Any loss in capacity can be recovered by operating the intermediate firing zones at a somewhat elevated temperature.

Consider a furnace designed to heat carbon steel slabs 6 in. thick from the top only to a final temperatures of 2300°F at the top and 2250°F at the bottom. To hold the exit flue gas temperature to about 2000°F, the wall temperature at the charge end will be about 1400°F. The furnace will be fired in four zones of length each 25 ft long for an effective total length of 100 ft. The preheat zone will be unfired, with a wall temperature tapering up to 2400°F at the load discharge end. That temperature will be held through the next two firing zones and dropped to 2333°F to balance final load temperatures in the fourth or soak zone. With overall heating

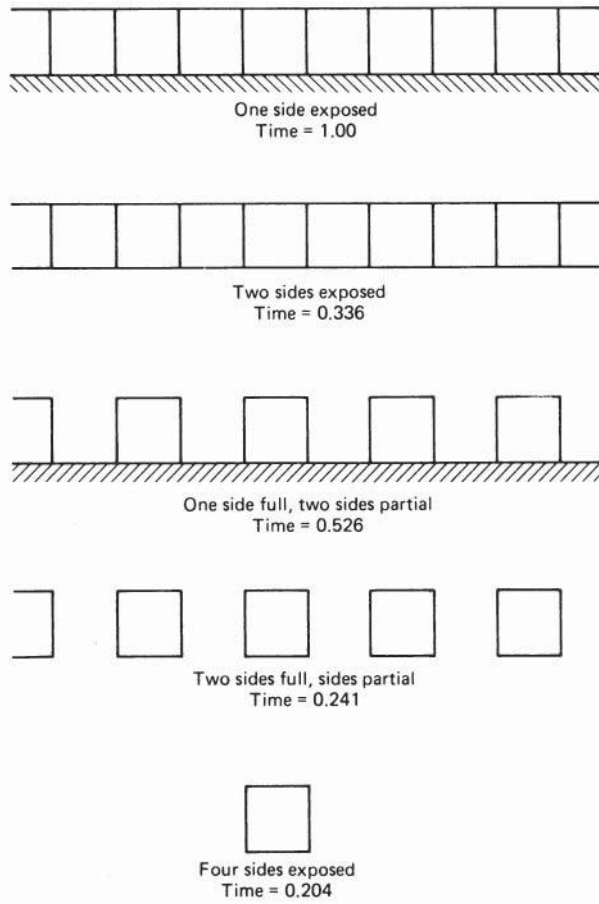


Figure 26 Heating time for carbon steel slabs to final surface temperature of 2300°F as function of thickness and final load temperature differential.^a

capacity equal to the integral of units of length times their absolute temperatures, effective heat input will be about 87% of that for a uniform temperature of 2400°F for the entire length.

Heat transfer from combustion gases to load will be by direct radiation from gas to load, including reflection of incident radiation from walls, and by radiation from gas to walls, absorbed and reradiated from walls to load. Assuming that wall losses will be balanced by convection heat transfer from gases, gas radiation to walls will equal solid-state radiation from walls to load:

$$A_w/A_s \times 0.1713 \times e_{gm} T_g^4 - T_w^4 = e_{ws} \times 0.1713(T_w^4 - T_s^4)$$

where A_w/A_s = exposed area ratio for walls and load
 e_{gm} = emissivity-absorptivity, gas to walls
 e_{ws} = emissivity-absorptivity, walls to load

At the midpoint in the heating cycle, MTD = 708°F and mean load surface temperature = $T_{sm} = 1698^\circ\text{F}$.

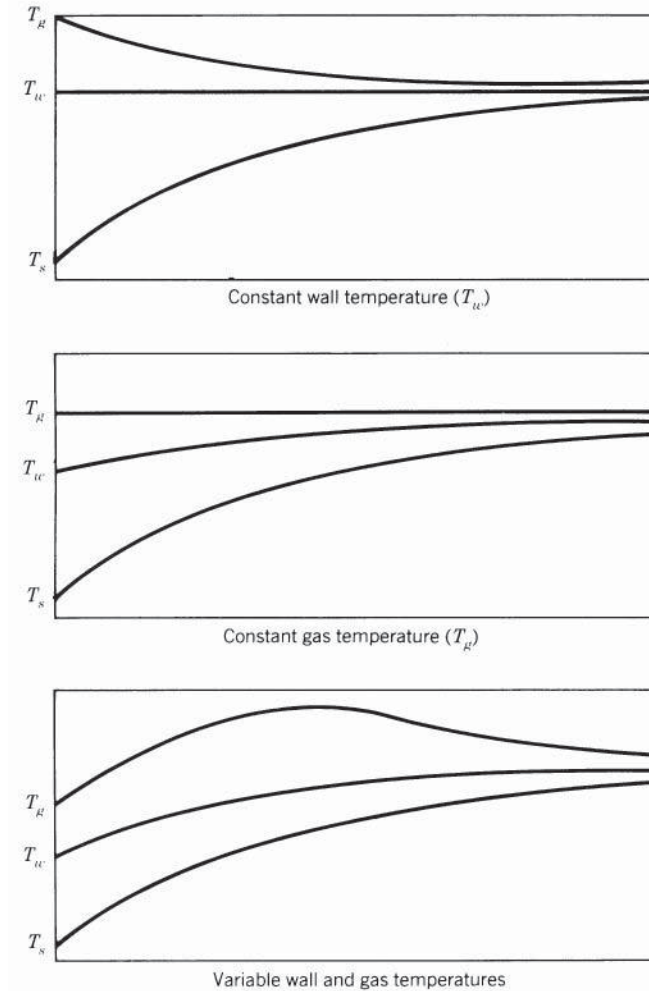


Figure 27 Furnace temperature profiles.

With $a_s = 0.85$ for refractory walls, 15% of gas radiation will be reflected to load, and total gas-to-load radiation will be

$$1.15 \times e_{gm} \times 0.1713(T_g^4 - T_s^4)$$

For $A_w/A_s = 2.5$, $e = 0.17$, and $e = 0.89$ from walls to load, the mean gas temperature = $T_g = 3108^\circ\text{F}$, net radiation gas to load = $47,042 \text{ Btu/h} \cdot \text{ft}^2$ and gas to walls = walls to load = $69,305 \text{ Btu/h} \cdot \text{ft}^2$ for a total of $116,347 \text{ Btu/h} \cdot \text{ft}^2$. This illustrates the relation shown in Fig. 21, since blackbody radiation from walls to load, without gas radiation, would be $77,871 \text{ Btu/h} \cdot \text{ft}^2$. Assuming blackbody radiation with a uniform wall temperature from end to end, compared to combined radiation with the assumed wall temperature, the overall heat transfer ratio will be

$$0.87 \times 116,347/77,871 = 1.30$$

As shown in Fig. 26, this ratio will vary with gas emissivity and wall-to-load areas exposed. For the range of possible values for these factors and for preliminary estimates of heating times, Fig. 26 can be used to indicate a conservative heating time as a function of final load temperature differential and depth of heat penetration for a furnace temperature profile depressed at either end.

Radiation factors will determine the mean coefficient of wall-to-load radiation and the corresponding non-steady-state conduction values. For blackbody radiation alone, H_r is about $77,871/708 = 110$. For combined gas and solid-state radiation, in the above example, it becomes $0.87 \times 116,347/708 = 143$. Values of R for use with Figs. 23 and 24 will vary correspondingly ($R = k/4H$).

8.14 Convection Heat Transfer

Heat transferred between a moving layer of gas and a solid surface is identified by "convection." Natural convection occurs when movement of the gas layer results from differentials in gas density of the boundary layer resulting from temperature differences and will vary with the position of the boundary surface: horizontal upward, horizontal downward, or vertical. A commonly used formula is

$$H_c = 0.27 (T_g - T_s)^{0.25}$$

where $H_c = \text{Btu/h} \cdot \text{ft}^2 \cdot ^\circ\text{F}$

$T_g - T_s =$ temperature difference between gas and surface, $^\circ\text{F}$

Natural convection is a significant factor in estimating heat loss from the outer surface of furnace walls or from uninsulated pipe surfaces. "Forced convection" is heat transfer between gas and a solid surface, with gas velocity resulting from energy input from some external source, such as a recirculating fan.

Natural convection can be increased by ambient conditions such as building drafts and gas density. Forced convection coefficients will depend on surface geometry, thermal properties of the gas, and Reynolds number for gas flow. For flow inside tubes, the following formula is useful:

$$H_c = 0.023 \frac{k}{D} \text{Re}^{0.8} \text{Pr}^{0.4} \text{Btu/h} \cdot \text{ft}^2 \cdot ^\circ\text{F}$$

where $k =$ thermal conductivity of gas

$D =$ inside diameter of tube, ft

Re = Reynolds number

Pr = Prandtl number

Forced convection coefficients are given in Fig. 28 for a Prandtl number assumed at 0.70.

For forced convection over plane surfaces, it can be assumed that the preceding formula will apply for a rectangular duct of infinitely large cross section, but only for a length sufficient to establish uniform velocity over the cross section and a velocity high enough to reach the Re value needed to promote turbulent flow.

In most industrial applications, the rate of heat transfer by forced convection as a function of power demand will be better for perpendicular jet impingement from spaced nozzles than for parallel flow. For a range of dimensions common in furnace design, the heat transfer coefficient for jet impingement of air or flue gas is shown in Fig. 29, calculated for impingement from slots 0.375 in. wide spaced at 18–24-in. centers and with a gap of 8 in. from nozzle to load.

Forced convection factors for gas flow through banks of circular tubes are shown in Fig. 30 for tubes spaced as follows:

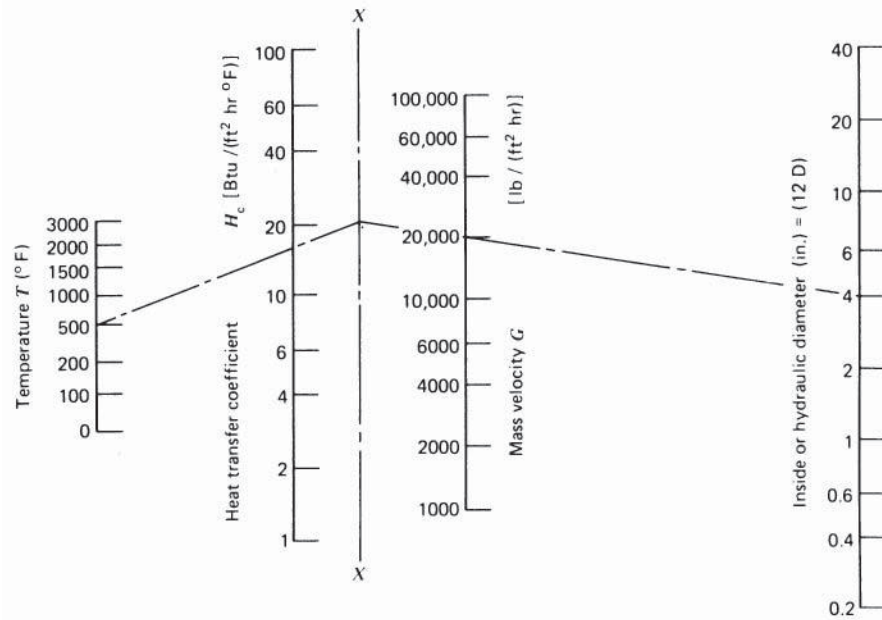


Figure 28 Convection coefficient (H_c) for forced convection inside tubes to air or flue gas.^a

- A: staggered tubes with lateral spacing equal to diagonal spacing
 B: tubes in line with equal spacing across and parallel to direction of flow
 C: tubes in line with lateral spacing less than half longitudinal spacing
 D: tubes in line with lateral spacing over twice longitudinal spacing

With F the configuration factor from Fig. 30, the heat transfer coefficients are

$$H_c = FkRe^{0.6}/D$$

Convection coefficients from this formula are approximately valid for 10 rows of tubes or more but are progressively reduced to a factor of 0.65 for a single row.

For gas-to-gas convection in a cross-flow tubular heat exchanger, overall resistance will be the sum of factors for gas to the outer diameter of tubes, tube wall conduction, and inside diameter of tubes to gas. Factors for the outer diameter of tubes may include gas radiation as calculated in Section 7.5.

8.15 Fluidized-Bed Heat Transfer

For gas flowing upward through a particular bed, there is a critical velocity when pressure drop equals the weight of bed material per unit area. Above that velocity, bed material will be suspended in the gas stream in a turbulent flow condition. With the total surface area of suspended particles on the order of a million times the inside surface area of the container, convection heat transfer from gas to bed material is correspondingly large. Heat transfer from suspended particles to load is by conduction during repeated impact. The combination can provide overall coefficients upward of 10 times those available with open convection, permitting the heating of thick and thin load sections to nearly uniform temperatures by allowing a low gas-to-load thermal head.

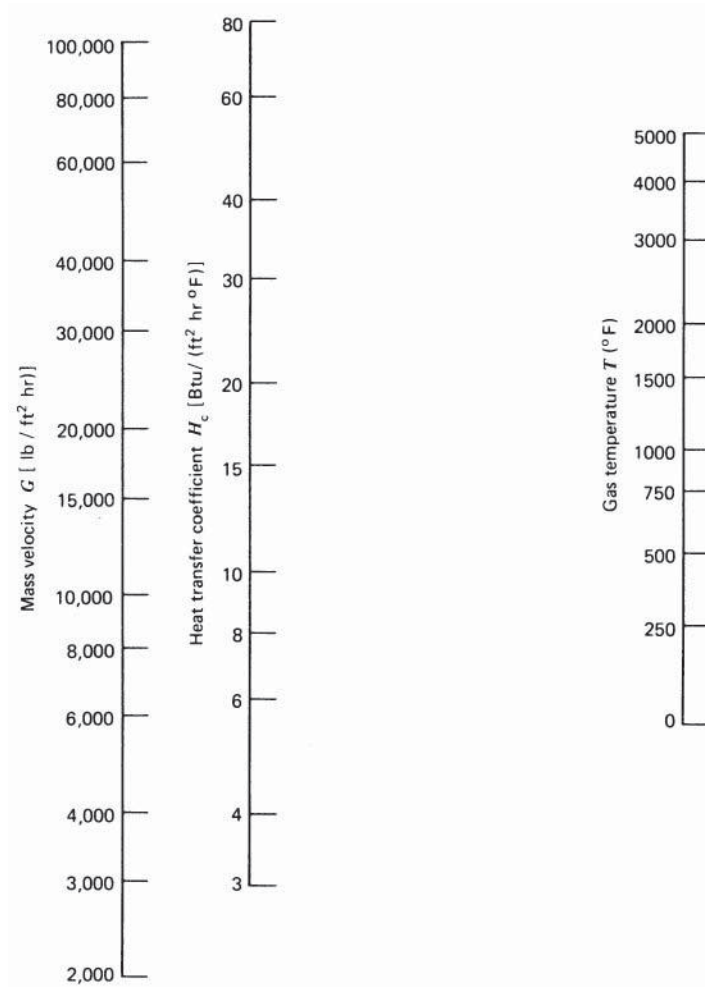


Figure 29 Convection coefficient (H_c) for jet impingement of air or flue gas on plane surfaces for spaced slots 0.375 in. wide at 18–24-in. centers 8 in. from load.^a

8.16 Combined Heat Transfer Coefficients

Many furnace heat transfer problems will combine two or more methods of heat transfer, with thermal resistances in series or in parallel. In a combustion chamber, the resistance to radiation from gas to load will be parallel to the resistance from gas to walls to load, which is two resistances in series. Heat flow through furnace walls combines a series of resistances in series, combustion gases to inside wall surface, consecutive layers of the wall structure, and outside wall surface to surroundings, the last a combination of radiation and convection in parallel.

As an example, consider an insulated, water-cooled tube inside a furnace enclosure. With a tube outside diameter of 0.5 ft and a cylindrical insulation enclosure with an outside diameter of 0.75 ft, the net thickness will be 0.125 ft. The mean area at midthickness is $1(0.5 + 0.75)/2$,

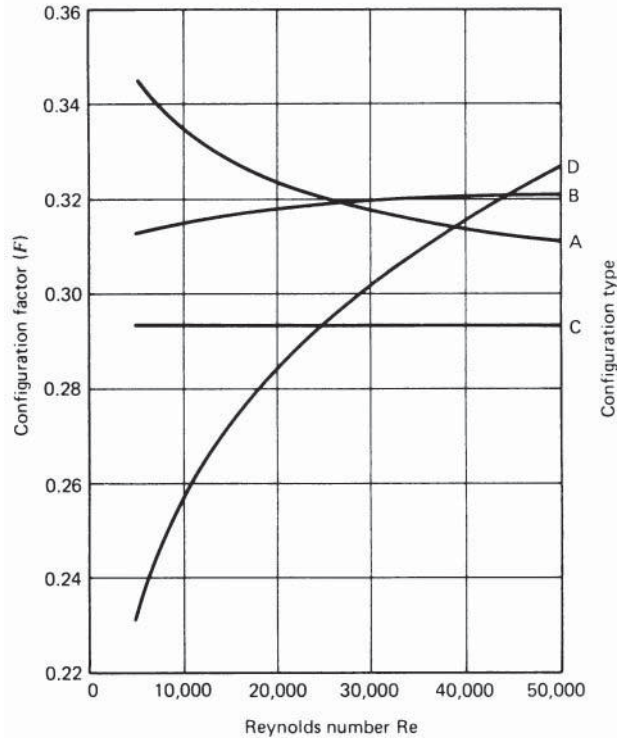


Figure 30 Configuration factors for convection heat transfer, air or flue gas through tube banks.⁴

or 1.964 ft² per foot of length. The outer surface area of insulation is 0.751, or 2.36 ft² per linear foot. Conductivity of insulation is $k = 0.20$. The effective radiation factor from gas to surface is assumed at 0.5 including reradiation from walls. For the two resistances in series,

$$0.1713 \times 0.5 \times 2.36(29.6^4 - T_s^4) = 1.964(T_s - 150) \times \frac{0.20}{0.125}$$

By trial, the receiver surface temperature is found to be about 2465°F. Heat transfer is about 7250 Btu/h·linear ft or 9063 Btu/h·ft² water-cooled tube surface.

If the insulated tube in the preceding example is heated primarily by convection, a similar treatment can be used to find receiver surface temperature and overall heat transfer.

For radiation through furnace wall openings, heat transfer in Btu/h·ft²·°F is reduced by wall thickness, and the result can be calculated similarly to the problem of two parallel planes of equal size connected by reradiating walls, as shown in Fig. 19.

Heat transfer in internally fired combustion tubes (“radiant tubes”) is a combination of convection and gas radiation from combustion gases to the tube wall. External heat transfer from tubes to load will be direct radiation and reradiation from furnace walls, as illustrated in Fig. 19. The overall factor for internal heat transfer can be estimated from Fig. 31, calculated for 6- and 8-in.-inside-diameter tubes. The convection coefficient increases with firing rate and to some extent with temperature. The gas radiation factor depends on temperature and inside diameter. The effect of flame luminosity has not been considered.

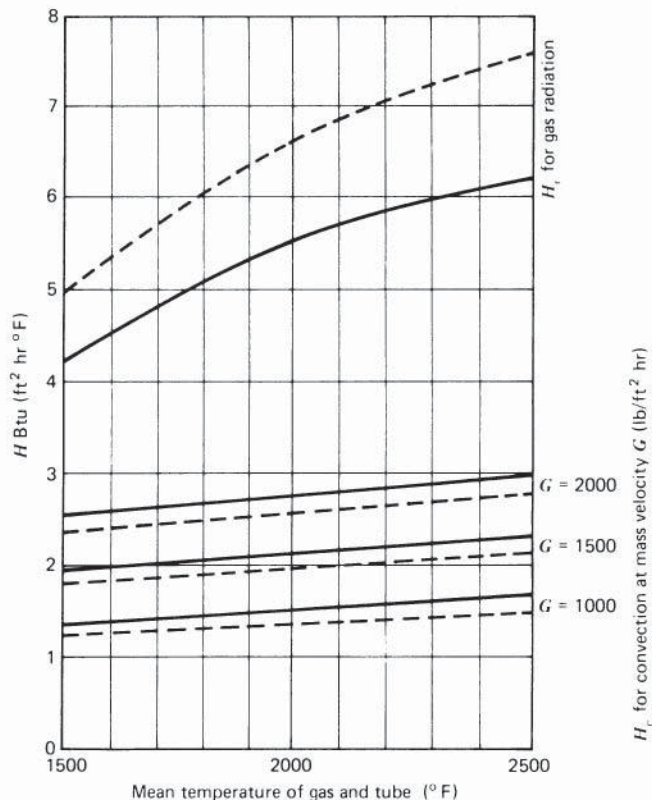


Figure 31 Gas radiation (H_r) and convection (H_c) coefficients for flue gas inside radiant tubes.^a

9 FLUID FLOW

Fluid flow problems of interest to the furnace engineer include the resistance to flow of air or flue gas over a range of temperatures and densities through furnace ductwork, stacks and flues, or recuperators and regenerators. Flow of combustion air and fuel gas through distribution piping and burners will also be considered. Liquid flow of water and fuel oil must also be evaluated in some furnace designs but will not be treated in this chapter.

To avoid errors resulting from gas density at temperature, velocities will be expressed as mass velocities in units of $G = \text{lb/h} \cdot \text{ft}^2$. Because the low pressure differentials in systems for flow of air or flue gas are usually measured with a manometer, in units of inches of water column (in. H_2O), that will be the unit used in the following discussion.

The relation of velocity head h_v in inches of H_2O to mass velocity G is shown for a range of temperatures in Fig. 32. Pressure drops as multiples of h_v are shown for some configurations used in furnace design in Figs. 33 and 34. The loss for flow across tube banks in multiples of the velocity head is shown in Fig. 35 as a function of the Reynolds number.

The Reynolds number Re is a dimensionless factor in fluid flow defined as $Re = DG/\mu$, where D is inside diameter or equivalent dimension in feet, G is mass velocity as defined above, and μ is viscosity as shown in Fig. 9. Values for Re for air or flue gas in the range of interest

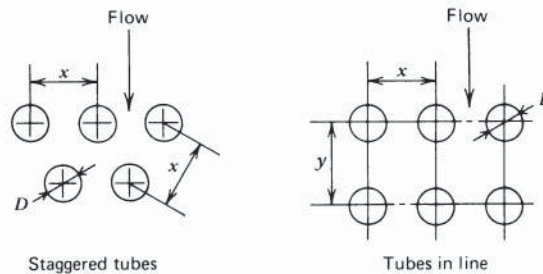
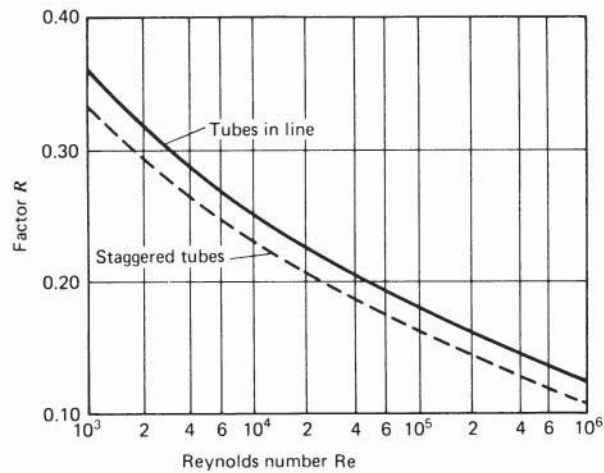


Figure 32 Heat loss for flow of air or flue gas across tube banks at atmospheric pressure (velocity head $\times F \times R$).

are shown in Fig. 36. Pressure drop for flow through long tubes is shown in Fig. 37 for a range of Reynolds numbers and equivalent diameters.

9.1 Preferred Velocities

Mass velocities used in contemporary furnace design are intended to provide an optimum balance between construction costs and operating costs for power and fuel; some values are as follows:

Medium	Mass Velocity G	Velocity Head (in H ₂ O)
Cold air	15,000	0.7
800°F air	10,000	0.3
2200°F flue gas	1,750	0.05
1500°F flue gas	2,000	0.05

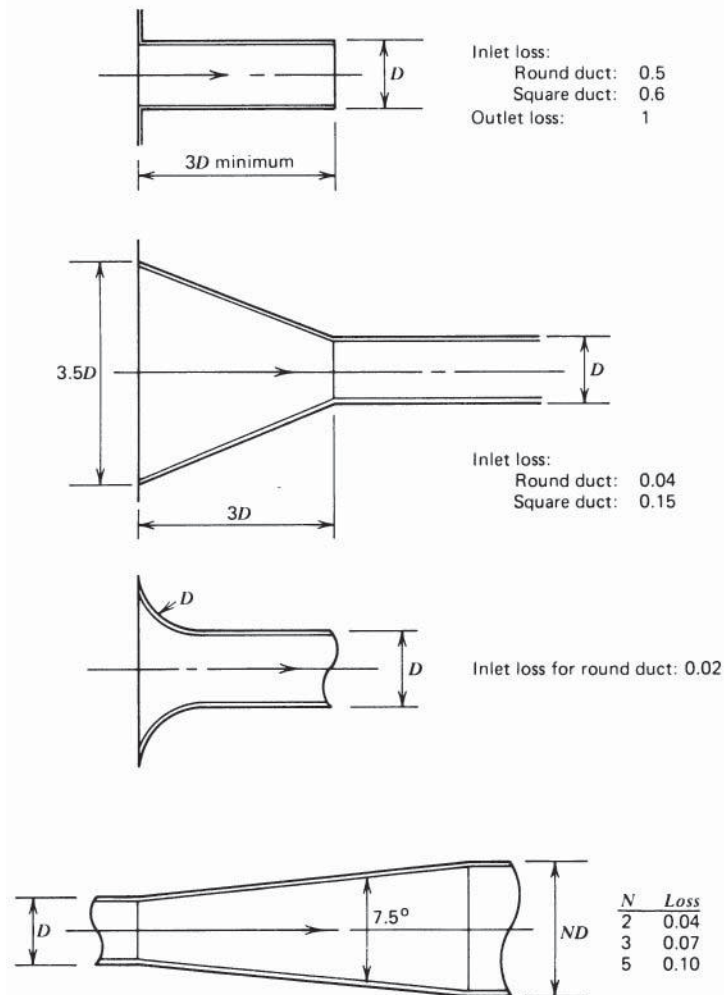


Figure 33 Pressure drop in velocity heads for flow of air or flue gas through entrance configurations or expansion sections.^a

The use of these factors will not necessarily provide an optimum cost balance. Consider a furnace stack of self-supporting steel construction lined with 6 in. of gunned insulation. For $G = 2000$ and $h_v = 0.05$ at 1500°F , an inside diameter of 12 ft will provide a flow of 226,195 lb/h. To provide a net draft of 1 in. H_2O with stack losses of about $1.75h_v$ or 0.0875 in., the effective height from Fig. 38 is about 102 ft. By doubling the velocity head to 0.10 in. H_2O , G at 1500°F becomes 3000. For the same mass flow, the inside diameter is reduced to 9.8 ft. The pressure drop through the stack increases to about 0.175 in., and the height required to provide a net draft of 1 in. increases to about 110 ft. The outside diameter area of the stack is reduced from 4166 ft^2 to $11 \times 3.1416 \times 110 = 3801 \text{ ft}^2$. If the cost per square foot of outside surface is the same for both cases, the use of a higher stack velocity will save construction costs. It is accordingly

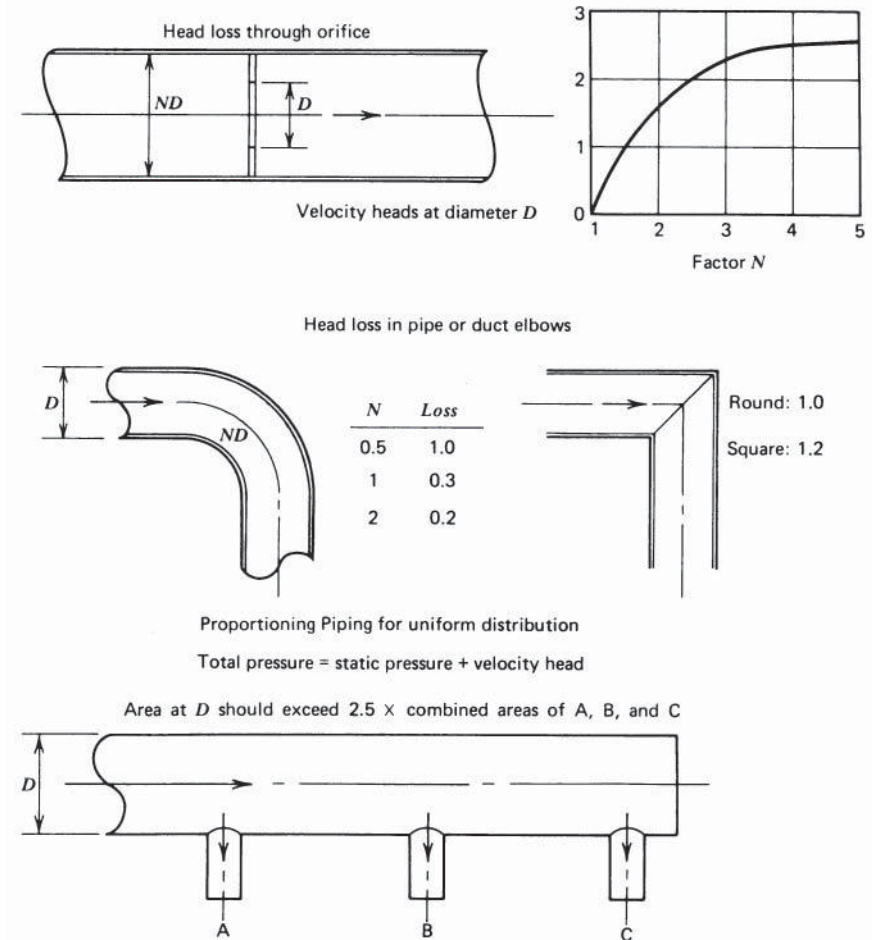


Figure 34 Pressure drop in velocity heads for flow of air or flue gas through orifices, elbows, and lateral outlets.^a

recommended that specific furnace designs receive a more careful analysis before selecting optimum mass velocities.

Staggered Tubes		Tubes in Line		Factor F for x/D		
x/D	Factor F	y/D	1.5	2	3	4
1.5	2.00	1.25	1.184	0.576	0.334	0.268
2	1.47	1.5	1.266	0.656	0.387	0.307
3	1.22	2	1.452	0.816	0.497	0.390
4	1.14	3	1.855	1.136	0.725	0.572
		4	2.273	1.456	0.957	0.761

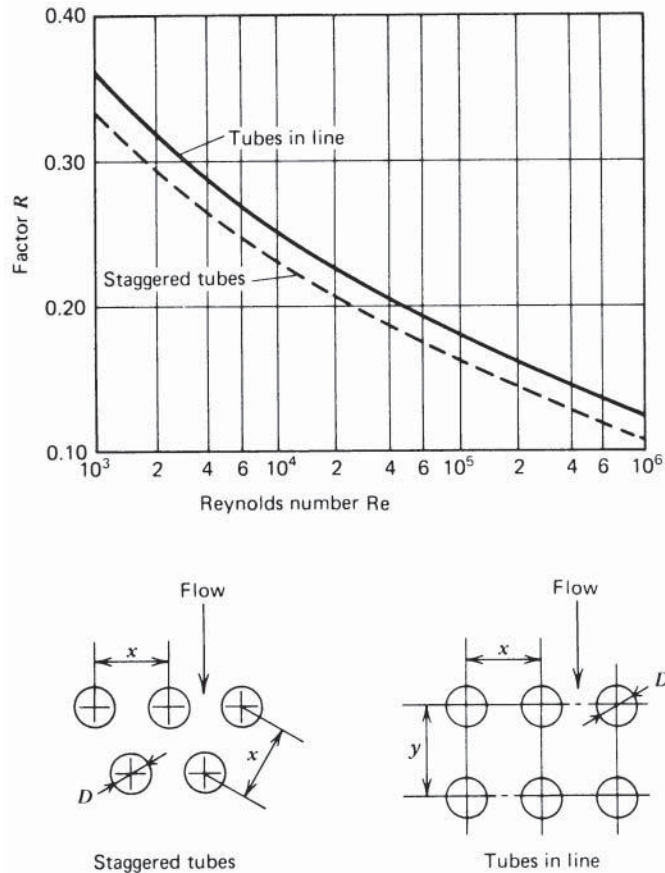


Figure 35 Pressure drop factors for flow of air or flue gas through tube banks.^a

Stack draft at ambient atmospheric temperature of 70°F is shown in Fig. 38 as a function of flue gas temperature. Where greater drafts are desirable with a limited height of stack, a jet-type stack can be used to convert the momentum of a cold air jet into stack draft. Performance data are available from manufacturers.

9.2 Centrifugal Fan Characteristics

Performance characteristics for three types of centrifugal fans are shown in Fig. 39. More exact data are available from fan manufacturers. Note that the backward curved blade has the advantage of limited horsepower demand with reduced back pressure and increasing volume and can be used where system resistance is unpredictable. The operating point on the pressure–volume curve is determined by the increase of duct resistance with flow matched against the reduced outlet pressure, as shown in the upper curve.

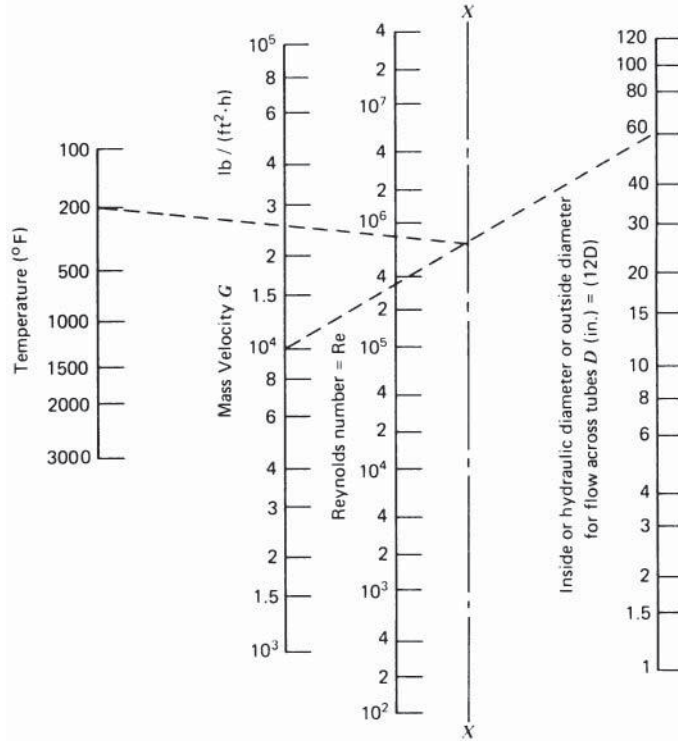


Figure 36 Reynolds number (Re) for flow of air or flue gas through tubes or across tube banks.^a

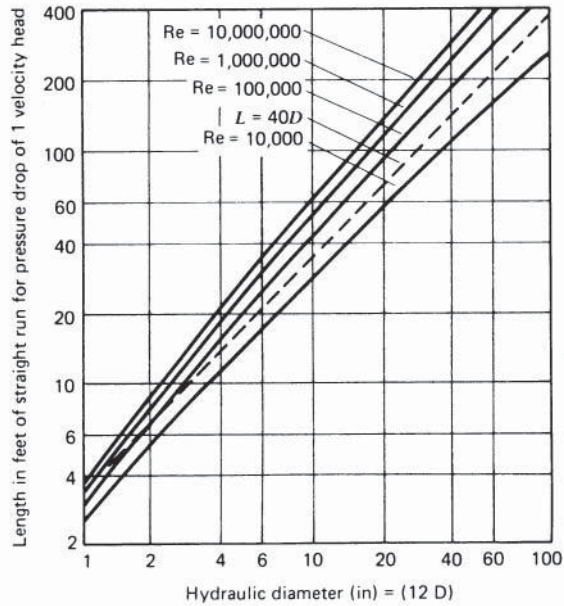


Figure 37 Length in feet for pressure drop of one velocity head for flow of air or flue gas as function of Re and D .^a

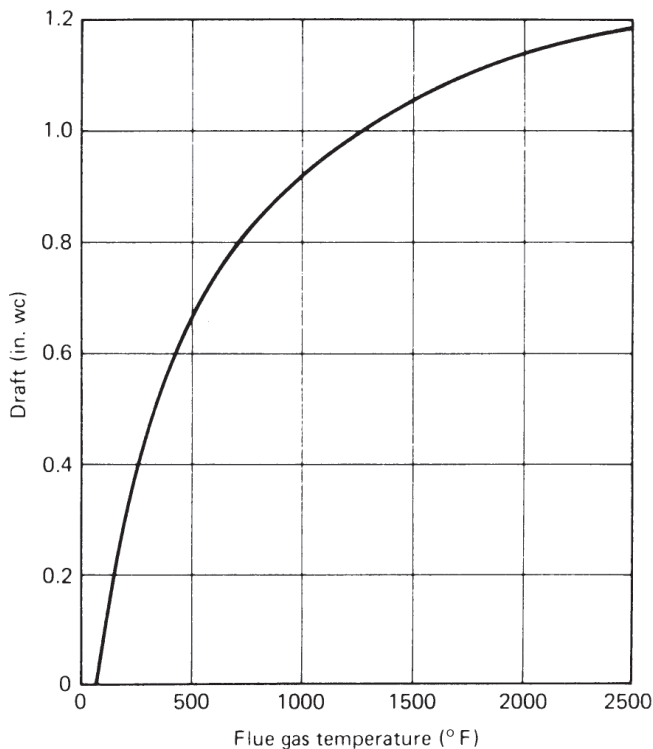


Figure 38 Stack draft for ambient $T_g = 70^\circ\text{F}$ and $\text{psia} = 14.7 \text{ lb} / \text{in}^2$.^a

9.3 Laminar and Turbulent Flows

The laminar flow of a fluid over a boundary surface is a shearing process with velocity varying from zero at the wall to a maximum at the center of the cross section or the center of the top surface for liquids in an open channel. Above a critical Reynolds number, between 2000 and 3000 in most cases, flow becomes a rolling action with a uniform velocity extending almost to the walls of the duct and is identified as turbulent flow.

With turbulent flow the pressure drop is proportional to D ; the flow in a large duct can be converted from turbulent to laminar by dividing the cross-sectional area into a number of parallel channels. If flow extends beyond the termination of these channels, the conversion from laminar to turbulent flow will occur over some distance in the direction of flow.

Radial mixing with laminar flow is by the process of diffusion, which is the mixing effect that occurs in a chamber filled with two different gases separated by a partition after the partition is removed. Delayed mixing and high luminosity in the combustion of hydrocarbon gases can be accomplished by “diffusion combustion,” in which air and fuel enter the combustion chamber in parallel streams at equal and low velocity.

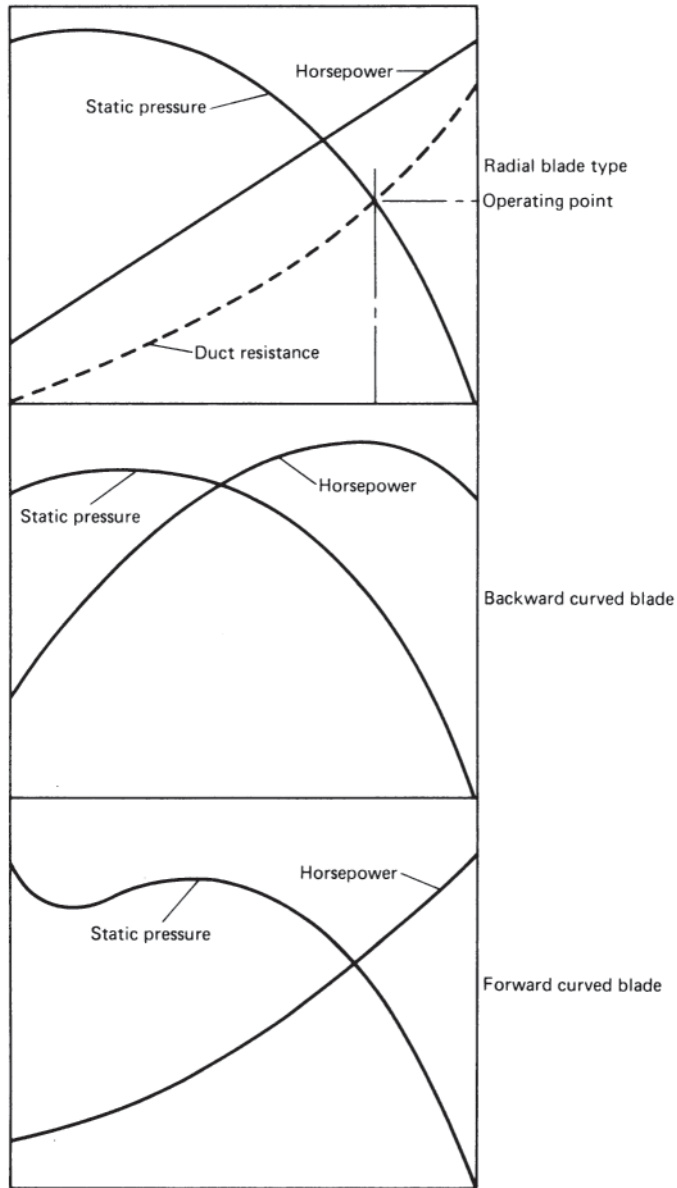


Figure 39 Centrifugal fan characteristics.^a

10 BURNER AND CONTROL EQUIPMENT

With increasing costs of fuel and power, the fraction of furnace construction and maintenance costs represented by burner and control equipment can be correspondingly increased.

Burner designs should be selected for better control of the flame pattern over a wider range of turndown and for complete combustion with a minimum excess air ratio over that range.

Furnace functions to be controlled, manually or automatically, include temperature, internal pressure, fuel/air ratio, and adjustment of firing rate to anticipated load changes. For intermittent operation or for a wide variation in required heating capacity, computer control may be justified to anticipate required changes in temperature setting and firing rates, particularly in consecutive zones of continuous furnaces.

10.1 Burner Types

Burners for gas fuels will be selected for the desired degree of premixing of air and fuel, to control flame pattern, and for the type of flame pattern, compact and directional, diffuse or flat flame coverage of adjacent wall area. Burners for oil fuels, in addition, will need provision for atomization of fuel oil over the desired range of firing rates.

The simplest type of gas burner comprises an opening in a furnace wall through which combustion air is drawn by furnace draft and a pipe nozzle to introduce fuel gas through that opening. The flame pattern will be controlled by gas velocity at the nozzle and by excess air ratio. The fuel/air ratio will be manually controlled for flame appearance by the judgment of the operator, possibly supplemented by continuous or periodic flue gas analysis. In regenerative furnaces, with firing ports serving alternately as exhaust flues, the open pipe burner may be the only practical arrangement.

For one-way fired furnaces, with burner port areas and combustion air velocities subject to control, fuel/air ratio control can be made automatic over a limited range of turndown with several systems, including:

Mixing in venturi tube, with energy supplied by gas supply inducing atmospheric air.

Allows simplest piping system with gas available at high pressure, as from some natural gas supplies.

Venturi mixer with energy from combustion air at intermediate pressure. Requires air supply piping and distribution piping from mixing to burners.

With both combustion air and fuel gas available at intermediate pressures, pressure drops through adjustable orifices can be matched or proportioned to hold desired flow ratios. For more accurate control, operation of flow control valves can be by an external source of energy.

Proportioning in venturi mixers depends on the conservation of momentum—the product of flow rate and velocity or of orifice area and pressure drop. With increased back pressure in the combustion chamber, the fuel/air ratio will be increased for the high-pressure gas inspirator or decreased with air pressure as the source of energy unless the pressure of the induced fluid is adjusted to the pressure in the combustion chamber.

The arrangement of a high-pressure gas inspirator system is illustrated in Fig. 40. Gas enters the throat of the venturi mixer through a jet on the axis of the opening. Air is induced through the surrounding area of the opening, and ratio control can be adjusted by varying the air inlet opening by a movable shutter disk. A single inspirator can supply a number of burners in one firing zone or a single burner.

For the air primary mixing system, a representative arrangement is shown in Fig. 41. The gas supply is regulated to atmospheric or to furnace gas pressure by a diaphragm-controlled valve. Ratio control is by adjustment of an orifice in the gas supply line. With air flow the only source of energy, errors in proportioning can be introduced by friction in the gas pressure control valve. Each mixer can supply one or more burners, representing a control zone.

With more than one burner per zone, the supply manifold will contain a combustible mixture that can be ignited below a critical port velocity to produce a backfire that can extinguish

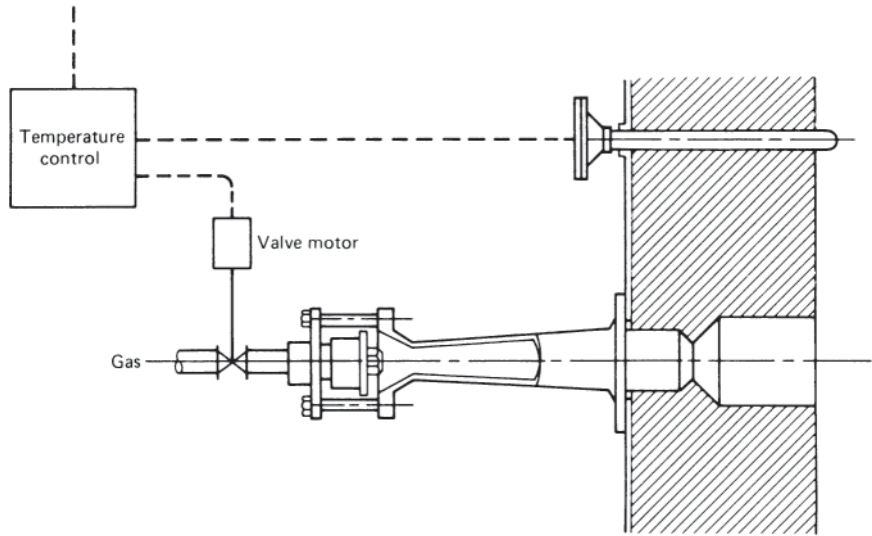


Figure 40 Air/gas ratio control by high-pressure gas inspirator.^a

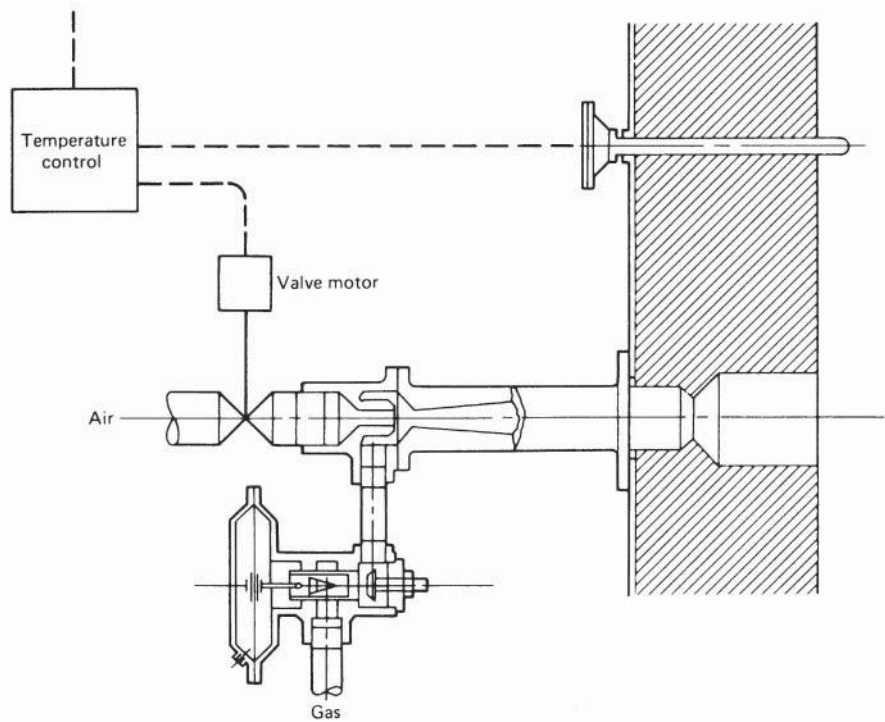


Figure 41 Air/gas ratio control by air inspirator.^a

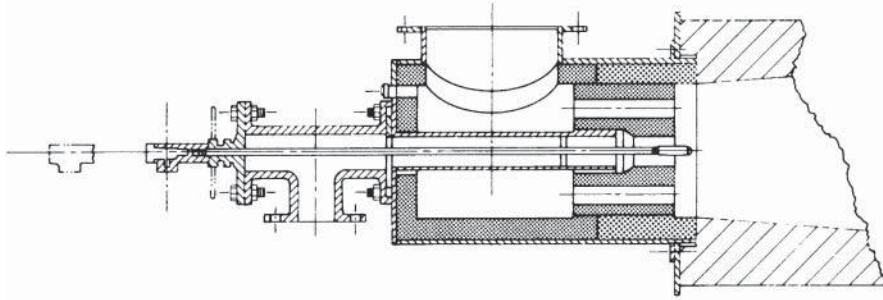


Figure 42 Dual fuel burner with removable oil nozzle.^a Courtesy of Bloom Engineering Company.

burners and possibly damage the combustion system. This hazard has made the single burner per mixer combination desirable, and many contemporary designs combine mixer and burner in a single structure.

With complete premixing of fuel and air, the flame will be of minimum luminosity, with combustion complete near the burner port. With delayed mixing, secured by introducing fuel and air in separate streams, through adjacent openings in the burner, or by providing a partial premix of fuel with a fraction of combustion air, flame luminosity can be controlled to increase flame radiation.

In a burner providing no premix ahead of the combustion chamber, flame pattern is determined by velocity differentials between air and fuel streams and by the subdivision of air flow into several parallel streams. This type of burner is popular for firing with preheated combustion air and can be insulated for that application.

Partial premix can be secured by dividing the air flow between a mixing venturi tube and a parallel open passage.

With the uncertainty of availability of contemporary fuel supplies, dual fuel burners, optionally fired with fuel gas or fuel oil, can be used. Figure 42 illustrates the design of a large burner for firing gas or oil fuel with preheated air. For oil firing, an oil-atomizing nozzle is inserted through the gas tube. To avoid carbon buildup in the oil tube from cracking of residual oil during gas firing, the oil tube assembly is removable.

Oil should be atomized before combustion in order to provide a compact flame pattern. Flame length will depend on burner port velocity and degree of atomization. Atomization can be accomplished by delivery of oil at high pressure through a suitable nozzle; by intermediate pressure air, part or all of the combustion air supply, mixing with oil at the discharge nozzle; or by high-pressure air or steam. For firing heavy fuel oils of relatively high viscosity, preheating in the storage tank, delivery to the burner through heated pipes, and atomization by high-pressure air or steam will be needed. If steam is available, it can be used for both tank and pipe heating and for atomization. Otherwise, the tank and supply line can be electrically heated, with atomization by high-pressure air.

10.2 Burner Ports

A major function of fuel burners is to maintain ignition over a wide range of demand and in spite of lateral drafts at the burner opening. Ignition can be maintained at low velocities by recirculation of hot products of combustion at the burner nozzle, as in the bunsen burner, but stability of ignition is limited to low port velocities for both the entering fuel/air mixture and lateral drafts at the point of ignition. Combustion of a fuel/air mixture can be catalyzed by contact with a hot refractory surface. A primary function of burner ports is to supply that source of ignition. Where combustion of a completely mixed source of fuel and air is substantially completed in

the burner port, the process is identified as “surface combustion.” Ignition by contact with hot refractory is also effective in flat flame burners, where the combustion air supply enters the furnace with a spinning motion and maintains contact with the surrounding wall.

Burner port velocities for various types of gas burners can vary from 3000 to 13,000 lb/h-ft², depending on the desired flame pattern and luminosity. Some smaller sizes of burners are preassembled with refractory port blocks.

10.3 Combustion Control Equipment

Furnace temperature can be measured by a bimetallic thermocouple inserted through the wall or by an optical sensing of radiation from furnace walls and products of combustion. In either case, an electrical impulse is translated into a temperature measurement by a suitable instrument and the result indicated by a visible signal and optionally recorded on a moving chart. For automatic temperature control, the instrument reading is compared to a preset target temperature, and the fuel and air supply is adjusted to match through a power-operated valve system.

Control may be on-off, between high and low limits; three position, with high, normal, and off valve openings; or proportional with input varying with demand over the full range of control. The complexity and cost of the system will, in general, vary in the same sequence. Because combustion systems have a lower limit of input for proper burner operation or fuel/air ratio control, the proportioning temperature control system may cut off fuel input when it drops to that limit.

Fuel/air ratios may be controlled at individual burners by venturi mixers or in multiple burner firing zones by similar mixing stations. To avoid back firing in burner manifolds, the pressures of air and gas supplies can be proportioned to provide the proper ratio of fuel and air delivered to individual burners through separate piping. Even though the desired fuel/air ratio can be maintained for the total input to a multiple burner firing zone, errors in distribution can result in excess air or fuel being supplied to individual burners. The design of distribution piping, downstream from ratio control valves, will control delayed combustion of excess fuel and air from individual burners.

In batch-type furnaces for interrupted heating cycles, it may be advantageous to transfer temperature control from furnace temperature to load temperature as load temperature approaches the desired level in order to take advantage of higher furnace temperatures in the earlier part of the heating cycle. An example is a furnace for annealing steel strip coils. Because heat flow through coil laminations is a fraction of that parallel to the axis of the coil, coils may be stacked vertically with open coil separators between them, to provide for heat transfer from recirculated furnace atmosphere to the end surfaces of coils. For bright annealing, the furnace atmosphere will be nonoxidizing, and the load will be enclosed in an inner cover during heating and cooling, with the atmosphere recirculated by a centrifugal fan in the load support base, to transfer heat from the inner cover to end faces of coils. There will also be some radiation heat transfer from the inner cover to the cylindrical surface of the coil stack.

Inner covers are usually constructed of heat-resisting alloy, with permissible operating temperatures well above the desired final load temperature. A preferred design provides for initial control of furnace inside wall temperature from a thermocouple inserted through the furnace wall, with control switched to a couple in the support base, in control with the bottom of the coil stack, after load temperature reaches a present level below the desired final temperature.

To avoid leakage of combustion gases outward through furnace walls, with possible overheating of the steel enclosure, or infiltration of cold air that could cause nonuniform wall temperatures, control of internal furnace pressure to slightly above ambient is desirable. This can be accomplished by an automatic damper in the outlet flue, adjusted to hold the desired pressure at the selected point in the furnace enclosure. In furnaces with door openings at either end, the point of measurement should be close to hearth level near the discharge end. A practical furnace pressure will be 0.01–0.05 in. H₂O.

With recuperative or regenerative firing systems, the preferred location of the control damper will be between the waste-heat recovery system and the stack to operate at minimum temperature. In high-temperature furnaces without waste-heat recovery, a water-cooled damper may be needed.

With combustion air preheated before distribution to several firing zones, the ratio control system for each zone will need adjustment to entering air temperature. However, if each firing zone has a separate waste-heat recovery system, the zone air supply can be measured before preheating to maintain the balance with fuel input.

The diagram of a combustion control system in Fig. 43 shows how these control functions can be interlocked with the required instrumentation.

For automatic furnace pressure control to be effective, it should be used in combination with proportioning-type temperature control. With on-off control, for example, the control of furnace pressure at zero firing rate cannot be accomplished by damper adjustment, and with a continuous variation in firing rate between maximum and minimum limits or between maximum and off, the adjustment of damper position to sudden changes in firing rate will involve a time lag factor that can make control ineffective.

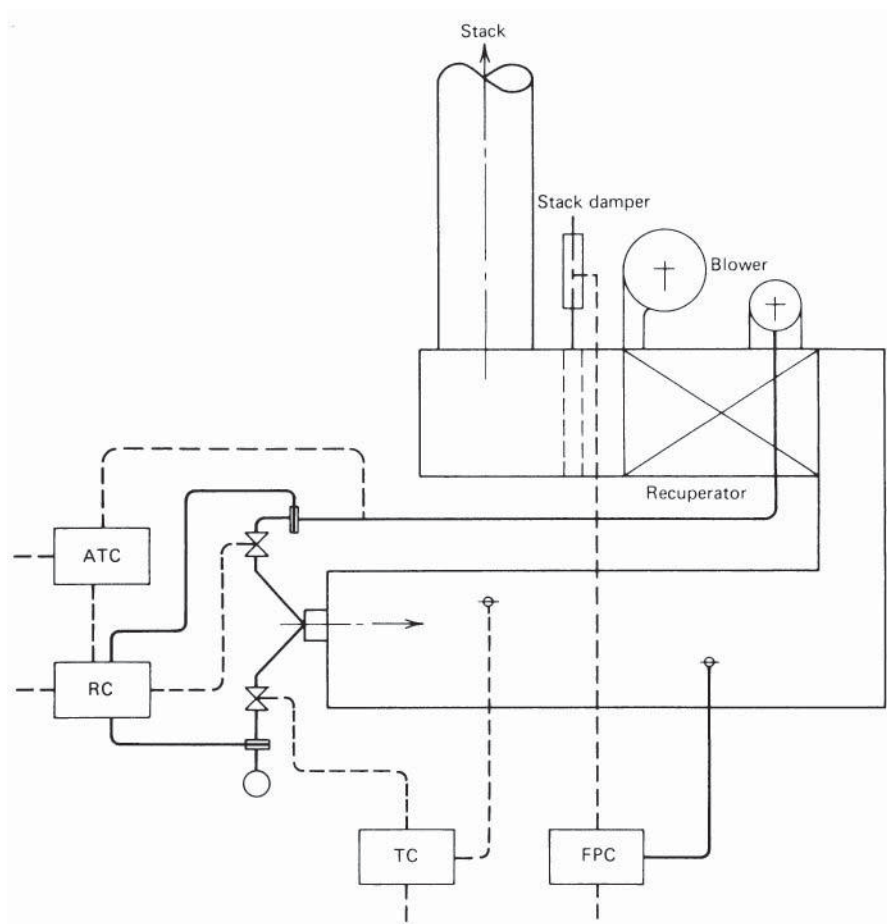


Figure 43 Combustion control diagram for recuperative furnace.^a

An important function of a furnace control system is to guard against safety hazards, such as explosions, fires, and personal injury. Requirements have been well defined in codes issued by industrial insurers and include provision for continuous ignition of burners in low-temperature furnaces, purging of atmosphere furnaces and combustion of hydrogen or carbon monoxide in effluent atmospheres, and protection of operating personnel from injury by burning, mechanical contact, electrical shock, poisoning by inhalation of toxic gases, or asphyxiation. Plants with extensive furnace operation should have a safety engineering staff to supervise selection, installation, and maintenance of safety hazard controls and to coordinate the instruction of operating personnel in their use.

10.4 Air Pollution Control

A new and increasing responsibility of furnace designers and operators is to provide controls for toxic, combustible, or particulate materials in furnace flue gases to meet federal or local standards for air quality. Designs for furnaces to be built in the immediate future should anticipate a probable increase in restrictions of air pollution in coming years.

Toxic contaminants include sulfur and chlorine compounds, nitrogen oxides, carbon monoxide, and radioactive wastes. The epidemic of "acid rain" in areas downwind from large coal-burning facilities is an example.

Combustible contaminants include unburned fuel, soot, and organic particulates from incinerators and the visible constituents of smoke, except for steam. Other particulates include suspended ash and suspended solids from calcination processes.

Types of control equipment include the following:

1. Bag filters or ceramic fiber filters to remove suspended solids. Filters require periodic cleaning or replacement and add to the pressure drop in flue gases leaving the system.
2. Electrostatic filters, in which suspended particles pass through a grid to be electrically charged and are collected on another grid or on spaced plates with the opposite potential. Smaller units are cleaned periodically by removal and washing. Large industrial units are cleaned in place. A possible objection to their use is a slight increase in the ozone content of treated air.
3. Wet scrubbers are particularly effective for removing water-soluble contaminants such as sulfur and chlorine compounds. They can be used in place of filters for handling heavy loads of solid particulates such as from foundry cupola furnaces, metal-refining processes, and lime kilns. Waste material is collected as a mud or slurry, requiring proper disposal to avoid solid-waste problems.
4. Combustible wastes, such as the solvent vapors from organic coating ovens, may be burned in incinerator units by adding combustion air and additional fuel as required. Fuel economy may be improved by using waste heat from combustion to preheat incoming gases through a recuperator. The same system may be used for combustible solid particulates suspended in flue gases.
5. Radioactive wastes from nuclear power plants will usually be in the form of suspended solids that can be treated accordingly if suitable facilities for disposal of collected material are available or as radioactive cooling water for which a suitable dumping area will be needed.

11 WASTE HEAT RECOVERY SYSTEMS

In fuel-fired furnaces, a fraction of the energy from combustion leaves the combustion chamber as sensible heat in waste gases and the latent heat of evaporation for any water vapor content resulting from the combustion of hydrogen. Losses increase with flue gas temperature and

excess air and can reach 100% of input when furnace temperatures equal theoretical flame temperatures.

Waste heat can be recovered in several ways:

1. Preheating incoming loads in a separate enclosure ahead of the furnace.
2. Generating process steam, or steam for electric power generation. Standby facilities will be needed for continuous demand to cover interruptions of furnace operation.
3. Preheating combustion air, or low-Btu fuels, with regenerative or recuperative firing systems.

11.1 Regenerative Air Preheating

For the high flue gas temperatures associated with glass- and metal-melting processes, for which metallic recuperators are impractical, air may be preheated by periodical reversal of the direction of firing, with air passing consecutively through a hot refractory bed or checker chamber, the furnace combustion chamber, and another heat storage chamber in the waste-gas flue. The necessary use of the furnace firing port as an exhaust port after reversal limits the degree of control of flame patterns and the accuracy of fuel/air control in multiple port furnaces. Regenerative firing is still preferred, however, for open hearth furnaces used to convert blast furnace iron to steel, for large glass-melting furnaces, and for some forging operations.

A functional diagram of a regenerative furnace is shown in Fig. 44. The direction of flow of combustion air and flue gas is reversed by a valve arrangement connecting the low-temperature

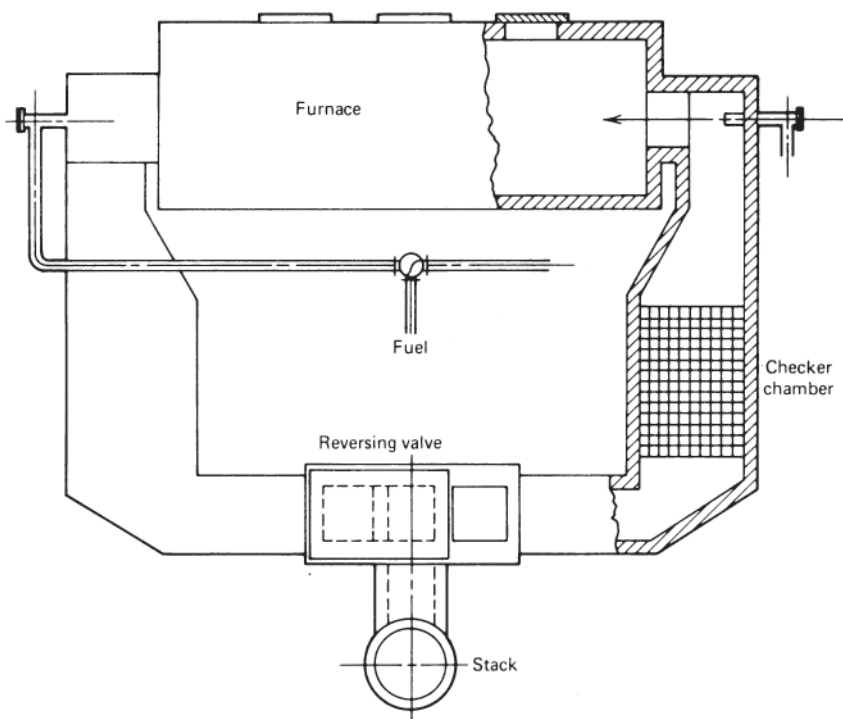


Figure 44 Regenerative furnace diagram.^a

end of the regenerator chamber to either the combustion air supply or the exhaust stack. Fuel input is reversed simultaneously, usually by an interlocked control. Reversal can be in cycles of from 10 to 30 min duration, depending primarily on furnace size.

11.2 Recuperator Systems

Recuperative furnaces are equipped with a heat exchanger arranged to transfer heat continuously from outgoing flue gas to incoming combustion air. Ceramic heat exchangers, built up of refractory tubes or refractory block units arranged for cross flow of air and flue gas, have the advantage of higher temperature limits for incoming flue gas and the disadvantage of leakage of air or flue gas between passages, with leakage usually increasing with service life and pressure

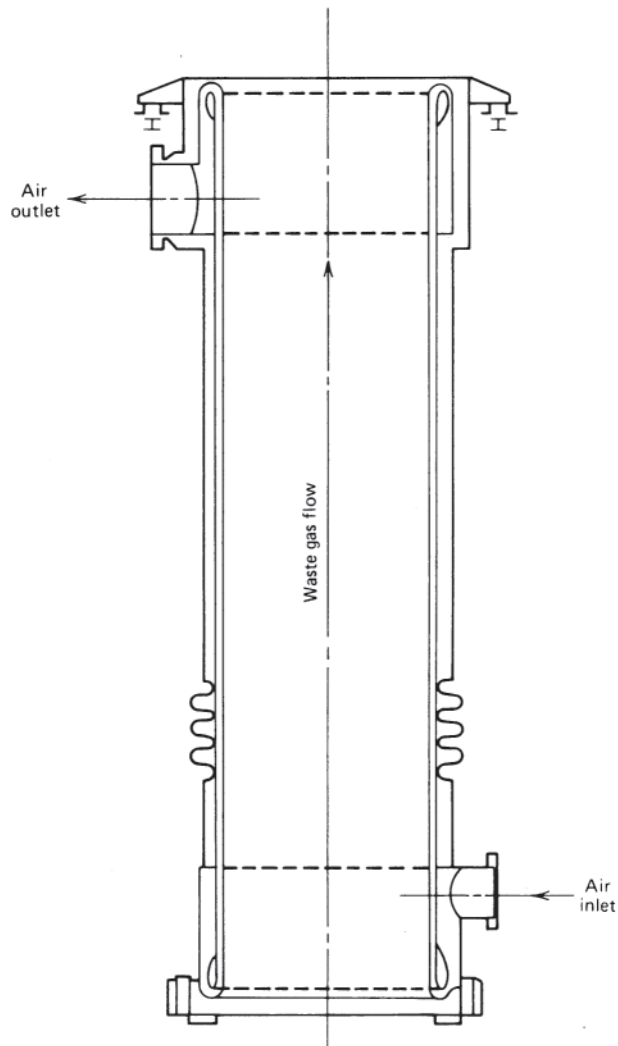


Figure 45 Stack-type recuperator.^a Courtesy of Morgan Engineering Company.

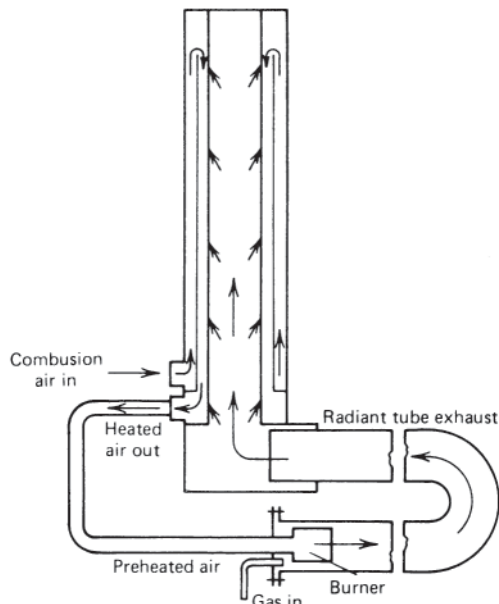


Figure 46 Radiant tube recuperator.^a Courtesy of Holcroft Division, Thermo-Electron Corp.

differentials. With the improvement in heat-resistant alloys to provide useful life at higher temperatures and with better control of incoming flue gas temperatures, metallic recuperators are steadily replacing ceramic types.

Metal recuperators can be successfully used with very high flue gas temperatures if entering temperatures are reduced by air dilution or by passing through a high-temperature waste-heat boiler.

Familiar types of recuperators are shown in Figures 45–47.

Figure 45 shows the radiation or stack type. Flue gases pass through an open cylinder, usually upward, with heat transfer primarily by gas radiation to the surrounding wall. An annular passage is provided between inner and outer cylinders, in which heat is transferred to air at high velocity by gas radiation and convection, or by solid-state radiation from inner to outer cylinders and convection. The radiation recuperator has the advantage of acting as a portion of an exhaust stack, usually with flue gas and air counterflow. Disadvantages are distortion and resulting uneven distribution of air flow, resulting from differential thermal expansion of the inner tube, and the liability of damage from secondary combustion in the inner chamber.

11.3 Recuperator Combinations

To provide preheated air at pressure required for efficient combustion without excessive air leakage from the air to the flue gas side in refractory recuperators, the air pressure can be increased between the recuperator and burner by a booster fan. Top air temperatures will be limited by fan materials. As an alternative, air temperatures can be boosted by a jet pump with tolerance for much higher temperatures.

In a popular design for recuperator firing of soaking pits, flue gases pass through the refractory recuperator at low pressure, with air flowing counterflow at almost the same pressure.

Air flow is induced by a jet pump, and, to increase the jet pump efficiency, the jet air can be preheated in a metal recuperator between the refractory recuperator and the stack. Because the metal recuperator can handle air preheated to the limit of the metal structure, power demand can be lowered substantially below that for a cold air jet.

Radiant tubes can be equipped with individual recuperators, as shown in Fig. 46. Some direct-firing burners are available with integral recuperators.

12 FURNACE COMPONENTS IN COMPLEX THERMAL PROCESSES

An industrial furnace, with its auxiliaries, may be the principal component in a thermal process with functions other than heating and cooling. For example, special atmosphere treatment of load surfaces to increase or decrease the carbon content of ferrous alloys can be accomplished in a furnace heated by radiant tubes or electrical heating elements or by electric induction. A source of the required controlled atmosphere is usually part of the furnace process equipment designed and supplied by the furnace manufacturer.

Continuous heat treatment of strip or wire to normalize or anneal ferrous materials followed by coating in molten metal, such as zinc or aluminum, or electroplating can be accomplished by one of two arrangements for furnace coating lines. One arrangement has a sequence of horizontal passes, with a final cooling zone to regulate strip temperature to the approximate temperature of the coating bath and an integral molten-metal container. Strip is heat treated in a controlled atmosphere to avoid oxidation, with the same atmosphere maintained to the point of immersion in molten metal. The second arrangement is for higher velocities and longer strands in heating and cooling passes. In this arrangement, strip may be processed in a series of vertical strands supported by conveyor rolls.

Furnace lines designed for either galvanizing or aluminum coating may be designed with two molten-metal pots with the entry strand arranged to be diverted to either one and with the cooling zone adjustable to discharge the strand to either pot at the required temperature.

Thermal processing lines may include furnace equipment for heating the load to the temperature required for annealing, normalizing, or hardening, a quench tank for oil or water cooling to develop hardness, a cleaning station to remove quench oil residues, and a separate tempering furnace to develop the desired combination of hardness and toughness. Loads may be in continuous strand form or in units carried by trays or fixtures that go through the entire process or carried on a series of conveyors. The required atmosphere generator will be part of the system.

Where exposure to hydrogen or nitrogen in furnace atmospheres may be undesirable, as in heat treatment of some ferrous alloys, heating and cooling can be done in a partial vacuum, usually with heat supplied by electrical resistors. Quenching can be done in a separate chamber with a controlled atmosphere suitable for brief exposure.

Systems for collecting operating data from one or more furnaces and transmitting the data to a central recording or controlling station may also be part of the responsibility of the furnace supplier.

13 FURNACE CAPACITY

Factors limiting the heating capacity of industrial furnaces include building space limitations, available fuel supplies, limited temperature of heat sources such as electric resistors or metal radiant tubes, and limits on final load temperature differentials. Other factors under more direct control by furnace designers are the choice between batch and continuous heating cycles; time-temperature cycles to reach specified final load temperatures; fuel firing arrangements; and control systems for furnace temperature, furnace pressure, and fuel/air ratios. In addition,

the skills and motivation of furnace operating personnel, as the result of training, experience, and incentive policies, will directly affect furnace efficiency.

14 FURNACE TEMPERATURE PROFILES

Time–temperature patterns can be classified as uniform wall temperature (T_w), uniform combustion gas temperature (T_g), or variable T_w and T_g designed to secure the best combination of heating capacity and fuel efficiency.

In a batch-type furnace with fairly massive loads, the temperature control system can be arranged to allow firing at the maximum burner capacity until a preset wall temperature limit is reached, adjusting the firing rate to hold that wall temperature, until the load temperature approaches the limit for the heated surface, and reducing the wall temperature setting to hold maximum load temperature T_s while the minimum T_c reaches the desired level.

In continuous furnaces, control systems have evolved from a single firing zone, usually fired from the discharge end with flue gas vented from the load charge end, to two or three zone firing arranged for counterflow relation between furnace loads and heating gases.

Progress from single to multiple zone firing has improved heating rates by raising furnace temperatures near the charge end while increasing fuel demand by allowing higher temperatures in flue gas leaving the preheat zone. Load temperature control has been improved by allowing lower control temperatures in the final zone at the discharge end.

With multiple zone firing, the control system can be adjusted to approach the constant gas temperature model, constant wall temperature, or a modified system in which both T_g and T_w vary with time and position. Because gas temperatures are difficult to measure directly, the constant-gas-temperature pattern can be simulated by an equivalent wall temperature profile. With increasing fuel costs, temperature settings in a three-zone furnace can be arranged to discharge flue gases at or below the final load temperature, increasing the temperature setting in the main firing zone to a level to provide an equilibrium wall and load temperature close to the desired final load temperature during operating delays and setting a temperature in the final or soak zone slightly above the desired final load surface temperature.

15 REPRESENTATIVE HEATING RATES

Heating times for various furnace loads, loading patterns, and time–temperature cycles can be calculated from data on radiation and non–steady-state conduction. For preliminary estimates, heating times for steel slabs to rolling temperatures, with a furnace temperature profile depressed at the entry end, have been estimated on a conservative basis as a function of thickness heated from one side and final load temperature differential and are shown in Fig. 26. The ratios for heating time required for square steel billets in various loading patterns are shown in Fig. 25. For other rectangular cross sections and loading patterns, heating times can be calculated by the Newman method.

Examples of heating times required to reach final load temperatures of $T_s = 2300^\circ\text{F}$ and $T_c = 2350^\circ\text{F}$ with constant furnace wall temperatures are as follows:

1. A 12-in.-thick carbon steel slab on refractory hearth with open firing: 9 h at 54.4 lb/h·ft².
2. A 4-in.-thick slab, same conditions as 1: 1.5 h at 109 lb/h·ft².
3. Carbon steel billets 4 in. square loaded 8 in. on center on a refractory hearth: 0.79 h at 103 lb/h·ft².
4. Billets 4 in. square loaded as in 3, but heated to $T_s = 1650^\circ\text{F}$ and $T_c = 1600^\circ\text{F}$ for normalizing: 0.875 h at 93 lb/h·ft².

5. Thin steel strip heated from both sides to 1350°F by radiant tubes with a wall temperature of 1700°F, total heating rate for both sides: 70.4 lb/h·ft².
6. Long aluminum billets, 6 in. diameter, are to be heated to 1050°F. Billets will be loaded in multiple layers separated by spacer bars, with wind flow parallel to their length. With billets in lateral contact and with wind at a mean temperature of 1500°F, estimated heating time is 0.55 h.
7. Small aluminum castings are to be heated to 1000°F on a conveyor belt by jet impingement of heated air. Assuming that the load will have thick and thin sections, wind temperature will be limited to 1100°F to avoid overheating thinner sections. With suitable nozzle spacing and wind velocity, the convection heat transfer coefficient can be $H_c = 15 \text{ Btu/h} \cdot \text{ft}^2$ and the heating rate 27 lb/h · ft².

16 SELECTING NUMBER OF FURNACE MODULES

For a given heating capacity and with no limits on furnace size, one large furnace will cost less to build and operate than a number of smaller units with the same total hearth area. However, furnace economy may be better with multiple units. For example, where reheating furnaces are an integral part of a continuous hot strip mill, the time required for furnace repairs can reduce mill capacity unless normal heating loads can be handled with one of several furnaces down for repairs. For contemporary hot strip mills, the minimum number of furnaces is usually three, with any two capable of supplying normal mill demand.

Rolling mills designed for operation 24 h per day may be supplied by batch-type furnaces. For example, soaking-pit-type furnaces are used to heat steel ingots for rolling into slabs. The mill rolling rate is 10 slabs/h. Heating time for ingots with residual heat from casting averages 4 h, and the time allowed for reloading an empty pit is 2 h, requiring an average turnover time of 6 h. The required number of ingots in pits and spaces for loading is accordingly 60, requiring six holes loaded 10 ingots per hole.

If ingots are poured after a continuous steelmaking process, such as open hearth furnaces or oxygen retorts, and are rolled on a schedule of 18 turns per week, it may be economical at present fuel costs to provide pit capacity for hot storage of ingots cast over weekends, rather than reheating them from cold during the following week.

With over- and underfired slab reheating furnaces, with slabs carried on insulated, water-cooled supports, normal practice has been to repair pipe insulation during the annual shutdown for furnace maintenance, by which time some 50% of insulation may have been lost. By more frequent repair, for example, after 10% loss of insulation, the added cost of lost furnace time, material, and labor may be more than offset by fuel savings, even though total furnace capacity may be increased to offset idle time.

17 FURNACE ECONOMICS

The furnace engineer may be called on to make decisions or submit recommendations for the design of new furnace equipment or the improvement of existing furnaces. New furnaces may be required for new plant capacity or addition to existing capacity, in which case the return on investment will not determine the decision to proceed. Projected furnace efficiency will, however, influence the choice of design.

If new furnace equipment is being considered to replace obsolete facilities or if the improvement of existing furnaces is being considered to save fuel or power or reduce maintenance costs, return on investment will be the determining factor. Estimating that return will require evaluation of these factors:

- Projected service life of equipment to be improved
- Future costs of fuel, power, labor for maintenance, or operating supervision and repairs for the period assumed
- Cost of production lost during operating interruptions for furnace improvement or strikes by construction trades
- Cost of money during the improvement program and interest available from alternative investments
- Cost of retraining operating personnel to take full advantage of furnace improvements

17.1 Operating Schedule

For a planned annual capacity, furnace size will depend on the planned hours per year of operation, and fuel demand will increase with the ratio of idle time to operating time, particularly in furnaces with water-cooled load supports. If furnace operation will require only a two- or three-man crew and if furnace operation need not be coordinated with other manufacturing functions, operating costs may be reduced by operating a smaller furnace two or three turns per day, with the cost of overtime labor offset by fuel savings.

On the other hand, where furnace treatment is an integral part of a continuous manufacturing process, the provision of standby furnace capacity to avoid plant shutdown for furnace maintenance or repairs may be indicated.

If furnace efficiency deteriorates rapidly between repairs, as with loss of insulation from water-cooled load supports, the provision of enough standby capacity to allow more frequent repairs may reduce overall costs.

17.2 Investment in Fuel-Saving Improvements

At present and projected future costs of gas and oil fuels, the added cost of building more efficient furnaces or modifying existing furnaces to improve efficiency can usually be justified. Possible improvements include better insulation of the furnace structure, modified firing arrangements to reduce flue gas temperatures or provide better control of fuel/air ratios, programmed temperature control to anticipate load changes, more durable insulation of water-cooled load supports and better maintenance of insulation, proportioning temperature control rather than the two-position type, and higher preheated air temperatures. For intermittent furnace operation, the use of low-density insulation to line furnace walls and roofs can result in substantial savings in fuel demand for reheating to operating temperature after idle periods.

The relative costs and availability of gas and oil fuels may make a switch from one fuel to another desirable at any future time, preferably without interrupting operations. Burner equipment and control systems are available, at some additional cost, to allow such changeovers.

The replacement of existing furnaces with more fuel-efficient designs or the improvement of existing furnaces to save fuel need not be justified in all cases by direct return on investment. Where present plant capacity may be reduced by future fuel shortages or where provision should be made for increasing capacity with fuel supplies limited to present levels, cost savings by better fuel efficiency may be incidental.

Government policies on investment tax credits or other incentives to invest in fuel-saving improvements can influence the return on investment for future operation.

REFERENCE

1. I.C. Cone, *Energy Management for Industrial Furnaces*, Wiley, New York, 1980.

CHAPTER 9

HEAT EXCHANGERS, VAPORIZERS, AND CONDENSERS

Joseph W. Palen
Consultant
Eugene, Oregon

1 HEAT EXCHANGER TYPES AND CONSTRUCTION	375	4 COMMON OPERATIONAL PROBLEMS	398
1.1 Shell-and-Tube Heat Exchangers	375	4.1 Fouling	398
1.2 Plate-Type Heat Exchangers	380	4.2 Vibration	399
1.3 Spiral Plate Heat Exchangers	380	4.3 Flow Maldistribution	400
1.4 Air-Cooled Heat Exchangers	381	4.4 Temperature Pinch	401
1.5 Compact Heat Exchangers	382	4.5 Critical Heat Flux in Vaporizers	402
1.6 Boiler Feedwater Heaters	382	4.6 Instability	402
1.7 Recuperators and Regenerators	382	4.7 Inadequate Venting, Drainage, or Blowdown	403
2 ESTIMATION OF SIZE AND COST	383	5 USE OF COMPUTERS IN THERMAL DESIGN OF PROCESS HEAT EXCHANGERS	403
2.1 Basic Equations for Required Surface	383	5.1 Introduction	403
2.2 Mean Temperature Difference	383	5.2 Incrementation	403
2.3 Overall Heat Transfer Coefficient	384	5.3 Main Convergence Loops	404
2.4 Pressure Drop	385	5.4 Rating, Design, or Simulation	405
3 RATING METHODS	386	5.5 Program Quality and Selection	406
3.1 Shell-and-Tube Single-Phase Exchangers	386	5.6 Determining and Organizing Input Data	407
3.2 Shell-and-Tube Condensers	388	NOMENCLATURE	410
3.3 Shell-and-Tube Reboilers and Vaporizers	392	REFERENCES	412
3.4 Air-Cooled Heat Exchangers	396		
3.5 Other Exchangers	398		

1 HEAT EXCHANGER TYPES AND CONSTRUCTION

Heat exchangers permit exchange of energy from one fluid to another, usually without permitting physical contact between the fluids. The following configurations are commonly used in the power and process industries.

1.1 Shell-and-Tube Heat Exchangers

Shell-and-tube heat exchangers normally consist of a bundle of tubes fastened into holes drilled in metal plates called tubesheets. The tubes may be rolled into grooves in the tubesheet, welded

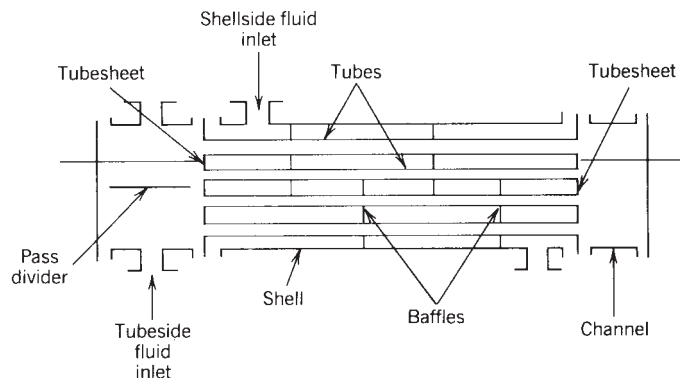


Figure 1 Schematic illustration of shell-and-tube heat exchanger construction.

to the tubesheet, or both to ensure against leakage. When possible, U-tubes are used, requiring only one tubesheet. The tube bundle is placed inside a large pipe called a shell; see Fig. 1. Heat is exchanged between a fluid flowing inside the tubes and a fluid flowing outside the tubes in the shell.

When the tubeside heat transfer coefficient is as high as three times the shellside heat transfer coefficient, it may be advantageous to use low integral finned tubes. These tubes can have outside heat transfer coefficients as high as plain tubes or even higher but increase the outside heat transfer area by a factor of about 2.5–4. For design methods using finned tubes, see Ref. 1 for single-phase heat exchangers and Ref. 1a for condensers. Details of construction practices are described by Saunders.²

The Tubular Exchanger Manufacturers Association (TEMA) provides a manual of standards for construction of shell-and-tube heat exchangers³ which contains designations for various types of shell-and-tube heat exchanger configurations. The most common types are summarized below.

E-Type

The E-type shell-and-tube heat exchanger (illustrated in Fig. 2) is the workhorse of the process industries, providing economical rugged construction and a wide range of capabilities. Baffles support the tubes and increase shellside velocity to improve heat transfer. More than one pass is usually provided for tubeside flow to increase the velocity (Fig. 2a). However, for some cases, notably vertical thermosiphon vaporizers, a single tubepass is used, as shown in Fig. 2b.

The E-type shell is usually the first choice of shell types because of lowest cost but sometimes requires more than the allowable pressure drop or produces a temperature “pinch” (see Section 4.4), so other, more complicated types are used.

F-Type Shell

If the exit temperature of the cold fluid is greater than the exit temperature of the hot fluid, a temperature cross is said to exist. A slight temperature cross can be tolerated in a multitubepass E-type shell (see below), but if the cross is appreciable, either units in series or complete countercurrent flow is required. A solution sometimes used is the F-type or two-pass shell, as shown in Fig. 3.

The F-type shell has a number of potential disadvantages, such as thermal and fluid leakage around the longitudinal baffle and high pressure drop, but it can be effective in some cases if well designed.

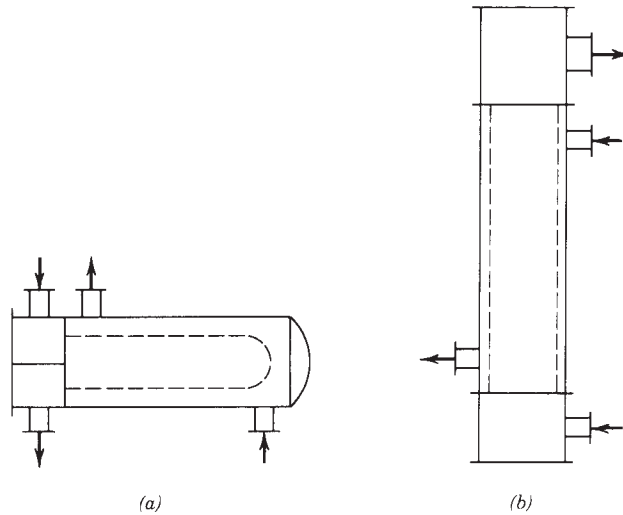


Figure 2 TEMA E-type shell: (a) horizontal multitubepass; (b) vertical single tubepass.

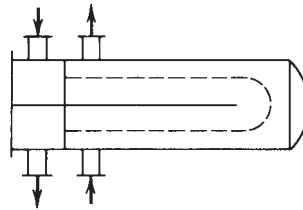


Figure 3 TEMA F-type shell.

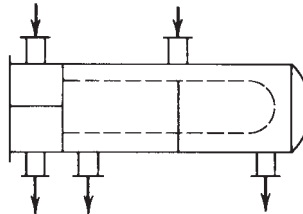


Figure 4 TEMA J-type shell.

J-Type

When an E-type shell cannot be used because of high pressure drop, a J-type or divided flow exchanger, shown in Fig. 4, is considered. Since the flow is divided and the flow length is also cut in half, the shellside pressure drop is only about one-eighth to one-fifth that of an E-type shell of the same dimensions.

X-Type

When a J-type shell would still produce too high a pressure drop, an X-type shell, shown in Fig. 5, may be used. This type is especially applicable for vacuum condensers and can be

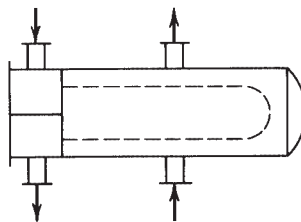


Figure 5 TEMA X-type shell.

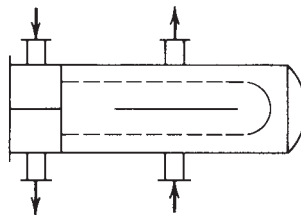


Figure 6 TEMA G-type shell.

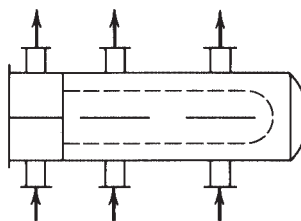


Figure 7 TEMA H-type shell.

equipped with integral finned tubes to counteract the effect of low shellside velocity on heat transfer. It is usually necessary to provide a flow distribution device under the inlet nozzle. When the ratio of tube length to shell diameter is greater than about 4.5, a second set of shellside nozzles should be added.

G-Type

This shell type, shown in Fig. 6, is sometimes used for horizontal thermosiphon shellside vaporizers. The horizontal baffle is used especially for boiling range mixtures and provides better flow distribution than would be the case with the X-type shell. The G-type shell also permits a larger temperature cross than the E-type shell with about the same pressure drop.

H-Type

If a G-type is being considered but pressure drop would be too high, an H-type may be used. This configuration is essentially just two G-types in parallel, as shown in Fig. 7.

K-Type

This type is used exclusively for kettle reboilers and vaporizers and is characterized by the oversized shell intended to separate vapor and liquid phases (Fig. 8). Shell-sizing relationships

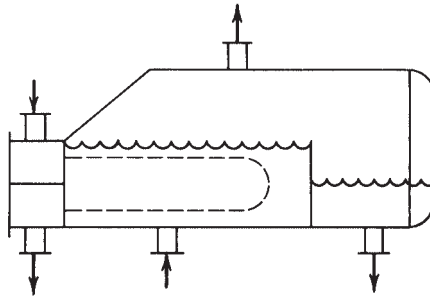


Figure 8 TEMA K-type shell.

are given in Ref. 4. Usually, the shell diameter is about 1.6–2.0 times the bundle diameter. Design should consider amount of acceptable entrainment, height required for flow over the weir, and minimum clearance in case of foaming.

Baffle Types

Baffles are used to increase the velocity of the fluid flowing outside the tubes (“shellside” fluid) and to support the tubes. Higher velocities have the advantage of increasing heat transfer and decreasing fouling (material deposit on the tubes) but have the disadvantage of increasing pressure drop (more energy consumption per unit of fluid flow). The amount of pressure drop on the shellside is a function of baffle spacing, baffle cut, baffle type, and tube pitch.

Baffle types commonly used are shown in Fig. 9, with pressure drop decreasing from Fig. 9a to Fig. 9c. The helical baffle (Section 6) has several advantages.

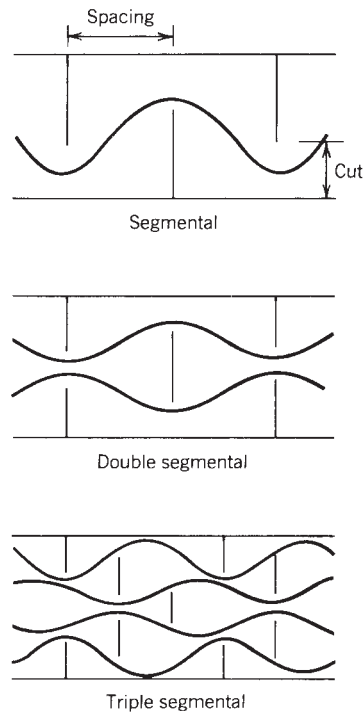


Figure 9 Baffle types.

Baffle spacing is increased when it is necessary to decrease pressure drop. A limit must be imposed to prevent tube sagging or flow-induced tube vibration. Recommendations for maximum baffle spacing are given in Ref. 3. Tube vibration is discussed in more detail in Section 4.2. When the maximum spacing still produces too much pressure drop, a baffle type is considered that produces less cross flow and more longitudinal flow, for example, double segmental instead of segmental. Minimum pressure drop is obtained if baffles are replaced by rod-type tube supports.⁵

1.2 Plate-Type Heat Exchangers

Composed of a series of corrugated or embossed plates clamped between a stationary and a movable support plate, these exchangers were originally used in the food-processing industry. They have the advantages of low fouling rates, easy cleaning, and generally high heat transfer coefficients and are becoming more frequently used in the chemical process and power industries. They have the disadvantage that available gaskets for the plates are not compatible with all combinations of pressure, temperature, and chemical composition. Suitability for specific applications must be checked. The maximum operating pressure is usually considered to be about 1.5 MPa (220 psia).⁶ However, welded plate versions are now available for much higher pressures. A typical plate heat exchanger is shown in Fig. 10. Welded plate exchangers and other compact types are discussed in Section 6.

1.3 Spiral Plate Heat Exchangers

These exchangers are also becoming more widely used, despite limitations on maximum size and maximum operating pressure. They are made by wrapping two parallel metal plates separated by spacers into a spiral to form two concentric spiral passages. A schematic example is shown in Fig. 11.

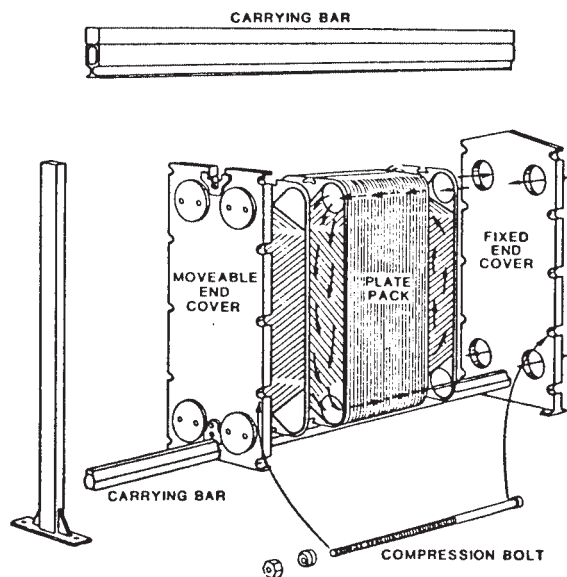


Figure 10 Typical plate-type heat exchanger.

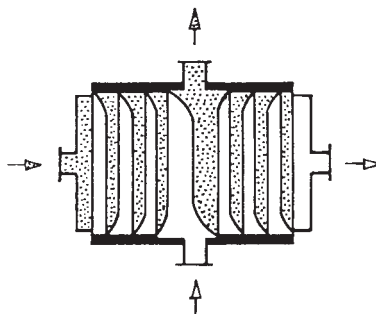


Figure 11 Spiral plate heat exchanger.

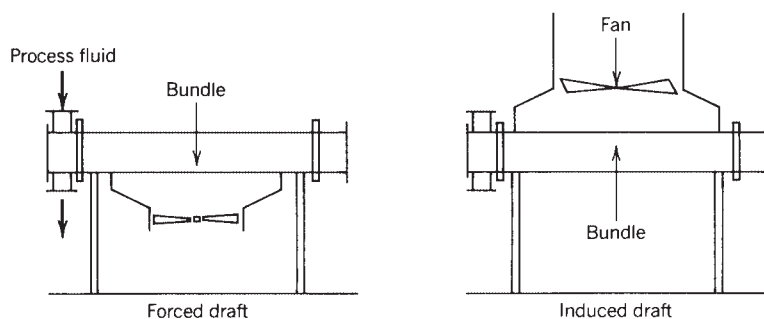


Figure 12 Air-cooled heat exchangers.

Spiral plate heat exchangers can provide completely countercurrent flow, permitting temperature crosses and close approaches while maintaining high velocity and high heat transfer coefficients. Since all flow for each fluid is in a single channel, the channel tends to be flushed of particles by the flow, and the exchanger can handle sludges and slurries more effectively than can shell-and-tube heat exchangers. The most common uses are for difficult-to-handle fluids with no phase change. However, the low-pressure-drop characteristics are beginning to promote some use in two-phase flow as condensers and reboilers. For this purpose the two-phase fluid normally flows axially in a single pass rather than spirally.

1.4 Air-Cooled Heat Exchangers

It is sometimes economical to condense or cool hot streams inside tubes by blowing air across the tubes rather than using water or other cooling liquid. They usually consist of a horizontal bank of finned tubes with a fan at the bottom (forced draft) or top (induced draft) of the bank, as illustrated schematically in Fig. 12.

Tubes in air-cooled heat exchangers (Fig. 12) are often 1 in. (25.4 mm) in outside diameter with $\frac{5}{8}$ in. (15.9 mm) high annular fins 0.4–0.5 mm thick. The fins are usually aluminum and may be attached in a number of ways, ranging from tension wrapped to integrally extruded (requiring a steel or alloy insert), depending on the severity of service. Tension wrapped fins have an upper temperature limit ($\sim 300^\circ\text{F}$) above which the fin may no longer be in good contact with the tube, greatly decreasing the heat transfer effectiveness. Various types of fins and attachments are illustrated in Fig. 13.

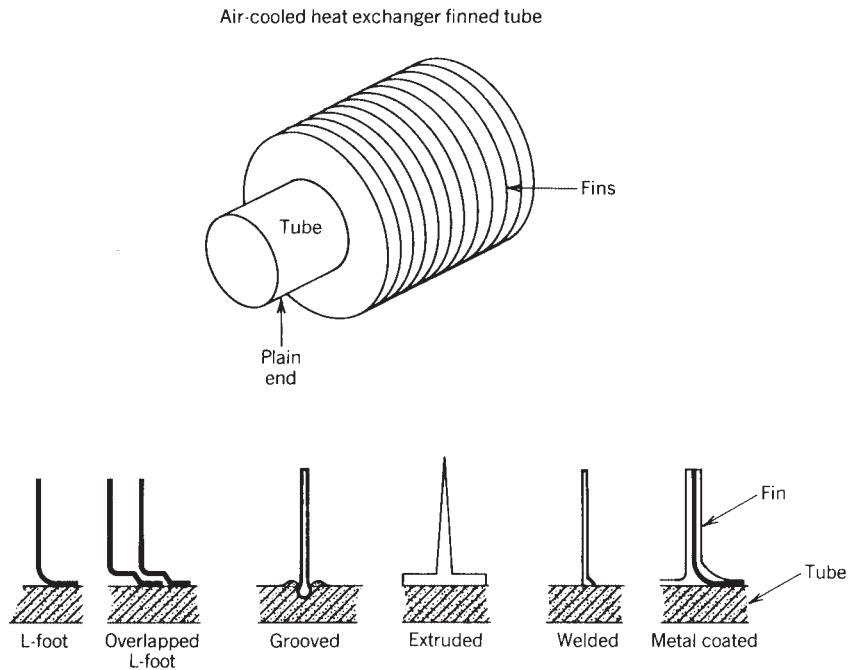


Figure 13 Typical finned tube and attachments.

A more detailed description of air-cooled heat exchanger geometries is given in Refs. 6 and 7.

1.5 Compact Heat Exchangers

The term *compact heat exchanger* normally refers to one of the many types of plate fin exchangers used extensively in the aerospace and cryogenics industries. The fluids flow alternately between parallel plates separated by corrugated metal strips that act as fins and that may be perforated or interrupted to increase turbulence. Although relatively expensive to construct, these units pack a very large amount of heat transfer surface into a small volume and are therefore used when exchanger volume or weight must be minimized. A detailed description with design methods is given in Ref. 8. Also see Section 6.

1.6 Boiler Feedwater Heaters

Exchangers to preheat feedwater to power plant boilers are essentially of the shell-and-tube type but have some special features, as described in Ref. 9. The steam that is used for preheating the feedwater enters the exchanger superheated, is condensed, and leaves as subcooled condensate. More effective heat transfer is achieved by providing three zones on the shellside: desuperheating, condensing, and subcooling. A description of the design requirements of this type of exchanger is given in Ref. 9.

1.7 Recuperators and Regenerators

These heat exchangers are used typically to conserve heat from furnace off-gas by exchanging it against the inlet air to the furnace. A recuperator does this in the same manner as any other

heat exchanger except the construction may be different to comply with requirements for low pressure drop and handling of the high-temperature, often dirty, off-gas stream. Heat pipes (Chapter 9) with fins are now sometimes used.

The regenerator is a transient batch-type exchanger in which packed beds are alternately switched from the hot stream to the cold stream. A description of the operating characteristics and design of recuperators and regenerators is given in Refs. 10 and 11.

2 ESTIMATION OF SIZE AND COST

In determining the overall cost of a proposed process plant or power plant, the cost of heat exchangers is of significant importance. Since cost is roughly proportional to the amount of heat transfer surface required, some method of obtaining an estimate of performance is necessary, which can then be translated into required surface. The term *surface* refers to the total area across which the heat is transferred. For example, with shell-and-tube heat exchangers “surface” is the tube outside circumference times the tube length times the total number of tubes. Well-known basic equations taken from Newton’s law of cooling relate the required surface to the available temperature difference and the required heat duty.

2.1 Basic Equations for Required Surface

The following well-known equation is used (equation terms are defined in the Nomenclature):

$$A_o = \frac{Q}{U_o \times \text{MTD}} \quad (1)$$

The required duty (Q) is related to the energy change of the fluids:

a. Sensible Heat Transfer

$$Q = W_1 C_{p1} (T_2 - T_1) \quad (2a)$$

$$= W_2 C_{p2} (t_1 - t_2) \quad (2b)$$

b. Latent Heat Transfer

$$Q = W\lambda \quad (3)$$

where W = flow rate of boiling or condensing fluid

λ = latent heat of respective fluid

The mean temperature difference (MTD) and the overall heat transfer coefficient (U_o) in Eq. 1 are discussed in Sections 2.2 and 2.3, respectively. Once the required surface, or area (A_o), is obtained, the heat exchanger cost can be estimated. A comprehensive discussion on cost estimation for several types of exchangers is given in Ref. 12. Cost charts for small- to medium-sized shell-and-tube exchangers, developed in 1982, are given in Ref. 13.

2.2 Mean Temperature Difference

The MTD in Eq. 1 is given by the equation

$$\text{MTD} = \frac{F(T_A - T_B)}{\ln(T_A/T_B)} \quad (4)$$

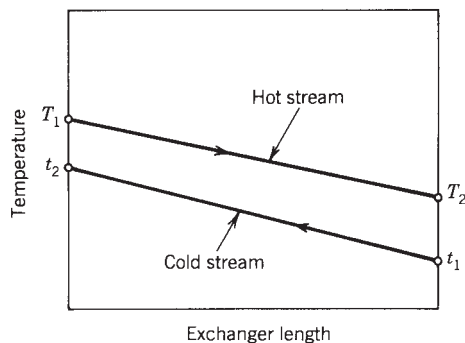


Figure 14 Temperature profiles illustrated for countercurrent flow.

where

$$T_A = T_1 - t_2 \quad (5)$$

$$T_B = T_2 - t_1 \quad (6)$$

The temperatures (T_1, T_2, t_1, t_2) are illustrated for the base case of countercurrent flow in Fig. 14.

The factor F in Eq. 4 is the multitubepass correction factor. It accounts for the fact that heat exchangers with more than one tubepass can have some portions in concurrent flow or cross flow, which produce less effective heat transfer than countercurrent flow. Therefore, the factor F is less than 1.0 for multitubepass exchangers, except for the special case of isothermal boiling or condensing streams for which F is always 1.0. Charts for calculating F are available in most heat transfer textbooks. A comprehensive compilation for various types of exchangers is given by Taborek.¹⁴

In a properly designed heat exchanger, it is unusual for F to be less than 0.7, and if there is no temperature cross ($T_2 > t_2$), F will be 0.8 or greater. As a first approximation for preliminary sizing and cost estimation, F may be taken as 0.85 for multitubepass exchangers with temperature change of both streams and 1.0 for other cases.

2.3 Overall Heat Transfer Coefficient

The factor U_o in Eq. 1 is the overall heat transfer coefficient. It may be calculated by procedures described in Section 3 and is the reciprocal of the sum of all heat transfer resistances, as shown in the equation

$$U_o = 1/(R_{h_o} + R_{f_o} + R_w + R_{h_i} + R_{f_i}) \quad (7)$$

where

$$R_{h_o} = 1/h_o \quad (8)$$

$$R_{h_i} = (A_o/A_i h_i) \quad (9)$$

$$R_w = \frac{A_o x_w}{A_m k_w} \quad (10)$$

Calculation of the heat transfer coefficients h_o and h_i can be time consuming since they depend on the fluid velocities, which, in turn, depend on the exchanger geometry. This is usually done now by computer programs that guess correct exchanger size, calculate heat transfer coefficients, check size, adjust, and reiterate until satisfactory agreement between guessed and calculated size is obtained. For first estimates by hand before size is known, values of h_o

Table 1 Approximate Values for Overall Heat Transfer Coefficient of Shell-and-tube Heat Exchangers (Including Allowance for Fouling)

Fluids	U_o	
	Btu/h-ft ² ·°F	W/m ² ·K
Water–water	250	1400
Oil–water	75	425
Oil–oil	45	250
Gas–oil	15	85
Gas–water	20	115
Gas–gas	10	60

and h_i as well as values of the fouling resistances R_{f_o} and R_{f_i} are recommended by Bell for shell-and-tube heat exchangers.¹⁵

Very rough, first approximation values for the overall heat transfer coefficient are given in Table 1.

2.4 Pressure Drop

In addition to calculation of the heat transfer surface required, it is usually necessary to consider the pressure drop consumed by the heat exchanger since this enters into the overall cost picture. Pressure drop is roughly related to the individual heat transfer coefficients by an equation of the form

$$\Delta P = Ch^n + EX \quad (11)$$

where ΔP = shellside or tubeside pressure drop

h = heat transfer coefficient

C = coefficient depending on geometry

m = exponent depending on geometry—always greater than 1.0 and usually about 3.0

EX = extra pressure drop from inlet, exit, and pass turnaround momentum losses

See Section 3 for actual pressure drop calculations.

Pressure drop is sensitive to the type of exchanger selected. In the final design it is attempted, where possible, to define the exchanger geometry so as to use all available pressure drop and thus maximize the heat transfer coefficient. This procedure is subject to some constraints, however, as follows. The product of density times velocity squared, ρv^2 , is limited to minimize the possibility of erosion or tube vibration. A limit often used is $\rho v^2 < 4000 \text{ lbm/ft}\cdot\text{s}^2$. This results in a velocity for liquids in the range of 7–10 ft/s. For flow entering the shellside of an exchanger and impacting the tubes, an impingement plate is recommended to prevent erosion if $\rho v^2 > 1500$. Other useful design recommendations may be found in Ref. 3.

For condensing vapors, pressure drop should be limited to a fraction of the operating pressure for cases with close temperature approach to prevent severe decrease of the MTD owing to lowered equilibrium condensing temperature. As a safe “rule of thumb,” the pressure drop for condensing is limited to about 10% of the operating pressure. For other cases, “reasonable” design pressure drops for heat exchangers roughly range from about 5 psi for gases and boiling liquids to as high as 20 psi for pumped nonboiling liquids.

3 RATING METHODS

After the size and basic geometry of a heat exchanger has been proposed, the individual heat transfer coefficients h_o and h_i may be calculated based on actual velocities, and the required surface may be checked, based on these updated values. The pressure drops are also checked at this stage. Any inadequacies are adjusted and the exchanger is rechecked. This process is known as “rating.” Different rating methods are used depending on exchanger geometry and process type, as covered in the following sections.

3.1 Shell-and-Tube Single-Phase Exchangers

Before the individual heat transfer coefficients can be calculated, the heat exchanger tube geometry, shell diameter, shell type, baffle type, baffle spacing, baffle cut, and number of tubepasses must be decided. As stated above, lacking other insight, the simplest exchanger—E-type with segmental baffles—is tried first.

Tube Length and Shell Diameter

For shell-and-tube exchangers the tube length is normally about 5–8 times the shell diameter. Tube lengths are usually 8–20 ft long in increments of 2 ft. However, very large size exchangers with tube lengths up to 40 ft are more frequently used as economics dictate smaller MTD and larger plants. A reasonable trial tube length is chosen and the number of tubes (NT) required for surface A_o (Section 2) is calculated as follows:

$$\text{NT} = \frac{A_o}{a_o L} \quad (12)$$

where a_o = surface/unit length of tube.

For plain tubes (as opposed to finned tubes),

$$a_o = \pi D_o \quad (13)$$

where D_o = tube outside diameter

L = tube length

The tube bundle diameter (D_b) can be determined from the number of tubes but also depends on the number of tubepasses, tube layout, and bundle construction. Tube count tables providing this information are available from several sources. Accurate estimation equations are given by Taborek.¹ A simple basic equation that gives reasonable first approximation results for typical geometries is the following:

$$D_b = P_t \left(\frac{\text{NT}}{\pi/4} \right)^{0.5} \quad (14)$$

where P_t = tube pitch (spacing between tube diameters). Normally, P_t/D_o equals 1.25, 1.33, or 1.5.

The shell diameter D_s is larger than the bundle diameter D_b by the amount of clearance necessary for the type of bundle construction. Roughly, this clearance ranges from about 0.5 in. for U-tube or fixed tubesheet construction to 3–4 in. for pull-through floating heads, depending on the design pressure and bundle diameter. (For large clearances, sealing strips are used to prevent flow bypassing the bundles.) After the bundle diameter is calculated, the ratio of length to diameter is checked to see if it is in an acceptable range, and the length is adjusted if necessary.

Baffle Spacing and Cut

Baffle spacing L_{bc} and cut B_c (see Fig. 9) cannot be decided exactly until pressure drop is evaluated. However, a reasonable first guess ratio of baffle spacing to shell diameter (L_{bc}/D_s) is about 0.45. The baffle cut (B_c , a percentage of D_s) required to give good shellside distribution may be estimated by the following equation:

$$B_c = 16.25 + 18.75 \left(\frac{L_{bc}}{D_s} \right) \quad (15)$$

For more detail, see the recommendations of Taborek.¹

Cross-Sectional Flow Areas and Flow Velocities

The cross-sectional flow areas for tubeside flow S_t and for shellside flow S_s are calculated as follows:

$$S_t = \left(\frac{\pi D_i^2}{4} \right) \left(\frac{NT}{NP} \right) \quad (16)$$

$$S_s = 0.785(D_b)(L_{bc})(P_t - D_o)/P_t \quad (17)$$

where L_{bc} = baffle spacing.

Equation 17 is approximate in that it neglects pass partition gaps in the tube field, it approximates the bundle average chord, and it assumes an equilateral triangular layout. For more accurate equations see Ref. 1.

The tubeside velocity V_t and the shellside velocity V_s are calculated as follows:

$$V_t = \frac{W_t}{S_t \rho_t} \quad (18)$$

$$V_s = \frac{W_s}{S_s \rho_s} \quad (19)$$

Heat Transfer Coefficients

The individual heat transfer coefficients h_o and h_i in Eq. 1 can be calculated with reasonably good accuracy (± 20 – 30%) by semiempirical equations found in several design-oriented textbooks.^{1,16} Simplified approximate equations are the following:

a. Tubeside Flow

$$\text{Re} = \frac{D_o V_t \rho_t}{\mu_t} \quad (20)$$

where μ_t = tubeside fluid viscosity.

If $\text{Re} < 2000$ (laminar flow),

$$h_i = 1.86 \left(\frac{k_f}{D_i} \right) \left(\text{Re} \text{Pr} \frac{D_i}{L} \right)^{0.33} \left(\frac{\mu_f}{\mu_w} \right)^{0.14} \quad (21)$$

If $\text{Re} > 10,000$ (turbulent flow),

$$h_i = 0.024 \left(\frac{k_f}{D_i} \right) \text{Re}^{0.8} \text{Pr}^{0.4} \left(\frac{\mu_f}{\mu_w} \right)^{0.14} \quad (22)$$

If $2000 < \text{Re} < 10,000$, prorate linearly.

b. Shellside Flow

$$\text{Re} = \frac{D_o V_s \rho_s}{\mu_s} \quad (23)$$

Table 2 Approximate Bypass Coefficient, C_b

Bundle Type	C_b
Fixed tubesheet or U-tube	0.70
Split-ring floating head, seal strips	0.65
Pull-through floating head, seal strips	0.55

where μ_s = shellside fluid viscosity.
 If $Re < 500$, see Refs. 1 and 16.
 If $Re > 500$,

$$h_o = 0.38 C_b^{0.6} \left(\frac{k_f}{D_o} \right) Re^{0.6} Pr^{0.33} \left(\frac{\mu_f}{\mu_w} \right)^{0.14} \quad (24)$$

The term Pr is the Prandtl number and is calculated as $C_p \mu/k$.

The constant (C_b) in Eq. 24 depends on the amount of bypassing or leakage around the tube bundle.¹⁷ As a first approximation, the values in Table 2 may be used.

Pressure Drop

Pressure drop is much more sensitive to exchanger geometry and, therefore, more difficult to accurately estimate than heat transfer, especially for the shellside. The so-called Bell–Delaware method¹ is considered the most accurate method in the open literature which can be calculated by hand. The following very simplified equations are provided for a rough idea of the range of pressure drop in order to minimize preliminary specification of unrealistic geometries:

- a. *Tubeside (contains about 30% excess for nozzles)*

$$\Delta P_t = \left[\frac{0.025(L)(NP)}{D_i} + 2(NP - 1) \right] \frac{\rho_t V_t^2}{g_c} \left(\frac{\mu_w}{\mu_f} \right)^{0.14} \quad (25)$$

where NP = number of tubepasses.

- b. *Shellside (contains about 30% excess for nozzles)*

$$\Delta P_s = \frac{0.24(L)(D_b)(\rho_s)(C_b V_s)^2}{g_c L_{bc} P_t} \left(\frac{\mu_w}{\mu_f} \right)^{0.14} \quad (26)$$

where g_c = gravitational constant (4.17×10^8 for velocity in ft/h and density in lb/ft³).

3.2 Shell-and-Tube Condensers

The condensing vapor can be on either the shellside or tubeside depending on process constraints. The “cold” fluid is often cooling tower water but can also be another process fluid which is sensibly heated or boiled. In this section, the condensing-side heat transfer coefficient and pressure drop are discussed. Single-phase coolants are handled, as explained in the previous section. Boiling fluids will be discussed in a later section.

Selection of Condenser Type

The first task in designing a condenser, before rating can proceed, is to select the condenser configuration. Mueller^{1a} presents detailed charts for selection based on the criteria of system

Table 3 Condenser Selection Chart

Process Condition	Suggested Condenser Type ^a
Potential coolant fouling	HS/E, J, X
High condensing pressure	VT/E
Low condensing pressure drop	HS/J, X
Corrosive or very high temperature vapors	VT/E
Potential condensate freezing	HS/E
Boiling coolant	VS/E or HT/K, G, H

^aV, vertical; H, horizontal; S, shellside condensation; T, tubeside condensation; E, J, H, K, X, TEMA shell styles.

pressure, pressure drop, temperature, fouling tendency of the coolant, fouling tendency of the vapor, corrosiveness of the vapor, and freezing potential of the vapor. Table 3 is an abstract of the recommendations of Mueller.

The suggestions in Table 3 may, of course, be ambiguous in case of more than one important criterion, for example, corrosive vapor together with a fouling coolant. In these cases, the most critical constraint must be respected as determined by experience and engineering judgment. Corrosive vapors are usually put on the tubeside, and chemical cleaning used for the shellside coolant, if necessary. Since most process vapors are relatively clean (not always the case!), the coolant is usually the dirtier of the two fluids and the tendency is to put it on the tubeside for easier cleaning. Therefore, the most common shell-and-tube condenser is the shellside condenser using TEMA types E, J, or X, depending on allowable pressure drop; see Section 1. An F-type shell is sometimes specified if there is a large condensing range and a temperature cross (see below), but, owing to problems with the F-type, E-type units in series are often preferred in this case.

In addition to the above condenser types the vertical E-type tubeside condenser is sometimes used in a “reflux” configuration with vapor flowing up and condensate flowing back down inside the tubes. This configuration may be useful in special cases, such as when it is required to strip out condensable components from a vent gas that is to be rejected to the atmosphere. The disadvantage of this type of condenser is that the vapor velocity must be very low to prevent carryover of the condensate (flooding), so the heat transfer coefficient is correspondingly low and the condenser rather inefficient. Methods used to predict the limiting vapor velocity are given in Refs. 1a and 18.

Temperature Profiles

For a condensing pure component, if the pressure drop is less than about 10% of the operating pressure, the condensing temperature is essentially constant and the log mean temperature difference (LMTD) applied ($F = 1.0$) for the condensing section. If there are desuperheating and subcooling sections,⁹ the MTD and surface for these sections must be calculated separately. For a condensing mixture, with or without noncondensables, the temperature profile of the condensing fluid with respect to fraction condensed should be calculated according to vapor–liquid equilibrium (VLE) relationships.¹⁹ A number of computer programs are available to solve VLE relationships; a version suitable for a programmable calculator is given in Ref. 20.

Calculations of the condensing temperature profile may be performed either integrally, which assumes vapor and liquid phases are well mixed throughout the condenser, or differentially, which assumes separation of the liquid phase from the vapor phase. In most actual condensers the phases are mixed near the entrance where the vapor velocity is high and separated near the exit where the vapor velocity is lower. The “differential” curve produces a lower MTD than the “integral” curve and is safer to use where separation is expected.

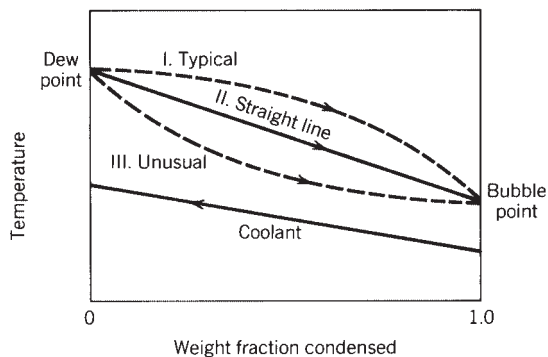


Figure 15 Condensation profiles illustrated.

For most accuracy, condensers are rated incrementally by stepwise procedures such as those explained by Mueller.^{1a} These calculations are usually performed by computers.²¹ As a first approximation, to get an initial size, a straight-line temperature profile is often assumed for the condensing section (not including desuperheating or subcooling sections!). As illustrated in Fig. 15, the true condensing curve is usually more like curve I, which gives a larger MTD than the straight line, curve II, making the straight-line approximation conservative. However, a curve such as curve III is certainly possible, especially with immiscible condensates, for which the VLE should always be calculated. For the straight-line approximation, the condensing heat transfer coefficient is calculated at average conditions, as shown below.

Heat Transfer Coefficients, Pure Components

For condensers, it is particularly important to be able to estimate the two-phase flow regime in order to predict the heat transfer coefficient accurately. This is because completely different types of correlations are required for the two major flow regimes.

Shear-Controlled Flow. The vapor shear force on the condensate is much greater than the gravity force. This condition can be expected, according to Ref. 22, when

$$J_g > 1.5 \quad (27)$$

where

$$J_g = \left[\frac{(Gy)^2}{gD_j \rho_v (\rho_l - \rho_v)} \right]^{0.5} \quad (28)$$

For shear-controlled flow, the condensate film heat transfer coefficient (h_{cf}) is a function of the convective heat transfer coefficient for liquid flowing alone and the two-phase pressure drop²²:

$$h_{cf} = h_l (\phi_l^2)^{0.45} \quad (29)$$

$$h_l = h_l (1 - y)^{0.8} \quad (30)$$

or

$$h_l = h_o (1 - y)^{0.6} \quad (31)$$

$$\phi_l^2 = 1 + \frac{C}{X_u} + \frac{1}{X_u^2}$$

$$C = 20 \text{ (tubeside flow)}, \quad C = 9 \text{ (shellside flow)} \quad (32)$$

$$X_{tt} = \left[\frac{1-y}{y} \right]^{0.9} \left[\frac{\rho_v}{\rho_l} \right]^{0.5} \left[\frac{\mu_l}{\mu_v} \right]^{0.1}$$

$$\mu_l = \text{liquid viscosity}, \quad \mu_v = \text{vapor viscosity} \quad (33)$$

Gravity-Controlled Flow. The vapor shear force on the condensate is small compared to the gravity force, so condensate drains by gravity. This condition can be expected, according to Ref. 22 when $J_g < 0.5$. Under gravity-controlled conditions, the condensate film heat transfer coefficient is calculated as follows:

$$h_{cf} = F_g h_N \quad (34)$$

The term h_N is the heat transfer coefficient from the well-known Nusselt derivation, given in Ref. 1a as

Horizontal Tubes

$$h_N = 0.725 \left[\frac{k_l^3 \rho_l (\rho_l - \rho_v) g \lambda}{\mu_l (T_s - T_w) D} \right]^{0.25} \quad (35)$$

where λ = latent heat.

Vertical Tubes

$$h_N = 1.1 k_l \left[\frac{\rho_l (\rho_l - \rho_v) g}{\mu_l^2 \text{Re}_c} \right]^{0.33} \quad (36)$$

$$\text{Re}_c = \frac{4W_c}{\pi D \mu_l} \quad (37)$$

The term F_g in Eq. 34 is a correction for condensate loading and depends on the exchanger geometry.^{1a}

On horizontal X-type tube bundles

$$F_g = N_{rv}^{-1/6} \quad (38)$$

(Ref. 16), where N_{rv} = number of tubes in a vertical row.

On baffled tube bundles (owing to turbulence)

$$F_g = 1.0 \quad (\text{frequent practice}) \quad (39)$$

In horizontal tubes

$$F_g = \left[\frac{1}{1 + (1/y - 1)(\rho_v/\rho_l)^{0.667}} \right]^{0.75} \quad (\text{from Ref. 1a}) \quad (40)$$

or

$$F_g = 0.8 \quad (\text{from Ref. 22}) \quad (41)$$

Inside or outside vertical tubes

$$F_g = 0.73 \text{Re}_c^{0.11} \quad (\text{rippled film region}) \quad (42)$$

or

$$F_g = 0.021 \text{Re}_c^{0.58} \text{Pr}^{0.33} \quad (\text{turbulent film region}) \quad (43)$$

Use a higher value of Eq. 42 or 43.

For quick hand calculations, the gravity-controlled flow equations may be used for h_{cf} and will usually give conservative results.

Correction for Mixture Effects

The above heat transfer coefficients apply only to the condensate film. For mixtures with a significant difference between the dewpoint and bubble point temperatures (condensing range), the vapor-phase heat transfer coefficient must also be considered as follows:

$$h_c = \frac{1}{(1/h_{cf} + 1/h_v)} \quad (44)$$

The vapor-phase heat transfer rate depends on mass diffusion rates in the vapor. The well-known Colburn–Hougen method and other more recent approaches are summarized by Butterworth.²³ Methods for mixtures forming immiscible condensates are discussed in Ref. 24.

Diffusion-type methods require physical properties not usually available to the designer except for simple systems. Therefore, the vapor-phase heat transfer coefficient is often estimated in practice by a “resistance-proration”-type method such as the Bell–Ghaly method.²⁵ In these methods the vapor-phase resistance is prorated with respect to the relative amount of duty required for sensible cooling of the vapor, resulting in the following expression:

$$h_v = \left(\frac{q_t}{q_{sv}} \right)^n h_{sv} \quad (44a)$$

The exponent n can range from about 0.7 to 1.0 depending on the amount of mixing of the light and heavy components. Use $n = 1.0$ for a well-mixed (high-velocity) vapor and decrease n for low-velocity systems with large molecular weight range.

For more detail in application of the resistance proration method for mixtures, see Ref. 1a or 25.

Pressure Drop

For the condensing vapor, pressure drop is composed of three components—friction, momentum, and static head—as covered in Ref. 1a. An approximate estimate on the conservative side can be obtained in terms of the friction component using the Martinelli separated flow approach:

$$\Delta P_f = \Delta P_l \phi_l^2 \quad (45)$$

where ΔP_f = two-phase friction pressure drop
 ΔP_l = friction loss for liquid phase alone

The Martinelli factor ϕ_l^2 may be calculated as shown in Eq. 32. Alternative methods for shellside pressure drop are presented by Diehl²⁶ and by Grant and Chisholm.²⁷ These methods were reviewed by Ishihara²⁸ and found reasonably representative of the available data. However, Eq. 32, also evaluated in Ref. 28 for shellside flow, should give about equivalent results.

3.3 Shell-and-Tube Reboilers and Vaporizers

Heat exchangers are used to boil liquids in both the process and power industries. In the process industry they are often used to supply vapors to distillation columns and are called reboilers. The same types of exchangers are used in many applications in the power industry, for example, to generate vapors for turbines. For simplicity these exchangers will all be called “reboilers” in this section. Often the heating medium is steam, but it can also be any hot process fluid from which heat is to be recovered, ranging from chemical reactor effluent to geothermal hot brine.

Selection of Reboiler Type

A number of different shell-and-tube configurations are in common use, and the first step in the design of a reboiler is to select a configuration appropriate to the required job. Basically, the type of reboiler should depend on the expected amount of fouling, operating pressure, MTD, and difference between temperatures of the bubble point and the dewpoint (boiling range).

The main considerations are as follows: (1) fouling fluids should be boiled on the tubeside at high velocity; (2) boiling either under deep vacuum or near the critical pressure should be in a kettle to minimize hydrodynamic problems unless means are available for very careful design; (3) at low MTD, especially at low pressure, the amount of static head must be minimized; (4) for wide boiling range mixtures, it is important to maximize both the amount of mixing and the amount of countercurrent flow. Often, fairly clean wide boiling mixtures are wrongly assigned a high fouling factor as a “safety” factor. This should not be done, and these fluids normally should be boiled on the shellside because of greater mixing.

These and other criteria are discussed in more detail in Ref. 4 and summarized in a selection guide, which is abstracted in Table 4.

In addition to the above types covered in Ref. 4, falling film evaporators²⁹ may be preferred in cases with very low MTD, viscous liquids, or very deep vacuum for which even a kettle provides too much static head.

Temperature Profiles

For pure components or narrow boiling mixtures, the boiling temperature is nearly constant and the LMTD applies with $F = 1.0$. Temperature profiles for boiling range mixtures are very complicated, and although the LMTD is often used, it is not a recommended practice and may result in underdesigned reboilers unless compensated by excessive design fouling factors. Contrary to the case for condensers, using a straight-line profile approximation always tends to give too high MTD for reboilers and can be tolerated only if the temperature rise across the reboiler is kept low through a high circulation rate.

Table 5 gives suggested procedures to determine an approximate MTD to use for initial size estimation based on temperature profiles illustrated in Fig. 16. It should be noted that the MTD values in Table 5 are intended to be on the safe side and that excessive fouling factors are not necessary as additional safety factors if these values are used. See Section 4.1 for suggested fouling factor ranges.

Heat Transfer Coefficients

The two basic types of boiling mechanisms that must be taken into account in determining boiling heat transfer coefficients are nucleate boiling and convective boiling. A detailed description

Table 4 Reboiler Selection Guide

Process Conditions	Suggested Reboiler Type ^a
Moderate pressure, MTD, and fouling	VT/E
Very high pressure, near critical	HS/K or (F)HT/E
Deep vacuum	HS/K
High or very low MTD	HS/K, G, H
Moderate to heavy fouling ^b	VT/E
Very heavy fouling ^b	(F)HT/E
Wide boiling range mixture	HS/G or /H
Very wide boiling range, viscous liquid	(F)HT/E

^aV, vertical; H, horizontal; S, shellside boiling; T, tubeside boiling; (F), forced flow, else natural convection;/E, G, H, K, TEMA shell styles.

^bTrue fouling demonstrated. Not just high fouling factor (which is often assigned for “safety”).

Table 5 Reboiler MTD Estimation

Reboiler Type ^a	T_A	T_B	MTD
HS/K	$T_1 - t_2$	$T_2 - t_2$	Eq. 4, $F = 1$
HS/X, G, H	$T_1 - t_1$	$T_2 - t_2$	Eq. 4, $F = 0.9$
VT/E	$T_1 - t_2$	$T_2 - t_1$	Eq. 4, $F = 1$
(F)HT/E or (F)HS/E	$T_1 - t_2$	$T_2 - t_1$	Eq. 4, $F = 0.9$
All types	Isothermal	$T_A = T_B$	T_A

^aV, vertical; H, horizontal; S, shellside boiling; T, tubeside boiling; (F), forced flow, else natural convection; E, G, H, K, TEMA shell styles.

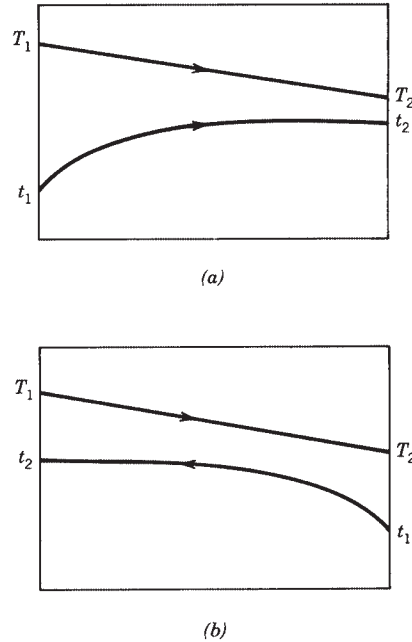


Figure 16 Reboiler temperature profiles: (a) use for kettle and horizontal thermosiphon; (b) use for tube-side boiling vertical thermosiphon.

of both types is given by Collier.³⁰ For all reboilers, the nucleate and convective boiling contributions are additive, as follows:

$$h_b = \alpha h_{nb} + h_{cb} \quad (46a)$$

or

$$h_b = [h_{nb}^2 + h_{cb}^2]^{0.5} \quad (46b)$$

Equation 46a includes a nucleate boiling suppression factor, α , that originally was correlated by Chen.³¹

Equation 46b is a simple asymptotic proration that was found to work well by Steiner and Taborek.³²

The convective boiling coefficient h_{cb} depends on the liquid-phase convective heat transfer coefficient h_l , according to the same relationship, Eq. 29, given for shear-controlled

condensation. For all reboiler types, except forced flow, the flow velocities required to calculate h_l depend on complex pressure balances for which computers are necessary for practical solution. Therefore, the convective component is sometimes approximated as a multiplier to the nucleate boiling component for quick estimations,⁴ as in the following equation:

$$h_b = h_{nb}F_b \quad (47)$$

$$F_b = \frac{h_{nb} + h_{cb}}{h_{nb}} \quad (48)$$

where F_b is approximated as follows:

For tubeside reboilers (VT/E thermosiphon)

$$F_b = 1.5 \quad (49)$$

For shellside reboilers (HS/X, G, H, K)

$$F_b = 2.0 \quad (50)$$

Equations 49 and 50 are intended to give conservative results for first approximations. For more detailed calculations see Refs. 33–35.

The nucleate boiling heat transfer coefficient (h_{nb}) is dependent not only on physical properties but also on the temperature profile at the wall and the microscopic topography of the surface. For a practical design, many simplifications must be made, and the approximate nature of the resulting coefficients should be recognized. A reasonable design value is given by the following simple equation⁴:

$$h_{nb} = 0.025F_c P_c^{0.69} q^{0.70} (P/P_c)^{0.17} \quad (51)$$

The term F_c is a correction for the effect of mixture composition on the boiling heat transfer coefficient. The heat transfer coefficient for boiling mixtures is lower than that of any of the pure components if boiled alone, as summarized in Ref. 30. This effect can be explained in terms of the change in temperature profile at the wall caused by the composition gradient at the wall, as illustrated in Ref. 36. Since the liquid-phase diffusional methods necessary to predict this effect theoretically are still under development and require data not usually available to the designer, an empirical relationship in terms of mixture boiling range (BR) is recommended in Ref. 4:

$$F_c = [1 + 0.018q^{0.15} \text{BR}^{0.75}]^{-1} \quad (52)$$

Where BR = difference between dewpoint and bubble point temperatures in degrees Fahrenheit.

Maximum Heat Flux

Above a certain heat flux, the boiling heat transfer coefficient can decrease severely, owing to vapor blanketing, or the boiling process can become very unstable, as described in Refs. 30, 36, and 37. Therefore, the design heat flux must be limited to a practical maximum value. For many years the limit used by industry was in the range of 10,000–20,000 Btu/h·ft² for hydrocarbons and about 30,000 Btu/h·ft² for water. These rules of thumb are still considered reasonable at moderate pressures, although the limits, especially for water, are considerably conservative for good designs. However, at both very high and very low pressures the maximum heat fluxes can be severely decreased. Also, the maximum heat fluxes must be a function of geometry to be realistic. Empirical equations are presented in Ref. 4; the equations give much more accurate estimates over wide ranges of pressure and reboiler geometry.

a For kettle (HS/K) and horizontal (HS/X, G, H) thermosiphons:

$$q_{\max} = 803P_c \left(\frac{P}{P_c} \right)^{0.35} \left(1 - \frac{P}{P_c} \right)^{0.9} \phi_b \quad (53)$$

$$\phi_b = 3.1 \left(\frac{\pi D_b L}{A_o} \right) \quad (54)$$

In the limit, for $\phi_b > 1.0$, let $\phi_b = 1.0$. For $\phi_b < 0.1$, consider a larger tube pitch or vapor relief channels.⁴ The design heat flux should be limited to less than $0.7 q_{\max}$.

b For vertical thermosiphon (VT/E):

$$q_{\max} = 16,080 \left(\frac{D_i^2}{L} \right)^{0.35} P_c^{0.61} \left(\frac{P}{P_c} \right)^{0.25} \left(1 - \frac{P}{P_c} \right) \quad (55)$$

c For tubeside forced circulation boiling: Recent research by Heat Transfer Research, Inc. has provided new proprietary data. For horizontal flow the phenomena are very complicated, involving preferential vapor flow at the top of the tube. The best published predictive methods are by Katto³⁸ and Kattan et al.³⁹

In addition to the preceding check, the vertical tubeside thermosiphon should be checked to ensure against mist flow (dryout). The method by Fair³³ was further confirmed in Ref. 40 for hydrocarbons. For water, extensive data and empirical correlations are available as described by Collier.³⁰ To determine the flow regime by these methods, it is necessary to determine the flow rate, as described, for example, in Ref. 33. However, for preliminary specification, it may be assumed that the exit vapor weight fraction will be limited to less than 0.35 for hydrocarbons and less than 0.10 for aqueous solutions and that under these conditions dryout is unlikely.

For some applications, such as liquefied natural gas (LNG) vaporization, it is required to fully vaporize and superheat the gas. For tubeside vaporization, this is very difficult due to droplet entrainment. Twisted tape inserts, such as supplied by Brown Fin Tube, solve the problem.

3.4 Air-Cooled Heat Exchangers

Detailed rating of air-cooled heat exchangers requires selection of numerous geometric parameters, such as tube type, number of tube rows, length, width, and number and size of fans, all of which involve economic and experience considerations beyond the scope of this chapter. Air-cooled heat exchangers are still designed primarily by the manufacturers using proprietary methods. However, recommendations for initial specifications and rating are given by Paikert⁷ and by Mueller.⁶ A preliminary rating method proposed by Brown⁴¹ is also sometimes used for first estimates owing to its simplicity.

Heat Transfer Coefficients

For a first approximation of the surface required, the bare-surface-based overall heat transfer coefficients recommended by Smith⁴² may be used. A list of these values from Ref. 6 is abstracted in Table 6. The values in Table 6 were based on performance of finned tubes, having a 1-in.-outside-diameter base tube on 2³/₈-in.-triangular-pitch, 5/₈-in.-high aluminum fins (1/₈-in. spacing between fin tips), with eight fins per inch. However, the values may be used as first approximations for other finned types.

Table 6 Typical Overall Heat Transfer Coefficients (U_o) Based on Bare Tube Surface for Air-Cooled Heat Exchangers

Service	U_o	
	Btu/h · ft ² · °F	W/m ² · K
<i>Sensible Cooling</i>		
Process water	105–120	600–680
Light hydrocarbons	75–95	425–540
Fuel oil	20–30	114–170
Flue gas, 10 psig	10	57
<i>Condensation</i>		
Steam, 0–20 psig	130–140	740–795
Ammonia	100–200	570–680
Light hydrocarbons	80–95	455–540
Refrigerant 12	60–80	340–455
Mixed hydrocarbons, steam, and noncondensables	60–70	340–397

As stated by Mueller, air-cooled heat exchanger tubes have had approximately the preceding dimensions in the past, but fin densities have tended to increase and now more typically range from 10 to 12 fins/in. For a more detailed estimate of the overall heat transfer coefficient, the tubeside coefficients are calculated by methods given in the preceding sections and the airside coefficients are obtained as functions of fin geometry and air velocity from empirical relationships such as given by Gnielinski et al.⁴³ Rating at this level of sophistication is now done mostly by computer.

Temperature Difference

Air-cooled heat exchangers are normally “cross-flow” arrangements with respect to the type of temperature profile calculation. Charts for determination of the F factor for such arrangements are presented by Taborek.¹⁴ Charts for a number of arrangements are also given by Paikert⁷ based on the “NTU method.” According to Paikert, optimum design normally requires the number of transfer units (NTU) to be in the range of 0.8–1.5, where

$$\text{NTU} = \frac{t_2 - t_1}{\text{MTD}} \quad (56)$$

For first approximations, a reasonable air temperature rise ($t_2 - t_1$) may be assumed, MTD calculated from Eq. 4 using $F = 0.9$ – 1.0 , and NTU checked from Eq. 56. It is assumed that if the air temperature rise is adjusted so that NTU is about 1, the resulting preliminary size estimation will be reasonable. Another design criterion often used is that the face velocity V_f should be in the range of 300–700 ft/min (1.5–3.5 m/s):

$$V_f = \frac{W_a}{L W_d \rho_v} \quad (57)$$

where W_a = air rate, lb/min
 L = tube length, ft
 W_d = bundle width, ft
 ρ_v = air density, lb/ft³

Fan Power Requirement

One or more fans may be used per bundle. Good practice requires that not less than 40–50% of the bundle face area be covered by the fan diameter. The bundle aspect ratio per fan should

approach 1 for best performance. Fan diameters range from about 4 to 12 ft (1.2 to 3.7 m), with tip speeds usually limited to less than 12,000 ft/min (60 m/s) to minimize noise. Pressure drops that can be handled are in the range of only 1–2 in. water (0.035–0.07 psi, 250–500 Pa). However, for typical bundle designs and typical air rates, actual bundle pressure drops may be in the range of only 1/4–1 in. water.

Paikert⁷ gives the expression for fan power as follows:

$$P_f = \frac{V(\Delta p_s + \Delta p_d)}{E_f} \quad (58)$$

where V = volumetric air rate, m³/s
 Δp_s = static pressure drop, Pa
 Δp_d = dynamic pressure loss, often 40–60 Pa
 E_f = fan efficiency, often 0.6–0.7
 P_f = fan power, W

3.5 Other Exchangers

For spiral, plate, and compact heat exchangers the heat transfer coefficients and friction factors are sensitive to specific proprietary designs and such units are best sized by the manufacturer. However, preliminary correlations have been published. For spiral heat exchangers, see Mueller⁶ and Minton.⁴⁴ For plate-type heat exchangers (Figs. 9 and 10), recommendations are given by Cooper⁴⁵ and Marriott.⁴⁶ For plate-fin and other compact heat exchangers, a comprehensive treatment is given by Webb.⁸ For recuperators and regenerators the methods of Hausen are recommended.¹⁰ Heat pipes are extensively covered by Chisholm.⁴⁷ Design methods for furnaces and combustion chambers are presented by Truelove.⁴⁸ Heat transfer in agitated vessels is discussed by Penney.⁴⁹ Double-pipe heat exchangers are described by Guy.⁵⁰

4 COMMON OPERATIONAL PROBLEMS

When heat exchangers fail to operate properly in practice, the entire process is often affected and sometimes must be shut down. Usually, the losses incurred by an unplanned shutdown are many times more costly than the heat exchanger at fault. Poor heat exchanger performance is usually due to factors having nothing to do with the heat transfer coefficient. More often the designer has overlooked the seriousness of some peripheral condition not even addressed in most texts on heat exchanger design. Although only long experience and numerous “experiences” can come close to uncovering all possible problems waiting to plague the heat exchanger designer, the following sections relating the more obvious problems are included to help make the learning curve less eventful.

4.1 Fouling

The deposit of solid insulating material from process streams on the heat transfer surface is known as fouling and has been called “the major unresolved problem in heat transfer.”⁵¹ Although this problem is recognized to be important (see Ref. 52) and is even being seriously researched,^{52,53} the nature of the fouling process makes it almost impossible to generalize. As discussed by Mueller,⁶ fouling can be caused by (1) precipitation of dissolved substances, (2) deposit of particulate matter, (3) solidification of material through chemical reaction, (4) corrosion of the surface, (5) attachment and growth of biological organisms, and (6) solidification by freezing. The most important variables affecting fouling (besides concentration of the fouling material) are velocity, which affects types 1, 2, and 5, and surface temperature, which

affects types 3–6. For boiling fluids, fouling is also affected by the fraction vaporized. As stated in Ref. 4, it is usually impossible to know ahead of time what fouling mechanism will be most important in a particular case. Fouling is sometimes catalyzed by trace elements unknown to the designer. However, most types of fouling are retarded if the flow velocity is as high as possible, the surface temperature is as low as possible (exception is biological fouling⁵⁴), the amount of vaporization is as low as possible, and the flow distribution is as uniform as possible.

The expected occurrence of fouling is usually accounted for in practice by assignment of fouling factors, which are additional heat transfer resistances; see Eq. 7. The fouling factors are assigned for the purpose of oversizing the heat exchanger sufficiently to permit adequate on-stream time before cleaning is necessary. Often in the past the fouling factor has also served as a general-purpose “safety factor” expected to make up for other uncertainties in the design. However, assignment of overly large fouling factors can produce poor operation caused by excessive overdesign.^{55,56}

For shell-and-tube heat exchangers it has been common practice to rely on the fouling factors suggested by TEMA.³ Fouling in plate heat exchangers is usually less and is discussed in Ref. 45. The TEMA fouling factors have been used for over 30 years and, as Mueller states, must represent some practical validity or else complaints would have forced their revision. A joint committee of TEMA and Heat Transfer Research, Inc. (HTRI) members has reviewed the TEMA fouling recommendations and slightly updated for the latest edition. In addition to TEMA, fouling resistances are presented by Bell¹⁵ and values recommended for reboiler design are given in Ref. 4. For preliminary estimation, the minimum value commonly used for design is $0.0005^\circ\text{F}\cdot\text{h}\cdot\text{ft}^2/\text{Btu}$ for condensing steam or light hydrocarbons. Typical conservative estimates for process streams or treated cooling water are around $0.001\text{--}0.002^\circ\text{F}\cdot\text{h}\cdot\text{ft}^2/\text{Btu}$, and for heavily fouling streams values in the range of $0.003\text{--}0.01^\circ\text{F}\cdot\text{h}\cdot\text{ft}^2/\text{Btu}$ are used. For reboilers (which have been properly designed) a design value of $0.001^\circ\text{F}\cdot\text{h}\cdot\text{ft}^2/\text{Btu}$ is usually adequate, although for wide boiling mixtures other effects in addition to fouling tend to limit performance. These commonly used estimates can contain large built-in safety factors and should not necessarily be accepted for modern computerized designs. A more realistic approach for most fluids is proposed in Section 5.6 under Fouling.

On the other hand, heavily fouling fluids such as crude oils may require even larger fouling factors for reasonable on-stream times than those given in TEMA. In this case, detailed physical characteristics of the fluid must be determined by experiment before realistic design fouling allowances can be assigned.

In cooperation with a task force of industry experts, HTRI has an ongoing research program to measure fouling rates over a range of process conditions and compare with fluid characteristics.

4.2 Vibration

A problem with shell-and-tube heat exchangers that is becoming more frequent as heat exchangers tend to become larger and design velocities tend to become higher is tube failure due to flow-induced tube vibration. Summaries including recommended methods of analysis are given by Chenoweth⁵⁷ and by Mueller.⁶ In general, tube vibration problems tend to occur when the distance between baffles or tube support plates is too great. Maximum baffle spacings recommended by TEMA were based on the maximum unsupported length of tube that will not sag significantly. Experience has shown that flow induced vibration can still occur at TEMA maximum baffle spacing, but for less than about 0.7 times this spacing most vibration can be eliminated at normal design velocities (see Section 2.4). Taborek¹ gives the following equations for TEMA maximum unsupported tube lengths (L_{su}) in inches:

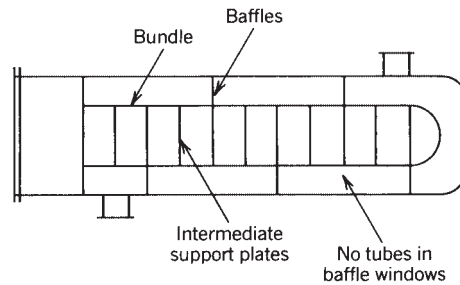


Figure 17 Segmental baffles with no tubes in window.

Steel and Steel Alloy Tubes

$$\begin{aligned} \text{For } D_o = 3/4 - 2 \text{ in.,} \\ L_{su} = 52D_o + 21 \end{aligned} \quad (59)$$

$$\begin{aligned} \text{For } D_o = 1/4 - 3/4 \text{ in.,} \\ L_{su} = 68D_o + 9 \end{aligned} \quad (60)$$

Aluminum and Copper Alloy Tubes

$$\begin{aligned} \text{For } D_o = 3/4 - 2 \text{ in.,} \\ L_{su} = 46D_o + 17 \end{aligned} \quad (61)$$

$$\begin{aligned} \text{For } D_o = 1/4 - 3/4 \text{ in.,} \\ L_{su} = 60D_o + 7 \end{aligned} \quad (62)$$

For segmental baffles with tubes in the windows (Fig. 9), the maximum baffle spacing is one-half the maximum unsupported tube length.

For very large bundle diameters, segmental or even double-segmental baffles may not be suitable, since the spacing required to prevent vibration may produce too high pressure drops. (In addition, flow distribution considerations require that the ratio of baffle spacing to shell diameter not be less than about 0.2.) In such cases, one commonly used solution is to eliminate tubes in the baffle windows so that intermediate support plates can be used and baffle spacing can be increased; see Fig. 17. Another solution with many advantages is the rod-type tube support in which the flow is essentially longitudinal and the tubes are supported by a cage of rods. A proprietary design of this type exchanger (RODbaffle) is licensed by Phillips Petroleum Co. Calculation methods are published in Ref. 5.

4.3 Flow Maldistribution

Several types of problems can occur when the flow velocities or fluid phases become distributed in a way not anticipated by the designer. This occurs in all types of exchangers, but the following discussion is limited to shell-and-tube and air-cooled exchangers, in which maldistribution can occur either shellside or tubeside.

Shellside Flow

Single-phase flow can be maldistributed on the shellside owing to bypassing around the tube bundle and leakage between tubes and baffle and between baffle and shell. Even for typical

well-designed heat exchangers, these ineffective streams can comprise as much as 40% of the flow in the turbulent regime and as much as 60% of the flow in the laminar regime. It is especially important for laminar flow to minimize these bypass and leakage streams, which cause both lower heat transfer coefficients and lower effective MTD.¹⁷ This can, of course, be done by minimizing clearances, but economics dictate that more practical methods include using bypass sealing strips, increasing tube pitch, increasing baffle spacing, and using an optimum baffle cut to provide more bundle penetration. Methods for calculating the effects of these parameters are described by Taborek.¹ One method to minimize leakage and bypass inefficiencies is to use helical baffles, which cause flow to proceed through the exchanger along a spiral path. Elimination of sharp flow reversals provides a much more uniform shellside distribution. A proprietary version of the helical baffle option is provided by the ABB Lummus Company.

Another type of shellside maldistribution occurs in gas–liquid two-phase flow in horizontal shells when the flow velocity is low enough that the vapor and liquid phases separate, with the liquid flowing along the bottom of the shell. For condensers this is expected and taken into account. However, for some other types of exchangers, such as vapor–liquid contactors or two-phase reactor feed effluent exchangers, separation may cause unacceptable performance. For such cases, if it is important to keep the phases mixed, a vertical heat exchanger is recommended. Improvement in mixing is obtained for horizontal exchangers if horizontal rather than vertical baffle cut is used.

Tubeside Flow

Several types of tubeside maldistribution have been experienced. For single-phase flow with axial nozzles into a single-tubepass exchanger, the dynamic head of the entering fluid can cause higher flow in the central tubes, sometimes even producing backflow in the peripheral tubes. This effect can be prevented by using an impingement plate on the centerline of the axial nozzle.

Another type of tubeside maldistribution occurs in cooling viscous liquids. Cooler tubes in parallel flow will tend to completely plug up in this situation, unless a certain minimum pressure drop is obtained, as explained by Mueller.⁵⁸

For air-cooled single-pass condensers, a backflow can occur owing to the difference in temperature driving force between bottom and top tube rows, as described by Berg and Berg.⁵⁹ This can cause an accumulation of noncondensables in air-cooled condensers, which can significantly affect performance, as described by Breber et al.⁶⁰ In fact, in severe cases, this effect can promote freeze-up of tubes or even destruction of tubes by water hammer. Backflow effects are eliminated if a small amount of excess vapor is taken through the main condenser to a backup condenser or if the number of fins per inch on bottom rows is less than on top rows to counteract the difference in temperature driving force.

For multipass tubeside condensers or tubeside condensers in series, the vapor and liquid tend to separate in the headers with liquid running in the lower tubes. The fraction of tubes filled with liquid tends to be greater at higher pressures. In most cases the effect of this separation on the overall condenser heat transfer coefficient is not serious. However, for multicomponent mixtures the effect on the temperature profile will be such as to decrease the MTD. For such cases, the temperature profile should be calculated by the differential flash procedure (Section 3.2). In general, because of unpredictable effects, entering a pass header with two phases should be avoided when possible.

4.4 Temperature Pinch

When the hot and cold streams reach approximately the same temperature in a heat exchanger, heat transfer stops. This condition is referred to as a temperature pinch. For shellside single-phase flow, unexpected temperature pinches can be the result of excessive bypassing

and leakage combined with a low MTD and possibly a temperature cross. An additional factor, the “temperature profile distortion factor,” is needed as a correction to the normal F factor to account for this effect.^{1,17} However, if good design practices are followed with respect to shellside geometry, this effect normally can be avoided.

In condensation of multicomponent mixtures, unexpected temperature pinches can occur in cases where the condensation curve is not properly calculated, especially when the true curve happens to be of type III in Fig. 15. This can happen when separation of liquid containing heavy components occurs, as mentioned above, and also when the condensing mixture has immiscible liquid phases with more than one dewpoint.²⁴ In addition, condensing mixtures with large desuperheating and subcooling zones can produce temperature pinches and must be carefully analyzed. In critical cases it is safer and may even be more effective to do desuperheating, condensing, and subcooling in separate heat exchangers. This is especially true of subcooling.⁶

Reboilers can also suffer from temperature pinch problems in cases of wide boiling mixtures and inadequate liquid recirculation. Especially for poorly designed thermosiphon reboilers, with the circulation rate less than expected, the temperature rise across the reboiler will be too high and a temperature pinch may result. This happens most often when the reboiler exit piping is too small and consumes an unexpectedly large amount of pressure drop. This problem normally can be avoided if the friction and momentum pressure drop in the exit piping is limited to less than 30% of the total driving head and the exit vapor fraction is limited to less than 0.25 for wide boiling range mixtures. For other recommendations, see Ref. 4.

4.5 Critical Heat Flux in Vaporizers

Owing to a general tendency to use lower temperature differences for energy conservation, critical heat flux problems are not now frequently seen in the process industries. However, for waste heat boilers, where the heating medium is usually a very hot fluid, surpassing the critical heat flux is a major cause of tube failure. The critical heat flux is that flux (Q/A_c) above which the boiling process departs from the nucleate or convective boiling regimes and a vapor film begins to blanket the surface, causing a severe rise in surface temperature, approaching the temperature of the heating medium. This effect can be caused by either of two mechanisms: (1) flow of liquid to the hot surface is impeded and is insufficient to supply the vaporization process or (2) the local temperature exceeds that for which a liquid phase can exist.³⁷ Methods of estimating the maximum design heat flux are given in Section 3.3, and the subject of critical heat flux is covered in great detail in Ref. 30. However, in most cases where failures have occurred, especially for shellside vaporizers, the problem has been caused by local liquid deficiency, owing to lack of attention to flow distribution considerations.

4.6 Instability

The instability referred to here is the massive large-scale type in which the fluid surging is of such violence as to at least disrupt operations, if not to cause actual physical damage. One version is the boiling instability seen in vertical tubeside thermosiphon reboilers at low operating pressure and high heat flux. This effect is discussed and analyzed by Blumenkrantz and Taborek.⁶¹ It is caused when the vapor acceleration loss exceeds the driving head, producing temporary flow stoppage or backflow, followed by surging in a periodic cycle. This type of instability can always be eliminated by using more frictional resistance, a valve or orifice, in the reboiler feed line. As described in Ref. 37, instability normally only occurs at low reduced pressures and normally will not occur if design heat flux is less than the maximum value calculated from Eq. 55.

Another type of massive instability is seen for oversized horizontal tubeside pure component condensers. When more surface is available than needed, condensate begins to subcool

and accumulate in the downstream end of the tubes until so much heat transfer surface has been blanketed by condensate that there is not enough remaining to condense the incoming vapor. At this point the condensate is blown out of the tube by the increasing pressure and the process is repeated. This effect does not occur in vertical condensers since the condensate can drain out of the tubes by gravity. This problem can sometimes be controlled by plugging tubes or injecting inert gas and can always be eliminated by taking a small amount of excess vapor out of the main condenser to a small vertical backup condenser.

4.7 Inadequate Venting, Drainage, or Blowdown

For proper operation of condensers it is always necessary to provide for venting of noncondensables. Even so-called pure components will contain trace amounts of noncondensables that will eventually build up sufficiently to severely limit performance unless vented. Vents should always be in the vapor space near the condensate exit nozzle. If the noncondensable vent is on the accumulator after the condenser, it is important to ensure that the condensate nozzle and piping are large enough to provide unrestricted flow of noncondensables to the accumulator. In general, it is safer to provide vent nozzles directly on the condenser.

If condensate nozzles are too small, condensate can accumulate in the condenser. It is recommended that these nozzles be large enough to permit weir-type drainage (with a gas core in the center of the pipe) rather than to have a full pipe of liquid. Standard weir formulas⁶² can be used to size the condensate nozzle. A rule of thumb used in industry is that the liquid velocity in the condensate piping, based on total pipe cross section, should not exceed 3 ft/s (0.9 m/s).

The problem of inadequate blowdown in vaporizers is similar to the problem of inadequate venting for condensers. Especially with kettle-type units, trace amounts of heavy, high-boiling, or nonboiling components can accumulate, not only promoting fouling but also increasing the effective boiling range of the mixture, thereby decreasing the MTD as well as the effective heat transfer coefficient. Therefore, means of continuous or at least periodic removal of liquid from the reboiler (blowdown) should be provided to ensure good operation. Even for thermosiphon reboilers, if designed for low heat fluxes (below about 2000 BTU/h/ft², 6300 W/m²), the circulation through the reboiler may not be high enough to prevent heavy components from building up, and some provision for blowdown may be advisable in the bottom header.

5 USE OF COMPUTERS IN THERMAL DESIGN OF PROCESS HEAT EXCHANGERS

5.1 Introduction

The approximate methods for the heat transfer coefficient and pressure drop given in the preceding sections will be used mostly for orientation. For an actual heat exchanger design, it only makes sense to use a computer. Standard programs can be obtained for most geometries in practical use. These allow reiterations and incrementation to an extent impossible by hand and also supply physical properties for a wide range of industrial fluids. However, computer programs by no means solve the whole problem of producing a workable efficient heat exchanger. Many experience-guided decisions must be made both in selection of the input data and in interpreting the output data before even the thermal design can be considered final. We will first review why a computer program is effective. This has to do with (1) incrementation and (2) convergence loops.

5.2 Incrementation

The method described in Section 2.1 for calculation of required surface can only be applied accurately to the entire exchanger if the overall heat transfer coefficient is constant and the

temperature profiles for both streams are linear. This often is not a good approximation for typical process heat exchangers because of variation in physical properties and/or vapor fraction along the exchanger length. The rigorous expression for Eq. 1 is as follows:

$$A_o = \int \frac{dQ}{U_o \text{ MTD}}$$

Practical solution of this integral equation requires dividing the heat transfer process into finite increments of ΔQ that are small enough so that U_o may be considered constant and the temperature profiles may be considered linear. The incremental area, ΔA_o , is then calculated for each increment and summed to obtain the total required area. An analogous procedure is followed for the pressure drop. This procedure requires determining a full set of fluid physical properties for all phases of both fluids in each increment and the tedious calculations can be performed much more efficiently by computer. Furthermore, in each increment several trial-and-error convergence loops may be required, as discussed next.

5.3 Main Convergence Loops

Within each of the increments discussed above, a number of implicit equations must be solved requiring convergence loops. The two main types of loops found in any heat exchanger calculation are as follows.

Intermediate-Temperature Loops

These convergence loops normally are used to determine either wall temperature or, less commonly, interface temperature. The discussion here will be limited to the simpler case of wall temperature. Because of the variation of physical properties between the wall and the bulk of the fluid, heat transfer coefficients depend on the wall temperature. Likewise, the wall temperature depends on the relative values of the heat transfer coefficients of each fluid. Wall temperatures on each side of the surface can be estimated by the following equations:

$$T_{w, \text{ hot}} = T_{\text{ hot}} - \frac{U_o}{h_{\text{ hot}}} (T_{\text{ hot}} - T_{\text{ cold}})$$

$$T_{w, \text{ cold}} = T_{\text{ cold}} + \frac{U_o}{h_{\text{ cold}}} (T_{\text{ hot}} - T_{\text{ cold}})$$

It is assumed in the above equations that the heat transfer coefficient on the inside surface is corrected to the outside area. Convergence on the true wall temperature can be done in several ways. Figure 18 shows a possible convergence scheme.

Pressure Balance Loops

These convergence loops are needed whenever the equations to be solved are implicit with respect to velocity. The two most frequent cases encountered in heat exchanger design are (1) flow distribution and (2) natural circulation. The first case, flow distribution, is the heart of the shell-and-tube heat exchanger shellside flow calculations and involves solution for the fraction of flow across the tube bundle, as opposed to the fraction of flow leaking around baffles and bypassing the bundle. Since the resistance coefficients of each stream are functions of the stream velocity, the calculation is reiterative. The second case, natural circulation, is encountered in thermosiphon and kettle reboilers where the flow rate past the heat transfer surface is a function of the pressure balance between the two-phase flow in the bundle, or tubes, and the liquid static head outside the bundle. In this case the heat transfer coefficients that determine the vaporization rate are functions of the flow velocity, which is in turn a function of the amount of vaporization. Figure 19 shows a flow velocity convergence loop applicable to the flow distribution case.

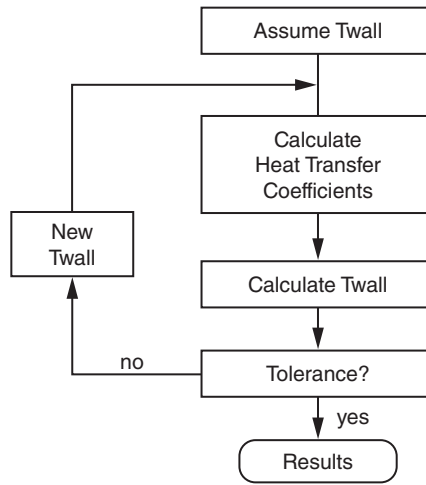


Figure 18 Temperature convergence loop.

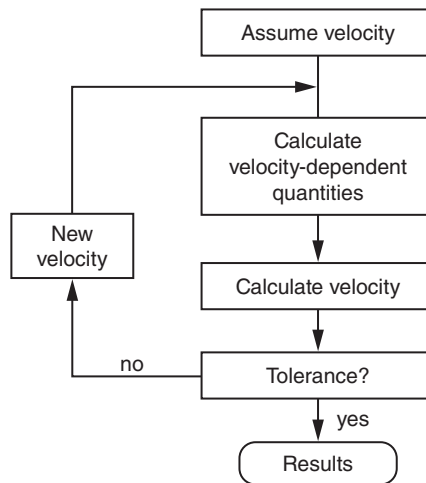


Figure 19 Velocity convergence loop.

5.4 Rating, Design, or Simulation

Several types of solutions are possible by computer. The better standard programs allow the user to choose. It is important to understand what the program is doing in order to properly interpret the results. The above three types of calculations are described as follows.

Rating

This is the normal mode for checking a vendor's bid. All geometry and all process conditions are specified. The program calculates the required heat transfer area and pressure drop and compares with the specified values. Normally this is done including the specified fouling factor. This means that on startup the amount of excess surface will be greater, sometimes

excessively greater, causing severe operating adjustments. It is therefore advisable to review clean conditions also.

Design

This mode is used by the process engineer to obtain a size based on process heat transfer requirements. In this case, most of the geometry specifications still are not determined by the program and must be determined by the designer based on experience. Required, but unknown, specifications, in addition to the process requirements of temperatures, flow rates, and pressure drops, include the following:

- Exchanger type (shell and tube, plate and frame, plate fin, air cooled, etc.)

If shell and tube

- TEMA shell type (E, F, J, G, H, X, K)
- TEMA front and rear head types (flat, dished, fixed tube sheet, split ring, pull-through)
- Baffle type (segmental, double segmental, triple segmental, rod, etc.)
- Tube type (plain, low finned, enhanced surface, etc.)
- Tube length (usually standard lengths of 8, 12, 16, 20 ft)
- Tube diameter (usually $\frac{5}{8}$, $\frac{3}{4}$, 1, $1\frac{1}{4}$ in. or 1.25 in.)
- Tube pitch (pitch ratios 1.25, 1.3, 1.5)
- Tube layout (30° , 45° , 60° , 90°)
- Tube material (carbon steel, stainless steel, copper alloys, titanium, etc.)
- Exchanger orientation (horizontal, vertical)

As shown, even with a good computer program, an overwhelming number of combinations of geometry parameters is possible and presently the engineer is required to select the best combination based on mechanical considerations, process considerations, fouling tendencies, and allowable pressure drop. Some general guidelines are given in Section 5.6. Once the above parameters are specified to the computer program, it can proceed to calculate the number of tubes required and the baffle spacing and number of tube passes consistent with the required pressure drops for both streams.

Simulation

This mode of calculation is used mostly to predict the performance of a field heat exchanger under different operating conditions. Usually the engineer “zeros” the program first by adjusting fouling factors and friction factor multipliers to match existing field performance. Then the adjusted process conditions are imposed and the computer program predicts the heat transfer rates and pressure drops under the new conditions. This mode of calculation can also be used to monitor apparent fouling resistance increase on operating units in order to better schedule maintenance.

5.5 Program Quality and Selection

All heat exchanger programs are not created equal. Heat exchange is not yet an exact science and all of the heat transfer coefficients and friction factors used in calculations are from correlations with empirically determined constants. Therefore, the database used for correlation development is important.

Methods Source

The methods used for the program should be available and documented in a readable form. Good methods will be based on theoretically derived equation forms that either are limited in range or automatically achieve theoretically justified limits. “Blackbox” methods, for which this may not be true, should be avoided.

Database

Good programs are also backed by a sizable data bank covering the range of conditions of interest as well as demonstrated successes in predicting field performance. No nontested methods, including so-called rigorous incremental methods, should be accepted without some data-based support.

Suitability

Completely general programs that apply to all geometries and process conditions and fulfill the above database requirements probably will not exist for some time. The program manual should list recommended ranges of applicability. When in doubt, consult the supplier.

5.6 Determining and Organizing Input Data

As of this writing, available programs still require a large number of input data decisions to be made by the user. The quality of the answers obtained is crucially dependent on the quality of these input decisions.

Process Data

The basis for the calculation is the heat duty, which usually comes from the process flow sheet. There must, of course, be a heat balance between the hot and cold sides of the exchanger. The temperature profiles are much more significant to a good design than are the heat transfer coefficients. Only in rare cases are these straight lines. For multicomponent phase change cases, the condensing or vaporization curves should be calculated by a good process simulator program containing state-of-the-art vapor–liquid equilibria methods. Most good heat exchanger programs will accept these curves as the basis for the heat transfer calculations.

It is important to specify realistic pressure drop limitations, since the heat transfer coefficient and the fouling rate are functions of the velocity, which is a function of the available pressure drop. For phase change, too much pressure drop can mean a significant loss in available temperature difference and one rule of thumb suggests a limit of 10% of the operating pressure. For liquid flow, erosion velocity often is the limiting factor, and this is usually taken to be in the range of 7–10 ft/s tubeside or 3–5 ft/s shellside. Velocities also are sometimes limited to a value corresponding to ρv^2 less than 4000, where ρ is in pounds per feet cubed and v is in feet per seconds.

Geometry Data

It is necessary for the program user to make a large number of geometry decisions, starting with the type of exchanger, which decides the type of program to be used. Only a brief list of suggestions can be accommodated in this chapter, so recommendations will be limited to some of the main shell-and-tube geometries mentioned in Section 5.4.

TEMA Shell Style. The types E, J, and X are selected based on available pressure drop, highest E, lowest X, and intermediate J. Types G and H are used mostly for horizontal thermosiphon reboilers, although they also obtain a slightly better MTD correction

factor than the E-type shell and are sometimes used even for single phases for that purpose. Pressure drops for G and E shells are about the same. For horizontal thermosiphon reboilers, the longitudinal baffle above the inlet nozzle prevents the light vaporizing component to shortcut directly to the exit nozzle. If the pressure drop for the less expensive G shell is too high, the H shell (two G's in parallel) is used. Type F is used when it is required to have a combination of countercurrent flow and two tube passes in a single shell. This type has the disadvantage of leakage around the longitudinal baffle, which severely decreases performance. A welded baffle prevents this but prevents bundle removal. Type K is used only for kettle reboilers.

TEMA Front and Rear Head Types. These are selected based on pressure and/or maintenance considerations. TEMA standards should be consulted. With respect to maintenance, rear heads permitting bundle removal should be specified for shellside fouling fluids. These are the split-ring and pull-through types.

Baffle Types. These are selected based on a combination of pressure drop and vibration considerations. In general, the less expensive, higher velocity segmental baffle is tried first, going to the double-segmental and possibly the triple-segmental types if necessary to lower pressure drop. Allowable pressure drop is a very important design parameter and should not be allocated arbitrarily. In the absence of other process limits, the allowable pressure drop should be about 10% of the operating pressure or the ρv^2 should be less than about 4000 (lb/ft³)(ft/s)², whichever gives the lower velocity. However, vibration limits override these limits. Good thermal design programs also check for tube vibration and warn the user if vibration problems are likely due to high velocity or insufficient tube support. In case of potential vibration problems, it is necessary to decrease velocity or provide more tube support, the latter being preferable. The two best ways of eliminating vibration problems within allowable pressure drop limitations are (1) no-tube-in-window baffles or (2) RoDbaffles, as discussed in Section 4.2. As mentioned in Section 4.3, the ABB Lummus Company offers software, based on Heat Transfer Research, Inc. technology, containing a helical baffle option. Helical baffles can both decrease vibration tendencies and improve shellside flow distribution.

Tube Types. For low-temperature differences and low heat transfer coefficients, low-finned or enhanced tubes should be investigated. In proper applications these can decrease the size of the exchanger dramatically. Previously, enhanced tubes were considered only for very clean streams. However, recent research is beginning to indicate that finned tubes fare as well in fouling services as plain tubes, and sometimes much better, providing longer on-stream time and often even easier cleaning. In addition, the trend in the future will be to stop assigning arbitrary fouling factors and rather to design for conditions minimizing fouling. A relatively new option available from the Brown Fin Tube Company is the twisted tube. This tube provides spiral corrugations through which fluids flow in spiral counterflow on the shellside and tubeside. No baffles are needed.

Tube Length. This is usually limited by plant requirements. In general, longer exchangers are economically preferable within pressure drop restrictions, except possibly for vertical thermosiphon reboilers.

Tube Diameter. Small diameters are more economical in the absence of restrictions. Cleaning restrictions normally limit outside diameters to not less than $\frac{5}{8}$ or $\frac{3}{4}$ in. However, some manufacturers now offer microchannel exchangers, which are very effective for some fluids, such as clean gases. Pressure drop restrictions, especially in vacuum, may require larger sizes. Vacuum vertical thermosiphon reboilers often require 1 $\frac{1}{4}$ -in. tubes, and vacuum falling film evaporators frequently use as large as 2-in.

tubes. Excessive pressure drop can be quickly decreased by going to the next standard tube diameter since pressure drop is inversely proportional to the fifth power of the inside diameter.

Tube Pitch. Tube pitch for shellside flow is analogous to tube diameter for tubeside flow. Small pitches are more economical and also can cause pressure drop or cleaning problems. In laminar flow, here too-small tube pitch can prevent bundle penetration and force more bypassing and leakage. A pitch-to-tube diameter ratio of 1.25 or 1.33 is often used in the absence of other restrictions depending on allowable pressure drop. For shellside reboilers operating at high heat flux, a ratio of as much as 1.5 is often required. Equation 54 shows that the maximum heat flux for kettle reboilers increases with increasing tube pitch.

Tube Layout. Performance is not critically affected by tube layout, although some minor differences in pressure drop and vibration characteristics are seen. In general, either 30° or 60° layouts are used for clean fluids, while 45° or 90° layouts are more frequently seen for fluids requiring shellside fouling maintenance.

Tube Material. The old standby for noncorrosive moderate-temperature hydrocarbons is the less expensive and sturdy carbon steel. Corrosive or very high temperature fluids require stainless steel or other alloys. Titanium and Hastelloy are becoming more frequently used for corrosion or high temperature despite the high cost, as a favorable economic balance is seen in comparison with severe problems of tube failure.

Exchanger Orientation. Exchangers normally are horizontal except for tubeside thermosiphons, falling film evaporators, and tubeside condensers requiring very low pressure drop or extensive subcooling. However, it is becoming more frequent practice to specify vertical orientation for two-phase feed-effluent exchangers to prevent phase separation, as mentioned in Section 4.3.

Fouling

All programs require the user to specify a fouling factor, which is the heat transfer resistance across the deposit of solid material left on the inside and/or outside of the tube surface due to decomposition of the fluid being heated or cooled. Considerations involved in the determination of this resistance are discussed in Section 4.1. Since there are presently no thermal design programs available that can make this determination, the specification of a fouling resistance, or fouling factor, for each side is left up to the user. Unfortunately, this input is probably more responsible than any other for causing inefficient designs and poor operation. The major problem is that there is very little relationship between actual fouling and the fouling factor specified. Typically, the fouling factor contains a safety factor that has evolved from practice, lived a charmed life as it is passed from one handbook to another, and may no longer be necessary if modern accurate design programs are used. An example is the frequent use of a fouling factor of $0.001 \text{ h ft}^2 \text{ }^\circ\text{F/Btu}$ for clean overhead condenser vapors. This may have evolved as a safety or correction from the failure of early methods to account for mass transfer effects and is completely unnecessary with modern calculation methods. Presently, the practice is to use fouling factors from TEMA standards. However, these often result in heat exchangers that are oversized by as much as 50% on startup, causing operating problems that actually tend to enhance fouling tendencies. Hopefully, with ongoing research on fouling threshold conditions, it will be possible to design exchangers to essentially clean conditions. In the meantime, the user of computer programs should use common sense in assigning fouling factors only to actual fouling conditions. Startup conditions should also be checked as an alternative case.

Industrial experience has shown for a long time that arbitrary fouling factors may actually contribute to fouling by greatly oversizing exchangers and lowering velocities. Gilmour⁶³

presented evidence of this years ago. In general, crude oils may need fouling factors, as may polymerizing fluids, but light hydrocarbons may not. We now recommend designing with no fouling factor, then adding about 20% surface, as length, and rechecking pressure drop.

NOMENCLATURE

Note: Dimensional equations should use U.S. units only.

	Description	U.S. Units	S.I. Units
A_i	Inside surface area	ft ²	m ²
A_m	Mean surface area	ft ²	m ²
A_o	Outside surface area	ft ²	m ²
a_o	Outside surface per unit length	ft	m
B_c	Baffle cut % of shell diameter	%	%
BR	Boiling range (dew–bubble points)	°F	(U.S. only)
C	Two-phase pressure drop constant	—	—
C_b	Bundle bypass constant	—	—
C_{p1}	Heat capacity, hot fluid	Btu/lb · °F	J/kg·K
C_{p2}	Heat capacity, cold fluid	Btu/lb · °F	J/kg·K
D	Tube diameter, general	ft	m
D_b	Bundle diameter	ft	m
D_i	Tube diameter, inside	ft	m
D_o	Tube diameter, outside	ft or in.	m or U.S. only
D_s	Shell diameter	ft	m
D_f	Effective length: = D_i for tubeside = $P_i - D_o$ for shellside	ft	m
E_f	Fan efficiency (0.6–0.7, typical)	—	—
F	MTD correction factor	—	—
F_b	Bundle convection factor	—	—
F_c	Mixture correction factor	—	—
F_g	Gravity condensation factor	—	—
g	Acceleration of gravity	ft/h ²	m/s ²
G	Total mass velocity	lb/h · ft ²	kg/s·m ²
g_c	Gravitational constant	4.17×10^8 lb _f ·ft/lb·h ²	1.0
h_{hot}	Heat transfer coeff., hot fluid	Btu/h·ft ² ·°F	W/m ² ·K
h_{cold}	Heat transfer coefficient, cold fluid	Btu/h·ft ² ·°F	W/m ² ·K
h_b	Heat transfer coeff., boiling	Btu/h·ft ² ·°F	W/m ² ·K
h_c	Heat transfer coeff., condensing	Btu/h·ft ² ·°F	W/m ² ·K
h_{cb}	Heat transfer coeff., conv. boiling	Btu/h·ft ² ·°F	W/m ² ·K
h_{cf}	Heat transfer coeff., cond. film	Btu/h·ft ² ·°F	W/m ² ·K
h_i	Heat transfer coeff., inside	Btu/h·ft ² ·°F	W/m ² ·K
h_l	Heat transfer coeff., liq. film	Btu/h·ft ² ·°F	W/m ² ·K
h_N	Heat transfer coeff., Nusselt	Btu/h·ft ² ·°F	W/m ² ·K
h_{nb}	Heat transfer coeff., nucleate boiling	Btu/h·ft ² ·°F	W/m ² ·K
h_o	Heat transfer coeff., outside	Btu/h·ft ² ·°F	W/m ² ·K
h_{sv}	Heat transfer coeff., sens. vapor	Btu/h·ft ² ·°F	W/m ² ·K

	Description	U.S. Units	S.I. Units
h_v	Heat transfer coeff., vapor phase	Btu/h·ft ² ·°F	W/m ² ·K
J_g	Wallis dimensionless gas velocity	—	—
k_f	Thermal conductivity, fluid	Btu/h·ft·°F	W/m·K
k_l	Thermal conductivity, liquid	Btu/h·ft·°F	W/m·K
k_w	Thermal conductivity, wall	Btu/h·ft·°F	W/m·K
L	Tube length	ft	m
L_{bc}	Baffle spacing	ft	m
L_{su}	Maximum unsupported length	in.	use U.S. only
MTD	Mean temperature difference	°F	K
NP	Number of tube passes	—	—
NT	Number of tubes	—	—
NTU	Number of transfer units	—	—
P	Pressure	psia	use U.S. only
P_c	Critical pressure	psia	use U.S. only
P_f	Fan power	use S.I. only	W
Pr	Prandtl number	—	—
P_t	Tube pitch	ft	m
q_{\max}	Maximum allowable heat flux	Btu/h·ft ²	use U.S. only
q	Heat flux	Btu/h ft ²	use U.S. only
Q	Heat duty	Btu/h	W
q_{sv}	Sensible vapor heat flux	Btu/h ft ²	W/m ²
q_t	Total heat flux	Btu/h ft ²	W/m ²
Re	Reynolds number	—	—
Re_c	Reynolds number, condensate	—	—
R_{fi}	Fouling resistance, inside	°F ft ² h/Btu	K m ² /W
R_{fo}	Fouling resistance, outside	°F ft ² h/Btu	K m ² /W
R_{hi}	Heat transfer resistance, inside	°F ft ² h/Btu	K m ² /W
R_{ho}	Heat transfer resistance, outside	°F ft ² h/Btu	K m ² /W
R_w	Heat transfer resistance, wall	°F ft ² h/Btu	K m ² /W
S_s	Cross-flow area, shellside	ft ²	m ²
S_t	Cross-flow area, tubeside	ft ²	m ²
t_1	Temperature, cold fluid inlet	°F	°C
T_1	Temperature, hot fluid inlet	°F	°C
t_2	Temperature, cold fluid outlet	°F	°C
T_2	Temperature, hot fluid outlet	°F	°C
T_A	Hot inlet—cold outlet temperature	°F	°C
T_B	Hot outlet—cold inlet temperature	°F	°C
T_{hot}	Temperature, hot fluid	°F	°C
T_{cold}	Temperature, cold fluid	°F	°C
T_s	Saturation temperature	°F	°C
T_w	Wall temperature	°F	°C
$T_{w, \text{hot}}$	Wall temperature, hot fluid side	°F	°C
$T_{w, \text{cold}}$	Wall temperature, cold fluid side	°F	°C
U_o	Overall heat transfer coefficient	Btu/h·ft ² ·°F	W/m ² ·K
V	Volumetric flow rate	use S.I. only	m ³ /s
V_f	Face velocity	ft/min	use S.I. only
V_s	Shellside velocity	ft/h	m/h

(continued)

	Description	U.S. Units	S.I. Units
V_t	Tubeside velocity	ft/h	m/h
W_a	Air flow rate	lb/min	use U.S. only
W_1	Flow rate, hot fluid	lb/h	kg/h
W_2	Flow rate, cold fluid	lb/h	kg/h
W_c	Flow rate, condensate	lb/h	kg/h
W_d	Air-cooled bundle width	ft	use U.S. only
W_s	Flow rate, shellside	lb/h	kg/h
W_t	Flow rate, tubeside	lb/h	kg/h
X_{tt}	Martinelli parameter	—	—
x_w	Wall thickness	ft	m
y	Weight fraction vapor	—	—
α	Nucleate boiling suppression factor	—	—
Δp_d	Dynamic pressure loss (typically 40–60 Pa)	use S.I.	Pa
ΔP_f	Two-phase friction pressure drop	psi	kPa
ΔP_l	Liquid-phase friction pressure drop	psi	kPa
Δp_s	Static pressure drop, air cooler	use S.I. only	Pa
ΔP_s	Shellside pressure drop	lb/ft ²	use U.S. only
ΔP_t	Tubeside pressure drop	lb/ft ²	use U.S. only
λ	Latent heat	Btu/lb	J/kg
μ	Viscosity, general	lb/ft · h	Pa
μ_f	Viscosity, bulk fluid	lb/ft · h	Pa
μ_w	Viscosity, at wall	lb/ft · h	Pa
ρ_l	Density, liquid	lb/ft ³	kg/m ³
ρ_s	Density, shellside fluid	lb/ft ³	kg/m ³
ρ_t	Density, tubeside fluid	lb/ft ³	kg/m ³
ρ_v	Density, vapor	lb/ft ³	kg/m ³
ϕ_b	Bundle vapor blanketing correction	—	—
ϕ_l	Two-phase pressure drop correction	—	—

REFERENCES

Note: Many of the following references are taken from Kuppan Thulukkanam, *Heat Exchanger Design Handbook* (HEDH), Hemisphere, Washington, DC, 1982, which will be referred to for simplicity as HEDH.

1. J. Taborek, "Shell and Tube Heat Exchangers, Single-Phase Flow," Section 3.3, HEDH.
- 1a. A. C. Mueller, "Condensers," Section 3.4, HEDH.
2. E. A. D. Saunders, "Shell and Tube Heat Exchangers, Elements of Construction," Section 4.2, HEDH.
3. *Standards of Tubular Heat Exchanger Manufacturers Association*, 6th ed., TEMA, New York, 1978.
4. J. W. Palen, "Shell and Tube Reboilers," Section 3.6, HEDH.
5. C. C. Gentry, R. K. Young, and W. M. Small, "RODbaffle Heat Exchanger Thermal-Hydraulic Predictive Methods," in *Proceedings of the 7th International Heat Transfer Conference*, Munich, 1982.
6. A. C. Mueller, in Rohsenow and Hartnet (Eds.), *Handbook of Heat Transfer*, McGraw-Hill, New York, 1983, Chapter 18.
7. P. Paikert, "Air-Cooled Heat Exchangers," Section 3.8, HEDH.
8. R. L. Webb, "Compact Heat Exchangers," Section 3.9, HEDH.
9. F. L. Rubin, "Multizone Condensers, Desuperheating, Condensing, Subcooling," *Heat Transfer Eng.*, **3**(1), 49–59, 1981.

10. H. Hausen, *Heat Transfer in Counterflow, Parallel Flow, and Crossflow*, McGraw-Hill, New York, 1983.
11. F. W. Schmidt, "Thermal Energy Storage and Regeneration," in J. Taborek et al. (Eds.), *Heat Exchangers Theory and Practice*, Hemisphere, McGraw-Hill, New York, 1983.
12. D. Chisholm et al., "Costing of Heat Exchangers," Section 4.8, HEDH.
13. R. S. Hall, J. Matley, and K. J. McNaughton, "Current Costs of Process Equipment," *Chem. Eng.*, **89**(7), 80–116, April 5, 1982.
14. J. Taborek, "Charts for Mean Temperature Difference in Industrial Heat Exchanger Configurations," Section 1.5, HEDH.
15. K. J. Bell, "Approximate Sizing of Shell-and-Tube Heat Exchangers," Section 3.1.4, HEDH.
16. D. Q. Kern, *Process Heat Transfer*, McGraw-Hill, New York, 1950.
17. J. W. Palen and J. Taborek, "Solution of Shellside Heat Transfer and Pressure Drop by Stream Analysis Method," *Chem. Eng. Prog. Symp. Ser.*, **65**(92), 1969.
18. K. W. McQuillan and P. B. Whalley, "A Comparison between Flooding Correlations and Experimental Flooding Data for Gas–Liquid Flow in Vertical Circular Tubes," *Chem. Eng. Sci.*, **40**(8), 1425–1440, 1988.
19. B. D. Smith, *Design of Equilibrium Stage Processes*, McGraw-Hill, New York, 1963.
20. V. L. Rice, "Program Performs Vapor-Liquid Equilibrium Calculations," *Chem. Eng.*, 77–86, June 28, 1982.
21. R. S. Kistler and A. E. Kassem, "Stepwise Rating of Condensers," *Chem. Eng. Prog.*, **77**(7), 55–59, 1981.
22. G. Breber, J. Palen, and J. Taborek, "Prediction of Horizontal Tubeside Condensation of Pure Components Using Flow Regime Criteria," *Heat Transfer Eng.*, **1**(2), 72–79, 1979.
23. D. Butterworth, "Condensation of Vapor Mixtures," Section 2.6.3, HEDH.
24. R. G. Sardesai, "Condensation of Mixtures Forming Immiscible Liquids," Section 2.5.4, HEDH.
25. K. J. Bell and A. M. Ghaly, "An Approximate Generalized Design Method for Multicomponent/Partial Condensers," *AIChE Symp. Ser.*, No. 131, 72–79, 1972.
26. J. E. Diehl, "Calculate Condenser Pressure Drop," *Pet. Refiner.*, **36**(10), 147–153, 1957.
27. I. D. R. Grant and D. Chisholm, "Two-Phase Flow on the Shell-Side of a Segmentally Baffled Shell-and-Tube Heat Exchanger," *Trans. ASME J. Heat Transfer*, **101**(1), 38–42, 1979.
28. K. Ishihara, J. W. Palen, and J. Taborek, "Critical Review of Correlations for Predicting Two-Phase Flow Pressure Drops across Tube Banks," *Heat Transfer Eng.*, **1**(3), 1979.
29. R. A. Smith, "Evaporators," Section 3.5, HEDH.
30. J. G. Collier, "Boiling and Evaporation," Section 2.7, HEDH.
31. J. C. Chen, "Correlation for Boiling Heat Transfer to Saturated Fluids in Convective Flow," *Ind. Eng. Chem. Proc. Design and Dev.*, **5**(3), 322–339, 1966.
32. D. Steiner and J. Taborek, "Flow Boiling Heat Transfer in Vertical Tubes Correlated by an Asymptotic Method," *Heat Transfer Eng.*, **13**(3), 43, 1992.
33. J. R. Fair, "What You Need to Design Thermosiphon Reboilers," *Pet. Refiner.*, **39**(2), 105, 1960.
34. J. R. Fair and A. M. Klip, "Thermal Design of Horizontal Type Reboilers," *Chem. Eng. Prog.*, **79**(3), 1983.
35. J. W. Palen and C. C. Yang, "Circulation Boiling Model of Kettle and Internal Reboiler Performance," paper presented at the 21st National Heat Transfer Conference, Seattle, WA, 1983.
36. J. W. Palen, A. Yarden, and J. Taborek, "Characteristics of Boiling Outside Large Scale Multitube Bundles," *Chem. Eng. Prog. Symp. Ser.*, **68**(118), 50–61, 1972.
37. J. W. Palen, C. C. Shih, and J. Taborek, "Performance Limitations in a Large Scale Thermosiphon Reboiler," in *Proceedings of the 5th International Heat Transfer Conference*, Tokyo, 1974, Vol. 5, pp. 204–208, The Science Council of Japan.
38. Y. Katto, "Generalized Correlation of Critical Heat Flux for Forced Convection Boiling in Vertical Uniformly Heated Round Tubes," *Int. J. Heat Mass Transfer*, **21**(12), 1527–1542, 1978.
39. N. Kattan, J. R. Thome, and D. Farrat, "Flow Boiling in Horizontal Tubes: Part 3—Development of a New Heat Transfer Model Based on Plow Pattern," *J. Heat Transfer*, **120**(1), 156–164, 1998.

40. J. W. Palen, C. C. Shih, and J. Taborek, "Mist Flow in Thermosiphon Reboilers," *Chem. Eng. Prog.*, **78**(7), 59–61, 1982.
41. R. Brown, "A Procedure for Preliminary Estimate of Air-Cooled Heat Exchangers," *Chem. Eng.*, **85**(8), 108–111, March 27, 1978.
42. E. C. Smith, "Air-Cooled Heat Exchangers," *Chem. Eng.*, November 17, 1958.
43. V. Gnielinski, A. Zukauskas, and A. Skrinska, "Banks of Plain and Finned Tubes," Section 2.5.3, HEDH.
44. P. Minton, "Designing Spiral-Plate Heat Exchangers," *Chem. Eng.*, **77**(9), May 4, 1970.
45. A. Cooper and J. D. Usher, "Plate Heat Exchangers," Section 3.7, HEDH.
46. J. Marriott, "Performance of an Alfaflex Plate Heat Exchanger," *Chem. Eng. Prog.*, **73**(2), 73–78, 1977.
47. D. Chisholm, "Heat Pipes," Section 3.10, HEDH.
48. J. S. Truelove, "Furnaces and Combustion Chambers," Section 3.11, HEDH.
49. W. R. Penney, "Agitated Vessels," Section 3.14, HEDH.
50. A. R. Guy, "Double-Pipe Heat Exchangers," Section 3.2, HEDH.
51. J. Taborek et al., "Fouling—The Major Unresolved Problem in Heat Transfer," *Chem. Eng. Prog.*, **65**(92), 53–67, 1972.
52. *Proceedings of the Conference on Progress in the Prevention of Fouling in Process Plants*, sponsored by the Institute of Corrosion Science Technology and the Institute of Chemical Engineers, London, 1981.
53. J. W. Suito, W. J. Marner, and R. B. Ritter, "The History and Status of Research in Fouling of Heat Exchangers in Cooling Water Service," *Can. J. Chem. Eng.*, **55**, August 1977.
54. R. B. Ritter and J. W. Suito, "Seawater Fouling of Heat Exchanger Tubes," in *Proceedings of the 2nd National Conference on Complete Water Reuse*, Chicago, 1975.
55. C. H. Gilmour, "No Fouling—No Fouling," *Chem. Eng. Prog.*, **61**(7), 49–54, 1965.
56. J. V. Smith, "Improving the Performance of Vertical Thermosiphon Reboilers," *Chem. Eng. Prog.*, **70**(7), 68–70, 1974.
57. J. C. Chenoweth, "Flow-Induced Vibration," Section 4.6, HEDH.
58. A. C. Mueller, "Criteria for Maldistribution in Viscous Flow Coolers," in *Proceedings of the 5th International Heat Transfer Conference*, HE 1.4, Tokyo, Vol. 5, pp. 170–174.
59. W. F. Berg and J. L. Berg, "Flow Patterns for Isothermal Condensation in One-Pass Air-Cooled Heat Exchangers," *Heat Transfer Eng.*, **1**(4), 21–31, 1980.
60. G. Breber, J. W. Palen, and J. Taborek, "Study on Non-Condensable Vapor Accumulation in Air-Cooled Condensers," in *Proceedings of the 7th International Heat Transfer Conference*, Munich, 1982.
61. A. Blumenkrantz and J. Taborek, "Application of Stability Analysis for Design of Natural Circulation Boiling Systems and Comparison with Experimental Data," *AIChE Symp. Ser.*, **68**(118), 1971.
62. V. L. Streeter, *Fluid Mechanics*, McGraw-Hill, New York, 1958.
63. C. H. Gilmour, "No Fouling, No Fouling," *Chem. Eng. Prog.*, **61**(7), 49–54, 1965.
64. A. Cooper, J. W. Suito, and J. D. Usher, "Cooling Water Fouling in Plate Exchangers," *Heat Transfer Eng.*, **1**(3), 1979.

CHAPTER 10

HEAT PIPES

Hongbin Ma

University of Missouri

Columbia, Missouri

1 INTRODUCTION	415	4.2 Working Fluid Selections	428
2 FUNDAMENTALS	417	4.3 Cleaning and Charging	429
2.1 Surface Tension	417	4.4 Testing	432
2.2 Contact Angle	417	5 OTHER TYPES OF HEAT PIPES	433
2.3 Laplace–Young Equation	417	5.1 Thermosyphon	433
2.4 Capillary Pressure	418	5.2 Loop Heat Pipes/Capillary Pumped Loop	434
2.5 Disjoining Pressure	418	5.3 Vapor Chamber	436
3 HEAT TRANSPORT LIMITATIONS	419	5.4 Micro Heat Pipes	437
3.1 Capillary Limit	419	5.5 Variable-Conductance Heat Pipes	438
3.2 Boiling Limit	422	5.6 Rotating Heat Pipes	438
3.3 Entrainment Limit	423	5.7 High-Temperature Heat Pipes (Metal Heat Pipes)	439
3.4 Viscous Limit	424	5.8 Cryogenic Heat Pipes	439
3.5 Sonic Limit	424	NOMENCLATURE	439
3.6 Effective Thermal Conductivity	424	REFERENCES	441
4 HEAT PIPE FABRICATION PROCESSES	428		
4.1 Wicks	428		

1 INTRODUCTION

The heat pipe is a device that utilizes the evaporation heat transfer in the evaporator and condensation heat transfer in the condenser in which the vapor flow from the evaporator to the condenser is caused by the vapor pressure difference and the liquid flow from the condenser to the evaporator is produced by the capillary force, gravitational force, electrostatic force, or other forces directly acting on it. The first heat pipe concept can be traced to the Perkins tube.^{1,2} Based on the structure, a heat pipe typically consists of a sealed container charged with a working fluid. Heat pipes operate on a closed two-phase cycle and only pure liquid and vapor are present in the cycle. The working fluid remains at saturation conditions as long as the operating temperature is between the triple point and the critical state. As illustrated in Fig. 1, a typical heat pipe consists of three sections: an evaporator or heat addition section, an adiabatic section, and a condenser or heat rejection section. When heat is added to the evaporator section of the heat pipe, the heat is transferred through the shell and reaches the liquid. When the liquid in the evaporator section receives enough thermal energy, the liquid vaporizes. The vapor carries the thermal energy through the adiabatic section to the condenser section, where the vapor is condensed into the liquid and releases the latent heat of vaporization.

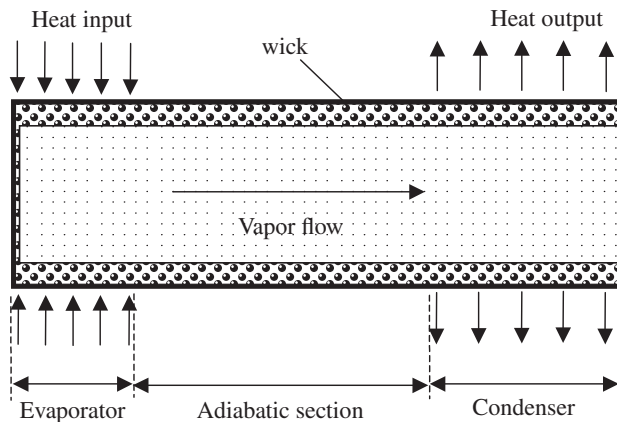


Figure 1 Schematic of a heat pipe.

The condensate is pumped back from the condenser to the evaporator by the driving force acting on the liquid.

In order for a heat pipe to be functional, the liquid in the evaporator is sufficient to be vaporized. There are a number of limitations to affect the return of the working fluid. When the pumping pressure produced by the surface tension cannot overcome the summation of the total pressures, the heat transport occurring in the heat pipe reaches a limit known as the capillary limit. There are several other limitations disconnecting the return of the working fluid from the evaporator to the condenser or from the condenser to the evaporator. Among these are the boiling limit, sonic limit, entrainment limit, and viscous limit. When the heat flux added to the evaporator is sufficiently high, nucleate boiling occurs. The bubble formed in the wick significantly increases the thermal resistance causing the heat transfer performance to be significantly reduced. More importantly, when the heat flux is so high, the bubbles block the return of the working fluid and lead to a dryout of the evaporator. The boiling limit plays a key role in a high-heat-flux heat pipe. When the vapor velocity is high and the cross-sectional area variation of the vapor space in a heat pipe cannot meet the flow condition, choked flow occurs, and the vapor flow rate will not respond with the amount of heat added in the evaporator. This will lead to a sonic limit. The entrainment limit is due to the frictional shear stresses caused by the vapor flow at the vapor–liquid interface. The viscous limit occurs in a low-heat-flux heat pipe, where the vapor pressure difference cannot overcome the vapor pressure drop in the vapor phase.

From a thermodynamics point of view, the thermal energy added to the evaporator in a functional heat pipe produces the mechanical work to pump the working fluid. No external power is needed for a typical heat pipe. The phase change heat transfer occurs almost in a quasi-equilibrium state. The heat pipe has a very high efficiency to transfer the thermal energy from a higher temperature heat source to a lower temperature heat source. An operational heat pipe can provide an extra high effective thermal conductivity and reach a higher level of temperature uniformity. The working fluid medium in a heat pipe can be selected from a variety of fluids depending on the operating temperature and compatibility with the shell material. The heat pipe can be operated from a temperature lower than 4 K to a high temperature up to 3000 K. Because the evaporator and condenser of a heat pipe function independently, the heat pipe can be made into any shape depending on the design requirement. Due to these unique features, the heat pipe has been used in a wide range of applications.

2 FUNDAMENTALS

2.1 Surface Tension

Surface tension is a force that operates on a surface and acts perpendicularly and inwardly from the boundaries of the surface, which tends to decrease the area of the interface. As a result, a liquid will form a shape having minimum area. In the case of zero gravity in vacuum, this liquid drop will be a perfect sphere. The surface tension can be viewed as a consequence of attractive and repulsive forces among molecules near the interface. From a thermodynamic point of view, it may be interpreted in terms of energy stored in the molecules near the interface. The surface tension can be considered as consisting of the dispersion force and other specific forces such as metallic or hydrogen bonding, i.e., $\sigma = \sigma_d + \sigma_m$. Surface tension in nonpolar liquids is entirely caused by dispersion forces. In hydrogen-bonded liquids, both dispersion forces and hydrogen bonding contribute to relatively larger values of surface tension. In liquid metals, the metallic force combining with the dispersion force results in higher values of surface tension. What naturally follows is the principle that surface tensions of liquid metals are higher than those of a hydrogen-bonded liquid such as water, which in turn are higher than those of nonpolar liquids such as pure hydrocarbons. The surface tension significantly depends on the temperature. As temperature increases, the surface tension decreases. For example, the surface tension of water decreases almost linearly with temperature, i.e., $\sigma = 75.83 - 0.1477T$ (mN/m), where T is temperature ($^{\circ}\text{C}$).

2.2 Contact Angle

A physical property closely related to the surface tension is the contact angle. The contact angle α is defined as the angle (measured in the liquid) formed between the liquid–vapor interface and the solid–liquid interface as shown in Fig. 2, which may be expressed as

$$\cos \alpha = \frac{\sigma_{sv} - \sigma_{sl}}{\sigma} \quad (1)$$

where σ_{sv} is the surface tension between the solid and vapor and σ_{sl} is the surface tension between the solid and liquid. The surface tension between the liquid and vapor is a function of temperature and decreases as the temperature increases. For a given solid surface and liquid, when the surface tension between the solid and liquid is a fixed constant, the contact angle will decrease as the temperature increases. Therefore, when the temperature increases, the wetting characteristic of a liquid on a given solid surface improves.

2.3 Laplace–Young Equation

For a liquid–vapor curved surface, there exists a pressure difference across the interface, which can be calculated by

$$p_1 - p_{II} = \sigma \left(\frac{1}{r_1} + \frac{1}{r_2} \right) \quad (2)$$

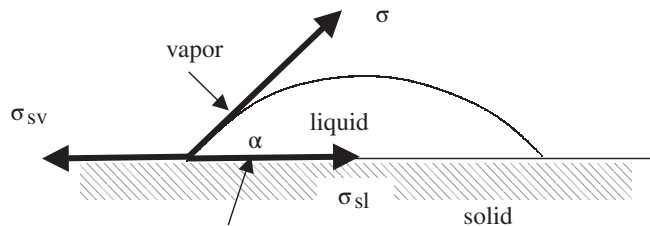


Figure 2 Contact angle.

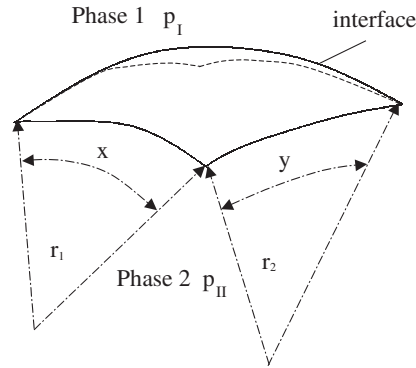


Figure 3 Curved interface between two phases.

where σ is surface tension, r_1 is the meniscus radius along the x direction and r_2 is the meniscus radius along the y direction, as shown in Fig. 3. This expression is known as the Laplace–Young Equation and was derived in 1805. Equation 2 can be used easily to find the pressure differences across the liquid–vapor interfaces for a number of structures shown in Table 1.

2.4 Capillary Pressure

When a curved surface with a meniscus radius at the liquid–vapor interface takes place, the pressure difference across the liquid–vapor interface exists. When a capillary tube with a radius of r_t is plugged into liquid as shown in Table 1, liquid is wicking up. The wicking height, h_w , can be determined by

$$h_w = \frac{2\sigma \cos \alpha}{r_t g (\rho_l - \rho_v)} \quad (3)$$

It should be noted that the wicking height determined by Eq. 3 is based on an assumption of constant meniscus radius at the liquid–vapor interface. This wicking height is due to the pressure difference across the liquid–vapor interface, $p_v - p_l$, caused by the meniscus radii existing at the liquid–vapor interface. This pressure difference is called the capillary pressure for this wicking height.

2.5 Disjoining Pressure

For a typical heat pipe, evaporation from liquid to vapor occurs at the liquid–vapor interface in the evaporator. Vapor is not formed by the nucleation process. If boiling takes place, the heat pipe reaches the boiling limit. During the phase change process in the evaporator, thin-film evaporation plays a key role. When liquid film becomes very thin, the pressure in the liquid film, p_l , is less than the bulk pressure, p_B . The pressure difference is known as the disjoining pressure, p_d , i.e.,

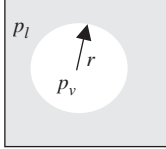
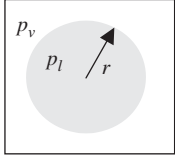
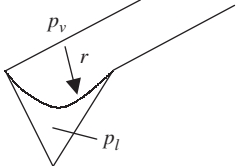
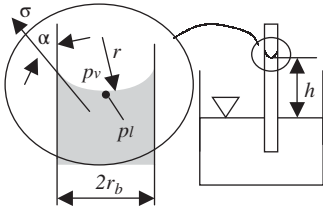
$$p_d = p_l - p_B \quad (4)$$

Because the pressure in the liquid film is less than the bulk pressure, the disjoining pressure is negative. The disjoining pressure basically is a function of film thickness, which can be calculated by

$$p_d = -\frac{A}{\delta^B} \quad \text{for nonpolar liquid and} \quad (5)$$

$$p_d = -\frac{A}{\delta^B} \ln(\delta/\delta_0) \quad \text{for polar liquid} \quad (6)$$

Table 1 Pressure Differences across Liquid–Vapor Curved Surfaces

Names/Structures	Pressure Difference across Liquid–Vapor Interface	Notes
Vapor bubble in liquid phase 	$p_v - p_l = \sigma \left(\frac{1}{r_1} + \frac{1}{r_2} \right) = \frac{2\sigma}{r}$	$r=r_1=r_2$
Liquid drop in vapor phase 	$p_l - p_v = \sigma \left(\frac{1}{r_1} + \frac{1}{r_2} \right) = \frac{2\sigma}{r}$	$r=r_1=r_2$
Liquid in a micro triangular groove 	$p_v - p_l = \sigma \left(\frac{1}{r_1} + \frac{1}{r_2} \right) = \frac{\sigma}{r}$	$r_2=\infty$ $r = \text{const}$
Capillary wicking in a capillary tube 	$p_v - p_l = \sigma \left(\frac{1}{r_1} + \frac{1}{r_2} \right) = \frac{2\sigma}{r} = \frac{2\sigma}{\frac{r_b}{\cos \alpha}} = \rho g h_w$	$r=r_1=r_2$

where A is the Hamaker constant (J). Because it is very difficult to find the accurate Hamaker constant, a number of correlations were experimentally obtained. For example, if water is on quartz, the disjoining pressure can be estimated by

$$p_d = \rho_l RT_{lv} \ln a \delta^b \quad (a = 1.5787, \quad b = 0.0243) \quad (7)$$

3 HEAT TRANSPORT LIMITATIONS

3.1 Capillary Limit

For a heat pipe to function, the capillary pressure difference occurring in the heat pipe must always be greater than the summation of all the pressure losses occurring throughout the liquid and vapor flow paths. When the heat transfer rate increases, the pressure losses increase, which will be overcome by the increase of the capillary pressure difference. The continuous increase of the heat transfer rate in a heat pipe will significantly increase the pressure losses, and at one

heat transfer rate, the total capillary pressure difference is no longer equal to or greater than the total pressure losses. This relationship, referred to as the capillary limit, can be expressed mathematically as

$$\Delta p_{c,\max} \geq \Delta p_l + \Delta p_v + \Delta p_g \quad (8)$$

where $\Delta p_{c,\max}$ = maximum capillary pressure difference generated within capillary wicking structure

Δp_l = sum of inertial and viscous pressure drops occurring in liquid phase

Δp_v = sum of inertial and viscous pressure drops occurring in vapor phase

Δp_g = hydrostatic pressure drop

When the maximum capillary pressure difference is equal to or greater than the summation of these pressure drops, the capillary structure is capable of returning an adequate amount of working fluid to prevent dryout of the evaporator wicking structure. This condition varies according to the wicking structure, working fluid, evaporator heat flux, vapor flow channel, and operating temperature.

Capillary Pressure. When the meniscus radius exists at a liquid–vapor interface, there is the pressure difference across the interface, which can be determined by the Laplace–Young equation shown in Eq. 2. During steady-state operation, it is generally defined that the maximum capillary pressure exists when the capillary radius in the condenser approaches infinity and the capillary radius in the evaporator reaches the smallest one. In order to generalize the application, the maximum capillary pressure can be expressed as a function of only the effective capillary radius of the evaporator wick, i.e.,

$$\Delta p_{c,\max} = \frac{2\sigma}{r_{c,e}} \quad (9)$$

where $r_{c,e}$ is the effective capillary radius depending on the wick structures. Table 2 lists effective capillary radii for four typical wicks. For other kinds of wicks, the effective capillary radii can be readily determined using the Laplace–Young equation.

Liquid Pressure Drop. The liquid pressure drop is the result of the combined effect of both viscous and inertial forces. If the flow rate in the wick is very small, the effect of inertial force can be neglected, and the pressure difference is caused in the liquid phase only by the frictional forces at the liquid–solid interface and in the liquid–vapor interface due to the vapor flow effect.

Table 2 Effective Capillary Radii

Structures	$r_{c,e}$	Note
Rectangular groove	$\frac{w}{\cos \alpha}$	w = groove width α = contact angle
Triangular groove	$\frac{3 \cos \theta w}{4 \cos \alpha}$	w = groove width α = contact angle θ = half groove angle
Wire screen	$\frac{w + d_w}{2 \cos \alpha}$	d_w = wire diameter w = mesh spacing α = contact angle
Packed or sintered particles	$0.41 r_s$	r_s = particle radius

Source: From Ref. 3.

The total liquid pressure drop can be determined by integrating the pressure gradient over the length of the flow passage, or

$$\Delta p_l(x) = - \int_0^x \frac{dp_l}{dx} dx \quad (10)$$

where the limits of integration are from the evaporator end ($x = 0$) to the condenser end ($x = L$), and dp_l/dx is the gradient of the liquid pressure resulting from the frictional forces from the solid wick, wall, and vapor flow at the liquid–vapor interface, which can be written as

$$\frac{dp_l}{dx} = \left(\frac{\mu_l}{KA_w \rho_l} \right) m_l \quad (11)$$

where m_l is the local mass flow rate in the wick and K , the permeability, can be expressed as

$$K = \frac{2\varepsilon r_{h,l}^2}{f_l \cdot \text{Re}_l} \quad (12)$$

The wick porosity ε in Eq. 12 is defined as the ratio of the pore volume V_{por} to the total volume V_{tot} of the wick structure. The hydraulic radius $r_{h,l}$ in Eq. 12 is defined as twice the cross-sectional area divided by the wetted perimeter, or $r_{h,l} = 2A_c/P$. It should be noted that Eq. 12 is valid for both the circular and noncircular channels/grooves. If the Reynolds number of the working fluid flowing through the wick structure is small and less than the critical value, then laminar flow is assumed. The product of the friction factor and Reynolds number, $f_l \cdot \text{Re}_l$, for laminar flow is constant and depends only on the passage shape. It should be noticed that when the liquid–vapor interface is affected by the vapor flow, the friction factor Reynolds number product, $f_l \cdot \text{Re}_l$, depends on the vapor flow in addition to the contact angle and channel angle.⁴

For uniform heat addition and rejection, Eq. 10 can be expressed as

$$\Delta p_l = \left(\frac{\mu_l}{KA_w h_{fg} \rho_l} \right) L_{\text{eff}} q \quad (13)$$

where $q = m_l h_{fg}$ and the effective heat pipe length can be found as

$$L_{\text{eff}} = 0.5L_e + L_a + 0.5L_c \quad (14)$$

In many cases, an analytical expression for the permeability K shown in Eq. 13 is not available. In such a case, semiempirical correlations based on experimental data are usually employed. For example, Marcus⁵ has described a method for calculating the permeability of wrapped, screened wicks. This expression, which is a modified form of the Blake–Kozeny equation, can be expressed as

$$K = \frac{d^2 \varepsilon^3}{122(1 - \varepsilon)^2} \quad (15)$$

In this expression, d is the wire diameter and ε is the wick porosity, which can be determined as

$$\varepsilon = 1 - \frac{1}{4} \pi S N d \quad (16)$$

where N is the mesh number per unit length and S is the crimping factor (approximately 1.05).⁶ For the sintered particles, this equation takes the form

$$K = \frac{d_s^2 \varepsilon^3}{37.5(1 - \varepsilon)^2} \quad (17)$$

where d_s is the average diameter of the sintered particles.

Vapor Pressure Drop. If the heat pipe is charged with an appropriate amount of working fluid and the wetting point occurs at the cap end of the condenser, the vapor pressure drop can be

calculated by the approach recommended by Peterson,⁶ Chi,⁷ and Dunn and Ready.⁸ Based on the one-dimensional vapor flow approximation, the vapor pressure drop can be determined by

$$\Delta p_v = \left(\frac{C (f_v \cdot \text{Re}_v) \mu_v}{2r_{h,v}^2 A_v \rho_v h_{fg}} \right) L_{\text{eff}} q \quad (18)$$

where C is the constant that depends on the Mach number defined by

$$\text{Ma}_v = \frac{q}{A_v \rho_v h_{fg} (R_v T_v \gamma_v)^{1/2}} \quad (19)$$

The ratio of specific heats, γ_v , in Eq. 19 depends on the molecule types and is equal to 1.67, 1.4, and 1.33 for monatomic, diatomic, and polyatomic molecules, respectively. Previous investigation summarized by Peterson⁶ has demonstrated that the friction factor Reynolds number product $f_v \cdot \text{Re}_v$ and the constant C shown in Eq. 18 can be determined by

$$\begin{aligned} \text{Re}_v < 2300 \quad \text{and} \quad \text{Ma}_v < 0.2 \\ f_v \cdot \text{Re}_v = \text{constant}, \quad C = 1.0 \end{aligned} \quad (20)$$

$$\begin{aligned} \text{Re}_v < 2300 \quad \text{and} \quad \text{Ma}_v > 0.2 \\ f_v \cdot \text{Re}_v = \text{constant}, \quad C = \left[1 + \left(\frac{\gamma_v - 1}{2} \right) \text{Ma}_v^2 \right]^{-1/2} \end{aligned} \quad (21)$$

$$\begin{aligned} \text{Re}_v > 2300 \quad \text{and} \quad \text{Ma}_v < 0.2 \\ f_v \cdot \text{Re}_v = 0.038 \left(\frac{2r_{h,v} q}{A_v \mu_v h_{fg}} \right)^{3/4}, \quad C = 1.0 \end{aligned} \quad (22)$$

It should be noted that Eq. 22 was determined based on a round channel. Because the equations used to evaluate both the Reynolds number and the Mach number are functions of the heat transport capacity, it is first necessary to assume the conditions of the vapor flow, and an iterative procedure must be used to determine the vapor pressure.

If the heat pipe is overcharged and/or the heat pipe is operating at a high cooling rate, the location of the wet point, where the pressures in the vapor and the liquid are equal, should be close to the beginning of the condensing section. In this case, only the total pressure drop in the evaporating and condensing sections are needed in the calculation of the capillary limitation.⁹ Equation 18 becomes

$$\Delta p_v = \left(\frac{C (f_v \cdot \text{Re}_v) \mu_v}{2r_{h,v}^2 A_v \rho_v h_{fg}} \right) q [0.5L_e (1 + F \text{Re}_r) + L_a] \quad (23)$$

where the correction factor F in Eq. 18 can be determined by

$$F = \frac{7}{9} - \frac{1.7 \text{Re}_r}{36 + 10 \text{Re}_r} \exp \left(-\frac{7.5 L_a}{\text{Re}_r L_e} \right) \quad (24)$$

The radial Reynolds number Re_r in Eqs. 18 and 19 is defined by

$$\text{Re}_r = \frac{\rho_v v_{lv} r_v}{\mu_v} \quad (25)$$

where v_{lv} is the interfacial velocity. For evaporation, $v_{lv} > 0$; for condensation, $v_{lv} < 0$.

3.2 Boiling Limit

When boiling occurs near the evaporating wall in the wick, two consequences result. First, the amount of thin-film evaporation at the solid–liquid–vapor interface dramatically decreases as

the boiling condition dominates the phase change behavior of the system. Second, the vapor forming at the base of the wick structure forms a blanket of vapor, preventing reentry of the working fluid. Since the vapor conductivity of working fluid is much lower than the fluid conductivity, the overall conductivity of the wick structure will experience a significant decrease. Obviously, boiling heat transfer in the wick should be avoided as this condition could lead to early dryout of the heat pipe.

If the wick is constructed such that the temperature difference between the wall temperature of the evaporator and the saturation temperature, $T_w - T_s$, remains less than the boiling superheat for a given pressure, bubble formation will not occur near the wall in the wick. When the local working fluid temperature inside the wick exceeds the saturation temperature corresponding to the local pressure and nucleation occurs, the bubbles that are formed will collapse and boiling will be avoided if the superheat is not sufficiently high enough. The equilibrium state for the bubbles, or the state at which the bubbles no longer collapse, is that thermodynamic state for which the Gibbs free energy between the liquid and vapor phases is minimized. Using the Clausius–Clapyeron relation, the superheat can be found as

$$T_l - T_s(p_l) = \frac{2\sigma T_s(p_l)}{h_{fg} r_e} \left(\frac{1}{\rho_v} - \frac{1}{\rho_l} \right) \quad (26)$$

If the vapor density is much smaller than the liquid density, Eq. 26 may be reduced to

$$T_l - T_s(p_l) = \frac{2\sigma T_s(p_l)}{\rho_v h_{fg} r_e} \quad (27)$$

where r_e is the meniscus radius of the vapor bubble formed in the wick structure of the heat pipe, which is directly related to the pore size of the wick structure. According to the theory presented by Hsu¹⁰ and the derivation presented by Carey,¹¹ an embryo bubble will grow and a cavity will become an active nucleation site if the equilibrium superheat becomes equaled or exceeded around the perimeter of the embryo. In order to avoid boiling near the base of the wick structure, the temperature difference between the wall and the saturation temperature must be less than the superheat required for bubble formation. Using the superheat obtained above, the critical heat flux related to the boiling limit can be found as

$$q'' = k_{\text{eff}}[T_l - T_s(p_l)] = \frac{k_{\text{eff}} 2\sigma T_s(p_l)}{\rho_v h_{fg} r_e}. \quad (28)$$

As can be seen, the boiling limit is sensitive to the effective thermal conductivity, k_{eff} , and the meniscus radius of the vapor bubble, r_e , at the wick–wall interface.

3.3 Entrainment Limit

In an operating heat pipe, when the vapor flow direction is opposite to the liquid flow direction, the frictional shear stress occurring at the liquid–vapor interface may slow down the return of liquid to the evaporator. As the vapor velocity increases, the vapor flow effect on the liquid–vapor interface increases depending on surface tension, viscosities, and densities of both the vapor and liquid phases. When the influence caused by the frictional shear stress acting on the liquid–vapor interface by the frictional vapor flow is large enough, the liquid flow cannot flow back to the evaporator. When this occurs, the liquid in the evaporator dries out. At this point the heat pipe reaches a heat transport limit, which is known as the entrainment limit. Based on a Weber number equal to unity, i.e., $We = F_{lv}/F_\sigma = 1$, where F_{lv} is the shear stress at the liquid–vapor interface and F_σ is the surface tension force, Cotter¹² developed an approximation of the entrainment limit as follows:

$$q_{\text{ent}} = A_v h_{fg} \left(\frac{\sigma \rho_v}{2r_{h,w}} \right)^{0.5} \quad (29)$$

where $r_{h,w}$ is the hydraulic radius of the wick surface pore.

3.4 Viscous Limit

When the vapor pressure from the evaporator to the condenser cannot overcome the vapor pressure drop caused by the viscous forces, the heat pipe reaches a heat transport limit, which is called the viscous limit. In particular, the viscous limit is reached when the vapor pressure in the condenser is equal to zero. Using assumptions of laminar flow, ideal gas, and zero pressure in the cap end of the condenser, the viscous limit can be determined by

$$q_{\text{vis}} = \frac{4r_v^2 h_{fg} \rho_{v,e} p_{v,e} A_v}{f_v \cdot \text{Re}_v \mu_v L_{\text{eff}}} \quad (30)$$

where $\rho_{v,e}$, $p_{v,e}$ are the vapor density and vapor pressure in the cap end of the evaporator, respectively.

3.5 Sonic Limit

When the vapor velocity at the exit of the evaporating section reaches the local sound speed, the vapor flow is choked. As the choked flow occurs, the vapor flow rate will not respond with the amount of heat added in the evaporator. The heat pipe has reached the maximum heat transport, which is called the sonic limit. If the vapor flow in the heat pipe can be approximated as one-dimensional flow with the assumptions of negligible frictional force and ideal gas, the sonic limit can be readily derived from the conservation of energy and momentum equations as follows:

$$q_s = A_v \rho_v h_{fg} \left[\frac{\gamma_v R_v T_0}{2(\gamma_v + 1)} \right]^{1/2} \quad (31)$$

where T_0 is the stagnation temperature and A_v and ρ_v are the cross-sectional area and vapor density, respectively, at the location where the local sound speed is reached. It should be noted that this might occur at the exit to the evaporator or any location in the condenser section if the cross-sectional area of the vapor flow path changes.

3.6 Effective Thermal Conductivity

While those operating limitations described above dominate the design of a heat pipe, the effective thermal conductivity provided by a heat pipe is a key factor for designing a highly efficient heat pipe cooling device. The effective thermal conductivity k_{eff} is related to the total temperature drop ΔT_{total} as

$$k_{\text{eff}} = \frac{q L_{\text{eff}}}{A_h \Delta T_{\text{total}}} \quad (32)$$

where A_h is the total cross-sectional area of the heat pipe. The total temperature drop ΔT_{total} across the heat pipe is the sum of: the temperature drop across the evaporator shell, $\Delta T_{e,\text{shell}}$; the temperature drop across the wick structure in the evaporator, $\Delta T_{e,\text{wick}}$; the temperature drop through the evaporating thin film, $\Delta T_{e,\text{film}}$; the temperature drop in the vapor flow, ΔT_v ; the temperature drop across the condensate film, $\Delta T_{c,\text{film}}$; the temperature drop across the wick structure at the condenser, $\Delta T_{c,\text{wick}}$; and the temperature drop across the condenser shell, $\Delta T_{c,\text{shell}}$, i.e.,

$$\Delta T_{\text{total}} = \Delta T_{e,\text{shell}} + \Delta T_{e,\text{wick}} + \Delta T_{e,\text{film}} + \Delta T_v + \Delta T_{c,\text{film}} + \Delta T_{c,\text{wick}} + \Delta T_{c,\text{shell}} \quad (33)$$

Temperature Drops across Shell and Wick. The temperature drop through the case shell material at both the evaporator and the condenser can be calculated by

$$\Delta T_{e,\text{shell}} = \frac{q_e' \delta_{e,\text{shell}}}{k_{\text{shell}}} \quad (34)$$

and

$$\Delta T_{c,\text{shell}} = \frac{q_c'' \delta_{c,\text{shell}}}{k_{\text{shell}}} \quad (35)$$

respectively. After heat travels through the wall, the heat reaches the working fluid in the wick. Provided that the wick is saturated with the working fluid and no boiling occurs in the wick, the heat will transfer through the wick, and evaporation will only occur at the liquid–vapor–solid interface. The heat transfer across the wick is dominated by the heat conduction. The temperature drop across the wick in the evaporator can be determined by

$$\Delta T_{e,\text{wick}} = \frac{q_e'' \delta_{\text{wick}}}{k_{\text{eff}}} \quad (36)$$

As shown in Eq. 36, the effective thermal conductivity of a wick plays a key role in the temperature drop in the wick. Since the effective thermal conductivity depends on the working fluid, porosity, and geometric configuration, it is very hard to find the exact effective thermal conductivity theoretically. Nevertheless, several approximations for the effective thermal conductivity have been developed. A list of common expressions for determining the effective thermal conductivity of the wick is presented in Table 3. It is clear from each of the listed expressions that the effective thermal conductivity of the wick is a function of the solid conductivity, k_s ; the working fluid conductivity, k_l ; and the porosity. However, in each of the relations

$$\lim_{\varepsilon \rightarrow 0} k_{\text{eff}} = k_s \quad \lim_{\varepsilon \rightarrow 1} k_{\text{eff}} = k_l$$

the manner by which the effective conductivity varies between the limiting cases is drastically different depending upon the type of arrangement of the wick structure. Comparing the various effective conductivity relations, as illustrated in Table 3 and Fig. 4, it becomes clear that sintering the metallic particles dramatically enhances the overall thermal conductivity.

Similar to the temperature drop calculation for the evaporator, the temperature drop across the wick in the condenser can be found as

$$\Delta T_{c,\text{wick}} = \frac{q_c'' \delta_{\text{wick}}}{k_{\text{eff}}} \quad (37)$$

Temperature Drop across Liquid–Vapor Interface. If heat is added to the wick structure, the heat is transferred through the wick filled with the working fluid, reaching the surface where the liquid–vapor–solid interface exists. There, by utilizing the thin-film evaporation, the heat is removed. The temperature drop across the evaporating thin film, as shown in Fig. 5, can be calculated from the thin-film thickness by solving the equations governing the heat transfer

Table 3 Expressions for Wick Effective Thermal Conductivities for Various Geometries

Wick Type	Expression for Effective Thermal Conductivity
Sintered Spheres	$k_{\text{Sintered}} = \frac{k_s[2k_s + k_l - 2\varepsilon(k_s - k_l)]}{2k_s + k_l + \varepsilon(k_s - k_l)}$
Packed Spheres	$k_{\text{PackedSpheres}} = \frac{k_l[(2k_l + k_s) - 2(1 - \varepsilon)(k_l - k_s)]}{(2k_l + k_s) + (1 - \varepsilon)(k_l - k_s)}$
Wick and Liquid in Series	$k_{\text{Series}} = \frac{k_l k_s}{k_s \varepsilon + k_l(1 - \varepsilon)}$
Wick and Liquid in Parallel	$k_{\text{Parallel}} = k_l \varepsilon + k_s(1 - \varepsilon)$
Wrapped Screens	$k_{\text{WrappedScreen}} = \frac{k_l[(k_l + k_s) - (1 - \varepsilon)(k_l - k_s)]}{(k_l + k_s) + (1 - \varepsilon)(k_l - k_s)}$

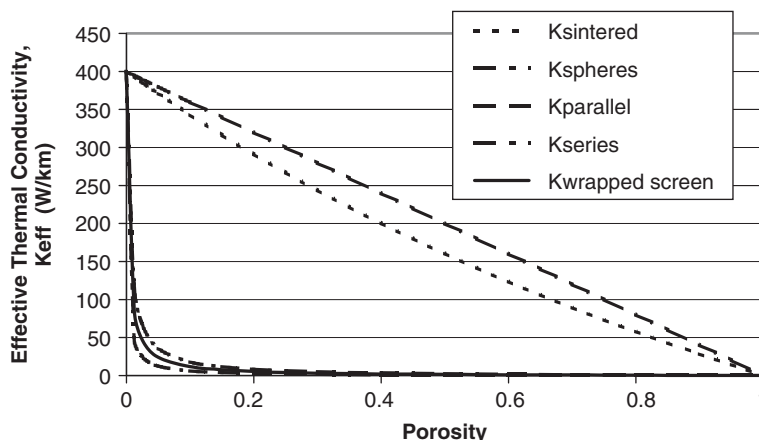


Figure 4 Effective thermal conductivities presented in Table 3.

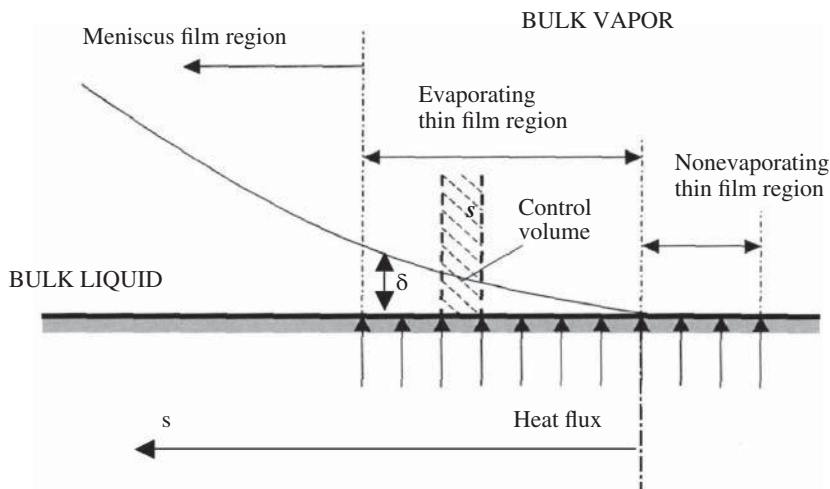


Figure 5 Thin-film evaporation.

and fluid flow in the thin-film region.¹³ The film thickness profile for a flat surface can be described by

$$\sigma \frac{dK}{ds} - \frac{dp_d}{ds} = - \frac{f_l^+ \cdot \text{Re}_\delta \mu_l \int_0^s \frac{q''(s)}{h_{fg}} ds}{2\delta^3(s)\rho_l} \tag{38}$$

for the steady-state evaporating process of a thin film, where the meniscus curvature K can be found by

$$K = \frac{\frac{d^2\delta}{ds^2}}{\left[1 + \left(\frac{d\delta}{ds}\right)^2\right]^{\frac{3}{2}}} \tag{39}$$

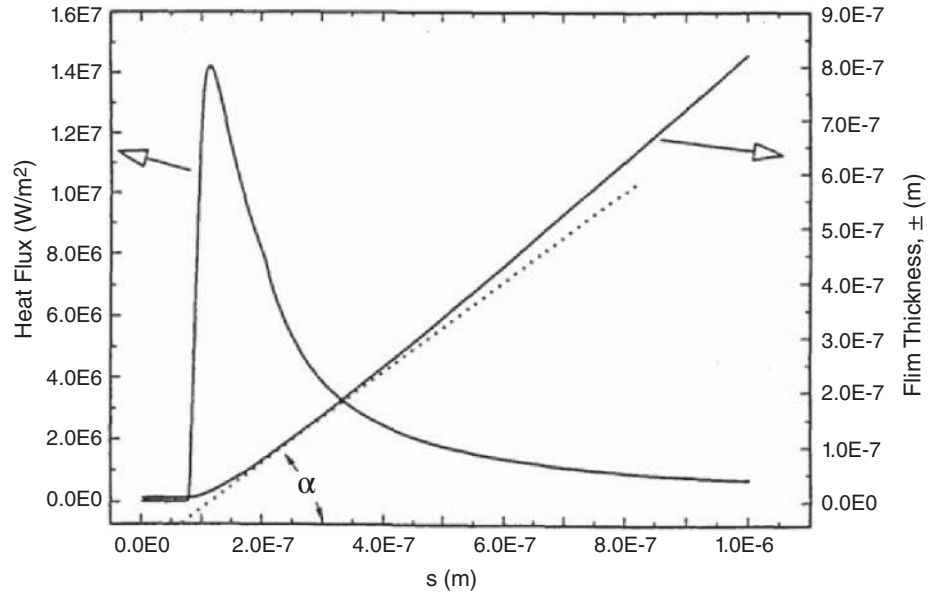


Figure 6 Heat flux distribution in thin-film region.

Using the conditions

$$\delta = \delta_0; \quad K = 0, \quad \frac{d\delta}{ds} = 0; \quad \text{at } s = 0 \quad (40)$$

with Eq. 38, the evaporating thin-film profile is obtained and the temperature drop across the evaporating thin film can be determined. As shown in Fig. 6, the heat flux level through the thin-film region can reach up to 1400 W/cm² with a superheat of 1.0°C. The optimization of thin-film evaporation in a high-heat-flux heat pipe design plays a key role.

Temperature Drop in Vapor Flow. In order to find the vapor velocity distribution and vapor pressure drop in a heat pipe, a three-dimensional model should be developed, particularly when the vapor space shape is irregular with evaporation occurring near the interline region. In order to obtain an effective tool, a simplified model can be used wherein the pressure drop at a given z location is found using a two-dimensional model, i.e.,

$$\frac{\partial^2 u_v}{\partial x^2} + \frac{\partial^2 u_v}{\partial y^2} = \frac{1}{\mu_v} \frac{dp_v}{dz} \quad (41)$$

The friction factor can be obtained based on the vapor channel cross section⁴ and the vapor flow along the z direction can be expressed as a one-dimensional momentum equation shown as

$$\frac{dp_v}{dz} + \rho_v g \sin \psi + \rho_v u_v \frac{du_v}{dz} = -f_v \frac{2\rho_v u_v^2}{d_{h,v}} \quad (42)$$

The vapor pressure varies from the evaporator section to the condenser section, due to frictional vapor flow, resulting in a temperature variation which can be predicted by the Clapeyron equation, i.e.,

$$T_v = \frac{T_{v,e}}{1 - \frac{RT_{v,e}}{h_{fg}} \ln \frac{p_e}{p_{v,e}}} \quad (43)$$

where $T_{v,e}$ is the vapor temperature in the evaporator and $p_{v,e}$ is the vapor pressure in the evaporator. Vapor flows through the adiabatic section to the condenser region. At the condensing section, vapor condenses due to the phase change driving force. The condensed fluid then is drawn into the wicking structure by a capillary force. Assuming that the heat pipe is charged with the proper amount of working fluid, the wick surface can be assumed to directly contact the saturated vapor. Therefore, the film thickness on the wicking structure is neglected while the temperature drop across the liquid–vapor interface in the condenser is equal to zero.

4 HEAT PIPE FABRICATION PROCESSES

4.1 Wicks

The wicks in a heat pipe are used to pump the condensate from the condenser to the evaporator. Figure 7 lists several wick structures currently being used in heat pipes. Among the wick structures shown in Fig. 7, the grooves, sintered metal, and wrapped screens are the most common wicks. The grooved wicks have been widely used in laptop computers for a relatively low heat load. The groove dimensions significantly affect the capillary limitation and effective thermal conductivity. When the groove configuration is different, as shown in Fig. 8, the heat transfer performance changes. For a given application, there exists an optimized groove configuration for the best heat transfer performance.

In addition to the grooved wick, another wick having higher effective thermal conductivity is the sintered metal. The sintered wick can be produced at a temperature of 50–200 °C below the melting point of the sintering material. The porosity of the sintered wick depends on the surrounding pressure, sintering temperature, and time. Also, the environmental gas can significantly help the sintering process. For example, when hydrogen is used as the environmental gas, it helps sinter the copper material. The heat transfer performance in a heat pipe with sintered wicks largely depends on the wick thickness, particle size, and porosity. For a given heat flux, there exists an optimum design for the evaporating heat transfer in a heat pipe with sintered wicks. As shown in Fig. 9, when the particle radius decreases, the optimum thickness increases.¹⁴ It is concluded that, if it is possible to decrease the particle radius while maintaining a constant porosity, the particle radius should be as small as possible. The impact of these results is that thicker sintered wicks, which are more readily manufactured and assembled into heat pipes, can provide heat removal capabilities equivalent to the thinner wicks.

The screen wick has been widely used in the conventional heat pipe. Stainless steel, copper, nickel, and aluminum meshes are commercially available for the screen wicks. Although the smallest pore size for the copper meshes is about 100 pores per inch, the smallest pore size for the stainless steel meshes can reach less than 5 μm in hydraulic diameter.

4.2 Working Fluid Selections

Because a heat pipe cannot function below the freezing point or above the critical temperature of its working fluid, the selected working fluid must be within this range. Table 4 lists some working fluids which can be used in the heat pipe for a given operating temperature. In addition, the vapor pressure, surface tension, contact angle, and viscosity in the heat pipe must be considered in the selection of working fluid. For example, the vapor pressure in the heat pipe should not be less than 0.1 atm or higher than 10 atm. Typical working fluids for cryogenic heat pipes include helium, argon, oxygen, and krypton. For most common low-temperature heat pipes ranging from 200 to 550 K, ammonia, acetone, and water are commonly employed. The typical working fluids being used in the high-temperature heat pipes are sodium, lithium, silver, and potassium. Furthermore, the more important factor in the selection of working fluid is the

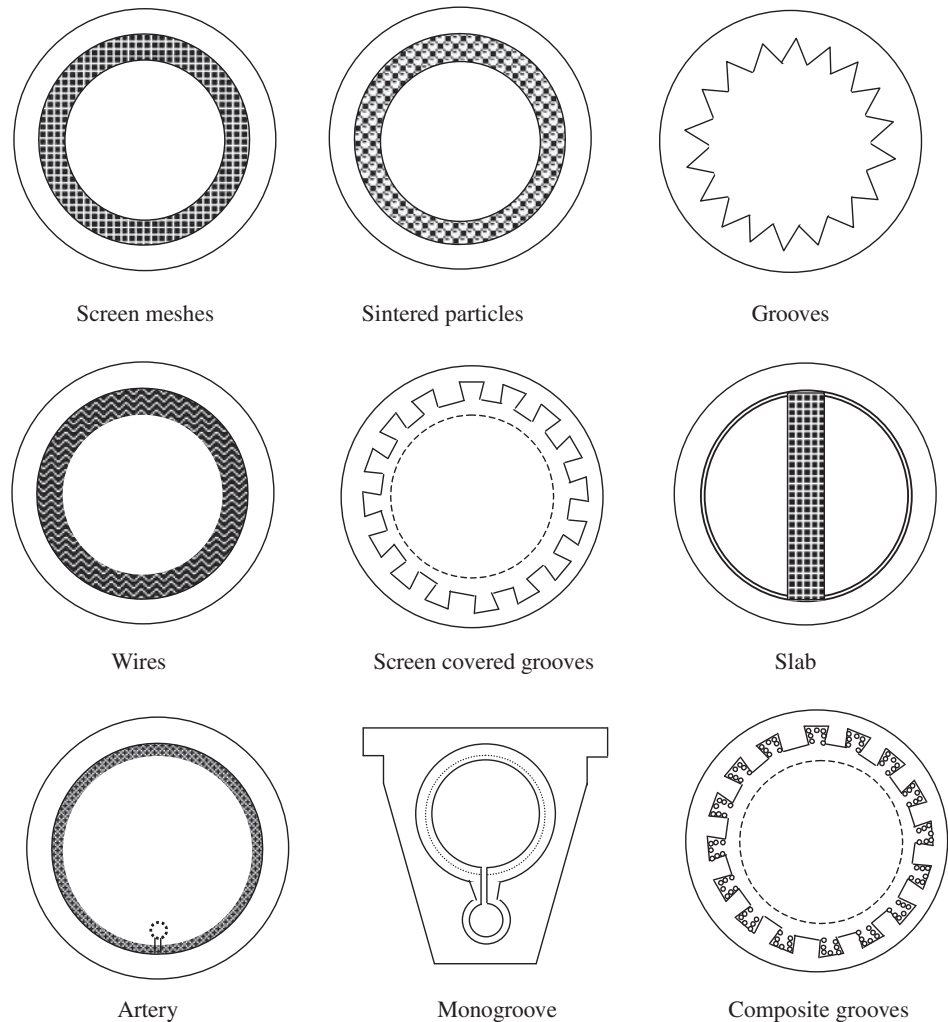


Figure 7 Some common wick structures.

compatibility with the case and wick materials. Table 5 lists results of compatibility tests of materials with some working fluids.

4.3 Cleaning and Charging

All of the materials used in a heat pipe must be clean. Cleanliness achieves two important objectives: 1 it ensures that the working fluid will wet the materials and 2 it keeps out any foreign matter that could hinder capillary action or create incompatibilities. The presence of contaminants in the solid, liquid, or gaseous state may be detrimental to heat pipe performance. If the interior of a heat pipe is not clean, degradation of the performance can result over time. Solid particles can physically block the wick structure, decreasing the liquid flow rate and increasing the likelihood of encountering the capillary limit. Oils from machining or from the human hand

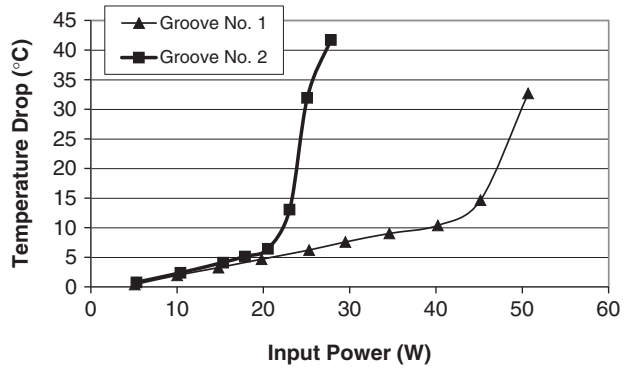
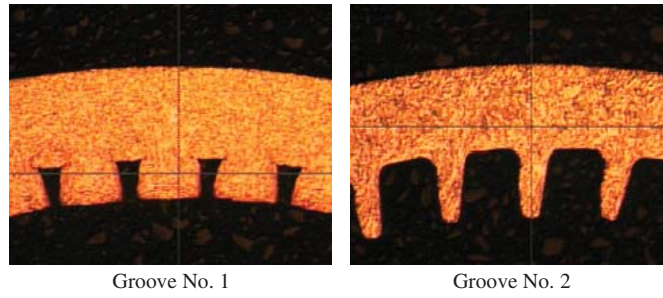


Figure 8 Groove configuration effect on temperature drops.

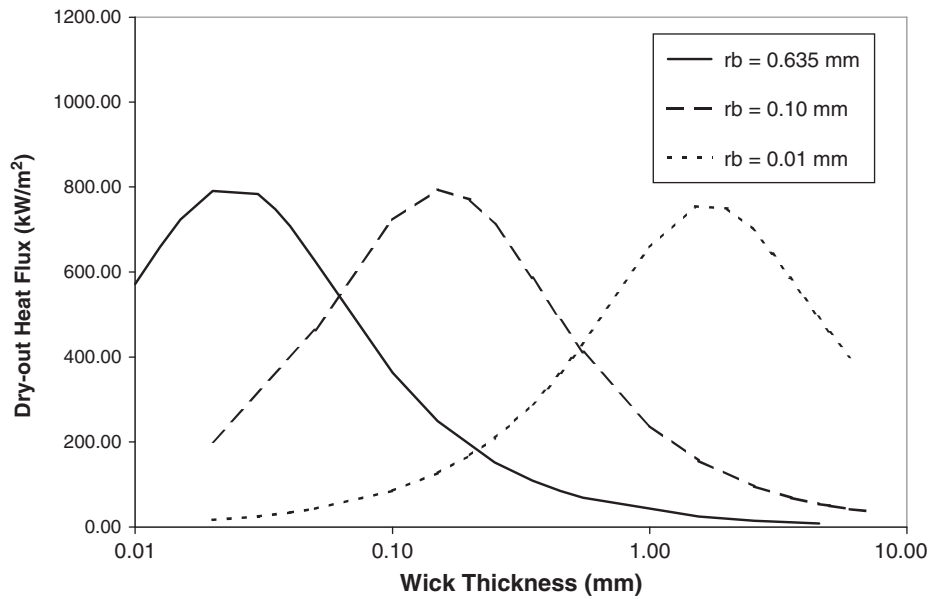


Figure 9 Particle size effect on dryout heat flux ($L = 0.254$ m; $\epsilon = 43\%$; $L_H = 0.01$ m; working fluid = water).

Table 4 Working Fluids and Temperature Ranges

Working Fluids	Melting Points, °K At 1 atm	Boiling Point, °K at 1 atm	Useful Range, °K
Helium	1	4.21	2–4
Hydrogen	13.8	20.38	14–31
Neon	24.4	27.09	27–37
Nitrogen	63.1	77.35	70–103
Argon	83.9	87.29	84–116
Oxygen	54.7	90.18	73–119
Methane	90.6	111.4	91–150
Krypton	115.8	119.7	116–160
Ethane	89.9	184.6	150–240
Freon 22	113.1	232.2	193–297
Ammonia	195.5	239.9	213–373
Freon 21	138.1	282	233–360
Freon 11	162.1	296.8	233–393
Pentane	143.1	309.2	253–393
Freon 113	236.5	320.8	263–373
Acetone	180	329.4	273–393
Methanol	175.1	337.8	283–403
Flutec PP2	223.1	349.1	283–433
Ethanol	158.7	351.5	273–403
Heptane	182.5	371.5	273–423
Water	273.1	373.1	303–473
Toluene	178.1	383.7	323–473
Flutec PP9	203.1	433.1	273–498
Naphthalene	353.4	490	408–478
Dowtherm	285.1	527	423–668
Mercury	234.2	630.1	523–923
Sulfur	385.9	717.8	530–947
Cesium	301.6	943	723–1173
Rubidium	312.7	959.2	800–1275
Potassium	336.4	1032	773–1273
Sodium	371	1151	873–1473
Lithium	453.7	1615	1273–2073
Calcium	1112	1762	1400–2100
Lead	600.6	2013	1670–2200
Indium	429.7	2353	2000–3000
silver	1234	2485	2073–2573

Source: From Ref. 9.

can decrease the wettability of the wick. Oxides formed on the wall and wick can also decrease the ability for the liquid to wet the surface. Therefore, proper cleaning of all of the parts in contact with the interior of the heat pipe (pipe, end caps, wick, and working fluid) is necessary for maximum reliability and performance. Several steps are needed in order to properly clean the heat pipe container and wick structure, such as solvent cleaning, vapor degreasing, alkaline cleaning, acid cleaning, passivation, pickling, ultrasonic cleaning, and vacuum baking. Many of these steps are used in a single cleaning operation.^{6,8}

It is necessary to treat the working fluid used in a heat pipe with the same care as that given to the wick and container. The working fluid should have the highest purity available, and further purification may be necessary following purchase. This may be carried out by distillation. The case of low-temperature working fluids, such as acetone, methanol, and ammonia

Table 5 Experimental Compatibility Tests

	Aluminum	Brass	Copper	Inconel	Iron	Nickel	Niobium	Silica	Stainless steel	Tantalum	Titanium	Tungsten
Acetone	C	C	C					C	C			
Ammonia	C		I		C	C			C			
Cesium							C				C	
Dowtherm			C					C	C			
Freon-11	C											
Heptane	C											
Lead				I		I	I		I	C	I	C
Lithium				I		I	C		I	C	I	C
Mercury					I	I	I		C	I	I	
Methanol		C	C		C			C	C			
Silver				I		I	I		I	C	I	C
Sodium				C		C	C		C		I	
Water	I		C	I		C		C	C		C	

Note: C, compatible; I, incompatible.

in the presence of water, can lead to incompatibilities, and the minimum possible water content should be achieved. The amount of working fluid required for a heat pipe can be approximately calculated by estimating the volume occupied by the working fluid in the wicking structure, including the volume of any arteries, grooves, cornered regions, and so on. The amount of working fluid charged to a heat pipe significantly affects the heat transfer performance of the heat pipe. For example, the heat transfer performance of a grooved heat pipe currently being used in a laptop computer is very sensitive to the charging amount of working fluid.

Once the required amount of working fluid is determined, the working fluid can be introduced into the heat pipe by an evacuation and back-filling technique, a liquid fill and vapor generation technique, a solid fill and sublimation technique, or a supercritical vapor technique.⁶ The most common among those for the low- or moderate-temperature working fluids currently being used for electronics cooling is the evacuation and back-fill techniques. All these charging methods are to prevent noncondensable gases from entering the heat pipe during the charging process. In order to charge the working fluid in, a suitable evacuation/filling rig must be applied. The rig must be able to evacuate the container to 10^{-4} torr or less. The filling rig is used to evacuate the pipe and charge it with the proper amount of working fluid. Details of the charging process depend on the state of the working fluid at the ambient temperature. The material of construction is generally glass, stainless steel, or plastic materials. Glass has advantages when handling liquids in that the presence of liquid droplets within the ductwork can be observed and their vaporization under vacuum noted. Stainless steel has obvious strength benefits. If plastic materials are chosen, the working fluid used in the charging process could not react with plastic.

4.4 Testing

The test facility needs to be established to test the heat transfer performance and heat transport limitations. Both transient and steady-state tests should be conducted for a heat pipe. For low-temperature heat pipes, however, the steady-state test is given the highest priority. A typical experimental system for low-temperature heat pipes, similar to the one shown in Fig. 10, would normally be used. The test facility shown in Fig. 10 consists of the heat pipe, a heat power supply and measuring unit, a cooling unit, and a data acquisition unit for the temperature measurements. The operating temperature of the heat pipe can be controlled by a cooling

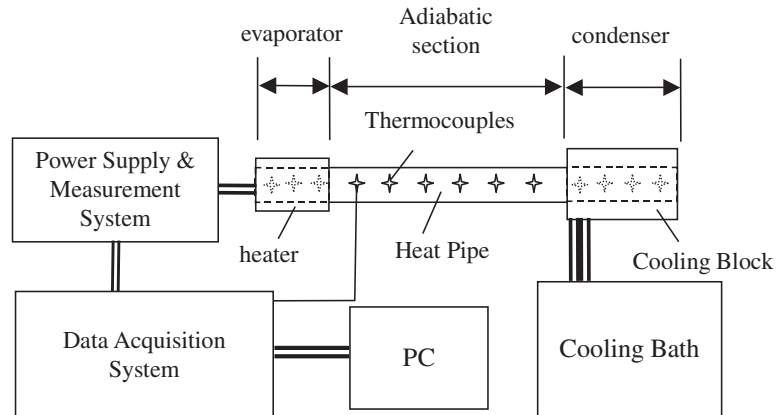


Figure 10 Heat pipe test apparatus

block connected to a cooling bath, where the temperature of the coolant is maintained at a constant temperature of a designed operating temperature. The heat source is directly connected to the evaporator. Power input can be supplied by an AC or DC power supply and recorded by multimeters with signals sent directly to a personal computer which can be used to control the entire system. The heat source should be well insulated to reduce convective losses. A number of temperature sensors are attached to the heat pipe surfaces to measure the temperature distribution on the heat pipe and temperature variation with the power input. All of the measured data are sent to the data acquisition system controlled by a personal computer. Prior to the start of the experiment, the system is allowed to equilibrate and reach steady state such that the temperatures of the cooling media and the heat pipe are constant. When this desired steady-state condition is obtained, the input power is then increased in small increments. Previous tests indicate that a time of approximately 5–30 min is necessary to reach steady state. To obtain the data for the next successive power level, the power is incremented every 5–30 min. During the tests, the power input and the temperature data are simultaneously recorded using a data acquisition system controlled by a personal computer.

5 OTHER TYPES OF HEAT PIPES

5.1 Thermosyphon

One of the simplest heat pipes is the thermosyphon. As shown in Fig. 11, a thermosyphon is a vertically oriented wickless heat pipe with a liquid pool at the bottom. A typical thermosyphon consists of three sections similar to the conventional heat pipe. As heat is added to the evaporator section where a liquid pool exists, the liquid vaporizes. The vapor rises and passes through the adiabatic section to the condenser section, where the vapor gives up its latent heat and condenses into liquid. The condensate is then pumped from the condenser to the evaporator by gravitational force. In a conventional thermosyphon, the evaporator must be located below the condenser for satisfactory operation because the device has to rely on gravity for condensate return. Therefore, thermosyphons are ineffective in zero gravity or microgravity. The thermosyphon has been widely used in the preservation of permafrost, electronics cooling, and heat pipe exchangers due to its highly efficient heat transfer performance, high level of temperature distribution, simplicity and reliability, as well as cost effectiveness. Heat transfer limitations such as the dryout limit, flooding and entrainment limit, and boiling limit should be

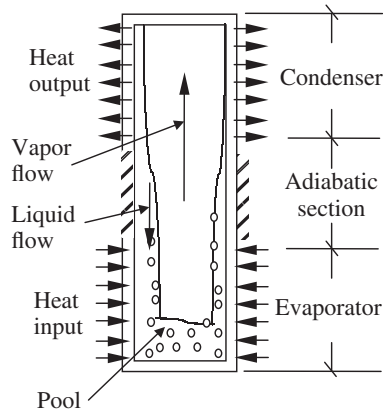


Figure 11 Schematic of thermosyphon.

considered during the design of thermosyphons. The dryout limitation might occur when the amount of working fluid in the evaporator is not sufficient and the heat added to the evaporator cannot be removed, which would result in a significant temperature increase. This is similar to the critical heat flux in pool boiling. Flooding and entrainment limits involve the interfacial shear stress between the countercurrent vapor and liquid flows. Boiling limitation can be found in a thermosyphon with large fill volumes and high radial heat flux in the evaporator.

5.2 Loop Heat Pipes/Capillary Pumped Loop

The loop heat pipe (LHP) and capillary pumped loop (CPL) utilize the capillary pressure developed in a fine pore wick to circulate the working fluid in a closed-loop system. Figure 12 shows the schematic of the CPL. The liquid phase flows through the liquid line from the condenser to the evaporator and the vapor flows from the evaporator to the condenser through the vapor line. The LHP or CPL can significantly reduce or eliminate the liquid pressure drop and vapor

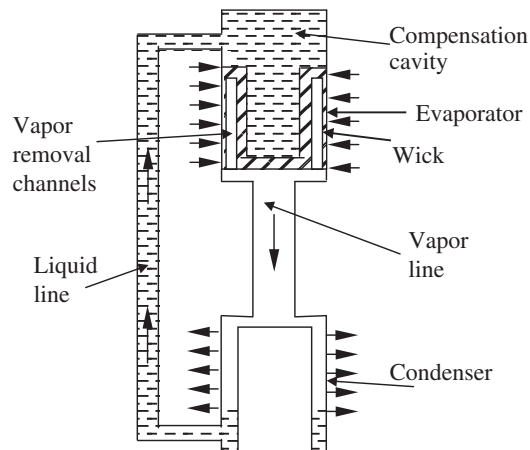


Figure 12 Schematic of capillary pumped loop/loop heat pipe.

flow effect on the liquid flow, resulting in a significant increase in the capillary pumping ability. Because the evaporator in a LHP or CPL is used not only as the heat sink to remove the heat but also as the source to provide the total capillary pumping pressure, a highly efficient evaporator is the key to success for a LHP or CPL. Compared to a conventional heat pipe, LHP or CPL systems have the potential to transport large amounts of heat over long distances at various orientations with minimal temperature drops and no external pumping power. Due to this unique feature, the LHP or CPL is especially suitable to the space station program, advanced communication satellite, high powered spacecraft, and electronics cooling, which require large heat dissipation. It is anticipated that the CPL or LHP will play an important role in the thermal management of space and terrestrial systems in the future.

Oscillating Heat Pipes

In 1990, Akachi¹⁵ invented the oscillating heat pipe (OHP). A typical OHP, as shown in Fig. 13, consists of a train of liquid plugs and vapor bubbles. The diameter of the OHP must be small enough so that liquid plugs can be separated by vapor bubbles. A typical OHP has three sections: an evaporating section, an adiabatic section, and a condensing section. As heat is added on the evaporating section, the vaporization in the evaporating section causes the vapor volume expansion, and the heat removal in the condensing section causes the vapor volume contraction. The expansion and contraction of vapor volume plus the thermal energy added on the system generate the oscillating motion of liquid plugs and vapor bubbles in the system. In addition to the oscillating motion observed in the system, the pulsating motions of liquid plugs and vapor bubbles exist at the same time. For this reason, the OHP is sometimes called a pulsating heat pipe (PHP). The oscillating motion in the OHP depends on the dimensions, working fluids, operating temperature, surface conditions, heat flux and total heat load, orientation, turns, and most importantly the filled ratio, V_l/V_t , where V_l is the liquid volume occupied by the liquid in the system and V_t is the total volume.^{16,17} Utilizing phase change heat transfer and forced convection, the heat is transferred from the evaporating section to the condensing section. Compared with the conventional heat pipe, the OHP has the following features: 1 an OHP is an “active” cooling device that converts heat from the heating area into the kinetic energy of liquid plugs to initiate and sustain the oscillating motion; 2 the liquid flow does not interfere with the vapor flow because both phases flow in the same direction; 3 the thermally driven oscillating flow inside the capillary tube effectively produces some free surfaces that significantly enhance evaporating and condensing heat transfer; 4 the oscillating motion in the capillary tube significantly improves the forced convection in addition to the phase change heat transfer; and 5 as the input power increases, the heat transport capability of an OHP dramatically increases. Because

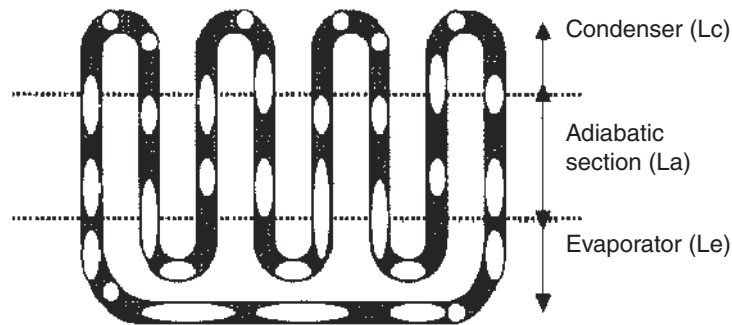


Figure 13 Schematic of oscillating heat pipe.

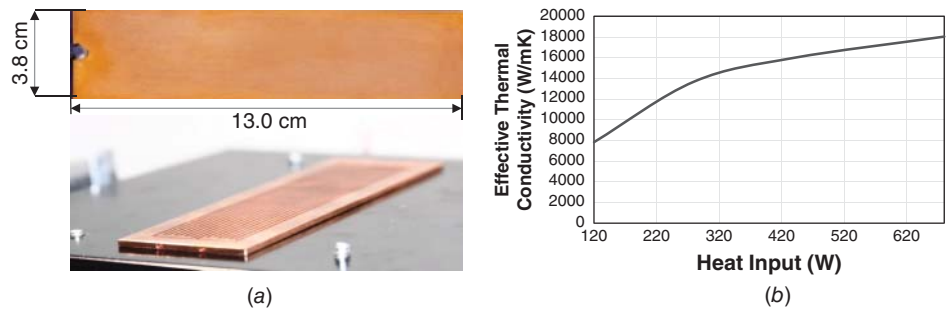


Figure 14 Heat transfer performance of flat-plate OHP: (a) photos and (b) effective thermal conductivity. Courtesy of ThermAvant Technologies, LLC.

of these features, the working mechanism and design of OHPs have been extensively investigated recently.^{18–22} When nanoparticles are added in an OHP, it can significantly increase the heat transfer performance.¹⁸ Check valves embedded in an OHP can improve the heat transfer performance.¹⁹ Most importantly, an OHP can be developed into a gravity-independent heat transfer device,²⁰ which is very different from the conventional heat pipe. Most recently, it has been demonstrated that when the tubular OHPs are developed into flat-plate OHPs, the heat flux level and total power can be significantly increased.^{21,22} For example, one OHP with dimensions of 130 mm × 38 mm × 2.0 mm as shown in Fig. 14 achieved an effective thermal conductivity higher than 18,000 W/mK with a heat flux level of 108 W/cm² and a total power up to 680 W.

5.3 Vapor Chamber

Vapor chambers (see Fig. 15), also named flat heat pipes, have the same primary components as a typical tubular heat pipe. These components consist of a hermetically sealed hollow chamber, a working fluid, and a wick structure. Compared to a one-dimensional tubular heat pipe, a typical vapor chamber is a two-dimensional heat pipe with a thickness much less than the other two dimensions. The thickness can be as thin as 0.5 mm. Due to this unique dimension feature, the vapor chamber has been widely used as heat spreaders to spread heat generated from microelectronic components or systems. When the thickness is very small, the cross-sectional area of vapor flow is significantly reduced, which directly limits the heat transport capability. In addition, the thickness reduction makes the wick thickness as thin as possible, which directly limits the capillary pressure in a vapor chamber. A number of new approaches, such as nanostructured wicks,^{23,24} have been taken to further increase the capillary pressure and enhance heat transfer.

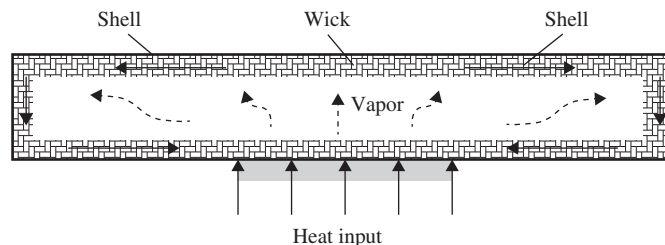


Figure 15 Schematic of cross sectional view of vapor chamber.

5.4 Micro Heat Pipes

In 1984, Cotter²⁵ first introduced the concept of very small “micro” heat pipes which were incorporated into semiconductor devices to promote more uniform temperature distributions and improve thermal control. The micro heat pipe was defined as a heat pipe in which the mean curvature of the liquid–vapor interface is comparable in magnitude to the reciprocal of the hydraulic radius of the total flow channel. Based on this definition, the hydraulic diameter of a typical micro heat pipe ranges from 10 to 500 μm . The fundamental operating principle of micro heat pipes is essentially the same as those occurring in relatively large conventional heat pipes. A typical micro heat pipe, shown in Fig. 16, is using the cornered region to pump the condensate from the condenser to the evaporator. As heat is added to the evaporating section, the liquid vaporizes and the vapor brings the heat through the adiabatic section to the condensing section, where the vapor condenses into liquid and releases latent heat. The heat addition on the evaporating section causes the liquid to recede into the cornered region and directly reduces the meniscus radius at the liquid–vapor interface in the evaporator. This vaporization and condensation process causes the liquid–vapor interface in the liquid arteries to change continually along the pipe and results in a capillary pressure difference between the evaporator and condenser regions. This capillary pressure difference promotes the flow of the working fluid from the condenser back to the evaporator. As the size of the heat pipe decreases, however, the micro heat pipe may encounter vapor continuum limitation. This limitation may prevent the micro heat pipe from working under lower temperatures. In addition to the vapor continuum limitation, the micro heat pipe is also subject to the operating limits occurring in the conventional

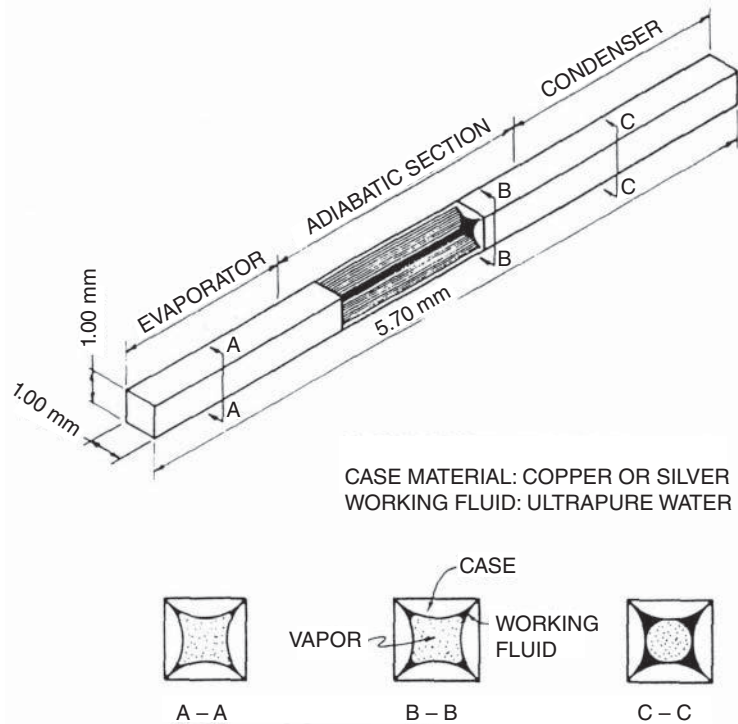


Figure 16 Schematic of micro heat pipe.

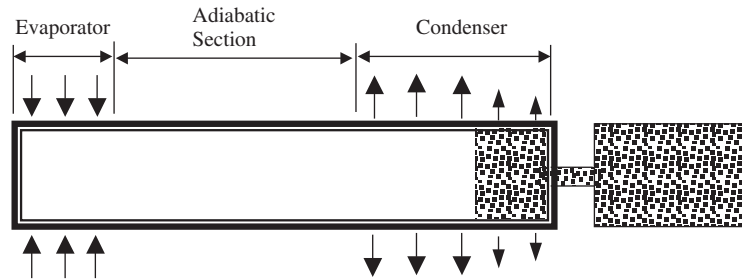


Figure 17 Schematic of variable-conductance heat pipe.

heat pipe. Of those operating limits, the capillary limitation remains the most important for the micro heat pipe. The micro heat pipes have been widely used in electronics cooling.

5.5 Variable-Conductance Heat Pipes

For a typical conventional heat pipe, the operating temperature can be determined by the heat removal rate from the condenser. When the heat load increases, the temperature drop from the evaporator to the condenser increases if the condensing area is constant. However, there are some applications where the evaporator or condenser temperature needs to be kept constant with a varying heat input. The variable-conductance heat pipe is suitable for this function design and its unique feature is the ability to maintain a device mounted at the evaporator at a near-constant temperature, independent of the amount of power being generated by the device. In order to keep the operating temperature independent of the heat input, the whole conductance of the heat pipe should be varied with the heat load. Figure 17 illustrates a typical variable-conductance heat pipe (VCHP). Compared to a conventional heat pipe, the VCHP as shown in Fig. 17 includes a gas reservoir containing noncondensable gas. When the input power is low, the vapor pressure inside the heat pipe is low. The volume of noncondensable gas expands and reduces the condensing area. When the input power is high, the vapor pressure increases, resulting in the contraction of vapor volume and directly increasing the condensing area. As a result, the temperature drop from the evaporator to the condenser is fairly constant. As shown in Fig. 15, the noncondensable gas is used to moderate the conductance as the input power is varied, giving the device the name gas-loaded variable heat pipe. Based on the same principle, several other VCHPs have been developed to moderate the conductance change in the heat pipe such as vapor-flow-modulated heat pipes, excess-liquid heat pipes, and liquid-flow-modulated heat pipes (thermal diodes)⁶.

5.6 Rotating Heat Pipes

The rotating heat pipe consists of a sealed hollow shaft which contains a fixed amount of working fluid. The rotating heat pipe can be divided into two types: with an internal taper and without an internal taper. Compared to a conventional heat pipe, the rotating heat pipe has the following advantages: (1) the condensate in the rotating heat pipe is returned to the evaporator by centrifugal force; (2) the rotational speed plays the most important role for its heat transfer performance; (3) the heat transfer performance is enhanced for a rotating heat pipe with an internal taper because the removal of the condensate from the cooled liquid surface by centrifugal action helps move the condensate back toward the evaporator; and (4) the sonic, entrainment, boiling, and condensing limits are the primary factors limiting the heat transfer capacity in the rotating heat pipe. For detailed information related to the rotating heat pipes, the reader is referred to the books written by Peterson⁶ and Fahgri.⁹

5.7 High-Temperature Heat Pipes (Metal Heat Pipes)

Because most working fluids in high-temperature heat pipes are metal, a high-temperature heat pipe is also called a metal heat pipe. Due to the higher surface tension, higher latent heat of vaporization, and higher thermal conductivity, the high-temperature heat pipes can transport large heat load and reach a very high level of temperature uniformity, and they have been employed for advanced energy systems such as advanced thermophotovoltaic advanced gas turbine engines and nuclear reactors. Table 4 lists some commonly used working fluids and their temperature ranges. However, compared with those heat pipes operating at other temperature ranges, the high-temperature heat pipe possesses some obstructions such as a corrosion/reliability concern, high chemical reactivity, start-up control, and severe work condition due to too high operating temperature.

5.8 Cryogenic Heat Pipes

Cryogenic fluids are used in the cryogenic heat pipe. These working fluids are either a chemically pure material such as helium, argon, krypton, nitrogen, or oxygen or a chemical compound such as methane, ethane, or Freon. The operating temperature ranges for these fluids are listed in Table 4. For cryogenic fluids at a low temperature, the surface tension, thermal conductivity, and latent heat of vaporization are relatively low and the liquid viscosity is much higher. As a result, the heat pipe optimized for zero-gravity operation would not properly prime in a 1g environment due to the low surface tension. The very high vapor pressure in the heat pipe during storage and the low operating temperature, where the cooling methods to remove heat from the condenser are limited, are also concerned for the cryogenic heat pipes. The capillary limit, sonic limit, entrainment limit, or boiling limit governs the heat transport limitation. Of those operating limits, the capillary limit from the low surface tension is the primary factor affecting the heat transfer performance in the cryogenic heat pipes. For this reason, considerable effort has been conducted to develop wicking structures that further increase the capillary limitation.

NOMENCLATURE

A	Cross-sectional area, m^2
C	Constant
c	Specific heat, $J/kg \cdot K$
d	Diameter, m
f	Friction factor
F	Correction factor
g	Gravitational acceleration, m/s^2
h_{fg}	Latent heat, J/kg
k	Thermal conductivity, $W/m \cdot K$
K	Curvature, m^{-1} ; permeability, m^2
L	Length, m
Ma	Mach number
m	Mass flow rate, kg/s
N	Mesh number
r	Radius, m
R	Universal constant, $J/kg \cdot K$
p	Pressure, N/m^2
P	Perimeter, m
q	Heat transfer, W

q''	Heat flux, W/m ²
Re	Reynolds number
s	Coordinate, m
S	Crimping factor
T	Temperature, °C
u	Vertical velocity, m/s
\bar{u}	Average velocity, m/s
We	Weber number
x	Coordinate, m
y	Coordinate, m
z	Coordinate, m

Greek Symbols

α	Contact angle, degree
δ	Film thickness, m
ε	Porosity
γ	Ratio of specific heats
ψ	Tilt angle, degree
μ	Dynamic viscosity, N · s/m ²
ρ	Mass density, kg/m ³
σ	Surface tension, N/m
τ	Shear stress, N/m ²

Subscripts

+	Normal direction
a	Adiabatic section
c	Capillary, condensation, condenser
d	Disjoining
e	Evaporation, evaporator
eff	Effective
ent	Entrainment
film	Film
g	Gravity
h	Hydraulic
l	Liquid
lv	Liquid–vapor
m	Meniscus
max	Maximum
r	Radial
s	Sintered particles, saturation, solid, sonic
shell	Shell
sl	Solid-liquid
sv	Solid-vapor
t	Capillary tube
total	Total
v	Vapor
vis	Viscous
w	Wire, wick

REFERENCES

1. L. P. Perkins and W. E. Buck, "Improvement in Devices for the Diffusion or Transference of Heat," U.K. Patent 22,272, London, England, 1892.
2. C. R. King, "Perkins Hermetic Tube Boiler," *The Engineer*, **152**, 405–406, 1931.
3. H. B. Ma, and G. P. Peterson, "The Minimum Meniscus Radius and Capillary Heat Transport limit in Micro Heat Pipes," *ASME J. Heat Transfer*, **120**(1), 227–233, 1998.
4. H. B. Ma, G. P. Peterson, and X. J. Lu, "The Influence of Vapor-Liquid Interactions on the Liquid Pressure Drop in Triangular Microgrooves," *Int. J. Heat Mass Transfer*, **37**(15), 2211–2219, 1994.
5. B. D. Marcus, "Theory and Design of Variable Conductance Heat Pipes," Report No. NASA CR, 2018, NASA, Washington, D.C., April 1972.
6. G. P. Peterson, *An Introduction to Heat Pipes*, Wiley, New York, 1994.
7. S. W. Chi, *Heat Pipe Theory and Practice*, McGraw-Hill, New York, 1976.
8. P. D. Dunn and D. A. Reay, *Heat Pipes*, Pergamon, New York, 1995.
9. A. Faghri, *Heat Pipe Science and Technology*, Taylor & Francis, New York, 1995.
10. Y. Y. Hus, "On the Size Range of Active Nucleation Cavities on a Heating Surface," *ASME J. Heat Transfer*, **84**, 207–213, 1962.
11. V. P. Carey, *Liquid-Vapor Phase-Change Phenomena*, Taylor & Francis, New York, 1992.
12. T. P. Cotter, "Heat Pipe Startup Dynamics," in *Proceedings of the SAE Thermionic Conversion Specialist Conference*, Palo Alto, CA, 1967.
13. H. B. Ma and G. P. Peterson, "Temperature Variation and Heat Transfer in Triangular Grooves with an Evaporating Film," *AIAA J. Thermophys. Heat Transfer*, **11**(1), 90–97, 1997.
14. M. A. Hanlon and H. B. Ma, "Evaporation Heat Transfer in Sintered Porous Media," *ASME J. Heat Transfer*, **125**, 644–653, August 2003.
15. H. Akachi, "Structure of a Heat Pipe," U.S. Patent No. 4,921,041. 1990.
16. H. B. Ma, M. R. Maschmann, and S. B. Liang, "Heat Transport Capability in Pulsating Heat Pipes," in *Proceedings of the 8th AIAA/ASME Joint Thermophysics and Heat Transfer Conference*, St. Louis, MO, June 24–27 2002.
17. H. B. Ma, M. A. Hanlon, and C. L. Chen, "Investigation of the Oscillating Motion in a Pulsating Heat Pipe," in *Proceedings of NHTC01, 35th National Heat Transfer Conference*, NHTC2001, 20149, Anaheim, CA. June 10–12 2001.
18. H. B. Ma, C. Wison, B. Borgmeyer, H. Park, Q. Yu, M. Tirumala, and S. Choi, "Nanofluid Effect on the Heat Transport Capability in an Oscillating Heat Pipe," *Appl. Phys. Lett.*, **88**(1–3), 143116, 2006.
19. S. M. Thompson, H. B. Ma, and C. Wilson, "Investigation of a Flat-Plate Oscillating Heat Pipe with Tesla-Type Check Valves," *J. Exp. Thermal Fluid Sci.*, **35**(7), 1265–1273, 2011.
20. S. M. Thompson, A. A. Hathaway, C. D. Smoot, C. A. Wilson, H. B. Ma, R. M. Young, L. Greenberg, B. R. Osick, S. Van Campen, B. C. Morgan, D. Sharar, and N. Jankowski, "Robust Thermal Performance of a Flat-Plate Oscillating Heat Pipe during High-Gravity Loading," *ASME J. Heat Transfer*, **133**(10), 1045041-5, 2011.
21. H. B. Ma, B. Borgmeyer, P. Cheng, and Y. Zhang, "Heat Transport Capability in an Oscillating Heat Pipe," *ASME J. Heat Transfer*, **130**, 0815011-7, 2008.
22. S. M. Thompson, H. B. Ma, R. A. Winholtz, and C. Wilson, "Experimental Investigation of Miniature Three-Dimensional Flat-Plate Oscillating Heat Pipe," *ASME J. Heat Transfer*, **131**, 0432101-9, 2009.
23. A. Chu, R. Xiao, and E. N. Wang, "Uni-Directional Liquid Spreading on Asymmetric Nanostructured Surfaces," *Nature Mater.*, **9**, 413–417, 2010.
24. J. A. Weibel, S. S. Kim, T. S. Fisher, and S. V. Garimella, "Carbon Nanotube Coatings for Enhanced Capillary-Fed Boiling from Porous Microstructures," *Nanoscale Microscale Thermophys. Eng.*, **16**, 1–17, 2012.
25. T. P. Cotter, "Principles and Prospects of Micro heat Pipes," in *Proceedings of the 5th International Heat Pipe Conference*, Tsukuba, Japan, 1984, pp. 328–335.

CHAPTER 11

AIR HEATING

Richard J. Reed
North American Manufacturing Company
Cleveland, Ohio

1	AIR-HEATING PROCESSES	443	4	BENEFITS	446
2	COSTS	445		REFERENCES	450
3	WARNINGS	445			

1 AIR-HEATING PROCESSES

Air can be heated by burning fuel or by recovering waste heat from another process. In either case, the heat can be transferred to air directly or indirectly. *Indirect air heaters* are heat exchangers wherein the products of combustion never contact or mix with the air to be heated. In waste heat recovery, the heat exchanger is termed a *recuperator*.

Direct air heaters, or *direct-fired air heaters*, heat the air by intentionally mixing the products or combustion of waste gas with the air to be heated. They are most commonly used for ovens and dryers. It may be impractical to use them for space heating or for preheating combustion air because of lack of oxygen in the resulting mixture (“vitiating air”). In some cases, direct-fired air heating may be limited by codes and/or by presence of harmful matter of undesirable odors from the heating stream. Direct-fired air heaters have lower first cost and lower operating (fuel) cost than indirect air heaters.

Heat requirements for direct-fired air heating. Table 1 lists the gross Btu of fuel input required to heat one standard cubic foot of air from a given inlet temperature to a given outlet temperature. It is based on natural gas at 60°F, having 1000 gross Btu/ft³, 910 net Btu/ft³, and stoichiometric air/gas ratio of 9.4:1. The oxygen for combustion is supplied by the air that is being heated. The hot outlet “air” includes combustion products obtained from burning sufficient natural gas to raise the air to the indicated outlet temperature.

Recovered waste heat from another nearby heating process can be used for process heating, space heating, or preheating combustion air (Ref. 1). If the waste stream is largely nitrogen, and if the temperatures of both streams are between 0 and 800°F, where specific heats are about 0.24, a simplified heat balance can be used to evaluate the mixing conditions: Heat content of the waste stream + heat content of the fresh air = heat content of the mixture, or

$$W_w T_w + W_f T_f = W_m T_m = (W_w + W_f) T_m$$

where W = weight and T = temperature of waste gas, fresh air, and mixture (subscripts w , f , and m).

Table 1 Heat Requirements for Direct-Fired Air Heating, Gross Btu of Fuel Input per scf of Outlet “Air”

Inlet Air Temperature, °F	Outlet Air Temperature, °F														
	100	200	300	400	500	600	700	800	900	1000	1100	1200	1300	1400	1500
-20	2.39	4.43	6.51	8.63	10.8	13.0	15.2	17.5	19.9	22.2	24.7	27.1	29.7	32.2	34.9
0	2.00	4.04	6.11	8.23	10.4	12.6	14.8	17.1	19.5	21.8	24.3	26.7	29.3	31.8	34.4
+20	1.60	3.64	5.71	7.83	9.99	12.2	14.4	16.7	19.0	21.4	23.8	26.3	28.8	31.4	34.0
40	1.20	3.24	5.31	7.43	9.58	11.8	14.0	16.3	18.6	21.0	23.4	25.9	28.4	31.0	33.6
60	0.802	2.84	4.91	7.02	9.18	11.4	13.6	15.9	18.2	20.6	23.0	25.5	28.0	30.6	33.2
80	0.402	2.43	4.51	6.62	8.77	11.0	13.2	15.5	17.8	20.2	22.6	25.1	27.6	30.1	32.7
100		2.03	4.10	6.21	8.36	10.6	12.8	15.1	17.4	19.8	22.2	24.6	27.2	29.7	32.3
200			2.06	4.17	6.31	8.50	10.7	13.0	15.3	17.7	20.1	22.5	25.0	27.6	30.2
300				2.10	4.23	6.41	8.63	10.9	13.2	15.5	17.9	20.4	22.9	25.4	28.0
400					2.13	4.30	6.51	8.76	11.1	13.4	15.8	18.2	20.7	23.2	25.8
500						2.16	4.36	6.61	8.90	11.2	13.6	16.0	18.5	21.0	23.6
600							2.19	4.43	6.71	9.03	11.4	13.8	16.3	18.8	21.3
700								2.23	4.50	6.81	9.16	11.6	14.0	16.5	19.0
800									2.26	4.56	6.91	9.30	11.7	14.2	16.7
900										2.29	4.63	7.01	9.43	11.9	14.4
1000											2.32	4.69	7.11	9.57	12.1

Example: Find the amount of natural gas required to heat 1000 scfm of air from 400 to 1400°F.

Solution: From the table, read 23.2 gross Btu/scf air. Then

$$\left(\frac{23.2 \text{ gross Btu}}{\text{scf air}} \times \frac{1000 \text{ scf air}}{\text{min}} \times \frac{60 \text{ min}}{1 \text{ h}} \right) \div \frac{1000 \text{ gross Btu}}{\text{ft}^3 \text{ gas}} = 1392 \text{ cfh gas.}$$

The conventional formula derived from the specific heat equation is

$$Q = wc\Delta T; \text{ so Btu/h} = \text{weight/h} \times \text{specific heat} \times \text{temp rise} = \frac{\text{scf}}{\text{min}} \times \frac{60 \text{ min}}{\text{h}} \times \frac{0.076 \text{ lb}}{\text{ft}^3} \times \frac{0.24 \text{ Btu}}{\text{lb } ^\circ\text{F}} \times ^\circ\text{rise} = \text{scfm} \times 1.1 \times ^\circ\text{rise.}$$

The table incorporates many refinements not considered in the conventional formulas: (a) % available heat which corrects for heat loss to dry flue gases and the heat loss due to heat of vaporization in the water formed by combustion, (b) the specific heats of the products of combustion (N_2 , CO_2 , and H_2O) are not the same as that of air, and (c) the specific heats of the combustion products change at higher temperatures.

For this example, the rule of thumb would give $1000 \text{ scfm} \times 1.1 \times (1400 - 400) = 1,100,000 \text{ gross Btu/h}$; whereas the example finds $1392 \times 1000 = 1,392,000 \text{ gross Btu/h}$ required. *Reminder:* The fuel being burned adds volume and weight to the stream being heated.

Example 1

If a 600°F waste gas stream flowing at 100 lb/h is available to mix with 10°F fresh air and fuel, how many pounds per hour of 110°F makeup air can be produced?

Solution:

$$(100 \times 600) + 10W_f = (100 + W_f) \times (110)$$

Solving, we find $W_f = 490 \text{ lb/h}$ of fresh air can be heated to 110°F, but the 100 lb/h of waste gas will be mixed with it; so the delivered stream, W_m , will be $100 + 490 = 590 \text{ lb/h}$.

If “indirect” air heating is necessary, a heat exchanger (recuperator or regenerator) must be used. These may take many forms, such as plate-type heat exchangers, shell-and-tube heat exchangers, double-pipe heat exchangers, heat pipe exchangers, heat wheels, pebble heater recuperators, and refractory checkerworks. The supplier of the heat exchanger should be able to predict the air preheat temperature and the final waste gas temperature. The amount of heat recovered is then given as $Q = Wc_p(T_2 - T_1)$, where W is the weight of air heated, c_p is the specific heat of air (0.24 when below 800°F), T_2 is the delivered hot air temperature, and T_1 is the cold air temperature entering the heat exchanger. Tables and graphs later in this chapter permit estimation of fuel savings and efficiencies for cases involving preheating of combustion air.

If a waste gas stream is only a few hundred degrees Fahrenheit hotter than the air stream temperature required for heating space, an oven, or a dryer, such uses of recovered heat are highly desirable. For higher waste gas stream temperatures, however, the second law of thermodynamics would say that we can make better use of the energy by stepping it down in smaller temperature increments, and preheating combustion air usually makes more sense. This also simplifies accounting, since it returns the recovered heat to the process that generated the hot waste stream.

Preheating combustion air is a very logical method for recycling waste energy from flue gases in direct-fired industrial heating processes such as melting, forming, ceramic firing, heat treating, chemical and petroprocess heaters, and boilers. (It is always wise, however, to check the economics of using flue gases to preheat the load or to make steam in a waste heat boiler.)

2 COSTS

In addition to the cost of the heat exchanger for preheating the combustion air, there are many other costs that have to be weighed. Retrofit or add-on recuperators or regenerators may have to be installed overhead to keep the length of heat-losing duct and pipe to a minimum; therefore, extra foundations and structural work may be needed. If the waste gas or air is hotter than about 800°F, carbon steel pipe and duct should be insulated on the inside. For small pipes or ducts where this would be impractical, it is necessary to use an alloy with strength and oxidation resistance at the higher temperature and to insulate on the outside.

High-temperature air is much less dense; therefore, the flow passages of burners, valves, and pipe must be greater for the same input rate and pressure drop. Burners, valves, and piping must be constructed of better materials to withstand the hot air stream. The front face of the burner is exposed to more intense radiation because of the higher flame temperature resulting from preheated combustion air.

If the system is to be operated at a variety of firing rates, the output air temperature will vary; so temperature-compensating fuel/air ratio controls are essential to avoid wasting fuel. Also, to protect the investment in the heat exchanger, it is only logical that it be protected with high-limit temperature controls.

3 WARNINGS

Changing temperatures from end to end of high-temperature heat exchangers and from time to time during high-temperature furnace cycles cause great thermal stress, often resulting in leaks and shortened heat exchanger life. Heat transfer surfaces fixed at both ends (welded or rolled in) can force something to be overstressed. Recent developments in the form of high-temperature slip seal methods combined with sensible location of such seals in cool air entrance sections are opening a whole new era in recuperator reliability.

Corrosion, fouling, and condensation problems continue to limit the applications of heat recovery equipment of all kinds. Heat transfer surfaces in air heaters are never as well cooled as those in water heaters and waste heat boilers; therefore, they must exist in a more hostile environment. However, they may experience fewer problems from acid-dew-point condensation. If corrosives, particulates, or condensables are emitted by the heating process at limited times, perhaps some temporary bypassing arrangement can be instituted. High waste gas design velocities may be used to keep particulates and condensed droplets in suspension until they reach an area where they can be safely dropped out.

Figure 1 shows recommended minimum temperatures to avoid "acid rain" in the heat exchanger.² Although a low final waste gas temperature is desirable from an efficiency standpoint, the shortened equipment life seldom warrants it. Acid forms from combination of water vapor with SO₃, SO₂, or CO₂ in the flue gases.

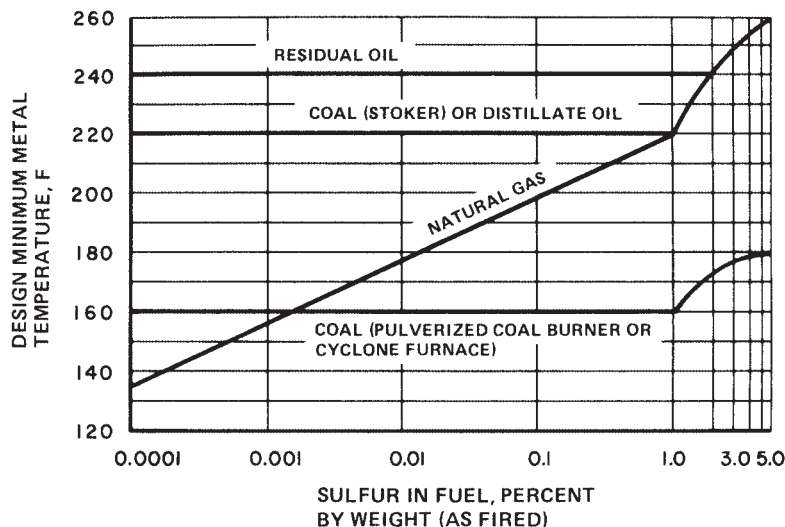


Figure 1 Recommended minimum temperatures to avoid "acid rain" in heat exchangers.

4 BENEFITS

Despite all the costs and warnings listed above, combustion air preheating systems *do* pay. As fuel costs rise, the payback is more rewarding, even for small installations. Figure 2 shows percent available heat³ (best possible efficiency) with various amounts of air preheat and a variety of furnace exit (flue) temperatures. All curves for hot air are based on 10% excess air.* The percentage of fuel saved by addition of combustion air preheating equipment can be calculated by the formula

$$\% \text{ fuel saved} = 100 \times \left(1 - \frac{\% \text{ available heat before}}{\% \text{ available heat after}} \right)$$

Table 2 lists fuel savings calculated by this method.¹

Preheating combustion air raises the flame temperature and thereby enhances radiation heat transfer in the furnace, which should lower the exit gas temperature and further improve fuel efficiency. Table 3 and the x intercepts of Fig. 2 show adiabatic flame temperatures when operating with 10% excess air,[†] but it is difficult to quantify the resultant saving from this effect.

Preheating combustion air has some lesser benefits. Flame stability is enhanced by the faster flame velocity and broader flammability limits. If downstream pollution control equipment is required (scrubber, baghouse), such equipment can be smaller and of less costly materials because the heat exchanger will have cooled the waste gas stream before it reaches such equipment.

* It is advisable to tune a combustion system for closer to stoichiometric air/fuel ratio *before* attempting to preheat combustion air. This is not only a quicker and less costly fuel conservation measure, but it then allows use of smaller heat exchange equipment.

† Although 0% excess air (stoichiometric air/fuel ratio) is ideal, practical considerations usually dictate operation with 5–10% excess air. During changes in firing rate, time lag in valve operation may result in smoke formation if some excess air is not available prior to the change. Heat exchangers made of 300 series stainless steels may be damaged by alternate oxidation and reduction (particularly in the presence of sulfur). For these reasons, it is wise to have an accurate air/fuel ratio controller with very limited time delay deviation from air/fuel ratio setpoint.

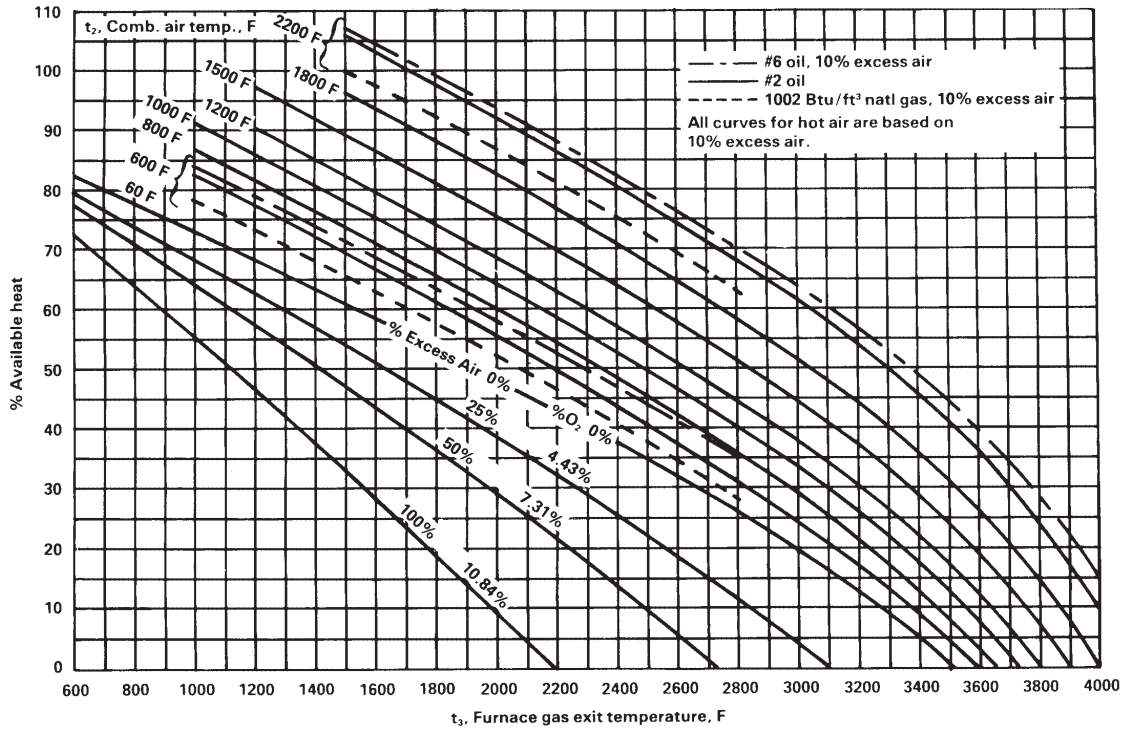


Figure 2 Available heat with preheated combustion air at 10% excess air. Applicable only if there is no unburned fuel in the products of combustion. Corrected for dissociation. See also Figs. 3 and 4 in Chapter 16. Reproduced with permission from Ref. 3.

Table 2 Fuel Savings (%) Resulting from Use of Preheated Air with Natural Gas and 10% Excess Air^a

t_3 , Furnace Gas Exit Temperature (°F)	t_2 , Combustion Air Temperature (°F)															
	600	700	800	900	1000	1100	1200	1300	1400	1500	1600	1800	2000	2200		
1000	13.4	15.5	17.6	19.6	—	—	—	—	—	—	—	—	—	—	—	
1100	13.8	16.0	18.2	20.2	22.2	—	—	—	—	—	—	—	—	—	—	
1200	14.3	16.6	18.7	20.9	22.9	24.8	—	—	—	—	—	—	—	—	—	
1300	14.8	17.1	19.4	21.5	23.6	25.6	27.5	—	—	—	—	—	—	—	—	
1400	15.3	17.8	20.1	22.3	24.4	26.4	28.4	30.2	—	—	—	—	—	—	—	
1500	16.0	18.5	20.8	23.1	25.3	27.3	29.3	31.2	33.0	—	—	—	—	—	—	
1600	16.6	19.2	21.6	24.0	26.2	28.3	30.3	32.2	34.1	35.8	—	—	—	—	—	
1700	17.4	20.2	22.5	24.9	27.2	29.4	31.4	33.4	35.3	37.0	38.7	—	—	—	—	
1800	18.2	20.9	23.5	26.0	28.3	30.6	32.7	34.6	36.5	38.3	40.1	—	—	—	—	
1900	19.1	21.9	24.6	27.1	29.6	31.8	34.0	36.0	37.9	39.7	41.5	44.7	—	—	—	
2000	20.1	23.0	25.8	28.4	30.9	33.2	35.4	37.5	39.4	41.3	43.0	46.3	—	—	—	
2100	21.2	24.3	27.2	29.9	32.4	34.8	37.0	39.1	41.1	43.0	44.7	48.0	51.0	—	—	
2200	22.5	25.7	28.7	31.5	34.1	36.5	38.8	40.9	42.9	44.8	46.6	49.9	52.8	—	—	
2300	24.0	27.3	30.4	33.3	36.0	38.5	40.8	42.9	45.0	46.9	48.7	52.0	54.9	57.5	—	
2400	25.7	29.2	32.4	35.3	38.1	40.6	43.0	45.2	47.2	49.2	51.0	54.2	57.1	59.7	—	
2500	27.7	31.3	34.7	37.7	40.5	43.1	45.5	47.7	49.8	51.7	53.5	56.8	59.6	62.2	—	
2600	30.1	33.9	37.3	40.5	43.4	46.0	48.4	50.6	52.7	54.6	56.4	59.6	62.4	64.9	—	
2700	33.0	37.0	40.6	43.8	46.7	49.4	51.8	54.0	56.1	58.0	59.7	62.8	65.5	67.9	—	
2800	36.7	40.8	44.5	47.8	50.8	53.4	55.8	58.0	60.0	61.9	63.5	66.5	69.1	71.3	—	
2900	41.4	45.7	49.5	52.8	55.7	58.4	60.7	62.8	64.7	66.4	68.0	70.8	73.2	75.2	—	
3000	47.9	52.3	56.0	59.3	62.1	64.6	66.7	68.7	70.4	72.0	73.5	75.9	78.0	79.8	—	
3100	57.3	61.5	65.0	68.0	70.5	72.7	74.6	76.2	77.7	79.0	80.2	82.2	83.8	85.2	—	
3200	72.2	75.6	78.3	80.4	82.2	83.7	85.0	86.1	87.1	87.9	88.7	89.9	90.9	91.8	—	

^aThese figures are for evaluating a proposed change to preheated air—not for determining system capacity.

Source: Reproduced with permission from Ref. 3.

Table 3 Effect of Combustion Air Preheat on Flame Temperature

Excess Air (%)	Preheated Combustion Air Temperature (°F)	Adiabatic Flame Temperature (°F)		
		With 1000 Btu/scf Natural Gas	With 137,010 Btu/gal Distillate Fuel Oil	With 153,120 Btu/gal Residual Fuel Oil
0	60	3468	3532	3627
10	60	3314	3374	3475
10	600	3542	3604	3690
10	700	3581	3643	3727
10	800	3619	3681	3763
10	900	3656	3718	3798
10	1000	3692	3754	3831
10	1100	3727	3789	3864
10	1200	3761	3823	3896
10	1300	3794	3855	3927
10	1400	3826	3887	3957
10	1500	3857	3918	3986
10	1600	3887	3948	4014
10	1700	3917	3978	4042
10	1800	3945	4006	4069
10	1900	3973	4034	4095
10	2000	4000	4060	4121
0	2000	4051	4112	4171

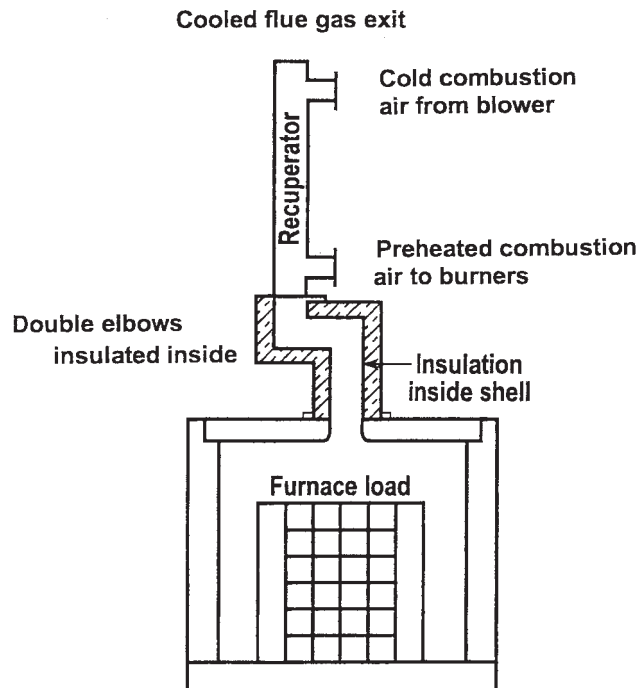


Figure 3 Recuperator using heat from waste flue gas to preheat combustion air to be fed to burners. The double elbow (insulated inside) in the flue uptake to the recuperator prevents (1) the recuperator from causing a cool spot on top of the furnace load and (2) the hot furnace load and interior walls from possibly radiating damaging overheating into the recuperator. Reproduced with permission from Ref. 4.

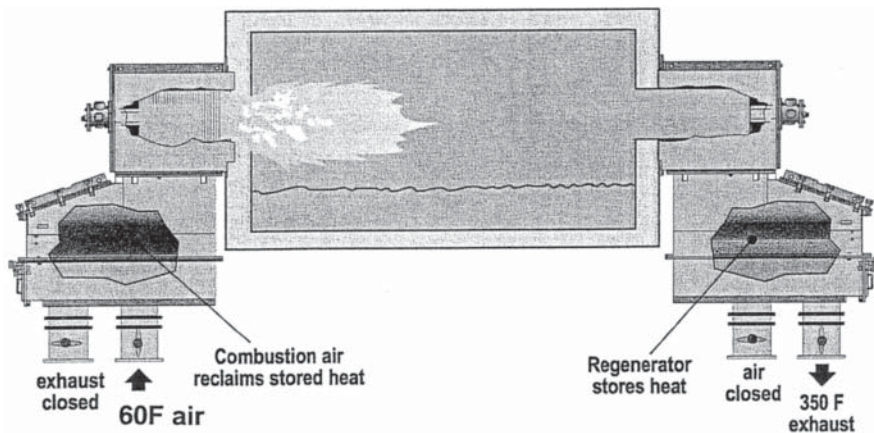


Figure 4 Melting furnace with a pair of compact regenerative burners. The regenerator on the right is storing waste heat in its bed of refractory nuggets. After 20 s of firing, as shown, the systems switch from firing from the left and exhausting through the right to firing from the right and exhausting through the left. At the moment shown, the regenerator on the right is storing waste heat, and the burner on the left is receiving reclaimed stored heat in the form of preheated combustion air. Reproduced with permission from Ref. 4.

Somewhat related to air heating (other than heating air for a subsequent process) is preheating combustion air for burners to make any heating process more efficient by recirculating waste heat through a heat exchange device (often built into a burner). This can be either a regenerator (steady-state heat exchanger, Fig. 3) or a recuperator (alternating flow heat exchanger, Fig. 4). Both use hot waste (flue) gases as the heat source to preheat combustion air being fed to the burners on almost any kind of furnace. Preheating air not only improves the thermal efficiency by recycling waste flue gas energy but also raises the flame temperature (Table 3), thereby increasing the heat transfer rate to the furnace loads.

REFERENCES

1. R. J. Reed, *Combustion Handbook*, 4th ed., Vol. 2, North American Manufacturing Co., Cleveland, OH, 1997.
2. *Steam—Its Generation and Use*, Babcock & Wilcox, New York, 1978.
3. R. J. Reed, *Combustion Handbook*, 3rd ed., Vol. 1, North American Manufacturing Co., Cleveland, OH, 1986.
4. W. Trinks, M. H. Mawhinney, R. A. Shannon, R. J. Reed, and J. R. Garvey, *Industrial Furnaces*, 6th ed., Wiley, Hoboken, NJ, 2003.
5. *Heat Requirements for Direct-Fired Air Heating*, North American Mfg. Co., Cleveland, OH, 1981.

CHAPTER 12

COOLING ELECTRIC EQUIPMENT

Allan Kraus
Beachwood, Ohio

Avram Bar-Cohen
University of Maryland
College Park, Maryland

Abhay A. Wative
Intel Corp.
Chandler, Arizona

1 THERMAL MODELING	451	2.2 Natural-Convection Heat Sinks	467
1.1 Introduction	451	2.3 Thermal Interface Resistance	470
1.2 Conduction Heat Transfer	451	2.4 Forced Convection	473
1.3 Convective Heat Transfer	455	3 THERMAL CONTROL TECHNIQUES	478
1.4 Radiative Heat Transfer	457	3.1 Extended Surface and Heat Sinks	478
1.5 Chip Module Thermal Resistances	458	3.2 Cold Plate	483
2 HEAT TRANSFER CORRELATIONS FOR ELECTRONIC EQUIPMENT COOLING	464	3.3 Thermoelectric Coolers	486
2.1 Natural Convection in Confined Spaces	464	3.4 Spray Cooling	490
		REFERENCES	494

1 THERMAL MODELING

1.1 Introduction

To determine the temperature differences encountered in the flow of heat within electronic systems, it is necessary to recognize the relevant heat transfer mechanisms and their governing relations. In a typical system, heat removal from the active regions of the microcircuit(s) or chip(s) may require the use of several mechanisms, some operating in series and others in parallel, to transport the generated heat to the coolant or ultimate heat sink. Practitioners of the thermal arts and sciences generally deal with four basic thermal transport modes: conduction, convection, phase change, and radiation.

1.2 Conduction Heat Transfer

One-Dimensional Conduction

Steady thermal transport through solids is governed by the Fourier equation, which, in one-dimensional form, is expressible as

$$q = -kA \frac{dT}{dx} \quad (\text{W}) \quad (1)$$

where q is the heat flow, k is the thermal conductivity of the medium, A is the cross-sectional area for the heat flow, and dT/dx is the temperature gradient. Here, heat flow produced by a negative temperature gradient is considered positive. This convention requires the insertion of the minus sign in Eq. (1) to assure a positive heat flow, q . The temperature difference resulting from the steady-state diffusion of heat is thus related to the thermal conductivity of the material, the cross-sectional area, and the path length L according to

$$(T_1 - T_2)_{\text{cd}} = q \frac{L}{kA} \quad (\text{K}) \quad (2)$$

The form of Eq. (2) suggests that, by analogy to Ohm's law governing electric current flow through a resistance, it is possible to define a thermal resistance for conduction, R_{cd} , as

$$R_{\text{cd}} \equiv \frac{T_1 - T_2}{q} = \frac{L}{kA} \quad (3)$$

One-Dimensional Conduction with Internal Heat Generation

Situations in which a solid experiences internal heat generation, such as that produced by the flow of an electric current, give rise to more complex governing equations and require greater care in obtaining the appropriate temperature differences. The axial temperature variation in a slim, internally heated conductor whose edges (ends) are held at a temperature T_o is found to equal

$$T = T_o + q_g \frac{L^2}{2k} \left[\left(\frac{x}{L} \right) - \left(\frac{x}{L} \right)^2 \right]$$

When the volumetric heat generation rate q_g in watts per cubic meter is uniform throughout, the peak temperature is developed at the center of the solid and is given by

$$T_{\text{max}} = T_o + q_g \frac{L^2}{8k} \quad (\text{K}) \quad (4)$$

Alternatively, because q_g is the volumetric heat generation, $q_g = q/LW\delta$, the center-edge temperature difference can be expressed as

$$T_{\text{max}} - T_o = q \frac{L^2}{8kLW\delta} = q \frac{L}{8kA} \quad (5)$$

where the cross-sectional area A is the product of the width W and the thickness δ . An examination of Eq. (5) reveals that the thermal resistance of a conductor with a distributed heat input is only one-quarter that of a structure in which all of the heat is generated at the center.

Spreading Resistance

In chip packages that provide for lateral spreading of the heat generated in the chip, the increasing cross-sectional area for heat flow at successive "layers" below the chip reduces the internal thermal resistance. Unfortunately, however, there is an additional resistance associated with this lateral flow of heat. This, of course, must be taken into account in the determination of the overall chip package temperature difference.

For the circular and square geometries common in microelectronic applications, an engineering approximation for the spreading resistance for a small heat source on a thick substrate or heat spreader (required to be 3 to 5 times thicker than the square root of the heat source area) can be expressed as¹

$$R_{\text{sp}} = \frac{0.475 - 0.62\varepsilon + 0.13\varepsilon^2}{k\sqrt{A_c}} \quad (\text{K/W}) \quad (6)$$

Where σ is the ratio of the heat source area to the substrate area, k is the thermal conductivity of the substrate, and A_c is the area of the heat source.

For relatively thin layers on thicker substrates, such as encountered in the use of thin lead frames or heat spreaders interposed between the chip and substrate, Eq. (6) cannot provide an acceptable prediction of R_{sp} . Instead, use can be made of the numerical results plotted in Fig. 1 to obtain the requisite value of the spreading resistance.

Interface/Contact Resistance

Heat transfer across the interface between two solids is generally accompanied by a measurable temperature difference, which can be ascribed to a contact or interface thermal resistance. For perfectly adhering solids, geometric differences in the crystal structure (lattice mismatch) can impede the flow of phonons and electrons across the interface, but this resistance is generally negligible in engineering design. However, when dealing with real interfaces, the asperities present on each of the surfaces, as shown in an artist's conception in Fig. 2, limit actual contact

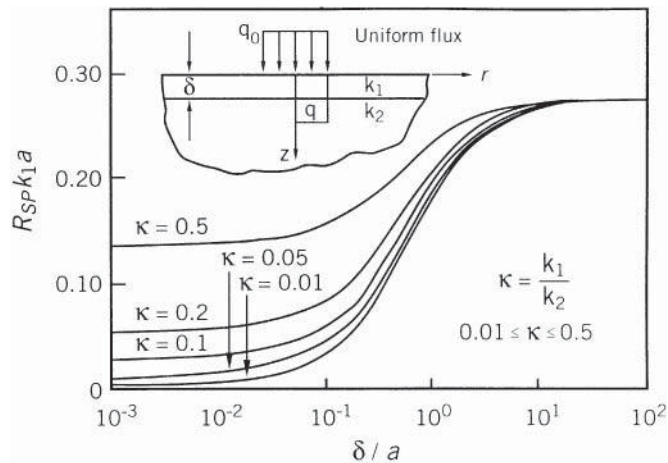


Figure 1 Thermal spreading resistance for circular heat source on two-layer substrate (from Ref. 2). Reprinted with permission of ASME International.

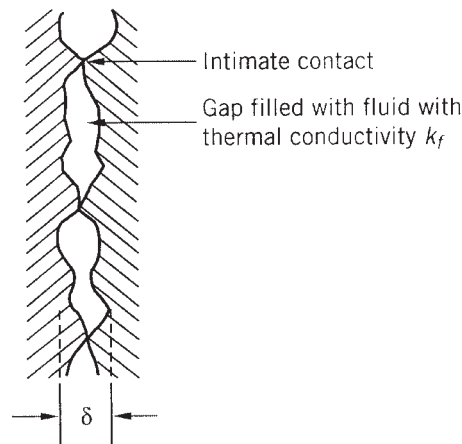


Figure 2 Physical contact between two nonideal surfaces.

between the two solids to a very small fraction of the apparent interface area. The flow of heat across the gap between two solids in nominal contact is thus seen to involve solid conduction in the areas of actual contact and fluid conduction across the “open” spaces. Radiation across the gap can be important in a vacuum environment or when the surface temperatures are high.

The heat transferred across an interface can be found by adding the effects of the solid-to-solid conduction and the conduction through the fluid and recognizing that the solid-to-solid conduction, in the contact zones, involves heat flowing sequentially through the two solids. With the total contact conductance h_{co} taken as the sum of the solid-to-solid conductance h_c and the gap conductance h_g ,

$$h_{co} = h_c + h_g \quad (\text{W/m}^2 \cdot \text{K}) \quad (7a)$$

the contact resistance based on the apparent contact area A_a may be defined as

$$R_{co} \equiv \frac{1}{h_{co}A_a} \quad (\text{K/W}) \quad (7b)$$

In Eq. (7a), h_c is given by

$$h_c = 54.25k_s \left(\frac{m}{\sigma}\right) \left(\frac{P}{H}\right)^{0.95} \quad (8a)$$

where k_s is the harmonic mean thermal conductivity for the two solids with thermal conductivities k_1 and k_2 ,

$$k_s = \frac{2k_1k_2}{k_1 + k_2} \quad (\text{W/m} \cdot \text{K})$$

σ is the effective rms surface roughness developed from the surface roughnesses of the two materials, σ_1 and σ_2 ,

$$\sigma = \sqrt{\sigma_1^2 + \sigma_2^2} \quad (\mu \cdot \text{m})$$

and m is the effective absolute surface slope composed of the individual slopes of the two materials, m_1 and m_2 ,

$$m = \sqrt{m_1^2 + m_2^2}$$

where P is the contact pressure and H is the microhardness of the softer material, both in newtons per square meter. In the absence of detailed information, the σ/m ratio can be taken equal to 5–9 μm for relatively smooth surfaces.^{1,2}

In Eq. (7a), h_g is given by

$$h_g = \frac{k_g}{Y + M} \quad (8b)$$

where k_g is the thermal conductivity of the gap fluid, Y is the distance between the mean planes (Fig. 2) given by

$$\frac{Y}{\sigma} = 54.185 \left[-\ln \left(3.132 \frac{P}{H} \right) \right]^{0.547}$$

and M is a gas parameter used to account for rarefied gas effects,

$$M = \alpha\beta\Lambda$$

where α is an accommodation parameter (approximately equal to 2.4 for air and clean metals), Λ is the mean free path of the molecules (equal to approximately 0.06 μm for air at atmospheric pressure and 15°C), and β is a fluid property parameter (equal to approximately 54.7 for air and other diatomic gases).

Equations (8a) and (8b) can be added and, in accordance with Eq. (7b), the contact resistance becomes

$$R_{co} \equiv \left\{ \left[1.25k_s \left(\frac{m}{\sigma}\right) \left(\frac{P}{H}\right)^{0.95} + \frac{k_g}{Y + M} \right] A_a \right\}^{-1} \quad (9)$$

1.3 Convective Heat Transfer

Heat Transfer Coefficient

Convective thermal transport from a surface to a fluid in motion can be related to the heat transfer coefficient h , the surface-to-fluid temperature difference, and the “wetted” surface area S in the form

$$q = hS(T_s - T_f) \quad (\text{W}) \quad (10)$$

The differences between convection to a rapidly moving fluid, a slowly flowing or stagnant fluid, as well as variations in the convective heat transfer rate among various fluids are reflected in the values of h . For a particular geometry and flow regime, h may be found from available empirical correlations and/or theoretical relations. Use of Eq. (10) makes it possible to define the convective thermal resistance as

$$R_{cv} \equiv \frac{1}{hS} \quad (\text{K/W}) \quad (11)$$

Dimensionless Parameters

Common dimensionless quantities that are used in the correlation of heat transfer data are the *Nusselt number* Nu , which relates the convective heat transfer coefficient to the conduction in the fluid where the subscript f pertains to a fluid property,

$$Nu \equiv \frac{h}{k_f/L} = \frac{hL}{k_f}$$

the *Prandtl number* Pr , which is a fluid property parameter relating the diffusion of momentum to the conduction of heat,

$$Pr \equiv \frac{c_p \mu}{k}$$

the *Grashof number* Gr , which accounts for the buoyancy effect produced by the volumetric expansion of the fluid,

$$Gr \equiv \frac{\rho^2 \beta g L^3 \Delta T}{\mu^2}$$

and the *Reynolds number* Re , which relates the momentum in the flow to the viscous dissipation,

$$Re \equiv \frac{\rho VL}{\mu}$$

Natural Convection

In natural convection, fluid motion is induced by density differences resulting from temperature gradients in the fluid. The heat transfer coefficient for this regime can be related to the buoyancy and the thermal properties of the fluid through the *Rayleigh number*, which is the product of the Grashof and Prandtl numbers,

$$Ra = \frac{\rho^2 \beta g c_p}{\mu k} L^3 \Delta T$$

where the fluid properties ρ , β , c_p , μ , and k are evaluated at the fluid bulk temperature and ΔT is the temperature difference between the surface and the fluid.

Empirical correlations for the natural-convection heat transfer coefficient generally take the form

$$h = C \left(\frac{k_f}{L} \right) (Ra)^n \quad (\text{W/m}^2 \cdot \text{K}) \quad (12)$$

where n is found to be approximately 0.25 for $10^3 < Ra < 10^9$, representing laminar flow; 0.33 for $10^9 < Ra < 10^{12}$, the region associated with the transition to turbulent flow; and 0.4 for

$Ra > 10^{12}$ when strong turbulent flow prevails. The precise value of the correlating coefficient C depends on the fluid, the geometry of the surface, and the Rayleigh number range. Nevertheless, for common plate, cylinder, and sphere configurations, it has been found to vary in the relatively narrow range of 0.45–0.65 for laminar flow and 0.11–0.15 for turbulent flow past the heated surface.³

Natural convection in vertical channels such as those formed by arrays of longitudinal fins is of major significance in the analysis and design of heat sinks and experiments for this configuration have been conducted and confirmed.^{4,5}

These studies have revealed that the value of the Nusselt number lies between two extremes associated with the separation between the plates or the channel width. For wide spacing, the plates appear to have little influence upon one another and the Nusselt number in this case achieves its *isolated plate limit*. On the other hand, for closely spaced plates or for relatively long channels, the fluid velocity attains its *fully developed* value and the Nusselt number reaches its *fully developed limit*. Intermediate values of the Nusselt number can be obtained from a form of a correlating expression for smoothly varying processes and have been verified by detailed experimental and numerical studies.^{6,7}

Thus, the correlation for the average value of h along isothermal vertical plates separated by a spacing z is given as

$$h = \frac{k_{\text{fl}}}{z} \left[\frac{576}{(\text{El})^2} + \frac{2.873}{(\text{El})^{1/2}} \right]^{1/2} \quad (13)$$

where El is the *Elenbaas number*

$$\text{El} \equiv \frac{\rho^2 \beta g c_p z^4 \Delta T}{\mu k_{\text{fl}} L}$$

and $\Delta T = T_s - T_{\text{fl}}$.

Several correlations for the coefficient of heat transfer in natural convection for various configurations are provided in Section 2.1.

Forced Convection

For forced flow in long or very narrow, parallel-plate channels, the heat transfer coefficient attains an asymptotic value (a fully developed limit), which for symmetrically heated channel surfaces is equal approximately to

$$h = \frac{4k_{\text{fl}}}{d_e} \quad (\text{W}/\text{m}^2 \cdot \text{K}) \quad (14)$$

where d_e is the *hydraulic diameter* defined in terms of the flow area A and the wetted perimeter of the channel, P_w ,

$$d_e \equiv \frac{4A}{P_w}$$

Several correlations for the coefficient of heat transfer in forced convection for various configurations are provided in Section 2.2.

Phase Change Heat Transfer

Boiling heat transfer displays a complex dependence on the temperature difference between the heated surface and the saturation temperature (boiling point) of the liquid. In nucleate boiling, the primary region of interest, the ebullient heat transfer rate can be approximated by a relation of the form

$$q_{\phi} = C_{\text{sf}} A (T_s - T_{\text{sat}})^3 \quad (\text{W}) \quad (15)$$

where C_{sf} is a function of the surface/fluid combination and various fluid properties. For comparison purposes, it is possible to define a boiling heat transfer coefficient h_ϕ as

$$h_\phi = C_{sf}(T_s - T_{sat})^2 \quad [\text{W}/\text{m}^2 \cdot \text{K}]$$

which, however, will vary strongly with surface temperature.

Finned Surfaces

A simplified discussion of finned surfaces is germane here and what now follows is not inconsistent with the subject matter contained in Section 3.1. In the thermal design of electronic equipment, frequent use is made of finned or “extended” surfaces in the form of *heat sinks* or *coolers*. While such finning can substantially increase the surface area in contact with the coolant, resistance to heat flow in the fin reduces the average temperature of the exposed surface relative to the fin base. In the analysis of such finned surfaces, it is common to define a fin efficiency η equal to the ratio of the actual heat dissipated by the fin to the heat that would be dissipated if the fin possessed an infinite thermal conductivity. Using this approach, heat transferred from a fin or a fin structure can be expressed in the form

$$q_f = hS_f\eta(T_b - T_s) \quad (\text{W}) \quad (16)$$

where T_b is the temperature at the base of the fin and T_s is the surrounding temperature and q_f is the heat entering the base of the fin, which, in the steady state, is equal to the heat dissipated by the fin.

The thermal resistance of a finned surface is given by

$$R_f \equiv \frac{1}{hS_f\eta} \quad (17)$$

where η , the fin efficiency, is 0.627 for a thermally optimum rectangular cross-sectional fin.⁸

Flow Resistance

The transfer of heat to a flowing gas or liquid that is not undergoing a phase change results in an increase in the coolant temperature from an inlet temperature of T_{in} to an outlet temperature of T_{out} according to

$$q = \dot{m}c_p(T_{out} - T_{in}) \quad (\text{W}) \quad (18)$$

Based on this relation, it is possible to define an effective flow resistance R_{fl} as

$$R_{fl} \equiv \frac{1}{\dot{m}c_p} \quad (\text{K}/\text{W}) \quad (19)$$

where \dot{m} is in kilograms per second.

1.4 Radiative Heat Transfer

Unlike conduction and convection, radiative heat transfer between two surfaces or between a surface and its surroundings is not linearly dependent on the temperature difference and is expressed instead as

$$q = \sigma S \mathcal{F} (T_1^4 - T_2^4) \quad (\text{W}) \quad (20)$$

where \mathcal{F} includes the effects of surface properties and geometry and σ is the Stefan–Boltzman constant, $\sigma = 5.67 \times 10^{-8} \text{ W}/\text{m}^2 \cdot \text{K}^4$. For modest temperature differences, this equation can be linearized to the form

$$q = h_r S (T_1 - T_2) \quad (\text{W}) \quad (21)$$

where h_r is the effective “radiation” heat transfer coefficient

$$h_r = \sigma \mathcal{F} (T_1^2 + T_2^2)(T_1 + T_2) \quad (\text{W/m}^2 \cdot \text{K}) \quad (22a)$$

and, for small $\Delta T = T_1 - T_2$, h_r is approximately equal to

$$h_r = 4\sigma \mathcal{F} (T_1 T_2)^{3/2} \quad (\text{W/m}^2 \cdot \text{K}) \quad (22b)$$

It is of interest to note that for temperature differences of the order of 10 K the radiative heat transfer coefficient h for an ideal (or “black”) surface in an absorbing environment is approximately equal to the heat transfer coefficient in natural convection of air.

Noting the form of Eq. (21), the radiation thermal resistance, analogous to the convective resistance, is seen to equal

$$R_r \equiv \frac{1}{h_r S} \quad (\text{K/W}) \quad (23)$$

1.5 Chip Module Thermal Resistances

Thermal Resistance Network

The expression of the governing heat transfer relations in the form of thermal resistances greatly simplifies the first-order thermal analysis of electronic systems. Following the established rules for resistance networks, thermal resistances that occur sequentially along a thermal path can be simply summed to establish the overall thermal resistance for that path. In similar fashion, the reciprocal of the effective overall resistance of several parallel heat transfer paths can be found by summing the reciprocals of the individual resistances. In refining the thermal design of an electronic system, prime attention should be devoted to reducing the largest resistances along a specified thermal path and/or providing parallel paths for heat removal from a critical area.

While the thermal resistances associated with various paths and thermal transport mechanisms constitute the “building blocks” in performing a detailed thermal analysis, they have also found widespread application as “figures-of-merit” in evaluating and comparing the thermal efficacy of various packaging techniques and thermal management strategies.

Definition

The thermal performance of alternative chip and packaging techniques is commonly compared on the basis of the overall (junction-to-coolant) thermal resistance R_T . This packaging figure of merit is generally defined in a purely empirical fashion,

$$R_T \equiv \frac{T_j - T_{fl}}{q_c} \quad (\text{K/W}) \quad (24)$$

where T_j and T_{fl} are the junction and coolant (fluid) temperatures, respectively, and q_c is the chip heat dissipation.

Unfortunately, however, most measurement techniques are incapable of detecting the actual junction temperature, that is, the temperature of the small volume at the interface of p -type and n -type semiconductors. Hence, this term generally refers to the average temperature or a representative temperature on the chip. To lower chip temperature at a specified power dissipation, it is clearly necessary to select and/or design a chip package with the lowest thermal resistance.

Examination of various packaging techniques reveals that the junction-to-coolant thermal resistance is, in fact, composed of an internal, largely conductive, resistance and an external, primarily convective, resistance. As shown in Fig. 3, the internal resistance R_{jc} is encountered in the flow of dissipated heat from the active chip surface through the materials used to support and bond the chip and on to the case of the integrated circuit package. The flow of heat from

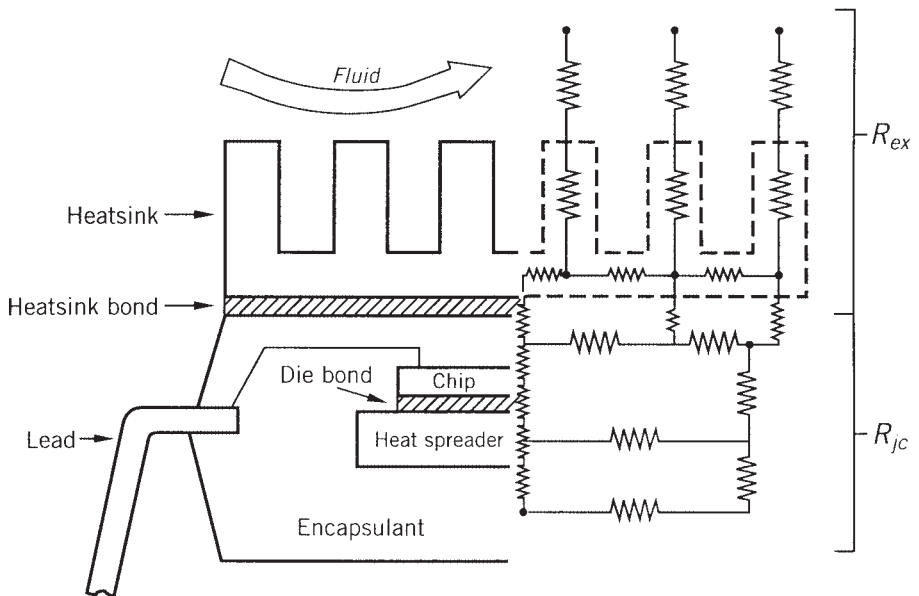


Figure 3 Primary thermal resistances in single-chip package.

the case directly to the coolant or indirectly through a fin structure and then to the coolant must overcome the external resistance R_{ex} .

The thermal design of single-chip packages, including the selection of die-bond, heat spreader, substrate, and encapsulant materials, as well as the quality of the bonding and encapsulating processes, can be characterized by the internal, or so-called junction-to-case, resistance. The convective heat removal techniques applied to the external surfaces of the package, including the effect of finned heat sinks and other thermal enhancements, can be compared on the basis of the external thermal resistance. The complexity of heat flow and coolant flow paths in a multichip module generally requires that the thermal capability of these packaging configurations be examined on the basis of overall, or chip-to-coolant, thermal resistance.

Internal Thermal Resistance

As discussed in Section 1.2, conductive thermal transport is governed by the Fourier equation, which can be used to define a conduction thermal resistance, as in Eq. (3). In flowing from the chip to the package surface or case, the heat encounters a series of resistances associated with individual layers of materials such as silicon, solder, copper, alumina, and epoxy, as well as the contact resistances that occur at the interfaces between pairs of materials. Although the actual heat flow paths within a chip package are rather complex and may shift to accommodate varying external cooling situations, it is possible to obtain a first-order estimate of the internal resistance by assuming that power is dissipated uniformly across the chip surface and that heat flow is largely one dimensional. To the accuracy of these assumptions,

$$R_{jc} = \frac{T_j - T_c}{q_c} = \sum \frac{x}{kA} \quad (\text{K/W}) \quad (25)$$

can be used to determine the internal chip module resistance where the summed terms represent the conduction thermal resistances posed by the individual layers, each with thickness x .

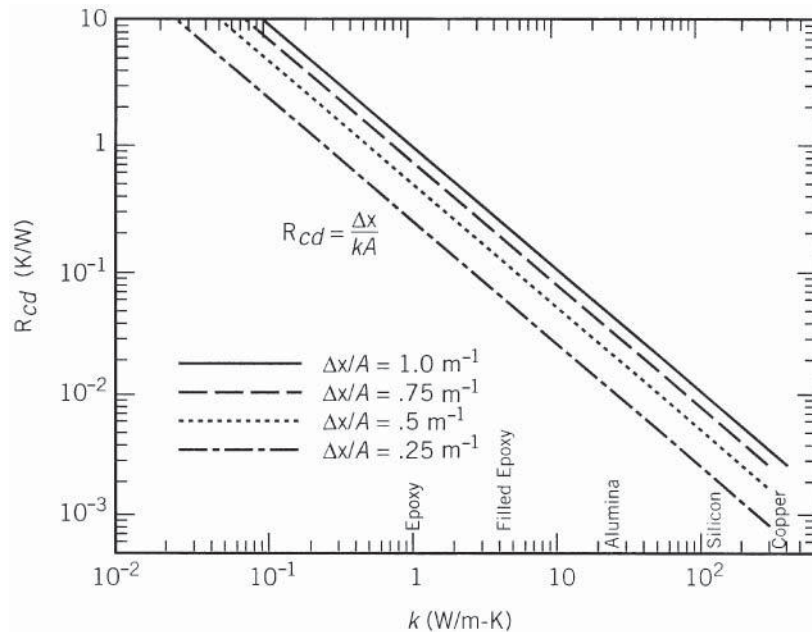


Figure 4 Conductive thermal resistance for packaging materials.

As the thickness of each layer decreases and/or the thermal conductivity and cross-sectional area increase, the resistance of the individual layers decreases. Values of R_{cd} for packaging materials with typical dimensions can be found via Eq. (25) or Fig. 4 to range from 2 K/W for a 1000-mm² × 1-mm-thick layer of epoxy encapsulant to 0.0006 K/W for a 100-mm² × 25- μ m (1-mil)-thick layer of copper. Similarly, the values of conduction resistance for typical “soft” bonding materials are found to lie in the range of approximately 0.1 K/W for solders and 1–3 K/W for epoxies and thermal pastes for typical x/A ratios of 0.25–1.0.

Commercial fabrication practice in the late 1990s yields internal chip package thermal resistances varying from approximately 80 K/W for a plastic package with no heat spreader to 15–20 K/W for a plastic package with heat spreader and to 5–10 K/W for a ceramic package or an especially designed plastic chip package. Large and/or carefully designed chip packages can attain even lower values of R_{jc} , down perhaps to 2 K/W.

Comparison of theoretical and experimental values of R_{jc} reveals that the resistances associated with compliant, low-thermal-conductivity bonding materials and the spreading resistances, as well as the contact resistances at the lightly loaded interfaces within the package, often dominate the internal thermal resistance of the chip package. It is thus necessary not only to determine the bond resistance correctly but also to add the values of R_{sp} obtained from Eq. (6) and/or Fig. 1 and R_{co} from Eq. (7b) or (9) to the junction-to-case resistance calculated from Eq. (25). Unfortunately, the absence of detailed information on the voidage in the die-bonding and heat sink attach layers and the present inability to determine, with precision, the contact pressure at the relevant interfaces conspire to limit the accuracy of this calculation.

Substrate or PCB Conduction

In the design of airborne electronic systems and equipment to be operated in a corrosive or damaging environment, it is often necessary to conduct the heat dissipated by the components down

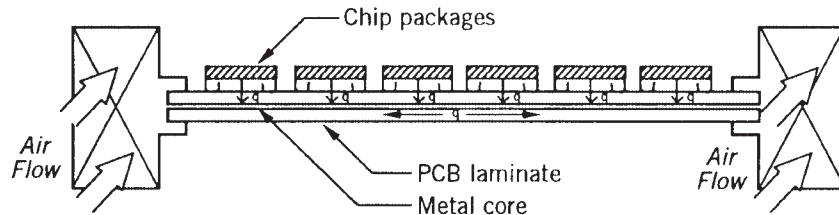


Figure 5 Edge-cooled PCB populated with components.

into the substrate or printed circuit board and, as shown in Fig. 5, across the substrate/printed circuit board (PCB) to a cold plate or sealed heat exchanger. For a symmetrically cooled substrate/PCB with approximately uniform heat dissipation on the surface, a first estimate of the peak temperature, at the center of the board, can be obtained by use of Eq. (5).

Setting the heat generation rate equal to the heat dissipated by all the components and using the volume of the board in the denominator, the temperature difference between the center at T_{ctr} and the edge of the substrate/PCB at T_o is given by

$$T_{\text{ctr}} - T_o = \left(\frac{Q}{LW\delta} \right) \left(\frac{L^2}{8k_e} \right) = \frac{QL}{8W\delta k_e} \quad (26)$$

where Q is the total heat dissipation, W , L , and δ are the width, length, and thickness, respectively, and k_e is the effective thermal conductivity of the board.

This relation can be used effectively in the determination of the temperatures experienced by conductively cooled substrates and conventional PCBs as well as PCBs with copper lattices on the surface, metal cores, or heat sink plates in the center. In each case it is necessary to evaluate or obtain the effective thermal conductivity of the conducting layer. As an example, consider an alumina substrate 0.20 m long, 0.15 m wide, and 0.005 m thick with a thermal conductivity of 20 W/m·K whose edges are cooled to 35°C by a cold plate. Assuming that the substrate is populated by 30 components, each dissipating 1 W, use of Eq. (26) reveals that the substrate center temperature will equal 85°C.

External Resistance

To determine the resistance to thermal transport from the surface of a component to a fluid in motion, that is, the convective resistance as in Eq. (11), it is necessary to quantify the heat transfer coefficient h . In the natural-convection air cooling of PCB arrays, isolated boards, and individual components, it has been found possible to use smooth-plate correlations, such as

$$h = C \left(\frac{k_{\text{fl}}}{L} \right) \text{Ra}^n \quad (27)$$

and

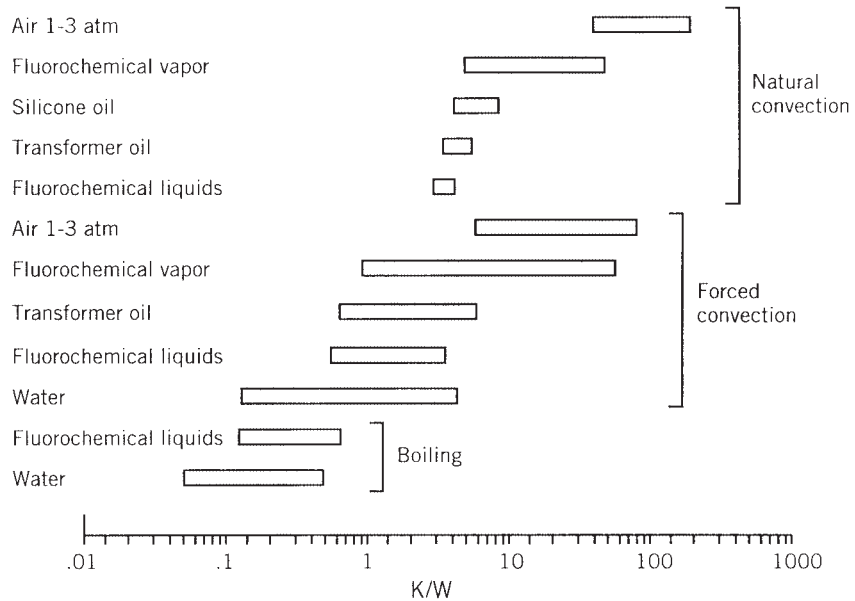
$$h = \frac{k_{\text{fl}}}{b} \left[\frac{576}{(\text{EI}^1)^2} + \frac{2.073}{(\text{EI}^1)^{0.5}} \right]^{-1/2} \quad (28)$$

to obtain a first estimate of the peak temperature likely to be encountered on the populated board. Examination of such correlations suggests that an increase in the component/board temperature and a reduction in its length will serve to modestly increase the convective heat transfer coefficient and thus to modestly decrease the resistance associated with natural convection. To achieve a more dramatic reduction in this resistance, it is necessary to select a high-density coolant with a large thermal expansion coefficient—typically a pressurized gas or a liquid.

When components are cooled by forced convection, the laminar heat transfer coefficient given later in Eq. (54) is found to be directly proportional to the square root of fluid velocity and inversely proportional to the square root of the characteristic dimension. Increases in the thermal conductivity of the fluid and in Pr, as are encountered in replacing air with a liquid coolant, will also result in higher heat transfer coefficients. In studies of low-velocity convective air cooling of simulated integrated circuit packages, the heat transfer coefficient h has been found to depend somewhat more strongly on Re (using channel height as the characteristic length) than suggested in Eq. (54) and to display a Reynolds number exponent of 0.54–0.72.^{9–11} When the fluid velocity and the Reynolds number increase, turbulent flow results in higher heat transfer coefficients, which, following Eq. (56), vary directly with the velocity to the 0.8 power and inversely with the characteristic dimension to the 0.2 power. The dependence on fluid conductivity and Pr remains unchanged.

An application of Eq. (27) or (28) to the transfer of heat from the case of a chip module to the coolant shows that the external resistance $R_{ex} = 1/hS$ is inversely proportional to the wetted surface area and to the coolant velocity to the 0.5–0.8 power and directly proportional to the length scale in the flow direction to the 0.5–0.2 power. It may thus be observed that the external resistance can be strongly influenced by the fluid velocity and package dimensions and that these factors must be addressed in any meaningful evaluation of the external thermal resistances offered by various packaging technologies.

Values of the external resistance, for a variety of coolants and heat transfer mechanisms are shown in Fig. 6 for a typical component wetted area of 10 cm² and a velocity range of 2–8 m/s. They are seen to vary from a nominal 100 K/W for natural convection in air, to 33 K/W for forced convection in air, to 1 K/W in fluorocarbon liquid forced convection, and to less than 0.5 K/W for boiling in fluorocarbon liquids. Clearly, larger chip packages will experience



Note: For wetted area = 10 cm²

Figure 6 Typical external (convective) thermal resistances for various coolants and cooling nodes.

proportionately lower external resistances than the displayed values. Moreover, conduction of heat through the leads and package base into the PCB or substrate will serve to further reduce the effective thermal resistance.

In the event that the direct cooling of the package surface is inadequate to maintain the desired chip temperature, it is common to attach finned heat sinks or compact heat exchangers to the chip package. These heat sinks can considerably increase the wetted surface area but may act to reduce the convective heat transfer coefficient by obstructing the flow channel. Similarly, the attachment of a heat sink to the package can be expected to introduce additional conductive resistances in the adhesive used to bond the heat sink and in the body of the heat sink. Typical air-cooled heat sinks can reduce the external resistance to approximately 15 K/W in natural convection and to as low as 5 K/W for moderate forced-convection velocities.

When a heat sink or compact heat exchanger is attached to the package, the external resistance accounting for the bond layer conduction and the total resistance of the heat sink, R_{sk} , can be expressed as

$$R_{ex} = \frac{T_c - T_{fl}}{q_c} = \sum \left(\frac{x}{kA} \right)_b + R_{sk} \quad (\text{K/W}) \quad (29)$$

where

$$R_{sk} = \left(\frac{1}{nhS_f\eta} + \frac{1}{h_bS_b} \right)^{-1}$$

is the parallel combination of the resistance of the n fins,

$$R_f = \frac{1}{nhS_f\eta}$$

and the *bare* or base surface not occupied by the fins,

$$R_b = \frac{1}{h_bS_b}$$

Here, the base surface is $S_b = S - S_f$ and the heat transfer coefficient h_b is used because the heat transfer coefficient that is applied to the base surfaces is not necessarily equal to that applied to the fins.

An alternative expression for R_{sk} involves and *overall surface efficiency* η_o defined by

$$\eta_o = 1 - \frac{nS_f}{S}(1 - \eta)$$

where S is the total surface composed of the base surface and the finned surfaces of n fins,

$$S = S_b + nS_f$$

In this case, it is presumed that $h_b = h$ so that

$$R_{sk} = \frac{1}{h\eta_o S}$$

In an optimally designed fin structure, η can be expected to fall in the range of 0.50–0.70.⁸ Relatively thick fins in a low-velocity flow of gas are likely to yield fin efficiencies approaching unity. This same unity value would be appropriate, as well, for an unfinned surface and, thus, serves to generalize the use of Eq. (29) to all package configurations.

Flow Resistance

In convectively cooled systems, determination of the component temperature requires knowledge of the fluid temperature adjacent to the component. The rise in fluid temperature relative to the inlet value can be expressed in a flow thermal resistance, as done in Eq. (19). When the coolant flow path traverses many individual components, care must be taken to use R_{fl} with the

total heat absorbed by the coolant along its path, rather than the heat dissipated by an individual component. For system-level calculations, aimed at determining the average component temperature, it is common to base the flow resistance on the average rise in fluid temperature, that is, one-half the value indicated by Eq. (19).

Total Resistance—Single-Chip Packages

To the accuracy of the assumptions employed in the preceding development, the overall single-chip package resistance relating the chip temperature to the inlet temperature of the coolant can be found by summing the internal, external, and flow resistances to yield

$$R_T = R_{jc} + R_{ex} + R_{fl} = \sum \frac{x}{kA} + R_{int} + R_{sp} + R_{sk} + \left(\frac{Q}{q}\right) \left(\frac{1}{2\rho Qc_p}\right) \quad (\text{K/W}) \quad (30)$$

In evaluating the thermal resistance by this relationship, care must be taken to determine the effective cross-sectional area for heat flow at each layer in the module and to consider possible voidage in any solder and adhesive layers.

As previously noted in the development of the relationships for the external and internal resistances, Eq. (30) shows R_T to be a strong function of the convective heat transfer coefficient, the flowing heat capacity of the coolant, and geometric parameters (thickness and cross-sectional area of each layer). Thus, the introduction of a superior coolant, use of thermal enhancement techniques that increase the local heat transfer coefficient, or selection of a heat transfer mode with inherently high heat transfer coefficients (boiling, for example) will all be reflected in appropriately lower external and total thermal resistances. Similarly, improvements in the thermal conductivity and reduction in the thickness of the relatively low-conductivity bonding materials (such as soft solder, epoxy, or silicone) would act to reduce the internal and total thermal resistances.

Frequently, however, even more dramatic reductions in the total resistance can be achieved simply by increasing the cross-sectional area for heat flow within the chip module (such as chip, substrate, and heat spreader) as well as along the wetted, exterior surface. The implementation of this approach to reducing the internal resistance generally results in a larger package footprint or volume but is rewarded with a lower thermal resistance. The use of heat sinks is, of course, the embodiment of this approach to the reduction of the external resistance.

2 HEAT TRANSFER CORRELATIONS FOR ELECTRONIC EQUIPMENT COOLING

The reader should use the material in this section that pertains to heat transfer correlations in geometries peculiar to electronic equipment.

2.1 Natural Convection in Confined Spaces

For natural convection in confined horizontal spaces the recommended correlations for air are¹²

$$\begin{aligned} \text{Nu} &= 0.195(\text{Gr})^{1/4}, \quad 10^4 < \text{Gr} < 4 \times 10^5 \\ \text{Nu} &= 0.068(\text{Gr})^{1/3}, \quad \text{Gr} > 10^5 \end{aligned} \quad (31)$$

where Gr is the Grashof number,

$$\text{Gr} = \frac{g\rho^2\beta L^2\Delta T}{\mu^2} \quad (32)$$

and where, in this case, the significant dimension L is the gap spacing in both the Nusselt and Grashof numbers.

For liquids¹³

$$\text{Nu} = 0.069(\text{Gr})^{1/3} \text{Pr}^{0.407}, \quad 3 \times 10^5 < \text{Ra} < 7 \times 10^9 \quad (33a)$$

where Ra is the Rayleigh number,

$$\text{Ra} = \text{GrPr} \quad (33b)$$

For horizontal gaps with $\text{Gr} < 1700$, the conduction mode predominates and

$$h = \frac{k}{b} \quad (34)$$

where b is the gap spacing. For $1700 < \text{Gr} < 10,000$, use may be made of the Nusselt–Grashof relationship given in Fig. 7.^{14,15}

The historical work of Elenbaas⁴ provides the foundation for much of the effort dealing with natural convection in such smooth, isothermal, parallel-plate channels. Many studies showing that the value of the convective heat transfer coefficient lies between two extremes associated with the separation distance between the plates or the channel width have been reported in literature.^{6,7,16} Adjacent plates appear to have little influence on one another when the spacing between them is large, and the heat transfer coefficient in this case achieves its isolated plate limit. When the plates are closely spaced or if the adjacent plates form relatively long channels, the fluid attains the fully developed velocity profile and the heat transfer rate reaches its fully developed value. Intermediate values of the heat transfer coefficient can be obtained from a judicious superposition of these two limiting phenomena, as presented in the composite expressions proposed by Bar-Cohen and Rohsenow.¹⁷ Composite correlations for other situations such as symmetrically heated isothermal or isoflux surfaces are available in the literature.³

Table 1 shows a compilation of these natural-convection heat transfer correlations for an array of vertically heated channels. The Elenbaas number used in these correlations is defined as

$$\text{El} = \frac{C_p \rho^2 g \beta (T_w - T_0) b^4}{\mu k_f L} \quad (35)$$

where b is the channel spacing, L is the channel length, and $T_w - T_0$ is the temperature difference between the channel wall and the ambient, or channel inlet. The equations for the uniform heat flux boundary condition are defined in terms of the modified Elenbaas number, El' , which is defined as

$$\text{El}' = \frac{C_p \rho^2 g \beta q'' b^5}{\mu k_f^2 L} \quad (36)$$

where q'' is the heat flux leaving the channel wall(s).

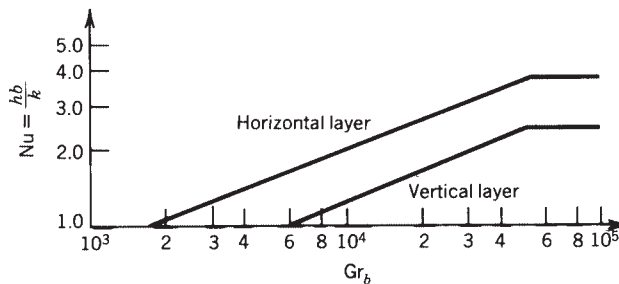


Figure 7 Heat transfer through enclosed air layers.^{14,15}

Table 1 Natural-Convection Heat Transfer Correlations for Array of Heated Vertical Channels

Condition	Fully Developed Limit	Composite Correlation
Symmetric isothermal plates	$Nu_0 = \frac{El}{24}$	$Nu_0 = \left(\frac{576}{El^2} + \frac{2.873}{\sqrt{El}} \right)^{(-1/2)}$
Asymmetric isothermal plates	$Nu_0 = \frac{El}{12}$	$Nu_0 = \left(\frac{144}{El^2} + \frac{2.873}{\sqrt{El}} \right)^{(-1/2)}$
Symmetric isoflux plates	$Nu_0 = \sqrt{\frac{El'}{48}}$	
Asymmetric isoflux plates	$Nu_0 = \sqrt{\frac{El'}{24}}$	
Symmetric isoflux plates based on midheight temperature	$Nu_0 = \sqrt{\frac{El'}{12}}$	$Nu_0 = \left(\frac{12}{El'} + \frac{1.88}{(El')^{2/5}} \right)^{(-1/2)}$
Asymmetric isoflux plates based on midheight temperature	$Nu_0 = \sqrt{\frac{El'}{6}}$	$Nu_0 = \left(\frac{6}{El'} + \frac{1.88}{(El')^{2/5}} \right)^{(-1/2)}$

Table 2 Nusselt Number for Symmetric Isothermal Walls at Different Temperatures

r_T	\overline{Nu}_0/El
1.0	1/24
0.5	17/405
0.1	79/1815
0.0	2/45

Source: From Ref. 16.

Asymmetry can also occur if adjacent channel walls are isothermal but at different temperatures or isoflux but dissipating different heat fluxes. Aung¹⁶ defined an asymmetry parameter for the case where the walls are isothermal but at different wall temperatures T_{w1} and T_{w2} as

$$r_T = \frac{T_{w1} - T_0}{T_{w2} - T_0} \quad (37)$$

in which T_0 is the air temperature at the channel inlet. Then the heat transfer could be calculated using the parameters listed in Table 2.

In the case of symmetric isoflux plates, if the heat flux on the adjacent walls is not identical, the equations in Table 1 can be used with an average value of the heat flux on the two walls. The composite relations listed in Table 1 can be used to optimize the spacing between PCBs in a PCB card array. For isothermal arrays, the optimum spacing maximizes the total heat transfer from a given base area or the volume assigned to an array of PCBs. In the case of isoflux parallel-plate arrays, the power dissipation may be maximized by increasing the number of plates indefinitely. Thus, it is more practical to define the optimum channel spacing for an array of isoflux plates as the spacing, which will yield the maximum volumetric heat dissipation rate per unit temperature difference. Despite this distinction, the optimum spacing is found in the same manner. The optimal spacing for different conditions is listed in Table 3.³

Table 3 Optimum Spacing for Natural-Convection Cooled Arrays of Vertical Plates or PCBs

Condition	Optimum Spacing
Symmetric isothermal plates	$b_{\text{opt}} = \frac{2.714}{P^{1/4}}$
Asymmetric isothermal plates	$b_{\text{opt}} = \frac{2.154}{P^{1/4}}$
Symmetric isoflux plates	$b_{\text{opt}} = 1.472R^{-0.2}$
Asymmetric isoflux plates	$b_{\text{opt}} = 1.169R^{-0.2}$

The parameter b_{opt} in Table 3 represents the optimal spacing, and the plate-to-air parameter P is given as

$$P = \frac{C_p(\rho_f)^2 g \beta \Delta T_0}{\mu_f k_f L} \quad (38)$$

where ΔT_0 is the temperature difference between the PCB and the ambient temperature at the inlet of the channel. The parameter R in Table 3 is given by

$$R = \frac{C_p(\rho_f)^2 g \beta q''}{\mu_f k^2 L} \quad (39)$$

These smooth-plate relations have proven useful in a wide variety of applications and have been shown to yield very good agreement with measured empirical results for heat transfer from arrays of PCBs. However, when applied to closely spaced PCBs these equations tend to underpredict heat transfer in the channel due to the presence of between-package “wall flow” and the nonsmooth nature of the channel surfaces.

2.2 Natural-Convection Heat Sinks

Despite the decades-long rise in component heat dissipation, the inherent simplicity and reliability of buoyantly driven flow continues to make the use of natural-convection heat sinks, the cooling technology of choice for a large number of electronic applications. An understanding of natural-convection heat transfer from isothermal, parallel-plate channels provides the theoretical underpinning for the conceptual design of natural-convection cooled plate-fin heat sinks. However, detailed design and optimization of such fin structures require an appreciation for the distinct characteristics of such phenomena as buoyancy-induced fluid flow in the interfin channels and conductive heat flow in the plate fins.

The presence of the heat sink “base,” or prime surface area, along one edge of the parallel-plate channel, contrasting with the open edge at the “tip” of the fins, introduces an inherent asymmetry in the flow field. The resulting three-dimensional flow pattern generally involves some inflow from (and possibly outflow through) the open edge. For relatively small fin spacings with long and low fins, this edge flow may result in a significant decrease in the air temperature between the fins and dramatically alter the performance of such heat sinks. For larger fin spacings, and especially with wide, thick fins, the edge flow may well be negligible.

Heat flow in extended surfaces must result in a temperature gradient at the fin base. When heat flow is from the base to the ambient, the temperature decreases along the fin, and the average fin surface excess temperature (i.e., $T_{\text{fin}} - T_{\text{air}}$) is typically between 50 and 90% of the base excess temperature. As a consequence of the temperature distribution on the fin surface, exact analytic determination of the heat sink capability requires a combined (or conjugate) solution of the fluid flow in the channel and heat flow in the fin. Due to the complexity of such a conjugate

analysis, especially in the presence of three-dimensional flow effects, the thermal performance of heat sinks is frequently based on empirical results. In recent years, extensive use has also been made of detailed numerical solutions to quantify heat sink performance. Alternatively, a satisfactory estimate of heat sink capability can generally be obtained by decoupling the flow and temperature fields and using an average heat transfer coefficient, along with an average fin surface temperature, to calculate the thermal transport from the fins to the ambient air.

Starner and McManus¹⁸ investigated the thermal performance of natural-convection heat sinks as a function of the geometry (spacing and height) and angle of base-plate orientation (vertical, horizontal, and 45°) in detail. Their configuration, with the present terminology, is shown in Fig. 8. They found that the measured heat transfer coefficients for the vertical orientation were generally lower than the values expected for parallel-plate channels. The inclined orientation (45°) resulted in an additional 5–20% reduction in the heat transfer coefficient. Results for the horizontal orientation showed a strong contribution from three-dimensional flow.

Welling and Wooldridge¹⁹ performed an extensive study of heat transfer from vertical arrays of 2–3-mm-thick fins attached to an identical 203 × 66.3-mm base. Their results revealed that, in the range of $0.6 < \text{El} < 100$, associated with 4.8–19-mm spacings and fin heights from 6.3 to 19 mm, the heat transfer coefficients along the total wetted surface were lower than attained by an isolated, flat plate but generally above those associated with parallel-plate flow. This behavior was explained in terms of the competing effects of channel flow, serving to preheat the air, and inflow from the open edge, serving to mix the heated air with the cooler ambient fluid. In this study it was observed, for the first time, that for any given interfin spacing there is an optimum fin height b beyond which thermal performance, per unit surface area, deteriorates.

In 1986 Bilitzky²⁰ completed a comprehensive investigation of natural-convection heat transfer from multiple heat sink geometries that differed, primarily, in fin height and spacing. The heat sinks were operated at different heat dissipations as well as different angles of inclination and orientation. Twelve distinct heat sinks and a flat plate were tested in a room within which extraneous convection had been suppressed. The base was first kept vertical, while the fins were rotated through four different positions (90°, 60°, 30°, and 0°). Then, the base was tilted backward toward the horizontal orientation through four different positions (90°, 60°, 30°, and 0°). Six of the heat sinks used 144-mm-long by 115-mm-wide bases to support plate fins, nominally 2 mm in thickness and 6–13.8 mm apart, ranging in height from 8.6 to 25.5 mm. Six additional heat sinks, with identical fin geometries, were supported on 280-mm-long and

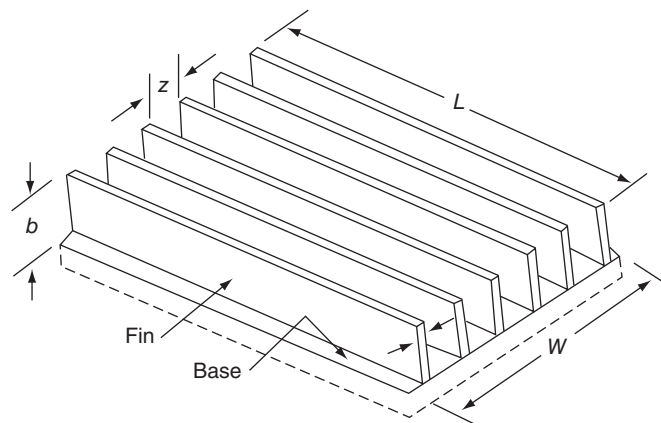


Figure 8 Geometric parameters for Starner and McManus¹⁸ fin arrays.

Table 4 Geometric Parameters for Bilitzky Fin Arrays

Array	L		W		b		z		δ	
	in.	mm	in.	mm	in.	mm	in.	mm	in.	mm
1	5.67	144	4.53	115	1.004	25.5	0.236	6.0	0.075	1.9
2	5.67	144	4.53	115	0.677	17.2	0.232	5.9	0.079	2.0
3	5.67	144	4.53	115	0.339	8.6	0.228	5.8	0.083	2.1
4	5.67	144	4.53	115	1.004	25.5	0.547	13.9	0.075	1.9
5	5.67	144	4.53	115	0.677	17.2	0.543	13.8	0.079	2.0
6	5.67	144	4.53	115	0.339	8.6	0.539	13.7	0.083	2.1
7	11.02	280	4.53	115	1.004	25.5	0.236	6.0	0.075	1.9
8	11.02	280	4.53	115	0.669	17.0	0.232	5.9	0.079	2.0
9	11.02	280	4.53	115	0.335	8.5	0.228	5.8	0.083	2.1
10	11.02	280	4.53	115	1.004	25.5	0.547	13.9	0.075	1.9
11	11.02	280	4.53	115	0.669	17.0	0.543	13.8	0.079	2.0
12	11.02	280	4.53	115	0.335	8.5	0.539	13.7	0.083	2.1

Source: From Ref. 20.

115-mm-wide bases. The geometric parameters of the 12 heat sinks were selected to span the base and fin dimensions encountered in electronics cooling applications and are summarized in Table 4.

In all 12 heat sinks studied, the vertical-vertical orientation, that is, a vertically oriented base with vertical fins and channels, yielded the highest heat transfer coefficients most often. However, in a relatively large number of situations, the thermal performance of the vertical-vertical arrays was indistinguishable from that attained by a vertical base plate with fins rotated 30° from the axis, a horizontal base plate, and a base plate inclined 60° from the horizontal with unrotated fins. On the other hand, the vertical-horizontal orientation, that is, the base plate vertical and the fins rotated 90° from the axis, led to the lowest heat dissipation rates. For the unrotated fins, the lowest heat transfer coefficients were almost always found to occur at a base-plate angle of 30° from the horizontal. The use of smoke revealed a relatively complex three-dimensional flow pattern around the heat sinks, with very substantial inflow from the direction of the fin tips when the base plate was strongly inclined and when the heat sinks were in the vertical base-horizontal fins orientation.

The influence of the spacing, between the fins for short and long base plates was examined by comparing pairs of heat sinks that differed only in geometric parameters, z (fin arrays 1 and 4, 2 and 5, 3 and 6, 7 and 10, 8 and 11, and 9 and 12 in Table 4). Bilitzky²⁰ observed that, in nearly all of the configurations and operating conditions examined, the highest heat transfer coefficients were attained with the larger fin spacing. However, the improvement in the heat transfer coefficient was not always sufficient to compensate for the loss of wetted fin surface area. Moreover, for the horizontal base-plate configuration, as well as for the vertical base with horizontal fins, the total array dissipation appeared not to depend on this parameter.

Analysis of data from the vertically oriented heat sinks led Bilitzky²⁰ to recognize that closely spaced fins, typical of actual heat sinks used for electronics cooling, display substantially higher heat transfer coefficients than predicted by the fully developed channel flow equations listed in Table 1. Bilitzky²⁰ proposed the following modification to the fully developed Nusselt number for symmetric isothermal plates:

$$\text{Nu}_0 = \frac{\text{El}}{24\psi} \quad (40)$$

where the correction factor ψ was given as

$$\psi = \frac{A_1}{[(1 + (a/2)(1 + A_2A_3))]^2} \quad (41)$$

The parameter a in Eq. (41) was the ratio of the fin pitch and the fin height and the parameters A_1 , A_2 , and A_3 were given as follows:

$$A_1 = 1 - 0.483e^{-0.17/a} \quad (42)$$

$$A_2 = (1 - e^{-0.83/a}) \quad (43)$$

$$A_3 = 9.14a^{1/2}e^{-1.25(1+a/2)} - 0.61 \quad (44)$$

Use of Eq. (40) was reported by Bilitzky²⁰ to yield agreement within 5% for his data.

2.3 Thermal Interface Resistance

Heat transfer across a solid interface is accompanied by a temperature difference caused by imperfect contact between the two solids. Even when perfect adhesion is achieved between the solids, the transfer of heat is impeded by the acoustic mismatch in the properties of the phonons on either side of the interface. Traditionally the thermal resistance arising due to imperfect contact has been called the “thermal contact” resistance. The resistance due to the mismatch in the acoustic properties is usually termed the “thermal boundary” resistance. The thermal contact resistance is a macroscopic phenomenon, whereas the thermal boundary resistance is a microscopic phenomenon. This section primarily focuses on thermal contact resistance and methods to reduce the contact resistance.

When two surfaces are joined, as shown in Fig. 9, asperities on each of the surfaces limit the actual contact between the two solids to a very small fraction, perhaps just 1–2% for lightly loaded interfaces, of the apparent area. As a consequence, the flow of heat across such an interface involves solid-to-solid conduction in the area of actual contact, A_{co} , and conduction through the fluid occupying the noncontact area, A_{nc} , of the interface. At elevated temperatures or in vacuum, radiation heat transfer across the open spaces may also play an important role.

The pressure imposed across the interface, along with the microhardness of the softer surface and the surface roughness characteristics of both solids, determines the interfacial gap δ and the contact area A_{co} . Assuming plastic deformation of the asperities and a Gaussian distribution of the asperities over the apparent area, Cooper et al.²¹ proposed the following relation

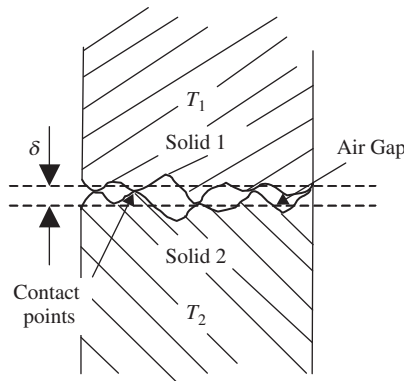


Figure 9 Contact and heat flow at a solid–solid interface.

for the contact resistance R_{co} :

$$R_{co} = \left(1.45 \frac{k_s (P/H)^{0.985}}{\sigma} |\overline{\tan \theta}| \right)^{-1} \quad (45)$$

where k_s is the harmonic mean thermal conductivity defined as $k_s = 2k_1k_2/(k_1 + k_2)$, P is the apparent contact pressure, H is the hardness of the softer material, and σ is the rms roughness given by

$$\sigma_1 = \sqrt{\sigma_1^2 + \sigma_2^2} \quad (46)$$

where σ_1 and σ_2 are the roughnesses of surfaces 1 and 2, respectively. The term $|\tan \theta|$ in Eq. (45) is the average asperity angle:

$$|\overline{\tan \theta}|^2 = |\tan \theta_1|^2 + |\tan \theta_2|^2 \quad (47)$$

This relation neglects the heat transfer contribution of any trapped fluid in the interfacial gap.

In the pursuit of a more rigorous determination of the contact resistance, Yovanovich and Antonetti²² found it possible to predict the area-weighted interfacial gap Y in the following form:

$$Y = 1.185\sigma \left[-\ln \left(\frac{3.132P}{H} \right) \right]^{0.547} \quad (48)$$

where σ is the effective root mean square (rms) as given by Eq. (46), P is the contact pressure (Pa), and H is the surface microhardness (Pa) of the softer material to a depth of the order of the penetration of the harder material. Using Y as the characteristic gap dimension and incorporating the solid–solid and fluid gap parallel heat flow paths, they derived the following equation for the total interfacial thermal resistance:

$$R_{co} = \left[1.25k_s \left(\frac{|\overline{\tan \theta}|}{\sigma} \right) \left(\frac{P}{H} \right)^{0.95} + \frac{k_g}{Y} \right]^{-1} \quad (49)$$

where k_g is the interstitial fluid thermal conductivity. In the absence of detailed information, $\sigma/|\overline{\tan \theta}|$ can be expected to range from 5 to 9 μm for relatively smooth surfaces.

In describing heat flow across an interface, Eq. (49) assumed the existence of a fluid gap, which provides a parallel heat flow path to that of the solid–solid contact. Because the noncontact area may occupy in excess of 90% of the projected area, heat flow through the interstitial spaces can be of great importance. Consequently, the use of high-thermal-conductivity interstitial materials, such as soft metallic foils and fiber disks, conductive epoxies, thermal greases, and polymeric “phase change” materials, can substantially reduce the contact resistance. The enhanced thermal capability of many of the high-performance epoxies, thermal greases, and phase change materials, commonly in use in the electronic industry, is achieved through the use of large concentrations of thermally conductive particles. Successful design and development of thermal packaging strategies thus require the determination of the effective thermal conductivity of such particle-laden interstitial materials and their effect on the overall interfacial thermal resistance.

Comprehensive reviews of the general role of interstitial materials in controlling contact resistance have been published by several authors, including Sauer.²³ When interstitial materials are used for control of the contact resistance, it is desirable to have some means of comparing their effectiveness. Fletcher²⁴ proposed two parameters for this purpose. The first of these parameters is simply the ratio of the logarithms of the conductances, which is the inverse of the contact resistance, with and without the filler:

$$\chi = \frac{\ln(\kappa_{cm})}{\ln(\kappa_{bj})} \quad (50)$$

in which κ is the contact conductance and c_m and b_j refer to control material and bare junctions, respectively. The second parameter takes the thickness of the filler material into account and is defined as

$$\eta' = \frac{(\kappa \delta_{\text{filler}})_{c_m}}{(\kappa \delta_{\text{gap}})_{b_j}} \quad (51)$$

in which δ is the equivalent thickness and η' is the effectiveness of the interstitial material.

The performance of an interstitial interface material as decided by the parameter defined by Fletcher,²⁴ in Eqs. (50) and (51) includes the bulk as well as the contact resistance contribution. It is because of this reason that in certain cases the thermal resistance of these thermal interface materials is higher than that for a bare metallic contact because the bulk resistance is the dominant factor in the thermal resistance. To make a clear comparison of only the contact resistance arising from the interface of the substrate and various thermal interface materials, it is important to measure it exclusively. Separation of the contact resistance and bulk resistance will also help researchers to model the contact resistance and the bulk resistance separately.

Equations (50) and (51) by Fletcher²⁴ show that the thermal resistance of any interface material depends on both the bond line thickness and thermal conductivity of the material. As a consequence, for materials with relatively low bulk conductivity, the resistance of the added interstitial layer may dominate the thermal behavior of the interface and may result in an overall interfacial thermal resistance that is higher than that of the bare solid–solid contact. Thus, both the conductivity and the achievable thickness of the interstitial layer must be considered in the selection of an interfacial material. Indeed, while the popular phase change materials have a lower bulk thermal conductivity (at a typical value of 0.7 W/mK) than the silicone-based greases (with a typical value of 3.1 W/mK) due to thinner phase change interstitial layers, the thermal resistance of these two categories of interface materials is comparable.

To understand the thermal behavior of such interface materials, it is useful to separate the contribution of the bulk conductivity from the interfacial resistance, which occurs where the interstitial material contacts one of the mating solids. Following Prasher,²⁵ who studied the contact resistance of phase change materials (PCMs) and silicone-based thermal greases, the thermal resistance associated with the addition of an interfacial material, R_{TIM} , can be expressed as

$$R_{\text{TIM}} = R_{\text{bulk}} + R_{\text{co}_1} + R_{\text{co}_2} \quad (52)$$

where R_{bulk} is the bulk resistance of the thermal interface material and R_{co} is the contact resistance with the substrate and subscripts 1 and 2 refer to substrates 1 and 2. Prasher²⁵ rewrote Eq. (52) as

$$R_{\text{TIM}} = \frac{\delta}{k_{\text{TIM}}} + \frac{\sigma_1}{2k_{\text{TIM}}} \left(\frac{A_{\text{nom}}}{A_{\text{real}}} \right) + \frac{\sigma_2}{2k_{\text{TIM}}} \left(\frac{A_{\text{nom}}}{A_{\text{real}}} \right) \quad (53)$$

where R_{TIM} is the total thermal resistance of the thermal interface material, δ the bond line thickness, k_{TIM} the thermal conductivity of the interface material, σ_1 and σ_2 the roughness of surfaces 1 and 2, respectively, A_{nom} the nominal area, and A_{real} the real area of contact of the interface material with the two surfaces. Equation (53) assumes that the thermal conductivity of the substrate is much higher compared to that of the thermal interface material. The first term on the right-hand side of Eq. (53) is the bulk resistance and other terms are the contact resistances.

Figure 10 shows the temperature variation at the interface between two solids, in the presence of a thermal interface material, associated with Eq. (53). Unlike the situation with the more conventional interface materials, the actual contact area between a polymeric material and a solid is determined by capillary forces, rather than the surface hardness, and an alternative approach is required to determine A_{real} in Eq. (53). Modeling each of the relevant surfaces

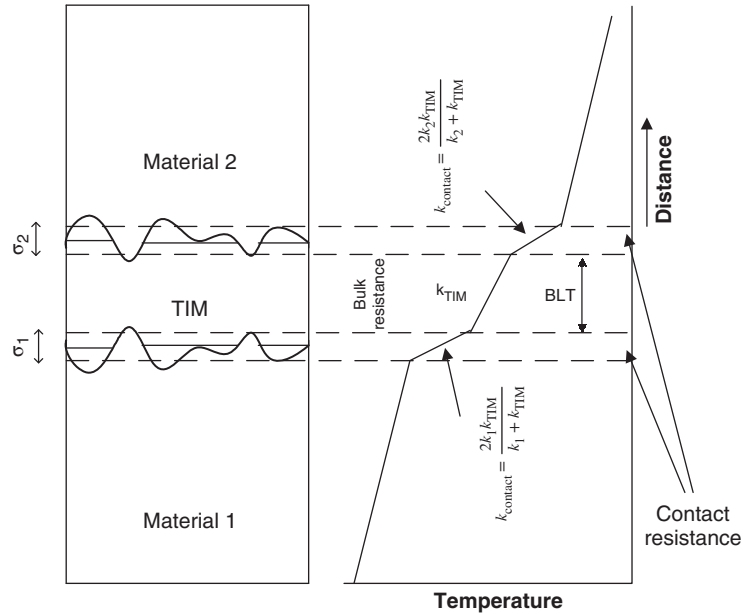


Figure 10 Schematic showing temperature drop across an interface.

as a series of notches and including the effects of surface roughness, the slope of the asperities, the contact angle of the polymer with each the substrates, the surface energy of the polymer, and the externally applied pressure, a surface chemistry model was found to match very well with the experimental data for PCMs and greases at low pressures.²⁵ Unfortunately, it has not been possible, as yet, to determine the contact area with a closed-form expression. It is also to be noted that Eq. (53) underpredicts the interface thermal resistance data at high pressures.

2.4 Forced Convection

External Flow on a Plane Surface

For an unheated starting length of the plane surface, x_0 , in laminar flow, the local Nusselt number can be expressed by

$$\text{Nu}_x = \frac{0.332\text{Re}^{1/2}\text{Pr}^{1/3}}{[1 - (x_0/x)^{3/4}]^{1/3}} \quad (54)$$

where Re is the Reynolds number, Pr is the Prandtl number, and Nu is the Nusselt number.

For flow in the inlet zones of parallel-plate channels and along isolated plates, the heat transfer coefficient varies with L , the distance from the leading edge,²⁶ in the range $\text{Re} \leq 3 \times 10^5$,

$$h = 0.664 \left(\frac{k_{fl}}{L} \right) \text{Re}^{0.5} \text{Pr}^{0.33} \quad (55)$$

and for $\text{Re} > 3 \times 10^5$

$$h = 0.036 \left(\frac{k_{fl}}{L} \right) \text{Re}^{0.8} \text{Pr}^{0.33} \quad (56)$$

Cylinders in Cross-Flow

For airflow around single cylinders at all but very low Reynolds numbers, Hilpert²⁷ has proposed

$$\text{Nu} = \frac{hd}{k_f} = B \left(\frac{\rho V_\infty d}{\mu_f} \right)^n \quad (57)$$

where V_∞ is the free stream velocity and where the constants B and n depend on the Reynolds number as indicated in Table 5.

It has been pointed out¹² that Eq. (57) assumes a natural turbulence level in the oncoming air stream and that the presence of augmentative devices can increase n by as much as 50%. The modifications to B and n due to some of these devices are displayed in Table 6.

Equation (57) can be extended to other fluids²⁸ spanning a range of $1 < \text{Re} < 10^5$ and $0.67 < \text{Pr} < 300$:

$$\text{Nu} = \frac{hd}{k} = (0.4\text{Re}^{0.5} + 0.06\text{Re}^{0.67})\text{Pr} \left(\frac{\mu}{\mu_w} \right)^{0.25} \quad (58)$$

where all fluid properties are evaluated at the free-stream temperature except μ_w , which is the fluid viscosity at the wall temperature.

Noncircular Cylinders in Cross-Flow

It has been found¹² that Eq. (57) may be used for noncircular geometries in cross-flow provided that the characteristic dimension in the Nusselt and Reynolds numbers is the diameter of a cylinder having the same wetted surface equal to that of the geometry of interest and that the values of B and n are taken from Table 7.

Flow across Spheres

For airflow across a single sphere, it is recommended that the average Nusselt number when $17 < \text{Re} < 7 \times 10^4$ be determined from²⁹

$$\text{Nu} = \frac{hd}{k_f} = 0.37 \left(\frac{\rho V_\infty d}{\mu_f} \right)^{0.6} \quad (59)$$

Table 5 Constants for Eq. (11)

Reynolds Number Range	B	n
1–4	0.891	0.330
4–40	0.821	0.385
40–4000	0.615	0.466
4000–40,000	0.174	0.618
40,000–400,000	0.0239	0.805

Table 6 Flow Disturbance Effects on B and n in Eq. (57)

Disturbance	Re Range	B	n
1. Longitudinal fin, 0.1 <i>d</i> thick on front of tube	1000–4000	0.248	0.603
2. 12 longitudinal grooves, 0.7 <i>d</i> wide	3500–7000	0.082	0.747
3. Same as 2 with burrs	3000–6000	0.368	0.86

Table 7 Values of B and n for Eq. (57)

Flow Geometry	B	n	Reynolds Number
	0.224	0.612	2,500–15,000
	0.085	0.804	3,000–15,000
◇	0.261	0.624	2,500–7,500
◇	0.222	0.588	5,000–100,000
□	0.160	0.699	2,500–8,000
□	0.092	0.675	5,000–100,000
○	0.138	0.638	5,000–100,000
○	0.144	0.638	5,000–19,500
○	0.035	0.782	19,500–100,000
	0.205	0.731	4,000–15,000

Source: From Ref. 12.

and for $1 < \text{Re} < 25$,³⁰

$$\text{Nu} = \frac{hd}{k} = 2.2 \text{Pr} + 0.48 \text{Pr} (\text{Re})^{0.5} \quad (60)$$

For both gases and liquids in the range $3.5 < \text{Re} < 7.6 \times 10^4$ and $0.7 < \text{Pr} < 380$ ²⁸

$$\text{Nu} = \frac{hd}{k} = 2 + (4.0\text{Re}^{0.5} + 0.06\text{Re}^{0.67})\text{Pr}^{0.4} \left(\frac{\mu}{\mu_w} \right)^{0.25} \quad (61)$$

Flow across Tube Banks

For the flow of fluids flowing normal to banks of tubes,³¹

$$\text{Nu} = \frac{hd}{k_f} = C \left(\frac{\rho V_\infty d}{\mu_f} \right)^{0.6} \left(\frac{c_p \mu}{k} \right)_f^{0.33} \phi \quad (62)$$

which is valid in the range $2000 < \text{Re} < 32,000$.

For in-line tubes, $C = 0.26$, whereas for staggered tubes, $C = 0.33$. The factor ϕ is a correction factor for sparse tube banks, and values of ϕ are provided in Table 8.

Table 8 Correlation Factor ϕ for Sparse Tube Banks

Number of Rows, N	In Line	Staggered
1	0.64	0.68
2	0.80	0.75
3	0.87	0.83
4	0.90	0.89
5	0.92	0.92
6	0.94	0.95
7	0.96	0.97
8	0.98	0.98
9	0.99	0.99
10	1.00	1.00

For air in the range where Pr is nearly constant (Pr ≈ 0.7 over the range 25–200°C), Eq. (62) can be reduced to

$$Nu = \frac{hd}{k_f} = C' \left(\frac{\rho V_\infty d}{\mu_f} \right)^{n'} \tag{63}$$

where C' and n' may be determined from values listed in Table 9. This equation is valid in the range $2000 < Re < 40,000$ and the ratios x_L and x_T denote the ratio of centerline diameter to tube spacing in the longitudinal and transverse directions, respectively.

For fluids other than air, the curve shown in Fig. 11 should be used for staggered tubes.²⁹ For in-line tubes, the values of

$$j = \left(\frac{hd_0}{k} \right) \left(\frac{c_p \mu}{k} \right)^{-1/3} \left(\frac{\mu}{\mu_w} \right)^{-0.14}$$

should be reduced by 10%.

Flow across Arrays of Pin Fins

For air flowing normal to banks of staggered cylindrical pin fins or spines,³²

$$Nu = \frac{hd}{k} = 1.40 \left(\frac{\rho v_\infty d}{\mu} \right)^{0.8} \left(\frac{c_p \mu}{k} \right)^{1/3} \tag{64}$$

Flow of Air over Electronic Components

For single prismatic electronic components, either normal or parallel to the sides of the component in a duct,³³ for $2.5 \times 10^3 < Re < 8 \times 10^3$,

$$Nu = 0.446 \left[\frac{Re}{(1/6) + (5A_n/6A_0)} \right]^{0.57} \tag{65}$$

where the Nusselt and Reynolds numbers are based on the prism side dimension and where A_0 and A_n are the gross and net flow areas, respectively.

Table 9 Values of Constants C' and n' in Eq. (63)

$x_L = \frac{S_L}{d_0}$	$x_T = \frac{S_T}{d_0} = 1.25$		$x_T = \frac{S_T}{d_0} = 1.50$		$x_T = \frac{S_T}{d_0} = 2.00$		$x_T = \frac{S_T}{d_0} = 3.00$	
	C'	n'	C'	n'	C'	n'	C'	n'
<i>Staggered</i>								
0.600							0.213	0.636
0.900					0.446	0.571	0.401	0.581
1.000			0.497	0.558				
1.125					0.478	0.565	0.518	0.560
1.250	0.518	0.556	0.505	0.554	0.519	0.556	0.522	0.562
1.500	0.451	0.568	0.460	0.562	0.452	0.568	0.488	0.568
2.000	0.404	0.572	0.416	0.568	0.482	0.556	0.449	0.570
3.000	0.310	0.592	0.356	0.580	0.440	0.562	0.421	0.574
<i>In Line</i>								
1.250	0.348	0.592	0.275	0.608	0.100	0.704	0.0633	0.752
1.500	0.367	0.586	0.250	0.620	0.101	0.702	0.0678	0.744
2.000	0.418	0.570	0.299	0.602	0.229	0.632	0.198	0.648
3.000	0.290	0.601	0.357	0.584	0.374	0.581	0.286	0.608

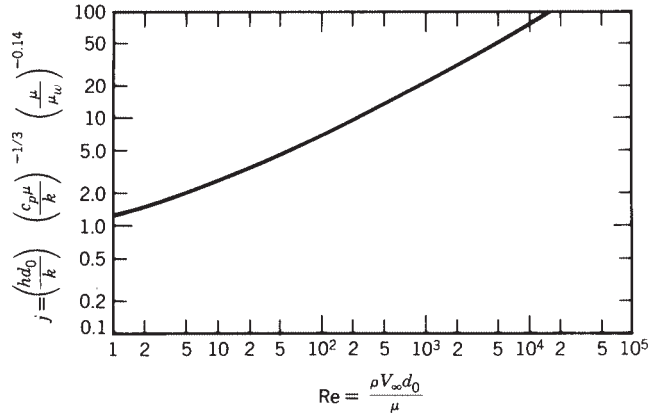


Figure 11 Recommended curve for estimation of heat transfer coefficient for fluids flowing normal to staggered tubes 10 rows deep. (From Ref. 29, © McGraw-Hill Education)

For staggered prismatic components, Eq. (65) may be modified to³³

$$\text{Nu} = 0.446 \left[\frac{\text{Re}}{(1/6) + (5A_n/A_0)} \right]^{0.57} \left[1 + 0.639 \left(\frac{S_T}{S_{T,\max}} \right) \left(\frac{d}{S_L} \right)^{0.172} \right] \quad (66)$$

where d is the prism side dimension, S_L is the longitudinal separation, S_T is the transverse separation, and $S_{T,\max}$ is the maximum transverse spacing if different spacings exist.

When cylindrical heat sources are encountered in electronic equipment, a modification of Eq. (57) has been proposed³⁴:

$$\text{Nu} = \frac{hd}{k_f} = FB \left(\frac{\rho V_\infty d}{\mu} \right)^n \quad (67)$$

where F is an arrangement factor depending on the cylinder geometry (see Table 10) and where the constants B and n are given in Table 11.

Forced Convection in Tubes, Pipes, Ducts, and Annuli

For heat transfer in tubes, pipes, ducts, and annuli, use is made of the equivalent diameter

$$d_e = \frac{4A}{WP} \quad (68)$$

Table 10 Values of F to Be Used in Eq. (67)^a

Single cylinder in free stream: $F = 1.0$

Single cylinder in duct: $F = 1 + d/w$

In-line cylinders in duct:

$$F = \left(1 + \sqrt{\frac{1}{S_T}} \right) \left\{ 1 + \left(\frac{1}{S_L} - \frac{0.872}{S_L^2} \right) \left(\frac{1.81}{S_T^2} - \frac{1.46}{S_T} + 0.318 \right) \left[\text{Re}^{0.526 - (0.354/S_T)} \right] \right\}$$

Staggered cylinders in duct:

$$F = \left(1 + \sqrt{\frac{1}{S_T}} \right) \left\{ 1 + \left[\frac{1}{S_L} \left(\frac{15.50}{S_T^2} - \frac{16.80}{S_T} + 4.15 \right) - \frac{1}{S_L} \left(\frac{14.15}{S_T^2} - \frac{15.33}{S_T} + 3.69 \right) \right] \text{Re}^{0.13} \right\}$$

^aRe to be evaluated at film temperature. S_L = ratio of longitudinal spacing to cylinder diameter. S_T = ratio of transverse spacing to cylinder diameter.

Table 11 Values of B and n for Use in Eq. (67)

Reynolds Number	B	n
1000–6000	0.409	0.531
6000–30,000	0.212	0.606
30,000–100,000	0.139	0.806

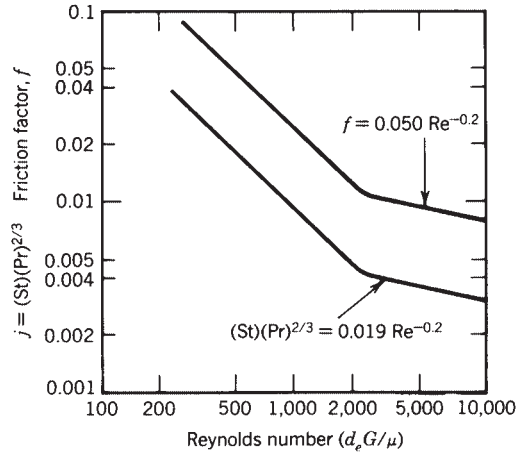


Figure 12 Heat transfer and friction data for forced air through rectangular ducts. St is the Stanton number, $St = hG/c_p$.

in the Reynolds and Nusselt numbers unless the cross section is circular, in which case d_e and $d_i = d$.

In the laminar regime³⁵ where $Re < 2100$,

$$Nu = hd_e/k = 1.86[RePr(d_e/L)]^{1/3} (\mu/\mu_w)^{0.14} \tag{69}$$

with all fluid properties except μ_w evaluated at the bulk temperature of the fluid.

For Reynolds numbers above transition, $Re > 2100$,

$$Nu = 0.023(Re)^{0.8}(Pr)^{1/3}(\mu/\mu_w)^{0.14} \tag{70}$$

and in the transition region, $2100 < Re < 10,000$,³⁶

$$Nu = 0.116[(Re)^{2/3} - 125](Pr)^{1/3}(\mu/\mu_w)^{0.14}[1 + (d_e/L)^{2/3}] \tag{71}$$

London³⁷ has proposed a correlation for the flow of air in rectangular ducts. It is shown in Fig. 12. This correlation may be used for air flowing between longitudinal fins.

3 THERMAL CONTROL TECHNIQUES

3.1 Extended Surface and Heat Sinks

The heat flux from a surface, q/A , can be reduced if the surface area A is increased. The use of extended surface or fins is a common method of achieving this reduction. Another way of

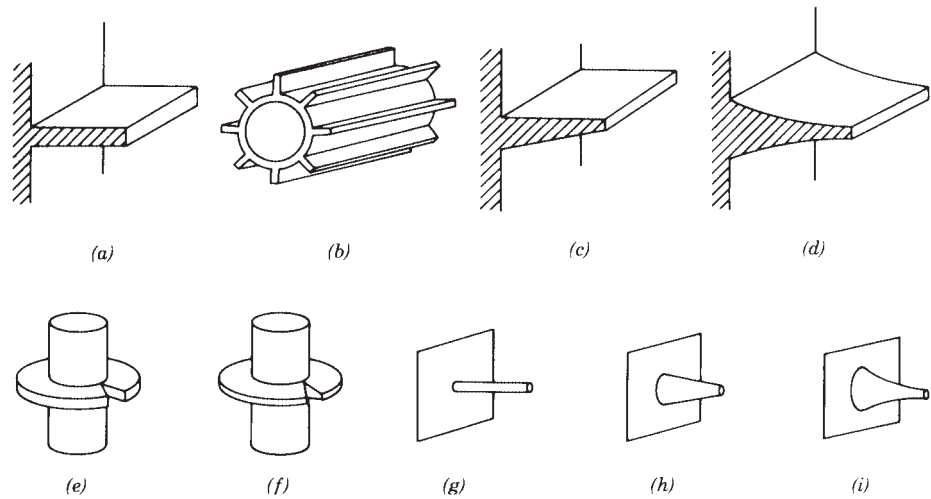


Figure 13 Some typical examples of extended surfaces: (a) longitudinal fin of rectangular profile; (b) cylindrical tube equipped with longitudinal fins; (c) longitudinal fin of trapezoidal profile; (d) longitudinal fin of truncated concave parabolic profile; (e) cylindrical tube equipped with radial fin of rectangular profile; (f) cylindrical tube equipped with radial fin of truncated triangular profile; (g) cylindrical spine; (h) truncated conical spine; (i) truncated concave parabolic spine.

looking at this is through the use of Newton's law of cooling,

$$q = hA \Delta T \quad (72)$$

and considering that ΔT can be reduced for a given heat flow q by increasing h , which is difficult for a specified coolant, or by increasing the surface area A .

The common extended surface shapes are the longitudinal fin of rectangular profile, the radial fin of rectangular profile, and the cylindrical spine shown, respectively, in Figs. 13a, e, and g.

Assumptions in Extended Surface Analysis

The analysis of extended surfaces is subject to the following simplifying assumptions^{38,39}:

1. The heat flow is steady; that is, the temperature at any point does not vary with time.
2. The fin material is homogeneous, and the thermal conductivity is constant and uniform.
3. The coefficient of heat transfer is constant and uniform over the entire face surface of the fin.
4. The temperature of the surrounding fluid is constant and uniform.
5. There are no temperature gradients within the fin other than along the fin height.
6. There is no bond resistance to the flow of heat at the base of the fin.
7. The temperature at the base of the fin is uniform and constant.
8. There are no heat sources within the fin itself.
9. There is a negligible flow of heat from the tip and sides of the fin.
10. The heat flow from the fin is proportioned to the temperature difference or temperature excess, $\theta(x) = T(x) - T_s$, at any point on the face of the fin.

Fin Efficiency

Because a temperature gradient always exists along the height of a fin when heat is being transferred to the surrounding environment by the fin, there is a question regarding the temperature to be used in Eq. (72). If the base temperature T_b (and the base temperature excess $\theta_b = T_b - T_s$) is to be used, then the surface area of the fin must be modified by the computational artifice known as the fin efficiency, defined as the ratio of the heat actually transferred by the fin to the ideal heat transferred if the fin were operating over its entirety at the base temperature excess. In this case, the surface area A in Eq. (54) becomes

$$A = A_b + \eta_f A_f \quad (73)$$

Longitudinal Fin of Rectangular Profile

With the origin of the height coordinate x taken at the fin tip, which is presumed to be adiabatic, the temperature excess at any point on the fin is

$$\theta(x) = \theta_b \frac{\cosh mx}{\cosh mb} \quad (74)$$

where

$$m = \left(\frac{2h}{k\delta} \right)^{1/2} \quad (75)$$

The heat dissipated by the fin is

$$q_b = Y_0 \theta_b \tan h mb \quad (76)$$

where Y_0 is called the characteristic admittance

$$Y_0 = (2hk\delta)^{1/2} L \quad (77)$$

and the fin efficiency is

$$\eta_f = \frac{\tan h mb}{mb} \quad (78)$$

The heat transfer coefficient in natural convection may be determined from the symmetric isothermal case pertaining to vertical plates in Section 2.1. For forced convection, the London correlation described in Section 2.2 applies.

Radial Fin of Rectangular Profile

With the origin of the radial height coordinate taken at the center of curvature and with the fin tip at $r = r_a$ presumed to be adiabatic, the temperature excess at any point on the fin is

$$\theta(r) = \theta_b \left[\frac{K_1(mr_a) I_0(mr) + I_1(mr_a) K_0(mr)}{I_0(mr_b) K_1(mr_a) + I_1(mr_a) K_0(mr_b)} \right] \quad (79)$$

where m is given by Eq. (75). The heat dissipated by the fin is

$$q_b = 2\pi r_b k m \theta_b \left[\frac{I_1(mr_a) K_1(mr_b) - K_1(mr_a) I_1(mr_b)}{I_0(mr_b) K_1(mr_a) + I_1(mr_a) K_0(mr_b)} \right] \quad (80)$$

and the fin efficiency is

$$\eta_f = \frac{2r_b}{m(r_a^2 - r_b^2)} \left[\frac{I_1(mr_a) K_1(mr_b) - K_1(mr_a) I_1(mr_b)}{I_0(mr_b) K_1(mr_a) + I_1(mr_a) K_0(mr_b)} \right] \quad (81)$$

Tables of the fin efficiency are available,⁴⁰ and they are organized in terms of two parameters, the radius ratio

$$\rho = \frac{r_b}{r_a} \quad (82a)$$

and a parameter ϕ ,

$$\phi = (r_a - r_b) \left(\frac{2h}{kA_p} \right)^{1/2} \quad (82b)$$

where A_p is the profile area of the fin:

$$A_p = \delta(r_a - r_b) \quad (82c)$$

For air under forced-convection conditions, the correlation for the heat transfer coefficient developed by Briggs and Young⁴¹ is applicable:

$$\frac{h}{2r_b k} = \left(\frac{2\rho V r_b}{\mu} \right)^{0.681} \left(\frac{c_p \mu}{k} \right)^{1/3} \left(\frac{s}{r_a - r_b} \right)^{0.200} \left(\frac{s}{\delta} \right)^{0.1134} \quad (83)$$

where all thermal properties are evaluated at the bulk air temperature, s is the space between the fins, and r_a and r_b pertain to the fins.

Cylindrical Spine

With the origin of the height coordinate x taken at the spine tip, which is presumed to be adiabatic, the temperature excess at any point on the spine is given by Eq. (72), but for the cylindrical spine

$$m = \left(\frac{4h}{kd} \right)^{1/2} \quad (84)$$

where d is the spine diameter. The heat dissipated by the spine is given by Eq. (76), but in this case

$$Y_0 = (\pi^2 h k d^3)^{1/2} / 2 \quad (85)$$

and the spine efficiency is given by Eq. (78).

Algorithms for Combining Single Fins into Arrays

The differential equation for temperature excess that can be developed for any fin shape can be solved to yield a particular solution based on prescribed initial conditions of fin base temperature excess and fin base heat flow, which can be written in matrix form^{42,43} as

$$\begin{bmatrix} \theta_a \\ q_a \end{bmatrix} = [\Gamma] \begin{bmatrix} \theta_b \\ q_b \end{bmatrix} = \begin{bmatrix} \gamma_{11} & \gamma_{12} \\ \gamma_{21} & \gamma_{22} \end{bmatrix} \begin{bmatrix} \theta_b \\ q_b \end{bmatrix} \quad (86)$$

The matrix $[\Gamma]$ is called the thermal transmission matrix and provides a linear transformation from tip to base conditions. It has been cataloged for all of the common fin shapes.⁴²⁻⁴⁴ For the longitudinal fin of rectangular profile

$$[\Gamma] = \begin{bmatrix} \cosh mb & -\frac{1}{Y_0} \sinh mb \\ -Y_0 \sinh mb & \cosh mb \end{bmatrix} \quad (87)$$

and this matrix possesses an inverse called the inverse thermal transmission matrix

$$[\Lambda] = [\Gamma]^{-1} = \begin{bmatrix} \cosh mb & \frac{1}{Y_0} \sinh mb \\ Y_0 \sinh mb & \cosh mb \end{bmatrix} \quad (88)$$

The assembly of fins into an array may require the use of any or all of three algorithms.^{3,44,45} The objective is to determine the input admittance of the entire array

$$Y_{in} = \left. \frac{q_b}{\theta_b} \right|_A \quad (89)$$

which can be related to the array (fin) efficiency by

$$\eta_f = \frac{Y_{in}}{hA_f} \tag{90}$$

The determination of Y_{in} can involve as many as three algorithms for the combination of individual fins into an array.

Cascade Algorithm. For n fins in cascade as shown in Fig. 14a, an equivalent inverse thermal transmission matrix can be obtained by a simple matrix multiplication, with the individual fins closest to the base of the array acting as permultipliers:

$$\{\Lambda\}_e = \{\Lambda\}_n \{\Lambda\}_{n-1} \{\Lambda\}_{n-2} \cdots \{\Lambda\}_2 \{\Lambda\}_1 \tag{91}$$

For the case of the tip of the most remote fin adiabatic, the array input admittance will be

$$Y_{in} = \frac{\lambda_{21,e}}{\lambda_{11,e}} \tag{92}$$

If the tip of the most remote fin is not adiabatic, the heat flow to temperature excess ratio at the tip, which is designated as μ ,

$$\mu = \frac{q_a}{\theta_a} \tag{93}$$

will be known. For example, for a fin dissipating to the environment through its tip designated by the subscript a :

$$\mu = hA_a \tag{94}$$

In this case, Y_{in} may be obtained through successive use of what is termed the reflection relationship (actually a bilinear transformation):

$$Y_{in,k-1} = \frac{\lambda_{21,k-1} + \lambda_{22,k-1}(q_a/\theta_a)}{\lambda_{11,k-1} + \lambda_{12,k-1}(q_a/\theta_a)} \tag{95}$$

Cluster Algorithm. For n fins in cluster, as shown in Fig. 14b, the equivalent thermal transmission ratio will be the sum of the individual fin input admittances:

$$\mu_e = \sum_{k=1}^n Y_{in,k} = \sum_{k=1}^n \left. \frac{q_b}{\theta_b} \right|_k \tag{96}$$

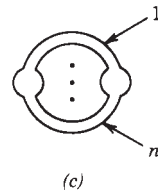
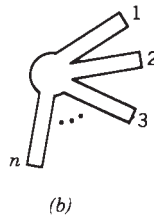
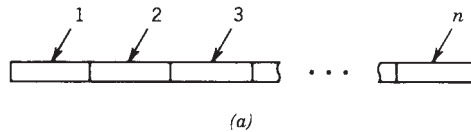


Figure 14 (a) n fins in cascade, (b) n fins in cluster, and (c) n fins in parallel.

Here, $Y_{in,k}$ can be determined for each individual fin via Eq. (93) if the fin has an adiabatic tip or via Eq. (95) if the tip is not adiabatic. It is obvious that this holds if subarrays containing more than one fin are in cluster.

Parallel Algorithm. For n fins in parallel, as shown in Fig. 14c, an equivalent thermal admittance matrix $[Y]_e$ can be obtained from the sum of the individual thermal admittance matrices:

$$[Y]_e = \sum_{k=1}^n [Y]_k \quad (97)$$

where the individual thermal admittance matrices can be obtained from

$$[Y] = \begin{bmatrix} y_{11} & y_{12} \\ y_{21} & y_{22} \end{bmatrix} = \begin{bmatrix} -\frac{\gamma_{11}}{\gamma_{12}} & \frac{1}{\gamma_{12}} \\ \frac{1}{\gamma_{12}} & \frac{\gamma_{12}}{\gamma_{22}} \end{bmatrix} = \begin{bmatrix} \frac{\lambda_{22}}{\lambda_{12}} & -\frac{1}{\lambda_{12}} \\ \frac{1}{\lambda_{12}} & -\frac{\lambda_{12}}{\lambda_{22}} \end{bmatrix} \quad (98)$$

If necessary, $[\Lambda]$ may be obtained from $[Y]$ using

$$[\Lambda] = \begin{bmatrix} \lambda_{11} & \lambda_{12} \\ \lambda_{21} & \lambda_{22} \end{bmatrix} = \begin{bmatrix} -\frac{y_{22}}{\Delta_Y} & \frac{1}{y_{21}} \\ \frac{y_{21}}{\Delta_Y} & \frac{y_{11}}{y_{21}} \end{bmatrix} \quad (99)$$

where $\Delta_Y = y_{11} y_{22} - y_{12} y_{21}$

Singular Fans. There will be occasions when a singular fin, one whose tip comes to a point, will be used as the most remote fin in an array. In this case the $[\Gamma]$ and $[\Lambda]$ matrices do not exist and the fin is characterized by its input admittance.⁴²⁻⁴⁴ Such a fin is the longitudinal fin of triangular profile where

$$Y_{in} = \frac{q_b}{\theta_b} = \frac{2hI_1(2mb)}{mI_0(2mb)} \quad (100)$$

where

$$m = \left(\frac{2h}{k\delta_b} \right)^{1/2} \quad (101)$$

3.2 Cold Plate

The cold-plate heat exchanger or forced cooled electronic chassis is used to provide a “cold wall” to which individual components and, for that matter, entire packages of equipment may be mounted. Its design and performance evaluation follows a certain detailed procedure that depends on the type of heat loading and whether the heat loading is on one or two sides of the cold plate. These configurations are displayed in Fig. 15.

The design procedure is based on matching the available heat transfer effectiveness ε to the required effectiveness ε determined from the design specifications. These effectivenesses are for, the isothermal case in Fig. 15a,

$$\varepsilon = \frac{t_2 - t_1}{T_s - t_1} = e^{-NTU} \quad (102)$$

and, for the isoflux case in Fig. 15b,

$$\varepsilon = \frac{t_2 - t_1}{T_2 - t_1} \quad (103)$$

where the “number of transfer units” is

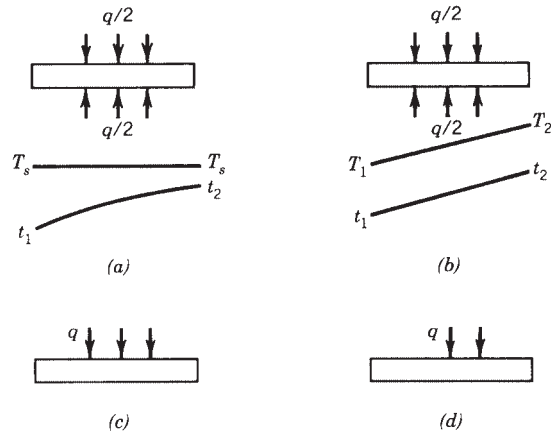


Figure 15 (a) Double-sided, evenly loaded cold plate—isotheermal case; (b) double-sided, evenly loaded cold plate—isoflux case; (c) single-sided, evenly loaded cold plate—isotheermal case; and (d) single-sided, evenly loaded cold plate—isoflux case.

$$NTU = \frac{h\eta_0 A}{Wc_p} \quad (104)$$

and the overall passage efficiency is

$$\eta_0 = 1 - \frac{A_f}{A}(1 - \eta_f) \quad (105)$$

The surfaces to be used in the cold plate are those described by Kays and London⁴⁵ where physical, heat transfer, and friction data are provided.

The detailed design procedure for the double-side-loaded isothermal case is as follows:

1. Design specification
 - a. Heat load, q , W
 - b. Inlet air temperature, t_1 , °C
 - c. Airflow, W , kg/s
 - d. Allowable pressure loss, cm H₂O
 - e. Overall envelope, H , W , D
 - f. Cold-plate material thermal conductivity, k_m , W/m·°C
 - g. Allowable surface temperature, T_s , °C
2. Select surface⁴⁵
 - a. Type
 - b. Plate spacing, b , m
 - c. Fins per meter, fpm
 - d. Hydraulic diameter, d_e , m
 - e. Fin thickness, δ , m
 - f. Heat transfer area/volume, β , m²/m³
 - g. Fin surface area/total surface area, A_f/A , m²/m³

3. Plot of j and f data⁴⁵

$$j = (\text{St})(\text{Pr})^{2/3} = f_1(\text{Re}) = f_1 \left(\frac{d_e G}{\mu} \right)$$

where St is the Stanton number

$$\text{St} = \frac{hG}{c_p} \quad (106)$$

and f is the friction factor

$$f = f_2(\text{Re}) = f_2 \left(\frac{d_e G}{\mu} \right)$$

4. Establish physical data

- a. $a = (b/H)\beta$, m^2/m^3
- b. $r_h = d_e/4$, m
- c. $\sigma = ar_h$
- d. $A_{fr} = WH$, m^2 (frontal area)
- e. $A_c = \sigma A_{fr}$, m^2 (flow areas)
- f. $V = DWH$ (volume)
- g. $A = aV$, m^2 (total surface)

5. Heat balance

- a. Assume average fluid specific heat, c_p , $\text{J/kg} \cdot ^\circ\text{C}$.
- b. $\Delta t = t_2 - t_1 = q/Wc_p$, $^\circ\text{C}$
- c. $t_2 = t_1 + \Delta t$, $^\circ\text{C}$
- d. $t_{av} = 1/2(t_1 + t_2)$
- e. Check assumed value of c_p . Make another assumption if necessary.

6. Fluid properties at t_{av}

- a. c_p (already known), $\text{J/kg} \cdot ^\circ\text{C}$
- b. μ , $\text{N/s} \cdot \text{m}^2$
- c. k , $\text{W/m} \cdot ^\circ\text{C}$
- d. $(\text{Pr})^{2/3} = (c_p \mu / k)^{2/3}$

7. Heat transfer coefficient

- a. $G = W/A_c$, $\text{kg/s} \cdot \text{m}^2$
- b. $\text{Re} = d_e G / \mu$
- c. Obtain j from curve (see item 3).
- d. Obtain f from curve (see item 3).
- e. $h = jGc_p / (\text{Pr})^{2/3}$, $\text{W/m}^2 \cdot ^\circ\text{C}$

8. Fin efficiency

- a. $m = (2h/k\delta)^{1/2}$, m^{-1}
- b. $mb/2$ is a computation
- c. $\eta_f = (\tanh mb/2)/mb/2$

9. Overall passage efficiency
 - a. Use Eq. (105).
10. Effectiveness
 - a. Required $\varepsilon = (t_2 - t_1)/(T_s - T_1)$
 - b. Form NTU from Eq. (104).
 - c. Actual available $\varepsilon = 1 - e^{-NTU}$
 - d. Compare required ε and actual ε and begin again with step 1 if the comparison fails. If comparison is satisfactory, go on to pressure loss calculation.
11. Pressure loss
 - a. Establish v_1 (specific volume), m^3/k .
 - b. Establish v_2 , m^3/kg .
 - c. $v_m = 1/2(v_1 + v_2)$, m^3/k .
 - d. Form v_m/v_1 .
 - e. Form v_2/v_1 .
 - f. Obtain K_c and K_e^{41}
 - g. Determine ΔP , cm:

$$\Delta P = 0.489 \frac{G^2 v_1}{2g} \left[(1 + K_c - \sigma^2) + f \frac{A}{A_c} \frac{v_m}{v_1} + 2 \left(\frac{v_2}{v_1} - 1 \right) - (1 - \sigma^2 - K_c) \frac{v_2}{v_1} \right] \quad (107)$$
 - h. Compare ΔP with specified ΔP . If comparison fails, select a different surface or adjust the dimensions and begin again with step 1.

If the cold plate is loaded on one side only, an identical procedure is followed except in steps 8 and 9. For single-side loading and for double and triple stacks, use must be made of the cascade and cluster algorithms for the combination of fins described in Section 3.1. Detailed examples of both of the foregoing cases may be found in Kraus and Bar-Cohen.⁸

3.3 Thermoelectric Coolers

Two thermoelectric effects are traditionally considered in the design and performance evaluation of a thermoelectric cooler:

The Seebeck effect concerns the net conversion of thermal energy into electrical energy under zero current conditions when two dissimilar materials are brought into contact. When the junction temperature differs from a reference temperature, the effect is measured as a voltage called the Seebeck voltage E_s .

The Peltier effect concerns the reversible evolution or absorption of heat that occurs when an electric current traverses the junction between two dissimilar materials. The Peltier heat absorbed or rejected depends on and is proportional to the current flow. There is an additional thermoelectric effect known as the Thomson effect, which concerns the reversible evolution or absorption of heat that occurs when an electric current traverses a single homogeneous material in the presence of a temperature gradient. This effect, however, is a negligible one and is neglected in considerations of thermoelectric coolers operating over moderate temperature differentials.

Equations for Thermoelectric Effects

Given a pair of thermoelectric materials, A and B , with each having a thermoelectric power α_A and α_B ,³ the Seebeck coefficient is

$$\alpha = |\alpha_A| + |\alpha_B| \quad (108)$$

The Seebeck coefficient is the proportionality constant between the Seebeck voltage and the junction temperature with respect to some reference temperature

$$dE_s = \pm \alpha dT$$

and it is seen that

$$\alpha = \frac{dE_s}{dT}$$

The Peltier heat is proportional to the current flow and the proportionality constant is Π , the Peltier voltage

$$q_p = \pm \pi I \quad (109)$$

The Thomson heat is proportional to a temperature difference dT and the proportionality constant is σ , the Thomson coefficient. With $dq_T = \pm \sigma I dT$, it is observed that σdT is a voltage and the Thomson voltage is defined by

$$E_T = \pm \int_{T_1}^{T_2} \sigma dT$$

Considerations of the second law of thermodynamics and the Kirchhoff voltage laws, show that the Peltier voltage is related to the Seebeck coefficient³

$$\pi = \alpha T \quad (110)$$

and if the Seebeck coefficient is represented as a polynomial³

$$\alpha = a + bT + \dots$$

then

$$\pi = aT + bT^2 + \dots$$

Design Equations

In Fig. 16, which shows a pair of materials arranged as a thermoelectric cooler, there is a cold junction at T_c and a hot junction at T_h . The materials possess a thermal conductivity k and an electrical resistivity ρ . A voltage is provided so that a current I flows through the cold junction from B to A and through the hot junction from A to B . This current direction is selected to guarantee that $T_c < T_h$.

The net heat absorbed at the cold junction is the Peltier heat

$$q_p = \pi T_c = \alpha I T_c \quad (111a)$$

minus one-half of the $I^2 R$ loss (known as the Joule heat or Joule effect),

$$q_j = 1/2 I^2 R \quad (111b)$$

and minus the heat regained at the cold junction (known as the Fourier heat or Fourier effect) due to the temperature difference $\Delta T = T_h - T_c$,

$$q_F = K \Delta T = K(T_h - T_c) \quad (111c)$$

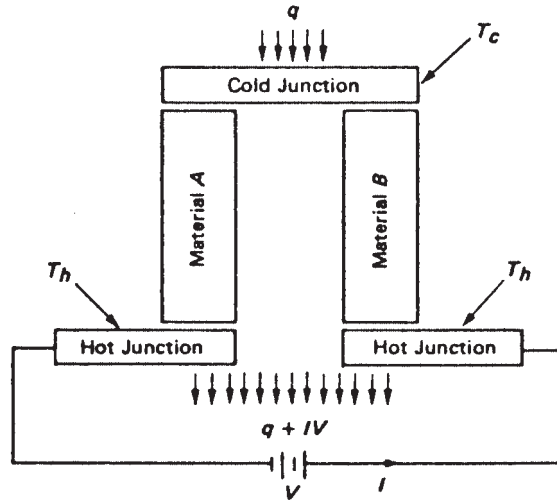


Figure 16 Thermoelectric cooler.

Thus, the net heat absorbed at the cold junction is

$$q = \alpha IT_c - \frac{1}{2}I^2R - K \Delta T \tag{112}$$

where the total resistance of the couple is the series resistance of material A and material B having areas A_A and A_B , respectively (both have length L),

$$R = \left(\frac{\rho_A}{A_A} + \frac{\rho_B}{A_B} \right) L \tag{113}$$

and where the overall conductance K is the parallel conductance of the elements A and B:

$$K = \frac{1}{L}(k_A A_A + k_B A_B) \tag{114}$$

To power the device, a voltage equal to the sum of the Seebeck voltages at the hot and cold junctions plus the voltage necessary to overcome the resistance drop must be provided:

$$V = \alpha T_h - \alpha T_c + RI = \alpha \Delta T + RI$$

and the power is

$$P = VI = (\alpha \Delta T + RI)I \tag{115}$$

The coefficient of performance (COP) is the ratio of the net cooling effect to the power provided:

$$\text{COP} = \frac{q}{P} = \frac{\alpha T_c I - \frac{1}{2}I^2R - K \Delta T}{\alpha \Delta T I + I^2 R} \tag{116}$$

Optimizations

The maximum possible temperature differential $\Delta T = T_h - T_c$ will occur when there is no net heat absorbed at the cold junction:

$$\Delta T_m = \frac{1}{2}zT_c^2 \tag{117}$$

where z is the figure of merit of the material,

$$z = \frac{\alpha^2}{KR} \tag{118}$$

The current that yields the maximum amount of heat absorbed at the cold junction can be shown to be³

$$I = I_m = \frac{\alpha T_c}{R} \quad (119)$$

and the coefficient of performance in this case will be

$$\text{COP}_m = \frac{1 - \Delta T / \Delta T_m}{2(1 + \Delta T / T_c)} \quad (120)$$

The current that optimizes or maximizes the coefficient of performance can be shown to be

$$I_0 = \frac{\alpha \Delta T}{R[(1 + zT_a)^{1/2} - 1]} \quad (121)$$

where $T_a = 1/2(T_h + T_c)$. In this case, the optimum coefficient of performance will be

$$\text{COP}_0 = \frac{T_c}{\Delta T} \left[\frac{\gamma - (T_h/T_c)}{\gamma + 1} \right] \quad (122)$$

where

$$\gamma = [1 + 1/2z(T_h + T_c)]^{1/2} \quad (123)$$

Analysis of Thermoelectric Coolers

In the event that a manufactured thermoelectric cooling module is being considered for a particular application, the designer will need to specify the number of junctions required. A detailed procedure for the selection of the number of junctions is as follows:

1. Design specifications
 - a. Total cooling load, q_T , W
 - b. Cold-side temperature, T_c , K
 - c. Hot-side temperature, T_h , K
 - d. Cooler specifications
 - (i) Materials A and B
 - (ii) α_A and α_B , V/°C
 - (iii) ρ_A and ρ_B , $\Omega \cdot \text{cm}$
 - (iv) k_A and k_B , W/cm·°C
 - (v) A_A and A_B , cm²
 - (vi) L , cm
2. Cooler calculations
 - a. Establish $\alpha = |\alpha_A| + |\alpha_B|$.
 - b. Calculate R from Eq. (113).
 - c. Calculate K from Eq. (114).
 - d. Form $\Delta T = T_h - T_c$, K or °C.
 - e. Obtain z from Eq. (118), 1/°C.
3. For maximum heat pumping per couple
 - a. Calculate I_m from Eq. (119), A.
 - b. Calculate the heat absorbed by each couple q , from Eq. (112), W.
 - c. Calculate ΔT_m from Eq. (117), K or °C.
 - d. Determine COP_m from Eq. (120).

- e. The power required per couple will be $p = q/\text{COP}_m$, W.
 - f. The heat rejected per couple will be $p + q$, W.
 - g. The required number of couples will be $n = q_T/q$.
 - h. The total power required will be $p_T = nP$, W.
 - i. The total heat rejected will be $q_{RT} = nq_R$, W.
4. For optimum coefficient of performance
- a. Determine $T_a = 1/2(T_h + T_c)$, K.
 - b. Calculate I_0 from Eq. (121), A.
 - c. Calculate the heat absorbed by each couple, q , from Eq. (112), W.
 - d. Determine γ from Eq. (123).
 - e. Determine COP_0 from Eq. (122).
 - f. The power required per couple will be $P = q/\text{COP}_0$, W.
 - g. The heat rejected per couple will be $q_R = P + q$, W.
 - h. The required number of couples will be $n = q_T/q$.
 - i. The total power required will be $P_T = nP$, W.
 - j. The total heat rejected will be $q_{RT} = nq_R$, W.

3.4 Spray Cooling

The use of impinging fluid jets for the thermal management of electronic components has received extensive attention in recent years. The high heat transfer coefficients that can be attained in this cooling mode, the ability to vary and control the heat transfer rates across a large substrate or printed circuit board with an appropriately configured distribution plate or nozzle array, and the freedom to tailor the jet flow to the local cooling requirements have made spray cooling one of the most promising alternatives for the cooling of high-heat-flux components.

Spray cooling may involve a single jet or multiple jets directed at a single component or an array of electronic components. The jets may be formed using circular or slot-shaped orifices or nozzles of various cross sections. The axis of the impinging jet may be perpendicular or inclined to the surface of the component. Moreover, in the application of liquid jets, a distinction can be made between “free jets,” which are surrounded by ambient air, and “submerged jets,” for which the volume surrounding the jet is filled with the working liquid. While heat transfer associated with gas jets has been the subject of active research since the mid-1950s, spray cooling with dielectric liquids is a far more recent development. Several reviews of the many pioneering and more recent studies on spray cooling can be found in the literature.^{46–51} This discussion focuses primarily on single-phase, forced convection.

Despite the complex behavior of the local heat transfer coefficient resulting from parametric variations in the impinging jet flow, it has been found possible to correlate the average heat transfer coefficient with a single expression for both individual jets and arrays of jets impinging on isothermal surfaces. Martin⁵² proposed a relation of the form shown below to capture the effects of jet Reynolds number, nondimensional distance of separation (H/D), impinging area ratio (f), Prandtl number (Pr), and fluid thermal conductivity on the jet Nusselt number:

$$\text{Nu}_D = \left[1 + \left(\frac{H/D}{0.6/\sqrt{f}} \right)^3 \right]^{0.05} \left[\frac{\sqrt{f} (1 - 2.2\sqrt{f})}{1 + 0.2(H/D - 6)\sqrt{f}} \right] \text{Re}_D^{0.667} \text{Pr}^{0.42} \quad (124)$$

The range of validity⁵² for this correlation, developed from extensive gas jet data, as well as some data for water and other, higher Prandtl number liquids, and including some high Schmidt number mass transfer data, is $2 \times 10^3 \leq Re_D \leq 10^5$, $0.6 < Pr(Sc) < 7(900)$, $0.004 \leq f \leq 0.04$, and $2 \leq H/D \leq 12$. This correlation has a predictive accuracy of 10–20% over the stated parametric range. The average Nu was also found to be nearly unaffected by the angle of inclination of the jet. It is to be noted that for jets produced by sharp-edged orifices, jet contraction immediately after the orifice exit must be taken into consideration in calculating the average velocity, jet diameter, and nozzle area ratio f . In applying this correlation to the cooling of electronic components, constituting discrete heat sources on a large surface, it is necessary to alter the definition of the jet area ratio f . Recognizing that, in this application, the impingement area is usually equal to the component area, f can be expressed as

$$f = \frac{nA_{\text{jet}}}{A} = \frac{0.785D^2n}{A} \quad (125)$$

Figure 17 shows a comparison correlations by Womac,⁵³ Brdlik and Savin,⁵⁴ and Sitharamayya and Raju⁵⁵ with the predictions from Eq. (43) for $f = 0.008$, $H/D = 3$, and $Pr = 13.1$. The maximum deviation of the data from predictions made using Eq. (24) was 32% in Figure 17. The Martin⁵² correlation [Eq. (124)] is recommended over these alternatives primarily because of the broad range of parameters in the database from which it was developed and because it often falls below the other correlations, making it a conservative choice.

The variation of the Nusselt number with each of the three primary factors influencing spray cooling in the range of the Martin⁵² correlation, Eq. (124), is shown in Figs 18–20. These figures show that the Nusselt number increases steadily with Reynolds number (Fig. 18) and decreases with the ratio of jet distance to jet diameter (Fig. 19). More surprisingly, the curves shown in Fig. 20 indicate that Nusselt number reaches an asymptote in its dependence on the ratio of jet area to component area.

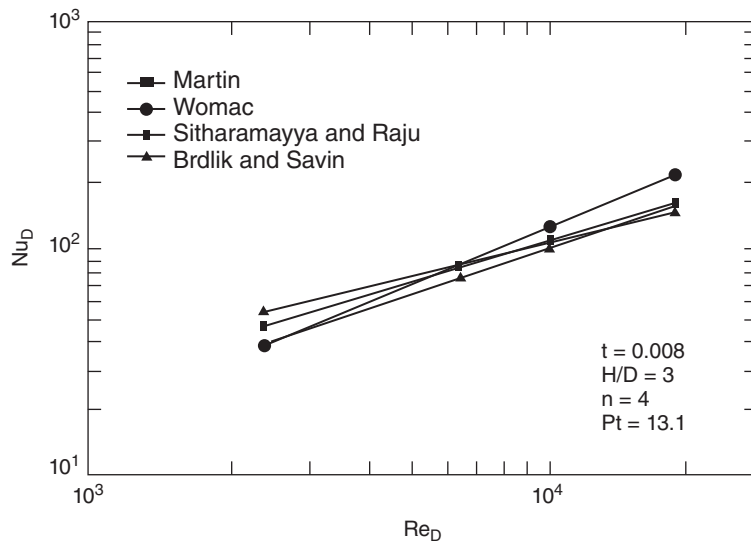


Figure 17 Comparison of various submerged jet correlations.

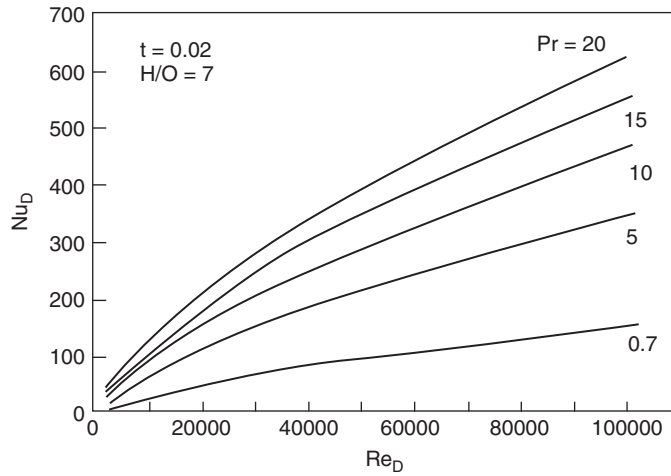


Figure 18 Effect of Reynolds and Prandtl numbers on heat transfer.

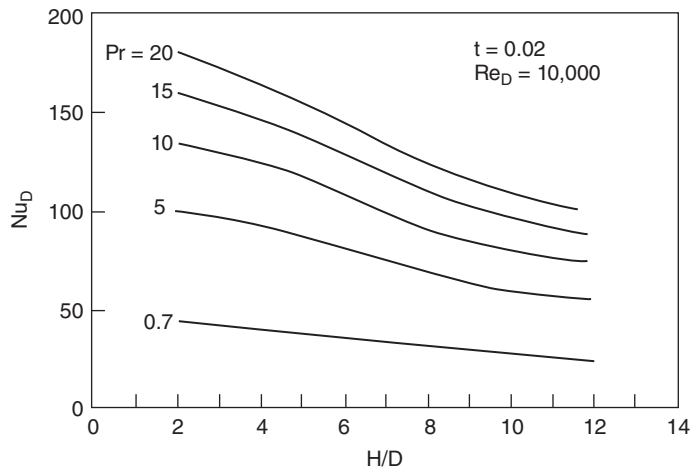


Figure 19 Effect of jet aspect ratio on heat transfer.

Returning to Eq. (124), it may be observed that, in the range of interest, the first term on the right side can be approximated as

$$\left\{ 1 + \left[\frac{H/D}{0.6/f^{0.5}} \right]^6 \right\}^{-0.05} \cong \left\{ \frac{H/D}{0.6/f^{0.5}} \right\}^{-0.3} \quad (126)$$

and that the second term is not far different from $0.6f^{0.5}$. Reexpressing Eq. (126) with these simplifications, the average heat transfer coefficient h is found to approximately equal

$$Nu \cong 0.5 \left(\frac{H}{D} \right)^{-0.3} f^{0.35} Re_D^{0.667} Pr^{0.42} \quad (127)$$

This approximation falls within 30% of Eq. (124) throughout the parametric range indicated but is within 10% for $H/D < 3$.

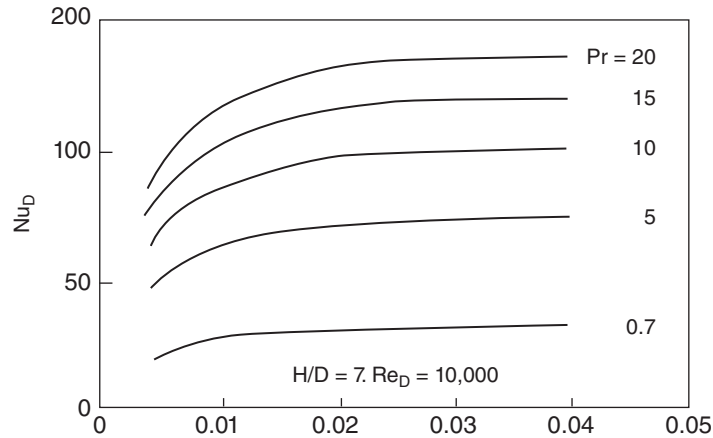


Figure 20 Effect of jet area–heater area ratio on heat transfer.

Recalling the definition of the jet Nusselt number, $Nu = hD/k$, and substituting for the area ratio f from Eq. (125), the heat transfer coefficient produced by impinging liquid jet(s) is found to be proportional to

$$h \propto kH^{-0.3} \left(\frac{n}{A}\right)^{0.35} Re_D^{0.67} Pr^{0.42} \quad (128)$$

Or, expanding the Reynolds and Prandtl numbers,

$$h \propto [k^{0.58} \rho^{0.67} \mu^{-0.25}] \left[\left(\frac{n}{A}\right)^{0.35} D^{0.67}\right] \left[\frac{V^{0.67}}{H^{0.3}}\right] \quad (129)$$

The first bracketed term in Eq. (129) represents a fluid figure of merit for submerged-jet heat transfer, the second term constitutes a thermal figure of merit for the jet plate, and the third the operating conditions of an impingement cooling system. Clearly, to maximize the jet heat transfer rate, it is desirable to choose a fluid with high thermal conductivity and density but relatively low viscosity. Within the accuracy of the approximations used to derive Eq. (129) (and especially in the low- f range), the thermally preferred jet plate would contain many large-diameter nozzles per component. Due to the strong dependence of the heat transfer rate on the jet Reynolds number, maximization of the heat transfer coefficient also requires increasing the fluid velocity at the nozzle and decreasing the distance of separation between the nozzle and the component. Alternatively, if a fluid has been selected and if the jet Reynolds number is to remain constant, a higher heat transfer coefficient can be obtained only by increasing n/A or decreasing H .

Although the thermal relations discussed in the previous section can be used to establish the gross feasibility of submerged spray cooling for high-power chips, successful implementation of this thermal management technique requires consideration of system-level issues and design trade-offs.⁵⁶ The minimization of life-cycle costs is a crucial element in electronic systems and, consequently, attention must be devoted to the “consumed” fluid flow rate, pressure drop, and pumping power as well as to the limitations imposed by manufacturing tolerances and costs. The gross impact of these considerations on the design of impinging jet cooling systems can be seen with the aid of Eq. (129).

The nozzle pressure drop and, hence, plenum pressure required to achieve a specified jet velocity have direct bearing on the choice and cost of the coolant circulation system and the structural design, as well as cost, of the jet plate. Since Eqs. (124) and (129) show the jet heat transfer coefficient to increase with velocity to the 0.67 power, while nozzle pressure losses

generally depend on the square of the velocity, concern about the plenum operating pressure would lead the designer to choose the lowest possible jet velocity.

Examination of the approximate relation for the jet heat transfer coefficient, Eq. (129), suggests that to maintain high heat transfer rates at low jet velocities would necessitate increasing the number of nozzles (n/A), increasing the diameter of each nozzle (D), or decreasing the spacing between the nozzle exit and the component (H). The minimum value of H is likely to be determined by the precision of assembly and deflection under pressure of the jet plate and, thus, it will benefit from reduced operating pressure. Since the maximum heat transfer rates are approached asymptotically as the total jet area increases to approximately 4% of the component area (see Fig. 20), there is coupling between the number of jets and the jet diameter. The heat transfer rate can, thus, be improved by increasing both jet diameter and the number of jets up to this value, but if operating near the maximum rate, the jet diameter is inversely related to the square root of n/A .

In the use of liquid jets, the operating costs are often dominated by the pumping power, or product of total volumetric flow rate and pressure drop, needed to provide a specified heat removal rate. The pumping power can be easily shown to vary with $D^2 V^3 n/A$. Examining this dependence in light of the approximate heat transfer coefficient relation, Eq. (48), it is again clear that reduced costs are associated with low liquid velocity and a relatively large total nozzle area.

These results suggest that optimum performance, based on system-level as well as thermal considerations and as represented by the average heat transfer coefficient, would be achieved by designing spray cooling systems to provide approximately 4% jet-to-component area ratios and operate at relatively low jet velocities. Improved surface coverage, more uniform heat removal capability, and decreased vulnerability to blockage of a single (or a few) nozzles would appear to be favored by the use of a relatively large number of jets per component, allowing reduction in the diameter of individual jets. Alternately, the cost of manufacturing and the probability of nozzle blockage can be expected to increase for small-diameter nozzles and, thus, place a lower practical limit on this parameter. Given the approximate nature of Eq. (129), these relationships must be viewed as indicative rather than definitive and the complete Martin⁵² correlation equation (124) should be used for any detailed exploration of these trends.

Heat transfer correlations for impingement-cooled, pin-fin heat sinks have also been reported in the literature.⁵⁷ Results were presented in terms of Nu_{base} , based on the heat sink footprint area, and on Nu_{HS} , based on the total heat sink surface area, as

$$Nu_{\text{base}} = 3.361 Re^{0.724} Pr^{0.4} \left(\frac{D}{d}\right)^{-0.689} \left(\frac{S}{d}\right)^{-0.210} \quad (130)$$

$$Nu_{\text{HS}} = 1.92 Re^{0.716} Pr^{0.4} \left(\frac{A_{\text{HS}}}{A_d}\right)^{-0.689} \left(\frac{D}{d}\right)^{0.678} \left(\frac{S}{d}\right)^{-0.181} \quad (131)$$

These equations are valid for $2000 \leq Re \leq 23,000$, $S/d = 2, 3$. The term D in the above equations refers to the jet diameter, whereas d refers to the pin diameter. The term S refers to the jet-to-jet pitch in the case of multiple jets.

REFERENCES

1. K. J. Negus, R. W. Franklin, and M. M. Yovanovich, "Thermal Modeling and Experimental Techniques for Microwave Bi-Polar Devices," in *Proceedings of the Seventh Thermal and Temperature Symposium*, San Diego, CA, 1989, pp. 63–72.
2. M. M. Yovanovich and V. W. Antonetti, "Application of Thermal Contact Resistance Theory to Electronic Packages," in A. Bar-Cohen and A. D. Kraus (Eds.), *Advances in Thermal Modeling of Electronic Components and Systems*, Hemisphere, New York, 1988, pp. 79–128.

3. A. D. Kraus and A. Bar-Cohen, *Thermal Analysis and Control of Electronic Equipment*, Hemisphere, New York, 1983.
4. W. Elenbaas, "Heat Dissipation of Parallel Plates by Free Convection," *Physica*, **9**(1), 665–671, 1942.
5. J. R. Bodoia and J. F. Osterle, "The Development of Free Convection between Heated Vertical Plates," *J. Heat Transfer*, **84**, 40–44, 1964.
6. W. Aung, L. S. Fletcher, and V. Sernas, "Developing Laminar Free Convection between Vertical Flat Plates with Asymmetric Heating," *Int. J. Heat Mass Transfer*, **15**, 2293–2308, 1972.
7. O. Miyatake, T. Fujii, M. Fujii, and H. Tanaka, "Natural Convection Heat Transfer between Vertical Parallel Plates—One Plate with a Uniform Heat Flux and the Other Thermally Insulated," *Heat Transfer Japan Res.*, **4**, 25–33, 1973.
8. A. D. Kraus and A. Bar-Cohen, *Design and Analysis of Heat Sinks*, Wiley, New York, 1995.
9. E. M. Sparrow, J. E. Niethammer, and A. Chaboki, "Heat Transfer and Pressure Drop Characteristics of Arrays of Rectangular Modules Encountered in Electronic Equipment," *Int. J. Heat Mass Transfer*, **25**(7), 961–973, 1982.
10. R. A. Wirtz and P. Dykshoorn, "Heat Transfer from Arrays of Flatpacks in Channel Flow," in *Proceedings of the Fourth Int. Electronic Packaging Society Conference*, New York, 1984, pp. 318–326.
11. S. B. Godsell, R. J. Dischler, and S. M. Westbrook, "Implementing a Packaging Strategy for High Performance Computers," *High Performance Syst.*, 28–31, January 1990.
12. M. Jakob, *Heat Transfer*, Wiley, New York, 1949.
13. S. Globe and D. Dropkin, "Natural Convection Heat Transfer in Liquids Confined by Two Horizontal Plates and Heated from Below," *J. Heat Transfer, Series C*, **81**, 24–28, 1959.
14. W. Mull and H. Rieher, "Der Warmeschutz von Luftschichten," *Gesundh-Ing. Beihefte*, **28**, 1930.
15. J. G. A. DeGraaf and E. F. M. von der Held, "The Relation between the Heat Transfer and the Convection Phenomena in Enclosed Plane Air Layers," *Appl. Sci. Res., Sec. A*, **3**, 393–410, 1953.
16. W. Aung, "Fully Developed Laminar Free Convection between Vertical Flat Plates Heated Asymmetrically," *Int. J. Heat Mass Transfer*, **15**, 1577–1580, 1972.
17. A. Bar-Cohen and W. M. Rohsenow, "Thermally Optimum Arrays of Cards and Fins in Natural Convection," *Trans. IEEE Chart, CHMT-6*, 154–158.
18. K. E. Starner and H. N. McManus, "An Experimental Investigation of Free Convection Heat Transfer from Rectangular Fin Arrays," *J. Heat Mass Transfer*, **85**, 273–278, 1963.
19. J. R. Welling and C. B. Wooldridge, "Free Convection Heat Transfer Coefficients from Rectangular Vertical Fins," *J. Heat Transfer*, **87**, 439–444, 1965.
20. A. Bilitzky, "The Effect of Geometry on Heat Transfer by Free Convection from a Fin Array," Thesis, Department of Mechanical Engineering, Ben-Gurion University of the Negev, Beer Sheva, Israel, 1986.
21. M. G. Cooper, B. B. Mikic, and M. M. Yovanovich, "Thermal Contact Resistance," *Int. J. Heat Mass Transfer*, **12**, 279–300, 1969.
22. M. M. Yovanovich and V. W. Antonetti, "Application of Thermal Contact Resistance Theory to Electronic Packages," in A. Bar-Cohen and A. D. Kraus (Eds.), *Advances in Thermal Modeling of Electronic Components and Systems*, Vol. 1, Hemisphere, New York, 1988.
23. H. J. Sauer, Jr., "Comparative Enhancement of Thermal Contact Conductance of Various Classes of Interstitial Materials," NSF/DITAC Workshop, Melbourne, Monash University, Victoria, Australia, 1992, pp. 103–115.
24. L. S. Fletcher, "A Review of Thermal Control Materials for Metallic Junctions," *J. Spacecrafts Rockets*, 849–850 (1972).
25. R. S. Prasher, "Surface Chemistry and Characteristics Based Model for the Contact Resistance of Polymeric Interstitial Thermal Interface Materials," *J. Heat Transfer*, **123**, 2001.
26. *Handbook of Chemistry and Physics (CRC)*, Chemical Rubber Co., Cleveland, OH, 1954.
27. R. Hilpert, "Warmeabgug von Geheizten Drahten und Rohren in Luftstrom," *Forsch. Ing-Wes*, **4**, 215–224, 1933.
28. S. Whitaker, "Forced Convection Heat Transfer Correlations for Flow in Pipes, Past Flat Plates, Single Cylinders, Single Spheres and for Flow in Packed Beds and Tube Bundles," *AIChE J.*, **18**, 361–371, 1972.
29. W. H. McAdams, *Heat Transmission*, 3rd ed., McGraw-Hill, New York, 1954.

30. F. Kreith, *Principles of Heat Transfer*, International Textbook Co., Scranton, PA, 1959.
31. A. P. Colburn, "A Method of Correlating Forced Convection Heat Transfer Data and a Comparison of Fluid Friction," *Trans AICHE*, **29**, 174–210, 1933.
32. W. Drexel, "Convection Cooling," *Sperry Eng. Rev.*, **14**, 25–30, December 1961.
33. W. Robinson and C. D. Jones, "The Design of Arrangements of Prismatic Components for Crossflow Forced Air Cooling," Report No. 47, Ohio State University Research Foundation, Columbus, OH, 1955.
34. W. Robinson, L. S. Han, R. H. Essig, and C. F. Heddleson, "Heat Transfer and Pressure Drop Data for Circular Cylinders in Ducts and Various Arrangements," Report No. 41, Ohio State University Research Foundation, Columbus, OH, 1951.
35. E. N. Sieder and G. E. Tate, "Heat Transfer and Pressure Drop of Liquids in Tubes," *Ind. Eng. Chem.*, **28**, 1429–1436, 1936.
36. H. Hausen, *Z VDI, Beih. Verfahrenstechn.*, **4**, 91–98, 1943.
37. A. L. London, "Air Coolers for High Power Vacuum Tubes," *Trans. IRE*, **ED-1**, 9–26, April 1954.
38. K. A. Gardner, "Efficiency of Extended Surfaces," *Trans. ASME*, **67**, 621–631, 1945.
39. W. M. Murray, "Heat Transfer through an Annular Disc or Fin of Uniform Thickness," *J. Appl. Mech.*, **5**, A78–A80, 1938.
40. D. Q. Kern and A. D. Kraus, *Extended Surface Heat Transfer*, McGraw-Hill, New York, 1972.
41. D. E. Briggs and E. H. Young, "Convection Heat Transfer and Pressure Drop of Air Flowing across Triangular Pitch Banks of Finned Tubes," *Chem. Eng. Prog. Symp. Ser.*, **41**(59), 1–10, 1963.
42. A. D. Kraus, A. D. Snider, and L. F. Doty, "An Efficient Algorithm for Evaluating Arrays of Extended Surface," *J. Heat Transfer*, **100**, 288–293, 1978.
43. A. D. Kraus, *Analysis and Evaluation of Extended Surface Thermal Systems*, Hemisphere, New York, 1982.
44. A. D. Kraus and A. D. Snider, "New Parametrizations for Heat Transfer in Fins and Spines," *J. Heat Transfer*, **102**, 415–419, 1980.
45. W. M. Kays and A. L. London, *Compact Heat Exchangers*, 3rd ed., McGraw-Hill, New York, 1984.
46. A. E. Bergles and A. Bar-Cohen, "Direct Liquid Cooling of Microelectronic Components," in A. Bar-Cohen and A. D. Kraus (Eds.), *Advances in Thermal Modeling of Electronic Components and Systems*, Vol. 2, ASME Press, New York, 1990, pp. 233–342.
47. J. Stevens and B. W. Webb, "Local Heat Transfer Coefficients under an Axisymmetric, Single-Phase Liquid Jet," paper presented at The National Heat Transfer Conference, Philadelphia, PA, 1989, pp. 113–119.
48. T. Nonn, Z. Dagan, and L. M. Jiji, "Boiling Jet Impingement Cooling of Simulated Microelectronic Heat Sources," ASME Paper 88-WA/EEP-3, ASME, New York, 1988.
49. X. S. Wang, Z. Dagan, and L. M. Jiji, "Heat Transfer between a Laminar Free-Surface Impinging Jet and a Composite Disk," in *Proceedings of the Ninth International Heat Transfer Conference*, Vol. 4, Hemisphere, New York, 1990, p. 137.
50. D. J. Womac, G. Aharoni, S. Ramadhyani, and F. P. Incropera, "Single Phase Liquid Jet Impingement Cooling of Small Heat Sources," in *Heat Transfer 1990 (Proceedings of the Ninth International Heat Transfer Conference)*, Vol. 4, Hemisphere, New York, 1990, pp. 149–154.
51. D. C. Wadsworth and L. Mudawar, "Cooling of a Multichip Electronic Module by Means of Confined Two Dimensional Jets of Dielectric Liquid," *J. Heat Transfer*, **112**, 891–898, 1990.
52. H. Martin, "Heat and Mass Transfer between Impinging Gas Jets and Solid Surfaces," in J. P. Hartnett and T. F. Irvine, Jr. (Eds.), *Advances in Heated Transfer*, Vol. 13, Academic, New York, 1977, pp. 1–60.
53. D. H. Womac, "Single-Phase Axisymmetric Liquid Jet Impingement Cooling of Discrete Heat Sources," Thesis, Department of Mechanical Engineering, Purdue University, Lafayette, IN, 1989.
54. P. M. Brdlik and V. K. Savin, "Heat Transfer between an Axisymmetric Jet and a Plate Normal to the Flow," *J. Eng. Phys.*, **8**, 91–98, 1965.

55. S. Sitharamayya and K. S. Raju, "Heat Transfer between an Axisymmetric Jet and a Plate Hold Normal to the Flow," *Can. J. Chem. Eng.*, **47**, 365–368, 1969.
56. D. E. Maddox and A. Bar-Cohen, "Thermofluid Design of Submerged-Jet Impingement Cooling for Electronic Components," in *Proceedings, ASME/AICHE National Heat Transfer Conference*, Minneapolis, MN, 1991.
57. H. A. El Sheikh and S. V. Garimella, "Heat Transfer from Pin-Fin Heat Sinks under Multiple Impinging Jets," *IEEE Trans. Advanced Packaging*, **23**(1), 113–120, 2000.

CHAPTER 13

REFRIGERATION

Dennis L. O’Neal
Texas A&M University
College Station, Texas

1 INTRODUCTION	499	5.2 Ammonia–Water Absorption Systems	517
2 BASIC PRINCIPLES	500	6 INDIRECT REFRIGERATION	518
3 REFRIGERATION CYCLES AND SYSTEM OVERVIEW	501	7 SYSTEM COMPONENTS	522
3.1 Closed-Cycle Operation	501	7.1 Compressors	522
3.2 Open-Cycle Operation	504	7.2 Condensers	528
3.3 Losses in Refrigeration Cycles	504	7.3 Evaporators	530
4 REFRIGERANTS	506	7.4 Expansion Devices	532
4.1 Regulations on Production and Use of Refrigerants	511	8 DEFROST METHODS	536
4.2 Refrigerant Selection for Closed Cycle	511	8.1 Hot Refrigerant Gas Defrost	536
4.3 Refrigerant Selection for Open Cycle	514	8.2 Air, Electric, and Water Defrost	537
5 ABSORPTION SYSTEMS	515	9 SYSTEM DESIGN CONSIDERATIONS	538
5.1 Water–Lithium Bromide Absorption Chillers	516	10 REFRIGERATION SYSTEM SPECIFICATION	539
		REFERENCES	541

1 INTRODUCTION

Refrigeration is the use of mechanical or heat-activated machinery for cooling purposes. The use of refrigeration equipment to produce temperatures below -150°C is known as cryogenics.¹ When refrigeration equipment is used to provide human comfort, it is called air conditioning. This chapter focuses primarily on refrigeration applications, which cover such diverse uses as food processing and storage, supermarket display cases, skating rinks, ice manufacture, and biomedical applications such as blood and tissue storage or hypothermia used in surgery.

The first patent on a mechanically driven refrigeration system was issued to Jacob Perkins in 1834 in London.² The system used ether as the refrigerant. The first viable commercial system was produced in 1857 by James Harrison and D. E. Siebe and used ethyl ether as the refrigerant.²

Refrigeration is used in installations covering a broad range of cooling capacities and temperatures. While the variety of applications results in a diversity of mechanical specifications and equipment requirements, the methods for producing refrigeration are well standardized.

2 BASIC PRINCIPLES

Most refrigeration systems utilize the vapor compression cycle to produce the desired refrigeration effect. A less common method used to produce refrigeration is the absorption cycle, which is described later in this chapter. With the vapor compression cycle, a working fluid, called the refrigerant, evaporates and condenses at suitable pressures for practical equipment designs. The ideal (no pressure or frictional losses) vapor compression refrigeration cycle is illustrated in Fig. 1 on a pressure–enthalpy diagram. This cycle has no pressure loss in the evaporator or condenser and no heat or frictional losses in the compressor.

There are four basic components in every vapor compression refrigeration system: (1) compressor, (2) condenser, (3) expansion device, and (4) evaporator. The compressor raises the pressure of the refrigerant vapor so that the refrigerant saturation temperature is slightly above the temperature of the cooling medium used in the condenser. The condenser is a heat exchanger used to reject heat from the refrigerant to a cooling medium. The refrigerant enters the condenser and usually leaves as a subcooled liquid. Typical cooling mediums used in condensers

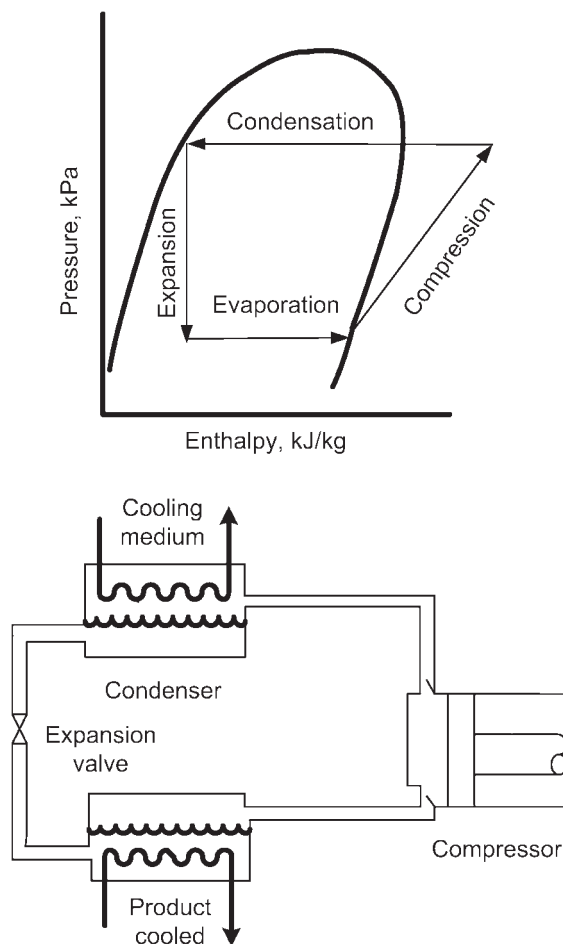


Figure 1 Simple vapor compression refrigeration cycle.³

are air and water. After leaving the condenser, the liquid refrigerant expands to a lower pressure in the expansion valve. The expansion valve can be a passive device, such as a capillary tube or short tube orifice, or an active device, such as a thermal expansion valve or electronic expansion valve. At the exit of the expansion valve, the refrigerant is at a temperature below that of the product to be cooled. As the refrigerant travels through the evaporator, it absorbs energy and is converted from a low-quality, two-phase fluid to a superheated vapor under normal operating conditions. The vapor formed must be removed by the compressor at a sufficient rate to maintain the low pressure in the evaporator and keep the cycle operating.

Pumped recirculation of a liquid secondary refrigerant rather than direct evaporation of a refrigerant is often used to service remotely located or specially designed heat exchangers. This technique is called indirect refrigeration and provides the user with wide flexibility in applying refrigeration to complex processes and greatly simplifies operation. Secondary refrigerants or brines are also commonly used for simple control and operation. Direct application of ice and brine storage tanks may be used to level off batch cooling loads and reduce equipment size. This approach provides stored refrigeration where temperature control is vital as a safety consideration to prevent runaway reactions or pressure buildup.

All mechanical cooling results in the production of a greater amount of heat energy than cooling energy. In many instances, this heat energy is rejected to the environment directly to the air in the condenser or indirectly to water where it is rejected in a cooling tower. Under some specialized applications, it may be possible to utilize this heat energy in another process at the refrigeration facility. This may require special modifications to the condenser. Recovery of this waste heat at temperatures up to 65°C can be used to achieve improved operating economy.

Historically, in the United States, capacities of mechanical refrigeration systems have been stated in tons of refrigeration, which is a unit of measure related to the ability of an ice plant to freeze one short ton (907 kg) of ice in a 24-h period. A ton is equal to 3.51 kW (12,000 Btu/h).

3 REFRIGERATION CYCLES AND SYSTEM OVERVIEW

Refrigeration can be accomplished in either closed-cycle or open-cycle systems. In a closed cycle, the refrigerant fluid is confined within the system and recirculates through the components (compressor, heat exchangers, and expansion valve). The system shown at the bottom of Fig. 1 is a closed cycle. In an open cycle, the fluid used as the refrigerant passes through the system once on its way to be used as a product or feedstock outside the refrigeration process. An example is the cooling of natural gas to separate and condense heavier components.

In addition to the distinction between open- and closed-cycle systems, refrigeration processes are also described as simple cycles, compound cycles, or cascade cycles. Simple cycles employ one set of components (compressor, condenser, evaporator, and expansion valve) in a single refrigeration cycle as shown in Fig. 1. Compound and cascade cycles use multiple sets of components and two or more refrigeration cycles. The cycles interact to accomplish cooling at several temperatures or to allow a greater span between the lowest and highest temperatures in the system than can be achieved with the simple cycle.

3.1 Closed-Cycle Operation

For a simple cycle, the lowest evaporator temperature that is practical in a closed-cycle system (Fig. 1) is set by the pressure ratio capability of the compressor and by the properties of the refrigerant. Most high-speed reciprocating compressors are limited to a pressure ratio of 9:1, so that the simple cycle is used for evaporator temperatures from 2 to -50°C . Below these temperatures, the application limits of a single-stage compressor are reached. Beyond that limit, there is a risk of excessively high temperatures at the end of compression, which

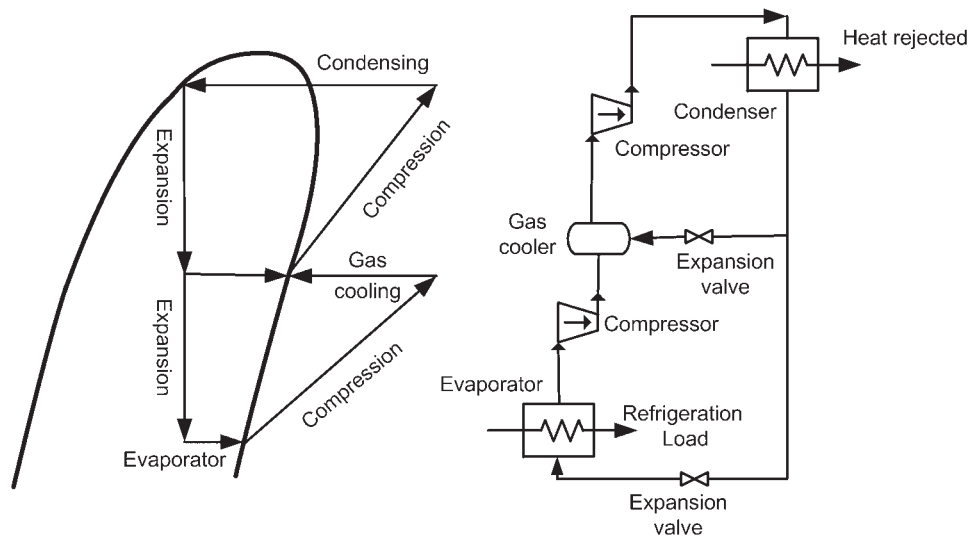


Figure 2 Ideal compound refrigeration cycle.³

may produce lubricant breakdown, high bearing loads, excessive oil foaming at startup, and inefficient operation because of reduced volumetric efficiency in the compressor.

Centrifugal compressors with multiple stages can generate a pressure ratio up to 18:1, but their high discharge temperatures limit the efficiency of the simple cycle at these high pressure ratios. As a result, they operate with evaporator temperatures in the same range as reciprocating compressors.

The compound cycle (Fig. 2) can achieve temperatures of approximately -100°C by using two or three compressors in series and a common refrigerant. This keeps the individual compressors within their application limits. A refrigerant gas cooler (also called a flash intercooler) is normally used between compressors to keep the final discharge temperature from the compressor at a satisfactory level. A common practice is to operate the gas cooler at about the geometric mean of the evaporating and condensing pressures. This provides nearly identical pressure ratios for the two compressors. Besides producing very low temperatures, the compound cycle can also be used in applications where multiple evaporators are needed to produce different temperatures.

Below -100°C , most refrigerants with suitable evaporator pressures have excessively high condensing pressures. For some refrigerants, the specific volume of refrigerant at low temperatures may be so great as to require compressors and other equipment of uneconomical size. With other refrigerants, the specific volume of refrigerant may be satisfactory at low temperature, but the specific volume may become too small at the condensing condition. In some circumstances, although none of the above limitations is encountered and a single refrigerant is practical, the compound cycle is not used because of oil return problems or difficulties of operation.

To satisfy these conditions, the cascade cycle is used (Fig. 3). This consists of two or more separate refrigerants, each in its own closed cycle. The cascade condenser–evaporator rejects heat to the evaporator of the high-temperature cycle, which condenses the refrigerant of the low-temperature cycle. Refrigerants are selected for each cycle with pressure–temperature characteristics that are well suited for application at either the higher or lower portion of the cycle. For extremely low temperatures, more than two refrigerants may be cascaded to

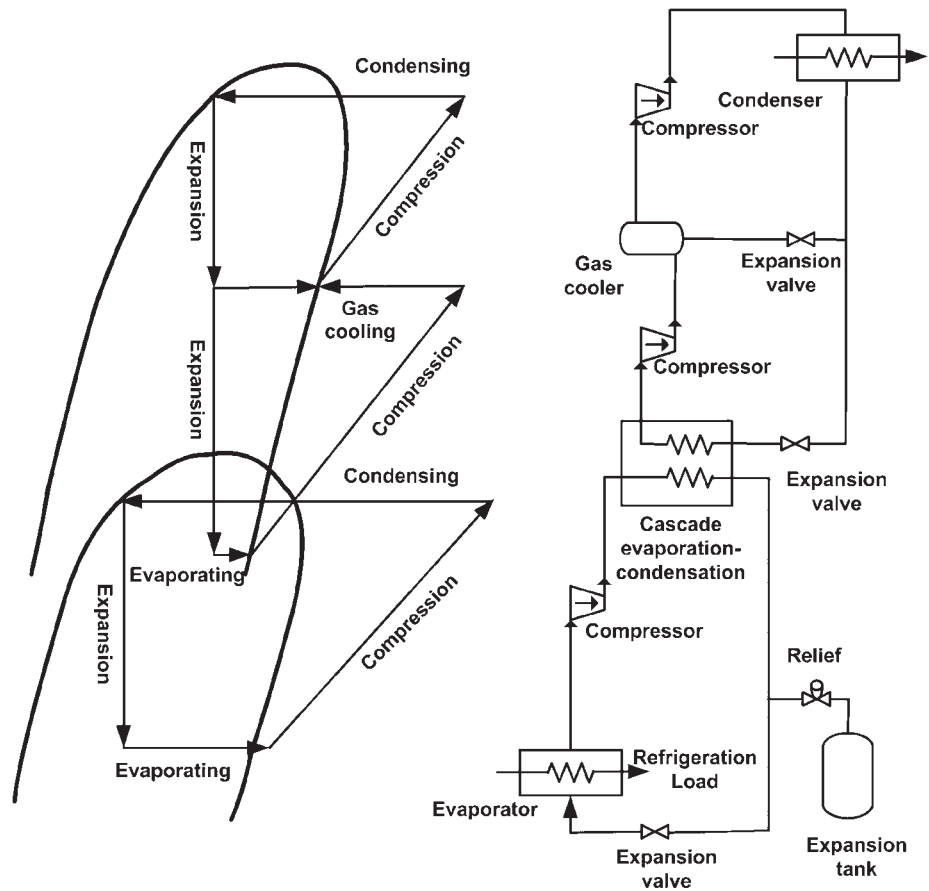


Figure 3 Ideal cascade refrigeration cycle.³

produce evaporator temperatures at cryogenic conditions (below -150°C). Expansion tanks, sized to handle the low-temperature refrigerant as a gas at ambient temperatures, are used during standby to hold pressure at levels suitable for economical equipment design.

Compound cycles using reciprocating compressors or any cycle using a multistage centrifugal compressor allows the use of economizers or intercoolers between compression stages. Economizers reduce the discharge gas temperature from the preceding stage by mixing relatively cool gas with discharge gas before entering the subsequent stage. Either flash-type economizers, which cool the refrigerant by reducing its pressure to the intermediate level, or surface-type economizers, which subcool refrigerant at the condensing pressure, may be used to provide the cooler gas for mixing. This keeps the final discharge gas temperature low enough to avoid overheating of the compressor and improves compression efficiency.

Compound compression with economizers also affords the opportunity to provide refrigeration at an intermediate temperature. This provides a further thermodynamic efficiency gain because some of the refrigeration is accomplished at a higher temperature, and less refrigerant must be handled by the lower temperature stages. This reduces the power consumption and the size of the lower stages of compression.

Figure 4 shows a typical system schematic with flash-type economizers. Process loads at several different temperature levels can be handled by taking suction to an intermediate compression stage as shown. The pressure–enthalpy diagram illustrates the thermodynamic cycle.

Flooded refrigeration systems are a version of the closed cycle that may reduce design problems in some applications. In flooded systems, the refrigerant is circulated to heat exchangers or evaporators by a pump. Figure 5 shows a liquid recirculator, which can use any of the simple or compound closed-refrigeration cycles.

The refrigerant recirculating pump pressurizes the refrigerant liquid and moves it to one or more evaporators or heat exchangers, which may be remote from the receiver. The low-pressure refrigerant may be used as a single-phase heat transfer fluid as in *A* of Fig. 5, which eliminates the extra heat exchange step and increased temperature difference encountered in a conventional system that uses a secondary refrigerant or brine. This approach may simplify the design of process heat exchangers, where the large specific volumes of evaporating refrigerant vapor would be troublesome. Alternatively, the pumped refrigerant in the flooded system may be routed through conventional evaporators as in *B* and *C* or special heat exchangers as in *D*.

The flooded refrigeration system is helpful when special heat exchangers are necessary for process reasons or where multiple or remote exchangers are required.

3.2 Open-Cycle Operation

In many chemical processes, the product to be cooled can itself be used as the refrigerating liquid. An example of this is in a natural gas gathering plant. Gas from the wells is cooled, usually after compression and after some of the heavier components are removed as liquid. This liquid may be expanded in a refrigeration cycle to further cool the compressed gas, which causes more of the heavier components to condense. Excess liquid not used for refrigeration is drawn off as product. In the transportation of liquefied petroleum gas (LPG) and of ammonia in ships and barges, the LPG or ammonia is compressed, cooled, and expanded. The liquid portion after expansion is passed on as product until the ship is loaded.

Open-cycle operations are similar to closed-cycle operations, except that one or more parts of the closed cycle may be omitted. For example, the compressor suction may be taken directly from gas wells, rather than from an evaporator. A condenser may be used, and the liquefied gas may be drained to storage tanks.

Compressors may be installed in series or parallel for operating flexibility or for partial standby protection. With multiple reciprocating compressors or with a centrifugal compressor, gas streams may be picked up or discharged at several pressures if there is refrigerating duty to be performed at intermediate temperatures. It always is more economical to refrigerate at the highest temperature possible.

Principal concerns in the open cycle involve dirt and contaminants, wet gas, compatibility of materials and lubrication circuits, and piping to and from the compressor. The possibility of gas condensing under various ambient temperatures either during operation or during standby must be considered. Beyond these considerations, the open-cycle design and its operation are governed primarily by the process requirements. The open system can use standard refrigeration hardware.

3.3 Losses in Refrigeration Cycles

The ideal cycles portrayed in Figs. 1–3 do not include frictional, heat transfer, or pressure losses found in real cycles. These reduce the overall performance of the cycle, in terms of both capacity and efficiency. For example, friction in the compressor produces higher discharge temperatures in the refrigerant than the ideal cycle. These higher temperatures require a larger condenser to reject heat energy from the cycle. Pressure losses in the evaporator and condenser

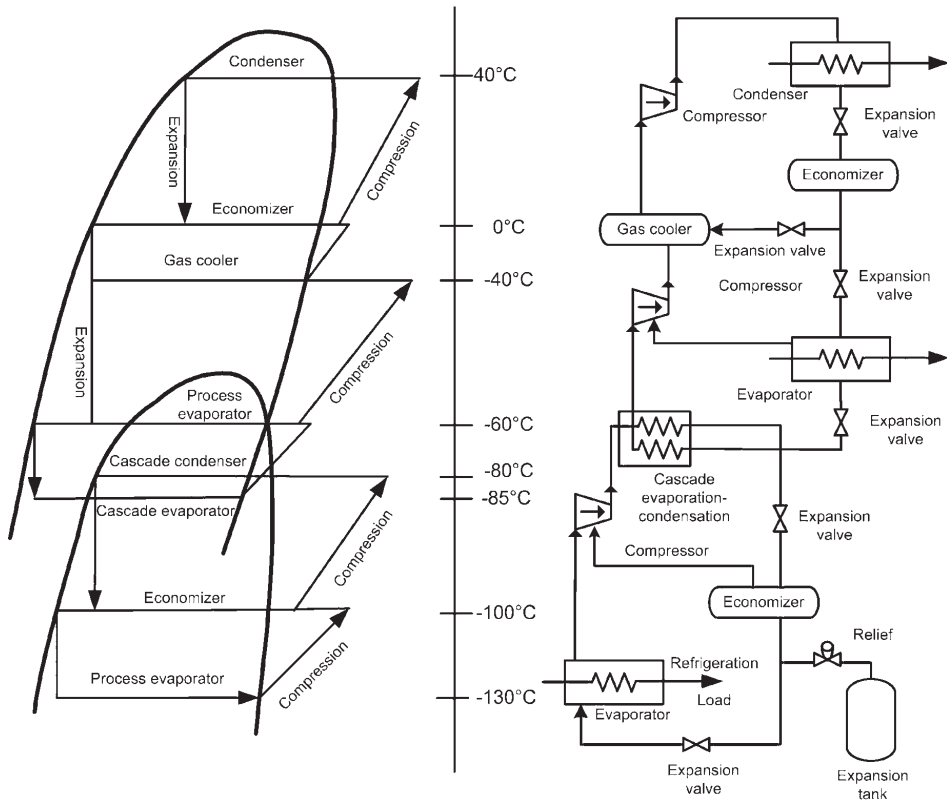


Figure 4 Refrigeration cycle with flash economizers.³

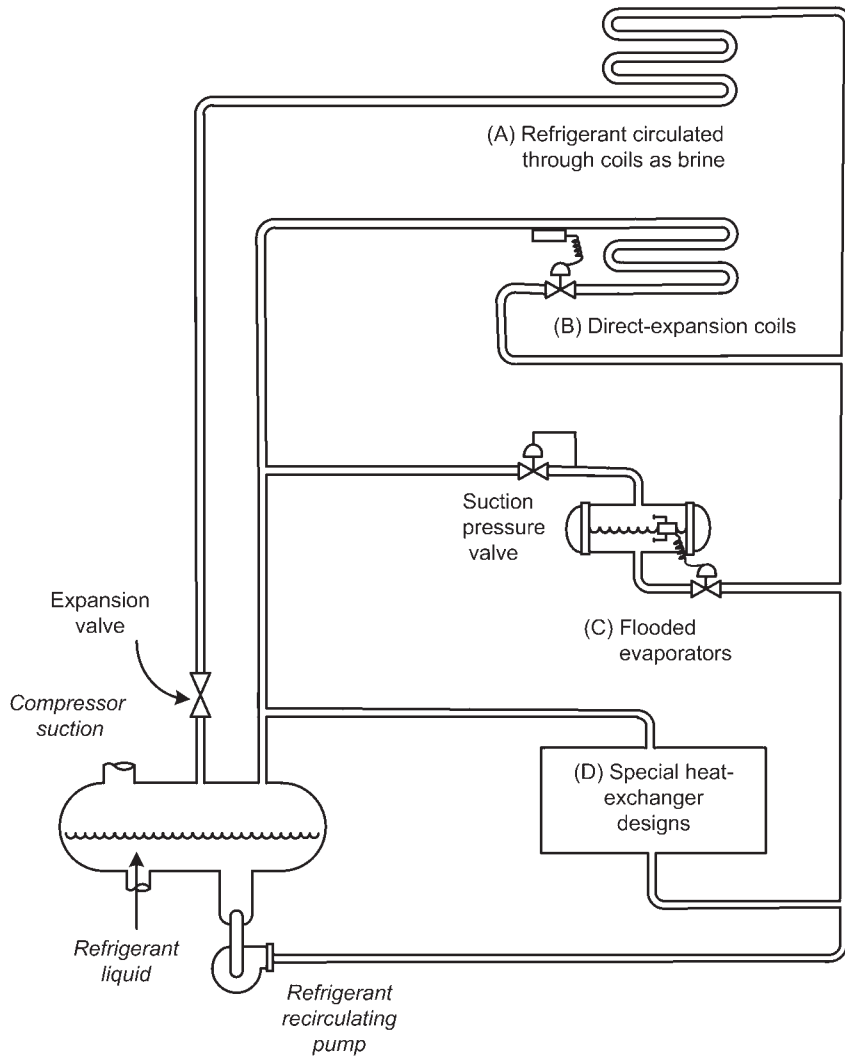


Figure 5 Liquid recirculator.

require the compressor to work harder to circulate refrigerant in the system. Predicting the performance of a real system must include these effects or the system capacity and efficiency will be overestimated.

4 REFRIGERANTS

No one refrigerant is capable of providing cost-effective cooling over the wide range of temperatures and the multitude of applications found in modern refrigeration systems. Ammonia is a popular refrigerant for many industrial and large warehouse applications.⁴ Both chlorofluorocarbons (CFCs) and hydrochlorofluorocarbon (HCFC) refrigerants have historically been used in many refrigeration applications, ranging from domestic refrigerators to supermarket and

food storage applications. Most of these refrigerants are generally nontoxic and nonflammable. Recent U.S. federal and international regulations⁵⁻⁷ have placed restrictions on the production and use of CFCs and HCFCs. Hydrofluorocarbons (HFCs) and HFC mixtures are now being used in some applications where CFCs and HCFCs have been used. Regulations affecting refrigerants are discussed in the next section.

The chemical industry uses low-cost fluids such as propane and butane whenever they are available in the process. These hydrocarbon refrigerants, often thought of as too hazardous because of flammability, are suitable for use in modern compressors and frequently add no more hazard than already exists in an oil refinery or petrochemical plant. These low-cost refrigerants are used in simple, compound, and cascade systems, depending on operating temperatures.

A standard numbering system, shown in Table 1, has been devised to identify refrigerants without the use of their cumbersome chemical names. There are many popular refrigerants in the methane and ethane series. These are called halocarbons or halogenated hydrocarbons because of the presence of halogen elements such as fluorine or chlorine.⁸ Halocarbons include CFCs, HCFCs, and HFCs.

Numbers assigned to the hydrocarbons and halohydrocarbons of the methane, ethane, propane, and cyclobutane series are such that the number uniquely specifies the refrigerant compound. The American National Standards Institute (ANSI) and American Society of Heating, Refrigerating and Air-Conditioning Engineers (ASHRAE) standard 34-2001 describes the method of coding.⁹

Zeotropes and azeotropes are mixtures of two or more different refrigerants. A zeotropic mixture changes saturation temperatures as it evaporates (or condenses) at constant pressure. This phenomenon is called temperature glide. For example, R-407C has a boiling (bubble) point of -44°C and a condensation (dew) point of -37°C , which means it has a temperature glide of 7°C . An azeotropic mixture behaves much like a single-component refrigerant in that it does not change saturation temperatures appreciably as it evaporates or condenses at constant pressure. Some zeotropic mixtures, such as R-410A, actually have a small enough temperature glide (less than 5.5°C) that they are considered a near-azeotropic refrigerant mixture.

Because the bubble point and dew point temperatures are not the same for a given pressure, some zeotropic mixtures have been used to help control the temperature differences in low-temperature evaporators. These mixtures have been used in the lowest stage of some liquefied natural gas (LNG) plants.¹⁰

Refrigerants are grouped by their toxicity and flammability (Table 2).^{9,11} Group A1 is nonflammable and least toxic, while group B3 is flammable and most toxic. Toxicity is quantified by the threshold limit value–time-weighted average (TLV-TWA), which is the upper safety limit for airborne exposure to the refrigerant. If the refrigerant is nontoxic in quantities less than 400 parts per million, then it is a class A refrigerant. If exposure to less than 400 parts per million is toxic, then the substance is given the class B designation. The numerical designation refers to the flammability of the refrigerant. The last column of Table 1 shows the toxicity and flammability rating of many of the common refrigerants.

The A1 group of refrigerants generally fulfills the basic requirements for an ideal refrigerant, with considerable flexibility as to refrigeration capacity. Many are used for comfort air conditioning since they are nontoxic and nonflammable. These refrigerants are also used extensively in refrigeration applications. Many CFCs are in the A1 group. With regulations banning the production and restricting the sale of all CFCs, the CFCs will eventually cease to be used. Common refrigerants in the A1 group include R-11, R-12, R-13, R-22, R-114, R-134a, and R-502.

Refrigerant 11, trichlorofluoromethane, is a CFC. It has a low-pressure–high-volume characteristic suitable for use in close-coupled centrifugal compressor systems for water or brine cooling. Its temperature range extends no lower than -7°C .

Table 1 Refrigerant Numbering System (ANSI/ASHRAE 34-2001)

Refrigerant Number Designation	Chemical Name	Chemical Formula	Molecular Mass	Normal Boiling Point, °C	Safety Group
<i>Methane Series</i>					
10	Tetrachloromethane	CCl ₄	153.8	77	B1
11	Trichlorofluoromethane	CCl ₃ F	137.4	24	A1
12	Dichlorodifluoromethane	CCl ₂ F ₂	120.9	-30	A1
13	Chlorotrifluoromethane	CClF ₃	104.5	-81	A1
22	Chlorodifluoromethane	CHClF ₂	86.5	-41	A1
32	Difluoromethane	CH ₂ F ₂	52.0	-52	A2
50	Methane	CH ₄	16.0	-161	A3
<i>Ethane Series</i>					
113	1,1,2-Trichlorotrifluoro-ethane	CCl ₂ FCClF ₂	187.4	48	A1
114	1,2-Dichlorotetrafluoro-ethane	CClF ₂ CClF ₂	170.9	4	A1
123	2,2-Dichloro-1,1,1-trifluoroethane	CHCl ₂ CF ₃	152.9	27	B1
125	Pentafluoroethane	CHF ₂ CF ₃	120.0	-49	A1
134a	1,1,1,2-Tetrafluoroethane	CH ₂ FCF ₃	102.0	-26	A1
170	Ethane	CH ₃ CH ₃	30.0	-89	A3
<i>Propane Series</i>					
290	Propane	CH ₃ CH ₂ CH ₃	44.0	-42	A3
<i>Zeotropes</i>					
<i>Composition</i>					
407C	R-32/R-125/R-134a (23/25/52 wt %)		95.0	-44	A1
410A	R-32/R-125 (50/50 wt%)		72.6	-53	A1
<i>Azeotropes</i>					
<i>Composition</i>					
500	R-12/152a (73.8/26.2 wt %)		99.31	-33	A1
502	R-22/115 (48.8/51.2 wt %)		112.0	-45	A1
<i>Hydrocarbons</i>					
600	Butane	CH ₃ CH ₂ CH ₂ CH ₃	58.1		
600a	Isobutane	CH(CH ₃) ₃	58.1	-12	A3
<i>Inorganic</i>					
<i>Compounds</i>					
717	Ammonia	NH ₃	17.0	-33	B2
728	Nitrogen	N ₂	28.0	-196	A1
744	Carbon dioxide	CO ₂	44.0	-78	A1
764	Sulfur dioxide	SO ₂	64.1	-10	B1
<i>Unsaturated</i>					
<i>Organic</i>					
<i>Compounds</i>					
1140	Vinyl chloride	CH ₂ —CHCl	62.5	-14	B3
1150	Ethylene	CH ₂ —CH ₂	28.1	-104	A3
1270	Propylene	CH ₃ CH—CH ₂	42.1	-48	A3

Source: From Ref. 9. Reprinted by permission from ASHRAE Standard 34-2001. Copyright © American Society of Heating, Refrigerating and Air-Conditioning Engineers, Inc., www.ashrae.org.

Table 2 ANSI/ASHRAE Toxicity and Flammability Rating System

Flammability	Group	Group
High	A3	B3
Moderate	A2	B2
None	A1	B1
Threshold limit value (parts per million)	<400	>400

Source: From Ref. 9.

Refrigerant 12, dichlorodifluoromethane, is a CFC. It was the most widely known and used refrigerant for U.S. domestic refrigeration and automotive air-conditioning applications until the early 1990s. It is ideal for close-coupled or remote systems ranging from small reciprocating to large centrifugal units. It has been used for temperatures as low as -90°C , although -85°C is a more practical lower limit because of the high gas volumes necessary for attaining these temperatures. It is suited for single-stage or compound cycles using reciprocating and centrifugal compressors.

Refrigerant 13, chlorotrifluoromethane, is a CFC. It is used in low-temperature applications to approximately -126°C . Because of its low volume, high condensing pressure, or both, and because of its low critical pressure and temperature, R-13 is usually cascaded with other refrigerants at a discharge pressure corresponding to a condensing temperature in the range of -56 to -23°C .

Refrigerant 22, chlorodifluoromethane, is an HCFC. It is used in many of the same applications as R-12, but its lower boiling point and higher latent heat permit the use of smaller compressors and refrigerant lines than R-12. The higher pressure characteristics also extend its use to lower temperatures in the range of -100°C .

Refrigerant 114, dichlorotetrafluoroethane, is a CFC. It is similar to R-11, but its slightly higher pressure and lower volume characteristic than R-11 extend its use to -17°C and higher capacities.

Refrigerant 123, dichlorotrifluoroethane, is an HCFC. It is a replacement refrigerant for R-11 in low-pressure centrifugal chillers. New centrifugal equipment designed for R-123 can provide exceptionally high energy efficiency. In retrofits of older existing centrifugal chillers, modifications are often needed to increase capacity or avoid material incompatibility (especially elastomers).

Refrigerant 125, pentafluoroethane, is an HFC. It is used in some refrigerant mixtures, including R-407C and R-410A.

Refrigerant 134a, 1,1,1,2-tetrafluoroethane, is an HFC. It is a replacement refrigerant for R-12 in both refrigeration and air-conditioning applications. It has operating characteristics similar to R-12. R-134a is commonly used in domestic refrigeration applications in the United States.

Refrigerants 407C and *410A* are both mixtures of HFCs. R-407C can be used in some retrofit applications for R-22. Because of its much higher operating pressures, R-410A cannot be used as a replacement refrigerant in an R-22 system. However, manufacturers have begun designing new systems that use R-410A, and these systems can be applied in situations where R-22 systems were used. The higher operating pressures as well as lubricant incompatibility with mineral oils has required manufacturers to completely redesign systems with R-410A.

Refrigerant 502 is an azeotropic mixture of R-22 and R-115. Its pressure characteristics are similar to those of R-22, but it has a lower discharge temperature.

The B1 refrigerants are nonflammable but have lower toxicity limits than those in the A1 group. *Refrigerant 123*, an HCFC, is used in many new low-pressure centrifugal chiller applications. Industry standards, such as ANSI/ASHRAE standard 15-1994, provide detailed guidelines for safety precautions when using R-123 or any other refrigerant that is toxic or flammable.¹¹

One of the most widely used refrigerants is *ammonia*, even though it is moderately flammable and has a class B toxicity rating. Ammonia liquid has a high specific heat, an acceptable density and viscosity, and high conductivity. Its enthalpy of vaporization is typically 6–8 times higher than that of the commonly used halocarbons. These properties make it an ideal heat transfer fluid with reasonable pumping costs, pressure drop, and flow rates. As a refrigerant, ammonia provides high heat transfer, except when affected by oil at temperatures below approximately -29°C , where oil films become viscous. To limit the ammonia-discharge-gas temperature to safe values, its normal maximum condensing temperature is 38°C . Generally, ammonia is used with reciprocating compressors, although relatively large centrifugal compressors (≥ 3.5 MW), with 8–12 impeller stages required by its low molecular weights, are in use today. Systems using ammonia should contain no copper (with the exception of Monel metal).

The flammable refrigerants (groups A3 and B3) are generally applicable where a flammability or explosion hazard is already present and their use does not add to the hazard. These refrigerants have the advantage of low cost. Although they have fairly low molecular weight, they are suitable for centrifugal compressors of larger sizes. Because of the high acoustic velocity in these refrigerants, centrifugal compressors may be operated at high impeller tip speeds, which partly compensates for the higher head requirements than some of the nonflammable refrigerants.

Flammable refrigerants should be used at pressures greater than atmospheric to avoid increasing the explosion hazard by the admission of air in case of leaks. In designing the system, it also must be recognized that these refrigerants are likely to be impure in refrigerant applications. For example, commercial propane liquid may contain about 2% (by mass) ethane, which in the vapor phase might represent as much as 16–20% (by volume) ethane. Thus, ethane may appear as a noncondensable. Either this gas must be purged or the compressor displacement must be increased about 20% if it is recycled from the condenser; otherwise, the condensing pressure will be higher than required for pure propane and the power requirement will be increased.

Refrigerant 290, propane, is the most commonly used flammable refrigerant. It is well suited for use with reciprocating and centrifugal compressors in close-coupled or remote systems. Its operating temperature range extends to -40°C .

Refrigerant 600, butane, occasionally is used for close-coupled systems in the medium-temperature range of 2°C . It has a low-pressure and high-volume characteristic suitable for centrifugal compressors, where the capacity is too small for propane and the temperature is within range.

Refrigerant 170, ethane, normally is used for close-coupled or remote systems at -87 to -7°C . It must be used in a cascade cycle because of its high-pressure characteristics.

Refrigerant 1150, ethylene, is similar to ethane but has a slightly higher pressure, lower volume characteristic, which extends its use to -104 to -29°C . Like ethane, it must be used in the cascade cycle.

Refrigerant 50, methane, is used in an ultralow range of -160 to -110°C . It is limited to cascade cycles. Methane condensed by ethylene, which is in turn condensed by propane, is a cascade cycle commonly employed to liquefy natural gas.

Refrigerant 744, carbon dioxide, is currently receiving attention as a possible refrigerant for use in cooling and refrigeration applications. It has the appeal of being a natural substance. Systems can be designed with R-744 but must operate at elevated pressures. Solid

carbon dioxide (dry ice) is commonly used in the food industry for chilling and freezing applications.

Table 3 shows the comparative performance of different refrigerants at conditions more typical of some freezer applications. The data show the relatively large refrigerating effect that can be obtained with ammonia. Note also that for these conditions both R-11 and R-123 would operate with evaporator pressures below atmospheric pressure.

4.1 Regulations on Production and Use of Refrigerants

In 1974, Molina and Rowland published a paper where they put forth the hypothesis that CFCs destroyed the ozone layer.¹³ By the late 1970s, the United States and Canada had banned the use of CFCs in aerosols. In 1985, Farmer noted a depletion in the ozone layer of approximately 40% over what had been measured in earlier years.⁴ This depletion in the ozone layer became known as the ozone hole. In September 1987, 43 countries signed an agreement called the Montreal Protocol⁷ in which the participants agreed to freeze CFC production levels by 1990, then to decrease production by 20% by 1994 and 50% by 1999. The protocol was ratified by the United States in 1988 and, for the first time, subjected the refrigeration industry to major CFC restrictions.

Recent regulations have imposed restrictions on the production and use of refrigerants.^{4,6,14} Production of CFCs in the United States was prohibited after January 1, 1996.¹⁴ A schedule was also imposed that started a gradual phase-out of the production of HCFCs in 2004 and will end complete production by 2030. Refrigerants are divided into two classes: class I, including CFCs, halons, and other major ozone-depleting chemicals, and class II, HCFCs.

Two ratings are used to classify the harmful effects of a refrigerant on the environment.¹⁵ The first, the ozone depletion potential (ODP), quantifies the potential damage that the refrigerant molecule has in destroying ozone in the stratosphere. When a CFC molecule is struck by ultraviolet light in the stratosphere, a chlorine atom breaks off and reacts with ozone to form oxygen and a chlorine/oxygen molecule. This molecule can then react with a free oxygen atom to form an oxygen molecule and a free chlorine. The chlorine can then react with another ozone molecule to repeat the process. The estimated atmospheric life of a given CFC or HCFC is an important factor in determining the value of the ODP. The ODP for CFC-11 is 1.0. All other ODP values for substances are normalized to that of CFC-11.

The second rating is known as the global warming potential (GWP), which represents how much a given mass of a chemical contributes to global warming over a given time period compared to the same mass of carbon dioxide.¹⁶ Carbon dioxide's GWP is defined as 1.0. The GWP of all other substances is normalized to that of carbon dioxide. Refrigerants such as CFCs, HCFCs, and HFCs can block energy from the earth from radiating back into space. One molecule of R-12 can absorb as much energy as 10,000 molecules of CO₂.

Table 4 shows the ODP and GWP for a variety of refrigerants. As a class of refrigerants, the CFCs have the highest ODP and GWP. Because HCFCs tend to be more unstable compounds and, therefore, have much shorter atmospheric lifetimes, their ODP and GWP values are much smaller than those of the CFCs. All HFCs and their mixtures have zero ODP because fluorine does not react with ozone. However, some of the HFCs, such as R-125, R-134a, and R-143a, do have GWP values that are as large or larger than some of the HCFCs. From the standpoint of ozone depletion and global warming, hydrocarbons provide zero ODP and GWP. However, hydrocarbons are flammable, which makes them unsuitable in many applications.

4.2 Refrigerant Selection for Closed Cycle

In any closed cycle, the choice of the operating fluid is based on the refrigerant with properties best suited to the operating conditions. The choice depends on a variety of factors,

Table 3 Comparative Refrigeration Performance of Different Refrigerants at -23°C Evaporating Temperature and $+37^{\circ}\text{C}$ Condensing Temperature

Refrigerant Number	Refrigerant Name	Evaporator Pressure (MPa)	Condenser Pressure (MPa)	Net Refrigerating Effect (kJ/kg)	Refrigerant Circulated (kg/h)	Compressor Displacement (L/s)	Power Input (kW)
11	Trichlorofluoromethane	0.013	0.159	145.8	24.7	7.65	0.297
12	Dichlorodifluoromethane	0.134	0.891	105.8	34.0	1.15	0.330
22	Chlorodifluoromethane	0.218	1.390	150.1	24.0	0.69	0.326
123	Dichlorotrifluoroethane	0.010	0.139	130.4	27.6	10.16	0.306
125	Pentafluoroethane	0.301	1.867	73.7	48.9	0.71	0.444
134a	Tetrafluoroethane	0.116	0.933	135.5	26.6	1.25	0.345
502	R-22/R-115 azeotrope	0.260	1.563	91.9	39.2	0.72	0.391
717	Ammonia	0.166	1.426	1057.4	3.42	0.67	0.310

Source: From Ref. 12. Reprinted by permission from 2001 ASHRAE Handbook of Fundamentals. Copyright © American Society of Heating, Refrigerating and Air-Conditioning Engineers, Inc., www.ashrae.org.

Table 4 Ozone Depletion Potential and Halocarbon Global Warming Potential of Popular Refrigerants and Mixtures

Refrigerant Number	Chemical Formula	Ozone Depletion Potential (ODP)	100-yr Global Warming Potential (GWP)
<i>Chlorofluorocarbons</i>			
11	CCl ₃ F	1.0	4,600
12	CCl ₂ F ₂	1.0	10,600
113	CCl ₂ FCClF ₂	0.80	14,000
114	CClF ₂ CClF ₂	1.0	9,800
115	CClF ₂ CF ₃	0.6	7,200
<i>Hydrochlorofluorocarbons</i>			
22	CHClF ₂	0.055	1,700
123	CHCl ₂ CF ₃	0.020	120
124	CHClF ₂ CF ₃	0.020	620
141b	CH ₃ CCl ₂ F	0.11	700
142b	CH ₃ CClF ₂	0.065	2,400
<i>Hydrofluorocarbons</i>			
32	CH ₂ F ₂	0	550
125	CHF ₂ CF ₃	0	3,400
134a	CH ₂ FCF ₃	0	1,100
143a	CH ₃ CF ₃	0	750
152a	CH ₃ CHF ₂	0	43
<i>Hydrocarbons</i>			
50	CH ₄	0	0
290	CH ₃ CH ₂ CH ₃	0	0
<i>Zeotropes</i>			
407C	R-32/125/134a (23/25/52%wt)	0	1,700
410A	R-32/125 (50/50%wt)	0	2,000
<i>Azeotropes</i>			
500	R-12/152a (73.8/26.2 wt%)	0.74	6,310
502	R-22/115 (48.8/51.2 wt%)	0.31	5,494

Source: Compiled from Refs. 4, 15, and 16.

some of which may not be directly related to the refrigerant's ability to remove heat. For example, flammability, toxicity, density, viscosity, availability, and similar characteristics are often deciding factors. The suitability of a refrigerant also depends on factors such as the kind of compressor to be used (i.e., centrifugal, rotary, or reciprocating), safety in application, heat exchanger design, application of codes, size of the job, and temperature ranges. The factors below should be taken into account when selecting a refrigerant.

Discharge (condensing) pressure should be low enough to suit the design pressure of commercially available pressure vessels, compressor casings, etc. However, discharge pressure, that is, condenser liquid pressure, should be high enough to feed liquid refrigerant to all parts of the system that require it.

Suction (evaporating) pressure should be above approximately 3.45 kPa (0.5 psia) for a practical compressor selection. When possible, it is preferable to have the suction pressure above atmospheric to prevent leakage of air and moisture into the system. Positive pressure normally is considered a necessity when dealing with hydrocarbons, because of the explosion hazard presented by any air leakage into the system.

Standby pressure (saturation at ambient temperature) should be low enough to suit equipment design pressure, unless there are other provisions in the system for handling the refrigerant during shutdown—for example, inclusion of expansion tanks.

Critical temperature and pressure should be well above the operating level. As the critical pressure is approached, less heat is rejected as latent heat compared to the sensible heat from desuperheating the compressor discharge gas, and cycle efficiency is reduced. Methane (R-50) and chlorotrifluoromethane (R-13) are usually cascaded with other refrigerants because of their low critical points.

Suction volume sets the size of the compressor. High suction volumes require centrifugal or screw compressors, and low suction volumes dictate the use of reciprocating compressors. Suction volumes also may influence evaporator design, particularly at low temperatures, since they must include adequate space for gas–liquid separation.

Freezing point should be lower than minimum operating temperature. This generally is no problem unless the refrigerant is used as a brine.

Theoretical power required for adiabatic compression of the gas is slightly less with some refrigerants than others. However, this is usually a secondary consideration offset by the effects of particular equipment selections, for example, line pressure drops, on system power consumption.

Vapor density (or molecular weight) is an important characteristic when the compressor is centrifugal because the lighter gases require more impellers for a given pressure rise, that is, head, or temperature lift. On the other hand, centrifugal compressors have a limitation connected with the acoustic velocity in the gas, and this velocity decreases with the increasing molecular weight. Low vapor densities are desirable to minimize pressure drop in long suction and discharge lines.

Liquid density should be taken into account. Liquid velocities are comparatively low, so that pressure drop is usually no problem. However, static head may affect evaporator temperatures and should be considered when liquid must be fed to elevated parts of the system.

Latent heat should be high because it reduces the quantity of refrigerant that needs to be circulated. However, large flow quantities are more easily controlled because they allow use of larger, less sensitive throttling devices and apertures.

Refrigerant cost depends on the size of the installation and must be considered from both the standpoint of initial charge and the composition owing to losses during service. Although a domestic refrigerator contains only a few dollars worth of refrigerant, the refrigerant in a cooling system for a typical chemical plant may cost thousands of dollars.

Other desirable properties: Refrigerants should be stable and noncorrosive. For heat transfer considerations, a refrigerant should have low viscosity, high thermal conductivity, and high specific heat. For safety to life or property, a refrigerant should be nontoxic and nonflammable, should not contaminate products in case of a leak, and should have a low-leakage tendency through normal materials of construction.

With a flammable refrigerant, extra precautions have to be taken in the engineering design if it is required to meet the explosion-proof classification. It may be more economical to use a higher cost but nonflammable refrigerant.

4.3 Refrigerant Selection for Open Cycle

Process gases used in the open cycle include chlorine, ammonia, and mixed hydrocarbons. These gases create a wide variety of operating conditions and corrosion problems. Gas

characteristics affect both heat exchangers and compressors, but their impact is far more critical on compressor operation. All gas properties and conditions should be clearly specified to obtain the most economical and reliable compressor design. If the installation is greatly overspecified, design features result that not only add significant cost but also complicate the operation of the system and are difficult to maintain. Specifications should consider the following:

Composition. Molecular weight, enthalpy–entropy relationship, compressibility factor, and operating pressures and temperatures influence the selection and performance of compressors. If process streams are subject to periodic or gradual changes in composition, the range of variations must be indicated.

Corrosion. Special materials of construction and types of shaft seals may be necessary for some gases. Gases that are not compatible with lubricating oils or that must remain oil free may necessitate reciprocating compressors designed with carbon rings or otherwise made oilless or the use of centrifugal compressors designed with isolation seals. However, these features are unnecessary on most installations. Standard designs usually can be used to provide savings in initial cost, simpler operation, and reduced maintenance.

Dirt and Liquid Carryover. Generally, the carryover of dirt and liquids can be controlled more effectively by suction scrubbers than by costly compressor design features. Where this is not possible, all anticipated operating conditions should be stated clearly so that suitable materials and shaft seals can be provided.

Polymerization. Gases that tend to polymerize may require cooling to keep the gas temperature low throughout compression. This can be handled by liquid injection or by providing external cooling between stages of compression. Provision may be necessary for internal cleaning with steam.

These factors are typical of those encountered in open-cycle gas compression. Each job should be thoroughly reviewed to avoid unnecessary cost and to obtain the simplest possible compressor design for ease of operation and maintenance. Direct coordination between the design engineer and manufacturer during final stages of system design is strongly recommended.

5 ABSORPTION SYSTEMS

Ferdinand Carré patented the first absorption machine in 1859.² He employed an ammonia–water solution. His design was soon produced in France, England, and Germany. By 1876, over 600 absorption systems had been sold in the United States. One of the primary uses for these machines was in the production of ice. During the late 1800s and early 1900s, different combinations of fluids were tested in absorption machines. These included such diverse combinations as ammonia with copper sulfate, camphor and naphthol with SO₂, and water with lithium chloride. The modern solution of lithium bromide and water was not used industrially until 1940.²

Absorption systems offer three distinct advantages over conventional vapor compression refrigeration. First, they do not use CFC or HCFC refrigerants, which are harmful to the environment. Second, absorption systems can utilize a variety of heat sources, including natural gas, steam, solar-heated hot water, and waste heat from a turbine or industrial process. If the source of energy is from waste heat, absorption systems may provide the lowest cost alternative for providing chilled water or refrigeration applications. Third, absorption systems do not require any mechanical compression of the refrigerant, which eliminates the need for a lubricant in the refrigerant. Lubricants can decrease heat transfer in evaporators and condensers.

Two different absorption systems are currently in use: (1) a water–lithium bromide system where water is the refrigerant and lithium bromide is the absorbent and (2) a water–ammonia system where the ammonia is the refrigerant and the water is the absorbent.

Evaporator temperatures ranging from -60° to 10°C are achievable with absorption systems.¹ For water-chilling service, absorption systems generally use water as the refrigerant and lithium bromide as the absorbent solution. For process applications requiring chilled fluid below 7°C , the ammonia–water pair is used with ammonia serving as the refrigerant.

5.1 Water–Lithium Bromide Absorption Chillers

Water–lithium bromide absorption machines can be classified by the method of heat input. *Indirect-fired* chillers use steam or hot liquids as a heat source. *Direct-fired* chillers use the heat from the firing of fossil fuels. *Heat recovery* chillers use waste gases as the heat source.

A typical arrangement for a single-stage water–lithium bromide absorption system is shown schematically in Fig. 6. The absorbent, lithium bromide, may be thought of as a carrier fluid bringing spent refrigerant from the low-pressure side of the cycle (the absorber) to the high-pressure side (the generator). There, the waste heat, steam, or hot water that drives the system separates the water from the absorbent by a distillation process. The regenerated

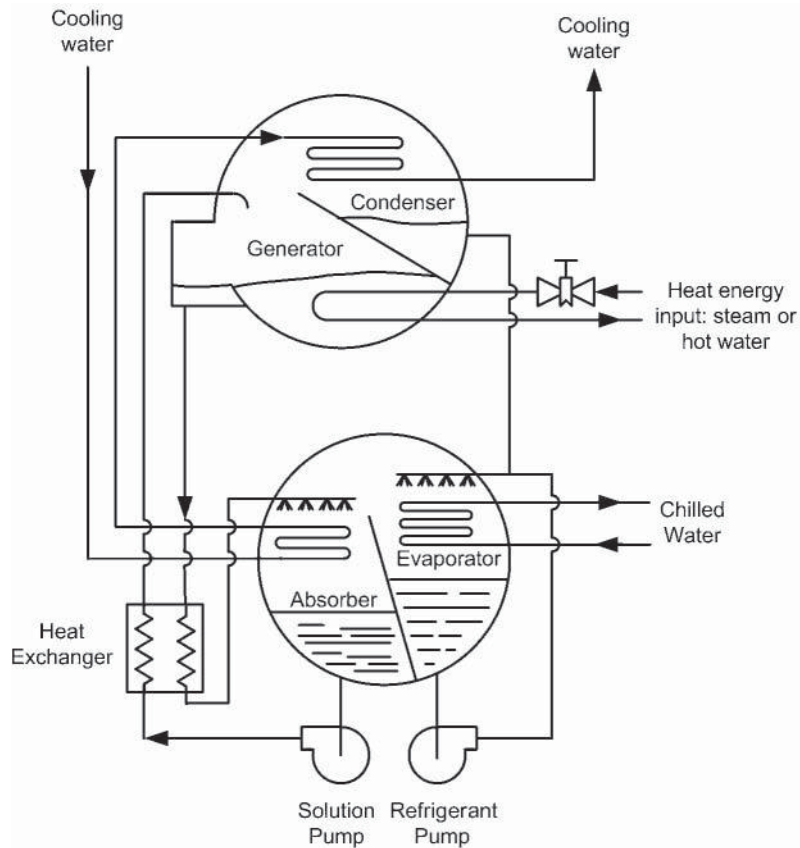


Figure 6 Single-stage water–lithium bromide absorption system.

absorbent returns to the absorber where it is cooled so it will absorb the refrigerant (water) vapor produced in the evaporator and, thereby, establish the low-pressure level, which controls the evaporator temperature. Thermal energy released during the absorption process is transferred to the cooling water flowing through tubes in the absorber shell.

The external heat exchanger shown in Fig. 6 saves energy by heating the strong liquid flowing to the generator as it cools the hot absorbent flowing from the generator to the absorber. If the weak solution that passes through the regenerator to the absorber does not contain enough refrigerant and is cooled too much, crystallization can occur. Leaks or process upsets that cause the generator to overconcentrate the solution are indicated when this occurs. The slushy mixture formed does not harm the machine, but it interferes with continued operation. External heat and added water may be required to redissolve the mixture.

Single-stage absorption systems are most common when generator heat input temperatures are less than 95°C. The coefficient of performance (COP) of a system is the cooling achieved in the evaporator divided by the heat input to the generator. The COP of a single-stage lithium bromide machine generally is 0.65–0.70 for water-chilling duty. The heat rejected by the cooling tower from both the condenser and the absorber is the sum of the waste heat supplied plus the cooling produced, requiring larger cooling towers and cooling water flows than for vapor compression systems.

Absorption machines can be built with a two-stage generator (Fig. 7) with heat input temperatures greater than 150°C. Such machines are called dual-effect machines. The operation of the dual-effect machine is the same as the single-effect machine except that an additional generator, condenser, and heat exchanger are used. Energy from an external heat source is used to boil the dilute lithium bromide (absorbent) solution. The vapor from the primary generator flows in tubes to the second-effect generator. It is hot enough to boil and concentrate absorbent, which creates more refrigerant vapor without any extra energy input. Dual-effect machines typically use steam or hot liquids as input. Coefficients of performance above 1.0 can be obtained with these machines.

5.2 Ammonia–Water Absorption Systems

Ammonia–water absorption technology is used primarily in smaller chillers and small refrigerators found in recreational vehicles.¹ Refrigerators use a variation of the ammonia absorption cycle with ammonia, water, and hydrogen as the working fluids. They can be fired with both gas and electric heat. The units are hermetically sealed. A complete description of this technology can be found in Ref. 1.

Ammonia–water chillers have three major differences from water–lithium bromide systems. First, because the water is volatile, the regeneration of the weak absorbent to strong absorbent requires a distillation process. In a water–lithium bromide system, the generator is able to provide adequate distillation because the absorbent material (lithium bromide) is nonvolatile. In ammonia absorption systems, the absorbent (water) is volatile and tends to carry over into the evaporator where it interferes with vaporization. This problem is overcome by adding a rectifier to purify the ammonia vapor flowing from the generator to the condenser.

A second difference between ammonia–water and water–lithium bromide systems is the operating pressures. In a water–lithium bromide system, evaporating pressures as low as 4–8 kPa are not unusual for the production of chilled water at 5–7°C. In contrast, an ammonia absorption system would run evaporator pressures of between 400 and 500 kPa.

A third difference focuses on the type of heat transfer medium used in the condenser and absorber. Most lithium bromide systems utilize water cooling in the condenser and absorber, while commercial ammonia systems use air cooling.

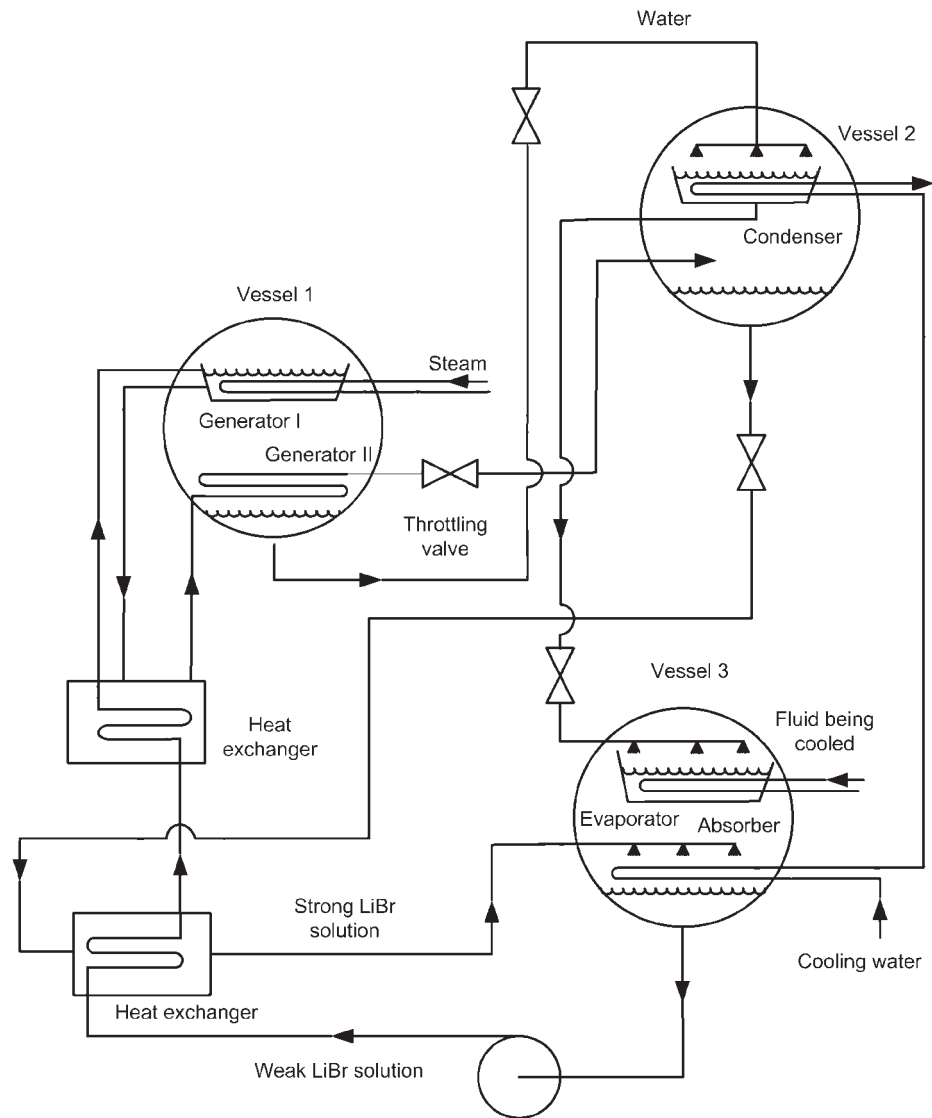


Figure 7 Two-stage water–lithium bromide absorption system.¹⁷

6 INDIRECT REFRIGERATION

For indirect refrigeration, the process or refrigeration load is cooled by an intermediate (secondary) liquid, which is itself cooled by refrigerant typically in a conventional vapor compression cycle (Fig. 8). The secondary liquid can be water, brine, alcohol, or refrigerant. The heat exchanger used to cool the process load may need to be capable of handling corrosive products, high pressures, or high viscosities and is usually not well suited as a refrigerant evaporator. Other problems preventing direct use of a vapor compression refrigeration cycle may be remote location, lack of sufficient pressures for the refrigerant liquid feed, difficulties with oil return, or

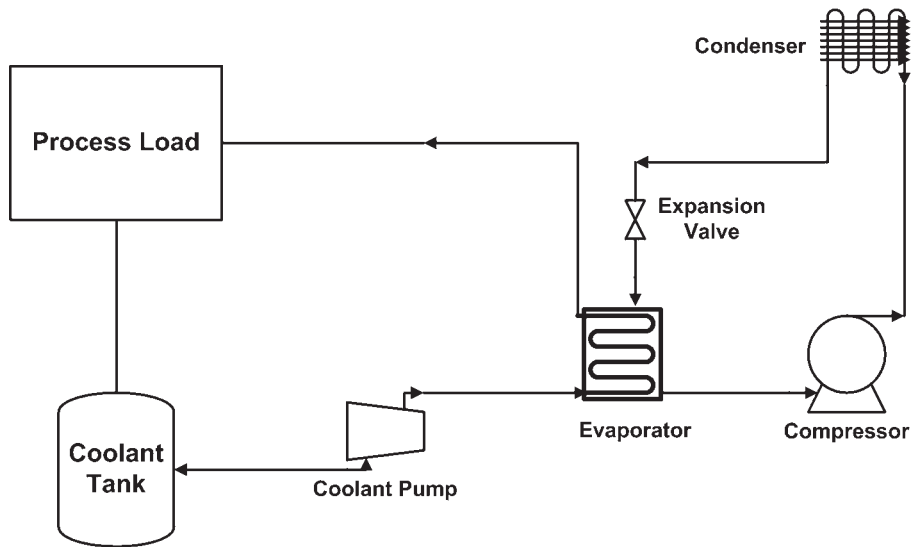


Figure 8 Indirect coolant refrigeration system.

inability to provide traps in the suction line to hold liquid refrigerant. Use of indirect refrigeration simplifies the piping system because it becomes a conventional single-phase liquid system design.

The indirect or secondary coolant (brine) is cooled in the refrigeration evaporator and then is pumped to the process load. The brine system may include a tank maintained at atmospheric pressure or may be a closed system pressurized by an inert, dry gas.

Secondary coolants can be separated into four categories:

1. *Coolants with a Salt Base.* These are water solutions of various concentrations and include the most common brines, that is, calcium chloride and sodium chloride.
2. *Coolants with a Glycol Base.* These are water solutions of various concentrations, most commonly ethylene glycol or propylene glycol.
3. *Coolants with an Alcohol Base.* Where low temperatures are not required, the alcohols are occasionally used in alcohol–water solutions.
4. *Coolants for Low-Temperature Heat Transfer.* These usually are pure substances such as methylene chloride, trichloroethylene, R-11, acetone, and methanol.

Coolants containing a mixture of calcium and sodium chloride are the most common refrigeration brines. These are applied primarily in industrial refrigeration and ice skating rinks. Glycols are used to lower the freezing point of water and used extensively as heat transfer media in cooling systems. Low-temperature coolants include some common refrigerants (R-11, R-30, and R-1120). Because R-11 is a CFC, it cannot be used in any new systems; however, it may still be found in some existing systems. Alcohols and other secondary refrigerants, such as *d*-limonene ($C_{10}H_{16}$), are primarily used by the chemical processing and pharmaceutical industries.

A coolant needs to be compatible with other materials in the system where it is applied. It should have a minimum freezing point approximately 8°C below the lowest temperature to which it is exposed.¹ Table 5 shows a performance comparison of different types of coolants. Some coolants, such as the salts, glycols, and alcohols, are mixed with water to lower the

Table 5 Secondary Coolant Performance Comparisons

Secondary Coolant	Concentration (by weight) %	Freezing Point (°C)	Flow Rate/Capacity [L/(s-kW)] ^a	Heat Transfer Factor ^b	Energy Factor ^c
<i>Salts</i>					
Calcium chloride	22	-22.1	0.0500	2.761	1.447
Sodium chloride	23	-20.6	0.0459	2.722	1.295
<i>Glycols</i>					
Propylene glycol	39	-20.6	0.0459	1.000	1.142
Ethylene glycol	38	-21.6	0.0495	1.981	1.250
<i>Alcohols</i>					
Methanol	26	-20.7	0.0468	2.307	1.078
<i>Low-Temperature Fluids</i>					
Methylene chloride (R-30)	100	-96.7	0.1146	2.854	3.735
Trichloroethylene (R-1120)	100	-86.1	0.1334	2.107	4.787
Trichlorofluoromethane (R-11)	100	-111.1	0.1364	2.088	5.022
<i>d</i> -Limonene	100	-96.7	0.1160	1.566	2.406

^aBased on inlet secondary coolant temperature at the pump of -3.9°C.

^bBased on a curve fit of the Sieder-Tate heat transfer equation values using a 27-mm-i.d. tube 4.9 m long and a film temperature of 2.8°C lower than the average bulk temperature with 2.134 m/s velocity. The actual i.d. and length vary according to the specific loading and refrigerant applied with each secondary coolant, tube material, and surface augmentation.

^cBased on the same pump head, refrigeration load, -6.7°C average temperature, 6 K range, and the freezing point (for water-based secondary coolants) 11–13 K below the lowest secondary coolant temperature.

Source: From Ref. 1. Reprinted by permission from 2002 *ASHRAE Handbook of Refrigeration*. Copyright © American Society of Heating, Refrigerating and Air-Conditioning Engineers, Inc., www.ashrae.org.

freezing point of water. Different concentrations than listed in Table 5 will result in different freezing temperatures. The flow rate divided by capacity gives a way to compare the amount of flow (L/s) that will be needed to produce a kilowatt of cooling. The low-temperature coolants have the highest flow requirements of the four types of coolants. The heat transfer factor is a value normalized to propylene glycol. It is based on calculations inside a smooth tube. The salt mixtures and R-30 provide the highest heat transfer factors of the fluids listed. The energy factor is a measure of the pumping requirements that will be needed for each of the coolants. The low-temperature fluids require the largest pumping requirements.

Table 6 shows the general areas of application for the commonly used brines. Criteria for selection are discussed in the following paragraphs. The order of importance depends on the specific application.

Corrosion problems with sodium chloride and calcium chloride brines limit their use. When properly maintained in a neutral condition and protected with inhibitors, they will give 20–30 years of service without corrosive destruction of a closed system. Preventing corrosions requires proper selection of materials, inhibitors, maintaining a clean system, and regular testing for the pH of the system.¹ Glycol solutions and alcohol-water solutions are generally less corrosive than salt brines, but they require inhibitors to suit the specific application for maximum corrosion protection. Methylene chloride, trichloroethylene, and trichlorofluoromethane do not show general corrosive tendencies unless they become contaminated with impurities such as moisture. However, methylene chloride and trichloroethylene must not be used with aluminum or zinc; they also attack most rubber compounds and plastics. Alcohol in high concentrations will attack aluminum. Reaction with aluminum is of concern because, in the event of leakage into the refrigeration compressor system, aluminum compressor parts will be attacked.

Toxicity is an important consideration in connection with exposure to some products and to operating personnel. Where brine liquid, droplets, or vapor may contact food products, as

Table 6 Application Information for Common Secondary Coolants

Secondary Coolant	Toxic	Explosive	Corrosive
<i>Salts</i>			
Calcium chloride	No	No	Yes
Sodium chloride	No	No	Yes
<i>Glycols</i>			
Propylene glycol	No	No	Some
Ethylene glycol	Yes	No	Some
<i>Alcohols</i>			
Methanol	Yes	Yes	Some
Ethanol	Yes	Yes	Some
<i>Low-Temperature Fluids</i>			
Methylene chloride (R-30)	No	No	No
Trichloroethylene (R-1120)	No	No	No
Trichlorofluoromethane (R-11)	No	No	No
<i>d</i> -Limonene	Yes	Yes	Yes

Source: From Refs. 1 and 3.

in an open spray-type system, sodium chloride and propylene glycol solutions are acceptable because of low toxicity. All other secondary coolants are toxic to some extent or produce odors, which requires that they be used only inside of pipe coils or a similar pressure-tight barrier.

Flash point and explosive-mixture properties of some coolants require precautions against fire or explosion. Acetone, methanol, and ethanol are in this category but are less dangerous when used in closed systems.

Specific heat of a coolant determines the mass rate of flow that must be pumped to handle the cooling load for a given temperature rise. The low-temperature coolants, such as trichloroethylene, methylene chloride, and trichlorofluoromethane, have specific heats approximately one-third to one-fourth those of the water-soluble brines. Consequently, a significantly greater mass of the low-temperature brines must be pumped to achieve the same temperature change.

Stability at high temperatures is important where a brine may be heated as well as cooled. Above 60°C, methylene chloride may break down to form acid products. Trichloroethylene can reach 120°C before breakdown begins.

Viscosities of brines vary greatly. The viscosity of propylene glycol solutions, for example, makes them impractical for use below -7°C because of the high pumping costs and the low heat transfer coefficient at the concentration required to prevent freezing. Mixtures of ethanol and water can become highly viscous at temperatures near their freezing points, but 190-proof ethyl alcohol has a low viscosity at all temperatures down to near the freezing point. Similarly, methylene chloride and R-11 have low viscosities down to -73°C . In this region, the viscosity of acetone is even more favorable.

Since a secondary coolant cannot be used below its freezing point, certain ones are not applicable at the lower temperatures. Sodium chloride's eutectic freezing point of -20°C limits its use to approximately -12°C . The eutectic freezing point of calcium chloride is -53°C , but achieving this limit requires such an accuracy of mixture that -40°C is a practical low limit of usage.

Water solubility in any open or semiopen system can be important. The dilution of a salt or glycol brine or of alcohol by entering moisture merely necessitates strengthening of the brine. But for a brine that is not water soluble, such as trichloroethylene or methylene chloride, precautions must be taken to prevent free water from freezing on the surfaces of the heat exchanger. This may require provision for dehydration or periodic mechanical removal of ice, perhaps accompanied by replacement with fresh brine.

Vapor pressure is an important consideration for coolants that will be used in open systems, especially where it may be allowed to warm to room temperature between periods of operation. It may be necessary to pressurize such systems during periods of moderate-temperature operation. For example, at 0°C the vapor pressure of R-11 is 39.9 kPa (299 mm Hg); that of a 22% solution of calcium chloride is only 0.49 kPa (3.7 mm Hg). The cost of vapor losses, the toxicity of the escaping vapors, and their flammability should be carefully considered in the design of the semiclosed or open system.

Environmental effects are important in the consideration of trichlorofluoromethane (R-11) and other chlorofluorocarbons. This is a refrigerant with a high ozone depletion potential and halocarbon global warming potential. The environmental effect of each of the coolants should be reviewed before seriously considering the use of it in a system.

Energy requirements of brine systems may be greater because of the power required to circulate the brine and because of the extra heat transfer process, which necessitates the maintenance of a lower evaporator temperature.

7 SYSTEM COMPONENTS

There are four major components in any refrigeration system: compressor, condenser, evaporator, and expansion device. Each is discussed below.

7.1 Compressors

Both positive-displacement and centrifugal compressors are used in refrigeration applications. With positive-displacement compressors, the pressure of the vapor entering the compressor is increased by decreasing the volume of the compression chamber. Reciprocating, rotary, scroll, and screw compressors are examples of positive-displacement compressors. Centrifugal compressors utilize centrifugal forces to increase the pressure of the refrigerant vapor. Refrigeration compressors can be used alone or in parallel and series combinations. Features of several of the compressors are described later in this section.

Compressors usually have a variety of protection devices for handling adverse conditions. These include high-pressure controls, high-temperature controls, low-pressure protection, time delay, low voltage and phase loss, and suction line strainer.¹⁸ High-pressure controls are required by Underwriters Laboratories. These can include a high-pressure cutoff or a relief valve. High-temperature devices are designed to protect against overheating and lubrication breakdown. Low-pressure protection is provided to protect the compressor against extremely low pressures, which may cause insufficient lubricant return, freeze-up, or too high a pressure ratio. Time delays are required to prevent damage to the compressor motor from rapid startup after a shutdown. A suction line strainer is used to remove dirt and other particles that may be in the refrigerant line. The specific protection devices will depend on the application and size of the compressor.

Reciprocating Compressors

High-speed, single-stage reciprocating compressors with displacements up to 0.283–0.472 m³/s (600–1000 cfm) generally are limited to a pressure ratio of about 9. The reciprocating compressor is basically a constant-volume variable-head machine. It handles various discharge pressures with relatively small changes in inlet volume flow rate as shown by the heavy line in Fig. 9.

Reciprocating compressors can also be found in an integral two-stage configuration.¹⁸ These can use R-22 or ammonia and can achieve low temperatures from –29 to –62°C. These

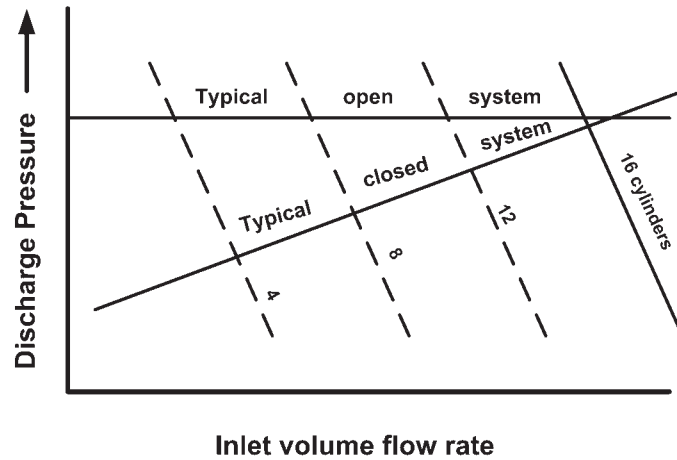


Figure 9 Volume–pressure relationships for a reciprocating compressor.

compressors will consist of multiple cylinders, with the cylinders divided so that the volumetric flow and pressure ratios are balanced. Capacity can be controlled with cylinder unloading.

Open systems and many processes require nearly fixed compressor suction and discharge pressure levels. This load characteristic is represented by the horizontal typical open-system line in Fig. 9. In contrast, condenser operation in many closed systems is related to ambient conditions, for example, through cooling towers, so that on cooler days the condenser pressure can be reduced. When the refrigeration load is lower, less refrigerant circulation is required. The resulting load characteristic is represented by the typical closed-system line in Fig. 9.

The compressor must be capable of matching the pressure and flow requirements imposed upon it by the system in which it operates. The reciprocating compressor matches the imposed discharge pressure at any level up to its limiting pressure ratio. Varying capacity requirements can be met by providing devices that unload individual or multiple cylinders. This unloading is accomplished by blocking the suction or discharge valves that open either manually or automatically. Capacity can also be controlled through the use of variable-speed or multispeed motors. When capacity control is implemented on a compressor, other factors at part-load conditions need to be considered, such as (1) effect on compressor vibration and sound when unloaders are used, (2) the need for good oil return because of lower refrigerant velocities, and (3) proper functioning of expansion devices at the lower capacities.

Reciprocating compressors employ a lubricant. Oil is pumped into the refrigeration system during operation. Systems must be designed carefully to return oil to the compressor crankcase to provide for continuous lubrication and also to avoid contaminating heat exchanger surfaces. At very low temperatures ($\sim -50^{\circ}\text{C}$ or lower, depending on refrigerant used) oil becomes too viscous to return, and provision must be made for periodic plant shutdown and warm-up to allow manual transfer of the oil.

Reciprocating compressors usually are arranged to start with the cylinders unloaded so that normal torque motors are adequate for starting. When gas engines are used for reciprocating compressor drives, careful torsional analysis is essential.

Rotary Compressors

Rotary compressors include both rolling piston and rotary vane compressors. Rotary vane compressors are primarily used in transportation air-conditioning applications, while rolling piston

compressors are usually found in household refrigerators and small air conditioners up to inputs of 2 kW. For a fixed-vane, rolling piston rotary compressor, the shaft is located in the center of the housing while the roller is mounted on an eccentric.⁸ Suction gas enters directly into the suction port. As the roller rotates, the refrigerant vapor is compressed and is discharged into the compressor housing through the discharge valve.

One difference between a rotary and a reciprocating compressor is that the rotary is able to obtain a better vacuum during suction.¹⁸ It has low reexpansion losses because there is no high-pressure discharge vapor present during suction as with a reciprocating compressor.

Because rotary vane compressors have a light weight for their displacement, they are ideal for transportation applications. Rotary vane compressors can be used in applications where temperatures drop down to -40 to -51°C , depending whether it is in a single- or two-stage system. Refrigerants R-22, R-404a, and R-717 are currently used with rotary vane compressors.¹⁸

Scroll Compressors

The principle of the scroll compressor was first patented in 1905.¹⁹ However, the first commercial units were not built until the early 1980s.²⁰ Scroll compressors are used in building air-conditioning, heat pump, refrigeration, and automotive air-conditioning applications. They range in capacity from 3 to 50 kW.¹⁸ Scroll compressors have two spiral-shaped scroll members that are assembled 180° out of phase (Fig. 10). One scroll is fixed while the other “orbits” the first. Vapor is compressed by sealing vapor off at the edge of the scrolls and reducing the volume of the gas as it moves inward toward the discharge port. Figure 10a shows the two scrolls at the instant that vapor enters the compressor and compression begins. The orbiting motion of the second scroll forces the pocket of vapor toward the discharge port while decreasing its volume (Figs. 10b–10h). In Figs. 10c and f, the two scrolls open at the ends and allow new pockets of vapor to be admitted into the scrolls for compression. Compression is a nearly continuous process in a scroll compressor.

Scroll compressors offer several advantages over reciprocating compressors. First, relatively large suction and discharge ports can be used to reduce pressure losses. Second, the separation of the suction and discharge processes reduces the heat transfer between the discharge and suction processes. Third, with no valves and reexpansion losses, they have higher volumetric efficiencies. Capacities of systems with scroll compressors can be varied by using variable-speed motors or by use of multiple suction ports at different locations within the two spiral members. Fourth, with a smaller number of moving parts, they have the potential to be more reliable and quieter than reciprocating compressors.

Screw Compressors

Screw compressors were first introduced in 1958.² These are positive-displacement machines available in the capacity range from 15 to 1100 kW, overlapping reciprocating compressors for lower capacities and centrifugal compressors for higher capacities. Both twin-screw and single-screw compressors are used for refrigeration applications.

Fixed suction and discharge ports, used instead of valves in reciprocating compressors, set the “built-in volume ratio” of the screw compressor. This is the ratio of the volume of fluid space in the meshing rotors at the beginning of the compression process to the volume in the rotors as the discharge port is first exposed. Associated with the built-in volume ratio is a pressure ratio that depends on the properties of the refrigerant being compressed. Peak efficiency is obtained if the discharge pressure imposed by the system matches the pressure developed by the rotors when the discharge port is exposed. If the interlobe pressure is greater or less than discharge pressure, energy losses occur but no harm is done to the compressor.

Capacity modulation is accomplished by slide valves that are used to provide a variable suction bypass or delayed suction port closing, reducing the volume of refrigerant actually compressed. Continuously variable capacity control is most common, but stepped capacity control

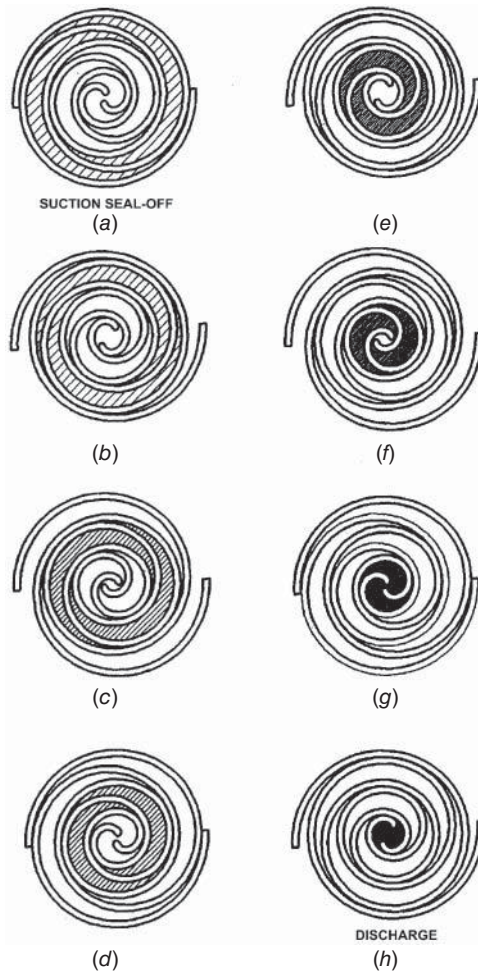


Figure 10 Operation of fixed and orbiting scrolls in a scroll compressor. Reprinted by permission from 2000 *ASHRAE Handbook of HVAC Systems and Equipment*. Copyright © American Society of Heating, Refrigerating, and Air-Conditioning Engineers, Inc., www.ashrae.org.

is offered in some manufacturers' machines. Variable discharge porting is available on a few machines to allow control of the built-in volume ratio during operation.

Oil is used in screw compressors to seal the extensive clearance spaces between the rotors, to cool the machines, to provide lubrication, and to serve as hydraulic fluid for the capacity controls. An oil separator is required for the compressor discharge flow to remove the oil from the high-pressure refrigerant so that performance of system heat exchangers will not be penalized and the oil can be returned for reinjection in the compressor.

Screw compressors can be direct driven at two-pole motor speeds (50 or 60 Hz). Their rotary motion makes these machines smooth running and quiet. Reliability is high when the machines are applied properly. Screw compressors are compact so they can be changed out readily for replacement or maintenance. Today, the efficiency of the best screw compressors matches that of reciprocating compressors at full load. Figure 11 shows the efficiency of a

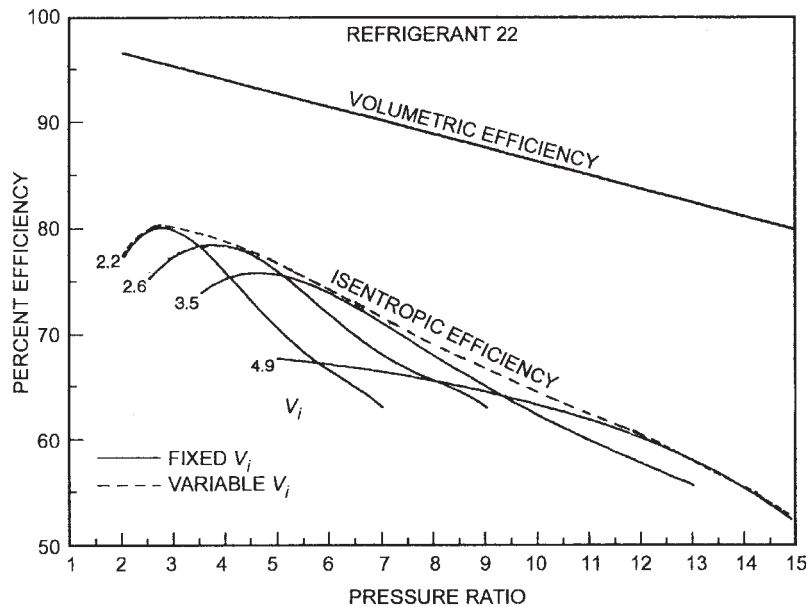


Figure 11 Typical performance of a single-screw compressor. Reprinted by permission from 2000 *ASHRAE Handbook of HVAC Systems and Equipment*. Copyright © American Society of Heating, Refrigerating, and Air-Conditioning Engineers, Inc., www.ashrae.org.

single-screw compressor as a function of pressure ratio and volume ratio (V_i). High isentropic and volumetric efficiencies can be achieved with screw compressors because there are no suction or discharge valves and small clearance volumes. Screw compressors have been used with a wide variety of refrigerants, including halocarbons, ammonia, and hydrocarbons.

Centrifugal Compressors

The centrifugal compressor is preferred whenever the gas volume is high enough to allow its use, because it offers better control, simpler hookup, minimum lubrication problems, and lower maintenance. Single-impeller designs are directly connected to high-speed drives or driven through an internal speed increaser. These machines are ideally suited for clean, noncorrosive gases in moderate-pressure process or refrigeration cycles in the range of 0.236–1.89 m³/s (5 cfm). Multistage centrifugal compressors are built for direct connection to high-speed drives or for use with an external speed increaser. Designs available from suppliers generally provide for two to eight impellers per casing covering the range of 0.236–11.8 m³/s (500–25,000 cfm), depending on the operating speed. A wide choice of materials and shaft seals to suit any gas composition, including dirty or corrosive process streams, is available.

The centrifugal compressor has a more complex head–volume characteristic than reciprocating machines. Changing discharge pressure may cause relatively large changes in inlet volume, as shown by the heavy line in Fig. 12a. Adjustment of variable inlet vanes or of a diffuser ring allows the compressor to operate anywhere below the heavy line to conditions imposed by the system. A variable-speed controller offers an alternative way to match the compressor's characteristics to the system load, as shown in the lower half of Fig. 12b. The maximum head capability is fixed by the operating speed of the compressor. Both methods have advantages: generally, variable inlet vanes or diffuser rings provide a wider range of capacity

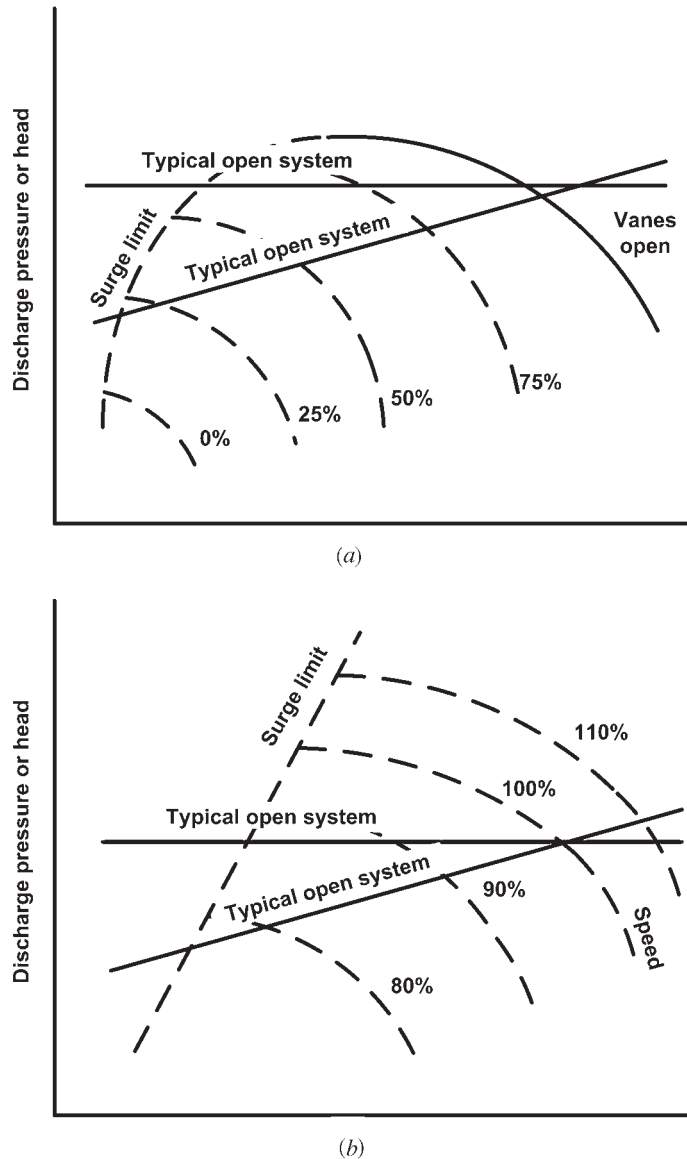


Figure 12 Volume–pressure relationships in a centrifugal compressor³: (a) with variable inlet-vane control at constant rotational speed; (b) with variable speed control at a constant inlet-vane opening.

reduction; variable speed usually is more efficient. Maximum efficiency and control can be obtained by combining both methods of control.

The centrifugal compressor has a surge point—that is, a minimum-volume flow below which stable operation cannot be maintained. The percentage of load at which the surge point occurs depends on the number of impellers, design–pressure ratio, operating speed, and variable inlet-vane setting. The system design and controls must keep the inlet volume

above this point by artificial loading, if necessary. This is accomplished with a bypass valve and gas recirculation. Combined with a variable inlet-vane setting, variable diffuser ring, or variable-speed control, the gas bypass allows stable operation down to zero load.

Compressor Operation

Provision for minimum-load operation is strongly recommended for all installations, because there will be fluctuations in plant load. For chemical plants, this permits the refrigeration system to be started up and thoroughly checked out independently of the chemical process.

Contrasts between the operating characteristics of the positive-displacement compressor and the centrifugal compressor are important considerations in plant design to achieve satisfactory performance. Unlike positive-displacement compressors, the centrifugal compressor will not rebalance abnormally high system heads. The drive arrangement for the centrifugal compressor must be selected with sufficient speed to meet the maximum head anticipated. The relatively flat head characteristics of the centrifugal compressor necessitates different control approaches than for positive-displacement machines, particularly when parallel compressors are utilized. These differences, which account for most of the troubles experienced in centrifugal compressor systems, cannot be overlooked in the design of a refrigeration system.

A system that uses centrifugal compressors designed for high-pressure ratios and that requires the compressors to start with high suction density existing during standby will have high starting torque. If the driver does not have sufficient starting torque, the system must have provisions to reduce the suction pressure at startup. This problem is particularly important when using single-shaft gas turbine engines or reduced-voltage starters on electric drives. Split-shaft gas turbines are preferred for this reason.

Drive ratings that are affected by ambient temperatures, altitudes, etc., must be evaluated at the actual operating conditions. Refrigeration installations normally require maximum output at high ambient temperatures, a factor that must be considered when using drives such as gas turbines and gas engines.

7.2 Condensers

The refrigerant condenser is used to reject the heat energy added to the refrigerant during compression and the heat energy absorbed in the evaporator. This heat energy is typically rejected to either water or air.

The amount of heat energy added to the refrigerant during compression depends on the compressor power and can become a significant part of the condenser load for low-temperature systems. Common types of water-cooled condensers include shell and tube, shell and coil, tube in tube, and brazed plate.¹⁸ Shell-and-coil condensers are smaller in size (3.5–50 kW) and circulate the cooling water through coiled tubes inside an external shell. The refrigerant condenses on the outside of the coiled tubes. Tube-in-tube condensers can be found in sizes up to 175 kW and consist of tubes within larger tubes. The refrigerant is condensed either in the annular space between the tubes or inside the inner tube. Brazed-plate condensers can be found in sizes up to 350 kW and are constructed of plates brazed together to form separate channels.¹⁸

Shell-and-tube condensers can be found in sizes from 3.5 to 35,000 kW. These condensers with finned tubes and fixed tube sheets provide an economical exchanger design for refrigerant use. Figure 13 shows an example of a shell-and-tube condenser. Commercially available condensers conforming to ASME Boiler and Pressure Vessel Code²¹ construction adequately meet both construction and safety requirements for this application.

Cooling towers and spray ponds are frequently used for water-cooling systems. These generally are sized to provide 29°C supply water at design load conditions. Circulation rates typically are specified so that design cooling loads are handled with a 5.6°C cooling-water

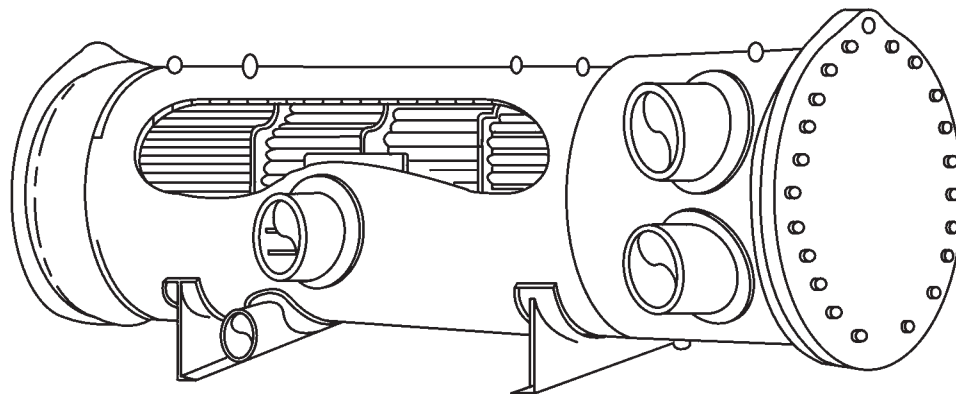


Figure 13 Typical shell-in-tube refrigerant condenser.³

temperature rise. Pump power, tower fans, makeup water (about 3% of the flow rate), and water treatment should be taken into account in operating cost studies. Water temperatures, which control condensing pressure, may have to be maintained above a minimum value to ensure proper refrigerant liquid feeding to all parts of the system.

River or well water, when available, provides an economical cooling medium. Quantities circulated will depend on initial supply temperatures and pumping cost but are generally selected to handle the cooling load with 8.3–16.6°C water temperature range. Water treatment and special exchanger materials frequently are necessary because of the corrosive and scale-forming characteristics of the water. Well water, in particular, must be analyzed for corrosive properties, with special attention given to the presence of dissolved gases, for example, H₂S and CO₂. These are extremely corrosive to many exchanger materials yet difficult to detect in sampling. Pump power, water treatment, and special condenser material should be evaluated when considering costs.

Allowances must be made in heat transfer calculations for fouling or scaling of exchanger surfaces during operation. This ensures sufficient surface to maintain rated performance over a reasonable interval of time between cleanings. Scale factor allowances are expressed in m²·K/kW as additional thermal resistance.

Commercial practice normally includes a scale factor allowance of 0.088 m² · K/kW. The long hours of operation usually associated with chemical plant service and the type of cooling water frequently encountered generally justify a greater allowance to minimize the frequency of downtime for cleaning. Depending on these conditions, an allowance of 0.18 or 0.35 m² · K/kW is recommended for chemical plant service. Scale allowance can be reflected in system designs in two ways: as more heat exchanger surface or as higher design condensing temperatures with attendant increase in compressor power. Generally, a compromise between these two approaches is most economical. For extremely bad water, parallel condensers, each with 60–100% capacity, may provide a more economical selection and permit cleaning one exchanger while the system is operating.

Air-cooled condensing equipment can also be used in refrigeration systems. With tighter restrictions on the use of water, air-cooled equipment is used even on larger centrifugal-type refrigeration plants, although it requires more physical space than cooling towers. Larger condensers include an array of propeller fans located at the top of the condenser that pull air over the condensing coil. Circulating fans and exchanger surface are usually selected to provide design condensing temperatures of 49–60°C when design ambient dry bulb temperatures range between 35 and 38°C.

The design dry bulb temperature should be carefully considered since most weather data reflect an average or mean maximum temperature. If full-load operation must be maintained at all times, care should be taken to provide sufficient condenser capacity for the maximum recorded temperature. This is particularly important when the compressor is centrifugal because of its flat-head characteristics and the need for adequate speed. Multiple-circuit or parallel air-cooled condensers must be provided with traps to prevent liquid backup into the idle circuit at light load. Pressure drop through the condenser coil must also be considered in establishing the compressor discharge pressure.

The condensing temperature and pressure must be controlled for the refrigeration system to function optimally. Too high a condensing temperature results in increased power and reduced capacity. Too low a condensing temperature can result in poor performance of the expansion device. Air-cooled condensers often employ fan cycling, modulating dampers, or fan speed control to maintain proper refrigerant condensing temperature and pressure.¹⁸ On condensers with multiple fans, one or more of the fans can each be cycled on and off to maintain refrigerant conditions. When modulating dampers are used, the airflow through the condenser can be controlled from 0 to 100%. Variable-speed drives can also be used to control fan speed and airflow through the condenser.

In comparing water-cooled and air-cooled condensers, the compression power at design conditions is usually higher with air-cooled condensing, because of the larger temperature differential required in air-cooled condensers. However, ambient air temperatures are considerably below the design temperature most of the time, and operating costs frequently compare favorably over a full year. In addition, air-cooled condensers usually require less maintenance, although dirty or dusty atmospheres may affect performance.

7.3 Evaporators

There are special requirements for evaporators in refrigeration service that are not always present in other types of heat exchanger design. These include problems of oil return, flash gas distribution, gas–liquid separation, and submergence effects.

Oil Return

When the evaporator is used with reciprocating–compression equipment, it is necessary to ensure adequate oil return from the evaporator. If oil will not return in the refrigerant flow, it is necessary to provide an oil reservoir for the compression equipment and to remove oil mechanically from the low side of the system on a regular basis. Evaporators used with centrifugal compressors do not normally require oil return from the evaporator, since centrifugal compressors pump very little oil into the system. However, even with centrifugal equipment, low-temperature evaporators eventually may become contaminated with oil, which must be reclaimed.

Two-Phase Refrigeration Distribution

As a general rule, the refrigerant is introduced into the evaporator by expanding it from a high-pressure liquid through the expansion device. In the expansion process, a significant portion of the refrigerant flashes off into vapor, producing a two-phase mixture of liquid and vapor that must be introduced properly into the evaporator for satisfactory performance. Improper distribution of this mixture can result in liquid carryover to the compressor and in damage to the exchanger tubes from erosion or from vibration.

Vapor–Liquid Separation

To avoid compressor damage, the refrigerant leaving the evaporator must not contain any liquid. The design should provide adequate separation space or include mist eliminators. Liquid carryover is one of the most common sources of trouble with refrigeration systems.

Submergence Effect

In flooded evaporators, the evaporating pressure and temperature at the bottom of the exchanger surface are higher than at the top of the exchanger surface, owing to the liquid head. This static head, or submergence effect, significantly affects the performance of refrigeration evaporators operating at extremely low temperatures and low-suction pressures.

Beyond these basic refrigeration design requirements, the chemical industry imposes many special conditions. Exchangers frequently are applied to cool highly corrosive process streams. Consequently, special materials for evaporator tubes and channels of particularly heavy wall thickness are dictated. Corrosion allowances in the form of added material thicknesses in the evaporator may be necessary in chemical service.

High-pressure and high-temperature designs on the process side of refrigerant evaporators are frequently encountered in chemical plant service. Process-side construction may have to be suitable for pressures seldom encountered in commercial service. Differences between process inlet and outlet temperatures greater than 55°C are not uncommon. In such cases, special consideration must be given to thermal stresses within the refrigerant evaporator. U-tube construction or floating-tube-sheet construction may be necessary. Minor process-side modifications may permit use of less expensive standard commercial fixed-tube-sheet designs. However, coordination between the equipment supplier and chemical plant designer is necessary to tailor the evaporator to the intended duty. Relief devices and safety precautions common to the refrigeration field normally meet chemical plant needs but should be reviewed against individual plant standards. It must be the mutual responsibility of the refrigeration equipment supplier and the chemical plant designer to evaluate what special features, if any, must be applied to modify commercial equipment for chemical plant service.

Refrigeration evaporators are usually designed to meet the ASME Boiler and Pressure Vessel Code,²¹ which provides for a safe, reliable exchanger at economical cost. In refrigeration systems, these exchangers generally operate with relatively small temperature differentials for which fixed-tube-sheet construction is preferred. Operating pressures in refrigerant evaporators also decrease as operating temperatures are reduced. This relationship results in extremely high factors of safety on pressure stresses, eliminating the need for expensive nickel steels from -59 to -29°C. Most designs are readily modified to provide suitable materials for corrosion problems on the process side.

The basic shell-and-tube exchanger with fixed-tube sheets (Fig. 14) is most widely used for refrigeration evaporators. Most designs are suitable for fluids up to 2170 kPa (300 psig) and for operation with up to 38°C temperature differences. Above these limits, specialized heat exchangers generally are used to suit individual requirements.

With the fluid on the tube side, the shell side is flooded with refrigerant for efficient wetting of the tubes (see Fig. 15). Designs must provide for distribution of flash gas and liquid refrigerant entering the shell and for separation of liquid from the gas leaving the shell before it reaches the compressor.

In low-temperature applications and large evaporators, the exchanger surface may be sprayed rather than flooded. This eliminates the submergence effect or static-head penalty, which can be significant in large exchangers, particularly at low temperatures. The spray cooler (Fig. 16) is recommended for some large coolers to offset the cost of refrigerant inventory or charge that would be necessary for flooding.

Where the Reynolds number in the process fluid is low, as for a viscous or heavy brine, it may be desirable to handle the fluid on the shell side to obtain better heat transfer. In these cases, the refrigerant must be evaporated in the tubes. On small exchangers, commonly referred to as direct-expansion coolers, refrigerant feeding is generally handled with a thermal expansion valve.

On large exchangers, this can best be handled by a small circulating pump to ensure adequate wetting of all tubes (Fig. 17). An oversized channel box on one end provides space for a liquid reservoir and for effective gas-liquid separation.

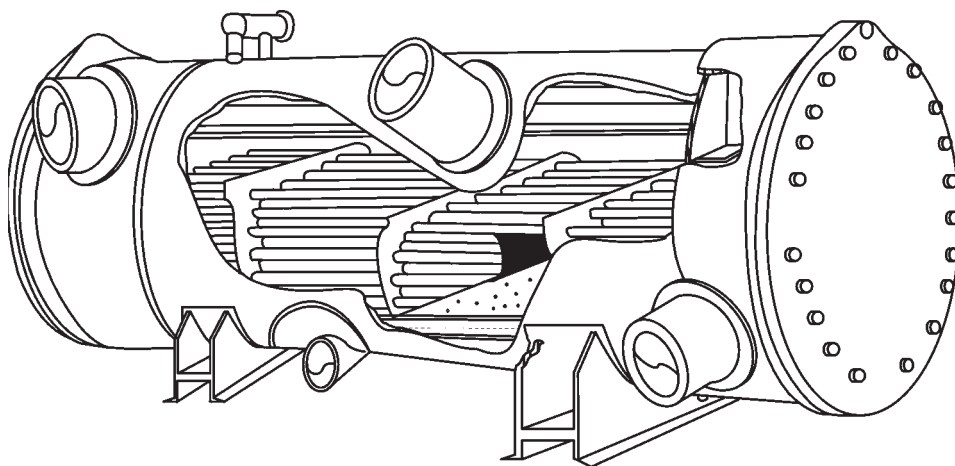


Figure 14 Typical fixed-tube-sheet evaporator.³

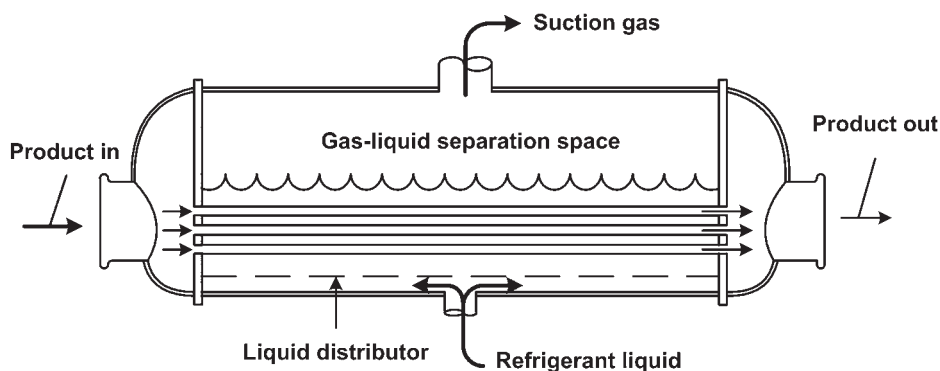


Figure 15 Typical flooded shell-and-tube evaporator.³

7.4 Expansion Devices

The primary purpose of an expansion device is to control the amount of refrigerant entering the evaporator. In the process, the refrigerant entering the valve expands from a relatively high-pressure, subcooled liquid to a saturated low-pressure mixture. Other types of flow control devices, such as pressure regulators and float valves, can also be found in some refrigeration systems. Discussion of these can be found in Ref. 1. Five types of expansion devices can be found in refrigeration systems: (1) thermostatic expansion valves, (2) electronic expansion valves, (3) constant-pressure expansion valves, (4) capillary tubes, and (5) short tube restrictors. Each is discussed briefly.

Thermostatic Expansion Valve

The thermostatic expansion valve (TXV) senses the superheat of the gas leaving the evaporator to control the refrigerant flow into the evaporator. Its primary function is to provide superheated vapor to the suction of the compressor. A TXV is mounted near the entrance to the evaporator

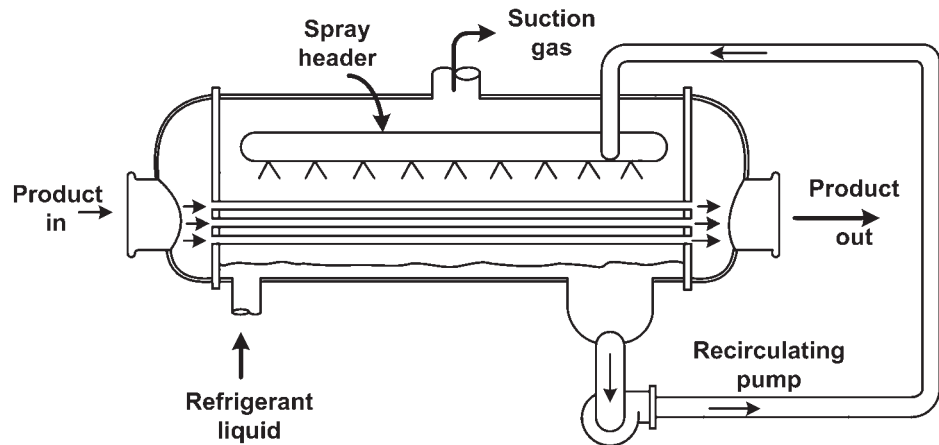


Figure 16 Typical spray-type evaporator.³

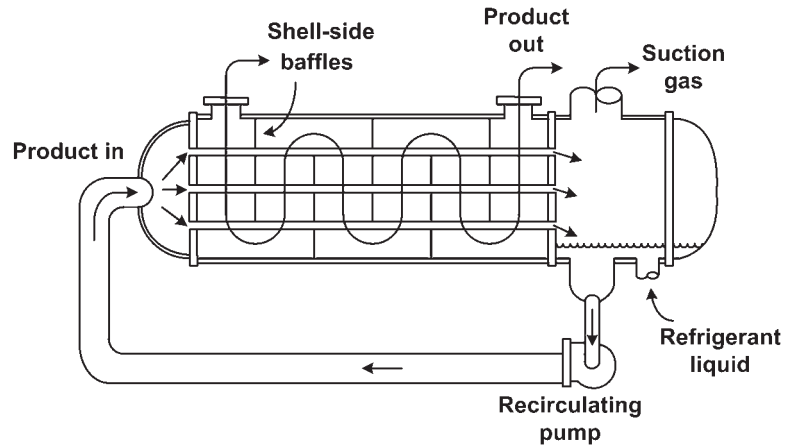


Figure 17 Typical baffled-shell evaporator.³

and has a capillary tube extending from its top that is connected to a small bulb (Fig. 18). The bulb is mounted on the refrigerant tubing near the evaporator outlet. The capillary tube and bulb are filled with a substance called the thermostatic charge.¹ This charge often consists of a vapor or liquid that is the same substance as the refrigerant used in the system. The response of the TXV and the superheat setting can be adjusted by varying the type of charge in the capillary tube and bulb.

The operation of a TXV is straightforward. Liquid enters the TXV and expands to a mixture of liquid and vapor at pressure P_2 . The refrigerant evaporates as it travels through the evaporator and reaches the outlet where it is superheated. If the load on the evaporator is increased, the superheat leaving the evaporator will increase. This increase in flow will increase the temperature and pressure (P_1) of the charge within the bulb and capillary tube. Within the top of the TXV is a diaphragm. With an increase in pressure of the thermostatic charge, a greater force is exerted on the diaphragm, which forces the valve port to open and allow more refrigerant

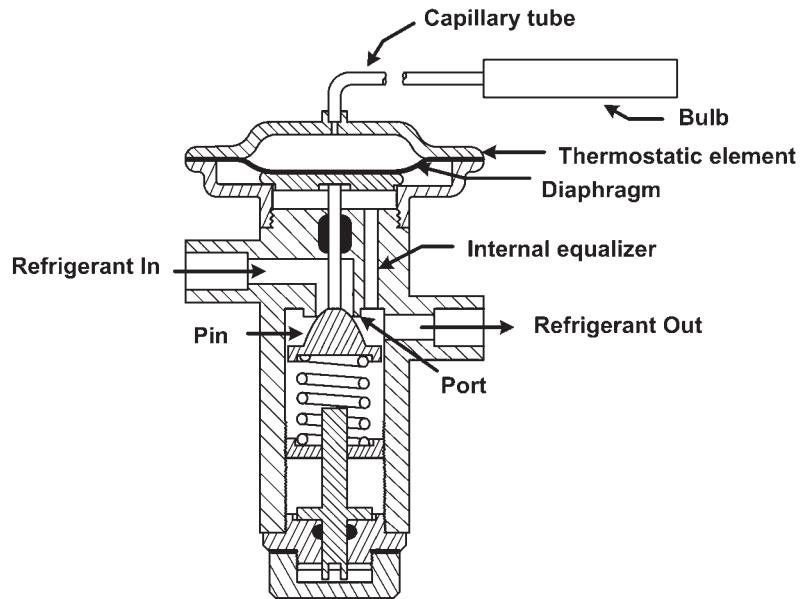


Figure 18 Cross section of thermal expansion valve. Reprinted by permission from 2002 *ASHRAE Handbook of Refrigeration*. Copyright © American Society of Heating, Refrigerating, and Air-Conditioning Engineers, Inc., www.ashrae.org.

into the evaporator. The larger refrigerant flow reduces the evaporator superheat back to the desired level.

The capacity of TXVs is determined on the basis of opening superheat values from 2 to 4°C. TXV capacities are published for a range in evaporator temperatures and valve pressure drops. TXV ratings are based on liquid only entering the valve. The presence of flash gas will reduce the capacity substantially.

Electronic Expansion Valve

The electronic expansion valve (EEV) has become popular in recent years on larger or more expensive systems where its cost can be justified. EEVs can be heat motor activated, magnetically modulated, pulse width modulated, and step motor driven.¹ EEVs can be used with digital control systems to provide control of the refrigeration system based on input variables from throughout the system.

Constant-Pressure Expansion Valve

A constant-pressure expansion valve controls the mass flow of the refrigerant entering the evaporator by maintaining a constant pressure in the evaporator. Its primary use is for applications where the refrigerant load is relatively constant. It is usually not applied where the refrigeration load may vary widely. Under these conditions, this expansion valve will provide too little flow to the evaporator at high loads and too much flow at low loads.

Capillary Tube

Capillary tubes are used extensively in household refrigerators, freezers, and small air conditioners. The capillary tube consists of one or more small-diameter tubes which connect the

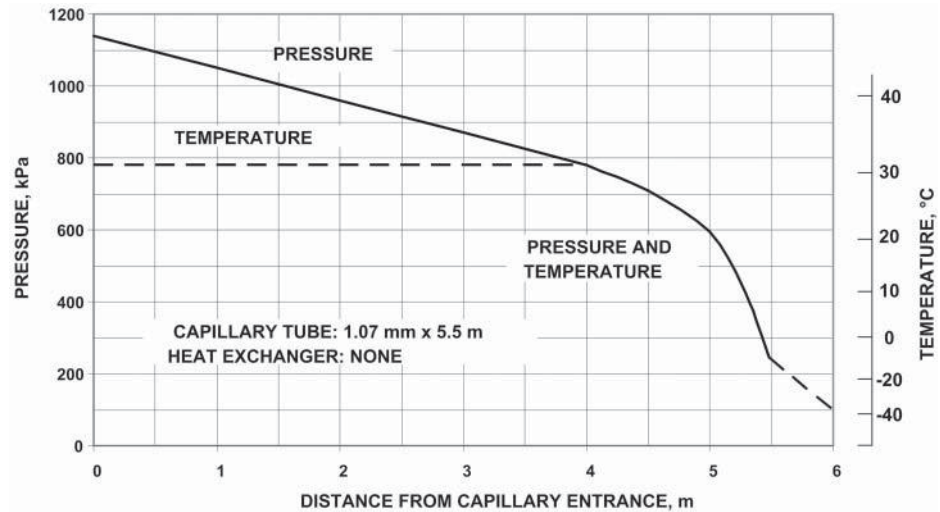


Figure 19 Typical temperature and pressure distribution in capillary tube. Reprinted by permission from 2002 *ASHRAE Handbook of Refrigeration*. Copyright © American Society of Heating, Refrigerating, and Air-Conditioning Engineers, Inc., www.ashrae.org.

high-pressure liquid line from the condenser to the inlet of the evaporator. Capillary tubes range in length from 1 to 6 m and diameters from 0.5 to 2 mm.¹⁷

After entering a capillary tube, the refrigerant remains a liquid for some length of the tube (Fig. 19). While a liquid, the pressure drops, but the temperature remains relatively constant (from point 1 to 2 in Fig. 19). At point 2, the refrigerant enters into the saturation region where a portion of the refrigerant begins to flash to vapor. The phase change accelerates the refrigerant and the pressure drops more rapidly. Because the mixture is saturated, its temperature drops with the pressure from 2 to 3. In many applications, the flow through a capillary tube is choked, which means that the mass flow through the tube is independent of downstream pressure.¹⁷

Because there are no moving parts to a capillary tube, it is not capable of making direct adjustments to variations in suction pressure or load. Thus, the capillary tube does not provide as good a performance as TXVs when applied in systems that will experience a wide range in loads.

Even though the capillary tube is insensitive to changes in evaporator pressure, its flow rate will adjust to changes in the amount of refrigerant subcooling and condenser pressure. If the load in the condenser suddenly changes so that subcooled conditions are no longer maintained at the capillary tube inlet, the flow rate through the capillary tube will decrease. The decreased flow will produce an increase in condenser pressure and subcooling.

The size of the compressor, evaporator, and condenser as well as the application (refrigerator or air conditioner) must all be considered when specifying the length and diameter of capillary tubes. Systems using capillary tubes tend to be much more sensitive to the amount of refrigerant charge than systems using TXVs or EEVs. Design charts for capillary tubes can be found in Ref. 1 for R-12 and R-22.

Short-Tube Restrictor

Short-tube restrictors are applied in many systems that formerly used capillary tubes. Figure 20 illustrates a short-tube restrictor and its housing. The restrictors are inexpensive, reliable, and easy to replace. In addition, for systems such as heat pumps, which reverse cycle, short-tube

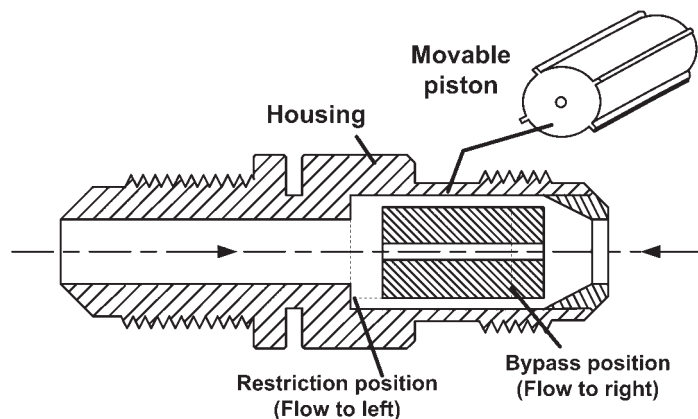


Figure 20 Schematic of short-tube restrictor. Reprinted by permission from 2002 *ASHRAE Handbook of Refrigeration*. Copyright © American Society of Heating, Refrigerating, and Air-Conditioning Engineers, Inc., www.ashrae.org.

restrictors eliminate the need for a check valve. Short tubes vary in length from 10 to 13 mm, with a length-to-diameter ratio from 3 to 20.¹ Current applications for short-tube restrictors are primarily in air conditioners and heat pumps.

Like a capillary tube, short-tube restrictors operate with choked or near-choked flow in most applications.²² The mass flow through the orifice is nearly independent of conditions downstream of the orifice. The flow rate does vary with changes in the condenser subcooling and pressure.

In applying short-tube restrictors, there are many similarities to capillary tubes. The size of the system components and type of system must be considered when sizing this expansion device. Sizing charts for the application of short-tube restrictors with R-22 can be found in Ref. 23.

8 DEFROST METHODS

When refrigeration systems operate below 0°C for extended periods of time, frost can form on the heat transfer surfaces of the evaporator. As frost grows, it begins to block the airflow passages and insulates the cold refrigerant from the warm/moist air that is being cooled by the refrigeration system. With increasing blockage of the airflow passages, the evaporator fan(s) are unable to maintain the design airflow through the evaporator. As airflow drops, the capacity of the system decreases and eventually reaches a point where the frost must be removed. This is accomplished with a defrost cycle.

Several defrost methods are used with refrigeration systems: hot refrigerant gas, air, and water. Each method can be used individually or in combination with the other.

8.1 Hot Refrigerant Gas Defrost

This method is the most common technique for defrosting commercial and industrial refrigeration systems. When the evaporator needs defrosting, hot gas from the discharge of the compressor is diverted from the condenser to the evaporator by closing control valve 2 and opening control valve 1 in Fig. 21. The hot gas increases the temperature of the evaporator and melts the frost. Some of the hot vapor condenses to liquid during the process. A special tank, such as an accumulator, can be used to protect the compressor from any liquid returning to the compressor.

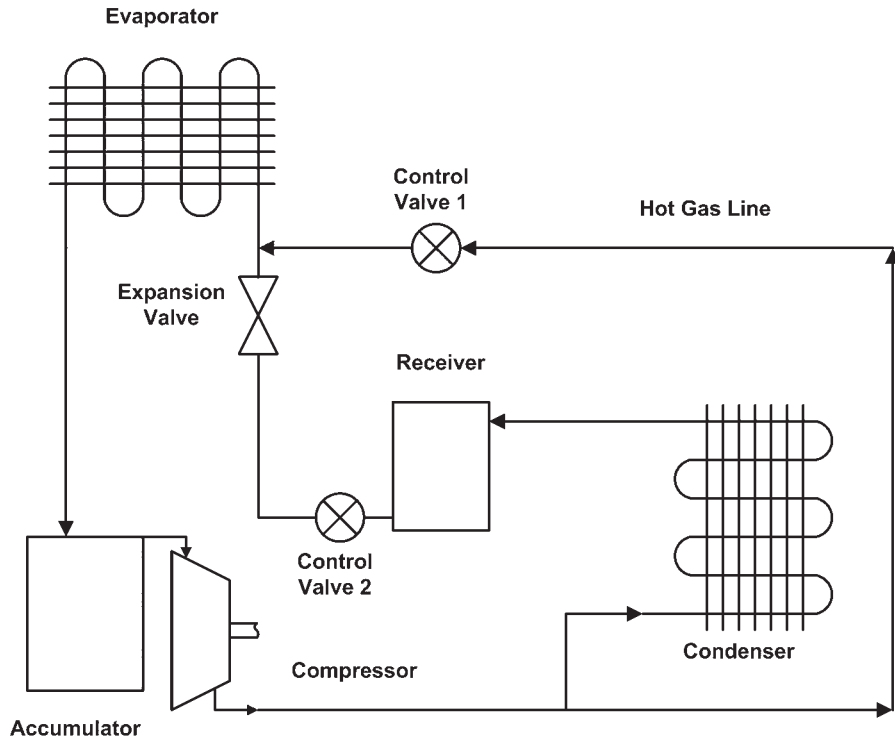


Figure 21 Simplified diagram of hot-refrigerant-gas defrost system.

During defrost operation, the evaporator fans are turned off, which increases the evaporator coil temperature faster. With the fans off, the liquid condensate drains from the coil faster and helps minimize the thermal load to the refrigerated space during defrost. In some instances, electrical heaters are added to increase the speed of the defrost.

Defrost initiation is usually accomplished via demand defrost or time-initiated defrost. Demand defrost systems utilize a variable, such as pressure drop across the air side of the evaporator or a set of temperature inputs, to determine if frost has built up enough on the coil to require a defrost. Time-initiated defrost relies on a preset number of defrosts per day. The number of defrosts and length of time of each defrost can be adjusted. Ideally, the demand defrost system provides the most efficient defrost controls on a system, because a defrost is only initiated if the evaporator needs it. Termination of the defrost cycle is accomplished by either a fixed-time interval or a set temperature of the coil.

8.2 Air, Electric, and Water Defrost

If the refrigerated space operates above 0°C , then the air in the space can be used directly to defrost the evaporator. Defrost is accomplished by continuing to operate the evaporator blower while the compressor is off. As the frost melts, some of it is evaporated into the airstream while the rest drains away from the coil as liquid water. The evaporated moisture adds an additional load to the evaporator when the compressor starts again.

Electric heat can be applied to the evaporator via a heating element. This technique is usually slower than hot-gas defrost. The heating element can be in direct contact with the evaporator or be located between the fan and evaporator.¹

Water can also be used to defrost the evaporator. The compressor and fans are shut off while water is sprayed over the evaporator. If the velocity of the water is kept high, it washes or melts the frost off the coil.

9 SYSTEM DESIGN CONSIDERATIONS

Associated with continuous operation are refrigeration startup and shutdown conditions that invariably differ, sometimes widely, from those of the process itself. These conditions, although they occupy very little time in the life of the installation, must be properly accommodated in the design of the refrigeration system. Consideration must be given to the amount of time required to achieve design operating conditions, the need for standby equipment, etc.

In batch processing, operating conditions are expected to change with time, usually in a repetitive pattern. The refrigeration system must be designed for all extremes. Use of brine storage or ice banks can reduce equipment sizes for batch processes.

Closed-cycle operation involves both liquid and gas phases. System designs must take into account liquid flow problems in addition to gas flow requirements and must provide for effective separation of the liquid and gas phases in different parts of the system. These factors require careful design of all components and influence the arrangement or elevation of certain components in the cycle.

Liquid pressures must be high enough to feed liquid to the evaporators at all times, especially when evaporators are elevated or remotely located. In some cases, a pump must be used to suit the process requirements. The possibility of operation with reduced pressures caused by colder condensing temperatures than the specified design conditions must also be considered. Depending on the types of liquid valves and relative elevation of various parts of the system, it may be necessary to maintain condensing pressures above some minimum level, even if doing so increases the compression power.

Provision must be made to handle any refrigerant liquid that can drain to low spots in the system upon loss of operating pressure during shutdown. It must not be allowed to return as liquid to the compressor upon startup.

The operating charge in various system components fluctuates depending on the load. For example, the operating charge in an air-cooled condenser is quite high at full load but is low, that is, essentially dry, at light load. A storage volume such as a liquid receiver must be provided at some point in the system to accommodate this variation. If the liquid controls permit the evaporator to act as the variable storage, the level may become too high, resulting in liquid carry over to the compressor.

Abnormally high process temperatures may occur during either startup or process upsets. Provision must be made for this possibility, for it can cause damaging thermal stresses on refrigeration components and excessive boiling rates in evaporators, forcing liquid to carry over and damage the compressor.

Factory-designed-and-built packages, which provide cooling as a service or utility, can require several thousand kilowatts of power to operate, but in most cases, they require no more installation than connection of power, utilities, and process lines. As a result, there is a single source of responsibility for all aspects of the refrigeration cycle involving the transfer and handling of both saturated liquids and saturated vapors throughout the cycle, oil return, and other design requirements. These packages are custom engineered, including selection of components, piping, controls, base designs, torsional and critical speed analysis, and individual chemical process requirements. Large packages are designed in sections for shipment but are readily interconnected in the field.

As a general rule, field-erected refrigeration systems should be close coupled to minimize problems of oil return and refrigerant condensation in suction lines. Where process loads are

remotely located, pumped recirculation or brine systems are recommended. Piping and controls should be reviewed with suppliers to assure satisfactory operation under all conditions.

10 REFRIGERATION SYSTEM SPECIFICATION

To minimize costly and time-consuming alterations owing to unexpected requirements, the refrigeration specialist who is to do the final design must have as much information as possible before the design is started. Usually, it is best to provide more information than thought necessary, and it is always wise to note where information may be sketchy, missing, or uncertain. Carefully spelling out the allowable margins in the most critical process variables and pointing out portions of the refrigeration cycle that are of least concern are always helpful to the designer. A checklist of minimum information (Table 7) needed by a refrigeration specialist to design a cooling system for a particular application may be helpful.

Process Flow Sheets. For chemical process designs, seeing the process flow sheets is the best overall means for the refrigeration engineer to become familiar with the chemical process for which the refrigeration equipment is to be designed. In addition to

Table 7 Information Needed for the Design of a Refrigeration System

Process Flow Sheets and Thermal Specifications

Type of process
 Batch
 Continuous
 Normal heat balances
 Normal material balances
 Normal material composition
 Design operating pressure and temperatures
 Design refrigeration loads
 Energy recovery possibilities
 Manner of supplying refrigeration (primary or secondary)

Basic Specifications

Mechanical system details
 Construction standards
 Industry
 Company
 Local plant
 Insulation requirements
 Special corrosion prevention requirements
 Special sealing requirements
 Process streams to the environment
 Process stream to refrigerant
 Operating environment

(continued)

Table 7 (Continued)

Indoor or outdoor location
Extremes
Special requirements
Special safety considerations
Known hazards of process
Toxicity and flammability constraints
Maintenance limitations
Reliability requirements
Effect of loss of cooling on process safety
Maintenance intervals and types that may be performed
Redundancy requirement
Acceptance test requirements
<i>Instrumentation and Control Requirements</i>
Safety interlocks
Process interlocks
Special control requirements
At equipment
Central control room
Special or plant standard instruments
Degree of automation: interface requirements
Industry and company control standards
<i>Off-Design Operation</i>
Process startup sequence
Degree of automation
Refrigeration loads vs. time
Time needed to bring process on-stream
Frequency of startup
Process pressure, temperature, and composition changes during startup
Special safety requirements
Minimum load
Need for standby capability
Peak-load pressures and temperatures
Composition extremes
Process shutdown sequence
Degree of automation
Refrigeration load vs. time
Shutdown time span
Process pressure, temperature, and composition changes
Special safety requirements

providing all of the information shown in Table 7, they give the engineer a feeling for how the chemical plant will operate as a system and how the refrigeration equipment fits into the process.

Basic Specifications. This portion of Table 7 fills in the detailed mechanical information that tells the refrigeration engineer how the equipment should be built, where it will be located, and specific safety requirements. This determines which standard equipment can be used and what special modifications need to be made.

Instrumentation and Control Requirements. These tell the refrigeration engineer how the system will be controlled by the plant operators. Particular controller types, as well as control sequencing and operation, must be spelled out to avoid misunderstandings and costly redesign. The refrigeration engineer needs to be aware of the degree of control required for the refrigeration system—for example, the process may require remote starting and stopping of the refrigeration system from the central control room. This could influence the way in which the refrigeration safeties and interlocks are designed.

Off-Design Operation. It is likely that the most severe operation of the refrigeration system will occur during startup and shutdown. The rapidly changing pressures, temperatures, and loads experienced by the refrigeration equipment can cause motor overloads, compressor surging, or loss of control if they are not anticipated during design.

REFERENCES

1. *ASHRAE Handbook of Refrigeration*, American Society of Heating, Refrigerating and Air-Conditioning Engineers, Atlanta, GA, 2002.
2. R. Thevenot, *A History of Refrigeration Throughout the World*, International Institute of Refrigeration, Paris, France, 1979, pp. 39–46.
3. K. W. Cooper and K. E. Hickman, “Refrigeration” in *Encyclopedia of Chemical Technology*, Vol. 20, 3rd ed., Wiley, New York, 1984, pp. 78–107.
4. C. E. Salas and M. Salas, *Guide to Refrigeration CFC’s*, Fairmont Press, Liburn, GA, 1992.
5. U.S. Environmental Protection Agency, “The Accelerated Phaseout of Ozone-Depleting Substances,” *Fed. Reg.*, **58**(236), 65018–65082, December 10, 1993.
6. U.S. Environmental Protection Agency, “Class I Nonessential Products Ban, Section 610 of the Clean Air Act Amendments of 1990,” *Fed. Reg.*, **58**(10), 4768–4799, January 15, 1993.
7. United Nations Environmental Program (UNEP), *Montreal Protocol on Substances That Deplete the Ozone Layer—Final Act*, UNEP, 1987.
8. G. King, *Basic Refrigeration*, Business News, Troy, MI, 1986.
9. *Number Designation and Safety Classification of Refrigerants*, ANSI/ASHRAE 34-2001, American Society of Heating, Refrigerating and Air-Conditioning Engineers, Atlanta, GA, 2001.
10. G. G. Haselden, *Mech. Eng.*, **44**, March 1981.
11. *Safety Code for Mechanical Refrigeration*, ANSI/ASHRAE 15-1994, American Society of Heating, Refrigerating and Air-Conditioning Engineers, Atlanta, GA, 1994.
12. *ASHRAE Handbook of Fundamentals*, American Society of Heating, Refrigerating and Air-Conditioning Engineers, Atlanta, GA, 2001, Chapter 19.
13. M. J. Molina and F. S. Rowland, “Stratospheric Sink for Chlorofluoromethanes: Chlorine Atoms Catalyzed Destruction of Ozone,” *Nature*, **249**, 810–812, 1974.
14. C. D. MacCracken, “The Greenhouse Effect on ASHRAE,” *ASHRAE J.*, **31**(6), 52–55, 1996.
15. U.S. Environmental Protection Agency (EPA), Ozone Depletion Website, <http://www.epa.gov/ozone/index.html>, 2004.
16. J. T. Houghton et al., *Climate Change 2001: The Scientific Basis*, Cambridge University Press, Cambridge, 2001.
17. W. F. Stoecker and J. W. Jones, *Refrigeration and Air Conditioning*, 2nd ed., McGraw-Hill, New York, 1982.

18. *ASHRAE Handbook of HVAC Systems and Equipment*, American Society of Heating, Refrigerating and Air-Conditioning Engineers, Atlanta, GA, 2000, Chapters 34 and 35.
19. K. Matsubara, K. Suefuji, and H. Kuno, "The Latest Compressor Technologies for Heat Pumps in Japan," in K. Zimmerman and R. H. Powell, Jr. (Eds.), *Heat Pumps*, Lewis, Chelsea, MI, 1987.
20. T. Senshu, A. Araik, K. Oguni, and F. Harada, "Annual Energy-Saving Effect of Capacity-Modulated Air Conditioner Equipped with Inverter-Driven Scroll Compressor," *ASHRAE Trans.*, **91**(2), 1985.
21. *ASME Boiler and Pressure Vessel Code*, Sect. VIII, Div. 1, American Society of Mechanical Engineers, New York, 1980.
22. Y. Kim and D. L. O'Neal, "A Comparison of Critical Flow Models for Estimating Two-Phase Flow of HCFC 22 and HFC 134a through Short Tube Orifices," *Int. J. Refrig.*, **18**(6), 1995.
23. Y. Kim and D. L. O'Neal, "Two-Phase Flow of Refrigerant-22 through Short-Tube Orifices," *ASHRAE Trans.*, **100**(1), 1994.

CHAPTER 14

CRYOGENIC ENGINEERING

J. G. Weisend II
European Spallation Source
Lund, Sweden

1 INTRODUCTION	543	6.1 Reducing Conduction Heat Transfer	555
2 PROPERTIES OF CRYOGENIC FLUIDS	544	6.2 Reducing Convection Heat Transfer	556
3 CRYOGENIC PROPERTIES OF MATERIALS	546	6.3 Reducing Radiation Heat Transfer	556
3.1 Suitable Materials for Cryogenic Applications	546	7 INSTRUMENTATION	561
3.2 Cryogenic Material Property Resources and Examples	548	7.1 Temperature Measurements	561
4 REFRIGERATION AND LIQUEFACTION	548	7.2 Pressure Measurements	562
4.1 Cascade Cooling System	548	7.3 Flow Measurements	562
4.2 Joule–Thomson Refrigeration	549	7.4 Level Measurements	564
4.3 Expansion Engine Cooling	551	7.5 Thermoacoustic Oscillations	564
5 CRYOCOOLERS	552	7.6 Summary	565
5.1 Regenerator Materials	553	8 AIR SEPARATION	565
6 CRYOSTAT DESIGN AND INSULATION	555	9 SAFETY	568
		10 HELIUM II	570
		11 SUB-KELVIN COOLING	574
		REFERENCES	575

1 INTRODUCTION

Cryogenics refers to the science and engineering associated with phenomena that occur below 120 K. A significant number of practical applications occur at these extremely low temperatures. These include the separation of air into its component gases, the liquefaction of natural gas, hydrogen and air components to allow efficient transport and storage, the cooling of superconducting magnets for use in magnetic resonance imaging (MRI) systems and fundamental research applications, and the use of liquid hydrogen and liquid oxygen for rocket propulsion. Annually, the worldwide cryogenic industry exceeds several billion dollars in revenues.

Cryogenic engineering involves the technology required to both produce and maintain these extremely low temperatures. It takes into account the unique properties of fluids and materials at cryogenic temperatures as well as the specific techniques required to operate safely and efficiently at these temperatures. Cryogenic engineering is broad based, using aspects of mechanical, electrical, chemical, and other engineering disciplines.

2 PROPERTIES OF CRYOGENIC FLUIDS

Cryogenic fluids, or cryogenes, may be defined as those whose boiling temperature at 1 bar (normal boiling point) is less than 120 K. Table 1 shows the normal boiling point, triple point, and critical point of typical cryogenic fluids. Notice in this table that of the two principal components of air oxygen has a higher boiling point than nitrogen. Thus, if a surface is cold enough to condense air, the liquid condensing on the surface will be oxygen rich. This effect can result in a significant fire hazard if the oxygen-rich fluid combines with a fuel and ignition source. Notice also that helium does not have a triple point. Due to the unique quantum properties of helium, there is no point where the liquid, gas, and solid phases coexist.

The properties of cryogenic fluids vary greatly as a function of temperature and pressure, and this variation of properties must be taken into account when designing and operating cryogenic systems. Properties of cryogenic fluids may be found in tabular form in reference books or reports¹⁻³ or, more commonly now, as the output of computer models. Sophisticated computer models exist based on semiempirical equations of state for a material that allow calculation of fluid properties over a wide range of temperatures and pressures. Examples of available programs include:

- NIST-12, from the National Institute for Standards and Technology (NIST), <http://www.nist.gov/srd/nist23.cfm>
- GASPAK and HEPAK, from CryoData, <http://www.htess.com/software.htm>

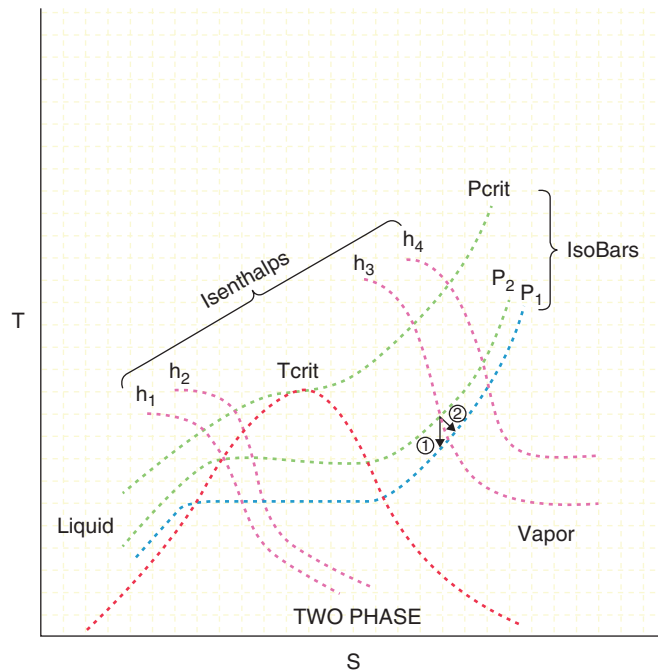
NIST also maintains an interactive website for the calculation of fluid properties (<http://webbook.nist.gov/chemistry/fluid/>). Fluid properties change rapidly near the critical point and care should be taken when using these programs in that region. In particular, extrapolating properties around the critical point can lead to significant errors.

Cryogenic fluid properties are frequently displayed on temperature–entropy (TS) or pressure–temperature (PT) diagrams. Such diagrams are also used to illustrate the processes in cryogenic refrigerators and cryocoolers (see Sections 4 and 5). Figure 1 is a schematic of a TS diagram showing lines of constant enthalpy (isenthalps) and pressure. Figure 1 also shows constant-enthalpy and constant-entropy expansions, processes that are critical for refrigeration cycles. Figure 2 is a TS diagram for pure nitrogen

Hydrogen and helium have unique fluid properties. In the case of molecular hydrogen, there are two forms of hydrogen due to differing nuclear spin states. In ortho hydrogen, the spins of the two atomic nuclei are parallel and in para hydrogen the spins of the two atomic nuclei are antiparallel. The practical result of this is that the fluid properties of these two forms of hydrogen can differ significantly and one must be aware of the form of the fluid with which

Table 1 Normal Boiling Point and Triple Point of Cryogenic Fluids

Fluid	Normal Boiling Point (K)	Triple-Point Temperature (K)	Critical Temperature (K)	Critical Pressure (kPa)
Krypton	119.8	115.8	209.4	5496
Methane	111.6	90.7	190.6	4599
Oxygen	90.2	54.4	154.6	5043
Argon	87.3	83.8	150.9	4906
Nitrogen	77.4	63.2	126.3	3399
Neon	27.1	24.6	44.4	2703
Hydrogen	20.3	13.8	32.9	1283.8
Helium	4.2	N/A	5.2	227.46



SCHEMATIC T-S DIAGRAM

- ① Isentropic Expansion
- ② Isenthalpic Expansion

Figure 1 Schematic temperature–entropy diagram for a pure fluid.

they are working. In addition, para hydrogen is the lower energy state and liquid hydrogen will naturally convert from a mixture of ortho and para hydrogen to 100% para hydrogen. This natural conversion process is very slow (on the order of hours to days) and releases heat, thus boiling off some of the liquid hydrogen. Modern hydrogen liquefiers solve this problem by using a chemical catalyst that speeds up the conversion from ortho to para hydrogen so that the resulting liquid hydrogen is 100% para hydrogen.

Liquid helium properties are strongly influenced by the effect of quantum mechanics. One example of this is the fact that helium remains a liquid all the way to 0 K.* In order to create solid helium, both low temperatures and pressures higher than 20 bars are required. This effect results from the zero point energy associated with the Heisenberg uncertainly principle in solid helium being greater than the energy required to melt the helium below 20 bars. This effect has a practical benefit in that helium can be used as a liquid coolant all the way down to the lowest temperatures achievable. Quantum mechanics has another important effect on helium. Below 2.2 K, helium has a second liquid phase known as He II (or somewhat imprecisely, superfluid helium). He II has unique heat transfer and fluid properties that make it an extremely valuable coolant for superconducting magnets and superconducting radio frequency (RF) cavities. Figure 3 is a pressure–temperature diagram of helium showing the vapor, solid, He I liquid,

* The third law of thermodynamics shows that it is impossible to reach 0 K (absolute zero) but we can get vanishingly close to it. The current record is approximately 100 pK (100×10^{-12} K).

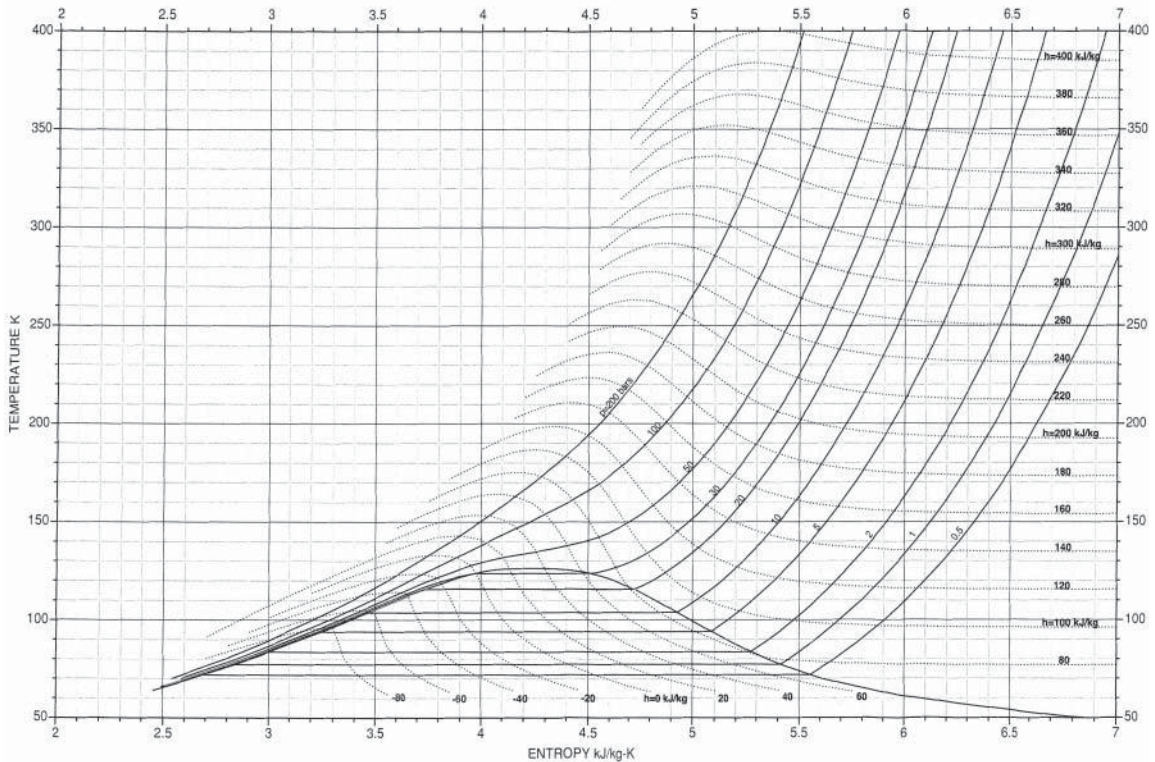


Figure 2 Temperature–entropy diagram for nitrogen.²

and He II liquid phases. He II is described in Section 10 and further details about the use of helium in cryogenics may be found in Ref. 4.

3 CRYOGENIC PROPERTIES OF MATERIALS

A key feature of cryogenic engineering is the successful use of appropriate materials. Many materials are not suitable for use at cryogenic temperatures and the properties of almost all materials change greatly between room temperature and cryogenic temperatures. It is fair to say that failures in cryogenic systems are frequently traced to the misuse of materials. Good cryogenic engineering practice includes never using materials at cryogenic temperatures unless their behavior at those temperatures is well understood and never extrapolating room temperature properties down to cryogenic temperatures.

3.1 Suitable Materials for Cryogenic Applications

Many materials cannot be used at cryogenic temperatures because the changes in their properties with temperature render them brittle or otherwise unsuitable. However, many workhorse engineering materials, such as austenitic stainless steels, do perform well at cryogenic temperatures. Table 2 gives a selection of suitable materials and Table 3 gives examples of unsuitable materials for use in cryogenics.

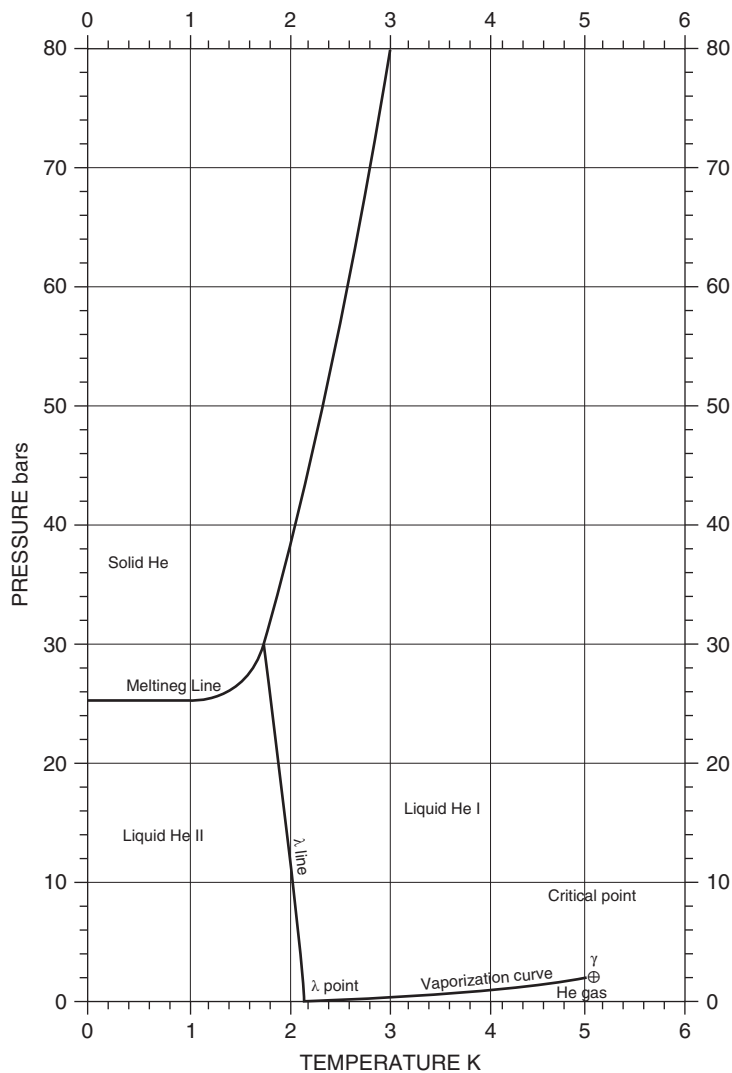


Figure 3 Phase diagram for helium.²

Table 2 Examples of Materials Suitable for Cryogenic Applications

Austenitic stainless steels (e.g., 304, 304L, 316, 321)
Aluminum alloys (e.g., 6061, 6063, 1100)
Copper
Brass
Some fiber-reinforced plastics such as G-10 and G-11
Niobium
Titanium
Indium (when used as an O-ring material)
Kapton and Mylar (used in multilayer insulation and as electrical insulation)
Quartz (frequently used in optical windows)

Table 3 Examples of Materials Unsuitable for Cryogenic Applications

Martensitic stainless steel—becomes brittle when cooled
Cast Iron—becomes brittle when cooled
Carbon steel ^a —becomes brittle when cooled
Rubber
Many polymers

^aCarbon steels are frequently used in the room temperature vacuum vessel surrounding a cryogenic device. This is alright as long as care is taken to ensure that the material is not cooled under various accident scenarios.

3.2 Cryogenic Material Property Resources and Examples

There are many resources available that provide properties of materials at cryogenic temperatures. Much of this work was done as part of the space program or in the development of superconductivity for scientific or industrial applications. Reference 5 is a good summary of available resources for cryogenic material properties. Other resources include the proceedings of the International Cryogenic Materials Conference and Refs. 6 and 7. There are also commercially available computer databases for cryogenic material properties. Two examples are:

- Cryocomp, from Eckels Engineering, <http://www.eckelsengineering.com/>
- METALPAK, CPPAK, and EXPAK, from CryoData, <http://www.htess.com/software.htm>

4 REFRIGERATION AND LIQUEFACTION

There are four principal ways to reduce the temperature of a pure fluid: (1) Transfer heat from the fluid to a colder surface. (2) Make the fluid perform work by expanding against an engine. This approximates isotropic expansion. (3) Make the fluid perform “internal work” by expanding through a valve or orifice. This is also known as Joule–Thomson expansion and approximates isenthalpic expansion. (4) Reduce the pressure of a boiling bath, thus reducing the saturated temperature of the bath. The refrigeration approaches described below use some or all of these techniques. There are some unique cooling techniques such as dilution refrigeration and adiabatic demagnetization refrigeration that are used to provide cooling below 1 K. More information about these techniques can be found in Section 11. Cryocoolers are small-scale refrigerators providing a few watts to a few hundred watts of cooling at cryogenic temperatures. They are described in Section 5. Reference 8 gives a very good overview of cryogenic refrigeration and liquefaction.

For large-scale cryogenic refrigeration, three common approaches are cascade cooling, Joule–Thomson cooling, and expansion engine cooling.

4.1 Cascade Cooling System

In this approach, a series of different refrigerants each with successively lower boiling temperatures are used. The first refrigerant is compressed so that its boiling point can be reached by air or chilled water cooling. The condensed liquid is then expanded in pressure, thus lowering its temperature, and this colder temperature fluid is then used to precool the next refrigerant in the cascade. In this way, lower and lower temperatures are achieved. Such an approach, shown in Fig. 4, is complicated, requiring many compressors, valves, and heat exchangers, and is limited in that there are regions in which overlapping refrigerants do not exist. This is particularly true below liquid nitrogen temperatures (77 K). Such an approach does not however require complicated cold turboexpanders. It can also be more efficient than other approaches.⁸

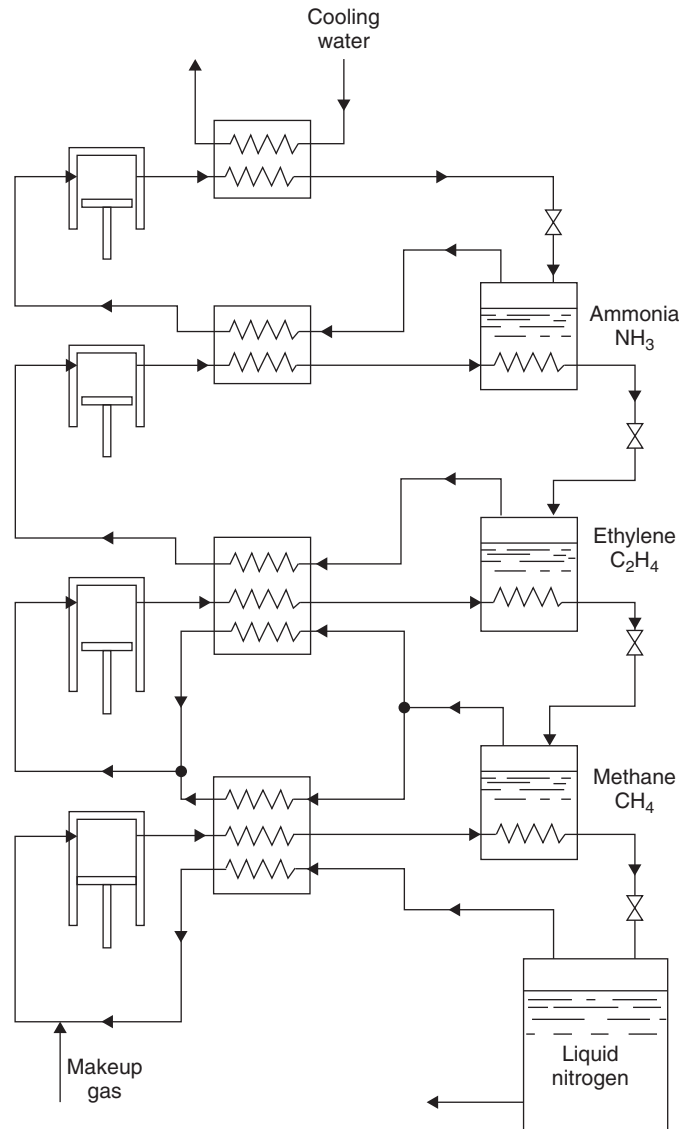


Figure 4 Schematic of a cascade cooling system. *Source:* Reprinted from Ref. 8 by permission of Oxford University Press.

4.2 Joule–Thomson Refrigeration

Joule–Thomson (JT) expansion occurs when a fluid expands along a line of constant enthalpy (see Fig. 1). When this happens, the fluid will either cool or warm depending on whether or not it is below its inversion temperature. If the fluid is below the inversion temperature, cooling will occur. Joule–Thomson expansion can be approximated by expanding the fluid through a valve or fixed orifice. A JT refrigerator uses this approach, combining a source of compressed gas (either a gas bottle or a mechanical compressor), a JT valve, and typically at least one heat

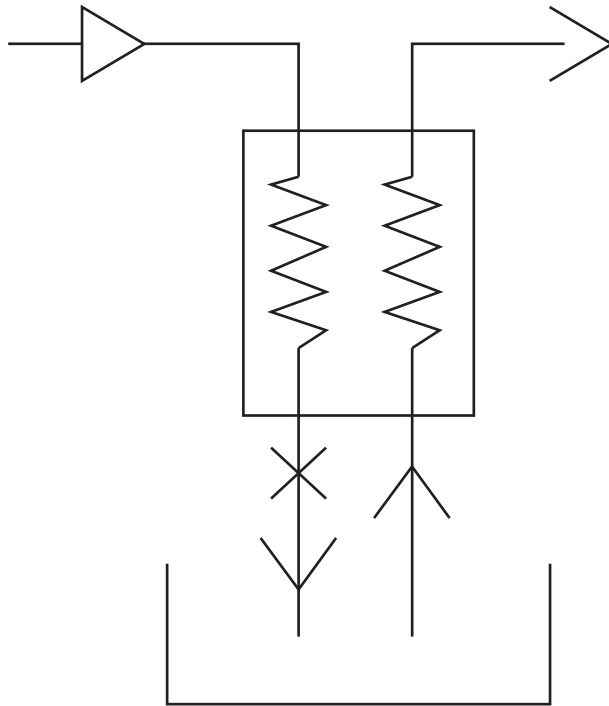


Figure 5 Schematic of a Joule–Thomson cooling system.

Table 4 Maximum Inversion Temperatures for Common Cryogenic Fluids

Fluid	Maximum Inversion Temperature (K)
Nitrogen	623
Argon	723
Hydrogen	202
He	43

exchanger. This is shown in Fig. 5. The compressed fluid expands through the JT valve and some of the colder fluid is routed via the heat exchanger where it pre-cools the incoming higher pressure fluid. In order for this to work, the fluid must be below the inversion temperature before it enters the JT valve. Table 4 lists the inversion temperatures of common cryogenic fluids. Note that nitrogen's inversion temperature is greater than room temperature. This means that nitrogen can be liquefied directly by a JT refrigerator. Helium, however, has an inversion temperature of 43 K so it will not cool when undergoing JT expansion, unless it has already been pre-cooled below 43 K. As will be seen, in modern helium refrigerators, the JT expansion valves are generally put at the lowest temperature portion of the refrigerator. Joule–Thomson refrigerators have a number of advantages: They are simple and do not require expensive cold turboexpanders, the JT valve handles two-phase flow without much trouble, and such systems

can be made in a wide range of capacities. Small cryocoolers (see Section 5) frequently use Joule–Thomson refrigeration. Microelectrochemical system (MEMS) techniques permit the miniaturization⁹ of JT refrigerators for aerospace and defense applications. Joule–Thomson refrigerators are also known as Linde–Hampson refrigerators.

4.3 Expansion Engine Cooling

Modern cryogenic refrigerators, particularly those operating below 77 K, use expansion engines as part of the cooling process. In this case, the working fluid is made to do work by pushing against an expansion engine. This is typically a turboexpander, though occasionally a piston expander is used. This technique approaches isentropic expansion. As seen in Fig. 1, for the same pressure difference, isentropic expansion provides a greater temperature drop than the isenthalpic expansion used in Joule–Thomson refrigeration. Expansion engine cooling also does not depend upon an inversion temperature and thus will provide cooling at any temperature. Turboexpanders generally do not work well with two-phase flows though some have been built that function in this regime.

Figure 6 is a schematic of one of the modern cryogenic refrigerators built for the CERN Large Hadron Collider Project.¹⁰ This plant provides the equivalent of up to 18 kW of cooling at 4.5 K. The working fluid is helium, which is compressed to high pressure (~ 20 bars) at room temperature and then expanded through a series of turboexpanders, providing cooling.

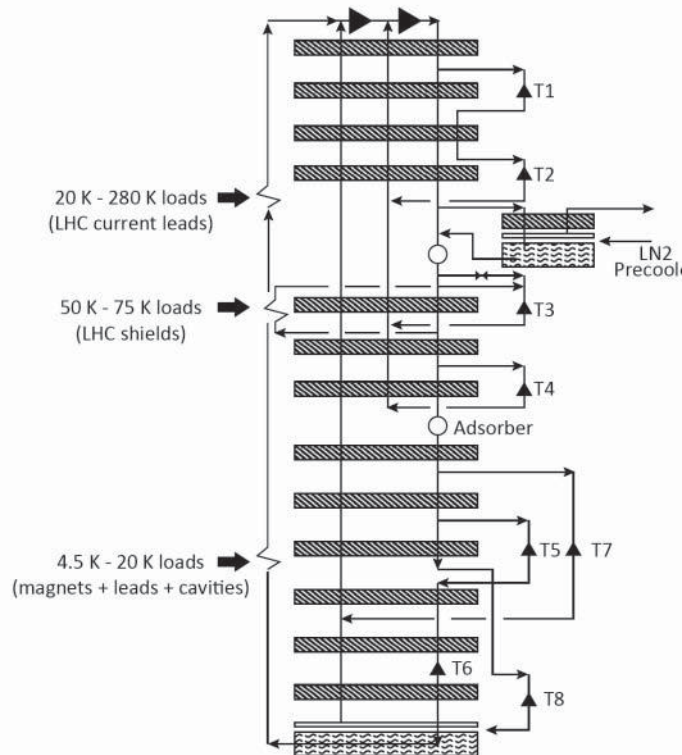


Figure 6 Large hadron collider cryogenic refrigerator.¹⁰

Note that at a number of locations, some of the colder, lower pressure helium is passed back through heat exchangers, precooling the incoming warmer gas. At the coldest part of this plant, the role of the JT valve is replaced with a dense fluid “wet” expander. Note in the schematic the large number of turboexpanders, the multiple pressure return paths, and the heat loads at different temperatures. All of these features are common in helium refrigerators of this size. The thermodynamic cycle for a plant of this type is known as the Collins cycle. Recently, a variant on the Collins cycle, the floating pressure process,¹¹ has been developed to increase the reliability and efficiency of helium refrigerators.

The performance of cryogenic refrigerators is described by the coefficient of performance (COP). The COP is defined as the heat removed from the cold sink divided by the net work required to remove that heat. For the ideal Carnot cycle, it can be shown that the COP can be determined from the high and low temperatures of the cycle:

$$\text{COP} = T_C / (T_H - T_C) \quad (1)$$

Keep in mind that the calculation of the COP for real cycles such as the Collins cycle or JT cycle is more complicated and depends upon the specific details of the plant design. Cryogenic engineers frequently talk in terms of the inverse of the COP, which gives the number of watts of work required to remove 1 W of heat at cryogenic temperature. For the ideal Carnot cycle operating between 300 and 4.2 K, this can be shown to be 70 W of work per watt of heat removed. Unfortunately, real world cycles come nowhere near this performance. The most modern helium refrigeration plants operate around 26–30% of Carnot or between 230 and 270 W of work per watt of heat removed at 4.2 K.

Whether a system is a refrigerator or a liquefier depends on how the cooling is used. In a refrigerator, the cooling is closed cycle, with the circulating helium absorbing heat at low temperature and returning back to the plant at a higher temperature. In a liquefier, the plant is used to make liquid helium, which is then transported elsewhere and used for cooling. In this case, additional gas must be added at room temperature to make up for the mass lost by the withdrawal of the liquid helium. In reality, most large helium plants can operate either as liquefiers or refrigerators or as a combination of both. As a rough estimate, a helium plant in liquefier mode can produce 1 g/s of liquid helium for every 100 W of cooling at 4.2 K while in the refrigerator mode.

5 CRYOCOOLERS

Cryocoolers are small (somewhat imprecisely defined as from less than 1 W to a few hundred watts of cooling power), stand-alone, closed-cycle, mechanical refrigeration systems. Cryocoolers can provide cooling from 4.2 K to up to 120 K. Advances in technology and materials have led to a greater interest in cryocoolers and to the development of a cryocooler industry. Cryocoolers are particularly useful in applications requiring portability or operation in remote sites (such as defense and aerospace applications), in applications where the cooling temperature is greater than 10 K, and in cases where there is a single cryogenic system within a larger noncryogenic system. Examples of cryocooler applications include cooling of night vision and infrared tracking systems, sample cooling in electron microscopes, reliquefaction of helium in MRI magnet systems, and cooling of high-temperature superconductor-based signal filters in cell phone towers. Disadvantages of cryocoolers include vibration near the object being cooled and low cooling capacity at liquid helium temperatures. References 12–14 are very good surveys of the theory and design of cryocoolers. A list of cryocooler vendors may be found in Ref. 15. Figure 7 displays both cryocooler applications and types as a function of their cooling capacity and temperature.

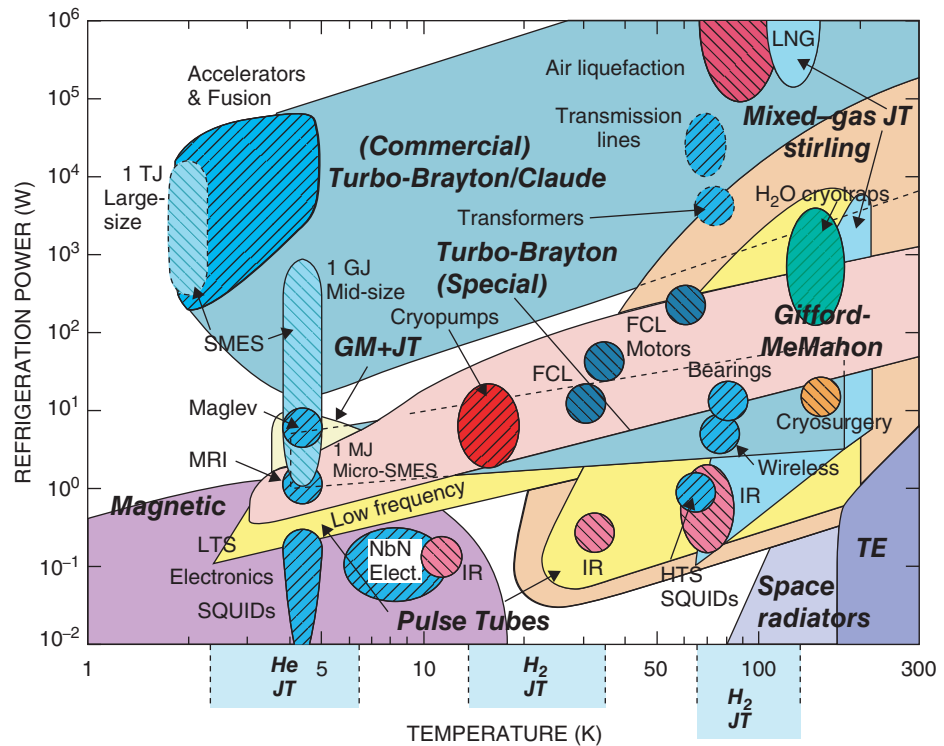


Figure 7 Cryocooler types and applications. Courtesy of R. Radebaugh (NIST).

5.1 Regenerator Materials

Cryocoolers typically use different thermodynamic cycles than those used by large cryogenic refrigerators/liquefiers. Two common features of cryocooler thermodynamic cycles are that they are oscillatory rather than continuous and they use regenerative heat exchangers. In regenerative heat exchangers both the warm and cold flow streams pass through the heat exchanger at different times, transferring heat to and from the regenerator material. Efficient regenerators must contain a large surface area for heat transfer while not producing high pressure drops in the working fluid. The regenerator material must have a large heat capacity over its operating range.

One of the advances that have enabled the growth of cryocoolers is the development of specialized erbium and gadolinium compounds that meet the requirements for regenerator materials. Figure 8 shows typical heat capacity–temperature curves for these materials.

Figure 7 shows that there are many different types of cryocoolers using different thermodynamic cycles. Two illustrative examples of cryocoolers are Stirling cycle and pulse tube cryocoolers. In a Stirling cycle cryocooler, there are four stages of the cycle (shown in Fig. 9):

1. Isothermal compression in which the working gas is compressed and heat is rejected to the outside environment ($a-b$)
2. Regenerative cooling in which heat is transferred from the fluid to the regenerator while pressure is decreased and the volume is kept constant ($b-c$)

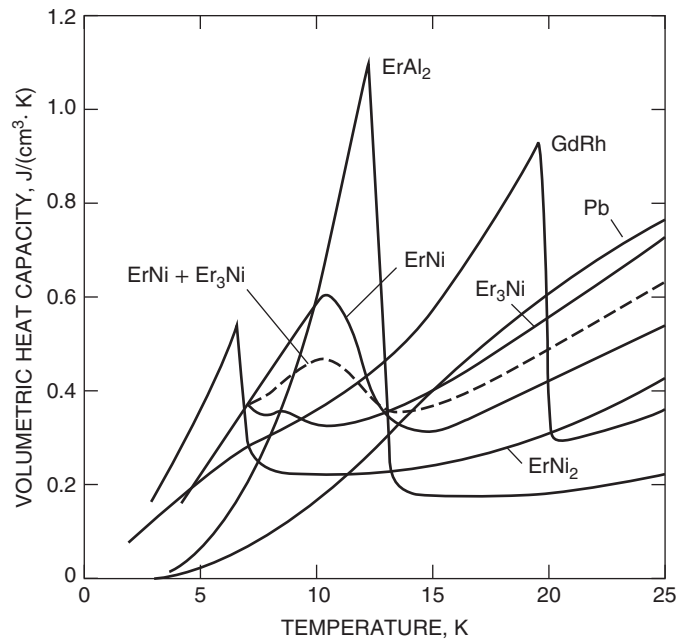


Figure 8 Heat capacity in regenerator materials. Courtesy of R. Radebaugh (NIST).

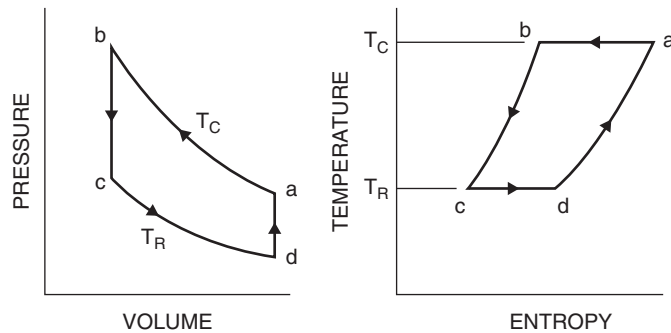


Figure 9 Stirling cycle. Courtesy of R. Radebaugh (NIST).

3. Isothermal expansion in which the gas is expanded and absorbs heat from the item being cooled ($c-d$)
4. Regenerative heating in which the fluid is compressed at a constant volume while absorbing heat from the regenerator ($d-a$)

In a Stirling cycle cryocooler, there is a warm compressor and a cold piston (typically called the displacer). The displacer adds complications to the mechanical design, adds inefficiencies to the cycle, and may impact reliability. In a pulse tube cryocooler, essentially the same cycle is used but the mechanical displacer is replaced with a column of the working gas inside the pulse tube. This can greatly simplify design and improve reliability. There have been significant developments in the theory and construction of pulse tube cryocoolers in the last decade.¹²⁻¹³ A schematic of a pulse tube cryocooler is shown in Fig. 10.

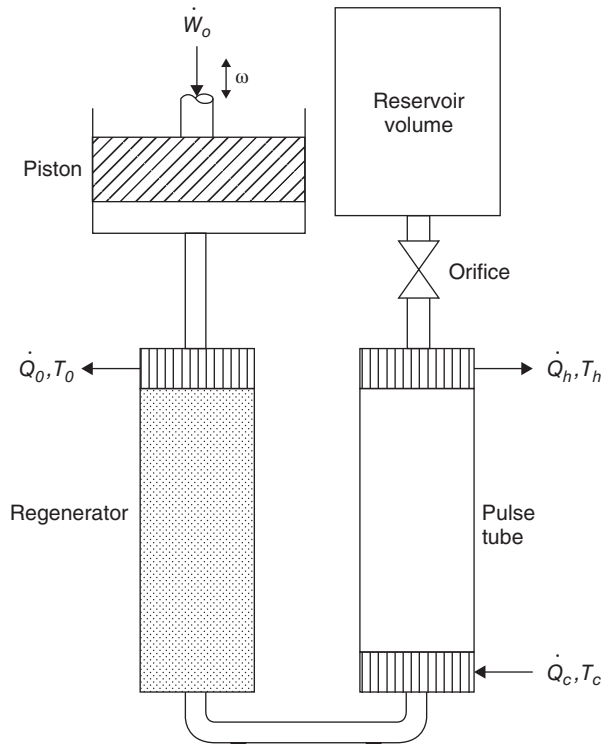


Figure 10 Pulse tube cryocooler. Courtesy of R. Radebaugh (NIST).

6 CRYOSTAT DESIGN AND INSULATION

Cryostats are devices or systems that maintain equipment or fluids at cryogenic temperatures. Cryostats that principally store cryogenic fluids are sometimes referred to as dewars, and the terms *dewar* and *cryostat* are frequently used interchangeably. Cryostats function by insulating the cryogenic equipment or fluid from heat leaking in from the outside environment. This is accomplished by reducing heat transfer via conduction, convection, and radiation. Techniques for this vary and the solutions chosen (and thus the design of the cryostat) depend upon the system requirements. Proper definition of the cryostat requirements is an essential first step for an optimum design. Cryostat requirements include operating temperatures, allowable heat leak, alignment and vibration limits, size and weight limits (particularly important for space systems), cost, ease of access to cryostat components, required instrumentation and feedthroughs, safety concerns, and expected life time. A significant design driver is whether the cryostat will be mass produced in large number or is a unique device. The varying importance of these requirements explains why the cryogenic insulation system for an LNG tanker is so different than that used in a satellite operating at 300 mK.

6.1 Reducing Conduction Heat Transfer

The general principle for reducing conduction heat leak into a cryostat is straightforward. Conduction heat leak is reduced by greatly increasing the resistance to thermal conduction between room temperatures and cryogenic temperatures. This is done by eliminating any unnecessary

connections between room and cryogenic temperatures and, for the remaining connections, using low-thermal-conductivity materials, increasing the length of the connection, and reducing the cross-sectional area of the connection.

The conduction heat leak to lower temperatures may also be greatly reduced by intercepting heat at intermediate temperatures. This not only reduces the heat leak to the lowest temperature but also is more thermodynamically efficient.

Complicating the calculation of conduction heat leak is the strong temperature dependence of thermal conductivity. Thus, the conduction heat leak for a connection of length L and constant cross-sectional area A is given by

$$Q = -A/L \int_{T_C}^{T_H} K(T) dT \quad (2)$$

This calculation may be simplified via the use of tabulated thermal conductivity integrals (θ_i) defined as

$$\theta_i = \int_0^{T_i} K(T) dT \quad (3)$$

Using these integrals, Eq. (2) becomes

$$Q = -A/L(\theta_{T_H} - \theta_{T_C}) \quad (4)$$

Table 5 shows typical values of thermal conductivity integrals for some common cryogenic engineering materials. The impact of low-conductivity materials on heat leak can be easily seen from this table.

6.2 Reducing Convection Heat Transfer

Cryostats, particularly those operating below 77 K, essentially eliminate convective heat transfer by separating the cold surface from the room temperature surface by a vacuum space. Pressures of 10^{-5} torr or less eliminate convective heat transfer. In a leak-tight vacuum space with a cold wall of 4 K these pressures can drop to 10^{-8} torr or less due to cryopumping of residual gases. Cryostat vacuum systems frequently employ getters of activated charcoal or other materials to remove residual gases and help reduce the impact of small leaks.

6.3 Reducing Radiation Heat Transfer

The governing equation for idealized (infinite parallel plates, surface emissivities equal to each other and $\ll 1$, N uncooled radiation shields between the cold and warm surfaces) thermal

Table 5 Thermal Conductivity Integrals for Typical Cryogenic Engineering Materials

Material	θ_{0-4} (W/m)	θ_{0-80} (W/m)	θ_{0-300} (W/m)
Stainless steel	0.4	300	3000
Cu (RRR ^a = 100)	1100	100,000	200,000
Cu (RRR ^a = 20)	225	50,000	150,000
Brass	6.5	3000	20,000
Al 6063	60	18,000	60,000
G-10	0.4	4	25
Phosphor-bronze	2.7	1100	9900
PTFE (Teflon)	0.06	3.5	60

^aResidual-resistivity ratio.

Source: Data from Ref. 16.

radiation heat transfer per unit area is given by

$$q = \frac{\epsilon}{(N + 1)2} \sigma (T_H^4 - T_L^4) \quad (5)$$

Thus, the heat leak may be reduced by decreasing the emissivity of the surfaces, increasing the number of uncooled thermal shields, or reducing the temperature of the warmer surface—typically done by installing an actively cooled thermal shield at an intermediate temperature.

Typical emissivities of materials are shown in Fig. 11. Note that the emissivities differ between 300 and 77 K and between 77 and 4.2 K. When using these data for actual systems, one should take care to allow for real surface finishes and tarnishing. Cryostat designs that have severe weight and space limits which do not permit the use of passive or actively cooled thermal radiation shields or those that have very strict heat leak requirements may minimize radiation heat leak by silver plating the warm and cold surfaces of the cryostat to reduce the emissivities.

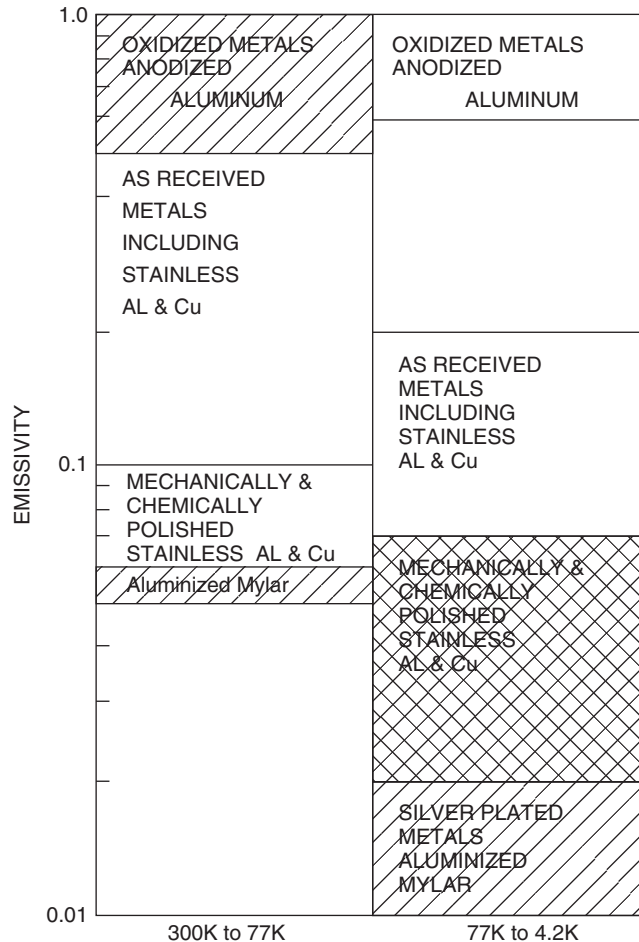


Figure 11 Emissivities of technical materials. *Source:* Reprinted from Ref. 4 with permission from Springer Science +Business Media B.V.

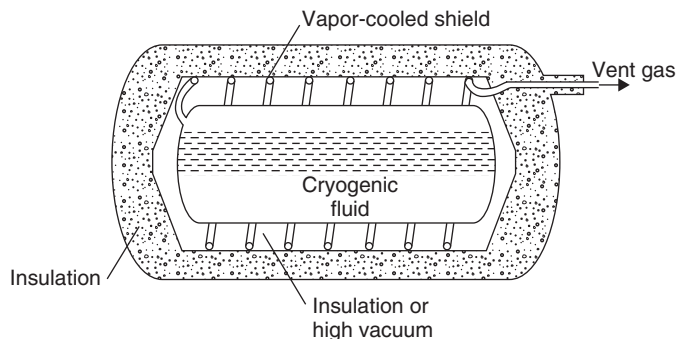


Figure 12 Cooling of intermediate shield via cold boil off gas.⁸

Actively cooled thermal shields at intermediate temperatures serve two main purposes: they reduce the thermal radiation heat leak to the lowest temperature equipment and they provide a convenient location to intercept conduction heat leaks, thus also reducing the conduction heat leak to the lowest temperature. These shields may be actively cooled by a separate cooling flow, by cold gas boiling off from the cryogenic liquid (see Fig. 12), or, increasingly today, by small stand-alone cryocoolers. The turn-to-turn spacing of a cooling tube on such a shield is given by¹⁷

$$\Delta T = \frac{qL^2}{2kt} \quad (6)$$

where ΔT is the maximum allowable between any point on the shield and the cooling tube, q is the expected heat flux on the shield, k is the thermal conductivity of the shield, t is the shield thickness, and L is $1/2$ the maximum tube spacing.

Multilayer insulation (MLI) consists of many thin layers of insulating material, typically Mylar or Kapton, that have been coated with a high-emissivity material, usually aluminum. MLI, also known as superinsulation, can be considered an extreme example of the use of uncooled thermal shields, which greatly increases the value of N in Eq (5), thus reducing the radiation heat leak. It is critical that the thermal conduction between the MLI layers is reduced and many MLI designs use an intermediate insulating spacer between layers. If MLI is packed too tightly within a vacuum space, its effectiveness may decrease due to increased conduction between the layers. Figure 13 shows the relationship of the total heat transfer (conduction and radiation) as a function of layer density for a typical MLI system operating between 77 and 4.2 K. Note that if the layer density increases much above 0.5 layers/mm the effectiveness of the MLI decreases due to the increasing importance of conduction heat transfer. In practical applications of MLI, the impact of seams, penetrations, and corners in the MLI can dominate the heat leak. Figure 14 shows the appropriate MLI installation in these cases. It is critical in these cases that sufficient overlap between layers exist so that gaps do not open up when the MLI shrinks during cooldown.

Not all cryostats use vacuum-insulated shells containing MLI and/or actively cooled shields. Systems, particularly those operating above 77 K, may use other solutions, including polystyrene foam, Perlite powder inside an inert gas space, and Perlite powder in a high-vacuum space. In recent years, Aerogel blankets^{19–20} have been used for cryogenic insulation. Table 6 shows typical values of the total heat flux transmitted through a variety of insulation schemes. Note that the cost and complexity of the insulation system increase as one moves from the top to the bottom of the table.

Figure 15 shows a cross section of the third-generation TESLA cryomodule developed at the DESY Laboratory in Hamburg, Germany.²¹ This figure illustrates a number of aspects of

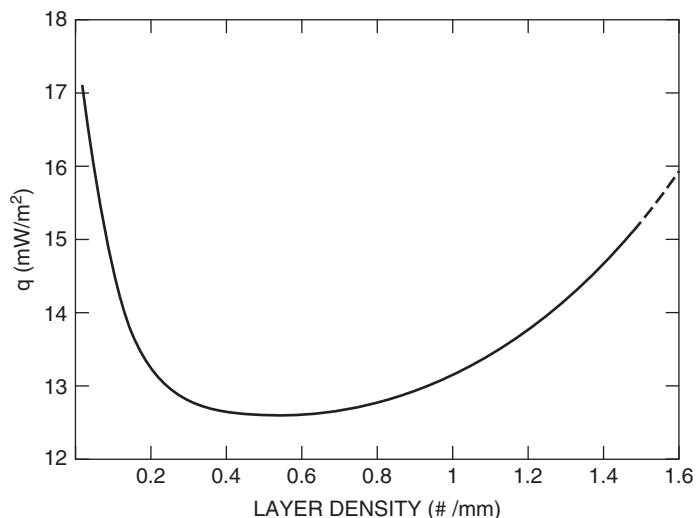


Figure 13 Total heat flux through MLI between 77 and 4.2 K as function of layer density. *Source:* Reprinted from Ref. 4 with permission from Springer Science +Business Media B.V.

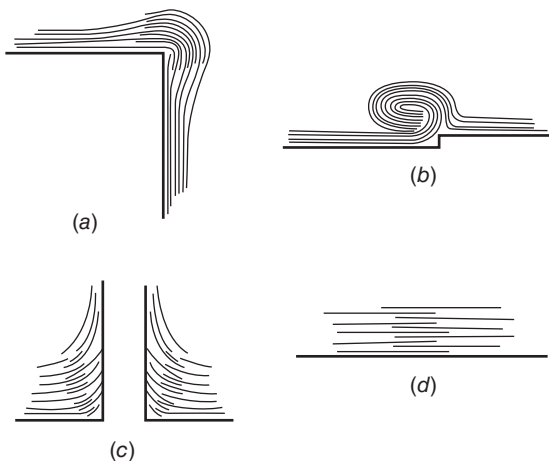


Figure 14 Examples of appropriate MLI installation.¹⁸

cryostat design. The TESLA cryomodule is designed to maintain a set of superconducting RF cavities at 1.8 K to provide acceleration of an electron beam for high-energy physics research. The cavities are surrounded by a bath of liquid helium at 1.8 K. These helium vessels are surrounded by thermal radiation shields actively cooled at 5 and 80 K. The helium vessels, thermal shields, and associated cryogenic piping are contained within a vacuum space that separates them from the 300 K vacuum vessel. MLI blankets within the vacuum space provide additional thermal insulation between the 300 K wall and the 80 K shield and between the 80 K shield and the 5 K shield. The cryogenic components are connected to the vacuum vessel via low-heat-leak supports constructed from thin-wall G-10 tubes. These supports and all other connections between 300 and 1.8 K are heat sunk to the 80 and 5 K temperature levels.

Table 6 Comparison of Thermal Insulation Approaches

Type of Insulation	Total Heat Flux (W/m ²)		
	300–77 K	77–20 K	
Polystyrene foam	48.3	5.6	
Gas-filled Perlite powder (5–6 lb/ft ³ filled with He)	184.3	21.8	
Perlite powder in vacuum (5–6 lb/ft ³)	1.6	0.07	↓ increasing Cost & Complexity
High vacuum (10 ⁻⁶ torr, $\epsilon=0.02$)	9	0.04	
Opaciated powder (Cu flakes in Santocel)	0.3	—	
MLI	0.03	0.007	

Note: Insulation 6 in. thick in all cases.

Source: From Ref. 8.

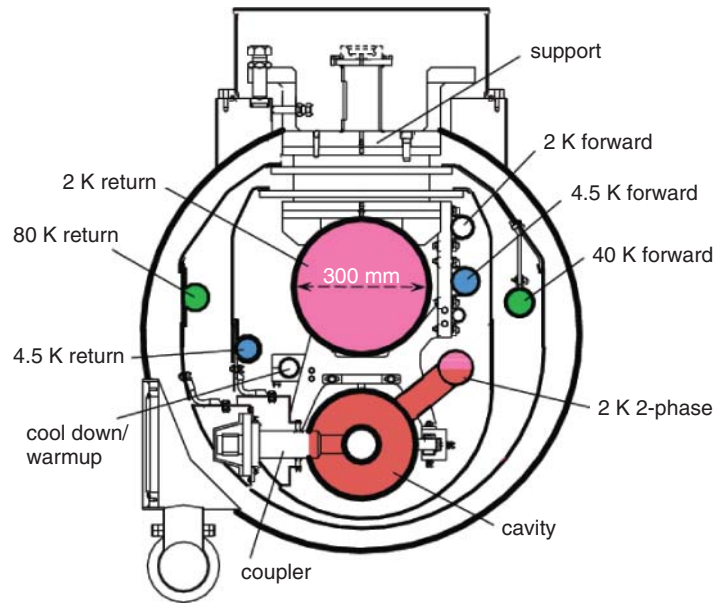


Figure 15 Cross section of third-generation TESLA cryomodule.²⁰

Together, techniques have resulted in a measured heat leak of 3–1.8 K for the entire 12-m-long cryomodule.

In summary, some general rules for successful cryostat design are:

- Define requirements first.
- Design in safety from the start.
- Use appropriate materials for cryogenic temperatures.
- Review the literature and learn from previous efforts.

- Use tested commercial solutions whenever possible.
- Avoid feedthroughs and demountable seals at cryogenic temperatures.
- Conduct prototype tests when required.

7 INSTRUMENTATION

Proper instrumentation is critical in cryogenic engineering. Measurements of properties such as temperature, pressure, flow, and level allow both verification of design and proper operation of cryogenic systems. It is important to design cryogenic instrumentation from the start as an integrated system consisting of sensor, wiring, data acquisition, and software. A good estimate is that a cryogenic measurement system will cost roughly \$1000 per measuring point when all costs are included. There is quite a lot of commercially available equipment for cryogenic measurements. There are also, however, many subtleties in the selection and installation of cryogenic sensors that must be observed to achieve a high-quality measurement.²²

7.1 Temperature Measurements

The most common measurement in cryogenics is temperature. Here there is a wide range of commercial devices available. Table 7 lists a number of sensor options along with their applicable temperature range and suitability for use in magnetic and ionizing radiation fields.

Figure 16 shows the dimensionless sensitivity [defined as $(T/V)(dV/dT)$ where T is the temperature and V is the output voltage] and Fig. 17 shows the relative temperature resolution of a variety of commercially available temperature sensors.

There are a number of errors that can lead to poor inaccurate temperature measurement in cryogenic systems. The small size and low heat capacity of sensors at cryogenic temperatures can lead to self-heating of the sensors by their excitation current. This can be avoided by always following the manufacturer's recommendations regarding sensor installation and excitation. Another significant problem, particularly for sensors mounted inside vacuum spaces and attached to cold surfaces, is the impact of heat leak down the sensor leads. Unless properly heat sunk, heat transmitted by the sensor leads can dominate the temperature of the sensor, leading to false readings. Figure 18 shows the minimum amount of length of heat sinking required for wires of various cross-sectional areas and materials to bring the sensor within 1 mK of the actual temperature. The value of using small-diameter and low-thermal-conductivity leads is clear.

Table 7 Cryogenic Temperature Sensor Options

Sensor Type	Applicable Temperature Range	Suitability for use in Magnetic Fields	Suitability for use in Ionizing radiation
Silicon diode	300 to ~1 K	Poor	Poor
Platinum resistor	300 to ~30 K	Poor	Good
Germanium resistor	100 to <1 K	Poor	Poor
Carbon glass Resistor	300 to ~1 K (best Below 100 K)	Fair	Good
Ruthenium oxide	40 to <1 K	Good	Good
Cernox	300 to <1 K	Good	Good
Thermocouple	300 to -2 K	Good	TBD
Cryogenic linear temperature sensors	300 to -4K	TBD	Good

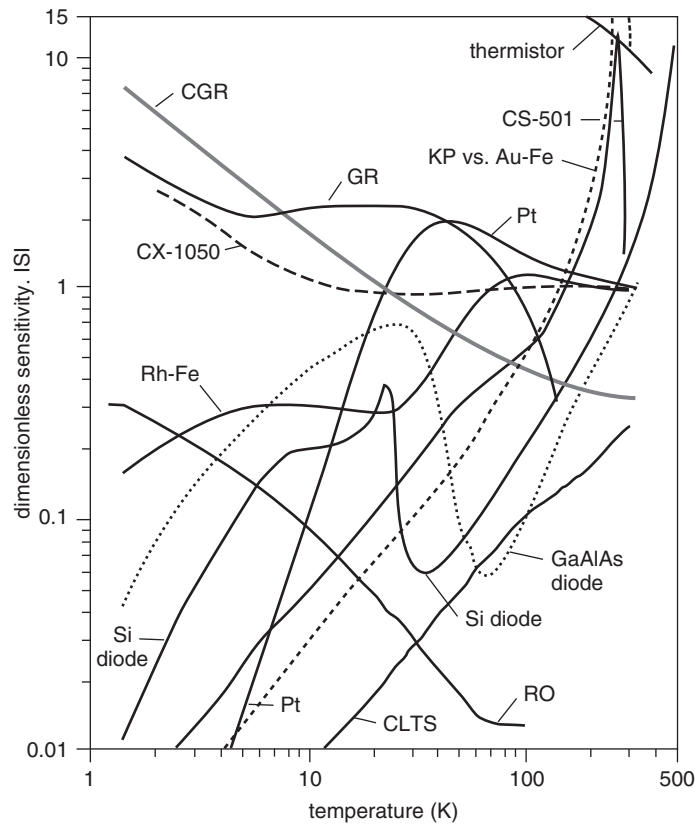


Figure 16 Dimensionless sensitivity of cryogenic temperature sensors.²¹

7.2 Pressure Measurements

Pressure measurements in cryogenic systems are typically carried out by room temperature pressure transducers connected to the cryogenic system by small capillary tubes. This approach permits the use of a wide range of pressure transducer types and allows for replacement of sensors without warming up the system. The disadvantage is that the time response of the pressure measurement is degraded by the presence of the capillary tubes. In the case of high-speed pressure measurements, such as those required in certain research applications, cryogenic pressure transducers will be required. There are a limited number of such devices commercially available.¹⁵

7.3 Flow Measurements

Flow measurements in cryogenic systems can be accomplished using typical techniques, including Venturi, orifice plate, turbine, fluidic, and Coriolis flowmeters. In all cases, the flowmeters must be calibrated to operate with the cryogenic fluids and must be constructed of materials suitable for use at cryogenic temperatures. Another concern in the measurement of flows at cryogenic temperatures is the creation of two-phase flow in reduced pressure locations, such as the throat of Venturi meters. Since many cryogenic systems operate near the saturation temperature, this is a possibility, and the resulting two-phase flow will affect the flow measurement. In many situations, such as refrigeration systems, it may be possible to measure the flows at room temperature, which simplifies the measurement.

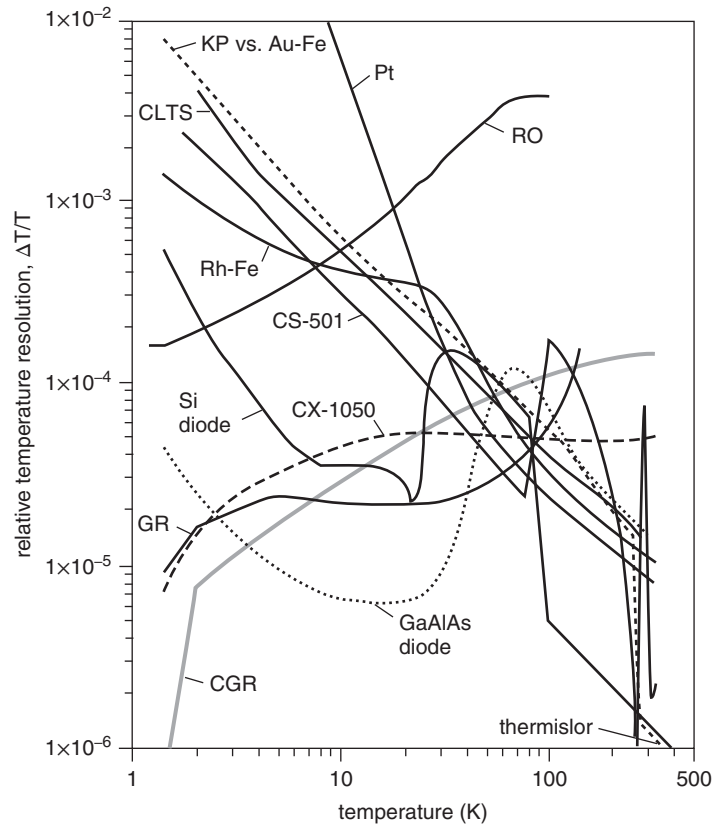


Figure 17 Temperature resolution of cryogenic temperature sensors.²¹

Material	T_1 [K]	T_s [K]	Heat-sinking length, L_2 (mm) for wire sizes			
			0.21 mm ² (24 AWG)	0.032 mm ² (32 AWG)	0.013 mm ² (36 AWG)	0.005 mm ² (40 AWG)
Copper	300	80	160	57	33	19
	300	4	688	233	138	80
Phosphor-Bronze	300	80	32	11	6	4
	300	4	38	13	7	4
Manganin	300	80	21	4	4	2
	300	4	20	7	4	2
304 ss	300	80	17	6	3	2
	300	4	14	5	3	2

Figure 18 Required heat sinking lengths for wire to achieve a measurement within 1 mK of the actual value.²¹ Note: Values are calculated assuming wires are in a vacuum environment, and the thermal conductivity of the adhesive is given by the fit to the thermal conductivity of GE 7031 varnish.

7.4 Level Measurements

The measurement of fluid level is frequently important in the control of cryogenic systems. Again, many standard techniques may apply, assuming proper calibration and materials. In helium systems, the use of superconducting level indicators is very common and commercial devices for this exist. Level indicators based on HTS superconductors have also been developed for liquid nitrogen systems. Superconducting level indicators, while accurate and simple to use, may fail and should be installed in such a way as to allow replacement without warming up the entire cryogenic systems. Where this is not possible, the installation of redundant sensors is recommended.

7.5 Thermoacoustic Oscillations

Cryogenic instrumentation systems frequently use tubes that are closed off at room temperature and extend to cryogenic temperatures containing a cryogenic fluid. Examples include pressure taps for room temperature pressure transducers or tubes containing wires and a cryogenic fluid extending up to a room temperature connector. Such scenarios also exist elsewhere in cryogenic systems, and this sort of installation can be susceptible to thermoacoustic oscillations (TAOs). These oscillations result from the temperature gradient in the tube setting up standing-pressure waves. These oscillations can cause very high pressure spikes as well as cause significant heating at the cryogenic end of the tube. TAOs should always be avoided. Design guidelines for avoiding these oscillations have been experimentally determined by Gu²³ for the case of a linear temperature gradient in the tube. Figure 19 shows the regions of stability determined. Here the parameters are

$$\alpha = T_H/T_C \quad (7)$$

$$\xi = L_H/L_C \quad (8)$$

where the division between length L_H and L_C is the point in the tube, $T = (T_H + T_C)/2$.

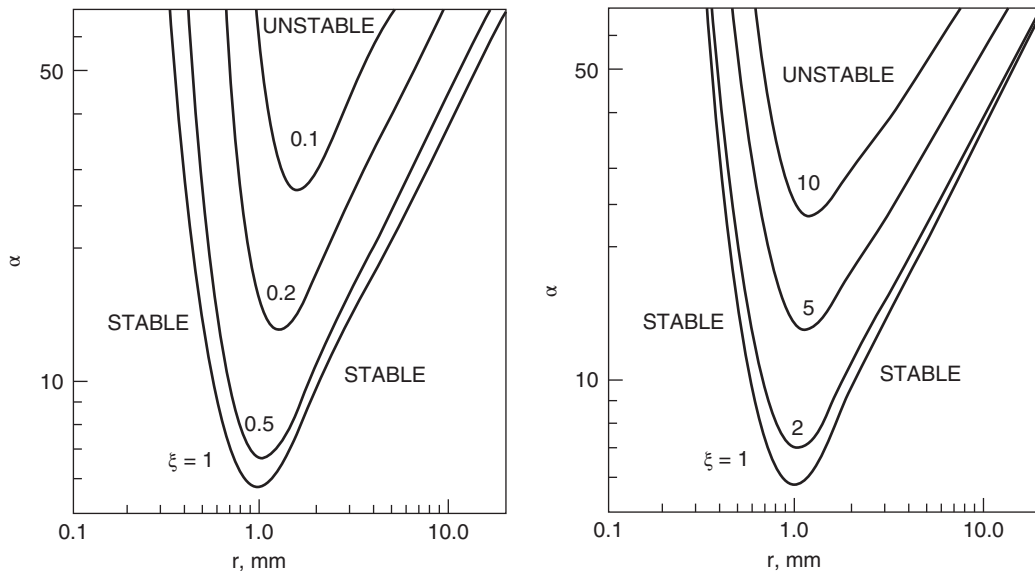


Figure 19 Stability maps for thermal acoustic oscillations in liquid helium systems.²²

These results are for a 1-m-long tube; to use them with other lengths, use the adjusted tube radius defined as the actual radius divided by the square root of the actual tube length.

Physically, the stability regions on the left-hand sides of the plots in Fig. 19 are caused by viscous damping while the stability regions on the right-hand side of the plots are caused by inertial damping.

7.6 Summary

A great deal of information on measurements in cryogenic systems has been developed. References 22 and 24 are detailed sources of information. Reference 15 is a good source for commercial suppliers of cryogenic instrumentation.

Some general guidelines for cryogenic instrumentation are:

- Do not use more accuracy and precision than required.
- Use commercially produced sensors whenever possible—there are a lot available.
- When possible, mount sensors outside cryostats at 300 K (e.g., pressure transducers, flowmeters).
- For critical devices inside of cryostats, install redundant sensors whenever feasible.
- Be sure to consider how to recalibrate sensors.
- If at all possible, avoid cold instrumentation feedthroughs. These are electrical connectors that have vacuum on one side and cryogenic fluids on the other.
- Once R&D is done, minimize the number of sensors in series production of cryostats.

8 AIR SEPARATION

*Courtesy Leonard A. Wenzel, Lehigh University.

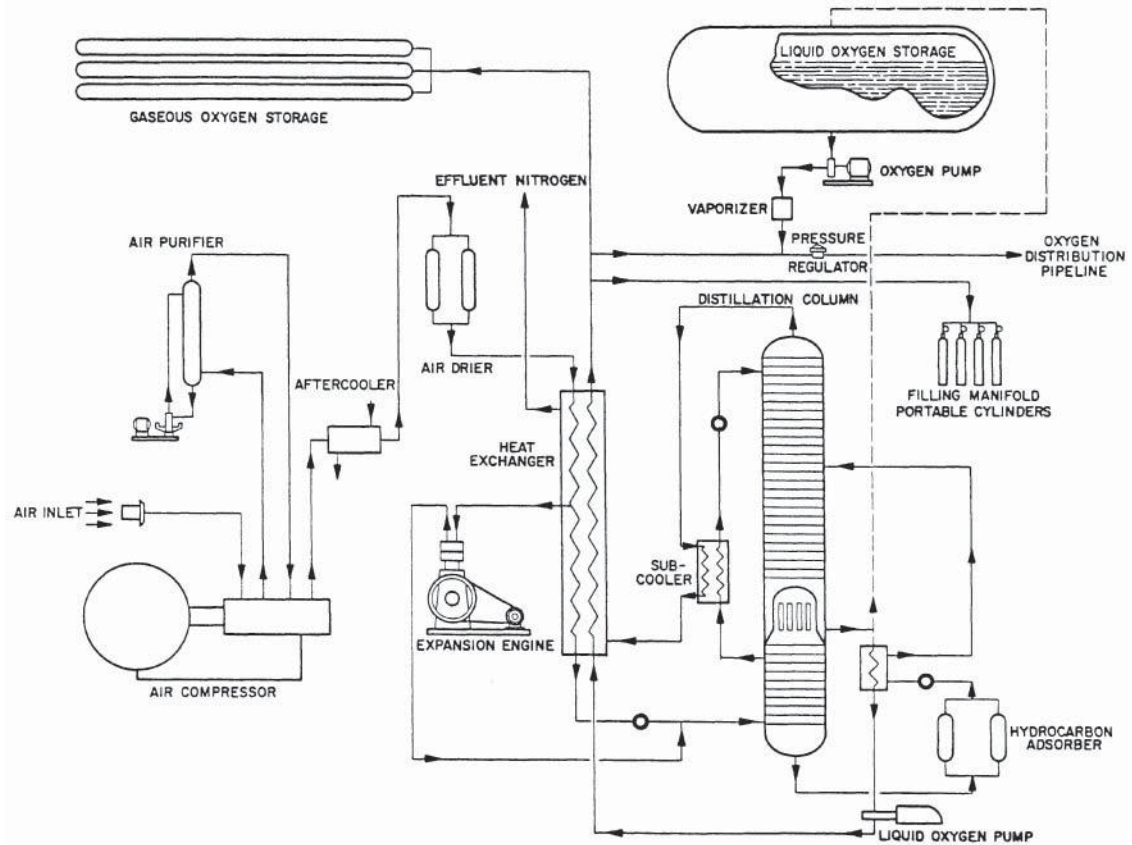
Among the products from air separation, nitrogen, oxygen, and argon are primary and are each major items of commerce. In 1994 nitrogen was second to sulfuric acid in production volume of industrial inorganic chemicals, with 932 billion standard cubic feet produced. Oxygen was third at 600 billion standard cubic feet produced. These materials are so widely used that their demand reflects the general trend in national industrial activity. Demand generally increases by 3–5% per year. Nitrogen is widely used for inert atmosphere generation in the metals, electronics and semiconductor, and chemical industries and as a source of deep refrigeration, especially for food freezing and transportation. Oxygen is used in the steel industry for blast furnace air enrichment, for welding and scarfing, and for alloying operation. It is also used in the chemical industry in oxidation steps, for wastewater treatment, for welding and cutting, and for breathing. Argon, mainly used in welding, in stainless steel making, and in the production of specialized inert atmospheres, has a demand of only about 2% of that of oxygen. However, this represents about 25% of the value of oxygen shipments, and the argon demand is growing faster than that of oxygen or nitrogen.

Since all of the industrial gases are expensive to ship long distances, the industry was developed by locating a large number of plants close to markets and sized to meet nearby market demand. Maximum oxygen plant size has now grown into the 3000-ton/day range, but these plants are also located close to the consumer with the product delivered by pipe line. Use contracts are often long-term take-or-pay rental arrangements.

Air is a mixture of about the composition shown in Table 8. In an air separation plant O_2 is typically removed and distilled from liquefied air. N_2 may also be recovered. In large plants argon may be recovered in a supplemental distillation operation. In such a plant the minor constituents (H_2 –Xe) would have to be removed in bleed streams, but they are rarely

Table 8 Approximate Composition of Dry-Air Component Composition (mol %)

Component	Composition (mol %)
N ₂	78.03
O ₂	20.99
Ar	0.93
CO ₂	0.03
H ₂	0.01
Ne	0.0015
He	0.0005
Kr	0.00011
Xe	0.000008

**Figure 20** Flow sheet of a merchant oxygen plant. Courtesy of Air Products & Chemicals.

collected. When this is done, the Ne, Kr, and Xe are usually adsorbed onto activated carbon at low temperature and separated by laboratory distillation.

Figure 20 is a simplified flow sheet of a typical small merchant oxygen plant meeting a variety of O₂ needs. Argon is not separated, and no use is made of the effluent N₂. Inlet air is filtered and compressed in the first of four compression stages. It is then sent to an air

purifier where the CO_2 is removed by reaction with a recycling NaOH solution in a counter-current packed tower. Usually the caustic solution inventory is changed daily. The CO_2 -free gas is returned to the compressor for the final three stages after each of which the gas is cooled and water is separated from it. The compressed gas then goes to an adsorbent drier where the remaining water is removed onto silica gel or alumina. Driers are usually switched each shift and regenerated by using a slip stream of dry, hot N_2 and cooled to operating temperature with unheated N_2 flow.

The compressed, purified air is then cooled in the main exchanger (here a coiled tube type, but more usually of the plate-fin type) by transferring heat to both the returning N_2 and O_2 . The process is basically a variation of that invented by Georges Claude where part of the high-pressure stream is withdrawn to the expansion engine (or turbine). The remainder of the air is further cooled in the main exchanger and expanded through a valve.

The combined air stream, nearly saturated or partly liquefied, enters the bottom of the high-pressure column. This distillation column condenses nearly pure N_2 at its top using boiling O_2 in the low-pressure column as the heat sink. If the low-pressure column operates at about 140 kN/m^2 (20 psia), the high-pressure column must operate at about 690 kN/m^2 (100 psia). The bottom product, called crude O_2 , is about 65 mol % N_2 . The top product from the high-pressure column, nearly pure N_2 , is used as N_2 reflux in the low-pressure column.

The crude O_2 is fed to an activated carbon bed where hydrocarbons are removed, is expanded to low-pressure column pressure, goes through a subcooler in which it supplies refrigeration to the liquid O_2 product, and is fed to the low-pressure column. The hydrocarbons removed in the adsorber may come in as impurities in the feed or may be generated by decomposition of the compressor oil. If they are not fully removed, they are likely to precipitate in the liquid O_2 at the bottom of the low-pressure column. They accumulate there and can form an explosive mixture with oxygen whenever the plant is warmed up. Acetylene is especially dangerous in this regard because it is so little soluble in liquid oxygen.

The separation of O_2 and N_2 is completed in the low-pressure column. In the column, argon accumulates below the crude O_2 feed and may be withdrawn at about 10 mol % for further distillation. If it is not so removed, it leaves as impurity in the N_2 product. Light contaminants (H_2 and He) must be removed periodically from the top of the condenser/reboiler. Heavy contaminants are likely to leave as part of the O_2 product.

This plant produces O_2 in three forms: liquid, high-pressure O_2 for cylinder filling, and lower pressure O_2 gas for pipe line distribution. The liquid O_2 goes directly from the low-pressure column to the storage tank. The rest of the liquid O_2 product is pumped to high pressure in a plunger pump after it is subcooled so as to avoid cavitation. This high-pressure liquid is vaporized and heated to ambient in the main heat exchanger. An alternate approach would be to warm the O_2 to ambient at high-pressure column pressure and then compress it as a gas. Cylinder pressure is usually too great for a plate-and-fin exchanger, so if the option shown in this flow sheet is used, the main exchanger must be of the coiled tube sort.

The nitrogen product, after supplying some refrigeration to the N_2 reflux, is warmed to ambient in the shell of the main exchanger. Here the N_2 product is shown as being vented to the atmosphere. However, some of it would be required to regenerate the adsorbents and to pressurize the cold box in which the distillation columns, condenser/reboiler, main exchanger, hydrocarbon adsorber, subcoolers, throttling valves, and liquid end of the liquid oxygen pump are probably contained.

This process is self-cooling. At startup refrigeration needed to cool the unit to operating temperatures is supplied by the expansion engine and the three throttling valves. During that time the unit is probably run at maximum pressure. During routine operation that pressure may be reduced. The lower the liquid O_2 demand, the less refrigeration is required and the lower the operating pressure may be.

9 SAFETY

Cryogenics presents some special safety issues. Most of these issues can be traced to either the unique properties of cryogenic fluids or to the behavior of materials at cryogenic temperatures. A frequent factor in accidents involving cryogenics is the use of inappropriate materials at these temperatures. References 25–27 are good general references on cryogenic safety. National laboratories in the United States have developed in-house policies on cryogenic safety. These are well thought out, vetted, and generally publically available. A good example of these is the chapter on cryogenic safety in the ES&H manual of the SLAC National Accelerator Laboratory.²⁸ Proper handling techniques for cryogenic fluids, including the use of appropriate personal protective equipment, are provided in the references above.

Overpressurization is a significant hazard in cryogenic systems. There is a very large volume ratio (typically 600–1300) between a cryogenic liquid at its normal boiling point and the resulting gas at standard temperature and pressure (STP). See Table 9. Thus, very large amounts of gas are evolved when cryogenic liquids warm up, which, unless properly released, will result in very high pressures and possible equipment failure, injury, and death. All cryogenic systems must have appropriately designed and reviewed pressure relief systems. Redundant systems are advisable and generally required, depending on local codes and policies. Under no circumstances should pressure reliefs be bypassed without proper review and approval. Cryogenic systems may leak and thus spaces such as insulation vacuum spaces that normally would not be expected to contain cryogenic liquids should also have appropriate pressure reliefs. Cryogenic fluids should only be transported or stored in containers specifically designed for that purpose.

Oxygen deficiency hazards (ODHs) stem from the inert nature of most cryogenic fluids and the large volume expansion between cryogenic liquids and their gases at STP. The ODH occurs when a gas such as nitrogen, helium, or argon displaces sufficient oxygen from an area to make it unable to support life. This is a very serious hazard and has resulted in fatalities over the years. Table 10 lists the symptoms of oxygen deficiency as a function of oxygen concentration. The Occupational Safety and Health Administration (OSHA) defines any oxygen concentration lower than 19.5% as oxygen deficient. A particularly dangerous aspect of ODH is that at sufficiently low oxygen concentrations the first symptom is unconsciousness, followed rapidly by coma and death; see Fig. 21. In small enough enclosures this can occur even with small amounts of cryogenic liquids. Owing to the severity of these hazards, any use of cryogenic fluid, no matter how small, must be analyzed for oxygen deficiency hazards. Some type of formal risk analysis must be carried out. Such an analysis generally looks at accident scenarios and then calculates the resulting oxygen concentration. An example of such a methodology is given in Ref. 28. Once the level of risk is understood, mitigations such as training, oxygen monitoring, alarms, and enhanced ventilation can be put into place.

Table 9 Volume Changes for Cryogenic Fluids from Normal Boiling Point to 300 K and 1 Bar

Substance	$V_{\text{gas}}/V_{\text{liquid}}$
Helium	701
Parahydrogen	788
Neon	1341
Nitrogen	646
Argon	779
CO ₂	762
Oxygen	797

Table 10 Effects of Oxygen Deficiency²⁸

Volume of Oxygen (at sea level)	Effect
17	Night vision reduced Increased breathing volume Accelerated heartbeat
16	Dizziness Reaction time for novel tasks doubled
15	Impaired attention Impaired judgment Impaired coordination Intermittent breathing Rapid fatigue
12	Loss of muscle control Very faulty judgment Very poor muscular coordination Loss of consciousness Permanent brain damage
10	Inability to move Nausea Vomiting
6	Spasmodic breathing Convulsive movements Death in 5–8 min

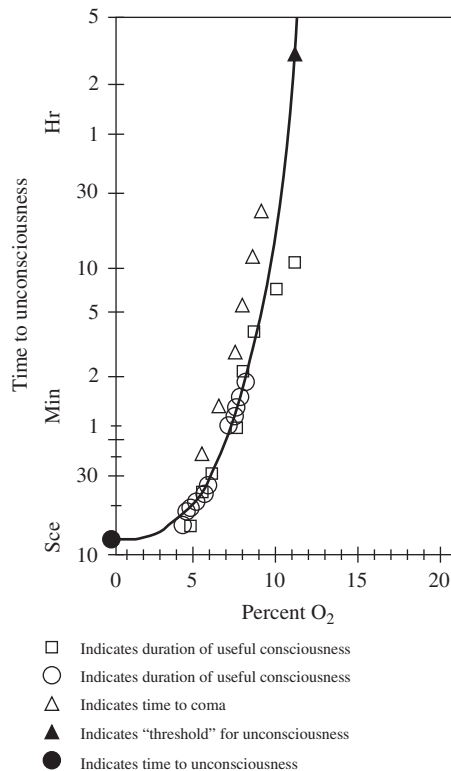


Figure 21 Approximate time of useful consciousness for a seated subject at sea level vs. % O₂.²⁸ Adapted from Compressed Gas Association, *Safe Handling of Cryogenic Liquids*, CGA P-12, 2009.

Systems using LNG and oxygen hydrogen have additional hazards associated with flammability. Care must be taken to avoid both the mixing of flammable cryogenics such as LNG or hydrogen with air or oxygen and the mixing of oxygen with other fuels. Many materials react with pure oxygen. Thus special attention must be paid in the selection of any materials that may be in contact with oxygen and in the cleaning of oxygen systems prior to use. The safe use and design of oxygen systems is a very detailed topic and Refs. 27, 29, and 30 should be consulted for further information. Additionally, if air condenses onto liquid nitrogen cooled surfaces, the resulting liquid will be oxygen rich (due to oxygen's higher boiling point). This condensate must be kept away from potential fuels and ignition sources. A better practice is to insulate cryogenic lines so that air will not condense on them.

10 HELIUM II

Sometimes known as superfluid helium, He II is the second liquid phase of the ^4He isotope. This second phase, hence the II, is formed when the temperature of the liquid helium is reduced below 2.17 K. The phase transition between He I and He II does not require latent heat and occurs instantaneously once the temperature of the liquid is reduced below 2.17 K. At the transition point, there is a sudden change in the specific heat whose plot versus temperature resembles the Greek letter λ . Thus, 2.17 K is known as the lambda point (T_λ) and the line separating the two liquid phases of helium is called the lambda line. Figure 3 is a phase diagram of helium showing the two liquid phases.

He II has significant technical applications due to both its lower temperature [which can result in higher performance superconducting magnets and lower wall losses in superconducting radio frequency (SRF) cavities] and its unique heat transfer and fluid properties. The lower temperature of He II is also valuable in infrared astronomy systems that study the 3 K background of the universe. He II cooling is a significant part of the Large Hadron Collider³¹ and of many SRF-based accelerators.³²⁻¹⁴

He II is formed due to the partial condensation of some of the atoms into the quantum ground state.⁴ The liquid is a macroscopic example of a quantum fluid and has been heavily studied by scientists interested in fundamental aspects of quantum mechanics, phase transitions, and turbulence. The properties of He II useful for engineering applications can be explained by the two-fluid model. The two-fluid model is divided into two interpenetrating fluids: the superfluid component representing the fraction of the fluid in the ground state and the normal fluid component representing the fraction of the fluid in the excited states. The superfluid component is taken to have zero viscosity and zero entropy while the normal fluid component has finite entropy and viscosity. The interplay between these components explains many of the properties of He II. Figure 22 shows the density fraction of the superfluid and normal fluid components as a function of temperature. Note that the fluid approaches 100% normal fluid component at T_λ and 100% superfluid component at 0 K.

Heat transfer within He II is driven by a unique mechanism known as internal convection, which can be described by the two-fluid model. In internal convection, the normal fluid component carries heat away from the heated surface to the cold sink. Simultaneously, the superfluid component flows from the cold sink to the heated surface, where it absorbs heat, is converted back to the normal fluid component, and flows back to the cold sink. This mechanism, illustrated in Fig. 23, can be extremely efficient, in some cases more than 1000 times more efficient than conduction through copper. Two things should be noted about internal convection. First, it is not conduction or convection; it is a mechanism unique to He II. Second, there is no net mass transfer occurring in this mechanism. A flowmeter put into the fluid in Fig. 23 would show zero flow.

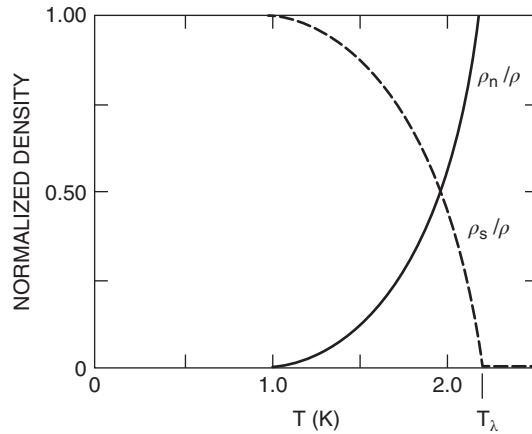


Figure 22 Density fractions of superfluid and normal fluid components in He II. *Source:* Reprinted from Ref. 4 with permission from Springer Science +Business Media B.V.

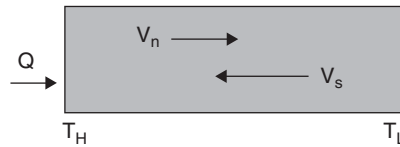


Figure 23 Schematic of internal convection flow in He II.

Heat transfer via internal convection occurs in two regimes. In the laminar regime, the heat transferred is given by

$$q = \frac{(psd^2)}{\beta\eta_n} \frac{dT}{dx}$$

where ρ is the density of the helium, s is the entropy, $\beta\eta_n$ is the viscosity, d is the diameter of the cooling channel, and β is a geometric factor

In the mutual friction regime, the superfluid component and normal fluid component interact with each other and the heat transferred is given by

$$q = \left[f^{-1}(P, T) \frac{dT}{dx} \right]^{1/3}$$

where $f^{-1}(P, T)$ is the heat conductivity function shown in Fig. 24.

The dividing line between these regimes is the velocity of the superfluid component, v_s ; if it is above a critical value, then the heat transfer is in the mutual friction regime. This critical value is approximately $d^{1/4}$ in cgs units, where d is the size of the cooling channel. This means that for most large-scale systems the heat transfer is usually in the mutual friction regime. These heat transfer rates, while high, do have limits. The physical limit is that the temperature at the heated surface cannot exceed T_λ . In the case of subcooled He II this limit, known as the peak heat flux (q^*), can easily be calculated by

$$q^* L^{1/3} = \left(\int_{T_b}^{T_\lambda} f^{-1}(T) dt \right)^{1/3} \quad (11)$$

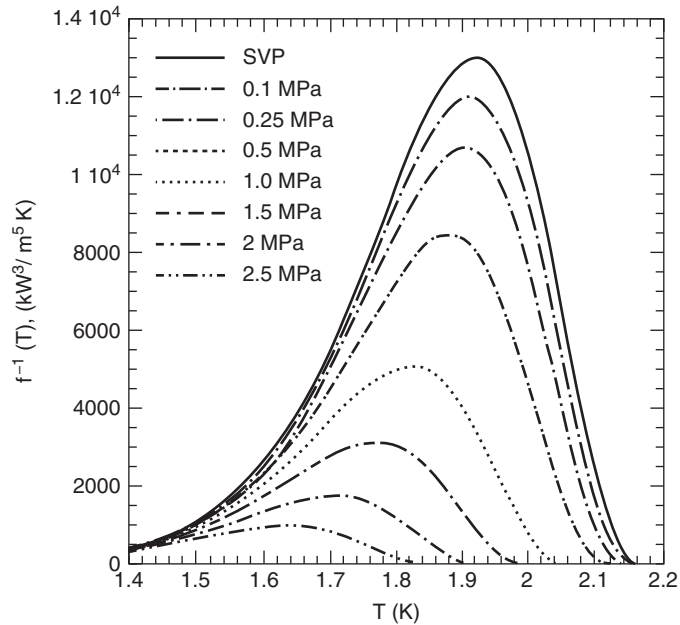


Figure 24 Heat conductivity function of He II. *Source:* Reprinted from Ref. 4 with permission from Springer Science +Business Media B.V.

At 1.9 K and 1 bar, $q^*L^{1/3} \sim 15 \text{ kW/m}^{5/3}$. In the case of saturated He II, the limit depends upon the height of the helium above the heated surface. This effect is described in Ref. 4.

Heat transfer from a heated surface into He II is also different than that typically seen in cryogenic systems. The surface heat transfer into He II is dominated by Kapitza conductance, which describes the problem of moving heat from a solid into a fluid at a fundamental level. This effect is dependent on the surface material, the surface finish, and the temperature, among other parameters. Interestingly, it is not dependent on the flow of the He II. There are no good fundamental predictive theories for Kapitza conductance so an empirical approach is taken. For a surface heat flux (q) of less than 1 kW/m^2 the heat transfer as a function of the surface temperature difference (ΔT_s) is given by

$$q = h_k \Delta T_s \quad (12)$$

Above roughly 1 kW/m^2 the surface heat transfer is given by

$$q = a(T_s^m - T_b^m) \quad (13)$$

where h_k , a , and m are all empirical parameters (typically $m \sim 3$) depending on material, surface finish, and temperature. Figure 25 shows some data for h_k .³⁵ Other data are available in the literature.

The nature of He II leads to unique fluid mechanics in certain specific conditions such as film flow and flow through porous media. However, in most engineering applications such

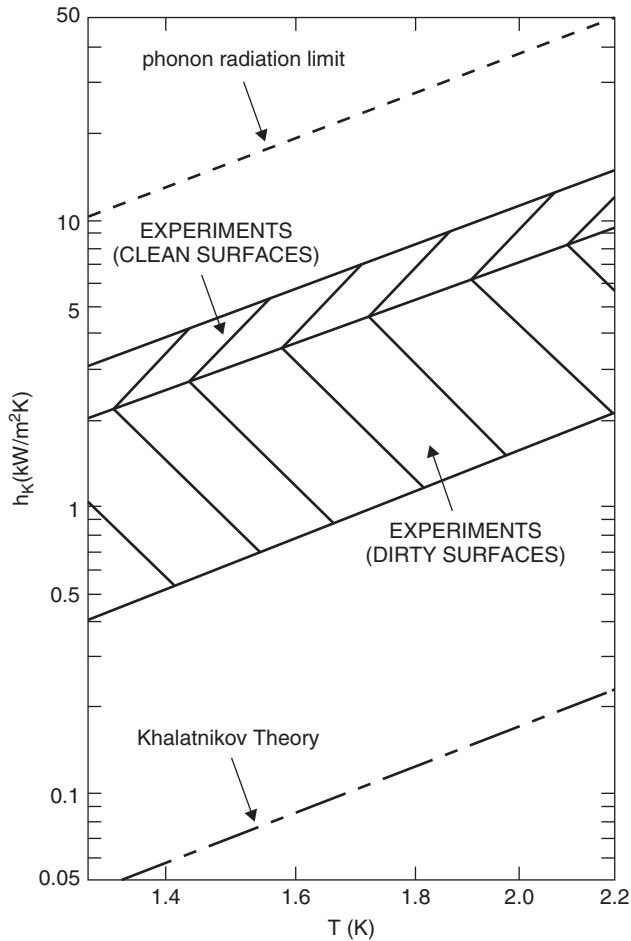


Figure 25 Values of h_k for Kapitza conductance.³⁴

as determining pressure drops, sizing of valves and pumps, and flow metering techniques, He II obeys the same rules as classical fluids^{4, 36} as long as the appropriate physical properties (density, viscosity, etc.) of the He II are used. Pumps in He II do tend to cavitate more readily than in He I and hot-wire anemometry will not work as a flow metering technique due to the lack of dependence of the Kapitza conductance on the He II flow.

The He II refrigeration systems produce He II by precooling a supercritical ~ 4.5 K helium flow to near the lambda point and then expanding it down to the He II subatmospheric pressure via a JT valve. Vapor is pumped off the saturated He II bath to maintain its operating temperature. This vapor provides the precooling of the incoming 4.5 K flow. In large systems, this pumping is carried out via cold compressors³⁴ or by a combination of cold and warm compressors.³¹ Figure 26 shows this process.

Much more information exists on He II and its applications. Reference 4 is an excellent survey of this topic.

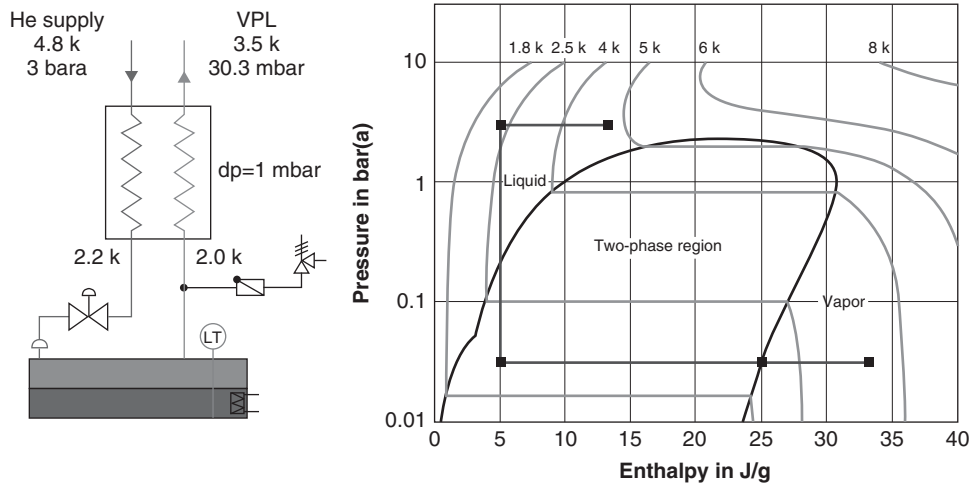


Figure 26 He II refrigeration process. Courtesy of T. Köttig, CERN.

11 SUB-KELVIN COOLING

Specialized cooling techniques are required for cooling systems below 1 K. Above ~ 1.2 K, temperatures can be reached by reducing the saturation pressure (and thus temperature) of a boiling bath of liquid helium. This is the technique used in most He II systems. Below 1.2 K, the vapor pressure of helium is so small that providing cooling in this manner is no longer effective. A number of more sophisticated techniques exist to reach temperatures well into the micro-Kelvin range.

The first of these techniques is pumping on the liquid phase of the isotope ^3He . This isotope has a higher vapor pressure at low temperatures than the standard ^4He and can be pumped down to between 200 and 300 mK. The ^3He isotope is quite rare and expensive and is always recycled. Pumping in these systems is frequently accomplished by sorption pumping using activated charcoal. Typical values for such systems are $400\ \mu\text{W}$ of cooling at 300 mK for a duration of 6 h.

Another technique, also using ^3He , is dilution refrigeration. These systems make use of a mixture of ^3He and ^4He and take advantage of three physical effects:

1. Below 0.8 K a ^3He - ^4He mixture will spontaneously separate into a ^3He -rich zone on top of a heavier ^4He -rich zone
2. It requires energy to move a ^3He atom from the ^3He -rich zone to the ^4He -rich zone. This energy reduces the temperature of the ^3He - ^4He mixture and whatever is attached to it.
3. Below 1 K the vapor pressure of ^3He is much higher than that of ^4He . Thus, pumping on the ^4He -rich zone will preferentially remove ^3He atoms.

These effects allow the construction of a closed-cycle refrigerator that, while complicated and expensive, can provide continuous cooling down to the tens of milli-Kelvin range. Dilution refrigerators are produced commercially,¹⁵ and typical capacities of them are 200 – $400\ \mu\text{W}$ at 100 mK. A very good explanation of the dilution refrigeration process, including animation, is given in Ref. 37.

A third approach is adiabatic demagnetization refrigeration (ADR). This technique takes advantage of the fact that the entropy of paramagnetic materials in a magnetic field is lower than when no field is present. The lower entropy comes from the magnetic regions in the paramagnetic material being aligned and thus more ordered in the presence of a magnetic field. A more ordered solid has lower entropy. In effect, the ADR transfers entropy between the random thermal vibrations of the paramagnetic material and the alignment of the magnetic regions. Consider an adiabatic (thermally isolated) sample. When the magnetic field is raised, the magnetic regions align and release entropy into the thermal vibrations heating the material. When the magnetic field is reduced, the regions drop out of alignment and absorb entropy from the thermal vibrations, cooling the material.

By combining this approach with heat switches that can thermally connect or disconnect an item to be cooled from the paramagnetic material, a cooling system can be created. ADRs are, by their nature, cyclic devices. Continuous cooling can be created by using multiple ADRs in parallel. ADRs can provide microwatt cooling capacity down to milli-Kelvin temperature levels. ADRs require both the presence of superconducting magnets and only work below about 2 K as higher temperatures result in too much thermal motion in the paramagnetic solid. In space applications,³⁸ where gravity is absent, ADRs have an advantage over dilution refrigerators that generally require gravity to establish the stratified ^3He - ^4He mixture.

Cryogenic engineering at sub-Kelvin temperatures poses a number of challenges. In particular, the heat capacities and available cooling at these temperatures is so small that even microwatt-scale heat leaks can result in unacceptable temperature rises. Great care must be taken in the design of thermal insulation and cryostats in this application. Reference 39 is a good source of information for cryogenics at these temperatures.

REFERENCES

1. V. Arp and J. G. Weisend II, "Properties of Cryogenic Fluids", in J. G. Weisand, Ed., *Handbook of Cryogenic Engineering*, Taylor & Francis, 1998, Chapter 1.
2. P. Cook, and B. A. Hands, *Cryogenic Fluids Databook*, British Cryoengineering Society, 2002.
3. R. T. Jacobsoen, S. G. Penoncello, and E. W. Lehmon, *Thermodynamic Properties of Cryogenic Fluids*, Springer, 1997.
4. S. W. Van Sciver, *Helium Cryogenics*, 2nd ed., Springer, 2012.
5. J. G. Weisend II, V. Flynn, E. Thompson, and R. P. Reed, "A Reference Guide for Cryogenic Properties of Materials," SLAC-TN-03-023, available: <http://www.slac.stanford.edu/cgi-wrap/getdoc/slac-tn-03-023.pdf>, accessed March 20, 2012.
6. T. F. Durham, R. M. McClintock, and R. P. Reed, *Cryogenic Materials Data Handbook*, U.S. Department of Commerce, National Bureau of Standards, Washington, DC, 1961.
7. R. P. Reed and A. F. Clark (Eds.), *Materials at Low Temperatures*, American Society of Metals, 1983.
8. R. Barron, *Cryogenic Systems*, Oxford University Press, 1985.
9. P. E. Bradley, R. Radebaugh, M. Huber, M. H. Lin, and Y. C. Lee, "Development of a Mixed- Refrigerant Joule-Thomson Microcooler," in S. D. Miller and R. G. Ross, Jr., Eds., *Cryocoolers 15*, ICC Press, 2009.
10. P. Dauguet, P. Briend, F. Delcayre, A. Ghisolfi, G. M. Gistau-Baguer, C. Guerin, B. Hilbert, G. Marot, and E. Monneret, "Design, Construction & Start Up of by Air Liquid of Two 18 kW at 4.5 K Helium Refrigerators for the New CERN Accelerator: LHC," *Adv. Cryo. Eng.*, **49A**, 2004.
11. V. Ganni and P. Knudsen, "Optimal Design & Operation of Helium Refrigeration Systems using the Ganni Cycle," *Adv. Cryo. Eng.*, **55B**, 2010.
12. R. Radebaugh, "Cryocoolers: The State of the Art and Recent developments," *J. Phys. Condens. Matter*, **21**, 2009.
13. A. T. A. M. de Wael, "Basic Operation of Cryocoolers and Related Thermal Machines," *J. Low Temp. Phys.*, **164**, 179–236, 2011.

14. L. Duband and A. Ravex "Small Cryocoolers," in J. G. Weisend II (Ed.), *Handbook of Cryogenic Engineering*, Taylor & Francis, 1998, Chapter 7.
15. *Cold Facts 2012 Buyer's Guide*, Cryogenic Society of America, available: http://www.cryogenic-society.org/buyers_guide/, accessed November 20, 2012.
16. P. Kittel, T. Nast, L. J. Salerno, M. Shiotsu, and J. G. Weisend II "Cryogenic Heat Transfer," in J. G. Weisend II (Ed.), *Handbook of Cryogenic Engineering*, Taylor & Francis, 1998, Chapter 3.
17. G. McIntosh, "Cryostat Design," in J. G. Weisend II (Ed.), *Handbook of Cryogenic Engineering*, Taylor & Francis, 1998, Chapter 5.
18. L. A. Wenzel, "Cryogenic Systems," in M. Kutz (Ed.), *Mechanical Engineer's Handbook*, Wiley, 2005, Chapter 13.
19. S. White, J. Demko, and A. Tomich, "Flexible Aerogel as a Superior Thermal Insulation for High Temperature Superconductors," *Adv. Cryo. Eng.*, **55A**, 2010.
20. B. E. Coffman, J. E. Fesmire, S. White, G. Gould, and S. Augustynowicz, "Aerogel Blanket Insulation Materials for Cryogenic Applications," *Adv. Cryo. Eng.*, **55B**, 2010.
21. J. G. Weisend II, C. Pagani, R. Bandelmann, D. Barni, A. Bosotti, G. Gygiel, R. Lange, P. Pierini, D. Sellmann, and S. Wolff, "The Tesla Test Facility (TTF) Cryomodule: A Summary of Work to Date," *Adv. Cryo. Eng.*, **45A**, 2000.
22. D. S. Holmes and S. S. Courts, "Cryogenic Instrumentation," in J. G. Weisend II (Ed.), *Handbook of Cryogenic Engineering*, Taylor & Francis, 1998, Chapter 4.
23. Y. Guo and K. D. Timmerhaus, "Experimental Verification of Stability Characteristics for Thermal Acoustic Oscillations in a Liquid Helium System," *Adv. Cryo. Eng.*, **39**, 1994.
24. J. W. Elkin, *Experimental Techniques for Low-Temperature Measurements*, Oxford, 2006.
25. F. J. Eduskuty and W. F. Stewart, *Safety in the Handling of Cryogenic Fluids*, Springer, 1996.
26. F. J. Eduskuty and M. Daugherty, "Safety," in J. G. Weisend II (Ed.), *Handbook of Cryogenic Engineering*, Taylor & Francis, 1998, Chapter 11.
27. *Safe Handling of Cryogenic Liquids*, CGA P-12, Compressed Gas Association, 2009.
28. "Cryogenic & Oxygen Deficiency Hazard Safety," SLAC ES&H Manual, Chapter 36, available: <http://www-group.slac.stanford.edu/esh/eshmanual/pdfs/ESHch36.pdf>, accessed June 19, 2012.
29. E. D. Beeson, S. R. Smith, and W. F. Stewart eds., *Safe Use of Oxygen and Oxygen Systems: Handbook for Design, Operation and Maintenance*, ASTM, West Conshohocken, PA, 2007.
30. *Cleaning Equipment for Oxygen Service*, GGA G4.1, Compressed Gas Association, 2009.
31. Ph. Lebrun, "Commissioning and First Operation of the Large Hadron Collider (LHC)," in *Proceedings ICEC 23*, Oficyna Wydawnicza Politechniki Wroclawskiej, 2011.
32. J. Casas-Cubillos et al., "Baseline Configuration of the Cryogenic System for the International Linear Collider," in *Proceedings of ICEC 21*, Icaris, 2007.
33. C. H. Rode, "Jefferson Lab 12 GeV CEBAF Upgrade," *Adv. Cryo. Eng.*, **55A**, 2010.
34. D. Hatfield et al., "SNS Cryogenic Systems Commissioning," *Adv. Cryo. En.*, **51B**, 2006.
35. N. S. Synder, "Heat Transport through He II: Kapitza Conductance," *Cryogenics*, **10**, 1970.
36. P. L. Walstrom, J. G. Weisend II, J. R Maddocks, and S. W. Van Sciver, "Turbulent Flow Pressure Drop in Various He II Transfer System Components," *Cryogenics*, **28**, 101, 1986.
37. <http://www.magnet.fsu.edu/education/tutorials/tools/dilutionfridge.html>, accessed November 2012.
38. J. Bartlett and I. Hepburn, "Design of a Continuous ADR for the ESA Mission XEUS Based on the ESA Engineering Model ADR," in *Proceedings of ICEC 21*, Icaris, 2007.
39. G. K. White and P. J. Meeson, *Experimental Techniques in Low Temperature Physics*, Oxford Science Publication, 2002.

CHAPTER 15

INDOOR ENVIRONMENTAL CONTROL

Jelena Srebric
The Pennsylvania State University
State College, Pennsylvania

1 INDOOR ENVIRONMENT PARAMETERS	578	5 BUILDING THERMAL LOADS	589
1.1 Moist Air Parameters	578	5.1 Heating Loads	591
1.2 The Psychrometric Chart	580	5.2 Cooling Loads	592
2 AIR-HANDLING PROCESSES	581	6 COMPUTER PROGRAMS	593
2.1 Typical HVAC Processes	581	6.1 Energy Calculation Programs	593
2.2 A Simple Air-Handling Unit	584	6.2 Airflow Simulation Programs	594
3 THERMAL COMFORT	585	6.3 Coupled Simulation Tools	595
3.1 First Law Applied to the Human Body	585	7 EQUIPMENT FOR ENVIRONMENTAL CONTROL	596
3.2 Thermal Comfort Indices	586	7.1 Air-Handling and Distribution Systems	596
4 INDOOR AIR QUALITY	587	7.2 Control Systems	596
4.1 Health Issues and Requirements	588	REFERENCES	597
4.2 Problem Mitigation	589		

The ability to control indoor environment parameters is vital to our every day lives because we spend most of our time indoors. The engineering systems that enable the control of environmental parameters are called heating, ventilating, and air-conditioning (HVAC) systems. Air-conditioning and refrigeration systems are considered to be one of the engineering achievements that transformed our lives in the past century.¹ The first applications of HVAC systems were industrial, primarily for ice production and food preservation in the nineteenth century. The first installations of air-conditioning systems for building environments dates to the early twentieth century and includes buildings such as the New York Stock Exchange (1905), the Central Park theater in Chicago (1917), and the U.S. Senate (1929). Residential air conditioning became affordable and popular after World War II. Today, air-conditioning systems are present everywhere in residential and commercial buildings and in different kinds of vehicles such as automobiles, space shuttles, and submarines. Based on the U.S. Energy Information Administration survey, 47% of all U.S. households use air conditioning.² Furthermore, in commercial buildings, more than half of the yearly energy consumption is for HVAC systems,³ including space heating, cooling, and ventilation. Largely, HVAC systems are major engineering systems that significantly affect the country's overall energy consumption and occupants' well-being through control of indoor air parameters.

1 INDOOR ENVIRONMENT PARAMETERS

The indoor environment parameters that are controlled by HVAC depend on the type of the building. In general, residential HVAC systems typically control indoor air temperature by heating in winter and cooling in summer. The humidity control is present in the form of humidification and dehumidification, but not always utilized due to energy costs associated with the addition or removal of this latent heat. Recently, air cleaners have become cheaper and, as a result, are installed more widely for their potential to remove dust and other potential allergens. Overall, the residential HVAC primarily controls the indoor air temperature. For the commercial buildings, HVAC systems are more sophisticated and may control many parameters such as pressure, temperature, humidity, carbon dioxide levels, and other gaseous or particulate contaminant concentrations.

1.1 Moist Air Parameters

HVAC systems supply treated outdoor air to building spaces via an air distribution system. The outdoor air conditions depend on location, elevation, and time of day. When designing an HVAC system, engineers use outdoor air parameters for U.S. standard atmosphere.⁴ The standard atmosphere contains the following components specified by volume fraction: 78.084% nitrogen (N₂), 20.948% oxygen (O₂), 0.934% argon (A), 0.031% carbon dioxide (CO₂), and 0.003% other minor gases. These components form a gas mixture called dry air. The atmospheric air, in addition to the dry air, includes water vapor and different gaseous and particulate contaminants. The standard design of HVAC systems accounts for the atmospheric air as a binary mixture of dry air and water vapor called moist air. Both of these moist air components are considered to obey the ideal gas law:

For dry air:

$$p_a v_a = R_a T \quad (1)$$

For water vapor:

$$p_v v_v = R_v T \quad (2)$$

where p is the gas partial pressure, v is the specific gas volume, T is the gas absolute temperature, and R is the specific gas constant [$R_a = 287 \text{ J}/(\text{kg} \cdot \text{K})$; $R_v = 462 \text{ J}/(\text{kg} \cdot \text{K})$].

The ideal gas law proves to be an excellent approximation for the real gas behavior of both moist air components. The following moist air parameters are commonly used in the design of HVAC systems: pressure p , dry-bulb temperature T_{DB} , wet-bulb temperature T_{WB} , dew point temperature T_{dp} , humidity ratio W , relative humidity ϕ , enthalpy i , and specific volume v .

The atmospheric pressure is the first consideration when designing an HVAC system. The standard barometric pressure at sea level is 101.325 kPa, which linearly decreases with the elevation based on the following equation⁵

$$p = 101.325 (1 - 2.25577 \times 10^{-5} H)^{5.2559} \quad (\text{kPa}) \quad (3)$$

where p is the barometric pressure in kilopascals and H is the elevation in meters.

The total barometric pressure is a sum of the partial pressures of the dry air p_a and water vapor p_v , based on the Gibbs–Dalton law for ideal gases:

$$p = p_a + p_v \quad (4)$$

The standard atmosphere also has defined standard air temperatures for different elevations, but when designing an HVAC system a more detailed temperature distribution is taken into account. The design temperature varies with geographic location, and it is tabulated for most of the U.S., Canada, and other world locations (ASHRAE, Chapter 14).⁵ In fact, two different temperatures, dry-bulb temperature and wet-bulb temperature, are specified for each location. To distinguish these two temperatures, it is necessary to introduce a condition called

the saturation of moist air. Saturation is a condition of moist air that occurs because the moist air can only contain a limited amount of water vapor. When saturation occurs, the excess water vapor condenses on nearby surfaces. By definition, the saturation of moist air is the condition where moist air may coexist in a neutral equilibrium with its condensed water on a flat surface.

The dry-bulb temperature represents the temperature of the moist air measured by a standard thermometer, while the wet-bulb temperature represents the temperature of the same moist air under adiabatic saturation. Adiabatic saturation could be achieved in an adiabatically insulated enclosure by the evaporation of water at wet-bulb temperature until the moist air is fully saturated. The wet-bulb temperature was named by the experiment that used a wet cloth wrapped around a regular thermometer rotated at a specific speed to achieve a condition close to that of adiabatic saturation. The wet-bulb temperature reflects the moisture content in the air: the lower the wet-bulb temperature for the same dry-bulb temperature, the lower the content of moisture. The wet-bulb temperature can only be equal to or lower than the dry-bulb temperature. Saturation occurs when these two temperatures are the same. The temperature for which the air is fully saturated is called the adiabatic saturation temperature, or wet-bulb temperature.

Saturation occurs due to the moist air's limited capacity to contain water vapor. It is possible to reach a fully saturated condition in the moist air by adding moisture or by decreasing the dry-bulb temperature under constant pressure. This process is different from adiabatic saturation because the moisture content stays constant. An example could be condensation on a window in a cold climate during the winter season. By decreasing the temperature of a surface such as the window, a first droplet of water appears as soon as the surface reaches the dew point temperature. This process is very useful for the dehumidification of moist air by condensation in HVAC system cooling coils.

The humidity ratio W represents the ratio of the mass of water vapor m_v to the mass of dry air m_a in the moist air binary mixture:

$$W = \frac{m_v}{m_a} = \frac{p_v R_a}{p_a R_v} = 0.622 \frac{p_v}{p_a} = 0.622 \frac{p_v}{p - p_v} \quad \left(\frac{\text{kg}_{\text{water vapor}}}{\text{kg}_{\text{dry air}}} \right) \quad (5)$$

The relative humidity ϕ is the ratio of the water vapor partial pressure p_v to the water vapor partial pressure in a saturated mixture under the same temperature p_s :

$$\phi = \frac{p_v}{p_s} \times 100 \quad (\%) \quad (6)$$

When compared to the wet-bulb temperature, both the humidity ratio and the relative humidity more explicitly define the moisture content in the moist air. In principle, the humidity ratio represents a nondimensional weight of the moisture, while the relative humidity represents a nondimensional degree of saturation. The humidity ratio ranges from zero or a few grams of water vapor per kilogram of dry air to 30 or more grams of water vapor per kilogram of dry air. The relative humidity ranges from zero for completely dry air to 100% for saturated moist air.

The enthalpy i of ideal gas mixtures is equal to the sum of the mixture component enthalpies. Therefore, the enthalpy of the moist air is a sum of the dry air enthalpy and the water vapor enthalpy:

$$i = c_{p,a}T + W(i_g + c_{p,v}T) = 1.01 T + W(2501.3 + 1.86T) \quad \left(\frac{\text{kJ}}{\text{kg}_{\text{dry air}}} \right) \quad (7)$$

where $c_{p,a}$ is the specific heat of dry air, $c_{p,v}$ is the specific heat of water vapor, and i_g is the enthalpy of saturated water vapor at 0°C.

The specific volume v of the moist air is a ratio of total volume to the mass of dry air, which also could be defined in terms of temperature and pressure based on the ideal gas law:

$$v = \frac{V}{m_{\text{dry air}}} = \frac{R_a T}{p_a} \quad \left(\frac{\text{m}^3}{\text{kg}_{\text{dry air}}} \right) \quad (8)$$

The above moist air parameters are expressed in terms of different units per kilogram of dry air, which is a convention adopted due to the small and volatile mass of the water vapor in the moist air mixture.

1.2 The Psychrometric Chart

All of the parameters defined in the previous section are put together in a chart called the psychrometric chart. The chart enables quick access to values of different moist air parameters without requiring the direct use of equations. This graphical approach to solving HVAC engineering problems is very popular in industry. Modern versions of the psychrometric chart are typically supplied in a software format to enable interactive reading of the parameters. The chart was more traditionally used in a paper-based version as presented in Fig. 1.⁵ To simplify the information presented in the psychrometric chart, Fig. 2 presents psychrometric parameters in six separate charts that are merged to form the chart presented in Fig. 1. The six charts present the pressure (elevation dependent), temperatures, humidity ratio, relative humidity, and specific volume.

The most commonly used chart is the sea-level chart for the standard barometric pressure of 101.325 kPa as shown in Fig. 1. Nevertheless, HVAC design for higher elevations should use ASHRAE charts for 750, 1500, and 2250 m or give an exact elevation to psychrometric software. The horizontal axis in the chart represents the dry-bulb temperature and the vertical

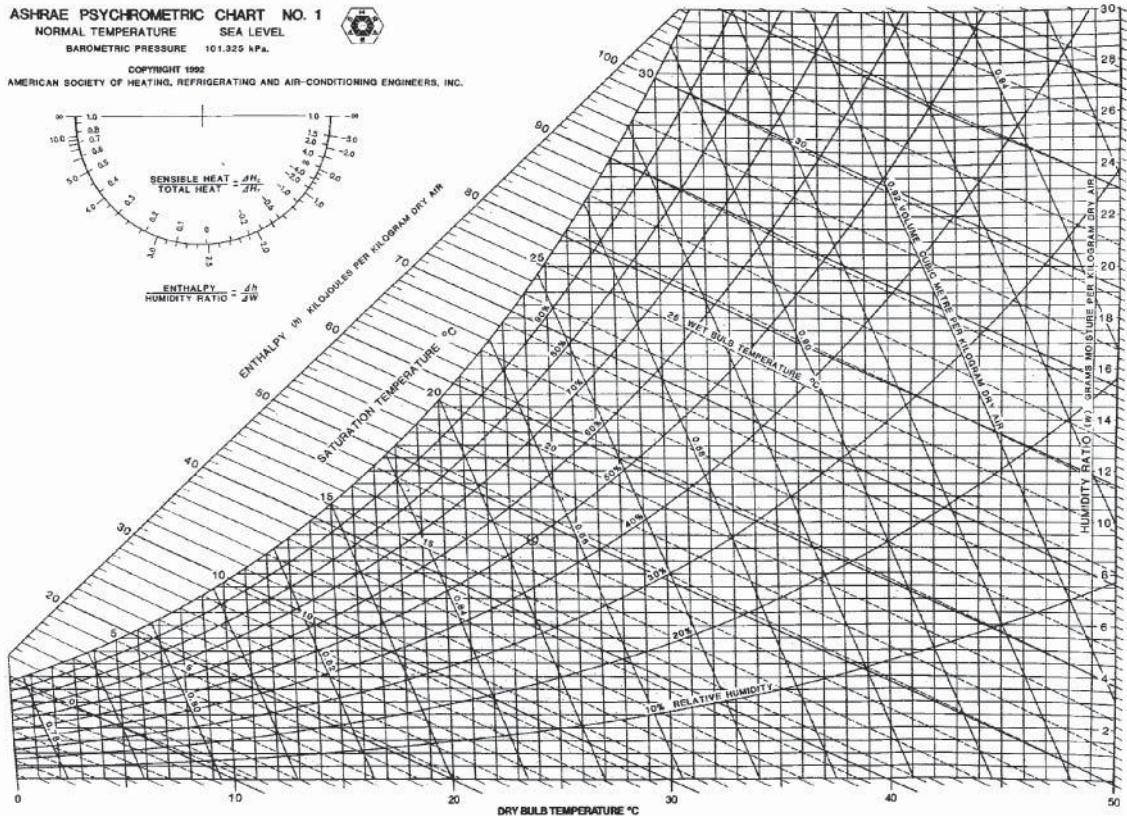


Figure 1 ASHRAE psychrometric chart.

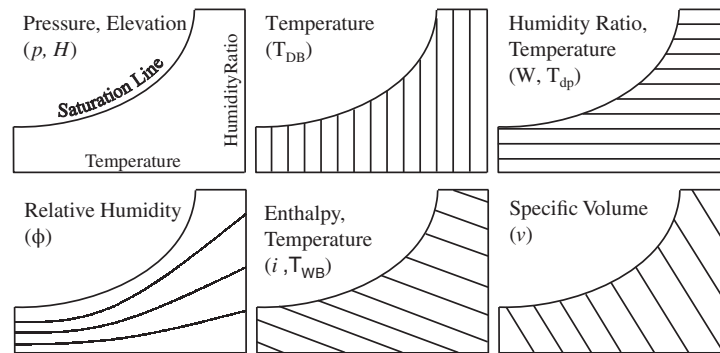


Figure 2 The psychrometric chart lines in separate diagrams.

axis represents the humidity ratio; see Fig. 2. The curved boundary on the left side of the chart is the saturation line representative of 100% relative humidity. The dry-bulb temperatures are straight, slightly inclined to the left, and not exactly parallel lines. The humidity ratio lines are straight, horizontal, and parallel. At the points where humidity ratio lines intersect the saturation line, a single dew point temperature T_{dp} can be obtained for all of the moist air states along that same humidity ratio line. The relative humidity lines are the only curves in the chart and are evenly spaced. The enthalpy and wet-bulb temperature lines are oblique and straight. It is important to notice that enthalpy and wet-bulb temperature lines are close to each other but do not coincide. The enthalpy lines are parallel to each other, while the wet-bulb temperature lines diverge from each other. Finally, the specific volume lines are oblique and not parallel.

The dry-bulb temperature in the standard psychrometric chart ranges from 0 to 50°C. For other temperature ranges, ASHRAE⁵ provides low temperature (−40 to 10°C), high temperature (10–120°C) and very high temperature (100–200°C) psychrometric charts.

The protractor shown in the upper left corner of the psychrometric chart (Fig. 1) gives two additional parameters. The inner scale of the protractor represents a sensible heat factor (SHF) and the outer scale gives a ratio of the enthalpy to humidity ratio change. Both parameters are important for air handling processes that take place in HVAC systems.

2 AIR-HANDLING PROCESSES

HVAC systems have different component devices to process and supply air to conditioned spaces. The part of any HVAC system that processes the moist air is called the air-handling unit (AHU). The psychrometric chart is used to study the energy and/or moisture transport that occurs in AHU processes.

2.1 Typical HVAC Processes

Several typical processes are present in most HVAC systems, although actual systems might differ significantly in appearance and arrangement. Depending on the role of an HVAC system, a certain process might be present or absent. Typical HVAC processes are:

- Sensible heating/cooling
- Cooling and dehumidification
- Heating and humidification
- Adiabatic humidification processes
- Adiabatic mixing of air

Each of the above processes is performed by an HVAC device and corresponds to a particular HVAC device, such as heating/cooling coils, humidifiers, or mixing boxes.

The analysis of these different processes uses the first law of thermodynamics and the conservation of mass principle. The first law is applied under the assumptions of steady-state processes and a negligible change in kinetic and potential energy, which are valid assumptions for an HVAC device. The first law for an HVAC device, which is an open thermodynamic system, becomes

$$\dot{Q}_{CV} - \dot{W}_{CV} = \sum_{\text{out}} \dot{m}_a i - \sum_{\text{in}} \dot{m}_a i \quad (9)$$

where \dot{Q}_{CV} is the heat added to the control volume, \dot{W}_{CV} is the shaft work done by the system (typically zero), \dot{m} is the mass flow rate, and i is the enthalpy of the moist air flowing through the control volume of a device. By convention, heat added to the control volume and work done by a device is positive.

Sensible heating/cooling occurs in a heat exchanger, which adds or removes heat without adding or removing the moisture content of the airstream. Figure 3 schematically shows the boundaries of the control volume and the corresponding process line in the psychrometric chart. The airstream changes its condition from state 1 to state 2 by flowing through the heat exchanger. The process is represented as a horizontal line in the psychrometric chart ($W = \text{const.}$). The walls of the heat exchanger and the air ducts are assumed to be adiabatically insulated. The first law for this control volume is

$$\dot{Q} = \dot{m}_a(i_1 - i_2) = \dot{m}_a(c_{p,a} + Wc_{p,v})(T_1 - T_2) = \dot{m}_a c_{p,a}(T_1 - T_2) \quad (10)$$

where $Wc_{p,v}$ is much smaller than $c_{p,a}$ and can be neglected for practical applications.

If the surface temperature of the cooling coil is lower than the dew point temperature of the moist air, condensation occurs, resulting in a cooling and dehumidification process. This process is very important and often used to dehumidify air in hot and humid climates. Figure 4 shows the dehumidification process that changes an airstream from state 1 to state 2. This process also results in water condensation. The first law for the cooling and dehumidification process is

$$\dot{Q} = \dot{m}_a(i_1 - i_2) - \dot{m}_a(W_1 - W_2)i_w \approx \dot{m}_a(i_1 - i_2) \quad (11)$$

where i_w is the enthalpy of the condensate (water) at the exit air temperature T_2 . The first term of the equation is much greater than the second one and can be neglected. Based on mass conservation, the flow rate for the condensate is

$$\dot{m}_w = \dot{m}_a(W_1 - W_2) \quad (12)$$

The process in the psychrometric chart could be represented by a straight line that connects the two air states, which is the dashed line in Fig. 4. Another way to represent this process is to draw a horizontal line to the saturation line and then a curve that follows the saturation line until point 2. Both sensible and latent heat are exchanged. The sensible heat is proportional to the change in dry-bulb temperature (ΔT), while the change in latent heat is proportional to the

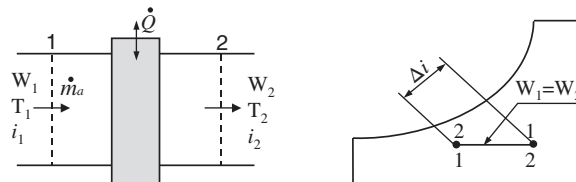


Figure 3 Sensible heating/cooling in a heating or cooling coil.

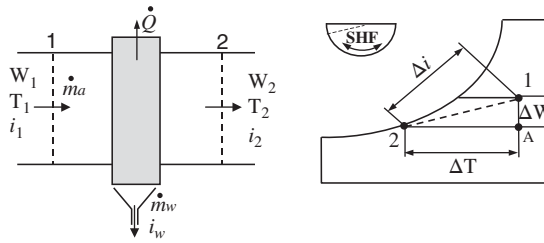


Figure 4 Cooling and dehumidification for hot and humid climates.

change in humidity ratio (ΔW). The total heat exchanged during the process is equal to the sum of the sensible and latent heat:

$$\dot{Q} = \dot{Q}_{\text{sensible}} + \dot{Q}_{\text{latent}} = \dot{m}_a(i_A - i_2) + \dot{m}_a(i_1 - i_A) = \dot{m}_a(i_1 - i_2) \quad (13)$$

Based on the definition of the sensible and latent heat portions, a new parameter called the sensible heat factor (SHF) is introduced as

$$\text{SHF} = \frac{\dot{Q}_{\text{sensible}}}{\dot{Q}} = \frac{i_A - i_2}{i_1 - i_2} \quad (14)$$

SHF defines the slope for the process line (dashed line in Fig. 4). The inner scale of the protractor in the upper left corner of the psychrometric chart gives SHF values. The line connecting the center of the protractor and SHF value is parallel to the process line in the chart.

Another typical process is heating and humidification for cold and dry climates. This process needs a heating coil and a humidifier as presented in Fig. 5. The heat exchanger heats up the air sensibly, while the humidifier adds moisture in either vapor or liquid form without heat exchange with the surroundings. The first law and the conservation of mass equations for this process are

$$\dot{m}_a i_1 + \dot{Q} + \dot{m}_w i_w = \dot{m}_a i_2 \quad (15)$$

$$\dot{m}_w = \dot{m}_a (W_2 - W_1) \quad (16)$$

When the moisture added is liquid at the wet-bulb temperature of the incoming airstream 1, the humidification process coincides with the constant enthalpy line ($i_A = i_2$).

Adiabatic humidification of the incoming airstream could be achieved with steam or liquid at an arbitrary temperature. Figure 6 schematically shows the adiabatic humidification process without heating process. The outgoing airstream could have different states represented as states 2, 3 or 4 in the example in Fig. 6. The constant enthalpy process 1–2, is achieved with a spray of water at the wet-bulb temperature ($T_{\text{WB},1}$). The air state 3 can be reached by adding saturated steam at the dry-bulb temperature of the incoming air (T_1). In general, the leaving air could be

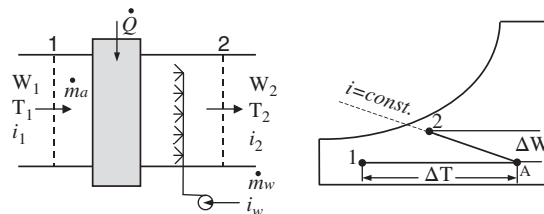


Figure 5 Heating and adiabatic humidification for cold and dry climates.

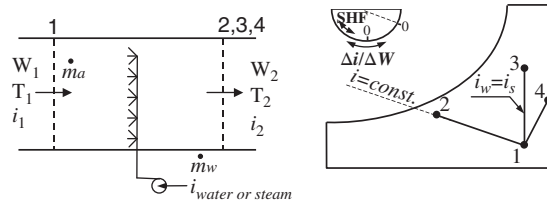


Figure 6 Adiabatic humidification processes.

humidified and cooled if the water enthalpy is between the enthalpy for $T_{WB,1}$ and the saturated liquid at T_1 , which would result in a process somewhere in between process 1–2 and process 1–3 on the psychrometric chart. Cooling happens when the water droplets fully evaporate by taking energy from the incoming airstream under the assumption of adiabatic process. The leaving air could be humidified and heated, such as in process 1–4, if the added steam has enthalpy greater than the saturated steam at T_1 . Except for process 1–2 and 1–3, the exact slope of an arbitrary adiabatic humidification process could be determined from the following equation, which is derived from Eqs. (15) and (16) ($\dot{Q} = 0$):

$$\frac{\Delta i}{\Delta W} = \frac{i_2 - i_1}{W_2 - W_1} = i_{\text{water or steam}} \quad (17)$$

The value of the ratio $\Delta i/\Delta W$ can be calculated and used in the protractor to determine the slope of the humidification process, in the same way as SHF factor was used. This ratio is plotted on the outer scale of the protractor.

Adiabatic mixing of two moist airstreams is a process often used in AHUs because it enables major energy savings for HVAC systems. For example, instead of taking the entire amount of circulated air from outside in a cold winter day, a certain portion can be recirculated at the room air temperature. A certain percentage of recirculated air intake versus fresh air intake is recommended based on indoor air quality requirements. A typical recirculation rate for U.S. commercial buildings is around 80%, which means about 20% fresh air is supplied to the building for dilution of contaminants and occupants' breathing. Figure 7 shows an example of adiabatic mixing for an airstream at state 1 (fresh air) and an airstream at state 2 (recirculated air). The resulting mixture is at state 3 on the mixing process line that connects states 1 and 2. The exact position of the state 3 is proportional to the ratio of the flow rates for the incoming airstreams.

2.2 A Simple Air-Handling Unit

A simple AHU incorporates all of the above-mentioned processes for climates that require heating and cooling in different seasons. Nevertheless, individual AHU components may be active only during certain seasons, such as a humidifier in winter and a cooling coil in summer.

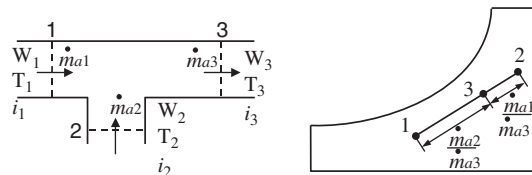


Figure 7 Adiabatic mixing of two moist airstreams.

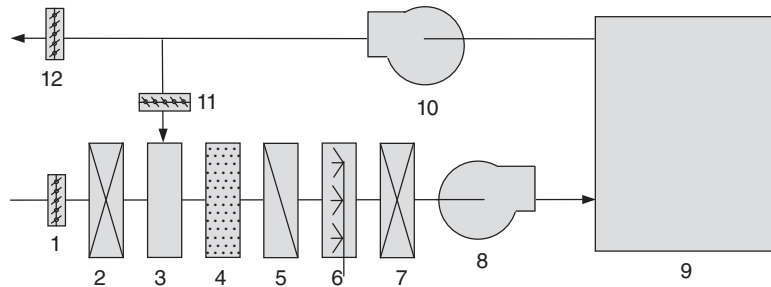


Figure 8 A simple single-zone air-handling system and conditioned space (1, fresh air louver; 2, preheat coil; 3, mixing box; 4, filter; 5, cooling coil; 6, humidifier; 7, reheat coil; 8, supply fan; 9, conditioned space; 10, return fan; 11, recirculation louver; and 12, exhaust louver).

The simplest AHU would serve a single zone, such as a single space (room), in a building and would be controlled by a thermostat placed in that zone. This kind of HVAC system is typically used for computer rooms, small department stores, or other small individual spaces with heating/cooling loads that are uniform and relatively stable throughout the zone. For nonuniform loads or larger spaces, multiple units could be installed with or without a duct system. Figure 8 presents an example of the single-zone system. Except for the cooling coil, filter, or supply fan, all other devices are optional depending on the type of space and purpose of the system. The separation of the heating coil into preheat and reheat coils has two basic functions. First, the reheat coil is used in summer for the control of the humidity level in the supply air by subcooling the air to a desired humidity ratio and then reheating the air to the desired supply temperature. Second, the preheat coil prevents freezing problems in the mixing box during cold winter days.

3 THERMAL COMFORT

The primary purpose of HVAC systems is to maintain thermal comfort for building occupants. ANSI/ASHRAE Standard 55-2010⁶ defines thermal comfort as the mind state that expresses satisfaction with thermal environment by a subjective evaluation. Due to the subjectivity of the thermal comfort, HVAC systems are currently designed to satisfy thermal comfort for 80% or more of the building occupants.

3.1 First Law Applied to the Human Body

The human body behaves similar to a heat engine, obeying the first law of thermodynamics. The chemical energy contained in food is converted into thermal energy through the process of metabolism. This thermal energy is used partially to perform work, while the other part has to be released to the surroundings to enable the normal functioning of the human body. The first law of thermodynamics for the human body has the following form:⁷

$$M - W = \dot{Q}_{\text{skin}} + \dot{Q}_{\text{respiration}} = (C_{\text{sk}} + R_{\text{sk}} + E_{\text{sk}}) + (C_{\text{res}} + E_{\text{res}}) \quad (18)$$

where M is the rate of metabolic heat production ($\text{W}/\text{m}^2_{\text{body surface area}}$), W is the rate of mechanical work, \dot{Q} represents the different heat losses, C is the convective heat losses, R is the radiative heat losses, and E is the evaporative heat losses. Fig. 9 schematically presents the energy balance components for the control volume presented by a dashed line.

The metabolic heat production, losses, and work are measured in $\text{W}/\text{m}^2_{\text{body surface area}}$ or in metabolic “met” units ($1 \text{ met} = 58.2 \text{ W}/\text{m}^2$). Table 1 gives a couple of examples for metabolic

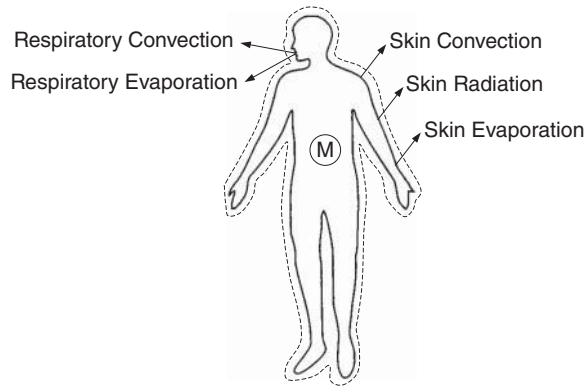


Figure 9 The energy balance for human body (M – metabolism).

Table 1 Metabolic Heat Production Rates for Typical Tasks

Activity	met	W/m ²
Reclining	0.8	46.6
Seated and quite	1.0	58.2
Sedentary activity (office, dwelling, lab, school)	1.2	69.8
Standing, relaxed	1.2	69.8
Light activity, standing (shopping, lab, light industry)	1.6	93.1
Medium activity, standing (shop assistant, domestic work, machine work)	2.0	114.4
High activity (heavy machine work, garage work, if sustained)	3.0	174.6

heat production rates based on activity levels (ANSI/ASHRAE Standard 55-2010).⁶ The table shows that the human body produces a total heat equivalent to one or several lightbulbs, depending on the activity level.

The main heat transfer mechanisms are convection, radiation, and evaporation; conduction is negligible due to the small surface area and high insulation of shoe soles. Each of the terms in Eq. (18) can be calculated.⁵ The equations for each term are based on the fundamentals of heat transfer, but also include empirical equations and coefficients. In general, the total heat transfer from the human body depends on environmental and personal factors.⁷ The environmental factors are air temperature (affects C), relative humidity (affects E), air velocity near the human body (affects C), and surface temperature of the enclosure and surrounding objects (affects R). The personal factors are activity rate and clothing (body insulation).

3.2 Thermal Comfort Indices

Several thermal comfort indices correlate the perception of thermal comfort with measured environmental parameters, i.e. dry-bulb temperature, mean radiant temperature, and humidity levels. The mean radiant temperature (T_{MR}) is a uniform temperature of an imaginary black enclosure that would exchange the same amount of radiative heat with an occupant as the actual nonuniform environment. Further, T_{MR} is used to define an operative temperature T_o , which includes combined radiative and convective heat transfer in the actual nonuniform environment. T_o is approximately equal to the average value of T_{MR} and dry-bulb temperature.

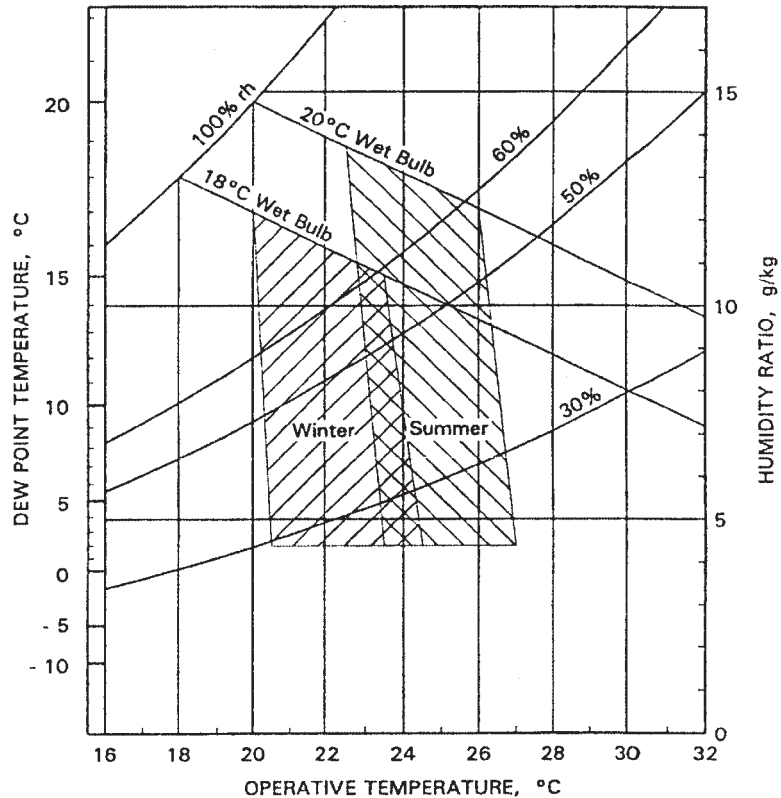


Figure 10 ASHRAE comfort zone. (After Ref.5.)

A rationally derived index, the operative temperature (T_o) is used to plot an ASHRAE comfort zone for winter and summer conditions (see Fig. 10). The “comfort zone” represents combinations of air temperature and relative humidity that most often produce thermal comfort for a seated North American adult in typical summer or winter clothing. An assumed level of dissatisfaction is 10% of all occupants. The vertical slender lines bordering the comfort zone represent acceptable operative temperatures for different indoor air dry-bulb temperatures and humidity levels forming two shaded areas, the left one for winter and the right one for summer outdoor environmental conditions. The upper and lower horizontal lines of the shaded areas represent the upper and lower boundaries of the comfort zone with acceptable humidity ratios for any set of the outdoor environmental conditions. The ASHRAE comfort zone can be adjusted for different clothing levels, air velocities, activity levels, and human adaptation. Overall, HVAC systems are designed to produce an indoor air state within the ASHRAE comfort zone.

4 INDOOR AIR QUALITY

In addition to the primary function of maintaining thermal comfort, HVAC systems have to maintain good indoor air quality. According to ANSI/ASHRAE Standard 62-2010,⁸ acceptable indoor air quality is achieved with air that contains known contaminants at harmful concentrations and the majority of occupants (more than 80%) express satisfaction. Indoor air quality

(IAQ) plays a significant role in occupants' well-being, satisfaction, and health, due to the prolonged time periods spent indoors in a modern society.

4.1 Health Issues and Requirements

Buildings with poor air quality have produced many occupant health complaints/illnesses/conditions that have been recorded and labeled "sick building syndrome" (SBS). SBS is discomfort/illness caused by indoor air. Symptoms are often comparable to a cold or influenza, such as headaches, drowsiness, eye irritation, and nose and throat infection. The main difference between SBS and a cold is that the SBS symptoms last much longer than cold symptoms and disappear after the occupant leaves the building. Approximately 30% of new or remodeled buildings produce health complaints as reported by the Environmental Protection Agency (EPA). Indoor air contaminant levels can be several magnitudes greater than the outdoor air contaminant levels due to the contaminant releases from building materials, occupants, or different building processes. Table 2 shows a few contaminant sources, permitted levels, and possible health effects according to EPA standards. Regardless of permitted levels, the actual response to a contaminant is based on the individual.

As listed in Table 2, indoor contaminants could be particles or gases and vapors. Particles could be allergens, molds, bacteria, dust, fumes, smoke, or mist and fog. Contaminant gases could be inorganic or organic. Harmful inorganic gases, such as radon (a radioactive gas), have the potential to cause lung cancer due to the particle deposition in lungs. Harmful organic vapors may cause major respiratory irritation and may be perceived as unpleasant odors. In the worst-case scenario, harmful vapors could be completely odorless. Many paints, waxes, varnishes, and cleaning products are rich in organic solvents that evaporate even without use. Table 3 shows human irritation responses to total volatile organic compound (TVOC) mixtures based on a human subject study in a controlled laboratory environment.⁹

Table 2 Contaminant Sources, Permitted Levels and Health Effects (EPA)

Contaminants	Sources	Permitted Levels	Health Effects
CO ₂	Human, combustion	1000 ppm	Stuffing
CO	Combustion, ETS	15 ppm	Body chemistry
SO _x	Combustion	100 µg/m ³	Irritation, Asthma,
NO _x	Combustion	4 picocuries/l	Lung cancer
Ra	Soil		
VOCs (Formaldehyde)	Combustion, pesticides, building materials, etc.	0.1 ppm	Eyes and mucous membrane irritation
Particulate	Outdoor air, Occupant activities, environmental tobacco smoke (ETS), furnishings, pets, etc.		Lung diseases, heart diseases, cancer

Table 3 Human Irritation Responses to TVOC Mixtures

Concentration (mg/m ³)	Health Effect Response	Exposure Definition
< 0.20	No irritation	Comfort
0.20–3.0	Irritation and discomfort	Multifactorial exposure range
3.0–25	Exposure effect and headache	Discomfort
> 25	Additional neurotoxic effects	Toxic

Table 4 Use of Different Filters for Different Types of Contaminants

	Media Filtration	HEPA Filters	Activated Carbon Adsorption	UV Photocatalytic Oxidation
Odors			X	X
VOCs			X	X
BioAerosols		X		X
Dust	X	X		

4.2 Problem Mitigation

Numerous indoor air quality investigations over the last decade by the National Institute for Occupational Safety & Health (NIOSH) have found that the primary sources of indoor air quality problems are:

- Inadequate ventilation 52%
- Contaminant from inside the building 16%
- Contaminant from outside the building 10%
- Microbial contamination 5%
- Contamination from building fabric 4%
- Unknown sources 13%

Appropriate design and maintenance of HVAC systems can eliminate the majority of indoor air quality problems. ANSI/ASHRAE Standard 62-2010⁸ has a prescriptive ventilation rate procedure that defines adequate ventilation. The standard uses CO₂ as an indicator for human occupancy rates. Typically required fresh air quantities for occupants are 8–10 l/(s person). An additional amount of fresh air is required based on the building floor area to dilute other potential indoor contaminants. The total required amount of fresh air combines the occupant and floor required amounts, while the rest of the air may be recirculated to save energy used by the HVAC system.

To solve IAQ problems, building owners or managers could use one of the following three strategies: (1) eliminate or modify the contaminant source, (2) dilute the contaminant with outdoor air and air distribution, or (3) use air cleaning (filtering). Even though these strategies sound straightforward, they may not be easy to implement. For example, for mold and fungi prevention, it is important to properly design HVAC systems for humidity control, but it is just as crucial to have a properly constructed building envelope. Effective use of air distribution requires proper maintenance and balancing of the building air distribution systems. Finally, the use of different types of filters and regular replacement of filters can significantly reduce IAQ problems. Table 4 uses an X to indicate the type of contaminants that certain filters are capable of removing; typically, two or more types of filters are combined to achieve proper removal of contaminants.

Recently, in addition to health concerns, HVAC systems have been charged with protecting buildings and occupants from internal or external releases of chemical, biological, or radiological contaminants. These new requirements for the removal of extremely harmful, high-concentration contaminants by HVAC systems are expected to transform the current design procedures.

5 BUILDING THERMAL LOADS

The building thermal loads represent the thermal energy that is removed (cooling loads) or added (heating loads) to a building in order to keep the occupants thermally comfortable, which

is the primary function of an HVAC system. Building thermal loads determine the capacity of the equipment and air distribution ducts used to condition a building. The procedures for the calculation of cooling and heating thermal loads are slightly different. Nevertheless, both procedures use concepts of indoor/outdoor design conditions and heat transfer through the multilayered building envelope assemblies to calculate the building thermal loads.

Indoor design conditions are based on thermal comfort for occupants⁶ and refer to all of the moist air parameters within the thermal comfort zone in winter or summer as shown in Figure 10. These conditions are maintained by a properly sized HVAC system.

Outdoor design conditions refer to the recommended weather data used for the design of HVAC systems. These data are available from ASHRAE⁵ and includes the United State, Canada, and world location data. The recommended data does not reflect the coldest or the hottest temperatures ever measured for a location because designing for ultimate extremes would cause the heating or cooling systems to be critically oversized. Instead, ASHRAE presents HVAC design weather data with statistically determined probability for the “worst” weather conditions to occur. For example, the heating design conditions are published for 99.6 and 99% probability levels, while the cooling design conditions are published for 0.4, 1.0, and 2.0% probability levels. These probability levels refer to the number of hours during a year (12 months = 8760 h) when the summer dry-bulb temperature is higher than the published design value or the winter dry-bulb temperature is lower than the published design value. A typical HVAC design would use 99% for heating and 1.0% for cooling probability levels. Therefore, depending on the year, the installed equipment might not have sufficient capacity to properly heat or cool the building during 88 h in summer and 88 h in winter, which is acceptable considering the initial costs and operating costs for an HVAC system.

The outdoor design conditions present the dry-bulb temperatures accompanied by other important coincident weather data. The heating design conditions include the coincident extreme and mean wind speed used for estimating infiltration airflow rates. Nevertheless, the outdoor moisture content is not presented because the winter humidity ratio is low and would not significantly influence the capacity of humidifiers. For the cooling conditions, coincident mean wet-bulb temperature, dew point temperature, and humidity ratio are used for sizing the cooling and dehumidification equipment.

Once indoor and outdoor design conditions for a particular building site are selected, heat transfer through the multilayered building envelope assemblies can be calculated. Heat transfer through building envelope, comprised of walls, windows, and roofs, includes all three heat transfer mechanisms: conduction, convection, and radiation. Heat transfer is dynamic due to the continuous change in weather data as well as the change in building occupancy rates, and uses of building equipment. Nevertheless, the simplest HVAC system design procedures assume one-dimensional steady-state heat transfer, a good approximation for practical purposes due to the complexity of the real building heat transfer phenomena.

Heat transfer calculations for a building wall assembly use the thermal transmittance, U factor, for envelope assembly components such as windows, walls, floors, or roofs. U factors are based on thermal resistances, R values, of building components obtained from standardized laboratory experiments that approximate building components as homogenous materials. Thermal transmittance and resistance values are available in published building material tables for standard building components⁵ or directly from the component manufacturers. The overall thermal transmittance U_o of the building envelope is

$$U_o = \frac{\sum U_i A_i}{A_o} \quad (19)$$

where A_o is the overall surface area of the envelope, U_i is the thermal transmittance, and A_i is the surface area of each envelope component. Based on the inverse relationship for thermal

transmittance and thermal resistance for a building envelope component:

$$U_i = \frac{1}{R_i} \quad R_i = R_{\text{in}} + \sum R_{\text{envelope}} + R_{\text{out}} \quad (20)$$

where R_{in} and R_{out} are the film resistances for the inner and outer envelope surfaces and R_{envelope} is the thermal resistance of the envelope assembly. The film resistances lump together the effects of thermal radiation and convection at the envelope surfaces, while the component resistance takes into account the conduction through the envelope. The envelope resistance is available in tables⁵ for standard components or could be calculated based on the resistance circuits representing the envelope component. The standard thermodynamic calculations for the R -value circuitry apply to the building components. For example, a side wall would have siding and sheathing connected in its series ($R = R_{\text{siding}} + R_{\text{sheathing}}$), while the wood studs and insulation would be thermally connected in parallel ($1/R = 1/R_{\text{wood studs}} + 1/R_{\text{insulation}}$).

The simplest thermal load calculations use U factors for envelope assemblies and the indoor and outdoor design conditions as described above. In general, heating and cooling loads are calculated differently for residential and nonresidential buildings. The main features of residential buildings are: 24-h conditioned small internal loads, single zone, small capacity, dehumidification for cooling only, and thermostats for temperature control.⁵ All other buildings are considered nonresidential. The following section discusses the calculations of residential and nonresidential building heating and cooling loads.

5.1 Heating Loads

The heating load calculation procedure for residential buildings is relatively simple. The two heating load components are the heat losses through the building envelope and the heat required for the heating of outdoor air. Building envelope heat losses occur through structural components such as the roof, windows, floors, walls, and walls below grade, while the outdoor air heat losses are introduced by infiltration through cracks around doors and windows, porous materials, and open doors and windows. The heating load through structural components and windows is

$$\dot{Q} = UA(T_o - T_i) \quad (21)$$

where U is the building envelope component transmittance, A is the component surface area, and T_o and T_i are the indoor and outdoor design temperatures.

The heating load through floors and walls below grade is

$$\dot{Q} = UA(T_{\text{earth}} - T_i) \quad (22)$$

where U is the transmittance, A is the area for the walls below grade, T_i is the indoor design temperature, and T_{earth} is design temperature for the ground.

The heating load by infiltration is

$$\dot{Q} = \rho \dot{V}_{\text{infiltration}}(T_o - T_i) \quad (23)$$

where ρ is the air density and $\dot{V}_{\text{infiltration}}$ is the volume flow rate of the infiltration. The infiltration flow rate can be estimated simply by assuming a certain flow rate for a building structure. This method is called the air exchange method and is suitable for experienced designers. Other methods such as the crack length method and basic LBNL method are also available for more detailed calculations.⁵

Nonresidential heating load calculations are similar to the residential building thermal load calculations because they do not include thermal storage effects or solar radiation heat gains. However, in nonresidential buildings, designers have to account for the fresh air heating required for occupant breathing and dilution of contaminants by ANSI/ASHRAE Standard 62-2010.⁷ In addition, nonresidential buildings should comply with ASHRAE/IES Standard

90.1-2010.¹⁰ This standard has been developed since the 1970s when the first energy crisis sparked energy-conscious building design. This building energy performance standard has already been adopted by more than a dozen states in the United States., with the idea that within a decade all of the states will have an energy code in compliance with this standard. The heating of nonresidential buildings is usually accompanied with the simultaneous requirement for cooling of the core building zones without external walls or windows.

5.2 Cooling Loads

Cooling loads occur through structural components, through windows, by infiltration, and due to occupants, appliances, lighting, and other equipment. For cooling load calculations, the thermal storage factor cannot be neglected. In fact, the building structure, whether light, medium, or heavy, plays a significant role in the building cooling load distribution. The cooling load is the heat transfer rate at which energy has to be removed from a space in order to maintain indoor design conditions within thermal comfort. As an opposite, a heat gain is the rate at which the thermal energy is transferred to or generated within a space. An instantaneous heat gain such as solar radiation is first absorbed by the building structure and later transferred to the indoor air by convection, when it becomes the cooling load. For example, the peak cooling load in a building typically occurs in the afternoon or early evening, which is much later than the time when the actual heat gain has a peak value, creating a thermal lag. The heavier the building structure, the longer the thermal lag.

Residential cooling loads account for the heat gain from the structural components, windows, ventilation (fresh air requirement), infiltration, and occupants. The calculation for structural components uses the cooling load temperature differences (CLTDs). This CLTD is equivalent to the actual indoor/outdoor temperature difference that would result in the same heating loads. Therefore, the building cooling load based on CLTD is:

$$\dot{Q} = UA(\text{CLTD}) \quad (24)$$

where U is the building envelope component transmittance for summer, A is the component surface area, and CLTD is available in tables for single-family and multifamily residences.⁵ CLTD depends on the building component type, orientation, outdoor design temperature, and daily temperature range.

To accurately account for the thermal radiation effects delayed by thermal storage, the cooling load through windows uses a glass load factor (GLF):

$$\dot{Q} = A(\text{GLF}) \quad (25)$$

where GLF is available in tables for single-family and multifamily residences.⁵ GLF also accounts for the air-to-air heat conduction and shading.

Another important cooling load is ventilation, which accounts for the air handling of the fresh air requirements for the building occupants.⁸ Infiltration in summer tends to be much lower than infiltration in winter because the wind velocities and the indoor/outdoor temperature difference are typically much smaller in summer than in winter. The actual infiltration exchange rate depends on whether the building is tight, medium, or loose, and on the indoor/outdoor temperature difference. Suggested infiltration flow rates are tabulated.⁵ Finally, each occupant gives off a certain amount of heat (approx. 70 W/person) that also needs to be included in the cooling load. The total cooling load is the sum of all defined sensible loads multiplied by the latent load multiplier (LF), which is based on the outdoor design humidity ratio and building air tightness.

In nonresidential buildings, it is important to consider not only the already listed heat gains but also the effects of multiple zones present in such buildings. An air-handling unit serves multiple zones in nonresidential buildings in contrast to a residential unit that conditions a

single zone. The zones are distinguished not only by their heating or cooling requirements but also by the schedule of these requirements. Therefore, the thermal load analysis for design of a nonresidential HVAC system should consider the simultaneous effects of different zones, diversification of heat gains for internal loads such as nonuniform occupancy rates, and other unique circumstances.⁵ Specifically, the calculation of nonresidential building thermal loads require detailed information on building characteristics (materials, size, and shape), configuration (location, orientation, and shading), outdoor design conditions, indoor design conditions, operating schedules (lighting, occupancy, and equipment), date and time, and additional considerations such as the type of air-conditioning system, fan energy, fan location, duct heat loss and gain, duct leakage, and the type and position of the air return system. In general, thermal load calculations for nonresidential buildings require use of computer programs no matter which calculation method is used.

6 COMPUTER PROGRAMS

The use of computer programs in building design is now a common practice. From the perspective of HVAC systems, building simulation programs can be classified as either building energy simulation programs or building airflow simulation programs. Building simulation programs are used for yearly HVAC system energy consumption calculations, while building airflow simulation programs are used for infiltration, thermal comfort, indoor air quality, and contaminant distribution calculations. Both simulation technologies enable the design of better buildings.

6.1 Energy Calculation Programs

Computer programs are often employed to perform nonresidential cooling/heating loads or yearly energy consumption analyses due to the complexity of heat transfer through building structures and variable weather data. The original manual methods for the calculation of yearly HVAC system energy consumption, degree day and bin methods, can provide only a general estimate based on the averaged weather data. Their use is limited to first-order energy consumption estimates. The introduction of computer methods in the early 1960s enabled the development of several different simulation methodologies and over a dozen energy simulation programs.

Energy simulation programs use two different methods for the calculation of heating/cooling loads: the weighting factor method and the energy balance method. The weighting factor method is older and simpler than the energy balance method. Based on building materials, weighting factors are precalculated for different building components. The weighting factors express the convective gains over the total heat gain incoming on a building element in a time sequence. The data based off of the weighting factor for different elements is used to calculate the cooling loads. The energy simulation programs DOE-1 and DOE-2 are the most popular representatives of this simulation technology.

The energy balance method is currently used by the most popular energy simulation programs such as EnergyPlus and ESP-r. The energy balance method uses a heat balance for each zone, typically a single space, in a building. Each building zone surface has conductive, convective, and radiative heat fluxes in balance. All of the energy balance equations are put together in a matrix to resolve all of the zone fluxes simultaneously. The energy balance equation for the zone air is

$$\sum_{i=1}^N \dot{q}_{i,c} A_i + \dot{Q}_{\text{lights}} + \dot{Q}_{\text{people}} + \dot{Q}_{\text{appliances}} + \dot{Q}_{\text{infiltration}} - \dot{Q}_{\text{heat_extraction}} = \frac{\rho \dot{V}_{\text{room}} c_p \Delta T}{\Delta t} \quad (26)$$

where $\sum_{i=1}^N \dot{q}_{i,c} A_i$ is the convective heat transfer from enclosure surfaces to room air, N is the number of enclosure surfaces, A_i is the area of surface i , \dot{Q}_{lights} , \dot{Q}_{people} , $\dot{Q}_{\text{appliances}}$, and $\dot{Q}_{\text{infiltration}}$

are the cooling loads of lights, people, appliances, and infiltration, respectively, $\dot{Q}_{\text{heat_extraction}}$ is the heat extraction via HVAC device (equal to cooling loads), $\rho \dot{V}_{\text{room}} c_p \Delta T / \Delta t$ is the room air energy change, ρ is the air density, \dot{V}_{room} is the room volume flow rate, c_p is the air specific heat, ΔT is the temperature change of room air, and Δt is the sampling time interval.

The energy balance method results not only in the energy requirement data to heat and cool a building hour by hour, but also the surface temperature distribution and an average air temperature needed to evaluate the thermal comfort in a building zone.

6.2 Airflow Simulation Programs

The first generation of airflow simulation programs for buildings used multizone models to estimate the building infiltration rates for energy simulation programs. Multizone models define a zone in a building that is connected to other zones by flow paths both among zones and to the outside environment. In each zone (room), perfect mixing is assumed with uniform density, temperature, velocities, and species concentration. Mass balance and energy conservation are applied to each zone:

Mass balance:

$$\frac{dM_i}{dt} = \sum_{j=1}^n m_{ij} + m_{\text{source}} + m_{\text{sink}} \quad (27)$$

Energy conservation:

$$\frac{dQ_i}{dt} = \sum_{j=1}^n q_{ij} + q_{\text{source}} + q_{\text{sink}} \quad (28)$$

where M_i is the mass in zone i ; Q_i is the thermal energy in zone i ; $\sum_{j=1}^n m_{ij}$ is the sum of mass transported to zone i from other zones, $i \neq j$; $\sum_{j=1}^n q_{ij}$ is the sum of thermal energy transferred to zone i from other zones, $i \neq j$; m_{source} is the mass (rate) generated by the source in zone i ; q_{source} is the thermal energy generated by the sources in zone i ; m_{sink} is the mass removed from the zone, and q_{sink} is the thermal energy removed from zone i .

Flow paths (elements) connect zones and allow airflow in one or both directions. The flow between different zones is usually driven by a pressure and/or temperature difference, so the wind data and outdoor temperatures can be used to estimate infiltration flow rates.

Multizone models have benefits and drawbacks. A major benefit of multizone models is that they can quickly calculate the airflow, heat flux, or contaminant transportation between different zones (rooms) in an entire building. Furthermore, specifying building zones is relatively simple because boundary conditions such as walls, windows, and supply/exhaust do not require detailed specifications. The simplicity of multizone models, on the other hand, does not allow them to provide detailed information on the airflow pattern, velocity, temperature, and concentration distributions in individual rooms (zones). However, more complicated programs based on computational fluid dynamics (CFD) are capable of predicting all those distributions with accuracy.

CFD programs numerically solve a set of partial differential equations for the conservation of mass, momentum (Navier–Stokes equations), energy, and species concentration. There are three groups of numerical methods for solving the equations: control volume, finite element, and spectral methods. The control volume method is widely used in CFD for building environment simulations. This CFD model divides a single room into fine control volumes, order(s) of magnitude smaller than the building zones. Typically, a control volume would be anywhere between 1 and 10 cm³. In each control volume, a uniform density, temperature, velocity, and species concentration is assumed. Also, each control volume has to satisfy mass (in the form of the continuity equation), momentum, energy, and species conservation. The major difference

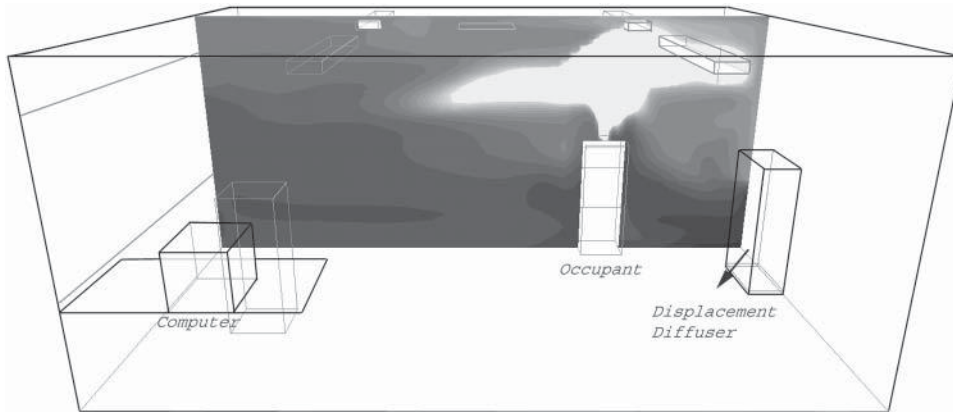


Figure 11 CFD result for CO₂ distribution in an office with displacement ventilation (blue, fresh air with CO₂ around 350 ppm; red, room air with CO₂ over 1000 ppm).

between the multizone and CFD models is the additional momentum equations used in the CFD model:

$$\frac{\partial \rho U_i}{\partial t} + \frac{\partial \rho U_i U_j}{\partial x_j} = -\frac{\partial P}{\partial x_i} + \frac{\partial}{\partial x_j} \left[\mu_{\text{eff}} \left(\frac{\partial U_i}{\partial x_j} + \frac{\partial U_j}{\partial x_i} \right) \right] + \rho \beta (T_0 - T) g_i \quad (28)$$

where U_j is the mean velocity component in the x_j direction, P is the mean pressure, μ_{eff} is the effective viscosity, β is the thermal expansion coefficient of air, T_0 is the temperature of the reference point, T is the mean temperature, and g_i is the gravity acceleration in the i direction.

The major benefit of CFD models is their capability to provide detailed results for three-dimensional distributions of air velocity, temperature, and species concentration in a room. Figure 11 shows a distribution of carbon dioxide from two occupants in an office with displacement ventilation, which has a supply diffuser at the floor level. However, CFD requires much more computing time and much more detailed boundary conditions compared to the multizone model. For example, the computing time for a single room would be several hours with the CFD model but only a few seconds with the multizone model. Furthermore, the boundary conditions such as walls, supply/exhaust, sources, and sinks must be defined not only by their properties but also by their detailed locations. As a result, and due to the extensive computation time, using CFD for practical engineering design is challenging, especially when an entire building is being analyzed.

6.3 Coupled Simulation Tools

Each of the building simulation programs has a function in improving building environment design. Due to the rapid increase in computation capacity, a new trend in building simulation technology is under way. Each building simulation program has advantages and disadvantages, so coupling of simulation tools is the way to mitigate respective weaknesses and create a new generation of building environment simulation programs. For example, coupled energy simulations and CFD can provide more accurate predictions of cooling loads for different cooling and heating systems. Furthermore, coupling of multizone and CFD models has shown how CFD models can help increase the accuracy of multizone models while the multizone model eliminates the requirement of applying CFD to the entire building.¹¹ Future generations of building simulation software will integrate all the components: energy, CFD, and multizonal modeling.

Such a sophisticated tool will allow building HVAC designers to accurately calculate the heating/cooling load, thermal comfort, indoor air quality, and contaminant concentrations while exploring different innovative HVAC solutions.

7 EQUIPMENT FOR ENVIRONMENTAL CONTROL

The capacity of the HVAC equipment based on indoor and outdoor design conditions and U factors for envelope assemblies or load simulation programs gives the HVAC equipment the capacity to handle the peak design conditions. It is important to notice that besides the performance requirements (removal of contaminants) and capacity requirements (building loads), an HVAC system also needs to satisfy spatial, initial cost, operating cost, reliability, flexibility, maintainability, and other special requirements. HVAC systems are typically coupled with heating/cooling production systems such as boilers for production of hot water or steam and chillers for production of cold refrigerant. Based on the fluid used to condition building spaces, an HVAC system can be all-air, air–water, or all-water systems. In the United States, all-air systems are the most widely used for environmental control. These systems include air-handling, air distribution, and control systems.

7.1 Air-Handling and Distribution Systems

Air-handling and distribution systems have a capacity calculated based on the design thermal loads. Heaters, coolers, and humidifiers are sized for the air-handling system, while supply/exhaust diffusers, ducts, and supply/return fans are sized for the air distribution systems. The air-handling unit calculations use the equations derived from the first law of thermodynamics and conservation of mass as outlined in Section 2 on basic air-handling processes. Once the air-handling unit is selected, the air distribution system is designed based on the airflow supply rate required by the air-handling unit. The procedure for diffuser design includes the selection of supply and return diffuser types, numbers, and locations. The diffuser selection is based on the diffuser manufacturer catalogs. From each of the diffusers, a duct branch has to be laid out. The duct and diffuser layout enables calculations of the total pressure drop in the distribution system based on the equal friction or static regain method. Finally, based on the total pressure drop, supply/return fans are selected. In this way, HVAC air-handling and distribution systems are designed for the peak loads.

7.2 Control Systems

The HVAC systems only occasionally operate under peak loads. Most of the time HVAC systems work under partial or so-called off-design loads. For off-design conditions, an HVAC system needs a control system to regulate its capacity, otherwise the building spaces would be too hot in winter or too cold in summer. Based on the first law of thermodynamics and under uniform indoor design conditions, the regulation could occur by changing the flow rate of the supply airstream while keeping all the other parameters constant. This system of control by variable air volume (VAV) flow rates is the most widely used system in the United States. Another way of controlling an all-air system is by modulating the supply air dry-bulb temperature. This system is called a constant air volume (CAV) control system. CAV offers fine regulation of indoor air parameters, but it is not often installed due to the high penalties in energy prices.

The essential components of a control system are controlled variable, sensor, controller, and controlled device. The controlled variable is a characteristic or parameter of HVAC systems to be regulated. In particular, a “set point” is the desired value, while a “control point” is the actual value of the regulated parameter. For example, the set point is the temperature set on

the dial of a thermostat, while the control point is the temperature measured by a thermocouple in the same zone with the thermostat. The “error” or “offset” is the difference between the set and control points. The sensor measures the actual value of the controlled variable such as the thermostat in the above-mentioned example. The controller modifies the action of the controlled device in response to error, and the controlled device acts to modify controlled variable as directed by the controller. The controller could be a valve controller connected to the thermocouple and thermostat, while the controlled device could be the steam valve regulating the flow rate of the steam for space heating.

The control system action control could be a two-position (on–off) control or a modulating control. The two-position system is commonly installed with HVAC systems due to its low cost, but it is relatively imprecise. Modulating control systems produce continuously variable output over a range. This is a finer control system than the two-position system, and is typically found in large HVAC systems. The modulating control system could be proportional, proportional plus integral (PI), or proportional plus integral plus derivative (PID). The simplest control system resulting in the control of only required parameters is typically selected. Overly complicated systems prove inefficient as they tend to be difficult and expensive to operate and maintain. Initial cost considerations also play an important role in the selection of a control system.

REFERENCES

1. G. Constable, and B. Somerville, *2003 A Century of Innovation: Twenty Engineering Achievements That Transformed Our Lives*, Joseph Henry Press, Washington, DC, 2003.
2. RECS, *The Residential Energy Consumption Survey*, U.S. Energy Information Administration, Washington, DC, 1997.
3. CBECS, *The Commercial Buildings Energy Consumption Survey*, U.S. Energy Information Administration, Washington, DC, 1990.
4. NASA, *U.S Standard Atmosphere*, National Oceanic and Atmospheric Administration, National Aeronautics and Space Administration, Washington, DC, 1976.
5. ASHRAE, *ASHARE Handbook of Fundamentals*, American Society of Heating, Ventilating and Air-Conditioning Engineers, Atlanta, GA, 2009.
6. ANSI/ASHRAE, Standard 55-2010, “Thermal Environmental Conditions for Human Occupancy,” American Society of Heating, Ventilating and Air-Conditioning Engineers, Atlanta, GA, 2010.
7. P. O. Fanger, *Thermal Comfort Analysis and Applications in Environmental Engineering*, McGraw-Hill, New York, 1970.
8. ANSI/ASHRAE, Standard 62-2010, “Ventilation for Acceptable Indoor Air Quality,” American Society of Heating, Ventilating and Air-Conditioning Engineers, Atlanta, GA, 2010.
9. L. Molhave, J. G. Jensen, and S. Larsen, “Subjective Reactions to Volatile Organic Compounds as Air Pollutants,” *Atmos. Environ.*, **25A**(7), 1283–1293, 1991.
10. ASHRAE/IES. Standard 90.1-2010, “Energy Standard for Buildings Except Low-Rise Residential Buildings,” American Society of Heating, Ventilating and Air-Conditioning Engineers, Atlanta, GA, 2010.
11. J. Srebric, “Building Performance Simulation for Design and Operation,” in J. L. M. Hensen and R. Lamberts, (eds.) *Ventilation Performance Prediction*, Taylor & Francis Group, Oxford, UK, 2011.

CHAPTER 16

THERMAL SYSTEMS OPTIMIZATION

Vikrant C. Aute
University of Maryland
College Park, Maryland

1 INTRODUCTION	599	4.1 Design of Experiment	616
2 OPTIMIZATION TOOLBOX	600	4.2 Metamodeling Techniques	616
2.1 System Evaluation	600	4.3 Verification	617
2.2 Engineering-Level System Simulation	600	4.4 Parallel Parameterized CFD	617
2.3 Optimization Drivers	605	4.5 Offline versus Online Approximation-Assisted Optimization	618
3 METHODOLOGY	607	4.6 Examples	618
3.1 Case Studies	607	REFERENCES	631
4 APPROXIMATION-ASSISTED OPTIMIZATION	614	BIBLIOGRAPHY	632

1 INTRODUCTION

Thermal systems include all functional groups of equipment and working fluids that are designed for the purpose of managing temperature and humidity conditions inside various spaces or materials. The purpose of the thermal management can be to provide comfort, to establish and maintain conditions necessary for the functionality of other equipment, or to utilize the change of thermophysical properties of materials for energy conversion. Examples reach from thermal management of electronic systems (electronic cooling) over space conditioning to power generation.

Optimization is the systematic procedure that guides the system designer in her/his choice of processes and components such that all requirements for the system are balanced in the best fashion possible. In most applications the designer has to balance several contradicting demands, such as high efficiency and reliability versus low costs and emissions, etc. In order to keep the design time and associated costs as low as possible, it is essential to take all requirements of the thermal system into account at the earliest possible design stage. Often a great amount of time and costs can be saved if the design engineer has means to evaluate the approximate costs of a design in the early stages of the development.

The optimization of thermal systems usually includes a mixture of technology decisions and the optimization of specific properties of selected components. An example is the decision between tube-fin and microchannel technology for an air-refrigerant heat exchanger in the air-conditioning system of a commercial building and the subsequent optimization of tube diameter/channel geometry and fin spacing. The system designer should find the least expensive designs for each technology that provide the required performance, in this example heat load at minimum fan power consumption. An informed decision can only be reached if the best options of all feasible technologies are compared. Additionally, other factors have to be considered: The best microchannel heat exchanger may be more expensive than the best fin-tube heat

exchanger but may require a smaller fan and thus lead to savings at other system components. This simple example shows that the optimization of thermal systems requires the evaluation of entire system performance and costs. The system designer must conduct the component optimization and selection with the system perspective in mind.

More advanced approximation-assisted optimization techniques are presented at the end of this chapter to efficiently optimize computationally expensive heat exchanger models. Two examples are presented for chevron plate heat exchanger segment optimization and the new generation of air-cooled heat exchanger optimization.

2 OPTIMIZATION TOOLBOX

Optimizing thermal systems requires evaluating, comparing, and modifying large numbers of design options. The system evaluation usually includes an evaluation on the engineering level, for instance, efficiency, reliability etc., and an evaluation on the accounting level, such as first and operating costs. In order to evaluate a large number of design options, it is helpful to employ a computer simulation tool (or a collection of tools) that is capable of predicting the system performance and system costs with sufficient accuracy. Section 2.1 describes a formulation of the simulation of general energy conversion systems.

The system designer must develop a basis of comparison for the various design options. This can be a single parameter of the system performance or cost but usually is a combination of many parameters. If the relative importance of the significant parameters is known in advance, the designer can formulate a weighted penalty function, which assigns a characteristic value to each design option. If the relative importance is not known a priori, the design task becomes a multiobjective optimization problem. In this case the optimization procedure should determine a Pareto-optimum set of solutions (see Section 2.3).

The optimization driver derives new design options based on the comparison of evaluated options. Section 2.3 illustrates a number of optimization drivers with their advantages and disadvantages. The selection of the appropriate driver for the optimization problem is essential for the success of the design process.

2.1 System Evaluation

In most design optimization problems the designer has to take into consideration engineering-level parameters of the thermal system as well as accounting-level parameters. The engineering-level evaluation includes parameters such as system efficiency, reliability, noise and vibration, emissions, etc. This level of evaluation requires a physics-based simulation of the system, which is sufficiently detailed to reflect the effects of relevant component variations on the system performance. The accounting-level evaluation requires a cost model for the system and its components that is sufficiently detailed to reflect the effect of component variations on the overall costs.

2.2 Engineering-Level System Simulation

Thermal systems can generally be described as networks of components and their interaction with the environment. System components are connected by junctions, through which they exchange flow rates as a result of driving forces imposed by the states of the junctions. A large number of component models typically encountered in thermal systems are presented throughout this volume of the handbook. The component models should be physics-based descriptions of the component with a level of detail that allows evaluating the effect of changes of optimization parameters on the component and system performance. If, for instance, the heat transfer

area of a heat exchanger is an optimization parameter, the model of the heat exchanger must reflect the effect of a change in heat transfer area on the performance (as opposed to using a constant heat exchanger effectiveness).

An appropriate mathematical description of the system results in a system of residual equations, which has to be solved numerically. The residuals can be formulated by the differences of flow rates (mass flow rates, heat flow rates, etc.) entering and leaving a junction. Figure 1 illustrates this on the example of a vapor compression system at steady-state conditions. Table 1 lists the residual equations. Flow rates leaving a component are associated with a negative sign, and flow rate entering a component has a positive sign. Table 2 gives examples for the forms of the component equations for steady-state conditions.

The residual equations can be passed to an equation solver. A list of solvers is given in the following section. If the network representation of the system is not very complex, in particular if there are no splits or mergers of streams, the residual equations can be simplified as illustrated in Table 3.

Alternative residual and component equations can be formulated, and the choice of the appropriate formulation can have a significant influence on the convergence of the simulation.

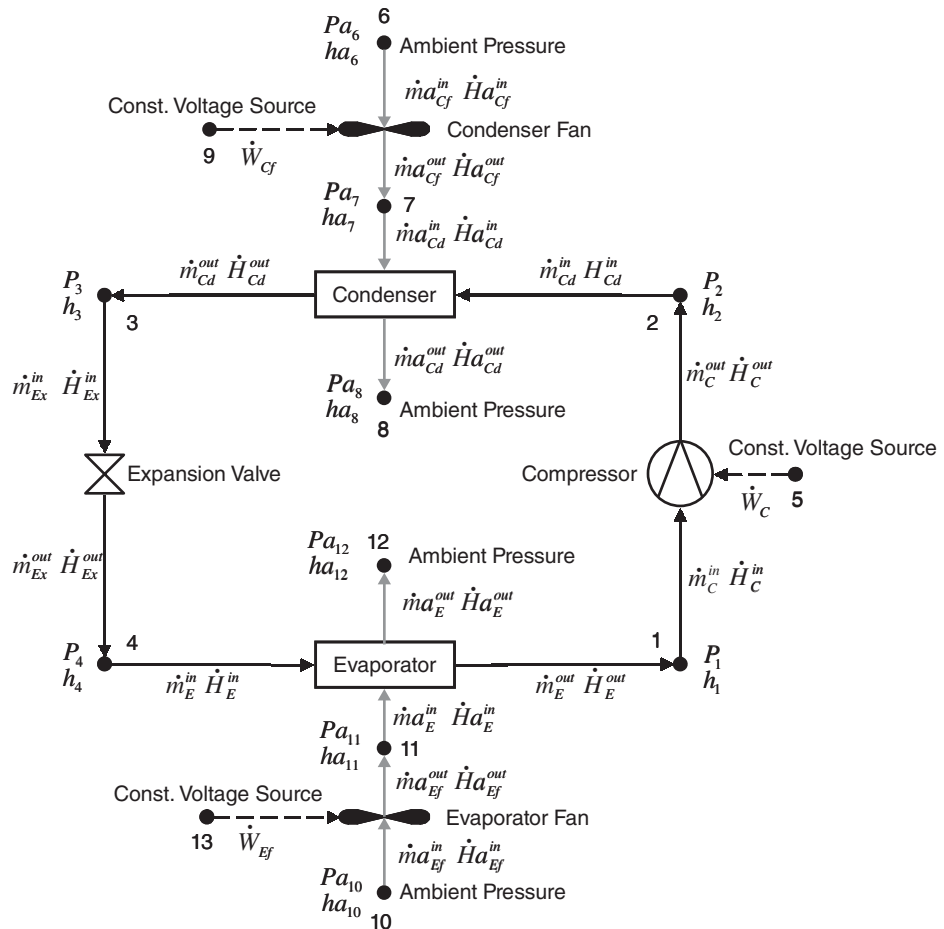


Figure 1 Network representation of vapor compression system with air fans.

Table 1 Residual Equations for Vapor Compression System

$R_1 = \dot{m}_C^{\text{out}} + \dot{m}_{Cd}^{\text{in}}$	$R_4 = -M_{\text{System}} + M_C + M_{Cd} + M_{Ex} + M_E$
$R_2 = \dot{m}_{Cd}^{\text{out}} + \dot{m}_{Ex}^{\text{in}}$	$R_5 = \dot{m}_{Cf}^{\text{out}} + \dot{m}_{Cd}^{\text{in}}$
$R_3 = \dot{m}_{Ex}^{\text{out}} + \dot{m}_E^{\text{in}}$	$R_6 = \dot{m}_{Ef}^{\text{out}} + \dot{m}_E^{\text{in}}$
$R_4 = \dot{m}_E^{\text{out}} + \dot{m}_C^{\text{in}}$	

Table 2 Examples for Forms of Component Equations at Steady State

$ \dot{m}_C^{\text{in}} = \dot{m}_C^{\text{out}} = \dot{m}_C$
$\dot{m}_C, h_2 = f_C(P_1, h_1, P_2, \text{compressor parameter})$
$ \dot{m}_{Cd}^{\text{in}} = \dot{m}_{Cd}^{\text{out}} = \dot{m}_{Cd}$
$ \dot{m}_{Cd}^{\text{in}} = \dot{m}_{Cd}^{\text{out}} = \dot{m}_{Cd}$
$\dot{m}_{Cd}, h_3, \dot{m}_{Cd}, ha_8 = f_{Cd}(P_1, h_1, P_2, Pa_7, ha_7, Pa_8, \text{condenser parameter})$
$ \dot{m}_{Cf}^{\text{in}} = \dot{m}_{Cf}^{\text{out}} = \dot{m}_{Cf}$
$\dot{m}_{Cf}, h_7 = f_{Cf}(Pa_6, ha_6, Pa_7, \text{condenser fan parameter})$
...

Table 3 Simplified Residual Equations for System without Splits and Mergers

$0 = \dot{m}_C^{\text{out}} + \dot{m}_{Cd}^{\text{in}}$	$R_2 = M_{\text{System}} + M_C + M_{Cd} + M_{Ex} + M_E$
$0 = \dot{m}_{Cd}^{\text{out}} + \dot{m}_{Ex}^{\text{in}}$	$R_3 = \dot{m}_{Cf}^{\text{out}} + \dot{m}_{Cd}^{\text{in}}$
$0 = \dot{m}_{Ex}^{\text{out}} + \dot{m}_E^{\text{in}}$	$R_4 = \dot{m}_{Ef}^{\text{out}} + \dot{m}_E^{\text{in}}$
$R_1 = \dot{m}_E^{\text{out}} + \dot{m}_C^{\text{in}}$	

The convergence of numerical equation solvers typically depends on the quality of the initial guess values. Special care must be given to provide good guess values to the equation solver. Other sources of divergence are invalid inputs to thermophysical property functions and invalid inputs to component models. Both instances can occur during the course of the iteration and may cause the termination of the simulation, which might have been successful if the functions would have handled the instance appropriately. For instance, instead of terminating the execution of the simulation if a function call attempts to compute the density of a fluid at negative absolute pressure, the function could return the lower limit of the density and report a warning to the user. The low density may produce a high value of the residual equation and may cause the iteration to step into a more appropriate direction. The success of a simulation can often be greatly enhanced when all functions and subroutines are as robust as possible and return appropriate outputs for all input values.

Other system parameters, such as reliability or noise and vibration, can be associated with the system design through specific correlations provided by component manufacturers, though test data that are accessible to the simulation through databases or other means available to the system designer.

The general approach illustrated on the example of a vapor compression system can be applied to all thermal systems by substituting the junction properties, flow rates, and component models with the appropriate variables and models.

Equation Solvers

Simultaneous equation solving is frequently an integral part of any mathematical model. The available equation solvers can be classified based on the types of equations they solve, as follows:

1. *Simultaneous linear equations.* These solve problems of the form $\mathbf{AX} = \mathbf{B}$, where \mathbf{A} , \mathbf{X} , and \mathbf{B} are matrices of order $\mathbf{m} \times \mathbf{n}$, \mathbf{m} , and \mathbf{n} , respectively. Many routines are available for these types of problems, like the LU decomposition, QR decomposition, etc.¹
2. *Simultaneous nonlinear equations.* These methods will be discussed here.

One-dimensional equation solving or problems with one variable and one unknown are seldom encountered in thermal systems simulation and optimization. This section discusses gradient-based algorithms for solving multiple simultaneous equations. Other methods for one-dimensional root finding are available but not discussed here. The reader is referred to Press et al.¹

The general algorithm for a gradient-based nonlinear equation solver can be summarized as follows:

1. Get an initial guess \mathbf{x}_0 .
2. Get an initial value for Jacobian matrix \mathbf{J} . \mathbf{J} is the transpose of the matrix of the gradients.
3. $\mathbf{x}_i = \mathbf{x}_0$.
4. Compute new direction and step \mathbf{s} .
5. Compute new \mathbf{x} and the length α .

$$\mathbf{x}_{i+1} = \mathbf{x}_i + \alpha \mathbf{s}_i$$
6. Test convergence.
7. Compute \mathbf{J}_{i+1} .
8. Repeat from step 4.

Several schemes are available for calculating the new direction \mathbf{s} , the step length α , and the convergence criteria and for computing the Jacobian for subsequent time steps. A summary of all of these schemes is provided in the following text. This list of equation-solving schemes is not meant to be complete.

Let

\mathbf{G} denote the gradient matrix of \mathbf{f} .

\mathbf{H} denote the inverse of \mathbf{J} , i.e., \mathbf{J}^{-1} .

\mathbf{f} denote the vector of function values and $\|\cdot\|$ denote the Euclidian norm.

$$\mathbf{y}_i = \mathbf{f}_{i+1} - \mathbf{f}_i$$

Other methods based on the second derivatives are also available in the literature.

Cost Estimation

In contrast to the engineering-level system simulation the cost estimation is less challenging on a mathematical level. The challenge in accurately estimating the cost of a thermal system arises from the availability and uncertainty of cost data. Cost data vary with the source that they are obtained from; they vary in time and may even be subject to the negotiation skills of the system designer. While most companies can accurately predict the cost of in-house manufacturing, equipment cost estimates from suppliers are less accurate. Fuel and other operating costs probably represent the most volatile cost category. Construction and installation costs can contribute significantly to the total costs depending on size and type of thermal system.

Table 4 Schemes for Calculation of Iteration Step

Scheme Name	Step Calculation	Comments
Steepest decent	$\mathbf{s}_{sd} \equiv \mathbf{s}_i = -\mathbf{G}\mathbf{f}_i$	Search is in the direction in which \mathbf{f} decreases rapidly.
Newton–Raphson	$\mathbf{s}_n \equiv \mathbf{s}_i = -\mathbf{H}_i\mathbf{f}_i$ $\alpha = 1$	The most basic method of all. Very efficient, with quadratic convergence close to the solution. Involves the calculation of \mathbf{H} at every iteration.
Broyden’s method (unmodified)	$\mathbf{s}_i = -\mathbf{H}_i\mathbf{f}_i$ $\alpha : \ \mathbf{f}_{i+1}\ < \ \mathbf{f}_i\ $ $\mathbf{H}_{i+1} = \mathbf{H}_i - (\mathbf{H}_i\mathbf{y}_i - \mathbf{s}_i\alpha_i)\mathbf{s}_i^T\mathbf{H}_i/\mathbf{s}_i^T\mathbf{H}_i\mathbf{y}_i$	The inverse of the Jacobian is required only at the first step of iterations. In subsequent steps, it is updated using the strategy shown.
Levenberg Marquardt method	$\mathbf{s}_{lm} \equiv$ Obtained by solving $(\mathbf{J}^T\mathbf{J} + \mu\mathbf{I})\mathbf{s}_{lm} = -\mathbf{G}\mathbf{f}$ μ is damping parameter, updated at each step.	Method used for nonlinear least-squares problem and nonlinear equation solving. Can be combined with secant updates to avoid repeated Jacobian calculations.
Powell’s dogleg method	Alternates between the Newton step and the steepest descent step. Radius of trust region updated at every iteration. ²	Based on the concept of trust region. Can be combined with secant updates to avoid repeated Jacobian calculations.

Table 5 Different Stopping Criteria Used in Nonlinear Equation Solving

Stopping Criteria	Representation	Comments
Function residuals	$\ \mathbf{f}\ \leq \epsilon$ ϵ is some tolerance value	Most used criteria
Change in solution in successive steps	$\text{rel}(\mathbf{x}_i)_j \leq \epsilon$ $\text{rel}(x_i)_j = \frac{ (x_i)_j - (x_{i-1})_j }{\max\{ (x_i)_j , \text{typ}(x_i)_j\}}$ $(\mathbf{x}_i)_j = j$ th component of x in the i th iteration.	Indication that the algorithm has stalled.
Maximum value of the components of \mathbf{f}	$\ \mathbf{f}\ _\infty \leq \epsilon$	

A large number of costs for components in thermal systems are provided in cost-estimating guides such as *Building Construction Cost Data* by RS Means,³ *Chemical Engineering Volume 6: Chemical Engineering Design*,⁴ and *Thermal Design and Optimization* by Bejan et al.⁵ along with methods for estimating fuel, operating, construction, and installation costs. These references generally provide component cost data associated with characteristic parameters for the equipment, such as heat transfer area as a parameter for the costs of the heat exchanger. Whenever possible it is recommended to obtain cost data directly from the equipment supplier.

Cost data typically present a discontinuous variable in the system simulation since they often do not scale continuously with equipment size. The optimization procedure can either interpolate over the discontinuities and round the optimization result to the closest available equipment size or can treat the cost as a discontinuous function. In this case, it is necessary to use an optimization driver that is capable of handling discontinuous variables, such as genetic algorithms.

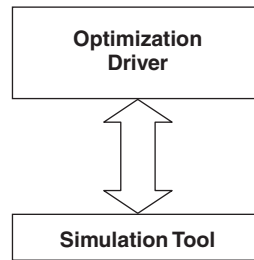


Figure 2 Engineering optimization process.

2.3 Optimization Drivers

An engineering optimization process in its simplest form can be visualized as show in Fig. 2.

There are two basic components, the optimization driver and the simulation tool. The optimization driver is a numerical implementation of some optimization algorithm. This optimization driver needs a function that can, with a given set of inputs (the design variables over which we optimize) provide the output (the objective value that we wish to optimize) and any other relevant simulation information, such as constraints.

From an implementation point of view, the above approach also demonstrates the power of component-based computer code development. Here we assume that eventually all of the optimization algorithms and the system and component models are used in the form of computer code. Ideally, the user would want to have a library of optimization routines or drives, from which the user can choose an optimization routine or adopt a hybrid approach wherein the intermediate results of one routine are fed to another more effective routine. Similarly the user would want to have a library of component models. For example, a shell-and-tube heat exchanger model, an air-cooled heat exchanger model, a turbine model, a compressor model, etc. These models can then be put together to assemble a thermal system or can be used individually to evaluate component performance. This component-based approach allows the user to achieve system-level objectives with the freedom of changing the lowest level (individual component) variables.

The simulation tool is the numerical model of the thermal system or the component, for example, the model of a vapor compression cycle or the model of an air-cooled heat exchanger.

Choosing an optimization driver

After having a library of optimization routines and the required component models to design and optimize a system, the next logical question is which optimization routine to choose. This section elaborates on several criteria that come into play when making such a decision.

Objectives. Objectives are performance measures that the designer wants to optimize. A vapor compression cycle system coefficient of performance (COP) is an example of an objective. Another example is the cost of the system. The objective function can be linear or nonlinear, continuous or discontinuous in its domain. The designer can have an analytical expression for the objective function or use a result of model simulation.

Independent variables. Independent variables are the variables over which the problem is optimized. These are the variables that are changed/varied during an optimization process to arrive at an optimal solution. The nature of the independent variables needs to be considered. They can be discrete or continuous? For example, the tube length of a heat exchanger is a

continuous variable, whereas the fan model number in an air-handling system is a discrete variable. Whether an objective function value exists for all possible values of the independent variables, or not, this needs to be gracefully conveyed to the optimization driver so that it can proceed in alternate search directions.

Derivative/Gradient Information. The gradient or the derivative information is required to improve the estimates of a solution in a nonlinear equation solving or an optimization process. Gradient computation can be simple if an analytical expression for the gradients is available. Alternatively, the designer can use a finite-difference technique. Using a finite-difference technique will involve additional function calls of the objective function, which might not be feasible when the objective function is computationally expensive.

Number of Objectives. Many real-world problems are multiobjective. Technically, multiobjective optimization is very different from single-objective optimization. In single-objective optimization the driver tries to find a solution that is usually the global minimum or maximum. In contrast, in a multiobjective optimization problem, there may not exist one solution that is superior to other solutions with respect to all the objectives, i.e., one solution might be better with regard to one objective but not with the other and so on. As a result the designer has to make a tradeoff between such solutions. Many times, in a multiobjective optimization problem, there exists a set of solutions that is better than the remaining solutions in the design space with respect to all the objectives, but within this set, the solutions are not better than each other with respect to all the objectives. Such a set is called the Pareto set or the tradeoff set, and the solutions are called Pareto solutions, tradeoff solutions, or nondominated solutions.

The case studies discussed in Section 3.1 will provide a practical example of the above decisions. In conclusion of this section, a relatively new search and optimization technique termed genetic algorithms is introduced, which is also used in the case studies discussed in Section 3.1.

Genetic Algorithms

Genetic algorithms (GA), first put forth by John Holland,⁶ are a part of a broader class of evolutionary computation methods. Based on the principal of natural evolution, they mimic on a mathematical level the biological principals of population, generations, inheritance, and selection of individuals based on the survival of the fittest.

Genetic algorithms maintain a population of candidate solutions. Each of these candidates is evaluated for their fitness in terms of the corresponding objective function value. Then the candidates with the best fitness are transformed, based on crossover and mutation, into new candidate solutions. Thus a new population is created and normally the fitness of the best individual increases from generation to generation.

Some of the advantages of genetic algorithms are explained below:

1. They need only one scalar value, which is the fitness or the objective value of the function that is being optimized. Thus the objective function is a black box object as far as the GA is concerned.
2. They do not need any gradient, i.e., first derivatives or second derivative information. This can result in significant computation savings, if the objective function is computationally expensive.
3. Genetic algorithms maintain a population of candidate solutions, i.e., they simultaneously search in multiple directions as opposed to deterministic search methods that search in one direction at a time.
4. They can handle discrete and continuous variables at the same time.

Representation and Genetic Operators. In a genetic algorithm (binary coded) a given candidate solution known as chromosome is represented as a series of binary digits, viz. 0's and 1's. These chromosomes are manipulated via genetic operators of selection, mutation, and crossover to form new chromosomes or candidate solutions.

The case studies in Section 3.1 demonstrate the use of genetic optimization algorithms for multiobjective optimization problems.

3 METHODOLOGY

The optimization of thermal systems requires the repeated evaluation of physics-based system simulations and cost functions. The number of system evaluations ranges from a few dozen for single-objective low-dimensional optimization tasks with deterministic algorithms to tens of thousands of evaluations for multiobjective high-dimensional tasks with nondeterministic schemes. Especially for optimization tasks with large numbers of system evaluations, it is critical to reduce the computational time for the system evaluation by implementing fast simulation methods or by increasing the computer capacity, possibly by parallel computing.

Whenever possible it is recommended to break out separate optimization tasks from the entire system simulation. This method is especially helpful for complex thermal systems. At a stage when the major technology decisions for a system are identified and the optimization focuses on the design of individual component parameters it is often possible to optimize functional groups of the thermal system under the assumption of constant boundary condition between the functional group and the rest of the system. In the design of the vapor compression system from Section 2.1 the optimization task may, for instance, be to find an evaporator–fan combination that provides a certain cooling capacity at minimum cost. Instead of evaluating the performance of the entire system for each evaporator–fan combination during the optimization, the designer can optimize the functional group evaporator, fan, and fan motor. By assuming reasonable values for the evaporator refrigerant inlet pressure and mass flow rate and minimizing the refrigerant pressure drop and cost of the functional group, the designer can find a design close to the optimum. The refrigerant inlet pressure and mass flow rate can be updated repeatedly by evaluating the system performance with the design found in the previous optimization of the functional group. This method can reduce the number of entire system evaluations. However, it may result in a higher number of component evaluations of the functional group, and the designer must base her/his decision for the optimization strategy on experience and sound judgment.

The following case studies illustrate optimization strategies for various thermal systems. The case studies are presented as examples to guide the designer in the development of successful optimization applications. While the general scheme for most optimization tasks is identical—find a system with maximum performance and minimum costs—each optimization task has its individual particularities that make a generalized approach very challenging. In the end the design engineer must use his/her sound understanding of the underlying physics, his/her experience, and creativity.

3.1 Case Studies

Case 1 – Constrained Single-Objective Optimization of an automotive Air-Conditioning System

The objective of this example is to maximize the efficiency measured as coefficient of performance (COP) of the automotive air-conditioning system. The constraint is the cooling capacity and the overall volume of the heat exchangers. Space is a valuable commodity in automotive applications, and the space available for the heat exchangers of the air-conditioning system can usually not be changed once the chassis and engine designs are completed.

The optimization follows the approach of optimizing functional groups separated from the rest of the system as laid out in the introduction of Section 3. While the overall goal of the optimization is maximum efficiency of the system, the heat exchangers are optimized separately from the rest of the system. Three performance parameters of the heat exchangers affect the system efficiency: heat load, refrigerant pressure drop, and air-side pressure drop. The heat load is a constraint determined by the capacity of the system and thus not an optimization objective. The refrigerant and air-side pressure drops are combined in a fitness function f of the form

$$f = \alpha \Delta P_{\text{Refrigerant}} + \beta \Delta P_{\text{Air}}$$

where α and β are weight functions, which must be determined by the designer based on experience or other parameters. The component with the smallest fitness value will perform best in the air-conditioning system.

The optimization is subject to the constraints of a given heat load and a maximum overall volume of the heat exchangers. The heat load for the evaporator is given by the required cooling capacity. The heat load for the condenser is given by the capacity and an estimated energy efficiency of the system:

$$\begin{aligned}\dot{Q}_{\text{Condenser}} &= \dot{Q}_{\text{Evaporator}} + \dot{W}_{\text{Compressor}} \\ \dot{W}_{\text{Compressor}} &= \dot{Q}_{\text{Evaporator}} / \text{COP}\end{aligned}$$

While the COP of the system depends on the performance of the heat exchangers and is thus not known a priori, an experienced designer can start with a good guess for the efficiency, perform the optimization, and update the guess to find a solution closer to the global optimum. For this case study only the first step of this iteration is shown.

The following geometric parameters are variables in this optimization (microchannel heat exchangers are used for the condenser and evaporator):

- Fin spacing
- Fin thickness
- Number of tubes per pass
- Number of ports per tube
- Port height

Figure 3 illustrates the geometric parameters of the microchannel heat exchangers. The heat exchangers are simulated with a detailed, segmented model. The heat exchanger geometry is coded as a binary string and passed to a genetic algorithm. Figure 4 illustrates the condenser and evaporator geometry. Figure 5 shows the network representation of the refrigerant circuit. The starting point for the optimization is the design of commercially available automotive condensers and evaporators.

Figure 6 shows the pressure drop and fitness value of the evaporator over the generation number. Note that the goal of the optimization was to minimize the value of the fitness function.

Table 6 lists the geometric parameters of the original system and the result of the optimization. Figure 7 shows the efficiency and capacity of the original and optimized systems at various temperature conditions and engine speeds. Figure 8 shows the relative performance improvement of the automotive air-conditioning system due to the optimized heat exchangers.

Case 2 – Constrained Multi-Objective Optimization of a Condensing Unit

This study performs a multi-objective optimization of a fan–coil unit with respect to minimizing cost and maximizing heat rejection capacity.⁷

The condensing unit in consideration is a traditional tube–fin heat exchanger. The individual components of the condensing unit include tubes, fins, fans, cabinet, etc. There is also a manufacturing cost associated with these components.

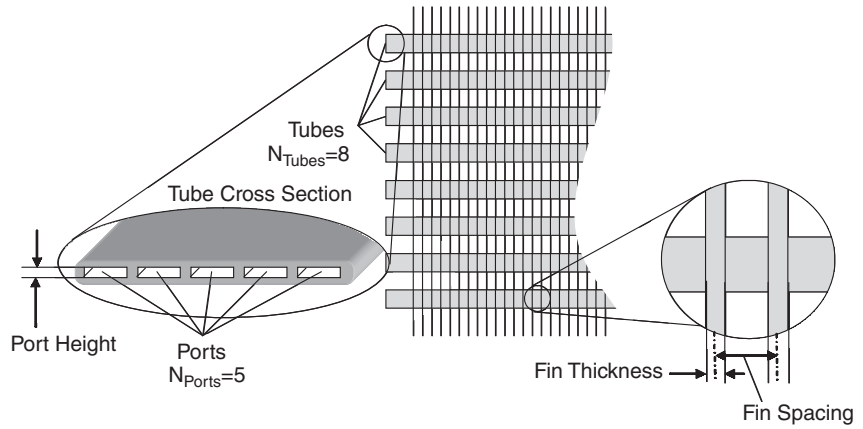


Figure 3 Geometric parameters of microchannel heat exchanger optimization.

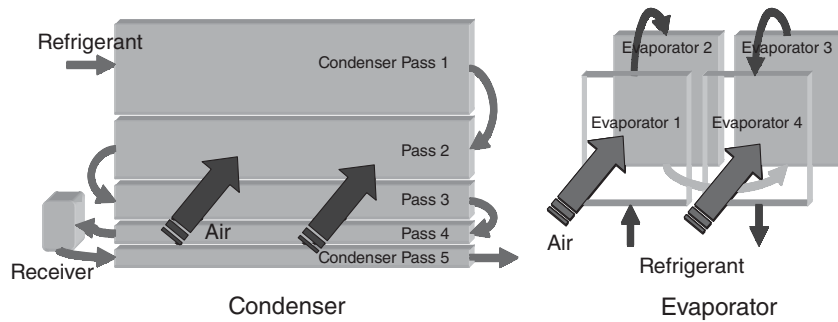


Figure 4 Condenser and evaporator geometry.

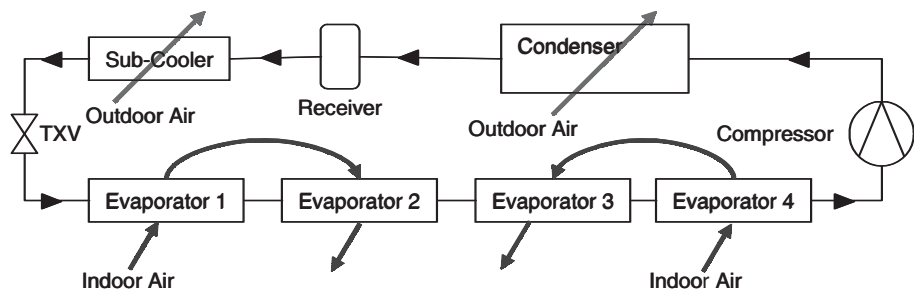


Figure 5 Network representation of automotive refrigerant circuit.

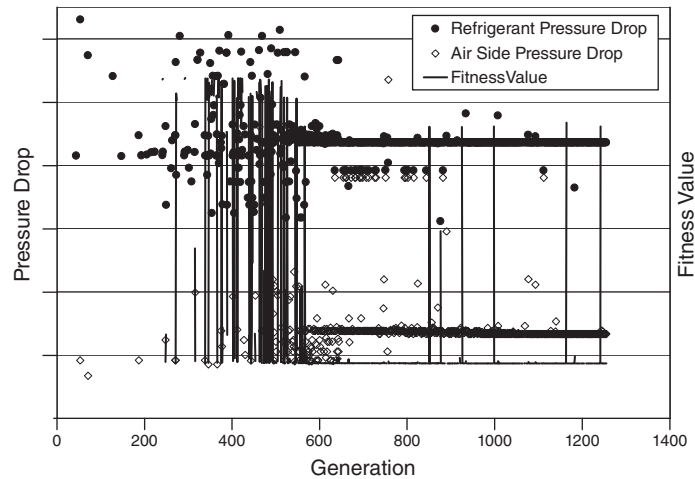


Figure 6 Performance of evaporator over generation number.

Table 6 Geometric Properties of Original and Optimized Heat Exchangers

	Fin Spacing (mm)	Fin Thickness (mm)	Port Height (mm)	No. of Tubes per Pass	No. of Ports per Tube
Original condenser	1.05	0.15	1	18/8/7/4/4	1
Optimized condenser	0.82	0.11	2.48	7/11/5/3/3	4
Original evaporator	0.81	0.15	2.9	9	2
Optimized evaporator	1.31	0.104	2.2	8	4

The independent variables are:

Tube Diameter (OD). Off-the-shelf four different tube sizes are available and being used in this study. The tube diameter sizes are not continuous; as a result there are four discrete choices.

Fin Spacing (FPI). Expressed in terms of fins per inch. The study uses 11 different values ranging from 6 to 16 fins per inch.

Tube Length. Tubes are cut from a coil of tubes; as a result any tube length is possible. This is a continuous variable. From a heat exchanger point of view, the heat rejection capacity increases as the tube length, but so does the cost.

Fan Models (Fan ID). For the particular coil, 20 different fan models are available, along with the required performance data such as static pressure drop, noise, power consumption, frame width, etc.

Number of Fans (NFan). The baseline coil length is fairly long, and hence multiple fans are required to drive the airflow across the coil.

Number of Parallel Circuits. The coil comprises of several parallel refrigerant circuits, with each circuit having a fixed number of tubes. The number of parallel circuits affects the coil height.

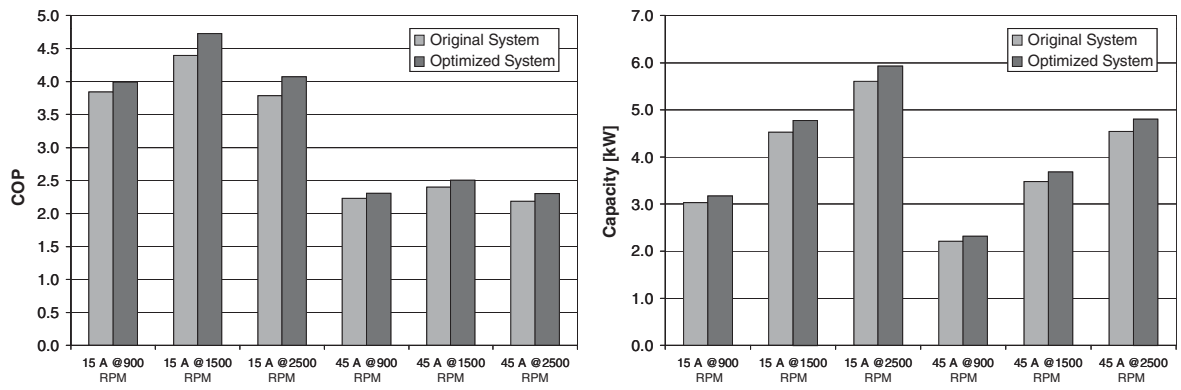


Figure 7 COP and capacity of original and optimized systems.

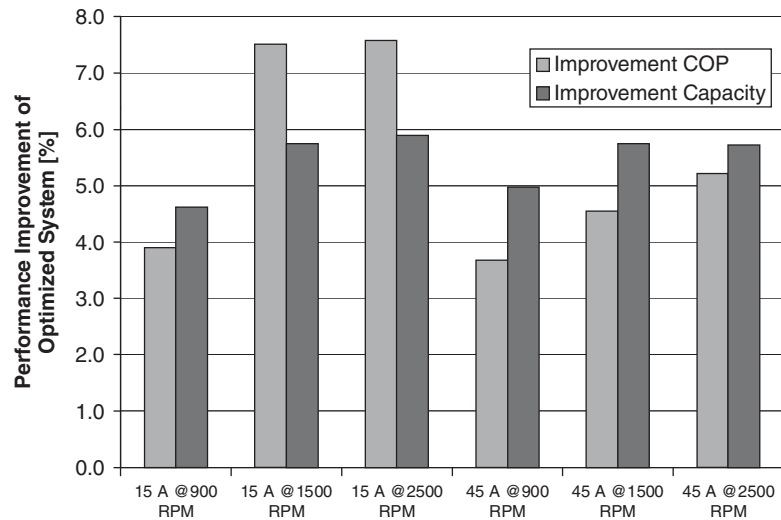


Figure 8 Relative performance improvement of optimized systems.

Table 7 Binary Representation of a Condensing Unit in a Genetic Algorithm

Nt	OD	Fan ID	FPI	NFan	Tube Length													
1	0	0	1	0	1	1	0	0	0	1	1	1	1	0	0	0	0	0

The constraints in this problem include manufacturing as well as performance-based constraints.

Constraint 1. The total combined width of the fans should be less than the specified cabinet width, so that the fans can fit into the cabinet.

Constraint 2. The fan chosen should be able to provide the required static pressure head for the coil, i.e., the fan pressure head should be equal to the air pressure drop through the coil.

Constraint 3. The coil height must be less than a specified maximum height.

Constraint 4. The refrigerant side pressure drop must be within acceptable lower and upper limits.

For this problem a multiobjective genetic algorithm is used. Table 7 shows the representation of a single condensing unit as seen by the genetic algorithm.

As seen from the independent variables and the constraints, the problem has two objectives, four constraints, one continuous variable, and four discrete variables. This is an example of constrained multiobjective optimization with mixed variables. A multiobjective genetic algorithm is used for this problem.

In Fig. 9, the inputs are generated by the optimization algorithms and are supplied to the condenser model. The condenser model is a very detailed simulation based on a segmented approach. After the condenser model is executed, the outputs are transferred to the multiobjective genetic algorithm (MOGA). The condenser model is coupled with the optimization algorithm, wherein the model is evaluated repeatedly with different input-variables until the termination criteria of the genetic algorithm is satisfied. Figure 10 Shows the pseudocode for the multiobjective genetic algorithm.

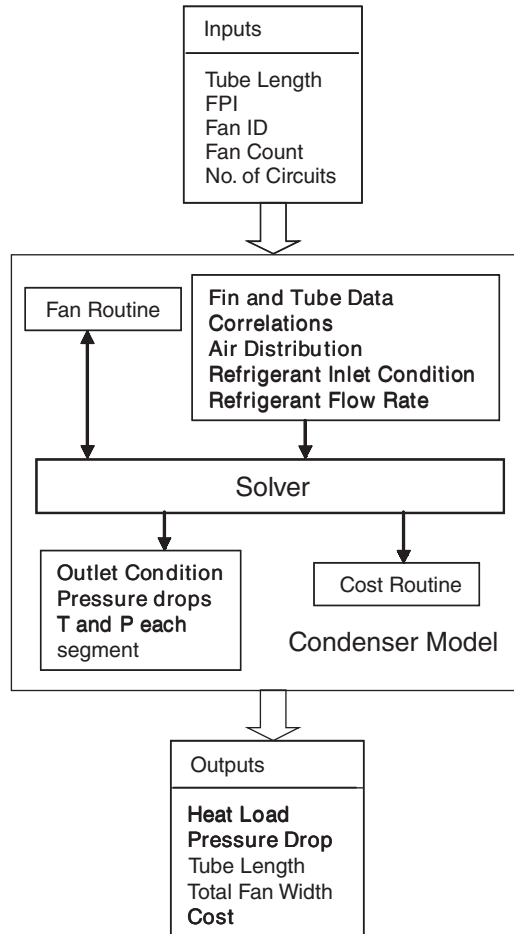


Figure 9 Flowchart of an air-cooled heat exchanger model.

```

Start
Initialize Condenser Model
Initialize GA
While (GA not done) {
  g = g + 1 "Update generation count"
  Evaluate {
    Decode Variables
    Run Condenser Model
    Calculate constraint violation
    Return (Cost, Heat load) and constraint violation
  }
  Perform Non-Dominated Sorting
  Assign Rank
  Assign Fitness
  Perform Selection, Crossover & Mutation
}
Print Results
End
  
```

Figure 10 Pseudocode for multiobjective genetic algorithm used in Case Study 1.

Considering all the choices the total solution space consists of over 125,000 different condensing units. The genetic algorithm evaluated only 5500 of them, which is 4.4% of the total solution space.

The results of the optimization runs are shown in Figs.11–13. Figure 11 shows how the number of Pareto solutions increases with respect to algorithm generations. This is consistent with the principle of natural evolution where successive generations are better or fitter than the previous. Figure 12 shows the Pareto curve for the solution. It can be seen from the figure that there are several different choices for the designer to pick from, and the decision will have to be based on other factors such as fan power requirements, pressure drops, etc. The baseline case is also shown in Fig. 12. It is found that for the same heat rejection capacity it is possible to reduce the coil cost by 16% or for the same coil cost, the heat rejection capacity can be increased by 12%. Figure 13 shows other condensing units evaluated by the genetic algorithm and that were found infeasible, i.e., they violated one or more of the constraints.

For all the given solutions the average reduction in cost is found to be 10% while the average increase in the heat rejection capacity is found to be 7%. It can be concluded that genetic algorithms are a very powerful tool for mixed variable optimization.

4 APPROXIMATION–ASSISTED OPTIMIZATION

It can be seen from the previous examples that, compared to exhaustive search, the use of systematic optimization techniques can yield better solutions to engineering design optimization problems. However, the computational cost is still prohibitive when applying optimization algorithms to computationally expensive simulations such as models based on finite element (FE) or computational fluid dynamics (CFD). One way to address this problem is to use

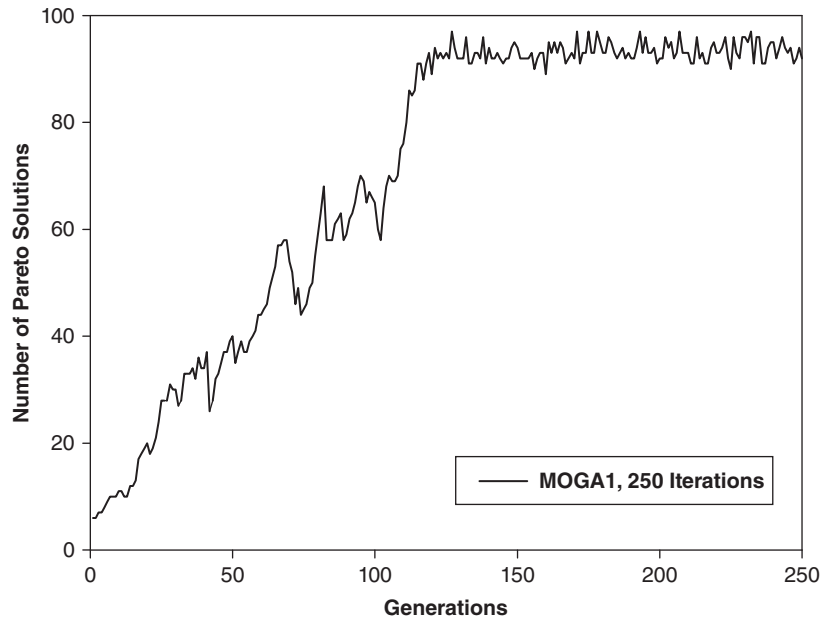


Figure 11 Number of Pareto solutions versus genetic algorithm generations.

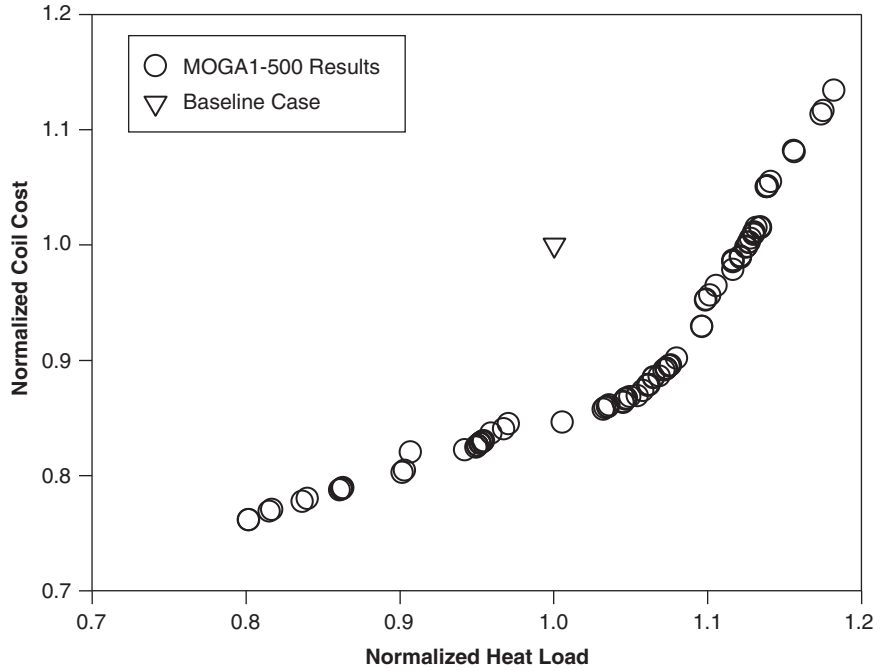


Figure 12 Pareto curve for the results from the multiobjective optimization of a condensing unit.

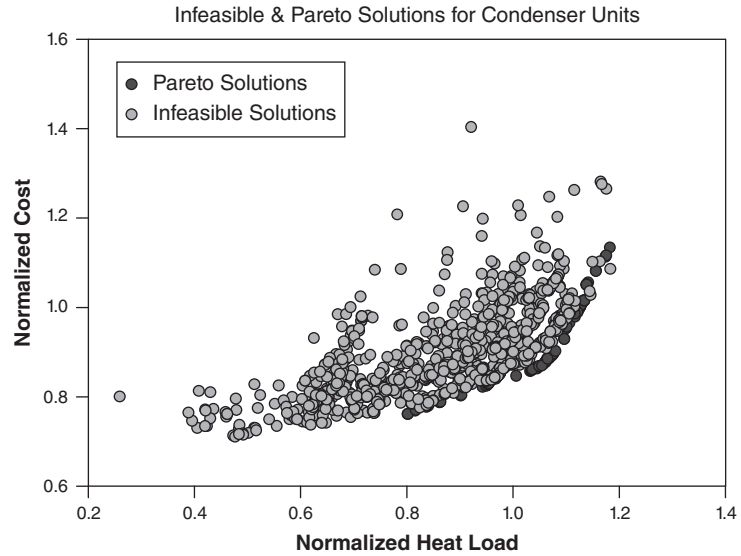


Figure 13 Infeasible and Pareto solution evaluated by genetic algorithm.

approximation-assisted optimization (AAO) techniques.⁸ In general, AAO approaches involve five steps:

1. Design of experiment (DOE) or sampling phase
2. Metamodels development phase
3. Metamodels verification
4. Optimization based on metamodels
5. Optimum solution verification

In the following sections, the main AAO steps are briefly described.

4.1 Design of Experiment

Design of experiment is the first step in any approximation technique. It involves sampling the design space in a proper way. DOE methods can be classified as classical methods, space-filling methods, and adaptive or sequential methods⁸ as presented in Table 8. Maximum Entropy Design (MED) method⁹ is one of the common space-filling methods. In this method, entropy as a measure of information¹⁰ is used to guide selection of sample points in order to increase the amount of information retrieved by adding new samples. Several comprehensive literature reviews of DOE and metamodeling approaches in engineering optimization have been reported.^{8,11,12}

4.2 Metamodeling Techniques

The samples are defined as the points generated using DOE techniques in the design space for which the response (i.e., objective and constraint values) from the computationally expensive simulation is to be evaluated. The samples along with responses are then used to construct simplified models or metamodels for the objective and constraint functions of an optimization

Table 8 Different Metamodeling Techniques

Design of Experiment Method (DOE)	Metamodeling Approach
Classical Methods	Polynomial (linear, quadratic, or higher)
(Fractional) factorial	Splines (linear, cubic, NURBS)
Central composite	Multivariate Adaptive Regression Splines (MARS)
Box–Behnken	Gaussian process
Alphabetical optimal	Kriging
Plackett–Burman	Radial basis functions (RBF)
Space-Filling Methods	Least interpolating polynomials
Simple grids	Artificial neural network (ANN)
Latin hypercube	Knowledge base or decision tree
Orthogonal arrays	Support vector machine (SVM)
Hammersley sequence	Hybrid models
Uniform designs	
Minimax and maxmin	
Hybrid methods	
Random or human selection	
Importance sampling	
Directional simulation	
Discriminative sampling	
Sequential or adaptive methods	

problem. Some popular metamodeling methods in AAO include response surface techniques¹³ such as quadratic polynomial, multilayer neural network, radial basis function, support vector machine, and Gaussian-based methods including Kriging.¹⁴ Several comprehensive reviews of metamodeling approaches in engineering optimization have been reported in the literature.^{8,11,12} Different metamodeling approaches according to sampling, model type, and model fitting are summarized in Table 8. The reader is referred to Wang and Shan¹² for more information.

Kriging¹⁵ is an interpolative Bayesian metamodeling technique. It can be viewed as a linear predictor that estimates the unknown value of a response for an input sample point based on the known value of the response and the distance of the sample from the known design points. Kriging treats the response from a deterministic simulation as a realization of a stochastic process Y :

$$Y = \mu + Z(x)$$

where Y is the unknown response, μ is a constant representing mean of all known response values, and $Z(x)$ represents the error that is modeled by a stochastic process with zero mean, variance of σ^2 , and a nonzero covariance. The quantity Y provides a global approximation of the design space while the term $Z(x)$ creates a localized deviation so that the Kriging metamodel interpolates with respect to the previous observed points. The prediction of the standard error is a unique advantage of Kriging over other metamodeling methods. This allows the metamodel to be dynamically updated based on the responses during a given optimization procedure. Furthermore, Kriging does not require a functional form, though the choice of the correlation functions used in Kriging is problem dependent and can require some trial and error. Simpson et al.⁸ found that Kriging is extremely flexible and suitable for deterministic computer experiments and recommend the use of Kriging metamodels when the number of input variables is less than 50. More detailed introduction about the Kriging method can be found in Jones.¹⁴

4.3 Verification

Once the metamodels are developed, they need to be verified for accuracy. In this step, the prediction from the metamodel is compared with the actual simulation response. There are two types of verifications involved in AAO. The first type is used to verify the globally accurate metamodels before running the optimizer based on metamodels. A set of random samples is generated and evaluated using both the actual simulation and the metamodels' prediction. If the metamodels are accurate enough, an optimizer can run directly based on metamodels; otherwise, more samples are added to improve the metamodels' performance. After running the optimizer based on metamodels, the results obtained are mainly based on metamodel predictions. Thus a second verification step is required to verify the accuracy of the approximated optimum solution.

4.4 Parallel Parameterized CFD

Any approximation-assisted optimization approach of a computationally expensive model especially those that are CFD based requires a large number of CFD simulations to be executed. In such a task, the majority of the engineering time is spent in developing 2D/3D models of the computational domain, meshing them, and setting boundary conditions. In some cases, the CFD runs may require topology change. Therefore, an engineer is required to re-create certain models instead of just scaling existing ones. In order to reduce the engineering time, Abdelaziz et al.¹⁶ introduced a methodology called Parallel parameterized CFD (PPCFD). For the purposes of explanation, we refer to Fluent® (ANSYS, 2010), a commercially available CFD package. Once implemented in computer code, the PPCFD algorithm automatically reads the normalized design variables and then generates the corresponding Gambit® journal files.

In this step, it is very important to correlate the Gambit® journal files to the corresponding design variables. Mesh refinement near the boundaries (boundary layer inflation) is applied based on the design dimensions. A finer mesh is applied as well in the locations where higher temperature gradients are expected, such as near the walls and the thermal and hydraulic entrance regions.

After generating the mesh, the PPCFD algorithm automatically generates Fluent® journal files to read the specified mesh, sets the appropriate boundary conditions, model parameters, and material properties. The materials and boundary conditions are defined in the Fluent® journal files. The main steps in PPCFD can be summarized as follows:

Step 1: Reading of the parametric values of all the CFD cases

Step 2: Automatic generation of Gambit® script files and Fluent® script files

Step 3: Running the scripts and performing postprocessing to summarize the results in terms of relevant thermal and hydraulic performance indicators

It is important to point out that the PPCFD methodology can be applied to any CFD package that supports scripting for all CFD tasks (e.g., modeling, preprocessing, execution, and postprocessing).

In this chapter, PPCFD is used to create the CFD models for the examples described in Section 4.6.

4.5 Offline versus Online Approximation-Assisted Optimization

Most AAO approaches can be classified into two main groups: offline and online. The main difference between these two groups is that metamodels are not updated during offline AAO while they are updated during online AAO. In offline AAO, the metamodels are built, verified, and if they are not accurate enough then more samples are added to improve the metamodels' accuracy. Then the optimization is performed using these metamodels. The offline approach can be computationally expensive as it requires numerous function evaluations to build globally accurate metamodels. Moreover, additional and separate function evaluations are needed to verify the metamodels. On the other hand, in online AAO there is a feedback from the optimizer to update the metamodel using additional and carefully chosen sample points. One significant advantage of online AAO is that the predictive capabilities of the metamodel are progressively improved in the area where the optimum is expected to be, as more sample points are evaluated and added to the sample set. However, one limitation of online AAO is that in the initial stage a poorly estimated metamodel for objective and/or constraint functions can mislead the optimization process into suboptimum or infeasible region of the design space. Depending upon how frequent the metamodels (for objective and constraint functions) are updated, some online AAO approaches update the metamodels only after a certain number of iterations while others update the metamodels at each iteration. Figure 14 shows the difference between offline and online AAO approaches.

4.6 Examples

In this section, two examples are presented for using AAO to optimize a chevron plate heat exchanger segment and an air-cooled heat exchanger with small dimensions.

Chevron Plate Heat Exchanger Optimization

In this example, an efficient online AAO method is used to optimize a chevron plate heat exchanger segment shown in Fig. 15. More details about the CFD model of the Chevron plate heat exchanger segment is presented in Han et al.¹⁷.

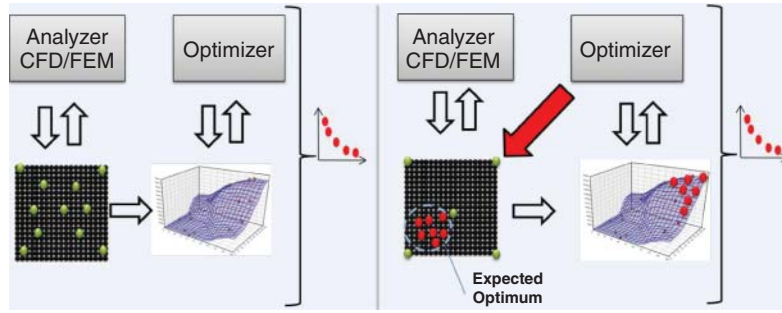


Figure 14 Offline vs. online AAO approaches:(a) offline and (b) online.

The chevron plate heat exchanger segment thermal and hydraulic performance is evaluated in terms of heat transfer coefficient h and pressure drop per unit length $\Delta P/L$, where L is the segment length and ΔP is reported directly from CFD simulation as given in the following equations:

$$h = \frac{Q}{ALMTD}$$

$$Q = \dot{m}C_p(T_{out} - T_{in})$$

$$LMTD = \frac{(T_{in} - T_w) - (T_{out} - T_w)}{\ln[(T_{in} - T_w)/(T_{out} - T_w)]}$$

$$\Delta P = P_{in} - P_{out}$$

From the CFD simulation, the mass flow rate (\dot{m}) and the outlet temperature (T_{out}) are calculated for the given inlet temperature ($T_{in} = 295$ K) and the wall temperature ($T_w = 300$ K) and the other design variables.

The goal of this example is to find optimized designs that have maximum heat transfer coefficient (h) and minimum pressure drop per unit length ($\Delta P/L$). The different design variables that define the chevron PHX segment are shown in Fig. 15. The four design variables along with their limits are defined in Table 9. The heat transfer coefficient and the PHX segment pressure drop are obtained by solving the continuity, the momentum, and the energy equations using a commercially available CFD tool such as Fluent®. For different designs, the solutions are obtained for a fixed wall temperature, $T_w = 300$ K, and constant coolant inlet temperature $T_{in} = 295$ K with variable coolant flow rate. Water is used in this study as the working fluid.

Individual metamodels are developed for each response, i.e., for heat transfer coefficient h and pressure drop per unit length $\Delta P/L$. The first objective is to maximize the heat transfer coefficient. The second objective is to reduce the pressure drop, thus reducing the pumping power required. The optimization problem can be summarized as shown in the following equation:

$$\begin{aligned} &\text{Maximize} && h && \text{W/m}^2\text{K} \\ &\text{Minimize} && \Delta P/L && \text{kPa/m} \\ &\text{Subject to:} && h \geq 5000 && \text{W/m}^2\text{K} \\ &&& \frac{\Delta P}{L} \leq 100 && \text{kPa/m} \end{aligned}$$

In offline AAO the following approach is used to optimize the chevron PHX segment as shown in Fig. 16. The stopping criterion used in this example is the maximum number of available simulations and can be set based on the available resources.

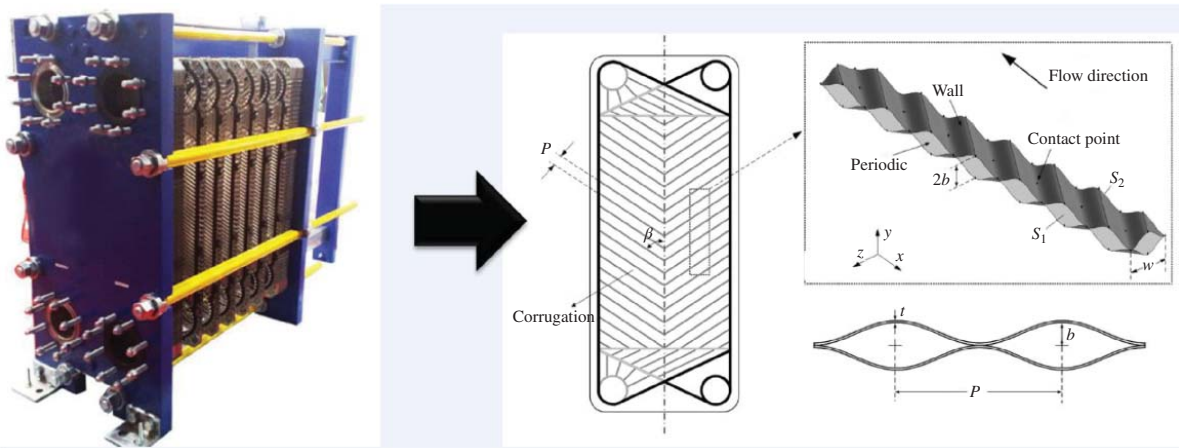
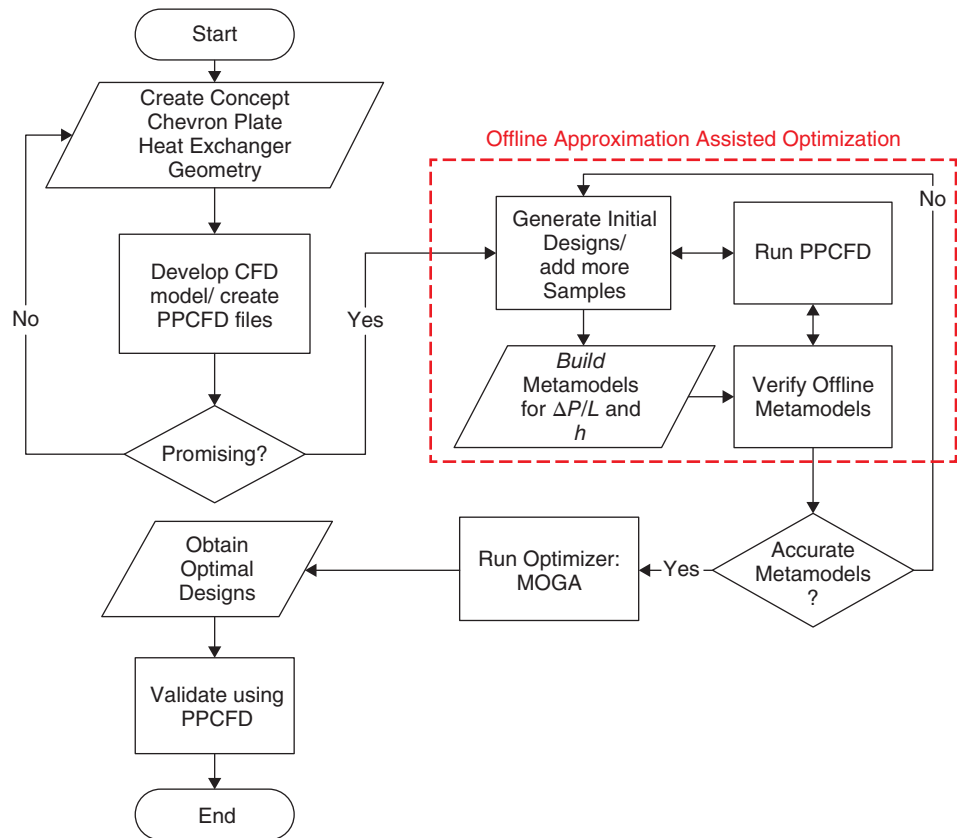


Figure 15 Chevron plate heat exchanger model and computational domain. (From Ref. 17.)

Table 9 Design Variables for Chevron Plate Heat Exchanger Segment Optimization

Design Variables	Lower limit	Upper limit
Corrugation height, b (mm)	3.18	6.35
Corrugation angle, β	22°	68°
Corrugation pitch, p (mm)	9.50	38.00
Coolant inlet velocity, u (m/s)	0.1	1.2

**Figure 16** Chevron plate heat exchanger optimization using offline AAO.

The steps used in offline AAO are as follows:

- Step 1: Generate an initial set of design points using the maximum entropy design method and observe the corresponding responses for the heat transfer coefficient (h) and the fluid pressure drop per unit length inside the PHX segment ($\Delta P/L$).
- Step 2: Develop a metamodel for each objective; i.e., h and $\Delta P/L$.
- Step 3: Test the accuracy of the metamodels using a set of random samples. If the metamodels are accurate enough, move to step 4, otherwise, add more samples to improve the metamodels' performance

Step 4: Formulate a multiobjective optimization problem based on the metamodels and solve it using MOGA and obtain optimum Pareto points

Step 5: Evaluate the true response of Pareto points (i.e., run the CFD simulations) and measure the accuracy of the optimum solutions.

In addition to the previous offline AAO, an adaptive online AAO approach can be used to optimize the chevron PHX segment as shown in Fig. 17. The stopping criterion is the maximum number of available simulations.

The steps used in online AAO are as follows:

Step 1: Generate an initial set of design points using the maximum entropy design method and evaluate the responses for the heat transfer coefficient (h) and the fluid pressure drop per unit length inside the PHX segment ($\Delta P/L$).

Step 2: Develop a metamodel for each objective; i.e., h and $\Delta P/L$.

Step 3: Formulate a multiobjective optimization problem based on the metamodels and solve it using MOGA.

Step 4: From all Pareto points, select points to improve the metamodel accuracy in the expected optimum region and to improve the diversity of the optimum designs both in the design space and the objective space.

Step 5: Evaluate the true response (i.e., run the CFD simulation) for the newly chosen points and then go to step 2.

Step 6: Repeat steps 2 to 5 until a limit on the number of function calls is achieved.

More details regarding online AAO approach and the selection criterion mentioned in step 4 can be found in Saleh et al.¹⁸.

In online AAO, an initial design comprising of 50 points was generated using the MED method, and then online AAO method was used to sample 62 additional points in 6 runs as presented in Fig. 18. In each run, the metamodels were built, then the optimizer run based on these metamodels and finally Pareto solutions were filtered to select the next samples to update the current metamodels.

As can be seen from Fig. 18, the performance of the online AAO is improved gradually by adding more samples in the expected optimum region. Generally speaking, having more sample points in the expected optimum region assists in improving the performance of any AAO approach. The relative error is given in the following equation, where $y(x)$ is the actual value from CFD simulation and $\hat{y}(x)$ is the predicted value using the metamodels:

$$\text{RError} = \frac{|y(x) - \hat{y}(x)|}{y(x)} \times 100\%$$

As can be seen from Table 10, online AAO gives accurate results while reducing significantly the computational cost. Compared to several thousands of actual simulations required for conventional MOGA (~5100 simulations), online AAO can reduce more than 97% of the computational cost.

In the next example, a similar online AAO approach is integrated with a multiscale simulation approach to optimize the entire heat exchanger design for a novel air-cooled heat exchanger.

Multiscale Simulation for New Generation of Heat Exchanger

In order to reduce the time associated with simulating and optimizing the new heat exchanger designs, a multiscale simulation concept is introduced by Abdelaziz et al.¹⁶ as shown in Fig. 20. By multiscale, we mean that two levels of simulations are required in order to evaluate the

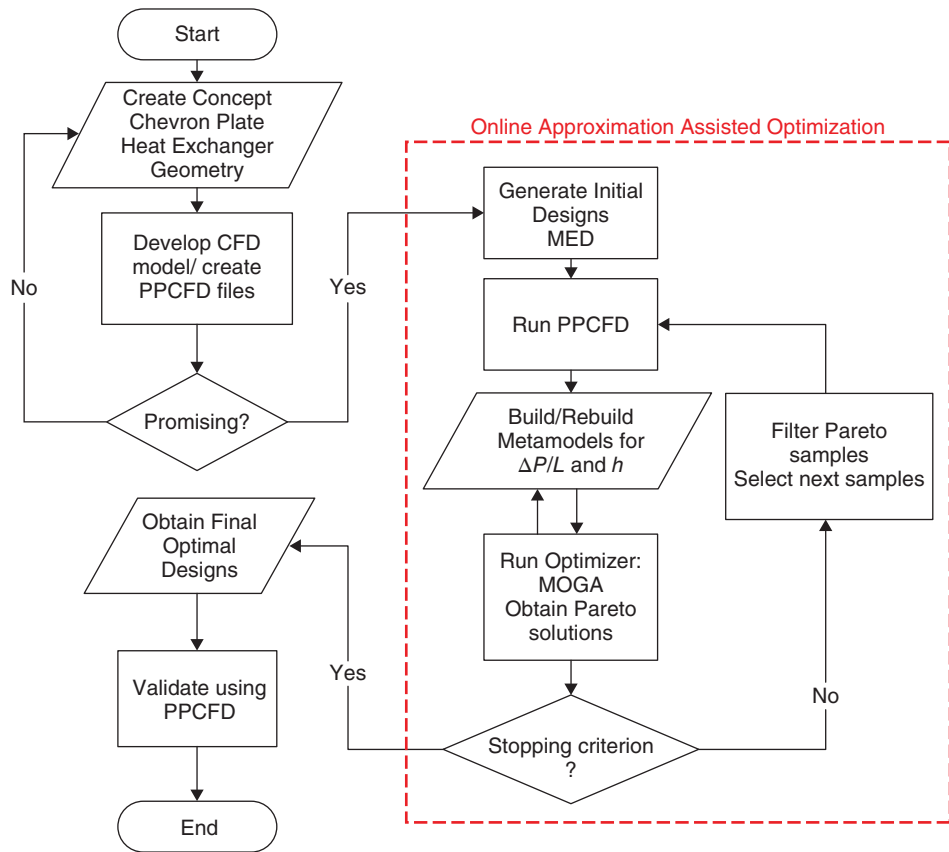


Figure 17 Chevron plate heat exchanger optimization using online AAO.

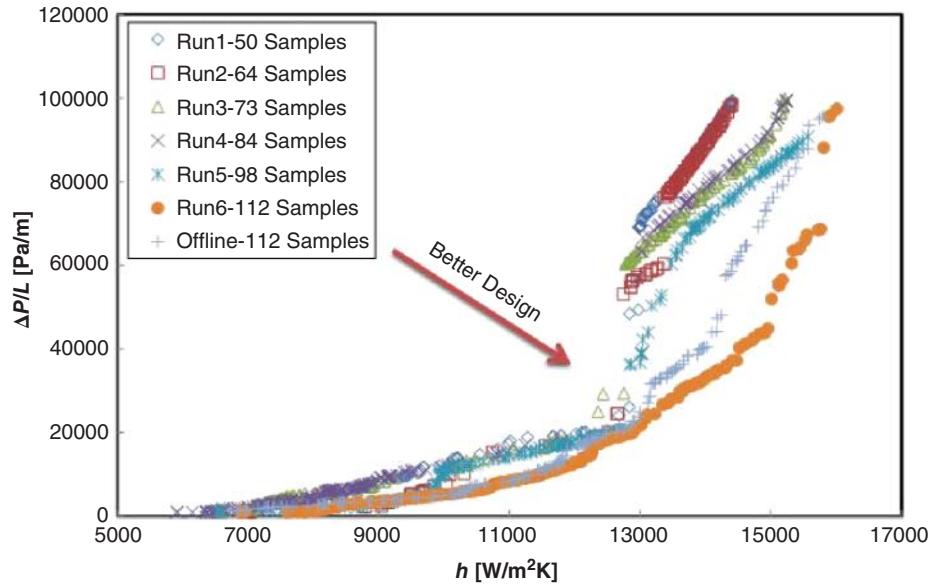
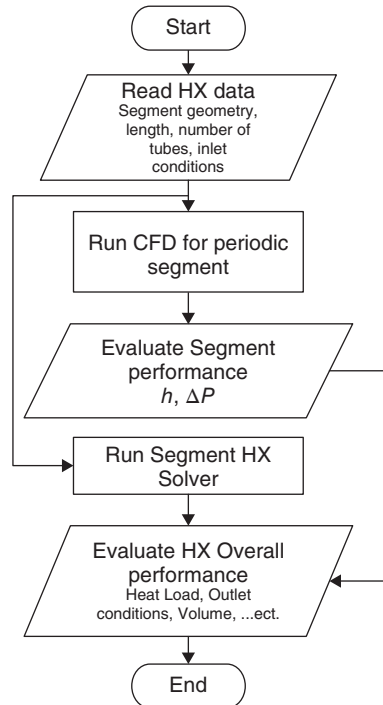


Figure 18 Chevron plate heat exchanger optimum designs using online AAO.

Table 10 Relative Absolute Error in Pareto Set

	h	$\Delta P/L$
Average	2.08	3.29
Maximum	4.56	6.43
Minimum	0.83	0.64
STD ^a	1.15	2.10

^aSTD: standard deviation.

**Figure 19** Multiscale simulation of a heat exchanger.

entire heat exchanger performance. The first level is the segment level where there are no valid correlations to calculate the thermal and the hydraulic characteristics of the flow regime. This is applicable for new heat exchanger geometries. Accordingly, CFD simulation is required in the segment level to evaluate the heat transfer coefficient and the pressure drop. On the other hand, in order to evaluate the entire heat exchanger performance, a segmented NTU solver is used to predict the performance of the entire heat exchanger. These two levels of simulations are integrated together under one framework, which is defined as multiscale simulation as presented in Fig. 19.

In the next example, multiscale simulation is used to optimize the new generation of an air-cooled heat exchanger shown in Fig. 20. The CFD simulations are performed for the HX segment level to predict the thermal and hydraulic performance of the new enhanced HX surfaces, whereas a segmented-based NTU solver such as CoilDesigner¹⁹ is used to predict the

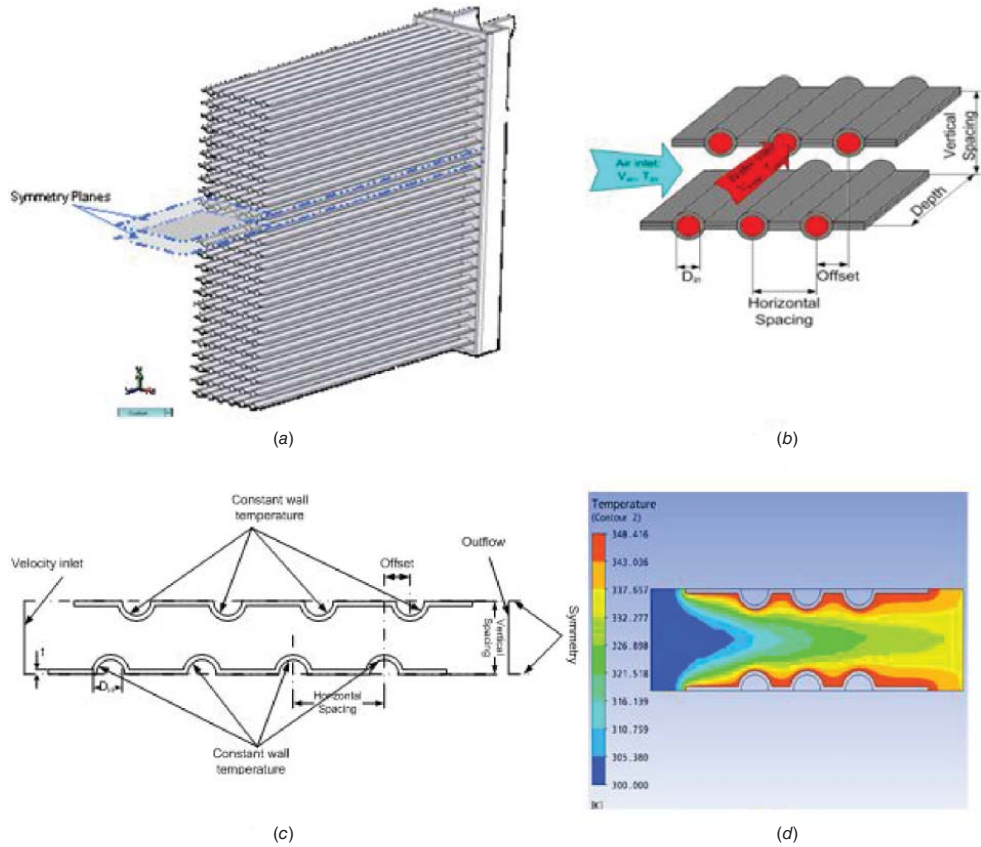


Figure 20 (a) Air-to-refrigerant heat exchanger, (b) heat exchanger segment, (c) schematic, and (d) computational domain and sample results. (From Ref. 16.)

performance of the entire heat exchanger. In order to apply the multiscale simulation approach, the following assumptions should be satisfied:¹⁶

1. Heat exchangers are periodic in nature.
2. Symmetry planes should be identified.
3. Neglecting the side wall effects.
4. The overall heat transfer coefficient is mainly dependent on the air-side performance.
5. Constant wall temperature for liquid inside the tubes.
6. Constant air properties and constant liquid in tube properties.

The optimization objectives are defined to minimize both the HX volume and the air-side pressure drop. These two objectives are conflicting in nature. The HX design configuration is shown in Fig. 20.¹⁶ There are six design variables as shown in Table 11.

The optimization problem can be summarized as shown in the following equation:

$$\begin{array}{ll}
 \text{Minimize} & \text{HX Volume} \\
 \text{Minimize} & \Delta P_{\text{air}} \\
 \text{Subject to:} & \Delta P_{\text{air}} < 100 \text{ Pa} \\
 & 0.25 < \text{Aspect Ratio} < 4 \\
 & 1000 < Q < 1050 \text{ W} \\
 & \text{HX Volum} < 240 \text{ cm}^3
 \end{array}$$

The main objectives are to minimize both the HX volume and the air-side pressure drop. This is subjected to a certain constraint on the pressure drop for the air side. Another constraint is defined for the aspect ratio, which is the ratio between the tube length (L) and the coil height ($N_t \times V.S$). In addition, two more constraints are defined for the heat load (Q) and the HX volume.

The multiscale simulation can be applied using offline or online AAO approaches as presented in the next section.

Multiscale Simulation Based on Offline Approximation Assisted Optimization

The flowchart for the overall approach using offline multiscale simulation is presented in Fig. 21 where the approach starts with building offline globally accurate metamodels. Then the metamodels are validated using a set of random samples. If these metamodels are accurate enough, we can use them later to predict the heat transfer coefficient and the pressure drop in the segment level. Otherwise, more samples are added to improve the accuracy of the metamodels until reaching a reasonable accuracy of the metamodels.

Table 11 Design Variables for Heat Exchanger Optimization

Design Variables	Lower Limit	Upper Limit
D_{in} (mm)	0.2	0.7
HS (Fraction of D_{in})	1.5	6
VS (Fraction of D_{in})	2.0	4.0
N_p	3	19
V_{air} (m/s)	0.5	3
Offset (Fraction of HS)	0	1

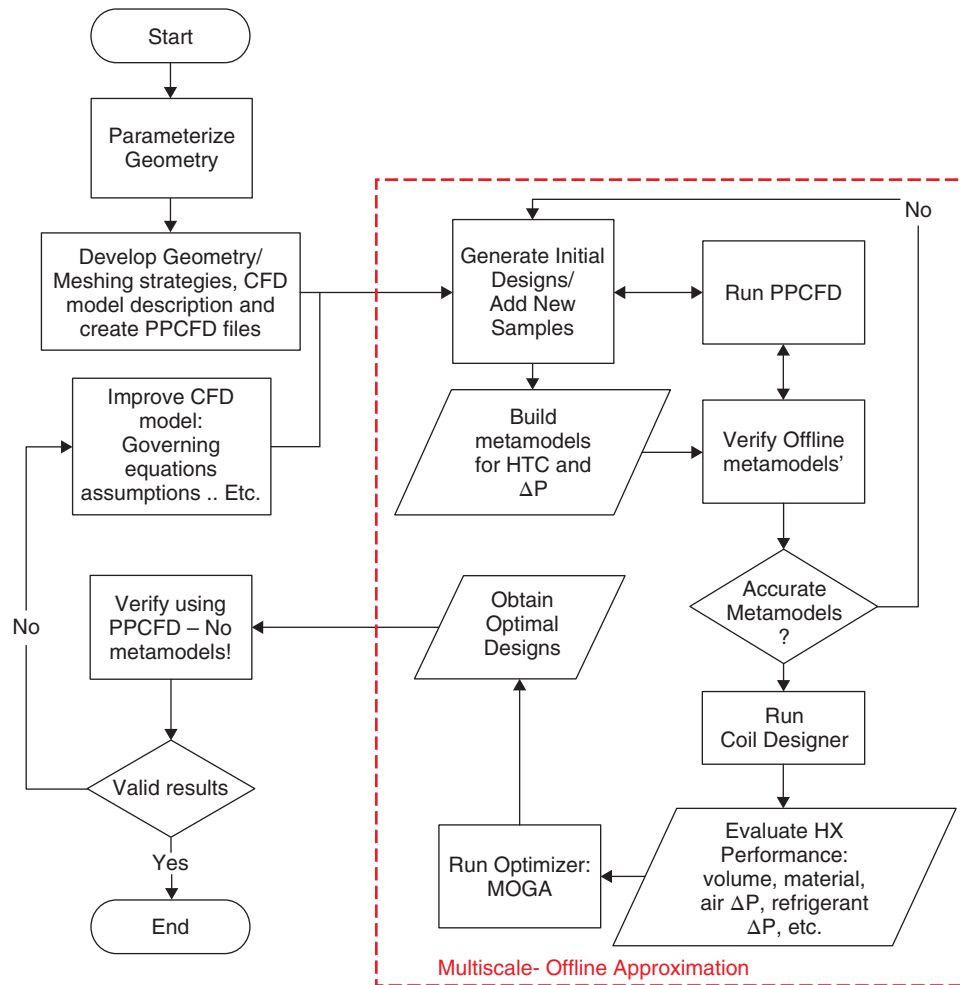


Figure 21 Flowchart of multiscale offline AAO approach.

In this case, the globally accurate metamodels are used to evaluate the performance of a segment, and then CoilDesigner is used to evaluate the performance of the entire heat exchanger.

Coupling the optimizer with CoilDesigner and running the MOGA, we can find the optimum Pareto solutions. As the results are generated based on the metamodels, PPCFD is used to validate the final results by running CFD simulation to measure the accuracy of the optimum Pareto solutions.

As it can be seen from Fig. 21, in multiscale simulation based on offline AAO, there is no feedback from the optimizer to update the metamodels. All metamodels are built and validated before running the optimizer.

After developing a robust CFD model that is valid for the entire range of design variables shown in Table 11, a set of 500 samples is selected based on the maximum entropy DOE method. The CFD runs are carried out using PPCFD. Based on CFD results, metamodels are built for both air heat transfer coefficient (h) and air pressure drop (ΔP_{air}) using the Kriging

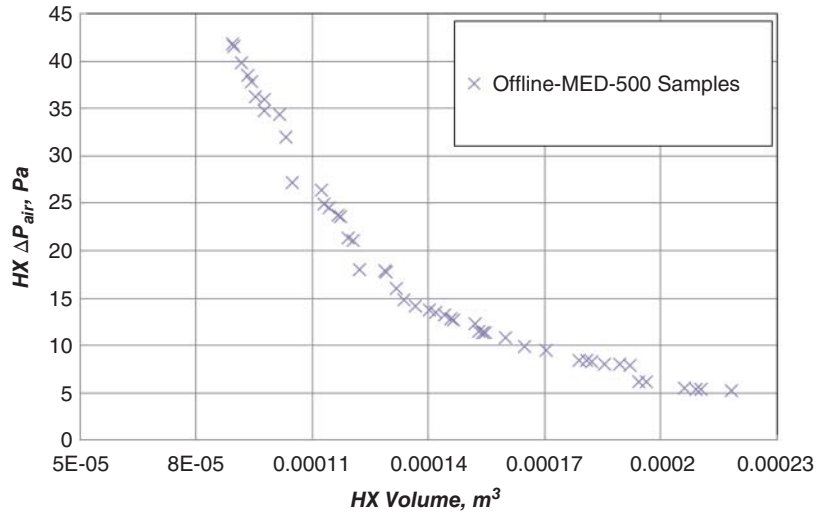


Figure 22 Multiscale offline AAO results.

Table 12 Pareto Optimal Design Verification Results

Method	RMSE		RRMSE	
	h (Pa)	ΔP_{air}	h %	ΔP_{air} %
Online multiscale approximation	3.8	18.32	16.7	14.82
Offline multiscale approximation	8.78	2.56	20.78	2.69

metamodeling method. Then the metamodels are validated using random samples. The validation results showed these metamodels are accurate enough. Having the globally accurate metamodels, CoilDesigner,¹⁹ a commercially available simulation tool for air-cooled HX, is used to predict h and ΔP_{air} based on the metamodels. After that, MOGA is used to optimize two design objectives: to minimize HX volume and minimize the air-side total pressure drop based on CoilDesigner simulations. Subsequently, the obtained optimum design solutions are validated using PPCFD. The validation results are presented in Table 12.

Multiscale based on online approximation-assisted optimization

As it can be shown in Fig. 23, there is a feedback from the optimizer to update the metamodels in multiscale online AAO approaches. After developing a robust CFD model that is valid for the entire range of design variables shown, a set of initial designs is generated based on the maximum entropy DOE method. The CFD runs are carried out using PPCFD. Based on CFD results, metamodels are built for both air heat transfer coefficient (h) and air pressure drop (ΔP_{air}) using the Kriging metamodeling method. CoilDesigner uses the metamodels to predict h and ΔP_{air} . After that, MOGA is used to optimize the HX based on two design objectives: minimizing HX volume and minimizing the air-side total pressure drop based on CoilDesigner simulations. Subsequently, the obtained optimum design solutions are filtered using online AAO approach presented earlier to select the new set of up to date metamodels. CFD simulations are performed for the new selected candidates using PPCFD and the metamodels are updated. The previous

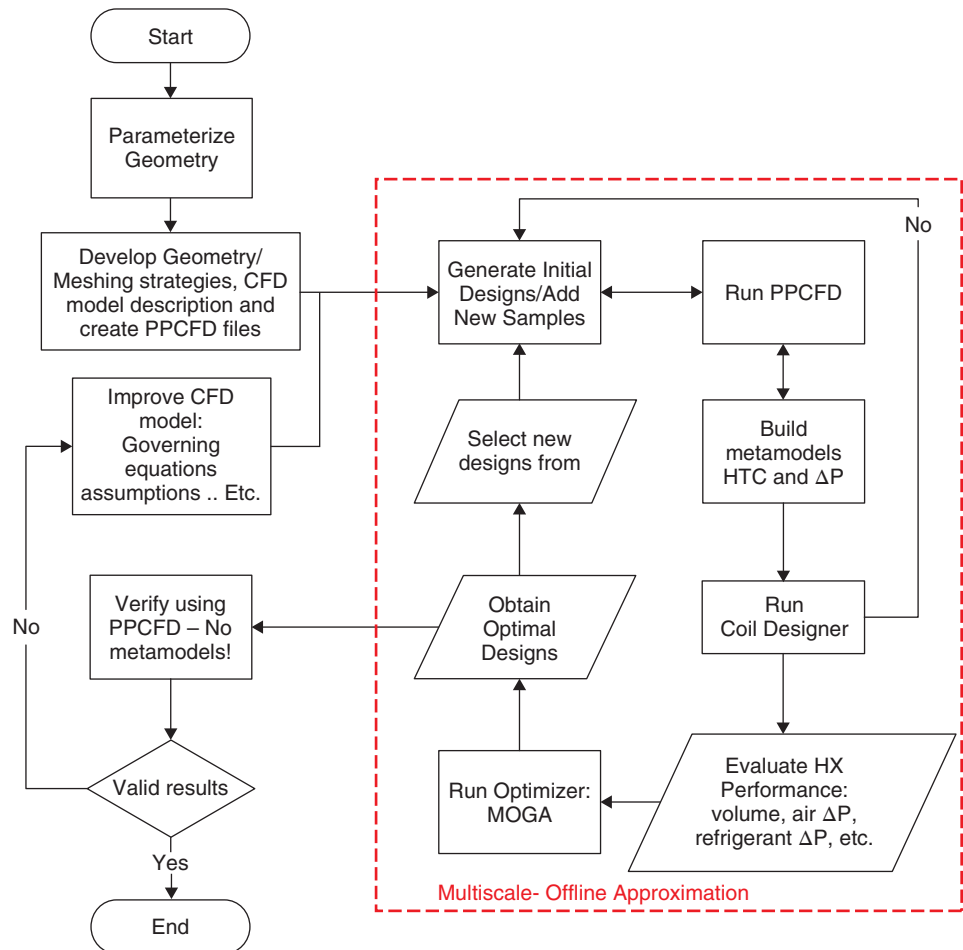


Figure 23 Flowchart of multiscale online AAO approach.

steps are repeated several times until a certain stopping criterion is met. In this example, a limited number of CFD runs is used as the stopping criterion. Finally, the optimum solutions are verified using CFD simulations.

The optimum results generated at different number of runs are presented. First, after running MOGA based on 65 samples, the optimum solutions, i.e., the approximated Pareto solutions, are presented as iteration 1 as shown in Fig. 24. Next, after different updates of the metamodels based on intermediate MOGA runs, the results are presented for a total number of samples of 95 and 120 as iteration 2 and iteration 3, respectively.

As is apparent from the results, better solutions can be obtained using a fewer number of CFD simulations. To compare the results with offline multiscale approximation approach, we built offline metamodels for both h and ΔP_{air} using 500 samples based on the MED method. As can be depicted from the results, the online multiscale approximation approach resulted in better optimum designs compared to the offline approach based on MED designs. Approximately 76% CFD simulations are saved when using the online multiscale approximation approach.

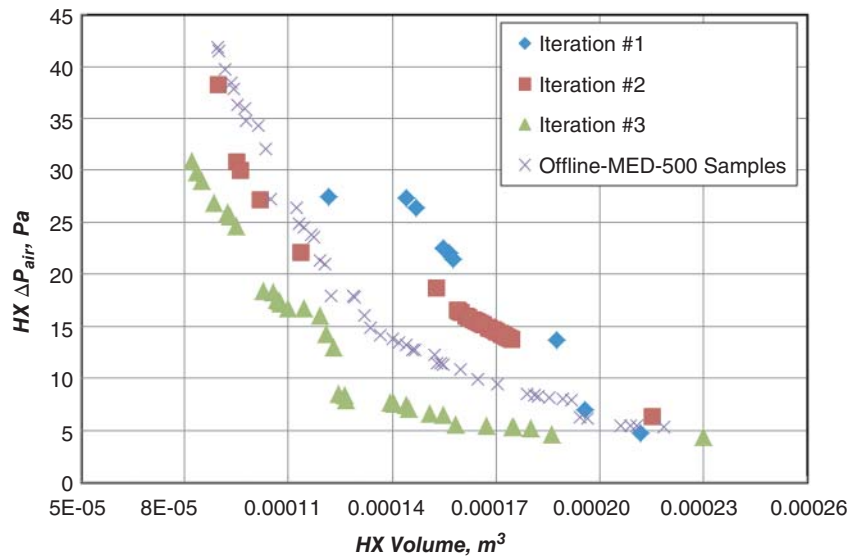


Figure 24 Online multiscale approximation results at different iterations and comparison with offline multiscale approximation.

In order to verify the accuracy of the obtained results, all Pareto solutions were verified using CFD runs. Based on the verification results, both root-mean-square error (RMSE) and relative root-mean-square error (RRMSE) are reported. Both RMSE and RRMSE are defined based on the actual CFD simulation results (y) and the metamodel predictions (\hat{y}_i) as presented in the following equations:

$$\text{RMSE} = \sqrt{\frac{1}{n} \sum_{i=1}^n (y_i - \hat{y}_i)^2}$$

$$\text{RRMSE} = \sqrt{\frac{1}{n} \sum_{i=1}^n \left(\frac{y_i - \hat{y}_i}{y_i} \right)^2}$$

By examining the results, it is obvious that the performance of the metamodels is improved by adding more samples; yet, the performance of online multiscale approximation gives acceptable results. This is the main advantage of using online approximation. In case of limitation in the computational resources, the online multiscale approximation approach gives reasonably accurate results in a shorter time. By adding more samples, the accuracy of the obtained results can be improved.

We conclude by making a few observations on the AAO techniques. AAO is a very powerful technique that can result in significant savings in computational costs and engineering time. However, at the same time it is important to choose the right tools and respective options for the metamodeling and optimization algorithms. The use of inappropriate metamodel can result in the model exhibiting nonphysical behavior that may or may not be obvious during analysis and optimization. Lastly comprehensive verification and validation is necessary before the results obtained from optimization can be used in a reliable manner. There is no substitute for prototype development and testing. The optimization techniques only assist us in getting the first prototype 90% right.

Symbols.

COP	coefficient of performance
f	function
G	gradient of function vector
H	inverse of Jacobian J
h, h_a	specific enthalpy, specific enthalpy of air
I	identity matrix
J	Jacobian matrix
M, \dot{m}	mass, mass flow rate
$P, P_a, \Delta P$	pressure, air pressure, pressure difference
\dot{Q}	heat flow rate
R	residual
W	work
\dot{W}, P	power
X	vector
α, β	step length, weight function
μ	damping parameter
ε	tolerance value
$\ \bullet\ , \ \bullet\ _\infty$	Euclidian norm, infinity norm

REFERENCES

1. W. H. Press, S. A. Teukolsky, W. T. Vetterling, and B. P. Flannery, *Numerical Recipes in C++ - The Art of Scientific Computing*, 2nd ed., Cambridge University Press, Cambridge, UK, 2002.
2. J. E. Dennis and R.B. Schnabel, *Numerical Methods for Unconstrained Optimization and Nonlinear Equations, Classics in Applied Mathematics*, Society of Industrial and Applied Mathematics, 1996.
3. P. R. Waier, *Building Construction Cost Data*, 62nd Annual Edition, R.S. Means, Kingston, MA, 2004.
4. R. S. Sinnott, *Chemical Engineering*, Butterworth-Heinemann, Oxford, Boston, 2003.
5. A. Bejan, M. J. Moran and G. Tsatsaronis, *Thermal Design and Optimization*, Wiley, New York, 1996.
6. J. H. Holland, *Adaptation in Natural and Artificial Systems: An Introductory Analysis with Applications to Biology, Control, and Artificial Intelligence*, MIT Press, Cambridge, MA, 1996.
7. V. Aute, R. Radermacher, and M. Naduvath "Constrained Multiobjective Optimization of a Condenser Coil Using Evolutionary Algorithms", Tenth International Refrigeration and Air Conditioning Conference at Purdue, July 2004.
8. T. W. Simpson, J. D. Peplinski, P. N. Koch, and J. K. Allen, "Metamodels for Computer-based Engineering Design: Survey and recommendations", *Eng. Comput.*, **17**(2), 129–150, 2001.
9. M. C. Shewry and H. P. Wynn, "Maximum Entropy Sampling", *J. Appl. Stat.*, **14**, 165–170, 1987.
10. C. E. Shannon, "A Mathematical Theory of Communication," *Bell Tech. J.*, **27**, 379–423, 623–656, 1948.
11. Y. Jin, M. Olhofer and B. Sendhoff, "A Framework for Evolutionary Optimization with Approximate Fitness Functions", *IEEE Trans. Evolution. Comput.*, **6**(5), 481–494, 2002.
12. G. G. Wang, and S. Shan, "Review of Metamodeling Techniques in Support of Engineering Design Optimization", *J. Mech. Design*, **129**(4), 369–463, 2007.
13. J. C. Otto, D. Landman and A. T. Patera, "A Surrogate Approach to the Experimental Optimization of Multi-element Airfoils", Proceedings of the Sixth AIAA/NASA/ISSMO Symposium on Multidisciplinary Analysis and Optimization, Bellevue, WA, September 4–6, AIAA 96-4138 CP, 1996.
14. D. R. Jones, "A Taxonomy of Global Optimization Methods Based on Response Surfaces", *J. Global Optimizat.*, **21**, 345–383, 2001.
15. N. A. C. Cressie, *Statistics for Spatial Data, Wiley Series in Probability and Mathematical Statistics*, Wiley, New York, 1993.

16. O. Abdelaziz, V. Aute, S. Azarm, and R. Radermacher, "Approximation Assisted Optimization for Novel Compact Heat Exchanger Designs", *HVAC&R Res.*, **16**(5), 707–728, 2010.
17. W. Han, K. Saleh, V. Aute, and R. Radermacher, "Numerical Simulation and Optimization of Single Phase Turbulent Flow in Chevron-type Plate Heat Exchanger with Sinusoidal Corrugations", *HVAC & R Res.*, **17**(2), 186–197, 2011.
18. K. Saleh, V. Aute, S. Azarm, and R. Radermacher, "Online Approximation Assisted Multiobjective Optimization with Space Filling", Variance and Pareto Measures, Thirteenth AIAA/ISSMO Multidisciplinary Analysis and Optimization Conference, AIAA-2010, Fort Worth, TX, 2010.
19. H. B. Jiang, V. Aute, and R. Radermacher, "CoilDesigner: A General Purpose Simulation and Design Tool for Air-to-Refrigerant Heat Exchangers", *Int. J. Refriger.*, **29**(4), 601–610, 2006.

BIBLIOGRAPHY

- P. D. Chaudhari, U. M. Diwekar, and J. S. Logsdon, "An Automated Approach for the Optimal Design of Heat Exchangers", *Ind. Eng. Chem. Res.*, **36**, 3685–3693, 1997.
- K. Deb, *Multi-Objective Optimization Using Evolutionary Algorithms*, Wiley, New York, 2001.
- D. H. Fax, and Mills, R. R., Jr., "Generalized Optimal Heat-Exchanger Design", ASME Gas Turbine and Power Division Semi-annual Meeting, Paper No 56-SA-19, June 1956.
- C. M. Fonseca, and P. J. Fleming, "Genetic Algorithms for Multiobjective Optimization: Formulation, Discussion and Generalization", *Proceedings of the Fifth International Conference on Genetic Algorithms*, Morgan Kaufmann, 1993, pp. 416–423.
- C. M. Fonseca and P. J. Fleming, "Multiobjective Genetic Algorithms Made Easy: Selection Sharing and Mating Restriction," *First International Conference on Genetic Algorithms in Engineering Systems: Innovations and Applications*, GALEZIA, Publ. No. 414, IEE, London, 1995, pp. 45–52.
- C. M. Fonseca, and P. J. Fleming, "Multiobjective Optimization and Multiple Constraint Handling with Evolutionary Algorithms – Part I: A Unified Formulation, Part II: Application Example", *IEEE Trans.Syst., Man Cybern. – Part A: Syst. Humans*, **28**(1), 1998.
- C. M. Fonseca, and P. J. Fleming, "An Overview of Evolutionary Algorithms in Multiobjective Optimization", *Evolution. Comput.*, **3**(1), 1–16, 1995.
- D. E. Goldberg, *Genetic Algorithms in Search Optimization and Machine Learning*, Addison-Wesley, Boston 1989.
- C. P. Hedderich, M. D. Kelleher, and G. N. Vanderplaats, "Design and Optimization of Air-Cooled Heat Exchangers", *ASME J. Heat Transfer*, **104**, 683–690, 1982.
- H. Jiang, V. Aute, and R. Radermacher, "A User-friendly Simulation and Optimization Tool for Design of Coils", Ninth International Refrigeration and Air Conditioning Conference at Purdue, July 2002.
- S. Narayanan, and S. Azarm, "On Improving Multiobjective Genetic Algorithms for Design Optimization", *Struct. Optimiz.*, **18**, 146–155, 1999.
- G. V. Reklaitis, A. Ravindran, and K. M. Ragsdell, *Engineering Optimization – Methods and Applications*, Wiley Interscience, New York, 1983.
- K. Saleh, R. Radermacher, V. Aute, and S. Azarm, "Online Approximation Assisted Optimization of a Novel Air-Cooled Heat Exchanger", Tenth IEA Heat Pump Conference, Tokyo, Japan, Paper No. 00272, 2011.
- N. Srinivas, and K. Deb, "Multiobjective Optimization Using Nondominated Sorting in Genetic Algorithms", *J. Evolution. Comput.*, **2**(3), 221–248, 1995.
- M. C. Tayal, Y. Fu, and U. M. Diwekar, "Optimal Design of Heat Exchangers: A Genetic Algorithm Framework", *Ind. Eng. Chem. Res.*, **38**, 456–467, 1999.
- E. Van den Bulck, "Optimal Design of Crossflow Heat Exchangers", *ASME J. Heat Transf.*, **113**, 341–347 1991.
- J. Wu, and S. Azarm, "Metrics for Quality Assessment of a Multiobjective Design Optimization Solution Set", *J. Mech. Design, Trans. ASME*, **123**, March 2001.

PART 2

POWER

CHAPTER 17

COMBUSTION

Eric G. Eddings
University of Utah
Salt Lake City, Utah

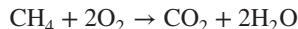
1 FUNDAMENTALS OF COMBUSTION	635	4.2 Liquid Fuels	658
1.1 Air–Fuel Ratios	635	4.3 Solid Fuels	659
1.2 Fuels	639	5 POLLUTANT EMISSIONS	665
2 THERMAL ASPECTS OF COMBUSTION	640	5.1 Control of Nitrogen Oxides	665
3 FLAME AERODYNAMICS	644	5.2 Control of Other Gaseous Emissions	665
3.1 Premixed Flames	644	5.3 Control of Particulate Emissions	666
3.2 Diffusion-Mixed Turbulent Flames	650	6 SAFETY CONSIDERATIONS	666
3.3 Turbulent Diffusion Flame Types	651	7 OXY-FUEL FIRING	670
4 FIRING SYSTEMS	654	ACKNOWLEDGMENTS	671
4.1 Gaseous Fuels	654	REFERENCES	671

1 FUNDAMENTALS OF COMBUSTION

1.1 Air–Fuel Ratios

Combustion is rapid oxidation, usually for the purpose of changing chemical energy into thermal energy—heat. This energy usually comes from oxidation of carbon, hydrogen, sulfur, or compounds containing C, H, and/or S. The oxidant is usually O₂—molecular oxygen from the air.

One can perform basic chemical reaction balancing to permit determination of the air required to burn a fuel. For example, consider the following reaction:



where the units are moles; therefore, 1 mol of methane (CH₄) produces 1 mol of CO₂; or 1000 mol of CH₄ requires 2000 mol of O₂ and produces 2000 mol of H₂O. Knowing that the atomic weight of C is 12, H is 1, N is 14, O is 16, and S is 32, one can determine molecular weights for each of the species involved in the reaction and thus predict weight flow rates: 16 lb/h CH₄ requires 64 lb/h O₂ to burn to 44 lb/h CO₂ and 36 lb/h H₂O. If the oxygen for combustion comes from air, it is necessary to know that dry air is 20.99% O₂ by volume and 23.20% O₂ by weight, most of the remainder being nitrogen (N₂).

It is convenient to remember the following ratios:

$$\text{Air}/\text{O}_2 = 100/20.99 = 4.76 \text{ by volume}$$

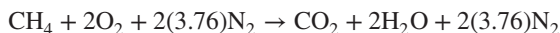
$$\text{N}_2/\text{O}_2 = 3.76 \text{ by volume}$$

$$\text{Air}/\text{O}_2 = 100/23.20 = 4.31 \text{ by weight}$$

$$\text{N}_2/\text{O}_2 = 3.31 \text{ by weight}$$

If there is significant humidity in the combustion air or if some combustion products have been recirculated into the combustion air stream, the moisture or other products will dilute the oxygen concentration. Therefore, the diluted oxygen concentration should be determined and used in the previous ratios as well as in the following calculations.

Rewriting the previous formula for combustion of methane gives



or



Table 1 lists the amounts of air or oxygen required for stoichiometric (quantitatively and chemically correct) combustion of a number of pure fuels calculated by the above method.

The stoichiometrically correct (perfect, ideal) air/fuel ratio from the above formula is therefore $2 + 2(3.76) = 9.52$ volumes of air per volume of the fuel gas. More than that is called a “lean” ratio and includes excess air and produces an oxidizing atmosphere. For example, if the actual air/fuel ratio were 10:1, the percentage of excess air would be

$$\frac{10 - 9.52}{9.52} \times 100 = 5.04\%$$

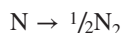
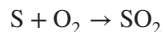
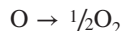
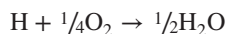
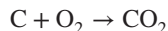
Some fuels (e.g., coal or fuel oil) do not have a simple molecular formula and cannot be analyzed by the method shown above. These fuels are typically described by an elemental analysis, weight percentages of C, H, O, N, and S, as well as percentages of moisture and noncombustible material (ash). In such a case, the required oxygen can be determined by calculating

Table 1 Proper Combining Proportions for Stoichiometric Combustion

Fuel	vol O ₂	vol Air	wt O ₂	wt Air	ft ³ O ₂	ft ³ Air	m ³ O ₂	m ³ Air
	vol Fuel	vol Fuel	wt Fuel	wt Fuel	lb Fuel	lb Fuel	kg Fuel	kg Fuel
Acetylene, C ₂ H ₂	2.50	11.9	3.08	13.3	36.5	174	2.28	10.8
Benzene, C ₆ H ₆	7.50	35.7	3.08	13.3	36.5	174	2.28	10.8
Butane, C ₄ H ₁₀	6.50	31.0	3.59	15.5	42.5	203	2.65	12.6
Carbon, C	—	—	2.67	11.5	31.6	150	1.97	9.39
Carbon monoxide, CO	0.50	2.38	0.571	2.46	6.76	32.2	0.422	2.01
Ethane, C ₂ H ₆	3.50	16.7	3.73	16.1	44.2	210	2.76	13.1
Hydrogen, H ₂	0.50	2.38	8.00	34.5	94.7	451	5.92	28.2
Hydrogen sulfide, H ₂ S	1.50	7.15	1.41	6.08	16.7	79.5	1.04	4.97
Methane, CH ₄	2.00	9.53	4.00	17.2	47.4	226	2.96	14.1
Naphthalene, C ₁₀ H ₈	—	—	3.00	12.9	35.5	169	2.22	10.6
Octane, C ₈ H ₁₈	—	—	3.51	15.1	41.6	198	2.60	12.4
Propane, C ₃ H ₈	5.00	23.8	3.64	15.7	43.1	205	2.69	12.8
Propylene, C ₃ H ₆	4.50	21.4	3.43	14.8	40.6	193	2.54	12.1
Sulfur, S	—	—	1.00	4.31	11.8	56.4	0.74	3.52
Coal, bituminous (avg.)	—	—	2.27	9.80	26.9	128	1.68	7.96

Source: Reproduced with permission from Ref. 1.

the number of moles for the elements of interest for a particular mass of fuel (say, 1 pound). Then, the required amount of oxygen can be determined for the moles of each element using the following balanced reactions:



The oxygen produced due to the presence of inherent oxygen in the fuel will result in an oxygen “credit” and should be subtracted from the stoichiometric oxygen requirement for complete combustion of C, H, and S. For some fuels like fuel oil No. 6, this oxygen will be negligible; however, for coal and wood this can be quite significant and needs to be taken in consideration when determining the stoichiometric air requirement. This type of calculation will determine the moles of oxygen required per pound of fuel, and this value can be converted to moles of air required using the ratios given above. The moles of air can be subsequently converted to mass using a molecular weight of 29.

Although a small amount of the nitrogen in the fuel can be oxidized, it is typically neglected in these calculations since it is generally a minor “sink” for oxygen. The majority of the nitrogen will combine with the N_2 from the combustion air and will pass through the system as a largely inert gas that dilutes the combustion products. This large amount of nitrogen results in a significant inefficiency in combustion systems, because much of the energy released in the combustion reactions is used to heat up this inert gas. Significant efforts have gone into the study of enriched oxygen combustion systems as a means to reduce the energy penalties associated with nitrogen in the air.

Communication problems sometimes occur because some individuals think in terms of air/fuel ratios, others in fuel/air ratios; some in weight ratios, others in volume ratios, and some in mixed metric units (such as normal cubic meters of air per metric tonne of coal), others in mixed American units (such as ft^3 air/gal of oil). To avoid such confusion, the following method is recommended.

It is more convenient to specify the air/fuel ratio in unitless terms such as percentage of excess air, equivalence ratio, or stoichiometric ratio. Those experienced in this field prefer to converse in terms of percentage of excess air. The scientific community favors equivalence ratio or stoichiometric ratio. The stoichiometric ratio is the most intuitive to use and explain to newcomers to the field. A stoichiometric ratio (SR) of 1.0 is the correct (stoichiometric) amount; SR = 2.0 air is twice as much as necessary, or 100% excess air, SR = 1.2 represents 20% excess air, and so on. The equivalence ratio (ER), widely used in combustion research, is the actual fuel/air ratio divided by the theoretical or stoichiometric fuel/air ratio. It is also the inverse of the stoichiometric ratio, or $\text{ER} = 1/\text{SR}$. The Greek letter phi, ϕ , is typically used for ER: $\phi < 1.0$ represents fuel-lean or excess-air conditions; $\phi > 1.0$ is fuel-rich or air-deficient conditions; and $\phi = 1.0$ is “on-ratio” or the stoichiometric point. Table 2 lists a number of equivalent terms for convenience in converting values from one method of categorization to another.

Significant levels of excess air are undesirable, because, like the residual N_2 , excess air passes through the combustion process without significant chemical reaction, yet it absorbs heat, which it carries out the flue. The percent available heat (best possible fuel efficiency) is highest with approximately zero excess air (see Fig. 1); however, thermodynamic and mixing considerations dictate some level of excess air (typically 10–20%) to achieve a high level of combustion efficiency, or near-complete conversion of fuel to oxidized products (CO_2 and H_2O).

Table 2 Equivalent Ways to Express Fuel-to-Air or Air-to-Fuel Ratios¹

	ϕ^a	SR ^b	% XS ^c
Fuel rich	2.50	0.40	
(air lean)	1.67	0.60	
	1.25	0.80	
	1.11	0.90	
	1.05	0.95	
Stoichiometric	1.00	1.00	0
Fuel lean	0.95	1.05	5
(air rich)	0.91	1.10	10
	0.83	1.20	20
	0.77	1.30	30
	0.71	1.40	40
	0.63	1.60	60
	0.56	1.80	80
	0.50	2.00	100
	0.40	2.50	150
	0.33	3.00	200
	0.25	4.00	300
	0.20	5.00	400
	0.167	6.00	500
	0.091	11.00	1000
	0.048	21.00	2000

^aEquivalence ratio.

^bStoichiometric ratio.

^c% excess air.

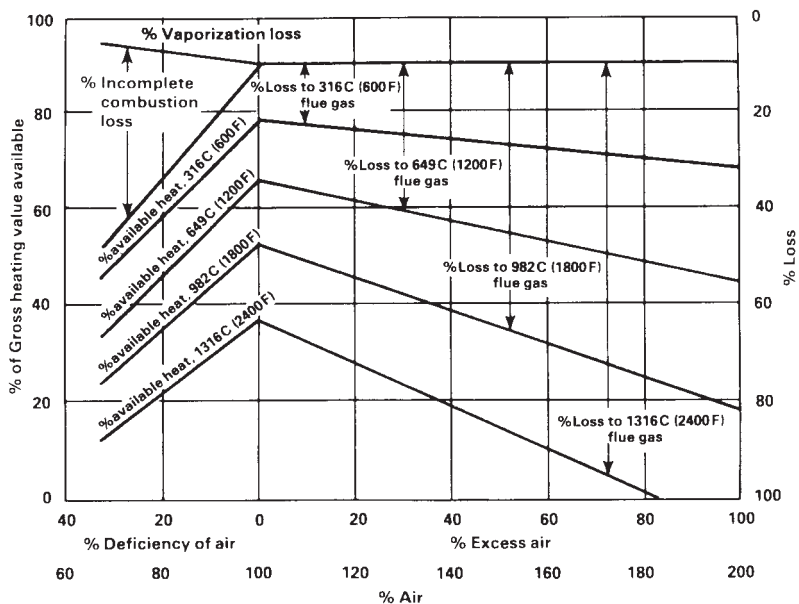


Figure 1 Percent available heat (best possible efficiency) peaks near the stoichiometric air/fuel ratio.¹

Excess fuel is even more undesirable because it means there is a deficiency of air and some of the fuel cannot be burned. This results in the emission of soot and smoke and carbon monoxide (CO). The accumulation of unburned fuel or partially burned fuel can represent an explosion hazard as well as a pollutant emission problem.

Enriching the oxygen content of the combustion “air” above the normal 20.9% reduces the nitrogen and thereby reduces the loss due to heat carried up the stack. This also raises the flame temperature, improving heat transfer, especially that by radiation.

Vitiated air (containing less than the normal 20.9% oxygen) results in less fuel efficiency and may result in flame instability. Vitiated air is sometimes encountered in incineration of fume streams or in staged combustion or with flue gas recirculation.

1.2 Fuels

Fuels used in practical industrial combustion processes have such a major effect on the combustion that they must be studied simultaneously with combustion. Fuels are covered in detail in later chapters, so the treatment here is brief, relating only to the aspects having direct bearing on the combustion process.

Gaseous fuels are generally easier to burn, handle, and control than liquid or solid fuels. Molecular mixing of a gaseous fuel with oxygen need not wait for vaporization or mass transport within a solid. Burning rates are limited only by mixing rates and the kinetics of the combustion reactions; therefore, combustion can be compact and intense. Reaction times as short as 0.001 s and combustion volumes from 10^4 to 10^7 Btu/h-ft³ are possible at atmospheric pressure.² Gases of low calorific value may be so dilute after mixing with air that their combustion rates will be limited by the mixing time.

Combustion stability means that a flame lights easily and then burns steadily and reliably after the pilot (or direct spark) is programmed off. Combustion stability depends on burner geometry plus air and fuel flow controls that maintain the point(s) of flame initiation (1) above the fuel’s minimum ignition temperature, (2) within the fuel’s flammability limits, and (3) with feed speed equal to flame speed—throughout the burner’s full range of firing rates and conditions. (Fuel properties are discussed and tabulated in Chapters 17–19.)

Liquid fuels are usually not as easily burned, handled, or controlled as gaseous fuels. Mixing with oxygen can occur only after the liquid fuel is evaporated; therefore, burning rates are limited by vaporization rates. In practice, combustion intensities are usually less with liquid fuels than with high calorific gaseous fuels such as natural gas.

Because vaporization is such an integral part of most liquid fuel burning processes, much of the emphasis in evaluating liquid fuel properties is on factors that relate to vaporization. One of the most critical properties is viscosity, which hinders good atomization, since atomization or the creation of small droplets is the primary method for enhancing vaporization. Much concern is also devoted to properties that affect storage and handling because, unlike gaseous fuels that usually come through public utility main pipelines, liquid fuels must be stored and distributed by the user.

The stability properties (ignition temperature, flammability limits, and flame velocity) are not readily available for liquid fuels, but flame stability is often less critical with liquid fuels.

Solid fuels are frequently more difficult to burn, handle, and control than liquid or gaseous fuels. After initial devolatilization or release of volatile matter, the combustion reaction rate depends on diffusion of oxygen into the remaining char particle and the diffusion of carbon monoxide back to its surface, where it burns as a gas. Reaction rates are usually low and required combustion volumes high, even with pulverized solid fuels burned in suspension. Some cyclone combustors have been reported to reach the intensities of gas and oil flames.²

Waste or by-product fuels and gasified solids are being used more as fuel costs rise. Operations that produce such materials should attempt to consume them as energy sources or to

sell them as a fuel to others. Problems with handling the lack of a steady supply and pollution problems often complicate such fuel usage.

For the precise temperature control and uniformity required in many industrial heating processes, the burning of solids, especially the variable quality solids found in wastes, presents a critical problem. Such fuels are often left to very large combustion chambers, particularly boilers and cement kilns. When solids and wastes must be used as heat sources in small and accurate heating processes, a better approach is to gasify them to produce a synthesis gas, which can be cleaned and then controlled more precisely.

2 THERMAL ASPECTS OF COMBUSTION

The purpose of combustion in industrial applications, for the most part, is to transform chemical energy, available in various types of fuels, to thermal energy or heat to be of use in the processing of gas or liquid streams or solid objects. Typical examples involve the heating of air, water, and steam for use in heating of other processes or equipment, the heating of metals and nonmetallic minerals during production and processing, the heating of organic streams for use in refining and processing, as well as heating of air for space comfort conditioning. For all of these, it is necessary to have a workable method for evaluating the heat available from a combustion process.

Available heat is the heat accessible for the load (useful output) and to balance all losses other than stack losses (see Fig. 2.). The available heat per unit of fuel is

$$AH = HHV - \text{Total stack gas loss} = LHV - \text{Dry stack gas loss}$$

$$\% \text{ available heat} = 100(AH/HHV)$$

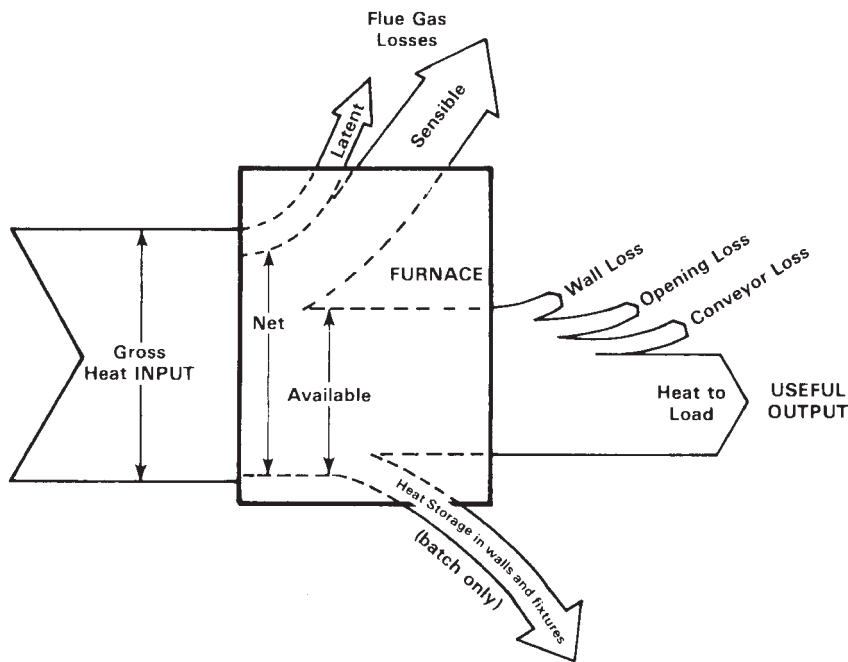


Figure 2 Sankey diagram for a furnace, oven, kiln, incinerator, boiler, or heater—a qualitative and roughly quantitative method for analyzing efficiency of fuel-fired heating equipment.

where AH = available heat, HHV = higher heating value, and LHV = lower heating value, as defined in Chapter 18. Figure 3 shows values of percentage of available heat for a typical natural gas, Fig. 4 for a typical heavy fuel oil.

Example Calculation

A process furnace is to raise the heat content of 10,000 lb/h of a load from 0 to 470 Btu/lb in a continuous furnace (no wall storage) with a flue gas exit temperature of 1400°F. The sum of wall loss and opening loss is 70,000 Btu/h. There is no conveyor loss. Estimate the fuel consumption using 1000 Btu/ft³ natural gas with 10% excess air.

Solution: From Fig. 3, the % available heat = 58.5%. In other words, the flue losses are 100% – 58.5% = 41.5%. The sum of other losses and useful output = 70,000 + (10,000 lb/h)(470 Btu/lb) = 4,770,000 Btu/h. This constitutes the “available heat” required. The required gross input is therefore 4,770,000/0.585 = 8,154,000 Btu/h, or 8154 ft³/h of natural gas (and about 81,540 ft³/h of air).

The use of the above precalculated percentage of available heat has proved to be a practical way to avoid long iterative methods for evaluating stack losses and what is therefore left for useful heat output and to balance other losses. For low exit gas temperatures such as encountered in boilers, ovens, and industrial dryers, the dry stack gas loss can be estimated by assuming the total exit gas stream has the specific heat of nitrogen, which is usually a major component of the “poc” (products of combustion):

$$\frac{\text{Dry stack loss}}{\text{Unit of fuel}} = \left(\frac{\text{lb dry proc}}{\text{Unit of fuel}} \right) \left(\frac{0.253 \text{ Btu}}{\text{lb poc } (^{\circ}\text{F})} \right) (T_{\text{exit}} - T_{\text{in}})$$

or

$$\left(\frac{\text{scf dry poc}}{\text{Unit of fuel}} \right) \left(\frac{0.0187 \text{ Btu}}{\text{scf poc } (^{\circ}\text{F})} \right) (T_{\text{exit}} - T_{\text{in}})$$

For a gaseous fuel, the “unit of fuel” is usually scf (standard cubic feet), where “standard” is at 29.92 in. Hg and 60°F or nm³ (normal cubic meter), where “normal” is at 1.013 bars and 15°C.

Heat transferred from combustion takes two forms: radiation and convection. Both phenomena involve transfer to a surface. Flame radiation comes from both particle and gas radiation. The visible yellow-orange light normally associated with a flame is actually from solid soot or char particles in the flame, and the “working” portion of this form of heat transfer is in the infrared wavelength range. Because oils have higher C/H ratios than gaseous fuels, oil flames are usually more yellow or luminous than gas flames (although oil flames can be made blue). Gas flames can be made more luminous, by a delayed-mixing burner design, for the purpose of increasing their radiating capability.

Particulate radiation follows the Stefan–Boltzmann law for solids but depends on the concentration of particles within the flame. Estimating or measuring the particle temperature and concentration in the flame can be difficult.

Gas radiation and blue flame radiation contain more ultraviolet radiation and tend to be less intense. Triatomic gases (CO₂, H₂O, and SO₂) emit radiation that is largely infrared. Gases beyond the tips of both luminous and nonluminous flames continue to emit this gas radiation. As a very broad generalization, blue or nonluminous flames tend to be hotter, smaller, and less intense radiators than luminous flames. Gas radiation depends on the concentrations (or partial pressures) of the triatomic molecules and the beam thickness of their “cloud.” Their temperatures are very transient in most combustion applications.

Convection from combustion products beyond the flame tip follows conventional convection formulas—largely a function of velocity. This is the reason for recent emphasis on high-velocity burners in some applications. Flame convection by actual flame impingement is more difficult to evaluate because (1) flame temperatures change so rapidly and are thus difficult

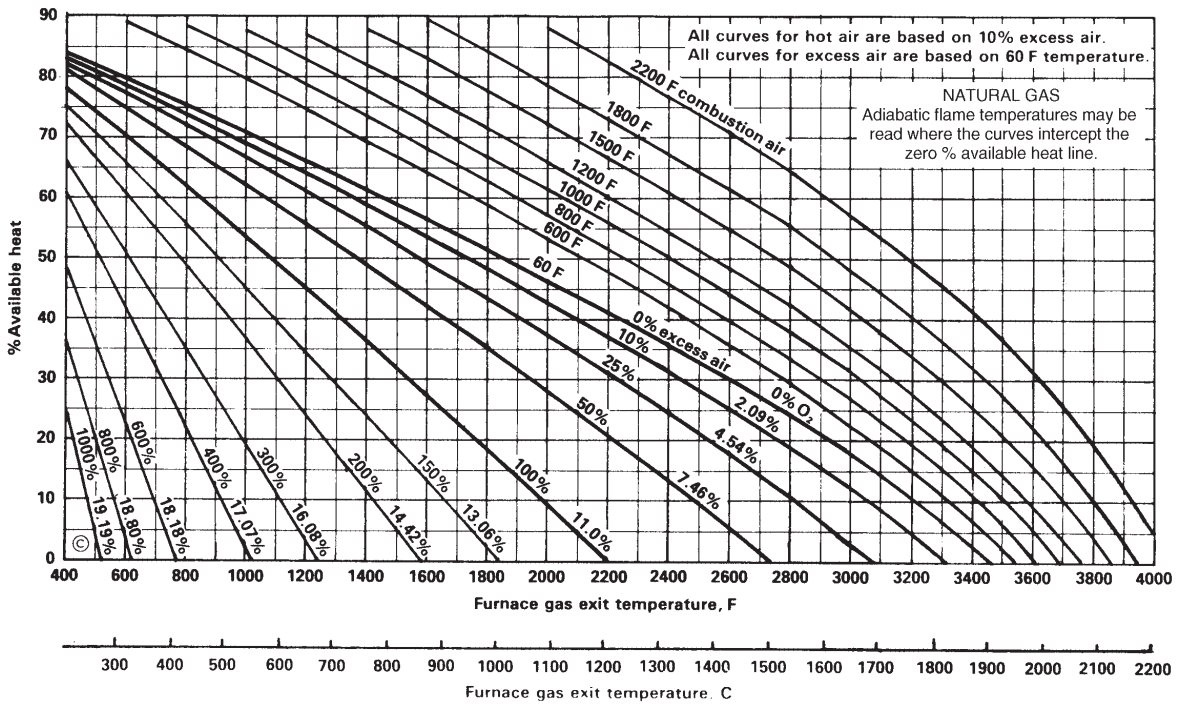


Figure 3 Available heat for 1000 Btu/ft³ natural gas. Examples: In a furnace with 1600°F flue temperature, 60°F air, and 10 % excess air, read that 54% of the gross heat input is available for heating the load and balancing the losses other than stack losses, and, at the *x* intercept, read that the adiabatic flame temperature will be 3310°F. If the combustion air were 1200°F instead of 60°F, read that the available heat would be 77% and that the adiabatic flame temperature would be 3760°F. It is enlightening to compare this graph with Figure 24 for oxy-fuel firing and oxygen enrichment.

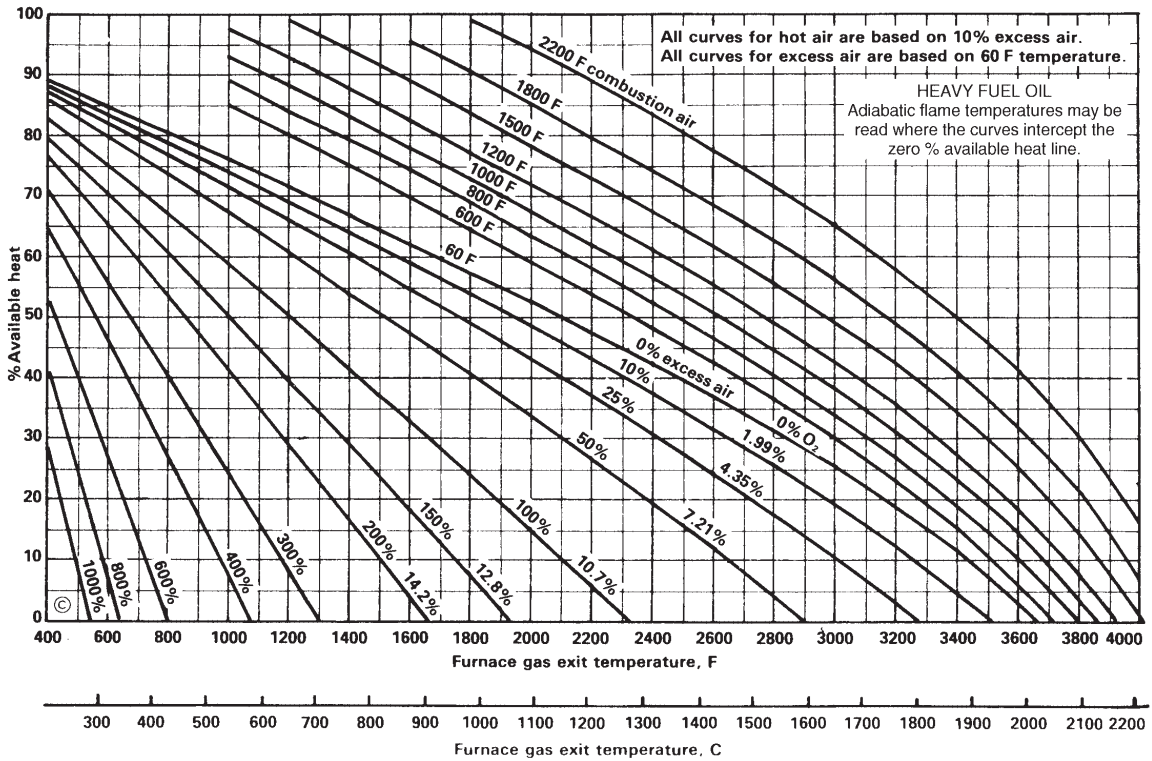


Figure 4 Available heat for 153,120 gross Btu/gal residual fuel oil (heavy, No. 6). With 2200°F gases leaving a furnace, 1000°F air entering the burners, and 10% excess air, 62% of the 153,120 is available; 100% – 62% = 38% stack loss.

to measure or predict and (2) it involves extrapolating many convection formulas into ranges where good data are lacking.

Refractory radiation is a second stage of heat transfer. The refractory must first be heated by flame radiation and/or convection. A gas mantle, so-called infrared burners, and “radiation burners” use flame convection to heat some solid (refractory or metal) to incandescence so that they become good radiators.

3 FLAME AERODYNAMICS

The functions of a properly designed burner can be listed as follows:

1. To introduce desired quantities of fuel and air into a furnace to release a given amount of heat
2. To release heat in a specified heat release pattern
3. To provide stable ignition and safe operation
4. To induce proper mixing of fuel and air
5. To allow for sufficient turndown range
6. To allow for fuel and oxidant composition variations
7. To be simple in operation
8. To have low pollutant omission and minimum noise
9. To maximize efficiency

In short, the burner must be designed so that the flame is retained in a fixed position with respect to the burner, with a predetermined flame pattern. It should have the ability to retain the flame in position over a range of firing rate. We will delineate how burner aerodynamics is often the most important factor influencing essentially all of the above factors.

3.1 Premixed Flames

Premixed Laminar Flame Speed

The premixed laminar flame speed is the rate at which a flame front propagates through a mixture of fuel and air. It is a fundamental physicochemical property of an oxidant fuel mixture. It is thus not influenced by burner aerodynamics. Very few industrial burners produce laminar flames and so the connection between laminar flame speed and burner throat velocity is indirect, if at all, and not direct. Figure 5 shows premixed laminar flame speeds for a variety of air/fuel mixtures. These speeds are controlled by molecular diffusion of species and heat upstream as well as the overall rate of reaction and are thus, with the notable exception of H_2 , quite low, of the order of 1–2 ft/s. Under adiabatic conditions, which are extremely rare in industry, the flame will flash back or blow off if the flame speed exceeds or is less than the incoming flow velocity determined by the operator. Under practical laminar flow conditions, the flame front, which is very thin, say about 1 mm, adjusts its position, so that the normal velocity to it is equal to the flame speed.

The simplest theory³ predicting laminar flame speed v_f uses an enthalpy balance to predict

$$v_f \text{ proportioned to } \left(\frac{k}{\rho C_p} \right)^{1/2} (RR)^{1/2} \quad (1)$$

where K = thermal conductivity of mixture

ρ = density of mixture

C = specific heat of mixture

RR = overall reaction rate

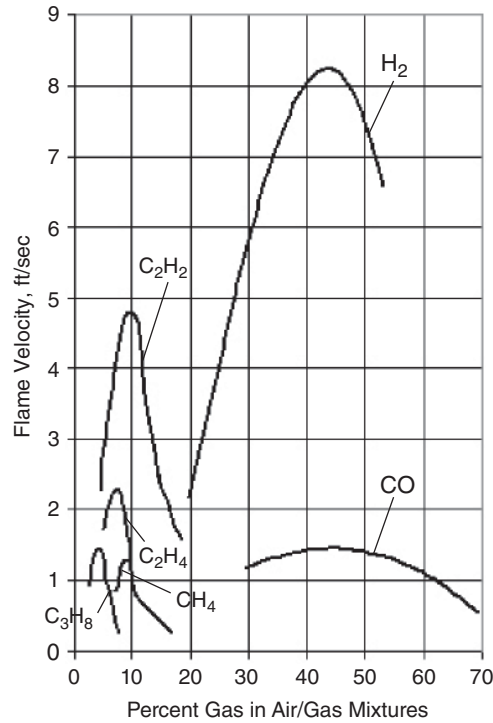


Figure 5 Laminar flame speeds.

Thus, the flame speed depends exponentially on the flame temperature because the reaction rate has this type of dependence.

Premixed Laminar Flame Stabilization on Tubes

In practice, the tube diameter plays an important role in laminar flame stabilization. This is because the tube walls act as a heat sink, quenching the reaction. When the flow velocity exceeds the flame speed, the flame begins to lift off the end of the tube, whereupon its heat loss to the tube is decreased, its temperature increased, and the flame speed thus also increased, allowing stabilization at a new position above the tube exit. Further increase in flow velocity will blow the flame off and extinguish it, due to increased dilution by the surroundings. At low flow velocities the flame may not necessarily flash back down the tube if the tube diameter is less than half the quenching distance, the latter defined by⁴

$$d_{\text{quenching}} = \frac{k/\rho C_p}{v_f} \quad (2)$$

The quenching distance $d_{\text{quenching}}$ is an important property; otherwise the flame would always propagate down the low-velocity regions of flow next to the tube wall. Thus, laminar premixed flames, stabilized on a tube, do allow a range in turndown, even though the adiabatic flame speed does not change. The home gas range is an example of this.

Turbulent Premixed Flames (No Recirculation)

In practice, under turbulent flow conditions, the mean incoming velocity capable of supporting a premixed flame is significantly higher than that of the laminar flame speed. This is because

turbulence produces eddies that grossly distort or wrinkle the laminar flame front. Thus, while the *mean* velocity is higher than the laminar flame speed, the local velocity normal to the (fluctuating) wrinkled flame front is equal to v_f . At high Reynolds numbers, the mean turbulent flame speed is typically a factor of four or five times the laminar flame speed, or about 10 ft/s, for methane/air mixtures.

From the foregoing it is clear that without recycle of heat via radiation or convective recirculation of hot products back into the ignition zone, it is impossible to stabilize premixed flames at high burner velocities. This introduces the subject of reverse flows. For the purpose of discussion we can define premixed flames as those in which the mixing of fuel and air is rapid and does *not* control flame length.

Aerodynamics of Premixed Flames

We now consider in detail how hot product gas recirculation can be accomplished through burner adjustments and flows. It is useful to consider (1) free jets, (2) confined jets with no swirl, (3) confined jets with swirl, and (4) flow past bluff bodies.

Free Jets. Consider a turbulent jet flowing into a quiescent medium as shown in Fig. 6. If the velocity along the center axis is denoted by u_m and the mean velocity leaving the jet is u_o , the following relationship holds for distances beyond five diameters from the exit:

$$\frac{u_m}{u_o} = A \frac{x-1}{d_o} \quad (3)$$

Thus, the velocity decay is inversely proportional to the distance downstream. The mean radial velocity has a Gaussian distribution

$$\frac{u(r)}{u_m} = \exp \left[-k \left(\frac{r}{x} \right)^2 \right] \quad (4)$$

The axial velocity decrease is due to entrainment from the surrounding fluid. If this fluid is cold, the ensuing dilution effect will rapidly cool down a hot jet. The entrained fluid influences the fluid at the center line of the jet at a distance equal to five times the jet diameter. The angle of spread is approximately 19° – 22° and is independent of u_o . According to Ricou and Spalding,⁵

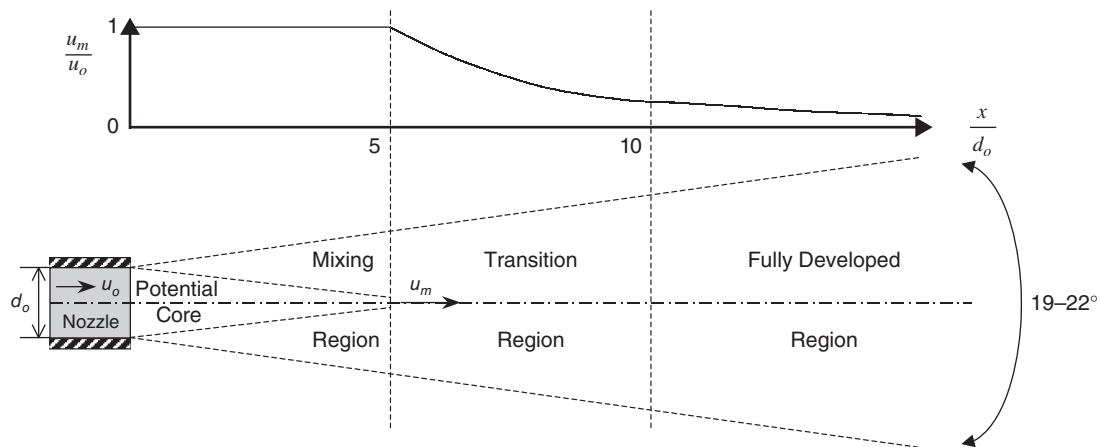


Figure 6 Free jet entrainment.

the rate of entrainment m_e is given by

$$\frac{\dot{m}_e}{\dot{m}_o} = 0.32 \left(\frac{\rho_e}{\rho_o} \right)^{1/2} \frac{x}{d_o} - 1 \quad (5)$$

where ρ_e = density of entrained fluid
 ρ_o = nozzle density
 \dot{m}_e = mass flow entrained
 \dot{m}_o = mass flow from nozzle
 d_o = nozzle diameter

Confined Jets: Creation of Secondary Recirculation. When the jet is confined, it still entrains surrounding fluid and spreads out. However, the fluid entrained must now consist of product gases, which are recirculated back along the walls. The walls also serve to prevent the jet from spreading out too rapidly. If the walls are hot, this secondary recirculation serves to recycle hot gases back into the ignition zone, which is good for flame stability. If the walls are cold, then heat is transferred by convection and the secondary recirculation acts like a cold diluent, thus providing for poor flame stability.

Confined jets have been analyzed by Thring and Newby⁶ (see Fig. 7). They assumed that a jet:

1. Expands as a free jet with an angle of 19.4° and thus impinges on a wall at a distance x_p .
2. Entrainment ceases at a point C , at position x_c (i.e., entrainment ceases and dis-entrainment begins) midway between the point where entrainment is zero, x_N , and the point where the jet hits the wall (see Fig. 8).

These assumptions lead to the following predictions for x_N , x_c , and x_p :

$$\frac{x_N}{d_o} = \frac{1}{0.32} \left(\frac{\rho_o}{\rho_e} \right)^{1/2} \quad (\text{see Eq. (5)}) \quad (6)$$

$$x_c = \frac{1}{2} \left[x_p + \frac{d_o}{0.32} \left(\frac{\rho_o}{\rho_e} \right)^{1/2} \right] \quad (7)$$

$$x_p = 5.85L \quad (\text{Free jet, } a = 19.4^\circ) \quad (8)$$

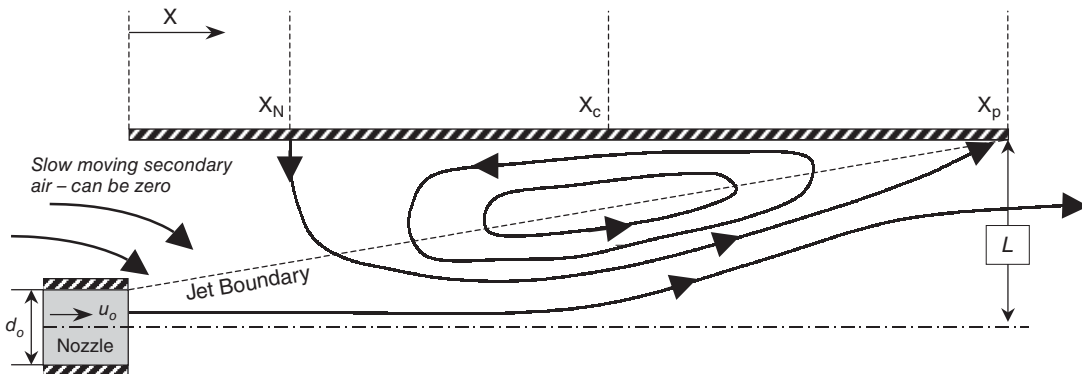


Figure 7 Axial confined jet and secondary recirculation.

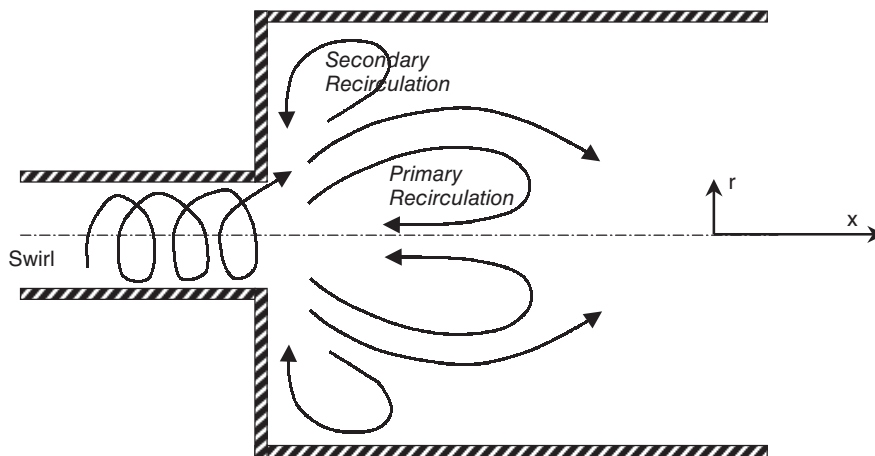


Figure 8 Creation of primary recirculation resulting from swirl.

The mass entrained between N and C is the mass of secondary recirculation and is given by

$$\frac{m_e}{m_o} = \frac{m_{\text{recirc}}}{m_o} = 0.32 \left(\frac{\rho_e}{\rho_o} \right)^{1/2} \frac{x_c}{d_o} - 1 \quad (\text{see Eq. (5)}) \quad (9)$$

Defining

$$\theta = \frac{d_o}{2L} \left(\frac{\rho_o}{\rho_e} \right)^{1/2} \quad (10)$$

yields

$$\frac{m_{\text{recirc}}}{m_o} = \frac{0.47}{\theta} - 0.5 \quad (11)$$

which agrees with experimental data to within about 10%.⁷ The parameter θ is a similitude parameter and can be used for nozzle/chamber scale-up purposes. We can conclude that both useful analytical predictions and scale-up criteria can be used for this simple premixed turbulent enclosed jet. The importance of secondary recirculation for flame stabilization should be again emphasized.

Confined Jets with Swirl: Recirculation. Some recirculation is essential for flame stability.

In many cases, secondary recirculation originating from confined jets is insufficient to maintain a constant supply of hot gases and/or active species to maintain ignition. In this case recirculation of hot gas must occur by some other means.

Swirl, or a tangential velocity at the burner exit, will cause a radial pressure gradient, given by

$$\frac{dP}{dr} = \rho \frac{v_\theta^2}{r} \quad (\text{centrifugal force}) \quad (12)$$

if radial velocity and viscosity are neglected but will in all cases be a positive number. This means that the pressure will be lowest in the center of the vortex. As the swirl dissipates in the combustor, the pressure along the center line increases. This adverse pressure gradient prompts a reverse flow down the center, creating primary recirculation of hot gases, as shown in Fig. 8.

The swirl number S is defined as $S = \text{axial flow of angular momentum} / \text{axial flow of axial momentum}$ and is given by

$$S = \frac{\left[\int_0^R \rho v_x r v_{\theta} r \, dr \right]}{\left[\int_0^R \rho v_x v_x r \, dr \right] R} \quad (13)$$

Unfortunately, v_{θ} is a strong function of r at the burner exit, and knowledge of this dependence is essential to calculate swirl numbers in practical instances. This functionality depends on how swirl is generated. The swirl number, however, is an important parameter describing the flow of swirling flames and can be used for scale-up.

For $S > 0.3$ a reverse flow can occur and increasing swirl will always shorten the flame jet and increase its spread. For weakly swirling flows ($S < 0.3$) the angle of spread is given by

$$a = 4.8 + 14S \quad (14)$$

Flame Stabilization by Bluff Bodies. When a bluff body is placed in the path of a fluid with velocity U , a low-pressure zone will form behind it and viscous forces in the boundary layer will result in flow separation. The result will be a recirculation zone or trailing wake (Fig. 9).

The blow-off velocity can be determined by equating the ignition time τ_i with the contact time in the recirculating wake, τ_c .

Thus,

$$\tau_c = \frac{D}{U_{bo}} = \tau_i \quad (15)$$

yielding

$$U_{bo} = \frac{D}{\tau_i} \quad (16)$$

(= 100D for $\tau_i = 10^{-2}$ sec)

Thus, for reasonable sized obstacle diameter D , the blow-off velocity can be many times the maximum turbulent flame speed described above.

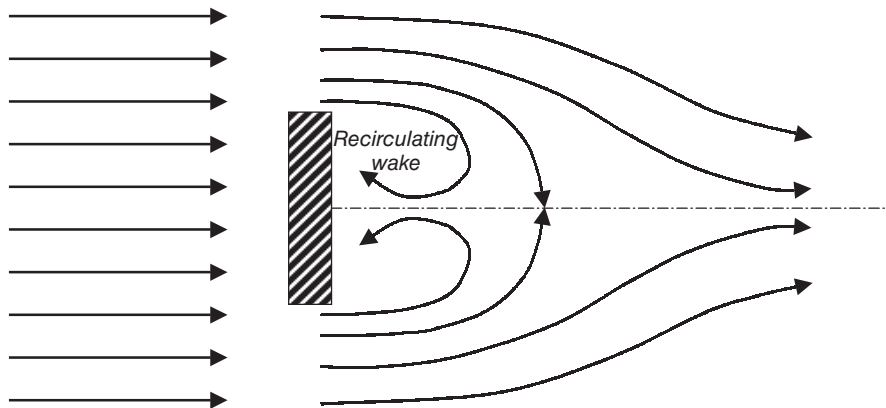


Figure 9 Recirculation caused by wake behind a bluff body.

The conclusions from this section on premixed turbulent flames are:

1. Recirculation of hot products or of heat is essential to maintain stable ignition at high burner velocities.
2. This can be achieved by secondary recirculation in a hot enclosure, where it can be modeled and predicted for scale-up purposes for axial jets only.
3. Swirl is always an effective technique to stabilize a flame but will also shorten it. Swirling flow cannot be easily modeled.
4. Bluff body stabilization is an inexpensive method to induce recirculating flows and allows high incoming blow-off velocities.

3.2 Diffusion-Mixed Turbulent Flames

An alternative to the premix burner is the diffusion-mixed type, also called the nozzle-mixed type. The majority of burners are of this type. Raw gas, atomized oil droplets, or pulverized coal is mixed with the air supply by a turbulent diffusion process occurring within the plume of flame. Figure 10 is a schematic representation of a diffusion flame gas burner with this mixing process taking place. Air is introduced through a register that can control the amount passing through, upon the pressure available; often the register is in the form of vanes, which will give the combustion air a swirling motion. Gas jets are introduced by a nozzle or a distributor ring placed in the air entry channel, with the jets disposed for mixing into the air. However, it is only some distance downstream from the gas jets where the velocity has slowed and where enough mixture within the combustible limits has been formed to support a flame. It is only within restricted limits of an air-to-fuel ratio that the burning will persist.

The actual burning process is an extremely complicated one, and many chemical and physical processes are occurring simultaneously. In the diffusion flame, the rate-controlling

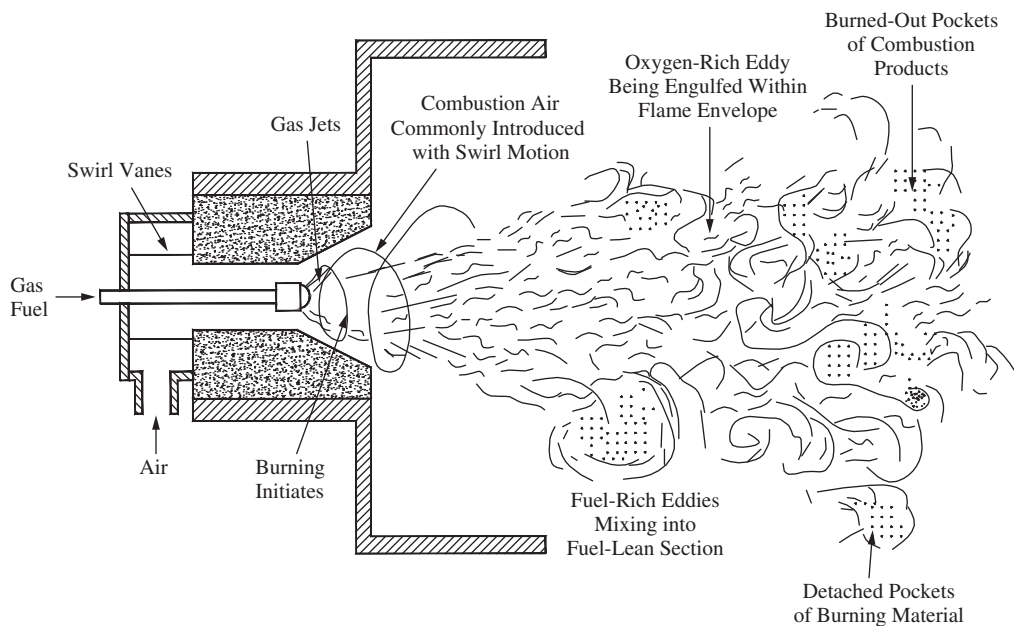


Figure 10 Schematic of a diffusion mixed burner.

process is that of the mixing between air and fuel, which involves a transport of both mass and momentum between regions of high velocity and regions of low velocity. Only in a relatively thin interface is there a combustible mixture, and this governs the formation of a sheet of flame. The sheet is very much warped and wrinkled as eddies of fuel are swept out into the air section or as eddies of oxygen-containing air move into the fuel. Pockets of flame will be carried into unignited regions, which will burst into new flames; or they will be projected into zones that have already been burned out, whereupon the flame is diluted and quenched. Since the flame front cannot move at a very high velocity, it remains always detached from the gas nozzle. A flame front will sweep through a stagnant mixture of cold gases at relatively low velocity, of the order of 2–30 ft/s. At too high a velocity the flame will actually blow out and away, and the flame will become extinguished; special provisions must therefore be made to hold the flame in place.

Some nozzle mix burners distribute the gas supply through a series of jets of from a pipe ring with many openings into the throat section of air inlet. In this way the air and fuel mixing are well under way before entering the combustion space. Such a burner is not clearly premix or a discrete diffusion-mixed type.

The size and shape of the flame are largely determined by the means used for mixing gas and fuel and for preheating it to ignition temperature. The resulting flame patterns differ widely from one burner to the next. This is the topic of a later section. The comments above pertain also to oil flame, with the added complications of atomization and liquid-phase pyrolysis.

As with the gas flame, many patterns of flame are possible with the oil burner. These depend partly on the spray pattern of the atomizing system and also on the manner of introducing the combustion air and its axial and tangential or swirl momentum.

3.3 Turbulent Diffusion Flame Types

Effect of Swirl

Consider the effect of swirl momentum and total (air and fuel) axial momentum. Recall that high swirl attempts to create a primary recirculation, backflow, up the center of the burner axis. However, this reverse flow may be countered by the axial momentum of the fuel jet and may or may not be sufficient to overcome this forward axial momentum. We consider four cases that are shown schematically in Fig. 11 (nomenclature follows naming conventions outlined by Beer and Chigier⁸).

Type 1A: Zero Swirl, Moderate Axial Momentum. The type 1 flame is long, poorly mixed, and highly luminous. The type 1A designation refers to an attached flame, and attachment with zero swirl is normally possible only when moderate axial momentum levels are used in conjunction with hot secondary recirculation. Burner throat velocities are typically on the order of 30 m/s (100 ft/s). This flame is utilized in cement kiln burners and other metal and product heating applications and in tangentially fired combustors.

Type 1B: Zero Swirl, Very High Axial Momentum. The type 1B designation refers to a high-axial-momentum, zero-swirl flame where ignition is delayed and the high velocity almost blows the flame off. If secondary recirculation causes cold gases (cold walls) to quench the ignition, the flame will go out. This “lifted” flame is not inherently stable.

Type 2: Moderate Swirl ($S < 0.6$), Moderate Axial Momentum. As swirl increases, primary recirculation zones attempt to form, but the axial fuel jet momentum is still sufficient to break through the reverse flow region. This behavior causes a toroidal recirculation zone to form, with primary jet penetration. This configuration is called a type 2 flame and is stable over a wide range of turndown ratios. This flame is typical of many wall-fired burner configurations. Increased swirl will broaden and shorten the flame. The direction of the fuel jet also clearly plays an important role in flame shape.

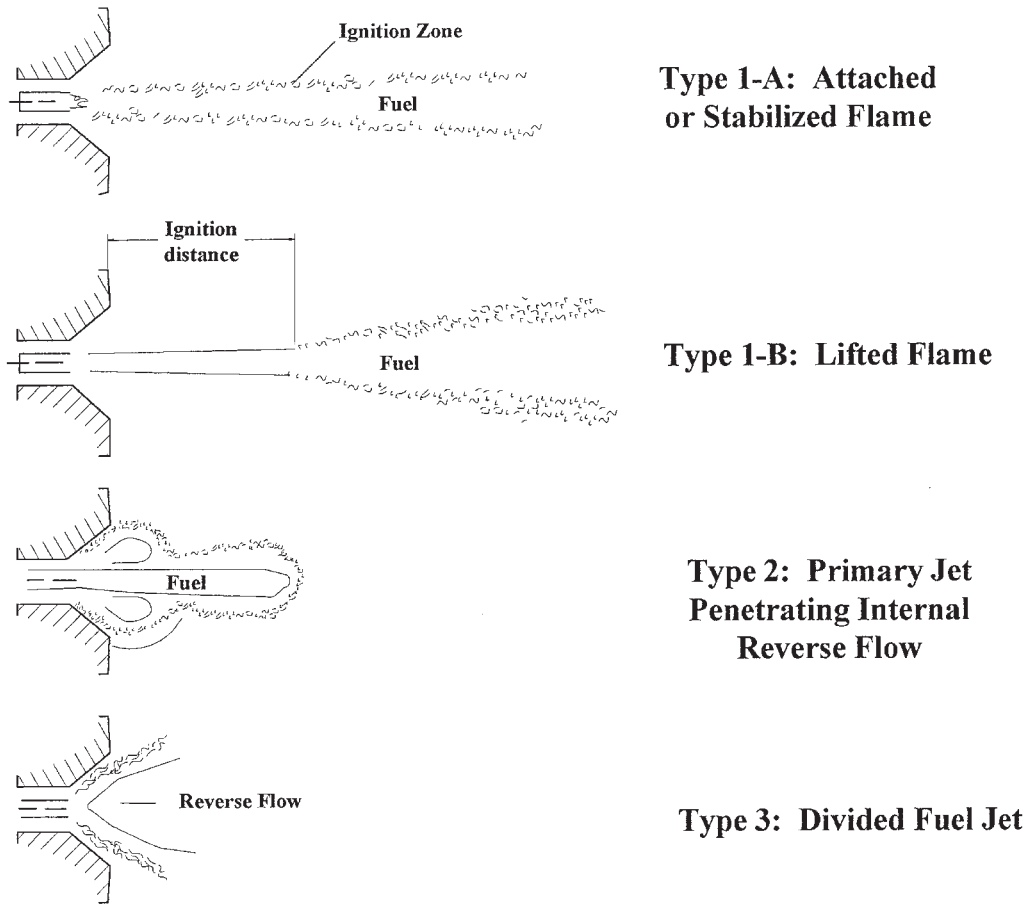


Figure 11 Simple flame classification scheme.

Type 3: High Swirl, Low Axial Momentum ($S > 0.6$). As swirl is increased or axial momentum of the fuel jet is decreased, the primary recirculation overcomes the forward thrust of fuel jet and divides it. This forms a type 3 flame, with recirculation down the center. As the swirl number increases, the flame shape can vary from a ball of flame to a conical flame to a flat flame along the walls. Thus, many type 3 flames may look quite different from one another. This flame is stable under most conditions, unless the fuel is injected too rapidly and there is sufficient momentum to penetrate the recirculation zone.

Other Methods of Stabilization

Holding a flame under a variety of operating and firing rates depends on maintaining a localized zone within or adjacent to the normal flame envelope, which will always lie within the combustion limits for the fuel and oxygen mixture, and in holding the zone where the fluid velocities are not sufficiently high to sweep the flame away. The following are examples of ways that are used to bring about improved stability.

Burner Tile (Fig. 12a). A conically shaped ceramix tile piece surrounds the burner opening. The diverging flow area slows the air velocity. The tile is heated by exposure to the flame to a glowing red temperature, and it reradiates and conducts to the incoming mixture. In addition, its conical or cup shape combined with a tangential swirl to the incoming air or fume stream may cause a recirculation zone in the flame center directly opposite the fuel nozzle, which brings hot combustion products and radicals back into contact with the fresh fuel and air mixture for ignition.

Target Rod and Plate (Figs. 12b and f). The flame is made to impinge on a cylindrical rod or a flat plate (made of ceramic or temperature-resistant alloy). Eddies form on the downstream side of this target, and these contain pockets of fuel-rich and air-rich mixture. Portions of these are swept off into the stream, forming multiple ignition sources; portions are retained and regenerated on the back of the target. The retained flame serves as a continuous pilot.

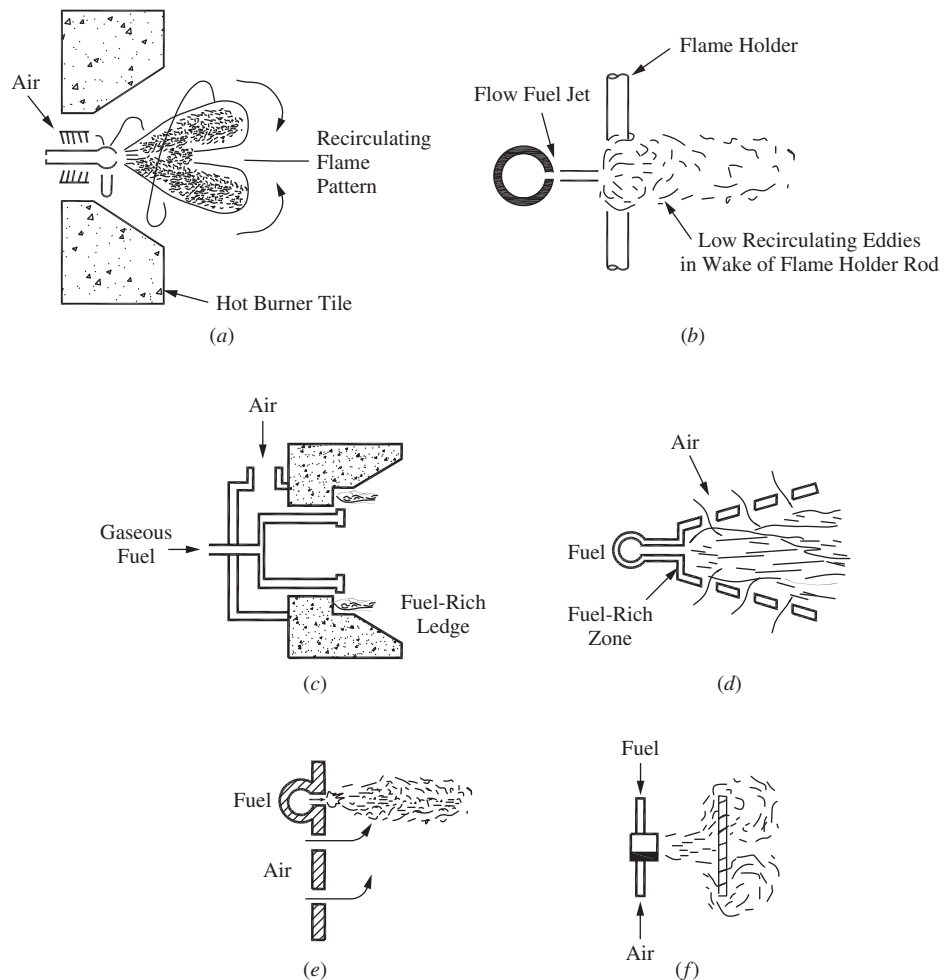


Figure 12 Examples of flame-holding arrangements: (a) recirculating flame and hot refractory tile; (b) target rod; (c) flameholder ledge; (d) grated air entry; (e) grated air entry, grid plate version; and (f) target plate.

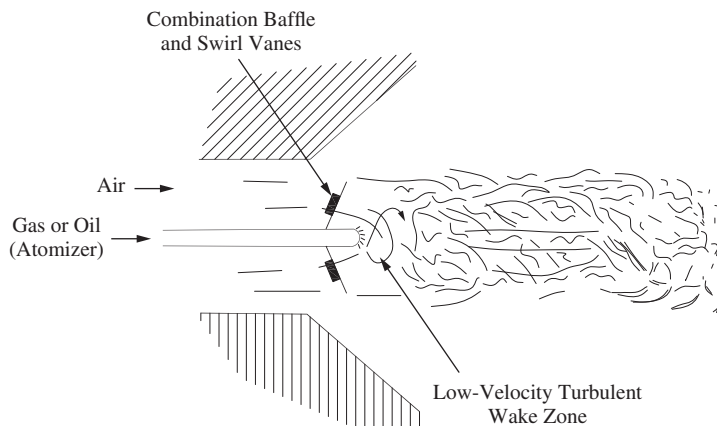


Figure 13 Flow pattern, axial jet burner, and conical oil fuel spray nozzle.

Fuel-Rich, Low-Velocity Pocket (Fig. 12c). The pocket is located downstream from the main fuel addition and has its own fuel supply. The low velocity in the pocket allows a flame to be retained and to act as a continuous pilot for the main stream. John Zink Company uses a ledge in the wall of the throat of one of its gas burners in this manner.

Graded Air Entry (Figs. 12d and e). The gas enters by a channel having a diverging cross section; air is introduced by holes that produce cross-stream jets of air. The diverging channel slows the mixture; meanwhile, some of the air jets are too fuel rich, some too fuel lean; at some point in the channel they are near optimum. Wake eddies are formed that retain the flame. Many jet engines use variants of this design.

Deflector Plate on Fuel Gun (Fig. 13). A vaned conical plate attached to the end of the fuel gun serves as a baffle and swirl-inducing device, holding a low-velocity turbulent wake zone immediately opposite the burner tip. Although the mixture in this region is generally fuel rich, pockets of burnable mixture recirculate in the zone to hold the flame in place. Additional air sweeps past the plate undisturbed and mixes with the central wake zone further out from the burner. This arrangement is commonly used with packaged pressure-atomized burner units.

Effects of Inner and Outer Swirl (Fig. 14). As noted before, type 3 flames can vary widely in shape. Some examples are shown in Fig. 14 (top). If a long, stable flame with primary recirculation is desired, then swirl in the center may be feasible (Fig. 14, bottom). This is a form of a delayed mixing flame, with type 1 attribute of luminosity, length, etc., but type 3 properties of stability. It is still essentially a type 3 flame.

4 FIRING SYSTEMS

The following sections describe the most commonly encountered firing systems for gaseous, liquid, and solid fuels. A firing system provides for mixing of fuel with an oxidizer (typically air) in a manner that promotes stable combustion and desired heat release rates.

4.1 Gaseous Fuels

Gaseous fuels are typically the simplest to use as they are typically supplied at pressure and do not require special pumping, heating, or atomizing (as is the case for liquid fuels) or crushing,

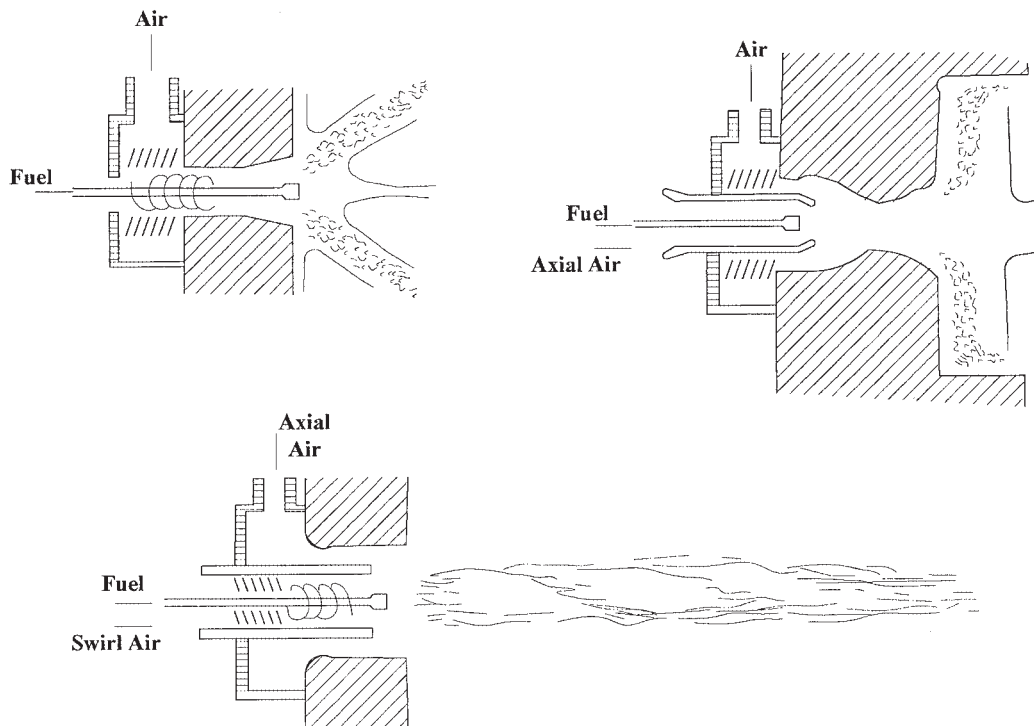


Figure 14 Effects of different swirl configurations.

grinding, or pulverizing (in the case of solid fuels). In general, it is easier to maintain a steady feed rate, and thus a more stable flame, with a gaseous fuel (unless the fuel has a very low heating value—e.g., blast furnace gas).

The previous section on flame aerodynamics discussed the basic principles underlying the shaping and stabilizing of both premixed and diffusion flames. Either of these flame types can be applied to gaseous fuels using the common burner types described below. Although presented under “Gaseous Fuels,” many of these burner types are also applicable for liquid and solid fuels.

Basic Burner Types

Open and natural draft-type burners rely on a negative pressure in the combustion chamber to pull in the air required for combustion, usually through adjustable shutters around the fuel nozzles. The suction in the chamber may be natural draft (chimney effect) or induced by draft fans. A crude “burner” may be nothing more than a gas gun and/or atomizer inserted through a hole in the furnace wall. Fuel–air mixing may be poor, and fuel–air ratio control may be nonexistent. Retrofitting for addition of preheated combustion air is difficult (see Fig. 15).

Sealed-in and power burners have no intentional “free” air inlets around the burner, nor are there air inlets in the form of louvers in the combustion chamber wall. All air inflow is controlled, usually by a forced draft blower or fan pushing the air through pipes or a windbox. These burners usually have a higher air pressure drop at the burner, so air velocities are higher, enabling more thorough mixing and better control of flame geometry. Air flow can be measured, so automatic air–fuel ratio control is easy (see Fig. 16).

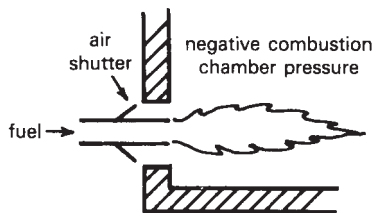


Figure 15 Open, natural draft-type burner.

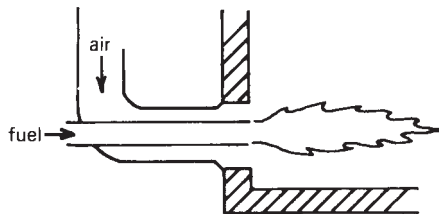


Figure 16 Sealed-in power burner.

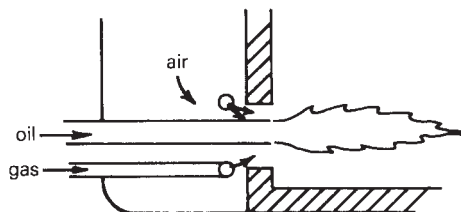


Figure 17 Windbox burner.

Windbox burners often consist of little more than a long atomizer and a gas gun or gas ring. These are popular for small industrial and large utility boilers where economic reasons have dictated that the required large volumes of air be supplied at very low pressure (2–10 in. we) (in. we = inches of water column). Precautions are necessary to avoid fuel flowback into the windbox (see Fig. 17).

Packaged burners usually consist of bolt-on arrangements with an integral fan and perhaps integral controls. These are widely used for new and retrofit installations from very small up to about 50×10^6 Btu/h (see Fig. 18).

Recommended Applications

Premix burner systems may be found in any of the above configurations. Most domestic appliances incorporate premixing using some form of gas injector or inspirator (gas pressure inducing air through a venturi). Small industrial multiport burners of this type facilitate spreading a small amount of heat over a large area, as for heating kettles, vats, rolls, small boilers, moving webs, and low-temperature processing of conveyORIZED products. Large single-port premix burners have been replaced by nozzle mix burners. Better fuel–air ratio control is possible by use of aspirator mixers. (Air injection provides the energy to draw in the proper proportion

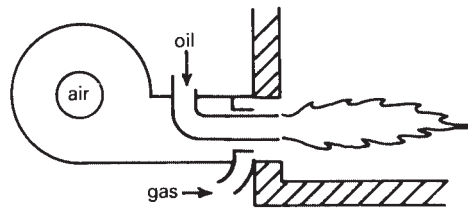


Figure 18 Integral fan burner.

of gas.) Many small units have undersized blowers, relying on furnace draft to provide secondary air. As fuel costs rise, the unwarranted excess air involved in such arrangements makes them uneconomical. Mixture manifold inside diameters larger than 4 in. (100 mm) are usually considered too great an explosion risk. For this reason, mixing in a fan inlet is rarely used.

Diffusion flame or nozzle mix burner systems constitute the most common industrial gas burner arrangement today. They permit a broad range of fuel–air ratios, a wide variety of flame shapes, and multifuel firing. A very wide range of operating conditions are now possible with stable flames using nozzle mix burners. For processes requiring special atmospheres, they can even operate with very rich (50% excess fuel) or lean (1500% excess air). They can be built to allow very high velocities (420,000 scfh/in.² of refractory nozzle opening) for emphasizing convection heat transfer.

Others use swirl to elicit centrifugal and coanda effects to cause the flame to scrub an adjacent refractory wall contour, thus enhancing wall radiation (see Fig. 14). By engineering the mixing configuration, nozzle mix burner designers are able to provide a wide range of mixing rates, from a fast, intense ball of flame ($L/D = 1$) to conventional feather-shaped flames ($L/D = 5\text{--}10$) to long flames ($L/D = 20\text{--}50$). Changeable flame patterns are also possible.

Aerodynamically staged or delayed-mixing burners are a special form of diffusion flame burners in which mixing is intentionally slow. (A raw gas torch is an unintentional form of delayed mixing.) Ignition of a fuel with a shortage of air results in polymerization or thermal cracking that forms soot particles only a few micrometers in diameter. These solids in the flame absorb heat and glow immediately, causing a delayed mix flame to be yellow or orange. The added luminosity enhances flame radiation heat transfer, which is one of the reasons for using delayed-mix flames. The other reason is that delayed mixing permits stretching the heat release over a great distance for uniform heating down the length of a radiant tube or a long kiln or furnace that can only be fired from one end. These types of long flames can also be beneficial for reducing nitrogen oxide (NO_x) emissions as peak temperatures are reduced with the staged heat release.

Gaseous fuels can sometimes provide a unique aerodynamic advantage over liquid or solid fuels. Most industrial process burners have traditionally used energy from the air stream to maintain flame stability and flame shape, as discussed previously. Now that higher pressure fuel supplies are readily accessible in most locations, there is an opportunity to use the energy in the fuel stream for controlling flame stability and shape, thereby permitting the use of lower pressure air sources.

Figure 19 shows a fuel-directed burner for gas and preheated air. Multiple supply passages and outlet port positions permit changing the flame pattern during operation for optimum heat transfer during the course of a furnace cycle. Oil burners or dual-fuel combination burners can be constructed in a similar manner using two-fluid atomizers with compressed air or steam as the atomizing medium.

In summary, desired flame shape, stability, and flexibility can be assured by the selection of an appropriate burner design. If maximum flexibility is needed, nozzle mix or diffusion flame

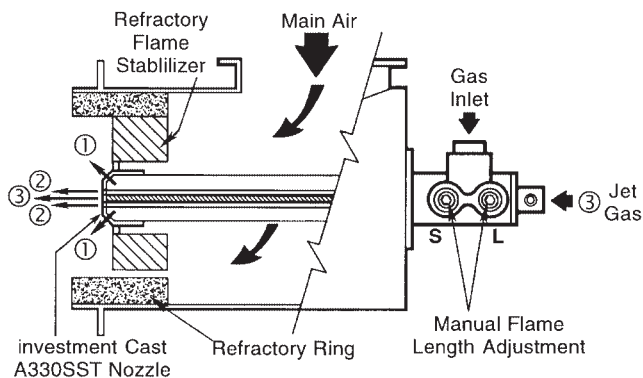


Figure 19 Low NO_x fuel-directed gas burner for use with preheated air. (1) Increasing tangential gas flow (adjustment screw S) shortens flame. (2) Increasing forward gas flow (adjustment screw L) lengthens flame. (3) Jet gas—to maintain flame definition as input is reduced. Courtesy of North American Mfg. Company

burners with *adjustable* swirl for secondary air are recommended. Together with flexibility in injector angle, this design allows just about any flame shape to be achieved and to be modified as desired heat flux distributions are varied. Such burners also allow for variation in fuels.

4.2 Liquid Fuels

Much of what has been said above for gas burners applies as well for oil or other liquid fuel burning. Liquids do not burn; therefore, they must first be vaporized and thus additional considerations must be addressed beyond those described above for gaseous fuels.

The liquid fuel can be prevaporized outside of the furnace to produce a hot vapor stream that is directly substitutable for gas in premix burners. Unless there are many burners or they are very small, it is generally more practical (less maintenance) to convert to combination (dual-fuel) burners of the nozzle mix type. For nozzle mix burners, the fuel is atomized inside the furnace to enhance vaporization rates as noted below.

Atomization of Liquid Fuel

Almost all industrial liquid fuel burners use atomization to aid vaporization by exposing the large surface area (relative to volume) of millions of droplets in the size range of 100–400 μm . Evaporation then occurs at a rapid rate even if the droplets are not exposed to furnace radiation or hot air due to enhanced mass transfer rates.

Pressure atomization (as with a garden hose) uses the pressure energy in the liquid stream to cause the kinetic energy to overcome viscous and surface tension forces. If input is turned down by reducing fuel pressure, however, atomizing quality suffers; therefore, this method of atomization is limited to on-off units or cases where more than 250 psi fuel pressure is available.

Two-fluid atomization is the method most commonly used in industrial burners. Viscous friction by a high-velocity second fluid surrounding the liquid fuel stream literally tears it into droplets. The second fluid may be low-pressure air (<2 psi, or <13.8 kPa), compressed air, gaseous fuel, or steam. Many patented atomizer designs exist, for a variety of spray angles, sizes, turndown ranges, and droplet sizes. Emulsion mixing usually gives superior atomization (uniformly small drops with relatively small consumption of atomizing medium), but control is complicated by interaction of the pressures and flows of the two streams. External mixing is

just the opposite. Tip emulsion atomization provides a compromise between these two mixing limits.

Rotary-cup atomization delivers the liquid fuel to the center of a fast-spinning cup surrounded by an air stream. Rotational speed and air pressure determine the spray angle. This is still used in some large boilers, but the moving parts near the furnace heat have proved to be too much of a maintenance problem in higher temperature process furnaces and on smaller installations where a strict preventive maintenance program could not be effected.

Sonic and ultrasonic atomization systems create very fine drops but impart very little motion to them. For this reason they do not work well with conventional burner configurations but require an all-new design.

Liquid Fuel Conditioning

A variety of additives can be used to reduce fuel degeneration in storage, minimize slagging, lessen surface tension, reduce pollution, and lower the dew point. Regular tank draining and cleaning as well as the use of filters are recommended.

Residual oils must be heated to reduce their viscosity for pumping, usually to 500 SSU (100 cSt). For effective atomization, burner manufacturers specify viscosities in the range of 100–150 SSU (22–32 cSt). In all but tropical climates, blended oils (Nos. 4 and 5) also require heating. In Arctic situations, distillate oils need heating. Figure 20 enables one to predict the oil temperature necessary for a specified viscosity. It is best, however, to install extra heating capacity because delivered oil quality may change.

Oil heaters can be steam or electric. If oil flow stops, the oil may vaporize or char. Either situation reduces heat transfer from the heater surfaces, which can lead to catastrophic failure in electric heaters. Oil must be circulated through heaters, and the system must be fitted with protective limit controls.

Hot oil lines must be insulated and traced with steam, induction, or resistance heating. The purpose of tracing is to balance heat loss to the environment. Rarely will a tracing system have enough capacity to heat up an oil line from ambient conditions. When systems are shut down, arrangements must be made to purge the heavy oil from the lines with steam, air, or (preferably) distillate oil. Oil standby systems should be operated regularly, whether needed or not. In cold climates, they should be started before the onset of cold weather and kept circulating all winter.

4.3 Solid Fuels

Solid fuel burns by a series of steps: (1) initial particle heatup and drying (most solid fuels have some degree of moisture), (2) evolution of volatile matter from the solid particle, (3) combustion of volatile gases, and (4) residual carbon or char oxidation. The design of a suitable firing system for a given solid fuel must take into account the relative importance of each of these steps, which will in turn depend on fuel characteristics and particle size. For gaseous fuels, only step 3 is required, and thus firing system design is focused on appropriate fuel–air mixing to achieve desired heat release and emission levels. For liquid fuels, steps 1–3 are required and thus firing systems must allow for droplet heatup and evaporation in addition to suitable fuel–air mixing.

Firing systems for solid fuels must provide for these steps as well as ensuring adequate burnout of the residual carbon material (which can be as high as 95% of the fuel in some cases). The time scales for these processes can vary greatly for solid fuels. For example, at typical combustion conditions, volatile release and combustion are on the order of 100s of milliseconds (represented by the luminous flame), whereas char oxidation can range from 1–2 s for pulverized char particles to several minutes for large chunks of fuel (the “burning embers” or flying sparklers visible in solid fuel furnaces). As a result, firing systems for solid fuels vary greatly, depending on the fuel characteristics and particle size.

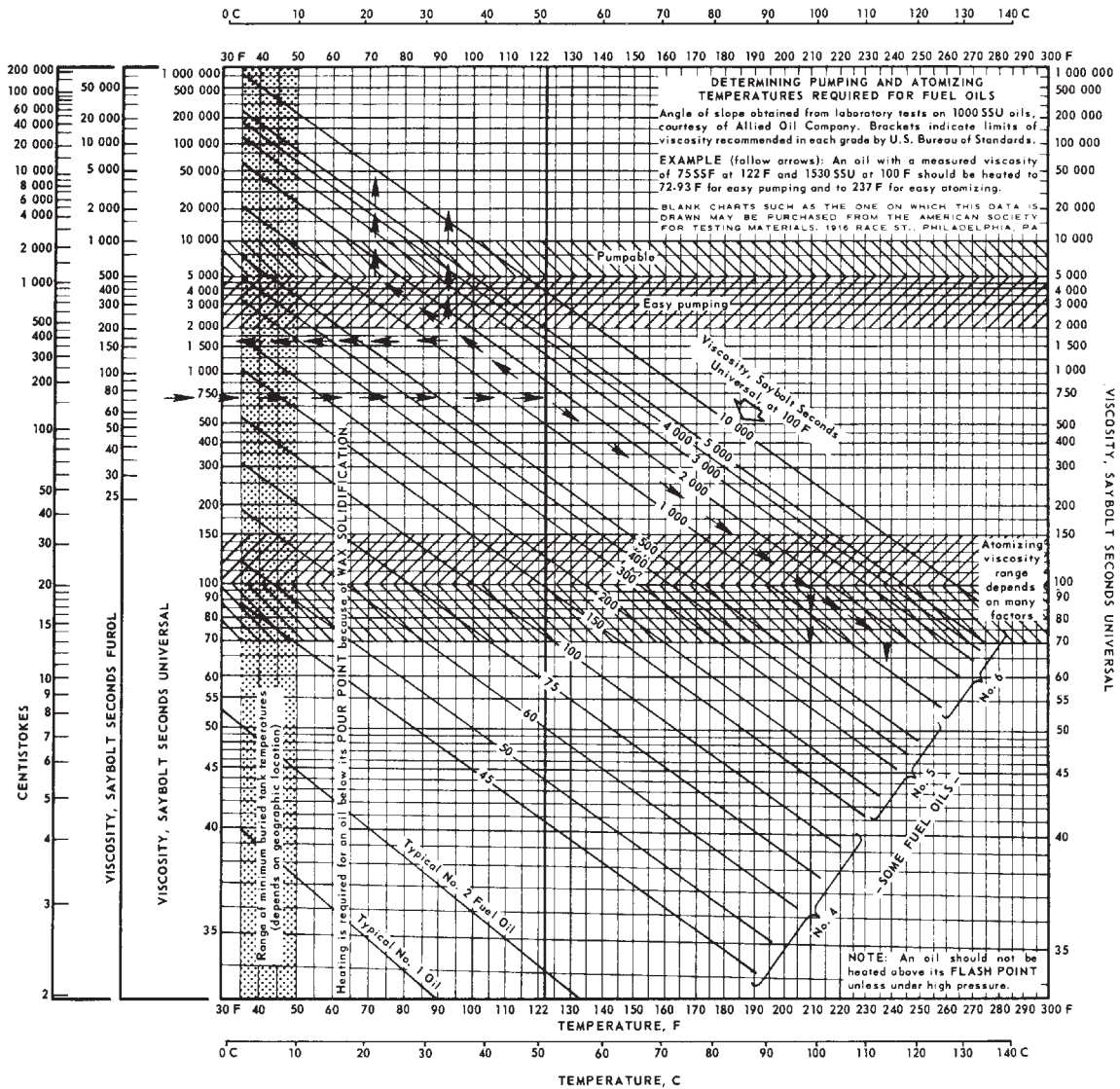


Figure 20 Viscosity-temperature relations for typical fuel oils.

Pulverized Fuels

The most commonly used pulverized fuel is coal, although a growing trend in the industrial and utility boiler industries is the cofiring of finely ground biomass fuels (e.g., wood, agricultural residues). Burners used with pulverized fuel tend to be either the windbox type (typical for boilers) or the sealed-in type (for smaller scale applications). Particle sizes typically range from tens to a few hundred micrometers, with a mean particle size occurring near 60 μm.

The most common type of burner for pulverized coal is a *circular burner*, which consists of a fuel feed pipe in the center and one, two, or even three annular air registers, as shown in Fig. 21. The figure illustrates a typical configuration for a modern low-NO_x burner. The

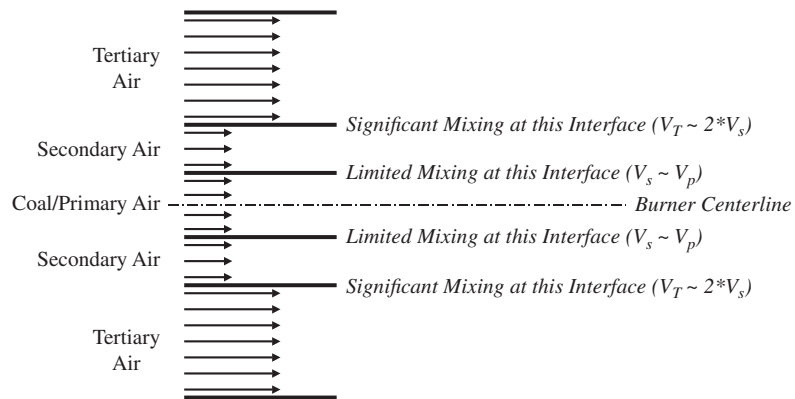


Figure 21 Cross-sectional schematic of a typical pulverized coal circular burner, configured for low- NO_x firing.

pulverized coal is introduced in the core, either with or without some sort of bluff body, and then air is introduced in the annular registers. By varying the degree of swirl and the relative velocities, a stable attached flame can be achieved. An example of a commercial circular burner is shown in Fig. 22, where the dual air registers and the vanes used to generate swirl are clearly evident in the cutaway view.

In addition, hardware modifications are often made to the fuel nozzle, including stabilizer rings, ledges, tabs, teeth, and bluff bodies to assist with flame stabilization. Also, burner quarls or tiles can provide additional stability by providing a hot surface for the heating of recirculating gases by convection and radiation. Some coal nozzles are designed to segregate fine and coarse particles prior to the nozzle exit, and the very fine coal particles can heat up rapidly and release volatiles more quickly to assist with flame stability and attachment. An example of such a nozzle is shown in Fig. 22. Combinations of all these hardware modifications have led to the apparent wide variety of burners commercially available.

Circular burners are commonly used in arrays along the front and rear walls in single- and opposed-wall-fired boilers and along the roof in arch-fired systems.

Tangentially fired burners differ in that the burners are generally located in the corners of the boiler and create helical flames in the center. The coal nozzles and air injection ports are stacked horizontally, as shown in Fig. 23, and can tilt their injection angle up or down to provide control over furnace outlet temperature (and thus steam reheat temperature) as boiler load changes. Tangentially fired systems provide delayed fuel–air mixing that results in long winding flames in the core of the boiler, and such flames have a significant benefit in terms of NO_x reduction. Circular burners can also be configured to provide long delayed-mixing flames for low- NO_x operation.

Granular and Larger Fuels

Solid fuels are typically less expensive than liquid or gaseous fuels, but the cost savings are mitigated by handling and fuel preparation costs. The power required for pulverizing coal can be a significant portion of the cost of operating a boiler; therefore, smaller scale units often utilize firing systems that require less fuel preparation.

Grate-fired systems are generally the simplest to operate and can handle a wide range of fuel sizes and fuel types. Particles ranging from fractions of inches to several inches in approximate diameter are reliable feed. The fuel is “spread” onto a perforated metal grate and

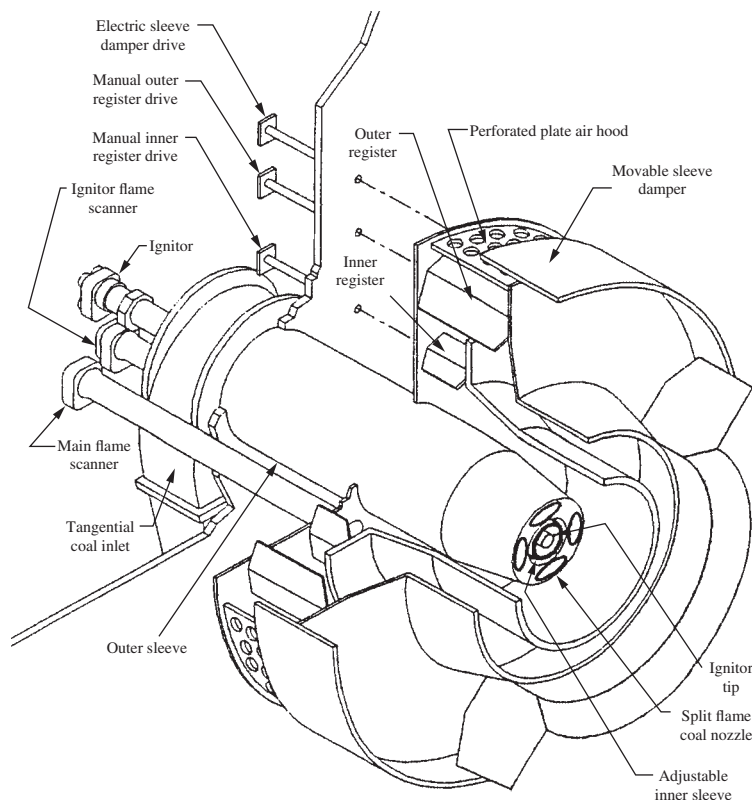


Figure 22 Typical low- NO_x pulverized coal circular burner. Adapted from Foster Wheeler Inc.

air is blown through the grate to provide oxygen for combustion and to assist in cooling the grate. In some designs, the grate is also water cooled. Grate-fired systems are among the oldest of solid fuel firing systems and were widely used in steamships, locomotives, and domestic heating until the advent of convenient means for distributing liquid and gaseous fuels. They are still commonly used for industrial boiler application (process steam generation and small-scale power production).

There are several grate designs, including (1) a traveling grate, in which the grate is moving at slow but constant velocity and the fuel slowly burns out before the residual ash is dumped off the end of the grate into a collecting hopper; (2) a reciprocating grate, which is typically a series of steps that are driven by reciprocating pistons that slowly move the fuel down the steps as it burns out; and (3) a vibrating grate, which is set at a slight angle and is operated by an electric motor with an eccentric cam. The vibrating grate is periodically cycled (every few minutes) to provide some stirring or mixing of the bed and to move fuel toward the end of the grate to dump into the ash hopper.

Typically, fuel size in grate-fired systems is dictated by feeding limitations and desired combustion efficiency targets. Larger fuel size requires greater residence time for acceptable consumption of residual carbon. In many cases, highly irregularly shaped particles are used (such as chipped or shredded wood products or fibrous biomass fuels), and the greatest

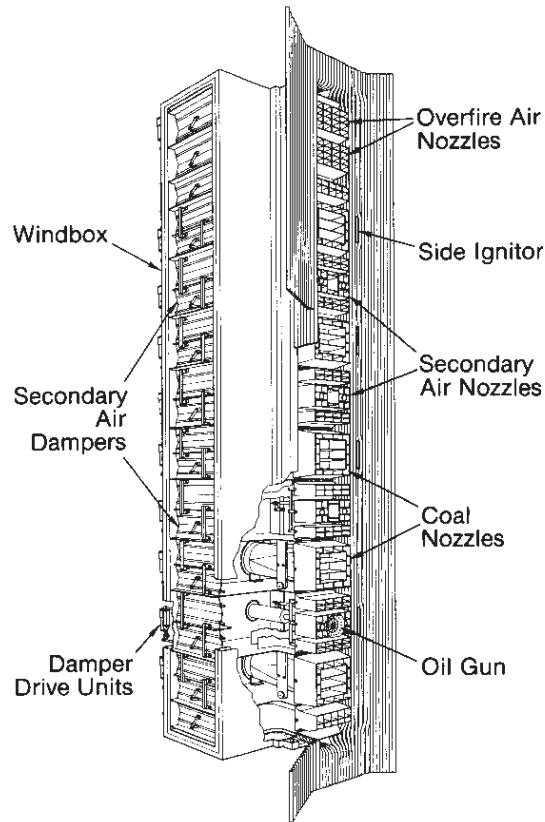


Figure 23 Typical tangentially fired pulverized coal burner arrangement. *Source:* Reproduced with permission of Alstom Power Inc., Windsor, CT, from *Combustion Fossil Power*. Copyright 1991.

challenge is often not combustion of the fuel but maintaining a reliable feed rate due to bridging and channeling in feed chutes, screws, and conveyors.

Fluidized bed systems provide the best environment for gas/solid contacting and utilize fuel that has been typically sized to millimeter-sized particles. A bed of (typically) inert material is fluidized by high-velocity air that is introduced through a distributor plate at the base of the furnace. The bubbling motion of the bed provides for a high degree of mixing and fuel is injected into the hot bubbling bed for combustion. If low-quality fuels are used (high ash content or low-reactivity carbon), increased residence times can be achieved by operating in *circulating* mode. Higher gas velocities are used and some of the bed material and fuel are entrained in the furnace and is separated in a cyclone and reinjected into the furnace.

Combustion temperatures are typically lower than in other combustion systems, and this provides some benefits in terms of NO_x emissions. Also, in many systems the bed material utilized is limestone, which can react with SO_2 generated from the combustion of sulfur in the fuel and form a benign calcium sulfate (gypsum) product.

A wide variety of fuels can be combusted in a fluidized bed, including coal, biomass, and sludges. A significant operational constraint is the melting temperature for the mineral matter present in the fuel. If the ash from the fuel becomes molten or even partially sticky, it may

cause the bed material to agglomerate and create particles that can no longer be fluidized by the current gas velocity. Such behavior can result in “defluidization” of the bed if a sufficient fraction of the bed becomes sticky and grows to form particles that cannot be entrained and simply fall to the bottom of the furnace.

Cyclone-fired systems utilize similar particle sizes as the fluidized bed systems but introduce the fuel in a cyclonic fashion into a horizontal barrel. Combustion air is also introduced tangentially to preserve the cyclonic motion. These cyclone barrels typically operate near adiabatic conditions (heat loss is typically <5%) and thus have very high temperatures to promote slagging of the mineral (ash) matter in the fuel. The molten slag runs down the walls of the horizontal barrel and exits through a tap at the bottom near the gas exit. Fuel that is thrown tangentially into the cyclone barrel is trapped in the molten slag layer and burns out as the slag runs down the walls. The hot exhaust gases exit the cyclone barrel and enter a water-wall boiler for subsequent heat extraction and steam production.

Cyclone-fired systems provide a high degree of fuel flexibility due to the slagging operation. Variations in ash composition when varying different fuel mixtures often create significant operational problems for other types of solid fuel firing systems due to the potential for a transition from dry ash to molten, deposit-forming ash.

Ash Handling

Solid fuels typically contain some fraction of noncombustible material (mineral matter or ash) that must be considered when selecting or designing a solid fuel firing system. Many wood or biomass materials have less than 1% ash; however, a typical coal will range from 6 to 30% ash, with some low-rank coals as high as 50–60% ash. The disposition of this ash is one of the greatest operational concerns for an operator of a solid-fuel firing system.

In general, the finer fractions of the ash (called “flyash”) will be entrained with the exhaust gases and need to be removed with some sort of particulate collection device (see Chapter 30). The larger ash particles (“bottom ash”) will be collected in some sort of hopper at the base of the furnace. Some ash particles will deposit on furnace walls, and if the wall is a heat transfer surface, the deposits must be periodically cleaned by an air or steam jet (“soot blowing”) to maintain furnace efficiency.

If ash particles become molten, the deposit will be difficult to remove and can grow to form an obstruction to flow as well as heat transfer. Thus, knowledge of the sticking temperature of the fuel or fuel mixtures being considered for firing is important to prevent deposition problems. It is for this reason that cyclone-fired systems are more forgiving of fuel switching than other firing systems.

In general, pulverized fuel systems will see approximately 80% of the ash end up as flyash, with 20% as bottom ash. Grate-fired systems are the reverse, with 20% flyash and 80% bottom ash. Cyclone-fired systems have very little flyash carryover (approximately 5%), as most of the ash is trapped in the slagging barrel.

The carbon content of the ash (often referred to as loss-on-ignition, or LOI, for the test performed to quantify it) should be monitored periodically. LOI provides an indication of combustion efficiency, since greater carbon-in-ash content implies less fuel is being completely burned out before exiting the furnace.

In addition, the carbon content often dictates the potential value of the flyash as a product. Flyash is often sold as a filler for use in concrete mixes (among other uses); however, carbon content greater than roughly 5% will often render it unusable for this purpose. Thus, flyash with low carbon-in-ash means good combustion efficiency and a ready revenue stream. Flyash with high carbon-in-ash results in poor combustion efficiency and a process waste stream that requires disposal—a financial liability on two counts. Many low- NO_x firing system modifications result in an increase in LOI, as most of these modifications delay fuel–air mixing and make it more difficult to completely oxidize the residual char before exiting the furnace.

5 POLLUTANT EMISSIONS

Combustion processes produce gaseous and particulate emissions that can be harmful to human health and the environment. The pollutants of primary concern with gaseous fuels are CO and various NO_x , since generally most sulfur-bearing species have been removed. For liquid fuels, the same pollutants come into play; however, many oils have significant sulfur contents and thus also produce sulfur oxides (SO_x). Solid fuels can also produce CO, NO_x , and SO_x emissions but also produce particulate emissions. Products of incomplete combustion (PICs) are possible with any of these fuels if the combustion process is poorly designed.

5.1 Control of Nitrogen Oxides

There are various sources of NO_x in a combustion system. All fuels have the potential to create *thermal* NO_x , which results from the oxidation of N_2 in the atmosphere at high temperatures. The air used for combustion is typically 79% N_2 , and at temperatures above roughly 2600 F, this N_2 can be readily oxidized to NO. In gas-fired systems and many liquid fuel-fired systems, this is the principal source of NO_x emissions. Control technologies focus on reducing peak temperatures to minimize significant NO formation. One common approach is the use of flue gas recirculation (FGR), either external recirculation with subsequent injection into the burner to dilute the combustion process or internal recirculation using eductive mixing.

Another source of NO_x stems from the presence of nitrogen in the fuel and is referred to as *fuel* NO_x . Fuel NO_x is the primary source of NO for coal combustion and represents approximately 80% of uncontrolled NO emissions, with thermal NO_x providing the balance. The primary method for controlling fuel NO_x is promoting fuel-rich or oxygen-starved combustion in the main burner zone, which allows the fuel-bound nitrogen (typically in the form of HCN or NH_3) to decay to N_2 . Once sufficient time has been given for nitrogen decay, then additional air can be introduced (*staging air*) to complete the combustion process. As more and more of the fuel NO is controlled through air staging, the NO emissions decrease and the percentage of the NO emissions represented by thermal NO_x increases.

The staging of air can be performed through burner aerodynamics using multiple air registers, as shown in Fig. 21. The innermost air register (secondary air) is operated with a small fraction of the total air, and its velocity is matched to the primary air/coal jet to minimize shear or mixing at the interface between the two streams. Sufficient air is provided in the secondary register to ensure ignition and attachment of the flame, however.

The tertiary stream, which contains the bulk of the combustion air, is operated at a velocity that is significantly higher than the secondary stream and thus promotes shearing or mixing between the secondary and tertiary air streams. The secondary air stream serves as a buffer between the fuel jet and the tertiary air stream and delays the mixing of most of the air with the fuel. The burner can be designed to optimize NO_x reduction and burner stability for a given fuel.

A small amount of NO is formed very early in the flame by reaction of fuel fragments with NO and is referred to as *prompt* NO. Prompt NO is difficult to control and is typically of concern only for gas burners designed to operate at very low NO emission levels (<20 ppm).

5.2 Control of Other Gaseous Emissions

Carbon monoxide emissions as well as other hydrocarbon emissions are generally controlled through good combustion practice. Providing adequate air/fuel mixing with sufficient residence time will generally minimize CO emissions. Many of the techniques for reducing NO emissions, however, can result in an increase in CO emissions due to a delay in air/fuel mixing. Thus, any emission strategy needs to be optimized for all pollutants of concern.

Sulfur oxides are formed through oxidation of the sulfur present in the fuel. Essentially all of the sulfur is oxidized to SO_2 , and there are no simple methods to convert fuel-bound sulfur

to benign products as there is for converting fuel-bound nitrogen to N_2 . In practice, fuel-bound sulfur is oxidized to SO_2 in the furnace and is then captured downstream through reaction with sorbents or caustic scrubber liquid. The notable exception is in-bed capture of SO_2 in fluidized beds using limestone.

Another option is eliminating the sulfur prior to combustion. Sulfur is generally removed from most gaseous and liquid fuels (with the exception of heavier fuel oils) through various “sweetening” processes at the well head or the refinery. Sulfur present in coal can be removed to some extent using beneficiation techniques; however, these processes may not be as economical as purchasing a lower sulfur coal from a more distant source.

5.3 Control of Particulate Emissions

Flyash formed during combustion processes typically has a bimodal size distribution. Larger flyash particles (1–10 μm) result from fragmentation and attrition processes or from molten ash particles that coalesce on the surface of a burning particle and are eventually liberated once the carbonaceous material is mostly consumed. Smaller flyash particles (less than 1 μm) are typically the result of vaporization/condensation processes. Burning coal particles create a locally reducing environment which promotes reduction of metal oxides to more volatile suboxide or base metal species. These volatile species vaporize, then oxidize as they diffuse away from the particle, and then condense as a submicrometer fume. Some of the more volatile elements will condense further downstream on the surface of this submicrometer fume, creating fine particulate that can be enriched in trace metals that are often toxic.

Particulate emissions are typically controlled using standard particulate collection devices such as cyclones, fabric filter baghouses, or electrostatic precipitators (ESPs). Cyclones are typically suitable for larger particles only (greater than 1 μm), whereas baghouses and ESPs will provide some measure of capture for submicrometer particulate.

6 SAFETY CONSIDERATIONS

Operations involving combustion must be concerned about all the usual safety hazards of industrial machinery, with additional consideration for the potential for explosions, fires, burns from hot surfaces, and asphyxiation. Less immediately severe but long-range health problems related to combustion result from overexposure to noise and pollutants.

Preventing explosions should be the primary operating and design concern of every person in any way associated with combustion operations, because an explosion can be so devastating as to eliminate all other goals of anyone involved. The requirements for an explosion include the first five requirements for combustion (Table 3); therefore, striving for efficient combustion also sets the stage for a potential explosion. The statistical probability of meeting all seven explosion requirements at the same time and place is so small that people often become careless, and therein lies the problem. Continual training and retraining are key to maintaining awareness.

The lower and upper limits of flammability are the same as the lower and upper explosive limits for any combustible gas or vapor. A summary of the most commonly encountered gases is given in Table 4, and a more extensive listing is provided in Table 3 in Chapter 17 on gaseous fuels. Table 5 lists flammability data for some common liquids. Dusts generated from solid fuel handling represent an explosion hazard as well; some typical values for carbonaceous fuels and other biomass materials are listed in Table 6. References 9–12 provide a more extensive source of explosion-related data for many industrial solvents, off-gases, and fugitive dusts.

Electronic safety control programs for most industrial combustion systems are generally designed to (1) prevent accumulation of unburned fuel when any source of ignition is present or (2) immediately remove any source of ignition when something goes wrong that may result in fuel accumulation.

Table 3 Requirements for Combustion and Explosion^a

Requirements for Combustion	Requirements for Explosion
1. Fuel	1. Fuel
2. Oxygen (air)	2. Oxygen (air)
3. Proper proportion (within flammability limits)	3. Proper proportion (within explosive limits)
4. Mixing	4. Mixing
5. Ignition	5. Ignition
	6. Accumulation
	7. Confinement

^aThere have been incidents of disastrous explosions of unconfined fast-burning gases, but most of the damage from industrial explosions comes from the fragments of the containing furnace that are propelled like shrapnel. Lightup explosions are often only “puffs” if large doors are kept open during startup.

Table 4 Flammability Limits for Common Gaseous Fuels¹³

Fuel	Lean or Lower Limit		Rich or Upper Limit	
	ϕ^a	SR ^b	ϕ	SR
Acetylene, C ₂ H ₂	0.19	5.26	∞	~ 0
Carbon monoxide, CO	0.34	2.94	6.76	0.15
Ethane, C ₂ H ₆	0.5	2	2.72	0.37
Ethylene, C ₂ H ₄	0.41	2.44	> 6.1	< 0.16
Hydrogen, H ₂	0.14	7.14	2.54	0.39
Methane, CH ₄	0.46	2.17	1.64	0.61
Propane, C ₃ H ₈	0.51	1.96	2.83	0.35

^aEquivalence ratio.

^bStoichiometric ratio.

Of course, the removal of an ignition source is very difficult in a furnace operating above 1400°F. If a burner in such a furnace should be extinguished because it suddenly became too fuel rich, requirement number 3 is negated and there can be no explosion until someone (untrained) opens a port or shuts off the fuel. The only safe procedure is to gradually flood the chamber with steam or inert gas (gradually, so as to not change furnace pressure and thereby cause more air in-flow).

For 1, the best way to prevent unburned fuel accumulation is to have a reliable automatic fuel–air ratio control system coordinated with automatic furnace pressure control. Such a system should also have input control so that the input cannot range beyond the capabilities of either automatic system. The emergency backup system consists of a trip valve that stops fuel flow in the event of flame failure or any of many other interlocks such as low air flow or high or low fuel flow.

For 2, removal of ignition sources is implemented by automatic shutoff of other burner flames, pilot flames, spark igniters, and glow plugs. In systems where a single flame sensor monitors either a main flame or a pilot flame, the pilot flame must be programmed out when the main flame is proven. If this is not done, such a “constant” or “standing” pilot can “fool” the flame sensor and cause an explosion.

Table 5 Flammability Data for Liquid Fuels

Liquid Fuel	Flash Point, °F (°C) (Closed Cup Method)	Flammability Limits (% Volume in Air)		Autoignition Temperature, °F (°C)	Vapor density, G (Air = 1)	Boiling Temperature, °F (°C)
		Lower	Upper			
Butane, -n	-76 (-60)	1.9	8.5	761 (405)	2.06	31 (-1)
Butane, -iso	-117 (-83)	1.8	8.4	864 (462)	2.06	11 (-12)
Ethyl alcohol (ethanol)	55 (13)	3.5	19	737 (392)	1.59	173 (78)
Ethyl alcohol, 30% in water	85 (29)	3.6	10	—	—	203 (95)
Fuel oil, #1	114-185 (46-85)	0.6	5.6	445-560 (229-293)	—	340-555 (171-291)
Fuel oil (diesel), #1-D	>100 (>38)	1.3	6.0	350-625 (177-329)	—	<590
Fuel oil, #2	126-230 (52-110)	—	—	500-705 (260-374)	—	340-640 (171-338)
Fuel oil (diesel), #2-D	>100	1.3	6.0	490-545 (254-285)	—	380-650 (193-343)
Fuel oil, #4	154-240 (68-116)	1	5	505 (263)	—	425-760 (218-404)
Fuel oil, #5	130-310 (54-154)	1	5	—	—	—
Fuel oil, #6	150-430 (66-221)	1	5	765 (407)	—	—
Gasoline, automotive	-50±	1.3-1.4	6.0-7.6	700 (371)	3-4	91-403 (33-206)
Gasoline, aviation	-50±	1	6.0-7.6	800-880 (427-471)	3-4	107-319 (42-159)
Jet fuel, JP-4	-2	0.8	6.2	468 (242)	—	140-490 (60-254)
Jet fuel, JP-5	105 (41)	0.6	4.6	400 (204)	—	370-530 (188-277)
Jet fuel, JP-6	127 (53)	—	—	500 (260)	—	250-500 (121-260)
Jet fuel, JP-8	100 (38)	0.7	4.7	410 (210)	5.7	330-510 (165-265)
Jet fuel, JP-10	106 (41)	0.9 ^a	6.0 ^a	552 ^a (289)	4.8	379 (193)
Kerosene	110-130 (43-54)	0.6	5.6	440-560 (227-293)	4.5	350-550 (177-288)
Methyl alcohol (methanol)	54 (12)	5.5	36.5	878 (470)	1.11	147 (64)
Methyl alcohol, 30% in water	75 (24)	—	—	—	—	167 (75)
Naphtha, dryclean	100-110 (38-43)	0.8	5.0	440-500 (227-260)	—	300-400 (149-204)
Naphtha, 76%, vm&p	20-45 (-7-+7)	0.9	6.0	450-500 (232-260)	3.75	200-300 (93-149)
Nonane, -n	88 (31)	0.74	2.9	403 (206)	4.41	303 (151)
Octane, -iso	10 (-12)	1.0	6.0	784 (418)	3.93	190-250 (88-121)
Propane	-156 (-104)	2.2	9.6	871 (466)	1.56	-44 (-42)
Propylene	-162 (-108)	2.0	11.1	927-952 (497-511)	1.49	-54 (-48)

^aEstimated.

Table 6 Explosion Characteristics of Various Dusts¹²

Type of Dust	Ignition Temperature		Minimum Cloud Explosion Concentration (g/m ³)	Limiting Oxygen Percentage ^a (Spark ignition)
	Cloud (°C)	Layer (°C)		
Cellulose, alpha	410	300	45	—
Cornstarch, commercial product	400	—	45	—
Lycopodium	480	310	25	C13
Wheat starch, edible	430	—	45	C12
Wood flour, white pine	470	260	35	—
Charcoal, hardwood mixture	530	180	140	—
Coal, Pennsylvania, Pittsburgh (Experimental Mine Coal)	610	170	55	—
Sulfur	190	220	35	C12
Aluminum flake, A 422 extra fine lining, polished	610	326	45	—
Magnesium, milled, Grade B	560	430	30	—
Acrylamide polymer	410	240	40	—
Methyl methacrylate polymer	480	—	30	C11
Cellulose acetate	420	—	40	C14
Polycarbonate	710	—	25	C15
Phenol formaldehyde molding compound, wood flour filler	500	—	30	C14

^aC = CO₂, numbers indicate percentages; e.g., C13 refers to dilution to 13% oxygen with carbon dioxide as the diluent.

Most operational codes and insuring authorities insist on the use of flame monitoring devices for combustion chambers that operate at temperatures below 1400°F. Some of these authorities point out that even high-temperature furnaces must go through this low-temperature range on their way to and from their normal operating temperature. Another situation where safety regulations and economic reality have not yet come to agreement involves combustion chambers with dozens or even hundreds of burners, such as refinery heaters, ceramic kilns, and heat transfer furnaces.

Avoiding fuel-fed fires first requires preventing explosions, which often start such fires (see previous discussion). Every building containing a fuel-fired boiler, oven, kiln, furnace, heater, or incinerator should have a spring-operated manual reset fuel shutoff valve outside the building with panic buttons at the guardhouse or at exits to allow shutting off fuel as one leaves the burning building.

Gas fuel lines should be overhead where crane and truck operators cannot rupture them or underground. If underground, keep and use records of their locations to avoid digging accidents. Overhead fuel lines must have well-marked manual shutoff valves where they can be reached without a ladder.

Liquid fuel lines should be underground; otherwise, a rupture will pour or spray fuel on a fire. The greatest contributor to fuel-fed fires is a fuel shutoff valve that will not work. All fuel shutoff valves, manual or automatic, must be tested on a regular maintenance schedule. Such testing may cause nuisance shutdowns of related equipment; therefore, a practical procedure is to have the maintenance crew do the day's end (or week's end) shutdown about once each month. The same test can check for leaking. If it is a fully automatic or manual reset automatic valve, shutdown should be accomplished by simulating flame failure and, in succession, each of the interlocks.

Because so much depends on automatic fuel shutoff valves, it makes sense (1) to have a backup valve (blocking valve) and (2) to replace it before it hangs up—at least every 5 years, or more often in adverse environments. Maintenance and management people must be ever alert for open side panels and covers on safety switches and fuel shutoff valves, which may be evidence that safety systems have been bypassed or tampered with in some way.

Storage of liquefied petroleum (LP) gas, oils, or solid fuels requires careful attention to applicable codes. If the point of use, an open line, or a large leak is below the oil storage elevation, large quantities may siphon out and flow into an area where there is a water heater or other source of ignition. Steam heaters in heavy oil tanks need regular inspections, or leaks can emulsify the oil, causing an overflow. It is advisable to make provision for withdrawing the heater for repair without having to drain the whole tank.

LP gas is heavier than air. Workers have been suffocated by this invisible gas when it leaked into access pits below equipment. Thus, the potential for accidental accumulation should be considered when designing and laying out equipment to avoid possible explosion or asphyxiation hazards.

Codes and regulations are proliferating, many by local authorities or insuring groups. Most refer, as a base, to publications of the National Fire Protection Association (NFPA), Batterymarch Park, Quincy, MA 02269. Their publications usually represent the consensus of technically competent volunteer committees from industries involved with the topic.

7 OXY-FUEL FIRING

Commercially “pure” oxygen (90–99% oxygen) is sometimes substituted for air (20.9% oxygen) in various mixture ratios up to pure oxygen to (1) achieve higher flame temperature, (2) get higher % available heat (best possible efficiency), or (3) try to eliminate nitrogen from the furnace atmosphere and thereby reduce the probability of NO_x formation.

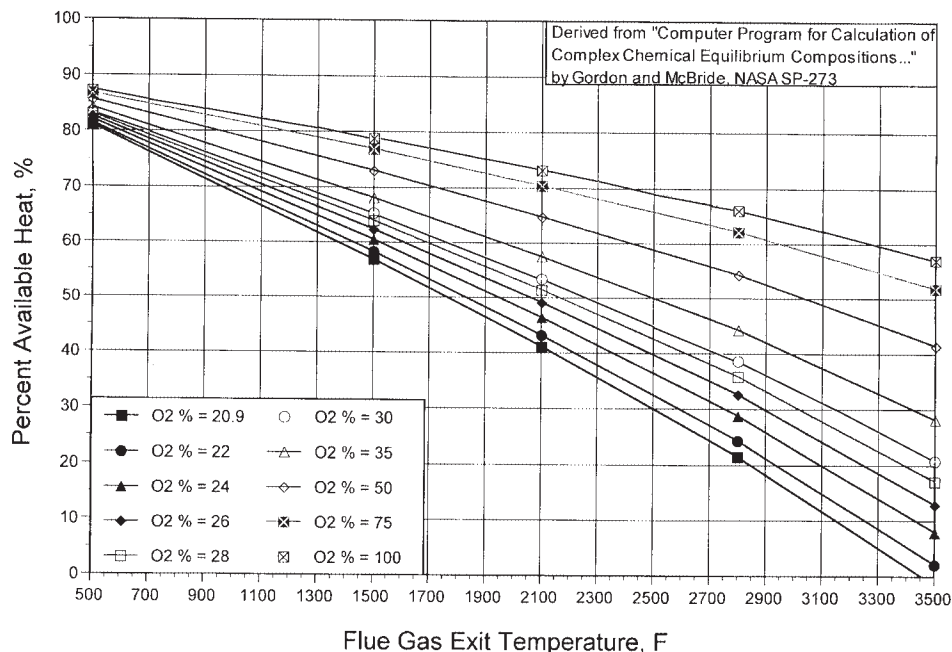


Figure 24 Percent available heat for $\phi = 0.95$ or 5% excess air with average natural gas, HHV = 1025 Btu/ft³, with various degrees of oxygen enrichment and for oxy-fuel firing (top curve).

Figure 24 shows percent available heat and adiabatic flame temperatures (x intercepts) for various amounts of oxygen enrichment of an existing air supply, and for “oxy-fuel firing” or 100% oxygen.

Oxy-fuel burners have been water cooled in the past, but their propensity to spring leaks and do terrible damage has led to use of better materials to avoid water cooling. Oxygen burner nozzles and tiles are subject to much higher temperatures and more oxidizing atmospheres than are air burner nozzles and tiles. Control valves, regulators, and piping for oxygen require special cleaning and material selection.

ACKNOWLEDGMENTS

The author would like to acknowledge Jost O.L. Wendt of the University of Arizona for his assistance with the flame aerodynamics section, Richard J. Reed of North American Manufacturing Company for contributions from previous editions of this chapter, and the many contributions of the International Flame Research Foundation (IFRF) for their vast body of work on flame stability, shaping, and aerodynamics.

REFERENCES

1. R. J. Reed (Ed.), *Combustion Handbook*, Vol. I, 3rd ed., North American Mfg. Co., Cleveland, OH, 1986.
2. R. H. Essenhigh, “An Introduction to Stirred Reactor Theory Applied to Design of Combustion Chambers,” in H. B. Palmer and J. M. Beer (Eds.), *Combustion Technology*, Academic, New York, 1974, pp. 389–391.
3. E. Mallard and H. L. Le Chatelier, *Ann. Mines*, **4**, 379, 1883.
4. B. Lewis and G. von Elbe, *Combustion, Flames and Explosion of Gases*, 2nd ed., Academic, New York, 1961, Chapter V.
5. F. P. Ricou and D. B. Spalding, *J. Fluid Mech.*, **11**, 21–32, 1961.
6. M. W. Thring and M. P. Newby, *Fourth International Symposium on Combustion*, Combustion Institute, Pittsburgh, PA, 1953, pp. 789–796.
7. M. A. Field, D. W. Gill, B. B. Morgan, and P. G. W. Hawksley, *Combustion of Pulverized Coal*, The British Coal Utilization Research Association, Letherhead, Surrey, UK, 1967, p. 58.
8. J. M. Beer and N. A. Chigier, *Combustion Aerodynamics*, Krieger, Malabar, FL, 1983.
9. National Fire Protection Association (NFPA), NFPA No. 86, *Standard for Ovens and Furnaces*, NFPA, Quincy, MA, 1995.
10. National Fire Protection Association (NFPA), *Flash Point Index of Trade Name Ligands*, NFPA, Quincy, MA, 1978.
11. National Fire Protection Association (NFPA), NFPA No. 325M, *Fire Hazard Properties of Flammable Liquids, Gases, Volatile Solids*, NFPA, Quincy, MA, 1994.
12. National Fire Protection Association (NFPA), *Fire Protection Handbook*, 18th ed., NFPA, Quincy, MA, 1997.
13. S. R. Turns, *An Introduction to Combustion*, McGraw Hill, New York, 1996.
14. Factory Mutual Engineering Corp., *Handbook of Industrial Loss Prevention*, McGraw-Hill, New York, 1967.

CHAPTER 18

GASEOUS FUELS

Richard J. Reed
North American Manufacturing Company
Cleveland, Ohio

1 INTRODUCTION	673	2.8 Flame Stability	678
2 NATURAL GAS	673	2.9 Gas Gravity	678
2.1 Uses and Distribution	673	2.10 Wobbe Index	678
2.2 Environmental Impact	674	2.11 Flame Temperature	679
2.3 Sources, Supply, and Storage	674	2.12 Minimum Ignition Temperature	680
2.4 Types and Composition	674	2.13 Flammability Limits	680
2.5 Properties	674	3 LIQUEFIED PETROLEUM GASES	681
2.6 Calorific Value or Heating Value	675	REFERENCES	682
2.7 Net Heating Value	678		

1 INTRODUCTION

Gaseous fuels are generally easier to handle and burn than are liquid or solid fuels. Gaseous fossil fuels include natural gas (primarily methane and ethane) and liquefied petroleum gases (LPGs; primarily propane and butane). Gaseous man-made or artificial fuels are mostly derived from liquid or solid fossil fuels. Liquid fossil fuels have evolved from animal remains through eons of deep underground reaction under temperature and pressure, while solid fuel evolved from vegetable remains. Figure 1 shows the ranges of hydrogen/carbon ratios for most fuels.

2 NATURAL GAS

2.1 Uses and Distribution

Although primarily used for heating, natural gas is also frequently used for power generation (via steam turbines, gas turbines, diesel engines, and Otto cycle engines) and as feedstock for making chemicals, fertilizers, carbon black, and plastics. It is distributed through intra- and intercontinental pipe lines in a high-pressure gaseous state and via special cryogenic cargo ships in a low-temperature, high-pressure liquid phase (LNG).

Final street-main distribution for domestic space heating, cooking, water heating, and steam generation is at regulated pressures on the order of a few inches of water column to a few pounds per square inch, gage, depending on local facilities and codes. Delivery to commercial establishments and institutions for the same purposes, plus industrial process heating, power generation, and feedstock, may be at pressures as high as 100 or 200 psig (800 or 1500 kPa absolute). A mercaptan odorant is usually added so that people will be aware of leaks.

Before the construction of cross-country natural gas pipe lines, artificial gases were distributed through city pipe networks, but gas generators are now usually located adjacent to the point of use.

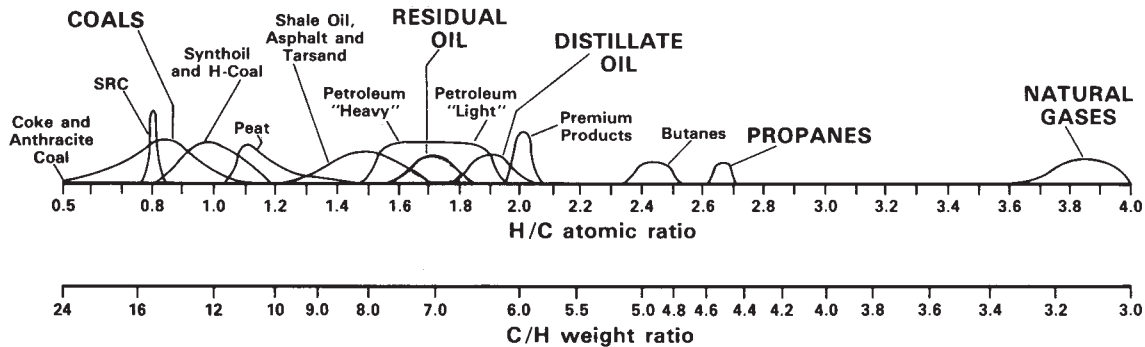


Figure 1 Hydrogen/carbon ratios of fossil and synthetic fuels. *Source:* Adapted from Ref. 1.

2.2 Environmental Impact

The environmental impact of natural gas combustion is generally less than that of liquid or solid fuels. Pollutants from natural gas may be (1) particulates, if burners are poorly adjusted or controlled (too rich, poor mixing, quenching), or (2) nitrogen oxides, in some cases with intense combustion, preheated air, or oxygen enrichment.

2.3 Sources, Supply, and Storage

Natural gas is found with oil deposits (animal fossils) and coal deposits (plant fossils). As-yet untapped supplies are known to exist (1) near the coast of the Gulf of Mexico in very deep geopressured/geothermal aquifers and (2) in difficult-to-separate Appalachian shale formations.

Except for these hard-to-extract supplies, U.S. natural gas supplies have been variously predicted to last 10–20 years, but such predictions are questionable because of the effects of economic and regulatory variations on consumption, production, and exploration. Except for transoceanic LNG vessels, distribution is by pipe line, using a small fraction of the fuel in compressors to provide pumping power.

Storage facilities are maintained by many local gas utilities as a cushion for changing demand. These may be low-pressure gas holders with floating bell-covers, old wells or mines (medium pressure), or cryogenic vessels for high-pressure liquefied gas.

2.4 Types and Composition

Natural gases are classified as “sweet” or “sour,” depending on their content of sulfur compounds. Most such compounds are removed before distribution. Odorants added (so that leaks can be detected) are usually sulfur compounds, but the amount is so minute that it has no effect on performance or pollution.

Various geographic sources yield natural gases that may be described as “high methane,” “high Btu,” or “high inert.”

2.5 Properties

Properties that concern most users of natural gases relate to the heat available from their combustion, flow characteristics, and burnability in a variety of burner types. Strangely, few people pay attention to the properties of their gas until they are forced to substitute another fuel for it. Some properties are listed in Tables 1a, 1b, and 1c.²

Table 1a Analyses of Typical Gaseous Fuels²

Type of Gas	Analysis in % by Volume								
	CH ₄	C ₂ H ₆	C ₃ H ₈	C ₄ H ₁₀	CO	H ₂	CO ₂	O ₂	N ₂
Acetylene, commercial				(97.1% C ₂ H ₂ , 2.5% C ₃ H ₆ O)				0.084	0.28
Blast furnace	—	—	—	—	27.5	1.0	11.5	—	60.0
Blue (water), bituminous	4.6	—	—	0.7	28.2	32.5	5.5	0.9	27.6
Butane, commercial, natural gas	—	—	6.0	70.7 <i>n</i> -, 23.3 iso-	—	—	—	—	—
Butane, commercial, refinery gas	—	—	5.0	50.1 <i>n</i> -, 16.5 iso-	—	—	(28.3% C ₄ H ₆)	—	—
Carbureted blue, low gravity	10.9	2.5	—	6.1	21.9	49.6	3.6	0.4	5.0
Carbureted blue, heavy oil	13.5	—	—	8.2	26.8	32.2	6.0	0.9	12.4
Coke oven, by-product Mapp	32.3	—	—	3.2	5.5	51.9	2.0	0.3	4.8
	—	—	15.0	10.0		(66.0% C ₃ H ₄ , 9.0% C ₃ H ₆)			
Natural, Alaska	99.6	—	—	—	—	—	—	—	0.4
Natural, Algerian LNG, Canvey	87.20	8.61	2.74	1.07	—	—	—	—	0.36
Natural, Gaz de Lacq	97.38	2.17	0.10	0.05	—	—	—	—	0.30
Natural, Groningen, Netherlands	81.20	2.90	0.36	0.14	—	—	0.87	—	14.40
Natural, Libyan LNG	70.0	15.0	10.0	3.5	—	—	—	—	0.90
Natural, North Sea, Bacton	93.63	3.25	0.69	0.27	—	—	0.13	—	1.78
Natural, Birmingham, AL	90.0	5.0	—	—	—	—	—	—	5.0
Natural, Cleveland, OH	82.9	11.9	—	0.3	—	—	0.2	0.3	4.4
Natural, Kansas City, MO	84.1	6.7	—	—	—	—	0.8	—	8.4
Natural, Pittsburgh, PA	83.4	15.8	—	—	—	—	—	—	0.8
Producer, Koppers–Totzek ^a	0.09	—	—	—	55.1	33.7	9.8	—	1.3
Producer, Lurgi ^b	5.0	—	—	—	16.0	25.0	14.0	—	40.0
Producer, W-G, bituminous ^b	2.7	—	—	—	28.6	15.0	3.4	0	50.3
Producer, Winkler ^b	1	—	—	—	10	12	22	—	55
Propane, commercial, natural gas	—	2.2	97.3	0.5	—	—	—	—	—
Propane, commercial, refinery gas	—	2.0	72.9	0.8	—	—	(24.3% C ₃ H ₆)	—	—
Sasol, South Africa	28.0	—	—	—	22.0	48.9	—	1.0	—
Sewage, Decatur	68.0	—	—	—	—	2.0	22.0	—	6.0
SNG, no methanation	79.9	—	—	—	1.2	19.0	0.5	—	—

^aO₂ blown.^bAir blown.

2.6 Calorific Value or Heating Value

The gross or higher heating value (HHV) is usually measured in a steady-state calorimeter, which is a small fire-tube heat exchanger with a water-cooled surface area so large that it cools the products of combustion to the temperature at which they entered as fuel and air (usually 60°F). HHV can be calculated from a volumetric analysis and the calorific values of the pure

Table 1b Properties of Typical Gaseous Fuels²

Type of Gas	Gas Gravity	Calorific Value				Gross Btu/ft ³ of Standard Air	Gross kcal/m ³ of Standard Air
		Btu/ft ³		kcal/m ³			
		Gross	Net	Gross	Net		
Acetylene, commercial	0.94	1,410	1,360	12,548	12,105	115.4	1,027
Blast furnace	1.02	92	91	819	819	135.3	1,204
Blue (water), bituminous	0.70	260	239	2,314	2,127	126.2	1,121
Butane, commercial, natural gas	2.04	3,210	2,961	28,566	26,350	104.9	932.6
Butane, commercial, refinery gas	2.00	3,184	2,935	28,334	26,119	106.1	944.2
Carbureted blue, low gravity	0.54	536	461	4,770	4,102	106.1	944.2
Carbureted blue, heavy oil	0.66	530	451	4,716	4,013	101.7	905.0
Coke oven, by-product	0.40	569	509	5,064	4,530	105.0	934
Mapp	1.48	2,406	2,282	21,411	20,308	1,13.7	1,011.86
Natural, Alaska	0.55	998	906	8,879	8,063	104.8	932.6
Natural, Algerian LNG, Canvey	0.64	1,122	1,014	9,985	9,024	104.3	928.2
Natural, Gaz de Lacq	0.57	1,011	911	8,997	8,107	104.1	927.3
Natural, Groningen, Netherlands	0.64	875	789	7,787	7,021	104.4	927.3
Natural, Libyan LNG	0.79	1,345	1,223	11,969	10,883	106.1	928.2
Natural, North Sea, Bacton	0.59	1,023	922	9,104	8,205	105.0	934.4
Natural, Birmingham, AL	0.60	1,002	904	8,917	8,045	106.1	945.1
Natural, Cleveland, OH	0.635	1,059	959	9,424	8,534	106.2	942.4
Natural, Kansas City, MO	0.63	974	879	8,668	7,822	106.3	946.0
Natural, Pittsburgh, PA	0.61	1,129	1,021	10,047	9,086	106.3	945.1
Producer, Koppers–Totzek ^a	0.78	288	271	2,563	2,412	135.2	1,203
Producer, Lurgi ^b	0.80	183	167	1,629	1,486	125.3	1,115
Producer, W-G, bituminous ^b	0.84	168	158	1,495	1,406	129.2	1,150
Producer, Winkler ^b	0.98	117	111	1,041	988	188.7	1,679
Propane, commercial, natural gas	1.55	2,558	2,358	22,764	20,984	107.5	956.6
Propane, commercial, refinery gas	1.77	2,504	2,316	22,283	20,610	108.0	961.1
Sasol, South Africa	0.55	500	448	4,450	3,986	114.9	1,022
Sewage, Decatur	0.79	690	621	6,140	5,526	105.3	936.2
SNG, no methanation	0.47	853	765	7,591	6,808	105.8	943.3

^aO₂ blown.^bAir blown.

compounds in the gas (Table 2). For example, for a natural gas having the analysis shown in column 2 below, the tabulation shows how a weighted average method can be used to determine the calorific value of the mixture:

Col. 1, Constituent	Col. 2, % Volume	Col. 3, HHV from Table 2 (Btu/ft ³)	Col. 4 = (Col. 3 × Col. 2)/100
Methane, CH ₄	90	1013	912
Ethane, C ₂ H ₆	6	1763	106
Nitrogen, N ₂	$\frac{4}{100}$	0	$\frac{0}{1018}$ Btu/ft ³
Total	100%		1018 Btu/ft ³

Table 1c Combustion Characteristics of Typical Gaseous Fuels²

Type of Gas	Wobbe Index	Vol. Air. Req'd per Vol. Fuel	Stoichiometric Products of Combustion			Total Vol.		Flame Temperature (°F) ^b
			% CO ₂ Dry ^a	% H ₂ O Wet	% N ₂ Wet	Vol. Fuel		
Acetylene, commercial	1559	12.14	17.4	8.3	75.8	12.66	3966	
Blast furnace	91.0	0.68	25.5	0.7	74.0	1.54	2559	
Blue (water), bituminous	310.8	2.06	17.7	16.3	68.9	2.77	3399	
Butane, commercial, natural gas	2287	30.6	14.0	14.9	73.2	33.10	3543	
Butane, commercial, refinery gas	2261	30.0	14.3	14.4	73.4	32.34	3565	
Carbureted blue, low gravity	729.4	5.05	14.0	18.9	69.8	5.79	3258	
Carbureted blue, heavy oil	430.6	5.21	15.7	16.6	70.3	6.03	3116	
Coke oven, by-product	961.2	5.44	10.8	21.4	70.1	6.20	3525	
Mapp	1947	21.25	15.6	11.9	74.4	22.59	3722	
Natural, Alaska	1352	9.52	11.7	18.9	71.6	10.52	3472	
Natural, Algeria LNG, Canvey	1423	10.76	12.1	18.3	71.9	11.85	3483	
Natural, Gaz de Lacq	1365	9.71	11.7	18.8	71.6	10.72	3474	
Natural, Groningen, Netherlands	1107	8.38	11.7	18.4	72.0	9.40	3446	
Natural, Kuwait, Burgan	1364	10.33	12.2	18.3	71.7	10.40	3476	
Natural, Libya LNG	1520	12.68	12.5	17.4	72.2	13.90	3497	
Natural, North Sea, Bacton	1345	9.74	11.8	18.7	71.7	10.77	3473	
Natural, Birmingham, AL	1291	9.44	11.7	18.6	71.8	10.47	3468	
Natural, East Ohio	1336	9.70	11.9	18.7	71.7	10.72	3472	
Natural, Kansas City, MO	1222	9.16	11.8	18.5	71.9	10.19	3461	
Natural, Pittsburgh, PA	1446	10.62	12.0	18.3	71.9	11.70	3474	
Producer, BCR, W. Kentucky	444	3.23	23.3	14.7	66.0	3.88	3514	
Producer, IGT, Lignite	562	4.43	18.7	17.5	67.0	5.24	3406	
Producer, Koppers–Totzek	326.1	2.13	27.7	12.6	63.2	2.69	3615	
Producer, Lurgi	204.6	1.46	18.4	15.5	68.9	2.25	3074	
Producer, Lurgi, subbituminous	465	2.49	23.4	19.6	61.5	3.20	3347	
Producer, W-G, bituminous	183.6	1.30	18.5	9.8	73.5	2.08	3167	
Producer, Winkler	118.2	0.62	24.1	9.3	68.9	1.51	3016	
Propane, commercial, natural gas	2029	23.8	13.7	15.5	73.0	25.77	3532	
Propane, commercial, refinery gas	2008	23.2	14.0	14.9	73.2	25.10	3560	
Sasol, South Africa	794.4	4.30	12.8	21.0	68.8	4.94	3584	
Sewage, Decatur	791.5	6.55	14.7	18.4	69.7	7.52	3368	
SNG, no methanation	1264	8.06	11.3	19.8	71.1	8.96	3485	

^aUltimate.^bTheoretical (calculated) flame temperatures, dissociation considered, with stoichiometrically correct air/fuel ratio. Although these temperatures are lower than those reported in the literature, they are all computed on the same basis; so they offer a comparison of the relative flame temperatures of various fuels.

It is a convenient coincidence that most solid fossil fuels release about 96–99 gross Btu/ft³ of standard *air*; liquid fossil fuels release about 101–104 Btu/ft³, gaseous fossil fuels about 104–108 Btu/ft³.

This would say that the natural gas in the example above should require about 1017 Btu/ft³ gas divided by 106 Btu/ft³ *air* = 9.6 ft³ *air*/ft³ gas. Precise stoichiometric calculations would say 0.909(9.53) + 0.06(16.7) = 9.58 ft³ *air*/ft³ gas.

Table 2 Calorific Properties of Some Compounds Found in Gaseous Fuels

Compound	Wobbe Index	Gross Heating Value ^d (Btu/ft ³)	Net Heating Value (Btu/ft ³)	Pounds, Dry poc ^a per std ft ³ of Fuel	Pounds H ₂ O per std ft ³ of Fuel	Air Volume per Fuel Volume
Methane, CH ₄	1360	1013	921	0.672	0.0950	9.56
Ethane, C ₂ H ₆	1729	1763	1625	1.204	0.1425	16.7
Propane, C ₃ H ₈	2034	2512	2328	1.437	0.1900	23.9
Butane, C ₄ H ₁₀	2302	3264	3034	2.267	0.2375	31.1
Carbon monoxide, CO	328	323	323	0.255	0	2.39
Hydrogen, H ₂	1228	325	279	0	0.0474	2.39
Hydrogen sulfide, H ₂ S	588	640	594	0.5855	0.0474	7.17
N ₂ , O ₂ , H ₂ O, CO ₂ , SO ₂	0	0	0	^b	^c	0

^apoc = products of combustion.

^bWeight of N₂, O₂, CO₂, and SO₂ in fuel.

^cWeight of H₂O in fuel.

^dHigher heating value (HHV).

2.7 Net Heating Value

Because a calorimeter cools the exit gases below their dew point, it retrieves the latent heat of condensation of any water vapor therein. But that latent heat is not recapturable in most practical heating equipment because of concern about corrosion; therefore, it is more realistic to subtract the latent heat from HHV, yielding a net or lower heating value, LHV. This is approximately

$$\frac{\text{LHV}}{\text{unit of fuel}} = \frac{\text{HHV}}{\text{unit of fuel}} - \left(\frac{970 \text{ Btu}}{\text{lb H}_2\text{O}} \times \frac{\text{lb H}_2\text{O}}{\text{unit of fuel}} \right)$$

Values for the latter term are listed in Table 2. (Note that available heat was discussed in Chapter 6.)

2.8 Flame Stability

Flame stability is influenced by burner and combustion chamber configuration (aerodynamic and heat transfer characteristics) and by the fuel properties tabulated in Table 3.

2.9 Gas Gravity

Gas gravity, G (Table 1), is the ratio of the actual gas density relative to the density of dry air at standard temperature and pressure (0.0765 lb/ft³). This should not be confused with “specific gravity,” which is the ratio of actual density relative to that of water. Gas gravity for natural gases typically ranges from 0.58 to 0.64 and is used in determination of flow rates and pressure drops through pipe lines, orifices, burners, and regulators:

$$\text{Flow} = \text{Flow coefficient} \times \text{Area}(\text{ft}^2) \times \sqrt{2g(\text{psf pressure drop})/\rho}$$

where $g = 32.2 \text{ ft/s}^2$ and $\rho = \text{gas gravity} \times 0.0765$. Unless otherwise emphasized, gas gravity is measured and specified at standard temperature and pressure (60°F and 29.92 in Hg).

2.10 Wobbe Index

The Wobbe index or Wobbe number (Table 2) is a convenient indicator of heat input considering the flow resistance of a gas-handling system. The Wobbe index is equal to the gross heating value divided by the square root of gas gravity; $W = \text{HHV}/\sqrt{G}$.

Table 3 Fuel Properties That Influence Flame Stability^{2,a}

Fuel	Minimum Ignition Temperature, °F (°C)	Calculated Flame Temperature, °F (°C) ^b		Flammability Limits, % Fuel Gas by Volume ^c		Laminar Flame Velocity, fps (m/s)		Percent Theoretical Air for Maximum Flame Velocity
		In Air	In O ₂	Lower	Upper	In Air	In O ₂	
Acetylene, C ₂ H ₂	581(305)	4770(2632)	5630(3110)	2.5	81.0	8.75(2.67)	—	83
Blast furnace gas	—	2650(1454)	—	35.0	73.5	—	—	—
Butane, commercial	896(480)	3583(1973)	—	1.86	8.41	2.85(0.87)	—	—
Butane, <i>n</i> -C ₄ H ₁₀	761(405)	3583(1973)	—	1.86	8.41	1.3(0.40)	—	97
Carbon monoxide, CO	1128(609)	3542(1950)	—	12.5	74.2	1.7(0.52)	—	55
Carbureted water gas	—	3700(2038)	5050(2788)	6.4	37.7	2.15(0.66)	—	90
Coke oven gas	—	3610(1988)	—	4.4	34.0	2.30(0.70)	—	90
Ethane, C ₂ H ₆	882(472)	3540(1949)	—	3.0	12.5	1.56(0.48)	—	98
Gasoline	536(280)	—	—	1.4	7.6	—	—	—
Hydrogen, H ₂	1062(572)	4010(2045)	5385(2974)	4.0	74.2	9.3(2.83)	—	57
Hydrogen sulfide, H ₂ S	558(292)	—	—	4.3	45.5	—	—	—
Mapp gas, C ₃ H ₄	850(455)	—	5301(2927)	3.4	10.8	—	15.4(4.69)	—
Methane, CH ₄	1170(632)	3484(1918)	—	5.0	15.0	1.48(0.45)	14.76(4.50)	90
Methanol, CH ₃ OH	725(385)	3460(1904)	—	6.7	36.0	—	1.6(0.49)	—
Natural gas	—	3525(1941)	4790(2643)	4.3	15.0	1.00(0.30)	15.2(4.63)	100
Producer gas	—	3010(1654)	—	17.0	73.7	0.85(0.26)	—	90
Propane, C ₃ H ₈	871(466)	3573(1967)	5130(2832)	2.1	10.1	1.52(0.46)	12.2(3.72)	94
Propane, commercial	932(500)	3573(1967)	—	2.37	9.50	2.78(0.85)	—	—
Propylene, C ₃ H ₆	—	—	5240(2893)	—	—	—	—	—
Town gas (Br. coal)	700(370)	3710(2045)	—	4.8	31.0	—	—	—

^aFor combustion with air at standard temperature and pressure.

^bFlame temperatures are theoretical—calculated for stoichiometric ratio, dissociation considered.

^cIn a fuel–air mix. Example for methane: the lower flammability limit or lower explosive limit, LEL = 5% or 95 volumes air/5 volumes gas = 19.1 air/gas ratio. From Table 2, stoichiometric ratio is 9.56:1. Therefore excess air is $19 - 9.56 = 9.44 \text{ ft}^3 \text{ air/ft}^3 \text{ gas}$ or $9.44/9.56 \times 100 = 99.4\%$ excess air.

If air can be mixed with a substitute gas to give it the same Wobbe index as the previous gas, the existing burner system will pass the same gross Btu/h input. This is often invoked when propane–air mixtures are used as standby fuels during natural gas curtailments. To be precise, the amount of air mixed with the propane should then be subtracted from the air supplied through the burner.

The Wobbe index is also used to maintain a steady input despite changing calorific value and gas gravity. Because most process-heating systems have automatic input control (temperature control), maintaining steady input may not be as much of a problem as maintaining a constant furnace atmosphere (oxygen or combustibles).

2.11 Flame Temperature

Flame temperature depends on burner mixing aerodynamics, fuel/air ratio, and heat loss to surroundings. It is very difficult to measure with repeatability. Calculated adiabatic flame temperatures, corrected for dissociation of CO₂ and H₂O, are listed in Tables 1a–c and 3 for 60°F air; in Chapter 15 it is listed for elevated air temperatures. Obviously, higher flame temperatures produce better heat transfer rates from flame to load.

2.12 Minimum Ignition Temperature

Minimum ignition temperature (Table 3) relates to safety in handling, ease of light-up, and ease of continuous self-sustained ignition (without pilot or igniter, which is preferred). In mixtures of gaseous compounds, such as natural gas, the minimum ignition temperature of the mixture is that of the compound with the lowest ignition temperature.

2.13 Flammability Limits

Flammability limits (Table 3, formerly termed “limits of inflammability”) spell out the range of air-to-fuel proportions that will burn with continuous self-sustained ignition. “Lower” and “upper” flammability limits [also termed lower explosive limit (LEL) and upper explosive limit (UEL)] are designated in percentage of gas in a gas–air mixture. For example, the flammability

Table 4a Physical Properties^a of LP Gases^{b,5}

	Propane	Isobutane	Butane
Molecular weight	44.09	58.12	58.12
Boiling point, °F	−43.7	+10.9	+31.1
Boiling point, °C	−42.1	−11.7	−0.5
Freezing point, °F	−305.8	−255.0	−216.9
Density of liquid			
Specific gravity, 60°F/60°F	0.508	0.563	0.584
Degrees, API	147.2	119.8	110.6
lb/gal	4.23	4.69	4.87
Density of vapor (ideal gas)			
Specific gravity (air = 1)	1.522	2.006	2.006
ft ³ gas/lb	8.607	6.53	6.53
ft ³ gas/gal of liquid	36.45	30.65	31.8
lb gas/1000 ft ³	116.2	153.1	153.1
Total heating value (after vaporization)			
Btu/ft ³	2,563	3,369	3,390
Btu/lb	21,663	21,258	21,308
Btu/gal of liquid	91,740	99,790	103,830
Critical constants			
Pressure, psia	617.4	537.0	550.1
Temperature, °F	206.2	272.7	306.0
Specific heat, Btu/lb, °F			
c_p , vapor	0.388	0.387	0.397
c_v , vapor	0.343	0.348	0.361
c_p/c_v	1.13	1.11	1.10
c_p , liquid 60°F	0.58	0.56	0.55
Latent heat of vaporization at boiling point, Btu/lb	183.3	157.5	165.6
Vapor pressure, psia			
0°F	37.8	11.5	7.3
70°F	124.3	45.0	31.3
100°F	188.7	71.8	51.6
100°F (ASTM), psig max	210		70
130°F	274.5	109.5	80.8

^aProperties are for commercial products and vary with composition.

^bAll values at 60°F and 14.696 psia unless otherwise stated.

limits of a natural gas are 4.3 and 15%. The 4.3% gas in a gas–air mixture means 95.7% must be air; therefore, the “lean limit” or “lower limit” air/fuel ratio is $95.7/4.3 = 22.3:1$, which means that more than 22.3:1 (volume ratio) will be too lean to burn. Similarly, less than $(100 - 15)/15 = 5.67:1$ is too rich to burn.

For the flammability limits of fuel mixtures other than those listed in Table 3, the Le Chatelier equation³ and U.S. Bureau of Mines data⁴ can be used.

3 LIQUEFIED PETROLEUM GASES

LP gases (LPGs) are by-products of natural gas production and of refineries. They consist mainly of propane (C_3H_8), with some butane, propylene, and butylene. They are stored and shipped in liquefied form under high pressure; therefore, their flow rates are usually measured in gallons per hour or pounds per hour. When expanded and evaporated, LPGs are heavier than air. Workmen have been asphyxiated by LPG in pits beneath leaking LPG equipment.

The rate of LPG consumption is much less than that of natural gas or fuel oils. Practical economics usually limit use to (a) small installations inaccessible to pipe lines, (b) transportation, or (c) standby for industrial processes where oil burning is difficult or impossible.

LPGs can usually be burned in existing natural gas burners, provided the air/gas ratio is properly readjusted. On large multiple burner installations an automatic propane–air mixing station is usually installed to facilitate quick changeover without changing air/gas ratios.

Table 4b Physical Properties^a of LP Gases^{b,5}

	Propane	Isobutane	Butane
Flash temperature, °F (calculated)	−156	−117	−101
Ignition temperature, °F	932	950	896
Maximum flame temperature in air, °F			
Observed	3497	3452	3443
Calculated	3573	3583	3583
Flammability limits, % gas in air			
Lower	2.37	1.80	1.86
Higher	9.50	8.44	8.41
Maximum rate flame propagation in 1-in. tube			
in./s	32	33	33
Percentage gas in air	4.6–4.8	3.6–3.8	3.6–3.8
Required for complete combustion (ideal gas)			
Air, ft ³ /ft ³ gas	23.9	31.1	31.1
lb/lb gas	15.7	15.5	15.5
Oxygen, ft ³ /ft ³ gas	5.0	6.5	6.5
lb/lb gas	3.63	3.58	3.58
Products of combustion (ideal gas)			
Carbon dioxide, ft ³ /ft ³ gas	3.0	4.0	4.0
lb/lb gas	2.99	3.03	3.03
Water vapor, ft ³ /ft ³ gas	4.0	5.0	5.0
lb/lb gas	1.63	1.55	1.55
Nitrogen, ft ³ /ft ³ gas	18.9	24.6	24.6
lb/lb gas	12.0	11.8	11.8

^aProperties are for commercial products and vary with composition.

^bAll values at 60°F and 14.696 psia unless otherwise stated.

(See the discussion of Wobbe index, Section 2.10.) Some fuel must be consumed to produce steam or hot water to operate a vaporizer for most industrial installations.

Tables 4a and 4b list some properties of commercial LPG, but it is suggested that more specific information be obtained from local suppliers.

REFERENCES

1. M. G. Fryback, "Synthetic Fuels—Promises and Problems," *Chem. Eng. Progr.*, May 1981.
2. R. J. Reed (Ed.), *Combustion Handbook*, Vol. I, North American Mfg. Co., Cleveland, OH, 1986, pp. 12, 36–38.
3. F. E. Vandever and C. G. Segeler, "Combustion," in C. G. Segeler (Ed.), *Gas Engineers Handbook*, Industrial Press, New York, 1965, pp. 2/75–2/76.
4. H. F. Coward and G. W. Jones, *Limits of Flammability of Gases and Vapors*, U.S. Bureau of Mines Bulletin 503, U.S. Government Printing Office, Washington, D.C., 1952, pp. 20–81.
5. E. W. Evans and R. W. Miller, "Testing and Properties of LP-Gases," in C. G. Segeler (Ed.), *Gas Engineers Handbook*, Industrial Press, New York, 1965, p. 5/11.
6. W. Trinks, M. H. Mawhinney, R. A. Shannon, R. J. Reed, and J. R. Garvey, *Industrial Furnaces*, 6th ed., Wiley, Hoboken, NJ, 2003.

CHAPTER 19

LIQUID FOSSIL FUELS FROM PETROLEUM

Richard J. Reed

North American Manufacturing Company

Cleveland, Ohio

1 INTRODUCTION	683	3 SHALE OILS	698
2 FUEL OILS	684	4 OILS FROM TAR SANDS	699
2.1 Kerosene	687	5 OIL-WATER EMULSIONS	700
2.2 Aviation Turbine Fuels	693	REFERENCES	701
2.3 Diesel Fuels	694		
2.4 Summary	698		

1 INTRODUCTION

The major source of liquid fuels is crude petroleum; other sources are shale and tar sands. Synthetic hydrocarbon fuels—gasoline and methanol—can be made from coal and natural gas. Ethanol, some of which is used as an automotive fuel, is derived from vegetable matter.

Crude petroleum and refined products are a mix of a wide variety of hydrocarbons—aliphatics (straight- or branched-chained paraffins and olefins), aromatics (closed rings, six carbons per ring with alternate double bonds joining the ring carbons, with or without aliphatic side chains), and naphthenic or cycloparaffins (closed single-bonded carbon rings, five to six carbons).

Very little crude petroleum is used in its natural state. Refining is required to yield marketable products that are separated by distillation into fractions including a specific boiling range. Further processing (such as cracking, reforming, and alkylation) alters molecular structure of some of the hydrocarbons and enhances the yield and properties of the refined products.

Crude petroleum is the major source of liquid fuels in the United States now and for the immediate future. Although the oil embargo of 1973–1974 intensified development of facilities for extraction of oil from shale and of hydrocarbon liquids from coal, the economics do not favor early commercialization of these processes. Their development has been slowed by an apparently adequate supply of crude oil. Tar sands are being processed in small amounts in Canada, but no commercial facility exists in the United States. (See Table 1.)

Except for commercial propane and butane, fuels for heating and power generation are generally heavier and less volatile than fuels used in transportation. The higher the “flash point,” the less hazardous is handling of the fuel. (Flash point is the minimum temperature at which the fuel oil will catch fire if exposed to naked flame. Minimum flash points are stipulated by law for safe storage and handling of various grades of oils.) (See Table 5 of Chapter 6.)

For most of the information in this chapter, the author is deeply indebted to John W. Thomas, retired Chief Mechanical Engineer of the Standard Oil Company (Ohio).

Properties of fuels reflect the characteristics of the crude. Paraffinic crudes have a high concentration of straight-chain hydrocarbons, which may leave a wax residue with distillation. Aromatic and naphthenic crudes have concentrations of ring hydrocarbons. Asphaltic crudes have a preponderance of heavier ring hydrocarbons and leave a residue after distillation. (See Table 2.)

Table 1 Principal Uses of Liquid Fuels

<i>Heat and Power</i>	
Fuel oil	Space heating (residential, commercial, industrial) Steam generation for electric power Industrial process heating Refinery and chemical feedstock
Kerosene	Supplemental space heating
Turbine fuel	Stationary power generation
Diesel fuel	Stationary power generation
Liquid propane ^a	Isolated residential space heating Standby industrial process heating
<i>Transportation</i>	
Jet fuel	Aviation turbines
Diesel fuel	Automotive engines Marine engines Truck engines
Gasoline	Automotive Aviation
Liquid propane and butane ^a	Limited automotive use

^aSee Chapter 8 on gaseous fossil fuels.**Table 2** Ultimate Chemical Analyses of Various Crudes^{a1}

Crude Petroleum Source	% wt of					Specific Gravity (at temperature, °F)	Base
	C	H	N	O	S		
Baku, USSR	86.5	12.0			1.5	0.897	
California	86.4	11.7	1.14			0.951 (at 59°F)	Naphthene
Colombia, South America	85.62	11.91	0.54				
Kansas	85.6	12.4				0.37	Mixed
Mexico	83.0	11.0	1.7			4.30	Naphthene
Oklahoma	85.0	12.9				0.76	Mixed
Pennsylvania	85.5	14.2					0.862 (at 59°F)
Texas	85.7	11.0	2.61			0.70	0.91
West Virginia	83.6	12.9			3.6		0.897 (at 32°F)

^aSee, also, Table 7.

2 FUEL OILS

Liquid fuels in common use are broadly classified as follows:

1. Distillate fuel oils derived directly or indirectly from crude petroleum
2. Residual fuel oils that result after crude petroleum is topped or viscous residua from refining operations
3. Blended fuel oils, mixtures of the above

Table 3 Some Properties of Liquid Fuels²

Property	Gasoline	Kerosene	Diesel Fuel	Light Fuel Oil	Heavy Fuel Oil	Coal Tar Fuel	Bituminous Coal (for Comparison)
Analysis, % wt							
C	85.5	86.3	86.3	86.2	86.2	90.0	80.0
H	14.4	13.6	12.7	12.3	11.8	6.0	5.5
N						1.2	1.5
O						2.5	7
S	0.1	0.1	1.0	1.5	2.0	0.4	1
Boiling range, °F	104–365	284–536	356 up	392 up	482 up	392 up	
Flash point, °F	–40	102	167	176	230	149	
Gravity specific at 59°F	0.73	0.79	0.87	0.89	0.95	1.1	1.25
Heat value, net							
cal/g	10,450	10,400	10,300	10,100	9,900	9,000	7,750
Btu/lb	18,810	18,720	18,540	18,180	17,820	16,200	13,950
Btu/U.S. gal	114,929	131,108	129,800	131,215	141,325		
Residue, % wt at 662°F			15	50	60	60	
Viscosity, kinematic							
Centistokes at 59°F	0.75	1.6	5.0	50	1,200	1,500	
Centistokes at 212°F		0.6	1.2	3.5	20	18	

The distillate fuels have lower specific gravity and are less viscous than residual fuel oils. Petroleum refiners burn a varying mix of crude residue and distilled oils in their process heaters. The changing gravity and viscosity require maximum oil preheat for atomization good enough to assure complete combustion. Tables 3–8 describe oils in current use. Some terms used in those tables are defined below.

Aniline point is the lowest Fahrenheit temperature at which an oil is completely miscible with an equal volume of freshly distilled aniline.

API gravity is a scale of specific gravity for hydrocarbon mixtures referred to in “degrees API” (for American Petroleum Institute). The relationships between API gravity, specific gravity, and density are

$$\text{sp gr } 60/60^{\circ}\text{F} = \frac{141.5}{^{\circ}\text{API} + 131.5}$$

where °API is measured at 60°F (15.6°C);

$$\text{sp gr } 60/60^{\circ}\text{F} = \frac{\text{lb/ft}^3}{62.3}$$

where lb/ft³ is measured at 60°F (15.6°C).

SSU (or SUS) is seconds, Saybolt Universal, a measure of kinematic viscosity determined by measuring the time required for a specified quantity of the sample oil to flow by gravity through a specified orifice at a specified temperature. For heavier, more viscous oils, a larger (Furol) orifice is used, and the results are reported as SSF (seconds, Saybolt Furol):

$$\text{kin visc in centistokes} = 0.226 \times \text{SSU} - 195/\text{SSU}, \text{ for SSU } 32 - 100$$

$$\text{kin visc in centistokes} = 0.220 \times \text{SSU} - 135/\text{SSU}, \text{ for SSU } > 100$$

$$\text{kin visc in centistokes} = 2.24 \times \text{SSF} - 184/\text{SSF}, \text{ for SSF } 25 - 40$$

$$\text{kin visc in centistokes} = 2.16 \times \text{SSF} - 60/\text{SSF}, \text{ for SSF } > 40$$

$$1 \text{ centistoke (cSt)} = 0.000001 \text{ m}^2/\text{sec}$$

Table 4 Gravities and Related Properties of Liquid Petroleum Products

Typical Ranges for		Specific Gravity		°API	lb/gal	kg/m ³	Gross		% H, wt ^e	Net Btu/ gal ^a	Net kcal/L ^a	Specific Heat @ 40°F	Specific Heat @ 300°F	Temperature Correction °API/°F ^a	ft ³ 60°F Air/gal	Ultimate % CO ₂
Aviation Turbine Fuels	Fuel Oils	60°F/60°F (15.6°C/ 15.6°C)	15.6°C/ 15.6°C)				Btu/gal ^a	kcal/L ^a								
0		1.076	8.969	1075	160,426	10,681	8.359	153,664	10,231	0.391	0.504	0.045	1581	—		
2		1.060	8.834	1059	159,038	10,589	8.601	152,183	10,133	0.397	0.508	—	—	—		
4		1.044	8.704	1043	157,692	10,499	8.836	150,752	10,037	0.397	0.512	—	—	18.0		
6		1.029	8.577	1028	156,384	10,412	9.064	149,368	9,945	0.400	0.516	0.048	1529	17.6		
8		1.014	8.454	1013	155,115	10,328	9.285	148,028	9,856	0.403	0.519	0.050	1513	17.1		
10 ^b		1.000 ^b	8.335 ^b	1000 ^b	153,881	10,246	10.00	146,351	9,744	0.406	0.523	0.051	1509	16.7		
12		0.986	8.219	985.0	152,681	10,166	10.21	145,100	9,661	0.409	0.527	0.052	1494	16.4		
14		0.973	8.106	971.5	151,515	10,088	10.41	143,888	9,580	0.412	0.530	0.054	1478	16.1		
16		0.959	7.996	958.3	150,380	10,013	10.61	142,712	9,502	0.415	0.534	0.056	1463	15.8		
18		0.946	7.889	945.5	149,275	9,939	10.80	141,572	9,426	0.417	0.538	0.058	1448	15.5		
20		0.934	7.785	933.0	148,200	9,867	10.99	140,466	9,353	0.420	0.541	0.060	1433	15.2		
22		0.922	7.683	920.9	147,153	9,798	11.37	139,251	9,272	0.423	0.545	0.061	1423	14.9		
24		0.910	7.585	909.0	146,132	9,730	11.55	138,210	9,202	0.426	0.548	0.063	1409	14.7		
26		0.898	7.488	897.5	145,138	9,664	11.72	137,198	9,135	0.428	0.552	0.065	1395	14.5		
28		0.887	7.394	886.2	144,168	9,599	11.89	136,214	9,069	0.431	0.555	0.067	1381	14.3		
30		0.876	7.303	875.2	143,223	9,536	12.06	135,258	9,006	0.434	0.559	0.069	1368	14.0		
32		0.865	7.213	864.5	142,300	9,475	12.47	134,163	8,933	0.436	0.562	0.072	1360	13.8		
34		0.855	7.126	854.1	141,400	9,415	12.63	133,259	8,873	0.439	0.566	0.074	1347	13.6		
36		0.845	7.041	843.9	140,521	9,356	12.78	132,380	8,814	0.442	0.569	0.076	1334	13.4		
38		0.835	6.958	833.9	139,664	9,299	12.93	131,524	8,757	0.444	0.572	0.079	1321	13.3		
40		0.825	6.887	824.2	138,826	9,243	13.07	130,689	8,702	0.447	0.576	0.082	1309	13.1		
42		0.816	6.798	814.7	138,007	9,189	—	—	—	0.450	0.579	0.085	—	13.0		
44		0.806	6.720	805.4	137,207	9,136	—	—	—	0.452	0.582	0.088	—	12.8		

^aFor gravity measured at 60°F (15.6°C) only.^bSame as H₂O.

Table 5 Heating Requirements for Products Derived from Petroleum³

Commercial Fuels	Specific Gravity at 60°F/ (15.6°C)	Distillation Range, °F (°C)	Vapor Pressure, ^a psia (mm Hg)	Latent Btu/ gal ^b to Vaporize	Btu/gal ^b to Heat from 32°F (0°C) to		
					Pumping Temperature	Atomizing Temperature	Vapor
No. 6 oil	0.965	600–1000 (300–500)	0.054 (2.8)	764	371	996	3619 ^c
No. 5 oil	0.945	600–1000 (300–500)	0.004 (0.2)	749	133	635	3559 ^c
No. 4 oil	0.902	325–1000 (150–500)	0.232 (12)	737	—	313	2725 ^c
No. 2 oil	0.849	325–750 (150–400)	0.019 (1)	743	—	—	2704 ^c
Kerosene	0.780	256–481 (160–285)	0.039 (2)	750	—	—	1303 ^c
Gasoline	0.733	35–300 (37–185)	0.135 (7)	772	—	—	1215 ^c
Methanol	0.796	148 (64)	4.62 (239)	3140	—	—	3400 ^d
Butane	0.582	31 (0)	31 (1604)	808	—	—	976 ^d
Propane	0.509	–44 (–42)	124 (6415)	785	—	—	963 ^d

^aAt the atomizing temperature or 60°F, whichever is lower. Based on a sample with the lowest boiling point from column 3.

^bTo convert Btu/U.S. gal to kcal/L, multiply by 0.666. To convert Btu/U.S. gal to Btu/lb, divide by 8.335 × sp gr, from column 2. To convert Btu/U.S. gal to kcal/kg, divide by 15.00 × sp gr, from column 2.

^cCalculated for boiling at midpoint of distillation range, from column 3.

^dIncludes latent heat plus sensible heat of the vapor heated from boiling point to 60°F (15.6°C).

Unlike distillates, residual oils contain noticeable amounts of inorganic matter, ash content ranging from 0.01 to 0.1%. Ash often contains vanadium, which causes serious corrosion in boilers and heaters. (A common specification for refinery process heaters requires 50% nickel–50% chromium alloy for tube supports and hangers when the vanadium exceeds 150 ppm.) The V₂O₅ also lowers the eutectic of many refractories, causing rapid disintegration. Crudes that often contain high vanadium are

Venezuela, Bachaqoro	350 ppm
Iran	350 – 440 ppm
Alaska, North Slope	80 ppm

2.1 Kerosene

Kerosene is a refined petroleum distillate consisting of a homogeneous mixture of hydrocarbons. It is used mainly in wick-fed illuminating lamps and kerosene burners. Oil for illumination and for domestic stoves must be high in paraffins to give low smoke. The presence of naphthenic and especially aromatic hydrocarbons increases the smoking tendency. A “smoke point” specification is a measure of flame height at which the tip becomes smoky. The smoke point is about 73 mm for paraffins, 34 mm for naphthalenes, and 7.5 mm for aromatics and mixtures.

Table 6 Analyses and Characteristics of Selected Fuel Oils³

Source	Ultimate Analysis (% Weight)							ppm if > 50	% wt Asphal- tine	% wt C Residue	° API at 60°F	Flash Point, °F	HV, Btu/lb		Pour Point, °F	Viscosity, SSU	
	C	H	N	S	Ash	O ^a	Gross						Net	At 140°F		At 210°F	
Alaska	86.99	12.07	0.007	0.31	< 0.001	0.62	—	—	—	33.1	—	—	—	—	33.0	29.5	
California	86.8	12.52	0.053	0.27	< 0.001	0.36	—	—	—	32.6	—	—	19,330	—	30.8	29.5	
West Texas	88.09	9.76	0.026	1.88	< 0.001	0.24	—	—	—	18.3	—	—	—	—	32.0	28.8	
Alaska	86.04	11.18	0.51	1.63	0.034	0.61	50 Ni 67 V	5.6	12.9	15.6	215	18,470	17,580	38	1071	194	
California	86.66	10.44	0.86	0.99	0.20	0.85	— ^b	8.62	15.2	12.6	180	18,230	17,280	42	720	200	
DFM (shale)	86.18	13.00	0.24	0.51	0.003	1.07	—	0.036	4.1	33.1	182	19,430	18,240	40	36.1	30.7	
Gulf of Mexico	84.62	10.77	0.36	2.44	0.027	1.78	—	7.02	14.8	13.2	155	18,240	17,260	40	835	181	
Indo/Malaysia	86.53	11.93	0.24	0.22	0.036	1.04	101 V	0.74	3.98	21.8	210	19,070	17,980	61	199	65	
Middle East ^c	86.78	11.95	0.18	0.67	0.012	0.41	—	3.24	6.0	19.8	350	19,070	17,980	48	490	131.8	
Pennsylvania ^d	84.82	11.21	0.34	2.26	0.067	1.3	65 Na 82 V	4.04	12.4	15.4	275	18,520	17,500	66	1049	240	
Venezuela	85.24	10.96	0.40	2.22	0.081	1.10	52 Ni 226 V	8.4	6.8	14.1	210	18,400	17,400	58	742	196.7	
Venezuela desulfurized	85.92	12.05	0.24	0.93	0.033	0.83	101 V	2.59	5.1	23.3	176	18,400	17,300	48	113.2	50.5	

^aBy difference.^b91 Ca, 77 Fe, 88 Ni, 66 V.^cExxon.^dAmerada Hess.

Table 7 ASTM Fuel Oil Specifications⁴

Grade of Fuel Oil ^a	Flash Point, °C(°F) Min	Pour Point, °C(°F) Max	Water and Sediment, Vol %		Carbon Residue on 10% Bottoms, % Max	Ash, % Max	Distillation Temperatures, °C(°F)		Saybolt Viscosity, S ^b		Kinematic Viscosity, cSt ^d						Sulfur, % Max		
			10% Point	90% Point			Universal at 38°C (100°F)	Furoil at 50°C (122°F)	At 38°C (100°F)		At 40°C (104°F)		At 50°C (122°F)		Specific Gravity, 60/60°F (deg API) Max	Copper Strip Corrosion No. 3 Max			
									Min	Max	Min	Max	Min	Max				Min	Max
No. 1 A distillate oil intended for vaporizing pot-type burners and other burners requiring this grade of fuel	38 (100)	-18° (0)	0.05	0.15	—	—	215 (420)	288 (550)	—	—	1.4	2.2	1.3	2.1	—	—	0.8499	No. 3	0.5
No. 2 A distillate oil for general-purpose heating for use in burners not requiring No. 1 fuel oil	38 (100)	-6° (20)	0.05	0.35	—	—	282° (540)	338 (640)	—	—	2.0°	3.6	1.9°	3.4	—	—	0.8762 (30 min)	No. 3	0.5 ^b

(continued)

No. 5 (Heavy) Preheating (130) may be required for burning and, in cold cli- mates, may be required for han- dling	55	—	1.00	—	0.10	—	—	—	(>300)	(900)	(23)	(40)	>65	194 ^f	58	168 ^f	(42)	(81)	—	—
No. 6 Preheating (140) required for burning and han- dling	60	g	2.00 ^e	—	—	—	—	—	(>900)	(9000)	(>45)	(300)	—	—	—	—	>92	638 ^f	—	—

^aIt is the intent of these classifications that failure to meet any requirement of a given grade does not automatically place an oil in the next lower grade unless in fact it meets all requirements of the lower grade.

^bIn countries outside the United States other sulfur limits may apply.

^cLower or higher pour points may be specified whenever required by conditions of storage or use. When pour point less than -18°C (0°F) is specified, the minimum viscosity for grade No. 2 shall be 1.7 cSt (31.5 SUS) and the minimum 90% point shall be waived.

^dViscosity values in parentheses are for information only and not necessarily limiting.

^eThe amount of water by distillation plus the sediment by extraction shall not exceed 2.00%. The amount of sediment by extraction shall not exceed 0.50%. A deduction in quantity shall be made for all water and sediment in excess of 1.0%.

^fWhere low-sulfur fuel oil is required, fuel oil falling in the viscosity range of a lower numbered grade down to and including No. 4 may be supplied by agreement between purchaser and supplier. The viscosity range of the initial shipment shall be identified and advance notice shall be required when changing from one viscosity range to another. This notice shall be in sufficient time to permit the user to make the necessary adjustments.

^gThis limit guarantees a minimum heating value and also prevents misrepresentation and misapplication of this product as Grade No. 2.

^hWhere low-sulfur fuel oil is required, Grade 6 fuel oil will be classified as low pour $+15^{\circ}\text{C}$ (60°F) max or high pour (no max). Low-pour fuel oil should be used unless all tanks and lines are heated.

Table 8 Application of ASTM Fuel Oil Grades as Described by One Burner Manufacturer

Fuel Oil	Description
No. 1	Distillate oil for vaporizing-type burners
No. 2	Distillate oil for general-purpose use and for burners not requiring No. 1 fuel oil
No. 4	Blended oil intended for use without preheating
No. 5	Blended residual oil for use with preheating; usual preheat temperature is 120–220°F
No. 6	Residual oil for use with preheaters permitting a high-viscosity fuel; usual preheat temperature is 180–260°F
Bunker C	Heavy residual oil, originally intended for oceangoing ships

Table 9 ASTM Chemical and Physical Requirements for Kerosene⁵

Property	Limit
Distillation temperature	
10% recovered	401 °F (205°C)
Final boiling point	572°F (300°C)
Flash point	100°F (38°C)
Freezing point	–22°F (–30°C)
Sulfur, % weight	
No. 1 K	0.04 maximum
No. 2 K	0.30 maximum
Viscosity, kinematic at 104°F (40°C), centistokes	1.0 min/1.9 max

Low sulfur content is necessary in kerosenes because:

1. Sulfur forms a bloom on glass lamp chimneys and promotes carbon formation on wicks.
2. Sulfur forms oxides in heating stoves. These swell and are corrosive and toxic, creating a health hazard, particularly in nonvented stoves.

Kerosene grades⁵ (see Table 9) in the United States are:

- No. 1 K: A special low-sulfur grade kerosene suitable for critical kerosene burner applications
- No. 2 K: A regular-grade kerosene suitable for use in flue-connected burner applications and for use in wick-fed illuminating lamps

2.2 Aviation Turbine Fuels

The most important requirements of aircraft jet fuel relate to freezing point, distillation range, and level of aromatics. Fluidity at low temperature is important to ensure atomization. A typical upper viscosity limit is 7–10 cSt at 0°F, with the freezing point as low as –60°F.

Aromatics are objectionable because (1) coking deposits from the flame are most pronounced with aromatics of high C/H ratio and less pronounced with short-chain compounds and (2) they must be controlled to keep the combustor liner at an acceptable temperature.

Jet fuels for civil aviation are identified as jets A and A1 (high-flash-point, kerosene-type distillates) and jet B (a relatively wide boiling range, volatile distillate).

Jet fuels for military aviation are identified as JP4 and JP5. The JP4 has a low flash point and a wide boiling range. The JP5 has a high flash point and a narrow boiling range. (See Table 10.)

Table 10 ASTM Specifications⁶ and Typical Properties⁷ of Aviation Turbine Fuels

Property	Specifications			Typical, 1979		
				26 Samples JP4	7 Samples JP5	60 Samples Jet A
	Jet A	Jet A1	Jet B			
Aromatics, % vol	20	20	20	13.0	16.4	17.9
Boiling point, final, °F	572	572	—	—	—	—
Distillation, max temperature, °F						
For 10% recovered	400	400	—	208	387	375
For 20% recovered	—	—	290	—	—	—
For 50% recovered	—	—	370	293	423	416
For 90% recovered	—	—	470	388	470	473
Flash point, min, °F	100	100	—	—	—	—
Freezing point, max, °F	–40	–53	–58	–110	–71	–56
Gravity, API, max	51	51	57	53.5	41.2	42.7
Gravity, API, min	37	37	45	—	—	—
Gravity, specific 60°F min	0.7753	0.7753	0.7507	0.765	0.819	0.812
Gravity, specific 60°F max	0.8398	0.8398	0.8017	—	—	—
Heating value, gross Btu/lb	—	—	—	18,700	18,530	18,598
Heating value, gross Btu/lb min	18,400	18,400	18,400	—	—	—
Mercaptan, % wt	0.003	0.003	0.003	0.0004	0.0003	0.0008
Sulfur, max % wt	0.3	0.3	0.3	0.030	0.044	0.050
Vapor pressure, Reid, psi	—	—	3	2.5	—	0.2
Viscosity, max SSU						
At –4°F	52	—	—	—	—	—
At –30°F	—	—	—	34–37	60.5	54.8

Table 11 Nonaviation Gas Turbine Fuel Grades per ASTM⁸

Grade	Description
No. 0-GT	A naphtha or low-flash-point hydrocarbon liquid
No. 1-GT	A distillate for gas turbines requiring cleaner burning than No. 2-GT
No. 2-GT	A distillate fuel of low ash suitable for gas turbines not requiring No. 1-GT
No. 3-GT	A low ash fuel that may contain residual components
No. 4-GT	A fuel containing residual components and having higher vanadium content than No. 3-GT

Table 12 ASTM Specifications⁸ for Nonaviation Gas Turbine Fuels

Property	Specifications				
	0-GT	1-GT	2-GT	3-GT	4-GT
Ash, max % wt	0.01	0.01	0.01	0.03	—
Carbon residue, max % wt	0.15	0.15	0.35	—	—
Distillation, 90% point, max °F	—	(550) ^a	(640)	—	—
Distillation, 90% point, min °F	—	—	(540)	—	—
Flash point, min °F	—	(100)	(100)	(130)	(150)
Gravity, API min	—	(35)	(30)	—	—
Gravity, spec 60°F max	—	0.850	0.876	—	—
Pour point, max °F	—	(0)	(20)	—	—
Viscosity, kinematic					
Min SSU at 100°F	—	—	(32.6)	(45)	(45)
Max SSU at 100°F	—	(34.4)	(40.2)	—	—
Max SSF at 122°F	—	—	—	(300)	(300)
Water and sediment, max % vol	0.05	0.05	0.05	1.0	1.0

^aValues in parentheses are approximate.

Gas turbine fuel oils for other than use in aircraft must be free of inorganic acid and low in solid or fibrous materials. (See Tables 11 and 12.) All such oils must be homogeneous mixtures that do not separate by gravity into light and heavy components.

2.3 Diesel Fuels

Diesel engines, developed by Rudolf Diesel, rely on the heat of compression to achieve ignition of the fuel. Fuel is injected into the combustion chamber in an atomized spray at the end of the compression stroke, after air has been compressed to 450–650 psi and has reached a temperature, due to compression, of at least 932°F (500°C). This temperature ignites the fuel and initiates the piston's power stroke. The fuel is injected at about 2000 psi to ensure good mixing.

Diesels are extensively used in truck transport, rail trains, and marine engines. They are being used more in automobiles. In addition, they are employed in industrial and commercial stationary power plants.

Fuels for diesels vary from kerosene to medium residual oils. The choice is dictated by engine characteristics, namely, cylinder diameter, engine speed, and combustion wall temperature. High-speed small engines require lighter fuels and are more sensitive to fuel quality variations. Slow-speed, larger industrial and marine engines use heavier grades of diesel fuel oil.

Ignition qualities and viscosity are important characteristics that determine performance. The ignition qualities of diesel fuels may be assessed in terms of their cetane numbers or diesel

indices. Although the diesel index is a useful indication of ignition quality, it is not as reliable as the cetane number, which is based on an engine test:

$$\text{Diesel index} = (\text{Aniline point, } ^\circ\text{F}) \times (\text{API gravity}/100)$$

The diesel index is an arbitrary figure having a significance similar to cetane number but with a value 1–5 numbers higher.

The cetane number is the percentage by volume of cetane in a mixture of cetane with an ethylnaphthalene that has the same ignition characteristics as the fuel. The comparison is made in a diesel engine equipped either with means for measuring the delay period between injection and ignition or with a surge chamber, separated from the engine intake port by a throttle in which the critical measure below which ignition does not occur can be measured. Secondary reference fuels with specific cetane numbers are available. The cetane number is a measure of ignition quality and influences combustion roughness.

The use of a fuel with a too low cetane number results in accumulation of fuel in the cylinder before combustion, causing “diesel knock.” A too high cetane number will cause rapid ignition and high fuel consumption.

The higher the engine speed, the higher the required fuel cetane number. Suggested rpm values for various fuel cetane numbers are shown in Table 13.⁹ Engine size and operating conditions are important factors in establishing approximate ignition qualities of a fuel.

Too viscous an oil will cause large spray droplets and incomplete combustion. Too low a viscosity may cause fuel leakage from high-pressure pumps and injection needle valves. Preheating permits use of higher viscosity oils.

To minimize injection system wear, fuels are filtered to remove grit. Fine-gauge filters are considered adequate for engines up to 8 Hz, but high-speed engines usually have fabric or felt filters. It is possible for wax to crystallize from diesel fuels in cold weather; therefore, preheating before filtering is essential.

To minimize engine corrosion from combustion products, control of fuel sulfur level is required. (See Tables 14, 15a, and 15b.)

Table 13 ASTM Fuel Cetane Numbers for Various Engine Speeds⁹

Engine Speed (rpm)	Cetane Number
Above 1500	50–60
500–1500	45–55
400–800	35–50
200–400	30–45
100–200	15–40
Below 200	15–30

Table 14 ASTM Diesel Fuel Descriptions¹⁰

Grade	Description
No. 1D	A volatile distillate fuel oil for engines in service requiring frequent speed and load changes
No. 2D	Distillate fuel oil of lower volatility for engines in industrial and heavy mobile service
No. 4D	A fuel oil for low and medium speed diesel engines
Type CB	For buses, essentially 1D
Type TT	For trucks, essentially 2D
Type RR	For railroads, essentially 2D
Type SM	For stationary and marine use, essentially 2D or heavier

Table 15a ASTM Detailed Requirements for Diesel Fuel Oils^{a,4,10}

Grade of Diesel Fuel Oil	Flash Point, °C		Cloud Point, °C (°F)		Water and Sediment, Vol%		Carbon Residue on, 10% Residuum, %		Ash, Weight %		Distillation Temperatures, °C (°F), 90% Point				Viscosity				Sulfur, ^d Weight %		Copper Strip Corrosion		Cetane Number ^e			
	Min	Max	Min	Max	Min	Max	Min	Max	Min	Max	Min	Max	Min	Max	Min	Max	Min	Max	Min	Max	Min	Max	Min	Max	Min	Max
	— ^b		— ^b		0.05		0.15		0.01		288 (550)		1.3 2.4		— 34.4		0.50		No. 3		40 ^f					
No. 1-D A volatile distillate fuel oil for engines in service requiring frequent speed and load changes	38 (100)	— ^b	0.05	0.15	0.01	0.01	288 (550)	1.3	2.4	—	34.4	0.50	40 ^f													
No. 2-D A distillate fuel oil of lower volatility for engines in industrial and heavy mobile service	52 (125)	— ^b	0.05	0.35	0.01	0.01	282 ^c (540)	1.9	4.1	32.6	40.1	0.50	40 ^f													
No. 4-D A fuel oil for low- and medium-speed engines	55 (130)	— ^b	0.50	—	0.10	—	—	5.5	24.0	45.0	125.0	2.0	30 ^f													

^aTo meet special operating conditions, modifications of individual limiting requirements may be agreed upon between purchaser, seller, and manufacturer.

^bIt is unrealistic to specify low-temperature properties that will ensure satisfactory operation on a broad basis. Satisfactory operation should be achieved in most cases if the cloud point (or wax appearance point) is specified at 6°C above the tenth percentile minimum ambient temperature for the area in which the fuel will be used. This guidance is of a general nature; some equipment designs, using improved additives, fuel properties, and/or operations, may allow higher or require lower cloud point fuels. Appropriate low-temperature operability properties should be agreed on between the fuel supplier and purchaser for the intended use and expected ambient temperatures.

^cWhen cloud point less than -12°C (10°F) is specified, the minimum viscosity shall be 1.7 cSt (or mm²/s) and the 90% point shall be waived.

^dIn countries outside the United States, other sulfur limits may apply.

^eWhere cetane number by Method D613 is not available, ASTM Method D976, Calculated Cetane Index of Distillate Fuels, may be used as an approximation. Where there is disagreement, Method D613 shall be the referee method.

^fLow-atmospheric temperatures as well as engine operation at high altitudes may require use of fuels with higher cetane ratings.

^gcSt = 1 mm²/s.

^hThe values stated in SI units are to be regarded as the standard. The values in U.S. customary units are for information only.

Table 15b ASTM Typical Properties of Diesel Fuels⁷

Property	All United States, 1981										Eastern United States, 1981									
	48 Samples			112 Samples			24 Samples			44 Samples			13 Samples			4 Samples				
	No. 1D	Min	Max	Min	Avg	Max	Min	Avg	Max	Min	Avg	Max	Min	Avg	Max	Min	Avg	Max		
Ash, % wt	0.000	0.001	0.005	0.000	0.002	0.020	—	0.001	0.005	—	0.002	0.015	—	0.000	0.001	—	0.001	0.001		
Carbon residue, % wt	0.000	0.059	0.067	0.000	0.101	0.300	—	—	0.21	0.101	—	0.25	—	0.121	0.23	—	0.148	0.21		
Cetane number	36	46.7	53.0	29.0	45.6	52.4	—	49.8	—	—	45.6	—	—	44.8	—	—	—	—		
Distillation, 90% point, °F	445	448	560	493	587	640	451	512	640	451	571	640	540	590	640	482	577	640		
Flash point, °F	104	138	176	132	166	240	120	140	240	120	162	240	156	164	192	136	162	180		
Gravity, API	37.8	42.4	47.9	22.8	34.9	43.1	—	41.5	—	—	36.3	—	—	33.8	—	—	35.3	—		
spec, 60/60 °F	0.836	0.814	0.789	0.917	0.850	0.810	—	0.818	—	—	0.843	—	—	0.856	—	—	0.848	—		
Sulfur, % wt	0.000	0.070	0.25	0.010	0.283	0.950	—	0.086	0.24	—	0.198	0.46	—	0.283	0.580	—	0.155	0.28		
Viscosity, SSU at 100 °F	32.6	33.3	35.7	33.8	36.0	40.3	32.9	34.3	40.2	32.9	35.7	40.2	34.2	36.0	37.8	36.0	—	37.8		

2.4 Summary

Aviation jet fuels, gas turbine fuels, kerosenes, and diesel fuels are very similar. The following note from Table 1 of Ref. 8 highlights this:

No. 0-GT includes naphtha, Jet B fuel, and other volatile hydrocarbon liquids. No. 1-GT corresponds in general to Spec D396 Grade No. 1 fuel and Classification D975 Grade No. 1-D Diesel fuel in physical properties. No. 2-GT corresponds in general to Spec D396 Grade No. 2 fuel and Classification D975 Grade No. 2 Diesel fuel in physical properties. No. 3-GT and No. 4-GT viscosity range brackets Spec D396 and Grade No. 4, No. 5 (light), No. 5 (heavy), No. 6, and Classification D975 Grade No. 4-D Diesel fuel in physical properties.

3 SHALE OILS

As this is written, there are no plants in the United States producing commercial shale oil. Predictions are that the output products will be close in characteristics and performance to those made from petroleum crudes.

Table 16 lists properties of a residual fuel oil (DMF) from one shale pilot operation and of a shale crude oil.¹¹ Table 17 lists ultimate analyses of oils derived from shales from a number of locations.¹² Properties will vary with the process used for extraction from the shale. The objective of all such processes is only to provide feedstock for refineries. In turn, the refineries' subsequent processing will also affect the properties.

If petroleum shortages occur, they will probably provide the economic impetus for completion of developments already begun for the mining, processing, and refining of oils from shale.

Table 16 Properties of Shale Oils¹¹

Property	DMF Residual	Crude
Ultimate analysis		
Carbon, % wt	86.18	84.6
Hydrogen, % wt	13.00	11.3
Nitrogen, % wt	0.24	2.08
Sulfur, % wt	0.51	0.63
Ash, % wt	0.003	0.026
Oxygen, % wt by difference	1.07	1.36
Conradson carbon residue, %	4.1	2.9
Asphaltene, %	0.036	1.33
Calcium, ppm	0.13	1.5
Iron, ppm	6.3	47.9
Manganese, ppm	0.06	0.17
Magnesium, ppm	—	5.40
Nickel, ppm	0.43	5.00
Sodium, ppm	0.09	11.71
Vanadium, ppm	0.1	0.3
Flash point, °F	182	250
Pour point, °F	40	80
API gravity at 60°F	33.1	20.3
Viscosity, SSU at 140°F	36.1	97
SSU at 210°F	30.7	44.1
Gross heating value, Btu/lb	19,430	18,290
Net heating value, Btu/lb	18,240	17,260

Table 17 Elemental Content of Shale Oils, % wt¹²

Source	Carbon, C			Hydrogen, H			Nitrogen, N			Sulfur, S			Oxygen, O		
	Min	Avg	Max	Min	Avg	Max	Min	Avg	Max	Min	Avg	Max	Min	Avg	Max
Colorado	83.5	84.2	84.9	10.9	11.3	11.7	1.6	1.8	1.9	0.7	1.2	1.7	1.3	1.7	2.1
Utah	84.1	84.7	85.2	10.9	11.5	12.0	1.6	1.8	2.0	0.5	0.7	0.8	1.2	1.6	2.0
Wyoming	81.3	83.1	84.4	11.2	11.7	12.2	1.4	1.8	2.2	0.4	1.0	1.5	1.7	2.0	2.3
Kentucky	83.6	84.4	85.2	9.6	10.2	10.7	1.0	1.3	1.6	1.4	1.9	2.4	1.8	2.3	2.7
Queensland	80.0	82.2	85.5	10.0	11.1	12.8	1.0	1.2	1.6	0.3	1.9	6.0	1.1	3.0	6.6
Australia (four locations)															
Brazil		85.3			11.2			0.9			1.1			1.5	
Karak, Jordan	77.6	78.3	79.0	9.4	9.7	9.9	0.5	0.7	0.8	9.3	10.0	10.6	0.9	1.4	1.9
Timahdit Morocco	79.5	80.0	80.4	9.7	9.8	9.9	1.2	1.4	1.6	6.7	7.1	7.4	1.8	2.0	2.2
Sweden	86.5	86.5	86.5	9.0	9.4	9.8	0.6	0.7	0.7	1.7	1.9	2.1	1.4	1.6	1.7

Table 18 Chemical and Physical Properties of Several Tar Sand Bitumens¹³

	Uinta Basin, Utah	Southeast Utah	Athabasca, Alberta	Trapper Canyon, WY ^a	South TX	Santa Rosa, NM ^a	Big Clifty, KY	Bellamy, MO
Carbon, % wt	85.3	84.3	82.5	82.4	—	85.6	82.4	86.7
Hydrogen, % wt	11.2	10.2	10.6	10.3	—	10.1	10.8	10.3
Nitrogen, % wt	0.96	0.51	0.44	0.54	0.36	0.22	0.64	0.10
Sulfur, % wt	0.49	4.46	4.86	5.52	~10	2.30	1.55	0.75
H/C ratio	1.56	1.44	1.53	1.49	1.34	1.41	1.56	1.42
Vanadium, ppm	23	151	196	91	85	25	198	—
Nickel, ppm	96	62	82	53	24	23	80	—
Carbon residue, % wt	10.9	19.6	13.7	14.8	24.5	22.1	16.7	—
Pour point, °F	125	95	75	125	180	—	85	—
API gravity	11.6	9.2	9.5	5.4	-2.0	5	8.7	10
Viscosities range from 50,000 to 600,000 SSF (100,000 to 1,300,000 cSt).								

^aOutcrop samples.

4 OILS FROM TAR SANDS

At the time that this is written, the only commercially practical operation for extracting oil from tar sands is at Athabaska, Alberta, Canada, using surface mining techniques. When petroleum supplies become short, economic impetus therefrom will push completion of developments already well under way for mining, processing, and refining of oils from tar sands.

Table 18 lists chemical and physical properties of several tar sand bitumens.¹³ Further refining will be necessary because of the high density, viscosity, and sulfur content of these oils.

Extensive deposits of tar sands are to be found around the globe, but most will have to be recovered by some in situ technique, fireflooding, or steam flooding. Yields tend to be small and properties vary with the recovery method, as illustrated in Table 19.¹³

Table 19 Elemental Composition of Bitumen and Oils Recovered from Tar Sands by Methods C and S^{a,13}

	Bitumen	Light Oil C ^b	Heavy Oil C 1–4 Mo.	Heavy Oil C 5–6 Mo.	Product Oil C	Product Oil S ^c
Carbon, % wt	86.0	86.7	86.1	86.7	86.6	85.9
Hydrogen, % wt	11.2	12.2	11.8	11.3	11.6	11.3
Nitrogen, % wt	0.93	0.16	0.82	0.66	0.82	1.17
Sulfur, % wt	0.45	0.30	0.39	0.33	0.43	0.42
Oxygen, % wt	1.42	0.64	0.89	1.01	0.55	1.21

^aThese percentages are site and project specific.

^bC = reverse-forward combustion.

^cS = steam flood.

Table 20 Orimulsion Fuel Characteristics

Density	63 lb/ft ³	
Apparent viscosity	41F/20 sec-1 — 700 mPa	
	86F/20 sec-1 — 450 mPa	
	158F/100 sec-1 — 105 mPa	
Flash point	266°F	
Pour point	32°F	
Higher heating value	12,683 Btu/lb	
Lower heating value	11,694 Btu/lb	
Weight analysis	Carbon	60%
	Hydrogen	7.5%
	Sulfur	2.7%
	Nitrogen	0.5%
	Oxygen	0.2%
	Ash	0.25%
	Water	30%
	Vanadium	300 ppm
	Sodium	70 ppm
	Magnesium	350 ppm

5 OIL–WATER EMULSIONS

Emulsions of oil have offered some promise of low fuel cost and alternate fuel supply for some time. The following excerpts from Ref. 14 provide introductory information on a water emulsion with an oil from the vicinity of the Orinoco River in Venezuela. It is being marketed as “Orimulsion” by Petroleos de Veneauels SA and Bitor America Corp of Boca Raton, Florida. It is a natural bitumen, like a liquid coal that has been emulsified with water to make it possible to extract it from the earth and to transport it.

Table 20 shows some of its properties and contents. Although its original sulfur content is high, the ash is low. A low C/H ratio promises less CO₂ emission. Because of handleability concerns, it will probably find use mostly in large steam generators.

REFERENCES

1. W. L. Nelson, *Petroleum Refinery Engineering*, McGraw-Hill, New York, 1968.
2. J. D. Gilchrist, *Fuels and Refractories*, Macmillan, New York, 1963.
3. R. J. Reed, *Combustion Handbook*, 3rd ed., Vol. 1. North American Manufacturing Co., Cleveland, OH, 1986.
4. *Standard Specification for Fuel Oils*, ANSI/ASTM D396, American Society for Testing and Materials, Philadelphia, PA, 1996.
5. *Standard Specification for Kerosene*, ANSI/ASTM D3699, American Society for Testing and Materials, Philadelphia, PA, 1996.
6. *Standard Specification for Aviation Turbine Fuels*, ANSI/ASTM D1655, American Society for Testing and Materials, Philadelphia, PA, 1996.
7. E. M. Shelton, *Diesel Oils*, DOE/BETC/PPS—81/5, U.S. Department of Energy, Washington, D.C., 1981.
8. E. M. Shelton, *Heating Oils*, DOE/BETC/PPS—80/4, U.S. Department of Energy, Washington, D.C., 1980.
9. E. M. Shelton, *Aviation Turbine Fuel*, DOE/BETC/PPS—80/2, Department of Energy, Washington, D.C., 1979.
10. *Standard Specification for Gas Turbine Fuel Oils*, ANSI/ASTM D2880, American Society for Testing and Materials, Philadelphia, PA, 1996.
11. *Kempe's Engineering Yearbook*, Morgan Grompium, London.
12. *Standard Specification for Diesel Fuel Oils*, ANSI/ASTM D975, American Society for Testing and Materials, Philadelphia, PA, 1996.
13. M. Heap et al., *The Influence of Fuel Characteristics on Nitrogen Oxide Formation—Bench Scale Studies*, Energy and Environmental Research Corp., Irvine, CA, 1979.
14. H. Tokairin and S. Morita, "Properties and Characterizations of Fischer-Assay-Retorted Oils from Major World Deposits," in *Synthetic Fuels from Oil Shale and Tar Sands*, Institute of Gas Technology, Chicago, IL, 1983.
15. K. P. Thomas et al., "Chemical and Physical Properties of Tar Sand Bitumens and Thermally Recovered Oils," in *Synthetic Fuels from Oil Shale and Tar Sands*, Institute of Gas Technology, Chicago, IL, 1983.
16. J. Makansi, "New Fuel Could Find Niche Between Oil, Coal," *POWER*, December 1991.

CHAPTER 20

COALS, LIGNITE, AND PEAT

James G. Keppeler
Progress Materials, Inc.
St. Petersburg, Florida

1 INTRODUCTION	703	4 PHYSICAL AND CHEMICAL PROPERTIES—DESCRIPTION AND TABLES OF SELECTED VALUES	709
1.1 Nature	703		
1.2 Reserves—Worldwide and United States	703		
1.3 Classifications	704		
2 CURRENT USES—HEAT, POWER, STEELMAKING, OTHER	707	5 BURNING CHARACTERISTICS	711
3 TYPES	707	6 ASH CHARACTERISTICS	713
		7 SAMPLING	715
		8 COAL CLEANING	716
		REFERENCES	718

1 INTRODUCTION

1.1 Nature

Coal is a dark brown to black sedimentary rock derived primarily from the unoxidized remains of carbon-bearing plant tissues. It is a complex, combustible mixture of organic, chemical, and mineral materials found in strata, or “seams,” in the earth, consisting of a wide variety of physical and chemical properties.

The principal types of coal, in order of metamorphic development, are lignite, subbituminous, bituminous, and anthracite. While not generally considered a coal, peat is the first development stage in the “coalification” process, in which there is a gradual increase in the carbon content of the fossil organic material and a concomitant reduction in oxygen.

Coal substance is composed primarily of carbon, hydrogen, and oxygen, with minor amounts of nitrogen and sulfur and varying amounts of moisture and mineral impurities.

1.2 Reserves—Worldwide and United States

According to the World Coal Study (see Ref. 1), the total geological resources of the world in “millions of tons of coal equivalent” (mtce) is 10,750,212, of which 662,932, or 6%, is submitted as “Technically and Economically Recoverable Resources.” Millions of tons of coal equivalent is based on the metric ton (2205 lb) with a heat content of 12,600 Btu/lb (7000 kcal/kg).

A summary of the percentage of technically and economically recoverable reserves and the percentage of total recoverable by country is shown in Table 1. As indicated in Table 1, the United States possesses over a quarter of the total recoverable reserves despite the low

Table 1 Geological Resources of Major Countries

	Percentage of Recoverable ^a of Geological Resources	Percentage of Total Recoverable Reserves
Australia	5.5	4.9
Canada	1.3	0.6
Peoples Republic of China	6.8	14.9
Federal Republic of Germany	13.9	5.2
India	15.3	1.9
Poland	42.6	9.0
Republic of South Africa	59.7	6.5
United Kingdom	23.7	6.8
United States	6.5	25.2
Soviet Union	2.2	16.6
Other countries	24.3	8.4
		100.0

^aTechnically and economically recoverable reserves. Percentage indicated is based on total geological resources reported by country.

Source: From Ref. 1.

percentage of recovery compared to other countries. The interpretation of “technical and economic” recovery is subject to considerable variation and also to modification, as technical development and changing economic conditions dictate. Also, there are significant differences in density and heating values in various coals, and, therefore, the mtce definition should be kept in perspective.

In 1977, the world coal production was approximately 2450 mtce,¹ or about $1/270$ th of the recoverable reserves. According to the U.S. Geological Survey, the remaining U.S. coal reserves total almost 4000 billion tons,² with overburden to 6000 ft in seams of 14 in. or more for bituminous and anthracite and in seams of $2\frac{1}{2}$ ft or more for subbituminous coal and lignite. The U.S. Bureau of Mines (USBM) and U.S. Geological Survey (USGS) have further defined “reserve base” to provide a better indication of the technically and economically minable reserves, where a higher degree of identification and engineering evaluation is available.

A summary of the reserve base of U.S. coal is provided in Table 2.³

1.3 Classifications

Coals are classified by “rank,” according to their degree of metamorphism, or progressive alteration, in the natural series from lignite to anthracite. Perhaps the most widely accepted standard for classification of coals is the American Society for Testing and Materials (ASTM) standard D388, which ranks coals according to fixed carbon and calorific value (expressed in Btu/lb) calculated to the mineral-matter-free basis. Higher rank coals are classified according to fixed carbon on the dry basis; the lower rank coals are classed according to calorific value on the moist basis. Agglomerating character is used to differentiate between certain adjacent groups. Table 3 shows the classification requirements.

Agglomerating character is determined by examination of the residue left after the volatile determination. If the residue supports a 500-g weight without pulverizing or shows a swelling or cell structure, it is said to be “agglomerating.”

The mineral-matter-free basis is used for ASTM rankings, and formulas to convert Btu, fixed carbon, and volatile matter from “as-received” bases are provided. The Parr

Table 2 Demonstrated Reserve Base^a of Coal in the United States in January 1980 by Rank (Millions of Short Tons)

State ^b	Anthracite	Bituminous	Subbituminous	Lignite	Total ^c
Alabama ^d	—	3,916.8	—	1,083.0	4,999.8
Alaska	—	697.5	5,443.0	14.0	6,154.5
Arizona	—	410.0	—	—	410.0
Arkansas	96.4	288.7	—	25.7	410.7
Colorado ^d	25.5	9,086.1	3,979.9	4,189.9	17,281.3
Georgia	—	3.6	—	—	3.6
Idaho	—	4.4	—	—	4.4
Illinois ^d	—	67,606.0	—	—	67,606.0
Indiana	—	10,586.1	—	—	10,586.1
Iowa	—	2,197.1	—	—	2,197.7
Kansas	—	993.8	—	—	993.8
Kentucky					
Eastern ^d	—	12,927.5	—	—	12,927.5
Western	—	21,074.4	—	—	21,074.4
Maryland	—	822.4	—	—	822.4
Michigan ^d	—	127.7	—	—	127.7
Missouri	—	6,069.1	—	—	6,069.1
Montana	—	1,385.4	103,277.4	15,765.2	120,428.0
New Mexico ^d	2.3	1,835.7	2,683.4	—	4,521.4
North Carolina	—	10.7	—	—	10.7
North Dakota	—	—	—	9,952.3	9,952.3
Ohio ^d	—	19,056.1	—	—	19,056.1
Oklahoma	—	1,637.8	—	—	1,637.8
Oregon	—	—	17.5	—	17.5
Pennsylvania	7,092.0	23,188.8	—	—	30,280.8
South Dakota	—	—	—	366.1	366.1
Tennessee ^d	—	983.7	—	—	983.7
Texas ^d	—	—	—	12,659.7	12,659.7
Utah ^d	—	6,476.5	1.1	—	6,477.6
Virginia	125.5	3,345.9	—	—	3,471.4
Washington ^d	—	303.7	1,169.4	8.1	1,481.3
West Virginia	—	39,776.2	—	—	39,776.2
Wyoming ^d	—	4,460.5	65,463.5	—	69,924.0
Total ^c	7,341.7	239,272.9	182,035.0	44,063.9	472,713.6

^aIncludes measured and indicated resource categories defined by USBM and USGS and represents 100% of the coal in place.

^bSome coal-bearing states where data are not sufficiently detailed or where reserves are not currently economically recoverable.

^cData may not add to totals due to rounding.

^dData not completely reconciled with demonstrated reserve base data.

equations 1–3 are appropriate in case of litigation, and the approximation equations 4–6 are otherwise acceptable:

Parr formulas

$$\text{Dry, MM-Free FC} = \frac{\text{FC} - 0.15S}{100 - (M + 1.08A + 0.55S)} \times 100 \quad (1)$$

$$\text{Dry, MM-Free VM} = 100 - \text{Dry, MM-Free FC} \quad (2)$$

$$\text{Moist, MM-Free Btu} = \frac{\text{Btu} - 50S}{100 - (1.08A + 0.55S)} \times 100 \quad (3)$$

Table 3 ASTM (D388) Classification of Coals by Rank^a

Class	Group	Fixed Carbon Limits, Percent (Dry, Mineral-Matter-Free Basis)		Volatile Matter Limits, Percent (Dry, Mineral-Matter-Free Basis)		Calorific Value Limits, Btu/lb Moist, Mineral-Matter-Free Basis)		Agglomerating Character
		Equal to or Less Than	Greater Than	Equal to or Less Than	Greater Than	Equal to or Less Than	Greater Than	
I Anthracitic	1. Metaanthracite	98	—	—	2	—	—	Nonagglomerating
	2. Anthracite	92	98	2	8	—	—	
	3. Semianthracite ^c	86	92	8	14	—	—	
II Bituminous	1. Low-volatile bituminous	78	86	14	22	—	—	Commonly agglomerating ^e
	2. Medium-volatile bituminous	69	78	22	31	—	—	
III Subbituminous	3. High-volatile A bituminous	—	69	31	—	14,000 ^d	—	Agglomerating
	4. High-volatile B bituminous	—	—	—	—	13,000 ^d	14,000	
	5. High-volatile C bituminous	—	—	—	—	11,500	13,000	
	1. Subbituminous A	—	—	—	—	10,500	11,500	
	2. Subbituminous B	—	—	—	—	10,500	10,500	
IV Lignite	3. Subbituminous C	—	—	—	—	9,500	10,500	Agglomerating
	1. Lignite A	—	—	—	—	8,300	9,500	
	2. Lignite B	—	—	—	—	6,300	8,300	6,300

^aThis classification does not include a few coals, principally nonbanded varieties, that have unusual physical and chemical properties and that come within the limits of fixed carbon or calorific value of the high-volatile bituminous and subbituminous ranks. All of these coals either contain less than 48% dry, mineral-matter-free fixed carbon or have more than 15,500 moist, mineral-matter-free British thermal units per pound.

^bMoist refers to coal containing its natural inherent moisture but not including visible water on the surface of the coal.

^cIf agglomerating, classify in the low-volatile group of the bituminous class.

^dCoals having 69% or more fixed carbon on the dry, mineral-matter-free basis shall be classified according to fixed carbon, regardless of calorific value.

^eIt is recognized that there may be nonagglomerating varieties in these groups of the bituminous class and that there are notable exceptions in the high-volatile C bituminous group.

Approximation formulas

$$\text{Dry, MM-Free FC} = \frac{\text{FC}}{100 - (M + 1.1A + 0.1S)} \times 100 \quad (4)$$

$$\text{Dry, MM-Free VM} = 100 - \text{Dry, MM-Free FC} \quad (5)$$

$$\text{Moist, MM-Free Btu} = \frac{\text{Btu}}{100 - (1.1A + 0.1S)} \times 100 \quad (6)$$

where MM = mineral matter
 Btu = British thermal unit
 FC = percentage of fixed carbon
 VM = percentage of volatile matter
 A = percentage of ash
 S = percentage of sulfur

Other classifications of coal include the International Classification of Hard Coals, the International Classification of Brown Coals, the “Lord” value based on heating value with ash, sulfur, and moisture removed, and the Perch and Russell Ratio, based on the ratio of moist, MM-free Btu to dry, MM-free VM.

2 CURRENT USES—HEAT, POWER, STEELMAKING, OTHER

According to statistics compiled for the 1996 *Keystone Coal Industry Manual*,² the primary use of coals produced in the United States in recent years has been for electric utilities, comprising almost 90% of the 926 million tons consumed in the United States in 1993. Industry accounted for about 8% of the consumption during that year in a variety of Standard Industrial Classification (SIC) Codes, replacing the manufacturing of coke (now about 3%) as the second largest coal market from the recent past. Industrial users typically consume coal for making process steam as well as in open-fired applications, such as in kilns and process heaters.

It should be noted that the demand for coal for coking purposes was greater than the demand for coal for utility use in the 1950s and has steadily declined owing to more efficient steelmaking, greater use of scrap metal, increased use of substitute fuels in blast furnaces, and other factors. The production of coke from coal is accomplished by heating certain coals in the absence of air to drive off volatile matter and moisture. To provide a suitable by-product coke, the parent coal must possess quality parameters of low ash content, low sulfur content, low coking pressure, and high coke strength. By-product coking ovens, the most predominant, are so named for their ability to recapture otherwise wasted by-products driven off by heating the coal, such as coke oven gas, coal-tar, ammonia, oil, and useful chemicals. Beehive ovens, named for their shape and configuration, are also used, albeit much less extensively, in the production of coke.

3 TYPES

Anthracite is the least abundant of U.S. coal forms. Sometimes referred to as “hard” coal, it is shiny black or dark silver-gray and relatively compact. Inasmuch as it is the most advanced form in the coalification process, it is sometimes found deeper in the earth than bituminous. As indicated earlier, the ASTM definition puts upper and lower bounds of dry, mineral-matter-free fixed carbon percent at 98 and 86%, respectively, which limits volatile matter to not more than 14%. Combustion in turn is characterized by higher ignition temperatures and longer burnout times than bituminous coals.

Excepting some semianthracites that have a granular appearance, they have a consolidated appearance, unlike the layers seen in many bituminous coals. Typical Hardgrove grindability index ranges from 20 to 60 and specific gravity typically ranges 1.55 ± 0.10 .

Anthracite coals can be found in Arkansas, Colorado, Pennsylvania, Massachusetts, New Mexico, Rhode Island, Virginia, and Washington, although by far the most abundant reserves are found in Pennsylvania.

Bituminous coal is by far the most plentiful and utilized coal form and within the ASTM definitions includes low-, medium-, and high-volatile subgroups. Sometimes referred to as “soft” coal, it is named after the word *bitumen*, based on its general tendency to form a sticky mass on heating.

At a lower stage of development in the coalification process, carbon content is less than the anthracites, from a maximum of 86% to less than 69% on a dry, mineral-matter-free basis. Volatile matter, at a minimum of 14% on this basis, is greater than the anthracites, and, as a result, combustion in pulverized form is somewhat easier for bituminous coals. Production of gas is also enhanced by their higher volatility.

The tendency of bituminous coals to produce a cohesive mass on heating lends them to coke applications. Dry, mineral-matter-free oxygen content generally ranges from 5 to 10%, compared to a value as low as 1% for anthracite. They are commonly banded with layers differing in luster.

The low-volatile bituminous coals are grainier and more subject to size reduction in handling. The medium-volatile bituminous coals are sometimes distinctly layered and sometimes only faintly layered and appearing homogeneous. Handling may or may not have a significant impact on size reduction. The high-volatile coals (A, B, and C) are relatively hard and less sensitive to size reduction from handling than low- or medium-volatile bituminous.

Subbituminous coals, like anthracite and lignite, are generally noncaking. “Caking” refers to fusion of coal particles after heating in a furnace, as opposed to “coking,” which refers to the ability of a coal to make a good coke, suitable for metallurgical purposes.

Oxygen content, on a dry, mineral-matter-free basis, is typically 10–20%.

Brownish black to black in color, this type coal is typically smooth in appearance with an absence of layers.

Although high in inherent moisture, these fuels are often dusty in handling and appear much like drying mud as they disintegrate on sufficiently long exposure to air.

The Healy coal bed in Wyoming has the thickest seam of coal in the United States at 220 ft. It is subbituminous, with an average heating value of 7884 Btu/lb, 28.5% moisture, 30% volatile matter, 33.9% fixed carbon, and 0.6% sulfur. Reported strippable reserves of this seam are approximately 11 billion tons.²

Lignites, sometimes referred to as “brown coal,” often retain a woodlike or laminar structure in which wood fiber remnants may be visible. Like subbituminous coals, they are high in seam moisture, up to 50% or more, and also disintegrate on sufficiently long exposure to air.

Both subbituminous coals and lignites are more susceptible than higher rank coals to storage, shipping, and handling problems, owing to their tendency for slacking (disintegration) and spontaneous ignition. During the slacking, a higher rate of moisture loss at the surface than at the interior may cause higher rates and stresses at the outside of the particles, and cracks may occur with an audible noise.

Peat is decaying vegetable matter formed in wetlands; it is the first stage of metamorphosis in the coalification process. Development can be generally described as anaerobic, often in poorly drained flatlands or former lake beds. In the seam, peat moisture may be 90% or higher, and, therefore, the peat is typically “mined” and stacked for drainage or otherwise dewatered prior to consideration as a fuel. Because of its low bulk density at about 15 lb/ft³ and low heating value at about 6000 Btu/lb (both values at 35% moisture), transportation distances must be short to make peat an attractive energy option.

In addition, it can be a very difficult material to handle, as it can arch in bins, forming internal friction angles in excess of 70°.

Chemically, peat is very reactive and ignites easily. It may be easily ground, and unconsolidated peat may create dusting problems.

4 PHYSICAL AND CHEMICAL PROPERTIES—DESCRIPTION AND TABLES OF SELECTED VALUES

There are a number of tests, qualitative and quantitative, used to provide information on coals; these tests will be of help to the user and/or equipment designer. Among the more common tests are the following, with reference to the applicable ASTM test procedure.

A “*Proximate*” analysis (D3172) includes moisture, “volatile matter,” “fixed carbon,” and ash as its components.

Percent moisture (D3173) is determined by measuring the weight loss of a prepared sample (D2013) when heated to between 219°F (104°C) and 230°F (110°C) under rigidly controlled conditions. The results of this test can be used to calculate other analytical results to a dry basis. The moisture is referred to as “residual” and must be added to moisture losses incurred in sample preparation, called “air-dry losses” in order to calculate other analytical results to an “as-received” basis. The method which combines both residual and air-dry moisture is D3302.

Percent volatile matter (D3175) is determined by establishing the weight loss of a prepared sample (D2013) resulting from heating to 1740°F (950°C) in the absence of air under controlled conditions. This weight loss is corrected for residual moisture and is used for an indication of burning properties, coke yield, and classification by rank.

Percent ash (D3174) is determined by weighing the residue remaining after burning a prepared sample under rigidly controlled conditions. Combustion is in an oxidizing atmosphere and is completed for coal samples at 1290–1380°F (700–750°C).

Fixed carbon is a calculated value making up the fourth and final component of a proximate analysis. It is determined by subtracting the volatile, moisture, and ash percentages from 100.

Also generally included with a proximate analysis are calorific value and sulfur determinations.

B *Calorific value*, Btu/lb (J/g, cal/g), is most commonly determined (D2015) in an “adiabatic bomb calorimeter” but is also covered by another method (D3286), which uses an “isothermal jacket bomb calorimeter.” The values determined by this method are called gross or high heating values and include the latent heat of water vapor in the products of combustion.

C *Sulfur* is determined by one of three methods provided by ASTM, all covered by D3177: the Eschka method, the bomb washing method, and a high-temperature combustion method.

The Eschka method requires that a sample be ignited with an “Eschka mixture” and sulfur be precipitated from the resulting solution as BaSO₄ and filtered, ashed, and weighed.

The bomb wash method requires use of the oxygen-bomb calorimeter residue, and sulfur is precipitated as BaSO₄ and processed as in the Eschka method.

The high-temperature combustion method produces sulfur oxides from burning of a sample at 2460°F (1350°C) which are absorbed in a hydrogen peroxide solution for analysis. This is the most rapid of the three types of analysis.

D *Sulfur forms* include sulfate, organic, pyritic, and, rarely, elemental sulfur. A method used to quantify sulfate, pyritic sulfur, and organic sulfur is D2492. The resulting data are sometimes used to provide a first indication of the maximum amount of sulfur potentially removable by mechanical cleaning.

E *Ultimate analysis* (D3176) includes total carbon, hydrogen, nitrogen, oxygen, sulfur, and ash. These data are commonly used to perform combustion calculations to estimate combustion air requirements, products of combustion, and heat losses such as incurred by formation of water vapor by hydrogen in the coal.

Chlorine (D2361) and phosphorus (D2795) are sometimes requested with ultimate analyses but are not technically a part of D3176.

F *Ash mineral analysis* (D2795) includes the oxides of silica (SiO_2), alumina (Al_2O_3), iron (Fe_2O_3), titanium (TiO_2), phosphorus (P_2O_5), calcium (CaO), magnesium (MgO), sodium (Na_2O), and potassium (K_2O).

These data are used to provide several indications concerning ash slagging or fouling tendencies, abrasion potential, electrostatic precipitator operation, and sulfur absorption potentiation.

See Section 8 for further details.

G *Grindability* (D409) is determined most commonly by the Hardgrove method to provide an indication of the relative ease of pulverization or grindability, compared to “standard” coals having grindability indexes of 40, 60, 80, and 110. As the index increases, pulverization becomes easier, that is, an index of 40 indicates a relatively hard coal; an index of 100 indicates a relatively soft coal.

Standard coals may be obtained from the USBM.

A word of caution is given: Grindability may change with ash content, moisture content, temperature, and other properties.

H *Free swelling index* (D720), also referred to as a “coke-button” test, provides a relative index (1–9) of the swelling properties of a coal. A sample is burned in a covered crucible, and the resulting index increases as the swelling increases, determined by comparison of the button formed with standard profiles.

I *Ash fusion temperatures* (D1857) are determined from triangular-core-shaped ash samples in a reducing atmosphere and/or in an oxidizing atmosphere. Visual observations are recorded of temperatures at which the core begins to deform, called “initial deformation”; where height equals width, called “softening”; where height equals one-half width, called “hemispherical”; and where the ash is fluid.

The hemispherical temperature is often referred to as the “ash fusion temperature.”

While not definitive, these tests provide a rough indication of the slagging tendency of coal ash.

Analysis of petrographic constituents in coals has been used to some extent in qualitative and semiquantitative analysis of some coals, most importantly in the coking coal industry. It is the application of macroscopic and microscopic techniques to identify maceral components related to the plant origins of the coal. The macerals of interest are vitrinite, exinite, resinite, micrinite, semifusinite, and fusinite. A technique to measure reflectance of a prepared sample of coal and calculate the volume percentages of macerals is included in ASTM standard D2799.

Table 4 shows selected analyses of coal seams for reference.

Table 4 Selected Values—Coal and Peat Quality

Parameter	East Kentucky, Skyline Seam (Washed)	Pennsylvania, Pittsburgh 8 Seam (Washed)	Illinois, Harrisburg 5 (Washed)	Wyoming, Powder River Basin (Raw)	Florida Peat, Sumter County	
					In situ	Dry
Moisture % (total)	8.00	6.5	13.2	25.92	86.70	—
Ash %	6.48	6.5	7.1	6.00	0.54	4.08
Sulfur %	0.82	1.62	1.28	0.25	0.10	0.77
Volatile %	36.69	34.40	30.6	31.27	8.74	65.73
Grindability (HGI)	45	55	54	57	36	69 ^a
Calorific value (Btu/lb, as received)	12,500	13,100	11,700	8,500	1,503	11,297
Fixed carbon	48.83	52.60	49.1	37.23	4.02	30.19
Ash minerals						
SiO ₂	50.87	50.10	48.90	32.02	58.29	
Al ₂ O ₂	33.10	24.60	25.50	15.88	19.50	
TiO ₂	2.56	1.20	1.10	1.13	1.05	
CaO	2.57	2.2	2.90	23.80	1.95	
K ₂ O	1.60	1.59	3.13	0.45	1.11	
MgO	0.80	0.70	1.60	5.73	0.94	
Na ₂ O	0.53	0.35	1.02	1.27	0.40	
P ₂ O ₅	0.53	0.38	0.67	1.41	0.09	
Fe ₂ O ₃	5.18	16.20	12.20	5.84	14.32	
SO ₃	1.42	1.31	1.96	11.35	2.19	
Undetermined	0.84	1.37	1.02	1.12	0.16	
Ash	7.04	7.0	8.23	7.53	4.08	
Hydrogen	5.31	5.03	4.95	4.80	4.59	
Carbon	75.38	78.40	76.57	69.11	69.26	
Nitrogen	1.38	1.39	1.35	0.97	1.67	
Sulfur	0.89	1.73	1.47	0.34	0.77	
Oxygen (by difference)	9.95	6.35	7.03	17.24	19.33	
Chlorine	0.05	0.10	0.40	0.01	0.30	
Ash Fusion						
Temperatures (°F)						
Initial deformation (reducing)	2800+	2350	2240	2204	1950	
Softening ($H = W$) (reducing)	2800+	2460	2450	2226	2010	
Hemispherical ($H = \frac{1}{2}W$) (reducing)	2800+	2520	2500	2250	2060	
Fluid (reducing)	2800+	2580	2700+	2302	2100	

^aAt 9% H₂O.

5 BURNING CHARACTERISTICS

The ultimate analysis, described in the previous section, provides the data required to conduct fundamental studies of the air required for stoichiometric combustion, the volumetric and weight amounts of combustion gases produced, and the theoretical boiler efficiencies. These data assist the designer in such matters as furnace and auxiliary equipment sizing. Among

the items of concern are draft equipment for supplying combustion air requirements, drying and transporting coal to the burners and exhausting the products of combustion, mass flow and velocity in convection passes for heat transfer and erosion considerations, and pollution control equipment sizing.

The addition of excess air must be considered for complete combustion and perhaps minimization of ash slagging in some cases. It is not uncommon to apply 25% excess air or more to allow operational flexibility.

As rank decreases, there is generally an increase in oxygen content in the fuel, which will provide a significant portion of the combustion air requirements.

The theoretical weight, in pounds, of combustion air required per pound of fuel for a stoichiometric condition is given by

$$11.53C + 34.34 \left(H_2 - \frac{1}{8}O_2 \right) + 4.29S \quad (7)$$

where C, H₂, O₂, and S are percentage weight constituents in the ultimate analysis.

The resulting products of combustion, again at a stoichiometric condition and complete combustion, are

$$CO_2 = 3.66C \quad (8)$$

$$H_2O = 8.94H_2 + H_2O \text{ (wt\% } H_2O \text{ in fuel)} \quad (9)$$

$$SO_2 = 2.00S \quad (10)$$

$$N_2 = 8.86C + 26.41 \left(H_2 - \frac{1}{8}O_2 \right) + 3.29S + N_2 \text{ (wt\% nitrogen in fuel)} \quad (11)$$

The combustion characteristics of various ranks of coal can be seen in Fig. 1, showing “burning profiles” obtained by thermal gravimetric analysis. As is apparent from this figure, ignition of lower rank coals occurs at a lower temperature and combustion proceeds at a more rapid rate than higher rank coals. This information is, of course, highly useful to the design engineer in determination of the size and configuration of combustion equipment.

The predominant firing technique for combustion of coal is in a pulverized form. To enhance ignition, promote complete combustion, and, in some cases, mitigate the effects of large particles on slagging and particulate capture, guidelines are generally given by the boiler manufacturer for pulverizer output (burner input).

Typical guidelines are as follows:

Coal Class/ Group	Percentage Passing a 200-mesh Sieve	Percentage Retained on a x 50-mesh Sieve	Allowable Coal/Air Temperature (°F)
Anthracite	80	2.0	200
Low-volatile bituminous	70–75	2.0	180
High-volatile bituminous A	70–75	2.0	170
High-volatile bituminous C	65–72	2.0	150–160
Lignite	60–70	2.0	110–140

These guidelines may vary for different manufacturers, ash contents, and equipment applications and, of course, the manufacturer should be consulted for fineness and temperature recommendations.

The sieve designations of 200 and 50 refer to U.S. standard sieves. The 200-mesh sieve has 200 openings per linear inch, or 40,000 per square inch. The ASTM designations for these sieves are 75 and 300 μm, respectively.

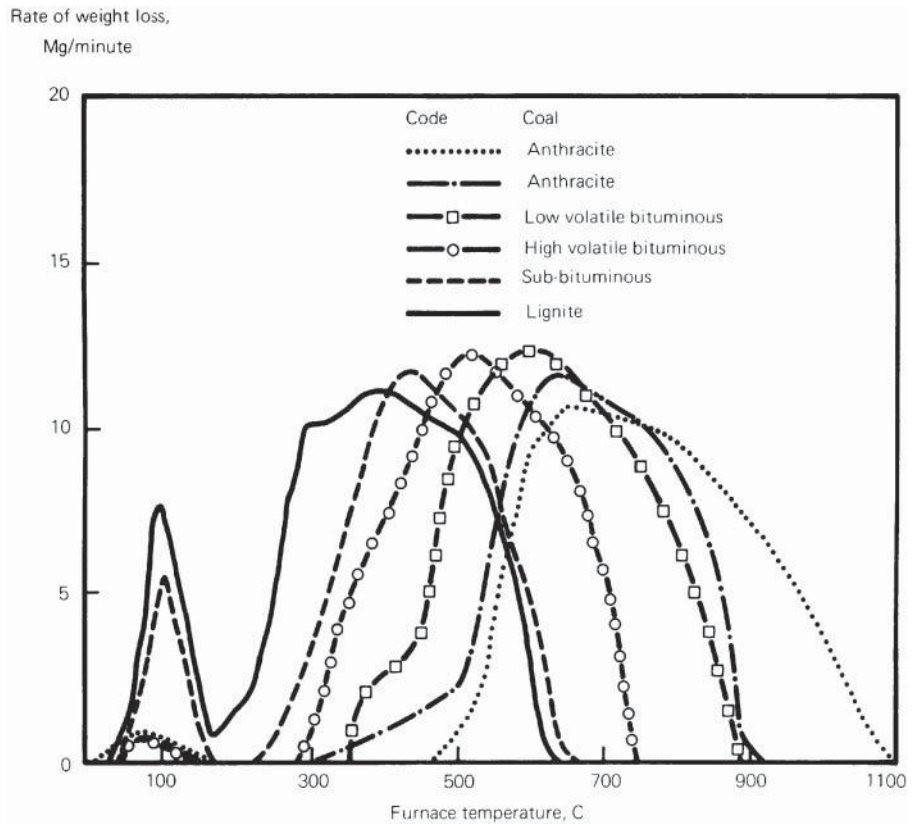


Figure 1 Comparison of burning profiles for coals of different rank. Courtesy of The Babcock and Wilcox Company.

Finally, agglomerating character may also have an influence on the fineness requirements, since this property might inhibit complete combustion.

6 ASH CHARACTERISTICS

Ash is an inert residue remaining after the combustion of coal and can result in significant challenges for designers and operators of the combustion, ash handling, and pollution control equipment. The quantity of ash in the coal varies widely from as little as 6% or less to more than 30% by weight. Additionally, diverse physical and chemical properties of ashes can pose substantial problems, with slagging, abrasion, and fouling of boilers. Electrostatic precipitators, used for pollution control, can experience material changes in collection efficiency depending on the mineral constituents of the ash.

“Slagging” is a term that generally refers to the formation of high-temperature fused ash deposits on furnace walls and other surfaces primarily exposed to radiant heat.

“Fouling” generally refers to high-temperature bonded ash deposits forming on convection tube banks, particularly superheat and reheat tubes.

Indication of ash-slagging tendencies can be measured by tests such as viscosity-temperature tests or by ash-softening tests. In addition, there are many empirical equations that are used to provide information as to the likelihood of slagging and fouling problems.

ASTM standard D1857 is the most common test used for slagging indication. In this test, ash samples are prepared as triangular cones and then are heated at a specified rate. Observations are then made and recorded of temperatures at prescribed stages of ash deformation, called initial deformation, softening temperature, hemispherical temperature, and fluid temperature. These tests are conducted in reducing and/or oxidizing atmospheres.

Another method used, although far more costly, involves measurement of the torque required to rotate a platinum bob suspended in molten slag. A viscosity–temperature relationship is established as a result of this test, which is also conducted in reducing and/or oxidizing atmospheres. A slag is generally considered liquid when its viscosity is below 250 poise, although tapping from a boiler may require a viscosity of 50–100 poise. It is plastic when its viscosity is between 250 and 10,000 poise. It is in this region where removal of the slag is most troublesome.

Ash mineral analyses are used to calculate empirical indicators of slagging problems. In these analyses are included metals reported as equivalent oxide weight percentages of silica, alumina, iron, calcium, magnesium, sodium, potassium, titania, phosphorus, and sulfur, as follows:



Some ratios calculated using these data are as follows:

Base: Acid Ratio, B/A

$$\frac{B}{A} = \frac{\text{Base}}{\text{Acid}} = \frac{\text{Fe}_2\text{O}_3 + \text{CaO} + \text{MgO} + \text{Na}_2\text{O} + \text{K}_2\text{O}}{\text{SiO}_2 + \text{Al}_2\text{O}_3 + \text{TiO}_2}$$

It has been reported⁴ that a base/acid ratio in the range of 0.4–0.7 results typically in low ash fusibility temperatures and, hence, more slagging problems.

Slagging Factor, R_s

$$R_s = B/A \times \%\text{sulfur, dry coal basis}$$

It has been reported⁵ that coals with bituminous-type ashes exhibit a high slagging potential with a slagging factor above 2 and severe slagging potential with a slagging factor of more than 2.6. Bituminous-type ash refers to those ashes where iron oxide percentage is greater than calcium *plus* magnesium oxide.

Silica/Alumina Ratio

$$\frac{\text{Silica}}{\text{Alumina}} = \frac{\text{SiO}_2}{\text{Al}_2\text{O}_3}$$

It has been reported⁴ that the silica in ash is more likely to form lower melting point compounds than is alumina and, for two coals having the same base/acid ratio, the coal with a higher silica/alumina ratio should result in lower fusibility temperatures. However, it has also been reported⁶ that for low base/acid ratios the opposite is true.

Iron/Calcium Ratio

$$\frac{\text{Iron}}{\text{Dolomite}} = \frac{\text{Fe}_2\text{O}_3}{\text{CaO} + \text{MgO}}$$

This ratio and its use are essentially the same as the iron/calcium ratio.

Silica Percentage (SP)

$$SP = \frac{\text{SiO}_2 \times 100}{\text{SiO}_2 + \text{Fe}_2\text{O}_3 + \text{CaO} + \text{MgO}}$$

This parameter has been correlated with ash viscosity. As silica ratio increases, the viscosity of slag increases. Graphical methods⁶ are used in conjunction with this parameter to estimate the T_{250} temperature—the temperature where the ash would

have a viscosity of 250 poise. Where the acidic content is less than 60% and the ash is lignitic, the *dolomite percentage* (*DP*) is used in preference to the silica percentage along with graphs to estimate the T_{250} :

$$DP = \frac{(\text{CaO} + \text{MgO}) \times 100}{\text{Fe}_2\text{O}_3 + \text{CaO} + \text{MgO} + \text{Na}_2\text{O} + \text{K}_2\text{O}}$$

where the sum of the basic and acidic components are adjusted, if necessary, to equal 100%. For bituminous ash or lignitic-type ash having acidic content above 60%, the base/acid ratio is used in conjunction with yet another graph.

Fouling Factor (R_F)

$$R_F = \text{Acid base} \times \% \text{Na}_2 \text{ (bituminous ash)}$$

or

$$R_F = \% \text{Na}_2\text{O (lignitic ash)}$$

For bituminous ash, the fouling factor⁷ is “low” for values less than 0.1, “medium” for values between 0.1 and 0.25, “high” for values between 0.25 and 0.7, and “severe” for values above 0.7. For lignitic-type ash, the percentage of sodium is used, and low, medium, and high values are <3.0, 3.0–6.0, and >6.0, respectively.

The basis for these factors is that sodium is the most important single factor in ash fouling, volatilizing in the furnace and subsequently condensing and sintering ash deposits in cooler sections.

Chlorine has also been used as an indicator of fouling tendency of eastern-type coals. If chlorine, from the ultimate analysis, is less than 0.15%, the fouling potential is low; if between 0.15 and 0.3, it has a medium fouling potential; and if above 0.3, its fouling potential is high.⁴

Ash resistivity can be predicted from ash mineral and coal ultimate analyses, according to a method described by Bickelhaupt.⁸ Electrostatic precipitator sizing and/or performance can be estimated using the calculated resistivity. For further information, the reader is referred to Ref. 8.

7 SAMPLING

Coals are by nature heterogeneous and, as a result, obtaining a representative sample can be a formidable task. Its quality parameters such as ash, moisture, and calorific value can vary considerably from seam to seam and even within the same seam. Acquisition of accurate data to define the nature and ranges of these values adequately is further compounded by the effects of size gradation, sample preparation, and analysis accuracy.

Inasmuch as these data are used for such purposes as pricing, control of the operations in mines, and preparation plants, determination of power plant efficiency, estimation of material handling and storage requirements for the coal and its by-products, and in some cases for determination of compliance with environmental limitations, it is important that samples be taken, prepared, and analyzed in accordance with good practice.

To attempt to minimize significant errors in sampling, ASTM D2234 was developed as a standard method for the collection of a gross sample of coal and D2013 for preparation of the samples collected for analysis. It applies to lot sizes up to 10,000 tons (9080 mg) per gross sample and is intended to provide an accuracy of $\pm 1/10$ th of the average ash content in 95 of 100 determinations.

The number and weight of increments of sample comprising the gross sample to represent the lot, or consignment, are specified for nominal top sizes of $5/8$ in. (16 mm), 2 in. (50 mm), and 6 in. (150 mm) for raw coal or mechanically cleaned coal. Conditions of collection include samples taken from a stopped conveyor belt (the most desirable), full and partial stream cuts from moving coal consignments, and stationary samples.

One recommendation made in this procedure and worth special emphasis is that the samples be collected under the direct supervision of a person qualified by training and experience for this responsibility.

This method does not apply to the sampling of reserves in the ground, which is done by core drilling methods or channel sampling along outcrops as recommended by a geologist or mining engineer. It also does not apply to the sampling of coal slurries.

A special method (D197) was developed for the collection of samples of pulverized coals to measure size consistency or fineness, which are controlled to maintain proper combustion efficiency.

Sieve analyses using this method may be conducted on No. 16 (1.18 mm) through No. 200 (750 mm) sieves, although the sieves most often referred to for pulverizer and classifier performance are the No. 50, the No. 100, and the No. 200 sieves. The number refers to the quantity of openings per linear inch.

Results of these tests should plot as a straight line on a sieve distribution chart. A typical fineness objective, depending primarily on the combustion characteristics, might be for 70% of the fines to pass through a 200-mesh sieve and not more than 2% to be retained on the 50-mesh sieve.

D2013 covers the preparation of coal samples for analysis or, more specifically, the reduction and division of samples collected in accordance with D2234. A “referee” method and a “nonreferee” method are delineated, although the nonreferee method is the most commonly used. The referee method is used to evaluate equipment and the nonreferee method.

Depending on the amount of moisture and, therefore, the ability of the coal to pass freely through reduction equipment, samples are either predried in air drying ovens or on drying floors or are processed directly by reduction, air drying, and division. Weight losses are computed for each stage of air drying to provide data for determination of total moisture, in combination with D3173 or 3302 (see Section 6).

Samples must ultimately pass the No. 60 (250 mm) sieve (D3173) or the No. 8 (2.36 mm) sieve (D3302) prior to total moisture determination.

Care must be taken to adhere to this procedure, including the avoidance of moisture losses while awaiting preparation, excessive time in air drying, proper use of riffing or mechanical division equipment, and verification and maintenance of crushing equipment size consistency.

8 COAL CLEANING

Partial removal of impurities in coal such as ash and pyritic sulfur has been conducted since before 1900, although application and development have intensified during recent years owing to a number of factors, including the tightening of emissions standards, increasing use of lower quality seams, and increasing use of continuous mining machinery. Blending of two or more fuels to meet tight emissions standards, or other reasons, often requires that each of the fuels is of a consistent grade, which in turn may indicate some degree of coal cleaning.

Coal cleaning may be accomplished by physical or chemical means, although physical coal cleaning is by far the most predominant.

Primarily, physical processes rely on differences between the specific gravity of the coal and its impurities. Ash, clay, and pyritic sulfur have a higher specific gravity than that of coal. For example, bituminous coal typically has a specific gravity in the range 1.12–1.35, while pyrite’s specific gravity is between 4.8 and 5.2.

One physical process that does not benefit from specific gravity differences is froth flotation. It is only used for cleaning coal size fractions smaller than 28 mesh ($1/2$ mm). Basically the process requires coal fines to be agitated in a chamber with set amounts of air, water, and chemical reagents, which creates a froth. The coal particles are selectively attached to the froth

bubbles, which rise to the surface and are skimmed off, dewatered, and added to other clean coal fractions.

A second stage of froth flotation has been tested successfully at the pilot scale for some U.S. coals. This process returns the froth concentrate from the first stage to a bank of cells where a depressant is used to sink the coal and a xanthate flotation collector is used to selectively float pyrite.

The predominant commercial methods of coal cleaning use gravity separation by static and/or dynamic means. The extent and cost of cleaning naturally depends on the degree of end product quality desired, the controlling factors of which are primarily sulfur, heating value, and ash content.

Although dry means may be used for gravity separation, wet means are by far the more accepted and used techniques.

The first step in designing a preparation plant involves a careful study of the washability of the coal. "Float and sink" tests are run in a laboratory to provide data to be used for judging application and performance of cleaning equipment. In these tests the weight percentages and composition of materials are determined after subjecting the test coal to liquid baths of different specific gravities.

Pyritic sulfur and/or total sulfur percent, ash percent, and heating value are typically determined for both the float (called "yield") and sink (called "reject") fractions.

Commonly, the tests are conducted on three or more size meshes, such as 1 1/2 in. \times 0 mesh, 3/8 in. \times 100 mesh, and minus 14 mesh, and at three or more gravities, such as 1.30, 1.40, and 1.60. Percentage recovery of weight and heating value are reported along with other data on a cumulative basis for the float fractions. An example of this, taken from a USBM study⁹ of 455 coals is shown in Table 5.

Many coals have pyrite particles less than 1 μ m in size (0.00004 in.), which cannot be removed practically by mechanical means. Moreover, the cost of coal cleaning increases as the particle size decreases, as a general rule, and drying and handling problems become more difficult. Generally, coal is cleaned using particle sizes as large as practical to meet quality requirements.

Table 5 Cumulative Washability Data^a

Product	Recovery Weight	% Btu	Btu/lb	Ash %	Sulfur (%)		lb SO ₂ / MBtu
					Pyritic	Total	
<i>Sample Crushed to Pass 1 1/2 in.</i>							
Float—1.30	55.8	58.8	14,447	3.3	0.26	1.09	1.5
Float—1.40	90.3	93.8	14,239	4.7	0.46	1.33	1.9
Float—1.60	94.3	97.3	14,134	5.4	0.53	1.41	2.0
Total	100.0	100.0	13,703	8.3	0.80	1.67	2.4
<i>Sample Crushed to Pass 3/8 in.</i>							
Float—1.30	58.9	63.0	14,492	3.0	0.20	1.06	1.5
Float—1.40	88.6	93.2	14,253	4.6	0.37	1.26	1.8
Float—1.60	92.8	96.8	14,134	5.4	0.47	1.36	1.9
Total	100.0	100.0	13,554	9.3	0.77	1.64	2.4
<i>Sample Crushed to Pass 14 Mesh</i>							
Float—1.30	60.9	65.1	14,566	2.5	0.16	0.99	1.4
Float—1.40	88.7	93.1	14,298	4.3	0.24	1.19	1.7
Float—1.60	93.7	97.1	14,134	5.4	0.40	1.29	1.8
Total	100.0	100.0	13,628	8.8	0.83	1.72	2.5

^aState: Pennsylvania (bituminous); coal bed: Pittsburgh; county: Washington; raw coal moisture: 2.0%.

It is interesting to note that a 50- μm pyrite particle (0.002 in.) inside a 14-mesh coal particle (0.06 in.) does not materially affect the specific gravity of a pure coal particle of the same size.

Washability data are usually organized and plotted as a series of curves, including:

1. Cumulative float–ash, sulfur %
2. Cumulative sink ash %
3. Elementary ash % (not cumulative)
4. Percent recovery (weight) versus specific gravity

Types of gravity separation equipment include jigs, concentrating tables, water-only cyclones, dense-media vessels, and dense-media cyclones.

In jigs, the coal enters the vessel in sizes to 8 in. and larger and stratification of the coal and heavier particles occurs in a pulsating fluid. The bottom layer, primarily rock, ash, and pyrite, is stripped from the mixture and rejected. Coal, the top layer, is saved. A middle layer may also be collected and saved or rejected depending on quality.

Concentrating tables typically handle coals in the $\frac{3}{8}$ in. \times 0 or $\frac{1}{4}$ in. \times 0 range and use water cascading over a vibrating table tilted such that heavier particles travel to one end of the table while lighter particles, traveling more rapidly with the water, fall over the adjacent edge.

In “water-only” and dense-media cyclones, centrifugal force is used to separate the heavier particles from the lighter particles.

In heavy-media vessels, the specific gravity of the media is controlled typically in the range of 1.45–1.65. Particles floating are saved as clean coal, while those sinking are rejected. Specific gravity of the media is generally maintained by the amount of finely ground magnetite suspended in the water, as in heavy-media cyclones. Magnetite is recaptured in the preparation plant circuitry by means of magnetic separators.

Drying of cleaned coals depends on size. The larger sizes, $\frac{1}{4}$ or $\frac{3}{8}$ in. and larger, typically require little drying and might only be passed over vibrating screens prior to stockpiling. Smaller sizes, down to, say, 28 mesh, are commonly dried on stationary screens followed by centrifugal driers. Minus 28-mesh particles, the most difficult to dry, are processed in vibrating centrifuges, high-speed centrifugal driers, high-speed screens, or vacuum filters.

REFERENCES

1. C. L. Wilson, *Coal—Bridge to the Future*, Vol. 1, Report of the World Coal Study, Ballinger, Cambridge, MA, 1980.
2. *Keystone Coal Industry Manual*, McGraw-Hill, New York, 1996.
3. *1979/1980 Coal Data*, National Coal Association and U.S. DOE, Washington, DC, 1982.
4. J. G. Singer, *Combustion—Fossil Power Systems*, Combustion Engineering, Inc., Windsor, CT, 1981.
5. R. C. Attig and A. F. Duzy, *Coal Ash Deposition Studies and Application to Boiler Design*, Babcock & Wilcox, Atlanta, GA, 1969.
6. *Stream—Its Generation and Use*, Babcock & Wilcox, New York, 1992.
7. E. C. Winegartner, *Coal Fouling and Slagging Parameters*, Exxon Research and Engineering, Baytown, TX, 1974.
8. R. E. Bickelhaupt, *A Technique for Predicting Fly Ash Resistivity*, EPA 600/7-79-204, Southern Research Institute, Birmingham, AL, August 1979.
9. J. A. Cavallaro and A. W. Deubrouch, *Sulfur Reduction Potential of the Coals of the United States*, RI8118, U.S. Dept. of Interior, Washington, DC, 1976.

CHAPTER 21

CLEAN POWER GENERATION FROM COAL

James W. Butler and Prabir Basu

Dalhousie University

Halifax, Nova Scotia

1 INTRODUCTION	719	3.5 Magnetohydrodynamics	739
1.1 Coal	720	3.6 Gasification	740
1.2 Potential Pollutants from Coal	722	4 POSTCONVERSION CLEAN-UP	745
1.3 Motivation for Cleaner Energy from Coal	724	4.1 Particulates	745
1.4 Cleaner Energy from Coal	725	4.2 Gaseous Emissions	748
2 PRECONVERSION	726	4.3 Heavy Metals	753
2.1 Physical Cleaning	726	4.4 Solid Waste	754
2.2 Chemical Cleaning	728	5 CARBON DIOXIDE	754
2.3 Biological Cleaning	729	5.1 CO ₂ Capture	755
3 COAL CONVERSION AND IN SITU POLLUTION CONTROL	729	5.2 Transportation	759
3.1 Pulverized Coal Combustion	731	5.3 Sequestration and Utilization	760
3.2 Fluidized Bed Combustion	733	5.4 Cost Implications	761
3.3 Supercritical Boilers	738	6 CONCLUSION	762
3.4 Cyclone Combustion	739	REFERENCES	763

1 INTRODUCTION

Coal has consistently accounted for about 40% of the world's total electricity generating capacity since the early 1970s (Fig. 1), despite the steady growth of the total generation capacity.¹ There is increased concern over global warming and emissions of sulfur dioxide, nitrogen oxides, and mercury from coal, but the low cost of electricity from coal has made it a necessary evil for many industries competing in the global marketplace. The world surely deserves pollution-free cleaner energy, at a cost that society can bear. Oil and gas provide a cleaner and more efficient means to generate electricity, but the cost is much higher. Geopolitical and economic factors make the price of oil and gas high and volatile, forcing utilities to rely on coal until other cleaner and more sustainable energy options mature and are available at competitive prices for the consumer.

Oil and gas prices show no signs of coming down significantly, public opposition to nuclear still remains strong, and renewable energies still remain a low-capacity option; electricity from coal is expected to increase to meet the rapidly increasing world energy demands. Low-cost electricity is crucial for the survival of some industries and is vital to the household expenditures of average people. So, instead of concentrating on the environmental ills of coal, it is worthwhile examining how clean we can make coal use while keeping the electricity price affordable.

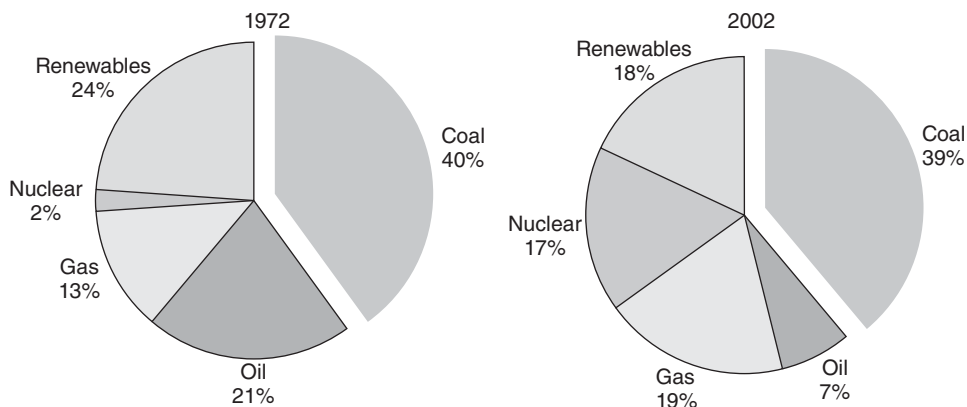


Figure 1 Worldwide energy production past and present. *Source:* Key World Energy Statistics, 2006, p. 24. Copyright © OECD/IEA.

Table 1 Roadmap of Pollution Reduction from Coal-Fired Power Plants Referred to Best Available Technology

		Reference (2003)	2010	2020
Pollution mitigation	SO ₂ , reduction	98%	99%	>99%
	NO _x , (lb/10 ⁶ Btu)	0.15	0.005	0.002
	Mercury capture	0%	90%	95%
	By-product utilization	30%	50%	100%
Plant efficiency (HHV)	Based on HHV	40%	45–50%	50–60%
Capital cost, \$/kW	In 2003 dollar	1000–1300	900–1000	800–900
Electricity cost, c/kWh	Based on coal \$1.2/mBtu	3.5	3.0–3.2	<3.0

Source: From Ref. 4. Courtesy of U.S. Department of Energy/NTL Electric Power Research Institute, and the Coal Utilization Research Council.

The term *clean coal technology* has drawn criticism from environmental groups as the use of coal can never be entirely clean. A more appropriate term would be *cleaner coal technology*. The ultimate goal of cleaner coal technology is to produce coal-fired electricity generating plants with near-zero harmful emissions. This is the goal of the U.S. Department of Energy's FutureGen project² and the Near Zero Emission fossil fuel power plant project of the European Union.³ Table 1 shows how the United States plans to meet the goal of zero emissions.⁴

1.1 Coal

Coal is formed from plant remains that have been compacted, hardened, chemically altered, and metamorphosed underground by heat and pressure over millions of years. It generally originates from swamp ecosystems. When plants die in a low-oxygen swamp environment, instead of decaying by bacteria and oxidation, their organic matter is preserved. Due to tectonic events, this organic material is buried by sedimentary loadings. Over time, heat and pressure remove

the water and transform the matter into coal. Depending on the geological age, the organic material will transform into the following members of the coal family:

1. *Lignite*. This contains considerable amount of water and volatiles and some mineral matters. It is youngest in geological age.
2. *Bituminous*. Moderate amount of moisture, volatiles, and inorganic materials are in bituminous coal.
3. *Anthracite*. This contains very little water or moisture but a large amount of carbon. It is the oldest in geological age.

Figure 2 shows the full spectrum of these plant-based fuels arranged in order of their geological age. It shows progressive changes in oxygen, volatile matter, and fixed carbon from wood to anthracite.

Nitrogen and sulfur appear in coal as organically bound pollutants that are oxidized during combustion to form harmful airborne gases such as nitric oxides (NO_x) and sulfur dioxide (SO_2).

Other impurities also become mixed with the coal during its formation:

- Ash—a quartz-based mineral and/or shale
- Pyretic sulfur (Fe_2S)
- Heavy metals either in elemental form or in the form of heavy metal ores, such as cinnabar (HgS), which releases mercury and sulfur upon heating

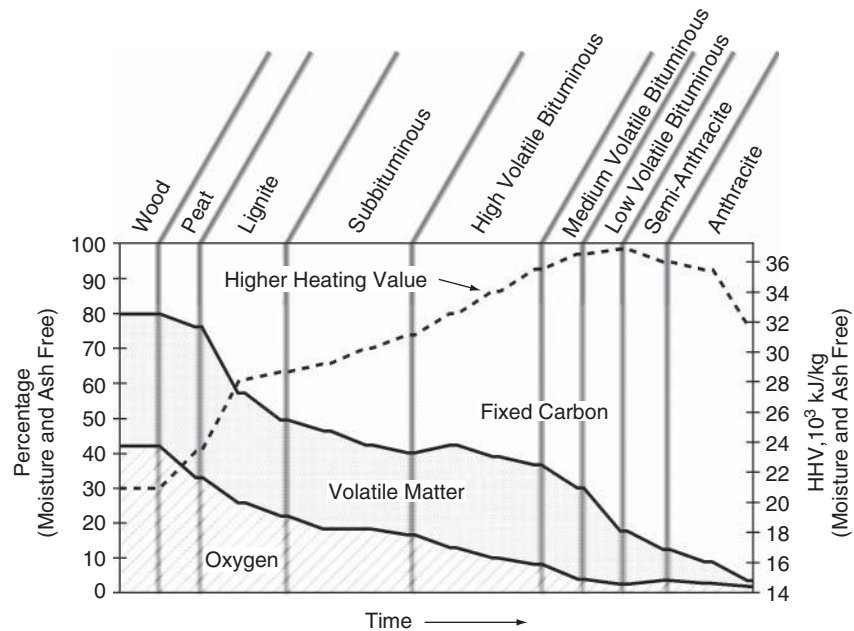


Figure 2 Properties of coallike fuel depends on the geological age of formation.

1.2 Potential Pollutants from Coal

Coal conversion generates a number of gaseous and solid pollutants:

1. Nitrogen oxides
2. Sulfur oxides
3. Carbon dioxide
4. Fine particulates
5. Heavy metals

The following sections briefly describe the generation and effect of these pollutants.

Nitrogen Oxides

When exposed to high temperatures, nitrogen in the air and the fuel could oxidize, forming a number of different compounds, such as NO, NO₂, and N₂O. Nitrogen oxides (NO_x), which represent nitric oxide (NO) and nitrogen dioxide (NO₂), are responsible for the formation of acid rain, photochemical smog, and ground-level ozone. It could also cause adverse health effects for those with respiratory problems. Nitrous oxide (N₂O) is a greenhouse gas and also causes depletion of stratospheric ozone. The formation of NO and NO₂ is favored at elevated temperatures (~1200°C) as found in pulverized coal (PC) flames, while N₂O is favored at lower temperatures (~800°C) like those found in fluidized bed combustors. The nitrogen in fuel is oxidized in all combustion temperatures, but that in air is oxidized generally above 1000°C.

Coal-fired plants are responsible for only a small portion of the anthropogenic NO_x emissions with the bulk coming from automobile emissions (Fig. 3).⁵

Sulfur Dioxide (SO₂)

Sulfur dioxide (SO₂) is formed when the sulfur in coal, either in pyretic or organically bonded form, is oxidized. SO₂ is the leading contributor to acid rain formation and is an irritant to the lungs. Coal combustion makes up the majority of SO₂ emissions from utilities, which in turn account for about a third of the total SO₂ emissions from all sources (Fig. 3).

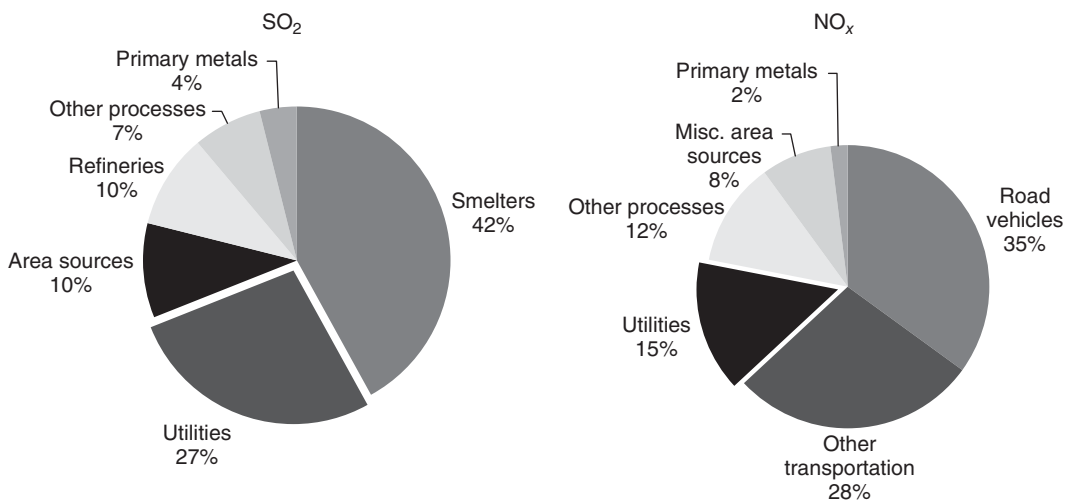


Figure 3 Man-made sources of NO_x and SO₂ in Ontario, Canada. *Source:* Adapted from Ref. 5.

Particulates

In a coal-burning plant a portion of the ash is released to the atmosphere through the stack, with the very fine particulates having harmful health effects. Particulate matter smaller than about $10\ \mu\text{m}$ can settle in the bronchial tubes and lungs; particles smaller than $2.5\ \mu\text{m}$ can penetrate directly into the lung; and particles smaller than $1\ \mu\text{m}$ can penetrate into the alveolar region of the lung and tend to be the most hazardous when inhaled. Fine particulates can have significant harmful health effects if exposure occurs over extended periods.

Heavy Metals

Most heavy metals like lead, tin, and magnesium are collected in particulate control systems, but due to its low vaporization point (356°C), much of the mercury found in coal escapes into the environment, making coal combustion the primary source for mercury emissions. The mercury concentration in coal is high compared to that in the rock surrounding it, because vegetation growing in very wet conditions absorbs large amounts of mercury and coal deposits are formed from such wet decaying vegetation (peat). Mercury vapor in the flue gas precipitates out into the environment and bioaccumulates in organisms such as fish, where it is often transformed into methylmercury, a highly toxic organic compound. Fish species that are high up on the food chain contain high concentrations of mercury, because they eat many smaller fish that have small amounts of mercury in them. The U.S. Food and Drug administration has an action level for methyl mercury in commercial marine and freshwater fish that is 1.0 parts per million (ppm),⁶ and in Canada the limit for the total of mercury content is 0.5 ppm.⁷

Carbon Dioxide

Carbon dioxide, a major greenhouse gas, is produced in all combustion processes involving fossil fuels as well in other industrial processes such as cement production and sweetening of natural gas. The absorption bands of CO_2 have a considerable overlap with the long-wave infrared region of radiation (Fig. 4). Thus, CO_2 allows the shorter wave radiation from the sun to pass through but traps the longer wavelength infrared radiation reflected from Earth's surface. This gives rise to the greenhouse-like warming of Earth, making CO_2 a greenhouse gas. Carbon dioxide stays in the atmosphere for hundreds of years, becoming a major threat

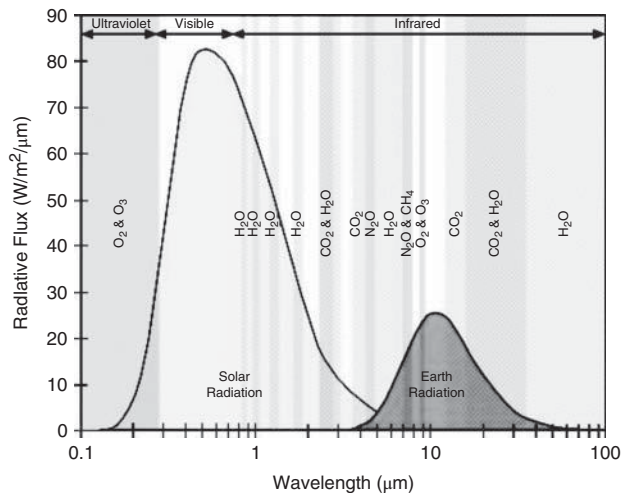


Figure 4 Atmospheric absorption spectrum.

to the biosphere, while water vapor, also having absorption bands in the infrared region, stays only for a few hours in the atmosphere before it is condensed. Thus, it is not considered a greenhouse gas.

The carbon content of coal is very high (50–89%) so it produces much larger amounts of CO₂ (carbon intensity) than produced by other fuels. Table 2 lists the amount of CO₂ produced per unit of energy released by different fossil fuels, with anthracite having the highest emission factor and natural gas having the lowest. Coal-fired power plants burning millions of tonnes of coal are therefore considered a major source of greenhouse gas. Since 1958, CO₂ in the atmosphere has seen a concentration increase of about 17% per year.

Despite divergent views on global warming, the scientific community largely accepts the temperature model that shows a large increase in average global temperature over the past century compared to that of the previous millennium. Either way, it would be prudent to reduce anthropogenic CO₂ emissions rather than wait for more conclusive proof before irreversible damage has been done.

1.3 Motivation for Cleaner Energy from Coal

In December 1952, London became encased in a thick fog caused by a combination of particulate and gaseous emissions from coal-fired power plants and coal furnaces in homes; an unusually cold month; and an unfortunate climatic condition that caused the air in London to become stagnant. The fog caused the deaths of 4000 people and led to Great Britain's Clean Air Act of 1956, resulting in a huge reduction in particulate emissions from coal-fired power plants. In 1963, the United States passed its own Clean Air Act.

As acid rain became an increasing problem in the eastern states and provinces, causing lakes and rivers to become barren and destroying forests, the United States signed the Convention on Long-Range Transboundary Air Pollution to help curb acid rain production. These regulations have helped to reduce the emissions of acid rain causing pollutants from coal-fired plants (Fig. 5).⁸ The major efforts came in the 1970s and 1980s with the creation of international agreements such as Europe's Long-Range Transboundary Air Pollution Treaty, signed by 32 countries in 1979, that called for limits on emissions of harmful airborne pollutants.

In recent years, concern has grown about the levels of mercury found in the environment, even in places that are thousands of miles from any coal-fired power plant. This concern has caused the U.S. EPA (Environmental Protection Agency) to introduce the first ever mercury emissions standards through the Clean Air Mercury Rule, which requires reduction of mercury emissions by 70% (from 1999 levels) from coal-burning plants by 2015.

Table 2 Emission Factors or Carbon Intensity (CO₂ Produced per Unit Amount of Heat Released) for Some Fuels

Fuel	Higher Heating Value (MJ/kg)	Emission Factor (g CO ₂ /MJ)
Anthracite coal	26.2	96.8
Bituminous coal	27.8	87.3
Subbituminous coal	19.9	90.3
Lignite	14.9	91.6
Wood (dry)	20.0	78.4
Distillate fuel oil (#1)	45.97	68.6
Residual fuel oil (#6)	42.33	73.9
Kerosene	37.62	67.8
Natural gas	37.30 MJ/m ³	50

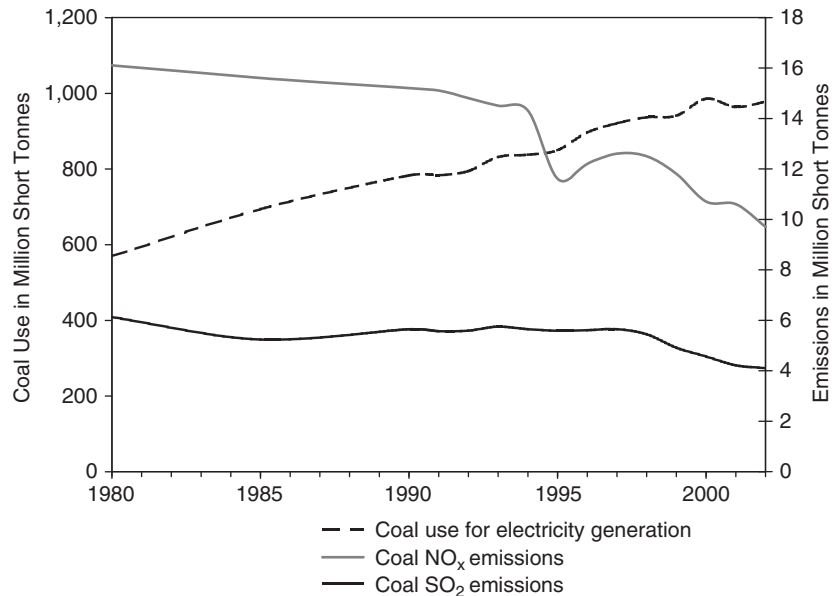


Figure 5 Improvements in emissions of acid rain causing pollutants from coal-fired power plants. *Source:* Adapted from Ref. 8.

Government-regulated emission standards have been largely reactionary, as they are motivated by public awareness brought about by the twentieth century environmental movement. The driving force behind all research and development of cleaner coal technologies has likewise been government regulations. As companies are driven by financial decisions, government regulations have turned the environment into a commodity and introduced a financial disincentive for polluting instead of traditional punitive measures for polluting.

Most scientists now agree that the unprecedented levels of carbon dioxide concentration in the atmosphere are contributing to global warming, though by how much and what the consequences will be is still up for debate. Climate change affects the entire world, and as such, the Kyoto Protocol to the United Nations Framework Convention on Climate Change was created in 1997 to reduce the amount of carbon dioxide and other greenhouse gases entering the atmosphere. Currently, 163 states have signed the agreement and set individual goals for reduction of carbon dioxide. Incentive-based carbon dioxide reduction schemes may encourage power generation companies to greatly reduce their CO₂ emissions or turn to its sequestration.

1.4 Cleaner Energy from Coal

A number of technologies are available or under development to make the process of converting coal into a transmittable form of energy a less polluting process. These technical options can be broadly divided into the following three categories, based on which stage of the conversion process the pollutant reduction takes place:

1. Preconversion technology
2. In situ control technology
3. Postconversion technologies

Preconversion technologies look to reduce the impurities from the raw coal before they are released in conversion and include physical, chemical, and biological cleaning. *In situ technologies* help reduce the amount of noxious gases released from the conversion process. Some of these technologies are low-NO_x burners (LNBs), fluidized bed combustion (FBC), supercritical boilers, gasification, and fuel cells. *Postconversion technologies* try to strip the flue gas of the harmful gases not eliminated through preconversion and conversion techniques. Some postconversion technologies are bag filters, electrostatic precipitators (ESPs), flue gas desulfurization (FGD), selective or selective noncatalytic reduction (SCR and SNCR), and carbon dioxide control involving CO₂ extraction and sequestration.

The purpose of this chapter is to present and explain the currently available cleaner coal technologies.

2 PRECONVERSION

An existing coal-fired power plant can improve its emissions to some extent without expensive modifications by using a cleaner variety of coal—that is, coal with a lower sulfur, ash, and heavy metals content. An added benefit of using a coal with low ash content is the savings on transportation cost of the raw coal to the plant and the ash to the disposal site. Cleaning the coal could potentially improve its utilization efficiency by up to 5%.⁹

High-quality coals are not as abundant as they were when electricity generation from coal first began. In addition, they are in high demand from the smelting industry. The end result is that using a cleaner raw coal is becoming less and less economical. This has led to a growth in coal cleaning or beneficiation, a process that makes possible the removal of mineral impurities that would otherwise be released in the conversion of the coal polluting the atmosphere.

Increased mechanization in coal mining and a shift from underground to open-pit mining resulted in a higher ash content in the coal, making coal cleaning essential. As well, increasingly stringent sulfur and mercury emissions standards have made the removal of these substances a priority in the cleaning process. Coal cleaning mainly focuses on reducing sulfur, ash, and heavy metal in the coal. It can be classified into three main types:

1. Physical (most widely used)
2. Chemical
3. Biological

2.1 Physical Cleaning

Gravity Separation

Gravity separation technologies rely on the differences in specific gravity between the coal and the impurities it contains. The specific gravity of bituminous coal is in the range of 1.12–1.35, whereas that for pyrite is between 4.8 and 5.2, and for ash it is around 2.3. Thus, denser ash and pyretic sulfur can be separated from the lighter coal by static or dynamic means. Gravity separation most often involves wet separation, although it can also be accomplished through a dry process, thus reducing the energy required to later dry the cleaned coal, a necessity for the pneumatic transportation of coal in PC-fired plants. Gravity separation is used to clean coal particles larger than 0.5 in. (12 mm), as smaller pyretic particles would not settle out. Four of the more widely used gravity separation equipment are as follows:

1. Rotating drums
2. Concentrating tables
3. Cyclones
4. Dense-media vessels

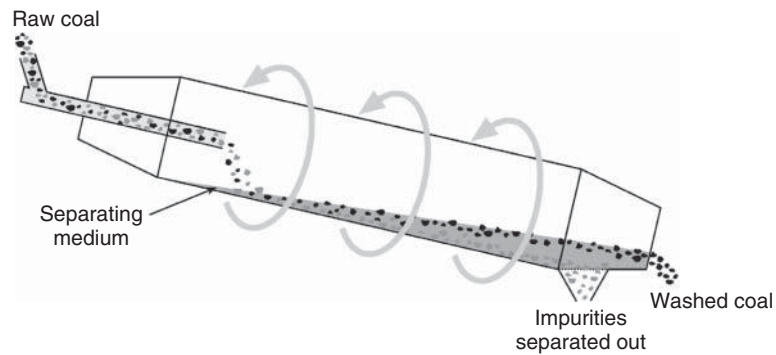


Figure 6 Rotating drum coal washing.

In rotating drums, water and raw coal travel down an incline, where less dense coal remains near the surface while the more dense ash and pyrite particles settle to the bottom (Fig. 6). At the exit, the top portion of the stream, containing mostly coal, is skimmed off and the rest is discarded.

Concentrating tables use flowing water to settle out the discard and carry the lighter coal particles across. The discard is periodically removed using moving riffles.

Cyclones using either water or a dense media separate the coal from the discard using the centrifugal forces from the tangential inlet of the cyclone. The lighter coal particles escape through the top of the cyclone, while the heavier discard is held to the walls by the tangential forces and spirals down and out the bottom.

In dense-media vessels, the raw coal flows through a large vessel with a liquid that has a specific gravity just higher than that of the coal (usually 1.45–1.65). The commonly used medium is water with finely ground magnetite suspended in it. After the mixture has passed through the vessel and the denser pyrite and ash have settled out, the magnetite is separated from the coal–water mixture using magnetic separators and is then recycled.

Agglomeration

Agglomeration is used to clean coal fines (<100 μm) and can recover very small coal particles <10 μm . The naturally hydrophobic coal fines are suspended in an aqueous solution, a light oil is added, and the solution is agitated. The oil preferentially wets the coal, and the agitation causes the fines to agglomerate into larger particles, 1–2 mm in size. These larger particles are then screened from the fine impurities.

The coal particles can be further agglomerated by pelletization with a binder such as asphalt. Agglomeration is becoming increasingly costly because it uses a large amount of expensive light oil to agglomerate the coal, which cannot be reused.

Froth Flotation

Froth flotation involves passing air up through an aqueous solution containing a frothing agent and pulverized coal (Fig. 7). The hydrophobic coal particles attach to the air bubbles, rise to the top, and are skimmed off with the froth, while the mainly hydrophilic impurities sink to the bottom. In some flotation processes, a modifier (i.e., fuel oil) is needed to increase the hydrophobicity of the coal. Froth flotation has three problems:

1. Entrainment of small ash particles by bubbles into the froth phase
2. Low probability of collision between small coal particles and air bubbles
3. Pyrites that have a natural hydrophobicity, causing them to attach to the bubbles

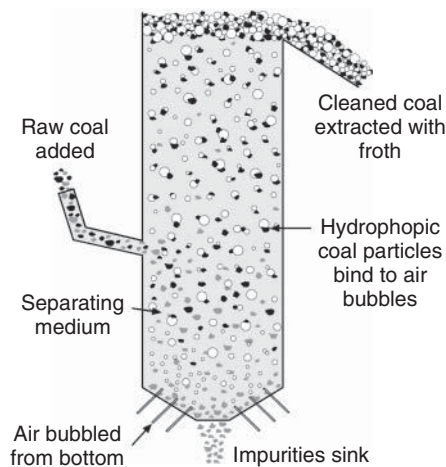


Figure 7 Column froth flotation coal cleaning.

Column flotation increases the likelihood that small coal particles will come in contact with air bubbles, lifting them to the surface, and that entrained ash particles will be dropped out (Fig. 7). Also, new microbubbling techniques can increase the coal particle recovery by increasing the odds that ultrafine coal particles will come into contact with air bubbles.

High Gradient Magnetic Separation (HGMS)

This process relies on the magnetic properties of pyrite (FeS_2) to separate it from the coal. A coal/liquid slurry is passed through high-intensity magnetic fields, where the magnetic impurities are drawn to the sides and discarded. The particles in the slurry must have a size distribution such that 70% are smaller than $76 \mu\text{m}$ to maximize the capture of mineral matter in the coal.¹⁰ The magnetic properties of the impurities can be enhanced by chemical fragmentation of the coal before going through the HGMS.¹¹ Problems with this process include the large capital investment required and its inability to remove the majority of ash particles that are nonmagnetic.

2.2 Chemical Cleaning

Cleaning of coal through chemical means is mainly concerned with removing the organically and inorganically (pyrite) bound sulfur from the coal prior to conversion. Some of the methods of chemically removing the sulfur from the coal follow:

- Chlorination
- Direct oxidization
- Indirect oxidation
- Mild hydrogenation

The operating conditions of chemical cleaning processes are very severe, with high temperature, long retention time, and high alkalinity leading to high-cost equipment and hazardous working conditions. On the one hand, chemical cleaning does have the benefit of removing organically bound sulfur, something physical cleaning cannot accomplish. On the other hand, chemical cleaning alone is unlikely to meet the sulfur removal standards required, so it is rarely used in commercial plants.

2.3 Biological Cleaning

A number of microorganisms (mainly bacterial species) can eliminate the pyretic and/or organically bound sulfur. These bacteria fall into three categories, depending on the type of sulfur they can remove:

1. *Obligate autotrophs*—oxidize pyretic sulfur only
2. *Facultative autotrophs*—oxidize pyretic sulfur and some organically bound sulfur compounds
3. *Heterotrophs*—oxidize organic compounds only.

Research has focused on the obligate autotrophs, as the majority of the sulfur found in coal is in the pyretic form. The reaction rates for sulfur removal are still too slow for commercial applications, so instead of using the bacteria to dissolve the pyrite, the hydrophilic bacteria is used to modify the surface chemistry of the pyrite in order to enhance the physical cleaning processes. Biological cleaning is still at a bench-scale stage and requires further research to assess its commercial viability for removing sulfur from coal.

3 COAL CONVERSION AND IN SITU POLLUTION CONTROL

As emission standards become more stringent, new and cleaner ways of converting coal to usable forms of energy are being developed and implemented (see Table 3).¹² Energy from coal follows one of two conversion routes: the combustion of coal to produce heat energy, which is used to drive a steam turbine, or the gasification of coal to produce a combustible gas (syngas) that can be used to generate heat, electricity, or hydrogen gas for sale.

Pulverized coal (PC) combustion, introduced in 1910, dominated as the most advanced coal-fired generating technology until fluidized bed combustion arrived on the scene in the 1980s. Advanced steam turbines with higher steam temperature greatly improved the overall power generation efficiency of such plants, raising it from 15 to 39%.^{*} Combined cycle power plants, which use both steam and gas turbines, could increase this efficiency to 48% using an integrated gasification combined cycle (IGCC)¹² and has the potential of raising it above 50% with a partial gasification system.¹³ Such higher efficiency plants cause less thermal as well

Table 3 Improvements in Emissions from Coal-Fired Power Plant

Plant Technology	Period of Use	Efficiency (HHV)	SO ₂ (g/kWh)	NO _x (g/kWh)	CO ₂ (g/kWh)	Ash + Sorbent (g/kWh)	Waste Heat in Cooling Water, MJ/kWh
PC	1950–70	30%	0.029	0.0034	1080	45 (ash only)	5.6
PC + FGD + SCR	Present	41%	0.0104	0.00029	770	84	4.0
PFBC combined cycle	Present	39%	0.0059	0.00058	815	99	3.6
IGCC	Present	42%	0.00015	0.00029	745	40.7	3.2
Natural-gas-fired combined cycle	Present without SCR	52%	0	0.00031			2.3

Source: Adapted from Ref. 12.

^{*} All efficiencies are expressed in terms of higher heating values (HHVs). Some efficiencies were converted from lower heating values (LHVs) using conversion factor of 0.8675, using HHV = 28,000 kJ/kg and [H] = 5%.

as gaseous pollutants per unit energy produced (Table 3). As shown in Table 1, efforts toward zero-emission power plants strive to reduce the emission and rejections to a near-zero level using the gasification route.

To meet the environmental regulations of governments and the economic need of the consumers, advanced power generation technologies strive to achieve two things:

1. Reduce the emission of harmful gases per kWh generated
2. Reduce the cost per kWh generated

These objectives are met either by increasing the energy conversion efficiency or by a conversion process with less inherent generation of pollutants. Some of the advanced technologies available for generation of cleaner energy conversion from coal are as follows:

- Rankine cycle plants operating on a supercritical steam cycle
- Integrated gasification or partial gasification combined cycle plants
- Pressurized fluidized bed combustion plants
- Fuel cells

Coal combustion is the high-temperature oxidation of carbon and hydrocarbon content of the coal. The basic equation is as follows:



These equations are the basis of mass balance or stoichiometric calculation needed to calculate the amount of air required and the amount of product produced, but these alone do not give the complete picture of the actual combustion process.

The combustion process requires transportation of the necessary amount of oxygen to the fuel surface, removal of product gases, a favorable temperature for reactions to occur, and a sufficient time for the reaction to complete. These three requirements led to the famous three *T* requirements for combustion:

1. Turbulence for efficient transport of oxidant and products
2. Temperature for necessary rate of reaction
3. Time for completion of the reactions

The transport of oxygen from the air to the surface of fuel is a major factor governing the combustion process. Coal being solid does not mix as easily with the oxygen as gaseous or liquid fuels do. As a result, a good gas–solid contact is vital for coal combustion. The furnace design also has to allow enough time for the coal particles to complete their combustion. Detailed discussion of the combustion process, though an integral part of clean coal technology, is beyond the scope of this chapter. Authors may be directed to Chapter 4 in Basu.¹⁴

Although coal combustion has been in use for centuries, it is only in the last few decades that efforts have been made to lessen the harmful effects of this process. Research has gone into developing advanced, more-efficient plants that produce less emissions. Figure 8 shows how the CO₂ emissions are reduced when the plant efficiency is increased above its 30% level of the 1970s.¹⁵

In order to reduce the pollutants generated, six in-situ coal conversion systems are available:

1. Pulverized coal boiler using a low-NO_x burner (LNB)
2. Fluidized bed combustion
3. Supercritical boiler technology

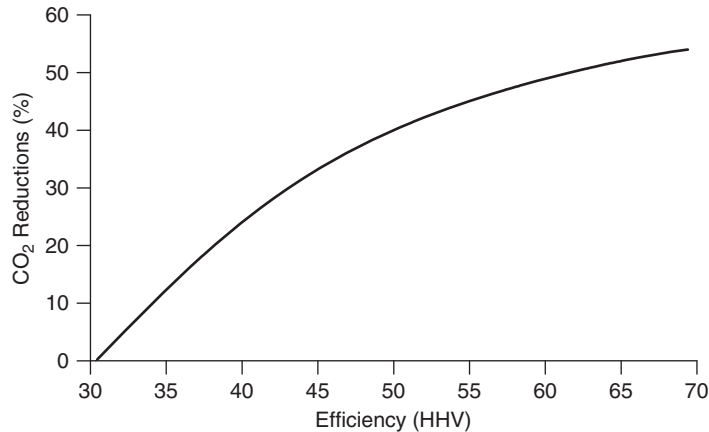


Figure 8 CO₂ emissions reductions with increased efficiency (referenced to a 30% efficient plant).
Source: Adapted from Ref. 15.

4. Cyclone combustion
5. Magnetohydrodynamics
6. Gasification

Brief descriptions of these technology options are given in this section.

3.1 Pulverized Coal Combustion

In this type of combustion, finely ground (pulverized) coal is burnt in a furnace to generate steam that either expands in a steam turbine to generate electricity (Carnot cycle) or provides process heat. Pulverized coal combustion started in the 1910s and is still the workhorse of coal-fired power plants around the world.

Energy conversion efficiency depends on the Carnot cycle efficiency, steam generation efficiency that includes combustion efficiency of coal, and the turbine efficiency. In the simplest form, the Carnot efficiency is written in terms of the highest (T_{\max}) and the lowest (T_{\min}) cycle temperatures of the working fluid. For Rankine cycle steam plants these are the temperatures of the steam at the inlet and exhaust of the turbine, respectively. In gas/steam turbine combined cycles, T_{\max} is the gas temperature at the inlet of the gas turbine (shown later in Fig. 13):

$$\eta_{\text{carnot}} = 1 - \frac{T_{\min}}{T_{\max}} \quad (3)$$

The condenser exhaust temperature (T_{\min}) is dependent on the condenser pressure and cooling water temperature, while the turbine inlet temperature (T_{\max}) is dependent on the maximum steam temperature the boiler can deliver.

The efficiency of early (1900s) plants was low, in the range of 15%, and steam temperature and pressure were modest, 180°C/1.0 MPa. The efficiency rose to about 29% steam temperature as pressure rose to 538°C/1.4 MPa and reheating/feedwater heating was introduced. The plants were still based on a very basic boiler arrangement without environment control systems.¹⁶

Up to the 1960s the primary design changes that led to increases in thermal efficiency included increasing the steam pressure, the number of reheat cycles, and the amount of feedwater heating using multiple extraction points.¹⁷ Subcritical pressure cycles (16.6 MPa and 538°C) with a single-stage reheat and feedwater heating pushed the efficiency to about 34.5%.

The advent of supercritical boilers pushed the frontier further to 38.9% with 27.5 MPa, 565°C steam. With further rise in steam pressures and temperatures (31.1 MPa, 604°C) and double reheat, ultra-supercritical plants are poised to raise the plant efficiency above 41%.¹⁸

Huge advances in control systems for coal-fired plants have also contributed to the increases in efficiency since the advent of the microprocessor in the 1970s.

The technology behind conventional pulverized coal-fired combustors is well developed, inexpensive, and capable of very large generating capacities. These types of combustors are likely to remain the dominant type of coal-fired furnace in the world for years to come. But, because of the unacceptable environmental performance of its basic form, new technologies have been developed to reduce the harmful emissions from PC boilers.

Pulverized coal-fired furnaces need high flame temperatures (~1500°C) for rapid combustion of very fine (90% <76 μm) coal particles.¹⁹ This rapid combustion is needed to prevent coal fines escaping the furnace unburnt, but its high flame temperatures cause the oxidation of nitrogen in the combustion air and in the fuel into NO_x. Furthermore, the high flame temperature does not allow for in situ sulfur capture through injection of limestone into the furnace.

Four means of mitigating the problem of NO_x formation in a PC furnace are as follows:

1. Using low excess air (low amount of air above the stoichiometric requirement)
2. Reducing the peak flame temperature
3. Firing a mixture of O₂ and recycled flue gas
4. Using low-NO_x burners

Low-NO_x Burners

Low-NO_x burners are the most cost-effective method of reducing NO_x emissions from an existing PC-fired power plant, but it can reduce NO_x emissions only up to 50%. In a typical low-NO_x burner (Fig. 9) the NO_x formation is reduced by two factors:

1. Staging the combustion air so that an inner fuel-rich zone is created, causing the fuel nitrogen to be released as N₂
2. Decreasing the temperature of the outer fuel-lean zone, reducing the formation of thermal NO_x

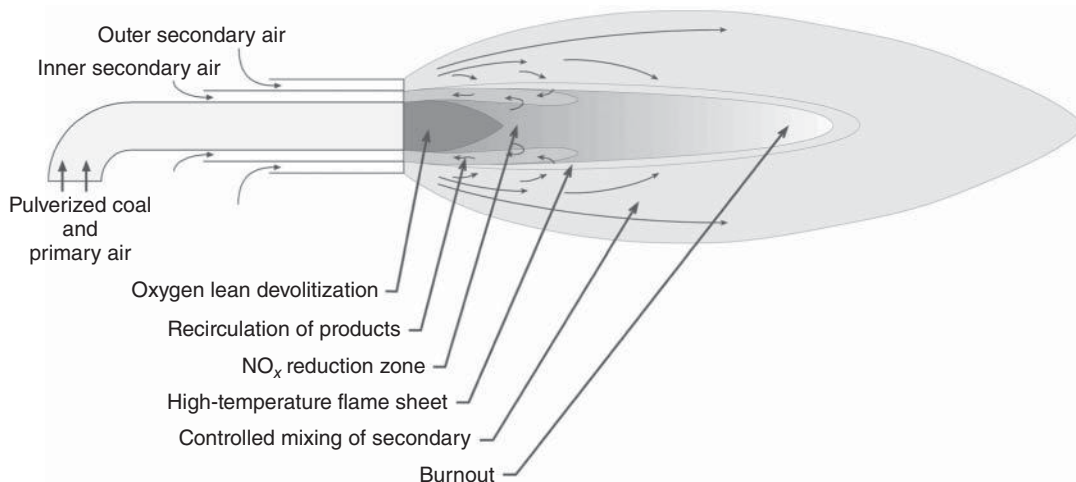
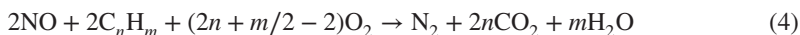


Figure 9 Low-NO_x burner.

The reduction of the flame temperature is difficult to achieve without sacrificing the combustion efficiency of char particles. Low excess air could reduce NO_x formation and is used in some boilers, but it also affects the combustion efficiency.

NO Reburning

For further NO_x reduction in the furnaces of PC boilers, a secondary fuel (CH₄, fuel oil, or high-volatile coal) can be burnt downstream of the main combustion zone to reduce the NO_x already formed by converting it to N₂. The NO_x is reduced by the combustion of hydrocarbon radicals in an oxygen-deficient environment:



Char can also react to reduce the NO_x. The problem with reburning is that its oxygen-deficient environment reduces the combustion efficiency and increases unburnt hydrocarbons or char.

3.2 Fluidized Bed Combustion

Fluidized bed combustion is the second revolution in the art of coal combustion after PC combustion. In a fluidized bed, air is passed through a grate supporting a mass of inert solids at a velocity such that the solid mass behaves as a fluid, giving it the name *fluidized bed*. In fluidized bed combustion, crushed coal burns in a suspension (bed) of highly agitated, hot, inert solids. Fuels constitute only a small fraction (typically 1–3%) of the total solids in this bed. The intense mixing, relatively uniform temperature, and large thermal inertia of the combustion zone allow fluidized bed combustion to burn most types of fuels, good or bad. This flexibility allows the generation of power from many inexpensive low-grade fuels such as petcoke, waste coal, and lignite, which cannot be burnt efficiently in pulverized coal-fired boilers.

Besides fuel flexibility, fluidized bed combustion offers reduced NO_x emission (due to the near absence of thermal NO_x formation) and the capability of sulfur capture in the furnace, 90% or more. Thus, a fluidized bed boiler can meet most of today's environmental standards without the postcombustion clean-up systems required by a PC boiler. These features are a direct result of its low (800–900°C) combustion temperature. However, this low temperature leads to increased emissions of N₂O, a greenhouse gas.

Thousands of subcritical fluidized bed boilers with capacities from a few hundred kilowatts up to 350 MW are in operation worldwide, with a 485-MWe supercritical boiler to begin operation in Lagisza, Poland.¹⁹

Fluidized bed boilers are of two principal types:

1. Bubbling fluidized bed (BFB)
2. Circulating fluidized bed (CFB)

Either type can be designed to operate at an elevated pressure, making it a pressurized fluidized bed combustor (PFBC) that can run a combined cycle plant.

Bubbling Fluidized Bed

The mean gas velocity through a bubbling fluidized bed combustor is typically in the range of 1.0–2.5 m/s. Coal particles with diameters of upward of 6 mm are fed into a fluidized bed and heated by the hot inert solids making up the bed. The heat energy produced from the combustion of the coal is absorbed by the inert solids and then transferred to tubes exposed to the bed (Fig. 10). Flue gas leaves the bed at about 800–900°C and passes through the relatively empty space above it (freeboard) before leaving the furnace to enter the back-pass of convective section of the boiler.

Some of the solids and fine char particles escape the bed and furnace as fly ash, but the majority of the ash is drained from the bottom of the bed (80%, compared to PC at 20%),

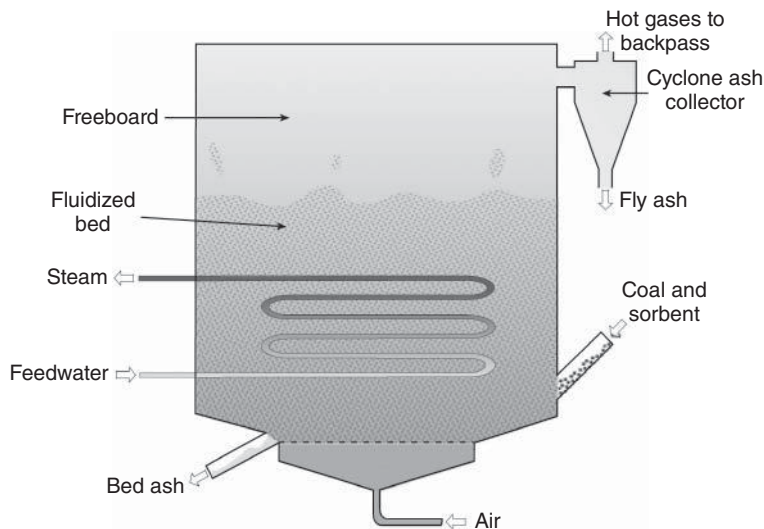
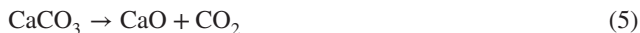


Figure 10 Bubbling fluidized bed combustor.

reducing the amount of particulates exiting the furnace. BFB boilers without heat absorption tubes in the bed are particularly suitable for biomass and waste firing because of their ability to sustain combustion of fuels of low calorific value.

Sulfur capture in the BFB furnace can be accomplished by using a sorbent such as limestone (CaCO_3) as the bed material. Limestone captures the sulfur dioxide generated from coal combustion through the following reactions:



These reactions progress best in the temperature range of 800–900°C, which exists in fluidized bed furnaces.

Rarely is calcium oxide converted completely into calcium sulfate, due to the plugging of sorbent particle pores caused by the increased molar volume of the sulfated sorbent molecules as the sulfur dioxide is captured, making most inner surface areas of the sorbent particle unavailable for sulfur capture (Fig. 11). Fine particles could increase the effective surface area for sulfur capture, but the entrainment of fine particles prevents the use of sorbents any finer than 500 μm in a bubbling fluidized bed. Thus, to capture 1 mol of sulfur a bubbling bed may need as much as 2.5–3.5 mol of CaO, meaning that 2.5–3.5 times the stoichiometric amount of sorbent is required for effective capture of the sulfur. This calcium-to-sulfur molar (Ca/S) ratio is an important parameter in fluidized bed sulfur capture.

From the reaction in equations (5) and (6), it is seen that for every mole of sulfur dioxide captured, 1 mol of carbon dioxide is released, but due to the plugging of pores, for every mole of sulfur captured about 3 mol of extra CO_2 is produced in a BFB boiler. This extra CO_2 emission is also present in PC boilers with a FGD scrubber, although to a lesser extent.

An atmospheric BFB combustor requires a large footprint, owing to its relatively low grate heat release rates of 1–2 MW/m^2 .²⁰ As well, in a BFB furnace, a large number of feed points are required. For example, a 160-MWe unit requires 120 feed points.²⁰ These two factors limit the capacity of BFB boilers to small industrial applications as well as for combustion of waste materials.

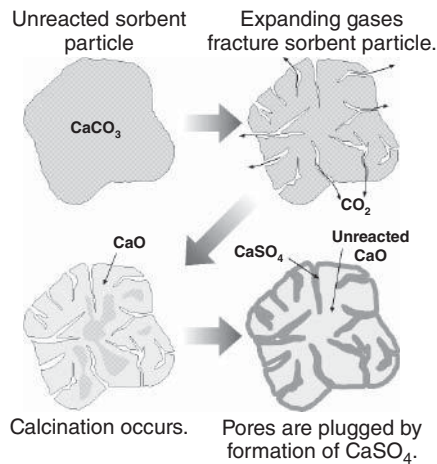


Figure 11 Sulfur capture process for a single sorbent particle.

Circulating Fluidized Bed Boiler

The other member of the fluidized bed family is the CFB, which uses much higher gas velocities (4–6 m/s), compared to BFBs in the furnace, causing the bed of solids to be entrained out of the furnace. The solids are then collected by a cyclone or other type of separator and recycled back at a sufficiently high rate by means of a solid recycle valve such as a loop seal (Fig. 12). This creates a special hydrodynamic condition known as a *fast bed* in the furnace, characterized by intense internal as well as external recirculation of solids.

The combustion air is fed into the furnace in stages. Thus, the lower section of the furnace, which operates in a substoichiometric condition, is refractory lined, while the enclosure of the upper furnace that operates with about 20% excess air is made of heat-absorbing evaporator tubes similar to that in PC boilers. Depending on the heat absorption requirements, additional tube panels in the furnace or an external bubbling bed heat exchanger may be needed to maintain the furnace in the desired temperature range (800–900°C) for a fluidized bed combustor.

The internal and external circulation of solids allows for long residence times even for very fine (~10- μm) coal and sorbent particles. Thus, a CFB boiler can use relatively fine (~200–300- μm) sorbent particles, increasing the effective surface area for capture and resulting in a reduced calcium to sulfur molar ratios of 1.5–2.0¹⁴ and as a result it achieves reduced CO_2 emissions compared to that for BFB boilers.

The high residence time also leads to an increase in combustion efficiency (~99%). Other advantages of CFB combustors include a small footprint owing to its higher grate heat release rate (3–5 MW/m²), fewer feed points (four points for a 190-MWe plant), and greater fuel flexibility.¹⁴ Furthermore, the staging of combustion air to provide favorable conditions for reduction in NO_x emission is possible in a CFB furnace.

FBC Repowering

One option for reducing the emissions from older PC-fired plants is to retrofit them for fluidized bed firing. This is an alternative to the addition of a scrubber and LNB to an old PC boiler. There are three main reasons for repowering an aging PC plant:

1. Deterioration of the fuel supply over time
2. Reducing the cost of expensive support fuel (oil/gas)
3. Reducing plant emissions to meet increasing standards

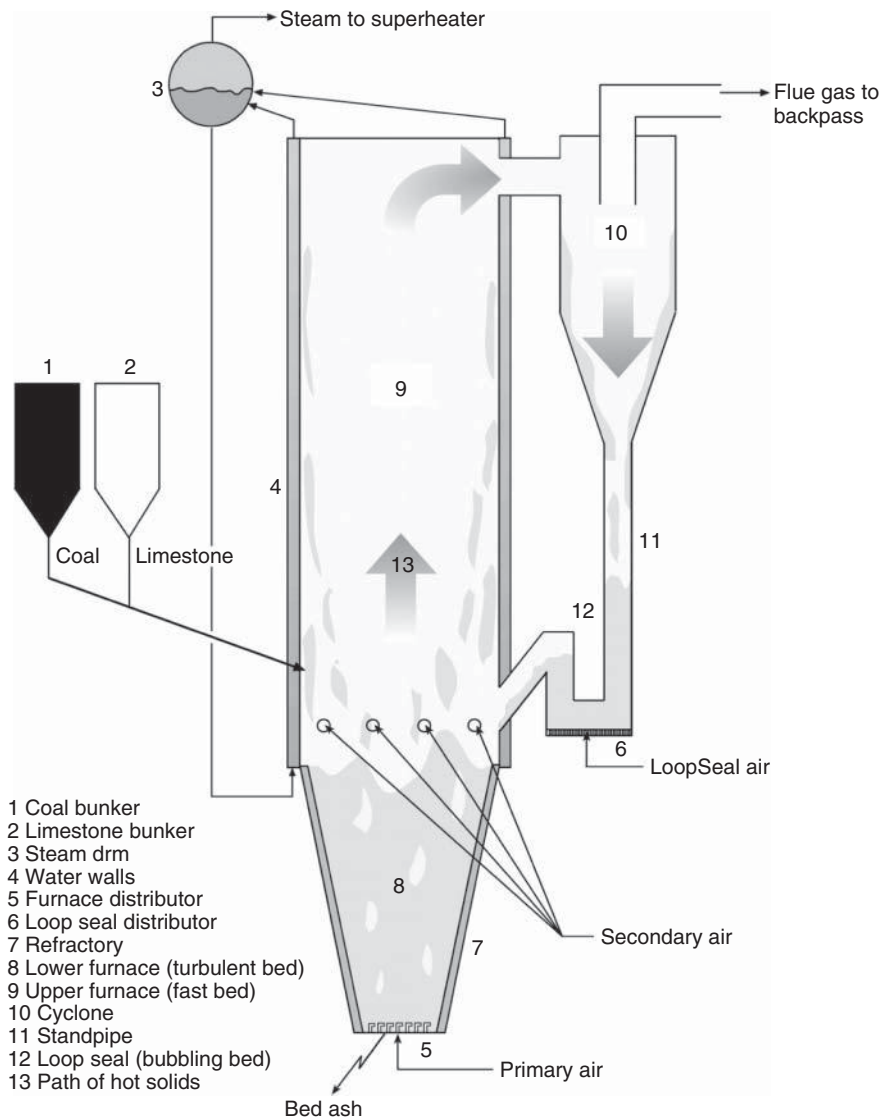


Figure 12 Circulating fluidized bed combustor.

The volumetric and grate heat release rates of a PC boiler significantly overlap those of a CFB boiler.¹³ As a result many old PC boilers can be adapted to CFB firing without major modifications to the plant, or a new CFB boiler can be built in the footprint of the existing PC boiler.²¹

The least invasive means of repowering would involve modification of the furnace to include a compact separator (cyclone or impact separator) and a solid recycle system.²²

In the other repowering option, the entire boiler is replaced with a new CFB boiler. Such a procedure can extend the life of older plants by as much as 25 years. In addition, auxiliary fuel consumption can be substantially reduced.²³

Repowering provides a PC plant with all the environmental and fuel flexibility benefits of a CFB plant for less cost than is needed to build a new CFB plant. These benefits include a reduction in NO_x as well as in situ sulfur capture potential. This may prove in some cases less expensive than adding a scrubber for environmental upgrade on an old PC plant.

Pressurized Fluidized Bed

In a PFBC the hot pressurized flue gas is filtered and enters the gas turbine at around 800°C for Brayton cycle power generation. The waste heat from the gas turbine and the combustion heat in the PFBC boiler are used to generate steam that drives a steam turbine in a traditional Rankine cycle. This combined cycle can attain efficiencies up to 40% with a subcritical boiler. The high efficiency is due to the higher turbine inlet temperature (T_{max}) of its working fluid [equation (3)].

Fig. 13 illustrates how the combination of Rankine and Brayton cycles reduces the relative losses to improve the cycle efficiency. It also illustrates how the addition of a reheater could improve plant efficiency.

The furnace of a pressurized fluidized bed boiler is operated at an elevated pressure such that the hot flue gas produced can be expanded in a gas turbine. Such a high-pressure operation gives a grate heat release rate several times higher than that of an atmospheric FBC and increased combustion efficiency.

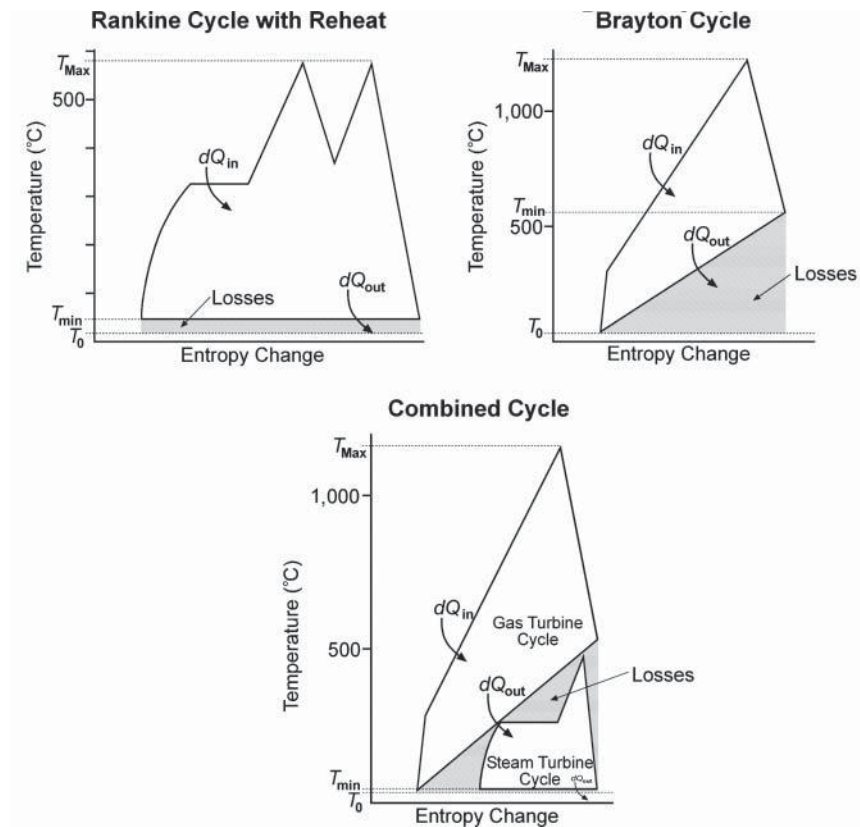


Figure 13 Thermodynamic representation of the improved efficiency of combined Rankine and Brayton cycles.

The hot flue gases from the PFBC must be stripped of both particulate matter and sulfur compounds to avoid erosion and corrosion, respectively, of the turbine blades. Currently, only six PCFB units are in operation around the world.¹⁹ Availability of higher efficiency systems such as IGCC or PGCC, which still use a fluidized bed for the coal conversion, reduced interest in this technology.

3.3 Supercritical Boilers

Supercritical or ultra-supercritical boiler technology can be applied to conventional PC-fired combustors as well as to fluidized bed combustors. Conventional boilers generate steam at around 16 MPa and 540°C, but supercritical boilers generate steam at much higher pressures (exceeding 22.1 MPa) and temperature (>374°C). Ultra-supercritical boilers operate with steam pressures and temperatures as high as 35 MPa and 760°C.²⁴ Owing to their high steam temperature and pressure supercritical boilers give plant efficiencies well exceeding 40% (HHV basis) compared to 35% for current subcritical units²⁵ leading to a reduction in emissions per kWh from the plant (Fig. 14).²⁶ For example, a 300-MWe supercritical boiler reduces carbon dioxide emissions by 137,000 tons/yr even with a very modest efficiency gain of 1.7%.¹⁹

Supercritical boilers use a once-through type of water/steam flow under forced circulation, eliminating the need to use expensive steam drums, downcomers, and so on. This is the main reason why supercritical boilers are within 3–5% of the cost of subcritical boilers, despite their need for high-pressure equipment and high-pressure pumps.

PC supercritical boilers suffer from the problem of very high and uneven heat flux distribution around the furnace. Uneven heating of steam/water in the evaporator panels could cause evaporator tube failure if the heat flux to one section is too high compared to another. In a PC boiler, this problem is overcome by several means, such as the use of the following three means:

1. An expensive spiral tube arrangement where the tubes wrap around the boiler, so that each tube is exposed to the same sections of varying heat flux
2. Riffled tubes, which help to reduce the surface temperature of the tubes
3. A multipass system where all tubes go up one wall of the boiler, meet at a header at the top, and go down another wall of the boiler.

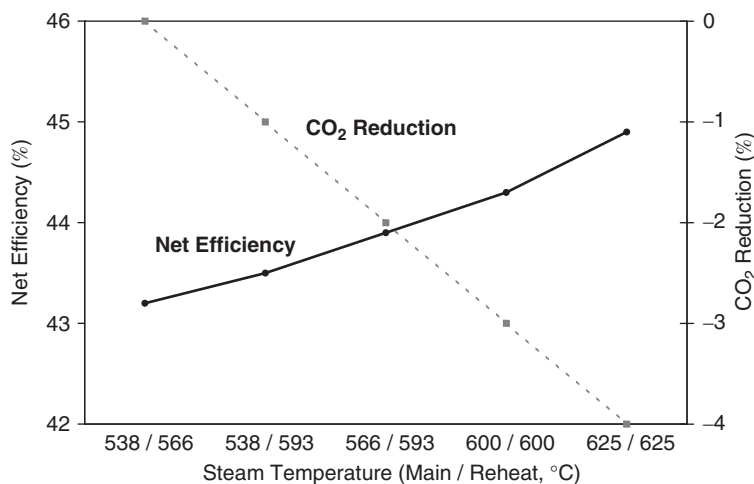


Figure 14 Steam condition and efficiency of a supercritical power plant. *Source:* Adapted from Ref. 2.

Circulating fluidized bed boilers are relatively free from these problems as its lower (compared to PC boiler) heat flux and relatively uniform distribution around the furnace periphery eliminate the need for complex tube construction.

CFB firing of a supercritical boiler is relatively new. In 2006, more than 500 PC supercritical plants were in operation around the world—most (46%) in the former Soviet Union.²⁷ Large increases in the number of additional units are expected with India and China choosing to adopt supercritical boilers as their standard for plants with generation above 800 MWe.⁹

Owing to their proven records, supercritical plants with postcombustion clean-up (for PC firing) and in situ cleaning (for CFB firing) may be more attractive to the utility industries than IGCC plants for generation of clean, reliable, and cost-effective power from coal. Unlike IGCC such plants are suitable for both high- and low-rank fuels.

3.4 Cyclone Combustion

Cyclone combustion technology offers high heat generation per volume ($18.5 \text{ GJ/h}\cdot\text{cm}^3$) and a good retrofit option for existing oil- and gas-fired plants as prices continue to increase.¹¹ It is useful for coals with a low ash melting temperature, which is difficult to burn in PC boilers. In a cyclone combustor, high-velocity air carrying coal particles is tangentially injected into a horizontal cyclone producing spiraling of the combustion gas around the furnace (Fig. 15). Its uncooled furnace generates high temperature (1650°C) causing the ash to slag and allowing for very high combustion efficiencies ($>99\%$).¹¹

Staged combustion can help to prevent the production of excessively high levels of NO_x in the high-temperature environment. The sulfur dioxide is removed only to a limited extent by injection of sorbents into the furnace along with the coal air stream. High temperatures also allow for removal of 70% of the ash, as liquid slag reducing the load on the particulate capture system.

In 2006, more than 100 cyclone combustion units were in use; however, owing to its high NO_x emission, no new units are planned or under construction in the United States.

3.5 Magnetohydrodynamics

Magnetohydrodynamics (MHD) uses very hot ($\sim 2500^\circ\text{C}$) combustion gases seeded with a compound that is easily ionized (K or Ce), passed at high velocities through a magnetic field to generate the flow of electrons. If combined with a Rankine cycle downstream of the MHD, efficiencies of 35–52% are expected.²⁸ MHD is still in the research stage with a number of hurdles to be overcome, such as the development of powerful superconductors, mitigation of thermal NO_x emissions, and the reduction of the high capital cost.

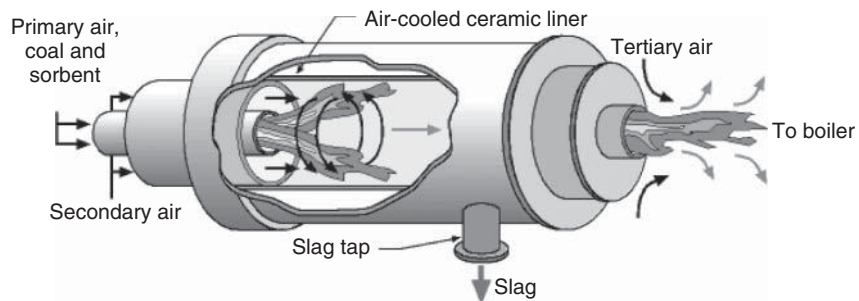
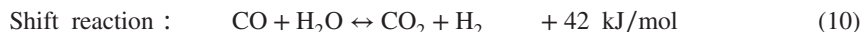
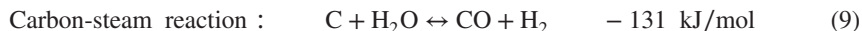


Figure 15 Cyclone combustor.

3.6 Gasification

Gasification is essentially the process of converting the organic material of coal into a gaseous form. This is accomplished by reacting coal in a gasifier operated in a substoichiometric or oxygen-deficient environment. It has a special place in the world of cleaner coal technology, as it is the centerpiece of near-zero-emission power plants and could provide valuable by-products such as hydrogen from coal. The energy density of hydrogen is very high (121 MJ/kg), about five times that of raw coal; therefore, it is suitable for many other applications such as transportation and use in fuel cells.

The first stage of gasification, called *pyrolysis*, occurs from 400°C and up in the absence of oxygen. Here coal is converted into char and hydrogen-rich volatiles. In the second stage (700°C and up), air or oxygen is added to gasify the char, yielding a combustible gas and ash. The key reactions involved in gasification are



Energy for the endothermic gasification reactions, shown in equations (8) and (9), is provided by a certain amount of combustion, shown in equation (7), also taking place in the gasifier. Regulating the amount of oxygen fed into the gasification chamber controls this extent of combustion. The shift reaction shown in equation (10) is encouraged if the desired product of gasification is hydrogen.

The air—in which nitrogen remains in the product gas, reducing its heating value—provides the oxygen for the reactions in equations (7)–(10). If gasification uses pure oxygen instead of air, a *syngas* consisting of CO₂, CO, and H₂ is produced that has twice the heating value obtained by air-blown gasification and about 20% the heating value of natural gas. Oxygen-blown gasification has the added benefit of carbon dioxide capture, as its end product is a high-pressure stream of water and carbon dioxide. A simple condensing out of the water would leave a stream of CO₂ for sale or sequestration. The thermal efficiency of an oxygen-blown gasifier, including carbon dioxide capture and sequestration, is about 73% [International Energy Agency (IEA²⁹)]. A combined cycle using such a gasifier would have an overall plant efficiency in the range of 43–52%.²⁸

There are three generic types of gasification reactors:

1. Fixed bed
2. Fluidized bed
3. Entrained flow reactors

The main difference between these types lies in the gas–solid contacting process employed in the gasification chamber. Table 4 shows that the mode of contact has important influences on the gasifier design and performance.³⁰

On the one hand, the gas velocity in a fixed-bed gasifier is below that required for fluidization of the coal or ash particles in it. Bubbling and circulating fluidized bed gasifiers, on the other hand, use gas velocities above the minimum fluidizing and terminal velocities of the average coal or ash particles, respectively. Entrained flow gasifiers operate similar to the burners of a PC boiler. The gasification medium (oxygen, steam, or air) transports pulverized coal particles through the gasifier at a velocity well above the transport velocity of the coal particles. Since the particles are not recycled, their residence time in the reactor is low.

Table 4 Important Characteristics of Generic Types of Gasifiers

	Moving-Bed Gasifier		Fluidized Bed Gasifier		Entrained Flow
	Dry Ash	Slagging	Dry Ash	Agglomerating	Slagging
Fuel characteristics	6–50 mm	6–50 mm	<6 mm	<6 mm	0.1 mm
Fuel size limits					
Preferred feedstock	Lignite, reactive bituminous coal, anthracite, wastes	Bituminous coal, anthracite, petcoke, wastes	Lignite, reactive bituminous coal, anthracite, wastes	Lignite, bituminous, anthracite, cokes, biomass, wastes	Lignite, reactive bituminous coal, anthracite, petcoke
Ash content limitations	None	<25%	None	None	<25%
Preferred ash melting temperature (°C)	>425	<650	>925	>925	<1035
Operating characteristics					
Exit gas temperature (°C)	425–650 ^a	425–650	925–1035	925–1035	>1260
Gasification pressure (MPa)	3.0+	3.0+	0.1	0.1–3.0	5.0
Oxidant requirement	Low	Low	Moderate	Moderate	High
Steam requirement	High	Low	Moderate	Moderate	Low
Unit capacities (MWth)	10–350	10–350	100–700	20–150	Up to 700
Key distinguishing characteristics	Hydrocarbon liquids in raw gas			Large char recycle	High sensible heat energy in raw gas
Key technical issues	Utilization of fines and hydrocarbon liquids			Carbon conversion	Raw gas cooling

^aMoving-bed gasifiers operating on low-rank fuels have temperatures lower than 425°C

Source: Adapted from Ref. 30.

Fixed beds are less expensive but are suitable only for small-capacity units. Fluidized beds are more expensive and are suitable for large- to medium-size units. Entrained bed gasifiers are generally used for large-capacity units.

A gasification-based plant can produce energy in the form of steam, electricity, or syngas for production of chemicals or hydrogen. It is especially important for the hydrogen economy of the future. Figure 16 shows a flow chart of one energy conversion option for gasification.

Integrated Gasification Combined Cycle

An integrated gasification combined cycle (IGCC), as the name implies, would gasify coal into fuel gas to fire a gas turbine and use the waste heat to generate steam to run a steam turbine. As such, it enjoys the benefit of higher peak working fluid temperature (T_{\max}) with higher efficiency power generation of the Brayton and Rankine combined cycle [see equation (3) and Fig. 14].

In a typical IGCC plant (Fig. 16), prepared coal is fed into a gasifier which could be of fluidized or entrained type. The coal is gasified into CO or H₂. Due to the reducing condition in the gasification chamber, the majority of the nitrogen and sulfur in the coal is not oxidized, reducing the production of the atmospheric pollutants NO_x and SO₂. The majority of the nitrogen from the coal is released as N₂ and NH₃. The latter is removed from the syngas prior to combustion to avoid corrosion of the gas turbine.

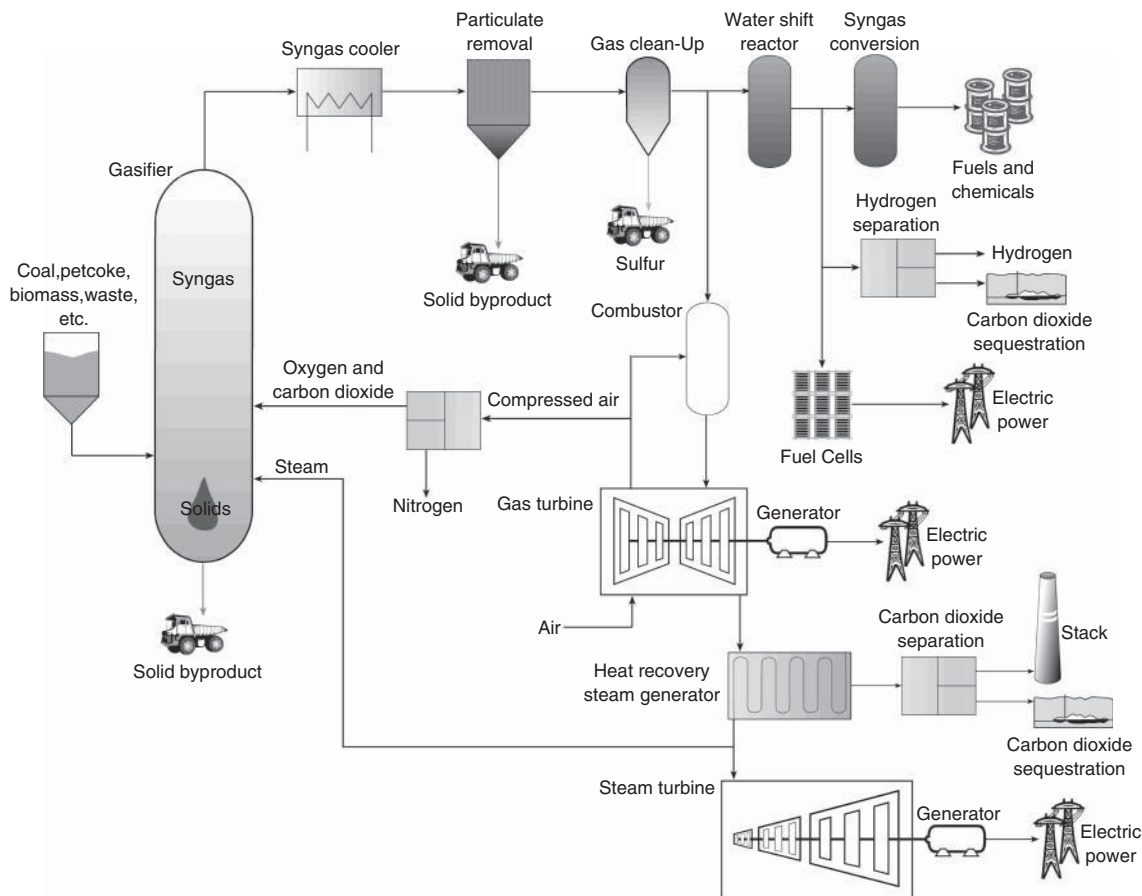


Figure 16 Gasification-based energy conversion options.

Sulfur reacts with hydrogen in the gasification chamber to produce H_2S , which is again removed from the flue gas prior to combustion to prevent corrosion. This is accomplished using amine scrubbers that generate organic sulfur or sulfuric acid, both of which are saleable by-products.

The particulates are removed using hot gas filters or a water scrubber that requires the temperature of the syngas to be greatly reduced. For sulfur removal the syngas must be cooled to 240–400°C. This is done by transferring the heat to a boiler. The cleaned gas expands in a gas turbine and its residual heat is used in the boiler again. Steam from the boiler drives a steam turbine.

Overall efficiency of an IGCC plant increases rapidly with an increase of cleaned syngas temperature up to 350°C³¹; however, sulfur capturing sorbents decrease in reactivity with temperature, making the development of high-temperature (>300°C) desulfurization techniques important.

Hot gas clean-up is a major issue of IGCC plants. Currently, ceramics are the material of choice for hot-gas filtration, as they can withstand high temperatures and maintain the extremely high collection efficiency required to prevent erosion of the gas turbine blades. However, ceramic filters are not ideal because they are brittle and susceptible to failure due to

mechanical or thermal shock. Current hot-gas filter research is focused on the development of sintered metal filters, which offer resistance to cracking. Preoxidized 2% chromium iron aluminide porous metal media is the preferred choice.

Chemical industries have been using IGCC for decades. Out of about one hundred operating gasification plants, there are only five large-scale IGCC plants operating on coal in the utility industry.³² Five major coal-fired IGCC plants are as follows:

1. Tampa Electric's Polk Power Station in Florida (Chevron Texaco Gasification Process, 250 MW)
2. PSI Energy's Wabash River Generating Station in Indiana (Global Energy's E-Gas Process, 262 MW)
3. NUON/Demkolec/Willem Alexander IGCC Plant in Buggenum, The Netherlands (Shell Gasification Process, 253 MW)
4. Elcogas/Puertollano IGCC Plant in Puertollano, Spain (Uhde's Prenflo Process, 298 MW)
5. NPRC in Negishi, Japan (342 MW Texaco gasifier, Shell gas clean-up technology)

These plants are of similar design, all using oxygen-blown entrained gasifiers. The performance of the five plants is detailed in Table 5.^{33,34}

Low-grade coal IGCCs tend to have higher heat rates (or lower efficiencies) than supercritical or ultra-supercritical plants. Overall plant availability is also an issue with IGCCs, unless the company takes the expensive route of buying a stand-by gasifier. Furthermore, gasifiers cannot be turned on and off rapidly without impunity due to the heavy refractory in the gasifiers.³²

Table 5 Operating Commercial Scale IGCC Plants Performance

	Polk Power (U.S.)	Wabash River (U.S.)	NUON/Demkolec (Netherlands)	ELCOGAS (Spain)	NPRC (Japan)
Gas turbine (MWe)	192	192	155	182	N/A
Steam turbine (MWe)	121	104	128	135	N/A
Net power output (MWe)	250	262	253	298	348
Efficiency (% HHV)	37.5	39.7	41.4	41.5	36
Total operating hours	>25,700 (09/2001)	21,991 (2001)	>23,000 (through 2000)	>6700 (03/2001)	4584 (08/2003) ⁱ
Coal usage (tons/day)	2,200	2544	2200	2400	N/A
Gasifier availability (%)	84.2 ^a	85 ^b	50	68 ^d	72.3 ⁱ
Power block availability (%)	94.4 ^a	89.9 ^b	(combined) ^c	84.6 ^d	80.7 ⁱ
Emissions					
SO ₂ (lb/MWh)	<1.35 ^e	1.08 ^f	0.44 ^g	0.15 ^g	<2 ppm
NO _x (lb/MWh)	0.86 ^h	1.09 ^f	0.7 ^g	0.88 ^g	<2.6 ppm
Particulates (lb/MWh)	<0.14 ^e	<0.10 ^f	0.01 ^g	0.044 ^g	<1.4 mg/m ₃
Sulfur removal (%)	>98	>97	>99	99.9	99.8

^aYear 5 operation, ending September 2001.

^bYear 5 operation in 2000.

^cAverage plant availability in 2000 through September.

^d2001 operating statistics through 9/2001.

^eReported emissions in 2000.

^fAverage emissions in 2001.

^gAverage emissions reported for 2001.

^hAverage of 14 months of CEMS data.

ⁱFrom gasifier first lit.

Source: Adapted from Ref. 33.

IGCC, however, has an edge over others when hydrogen, sulfur, and other by-products of gasification can be sold easily.

Partial Gasification Combined Cycle

Much the same as the IGCC, partial gasification combined cycle (PGCC) plants generate both gas for use in a gas turbine and steam—the difference being in the gasification of the coal. A partial gasifier uses air instead of oxygen to pyrolyze or partially gasify the coal into a lean gas in a pressurized gasifier. The remaining char particles are then captured and fed into a pressurized circulating fluidized bed boiler. The boiler produces steam at supercritical pressure to drive a steam turbine as well as high-pressure hot flue gas containing excess oxygen that helps burn the lean gas in the combustion chamber to drive a gas turbine.

This process is more efficient (>50%) than the IGCC because the steam turbine inlet temperature is not limited by the exhaust gas temperature of the gas turbine, thus resulting in lower emissions per kilowatts. The PGCC also has the potential to have a lower capital cost and higher reliability than the IGCC due to the absence of an oxygen separation unit and complete gasifier and increased simplicity of the system.³⁵ However, the PGCC is not suitable for hydrogen production and is less proven than the IGCC as there are no industrial-scale plants currently in operation. It can work with a CO₂ sequestration system.

Fuel Cells

Fuel cells are direct energy conversion systems with a very high conversion efficiency. The gasification of coal to produce hydrogen for use in fuel cells offers an efficient means of electricity generation from coal. If a solid oxide fuel cell (SOFC) was run off the syngas produced from coal gasification (Fig. 17) and the heat from the fuel cell (SOFCs operate between 850 and 1000°C) recovered for use in a Brayton/Rankine combined cycle, then efficiencies of up to 60% could be realized.²⁷

Fuel cells are a viable option for future power generation but still need to overcome major reliability obstacles and find ways to decrease the capital and operational costs.

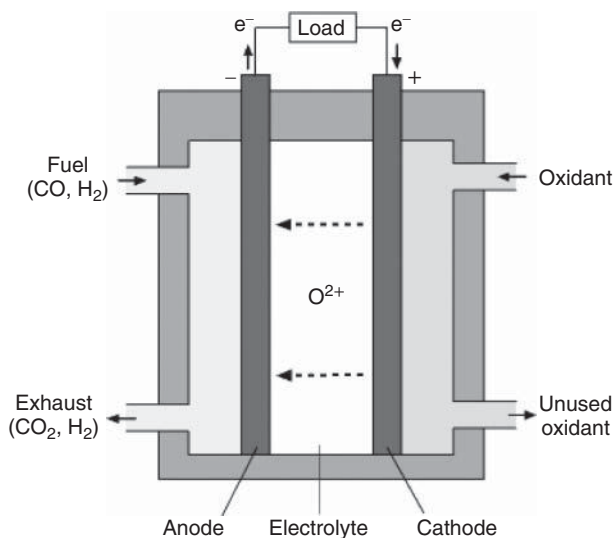


Figure 17 SOFC operation.

4 POSTCONVERSION CLEAN-UP

Postconversion clean-up is necessary for all types of coal-fired plants to reduce their environmental impact. Control technologies currently exist to remove particulates, NO₂, SO₂, N₂O, and CO₂ from the flue gas. Technologies for the control of heavy-metal emissions are under development. The following sections discuss control options for these pollutants, with the exception of carbon dioxide, which is discussed separately in Section 5.

4.1 Particulates

Particulates in the flue gas include very fine ash and unburnt carbon particles released during the combustion or conversion of coal. The amount of particulates depends on the firing method and ash content of the coal fired. Typically, a PC-fired boiler, using very fine (75% below 75 μm) coal particles, will see 80% of the ash in the coal released as fly ash, with the other 20% collected as slag or bed ash at the bottom of the boiler.³⁶ For a fluidized bed combustor the ratio could be reversed due to the much larger size (75% below 6000 μm) of coal particles fired in these types of systems.

Two common types of control technologies are used in coal-fired plants to reduce particulate emissions:

1. Bag filters
2. Electrostatic precipitators

Cyclones are used to collect only large particles and will not be discussed here.

Bag Filter

A bag filter offers a porous barrier to the dust-laden flue gas, capturing the particulate matter while allowing gases to pass through it (Fig. 18). Individual bag filters are arranged in rows in bag houses, where cooled flue gas flows from high to low pressure (keeping the bags inflated) trapping particulates, allowing only the flue gases through. There are two types of dust filtration systems:

1. Depth filtration
2. Surface filtration

In depth filtration the mesh in the fabric bag is generally not fine enough to capture the smallest particles, which pass through the pores in the mesh. However, as particles pass through, a cake of fly ash forms on the fibers of the mesh, restricting the pore size, trapping finer particles, and at the same time increasing the pressure drop across the bags (Fig. 19). Thus, the dust particulates trapped in the filter media facilitate the actual filtering.

In contrast, surface filtration occurs mainly on the surface of the filter media, with little penetration of dust onto the interstices of the filter media because the fabric has extremely small pores. Gor-Tex[®] and P84 are examples of surface filtration materials.³⁷ These filters can tolerate higher air-to-cloth ratios and even a small amount of condensation, which would cause normal bag filters to clog and cease operating. These types of microporous filter materials are still in the testing stage, and wide-scale implementation has yet to take place.

The dust cake formed on either depth or surface filters must be shed through either of the following two methods:

1. Periodical pulse cleaning of the bags when off-line
2. Back-flushing of each bag using high-pressure air

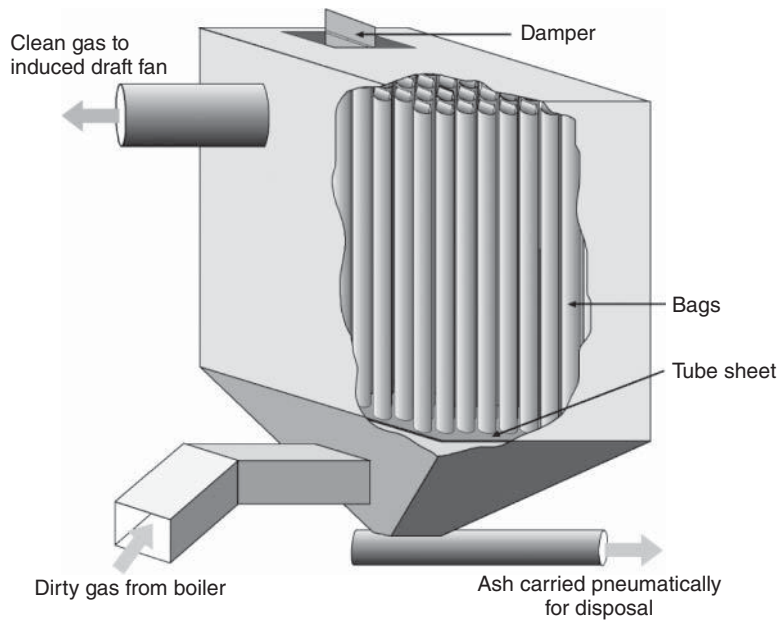


Figure 18 Typical bag house.

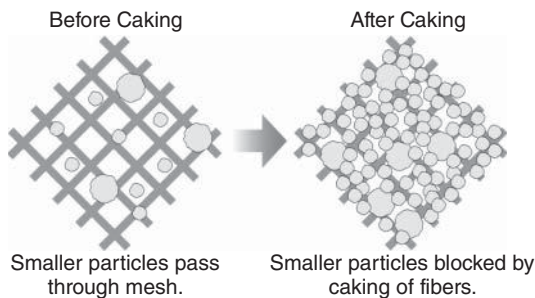


Figure 19 Depth filtration caking.

Failure to do this will result in clogging and/or rupturing of the bag. The problem with depth filters is the reduction in filtration efficiency immediately after the cleaning of the bags, when no cake is present. Surface filtration medium such as Gor-Tex[®] could allow for collection of finer particles without a drop in the collection efficiency immediately after cleaning.³⁸

Bag houses have collection efficiencies of greater than 99% even for very small particles. As well, they have the advantage of modular design, reducing costs. The disadvantages of bag houses are that they occupy a great deal of space, as tens of thousands of bag filters are required in large plants to handle the large volume of flue gas. Also, the bags can be harmed by high-temperature or corrosive conditions; as such they cannot operate in humid conditions. A large pressure drop resulting in higher auxiliary power consumption is another disadvantage of the bag house. Despite this, bag houses still remain a strong technology of choice for particulate collection.

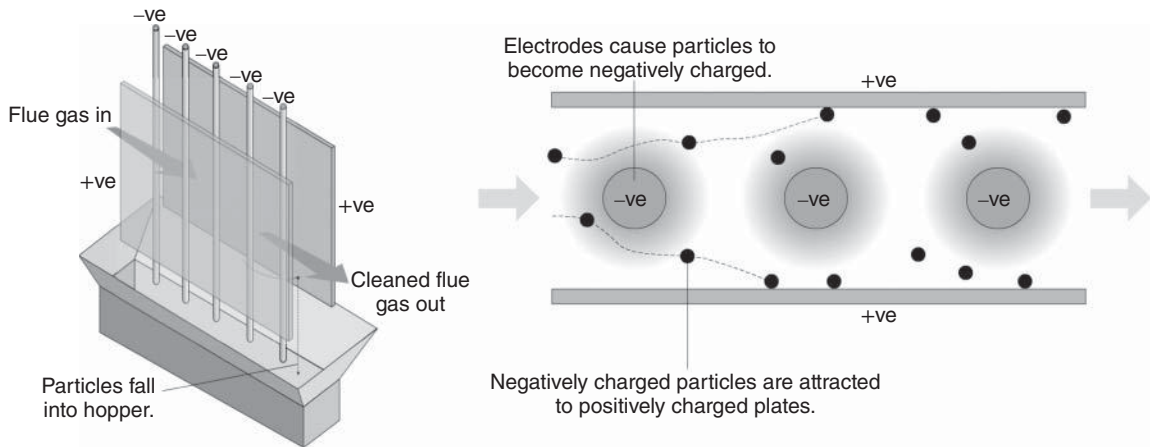


Figure 20 Operation of an electrostatic precipitator.

The air-to-cloth ratio (cm^3/s per cm^2) is an important design parameter for a bag filter. In a typical coal-fired plant, it may range from 0.75 to 1.1 cm^3/s with reverse air cleaning and from 1.5 to 2.0 cm^3/s for pulsed jet cleaning.¹⁶

Electrostatic Precipitators

Electrostatic precipitators collect particulate matter by applying a static charge to the fly ash particles and drawing them out of the flue gas stream with the opposite charge. As the flue gas passes through a chamber containing anode plates or rods with a potential of 30–75 kV,¹¹ the particles in the flue gas pick up the charge and are collected downstream by positively charged cathode collector plates (Fig. 20). Grounded plates or walls also attract the charged particles and are often used for design simplicity. Although the collection efficiency does not decrease, as particles build up on the plates, periodic mechanical wrapping is required to clean the plates to prevent the impediment of the gas flow or the short circuiting of the electrodes through the built-up ash.

The resistivity of the ash particles is a very important parameter influencing the collection efficiency of ESPs. An ash of high resistivity will not take the charge from the anodes as easily as a less-resistive ash will. If the resistivity is too low, the particles will lose their charge before coming in contact with the collector plates. ESPs can attain efficiencies exceeding 99.5% for ash resistivity in the range of 10^4 and 10^{11} Ω/cm . Resistivity of ash is highest around 200°C and drops sharply above or below this temperature, so the ESP is best operated near this temperature.¹⁶ Higher moisture, sulfur, sodium, and potassium in the coal are favorable for ash collection in an ESP due to their favorable resistivity. Higher calcium and magnesium content in the coal and nonuniform gas distribution in the collector contribute to lower collection efficiencies.

The collection area of the plates also has a direct effect on the collection efficiency, as can be seen in the Deutsch–Anderson equation:

$$\eta = 1 - e^{-\omega A/Q} \quad (11)$$

where η = efficiency of the collector
 A = collection area (m^2)
 ω = particle migration velocity (determined from experiments, m/s)
 Q = flue gas flow rate (m^3/s)

The main advantages of ESPs are their low operation and maintenance costs, the relatively small footprint (versus bag houses) for large flue gas flows, minimal pressure drop, and constant collection efficiency. A major disadvantage of an ESP is its low collection efficiency for submicrometer particles that are of the greatest health concern as well its sensitivity to the flue gas velocity distribution inside the collector and gas temperature. Even a well-designed ESP can operate poorly if proper conditions are not maintained.

If slagging conditions are present in PC-fired plants, molten ash can vaporize and condense in the backpass, forming submicrometer-size inorganic particles, which cannot be captured by conventional particulate control technologies such as ESP or depth filtration bag houses.

Wet Scrubber

Scrubbers are used to clean the flue gas of gaseous pollutants as well as particulates. When only particulate matter control is needed, water is used as the scrubbing solution. The water is misted into the flue gas stream, coming into contact with the particulate matter, capturing the particles and condensing out with the particulates.

Wet scrubbers also have high collection efficiencies, upward of 99%, but their major disadvantage is the large increase in possibly toxic wastewater produced.

There are a number of different types of wet scrubbers. All try to maximize the surface area of the scrubber solution and increase the residence time of flue gas in the scrubber to improve efficiency. Three types of scrubber are shown in Fig. 21.

4.2 Gaseous Emissions

The oldest method of reducing the harmful effects of gaseous emissions was to disperse them over a wider area using a very tall stack, making the immediate surroundings less toxic while doing nothing for the reduction in acid rain, smog, or ground-level ozone formation. Regulatory authorities in some countries (e.g., India), for that reason, still relate SO₂ capture with stack height.

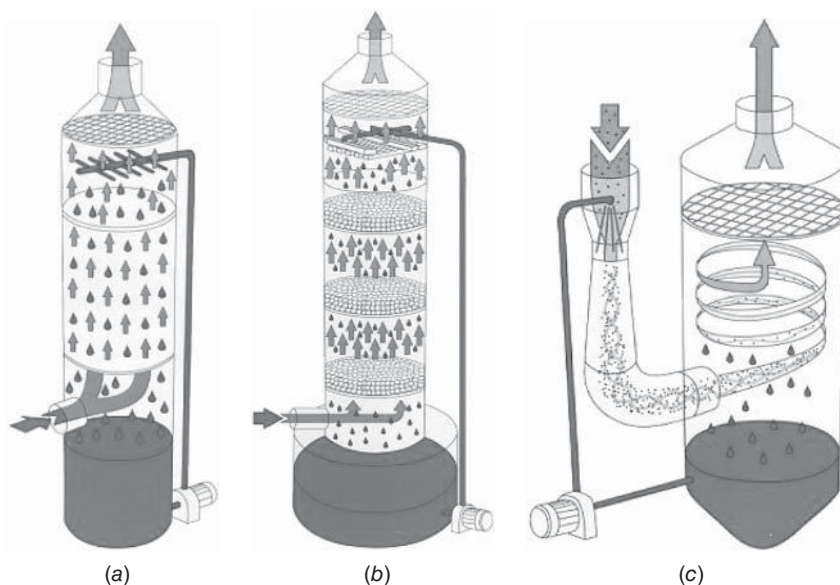


Figure 21 Various types of wet scrubbers: (a) typical wet scrubber, (b) fluidized bed scrubber, and (c) venture scrubber. Courtesy Forbes—Plastic Tanks and Environmental Technologies.

Advanced combustion technologies produce less amounts of harmful gases, yet some plants might still need a certain amount of postconversion clean-up of the flue gas.

Sulfur Dioxide

The emission of SO₂ can be reduced either by using fluidized bed combustion in a bed of limestone (see Section 3.2) or by scrubbing the flue gas with sorbents for postcombustion removal.

For PC-fired plants, scrubbing is the accepted means for SO₂ reduction. Flue gas desulfurization removes the SO₂ from the flue gas stream with a chemical absorbent before it is released into the atmosphere. Sulfur capture is effected using alkaline sorbents such as NH₄, NaOH, or a lime [CaCO₃, CaMg(CO₃)₂]. The ammonia species has the added benefit of capturing NO_x as well. NaOH is generally used as a sulfur carrier and regenerated using lime. Equations (12)–(16) are the reactions involved with respective sorbents:

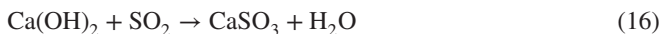
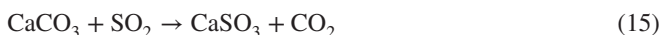
Sodium hydroxide:



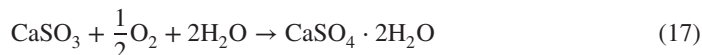
Ammonium:



Limestone:



Additional limestone is added to the effluent holding tank for precipitation of CaSO₃, which can be subsequently oxidized and hydrated with the additional air and water, creating gypsum (CaSO₄·2H₂O), as seen in equation (17):



Lime is the most efficient scrubbing agent. Therefore, the subsequent discussion will be based on lime scrubbing, which can be either a wet or dry FGD process.

Wet FGD Process. Wet FGD involves spraying finely ground limestone in aqueous slurry, as a mist into the flue gas stream. The water/calcium sulfite mixture produced is then collected in an effluent holding tank and can be further oxidized and hydrated to form calcium sulfate dehydrate (gypsum), which can be a saleable by-product if impurity levels are low enough (Fig. 22). However, there is a limited market for low-quality gypsum and as such much of the gypsum produced from FGD processes is simply land filled. However, if ammonia is used as the scrubbing agent its by-product will be (NH₄)₂SO₄, which can be used as a fertilizer.

One of the problems with using wet FGD is the formation of sulfuric acid from reactions between the water and SO₂, requiring the use of more expensive stainless steel or other corrosion-resistant material. Energy consumption of the wet FGD process ranges from 1 to 4% of the total plant-generating capacity.²⁹ A benefit of using wet FGD is that it also functions as a wet scrubber for particulate matter, as discussed in Section 4.1.3.

Dry Scrubbing. There are two different types of dry scrubbing:

1. Spray dry scrubbing using sorbent slurries
2. Dry sorbent injection

Spray drying FGD involves atomizing the sorbent slurry in the hot flue gas stream creating a large sorbent-gas surface area for SO₂ absorption (Fig. 23). The mixture is then dried in the hot flue gas stream enabling the removal of spent sorbents as a dry powder by means of appropriate

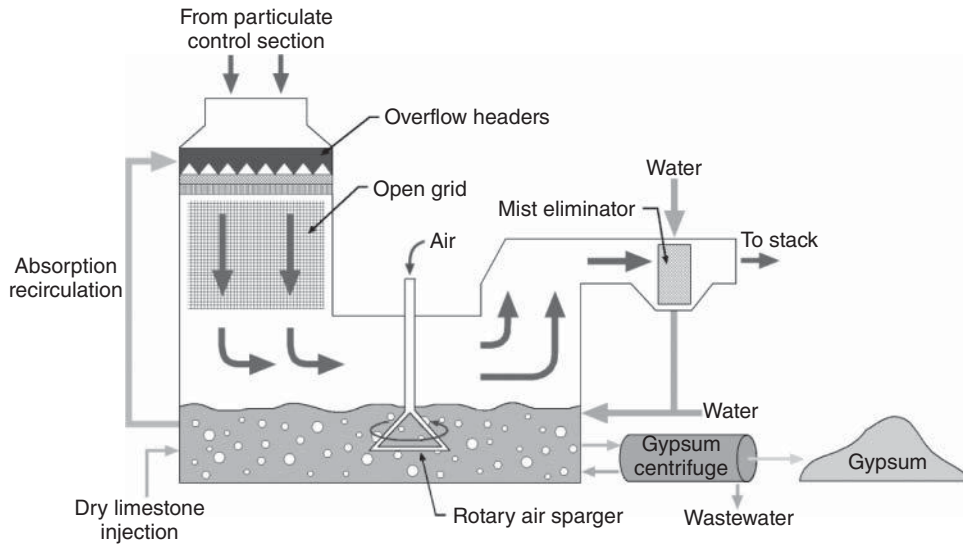


Figure 22 Wet FGD process.

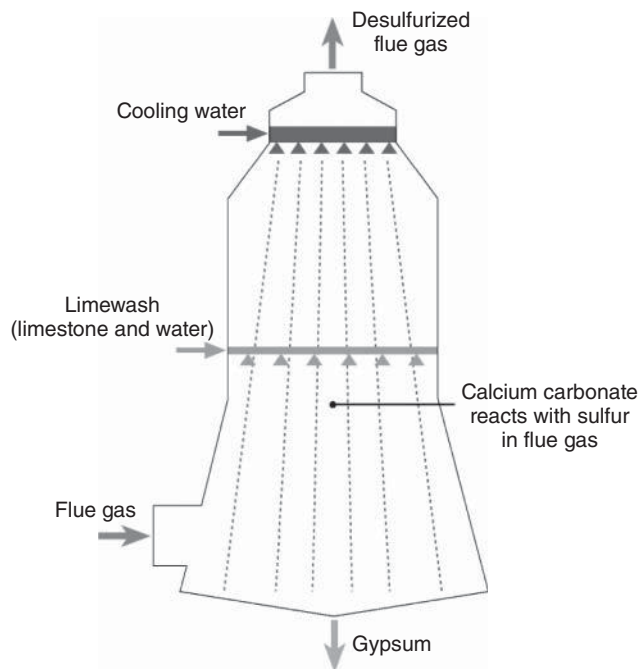


Figure 23 Spray drying FGD process.

particulate control technologies. If a bag filter is used, then the flow of flue gases through caked sorbents increases the removal of SO_2 by roughly 10%, due to the increased contact time between the sorbents and the flue gas. Spray drying sulfur removal rates are upward of 90%.²⁹

A typical dry injection system injects pulverized lime directly into the hot flue gas stream just after it exits the furnace. As in spray drying, the spent sorbent, along with fly ash, is collected in the particulate control system. Electrostatic precipitators cannot be used here, as they will not collect the sulfate product. The main drawbacks of dry FGD are the high temperatures and high Ca:S ratios required for an adequate level of sulfur capture. Impurities in the fly ash, such as chlorine, could bind to the calcium, lowering the melting temperature of the fly ash and causing fouling problems due to the high temperatures immediately after the furnace.

Benefits of dry FGD over wet FGD include reduced pumping requirements (less water use), elimination of flue gas reheating, reduced corrosion of equipment (little to no acid products are produced), and ease of handling a dry product. However, it requires a relatively high Ca:S ratio, which leads to high-alkalinity by-products that require special handling and disposal. The Ca:S ratio could be reduced if unspent sorbents were recycled.

Nitrogen Oxides

During combustion the nitrogen in both fuel and combustion air could oxidize to form the following three air pollutants:

1. NO (nitric oxide)
2. NO_2 (nitrogen dioxide)
3. N_2O (nitrous oxide)

These compounds cause a number of problems, such as:

1. Formation of ground level ozone (NO)
2. Production of photochemical smog (NO_2)
3. Formation of acid rain (NO)
4. Destruction of stratospheric ozone (N_2O)
5. Acting as a greenhouse gas (N_2O)

The oxidation of nitrogen in air (thermal NO_x) below 1000°C is generally very small. For this reason, fluidized bed boilers operating at around 850°C emit very low amounts of NO_x (Table 6).⁴² Furthermore, a number of other reactions occur, especially in the circulating fluidized bed furnace, to reduce the NO_x generated from fuel nitrogen.

The emissions from tangential fired PC boilers (350–500 ppm*) are lower than other types of PC boilers, which can have NO_x emissions as high as 1500 ppm.³⁹ Table 6 shows how the uncontrolled NO_x emissions vary with the types of firing method adopted. The two postcombustion NO_x control technologies are:

1. Selective catalytic reduction (SCR)
2. Selective noncatalytic reduction (SNCR)

Both processes use ammonia (NH_3) or urea ($(\text{NH}_2)_2\text{CO}$) to reduce NO_x back to the stable form of N_2 . The reaction is as follows:



* ppm = parts per million

Table 6 Uncontrolled NO_x Emissions

Types of Boiler	Fuel Types	Firing Type	Emission Factor, kg NO_x /tonne Coal
Pulverized firing	Anthracite	All types	9
		Front	10.5
	Bituminous	Tangential	7.5
		Front	6.5
	Lignite	Tangential	4
		Vertical firing	12.6 kg/1000 L
Residual oil	Tangential firing	5 kg/1000 L	
	Natural gas	All types	8.8 kg/1000 m ³
Fluidized bed	Bituminous	Circulating fluidized bed	100–200 ppm

Source: Adapted from Ref. 39.

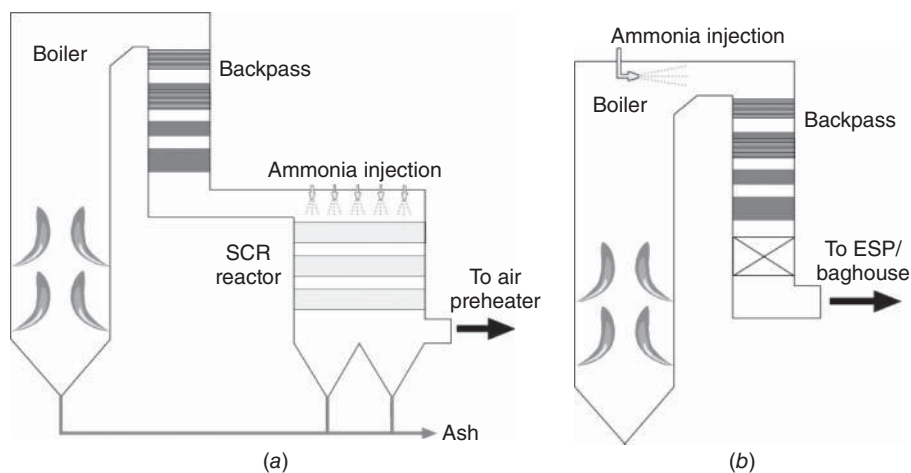


Figure 24 (a) Selective catalytic reduction (SCR) and (b) Selective noncatalytic reduction (SNCR).

Selective Catalytic Reduction. SCR occurs in a separate reactor (Fig. 24) at lower temperatures (300–400°C) in the presence of a catalyst (i.e., vanadium or a catalyst with zeolites in the wash coat). To move the reaction forward activated carbon can also be used as a catalyst and it can drive the reaction at even lower temperatures (150°C) with the added benefit of absorbing SO_2 .⁴⁰ On the downside, SCR has a high installation cost as well as high maintenance and operation costs due to the required periodic replacement of expensive catalysts. Another problem with SCR is that the ammonia injected may not be entirely consumed. The emission of NH_3 through the stack (referred to as ammonia slip) is a common problem for SCR and attention must be paid to the reagent dosage and good mixing must be present in the reaction chamber. A NO_x reduction of 90% or more is achievable using a SCR process.²⁸

Selective Noncatalytic Reduction. In SNCR, the reducing agent is injected directly into the furnace above the combustion zone in the temperature range of 900–1100°C without any catalyst. Sufficient residence time in this temperature range and uniform distribution and mixing of the reagent are required for efficient NO_x capture. The capital cost of SNCR is about half of that of SCR due to the absence of catalysts and the separate reaction chamber needed for SCR.²⁷

One problem with SNCR is the production of ammonia sulfate $[(\text{NH}_4)_2\text{SO}_4]$, which can corrode boiler tubes in the backpass. Tests done on direct ammonia injection (SNCR) in combination with a calcium sorbent have shown reductions of emissions of 85% for NO_x and 90% for SO_2 .²⁷

Nitrous Oxide

Nitrous oxide (N_2O) is a major greenhouse gas with a global warming potential 310 times (100-yr basis) higher than that of carbon dioxide, but it cannot be captured using SCR or SNCR. The intermediate combustion product hydrogen cyanide (HCN) plays an important role in reducing NO into N_2O , which can be reduced back to molecular nitrogen (N_2) if hydrogen radicals are present⁴¹:



The extent of the reduction of N_2O into N_2 as shown in equation (19) increases with combustion temperature; therefore, a higher combustion temperature favors lowering the N_2O emissions. As such, the N_2O emission from PC-fired boilers with combustion temperatures $\sim 1300^\circ\text{C}$ is in the range of 1–20 ppm, while that in fluidized bed boilers with combustion temperatures $\sim 850^\circ\text{C}$ is in the range of 20–200 ppm.¹⁴ It may be noted that NO increases with the combustion temperature, but N_2O decreases with it.

Fossil fuels with a higher volatile content decrease N_2O formation but increase NO formation. Biomass fuels emit relatively low N_2O .⁴²

4.3 Heavy Metals

A total of 11 heavy metals, classified as hazardous air pollutants (HAPs), have been detected in the flue gases of coal-fired power plants. The majority are removed using conventional particulate and gaseous control technologies, with the exception of vaporous mercury.

In 2010 the United States will implement the first emissions controls on heavy metals produced from coal-fired plants. The Clean Air Mercury Rule (CAMR) will implement mercury emissions trading and force a reduction of mercury emissions by 23% from 1999 levels and a further reduction to 69% of 1999 levels by 2018.⁴³ These regulations will force coal-fired plants in the United States to either reduce mercury emissions or pay for producing them. This has resulted in a great deal of research into mercury emissions reduction techniques in the United States in recent years.

Mercury in coal appears in three different forms. Solid mercury compound (Hg_p) is effectively removed using existing particulate control technology, with ESPs being most effective due the conductive properties of the compounds. Elemental mercury (Hg^0) and ionic mercury (Hg^{2+}) are in the form of a vapor in the flue gas and represent 90% of the mercury emissions. In coals with some chlorine the ionic mercury will be oxidized to produce mercury chloride (HgCl_2). Although HgCl_2 can be captured by conventional means, it is a very toxic substance and could pose a major waste-handling problem. Plants with wet scrubbers have shown a reduction in ionic mercury compounds but not elemental mercury, as it is insoluble in water. SCR may allow a small reduction in the elemental mercury.

The best method to remove the remaining high concentrations of elemental mercury in the flue gas stream is through the injection of a sorbent. One sorbent being investigated is Na_2CO_3 , which oxidizes the elemental mercury, making it easy to capture using a wet scrubber.⁴⁴ Activated carbon, injected either as powdered activated carbon (PAC) or as fixed-bed granular activated carbon, is an effective absorber of mercury. It has been shown that even

without activated carbon injection, 12% of the total mercury was absorbed on carbon-rich ash.⁴⁴ Through the use of sulfur-impregnated active carbon, elemental mercury reductions of more than 99%, with a relatively small mass loading, have been observed in laboratory testing.⁴⁵

Testing on existing coal-fired plants has shown that changes to combustion, air preheater, and ESP operation can reduce mercury emissions; however, a trade-off exists between emissions of Hg and NO_x.

4.4 Solid Waste

In Germany and Japan the by-products from coal combustion must be used in some way, as land filling of viable products from coal combustion is illegal. In India, where 75% of electricity is generated from fossil fuel combustion, 106 million tons of coal combustion residue is produced annually and 73% of this is put into landfills, showing the need to make use of this waste.⁴⁶

Solid wastes include fly ash, bottom ash, boiler slag, FGD waste, and SCR waste. Ash produced from regular PC-fired boilers has use as an aggregate for concrete, road construction, and general fill. Currently, the U.S. EPA does not classify this waste as a hazardous material, even though it contains trace amounts of heavy metals, which could leach out of a landfill site and cause environmental problems.

The solid residues from a fluidized bed boiler with sulfur capture are composed of spent sorbent CaSO₄, which can be hydrated to make gypsum (CaSO₄·2H₂O), but due to the presence of ash from the coal, the quality of the gypsum is reduced and thus the main use for bed ash would be as a low-grade cement or soil remediation. Boilers firing low-sulfur coal without limestone feed produce ash particularly suitable for cement production.

FGD processes using a lime-based sorbent produces gypsum as a by-product, which can be used in low-quality concrete or wall board manufacture. If the combustion efficiency of the process is low and a large amount of carbon fines remain with the gypsum, then the product is unusable unless the carbon can be removed. In addition, heavy metals and high alkalinity due to unreacted CaO could make solid by-products toxic and difficult to use or handle. Dry FGD, which uses a higher Ca:S ratio, is more prone to this problem than wet FGD is. If the material has a high alkalinity, it could see alternate usage as a soil amendment to neutralize soil acidity.

The IGCC plants can capture sulfur as either sulfuric acid or elemental sulfur. Sulfuric acid is an important commodity chemical. The major use (60% of total worldwide) for sulfuric acid is in the production of phosphoric acid, used for manufacture of phosphate fertilizers, and as trisodium phosphate for detergents. It also finds use in sulfate fertilizers, nylon, and lead-acid battery manufacturing. Elemental sulfur has a large number of uses, a few being gunpowder, vulcanized tires, and Epsom salts.

5 CARBON DIOXIDE

Coal produces more CO₂ than any other fossil fuel, and as such, the concern over global warming is a major issue with coal-fired power plants. The easiest means for reducing CO₂ emissions from coal-fired plants is to increase the efficiency of the plant, thus emitting less CO₂ for a given amount of power produced. This alone may not be enough to curb the rising levels of CO₂ in the atmosphere. Emissions must be not only reduced but also eliminated to curb rising greenhouse gas levels in the atmosphere. To do this an almost pure stream of CO₂ must be produced and transported to a proper disposal site for permanent storage, as is done for nuclear wastes.

Figure 25 outlines management plans for reducing CO₂ emissions from coal-fired power plants and its sequestration. Reduction in emissions through improved efficiency and cofiring of

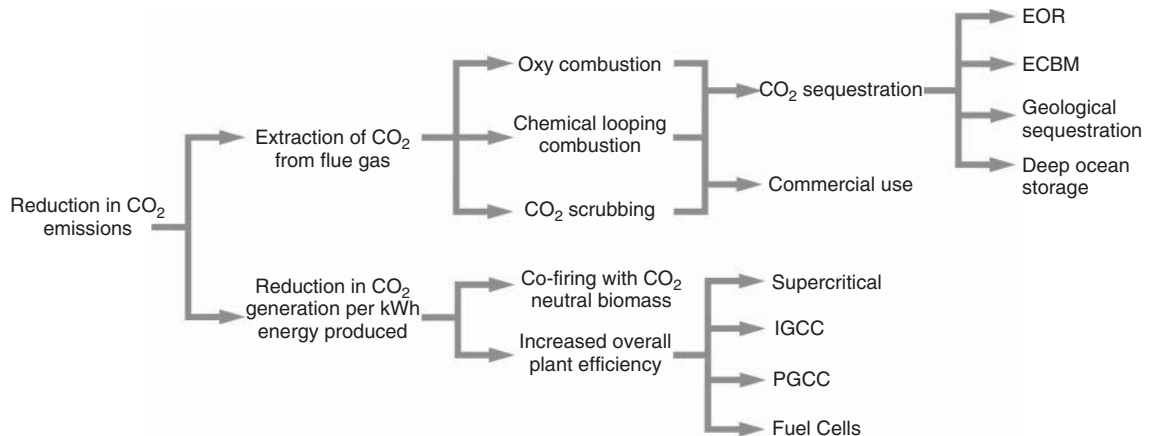


Figure 25 Means for reduction of CO₂ emissions from coal-fired power plants and its sequestration.

carbon neutral biomass in coal-fired plants are not discussed here. Carbon dioxide management has three steps:

1. Capture
2. Transportation
3. Disposal (sequestration)

5.1 CO₂ Capture

The systems for CO₂ capture can be grouped under three categories:

1. Precombustion
2. During combustion (oxygen-fired or chemical looping combustion)
3. Postcombustion

Precombustion

Precombustion capture of CO₂ involves separation of carbon dioxide from the fuel before it is burnt. Gasification is an example of a precombustion process. Here a synthesis gas is produced in a gasifier through reaction of the coal with air, steam, or oxygen to produce a synthesis gas composed of hydrogen and carbon monoxide.¹⁴ Refer to equations (7)–(10) for gasification reactions.

The CO₂ can be separated from the product gas by a suitable separation technique to produce a carbon-free hydrogen stream, carrying the energy from the fuel. This hydrogen can be either used in fuel cells or gas turbine engines for energy production.

The flue gas from air-blown coal-fired plants is only 13–15% carbon dioxide, insufficient for cost-effective transportation and sequestration. The simplest way to obtain an almost pure stream of CO₂ is to use a nitrogen-free combustion process, which results in a concentrated stream of CO₂ and water (Fig. 26). The CO₂ could then be easily dehydrated, pressurized, and pumped to the sequestration site.

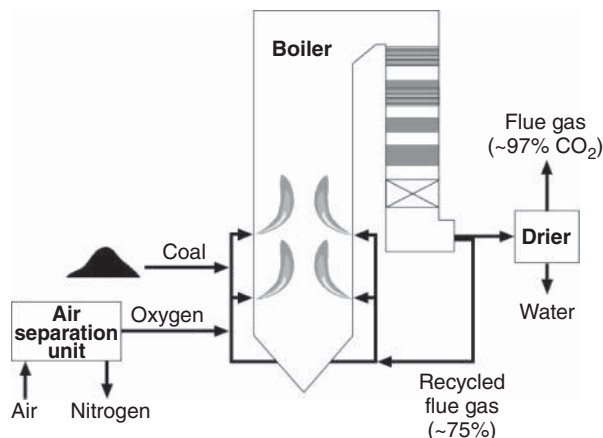


Figure 26 High-concentration carbon dioxide stream produced using oxygen fuel combustion.

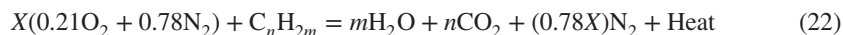
Combustion

There are two main methods of separating CO₂ during combustion:

1. Oxy-fuel combustion
2. Chemical looping combustion

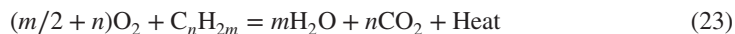
Oxy-Fuel Combustion. Traditionally, oxygen in air is used as the oxidant for combustion. This produces a flue gas containing large amounts of nitrogen, making it unsuitable for CO₂ sequestration or for commercial use. The nitrogen content in the flue gas can be reduced by adding oxygen to the combustion air⁴⁷ or even eliminated by burning the fuel in pure oxygen. In oxy-fuel combustion plants, oxygen is separated from air and used in the boiler instead of air for combustion. Equations (22) and (23) illustrate the process:

Air combustion



where $0.42X = m + 2n$

Pure oxy-combustion



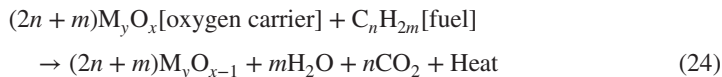
In oxy-fuel combustion plants, oxygen is separated from air and used in the boiler instead of air for combustion. Elimination of nitrogen in the oxidant brings with it a number of benefits, including pure carbon dioxide in flue gas:

1. The flue gas is composed of CO₂ and water vapor. After condensing out the water, the flue gas available is pure carbon dioxide that is ready for transport and sequestration or sale.
2. Thermal efficiency of the boiler is enhanced due to reduced flue gas volume and, hence, lower dry flue gas loss.
3. A higher percentage of CO₂ and/or H₂O in the flue gas enhances the nonluminous radiation from flue gas and results in a higher specific heat than that of nitrogen, the main diluent of normal flue gas. This increases the heat transfer rates in the backpass and reduces the required size of heat transfer surfaces.
4. High volumetric and grate heat release rates are obtained, and therefore the size of the boiler furnace could be reduced.⁴⁸

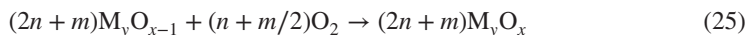
Chemical Looping Combustion. In a chemical looping combustion process, the oxygen for combustion is provided by a metal oxide which absorbs oxygen from air in a separate reactor. Chemical looping combustion processes result in pure nitrogen in one reactor and pure carbon dioxide, after combustion, in the other.

Figure 27 shows the principle of chemical looping combustion. In reactor A, the fuel, C_nH_{2m} , reacts with the oxygen carrier metal oxide, M_yO_x , to produce CO_2 and H_2O . This exothermic reaction generates the combustion heat. In reactor B, the reduced oxygen carrier M_yO_{x-1} reacts with the oxygen in air, regenerating the oxygen-carrying metal oxide, M_yO_x .⁵⁰ The reaction is expressed in equations (24) and (25):

Fuel reactor A



Air reactor B



The major advantage of chemical looping combustion over the oxy-fuel option is that it does not require the expensive oxygen separation plant. Furthermore, the extra power consumption and hence extra CO_2 generation for oxygen separation are avoided.

Metal oxides such as Fe_2O_3 , Mn_3O_4 , CuO , and NiO impregnated on quartz, alumina, or other inert materials act as the oxidant for combustion by transporting the O_2 .⁵¹ Johansson et al.⁵⁰ studied the reactivity and crushing strengths of 58 different oxygen carriers in a

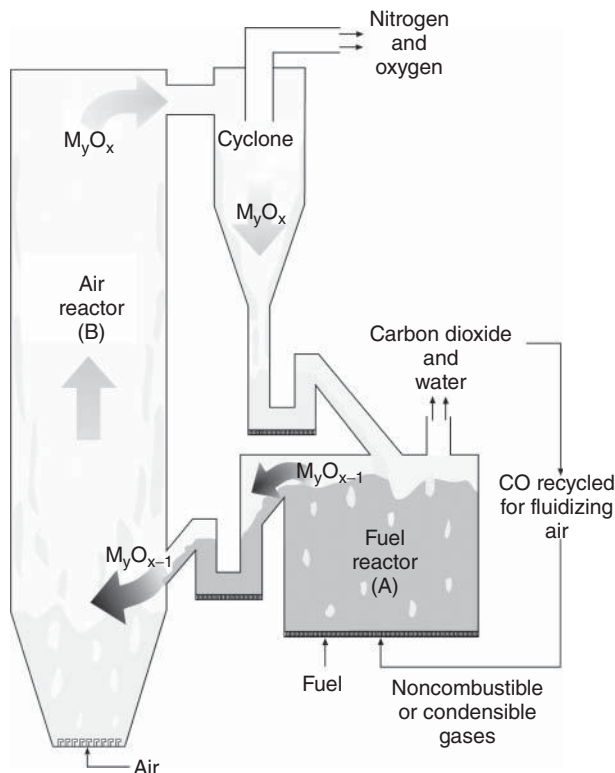


Figure 27 Chemical looping combustion.

circulating fluidized bed burning methane.⁵² Nickel-based particles were most active, followed by copper, manganese, and iron.

Chemical looping combustion is in its early stage of development, and issues around solid fuel combustion and burning in large furnaces are yet to be sorted out.

Postcombustion CO₂ Extraction

Available processes for stripping CO₂ from the flue gas can be classified into three groups:

1. Separation with sorbent/solvents
2. Membrane separation
3. Separation by cryogenic distillation

Separation with Sorbent/Solvents. Currently, the sorbent/solvent absorption method is more advanced and closer to commercialization than other options. With this process, the separation is achieved by passing the flue gas through a reaction chamber in intimate contact with a liquid or solid sorbent that is capable of capturing the CO₂. The sorbent with dissolved CO₂ is then transported to a different vessel where, due to changes in pressure, temperature, or other conditions, it releases the CO₂. The regenerated sorbent is sent back to the first vessel to capture more CO₂ in a cyclic process.

In some processes that use this type of separation, the solid sorbent does not circulate between vessels; the sorption and regeneration are achieved by cyclic changes in pressure. This process is called *pressure swing adsorption* (PSA). In PSA a high-pressure flue gas stream is passed through a porous material, where the CO₂ is preferentially adsorbed. When the pressure is decreased, the CO₂ is desorbed from the porous sorbent for sequestration. Three sorbents recently studied for use in PSA were molecular sieve 13X, natural zeolite ZS500A, and activated carbon.⁵²

In amine scrubbing, the flue gas is passed through a large vessel, usually an absorbing tower, and mixed with an amine-based solvent (organic molecule with nitrogen at the core, such as NH₄, NCH₅, etc.), which captures the CO₂ (Fig. 28). The CO₂ is then stripped off the amine using large amounts of low-quality heat, producing a stream of concentrated CO₂. This heat is provided by low-temperature steam generated through the burning of extra fuel. The CO₂ must be compressed to 150 bars to facilitate transport and sequestration.⁵³ The amine is

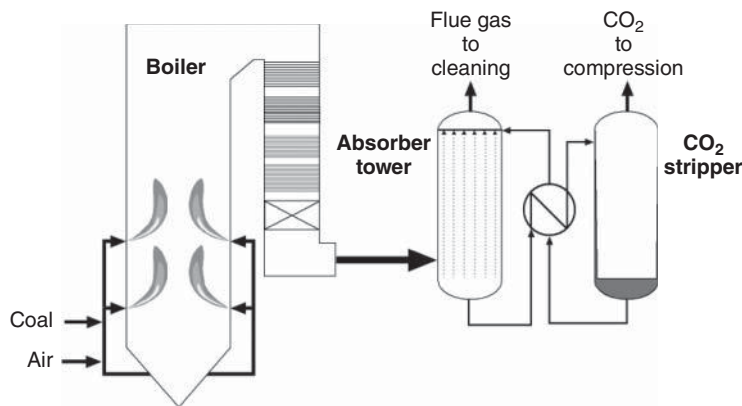


Figure 28 CO₂ capture using an amine scrubber.

regenerated and fed back to the absorbing tower. One drawback to this would be the possible capture of not only CO₂ but also NO_x and SO₂. Although this is good for boiler emissions, it contaminates the CO₂ stream produced, preventing its commercial use.

Membrane Separation. Gas separation membranes, used commercially for separation of CO₂ from natural gas, are being considered for flue gas separation. This method relies on differences in physical or chemical interactions between the different substances in a gas mixture and a membrane material that allow one gas to move through the membrane at a faster rate than another. Such a membrane would allow carbon dioxide gas to pass through while excluding the other parts of the flue gas emitted from industry or power plants. If a pressure differential is set up on opposing sides of a membranelike polymeric film, gas transport across the film (permeation) will occur. The CO₂ will permeate through the membrane at a faster rate than the nitrogen or other flue gas components, producing a CO₂-rich stream. Polymers such as cellulose acetate, hollow-fiber polyimides,⁵⁴ and polypropylene⁵⁵ are also being considered as membrane materials.

Separation by Cryogenic Distillation. Distillation is the separation of various gases through the differences in their relative volatility or boiling points. The CO₂-containing flue gas is compressed and cooled below the boiling point of the CO₂. The liquid carbon dioxide is distilled out of the cooled flue gas and separated for storage or use. Carbon dioxide has a relatively high boiling point (−78°C at 1.0 atm) compared to other components of the flue gas, such as nitrogen (−196°C at 1.0 atm). A second distillation of the carbon dioxide stream may be necessary to remove other gases that also have lower boiling points, such as sulfur dioxide (−10°C at 1.0 atm).

Cost of Separation

The oxy combustion process needs power for the oxygen separation, requiring additional fuel to be burnt to produce this extra energy. On a fuel-equivalent basis, oxy combustion requires about 1.32 MWth (MW thermal) per tonne of CO₂ avoided, compared to amine scrubbing, which requires 2.8 MWth per tonne of CO₂ avoided.⁵³ Taking into account an air infiltration (~3%), 95% oxygen purity and extra CO₂ produced for extra auxiliary power, the oxy combustion can avoid about 66% of the original CO₂ emission compared to 58% for amine scrubbing, both with 90% capture.⁵³

5.2 Transportation

For transportation of the captured CO₂ two options are available:

1. *Pipeline Transportation.* This is suitable for transportation of large amounts of CO₂ (>40 million tonnes/yr) over small distances (<2500 km).⁵⁶
2. *Use of Ships.* This is suitable for small amounts of CO₂ (<few million tonnes/yr) over large distances (overseas).

In the United States, approximately 2500 km of CO₂ pipeline already supplies several million tons of CO₂ per year to enhanced oil recovery (EOR) projects.⁵⁷ Transportation of carbon dioxide through pipelines is done in the gaseous phase to avoid problems associated with two-phase flow as pressure drops in the pipeline. Due to similar chemical properties with propane, transportation of liquid CO₂ in trucks and ships is a readily available transportation option. However, the large amounts of CO₂ produced from coal-fired plants make these methods inadequate, as they can transport only small quantities at a time.

There are a few health concerns with transportation of CO₂ because it is toxic in concentrations above 10% and is heavier than air, allowing it to accumulate in low-lying areas. This makes

opposition to onshore CO₂ pipelines high; however, offshore pipelines would require longer transport distances as well as more complex and costly infrastructure.⁵⁸

5.3 Sequestration and Utilization

Carbon dioxide sequestration is the process of keeping anthropogenic CO₂ out of the atmosphere by storing it deep underground. If the CO₂ stream contains other gases, it will make carbon sequestration more costly. These gaseous impurities also increase the minimum miscibility pressure, meaning that the CO₂ stream will have to be pumped to a higher pressure for EOR applications, so a nearly pure stream of CO₂ is required. The CO₂ can be stored permanently either in deep onshore/offshore geological formations or at the bottom of the ocean. Several options are available for sequestration of carbon dioxide, as discussed below. Carbon sink management and industrial use are other CO₂ reduction methods.

Underground Sequestration

There are a number of ways to sequester a high-pressure stream of carbon dioxide. For example, it can be pumped deep (~800 m) into any of the following:

- Empty oil wells or other geological formations
- Saline aquifers, as done in the Sleipner and Snøhvit projects in Norway
- Active oil wells for EOR, as done in the Weyburn project in Canada
- Active gas fields, as in the In-Salah project in Algeria (Fig. 29)

Carbon dioxide can also be pumped to shallower depths into unrecoverable coal seams where it is adsorbed on the coal surface. This also has the potential for enhanced coal bed methane (ECBM) extraction.

Enhanced oil recovery is the preferred technology, as it has a value-added effect over geological sequestration and is more proven than ECBM extraction, which does not have any pilot-scale testing yet. EOR is being used at the Weyburn oil field in Saskatchewan, Canada, with the pressurized carbon dioxide being pumped 400 km north from the Great Plains synfuel plant in North Dakota at a rate of 5000 tons/day.

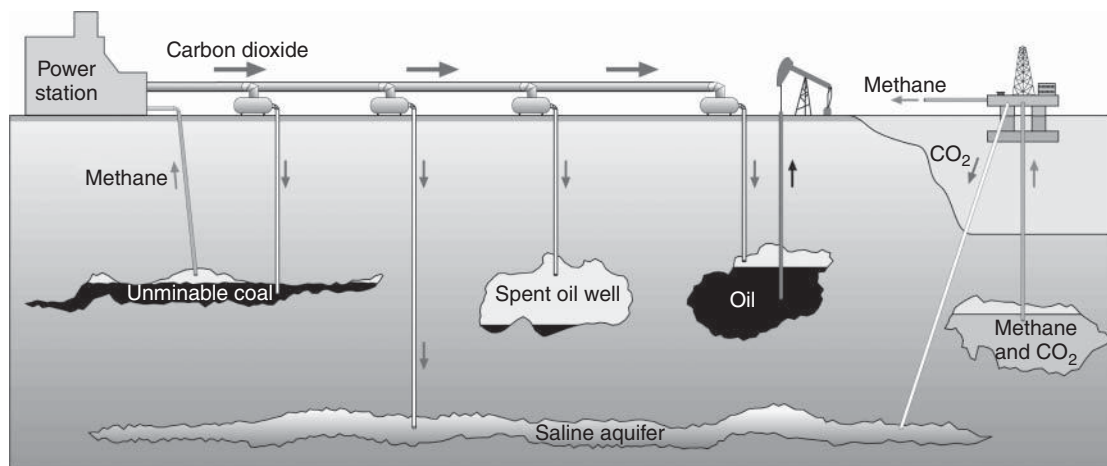


Figure 29 Carbon dioxide sequestration options.

Undersea Sequestration

At atmospheric temperature and pressure, carbon dioxide remains in the gaseous state, but it can be turned into a liquid by compression within the temperature range of -56.5 and $+31.1^{\circ}\text{C}$. Above its critical temperature (31.1°C), the gaseous CO_2 can be compressed to a very high density, even exceeding that of water. Thus, CO_2 can be stored under the ocean floor, where the pressure is very high, without the risk of being released to the atmosphere above. Carbon dioxide is soluble in water, but its solubility (0.25 kg CO_2 /100 kg water at 20°C and 1 bar pressure) decreases with temperature, pressure, and the salinity of water. At depths below 3000 m, the pressurized liquid CO_2 is denser than water and will form an undersea lake and not rise to the surface.

There is great concern over this type of CO_2 storage, as there is a chance the CO_2 will dissolve into the surrounding water over the long term, acidifying the water and destroying aquatic life.

Industrial Utilization

Industrial use of CO_2 is the only disposal/sequestration option with direct revenues. With this option, the captured CO_2 is used as a feedstock in chemical processes. Pure CO_2 finds use in the industry as a coolant, to carbonate beverages, and in the pharmaceutical industry as a nontoxic solvent. These uses can absorb only a fraction of the CO_2 generated by even a medium-size coal-fired plant, which generates about 8000 tons/day. About 100,000 tons of CO_2 is used by U.S. industry annually.⁵⁸ Using CO_2 for such purposes does not eliminate the CO_2 emissions as it is still released into the atmosphere in the end.

Carbon Sink Management

The Kyoto Protocol and Marrakesh Accords to the United Nations Framework Convention on Climate Change recognize land use, land use change, and forestry activities—mainly afforestation and reforestation—as a potential means to reduce carbon dioxide concentration in the atmosphere and help developed countries to meet the reduction targets allocated through Kyoto.⁵⁹

5.4 Cost Implications

The additional energy required and the cost involved in CO_2 separation and sequestration are preventing immediate commercial implementation of carbon dioxide separation and its sequestration from coal-fired power plants. The National Energy and Technology Laboratory (NETL) of the United States, along with other groups around the world, are currently studying this issue in the hope of developing viable solutions to reduce the cost of CO_2 separation and sequestration. For example, in a 400-MW net power plant, using oxy-fuel combustion of pulverized coal with cryogenic oxygen separation, the base plant power consumption was 30 MW, while that for CO_2 capture was 102 MW (CO_2 compression = 37 MW, CO_2 transport over 10 miles is greater than 1 MW, storage in an aquifer is 3 MW).⁶¹ Ciferno and Plasynski⁶¹ compared different technologies for CO_2 capture and their costs (Table 7). It is noteworthy that the rise in cost of electricity ranged from 37 and 66% for different CO_2 capture technologies used. Another study compared the CO_2 capture cost for three technologies and found amine scrubbing to be least expensive (Table 8).⁶²

Richards and Stokes⁶³ analyzed data from several countries ranging from India to the United States for the cost of carbon sequestration through forestation, it being highly country and geography specific. In general, the cost is lower than that for sequestration under the sea or ground.

Table 7 Cost of Carbon Capture and Sequestration^a

	Amine Scrubbing	Aqueous Ammonia CO ₂ Capture	Oxy-Fuel PC Combustion with Cryogenic ASU	Oxy-Fuel PC Combustion, Membrane ASU
Units in Operation	1	4	6	7
Increase in COE, %	66	37	64	40
CO ₂ avoidance cost, \$/tonne	42	24	42	25
Increase in capital cost, %	64.6	43.7	77.8	46.3
Efficiency, ^b % (HHV)	29	34	30	32
Auxiliary load, MW	85	78	172	125

^aFor a double reheat supercritical plant with 400 MW net power, 80% capacity factor firing bituminous #6 coal, 90% CO₂ capture, compressed to 2200 psia, transported 10 miles and stored in a saline formation

^bBase case efficiency and auxiliary load are 41% and 21 MW, respectively

Source: Adapted from Ref. 61.

Table 8 Techno-Economic Comparison of CO₂ Capture Technologies

Fuel Technology		Bituminous Gasification	Subbituminous Gasification	Lignite Gasification	Lignite Amine scrubbing	Lignite Oxy-fuel combustion
COE, ^a	\$/MWh	107	97	131	116	152
CO ₂ emitted,	tonnes/MWh	0.116	0.111	0.182	0.06	0.145
CO ₂ avoided,	tonnes/MWh	0.65	0.74	0.71	0.82	0.74
Cost of CO ₂ avoided,	\$/Tonne	47	52	88	57	112
Capacity	MW net	594	437	361	311	373
Net heat rate,	kJ/kWh	11,410	13,810	13,240	12,530	14,880
Unit cost,	\$/kW net	3,000	3,400	4,400	4,400	6,200

^aCost of electricity for 90% capacity factor.

Source: From Ref. 62.

The sequestration cost depends to a great extent on the pipeline length, sequestration site, geological formation, amount of carbon dioxide sequestered, and so on. Cudnik⁶⁴ predicted a cost of \$1–\$70/tons CO₂ for 100–3500 Mt of CO₂, but it went sharply up to about \$700 when the requirement exceeded 3500 Mt, as capacities were not available at the site. The Canadian Clean Power Coalition (CCPC)⁶² studied three specific sites in Canada and predicted a cost of \$38/tons CO₂ for enhanced oil recovery sequestration 200 km away, \$10/tons CO₂ for sequestration for enhanced coal bed methane extraction 100 km away, and \$4/tons CO₂ for geological sequestration 75 km away. Another study for a 500-MW plant in Ontario predicts a cost \$7.5–\$11.5/tons CO₂ for sequestration at 1000 m depth in sea 150 km away.⁶⁵ The sequestration cost was 10–30% of the total cost of CO₂ capture and sequestration.

6 CONCLUSION

Coal currently supplies 38% of the world's electricity needs, and this number is expected to grow by 1.4% per year over the next 30 years.¹ This growth in coal usage could occur in an environmentally responsible way, because available *cleaner coal technologies* can meet even the most stringent emission requirements with only a modest increase in the price of electricity.

Utilities have made great improvements in the reduction of particulates, SO₂, and NO_x emissions from coal-fired power plants, and this will likely continue to improve in the coming decades. The improvements will be driven by the economic disincentives associated with polluting brought about by government legislation. In the near term, supercritical plants with PC or CFB firing will dominate coal-based power generation, followed by IGCC. More advanced technologies like partial gasification combined cycle and fuel cell may take some time to come to the mainstream utility market.

Reducing and eventually eliminating carbon dioxide emissions will be a very challenging, although not impossible, task for the coal industry. The positive news is that the utility industry has been able to meet every emission challenge in the past, and this new challenge should be no different. The need to avoid potentially drastic, irreversible changes to our climate is imperative and is reflected in the following quote: "There is broad agreement within the scientific community that amplification of the Earth's natural greenhouse effect by the build-up of various gases introduced by human activity has the potential to produce dramatic changes in climate."*

In 1990, the CO₂ concentration in the atmosphere was 350 ppm.⁶⁶ By 2006, the concentrations rose to about 380 ppm, a dramatic 8.5% increase in 16 years. Technologies for separation and disposal of the CO₂ from coal-fired plants are available to arrest this dramatic rise in CO₂ concentration within a reasonable cost. "Only by taking action now can we ensure that future generations will not be put at risk."*

REFERENCES

1. International Energy Agency (IEA), "World Energy Outlook," IEA, Paris, France, 2006.
2. U.S. Department of Energy, "FutureGen—Tomorrows Pollution Free Power Plant," available: www.fossil.energy.gov/programs/powersystems/futuregen, accessed 2003.
3. European Commission, "Outline Concept and Tentative Structure for the Technology Platform—Zero Emission Fossil Fuel Power Plants," Report noTP-ZE-AC-4/2005, Advisory Council Meeting, September 9, 2005, available: http://ec.europa.eu/research/energy/nn/nn_rt/nn_rt_co/article_2268_en.htm.
4. M. Eastman, "Clean Coal Power Initiative," paper presented at the US–PRC Conference on Clean Energy, U.S. Department of Energy, NETL, Washington, D.C., November 2003.
5. Ontario Ministry of the Environment, "Air Quality in Ontario—2004 Report," Environmental Monitoring and Reporting Branch, 2004.
6. U.S. Food and Drug Administration (FDA), *What You Need to Know about Mercury in Fish and Shellfish*, FDA, Washington, D.C., March 2004.
7. J. B. Calvert, "Mercury: The Lore of Mercury, Especially Its Uses in Science and Engineering," University of Denver, available: <http://www.du.edu/~jcalvert/phys/mercury.htm#Pois>, accessed May 2004.
8. National Mining Association, "Clean Coal Technology: Current Progress, Future Promise," available: www.nma.org/technology/environmental.asp, 2002–2007.
9. World Coal Institute, available: <http://www.worldcoal.org/pages/content/index.asp?PageID=19>, accessed 2006.
10. International Energy Agency (IEA), "Clean Coal Technologies," IEA Clean Coal Center, available: <http://www.iea-coal.org.uk/content/default.asp?PageId=62&LanguageId=0>, 2007.
11. N. Berkowitz, *An Introduction to Coal Technology*, 2nd ed., Academic, San Diego, CA, 1994.
12. H. Termuehlen and W. Emsperger, *Clean and Efficient Coal-Fired Power Plants*, ASME Press, New York, 2003.
13. P. Basu, "An Arrangement for Conversion of Existing Fossil Fuel Fired Boiler into Circulating Fluidized Bed Firing," Canadian Patent No. 2159949, November 5, 2005.
14. P. Basu, *Combustion and Gasification in Fluidized Beds*, Taylor & Francis, CRC Press, Boca Raton, FL, 2006.

* Statement by 49 Nobel Prize winners and 700 members of the National Academy of Sciences, 1990.

15. U.S. Department of Energy (DOE), NETL, "Clean Coal Technology Roadmap," Electric Power Research Institute and the Coal Utilization Research Council, available: <http://www.netl.doe.gov/technologies/coalpower/cctc/pubs/CCT-Roadmap.pdf>, 2006.
16. S. C. Stultz, (Ed.), *Steam*, 41st ed., Babcock & Wilcox, Barberton, OH, 2005.
17. Natural Resources Canada (NRCAN), CANMET Energy Technology Center, available: http://www.nrcan.gc.ca/es/etb/cctc/cctc01/htmldocs/home_e.htm, 2007.
18. S. J. Goidich, S. Wu, and Z. Tan, "Design Aspects of the Ultra-Supercritical CFB Boiler," in *Proceedings of the International Pittsburgh Coal Conference*, Pittsburgh, PA, September 12–15, 2005.
19. J. M. Beér, "Combustion Technology Developments in Power Generation in Response to Environmental Challenges," *Progr. Energy Combustion Sci.e.*, **26**, 301–327, 2000.
20. S. Azuhata, "Advanced Clean Coal Technology," IEEE, 2000.
21. P. Basu and P. K. Halder, "A New Concept for Operation of Pulverized Coal Fired Boiler Using Circulating Fluidized Bed Firing," *Trans. ASME*, 626–630, October 1989.
22. P. Basu and J. Talukdar, "Revamping of a 120 Mwe Pulverized Coal Fired Boiler with Circulating Fluidized Bed Firing," in D. W. Geiling (Ed.), *Proceedings of the 16th International Fluidized Bed Combustion Conference*, Reno, NV, May 13–16, ASME, 2001.
23. S. Kavidass, D. J. Walker, and G. S. Norton Jr., "IR-CFB Repowering: A Cost-Effective Option for Older PC-Fired Boilers," *Power-GE Int.* 1999, November 30–December 2, 1999.
24. R. Viswanathan, J. F. Henry, J. Tanzosh, G. Stanko, J. Shingledecker, B. Vitalis, and R. Purgert, "U.S. Program on Materials Technology for Ultra-supercritical Coal Power Plants," *J. Mater. Eng. Perform.*, **14**(3), 281–292, June 2005.
25. G. Sormani, and G. Moscatelli, "AVEDORE no. 2—The Most Advanced Steam Turbine Generator in the World," paper presented at the International Exhibition & Conference for the Power Generation Industries, 1997.
26. G. Sormani, and G. Moscatelli, "AVEDORE no. 2—The Most Advanced Steam Turbine Generator in the World," paper presented at the International Exhibition & Conference for the Power Generation Industries—Power-Gen, 81, 1997.
27. M. K. MacRae, *New Coal Technology and Electric Power Development*, Canadian Energy Research Institute, 1991.
28. B. Davidson, "Clean Coal Technologies for Electricity Generation," *Power Eng. J.*, **7**(6), 257–263, December 1993.
29. IEA, "China Makes a Start on Advanced 'Clean Coal' Generation," *Review, News*, February 2005, p. 12.
30. D. R. Simbeck, N. Korens, F. E. Biasca, S. Vejtsa, and R. L. Dickenson, "Coal Gasification Guidebook: Status, Applications, and Technologies," TR-102034, Final Report, Prepared for Electric Power Research Institute, December 1993.
31. K. Jothimurugesan, S. K. Gangwal, R. Gupta, and B. S. Turk, "Advanced Hot-Gas Desulphurization Sorbent," paper presented at the Advanced Coal-Based Power and Environmental Systems '97 Conference, July 1997.
32. S. Blankinship, "Amid All the IGCC talk, PC Remains the Go-to-guy," *Power Eng.*, 16–22, April 2006.
33. J. Ratafia-Brown, L. Manfredo, J. Hoffmann, and M. Ramezan, "Major Environmental Aspects of Gasification-Based Power Generation Technologies," Final Report, Gasification Technologies Program National Energy Technology Laboratory, U.S. DOE, Washington, DC, December 2002.
34. World Coal Institute, "Clean Coal: Building a Future through Technology," World Coal Institute, available: <http://www.worldcoal.org/pages/content/index.asp? PageID =36>, July 2004.
35. A. Robertson, Z. Fan, D. Horazak, R. Newby, H. Goldstein, and A. C. Bose, "2nd Generation PFB Plant with W501G Gas Turbine," in *Proceedings of FBC2005, 18th International Conference on Fluidized Bed Combustion*, 2005.
36. P. Basu, C. Kefa, and L. Jestin, *Boilers & Burners—Design and Theory*, Springer, New York, 2000, p. 57.
37. G. E. Tooker, "Troubleshooting Dust Collection Systems," Air Control Science Inc., available: www.aircontrolscience.com/uploads/publications/, 1996.

38. S. J. Miller, G. L. Schelkoph, G. E. Dunham, K. Walker, and H. Krigmont, "Advanced Hybrid Particulate Collector, A New Concept for Air Toxics and Fine-Particle Control," Topical Report prepared for Program Research and Development Program, U.S. Department of Energy, Washington, DC, 2002.
39. U.S. Environmental Protection Agency (EPA), *Control Techniques for Nitrogen Oxide Emissions from Stationary Sources*, 2nd rev. ed., EPA-450/3-83-002, EPA, Research Triangle Park, NC, 1983.
40. K. Knoblauch, E. Richter, and H. Juentgen, "Application of Active Coke in Processes of SO₂ and NO_x Removal from Flue Gasses," *Fuel*, **60**(9), 832–838, September 1981.
41. L. E. Amand and S. Andersson, "Emissions of Nitrous Oxide from Fluidized Bed Boilers," in *Proceedings of the 10th International Conference on Fluidized Bed Combustion*, 1989.
42. B. Leckner, M. Karlsson, M. Mjornell, and U. Hagman, "Emissions from a 165 MWth Circulating Fluidized Bed Boiler," *J. Inst. Energy*, **65**(464), 122–130, 1992.
43. J. Winters, "News and Notes—Quashing Quicksilver," *Mech. Eng.*, **127**(11), November 2005.
44. Y. Tan, R. Mortazavi, B. Dureau, and M. A. Douglas, "An Investigation of Mercury Distribution and Speciation During Coal Combustion," *Fuel*, **83**, 2229–2236, 2004.
45. R. Yan, D. T. Liang, L. Tsen, Y. P. Wong, and Y. K. Lee, "Bench-Scale Experimental Evaluation of Carbon Performance on Mercury Vapour Adsorption," *Fuel*, **83**, 2401–2409, 2004.
46. P. Asokan, M. Saxena, and S. R. Asolekar, "Coal Combustion Residues—Environmental Implications and Recycling Potentials," *Resour. Conservation Recycling*, **43**, 239–262, 2005.
47. R. Hugh, L. Jia, Y. Tan, E. J. Anthony, and A. Macchi, "Oxy-Fuel Combustion of Coal in a Circulating Fluidized Bed Combustor," in F. Winter (Ed.), *Proceedings of the 19th International Conference on Fluidized Bed Combustion*, Vienna, Part—I, May 22–24, 2006.
48. J. Saastamoinen, A. Tourunen, T. Pikkarainen, H. Hasa, J. Miettinen, T. Hyppanen, and K. Myohanen, "Fluidized Bed Combustion in High Concentrations of O₂ and CO₂," in F. Winter (Ed.), *Proceedings of the 19th International Conference on Fluidized Bed Combustion*, Vienna, Part—I, May 22–24, 2006.
49. International Energy Agency (IEA), "Clean Coal Technologies," IEA Briefing Paper No. 83, IEA, November 2004.
50. M. Johansson, T. Mattison, and A. Lyngfelt, "Comparison of Oxygen Carriers for Chemical-looping of Methane-Rich Fuels," in F. Winter (Ed.), *Proceedings of the 19th International Conference on Fluidized Bed Combustion*, Vienna, F. Part—I, May 22–24, 2006.
51. J. Adanez, P. Gayan, J. Celaya, L. F. de Diego, F. Garcia-Labiano, and A. Abad, "Behavior of a Cuo-Al₂O₃ Oxygen Carrier in a 10kW Chemical-looping combustion plant," in F. Winter (Ed.), *Proceedings of the 19th International Conference on Fluidized Bed Combustion*, Vienna, May 22–24, 2006.
52. R. Siriwardane, M. Shen, E. Fisher, J. Poston, and A. Shamsi, "Adsorption and Desorption of CO₂ on Solid Sorbents," Prepared for U.S. Department of Energy, National Energy and Technology Laboratory, 2002.
53. D. J. Singh, E. Croiset, P. L. Douglas, and M. A. Douglas, "CO₂ Capture Options for an Existing Coal Fired Power Plant: O₂/CO₂ Recycle Combustion vs. Amine Scrubbing," paper presented at the First National Conference on Carbon Sequestration, National Energy and Technology Laboratory, May 14–17, 2001.
54. K. Nagao, N. Booker, A. Mau, J. Hodgkin, S. Kentish, G. Stevens, and P. Geertsema, "Gas Permeation Properties of Polyimide/epoxy Composite Materials," paper presented at the 22nd ACS Fall National Meeting, Chicago, August 26–30, 2001.
55. Z. Zhikang, W. Jianli, C. Wei, and X. Youyi, "Separation and Fixation of Carbon Dioxide Using Polymeric Membrane Contactor," paper presented at the First National Conference on Carbon Sequestration, U.S. Department of Energy, NETL, May 14–17, 2001.
56. B. Metz, O. Davidson, H. Coninck, M. Loos, and L. Meyer, "Carbon Dioxide Capture and Storage," Special Report, Intergovernmental Panel on Climate Change, September, 2005.
57. R. W. Luhnning, J. H. Glanzer, P. Noble, and H.-S. Wang, "Pipeline Backbone for Carbon Dioxide for Enhanced Oil Recovery in Western Canada," *J. Can. Petroleum Technol.*, **44**(8), 55–58, August 2005.
58. R. Svensson, M. Odenberger, F. Johnsson, and L. Stromberg, "Transportation Systems for CO₂—Application to Carbon Capture and Storage," *Energy Conversion Manag.*, **45**, 2343–2353, 2004.

59. S.-E. Ahn, "An Econometric Analysis on the Costs of Carbon Sequestration in Korea," Korea Environment Institute, Seoul, Korea, 2005.
60. Z. Xu, J. Wang, W. Chen, and Y. Xu, "Separation and Fixation of Carbon Dioxide Using Polymeric Membrane Contactor," paper presented at the First National Conference on Carbon Sequestration, U.S. Department of Energy, NETL, May 14–17, 2001.
61. J. P. Ciferno and S. I. Plasynski, "System Analyses of CO₂ Capture Technologies Installed on Pulverized Coal Plants," Technical Facts, U.S. DOE, National Energy Technology Laboratory, Sequestration, December 2005.
62. Canadian Clean Power Coalition, "Summary Report on the Phase I Feasibility Studies," May 2004.
63. K. R. Richards and C. Stokes, "A Review of Forest Carbon Sequestration Cost Studies: A Dozen of Years of Research," *Climate Change*, **63**, 1–48, 2004.
64. R. Cudnik, "Managing Climate Change and Securing a Future for the Midwest's Industrial Base," paper presented at the Battelle Columbus Operations, Regional Carbon Sequestration Partnership Meeting, November 3–4, 2003.
65. A. Shafeen, "CO₂ Sequestration Opportunities for Ontario," Fossil Fuels & Climate Change Group, CEPG, CANMET Energy Technology Centre, Ottawa, Ontario, Canada, 2003.
66. NOAA, "Atmospheric CO₂ at Mauna Loa Observatory," ESRL Global Monitoring Division, available: http://www.cmdl.noaa.gov/ccgg/trends/co2_data_mlo.php, 20.

CHAPTER 22

BIOFUELS FOR TRANSPORTATION

Aaron Smith, Cesar Granda, and Mark Holtzaple

Texas A&M University

College Station, Texas

1 INTRODUCTION	767	3.10 Current Availability	783
2 ETHANOL	768	3.11 Production Capacity	783
2.1 Introduction	768	3.12 Subsidy	784
2.2 Biomass Sources	769	3.13 Safety	784
2.3 Manufacturing Methods	769	3.14 Current Research and Future of Biodiesel	784
2.4 Manufacturing Research and Development	770	4 HYDROGEN	785
2.5 Quality Standards	770	4.1 Introduction	785
2.6 Vehicle Modifications and Use	770	4.2 Manufacturing Methods	786
2.7 Performance	773	4.3 Quality Standards	788
2.8 Emissions	774	4.4 Hydrogen Vehicles	788
2.9 Fuel Transportation and Distribution	774	4.5 Emissions	792
2.10 Fuel Storage	775	4.6 Fuel Transmission and Distribution	793
2.11 Safety	775	4.7 Storage Issues	794
2.12 Subsidy	775	4.8 Current Availability	797
2.13 Current Availability	775	4.9 Safety	797
2.14 Ethanol Links	777	4.10 Current Research	798
3 BIODIESEL AND VEGETABLE OIL	777	4.11 Hydrogen Links	798
3.1 Introduction	777	5 OTHER BIOFUELS	799
3.2 Biomass Source	777	5.1 Methanol	799
3.3 Manufacturing Methods	777	5.2 Butanol	799
3.4 Quality Standards	779	5.3 Mixed Alcohols	799
3.5 Vehicle Modifications	779	5.4 Petroleumlike Biofuels	799
3.6 Performance	779	5.5 Synthesis Hydrocarbons	800
3.7 Emissions	780	5.6 Methane	800
3.8 Fuel Transportation Issues	782	6 CLOSING REMARKS	800
3.9 Storage Issues	782	REFERENCES	800

1 INTRODUCTION

Why biofuels? Biofuels offer a responsible solution to potential crises in the near future. Fossil fuels have been the dominant energy source since the Industrial Revolution because they are inexpensive, energy dense, and easy to use. Biofuels are renewable and provide a means to become independent from fossil fuels. Oil exploration is becoming more costly as more remote locations must be explored to find oil. As oil prices increase, biofuels will become economically competitive. The United States depends on foreign oil, so its oil supplies are not secure. There

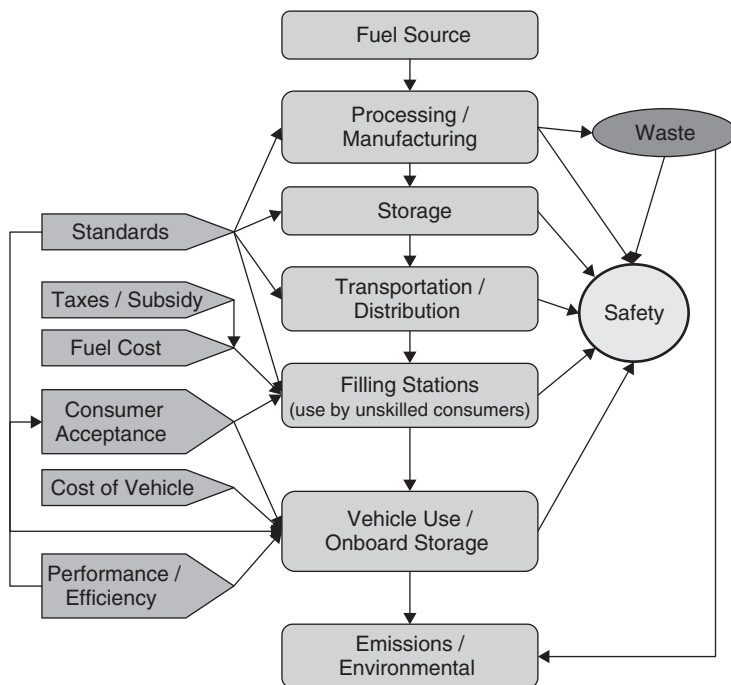


Figure 1 Considerations when selecting a biofuel.

is a growing consensus that carbon emissions from fossil fuels are a large contributor to global warming. Biofuels are carbon neutral and, therefore, address global warming. Other benefits of biofuels are improved emissions, healthier rural economies, and the potential to reduce waste.

The purpose of this chapter is to educate practicing engineers and students about biofuels for transportation. Biofuels are made from renewable materials such as plants and organic waste. Conventional transportation fuels such as gasoline or diesel are made from petroleum. Although biofuels are alternative fuels, not all alternative fuels are biofuels. For example, natural gas and propane are alternative fuels, but not biofuels.

In this chapter, ethanol, biodiesel, and hydrogen will be discussed in detail. A fourth section is included to enumerate other biofuels that are less well known yet potentially valuable. Each of the three central biofuels is reviewed objectively. Advantages and disadvantages are discussed as well as engineering and research issues. Although some detailed information is provided, our goal is for the reader to see the big picture.

Figure 1 illustrates the major considerations when selecting a biofuel. After reading this chapter, you should have a firm understanding of the ins and outs of each biofuel described.

It is the view of the authors that no single biofuel is a silver bullet; however, alcohols and vegetable oils have clear advantages. We believe the future of biofuels will be diverse, and each fuel will be selected for specific applications.

2 ETHANOL

2.1 Introduction

In 1826, Samuel Morey of Oxford, New Hampshire, built the first prototype internal combustion engine in the United States. He used alcohol biofuel in his experiments.^{1,2} In 1876, when

Nikolaus Otto invented the four-stroke internal combustion engine, he designed it to run on ethanol.² Why? Because gasoline did not exist. Henry Ford promoted ethanol and built the famous model-T to run on ethanol, gasoline, or any ratio of the two with manual adjustment to the carburetor. Ford felt so strongly about ethanol fuel that he built an ethanol plant in the Midwest.^{1,2} Eventually, the plant was closed due to competition with petroleum. In modern times, gasoline has been cheaper than alcohol, so it dominated; however, alcohols such as ethanol are excellent motor fuels.³

Ethanol is typically blended with gasoline rather than used *neat*. Throughout this section, blends such as E10 are mentioned. This nomenclature indicates that the blend is 10% ethanol by volume. Likewise, E20 is 20% ethanol by volume, E85 is 85% ethanol, and so on.

2.2 Biomass Sources

Ethanol can be produced from any biodegradable source if the appropriate method for conversion is used. At present, sucrose (e.g., from sugarcane) and starch (e.g., from corn) are the main feedstock for fuel ethanol. Sucrose is squeezed or extracted from sucrose-bearing crops and fermented into ethanol. Before starches can be fermented, they must be enzymatically *saccharified*, or converted into simple sugars. Both of these two sources directly compete with food. Further, they have a relatively low productivity because only a portion of the crop is converted to ethanol.

Sugar and corn alone cannot significantly impact the world energy economy. A more prolific feedstock is needed, such as lignocellulose. The most abundant biological material, it is composed of lignin, cellulose, and hemicellulose. The conversion of lignocellulose to ethanol is the future of ethanol manufacturing, and many methods to achieve this conversion are being investigated.

There are obvious advantages of being able to convert the entire plant, and not just the easily digestible biomass (e.g., sucrose or starch) into liquid fuels. For example, on a dry basis, sugarcane is roughly 40% sugars and 60% fiber (i.e., lignocellulose), including tops and leaves. Using only sugars, the average ethanol yield is about 6370 L/(ha·yr) [680 gal/(acre·yr)] in Brazil.⁴ Using the lignocellulose adds about 5930 L/(ha·yr) [630 gal/(acre·yr)], assuming 85% of theoretical yield for bagasse,⁵ giving a total of 12,300 L/(ha·yr) [1310 gal/(acre·yr)]. Furthermore, other cane varieties, known as *energy cane*, are only 30% sugars and 70% lignocellulose but yield about twice the biomass.⁶ With lignocellulose conversion technologies, ethanol yields can be as high as 23,400 L/(ha·yr) [2500 gal/(acre·yr)]. In addition, energy crops tend to be easier to grow because they are more rugged, resisting drought and pests. They often have a much lower environmental impact because they do not need as much herbicides, pesticides, and fertilizer and cause less soil erosion. Other high-yield lignocellulosic crops under investigation include sorghum, switchgrass, miscanthus, and hybrid poplar.^{7–10}

2.3 Manufacturing Methods

The only established method for producing ethanol from biomass is yeast fermentation of sugars. The sugar source may vary, but the fermentation is virtually identical in all practiced processes. Figure 2 shows two common ways to obtain sugars:

1. *Sugar Extraction from Sugar-Bearing Crops.* The juice from sugarcane or sweet sorghum can be fermented directly or from the molasses, after crystallized sugar has been produced.
2. *Starch Saccharification from Starch-Bearing Crops.* Grains from corn, sorghum, rice, or wheat are converted into sugars using enzymes (i.e., amylases).

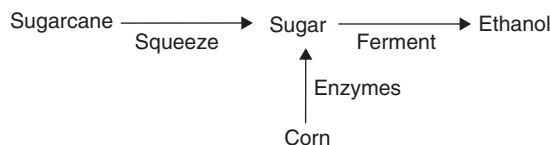


Figure 2 Schematic of established methods for ethanol production.

Yeasts, such as *Saccharomyces cerevisiae*, convert sugars into ethanol and carbon dioxide. The ethanol-rich fermentation broth, known as wine or beer, is then distilled to concentrate the ethanol. The distillation yields an azeotrope, which is about 96% ethanol by volume. In Brazil, this hydrated or hydrous ethanol is used in flexible fuel vehicles (FFVs) or ethanol-only vehicles. However, water must be removed for blending with gasoline as a gasoline oxygenate (e.g., 5, 10, 20% ethanol by volume). The most common method for producing anhydrous ethanol is to use a molecular sieve, such as zeolites. Alternatively, azeotropic distillation or extractive distillation may be employed. In the United States, the anhydrous ethanol must be denatured with gasoline before it can be marketed.

Ethanol from corn is the most utilized method in United States,¹¹ whereas ethanol from sugarcane is the basis for Brazil's ethanol industry. Ethanol production from corn differs from sugarcane, because yeasts cannot metabolize starch. Corn starches must be saccharified (hydrolyzed into sugars) using enzymes prior to fermentation. Additionally, the distillation stillage from sugar-derived ethanol, known as *vinasse*, is commonly returned to the fields for fertilization and irrigation. In contrast, the distillation stillage from starch-derived ethanol (i.e., distiller's dry grain) is dried and sold as animal feed. Ethanol from corn is less energy efficient than ethanol from sugarcane because the sugarcane process has leftover fiber (i.e., bagasse), which is used to provide energy for the process.

2.4 Manufacturing Research and Development

Many lignocellulose-to-ethanol processes are under research and development. Some of these processes saccharify lignocellulose into simple sugars using acids or enzymes, known as cellulases.^{12,13} The sugars are then converted into ethanol. One process ferments the hydrolyzed sugars into acetic acid, which is then hydrogenated into ethanol.¹⁴ This process produces higher yields, because, unlike ethanol fermentation, mass is not lost as carbon dioxide. The hydrogen can be obtained by gasifying undigested residue; this way, more biomass energy is contained in liquid fuel. The MixAlco process is a similar method under development that produces ethanol. Because it produces a mixture of alcohols, it is discussed in the "Other Fuels" section.¹⁵ Finally, lignocellulose can be gasified to produce syngas (carbon monoxide and hydrogen), which can be converted into mixed alcohols, mainly ethanol, using a catalyst.^{16,17} Alternatively, syngas can be fermented to ethanol using selected microorganisms.^{18,19}

2.5 Quality Standards

Ethanol is a well-developed automotive fuel. Table 1 shows the American Society for Testing and Materials (ASTM) D 5798 standard specification for denatured fuel ethanol (E75–85) for automotive spark ignition engines.^{20,21} Hydrocarbons used to denature fuel ethanol must meet the requirements of ASTM D 4806.^{20,22}

2.6 Vehicle Modifications and Use

Ethanol may be used in spark ignition engines as a pure fuel or blended with gasoline. However, to take full advantage of ethanol's unique properties, engines should be specifically designed

Table 1 ASTM D 5798 Standard Specification for Denatured Fuel Ethanol (E75–E85) for Automotive Spark Ignition Engines

Property	Value for Class			Test Method
ASTM volatility class	1	2	3	N/A
Ethanol, plus higher alcohols (minimum, volume %)	79	74	70	ASTM D 5501
Hydrocarbons (including denaturant)/(volume %)	17–21	17–26	17–30	ASTM D 4815
Vapor pressure at 37.8°C kPa	38–59	48–65	66–83	ASTM D 4953, D 5190, D 5191
psi	5.5–8.5	7.0–9.5	9.5–12.0	
Lead (maximum, mg/L)	2.6	2.6	3.9	ASTM D 5059
Phosphorus (maximum, mg/L)	0.3	0.3	0.4	ASTM D 3231
Sulfur (maximum, mg/kg)	210	260	300	ASTM D 3120, D 1266, D 2622
Methanol (maximum, volume %)		0.5		N/A
Higher aliphatic alcohols, C3–C8 (maximum, volume %)		2		N/A
Water (maximum, mass %)		1		ASTM E 203
Acidity as acetic acid (maximum, mg/kg)		50		ASTM D 1613
Inorganic chloride (maximum, mg/kg)		1		ASTM D 512, D7988
Total chlorine as chlorides (maximum, mg/kg)		2		ASTM D 4929
Gum, unwashed (maximum, mg/100 mL)		20		ASTM D 381
Gum, solvent washed (maximum, mg/100 mL)		5		ASTM D 381
Copper (maximum, mg/L)		0.07		ASTM D 1688
Appearance	Product shall be visibly free of suspended or precipitated contaminants (shall be clear and bright).			Appearance determined at ambient temperature or 21°C (70°F), whichever is higher.

Source: From Refs. 20–22.

for it.²³ Vehicles manufactured after 1990 may use E10 or less without modification. Vehicles manufactured before 1990 may require a new carburetor to operate with blends between E5 and E10.²⁴ Ethanol has poor cold-start properties, so vehicles that run on blends greater than E85 must have a gasoline reservoir for cold starts. Aftermarket conversion of gasoline-powered vehicles to ethanol-fueled vehicles is possible but not recommended because of the necessary changes in component materials, the high cost, and need for extensive engine recalibration.²⁵ Table 2 shows component modifications required to operate vehicles manufactured after 1990 on blends higher than E10.

The FFVs available in the United States may run on gasoline and ethanol blends up to E85. These vehicles use an electronic control unit (ECU) and several sensors to adjust the engine. In Brazil, FFVs operate with E20, hydrous E100 (96% ethanol v/v, 4% v/v water) and any ratio of the two. In the United States and Brazil, FFVs are different. The Brazilian ECU can tolerate some water to accommodate use of hydrous ethanol.

Table 2 Vehicle Modifications for Vehicles after 1990

Ethanol Content in Fuel	Carburetor	Fuel Injection	Fuel Pump	Fuel Pressure Device	Filter	Ignition System	Evaporative System	Fuel Tank	Catalytic Converter	Basic Engine	Motor Oil	Intake Manifold	Exhaust System	Cold-Start System
≤10%														
10–25%														
25–85%														
≥85%														

Source: From Ref. 24.

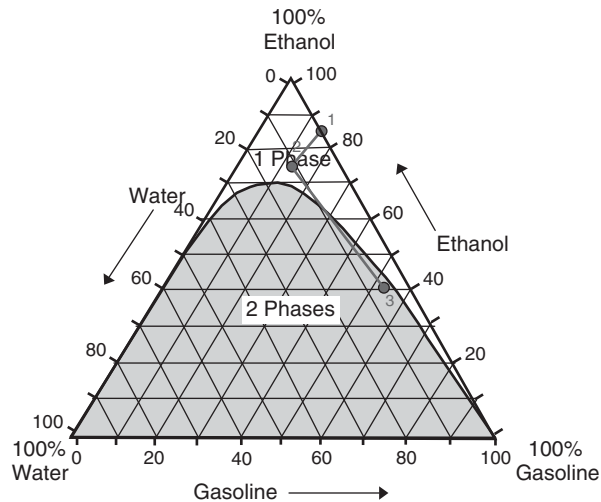


Figure 3 Gasoline/water/ethanol ternary phase diagram. Point 1—E85; Point 2—E85 contaminated with water; Point 3—contaminated E85 blended with pure gasoline (phase separates). *Source:* From Ref. 26.

Water in gasoline/ethanol can be problematic. Large amounts of water will cause an engine to run poorly or not at all. Additionally, water can cause blends to separate into two phases, which will also cause poor engine operation. There is concern that high-ethanol blends could be contaminated with water yet remain a single phase. If this contaminated E85 were added to a half-full tank of gasoline in a FFV, it could phase separate depending on the percentage of water. Figure 3 is a ternary phase diagram for gasoline/water/ethanol mixtures and illustrates how phase separation might occur.²⁶ The minimum blend in Brazil is E20, which may be mixed with higher water content without phase separating. In the United States, anhydrous ethanol is used for blending to avoid phase separation problems.

Ethanol is hygroscopic and can be corrosive to common metals used in fuel systems. Additionally, plastics and elastomers may deteriorate or soften in the presence of ethanol.²³ Table 3 lists metallic and nonmetallic materials that are compatible and incompatible with high blends of ethanol.

2.7 Performance

Ethanol (76,000 Btu/gal) contains less energy than gasoline (114,132 Btu/gal).²⁷ It takes 1.5 gal of ethanol to equal the energy of 1 gal of gasoline. Because ethanol and ethanol blends have a lower volumetric energy density than gasoline, fuel economy will be lower. For blends of E10 or less, the difference in fuel economy is generally not noticeable.²⁸

Ethanol (E100) is an excellent fuel for internal combustion engines (ICEs).³ It has a higher octane rating than gasoline, 113,²⁹ which gives it excellent antiknock properties and allows ethanol (E100) to be used in engines with higher compression ratios. Ethanol burns faster, allows more efficient torque development, and gives a vehicle increased power (5% for pure ethanol, 3–5% for E85).^{20,23}

Compared to gasoline, ethanol has poor cold-start properties due to its high heat of vaporization.³⁰ Gasoline requires less heat to vaporize than ethanol and is blended with ethanol to

Table 3 Incompatible and Compatible Materials with High-Ethanol Blends Like E85

	Incompatible	Acceptable Compatibility	
Metallic	Zinc	Unplated steel	
	Brass	Stainless steel	
	Lead	Black iron	
	Aluminum	Bronze	
	Terne (lead–tin alloy) plated steel		
	Lead-based solder		
	Copper		
	Magnesium		
	Nonmetallic	Natural rubber	Buna-N
		Polyurethane	Neoprene rubber
Cork gasket		Polyethylene	
Leather		Nylon	
Polyester-bonded fiberglass		Polypropylene	
Polyvinylchloride (PVC)		Nitrile	
Polyamides		Viton	
Methyl-methacrylate plastics		Flourosilicones	
Fiberglass-reinforced plastic laminate		Teflon	

Source: From Refs. 20 and 32.

improve its cold-start properties.³⁰ E85 has similar cold-start properties as 87 octane gasoline.²⁰ In the winter months to improve cold starts, fuel that is sold as E85 is, in fact, 70% ethanol and 30% gasoline by volume.²⁵

Ethanol has been tested and used in diesel engines; however, the physical and thermodynamic characteristics of alcohols do not make them particularly suitable fuels for compression ignition engines; therefore, we have limited our discussion to ethanol's performance in spark ignition engines.²³

2.8 Emissions

The blend of gasoline affects emissions. Ethanol does not have sulfur; therefore, it does not contribute to SO_x . Emission trends that are typical of all ethanol/gasoline blends are decreased CO, decreased particulate matter, decreased total hydrocarbon emissions, increased NO_x , and increased aldehydes.^{23,31,32} Ethanol has a higher vapor pressure than gasoline; therefore, evaporative emissions tend to increase with increasing percentages of ethanol.

2.9 Fuel Transportation and Distribution

Ethanol/gasoline blends cannot use existing petroleum pipeline systems because of possible contamination by water and residues from other petroleum products or incompatibility with the system due to the corrosive properties of alcohols.²⁰ In the United States, ethanol is transported either by rail or truck. Generally, rail is used for transmission of anhydrous denatured ethanol from the manufacturing facility to the distribution/blending stations. Trucks are used for distribution to the fueling stations.

Blending occurs at the distribution center, although sometimes it may also occur at the fueling stations. Transportation containers must be free of water and other contaminants. If other fuels have been transported in the same container, it should be washed with solvent and air dried.²⁵

The same technologies used for dispensing gasoline and diesel fuel may be employed with ethanol and ethanol blends.²⁵ However, care should be taken to ensure material compatibility of ethanol and higher blends with containers and transferring equipment. Table 3 lists materials that are incompatible and compatible with high blends of ethanol.

2.10 Fuel Storage

Ethanol is stored and handled in a similar fashion as gasoline. Above-ground and below-ground storage systems are both viable. Larger storage volumes will be required to house the same energy equivalent as gasoline.²³ Materials used may be different due to compatibility issues.²⁰ For example, metal-plated tanks should not be used. Fiberglass tanks maybe used, but must be coated with a chemical-resistant rubber. Table 3 lists some materials that are incompatible and compatible with high blends of ethanol like E85. Additionally, extra precautions may be necessary to prevent contamination with water and evaporative emissions.

2.11 Safety

The safety standards for handling and storing ethanol and its gasoline blends are the same as those for gasoline.²⁰ Special attention should be given, however, to material compatibility.

2.12 Subsidy

Currently, ethanol and biodiesel are commercially being used to curb gasoline and diesel use, respectively. According to the Energy Information Agency (EIA), 140 billion gallons of gasoline were used in the United States during 2006. The current U.S. capacity for ethanol production is 5–6 billion gallons (3–4% of the gasoline market).²⁹ For ethanol to be competitive, government subsidy is required. The Volumetric Ethanol Excise Tax Credit (VEETC) provides ethanol blenders/retailers with \$0.51 per pure gallon of ethanol blended, or \$0.0051 per percentage point of ethanol blended (i.e., E10 is eligible for \$0.051/gal; E85 is eligible for \$0.4335/gal). The incentive is available until 2010.³³

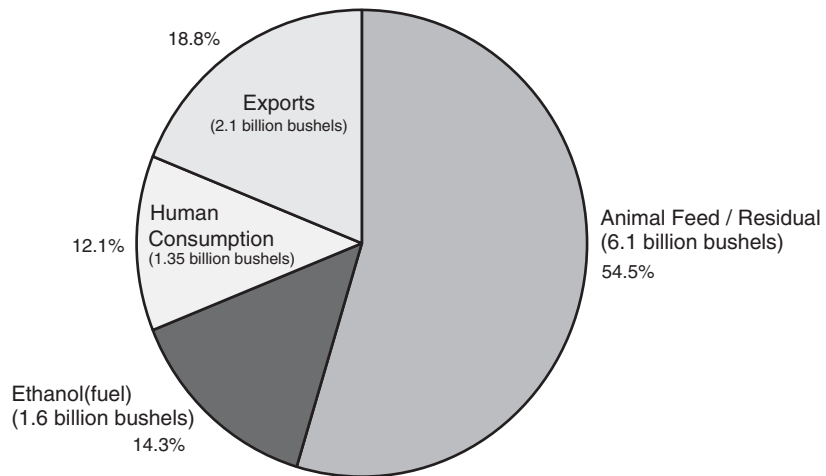
Skeptics criticize subsidies as a waste of tax money; however, biofuel subsidies return more revenue to the U.S. Treasury than they cost.²⁹ The benefit to taxpayers is that this tax credit is usually passed on to the consumer as lower pump prices for high-octane, ethanol-enriched fuel. According to the Consumer Federation of America, consumers who purchase gasoline with 10% ethanol could be saving as much as \$0.08 per gallon compared to straight gasoline.³⁴ Biofuels stimulate the economy by creating jobs, which increases wages and taxes and reduces unemployment benefits and farm program payments.²⁹

Many argue that corn-derived ethanol is causing a food shortage because it competes with corn grown for human consumption. According to iowacorn.org, only about 12% of the corn grown in the United States is used for human consumption. Figure 4 shows the distribution of corn usage in the United States for 2005/2006. Ethanol fuel comprises a significant portion of U.S. corn production, but it is not creating a food shortage.

The Energy Policy Act of 2005 included a historic provision—the Renewable Fuels Standard (RFS). The RFS is a directive for the United States to increase its renewable fuel usage each year. The schedule begins with 4 billion gallons per year in 2006, increasing annually to 7.5 billion gallons per year in 2012.³⁵

2.13 Current Availability

Ethanol production has increased annually and will continue to grow to meet the Renewable Fuels Standard. Figure 5 shows the annual U.S. production of ethanol. In 2006, 46% of



http://www.iowacorn.org/cornuse/cornuse_3.html

Figure 4 Corn usage in the United States (2005/2006 statistics). *Source:* From Ref. 36.

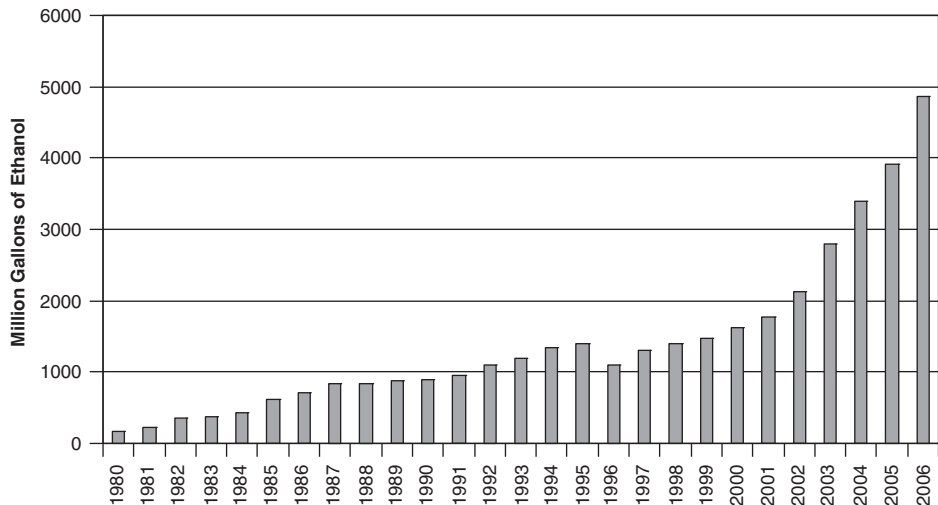


Figure 5 Annual ethanol production in the United States. *Source:* From Ref. 29.

America’s gasoline was blended with ethanol, and approximately one-third of all gasoline in the United States is E10.^{25,35} All gasoline vehicles since 1990 are approved to use blends up to 10% ethanol (E10).^{28,35} As a result, fueling stations that dispense E10 blends may not label the pumps. This rule varies, depending on the state. All E85 pumps are labeled with a bronze E85 pentagon.²⁵ As of April 2007, the U.S. Department of Energy Office of Energy Efficiency and Renewable Energy (DOE EERE) listed more than 1100 E85 fueling stations across 40 states serving approximately 6 million FFVs.^{27,33} To find an E85 fueling station, the Alternative Fuels Data Center has a station locator at www.eere.energy.gov/afdc/infrastructure/locator.html. Additionally, the National Ethanol Vehicle Coalition provides a flexible fuel vehicle guide on its website, e85fuel.com.

2.14 Ethanol Links

National Ethanol Vehicle Coalition (NEVC)	www.e85fuel.com
Renewable Fuels Association (RFA)	www.ethanolrfa.org
Governors' Ethanol Coalition	www.ethanol-gec.org
U.S. DOE EERE	www.eere.energy.gov
Ethanol Promotion and Information Council (EPIC)	www.drivingethanol.org/
American Coalition for Ethanol	www.ethanol.org
Iowa Corn Growers Association	www.iowacorn.org
Energy Information Administration	www.eia.doe.gov

3 BIODIESEL AND VEGETABLE OIL

3.1 Introduction

Rudolf Diesel first developed his engine to run off peanut oil; however, petroleum became less expensive and the use of vegetable oil as fuel was abandoned. More recently, petroleum reserves are becoming more difficult to find, so exploration and drilling costs are increasing. Diesel was a visionary and knew that vegetable oils, though not considered important in 1912, would “in the course of time become as important as petroleum and coal tar products of the present time.”³⁷ If Rudolf Diesel were alive today, he likely would run his diesel on pure biodiesel.

Biodiesel is an attractive biofuel, made from vegetable oils and fats. It may be used in diesel engines without modification. In many ways, biodiesel is a wonder fuel. Compared to petroleum-derived diesel, biodiesel extends the life of diesel engines, has lower emissions, is biodegradable and nontoxic, and has a higher flash point (making it safer to transport). Vegetable oil (VO) can be run directly in a diesel engine but requires an additional fuel tank and modification to the fuel system.

This section focuses on biodiesel because it is a more developed technology and more practical than vegetable oil. Because these two fuels are very closely related, they are combined into one section.

3.2 Biomass Source

Biodiesel can be made from virgin and waste vegetable oils and animal fats. There are hundreds of species of oil-producing plants that may be used to produce biodiesel.³⁷ Those with the greatest yields per acre are preferred for fuel production. Increasing yield per acre is a dominant area in biodiesel research. Rapeseed (canola) and soybean oils are the two most common crops used to produce biodiesel. Rapeseed is the primary oil crop used for biodiesel in Europe. In the United States, soybean is the dominant oil crop. Table 4 lists 48 common oil-producing plants with annual production averages.

3.3 Manufacturing Methods

According to the National Biodiesel Board, “Biodiesel is defined as the mono alkyl ester of long-chain fatty acids derived from VOs or animal fats, for use in compression-ignition (diesel) engines.”³⁸ Oils are triglycerides; a glycerol molecule bonded to three long-chain fatty acids. Transesterification chemically converts oil and alcohol into biodiesel. Fatty acids are hydrolyzed from the triglyceride and transformed into esters (biodiesel).^{1,37,38} Figure 6 illustrates this chemical reaction. A strong acid or base may be used as a catalyst. Sodium hydroxide (NaOH) is the most common catalyst because it is the least expensive. Typically,

Table 4 Oil-Producing Plants with Average Production Yields

	Plant	Latin Name	kg Oil/ha
1	Oil palm	<i>Elaeis guineensis</i>	5000
2	Macauba palm	<i>Acrocomia aculeata</i>	3775
3	Pequi	<i>Caryocar brasiliense</i>	3142
4	Buriti palm	<i>Mauritia flexuosa</i>	2743
5	Oiticia	<i>Licania rigida</i>	2520
6	Coconut	<i>Cocos nucifera</i>	2260
7	Avacado	<i>Persea americana</i>	2217
8	Brazil nut	<i>Bertholletia excelsa</i>	2010
9	Macadamia nut	<i>Macadamia terniflora</i>	1887
10	Jatropha	<i>Jatropha curcas</i>	1590
11	Babassua palm	<i>Orbignya martiana</i>	1541
12	Jojoba	<i>Simmondsia chinensis</i>	1528
13	Pecan	<i>Carya illinoensis</i>	1505
14	Bacuri	<i>Platonia insignis</i>	1197
15	Castor bean	<i>Ricinus communis</i>	1188
16	Gopher plant	<i>Euphorbia lathyris</i>	1119
17	Piassava	<i>Attalea funifera</i>	1112
18	Olive tree	<i>Olea europaea</i>	1019
19	Rapeseed	<i>Brassica napus</i>	1000
20	Opium poppy	<i>Papaver somniferum</i>	978
21	Peanut	<i>Arachis hypogea</i>	890
22	Cocoa	<i>Theobroma cacao</i>	863
23	Sunflower	<i>Helianthus annus</i>	800
24	Tung oil tree	<i>Aleurites fordii</i>	790
25	Rice	<i>Oriza sativa</i>	696
26	Buffalo gourd	<i>Cucurbita foetidissima</i>	665
27	Safflower	<i>Carthamus tinctorius</i>	655
28	Crambe	<i>Crambe abyssinica</i>	589
29	Sesame	<i>Seasmum indicum</i>	585
30	Camelina	<i>Camelina sativa</i>	490
31	Mustard	<i>Brassica alba</i>	481
32	Coriander	<i>Coriandrum sativum</i>	450
33	Pumkin seed	<i>Cucurbita pepo</i>	449
34	Euphorbia	<i>Euphorbia lagascae</i>	440
35	Hazelnut	<i>Corylus avellana</i>	405
36	Linseed	<i>Linum usitatissimum</i>	402
37	Coffee	<i>Coffea arabica</i>	386
38	Soybean	<i>Glycine max</i>	375
39	Hemp	<i>Cannabis Sativa</i>	305
40	Cotton	<i>Gossypium hirsutum</i>	273
41	Calendula	<i>Calendula officinalis</i>	256
42	Kenaf	<i>Hibiscus cannabinus L.</i>	230
43	Rubber seed	<i>Hevea brasiliensis</i>	217
44	Lupine	<i>Lupinus albus</i>	195
45	Palm	<i>Erythea salvaorensis</i>	189
46	Oat	<i>Avena sativa</i>	183
47	Cashew nut	<i>Anacardium occidentale</i>	148
48	Corn	<i>Zea mays</i>	145

Note: These figures are based on international averages and may vary with climate, region, and subspecies grown. Those listed in bold are the 10 most common plants used.
From Ref. 37.

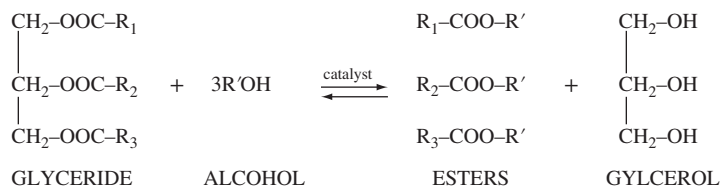


Figure 6 Transesterification of triglycerides with alcohol. *Source:* Adapted from Ref. 3.

methanol is used due to cost and reaction performance; however, ethanol and higher alcohols could be used.³⁸

The result of transesterification is two separate liquid phases. The bottom phase is glycerol and the top phase is alkyl esters (biodiesel). The biodiesel is separated from the glycerol and then washed to remove remaining alcohol, catalyst, and soap that may have formed. Typically, water washing is necessary to meet the ASTM standards.³⁷

Other methods for using VO in diesel engines include direct use of VO, blends of VO with diesel or kerosene, microemulsions of VO with various solvents, as well as other methods of transesterification.³⁹ The details of these methods are not discussed as base-catalyzed transesterification of VO to biodiesel is superior.

3.4 Quality Standards

Biodiesel is a well-developed biofuel. The ASTM approved quality standards for biodiesel in December 2001 under the designation of D-6751.^{1,38} The ASTM standards are shown in Table 5. Commercially sold biodiesel must meet this standard. BQ-9000 is a quality assurance program analogous to systems established by the International Organization for Standardization (ISO).⁴⁰ Both producers and distributors of biodiesel are encouraged to participate in the BQ-9000 program. The maintenance of quality fuel is essential for customer acceptance and industrial growth. Advantages and disadvantages of biodiesel use are shown in Table 6.

3.5 Vehicle Modifications

Biodiesel can be run in any diesel engine without modification. If the engine is older than 1994, engine gaskets and hoses may need replacement because biodiesel can deteriorate rubber hoses and gaskets.¹ Biodiesel helps maintain fuel systems by dissolving buildup. This may require changing the fuel filter frequently until the system is clean.

For a diesel to run on VO, the kinematic viscosity must be below 20 centistokes (cSt). To achieve this, a second fuel tank must be added and heated by routing the radiator cooling lines through the VO fuel tank. These vehicles must be started with conventional diesel fuel. Once the VO viscosity is below 20 cSt (160°F), the fuel line is switched via a solenoid valve. In a converse manner, the vehicle must be shut off using conventional diesel to ensure proper startup.³⁷

3.6 Performance

Pure biodiesel (B100) has 12% less energy per kilogram than conventional diesel (37 vs. 42 MJ/kg) but 7% higher combustion efficiency.³⁷ As a result, performance and fuel efficiency decrease by about 5%.³⁷ In most cases, the difference is hardly noticeable. The power and torque curve for B100 is shown in Fig. 7.

In the case of biodiesel blends, there have been reports that fuel efficiency increased. St. Johns Schools in Michigan report that using B20 (20% biodiesel by volume) increased fuel

Table 5 Specification for Biodiesel^a (B100)—ASTM D6751-07b (March 2007)

Property ^b	ASTM Method	Limits	Units
Calcium and magnesium, combined	EN 14538	5 max.	ppm (µg/g)
Flash point (closed cup)	D 93	93 min	°C
Alcohol control (one of the following must be met)			
1. Methanol content	EN14110	0.2 max.	% volume
2. Flash point	D93	130 min	°C
Water and sediment	D 2709	0.05 max.	% vol.
Kinematic viscosity, 40°C	D 445	1.9–6.0	mm ² /s
Sulfated ash	D 874	0.02 max.	% mass
Sulfur			
S 15 Grade	D 5453	0.0015 max. (15)	% mass (ppm)
S 500 Grade	D 5453	0.05 max. (500)	% mass (ppm)
Copper strip corrosion	D 130	No. 3 max.	
Cetane	D 613	47 min	
Cloud point	D 2500	Report	°C
Carbon residue 100% sample	D 4530 ^c	0.05 max.	% mass
Acid number	D 664	0.50 max.	mg KOH/g
Free glycerin	D 6584	0.020 max.	% mass
Total glycerin	D 6584	0.240 max.	% mass
Phosphorus content	D 4951	0.001 max.	% mass
Distillation, T90 AET	D 1160	360 max.	°C
Sodium/potassium, combined	EN 14538	5 max.	ppm
Oxidation stability	EN 14112	3 min	h
Workmanship	Free of undissolved water, sediment, and suspended matter		

^aBiodiesel is defined as the mono alkyl esters of long-chain fatty acids derived from vegetable oils or animal fats, for use in compression-ignition (diesel) engines. This specification is for pure (100%) biodiesel prior to use or blending with diesel fuel. A considerable amount of experience exists in the United States with a 20% blend of biodiesel with 80% diesel fuel (B20). Although biodiesel (B100) can be used, blends of over 20% biodiesel with diesel fuel should be evaluated on a case-by-case basis until further experience is available.

^bBoldface = BQ-9000 Critical Specification Testing Once Production Process Under Control.

^cThe carbon residue shall be run on the 100% sample.

mileage from 8.1 to 8.8 miles per gallon.⁴¹ However, this is a singular report and may not be true for all users of B20. The exact performance of biodiesel depends on the specific engine, its condition, and the blend of biodiesel used. In any case, the performance of biodiesel is similar to that of conventional diesel.

Biodiesel has a higher cloud point than conventional diesel, making it less tolerant to cold temperatures (<32°F). Below-freezing temperatures can be tolerated when using blends of B20 or less.⁴² Figure 8 shows how cloud point varies with blend percentage. Free fatty acids increase the biodiesel cloud point; therefore, biodiesel made from waste vegetable oil will have a higher cloud point than that made from virgin oil.³⁷

3.7 Emissions

“Biodiesel is the first and only alternative fuel to have a complete evaluation of emission results and potential health effects submitted to the U.S. Environmental Protection Agency under the Clean Air Act Section 211(b).”³⁸ Biodiesel contains about 10% oxygen by mass, which makes it burn cleaner than conventional diesel. Biodiesel has lower hydrocarbon (HC), particulate matter (PM), and carbon monoxide (CO) emissions. Biodiesel does not contain sulfur and does not

Table 6 Advantages and Disadvantages of Biodiesel (B100) Usage

Advantages	Disadvantages
<ul style="list-style-type: none"> • Nontoxic • Higher flash point (less flammable) • Biodegradable • Extends engine life • Cleans fuel system • Easily made • Small performance gain^a • Adds value to agriculture • Safe to handle • Compatible with engines made since 1994^b • Sulfur free • Increased cetane number • No offensive odor • Lower hydrocarbon, particulate matter, and CO emissions • Improved lubricity • Minimal change in infrastructure and distribution systems 	<ul style="list-style-type: none"> • Slightly higher cost (2006) • Higher cloud point • Small performance loss^a • Increased NO_x emissions • Availability is not widespread • Could invalidate warranty of fuel systems • Six-month shelf life • May require hose and gasket replacement • Currently requires government subsidy

^aDepends fuel blend and engine used

^bRefers to OEM gaskets and hoses

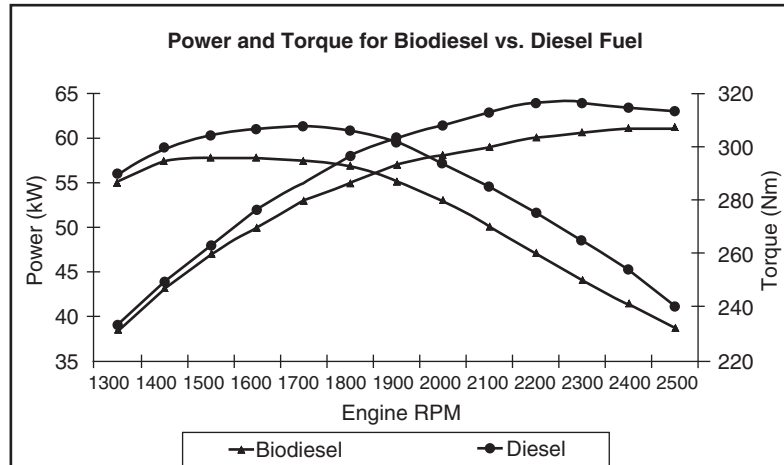


Figure 7 Power torque curve for B100.

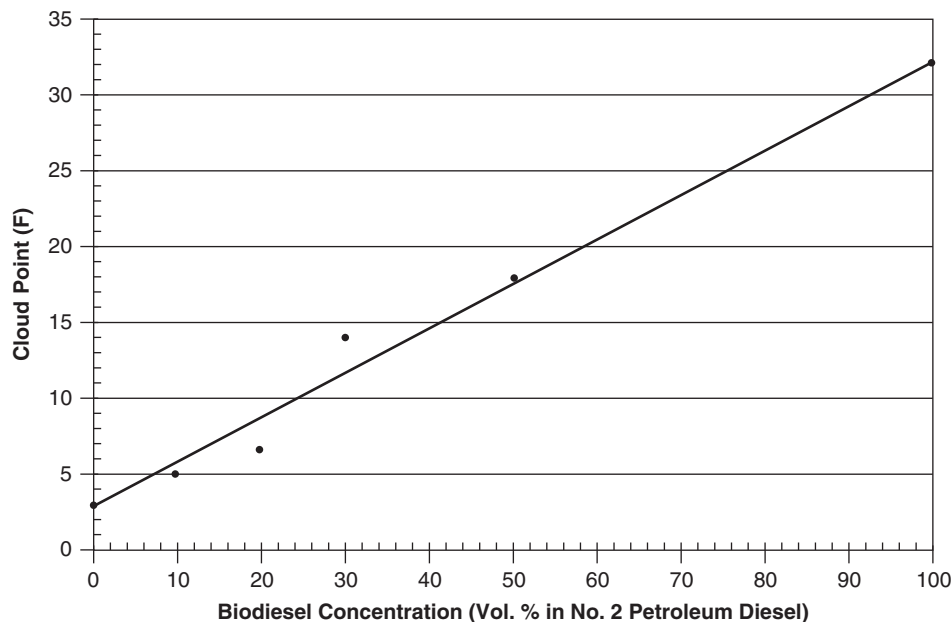


Figure 8 Cloud point variation with biodiesel concentration. *Source:* From Ref. 7.

contribute to SO_x emissions. Figure 9 shows the percent change in emissions from conventional diesel as a function of blend percentage. These changes are not absolute and depend on the feedstock and the specific engine.^{43,44} Figure 9 is only representative of heavy-duty highway engines on soy biodiesel; however, the general trends are representative of biodiesel usage.⁴³

The effect of biodiesel on NO_x emissions is debated. Nitrogen oxides are formed when nitrogen is oxidized. The use of oxygenated fuels increases the production of NO_x emissions. Several factors affect NO_x emissions: blend percentage, degree of saturation, and engine technology/age.^{43,44} In 2006, the National Renewable Energy Laboratory (NREL) published a report in which it had tested 43 heavy-duty engines running on B20 and concluded “that B20 has no net impact on NO_x .”⁴³ Some engines decrease NO_x and others increase NO_x , the difference being the technology of each vehicle. Unsaturated fatty acids increase NO_x emissions.^{1,44} Therefore, feedstocks with more unsaturated fatty acids will produce more NO_x emissions. Most reports conclude that biodiesel increases NO_x emissions by a small percentage and that future engine technology can correct this increase.^{1,37,38,43,44}

3.8 Fuel Transportation Issues

Because biodiesel has a higher flash point than conventional diesel [150°C (300°F) and 52°C (125°F), respectively], it is easier and safer to transport. Regular shipping services such as FedEx and UPS can transport biodiesel.^{1,37} Shipping methods used for conventional diesel may also be used.

3.9 Storage Issues

Biodiesel can be handled and stored in the same containers and places as conventional diesel.³⁷ Biodiesel has a shelf life ranging from about one year in warm climates to indefinitely in cold

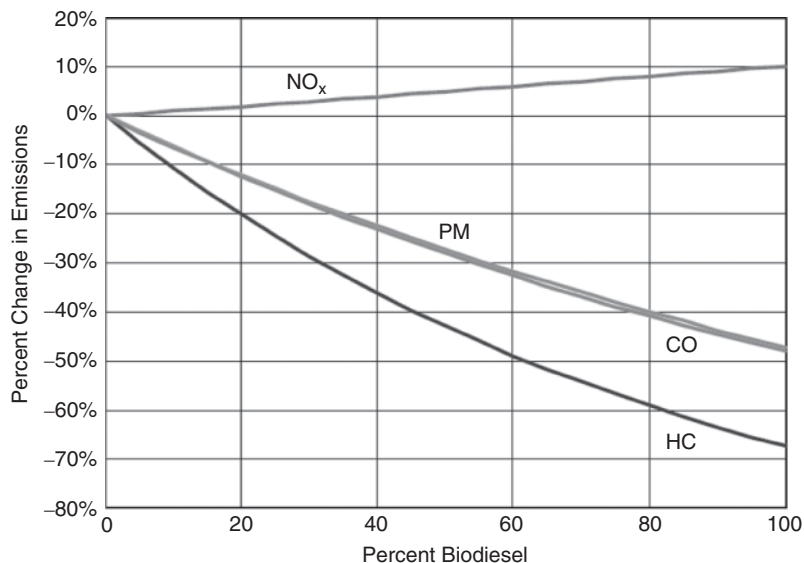


Figure 9 Average emissions impacts of biodiesel for heavy-duty highway engines. *Source:* From Ref. 8.

climates.³⁷ Because biodiesel is derived from VO, it may serve as a carbon source for microorganisms. To prevent microbial growth in warm humid climates, it is recommended to add a biocide or biostat.³⁷ Additionally, it is important to minimize biodiesel exposure to air and oxidizing agents. Waste vegetable oil should not be stored for extended periods of time because it may spoil.³⁷

3.10 Current Availability

Biodiesel is sold just like conventional diesel. Biodiesel is typically blended with conventional diesel and is labeled “B#.” The “B” indicates biodiesel and the number is the volume percentage of biodiesel. Figure 10 shows a fueling station that sells biodiesel (B20) and ethanol (E85 and E10).⁴⁵ Various retailers carry one or more of the following blends: B2, B5, B10, B11, B50, B98, B99, B100. To find a retailer near you, the National Biodiesel Board has a retailer locator on its website, <http://www.biodiesel.org/buyingbiodiesel/retailfuelingsites/.38>.

The availability of vegetable oil for the end consumer is very limited. Food-grade oil may be purchased in supermarkets at a premium price. Waste vegetable oil may be available from a local restaurant. Otherwise, vegetable oil is not commercially available to the consumer for use as fuel.

3.11 Production Capacity

Vegetable oil production capacity will limit the growth of the biodiesel industry. According to the EIA, the United States uses 50–60 billion gallons of diesel fuel every year.⁴⁶ In 2006, The United States produced approximately 250 million gallons of biodiesel (~0.5% of diesel market).³⁸ As of November 2006, the National Biodiesel Board reported that the *capacity* of U.S. biodiesel plants is 582 million gallons (~1% of biodiesel market). If the United States were to use all its waste cooking oil and animal fats and fallow farm land were planted with high-yield rapeseed to produce biodiesel, the result would displace about 24% of the annual



Figure 10 Biofuel gas station. *Source:* From Ref. 10, with permission from Elsevier.

diesel fuel usage by the most generous estimates.³⁷ For the biodiesel industry to grow past this limit, breakthroughs must be made with a high-yield oil crop.

3.12 Subsidy

Energy Policy Act of 2005 Section 1344 extends the tax credit for biodiesel through 2008. A subsidy of \$1.00 per gallon is given for biodiesel made from virgin VO and \$0.50 for biodiesel from waste cooking oils.⁴⁷

3.13 Safety

Comprehensively, biodiesel is the safest fuel available. It is “more biodegradable than sugar and less toxic than salt.”¹ It produces fewer carcinogens and has a higher flash point than conventional diesel. Figure 11 compares biodiesel’s flash point to other conventional fuels. Because biodiesel is very safe and environmentally friendly, it is excellent for use in marine environments and sensitive areas such as national parks and forests.³⁷ Because biodiesel has lower emissions, it is an attractive fuel for use in school buses.

3.14 Current Research and Future of Biodiesel

Biodiesel is well established and has been defined with standards. Most engine manufactures have warmed up to biodiesel and have begun covering biodiesel under vehicle warranty. The

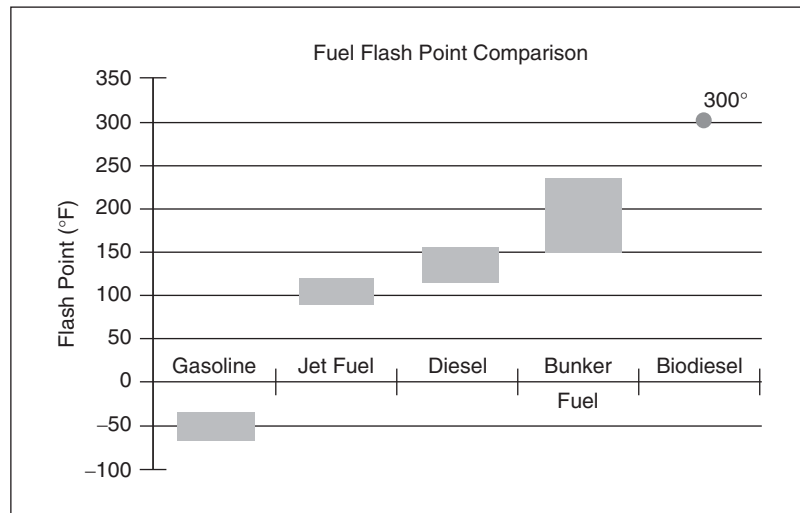


Figure 11 Fuel flash point comparison. *Source:* From Ref. 7, Copyright © 1996 Published by Elsevier Ltd. Reprinted with permission from Elsevier.

main challenges for the future of biodiesel will be production volume, education of the public, maintenance of fuel quality, improvement of government policy and incentives, and, most importantly, economics.

Current biodiesel research is focused on increasing vegetable oil production. Algae show great potential as a mass biooil producer and could provide enough oil to completely replace conventional diesel.³⁷ Currently, several engineering issues must be addressed before algae can become an economical player as a feedstock for biodiesel. These include issues regarding economy of scale, diffusion of CO₂ into the growth solution, solar efficiency of algae, oil yield along with economical extraction methods, and ecological implications of genetically modified algae.

4 HYDROGEN

4.1 Introduction

On a mass basis, hydrogen has more energy than any other fuel. On a volume basis, hydrogen has the least energy of any fuel. This comparison, in short, is the life story of hydrogen.

Hydrogen is a mammoth. The advantages and prospects of realizing the *hydrogen economy* are enormous. Likewise, the hurdles and engineering issues that must be overcome to get there are equally great. From a theoretical viewpoint, it is easily argued that hydrogen is the perfect fuel, which is why hydrogen research continues to draw entrepreneurs, investors, government support, and environmentalists. From a practical viewpoint, hydrogen is far from perfect. Many experts agree that realizing the hydrogen economy is many decades away by the most optimistic estimates.

This section will only scratch the surface of information about hydrogen. We will only mention that which pertains to hydrogen used as a transportation fuel. Furthermore, our focus is on hydrogen produced in a “green” fashion.

4.2 Manufacturing Methods

Hydrogen is an energy carrier rather than an energy source. Despite being the most abundant element in the universe and the third most abundant element in Earth's crust, pure hydrogen gas is not readily available. Hydrogen is molecularly bound in many organic and inorganic compounds. The primary resources for hydrogen production are water, biomass, and hydrocarbons. To liberate hydrogen takes energy. Once made, the hydrogen is *stored* energy; thus, hydrogen is an energy carrier.

There are many hydrogen sources and production methods. For hydrogen to be green, it should be produced from water or biomass. Figure 12 illustrates the various pathways that may be used to produce hydrogen from these resources. The following is a brief description of each process.

Photolytic/Photoelectrolysis

Photoelectrolysis employs catalysts that absorb photons from sunlight to split water into hydrogen and oxygen.^{48,49} Photoelectrolysis is described as running a fuel cell in reverse.⁴⁹ This technology is still under research and is considered the Holy Grail of hydrogen production, because it would directly convert sunlight into hydrogen.⁴⁸

Electrolysis

Electrolysis is the decomposition of water using an electrical current. An anode and cathode are placed in water with an electrolyte. When current is applied, hydrogen is formed at the cathode and oxygen at the anode. Equation (1) describes the chemistry of electrolysis. Electrolysis is a

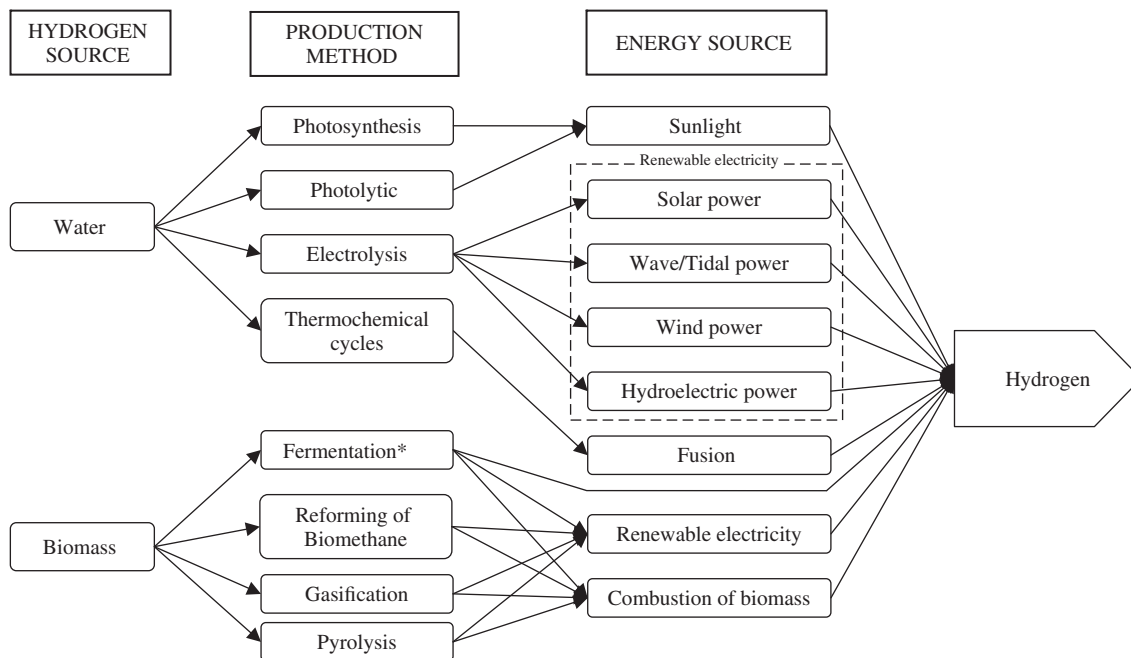
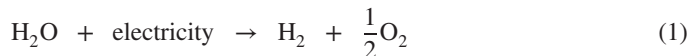


Figure 12 Green routes to hydrogen production. Fermentation may not require a heat source. Gasification and pyrolysis may only require initial heat source. *Source:* From Refs. 1 and 4.

well-known technology and produces very pure hydrogen. Of the renewable paths to hydrogen, electrolysis is the only one commercially used.^{50,51}

Electrolysis is very energy intensive. In principle, operating at high temperatures (900–1000°C) can reduce the energy requirement.⁵² Commercial electrolysis plants achieve efficiencies of 70–75% (electrolyzers range from 75 to 90%).^{50,53} There are other variations of electrolysis such as alkaline electrolysis, polymer electrolyte membrane electrolysis, and high-temperature electrolysis. Regardless of the method, the net reaction is that described by the equation⁵²



Thermochemical Cycles

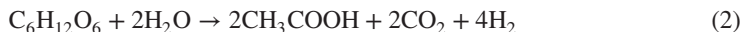
Thermochemical cycles produce hydrogen using high-temperature cycling of chemical reactions that split water. Thermochemical cycles operating in conjunction with a high-temperature reactor offer high-efficiency hydrogen generation comparable to high-temperature steam electrolysis. This is well suited for use with nuclear power or future fusion power generation.⁵⁵

Photosynthesis

Photosynthetic production of hydrogen uses modified green algae that produces hydrogenase enzymes to strip hydrogen from water.⁵³ This technology is still in the initial stages of research but could prove to be a key player in the direct conversion of light to hydrogen.⁵⁵

Fermentation

The fermentation path to hydrogen production would employ microorganisms that consume biomass. This route to hydrogen is attractive because it does not require sterile conditions or sunlight, and it may use a wide variety of feedstocks. The conversion of glucose to hydrogen by anaerobic fermentation is shown by the equation⁵³



This technology is still under research. This route to hydrogen would have a low external energy requirement because the microorganisms consume energy from the biomass.

Reforming of Biomethane

Steam reforming of natural gas accounts for 48% of the hydrogen produced in the United States.⁵¹ High-temperature steam is used to strip the hydrogen from methane. This conventional technology could be modified to use methane produced from manure or other biomass resources. The primary hurdle is increasing methane production.

Gasification/Pyrolysis

Gasification is the thermal decomposition of organic material (biomass) in a low-oxygen environment that employs 20–40% of the stoichiometric oxygen needed for combustion.⁵² The production gas (synthesis gas) contains hydrogen, carbon monoxide, carbon dioxide, low-molecular-weight alkanes, as well as other compounds. Gasification temperature ranges from about 700°C with a catalyst, to about 900°C without a catalyst.⁵² This production route requires purification if high-purity hydrogen is required. Pyrolysis is similar to gasification, except that the biomass is heated in the absence of oxygen.

“The cost of producing hydrogen ... is one of the biggest barriers on the path toward a hydrogen economy.”⁵⁰ Furthermore, the cost of producing hydrogen in an environmentally friendly way is an even larger hurdle. Currently, steam reforming of natural gas is the most

economical route to hydrogen production. Steam reforming of fossil fuels, primarily methane and naphtha, accounts for 96% of all hydrogen produced.⁵¹ Breakthroughs must be made for green hydrogen to compete with fossil fuel hydrogen.

4.3 Quality Standards

Fuel cells require high-purity hydrogen to prevent poisoning. Because hydrogen is not a conventional fuel, new standards must be developed for storage, delivery, infrastructure, and end use. Fuelcellstandards.com is a site “dedicated to assist the worldwide community working to develop and interpret fuel cell codes and standards.”⁵⁶ “The key players in this area are SAE, ISO TC 22 SC 21, and ISO TC 197.”⁵⁷ These organizations are actively forming committees to develop and evaluate standards for all aspects of hydrogen. In 2004, ASTM formed a subcommittee (D03) to develop standards on hydrogen and fuel cells.⁵⁸ Standards are important to the development of any commercialized product. In the case of hydrogen, standards are essential for public acceptance and safety. Links to hydrogen standards websites are listed in the hydrogen links in Section 4.11.

4.4 Hydrogen Vehicles

Hydrogen is unique as a transportation fuel. Transportation during the Industrial Revolution was powered by pistons. The steam locomotive, the model-T Ford, and the diesel engine all operate via piston-driven engines. Hydrogen-powered vehicles can employ an ICE, too; however, the fuel cell is the most efficient way to convert hydrogen to power. Fuel cells do not involve direct combustion nor do they require high operating temperatures. A fuel cell extracts the electrochemical potential from hydrogen to create electricity.

How much hydrogen is equal to a gallon of gasoline? Comparing heat of combustion, 1 lb (0.45 kg) of hydrogen has the equivalent energy of approximately 19.5 lb of gasoline (3.1 gal).⁵⁹ Table 7 compares the fuel economy and fuel equivalents to a kilogram of hydrogen for a proton exchange membrane fuel cell vehicle (PEMFCV), ICE gasoline vehicle, and a hybrid electric vehicle (HEV) running on gasoline. For a better illustration, the hydrogen contained in a gallon of water (0.92 lb, or 0.42 kg) will provide the same traveling capacity for a PEMFCV as a gallon of gasoline in a typical car.^{50,60}

Fuel Cells

Hydrogen used in vehicles is likely to employ a PEMFC. Fuel cells (FCs) produce electricity through an electrochemical reaction rather than direct combustion in a heat engine. As shown in Table 8 and Fig. 13, there are many types of FCs each classified by the electrolyte used; however, the PEMFC is currently the only practical FC for vehicular applications.^{50,61,62} Figure 14 illustrates the internals of a PEMFC. The DOE describes the PEMFC as follows:

When hydrogen is fed to a PEM fuel cell and encounters the first catalyst-coated electrode, called the anode, the hydrogen molecules release electrons and protons. The protons migrate through the

Table 7 Fuel Economy and Fuel Equivalents for PEMFC, ICE, and HEV




	PEMFCV	ICE	HEV
Fuel	H ₂	Gasoline	Gasoline
Fuel economy	55 mpg	24 mpg	34 mpg
Equivalence to 1 kg hydrogen	1.00 kg	2.29 gal	1.62 gal

Source: From Ref. 61.

Table 8 Fuel Cell Technologies

Fuel Cell Type	Temperature Range	Efficiency	Capacities	Primary Application	Notes
Polymer electrolyte or proton exchange membrane	<100°C (<212°F)	50–60%	Polymer membrane (thin plastic film)	100 W to 250 kW per cell	Transportation, stationary Fast startup, high power density, rapid response to power demand, relatively rugged
Phosphoric acid	160–220°C (320–430°F)	37–55%; up to 72–80% with heat recovery	Concentrated phosphoric acid	25–250 kW per cell	Stationary Fuel of choice is natural gas
Solid oxide	800–1000°C (1500–1800°F)	45–65%; up to 70–85% with heat recovery	Solid nonporous ceramic materials	200 W per cell; 300 kW–3 MW per module	Stationary, utility Typically applied in stacks of hundreds; a plant might produce up to 10 MW
Alkaline	23–250°C (70–482°F)	50–60%	Potassium hydroxide solution (35–50% KOH)	2.2 kW	Spacecraft Being developed for other applications
Molten carbonate	650–660°C (1200°F)	45–60%; 70–85% with heat recovery	Melted carbonate salt mixture	250 kW to >1 MW	Stationary, utility Corrosive electrolyte limits durability

^aWithout recovery of cogenerated heat, unless otherwise noted
Source: From Ref. 50.

			
OEM	Honda	GM	Daimler Chrysler
Model	FCX	Equinox	F-Cell A-type car
Year of manufacture	2006	2006	2002
Energy efficiency	60%	----	----
FC power output (max)	134 hp	125 hp	92 hp
Motor power output (max)	127 hp	126 hp	87 hp
Motor torque	201 ft*lb _f	236 ft*lb _f	----
Range	270 ^A - 350 ^B miles	200 mi	93 miles
Fuel tank capacity	171 liters	----	----
Gas pressure	5,100 psi	10,000 psi	5075 psi
Max speed	93 mph	100	87 mph
Acceleration 0–60 mph	----	12 s	16 s
Operating range, low/high	-22°F /	-13°F / 113°F	----
Payload	----	750 lbs	----
Seating	4	4	----

A Determined using EPA calculation method

B When driven in LC4 mode (calculated by Honda)

Figure 13 Comparison of FC vehicle specifications.

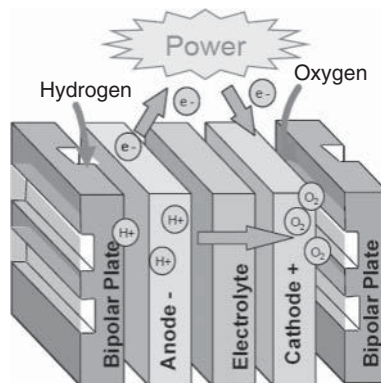


Figure 14 Illustration of how a proton exchange membrane (PEM) fuel cell works. *Source:* From Ref. 60.

electrolyte membrane to the second catalyst-coated electrode, called the cathode, where they react with oxygen to form water. The electrons, however, can't pass through the electrolyte membrane to the cathode. Instead they must travel around it—this movement of electrons is an electrical current."⁶¹

Depending on the area, a single FC will produce an electric potential around 0.7 V.⁵³ In applications, many individual FCs are connected in a stack to produce the power necessary to propel a vehicle. In Fig. 15, the FC stack produces 5 kW.

FC vehicles have been developed by GM, Honda, Ford, DaimlerChrysler, Toyota, Nissan, as well as others (see Ref. 50). Figure 13 compares three FC vehicles and their specifications. Although hydrogen FC vehicle prototypes have been developed and successfully demonstrated,

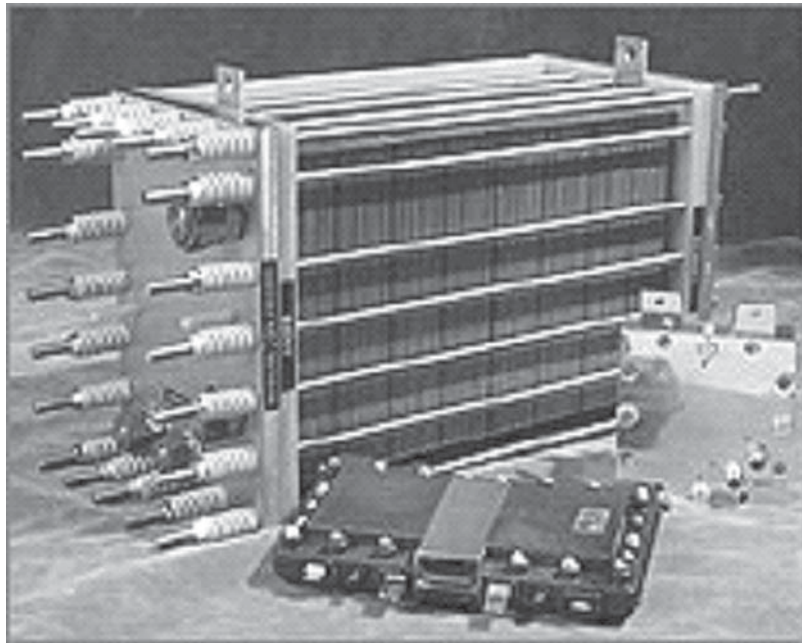


Figure 15 Fuel cell (5 kW) manufactured by plug power.

the cost is prohibitive. To put this in perspective, prototype FCs cost \$2000–\$3000/kW with high-volume production FCs costing approximately \$225/kW,⁶¹ whereas the ICE is on the order of \$25–\$35/kW, an order of magnitude less. According to the DOE, FCs must approach \$50/kW to be competitive.^{61,62}

Advantages of FCs

- Not limited by Carnot efficiency
- Low operating temperature ($\sim 80^{\circ}\text{C}$)⁶⁰
- Most efficient way to use hydrogen (65–85%)⁴⁸
- High power density
- Reliable power generation⁴⁸
- No harmful emissions^{48,50}
- Quiet⁴⁸
- Can serve as remote electrical power⁵⁵

Disadvantages of FCs

- Require high-purity gas; CO poisoning⁵³
- Expensive⁶¹
- Material and component are not durable⁴⁸
- Air, heat, and water management⁶⁰

Internal Combustion Engines

Although FCs are the cleanest, most efficient way to use hydrogen, ICEs offer the potential of a less expensive route to hydrogen use.⁶⁹ Hydrogen-powered ICEs have approximately 20% greater efficiency than those running on gasoline.⁵³ Even though hydrogen may increase efficiency, power is lost due to the low volumetric energy density of hydrogen gas. To compensate for the loss of power, engine displacement volumes must increase.⁵² ICEs must be redesigned to accommodate the combustion properties of hydrogen, particularly its fast flame speed.⁷⁰ Combustion of hydrogen *does* produce NO_x emissions; however, NO_x emissions may be reduced to levels less than gasoline engines using exhaust gas recirculation.⁶⁹

The excellent paper by Karim lists the following advantages of hydrogen-powered ICEs⁷¹:

- Reduced cyclic variations which reduced emissions, improves efficiency, and allows quieter and smoother operation.
- High-octane number
- Excellent cold-start characteristics
- High-speed engine operation
- Higher efficiency than other ICE fuels
- Lean-mixture operation
- Tolerates impure gas

Karim⁷¹ also describes the following disadvantages:

- Low-volumetric energy density, which leads to power loss—compressed hydrogen (200 atm) has approximately 5% of the energy as the same volume of gasoline
- Potential problems with uncontrolled preignition and backfiring into the intake manifold
- Serious limitations to the application of cold exhaust gas recirculation for exhaust emissions control
- Serious limitations to effective turbocharging
- Safety problems
- Material compatibility issues
- Ice formation from exhaust in extreme cold
- Potential durability issues
- A hydrogen-powered engine must be 40-60% larger in size than for gasoline-powered engine with the same power output

4.5 Emissions

Hydrogen is the cleanest fuel on the planet. This hallmark quality motivates hydrogen research and development. FCs have zero emissions producing only water and heat.⁶⁰ Only when combusted does hydrogen produce NO_x.⁵⁰

Because hydrogen is an energy carrier, the hydrogen production method must be considered. Hydrogen produced from reformed fossil fuels produces carbon dioxide. Likewise, hydrogen produced via electrolysis indirectly contributes to carbon dioxide emissions if the electricity is produced from fossil fuels. For this reason, many environmentalists only favor hydrogen produced from renewable sources (water and biomass) using renewable energies (wind, solar, hydropower, etc.).

Emissions from a manufacturing plant are easier to remove than from a tail pipe. Carbon sequestration methods could capture CO₂. The most responsible technologies will avoid emission production. Interestingly, if all passenger vehicles in the United States ran on reformed

hydrogen (without carbon sequestration) using FCs, 30–50% less CO₂ would be emitted than if the fossil fuel were burned in ICEs.⁵⁰ This results from the high efficiency of FCs. Even though hydrogen from fossil fuels is not completely clean or green, it is an improvement over direct use of fossil fuels regarding emissions.

4.6 Fuel Transmission and Distribution

Currently, hydrogen is only used as a transportation fuel where municipalities, organizations, or corporations have established pilot programs for research and/or demonstration.^{50,72} Distribution and storage are very costly due to the lack of infrastructure and hydrogen's low volumetric density. Hydrogen transportation is arguably the biggest economic hurdle facing the commercialization of hydrogen vehicles. Figures 16, 17, and 18 show that transportation costs can add \$0.50–\$3.50 to the cost of a kilogram of hydrogen. Compared to gasoline, this is enormous. According to the EIA, "Distribution, marketing and retail dealer costs and profits combined make up 9% (\$0.204) of the cost of a gallon of gasoline (\$2.27 in 2005)."⁷³

Bulk hydrogen must be delivered from a production facility to a single point and then distributed to many smaller refueling stations. Yang and Ogden evaluated transmission and distribution costs by three modes: pipelines, compressed-gas trucks, and cryogenic liquid H₂ trucks.⁷⁴ Each mode has its own advantages and disadvantages. Determining which mode is the most economical depends on two key parameters: transportation distance and flow rate.⁷⁴ Figure 16 shows the minimum transmission cost as a function of flow rate and transport distance. From Fig. 16, pipelines are favored at high flow rates and trucking is favored at low flow rates, compressed gas for short distances and liquefied hydrogen for long distances. Figures 17 and 18 show distribution costs as a function of the number of refueling stations and the city radius for 1800- and 500-kg/day-capacity fueling stations, respectively. Distribution may contribute \$0.80–\$1.80 per kilogram of hydrogen.

The models used by Yang and Ogden are based on idealized assumptions; their predictions have not been compared to real scenarios because none exist.⁷⁴ Nonetheless, their models

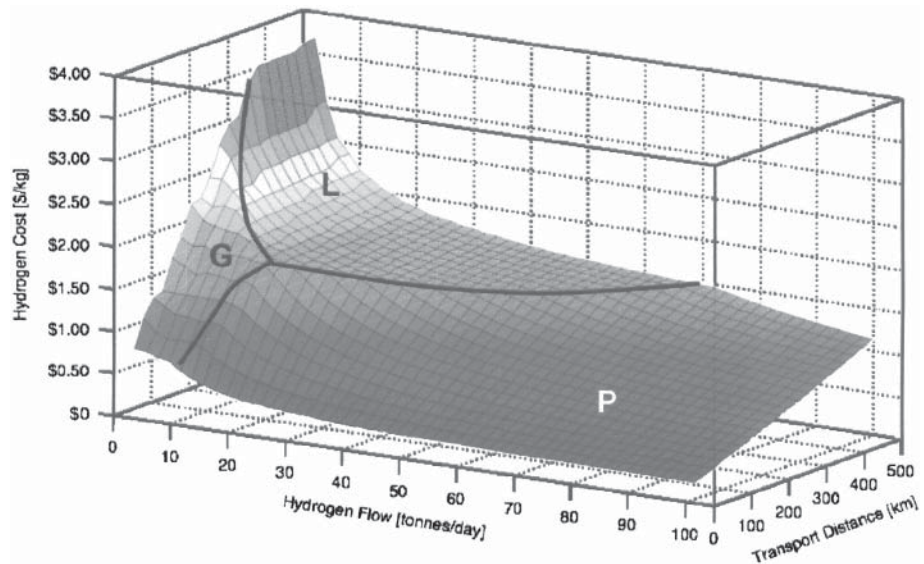


Figure 16 Minimum hydrogen transmission costs as a function of H₂ flow and transport distance. *Source:* From Ref. 27.

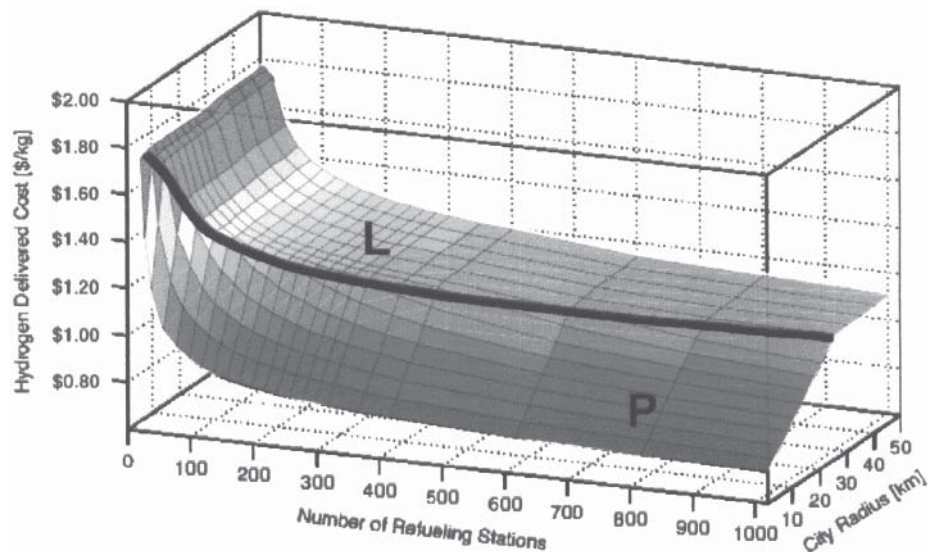


Figure 17 Distribution cost for a network of fueling stations with 1800 kg/day capacity as a function of number of refueling stations and city radius. *Source:* From Ref. 27.

provide valuable insights. For Figs. 17 and 18, note that the region of many refueling stations within a small radius is very unlikely.⁷⁴ In the future, advances in fuel storage (e.g., carbon nanotubes, metal hydrides) may create more cost-efficient distribution modes.

Distributed manufacturing (on-site hydrogen production) is an alternative to hydrogen transport. Although the transmission and distribution are reduced, the generation cost increases.⁵²

4.7 Storage Issues

Hydrogen has a very low volumetric density. Increasing its density consumes energy, thus reducing energy efficiency. This section focuses on hydrogen storage on board vehicles. The fuel tank is central to any vehicle fuel system. Following is a list of key requirements for on-board hydrogen storage systems:

- Refueling time less than 3 min⁵⁴
- Range of 300 miles or greater (5–13 kg storage capacity)^{54,55}
- Low volume; high density⁵⁴
- Safety (fueling, accidents, etc.)⁵⁴
- Hydrogen discharge temperatures below FC temperature⁵⁴
- Operating temperatures range from -50 to 150°C ⁴⁸
- Fast kinetics of hydrogen uptake and release⁴⁸

There are many on-board storage schemes. Figure 19 compares the volumetric and gravimetric energy densities for hydrogen storage technologies, and Fig. 20 compares their cost. The 2010 and 2015 target goals are listed in these figures. None of the current technologies have met the target goals. The following is a brief overview of each hydrogen storage systems.

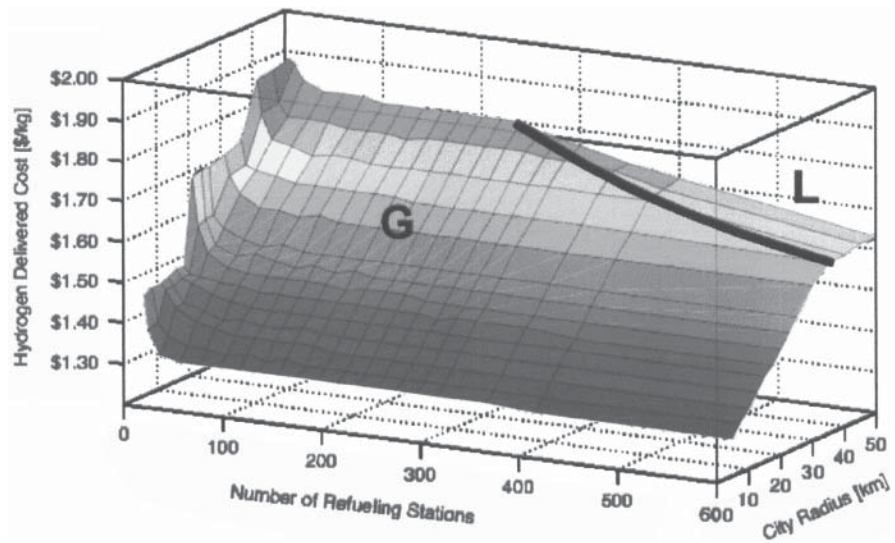


Figure 18 Distribution cost for a network of fueling stations with 1800 kg/day capacity as a function of number of refueling stations and city radius. *Source:* From Ref. 27.

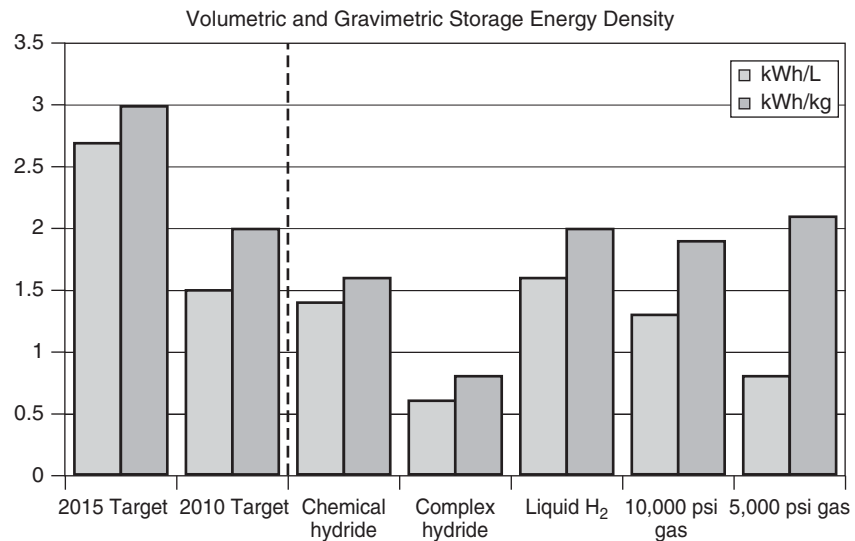


Figure 19 Volumetric and gravimetric energy densities for hydrogen storage technologies. *Source:* From Ref. 15.

Pressurized Hydrogen in Composite Tanks

A composite carbon fiber tank is used to store gaseous hydrogen at pressures of 5000–10,000 psi.⁵⁴ Compression consumes 2–10% of the energy content of hydrogen fuel, depending on the starting pressure and compression efficiency.^{50,55,74} This is the storage system used in Honda's FCX FC vehicle and is commercially available.⁶⁴ According to the International Energy Agency (IEA), composite pressurized tanks cost \$500–\$600/kg H₂.⁵⁴

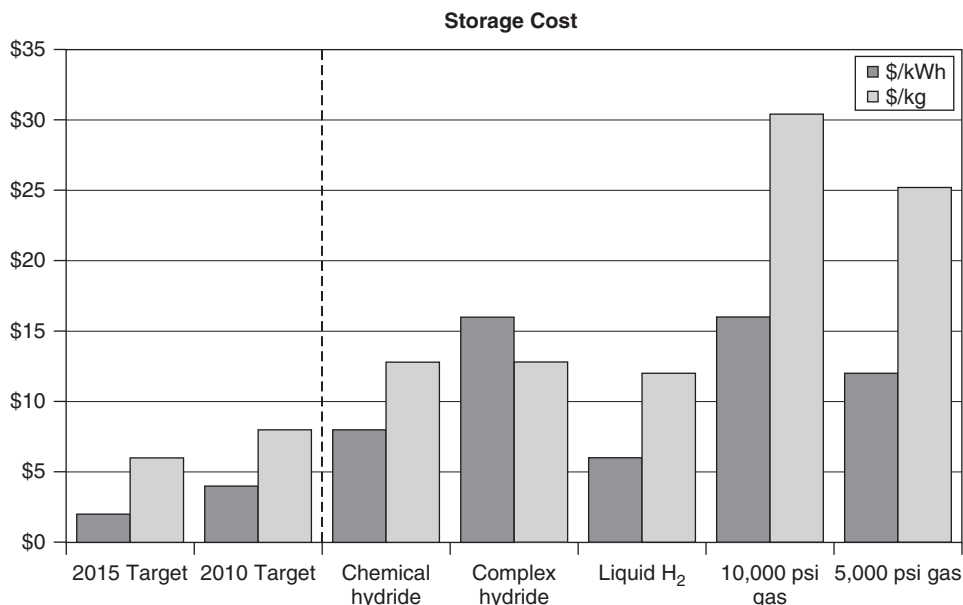


Figure 20 Hydrogen storage costs. *Source:* From Ref. 15.

Glass Microspheres

Microscale glass spheres are filled with hydrogen at high pressure (5000–10,000 psi) and high temperature (300°C).⁵⁴ Then, the spheres are cooled and transferred to a low-pressure fuel tank. To release the hydrogen, the microspheres are heated to 200–300°C. The main advantages of this system are low operating pressure and conformable fuel tanks.⁵⁴ The liberation temperature is higher than the FC temperature; thus, additional heating is required, reducing fuel efficiency. Additionally, there are challenges to prevent breakage while recharging the microspheres.⁵⁴

Cryogenic Liquid Tanks

Liquid hydrogen is the highest energy density storage system (~20% hydrogen of system mass) and may be kept at low pressures.⁵⁴ Liquid hydrogen is extremely cold (–253°C, 20 K). Liquefaction requires 30–40% of the energy content of hydrogen.^{48,50,54} Boil-off is another problematic issue; 1–3% is lost per day.^{48,53}

Chemical Cycling

Another way to store hydrogen as a liquid is to use a chemical cycling system. A few common chemical cycling systems are borohydride (NaBH₄), rechargeable organic liquids, and anhydrous ammonia (NH₃). In each of these systems, a reversible chemical reaction releases hydrogen. The key advantages of chemical cycling are medium-density storage and control. Except for NH₃, spent chemicals must be returned to a filling station for off-board regeneration.⁵⁴ Depending on the chemicals used, safety and toxicity may also be a concern.

On-Board Reforming

On-board reforming strips hydrogen-rich compounds (gasoline, methanol, ethanol, etc.) to form hydrogen gas. The advantage is that a liquid fuel would be stored on board and hydrogen would

be produced as needed. However, as the National Research Council (NRC) points out, “Significant technical barriers exist, such as size, weight, cost and long start-up times.”⁵⁵

Solid-State Storage

Solid-state storage of hydrogen would be safe and efficient.⁵⁴ These systems fall into two subcategories: carbon nanostructures and metal hydride systems. These systems physically or chemically absorb hydrogen into small structures or interstitial areas, where it is bound in the solid medium. Hydrogen may be liberated for use at elevated temperatures (100–500°C) or by adding water (water-reactive metal hydrides).⁵⁴ These systems are still in development. The main challenges are to maximize storage density, lower liberation temperatures, increase absorption kinetics, and increase durability.⁵⁴

4.8 Current Availability

Hydrogen vehicles have been created for demonstrations by many developers.^{50,64–67} Various hydrogen production schemes and fueling systems have also been created and tested successfully.^{50,54,55} However, in all scenarios, the primary limiting factor to commercial development has been cost. A close second is practical engineering hurdles such as storage and distribution, which also contribute high costs.

Hydrogen fueling stations are few and far between. Only a few key regions (e.g., Washington, D.C., California) have public hydrogen fueling stations. Busby includes a table of worldwide hydrogen fueling stations.⁵⁰ The DOE provides an excellent alternative fueling station locator on its website, www.eere.energy.gov/afdc/infrastructure/locator.html.

Each year, the United States produces 90 million tons of hydrogen, and the vast majority is used in refining and fertilizer production.⁷⁵ Of the hydrogen produced, very little is green. Steam reforming of natural gas is the least expensive route to hydrogen production and accounts for 48% of the hydrogen market.⁵¹ The remainder is reformed coal and oil; only 4% is from electrolysis. Furthermore, “to replace all the gasoline sold in the United States with hydrogen from electrolysis would require more electricity than is sold in the United States at the present time.”⁵¹

In some ways, a hydrogen economy would be similar to our current gasoline economy. Consumers would purchase hydrogen at fueling stations, and outwardly vehicles will likely look much the same as gasoline vehicles. However, much research, development, and cost reduction must be accomplished for it to become a reality. “Of the three primary markets (transportation, portable applications, and micropower generation) for fuel cells, transportation is the furthest from mass production and widespread use, but hydrogen fuel-cell vehicles seem to generate the most excitement, by virtue of their visibility and lavish publicity.”⁵⁰

4.9 Safety

The public perceives hydrogen to be an extremely dangerous fuel; however, the literature generally accepts the hazards of hydrogen to be similar to gasoline.

“It is now reasonably well established that the hazards of hydrogen use in transportation would be different from, but not necessarily worse than, the hazards of using petroleum fuels.”⁷⁶

“In general, hydrogen is neither more nor less inherently hazardous than gasoline, propane or methane.”⁷⁷

“In general, however, hydrogen is neither more nor less inherently dangerous than conventional fuels. Some of its properties make it safer, while others make it more dangerous. With proper handling and controls, hydrogen can be as safe as other fuels in common use, or even safer.”⁵⁰

“Hydrogen is neither more nor less dangerous than most other energy carriers. In some respects, hydrogen has qualities that make it safer than most. Hydrogen is not poisonous, it burns rapidly with low radiation heat, and due to its low density compared to air, has the ability to spread rapidly in open surroundings.”⁷⁸

“It is possible to manufacture and utilize hydrogen just as safely as with today’s gasoline systems.”⁷⁸

Because hydrogen is a gas, its safety issues are different than for liquid fuels. “The approach to handling safety issues for hydrogen applications ... requires consistent standards in several areas from production to use and also requires a way of handling the unanticipated safety-related events bound to occur in a technology that is significantly different from that currently used.”⁵² Until hydrogen is a mainstream fuel and used by the public, hydrogen safety will remain a debate. Below are safety advantages of hydrogen:

- Lighter than air, disperses easily⁷⁶
- Burns rapidly with little radiant heat; therefore, risk of secondary fires is low^{76,77}
- Nontoxic
- Nonpoisonous⁷⁷
- Noncarcinogenic⁷⁷
- Not an air or water pollutant⁷⁷
- Proven safety track record in industry⁷⁷

However, hydrogen also has the following safety disadvantages:

- Hard to detect—colorless, odorless, tasteless^{76,77}
- Very hot clear flames⁷⁶
- Large range of ignitability—4–74% hydrogen to air by volume⁷⁶
- Requires little energy to ignite⁷⁶

4.10 Current Research

For hydrogen to become mainstream fuel, it must be economical and practical. Hydrogen production is a proven technology; it can be produced through various methods. Many companies have developed fuel cells and have made hydrogen demonstration vehicles. Hydrogen fueling stations have also been created and are available in a few locations. So why is hydrogen not more prevalent? The reason is simple: cost. Every step of hydrogen, from *well to wheel*, is very expensive. Hydrogen research is not about making it work; it is about making it practical. The hydrogen economy will only become a reality when fuel prices have risen and hydrogen costs have decreased.

4.11 Hydrogen Links

Fuel cell/Hydrogen Infrastructure Codes & Standards	www.fuelcellstandards.com
U.S. Fuel Cell Council	www.usfcc.com/
Fuel Cell Today	http://fuelcelltoday.com/index/
National Renewable Energy Laboratory	www.nrel.gov/
National Hydrogen Association	www.hydrogenassociation.org/
Hydrogen Safety Report	www.hydrogensafety.info/
Hydrogen.gov	www.hydrogen.gov/index.html

American Hydrogen Association	www.clean-air.org/
International Electrotechnical Commission	www.iec.ch/
U.S. DOE EERE	www.eere.energy.gov
Union of Concerned Scientists	www.ucsusa.org
American National Standards Institute	www.hcsp.ansi.org
Wikipedia.org	http://en.wikipedia.org/wiki/Hydrogen
Sandia Nat. Lab., Hydride Info. Center	http://hydpark.ca.sandia.gov/

5 OTHER BIOFUELS

Ethanol, biodiesel, and hydrogen are the dominant biofuels; however, there are other potential biofuels for transportation. Below, we briefly describe additional possibilities.

5.1 Methanol

Methanol, like ethanol, is an excellent automobile fuel.⁷⁹ Because of its excellent combustion properties (e.g., high octane rating), it is used as a racing fuel.⁷⁹ Many characteristics of methanol fuel are similar to ethanol. Methanol is synthesized from gasification or anaerobic digester gases.⁸⁰ Some advantages of methanol are increased power, increased efficiency, and reduced knock.^{79,80} Disadvantages include health hazards, such as blindness and acidosis, poor cold-start properties, corrosion, low lubricity, and formaldehyde production.^{23,80}

5.2 Butanol

Butanol is an alcohol that can be produced via fermentation. Historically, butanol was fermented using *Clostridium acetobutylicum* in the acetone-butanol-ethanol (ABE) fermentation, which produces acetone, butanol, and ethanol.⁸¹ Environmental Energy Inc. (EEI) has developed a patented process that produces only butanol and hydrogen.⁸² In both fermentations, sugars and starches are feedstocks.^{81,82}

Butanol may be blended with gasoline or used directly.^{82,83} Compared to ethanol, butanol has more favorable physical properties, such as higher energy content and less susceptibility to water contamination.

5.3 Mixed Alcohols

The MixAlco process anaerobically ferments any biodegradable material into mixed organic acids, which are then chemically converted into mixed alcohols. The MixAlco process is very robust; all process steps have been demonstrated on the laboratory scale and some at the pilot scale. Because the MixAlco process does not require sterility, costs are very low.¹⁵ Another route to mixed alcohols involves gasifying lignocellulose to syngas (carbon monoxide and hydrogen), which can be converted into mixed alcohols using a catalyst.^{16,17}

5.4 Petroleumlike Biofuels

Petroleumlike compounds may be extracted from hydrocarbon-producing plants and used as fuel. For example, *Euphorbiaceae* and *Asclepiadaceae* have several species that produce these compounds.⁸⁴ Biocrude extracted from *Euphorbiaceae lathyris* “contained ethylene (10%), propylene (10%), toluene (20%), xylene (15%), C5–C20 non-aromatics (21%), coke (5%), C1–C4 alkenes (10%) and fuel oil (10%).”⁸⁴ Biocrude will be processed much like petroleum crude to produce fuel.

5.5 Synthesis Hydrocarbons

Fisher-Tropsch is a well-known synthesis process that converts syngas to gasoline, diesel, and waxes.⁸⁵ Unfortunately, Fisher-Tropsch is an expensive technology and is practiced only at large scales where economies can be realized. Another gas-to-liquid (GTL) technology can oligomerize methane or alcohols into gasoline, diesel, or jet fuel. SynFuels International Inc. is developing the technology and estimates production costs of \$25–\$28 per barrel from low-cost feedstocks.⁸⁶

5.6 Methane

Anaerobic digesters are a common route to methane production. Typically, these systems do not generate enough methane to run more than a small generator.⁸⁷ Biomethane could be used as a transportation fuel.

6 CLOSING REMARKS

Currently, none of the biofuels mentioned in this chapter significantly displace petroleum. Some require subsidy, some are too expensive, and others are still under research and development. Displacing petroleum will require parallel use of renewable energy and biofuels. Renewable experts agree that there is no single silver bullet. In recent years, biofuels have gained momentum and will continue to grow as long as the sun shines.

REFERENCES

1. G. Pahl, *Biodiesel: Growing a New Economy*, Chelsea Green, 2005.
2. Energy Information Agency, “EIA Kids Page Ethanol Energy Timeline—Milestone in Ethanol Energy History,” available: www.eia.doe.gov/kids/history/timelines/ethanol.html, accessed January 15, 2007.
3. S. W. Mathewson, *The Manual for the Home and Farm Production of Alcohol Fuel*, Ten Speed Press, 1980.
4. J. Finguerut, “Ethanol Production in a Cane Sugar Mill,” paper presented at Workshop—Louisiana State University, Baton Rouge, LA, 2005.
5. U.S. Department of Energy (DOE), “Energy Efficiency and Renewable Energy, Biomass Program,” available: http://www1.eere.energy.gov/biomass/ethanol_yield_calculator.html, accessed December 7, 2007.
6. A. G. Alexander, *The Energy Cane Alternative* (Sugar Series 6), Elsevier, Amsterdam, 1985.
7. M. H. Nguyen and R. G. H. Prince, “A Simple Rule for Bioenergy Conversion Plant Size Optimization: Bioethanol from Sugar Cane and Sweet Sorghum,” *Biomass Bioenergy*, **10**(5/6), 361–365, 1996.
8. M. Wu, Y. Wu, and M. Wang, “Energy and Emission Benefits of Alternative Transportation Liquid Fuels Derived from Switchgrass: A Fuel Life Cycle Assessment,” *Biotechnol. Progr.*, **22**(4), 1012–1024, 2006.
9. H. Hartmann, “Environmental Aspects of Energy Crop Use—A System Comparison,” in P. Chartier, A. A. C. M. Beenackers, and G. Grassi (Ed.), *Biomass for Energy, Environment, Agriculture and Industry, Proceedings of the 8th European Biomass Conference*, Vienna, October 3–5, 1994, 1995.
10. C. Luo, D. L. Brink, and H. W. Blanch, “Identification of Potential Fermentation Inhibitors in Conversion of Hybrid Poplar Hydrolyzate to Ethanol,” *Biomass Bioenergy*, **22**(2), 125–138, 2002.
11. Renewable Fuels Association, “Ethanol Industry Outlook,” available: www.ethanolrfa.org, 2006.
12. M. M. Rabbani, “Acid Hydrolysis Processes for Cellulosic Biomass,” *Esc. Univ. Ing. Tec. Agric.*, Villava, Spain, *Ingenieria Quimica* (Madrid, Spain), **21**(245), 139–146, 1989.
13. L. Laureano-Perez, F. Teymouri, H. Alizadeh, and B. E. Dale, “Understanding Factors That Limit Enzymatic Hydrolysis of Biomass. Characterization of Pretreated Corn Stover,” *Appl. Biochem. Biotechnol.*, 121–124, 2005.

14. T. Eggeman, and D. Verser, "The Importance of Utility Systems in Today's Biorefineries and a Vision for Tomorrow," *Appl. Biochem. Biotechnol.* **129–132**, 361–381, 2006.
15. M. T. Holtzapple, "Advanced Biomass Refinery: Third-Generation Technology," Abstracts, presented at the 62nd Southwest Regional Meeting of the American Chemical Society, Houston, October 19–22, 2006, SRM-156, American Chemical Society, Washington, D.C.
16. M. Xiang, D. Li, W. Li, B. Zhong and Y. Sun, "Potassium and Nickel Doped β - Mo_2C Catalysts for Mixed Alcohols Synthesis Via Syngas," *Catal. Commun.*, **8**(3), 513–518, 2007.
17. J. M. Campos-Martin, A. Guerrero-Ruiz, and J. L. G. Fierro, "Structural and Surface Properties of $\text{CuO-ZnO-Cr}_2\text{O}_3$ Catalysts and Their Relationship with Selectivity to Higher Alcohol Synthesis," *J. Catal.*, **156**, 208–218, 1995.
18. G. Najafpour and H. Younesi, "Ethanol and Acetate Synthesis from Waste Gas Using Batch Culture of *Clostridium ljungdahlii*," *Enz. Microbial Technol.*, **38**(1–2), 223–228, 2006.
19. K. T. Klasson, M. D. Ackerson, E. C. Clausen, and J. L. Gaddy, "Bioconversion of Synthesis Gas into Liquid or Gaseous Fuels," *Enz. Microbial Technol.*, **14**(8), 602–608, 1992.
20. *Guidebook for Handling, Storing, & Dispensing Fuel Ethanol*, prepared for the U.S. Department of Energy, Center for Transportation Research Energy Systems Division, Argonne National Laboratory, Lemont, IL.
21. Renewable Fuels Association, *Guidelines for Establishing Ethanol Plant Quality Assurance and Quality Control Programs*, RFA Publication #040301, available: www.ethanolrfa.org, accessed August 1, 2007.
22. "D4806-98 for Denatured Fuel Ethanol for Blending with Gasoline," available: <http://www.distill.com/specs/US-1.html>, accessed May 11, 2007.
23. K. Owen and T. Coley, *Automotive Fuels Reference Book*, 2nd ed., Society of Automotive Engineers, Warrendale, PA, 1995.
24. H. Joseph, "ANFAVEA," available: anfavea@anfavea.com.br, henry.joseph@volkswagen.com.br, accessed March 5, 2007.
25. U.S. Department of Energy EERE, *Handbook for Handling, Storing, and Dispensing E85*, available: www.e85fuel.com/pdf/e85_technical_booklet.pdf, accessed May 12, 2007.
26. E de Oliveira, Ph.D. Dissertation, University of Waterloo, Ontario, 1997.
27. National Ethanol Vehicle Association, available: <http://www.e85fuel.com>, accessed April 30, 2007.
28. "Low-Level Ethanol Blends," available: <http://www.nrel.gov/docs/fy05osti/37135.pdf>, accessed April 30, 2007.
29. Renewable Fuels Association, available: <http://www.ethanolrfa.org>, accessed April 30, 2007.
30. M. Gautam and D.W. Martin II, "Combustion Characteristics of Higher-Alcohol/Gasoline Blends," *Proc. Inst. Mech. Eng.*, **214** Part A, 2000.
31. R. K. Niven, "Ethanol in Gasoline: Environmental Impacts and Sustainability," *Renewable Sustainable Energy Rev.*, **9**, 535–555, 2005.
32. R. L. Bechtold, *Alternative Fuel Guidebook: Properties, Storage, Dispensing and Vehicle Facility Modifications*, Society of Automotive Engineers, 1997.
33. U.S. Department of Energy, Efficiency and Renewable Energy (EERE), available: <http://www.eere.energy.gov/>, accessed April 30, 2007.
34. M. Cooper, "Over a Barrel: Why Aren't Oil Companies Using Ethanol to Lower Gasoline Prices?" Confederation of America, May 2005.
35. American Coalition for Ethanol, available: www.ethanol.org, accessed May 1, 2007.
36. Iowa Corn Growers Association, available: www.iowacorn.org, accessed May 1, 2007.
37. J. Tickell, *From Fryer to Fuel Tank: The Complete Guide to Using Vegetable Oil as an Alternative Fuel*, 3rd ed., Ticknell Energy, Hollywood, CA, 2003.
38. The National Biodiesel Board., available: www.biodiesel.org, accessed July 21, 2007.
39. F. Ma and M. A. Hanna., "Biodiesel Production: A Review," *Bioresour. Technol.*, **70**, 1999.
40. BQ 9000 Quality Management Program, available: www.bq-9000.org, accessed January 15, 2007.
41. G.I R. Frahm, "St. Johns School Buses Rolling 1 Million Miles on Biodiesel," Michigan Soybean Promotion Committee press release, April 27, 2004.
42. S. Howell, "Rigorous Standards Ensure Biodiesel Performance," *Biodiesel: On The Road to Fueling the Future*, Biodiesel Report, National Biodiesel Board, 2001.

43. R. L. McCormick et al., "Effects of Biodiesel Blends on Vehicle Emissions," NREL Milestone Report NREL/MP-540-40554, October 2006.
44. K. S. Tyson, "2004 Biodiesel Handling and Use Guide," DOE/GO-102004-1999, November 2004.
45. Picture of biofuels fuel pump, National Renewable Energy Laboratory, Image Library, available: <http://www.nrel.gov/data/pix/Jpegs/13531.jpg>, accessed March 20, 2007.
46. Energy Information Administration, available: www.eia.doe.gov, accessed March 20, 2007.
47. U.S. Congress, Safe, Accountable, Flexible, and Efficient Transportation Act of 2004, Section 5102.
48. P.P. Edwards et al., "Hydrogen Energy," *Phil. Trans. R. Soc. A*, **365**, 1043–1056, 2007.
49. R. F. Service, "Profile: Daniel Nocera, Hydrogen Economy? Let Sunlight Do the Work," *Science*, **315**, February 9, 2007, available: www.sciencemag.org.
50. R. L. Busby, *Hydrogen and Fuel Cells: A Comprehensive Guide*, PennWell, Tulsa, OK, 2005.
51. M. F. Hordeski, *Alternative Fuels: The Future of Hydrogen*, Fairmont Press, Lilburn, GA, 2007.
52. B. Sorenson, *Hydrogen and Fuel Cells*, Elsevier, Amsterdam, 2005.
53. A. G. Dutton, "Hydrogen Energy Technology," Tyndall Working Paper TWP 17, Tyndall Centre for Climate Change, p. 30, available: http://www.tyndall.ac.uk/publications/working_papers/wp17.pdf, accessed March 12, 2007.
54. International Energy Agency, "2006 Hydrogen Production and Storage, R&D Priorities and Gaps," available: <http://www.iea.org/Textbase/papers/2006/hydrogen.pdf>, accessed March 12, 2007.
55. National Research Council, *The Hydrogen Economy: Opportunities, Costs, Barriers, and R&D Needs*, The National Academies Press, 2004, available: www.nap.edu.
56. www.fuelcellstandards.com, accessed December 7, 2007.
57. K. Hall, Personal e-mail communication, March 23, 2007, khall@ttcorp.com.
58. Committee on Gaseous Fuels Forms, "Subcommittee on Hydrogen and Fuel Cells," *Standardization News*, December 2004, available: www.astm.org.
59. Energy Information Administration (EIA), "Alternatives to Traditional Transportation Fuels: An Overview," June 1994, available: ftp://ftp.eia.doe.gov/pub/solar.renewables/alt_over.pdf#page=58.
60. U.S. Department of Energy, Energy Efficiency and Renewable Energy, available: http://www1.eere.energy.gov/hydrogenandfuelcells/education/pdfs/fuel_cell_facts.pdf, accessed March 20, 2007.
61. R. Rose, "Questions and Answers about Hydrogen and Fuel Cells," available: www.fuelcells.org, accessed April 10, 2007.
62. U.S. Department of Energy, Energy Efficiency and Renewable Energy, available: http://www1.eere.energy.gov/hydrogenandfuelcells/pdfs/01_paster_hydrogen_prog.pdf.
63. I. Dincer, "Environmental and Sustainability Aspects of Hydrogen and Fuel Cells," *Int. J. Energy Res.*, **31**, 29–55, 2007.
64. Honda Worldwide, available: <http://world.honda.com/news/2007/4070108FCXConcept/>, accessed 2007.
65. General Motors Corporation, "Chevrolet Equinox specifications," available: http://www.gm.com/company/gmability/adv_tech/400_fc/fact_sheets.html.
66. Tokyo Gas Co., Ltd., "Corporate Communications Dept. Introduction of DaimlerChrysler F-Cell Fuel Cell Vehicle," October 16, 2003, available: http://www.tokyo-gas.co.jp/Press_e/20031016-1e.pdf.
67. S. Geiger, "Opening Doors to Fuel Cell Commercialisation: DaimlerChrysler F-Cell," *Fuel Cell Today*, April 5, 2004, available: http://www.fuelcelltoday.com/FuelCellToday/FCTFiles/FCTArticleFiles/Article_788_DCF-Cell0404.pdf.
68. National Renewable Energy Lab (NREL), "Fuel Cell," available: <http://www.nrel.gov/data/pix/Jpegs/12508.jpg>, accessed April 10, 2007.
69. J. W. Heffel, "NO_x Emission and Performance Data for a Hydrogen Fueled Internal Combustion Engine at 1,500rpm Using Exhaust Gas Recirculation," *Int. J. Energy Res.*, **28**, 901–908, 2003.
70. J. A. A. Yamin, "Comparative Study Using Hydrogen and Gasoline as Fuels: Combustion Duration Effect," *Int. J. Energy Res.*, **30**, 1175–1187, 2006.
71. G. A. Karim, "Hydrogen as a Spark Ignition Engine Fuel," *Int. J. Hydrogen Energy*, **28**, 569–577, 2003.
72. Arizona Public Service, "Alternative Fuel Pilot Plant & Hydrogen Internal Combustion Engine Vehicle Testing," available: <http://avt.inl.gov/pdf/hydrogen/h2factsheet.pdf>, accessed April 11, 2007.

73. Energy Information Agency (EIA), "A Primer on Gasoline Prices," available: http://www.eia.doe.gov/pub/oil_gas/petroleum/analysis_publications/primer_on_gasoline_prices/html/petbro.html, accessed December 7, 2007.
74. C. Yang and J. Ogden, "Determining the Lowest-Cost Hydrogen Delivery Mode," *Int. J. Hydrogen Energy*, **32**, 268–286, 2007.
75. U.S. Department of Energy Hydrogen Program, "Hydrogen Production," available: www.hydrogen.energy.gov, accessed December 7, 2007.
76. D. Sperling (Ed.), *Alternative Transportation Fuels: An Environmental and Energy Solution*, Greenwood Press, Westport, CT, 1989.
77. U.S. Department of Energy (DOE), EERE., "Regulators' Guide to Permitting Hydrogen Technologies," Version 1.0 PNNL-14518, DOE, Washington, DC, released January 12, 2004.
78. Bellona, "Hydrogen Report," 2002, available: <http://www.bellona.org/reports/hydrogen>.
79. J. H. Perry and C. P. Perry, *Methanol: Bridge to a Renewable Energy Future*, University Press of America, 1990.
80. M. A. Deluchi, D. Sperling, and R. A. Johnston, "A Comparative Analysis of Future Transportation Fuels," Research Report UCB-ITS-RR-87-13, Institute of Transportation Studies, University of California, Berkeley, CA, 1987.
81. Wikipedia, "Clostridium acetobutylicum," available: http://en.wikipedia.org/wiki/Clostridium_acetobutylicum, accessed December 7, 2007.
82. Environmental Energy, Inc, available: <http://www.butanol.com/>, accessed December 7, 2007.
83. Dupont, "Biobutanol Fact Sheet," available: http://www.dupont.com/ag/news/releases/BP_DuPont_Fact_Sheet_Biobutanol.pdf, accessed December 7, 2007.
84. D. Kalita, "Hydrocarbon Plant—New Source of Energy for Future, Renewable & Sustainable Energy Reviews," 2006, available: www.elsevier/locate/rser.
85. A. Demirbas, "Progress and Recent Trends in Biofuels," *Progr. Energy Combustion Sci.*, **33**, 1–18, 2007.
86. K. R. Hall, "A New Gas to Liquids (GTL) or Gas to Ethylene (GTE) Technology," Texas A&M University, College Station, TX, 2007.
87. F. T. Varani and J. J. Buford, Jr., *Fuels from Waste Chapter VI: The Conversion of Feedlot Wastes into Pipeline Gas*, Academic, 1977.

CHAPTER 23

SOLAR ENERGY MEASUREMENTS

Tariq Muneer and Yieng Wei Tham
Edinburgh Napier University
Edinburgh, Scotland

1 INTRODUCTION	805	7 MODERN DEVELOPMENTS	827
1.1 Radiation Measurement			
History	805		
1.2 Solid Angle	806	8 DATA QUALITY	829
1.3 Intensity and Flux	807	ASSESSMENT	
1.4 Radiation Units	808	8.1 U. S. National Renewable	
1.5 Radiation Laws	808	Energy Laboratory (NREL),	
1.6 Thermal Detector	809	1993	829
1.7 Photo Detectors	809	8.2 Commission Internationale de	
1.8 Classification of		l'Éclairage (CIE) Automatic	
Pyrheliometer	810	Quality Control	830
1.9 Working Standard	811	8.3 Page Model	830
		8.4 Muneer and Fairouz Quality	
		Control Procedure	830
2 MEASUREMENT			
EQUIPMENT	811	9 STATISTICAL EVALUATION OF	831
2.1 Pyranometer	811	MODELS	
2.2 Pyranometer with Shading		9.1 Slope of the Best-Fit Line, s	832
Device	813	9.2 Coefficient of	
2.3 Pyrheliometer	814	Determination, r^2	832
2.4 Pyrgeometer	814	9.3 Coefficient of Correlation, r	833
2.5 Albedometer	815	9.4 Student's t Distribution	833
2.6 Sunshine Recorder	817	9.5 Root-Mean-Squared Error	833
		9.6 Mean Bias Error	833
3 EQUIPMENT ERROR AND		9.7 Mean of Absolute	
UNCERTAINTY	819	Deviations	834
		9.8 Nondimensional MBE, MAD,	
4 OPERATIONAL ERRORS	820	and RMSE	834
		9.9 Figure of Merit, Ψ	835
5 DIFFUSE RADIATION DATA			
MEASUREMENT ERRORS	821	10 OUTLIER ANALYSIS	835
5.1 Description of Models	822		
		REFERENCES	836
6 TYPES OF SENSORS AND			
THEIR ACCURACY	825		

1 INTRODUCTION

1.1 Radiation Measurement History

The Basra-born physicist Abu Ali al-Hasan ibn al-Hasan ibn al-Haytham was one of the first scientists who made a systematic attempt at understanding the transmission of solar radiation through terrestrial atmosphere. Al-Haytham was born in the year 965 and in his treatise *Balance of Wisdom*, he discusses the density of the atmosphere and the phenomenon of atmospheric

refraction. He also attempted to measure the height of the atmosphere, which has now been confirmed to be 99% accurate.¹

The invention of the telescope by Galileo in the sixteenth century was probably when the sun was investigated with any reported significance. Since then, first a great many discoveries have been made and physical laws formulated and explained such as radiation electromagnetic theory, color of sunlit sky, solar radiation absorption by water vapor, and the wave theory of light.

The electrical compensation pyrheliometer invented by Knut Ångström in 1893 was among the earliest radiation measurement instruments. This instrument is still used in many countries as the standard for absolute radiant energy determination.²

The advancement of measurement instrument development started after World War II when technology was furthered. The replacement of conventional resistance strips in Ångström-type pyrheliometers with thermopile is one of the many examples. Furthermore, the use of computerized data logging and data acquisition has replaced conventional manual, time-consuming methods.

The World Meteorological Organization (WMO) has recommended a standard terminology for various radiation fluxes and the classification of the associated instruments. The units have been chosen on the basis of standard use and ease of physical interpretation. Some of the relevant basic concepts are explained in the following sections.

1.2 Solid Angle

Refer to Fig. 1 where an elemental solid angle, $d\omega$, is shown. The concept of solid angle can be illustrated as a straight line through point 0 moving in space and intersecting an arbitrary surface located at some distance s from point 0. If the locus of the point of intersection forms a closed path on the surface but does not intersect itself, then a unique area is defined on the surface.

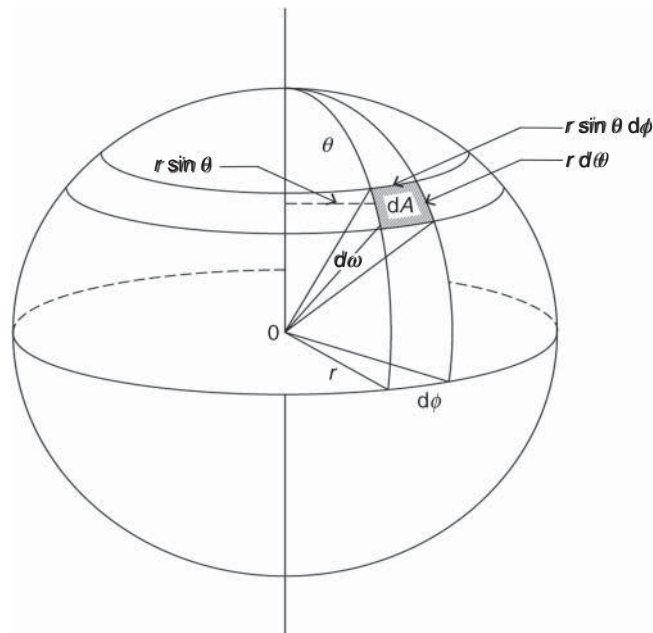


Figure 1 Illustration of solid angle and its interpretation in spherical coordinates.

Assume the area is an elemental area, da , the surface normal of which makes an angle with the direction to point 0.

For purpose of illustration, assume it is the surface of a sphere of radius r , as shown in Fig. 1. For this case, the solid angle subtended at the center of the sphere by area dA on its surface is $d\omega = dA/r^2$. For the special case of a unit sphere ($r = 1$), $d\omega$ and dA have the same numerical value if $d\omega$ is expressed in steradians (sr) and dA and r are expressed in the same system of units. Because the area of the surface of a sphere is $4\pi r^2$, the total solid angle subtended at a point by the entire surrounding sphere is $4\pi r^2/r^2 = 4\pi$ sr.

A hemispheric solid angle is 2π sr. As can be seen from Fig. 1, an elemental solid angle is conveniently expressed in a spherical coordinate system as

$$d\omega = \frac{(r \, d\theta)(r \sin \theta \, d\phi)}{r^2} \quad (1)$$

1.3 Intensity and Flux

Consider a line of radiation crossing the elemental area $d\sigma$ of Fig. 2 and confined to the elemental angle $d\omega$, which is oriented at some angle θ to the normal of $d\sigma$. The energy dE_v contained in the frequency interval dv , which crosses $d\sigma$ in the time increment dt , is given by

$$dE_v = I_v \, dv \, dt \, d\omega \, d\sigma \cos \theta \quad (2)$$

This relation defines the monochromatic specific intensity in the most general way as

$$I_v = \frac{dE_v}{dv \, dt \, d\omega \, d\sigma \cos \theta} \quad (3)$$

Thus, the definition of specific intensity implies directionality. The term flux, however, is flow of energy, and it may or may not have an implied direction. For instance, the monochromatic flux of energy across $d\sigma$ is given by the integration of the normal component of I_v , over the entire spherical solid angle Ω . Thus,

$$F_v = dv \, dt \, d\sigma \int_{\Omega} I_v(\omega) \cos \theta \, d\omega \quad (4)$$

or, in terms of spherical coordinates,

$$F_v = dv \, dt \, d\sigma \int_0^{2\pi} \int_0^{\pi} I_v(\theta, \phi) \sin \theta \cos \theta \, d\theta \, d\phi \quad (5)$$

Terminology in Radiation Instruments

Considerable confusion in the terminology applied to various types of solar radiation instruments has built up over the years. For instance, an instrument measuring the total

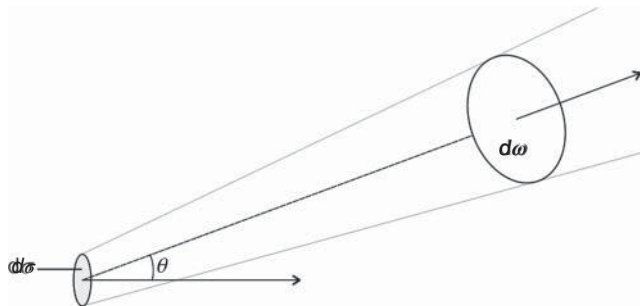


Figure 2 Beam of radiation passing through an elemental area.

hemispherical flux of solar radiation has been variously called pyrheliometer, pyranometer, solarimeter, actinograph, and sunshine recorder.

To standardize terminology, the WMO, through its Commission for Instruments and Method of Observation, has recommended the following classification of radiation instruments:

Pyrheliometer: An instrument for measuring “the intensity of direct solar radiation at normal incidence.”

Pyranometer: An instrument for measuring “the solar radiation received from the whole hemisphere. It is suitable for the measurement of the global or sky radiation.” A pyranometer for measuring the radiation on a spherical surface is a “spherical pyranometer.”

Pyrgeometer: An instrument for measuring “the net atmospheric radiation on a horizontal upward-facing black surface at ambient air temperature.”

Pyrradiometer: An instrument for measuring “both the solar and terrestrial radiation (total radiation).”

Net Pyrradiometer: An instrument for measuring “the net flux downward and upward total (solar, terrestrial, surface, and atmospheric) radiation through a horizontal surface.” A net radiometer is sometimes termed a balance pyrradiometer or radiation balance meter.

1.4 Radiation Units

The principal units of radiation are given in Table 1.

1.5 Radiation Laws

1. *Planck's Law*. Max Planck showed that the spectral density emitted by a blackbody at temperature T is given by the Planck function to the following, the first being expressed on the basis of frequency ν and the second on the basis of wavelength λ of the radiation:

$$B_{\nu}(T) = \frac{2h\nu^3}{c^2(e^{h\nu/kt} - 1)} \quad (6)$$

$$B_{\lambda}(T) = \frac{C_1\lambda^{-5}}{(e^{c_2/\lambda T} - 1)} \quad (7)$$

Table 1 Principal Units of Radiation

Quantities	Units
Wavelength	Micrometer (μm) or Ångstrom (Å)
Frequency (ν)	s^{-1}
Wave number	cm^{-1}
Specific intensity: spectral	$\text{W}/\text{cm}^2/\text{sr}/\text{cm}$
Specific intensity: total	$\text{W}/\text{cm}^2/\text{sr}$
Radian flux: spectral	$\text{W}/\text{cm}^2/\mu\text{m}$
Radian flux: total	W/cm^2

where h	=	Planck's constant = 6.6256×10^{-27} erg s
k	=	Boltzmann's constants = 1.3805×10^{-16} erg deg $^{-1}$
c	=	speed of light in vacuo = 2.998×10^{10} cm s $^{-1}$
C_1	=	first radiation constant = $2hc^2 = 3.74150 \times 10^{-5}$ erg cm 2 s $^{-1}$
C_2	=	second radiation constant = $hc/k = 1.43879$ cm deg

2. *Kirchhoff's Law.* Gustav Kirchhoff stated that for a medium in thermodynamic equilibrium, the ratio between the mass emission coefficient and mass absorption coefficient has a value, which is independent of the nature of the material and is dependent only on wavelength of the radiation and temperature of the medium.

A note on the limits of applicability of Kirchhoff's law to the terrestrial radiation field of the atmosphere is appropriate. The law requires thermodynamic equilibrium, one characteristic of which is that the radiation field be isotropic. Obviously, the radiation field for the atmosphere as a whole is not isotropic. On the other hand, the field in the localized volume of the troposphere or stratosphere is approximately isotropic, and it is in the context of this local thermodynamic equilibrium that Kirchhoff's law is applicable to the atmosphere. A second characteristic of local thermodynamic equilibrium is that the populations of atomic and molecular states be those of their equilibrium distribution. In such a case, the energy transitions are controlled by molecular collisions and not by interaction of particles with the radiation field itself. In the atmosphere, molecular collisions dominate the energy transitions at all altitudes below 60–70 km, indicating that local thermodynamic equilibrium is a good approximation through more than 90% of the mass of the atmosphere.

3. *Stefan–Boltzmann Law.* By integrating the monochromatic blackbody function of Eq. 7 over the entire wavelength range from 0 to ∞ , an expression for the total rate of energy emission E by a unit area of blackbody surface in terms of its absolute temperature T may be derived as

$$E = \sigma T^4 \quad (8)$$

where σ is the Stefan–Boltzmann constant, which is 5.6704×10^{-8} W/m 2 /K 4 .

4. *Wien Displacement Law.* Wien's displacement law is obtained by differentiating the Planck function with respect to wavelength, setting the result equal to 0 and thereby determining the value λ_{\max} at which $B_\lambda(T)$ is a maximum. Hence,

$$\lambda_{\max} T = \text{const} \quad (9)$$

The value of the constant is 0.2897 cm deg if λ is in centimeters. Important dates related to solar radiation measurement are provided in Table 2.

1.6 Thermal Detector

The mode of operation of a thermal detector starts when the radiant energy transfers into heat energy, with consequent rise of temperature of some materials. They respond only to total energy absorbed and are thus, at least theoretically, nonselective as to the spectral distribution of the energy. Because of the limitation of the absorbing materials, this nonselective feature is difficult to achieve completely in operation, but it is more closely achieved in thermal detectors than in any other type. The main types of thermal detectors are calorimeters, thermocouples or thermopiles, and bolometers.

1.7 Photo Detectors

The advantage of photo detectors is that the sensor is activated by discrete events of photons striking the material and not by a change in temperature because of the absorption of radiation, as in the thermal detectors. The advantage of sensing discrete events is that much faster

Table 2 Highlights of Solar Radiation Instruments Development

Year	Events
1825	Herschel's pyrheliometer (actinometer) developed
1837	Invention of Pouillet's pyrheliometer
1840	Invention of first photographic sunshine recorder by Jordan
1879	Campbell–Stokes sunshine recorder started in use
1885	Invention of photographic sunshine recorder by Jordan
1885	Invention of new form polarimeter and of pole-star recorder by Pickering
1886	Invention of new type of radiometer by Ångstrom
1891	Concept of Maring–Marvin sunshine recorder by Maring
1893	Invention of electric compensation pyrheliometer by Ångstrom
1898	Invention of Callender pyranometer
1902	Secondary standard silver-disk pyrheliometer developed by Abbot
1905	Ångstrom electrical compensation pyrheliometer adopted as a WMO standard
1908	Invention of Michelson pyrheliometer
1910	Invention of Marvin pyrheliometer
1915	First bolometer constructed
1916	Pyranometer for measuring global radiation devised
1917	Ultrasensitive vacuum bolometer constructed
1919	Honeycomb (melikeron) pyranometer constructed
1922	Dorno's pyrheliograph invented
1923	Invention of Kimball–Hobbs pyranometer (forerunner of first Eppley pyranometers)
1923	Invention of Moll thermopile
1924	Moll thermopile used by Gorczynski, later known as Kipp solarimeter
1927	Double water-flow pyrheliometer developed by Shulgin
1932	First standard design of Robitzsch pyranometer developed
1948	Menzel developed sensitive sky photometer
1953	Invention of sunshine switch by Foster and Foskett of U.S Weather Bureau
1957	International Pyrheliometric Scale (1956) put into effect; original Ångstrom scale increased by 1.5% and (1913) Smithsonian scale decreased by 2.0%
1962	Adoption of the Campbell–Stokes sunshine recorder as an "Interim Reference Sunshine Recorder" by the Commission on Instruments and Methods of Observation, WMO
1965	Introduction of Eppley precision pyranometer
1965	Development of automatic control of Ångstrom pyrheliometer by Marsh
1969	Introduction of Eppley black and white (star-type) pyranometer
1990	Wide-scale use of programmable data loggers for recording irradiance
2001	Invention of BF3 sensor by Delta-T of Cambridge, England. The instrument integrates sunshine duration recorder with global and diffuse irradiance measurement

responses and higher sensitivities can be achieved than with thermal devices. There are three principal types of photo detectors, namely, photovoltaic, photoconductive, and photoemissive cells.

1.8 Classification of Pyrheliometer

The Commission for Instruments and Method of Observation of the WMO (1965) classified pyrheliometers as standard, first, or second class, in accordance with the criteria given in Table 3. On the basis of these criteria, the commercially available pyrheliometer are classified as in Table 4.

Table 3 Classification of Pyrheliometers by WMO

	Standard	First Class	Second Class
Sensitivity (mW/cm ²)	±0.2	±0.4	±0.5
Stability (% change in year)	±0.2	±1	±2
Temperature (maximum error due to changes of ambient temperature, %)	±0.2	±1	±2
Selectivity (maximum error due to departure from assumed spectral response, %)	±1	±1	±2
Linearity (maximum error due to nonlinearity not accounted for, %)	±0.5	±1	±2
Time constant (maximum)	25 s	25 s	1 min

Table 4 Classification of Commercial Pyrheliometers

Class	Type
First class	Ångstrom electrical compensation pyrheliometer Abbot silver-disk pyrheliometer
Second class	Michelson bimetallic pyrheliometer Linke–Feussner iron-clad pyrheliometer New Eppley pyrheliometer (temperature compensated) Yanishevsky thermoelectric pyrheliometer
Third class	Moll-Gorczyński pyrheliometer Old Eppley pyrheliometer

1.9 Working Standard

Working standard pyrheliometers of Ångstrom type (referenced to Davos) are maintained at the regional and national centers designated by the WMO for the purpose of reproducing the International Pyrheliometric Scale 1956 (IPS). To a limited extent, the Abbot silver-disk pyrheliometer is still used at such centers. The secondary transfer instruments in current use are the other Ångstrom pyrheliometer and instruments of Eppley, Linke–Feussner, and Michelson types.

2 MEASUREMENT EQUIPMENT

According to the European Solar Radiation Atlas (ESRA), solar radiation measurements can be broadly classified as ground-based measurements derived from geostationary satellites, which measures the energy reflected by the system (earth/atmosphere) in different wavelength bands.³

2.1 Pyranometer

This instrument measures global solar radiation. Figure 3 shows the structure of the CM11 Kipp and Zonen pyranometer. The pyranometer has the spectral response of between 335 and 2200 nm. A thermal detector in the sensing element responds to the total power absorbed from the solar radiation at any spectral distribution. The absorption of radiation on the black disk generates heat, and the heat energy flows to the heat sink through a thermal resistance.

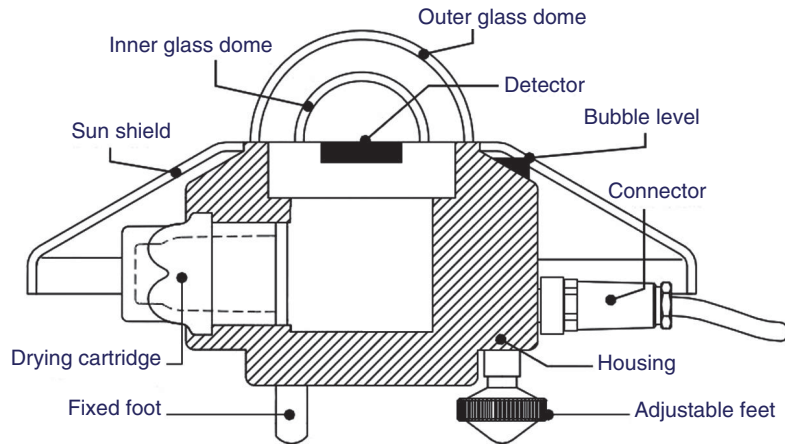


Figure 3 Kipp and Zonen CMP11 pyranometer. Image courtesy of Kipp and Zonen.

The temperature difference across the thermal resistance of the disk is converted into a small voltage, which can be detected by the logging system or computer. To avoid temperature fluctuation and reduce thermal radiation losses to the atmosphere, the pyranometer is built with a double-glass envelope. Furthermore, silica gel crystal is used to prevent moisture within the pyranometer. Periodic cleaning of the glass dome is recommended as debris may collect over time. The working principle of the pyranometer given here is as discussed by Muneer.⁵



Figure 4 Kipp and Zonen pyranometer with shading device. (From Ref. 6.)

2.2 Pyranometer with Shading Device

This type of pyranometer measures the diffuse solar radiation. The shadow ring or disk shades the sun's direct beam from the pyranometer. Figure 4 shows a Kipp and Zonen CM11 pyranometer with shadow ring. The shadow ring needs to be adjusted according to the sun's declination angle. A more expensive approach has been designed to track the sun's declination, where the disk will move accordingly or synchronous with the sun's movement. Hence, it produces a more accurate estimation of diffuse radiation.

The WMO classified pyranometers according to features like stability, sensitivity, and so on. Classifications of pyranometers are divided into three classes, that is, first, second, and third class. The same features of classification apply to pyrhemimeters where they are divided only into two classes, first and second class as mentioned before. The WMO characteristics of operational pyranometers are given in Table 5. Figure 5 shows the shade ring correction factors for the measurement of diffuse sky radiation.

Table 5 WMO Characteristic of Operational Pyranometer

Characteristic	High Quality ^a	High Quality ^b	High Quality ^c
Response time (95% response)	< 15 s	< 30 s	< 60 s
Zero offset: (a) Response to 200 W/m ² net thermal radiation (ventilated)	7 W/m ²	15 W/m ²	30 W/m ²
(b) Response to 5 K/h change in ambient temperature	2 W/m ²	4 W/m ²	8 W/m ²
Resolution (smallest detectable change)	1 W/m ²	5 W/m ²	10 W/m ²
Stability (change per year, percentage of full scale)	0.8	1.5	3
Directional response for beam radiation (the range of errors caused by assuming that the normal incidence responsivity is valid for all directions when measuring, from any direction, a beam radiation whose normal incidence irradiance is 1000 W/m ²)	10 W/m ²	20 W/m ²	30 W/m ²
Temperature response (percentage maximum error due to any change of ambient temperature within an interval of 50 K)	2	4	8
Nonlinearity (percentage deviation from the responsivity at 500 W/m ² due to any change of irradiance within the range 100–1000 W/m ²)	0.5	1	3
Spectral sensitivity (percentage deviation of the product of spectral absorptance and spectral transmittance from the corresponding mean within the range 0.3–3 μm)	2	5	10
Tilt response (percentage deviation from the responsivity at 0° tilt (horizontal) due to change in tilt from 0° to 90° at 1000 W/m ² irradiance)	0.5	2	5
Achievable uncertainty, 95% confidence level:			
Hourly totals	3%	8%	20%
Daily totals	2%	5%	10%

^aNear state of the art, suitable for use as a working standard; maintainable only at stations with special facilities and staff.

^bAcceptable for network operations.

^cSuitable for low-cost networks where moderate to low performance is acceptable.

Source: Adapted from Ref. 7.

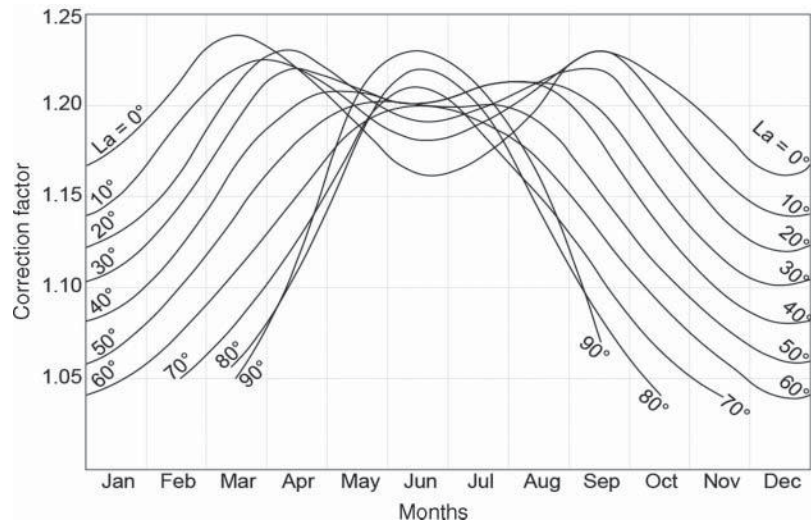


Figure 5 Shade ring correction factors for measured sky diffuse radiation.

2.3 Pyrheliometer

A pyrheliometer is used to measure beam (direct) radiation at normal incidence. Figure 6 shows a DN5 pyrheliometer used in an automatic tracking system. The long barrel of the pyrheliometer may be seen on the right in this picture. This equipment is equipped with a sun tracking system to enable it to measure direct radiation as the sun moves. Inside the pyrheliometer there is a collimator with an optimum aperture of 6° , which can completely include the sun's disk. A multijunction thermopile, which converts the heat from the sun's radiation to an electrical signal, is used so that the data can be read and recorded by data logger. To obtain the equivalent radiant energy flux (W/m^2) a calibration factor is applied. Other types of pyrheliometer are shown in Fig. 7 and 8. Table 6 gives the characteristics of operational pyrheliometers.

The direct equipment cost of a pyrheliometer is approximately six times that of a shaded pyranometer.⁵ Because the measurement cost of direct normal radiation is high, a simple relationship relating horizontal of global (I_G), diffuse (I_D), and beam (I_B) radiation may be used to estimate the latter component. The relation can be given as

$$I_G = I_D + I_B \sin \text{SOLALT} \quad (10)$$

where SOLALT is the solar altitude.

According to Perez et al.¹⁰ and Gueymard,¹¹ the present state of solar radiation and daylight model is such that they are approaching the accuracy limits set out by the measuring equipment. Hence, modeling procedures are now used to cross-check the measurements.

2.4 Pyrgeometer

Pyrgeometer is used to measure long-wave radiation, which falls within the infrared radiation spectrum ($4.5\text{--}100\ \mu\text{m}$). It consists of a thermopile with a $200\text{--}100\ \mu\text{m}$ radiation band sensitivity, a dome mirror with solar blind filter coating, which eliminates short-wave radiation, a temperature sensor that measures the body temperature of the instrument, and a sun shield to reduce heat from radiation. Figure 9 shows an EKO MS-202 pyrgeometer.

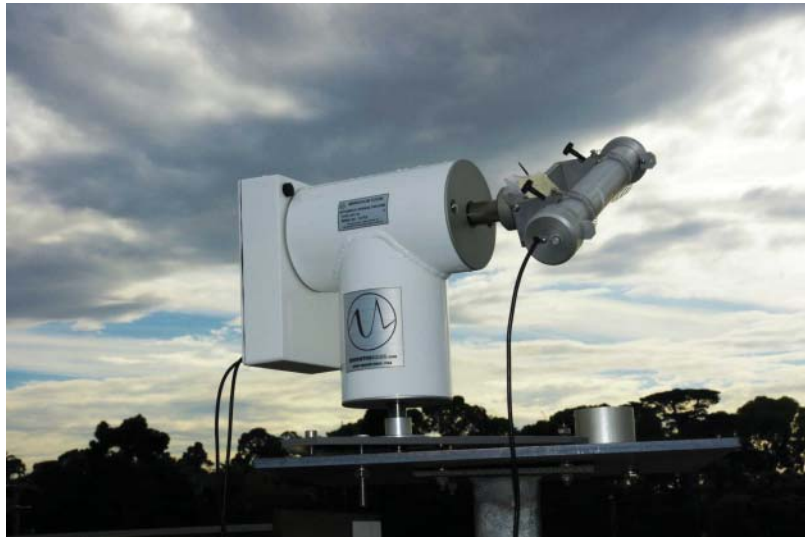


Figure 6 Middleton Solar-DN5 pyrheliometer (in automatic solar tracking system). (From Ref. 8.)



Figure 7 Eppley normal incidence pyrheliometer. (From Ref. 9.)

2.5 Albedometer

The term “ground albedo” or simply “albedo” is often used interchangeably with “ground reflectance.” On the other hand, as Monteith¹³ has pointed out, the term “albedo” or “whiteness” refers to the reflection coefficient in the visible range of the spectrum, whereas “reflectance” denotes the reflected fraction of short-wave energy. In this book, the term “albedo” has been used synonymously with reflectance, applying to the total short-wave energy.



Figure 8 The EKO-instrument's Sky scanner MS-321LR. (From Ref. 4.)



Figure 9 EKO M-S202 pyrgeometer. (From Ref. 12.)

The importance of knowing the albedo for the determination of radiation balance of macro- and microclimates is well known. A good estimate of albedo of the surrounding terrain is a prerequisite for representative calculations related to the energy balance of vegetation, amount of potential transpiration, energy interception of walls, windows, roofs, and solar energy collectors. Therefore, the small- and large-scale variation of albedo is of interest. The variation in

Table 6 WMO Characteristic of Operational Pyrheliometers

Characteristic	High Quality ^a	High Quality ^b
Response time (95% response)	< 15 s	< 30 s
Zero offset (response to 5 K/h change in ambient temperature)	2 W/m ²	4 W/m ²
Resolution (smallest detectable change)	0.5	1
Stability (change per year, percentage of full scale)	1	0.5
Temperature response (percentage maximum error due to change of ambient temperature within an interval of 50 K)	1	2
Nonlinearity (percentage deviation from the responsivity at 500 W/m ² due to any change of irradiance within the range 100–1000 W/m ²)	0.2	0.5
Spectral sensitivity (percentage deviation of the product of spectral absorptance and spectral transmittance from the corresponding mean within the range 0.3–3 μm)	0.5	1
Tilt response (percentage deviation from the responsivity at 0° tilt (horizontal) due to change in tilt from 0° to 90° at 1000 W/m ² irradiance)	0.2	0.5
Achievable uncertainty, 95% confidence level (see above)		
1 min totals		
Percent	0.9	1.8
kJ/m ²	0.56	1
1 h totals		
Percent	0.7	1.5
kJ/m ²	21	54
Daily totals		
Percent	0.5	1
kJ/m ²	200	400

^aNear state of the art, suitable for use as a working standard; maintainable only at stations with special facilities and staff.

^bAcceptable for network operations.

Source: Adapted from Ref. 7.

albedo is spatial and temporal owing to the changing landscapes of the Earth and due to the seasonal presence of snow and to some extent moisture deposition.

As the name of the instrument suggest, it measures the reflected radiation as well as the global radiation. Figure 10 shows an albedometer. Generally, albedometer is constructed with two pyranometers. One is facing upward to measure incident global radiation and the other facing downward to measure the ground-reflected radiation. Both pyranometers provide output individually. Albedo can be calculated from the output data of the two pyranometers. To obtain the albedo value, the following equation may be used:

$$\text{Albedo} = \frac{\text{reflected radiation}}{\text{global radiation}} \quad (11)$$

2.6 Sunshine Recorder

According to the WMO, the definition of sunshine duration is “sunshine duration during a given period is defined as the sum of that sub-period for which the direct solar irradiance exceeds 120 W/m²”¹⁵

In many countries, diurnal duration of bright sunshine is measured in numerous places. For over a century, these data have been measured using the well-known Campbell–Stokes sunshine recorder which uses a solid glass spherical lens to burn a trace of the sun on a treated paper,



Figure 10 Kipp and Zonen CMA 11 Albedometer. (From Ref. 14.)

the trace being produced whenever the beam irradiation is supposedly above the aforementioned critical level. Although the critical threshold varies loosely with the prevailing ambient conditions, the sunshine recorder is an economic and robust device and hence used widely.

The limitations of the Campbell–Stokes sunshine recorder are well known and have been discussed in *Observers' Handbook*,¹⁷ Painter,¹⁸ and Rawlins.¹⁹ Some of the associated limitations with this device are that the recorder does not register a burn on the card below a certain level of incident radiation (about 150–300 W/m²). On a clear day with a cloudless sky, the burn does not start until 15–30 min after sunrise and usually ceases about the same period before sunset. This period varies with the season. On the other hand, under periods of intermittent bright sunshine the burn spreads. The diameter of the sun's image formed by the spherical lens is only about 0.7 mm. However, a few seconds' exposure to bright sunshine may produce a burnt width of about 2 mm. As such, intermittent sunshine may be indistinguishable from a longer period of continuous sunshine. In the past, a more sophisticated photoelectric sunshine recorder called the Foster sunshine switch²⁰ has been used by the U.S. Weather Service. This device incorporates two photovoltaic cells, one shaded and the other exposed to solar beam. Incident beam irradiation above a given threshold produces a differential output from the above two cells, the diurnal duration of which determines the hours of bright sunshine.

Suehrcke²¹ has presented an elegant and simple relationship that enables estimation of \overline{G} from the monthly averaged daily bright sunshine fraction and clear sky clearness index, $\overline{G}_{\text{clear}}/\overline{E}$. Thus,

$$\frac{\overline{G}}{\overline{E}} = \left(\frac{n}{N}\right) \left(\frac{\overline{G}_{\text{clear}}}{\overline{E}}\right) \quad (12)$$

where \overline{G} and \overline{E} are the monthly averaged daily terrestrial and extraterrestrial irradiation, $\overline{G}_{\text{clear}}$ the monthly averaged daily terrestrial irradiation on a clear day, n the average daily hours of bright sunshine, and N the day length.

Suehrcke has argued that $\overline{G}_{\text{clear}}/\overline{E}$ varies narrowly between 0.65 and 0.75. Given this small range of variation, in the absence of specific site information, an average value of 0.7 may be assumed for $\overline{G}_{\text{clear}}/\overline{E}$, thus giving Eq. (12) the potential for worldwide application.

Driesse and Thevenard²² have evaluated the above claim. They have used measurements from 700 sites, compiled by the World Radiation Data Center with over 70,000 sunshine and radiation data. It may be noted that there is a considerable dispersion in the values of solar radiation. This variation (root-mean-square errors, RMSEs) was found to be around 12%. The

latter team has fitted the above data to find regressed values of globally applicable Ångström a and b coefficients. These values are 0.2336 and 0.4987, respectively. Using the latter “universal” coefficients the performance of Suehrcke and Ångström procedures for estimating \overline{G} was found to be on par.

3 EQUIPMENT ERROR AND UNCERTAINTY

With any measurement there exist errors, some of which are systematic and others inherent of the equipment used. Angus²³ has provided an account of the measurement errors associated with solar irradiance and illuminance measurements. These are summarized herein. The most common sources of error arise from the sensors and their construction. These are broken down into the most general types of error as follows:

1. Cosine response
2. Azimuth response
3. Temperature response
4. Spectral selectivity
5. Stability
6. Nonlinearity
7. Thermal instability
8. Zero offset due to nocturnal radiative cooling

To be classed as a secondary standard instrument (such as the CM11) pyranometers have to meet the specifications set out by WMO.

Of all the aforementioned errors, the cosine effect is the most apparent and widely recognized. This is the sensor’s response to the angle at which radiation strikes the sensing area. The more acute the angle of the sun, that is, at sunrise and sunset, the greater the error is (at altitude angles of sun below 6°). Cosine error is typically dealt with through the exclusion of the recorded data at sunrise and sunset times.

The azimuth error is a result of imperfections of the glass domes and in the case of solarimeters the angular reflection properties of the black paint. This is an inherent manufacturing error, which yields a similar percentage error as the cosine effect. Like the azimuth error, the temperature response of the sensor is an individual fault for each cell. The photometers are thermostatically controlled, and hence the percentage errors due to fluctuations in the sensor’s temperature are reduced. However, the CM11 pyranometers have a much less elaborate temperature control system. The pyranometers rely on the two glass domes to prevent large temperature swings. Ventilation of the instrument is an additional recommended option.

The spectral selectivity of the CM11 is dependent on the spectral absorptance of the black paint and the spectral transmission of the glass. The overall effect contributes only a small percentage error to the measurements. Each sensor possesses a high level of stability with the deterioration of the cells resulting in approximately $\pm 1\%$ change in the full-scale measurement per year. Finally, the nonlinearity of the sensors is a concern especially with photometers. It is a function of illuminance or irradiance levels. It, however, tends to contribute only a small percentage error toward the measured values. In addition to the above sources of equipment-related errors, care must be taken to avoid operational errors such as incorrect sensor leveling and orientation of the vertical sensors, as well as improper screening of the vertical sensors from ground-reflected radiation.

4 OPERATIONAL ERRORS

In Section 3, the likely errors resulting from equipment were introduced. Understanding and an assessment of operational errors are also of equal importance, and these are addressed below:

1. Complete or partial shade-ring misalignment
2. Dust, snow, dew, water droplets, bird droppings, and so on
3. Incorrect sensor leveling
4. Shading caused by building structures
5. Electric fields in the vicinity of cables
6. Mechanical loading on cables
7. Orientation and/or improper screening of the vertical sensors from ground-reflected radiation
8. Station shutdown
9. Improper application of diffuse shade-ring correction factor
10. Inaccurate programming of calibration constants

The sources of operation-related errors itemized above are self-explanatory. It is good practice to protect cables from strong electric fields such as elevator shafts. Another source of error that may arise is from cables under mechanical load (piezoelectric effects). The piezoelectric effect is the production of electrical polarization in a material by the application of mechanical stress. Failure to protect cables from the above sources may produce “spikes” in the data, and these are shown as unusually high values of irradiance. Figure 11 demonstrates the sources of error categorized under items 1 and 2 discussed above. Such errors are best highlighted via cross plotting the diffuse ratio (the ratio of horizontal sky diffuse and the total or global irradiance) against clearness index (the ratio of horizontal global to extraterrestrial irradiance). Any serious

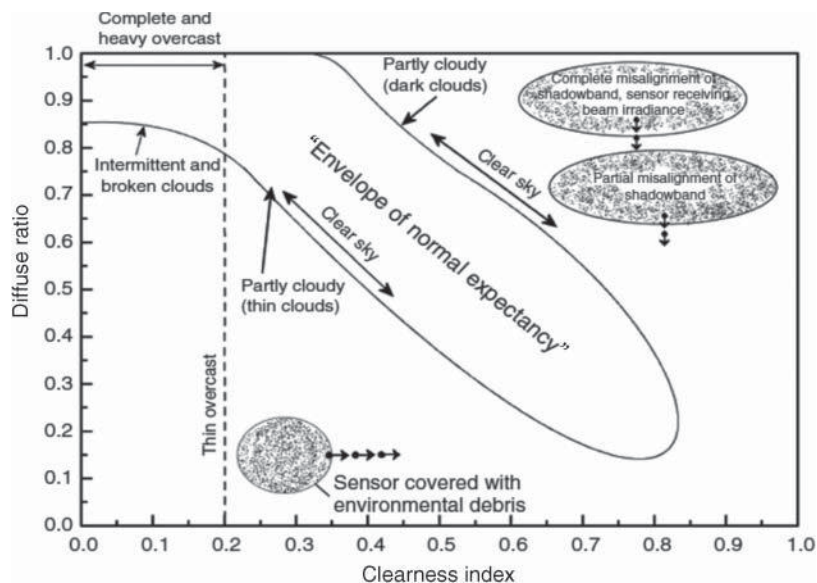


Figure 11 Demonstration of the sources of measurement errors.

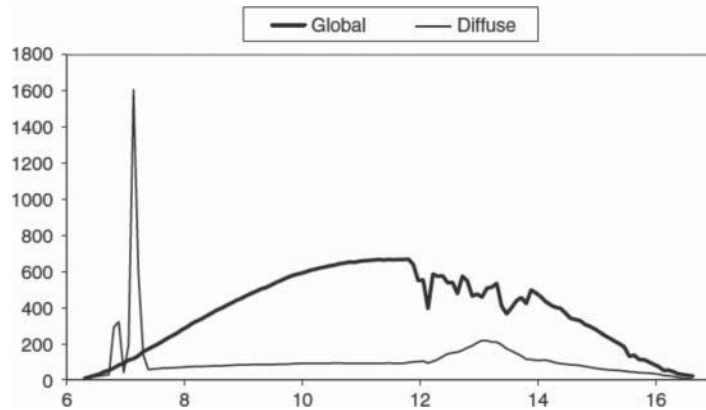


Figure 12 Demonstration of problems associated with mechanical loading on cables connecting data logger to irradiance sensor. Note: 5 min averaged data for Bahrain for December 12, 2001 (x axis: the time of the day, y axis: irradiance, W/m^2).

departure of data from the normally expected envelope is thus identified. Figure 12 highlights the error categorized under item 6.

5 DIFFUSE RADIATION DATA MEASUREMENT ERRORS

Historically, meteorological offices worldwide have used the shade-ring correction procedure, which is based on the assumption of an isotropic sky. However, during the past 15 years, a number of alternate, more precise methods that are based on a realistic, anisotropic sky have been established. The older, isotropic-sky-corrected diffuse irradiance records are slightly higher for overcast conditions and lower by up to 10% for clear sky conditions. It is imperative that due care is taken in using a precise and validated shade-ring correction procedure since any errors in horizontal diffuse irradiance records will be multiplied by a large factor when horizontal beam irradiance and subsequently the total slope energy computations are undertaken.

The diffuse irradiance can be calculated from measurements of global parameter and the beam normal irradiance by using the following equation:

$$I_d^{\text{true}} = I_g - I_n \sin \alpha \quad (13)$$

where I_d^{true} is the diffuse horizontal irradiance, which is referred to hereafter as “true” diffuse, I_g the global irradiance on a horizontal surface; I_n the beam normal irradiance, and α the solar altitude. Measurements of beam normal irradiance are made using a pyrheliometer.

Unfortunately, the collection of pyrheliometric data can be very expensive; the direct equipment cost alone is almost six times the expense of alternate collection methods, for example, prices quoted for Kipp and Zonen, premium-grade equipment (> ISO 9000 standard) in February of 2003, were (US\$) \$18,909 for a pyrheliometric system and \$3245 for a pyranometer with a shadow band.²⁴ The overall expense is most certainly directly related to the equipment cost but has a significant indirect cost, which is linked to the high level of daily maintenance required while using the system. An alternate and relatively inexpensive approach is to use a pyranometer with an occulting device to block the beam direct component from reaching the sensor. The most commonly used occulting devices are shadow bands or shade rings. All shading devices are usually coated with a low albedo black paint to reduce any reflected radiation from the shadow band. The shadow bands are aligned and fixed

parallel to the Earth's polar axis, matching the sun's track in the sky. This method produces a constant shadow on the pyranometer's sensor, effectively blocking the beam direct irradiance and theoretically leaving only the diffuse irradiation. Shadow-band use is economical and effectively shades direct beam irradiation. Regrettably, shadow bands also shade a portion of the sky and the corresponding slice of the diffuse irradiance that is obscured by the band itself. This shading introduces errors that can markedly influence the accuracy of measurements. Because of this error, a correction factor needs to be introduced to the diffuse irradiance readings. The correction factor can be derived by accounting for the physical amount of sky that is blocked by the band and the amount of diffuse irradiance that is representative of that blocked portion. Various authors^{25–35} have proposed many models, isotropic and anisotropic in nature, to correct the diffuse irradiance component when deploying a shadow band.

Historically, Drummond²⁵ suggested a theoretical, isotropic model based on solar geometric calculations for shadow-band correction. The model could be applied anywhere in the world, but Drummond noted that as much as 7% additional correction was needed under a cloudless sky to account for anisotropic conditions. The additional correction required for overcast or cloudy skies was 3%. Stanhill²⁶ found that additional corrections for anisotropic conditions actually ranged between 14 and 30% to the isotropic correction. Other models have been investigated using various parameters such as solar declination, clearness index, cloud cover, and atmospheric turbidity.²⁷ Dehne²⁸ reported that attempts to use these models or duplicate the results proved disappointing for sites other than the site that was used to develop the models. LeBaron et al.²⁹ suggested a model using four parameters covering both isotropic and anisotropic conditions. More recently, Batlles et al.³⁵ and Muneer and Zhang³¹ introduced correction models describing an improved methodology accounting for both the isotropic and anisotropic correction contribution to “true” diffuse irradiance. The objective of this work is to evaluate the overall performance of the shadow-band correction models proposed by LeBaron et al.,²⁹ Batlles et al.,³⁵ and Muneer and Zhang,³¹ against the benchmark Drummond's model,²⁵ using data collected in disparate locations to those where models were originally developed.

5.1 Description of Models

All four of the diffuse shadow-band correction models considered herein^{25,29,31,35} are well established and widely used by metrological offices worldwide. They have been adequately described in sufficient detail in the previously cited references. For the sake of brevity, these models are described in the following sections. Hereafter, we refer to each model by the name of the first author.

1. *Drummond*²⁵ Drummond's model assumes an isotropic sky condition. The portion of the horizontal irradiance intercepted for the shadow band X is calculated according to the following equation:

$$X = \frac{2b}{\pi r} \cos^3 \delta \left[\left(\frac{\pi}{180} \varpi_0 \right) \sin \phi \sin \delta + \cos \phi \cos \delta \sin \varpi_0 \right] \quad (14)$$

where r is the radius of the shadow band, b the width of the shadow band, ϖ_0 the sunset/sunrise hour angle, ϕ the latitude, and the δ declination. The Drummond correction factor C_D is then expressed as

$$C_D = \frac{1}{1 - X} \quad (15)$$

By using Drummond's model, the corrected diffuse irradiance I_{dD} may be obtained by applying the following formula:

$$I_{dD} = C_D I_d \quad (16)$$

2. *LeBaron et al.*²⁹: This model uses four parameters that take into account varying (isotropic and anisotropic) sky conditions. Three of the parameters used within this method are solar altitude and two dimensionless indices introduced by Perez et al.¹⁰ and Pollard and Langevine,²⁷ termed, respectively, as the clearness of the sky, ϵ , and the brightness of the sky, Δ . The fourth parameter is Drummond's correction factor C_D described earlier. Using these four parameters, LeBaron et al.²⁹ Gueymard¹¹ clustered the data according to 256 categories. For each one of these categories, they determined an appropriate value of the correct factor.
3. *Batlles et al.*³: Batlles et al.¹⁵ developed a piecewise multiple linear model using the same four parameters used in LeBaron's approach. The correction factor C_B is then expressed as an analytical function of C_D , α , and Δ , which is parameterized against ϵ . The set of equations are

$$\epsilon \leq 3.5C_B = 1.178C_D + 0.207 \log \Delta + 0.122e^{-1/\sin \alpha} \quad (17a)$$

$$3.5 \leq \epsilon \leq 8C_B = 1.454C_D + 0.665 \log \Delta + 0.4756e^{-1/\sin \alpha} \quad (17b)$$

$$8 \leq \epsilon \leq 11C_B = 1.486C_D + 0.495 \log \Delta \quad (17c)$$

$$\epsilon > 11C_B = 1.384C_D + 0.363 \log \Delta \quad (17d)$$

Measurements of diffuse irradiance are then corrected for isotropic and anisotropic conditions using:

$$I_{dB} = C_B I_d \quad (18)$$

4. *Muneer and Zhang*³¹: This model is based on the sky patch radiance distribution work of Moon and Spencer.²⁸ The model incorporates both isotropic and anisotropic elements by means of the following equation:

$$D = \left(\frac{\pi L_z}{6} \right) \left(\frac{3 + 2b_1}{1 + b_1} + \frac{3 + 2b_2}{1 + b_2} \right) \quad (19)$$

where D is the diffuse irradiance calculated in terms of the radiance indices and L_z . Parameters b_1 and b_2 are the radiance distribution indices for the two sky quadrants containing sun and opposed to sun, given as for $k > 0.2$,

$$b_1 = \frac{3.6 - 10.462k_t}{-0.4 + 6.974k_t} \quad (20)$$

$$b_2 = \frac{1.565 - 0.990k_t}{0.957 - 0.660k_t} \quad (21)$$

for $k \leq 0.2$, $b_1 = b_2 = 1.68$. The correction factor C_M may be calculated as follows:

$$I_1 = \cos \theta \cos \delta \sin \omega_0 + \omega_0 \sin \theta \sin \delta \quad (22)$$

$$I_2 = \omega_0 \sin^2 \theta \sin^2 \delta + 2 \sin \omega_0 \sin \theta \cos \theta \sin \delta \cos \delta + \cos^2 \theta \cos^2 \delta \left(\frac{\omega_0}{2} + \frac{\sin 2\omega_0}{4} \right) \quad (23)$$

$$F = \frac{2b}{r} L_z \cos^3 \delta \frac{I_1 + b_1 I_2}{1 + b_1} \quad (24)$$

$$CM = \frac{1}{1 - (F/D)} \quad (25)$$

Tables 7-9 give the statistical results of the models discussed above for different types of sky condition. Figure 13 shows corrected diffuse irradiance versus true diffuse irradiance.

Table 7 Statistical Results for All-Sky Conditions (Mean Value of the True Diffuse Irradiance is 153.8 W/m²)

Correction Model	R^2	RSME(%)	MBE (%)
Uncorrected	0.96	26.8	-20.9
Drummond	0.96	16.6	-10.2
LeBaron	0.96	15.8	-8.7
Battles	0.96	13.6	-2.1
Muneer	0.96	12.9	-4.9

Table 8 Statistical Results for Cloudy to Part-Cloudy Sky Conditions (Mean Value of the True Diffuse Irradiance is 207.4 W/m²)

Correction Model	R^2	RSME(%)	MBE (%)
Uncorrected	0.97	23.5	-18.0
Drummond	0.96	12.4	-7.2
LeBaron	0.96	8.9	-3.1
Battles	0.96	9.7	2.2
Muneer	0.96	9.0	-3.6

Table 9 Statistical Results for Cloudless Sky Condition (Mean Value of the True Diffuse Irradiance is 124.1 W/m²)

Correction Model	R^2	RSME(%)	MBE (%)
Uncorrected	0.89	29.4	-23.5
Drummond	0.89	20.5	-13.0
LeBaron	0.87	21.7	-13.9
Battles	0.88	17.2	-6.0
Muneer	0.89	16.4	-6.1

The performance of the models considered are analyzed by the residual differences (calculated as corrected diffuse irradiance minus true diffuse irradiance values) against clearness index and solar altitude. Figures 14*a, b* and 15 *a, b* show the residuals expressed as percentage of the mean value of true diffuse irradiance, respectively, for each interval of k_t and solar altitude. Uncorrected measurements of diffuse irradiance present estimates ranging from -5% for low k_t values to -20% for k_t values around 0.8. Residuals from Drummond's isotropic model present almost no deviation for $k_t < 0.2$, whereas an accentuated underestimation is noted for $k_t > 0.6$ with residuals lower than -8 to -10%. This result shows that under cloudy conditions, diffuse irradiance can be considered isotropic, and thus, a correction factor accounting only for isotropic conditions, such as the one proposed by Drummond, leads to fairly accurate corrections. Under cloudless conditions, sky anisotropy plays a major role, and an isotropic correction factor is not enough. It is interesting to note that residuals from LeBaron's and Muneer's model present a similar profile, with the worst performers being the Drummond and Battles models.

Four models for correcting diffuse irradiance measurements using shadow band have been analyzed. The Drummond model treats the sky as an isotropic entity, while the other three newer models are of an anisotropic nature. As shown above, using an isotropic correction

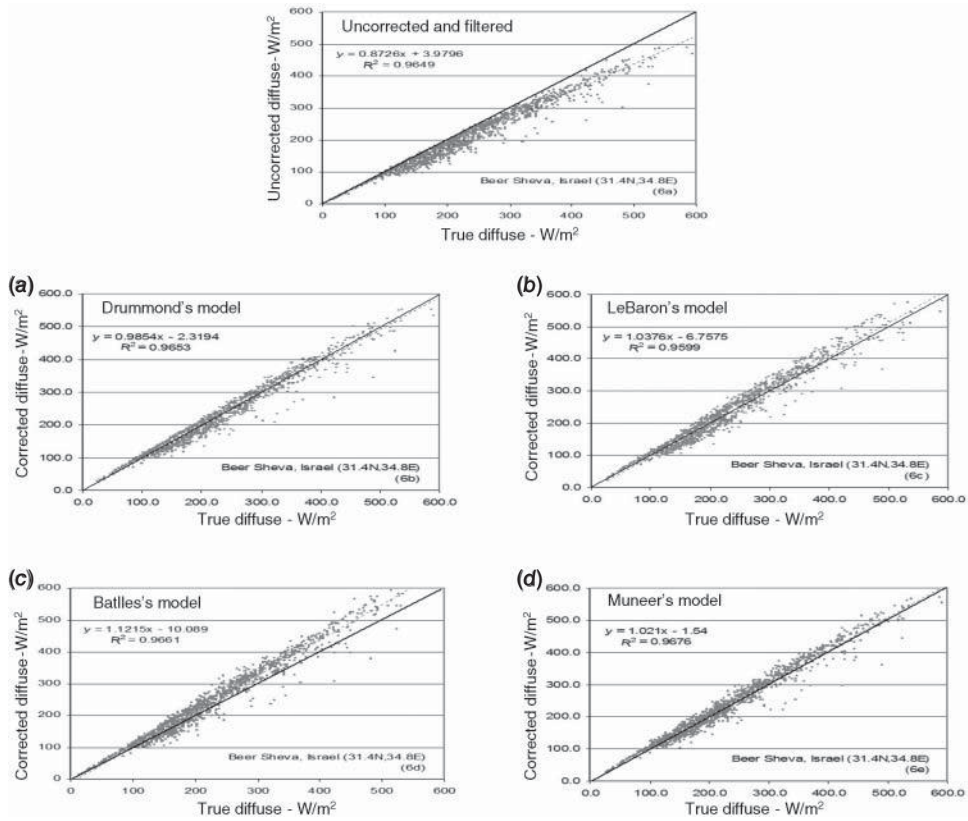


Figure 13 Shadow-band diffuse irradiance corrected using (a) Drummond's, (b) LeBaron's, (c) Batlles's, and (d) Muneer's models against true diffuse irradiance.

factor leads to an overall underestimation of the actual diffuse irradiation of 4–11%. The use of anisotropic correction schemes will considerably reduce the above underestimation depending on the model that is chosen. The results showed that the improvement in accuracy is even further improved under a cloudless sky and that the LeBaron and Muneer models were better in performance than the Drummond and Batlles procedures. Finally, owing to the large errors it generates, particularly in the higher clearness index range where the capture of solar energy is most crucial, it is recommended that Drummond's model is dropped as the de facto procedure currently used by numerous meteorological organizations.

6 TYPES OF SENSORS AND THEIR ACCURACY

A survey of radiation instruments undertaken by Lof et al.³⁶ showed that of the 219 sensors in use across Europe, 65 were of the CM11-type pyranometers while 107 sensors were the simpler and less expensive Robitzch actinographs with a bimetallic temperature element. The latter instrument is also quite popular in the developing Asian (89 such sensors were reported to be in use), African (20.16 sensors), and South American (20.47 sensors) countries where maintenance is often the key factor. The lead author (Muneer) has in the past visited a solar radiation measurement station in the middle of the Sahara desert and seen the Robitzch actinograph

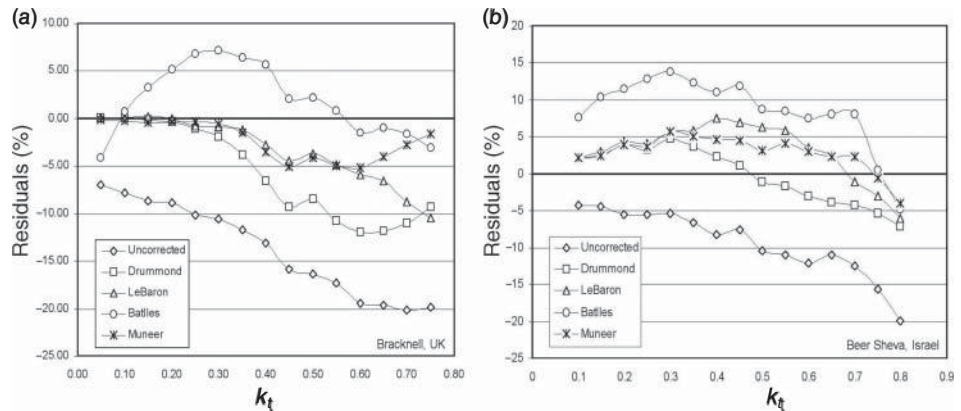


Figure 14 Residual differences against clearness index. (a) Bracknell, UK, and (b) Beer Sheva, Israel.

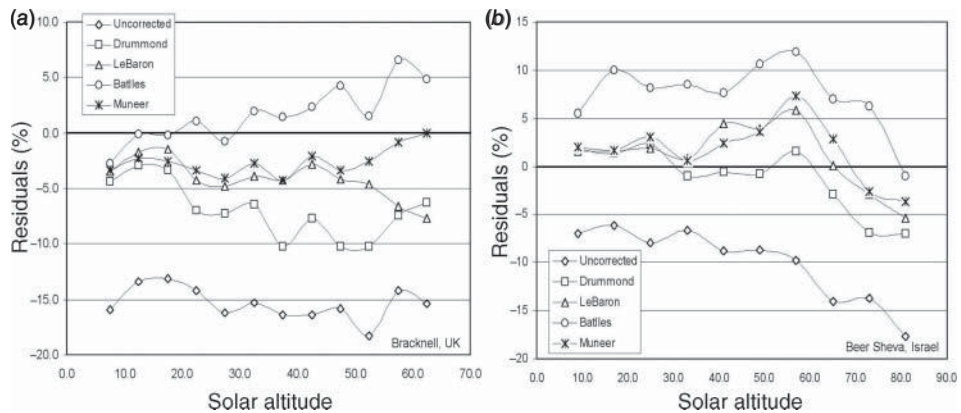


Figure 15 Residual differences against solar altitude. (a) Bracknell, UK, and (b) Beer Sheva, Israel. [c23f017.tif]

faithfully recording a regular trace of irradiation. The weekly changeover of the recording chart makes this instrument an ideal choice for remote locations. Although not in use with the North American meteorological network, it is known to be of use over there in biological and agriculture-related work.² Drummond³⁷ estimates that accuracies of 2–3% are attainable for daily summations of radiation for pyranometers of first-class classification. Individual hourly summations even with carefully calibrated equipment maybe in excess of 5%. Coulson² infers that the errors associated with routine observations may be well in excess of 10%. Isolated cases of poorly maintained equipment that are in the regular network may exhibit monthly averaged errors of 10% or more. The Robitzsch actinograph, even with all the modifications to improve its accuracy, is suitable only for daily summations. At this interval, it provides an accuracy of around 10%. However, not all designs of the latter sensor can claim even this level of accuracy. These figures must be borne in mind when evaluating the accuracy of the relevant computational models.

7 MODERN DEVELOPMENTS

Delta-T Device of Cambridge, England, has produced a relatively new instrument that measures the horizontal global and diffuse irradiance as well as sunshine duration from a single, stationary sensor. Unlike the Campbell–Stokes sunshine recorder, the Delta-T device neither requires any cards or shade ring for the measurement of sky-diffuse irradiance. The BF3 model enables simultaneous recording of the above mentioned three sets of data in a sensor that used no moving parts and required no specific polar alignment or routine adjustment. The electronic outputs are compatible with electronic data loggers and work at any latitude.

The device uses a system of photodiodes and a shading pattern such that wherever the sun is in the sky at least one photodiode is always exposed to the full solar beam and at least another diode is always completely shaded. All photodiodes receive an equal sampling of diffuse light from the rest of the sky hemisphere. A special layout of seven photodiodes on a hexagonal grid, covered by a hemispherical shading pattern, ensures the satisfaction of the above constraints. A sketch of the shading pattern of BF3 is shown in Fig. 16, plotted in a 180° fisheye lens view.

The sensor has a digital output of sunshine presence. As pointed out above, bright sunshine is defined by the WMO as the duration with irradiance greater than 120 W/m^2 in the direct beam measured perpendicular to the beam. The microprocessor algorithm within the BF3 sensor uses the measured global and diffuse irradiance to provide an estimate of sunshine duration. An account of BF3's performance, evaluated against Kipp and Zonen irradiance sensors and Campbell–Stokes sunshine recorders, has been presented by Wood et al.³⁹

Table 10 gives the results of regression analysis of the BF3 sensor with respect to the Kipp CM11 using the following indicators:

1. Calibration error, the deviation of the slope of the line of best fit from unity (expressed in percentage terms)
2. Coefficient of determination (R^2)
3. Standard error, the root mean square deviation of the measured BF3 values from the line of best fit



Figure 16 Hemispherical shading pattern for Delta-T BF3 irradiance sensor.

Table 10 Statistical Summary of BF3 Hourly Average with Respect to Kipp CM11 Readings, Feb 22–Jul 3, 2000

	Calibration Error (%)	R^2	Standard Error (W/m^2)
Global	4.7	0.994	16.5
Diffuse	1.4	0.980	13.4

Table 11 Sunshine Hour Regressions

Regression	Calibration Error (%)	R^2	Standard Error (h)
BF3 v WMO	-0.2	0.993	0.23
CS1(JW) v WMO	1.3	0.902	0.86
CS1(SY) v WMO	7.5	0.893	0.91
CS2(SY) v WMO	6.3	0.893	0.90
CS1(JW) v CS1(SY)	6.1	0.980	0.38
CS1(SY) v CS2(SY)	1.1	0.999	0.09

These results show a good match between the global and diffuse outputs of the BF3, and those measured using the Kipps and shade ring.

For evaluation against Campbell–Stokes recorders, two recorders were placed adjacent to each other, namely, CS1 and CS2. These are compared to each other and also to the WMO reference, for the days when all the data are available. Cards from the CS1 were independently analyzed by two different people, giving results CS1 (SY) and CS1 (JW). Table 11 gives a summary of these different regressions. Figure 17 shows the BF3 and CS1 values plotted against the WMO reference.

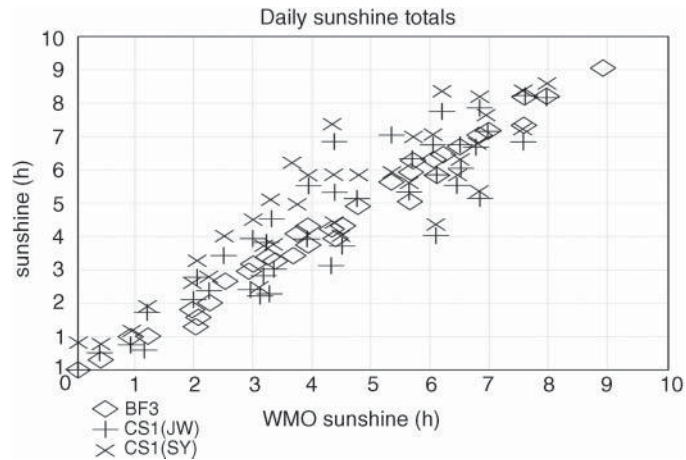


Figure 17 BF3 and Campbell–Stokes recorders compared to WMO reference. Note: BF3 = Delta -T BF3 irradiance sensor, CS1 (JW) = Campbell–Stokes recorder 1, CS1 (SY) = Campbell–Stokes recorder 2. Names of observers: John Wood (JW) and Serge Younes (SY).

These results show that the Campbell–Stokes recorder is a relatively poor performer when judge against the WMO sunshine definition. It shows a typical error of nearly an hour, some four times greater than the BF3. Although the two adjacent C–S recorders gave fairly consistent results when interpreted by the same person, the two independent operators gave very different interpretations of the same set of record cards, despite working from the same set of guidelines. The variability in interpretation was nearly half as much as the total error relative to the WMO standard, though neither operator was in fact consistently more accurate than the other.

8 DATA QUALITY ASSESSMENT

Data quality assessment is a process or a procedure to avoid spurious data to be included in the data set. Gueymard and Kembezidis⁴⁰ pointed out that even though a data set has passed the quality assessment process or procedure, the data must be examined for its uncertainty that has been transferred from a measuring sensor to the actual measurement. Here, in this section, a summary of a few assessment methods will be discussed.

8.1 U. S. National Renewable Energy Laboratory (NREL), 1993

The U.S. NREL⁴¹ developed a quality assessment procedure named SERI QC. This procedure will assess the three radiation data elements, namely, global horizontal, diffuse horizontal, and direct normal. Summary of the key features are discussed as follows:

- At the beginning, SERI QC will perform one-element test by defining a range of acceptable values for K_t , K_d , or K_n between minimum and maximum, which depends on the element that is being tested, based on air mass regimes and month of the year.
- If the zenith angle is less than or equal to 80° and all three elements are present, then SERI QC will perform a three-element test. A range of acceptable values will be defined so that the equation $K_t = K_d + K_n$ is satisfied within the arbitrary error limit of ± 0.03 , which accounts for the measurement uncertainties.
- If the data pass the three-element test or two elements pass the one-element test, SERI QC will perform a two-element test by defining a range of acceptable values within the boundaries empirically to determine three different air mass regimes for each month using data collected from the site.
- Flags are assigned to the data after the test. The flagging system of SERI QC permits the assignment of uncertainties that depend on the nature of the test performed (one, two, or three elements) and the distance by which the data points exceed the expected limit.

The values of K_t , K_d , K_n can be defined as follows:

- K_t = clearness index or global horizontal transmittance or global horizontal radiation/extraterrestrial horizontal radiation,
- K_d = diffuse horizontal transmittance or diffuse horizontal radiation/extraterrestrial horizontal radiation,
- K_n = direct normal transmittance or direct normal radiation/extraterrestrial direct normal radiation.

For more in-depth information regarding the procedure, readers are referred to the following website: http://rredc.nrel.gov/solar/pubs/seri_qc/.

8.2 Commission Internationale de l'Éclairage (CIE) Automatic Quality Control

A brief summary of the five tests in CIE⁴² quality control for radiation and illuminance is presented below:

1. A rough boundary limits for global and diffuse irradiance and direct irradiance is set to be less than the extraterrestrial irradiance.
2. To ensure consistency, it utilizes the redundancy among three solar radiation components or the diffuse component to be less than the global component plus a 10% allowance for shade ring correction where beam component is not measured.
3. Each aspect of the global irradiance and illuminance is tested, that is, north, east, south, and west.
4. Intercomparison test is done between irradiance and illuminance.
5. Tests to compare the zenith luminance with either diffuse irradiance or illuminance were also included.

Bear in mind that CIE noted that automatic testing should not be performed when global irradiance is below 20 W/m^2 and solar elevation is less than 4° .

8.3 Page Model

The Page model is based on the work undertaken for the production of the European Solar Radiation Atlas (ESRA) and the Chartered Institution of Building Services Engineers (CIBSE) Guide on weather and solar data.^{43,44} Page sets out the following steps to control all daily totals of solar radiation data:

- Values for global solar radiation have to be less than the extraterrestrial radiation, and sunshine values have to be less than or equal to corresponding astronomical values.
- Solar radiation values have to lie within the range of the expected clear sky extreme values by considering the influence of the atmospheric layer.
- Basic relationship between different radiation components should be fulfilled.
- Values of solar radiation parameters have to be in a specific range compared to nearby station's value with allowance for spatial variability.
- The variation of relative terms (G/E) of the Ångström regression should lie within a defined range.

Note that further details and software for the Page model are provided by Muneer⁵

8.4 Muneer and Fairouz Quality Control Procedure

This quality control procedure⁴⁵ consists of four levels of tests, which emphasize the global and diffuse radiation. The procedure was developed based on CIE recommendations for first-level test and Page irradiance model for fourth-level test. Those levels of tests are summarized as follows:

1. Adopted from CIE quality control:

$$0 < G < 1.2E_n$$

$$0 < D < 0.8E_n$$

where E_n is the normal incidence extraterrestrial irradiance.

2. Consistency test that compares diffuse and global irradiation and global and horizontal extraterrestrial irradiation.
3. Test based on an expected diffuse ratio clearness index envelope. This check is to make sure that the diffuse irradiation data conforms to the limit set out by the envelope of acceptance.
4. Check on the quality of diffuse irradiance is performed by comparing its value with the diffuse irradiance under two extreme conditions as define by Page.

A further test is carried out on the diffuse and global irradiance by investigating the Linke turbidity values. For example, when the Linke turbidity value is less than 2.5 or greater than 12, a close inspection of the corresponding data is required.

Refer to the graphical procedure as mentioned in third-level tests above. Younes et al.⁴⁶ proposed a new standard deviation procedure to produce an envelope of acceptance. This procedure basically categorizes diffuse ratio clearness index in the band of k_t . For any given band of k_t , outliers are identified as data points lying outside the envelope, which is defined by $\bar{k} \pm 2\sigma_k$ boundaries. For more in-depth discussion, readers are referred to Ref.46.

9 STATISTICAL EVALUATION OF MODELS

As pointed out in Section 1, the accuracy of mathematical models for estimating solar radiation is approaching the measurement accuracy of instruments. A number of routines, therefore, now use mathematical models for assessing the quality of measured data. Thus, in this section, an account of cross-checking the two set of procedures, that is, relationship or trend between the two sets of quantities, that is, models and measured data, is presented.

Checking on the adequacy of the mathematical model describing any physical process such as a given solar radiation model is important not only in the final stages of the work program but more particularly in the initial phase. An examination of residuals is recommended. The procedure is to produce a graph of the residuals d (the difference between observed Y_o and calculated Y_c values of the dependent variable) plotted against the independent variable X or the observed value Y_o .

If the residuals fall in a horizontal band as shown in Fig. 18a, the model may be judged as adequate. If the band widens as X or Y_o increases, displayed in Fig. 18b, it indicates a lack of constant variance of the residuals. The corrective measure in this case is a transformation of the Y variable. A plot of the residuals such as Fig. 18c indicates the absence of an independent variable in the model under examination. If, however, a plot such as Fig. 18d is obtained, a linear or quadratic term would have to be added.

Often correlation between two quantities is also to be examined. In solar energy literature, it has become a common practice to refer to regression models as “correlation equations.” Strictly speaking, this is wrong usage of statistician’s language. Correlation is the degree of relationship between variables, and one seeks to determine how well a linear or other model describes the relationship. On the other hand, regression is a technique of fitting linear or nonlinear models between a dependent and a set of independent variables. Thus, fitting an equation of the form:

$$Y = a_0 + a_1X \quad (26)$$

for n pairs of (X,Y) is an example of linear regression. On the other hand, fitting

$$Y = a_0 \exp(a_1X) + b_0 \sin(b_1X) \quad (27)$$

is an example of a nonlinear model. A number of low-priced software packages are available that adequately cover the requirements of fitting linear and nonlinear models. Popular spreadsheet packages such as Lotus 1-2-3 (a product of Lotus Corporation) and Excel (a product

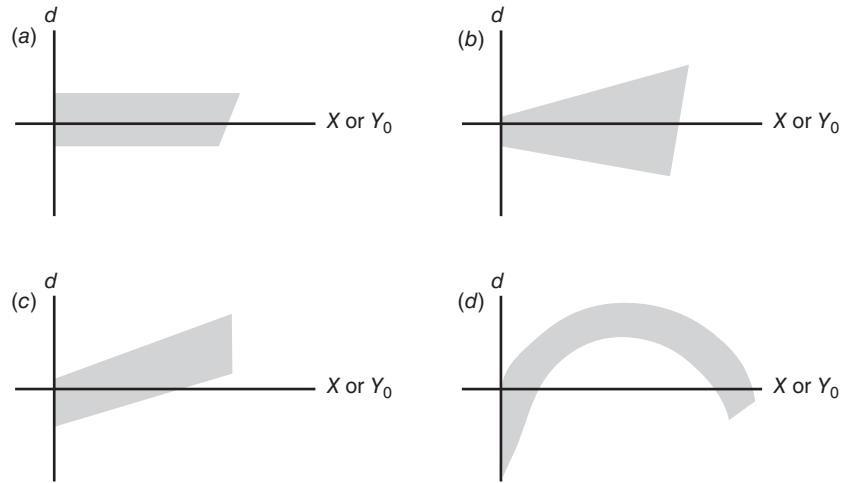


Figure 18 Plot of residuals for evaluating the adequacy of the model: (a) adequacy, (b) Y_o needs transformation, (c) missing linear independent variable, and (d) missing linear or quadratic independent variable.

of Microsoft Corporation) as well as more specialist statistical packages such as SOLO and BMDP (products of BMDP Statistical Software Inc., California) are a few examples. For handling very large data arrays, one has to resort to FORTRAN and C environments. The text *Numerical Recipes* by Press et al.,⁴⁷ with its companion electronic suite of programs, offers solutions at this end. All of the above packages use robust and efficient routines, which obviate any particular need for developing optimization programs from scratch. In the following paragraphs, a brief discussion on the statistical examination of models is provided.

9.1 Slope of the Best-Fit Line, s

The slope of the best-fit line, given by Eq. (28), between the computed and measured variable is desired to be as close as possible to unity. Slope values exceeding 1 indicate overestimation, while slope values under 1 indicate underestimation of the computed variable,

$$s = \frac{\Sigma(Y_m - \bar{Y}_m)(Y_c - \bar{Y}_c)}{\Sigma(Y_m - \bar{Y}_m)^2}$$

Note that $\frac{Y_c}{Y_m}$ is the calculated value of the dependent variable, Y_m the measured or observed value, and \bar{Y}_m the mean value of the measured variable.

9.2 Coefficient of Determination, r^2

The coefficient of determination (r^2) is the ratio of explained variation to the total variation; r^2 lies between zero and one,

$$r_2 = \left[\frac{\Sigma(Y_m - \bar{Y}_m)(Y_c - \bar{Y}_c)}{\sqrt{\Sigma(Y_m - \bar{Y}_m)^2 \Sigma(Y_c - \bar{Y}_c)^2}} \right]^2 \quad (29)$$

A high value of r^2 , thus indicating a lower unexplained variation, is desirable; r^2 is often used to judge the adequacy of a regression model, but it should not be the sole criterion for

choosing a particular model. In the present context, r^2 provides an indication of the order of scatter between Y_c and Y_m . Further information may be obtained in Montgomery and Peck⁴⁸ and Draper and Smith⁴⁹.

9.3 Coefficient of Correlation, r

The square root of the coefficient of determination is defined as the coefficient of correlation r . It is a measure of the relationship between the variables based on a scale ranging between +1 and -1. Whether r is positive or negative depends on the interrelationship between x and y , that is, whether they are directly proportional (y increases and x increases) or vice versa. Once r has been estimated for any fitted model, its numerical value may be interpreted as follows. Let us assume that for a given regression model $r = 0.9$. This means $r^2 = 0.81$. It may be concluded that 81% of the variation in Y has been explained (removed) by the model under discussion, leaving 19% to be explained by other factors.

9.4 Student's t Distribution

Often the modeler is faced with the question as to what quantitative measure is to be used to evaluate the value of r^2 obtained for any given model.⁵⁰ Clearly, r^2 would depend on the size of the data population. For example, a lower value of r^2 obtained for a model fitted against a large database may or may not be better than another model that used a smaller population. In such situations, the Student's t test may be used for comparing the above two models. The following example demonstrates the use of this test of significance for r^2 .

Example 1. For a given location, a regression model between average clearness index (\bar{K}_T) and monthly averaged sunshine fraction (n/N) gives $r^2 = 0.64$ for 12 pairs of data points. Using Student's t test investigates the significance of r .

The test statistic $t = (n - 2)^{0.5}[r/\sqrt{1 - r^2}]$, where n is the number of data points and $(n - 2)$ is the degrees of freedom (df).

Thus,

$$\text{Test statistic } t = (12 - 2)^{0.5}[0.8/\sqrt{(1 - 0.64)}] = 4.216$$

In this example there are 10° df. Thus from Table 12, the value of $r = 0.8$ is significant at 99.8% but not at 99.9% (note that for df = 10 and $t = 4.216$ lies between 4.144 and 4.587, corresponding to columns for 0.998 and 0.999, respectively). In laymans terms, this means that using the above regression model, K_T may be estimated with a 99.8% confidence.

9.5 Root-Mean-Squared Error

The root mean squared error (RMSE) gives a value of the level of scatter that the model produces. This is an important statistical test as it highlights the readability and repeatability of the model. It provides a term-by-term comparison of the actual deviation between the predicted and the measured values. Because it is a measure of the absolute deviation, RMSE is always positive. A lower absolute value of RMSE indicates a better model. Mathematically, it is given by the following equation:

$$\text{RMSE} = \sqrt{\Sigma \left[\frac{(Y_c - Y_m)^2}{n} \right]} \quad (30)$$

9.6 Mean Bias Error

The mean bias error (MBE) provides an indication of the trend of the model, whether it has a tendency to underpredict or overpredict the modeled values. MBE can be expressed either as

Table 12 Percentile Values for Student's t Distribution

df	$P = 0.95$	0.98	0.99	0.998	0.999
1	12.706	31.821	63.657	318.310	636.620
2	4.303	6.965	9.925	22.327	31.598
3	3.182	4.541	5.841	10.214	12.924
4	2.776	3.747	4.604	7.173	8.610
5	2.571	3.365	4.032	5.893	6.869
6	2.447	3.143	3.707	5.208	5.959
7	2.365	2.998	3.499	4.785	5.408
8	2.306	2.896	3.355	4.501	5.041
9	2.262	2.821	3.250	4.297	4.781
10	2.228	2.764	3.169	4.144	4.587
15	2.131	2.602	2.947	3.733	4.073
20	2.086	2.528	2.845	3.552	3.850
25	2.060	2.485	2.787	3.450	3.725
30	2.042	2.457	2.750	3.385	3.646
40	2.021	2.423	2.704	3.307	3.551
60	2.000	2.390	2.660	3.232	3.460
120	1.980	2.358	2.617	3.160	3.373
200	1.972	2.345	2.601	3.131	3.340
500	1.965	2.334	2.586	3.107	3.310
1000	1.962	2.330	2.581	3.098	3.300
∞	1.960	2.326	2.576	3.090	3.291

Source: From Ref. 9.

a percentage or as an absolute value. Nevertheless, within a data set, an overestimation of one observation can cancel an underestimation of another. An MBE nearest to zero is desired. It is given by the following equation:

$$\text{MBE} = \frac{\sum(Y_c - Y_m)}{n} \quad (31)$$

9.7 Mean of Absolute Deviations

Another metric that is often used in such analysis is the mean of absolute deviations (MAD) and is given by

$$\text{MAD} = \frac{\sum|(Y_c - Y_m)|}{n} \quad (32)$$

Unlike MBE, the MAD metric provides an insight into the scatter between Y_c and Y_m . Note that the MAD is similar to RMSE and provides a measure of absolute deviations.

9.8 Nondimensional MBE, MAD, and RMSE

The above formulas provide MBE, MAD, and RMSE, which have the same physical units as the dependent variable, Y . In some instances, nondimensional MBE (NDMBE), MAD (NDMAD), and RMSE (NDRMSE) are required. These are obtained as follows:

$$\text{NDMBE} = \frac{\sum \left[\frac{(Y_c - Y_m)}{Y_m} \right]}{n} \quad (33)$$

$$\text{NDMAD} = \frac{\sum \left| \left[\frac{(Y_c - Y_m)}{Y_m} \right] \right|}{n} \quad (34)$$

$$\text{NDRMSE} = \sqrt{\frac{\sum \left[\frac{(Y_c - Y_o)}{Y_m} \right]^2}{n}} \quad (35)$$

9.9 Figure of Merit, Ψ

One of the important steps in the evaluation of different functions is the interpretation of different statistical parameters, namely, slope, r^2 , MBE, MAD, and RMSE. Often when two or more models are intercompared for their relative strengths and weaknesses, there may be a tie between the above-mentioned metrics. For example, a model may have a lower MBE but a higher RMSE. Therefore, an overall accuracy score is highly desirable to facilitate a discrete comparison between different models. In this chapter, a novel statistical tool combines the five metrics mentioned above to produce an overall score. With the view to demonstrate this point, Fig. 19a shows a slope that has a large deviation from the ideally sought value of 1 but a high value of r^2 , whereas in Fig. 19b the slope is very close to the ideal value, but a low value of r^2 is realized due to large data scatter. Therefore, the case in Fig. 19b would be preferable over the case in Fig. 19a. Similarly, Fig. 19c presents a smaller but systematic trend of deviation, notice the negative deviations in the middle range, with positive outcomes at the lower and higher ends. In the case of Fig. 19d, an almost equal spread of positive and negative but larger deviations is noticed. Although the case in Fig. 19d would provide a much higher value of MBE, the case in Fig. 19d would, however, be preferable over the case in Fig. 19c. Overall, it can be concluded that the slope parameter provides a much more important indication of the validity of any given model. The r^2 of the line fitted between computed and observed data, MBE, MAD, and RMSE for the given model's deviation provide second-order information as higher values of r^2 or lower values of MBE, MAD, and RMSE do not warrant a better model. Ideally, the latter four parameters ought to be examined in conjunction with the value of slope. The following overall accuracy score is proposed with varying weighing factors of 3, 1, 1, 1, and 1 for s , r , RMSE, MBE, and MAD, respectively,

$$\Psi = 3[s] + [r] + \left[1 - \frac{\text{RMSE}}{\text{RMSE}_{\max}} \right] + \left[1 - \frac{|\text{MBE}|}{|\text{MBE}|_{\max}} \right] + \left[1 - \frac{\text{MAD}}{\text{MAD}_{\max}} \right] \quad (36)$$

Note that s and r are dimensionless, unlike RMSE, MBE, and MAD, and, therefore, the latter three are, respectively, divided by the values of RMSE_{\max} , $|\text{MBE}|_{\max}$, and MAD_{\max} . Ψ is a convenient figure of merit, by means of which it is possible to compare the performance of any suite of models. Therefore, for a perfect fit, the overall accuracy score Ψ will be 7.

10 OUTLIER ANALYSIS

Often in solar radiation studies, we encounter data that lie unusually far removed from the bulk of the data population. Such data are called "outliers." One definition of an outlier is that it lies three or four standard deviations or more from the mean of the data population. The outlier indicates peculiarity and suggests that the datum is not typical of the rest of the data. As a rule, an outlier should be subjected to particularly careful examination to see whether any logical explanation may be provided for its peculiar behavior. Automatic rejection of outliers is not always very wise. Sometimes, an outlier may provide information that arises from unusual conditions. Outliers may, however, be rejected if the associated errors may be traced to erroneous observations due to any one or a combination of factors described in previous sections of statistical analysis.

Statistically, a "near outlier" is an observation that lies outside 1.5 times the interquartile range. The interquartile is the interval from the first quartile to the third quartile.

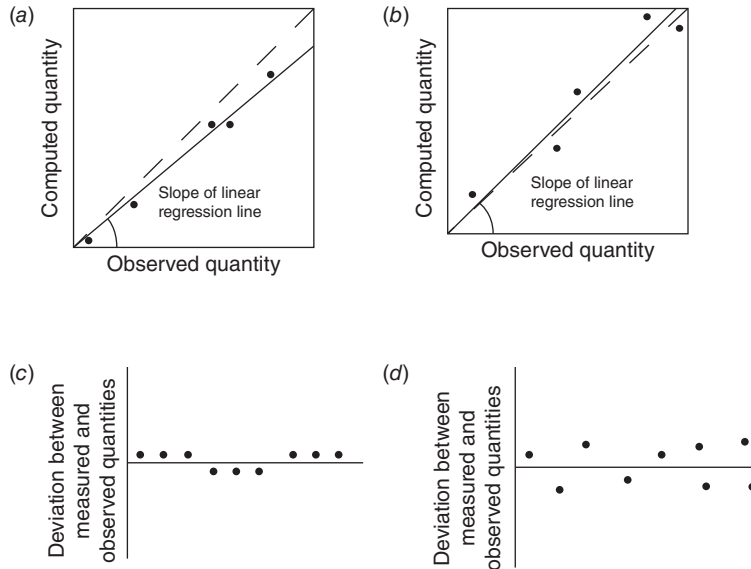


Figure 19 Basic concepts for the statistical parameters used. (a) Slope has a large deviation but with a reduced data scatter about the fitted line. (b) Slope is very close to ideal value but with an enhanced data scatter. (c) Smaller but a systematic trend of deviations. (d) An almost equal spread of positive and negative but larger deviations.

The *near outlier* limits are mathematically defined by:

$$\text{Lower outlier limit: } 1\text{st quartile} - 1.5 (3\text{rd quartile} - 1\text{st quartile}) \quad (37)$$

$$\text{Upper outlier limit: } 3\text{rd quartile} + 1.5 (3\text{rd quartile} - 1\text{st quartile}) \quad (38)$$

Likewise, *far outliers* are defined as the data whose limits are defined below:

$$\text{Lower limit: } 1\text{st quartile} - 3 (3\text{rd quartile} - 1\text{st quartile}) \quad (39)$$

$$\text{Upper limit: } 3\text{rd quartile} + 3 (3\text{rd quartile} - 1\text{st quartile}) \quad (40)$$

A high number of outliers in a given data set signify that the observations have a high degree of variability or a large set of suspect data indicating poor station operation. For a more rigorous discussion on outlier analysis, readers are referred to the reference made to Draper and Smith⁴⁹ and Montgomery and Peck.⁴⁸

Acknowledgments

This contribution has relied heavily on the work of a number of contributions, all of which have been presently referenced. However, the three sources that were of particular and significant use were the following: *Solar and Terrestrial Radiation* by Coulson,² *Solar Radiation and Daylight Models* by Muneer,⁵ and photographs of sensors and equipment that were obtained from Delta-T of England, EKO Instruments of USA, Eppley of USA, Kipp and Zonen of Netherlands, and Middleton Solar of Australia.

REFERENCES

1. G. V., Rozenberg *Twilight – A Study in Atmospheric Optics*, New York: Plenum, New York, 1966.
2. K. L., Coulson *Solar and Terrestrial Radiation*, Academic Press, New York, 1975.

3. ESRA, *European Solar Radiation Atlas*, Ecole des Mines, Paris, 2000.
4. Kipp and Zonen, *Instruction Manual CMP series Pyranometer and CMA series Albedometer*, 11, 2013.
5. T. Muneer, *Solar Radiation and Day light model*, Elsevier, Amsterdam, 2004.
6. Instruments, *CM 121B/C Shadow Ring*, accessed December 16, 2014, www.kippzonen.com/Product/42/CM-121B-C-Shadow-Ring.
7. Instruments, E. *Sky Scanner MS-321LR*. 2004, accessed December 8, 2010, available <http://www.eko-usa.com/products/am/MS-321LR/MS-321LR.html>.
8. Instruments, *APT-01 Automatic Solar Tracker with DN5 Pyrheliometer*, accessed December 16, 2014, www.middletonsolar.com/products/product13.htm.
9. EPLAP, *Normal Incidence Pyrheliometer*, accessed December 6, 2010, available <http://www.eppleylab.com/>.
10. R., Perez P., Ineichen and R. Seals "Modelling Daylight Availability and Irradiance Components from Direct and Global Irradiance", *Solar Energy*, **44**, 271, 1990.
11. C. A., Gueymard "Direct Solar Transmittance and Irradiance Predictions with Broadband Models Part 1: Detailed Theoretical Performance Assessment," *Solar Energy*, (74), 355–379, 2003.
12. Instruments, E. *Pyrgometer: MS-202/MS-202F*, 2005, accessed November 25, 2010 available: http://www.eko-usa.com/products/am/MS-202_MF-11/MS-202/MS-202.html.
13. J. L., Monteith "The Reflection of Short-Wave Radiation by Vegetation," *Quart. J. Roy. Meteorol. Soc.* **85**, 392, 1959.
14. Instruments, *CMA 11 Albedometer*, accessed December 16, 2014, www.kippzonen.com/Product/23/CMA-11-Albedometer#.VJC4ZtLF_xo.
15. World Meteorological Organization, *Manual on the Global Observing System*. Geneva, 2003.
16. Corporation, N. *240–1070-L Campbell–Stokes Pattern Sunshine Recorder*, accessed November 25, 2010, available <http://www.novalynx.com/240-1070.html>.
17. *Observers Handbook*, HSMO, London, 1969.
18. H. E., Painter "The Performance of a Campbell–Stokes Sunshine Recorder Compared with a Simultaneous Record of the Normal Incidence Irradiance," *Met. Mag.*, **110**, 102–187, 1987.
19. F., Rawlins "The Accuracy of Estimates of Daily Global Irradiation from Sunshine Records for the United Kingdom," *Meteorol. Mag.* (20.20.113), 187, 1984.
20. N. B., Foster and L.W. Foskett, "A Photoelectric Sunshine Recorder," *Bull. Am. Meteorol. Soc.*, (20.34), 212, 1953.
21. H., Suchrcke "On the Relationship between Duration of Sunshine and Solar Radiation on the Earth's Surface: Ångström's Equation Revisited," *Solar Energy*, **68**, 417, 2000.
22. A., Driesse and D., Thevenard "A Test of Suehrcke's Sunshine–Radiation Relationship Using a Global Data Set," *Solar Energy*, **72**, 167, 2002.
23. R. C., Angus *Illuminance Models for the United Kingdom*. Edinburgh Napier University, Edinburgh, 1995.
24. Omni Instruments, *Kipp and Zonen Retail Prize*, Dundee, Scotland, 2012.
25. A. J., Drummond "On the Measurement of Sky Radiation," *Arch. Meteorol., Geophys. Bioclimatol.* **B7**, 413–436, 1956.
26. G., Stanhill "Observations of the Shade Ring Corrections for Diffuse Sky Radiation Measurements at the Dead Sea." *Quart. J. Roy. Meteorol. Soc.* **111**, 1125–1130, 1985.
27. D. G., Pollard and L. P. Langevine "An Anisotropic Correction for Diffuse Irradiance Measurements in Guyana," in Proceedings of the 1988 Annual Meeting, ASES, Cambridge.
28. K., Dehne *Diffuse Solar Radiation Measured by Shade Ring Method Improved by a Correction Formula*, World Meteorological Organization, 1984.
29. B. A., LeBaron J. J., Michalsky, and R., Perez "A Simple Procedure for Correcting Shadowband Data for all Sky Conditions," *Solar Energy*, **44**(20.5), 249–256, 1990.
30. F. J., Batlles and F. J., Olmo "On Shadowband Correction Methods for diffuse Irradiance Measurements," *Solar Energy*, **54**, 105–114, 1995.
31. T., Muneer and X. Zhang "A New Method for Correcting Shadowband Diffuse Irradiance Data." *ASME*, **124**, 34–43, 2002.

32. H. E., Painter “The Shade Ring Correction for Diffuse Irradiation Measurements,” *Solar Energy*, **26**, 361, 1981.
33. F., Kasten K., Dehne and W. Brettschneider, “Improvement of Measurement of Diffuse Solar Radiation,” in *Solar Radiation Data Series F*, p. 221, 1983.
34. A. I., Kudish and A. Ianetz, “Analysis of Diffuse Radiation Data for Beer Sheva: Measured (Shadow Ring) versus Calculated (Global-Horizontal Beam) Values,” *Solar Energy*, **51**, 495–503, 1993.
35. F. J., Batlles J., Barbero G., Lopez M., Perez F., Rodrigo and M. A., Rubio *Fundamentos de la radiacion solar y aspectos climatologicos de Almeria, 1990–1996* (in Spanish); Servicio de Publicaciones de la Universidad de Almeria, 1998.
36. G. O. G., Lof J. A., Duffie and C.O. Smith “World Distribution of Solar Radiation,” in *Engineering Experiment Station Report*, University of Wisconsin, Madison, 1965.
37. A. J., Drummond “Techniques for the Measurement of Solar and Terrestrial Radiation Fluxes in Plant Biological Research: A Review with Special Reference to Arid Zones”, in Montpiller Symposium 1965, UNESCO.
38. D.-T Devices, *Sunshine Sensor—BF3*. 2010, accessed November 25, 2010, available <http://www.delta-t.co.uk/products.html?product2005092016583>.
39. J., Wood T., Muneer J., Kubie Evaluation of a New Photodiode Sensor for Measuring Global and Diffuse Irradiance, and Sunshine Duration”. *J. Solar Energy Eng.* **125**(20.20.1), 43–48, 2003.
40. C., Geuymard and H. D. Kambezidis, “Solar Spectral Radiation.” in: T. Muneer (ed.), *Solar Radiation and Daylight Models*, Elsevier, Oxford, pp. 221–302, 2004.
41. NREL, *Quality Assessment with SERI_QC*, 1993, accessed November 25, 2010, available http://rredc.nrel.gov/solar/pubs/seri_qc/.
42. D. E. A. Kendrick *Guide to Recommended Practice of Daylight Measurement*, International Commission on Illumination (CIE), Wein, Austria, 1994.
43. ESRA. *European Solar Radiation Atlas 2000. Vol. 1, Fundamentals and Maps*, 4th ed., Ecole des mines de Paris, Les Presse de l’Ecole, Chapters 3 and 4, pp. 17–40, 2000.
44. J. K., Page *Proposed Quality Control Procedures for the Meteorological Office Data Tapes Relating to Global Solar Radiation, Diffuse Solar Radiation, Sunshine and Cloud in UK*, London, Chartered Institution of Building Services Engineers, UK 1997.
45. T., Muneer and F. Fairouz “Quality Control of Solar Radiation and Sunshine Measurements — Lessons Learnt from Processing Worldwide Databases,” *Build. Ser. Eng. Res.* **23**(20.3), 151–166, 2002.
46. S., Younes R., Claywell and T. Muneer “Quality Control of Solar Radiation Data: Present Status and Proposed New Approaches,” *Energy*, **30**, 1533–1549, 2005.
47. W. H., Press et al., *Numerical Recipes in FORTRAN: The Art of Scientific Computing*. Cambridge University Press, Cambridge, 1992.
48. D., Montgomery and E. Peck *Introduction to Linear Regression Analysis*, Wiley, New York, 1992.
49. N., Draper and H. Smith *Applied Regression Analysis*, Wiley, New York, 1998.
50. F., Owen and R. Jones *Statistics*, Pitman London, 1990.
51. World Meteorological Organization, *Guide to Meteorological Instruments and Methods of Observation. Preliminary*, 7th ed., Geneva, 2006.

CHAPTER 24

GEOTHERMAL RESOURCES AND TECHNOLOGY: INTRODUCTION

Peter D. Blair*
National Academy Sciences
Washington, DC

1 INTRODUCTION	839	3 GEOTHERMAL ENERGY CONVERSION	846
2.1 U.S. Geothermal Resource Base	841	3.1 Direct Uses of Geothermal Energy	847
2.2 Hydrothermal Resources	842	3.2 Electric Power Generation	847
2.3 Vapor-Dominated Resources	842	3.3 Direct Steam Conversion	848
2.4 Liquid-Dominated Resources	844	3.4 Flashed Steam Conversion	849
2.5 Enhanced Geothermal Systems	844	3.5 Binary Cycle Conversion	850
2.6 Geothermal Energy from Magma Intrusions	845	3.6 Some Additional System Selection Considerations	852
2.7 Geopressured Resources	845	3.7 Hybrid Geothermal/Fossil Energy Conversion	853
		3.8 Geothermal Heat Pumps	853
		3.9 Ground Loop GHP Systems	854
		REFERENCES	854

1 INTRODUCTION

Geothermal energy is heat from Earth's interior. Nearly all of geothermal energy refers to heat derived from Earth's molten core. Some of what is often referred to as geothermal heat derives from solar heating of the surface of Earth, although it amounts to a very small fraction of the energy derived from Earth's core. For centuries, geothermal energy was only apparent through anomalies in Earth's crust that permit the heat from Earth's molten core to venture close to the surface. Volcanoes, geysers, fumaroles, and hot springs are the most visible surface manifestations of these anomalies.

Earth's core temperature is estimated by most geologists to be around 5000–7000°C. For reference, that is nearly as hot as the surface of the sun (although substantially cooler than the sun's interior). And while Earth's core is cooling, it is doing so very slowly in a geologic sense, since the thermal conductivity of rock is very low and, further, the heat being radiated from Earth is being substantially offset by radioactive decay and solar radiation. Some scientists estimate that over the past three billion years, Earth may have cooled several hundred degrees.

* Peter D. Blair, Ph.D. is Executive Director of the Division on Engineering and Physical Sciences of the National Academy of Sciences (NAS) in Washington, DC. The views expressed in the chapter, however, are his own and not necessarily those of the NAS.

Table 1 Worldwide Geothermal Power Generation, 2010

Country	Installed Capacity (MW)
United States	3,086
Philippines	1,904
Indonesia	1,197
Mexico	958
Italy	843
New Zealand	628
Iceland	575
Japan	536
El Salvador	204
Kenya	167
Costa Rica	166
Nicaragua	88
Russia	82
Turkey	82
Papua New Guinea	56
Guatemala	52
Portugal	29
China	24
France	16
Ethiopia	7.3
Germany	6.6
Austria	1.4
Australia	1.1
Thailand	0.3
Total	10,710

Source: From Ref. 1.

Geothermal energy has been used for centuries, where it is accessible, for aquaculture, greenhouses, industrial process heat, and space heating. It was first used for production of electricity in 1904 in Lardarello, Tuscany, Italy, with the first commercial geothermal power plant (250 kWe) developed there in 1913. Since then geothermal energy has been used for electric power production all over the world, but most significantly in the United States, the Philippines, Mexico, Italy, Japan, Indonesia, and New Zealand. Table 1 lists the current levels of geothermal electric power generation installed worldwide.

2 GEOTHERMAL RESOURCES

Geothermal resources are traditionally divided into the following three basic categories or types that are defined and described later in more detail:

1. Hydrothermal convection systems, which include thermal aquifers that are so-called vapor-dominated or liquid-dominated systems.
2. Hot igneous resources, which include hot dry rock and geologic magna systems.
3. Conduction-dominated resources, which include geopressed and radiogenic resources.

These basic resource types are distinguished by basic geologic characteristics and the manner in which heat is transferred to Earth's surface, as noted in Table 2. At present only

Table 2 Geothermal Resource Classification

Resource Type	Temperature Characteristics
Hydrothermal convection resources (heat carried upward from depth by convection of water or steam)	
a. Vapor dominated	~240°C
b. Liquid (hot-water) dominated	
1. High temperature	150–350°C
2. Intermediate temperature	90–150°C
3. Low temperature	<90°C
Hot igneous resources (rock intruded in molten form from depth)	
a. Molten material present—magma systems	>659°C
b. No molten material—hot dry-rock systems	90–650°C
Conduction-dominated resources (heat carried upward by conduction through rock)	
a. Radiogenic (heat generated by radioactive decay)	30–150°C
b. Sedimentary basins (hot fluid in sedimentary rock)	30–150°C
c. Geopressured (hot fluid under high pressure)	150–200°C

hydrothermal resources are exploited commercially, but research and development activities around the world are developing the potential of the other categories, especially hot dry rock. Estimates of the world potential vary considerably, but one 1998 analysis (Ref. 2) estimates the world geothermal energy resource base as 130 billion barrels of oil equivalent (bboe) for thermal aquifers, 410,000 bboe for geopressured resources (recoverable oil plus hydrothermal potential), 2.4 million bboe for magma systems, and 79 million bboe for other crustal heat (excluding thermal aquifers, geopressured resources, and magma systems).

The following discussion includes a description of and focuses on the general characterization of the features and location of each of these resource categories in the United States.

2.1 U.S. Geothermal Resource Base

In 2008 the U.S. Geological Survey (USGS) compiled its first assessment of geothermal resources in the United States in over 30 years,³ following earlier assessments in 1975,⁴ which was updated in 1978.⁵ All of these assessments characterize a “geothermal resource base” for the United States based on geologic estimates of all stored heat in Earth above 15°C within six miles of the surface. The defined base does not address the practical “recoverability” of the resource but provides to first order a sense of the scale, scope, and location of the geothermal resource base in the United States.

The U.S. geothermal resource base, as most recently defined by USGS, includes 241 identified geothermal systems located on private or accessible public lands classified as either moderate-temperature (90–150°C) or high-temperature (greater than 150°C) resources that are suitable as a source for electric power production. These systems span the states of Alaska, Arizona, California, Colorado, Hawaii, Idaho, Montana, Nevada, New Mexico, Oregon, Utah, Washington, and Wyoming. This inventory excludes systems located on closed public lands, such as national parks, or lower grade resources less suitable for electric power generation but possibly applicable for direct uses (space heating, greenhouses, etc.). These lower grade resources essentially blanket the entire geography of the nation, although once again ignoring the issues of practical recoverability. However, in this latest USGS inventory,

seven low-temperature (less than 90°C) systems in Alaska are included for which local circumstances suggest electric power generation may be feasible with technologies currently being developed. Finally, the latest inventory also includes provisional estimates of the power generation potential of a number of unconventional resource locations in Arizona, California, Colorado, Idaho, Montana, Nevada, New Mexico, Oregon, Utah, Washington, and Wyoming that are potentially suitable for so-called Enhanced Geothermal Systems (EGS) technology discussed later in this chapter.

Since the 1970s, many of the resource areas identified by USGS have been explored extensively and some developed commercially for electric power production, discussed in more detail by Blair et al.⁶ Virtually all the geothermal resources developed in the United States for electric power generation are hydrothermal resources where a water aquifer is collocated with a geothermal heat source. These production facilities comprise a power production capacity of approximately 2500 megawatts electric (mWe) from geothermal power plants in five western states: Alaska, California, Hawaii, Idaho, Nevada, and Utah. In 2005, electricity generated from these plants accounted for a quarter of all non-hydroelectric renewable electric power generation in the United States. The most recent USGS estimate is that the power generation potential for known geothermal resources is over 9000 mWe.

2.2 Hydrothermal Resources

Hydrothermal convection systems are formed when underground reservoirs carry Earth's heat toward the surface by convective circulation of steam in the case of so-called *vapor-dominated resources* or water in the case of *liquid-dominated resources*. Vapor-dominated resources are extremely rare on Earth. Three are located in the United States: The Geysers and Mount Lassen in California and the Mud Volcano system in Yellowstone National Park.* All remaining known geothermal resources in the United States are liquid-dominated resources. Figure 1 shows major known geothermal resources in the continental United States; there are substantial known geothermal resources in Alaska and Hawaii as well.

2.3 Vapor-Dominated Resources

In vapor-dominated hydrothermal systems, deep subsurface water boils to produce water vapor, which is also often superheated by hot surrounding rock. Many geologists speculate that as the vapor moves toward the surface, a level of cooler near-surface rock induces condensation, which along with the cooler groundwater from the margins of the reservoir serves to recharge the reservoir. Since fluid convection takes place constantly, the temperature in the vapor-filled area of the reservoir is relatively uniform and a well drilled into this region will yield high-quality[†] superheated steam, which can be circulated directly in a steam turbine-generator to produce electricity.

The most commercially developed geothermal resource in the world today is known as The Geysers in northern California, which is a very high-quality, vapor-dominated hydrothermal convection system. At The Geysers steam is delivered from the reservoir from a depth of 5000-10,000 ft and piped directly to turbine-generators to produce electricity.

* Other known vapor-dominated resources are located at Larderello and Monte Amiata, Italy, and at Matsukawa, Japan.

† High-quality steam is often referred to as *dry* steam since it contains no entrained liquid water spray. Most steam boilers are designed to produce high-quality steam. Steam with entrained liquid has significantly lower heat content than dry steam. Superheated steam is steam generated at a higher temperature than its equivalent pressure, created either by further heating of the steam (known as *superheating*), usually in a separate device or section of a boiler known as a *superheater*, or, alternatively, by dropping the pressure of the steam abruptly, which allows the steam to drop to a lower pressure before the extra heat can dissipate.



Figure 1 U.S. known geothermal resource location. Based on USGS resource assessment and spatial modeling, the black dots on this map identify known geothermal systems in the western contiguous United States. *Source:* From Ref. 3.

Power production at The Geysers began in 1960 growing to a peak generating capacity in 1987 of over 2000 MWe, but since then has declined to around 1000 MWe, but still accounting for over half of the total U.S. geothermal electric generating capacity (see Refs. 7 and 8).

Commercially produced vapor-dominated systems at The Geysers, Lardarello (Italy), and Matsukawa (Japan) all are characterized by reservoir temperatures in excess of 230°C.* Accompanying the water vapor in these resources are very small concentrations (less than 5%) of noncondensable gases (mostly carbon dioxide, hydrogen sulfide, and ammonia). The Mount Amiata Field in Italy is actually a different type of vapor-dominated resource, characterized by somewhat lower temperatures than The Geysers-type resource and by much higher concentrations of noncondensable gases. The geology of Mount Amiata-type resources is less well understood than The Geysers-type vapor-dominated resources but may turn out to be more common because its existence is more difficult to detect.

2.4 Liquid-Dominated Resources

Hot-water or wet-steam hydrothermal resources are much more commonly found around the globe than dry-steam deposits. Hot-water systems are often associated with a hot spring that discharges at the surface. When wet-steam deposits occur at considerable depths (also relatively common), the resource temperature is often well above the normal boiling point of water at atmospheric pressures. These temperatures are known to range from 100 to 700°C at pressures of 50-150 psig. When water from such resources emerges at Earth's surface, either through wells or natural geologic anomalies (e.g., geysers), it flashes to wet steam. As described in more detail later, converting such resources to useful energy forms requires more complex technology than from vapor-dominated resources.

One reason dealing with wet-steam resources is more complex is that the types of impurities found in them vary considerably. Commonly found dissolved salts and minerals include sodium, potassium, lithium, chlorides, sulfates, borates, bicarbonates, and silica. Salinity concentrations can vary from thousands to hundreds of thousands of parts per million. The Wairekei Fields in New Zealand and the Cerro Prieto Fields in Mexico are examples of currently well-developed liquid-dominated resources and in the United States many such resources are in development or under consideration for development.

2.5 Enhanced Geothermal Systems

In some areas of the western United States, geologic anomalies such as tectonic plate movement and volcanic activity have created pockets of impermeable rock covering a magma chamber within 6 or so miles of the surface. The temperature in these pockets increases with depth and the proximity to the magma chamber, but, because of the impermeability of the rock, they lack a water aquifer. Hence, they are often referred to as *hot dry-rock* (HDR) deposits. To enable electric power generation from such resources with current technology, some form of engineering to develop sufficient permeability for circulation of hot water or steam is necessary.

A number of schemes for useful energy production from HDR resources, known as EGS, have been proposed and tested, but most of them basically involve creation of an artificial aquifer that is used to bring the heat to the surface. The basic idea is to introduce artificial fractures that connect a production and injection well. Water is injected from the surface into the artificial reservoir where it is heated and then returned to the surface through a production well for use in direct-use or geothermal power generation applications. Some researchers consider EGS very promising, despite the many challenges remaining.⁹

* The temperature of dry steam is 150°C, but steam plants are most cost-effective when the resource temperature is above about 175°C.

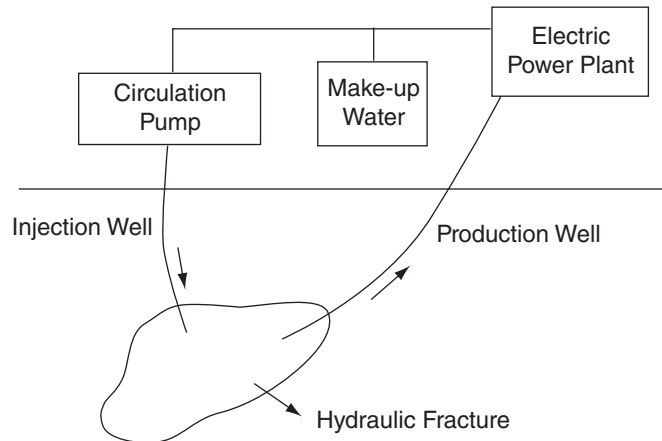


Figure 2 Hot dry-rock geothermal resource conversion.

A typical EGS design is shown in Fig. 2. The critical parameters affecting the ultimate commercial feasibility of HDR resources are the geothermal gradient throughout the artificial reservoir that is developed and the achievable well flow rate from the production well as well as the drilling and development costs. In addition, there are a number of additional challenges in developing an EGS such as perhaps especially the potential of induced seismicity as the artificial reservoirs are created and developed.

2.6 Geothermal Energy from Magma Intrusions

Magma is subsurface molten rock often mixed with suspended crystals and dissolved gas, collecting in so-called magma chambers that often feed volcanoes. Perhaps even more challenging than HDR resource extraction is extracting thermal energy directly from shallow (several kilometers in depth) magma intrusions beneath volcanic regions. Little has been done to date to develop this kind of resource although some studies have indicated the scientific feasibility deserves further investigation as a source for power generation.¹⁰

2.7 Geopressured Resources

Near the Gulf Coast of the United States are a number of deep sedimentary basins that are geologically very young, i.e., less than 60 million years. In such regions, fluid located in subsurface rock formations carry a part of the overburden load, thereby increasing the pressure within the formation. If the water in such a formation is also confined in an insulating clay bed, the normal heat flow of Earth can raise the temperature of the water considerably. The water in such formations is typically of somewhat lower salinity as well, compared to adjacent aquifers and, in many cases, is saturated with large amounts of recoverable methane. Such formations are referred to as *geopressured* and are considered by some geologists to be promising sources of energy in the coming decades.

The promise of geopressured geothermal resources lays in the fact that they may be able to deliver energy in three forms: (1) mechanical energy, since the gas and liquids are resident in the formations under high hydraulic pressure, (2) the geothermal energy stored in the liquids, and (3) chemical energy since, as noted above, many geopressured resources are accompanied by high concentrations of methane or natural gas.

Geopressed basins exist in several areas within the United States, but those considered the most promising are located in the Texas–Louisiana coast. They are of particular interest because they are very large in terms of both areal extent and thickness and because the geopressed liquids (mostly high-salinity brine) are suspected to include high concentrations of methane.

In past evaluations of the Gulf Coast region, a number of so-called geopressed fairways were identified, which are thick sandstone bodies expected to contain geopressed fluids of at least 150°C. Detailed studies of the fairways of the Frio Formation in East Texas were completed in 1979, although only one, Brazoria, met the requirements for further well testing and remains the subject of interest by researchers. More recent assessments, such as by Griggs,¹¹ indicate more promising results but the economic viability varies considerably according to the characteristics being discovered at known resources.

3 GEOTHERMAL ENERGY CONVERSION

As a source of energy for modern society, geothermal has a number of important advantages. While not immediately renewable like solar and wind resources, the energy within Earth is vast and essentially inexhaustible, i.e., with a lifetime of billions of years; environmental impacts associated with geothermal energy conversion are generally modest and local compared with other alternatives; and energy production is generally very reliable and available day and night. In addition, geothermal energy is not generally affected by weather, although there may be seasonal differences in plant efficiency. Finally, geothermal plants take little space and can be made unobtrusive even in areas of high scenic value, where many geothermal resources are located.

Most economical applications of geothermal energy, at least at this point in the development of the necessary technology, hinge on the availability and quality of the resource. On the one hand, geothermal resources are far less pervasive than solar or wind resources, but, on the other hand, as technology continues to develop, the use of lower quality but much more common geothermal resources may increase their development substantially.

Since use of geothermal energy involves interaction with a geologic system, the characteristics and quality of the resource involve some natural variability (far less than with solar or wind) but, more importantly, the utilization of the geothermal resource can be affected profoundly by the way in which the resource is tapped. In particular, drawing steam or hot water from a geothermal aquifer at a rate higher than the rate at which the aquifer is refreshed will reduce the temperature and pressure of the resource available for use locally and can precipitate geologic subsidence evident even at the surface. The consequences of resource utilization for the quality of the resource are especially important since geothermal energy is used immediately and not stored, in contrast to the case of oil and gas resources, and would undermine the availability, stability, and reliability of the commercially produced energy from the resource and diminish its value.

Reinjecting geothermal fluids that remain after the water (or steam) has been utilized in a turbine (or other technology that extracts the useful heat from the fluid) helps preserve the fluid volume of the reservoir and is now a common practice for environmental reasons and to mitigate subsidence.* Nonetheless, even with reinjection, the heat content of a well-developed geothermal reservoir will gradually decline, as typified by the history at The Geysers.

* Reinjection of water is common in oil and gas field maintenance to preserve the volume and pressure of the resource in those fields and the basic concept is applicable in geothermal fields as well to both mitigate the environmental impacts of otherwise disposing spent geothermal liquids and to maintain the volume, temperature, and pressure of the geothermal aquifer.

A variety of technologies are in current use to convert geothermal energy to useful forms. These can very generally be grouped into three basic categories: (1) direct use, (2) electric power generation, and (3) geothermal heat pumps. Each category utilizes the geothermal resource in a very different way.

3.1 Direct Uses of Geothermal Energy

The heat from geothermal resources is frequently used directly without a heat pump or to produce electric power. Such applications generally use lower temperature geothermal resources for space heating (commercial buildings, homes, greenhouses, etc.), industrial processes requiring low-grade heat (drying, curing, food processing, etc.), or aquaculture.

Generally, these applications use heat exchangers to extract the heat from geothermal fluids delivered from geothermal wells. Then, as noted earlier, the spent fluids are injected back into the aquifer through reinjection wells. The heat exchangers transfer the heat from the geothermal fluid usually to fresh water that is circulated in pipes and heating equipment for direct-use applications.

Such applications can be very efficient in small end-use applications such as greenhouses, but it is generally necessary for the applications to be located close to the geothermal heat source. Perhaps the most spectacular and famous example of direct use of geothermal energy is the city of Reykjavik, Iceland, which is heated almost entirely with geothermal energy.

3.2 Electric Power Generation

Geothermal electric power generation generally uses higher temperature geothermal resources (above 110 °C). The appropriate technology used in power conversion depends on the nature of the resources.

As noted earlier, for vapor-dominated resources, it is possible to use direct steam conversion. For higher quality liquid-dominated hydrothermal resources, i.e., with temperatures greater than 180 °C, power plants that separate steam (flashed) from the geothermal fluid and then feed the steam into a turbine which turns a generator can be used. For lower quality resources so-called *binary* power plants can increase the efficiency of electric power production from liquid-dominated resources.

In a manner similar to direct uses of geothermal energy, binary power plants use a secondary working fluid which is heated by the geothermal fluid in a heat exchanger. In binary power plants, however, the secondary working fluid is usually a substance such as isobutane, which is easily liquefied under pressure but immediately vaporizes when the pressure is released at lower temperatures than water. Hence, the working fluid vapor turns the turbine and is condensed prior to reheating in a heat exchanger to form a closed-loop working cycle.

In all currently envisioned versions of geothermal electric power generation, the spent geothermal fluids are ultimately injected back into the reservoir. Geothermal power plants vary in capacity from several hundred kWe to hundreds of mWe. In the United States, in 2012, there are 147 geothermal power plant projects in development, mostly located in California and Nevada, but plants are also operating and being developed in Alaska, Hawaii, Idaho, Oregon, Utah, and Wyoming. The power-generating capacity at The Geysers remains the largest concentration of geothermal electric power production in the world, accounting for almost 50% of the total U.S. geothermal installed capacity.

Kutscher¹² observes that if hot dry-rock resources utilizing enhanced geothermal systems technology become economic, the United States would be “sufficient to provide our current electric demand for tens of thousands of years,” although currently economically tapping hot dry-rock resources remains largely elusive and speculative. To explore that potential, a variety of research and development program activities are underway sponsored by the U.S. government.¹³

The following explores more specifically the technologies of direct steam, flash, and binary geothermal energy conversion along with the strategy of combining geothermal energy with fossil (oil, coal, or natural gas) in power generation.

3.3 Direct Steam Conversion

Electric power generation using the geothermal resources at The Geysers in California and in central Italy, which were referred to earlier as The Geysers-type vapor-dominated resources, is a very straightforward process relative to the processes associated with other kinds of geothermal resources. A simplified flow diagram of direct steam conversion is shown in Fig. 3. The key components of such a system include the steam turbine–generator, condenser, cooling towers, and some smaller facilities for degassing and removal of entrained solids and for pollution control of some of the noncondensable gases.

The process begins when the naturally pressurized steam is piped from production wells to a power plant, where it is routed through a turbine–generator to produce electricity. The geothermal steam is supplied to the turbine directly, except for the relatively simple removal of entrained solids in gravity separators or the removal of noncondensable gases in degassing vessels. Such gases include carbon dioxide, hydrogen sulfide, methane, nitrogen, oxygen, hydrogen, and ammonia. In modern geothermal plants additional equipment is added to control, in particular, the hydrogen sulfide and methane emissions from the degassing stage. Release of hydrogen sulfide is generally recognized as the most important environmental issue associated with direct steam conversion plants at The Geysers’ generating facilities. The most commonly applied control technology for abatement of toxic gases such as hydrogen sulfide in geothermal power plants is known as the Stratford process.

As the “filtered” steam from the gravity separators and degassing units expands in the turbine, it begins to condense. It is then exhausted to a condenser, where it cools and condenses completely to its liquid state and is subsequently pumped from the plant. The condensate is then almost always reinjected into the subterranean aquifer at a location somewhat removed from the production well. Cooling in the condenser is provided by a piping loop between the condenser and the cooling towers. The hot water carrying the heat extracted from the condensing steam line from the turbine is routed to the cooling tower where the heat is rejected to the atmosphere. The coolant fluid, freshly cooled in the cooling tower, is then routed back to the condenser forming the complete cooling loop (as shown in Fig. 3).

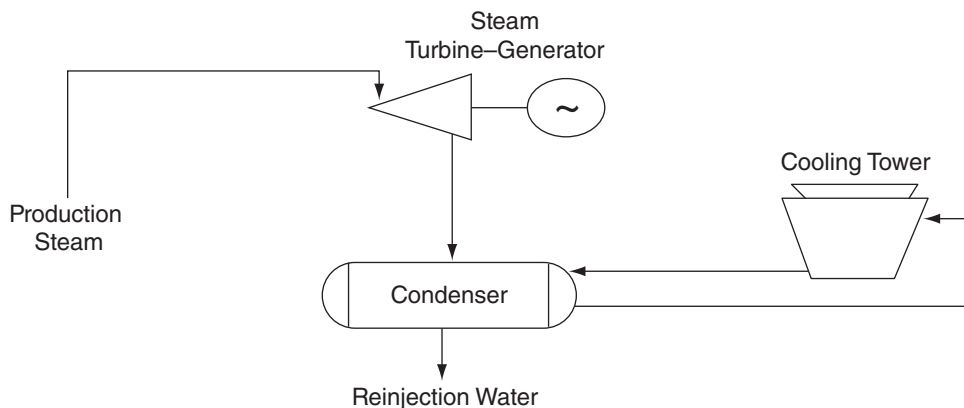


Figure 3 Direct steam conversion.

Reinjection of geothermal fluids in modern geothermal systems is almost always employed to help preserve reservoir volume and to help mitigate air and water pollutant emissions on the surface. However, as the geothermal well field is developed and the resource produced, effective reservoir maintenance becomes an increasingly important issue. For example, in The Geysers, noted earlier as a highly developed geothermal resource, as the geothermal fluids are withdrawn and reinjected, the removal of the heat used in power generation causes the reservoir temperature to decline. The cooling reservoir then contracts* and this is observed at the surface as subsidence. Geophysicists Mossop and Segall¹⁴ observe that subsidence at The Geysers has been on the order of 0.05 m/year since the early 1970s.

Because of the quality of the resource and the simplicity of the necessary equipment, direct steam conversion is the most efficient type of geothermal electric power generation. A typical measure of plant efficiency is the amount of electric energy produced per pound of steam at a standard temperature (usually around 175°C). For example, the power plants at The Geysers produce 50–55 Wh of electricity per pound of 176°C steam used, which is a very high quality geothermal resource. Another common measure of efficiency is known as the geothermal resource utilization efficiency (GRUE), defined as the ratio of the net power output of a plant to the difference in the thermodynamic availability of the geothermal fluid entering the plant and that of that fluid at ambient conditions. Power plants at The Geysers operate at a GRUE of 50–56%.

3.4 Flashed Steam Conversion

Most geothermal resources do not produce dry steam; rather they produce a pressurized two-phase mixture of steam and water often referred to as wet steam. When the temperature of the geothermal fluid in this kind of resource regime is greater than about 180°C, plants can use the so-called flashed steam energy conversion process. Figure 4 is a simplified schematic that illustrates the flashed steam power generation process used in such plants. In addition to the key components used in direct steam conversion plants (i.e., turbine, condenser, and cooling towers), flashed steam plants include a component called a separator or flash vessel.

The flash conversion process begins with the geothermal fluid from the production well(s) flowing under its own pressure into the separator, where saturated steam is flashed from the liquid brine. That is, as the pressure of the fluid emerging from the resource decreases in the separator, the water boils, or “flashes,” to steam and the water and steam are separated. The steam is diverted into the power production facility and the spent steam and remaining water are then reinjected into the aquifer.

Many geothermal power plants use multiple stages of flash vessels to improve the plant efficiency and raise power generation output. Figure 5 is a simplified schematic illustrating a two-stage or “dual-flash” system. Such systems are designed to extract additional energy from geothermal resource by capturing energy from both high and lower temperature steam.

In the two-stage process, the unflashed fluid leaving the initial flash vessel enters a second flash vessel that operates at a lower pressure, causing additional steam to be flashed. This lower pressure steam is supplied to the low-pressure section of the steam turbine, recovering energy that would have been lost if a single-stage flash process had been used. The two-stage process can result in a 37% or better improvement in plant performance compared with a single-stage process. Additional stages can be included as well, resulting in successively diminishing levels of additional efficiency improvement. For example, addition of a third stage can add an additional 6% in plant performance.

* Most researchers conclude that the extraction, reinjection, and associated temperature decline causes strain due to a combination of thermoelastic and poroelastic deformations, which results in surface subsidence, e.g., Mossop and Segall (Ref. 14).

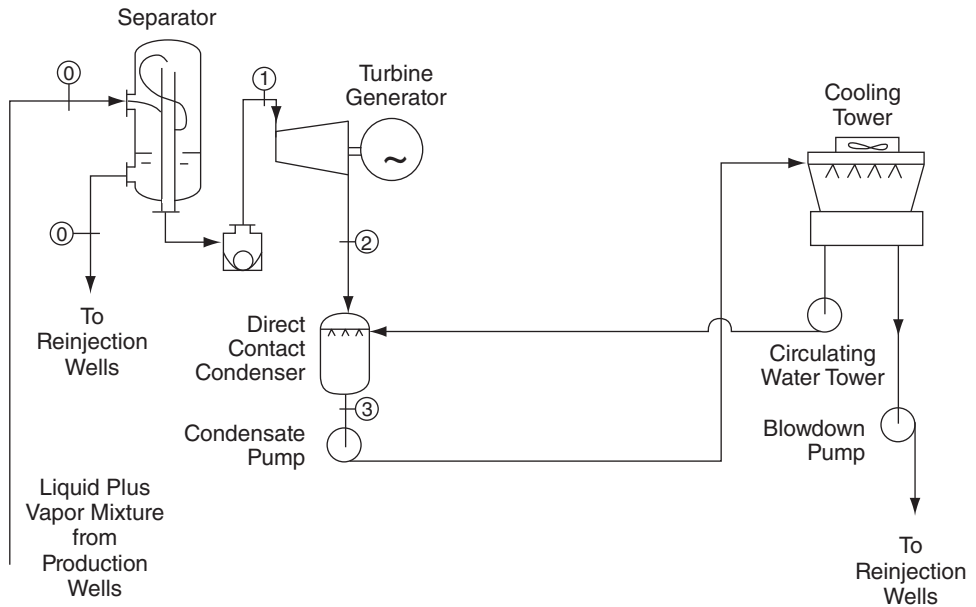


Figure 4 Flashed steam conversion.

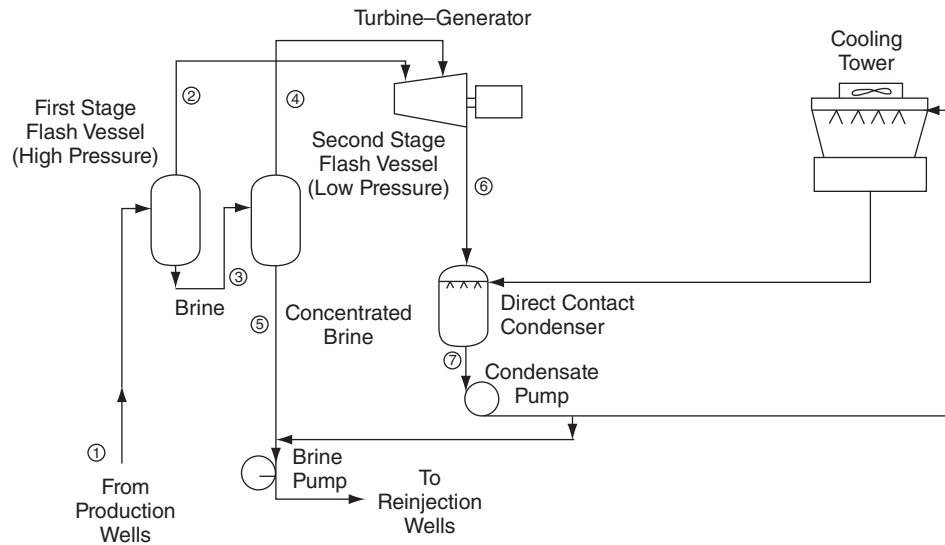


Figure 5 Two-stage flash conversion.

3.5 Binary Cycle Conversion

For lower quality geothermal resource temperatures, i.e., usually below about 175°C, flash power conversion is not efficient enough to be cost effective. In such situations, it becomes more efficient to employ a so-called binary cycle. In the binary cycle, heat is transferred from the geothermal fluid to a volatile working fluid (usually a hydrocarbon such as iobutane or

isopentane) that vaporizes and is passed through a turbine. Such plants are called binary since the secondary fluid is used in a Rankine power production cycle, and the primary geothermal fluid is used to heat the working fluid. These power plants generally have higher equipment costs than flash plants because the system is more complex.

Figure 6 is a simplified schematic illustrating the key components in the binary cycle conversion process. Geothermal brine from the production well(s) passes through a heat exchanger, where it transfers heat to the secondary working fluid. The cooled brine is then reinjected into the aquifer. The secondary working fluid is vaporized and superheated in the heat exchanger and expanded through a turbine, which drives an electric generator. The turbine exhaust is condensed in a surface condenser, and the condensate is pressurized and returned to the heat exchanger to complete the cycle. A cooling tower and a circulating water system reject the heat of condensation to the atmosphere.

A number of variations of the binary cycle have been designed for geothermal electric power generation. For example, a regenerator may be added between the turbine and condenser to recover energy from the turbine exhaust for condensate heating and to improve plant efficiency. The surface-type heat exchanger, which passes heat from the brine to the working fluid, may be replaced with a direct contact or fluidized-bed type exchanger to reduce plant cost. Hybrid plants combining the flashed steam and binary processes have also been evaluated in many geothermal power generation applications.

The binary process is proving to be an attractive alternative to the flashed steam process at geothermal resource locations that produce high-salinity brine. First, since the brine can remain in a pressurized liquid state throughout the process and does not pass through the turbine, problems associated with salt precipitation and scaling as well as corrosion and erosion can be greatly reduced. In addition, binary cycles offer the additional advantage that a working fluid can be selected that has superior thermodynamic characteristics to steam, resulting in a more efficient conversion cycle. Finally, because all the geothermal brine is reinjected into the aquifer, binary cycle plants do not require mitigation of gaseous emissions and reservoir fluid volume is maintained. Larger binary plants are typically constructed as a series of smaller units or modules, so maintenance can be completed on individual modules without shutting down the entire plant, thereby minimizing the impact on total plant output.

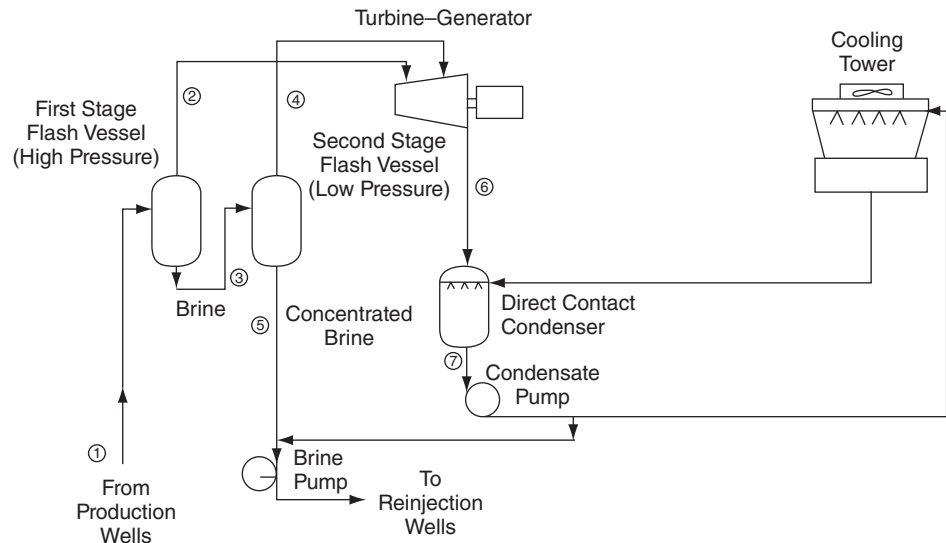


Figure 6 Binary cycle conversion.

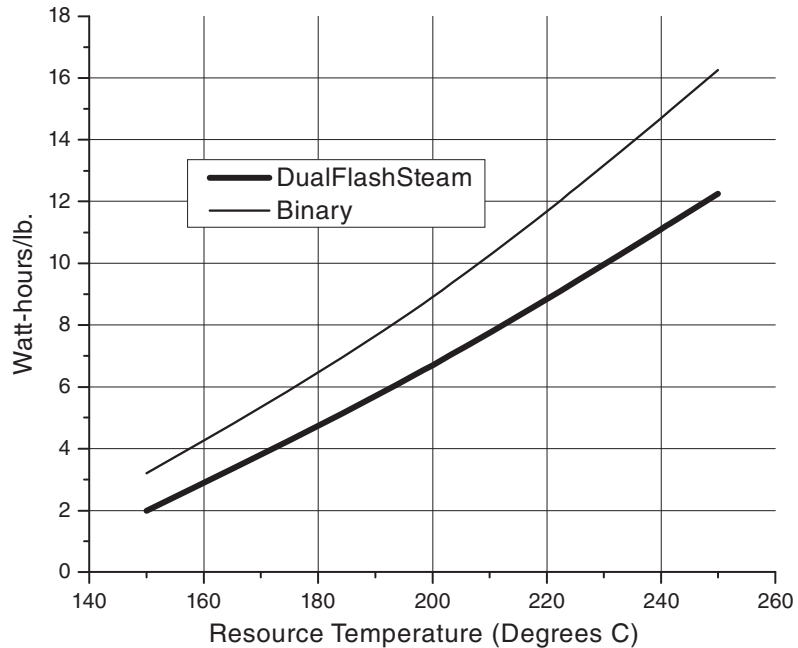


Figure 7 Net geothermal brine effectiveness.

3.6 Some Additional System Selection Considerations

The overall efficiency of energy conversion processes for liquid-dominated resources is dependent primarily on the resource temperature and to a lesser degree on brine salinity and the concentration of noncondensable gases. System efficiency can generally be improved by system modifications, but such modifications usually involve additional cost and complexity. Figure 7 shows an empirical family of curves relating power production per unit of geothermal brine consumed for both two-stage flash and binary conversion systems.

The level of hydrogen sulfide emissions is an important consideration in geothermal power plant design. Emissions of hydrogen sulfide at liquid-dominated geothermal power plants are generally lower than for direct steam processes. For example, steam plants emit 30–50% less hydrogen sulfide than direct steam plants. Binary plants would generally not emit significant amounts of hydrogen sulfide because the brine remains contained and pressurized throughout the entire process.

Finally, the possibility of land surface subsidence caused by withdrawal of the brine from the geothermal resource can be an important design consideration. ReInjection of brine is the principal remedy for avoiding subsidence by maintaining reservoir volume and has the added environmental benefit of minimizing other pollution emissions to the atmosphere. However, faulty reInjection can contaminate local fresh groundwater. Also, in some plant designs, if all brine is reInjected, an external source of water is required for plant cooling water makeup.

Evaluating the power plant design most suitable to the characteristics of a particular geothermal resource can be very complex (see Ref. 15), and very sophisticated computer models have been developed to tune designs to resources characteristics, as in Ref. 16.

3.7 Hybrid Geothermal/Fossil Energy Conversion

Hybrid fossil/geothermal power plants use both fossil energy and geothermal heat to produce electric power. A number of alternative designs exist. First, a geothermal preheat system involves using geothermal brine to preheat the feedwater in an otherwise conventional fossil-fired power plant. Another variation is a fossil superheat concept that incorporates a fossil-fired heater to superheat geothermal steam prior to expansion in a turbine.

3.8 Geothermal Heat Pumps

Geothermal heat pumps (GHPs), sometimes also referred to as groundwater heat pumps, use the earth's typical diffuse low-grade heat found in the very shallow subsurface (usually between 30 and 300 ft in depth) usually in space heating applications. In most geographic areas in the United States, GHPs can deliver three to four times more energy than it consumes in the electricity needed to operate and can be used over a wide range of Earth temperatures.

The GHP energy conversion process works much like a refrigerator, except that it is reversible, i.e., the GHPs can move heat either into the earth for cooling or out of the earth for heating, depending on whether it is summer or winter. GHPs can be used instead of or in addition to direct uses of geothermal energy for space or industrial process heating (or cooling), but the shallow resource used by GHPs is available essentially anywhere, constrained principally by land use and economics, especially initial installation costs.

The key components of the GHP system include a ground refrigerant-to-water heat exchanger, refrigerant piping and control valves, compressor, an air coil (used to heat in winter and cool and dehumidify in summer), a fan, and control equipment. This system is illustrated in Fig. 8.

The GHP energy conversion process begins with the ground heat exchanger, which is usually a system of pipes configured as either a closed- or open-loop system. The most common configuration is the closed loop, in which high-density polyethylene pipe is buried horizontally at a depth of at least 4–6 ft deep or vertically at a depth of 100–400 ft. The pipes are typically filled with a refrigerant mixture of antifreeze and water solution that acts as a heat exchanger. That is, in winter, the fluid in the pipes extracts heat from the earth and carries it into the building. In the summer, the system reverses the process and takes heat from the building and transfers it to the cooler ground.

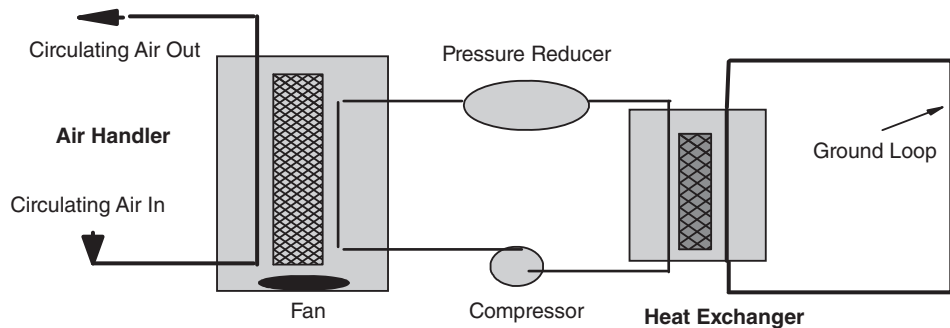


Figure 8 Geothermal heat pump system configuration.

GHP systems deliver heated or cooled air to residential or commercial space through ductwork just like conventional heating, ventilating, and air conditioning (HVAC) systems. An indoor coil and fan is called an air handler and contains a large blower and a filter just like conventional air conditioners.

3.9 Ground Loop GHP Systems

There are four basic types of ground loop GHP systems: (1) horizontal, (2) vertical, (3) pond/lake, and (4) open-loop configurations. The first three of these are all closed-loop systems. Selection of one of these system types depends on climate, soil conditions, available land, and local installation costs. The following briefly describes each of the approaches to GHP ground loop systems:

- *Horizontal.* Considered generally most cost-effective for residential installations, especially for new construction where sufficient land is available, the installation entails two pipes buried in trenches that form a loop.
- *Vertical.* Vertically oriented systems are often used for large commercial buildings and schools where the land area required for horizontal loops would be prohibitive or where the surrounding soil is too shallow for trenching in a horizontal system or when a goal is to minimize the disturbance to existing landscaping. In such systems holes are drilled about 20 ft apart and 100–400 ft deep and pipes are installed and connected at the bottom to form the loop.
- *Pond/Lake.* If the site has a suitable water body accessible, a supply line pipe can be run from the building to the water and coiled under the surface of the water body to prevent freezing in winter.
- *Open Loop.* An open-loop system uses water from well(s) or a surface body of water as the heat exchange fluid that circulates directly through the GHP system. Once the water has circulated through the heat exchanger, the water returns to the ground through another well or by surface discharge. This option can only be used where there is an adequate supply of relatively clean water and use of it is permitted under local environmental codes and regulations.

REFERENCES

1. A. Holm, L. Blodgett, D. Jennejohn, and K. Gawell, *Geothermal Energy: International Market Update*, Geothermal Energy Association, Washington, DC, May 2010.
2. P. M. Wright, “The Sustainability of Production from Geothermal Resources,” *GHC Bulletin*, Oregon Institute of Technology, Geo-Heat Center, Klamath Falls, OR, June 1998.
3. C. F. Williams, M. J. Reed, J. Marshall, R. H. Mariner, J. DeAngelo, and S. P. Galanis, Jr., “Assessment of Moderate- and High-Temperature Geothermal Resources of the United States,” Fact Sheet 2008-3082, U.S. Geological Survey, Arlington, VA, 2008.
4. D. E. White and D. L. Williams (Eds.), “Assessment of Geothermal Resources of the United States—1975,” Circular 726, U.S. Geological Survey, Arlington, VA, 1975.
5. L. J. P. Muffler (Ed.), “Assessment of Geological Resources of the United States—1978,” Circular 790, U.S. Geological Survey, Arlington, VA, 1979.
6. P. D. Blair, T. A. V. Cassel, and R. H. Edelstein, *Geothermal Energy: Investment Decisions and Commercial Development*, Wiley, New York, 1982.
7. S. Sanyal and S. L. Eney, “Fifty Years of Power Generation at the Geysers Geothermal Field, California—The Lessons Learned,” in *Proceedings of the Thirty-Sixth Workshop on Geothermal Reservoir Engineering*, SGP-TR-191, Stanford University, Stanford, CA, January 31–February 2, 2011.

8. Geothermal Energy Association (GEA), *Annual U.S. Geothermal Power Production and Development Report*, GEA, Washington, DC, April 2012.
9. Massachusetts Institute of Technology, *The Future of Geothermal Energy Impact of Enhanced Geothermal Systems (EGS) on the United States in the 21st Century*, Prepared under U.S. Department of Energy Contract DE-AC07-05ID14517, 2006.
10. J. L. Colp, "Final Report—Magma Energy Research Project," SAND82-2377, Geophysics Division, Sandia National Laboratories, Albuquerque, NM, October 1982.
11. J. Griggs, "A Reevaluation of Geopressured-Geothermal Aquifers as an Energy Sources," in *Proceedings of the Thirtieth Workshop on Geothermal Reservoir Engineering*, Stanford University, Stanford, CA, January 31–February 2, 2005.
12. C. F. Kutscher, "The Status and Future of Geothermal Electric Power," NREL/CP-550-28204, National Renewable Energy Laboratory, Golden, CO, August 2000.
13. U.S. Department of Energy (DOE), Office of Energy Efficiency and Renewable Energy, Strategic Plan, DOE/GO-102002-1649, DOE, Washington, DC, October 2002.
14. A. Mossop and P. Segall, "Subsidence at The Geysers Geothermal Field," *Geophys. Res. Lett.*, **24**(14), 1839–1842, July 15, 1997.
15. S. L. Milora and J. W. Tester, *Geothermal Energy as a Source of Electrical Power, Thermodynamic and Economic Design Criteria*, MIT Press, Cambridge, MA, 1976.
16. D. Entingh, "DOE Geothermal Electricity Technology Evaluation Model (GETEM): Volume III—Detailed Technical Appendixes," U.S. Department of Energy, Washington, DC, 2006.

CHAPTER 25

PUMPS, FANS, BLOWERS, AND COMPRESSORS

Keith Marchildon and David Mody
Queen's University
Kingston, Ontario, Canada

1 LIQUID MOVERS—PUMPS	857	2.3 Axial-Flow Fans	887
1.1 Centrifugal Pumps	858	2.4 Ejectors	888
1.2 Other Dynamic Pumps: Axial Flow, Mixed Flow, Jet	871	2.5 Compression	892
1.3 Positive-Displacement Pumps	873	3 THERMODYNAMICS OF GAS COMPRESSION	897
2 GAS MOVERS	878	REFERENCES	900
2.1 Fans and Blowers—General	880	BIBLIOGRAPHY	900
2.2 Centrifugal Fans	881		

The continuous transport of a liquid requires a pump, and the continuous transport of a gas or vapor requires a fan, blower, or compressor. All of these devices are described by the general term *fluid movers*. Specialized fluid movers are required for the transport of liquid-and-gas mixtures and of slurries and suspensions of solids in liquid or gas. The vast majority are mechanically driven. A few—eductors and ejectors—use another fluid as the motive source. In all cases the fundamental action of the device is to generate a localized increase of pressure, which then allows the fluid to overcome adverse differences and gradients of pressure that oppose its movement from source to destination.

There are two general types of fluid movers, the *dynamic* and the *positive displacement*. The former imparts momentum to the fluid through principles of fluid dynamics, and the scale and direction of the momentum is usually different from that of the impelling element. The latter simply displaces the fluid, giving the fluid the velocity and direction of the impelling element.

Another major distinction is between the type of fluid being transported, i.e., liquid or gas. Liquids are somewhat simpler, but they require considerations of viscosity and of any tendency to vaporize under conditions of pressure at the inlet of the pump. Gases are subject to compression and to attendant changes in volume and temperature. The present account is organized into two broad sections—on liquid transport and on gas transport—and within each section it describes the technology of both the dynamic and the positive-displacement devices. In the case of gas compression, where pressure, volume, and temperature are all in flux, an outline of the relevant thermodynamics is provided.

1 LIQUID MOVERS—PUMPS

Many ingenious devices for pumping liquids have been used over the ages. As stated, current pumps fall into one of two general types: the *dynamic* and the *positive displacement*.

Dynamic devices include *centrifugal*, *axial*, *mixed flow*, and *jet pumps*. Positive-displacement devices comprise *gear*, *screw*, *progressive cavity*, *peristaltic*, and *reciprocating pumps*. Dynamic pumps, especially centrifugal, are by far the most widely used. If an application can be served by either type, the dynamic is chosen because of its lower cost.

Dynamic pumps are subject to inner losses of pressure because of, for instance, fluid acceleration and frictional forces. Achievable pressure rise across the pump decreases as liquid rate increases. There is generally a combination at which efficiency (to be defined) is greatest and close to which it is desired to operate

The capacity of a positive-displacement pump is largely independent of pressure rise across the pump, being subject only to backflow through clearances. An exception is that some types of screw pump allow backflow through the screw channels, which causes their capacity to depend significantly on the pressure rise.

1.1 Centrifugal Pumps

The centrifugal pump uses an *impeller*, a rotor with radial vanes, to impart a rotational velocity to the liquid. The impeller and liquid are contained in a circular casing, the outer part of which exerts pressure to oppose centrifugal force of the liquid. The liquid enters at the center of rotation and leaves through a port at the periphery of the casing, carrying the above pressure. Pumps may be single staged or they may have several stages in series in order to build stepwise to high pressure. As seen in Fig. 1, the vanes are convex in the direction of rotation. They may also be twisted along their length. Pump designers continually strive to improve the design of impellers and of casings in order to achieve optimum combinations of capacity and pressure.

Figure 2 shows the exterior of a typical centrifugal pump, and Fig. 3 shows the impellor and its backward-curving vanes.

Basis of Centrifugal Operation

Flow in a centrifugal pump is complex and difficult to describe mathematically. The following simplified description captures the main features and leads to the derivation of key relationships and rules.

The peripheral pressure P_o exerted by a volume of liquid of diameter D , with density ρ and rotating at speed N may be calculated by integrating outward from the center. The result is

$$(\Delta P)_o = \frac{1}{3} \rho (N\pi D)^2 g_c^{-1} \quad (1)$$

where $(\Delta P)_o$ is the pressure increase between center and periphery, g_c is the conversion factor for Newton's second law: $1 \text{ kg m s}^{-2} \text{ N}^{-1}$ or $32.16 \text{ lb ft s}^{-2} \text{ lbf force}^{-1}$.

This is the pressure rise that should be seen when the pump exit is sealed or "dead headed." In practice the measurement is usually somewhat higher, most likely because of deceleration in

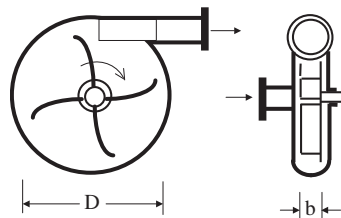


Figure 1 Centrifugal pump schematic.

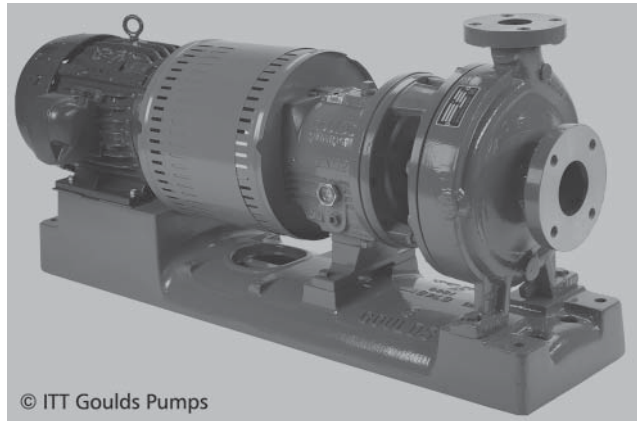


Figure 2 Centrifugal pump exterior. (Courtesy of Goulds Pumps.)



Figure 3 Centrifugal pump impeller. (Courtesy of Goulds Pumps.)

the vicinity of the gauge. Equation (1) is useful as a rough estimate but is converted to a more general form:

$$(\Delta P)_O = K_P \rho N^2 D^2 g_C^{-1} \quad (2)$$

Once flow begins, some of this pressure starts being depleted because of frictional losses as the liquid travels outward between the vanes. Application of standard frictional relations for turbulent flow and the assumption that pump width is proportional to diameter results in a proportionality for the pressure decrease $(\Delta P)_L$:

$$(\Delta P)_L = K'_Q \rho Q^2 D^{-4} g_C^{-1} \quad (3)$$

where Q is volumetric flow rate.

The net pressure change is the difference between $(\Delta P)_O$ and $(\Delta P)_L$:

$$\begin{aligned} \Delta P &= K_P \rho N^2 D^2 g_C^{-1} - K'_Q \rho Q^2 D^{-4} g_C^{-1} \\ &= K_P \rho N^2 D^2 g_C^{-1} (1 - K'_Q K_P^{-1} D^{-6} N^{-2} Q^2) \end{aligned} \quad (4)$$

The bracketed factor is thus the fraction of the zero-throughput pressure rise that remains when the throughput is Q . In this simplified picture, pressure rise falls off as the square of

volumetric throughput. This behavior is followed at least approximately by many centrifugal pumps. A more general examination is made later of patterns of pressure versus throughput, P vs. Q .

Equation (4) provides a way of predicting the effect on pressure rise of a change or combination of changes in liquid density, impeller speed, pump diameter, and throughput, based on the two constants K_P and K'_Q , which are best evaluated by onsite experience with the pump or from the manufacturer's data.

The power, Pwr, which the pump delivers to the liquid is given by

$$\text{Pwr} = \Delta P \times Q \quad (5)$$

The pumping efficiency, Eff, of the operation is defined as

$$\text{Eff} = \text{Pwr} \times \text{BPwr}^{-1} \quad (6)$$

where BPwr is the brake power, i.e., the power delivered from the shaft to the impeller.

From these two definitions the efficiency is zero when there is no flow (Q equal to zero) and also when the flow is so large as to make ΔP , as calculated in Eq. (4), zero. Between these two extremes the efficiency passes through a maximum, and this is the condition at or near which it is desired to operate. For a given style of pump, maximum efficiency occurs when the fraction of zero-throughput pressure rise [i.e., the bracketed factor in Eq. (4)] is around a common value, generally in the range 0.5–0.75. For any value, qf , of this fraction, whether at the point of maximum efficiency or not,

$$\Delta P = K_P \rho N^2 D^2 g_C^{-1} (qf) \quad (7)$$

The value of throughput at this operating point is the value that makes the second factor in Eq. (4) equal to qf , i.e.,

$$1 - K'_Q K_P^{-1} D^{-6} N^{-2} Q^2 = qf$$

or

$$Q = K_Q D^3 N (1 - qf)^{0.5} \quad (8)$$

where K_Q is $K_P (K'_Q)^{-1}$

The pumping power at this condition is the product of ΔP and Q and, therefore, from Eqs. (7) and (8) Pwr is proportional to $(\rho N^2 D^2) (D^3 N)$, that is,

$$\text{Pwr} = K_{\text{PWR}} (\rho N^3 D^5) \quad (9)$$

where K_{PWR} is a third constant.

The pressure rise across a pump is often expressed as *head of fluid*, H , where H is the height of liquid that would be supported (on planet Earth) by a pressure equal to ΔP . The relation between H and ΔP is given by

$$H = \Delta P g_C \rho^{-1} g^{-1} \quad (10)$$

where g is acceleration due to Earth's gravity, 9.8 m s⁻² or 32.2 ft s⁻².

Substituting from Eq. (7) for ΔP

$$H = K_P N^2 D^2 g^{-1} qf \quad (11)$$

Equations (11), (8), and (9) express what are known as the *affinity laws* for rotating machines:

1. Head rise varies as (speed)² and as (diameter)².
2. Throughput varies as (speed)¹ and as (diameter)³.
3. Power required varies as (speed)³ and as (diameter)⁵.

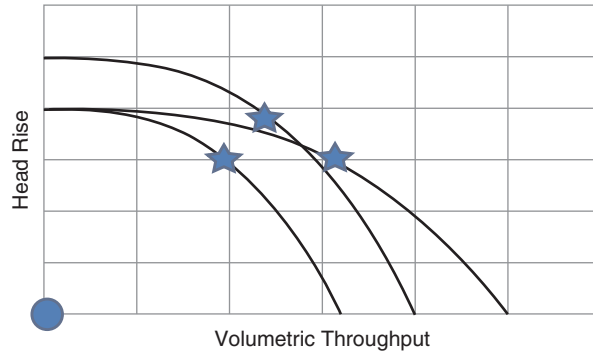


Figure 4 Centrifugal pump head characteristic.

The first and third laws are valid only if the throughput is adjusted to satisfy the second law, i.e., to maintain the equality in Eq. (8). These laws describe any situation where the throughput is adjusted to maintain a constant value of qf , the fraction of the zero-throughput head rise. Equation (4) is a more general relation and describes the reaction to any change, without this restriction.

Figure 4 shows schematically some head-versus-throughput patterns, H vs. Q , based on the square-law equation. In the diagram, the “stars” show the points where qf is 0.75. This simple relationship is a good approximation for many pumps but is not followed as well for others, as is seen subsequently.

The affinity laws provide a way of using the performance of one size of pump operating at a given speed to predict the performance of a pump of similar proportions but of different size and/or operating at a different speed. In many cases the pump body retains its size but the dimension D changes because an impeller of different diameter gets installed.

Specific Speed

The constants of proportionality, K_p , K_Q , and K_{PWR} , are descriptive of pump operation, but they are not in common use by vendors or users. But a combination of K_Q and K_p produces a useful and widely used descriptor, chiefly because it is independent of pump size and it describes whole classes of similarly proportioned pumps. From the definitions in Eqs. (8) and (11), dropping the qf factors, at the optimum condition of maximum efficiency,

$$K_Q^{0.5} K_p^{-0.75} = \left\{ \frac{Q_{OPT}}{(D^3 N)} \right\}^{0.5} \left\{ \frac{H_{OPT}}{(N^2 D^2 g^{-1})} \right\}^{-0.75} = N Q_{OPT}^{0.5} H_{OPT}^{-0.75} g^{-0.75} \quad (12)$$

This quantity is the *specific speed*. Generally the $g^{0.75}$ factor is omitted (but if it is included it makes the specific dimensionless). The common definition is simply

$$N_S = N Q^{0.5} H^{-0.75} \quad (13)$$

where the flow and head, if not exactly at the optimum, are in the general vicinity.

Common units for pump speed are revolutions per minute or per second, for flow are gallons per minute, liters per second, cubic meters per second, and for head are feet or meters. The quantity can be made dimensionless by including the factor $g^{-0.75}$. For a specific case a comparison of N_S values in different sets of units is given in Table 1.

In the present discussion N_S is expressed in the units of the third line: pump speed in revolutions per minute, liquid flow in liters per second, and head in meters:

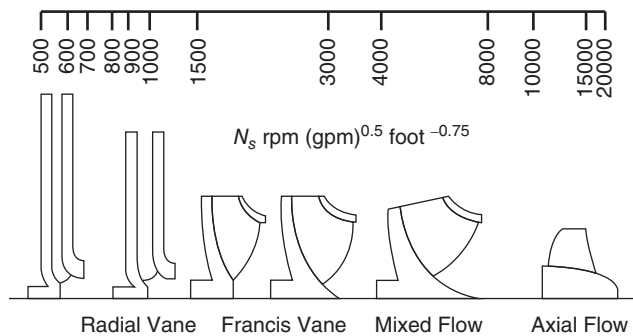
$$N_S = \text{rpm} \times (\text{liters s}^{-1})^{0.5} \times \text{meters}^{-0.75}$$

Table 1a Units of Specific Speed

Pump Speed, N	Liquid Rate, Q	Head, H	Specific Speed, N_s
minute ⁻¹	gallons · minute ⁻¹	Feet	1632
minute ⁻¹	meter ³ · second ⁻¹	Meters	32
minute ⁻¹	liters · second ⁻¹	Meters	1000
Nondimensional			0.095

Table 1b Units of Specific Speed—Comparison

Pump Speed, N	Liquid Rate, Q	Head, H	Specific Speed, N_s
minute ⁻¹	gallons · minute ⁻¹	Feet	1632
minute ⁻¹	meter ³ · second ⁻¹	Meters	32
minute ⁻¹	liters · second ⁻¹	Meters	1000
Non-dimensional			0.095

**Figure 5** Specific speeds of various pump types. (Courtesy of Goulds Pumps.)

Equation (13) gives the impression that specific speed depends on the speed of rotation. This is not the case. The affinity laws show that, for any change in speed, the values of H_{OPT} and Q_{OPT} also change, and in such a way as to keep N_s constant. Specific speed depends only on the style and proportions of the pump. Specific speed provides a guide to pump selection for a given application: Knowing the required head and throughput and the likely pump speed (generally 1750 or 3500 rpm), the purchaser calculates N_s and seeks the style of pump that best matches. The size of pump depends on throughput.

Figure 5 shows that N_s depends mainly on the length of the path from center to periphery of the impeller.

Centrifugal Pump Performance Curves

For any pump the variation of head with liquid rate is important but not the only important characteristic of the operation. Figure 6 shows four quantities, including head H , all plotted as functions of the flow Q . Brake power is specific to water, requiring a correction if a liquid of different density is being pumped.

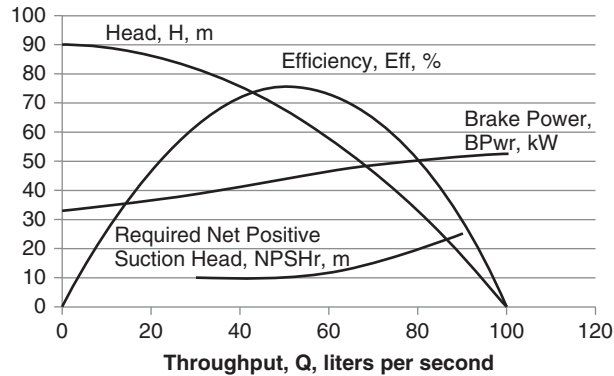


Figure 6 Centrifugal pump performance.

$NPSH_R$ is the required *net positive suction head*, the minimum amount that the head at the pump inlet must exceed the vapor pressure of the liquid at the temperature of the liquid. This requirement is imposed in order to avoid vaporization and subsequent collapse of the vapor phase as pressure rises in the pump. The latter occurrence is known as *cavitation* and is potentially damaging to the pump. In setting values for $NPSH_R$, pump designers sometimes judge vapor formation as beginning when discharge head drops by 3%. Another approach is to use audio tools to detect the onset of “roughness” in the entrance flow, as caused by the presence of bubbles. To avoid vaporization and cavitation, it is necessary to properly design the system upstream of the pump. Difficulties can arise when there is a large frictional pressure drop in the piping, when there is a large positive change in elevation on the way to the pump, or where the liquid rises in temperature and therefore vapor pressure. Good design requires that $NPSH_A$, the *available* net positive suction head at the pump, significantly exceed $NPSH_R$. The pump supplier can advise on how much the margin should be. One rule is to provide the maximum of either $1.2 \times NPSH_R$ or 3 ft of head.

BPwr is *brake power*, the power delivered by the system drive to the impeller. It is not measurable in operation but is inferred from previous testing with a de Prony brake that allows delivered power to be correlated with electrical power to the drive motor.

The power that is received by the liquid is given in Eq. (5) as

$$Pwr = \Delta P Q$$

or, substituting from Eq. (10),

$$Pwr = HQ\rho g g_C^{-1} \quad (14)$$

In terms of units

$$Pwr(\text{Watts}) = \Delta P(\text{Pa}) \times Q(\text{liters s}^{-1}) \times 10^{-3}(\text{m}^3 \text{ liter}^{-1})$$

$$Pwr(\text{horsepower}) = \Delta P(\text{psi}) \times Q(\text{gpm}) \times 0.1337(\text{ft}^3/\text{gal})/33000[(\text{ft}\cdot\text{lb}/\text{min})/\text{hp}]$$

From Eq. (6), efficiency, Eff, is the ratio of Pwr to BPwr.

A more generalized performance plot is presented, taking into account the fact that the same pump casing may be fitted with impellers of different diameters. This is common practice for shifting the H -vs.- Q range of a pump. Figures 7 and 8 show data for a pump operating at a fixed speed of 1750 rpm, employing five different impeller diameters. Figure 7 shows not only the head-versus-throughput curves but also the expected efficiency and the required suction head ($NPSH_R$). Figure 8 shows the brake power (again assuming water) that each of these impellers require, with the lines in descending order of impeller diameter corresponding to the

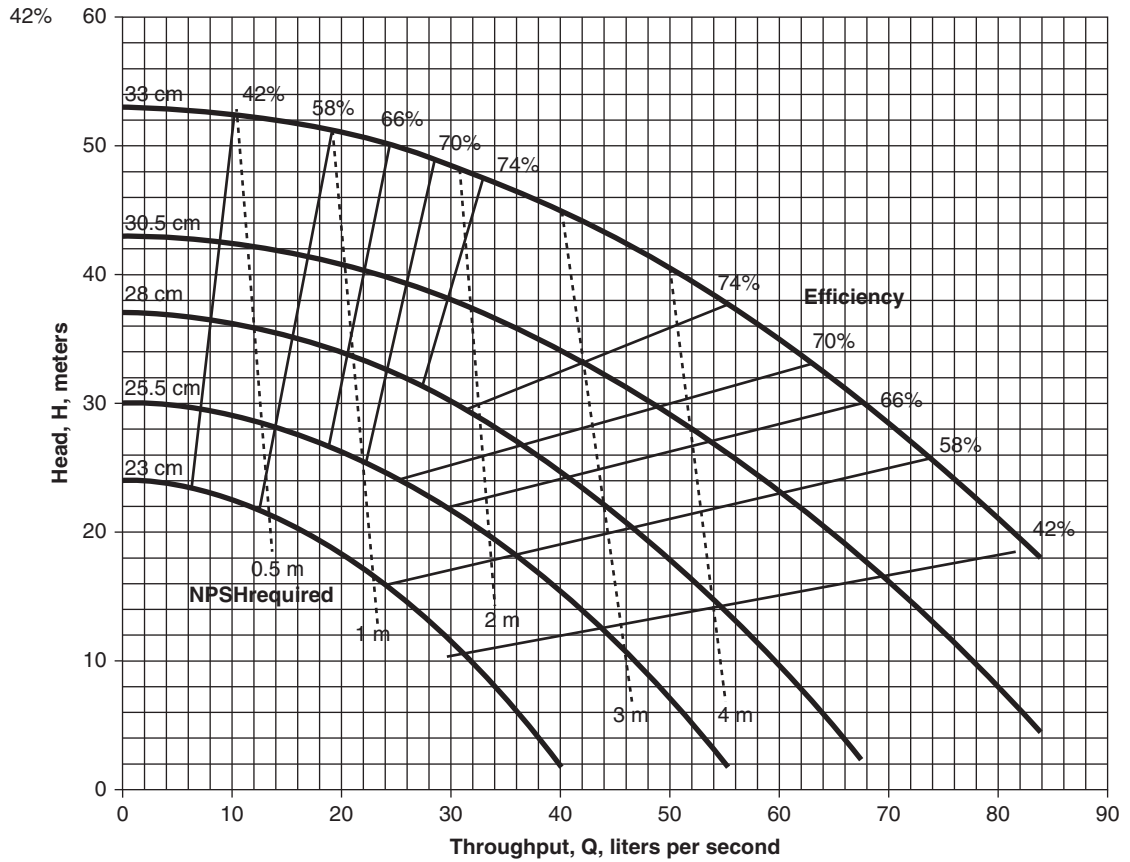


Figure 7 Centrifugal pump impeller diameter effects.

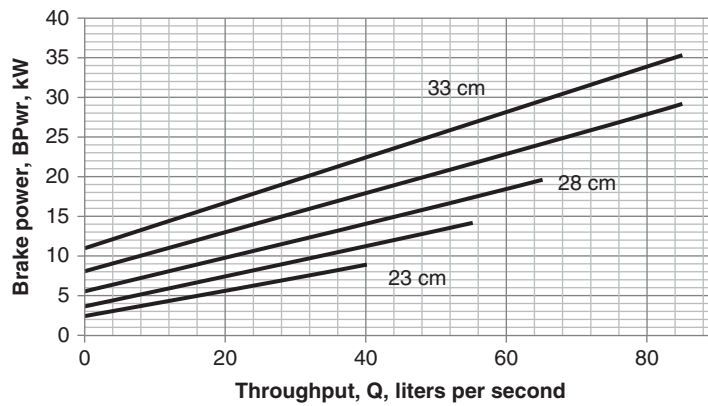


Figure 8 Impeller diameter effect on centrifugal power.

sizes in Fig. 7. Using this flexibility with impeller diameters allows an oversized pump to be installed with a view to future capacity requirements.

Generalized Head Loss with Throughput

Equation (4) shows a square-law decrease in head with throughput, which is a reasonable approximation for pumps with specific speed less than about 1500. Stepanoff¹ states that the actual shape of the H -vs.- Q curve depends strongly on the specific speed, and he has presented a graph illustrating and quantifying this effect. To normalize the curves, he plotted them in the form of h -vs.- q , where h is H/H_{OPT} and q is Q/Q_{OPT} . All curves thus pass through a common point (1, 1). At least one other author, Gulich,² has presented a plot of the same nature but with the individual curves somewhat displaced. Pump manufacturers may have versions of their own.

A generalized equation has been fitted to the curves of Stepanoff, of form

$$h = A_0 + A_1q + A_2q^2 \quad (15)$$

where the coefficients A_0 , A_1 , and A_2 are functions of N_S , as follows:

$$A_0 = 6.75 \times 10^{-8}N_S^2 + 0.0000421N_S + 1.0093 \quad (16)$$

$$A_1 = -1.393 \times 10^{-7}N_S^2 + 0.0002072N_S + 0.1108 \quad (17)$$

$$A_2 = 7.184 \times 10^{-8}N_S^2 - 0.000249N_S - 0.12014 \quad (18)$$

where N_S is in units of $\text{min}^{-1}(\text{liters s}^{-1})^{0.5} \text{ meter}^{-0.75}$.

Figure 9 presents the results of these equations graphically. There is a close match with Stepanoff's curves and provide a reasonable fit to pump performance.

Centrifugal Pump Flow Control

A pump is just one part of an overall system. Its performance, i.e., the head and throughput that it delivers, are determined jointly by its own H -vs.- Q curve and by the pressure characteristics of the equipment upstream and downstream of itself. Assuming that the upstream pressure is sufficient to meet NPSH requirements, that pressure also affects downstream pressure because it adds to the head developed by the pump. To clarify, by "pump head," H , is meant the *increase* in head across the pump. Because of frictional losses in piping, fittings, and equipment, the pressure rise that the pump must generate often depends on throughput, as well as on the overall source and destination pressures of the system, which themselves may change with time. Without control, the pump assumes a head and flow that is compatible hydrodynamically with the rest of the system but not generally satisfying the requirements of the system. Figure 10 shows a pump settling out at two different points of operation, in response to two different characteristics of the rest of the system, i.e., two system curves 1 and 2. As the system curves change, the point of intersection changes and the head and throughput of the pump change. Because the throughput is unlikely to be that which is desired, a means of control must be added to the system to regulate liquid flow.

Two possible approaches involve changing the location of the pump H -vs.- Q curve, so that the point of intersection is at the desired throughput. One of these ways is to alter the speed N of the pump and to continue altering it as part of a control "loop" to maintain the desired flow. As seen from Eq. (11), H changes with N and therefore the location of the whole H -vs.- Q curve changes. But most pumps operate at a fixed standard speed (e.g., 1750 or 3500 rpm) and, in general, it is too expensive to equip them with a variable-speed drive. A second way is to switch to an impeller of different diameter. From Fig. 7 it is seen that diameter has a profound effect on the whole pump curve. This is a good solution if an oversized pump must have its

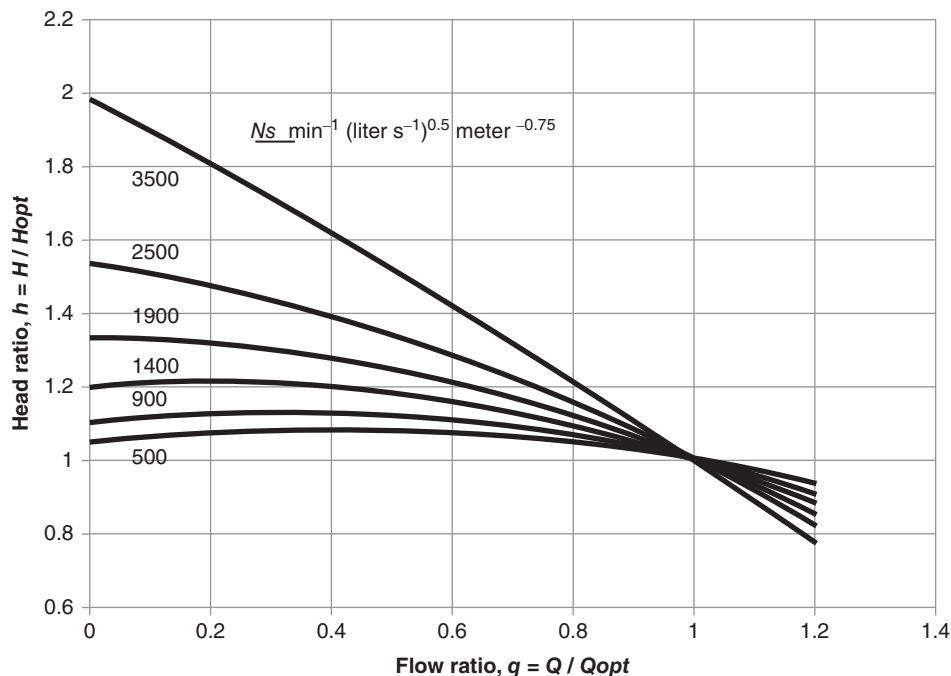


Figure 9 Specific speed effect on centrifugal head behavior.

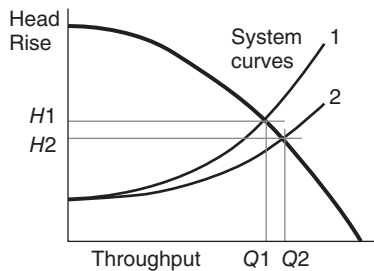


Figure 10 Pump and system interaction.

capacity reduced for an extended period of time but obviously not a way to provide continuous control of flow.

The standard way to control flow is to interpose, between the pump and the destination, a flow measuring device and an adjustable valve. The valve varies its opening to maintain the desired flow, concurrently adjusting the pressure upstream of itself and at the exit of the pump. The pump is operated at constant speed, with its operating point running up and down its H -vs.- Q curve as the required Q changes. Since there is always the possibility of the valve closing completely, either through malfunction or because zero flow is called for, provision must be provided for maintaining some amount of flow through the pump: This is done by allowing a small flow of liquid back around the pump to its inlet through a line that is fitted with an orifice to regulate the flow. The whole arrangement is shown schematically in Fig. 11.

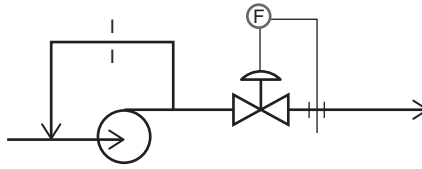


Figure 11 Pump outfitted for flow control and relief.

The pump has to expend extra energy in overcoming the pressure drop through the control valve, so it is advantageous to install the largest possible valve that still has enough range to regulate over the range of expected flow rates.

Every valve has a coefficient of flow CV such that when it is fully open

$$Q_v = CV \times [(\Delta P)_v]^{0.5} \quad (19)$$

where Q_v is the flow through the valve in units of gallons per minute, and $(\Delta P)_v$ is the pressure drop across the valve, expressed in units of pounds force per square inch.

For the present purpose it is desired to express Q_v in units of liters per second and pressure drop in meters of the flowing liquid, water:

$$Q_v = CVO \times [(\Delta H)_v]^{0.5} \quad (20)$$

where

$$CVO = 0.0752 \times CV \quad (21)$$

At any lesser opening

$$Q_v = cv \times CVO \times [(\Delta H)_v]^{0.5} \quad (22)$$

where cv is a fraction less than one. Note that cv is not the same thing as fraction of valve opening.

For the present purpose a valve should be chosen so the cv is high (e.g., 0.7) at maximum liquid flow and low (e.g., 0.05) at minimum flow. This choice can only be made in conjunction with the choice of the pump, and it also depends on the way in which system (e.g., piping) pressure drop depends on flow rate. The following stepwise procedure explains how to choose valve and pump. It is referenced to Fig. 12 where it is assumed that pump and valve are close enough to each other that the exit pressure of the pump is the entrance pressure of the valve. The calculations can easily be set up on a spreadsheet.

1. Determine the liquid density ρ , kg liter^{-1} , and choose the pump speed N , min^{-1} .
2. Determine the head at source H_S and destination H_D and the details of the piping upstream and downstream of the pump.
3. Specify the minimum and maximum liquid rates passing through the valve and reaching the destination, Q_N and Q_X , liters s^{-1} .

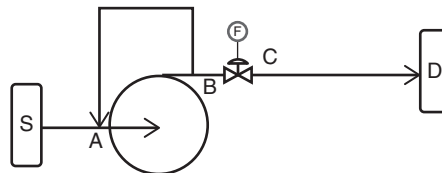


Figure 12 Pressure map in centrifugal pump system.

4. Specify the fraction, cv_N and cv_X (e.g., 0.05 and 0.7) of the fully open valve CVO for minimum and maximum throughputs.
5. Specify a ratio, f_{ret} , of return flow to pump design flow, Q_{OPT} . Suggested ratio is 0.15.
6. Choose a value for the pump rate of maximum efficiency, Q_{OPT} . A good choice is Q_X or a rate close to it.
7. For the minimum and maximum flow rates calculate the head upstream of the pump, Ha_N and Ha_X , and downstream of the valve, Hc_N and Hc_X .
8. Make an initial estimate of pump specific speed, N_S . It gets refined as part of the procedure.
9. Calculate q_N and q_X as $(Q_N + f_{ret} \cdot Q_{OPT})/Q_{OPT}$ and $(Q_X + f_{ret} \cdot Q_{OPT})/Q_{OPT}$, and for these values, find the values of h_N and h_X from the h -vs- q curve for the chosen specific speed [see Eqs. (15) to (18)].
10. Set up the valve equations for the two flows:

$$Q_N = cv_N \times CVO \times \{Ha_N + h_N H_{OPT} - Hc_N\}^{0.5}$$

and

$$Q_X = cv_X \times CVO \times \{Ha_X + h_X H_{OPT} - Hc_X\}^{0.5}$$

Solve for H_{OPT} as

$$\frac{(cv_N/Q_N)^2 (Ha_N - Hc_N) - (cv_X/Q_X)^2 (Ha_X - Hc_X)}{(cv_X/Q_X)^2 h_X - (cv_N/Q_N)^2 h_N}$$

11. Reestimate specific speed as $NQ_{OPT}^{0.5} H_{OPT}^{-0.75}$ where N is the (constant) speed at which it is intended to operate the pump, and return to step 9.
12. Calculate CVO from one or the other of the above two equations.
13. Calculate the return orifice coefficient CRET, liters s^{-1} meter $^{-0.5}$, as $f_{ret} \times Q_{OPT} \times (H_{DEADHEAD})^{-0.5} = f_{ret} \times Q_{OPT} \times (H_{OPT} \times A_0)^{-0.5}$ where A_0 is calculated in Eq. (16).

This calculation provides valve size CVO, pump design specs H_{OPT} and Q_{OPT} , and orifice coefficient CRET.

Table 2 shows the results, with reference to Fig. 12, for a specific case.

Using Eq. (21) the calculated CVO is converted back to CV in conventional units and a table of valve sizes and characteristics can be consulted. If the valve openings are unrealistic, then new values for cv_N and cv_X can be tried.

Effect of Viscosity on Centrifugal Pumps

Most centrifugal pumps are used for the movement of liquids of low, waterlike viscosity, and, in fact, performance curves are based on the pumping of water as the test liquid. For liquids of high viscosity direct-action devices such as screw pumps and gear pumps are employed. However, between low and high viscosity there is a gray area where a centrifugal pump may still be suitable. As would be expected, viscosity tends to interfere with the dynamic or momentum-imparting action of the pump. A quantitative assessment of these effects must be made. It has been found that it is the *combination* of viscosity, throughput, and head that determine the viscous effects. The Hydraulic Institute Standards provide a nomograph into which the values of these three variables is entered and from which three *attenuation factors* are received:

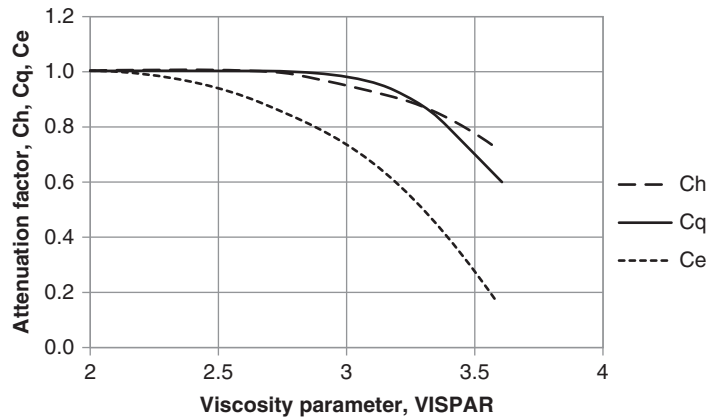
C_H , the fraction of the head that would be predicted for water that is actually attained

C_Q , the fraction of the throughput that would be predicted for water that is actually attained

C_E , the fraction of the efficiency that is predicted for water that is actually attained

Table 2 Specification and Results for Pump–Valve Combination

System Specification	Liquid Density, ρ (kg L ⁻¹)	Source Pressure, H_S (m)	Destination Pressure, H_D	Upstream Piping
	1.0	5	25	0.5 m, 8.5-cm pipe
	Downstream piping	Pump speed, N (rpm)	Minimum throughput, Q_N (liters s ⁻¹)	Maximum throughput, Q_X , (liters s ⁻¹)
	50 m, 12 cm pipe	1750	20	100
Control Settings	Fraction of fully open CVO at minimum throughput, cv_N	Fraction of fully open CVO at maximum throughput, cv_X	Ratio return flow to optimum pump flow, f_{ret}	Optimum pump flow (best operating point), Q_{OPT}
	0.05	0.7	0.15	40
Results	Pump head rise at optimum, H_{OPT}	Specific speed, N_S	Valve fully open coefficient, CVO	Return orifice coefficient, CRET
	40.9	685	85	0.91
	Point:	A	B	C
	Head at min. TP:	4.9	49.1	27
	Head at max TP:	4.4	38.2	37.5

**Figure 13** Viscosity effect on head, throughput, and efficiency.

Examination of the nomograph reveals that these three fractions (or *attenuation factors*) depend on a single nondimensional ratio:

$$VR = \eta^{0.5} Q^{-0.25} (H g)^{-0.125} \quad (23)$$

where η is the kinematic viscosity of the liquid, expressed in meter² second⁻¹ or in centistokes (10^{-6} m²s⁻¹) where water has viscosity 1 centistoke, Q is the desired volumetric throughput, H is the desired increase in head across the pump, and G is acceleration due to gravity.

The parameter

$$VISPAR = \log_{10}(K_V \eta^{0.5} Q^{-0.25} H^{-0.125}) \quad (24)$$

is related to VR and is conveniently used as the determinant of C_h , C_q and C_e , as seen in Fig. 13. The value of K_V depends on the choice of units for the variables. This is shown in Table 3.

Table 3 Units for viscosity parameter

η	Q	H	K_V
Centistokes	Gallons per minute	Feet	872.3
Centistokes	Liters per second	Meters	376.8
Centistokes	Cubic meters per second	Meters	67.01
Square meters per second	Cubic meters per second	Meters	67006
Square feet per second	Cubic feet per second	Feet	57758

The procedure for applying this method is:

1. Establish the desired throughput Q and head rise H .
2. Form the parameter VISPAR.
3. Find the values of the attenuation factors, C_h , C_q , and C_e , either from Fig. 13 or from Eqs. (25), (26), and (27)
4. Choose a pump for which, at best operating point, the water-based head is H/C_h and the water-based throughput is Q/C_q
5. Provide mechanical power at the pump equal to the water-based required *brake power* divided by C_e .

The curves of Fig. 13 are approximated by the following equations:

$$C_h = 1 - 0.00240 \times \text{Exp}(3 \times \text{VISPAR}) \quad (25)$$

$$C_q = 1 - 0.000680 \times \text{Exp}(4 \times \text{VISPAR}) \quad (26)$$

$$C_e = 1 - 0.0375 \times \text{Exp}(2 \times \text{VISPAR}) \quad (27)$$

By way of example, a pump with throughput 64.6 liters s^{-1} (1000 gpm) and head 30.48 m (100 ft) can tolerate a viscosity of 20 cst with only a 10% reduction in efficiency; a pump with 646 l s^{-1} and 183 m (600 ft) can similarly tolerate viscosity of 100 cst, i.e., 100 times that of water.

Kinematic viscosity equals dynamic viscosity divided by fluid density. Dynamic viscosity is the ratio of shear stress to shear rate and is what is measured by viscometers.

Pumping of Slurries

A slurry is a mechanical mixture of liquid and solid particles. A slurry may occur incidentally as when a liquid happens to contain some solids contamination, or it may be the form in which it is chosen to transport a solid, in which case the liquid may be incidental. The important characteristics of a slurry are:

- Solids concentration
- Particle size—microns to millimeters
- Particle shape—compact, flakey, stringy
- Particle and liquid densities—similar or disparate
- Particle abrasivity and particle friability

All of these considerations enter into the choice of a fluid mover. There are many companies that provide suitable equipment and also that provide useful manuals dealing with the technology of slurries. One of the key choices is whether a centrifugal pump can handle the flow or whether a direct action, positive-displacement device is needed. As part of assessing the

situation, it is necessary to determine the pressure losses in upstream and downstream piping and fittings that will occur with such a mixture since this will affect the required head rise from the pump.

Centrifugal pumping will generally suffer a loss of head capability and of efficiency, mainly because of modifications that must be made to accommodate the slurry. The most common steps to handle slurries are as follows:

- Operate at lower speed, typically less than 1200 rpm.
- As a result of the lower speed, specify a larger pump.
- Reduce the number of vanes to allow easier passage between them.
- Provide wider impeller-to-casing clearance to avoid clogging.
- Design for heavier duty of impeller, casing, and drive.
- Provide nonclogging seals.
- Provide replaceable sacrificial surfaces where abrasive wear is expected.
- Line some surfaces with rubber to cushion particle-to-surface impact.
- Recess the impeller if the particles are shear sensitive—let the vortex do the work.
- Provide an upstream gas separator if the slurry also contains dispersed gas.

1.2 Other Dynamic Pumps: Axial Flow, Mixed Flow, Jet

Centrifugal pumps are greatly dominant among pumps that operate on the dynamic principle. Two other types follow the same principle, one using mechanical power and the other powered by a second liquid.

Axial-Flow Pumps

One definition of an axial-flow pump is that the inlet and the outlet are collinear. This categorization would include “in-line” centrifugal pumps, pumps that have their inlet and outlet lines routed so that they line up with each other, but which are the same internally as any other centrifugal pump. The pumps considered in the present section operate on a different principle—that of *aerodynamic lift*—or on a combination of aerodynamic lift and centrifugal principles. The impeller, with its blades, is commonly known as a *propeller*. The propulsive pressure comes from the fact that when a thin solid body (i.e., the blades) and a fluid move relative to each other and when the body is inclined at a slight angle to the motion, there arises a mutual force F_L *perpendicular* to the direction of motion that is much larger than the force F_D in the direction of motion. These forces are illustrated in Fig. 14 for a body of aerodynamically favorable shape, by the

$$\text{Coefficient of lift} = C_L = 2F_L g_C \rho^{-1} U^{-2} A_p^{-1} \quad (28)$$

and

$$\text{Coefficient of drag} = C_D = 2F_D g_C \rho^{-1} U^{-2} A_p^{-1} \quad (29)$$

where ρ is the density of the fluid, U is the relative velocity between fluid and solid, and A_p is the area of the solid body projected in the direction of motion.

An axial-flow pump may operate in the open, as when it serves as the propulsion screw for a boat, in which case the blades are curved in such a way as to direct the forced liquid as directly backward as possible. More commonly an axial pump is enclosed. In this case the blades may have some component of radial thrust, producing a measure of centrifugal force so that the unit becomes a *mixed-flow* pump.

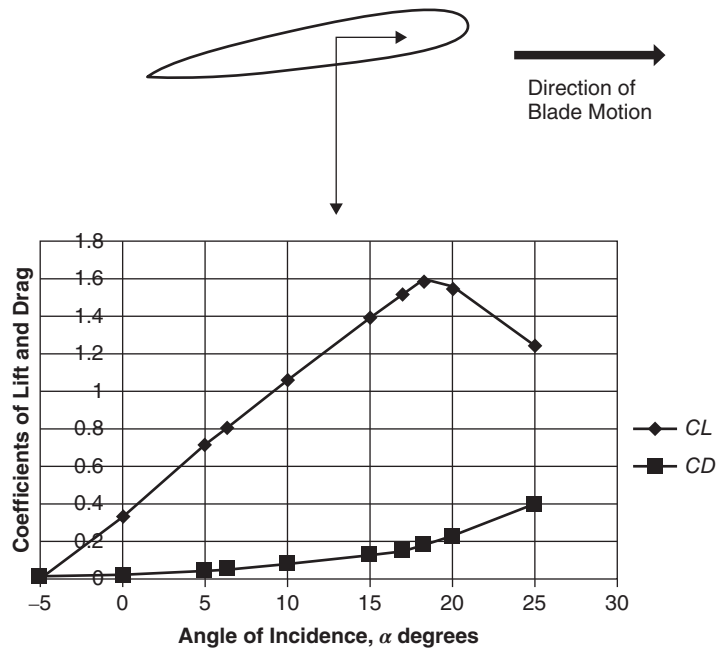


Figure 14 Aerofoil lift and drag.

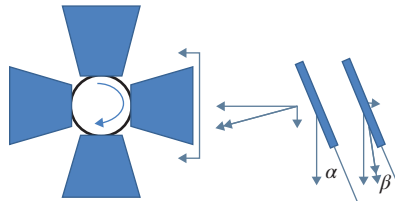


Figure 15 Effect of axial flow on lift.

As seen in Fig. 14, the lift force depends on the angle (*angle of incidence*) between the blade and its direction of motion relative to the fluid. When fluid begins to flow in the axial direction, the vector of relative motion changes in such a way as to reduce the angle of incidence. This effect is illustrated in Fig. 15. The result is that the head H developed by the pump decreases with throughput Q in much the same way as it does for centrifugal pumps. In fact the specific speed of axial pumps is generally high and, as seen in Fig. 9, the H -vs.- Q curve is quite steep.

Two common places where axial-flow or mixed-flow pumps are found are at the bottom of wells and in the jet-producing unit of personal watercraft. Application of these pumps is generally for uses where relatively high throughput and only moderate head are required.

Jet Pumps

Like the centrifugal and axial-flow pumps, the jet pump operates on the Bernoulli principle, but unlike those pumps it uses fluid power instead of mechanical power (Fig. 16). The fluid

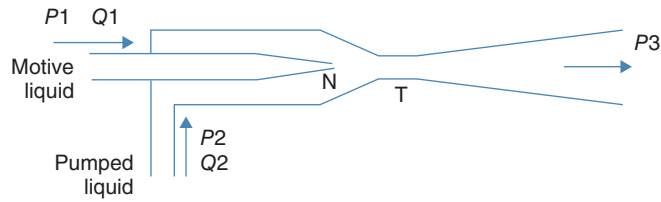


Figure 16 Liquid-flow eductor.

power is provided by a high-pressure *motive* liquid stream that accelerates through a nozzle to create a local zone of low pressure. The liquid that is to be pumped is drawn into this zone, and then the combined stream decelerates through a diffuser and rises to the desired intermediate pressure. Calculations are done to determine the pressure, P_1 and flow rate Q_1 of motive liquid that are required for the raising of Q_2 liquid flow from pressure P_2 to P_3 . The arrangement is shown schematically in Figure 16.

The performance of a jet pump is described by two equations:

$$\begin{aligned} \text{NUM} = & 2 \left(\frac{A_N}{A_T} \right) + 2 \left(\frac{\rho_2}{\rho_1} \right) \left(\frac{Q_2}{Q_1} \right)^2 \left(\frac{A_N}{A_T} \right)^2 \\ & - \left(\frac{A_N}{A_T} \right)^2 (1 + K_3) \left[1 + \left(\frac{Q_2}{Q_1} \right) \right]^2 - \left[\left(\frac{Q_2}{Q_1} \right) \left(\frac{A_N}{A_T - A_N} \right)^2 (1 + K_2) \right] \end{aligned} \quad (30)$$

and

$$\text{PR} = \frac{\text{NUM}}{1 + K_1 - \text{NUM}} \quad (31)$$

where ρ is liquid density of the motive and pumped liquids;

K is the number of heads lost due to friction in channels 1, 2, and 3;

PR is the pressure ratio $(P_3 - P_2)/(P_1 - P_3)$;

A_N and A_T are, respectively, the cross-sectional areas of the nozzle and throat. Recommended design is for an area ratio, A_N/A_T , of 0.2–0.3.

The pressure losses in the piping, reflected in the K values, lessen the efficiency of the pump and are kept low by shortening and streamlining the ports. Efficiency, Eff, is defined as

$$\text{Eff} = \frac{Q_2(P_3 - P_2)}{Q_1(P_1 - P_3)} = \text{PR} \left(\frac{Q_2}{Q_1} \right) \quad (32)$$

For choices of A_N/A_T equal to 0.2 and all K values equal to 0.1, the variation of PR and Eff with flow ratio Q_2/Q_1 is plotted in Fig. 17.

Consider a stream of water of 10 liters per second at absolute pressure 101.3 kPa, which is required to raise to 300 kPa using this jet pump. It is recommended that the pump be operated at a flow ratio 2/3 that of maximum efficiency in order to avoid the possibility of cavitation: in this case Q_2/Q_1 is set as 1.0. The corresponding value of pressure ratio, PR, is 0.3, so that

$$P_1 = \frac{390 - 101.3}{0.3}, \text{ i.e., } 962 \text{ kPa}$$

and

$$Q_1 = 10 \text{ liters s}^{-1}$$

1.3 Positive-Displacement Pumps

Positive-displacement devices constitute only a small fraction of all pumps but, in some situations, they are competitive, sometimes preferable, and sometimes essential. In the case of a

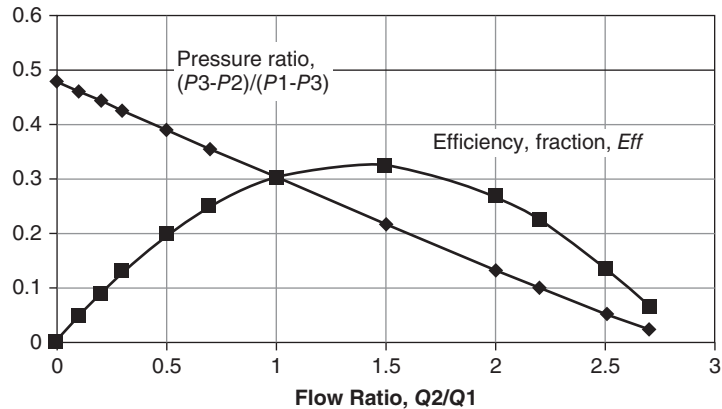


Figure 17 Performance of eductor.

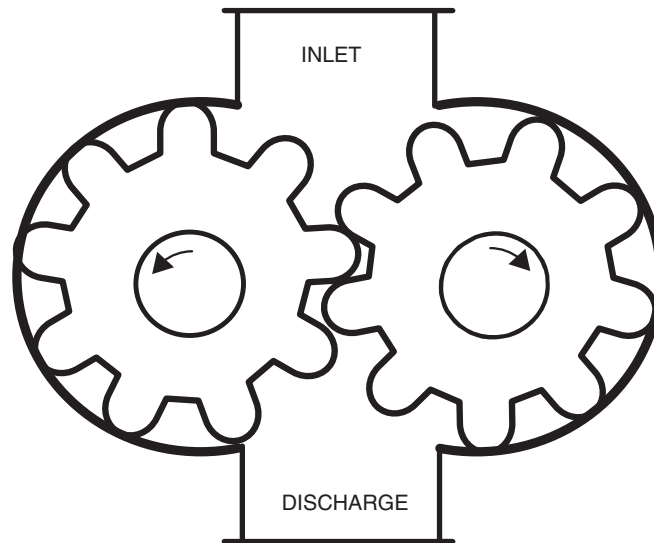


Figure 18 Gear pump.

highly viscous liquid the dynamically based pumps become inoperable. In the case of extreme head requirement a single-stage positive-displacement pump may be a good alternative to a multistage dynamic device. In the case where very precise control over delivery rate is needed, a positive-displacement pump with speed control may be chosen over a dynamic device with control valve.

Gear Pumps

The gear pump is a rotary device in which the liquid is impelled by intermeshing gears (usually two, as in Fig. 18), which trap and move the liquid in pockets around the casing wall. The effectiveness of the pump relies on tight clearances to avoid backflow of liquid between the gears or over the tips of the teeth or over the upper and lower surfaces of the gears. This leakage

depends directly on the head rise across the pump. The action of a gear pump is described by the following equation:

$$Q = \alpha N - \frac{\beta \Delta P}{\mu} \quad (33)$$

where Q is volumetric throughput; N is pump rotational speed; ΔP is pressure rise across the pump; μ is liquid dynamic viscosity; α is a geometric constant calculable from the number and size of the pockets of liquid carried around the casing during one rotation of the gears, and β is a constant that depends on the combined size of leakage paths.

It is desirable to keep the second term as small as possible. The value of β is difficult to predict and is accurately known only by test. If the pump becomes worn, β will increase. Gear pumps are widely used in the polymer industries where viscosities of thousands of pascal-seconds and pressures of tens of megapascals are common.

Screw Pumps

Screw pumps are much more varied in design and function than gear pumps. Some key facts are:

- Along with pumping they usually perform other tasks such as melting of solid feed material, blending, dispersion of solids into liquid, chemical reaction, and devolatilization.
- They are generally fed with some form of solid rather than a liquid.
- They often require heating or cooling along their length.
- They have three main types: single screw, twin co-rotating screw, and twin counterrotating screw.

Because of all these considerations, screw pumps constitute a major area of technology with applications mainly for high-viscosity liquids such as in the production and forming of plastics. They would rarely be used solely as pumps in situations where a gear pump would suffice, but their pumping characteristics are nonetheless of importance.

The single screw is the simplest and least expensive. A screw of this type is shown in Fig. 19. It comprises a spiral auger rotating with close clearance in a circular barrel. The screw turns in the direction that moves the liquid forward along the barrel, at a rate independent of liquid viscosity and of any pressure gradient. At the same time liquid is free to move backward along the screw channels, at a rate proportional to positive pressure gradient and inversely proportional to viscosity. The operation is described by the equation

$$Q = \alpha N - \frac{\beta x(\Delta P/\Delta L)}{\mu} \quad (34)$$

where $(\Delta P/\Delta L)$ is the pressure gradient along the pump and α and β are constants calculable from the geometry of the screw and its clearance with the barrel.

The screw is rotated at sufficient speed to satisfy the twin requirements of throughput and delivery pressure at its end. In practice, the depth and pitch of the screw thread may be

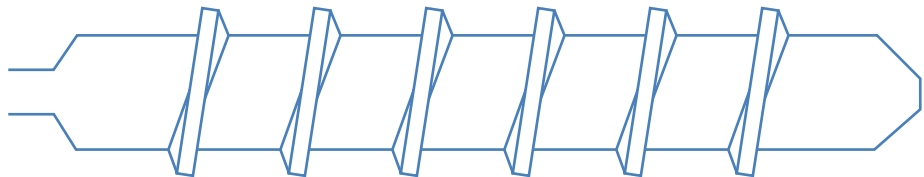


Figure 19 Single-screw extruder.

varied along the length, in order to achieve solids melting at the upstream end and pressure development at the downstream end. Screws of conical shape, with diameter decreasing along the length, are also used. Inverting Eq. (34) shows how pressure is built:

$$\Delta P = (\alpha N - Q) \left(\frac{\mu}{\beta} \right) (x \Delta L) \quad (35)$$

where ΔL is liquid-filled length.

A twin-screw *co-rotating* device is shown in Fig. 20. This pump has the same operating principle as the single screw and the same descriptive equation. Most of these pumps are intermeshing, such that the tips of each screw pass across the faces of the other screw. The cross section of a trilobal screw that accomplishes this goal is shown in Fig. 20. Other cross sections also can be made intermeshing. The advantage is that there is reduced opportunity for stagnation and buildup of degraded material on the screws. The extra expense of a twin-screw pump (or twin-screw “extruder”) is justified on other considerations than pumping, typically its ability to blend materials and to provide uniform residence time for chemical reaction. Along the screws the pitch may be varied, and sections of neutral and even reverse pumping may be provided. Because of this variation and the fact that there is a certain amount of trial and error in screw design, the screws are generally built up modularly from smaller elements slipped onto a splined shaft.

A different design of screw is used in twin-screw *counterrotating* devices. When fully intermeshing, this pump has no backflow apart from clearance leakage, and its throughput is simply proportional to the speed of rotation of the screws. Apart from its pumping capability, it is effective in dispersing solid particles in the viscous liquid, a step frequently required in plastics processing.

Progressive Cavity Pumps

This pump is also a screw-type rotational device, formulated on a principle devised by Rene Morneau in 1921 and, based on the name of the inventor, usually referred to as a Moyno pump. It consists of a single-helix rotor of circular cross section and a barrel or stator with internal wall formed into two intertwined helices. The rotor fits accurately into one of the two helices, say helix A. The centerlines of the stator helices are offset in such a manner that the rotor, at any instant, seals off a succession of cavities in helix B. As the rotor turns, these cavities *progress* axially and thus convey the liquid to the end of the pump. The direction is reversed if the rotation is reversed. The device can deliver high pressures. It can handle liquids of high viscosity as

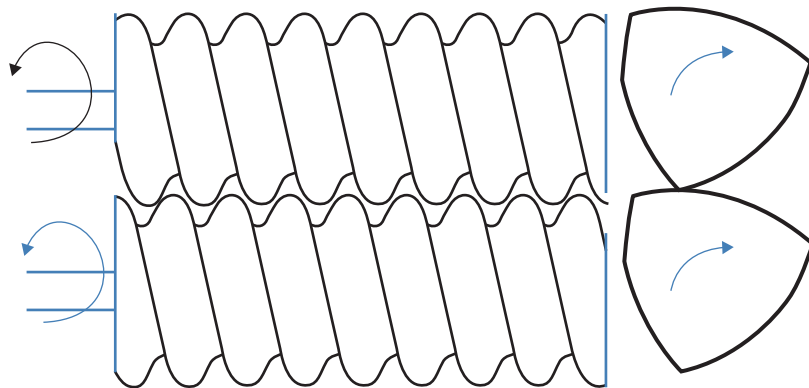


Figure 20 Twin-screw co-rotating extruder.

well as high concentration slurries including suspensions of stringy materials and of abrasive particles. The rotor is made typically of steel with a highly polished surface, and the stator is usually an elastomeric composition bonded to the inside of a metal casing. A progressive cavity pump is shown schematically in Fig. 21.

Peristaltic Pumps

The peristaltic pump mimics an action of the human body where materials are moved through various passages through the action of a sequence of muscle contractions. As shown in Fig. 22, the liquid is contained in an elastomeric tube and is pushed along by moving pinch points in the tube. The direction can be reversed by reversing the rotation of the rotor. There is no contact between rotor and liquid. This type of pump cannot handle high pressures or deliver significant rise in pressure.

Piston and Diaphragm Pumps

Piston pumps and diaphragm pumps operate with a reciprocating motion in which liquid is alternately admitted into a cylindrical space and then forced out into a region of higher pressure. The piston may be in actual contact with the liquid, in which case it fits with tight clearance into the cylinder in which it moves, or it may be separated from the liquid by a flexible inert diaphragm. The latter arrangement avoids leakage around the piston and avoids contamination of the liquid or corrosion of the piston. The piston type is illustrated in Fig. 23. The action

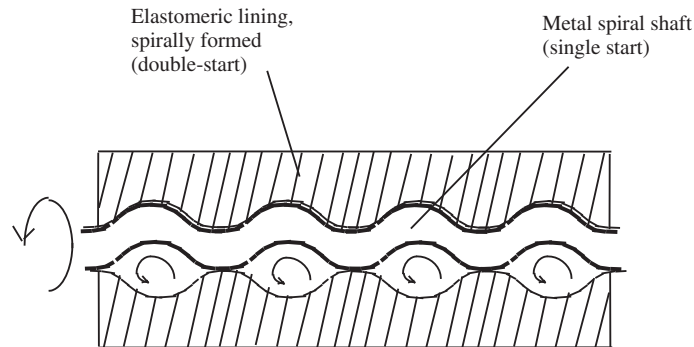


Figure 21 Moyno-type pump.

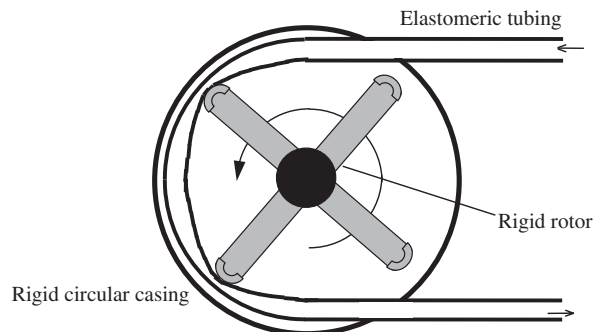


Figure 22 Peristaltic pump.

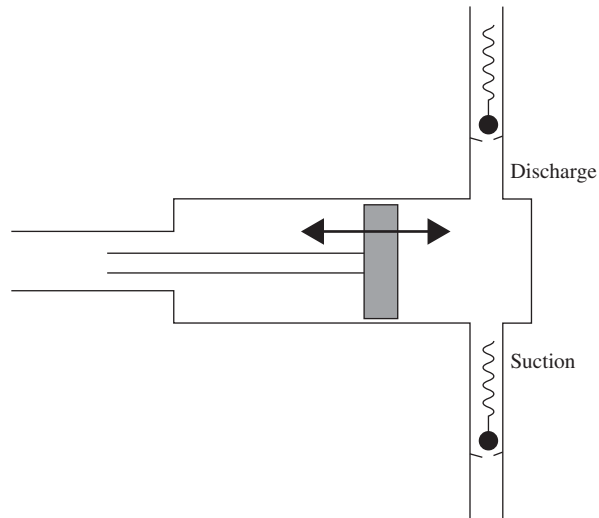


Figure 23 Piston pump.

is made possible by the use of check valves at the entrance and exit of the pump, the valves opening only when they experience a higher pressure upstream than downstream. This type of pump is not suitable for liquids of very high viscosity, which would impede the action of the valves.

The throughput of a reciprocating pump may be changed in two ways: on the short term by varying the speed of reciprocation and on the longer term by varying the stroke length or chamber size. Sometimes a group of liquids are being supplied to a common destination, with fixed proportions to one another but with varying overall rate. One arrangement is to have each liquid fed by an individual reciprocating pump, with cylinder diameter chosen for its average rate, and with all pumps operating at the same speed set by a common drive. If it is desired to change the proportions from time to time, this can be done by adjusting the stroke length of selected pumps.

It may be necessary in some applications to install a pulsation dampener downstream of the piston or diaphragm pump because of the intermittency of the output, which goes from zero to as much as π times the average flow during each cycle of reciprocation. The maximum flow in this cycle should be used to calculate pressure drop on the inlet side in determining net positive suction head.

2 GAS MOVERS

Gases and liquids share the common designation of *fluids*, and they share many of the same methods of being moved. However, there are several differences in their characteristics that make the technology different:

- Gases are compressible, unlike liquids which have close to constant density even under conditions of extreme pressure.
- In moving a gas there may be appreciable $\int P dV$ work of compression.
- The work of compression may be accompanied by significant temperature rise.

- Pressures can range from high vacuum, e.g., 10^{-6} atmospheres absolute to as high as anything encountered in liquid transport, e.g., 10^4 atmospheres, giving an overall range of 10^{10} .
- If the gas is a vapor, that is, if it is below its critical temperature, then compression may bring on liquefaction.

A key parameter is CR, the compression ratio, $P_{\text{DISCHARGE}}/P_{\text{INLET}}$, P_2/P_1 , where the pressures are absolute. If the gas is ideal or if its compressibility factor Z is close to constant, then the ratio of absolute temperatures entering and leaving is given by

$$\frac{T_2}{T_1} = \left(\frac{P_2}{P_1} \right)^{(\gamma-1)/\gamma} \quad (36)$$

where γ is the ratio of specific heat at constant pressure to specific heat at constant volume and is around 1.4 for many common gases.

The consequences of this relation can be seen in Table 4.

Two observations may be made:

- For large compression ratios, overheating may cause (a) damage to the equipment, (b) higher gas volumes that lower the efficiency of the operation, and (c) possibly dangerous conditions in the gas. Cooling is required and, in multistage compression, cooling must be done between stages.
- For small pressure ratios, it may be permissible to ignore these effects.

In fact, small pressure ratios are found in many gas movers, namely the *fans* and *blowers*. Although the demarcation is arbitrary, one definition has fans operating at CR up to 1.1, and blowers from 1.1 to 1.2. For the present discussion all these devices are denoted simply as fans. Fans (including blowers) are dynamic (as opposed to positive displacement) devices and come in two types, centrifugal and axial. As with pumps, there are fundamental differences between the two types and, as with pumps, they are considered separately.

Compressors are considered to start at ratios above 1.2 or 1.3. In general the devices are mechanically driven, and they comprise both dynamic and positive-displacement types. Another gas mover/compressor is the *ejector*, a nonmechanical system in which a high-pressure motive gas entrains a gas stream of lower pressure and produces a combined stream of intermediate pressure. The ejector is similar to the liquid-flow *eductor* but is more powerful because of the ability of the motive gas to become supersonic and assume extremely low pressure.

The areas of operation of the various classes of device are shown in Fig. 24, where the logarithm of discharge absolute pressure P_2 is plotted against the logarithm of inlet absolute pressure P_1 . The pressure unit of *atmospheres* is chosen so that the origin is at 1 atmosphere.

Table 4 Temperature Rise in Gas Compression

Compression Ratio, P_2/P_1	Temperature Ratio, T_2/T_1	Temperature rise for T_1 of 273 K
1.05	1.014	3.8
1.2	1.05	14.6
1.3	1.078	21.3
2	1.22	60
5	1.58	159

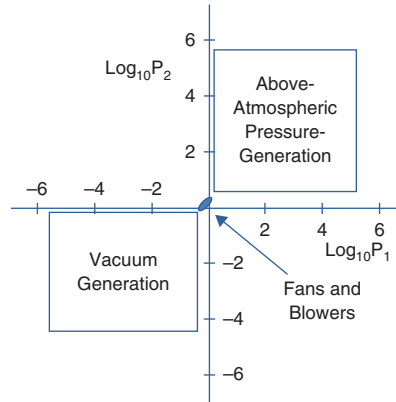


Figure 24 Pressure ratio map.

2.1 Fans and Blowers—General

The term *blower* is used in different ways by workers in the gas-moving business. In the present account blowers are simply included with fans as devices of low compression ratio.

Although fans (and blowers) occupy only a tiny fraction of the space in Fig. 24, they make up a large fraction of gas movers. They are similar in many ways to the centrifugal and axial pumps that are used for liquids. Many of the same relationships carry over, based on the fact that at low ratios of discharge pressure to entrance pressure the density may be considered constant, either at the inlet value or the discharge value or at an average of the two.

In the present account no distinction is made between the terms *fan* and *blower* and all are referred to as fans. The criterion for distinguishing between these devices and *compressors* has been proposed by the International Standards Organization as the mechanical energy, W_f , expended per unit weight of flowing gas. Fans (i.e., including blowers) are considered to be those devices having a value less than 25,000 J/kg.

Thermodynamics teaches that, in the most general case, the work or energy required is

$$W_f = P_2 V_2 - \left(P_1 V_1 + \int P dV \right) = \int V dP = \int \left(\frac{1}{\rho} \right) dP \quad (37)$$

where V is the specific volume of the gas, i.e., the volume per unit mass, $\text{m}^3 \text{kg}^{-1}$, and ρ is the density of the gas.

If density is assumed constant, then

$$W_f = \left(\frac{1}{\rho} \right) (P_2 - P_1) = \left(\frac{1}{\rho} \right) \Delta P \quad (38)$$

and the power expended by the device is

$$\text{Pwr} = W W_f = W \left(\frac{1}{\rho} \right) \Delta P = Q \Delta P \quad (39)$$

where W = weight flow
 Q = volumetric flow, $\text{m}^3 \text{s}^{-1}$
 ΔP = pressure rise, Pa
 Pwr = power, W

Alternatively,

$$\text{Pwr (horsepower)} = 0.000157 Q \text{ (cubic feet per minute)} \Delta P \text{ (inches of water)} \quad (40)$$

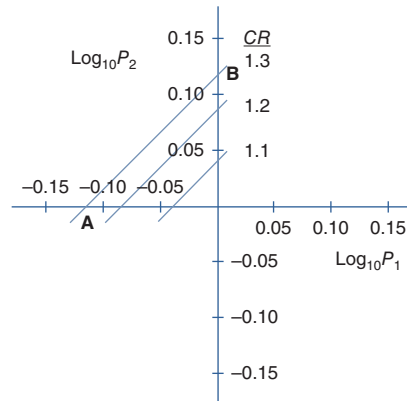


Figure 25 Pressure ratios for fans and blowers.

From Eq. (38) it is seen that the ISO definition requires a fan to have a pressure rise ΔP no greater than $25,000\rho$. Considering the very common case of air being moved at a pressure in the vicinity of one atmosphere absolute, the density is 1.2 kg m^{-3} , so the maximum allowed pressure is 30,000 Pa. The compression ratio, CR, is $(101,325 + 30,000)/101,325$ or 1.3. Table 4 shows a temperature rise of 21°C .

Figure 25 is an abbreviated version of Fig. 24, showing the combinations of inlet and discharge pressures, P_1 and P_2 , typical of fans. Two common situations are denoted by points A and B. Point A shows a fan exhausting gas from a subatmospheric region and discharging to atmospheric pressure. Point B shows a fan forcing gas from atmospheric pressure into a region above atmospheric. Both operations are seen to be occurring at a compression ratio of 1.3. Between points A and B are other less likely possibilities, also at CR of 1.3, where gas is being moved from below atmospheric to above atmospheric pressure. Operations at lesser values of CR are shown by the other two loci lines.

2.2 Centrifugal Fans

Centrifugal fans (and blowers) are entirely analogous to centrifugal pumps. They use a vaned rotor to impart rotational velocity and centrifugal force to the gas, which is opposed by pressure exerted by the fan casing. The gas undergoes a 90° change in direction, entering at the center of the rotor and leaving tangentially from the outer periphery of the casing. A typical fan and impeller is shown in Fig. 26.

The vanes can take one of five different forms, as shown in Fig. 27. Qualitative performance curves are shown for each style of vane, where SP is *static pressure*, which is the term used in practice to denote the pressure rise across the fan, i.e., ΔP , BPwr is *brake power*, which is the term used in practice to denote the power delivered to the rotor impeller, and Q is volumetric throughput of gas.

The characteristics of the various vane types are described as follows:

- Radial vanes
 - Simple, robust, inexpensive
 - Wide range of applicability and in common use
 - Can handle significant particulate load without fouling
 - Relatively low speed of operation
 - Stable because of no region of rising SP with throughput

- Relatively low efficiency
- Monotonic increase in power requirement with throughput, making it important to provide adequate drive power
- Backward inclined vanes
 - In common use
 - Quiet
 - Good efficiency
 - Falling power requirement at high throughput
 - May be straight or curved
- Aerodynamically shaped vanes
 - A streamlined version of the backward inclined vanes
 - Better efficiency and quietness
 - More expensive to make
- Forward curved vanes
 - Operate at lower speed than other types
 - Quiet
 - Used for medium throughputs at low SP
 - Monotonic increase in power requirement with throughput
 - Complex SP-vs.- Q relation, important to operate in the falling SP region
- Radially tipped vanes
 - A hybrid between radial and backward inclined
 - Efficiency is better than that of radial vanes
 - Can handle moderate particulate load
 - Monotonic increase in power requirement with throughput

The fan shown in Fig. 26 is equipped with curved backward inclined vanes.



Figure 26 Centrifugal fan with impeller.

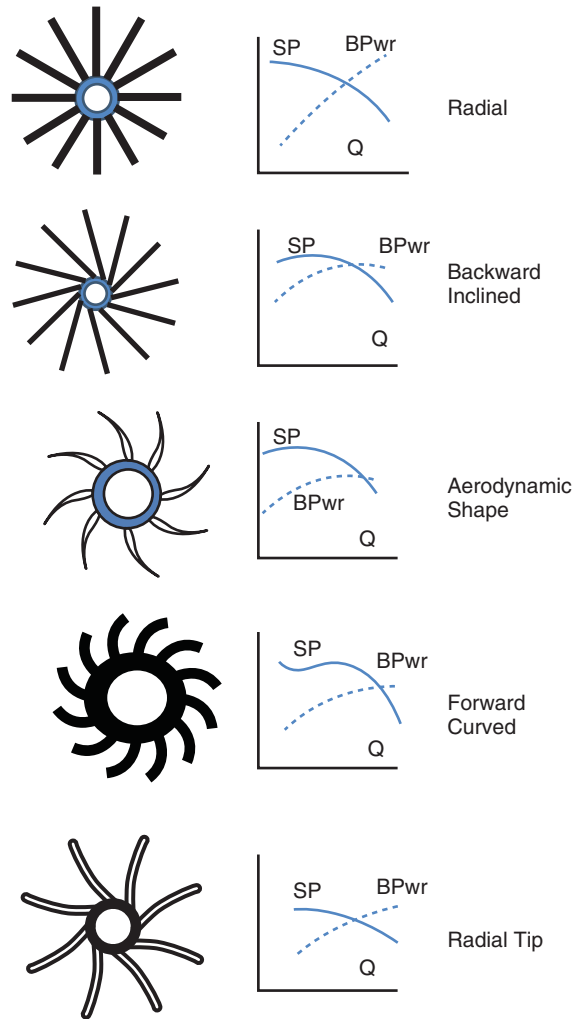


Figure 27 Centrifugal fan vane types.

Fundamental Relationships for Centrifugal Fans

For a centrifugal pump, Eq. (1) related the zero-flow (or “dead-head”) pressure rise to fluid density ρ , speed of rotation N , and impeller diameter D . The same equation applies to centrifugal fans. An indication of the accuracy of this prediction is shown in Table 5.

Similarly, Eq. (4) applies to fans, showing the square-law decrease in pressure generation with throughput. Similarly to pumps, these relationships lead to three *affinity laws* that describe a fan operating at a fixed fraction of zero-throughput SP, including the optimal or best-operating condition:

$$\text{SP is proportional to } \rho N^2 D^2 \quad (41)$$

$$Q \text{ is proportional to } D^3 N \quad (42)$$

$$\text{Pwr is proportional to } \rho N^3 D^5 \quad (43)$$

This optimal or best-operating condition occurs where the efficiency, Pwr/BPwr , is at a maximum, generally about $\frac{1}{4}$ to $\frac{1}{3}$ of the way down the SP-vs.- Q curve.

Table 5 Prediction of Zero-Throughput Pressure Rise in Centrifugal Fans

Gas Density, ρ	Rotational Speed, N	Impeller Diameter, D	Pressure Rise From Eq. (1)	Measured Pressure Rise
kg m^{-3}	s^{-1}	m	Pa	Pa
1.2	53.4	0.305	1047	1269
1.2	22.1	0.762	1120	1269

Table 6 Speed and Power Requirement for Centrifugal Fan

Air Flow	Static Pressure, SP , Pascals					
	125		500		2000	
	Speed of Rotation	Brake Power	Speed of Rotation	Brake Power	Speed of Rotation	Brake Power
$\text{m}^3 \text{s}^{-1}$	s^{-1}	kW	s^{-1}	kW	s^{-1}	kW
4.0	11.3	1.0	14.8	2.6	27.3	12.0
5.2	14.1	1.8	16.8	3.7	27.2	13.9
7.1	18.3	3.7	20.5	6.2	28.3	17.7
8.3	21.3	5.5	23.2	8.4	30.0	21.0

The affinity laws lead to a *specific speed* for fans, defined in nondimensional form as

$$N_S = NQ^{0.5}[\rho(SP \times g_C)^{-1}]^{0.75} \quad (44)$$

- where N = rotor speed, s^{-1}
 Q = gas throughput, $\text{m}^3 \text{s}^{-1}$
 ρ = gas density, kg m^{-3}
 SP = pressure rise, Pa
 g_C = conversion, $\text{kg m s}^{-2} \text{N}^{-1}$, which is 1.0

In other units

$$N'_S = N(\text{rpm})[Q(\text{ft}^3/\text{min})]^{0.5} \times \{\rho(\text{lb}/\text{ft}^3) \times [SP(\text{inches of water})]^{-1}\}^{0.75} \quad (45)$$

N_S and N'_S are related as

$$N'_S = 21602N_S \quad (46)$$

Performance of Centrifugal Fans

The purchaser of a fan has specific requirements for throughput and pressure rise, and so the supplier of fans provides performance information that allows the buyer to determine rotational speed and brake power to meet these requirements with various models and sizes of fans. Table 6 shows typical data, in abbreviated form.

By examining similar tables for a range of fans, the purchaser and supplier are able to arrive at the best choice.

This mode of presentation is useful for choosing a fan but not for understanding the fundamentals of the operation. The data were originally taken by the manufacturer from testing with a range of airflows and rotor speeds and measurement of the resulting static pressure and

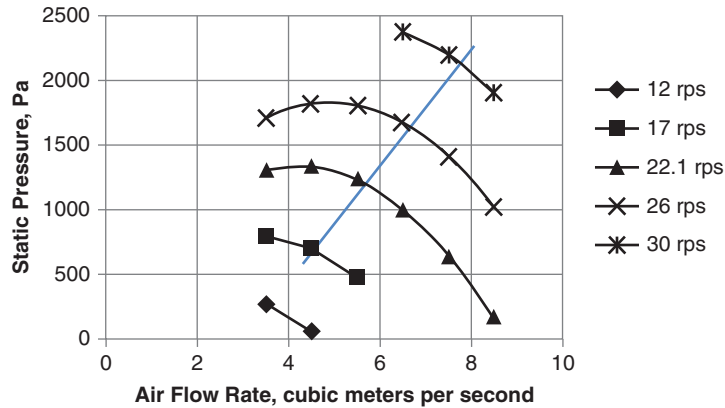


Figure 28 Effect of speed on fan head.

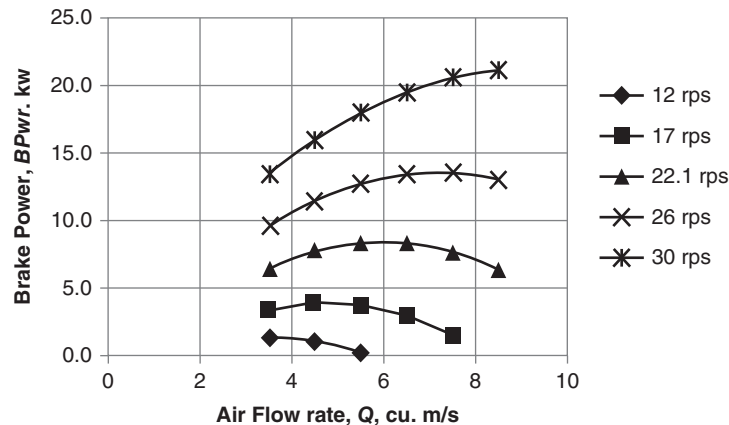


Figure 29 Effect of speed on fan brake power.

brake power. The air would be at *standard conditions*, 68°F, 14.70 psia, 36% relative humidity. The table can be reversed to recover the original form, as shown in Figs. 28 and 29.

The SP-vs.- Q curves display roughly the square-law decrease in pressure with throughput. The straight-line locus drawn on each plot corresponds to the optimal, maximum-efficiency or best-operating condition for each fan speed. In Fig. 28 the ratio SP/N^2 and the ratio Q/N stay approximately constant for the five curves, indicating agreement with *affinity laws* 1 and 2. In Fig. 29 the ratio $BPwr/N^3$ is close to constant, agreeing with *affinity law* 3.

Figure 30 shows, for one fan speed, the comparison of brake power BPwr with power actually transmitted to the gas, i.e., $Q \times SP$, along with the efficiency, which is the ratio of the two.

For the same style of fan but at one-half the diameter, a similar calculation may be done and, when the data for the two fans are compared, the ratios SP/D^2 , Q/D^3 , and $BPwr/D^5$ stay constant, again in agreement with *affinity laws* 1, 2, and 3, respectively.

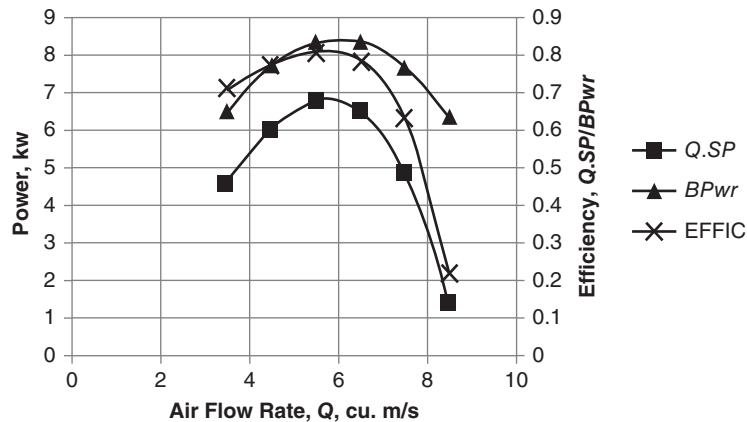


Figure 30 Centrifugal fan power and efficiency.

It should be noted that the data in the performance tables are for the flow of air. Air at standard conditions of temperature and pressure and at a density of 1.2 kg m^{-3} or 0.075 lb ft^{-3} is the standard test gas. If gas at a different density ρ is to be moved, then the following procedure is applied to the supplier's tables (e.g., Table 6):

- Given that the requirement is for throughput Q and pressure rise SP .
- Multiply SP by $1.2/\rho$ and obtain SP' .
- Enter the table with Q and static pressure SP' and determine the required speed N and a value for brake power $BPwr'$.
- Multiply $BPwr'$ by $\rho/1.2$ to determine $BPwr$, the required brake power.

This procedure is consistent with the way in which density appears in the affinity laws.

Control of Centrifugal Fan Throughput

A fan forms part of a larger system in which other parts also have an influence on the pressure profile. There may be a difference in pressure between the source and destination of the flow and there may be frictional pressure losses that generally vary as approximately the square of flow rate. The pressure requirement of the system, apart from the fan, can be represented as a function of throughput on a "system" curve on the same plot as the pump SP -vs.- Q characteristic is represented. Figure 31 shows two such curves, Syst.1 and Syst.2 along with performance curves of the fan for different fan speeds (from Fig. 28).

Because the fan's pressure must match the system losses, the point of operation is where the fan and system curves intersect. If the indicated throughput is not what is desired, then there are three ways of altering the overall system to make it so:

- Change the speed of the fan. If the change is to be infrequent, changes can be made to the drive gearing or pulleys. If the change is to be continuous, then a variable-speed drive is needed.
- Downstream: Install an adjustable louver downstream of the fan, to provide an additional source of pressure loss, which can be varied to move the system curve up and down. This is the option that was examined for liquids, where a pump-and-valve combination allowed continuous adjustment of flow by manipulating the valve. The disadvantage is that energy is wasted in pressure loss through the louver.

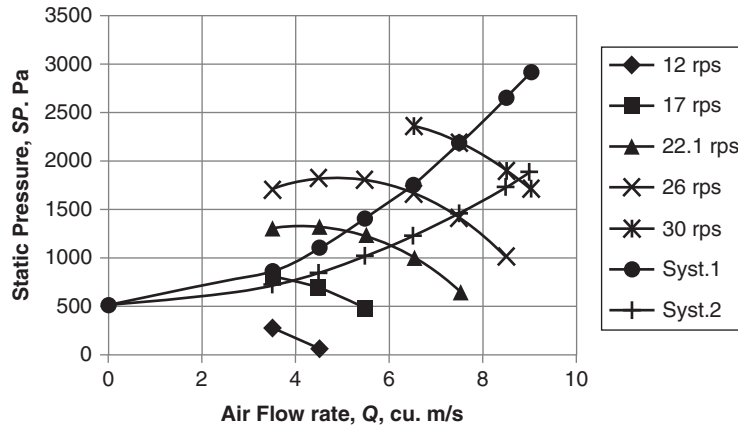


Figure 31 System and fan interaction.

- Upstream: Install an adjustable louver or, better, have the supplier equip the fan with inlet vanes, which cause swirl in the incoming flow and weaken the ability of the fan to develop pressure. For a given fan speed the SP-vs.- Q curve is bent more sharply downward. An advantage is that, compared with louvers, the power requirement is actually reduced.

2.3 Axial-Flow Fans

As was seen with liquids, it is possible to move a fluid using an impeller designed on the principle of aerodynamic lift. The principle is shown in Fig. 14. The main motion is in the same direction as the axis of rotation, hence the designation *axial flow*. Gases are also moved in this manner. As was seen with liquids, axial-flow gas movers also display the same decrease in head with throughput and the same affinity laws as centrifugal devices. The specific speed of axial fans is high because they tend to be movers of gas rather than builders of pressure.

Axial Fan Types

Axial fans have three general types: propeller, tube axial, and vane axial. Propeller fans are common as domestic air movers with no requirement for generating pressure. They may be completely in the open or they may be equipped with a stationary plate extending out from the periphery to help reduce backflow. Static pressure rise is 1 in. of water or less. Large fans of this type are used industrially to impart velocity to air to make it more effective in heat exchange or in cooling towers.

A tube-axial fan is shown in Fig. 32. It is mounted in a tube, which provides better directionality and which allows pressures of 3–4 in. of water to be generated. The ends of the tube are streamlined to minimize friction losses and the unit is intended to be connected into a more extensive system of piping.

Vane-axial fans deal with the fact that the drag force of the impeller blades, while small compared to the lift force, is enough to impart tangential swirl to the gas. As seen in Fig. 14, the drag force becomes larger the higher the angle of incidence is set, and the angle of incidence is desired to be high to achieve lift and capacity. The vane-axial fan adds, to the tube-axial design, a set of vanes in the surrounding tube. These vanes not only counteract the tangential component but also convert some of it into the desired axial motion. This feature allows the angle

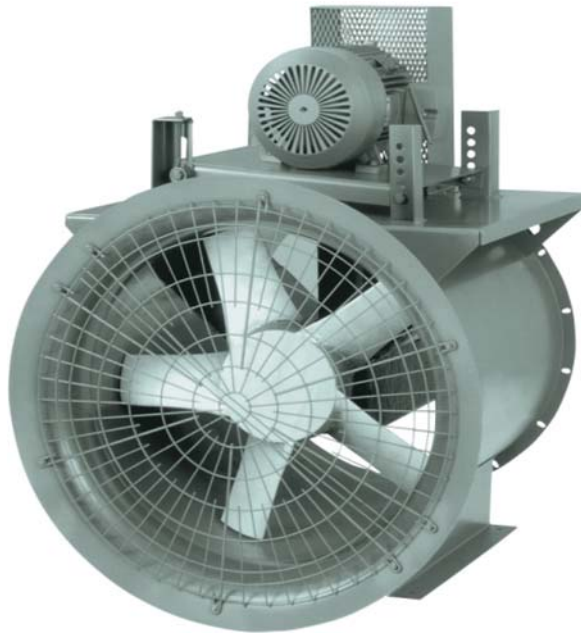


Figure 32 Tube-axial fan.

of incidence to be set close to a maximum and it imparts a somewhat higher head capability compared with nonvaned tube-axial fans.

In fan parlance the “angle of incidence” is referred to as the *pitch* of the blades. Some manufacturers provide choice of pitch in their commercial offerings. In the case of some large fans the capability of pitch adjustment is provided, either manually when the fan is shut down or, more ideally, online during operation.

Flow Control of Axial Fans

Centrifugal fans were seen to have three ways of controlling their throughput: speed manipulation, downstream adjustable louvers, and inlet vane swirl interference with pressure development. Axial fans use the first two methods, with their respective advantages and disadvantages, and they have a third manipulatable variable, namely blade pitch. Figure 33 is taken from Monroe³ and shows the performance of a specific axial fan operating with different pitches. Also shown is a “system line,” the intersection of which with the fan curves defines the conditions of operation. If the fan has been delivering $140 \text{ m}^3\text{s}^{-1}$ with pitch at 14° and is then required to cut back to 115, Fig. 33 shows two ways of doing so. One is to shift the location of the system line by further closing of a downstream louver. The operating condition moves from point A to point B', with considerable increase in brake power. On the other hand achieving the throughput reduction by reducing the blade pitch to 6° avoids the wasteful increase in static pressure and brake power caused by louvers.

2.4 Ejectors

Ejectors, sometimes known as *thermoc compressors* or *re-compressors*, accomplish the feat of combining two gases or vapors of unequal pressure into a single stream of intermediate pressure. *Eductors* do the same for liquids. Both operate by accelerating, in a nozzle, a high-pressure

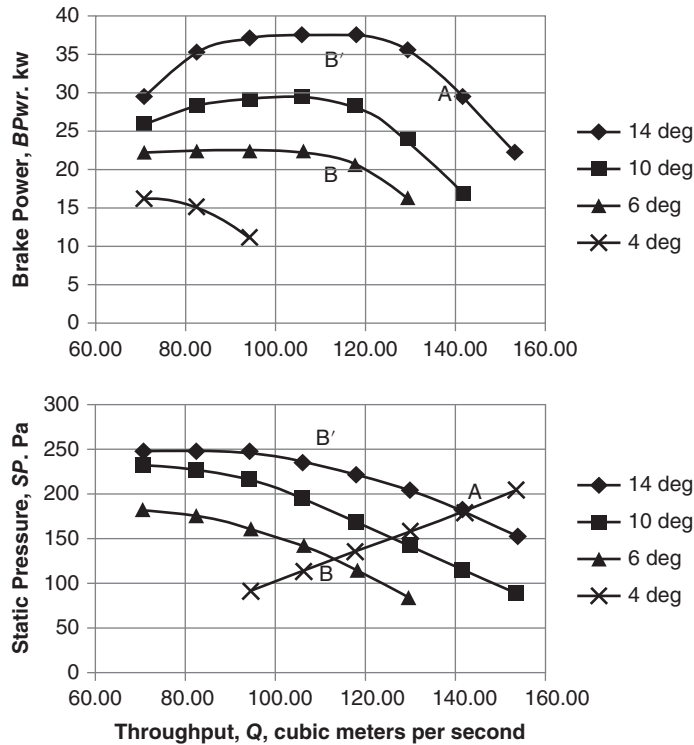


Figure 33 Axial fan vane-angle flow control.

stream of *motive fluid*, which creates a zone of sufficiently low pressure that the lower-pressure stream is drawn into it. The mixed fluid then passes through a divergent zone to recover some of the pressure. Both devices observe Bernoulli's principle, but the ejector has the added feature that the density of the gas varies almost directly with the pressure. The device is designed so that the motive gas reaches sonic velocity in the nozzle so that, after the nozzle, it becomes supersonic with attendant ultralow pressure. The arrangement is shown schematically in Fig. 34, including an indication of how velocity and pressure vary along the path of flow. The ability to enter the sonic and supersonic region makes the ejector a more powerful device than the eductor.

Ejectors are used primarily in two situations:

- Raising the pressure of waste streams in order to reuse them
- Creating and maintaining vacuum

Typical of the first application is the combination of plant waste steam at atmospheric pressure with high-pressure steam (e.g., at 2000 Pa) to make a combined stream of sufficient pressure (e.g., 250 kPa) to be useful in area heating. All pressures are absolute.

The second application is the more common, where ejectors compete with other methods of achieving vacuum. The lack of moving parts and the low cost make ejectors competitive. Steam is the preferred motive fluid, particularly if ejectors are to be used in series, which requires condensation of most of the steam between the stages. An example of such an arrangement is shown in Fig. 35.

Ejectors can be designed with reasonable confidence. The chief variable is the ratio of the area of the throat to the area of the nozzle, A_T/A_N . The right-hand part of the graph in

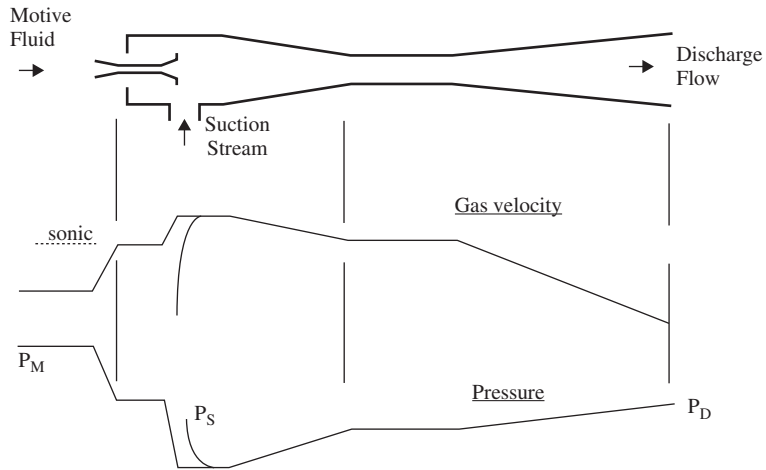


Figure 34 Ejector.

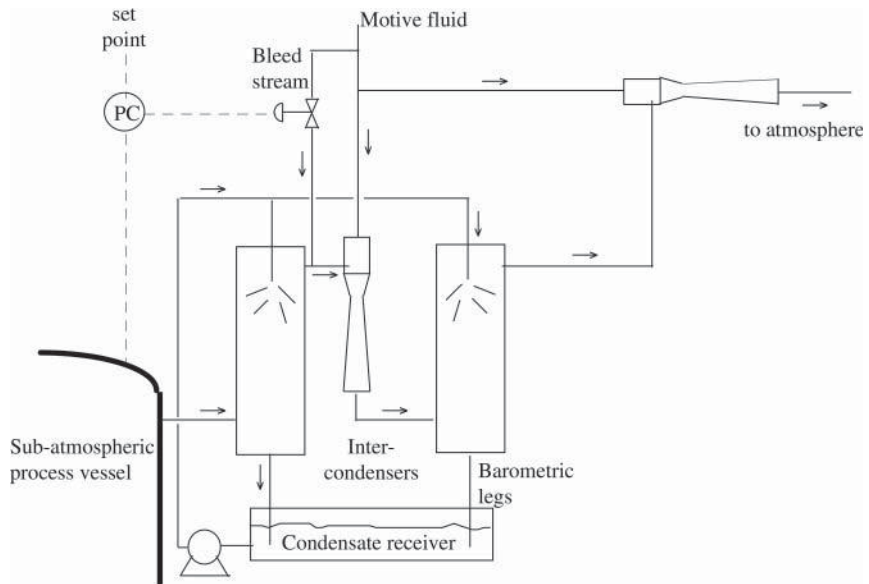


Figure 35 Two-stage ejector with condenser.

Fig. 36 is used to determine the value of this ratio, based on the ratio of discharge pressure to suction pressure P_D/P_S and the ratio of suction pressure to motive pressure P_S/P_M . For this combination of A_T/A_N and P_S/P_M the left-hand part of the graph indicates what is the ratio of suction to motive weight flow. Two examples may be helpful.

Vapor Recompression

A plant has a stream of waste steam at atmospheric pressure (101.3 kPa abs) and wishes to recompress it to 20 lb in.⁻² gauge or 239 kPa absolute. A high-pressure source of steam is available at 250 lb in.⁻² gauge, or 1825 kPa abs. The recompression will therefore have P_D/P_S

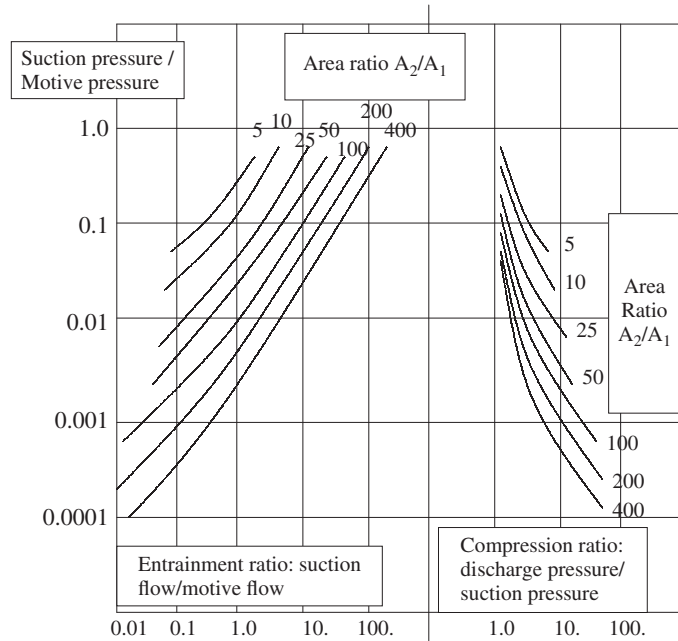


Figure 36 Ejector performance map.

of 239/101.3, i.e., 2.4 and P_S/P_M of 101.3/1825, i.e., 0.056. The right-hand side of Fig. 36 specifies an area ratio A_T/A_N of 20. From the left-hand side of the graph it is determined that approximately one weight unit of motive steam will be required for each weight unit of waste steam.

Vacuum Generation with Ejectors

Consider the two-stage ejection system shown in Fig. 35. Assume that steam is being handled and that essentially all the steam from the first stage is condensed in the interstage condenser. The absolute pressure is to be 10 mm Hg abs, the motive steam is at 1000 kPa or approximately 7500 mm Hg abs, and the final discharge pressure is atmospheric, 760 mm Hg abs. Design of the two individual ejectors requires a choice of intermediate pressure. This value would be chosen on the recommendation of the supplier but, for interest, a value of 150 is tested. The results are shown in Table 7.

For sizing, the following two relationships may be used:

$$W_M = 146,000 P_M A_N (T_M)^{-0.5} \text{ if air is the motive fluid} \tag{47}$$

$$W_M = 113,000 P_M A_N (T_M)^{-0.5} \text{ if steam is the motive fluid} \tag{48}$$

Table 7 Ejector Staging in Vacuum Service

Stage	Entrance Pressure, P_S	Exit Pressure, P_D	P_D/P_S	P_S/P_M	A_T/A_N	W_S/W_M
	mm Hg abs	mm Hg abs				
1.	10	150	15	0.0013	71	0.032
2.	150	760	5.1	0.02	15	0.110

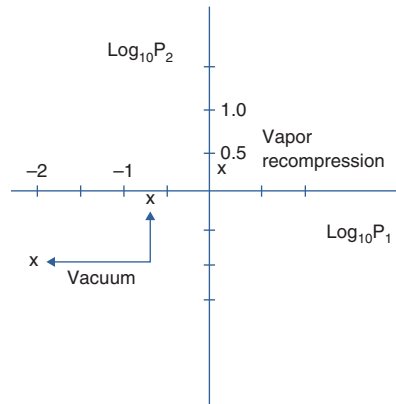


Figure 37 Pressure ratios for ejector systems.

For the ejector in the first example and the two ejectors in the second example, the locations on the discharge-versus-inlet pressure plot are shown in Fig. 37.

2.5 Compression

The determinant of whether a gas mover is a fan, blower, or compressor is the compression ratio CR. CR of 1.3 or greater is a reasonable starting point for compressors. The actual pressures may be below or above atmospheric. Ejectors qualify as compressors and, as was seen, they may be used in ranges both below and above atmospheric. Seven mechanical devices are commonly used for compression. Three of them are used mainly for vacuum service and are considered first.

Vacuum Generation

The need for vacuum or subatmospheric pressure can take several forms. It may be transient, where a region needs to be “pumped down” to a low pressure. It may be low volume, where vacuum must be held in the face of slight infiltration of outside gas. It may be steady, where gas continuously enters or is generated within the region. It may be mild, where the absolute pressure is a significant fraction of one atmosphere or it may be “hard,” where the absolute pressure is 1 mm Hg or less. Vacuum may be expressed quantitatively as the difference between atmospheric and system pressure or it may be expressed as the system absolute pressure: atmospheres, millimeters of mercury, pascals. The latter convention, absolute pressure, is used here. Three devices are described. First, it should be noted that staged ejectors, already described, are capable of producing absolute pressures as low 0.003 mm Hg abs or 0.4 Pa. With six stages, this implies an average CR per stage of 8.

Rotary Lobe Two or more rotors, each with two or more intermeshing lobes, trap the gas on the suction side and deliver it to a higher pressure destination. The original version is the Roots Blower. They can be used to generate pressures up to 2 atm absolute and to generate vacuum as low as 60 mm Hg abs (8000 Pa, 0.08 atm). Capacities are from 30 to 30,000 ft³/min, 0.015–15 m³s⁻¹. A schematic is shown in Fig. 38.

Rotary Sliding Vane The rotor in this compressor is eccentrically mounted in the casing but has spring-loaded sliding vanes that extend to the casing wall. Gas enters at a point where the vanes are most extended, then is carried around as the vanes recede and as the rotor-to-wall distance decreases. The gas is thus compressed and then expelled at the point of minimum

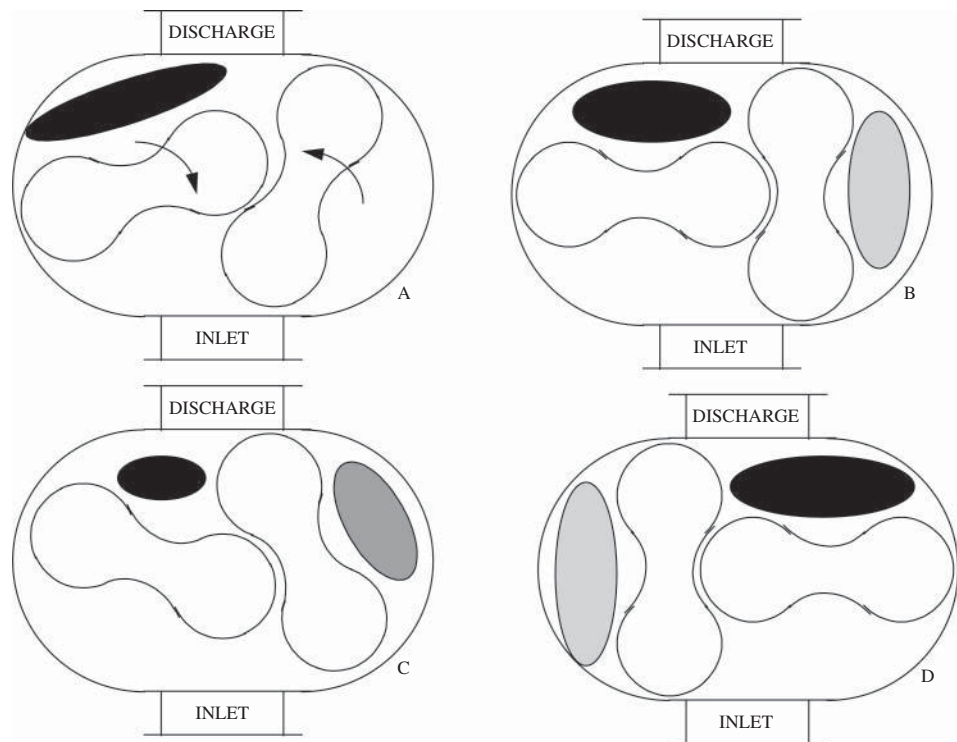


Figure 38 Rotary lobe compressor.

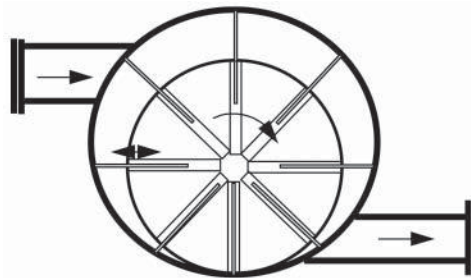


Figure 39 Rotary sliding vane compressor.

vane extension. A single stage can create a vacuum of 15–20 mm Hg abs, two stages can produce 0.5 mm, and multiple stages can take pressure as low as 0.001 mm or 0.13 Pa. Oil is usually passed through the compressor to lubricate, seal, and cool. Capacities are listed from 3 to 1100 ft³/min (0.5 m³ s⁻¹). A schematic is given in Fig. 39, showing 8 vanes: up to 12 are sometimes used.

Liquid Ring A rotor with vanes is used to circulate liquid around the periphery of a non-circular (e.g., elliptical) casing. The spacing between liquid surface and rotor varies as the distance between rotor and casing increases and decreases. Gas enters the zone between rotor and casing at its two points I of greatest spacing, gets compressed as the spacing shrinks, and then gets expelled at the two points D of minimum spacing. Vacuum down to 100 mm Hg and lower is

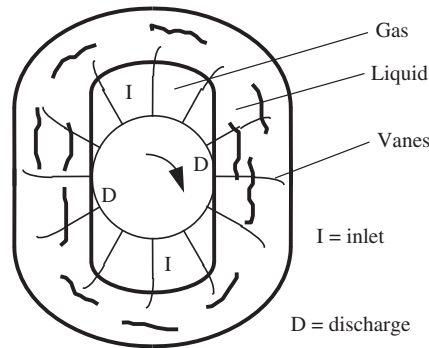


Figure 40 Liquid ring compressor.

achieved but may be limited by the vapor pressure of the liquid. It is sometimes used in tandem with a different type of device, delivering the gas to its atmospheric pressure termination. If the gas is a condensable vapor the liquid may simply be the same substance (e.g., steam and liquid water). Capacities are listed as 3–10,000 ft³/min or 0.0015–5 m³s⁻¹. The device is shown schematically in Fig. 40.

Above-Atmospheric Compression

Rotary lobe, rotary sliding vane, and liquid ring compressors are all positive-displacement devices. Two more *positive-displacement* devices, which are often used for above-atmospheric pressurization, are the reciprocating compressor and the screw compressor. Two *dynamic*-type compressors are the centrifugal and the axial.

Reciprocating Compressor. Reciprocating devices take two types, the *piston* and the *diaphragm*. The former is illustrated in Fig. 23. In both types a movable surface alternately allows fluid into a chamber and then expels it into a region of higher pressure. The directions of the inflow and outflow are regulated by a pair of check valves, which open only when the pressure upstream exceeds the pressure downstream. Piston pumps may have two chambers, one on each side of the piston, with the cycles 180° out of synchronization with each other. Piston pumps have maximum compression ratios of 4–8. Small domestic compressors generally are the piston type.

Diaphragm compressors make use of the motion of a flexible membrane (usually metallic) to admit, pressurize, and then expel gas. The membrane is sealed around the edges so that there is no leakage of gas (or lubricant) as there might be around a piston. The membrane may be directly attached to a piston or it may be driven by oil, which in turn is driven by a piston, as shown in Fig. 41. Diaphragm compressors can have compression ratios much higher than piston units, e.g., 10 and higher. They can reach pressures of 60,000 lb/in.², which is higher than any other compressor; however, they have relatively low capacity compared to piston units.

Screw Compressor Screw compressors employ two counterrotating screws to trap, pressurize, and expel gas. Examining the cross sections of the two screws shows that they are dissimilar, with the lobes of one screw fitting closely into the cavities of the other. Typically, the number of lobes does not equal the number of cavities, so that the screws rotate at different speed: In Fig. 42, screw A would rotate 50% faster than screw B. The screws have very tight clearances but are driven using timing gears to prevent them from touching each other. They can be run

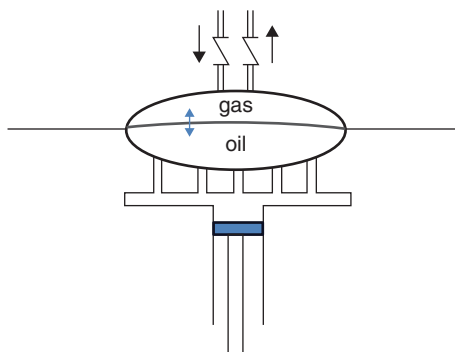


Figure 41 Diaphragm compressor.

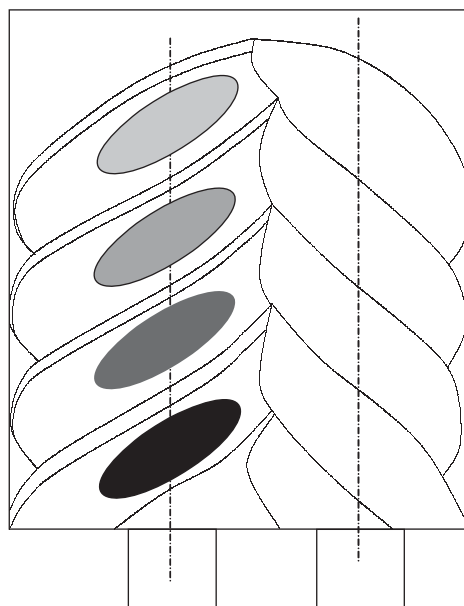


Figure 42 Screw compressor.

dry, in which case they may have compression ratio of up to 5, or run with oil to lubricate, cool, and seal, in which case they may have compression ratio 20 and higher. One manufacturer advertises a dry-running unit that delivers $120,000 \text{ m}^3 \text{ h}^{-1}$ or $67,000 \text{ ft}^3 \text{ min}^{-1}$. Oil-sealed units have lesser capacities; they are sometimes also used for vacuum generation.

Scroll Compressor. The scroll compressor or pump is a century-old concept made practical more recently by the ability to machine the parts to the tight required tolerances. It consists of two interleaved spiral elements, one fixed and the other moving eccentrically in contact with it. Pockets of gas (or liquid) are trapped and moved along from inlet to discharge. It can be used at pressures below or above atmospheric. Usual compression ratio is 3–4 but some uses are reported where CR is 8 or 9. It is used extensively in automotive, air-conditioning and refrigeration applications, especially where a compact quiet device is required.

Centrifugal Compressor. Unlike the positive devices, the centrifugal compressor is dynamic and operates in terms of head rise rather than compression ratio. This compressor has the same principle as centrifugal pumps and centrifugal fans and blowers and it follows the same affinity rules. It is differentiated from the fans by always using backward-inclined vanes, employing static vanes in the casing to help direct the peripheral flow, and having a spiral volute-shaped casing. These features are shown in Fig. 43. Operating speeds are also higher than for fans and blowers. Single-stage compression ratio is usually in the 1.5–3 range: Higher CR can cause undue mechanical stress. Multistaged, the compressor delivers higher throughput than the positive-displacement devices. Eight stages are typical. The centrifugal compressor is unsuitable for gases of low molecular weight because unrealistic heads, as calculated in Eq. (49), are required to achieve desired discharge pressure:

$$H(\text{m}) = \Delta P(\text{N m}^{-2}) \rho^{-1}(\text{m}^3 \text{kg}^{-1})g^{-1}(\text{kgf N}^{-1}) \quad (49)$$

The head-versus-volumetric throughput curve has a rising portion at low throughput, which must be avoided to prevent instability known as *surging*. This serious phenomenon limits the turn-down range: single stages down to 50%, multiple stages down to 75%.

Axial-Flow Compressor Like the axial-flow pumps, fans, and blowers, the axial-flow compressor uses the principle of aerodynamic lift to create head rise. Inclined blades on a rotor, the axis of which lays in the direction of flow, impart lift and a small amount of tangential swirl to the gas. Intervening rows of static vanes help to redirect the swirl into the axial direction. All blades and vanes are designed to maximize lift and minimize drag. Axial compressors are typically 8–10% more efficient than centrifugal compressors. Axial units have the highest capacity of all compressors. Figure 44 is a schematic.

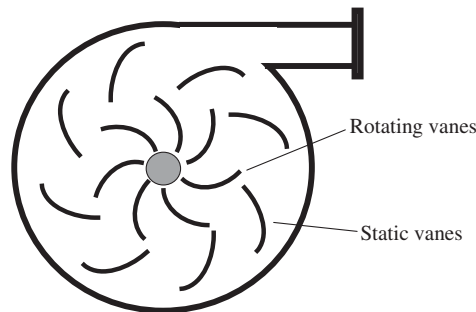


Figure 43 Centrifugal compressor.

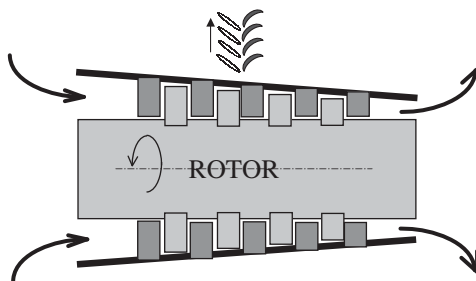


Figure 44 Axial-flow compressor.

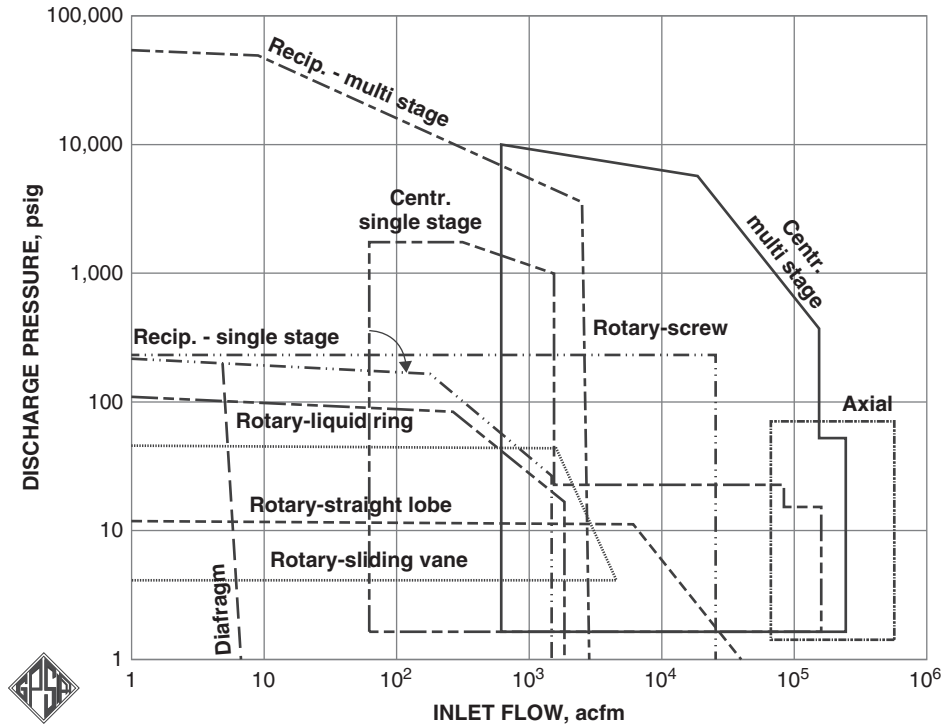


Figure 45 Compressor map. (Courtesy of Gas Processors Suppliers Association.)

Figure 45 shows a useful graphic comparison of the range of discharge pressures and of throughputs for the compressors that have been discussed.

3 THERMODYNAMICS OF GAS COMPRESSION

Raising the pressure of any fluid requires energy, and the work per unit weight of a fluid was given by Eq. (37) as

$$W_f = \int \left(\frac{1}{\rho} \right) dP \quad (37)$$

If the fluid is liquid or if, in the case of a gas, the pressure change is small, then density ρ may be taken as constant and Eq. (38) applies

$$W_f = \left(\frac{1}{\rho} \right) \Delta P \quad (38)$$

For a liquid, because density is relatively large, the energy is relatively small. Likewise, for a gas at low pressure rise, the energy expended is small.

For a gas undergoing significant compression, the energy cost is significant. Also, since the expended energy has little chance to dissipate, it appears as temperature rise in the gas. This compression energy must be removed by cooling the gas after compression or between sequential stages of compression. These effects and requirements must be estimated. The calculation starts with Eq. (37). And, it is assumed, conservatively, that *all* of the compression work is converted into gas temperature, with no heat transfer to the surroundings.

Adiabatic Calculation

A first examination of the compression is to consider it reversible and therefore described by the equations of an adiabatic, isentropic process. The relation between gas pressure and gas density is

$$\frac{P}{\rho^\gamma} = \frac{P_1}{\rho_1^\gamma} \quad (50)$$

where γ equals C_p/C_v with C_p being the specific heat at constant pressure and C_v being the specific heat at constant volume.

Substituting into Eq. (37) and integrating between P_1 and P_2 gives the following expression for work input based on an adiabatic reversible process:

$$(W_f)_{\text{ad}} = \left(\frac{\gamma}{\gamma - 1} \right) \left(\frac{P_1}{\rho} \right) \left[\left(\frac{P_2}{P_1} \right)^{(\gamma-1)/\gamma} - 1 \right] \quad (51)$$

The temperature rise is calculated from Eq. (36):

$$\frac{T_2}{T_1} = \left(\frac{P_2}{P_1} \right)^{(\gamma-1)/\gamma} \quad (36)$$

From Eqs. (36) and (51) it is shown that

$$(T_2)_{\text{ad}} - T_1 = C_p^{-1} (W_f)_{\text{ad}} \quad (52)$$

In practice, the required work and the rise in temperature are higher than these predictions because of irreversible energy losses in the compressor. An efficiency factor is defined for the process as

$$\eta_{\text{ad}} = \frac{(T_2)_{\text{ad}} - T_1}{(T_2)_{\text{actual}} - T_1} \quad \text{or} \quad \frac{(W_f)_{\text{ad}}}{(W_f)_{\text{actual}}} \quad (53)$$

For example, if P_2/P_1 is 5 and γ is 1.4 and T_1 is 50°C or 323 K, then from Eq. (36) T_2/T_1 is 1.58 and $(T_2)_{\text{ad}}$ is 512 K or 239°C. But if η_{ad} is 0.75, then from Eq. (53)

$$(T_2)_{\text{actual}} = \frac{(T_2)_{\text{ad}} + (\eta_{\text{ad}} - 1)T_1}{\eta_{\text{ad}}} = 575 \text{ K} \quad \text{or} \quad 302^\circ\text{C}$$

Polytropic Calculation

A different approach, favored by compressor manufacturers, is to recognize the considerable misprediction of the adiabatic assumption and to base the calculation on an altered form of Eq. (50), namely

$$\frac{P}{\rho^n} = \frac{P_1}{\rho_1^n} \quad (54)$$

where the index n is chosen to produce a better match with the temperature rise than is experienced in practice. For instance, if n were chosen as 1.56 (instead of 1.4) in the above example, then there would be equality between T_{actual}/T_1 and $(P_2/P_1)^{(n-1)/n}$

Since it is impossible to choose a value of n that would fit all cases, the manufacturer specifies a common value and uses a *polytropic efficiency* η_p to cover any mismatch. η_p is always closer than η_{ad} to 1.0.

$$(W_f)_p = \left(\frac{n}{n-1} \right) \left(\frac{P_1}{\rho_1} \right) \left[\left(\frac{P_2}{P_1} \right)^{(n-1)/n} - 1 \right] \quad (55)$$

$$(W_f)_{\text{actual}} = \frac{(W_f)_p}{\eta_p} \quad (56)$$

$$T_{\text{actual}} = T_1 + \frac{[(P_2/P_1)^{(n-1)/n}] T_1 - T_1}{\eta_p} \quad (57)$$

The units of W_f are typically joules per kilogram (if P_1 is in pascals and ρ_1 is in kg m^{-3}) or foot pounds-force per pound. In the latter case the work is expressed simply as “feet of head.” For head in meters,

$$H(\text{m}) = (W_f)_{\text{actual}} g_c g^{-1} \quad (58)$$

Use of Thermodynamic Charts

The above treatment assumes a constant value for Z , the compressibility factor in the equation of state for the gas,

$$P V = Z(W/\text{mol wt}) RT \quad (59)$$

For many gases such as hydrocarbons this assumption becomes inaccurate over significant increases of pressure and temperature. If thermodynamic charts are available, they may be used directly to make the adiabatic estimate and then to correct it for efficiency. This is the preferred way to calculate power and discharge temperature. In Fig. 46 a portion of the enthalpy-versus-entropy chart is shown for steam. The line 1 – 2 shows adiabatic compression of steam from 30 psia and 320°F to a pressure of 50 psia. The enthalpy rises from 1200 Btu per pound to 1245, an increase of 45. If the adiabatic efficiency for this compressor were only 50%, then the final enthalpy would be 1290, shown by the point at 3, still at 50 psia but with discharge temperature 514°F. Total energy expended would be

$$90 \text{ Btu lb}^{-1} \quad \text{or} \quad 70020 \text{ ft-lbf lb}^{-1} \quad \text{or} \quad 127.3 \text{ hp lb}^{-1} \quad \text{or} \quad 209 \text{ kJ kg}^{-1}$$

or 21327 m head

The Gas Processors Suppliers Association is a good source for thermodynamic charts for hydrocarbons.

Total Compressor Power

The power calculated above is the *gas power*, GP, the power that shows up as temperature rise. To obtain the total power requirement the losses due to friction in bearings, seals, and speed-increasing gears must be added. An approximate equation is

$$\text{Total power} = \text{gas Power, GP} + \text{mechanical losses} \quad (60)$$

where

$$\text{Mechanical losses (hp)} = \text{GP}(\text{hp})^{0.4} \quad (61)$$

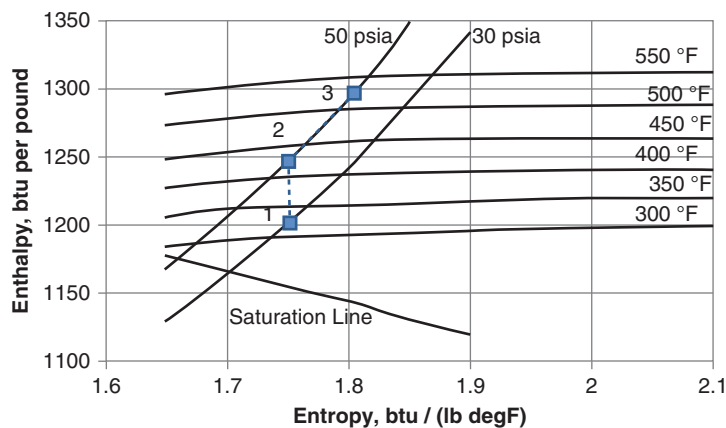


Figure 46 Path of a steam compression.

Field Determination of Compressor Power

In the absence of good estimates for the various efficiencies, the above calculations are sometimes circumvented by using experiential data for various compressions. These data are obtained from measurements of electrical power used by existing units and they provide a quick indication of what will be needed in a future installation. For instance, typical values for air compression are 6 standard cubic feet per minute per kilowatt for 100 psig air and 4.2 for 175 psig air. By way of comparison, the ratio for the above example of steam compression from 30 to 50 psia has a value of 8.4 based on gas power alone and somewhat less when mechanical losses are included.

Required Number of Stages

Compressing a gas in stages, with cooling between stages, brings the operation closer to the ideal of isothermal compression, minimizing high temperatures and minimizing operating cost. However, capital cost increases with the number of stages. It is desired to know how many are needed. One factor is the achievable compression ratio per stage. Depending on the type of compressor, it may vary from, say, 1.05–7, but a reasonable assumption is 3–4 for most units. Another factor is the allowable gas temperature. Compressor sealing systems are usually limited to about 300°F (148°C). Some gases such as oxygen, chlorine, and acetylene require temperature below 200°F (93°C). With these limits in mind, the necessary staging can be specified. Theoretically, the minimum operating power occurs when all stages have the same compression ratio, so that

$$\text{CR per stage} = (\text{Total CR})^{1/(\text{required number of stages})} \quad (62)$$

REFERENCES

1. A. J. Stepanoff, *Centrifugal and Axial Flow Pumps: Theory, Design and Application*, 2nd ed., Krieger, Malabar, FL, 1993.
2. J. F. Gulich, *Centrifugal Pumps*, 2nd ed., Springer, New York, 2010.
3. R. C. Monroe, Hudson Products Corporation, "Minimizing Fan Energy Costs," *Chem. Eng. Cost File*, 1993.

BIBLIOGRAPHY

- American Petroleum Institute Standard 610, *Centrifugal Pumps for Petroleum, Petrochemical and Natural Gas Industries*, 11th ed. American Petroleum Institute, Washington, DC, 2009.
- ANSI/AMCA Standards 99-10, 210, 300, 301, 320, *Standards Handbook*, Air Movement and Control Association International, Arlington Heights, IL.
- ANSI/Hydraulic Institute Standards, www.pumps.org.
- Gas Processors Suppliers Association, *Data Book*, 12th ed., Tulsa, OK, 2004.
- I. Karassik, J. Messina, P. Cooper, and C. Heald, *Pump Handbook*, 4th ed., McGraw-Hill, New York, 2007.
- The New York Blower Company, Bulletin 051, "General Purpose Packaged Fans," 2009; available at www.nyb.com.

CHAPTER 26

GAS TURBINES

Harold E. Miller and Todd S. Nemeć
GE Energy
Schenectady, New York

1 INTRODUCTION	901		
1.1 Basic Operating Principles	901		
1.2 Brief History of Gas Turbine Development and Use	906		
1.3 Subsystem Characteristics and Capabilities	908		
1.4 Controls and Accessories	919		
1.5 Gas Turbine Operation	923		
2 GAS TURBINE PERFORMANCE	924		
2.1 Gas Turbine Configurations and Cycle Characteristics	924		
2.2 Trends in Gas Turbine Design and Performance	931		
3 APPLICATIONS	934		
3.1 Use of Exhaust Heat in Industrial Gas Turbines	934		
		3.2 Integrated Gasification Combined Cycle	938
		3.3 Applications in Electricity Generation	940
		3.4 Engines in Aircraft	941
		3.5 Engines for Surface Transportation	946
		4 EVALUATION AND SELECTION	947
		4.1 Maintenance Intervals, Availability, and Reliability	947
		4.2 Selection of Engine and System	949
		REFERENCES	953

1 INTRODUCTION

1.1 Basic Operating Principles

Gas turbines are heat engines based on the Brayton thermodynamic cycle, which is one of the four cycles that account for most heat engines in use. The other three cycles are the Otto, Diesel, and Rankine. The Otto and Diesel cycles are cyclic in regard to energy content, while the Brayton (gas turbine) and Rankine (steam turbine) cycles are steady-flow, continuous energy transfer cycles. The Rankine cycle involves condensing and boiling of the working fluid (steam) and utilizes a boiler to transfer heat to the working fluid. The working fluid in the Otto, Diesel, and Brayton cycles is generally air, or air plus combustion products; these cycles are usually internal combustion cycles wherein the fuel is burned in the working fluid. In summary, the Brayton cycle is differentiated from the Otto and Diesel cycles in that it is continuous and from the Rankine in that it relies on internal combustion and does not involve a phase change in the working fluid.

In all cycles, the working fluid experiences induction, compression, heating, expansion, and exhaust. In a nonsteady cycle, these processes are performed in sequence in the same closed space—one formed by a piston and cylinder—and operate on the working fluid one mass at a time. In contrast, the working fluid flows without interruption through a steam turbine power plant or gas turbine engine, passing continuously from one single-purpose device to the next.

Gas turbines are used to power aircraft and land vehicles, to drive generators (alternators) to produce electric power, and to drive other devices such as pumps and compressors. Gas turbines in production range in output from below 50 kW to over 200 MW. Design philosophies and engine configurations vary significantly across the industry. For example, aircraft engines are optimized for high power-to-weight ratios, while heavy-duty, industrial and utility gas turbines are heavier, since they are designed for low cost and long life in severe environments.

Figure 1 shows the arrangement of a simple gas turbine engine. The rotating compressor acts to raise the pressure of the working fluid and force it into the combustor. The turbine is rotated by fluid expanding from a high pressure at the combustor discharge to ambient

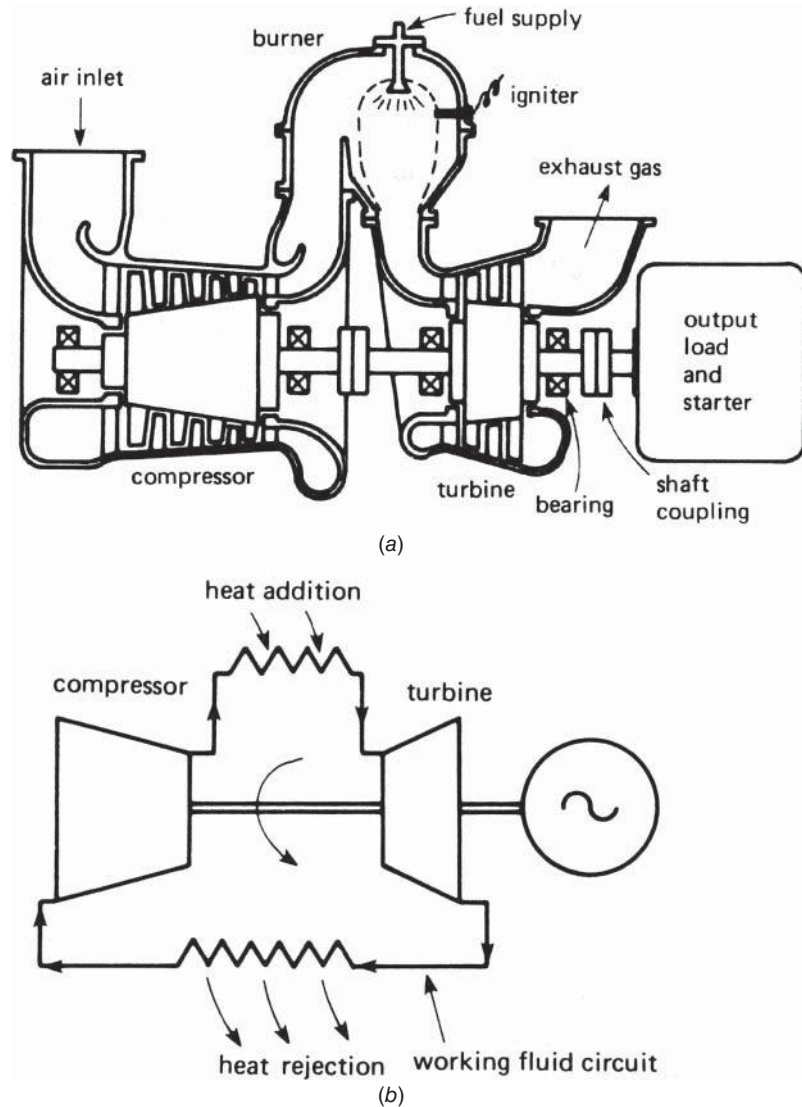


Figure 1 Simple engine types: (a) open cycle and (b) closed cycle.

air pressure at the turbine exhaust. The resulting mechanical work drives the mechanically connected compressor and output load device.

The nomenclature of the gas turbine is not standardized. In this chapter the following descriptions of terms apply:

- *Blading* refers to all rotating and stationary airfoils in the gas path.
- *Buckets* are turbine (expander) section rotating blades; the term is derived from steam turbine practice.
- *Nozzles* are turbine section stationary blades.
- *Combustors* are the combustion components in contact with the working fluid; major combustor components are *fuel nozzles* and *combustion liners*. The combustor configurations are *annular*, *can-annular*, and *silo*. Can-annular and silo-type combustors have transition pieces which conduct hot gas from the combustion liners to the first-stage nozzles.
- A *compressor stage* consists of a row of rotor blades, all at one axial position in the gas turbine, and the stationary blade row downstream of it.
- A *turbine stage* consists of a set of nozzles occupying one axial location and the set of buckets immediately downstream.
- *Discs* and *wheels* are interchangeable terms; rotating blading is attached either to a monolithic rotor structure or to individual discs or wheels designed to support the blading against centrifugal force and the aerodynamic loads of the working fluid.

Gas turbine performance is established by three basic parameters: mass flow, pressure ratio, and firing temperature. Compressor, combustor, and turbine efficiency have significant, but secondary, effects on performance, as do inlet and exhaust systems, turbine gas path and rotor cooling, and heat loss through turbine and combustor casings. In gas turbine catalogues and other descriptive literature, mass flow is usually quoted as compressor inlet flow, although turbine exit flow is sometimes quoted. Output is proportional to mass flow.

Pressure ratio is quoted as the compressor pressure ratio. Aircraft engine practice defines the ratio as the total pressure at the exit of the compressor blading *divided by* the total pressure at the inlet of the compressor blading. Industrial/utility turbine manufacturers generally refer to the static pressure in the plenum downstream of the compressor discharge diffuser (upstream of the combustor) *divided by* the total pressure downstream of the inlet filter and upstream of the inlet of the gas turbine. Similarly, there are various possibilities for defining turbine pressure ratio. All definitions yield values within 1 or 2% of one another. Pressure ratio is the primary determiner of simple-cycle gas turbine efficiency. High pressure results in high simple-cycle efficiency.

Firing temperature is defined differently by each manufacturer, and the differences are significant. Heavy-duty gas turbine manufacturers use three definitions:

1. There is an International Organization for Standardization (ISO) definition of firing temperature, which is a calculated temperature. The compressor discharge temperature is increased by a calculated enthalpy rise based on the compressor inlet air flow and the fuel flow. This definition is valuable in that it can be used to compare gas turbines or to monitor changes in performance on through calculations made on the basis of field measurements. Knowledge of the secondary flows within the gas turbine is not required to determine ISO firing temperature.
2. A widely used definition of firing temperature is the average total temperature in the exit plane of the first-stage nozzle. This definition is used by General Electric for its industrial engines.

3. Westinghouse (now part of Siemens-Westinghouse) and several other manufacturers refer to “turbine inlet temperature,” the temperature of the gas entering the first-stage nozzle. Turbine inlet temperature is approximately 100°C above nozzle exit firing temperature, which is in turn approximately 100°C above the ISO firing temperature.

Since firing temperature is commonly used to compare the technology level of competing gas turbines, for comparison purposes it is important to use one definition of this parameter.

Aircraft engines and aircraft derivative industrial gas turbines have other definitions. One nomenclature establishes numerical stations (in which station 3.9 is combustor exit and station 4.0 is first-stage nozzle exit). Thus, $T_{3.9}$ is very close to turbine inlet temperature and $T_{4.0}$ is approximately equal to GE’s firing temperature. There are some subtle differences that relate to the treatment of the leakage flows near the first-stage nozzle.

Firing temperature is a primary determiner of power density (specific work) and combined-cycle (Brayton–Rankine) efficiency. High firing temperature increases the power produced by a gas turbine of a given physical size and mass flow. The pursuit of higher firing temperatures by all manufacturers of the large, heavy-duty gas turbines used for electrical power generation is driven by the economics of high combined-cycle efficiency.

Pressures and temperatures used in the following descriptions of gas turbine performance will be total pressures and temperatures. Absolute, stagnation, or total values are those measured by instruments that face into the approaching flow to give an indication of the energy in the fluid at any point. The work done in compression or expansion is proportional to the change of stagnation temperature in the working fluid in the form of heating during a compression process or cooling during an expansion process. The temperature ratio between the temperatures before and after the process is related to the pressure ratio across the process by the expression $T_b/T_a = (P_b/P_a)^{(\gamma-1)/\gamma}$, where γ is the ratio of working fluid specific heats at constant pressure and volume. The temperature and pressure are stagnation values. It is the interaction between the temperature change and ratio at different starting temperature levels which permits the engine to generate a useful work output.

This relationship between temperature and pressure can be demonstrated by a simple numerical example using the Kelvin scale for temperature. For a starting temperature of 300 K (27°C), a temperature ratio of 1.5 yields a final temperature of 450 K and a change of 150°C. Starting instead at 400 K, the same ratio would yield a change of 200°C and a final temperature of 600 K. The equivalent pressure ratio would ideally be 4.13, as calculated from solving the preceding equation for P_b/P_a : $P_b/P_a = T_b/T_a^{\gamma/\gamma-1} = 1.5^{1.4/0.4} = 4.13$. These numbers show that, working over the same temperature ratio, the temperature change and, therefore, the work involved in the process vary in proportion to the starting temperature level.¹

This conclusion can be depicted graphically. If the temperature changes are drawn as vertical lines ab and cd and are separated horizontally to avoid overlap, the resultant is Fig. 2a. Assuming the starting and finishing pressures to be the same for the two processes, the thin lines through ad and bc depict two of a family of lines of constant pressure which diverge as shown. In this ideal case, expansion processes could be represented by the same diagram, simply by proceeding down the lines ba and cd . Alternatively, if ab is taken as a compression process, bc as heat addition, cd as an expansion process, and da as a heat rejection process, then the figure $abcd$ represents the ideal cycle to which the working fluid of the engine is subjected.

Over the small temperature range of this example, the assumption of constant gas properties is justified. In practice, the 327°C (600 K) level at point d is too low a temperature from which to start the expansion. Figure 2b is more realistic. Here, the lines of constant pressure have been constructed for ideal gas–air properties, which are dependent on temperature. Expansion begins from a temperature of 1250°C. With a pressure ratio of 16:1, the end point of the expansion is approximately 480°C. Now, ab represents the work input required by the compressor. Of the expansion work capacity cd , only the fraction cd' is required to drive the compressor.

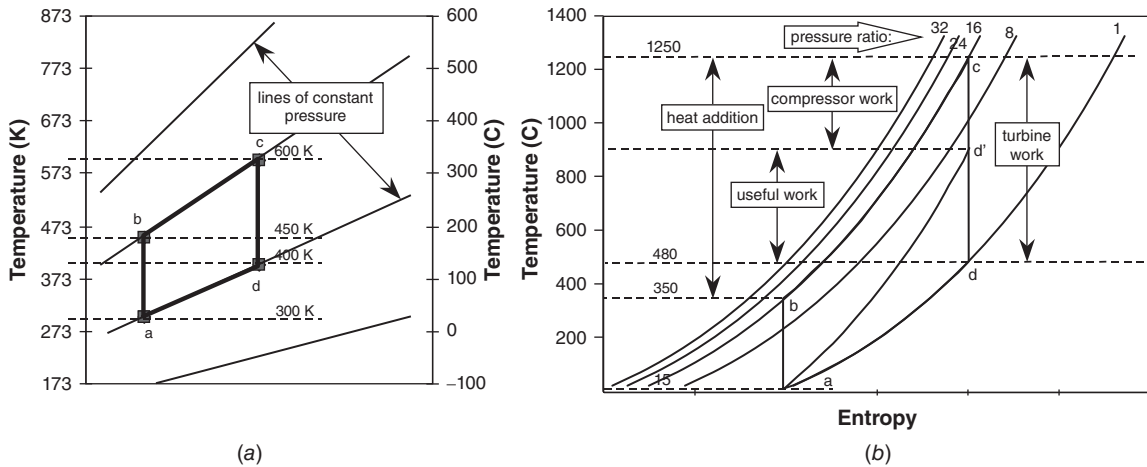


Figure 2 (a) Temperature changes and (b) temperature–entropy diagram for ideal simple gas turbine cycles.

An optical illusion makes it appear otherwise, but line ad' is displaced vertically from line bc by the same distance everywhere. The remaining 435°C , line $d'd$, is energy that can be used to perform useful external work, by further expansion through the turbine or by blowing through a nozzle to provide jet thrust.

Now consider line bc . The length of its vertical projection is proportional to the heat added. The ability of the engine to generate a useful output arises from its use of the energy in the input fuel flow, but not all of the fuel energy can be recovered usefully. In this example, the heat input proportional to $1250 - 350 = 900^\circ\text{C}$ compares with the excess output proportional to 435°C (line $d'd$) to represent an efficiency of $435/900$, or 48%. If more fuel could be used, raising the maximum temperature level at the same pressure, then more useful work could be obtained at nearly the same efficiency.

The line da represents heat rejection. This could involve passing the exhaust gas through a cooler, before returning it to the compressor, and this would be a closed cycle. However, almost universally, da reflects discharge to the ambient conditions and intake of ambient air (Fig. 1b). Figure 1a shows an open-cycle engine, which takes air from the atmosphere and exhausts back to the atmosphere. In this case, line da still represents heat rejection, but the path from d to a involves the whole atmosphere and very little of the gas finds its way immediately from e to a . It is fundamental to this cycle that the remaining 465°C , the vertical projection of line da , is wasted heat because point d is at atmospheric pressure. The gas is therefore unable to expand further and so can do no more work.

Designers of simple-cycle gas turbines—including aircraft engines—have pursued a course of reducing exhaust temperature through increasing cycle pressure ratio, which improves the overall efficiency. Figure 3 is identical to Fig. 2b except for the pressure ratio, which has been increased from 16:1 to 24:1. The efficiency is calculated in the same manner. The total turbine work is proportional to the temperature difference across the turbine, $1250 - 410 = 840^\circ\text{C}$. The compressor work, proportional to $430 - 15 = 415^\circ\text{C}$, is subtracted from the turbine temperature drop $840 - 415 = 425^\circ\text{C}$. The heat added to the cycle is proportional to $1250 - 430 = 820^\circ\text{C}$. The ratio of the net work to the heat added is $425/820 = 52\%$. The approximately 8% improvement in efficiency is accompanied by a 70°C drop in exhaust temperature. When no use is made of the exhaust heat, the 8% efficiency may justify the mechanical complexity associated with higher pressure ratios. Where there is value to the

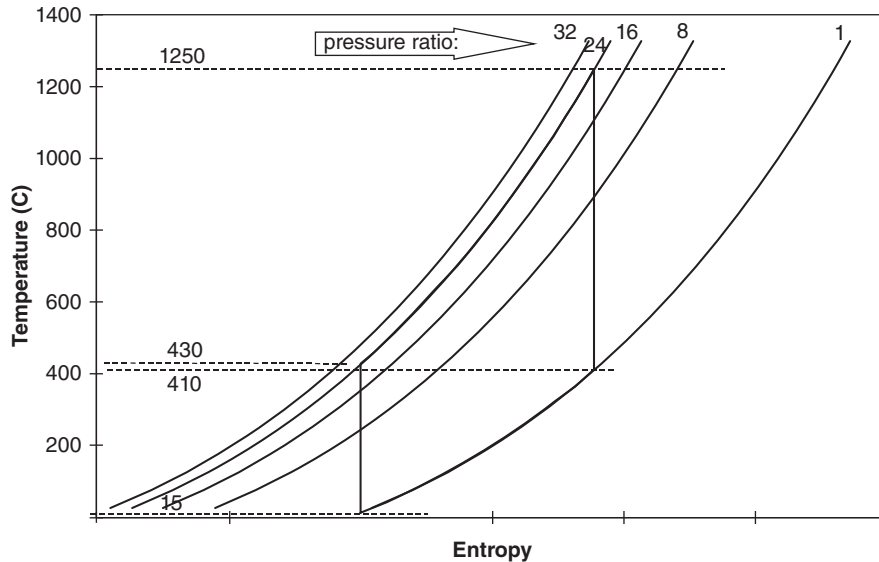


Figure 3 Simple-cycle gas turbine temperature–entropy diagram for high pressure ratio (24:1) and 1250°C firing temperature.

exhaust heat, as there is in combined Brayton–Rankine cycle power plants, the lower pressure ratio may be superior. Manufacturers forecast their customer requirements and understand the costs associated with cycle changes and endeavor to produce gas turbines featuring the most economical thermodynamic designs.

The efficiency levels calculated in the preceding example are very high because many factors have been ignored for the sake of simplicity. Inefficiency of the compressor increases the compressor work demand while turbine inefficiency reduces turbine work output, thereby reducing the useful work output and efficiency. The effect of inefficiency is that, for a given temperature change, the compressor generates less than the ideal pressure level while the turbine expands to a higher temperature for the same pressure ratio. There are also pressure losses in the heat addition and heat rejection processes. There may be variations in the fluid mass flow rate and its specific heat (energy input divided by consequent temperature rise) around the cycle. These factors can easily combine to reduce the overall efficiency.

1.2 Brief History of Gas Turbine Development and Use

It was not until the year 1791 that John Barber patented the forerunner of the gas turbine, proposing the use of a reciprocating compressor, a combustion system, and an impulse turbine. Even then, he foresaw the need to cool the turbine blades, for which he proposed water injection.

The year 1808 saw the introduction of the first explosion type of gas turbine, which in later forms used valves at the entry and exit from the combustion chamber to provide intermittent combustion in a closed space. The pressure thus generated blew the gas through a nozzle to drive an impulse turbine. These operated successfully but inefficiently for Karavodine and Holzwarth from 1906 onward, and the type died out after a Brown, Boveri model was designed in 1939.¹

Developments of the continuous-flow machine suffered from lack of knowledge, as different configurations were tried. In 1872 Stolze designed an engine with a seven-stage axial-flow compressor, heat addition through a heat exchanger by external combustion, and a 10-stage

reaction turbine. It was tested from 1900 to 1904 but did not work because of its very inefficient compressor. Parsons was equally unsuccessful in 1884, when he tried to run a reaction turbine in reverse as a compressor. These failures resulted from the lack of understanding of aerodynamics prior to the advent of aircraft. As a comparison, in typical modern practice, a single-stage turbine drives about six or seven stages of axial compressor with the same mass flow.

The first successful dynamic compressor was Rateau's centrifugal type in 1905. Three assemblies of these (with a total of 25 impellers in series giving an overall pressure ratio of 4) were made by Brown, Boveri and used in the first working gas turbine engine, which was built by Armengaud and Lemale in the same year. The exhaust gas heated a boiler behind the turbine to generate low-pressure steam, which was directed through turbines to cool the blades and augment the power. Low component efficiencies and flame temperature (828 K) resulted in low work output and an overall efficiency of 3%. By 1939, the use of industrial gas turbines had become well established and experience with the Velox boiler led Brown, Boveri into diverging applications; a Hungarian engine (Jendrassik) with axial-flow compressor and turbine used regeneration to achieve an efficiency of 0.21; and the Sun Oil Co. (USA) was using a gas turbine engine to improve a chemical process.¹

The history of gas turbine engines for aircraft propulsion dates from 1930, when Frank Whittle saw that its exhaust gas conditions ideally matched the requirements for jet propulsion and took out a patent.¹ His first model was built by British Thomson-Houston and ran as the Power Jets Type U in 1937, with a double-sided centrifugal compressor, a long combustion chamber that was curled round the outside of the turbine, and an exhaust nozzle just behind the turbine. Problems of low compressor and turbine efficiency were matched by hardware problems and the struggle to control the combustion in a very small space. In 1938 reverse-flow can-annular combustors were introduced with the aim still being to keep the compressor and turbine as close together as possible to avoid shaft whirl problems (Fig. 4). Whittle's first flying engine was the W1, with 850 lb thrust, in 1941. It was made by Rover, whose gas turbine establishment was taken over by Rolls-Royce in 1943. A General Electric version of the W1 flew in 1941. A parallel effort at General Electric led to the development of a successful axial-flow compressor. This was incorporated in the first turboprop engine, the TG100, later designated

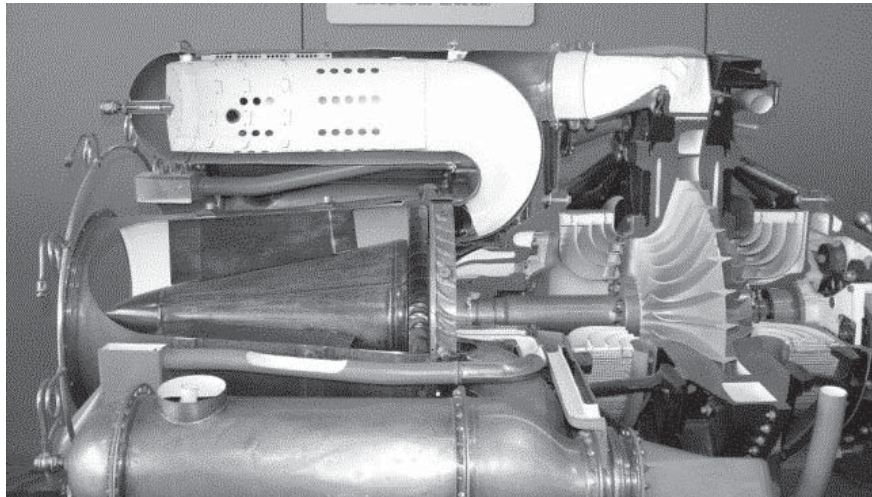


Figure 4 Photo of an early Whittle-type jet engine with portions cut away to show double-sided compressor and reverse-flow combustion chambers. Photo by Mark Doane of General Electric.

the T31. This engine was first tested in May 1943 and produced 1200 hp from an engine weighing under 400 kg. Flight testing followed in 1949. An axial-flow compressor turbojet version was also constructed. Designated the J35, it flew in 1946. The compressor of this engine evolved to the compressor of the GE MS3002 industrial engine that was introduced in 1950 and is still commercially available.²

A Heinkel experimental engine flew in Germany in 1939. Several jet engines were operational by the end of the World War II, but the first commercial engine did not enter service until 1953—the Rolls-Royce Dart turboprop in the Viscount, followed by the turbojet de Havilland Ghost in the Comet of 1954. The subsequent growth of the use of jet engines has been visible to most of the world and has forced the growth of design and manufacturing technology.¹ By 1970 a range of standard configurations for different tasks had become established, and some aircraft engines were established in industrial applications and in ships.

Gas turbines entered the surface transportation fields also during their early stages of development. The first railway locomotive application was in Switzerland in 1941, with a 2200-hp, Brown, Boveri engine driving an electric generator and electric motors driving the wheels. The engine efficiency approached 19% using regeneration. The next decade saw several similar applications of gas turbines by some 43 different manufacturers. A successful application of gas turbines to transportation was the 4500 draw-bar horsepower engine based on the J35 compressor. Twenty-five locomotives so equipped were delivered to the Union Pacific Railroad between 1952 and 1954. The most powerful locomotive gas turbine was the 8500-hp unit offered by General Electric to the Union Pacific Railroad for long-distance freight service.³ This became the basis of the MS5001 gas turbine, which is the most common heavy-duty gas turbine in use today. Railroad applications continue today, but they rely on a significantly different system. Japan Railway operates large, stationary gas turbines to generate power transmitted by overhead lines to their locomotives.

Automobile and road vehicle use started with a Rover car of 1950, followed by Chrysler and other companies, but commercial use has been limited to trucks, particularly by Ford. Automotive gas turbine development has been largely independent of other types and has forced the pace of development of regenerators. Of course, no history would be complete without mention of the Pratt & Whitney-engined race car campaigned by Andy Granatelli and driven by Parnelli Jones at the 1967 Indianapolis 500, which led most of the race before being sidelined by a bearing failure.

1.3 Subsystem Characteristics and Capabilities

The three subsystems that comprise the gas turbine proper are the compressor, combustor, and turbine. Technologies developed for these subsystems enable the operation and contribute to the value of the gas turbine.

Compressors

Compressors used in gas turbines are of the dynamic type, wherein air is continuously ingested and raised to the required pressure level—usually, but not necessarily, between 8 and 40 atm. Larger gas turbines use axial types; smaller ones use radial outflow, centrifugal compressors. Some smaller gas turbines use both—an axial-flow compressor upstream of a centrifugal stage.

Axial compressors feature an annular flow path, larger in cross-sectional area at the inlet than at the discharge. Multiple stages of blades alternately accelerate the flow of air and allow it to expand, recovering the dynamic component and increasing pressure. Both rotating and stationary stages consist of cascades of airfoils, as can be seen in Fig. 5. Physical characteristics of the compressor determine many aspects of the gas turbine's performance. Inlet annulus area establishes the mass flow of the gas turbine. Rotor speed and mean blade diameter

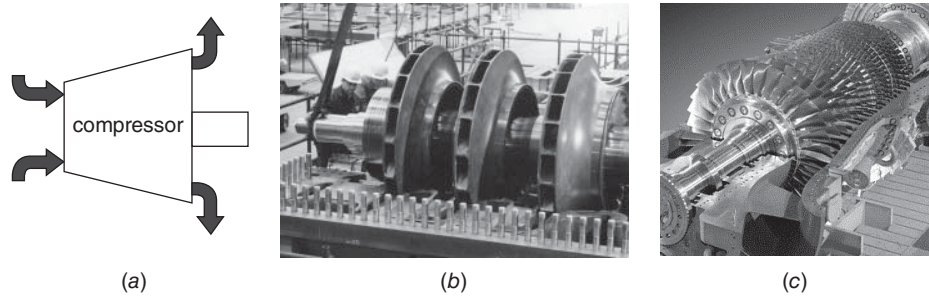


Figure 5 Diagram and photos of centrifugal compressor rotor and axial compressor during assembly. Courtesy of General Electric © GE.

are interrelated since optimum blade velocities exist. A wide range of pressure ratios can be provided, but today's machines feature compressions from below 8:1 to as high as 40:1. The higher pressure ratios are achieved using two compressors operating in series at different rotational speeds. The number of stages required is partially dependent on the pressure ratio required, but also on the sophistication of the blade aerodynamic design that is applied. Generally, the length of the compressor is a function of mass flow and pressure ratio, regardless of the number of stages. Older designs have stage pressure ratios of 1.15:1. Low-aspect-ratio blading designed with three-dimensional analytical techniques has stage pressure ratios of 1.3:1. There is a trend toward fewer stages of blades of more complicated configuration. Modern manufacturing techniques make more complicated forms more practical to produce, and minimizing parts count usually reduces cost.

Centrifugal compressors are usually chosen for machines of below 2 or 3 MW in output, where their inherent simplicity and ruggedness can largely offset their lower compression efficiency. Such compressors feature a monolithic rotor with shaped passages leading from the inlet circle or annulus to a volute at the outer radius where the compressed air is collected and directed to the combustor. The stator contains no blades and only interconnecting passages and simply provides a boundary to the flow path (three sides of which are machined or cast into the rotor). Two or more rotors can be used in series to achieve the desired pressure ratio within the mechanical factors that limit rotor diameter at a given rotational speed.⁴

Two efficiency definitions are used to describe compressor performance. Polytropic efficiency characterizes the aerodynamic efficiency of low-pressure-ratio individual stages of the compressor. Isentropic, or adiabatic, efficiency describes the efficiency of the cycle's first thermodynamic process shown in Fig. 6 (the path from *a* to *b*). From the temperatures shown for the compression process on this figure, the isentropic efficiency can be calculated. The isentropic temperature rise is for the line *ab*: 335°C. The actual rise is shown by line *ab'*, and this rise is 372°C. The compressor efficiency η_c is 90%.

Successful compressor designs achieve high component efficiency while avoiding compressor surge or stall—the same phenomenon experienced when airplane wings are forced to operate at too high an angle of attack at too low a velocity. Furthermore, blade and rotor structures must be designed to avoid vibration problems. These problems occur when natural frequencies of components and assemblies are coincident with mechanical and aerodynamic stimuli, such as those encountered as blades pass through wakes of upstream blades. The stall phenomenon may occur locally in the compressor or even generally, whereupon normal flow through the machine is disrupted. A compressor must have good stall characteristics to operate at all ambient pressures and temperatures and to operate through the start, acceleration, load, load change, unload, and shutdown phases of turbine operation. Compressors are designed

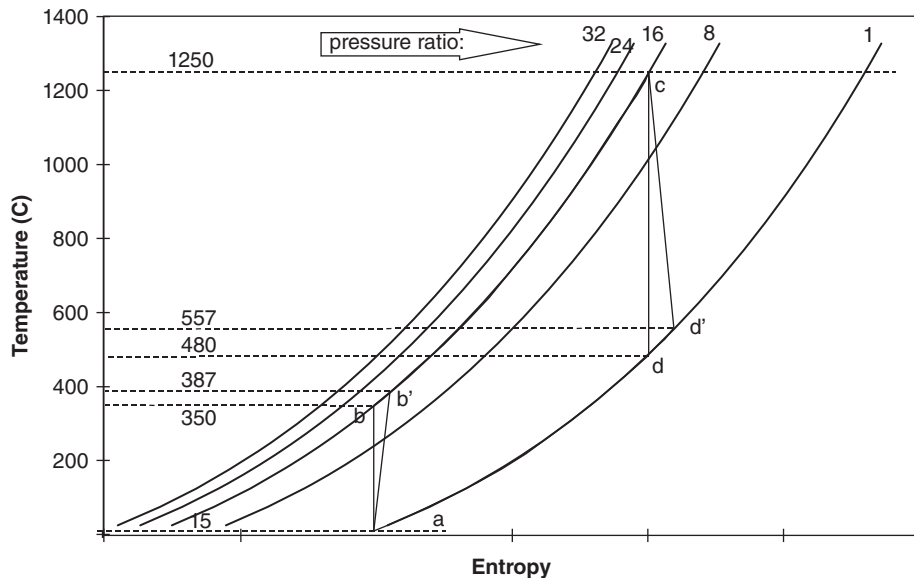


Figure 6 Temperature–entropy diagram showing the effect of compressor and turbine efficiency.

with features and mechanisms for avoiding stall. These include air bleed at various points, variable-angle stator (as opposed to rotor) blades, and multiple spools.

Recent developments in the field of computational fluid dynamics (CFD) provide analytical tools that allow designers to substantially reduce aerodynamic losses due to shock waves in the supersonic flow regions. Using this technique, stages that have high tip Mach numbers can attain efficiencies comparable to those of completely subsonic designs. With these tools, compressors can be designed with higher tip diameters, hence higher flows. The same tools permit the design of low-aspect-ratio, high-stage-pressure-ratio blades for reducing the number of blade rows. Both capabilities contribute to lower cost gas turbine designs with no sacrifice in performance.

Gas Turbine Combustors

The gas turbine combustor is a device for mixing large quantities of fuel and air and burning the resulting mixture. A flame burns hottest when there is just enough fuel to react with the available oxygen (which is called a stoichiometric condition). Here combustion produces the fastest chemical reaction and the highest flame temperatures, compared with excess-air (fuel-lean) and excess-fuel (fuel-rich) conditions, where reaction rates and temperatures are lower. The term “equivalence ratio” is used to describe the ratio of fuel to air relative to the stoichiometric condition. An equivalence ratio of 1.0 corresponds to the stoichiometric condition. At fuel-lean conditions, the ratio is less than 1; conversely, when fuel rich, it is greater than 1. The European practice is to use the reciprocal, which is the lambda value (λ). In a gas turbine—since air is extracted from the compressor for cooling the combustor, buckets, nozzles, and other components and to dilute the flame (as well as support combustion)—the overall equivalence ratio is far less than the value in the flame zone, ranging from 0.4 to 0.5 (λ from 2.5 to 2).⁵

Historically, the design of combustors required providing for the near-stoichiometric mixture of fuel and air locally. The combustion in this near-stoichiometric situation results in a diffusion flame of high temperature. Near-stoichiometric conditions produce a stable

combustion front without requiring designers to provide significant flame-stabilizing features. Since the temperatures generated by the burning of a stoichiometric mixture greatly exceed those at which materials are structurally sound, combustors have to be cooled, and also the gas heated by the diffusion flame must be cooled by dilution before it becomes the working fluid of the turbine. Emissions implications are discussed below.

Gas turbine operation involves a start-up cycle that features ignition of fuel at 20% of rated operating speed, where air flow is proportionally lower. Loading, unloading, and part-load operation, however, require low fuel flow at full compressor speed, which means full air flow. Thermodynamic cycles are such that the lowest fuel flow per unit mass flow of air through the turbine exists at full speed and no load. The fuel flow here is about 1/6 of the full-load fuel flow. Hence, the combustion system must be designed to operate over a 6:1 range of fuel flows with full rated air flow.

Manufacturers have differed on gas turbine combustor construction in significant ways. Three basic configurations have been used: annular, can-annular, and silo combustors. All have been used successfully in machines with firing temperatures up to 1100°C. Annular and can-annular combustors feature a combustion zone uniformly arranged about the centerline of the engine. All aircraft engines and most industrial gas turbines feature this type of design. A significant number of units equipped with silo combustor have been built as well. Here, one or two large combustion vessels are constructed on top or beside the gas turbine. All manufacturers of large machines have now abandoned silo combustors in their state-of-the-art large gas turbine products. The can-annular, multiple-combustion chamber assembly consists of an arrangement of cylindrical combustors, each with a fuel injection system, and a transition piece that provides a flow path for the hot gas from the combustor to the inlet of the turbine. Annular combustors have fuel nozzles at their upstream end and an inner and outer liner surface extending from the fuel nozzles to the entrance of the first-stage stationary blading. No transition piece is needed.

The current challenge to combustion designers is to provide the cycle with a sufficiently high firing temperature while simultaneously limiting the production of oxides of nitrogen, NO_x , which refers to NO and NO_2 . Very low levels of NO_x have been achieved in special low-emission combustors. NO_x is formed from the nitrogen and oxygen in the air when it is heated. The nitrogen and oxygen combine at a significant rate at temperatures above 1500°C, and the formation rate increases exponentially as temperature increases. Even with the high gas velocities in gas turbines, NO_x emissions will reach 200 parts per million by volume, dry (ppmvd), in gas turbines with conventional combustors and no NO_x abatement features. Emissions standards throughout the world vary, but many parts of the world require gas turbines to be equipped to control NO_x to below 25 ppmvd at base load.

Emissions

Combustion of common fuels necessarily results in the emission of water vapor and carbon dioxide. Combustion of near-stoichiometric mixtures results in very high temperatures. Oxides of nitrogen are formed as the oxygen and nitrogen in the air combine, and this happens at gas turbine combustion temperatures. Carbon monoxide forms when the combustion process is incomplete. Unburned hydrocarbons (UHCs) are discharged as well when combustion is incomplete. Other pollutants are attributed to fuel; principal among these is sulfur. Gas turbines neither add nor remove sulfur; hence, what sulfur enters the gas turbine in the fuel exits as SO_2 in the exhaust.

Carbon dioxide emissions are no longer considered totally benign due to global concern for the “greenhouse effect” and global warming. Carbon in fuel is converted to CO_2 in the combustion process, so for any given fuel, increasing cycle efficiency is the only means of reducing exhaust of the CO_2 associated with each megawatt generated. Figure 7 gives the relationship

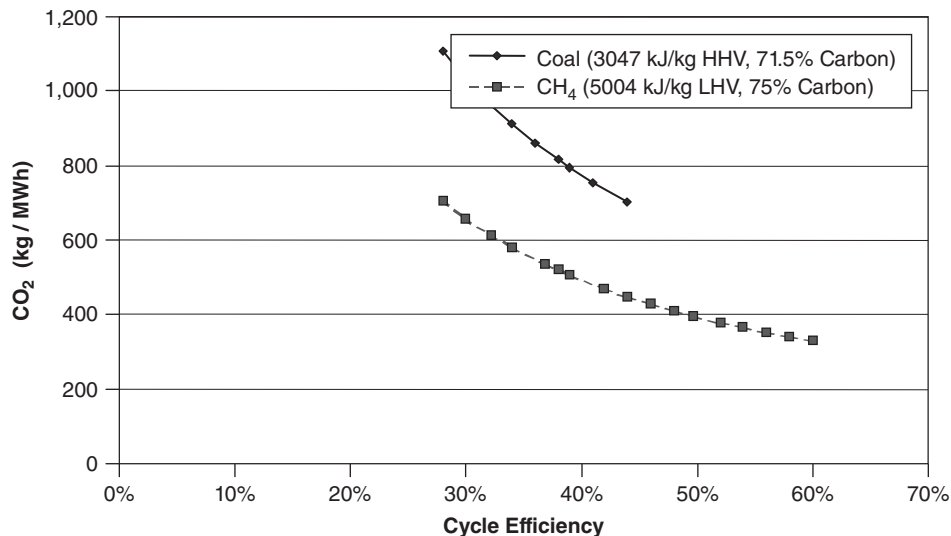


Figure 7 Coal versus natural gas: kg CO₂ per MWh. (Coal and CH₄ quoted at different heating values; published efficiencies are consistent with each definition.)

between efficiency and exhaust CO₂ for a gaseous and a solid fuel. Several studies have been made for further reducing the release of CO₂ to the environment, and these involve either removing the carbon from the fuel or removing the CO₂ from the exhaust. In either case, the scheme requires an enabling technology for sequestering the carbon or carbon dioxide. Some schemes involve gas turbine design considerations, as they require some integration with air separation processes or working fluids with high water content, hence high thermal transport properties.

Much of the gas turbine combustion research and development since the 1980s focused on lowering NO_x production in mechanically reliable combustors while maintaining low CO and UHC emissions. Early methods of reducing NO_x emissions included removing it from the exhaust by selective catalytic reduction (SCR) and by diluent injection, which is the injection of water or steam into the combustor. These methods continue to be employed. The lean-premix combustors now in general use are products of ongoing research.

Thermal NO_x is generally regarded as being generated by a chemical reaction sequence called the Zeldovich mechanism,⁶ and the rate of NO_x formation is proportional to temperature, as shown in Fig. 8. In practical terms, a conventional gas turbine emits approximately 200 ppmvd when its combustors are not designed to control NO_x. This is because a significant portion of the combustion zone has stoichiometric or near-stoichiometric conditions and temperatures are high. Additional oxygen and, of course, nitrogen on the boundary of the flame are heated to sufficiently high temperatures and held at these temperatures for sufficient time to produce NO_x.

Water- and steam-injected combustors achieve low flame temperatures by placing diluent in the neighborhood of the reacting fuel and air. Among low-NO_x combustion systems operating today, water and steam injection are the most common means of flame temperature reduction. Several hundred large industrial turbines operating with steam or water injection have accumulated over 2.5 million hours of service. Water is not the only diluent used for NO_x control. In the case of integrated gasification combined-cycle (IGCC) plants, nitrogen and CO₂ are available and can be introduced into the combustion region.⁷

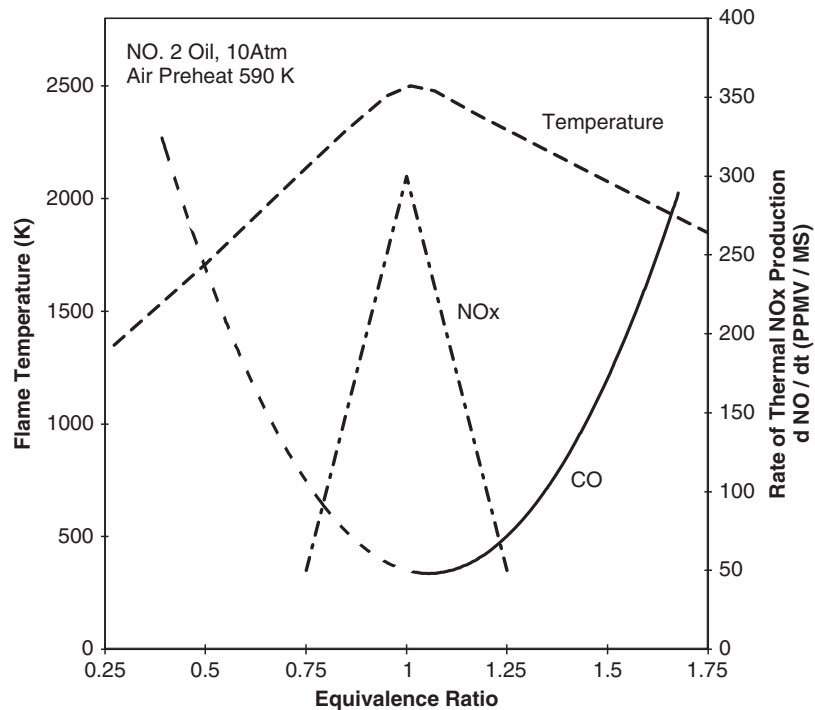


Figure 8 NO_x formation rate driven by temperature. *Source:* From Ref. 5, Courtesy of Westinghouse Corporation.

Water or steam injection can achieve levels that satisfy many current standards, but water consumption is sometimes not acceptable to the operator because of cost, availability, or impact on efficiency. Steam injection sufficient to reduce NO_x emissions to 25 ppmvd can increase fuel consumption in combined-cycle power plants by over 3%. Water injection increases fuel use by over 4% for the same emissions level. In base-load power plants, fuel cost is so significant that it has prompted the development of systems that do not require water.⁸

In all combustion processes, when a molecule of methane combines with two molecules of oxygen, a known and fixed amount of heat is released. When only these three molecules are present, a minimum amount of mass is present to absorb the energy not radiated and the maximum temperature is realized. Add to the neighborhood of the reaction the nitrogen as found in air (four times the volume of oxygen involved in the reaction) and the equilibrium temperature is lower. By adding even more air to the combustion region, more mass is available to absorb the energy, and the resulting observable temperature is lower still. The same can be achieved through the use of excess fuel. Thus, by moving away from the stoichiometric mixture, observable flame temperature is lowered, and the production of NO_x is also reduced. On a microscopic level, lean-burning, low-NO_x combustors are designed to force the chemical reaction to take place in such a way that the energy released is in the neighborhood of as much mass not taking part in the reaction as possible. By transferring heat to neighboring material immediately, the time at temperature is reduced. On a larger scale, a high measurable temperature will never be reached in a well-mixed lean system. Thus, NO_x generation is minimized. Both rich-mixture and lean-mixture systems have led to low-NO_x schemes. Those featuring rich flames followed by lean-burning zones are sometimes suggested for situations where there is nitrogen in the fuel; most of today's systems are based on lean burning.

Early lean, premix, dry, low- NO_x combustors were operated in GE gas turbines at the Houston Light and Power Wharton Station (U.S.) in 1980 and in Mitsubishi units in Japan in 1983 and were introduced in Europe in 1986 by Siemens KWU. These combustors control the formation of NO_x by premixing fuel with air prior to its ignition while conventional combustors mix essentially at the instant of ignition. Dry low- NO_x combustors, as the name implies, achieve NO_x control without consuming water and without imposing efficiency penalties on combined-cycle plants.

Figures 9 and 10 show dry low- NO_x combustors developed for large gas turbines. In the GE system, several premixing chambers are located at the head end of the combustor. A fuel nozzle assembly is located in the center of each chamber. By manipulating valves external to the gas turbine, fuel can be directed to several combinations of chambers and to various parts of the fuel nozzles. This is to permit the initial ignition of the fuel and to maintain a relatively constant local fuel-air ratio at all load levels. There is one flame zone, immediately downstream of the premixing chambers. The Westinghouse combustor illustrated in Fig. 10 has three concentric premixing chambers. The two nearest the centerline of the combustor are designed to swirl the air passing through them in opposite directions and discharge into the primary combustion zone. The third, which has a longer passage, is directed to the secondary zone. Modulating fuel flow to the various mixing passages and combustion zones ensures low- NO_x production over a wide range of operating temperatures. Both the combustors shown are designed for state-of-the-art, high-firing-temperature gas turbines.

Low- NO_x combustors feature multiple premixing features and a more complex control system than more conventional combustors to achieve stable operation over the required range of operating conditions. Conventional combustors operate with stability over a wide range of fuel-air mixtures between the rich and lean flammability limits. A sufficiently wide range of fuel flows could be burned in a combustor with a fixed air flow to match the range of load

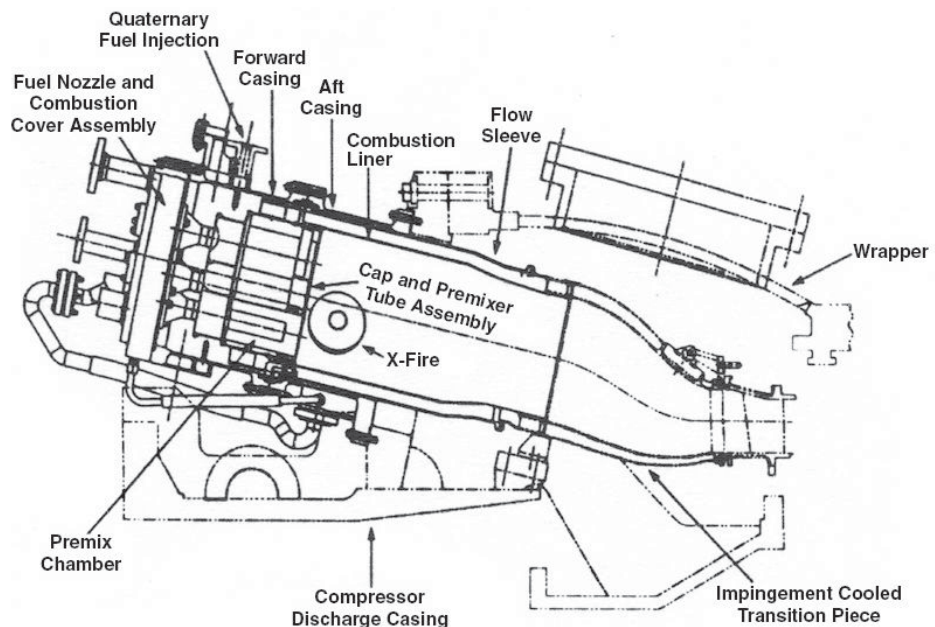


Figure 9 GE DLN-2 lean-premix combustor designed for low emissions at high firing temperatures. Courtesy of General Electric Company.

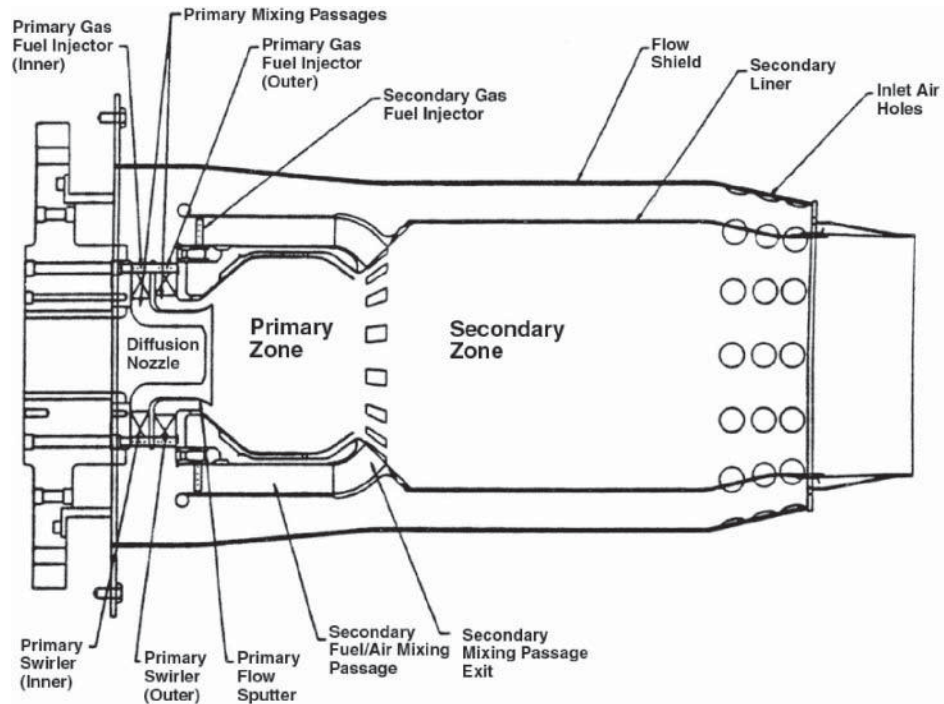


Figure 10 Westinghouse dry low- NO_x combustor for advanced gas turbines. Courtesy of Westinghouse Corporation.

requirements from no load to full load. In a low- NO_x combustor, the fuel–air mixture feeding the flame must be regulated between the point of flame loss and the point where the NO_x limit is exceeded. When low gas turbine output is required, the air premixed with the fuel must be reduced to match the fuel flow corresponding to the low power output. The two combustors shown previously hold nearly constant fuel–air ratios over the load range by having multiple premixing chambers, each one flowing a constant fraction of the compressor discharge flow. By directing fuel to only some of these passages at low load, the design achieves both part load and optimum local fuel–air ratio. Three, four, or more sets of fuel passages are not uncommon, and premixed combustion is maintained to approximately 50% of the rated load of the machine.^{5,9}

Catalytic combustion systems are under investigation for gas turbines. These systems have demonstrated stable combustion at lower fuel–air ratios than those using chamber or nozzle shapes to stabilize flames. They offer the promise of simpler fuel regulation and greater turn-down capability than low- NO_x combustors now in use. In catalytic combustors, the fuel and air react in the presence of a catalytic material, which is deposited on a structure having multiple parallel passages or mesh. Extremely low NO_x levels have been observed in laboratories with catalytic combustion systems.

Turbine

Figure 11 shows an axial-flow turbine. Radial in-flow turbines similar in appearance to centrifugal compressors are also produced for some smaller gas turbines. By the time the extremely hot gas leaves the combustor and enters the turbine, it has been mixed with compressor discharge air to cool it to temperatures that can be tolerated by the first-stage blading in the turbine:

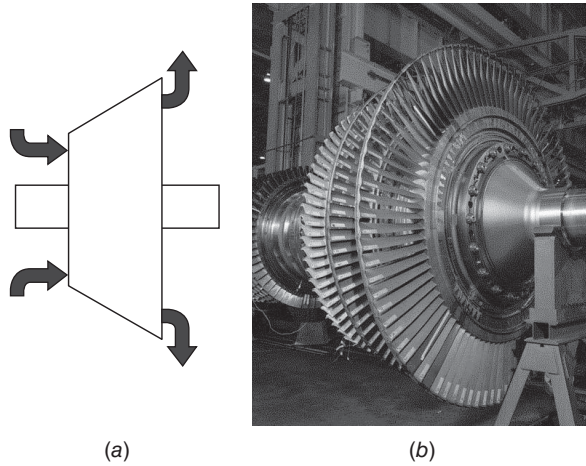


Figure 11 Turbine diagram and photograph of an axial-flow turbine during assembly. Courtesy of General Electric Company.

temperatures ranging from 950°C in first-generation gas turbines to over 1500°C in turbines are currently being developed and in state-of-the-art aircraft engines. Less dilution flow is required as firing temperatures approach 1500°C .

The first-stage stationary blades, or nozzles, are located at the discharge of the combustor. Their function is to accelerate the hot working fluid and turn it so as to enter the following rotor stage at the proper angle. These first-stage nozzles are subjected to the highest gas velocity in the engine. The gas entering the first-stage nozzle can regularly be above the melting temperature of the structural metal. These conditions produce high heat transfer to the nozzles, so that cooling is necessary.

Nozzles are subjected to stresses imposed by aerodynamic flow of the working fluid, pressure loading of the cooling air, and thermal stresses caused by uneven temperatures over the nozzle structure (Fig. 12). First-stage nozzles can be supported at both ends by the inner and

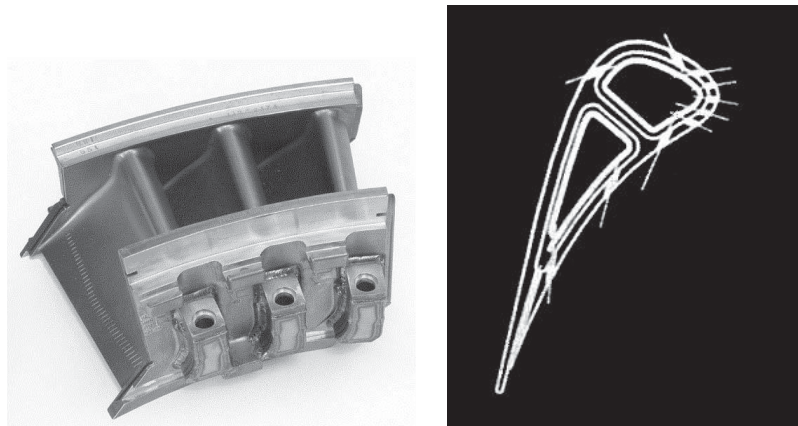


Figure 12 Gas turbine nozzle. Sketch shows cooling system of one airfoil. Courtesy of General Electric Company.

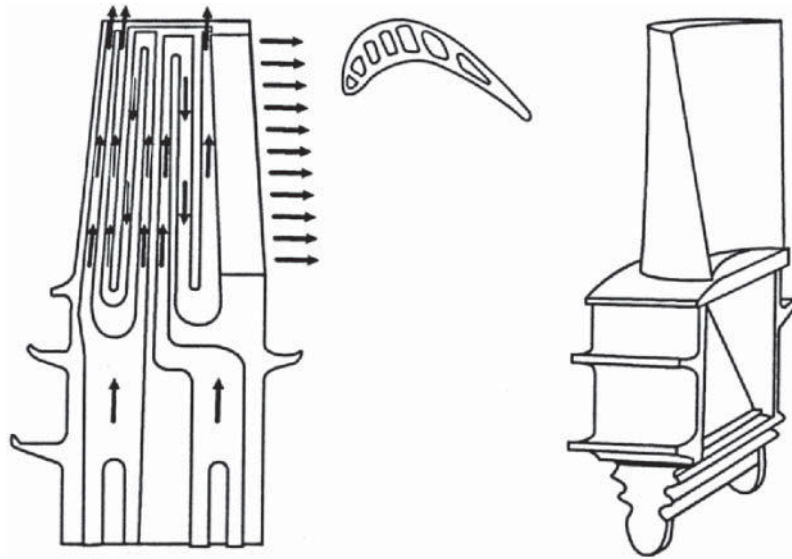


Figure 13 Gas turbine first-stage air-cooled bucket. Cutaway view exposes serpentine cooling passages. Courtesy of General Electric Company.

outer sidewalls. But later stage nozzles, because of their location in the engine, can be supported only at the outer end, intensifying the effect of aerodynamic loading.

The rotating blades of the turbine, or buckets, convert the kinetic energy of the hot gas exiting the nozzles to the shaft power used to drive the compressor and load devices (Fig. 13). The blade consists of an airfoil section in the gas path, a dovetail or other type of joint connecting the blade to the turbine disk, and often a shank between the airfoil and dovetail allowing the dovetail to run at lower temperature than the root of the airfoil. Some bucket designs employ tip shrouds to limit deflection at the outer ends of the buckets, raise natural vibratory frequencies, and provide aerodynamic benefits. Exceptions from this configuration are radial inflow turbines like those common to automotive turbochargers and axial turbines, wherein the buckets and wheels are made of one piece of metal or ceramic.

The total temperature of the gas relative to the bucket is lower than that relative to the preceding nozzles. This is because the tangential velocity of the rotor-mounted airfoil is in a direction away from the gas stream and thus reduces the dynamic component of total temperature. Also, the gas temperature is reduced by the cooling air provided to the upstream nozzle and the various upstream leakages.

Buckets and the disks on which they are mounted are subject to centrifugal stresses. The centrifugal force acting on a unit mass at the blades' midspan is 10,000–100,000 times that of gravity. Midspan airfoil centrifugal stresses range from 7 kg/mm^2 (10,000 psi) to over 28 kg/mm^2 (40,000 psi) at the airfoil root in the last stage (longest buckets).

Turbine efficiency is calculated similarly to compressor efficiency. Figure 6 also shows the effect of turbine efficiency. Line cd represents the isentropic expansion process and cd' the actual. Turbine efficiency η_t is the ratio of the vertical projections of the lines. Thus, $(1250 - 557)/(1250 - 480) = 90\%$. It is possible at this point to compute the effect of a 90% efficient compressor and a 90% efficient turbine upon the simple-cycle efficiency of the gas turbine represented in the figure. The turbine work is proportional to 693°C and the compressor work to 372°C . The heat added by combustion is proportional to 887°C , the temperature rise from

b' to c . The ratio of the useful work to the heat addition is thus 36.2%. It was shown previously that the efficiency with ideal components is approximately 48.3%.

The needs of gas turbine blading have been responsible for the rapid development of a special class of alloys. To tolerate higher metal temperatures without decrease in component life, materials scientists and engineers have developed and continue to advance families of temperature-resistant alloys, processes, and coatings. The “superalloys” were invented and continue to be developed primarily in response to turbine needs. These are usually based on group VIIIA elements: cobalt, iron, and nickel. Bucket alloys are austenitic with gamma/gamma-prime, face-centered-cubic structure (Ni_3Al). The elements titanium and columbium are present and partially take the place of aluminum with beneficial hot corrosion effect. Carbides are present for grain boundary strength, along with some chromium to further enhance corrosion resistance. The turbine industry has also developed processes to produce single-crystal and directionally solidified components, which have even better high-temperature performance. Coatings are now in universal use, which enhance the corrosion and erosion performance of hot-gas path components.¹⁰

Cooling

Metal temperature control is addressed primarily through airfoil cooling, with cooling air being extracted from the gas turbine flow ahead of the combustor. Since this air is not heated by the combustion process and may even bypass some turbine stages, the cycle is less efficient than it would be without cooling. Further, as coolant reenters the gas path, it produces quenching and mixing losses. Hence, for efficiency, the use of cooling air should be minimized. Turbine designers must make trade-offs among cycle efficiency (firing temperature), parts lives (metal temperature), and component efficiency (cooling flow).

In early first-generation gas turbines, buckets were solid metal, operating at the temperature of the combustion gases. In second-generation machines, cooling air was conducted through simple, radial passages, to keep metal temperatures below those of the surrounding gas. In today’s advanced-technology gas turbines, most manufacturers utilize serpentine air passages within the first-stage buckets, with cooling air flowing out the tip, leading, and trailing edges. Leading-edge flow is used to provide a cooling film over the outer bucket surface. Nozzles are often fitted with perforated metal inserts attached to the inside of hollow airfoils. The cooling air is introduced inside of the inserts. It then flows through the perforations, impinging on the inner surface of the hollow airfoil. The cooling thus provided is called impingement cooling. The cooling air then turns and flows within the passage between the insert and the inner surface of the airfoil, cooling it by convection until it exits the airfoil in either leading-edge film holes or trailing-edge bleed holes.

The effectiveness of cooling, η , is defined as the ratio of the difference between gas and metal temperatures to the difference between the gas temperature and the coolant temperature:

$$\eta = (T_g - T_m)/(T_g - T_c)$$

Figure 14 portrays the relationship between this parameter and a function of the cooling air flow. It can be seen that, while increased cooling flows have improved cooling effectiveness, there are diminishing returns with increased cooling air flow.

Cooling can be improved by precooling the air extracted from the compressor. This is done by passing the extracted air through a heat exchanger prior to using it for bucket or nozzle cooling. This does increase cooling but presents several challenges, such as increasing temperature gradients and the cost and reliability of the cooling equipment. Recent advanced gas turbine products have been designed with both cooled and uncooled cooling air.

Other cooling media have been investigated. In the late 1970s, the U.S. Department of Energy sponsored the study and preliminary design of high-temperature turbines cooled by

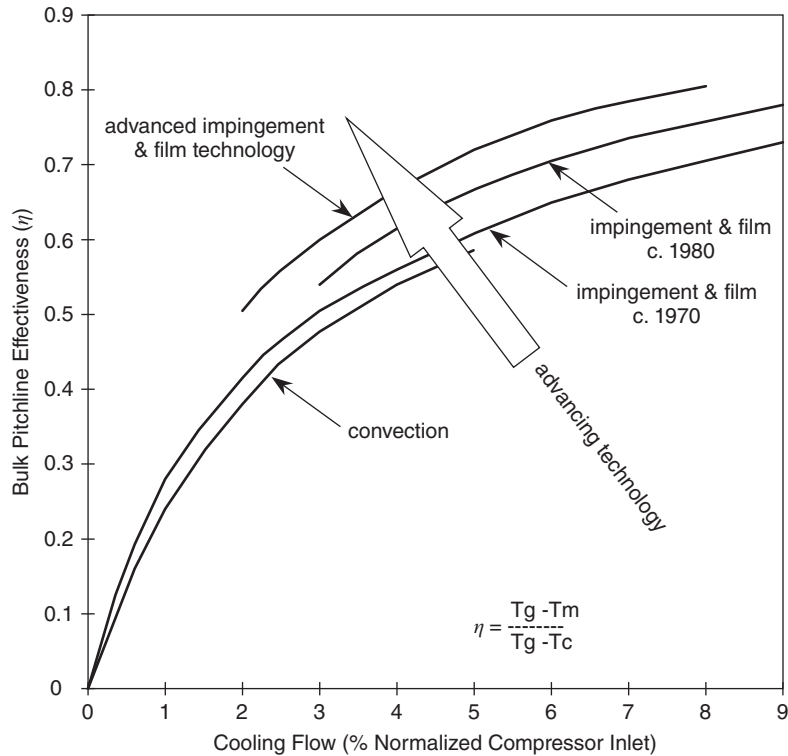


Figure 14 Evolution of turbine airfoil cooling technology.

water and steam. Nozzles of the water-cooled turbine were cooled by water contained in closed passages and kept in the liquid state by pressurization; no water from the nozzle circuits entered the gas path. Buckets were cooled by two-phase flow; heat was absorbed as the coolant was vaporized and heated. Actual nozzles were successfully rig tested. Simulated buckets were tested in heated, rotating rigs. Recent advanced land-based gas turbines have been configured with both buckets and nozzles cooled with a closed steam circuit. Steam, being a more effective cooling medium than air, permits high firing temperatures and, since it does not enter the gas path, eliminates the losses associated with cooling air mixing with the working fluid. The coolant, after being heated in the buckets and nozzles, returns to the steam cycle of a combined-cycle plant. The heat carried away by the steam is recovered in a steam turbine.

Steam cooling of gas path airfoils—both stationary and rotating—has been reduced to practice in gas turbines, and such gas turbines are available commercially. The first so-called “H” technology, the 50-Hz power plant operated at Baglan Bay in the United Kingdom, has been observed to produce more than 530 MW when operated at an ambient temperature of 4.5°C. The level of power was produced by a single-gas-turbine, single-steam-turbine combined-cycle plant.

1.4 Controls and Accessories

Controls

The control system is the interface between the operator and the gas turbine. More correctly, the control system of modern industrial and utility gas turbines interfaces between the operator

and the entire power plant, including the gas turbine, generator, and all related accessories. In combined-cycle power plants where in addition a steam turbine, heat recovery steam generator, condensing system, and all related accessories are present, the control system interfaces with these as well.

Functions provided are described in Section 1.5 plus protection of the turbine from faults such as overspeed, overheating, combustion anomalies, cooling system failures, and high vibrations. Also, controls facilitate condition monitoring, problem identification and diagnosis, and monitoring of thermodynamic and emissions performance. Sensors placed on the gas turbine include speed pickups, thermocouples at the inlet, exhaust, compressor exit, wheelspaces, bearings, oil supplies, and drains. Vibration monitors are placed on each bearing. Pressures are also monitored at the compressor exit. Multiple thermocouples in the exhaust can detect combustor malfunction by noting abnormal differences in exhaust temperature from one location to another. Multiple sensors elsewhere allow the more sophisticated control systems to self-diagnose, to determine if a problem reading is an indication of a dangerous condition or the result of a sensor malfunction.

Control system development over the past two decades has contributed greatly to the improved reliability of power generation gas turbines. The control systems are now all computer based. Operator input is via keyboard and cursor movement. Information is displayed to the operator via color graphic displays and tabular and text data on color monitors.

Inlet Systems

Inlet systems filter and direct incoming air and provide attenuation of compressor noise. They also can include heating and cooling devices to modify the temperature of the air drawn into the gas turbine. Since fixed-wing aircraft engines operate most of the time at high altitudes where air is devoid of heavier and more damaging particles, these engines are not fitted with inlet air treatment systems performing more than an aerodynamic function. The premium placed on engine weight makes this so. Inertial separators have been applied to helicopter engines to reduce their ingestion of particulates.

Air near the surface of the earth contains dust and dirt of various chemical compositions. Because of the high volume of air taken into a gas turbine, this dirt can cause erosion of compressor blades, corrosion of turbine and compressor blades, and plugging of passages in the gas path as well as cooling circuits. The roughening of compressor blade surfaces can be due to particles sticking to airfoil surfaces, erosion, or because of corrosion caused by their chemical composition. This fouling of the compressor can, over time, reduce mass flow and lower compressor efficiency. Both effects will reduce the output and efficiency of the gas turbine. "Self-cleaning" filters collect airborne dirt. When the pressure drop increases to a preset value, a pulse of air is used to reverse the flow briefly across the filter medium, cleaning the filter. More conventional, multistage filters also find application.

Under low-ambient-temperature, high-humidity conditions, it is possible to form frost or ice in the gas turbine inlet. Filters can be used to remove humidity by causing frost to form on the filter element; this frost is removed by the self-cleaning feature. Otherwise, a heating element can be installed in the inlet compartment. These elements use higher temperature air extracted from the compressor. This air is mixed with the ambient air raising its temperature. Compressors of most robust gas turbines are designed so that these systems are required only at part load or under unusual operating conditions.

Inlet chillers have been applied on gas turbines installed in high-ambient-temperature, low-humidity regions of the world. The incoming air is cooled by the evaporation of water. Cooling the inlet air increases its density and increases the output of the gas turbine.

Exhaust Systems

The exhaust systems of industrial gas turbines perform three basic functions. Personnel must be protected from the high-temperature gas and from the ducts that carry it. The exhaust gas must be conducted to an exhaust stack or to where the remaining heat from the gas turbine cycle can be effectively used. The exhaust system also contains baffles and other features employed to reduce the noise generated by the gas turbine.

Enclosures and Lagging

Gas turbines are enclosed for four reasons: noise, heat, fire protection, and visual aesthetics. Gas turbines are sometimes provided for outdoor installation, where the supplier includes a sheet metal enclosure, which may be part of the factory-shipped package. Other times, gas turbines are installed in a building. Even in a building, the gas turbine is enclosed for the benefit of maintenance crews or other occupants. Some gas turbines are designed to accommodate an insulating wrapping that attaches to the casings of the gas turbine. This prevents maintenance crews from coming into contact with the hot casings when the turbine is operating and reduces some of the noise generated by the gas turbine. Proponents cite the benefit of lowering the heat transferred from the gas turbine to the environment. Theoretically, more heat is carried to the exhaust, which can be used for other energy needs. Others contend that the larger internal clearances resulting from hotter casings would offset this gain by lower component efficiencies.

Where insulation is not attached to the casings—and sometimes when it is—a small building-like structure is provided. This structure is attached to either the turbine base or the concrete foundation. Such a structure provides crew protection and noise control and assists in fire protection. If a fire is detected on the turbine, within the enclosure, its relative small volume makes it possible to quickly flood the area with CO₂ or other fire-fighting chemical. The fire is thereby contained in a small volume and more quickly extinguished. Even in a building, the noise control provided by an enclosure is beneficial, especially in buildings containing additional gas turbines or other equipment. By lowering the noise 1 m from the enclosure to below 85 or 90 dBA it is possible to safely perform maintenance on this other equipment, yet continue to operate the gas turbine. Where no turbine enclosure is provided within a building, the building becomes part of the fire protection and acoustic system.

Fuel Systems

The minimum function required of a gas turbine fuel system is to deliver fuel from a tank or pipeline to the gas turbine combustor fuel nozzles at the required pressure and flow rate. The pressure required is somewhat above the compressor discharge pressure, and the flow rate is that called for by the controls. On annular and can-annular combustors, the same fuel flow must be distributed to each nozzle to ensure minimum variation in the temperature to which gas path components are exposed. Other fuel system requirements are related to the required chemistry and quality of the fuel.

Aircraft engine fuel quality and chemistry are closely regulated, so extensive on-board fuel-conditioning systems are not required. Such is not the case in many industrial applications. Even the better grades of distillate oil may be delivered by ocean-going tankers and run the risk of sodium contamination from the saltwater sometimes used for ballast. Natural gas now contains more of the heavier liquefied petroleum gases. Gas turbines are also fueled with crude oil, heavy oils, and various blends. Some applications require the use of nonlubricating fuels such as naphtha. Most fuels today require some degree of on-site treatment.

Complete liquid fuel treatment includes washing to remove soluble trace metals such as sodium, potassium, and certain calcium compounds. Filtering the fuel removes solid oxides and silicates. Inhibiting the vanadium in the fuel with magnesium compounds in a ratio of three parts of magnesium by weight to one part of vanadium, limits the corrosive action of vanadium on the alloys used in high-temperature gas path parts.

Gas fuel is primarily methane, but it contains varying levels of propane, butane, and other heavier hydrocarbons. When levels of these heavier gases increase, the position of the flame in the combustor may change, resulting in local hot spots, which could damage first-stage turbine stator blades. Also, sudden increases could cause problems for dry low- NO_x premixed combustors. These combustors depend on being able to mix fuel and air in a combustible mixture before the mixture is ignited. Under some conditions, heavier hydrocarbons can self-ignite in these mixtures at compressor exit temperatures, thus causing flame to exist in the premixing portion of the combustor. The flame in the premixing area would have to be extinguished and reestablished in the proper location. This process interferes with normal operation of the machine.

Lubricating Systems

Oil must be provided to the bearings of the gas turbine and its driven equipment. The lubricating system must maintain the oil at sufficiently low temperature to prevent deterioration of its properties. Contaminants must be filtered out. Sufficient volume of oil must be in the system so that any foam has time to settle out. Also, vapors must be dealt with; preferably they are recovered and the oil returned to the plenum. The oil tank for large industrial turbines is generally the base of the lubricating system package. Large utility machines are provided with tanks that hold over 12,000 L of oil. The oil is generally replaced after approximately 20,000 h of operation. More oil is required in applications where the load device is connected to the gas turbine by a gearbox.

The lubrication system package also contains filters and coolers. The turbine is fitted with mist elimination devices connected to the bearing air vents. Bearings may be vented to the turbine exhaust, but this practice is disappearing for environmental reasons.

Cooling Water and Cooling Air Systems

Several industrial gas turbine applications require the cooling of some accessories. The accessories requiring cooling include the starting means, lubrication system, atomizing air, load equipment (generator/alternator), and turbine support structure. Water is circulated in the component requiring cooling, then conducted to where the heat can be removed from the coolant. The cooling system can be integrated into the industrial or power plant hosting the gas turbine or can be dedicated to the gas turbine. In this case the system usually contains a water-to-air heat exchanger with fans to provide the flow of air past finned water tubes.

Water Wash Systems

Compressor fouling related to deposition of particles that are not removed by the air filter can be dealt with by water washing the compressor. A significant benefit in gas turbine efficiency over time can be realized by periodic cleaning of the compressor blades. This cleaning is most conveniently done when the gas turbine is fitted with an automatic water-wash system. Washing is initiated by the operator. The water is preheated and detergent is added. The gas turbine rotor is rotated at a low speed and the water is sprayed into the compressor. Drains are provided to remove wastewater.

1.5 Gas Turbine Operation

Like other internal combustion engines, the gas turbine requires an outside source of starting power. This is provided by an electrical motor or diesel engine connected through a gear box to the shaft of the gas turbine (the high-pressure shaft in a multishaft configuration). Other devices can be used (including the generator of large, electric utility gas turbines) by using a variable-frequency power supply. Power is normally required to rotate the rotor past the gas turbine's ignition speed of 10–15%, on to 40–80% of rated speed where the gas turbine is self-sustaining, meaning the turbine produces sufficient work to power the compressor and overcome bearing friction, drag, etc. Below self-sustaining speed, the component efficiencies of the compressor and turbine are too low to reach or exceed this equilibrium.

When the operator initiates the starting sequence of a gas turbine, the control system acts by starting auxiliaries such as those that provide lubrication and the monitoring of sensors provided to ensure a successful start. Then the control system calls for application of torque to the shaft by the starting means. In many industrial and utility applications, the rotor must be rotated for a period of time to purge the flow path of unburned fuel which may have collected there. This is a safety precaution. Thereafter, the light-off speed is achieved; ignition takes place and is confirmed by sensors. Ignition is provided by either a spark-plug-type device or a liquefied petroleum gas torch built into the combustor. Fuel flow is then increased to increase the rotor speed. In large gas turbines, a warm-up period of 1 min or so is required at approximately 20% speed. The starting means remains engaged, since the gas turbine has not reached its self-sustaining speed. This reduces the thermal gradients experienced by some of the turbine components and extends their low-cycle fatigue life.

The fuel flow is again increased to bring the rotor to self-sustaining speed. For aircraft engines, this is approximately the idle speed. For power generation applications, the rotor continues to be accelerated to full speed. In the case of these alternator-driving gas turbines, this is set by the speed at which the alternator is synchronized with the power grid to which it is to be connected.

The speed and thrust of aircraft engines are interrelated. The fuel flow is increased and decreased to generate the required thrust. The rotor speed is principally a function of this fuel flow but also depends on any variable compressor or exhaust nozzle geometry changes programmed into the control algorithms. Thrust is set by the pilot to match the current requirements of the aircraft—through takeoff, climb, cruise, maneuvering, landing, and braking.

At full speed, the power generation gas turbine and its generator (alternator) must be synchronized with the power grid in both speed (frequency) and phase. This process is computer controlled and involves making small changes in turbine speed until synchronization is achieved. At this point, the generator is connected with the power grid. The load of a power generation gas turbine is set by a combination of generator (alternator) excitement and fuel flow. As the excitation is increased, the mechanical work absorbed by the generator increases. To maintain a constant speed (frequency) the fuel flow is increased to match that required by the generator. The operator normally sets the desired electrical output and the turbine's electronic control increases both excitation and fuel flow until the desired operating conditions are reached.

Normal shutdown of a power generation gas turbine is initiated by the operator and begins with the reduction of load, reversing the loading process described immediately previous. At a point near zero load, the breaker connecting the generator to the power grid is opened. Fuel flow is decreased, and the turbine is allowed to decelerate to a point below 40% speed, whereupon the fuel is shut off and the rotor is allowed to a stop. The rotors of large turbines should be turned periodically to prevent temporary bowing from uneven cooldown, which will cause vibration on subsequent start-ups. Turning of the rotor for cooldown is accomplished by a ratcheting mechanism on smaller gas turbines or by operation of a motor associated with shaft-driven

accessories or even the starting mechanism on others. Aircraft engine rotors do not tend to exhibit the bowing just described. Bowing is a phenomenon observed in massive rotors left stationary surrounded by cooling, still air, which, due to free convection, is cooler at the 6:00 position than at the 12:00 position. The large rotor assumes a similar gradient and because of proportional thermal expansion assumes a bowed shape. Because of the massiveness of the rotor, this shape persists for several hours and could remain present at the time when the operator wishes to restart the turbine.

2 GAS TURBINE PERFORMANCE

2.1 Gas Turbine Configurations and Cycle Characteristics

There are several possible mechanical configurations for the basic simple-cycle, or open-cycle, gas turbine. There are also some important variants on the basic cycle—intercooled, regenerative, and reheat cycles.

The simplest configuration is shown in Fig. 15. Here the compressor and turbine rotors are connected directly to one another and to shafts by which turbine work in excess of that required to drive the compressor can be applied to other work-absorbing devices. Such devices are the propellers and gear boxes of turboprop engines, electrical generators, ships' propellers, pumps, gas compressors, vehicle gear boxes and driving wheels, and the like. A variation is shown in Fig. 16, where a jet nozzle is added to generate thrust. Through aerodynamic design, the pressure drop between the turbine inlet and ambient air is divided so that part of the drop occurs across the turbine and the remainder across the jet nozzle. The pressure at the turbine exit is set so that there is only enough work extracted from the working fluid by the turbine

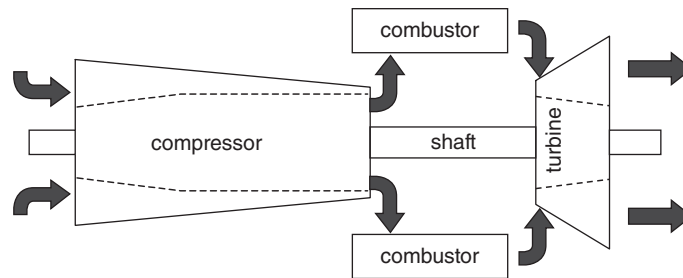


Figure 15 Simple-cycle, single-shaft gas turbine schematic.

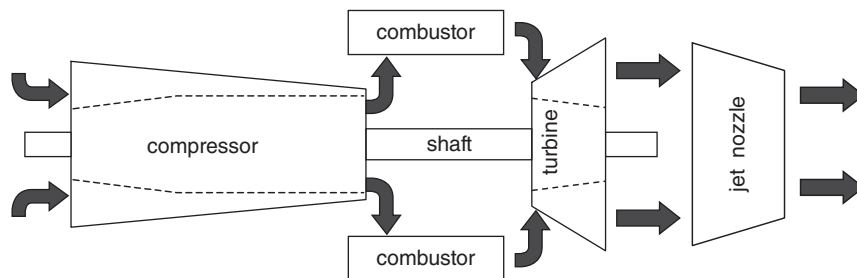


Figure 16 Single-shaft, simple-cycle gas turbine with jet nozzle; simple turbojet engine schematic.

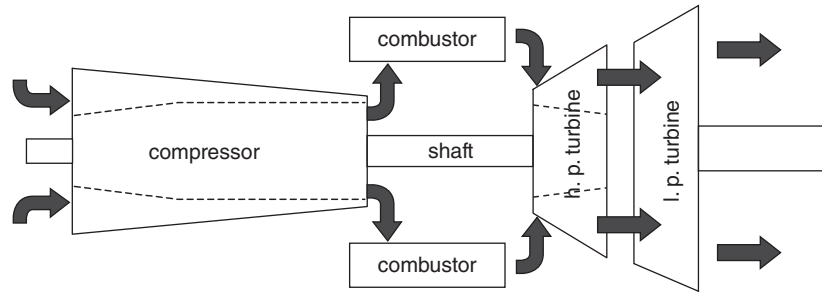


Figure 17 Industrial two-shaft gas turbine schematic showing high-pressure gas generator rotor and separate, free-turbine low-pressure rotor.

to drive the compressor (and mechanical accessories). The remaining energy accelerates the exhaust flow through the nozzle to provide jet thrust.

The simplest of multishaft arrangements appears in Fig. 17. For decades, such arrangements have been used in heavy-duty turbines applied to various petrochemical and gas pipeline uses. Here, the turbine consists of a high-pressure and a low-pressure section. There is no mechanical connection between the rotors of the two turbines. The high-pressure (h.p.) turbine drives the compressor and the low-pressure (l.p.) turbine drives the load—usually a gas compressor for a process, gas well or pipeline. Often, there is a variable nozzle between the two turbine rotors, which can be used to vary the work split between the two turbines. This offers the user an advantage. When it is necessary to lower the load applied to the driven equipment—for example, when it is necessary to reduce the flow from a gas pumping station—fuel flow would be reduced. With no variable geometry between the turbines, both would drop in speed until a new equilibrium between low- and high-pressure speeds occurs. By changing the nozzle area between the rotors, the pressure drop split is changed, and it is possible to keep the high-pressure rotor at a high, constant speed and have all the speed drop occur in the low-pressure rotor. By doing this, the compressor of the gas turbine continues to operate at or near its maximum efficiency, contributing to the overall efficiency of the gas turbine and providing high part-load efficiency. This two-shaft arrangement is one of those applied to aircraft engines in industrial applications. Here, the high-pressure section is essentially identical to the aircraft turbojet engine, or the core of a fan-jet engine. This high-pressure section then becomes the “gas generator,” and the free turbine becomes what is referred to as the “power turbine.” The modern turbofan engine is somewhat similar in that a low-pressure turbine drives a fan, which forces a concentric flow of air outboard of the gas generator aft, adding to the thrust provided by the engine. In the case of modern turbofans, the fan is upstream of the compressor and is driven by a concentric shaft inside of the hollow shaft connecting the high-pressure compressor and high-pressure turbine.

Figure 18 shows a multishaft arrangement common to today’s high-pressure turbojet and turbofan engines. The high-pressure compressor is connected to the high-pressure turbine, and the low-pressure compressor to the low-pressure turbine, by concentric shafts. There is no mechanical connection between the two rotors (high pressure and low pressure) except via bearings and the associated supporting structure and the shafts operate at speeds mechanically independent of one another. The need for this apparently complex structure arises from the aerodynamic design constraints encountered in very high pressure ratio compressors. By having the higher pressure stages of a compressor rotating at a higher speed than the early stages, it is possible to avoid the low annulus height flow paths that contribute to poor compressor efficiency. The relationship between the speeds of the two shafts is determined by the aerodynamics of

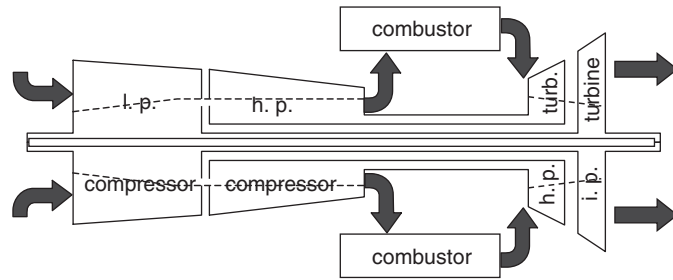


Figure 18 Schematic of multishaft gas turbine arrangement typical of those used in modern, high-pressure-ratio aircraft engines. Either a jet nozzle, for jet propulsion, or a free power turbine, for mechanical drive, can be added aft of the low-pressure turbine.

the turbines and compressors, the load on the loaded shaft, and the fuel flow. The speed of the high-pressure rotor is allowed to float but is generally monitored. Fuel flow and adjustable compressor blade angles are used to control the low-pressure rotor speed. Turbojet engines, and at least one industrial aeroderivative engine, have been configured just as shown in Fig. 18.

Additional industrial aeroderivative engines have gas generators configured as shown and have power turbines as shown in Fig. 17.

The next three configurations reflect deviations from the basic Brayton gas turbine cycle. To describe them, reference must be made back to the temperature–entropy diagram.

Intercooling is the cooling of the working fluid at one or more points during the compression process. Figure 19 shows a low-pressure compression from points *a* to *b*. At point *b*, heat is removed at constant pressure, moving to point *c*. At point *c*, the remaining compression takes place (line *cd*), after which heat is added by combustion (line *de*). Following combustion,

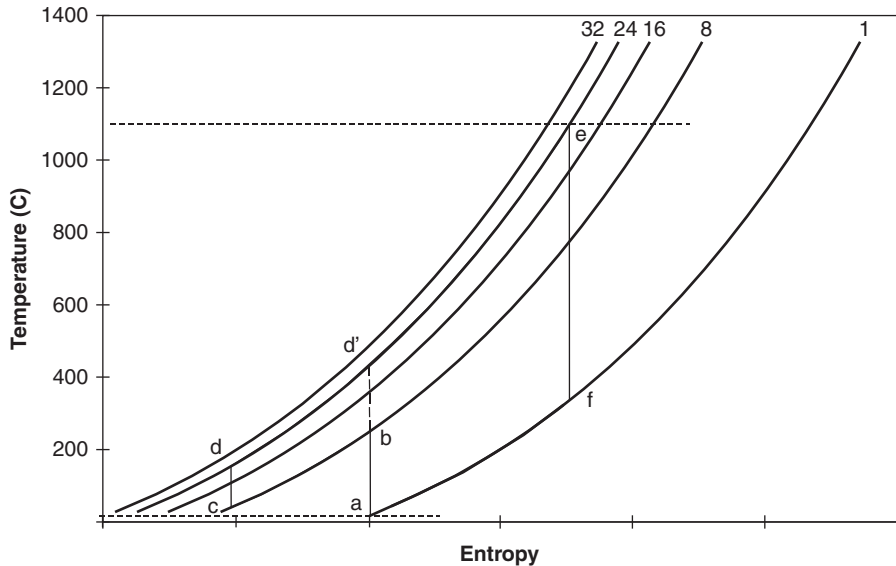


Figure 19 Temperature–entropy diagram for intercooled gas turbine cycle. Firing temperature arbitrarily selected at 1100°C and pressure ratio at 24:1.

expansion takes place (line ef) and finally the cycle is closed by discharge of air to the environment (line fa), closing the cycle. Intercooling lowers the amount of work required for compression, because work is proportional to the sum of line ab and line cd , and this is less than that of line ad' , which would be the compression process without the intercooler. Lines of constant pressure are closer together at lower temperatures, due to the same phenomenon that explains higher turbine work than compressor work over the same pressure ratio. Although the compression process is more efficient with intercooling, more fuel is required by this cycle. Note the line de as compared with the line $d'e$. It is clear that the added vertical length of line de versus $d'e$ is greater than the reduced vertical distance achieved in the compression cycle. For this reason, when the heat in the partially compressed, air is rejected, the efficiency of an intercooled cycle is generally lower than a similar simple cycle. Some benefit may be observed when comparing real machinery with intercooling applied early in the compression process, but it is, arguably, small. Furthermore, attempts to utilize low-quality heat in a cost-effective manner are usually not successful.

The useful work, which is proportional to ef less the sum of ab and cd , is greater than the useful work of the simple $ad'efa$ cycle. Hence, for the same turbomachinery, more work is produced by the intercooled cycle—an increase in power density. This benefit is somewhat offset by the fact that relatively large heat transfer devices are required to accomplish the intercooling. The intercoolers are roughly the size and volume of the turbomachinery and its accessories.

The preceding comments compare intercooled with simple cycles at fixed pressure ratio and firing temperature. The comparison ignores a potential benefit. Supercharging existing compressors and adding intercooling means pressure ratio can be increased without the mechanical implications of high compressor exit temperature. Higher cycle efficiency will follow from a higher pressure ratio.

An intercooled gas turbine is shown schematically in Fig. 20. A single-shaft arrangement is shown to demonstrate the principal, but a multishaft configuration could also be used. The compressor is divided at some point where air can be taken off-board, cooled, and brought back to the compressor for the remainder of the compression process.

The compressor discharge temperature of the intercooled cycle (point d) is lower than that of the simple cycle (point d'). Often, cooling air used to cool turbine and combustor components is taken from, or from near, the compressor discharge. An advantage often cited for intercooled cycles is the lower volume of compressor air that has to be extracted. Critics of intercooling point out that the cooling of the cooling air only, rather than the full flow of the machine, would

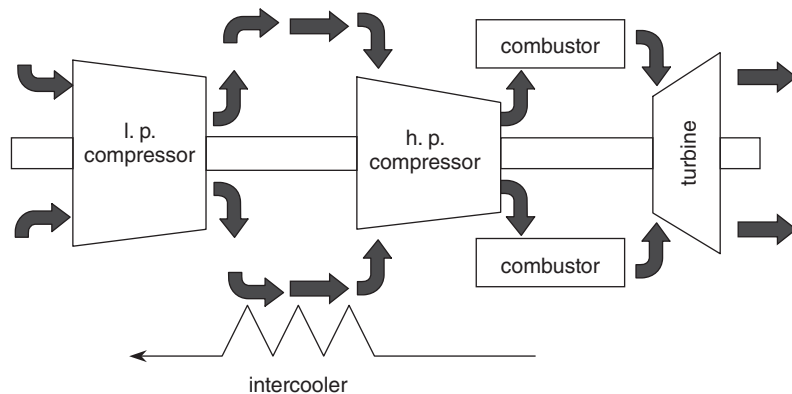


Figure 20 Schematic of a single-shaft, intercooled gas turbine. In this arrangement, both compressor groups are fixed to the same shaft. Concentric, multishaft, and series arrangements are also possible.

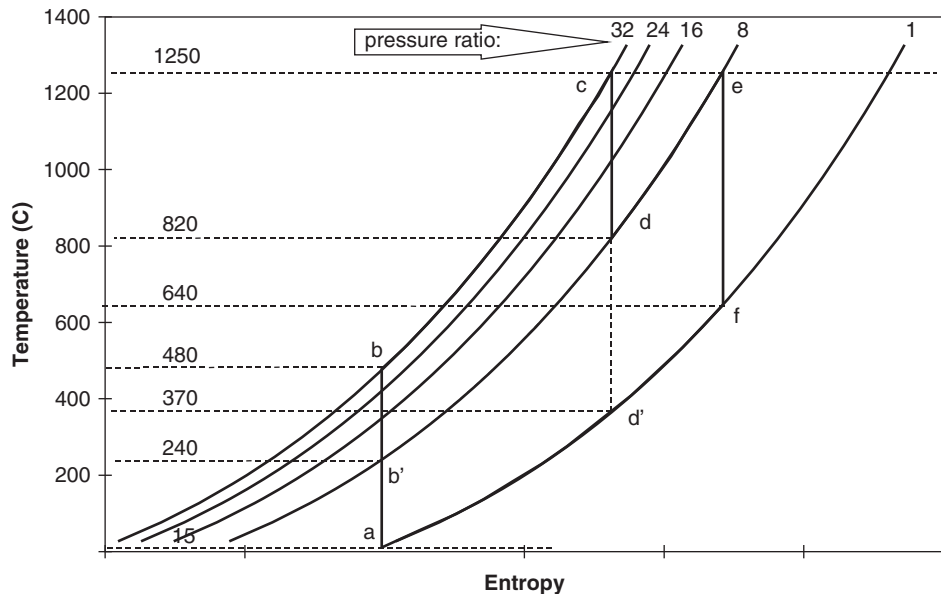


Figure 21 Temperature–entropy diagram for a reheat, or refired, gas turbine. Firing temperatures were arbitrarily chosen to be equal and to be 1250°C. The intermediate pressure ratio was chosen to be 8:1, and the overall pressure ratio was chosen to be 32:1. Dashed lines are used to illustrate comparable simple gas turbine cycles.

offer the same benefit with smaller heat exchangers. Only upon assessment of the details of the individual application can the point be settled.

The temperature–entropy diagram for a reheat or refired gas turbine is shown in Fig. 21. The cycle begins with the compression process shown by line *ab*. The first combustion process is shown by line *bc*. At point *c*, a turbine expands the fluid (line *cd*) to a temperature associated with an intermediate pressure ratio. At point *d*, another combustion process takes place, returning the fluid to a high temperature (line *de*). At point *e*, the second expansion takes place, returning the fluid to ambient pressure (line *ef*); thereafter, the cycle is closed by discharge of the working fluid back to the atmosphere.

An estimate of the cycle efficiency can be made from the temperatures corresponding to the process end points of the cycle in Fig. 21. By dividing the turbine temperature drops less the compressor temperature rise by the sum of the combustor temperature rises, one calculates an efficiency of approximately 49%. This, of course, reflects perfect compressor, combustor, and turbine efficiency and pure air as the working fluid. Actual efficiencies and properties and consideration of turbine cooling produce less optimistic values.

A simple cycle with the same firing temperature and exhaust temperature would be described by the cycle *ab'efa*. The efficiency calculated for this cycle is approximately 38%, significantly lower than for the reheat cycle. This is really not a fair comparison, since the simple cycle has a pressure of only 8:1, whereas the refired cycle operates at 32:1. The ALSTOM GT26 shown in Fig. 22 and the 60-Hz version, the GT24, are current examples of refired gas turbines.

A simple-cycle gas turbine with the same pressure ratio and firing temperature would be described by the cycle *abcd'a*. Computing the efficiency, one obtains a value of approximately 54%, more efficient than the comparable reheat cycle. However, there is another factor to

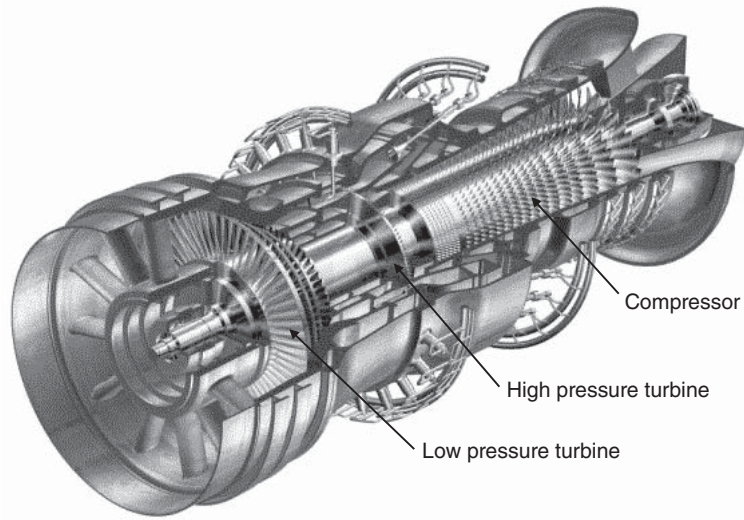


Figure 22 ALSTOM GT26 gas turbine. Courtesy of ALSTOM.

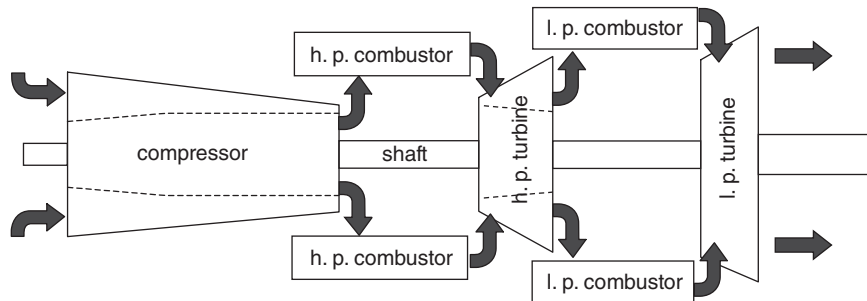


Figure 23 Schematic of a reheat, or fired, gas turbine. This arrangement shows both turbines connected by a shaft. Variations include multiple-shaft arrangements and independent components or component groups arranged in series.

be considered. The exhaust temperature of the reheat cycle is 270°C higher than for the simple-cycle gas turbine. When applied in combined-cycle power plants (these are discussed later) this difference is sufficient to allow optimized reheat cycle-based plants more efficient than simple-cycle-based plants of similar overall pressure ratio and firing temperature. Figure 23 shows the arrangement of a single-shaft, reheat gas turbine.

Regenerators, or recuperators, are devices used to transfer the heat in a gas turbine exhaust to the working fluid, after it exits the compressor but before it is heated in the combustor. Figure 24 shows the schematic arrangement of a gas turbine with regenerator. Such gas turbines have been used extensively for compressor drives on natural gas pipelines and have been tested in wheeled vehicle propulsion applications. Regeneration offers the benefit of high efficiency from a simple, low-pressure gas turbine without resort to combining the gas turbine with a steam turbine and a boiler to make use of exhaust heat. Regenerative gas turbines with modest firing temperature and pressure ratio have comparable efficiency to advanced, aircraft-derived simple-cycle gas turbines.

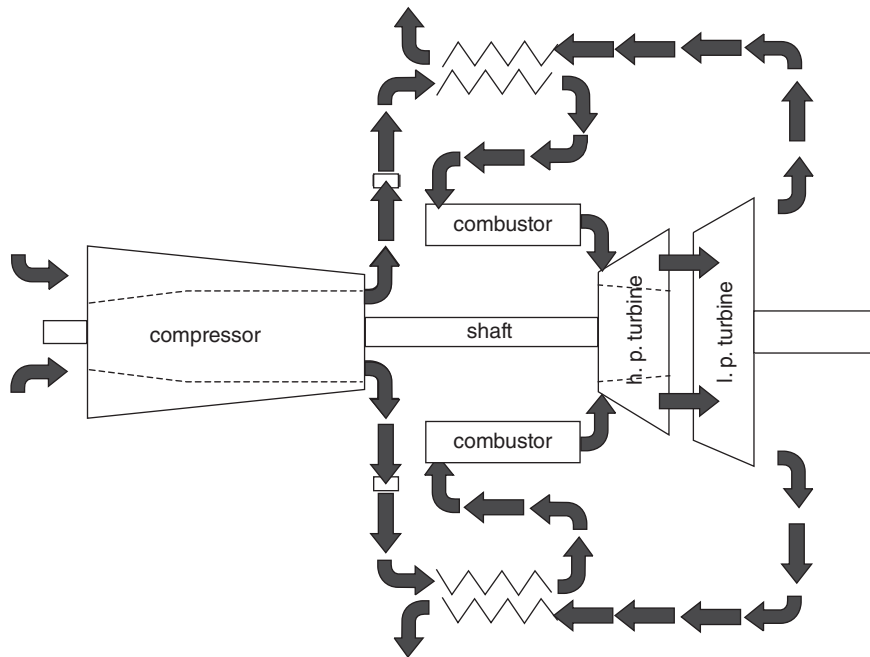


Figure 24 Regenerative, multishaft gas turbine.

The temperature–entropy diagram for an ideal, regenerative, gas turbine appears in Fig. 25. Without regeneration, the 8:1 pressure ratio, 1000°C firing temperature gas turbine has an efficiency of $[(1000 - 480) - (240 - 15)] / (1000 - 240) = 38.8\%$ by the method used repeatedly above. Regeneration, if perfectly effective, would raise the compressor discharge temperature to the turbine exhaust temperature, 480°C. This would reduce the heat required from the combustor, reducing the denominator of this last equation from 760 to 520°C and thereby increasing the efficiency to 56.7%. Such efficiency levels are not realized in practice because of real component efficiencies and heat transfer effectiveness in real regenerators. The relative increase in efficiency between simple and regenerative cycles is as indicated in this example.

Figure 25 has shown the benefit of regeneration in low-pressure ratio gas turbines. As the pressure ratio is increased, the exhaust temperature decreases, and the compressor discharge temperature increases. The dashed line $ab'cd'a$ shows the effect of increasing the pressure to 24:1. Note that the exhaust temperature d' is lower than the compressor discharge temperature b' . Here regeneration is impossible. As the pressure ratio (at constant firing temperature) is increased from 8:1 to nearly 24:1, the benefit of regeneration decreases and eventually vanishes. There is, of course, the possibility of intercooling the high-pressure-ratio compressor, reducing its discharge temperature to where regeneration is again possible. Economic analysis and detailed analyses of the thermodynamic cycle with real component efficiencies is required to evaluate the benefits of the added costs of the heat transfer and air-handling equipment.

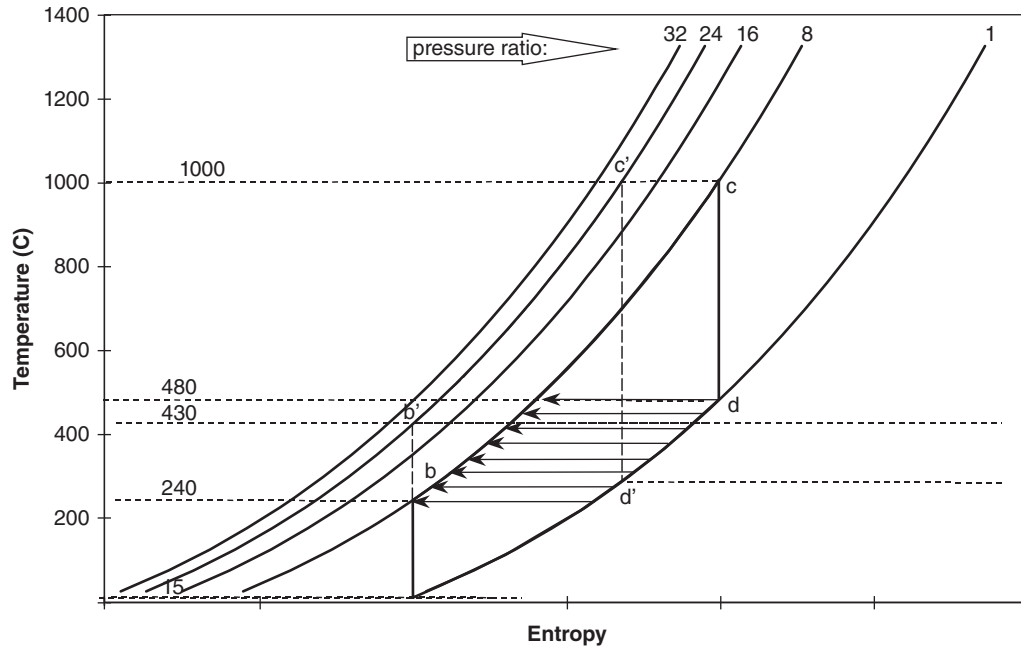


Figure 25 Temperature–entropy diagram comparing an 8:1 pressure ratio, ideal, regenerative cycle with a 24:1 pressure ratio simple cycle, both at a firing temperature of 1000°C.

2.2 Trends in Gas Turbine Design and Performance

Output or Size

Higher power needs can be met by increasing either the number or the size of gas turbines. Where power needs are high, economics generally favor large equipment. The specific cost (cost per unit power) of gas turbines decreases as size increases, as can be shown in Fig. 26. Note that the cost decreases, but at a decreasing rate; the slope remains negative at the maximum current output for a single gas turbine, around 300 MW. Output increases are accomplished by increased mass flow and increased firing temperature. Mass flow is roughly proportional to the inlet annulus area of the compressor. There are four ways of increasing this:

1. *Lower rotor speed while scaling root and tip diameter proportionally.* This results in geometric similarity and low risk but is not possible in the case of synchronous gas turbines where the shaft of the gas turbine must rotate at either 3600 or 3000 rpm to generate 60 or 50 Hz (respectively) alternating current.
2. *Increase tip diameter.* Designers have been moving the tip velocity into the transonic region. Modern airfoil design techniques have made this possible while maintaining good aerodynamic efficiency.
3. *Decrease hub diameter.* This involves increasing the solidity near the root, since the cross section of blade roots must be large enough to support the outer portion of the blade against the centrifugal force. The increased solidity interferes with aerodynamic efficiency. Also, where a drive shaft is designed into the front of the compressor

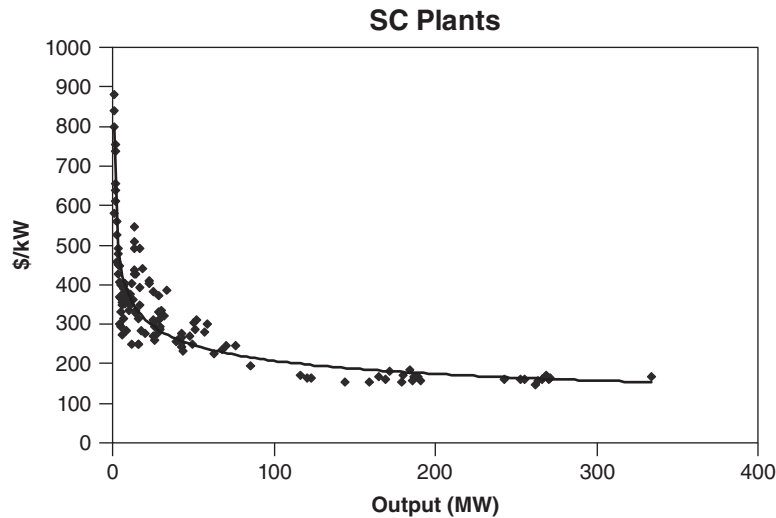


Figure 26 Cost of simple-cycle, generator-drive electric power generation equipment. *Source:* From Ref. 11, R. Farmer, ed., Gas Turbine World 2003 Handbook, Vol. 23, Pequot Publishing Inc. © Gas Turbine World.

(cold end drive) and where there is a large bearing at the outboard end of the compressor, there are mechanical limits to reducing the inlet inner diameter.

4. *Reduce the thickness of the blades themselves.*

Firing Temperature

Firing temperature increases provide higher output per unit mass flow and higher combined-cycle efficiency. Efficiency is improved by increased firing temperature wherever exhaust heat is put to use. Such uses include regeneration/recuperation, district heating, supplying heat to chemical and industrial processes, Rankine bottoming cycles, and adding a power turbine to drive a fan in an aircraft engine. The effect of firing temperature on the evolution of combined Brayton–Rankine cycles for power generation is illustrated in Fig. 27.

Firing temperature increases when the fuel flow to the engine’s combustion system is increased. The challenge faced by designers is to increase firing temperature without decreasing the reliability of the engine. A metal temperature increase of 15°C will reduce bucket creep life by 50%. Material advances and more increasingly more aggressive cooling techniques must be employed to allow even small increases in firing temperature. These technologies have been discussed previously.

Maintenance practices represent a third means of keeping reliability high while increasing temperature. Sophisticated life prediction methods and experience on identical or similar turbines are used to set inspection, repair, and replacement intervals.

Coupled with design features that reduce the time required to perform maintenance, both planned and unplanned downtime can be reduced to offset shorter parts lives, with no impact on reliability. Increased firing temperature usually increases the cost of the buckets and nozzles (developments involve exotic materials or complicated cooling configurations). Although these parts are expensive, they represent a small fraction of the cost of an entire power plant. The increased output permitted by the use of advanced buckets and nozzles is generally much higher, proportionally, than the increase in power plant cost and maintenance cost, and hence increased firing temperature tends to lower specific power plant cost.

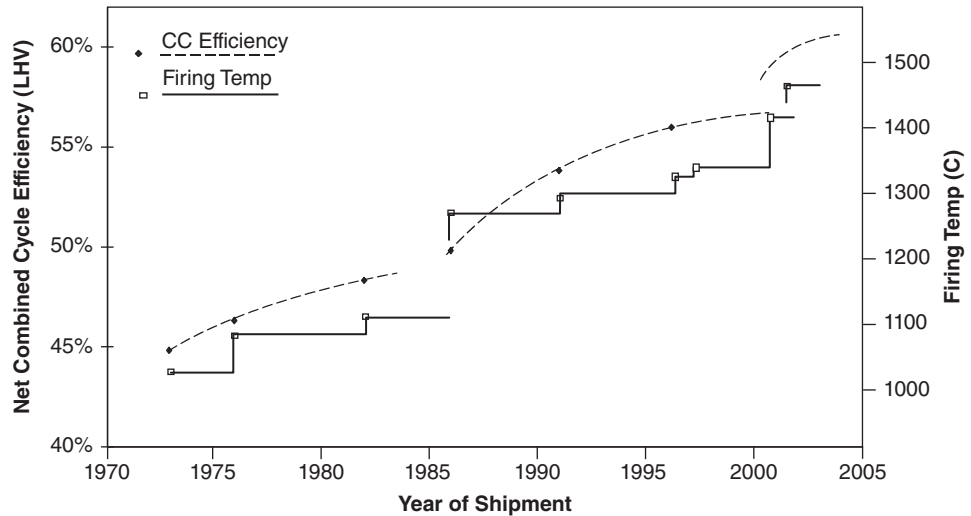


Figure 27 History of power generation, combined-cycle efficiency and firing temperature, illustrating the trends to higher firing temperature and its effect on efficiency.

Pressure Ratio

Two factors drive the choice of pressure ratio. First is the primary dependence of simple-cycle efficiency on pressure ratio. Gas turbines intended for simple-cycle application, such as those used in aircraft propulsion, emergency power, or power where space or weight is a primary consideration, benefit from higher pressure ratios.

Combined-cycle power plants do not necessarily benefit from high pressure ratios. At a given firing temperature, an increase in pressure ratio lowers the exhaust temperature. Lower exhaust temperature means less power from the bottoming cycle and a lower efficiency bottoming cycle. So, as pressure ratio is increased, the gas turbine becomes more efficient and the bottoming cycle becomes less efficient. There is an optimum pressure ratio for each firing temperature, all other design rules held constant. Figure 28 shows how specific output and combined-cycle efficiency are affected by gas turbine firing temperature and pressure ratio for a given type of gas turbine and steam cycle. At each firing temperature there is a pressure ratio for which the combined-cycle efficiency is highest. Furthermore, as firing temperature is increased, this optimum pressure ratio is higher as well. This fact means that, as firing temperature is increased in pursuit of higher combined-cycle efficiency, pressure ratio must also be increased.

Reducing the flow area through the first-stage nozzle of the turbine increases pressure ratio. This increases the pressure ratio per stage of the compressor. There is a point at which increased pressure ratio causes the compressor airfoils to stall. Stall is avoided by either adding stages (reducing the pressure ratio per stage) or increasing the chord length and applying advanced aerodynamic design techniques. For a very high pressure ratio a simple, single-shaft rotor with fixed stationary airfoils cannot deliver the necessary combination of pressure ratio, stall margin, and operating flexibility. Features required to meet all design objectives simultaneously include variable-angle stationary blades in one or more stages; extraction features, which can be used to bleed air from the compressor during low-speed operation; and multiple rotors that can be operated at different speeds.

Larger size, higher firing temperature, and higher pressure ratio are pursued by manufacturers to lower cost and increase efficiency. Materials and design features evolve to accomplish these advances with only positive impact on reliability.

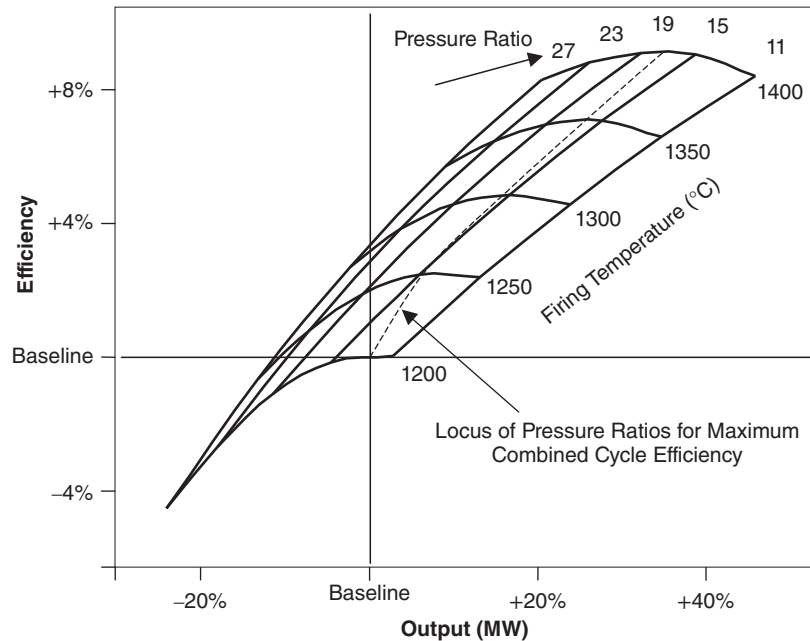


Figure 28 Effect of pressure ratio and firing temperature on combined-cycle efficiency and output for fixed air flow and representative gas and steam turbine designs.

3 APPLICATIONS

3.1 Use of Exhaust Heat in Industrial Gas Turbines

By adding equipment for converting exhaust energy to useful work, the thermal efficiency of a gas-turbine-based power plant can be increased by 10% to over 30%. Of these numerous schemes, the most significant is the fitting of a heat recovery steam generator (HRSG) to the exhaust of the gas turbine and delivering the steam produced to a steam turbine. Both the steam turbine and gas turbine drive one or more electrical generators.

Figure 29 displays the combining of the Brayton and Rankine cycles. The Brayton cycle *abcd* has been described already. It is important to point out that the line *da* now represents heat transferred in the HRSG. In actual plants, the turbine work is reduced slightly by the back pressure associated with the HRSG. Point *d* would be above the 1:1 pressure curve, and the temperature drop would be proportionately reduced.

The Rankine cycle begins with the pumping of water into the HRSG, line *mn*. This process is analogous to the compression in the gas turbine, but rather than absorbing 50% of the turbine work, consumes only about 5%, since the work required to pump a liquid is less than that required to compress a gas. The water is heated (line *no*) and evaporated (*op*). The energy for this is supplied in the HRSG by the exhaust gas of the gas turbine. More energy is extracted to superheat the steam as indicated by line *pr*. At this point, superheated steam is delivered to a steam turbine and expanded (*rs*) to convert the energy therein to mechanical work.

The addition of the HRSG reduces the output of the gas turbine only slightly. The power required by the mechanical devices (like the feedwater pump) in the steam plant is also small. Therefore, most of the steam turbine work can be added to the net gas turbine work with almost no increase in fuel flow. For combined-cycle plants based on industrial gas turbines where

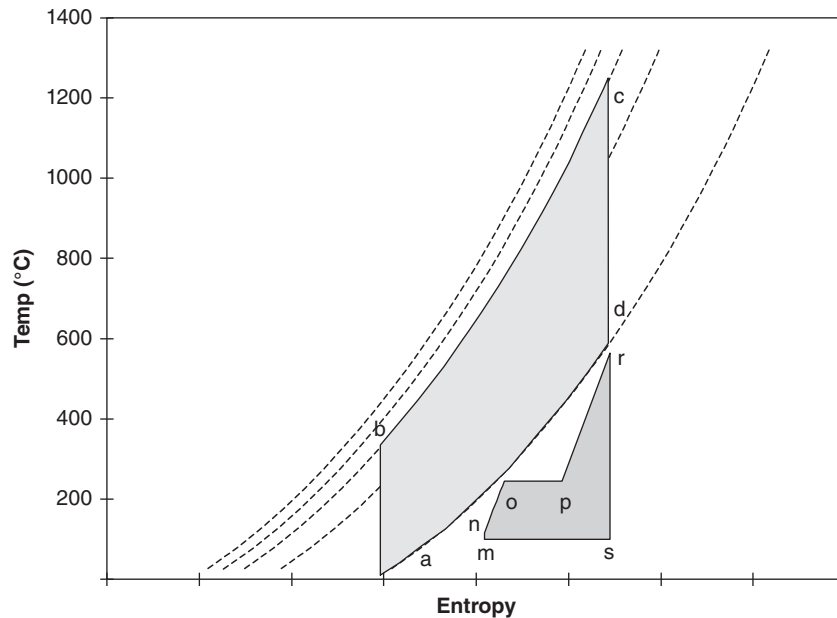


Figure 29 Temperature–entropy diagram illustrating the combining of a gas turbine (*abcda*) and steam turbine cycle (*mnoprsm*). The heat wasted in process *da* in simple-cycle turbines supplies the heat required by processes *no*, *op*, and *pr*.

exhaust temperature is in the 600°C class, the output of the steam turbine is about half that of the gas turbine. Their combined-cycle efficiency is approximately 50% higher than simple-cycle efficiency. For high-pressure-ratio gas turbines with exhaust temperature near 450°C the associated steam turbine output is close to 25% of the gas turbine output, and efficiency is increased by approximately 25%. The thermodynamic cycles of the more recent large, industrial gas turbines have been optimized for high combined-cycle efficiency. They have moderate to high simple-cycle efficiency and relatively high exhaust temperatures. Figure 30 has shown that net combined-cycle efficiency (lower heating value) of approximately 55% has been realized as of this writing, and levels of 60% and beyond are under development.

Figure 30 shows a simple combined-cycle arrangement where the HRSG delivers steam at one pressure level. All the steam is supplied to a steam turbine. Here, there is neither steam reheat nor additional heat supplied to the HRSG. There are many alternatives.

Fired HRSGs have been constructed where heat is supplied both by the gas turbine and by a burner in the exhaust duct. This practice lowers overall efficiency but accommodates the economics of some situations of variable load requirements and fuel availability. In other applications steam from the HRSG is supplied to nearby industries or used for district heating, lowering the power generation efficiency but contributing to the overall economics in specific applications.

Efficiency of electric power generation benefits from more complicated steam cycles. Multiple-pressure, nonreheat cycles improve efficiency as a result of additional heat transfer surface in the HRSG. Multiple-pressure, reheat cycles, such as shown in Fig. 31, match the performance of higher exhaust temperature gas turbines (600°C). Such systems are the most efficient currently available but are also the most costly. The relative performance for several combined-cycle arrangements is shown in Table 1.¹² The comparison was made for plants using a gas turbine in the 1250°C firing temperature class.

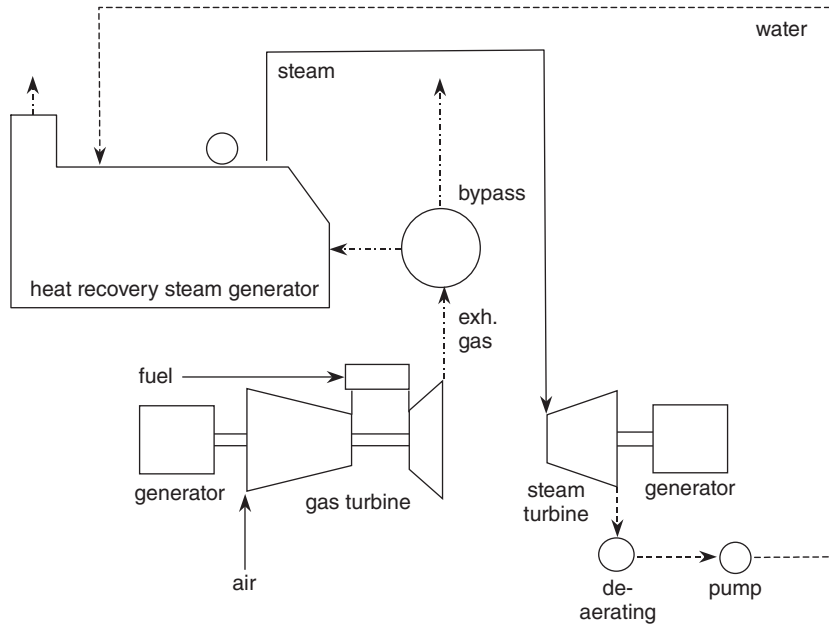


Figure 30 Schematic of simple combined-cycle power plant. A single-pressure, nonreheat cycle is shown.

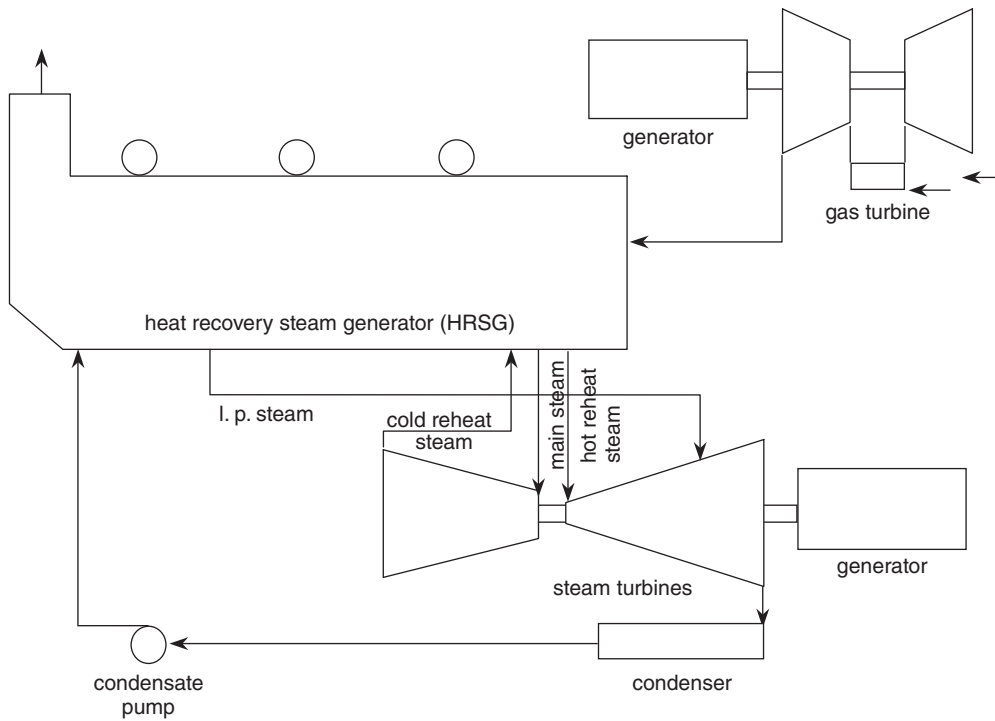


Figure 31 Three-pressure, reheat combined-cycle arrangement. The highest power generation efficiency is currently achieved by such plants.

Table 1 Comparison of Performance for Combined-Cycle Arrangements Based on Third-Generation (1250°C Firing Temperature) Industrial Gas Turbines

Steam Cycle	Relative Net Plant Output (%)	Relative Net Plant Efficiency (%)
Three pressure, reheat	Base	Base
Two pressure, reheat	-1.1	-1.1
Three pressure, nonreheat	-1.2	-1.2
Two pressure, nonreheat	-2.0	-2.0

Table 2 Recent Large Multiunit Gas-Turbine-Based Combined-Cycle Power Plants

Station	Country	Number of GTs	Rating (MW)
Seo-Inchon 1-4	Korea	16	3950
Chiba 2-3	Japan	8	2850
Hsinta 1-5	Taiwan	15	2450
Gila River 1-4	United States	8	2350
El Dorado 1-4	United States	8	2330
Ratchaburi	Thailand	6	2310
Lumut	Malaysia	9	2230
Phu My 1-3	Vietnam	7	2190
Black Point	Hong Kong	6	2080

Plant costs for simple-cycle gas turbine generators is lower than that for steam turbines and most other types of power plant. Since combined-cycle plants generate two-thirds of their power with the gas turbine, their cost is between that of simple-cycle gas turbine plants and steam turbine plants. Their efficiency is higher than either. The high efficiency and low cost make combined-cycle plants extremely popular. Very large commitments to this type of plant have been made around the world. Table 2 shows some of the more recent to be put into service.

There are other uses for gas turbine exhaust energy. Regeneration, or recuperation, uses the exhaust heat to raise the temperature of the compressor discharge air before the combustion process. Various steam injection arrangements have been used as well. Here, an HRSG is used as in the combined-cycle arrangements shown in Fig. 31, but instead of expanding the steam in a steam turbine, it is introduced into the gas turbine, as illustrated in Fig. 32. It may be injected into the combustor, where it lowers the generation of NO_x by cooling the combustion flame. This steam increases the mass flow of the turbine and its heat is converted to useful work as it expands through the turbine section of the gas turbine.

Steam can also be injected downstream of the combustor at various locations in the turbine, where it adds to the mass flow of the working fluid. Many gas turbines can tolerate steam injection levels of 5% of the mass flow of the air entering the compressor; others can accommodate 16% or more if distributed appropriately along the gas path of the gas turbine. Gas turbines specifically designed for massive steam injection have been proposed and studied. These proposals arise from the fact that the injection of steam into gas turbines of existing designs has significant reliability implications. There is a limit to the level of steam injection into combustors without flame stability problems and loss of flame. Adding steam to the gas flowing through the first-stage nozzle increases the pressure ratio of the machine and reduces the

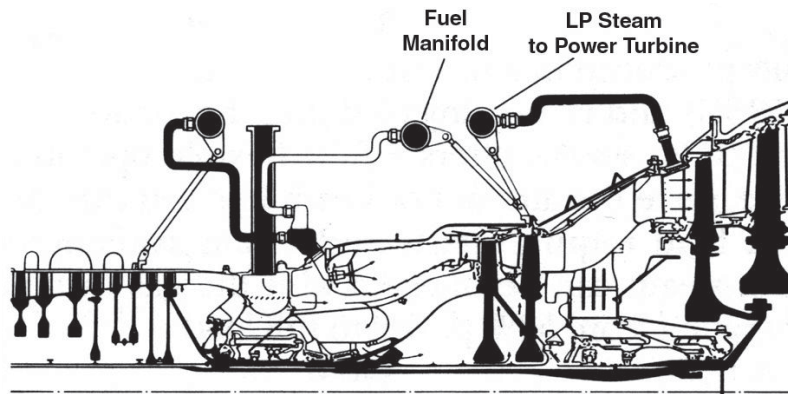


Figure 32 LM500 aeroderivative gas turbine with steam injection. Courtesy of General Electric Company.

stall margin of the compressor. Addition of steam to the working fluid expanding in the turbine increases the heat transfer coefficient on the outside surfaces of the blading, raising the temperature of these components. The higher work increases the aerodynamic loading on the blading, which may be an issue on later stage nozzles, and increases the torque applied to the shafts and rotor flanges. Design changes can be made to address the effects of steam in the gas path.¹³

Benefits of steam injection are an increase in both efficiency and output over those of the simple-cycle gas turbine. The improvements are less than those of the steam turbine and gas turbine combined cycles, since the pressure ratio of the steam expansion is much higher in a steam turbine. Steam turbine pressures may be greater than 100 atm and gas turbines no higher than 40 atm. Steam injection cycles are less costly to produce since there is no steam turbine. There is, of course, higher water consumption with steam injection, since the expanded steam exits the plant in the gas turbine exhaust.

3.2 Integrated Gasification Combined Cycle

In many parts of the world, coal is the most abundant and inexpensive fuel. Coal-fired boilers raising steam that is expanded in steam turbine generators is the conventional means of converting this fuel to electricity. Pulverized coal plants with flue gas desulfurization operate at over 40% overall efficiency and have demonstrated the ability to control sulfur emissions from conventional boiler systems. Gas turbine combined-cycle plants are operating with minimal environmental impact on natural gas at 55% efficiency, and 60% is expected with new technologies. A similar combined-cycle plant that could operate on solid fuel would be an attractive option.

Competing means of utilizing coal with gas turbines have included direct combustion, indirect firing, and gasification. Direct combustion in conventional, on-engine combustors has resulted in rapid, ash-caused erosion of bucket airfoils. Off-base combustion schemes—such as pressurized fluidized bed combustors—have not simultaneously demonstrated the high exit temperature needed for efficiency and low emissions. Indirect firing raises compressor discharge temperature by passing it through a heat exchanger. Metal heat exchangers are not compatible with the high turbine inlet temperature required for competitive efficiency. Ceramic heat exchangers have promise, but their use will necessitate the same types of emission controls required on conventional coal-fired plants. Power plants with the gasification process, desulfurization, and the combined-cycle machinery integrated have been successfully demonstrated,

with high efficiency, low emissions, and competitive first cost. Significant numbers of integrated gasification combined-cycle (IGCC) plants are operating or under construction.

Fuels suitable for gasification include several types of coal and other low-cost fuels. Those studied include:

- Bituminous coal
- Subbituminous coal
- Lignite
- Petroleum coke
- Heavy oil
- Orimulsion
- Biomass

Fuel feed systems of several kinds have been used to supply fuel into the gasifier at the required pressure. Fuel type, moisture content size, and the particular gasification process need to be considered in selecting a feed system.

Several types of gasifiers have been designed to produce fuel with either air or oxygen provided. The system shown in Fig. 33 features a generic oxygen-blown gasifier and a system for extracting some of the air from the compressor discharge and dividing it into oxygen and nitrogen. An oxygen-blown gasifier produces a fuel about one-third of the heating value of natural gas. The fuel produced by the gasifier (after sulfur removal) is about 40% CO, 30% H₂. Most of the remaining 30% is H₂O and CO₂ which are inert and act as diluents in the gas turbine combustor, reducing NO_x formation. A typical lower heating value is 1950 K-cal/m³. The fuel

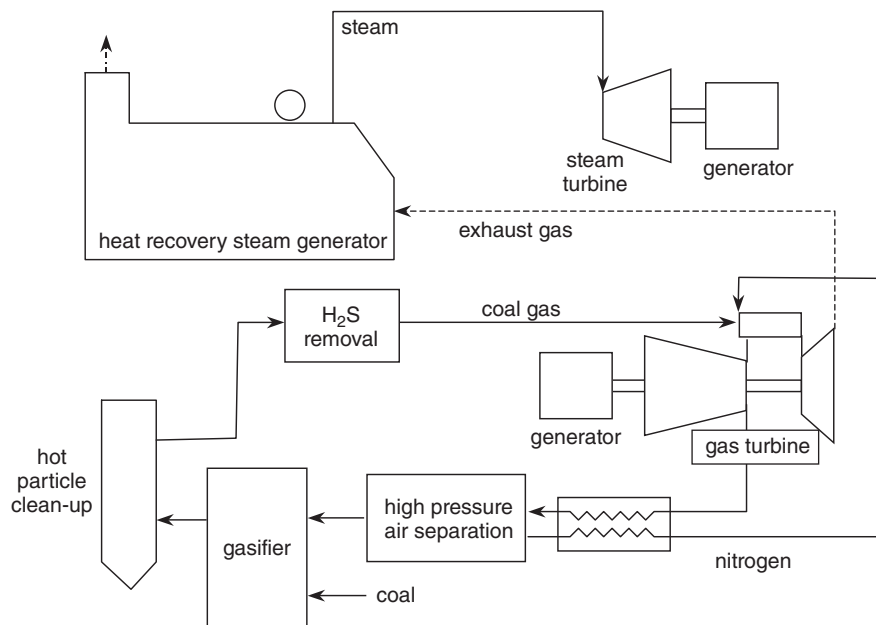


Figure 33 Integrated gasification combined-cycle diagram. Air compressed in the gas turbine is cooled, then separated into oxygen and nitrogen. Oxygen is fed to the gasifier while the nitrogen is sent back to the gas turbine for NO_x control. Coal is partially burned in the gasifier. The gas produced is cleaned and flows to the gas turbine as fuel.

exits the gasifier at a temperature higher than that at which it can be cleaned. The gas is cooled by either quench or heat exchange and cleaned. Cleaning is done by water spray scrubber or dry filtration to remove solids that are harmful to the turbine and potentially harmful to the environment. This is followed by a solvent process that absorbs H_2S .

Some gas turbine models can operate on coal gas without modification. The implications for the gas turbine relate to the volume of fuel, which is three times or more higher than that of natural gas. When the volume flow through the first-stage nozzle of the gas turbine increases, the back pressure on the compressor increases. This increases the pressure ratio of the cycle and decreases the stall margin of the compressor. Gas turbines with robust stall margins need no modification. Others can be adapted by reducing inlet flow by inlet heating or by closing off a portion of the inlet. (Variable inlet stator vanes can be rotated toward a closed position.) The volume flow through the turbine increases as well. This increases the heat transfer to the buckets and nozzles. To preserve parts lives, depending on the robustness of the original design, the firing temperature may have to be reduced. The increased flow and decreased firing temperature, if required, result in higher gas turbine output than developed by the same gas turbine fired on natural gas.

3.3 Applications in Electricity Generation

Before 1965, the generating capacity of gas turbines shipped per year was below 2 GW. In 2003, in sharp contrast, about 75 GW of electrical generation power plants were commissioned. Approximately 16% of the entire world's current generating capacity is now produced by gas turbines, either in simple cycle or combined cycle. In 2003, over 12% of new power plants featured simple-cycle gas turbines, and over 50% were combined-cycle plants, which derive two-thirds of their capacity from gas turbines. Thus, 45% of new power plant capacity is provided by gas turbine generators. This compares to 40% for steam turbine generators, either alone or in combined cycle. Hydroelectric plants, nuclear and other means, provide the remaining additions.

The 30-fold increase in the rate of gas turbine installations between 1965 and 2003 was due to several factors. In the late 1960s and early 1970s, there was an increasing need for peaking power, particularly in the United States. Gas turbines, because of their low cost, low operating crew size, and fast installation time, were the engine of choice. Because of the seasonal and daily variations in the demand for electric power, generating companies could minimize their investment in plant and equipment by installing a mixture of expensive but efficient base-load plants (steam and nuclear) run over 8000 hours per year and far less expensive (but less efficient) plants, which would operate only a few hundred hours per year. However, rapid progress in efficiency, reliability, availability, and environmental impact would soon follow.

Existing industrial gas turbines and newly designed larger units, whose operating speed was chosen to match the requirements of a directly coupled alternator, met the demand for peaking power. The experience on these early units resulted in improvements in efficiency, reliability, and cost-effectiveness. Much of the technology needed to improve the value of industrial gas turbines came from aircraft engine developments, as it still does. Beginning in the 1970s, with the rapid rise in oil prices and associated natural gas prices, electric utilities focused on ways of improving the efficiency of generating plants. Combined-cycle plants are the most thermally efficient fuel-burning plants. Furthermore, their first cost is lower than all other types of plants except for simple-cycle gas turbine plants.

The only drawback to gas turbine plants was the requirement for more noble fuels; natural gas and light distillates are usually chosen to minimize maintenance requirements. Coal is abundant in many parts of the world and costs significantly less than oil or gas per unit energy. Experiments in the direct firing of gas turbines on coal have been conducted without favorable results. Other schemes for using coal in gas turbines include indirect firing, integrating

with a fluidized bed combustor, and integrated gasification. The last of these offers the highest efficiency due to its ability to deliver the highest temperature gas to the turbine blading. Furthermore, integrated gasification is the most environmentally benign means of converting coal to electricity. The technology has been demonstrated in several plants, including early technology demonstration plants and commercial power-generating facilities.

3.4 Engines in Aircraft

Like electricity generation, gas turbine design for aircraft engines begins with an understanding of customer requirements. Utility metrics, such as cost of electricity, internal rate of return, and project net present value, are equivalent to cost per seat-mile for a commercial turbofan, or specific mission performance objectives for a military engine.

In addition to optimizing for best economics or performance, electric power and aircraft engine designs are usually subject to a number of constraints. From the utility perspective, these could include kilowatts or fuel consumption on a hot or cold day or power response during grid events. For an aircraft engine customer, mission objectives such as airspeed, range, payload, maneuverability, runway length, or engine-out rate of climb may limit the available solutions. For both design environments, engineers will optimize the cycle selection variables (such as overall pressure ratio, firing temperature, and bypass ratio) in conjunction with technology (materials, cooling, airfoil aerodynamics) to produce a solution that optimizes economics for an acceptable risk.

Three of the key propulsion parameters to an aircraft are thrust, thrust-specific fuel consumption (SFC, or lbm/h fuel flow/lbf thrust), and weight. Gas turbines currently provide the best combination of these three parameters for flight Mach numbers ranging from about 0.3 through supersonic speeds. Normally, aspirated piston engines (both Otto and Diesel cycles) are favored for aircraft operating at low speeds and altitudes; turbocharged versions are used at higher speeds and at higher altitudes, up to about 400–500 km/h. Pulse jet, scramjet, and rocket propulsion take over from gas turbines at high supersonic and hypersonic speeds. The two most commonly used aircraft gas turbine configurations are the turboprop and turbofan. Gas turbines are particularly appropriate for aircraft applications because of their efficiency at high airspeeds, high power-to-weight ratios, and good high-power efficiency.

Equations for thrust and SFC are shown below:

$$\begin{array}{ll}
 \text{Net Thrust :} & F_n = W_1(V_j - V_o) + A_e(P_j - P_o) \quad \text{for turbojet} \\
 & F_n = W_c(V_j - V_o) + W_d(V_d - V_o) + A_e(P_j - P_o) \quad \text{for turbofan} \\
 \text{Specific Thrust :} & ST = F_n/W_1 \\
 \text{Specific Fuel Consumption :} & \text{SFC} = W_f/F_n \quad \text{general definition} \\
 & \text{SFC}_{\text{tp}} = W_f/\text{hp/h} \quad \text{sometimes applied to} \\
 & \quad \quad \quad \text{turboprop and shaft engines}
 \end{array}$$

where W_1 = total inlet mass flow rate,
 W_c = portion of W_1 passing through the core engine,
 W_d = portion of W_1 passing through bypass duct,
 V_o = flight velocity,
 V_j = exhaust jet velocity,
 A_e = exhaust area,
 P_j = exhaust jet static pressure,
 P_o = ambient pressure,
and W_f = fuel flow rate.

The gas turbine flight speed range mentioned above is not met with a single gas turbine configuration, however. The equations above show that to produce thrust at higher flight velocity, higher exhaust velocity is required. Each configuration—turbo-prop, turbofan, and turbojet—has its own range of potential and optimum exhaust velocities, which, in addition to thrust, are set as a function of SFC and weight objectives.

While the prior power generation thermal efficiency conclusions still hold true for aircraft turbines, higher firing temperature and overall pressure ratio are selected in conjunction with cooling component efficiency technology to select the right balance between specific power and thermal efficiency. Two new efficiency definitions are required, however, to quantify the aircraft fuel efficiency metric (SFC): overall and propulsive efficiency. SFC is proportional to the flight velocity times the inverse of overall efficiency, while overall efficiency is the product of thermal and propulsive efficiencies:

$$\text{SFC} \approx V_o / \eta_{\text{overall}}$$

$$\text{where } \eta_{\text{overall}} = \eta_{\text{thermal}} \times \eta_{\text{ps}} \\ \eta_{\text{ps}} = \text{const} \times (F_n V_o) / W_f \text{ or } \eta_{\text{ps}} = \text{const} \times V_o / \text{SFC}$$

This more extensive efficiency definition adds computational complexity and new design variables to mission design and optimization problems: bypass ratio and fan pressure ratio.

Because of its high exhaust velocity, the twin-spool turbojet shown in Fig. 19 will have a high specific thrust and low frontal area, which are ideal for high flight speeds. To improve the fuel consumption at lower speeds, the exhaust velocity could be lowered to the ideal level for a turbojet (two times flight velocity) by extending the low-pressure compressor blades and adding a duct around this extension, creating a turbofan. The duct airflow divided by core airflow is defined as the bypass ratio. The pressure ratio of the low-pressure compressor (now called the fan) is now available to optimize efficiency but is also available to meet other mission objectives, such as specific power. For unmixed core and exhaust streams, the fan pressure ratio impacts the turbine specific power and relative exhaust velocities between the two streams. In a mixed-flow exhaust, common to military turbofans, fan pressure ratio communicates to the core exhaust through a common static pressure during mixing of the two streams. This communication can be controlled by area sizing before these flows mix, and can be used to modify the cycle performance match at both design and off-design flight conditions.

In this example, thrust has increased because core flow was unchanged. If bypass ratio were increased at constant thrust, the total flow will increase faster than the core flow decreases, driving up weight. As technology has improved, however (with better materials, aerodynamics, manufacturing, and heat transfer technologies), core specific power has gone up, leading to increased bypass ratio and lower weight at a given thrust.

Trends in specific thrust and SFC with flight Mach number are shown in Figs. 34 and 35. The figures show that at lower Mach numbers, the turbofan engines have relatively high propulsion efficiency (low SFC). The need for improved efficiency in the high-subsonic-speed regime has produced a focus on turbofan engines rather than turbojets. At lower speeds, turbo-prop engines are preferred.

Installation Effects

Specific thrust curves shown in Fig. 34 and most other gas-turbine-only comparisons are done on an uninstalled basis. Here, thrust means net thrust as it is used in the equations above. The curves are particularly convenient for showing generic effects of technology or of changing design parameters. For actual cycle design, optimization, control scheduling, operability studies, and aircraft performance calculations, however, installation effects must be considered

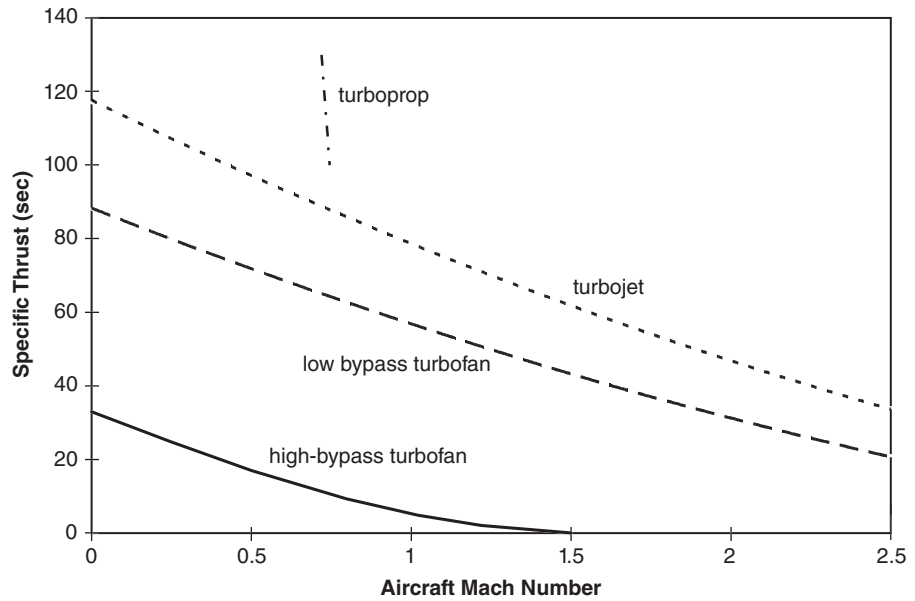


Figure 34 Low values of specific thrust give higher propulsive efficiency at low Mach numbers. *Source:* Adapted Ref. 14, Courtesy of General Electric. GE aircraft Engines © 1989.

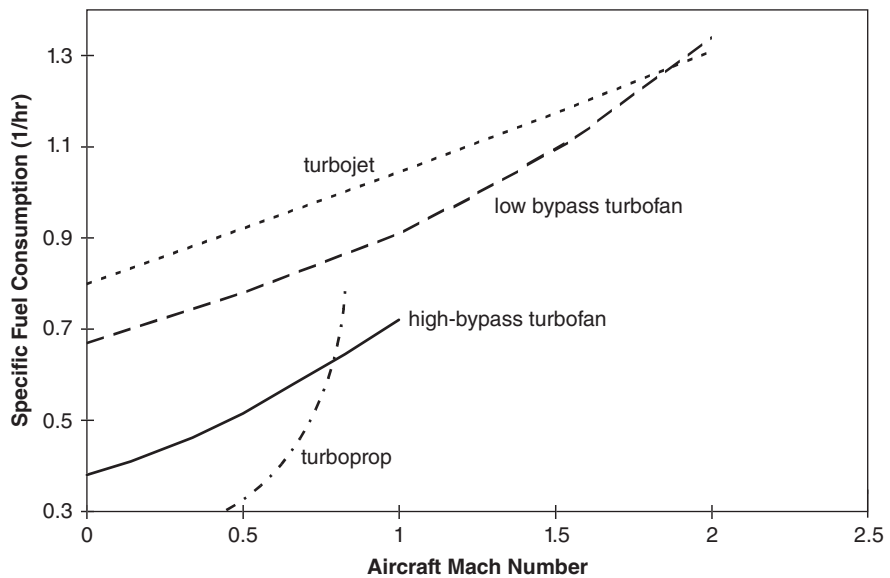


Figure 35 As flight Mach number increases, higher specific thrusts are necessary to maintain high propulsive efficiency and reduce SFC. *Source:* Adapted Ref. 14, Courtesy of General Electric. GE aircraft Engines © 1989.

to develop the optimum propulsion system. The effect of installation parameters and features on performance is more significant in aircraft applications than in power generation. Aircraft engine installation effects include items such as inlet and nozzle drag, inlet ram recovery, horsepower and bleed extraction, and inlet pressure distortion.

Inlets and Nozzles

For aircraft and propulsion performance analysis, thrust is converted from gross levels (produced by the exhaust) to net, which subtracts inlet ram drag. Installed corrections also account for real losses and are used to align the bookkeeping between aircraft and propulsion manufacturers. These corrections include inlet spillage drag, inlet ram recovery (pressure losses), and nozzle drag. The design of inlets and nozzles and scheduling of inlet airflow represent a compromise between performance and aeromechanical considerations. Supersonic inlets can become more complex in an effort to reduce shock losses.

As design speeds increase, inlets increase in complexity from a normal shock design, used for subsonic, transonic, and low supersonic designs, to external compression, to mixed internal/external compression designs. Military aircraft such as the Boeing F-15 use variable-geometry inlet ramps to reduce recovery losses, which improves performance and operability across its flight envelope while paying a penalty in weight and cost.

Exhaust nozzle configurations are driven by the throat area, efficiency, and cost requirements of the propulsion system. Fixed-area convergent nozzles are satisfactory for subsonic, nonafterburning designs. Variable-area convergent nozzles maintain high efficiency up to low supersonic speeds with afterburning engines. Variable-area convergent–divergent nozzles are required for good performance for afterburning engines operating at higher supersonic speeds.

Figures of Merit and Cycle Design Variables

Business, Commercial, and Transport Aircraft. Turbofans use two or three concentric spools and bypass the fan exit air from the outer spool, usually through an independent duct nozzle. Commercial aircraft are characterized by requirements for relatively low thrust-to-weight ratio, high efficiency during cruise, low noise, and low emissions. The low thrust-to-weight requirement means gas turbine size, or scale factor, is set by the takeoff thrust specification. Cruise conditions are generally at a high fraction of full power, which is ideal for high gas turbine thermal efficiency.

Military Turbofans. Most modern military aircraft use a twin-spool turbofan configuration similar to commercial aircraft but will have additional complexity driven by requirements across a larger flight envelope. Military aircraft designed for supersonic operation and high thrust-to-weight ratio require low drag and low weight. Emerging military aircraft designs include the engines as an integral part of the fuselage and associated engine designs with higher specific power as opposed to the pylon-mounted large-fan engines used in commercial and transport aircraft. Military engine cruise thrust is usually a lower fraction of peak thrust, and cruise operation is frequently interrupted by maximum power operation during the mission, decreasing its significance and adding to the frequency and severity of fatigue loading cycles.

Afterburners are designed to be a cost-effective means of achieving high thrust for short duration. During afterburner operation (referred to as augmentation) fuel is introduced and burned downstream of the last turbine stage and diffuser to increase thrust through higher exhaust exit velocity. The temperature increase causes the exiting gas to expand. Since mass flow is fixed and set by the compressor and fan, exit velocity must increase to satisfy continuity. Afterburner performance is measured by percentage increase in thrust due to augmentation.

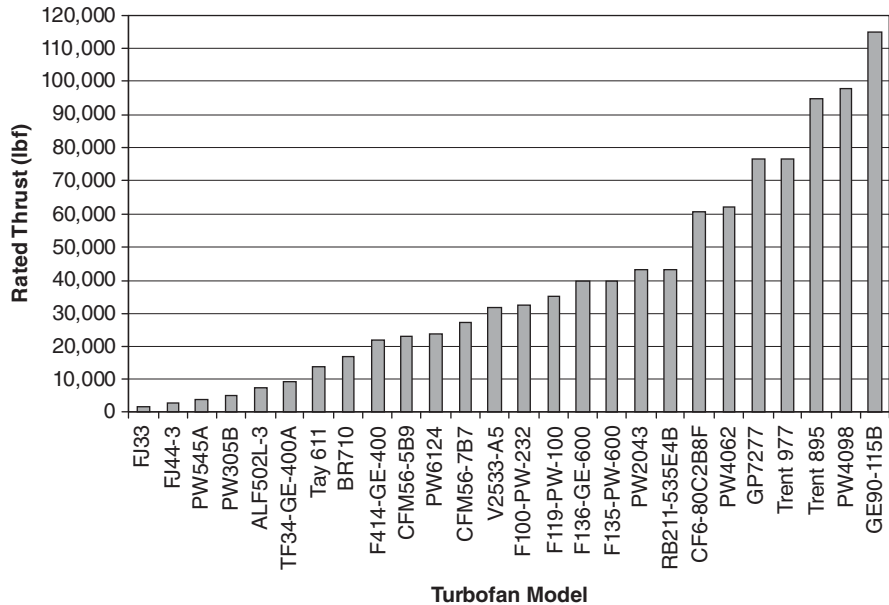


Figure 36 Rated thrust of current aircraft engines.

Turbojets, low-bypass-ratio turbofans, and gas turbines with high exit fuel-air from the gas generator core have reduced potential for augmentation percentage because of stoichiometric fuel/air ratio and exhaust temperature limits.

Military turbofans have historically led the development of gas turbine technologies. Absolute performance metrics have driven materials development, advanced turbine cooling schemes, variable cycle technology, and control software.

Figure 36 compares the engines selected or competing for recent applications. All of the larger commercial transport applications and newer military applications are met by turbofan engines.¹⁶

There are multiple ratings for several basic engine designs. The range of ratings is due to the practice of fine tuning engine performance for particular applications, incremental performance gains over time, and optional features. This comparison is a snapshot of performance over a particular time. Relative ratings change often as manufacturers continue to apply new technologies and improve designs. One of the newest and most powerful turbofan engines is shown in Fig. 37. It is a two-rotor engine. The 1-stage fan and 3-stage, low-pressure compressor are joined on one shaft connected to a 6-stage, low-pressure turbine. The 10-stage, high-pressure compressor is driven by the 2-stage, high-pressure turbine, both joined on another shaft that can rotate at a higher speed. The ratio of the air mass flow through the duct to the air flowing through the compressor, combustor, and turbines is 9:1. The overall pressure ratio is 40:1, and the rated thrust is in the 85,000-lb class. The engine is over 3 m in diameter. A new feature for aircraft engines is the double-domed, lean-premixed, fuel-staged dry low- NO_x combustor. The GE 90, PW4084, and 800-series RB.211 Trent high-bypass-ratio turbofan engines have been built for use on the Boeing 777 aircraft.

Control Scheduling. Aircraft engine control scheduling has also led the field in gas turbine development. Fast thrust transients, wide ranges of inlet conditions, airframe

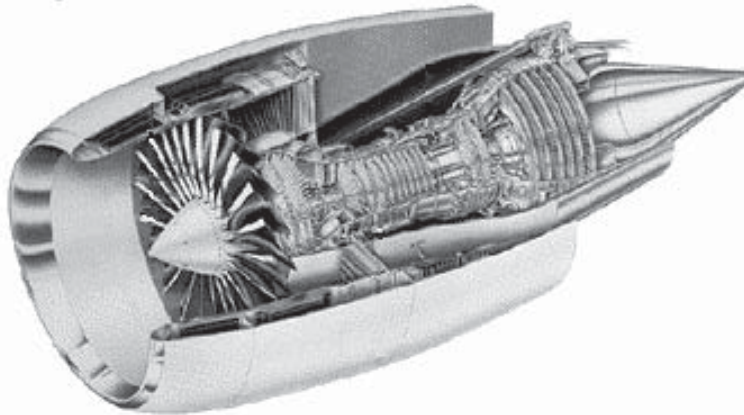


Figure 37 Sectional view of the GE 90, a high-bypass-ratio, two-shaft, turbofan engine rated at over 80,000 lbf thrust. Courtesy of General Electric Company.

bleed and power demands, mission demands such as in-flight refueling, and high reliability have necessitated more reliable and smarter controls. To create such controls, designers make the best use of a wide range of control effectors, including primary combustor and augmentor fuel flow, fan and compressor vane angles, bleed valves, exhaust nozzle area and area ratio, and other variable geometry. The advent of digital electronic controls in the early 1980s led to significant improvements in this regard. Controls technology has produced increased monitoring and diagnostic capability, which allows real-time sensor fault identification and corrective action.

Auxiliary Power Units. Another aircraft engine type is the auxiliary power unit (APU). It is a small turboshaft engine that provides air-conditioning and electric and hydraulic power while the main engines are stopped, but its main function is to start the main engines without external assistance. The APU is usually started from batteries by an electric motor. When it reaches its operating speed, a substantial flow of air is bled from its compressor outlet and is ducted to drive the air turbine starters on the main engines. The fuel flow is increased when the turbine air supply is reduced by the air bleed to provide the energy required for compression. These engines are also found on ground carts, which may be temporarily connected to an aircraft to service it. They may also have uses in industrial plants requiring air pressure at 3 or 4 bars.

3.5 Engines for Surface Transportation

This category includes engines for rail, road, off-road, and over-water transport. The low weight and high power density of gas turbines are assets in all cases, but direct substitution for Diesel or Otto cycle engines is unusual. When the economics of an application favor high power density or high driven-device speed, or when some heat recovery is possible, gas turbines become the engines of choice. Surface vehicle engines include the array of turboshaft and turboprop derivatives, free-turbine aeroderivative and industrial gas turbines, and purpose-built gas turbines. Applications exist for engines ranging from around 100 hp to nearly 40,000 hp.

Truck, bus, and automobile gas turbine engines are, for the most part, in the development stage. Current U.S. Department of Energy initiatives are supporting development of gas turbine automobile engines of superior efficiency and low emissions. Production cost similar to

current power plants is also a program goal. Additional requirements must be met, such as fast throttle response and low fuel consumption at idle. The balancing of efficiency, first cost, size, and weight have led to different cycle and configuration choices than for aircraft or power generation applications. Regenerative cycles with low pressure ratios have been selected. Parts count and component costs are addressed through the use of centrifugal compressors, integral blade-disk axial turbines, and radial inflow turbines. Low-pressure-ratio designs support the low stage count. It is possible to achieve the necessary pressure ratio with one centrifugal compression stage, and in one turbine stage, or one each high pressure and power turbine. The small size of parts and the selection of radial inflow or integral blade-disk turbines make ceramic materials an option. Single-can combustors are also employed to control cost. Prototypes have been built and operated in the United States, Europe, and Japan.¹⁷

The most successful automotive application of gas turbines is the power plant for the M1 Abrams Main Battle Tank. The engine uses a two-spool, multistage, all-axial-flow, gas generator plus power turbine. The cycle is regenerative. Output and cost appear too high for highway vehicle application.

Ship propulsion by gas turbine is more commonplace. One recent report summarizing orders and installations over an 18-month period listed 10 orders for a total of 64 gas turbines—75 MW in all. Military applications accounted for 55% of the total. The remaining 45% were applied to fast ferries and similar craft being built in Europe, Australia, and Hong Kong.¹¹ Gas turbine outputs in the 3–5-MW range, around 10 MW, and in the 20–30-MW range account for all the applications. Small industrial engines were selected in the 3–5-MW range and aeroderivative, free-turbine engines accounted for the remainder.

Successful application of gas turbines aboard ship requires protection from the effects of saltwater and, in the case of military vessels, maneuver and sudden seismic loads. In addition to the common problems with saltwater-induced corrosion of unprotected metal, airborne sodium (in combination with sulfur usually found in the fuel or air) presents a problem for buckets, nozzles, and combustors. Hot corrosion—also called sulfidation—has led to the development of alloys that combine the creep strength of typical aircraft engine bucket and nozzle alloys, with superior corrosion resistance. Inconel 738 was the first such alloy, and this set of alloys is used in marine propulsion engines. Special corrosion-resistant coatings are applied to further improve the corrosion resistance of nickel-based superalloy components. The level of sodium ingested by the engine can also be controlled with proper inlet design and filtration.¹⁰

Although there was a period when gas turbines were being applied as prime movers on railroad locomotives, the above report contained only one small railroad application.

4 EVALUATION AND SELECTION

4.1 Maintenance Intervals, Availability, and Reliability

Service requirements of aircraft and industrial gas turbines differ from other power plants principally in the fact that several key components operate at very high temperatures and thus have limited lives and have to be repaired or replaced periodically to avoid failures during operation. Components that must be so maintained include combustion chambers, buckets, and nozzles. Occasionally, other components, such as wheels or casings, may require inspection or retirement.

Wear-out mechanisms in hot gas path components include creep, low cycle fatigue, corrosion, and oxidation. All combustors, buckets, and nozzles have a design life and, if operated for significantly longer than this design life, will fail in one these modes. Repair or replacement is required to avoid failure. Most of the failure mechanisms give some warning prior to loss of component integrity. Corrosion and oxidation are observable by visual inspection, and affected parts can be repaired or replaced. The creep deflection of nozzles can be detected by

measuring changes in clearances. Low-cycle fatigue cracks can occur in nozzles, buckets, and combustors without causing immediate failure of these components. These can be detected visually or by more sophisticated nondestructive inspection techniques. Tolerance of cracks depends on the particular component design, service conditions, and what other forces or temperatures are imposed on the component at the location of the crack. Inspection intervals are set by manufacturers (based on analysis, laboratory data, and field experience) so that components with some degree of distress can be removed from service or repaired prior to component failure.

Bucket creep often gives no advance warning. There are several factors that make this so. First, the ability of bucket alloys to withstand alternating stress and the rate of creep progression are both affected by the existence of creep void formation. Local creep void formation is difficult to observe even in individual buckets subjected to radiographic and other nondestructive inspections. Destructive inspection of samples taken from a turbine are not useful in predicting the conditions of a particular bucket in a stage suffering the most advanced creep damage. This is due to the statistical distribution of creep conditions in a sample set. Such a large number of samples would be required to accurately predict the condition of the worst part in a set that the cost of such an inspection would be higher than the set of replacement components. Because of this, creep failure can be avoided by the retirement of sets of buckets as the risk of the failure of the weakest bucket in the set increases to a preselected level.

Some of the wear-out mechanisms are time related while others are start related. Thus, the actual service profile is significant to determining when to inspect or retire gas path components. Manufacturers differ in the philosophy applied. Some aircraft engine maintenance recommendations have been based on a particular number of mission hours of operation. Each mission contains a number of hours at takeoff conditions, a number at cruise, a number of rapid accelerations, thrust reversals, etc. Components' lives have been calculated and expressed in terms of a number of mission cycles. Thus, the life of any component can be expressed in hours, even if the mechanism of failure expected is low cycle fatigue, related to the number of thermal excursions to which the component is exposed. Inspection and component retirement intervals (based on mission-hours) can be set to detect distress and remove or repair components before the actual failure is likely to occur. Actual starts and actual hours are becoming more commonplace measures for aircraft engines.

Industrial gas turbine manufacturers have historically designed individual products to be suitable for both continuous duty and frequent starts and stops. A particular turbine model may be applied to missions ranging from twice-daily starts to continuous operation for over 8000 h per year and virtually no start cycles. To deal with this, manufacturers of industrial gas turbines have developed two ways of expressing component life and inspection intervals. One is to set two criteria for inspection—one based on hours and one based on starts. The other is to develop a formula for "equivalent hours," which counts each start as a number of additional hours of operation. These two methods are illustrated in Fig. 39. The figure is a simplification in that it considers only normal starts and base-load hours. Both criteria evaluate hours of operation at elevated firing temperature, fast starts, and emergency shutdown events as more severe than normal operating hours and starts. Industry practice is to establish maintenance factors that can be used to account for effects that shorten the intervals between inspections. Table 3 gives typical values. The hours to inspection or starts to inspection in Fig. 38 would be divided by the factor in Table 3.

The values shown here are similar to those used by manufacturers, but are only approximate, and recommendations are modified and updated periodically. Also, the number, extent, and types of inspections vary across the industry. To compare the frequency of inspection recommended for competing gas turbines, the evaluator must forecast the number of starts and hours expected during the evaluation period and, using the manufacturers' recommendation and other experience, determine the inspection frequency for the particular application.

Table 3 Maintenance Factors—Industrial Gas Turbine Nozzles and Buckets

		Hours Factors
Fuel	Natural gas	1
	Distillate	1–1.5
	Residual	3–4
Peak load	Elevated firing temperature	5–10
Diluent injection	Water or steam	1–2
		Starts Factors
Trip from full load		6–10+
Fast load		2–4
Emergency start		10–20

Reliability and availability have specific definitions when applied to power generation equipment¹⁸:

Reliability = $1 - (\text{FOH}/\text{PH})$, expressed as a percentage.

FOH = total forced outage hours

PH = period hours(8760 hr per year).

Reliability is used to reflect the percentage of time for which the equipment is not on forced outage. It is the probability of not being forced out of service when the unit is needed and includes forced outage hours while in service, while on reserve shutdown, and while attempting to start.

Availability = $1 - (\text{UH}/\text{PH})$, expressed as a percentage.

UH = total unavailable hours(forced outage, failure to start, unscheduled maintenance hours, maintenance hours)

PH = period hours

Availability reflects the probability of being available, independent of whether or not the unit is needed, and includes all unavailable hours normalized by period hours.

There are some minor differences in the definitions across the industry, which reflect the way different databases treat particular types of events, but the equations given above reasonably represent industry norms. Availability and reliability figures used in the power generation industry literature reflect the performance of not only the turbomachinery but also the generator, control system, and accessories. Historically, less than half of the unavailability and forced outage hours are due to the turbomachinery.

Availability is affected by the frequency of inspections, duration of inspections, as well as the duration of forced outages. Improvements in analytical capability, understanding of material behavior, operating practices, and design sophistication have led to improvements in both availability and reliability over the past decades. The availability of industrial gas turbines has grown from 80% in the early 1970s to better than 95% in the mid-1990s.

4.2 Selection of Engine and System

In the transportation field, gas turbines are the engine of choice in large, and increasingly in small, aircraft where the number of hours per year flown is sufficiently high that the higher speed

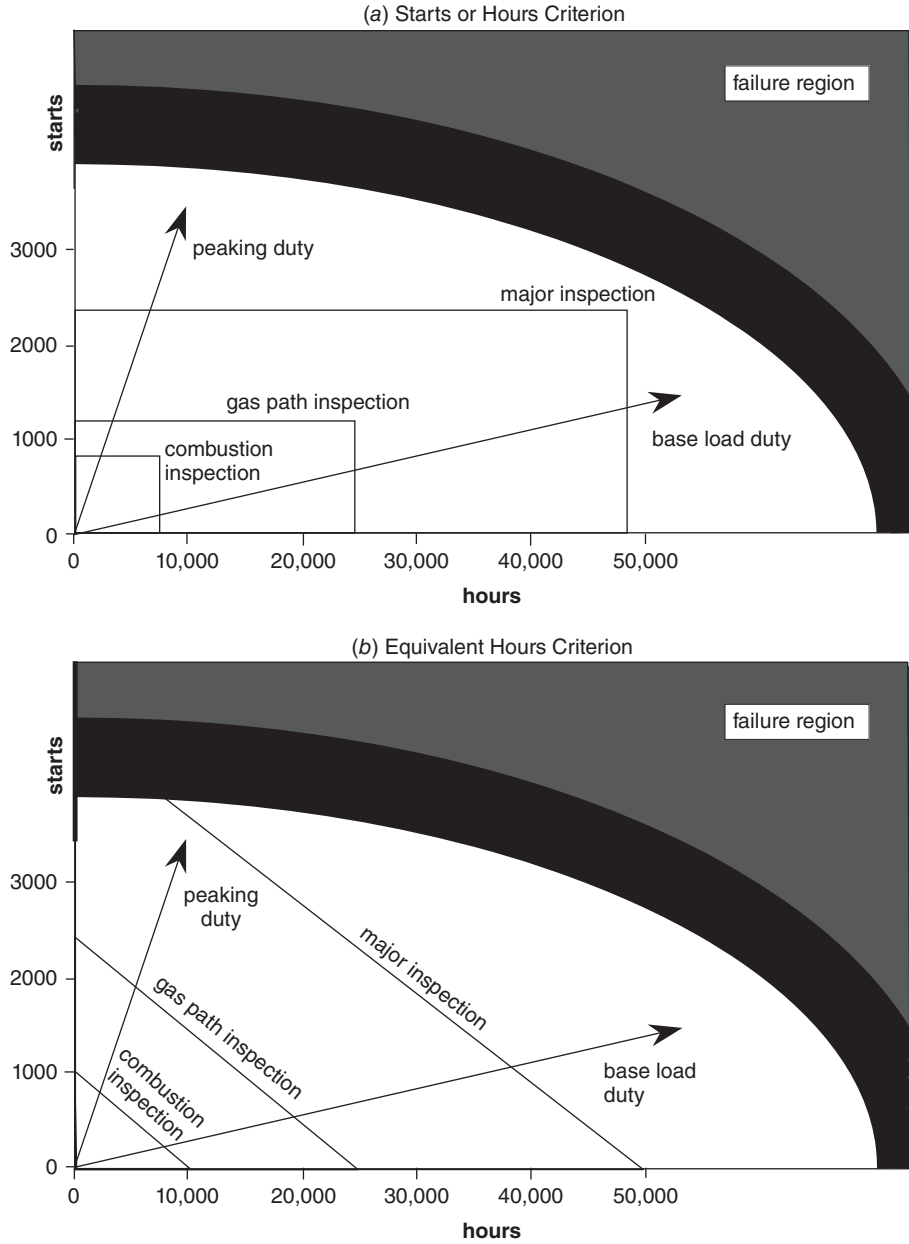


Figure 38 Inspection interval criteria compared. Starts-or-hours criterion shown requires major inspection after 48,000 h or 2400 starts. Equivalent-hours criterion shown reflects each start being equivalent to 10 h, and major inspection required after 50,000 equivalent hours.

and lower fuel and service costs attributable to gas turbines justifies the higher first cost. Private automobiles, which operate nominally 400 hours per year, and where operating characteristics favor the Otto and Diesel cycles, are not likely to be candidates for gas turbine power, since exhaust-driven superchargers are a more acceptable application of turbomachinery technology to this market. Long-haul trucks, buses, and military applications may be served by gas turbines if the economics that made them commonplace on aircraft can be applied.

Gas turbine technology finds application in mechanical drive and electric power generation. In mechanical drive application, the turbine rotor shaft typically drives a pump, compressor, or vehicle drive system. Mechanical drive applications usually employ “two-shaft” gas turbines in which the output shaft is controllable in speed to match the varying load/speed characteristic of the application. In electric power generation, the shaft drives an electric generator at a constant synchronous speed. Mechanical drive applications typically find application for gas turbines in the 5–25-MW range and over the last four years this market was over 3000 MW per year. Power generation applications are typically in the larger size ranges, from 25 to 250 MW, and have recently averaged over 60,000 MW per year.

Gas turbine technology competes with other technologies in both power generation and mechanical drive applications. In both applications, the process for selecting which thermodynamic cycle or engine type to apply is similar. Table 4 summarizes the four key choices in electric power generation.

Steam turbine technology utilizes an externally fired boiler to produce steam and drive a Rankine cycle. This technology has been used in power generation for nearly a century. Because the boiler is fired external to the working fluid (steam), any type of fuel may be used, including coal, distillate oil, residual oil, natural gas, refuse, and biomass. The thermal efficiencies are typically in the 30% range for small (20–40-MW) industrial and refuse plants to 35% for large (400-MW) power generation units, to 40% for large, ultraefficient, ultrasupercritical plants. These plants are largely assembled and erected at the plant site and have relatively high investment cost per kilowatt of output. Local labor costs and labor productivity influence the plant cost. Thus, the investment cost can vary considerably throughout the world.

Diesel technology uses the Diesel cycle in a reciprocating engine. The diesels for power generation are typically medium speed (800 rpm). The diesel engine has efficiencies from 40 to 45% on distillate oil. If natural gas is the fuel, the Diesel cycle is not applicable, but a spark

Table 4 Fossil Fuel Technologies for Mechanical Drive and Electric Power Generation

Technology	Power Cycle	Performance Level	Primary Advantages	Primary Disadvantages
Steam turbine	Rankine cycle	30–40%	Custom size Solid fuels Dirty fuels	Low efficiency Relatively high \$/kW Slow load change
Gas turbine	Brayton cycle	30–40%	Packaged power plant Low \$/kW Medium fast starts Fast load delta	Clean fuels Ambient dependence
Combined cycle	Brayton topping/ Rankine bottoming	45–60%	Highest efficiency Medium \$/KW Limited fast load delta	Clean fuels Ambient dependence Medium start times
Diesel	Diesel cycle	40–50%	Relatively high efficiency Packaged power plant Fast start Fast construction	High maintenance Small size (5 MW)

ignition system based on the Otto cycle can be employed. The Otto cycle leads to three percentage points lower efficiency than the diesel. Diesel engines are available in smaller unit sizes than the gas turbines that account for most of the power generated for mechanical drive and power generation (1–10 MW). The investment cost of medium-speed diesels is relatively high per kilowatt of output, when compared with large gas turbines, but is lower than that of gas turbines in this size range. Maintenance cost of diesels per kilowatt of output is typically higher than gas turbine technology.

The *life-cycle cost* of power generation technology projects is the key factor in their application. The life-cycle cost includes the investment cost charges and the present worth of annual fuel and operating expenses. The investment cost charges are the present-worth costs of financing, depreciation, and taxes. The fuel and operating expenses include fuel consumption cost, maintenance expenses, operational material costs (lubricants, additives, etc.), and plant operation and maintenance labor costs. For a combined-cycle technology plant, investment charges can contribute 20%, fuel 70%, and operation and maintenance costs 10%. The magnitude and composition of costs are very dependent on technology and geographic location.

One way to evaluate the application of technology is to utilize a *screening curve* as shown in Fig. 39. This chart represents one particular power output and set of economic conditions and is used here to illustrate a principle, not to make a general statement on the relative merits of various power generation means. The screening curve plots the total \$/kW/year annual life-cycle cost of a power plant versus the number of hours per year of operation. At zero hours of operation (typically of a standby plant used only in the event of loss of power from other sources), the only life-cycle cost component is from investment financing charges and any operating expense associated with providing manpower to be at the site. As the operating hours increase toward 8000 h/year, the costs of fuel, maintenance, labor, and direct materials are added into the annual life-cycle cost.

If the application has only a few hours per year of operation (less than 2000), the simple-cycle gas turbine technology has typically the lowest annual life-cycle cost and is therefore chosen. The simple-cycle gas turbine has the lowest annual life-cycle cost in this

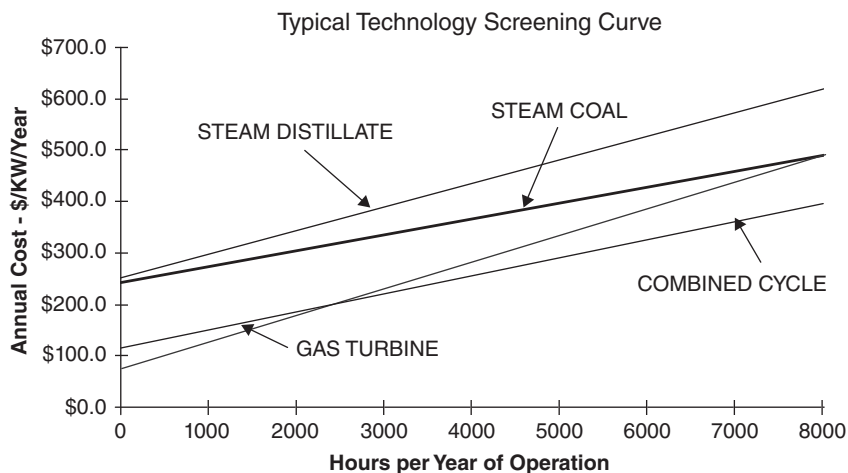


Figure 39 Hypothetical screening curve for selecting power generation technology from among various thermodynamic cycles and fuel alternatives. This curve would indicate the most economic choice for few operating hours per year is the simple-cycle gas turbine and the combined cycle for base-load applications. Position of the lines depends greatly on anticipated relative fuel costs. Source: From <http://www.asme.org/igt/resources/articles/hybrid6.html>.

region in view of its low investment cost. If the application has more than 2000 h/year of operation, then the combined-cycle technology provides the lowest annual life-cycle cost and is selected for application.

Other technology choices are the higher investment cost alternatives of the coal-fired steam turbine technology and the IGCC technology. In the example of Fig. 39 these technologies do not have the lowest annual life-cycle cost in any region. Consequently, they would not find application. However, the screening curve of Fig. 39 is based on a specific set of fuel prices and investment costs. In other regions of the world, coal prices may be less or natural gas prices may be higher. In this case, the coal technologies may be the lowest annual life-cycle cost in the 6000–8000-h range. These technologies would then be selected for application.

In summary, there is a range of fuel prices and investment costs for power generation technology. This range influences the applicability of the power generation technology. In some countries with large low-priced coal resources, coal steam turbine technology is the most widely used. Where natural gas is available and modestly priced, gas turbine and combined-cycle technology is frequently selected.

REFERENCES

1. R. Harman, "Gas Turbines," in M. Kutz (Ed.), *Mechanical Engineers' Handbook*, Wiley, New York, 1986, pp. 1984–2013.
2. D. E. Brandt, "The History of the Gas Turbine with an Emphasis on Schenectady General Electric Developments," GE Company, Schenectady, NY, 1994.
3. A. N. Smith and J. D. Alrich, "Gas Turbine Electric Locomotives in Operation in the USA," in *Combustion Engine Progress*, c. 1957.
4. H. E. Miller and E. Benvenuti, "State of the Art and Trends in Gas-Turbine Design and Technology," paper presented at the European Powerplant Congress, Liège, 1993.
5. L. B. Davis, "Dry Low NO_x Combustion Systems for GE Heavy-Duty Gas Turbines," paper presented at the 38th GE Turbine State-of-the-Art Technology Seminar, GE Company, Schenectady, NY, 1994.
6. J. Zeldovich, "The Oxidation of Nitrogen in Combustion and Explosions," *Acta Physicochim. USSR*, **21**(4), 577–628, 1946.
7. D. M. Todd and H. E. Miller, "Advanced Combined Cycles as Shaped by Environmental Externality," paper presented at the Yokohama International Gas Turbine Congress, Yokohama, Japan, 1991.
8. G. Leonard and S. Correa, "NO_x Formation in Premixed High-Pressure Lean Methane Flames," paper presented at the ASME Fossil Fuel Combustion Symposium, New Orleans, ASME/PD Vol. 30, S. N. Singh (Ed.), 1990, pp. 69–74.
9. R. J. Antos, "Westinghouse Combustion Development 1996 Technology Update," Westinghouse Electric Corporation Power Generation Business Unit, Orlando, FL, 1996.
10. C. T. Sims, N. S. Stoloff, and W. C. Hagel (Eds.), *Superalloys II*, Wiley, New York, 1987.
11. R. Farmer (Ed.), *Gas Turbine World 2003 Handbook*, Vol. 23, Pequot, Fairfield, CT, 2003.
12. D. L. Chase et al., "GE Combined Cycle Product Line and Performance," Publication GER-3574E, GE Company, Schenectady, NY, 1994.
13. M. W. Horner, "GE Aeroderivative Gas Turbines—Design and Operating Features," paper presented at the 38th GE Turbine State-of-the-Art Technology Seminar, GE Company, Schenectady, NY, 1994.
14. T. W. Fowler (Ed.), *Jet Engines and Propulsion Systems for Engineers*, University of Cincinnati, Cincinnati, OH, 1989.
15. P. G. Hill and C. R. Peterson, *Mechanics and Thermodynamics of Propulsion*, Addison-Wesley, Reading, MA, 1965.
16. A. L. Velocci, Jr. (Ed.), *2004 Aviation Week & Space Technology Aerospace Source Book*, McGraw-Hill, New York, 2004, pp. 126–140.
17. D. G. Wilson, "Automotive Gas Turbines: Government Funding and the Way Ahead," *Global Gas Turbine News*, **35**(4), ASME IGTI, Atlanta, 1995.

18. R. F. Hoefl, "Heavy-Duty Gas Turbine Operating and Maintenance Considerations," paper presented at the 38th GE Turbine State-of-the-Art Technology Seminar, GE Company, Schenectady, NY, August 1994.
19. H. Roxbee Cox, "British Aircraft Gas Turbines," *J. Aeronaut. Sci.*, **13**(2) (1946).
20. R. Gusso and H. E. Miller, "Dry Low NO_x Combustion Systems for GE/Nuovo Pignone Heavy Duty Gas Turbines," paper presented at the Flowers '92 Gas Turbine Congress, Florence, Italy, 1992.
21. C. Houllier, "The Limitation of Pollutant Emissions into the Air from Gas Turbines—Draft Final Report," CITEPA No. N 6611-90-007872, Paris, 1991.

CHAPTER 27

WIND POWER GENERATION

Todd S. Nemec
GE Energy
Schenectady, New York

1	MARKET AND ECONOMICS	955	4	ROTOR AND DRIVE TRAIN DESIGN	959
2	CONFIGURATIONS	955	5	SITE SELECTION	960
3	POWER PRODUCTION AND ENERGY YIELD	957		REFERENCES	962

1 MARKET AND ECONOMICS

Wind power has long been used for grain-milling and water-pumping applications. Significant technical progress since the 1980s, however, driven by advances in aerodynamics, materials, design, controls, and computing power, has led to economically competitive electric energy production from wind turbines. Technology development, favorable economic incentives (due to its early development status and environmental benefits), and increasing costs of power from traditional fossil sources have led to significant worldwide sales growth since the early 1980s. Production has progressed at an even faster pace beginning in the late 1990s. Figure 1 shows the U.S. wind turbine installations (MW, net) since 1981.

The spike in U.S. wind turbine installations from 1982 to 1985 was due to generous tax incentives (up to 50% in California²), access to excellent wind resources, and high fossil fuel prices. Today, Germany, the United States, Spain, and Denmark lead in installed MW, although significant growth is occurring worldwide.³ From an energy-share standpoint, the northern German state, Shleswig-Holstein, produces approximately 30% of its electric energy from wind power, while Denmark produces about 20%.⁴

Like other power-producing technologies, wind turbines are measured on their ability to provide low cost of electricity (COE) and high project net present value (NPV). Unlike fossil fuel plants, however, fuel (wind energy) is free. This causes COE to be dominated by the ratio of costs per unit energy, rather than a combination of capital costs, fuel cost, and thermal efficiency. For customers purchasing based on highest NPV, high power sale prices and energy production credits can drive turbine optimization to a larger size (and/or energy capture per rated MW) and higher COE than would be expected from a typical optimization for lowest COE. Operation and maintenance costs (in cents per kWh) for wind turbines trend higher than those for fossil plants, primarily due to their lower power density. The ability to predict and trade life-cycle costs versus energy improvement from new technologies is a key contributor to efficient technology development and market success.

2 CONFIGURATIONS

The most popular configuration for power-generating wind turbines is the upwind three-bladed horizontal-axis wind turbine (HAWT), shown in Fig. 2. *Upwind* refers to the position of the blades relative to the tower.

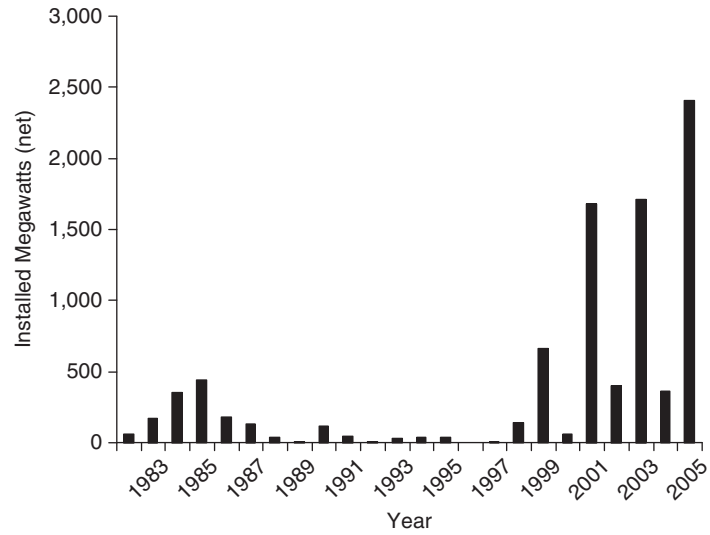


Figure 1 U.S. wind turbine installations (MW) by year. From Ref. 1



Figure 2 Horizontal Access Wind Turbine (HAWT). Copyright © tln/Shutterstock.

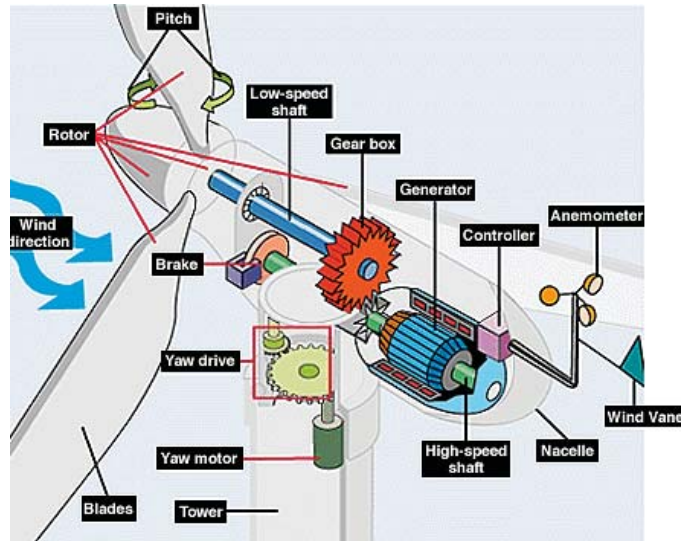


Figure 3 Nacelle cutaway view of a horizontal-axis turbine. © A. Guzzetta, G. Myers, A. Purse via Wikidot. Accessed at <http://me1065.wikidot.com/types-of-wind-turbines-and-associated-advantages>.

Wind turbine configurations can be traced back to vertical-axis drag-type machines used for milling grain, which had the theoretical potential to achieve an 8% power coefficient, or percent energy extracted from the wind.⁵ Modern vertical-axis wind turbines (VAWT), like HAWTs, use the much more effective *lift principle* to produce power. VAWTs have been built in both Darrieus (curved blades connected at one or both ends) and H (separate vertical blades; also called giromill) configurations, although neither has been put into widespread use. VAWT aerodynamics are somewhat more complex, with a constantly changing angle of attack, and analyses have generally concluded that their power coefficient entitlement is lower than HAWTs.⁴⁶ Figure 3 shows the nacelle cutaway view of a horizontal-axis turbine.

The rotor, made up of the blades and hub, rotates a drive train through the low-speed shaft connected to a gearbox, high-speed shaft, and generator (or from the low-speed shaft to a direct-drive generator). The nacelle consists of the base frame and enclosure; it houses the drive train, various systems, and electronics required for turbine operation. Towers are made of steel or steel-reinforced concrete. Steel towers use either a tubular or lattice-type construction. Today's turbine configuration has evolved from both scaling-up and adding features to small wind turbine designs and from private and government-sponsored development of large machines.

3 POWER PRODUCTION AND ENERGY YIELD

Turbines extract energy from the wind according to following formula, derived from the first law of thermodynamics:

$$P = C_p \frac{1}{2} \rho A U^3$$

where P = power
 C_p = power coefficient
 ρ = air density
 A = rotor swept area
 U = air velocity at hub height

This equation shows power to be a function of air density and swept area while varying by the cube of wind speed. These functions are not exact in real calculations, however, as aerodynamic and drive-train characteristics restrict the power coefficient over much of the operating range. The maximum theoretical power coefficient with zero airfoil drag and other simplifying assumptions is 59.3%, while modern turbines deliver peak coefficients in the mid-40% range.

The peak efficiency corresponds to a rotor exit air velocity of one-third the initial wind speed. This wake effect—along with site geographic, turbulence, and wind rose data—is significant when planning turbine spacing and arrangement on a multiturbine wind farm. Turbulence acts to reduce the velocity reduction immediately behind the turbine by reenergizing the wake, while it also spreads the energy loss over a larger area.⁵ Crosswind spacing, depending on wind characteristics, can usually be much closer than downwind spacing—crosswind tower spacing is on the order of three to five rotor diameters.

The power equation also provides insight into the basic power and mass scaling relationships. Power increases as a function of area, a function of diameter squared, while mass is a function of volume, or diameter cubed. This is true for aerodynamically load-limited components. Most electrical capacities and costs scale with rated power, while some part sizes are independent of turbine size. The cubed–squared relationship between component mass and power is the same found in most power generation cycles, such as gas turbines. Larger wind turbines are made economically possible by both reducing this $3/2$ exponent, by improving technology and design strategy, such as using more advanced materials, and from increased leverage over fixed costs.

Wind turbine performance is characterized by its power curve, in Fig. 4, which shows the gross power produced as a function of wind speed. This curve assumes clean airfoils, standard control schedules, a given wind turbulence intensity, and a sea-level air density. Three items

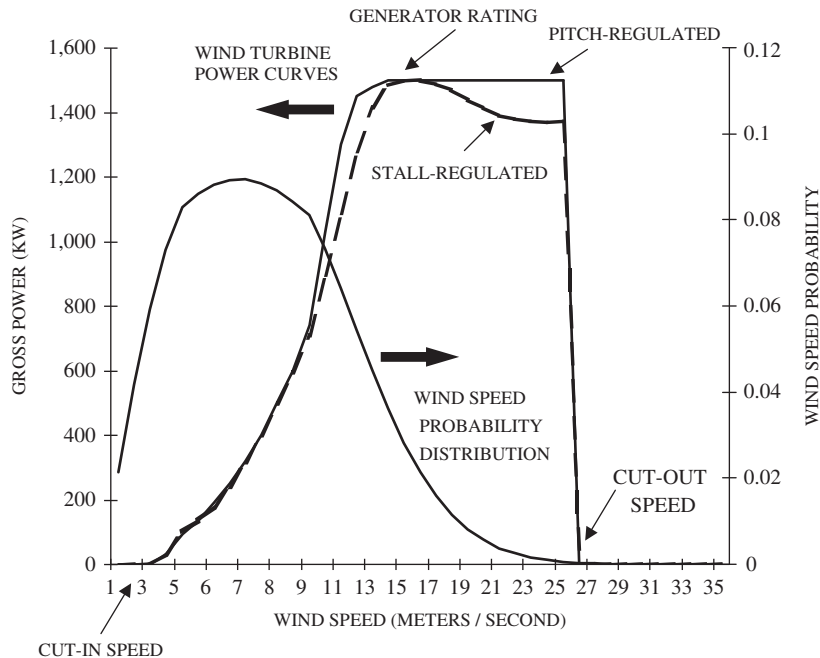


Figure 4 Wind speed probability distribution and notional power curves. Adapted from General Electric Company.

to note on the power curve are the cut-in speed, cut-out speed, and generator rating. Cut-in speed is determined by the wind speed where the aerodynamic torque is enough to overcome losses. Cut-out speed is set to balance the power production in high winds with design loads and costs. Both speeds have dead-band regions around them to minimize the number of start–stop transients during small changes in wind speed.

Like cut-out speed, selecting the rotor diameter relative to generator rating requires balancing higher energy production at high wind speeds while minimizing costs.

Economic and design analysis has proven that turbines designed for high-wind-speed operation should have a larger generator relative to rotor size, while those designed for low wind speed will have a larger rotor for a given generator size.⁷ Advances in design and controls technology have not only helped turbines scale economically to larger sizes but also have allowed turbines to run larger rotor diameters at a given rating.⁴

Representative power curves are shown for two methods of limiting power in high winds. The pitch-controlled blade curve shows a constant generator output above rated power, while the curve for a stall-controlled (fixed-pitch) turbine delivers a peaked profile. Gross annual energy production (in kilowatt-hours, kWh) is calculated by multiplying the wind probability (in annual hours) at each wind speed by the power curve kW at that same wind speed, then adding up the total. Because of the higher probability for low wind speeds and turbine design/economic tradeoffs, wind turbines operate at 25–45% plus net capacity factor, depending on the turbine and site. Capacity factor is the fraction of energy produced relative to the rated capacity. This is much lower than the 95% plus levels achieved by dispatchable fossil fuel power plants:

$$\text{Annual energy yield} = 5,000,000 \text{ kWh (assumed: measured from a kWh meter, or calculated based on turbine and wind conditions)}$$

$$\text{Rated capacity} = 1500 \text{ kW (Rating)} \times 8,760 \text{ hours/year}$$

$$\text{Capacity Factor} = 5,000,000 / (1,500 \times 8,760) = 38\%$$

Some of the gross-to-net loss is bookkept as availability losses (1–4% of energy produced), which are caused by both forced and scheduled outages. Other losses can total less than 15% and include array interference effects, electrical collection losses, blade soiling, and control losses.

Predictive performance analysis generally assumes that wind speed probability follows a Rayleigh distribution (Weibull distribution with shape factor equal to 2), along with an average wind speed at the hub height. In-depth and site analyses will use modifications to this statistical model or will use data unique to a given site. Although the previous example considers the effects of vertical wind shear on average wind speed at hub height, detailed energy yield analysis and loads calculations need to consider the effects of vertical velocity distribution. Taller towers allow turbines to see a higher average wind speed due to reduced friction with the ground and other objects at lower heights.

4 ROTOR AND DRIVE TRAIN DESIGN

The rotor and drive train are ultimately optimized to yield the best economics for the turbine’s mission. This is part of a multidisciplinary process involving aerodynamics, weight, materials, aeroelasticity, life, first cost, operating cost, frequency response, controls strategy, configuration options/technology availability, noise, site characteristics, supply chain, and a customer value equation. One modern mission requirement is quieter operation for land-based turbines—various noise sources correlate with tip speed raised to powers as high as 5, among other variables.⁵ Aerodynamic characteristics that are selected include number of blades, tip speed ratio, blade radius, solidity, blade twist, chord length, airfoil section, and so on, in

greater detail. As an example of this process, consider that at a given rated power, higher tip speed ratio (higher rotor speed at a given wind speed) does the following:

- It reduces main shaft torque requirements and component sizes (costs).
- It increases noise.
- It decreases rotor solidity (to maintain or increase the power coefficient), which reduces blade chord length and thickness (for a given number of blades).
- It makes it more difficult to fabricate blades and achieve strength objectives.

Prior to generating power, wind turbines were generally configured as direct-drive units to pump water or mill grain. These applications place a high emphasis on torque coefficient at zero rotor speed, defining their ability to start under load. A high-power coefficient was sacrificed by using high blade solidity (blade area divided by rotor disk area) and low tip speed ratios (tip speed divided by wind speed) in order to achieve high torque.⁸ When transferring power through an electrical connection, such as a generator, rotor design generally favors higher power coefficients via low solidity and high tip speed ratio, resulting in modern high-aspect-ratio blade shapes. Three blades have generally been favored over two because power coefficient is higher at lower tip speed ratios and for several structural dynamic considerations: Out-of-plane bending loads are higher on two-blade designs due to wind shear, tower shadow effect, effects of an upward-tiled shaft (to improve tower clearance), and from yaw-induced moments due to a changing moment of inertia.⁹ Several of these loads can be eliminated in two-blade rotors with the use of a teetering hub.

As already described above, a wind turbine will generally be designed with little excess weight, or structural design, margin in order to optimize life-cycle economics. Design misses, such as higher weight blades, have subsequent effect in weight, cost, and/or life of drive train, tower, and foundation components. Turbine fatigue and ultimate loads are driven by four categories: aerodynamic, gravity, dynamic interactions, and control.¹⁰

Drive trains absorb the rotor loads and distribute them to the bedplate for transmission to the tower and foundation. They also serve to convert torque into electrical power via the nacelle-mounted generator. Direct-drive generators, used by some manufacturers, turn at the rotor RPM, use a higher number of generator poles, and use power electronics to convert this rotor RPM into 50 or 60 Hz alternating current. Geared drive trains use a gearbox to drive a high-speed shaft connected to a smaller generator (with a fewer number of poles). Most manufacturers are employing variable-speed and pitch control using power electronics, pitch controllers, gearboxes, and induction (asynchronous) generators to optimize cost, energy yield, and grid power quality.

Design advances are evident in the lighter and more compact drive trains. ENERCON GmbH has used direct-drive generators since the early 1990s.¹¹ These, and mixed solutions that use a single-stage gearbox to step up to a smaller low-speed generator, have been receiving more attention by other manufacturers as power electronic costs have come down.

5 SITE SELECTION

Turbine siting tasks are designed to solve a wide range of economic, environmental, social, and technical issues. Computer modeling of wind farm concepts can both help estimate the wind resource and improve understanding of visual, acoustic, and environmental issues. Some of the early site election activities include the following:

1. Wind resource
 - Determining location(s) with highest average wind speeds
 - Estimating array losses and terrain effects

2. Revenue
 - Energy
 - Capital, energy, and/or emissions incentives
3. Costs
 - Transportation and construction access
 - Grid interconnection costs and transmission impact
 - Land-lease and/or opportunity costs
 - Foundation costs and geological compatibility
4. Site access and environmental
 - Noise and visual restrictions
 - Access rights
 - Impact on wildlife such as birds, bats, or endangered species
 - Interference with aviation flight routes or radar

Micrositing optimizes turbine placement at a given site through the detailed evaluation of energy resource and iteration for best energy yield and/or farm economics. It can be performed after or during the early selection process. State-of-the-art micrositing utilizes macro- and microlevel weather and flow models that are correlated to both long-term (usually low-resolution data, such as airport weather stations) and shorter term high-resolution data taken from meteorological masts. Models will include topographical features and turbulence estimates and should be able to produce uncertainty estimates that are useful in financial risk calculations. Ideally, micrositing optimization will include the impact of cost, such as roads and electrical collection, and noise/control strategy in addition to energy yield.

Although it pays for large farms to expend considerable resources to optimize farm layout, smaller installations consisting of one or a few small turbines may not want to cover the cost of detailed analysis. For these cases, rules of thumb can be used to optimize siting to account for turbulence and boundary layer effects caused by surface roughness and interference, topographical features in the terrain, and turbine wakes. Boundary layer impact on wind velocity is usually expressed by a power law equation, often using a default one-seventh exponent to model a typical vertical wind shear profile:

$$V(z)/V(z_r) = (z/z_r)^\alpha$$

where $\alpha = 1/7 = 0.143$

$V(z)$ = Average wind velocity (m/s) at hub height

$V(z_r)$ = average wind velocity (m/s) at reference elevation

z = elevation, m

z_r = reference elevation, m

This allows correcting from a measured (reference) wind location, such as a 10-m weather tower to a much taller wind turbine hub height. The actual exponent will be calculated from meteorological mast data, extending to a much taller height, and will vary with wind direction and speed (topography, array interference), among other factors. For improved—but still approximate—calculations, the exponent equation can be replaced with an expression based on terrain features:

$$V(z)/V(z_r) = \ln(z/z_0)/\ln(z_r/z_0)$$

where $V(z)$ = average wind velocity (m/s) at hub height
 $V(z_r)$ = average wind velocity (m/s) at reference elevation
 z = elevation, m
 z_0 = roughness length, m
 z_r = reference elevation, m

Terrain	z_0 , Roughness Length (m)
Cities, forests	0.7
Suburbs, wooded countryside	0.3
Villages, countryside with trees and hedges	0.1
Open farmland	0.03
Flat, grassy plains	0.01
Flat desert, rough sea	0.001
Calm open sea	0.0002

As both equations show, wind speed will be higher at a given hub height when there is reduced interference or vertical shear. This is favorable for energy yield, allowing lower hub heights to collect the same wind energy, reducing tower, foundation, and installation costs. Expected revenue should be weighed versus these costs to guide the micro-siting turbine placement and farm design.

REFERENCES

1. Wind Energy Program and AWEA Global Market Reports, U.S. DOE, Office of Energy Efficiency and Renewable Energy, Wind and Hydropower Technologies Program and AWEA data, available: http://www.eere.energy.gov/windandhydro/windpoweringamerica/wind_wind_installed_capacity.asp, accessed October 11, 2006
2. M. Gielecki et al., "Renewable Energy 2000, Issues and Trends: Incentives, Mandates, and Government Programs for Promoting Renewable Energy," U.S. DOE Energy Information Association (EIA), Washington, DC, 2001.
3. "Global Wind Power Growth Continues to Strengthen," Joint EWEA/AWEA press release, March 10, 2004.
4. European Wind Energy Association (EWEA), "Wind Energy—The Facts; An Analysis of Wind Energy in the EU-25," 2003, available: www.ewea.org, accessed October 15, 2004.
5. D. Spera (Ed.), *Wind Turbine Technology*, ASME Press, New York, 1995.
6. R. Harrison et al., *Large Wind Turbines, Design and Economics*, Wiley, New York, 2000.
7. D. J. Malcolm and A. C. Hansen, "WindPACT Turbine Rotor Design, Specific Rating Study," National Renewable Energy Laboratory (NREL), 2003.
8. J. A. C. Kentfield, *The Fundamentals of Wind-Driven Water Pumps*, Gordon and Breach Science, Amsterdam, 1996.
9. T. Burton et al., *Wind Energy Handbook*, Wiley, New York, 2001.
10. J. F. Manwell et al., *Wind Energy Explained, Theory, Design and Application*, Wiley, West Sussex, England, 2003.
11. "ENERCON History," available: www.enercon.de, accessed October 21, 2004.

CHAPTER 28

COGENERATION

Jerald A. Caton
Texas A&M University
College Station, Texas

1 INTRODUCTION	963	6 REGULATORY CONSIDERATIONS	977
1.1 History of Cogeneration	964	6.1 Federal Regulations Related to Cogeneration	977
1.2 Constraints on Cogeneration	965	6.2 Energy Policy Act of 2005	979
2 BASIC COGENERATION SYSTEMS	965	6.3 2008 and 2009 Legislation	979
2.1 Topping Cycles	965	6.4 Air Pollution Regulations	979
2.2 Bottoming Cycles	966	6.5 Equipment Specific Regulations	980
2.3 Combined Cycles	967	6.6 Water Quality and Solid Waste Disposal	981
2.4 Applications of Cogeneration Systems	967	6.7 Permits and Certificates for Cogeneration	982
3 DESCRIPTIONS OF PRIME MOVERS	968	7 ECONOMIC EVALUATIONS	983
3.1 Steam Turbines	968	7.1 Operating Costs of Current System	983
3.2 Gas Turbines	969	7.2 Operating Costs of the Proposed Cogeneration System	984
3.3 Reciprocating Engines	970	7.3 Economic Merit	985
3.4 Other Possible Prime Movers	971	8 OWNERSHIP AND FINANCIAL ARRANGEMENTS	986
4 DESCRIPTION OF OTHER EQUIPMENT AND COMPONENTS	971	8.1 Overall Considerations	986
4.1 Electrical Equipment	971	8.2 Conventional Ownership and Operation (100% Ownership)	987
4.2 Heat Recovery Equipment	972	8.3 Partnership Arrangements	988
4.3 Absorption Chillers	972	8.4 Third-Party Ownership	988
4.4 Balance of Plant Equipment	974	8.5 Final Comments on Financial Aspects	989
5 TECHNICAL DESIGN ISSUES	974	9 SUMMARY AND CONCLUSIONS	989
5.1 Selecting and Sizing Prime Mover	974	REFERENCES	990
5.2 Matching Electrical and Thermal Loads	975		
5.3 Dynamic Power and Thermal Matching	976		
5.4 Packaged Systems	976		

1 INTRODUCTION

The term “cogeneration” refers to the combined production of electrical power and useful thermal energy by the sequential use of a fuel or fuels. The electrical power is produced by an electrical generator which is most often powered by a prime mover such as a steam turbine, gas

turbine, or reciprocating engine. Examples of useful thermal energy include hot exhaust gases, hot water, steam, or chilled water.

Cogeneration is important because of the potential for monetary and energy savings and emission reductions. Any facility that uses electrical power and has thermal energy needs is a candidate for cogeneration. Although many considerations are involved in determining if cogeneration is feasible for a particular facility, the basic consideration is if the savings on thermal energy costs is sufficient to justify the capital expenditures for a cogeneration system. Facilities that may be considered for cogeneration include those in the industrial, commercial, and institutional sectors.

The technology for cogeneration exists for a range of sizes: from less than 50 kW to over 100 MW. The major equipment requirements include a prime mover, electrical generator, electrical controls, heat recovery systems, and other typical power plant equipment. These components are well developed, and the procedures to integrate these components into cogeneration systems are well established.

In addition to the economic and technical considerations, the application of cogeneration systems involves an understanding of the governmental regulations and legislation on electrical power production and on environmental impacts. With respect to electrical power production, certain governmental regulations were passed during the late 1970s which removed barriers and provided incentives to encourage cogeneration development. Finally, no cogeneration assessment would be complete without an understanding of the financial arrangements, contracts, and agreements that are possible.

The sections of this brief overview of cogeneration systems will include introductory comments, descriptions of basic systems and terminology, descriptions of prime movers and major equipment, some comments on technical designs, a summary of relevant regulations, descriptions of economic evaluations, and comments on financial and ownership aspects. A number of references exist that cover various aspects of cogeneration systems (e.g., Refs. 1–7).

1.1 History of Cogeneration

At the beginning of the twentieth century, electrical power generation was in its infancy. Most industrial facilities generated all their own electrical power and often supplied power to nearby communities. They used the thermal energy which was available during the electrical power production to provide or supplement process or building heat. These industrial facilities, therefore, were the first “cogenerators.” The dominant prime mover at this time was the reciprocating steam engine, and the low-pressure exhaust steam was used for heating applications.

Between the early 1920s and through the 1960s, the public electric utility industry grew rapidly because of increasing electrical power demands. Coincident with this rapid growth was a general reduction in the costs to produce the electrical power mainly due to the economies of scale, more efficient technologies, and decreasing fuel costs. During this period, industry often abandoned their own electrical power generation because of (1) the decreasing electrical rates charged by public utilities, (2) income tax regulations which favored expenses instead of capital investments, (3) increasing costs of labor, and (4) the desire of industry to focus on their product rather than the side issue of electrical power generation. Estimates are available that suggest that industrial cogenerated electrical power decreased from about 25 to 9% of the total electrical power generated in the country between the years of 1954 and 1976. Since about the mid-1980s, this percentage has been fairly constant at about 5%. For example, at the end of 1992, 5.1% of the total U.S. electrical capacity was due to cogeneration systems.

In late 1973 and again in 1979, America experienced major “energy crises” which were largely a result of reduced petroleum imports. Between 1973 and 1983, the prices of fuels and electrical power increased by a factor of about five (5). Any facility purchasing electrical power began to consider (or reconsider) the economic savings associated with cogeneration.

These considerations were facilitated by federal regulations which were enacted in 1978 to ease or remove barriers to cogeneration.

As of 2010, cogeneration accounts for about 9% of total generating capacity in the United States. Texas, California, Louisiana, New York, and Florida are the top five U.S. states in terms of cogeneration capacity. About 88% of the U.S. cogeneration capacity is located at industrial or manufacturing facilities. Natural gas is used in about 73% of these cogeneration plants, and about 66% of all capacity uses gas turbines. Interestingly, in terms of numbers, reciprocating engines account for 42% of all plants, but due to their smaller sizes they only account for 2% of electrical capacity.

Cogeneration is widely used throughout the world. In some European countries, cogeneration may account for 30–50% of their total generating capacity. In China and India, cogeneration accounts for about 13 and 5%, respectively, of their total generating capacity. The International Energy Agency (IEA) projects that, by 2030, cogeneration in China and India could increase to 28 and 26%, respectively. A large majority (~80%) of the cogeneration worldwide is sited at industrial and manufacturing locations.

1.2 Constraints on Cogeneration

Although the arguments for cogeneration technology are persuasive, a number of obstacles may exist which constrain the implementation of these systems:

- *High Cost of Capital Investment.* Costs of cogeneration systems vary depending upon the size and the type of facility, and for relatively large systems, these costs can be millions of dollars.
- *High Cost of Fuel.* The fuel cost can be the major operating expense of a cogeneration facility.
- *Low Cost of Electricity.* Despite the rate increases of recent years, the cost of electricity still remains low in many areas of the country and for certain sectors (such as for large industrial users due to the declining block rate structuring approach used by some utilities).
- *Environmental Concerns.* The regulations on environmental emissions continue to impede the implementation of new power facilities. In some areas of the country (e.g., California), new power plant construction has slowed or stopped for some periods of time.
- *Restricted Revenue from Electricity Sales.* The Federal Energy Regulatory Commission (FERC) has required utilities to purchase cogenerated electricity, minimizing this obstacle, but the utilities pay a rate on an “avoided cost” basis.
- *High Back-Up Rates.* Electric utilities have traditionally charged high rates to provide stand-by power. The FERC has ruled that electric utilities must apply the theory of load diversity in a nondiscriminatory fashion to establish stand-by rates.
- *Business Uncertainty.* A company must be certain that a particular location will be economically viable long enough to support the investment.

2 BASIC COGENERATION SYSTEMS

2.1 Topping Cycles

A cogeneration system may be classified as either a topping-cycle system or a bottoming-cycle system. Figure 1 illustrates a topping-cycle system. As shown, a prime mover uses fuel to power

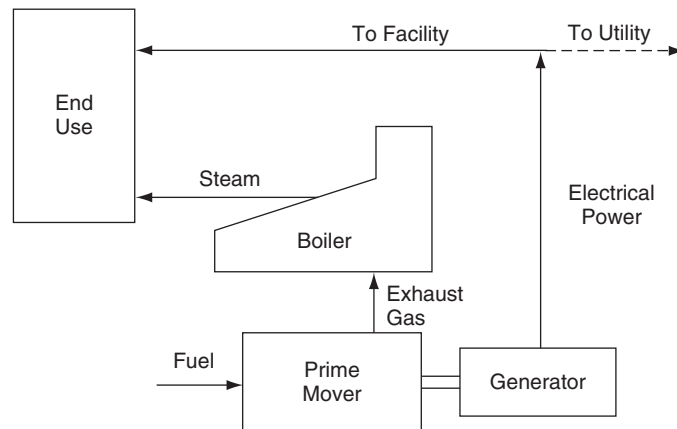


Figure 1 Cogeneration topping-cycle system.

an electrical generator to produce electricity. This electricity may be used completely on-site or may be tied into an electrical distribution network for sale to the local utility or other customers. The hot exhaust gases are directed to a heat recovery steam generator (HRSG)* to produce steam or hot water. This steam or hot water is used on-site for process or building heat. This cogeneration system is classified as a topping-cycle because the electrical power is generated first at the higher (“top”) temperatures associated with the fuel combustion process, and then, the rejected or exhausted energy is used to produce useful thermal energy. The majority of cogeneration systems are based on topping cycles.

2.2 Bottoming Cycles

The other classification of cogeneration systems is bottoming-cycle systems. Figure 2 illustrates a bottoming-cycle system. As shown, the high-temperature combustion gases are used first in a high-temperature thermal process (such as high-temperature metal treatment), and then, the lower temperature gases are used in a special low-temperature cycle to produce electrical power. After the energy is removed at the high temperatures, the energy available at the “bottom” or lower temperatures is then used to produce electrical power.†

Bottoming-cycle cogeneration systems have fewer applications than topping-cycle systems and must compete with waste heat recovery systems such as feedwater heaters, recuperators, and process heat exchangers. One of the difficulties with bottoming-cycle systems is the low-temperature electrical power producing cycle. One example, depicted in Fig. 2, is a low-temperature Rankine cycle. The low-temperature Rankine cycle is a power cycle similar to the conventional steam Rankine cycle, but a special fluid such as an organic substance (like a refrigerant) is used in place of water. This fluid vaporizes at a lower temperature compared to water, and therefore, this cycle is able to utilize the low-temperature energy. These cycles are generally much less efficient than conventional power cycles, often involve special equipment, and use more expensive working fluids.

* Many other terms for this boiler are common: e. g., waste heat boiler (WHB) and heat recovery boiler (HRB).

† Other definitions of bottoming cycles are common. These other definitions often include any second use of the energy. For example, some authors refer to the steam turbine in a combined cycle as using a bottoming cycle. The more precise thermodynamic definition employed here is preferred, although fewer applications meet this definition.

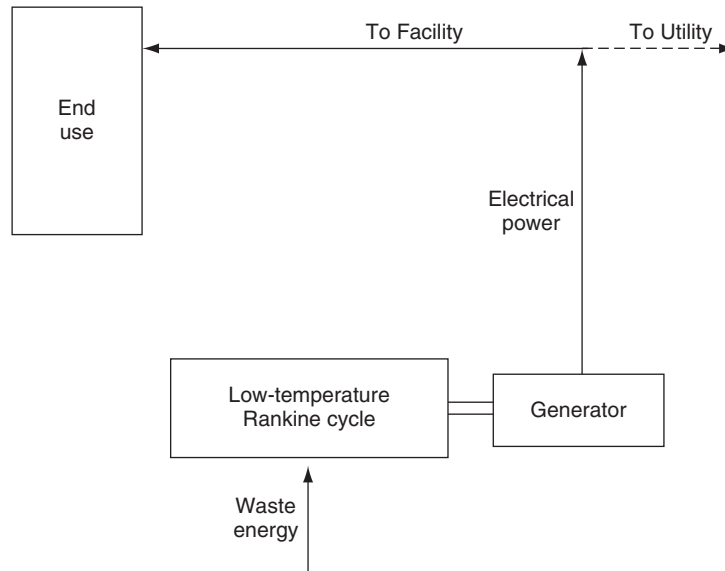


Figure 2 Cogeneration bottoming-cycle system.

2.3 Combined Cycles

One power plant configuration which is based on a form of a topping cycle and is widely used in industry and by electrical utilities is known as a combined cycle. Figure 3 illustrates a possible combined-cycle cogeneration system. In this example, a gas turbine generates electrical power, and the exhaust gas is ducted to an unfired heat recovery boiler. The produced steam then drives a steam turbine which produces additional electrical power. The exhaust steam from the steam turbine is at a high enough pressure and temperature to supply thermal energy for process or building heat. In this example, the steam is then condensed and pumped back into the boiler. For such a combined-cycle gas turbine (CCGT) power plant to qualify as a cogeneration application, some steam would need to be used to satisfy a thermal requirement. If no thermal commodity is produced and used, the facility could not be considered a cogeneration system.

As might be expected, combined cycles have high power-to-heat ratios and high electrical efficiencies. Current designs may have electrical efficiencies as high as 60% depending on the equipment, location, and details of the specific application. These current designs for combined-cycle plants result in the gas turbine power to be between 1.5 and 3.5 times the power obtained from the steam turbine. These plants are most often base-load systems operating more than 6000 hours per year. More details on gas turbines and steam turbines are provided in the following sections on the prime movers.

2.4 Applications of Cogeneration Systems

Cogeneration systems may involve different types of equipment and may be designed to satisfy specific needs at individual sites. On the other hand, many sites have similar needs and packaged (preengineered) cogeneration systems may satisfy these needs and are less expensive than custom engineered systems.

Cogeneration systems are found in all economic sectors of the world. For convenience, cogeneration systems are often grouped into one of three sectors: (1) industrial, (2) institutional, or (3) commercial. The types and sizes of the cogeneration systems in these sectors

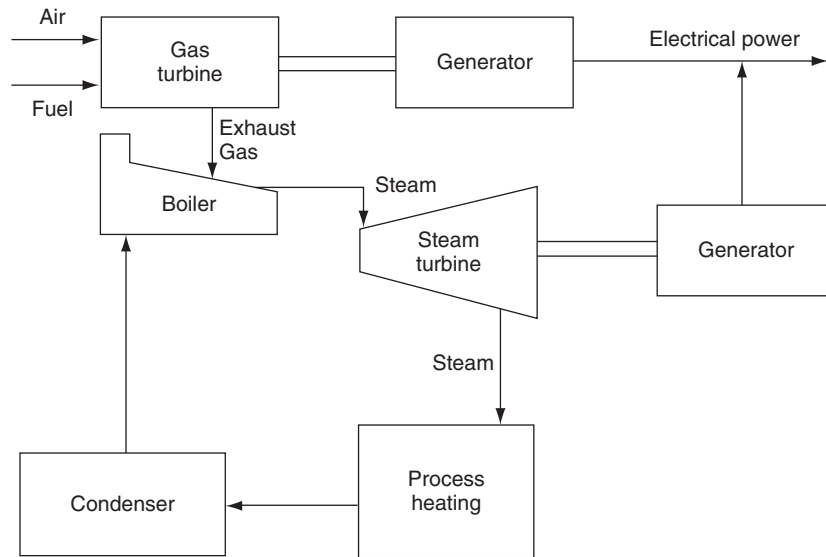


Figure 3 Possible combined-cycle cogeneration system.

overlap to varying degrees, but nonetheless, these sectors are convenient for describing various applications of cogeneration. Examples of successful applications are often found for universities (and other similar campuses), hospitals, other medical facilities, military bases, industrial sites, laundries, hotels, and airports.

3 DESCRIPTIONS OF PRIME MOVERS

Cogeneration systems consist of several major pieces of equipment and many smaller components. This section will describe the prime movers, and the following section will describe the other major equipment (electrical equipment, heat recovery devices, absorption chillers, and balance of plant equipment).

Prime movers include those devices that convert fuel energy into rotating shaft power to drive electrical generators. The prime movers that are used most often in cogeneration systems are steam turbines, gas turbines, and reciprocating engines. Each of these prime movers are described below. Important distinctions between the prime movers are the fuels that they may use, their combustion processes, their pollutant emissions, their overall thermal efficiency, and the type, amount, and temperature of their rejected thermal energy. In cogeneration applications, a significant parameter for each type of prime mover is the ratio of the rate of supplied thermal energy and the output power. This ratio is called the heat-to-power ratio. Knowing the value of the heat-to-power ratio assists in matching a particular prime mover to a particular application. This matching is discussed in a subsequent section.

3.1 Steam Turbines

Steam turbines are widely used in power plants throughout industry and electric utilities. Steam turbines use high-pressure, high-temperature steam from a boiler. The steam flows through the turbine, forcing the turbine wheel to rotate. The steam exits the turbine at a lower pressure and temperature. A major advantage of the steam turbine relative to reciprocating engines and gas

turbines is that the combustion occurs externally in a separate device (boiler). This allows a wide range of fuels to be used, including solid fuels such as coal or solid waste materials. The turbine's exit steam, of course, can be used for thermal heating or to supply the energy to an absorption chiller.

Steam turbines are available in a multitude of configurations and sizes. A major distinction is whether the machine is a condensing or noncondensing (back-pressure) steam turbine. Condensing steam turbines are steam turbines designed so that the steam exits at a low pressure (less than atmospheric) such that the steam may be condensed in a condenser at near-ambient temperatures. Condensing steam turbines provide the maximum electrical output and hence are most often used by central plants and electric utilities. Since the exiting steam possesses little available energy, applications of condensing steam turbines for cogeneration would require the extraction of steam prior to the exhaust.

Noncondensing steam turbines are those steam turbines which are designed so that the exiting steam is at a pressure above atmospheric. The exiting steam possesses sufficient energy to provide process or building heat. Either type of steam turbine may be equipped with one or more extraction ports so that a portion of the steam may be extracted from the steam turbine at pressures between the inlet and exit pressures. This extracted steam may be used for heating or thermal processes which require steam at higher temperatures and pressures than that which is available from the exiting steam.

Noncondensing steam turbines are available in a wide range of outputs beginning at about 50 kW and increasing to over 100 MW. Inlet steam pressures typically range from 150 to 2000 psig, and inlet temperatures range from 500 to 1100°F. Depending on the specific design and application, the heat-to-power ratio for steam turbines could range from 4 to over 10. The thermal efficiency typically increases with size (or power level). Although the major source of thermal energy is the exit or extracted steam, the boiler exhaust may be a possible secondary source of thermal energy in some cases.

3.2 Gas Turbines

As with steam turbines, stationary gas turbines are major machines in many power plants. Stationary gas turbines share many of the same components with the familiar aircraft gas turbines. In fact, both stationary (or industrial) and aircraft (or aeroderivative) gas turbines are used in cogeneration systems. The major components of a gas turbine are the air compressor, the combustor, and the turbine. A significant fraction of the turbine power is used internally to drive the compressor. This brief description will highlight the important characteristics of gas turbines as applied to cogeneration.

Many configurations, designs, and sizes of gas turbines are available. The simple-cycle gas turbine uses no external techniques such as regeneration to improve its efficiency. The thermal efficiency of simple-cycle gas turbines may be increased, therefore, by the use of several external techniques, but the designs and configurations become more complex. Many of these modifications to the simple-cycle gas turbine are directed at using the energy in the exhaust gases to increase the electrical output and efficiency. Of course, such modifications will decrease the available energy in the exhaust. For some cogeneration applications, therefore, the most efficient gas turbine may not always be the appropriate choice.

The single shaft, single turbine described above is the configuration of the simple-cycle gas turbine. Other configurations are available. Gas turbines may be designed with two or more turbines. This permits one turbine to be designed for high rotating speeds to drive the compressor and a second (mechanically uncoupled) turbine to be operated at generator speeds. This flexibility permits a more overall efficient design. These gas turbines are known as two- or three-shaft machines. The multiple-shaft machines are more complex and hence more costly than the simple single-shaft machines.

A gas turbine may also be equipped with regeneration,* intercooling, and reheating. *Regeneration* is the process of using exhaust gas energy to heat the air from the compressor before the air enters the combustor. This lowers the fuel consumption of the gas turbine for the same combustor outlet gas temperature, but regeneration will reduce the energy (temperature) of the exhaust gases for cogeneration applications. *Intercooling* is the process of cooling the partially compressed air. Intercooling would normally be installed between stages of a gas turbine which used two or more compressor stages. The use of intercooling reduces the required compressor power and therefore increases the turbine output power. *Reheating* is the process of providing other combustors after the main combustor. Reheating is especially effective where two or more turbines are used. The gases may be reheated between the multiple turbines. Other modifications and variations of gas turbines are available, but these are the most common.

A variety of combustor designs are used in different gas turbines. These designs are aimed at providing stable combustion, long life, and low emissions. Typically, the combustor has a primary zone that operates near stoichiometric, and then the product gases are diluted with additional air. This dilution is necessary to reduce the gas temperatures to acceptable levels for the turbine blades. The final product gas mixture will represent a high air–fuel mass ratio (for some cases, the total air mass flow rate may be on the order of 100 times the fuel mass flow rate). In other words, the gas turbine operates with high levels of overall excess air. Due to the large amount of excess air used in the combustion process of gas turbines, the exiting exhaust gas contains a relatively high concentration of nitrogen and oxygen. Hence, the gas turbine exhaust may be characterized as mostly heated air and is nearly ideal for process or heating purposes.

Gas turbines may use liquid fuels such as jet fuel or kerosene or they may use gaseous fuels such as natural gas or propane. The highest performance is possible with liquid fuels, but the lowest emissions have been reported for natural gas operation.

3.3 Reciprocating Engines

A third category of prime movers for cogeneration systems is internal combustion (IC), reciprocating engines.† These engines are available in several forms. Probably the most familiar form of the reciprocating engine is the typical spark-ignited gasoline engine used in automobiles. For cogeneration applications, the spark-ignited gasoline engine must be converted to operate in a stationary, continuous mode with fuels such as natural gas. Such engines are typically for small cogeneration systems with less than about 100 kW of electrical output. One major group of reciprocating engines for mid- to large-sized cogeneration systems are stationary diesel engines operating with either diesel fuel or in a dual-fuel mode with natural gas. Another large number of reciprocating engines for cogeneration systems are stationary gas engines using natural gas fuel and spark ignition. All of these engines share some common characteristics for cogeneration applications and some distinctive features as well.

Power ratings for reciprocating engines are similar to those for gas turbines in that both continuous and intermittent duty cycle ratings are provided. As with the gas turbines, these power ratings are provided for a set of standard conditions for ambient temperature and pressure and elevation. The standard power ratings need to be adjusted for the local conditions at the site of the installation. Reciprocating engines are not as adversely affected by high inlet air temperatures as are gas turbines. Furthermore, many larger reciprocating engines are equipped with turbochargers and after coolers which minimize the effects of inlet air conditions. For cogeneration applications, reciprocating engines are available in many power levels and designs.

* Regeneration also is known as recuperation.

† Although rotary engines could be used in cogeneration systems, at this time no significant applications are known. The remaining discussion will focus on reciprocating engines.

These power levels range from less than 50 kW to over 60 MW for single engines. Some manufacturers even offer “mini” cogeneration systems with outputs as low as 6 kW.

The portion of the fuel energy which is not converted into mechanical power ultimately is rejected to the surroundings. This energy is rejected to the cooling water and lubricating oil, and to the surroundings by radiation from the engine block and by the hot exhaust gases. The fraction of energy rejected in these different manners depends on the engine design and operating conditions. As an example, if 35% of the fuel energy is converted to shaft power output, then 30% of the fuel energy may be rejected to the cooling liquid, 27% may be rejected with the exhaust gas, and 8% may be rejected as radiation and miscellaneous other energy rejections.

For those reciprocating internal combustion engines that are liquid cooled (the majority of the engines considered here), the cooling liquid is a secondary source of thermal energy. Although not at the high temperatures of exhaust gas, this energy can be used to produce hot water. Several designs are available for recovering the energy in the cooling liquid. These designs use one or more direct or indirect heat exchangers to generate the hot water or low-pressure steam. Liquid-to-liquid heat exchangers can have high efficiencies, and most of this energy is recoverable (but at relatively low temperatures). Other sources of energy from a reciprocating engine are sometimes possible to recover such as from oil coolers and turbocharger after-coolers. This energy is usually at temperatures below 160°F and would only be practical to recover for low-temperature requirements.

Another benefit of the reciprocating engine is that the maintenance and repair are less specialized than for gas turbines. On the other hand, the maintenance may be more frequent and more costly.

3.4 Other Possible Prime Movers

Although most cogeneration systems are based on the above prime movers, some other possibilities exist. Some cogeneration systems are based on fuel cells. Fuel cells generally use hydrogen to produce electricity. During this conversion process, thermal energy must be removed. This energy can be captured and used to produce hot water. Such a system would be a cogeneration plant.

Microturbines are also used in cogeneration systems. Although actually a subclassification of gas turbines, since they represent a relatively new technology, they are often described as a separate category of prime mover. The generic description above for gas turbines would apply in general to microturbines. As small as about the size of a refrigerator, a microturbine may produce something on the order of 25–300 kW of electricity. Thermal energy in the exhaust is generally used to produce hot water.

4 DESCRIPTION OF OTHER EQUIPMENT AND COMPONENTS

In addition to the prime mover, cogeneration systems consist of several major pieces of equipment and many smaller components: (1) electrical equipment, (2) heat recovery devices, (3) absorption chillers, and (4) balance of plant equipment.

4.1 Electrical Equipment

The electrical equipment for cogeneration systems includes electrical generators, transformers, switching components, circuit breakers, relays, electric meters, controls, transmission lines, and related equipment. In addition to the equipment which supports electrical production, cogeneration systems may need equipment to interconnect with an electric utility to operate in parallel for obtaining supplementary power, the use of back-up (emergency) power, or for electrical sales to the utility.

The electric generator is a device for converting the rotating mechanical energy of a prime mover to electrical energy. The basic principle for this process, known as the Faraday effect, is that when an electrically conductive material such as a wire moves across a magnetic field, an electric current is produced in the wire. This can be accomplished in a variety of ways, and therefore, there are several types of electric generators. The frequency of the generator's output depends on the rotational speed of the assembly.

Most often the manufacturer of the prime mover will provide the prime mover and generator as an integrated, packaged assembly (called a "gen-set"). Performance characteristics of generators include power rating, efficiency, voltage, power factor, and current ratings. Each of these performance characteristics must be considered when selecting the proper generator for a given application. Electric generators may have conversion efficiencies of between about 50 and 98%, and, in general, the efficiency increases with increases in generator size (power level). Only the largest electric generators (say, on the order of 100 MW) attain efficiencies of 98%.

4.2 Heat Recovery Equipment

The primary heat recovery equipment used in cogeneration systems includes several types of steam and hot-water production facilities. In addition, absorption chillers could be considered in this section, but for organizational reasons, absorption chillers will be discussed in the following section.

Several configurations of heat recovery devices are available. As mentioned above, these devices may be referred to as "heat recovery steam generators" or HRSGs. HRSGs are often divided into the following categories: (1) unfired, (2) partially fired, and (3) fully fired. An unfired HRSG is essentially a convective heat exchanger. A partially fired HRSG may include a "duct burner" which often uses a natural gas burner upstream of the HRSG to increase the exhaust gas temperature. A fully fired HRSG is basically a boiler which simply uses the exhaust gas as preheated air. Figure 4 is a schematic of one configuration of an unfired HRSG. As shown in this schematic, gas turbine exhaust flows up through the device and exits at the top. Energy from the exhaust gas is used to heat and vaporize the water and to superheat the steam.

Figure 5 shows the water/steam and exhaust gas temperatures for the three sections of a typical unfired HRSG: economizer, evaporator, and superheater. The top line shows the exhaust gas temperature decreasing from left to right as energy is removed from the gas to heat the water. The lower line represents the water heating up from right to left in the diagram. The lower temperature exhaust is used to preheat the water to saturation conditions in the economizer. The intermediate temperature exhaust is used to vaporize (or boil) the water to form saturated steam. Finally, the highest temperature exhaust is used to superheat the steam.

The temperature difference between the exhaust gas and the water where the water first starts to vaporize is referred to as the pinch point temperature difference. This is the smallest temperature difference in the HRSG and may limit the overall performance of the heat recovery device. Since the rate of heat transfer is proportional to the temperature difference, the greater this difference, the greater the heat transfer rate. On the other hand, as this temperature difference increases, the steam flow rate must decrease and less of the exhaust gas energy will be utilized. To use smaller temperature differences and maintain higher heat transfer rates, larger heat exchanger surfaces are required. Larger heat transfer surface areas result in higher capital costs. These, then, are the types of trade-offs that must be decided when incorporating a heat recovery device into a cogeneration system design.

4.3 Absorption Chillers

Absorption chillers may use the thermal energy from cogeneration systems to provide cooling for a facility. Absorption chillers use special fluids and a unique thermodynamic cycle which produces low temperatures (for the cooling) without the requirement of a vapor compressor

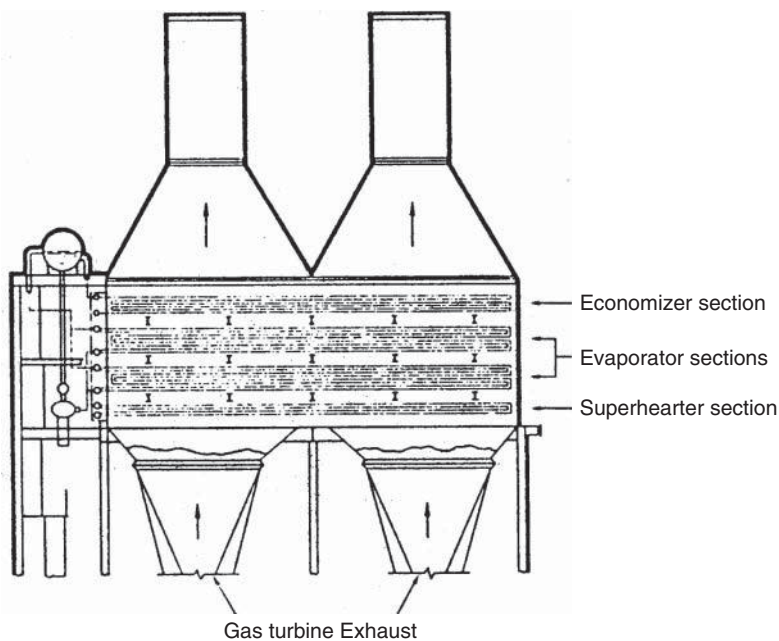


Figure 4 Schematic of an unfired HRSG.

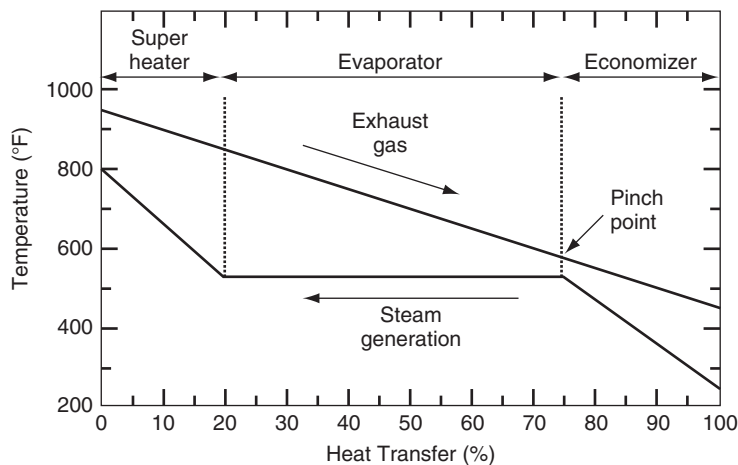


Figure 5 Temperature as a function of heat transfer (or position) for the three sections (economizer, evaporator, and superheater) of a typical unfired HRSG.

which is used in mechanical chillers. Instead of the vapor compressor, an absorption chiller uses liquid pumps and energy from hot water, steam, or exhaust gas.

For cogeneration applications, the important feature of absorption chillers is that they use relatively low-temperature energy available directly or indirectly from the prime mover and produce chilled water for cooling. The use of absorption chillers is particularly advantageous for locations where space and water heating loads are minimal during a good part of the year.

For these situations, the thermal output of a cogeneration system can be used for heating during the colder part of the year and, using an absorption chiller, for cooling during the warmer part of the year. Furthermore, by not using electric chillers, the electric loads are more constant throughout the year. In warm climates, absorption chillers are often an important, if not an essential, aspect of technically and economically successful cogeneration systems.

Some absorption chillers are designed as indirect-fired units using hot water or steam. As examples of typical numbers, a single-stage unit could use steam at 250°F to produce a ton of cooling for every 18 lb of steam flow per hour. A dual-stage unit would need 365°F steam to produce a ton of cooling for every 10 lb of steam flow per hour. If hot water is available, a ton of cooling could be produced for every 220 lb of 190°F hot water per hour.

Other absorption chillers use the exhaust gas directly and are called direct-fired units. Direct-fired absorption chillers are particularly advantageous when a steam or hot-water system does not exist. For a direct-fired absorption chiller, the exhaust gas temperature needs to be 550–1000°F. The higher the exhaust temperature, the less energy (or exhaust gas flow) is needed per ton of cooling. For example, for 1000°F exhaust gas, a ton of cooling requires 77 lb per hour of flow whereas for 550°F exhaust gas a ton of cooling requires 313 lb per hour of flow.

4.4 Balance of Plant Equipment

Balance of plant (BOP) equipment includes those components not explicitly described already. The BOP equipment for cogeneration systems is similar to that for conventional power plants. This includes other controls, emergency devices, exhaust systems and stacks, natural gas compressors, any thermal energy storage equipment, water treatment devices, concrete bases or pads, fuel supply system components, any necessary building modifications, other piping and fittings, mechanical system interfaces, condensers, cooling systems, feedwater tanks, deaerators, feedwater pumps, other pumps, flue gas bypass valves, dampers and ducts, and other such equipment.

5 TECHNICAL DESIGN ISSUES

5.1 Selecting and Sizing Prime Mover

The selection of a prime mover for a cogeneration system involves the consideration of a variety of technical and nontechnical issues. Technical issues which often dominate the selection process include the operating mode or modes of the facility, the required heat-to-power ratio of the facility, the overall power level, and any special site considerations (e. g., low noise). Other issues, which may play a role in the selection process, include the desire to match existing equipment and to utilize the skills of existing plant personnel. Of course, the final decision is often dominated by the economics.

Steam turbines and boilers usually are selected for a cogeneration system if the fuel of choice is coal or another solid fuel. For certain situations, a steam turbine system may be selected even for a liquid or gaseous fuel. Also, steam turbines and boilers would be selected if a high heat-to-power ratio is needed. Steam turbines also may be selected for a cogeneration system in certain specialized cases. For example, a large pressure reduction valve in an existing steam system could be replaced with a steam turbine and thereby provide electrical power and thermal energy. In other applications, steam turbines are selected to be used in conjunction with a gas turbine in a combined-cycle power plant to increase the electrical power output. Combined-cycle gas turbine power plants for cogeneration system applications were described in an earlier section.

Gas turbines are selected for many cogeneration systems where the required heat-to-power ratio and the electrical power need are high. Also, gas turbines are the prime mover of choice

where minimal vibration or low weight-to-power ratio (such as for a roof installation) is required. Reciprocating engines are selected where the heat-to-power ratio is modest, the temperature level of the thermal energy is low, and the need for the highest electrical efficiency is necessary for the economics. Usually, for the smaller size systems, reciprocating engines will result in the most favorable economics. Additionally, reciprocating engines may be selected if the plant personnel are more suited to the operation and maintenance of these engines.

Selecting the appropriate size prime mover involves identifying the most economic cogeneration operating mode. This is accomplished by first obtaining the electrical and thermal energy requirements of the facility. Next, various operating modes are considered to satisfy these loads. By conducting a comprehensive economic analysis, the most economic operating mode and prime mover size can be identified. The process of matching the prime mover and the loads is described next.

5.2 Matching Electrical and Thermal Loads

To properly select the size and operating mode of the prime mover, the electric and thermal loads of the facility need to be obtained. For the most thorough “matching,” these loads are needed on an hourly, daily, monthly, and yearly basis. As an example, Fig. 6 shows the month totals for the electrical and thermal loads for a hypothetical facility. For the summer months (numbers 5–9), the heating loads are minimum, and then for the winter months, the heating loads are higher. The electrical loads are highest for the summer months reflecting the use of air conditioning. In addition, this figure shows dashed lines which represent the “base loads” for the electrical and heating loads, respectively. The base loads are the minimum loads during the year and form a floor or base for the total loads. Often a cogeneration system may be sized so as to provide only the base loads. In this case, auxiliary boilers would provide the additional heating needed during the days where the heating needs exceeded the base amount. Similarly, electrical power would need to be purchased to supplement the base power provided by the cogeneration system.

The possible overall operating modes for a cogeneration power plant are often categorized into one of three classes. (1) The plant may operate as a *base-load system* with little or no

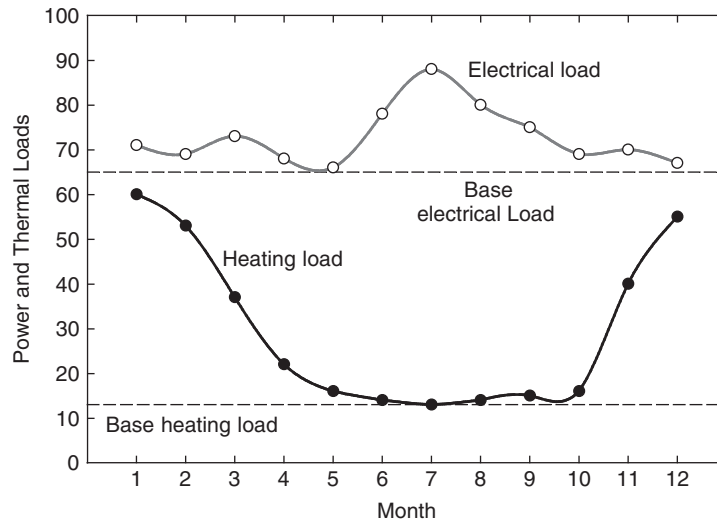


Figure 6 Example of monthly electrical and thermal loads.

variation in power output. Base-load plants operate in excess of 6000 hours per year. Power needs above the base load are typically provided by interconnections to a local utility or by an auxiliary power plant. (2) The plant may operate as an *intermediate system* for 3000–4000 hours per year. These systems are less likely than base-load systems, but if the economics are positive, they may have application for facilities that are not continuously operated, such as some commercial enterprises. (3) Finally, a third class of plant is a *peaking system* which operates only for 1000 hours or less per year. Utility plants often use peaking systems to provide peaking power during periods of high electrical use. For cogeneration applications, peaking units may be economical where the costs of the electricity above a certain level is unusually high. These units are sometimes referred to as “peak shaving” systems.

5.3 Dynamic Power and Thermal Matching

In addition to selecting and sizing the prime mover for the average loads, consideration must be given to dynamic operation of the cogeneration system. Dynamic operation refers to the necessity of satisfying the “minute-by-minute” electrical power and thermal needs of a facility.

The options for electrical power modulation include operating the prime mover at part load as needed. This is essentially “load following.” The disadvantage to this approach is the lower efficiencies at part load. The second option is to use multiple prime movers. This option allows the prime movers to be operated near full load more often. When the power requirements increase, one or more additional prime movers would be activated. One disadvantage of this option is that the economics may be less attractive since multiple units are generally more expensive than a single, larger unit. Another disadvantage is the additional wear and deterioration of the prime mover due to the more frequent starting and stopping of individual prime movers. A third option (and often the most common) is to use the utility power to make up any power needed in excess of what the prime mover can supply. The disadvantage is the utility charges for electrical power and the dependence on the utility.

The options for providing the dynamic thermal loads of a facility include the use of one or more supplementary boilers. This is the most common form of thermal modulation and simply requires the supplementary boiler or boilers to “follow” the thermal loads and provide the thermal requirements in excess of what can be supplied by the cogeneration system. The next option is heat dumping, which is simply discharging the thermal energy not needed. This is obviously not attractive from an energy conservation or economic perspective but may be acceptable as a short-term solution in cases where future thermal needs are expected to increase. The last option is to utilize some form of thermal storage. In this case, thermal energy is stored during periods of excessive production of thermal energy. The storage options are varied, but a common technique is the use of hot-water tanks.

The overall topic of dynamic matching of the electrical power and thermal needs is complex and is central to the overall issue of selecting and sizing the prime movers for a given facility. Many scenarios need to be explored and the resulting economics examined. Once all the issues are fully explored, decisions may be made on what technical design makes the most sense for a given facility.

5.4 Packaged Systems

In general, facilities with low electrical power needs cannot utilize customized cogeneration systems because of the relatively high initial costs that are associated with any size system. These initial costs include at least a portion of the costs related to the initial design, engineering,

and related development and installation matters. Also, smaller facilities often do not have the specialized staff available to develop and operate complex power plants.

To solve some of these above problems, preengineered, factory-assembled, “packaged” cogeneration systems have been developed. The major advantage of packaged cogeneration systems is the fact that the initial engineering, design, and development costs can be spread over many units, which reduces the capital cost (per kW) for these systems. Other advantages of packaged cogeneration systems include factory assembly and testing of the complete system. If there are any problems, they can be fixed while the system is still at the manufacturer’s plant. The standard design and reduced installation time result in short overall implementation times. In some cases, a packaged cogeneration system could be operational within a few months after the order is received. This short implementation time reduces the project’s uncertainty, which eases making decisions and securing financing.

Another advantage of packaged cogeneration systems is the fact that the customer only interacts with one manufacturer. In some cases, the packaged cogeneration system manufacturer will serve as project engineer and take the project from initial design to installation to operation. The customer often may decide to purchase a “turn-key” system. This provides the customer with little uncertainty and places the burden of successful project completion on the manufacturer. Also, the manufacturer of a packaged cogeneration system will have experience interacting with regulating boards, financing concerns, and utilities and may assist the customer in these interactions.

The major disadvantage of packaged cogeneration systems is that the system is not customized for a specific facility. This may mean some compromise and lack of complete optimization. Specialized configurations may not be available. Also, beyond a certain size, packaged cogeneration systems are simply not offered and a customized unit is the only alternative.

6 REGULATORY CONSIDERATIONS

This section includes brief overviews of the relevant federal regulations on electric power generation by cogenerators and the related environmental constraints. Specifically, this section contains the following sections: federal regulations on power generation related to cogeneration, air pollution regulations, water and waste pollution regulations, and permitting and certificates for cogeneration.

6.1 Federal Regulations Related to Cogeneration

The passage of the Public Utility Regulatory Policies Act (PURPA), in 1978, helped cogeneration to become a much more attractive option for electric power generation for a variety of facilities. Prior to the passage of PURPA, the three most common barriers to cogeneration were (1) no general requirement by electric utilities to purchase electric power from cogenerators, (2) discriminatory back-up power for cogenerators, and (3) fear on the part of the cogenerator that they might become subject to the same state and federal regulations pertaining to electric utilities. The passage of PURPA helped to remove these obstacles to development of cogeneration facilities.

Although PURPA was passed in 1978, it was not until 1980 that the FERC issued its final rulemakings and orders on PURPA. In the National Energy Act, FERC was designated as the regulatory agency for implementation of PURPA. The regulations dealing with PURPA are contained in Part 292 of the FERC regulations, and Sections 201 and 210 are the two primary sections relevant to small power production and cogeneration.

Section 201 contains definitions of cogeneration and sets annual efficiency standards for new topping-cycle* cogeneration facilities which use oil or natural gas.† For a cogenerating facility to qualify for the privileges and exclusions specified in PURPA, the facility must meet these legislated standards. These standards define a legislated or artificial “efficiency” which facilities must equal or exceed to be considered a “qualified facility” (QF). A qualified facility is eligible to use the provisions outlined in PURPA regarding nonutility electric power generation. This legislated “efficiency” is defined as:

$$\eta_{\text{PURPA}} = \frac{P + 1/2T}{F}$$

where P is the electrical energy output, T is the used thermal energy, and F is the fuel energy used (all items in consistent units). The $1/2$ in the relation helps to encourage systems to have significant electrical power to obtain acceptable PURPA efficiencies (see more below).

Table 1 lists the standards for the PURPA efficiencies. These standards state that a facility must produce at least 5% of the site energy in the form of useful thermal energy. For cases where the useful thermal energy percentage is between 5 and 15%, the facility must have a PURPA efficiency of at least 45.0%. If the thermal fraction is greater than 15%, the facility meets the standards if it has an efficiency of at least 42.5%. Values for the thermal percentage and the PURPA efficiency are based upon projected or estimated annual operations.

The purpose of introducing the “artificial” standards was to ensure that useful thermal energy was produced on-site in sufficient quantities to make the cogenerator more efficient than the electric utility. Any facility which meets or exceeds the required efficiencies will be more efficient than any combination of techniques producing electrical power and thermal energy separately. Section 201 also put limitations on cogenerator ownership, i. e., electric utilities could not own a majority share of a cogeneration facility, nor could any utility holding company or a combination thereof. These ownership restrictions were removed in the Energy Act of 2005 (described below).

Section 210 defines the procedures for obtaining QF status. An owner or operator of a generating facility may obtain QF status by either submitting a self-certification or applying for and obtaining a Commission certification of QF status. The choice of whether to certify a facility through a self-certification or Commission certification is up to the applicant. In some instances, negotiations with a lender or utility purchaser may proceed more smoothly if the facility has been certified by the Commission.

Table 1 Required Efficiency Standards for Qualified Facilities

If the Useful Thermal Energy Fraction Is:	The Required η_{PURPA} Must Be:
$\geq 5.0\%$	$\geq 45.0\%$
$\geq 15.0\%$	$\geq 42.5\%$

* Since bottoming-cycle cogeneration facilities do not use fuel for the primary production of electrical power, these facilities are only regulated when they use oil or natural gas for supplemental firing. The standard states that during any calendar year the useful power output of the bottoming-cycle cogeneration facility must equal or exceed 45% of the energy input if natural gas or oil is used in the supplementary firing. The fuels which are used first in the thermal process prior to the bottoming-cycle cogeneration facility are not taken into account for satisfying PURPA requirements.

† For topping-cycle cogeneration facilities using energy sources other than oil or natural gas (or facilities installed before March 13, 1980), no minimum has been set for efficiency.

Section 210 of the PURPA regulations specifically addressed the above three major obstacles to developing cogeneration facilities. The principal issues in Section 210 include the following legal obligations of the electric utility toward the cogenerator: (1) obligation to purchase cogenerated energy and capacity from QFs, (2) obligation to sell energy and capacity to QFs, (3) obligation to interconnect, (4) obligation to provide access to transmission grid to “wheel” to another electric utility, (5) obligation to operate in parallel with QFs, and (6) obligation to provide supplementary power, back-up power, maintenance power, and interruptible power.

Section 210 also exempted QFs from utility status and established a cost basis for purchase of the power from QFs. FERC specified that the price paid to the QF must be determined both on the basis of the utility’s avoided cost for producing that energy and, if applicable, on the capacity deferred as a result of the QF power (i.e., the cost savings from not having to build a new power plant). Other factors, such as QF power dispatchability, reliability, and cooperation in scheduling planned outages, could also be figured into the price paid to the QFs by the electric utilities. The state public utility commissions were responsible for determining the value of these avoided cost rates.

6.2 Energy Policy Act of 2005

The Energy Policy Act (EPAct) of 2005 contained several items that specifically concerned cogeneration. In particular, EPAct eliminated the ownership limitations on qualifying facilities which were part of the original PURPA. This means, for example, that utilities are allowed to own up to 100% of a cogeneration plant (while the original PURPA restricted utilities to less than 50% ownership). For qualifying facilities that have nondiscriminatory access to other sources of electric power (such as from wholesale markets), EPAct relaxed the requirements that utilities must purchase cogenerated power and must sell electric energy to qualifying facilities. EPAct also contains new language which encourages the thermal output of cogeneration plants to be productive and useful (and to avoid situations where no real need existed for the thermal energy).

6.3 2008 and 2009 Legislation

The Energy Improvement and Extension Act (EIEA) of 2008 and the American Recovery and Reinvestment Act (ARRA) of 2009 includes wording that encourages cogeneration. This encouragement is in the form of tax incentives such as the CHP tax credit and accelerated depreciation and funding programs for select CHP projects.

6.4 Air Pollution Regulations

Legislation to limit pollutant emissions has a long history. In the United States, the first major national legislation was the Air Pollution Control Act in 1955. This legislation was motivated largely by the recognition of the air quality concerns in California, particularly in the Los Angeles area. This act was narrow in scope and provided no specific limitations on pollutant emissions.

The current era of air pollution regulation was started with the Clean Air Act (CAA) of 1963. The CAA was considered the first major modern environmental law established by the U.S. Congress and set the groundwork for the present regulation format. The original CAA has been revised by Congress six times since it became law, with major amendments in 1967, 1970, 1977, and 1990. These amendments are referred to as the Clean Air Act Amendments (CAAA). Each of these subsequent amendments continued to increase the strength of the original law by lowering the acceptable levels of emissions. The CAA and the subsequent CAAA apply to a

wide range of applications, and they have a significant impact on the design and operation of power generation facilities.

The first major revision to the CAA occurred in 1967 and established the National Ambient Air Quality Standards (NAAQS) and required State Implementation Plans (SIPs) to verify compliance on the state level. In addition, the amendment established Air Quality Control Regions (AQCR) to interconnect different states into larger regional areas since air pollution is not restricted to state boundaries. The NAAQS established maximum safe levels for the different pollutants designated under the original CAA. Although these standards did not have a direct effect on power generation facilities, it was the precursor to several minor amendments between 1970 and 1975 that established federal emission limits for specific equipment. These amendments were used as a basis for the new source performance standards (NSPSs), which apply to both new and modified stationary sources. These stationary sources include not only power generation facilities but also a larger number of industrial operations such as municipal waste combustors, sulfuric acid production units, and grain elevators. These intermediate amendments also established regulations for mobile sources of air pollution such as automobiles and also for hazardous air pollutants. The NSPS regulation only takes into account the pollutant emissions from the source regardless of the surrounding environment. This required facilities to control or reduce pollutant emissions even though the ambient air pollution levels may be significantly lower than the NAAQS amounts.

One of the major amendments to the CAA was passed in 1977 and added two additional regulatory programs: the nonattainment (NA) program and the prevention of significant deterioration (PSD) program. These two programs addressed the issue of meeting the previously established ambient air quality standards for the air quality control regions. The NA program applied to the regions that failed to meet the ambient air standards and the PSD program was design to preserve and protect air quality in regions surpassing the national standards. The PSD program set the allowable pollutant levels lower than the NA areas to prevent previously clean or unpolluted areas from becoming polluted. The PSD program also required the large-size facilities (facilities producing over 100 tons/yr of a controlled pollutant) to include the best available control technology (BACT) to reduce emission levels below that required by the NSPS. Under the NA program, new facilities in NA zones must be equipped with controls to assure the lowest achievable emissions rate (LAER). The facility must also show that some other source of pollutants must be reduced or eliminated to provide a net increase in air quality. The NA program also affects existing facilities by requiring timely reduction of emissions using reasonable available control technology (RACT). The difference between BACT, RACT, and LAER is that the first two include economic considerations when determining the required control equipment while LAER is based on the most advanced equipment to achieve the lowest emissions without regard to cost. The addition of these two programs increased the complexity of determining the emission limits for new and modified power generation facilities significantly.

The regulation of emission levels for power generation facilities is determined by several different agencies at the federal, state, and local levels. State and local agencies can require lower emission levels but can never require higher levels than the federal requirements. The Clean Air Act also allowed state and local authorities to reduce the acceptable levels to meet specific local air quality standards. For example, the Los Angeles basin area is regulated by the South Coast Air Quality Management District (SCAQMD) and has stricter standards than those set by the federal government.

6.5 Equipment Specific Regulations

In addition to the above requirements, regulations exist for specific equipment. In terms of power generation, the specific equipment which is regulated are stationary gas turbines and boilers (steam systems). Stationary reciprocating engines are not specifically covered by NSPS

since they have a much smaller impact on the overall generation capacity.* The emissions from reciprocating engines will, of course, need to satisfy any local, state, or federal limits at the installation site.

Stationary gas turbines have become one of the prominent types of power generation facilities. As a result of this growth, the Code of Federal Regulations (CFR) includes specific requirements for the emission levels of gas turbines. The NO_x emission limits are divided into two levels depending on the energy input rate of the plant and are increased if the fuel contains nitrogen. For natural-gas-fired units, neither fuel bound nitrogen nor sulfur dioxide exist in significant quantities. Also, the NSPS limits do not cover particulates or unburned hydrocarbon emissions for gas turbines since neither exist in significant amounts.

Steam-based Rankine cycle electric power generation facilities are also covered under the NSPS regulations. The allowable emission levels vary based on the type of fuel used with substantially lower limits for liquid and gaseous fuels. The nitrogen oxide limits also vary between the different types of solid fuel consumed. This variation in the limits is due to the different amounts of fuel bound pollutants in each of the different fuel sources.

In 1998, revised nitric oxide emission limits for steam power plants were introduced. In addition to lower limits, the limits for new utility boilers are expressed per “MWh,” in contrast with the other limits, which are expressed per “MMBtu.” The use of these new units (MWh) is referred to as “output-based” format where emissions are linked to the amount of power generated. This was used to promote energy efficiency as well as pollution prevention. The use of “MMBtu” is referred to as an “input-based” format where emissions are linked to the amount of fuel energy used.

The standards for the stationary gas turbine and Rankine cycle electric utilities are for that particular source unit and do not cover the ambient air quality limits. The total pollutant levels for a given region must also be considered, and at this point, even facilities not covered by the NSPS are considered, including reciprocating engines. The ambient air quality is regulated by the NAAQS discussed previously and varies from region to region. The NAAQS determines if a region is governed by the PSD or NA program and therefore if BACT or LAER control equipment is required. Different types of pollution control technologies are often required for each of the three power generation facilities discussed in this section (gas turbine, reciprocating engine, and Rankine cycle), and these are described in numerous references.

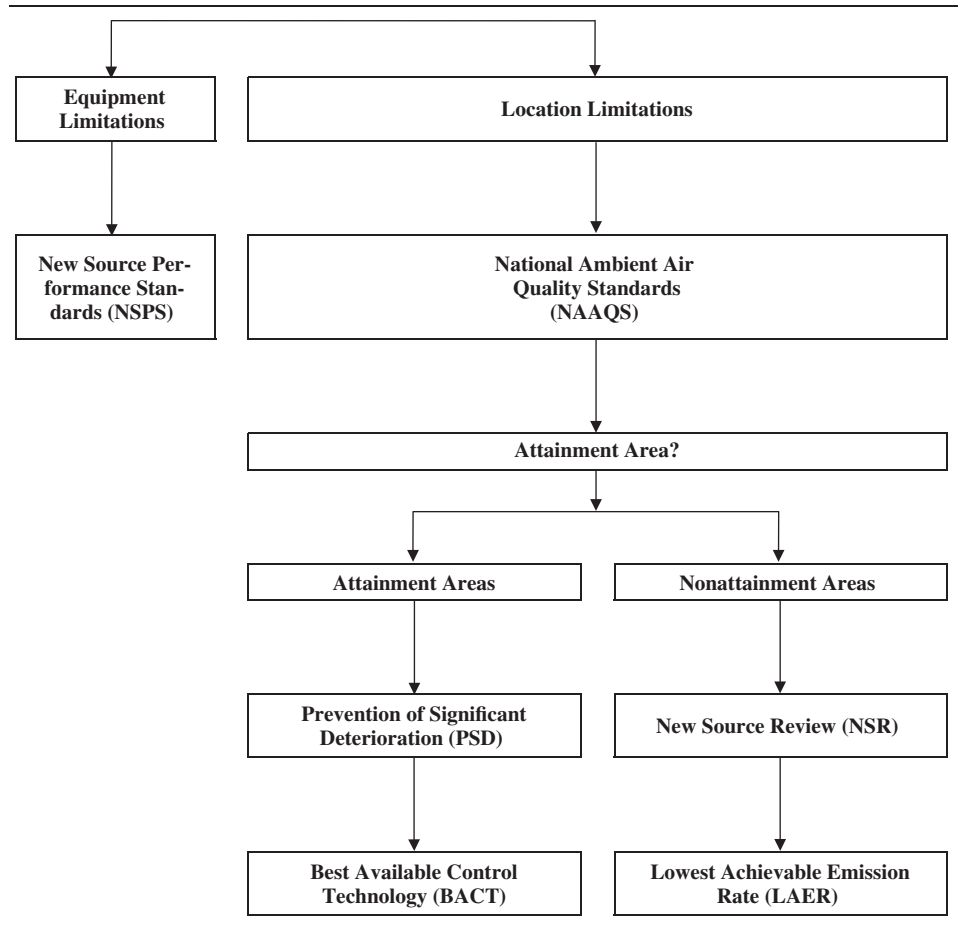
As described, the regulations for air pollutants relative to power generation are complex and numerous. To help clarify this situation, Table 2 is a flow chart of the various regulations and their interactions. As shown, the regulations that govern a given situation depend on several factors. First, the most restrictive limits are applicable. These limitations could be those due to local regulations or due to original equipment regulations. For local regulations, the NAAQS must be met. These limits depend on whether the location is in an attainment zone or a NA zone. Depending on the specific “zone,” the facility might have to meet limits imposed by new source review (NSR), or PSD. The technologies that will be needed are BACT for PSD and LAER for NSR.

6.6 Water Quality and Solid Waste Disposal

The main legislative basis for managing water pollution is the Federal Water Pollution Control Act of 1956, as amended by the Water Quality Act of 1965, the Federal Water Pollution Control Act amendments of 1972, and the Clean Water Act of 1977. Discharge water will often be monitored and will often require both state and federal permits if the wastewater is discharged

* Emissions from reciprocating engines are, of course, regulated extensively for mobile and some off-highway applications.

Table 2 Federal Air Quality Regulations (Most Restrictive Limits Apply)



into a public waterway. In some cases, both the temperature and the pH of the discharged water will need to be controlled.

Solid waste disposal is generally not a problem with either natural gas or oil-fired cogeneration plants but could be a problem for a coal-fired, coal gasification, or waste-to-energy cogeneration system. In some states the bottom ash from waste-to-energy plants has been considered hazardous waste, and the ash disposal cost per ton was more expensive than the refuse disposal cost. All states have different standards for both the quality of the water discharged and the requirements for solid waste disposal, and all project planners should check with the appropriate regulatory agencies in the state where the project is planned to ensure what air, water, and solid waste (if applicable) permits are required.

6.7 Permits and Certificates for Cogeneration

A number of certifications are required to get a cogeneration plant approved. These include not only a FERC certificate but also various state permits. Since each state will set its own permitting requirements, it is not possible to generalize what is required on each application.

As described above, different requirements must be met if the proposed site is in an “attainment” or “NA” zone. An attainment area will require sufficient modeling of ambient air conditions to ensure that no significant deterioration of existing air quality occurs. For a “nonattainment” area, no new emissions can be added unless they are offset by the removal of existing emissions. This has led to the selling or trading of emissions by industrial facilities and utilities.

Satisfying the emission regulations has become one of the most important factors in determining whether a cogeneration system is feasible for a specific application. The type of prime mover is a major consideration. Gas turbines have often been easier to permit than other prime movers, but each application is unique. Also, the offset of emissions from existing central plant boilers (which are shut down) can often be important in satisfying the overall emission levels.

7 ECONOMIC EVALUATIONS

A decision to install a cogeneration system often is based primarily on economic considerations. Since a cogeneration system requires that funds be spent for the system (capital expense), the monetary earnings and savings resulting from the cogeneration system must be sufficient by some criteria to justify the expenditures. To determine if a cogeneration system is economically justifiable requires a wide range of input information about both the current mode of operation and the proposed system. This section is a brief overview of the considerations that are necessary to complete an economic evaluation of a cogeneration system installation. Fundamentals of completing engineering economic assessments may be found in a number of references (e.g., Ref. 8).

Some of the aspects needed to complete economic evaluations include the computation of charges from the utility for electrical power before and after the installation of the cogeneration system. In addition, both the capital and the operating costs incurred with the installation and operation of a cogeneration system are needed. Finally, all of the economic information must be analyzed to determine the economic feasibility of cogeneration systems. Economic performance measures will be described and compared for use in these economic evaluations.

When discussing and completing economic evaluations for cogeneration systems, several important terms need to be defined. Unlike some engineering projects, installation of a cogeneration system may result in annual savings (for example, as a result of reducing thermal energy costs) in addition to generating annual income (for example, as a result of electrical or thermal energy sales). For this reason, economic evaluations for cogeneration systems must be based on revenue which is defined as the sum of any income and savings cash flows minus the associated costs.

The process of conducting an economic evaluation of a cogeneration system involves a variety of actions. These actions include (1) determining the current electrical and thermal loads, (2) determining the current or base case operating costs, (3) estimating the future electrical and thermal loads, (4) estimating the future operating costs, (5) estimating the capital costs of the cogeneration system, (6) estimating the new electrical and thermal loads with the cogeneration system, (7) estimating the new operating costs with the cogeneration system, (8) estimating the savings and revenues as a result of the cogeneration system, and (9) using this information to complete the overall economic evaluation of the project. For simplicity, the following discussion will consider the above items in three categories.

7.1 Operating Costs of Current System

A successful economic analysis must be based on accurate values for current and future (projected) electrical and thermal operating costs. This means that the current and future electrical

and thermal loads are needed. Depending on the facility, the appropriate values for the electrical and thermal loads may or may not be easy to obtain. Electrical and thermal loads will generally vary with time and will possess specific profiles on an hourly, daily, monthly, and seasonal basis. For different facilities, the variation may be negligible or significant for one or another of these time periods. For example, in a large industrial plant that operates seven days a week on a 24-hour per day basis, the electrical and process steam loads are often nearly constant. On the other hand, for small manufacturing facilities, schools, and many commercial enterprises, the electrical and thermal loads will vary significantly on an hourly, daily, monthly, and seasonal basis. Whenever an accurate economic analysis is required, the electrical and thermal loads need to be obtained for each of these time periods.

For large industrial facilities, the process steam and electric data often are available on an hourly (or even on a 15-min) basis. For many other facilities, however, obtaining the required load information (particularly on an hourly basis) is difficult. For example, for universities, small manufacturing plants, and many commercial enterprises, this type of data is not always available. Typically whole campus/facility electrical data are available on a monthly basis only (from utility bills), and hourly electrical profiles may have to be “constructed” from monthly energy and demand data. Hourly thermal data, also, may not exist. Boiler operators may have daily logs, but these may not provide enough detail and may not be in electronic form. Constructing accurate hourly thermal energy profiles can involve hours of tedious work pouring over graphs and boiler operator logs. In the worst case scenario, only monthly gas bills may be available, and it may be necessary to construct hourly thermal profiles from monthly bills, boiler efficiencies, and heating value content of the fuel. Since the monthly utility charges have to be matched, there is often a great deal of “trial and error” involved before there is a match between assumed hourly energy profiles and monthly energy consumption and costs from the utility bills.

While “first cut” energy and cost analyses may be completed using monthly load profiles, more exact analyses require more detailed load profiles. These more detailed load profiles often consist of hourly data for a typical work day and a typical nonwork day. Although for an industrial facility that operates seven days a week, 24 hours a day, such detail data may not be needed. That is not the case for many other facilities such as a university, a commercial building complex, or a one- or two-shift manufacturing facility. In these latter cases, the energy loads are highly variable, and hourly analyses are required. In these cases, there will often be a significant difference between weekday and weekend loads. This means that the analysis needs to distinguish between the typical week day and weekend day.

Once a valid energy profile (hourly preferred) is constructed, the current operating costs are determined. This is the annual cost of doing business without the cogeneration system, including annual purchased electrical energy sales, electrical demand charges, boiler fuel costs, boiler maintenance, direct and contract labor, insurance, and other such items. This total number is the baseline to which the cogeneration economics are compared.

Since the economic analysis will be completed for the life of the project, the future electrical and thermal loads are needed. Although these factors are often uncertain, the best estimates should be used. The future electrical and thermal loads should be obtained for each of the years of the cogeneration system life. Based on the future electrical and thermal loads, the projected (nongeneration) operating costs should be estimated.

7.2 Operating Costs of the Proposed Cogeneration System

Determining the new electrical and thermal loads associated with a cogeneration system will depend on the type and size of system selected. Ideally, the cogeneration system could be sized to match the electrical and thermal loads exactly; however, seldom is there an “exact” match.

Based on the new electrical and thermal loads for the cogeneration installation, the projected operating costs should be estimated. For the cogeneration system, these operating costs include the costs of fuels and maintenance. Also, estimates of the new utility costs are needed. Costs of both the electrical energy (per kWh) and the electrical demand (kW) are needed. Since utility rates are often dependent on the total power (demand) used, the utility rates and costs may be different not only because of the reduction of utility electrical energy consumption but also because of the reduction in electrical demand. Another important cost may be a back-up or stand-by charge imposed by the utility to have power available for the facility in case of an emergency shutdown of the cogeneration system.

As for the current system, the estimated projected future electrical and thermal loads need to be used for the cogeneration system for each of the project years. Based on these future electrical and thermal loads, the projected operating costs for the cogeneration system should be estimated.

7.3 Economic Merit

By comparing the operating costs of the current system with the costs associated with the cogeneration system, the project savings can be estimated. The savings and income from the cogeneration system must be determined as well as the additional costs associated with such items as the additional fuel and the additional maintenance. At this point, all the necessary information is available to complete a detailed economic assessment of the cogeneration project for the economic life of the project. Several economic measures may be used to judge the economic feasibility of a specific project.

For some situations, a simple payback (or investor's rate of return) approach is often sufficient. Once an acceptable payback period is defined, a decision can be made on the feasibility of the cogeneration project. If the simple payback period is fairly short (e.g., two to three years), then small variations in the assumptions, approximations, or prices will have little effect on the decision. As the payback period lengthens (e.g., more than four years), other more complete economic measures should be examined. For these longer periods, the time value of money has to be considered, as well as projected energy rates, and projected changes in energy needs for the facility. For projects with these longer payback periods, other economic measures should be used.

An example of a more detailed evaluation would be the use of a net present-value analysis. For this approach, all costs and income (including savings) streams are "brought to the present" using a discount factor and summed. This process starts with the initial investment which is often the only entry for the first year. For each subsequent year, the operating income or savings, depreciation, and taxes are listed. These amounts are used to determine the net cash flow for each year. These values are then adjusted with the discount factor for each year to obtain "present" values. A final net present value at the end of the project can then be determined and compared to the net present values of other alternatives.

Table 3 is a simple "template" of the type of final evaluation that may be developed. As shown, tax considerations are a part of the evaluation for "for profit" facilities. The number of years will be dictated by the economic life of the project. Typically, the numbers that are needed for each item in Table 3 are supplied from earlier tables that can be arranged to provide the numbers automatically. If set up in such a fashion, a number of studies can be completed rather easily.

Once the first case is completed, various sizing and operating modes for the cogeneration system should then be evaluated. The case with the highest net present value would then be the most favorable economic choice. With any potential operating mode considered, the use of the thermal energy is what generally makes a cogeneration system feasible. If electricity production were the primary output, the cogenerator could not typically compete with the local

Table 3 Template for Final Economic Evaluation

		Year 0	Year 1	Year 2	—
	Investment		—	—	—
Income calculations	Operating income	—			
	Depreciation (%)	—			
	Depreciation (\$)	—			
	Adjusted income	—			
Tax calculations	Tax (%)	—			
	Tax (\$)	—			
	Investment tax credits (if any)	—			
	Adjusted tax	—			
Present-value calculations	Income after tax (operating income minus the adjusted tax)	—			
	Discount factor	—			
	Discounted revenue	—			
	Net present value	—			

electric utility. The simultaneous production of and need for the thermal energy is what makes a cogeneration project economically attractive.

A final aspect of any comprehensive economic evaluation is to conduct a series of “sensitivity analyses.” These sensitivity analyses are designed to detect the sensitivity of the results to the assumptions and approximations used in the analysis. For example, the future cost of fuels and electric rates should be varied (by, say, $\pm 20\%$) to determine the effect on the final net present value or other economic measures. In a similar manner, the effect of inflation on specific items on the final results should be explored. A comprehensive sensitivity study will include most of the parameters of the economic evaluation and can be quite extensive.

In general, an economic analysis of a cogeneration system is complicated, and the results will vary greatly depending on values for most of the parameters (such as interest rates, cost of fuel, permitting requirements, cost of electricity sales, and other factors). To complete detailed studies with all of these considerations in a reasonable manner requires the use of computer programs of one nature or another. Commercial computer programs and simulations for cogeneration systems are available, and “spreadsheet”-type programs can be constructed for specific uses (e.g., Ref. 4).

8 OWNERSHIP AND FINANCIAL ARRANGEMENTS

8.1 Overall Considerations

Even with a reliable technical design and favorable economics, the successful completion of a cogeneration project often will depend on acceptable financial arrangements. Financing is critical to the success of a cogeneration project, and it is best to determine, early on, the financial arrangement to be used. The selected financial arrangement will be intimately linked to the ownership structure. A cogeneration system may be owned by the facility,* by a third-party† entity, or by a partnership. The ownership may be structured in a variety of ways. By increasing

* In this section, “facility” refers to the entity with the electric and thermal loads. This is sometimes called the thermal consumer, heat consumer, or thermal host.

† A “third-party” refers to an entity separate from the thermal load owner (first party) and from the local utility (second party).

the number of participants in the project, the individual risk decreases, but the venture is more difficult to organize and the individual potential gains decrease.

The thermal and electric loads of a facility are the items that might motivate others to be involved in developing a cogeneration system. In one respect, these loads represent the opportunity for financial gains. There are a number of potential project participants that could conceivably have an interest in the development of the cogeneration system. These potential participants include equipment manufacturers, power plant operators, investors (such as banks, insurance companies, and pension funds), electric utilities, fuel suppliers, engineering firms, and governmental agencies. In general, the goal of the selected ownership structure and the related financial arrangements is to result in some combination of maximum profits, minimal risk, and maximum tax benefits.

External participants, partners, and investors will examine a number of issues before deciding to be involved in the project. These issues include the overall economics, the revenue from thermal and electricity sales, the accuracy of the capital costs and operating expenses, the experience of the participants, the projected availability of the plant, the previous success of the proposed technology, the assurance that permits, contracts, and agreements will be obtained on a timely basis, and the availability and cost of fuel. A net positive assessment of these issues will be necessary for any external participation.

Cogeneration projects can be financed by a variety of options. The traditional approach to financing is owner financing; however, cogeneration facilities are expensive and complex, and a number of alternatives are available for financing. When deciding on the most favorable financial arrangement, the owners of a facility will often consider the following questions:

- Do the owners have adequate capital to finance the whole project?
- If borrowing the money to finance the plant, will the effect on the owners' credit rating be acceptable?
- How will the financing impact the owners' balance sheet?
- Do the owners desire to receive guaranteed savings (and minimize their risk)?
- If the owners finance the project, do they have the ability to utilize available tax benefits?
- Do the owners have an interest in operating or owning the plant (since this is probably not their main line business)?

Answers to these questions will help the owners of a facility select the most attractive ownership and financial structures for their needs. They will evaluate the possible options and select the ones that will have the most favorable impact on their business.

The following are descriptions of examples of possible financial arrangements. They are grouped according to three major ownership structures. For the first category, the owners of the thermal load may own and operate the cogeneration system and use conventional financing. In the second category, the owners of the thermal load may develop a partnership arrangement for the ownership and financing of the cogeneration system. For the third category, the owners may offer a third party the opportunity to develop the cogeneration project. A third-party ownership structure has the greatest variety of financing arrangements. Examples of these various financial structures are described below. Other financing arrangements may be possible, including combinations of these, but most financial arrangements will possess characteristics represented by one or more of the following arrangements.

8.2 Conventional Ownership and Operation (100% Ownership)

The owner of the electric and thermal loads has two basic financing options in a conventional owner/operator structure: (1) fund the project internally from profits in other areas of the business or (2) fund part of the project from internal sources and borrow the remainder from a

conventional lending institution. Sole ownership offers the largest degree of control and rewards but also results in the largest exposure to risk. All external participants (e.g., utilities, engineering and construction firms, and operating and maintenance organizations) must interact with the facility owner.

Most businesses have a minimum internal rate of return on equity that they require for any investment. They may not be willing to fund any project which does not meet the internal hurdle rate using 100% equity (internal) financing. With 100% internal financing the company avoids the problems of arranging external financing (perhaps having to add partners). If there is a marginal return of equity, however, the company will not finance the project, especially if the money could be used to expand a product line or create a new product which could provide a greater return on equity.

Because the cost of borrowed money is typically lower than a business's own return on equity requirements, the combination of partial funding internally and conventional borrowing is often used. By borrowing most of the funds, the internal funds can be leveraged for other projects, thus magnifying the overall return on equity.

External contract issues are simpler in conventional ownership. Contracts will be required for the gas supply, excess power sales to the local utility, possible operating and maintenance agreements, and any agreements with possible lenders. For conventional ownership and financing, no contracts may be needed for the thermal energy and electricity if all is used internally.

8.3 Partnership Arrangements

One alternative to 100% ownership is to share ownership with partners. A variety of partnership arrangements are possible. These arrangements include conventional partnerships, limited partnerships, jointly owned corporation, unincorporated associations, and others. Partners might include a gas utility, a major equipment vendor (such as a gas turbine manufacturer), investors, and engineering firms.

The major advantage of a partnership is the sharing of risks and credit. The disadvantages are that profits are also shared and that contract complexity increases. Since the partnership is the "owner" of the cogeneration system, thermal and power sales agreements have to be arranged with the owners of the facility, in addition to the other contracts required under conventional ownership. The joint venture company must develop agreements and contracts with the utilities, engineering and construction firms, possible operating and maintenance firms, and lenders (if any).

8.4 Third-Party Ownership

As mentioned above, the potential for financial gain may attract third parties to develop and operate a cogeneration system where the owner of the thermal load would contract for at least a portion of the electrical and thermal outputs of the plant. In third-party ownership, the entity with the electric and thermal loads distances himself from both the financing and construction of the cogeneration facility. A third party arranges the finances, develops the project, arranges for gas supply, power sales for any excess power produced, thermal sales to the heat consumer, and operating and maintenance agreements. Under the 1992 National Energy Policy Act, the third party may also be able to enter into an electric power sales contract with the heat consumer as well. The third party might operate the facility and sell the thermal and electric to customers, or the third party might lease the facility to the entity with the electric and thermal loads. Often, the facility is colocated on or in close proximity to the thermal owners' facility.

A number of third-party ownership and financing arrangements are possible. Three of the more common forms are lease arrangement, guaranteed savings arrangement, and energy services contract arrangement.

Table 4 Summary of Main Characteristics of Major Ownership/Financing Structures

Characteristic	Self-Owned, Self-Operated	Not Owned, Self-Operated	Not Owned, Not Self-Operated
Typical financing	Conventional	Leased	Third party
Capital requirements	Maximum	None	None
Balance sheet impact	Maximum	Some	None
Risk	Maximum	Some	Least
Rate of return	Depends, probably highest	Depends, probably moderate	Depends, probably lowest
Personnel required	Maximum	Some	Least
Control of supply of electric power and thermal	Yes	Yes	No
Fuel contracts	Required	Required	For others

8.5 Final Comments on Financial Aspects

Financing arrangements are a crucial aspect of most cogeneration developments. These arrangements may range from simple to highly complex. They are affected by internal factors such as ownership arrangements, credit ratings, and risk tolerance. In addition, these financial aspects are affected by external factors such as the financial and credit markets, tax laws, and cogeneration regulations. A variety of initial financial arrangements have been outlined in this section to illustrate the nature of these arrangements. Much more detailed arrangements are possible and often necessary, but these are beyond the scope of this chapter. Table 4 is a summary of the main characteristics of the major ownership/financing structures.

To reduce the costs, risk, and uncertainties associated with financing, a number of actions should be considered. These include establishing reliable and robust contracts and agreements with engineering and construction firms, fuel suppliers, and the local utility. Also, actions to minimize any volatility (or perceived volatility) will enhance the situation and should include using reliable and well-known firms. Other actions that will be useful include emphasizing profitability, flexibility, detail work, and careful understanding of the governing regulations.

9 SUMMARY AND CONCLUSIONS

This chapter has provided a brief overview of cogeneration systems. Cogeneration systems are attractive options for facilities where electrical power and thermal energy are used. The major motivations for considering cogeneration systems are the potential savings in money and energy and the potential for lower emissions.

The technology for cogeneration exists for a range of sizes, and the procedures to integrate these components into cogeneration systems are well established. The key item in the design of a cogeneration system is the prime mover, which is typically a steam turbine, gas turbine, or reciprocating engine. Other important components are the HRSG, possibly adsorption chillers, and other power plant equipment. The arrangements of the equipment are quite varied, particularly for larger systems. An important aspect of the technical design of a cogeneration system is the selection of the size of the system to match the electrical and thermal energy needs.

In addition to the technical considerations, the application of cogeneration systems involves completing an economic evaluation and an understanding of the governmental regulations and legislation on electrical power production and on environmental impacts. With respect to electrical power production, certain governmental regulations (PURPA) were passed during the late 1970s which removed barriers and provided incentives to encourage

cogeneration development. Finally, no cogeneration assessment would be complete without an understanding of the financial arrangements that are possible and the contracts and agreements that are needed.

REFERENCES

1. M. P. Boyce, *Handbook for Cogeneration and Combined Cycle Power Plants*, American Society of Mechanical Engineers, New York, 2002.
2. B. F. Kolanowski, *Small-Scale Cogeneration Handbook*, Fairmont Press, Lilburn, GA, 2000.
3. S. A. Spiewak, and L. Weiss, *Cogeneration and Small Power Production Manual*, 5th ed., Pearson Professional Education, 1999.
4. G. R. Baxter and J. A. Caton “Technical and Economic Assessments of Cogeneration Systems: An Overview of the Development and Application of a Generalized Computer Simulation,” in *Proceedings of the 1997 Power-Gen International Conference*, Dallas Convention Center, Dallas, TX, December 9–11, 1997.
5. R. G. Tessmer, J. R. Boyle, J. H. Fish, and W. A. Martin, *Cogeneration and Wheeling of Electric Power*, PennWell Books, Tulsa, OK, 1995.
6. J. A. Caton, N. Muraya, and W. D. Turner, “Engineering and Economic Evaluations of a Cogeneration System for the Austin State Hospital,” Paper No. 910444, in *Proceedings of the 26th Intersociety Energy Conversion Engineering Conference*, Vol. 5, Boston, MA, August 1991, pp. 438–443.
7. J. H. Horlock, *Cogeneration: Combined Heat and Power—Thermodynamics and Economics*, Pergamon, Oxford, England, 1987.
8. L. Blank and A. Tarquin, *Engineering Economy*, McGraw-Hill, New York, 2002.

CHAPTER 29

HYDROGEN ENERGY

E. K. Stefanakos and D. Y. Goswami
Clean Energy Research Center
University of South Florida
Tampa, Florida

S. S. Srinivasan
College of Innovation and Technology
Florida Polytechnic University
Lakeland, Florida

1 INTRODUCTION	991	3 HYDROGEN STORAGE	1001
2 HYDROGEN PRODUCTION	992	3.1 Hydrogen Storage Options	1003
2.1 Steam Reforming of Natural Gas	992	4 HYDROGEN UTILIZATION	1015
2.2 Partial Oxidation of Heavy Hydrocarbons	994	4.1 Fuel Cells	1016
2.3 Coal Gasification	995	4.2 Internal Combustion Engines	1019
2.4 Hydrogen Production from Biomass	995	4.3 Hydrogen Burner Turbines	1020
2.5 Electrolysis	997	5 HYDROGEN SAFETY	1021
2.6 Thermochemical Processes	998	5.1 The Nature of Hydrogen	1021
2.7 Photoelectrochemical Hydrogen Production	1000	5.2 How to Handle Hydrogen	1021
2.8 Biological Methods	1000	6 CONCLUSIONS	1022
		REFERENCES	1023

1 INTRODUCTION

Fossil fuels are not renewable. They are limited in supply, their economic cost is continuously increasing, and their use is growing exponentially. Moreover, combustion of fossil fuels is causing global climate change and harming the environment in other ways as well, which points to the urgency of developing environmentally clean alternatives to fossil fuels.¹

Hydrogen is a good alternative to fossil fuels for the production, distribution, and storage of energy.^{2,3} Automobiles can run on hydrogen either used as fuel in internal combustion (IC) engines or fuel cell cars or in hybrid configurations. Hydrogen is not a primary energy source but an energy carrier that holds tremendous potential to use renewable and clean energy options. It is not available in free form and must be dissociated from other molecules containing hydrogen, such as natural gas or water. Once produced in free form, it must be stored in a compressed or liquefied form or in solid-state materials.

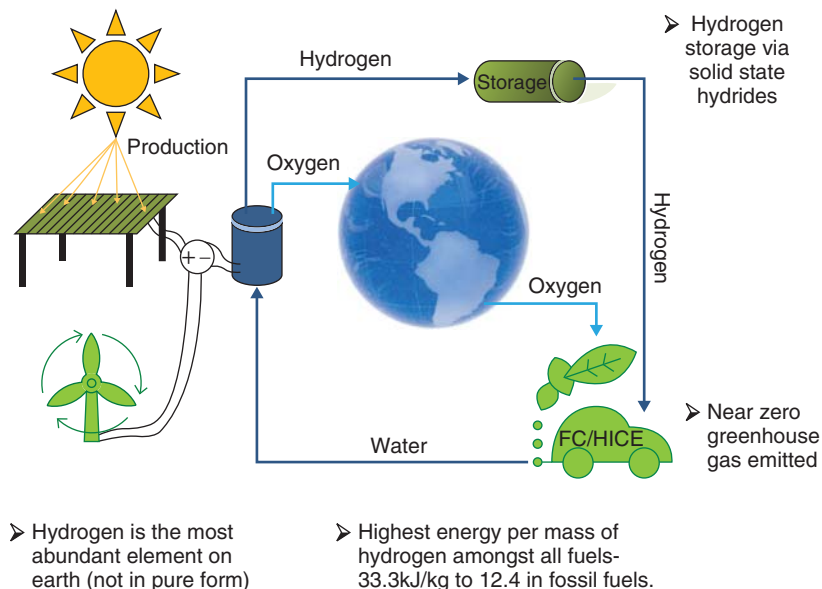
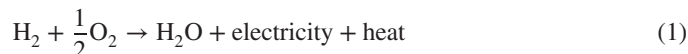


Figure 1 Schematic diagram to demonstrate hydrogen production, storage, and utilization in IC engine/fuel cell vehicles.

There are a number of advantages in using hydrogen as a universal energy medium.⁴ The conversion of hydrogen by combustion or fuel cells results in only heat or electricity and water, as represented by the following equation:



Hydrogen is nontoxic and is easily absorbed in the biosphere. It can be readily produced (albeit at high cost) from water by electrolysis. However, additional research is needed for the production from nonfossil resources, storage, and transportation of hydrogen before it becomes commercially viable as an alternative to conventional fuels (see Fig. 1).⁵⁻⁷

The following sections cover the production, storage, utilization, and safety of hydrogen.⁸ The standards and codes are also discussed at the very end.

2 HYDROGEN PRODUCTION

As hydrogen is not readily available in its natural state, it must be produced at low cost, without creating any imbalance in global ecology. The conventional technologies used by industry to produce hydrogen are steam reforming of natural gas, partial oxidation of heavy hydrocarbons, gasification, and water electrolysis (driven by fossil fuel electricity production). All these processes are heavily dependent on fossil fuels. Thus, they have the inherent pollution and availability problems. The other potential ways of producing hydrogen include photoelectrochemical, photochemical, thermochemical, photocatalytic, and biological methods using renewable energy sources.

2.1 Steam Reforming of Natural Gas

Steam reforming of natural gas, or *steam methane reformation* (SMR), is one of the most developed and commercially used technologies. A block diagram of the SMR process is shown

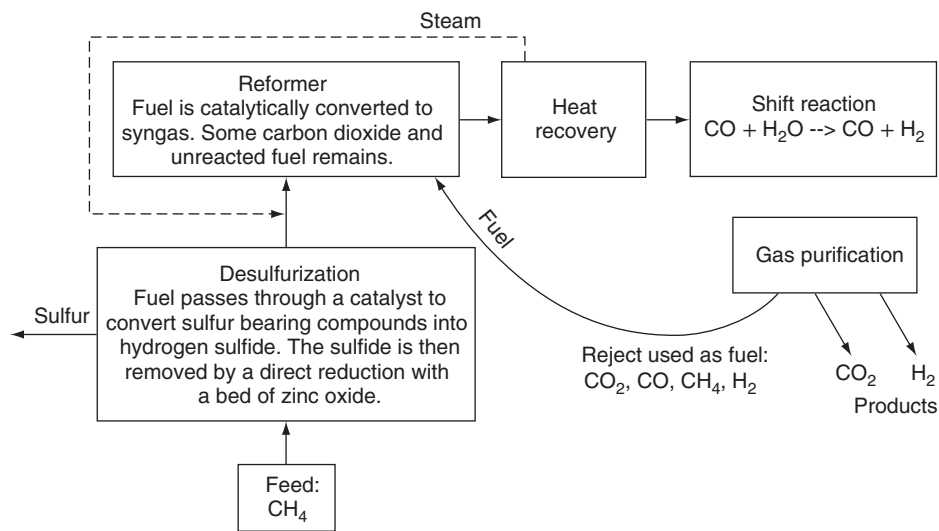
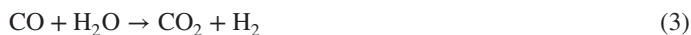
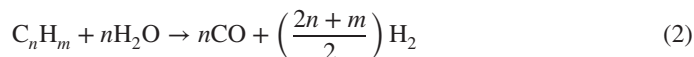


Figure 2 Block diagram of hydrogen production by steam reforming process. (Adapted from Ref. 11.)

in Fig. 2. Steam reforming of natural gas involves two steps. The first step is for the feedstock consisting of light hydrocarbons, usually methane, to react with steam at elevated temperatures (700–925°C) to produce *syngas* —a mixture of hydrogen (H₂) and carbon monoxide (CO). The process is endothermic, and heat of reaction is supplied by the combustion of fossil fuels. This process requires a catalyst inside the reformer for the reactions to occur. To protect the catalyst from corrosion, the feedstock must pass through a desulfurization process prior to entering the reformer. The second step, a water–gas shift reaction helps reacting carbon monoxide with steam to produce additional H₂ and carbon dioxide (CO₂) at around 350°C. This reaction is known as a shift reaction and is used to increase the H₂ content. Finally, a mixture of CO₂ and H₂ is sent to a gas purifier, where the hydrogen is separated from CO₂ via one of many methods (pressure swing absorption, wet scrubbing, or membrane separation). The chemical reactions involved in the SMR process are shown in Eqs (2) and (3):



For effective H₂ production using SMR, high temperatures at the reformer exit and an excess of steam to the reactor are required. Temperatures of 800–900°C and a molar steam to carbon ratio of $S/C = 2.5\text{--}3.0$ are considered the optimum conditions.⁹ Overall, SMR produces hydrogen with a purity of 96–98% and with operating efficiencies ranging from 65–75% as estimated by Sherif et al.^{10,11}

SMR is the most widely used and cheapest process for producing H₂ and is used to produce 48% of the world's hydrogen.¹² The price of hydrogen production from the SMR process strongly depends on the cost and availability of the natural gas feedstock. Kirk and Ledas estimated that feedstock cost contributes 52 – 68% of the overall hydrogen production expense.¹³ Basye and Swaminathan reported the cost division as 60% on feedstock, 30% from capital related charges, and 10% owing to operation and maintenance costs.¹⁴

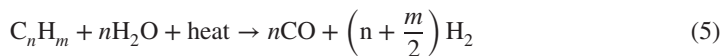
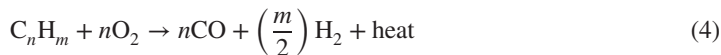
The SMR process is heavily dependent on fossil fuels. Moreover, it is not 100% efficient and some of the energy value of the hydrocarbon fuel is lost while in the conversion to hydrogen. The emissions of CO₂ from the SMR process can be reduced to some extent by sequestering the CO₂ (by storing it underground or in canisters). This capture and storage of CO₂ increases the

capital and operational costs by about 25–30%.¹⁵ However, according to Padro and Putsche, even after the inclusion of these costs, SMR is still less expensive than producing hydrogen from electrolysis (using large-scale hydropower plants).¹⁶ It has also been found with the SMR process that heavier feedstocks (e.g., oil) cannot be used to supply the reformer due to the need for the feed to be vapor.¹⁷ The possible areas of efficiency improvement include pre-reformers and medium-temperature shift reactors.¹⁷

2.2 Partial Oxidation of Heavy Hydrocarbons

Partial oxidation (POX) refers to the conversion of heavy hydrocarbon feedstocks (e.g., residual oil from the treatment of crude oil) into a mixture of H₂, CO, and CO₂ using superheated steam and oxygen. Figure 3 provides a schematic representation of the POX process. The external energy required to drive the process is obtained through the combustion of the feedstock itself. This necessitates controlling the quantity of O₂ and water vapor required for the reactions. To increase the H₂ content, the mixture of H₂, CO, and CO₂ is subjected to the shift reaction. This results in the formation of H₂ and CO₂.

The reactions involved in a POX process are as follows:



where $n = 1$ and $m = 1.3$ for residual oils.¹¹ POX produces hydrogen with a purity of 96–98%.¹⁰

The process works with any liquid or gaseous hydrocarbon. The overall efficiency of the process is about 50%.^{11,16} Like natural gas reforming, production cost of hydrogen is influenced by the price of feedstock. Some problems with POX include the need for an air separation unit. The air separation unit is needed to supply the pure oxygen to the process in order to prevent the release of nitrous oxide to the environment.¹⁴ The addition of this unit increases the system's capital cost thus increasing the hydrogen product cost.

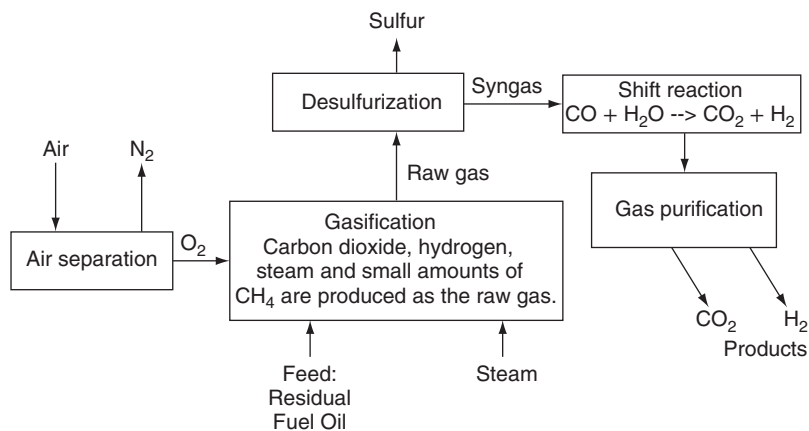
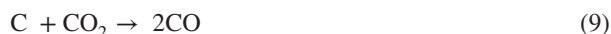
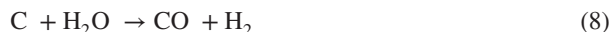


Figure 3 Block diagram of hydrogen production by partial oxidation. (Adapted from Ref. 11.)

2.3 Coal Gasification

Gasification is similar to partial oxidation except it has two main differences: gasification occurs at much higher temperature (1100–1300°C), and it uses a wide range of solid feedstocks (coal, heavy refinery residuals, biomass). In this process, a dry or slurried form of the feedstock is subjected to elevated temperature and pressure conditions in an oxygen-starved environment. The schematic flow diagram of the coal gasification process to produce either transportation fuel or electric power is shown in Fig. 4.¹⁸

This leads to an efficient and clean conversion of carbonaceous substances into a mixture of gas, containing mainly carbon monoxide and hydrogen. Inorganic materials in the feed are finally removed as a molten slag at the bottom of the reactor. The entire gasification process can be represented by the following reactions:



Coal is the most abundant fossil fuel. Gasification of coal offers higher thermal efficiencies than conventional coal-fired power generation and also has less impact on the environment. Low-grade coal types can be effectively used in coal gasification, expanding the available fossil fuel options.

2.4 Hydrogen Production from Biomass

Biomass represents a large potential feedstock resource for environmentally clean hydrogen production.¹⁹ It lends itself to both biological and thermal conversion processes. In the thermal path hydrogen can be produced in two ways: *direct gasification* and *pyrolysis* to produce liquid bio-oil, followed by steam reforming.

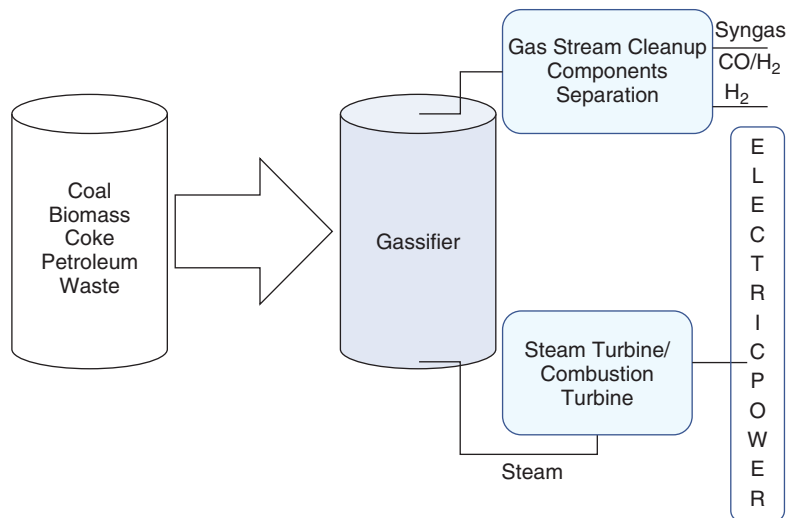


Figure 4 Block diagram of coal gasification for production of hydrogen for transportation or electric power. (Adapted from Ref. 18.)

Direct gasification of biomass is in many ways similar to coal gasification (see Section 2.3). The process occurs broadly in three steps:

1. Biomass is gasified (using steam or air) to produce an impure syngas mixture composed of hydrogen, CO, CO₂, CH₄, small amounts of higher hydrocarbons, tar, and water vapor. The gas may also contain particulate matter, which is removed using cyclones and scrubbers. The particulate free gas is compressed and then catalytically steam reformed to eliminate the tars and higher hydrocarbons.
2. High- and low-temperature shift conversions convert the CO to CO₂ and thereby produce additional hydrogen.
3. The hydrogen is separated from other products by PSA (pressure swing adsorption).²⁰

Figure 5 illustrates the sequence of processes.

The main reactions taking place in biomass gasification are as follows:



Biomass typically contains about 6% hydrogen by weight. However, in the presence of hydrogen-bearing species (steam), the hydrogen yield can be considerably improved above the 6% minimum.²¹ Gasification temperatures encountered are typically in the range 600–850°C, which is lower than many thermochemical water-splitting cycles, thereby making biomass gasification an attractive technology to produce hydrogen. Steam gasification of biomass is endothermic. The energy required for the process is supplied by burning part of the biomass feedstock or uncombusted char. Tars are polyaromatic hydrocarbons (PAHs) produced during gasification of biomass. However, tars are undesirable co-products, as they clog filters, pipes, and valves and damage downstream equipment such as engines and turbines. Efforts are being made to minimize or reform the tars to additionally produce hydrogen.^{22,23}

Hydrogen can alternately be produced by reforming the biomass to a liquid bio-oil in a process called *pyrolysis*. Pyrolysis is an endothermic thermal decomposition of biomass carried out in an inert atmosphere at 450–550°C.²⁴ The bio-oil so produced is a liquid composed of 85% oxygenated organics and 15% water. The bio-oil is then steam reformed in the presence of a nickel-based catalyst at 750–850°C, followed by shift conversion to convert CO to CO₂.²⁵ The reactions can be written as follows:

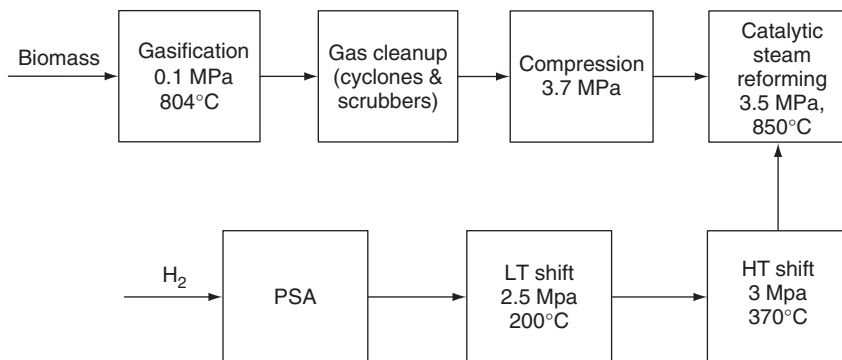
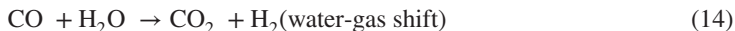
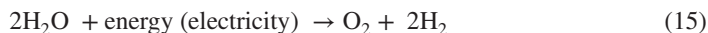


Figure 5 Gasification followed by steam reforming. (Adapted from Ref. 20).

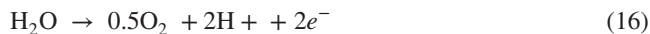
2.5 Electrolysis

Hydrogen production by electrolysis of water is a mature and efficient technology. The electrodes are separated by an ion-conducting electrolyte, as shown in Fig. 6. Hydrogen and oxygen are produced at the cathode and the anode, respectively. To keep the produced gases isolated from each other, an ion-conducting diaphragm is used to separate the two chambers.

Equation (15) shows the overall chemical equation for electrolysis:



Reaction at the anode:



Reaction at the cathode:



The reversible decomposition potential of Eq. (15) is 1.229 V at standard conditions of 1 atm pressure and 25°C. However, the total theoretical water decomposition potential is 1.480 V corresponding to hydrogen's enthalpy. The actual potential is typically between 1.75 and 2.05 V due to irreversibility and internal resistance. Typical efficiencies are of the order of 80%.

Electrolysis cells are normally characterized by their electrolytes [e.g., alkaline electrolyzer, solid polymer electrolyte (SPE) electrolyzer, or solid oxide electrolyzer].

Alkaline Water Electrolyzer

Alkaline water electrolysis is the most common type of electrolysis currently in use for large-scale electrolytic hydrogen production. The most common electrolyte used in alkaline water electrolysis is aqueous potassium hydroxide (KOH) at 30% concentration owing to the high conductivity and high resistance to corrosion of stainless steel at this concentration.²⁶ These electrolyzers work effectively under the operating conditions of 70–100°C and 1–30 bars. Asbestos has commonly been used as a diaphragm material to prevent hydrogen and oxygen gases from mixing together inside the cell. The principle of alkaline water electrolysis is shown schematically in Fig. 6. Commercial alkaline water electrolyzers are typically classified into two main types, unipolar and bipolar.²⁷

Solid Polymer Electrolyte Electrolyzer

SPE electrolyzers, as the name suggests, use solid polymer electrolytes, which are made up of special materials also called *perfluorocarbon ion exchange membranes*. This ion exchange membrane is sandwiched between catalyst-loaded electrodes. Water is fed to the anode of an

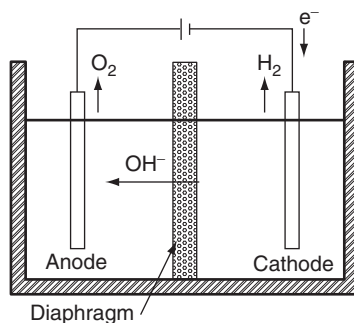


Figure 6 Electrolysis of water in an alkaline electrolyzer.

electrolysis cell, which is generally made up of porous titanium and activated by a mixed noble metal oxide catalyst. At the anode, water splits into oxygen and protons. The protons migrate through the ion exchange membrane to the cathode, where they are reduced to hydrogen. Figure 7 shows a simplified schematic of the SPE electrolyzer. SPE electrolyzers are also referred to as proton or polymer exchange membrane (PEM) electrolyzers.

The most common proton-conducting solid electrolytes are perfluoroalkyl sulfonic acid polymers, such as Nafion. Because of the dehydration of the membrane, the operating temperature of the SPE devices is limited to about 80°C.²⁸ To raise the dehydration temperature, several aromatic sulfonic acid polymers were synthesized and characterized. These were polyetheretherketone (PEEK), polyethersulfone (PES), polyphenylquinoxaline (PPQ), and polybenzimidazole (PBI).

2.6 Thermochemical Processes

Thermochemical hydrogen production is a means of splitting water via a series of chemical reactions. All chemical intermediates are recycled internally within the process so that water is the only raw material and hydrogen and oxygen are the only products. The maximum temperature requirements for most thermochemical cycles lie within a temperature range of 650–1100°C, thus eliminating use of lower temperature heat sources.²⁹ Figure 8 illustrates the concept of splitting water by a thermochemical cycle.

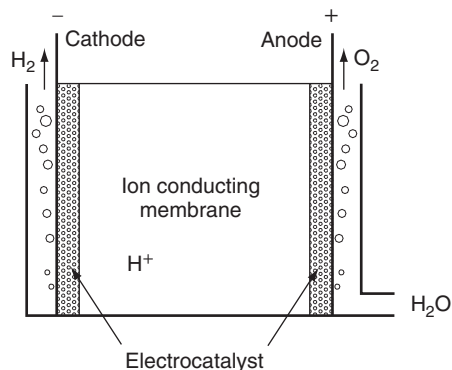


Figure 7 Schematic representation of an SPE electrolyzer.

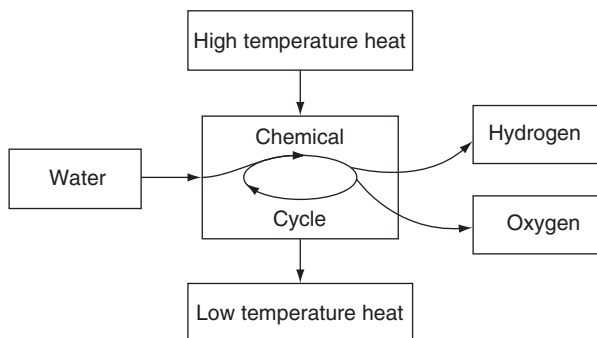


Figure 8 Schematic diagram of thermochemical cycle. (Adapted from Ref. 29.)

Wendt claims that 2000 – 3000 different theoretical cycles have been proposed and evaluated.²⁶ They can all be subdivided into four basic steps: water-splitting reaction, hydrogen production, oxygen production, and material regeneration.

The ability to reuse almost all of the components involved in the cycle (except feedwater) makes the thermochemical process attractive. Among the 2000–3000 possible thermochemical cycles, fewer than 10 have been studied extensively. The important ones under research now are described below.

ZnO/Zn Cycle

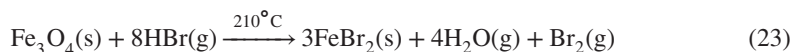
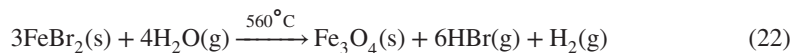
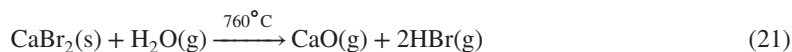
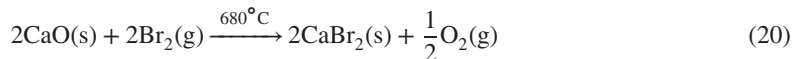
The ZnO/Zn cycle is a two-step water-splitting sequence based on the thermal redox pairs of metal oxides. As shown in the following reactions, the process relies on the endothermic thermal dissociation of ZnO, followed by the exothermic hydrolysis of Zn:



Theoretical conversion efficiencies for this cycle are of the order of 50%.³⁰ This cycle is in its preliminary stage. The current work is focused on the quenching step and decomposition rate measurements. The success of this cycle will depend on the development of an efficient mechanism for separating the Zn–H₂ mixture.

UT-3 Cycle

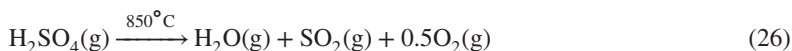
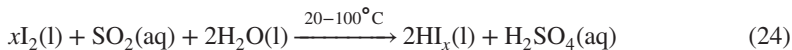
The UT-3 cycle, invented at University of Tokyo, consists of Ca, Fe, and Br compounds. It involves the use of solid and gaseous phases of reactants and products. The predicted first law and second law efficiencies of the adiabatic UT-3 cycle are 49 and 53%, respectively.³¹ This cycle is composed of the following reactions:



A substantial amount of research work, including bench-scale laboratory tests,³² solid reactants development, and reaction kinetic measurements have been performed on this cycle.^{33–35}

Iodine–Sulfur Cycle

The iodine–sulfur cycle is a three-step thermochemical process for decomposing water into H₂ and O₂. The cycle proposed by General Atomic (GA) Co. is one of the most extensively studied cycles. The chemical reactions involved in the process are shown in Eqs. (24)–(26).³⁶



The maximum hydrogen production efficiency as estimated by GA was around 50%.³⁷ Practical implementation of this cycle has been limited by the effective separation of HI and H₂ from HI–I₂–H₂O and H₂–H₂O–HI–I₂ mixtures, respectively. Moreover, the severe corrosion issue associated with high-temperature hydriodic acid and sulfuric acid needs to be addressed.

2.7 Photoelectrochemical Hydrogen Production

Photoelectrochemical (PEC) systems combine both photovoltaics and electrolysis into a one-step water-splitting process. These systems use a semiconductor electrode exposed to sunlight in combination with a metallic or semiconductor electrode to form a PEC cell. A schematic illustration of a PEC hydrogen production driven by solar energy is shown in Fig. 9.

In general, the semiconductor electrode (photoanode) is activated by solar radiation, which drives the reaction in an aqueous solution. Looking closely into the reaction involved in the photoelectrochemical process, we find that, due to bandgap illumination, electrons and holes are formed in the conduction and valence bands, respectively, at the photoanode.



where h is Planck's constant, ν the frequency, e^{-} the electron, and h^{+} the hole. The photogenerated holes at the anode split the water molecules into hydrogen ions and oxygen. The released hydrogen ions migrate to the cathode through the aqueous electrolyte.



Electrons generated at photoanode are transferred over the external circuit to the cathode, where they reduce hydrogen ions into gaseous hydrogen:



Thus, solar energy is utilized to produce hydrogen. Ideally, electrochemical decomposition of water takes place when the electromotive force of the cell is equal to 1.23 eV. If we consider internal losses in the PEC, a minimum bandgap of 1.8 eV is required to run the reaction.³⁸

The PEC devices have an advantage over conventional "photovoltaics (PV)," since they don't require semiconductor/semiconductor p - n junctions. In PEC, the junction is formed intrinsically at the semiconductor–electrolyte interface. Chemical photocorrosion and high costs have so far prevented the commercial utilization of photoelectrochemical devices.

2.8 Biological Methods

Hydrogen can also be obtained from biological process involving organic compounds. Figure 10 shows one of the techniques for hydrogen production using biological means.

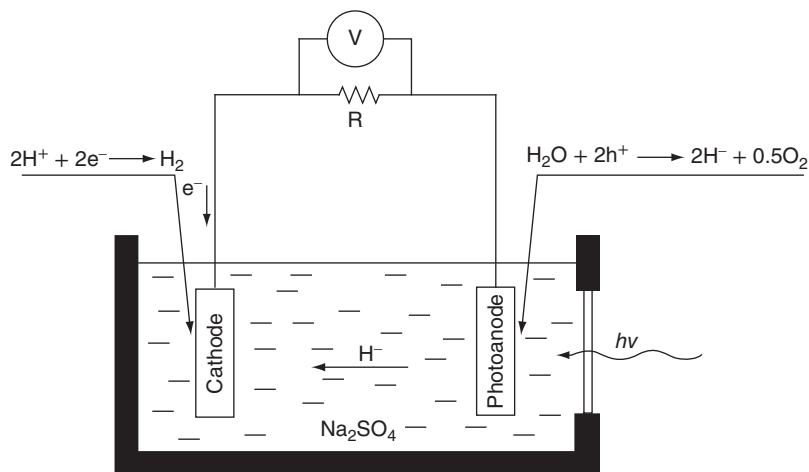


Figure 9 Schematic representation of Photoelectrochemical cell (PEC).³⁹

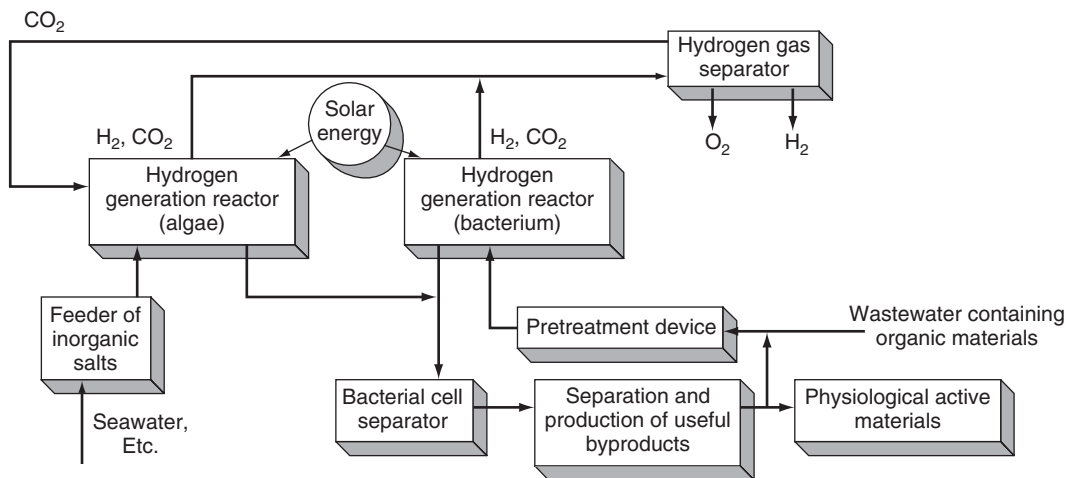


Figure 10 Concept of biological hydrogen production. (Adapted from Miyake et al., *J. Biotech.*, 70, 90, 1999, Fig. 1.)

There are two fundamental ways of biological hydrogen production:

1. Fermentation of the bacteria, which is an anaerobic process that converts organic substances such as starch, cellobiose, sucrose, and xylose to H_2 and CO_2 without the need of sunlight and oxygen
2. Biophotolysis, a process that uses microalgae-cynobacteria and green algae to produce hydrogen in the presence of sunlight and water

Both of these processes are being researched.

3 HYDROGEN STORAGE

An intermediate storage of hydrogen is mandatory for on-board vehicular applications, and this is schematically represented in Fig. 11.^{40–45}

The barriers and limitations of the existing and new hydrogen storage technologies (Table 1) delay its practical use for commercial applications.⁴⁶ The development and commercialization of new technologies are required to meet the U.S. Department of Energy (DOE) milestones and FreedomCAR technical target performance (Table 2).^{47,48}

Several critical properties of the hydrogen storage materials can be evaluated for automotive applications:

- Light weight
- Cost and availability
- High volumetric and gravimetric density of hydrogen
- Fast kinetics
- Ease of activation
- Low temperature of dissociation or decomposition
- Appropriate thermodynamic properties
- Long-term cycling stability
- High degree of reversibility

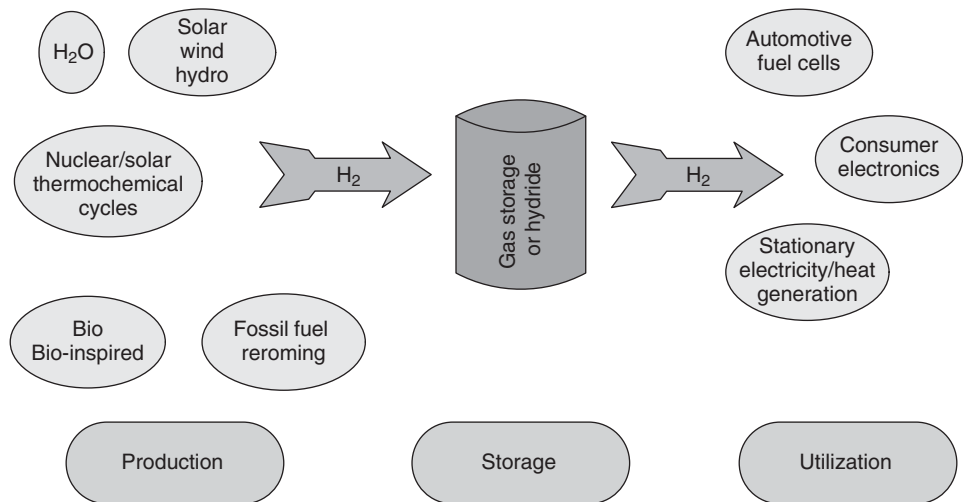


Figure 11 The hydrogen economy consists of production, storage and use.

Table 1 Hydrogen Storage Methods and Phenomena (gravimetric density, ρ_m , the volumetric density ρ_v , the working temperature T , and pressure P)

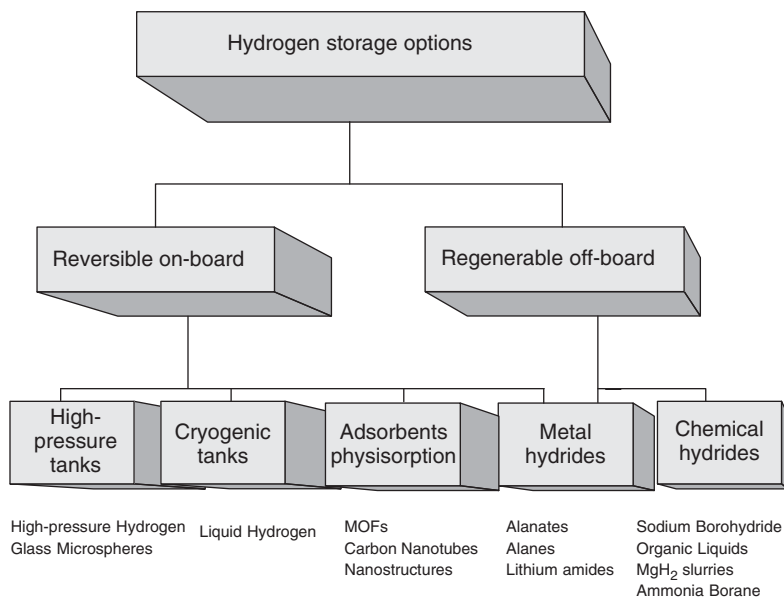
Storage Method	ρ_m (mass %)	ρ_v (kg H ₂ m ⁻³)	T (°K)	P (bar)	Phenomena and Remarks
High-pressure gas cylinders	13	<40	303	800	Compressed gas (molecular H ₂) in lightweight composite cylinders (tensile strength of the material is 2000 MPa)
Liquid hydrogen in cryogenic tanks	Size dependent	70.8	21	1	Liquid hydrogen (molecular H ₂) continuous loss of a few % per day of hydrogen at room temperature
Adsorbed hydrogen (carbon nanotube)	2	20	193	100	Physisorption (molecular H ₂) on materials (e.g., carbon with a very large specific surface area), reversibility problems
Absorbed on interstitial sites in a host metal (Metal hydrides)	2	150	303	1	Hydrogen (atomic H) intercalation in host metals, metallic hydrides working at room temperature are fully reversible
Complex compounds	<18	150	>373	1	Complex compounds ([AlH ₄] ⁻ or [BH ₄] ⁻), desorption at elevated temperature, absorption at high pressures
Metals and complexes together with water	<40	>150	303	1	Chemical oxidation of metals with water and liberation of hydrogen, not directly reversible

Source: Adapted from Ref. 46.

Table 2 U.S. DOE Hydrogen Storage Milestones

Technical Targets	Units	Year 2017
Gravimetric capacity (GrC)	kg H ₂ /kg	0.055
(net useful energy/max system mass)	kWh/kg	1.8
Volumetric capacity (VC)	kg H ₂ /L	0.040
(net useful energy/max system volume)	kWh/kg	1.3
Fuel cost	\$/gauge at pump	2–4
Min/Max delivery temperature	°C	–40/85
Cycle life	Cycles	1500
Refueling rate	kg H ₂ /min	1.5

Source: Adapted from Ref. 48.

**Figure 12** Options for vehicular hydrogen storage.

3.1 Hydrogen Storage Options

Current hydrogen storage technologies include high-pressure tanks, cryogenic storage, metal hydrides, chemical hydrides, and high surface adsorbents such as nanostructured carbon-based materials. High pressure and cryogenic tanks, high surface adsorbents, and many metal hydrides fall in the category of reversible on-board hydrogen storage since refueling with hydrogen can take place directly on board the vehicle. For chemical hydrogen storage and some high-temperature metal hydrides, hydrogen regeneration is not possible on board the vehicle, and thus these systems must be regenerated off board (see Fig. 12).

Hydrogen can be stored as a gas or liquid in pressure vessels. Gaseous storage requires large volume and pressure (up to 10,000 psi). Liquid storage requires low temperatures (–423°C) with cryogenic systems. Hydrogen can also be stored in advanced solid-state materials—within the structure or on the surface of certain materials, as well as in the form

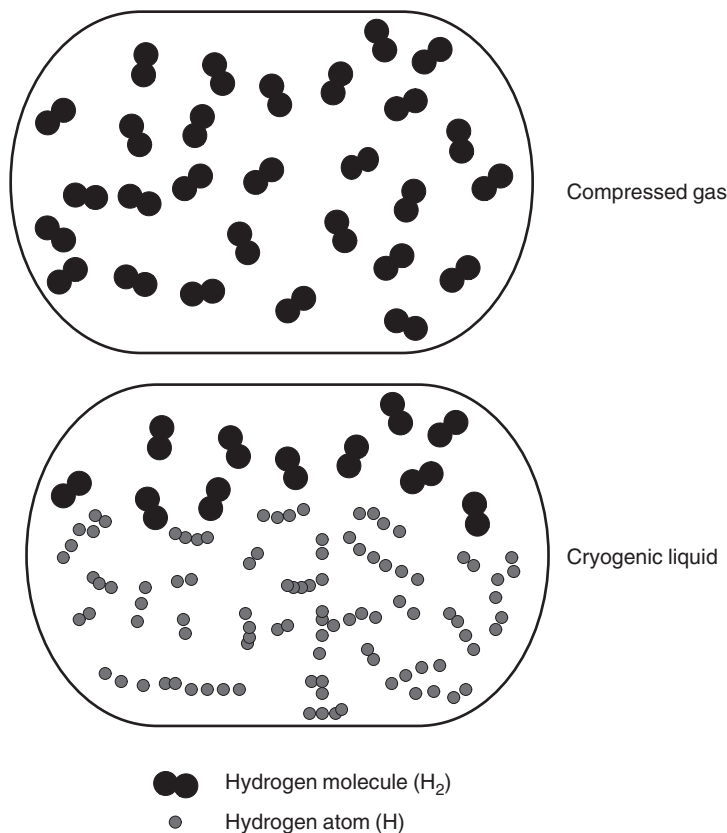


Figure 13 Different types of hydrogen storage methods.

of chemical precursors that undergo a chemical reaction to release hydrogen.^{49–52} Figures 13 and 14 demonstrate these processes in the atomic or molecular scale.

The volume storage efficiencies of gaseous and liquid hydrogen storage are generally very low compared to the solid-state hydrogen storage.⁵³ Figure 14 shows the hydrogen storage methods in solids (by adsorption) or within solids (by absorption). In *adsorption* (a), hydrogen attaches to the surface of a material either as hydrogen molecules (H_2) or hydrogen atoms (H). In *absorption* (b), hydrogen molecules dissociate into hydrogen atoms that are incorporated into the solid lattice framework. This method may make it possible to store large quantities of hydrogen in smaller volumes at low pressure and room temperature. Finally, hydrogen can be bound strongly within molecular structures as chemical compounds containing hydrogen atoms (c).

High-Pressure Gaseous Hydrogen Storage

The energy density of gaseous hydrogen can be improved by storing hydrogen at higher pressures. This requires material and design improvements in order to ensure tank integrity. Advances in compression technologies are also required to improve efficiencies and reduce the cost of producing high-pressure hydrogen.

Carbon fiber–reinforced 5000-psi and 10,000-psi compressed hydrogen gas tanks are developed by Quantum Technologies and others.⁵⁴ Such tanks are already used in prototype

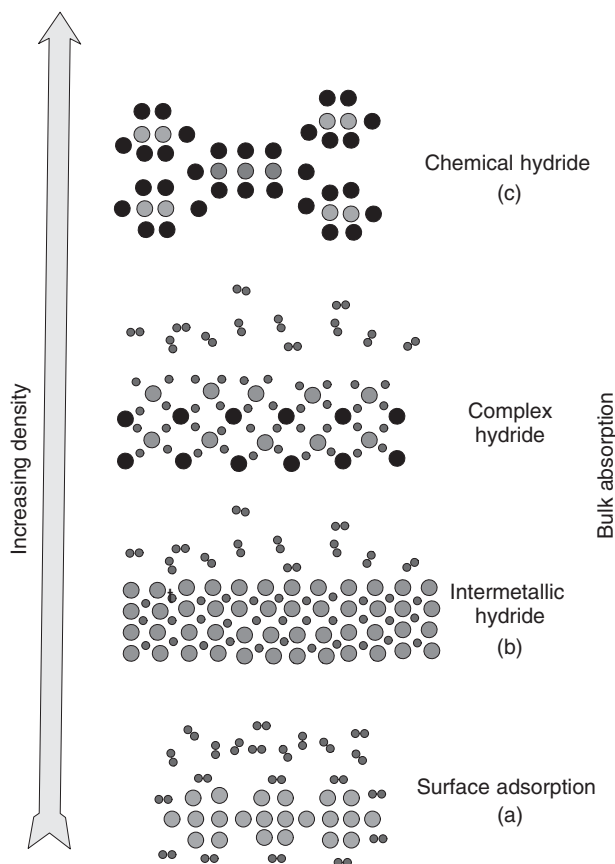


Figure 14 Hydrogen storage in carbon, metal/complex hydrides, and chemical compounds.

hydrogen-powered vehicles. The inner liner of the tank is a high-molecular-weight polymer that serves as a hydrogen gas permeation barrier. A carbon fiber–epoxy resin composite shell is placed over the liner and constitutes the gas pressure load-bearing component of the tank. Finally, an outer shell is placed on the tank for impact and damage resistance. The pressure regulator for the 10,000 psi tank is located in the interior of the tank. There is also an in-tank gas sensor to monitor the tank temperature during the gas-filling process when the tank is heated.

Issues with compressed hydrogen gas tanks revolve around high pressure, weight, volume, conformability, and cost. The cost of high-pressure compressed gas tanks is essentially dictated by the cost of the carbon fiber that must be used for lightweight structural reinforcement. Efforts are underway to identify lower cost carbon fibers that can meet the required high-pressure and safety specifications for hydrogen gas tanks. However, lower cost carbon fibers must still be capable of meeting tank thickness constraints in order to help meet volumetric capacity targets. Thus, lowering cost without compromising weight and volume is a key challenge.

Two approaches are being pursued to increase the gravimetric and volumetric storage capacities of compressed gas tanks from their current levels. The first approach involves cryo-compressed tanks. This is based on the fact that, at fixed pressure and volume, gas tank volumetric capacity increases as the tank temperature decreases. Thus, cooling a tank from room temperature to liquid nitrogen temperature (77 K) will increase its volumetric capacity

by a factor of 4, although system volumetric capacity will be less than this due to the increased volume required for the cooling system.

The second approach involves the development of conformable tanks. Current liquid gasoline tanks in vehicles are highly conformable in order to take maximum advantage of available vehicle space. Concepts for conformable tank structures are based on the location of structural supporting walls. Internal cellular-type load-bearing structures may also be a possibility for greater degree of conformability.

Compressed hydrogen tanks [5000 psi \sim 35 MPa and 10,000 psi \sim 70 MPa] have been certified worldwide according to ISO 11439 (Europe), NGV-2 (United States), and Reijikijun Betten (Iceland) standards and approved by TUV (Germany) and the High-Pressure Gas Safety Institute of Japan (KHK). Tanks have been demonstrated in several prototype fuel cell vehicles and are commercially available. Composite, 10,000-psi tanks have demonstrated a 2.35 safety factor (23,500-psi burst pressure), as required by the European Integrated Hydrogen Project specifications.

Liquid Hydrogen Storage

The energy density of hydrogen can be improved by storing hydrogen in a liquid state. However, the issues with liquid hydrogen (LH₂) tanks are hydrogen boil-off, the energy required for hydrogen liquefaction, volume, weight, and tank cost.^{4,55} There are four contributing mechanisms to boil-off losses in cryogenic hydrogen storage systems:

1. Ortho-para conversion
2. Heat leak (shape and size effect, thermal stratification, thermal overfill, insulation, conduction, radiation, cool-down)
3. Sloshing
4. Flashing

Typically, 30% of the heating value of hydrogen is required for liquefaction. New approaches, which can lower these energy requirements and thus the cost of liquefaction, are needed. Hydrogen boil-off must be minimized or eliminated for cost, efficiency, and vehicle range considerations, as well as for safety considerations when vehicles are parked in confined spaces. Insulation is required for LH₂ tanks, and this reduces system gravimetric and volumetric capacity.

Liquid hydrogen tanks can store more hydrogen in a given volume than compressed gas tanks. The volumetric capacity of liquid hydrogen is 0.070 kg/L, compared to 0.030 kg/L for 10,000-psi gas tanks. Liquid tanks are being demonstrated in hydrogen-powered vehicles, and a hybrid tank concept combining both high-pressure gaseous and cryogenic storage is being studied.

Metal-Complex Hydrides

Hydrogen can be packed and stored in a solid state by forming a metal hydride.⁵⁶⁻⁶⁴ During the formation of the metal hydride, hydrogen molecules are dissociated into hydrogen atoms, which insert themselves into interstitial spaces inside the lattice of intermetallic compounds and/or alloys (Fig. 15). The typical reversible metal-hydrogen interaction occurs either as a gas-phase reaction or as an electrochemical reaction.

In such a way, an effective storage comparable to the density of liquid hydrogen is created. However, when the mass of the metal or alloy is taken into account, the metal hydride gravimetric storage density is comparable to storage of pressurized hydrogen. The best achievable gravimetric storage density is about 0.07 kg of H₂/kg of metal, for a high-temperature hydride

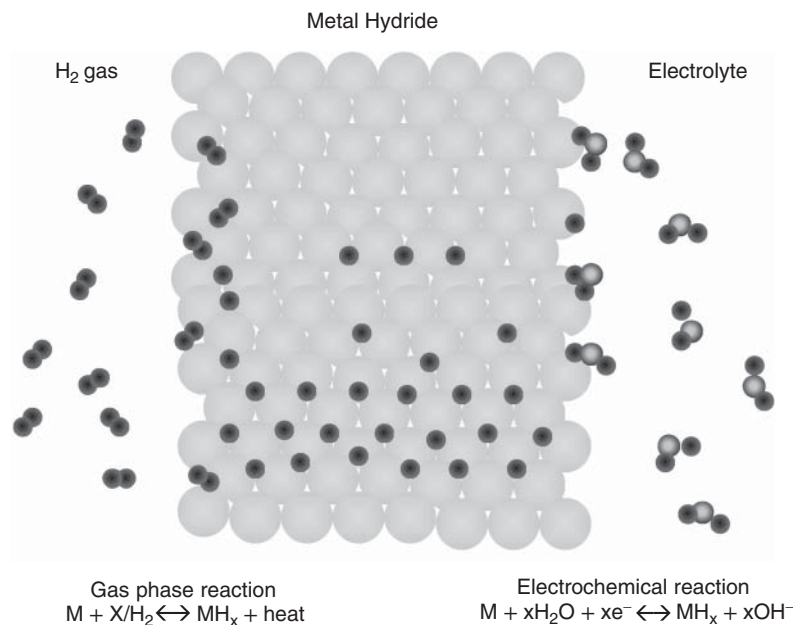


Figure 15 Hydrogen in atomic form on interstitial lattice sites of an intermetallic alloy.

Table 3 Theoretical Capacities of Hydriding Substances as Hydrogen Storage Media

Medium	Content kg/kg	Hydrogen Storage Capacity, kg/liter of vol.	Energy Density kJ/kg	Energy Density kJ/liter of vol.
MgH ₂	0.070	0.101	9,933	14,330
Mg ₂ NiH ₄	0.0316	0.081	4,484	11,494
VH ₂	0.0207		3,831	
FeTiH _{1.95}	0.0175	0.096	2,483	13,620
TiFe _{0.7} Mn _{0.2} H _{1.9}	0.0172	0.090	2,440	12,770
LaNi ₅ H _{7.0}	0.0137	0.089	1,944	12,630
R.E.Ni ₅ H _{6.5}	0.0135	0.090	1,915	12,770
Liquid H ₂	1.00	0.071	141,900	10,075
Gaseous H ₂ (100 bars)	1.00	0.0083	141,900	1,170
Gaseous H ₂ (200 bars)	1.00	0.0166	141,900	2,340
Gasoline	—	—	47,300	35,500

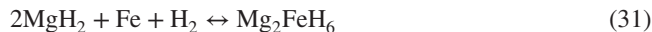
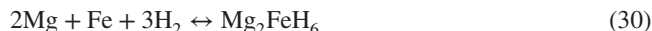
such as MgH₂, as shown in Table 3, which gives a comparison of some hydriding substances with liquid hydrogen, gaseous hydrogen, and gasoline.¹⁹

The potential to use hydrides for energy storage and applications has stimulated extensive theoretical and experimental research on the fundamental aspects of hydrogen sorption, and several reversible storage intermetallics⁶⁵ such as FeTi,⁶⁶ LaNi₅, MmNi_{4.5}Al_{0.5},⁶⁷ and Mg₂Ni.⁶⁸ Since the maximum weight percentage storage for these intermetallics is ~1.8 wt % at ambient conditions and ~3.8 wt % at high temperature (300–400°C) there is ongoing

research to find better hydride materials with higher storage capacity at ambient as well as high-temperature conditions. To achieve this, two prominent routes are being followed: first, to modify and optimize the present storage materials such as FeTi, LaNi₅ and the high-temperature hydride Mg₂Ni, and second, to develop altogether new storage materials, e.g., transition metal complexes, composite materials, nanoparticle and nanostructured materials, and new carbon variants (fullerenes, C₆₀ and other higher versions, graphitic nanofibers, and nanotubes).

Magnesium has the highest theoretical hydrogen storage capacity of ~ 7.6 wt %. However, it has two significant disadvantages: (1) the Mg–H₂ reaction has poor kinetics; and (2) the resulting hydride is not reversible under ambient or moderate temperature and pressure conditions.⁶⁹ A possible way to achieve Mg-like storage capacity but with reversible hydrogenation characteristics is to form composites with Mg as one of the components. The other component may be one of the known hydrogen storage intermetallic alloys.⁷⁰

An important feature of the metallic hydrides is the high volumetric density of the hydrogen atoms present in the host atomic lattice.⁷¹ The highest theoretical volumetric hydrogen density known today is 150 kg · m⁻³ for Mg₂FeH₆ and Al(BH₄)₃. The Mg₂FeH₆ hydride belongs to the family of Mg–transition metal complex hydrides with [FeH₆]⁴⁻ octahedral surrounded by Mg atoms in cubic configuration.⁷² Interestingly, iron does not form intermetallic compounds with Mg, but it readily combines with hydrogen and Mg to form ternary hydride Mg₂FeH₆ according to these reactions:



During the storage process (charging or absorption) heat is released that must be removed in order to achieve the continuity of the reaction. During the hydrogen release process (discharging or desorption) heat must be supplied to the storage tank. The thermodynamic aspects of hydride formation from gaseous hydrogen are described by means of pressure–composition isotherms as shown in Fig. 16. While the solid solution and hydride phase coexist, the isotherms show a flat plateau, the length of which determines the amount of H₂ stored. The stability of metal hydrides is usually presented in the form of Van't Hoff equation (32):

$$\ln P_{\text{H}_2}(\text{atm}) = \frac{2\Delta H_f}{SRT} + C \quad (32)$$

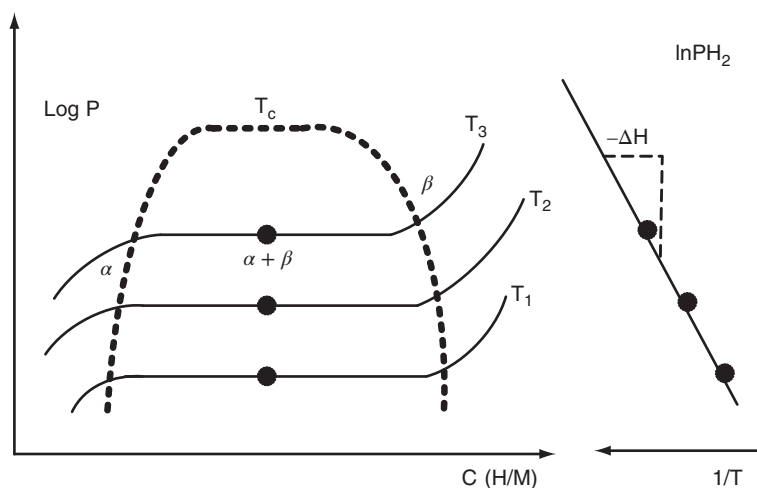
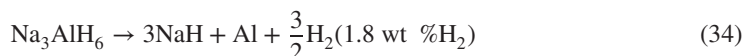
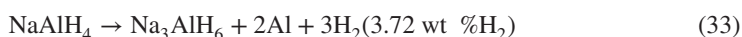


Figure 16 P–C isotherms and Van't Hoff curve for the LaNi₅ metal hydride.

systems for hydrogen storage.⁷⁵ However, reduced availability of reversible hydrogen (~4–5 wt %), poor cyclic stability, loss of the catalytic function of Ti species, necessitates the search for new and efficient complex hydride systems.⁷⁶ There are about 234 complex chemical hydrides that have been reported with theoretical hydrogen storage capacity.⁷⁷ Table 4 lists the complex chemical hydrides and their available capacities and operating temperatures.

The hydride complexes such as NaAlH₄ and NaBH₄ are known to be stable and decompose only at elevated temperatures, often above the melting point of the complex. However, the addition of a few mole concentrations of titanium species to NaAlH₄ eases the release of hydrogen at moderate temperatures and ambient pressure.⁷⁵ The decomposition of Ti-doped NaAlH₄ proceeds in two steps with the total released hydrogen of ~5.5 wt % at 100–150°C, as given in Eqs. (33) and (34):



Following this breakthrough discovery, an effort was initiated at the U.S. DOE hydrogen program to develop NaAlH₄ and related alanes as hydrogen storage materials.^{78,79} Another complex hydride, Mg(AlH₄)₂, contains 9.6 wt % of hydrogen that decomposes below 200°C.⁸⁰ Some of the new complex hydrides and their theoretical capacities are listed in Table 5.

Borohydride complexes with suitable alkali or alkaline earth metals are a promising class of compounds for hydrogen storage. The hydrogen content can reach values of up to 18 wt % for LiBH₄.⁸¹ The total amount of hydrogen desorbed up to 600°C is 9 wt %. Mixing LiBH₄ with SiO₂ powder lowers the desorption temperature, so that 9 wt % of hydrogen is liberated below 400°C.⁷¹ Recently, Chen et al. reported a new hydrogen storage system, lithium nitride

Table 4 Theoretical Hydrogen Storage Capacities of Complex Hydrides

No.	Complex Chemical Hydride	Theoretical Capacity (wt %)	Reversible Capacity (wt %)	Operating Temperature (°C)	Remarks
1.	Ti-doped NaAlH ₄	7.5	5.5	100–150	High rehydrogenation pressure, poor cycle life, loss of catalytic activity, less available capacity
2.	Undoped and Ti-doped LiAlH ₄	10.5	6.3	120–170	Problems with reversibility, and reduced thermodynamic stability
3.	Undoped and doped LiBH ₄	18.2	9.0	200–400	High operating temperature, rehydrogenation problem, possible borane gas evolution
4.	Mg(AlH ₄) ₂	9.3	6.6	200–250	High operating temperature, thermodynamic stability
5.	NaBH ₄ /H ₂ O	10.5	9.2	Ambient	Hydrolysis reaction, irreversibility, one-time use
6.	Li ₃ N (LiNH ₂ /LiH)	11.3	6.5–7.0	255–285	High operating temperature, possible ammonia evolution
7.	B-H-Li-N	10.0		80–150	Rehydrogenation problem
8.	AlH ₃	10.5		150	Ball milling induced decomposition, irreversible
9.	H ₃ BNH ₃	18.3	12.6		Ammonia evolution possibility, irreversible

Table 5 New Complex Hydrides and Their Hydrogen Storage Capacity

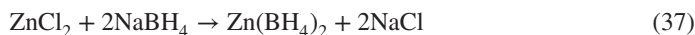
Serial Number	Complex Hydride	Theoretical Capacity, (wt %)	Decomposition Temperature, (T_{dec} °C)
1.	$\text{LiAlH}_2(\text{BH}_4)_2$	15.2	
2.	$\text{Mg}(\text{BH}_4)_2$	14.8	260–280
3.	$\text{NH}_4\text{Cl} + \text{LiBH}_4$	13.6	>ambient
4.	$\text{Ti}(\text{BH}_4)_3$	12.9	ca. 25
5.	$\text{Fe}(\text{BH}_4)_3$	11.9	–30 to –10
6.	$\text{Ti}(\text{AlH}_4)_4$	9.3	–85
7.	$\text{Zr}(\text{BH}_4)_3$	8.8	<250
8.	$\text{Zn}(\text{BH}_4)_2$	8.4	85

(Li_3N), which absorbs 11.5 wt % of hydrogen reversibly.^{82,83} The hydrogenation of lithium nitride is a two-step reaction as shown in Eqs. (35) and (36):



Li_3N absorbs 5.74 wt % of hydrogen in the first step and 11.5 wt % in the second step. Since the hydrogen pressure for the reaction corresponding to the first step is very low (about 0.01 bar at 255°C), only the second step reaction of Li_2NH (lithium imides) with H_2 leads to the reversible storage capacity. According to Chen et al., the plateau pressure for imides hydrogenation is 1 bar at the relatively high temperature of 285°C.⁸² However, the temperature of this reaction can be lowered to 220°C with magnesium substitution, although at higher pressures.⁸⁴ Further research on this system may lead to additional improvements in operating conditions with improved capacity.

$\text{Zn}(\text{BH}_4)_2$ is a ternary complex metal borohydride with a decomposition temperature of around 85°C.⁸⁵ Its theoretical hydrogen capacity is about 8.5 wt %, and it can be synthesized by metathesis reaction of NaBH_4 and ZnCl_2 in diethyl ether.⁸⁶ A recent report from Jeon and Cho.⁸⁷ indicates that zinc borohydride was successfully synthesized by ball milling zinc chloride and sodium borohydride without the use of a solvent, see reaction (37):



An example of the decomposition of a borohydride [$\text{Zn}(\text{BH}_4)_2$] is given by.⁸⁵



which shows $\text{Zn}(\text{BH}_4)_2$ thermally decomposing into the constituent elements with release of hydrogen. The main reason that complex hydride compounds have not been considered for hydrogen storage before is their reported lack of reversibility.

Chemical Hydrogen Storage

The term *chemical hydrogen storage* is used to describe storage technologies in which hydrogen is generated through a chemical reaction. Common reactions involve chemical hydrides with water or alcohols. Typically, these reactions are not easily reversible on board a vehicle. Hence, the “spent fuel” or by-products must be removed from the vehicle and regenerated off board.

Hydrolysis Reactions. Hydrolysis reactions involve the oxidation reaction of chemical hydrides with water to produce hydrogen. The reaction of sodium borohydride has been the most studied to date. This reaction is



In the first embodiment, slurry of an inert stabilizing liquid protects the hydride from contact with moisture and makes the hydride pumpable. At the point of use, the slurry is mixed with water, and the consequent reaction produces high-purity hydrogen. The reaction can be controlled in an aqueous medium via pH and the use of a catalyst. Although the material hydrogen capacity can be high and the hydrogen release kinetics fast, the borohydride regeneration reaction must take place off board. Regeneration energy requirements cost and life-cycle impacts are key issues currently being investigated.

Millennium Cell has reported that its NaBH_4 -based hydrogen-on-demand system possesses a system gravimetric capacity of about 4 wt %.⁸⁸ Similar to other material approaches, issues include system volume, weight and complexity, and water availability.

Another hydrolysis reaction currently being investigated by Safe Hydrogen is the reaction of MgH_2 with water to form Mg(OH)_2 and H_2 .⁸⁹ In this case, particles of MgH_2 are contained in nonaqueous slurry to inhibit premature water reactions when hydrogen generation is not required. Material-based capacities for the MgH_2 slurry reaction with water can be as high as 11 wt %. However, as with the sodium borohydride approach, water must be carried on board the vehicle in addition to the slurry, and the Mg(OH)_2 must be regenerated off board.

New Chemical Approach. A new chemical approach may provide hydrogen generation from ammonia–borane materials by the following reactions:



The first reaction, which occurs at less than 120°C releases 6.1 wt % hydrogen, while the second reaction, which occurs at approximately 160°C, releases 6.5 wt % hydrogen.⁹⁰ Recent studies indicate that hydrogen-release kinetics and selectivity are improved by incorporating ammonia–borane nanosized particles in a mesoporous scaffold.

Carbonaceous Materials for Hydrogen Storage

Carbonaceous materials are attractive candidates for hydrogen storage because of a combination of adsorption ability, high specific surface, pore microstructure, and low mass density. In spite of extensive results available on hydrogen uptake by carbonaceous materials, the actual mechanism of storage still remains a mystery. The interaction may either be based on van der Waals attractive forces (physisorption) or on the overlap of the highest occupied molecular orbital of carbon with occupied electronic wave function of the hydrogen electron, overcoming the activation energy barrier for hydrogen dissociation (chemisorption).

The physisorption of hydrogen limits the hydrogen-to-carbon ratio to less than one hydrogen atom per two carbon atoms (i.e., 4.2 mass %). While in chemisorption, the ratio of two hydrogen atoms per one carbon atom is realized, as in the case of polyethylene.^{46,91,92} Physisorbed hydrogen has a binding energy normally of the order of 0.1 eV, while chemisorbed hydrogen has C–H covalent bonding, with a binding energy of more than 2–3 eV.

Dillon et al. presented the first report on hydrogen storage in carbon nanotubes and triggered a worldwide tide of research on carbonaceous materials.⁹³ Hydrogen can be physically adsorbed on activated carbon and be “packed” on the surface and inside the carbon structure more densely than if it has just been compressed. The best results achieved with carbon nanotubes to date confirmed by the National Renewable Energy Laboratory is hydrogen storage density corresponding to about 10% of the nanotube weight.⁹⁴

Hydrogen can be stored in glass microspheres of approximately 50 μm diameter. The microspheres can be filled with hydrogen by heating them to increase the glass permeability to hydrogen (see Fig. 18).⁹⁵ At room temperature, a pressure of approximately 25 MPa is achieved, resulting in storage density of 14% mass fraction 10 $\text{kg H}_2/\text{m}^3$.⁹⁶ At 62 MPa, a bed of glass microspheres can store 20 $\text{kg H}_2/\text{m}^3$. The release of hydrogen occurs by reheating the spheres to again increase the permeability.

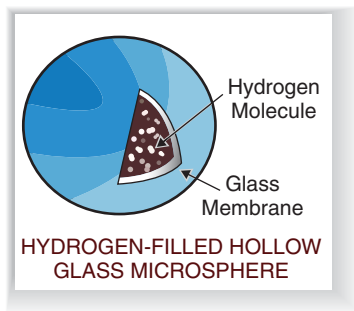


Figure 18 Schematic of a hydrogen-filled hollow glass microsphere.

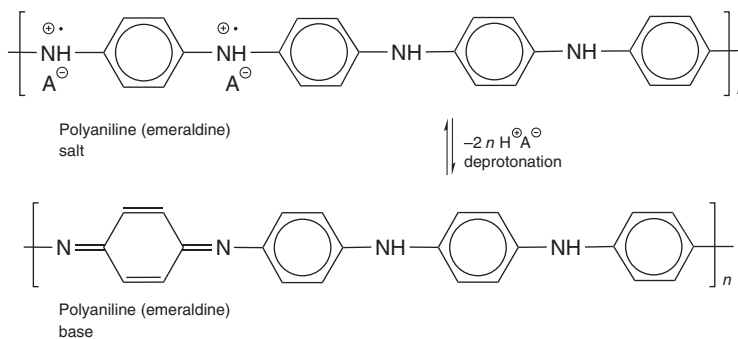


Figure 19 Chemical structure of polyaniline (emeraldine) in its salt and base form.

Polymer Nanostructures

Novel nanocomposite materials consist primarily of polyaniline, a conducting polymer, which has conductivity on the order of 1 S/cm.⁹⁷ Figure 19 shows the chemical structure of polyaniline in its emeraldine form. The salt form of the polyaniline has anions, which allow hydrogen ions to bond to the material very well. Due to its porosity, the surface area of the conducting polymeric matrix material will allow for additional hydrogen binding in the form of physisorption.

Conducting polymer nanostructures combine the advantages of organic conductors and low dimensional systems having interesting physicochemical properties^{98–101} and useful applications.^{102–104} Among the conducting polymers, polyaniline is considered important because of its extraordinary properties of electrical and optical behavior. It was recently reported that polyaniline can store as much as 6–8 wt % of hydrogen,¹⁰⁵ which was later refuted by Panella et al.¹⁰⁶ Though many controversial results were reported in terms of hydrogen uptake^{107–110} in polymer nanocomposites, there are still a number of parameters, tailor-made properties, surface morphologies, and their correlation with hydrogen sorption behavior to be investigated before these materials can be commercially deployed for on-board hydrogen storage. Similarly, nanotubes¹¹¹ or nanofibers¹¹² have attracted more interest because of their novel properties and wide potential application for nanometer-scale engineering applications. It is known that the nanofibrillar morphology significantly improves the performance of polyaniline in many conventional applications involving polymer interactions with its environment.¹¹³ This leads to faster and more responsive chemical sensors,¹¹⁴ new organic/polyaniline nanocomposites,¹¹⁵ and ultrafast nonvolatile memory devices.¹¹⁶ Nanofibers with diameters of tens of nanometers appear to be an intrinsic morphological unit that was found to naturally form in the early stage

of chemical oxidative polymerization of aniline. In conventional polymerization, nanofibers are subject to secondary growth of irregularly shaped particles that form the final granular agglomerates. The key to producing pure nanofibers is to suppress secondary growth. Based on this, two methods (interfacial polymerization and rapidly mixed reactions) have been developed that can readily produce pure nanofibers by slightly modifying the conventional chemical synthesis of polyaniline without the need for any template or structural directing material. With this nanofiber morphology, dispensability and processability of polyaniline are now greatly improved. On the other hand, the template synthesis method is an effective way to grow the nanotubes of various conducting polymers.¹¹⁷ The preparation conditions and their effect on morphology, size, and electrical properties of nanofibers have been reported by Zhang and Wang.¹¹⁸ We have recently observed excellent hydrogen sorption characteristics in polyaniline nanofibers^{119,120} prepared by an electrospinning process as shown in Fig. 20. Hydrogen uptake of 10 wt % followed by the coexistence of physisorption and chemisorptions, during hydrogen release, has been correlated with unique nanofibrous morphologies (see Fig. 21). Though the initial hydrogen storage capacity and kinetics are excellent in these materials, they diminish in consecutive cycles, fundamental gas–solid reaction, and the rate-limiting factors are currently under investigation.

Additive materials, such as carbon nanotubes and fullerenes, as well as catalyst materials will also allow the formation of chemical and physical bonds at the matrix material. By combining various carbon structures in a nanocomposite, a new hydrogen storage system can be developed that exceeds the performance of the existing state-of-the-art materials and facilitates rapid commercialization of high-energy density hydrogen storage devices. These new catalyst-enhanced hydrogen storage materials can be described as porous nanocomposites of a conducting polymer with modified fullerene compounds and carbon nanotubes, as well as kinetics enhancing catalyst materials. The combination of the high surface area of carbon nanotubes

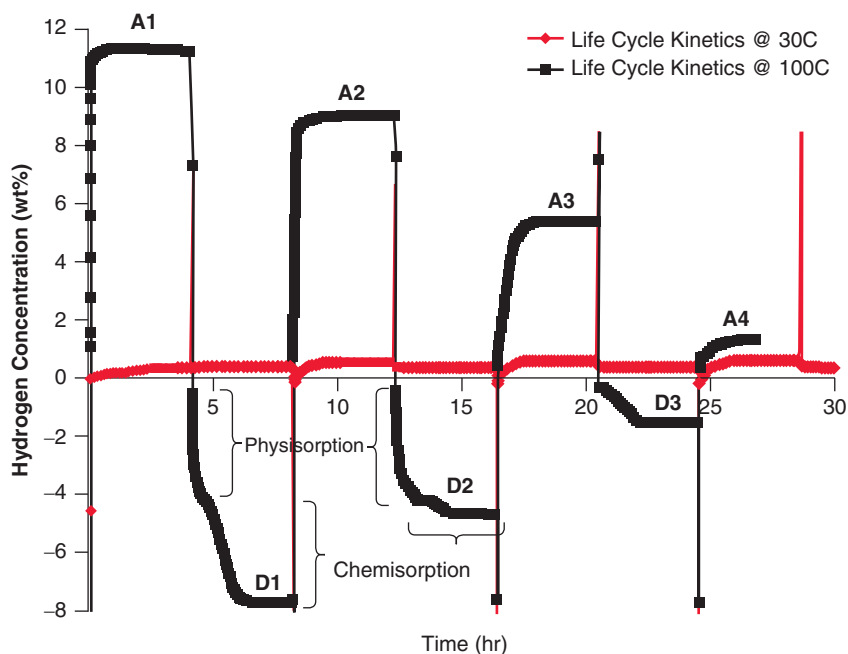


Figure 20 Hydrogen absorption and desorption cycling of electrospun polyaniline nanofiber at around 100°C.

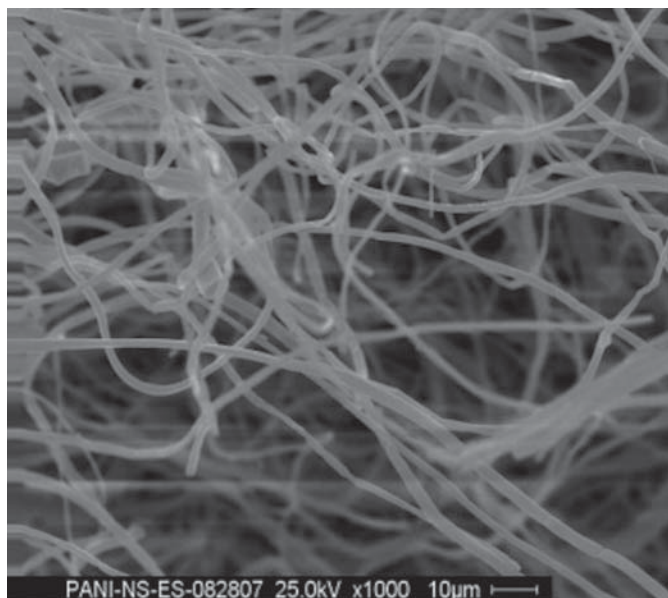


Figure 21 Surface morphology of electrospun polyaniline nanofiber as obtained from scanning electron microscopy (SEM).

and modified fullerenes¹²¹ with the tunable redox behavior of the conducting polymer potentially offers enhanced performance as a hydrogen storage system.

High Surface Area Sorbents and New Materials Concepts

There is a pressing need for the discovery and development of new reversible materials. One new area that may be promising is that of high surface area hydrogen sorbents based on microporous metal–organic frameworks (MOFs). Such materials are synthetic, crystalline, and microporous and are composed of metal–oxide groups linked together by organic struts. Hydrogen storage capacity at 78 K (-195°C) has been reported as high as 4 wt % via an adsorptive mechanism, with a room temperature capacity of approximately 1 wt %.¹²² However, due to the highly porous nature of these materials, the volumetric capacity may still be a significant issue.

Another class of materials for hydrogen storage may be clathrates, which are primarily hydrogen-bonded H_2O frameworks.¹²³ Initial studies have indicated that significant amounts of hydrogen molecules can be incorporated into the sII clathrate. Such materials may be particularly viable for off-board storage of hydrogen without the need for high-pressure or liquid-hydrogen tanks.

4 HYDROGEN UTILIZATION

Today, hydrogen is used primarily in ammonia production, petroleum refinement, and the synthesis of methanol. It is also used in the U.S. National Aeronautics and Space Administration's (NASA) space program as fuel for the space shuttles and in fuel cells that provide heat, electricity, and drinking water for the astronauts. Current thinking suggests that fuel cells are the way to use hydrogen and that the fuel cell industry is the driving force toward a hydrogen economy. This may be true, but it loses sight of other, less costly opportunities. Hydrogen can also be used in internal combustion engines (ICE), turbines, and gas boilers. In many parts of the world, the

gas that is used to fuel lights and furnaces is a hydrogen-rich mixture called *town gas*, mainly consisting of hydrogen and methane. In the very near future, hydrogen could be used to fuel vehicles and aircraft, and provide power for our homes and offices.¹²⁴ Hydrogen's potential use as a fuel and an energy carrier includes powering vehicles, running turbines or fuel cells to produce electricity, and cogenerating heat and electricity for buildings, among others.

4.1 Fuel Cells

Fuel cells are significantly more energy efficient than combustion-based power generation technologies. A conventional combustion-based power plant typically generates electricity at efficiencies of 33–35%, while fuel cell plants can generate electricity at efficiencies of up to 60%. When fuel cells are used to generate electricity and heat (cogeneration), they can reach efficiencies of up to 85%. Internal combustion engines in today's automobiles convert less than 30% of the energy in gasoline into power that moves the vehicle. Vehicles using electric motors powered by hydrogen fuel cells are much more energy efficient, utilizing 40–60% of the fuel's energy. Even fuel cell vehicles that reform hydrogen from gasoline can use about 40% of the energy in the fuel.¹²⁵

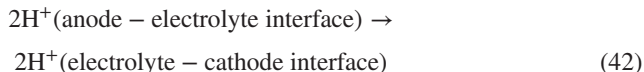
A fuel cell can be thought of as an *electrochemical combustor*. Hydrogen is oxidized, some heat is released, and, as in any chemical reaction, electrons change hands (i.e., chemical bonds are broken). However, in a fuel cell, the fuel and oxidant react separately in different regions that are connected to each other by two different conduits for charged particles. This consists of a catalytically activated electrode for the fuel (anode) and the oxidant (cathode), and an electrolyte to conduct ions between the two electrodes. The exchange of electrons among the reagents occurs through an electrical circuit outside the cell. The fuel cell converts chemical potential energy to usable electrical energy in the form of moving electrons. For electrons to journey through the external circuit, they must overcome any electrical barriers, such as impedance, to their transmission in order to do electrical work. Electrochemical reactions for use in fuel cells are purposely chosen so that the amount of electrical work attainable is sufficient to overcome the resistance of electron flow inherent in any circuit, but also to allow the electron flow to carry out useful electrical tasks. The second conduit for charged particles is inside the cell and is called an *electrolyte*. This can be an aqueous or other solution, a solid polymer, or an ion-conducting ceramic. The electrolyte allows particles much more massive than electrons, such as H^+ or OH^- , respectively, for acidic and basic electrolytes or O^{2-} in the case of solid oxide ceramics to pass between the two electrodes. Figure 22 shows an illustration of an acidic electrolyte fuel cell in which H_2 is converted to electricity using O_2 as the oxidant.

This cell requires four chemical and physical processes in order to operate:

1. Oxidation of the fuel, gaseous $H_{2(g)}$, at a region of the anode in interfacial contact with the electrolyte:



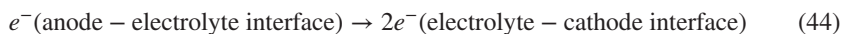
2. Physical transport of H^+ from the anode through the electrolyte to the cathode:



3. Reduction of gaseous O_2 , the oxidant, at a region of the cathode in interfacial contact with the electrolyte:



4. Physical transport of electrons from the anode to the cathode through the external circuit:



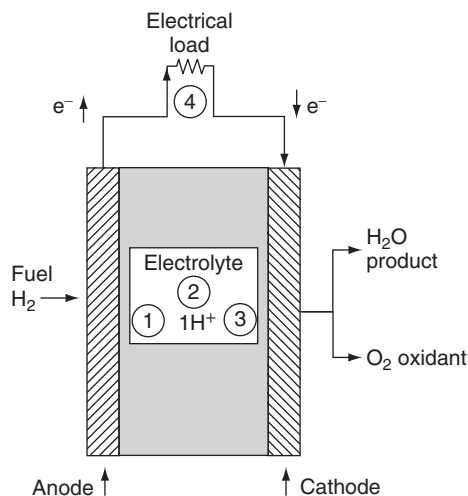


Figure 22 Schematic of an acidic electrolyte hydrogen–oxygen fuel cell illustrating the numbered processes as outlined in the text.

Summarizing Eqs. (38)–(41) one obtains the same overall reaction as direct combustion of hydrogen:



However, through the use of the fuel cell, electricity is generated directly. Fuel cells now command great interest as clean energy converters for use in producing electricity for consumers and as the energy source for electric vehicles. This interest is motivated by the potential for high fuel-to-electricity conversion efficiencies and that fuel cells run with hydrogen emit only water and waste heat. Since fuel cells operate at lower than typical combustion processes, NO_x emissions are eliminated. Fuel cells are also attractive because of their potential for low maintenance, high reliability, and low noise levels.

Table 6 summarizes several common types of fuel cells under development for stationary electric power systems and vehicle propulsion applications, together with estimates of their fuel-to-electricity conversion efficiencies, assuming that H_2 is the fuel.¹²⁶ The ion flowing through the electrolyte may be H^+ or any of several negatively charged species (anions), such as OH^- , CO_3^{2-} , or O^{2-} (the anions flow from the cathode to the anode). Advanced electrolyte systems such as proton-conducting inorganic oxides (i.e., ceramics) may enable fuel-to-electricity efficiencies as high as 70% based on H_2 and its low heat value. Because each fuel cell unit generates approximately 1 V, fuel cell systems are composed of stacks of individual fuel cells that are interconnected to produce the desired voltage and power densities for specific application.

Although larger fuel cells (greater than 200 kw) are being commercialized for on-site cogeneration of electricity and steam heat, fuel cells for transportation are in much earlier stages of development. Fuel cells are currently too large, too heavy, and too expensive to produce for a commercial application in powering vehicles. With the resolution of these problems, however, hydrogen-powered fuel cell vehicles will be pollution free and about three times as energy efficient as comparable gasoline-fueled vehicles. There are several configurations of fuel cells, classified by the type of electrolyte used. The most mature technology for near-term use in large vehicles is the phosphoric acid fuel cell. The proton-exchange membrane fuel cell is a prime candidate for midterm use in several areas, including automobiles. Solid oxide fuel cells are being developed for longer term utility applications.¹²⁷ Descriptions of the most common fuel cells from Table 6 are presented below.

Table 6 Summary of Several Common Fuel Cell Technologies

Fuel Cell	Anode Reaction	Electrolyte	Transfer ion ^a	Cathode Reaction	Operating Temp. (°C)	Conditions Pressure (atm)	H ₂ -to-Electrical Efficiency, %
Proton exchange membrane (PEM) ^b	$H_2 \rightarrow 2H^+ + 2e^-$	Solid polymer	H ⁺	$2H^+ + \frac{1}{2}O_2 + 2e^- \rightarrow H_2O$	80–100	1–8 ^c	36–38
Phosphoric acid (PAFC)	$H_2 \rightarrow 2OH^- + 2H_2O + 2e^-$	Phosphoric acid	H ⁺	$2H^+ + \frac{1}{2}O_2 + 2e^-$	150–250	1–8 ^c	40
Alkaline (AFC)	$H_2 \rightarrow 2H^+ + 2e^-$	Aqueous base	OH ⁻	$H_2O + \frac{1}{2}O_2 + 2e^- \rightarrow 2OH^-$	80–250	1–10 ^c	50 to >60
Molten carbonate (MCFC)	$H_2 + CO_3^{2-} \rightarrow H_2O + CO_2 + 2e^-$	Molten salt (metal Carbonate)	CO ₃ ²⁻	$CO_2 + \frac{1}{2}O_2 + 2e^- \rightarrow CO_3^{2-}$	600–700	1–10	50–55
Solid oxide (SOFC)	$H_2 + O^{2-} \rightarrow H_2O + 2e^-$	Solid ceramic oxide	O ²⁻	$2H^+ + \frac{1}{2}O_2 + 2e^- \rightarrow H_2O$	800–1000	1	50–55

Source: Adapted from Ref. 114.

^aPositively charged ions (cations) travel through the electrolyte from the anode to the cathode; negatively charged ions (anions) transverse the electrolyte in the opposite direction.

^bAlso called polymer electrolyte fuel cell.

^cPressure must be sufficiently high to prevent boiling of water in PEM or aqueous electrolytes in PAFCs and AFCs.

Phosphoric Acid Fuel Cells

A phosphoric acid fuel cell (PAFC) consists of an anode and a cathode made of finely dispersed platinum catalyst on carbon paper and a silicon carbide matrix that holds the phosphoric acid electrolyte. PAFCs produce a cell voltage of 0.66 V at atmospheric pressure and 200°C and a current density of 240 mA/cm². Overall fuel-to-electricity energy conversion efficiency is about 40%. PAFCs are the most advanced of the fuel cell designs and are being commercialized for stationary power applications and for demonstrations in larger fleet vehicles, such as buses. The power density of a PAFC is too low for use in an automobile, however, and it cannot generate power at room temperature. Because of these limitations, the optimum use of PAFCs is in steady-state operating modes. Researchers are studying other fuel cell alternatives for vehicle applications.

Proton Exchange Membrane Fuel Cells

The proton exchange membrane (PEM) fuel cell uses a fluorocarbon ion exchange with a polymeric membrane as the electrolyte. The hydrogen proton migrates across the membrane, and water is evolved at the cathode. The PEM operates at a relatively low temperature of about 80°C and can start up from ambient temperature at partial load. These characteristics, plus its high-power density, make the PEM cell more adaptable to automobile use than the PAFC. Current densities of up to 4 A/cm² have been reported for single PEM cells. An assembly of PEM cells has not been able to achieve this level because at high current densities localized overheating limits the attainable density to about 1 A/cm². As research overcomes this problem, higher current densities will allow the weight and volume of a PEM fuel cell to be more practical for vehicle use.

Solid Electrolyte Fuel Cells

Solid oxide fuel cells (SOFC) currently under development use a thin layer of zirconium oxide as a solid electrolyte, a lanthanum manganite cathode, and a nickel–zirconia anode. When heated to about 1000°C, the oxide becomes a suitable conductor of oxygen ions but not electrons. A tubular arrangement of the cathode, anode, and electrolyte is the most advanced of the SOFC designs; 20-kw demonstration units have been installed in Japanese utilities. A planar configuration consists of alternating flat plates of a trilayer containing an anode, an electrolyte, and a cathode. A monolithic configuration adds a layer of anode and cathode material corrugated on either side of the trilayers to form flow channels for the fuel and airstreams. Planar SOFCs are easier to fabricate than the monolithic configuration, which is co-sintered into a solid, ceramic structure, but monolithic configurations have the highest power density of the designs. All SOFC designs have fewer components and ultimately may need less maintenance and be less expensive than other fuel cell types.

Fuel cells are but one of many opportunities for hydrogen energy utilization. As described next, internal combustion engines and hydrogen burners are relatively low-cost hydrogen utilization technologies.

4.2 Internal Combustion Engines

Hydrogen use in an internal combustion (IC) engine was demonstrated more than 100 years ago. Hydrogen-fueled IC engines offer the potential of no carbon and very low nitrogen oxide emissions, combined with high thermal efficiency. To be competitive and cost effective, however, key problems must be solved in engine combustion, fuel delivery, and practical storage. The primary research goal is to develop an optimized hydrogen IC engine with about 80 miles

per gallon (mpg) equivalent performance in an ultra-low emission vehicle. Fuel efficiencies of 80–90 (mpg) energy equivalent have been realized in simulations using a hybrid hydrogen electric vehicle. The research challenge is to achieve high efficiency and low emissions while overcoming the problems of preignition and flashback that have been common with hydrogen fuel in the past. *Flashback* is the improperly timed explosion of the fuel and air mixture that occurs when the exhaust valve of the IC engine is open. This risk is more significant with hydrogen fuel than hydrocarbon fuels because hydrogen's flame speed is 2–10 times greater than that of hydrocarbons. Two key areas of investigation are the fuel delivery system and the ignition system. In a carburetion system, premixing creates a lean, homogeneous charge that keeps nitrogen oxide emissions low. A fuel-injected system better prevents preignition of the fuel–air mixture and flashback. These engines can be used for both transportation and stationary power applications. Researchers are studying direct power from an IC engine fueled by hydrogen or mixed fuels (such as hydrogen–methane) and hybrid power systems, where an IC engine operating at a single speed and load runs an electric motor.

Research is also focused on reducing nitrogen oxide emissions in fuel-injection systems by diluting the intake air charge in a direct-injection IC engine. Dilution can be accomplished by recirculating exhaust gases or by scavenging. These techniques work by reducing the flame temperature and oxygen availability of the hydrogen/oxidizer mixture. This subsequently reduces the formation of nitrogen oxides, which is highly sensitive to temperature. It is anticipated that hydrogen ICEs will provide a high-volume usage of hydrogen prior to the low-cost mass production of fuel cells for transportation. In this light, the use of hydrogen or hydrogen–methane mixtures in ICEs could result in an acceleration of hydrogen demand into the nearer term economy, particularly in terms of hydrogen production and delivery. Several programs are currently underway to define baseline emissions and operational ranges for hydrogen and hydrogen–methane mixtures. Examples of these types of programs are studies being conducted by the U.S. National Energy Technology Laboratory's (NETL) Office of Science and Engineering Research (OSER) on lubricant life in hydrogen ICEs, injector performance, and ignition systems.¹²⁸

4.3 Hydrogen Burner Turbines

Research is focusing on the development of a safe and environmentally benign hydrogen burner that can generate electricity for utilities and provide heat to industry and homes. Burning hydrogen eliminates most emissions that come from carbon-based fuels, including carbon dioxide and carbon monoxide. The burning of any fuel in air, however, produces some amount of nitrogen oxides, and burner research is focusing on eliminating these emissions from hydrogen combustion. One way to do this is to remove nitrogen from the fuel mix completely, by burning pure hydrogen and pure oxygen derived directly from the electrolysis process. This is an expensive alternative, however, and researchers are looking at more cost-effective methods. Nitrogen oxide emissions can be minimized by reducing the peak combustion temperature and the time spent at the peak temperature. Typical thermal efforts reduce the peak temperature by recirculating cooler inert gases through the combustion process or injecting steam. Nitrogen oxides can also be reduced to essentially zero by premixing the fuel and oxidizer to reduce the amount of fuel in proportion to the oxidizer—a *lean* mixture. A sufficiently lean mixture can reduce the combustion temperatures to 1400–1500°C, although it can also increase the occurrence of flashback. Researchers are investigating the combustion fluid dynamics required to completely oxidize hydrocarbon and hydrogen fuels. Because the momentum flux of the oxidizer (air) is the primary variable in resolving these problems, an improved hydrogen burner will also work efficiently with natural gas and liquid petroleum gas. This flexibility should accelerate the utilization of hydrogen by facilitating the use of hybrid fuels.¹²⁹

5 HYDROGEN SAFETY

Hydrogen has been safely used for a long time in industrial and aerospace applications. Through this experience, a great deal of relevant knowledge exists. However, in the preliminary stages of a hydrogen economy, great care must be taken to assure a high degree of safety in all hydrogen applications because a loss in public confidence could have a significant impact on future developments.

5.1 The Nature of Hydrogen

Hydrogen is less flammable than gasoline. The self-ignition temperature of hydrogen is 585°C. The self-ignition temperature of gasoline varies from 228 to 501°C, depending on the grade (Table 7). Hydrogen disperses quickly and, being the lightest element (15 times lighter than air), it rises and spreads out quickly in the atmosphere. So when a leak occurs, the hydrogen gas quickly becomes so sparse that it cannot burn. Even when ignited, hydrogen burns upward, and is quickly consumed. By contrast, materials such as gasoline or natural gas are heavier than air, and will not disperse, remaining a flammable threat for a longer period of time. Hydrogen is a nontoxic, naturally occurring element in the atmosphere. By contrast, all fossil fuels are poisonous to humans. Hydrogen combustion produces only water. Compared with the toxic compounds (carbon monoxide, nitrogen oxides, and hydrogen sulfide) produced by petroleum fuels, the products of hydrogen burning are much safer. Hydrogen can be stored safely in gaseous, liquid, or solid state form (see hydrogen storage section). Tanks currently in use for storage of compressed hydrogen (similar to compressed natural gas tanks) have survived intact through testing by various means, such as bullets, fires, and shocks.¹³⁰

Other properties of hydrogen necessitate special considerations when handling. Hydrogen consists of small molecules, which require special qualities in materials used in storage and transportation. Hydrogen creates flammable and explosive mixtures of air over a broad spectrum (Table 7).¹³¹ These mixtures need very little energy to ignite. Ventilation is therefore an important factor in areas where hydrogen is used.

5.2 How to Handle Hydrogen

The wide flammability ranges of hydrogen imply that a mixture of hydrogen and air might ignite more easily than other fuels. Consequently, the following precautions must be adhered to:

- Hydrogen should not be mixed with air.
- Contact of hydrogen with potential ignition sources should be prevented.

Table 7 Summary of Safety Statistics for Hydrogen and Other Fuels

Characteristic	Hydrogen	Natural Gas	Gasoline
Lower heating value (kJ/g)	120	50	44.5
Self-ignition temperature (°C)	585	540	228–501
Flame temperature (°C)	2045	1875	2200
Flammability limits in air (vol %)	4–75	5.3–15	1.0–7.6
Minimum ignition energy in air (μJ)	20	290	240
Detonability limits in air (vol %)	18–59	6.3–13.5	1.1–3.3
Theoretical explosive energy (kg TNT/m ³ gas)	2.02	7.03	44.22
Diffusion coefficient in air (cm ² /s)	0.61	0.16	0.05

Source: Adapted from Ref. 118.

- Purging hydrogen systems should be performed with an inert gas such as nitrogen.
- Venting hydrogen should be done according to standards and regulation.
- Because the hydrogen flame is invisible, special flame detectors are required.

Hydrogen should be handled with special care in confined, unvented areas. Various safety assessments (safety codes and standards) are available or under development to serve as a guide in setting up and designing hydrogen systems.¹³²

Codes and Standards

The subject of codes and standards is covered in a different section of this handbook. However, it is important to note that the Hydrogen, Fuel Cells, and Infrastructure Technologies (HFCIT) Program of the U.S. DOE and the National Renewable Energy Laboratory (NREL) are developing hydrogen codes and standards to expedite the future construction of a hydrogen infrastructure. HFCIT has developed a Web-based bibliographic database that is intended to provide easy public access to a wide range of hydrogen safety aspects. The database includes references related to the following topics¹³³:

- Hydrogen properties and behavior
- Safe operating and handling procedures
- Leaks, dispersion, and flammable vapor cloud formation
- Embrittlement and other effects on material properties
- Fuel cells and other energy conversion technologies
- Sensors, tracers, and leak detection technologies
- Accidents and incidents involving hydrogen

Also, the National Fire Protection Association (NFPA) has incorporated hydrogen safety requirements in its family of codes and standards.¹³⁴ In Europe, a HySafe Network of Excellence for Hydrogen Safety has been formed. The network is composed of 24 partners from 12 European countries and Canada, representing private industries, universities, and research institutions.¹³⁵ The website www.hysafe.net offers a wealth of information on hydrogen safety. The New Energy and Industrial Technology Development Organization (NEDO) in Japan is pursuing a large number of projects on the safety of hydrogen infrastructure and building frames in case of hydrogen explosion and earthquakes.^{136–138}

Other organizations are also involved in new standards activities. The National Hydrogen Association (NHA) has created Codes and Standards Working Groups on topics such as hydride storage, electrolyzers for home use, transportation infrastructure issues, and maritime applications. The Society of Automotive Engineers, through a Fuel Cell Standards Forum Safety Task Force, is collaborating with NHA on the transportation issues. The International Organization for Standardization (ISO) level in ISO Technical Committee 197 (Hydrogen Technologies) is actively pursuing the development of codes and standards with input from national organizations.¹³⁹

6 CONCLUSIONS

Fossil fuels, electricity, biomass, and sunlight are four potential resources to use in H₂ production. So far, hydrogen has been produced principally from methane (a depleting energy resource) using steam reforming. Although several possibilities exist for hydrogen production, solar-based hydrogen would be desirable. Further, hydrogen represents a good storage medium of solar energy. Producing hydrogen from water using solar energy appears to be an attractive

step toward this approach. However, relatively few water-based solar hydrogen-producing systems are currently available: thermochemical cycle, photoelectrochemical system, photochemical process, and solar-assisted electrolysis.

Even though thermochemical systems have high theoretical limits, they exhibit problems with materials and separation at high temperatures. Photochemical and photoelectrochemical systems are currently at a very early stage of development. The difficulties that still need to be addressed with photoelectrochemical systems are semiconductor stability, efficient light absorption, and interfacial kinetics. Currently, biophotolysis processes demonstrate very low solar conversion efficiencies, and they can be sustained only for short periods of time. Among the various hydrogen production methods, water electrolysis is the only developed nonpolluting technology. Electrolysis efficiency of 85–95% is currently possible.

Hydrogen storage is essential, especially for the on-board vehicular applications that lead to a hydrogen-based economy. Various hydrogen storage methods have been presented in this chapter with respect to their physical and chemical phenomena. Currently, none of the storage methods are mature enough to address all the technological barriers and targets of the U.S. DOE's FreedomCAR goals and require additional basic and applied research.

Some technologies are currently available for the practical and cost-effective utilization of hydrogen as an energy carrier. Additional technologies need to be developed as hydrogen production, transport, and storage capabilities become integrated into the energy economy.

Clean energy and a healthy environment are the concerns of everyone. Aggressive improvement in energy efficiency, along with well-thought-out and executed transitional strategies, are essential to enable the growth of hydrogen utilization and the development of technologies, markets, and infrastructure to support a green hydrogen economy.

REFERENCES

1. R. M. Zweig, "Pollution Solution/Revisited," *Int. J. Hydrogen Energy*,
2. J. O. M. Bockris, T. N. Veziroglu, and D. Smith, *Solar Hydrogen Energy: The Power to Save the Earth*, Macdonald Optima, London, 1991.
3. S. Dunn, "Hydrogen Futures: Toward a Sustainable Energy System," *Int. J. Hydrogen Energy*, **27**, 235–264, 2002.
4. S. A. Sherif, F. Barbir, T. N. Veziroglu, M. Mahishi, and S. S. Srinivasan, in *Hydrogen Energy Technologies*, Y. Goswami (Ed.), CRC Handbook of Hydrogen Energy Technologies, Boca Raton, FL, 2006.
5. J. M. Ogden, "Hydrogen: The Fuel of the Future?" *Phys. Today*, **55**(4), 69–75, 2002.
6. U.S. DOE, Hydrogen Program, 2006; available: <http://www.hydrogen.energy.gov>.
7. U.S. DOE Hydrogen Program website, 2006, available: <http://www.hydrogen.energy.gov>.
8. S. A. Sherif, F. Barbir, and T. N. Veziroglu, "Principles of Hydrogen Energy Production, Storage and Utilization," *J. Sci. Ind. Res.*, **62**, 46–63, January–February, 2003.
9. A. Raissi, "Technoeconomic Analysis of Area II Hydrogen Production—Part 1," Proceedings of the 2001 U.S. DOE Hydrogen Program Review, NREL/CP/570-30535, 2006.
10. R. Minet and K. Desai, "Cost-Effective Methods for Hydrogen Production," *Int. J. Hydrogen Energy*, **8**, 285–290, 1983.
11. S. Sherif, T. N. Veziroglu, and F. Barbir, "Hydrogen Energy Systems," in J. G. Webster (Ed.), *Wiley Encyclopedia of Electrical and Electronics Engineering*, vol. 9, Wiley, New York, 1999, pp. 370–402.
12. B. Gaudernack and Lynum, S. "Hydrogen from Natural Gas without Release of CO₂ to the Atmosphere," Proceedings of the 11th World Hydrogen Energy Conference: Hydrogen Energy Progress, Germany, pp. 511–523, 1996.
13. D. W. Kirk and A. E. Ledas, "Precipitate Formation during Sea-Water Electrolysis," *Int. J. Hydrogen Energy*, **7**, 925–932, 1982.
14. L. Basye and S. Swaminathan, "Hydrogen Production Costs—A Survey," U.S. Department of Energy, DOE/GO/10170-T18, 1997.

15. H. Audus, O. Kaarstad, and M. Kowal. "Decarbonization of Fossil Fuels: Hydrogen as an Energy Carrier," Proceedings of the 11th World Hydrogen Energy Conference: Hydrogen Energy Progress, **1**, 525–534, 1996.
16. C. E. G. Padro and V. Putsche, "Survey of the Economics of Hydrogen Technologies," National Renewable Energy Laboratory, NREL/TP-570-27079, 1999.
17. S. Leiby, "Options for Refinery Hydrogen," Private report by The Process Economics Program, Report No. 212, SRI International, Menlo Park, CA, 1994.
18. <http://www.fossil.energy.gov/programs/powersystems/gasification/howgasificationworks.html>.
19. T. N. Veziroglu, "Hydrogen Technology for Energy Needs of Human Settlements," *Int. J. Hydrogen Energy*, **12**(2), 99–129, 1987.
20. S. Turn, C. Kinoshita, Z. Zhang, D. Ishimura, and J. Zhou, "An Experimental Investigation of Hydrogen Production from Biomass Gasification," *Int. J. Hydrogen Energy*, **23**(8), 641–648, 1998.
21. P. L. Spath, M. K. Mann, and W. A. Amos, "Update of Hydrogen from Biomass: Determination of the Delivered Cost of Hydrogen," NREL/MP-510-33112, 2000.
22. D. Dayton, "A Review of the Literature on Catalytic Biomass Tar Destruction: Milestone Completion Report," NREL/TP-510-32815, December 2002.
23. L. Devi, K. J. Ptasinski, and F. J. J. G. Janssen, "A Review of the Primary Measures for Tar Elimination in Biomass Gasification Process," *Biomass Bioenergy*, **24**, 125–140, 2003.
24. M. K. Mann, "Technical and Economic Analysis of Hydrogen Production via Indirectly Heated Gasification and Pyrolysis," Proceedings of the 1995 USDOE Hydrogen Program Review, NREL/CP-430-20036, **1**, 205–236, 1995.
25. T. A. Milne, C. C. Elam, and R. J. Evans, "Hydrogen from Biomass: State of the Art and Research Challenges," NREL IEA/H2/TR-02/001, 2001.
26. H. Wendt, *Electrochemical Hydrogen Technologies: Electrochemical Production and Combustion of Hydrogen*, Elsevier, New York, 1990.
27. S. M. El-Haggar and M. Khalil, "Parametric Study of Solar Hydrogen Production from Saline Water Electrolysis," *Int. J. Environ. Poll.*, **8**, 164–173, 1997.
28. S. Zhuiykov, "Research on Proton-Conducting Materials in the Hydrogen Partial Pressure Sensors," *Herald Kiev Polytech. Inst. Instrum.*, **19**, 7–9, 1989.
29. M. S. Casper, *Hydrogen Manufacture by Electrolysis, Thermal Decomposition and Unusual Techniques*, Noyes Data Corporation, New Jersey, 1978.
30. A. Weidenkaff, A. Reller, A. Wokaun, and A. Steinfeld, "Thermogravimetric Analysis of the ZnO/Zn Water Splitting Cycle," *Thermochim. Acta*, **359**, 69–75, 2000.
31. M. Sakurai, E. Bilgen, A. Tsutsumi, and Yoshida, K. "Adiabatic UT-3 Thermochemical Process for Hydrogen Production," *Int. J. Hydrogen Energy*, **21**, 865–870, 1996.
32. T. Nakayama, H. Yoshioka, H. Furutani, H. Kameyama, and K. Yoshida, "Mascot—A Bench Scale Plant for Producing Hydrogen by the UT-3 Thermochemical Decomposition Cycle," *Int. J. Hydrogen Energy*, **9**, 187–190, 1984.
33. M. Sakurai, N. Miyake, A. Tsutsumi, and Yoshida, K. "Analysis of a Reaction Mechanism in the UT-3 Thermochemical Hydrogen Production Cycle," *Int. J. Hydrogen Energy*, **21**, 871–875, 1996.
34. R. Amir, S. Shizaki, K. Tamamoto, T. Kabe, and H. Kameyama, "Design Development of Iron Solid Reactants in the UT-3 Water Decomposition Cycle Based on Ceramic Support Materials," *Int. J. Hydrogen Energy*, **18**, 283–286, 1993.
35. M. Sakurai, M. Aihara, N. Miyake, A. Tsutsumi, and K. Yoshida, "Test of One-Loop Flow Scheme for the UT-3 Thermochemical Hydrogen Production Process," *Int. J. Hydrogen Energy*, **17**, 587–592, 1992.
36. M. Sakurai, H. Nakajima, K. Onuki, K. Ikenoya, and S. Shimizu, "Preliminary Process Analysis for the Closed Cycle Operation of the Iodine-Sulfur Thermochemical Hydrogen Production Process," *Int. J. Hydrogen Energy*, **24**, 603–612, 1999.
37. K. R. Schulz, L. C. Brown, and C. J. Hamilton, "Production of Hydrogen by Nuclear Energy: The Enabling Technology for the Hydrogen Economy," American Nuclear Energy Symposium, Miami, Florida, October 16–18, 2002.
38. T. Bak, J. Nowotny, M. Rekas, and C. C. Sorrell, "Photo-Electrochemical Hydrogen Generation from Water Using Solar Energy. Materials-Related Aspects," *Int. J. Hydrogen Energy*, **27**, 991–1022, 2002.

39. J. R. Bolton, S. J. Strickler, and J. S. Connolly, "Limiting and Realizable Efficiencies of Solar Photolysis of Water," *Nature*, **316**, 495–500.
40. Argonne National Laboratory, Report of the Basic Energy Science Workshop on Hydrogen Production, Storage and Use, Rockville, MAD, May 13–15, 2003.
41. C. Read, J. Petrovic, G. Ordaz, and S. Satyapal, "The DOE National Hydrogen Storage Project: Recent Progress," Proceedings of the On-Board Vehicular Hydrogen Storage, Materials Research Symposium, 885E, A05–1.1, 2006.
42. W. Grochala and P. P. Edwards, "Thermal Decomposition of the Non-Interstitial Hydrides for the Storage and Production of Hydrogen," *Chem. Rev.*, **104**, 1283–1315, 2004.
43. F. E. Pinkerton and B. G. Wicke, "Bottling the Hydrogen Genie," *Ind. Phys.*, Feb./March, 20–25, 2004.
44. L. Schlapbach, and A. Zuttel, "Hydrogen-Storage Materials for Mobile Applications," *Nature*, **414**(15), 353, Nov. 2001.
45. A. K. Shukla, "Fuelling Future Cars," *J. Indian Inst. Sci.*, **85**, 51–65, March–April, 2005.
46. A. Zuttel, "Hydrogen Storage Methods," *Naturwissenschaften*, **91**, 157–172, 2004.
47. U.S. DOE Energy Efficiency and Renewable Energy (EERE), "Hydrogen and Fuel Cells", 2006, available: [http://www.eere.energy.gov/hydrogenandfuelcells/storage/doe rd.html](http://www.eere.energy.gov/hydrogenandfuelcells/storage/doe_rd.html).
48. U.S. Department of Energy Office of Energy Efficiency and Renewable Energy and The Freedom-CAR and Fuel Partnership, "Targets for Onboard Hydrogen Storage Systems for Light-Duty Vehicles," 2009.
49. D. Chandra, J. J. Reilly, and R. Chellappa. "Metal Hydrides for Vehicular Applications: The State of the Art," *J. Mat.*, February 26–32, 2006.
50. M. Fichtner, "Nanotechnological Aspects in Materials for Hydrogen Storage," *Adv. Eng. Mat.*, **7**(6), 443–455, 2005.
51. M. V. C. Sastry, B. Viswanathan, and S. Srinivasan Murthy, *Metal Hydrides, Fundamentals and Applications*, Springer, Narosa Publishing, Berlin, 1998.
52. L. Zhou, "Progress and Problems in the Hydrogen Storage Methods," *Renew. Sustain. Energy Rev.*, **9**, 395–408, 2005.
53. U.S. DOE Energy Efficiency and Renewable Energy (EERE), "Hydrogen and Fuel Cells," 2006, available: [http://www.eere.energy.gov/hydrogenandfuelcells/posture plan04.html](http://www.eere.energy.gov/hydrogenandfuelcells/posture_plan04.html).
54. J. Ko, K. Newell, B. Geving, and W. Dubno, U.S. DOE Hydrogen Program, FY 2005 Progress Report, accessed 2005, available: [http://www.hydrogen.energy.gov/pdfs/progress05/vi e 1 ko.pdf](http://www.hydrogen.energy.gov/pdfs/progress05/vi_e_1_ko.pdf).
55. M. Lordgooei, S. A. Sherif, and T. N. Veziroglu, "Analysis of Liquid Hydrogen Boil-Off Losses," *Energy Environ. Prog.*, **1**, D 241–266, 1991.
56. Y. Fukai, *The Metal-Hydrogen System, Basic Bulk Properties*, Springer, Berlin, Heidelberg, 1993.
57. G. G. Libowitz and A. J. Maeland, "Hydrides of Rare Earths," in K. A. J. Gschneidner and L. Eyring (Eds.), *Handbook on the Physics and Chemistry of Rare Earths*, North Holland, Amsterdam, 1979.
58. W. M. Muller, J. P. Blackledge, and G. G. Libowitz, *Metal Hydrides*, Academic, New York, 1968.
59. K. J. Gross, *Intermetallic Materials for Hydrogen Storage*, Ph.D. Thesis, University of Fribourg, Fribourg, Switzerland, 1998.
60. S. S. S. Raman, *Synthesis and Characterization of Some Mg Bearing Hydrogen Storage (Hydride) Materials*, Ph.D. Thesis, Banaras Hindu University, Varanasi, India, 2006.
61. J. J. Reilly, *Metal Hydrides as Hydrogen Storage and Their Applications*, CRC Press, Cleveland, OH, pp. 2, 13, 1977.
62. G. D. Sandroch, "The Metallurgy and Production of Rechargeable Hydrides," in A. F. Anderson and A. J. Maeland (Eds.), *Hydrides for Energy Storage*, Pergamon, Oxford, p. 353, 1978.
63. L. Schlapbach, A. Seiler, F. Stucki, and H. C. Siegman, "Surface Effects and the Formation of Metal Hydrides," *J. Less Common Metals*, **T3**, 145, 1980.
64. B. L. Shaw, *Inorganic Hydrides*, Pergamon, United Kingdom, 1967.
65. R. Griessen, and T. Rieusterer, "Hydrogen in Intermetallic Compounds," in I. L. Schlapbach (Ed.), *Hydrogen in Intermetallic Compounds*, New York, Springer Verlag, p. 219, 1988.
66. J. J. Reilly, and R. H. Wiswall, Jr., "Formation and Properties of Iron Titanium Hydride," *Inorg. Chem.*, **13**, 218, 1974.

67. J. H. N. Van Vucht, F. A. Kuijpers, and H. C. A. M. Burning, "AB₅ Intermetallic Hydrides," *Philips Res. Rep.*, pp. 133, 1970.
68. J. J. Reilly and R. H. Wiswall, Jr., "Reaction of Hydrogen with Alloys of Magnesium and Nickel and the Formation of Mg₂NiH₄," *Inorg. Chem.*, **7**, 225, 1968.
69. P. Selvam, "Energy and Environment—An All Time Research," *Int. J. Hydrogen Energy*, **16**(1), 35–45, 1991.
70. S. S. S. Raman and O. N. Srivastava, "Hydrogenation Behavior of the New Composite Storage Materials, Mg-Xwt.% CFMmNi₅," *J. Alloys Comp.*, **241**, 167–174, 1996.
71. A. Zuttel, P. Wenger, S. Rentsch, P. Sudan, P. Mauron, and C. Emmenegger, "LiBH₄: A New Hydrogen Storage Material," *J. Power Sources*, **118**(1–2), 1–7, 2003.
72. J. J. Didisheim, P. Zolliker, K. Yvon, P. Fischer, J. Schefer, M. Gubelmann, and A. Williams, "Dimagnesium Iron (II) Hydride Mg₂FeH₆ Containing Octohedral [FeH₆]₄– Anions," *Inorg. Chem.*, **23**(13), 1953–1957, 1984.
73. L. Schlapbach, I. Anderson, and J. P. Burger, "Heats of Formations of Metal Hydrides," in K. H. J. Buschow (Ed.), *Material Sci. Techn.*, VCH Mbh Publishing, York, UK, p. 63, 1988.
74. G. Sandrock, "A Panoramic Overview of Hydrogen Storage Alloys from a Gas Reaction Point of View," *J. Alloys Comp.*, **877**, 293–295, 1999.
75. B. Bogdanovic and M. Shwickardi, "Ti-Doped Alkali Metal Aluminum Hydrides as Potential Novel Reversible Hydrogen Storage Materials," *J. Alloys Comp.*, **1**, 253–254, 1997.
76. F. Schuth, B. Bogdanovic, and M. Felderhoff, "Light Metal Hydrides and Complex Hydrides for Hydrogen Storage," *Chem. Commun.*, **20**, 2249–2258, 2004.
77. Sandia National Laboratory Hydpark, accessed 2006, available: <http://hydpark.ca.sandia.gov>.
78. C. M. Jensen and R. A. Zidan, "Sodium Alanates for Reversible Hydrogen Storage," Proceedings of the 1998 U.S. Hydrogen Program Review, Alexandria, VA, p. 449, 1998.
79. C. M. Jensen and K. J. Gross, "Development of Catalytically Enhanced Sodium Aluminum Hydride as a Hydrogen-Storage Material," *Appl. Phys. A*, **72**, 213, 2001.
80. M. Fichtner, "Synthesis and Structure of Magnesium Alanates and Two Solven Adducts," *J. Alloys and Comp.*, **345**(1–2), 286–296, 2002.
81. E. M. Fedneva, V. L. Alpatova, and V. I. Mikheeva, "LiBH₄ Complex Hydride Materials," *Russian J. Inorg. Chem.*, **9**, 826, 1964.
82. P. Chen, Z. Xiong, J. Luo, J. Lin, and K. L. Tan. "Interaction of Hydrogen with Metal Nitrides and Imides," *Nature*, **420**(2), 302, 2002.
83. P. Chen, Z. Xiong, J. Luo, J. Lin, and K.L. Tan. "Interaction between Lithium Amide and Lithium Hydride," *J. Phys. Chem. B*, **107** 10967, 2003.
84. W. F. Luo, "LiNH₂-MgH₂: A Viable Hydrogen Storage System," *J. Alloys Comp.*, **381**, 284–287, 2004.
85. W. Grochala, and P. P. Edwards, "Thermal Decomposition of the Non-Interstitial Hydrides for the Storage and Production of Hydrogen," *Chem. Rev.*, **104** 1283, 2004
86. T. J. Marks, and J. R. Kolb, "Covalent Transition Metal, Lanthanide, and Actinide Tetrahydroborate Complexes," *Chem. Rev.*, **77** 263, 1977.
87. E. Jeon and Y. W. Cho, "Mechanochemical Synthesis and Thermal Decomposition of Zinc Borohydride," *J. Alloys Comp.*, **422** 273–275, 2006.
88. Stanford University Global Climate and Energy Project, 2003, available: [http://gcep.stanford.edu/pdfs/hydrogen workshop/wu.pdf](http://gcep.stanford.edu/pdfs/hydrogen%20workshop/wu.pdf). 2003.
89. U.S. DOE Energy Efficiency and Renewable Energy (EERE), Hydrogen and Fuel Cells, 2006, available: http://www1.eere.energy.gov/hydrogenandfuelcells/pdfs/review04/st_6_mccaine.pdf.
90. U.S. DOE Energy Efficiency and Renewable Energy (EERE), Hydrogen and Fuel Cells, 2006, available: http://www1.eere.energy.gov/hydrogenandfuelcells/pdfs/review04/st_p2_autrey_04.pdf.
91. B. Viswanathan, M. Sankaran, and M. A. Schibioh, "Carbon Nanomaterials: Are They Appropriate Candidates for Hydrogen Storage?" *Bull. Catalysis Soc. India*, **2**, 12, 2003.
92. M. G. Nijkamp, J. E. M. J. Raaymakers, A. J. Van Dillen, and K. P. De Jong, "Hydrogen Storage by Using Physisorption Materials Demand," *Appl. Phys. A* **72**, 619, 2001.
93. A. C. Dillon, K. M. Jones, T. A. Bekkedahl, C. H. Kiang, D. S. Bethune, and M. J. Heben, "Storage of Hydrogen in Single-Walled Carbon Nanotubes," *Nature (London)*, **386**(6623), 377–379, 1997.

94. P. M. F. J. Costa, K. S. Coleman, and Green, M. L. J. "Influence of Catalyst Metal Particles on the Hydrogen Sorption of Single-Wall Carbon Nanotube Materials," *Nanotechnology*, **16**, 512, 2005.
95. R. Mohtadi, K. Tange, G. Wicks, K. Heung, and, R. Schumacher, "A New Way for Storing Reactive Complex Hydrides on Board of Automobiles," *Ceramic Trans.*, **202**, 91–96, 2009.
96. Y. Kojima, Y. Kawai, A. Koiwai, N. Suzuki, T. Haga, T. Hioki, and K. Tange, "IR Characterizations of Lithium Imide and Amide," *J. Alloys Comp.*, **395**(1–2), 236–239, 2005.
97. J. Stejskal, "Polyaniline. Preparation of a Conducting Polymer (IUPAC Technical Report)," *Int. Union Pure Appl. Chem.*, **75**(5), 857, 2002.
98. A. G. MacDiarmid and A. J. Epstein, "A Novel Class of Conducting Polymers," *Faraday Discuss. Chem. Soc.*, **88**, 317, 1989.
99. J. Stejskal, P. Kratochvil, and A. D. Jenkins, "The Formation of Polyaniline and the Nature of Its Structures," *Polymer*, **37**(2), 367, 1996.
100. D. C. Trivedi, *Handbook of Organic Conductive Molecules and Polymers*, H. S. Nalwa (Ed.), Wiley, Chichester, vol. 2, p. 505, 1997.
101. J. Stejskal and R.G. Gilbert, "Preparation of a Conducting Polymer," *Pure App. Chem.*, **74**, 857, 2002.
102. S. Virji, R. B. Kaner, and B. H. Weiller, "Hydrogen Sensors Based on Conductivity Changes in Polyaniline Nanofibers," *J. Phys. Chem. B*, **110**(44), 22266, 2006.
103. F. Fusalba, P. Gouerec, D. Vellers, and D. J. Belanger, "Electrochemical Characterization of Polyaniline in Nonaqueous Electrolyte and Its Evaluation as Electrode Material for Electrochemical Supercapacitors," *Electrochem. Soc.*, **148**(1), A1–6, 2001.
104. K. Rossberg, G. Paasch, and L. J. Dunsch, "The Influence of Porosity and the Nature of the Charge Storage Capacitance on the Impedance Behaviour of Electropolymerized Polyaniline Films," *Electroanal. Chem.*, **443**(1), 49, 1998.
105. S. J. Cho, K. S. Song, J. W. Kim, T. H. Kim, and K. Choo, "Hydrogen Sorption in HCl Treated Polyaniline and polypyrrole, new potential hydrogen Storage Media," Preprints of Symposia — *American Chemical Society*, Division of Fuel Chemistry, **47**(2), 790, 2002.
106. B. Panella, L. Kossykh, U. Dettlaff-Weglikowska, M. Hrischer, G. Zerbi, and S. Roth, "Volumetric Measurement of Hydrogen Storage in HCl-Treated Polyaniline and Polypyrrole," *Synth. Metals*, **151**(3), 208, 2005.
107. N. B. McKeown, P. M. Budd, and D. Book. "Microporous Polymers as Potential Hydrogen Storage Materials," *Macromol. Rapid Commun.*, **28**(9), 995, 2007.
108. S. J. Cho, K. Choo, D. P. Kim, and J. W. Kim, "H₂ Sorption in HCl-Treated Polyaniline and Polypyrrole," *Catalysis Today*, **120**(3–4), 336, 2007.
109. M. U. Jurczyk, A. Kumar, S. Srinivasan, and E. Stefanakos, "Polyaniline-Based Nanocomposite Materials for Hydrogen Storage," *Int. J. Hydrogen Energy*, **32**(8), 1010, 2007.
110. J. Germain, J. M. J. Frechet, and F. J. Svec, "Hypercrosslinked Polyanilines with Nanoporous Structure and High Surface Area: Potential Adsorbents for Hydrogen Storage," *Mater. Chem.*, **17**(47), 4989, 2007.
111. A. Nikitin, X. Li, Z. Zhang, H. Ogasawara, H. Dai, and A. Nilsson, "Hydrogen Storage in Carbon Nanotubes through the Formation of Stable C–H Bonds," *Nano Lett.*, **8**(1), 162, 2008.
112. J. Y. Hwang, S. H. Lee, K. S. Sim and J. W. Kim, "Synthesis and Hydrogen Storage of Carbon Nanofibers," *Syn. Metals*, **126**(1), 81, 2002.
113. Y. Wang and X. J. Jing, "Synthesis and Hydrogen Storage of Carbon Nanofibers. *Synth. Metals*," *Phys. Chem. B*, **112**(4), 1157, 2008.
114. A. Z. Sadek, A. Trinchi, W. Wlodarski, K. Kalantar-zadeh, K. Galatsis, C. Baker, and R. B. Kaner, "A Room Temperature Polyaniline Nanofiber Hydrogen Gas Sensor," *IEEE Sensors*, **3**, 207, 2005.
115. A. A. Athawale and S. V. J. J. Bhagwat, "Synthesis and Characterization of Novel Copper/Polyaniline Nanocomposite and Application as a Catalyst in the Wacker Oxidation Reaction," *J. Appl. Polym. Sci.* **89**(9), 2412, 2003.
116. Y. Yang, J. Ouyang, L. Ma, R. J. Tseng, and C. W. Chu, "Electrical Switching and Bistability in Organic/Polymeric Thin Films and Memory Devices," *Adv. Funct. Mat.*, **16**(8), 1001, 2006.
117. A. Huczko, "Template-Based Synthesis of Nanomaterials," *Appl. Phys. A: Mat. Sci. & Process*, **70**(4), 365, 2000.

118. D. Zhang and Y. Wang, "Synthesis and Applications of One-dimensional Nanostructured Polyaniline: An Overview," *Mat. Sci. Eng. B*, **134**(1), 9, 2006.
119. S. S. Srinivasan, R. Ratnadurai, M. U. Niemann, A. R. Phani, D. Y. Goswami, and E. K. Stefanakos, "Reversible Hydrogen Storage in Electrospun Polyaniline Fibers," *Int. J. Hydrogen Energy*, **35**, 225, 2010.
120. M. U. Niemann, S. S. Srinivasan, A. R. Phani, A. Kumar, D. Y. Goswami, and E. K. Stefanakos, "Room Temperature Hydrogen Storage in Polyaniline (PANI) Nanofibers," *J. Nanosci. Nanotech.*, **9**, 1–5, 2009.
121. H. Zhang, L. Fan, Y. Fang, and S. Yang, "Electrochemistry of Composite Films of C₆₀ and Multi-walled Carbon nanotubes: A Robust Conductive Matrix for the Fine Dispersion of Fullerenes," *Chem. Phys. Lett.* **413**, 346, 2005.
122. J. L. C. Rowsell, E. C. Spencer, J. Eckert, J. A. K. Howard, and O. M. Yaghi, "Gas Adsorption Sites in a Large Pore Metal-Organic Framework," *Science*, **309**, 1350–1354, 2005.
123. F. Schuth, "Technology: Hydrogen and Hydrates," *Nature*, **434**(7034), 712–713, April 2005.
124. C. E. G. Padro and V. Putsche, "Survey of the Economics of Hydrogen Technologies," National Renewable Energy Laboratory, NREL/TP-570-27079, 1999.
125. M. Momirlan and T. N. Veziroglu, "The Properties of Hydrogen as Fuel for Tomorrow as Sustainable Energy System for a Cleaner Planet," *Int. J. Hydrogen Energy*, **30**, 795–802, 2005.
126. J. B. O'Sullivan, "Hydrogen Technical Advisory Panel Report and Fuel Cell Development Status." *National Research Council Committee*, May **11**, 1999.
127. National Academies Press, *The Hydrogen Economy: Opportunities, Costs, Barriers, and Needs*, 2004, available: <http://www.nap.edu>.
128. U.S. DOE, *Hydrogen from Coal Program—Research, Development, and Demonstration Plan*, 2004–2015, September, 2005, available: http://www.netl.doe.gov/technologies/hydrogen_clean_fuels/refshelf/myrddp.html
129. C. Y. Termaath, E. G. Skolnik, R. W. Schefer, and J. O. Keller, "Emissions Reduction Benefits from Hydrogen Addition to Midsize Gas Turbine Feedstocks," *Int. J. Hydrogen Energy*, **31**, 1147–1158, 2006.
130. A. Bain, *The Freedom Element—Living with Hydrogen*, Blue Note Publications, Cocoa Beach, FL, 2001.
131. Bellona, "Hydrogen—Status and Possibilities," *Bellona Report*, **4**, 2004, accessed February 1, 2002, available: 193.71.199.52/en/energy/hydrogen/report_6-2002/22966.html.
132. National Aeronautics and Space Administration (NASA), "Safety Standards for Hydrogen Safety and Hydrogen Systems," accessed 2006, available: <http://www.nasa.gov>.
133. B. Kinzey, P. Davis, and A. Ruiz, "The Hydrogen Safety Program of the U.S. Department of Energy," Proceedings of the 16th World Hydrogen Energy Conference (WHEC), June 13–16, Lyon, France, 2006.
134. J. Ohi, "Hydrogen Codes and Standards: An Overview of the U.S. DOE Activities," Proceedings of the 16th World Hydrogen Energy Conference (WHEC), Lyon, France, June 13–16, 2006.
135. T. Jordan, "Hysafe—The Network of Excellence for Hydrogen Safety" Proceedings of the 16th World Hydrogen Energy Conference (WHEC), June 13–16, Lyon, France, 2006.
136. NEDO, "Research on the Safety of Hydrogen Infrastructure and Building Frame Structure against Hydrogen Explosion and Earthquake," NEDO-03002978-0 and NEDO-04000481-1, accessed 2005, available: <http://www.nedo.go.jp/>.
137. H. Miyahara, K. Kubo, M. Saito, Y. Suwa, K. Yonezawa, K. Naganuma, and K. Imoto, "Research on the Safety of Hydrogen Infrastructure and Building Frame Structure against Hydrogen Explosion and Earthquake," Proceedings of the 15th World Hydrogen Energy Conference (WHEC), Yokohama, Japan, 2006.
138. Y. Suwa, H. Miyahara, K. Kubo, K. Yonezawa, Y. Ono, and K. Mikoda, "Design of Safe Hydrogen Refueling Stations against Gas-Leakage, Explosion and Accidental Automobile Collision," Proceedings of the 16th World Hydrogen Energy Conference (WHEC) June 13–16, 2006, Lyon, France.
139. The Hydrogen Community, accessed February 1, 2007, available: <http://www.hydrogensociety.net>.

CHAPTER 30

STEAM TURBINES

William W. Peng
California State University
Fresno, California

1 INTRODUCTION	1029	5.3 Basic Stage Performance	1046
2 HISTORICAL EVOLUTION OF STEAM TURBINES	1033	5.4 Part-load Operation	1046
3 TURBINE STAGES	1036	6 COGENERATION AND COMBINED-CYCLE PLANTS	1048
3.1 Velocity-Compounded Stage	1036	7 APPLICATIONS	1049
4 CLASSIFICATION OF STEAM TURBINES	1039	8 OTHER RELATED TOPICS	1051
5 STEAM TURBINE PARAMETERS AND PERFORMANCE	1043	8.1 Turbine Control	1051
5.1 Efficiencies	1043	8.2 Gland Seals	1051
5.2 Nondimensional Parameters	1044	8.3 Turbine Blade Erosion	1051
		8.4 Axial Thrust	1052
		REFERENCES	1053

1 INTRODUCTION

Energy conversion from thermal form (heat) to mechanical form (force or torque) are generally done through the fluid medium of either water/steam or air/gas. Since water has to be reused, it has to be vaporized (boiled) and condensed in a closed loop. Air, however, can be directly sucked-in from and rejected-out to ambient atmosphere. It can be processed in an open loop. The water/steam system of the former case is generally more complicated and heavy, hence it is limited to the ground or marine applications, while the latter can be employed in air flight. The turbomachines, steam turbines, and gas turbines are some examples. Although other types of heat engines, such as steam engines, Otto and diesel engines, etc. are also commonly employed, their choices normally depend on the magnitude of power output required and types of fuel available.

The thermodynamic properties of water/steam flowing through the power plant with steam turbine can be described with a Rankine cycle in a Mollier diagram, as shown in Fig. 1, for the simplest case. Each point on the diagram represents the properties of water/steam at a certain location in the plant. The curve from point 3 to 4 represents how the water/steam properties change when it passes through a steam turbine. While 1 to 2 is through a pump, 2 to 3 is through a boiler (steam generator), and 4 to 1 is through a condenser. To improve the plant efficiency, the system and cycle phase diagram can be modified. The typical diagram of a real plant is shown in Fig. 2. Detailed explanations of these diagrams are given in the typical thermodynamics texts^{1,2} and other chapters of this handbook.

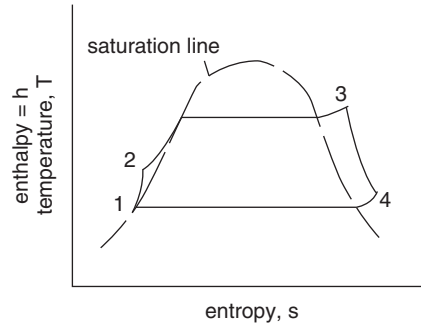


Figure 1 Mollier diagram of basic Rankine cycle with water/steam.

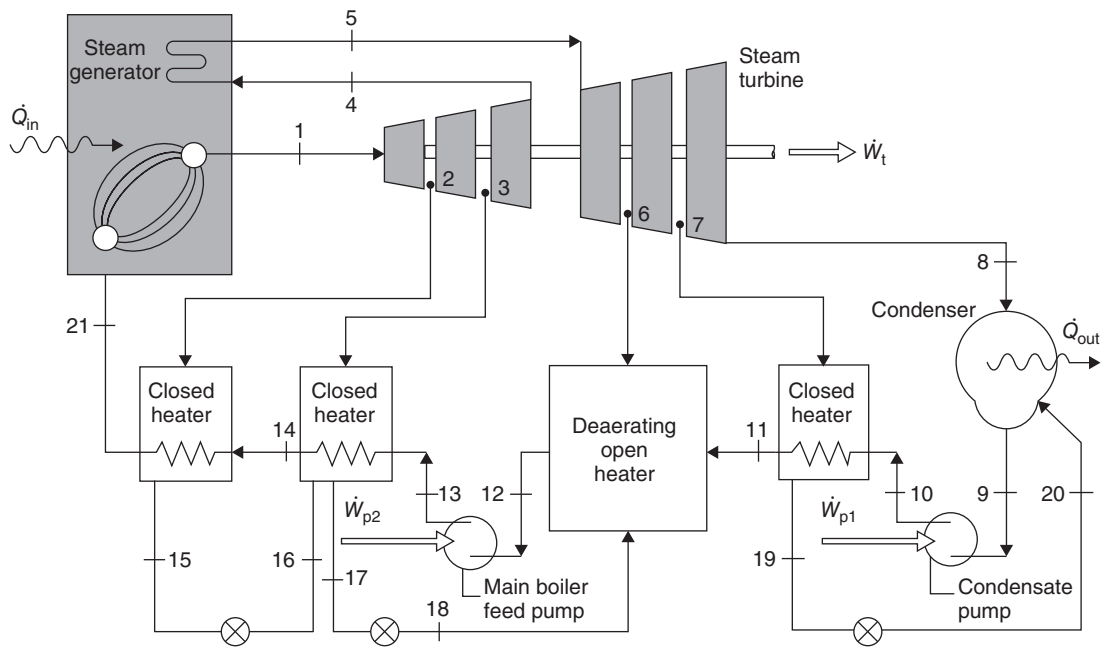


Figure 2 Schematic diagram of typical Rankine cycle with reheating and regeneration. (Reprinted by permission from Ref. 1.)

Many of the basic theories for gas turbines are also applicable to steam turbines. But the steam can only be treated as an ideal gas when it is highly superheated. The criteria can be expressed in terms of the compressibility factor $Z \equiv p / (\rho RT)$. The compressibility factor is a function of p_R and T_R , that is, $Z = f(p_R, T_R)$, where the reduced pressure and temperature are defined as $p_R \equiv p / p_c$ and $T_R \equiv T / T_c$. The critical pressure and critical temperature p_c , T_c of steam are 3207 psia and 1165°R, respectively. When Z is close to unity, the steam can be treated as an ideal gas with the specific heat capacities ratio $k = 1.30$. Otherwise the chart (Mollier diagrams as shown in Fig. 3), steam table, or other empirical formula has to be used to relate the thermodynamic properties of fluid.

Another special characteristic of a steam turbine is that the fluid flowing through a steam turbine can be a two-phase mixture of vapor and liquid droplets, especially in the low-pressure

turbines, if it expands into the saturated region. The state of mixture is identified with a parameter called moisture content, $y = m_{\text{liq}} / m_{\text{mx}}$ (ratio of liquid mass over total mixture mass per unit volume, if two-phase mixture is homogeneous). The effects of liquid droplets on steam turbine performance are twofold. First, the liquid droplets move slower than the vapor and may impinge on the blade surface, causing additional friction loss and damaging the blades in the long run. Second, in the fast expansion regions (pressure/temperature reduction) through the turbine, some vapor condensation can be delayed, even when the mixture pressure

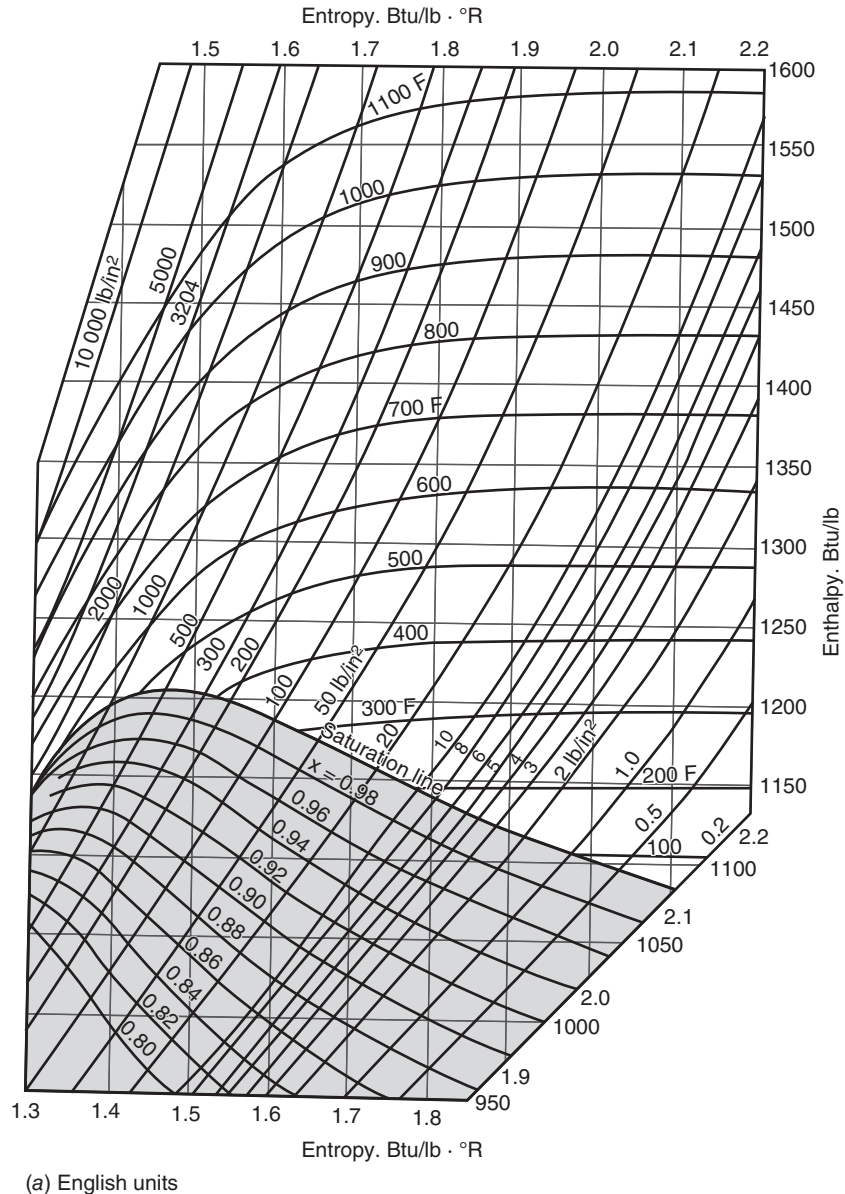
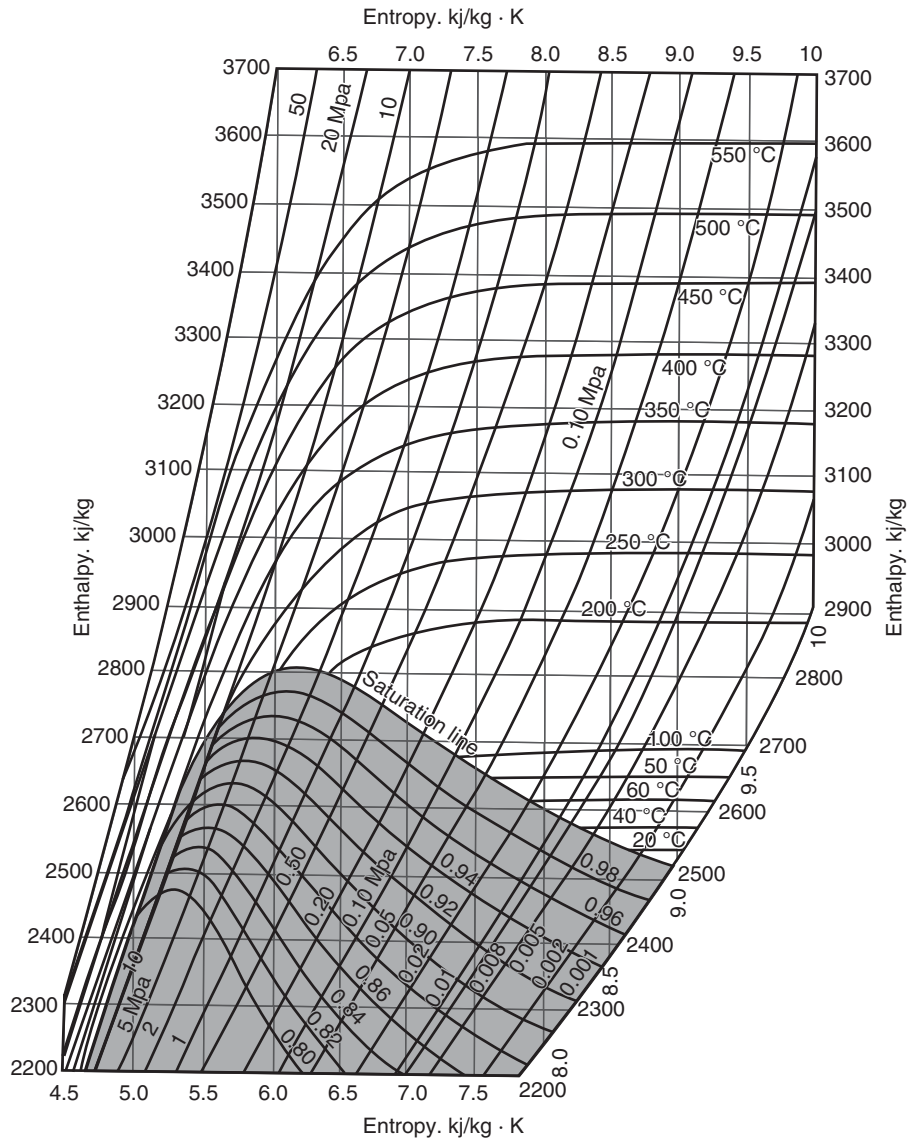


Figure 3 Mollier diagrams for steam: (a) English and (b) SI units. (Reprinted by permission from Ref. 2.)



(b) SI units

Figure 3 (Continued)

drops into the saturated condition. This phenomenon is called *nonequilibrium* process or *supersaturation*. Less energy in the vapor is released to do work than the slow expansion under equilibrium process.

In central electricity generation power plants, steam turbines are predominantly employed. This is so because steam can be conveniently generated with different types of fuel. Since the water is separated from the combustion gas in the steam generator/boiler, the fuel can be fossil, nuclear, solid waste, geothermal, or others. The pollutants from combustion can be treated

separately. Also compared to the gas turbine, pumping liquid water in the steam power plant is more efficient than pressurizing air in the gas turbine plant.

In the process plants where steam is needed, the steam can be produced economically at a pressure and temperature higher than that needed. Sometimes the steam of different pressure/temperature levels is needed. In these cases, steam turbines can be used to reduce the pressure and produce mechanical power simultaneously, instead of using other pressure-reducing devices through friction. In addition to these advantages, steam turbines are more flexible for power and speed variations compared to electrical motors, especially for medium- and high-power applications. Also steam turbines are spark proof in hazardous environments, have higher starting torque, and are inherently self-limiting against overloading.

The disadvantage of steam turbine compared to the gas turbine at high-power and the electric motor at low-power applications is its bulky size. Since it is generally a closed-loop machine, a condenser and its accessories are required. Also the steam generator/boiler is heavier than the combustion chamber in a gas turbine. Since the pressure of superheated steam is higher than that of the air at the comparable temperature and density, as indicated from the ideal gas equation, $p = \rho(R_0 / M_w)T$, where M_w is the molecular weight, and R_0 is the universal gas constant.

Cogeneration and combined-cycles plants have become more popular in recent years due to their higher overall plant efficiency. A detailed schematic is shown in Fig. 4. In this plant, natural gas is burnt in the gas turbine. The residual heat in its exhaust gas is used to produce steam in a heat recovery steam generator (HRSG), also called a waste heat boiler (WHB). The steam is used to drive a steam turbine. Both turbines drive generator sets or other machinery. Some steam is extracted for space heating, industrial processes, or gas turbine blade cooling.

2 HISTORICAL EVOLUTION OF STEAM TURBINES

The Greek geometrician Hero devised the first steam turbine more than 2000 years ago. A simple closed spherical vessel mounted on bearings discharges steam from a boiler through one or more pipes tangentially at the vessel's periphery, as shown in Fig 5. He called it "Aeolipile" (wind ball). It is a pure reaction machine. In 1629, Giovanni de Branca in Italy developed an impulse-type steam turbine like a horizontal water wheel, as shown in Fig. 5*b*.

Not until the early nineteenth century did steam turbines attract any interest for power generation. In 1831, William Avery in the United States produced some Hero's steam turbines to drive circular saws. In 1848, Robert Wilson of Scotland patented a radial-inflow steam turbine. In 1875, Osborne Reynolds of England, who invented the turbine pump, also made a multistage axial-flow steam turbine, running at 12,000 rpm. While in 1884, Charles Parsons, also of England, made a multistage axial-flow reaction turbine, running at 18,000 rpm to produce 10 hp. He also tried to produce a multistage radial-inflow turbine but failed because of some mechanical problems. In the following few years, he devoted his effort in the further development of the axial-flow machines. His machines were used for marine propulsion and electrical power generation.

Development of steam turbine was closely related to that of gas turbine. In the early stage of gas turbine engine development, the failure was mostly due to the difficulty to design an efficient compressor (pumping liquid water in a steam turbine engine is easier, as mentioned). To produce a net positive output power, it requires that the turbine output power be greater than the power required by the compressor or pump. This can be achieved by having either a higher efficient compressor/pump or a higher gas/steam inlet temperature to turbine.

In 1903, Aegidus Eilling, in Norway, constructed the world's first gas turbine that produced net power output of 11 hp. His machine consisted of a 6-stage centrifugal compressor and a single-stage radial-inflow turbine. While in France, August Rateau in 1905, designed a gas

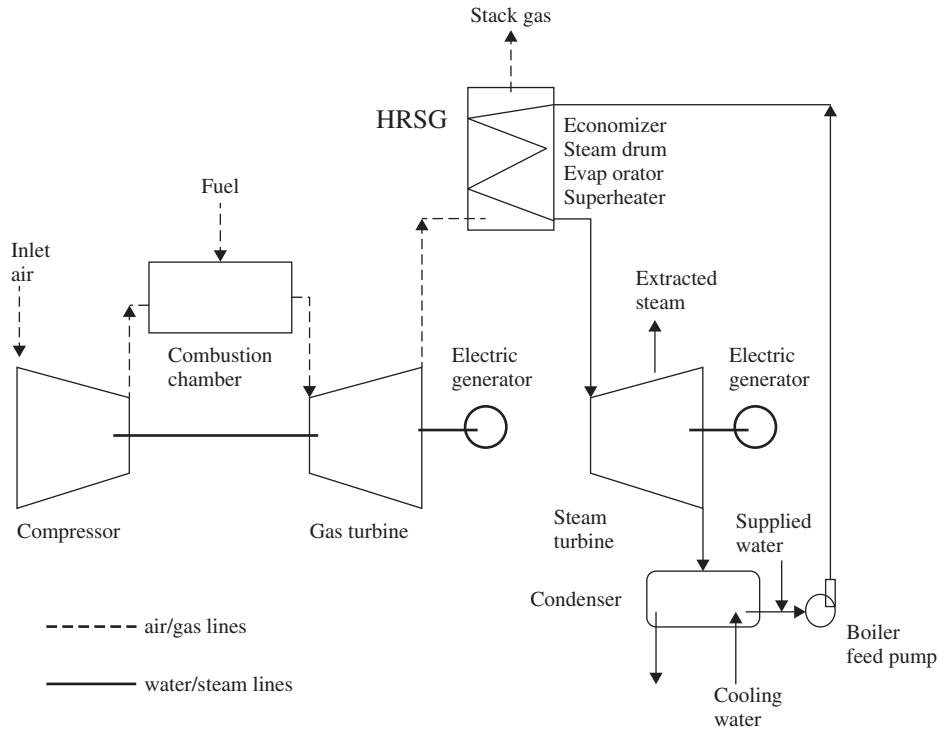


Figure 4 Combined cycle and cogeneration plant. (Reprinted by permission from Ref. 3.)

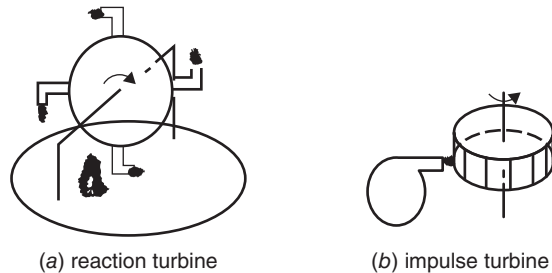
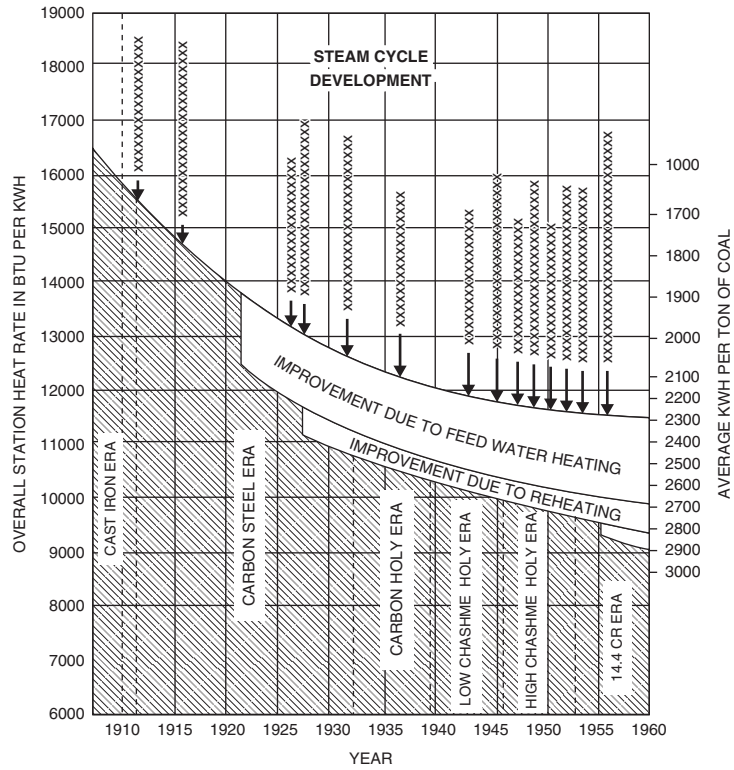


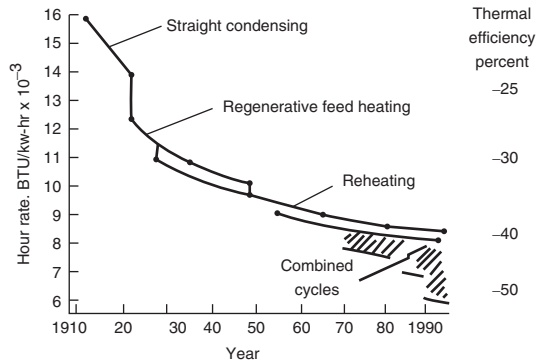
Figure 5 Ancient steam turbines by Hero and Giovanni de Branca. (Reprinted by permission from Ref. 3.)

turbine with total power output of 400 hp. It consisted of a 25-stage centrifugal compressor with intercooling and a 2-stage axial-flow turbine of impulse type.

Thermal efficiency or heat rate, HR is strongly related to the peak temperature of fluid entering the turbine (T_3 in Fig. 1). In the past few decades, efforts in steam turbine development have been made to increase the turbine inlet pressure/temperature with better materials and blade cooling. Up to 1920, they were 200 psia/550°F; around 1980, they were 2400 psia/1000°F. These efforts resulted in the thermal efficiency/heat rate being improved, as shown in Fig. 6³.



(a) Steam cycle development



(b) Fossil fuel unit heat rate as a function of time

Figure 6 (a) Development of steam turbines. (b) Fossil fuel unit heat rate as a function of time. (Reprinted by permission from Ref. 4.)

Further improvement in thermal cycle efficiency has been achieved by combining gas turbine and steam turbine in a combined cycle or cogeneration plant, to be discussed in Section 6.

3 TURBINE STAGES

Steam turbine is a type of turbomachine that converts energy through the continuously dynamic interaction between fluid medium and a rotating impeller called a rotor. Other stationary components are also required to convert thermal to kinetic energy of fluid or simply to change the flow direction. They are called nozzles or stators.

According to the types of rotor and stator, most of the steam turbines can be either radial-inflow or axial-flow type. The former is mainly used for the low-power units, while the later is employed for the medium- or high-power units and is generally arranged in a multistage, where each pair of stator and rotor is called a stage. The rotor can be either impulse or reaction type. They are shown in Fig. 7 schematically.

In the impulse types (also called Rateau type after its inventor), steam pressure and enthalpy drop predominantly in the stator in each stage, and only negligible expansion takes place in the rotor due to friction. Hence the rotor flow passage area is almost constant. In the reaction type (also called Parsons type), steam expands almost equally in stator and rotor. In general, the reaction type is more efficient, but it transfers less energy than the impulse type each stage for the same size and rotating speed. Under the maximum ideal situation, we have energy transfer per stage, $\Delta E_{r,\max} = U^2$ and $\Delta E_{i,\max} = 2U^2$, respectively, where U is the tangential velocity of the blades at mean radius.

Using the quasi-steady, one-dimensional flow analysis, the energy transfer equation across each stage (called Euler's equation in turbomachinery) can be expressed as

$$\Delta h_0 = \Delta E = U_i V_{ui} - U_o V_{uo} \quad (1)$$

where Δh_0 is the stagnation enthalpy drop of steam across each stage, V_u is the tangential component of steam absolute flow velocity at mean radius, subscripts i and o designate inlet and outlet of the rotor. For the axial-flow bladings, we have $U_i = U_o = U$.

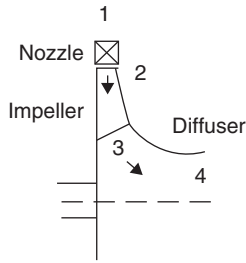
More detailed discussions on these topics can be found in the typical turbomachinery texts, such as Ref. 3 and 5.

3.1 Velocity-Compounded Stage

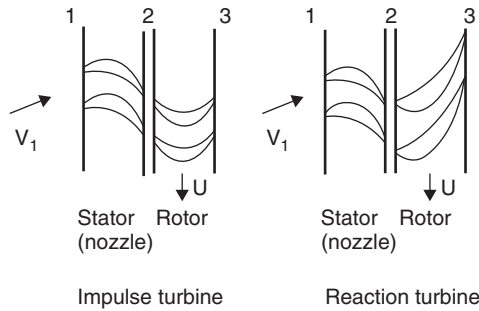
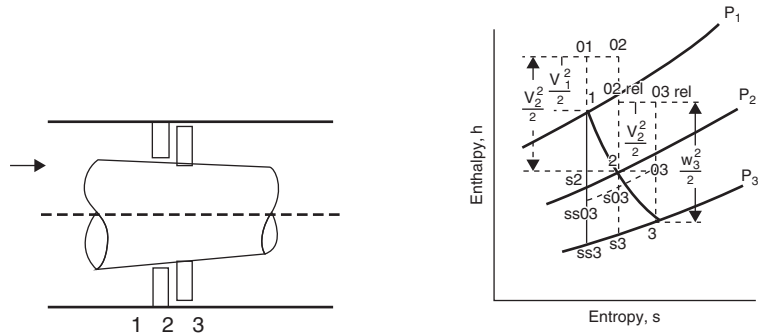
As mentioned, for the same size and rotating speed, an impulse turbine stage converts more energy per stage than a reaction turbine stage. Hence in a multistage turbine, the impulse stages are placed upstream to reduce the fluid pressure/temperature faster. So the total number of stages required can be reduced. This is especially advantageous for the steam turbine because the steam boiler pressure is much higher. To facilitate the pressure drop even further, a velocity-compounded stage arrangement is sometimes used for the first few stages of a multistage steam turbine. It can be either a Curtis stage or a reentry stage, as shown in Fig. 8. Most pressure drop occurs in the nozzle (normally a convergent–divergent nozzle), and hence higher velocity is obtained at the rotor inlet.

In a Curtis stage, two rows of impulse rotor blades are used with a row of stator blades in between to change the flow direction. Sometimes, a second row of stators and a third row of rotors are added. The velocity and h - s diagrams across both rotors are shown in Fig. 9.

The required conversion of enthalpy to kinetic energy takes place in the nozzle, and the static enthalpies downstream of station 1 are constant, as shown. For the ideal case of flow without friction losses, the static pressure will also be constant. This can be shown in the h - s diagram when all points 1, 2, 3, 4 and s_2 , s_3 , s_4 collapse into one single point s_1 .



(a) Typical radial-inflow turbine



(b) Axial-flow turbine stage

Figure 7 Types of turbine stages: (a) Typical radial-inflow turbine and (b) axial-flow turbine stage. (Reprinted by permission from Ref. 3.)

The energy transfer of both rotors from Eq. (1), can be written as

$$\begin{aligned} \Delta E_1 &= U(V_1 \sin \alpha_1 + V_2 \sin \alpha_2) = U(V_1 \sin \alpha_1 + W_2 \sin \beta_2 - U) \\ &= U[V_1 \sin \alpha_1 + (V_1 \sin \alpha_1 - U) - U] = 2U(V_1 \sin \alpha_1 - U) \end{aligned}$$

$$\begin{aligned} \Delta E_2 &= U(V_3 \sin \alpha_3) = 2U(W_3 \sin \beta_3) = 2U(V_3 \sin \alpha_3 - U) = 2U(V_2 \sin \alpha_2 - U) \\ &= 2U(W_2 \sin \beta_2 - 2U) = 2U(W_1 \sin \beta_1 - 2U) = 2U(V_1 \sin \alpha_1 - 3U) \text{ hence} \end{aligned}$$

$$\Delta E_c = \Delta E_1 + \Delta E_2 = 4U(V_1 \sin \alpha_1 - 2U).$$

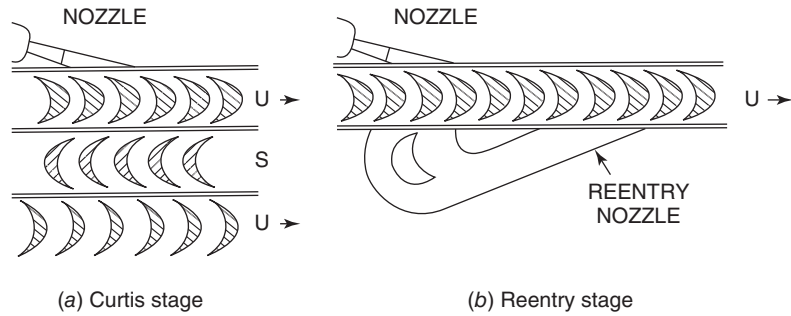


Figure 8 Velocity compounded stages: (a) curtis stage and (b) reentry state. (Reprinted by permission from Ref. 6, © McGraw-Hill Education.)

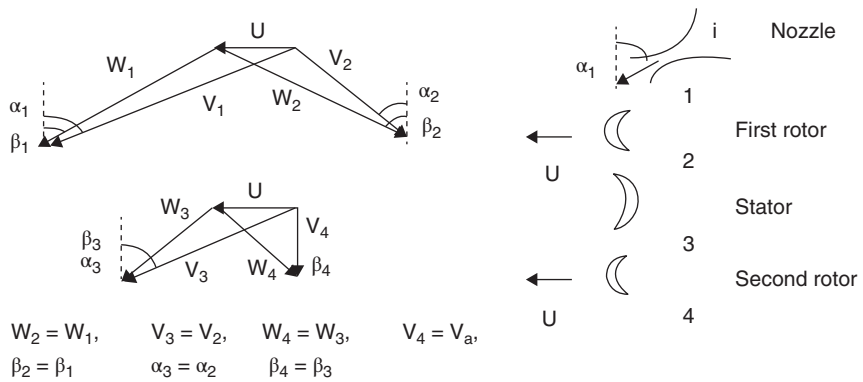


Figure 9 Curtis stage velocity and h - s diagrams. (Reprinted by permission from Ref. 3.)

Expressed in terms of the utilization factor, we have

$$\epsilon = \frac{\Delta E_c}{\Delta E_c + V_4^2/2} = \frac{\Delta E_c}{V_1^2/2} = 8 \left(\frac{U}{V_1} \right) \left[\sin \alpha_1 - 2 \left(\frac{U}{V_1} \right) \right]$$

where $V_1^2/2 = \Delta E_c + V_4^2/2$ is the total available energy, since $h_1 = h_4$ as shown in the h - s diagram.

To find the condition of maximum ϵ , we set $d\epsilon/d(U/V_1) = 0$, that is,

$$8 \sin \alpha_1 - 32 \left(\frac{U}{V_1} \right) = 0 \text{ or } \left(\frac{U}{V_1} \right)_{\max} = \frac{\sin \alpha_1}{4}. \quad (2)$$

The corresponding maximum ϵ and ΔE_c are obtained as

$$\epsilon_{\max} = 2 \sin \alpha_1 \left(\sin \alpha_1 - \frac{\sin \alpha_1}{2} \right) = \sin^2 \alpha_1 \quad (3)$$

$$\Delta E_{c,\max} = 4U(2U) = 8U^2 \quad (4)$$

For the regular impulse and reaction turbines, the maximum energy transfer per stage are $\Delta E_{i,\max} = 2U^2$ and $\Delta E_{r,\max} = U^2$, as mentioned. Hence the advantage of a Curtis stage is obvious.

4 CLASSIFICATION OF STEAM TURBINES

Steam turbines can be classified according to several different schemes:

1. Based on steam flow direction, a steam turbine can be an axial-flow, radial-inflow, radial-outflow (also called Ljungstrom turbine), or tangential-flow machine.
 - a. The construction of an axial-flow steam turbine is similar to that of the axial-flow gas turbine. The flow through the stator and rotor is substantially in the axial direction. This type of design is predominantly adapted in the medium- and high-power units as mentioned, except the single-stage impulse turbine for high-flow, low-pressure drop steam. Any reasonable number of stages can be used for the expansion of high-pressure/temperature steam in a compact arrangement. Some different arrangements normally adopted are:
 - (i) All regular impulse stages, also called pressure stage
 - (ii) All reaction stages
 - (iii) Curtis stage, also called velocity stage
 - (iv) Several Curtis stages, with a nozzle for each stage; also called pressure and velocity stage
 - (v) A Curtis stage followed with several reaction stages
 - (vi) A few impulse stages followed with several reaction stages.

Some turbines have extraction or induction at the intermediate stages.

The schematic diagram of a typical multistage steam turbine is shown in Fig. 10. As mentioned, each stage consist of a row of rotor blades fixed on the shaft and a row of stator blades. The stator blades can be directly inserted to the casing, individually or in groups. Or they can be part of an integral component called a diaphragm fixed to the casing as shown in Fig. 11. The diaphragm design of higher structure integrity is normally employed in the impulse stages, to accommodate the high-pressure drop across the stators.

- b. The radial-inflow turbine, as discussed, is primarily designed for the lower power units. As indicated in the Euler equation for turbines [Eq. (1)], radial-inflow is a logical arrangement to maximize the energy transfer for radial-flow turbines since it results in $U_i > U_o$.
- c. The radial-outflow turbine, also called Ljungstrom turbine, is shown in Fig. 12. The steam enters the blades through the hollow shaft radially. Two rotors, with blades arranged alternatively, rotate in opposite directions. There is no stator between the rotor blades. The velocity diagrams shown are for the first two inner rings of blades. It is noted that the peripheral velocity U changes direction, hence $U_3 = -U_2$, and the absolute velocity $V_3 = V_2$.

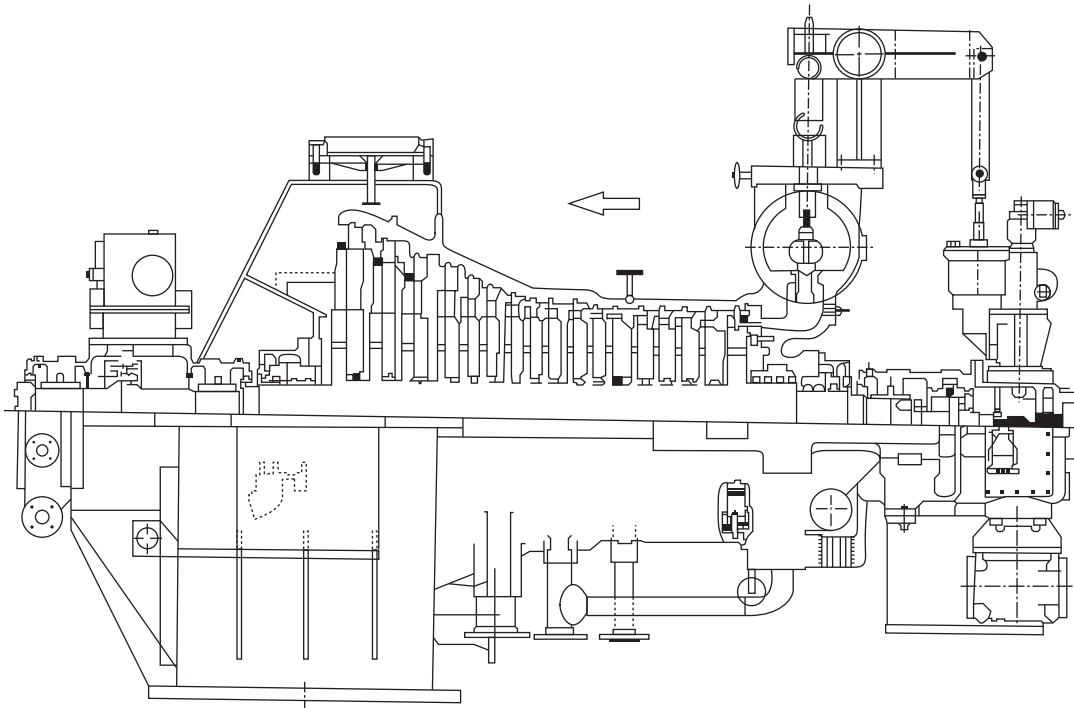


Figure 10 Typical axial-flow multistage steam turbine. (Reprinted by permission from Ref. 6, © McGraw-Hill Education.)

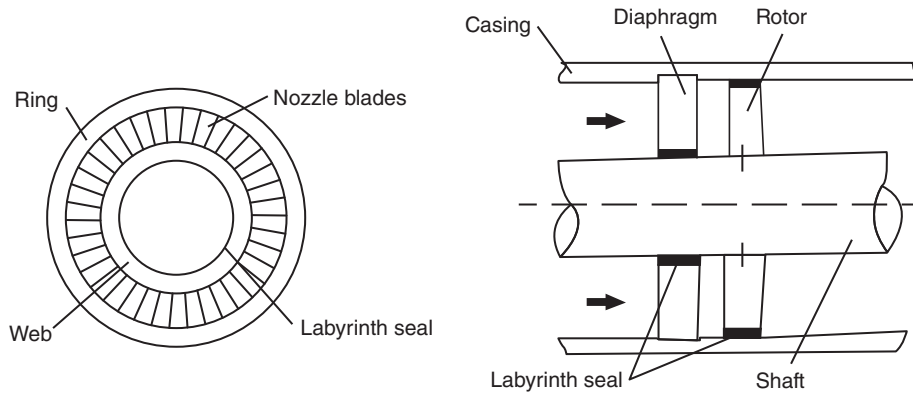


Figure 11 Typical diaphragm with nozzles and seals.

The energy transfer based on the Euler equation across each rotor is always positive, that is, $\Delta E = U_i V_i - U_o V_o > 0$. This type of turbine has high efficiency, but is complicated mechanically and expensive to construct. Hence its development has not been widely received.

- d. The tangential-flow turbine, as shown in Fig. 13 is similar to the Pelton wheel of hydraulic turbine. The steam exiting from nozzles that are arranged almost tangent

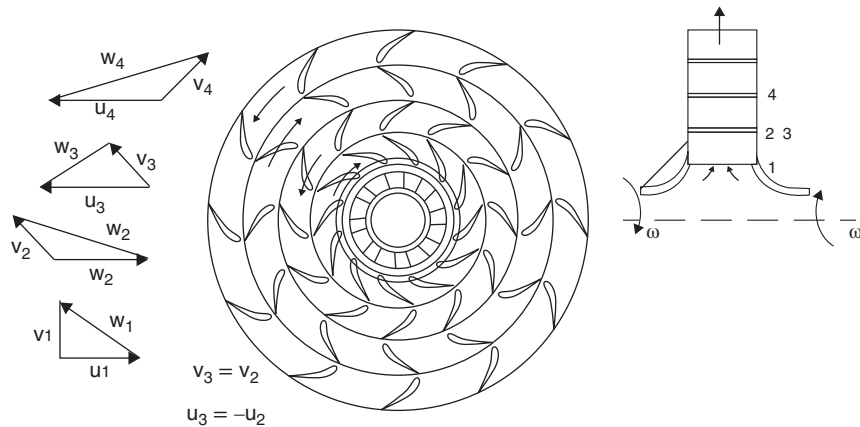


Figure 12 Radial-outflow steam turbine (Ljungstrom turbine). (Reprinted by permission from Ref. 3.)

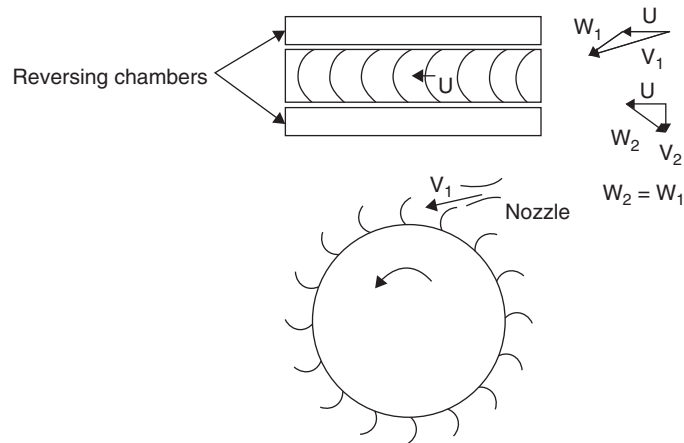


Figure 13 Tangential flow steam turbine. (Reprinted by permission from Ref. 3.)

to the periphery of the rotor impinges on a semicircular rotor blade (or bucket). It then discharges to a reversing chamber and reenters the rotor blades.

2. Based on the exhausting condition, the steam turbines can be classified as
 - a. Condensing
 - b. Noncondensing, or topping

The condenser pressure ranges from 26 to 29 in. Hg VAC (0.5– 2 psia). In the noncondensing turbine, the exhausting steam is used for processing or heating, and hence it is an open-cycle machine. The topping turbine exhausts steam to another steam turbine.

3. Steam turbines can also be classified according to
 - a. Orientation of their shaft, either horizontal or vertical
 - b. Connection with load, either directly connected or geared.

The choice will depend on the application, installation, and space available.

4. For the high-power systems, more than one casing or one shaft may be needed. Hence, the steam turbines can be classified as

- a. Tandem-compound unit
- b. Cross-compound unit.

The tandem-compound unit has all turbines driving the same shaft, while the cross-compound unit has the turbines driving the separate shafts, as shown in Fig. 14. In the large plants, steam turbines may be divided into three sections, according to their pressure ranges:

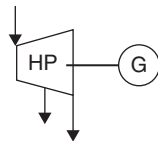
- a. High-pressure turbine (HP) with pressure ranging from 400 to 4500 psia (2.8–31 MPa)
- b. Intermediate-pressure turbine (IP) with pressure ranging from 300 to 1300 psia (2–9 MPa)
- c. Low-pressure turbine (LP) with pressure below 300 psia (2 MPa)

In the LP sections, typically, the steam is split into two flows to drive two identical turbines, because the low-pressure/density steam requires more flow passage area. This arrangement also helps to minimize the axial thrust on the shaft and bearings.

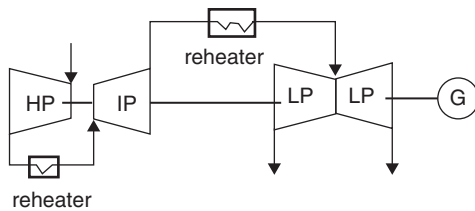
5. Based on the arrangement of the first-stage nozzles, the steam turbines can be classified as

- a. Full admission
- b. Partial admission

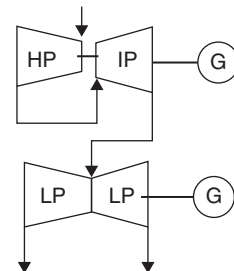
The turbines with full admission have the nozzles arranged around a complete circle upstream of the first-stage rotor. In general, the partial admission arrangement is employed in the HP turbines since the high-pressure/density steam requires less flow passage area.



(a) Single casing with extraction



(b) Tandem-compound with reheat and double flow



(c) Cross-compound with double flow

Figure 14 Arrangement of steam turbine casing and shaft: (a) single casing with extraction, (b) tandem compound with reheat and double flow, and (c) cross compound with double flow.

5 STEAM TURBINE PARAMETERS AND PERFORMANCE

5.1 Efficiencies

Similar to other types of turbomachines, the efficiencies of a steam turbine can be defined to account for several mechanisms of energy losses in converting input power to output power. The overall efficiency (also called engine efficiency or brake engine efficiency) is defined as $\eta_{o/a} \equiv P_s / (m_t \Delta H_s)$, where P_s is the output shaft power, m_t is the total steam mass flow rate through the turbine stages, (excluding leakage through the shaft/packing seals and assuming no extraction) and ΔH_s is the isentropic stagnation enthalpy drop per unit mass of steam from inlet condition to exhaust pressure. Or $m_t \Delta H_s$ is the maximum possible energy conversion for the given inlet/outlet conditions.

The energy losses contributing to the fact that $\eta_{o/a}$ being less than 100%, can be divided into

1. Losses due to the flow friction and secondary flow through the flow passages, ΔH_f
2. Losses due to the flow leakage through the rotor/casing clearances, m_l
3. Losses due to the friction of rotor disk, bearings, seals of rotor blading, transmission gear, and the power to drive the accessory devices, such as governor and oil pump, if there is any, ΔP_m

The efficiencies associated with these losses are defined as adiabatic efficiency $\eta_{ad} = \Delta H_a / \Delta H_s = (\Delta H_s - \Delta H_f) / \Delta H_s$, volumetric efficiency $\eta_v = (m_t - m_l) / m_t$, and mechanical efficiency (also called rotational efficiency in some studies) $\eta_m = P_s / (P_s + \Delta P_m) = P_s / [(m_t - m_l) \Delta H_a]$, respectively, where ΔH_a is actual stagnation enthalpy drop per unit mass of steam. The overall efficiency can, therefore, be related as $\eta_{o/a} \equiv P_s / (m_t \Delta H_s) = P_s / (m_t \Delta H_s) [(\Delta H_a / \Delta H_s) [(m_t - m_l) / (m_t - m_l)]] = \eta_{ad} \eta_v \eta_m$. Sometimes, the internal efficiency defined as $\eta_i \equiv \eta_{ad} \eta_v$ is used, especially in designing the turbine itself.

For the machine users, a parameter called *steam rate* (SR) is more relevant than the efficiencies defined above. It is defined as the steam mass flow rate required to produce one unit of shaft power, expressed in the units of $\text{lb}_m / (\text{hp}\cdot\text{h})$ or $\text{kg} / (\text{kW}\cdot\text{h})$. It is inversely proportional to the overall efficiency for a given set of steam inlet/outlet conditions. Since we have $\text{SR} \equiv m_i / P_s = (m_i m_t / m_t) / P_s = (m_i / m_t) / (\Delta H_s \eta_{o/a})$ from the definition, where m_i is steam mass flow rate at turbine inlet, which includes leakage through the shaft/packing seals, m_{ls} or $m_i = m_t + m_{ls}$. This is true only for the basic turbine without extraction and reheating. Or the *heat rate* (HR) can be defined as the heat supply required to produce unit work in terms of $\text{Btu} / (\text{kW}\cdot\text{h})$, $\text{Btu} / (\text{hp}\cdot\text{h})$ or $\text{kJ} / (\text{kW}\cdot\text{h})$. It is a more useful measure of performance, as it is directly proportional to the cost of fuel for each unit of work output. Of course, both mass rate and heat rate are dimensional, some conversion factors are needed to relate them with thermal efficiency.

Thermal efficiencies are slightly different from the efficiencies defined above. They are based on the heating value per unit mass of steam at turbine inlet, Q_i , as follows:

1. Brake thermal efficiency, $\eta_{th,b} = P_s / (m_i Q_i)$
2. Internal thermal efficiency, $\eta_{th,i} = \Delta H_a / Q_i$
3. Rankine-cycle efficiency, $\eta_{th,r} = \Delta H_s / Q_i$

Hence, we have adiabatic efficiency, $\eta_{ad} \equiv \Delta H_a / \Delta H_s = \eta_{th,i} / \eta_{th,r}$. Then, the heat rate (HR) and brake thermal efficiency can be related as $\eta_{th,b} = P_s / (m_i Q_i) [\text{kW} / \text{kJ/s}] = 3600 P_s / (m_i Q_i) [\text{kW} / (\text{kJ/h})] = (3600 / 1.055) P_s / (m_i Q_i) [\text{kW} / (\text{Btu/h})] = 3413 / \{\text{HR} [\text{Btu} / (\text{kW}\cdot\text{h})]\} = 2545 / \{\text{HR} [\text{Btu} / (\text{hp}\cdot\text{h})]\}$. The numerical values of “3413” and “2545” come from the unit

conversion and are actually the theoretical heat rate (THR), corresponding to the turbine efficiency of 100%.

For a condensing closed-loop system without extraction, Q_i can be evaluated from $Q_i = h_i - h_f$, where h_i and h_f are the enthalpies of steam at turbine inlet and water at boiler inlet, respectively. Or it can be related as $m_i Q_i = \eta_b m_f Q_f$, where η_b is the boiler efficiency, m_f and Q_f are the fuel mass flow rate and fuel heating value, respectively. Alternative definitions are used, especially for the open noncondensing systems.

5.2 Nondimensional Parameters

From dimensional analysis the typical non-dimensional parameters used in relating a steam turbine performance can be obtained as:

1. Pressure ratio between outlet and inlet, p_{0e} / p_{0i}
2. Power coefficient, $P_s / (p_{0i} D^2 \sqrt{RT_{0i}})$ (or temperature ratio, T_{0e} / T_{0i})
3. Mass coefficient, $m \sqrt{RT_{0i}} / (p_{0i} D^2)$ (or flow Mach number, V_i / a_{0i})
4. Rotational speed coefficient, $ND / \sqrt{RT_{0i}}$ (or velocities ratio, U / V_i , or rotational Mach number, U / a_{0i})
5. Torque coefficient, $\tau / (p_{0i} D^3)$
6. Overall efficiency, $\eta_{o/a} = P_s / (m \Delta H_s)$

The detailed derivation can be found in Ref. 3. For a given machine and fluid medium, the characteristic dimension (rotor diameter), D , and gas constant, R , are constants, hence they are generally ignored in the parameters for correlating its own performance.

The average efficiencies of typical steam turbines can be correlated with a parameter called *quality factor* (QF). The situation is similar to the specific speeds used in the other turbomachines. The quality factor is defined as $QF \equiv \Sigma U_i^2 / \Delta H_s$, where U_i is the rotor tip velocity of the stages. It can be related to the other parameters as follows.

Across each stage, we have the enthalpy drop Δh_s related as $f \Delta h_s = V_s^2 / (2g_c) = U_i^2 / (2g_c \lambda^2)$, or $U_i^2 / \Delta h_s = 2g_c f \lambda^2$, where V_2 is the absolute flow velocity at the nozzle outlet (rotor inlet), g_c is the conversion factor, f is the fraction of stagnation enthalpy drop converted to kinetic energy through the nozzle. It is recalled that $f \approx 1.0$ and $\lambda \approx U_i / V_2 = \sin \alpha_2 / 2 \approx 0.5$ for impulse blading or $f \approx 0.5$ and $\lambda = \sin \alpha_2 \approx 1.0$ for reaction blading under the maximum efficiency condition.

Assuming identical stages, the above expressions can be summed over all stages in the form $\Sigma U_i^2 = 2g_c f \lambda^2 \Sigma \Delta h_s = 2g_c f \lambda^2 R_H \Delta H_s$, where R_H is the reheat factor for steam, defined as $R_H = \Sigma \Delta h_s / \Delta H_s$. Hence the quality factor can be related as $QF \equiv \Sigma U_i^2 / \Delta H_s = 2g_c f \lambda^2 R_H$. The reheat factor, R_H also relates the overall adiabatic efficiency of a multistage turbine with the individual stage efficiency as $\eta_{ad} = R_H \eta_s$, if η_s is the same for all stages. Typical values for R_H and η_s are $R_H = 1.04 \sim 1.10$, $\eta_s = 0.84 \sim 0.90$. A simplified and straightforward procedure to determine R_H is discussed in Ref. 7.

A chart relating the average engine efficiency and quality factor for multistage steam turbines is given in Fig. 15. Here the conversion factor g_c is $g_c = 778 \times 32.2 = 25,052 (ft/s)^2 / (Btu/lb_m)$ in the English system of units, and $g_c = 1000 (m/s)^2 / (kJ/kg)$ in the SI system.

For the convenience of machine selection, the manufactures also plot their machines performance at the rated power under different inlet/outlet conditions. Typical performance curves of axial-flow multistage steam turbines of both condensing and noncondensing types are shown in Fig. 16. The effects of steam inlet pressures, degrees of superheat and vacuum at the condenser on turbine performance are also included.

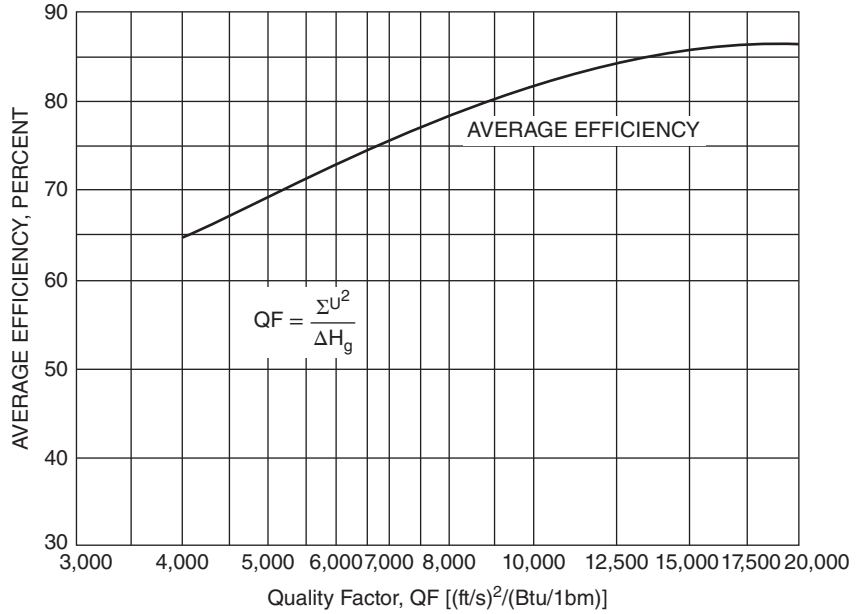


Figure 15 Typical correlation of average efficiency with quality factor for multistage steam turbines. (Reprinted by permission from Ref. 6, © McGraw-Hill Education.)

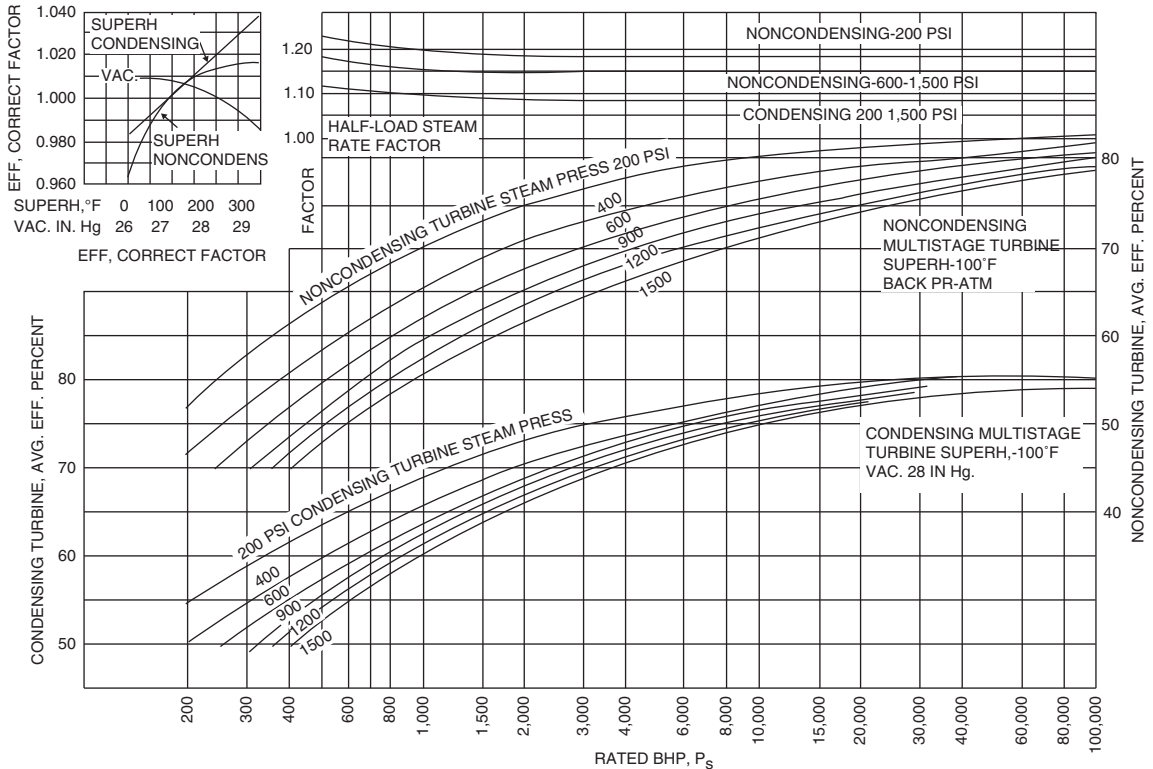


Figure 16 Typical axial-flow multistage steam turbine performance at rated power. (Reprinted by permission from Ref. 6, © McGraw-Hill Education.)

5.3 Basic Stage Performance

Similar to other types of turbines (such as gas, hydraulic, and wind turbines), the basic performance of a steam turbine stage can be expressed in terms of shaft power or efficiency versus the rotational speed under constant steam mass flow rate and inlet/outlet conditions. They are shown in Fig. 17 qualitatively. It results from the energy transfer equation (Euler's equation) with the appropriate changes of velocity diagram as the rotational speed of rotor changes. Under maximum efficiency condition, the steam relative flow direction matches with the rotor blades with minimum interference and losses, which is the design condition. The shaft torque, $\tau = P_s/\omega$ is also shown with maximum at the stationary condition. It reaches zero at the run-away speed, when both torque and power become zero.

As mentioned, for reaction turbine stage, the maximum efficiency occurs around $U/V_2 \approx 1$; for impulse type, it is around $U/V_2 \approx 0.5$, where U is the blade tangential velocity, and V_2 is the steam flow velocity at nozzle outlet (rotor inlet).

5.4 Part-load Operation

Most turbines are designed at the high-power condition (but not the maximum power) and are required to operate at a constant speed for some variation of output power. For gas turbines, the output power can be changed by injecting different amount of fuel, hence changing the air-fuel ratio and turbine inlet temperature. For steam turbines, the boiler condition and hence the steam pressure/temperature at turbine inlet are usually kept constant. The variation of output power must be affected by either (1) reducing the steam pressure with throttling or (2) partial admission, that is, admitting steam into only some of the nozzles, upstream of the first stage of turbine. In the other cases, if the turbines have to be operated with overload for a short period of time, the steam can bypasses the first one or two stages with full pressure. This will cause the mass flow rate, hence output power, to increase since the flow passage area normally increases from upstream to downstream in order to accommodate the increasing specific volume of steam. Of course, all of these operations under off-design conditions will result in a slight decrease in plant efficiency.

Throttling is a process to cause pressure reduction with flow friction, while enthalpy is constant and entropy increases, so the available energy in steam drops. It is simple but inefficient, so it is primarily used in the small turbines, where initial cost is more important than operating efficiency.

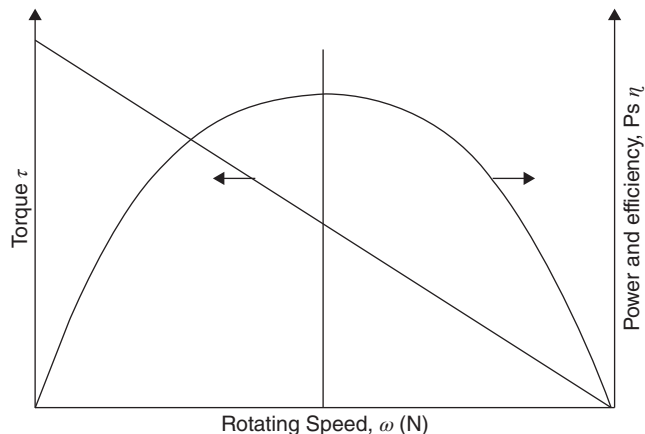


Figure 17 Theoretical shaft torque, power, and efficiency of a turbine versus rotating speed.

Partial admission is more complicated but causes less drop in efficiency. Steam supply following the main valve is split into two or more streams, each with its own control valve. Under part-load operation, the steam is admitted only to some of the nozzles, with the design pressure maintained (but the mass flow rates in the other parts of the plant have to be adjusted accordingly). No extra energy loss is incurred, except that due to the windage and turbulence in the rotors as steam passes “idle nozzles.” Partial admission is commonly used in the large turbines.

In both methods, however, the parameter that changes significantly with output power is steam mass flow rate. The efficiency and enthalpy changes are relatively minor. Hence under the off-design operation, shaft power and steam flow rate are related almost linearly. This relationship as shown in Fig. 18 is called Willans line. With this simple relationship, the complete off-design performance of a steam turbine can be obtained with the tests at two conditions. Then a straight line is plotted through them. The intercept on abscissa (point 1) indicates the no-load loss, P_1 , that is external power required to drive the turbine without steam flow supplied, or the power losses ΔP_m mentioned earlier, while that on ordinate (point 2) represents the flow required for no-load, m_o . The steam rate $SR = m_i / P_s$ is also plotted as shown. They can be expressed mathematically as

$$m_i = m_o(1 + P_s/P_1) \quad SR \equiv \frac{m_i}{P_s} = m_o \left(\frac{1}{P_s} + \frac{1}{P_1} \right)$$

The heat rate ($HR \equiv m_i Q_i / P_s$) curve is similar to the steam rate curve since the inlet steam condition is kept constant and the heat required to produce unit mass of steam Q_i (called heating value) is constant. While the thermal efficiency is reciprocal to the heat rate with a conversion factor since we have $\eta_{th,b} = P_s / (m_i Q_i)$. These two curves are shown in Fig. 19 qualitatively. Considering the combustion processes and boiler performance, the heating value Q_i , if not available, can be treated as approximately equal to the steam enthalpy drop ΔH_s , and $m_i \approx m_t$, hence we have $\eta_{t,b} \approx \eta_o/a$.

Another curve, called incremental heat rate curve (dHR/dP_s versus P_s) can also be developed. It is useful in an economic load dispatch procedure for the major utility networks.

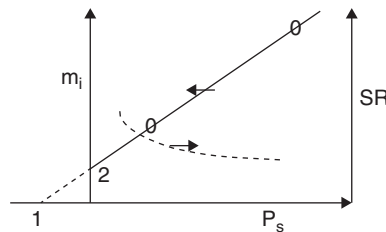


Figure 18 Willans line (steam mass flow rate versus shaft power).

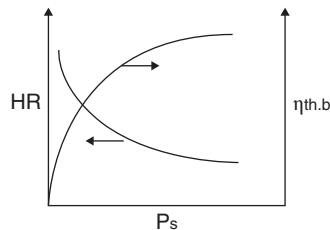


Figure 19 Qualitative heat rate and thermal efficiency versus shaft power for part load with constant rotating speed and steam inlet/outlet conditions.

With a fixed exhaust pressure, the steam mass flow rate is approximately proportional to the turbine inlet pressure. For choked flow, as is likely in an impulse turbine stage, the mass flow rate can be calculated from

$$m_t = \rho_1 V_1 A_1 = \rho_1 a_1 A_1 \sim \left(\frac{p_1}{RT_1} \right) \sqrt{(kRT_1)} \sim \frac{p_1}{\sqrt{T_1}}$$

where a_1 is the sonic speed of steam, if the superheated steam can be treated as an ideal gas.

For nonchoking flow, the manipulation given below also shows a linear relationship. Across each stage, we have $\Delta h \sim (V_2^2 - V_1^2) - V_1^2(C_1 - 1)$, where $C_1 \equiv (V_2/V_1)^2 \cong (A_1/A_2)^2$ is approximately constant for low subsonic flow. Or we have $V_1^2 \sim \Delta h \sim \Delta p/\rho$. And from $m_t = \rho VA$ across each stage, we have

$$\begin{aligned} m_t^2 &= (\rho VA)^2 = \frac{(\rho_1 V_1)^2}{(1/A_1)^2} = \frac{(\rho_2 V_2)^2}{(1/A_2)^2} \\ &= \frac{(\rho_n V_n)^2}{(1/A_n)^2} \end{aligned}$$

hence,

$$m_t^2 = \frac{\Sigma(\rho_i V_i)^2}{\Sigma(1/A_i)^2} = \frac{\Sigma(\rho_i \Delta p_i)}{\Sigma(1/A_i)^2}$$

Also from $\Delta(\rho p) = \rho \Delta p + p \Delta \rho$ and $p = C \rho^k$, or $\rho \Delta p = k p \Delta \rho$, we have $\Delta(\rho p) = \rho \Delta p + \rho \Delta p/k = [(k+1)/k] \rho \Delta p$

Or substituting it back, we have $m_t^2 = [k/(k+1)] \Sigma[\Delta(\rho_i p_i)] / \Sigma(1/A_i)^2 = [k/(k+1)] [(\rho_1 p_1 - \rho_2 p_2) + (\rho_2 p_2 - \rho_3 p_3) + \rho_n p_n] / \Sigma(1/A_i)^2 \cong [k/(k+1)] (\rho_1 p_1) / \Sigma(1/A_i)^2$, or $m_t^2 \sim \rho_1 p_1 = p_1^2 / (RT_1)$ So it is concluded that $m_t \sim p_1$.

6 COGENERATION AND COMBINED-CYCLE PLANTS

Cogeneration is a system in which fuel energy is used to generate shaft power and steam thermal energy simultaneously. So the overall efficiency of the plant can be improved.

It can be either a topping cycle or a bottom cycle system. They are shown schematically in Fig. 20. In the topping cycle, fuel is burnt to produce high-pressure/temperature gas or steam to drive a gas/steam or combined-cycle turbine. Then the exhaust gas from the gas turbine is used to produce steam through a heat recovery steam generator (HRSG) (also called waste heat recovery boiler in the literature). Or the steam is extracted from the intermediate stages of the steam turbine and from its final exhaust for process/heating. In the bottom cycle system, the fuel is burnt to produce the steam for industrial plant processes. Then the waste heat from the exhaust steam is used to drive a steam turbine for shaft power production. The exhaust steam from turbine can be used for another process/heating.

In a combined-cycle power plant, the hot gas exhausted from a shaft power gas turbine is used to generate steam to drive a steam turbine. It can generally be designed such that the required equipment can be selected from the existing models (including gas turbine, steam turbine, and HRSG). Additional fuel can be burnt in HRSG to make up the discrepancy between the gas turbine exhaust condition and the design inlet condition for the steam turbine.

The definition of thermal efficiency (also called utilization factor in some studies) for a cogeneration system is not straightforward since the mechanical energy of shaft is worth more than the steam heating energy from a thermodynamics point of view. Hence two types of definition are devised, namely,

$$\eta_{th} = \frac{P_s + m_{ex} Q_{th}}{m_i Q_{in}} \quad \text{or} \quad \eta_{th} = \frac{A_s + A_{th}}{A_i}$$

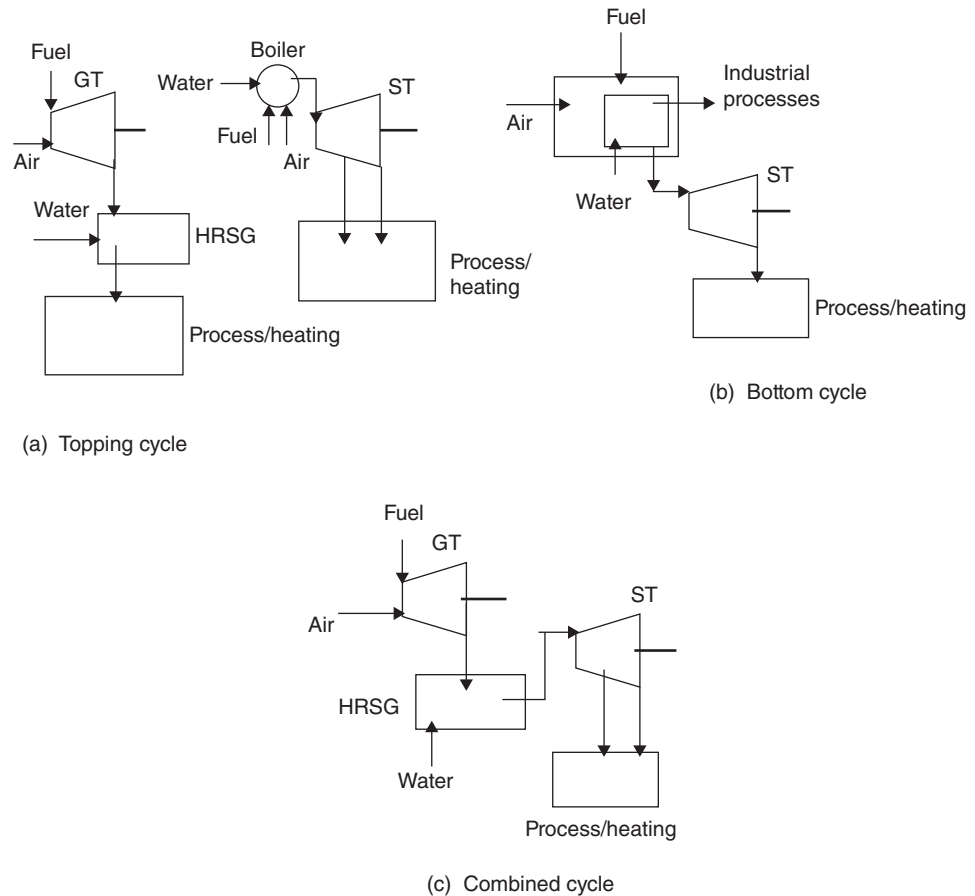


Figure 20 Cogeneration systems: (a) topping cycle, (b) bottom cycle, and (c) combined cycle. (Reprinted by permission from Ref. 3.)

where P_s is mechanical shaft power, m_{ex} , and Q_{th} are the mass flow rate and heating value of steam produced, m_i and Q_{in} are the mass flow rate and heating value of steam at turbine inlet. While A_s , A_{th} and A_i are the equivalent availabilities of shaft power, produced steam, and inlet steam required.

Discussion on the basic concept of availability and thermodynamic cycles of the cogeneration or combined-cycle plants can be found in typical thermodynamics texts, such as Ref. 1 and 2. More detailed information about cogeneration and combined cycle plants can be found in Ref. 8.

7 APPLICATIONS

As mentioned earlier, the steam turbines are commonly used in the following industries.

Electric Utility. Due to their capabilities of using multiple types of fuel and quick starting up, the steam turbines are predominantly used to drive electric generators. They can be either for base load or peaking services with a rating up to 1200 MW. To meet the large load demand,

many turbines run in parallel, or cross-compound arrangements as mentioned earlier. Other smaller units are used to drive the auxiliary equipment, such as the boiler-feed pump in the plant. Main considerations in selection are economics, reliability, load cycles, and peak demand.

Process Industry. Steam turbines are widely used in the petrochemical plants, as the mechanical drives for centrifugal pumps, turbofans, blowers, and compressors, especially those high-power units with size up to 15,000 hp. They are also used to drive the pumps and compressors for the oil and gas pipelines. Main considerations in selection are process requirements and possible growth, reliability and economics. Some small units (called turboexpanders) are used to reduce the steam pressure from high-pressure source for processes in the plants. Cogenerations and combined cycles are commonly employed. Typical cogeneration service employs small size units up to 3500 hp, using steam from boiler with pressure up to 1400 psia in topping service.

Marine Applications. Steam turbines are used for ship propulsions and auxiliary equipment drives. Their selection considerations are compactness/weight, reliability, and fast speed change capability. Typically, impulse or Curtis stage turbines are employed since they are more compact.

Geothermal. Geothermal fluid from wells can be either dry steam or two-phase mixture of water and steam. Two-phase mixture has to be flashed in a separator to produce pure steam before being admitted into the turbine. Steam turbines used in the geothermal powers require special construction materials, such as stainless steel or titanium, for the critical parts due to the corrosive steam with sulfur. They require more frequent cleaning due to the scaling problems associated with silica, calcium, carbonate, sulfate, and heavy-metal ions in the steam. Due to the low-energy content per unit mass of steam (low pressure/temperature), the steam turbine size is larger. The longer blades are required to accommodate higher flow rate. A typical 60-MW turbine for geothermal power has a size about 2.5 times an equivalent fossil unit turbine.

Ocean Thermal Energy Conversion (OTEC). Special fluid medium and design characteristics are required for the low temperature difference (around 22°C) between ocean surface and bottom floor. The closed-cycle type OTEC uses ammonia, sulfur dioxide, or Freon compounds as the working fluid medium. It is more compact, but some special materials and equipment are needed to handle the corrosive fluids. In the open-cycle-type OTEC, water/steam is used directly as the working fluid medium. The warmer water from the ocean surface is flashed into steam in a low-pressure evaporator to drive the steam turbine. The exhaust steam is condensed with the cooler water from ocean bottom. Then the condensate is pressurized to ambient atmospheric pressure, before being rejected. The system will be bulky, but fresh water can be produced as a by-product. More information on geothermal and OTEC systems are available in Ref. 9.

Solar Rankine Cycle System. Solar energy can be converted into electricity directly through the photovoltaic process. It can also be converted to mechanical energy through a thermal conversion process with gas or steam turbine. The choice is mainly an economical consideration.

However, due to the relatively low temperature of the fluid medium that solar energy can produce, special fluid medium has to be used in a closed loop with a gas/steam turbine. Similar to the OTEC system, the Rankine cycle system also employs ammonia, sulfur dioxide, and Freon compounds or their mixtures with water (hence it is also called an organic Rankine cycle).

Table 1 Rankine Cycle System Substance Properties

Substance	Critical Properties		Saturation Properties					
	p_c (psia)	T_c (R)	p_c (psia)	T_s (°F)	p_s (psia)	T_s (°F)	p_s (psia)	T_s (°F)
Ammonia	1637	730	14.7	-28.1	100	56	200	96
Freon 134A	591	673	14.7	-15	100	79	200	125
Water	3207	1165	14.7	212	100	328	200	382

It is so since the superheated vapors of these substances have lower temperatures than that of water at the comparable pressure, as shown with the sample data in table.1.

One example of studies on this type of system is given in Ref. 10.

8 OTHER RELATED TOPICS

8.1 Turbine Control

Control systems (also called governing systems) can be mechanical, hydraulic, analog, or digital or a combination of them, depending on the size and complexity. In steam turbines, the main function of a control system is to maintain a constant rotating speed of shafts or a constant pressure at some points.

For the steam turbine driving an electric generator, the shaft rotating speed has to be constant in order to generate electrical output of constant frequency. But when the load changes, the shaft speed will change, hence the steam flow entering the turbine has to be adjusted. Also, under normal operating conditions, steam flow through the unit is controlled by positioning the main steam control valves. If an unsafe condition develops, either the analog/digital system or a mechanical backup system will close the main and reheat steam valves.

Examples of pressure control are (1) pressure upstream of the control valves, (2) back pressure, and (3) pressure at extraction points.

8.2 Gland Seals

Seals are required at the rotor and nozzle blades to minimize leakage as mentioned. Gland seals are also provided, where the turbine shaft passes through the casing. In steam turbines, labyrinth seals are typically employed, due to their high rotating speed and high-temperature environment. They are used to minimize air leaking into LP turbines and steam leaking out in HP and IP turbines. To further reduce or completely eliminate the leaking in or out, low-pressure or high-pressure headers located next to the seals can be used to collect or inject steam. The collected steam in steam-air mixture is condensed in a gland steam condenser.

8.3 Turbine Blade Erosion

Erosion of turbine blades can occur if moisture is present in the steam. This is especially possible for LP turbines. Moisture removal and reheating is accomplished either by rerouting the steam back to the boiler or by a moisture separator reheater. It can be a separately fired heat exchanger or an open heater mixed with the superheated steam extracted from HP turbines.

8.4 Axial Thrust

Due to the differences in pressure and steam flow momentum flux across each row of rotor blading, the whole rotor assembly is subject to an unbalanced axial thrust force. This is especially pronounced in the multistage turbines with predominant reaction type of blading. The magnitude and direction of this force can vary with the operating condition. Typically, this net axial thrust is taken care of with the Kingsbury thrust bearings. To reduce the load of thrust bearing, some design schemes are incorporated if possible. They can be:

1. Balance holes in the rotor disk
2. Thrust compensator (or called dummy piston) with two sides of the disk exposed to different pressure
3. Double-flow turbines driving one shaft, with steam flowing in opposite directions as mentioned earlier.

Normally, the axial position of the thrust bearing can be adjusted to change the clearance between rotor and stator (or casing). The clearance can change due to wearing of some parts from the machine operation.

Symbols.

A	flow passage area (in ² cm ³)
a	acoustic speed (ft/s, m/s)
C	constant
GT	gas turbine
g_c	conversion factor (= 32.174 lb _m /slug, = 1 for SI system)
ΔH_s	isentropic enthalpy change per unit mass flow rate, across a multistage machine
h	enthalpy of fluid per unit mass (Btu/lbm, kJ/kg)
Δh_{0s}	stagnation enthalpy change per unit mass flow rate across each stage
k	ratio of specific heats
M_w	molecular weight
m	mass flow rate (lb _m /s, kg/s)
p	pressure (psi, Pa)
P_s	shaft power (lb _f -ft/s, hp, kW)
Δp	pressure rise or change (psi, Pa)
Q	heating value (Btu/lb _m , kJ/kg)
R	gas constant [Btu/(lb _m -R), kJ/(kg-K)]; Rankine (absolute temperature scale in English system)
R_h	reheat factor
ST	steam turbine
s	entropy of fluid per unit mass [Btu/(lb _m -R), kJ/(kg-K)]
T	temperature (°F, R, °C, K)
U, U	impeller peripheral velocity (ft/s, m/s)
V, \mathbf{V}	absolute flow velocity (ft/s, m/s)
W, \mathbf{W}	relative flow velocity with respect to impeller (ft/s, m/s)
y	moisture content of two-phase mixture
Z	elevation (ft, m); compressibility factor

Greek Letters.

ε	utilization factor
ρ	fluid density (lbm/ft ³ , kg/m ³)
π	3.14159
ω	rotating speed (rad/s)
η	efficiency
λ	turbine tip speed ratio ($= U_t / V$)
τ	shaft torque (lb _f -ft, Nt-m)

Subscripts.

1	inlet of nozzle/stator for turbines; condition 1
2	inlet of turbine impeller/rotor; condition 2
3	outlet of turbine impeller/rotor, condition 3
<i>a</i>	actual
ad	adiabatic process
o/a	overall
<i>c</i>	critical property
<i>f</i>	frictional, fuel
<i>h</i>	heating
<i>i</i>	inlet; ideal condition; input; internal
<i>l</i>	leakage
lq	liquid
<i>m</i>	mechanical
mx	mixture
<i>n</i>	nozzle
<i>o</i>	outlet; output; universal
0	stagnation (or total) property
01	stagnation (or total) property at inlet
02	stagnation (or total) property at discharge
<i>b</i>	brake
<i>R</i>	reduced property
<i>s</i>	stator; per stage; properties along isentropic process
<i>t</i>	turbine; tip; tank; total
th	theoretical; thermal
<i>u</i>	tangential direction
<i>v</i>	volumetric; viscous

REFERENCES

1. M. J. Moran and H. N. Shapiro, *Fundamentals of Engineering Thermodynamics*, 3rd ed., Wiley, New York, 1995.
2. J. B. Jones and G. A. Hawkins, *Engineering Thermodynamics*, 2nd ed., Wiley, 1986.
3. W. W. Peng, *Fundamentals of Turbomachinery*, Wiley, Hoboken, NJ, 2008.
4. M. Kutz, (Ed.), *Mechanical Engineers' Handbook*, 3rd ed., Wiley, Hoboken, NJ, 2006.
5. S. L. Dixon, and C. A. Hall, *Fluid Mechanics and Thermodynamics of Turbomachinery*, 6th ed., Elsevier Burlington, MA, 2010.

1054 Steam Turbines

6. H. Gartmann, (Ed.), *De Laval Engineering Handbook*, 3rd ed, McGraw-Hill, New York, 1970.
7. E. F. Church, *Steam Turbines*, McGraw-Hill, New York, 1950.
8. M. P. Boyce, *Handbook for Cogeneration and Combined Cycle Power Plants*, ASME Press, New York, 2002.
9. L. C. Wilbur, (Ed.), *Handbook of Energy Systems Engineering*, Wiley, New York, 1985.
10. S. C. Kaushik, A. Dubey, and M. Singh, "Steam Rankine Cycle Cooling System: Analysis and Possible Refinements," *Energy Con. Manage.* **35**(10), 871–886, 1994.

CHAPTER 31

FUEL CELLS

Matthew M. Mench

University of Tennessee

Knoxville, Tennessee

and

Oak Ridge National Laboratory

Oak Ridge, Tennessee

Feng-Yuan Zhang

University of Tennessee Space Institute

Tullahoma, Tennessee

1 INTRODUCTION	1055	2.4 H ₂ PEFC Performance	1070
2 BASIC OPERATING PRINCIPLES, EFFICIENCY, AND PERFORMANCE	1060	2.5 Technical Issues of the DMFC	1075
2.1 Description of a Fuel Cell Stack	1062	3 THE SOLID OXIDE FUEL CELL	1076
2.2 Performance and Efficiency Characterization	1063	3.1 Technical Issues of the SOFC	1077
2.3 Heat Management	1068	3.2 Performance and Materials	1077
		REFERENCES	1085

1 INTRODUCTION

In 1839, Sir William Grove conducted the first known demonstration of the fuel cell. It operated with separate platinum electrodes in oxygen and hydrogen submerged in a dilute sulfuric acid electrolyte solution, essentially reversing a water electrolysis reaction. Early development of fuel cells had a focus on use of coal to power fuel cells, but poisons formed by the gasification of the coal limited the fuel cell usefulness and lifetime.^{1,2} High-temperature solid oxide fuel cells (SOFC) began with Nernst's 1899 demonstration of the still-used yttria-stabilized zirconia solid-state ionic conductor, but significant practical application was not realized.³ The molten carbonate fuel cell (MCFC) utilizes a mixture of alkali metal carbonates retained in a solid ceramic porous matrix that become ionically conductive at elevated (> 600°C) temperatures and was first studied for application as a direct coal fuel cell in the 1930s.⁴ In 1933, Sir Francis Bacon began development of an alkaline-based oxygen–hydrogen fuel cell that achieved a short-term power density of 0.66 W/cm², relatively high even for today's standards. However, little additional practical development of fuel cells occurred until the late 1950s, when the space race between the United States and the Soviet Union catalyzed development of fuel cells for auxiliary power applications. Low-temperature polymer electrolyte fuel cells (PEFCs) were first invented by William Grubb at General Electric in 1955 and generated power for NASA's Gemini space program. However, short operational lifetime and high catalyst loading contributed to a shift to alkaline fuel cells (AFCs) for the NASA Apollo program, and AFCs still serve as auxiliary power units (APUs) for the space shuttle orbiter.

After the early space-related application, development of fuel cells went into relative abeyance until the 1980s. The phosphoric acid fuel cell (PAFC) became the first fuel cell system to reach commercialization in 1991. Although only produced in small quantities (twenty to forty 200-kW units per year) by United Technologies Company (UTC), UTC has installed and operated over two-hundred forty five 200-kW units in 19 countries worldwide, for applications such as reserve power for the First National Bank of Omaha. By 2002, these units logged over 5 million hours of operation with 95% fleet availability.²

Led by researchers at Los Alamos National Laboratory in the mid 1980s, resurgent interest in PEFCs was spawned through the development of a carbon-supported catalyst electrode assembly technique that enabled an order-of-magnitude reduction in noble-metal catalyst loading. This major breakthrough and ongoing environmental concerns, combined with availability of a nonhydrocarbon-based electrolytes with substantially greater longevity than those used in the Gemini program, has resurrected research and development of PEFCs for stationary, automotive, and portable power applications.

Research and development toward commercialization of high-temperature fuel cells including MCFC and SOFC systems has also grown considerably in the past two decades, with a bevy of demonstration units in operation and commercial sales of MCFC systems.

The science and technology of fuel cell engines is both fascinating and constantly evolving. This point is emphasized by Fig. 1, which shows the number of annual granted patents of fuel cells along with other renewable energy resources. Fuel cell technology has dominated intellectual property development in the renewable energy field based on patents granted, easily outpacing solar, wind, hybrid/electric, biofuel, and geothermal technologies.

Potential applications of fuel cells can be grouped into four main categories: (1) transportation, (2) portable power, (3) stationary or grid-based power, and (4) niche applications. As shown in Fig. 2, the total installed megawatts shipped of fuel cells has continually grown, with a slowdown in 2010 due to the global financial crisis. Automotive commercialization is

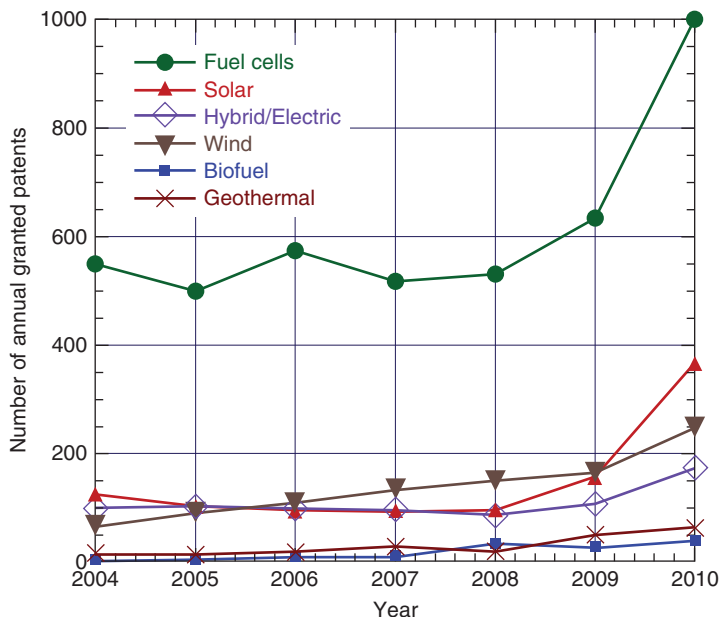


Figure 1 Timeline of worldwide patents in renewable energy resources. (Adapted from Ref. 5.)

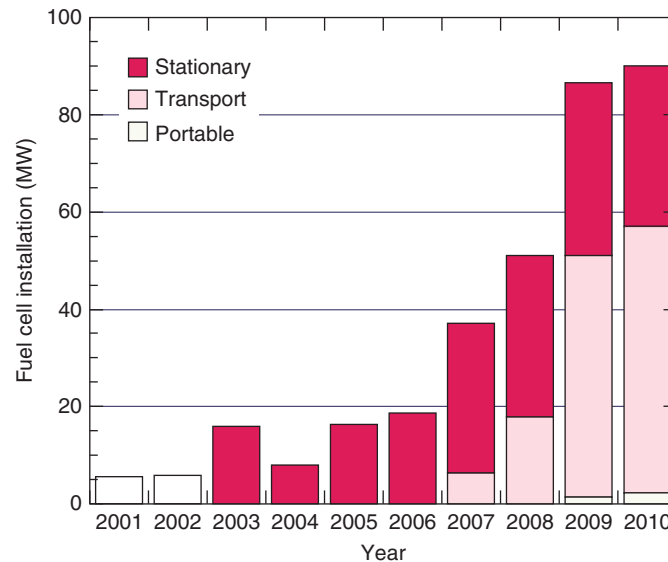


Figure 2 Fuel cell installations. (Based on data from Refs. 7 and 8, Reprinted with permission of ASME International.)

underway, and several major auto manufacturers have worked with governments in Europe and Asia to introduce early hydrogen fueling infrastructures and commercial vehicles in the 2015 time frame. Figure 3 shows a Department of Energy (DOE) projected fuel cell system cost for transportation, which is based on a high volume manufacturing of about 500,000 vehicles per years. The cost has been decreased over 80% since 2002 due to significant technical achievements, including cell performance, and reductions in catalyst loading and redesign of associated systems. The current cost of \$49/kW is now close to the target of \$30/kW established for 2015.⁶ The existing combustion engine technology market dominance will be difficult to usurp, considering its slight lower cost (\$20–30/kW), high durability, high power density, suitability for rapid cold start, and high existing degree of optimization. Additionally, the recent success of high-efficiency hybrid electric/combustion engine technology adds another rapidly evolving target fuel cells must match to compete.

Arguably where fuel cells show the most promise for ubiquitous near-term implementation is in portable power applications, such as cell phones and laptop computers. Toshiba and other companies have already developed a handheld direct methanol fuel cell for portable power. The 8.5-g direct methanol fuel cell (DMFC) developed by Toshiba is rated at 100 mW continuous power (up to 20 h) and measures 22 mm × 56 mm × 4.5 mm with a maximum of 9.1 mm for the concentrated methanol fuel tank.⁹ Passive portable fuel cells can potentially compete favorably with advanced Li ion batteries in terms of gravimetric energy density of ~120–160 Wh/kg and volumetric energy density from ~230 to 270 Wh/L. Additionally, the cost of existing premium power battery systems is already on the same order as contemporary fuel cells, with additional development anticipated. With replaceable fuel cartridges, portable fuel cell systems have the additional advantage of instant and remote rechargeability that can never be matched with secondary battery systems. However, engineering, legal, and compatibility issues have hindered market application to date, although it is fair to say small handheld portable fuel cell units have reached the early commercialization stage.

Stationary and distributed power applications include power units for homes or auxiliary and backup power generation units. Stationary applications (1–500 kW) are designed for nearly

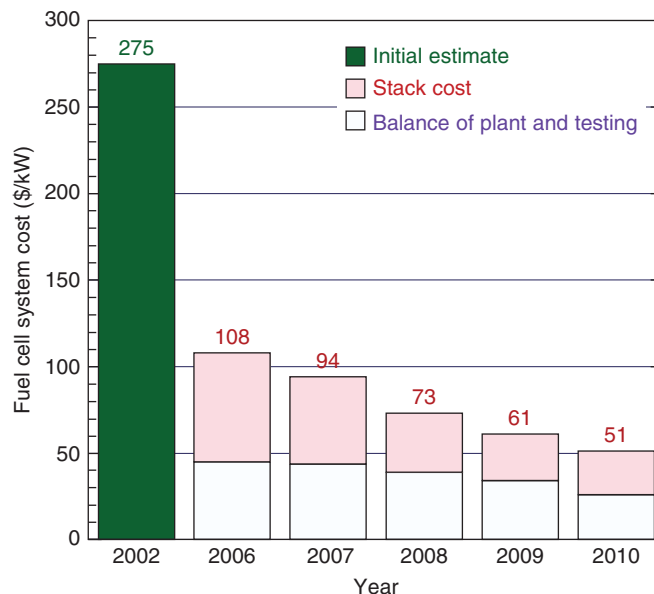


Figure 3 Projected cost of an 80-kW_{net} proton exchange membrane (PEM) fuel cell system. (Based on data from Ref. 6.)

continuous use and, therefore, must have far greater lifetime than automotive units. Distributed power plants are designed for megawatt-level capacity, and some have been demonstrated to date. In particular, a 2-MW MCFC was demonstrated by Fuel Cell Energy in California.¹⁰ As shown in Fig. 2, the fuel cell power installed for stationary power has steadily increased, especially in Japan and Europe. Earlier growth corresponded mostly to PAFC units, although recently most additional units have been PEFC. Not surprisingly, the exponential growth in the number of online units follows a similar qualitative trend to the available patents granted for various fuel cell technologies shown in Fig. 1. The early rise in stationary units in 1997 was primarily PAFC systems sold by United Technologies Center Fuel Cells, as shown in Fig. 4. Data are estimated from the best available compilation available online at Ref. 7, and some manufacturers do not advertise prototype demonstrations, so that numbers are not exact, however, the trend is clear.

The fundamental advantages common to all fuel cell systems include:

1. A potential for a relatively high operating efficiency, scalable to all size power plants.
2. If hydrogen is used as fuel, greenhouse gas emissions are strictly a result of the production process of the fuel stock used.
3. No moving parts, with the significant exception of pumps, compressors, and blowers to drive fuel and oxidizer.
4. Multiple choices of potential fuel feedstocks, from existing petroleum, natural gas, or coal reserves to renewable ethanol or biomass hydrogen production.
5. A nearly instantaneous recharge capability compared to batteries.

The following technical limitations common to all fuel cell systems must be overcome before successful implementation can occur:

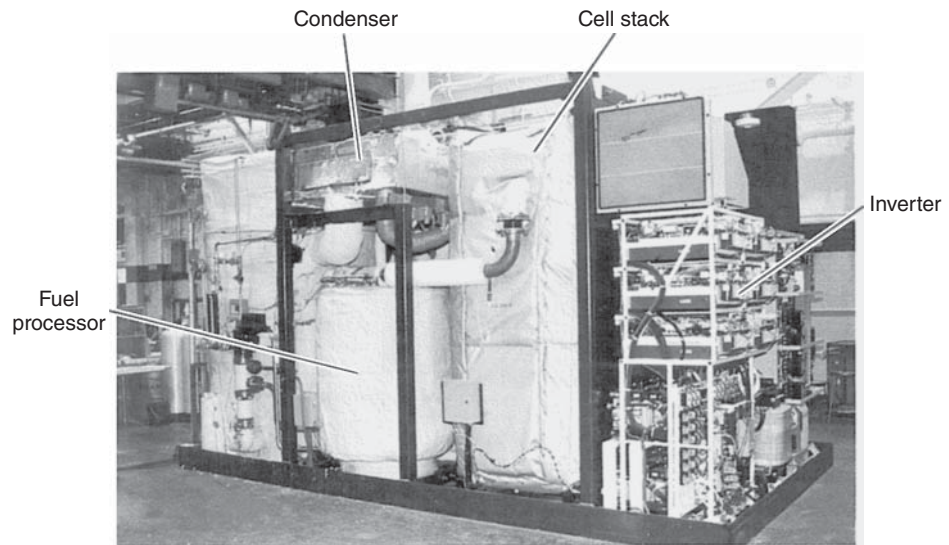


Figure 4 Picture of 200-kW PC25 PAFC power plant manufactured by United Technologies Corporation. (From Ref. 11.)

1. Alternative materials and construction methods must be developed to reduce fuel cell system cost to be competitive with the automotive combustion engine ($\sim \$30/\text{kW}$) and stationary power systems ($\sim \$500/\text{kW}$). The cost of the catalyst no longer dominates the price of most fuel cell systems, as residual system and stack costs are now comparable. Manufacturing and mass production technology is now a key component to the commercial viability of fuel cell systems.

2. Suitable reliability and durability must be achieved. The performance of every fuel cell gradually degrades with time, due to a variety of phenomena. The automotive fuel cell must withstand load cycling and freeze/thaw environmental swings with an acceptable level of degradation from the beginning-of-lifetime (BOL) performance over a lifetime of 5500 or more hours. A stationary fuel cell must withstand over 40,000 h of steady operation under vastly changing external temperature conditions.¹²

3. Suitable system power density and specific power must be achieved. The U. S. Department of Energy year 2015 targets for system power density and specific power are 650 W/kg and 650 W/L for automotive (80 kW) applications, 100 W/kg and 100 W/L for auxiliary (5–10 kW peak) applications, and 100 W/kg and 100 W/L for portable (mW–50 W) power systems.¹³ Current systems fall well short of these targets.

4. Fuel storage and delivery technology must be advanced if pure hydrogen is to be used. The issue of hydrogen infrastructure, i.e., production, storage, and delivery, is not addressed herein but is nevertheless critical. This topic is addressed in detail in Ref. 14.

5. Fuel reformation technology must be advanced if a hydrocarbon fuel is to be used for hydrogen production.

6. Desired performance and longevity of ancillary system components must be achieved. New hardware (e.g., efficient transformers and high-volume blowers) will need to be developed to suit the needs of fuel cell power systems.

The particular limitations and advantages of several different fuel cell systems will be discussed in this chapter in greater detail.

2 BASIC OPERATING PRINCIPLES, EFFICIENCY, AND PERFORMANCE

Figure 5 shows a schematic of a generic fuel cell. Electrochemical reactions for the anode and cathode are shown for the most common fuel cell types. Table 1 presents the various types of fuel cells, operating temperature, electrolyte material, and likely applications. The operating principle of a fuel cell is similar to a common battery, except that a fuel (hydrogen, methanol, or other) and oxidizer (commonly air or pure oxygen) are brought separately into the electrochemical reactor from an external source, whereas a battery has stored reactants. Referring to Fig. 5, separate liquid- or gas-phase fuel and oxidizer streams enter through flow channels, separated by the electrolyte/electrode assembly. Reactants are transported by diffusion and/or convection to the catalyzed electrode surfaces, where electrochemical reactions take place. Some fuel cells (alkaline and polymer electrolyte) have a porous (typical porosity $\sim 0.5\text{--}0.8$) contact layer between the electrode and current collecting reactant flow channels that functions to transport electrons and species to and from the electrode surface. In PEFCs, an electrically conductive carbon paper or cloth diffusion medium (DM) layer [also called gas diffusion layer (GDL), or porous transport layer (PTL)], serves this purpose and covers the anode and cathode catalyst layer.

At the anode electrode, the electrochemical oxidation of the fuel produces electrons that flow through the bipolar plate (a.k.a. cell interconnect) to the external circuit, while the ions migrate through the electrolyte. The electrons in the external circuit drive the load and return to

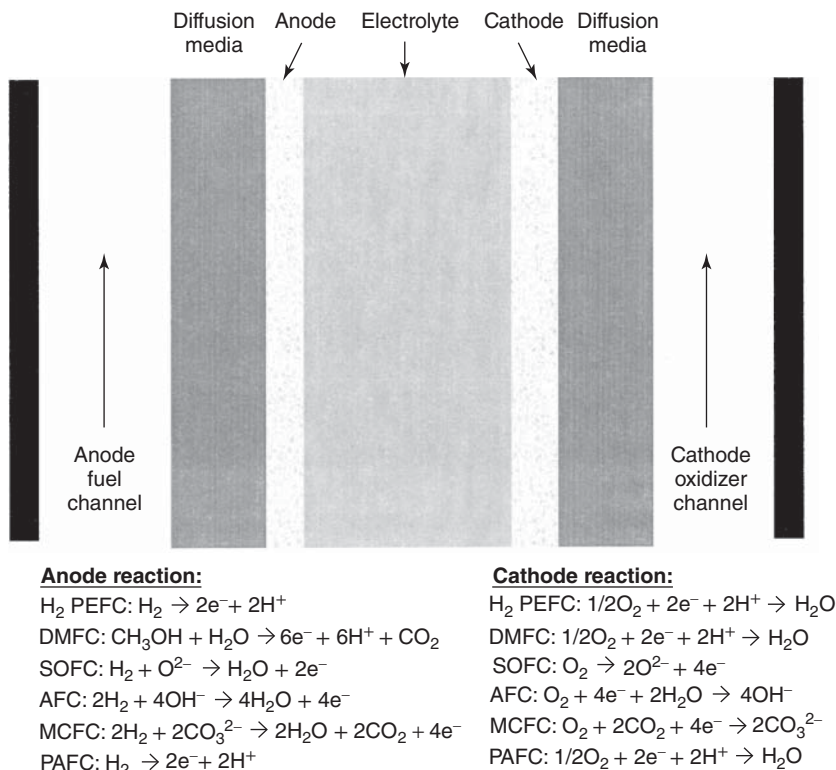


Figure 5 Schematic of a generic fuel cell.

Table 1 Fuel Cell Types, Descriptions, and Basic Data

Fuel Cell Type	Electrolyte Material	Operating Temp.	Major Poison	Advantages	Disadvantages	Most Promising Applications
Alkaline Fuel Cell (AFC)	Solution of potassium hydroxide in water	60-250°C* *modern AFCs < 100°C	CO ₂	High efficiency, low oxygen reduction reaction losses	Must run on pure oxygen without CO ₂ contaminant	Space applications with pure O ₂ /H ₂ available
Phosphoric Acid Fuel Cell (PAFC)	Solution of phosphoric acid in porous silicon carbide matrix	160-220°C	Sulfur, high levels of CO	1-2% CO tolerant Good quality waste heat Demonstrated durability	Low power density, expensive Platinum catalyst used Slow start-up Loss of electrolyte	Premium stationary power
Solid Oxide Fuel Cell (SOFC)	yttria (Y ₂ O ₃) stabilized zirconia (ZrO ₂)	600-1000°C	Sulfur	CO tolerant Fuel flexible High quality waste heat Inexpensive catalyst	Long start-up time Durability under thermal cycling Inactivity of electrolyte below -800°C	Stationary power with cogeneration Continuous power applications
Molten Carbonate Fuel Cell (MCFC)	molten alkali metal (Li/K or Na) carbonates, in porous matrix	600-800°C	Sulfur	CO tolerant Fuel flexible High quality waste heat Inexpensive catalyst	Electrolyte dissolves cathode catalyst Extremely long start-up time Carbon dioxide must be injected to cathode Electrolyte maintenance	Stationary power with cogeneration Continuous power applications
Polymer Electrolyte Fuel Cell (PEFC)*	Flexible solid perfluorosulfonic acid polymer	30-100°C	CO, Sulfur, Metal Ions Peroxide	Low temperature operation High efficiency High H ₂ power density Relatively rapid start-up	Expensive catalyst Durability of components not yet sufficient Poor quality waste heat Intolerance to CO Thermal and water management	Portable, automotive, and stationary applications

* Includes direct methanol fuel cell (DMFC) and direct alcohol fuel cells (DAFC)

the cathode catalyst where they recombine with the oxidizer in the cathodic oxidizer reduction reaction (ORR). The outputs of the fuel cell are thus threefold: (1) chemical products, (2) waste heat, and (3) electrical current.

A number of fuel cell varieties have been developed to differing degrees, and the most basic nomenclature of fuel cells is related to the electrolyte utilized. For instance, an SOFC has a solid ceramic oxide electrolyte, and a PEFC has a flexible polymer electrolyte, etc. Additional subclassification of fuel cells beyond the basic nomenclature can be assigned in terms of fuel used (e.g., hydrogen PEFC or direct methane SOFC) or the operating temperature range.

Each fuel cell variant has particular advantages that engender use for particular applications. In general, low-temperature fuel cells (e.g., PEFC, AFC) have advantages in startup time and potential efficiency, while high-temperature fuel cells (e.g., SOFC, MCFC) have an advantage in raw materials (catalyst) cost and quality and ease of rejection of waste heat. Medium-temperature fuel cells (e.g., PAFC) have some of the advantages of both high- and low-temperature classification. Ironically, a trend in SOFC development is to enable lower temperature (<600°C) operation, while a focus of current PEFC research is to operate at a higher (>120°C) temperature. Although the alkaline and phosphoric acid fuel cell had much research and development in the past, and the molten carbonate fuel cell is still under development, fuel cell technologies under the most aggressive development are still the polymer electrolyte and the solid oxide fuel cells.¹

2.1 Description of a Fuel Cell Stack

A single cell can theoretically be made to achieve whatever current and power is required, simply by increasing the size of the active electrode area and reactant flow rates. The output voltage of a single fuel cell is always less than one volt for realistic operating conditions, limited by the fundamental electrochemical potential of the reacting species involved. Therefore, for most applications and for compact design, a fuel cell stack of several individual cells connected in series is utilized. Figure 6 is a schematic of a generic planar fuel cell stack assembly and shows

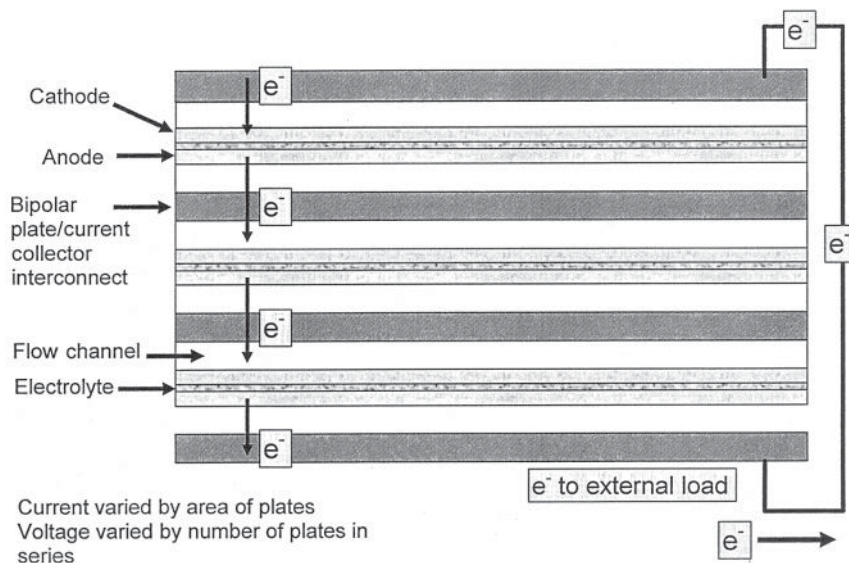


Figure 6 Schematic of the fuel cell stack concept.

the flow of current through the system. For a stack in series, the total current is proportional to the active electrode area of the cells in the stack, and is the same through all cells in the stack, and the total stack voltage is the sum of the individual cell voltages. For applications that benefit from higher voltage output, such as automotive stacks, over 200 fuel cells in a single stack is typical. In many systems, additional stacks in parallel are added to provide reliability through redundancy.

Other components necessary for fuel cell system operation include subsystems for oxidizer delivery, electronic control including voltage regulation, fuel storage and delivery, fuel recirculation/consumption, stack temperature control, and systems sensing of control parameters. For the PEFC, separate humidification systems are also needed to ensure optimal performance and stability. A battery is often used to start reactant pumps/blowers during startup. In many fuel cells operating at high temperature, such as an SOFC or MCFC, a preheating system is needed to raise cell temperatures during startup. This is typically accomplished with a combustion chamber that burns fuel and oxidizer gases. In all commercial fuel cells, provision must be made for effluent recovery. Fuel utilization efficiency is not 100% due to concentration polarization limitation on performance, so that unused fuel must be actively recycled, utilized, or converted prior to exhaust to the environment. Potential effluent management schemes include the use of recycling pumps, condensers (for liquid fuel), secondary burners, or catalytic converters.

2.2 Performance and Efficiency Characterization

The single cell combination shown in Fig. 5 provides a voltage dependent on operating conditions such as temperature, pressure, applied load, and fuel/oxidant flow rates. The thermal fuel cell voltage corresponds to a 100% efficient fuel cell and is shown as

$$E_{\text{th}} = -\frac{\Delta H}{nF} \quad (1)$$

This is the total thermal voltage potential available, if all chemical energy was converted to electrical potential. This is not possible, however, due to entropy change during reaction.

Consider a generalized global fuel cell reaction:



the maximum possible electrochemical potential can be calculated from the Nernst equation as

$$E^\circ = \frac{-\Delta G^\circ(T)}{nF} + \frac{RT}{nF} \ln \left[\frac{a_A^{v_A} a_B^{v_B}}{a_C^{v_C} a_D^{v_D}} \right] \quad (3)$$

where the $\Delta G^\circ(T)$ is evaluated at the fuel cell temperature and standard pressure, and the pressure dependency is accounted for in the second term on the right. The activity of gas-phase reactants, besides water vapor, can be calculated from

$$a_i = \frac{y_i P}{P^\circ} \quad (4)$$

where P° is a standard pressure of 1 atm. Under less than fully saturated local conditions, the activity of water vapor can be shown to be the relative humidity (RH):

$$a_{\text{H}_2\text{O}} = \frac{y_{\text{H}_2\text{O}} P}{P_{\text{sat}}(T)} = \text{RH} \quad (5)$$

where P_{sat} is the saturation pressure of water vapor at the fuel cell temperature. Because water is a product of the reaction and Eq. (5) references the local activity on the catalyst surface as opposed to free stream values, local values of $\text{RH} = 1$ are normally used.

Because a fuel cell directly converts chemical energy into electrical energy, the maximum theoretical efficiency is not bound by the Carnot cycle but is still not 100% due to entropy

change via reaction. The maximum thermodynamic efficiency is simply the ratio of the maximum achievable electrochemical potential to the maximum thermal potential:

$$\eta_{\text{th}} = \frac{E^{\circ}}{E_{\text{th}}} = \frac{\Delta G}{\Delta H} = \frac{\Delta H - T \Delta S}{\Delta H} = 1 - \frac{T \Delta S}{\Delta H} \quad (6)$$

The actual operating thermodynamic (voltaic) efficiency of the fuel cell is the actual fuel cell voltage, E_{fc} divided by E_{th} . The operating efficiency is really a ratio of the useful electrical output and heat output. If water is generated by reaction, as is the case with most fuel cell systems, efficiency and voltage values can be based on the low heating value (LHV) (all water generated is in the gas phase) or the high heating value (HHV) (all water generated is in the liquid phase). Representation with respect to the LHV accounts for the latent heat required to vaporize liquid water product, which is the natural state of the fuel cell system. Selection of the LHV or HHV representations are arbitrary, and do not necessarily represent the actual physical state of a portion of all of the product water.

Table 2 shows a selection of fuel cell reactions and the calculated maximum theoretical efficiency at 298 K. Typical values for maximum efficiency at open circuit calculated from Eq. (6) range from 60 to 90%, and vary with temperature according to the sign of the net entropy change. That is, according to Eq. (6), the efficiency will decrease with temperature if the net entropy change is negative and increase with temperature if ΔS is positive (since ΔH is negative for an exothermic reaction). Based on the Le Chatelier principle, we can predict the qualitative trend in the functional relationship between maximum efficiency and temperature. If the global fuel cell reaction ($\nu_A + \nu_B = \nu_C + \nu_D$) has more moles of gas-phase products than reactants (e.g., $\nu_C + \nu_D > \nu_A + \nu_B$), ΔS will be positive, and η_{th} will *increase* with temperature. Liquid- or solid-phase species have such low relative entropy compared to gas-phase species they have negligible impact on ΔS . These fuels yield a theoretical maximum efficiency greater than 100%! Physically, this means the reaction would absorb heat from the environment and convert the energy into voltage potential. An example of this is a direct carbon fuel cell. Although use of ambient heat to generate power with an efficiency greater than 100% seems like an amazing possibility, the entropy of the universe still increases as it must, and a practical efficiency near 100% is not realistic due to various losses. If the number of gas-phase moles is the same between products and reactants, the η_{th} is basically invariant with temperature and near 100%, as in the methane-powered fuel cell with gas-phase water produced. Most fuel cells, including those with hydrogen fuel, have less product gas-phase moles compared to the reactants, and the ΔS is negative. Thus, for these fuel cells the η_{th} will *decrease* with operating temperature.

Figure 7 shows the calculated maximum thermodynamic efficiency of a hydrogen–air fuel cell with temperature compared to that of a heat engine. Since the maximum heat engine efficiency is the Carnot efficiency, it is an increasing function of temperature. It is important to realize that fuel cell systems are not inherently more efficient than all heat engine alternatives. Note that at a certain temperature above 600°C, the theoretical maximum

Table 2 Some Common Fuel Cell Reactions and Maximum Theoretical Efficiency at 298 K

Fuel	Global Reaction	n (electrons per mole fuel)	Maximum η_{th} (HHV)
Hydrogen	$\text{H}_2 + 1/2\text{O}_2 \rightarrow \text{H}_2\text{O}_1$	2	83
Methanol	$\text{CH}_3\text{OH} + 3/2\text{O}_2 \rightarrow \text{CO}_2 + 2\text{H}_2\text{O}_1$	6	97
Methane	$\text{CH}_4 + 2\text{O}_2 \rightarrow \text{CO}_2 + 2\text{H}_2\text{O}_1$	8	92
Formic acid	$\text{HCOOH} + 1/2\text{O}_2 \rightarrow \text{CO}_2 + \text{H}_2\text{O}_1$	2	106
Carbon monoxide	$\text{CO} + 1/2\text{O}_2 \rightarrow \text{CO}_2$	2	91
Carbon	$\text{C}_s + 1/2\text{O}_2 \rightarrow \text{CO}$	2	124

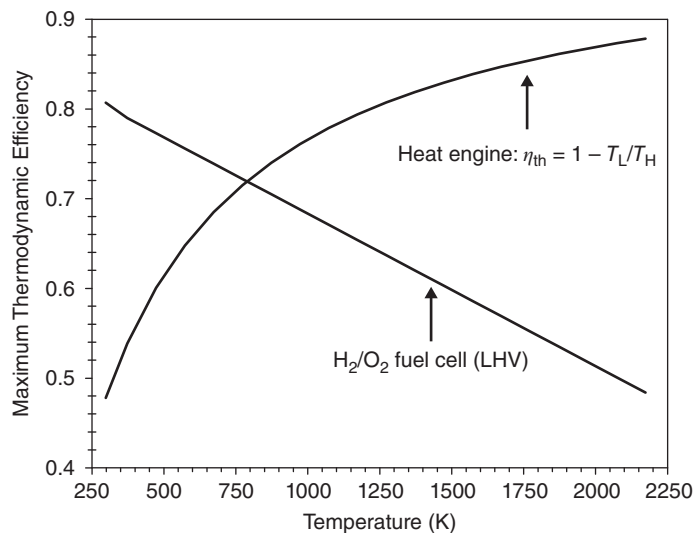


Figure 7 Maximum thermodynamic efficiency of a fuel cell and heat engine.

efficiency of the hydrogen–air fuel cell actually becomes *less* than that of a heat engine. In fact, high-efficiency combined-cycle gas turbines can now achieve power conversion efficiencies that rival high-temperature SOFCs. In practice, a 100-kW system operated by Dutch and Danish utilities has demonstrated an operating efficiency of 46% (LHV) over more than 3700 h of operation.¹⁵ Combined fuel cell/bottoming cycle and cogeneration plants can achieve operational efficiencies as high as 80%, with very low pollution. Another major advantage of fuel cells compared to heat engines is that efficiency is not a major function of device size, so that high-efficiency power for portable electronics can be realized, whereas small-scale heat engines have very low efficiencies due to heat transfer from high surface area to volume ratio. In terms of automotive applications, fuel cell hybrid and stand-alone systems operating with a variety of, but not all, fuel feedstocks have the potential for greater than double the equivalent mileage as conventional vehicles.¹⁶

Thermodynamic efficiency is not the entire picture, however, as the overall fuel cell efficiency must consider the utilization of fuel and oxidizer. The appropriate mass flow rate of reactants into the fuel cell is determined by several factors related to the minimum requirement for electrochemical reaction, thermal management, and issues related to the particular type of fuel cell. However, the *minimum* flow requirement is prescribed by the electrochemical reaction. An expression for the molar flow rate of species required for electrochemical reaction can be shown from Faraday's law as¹⁷

$$\dot{n}_k = \frac{iA}{n_k F} \quad (7)$$

where i and A represent the current density and total electrode area, respectively, and n_k represents the electrons generated in the global electrode reaction per mole of reactant k . For fuel cells, the stoichiometric ratio or stoichiometry for an electrode reaction is defined as the ratio of reactant delivered to that required for the electrochemical reaction.

$$\text{Anode: } \xi_a = \frac{\dot{n}_{\text{fuel,actual}}}{\dot{n}_{\text{fuel,required}}} = \frac{\dot{n}_{\text{fuel,actual}}}{iA/n_{\text{fuel}}F} \quad \text{Cathode: } \xi_c = \frac{\dot{n}_{\text{ox,actual}}}{\dot{n}_{\text{ox,required}}} = \frac{\dot{n}_{\text{ox,actual}}}{iA/n_{\text{ox}}F} \quad (8)$$

The stoichiometry can be different for each electrode and must be greater than unity. This is due to the fact that zero concentration near the fuel cell exit will result in zero voltage from Eq. (3). Since the current collectors are electrically conductive, a large potential difference cannot exist and cell performance will decrease to zero if reactant concentration goes to zero. As a result of this requirement, fuel and oxidizer utilization efficiency is never 100%, and some system to recycle or consume the effluent fuel from the anode is typically required to avoid releasing unused fuel to the environment. Thus, the overall operating efficiency of a fuel cell can be written as the product of the voltaic and Faradaic (fuel utilization) efficiencies:

$$\eta_{fc} = \eta_{th} \cdot \frac{1}{\xi_a} \frac{1}{\xi_c} \quad (9)$$

Polarization Curve

Figure 8 is an illustration of a typical polarization curve for a fuel cell with negative ΔS , such as the hydrogen–air fuel cell, showing five regions labeled I–V. The polarization curve, which represents the cell voltage versus current relationship, is the standard figure of merit for evaluation of fuel cell performance. Also shown in Fig. 8 are the regions of electrical and heat generation. Since the thermodynamically available power not converted to electrical power is converted to heat, the relationship between current and efficiency can be clearly seen by comparing the relative magnitude of the voltage potential converted to waste heat and to electrical power. Region V is the departure from the maximum thermal voltage, caused by entropy generation. In practice, the open-circuit voltage achieved is somewhat less than that calculated from the Nernst equation. Region IV represents this departure from the calculated maximum open-circuit voltage. This loss can be very significant and for PEFCs is due to undesired species crossover through the thin-film electrolyte and resulting mixed potential at the electrodes. For other fuel cells, there can be some loss generated by internal currents from electron leakage through the electrolyte. This is especially a challenge in SOFCs. Beyond the departure from

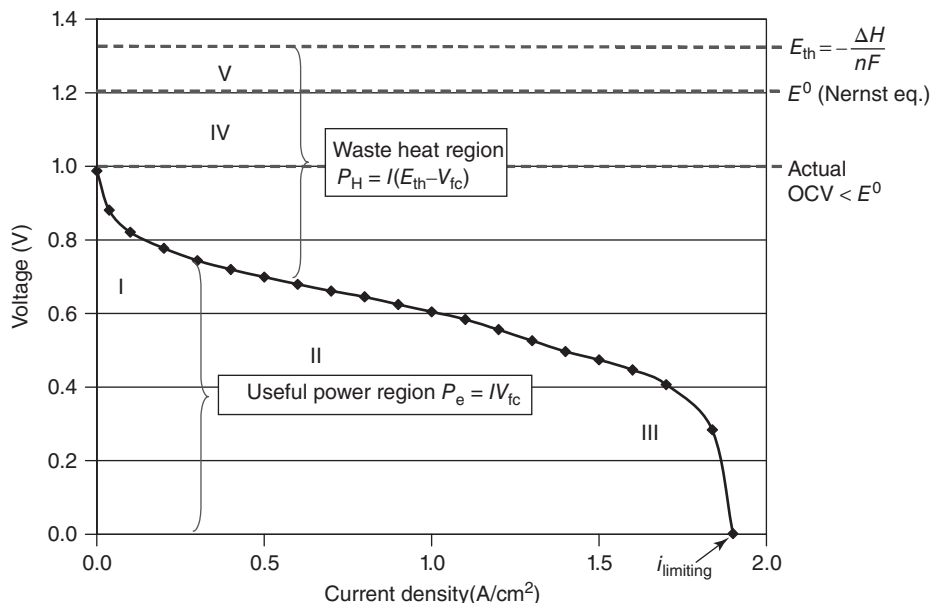


Figure 8 Illustration of a typical polarization curve for a fuel cell.

the theoretical open-circuit potential, there are three major classifications of losses that result in a drop of the fuel cell voltage potential, shown in Fig. 8: (1) activation (kinetic) polarization (region I), (2) ohmic polarization (region II), and (3) concentration polarization (region III). It should be noted that voltage loss, polarization, and overpotential are all interchangeable and refer to a voltage loss. The operating voltage of a fuel cell can be represented as the departure from ideal voltage caused by these polarizations:

$$E_{fc} = E^0 - \eta_{a,a} - |\eta_{a,c}| - \eta_r - \eta_{m,a} - |\eta_{m,c}| \quad (10)$$

where E^0 is the theoretical Nernst open-circuit potential of the cell, and the activation overpotential at the anode and cathode are represented by $\eta_{a,a}$ and $\eta_{a,c}$, respectively. The ohmic (resistive) polarization is shown as η_r . The concentration overpotential at the anode and cathode are represented as $\eta_{m,a}$ and $\eta_{m,c}$, respectively. Cathode polarization losses are negative relative to the standard hydrogen electrode, so the absolute value is taken. Additional losses in region IV of Fig. 8 attributed to species crossover or internal currents can also be added to Eq. (10) as needed. Activation and concentration polarizations occur at both anode and cathode, while the resistive polarization represents ohmic losses throughout the fuel cell, and thus includes ionic, electronic, and contact resistance between all fuel cell components carrying current. It is important to note that the regions on the polarization curve of dominance kinetic, ohmic, or mass transfer polarizations are not discrete. That is, all modes of loss contribute throughout the entire current density range and there is no discrete “ohmic loss” region where other polarizations are not also contributing to total deviation below the Nernst potential. Although the activation overpotential dominates in the low current region, it still contributes to the cell losses at higher current densities where ohmic or concentration polarization dominates. Thus, each region is not discrete, and all types of losses contribute throughout the operating current regime.

Activation polarization, which dominates losses at low current density, is the voltage overpotential required to overcome the activation energy of the electrochemical reaction on the catalytic surface, and is commonly represented by a Butler–Volmer equation at each electrode¹:

$$i_{fc} = i_o \left\{ \exp\left(\frac{\alpha_a F n \eta}{RT}\right) - \exp\left(\frac{\alpha_c F n \eta}{RT}\right) \right\} \quad (11)$$

where α_a and α_c are the charge transfer coefficients for the anode and cathode, respectively. The fraction of the electrical overpotential (η) resulting in a change of the rate of reaction for the reduction branch of this electrode is shown as α_c . Obviously, $\alpha_a + \alpha_c = 1$. Here, n is the number of exchange electrons involved in the elementary electrode reaction, which is typically different from the n used in Eqs. (3) and (7). The exchange current density, i_o , represents the activity of the electrode for a particular reaction. In hydrogen PEFCs, the anode i_o for hydrogen oxidation is so high relative to the cathode i_o for oxygen reduction, that the anode contribution to this polarization is often neglected for pure hydrogen fuel. On the contrary, if neat hydrogen is not used, significant activation polarization losses at both electrodes are typical (e.g., the DMFC). It appears from Eq. (11) that activation polarization should increase with temperature. However, i_o is a highly nonlinear function of the kinetic rate constant of reaction and the local reactant concentration and can be modeled with an Arrhenius form as

$$i_o = i_o^0 \exp(-E_A/RT) \left(\frac{C_{ox}}{C_{ref}}\right)^\gamma \left(\frac{C_f}{C_{ref}}\right)^v \quad (12)$$

Thus, i_o is an exponentially increasing function of temperature, and the net effect of increasing temperature is to decrease activation polarization. For this reason, high-temperature fuel cells such as SOFC or MCFC typically have very low activation polarization and can use less exotic catalyst materials. Accordingly, the effect of an increase in electrode temperature is to decrease the voltage drop within the activation polarization region shown in Fig. 8. For various fuel cell systems, however, the operating temperature range is dictated by the electrolyte and materials properties, so that temperature cannot be arbitrarily increased to reduce activation losses.

At increased current densities, a primarily linear region is evident on the polarization curve. In this region, reduction in voltage is dominated by internal ohmic losses (η_r) through the fuel cell, which can be represented as

$$\eta_r = iA \left(\sum_{k=1}^n r_k \right) \quad (13)$$

where each r_k value is the area-specific resistance of individual cell components, including the ionic resistance of the electrolyte, and the electric resistance of bipolar plates, cell interconnects, contact resistance between mating parts, and any other cell components. With proper design and assembly, ohmic polarization is typically dominated by electrolyte conductivity for all fuel cell types.

At very high current densities, mass transport limitation of fuel or oxidizer to the corresponding electrode causes a sharp decline in the output voltage. This is referred to as concentration polarization. This region of the polarization curve is really a combined mass transport/kinetic related phenomenon, as the surface reactant concentration is functionally related to the exchange current density as shown in Eq. (12). In general, reactant transport to the electrode is limited to some value depending on operating conditions, porosity and tortuosity of the porous media, input stoichiometry, etc.¹⁸ If this limiting mass transport rate is approached by the consumption rate of reactant [Eq. (7)], the surface concentration of reactant will approach zero, and, from Eq. (3), the fuel cell voltage will also approach zero. The Damköler number (Da) is a dimensionless parameter that is the ratio of the characteristic electrochemical reaction rate to the rate of mass transport to the reaction surface. In the limiting case of infinite kinetics (high Damköler number), one can derive an expression for η_m as¹

$$\eta_m = -\frac{RT}{nF} \ln \left(1 - \frac{i}{i_l} \right) = -B \ln \left(1 - \frac{i}{i_l} \right) \quad (14)$$

where i_l is the limiting current density and represents the maximum current produced when the surface concentration of reactant is reduced to zero at the reaction site. The limiting current density (i_l) can be determined by equating the reactant consumption rate to the mass transport rate to the surface, which in itself can be a complex calculation. The strict application of Eq. (14) results in a predicted voltage drop-off that is much more abrupt than actually observed. To accommodate a more gradual slope, an empirical coefficient B is often used to fit model to experiment.¹⁹ Concentration polarization can also be incorporated into the exchange current density and kinetic losses as in Eq. (12).

2.3 Heat Management

While PEFC systems can achieve a high relative operating efficiency, the inefficiencies manifest as dissipative thermal losses. At the cell level, if waste heat is not properly managed, accelerated performance degradation or catastrophic failure can occur.²⁰ The total waste heat rate per cell can be shown as

$$P_{\text{waste}} = I(E_{\text{th}} - E_{\text{fc}}) \quad (15)$$

This heat generation can be broken into components and shown as²⁰

$$\begin{aligned} q'' = -i_{\text{fc}} \left[\frac{\Delta H}{nF} - \frac{\Delta G}{nF} - \eta_{a,a} - |\eta_{a,c}| - i_{\text{fc}} \sum_{k=1}^n r_k \right] \\ + i_{\text{fc}}^2 \sum_{k=1}^n r_k - i_{\text{fc}} \left(-\eta_{a,a} - |\eta_{a,c}| + \frac{T}{nF} \Delta S \right) \end{aligned} \quad (16)$$

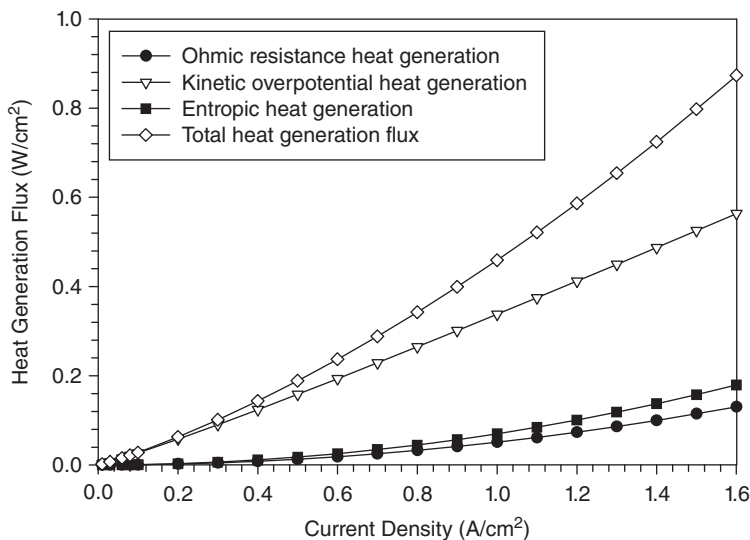


Figure 9 Calculated heat generation from activation, ohmic, and entropic sources as a function of current for a typical PEFC.

The first term on the right-hand side of Eq. (16) is Joule heating and is thus an i^2r relationship. The second and third terms of Eq. (16) represent the heat flux generated by activation polarization in the anode and cathode catalyst layers. This assumes the concentration dependence on exchange current density is included in the activation polarization terms. The third term in Eq. (16) is a linearly varying function of current density and represents the total Peltier heat generated via entropy change by reaction. The functional relationship derived in Eq. (16) is shown in Fig. 9, a plot of the heat generation via Peltier, Joule, and kinetic heating as a function of current density for a typical PEFC.²¹ The ionic conductivity for the electrolyte was chosen to be 0.1 S/cm, based on the assumption of a fully humidified membrane in contact with vapor-phase water,²² and other parameters were chosen as typical values. This plot should be viewed only as a guide to the qualitative behavior of the heat generation with current density, as each fuel cell and different operating condition will have much different distributions. For example, the SOFC typically has quite low activation polarization generated heat, due to the high operating temperatures. Note that an assumption of ohmic heating dominance is not always accurate, and entropic heat generation can be quite significant and cannot be ignored. For higher temperature fuel cells with low activation overpotential, the heat generation is dominated by ohmic and entropic terms.

Degradation

The lifetime of a fuel cell is expected to compete with existing power systems it would replace.¹² As a result, the automotive fuel cell must withstand load cycling and freeze–thaw environmental swings with minimal degradation over a lifetime of 5000 h.^{23,24} A stationary fuel cell, meanwhile, must withstand over 40,000 h of steady operation with minimal downtime. The fuel cell environment is especially conducive to degradation since a voltage potential difference exists that can promote undesired reaction, and some fuel cells operate at high temperature or have corrosive electrolytes.²⁵ Transient load cycling between high and low power points has also been shown to accelerate degradation, so that steady-state degradation rates may not be truly representative for transient systems. Many different modes of physicochemical degradation are known to exist, including:

1. *Catalyst or electrolyte poisoning and degradation.* Since the catalyst and electrolyte control the reaction and ohmic polarization, any poisoning or other degradation of these components will adversely affect cell performance.^{26,27} Some minor species in air and reformed gas product, such as carbon monoxide, will foul a platinum catalyst operating at low temperatures ($< 150^{\circ}\text{C}$). As a result, PEFCs are extremely susceptible to CO poisoning. Some surface absorption of species can be reversible, including adsorbed CO.²⁸ Sulfur is also a major contaminant that will greatly reduce performance in most fuel cells in extremely low ($< \text{ppb}$) concentrations. Many other low-level impurities can greatly harm fuel cell performance, e.g., CO_2 will degrade the electrolyte in AFCs. Given that the electrolyte is an ion conductor, when unintended ions are present in the fuel cell system by corrosion or other impurities, the electrolyte will absorb these impurities, which can alter the ionic conductivity of the media. In SOFCs, carbonaceous residue from internal performance can foul the anode catalyst.

2. *Electrolyte loss.* In some cases, electrolyte material is lost through a variety of physicochemical mechanisms.^{27,29} For polymer electrolyte fuel cells, the polymer itself can degrade physically and chemically, particularly from peroxide radical attack.³⁰ This results in loss of mass and conductivity in the electrolyte and possible catastrophic pinhole formation. For liquid electrolyte systems such as the AFC, PAFC, and MCFC, the finite vapor pressure of the liquid phase results in a steady but predictable loss of electrolyte through the reactant flow streams, which must be replenished with regularity or performance will suffer.

3. *Morphology changes or loss in the catalyst layer or other components.* For all fuel cells, the catalyst layer electrochemical active surface area (ECSA) is a determining factor in overall power density, and nano-sized catalysts and supports are present in a complex three-dimensional electrode structure designed to simultaneously optimize electron, ion, and mass transfer.^{26,31–33} As a result, any morphological changes can result in reduced performance. Commonly observed phenomena include catalyst sintering, dissolution and migration, catalyst oxidation,³⁴ supporting material oxidation (e.g., carbon corrosion for carbon-supported catalysts), and Oswald ripening.³⁵ These effects are most often irreversible. Other components can also be chemically or physically altered, such as the porosity distribution or hydrophobicity of the gas diffusion layer in a PEFC.^{24,36}

4. *Corrosion of other components.* Oxidation of other components such as the current collector can become a major loss in fuel cells over time.^{37,38} This is especially relevant in high-temperature MCFCs and SOFCs, where the corrosion process is accelerated by the high temperature. Chromium used in SOFCs in stainless steel interconnects is believed to cause cathode degradation. Low-temperature PEFCs can also suffer losses from current collector corrosion, and proper coatings with high electronic conductivity must be used.³⁹

The Hydrogen PEFC

The hydrogen polymer electrolyte fuel cell (H_2 PEFC) is seen by many as the most viable alternative to heat engines and battery replacement for automotive, stationary, and portable power applications. The H_2 PEFC is fueled either by pure hydrogen or from a diluted hydrogen mixture generated from a hydrocarbon reformation process. An H_2 PEFC fuel cell stack power density of greater than 1.0 kW/L is typical.

2.4 H_2 PEFC Performance

H_2 PEFCs operate at $60\text{--}100^{\circ}\text{C}$. The anode and cathode catalyst is commonly $\sim 2\text{-nm}$ platinum or platinum–alloy powder supported on significantly larger size carbon particles with a total (anode and cathode) platinum loading of less than 0.4 mg/cm^2 . Recently, 2.0 A/cm^2 at 0.55 V/cell was obtained at 0.2 mg/cm^2 platinum loading.⁴⁰ This represents a major breakthrough in required catalyst loading from the 28 mg/cm^2 of the original 1960s H_2 PEFC. As a

result, the catalyst is no longer the dominating factor in fuel cell cost, although it is still higher than needed to reach long-term goals of another 20-fold reduction in loading or elimination of precious metals.⁴⁰ The state-of-the-art H₂ PEFC can reach nearly 0.7 V at 1 A/cm², under pressurized conditions at 80°C. There is always a desire to operate at high voltages because of increased efficiency and reduced flow requirements. However, power density typically peaks below 0.6 V, and high-voltage operation or heat generation can cause accelerated degradation, so there is a size tradeoff for high-voltage operation. Typical single-pass anode and cathode stoichiometry values are 2 for the cathode and around 1.2 for the anode, although the residual hydrogen is recycled.

Technical Issues in the Hydrogen PEFC

The H₂ PEFC has many technical issues that complicate performance and control. Besides issues of manufacturing, ancillary system components, cost, and market acceptance, the main remaining technical challenges for the fuel cell itself include (1) water and heat management, (2) durability, and (3) freeze–thaw cycling capability.

Water and Heat Management. For PEFCs, waste heat affects the water distribution by increasing temperature and thus the local equilibrium saturation pressure of the gases. At a typical PEFC operating temperature of 80°C and atmospheric pressure, each 1°C change in temperature results in an approximately 5% change in equilibrium saturation pressure.^{41–43} Thus, the thermal and water management and control are inexorably coupled at the individual cell and stack level, and even small variations in temperature can dramatically affect optimal humidity, locations of condensation/vaporization, membrane longevity, and a host of other phenomena. Due to heat generation, relatively high temperature gradients up to 10°C between the electrolyte and current collector can occur.⁴⁴ Analysis has shown that the through-plane thermal conductivity of carbon cloth gas diffusion media and Nafion[®] electrolyte material are approximately 0.15 and 0.1 W/m K, respectively.^{45,46} The main barrier to the heat transport is generally through the gas diffusion layer (GDL), which acts as a thermal insulator to limit conductive heat transfer. Once through the GDL, the majority of heat transfer is typically through the landings and not to the reactant in the flow channels.^{21,47}

For high-power (>kW) fuel cell stacks, waste heat must be properly managed with cooling channels, which take up space and require parasitic pumping losses. The choice of coolant is based on the necessary properties of high specific heat, nonconductive, noncorrosive, sufficient boiling/freezing points for operation in all environments, and low viscosity. Laboratory systems typically use deionized water, although practical systems exposed to the environment must use a lower freezing point nonconductive solution.

Water management and humidification is a major issue in H₂ PEFC performance. The most common electrolyte used in PEFCs is a perfluorosulfonic acid–polytetrafluoro ethylene (PTFE) copolymer in the acid (H⁺) form, known commercially as Nafion[®] (E. I. du Pont de Nemours). Nafion[®] electrolyte conductivity is primarily a function of water content and temperature, shown as²²

$$\sigma_e = 100 \exp \left[1268 \left(\frac{1}{303} - \frac{1}{T(K)} \right) \right] (0.005139\lambda - 0.00326) \quad (\text{in } 1/\Omega\text{m})$$

$$\text{where } \lambda = 0.043 + 17.18a - 39.85a^2 + 36.0a^3 \quad \text{for } 0 < a \leq 1$$

$$\lambda = 14 + 14(a - 1) \quad \text{for } 0 \leq a \leq 3$$

$$a = \text{water activity} = \frac{y_{\text{H}_2\text{O}}}{P_{\text{sat}}(T)} = \text{RH} \quad (17)$$

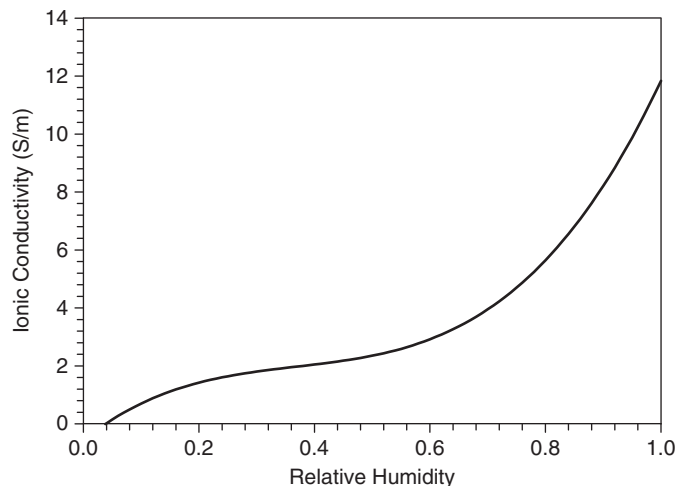


Figure 10 Electrolyte conductivity of Nafion® as a function of relative humidity at 80°C.

A plot of Nafion® conductivity as a function of humidity, based on Eq. (17), is given in Fig. 10. It is obvious that ionic conductivity is severely depressed without sufficient water. Alternatively, excessive water at the cathode can cause flooding, i.e., liquid water accumulation at the cathode surface that prevents oxygen access to the reaction sites. Flooding is most likely near the cathode exit under high-current-density, high-humidification, low-temperature, and low-flow-rate conditions. However, the term “flooding” has been rather nebulously applied in the literature to date, representing a general performance loss resulting from liquid water accumulation blocking reactant transport to the electrode. There are actually many discrete regions that can suffer flooding losses in the PEFC, the anode and cathode catalyst layers, the anode and cathode gas diffusion layers, interfaces between the various component layers, and the anode and cathode flow channels.^{48–54} Figure 11 is a radiograph image of a PEFC under severely flooded conditions, with significant diffusion media and channel-level flooding. In this image, the water accumulation was determined to be primarily in the anode flow channels. This phenomena can occur for low-flow-rate, low-power, and high-fuel-utilization conditions, which indicates that channel level flooding is not solely a cathode issue.

Depending on operating conditions, flow field design, and material properties, a membrane can have a highly nonhomogeneous water (and therefore ionic conductivity) distribution. The membrane beneath a long channel may be dried by hot inlet flow, ideally saturated near the middle of the cell, and experiencing flooding near the exit. It is difficult in practice to maintain an ideal water distribution throughout the length of the cell. Thus water transport is an especially important issue in PEFC design. Even a slight reduction in ohmic losses through advanced materials, thinner electrolytes, or optimal temperature–water distribution can significantly improve fuel cell performance, durability, and power density.

Figure 12 shows a schematic of the water transport and generation modes in the PEFC electrolyte membrane. At the cathode surface, the oxygen reduction reaction results in water production proportional to the current density via Faraday’s law. Water transport through the electrolyte occurs by diffusion, electroosmotic drag, thermoosmotic drag, and hydraulic permeation from a pressure difference across the anode and cathode. Diffusion through the electrolyte can be represented with Fick’s law, and appropriate expressions relating to diffusion coefficients for Nafion® can be found.⁵⁶ An electroosmotic drag coefficient (λ_{drag}) of 1–5 $\text{H}_2\text{O}/\text{H}^+$

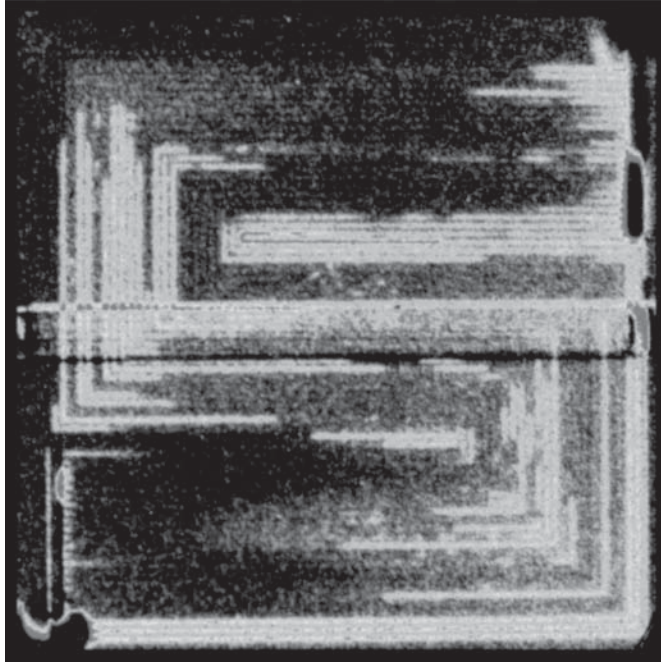


Figure 11 Neutron radiograph of 50 cm² active area fuel cell showing severe channel level flooding at low current density for an H₂ PEFC. (From Ref. 55.)

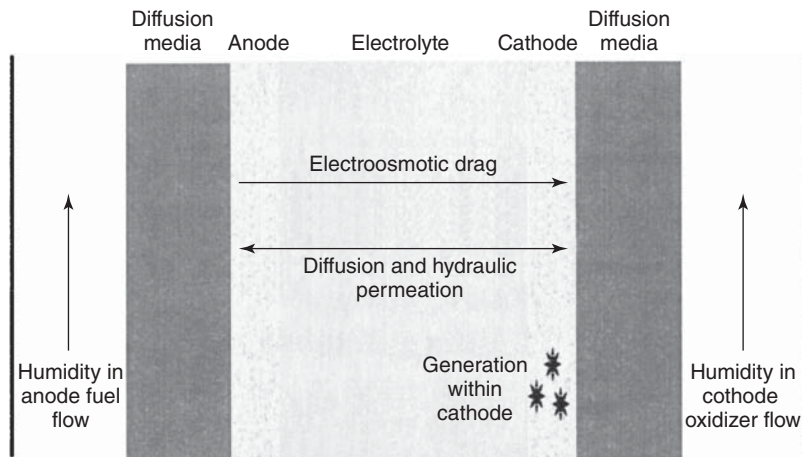


Figure 12 Schematic of water transport and generation modes in the PEFC.

of Nafion® membranes has been shown for a fully hydrated Nafion® 117 membrane.⁵⁷ The drag coefficient was shown to be a nearly linearly increasing function of temperature from 20 to 120°C. Thus, the water delivered to the cathode by this transport mode can be 2–10 times greater than that generated by reaction. Hydraulic permeation of water through the membrane under gas-phase pressure difference between the anode and cathode is usually small for H₂ PEFCs due to small pressure differences in the anode and cathode compartments. However, capillary pressure differences can result in a net flux of water via this mode of transport.⁵⁸ Combining the different forms of water transport through the membrane, the bulk molar water transport and creation at the cathode can be shown as

$$\dot{n}_{\text{H}_2\text{O}} = -DA \frac{\Delta C_{c-a}}{\Delta x} + \frac{iA}{F} (\lambda_{\text{drag}} + 0.5) - \dot{n}_{\text{pressure-driven, } a-c} + \dot{n}_{\text{thermo}} \quad (18)$$

where the last term on the right represents the flow of water by imbalanced pressure forces, which can be further represented by capillary and gas-phase pressure terms. Since the reduction reaction and electroosmotic drag result in water transport to and generation at the cathode surface, the flux of water by diffusion can be either to or from the anode surface, depending on local flow and humidity conditions. The flux by pressure difference is a function of tailorable material and operating properties and can flow toward either electrode, depending on the desire of the designer. The thermoosmotic term is normally small for low current or thin membranes,⁵⁹ but new, high-power fuel cells have been designed in which the temperature difference across the membrane is enough to cause significant thermoosmotic drag.⁶⁰

In order to achieve a proper water balance, many technologies have been employed, including tailored temperature or pressure gradients to absorb the net water generated. Flow field design also has a profound effect on the local liquid water distribution, and it is too detailed a topic to discuss in this chapter. The ambient relative humidity also should affect the system water balance; however, this effect is typically quite small due to the vast difference between typical ambient temperature and operating temperature $P_{g,\text{sat}}$ values. For example, even fully saturated inlet flow drawn from an ambient air source at 20°C ($P_{g,\text{sat}} = 2.338$ kPa) contains only 5% of the water required for saturation in a fuel cell operating at 80°C ($P_{g,\text{sat}} =$ kPa).⁵⁰

Durability and Freeze–Thaw Cycling. For PEFCs, durability and freeze–thaw cycling capability are major issues.²⁴ Durability issues in PEFCs have been discussed for fuel cells in general.⁶¹ For PEFCs, carbon support corrosion, morphological changes, susceptibility to chemical poisoning (especially carbon monoxide), catalyst loss, and electrolyte degradation all contribute to an operational degradation rate that is on the order of microvolts per hour under ideal steady conditions, which is still too high.⁶² Load cycling is known to initiate even greater degradation rate for a variety of reasons, so that steady-state laboratory testing typically underestimates true performance loss. Under nonoptimal higher temperature or low-humidity conditions, longevity is even less. Additionally, further system size and weight reductions are needed for automotive packaging requirements.

For automotive and stationary applications, PEFCs must withstand vastly changing environments as low as –40°C. Because the electrolyte contains water, freezing results in some ice formation and volume change, which can easily result in damage to the electrode structure and interfacial contact between the various layer structures. To compete with existing combustion-based technology, fuel cell stacks must achieve over 100 cold starts at –20°C with drivable power in under 5 s

The Direct Methanol Fuel Cell

The liquid-fed DMFC is seen by many as the most viable alternative to lithium ion batteries in portable applications because DMFC systems require less ancillary equipment and can

therefore be more simplified compared to an H₂ PEFC. While both H₂ PEFC and DMFC are strictly PEFCs (same electrolyte), the DMFC feeds a liquid solution of methanol and water to the anode as fuel. The additional complexities of the low-temperature internal reformation prevent the DMFC from obtaining the same level of fuel cell power density as the H₂ PEFC. For the DMFC, both anode and cathode activation polarizations are significant and are the same order of magnitude. However, reduced performance compared to the H₂ PEFC is tolerable in light of other advantages of the DMFC, namely:

1. Because the anode flow is mostly liquid (gaseous CO₂ is a product of methanol oxidation), there is no need for a separate cooling or humidification subsystem.
2. Liquid fuel used in the anode results in lower parasitic pumping requirements compared to gas flow. In fact, an emerging class of passive DMFC designs operate without any external parasitic losses, instead relying on natural forces such as capillary action, buoyancy, and diffusion to deliver reactants.^{63–65}
3. The highly dense liquid fuel stored at ambient pressure eliminates problems with fuel storage volume. With highly concentrated methanol as fuel (>10 M), passive DMFC system power densities can compare favorably to advanced Li ion batteries.

2.5 Technical Issues of the DMFC

Four main technical issues affecting performance remain, including: (1) water management, (2) methanol crossover, (3) managing two-phase transport in the anode, and (4) high activation polarization losses and catalyst loading. While significant progress has been made by various groups to determine alternative catalysts, total catalyst loading is still on the order of 10 mg/cm². Typically a platinum–ruthenium catalyst is utilized on the anode to reduce polarization losses from CO intermediate poisoning, and a Pt catalyst is used on the cathode.⁶⁶

External humidification is not needed in the DMFC, due to the liquid anode solution, but prevention of cathode flooding is critical to ensure adequate performance. Flooding is more of a concern for DMFCs than H₂ PEFCs because of constant diffusion of liquid water to the cathode. To prevent flooding, cathode airflow must be adequate to remove water at the rate that it arrives and is produced at the cathode surface. Assuming thermodynamic equilibrium, the minimum stoichiometry required to prevent liquid water accumulation in the limit of zero water diffusion through the membrane can be shown as⁶⁷

$$\xi_{c,\min} = \frac{2.94}{(p_{g,\text{sat}}/P_t - P_{g,\text{sat}})} + 1 \quad (19)$$

The factor of 1 in Eq. (21) is a result of the consumption of oxygen in the cathode by an electrochemical oxygen reduction reaction. For most cases, the minimum cathode stoichiometry for a DMFC is determined by flooding avoidance rather than electrochemical requirements. Therefore, optimal cathode stoichiometries are significantly greater than unity. It should be noted that Eq. (21) is purely gas phase and therefore does not allow for water removal in liquid phase, as droplets, a capillary stream out of the cathode or to the anode, or even entrained as a mist in the gas flow. Some recirculation of the water is needed from the cathode to the anode if neat methanol solution is used. In a totally passive system design, the hydrophobicity of the gas diffusion layer and catalyst can be tailored to pump water back to the anode via capillary action.

Another critical issue in the DMFC is methanol crossover from the anode to cathode. This is a result of diffusion, electroosmotic drag, and permeation from pressure gradients. Therefore, an expression for the methanol crossover through the membrane can be written similar to Eq. (18), with different transport properties. When crossover occurs, the mixed potential, caused by the anodic reaction on the cathode electrode, reduces cell output and the true stoichiometry of the cathode flow.

Of the three modes of methanol crossover, diffusion (estimated as $10^{-5.4163-999.778/T} \text{ m}^2/\text{s}$)⁶⁸ is dominant under normal conditions, especially at higher temperatures. Since the driving potential for oxidation is so high at the cathode, the methanol that crosses over is almost completely oxidized to CO_2 , which sets up a sustained maximum activity gradient in methanol concentration across the electrolyte. The electroosmotic drag coefficient of methanol (estimated as $0.16 \text{ CH}_3\text{OH}/\text{H}^+$,⁶⁹ or $2.5y$, where y is mole fraction of CH_3OH in solution⁷⁰) is relatively weak, owing to the nonpolar nature of the molecule. In order to prevent crossover so that more concentrated (and thus compact) solutions of methanol can be utilized as fuel, use of various diffusion barriers have been developed.^{71–73} That is, a porous filter in the GDL or separating the fuel from the fuel channel can be used to separate concentrated methanol solution from the membrane electrode assembly (MEA), greatly reducing crossover through the electrolyte.^{73,74} An earlier solution was used of a thicker electrolyte to reduce methanol crossover, but the concomitant loss in performance via increased ohmic losses through the electrolyte is unsatisfactory.

Several other transport-related issues are important to DMFC performance. The anode side is a two-phase system primarily consisting of methanol solution and product CO_2 . The methanol must diffuse to the catalyst, while the reaction-generated CO_2 must diffuse outward from the catalyst. At high current densities, CO_2 can become a large volume fraction ($> 90\%$) in the anode flow field. CO_2 removal from the catalyst sites is critical to ensure adequate methanol oxidation. Other disadvantages of the DMFC are related to use of methanol. Methanol is toxic, can spread rapidly into groundwater, has a colorless flame, and is more corrosive than gasoline.

3 THE SOLID OXIDE FUEL CELL

The SOFC and MCFC represent high-temperature fuel cell systems. The current operating temperature of most SOFC systems is around $800\text{--}1000^\circ\text{C}$, although new technology has demonstrated 600°C operation, where vastly simplified system sealing and materials solutions are feasible. High electrolyte temperature is required to ensure adequate ionic conductivity (of O^{2-}) in the solid-phase ceramic electrolyte and reduces activation polarization so much that cell losses are typically dominated by internal cell ohmic resistance through the electrolyte. Typical SOFC open-circuit cell voltages are around 1 V, very close to the theoretical maximum, and operating current densities vary greatly depending on design. While the theoretical maximum efficiency of the SOFC is less than the H_2 PEFC because of increased temperature, activation polarization is extremely low, and operating efficiencies as high as 60% have been attained for a 220-kW cogeneration system.⁷⁵

There has been much recent development in the United States on SOFC systems, incubated by the Department of Energy Solid State Energy Conversion Alliance (SECA) program. The 10-year goal of the SECA program is to develop kilowatt-sized SOFC APU units at \$400/kW with rated performance achievable over the lifetime of the application with less than 0.1% loss per 500 h operation by 2021.

The solid-state, high-temperature ($600\text{--}1000^\circ\text{C}$) SOFC system eliminates many of the technical challenges of the PEFC, while suffering unique limitations. SOFC power density varies greatly depending on cell design but can achieve above $400 \text{ mW}/\text{cm}^2$ for some designs. In general, an SOFC system is well suited for applications where a high operating temperature and a longer startup transient are not a limitation, or where conventional fuel feedstocks are desired.

The main advantages of the SOFC system include the following:

1. High operating temperature greatly reduces activation polarization and eliminates the need for expensive catalysts. This also provides a tolerance to a variety of fuel stocks and enables internal reformation of complex fuels.

2. High-quality waste heat, enabling a potential for high overall system efficiencies ($\sim 80\%$) utilizing a bottoming or cogeneration cycle.⁷⁶
3. Tolerance to carbon monoxide (CO), which is a major poison to Pt-based low-temperature PEFCs.

3.1 Technical Issues of the SOFC

Besides manufacturing and economic issues beyond the scope of this chapter, the main technical limitations of the SOFC include operating temperature, long startup time, durability, and cell sealing problems resulting from mismatched thermal expansion of materials. For additional details, an excellent text for SOFC was written by Minh and Takahashi.⁷⁷

The high operating temperature of the SOFC requires long startup time to avoid damage due to nonmatched thermal expansion properties of materials. Another temperature-related limitation is that no current generation is possible until a critical temperature is reached in the solid-state electrolyte, where oxygen ionic conductivity of the electrolyte becomes nonnegligible. Commonly used electrolyte conductivity is nearly zero until around 650°C ,¹⁹ although low-temperature SOFC operation at 500°C using doped ceria (CeO_2) ceramic electrolytes have shown feasibility.⁷⁸ In many SOFC designs, a combustor is utilized to burn fuel and oxidizer effluent to preheat the cell to light-off temperature and hasten startup, and provide a source of heat for cogeneration. In addition, the combustor effectively eliminates unwanted hydrogen or CO, which is especially high during startup when fuel cell performance is low. Additionally, electrolyte, electrode, and current collector materials must have matched thermal expansion properties to avoid internal stress concentrations and damage during both manufacture and operation.

The desire for lower temperature operation of the SOFC is ironically opposite to the PEFC, where higher operating temperature is desired to simplify water management and CO poisoning issues. Lower temperature ($\sim 400 - 500^\circ\text{C}$) operation would enable rapid startup, use of common metallic compounds for cell interconnects, reduce thermal stresses, reduce the rate of some modes of degradation, and increase reliability and reduced manufacturing costs. Despite the technical challenges, the SOFC system is a good potential match for many applications, including stationary cogeneration plants and auxiliary power.

Durability of SOFCs is not solely related to thermal mismatch issues. The electrodes suffer a strong poisoning effect from sulfur (in the ppb), requiring the use of sulfur-free fuels. Additionally, anode oxidation of nickel catalysts can decrease performance, and will do so rapidly if the SOFC is operated below 0.5 V. As SOFC reduced operating temperature targets are achieved and use of inexpensive metallic interconnects become feasible, accelerated degradation from metallic interaction is possible. Metals utilizing chromium (e.g., stainless steels) have shown limited lifetimes in SOFC and can degrade the cathode catalyst through various physicochemical pathways.⁷⁹

3.2 Performance and Materials

In the SOFC system, yttria- (Y_2O_3) stabilized zirconia (ZrO_2) is most often used as the electrolyte. In contrast to PEFCs, O^{2-} ions are passed from the *cathode* to *anode* via oxygen vacancies in the electrolyte instead of H^+ ions from *anode* to *cathode*. Other cell components such as interconnects and bipolar plates are typically doped ceramic, cermet, or metallic compounds.

There are four different basic designs for the SOFC system: the planar, seal-less tubular, monolithic, and segmented cell-in-series design. Two of the designs, planar and tubular, are the most promising for continued development. The other designs have been comparatively limited in development to date. The planar configuration looks geometrically similar to the

generic fuel cell shown in Fig. 5. The three-layer anode–electrolyte–cathode structure can be anode-, cathode-, or electrolyte-supported design, meaning the structural support is provided by a thicker layer of one of the structures (anode, cathode, or electrolyte supported). Since excessive ionic and concentration losses result from electrolyte- and cathode-supported structures, respectively, many designs utilize an anode-supported structure, although ribbed supports or cathode-supported designs are utilized in some cases.

For the planar design, the flow channel material structure is used as support for the electrolyte, and a stacking arrangement is employed. Although this design is simple to manufacture, one of the major limitations is difficulty sealing the flow fields at the edges of the fuel cell. Sealing is a key issue in planar SOFC design because it is difficult to maintain system integrity over the large thermal variation and reducing/oxidizing environment over many startup and shutdown load cycles. Compressive, glass, cermet, glass–ceramic, and hybrid seals have been used with varied success for this purpose.

The second major design is the seal-less tubular concept pioneered by Westinghouse (now Siemens-Westinghouse) in 1980. A schematic of the general design concept is shown in Fig. 13. Air is injected axially down the center of the fuel cell, which provides preheating of the air to operation temperatures before exposure to the cathode. The oxidizer is provided at adequate flow rates to ensure negligible concentration polarization at the cathode exit, to maintain desired cell temperature, and to provide adequate oxidizer for effluent combustion with unused fuel. The major advantage of the tubular configuration is that the difficult high-temperature seals needed for the planar SOFC design are eliminated. Tubular designs have been tested in 100-kW atmospheric pressure and 250-kW pressurized demonstration systems with little performance degradation with time (less than 0.1% per 1000 h) and efficiencies of 46 and 57% (LHV), respectively.⁷⁶

One drawback of this type of tubular design is the more complex and limited range of cell fabrication methods. Another drawback is high internal ohmic losses relative to the planar design, due to the relatively long in-plane path that electrons must travel along the electrodes to and from the cell interconnect. Some of these additional ionic transport losses have been reduced by use of a flattened tubular SOFC design with internal ribs for current flow, called the high-power-density (HPD) design by Siemens-Westinghouse and shown schematically in Fig. 14.⁸⁰ This design can also experience significant losses due to limited oxygen transport through the porous (~35% porosity) structural support tube used to provide rigidity to the assembly. The internal tube can also be used as the anode, reducing these losses through the higher diffusivity of hydrogen.

The monolithic and segmented cell-in-series designs are less developed, although demonstration units have been constructed and operated. A schematic of the monolithic cell design is shown in Fig. 15. In the early 1980s, the corrugated monolithic design was developed, based on the advantage of HPD compared to other designs. The HPD of the monolithic design is a result of the high active area exposed per volume and the short ionic paths through the electrolyte, electrodes, and interconnects. The primary disadvantage of the monolithic SOFC design, preventing its continued development, is the complex manufacturing process required to build the corrugated system.

The segmented cell-in-series design has been successfully built and demonstrated in two configurations: the bell-and-spigot and the banded configuration shown schematically in Fig. 16. The bell-and-spigot configuration uses stacked segments with increased electrolyte thickness for support. Ohmic losses are high because electron motion is along the plane of the electrodes in both designs, requiring short individual segment lengths (~1–2 cm). The banded configuration avoids some of the high ohmic losses of the bell-and-spigot configuration with a thinner electrolyte but suffers increased mass transport losses associated with the porous support structure used. The main advantage of the segmented cell design is a higher operating efficiency than larger-area single-electrode configurations. The primary disadvantages limiting development of the segmented cell designs include the necessity for many high-temperature

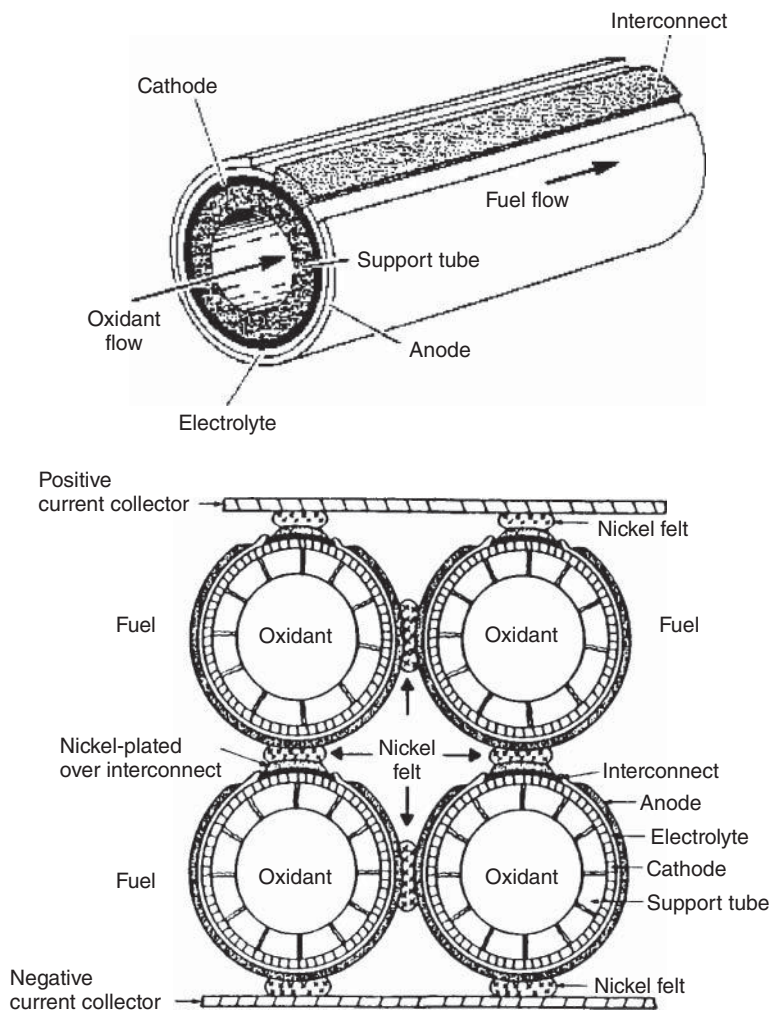


Figure 13 Schematic of seal-less tubular SOFC design. (From Ref. 77.)

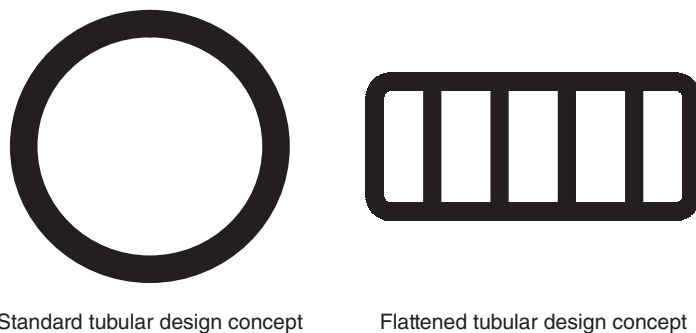


Figure 14 End-view schematic of conventional tubular and flattened high-power density SOFC concepts for reduced ionic transport losses. (From Ref. 80.)

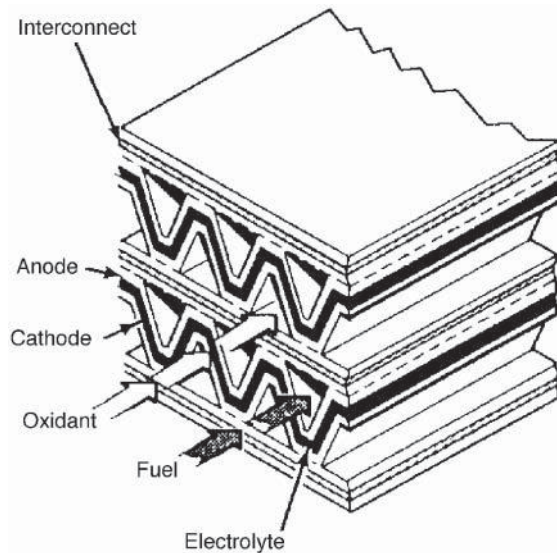


Figure 15 Schematic of the monolithic SOFC design. (From Ref. 77.)

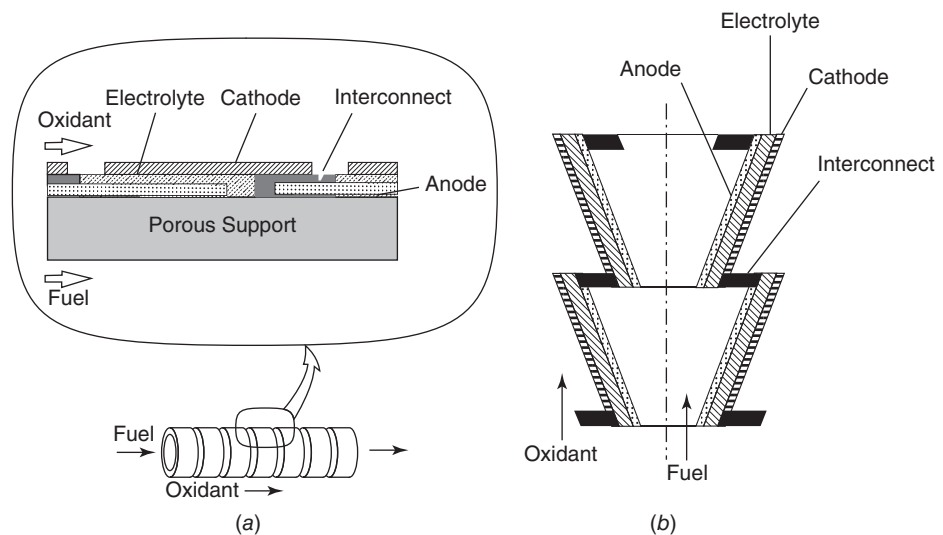


Figure 16 Schematic of the segmented cell-in-series design: (a) banded and (b) bell-and-spigot configuration. (From Ref. 77.)

gas tight seals, relatively high internal ohmic losses, and requirement for manufacture of many segments for adequate power output. Other cell designs, such as radial configurations, and more recently microtubular designs have been developed and demonstrated to date.

Many other fuel cell varieties and configurations, too numerous to enumerate here, have been developed to some degree. The most developed to date have been the phosphoric acid, alkaline, and molten carbonate fuel cells, all three of which have had some applied and commercial success.

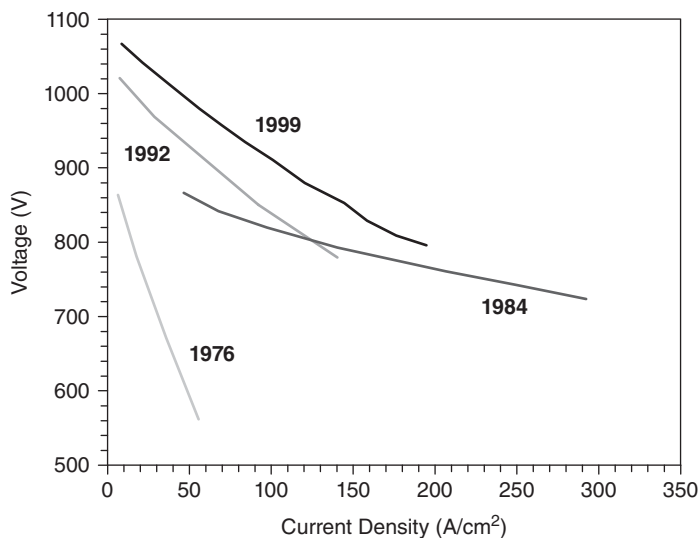


Figure 17 Relative performance of MCFCs at 1 atm pressure. (Adapted from Ref. 19.)

Alkaline Fuel Cells. Alkaline fuel cells (AFCs) utilize a solution of potassium hydroxide in water as an alkaline, mobile (liquid) electrolyte. Alkaline fuel cells were originally developed as an alternative power unit (APU) for space applications by the Soviet Union and the United States in the 1950s, and served on the Apollo program as well as the space shuttle orbiter.

Alkaline fuel cells were installed in Apollo mission service modules in 1964.⁸¹ AFCs were chosen for space applications for their high efficiency and robust operation. Both circulated and static electrolyte designs have been utilized. The AFC operates around 60–250°C with greatly varied electrode design and operating pressure. More modern designs tend to operate at the lower range of temperature and pressure. The primary advantages of the AFC are the cheaper cost of materials and electrolyte, and high operating efficiency (60% demonstrated for space applications) due to use of an alkaline electrolyte. For alkaline electrolyte, the oxidation reduction reaction (ORR) kinetics are much more efficient than acid-based electrolytes (e.g., PEFC, PAFC) enabling high relative operating efficiencies. Since space applications typically utilize pure oxygen and hydrogen for chemical propulsion, the AFC was well suited. However, the electrolyte suffers an intolerance to even small fractions of carbon dioxide found in air, which react to form potassium carbonate (K_2CO_3) in the electrolyte, gravely reducing performance over time. For terrestrial applications, CO_2 poisoning has limited the lifetime of AFC systems to well below that required for commercial application, and filtration of carbon dioxide is too expensive for practical use. Due to this limitation, relatively little commercial development of the AFC beyond space applications has been realized.

Molten Carbonate Fuel Cells. Currently MCFCs are commercially available from several companies, including a 250-kW unit from Fuel Cell Energy, Inc. in the United States and several other companies in Japan. Some MW-sized demonstration units are installed worldwide, based on natural gas or coal-based fuel sources that can be internally reformed within the anode of the MCFC. MCFCs operate at high-temperature (600–800°C) with a molten mixture of alkali metal carbonates (e.g., lithium and potassium) or lithium and sodium carbonates, retained in a porous ceramic matrix. In the MCFC, CO_3^{2-} ions generated at the cathode migrate to the

anode oxidation reaction. The MCFC design is similar to a phosphoric acid fuel cell (PAFC) in that both have liquid electrolytes maintained at precise levels within a porous ceramic matrix and electrode structure by a delicate balance of gas-phase and capillary pressure forces. A major advantage of the MCFC compared to the PAFC is the lack of precious-metal catalysts, which greatly reduce the system raw material costs. Original development on the MCFC was mainly funded by the U. S. Army in the 1950s and 1960s, and significant advances of this liquid electrolyte high-temperature fuel cell alternative to the SOFC were made.⁸² The U.S. Army desired operation of power sources from logistic fuel, thus requiring high temperatures with internal fuel reformation that can be provided by the MCFC. Development waned somewhat after this early development, but advances have continued and initial commercialization has been achieved. The steadily increasing performance of MCFCs throughout years of development is illustrated in Fig. 17. The main advantages of MCFCs include the following:

1. The MCFC can consume CO as a fuel and generates water at the anode, thus making it ideal for internal reformation of complex fuels.
2. As with the SOFC, high-quality waste heat is produced for bottom cycle or cogeneration applications.
3. Nonnoble metal catalysts are used, typically a nickel–chromium or nickel–aluminum on the anode, and a lithiated nickel oxide on the cathode.

The main disadvantages of MCFCs include the following:

1. Versus the SOFC (*the other high-temperature fuel cells*), the MCFC has a highly corrosive electrolyte that, coupled with the high operating temperature, accelerates corrosion and limits longevity of cell components, especially the cathode catalyst. The cathode catalyst (nickel oxide) has a significant dissolution rate into molten carbonate electrolyte.
2. Extremely long startup time (the MCFC is generally suitable only for continuous power operation) and nonconductive electrolyte at low temperatures.
3. Carbon dioxide must be injected to the cathode to maintain ionic conductivity. This can be accomplished with recycling from the anode effluent, or injection of combustion product, but complicates the system design.
4. Electrolyte maintenance is an engineering technical challenge. The liquid electrolyte interface between the electrodes is maintained by a complex force balance involving gas-phase and electrolyte–liquid capillary pressure between the anode and cathode. Significant spillage of the electrolyte into the cathode can lead to catalyst dissolution but is difficult to eliminate.
5. Vapor pressure of the electrolyte is nonnegligible and leads to loss of electrolyte through reactant flows.

Phosphoric Acid Fuel Cells. The PAFC was originally developed for commercial application in the 1960s. The PAFC has an acidic, mobile (liquid) electrolyte of phosphoric acid contained by a porous silicon carbide ceramic matrix and operates at around 160–220°C. Like the MCFC, the electrolyte is bound by capillary and gas pressure forces between porous electrode structures. The PAFC is in many ways similar to the PEFC, except the acid-based electrolyte is in liquid form, and the operating temperature is slightly higher. Over two hundred 200-kW commercial PAFC units were developed and sold by International Fuel Cells (now United Technologies Research Fuel Cells) and many are still in operation. However, ubiquitous commercial application has not been achieved, primarily due to high cost of approximately \$4500 per kW, about five times greater than cost targets for conventional stationary applications. The main advantages of the PAFC include the following:

1. The high operating temperature provides better waste heat than PEFC and allows operation with 1–2% CO in fuel stream, which is much better for use of reformed fuel compared to the PEFC, which cannot tolerate more than 10 ppm of CO without significant performance loss.¹⁰
2. The acid electrolyte does not need water for conductivity, making water management very simple compared to PEFC. Only the product water from the cathode reduction reaction needs to be removed, a relatively simple task at elevated temperature.
3. The demonstrated long life and commercial success for premium stationary power of the PAFC.

The main disadvantages of the PAFC include the following:

1. The PAFC is a bulky, heavy system compared to PEFC. Area specific power (0.2–0.3 W/cm²) is much less than PEFC.⁸³
2. The use of platinum catalyst with nearly the same loading as PEFCs.
3. The liquid electrolyte has finite vapor pressure, resulting in continual loss of electrolyte in vapor phase and a continual need for replenishment or recirculation. Modern PAFC design includes cooling and condensation zones to mitigate this loss.
4. The relatively long warmup time until electrolyte is conductive at ~160°C (although much less than the MCFC or SOFC).

Other Fuel Cells. Many other fuel cell systems exist, and new versions are constantly being developed. Most of these are simply existing fuel cell systems with a new fuel. For example, PEFCs based on a direct alcohol solution offer alternatives to DMFCs for portable power application and include those based on formic acid,⁸⁴ dimethyl ether,⁸⁵ ethylene glycol, dimethyl oxalate, and others.⁸⁶ A completely different concept is the biological or microbial fuel cell (MFC).^{87,88} In the MFC, electricity is generated by anerobic oxidation of organic material by bacteria. The catalytic activity and transport of protons is accomplished using biological enzymes or exogenous mediators.^{89,90} Although relative performance is very low, on the order of 1–100 mW/m², the potential for generating some power or simply power-neutral decomposition and treatment of organic waste matter such as sewage water is potentially quite significant to society.^{91,92}

Based on the continued growth and expansion of fuel cell science, it is evident that, despite lingering cost and technical challenges, continued growth and development of a variety of fuel cell systems will evolve toward implementation in many, but certainly not all, potential applications. In some cases, development of existing or new power sources or the exiting technical barriers will ultimately doom application of fuel cells, while some applications are likely to enjoy long-term commercial success.

Nomenclature.

<i>a</i>	activity coefficient of species, unitless
<i>A</i>	area term, cm ²
<i>C</i>	molar concentration, mol/cm ³
<i>D</i>	diffusion coefficient, cm ² /s
<i>E</i>	voltage, V
<i>E_a</i>	activation energy of electrochemical reaction, J/mol
<i>F</i>	Faraday constant, charge on 1 mol of electrons, 96,485 A · s/mol electron
<i>G</i>	Gibb's free energy, kJ/kg
<i>H</i>	enthalpy, kJ/kg

I	current, A
i	current density, A/cm ²
i_o	exchange current density, A/cm ²
i_l	mass limited current density, A/cm ²
M	solution molarity, mol/liter
n	electrons per mole oxidized or reduced, e ⁻ /mol
\dot{n}	molar flow rate, mol/s
P	pressure, Pa, and power, W
q''	heat flux, W/cm ²
r	area specific resistance, Ω /cm ²
R	universal gas constant, 8.314 J/mol · K
RH	relative humidity, unitless
S	entropy, kJ/kg · K
T	temperature, K
y	mole fraction, unitless

Greek letters.

α	charge transfer coefficient
$\Delta(x)$	change of parameter x
γ	reaction order for elementary oxidizer reaction
η	polarization, V
λ	electroosmotic drag coefficient, mol/mol H ⁺ , and water saturation in electrolyte
σ	conductivity, 1/ $\Omega \cdot \text{cm}$
ν	stoichiometric coefficient of balanced equation, and reaction order for elementary fuel reaction
ξ	stoichiometric flow ratio

Superscripts.

^o	standard conditions
--------------	---------------------

Subscripts.

a	activation or anode
c	cathode
e	electrolyte
fc	fuel cell
f	fuel
H ₂ O	water
i	species i
k	individual cell components, and number of cells in a stack
m	mass transport
ox	oxidizer
r	resistive
ref	reference
sat	at saturation conditions
th	thermal
thermo	thermo-osmotic

REFERENCES

1. M. M., Mench, *Fuel Cell Engines*, Wiley Online Library, 2008.
2. M. L., Perry and T. F. Fuller, "A Historical Perspective of Fuel Cell Technology in the 20th Century." *J. Electrochem. Soc.*, **149**, S59, 2002.
3. W., Nernst, "Über die elektrolytische Leitung fester Körper bei sehr hohen Temperaturen," *Zeitschrift Elektrochem.*, **6**(2), 41–43, 1899.
4. E., Baur and J. Tobler, "Brennstoffketten" *Zeitschrift Elektrochem. Angewandte Physikal. Chem.*, **39**(3), 169–180, 1933.
5. S., Satyapal, *Fuel Cell Technologies Overview*, Fuel Cell Seminar, Orlando, FL, 2011.
6. Available at: http://www1.eere.energy.gov/hydrogenandfuelcells/pdfs/2010_market_report.pdf.
7. Available at: <http://www1.eere.energy.gov/hydrogenandfuelcells/pdfs/48219.pdf>.
8. Available: http://www1.eere.energy.gov/hydrogenandfuelcells/pdfs/2011_market_report.pdf.
9. Toshiba Press Release of June 24, available at: http://www.toshiba.com/taec/press/dmfc_04_222.shtml.
10. R., Breault, "Stack Materials and Stack Design" in *Handbook of Fuel Cells—Fundamentals, Technology and Applications*, Vielstich, Gasteiger, Lamm, **4**: pp. 797–810, 2003.
11. J., King and B. McDonald, "Experience with 200 kW PC25 Fuel Cell Power Plant," in *Handbook of Fuel Cells: Fundamentals, Technology and Applications*, vol. **4**, Wiley, Hoboken, NJ, 2003.
12. M. M., Mench, E. C. Kumbur, and T. N. Veziroglu, "Polymer Electrolyte Fuel Cell Degradation," *Recherche*, **67**, 02, 2011.
13. Available at: http://www1.eere.energy.gov/hydrogenandfuelcells/wkshp_fuelcell_jan08.html.
14. D., Sperling, J. S. Cannon, and I. NetLibrary, *The Hydrogen Energy Transition: Moving toward the Post Petroleum Age in Transportation*, Elsevier, Amsterdam, 2004.
15. O., Yamamoto, "Solid Oxide Fuel Cells: Fundamental Aspects and Prospects," *Electrochim. Acta*, **45**(15–16), 2423–2435, 2000.
16. M., Wang, "Fuel Choices for Fuel-Cell Vehicles: Well-to-Wheels Energy and Emission Impacts." *J. Power Sources*, 2002. **112**(1), 307–321, 2002.
17. A. J., Bard and L. R. Faulkner, *Electrochemical Methods: Fundamentals and Applications*, Wiley, Hoboken, NJ, 2006.
18. M. M., Mench, C. Y. Wang, and S. T. Thynell, "An Introduction to Fuel Cells and Related Transport Phenomena," *Int. J. Transp. Phenom.*, **3**, 151–176, 2001.
19. J., Larminie and A. Dicks, *Fuel Cell Systems Explained*, Wiley, Hoboken, NJ, 2003.
20. A., LaConti, M. Hamdan, and R. McDonald, "Mechanisms of Membrane Degradation," in *Handbook of Fuel Cells—Fundamentals, Technology, and Applications*, Vol. **3**, pp. 647–662, 2003.
21. S., He, M. M. Mench, and S. Tadigadapa, "Thin Film Temperature Sensor for Real-Time Measurement of Electrolyte Temperature in a Polymer Electrolyte Fuel Cell," *Sensors Actuators A: Phys.*, **125**(2), 170–177, 2006.
22. T. E., Springer, T. Zawodzinski, and S. Gottesfeld, "Polymer Electrolyte Fuel Cell Model," *J. Electrochem. Soc.*, **138**(8), 2334–2342, 1991.
23. S., Kim and M. Mench, "Physical Degradation of Membrane Electrode Assemblies undergoing Freeze/Thaw Cycling: Micro-Structure Effects," *J. Power Sources*, **174**(1), 206–220, 2007.
24. A. K., Srouji and M. M. Mench, "Freeze Damage to Polymer Electrolyte Fuel Cells," in *Polymer Electrolyte Fuel Cell Degradation*, M. M. Mench, E. C. Kumbur, and T. N. Veziroglu (Eds.), Elsevier, Amsterdam, p. 293, 2011.
25. E., Wargo, C. Dennison, and E. Kumbur, "Durability of Polymer Electrolyte Fuel Cells: Status and Targets," in M. M. Mench, E. C. Kumbur, and T. N. Veziroglu (Eds.), *Polymer Electrolyte Fuel Cell Degradation*, Elsevier., Amsterdam, p.1, 2011.
26. C. S., Gittleman, F. D. Coms, and Y. H. Lai, "Membrane Durability: Physical and Chemical Degradation," in M. M. Mench, E. C. Kumbur, and T.N. Veziroglu (Eds.), *Polymer Electrolyte Fuel Cell Degradation*, Elsevier., Amsterdam, p. 15. 2011.

27. S. S., Kocha, "Electrochemical Degradation: Electrocatalyst and Support Durability". in M. M. Mench, E. C. Kumbur, and T. N. Veziroglu (Eds.), *Polymer Electrolyte Fuel Cell Degradation*, Elsevier., Amsterdam, p. 89, 2011.
28. K. S., Bhambare, et al., "A Carbon Monoxide Sensor in Polymer Electrolyte Fuel Cells Based on Symbolic Dynamic Filtering", *Sensors Actuators B: Chem.*, **134**(2), 803–815, 2008.
29. F. Y., Zhang, S. G. Advani, and A. K. Prasad, "Advanced High Resolution Characterization Techniques for Degradation Studies in Fuel Cells," in M. M. Mench, E.C. Kumbur, and T.N. Veziroglu (Eds.), *Polymer Electrolyte Fuel Cell Degradation*, Elsevier., Amsterdam, p. 365, 2011.
30. S., Kim, et al., "Investigation of the Impact of Interfacial Delamination on Polymer Electrolyte Fuel Cell Performance." *J. Electrochem. soc.*, **156**, B99, 2009.
31. S., Kim, B. K. Ahn, and M. Mench, "Physical Degradation of Membrane Electrode Assemblies undergoing Freeze/Thaw Cycling: Diffusion Media Effects," *J. Power Sources*, **179**(1), 140–146, 2008.
32. J., Divisek, "Low Temperature Fuel Cells" in W. Vielstich, A. Lamm, and H. A. Gasteiger (Eds.) *Handbook of Fuel Cells—Fundamentals, Technology and Applications*, Vol. 1, Wiley, Hoboken, NJ, pp. 99–114, 2003.
33. Y. Morimoto and S. Yamakawa, "Computational Modeling Aspects of PEFC Durability," in M. M. Mench, E. C. Kumbur, and T. N. Veziroglu (Eds.), *Polymer Electrolyte Fuel Cell Degradation*, Elsevier, Amsterdam, p. 423, 2011.
34. F. Y., Zhang, et al., "Quantitative Characterization of Catalyst Layer Degradation in PEM Fuel Cells by X-ray Photoelectron Spectroscopy," *Electrochim. Acta*, **54**(16), 4025–4030, 2009.
35. D., Wilkinson and J. St-Pierre, *Durability. Handbook of Fuel Cells*, Wiley, Hoboken, NJ, 2003.
36. A., El-kharouf and B. G. Pollet, "Gas Diffusion Media and their Degradation" in M. M. Mench, E. C. Kumbur, and T. N. Veziroglu (Eds.), *Polymer Electrolyte Fuel Cell Degradation*, Elsevier, Amsterdam, p. 215, 2011.
37. H., Tawfik, et al., "Bipolar Plate Durability and Challenges," In M. Mench, E. C. Kumbur, and T. N. Veziroglu (Eds.), *Polymer Electrolyte Fuel Cell Degradation*, Elsevier, Amsterdam, p. 249, 2011.
38. M. L., Perry, R. Balliet, and R. M. Darling, "Experimental Diagnostics and Durability Testing Protocols," in M. M. Mench, E. C. Kumbur, and T. N. Veziroglu (Eds.), *Polymer Electrolyte Fuel Cell Degradation*, Elsevier, Amsterdam, p. 335, 2011.
39. D., Shores and G. Deluga, "Basic Materials Corrosion Issues," *Handbook of Fuel Cells*, **3**, 273–285, 2003.
40. Available: http://www.hydrogen.energy.gov/pdfs/progress11/v_e_5_blanchet_2011.pdf.
41. M. J., Moran and H. N. Shapiro, *Fundamentals of engineering Thermodynamics*, Wiley, New York, 2000.
42. M., Khandelwal, S. H. Lee, and M. M. Mench, "One-Dimensional Thermal Model of Cold-Start in a Polymer Electrolyte Fuel Cell Stack," *J. Power Sources*, **172**(2), 816–830, 2007.
43. Q., Dong, et al., "Distributed Performance of Polymer Electrolyte Fuel Cells under Low-Humidity Conditions," *J. Electrochem. Soc.*, **152**(11), A2114–A2122, 2005.
44. M., Mench, D. Burford, and T. Davis, "IMECE2003-42393 In Situ Temperature Distribution Measurement in an Operating Polymer Electrolyte Fuel Cell," *ASME Publications-HTD*, **374**(2), 415–428, 2003.
45. M., Khandelwal and M. M. Mench, "Direct Measurement of Through-Plane Thermal Conductivity and Contact Resistance in Fuel Cell Materials," *J. Power Sources*, **161**, 1106–1115, 2006.
46. P. J. S., Vie and S. Kjelstrup, "Thermal Conductivities from Temperature Profiles in the Polymer Electrolyte Fuel Cell," *Electrochim. Acta*, **49**(7), 1069–1077, 2004.
47. F. E., Hizir, et al., "Characterization of Interfacial Morphology in Polymer Electrolyte Fuel Cells: Micro-porous Layer and Catalyst Layer Surfaces," *J. Power Sources*, **195**(11), 3463–3471, 2010.
48. R. P., Ramasamy, et al., "Investigation of Macro- and Micro-porous Layer Interaction in Polymer Electrolyte fuel Cells," *Int. J. Hydrogen Energy*, **33**(13), 3351–3367, 2008.
49. A., Turhan et al., "Passive control of Liquid Water Storage and Distribution in a PEFC through Flow-Field Design," *J. Power Sources*, **180**(2), 773–783, 2008.
50. J. J., Kowal, et al., "Liquid Water Storage, Distribution, and Removal from Diffusion Media in PEFCs," *J. Electrochem. Soc.*, **153**(10), A1971–A1978, 2006.

51. E. C., Kumbur, K.V. Sharp, and M. M. Mench, "Validated Leverett Approach for Multiphase Flow in PEFC Diffusion Media," *J. Electrochem. Soc.*, **154**(12), B1295–B1304, 2007.
52. T., Swamy, E. C. Kumbur, and M. M. Mench, "Investigation of Bipolar Plate and Diffusion Media Interfacial Structure in PEFCs: A Fractal Geometry Approach," *Electrochim. Acta*, **56**(8), 3060–3070, 2011.
53. T., Swamy, E. C. Kumbur, and M. M. Mench, "Characterization of Interfacial Structure in PEFCs: Water Storage and Contact Resistance Model," *J. Electrochem. Soc.*, **157**(1), B77–B85, 2010.
54. F.Y., Zhang, et al., "In Situ Characterization of the Catalyst Layer in a Polymer Electrolyte Membrane Fuel Cell," *J. Electrochem. Soc.*, **154**(11), B1152–B1157, 2007.
55. N., Pekula, et al., "Study of Water Distribution and Transport in a Polymer Electrolyte Fuel Cell Using Neutron Imaging," *Nuclear Instrum. Methods Phys. Res. Section A: Accelerators, Spectrometers, Detectors Associated Equipment*, **542**(1), 134–141, 2005.
56. S., Motupally, A. J. Becker, and J. W. Weidner, "Diffusion of Water in Nafion 115 Membranes," *J. Electrochem. Soc.*, 3171, 2000.
57. X., Ren and S. Gottesfeld, "Electro-osmotic Drag of Water in Poly (perfluorosulfonic Acid) Membranes," *J. Electrochem. Soc.*, **148**, A87, 2001.
58. U., Pasaogullari and C. Y. Wang, "Two-Phase Transport and the Role of Micro-porous Layer in Polymer Electrolyte Fuel Cells," *Electrochim. Acta*, **49**(25), 4359–4369, 2004.
59. S., Kim and M. Mench, "Investigation of Temperature-Driven Water Transport in Polymer Electrolyte Fuel Cell: Thermo-osmosis in Membranes," *J. Membr. Sci.*, **328**(1), 113–120, 2009.
60. L., Zheng, et al., "Computational Exploration of Ultra-High Current PEFC Operation with Porous Flow Field," *J. Electrochem. Soc.*, **159**(7), F267–F277, 2012.
61. R., Borup, et al., "Scientific Aspects of Polymer Electrolyte Fuel Cell Durability and Degradation," *Chem. Rev.*, **107**(10), 3904–3951, 2007.
62. S., Cleghorn, J. Kolde, and W. Liu, "Catalyst Coated Composite Membranes," in *Handbook of Fuel Cells*, Wiley, Hoboken, NJ, 2003.
63. W. M., Yang, S. K. Chou, and C. Shu, "Effect of Current-Collector Structure on Performance of Passive Micro Direct Methanol Fuel Cell," *J. Power Sources*, **164**(2), 549–554, 2007.
64. Q. X., Wu, et al., "A Microfluidic-Structured Flow Field for Passive Direct Methanol Fuel Cells Operating with Highly Concentrated Fuels," *J. Micromech. Microeng.* **20**(4), 2010.
65. G. Q., Lu and C. Y. Wang, "Development of High Performance Micro DMFCs and a DMFC Stack," *J. Fuel Cell Sci. Tech.*, **3**(2), 131–136, 2006.
66. J., Müller, et al., "Transport/Kinetic Limitations and Efficiency Losses," in *Handbook of Fuel Cells*, pp. 847–855, 2003.
67. M. M., Mench and C. Wang, "An in Situ Method for Determination of Current Distribution in PEM Fuel Cells Applied to a Direct Methanol Fuel Cell," *J. Electrochem. Soc.*, **150**, A79, 2003.
68. C. L., Yaws, *Handbook of Transport Property Data: Viscosity, Thermal Conductivity, and Diffusion Coefficients of Liquids and Gases*, Gulf Pub. Co, 1995.
69. J., Cruickshank and K. Scott, "The Degree and Effect of Methanol Crossover in the Direct Methanol Fuel Cell," *J. Power Sources*, **70**(1), 40–47, 1998.
70. X., Ren, et al., "Methanol Transport through Nafion Membranes. Electro-osmotic Drag Effects on Potential Step Measurements," *J. Electrochem. Soc.*, **147**, 466, 2000.
71. S., Arisetty, S. G. Advani, and A. K. Prasad, "Methanol Diffusion Rates through the Anode Diffusion Layer in Direct Methanol Fuel Cells from Limiting Current Measurements," *Heat Mass Transfer*, **44**(10), 1199–1206, 2008.
72. F. Q., Liu, G. Q. Lu, and C. Y. Wang, "Low Crossover of Methanol and Water through Thin Membranes in Direct Methanol Fuel Cells," *J. Electrochem. Soc.*, **153**(3), A543–A553, 2006.
73. F. Q., Liu and C. Y. Wang, "Water and Methanol Crossover in Direct Methanol Fuel Cells — Effect of Anode Diffusion Media," *Electrochim. Acta*, **53**(17), 5517–5522, 2008.
74. Y., Pan, Integrated Modeling and Experimentation of Electrochemical Power Systems, Ph. D. Dissertation, Pennsylvania State University, 2004.
75. R., Service, "MATERIALS SCIENCE: New Tigers in the Fuel Cell Tank," *Science*, **288**(5473), 1955–1957, 2000.
76. S., Singhal, "Science and Technology of Solid-Oxide Fuel Cells," *MRS bull.*, **25**(3), 16–21, 2000.

77. N. Q., Minh and T. Takahashi, *Science and Technology of Ceramic Fuel Cells*, Vol. 9, Elsevier, Amsterdam, 1995.
78. R., Doshi, et al., "Development of Solid-Oxide Fuel Cells That Operate at 500 C," *J. Electrochem. Soc.*, **146**, 1273, 1999.
79. Y., Matsuzaki and I. Yasuda, "Dependence of SOFC Cathode Degradation by Chromium-Containing Alloy on Compositions of Electrodes and Electrolytes," *J. Electrochem. Soc.*, **148**, A126, 2001.
80. D., Stöver, H. Buchkremer, and J. Huijsmans, "MEA/Cell Preparation Methods: Europe/USA," Eds. Wolf Vielstich, Arnold Lamm, Hubert A. Gasteiger, in *Handbook of Fuel Cells*, vol. 4, pp. 1013–1031, 2003.
81. Available: <http://americanhistory.si.edu/fuelcells/alk/alk3.htm>.
82. B. S., Baker, *Hydrocarbon Fuel Cell Technology*, Academic, New York, 1955.
83. F. C., Handbook, *EG&G Services Parsons*. Science Applications International Corporation, 2000.
84. M., Zhao, et al., "Kinetic Study of Electro-oxidation of Formic Acid on Spontaneously-Deposited Pt/Pd Nanoparticles," *J. Electrochem. Soc.*, **151**, A131, 2004.
85. M., Mench, H. Chance, and C. Wang, "Direct Dimethyl Ether Polymer Electrolyte Fuel Cells for Portable applications," *J. Electrochem. Soc.*, **151**, A144, 2004.
86. E., Peled, et al., "New Fuels as Alternatives to Methanol for Direct Oxidation Fuel Cells," *Electrochem. Solid-State Lett.*, **4**, A38, 2001.
87. S., Jung, M. M. Mench, and J. M. Regan, "Impedance Characteristics and Polarization Behavior of a Microbial Fuel Cell in Response to Short-Term Changes in Medium pH," *Environ. Sci. Tech.*, **45**(20), 9069–9074, 2011.
88. Z. Y., Ren, et al., "Characterization of Microbial Fuel Cells at Microbially and Electrochemically Meaningful Time Scales," *Environ. Sci. Tech.*, **45**(6), 2435–2441, 2011.
89. H., Liu, R. Ramnarayanan, and B. E. Logan, "Production of Electricity During Wastewater Treatment Using a Single Chamber Microbial Fuel Cell," *Environ. Sci. Tech.*, **38**(7), 2281–2285, 2004.
90. T., Chen, et al., "A Miniature Biofuel Cell," *J. Am. Chem. Soc.*, **123**(35), 8630–8631, 2001.
91. Z. Y., Ren, et al., "Time-Course Correlation of Biofilm Properties and Electrochemical Performance in Single-Chamber Microbial Fuel Cells," *Biore. Tech.*, **102**(1), 416–421, 2011.
92. R. P., Ramasamy, et al., "Impact of Initial Biofilm Growth on the Anode Impedance of Microbial Fuel Cells," *Biotech. Bioen.*, **101**(1), 101–108, 2008.

CHAPTER 32

FLUID POWER SYSTEMS

Andrew Alleyne
University of Illinois, Urbana–Champaign
Urbana, Illinois

1 INTRODUCTION	1089	4 SYSTEM DYNAMIC BEHAVIOR	1116
2 SYMBOLS AND TERMINOLOGY	1090	5 COMMON NONLINEARITIES	1119
3 SYSTEM COMPONENTS	1095	5.1 Saturations and Dead Zones	1119
3.1 Hydraulic Oils	1095	5.2 Hysteresis and Asymmetry	1119
3.2 Hydraulic Hoses	1097	5.3 Friction	1121
3.3 Hydraulic Pumps	1099	REFERENCES	1122
3.4 Hydraulic Valves	1105		
3.5 Cylinders and Motors	1113		
3.6 Other Components	1115		

1 INTRODUCTION

The use of fluids for power delivery has been a part of human civilization for many centuries. For example, much of the growth in the U.S textile industry in the 1820s and 1830s can be credited to the abundant supply of hydraulic power available in the northeastern United States through lakes and man-made canals.¹ Early hydraulic systems utilized gravitational potential to convert the energy stored in the fluid to some type of useful mechanical energy. Currently, fluid power systems are ubiquitous in our everyday society. All facets of our lives are touched by some form of pressurized fluid distributing power. Simple transportation examples would be fuel delivery systems or braking systems in cars and buses. Many manufacturing systems also use fluid power for presses and other types of forming applications. In fact, fluid power is seen as a vital and necessary component for many types of engineering systems. This is particularly true in mobile applications where a power generation component, such as an internal combustion engine, is coupled to the fluid power system. In these cases, the inherent power density advantages of fluid power make it a very attractive choice over other types of actuation.

One key advantage of fluid power systems is the high power density available. This means a very large force can be generated in a very compact space; something that is useful for applications such as aircraft where weight and volume are at a premium. Another advantage is the ability to hold loads for long periods of time, since a continuous load can be applied without requiring power flow. Any possible heat generated near the point of power application can be drawn away to a remote location for heat rejection. A third advantage is the ability to move large inertias very rapidly. The bandwidth versus power characteristics of modern fluid power systems gives them an advantage over other types of actuation systems at higher loads.

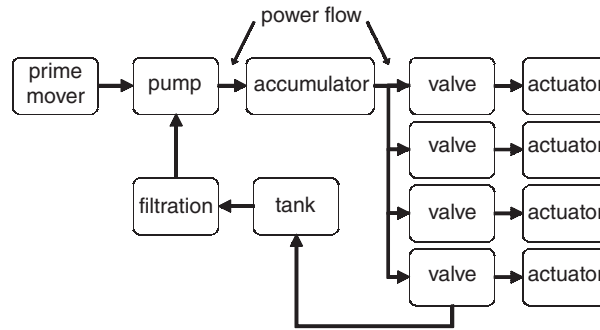


Figure 1 Schematic of a fluid power system.

Analysis of a typical fluid power application requires a complete systems-level understanding. Figure 1 illustrates the interconnection of several different components to form an overall system as would be found in a mobile application. Each interconnected component is itself a complex system made up of various subsystems, as will be described in subsequent sections.

Most fluid power systems have the basic components of *power generation*, *power distribution*, *power modulation*, and *power application*. Using Fig. 1 as an example, the power generation component consists of the prime mover coupled to the pumping device to convert stored chemical energy such as diesel fuel to mechanical power and, subsequently, to high-pressure fluid power. The variables of power in this system include the fluid pressure and flow rate since $\text{power} = \text{pressure} \times \text{flow}$. The power distribution aspect of the system is depicted by the interconnections, which usually consist of hoses and couplings. These conduits of power transport the high-pressure fluid to various locations within the system. At a specific location, the available power is modulated, or metered, often by the use of a valve device. The valve device determines how much power is actually applied to a particular load. The power application component is some type of actuator, usually a piston or motor, which converts the fluid power to mechanical power and applies it to some load. The following sections elaborate in detail on the basic components outlined here.

In addition to the four primary classes of components, several other subsystems are critical to proper overall functionality and are illustrated in Fig. 1. These include the filters for maintaining fluid cleanliness, accumulators for temporarily storing energy, as well as tank storage systems for containing the bulk of the fluid used in the system and providing some centralized place for heat rejection. These subsystems are addressed after the primary components and in less detail. For a more in-depth understanding of these system components, the reader is referred to the excellent and comprehensive book of Yeaple.²

2 SYMBOLS AND TERMINOLOGY

As is the case in many other fields, fluid power systems have their own unique symbols and terminology. The following tables illustrate some of the basic hydraulic symbols and terms that are commonly encountered and are referred to later on in this chapter. Section 3 gives more detail on the physical realization of these different system components. Table 1 gives symbols used for representing the hydraulic lines that carry pressurized fluid between different components. Table 2 illustrates symbols for fluid power motors and pumps. These are the components that convert rotary mechanical power to fluid power (pumps) or convert fluid power to rotary mechanical power (motors). Table 3 illustrates symbols for different energy or fluid storage

Table 1 Hydraulic Line Symbols





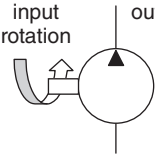
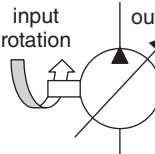
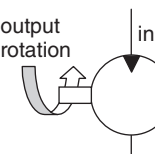

	Main line
	Pilot line
	Fluid flow direction
	Hydraulic line with in-line filter

Table 2 Motors and Pumps



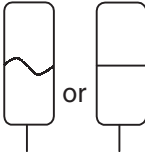

	Pump (fixed displacement)
	Pump (variable displacement)
	Unidirectional motor
	Electric motor

elements. Table 4 gives the symbols for a wide assortment of valves as well as the types of mechanical or electromechanical devices that move the valves. Table 5 illustrates the symbols used to describe cylinders which, like motors, are also used to transform fluid power to mechanical power. However, unlike fluid power motors, the cylinders in Table 5 convert fluid power into rectilinear mechanical power.

The symbols shown in the tables can be connected to form complicated hydraulic diagrams. A simple example, which is revisited in Section 3 when discussing valves, can be seen in Fig 2. Here we see a 4-way, 3-position valve with a solenoid actuator and a spring return that is connected to a bidirectional hydraulic motor. The work ports on the valve are labeled as follows: P = pump pressure, T = tank or reservoir, A = work port connected to one side of the motor, and B = work port connected to other side of the motor.

As stated before, fluid power systems deal with the flow of power in terms of pressure and volumetric flow. Therefore, in a system dynamics sense they can easily be seen to be quite

Table 3 Reservoirs and Energy Storage Elements

	Vented reservoir or tank
	Pressurized reservoir or tank
	Gas-charged accumulator
	Spring-loaded accumulator

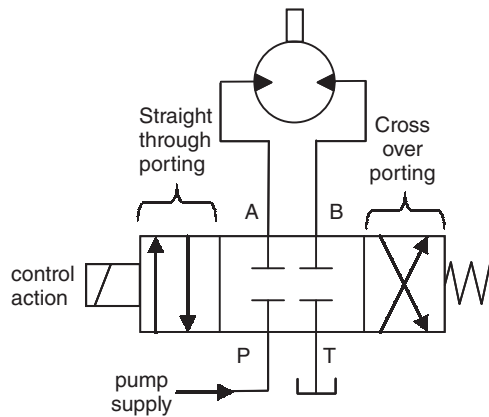


Figure 2 Diagram of a valve-driven motor.

analogous to electrical systems. The pressure is analogous to voltage and flow is analogous to current. An engineer who is comfortable with creating and analyzing simple electronic circuits could perform similar tasks with a fluid power system once the symbols are clearly understood. Table 6 gives a better comparison between the electrical and fluid power systems.

In addition to the analogous components shown in Table 6 there are several other parallels between electrical and fluid power systems. The hydraulic pump could be connected to a pressure relief valve to give a constant pressure supply, much like a direct-current (dc) battery or other constant voltage source. Moreover, instrumentation devices such as ammeters or voltmeters are analogous to flow meters and pressure sensors, respectively.

Table 4 Common Valves and Valve Actuators





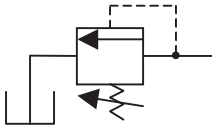
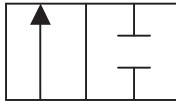


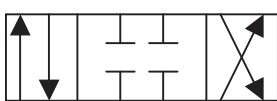


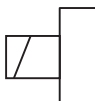
	Fixed orifice
	Variable orifice
	Check valve (not spring loaded)
	Check valve (spring loaded)
	Variable relief valve
	2-way, 2-position valve
	3-way, 2-position valve
	4-way, 2-position valve
	4-way, 3-position valve
	Valve return spring
	Manual or lever valve actuation
	Solenoid or electric actuation

Table 5 Cylinders

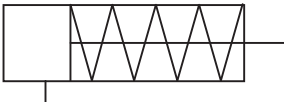
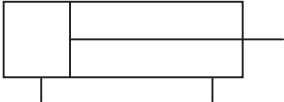
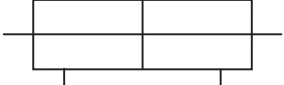
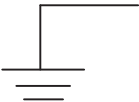




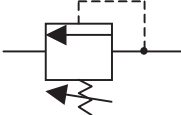
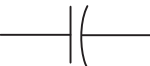







	Single rod, single acting, spring return
	Single rod, double acting
	Double rod, double acting

Table 6 Electrical–Hydraulic Analogy

Electrical Components	Electrical Diagram	Fluid Power Diagram	Fluid Power Components
Ground			Reservoir or tank
Current source			Pump
Voltage regulator			Relief valve
Capacitor			Accumulator
Resistor			Orifice
Diode			Check valve
Electric motor			Hydraulic motor

3 SYSTEM COMPONENTS

3.1 Hydraulic Oils

The oil used in a hydraulic circuit is designed to withstand high pressures and large pressure drops without deterioration in performance. The majority of common fluids are petroleum-based, often called mineral oil, with other fluids developed for targeted applications. The primary other types of common fluids are synthetic ones, including phosphate ester or silicone-based fluids. A primary advantage of these types of synthetic fluids is their fire-resistant nature, making them essential in applications where volatility is catastrophic (e.g., aircraft, submarines). The most fire-resistant type of fluid that can be used is a water–glycol mixture that has the low volatility of water but yet does not have the drawback of freezing in low-temperature applications. In addition to the basic types of hydraulic oil, many additives are used to aid in fluid performance. For example, metal dithiophosphates are often added to inhibit oxidation and to serve as wear-reducing agents. High-molecular-mass compounds such as polysiloxanes can act as antifoaming agents to reduce the amount of foam developed in the tank or reservoir. Further information on oil types can be found in Refs. 2 and 3 or from product literature available from major oil manufacturers.

Regardless of their chemical makeup, all of the oils must satisfy basic performance criteria. Critical criteria are (1) viscosity and lubricity, (2) stability (thermal, absorption), and (3) incompressibility. Viscosity of a fluid indicates the amount of shear stress necessary for relative motion between two adjacent surfaces with the fluid between them. Figure 3 illustrates a block sliding on a patch of fluid.

Area A is the underside of the block and t is the thickness of the fluid patch. The force required to move the block is proportional to the velocity of the block and inversely proportional to the fluid thickness:

$$F = \nu A \frac{\dot{x}}{t} \quad (1)$$

The viscosity term ν determines the resistance to motion determined by the internal friction of the fluid. Viscosity is important because of the relatively close tolerances of fluid power components such as valves and pumps. Highly viscous fluids will have a resistance to shear flow and will tend to damp the motion of the various components, thereby making it more difficult to pump fluid up to higher pressure. Simultaneously, low-viscosity fluids tend to leak easily around passages within fluid power components and reduce overall system efficiency. Related to the concept of viscosity is that of lubricity. High-lubricity fluids are able to reduce the wear on the moving mechanical components, thereby increasing the life of the overall system. Low-lubricity fluids, like water, need to have additives present to prevent excessive metal on metal contact.

Stability is an important aspect of a hydraulic fluid. Essentially, the ideal hydraulic fluid would satisfy the performance requirements and do so irrespective of its operating environment. That is not the case in practice. The viscosity and lubricity of most oils change dramatically with temperature, going from high viscosity at low temperatures to low viscosity

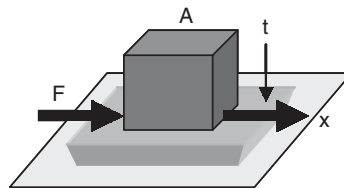


Figure 3 Viscosity schematic.

at high temperatures. The extreme operating limits for viscosity on most systems range between 1.0 and 5000 cst (centistokes). Anything outside those limits will not be practical. In general, good fluids are less sensitive in their viscosity or lubricity to changes in temperature. Similar aspects apply for insensitivity to pressure. In addition to being stable with respect to physical properties, it is usually desirable for the oil to be environmentally insensitive with respect to its chemical properties. In particular, for reasons to be discussed shortly, the oil should not absorb much air from the surrounding environment if it is exposed. The oil should have a minimal reaction to materials (e.g., rubber, polymers, metals) contained in hoses, seals, filters, valves, or pumps. One example of an undesirable interaction is the potential for swelling of most elastomer seals in contact with typical hydraulic fluids, which can cause unwanted internal stresses on components. In addition to the desired inertness with respect to the components it affects, a good hydraulic fluid should remain chemically stable with little settling of any additives introduced so that its performance will be unaffected by periods of inactivity.

Fluid compressibility is crucial to the overall performance of the system. Thinking of the fluid in a closed chamber (e.g., cylinder) as a spring to store energy, it becomes apparent that a more compressible fluid will act as a softer spring, thereby reducing the natural frequency of the closed chamber. This can be seen in practice as a change in resonant frequency for fluid power systems when the oil properties change. In most cases, it is better to have higher resonant frequencies due to the fluid compressibility rather than lower resonant frequencies.

Unfortunately, the natural tendency of hydraulic fluids is to absorb air from the environment. This air becomes dissolved in the hydraulic fluid, causing it to become more compressible than if there were no air. The compressibility of the fluid is usually defined by the *bulk modulus*, which is defined as the percentage change in volume of a fluid for a given change in pressure. Define a volume, V , under some pressure, P , as shown in Fig 4. Using Δ to denote the change in a variable, the definition of the fluid's bulk modulus, β , is

$$\frac{1}{\beta_{\text{fluid}}} = -\frac{\Delta V}{V} \frac{1}{\Delta P} \quad (2)$$

where the negative sign indicates that an increase in pressure results in a decrease in fluid volume. If the hydraulic oil has air dissolved in it, the air and the oil act as separate springs in series for the purpose of the overall compressibility. An examination of Fig 5 illustrates this concept. On the right, the air can be seen to be a compressible volume in series with the oil. A force on the piston will act to compress the air more than the oil, as would be the case if there were two mechanical springs in series.

Therefore,

$$\frac{1}{\beta_{\text{total}}} = \frac{1}{\beta_{\text{fluid}}} + \frac{V_{\text{air}}}{V_{\text{total}}} \frac{1}{\beta_{\text{air}}} \quad (3)$$

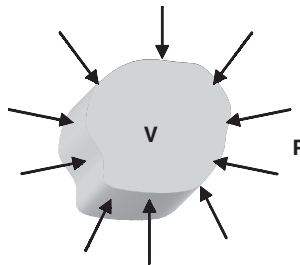


Figure 4 Fluid volume under pressure.

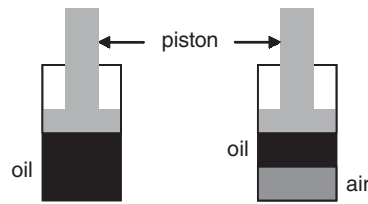


Figure 5 Schematic of a fluid chamber with and without dissolved air.

Since the air is so much more compressible than the fluid, a small amount of air ($< 1\%$) can have a drastic effect on the overall system stiffness. For example,⁴ suppose we have a fluid with 1% entrained air, by volume, that is under 500 psi pressure. If the ratio of specific heat for air is 1.4, then the bulk modulus of the air equals $1.4 \times 500 = 700$ psi. A typical bulk modulus for a petroleum-based fluid is approximately 2×10^5 psi. Therefore,

$$\frac{1}{\beta_{\text{total}}} = \frac{1}{2 \times 10^5} + 0.01 \times \frac{1}{700} = 1.9 \times 10^{-5} \frac{\text{in}^2}{\text{lb}} \quad (4)$$

$$\Rightarrow \beta_{\text{total}} = 5.2 \times 10^4 \text{ psi} \quad (5)$$

Addition of 1% dissolved air reduces the total bulk modulus to only one-fourth of the ideal value of the oil with no air. In practice, it is not uncommon to have much more than 1% air dissolved in a fluid, which will have serious consequences for high-performance hydraulics relying on very low compressibility to achieve high bandwidth and high performance. Therefore, it is important for the designer of the overall system to fully understand the role that oil properties, and the cause for their changes, can have on system performance.

Another oil property that needs to be understood by the system designer is environmental toxicity, which has serious impact on where fluid power systems can be applicable. For example, due to the chemical nature of mineral oil hydraulic fluids, typical fluid power systems are not employed in the food processing industry. Instead, more exotic types of fluid power systems need to be used, including water-based hydraulics, to maintain the necessary system sterility. A final issue of concern is the flammability of the fluid, since many connection or component failures can result in a rapid dispersal of a fine fluid mist, which can be a significant hazard. Further discussion on oil characteristics can be found in Refs. 2–4.

3.2 Hydraulic Hoses

Hoses are a component of fluid power systems that are often overlooked in an overall systems analysis, but they are important to overall system performance. In a systems sense, the hoses are responsible for distributing the power of the pressurized fluid from a central generation location to remote locations where the power is then converted to mechanical power for application to some load. If the hoses are inefficient, then the system will use more energy than necessary. More critically, if the hoses are not properly suited to carry the power being distributed, then failure can result. This would be analogous to sending more electrical current through a wire than is rating allowed.

Most hoses in typical hydraulic fluid power systems are relatively complex composite devices constructed from multiple layers of material. Figure 6 illustrates two separate types of hoses with the primary difference being the reinforcing material. The core tube transports the high-pressure fluid and is fabricated from a material that will not react with the fluid being carried. This tube can be made from rubber or some type of thermoplastic polymer. This core is then surrounded by one or more layers of reinforcing material that adds rigidity and strength

to the hose. The figure on the left uses reinforcing wire spirals to strengthen the tube, while the one on the right uses reinforcing braids. The braids can be either metal or some synthetic fiber, whereas the spirals are primarily metal. The design of the reinforcing material ensures that the hose can be both strong and flexible. Wire reinforcement gives higher strength, whereas fiber reinforcement gives lower weight and greater flexibility. Flexibility is often desired in hydraulic hose for several reasons. First, it often needs to move with the system that it is attached to, for example, as cylinders extend on an earthmoving vehicle. Second, flexibility aids in the design and construction of the overall systems into which these hoses get integrated because a flexible hose is easier to route throughout a machine. Finally, a small amount of flexibility with associated viscoelastic behavior can aid in the damping of pressure pulsations occurring in the system, although this usually means reduced efficiency due to hose losses. If maximum efficiency is desired, and flexibility is not needed, then the hoses can be replaced by solid metal tubing.

There are intermediate separating layers between the reinforcing layers and this is particularly true for wire reinforcements. The separation layer ensures that there is no fretting or wear due to relative motion of two wire layers adjacent to each other. If the reinforcing layers are made of a synthetic fiber braid, then the need for a separating layer is lessened. The total system is then housed by a cover layer that is primarily for protection and resistance to abrasion caused by the external environment.

As mentioned, the flexibility of the hoses depicted in Fig. 6 can be a system advantage. However, the flexibility also means compliance in the hose. For example, Table 7 illustrates

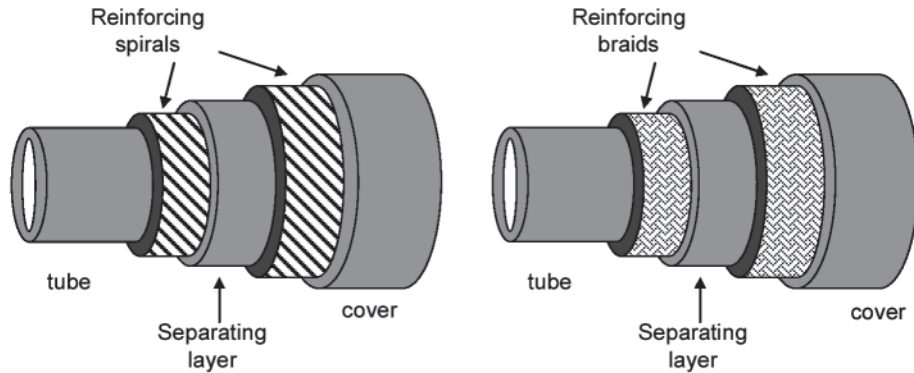


Figure 6 Hydraulic hose construction.

Table 7 Volumetric Expansion of Hydraulic Hose Types

Hose Model	Volumetric Expansion at Maximum Working Pressure		Equation for Volumetric Expansion
	psi	cm ³ /ft	y = (cm ³ /ft); x = (psi)
77C-06	4000	0.8	y = 0.0002x
77C-08	4000	1.2	y = 0.0003x
701-12	5000	7.42	y = 0.0007x + 3.76
701-8	6000	5.61	y = 0.0004x + 3.295
701-6	6500	5.6	y = 0.0003x + 3.87

Source: From Ref. 5.

the volumetric expansion for several particular hoses made by a major U.S. manufacturer.⁵ This compliance can introduce an additional dynamic element to the overall system since the fluid inertia contained in the hose, along with the hose inertia itself, can couple with the hose compliance to produce resonant modes within the hose. Therefore, if pressure pulsations from a pumping device happen to occur at one of the resonant frequencies of the hose section, then severe performance degradation, and possible hose/connector failure, can occur. An excellent and detailed analysis on the resonant modes found in hydraulic hoses, termed transmission line dynamics, can be obtained in Ref. 3.

If the pressurized fluid is to be transported through hoses where the length is significantly greater than the inner diameter, then there is likely to be some power loss due to the friction between the fluid and the walls of the hose tube. This power loss manifests itself as a pressure drop or head loss between two points in the hose. A pressure drop or pipe head loss (h_l) correlation can be obtained by the Darcy–Weisbach equation⁶:

$$h_l = f \frac{L}{D} \frac{V^2}{2g} \quad (6)$$

Where f = friction factor
 L = pipe length
 D = pipe inner diameter
 V = fluid velocity
 g = gravitational constant (9.81 m/s²)

The empirical relationship given in Eq. (6) is quite general and is valid for pipe flow of any cross section. It applies to both laminar and turbulent flow with the basic assumptions of a straight hose, a constant cross-sectional area, and a constant friction factor. The key term to be empirically determined is the friction factor f . There exist well-established correlations for both laminar and turbulent flow:

$$f = \begin{cases} \frac{64}{Re_d} & \text{Hagen – Poiseuille relation (laminar flow)} \\ \frac{0.316}{(Re_d)^{1/4}} & \text{Blassius relation (turbulent flow)} \end{cases} \quad (7)$$

The friction factor has been modeled in the literature by various methods and is dependent on factors like pipe roughness and flow condition. In addition, there exist correlations specifically for flow conditions that are in the transition between laminar and turbulent flow. The reader is referred to Ref. 6 for further details on pipe losses. This includes correction factors to account for bends in the piping, which cause additional losses due to momentum changes in the fluid. Although these pipe losses may be small, it is still important to minimize them to achieve maximum overall system efficiency.

3.3 Hydraulic Pumps

The purpose of a pump is to take mechanical power, in the form of a rotational shaft powered by a combustion engine or electric machine, and convert that to fluid power, in the form of high-pressure fluid moving at some flow rate. The majority of pumping devices in use are termed positive-displacement pumps. This means that for a given rotation of a pump's input shaft, there is an amount of fluid expelled out of the pump's discharge port that is primarily related to the size or displacement of the pumping components. The amount of fluid displaced per revolution is much less sensitive to aspects such as the pressure in the line resulting in the terminology of positive displacement. Two basic classes of pumps are available in current fluid power systems: fixed-displacement pumps and variable-displacement pumps.

Fixed-displacement pumps are usually less costly than variable-displacement pumps because they have fewer components. The most basic types of fixed-displacement pumps are gear pumps, vane pumps, lobe pumps, and piston pumps. Figure 7 demonstrates the working of the gear pump. As the input shaft turns, fluid on the suction side of the pump is pulled into the gears. Then small portions of fluid are carried over the gears, much like a waterwheel, to the discharge side of the pump. The space between each gear tooth acts as a separate volume to transport fluid from the low-pressure suction side to the high-pressure discharge side.

As the speed of the input shaft increases, the flow rate at the discharge port also increases. This increase is usually proportional to the speed across the rated range of the pump, and the proportionality constant is fixed for a given pressure at the discharge port. A similar type of action is responsible for the pumping behavior of both vane or lobe pumps. Figure 8 illustrates the constant proportionality between flow and speed for a vane pump. As can be seen, for a fixed discharge pressure the output flow scales linearly with the input shaft rotational speed.

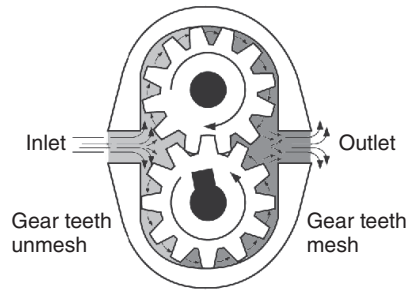


Figure 7 Gear pump schematic.

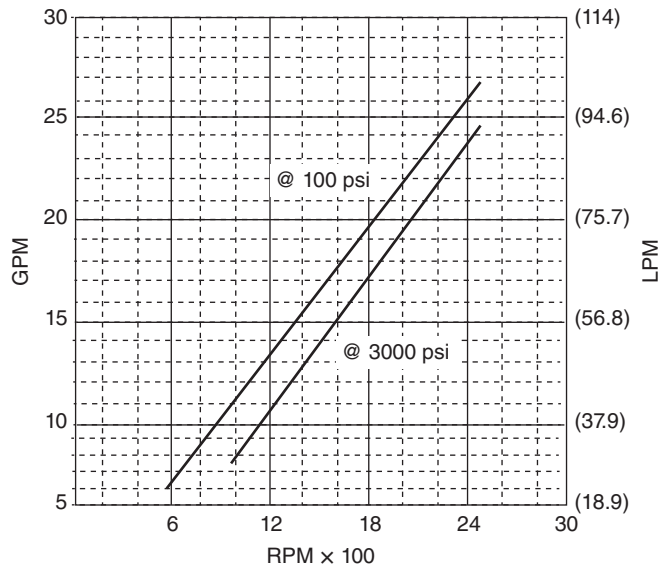


Figure 8 Parker PFVH25 series vane pump flow data (displacement = 40 cm³/rev).

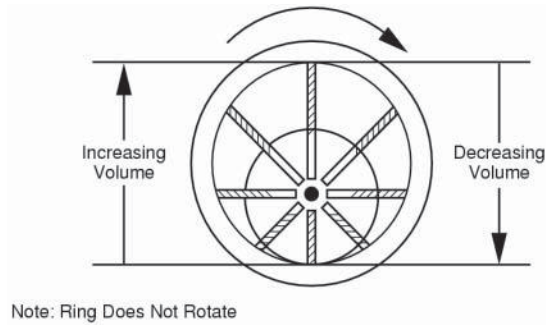


Figure 9 Vane pump schematic.

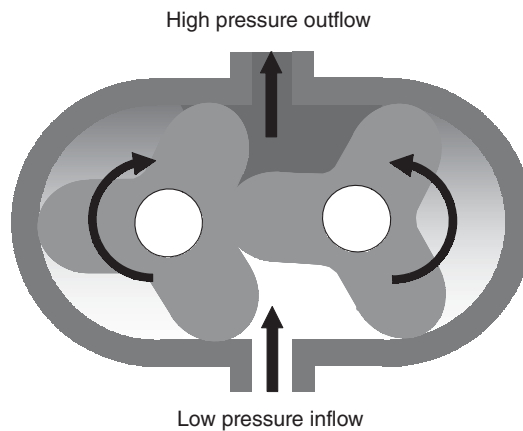
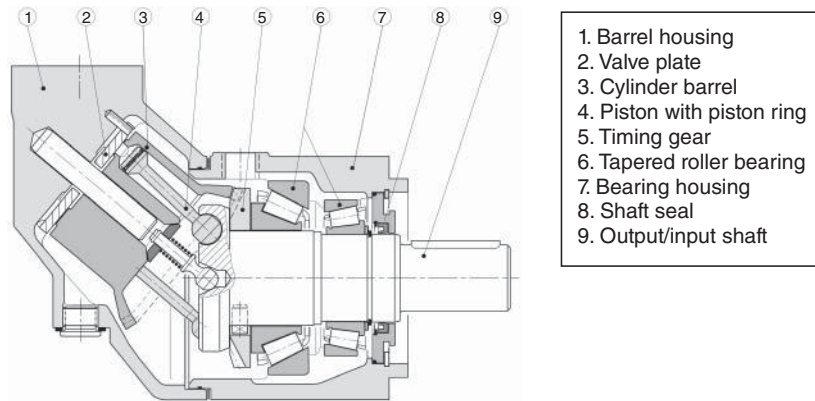


Figure 10 Lobe pump schematic.

Figure 9 shows a schematic similar to Fig. 7 for a vane pump and Fig. 10 does so for a lobe pump. Similar to the gear pump, the vane pump uses vanes or fins to sweep the fluid from the suction inlet around to the discharge section of the pump. The lobe pump uses the lobes much like the gear pump uses teeth to do the same thing.

The primary differences between these types of fixed-displacement pumps are the applications for which they are best suited. For example, the gear pump is better suited for higher pressure applications than the vane pump because of the ability of the gear teeth to hold higher loads than the vanes. However, the vane pump may be better suited for pumping fluids with low lubricity due to the reduced metal to metal contact. The relatively large volumes between the lobes on the lobe pump allow it to handle small bits of solids or contaminants better than the vane or the gear pumps.

Should high pressures be needed (e.g., 3000 psi or more), then the choice of positive-displacement pumps is the piston pump. In this subsystem, individual pistons move back and forth to pump fluid from the low-pressure side of the pump to the high-pressure side. Typical piston pumps are axial and radial piston pumps. A fixed-displacement axial piston pump is usually constructed with the pumping pistons and input shaft offset by an angle. This is termed a bent-axis piston pump and is shown in Fig 11. As the input shaft rotates, the distance between the piston and the intake section of the valve plate increases. This draws fluid into the piston



1. Barrel housing
2. Valve plate
3. Cylinder barrel
4. Piston with piston ring
5. Timing gear
6. Tapered roller bearing
7. Bearing housing
8. Shaft seal
9. Output/input shaft

Figure 11 Axial piston pump schematic. (Reprinted Courtesy of Parker Hannifin Corp. Copyright © Parker Hannifin Corp.)

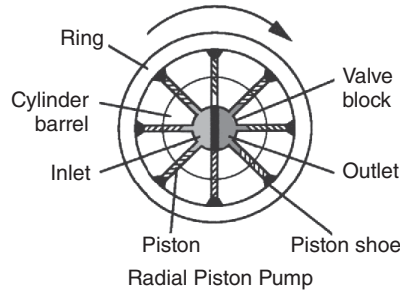


Figure 12 Radial piston pump schematic.

chamber. After the piston has reached its maximum displacement it enters the discharge section of the valve plate where its distance to the plate decreases. This decrease forces fluid out of the high-pressure side of the pump.

As illustrated in Fig 12, a radial piston pump operates similarly to an axial piston pump except that the pistons are now arranged radially. An eccentricity between the pump outer housing, or stator, and the piston housing, or rotor, performs the same actions as the swashplate in terms of moving the pistons in and out of their pumping chambers. Reciprocating devices like piston pumps are very good for generating higher pressures than the continuous devices such as the vane or gear pumps and they tend to be more efficient. On the other hand, the gear and vane pumps tend to be quieter and less expensive to produce.

In many fluid power systems, there is a need to provide a relatively continuous supply pressure from the pump even while the amount of flow, and hence power, demanded can be varying. This would be analogous to having a constant electrical supply voltage while drawing a varying load. Fixed-displacement devices can solve this problem by running at varying speeds or by running at a fixed speed and incorporating a relief valve device at the pump outlet. The relief valve simply diverts high-pressure flow back to the tank when it is not needed and is usually a cheaper option than the variable-speed device to drive the pump. Unfortunately, generating high-pressure fluid and then dumping it over a relief device is not a very efficient use of energy. Therefore, one option that is common is to have a variable-displacement pumping device. Of the different types of positive-displacement pumping devices given above, the most

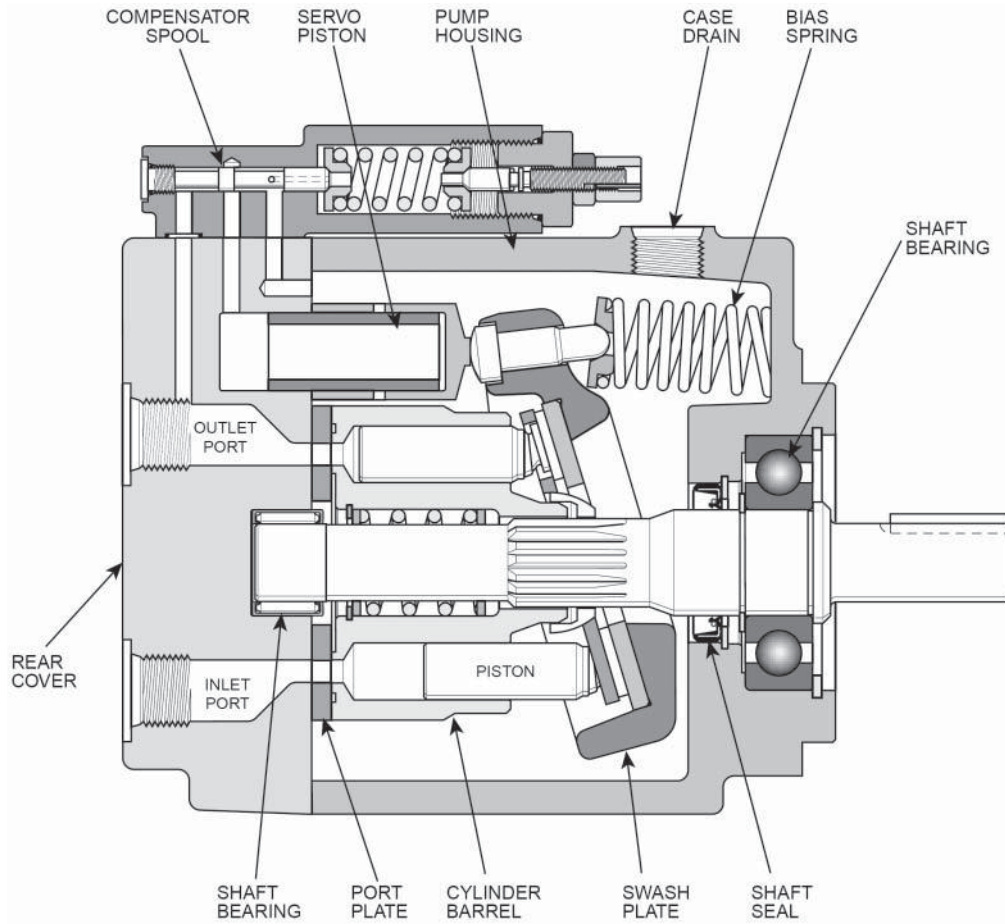


Figure 13 Variable-displacement axial piston pump schematic.

amenable to variation of displacement is the axial piston pump. A variable-displacement axial piston pump contains a swashplate, or wobble plate, attached to the pump input shaft. This allows variation of the relative angle of the pistons and the input shaft that the bent-axis configuration in Fig. 11 could not achieve. By varying the angle of the swashplate, it is possible to vary the amount of fluid that is drawn into and expelled from the pump during each revolution. Figure 13 shows a variable-displacement pumping device illustrating the movable swashplate.

The swashplate setting can be altered to affect the displacement. A very common usage for this type of variable-displacement device is to incorporate *load sensing* into its behavior. A mechanical feedback path from the pump outlet can be used to drive a spring-loaded pilot valve, which in turn provides a flow to pivot the swashplate. Should the flow out of the pump be too great for the current application's usage, an excessive pressure buildup will occur at the pump discharge outlet. Through the pressure feedback mechanism, this will then cause the pump to destroke or reduce its displacement. In turn, this will lower the flow coming out of the pump per revolution and reduce the output pressure the level set by the spring preload on the pilot valve. A similar sequence of events will regulate the pump displacement to increase should the output pressure drop below some desired value. This mechanical feedback system

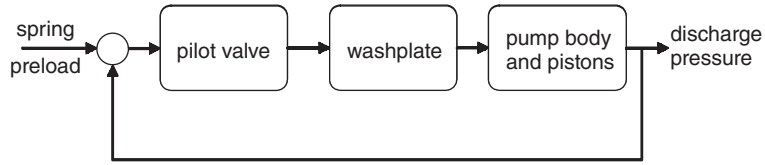


Figure 14 Load sensing axial piston pump diagram.

can therefore provide the correct amount of fluid power for a given application without under-supplying or wasting any fluid that can lead to a large increase in efficiency. A block diagram of a load-sensing variable-displacement pump is shown in Fig 14.

In addition to the mechanical feedback device, it is possible to have an electronically controlled pilot valve to drive the pump displacement. This electrohydraulic pump arrangement has an increased cost and complexity but also provides increased flexibility. It is possible to electronically sense the pump pressure output and feed that information back to the valve driving the washplate displacement. This would mimic the mechanical load-sensing behavior mentioned earlier. In addition, direct electronic control of the pump displacement can be used to provide user-specified flow to a system such as a hydrostatic transmission.⁷ The variable displacement can be used as a variable transmission to drive a hydraulic motor at different speeds.

When considering pump characteristics the end user should consider the efficiency of the pump, since that will have a direct effect on the overall efficiency of the system. Two types of efficiencies are associated with hydraulic pumps: volumetric efficiency and overall efficiency. Theoretically, the output flow of a pump would be equal to the pump rotational speed (Ω) multiplied by the pump displacement (D):

$$Q_{\text{theoretical}} = D\Omega \quad (8)$$

However, there are many internal passages within pumps and, with high pressure at the outlet, leakage can occur within these passages such that not all of the flow coming into the pump actually makes it to the pump exit. The volumetric efficiency of a pump is the ratio of actual output flow of the pump to the theoretical output flow:

$$\eta_{\text{volumetric}} = \frac{Q_{\text{actual}}}{D\Omega} \quad (9)$$

Volumetric efficiency is affected greatly by internal leakages, which are in turn affected by the pressure at the discharge of the pump. As discharge pressures increase, the volumetric efficiency of a pump will decrease. Due to good design and close manufacturing tolerances, modern pumps have volumetric efficiencies that tend to be quite high; usually above 90% for a properly functioning pump.

The overall efficiency of a pump is determined by the ratio between the mechanical power input (torque \times speed) to the driving shaft and the fluid power (pressure \times flow) that exits the pump discharge:

$$\eta_{\text{total}} = \frac{PQ}{\tau\Omega} \quad (10)$$

The overall efficiency of a pump is related to the volumetric efficiency but they are not the same. Overall efficiency is primarily governed by the energy losses associated with the pump. The principal losses are due to friction. This includes viscous friction, which hinders the movement of pump parts within the fluid, particularly if the pump parts are moving a thin film of hydraulic fluid. Energy losses are also due to friction contained in bearings and seals. The fluid viscosity has a large part to play in both the volumetric and overall efficiency. Low-viscosity fluid means easy pumping and a higher overall efficiency. However, low viscosity also means more internal leakage and therefore lower volumetric efficiency.

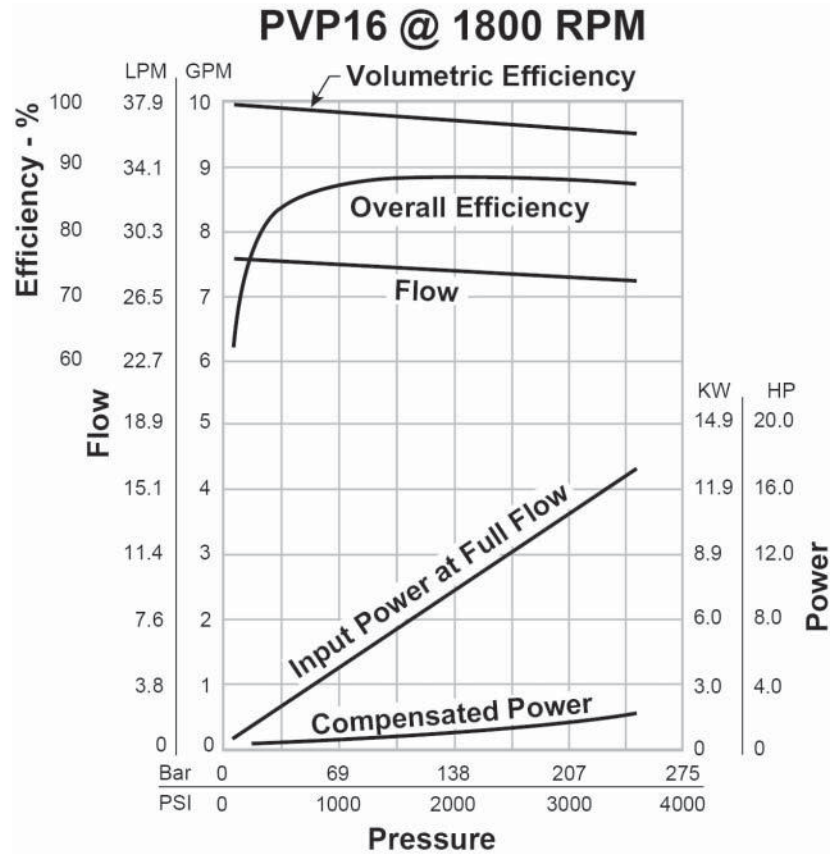


Figure 15 Performance of a pressure-compensated variable-displacement axial piston pump.

Typically, the construction of different pumps will affect their efficiency levels. All pumps have low overall efficiencies at flow rates far below their rated pressures. Typically, gear and vane pumps will have a lower overall efficiency at higher pressures than a piston pump. Figure 15 illustrates a typical performance chart for a variable-displacement axial piston pump.

3.4 Hydraulic Valves

In a fluid power system, the hydraulic valve serves to restrict the flow of fluid through the system. In this sense, it is analogous to the electrical resistance as depicted in Table 6. This flow restriction can be used to modulate or meter the amount of fluid going into the chamber of a cylinder or motor. Additionally, this restriction can act to divert the flow of fluid from one path to another. An example of this is the relief valve that diverts flow from the main pressurized line back to the low-pressure tank. Since all valves act as a restriction, it is simplest to consider them as orifices from the point of view of basic fluid mechanics.⁶ If a further assumption is made that the fluid is incompressible, this allows for the simple approximation of the valve opening as a sharp-edged orifice. From Bernoulli's principle⁶ we can determine the relative velocity downstream of an orifice if we are given flow conditions across the orifice. Considering u to

denote upstream of the orifice and d to denote downstream we can calculate

$$v_d^2 - v_u^2 = \frac{2}{\rho} (P_u - P_d) \quad (11)$$

The fluid density is denoted as ρ and the pressures by P . The volumetric fluid flow can be determined from the fluid velocities (v) depicted in Eq. (11). It is essentially the velocity times the area of the pipe or channel carrying the fluid. Then, assuming incompressible flow,

$$A_u v_u = A_d v_d \quad (12)$$

This can be used with (11) to determine the velocity downstream:

$$A_u v_u = A_d v_d = Q = \frac{A_d}{\sqrt{1 - (A_d/A_u)^2}} \sqrt{\frac{2}{\rho} (P_u - P_d)} \quad (13)$$

Equation (13) is an idealization, and it is necessary to add an empirical correction factor to account for the loss in energy due to the internal fluid friction. In addition, the downstream area used is the *vena contracta*⁴ rather than the area of the actual orifice itself, thereby necessitating another correction factor. These two correction factors can be lumped together into a *discharge coefficient*, C_d :

$$Q = C_d A_o \sqrt{\frac{2}{\rho} (P_u - P_d)} \quad \text{or} \quad Q = C_d A_o \sqrt{(P_u - P_d)} \quad (14)$$

where A_o is the physical orifice area. Either one of the equations in (14) can be used as long as the correct definition of discharge coefficient accompanies it:

$$C_d = \frac{C_v C_c}{\sqrt{1 - C_c^2 (A_o/A_u)^2}} \quad \text{or} \quad C_d = \frac{C_v C_c}{\sqrt{1 - C_c^2 (A_o/A_u)^2}} \sqrt{\frac{2}{\rho}} \quad (15)$$

Where C_v (~ 1.0) is the correction coefficient due to internal friction losses, and C_c is the contraction coefficient, which is the ratio of the vena contracta to the orifice area A_o . The two empirical coefficients, C_v and C_c , are usually difficult to determine analytically. Oftentimes, the discharge coefficient is simply determined as a lumped parameter from calibrated pressure versus flow data. Reasonable values of C_d for most conditions would range between 0.5 and 0.8.

Many different types of valves are available. Three of the most common ones that will be mentioned briefly here are related to the shape of the metering orifice: the ball valve, poppet valve, and spool valve. The ball valve and poppet valve operate similarly in that there is an opening or orifice on which the ball or poppet is seated. The name of the valve comes from the device that seals the opening. Figure 16 illustrates both a ball valve and poppet valve. As either the ball or poppet lift off of the seat, an annular area is uncovered through which fluid can pass. This annulus is a metering orifice. Usually, flow will come from the passage below the ball or poppet as drawn in Fig. 16. As will be shown shortly with a relief valve example, the ball or poppet is usually connected to a spring that applies a load, attempting to keep the valve in a

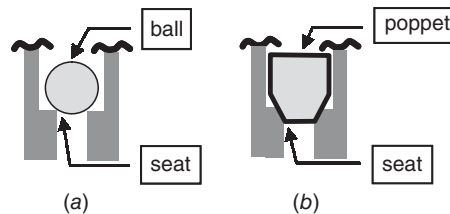


Figure 16 (a) Ball valve and (b) poppet valve.

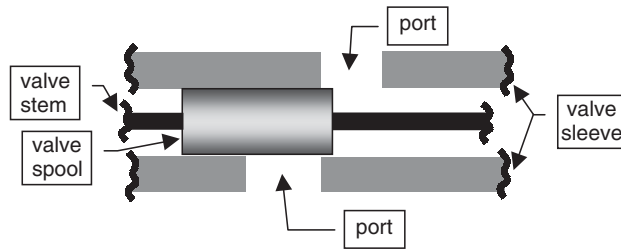


Figure 17 Spool-in-sleeve valve.

normally closed when insufficient pressure is present below the seat. The benefit of the poppet style valve over the ball valve is the ability to seal better with less leakage across the valve.

A third class of valve is called a spool valve. This is because the metering orifice is created by the sliding of a spool within a sleeve as illustrated in Fig 17. The spool is usually cylindrical in geometry. As it moves within the sleeve it will cover or uncover different ports. In Fig 17 the valve spool covers up the lower port while potentially allowing fluid to flow through the upper port. These ports are connected to different components within the overall fluid power system, thereby allowing this type of a valve to be used to redirect flow from one path to another. This will be further described shortly.

One common function for a ball or poppet type of hydraulic valve is the simple pressure relief valve. The simplest representation of a pressure relief valve is shown schematically in Fig 18. When the pressure in the pressure port becomes large enough, the force on the ball will overcome the preloaded spring force and open a direct flow connection between the high-pressure line and the return line to the low-pressure tank or reservoir. Therefore, the pressure in the high-pressure line will be maintained at some preset level that is based on the spring preload. The spring preload may be set manually by means of a screw that would be located at the top of the valve. Alternatively, the spring preload could be set by a solenoid, which would enable an electronically adjustable relief pressure setting. This would result in a pressure control valve rather than just a relief valve.

Probably the most common function for a sliding spool valve is the directional control valve. This valve is called directional because it is used to direct the flow from a high-pressure source, such as a pump, to a motor or cylinder to perform work on an external environment. A schematic diagram of a four-way directional control valve can be seen in Fig 19, and its connection to a load was shown earlier in Table 4 and Fig. 2. By shifting the direction of the valve, different connections between the pump, tank, and work ports (A and B) of the valve can be

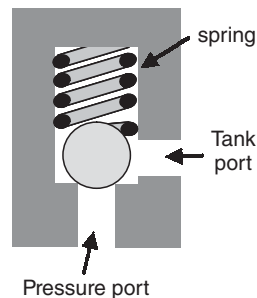


Figure 18 Relief valve schematic.

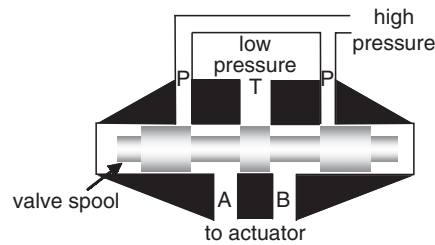


Figure 19 Four-way directional control valve.

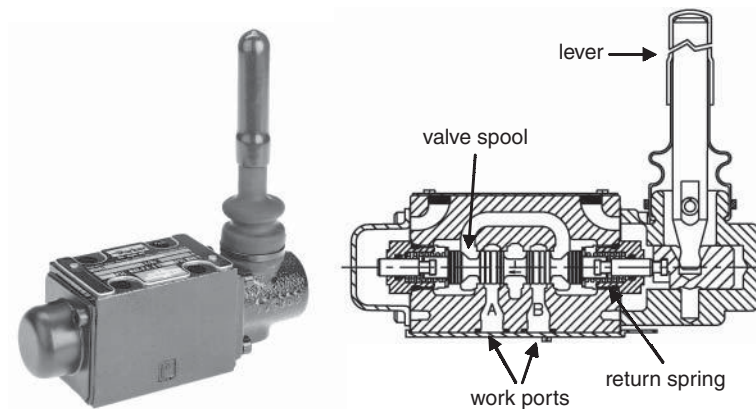
established. For example, if the valve in Fig 19 is shifted to the right, there will be a connection between port A and the tank as well as a connection between port B and the high-pressure supply from the pump. Therefore, the fluid will flow into the side of the actuator connected with B causing motion to occur. A motion of the valve to the left will cause a connection between port B and the tank as well as port A and the supply.

Several different terms or characteristics can be used to describe valve construction and their function. As depicted in Table 4 valves can often be defined by their *ways*; there are two-way, three-way, and four-way valves. A two-way valve is essentially an on-off valve. The valve is either opened or closed and the flow path cannot be changed. The flow simply moves between the pressure supply port and the exhaust port. The relief valve or ball and poppet valves illustrated in Figs. 16 and 18 are examples of two-way valves. A three-way valve is one that has a pressure port, an exhaust port, and a work port that meters fluid to some actuator in order to enable it to perform work. A four-way valve will have a supply port, an exhaust port, and two outlet ports. Figure 19 is an illustration of a four-way valve because there are four basic ports: two work ports plus a supply port (P) and an exhaust port (T). Here, P and T are commonly used to represent *pump* and *tank*.

Another valve characteristic associated with directional valves is the type of center configuration: open centered or closed centered. An open-centered valve has a direct path between the tank and the pump when the valve spool is centered. This is useful when the pump is fixed displacement because it minimizes the power loss from the pump during zero valve position. Also, the open-centered valves can provide a faster response from valve command input to flow output. Oftentimes open-centered valves are also referred to as *underlapped* valves. The closed-centered valves block the flow from pump to tank when the valve is in the centered position. This is inadvisable with a fixed-displacement pump because it ends up dumping high-pressure flow over the relief valve with a large waste of energy. In this case, a pressure-compensated pump is advised. Closed-centered valves are good for holding loads in place, even when the pump is not providing power, because very little leakage can occur across the valve. Closed-centered valves are also called *overlapped* valves. In Fig. 19 the spool dimensions are drawn so as to just cover the pressure and return ports exactly. This is termed *critically lapped*. This means there is flow for a given valve motion away from center and no flow for valve at its center position. Table 8 illustrates the flow characteristics of differently lapped valves. It should be noted that the flow characteristics depicted do not differentiate whether the high-pressure fluid is directed toward port A or B; only the magnitude of the flow is shown. If the spool lands did not sufficiently block the P and T ports, the valve would be considered underlapped. For an underlapped valve, there will always be flow through the valve. This leakage flow can be undesirable in some cases because it represents power that is not utilized for useful work. If the spool lands completely covered the P and T ports with plenty of room to spare, the valve would be considered overlapped. Overlapped valves minimize leakage through the valve, thereby leading to higher overall system efficiency. However, the cost of doing so is

Table 8 Configurations for Four-Way Directional Control Valves

Valve Lap	Valve Schematic	Valve Flow
Underlapped		
Overlapped		
Critically lapped		

**Figure 20** Manual four-way directional control valve. (Reprinted Courtesy of Parker Hannifin Corp. Copyright © Parker Hannifin Corp.)

to introduce a dead zone or dead band in the relationship between valve motion and flow. This dead band can have serious consequences for closed-loop control schemes utilizing this valve.

As illustrated in Table 4, there is more than one way to move a valve to generate flow. Manual control of valve motion can be accomplished by connecting the valve, through some type of linkage, to a lever or device that can be operated by a human. Figure 20 illustrates a Parker Hannifin D1VL-series four-way directional control valve operated by a lever. The valve is centered by springs on either side of the valve spool. By shifting the lever in or out, flow can

be directed from a high-pressure source to either the A or B work ports. Other manual methods for moving a spool include foot pedals and buttons (for two-way valves).

If electronic control or automation is required from the fluid power system, then the input can no longer be manual but must be generated electronically. This leads to electrohydraulic fluid power systems. The simplest and most common electronic actuator to generate valve motion or spring preloading is a solenoid. A solenoid consists of a wire coil surrounding a metal plunger. When current flows through the solenoid, it generates a magnetic field that produces a force on the plunger. Depending on the configuration of the solenoid, its energized state can either retract or extend the plunger. Often, for directional control valves, two separate solenoids are used as shown in Fig 21 for a Parker Hannifin D1FW-series valve. The left solenoid is used to actuate the valve to the right in the figure and vice versa for the other solenoid. If neither solenoid is engaged, the return springs on either side of the valve will bring it back to a neutral position. The use of dual solenoids is due to the fact that it is simpler to have two single-action solenoids than one electromagnetic device that can retract and extend the plunger attached to the valve spool. For a two-way valve, such as a relief valve, a single solenoid is sufficient for it acts only to provide a preload to the spring that seats the valve.

Although solenoids are rugged and cost effective, one disadvantage is their nonlinear behavior. As the plunger moves further out of the energized coil, the electromagnetic force decreases in a nonlinear fashion. This is shown schematically in Fig 22. Additionally, the force generation characteristics associated with the solenoid are greatly affected by temperature, which can change if the solenoid is repeatedly energized or held on for an extended period of time. This temperature dependence is also a nonlinear one. Vaughan and Gamble⁸ develop a

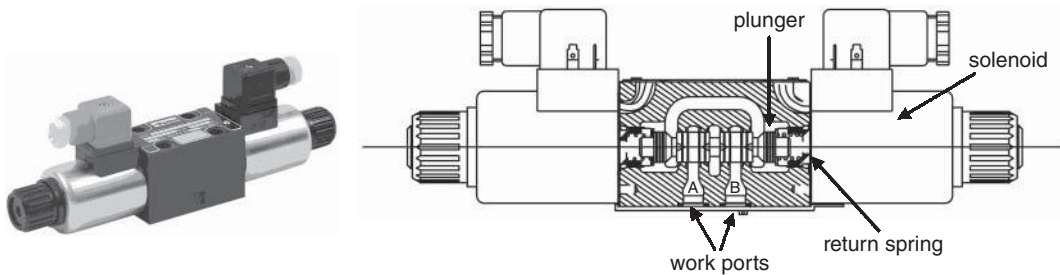


Figure 21 Solenoid operated four-way directional control valve. (Reprinted Courtesy of Parker Hannifin Corp. Copyright © Parker Hannifin Corp.)

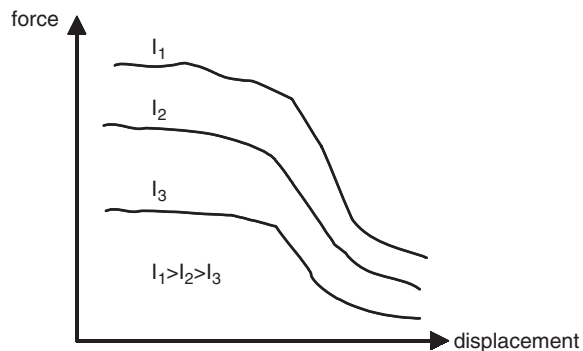


Figure 22 Nonlinear force generation characteristics for a solenoid.

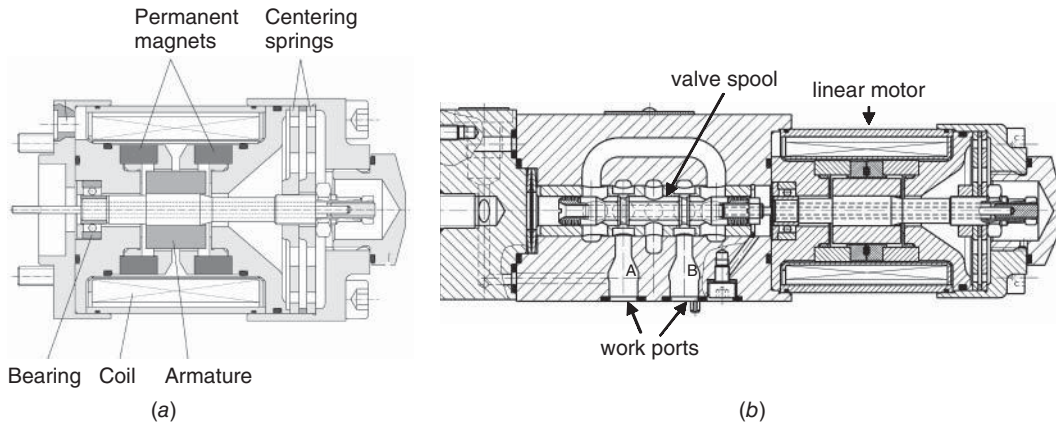


Figure 23 Direct-drive linear motor for electrohydraulic valve. (Courtesy of Moog, Inc.)

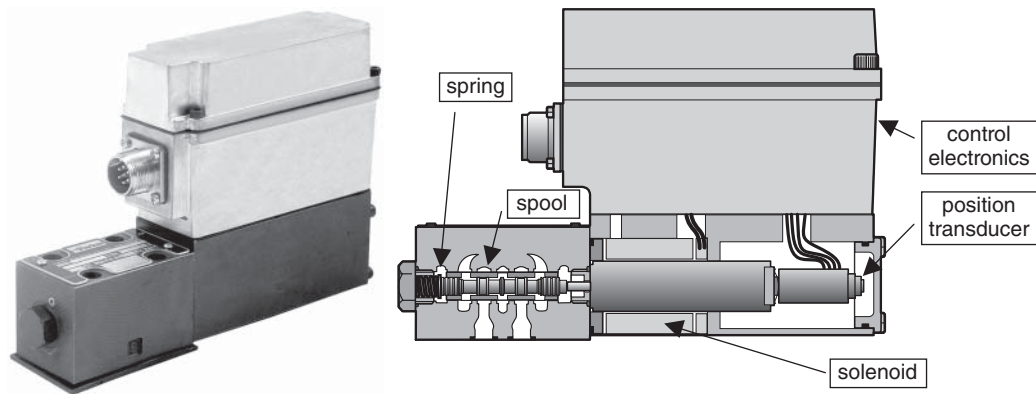


Figure 24 Parker D1FH proportional valve with closed-loop spool feedback. (Reprinted Courtesy of Parker Hannifin Corp. Copyright © Parker Hannifin Corp.)

good model of solenoid characteristics for use in an electrohydraulic system. These shortcomings make it difficult to provide high-performance precision control from a simple solenoid valve. One method to compensate for this is to use a more expensive direct-drive linear motor in place of a solenoid. A single direct-drive motor can actuate a plunger in two directions. Figure 23a shows a cross section of a direct-drive linear motor for electrohydraulic valve actuation. Figure 23b shows the single-sided attachment of the linear motor to a valve spool. This type of arrangement gives a much more linear response than the solenoid depicted in Fig. 21.

Another method to compensate for the valve nonlinearity is to close a feedback loop locally about the valve position. Figure 24 shows a schematic of a valve where a lower precision solenoid actuation is used to move a spool valve. However, the nonlinearity of the solenoid is compensated by the closed loop feedback of the spool position using an integrated position sensor. The actual control electronics depicted in Fig. 24 can be either digital or analog, depending on the sophistication of the valve. Proportional valves with closed-loop feedback are often called servo valves. This term comes from the fact that the valve position is only a function of the command given. The closed-loop electronics eliminate nearly all of the variability in spool position as a function of commanded reference. Additionally, this effect can be enforced

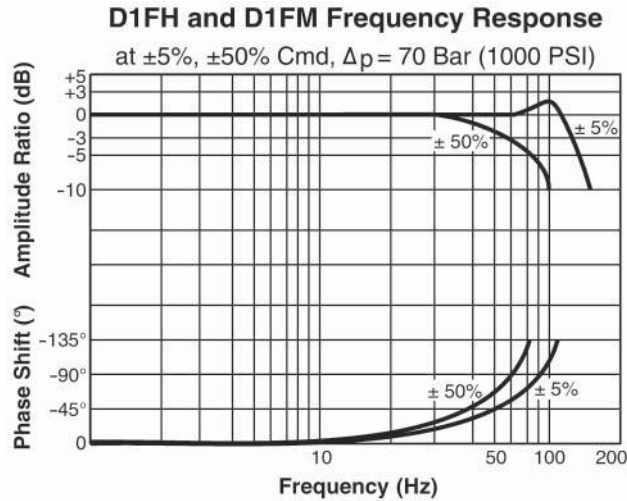


Figure 25 Parker D1FH and D1FM proportional valve frequency response. (Reprinted Courtesy of Parker Hannifin Corp. Copyright © Parker Hannifin Corp.)

up to very high frequency motions. Figure 25 illustrates a frequency response of a particular proportional servo valve for different amplitudes of motion. As can be seen, the valve responds reliably to reference command changes up to 100 Hz for small signal amplitudes, which is fast enough for many applications. In addition to being fast, this electronic feedback allows the valve to be programmable. For instance, the valve motion could be made nonlinear with respect to command so that it was very sensitive to commands (high gain) around null and less sensitive (low gain) once the valve was open a certain percentage.

In addition to the electronic position sensing feedback for valve positioning, it is also possible to have an internal mechanical valve feedback. Typically this is obtained by a mechanical feedback device, such as a spring, between a light and fast first stage and a heavier second stage that contains the actual spool. Figure 26 shows a classical servo valve that operates with a flapper-nozzle arrangement.⁹ The fast first stage is actually a torque motor that provides a rotation for a given torque input. This electrical effect produces flapper motion that uses differential pressure to generate a hydraulic amplification, which then affects the spool motion. The motion of the main spool is communicated back to the first-stage torque motor by means of a slim wire attached to the middle of the main spool. The flexure of this wire has a force effect on the spool that is proportional to displacement, thereby providing a proportional mechanical feedback. These types of valves can be designed to have very rapid responses, even beyond those depicted in Figs. 23 and 24. However, they are susceptible to contamination because of the very fine manufacturing tolerances. These manufacturing tolerances also make them generally more expensive than their electronic feedback counterparts. There are other mechanical servo valve designs using jet pipe feedback or other means. The reader is referred to Refs. 4 and 9 for further insight into mechanical servo valve design and construction.

The basic idea behind the mechanical servo valve in Fig. 26 is the idea of a multistage hydraulic valve. This idea is often used when a fast response is needed in conjunction with a high flow rate. A high flow rate for a directional valve indicates a large spool inertia. For example, the directional valves on large earthmoving equipment can have spools weighing several kilograms. Solenoids would not be sufficiently powerful to move such an inertia or resist the flow forces⁴ that would arise. Therefore, it is common in these cases to use a small

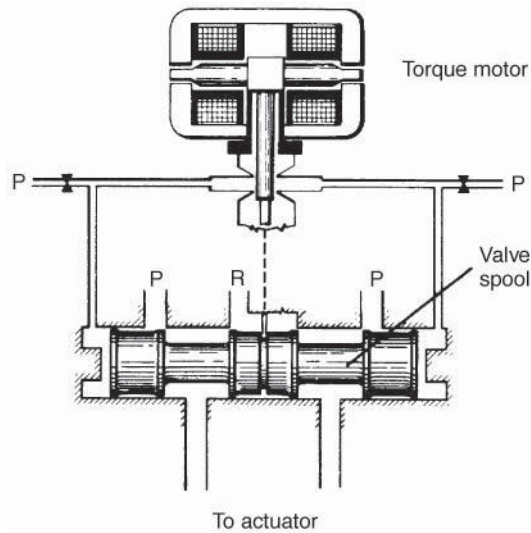


Figure 26 Two-stage flapper-nozzle servo valve. (Courtesy Moog Inc.)

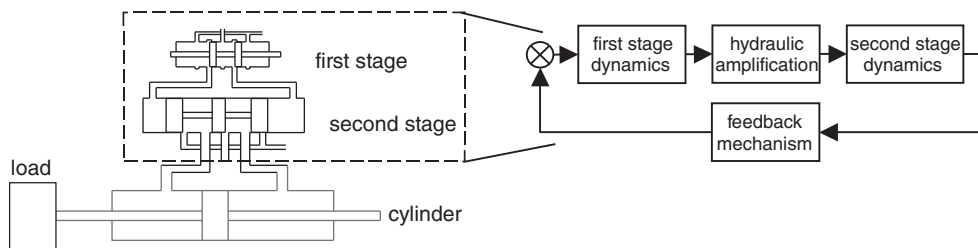


Figure 27 General multistage valving.

valve to drive a large valve. This is depicted conceptually in Fig 27. The small quick valve utilizes the hydraulic amplification of pressure against the second-stage spool end to gain a valve system with high flow and fast response.

3.5 Cylinders and Motors

Hydraulic cylinders and motors are the components that convert fluid power into mechanical power by applying forces and torques to some load environment. Hydraulic cylinders convert fluid power into linear mechanical power and hydraulic motors convert fluid power into rotary mechanical power. The basic hydraulic cylinder consists of a piston and a rod inside of a sleeve or barrel with two end caps. This configuration was shown schematically in Table 5. A more detailed schematic is shown in Fig 28 for a single-rod cylinder.

The piston can have rods on either end (double acting) or only on one end (single acting) although only one rod is shown in Fig. 28. The price to be paid for a double-acting rod is a more complicated and expensive device that occupies more volume, since allowances have to be made for extensions of rods in two directions. The benefits to be gained are uniformity in behavior during retraction and extension. The hydraulic cylinder is capped at two ends and,

as shown in the figure, sometimes reinforced by tie rods that hold the end caps on and provide additional strength. Ports at either end of the cylinder allow fluid to flow into and out of the actuator on either side of the piston. High-performance seals between the piston circumference and the cylinder body ensure that minimal amounts of fluid leak across the piston between the low- and high-pressure chambers. There are also seals on the end cap through which the rod extends to prevent the leakage of fluid to the external environment. Additionally, modern cylinders often have wipers at the seal interface between the rods and the end caps to ensure that dirt and contamination from the external environment do not find their way into the hydraulic fluid.

Figure 28 shows a relatively simple schematic of a hydraulic cylinder. In addition to the aspects shown above, the normal seals on the piston can be replaced by hydrodynamic seals if seal friction is to be reduced for high-performance systems. Additionally, many hydraulic cylinders incorporate “snubbers” or hydraulic cushioning devices to minimize shock induced by reaching the end of the cylinder’s stroke. Further details may be found in Ref. 2.

Hydraulic motors primarily come in several varieties. In most cases, the motors simply act like pumps running in reverse. For example, consider the gear motor schematic shown in Fig 29. The high-pressure inlet flow acts on the lower sets of gear teeth and forces them to rotate in the directions of the arrows. The segments of two meshing teeth tend to oppose rotation, making

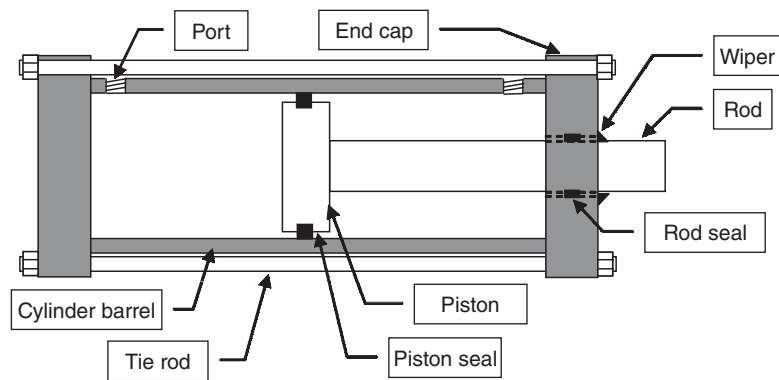


Figure 28 Schematic of a single-rod hydraulic cylinder.

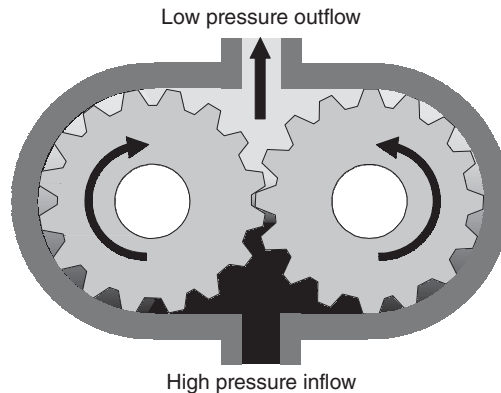


Figure 29 Schematic of a gear motor.

the net torque available be an effective function of one tooth. Pressure on the outer gear teeth that ride along the casing of the motor is effectively neutralized because of the identical teeth. The net torque from this section is zero as the oil is carried around and over to the exit port. The teeth at the top of the motor have only tank low pressure that they face to oppose them, which leads to the pressure difference between the inlet high pressure and the outlet tank pressure to provide torque to move the gears. For the actual motor, one of the gears would be coupled to an output shaft that would rotate and provide the external torque to whatever load was attached. As we can see, the basic principle is exactly the same as the gear pump except the input and output are reversed. For the gear pump, the input is shaft torque to the gears and the output is the high-pressure fluid. For the gear motor, the input is the high-pressure fluid and the output is the shaft torque.

Similar to the gear motor, most other hydraulic motors act with a dual relationship to their hydraulic pumping counterparts. For example, the hydraulic axial piston motor uses high-pressure fluid to force pistons to move. The piston motion causes a swashplate to rotate. Additionally, the pitch of the swashplate can be made variable, just as in a pump, so that the displacement per revolution of the motor can be altered. This would result in a variable-displacement motor that can give a significant control degree of freedom to an overall system. Since the basic behavior of the other types of motors (e.g., axial piston, radial piston, vane, etc.) are so similar to their pumping counterparts, the reader is referred to Ref. 2 for further detailed discussion.

3.6 Other Components

There are several components, other than the primary ones described above, that make up an overall fluid power system such as the one depicted in Fig. 1. Without these other components, the behavior of most fluid power systems would be either impossible or very suboptimal. One of the key components in many fluid power systems is the accumulator. This is effectively the same as an electric capacitor and is used for direct storage of fluid power in the form of highly pressurized fluid. Physically, an accumulator consists of a chamber with a movable interface separating the hydraulic fluid from some other type of gas, often nitrogen. There are two primary types of accumulators, piston and bladder types. Figure 30 shows schematics of both types of systems. For the piston types of accumulators, a linear spring element could be substituted instead of the inert gas to act as an energy storage element.

Accumulators serve many different purposes in fluid power systems. If they are placed immediately downstream of a positive-displacement pumping device, such as an axial piston pump, they can act to smooth out pressure ripples that may come from the individual piston strokes. Schematically, this is shown in Fig 31. In addition to smoothing out pressure pulsations from pumps, accumulators can be placed immediately upstream of valves. In doing so, they will absorb any system shocks that might occur from sudden valve closings. This is often called

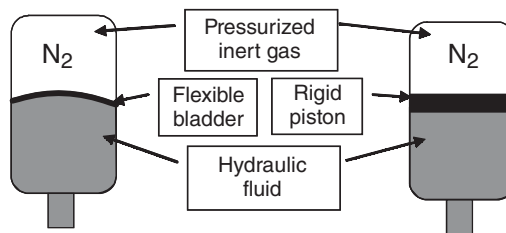


Figure 30 Bladder (*left*) and piston (*right*) types of accumulators.

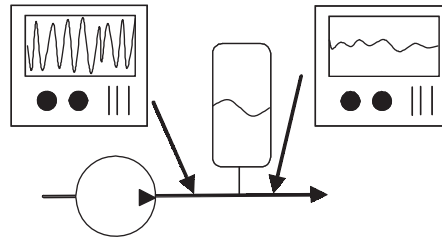


Figure 31 Filtering action of an accumulator placed at a pump exit.

surge compensation. Accumulators can also be used to store fluid power that can be used to briefly run safety-critical systems in the event of a power failure. In this role, the energy stored in the accumulator can be used to safely bring the system or machine to a shutdown condition in a properly controlled fashion. Finally, accumulators can often be used to provide additional flow to a system so that maximum flow available is greater than the instantaneous flow the pump can provide. Therefore, mobile systems, such as aircraft, can be made lighter and more efficient by using smaller pumping and reservoir components.

Another component associated with fluid power systems that should be considered in the overall design is the tank or oil reservoir. The tank serves as more than a repository for oil. Tanks must be appropriately sized so as to provide a suitable heat sink for rejection of the heat developed as the fluid is worked throughout the system. As the fluid goes over several pressure drops, it can become heated. As it returns to the tank, it has the opportunity to cool down before going into the system again. It is often sufficient in stationary applications to size the tank appropriately to be an effective source of heat rejection using passive means. However, in mobile applications such as aerospace where space is at a premium, active cooling by means of embedded heat exchangers is often necessary to get by with a smaller tank size.

Several of the components mentioned in this section are given to the reader in an introductory form. That does not mean that they are not crucial to the overall system performance. Rather, given the compact nature of this chapter, there is insufficient space to detail all of the system components in depth. However, there are several excellent texts the reader may turn to for further details on these components and others.²⁻⁴ Some of the other components include filters for keeping contamination out of the oil and couplings for connecting hoses to components.

4 SYSTEM DYNAMIC BEHAVIOR

The previous section detailed several of the components that make up a fluid power system. These components are useful only when they are combined and integrated into an overall system. As mentioned at the beginning of this chapter, care must be exercised when connecting each of these subsystems since the interconnected system can exhibit dynamics that were not apparent in the individual subsystem.

Each component has its own dynamic behavior that can be examined separately before interconnection. Here we can consider the dynamics of a variable-displacement axial piston pump. The simplest dynamic models are the linear input–output transfer functions.¹⁰ Under many situations, the pump can be treated as a constant gain between input rotational speed and output flow. This is the case when the pump is operating in a steady-state environment:

$$Q_{\text{pump}} = D_{\text{pump}}\omega_{\text{pump}} \quad (16)$$

As mentioned in relation to Fig. 31, slight variations in flow due to individual motion of the pistons are usually smoothed out by the inclusion of an accumulator at the pump output. There are cases where the pump displacement D_{pump} can be varied to change the output flow in a controlled manner. For these systems, the pump displacement is varied by changing the swashplate angle, termed here as α :

$$D_{\text{pump}} = K_{\text{displ}} \alpha \quad (17)$$

In electrohydraulic pumps, the swashplate angle can be changed electronically by means of a solenoid valve providing a pilot force to the swashplate. The simplified swashplate dynamics can usually be modeled as a simple second-order transfer function¹¹ about some nominal operating position, α_0 :

$$\left. \frac{\alpha(s)}{u(s)} \right|_{\alpha_0} = \frac{K_{\text{swashplate}}(\alpha_0)}{s^2 + 2\xi(\alpha_0)\omega_n(\alpha_0)s + \omega(\alpha_0)_n^2} \quad (18)$$

The actual system dynamics are nonlinear, so Eq. (18) is valid for a specific displacement angle since the damping ratio and natural frequency often change as a function of the swashplate displacement angle. The input signal is usually amplified and sent to a control valve, which operates against a spring-loaded hydraulic amplification to affect a net torque on the swashplate. Depending on the internal pump configuration and the operating pressure set by the relief valve, the dynamics can be either underdamped or overdamped. Many manufacturers design the pump to be significantly overdamped and so the dynamics can be further simplified as a first-order system if the faster pole is neglected. Additionally, flow limitations in the internal pump feedback often will limit the pump to a rate-limited dynamic behavior.

For electronically driven single-stage valve components with centering springs the valve usually acts as a simple second-order system. Therefore, the relationship between the valve motion (x_v) and the input signal from some pulse-width-modulated amplifier is given as

$$\frac{x_v(s)}{u(s)} = \frac{G_v}{m_v s^2 + b_v s + k_v} \quad (19)$$

Where G_v = valve gain
 m_v = valve mass
 k_v = valve centering spring
 b_v = valve damping
 u = control voltage

A two-stage servo valve, such as the one shown in Fig. 26, possesses different dynamics than the single-stage directional valves. A simplified block diagram is given in Fig 32,⁹ with the related system parameters given subsequently:

K_t = torque motor gain
 K_h = hydraulic amplification gain
 A_v = spool end area
 k_f = net stiffness on armature
 ω_n = 1st – stage (flapper) natural freq.
 ζ = 1st – stage (flapper) damp. ratio
 K_w = feedback wire stiffness

This representation ignores the nonlinear effects of the two-stage valve such as flow saturation in the first stage due to flapper rotation limits but is useful for analyzing small signal

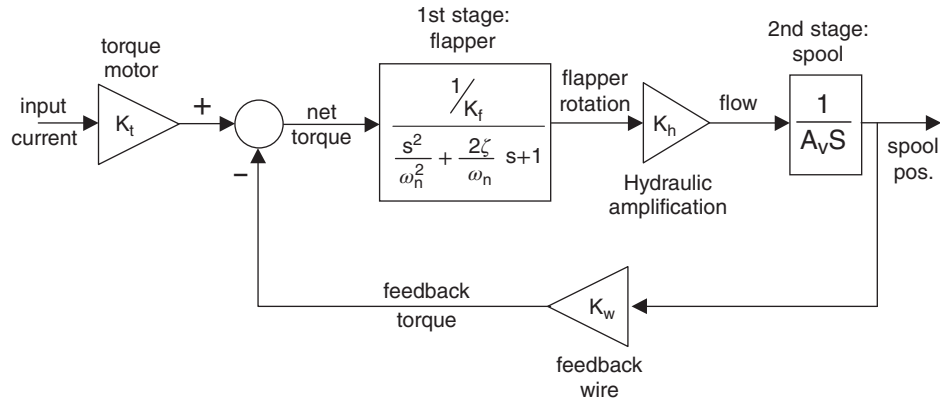


Figure 32 Two-stage servo valve dynamics. (From Ref. 9.)

valve response. The transfer function from input current, $i(s)$, to output valve position, $x_v(s)$, can be written as

$$\frac{x_v(s)}{i(s)} = \frac{\left(\frac{K_f K_h}{K_f A_v}\right)}{s \left(\frac{s^2}{\omega_n^2} + \frac{2\zeta}{\omega_n} s + 1\right) + \left(\frac{K_f K_h}{K_f A_v}\right)} \quad (20)$$

The simplified transfer function for a two-stage servo valve usually has three poles, two complex and one real. The response due to the two complex roots is often much faster than the response due to the real root. Consequently, the model could be simplified to a first-order system for lower-frequency analysis.

Examples of the components given above can be put together to form an overall system to perform a given task. Consider, for example, the electrohydraulic valve-driven, double-ended hydraulic cylinder moving an inertia with both damping and a spring resistance. The overall block diagram for the system's dynamics appears as shown in Fig. 33

- where A = piston area
- m = load mass
- b = viscous damping on load
- x = cylinder position
- F = cylinder force generated

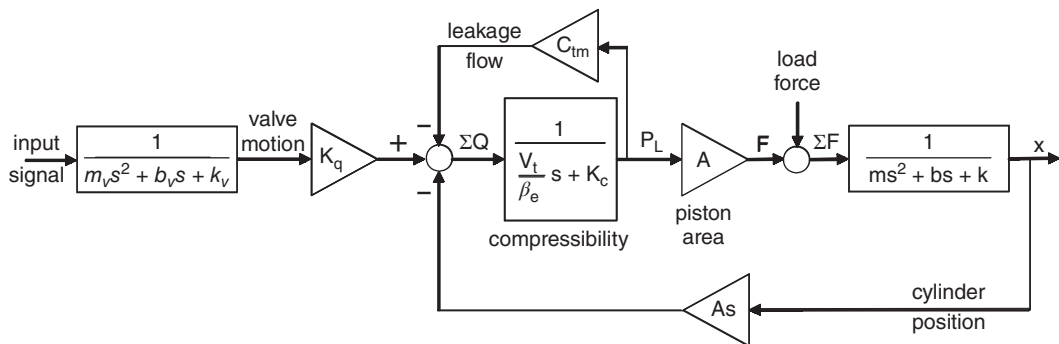


Figure 33 Linearized dynamics of a hydraulic cylinder.

In the absence of load forces, the transfer function from valve command input to cylinder position output is given as a fifth-order transfer function:

$$\frac{x(s)}{u(s)} = \frac{1}{m_v s^2 + b_v s + k_v} \times \frac{K_q/A}{\left(\frac{V_t m}{\beta_c A^2}\right) s^3 + \left(\frac{(K_c + C_m)m}{A^2} + \frac{bV_t}{\beta_c A^2}\right) s^2 + \left(1 + \frac{(K_c + C_m)b}{A^2} + \frac{kV_t}{\beta_c A^2}\right) s + \frac{(K_c + C_m)k}{A^2}} \quad (21)$$

As can be seen by Eq. (21), the dynamics of this relatively simple fluid power system can be quite complex, with dynamic behavior more intricate than the behavior of a single component. If one were to try and close a control loop around this system, one would have to take into account all the dynamics associated with the system. Moreover, if this simple cylinder linear motion system were to be incorporated into an overall system, such as a primary flight control surface on an aircraft, it could become even more complex. A thorough knowledge of system dynamics is an engineer's best tool in this situation.

5 COMMON NONLINEARITIES

The description of fluid power systems in the previous section was simplified to determine linear, time-invariant, dynamic models. There are some key nonlinearities that are common in fluid power systems and greatly affect their dynamic performance. Here we mention several of the major ones that can affect dynamic system performance.

5.1 Saturations and Dead Zones

One of the primary nonlinearities in any hydraulic system is saturation. This can occur at several places. The valve has a finite displacement, which leads to a saturation. Similarly, a cylinder will have a constraint on its motion. Finally, the system pressure is usually limited to be below 3000 psi in most operating systems through the use of a relief valve at the pressure supply as shown in Fig. 5. If these saturations were to be incorporated into the dynamics of a valve-controlled cylinder, the modified block diagram would be as shown in Fig 34.

Another nonlinearity mentioned in the section on components is the characteristic associated with the valve's center position. As mentioned earlier, the valve can be underlapped, critically lapped, or overlapped. This corresponds to the covering of the ports by the spool lands. An overlapped valve, while minimizing fluid leakage and hence system power, does produce a dead zone in the relationship between valve displacement and fluid flow. An underlapped valve allows flow between the pump and tank even when the valve is in its center position, thereby wasting some energy. However, an underlapped valve has a higher flow gain at low valve displacements, thereby making the system response faster. Figure 35 depicts flow gains for these different conditions.

5.2 Hysteresis and Asymmetry

Another nonlinear valve characteristic that will be present is the hysteresis in the valve motion. This hysteresis can be significant for low-performance, solenoid-operated, proportional valves. However, for most high-performance servo valves or electronically controlled directional valves the hysteresis problem is negligible. An additional nonlinearity of fluid power systems is their asymmetry. Frequently these systems are asymmetric, due to either intentional design or imperfections in the actual components. The single-ended cylinder of Fig. 28 is intentionally designed to have a different flow-to-velocity characteristic during retraction and

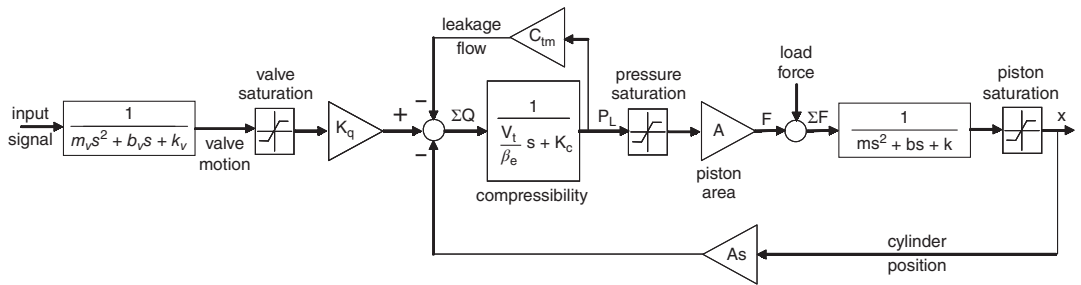


Figure 34 Saturations in hydraulic cylinder model.

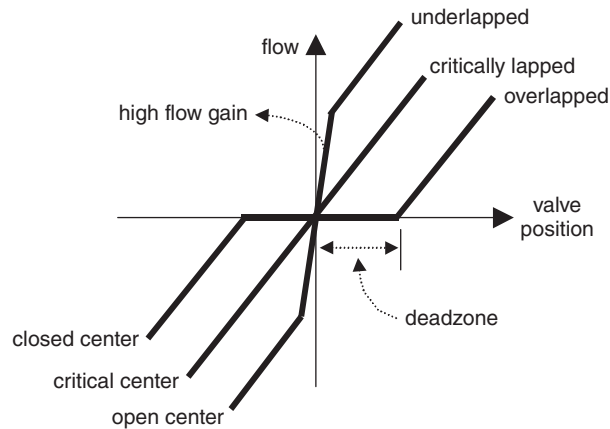


Figure 35 Valve flow characteristics near center.

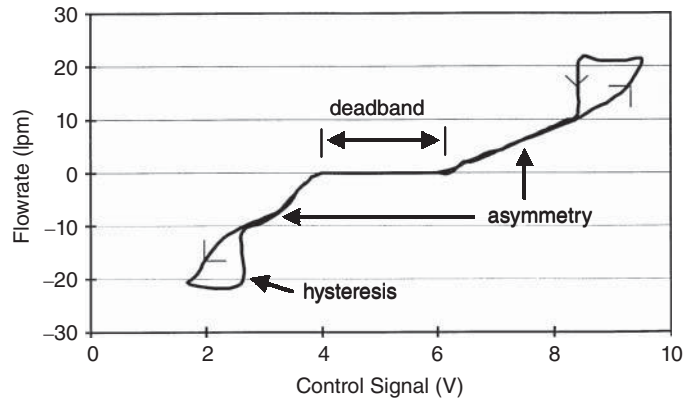


Figure 36 Steering valve flow characteristics.

extension to minimize the space necessary for the actuator. Quite often, valves will display asymmetrical flow profiles from valve position to flow. This can be done intentionally to match a single-ended cylinder with an asymmetric valve in order to have an input–output system relationship that is symmetric. The valve flow characteristics can also be asymmetric due to imperfectly manufactured valves, valve tolerances, or component wear. Figure 36 shows the flow rate response of a large electrohydraulic steering valve for an 8000-kg farm tractor.¹² This is a solenoid-operated valve; therefore, it has a large amount of hysteresis. The asymmetry in the flow characteristic is very easy to see, as is the dead band. Figure 36 also illustrates a valve that shifts entirely to one side if the input signal is zero. The spring loading is only on one side, so a nonzero input is required to maintain zero flow.

5.3 Friction

The final nonlinearity that is discussed is friction. This is present to some degree in all fluid power systems, particularly in piston or motor seals as well as the sliding valve spool itself. As with purely electromechanical systems, it can be the key barrier to precise motion control.

For all its importance, there are still widely varying models of friction for systems analysis. The simplest is the Coulomb model. However, this does not capture the complicated stick-slip motion of friction. This stick-slip motion necessitates the inclusion of a presliding displacement in the frictional model. A good analytical model that captures the stick-slip phenomenon as well as the dynamic behavior of the sliding friction is given by Lischinsky et al.¹³

REFERENCES

1. D. Billington, *The Innovators: The Engineering Pioneers Who Made America Modern*, Wiley, New York, 1996.
2. F. Yeaple, *Fluid Power Design Handbook*, 3rd ed., Marcel Dekker, New York, 1996.
3. J. Watton, *Fluid Power Systems: Modeling, Simulation, Analog and Microcomputer Control*, Prentice-Hall, Englewood Cliffs, NJ, 1989.
4. H. E. Merritt, *Hydraulic Control Systems*, Wiley, New York, 1967.
5. Parker Hannifin Hose Products Tech Alert #42, Parker Hannifin Corp., 2004.
6. F. White, *Fluid Mechanics*, 5th ed., McGraw-Hill, New York, 2002.
7. R. Zhang, A. Alleyne, and E. Prasetyawan, "Modeling and H-2/H-infinity MIMO Control of an Earth-moving Vehicle Powertrain," *ASME J. Dyn. Syst., Measure. Control*, **124**, 625–636, 2002.
8. N. D. Vaughan and J. B. Gamble, "The Modelling and Simulation of a Proportional Solenoid Valve" *ASME J. Dyn. Syst., Measure. Control*, **118**, 120–125, 1996.
9. W. Thayer, "Transfer Functions for Moog Servovalves," Moog Technical Bulletin **103**, 1965.
10. G. Franklin, J. Powell, and A. Emani-Naeini, *Feedback Control of Dynamic Systems*, 4th ed., Prentice-Hall, Upper Saddle River, NJ, 2002.
11. G. Schoenau, R. Burton, and G. Kavanagh, "Dynamic Analysis of a Variable Displacement Pump," *ASME J. Dyn.Syst., Measure. Control*, **112**, 122–132, 1990.
12. T. Stombaugh, Automatic Guidance of Agricultural Vehicles at Higher Speeds, Thesis, University of Illinois, Urbana, 1997.
13. P. Lischinsky, C. Canudas de Wit, and G. Morel, "Friction Compensation for an Industrial Hydraulic Robot." *IEEE Control Syst. Mag.*, **19**, 25–32, 1999.

Index

A

- ABB Lummus Company, 401, 408
- ABE (acetone-butenol-ethanol) fermentation, 799
- Above-atmospheric compression, 894–897
- Absolute deviations, mean of, 834
- Absolute pressure, 52
- Absolute roughness, 87
- Absolute (dynamic) viscosity, 48, 49, 119, 870
- Absorption, 1004
- Absorption chillers, 516–518, 972–974
- Absorption spectrum, atmospheric, 723
- Absorption systems, refrigeration, 515–518
- Absorptivity, 219–224
 - evaluation of, 338–339
 - for low-temperature thermal radiation, 224
 - for solar incident radiation, 222–224
 - for solid-state radiation, 331–332
 - spectral hemispherical, 219
 - total, 221
 - total hemispherical, 220
- Acceleration:
 - convective, 63
 - of fluid masses without relative motion, 57–58
 - local, 63
- Accumulators, 1115–1116
- Accuracy, 250, 617
- Acetone-butenol-ethanol (ABE)
 - fermentation, 799
- “Acid rain,” 367, 445
- Active cooling devices, 435
- Active heating methods, 302–305
- Additive property (of configuration factors), 227
- Adequacy, of models, 831, 832
- Adiabatic boundary, 138
- Adiabatic calculation, for gas compression, 898
- Adiabatic demagnetization refrigeration (ADR), 575
- Adiabatic ducts, 153–155
- Adiabatic efficiency, 898, 1043
- Adiabatic humidification, 583–584
- Adiabatic mixing, 584
- Adiabatic region (heat pipes), 239
- Adiabatic surface temperature, 210
- ADR (adiabatic demagnetization refrigeration), 575
- Adsorption, 1004
- Adverse slope, channels with, 112
- Aeolipile, 1033
- Aerodynamics, of premixed flames, 646–650
 - confined jets, 647–649
 - flame stabilization in bluff bodies, 649–650
 - free jets, 646
- Aerodynamically shaped vanes, 882, 883
- Aerodynamically staged burners, 657
- Aerodynamic lift, 871, 872
- AFCs, *see* Alkaline fuel cells
- Affinity laws:
 - for fans, 883–885
 - for rotating machines, 860–862
- Afterburners, 944, 945
- Agglomerating character (of coal), 704, 706, 713
- Agglomeration, 727
- AHUs, *see* Air-handling units
- Air:
 - air–fuel ratio, 362–365, 635–639
 - dry, 578
 - ideal gas thermophysical properties of, 8–9
 - moist, 578–580
 - quality of indoor, 587–589
 - staging of, 665
 - thermodynamic properties of, 328, 329
 - vapor, 7–8
 - vitiated, 639

- Air atomization, 323
- Air combustion, 756
- Air-cooled condensers, 529–530
- Air-cooled heat exchangers, 381–382, 396–398
 - fan power requirement for, 397–398
 - flow chart of, 613
 - heat-transfer coefficients for, 396–397
 - temperature difference in, 397
- Air cooling, 922
- Aircraft-engine gas turbines, 907–908, 941–946
 - figures of merit/cycle design variables, 944–946
 - fuel systems, 921–922
 - inlets/nozzles, 944
 - installation effects, 942–944
- Air defrost, 537
- Airflow simulation programs, 594–595
- Air–fuel ratio:
 - for combustion, 635–639
 - controlling, 362–365
- Air handling and distribution systems, 596
- Air-handling units (AHUs), 581, 584–585
 - HVAC, 581–584
 - simple, 584–585
- Air heating, 443–450
 - available heat with preheated, 447
 - benefits of, 445–450
 - costs of, 445
 - heat requirements for direct-fired, 444
 - recommended minimum temperatures for, 445
 - types of, 443
 - warnings about, 445
- Air inspirators, 362, 363
- Air pollution:
 - controlling, in furnaces, 367
 - regulations on, 979–980
- Air Pollution Control Act of 1955, 979
- Air separation, 565–567
- Air-to-cloth ratio, bag filter, 747
- Air-to-refrigerant heat exchanger, 625
- Albedometers, 815–818
- Albedo value, 817
- Alcohol-based coolants, 519–521
- Al-Haytham, Abu Ali al-Hasan ibn al-Hasan ibn, 805–806
- Aligned parallel rectangles, 226
- Aligned tubes, 209
- Alkaline fuel cells (AFCs):
 - applications of, 1055, 1061
 - characteristics of, 1018, 1061, 1062
 - electrolyte loss in, 1070
 - performance of and materials in, 1081
- Alkaline water electrolyzers, 997
- ALSTOM GT26 gas turbine, 928, 929
- American National Standards Institute (ANSI), 507–510, 589, 591
- American Petroleum Institute (API), 685
- American Recovery and Reinvestment Act of 2009 (ARRA), 979
- American Society for Testing and Materials (ASTM), 689–691. *See also specific ASTM standards*
- American Society of Heating, Refrigerating and Air-conditioning Engineers (ASHRAE), 507–510, 580–581, 587, 589–591
- Amine scrubbing, 758–759
- Ammonia, 510, 512
- Ammonia–borane, 1012
- Ammonia–water absorption systems, 517
- Ammonium, 749
- Anemometers, 122–125
- Angle factor, *see* Configuration factor(s)
- Angle of incidence, 872, 888
- Ångström, Knut, 806
- Aniline point, 685
- Anisotropic thermoelements, 293
- Annuli, forced convection in, 477–478
- ANSI, *see* American National Standards Institute
- Anthracite, 703, 705–708, 721
- API (American Petroleum Institute), 685
- API gravity (sg), 685, 686
- Apollo space program, 1055, 1081
- Approximation-assisted optimization of thermal systems, 614, 616–631
 - chevron plate heat exchanger example, 618–623
 - design of experiment in, 616
 - metamodeling techniques for, 616–617

- multiscale simulation for heat exchanger, 622, 624–630
 - offline, 618, 619, 621–622, 626–628
 - online, 618, 619, 622, 623, 628–630
 - parallel parameterized CFD in, 617–618
 - symbols for, 631
 - verification in, 617
 - Approximation formulas, 707
 - APUs, *see* Auxiliary power units
 - “A” refrigerants, 507–510
 - Argon, 565
 - Aromatics, 693
 - ARRA (American Recovery and Reinvestment Act of 2009), 979
 - Ash:
 - bottom, 664
 - coal, 713–715
 - flyash, 664, 666
 - percent ash test, 709
 - in residual oils, 687
 - Ash fusion temperatures (D1857), 710
 - Ash handling, 664
 - Ash mineral analysis, 710, 714
 - ASHRAE, *see* American Society of Heating, Refrigerating and Air-conditioning Engineers
 - Ash resistivity, 715
 - ASME Boiler and Pressure Vessel Code, 528, 531
 - Asphaltic crudes, 683
 - ASTM (American Society for Testing and Materials), 689–691
 - ASTM D388 standard, 704, 706
 - ASTM D5798 standard, 770, 771
 - ASTM D6751–07b standard, 780
 - Asymmetry (in fluid power systems), 1119, 1121
 - Atmosphere (unit), 879
 - Atmospheric absorption spectrum, 723
 - Atmospheric pressure:
 - and HVAC, 578
 - ratio of principal specific heats for liquids/gases at, 32
 - thermal properties of gases at, 192
 - thermophysical properties of fluids at, 16, 17, 26–27
 - Atomization:
 - air, 323
 - liquid fuel, 658–659
 - oil, 364
 - steam, 323
 - Attenuation factors, pump, 868, 869
 - Automotive air-conditioning systems, 607–612
 - Automotive applications, hydrogen storage for, 1001, 1003
 - Auxiliary power units (APUs), 946, 1055, 1081
 - Availability, gas-turbine, 949
 - Available heats, 322, 323
 - Available heat ratios, 323–325, 638, 640–643
 - Average efficiency, steam turbine, 1044, 1045
 - Average Nusselt number, 207
 - Avery, William, 1033
 - Aviation turbine fuels, 693
 - Axial-flow compressors:
 - gas compression in, 896
 - in gas turbines, 908–909
 - Axial-flow fans, 887–889
 - flow control for, 888, 889
 - types of, 887–888
 - Axial-flow pumps, 858, 871–872
 - Axial-flow turbines:
 - gas, 915, 916
 - steam, 1036, 1037, 1039, 1040
 - Axial piston pumps, 1103–1105
 - Axial thrust, 1052
 - Azeotropes, 507–509, 512, 513
 - Azimuth error, 819
- ## B
- Backflow effects, 401
 - Backward inclined vanes, 882, 883
 - BACT (best available control technology), 980
 - Baffles:
 - and heat exchanger programs, 408
 - in shell and tube heat exchangers, 376–380
 - spacing and cut of, 387
 - and vibration, 399–400
 - Baffled-shell evaporators, 533
 - Baffled tube bundles, 391

- Bag filters, 367, 745–747
- Balance of plant (BOP) equipment, 974
- Ball valves, 1106, 1107
- Bands, spectral, 230. *See also* Diffuse shadow-band correction models
- Barometric pressure, sea level chart for, 580–581
- Base-load systems, 975, 976
- Basic stage performance, steam turbine, 1046
- Battles et al. model of diffuse shadow-band correction, 823–826
- Bead formation, thermocouple, 263, 264
- Beam lengths, 338
- Bernoulli equation for one-dimensional flow, 60–61
- Best available control technology (BACT), 980
- Best fit line, 832
- BFBs (bubbling fluidized beds), 733–735
- Bilitzky fin arrays, 468–470
- Bimetallic thermometers, 254–255
- Binary cycle conversion, 850–851
- Binary hydrides, 1009
- Biocrude, 799
- Biodiesel, 777–785
 - biomass sources of, 777, 778
 - current availability of, 783
 - emissions from, 780, 782, 783
 - manufacturing methods, 777, 779
 - performance of, 779–782
 - production capacity for, 783–784
 - quality standards for, 779–781
 - research on, 784, 785
 - safety issues with, 784, 785
 - storage of, 782, 783
 - subsidies for, 784
 - transportation of, 782
 - vehicle modifications for use of, 779
- Biofuels, 767–800
 - biodiesel, 777–785
 - butanol, 799
 - ethanol, 768–777
 - hydrogen, 785–799
 - methane, 800
 - methanol, 799
 - mixed alcohols, 799
 - petroleumlike, 799
 - synthesis hydrocarbons, 800
 - vegetable oil, 777, 779, 783–785
- Biological cleaning of coal, 729
- Biological hydrogen production, 1000, 1001
- Biomass:
 - biodiesel from, 777, 778
 - ethanol from, 769
 - hydrogen from, 995, 996
- Biomethane, 787, 800
- Biophotolysis, 1001
- Bitor America Corp, 700
- Bituminous coal, 703, 705, 706, 708, 721
- Blackbodies, 216
- Blackbody radiation, 216–220
 - in furnaces, 331, 333
 - Planck's distribution law, 217–220
 - Stefan–Boltzmann law, 217
 - Wien's displacement law, 218
- Black enclosures, 233
- Bladder accumulators, 1115
- Blade erosion, 1051
- Blade thickness, 932
- Blading, 903
- Blassius relation, 1099
- Blast furnace gas, 320, 322, 324, 325
- Blowdown, inadequate, 403
- Blowers:
 - compression ratios for, 879
 - general features of, 880–881
- Blue flame radiation, 641
- Bluff bodies, 649–650
- Boeing F-15, 944
- Boilers. *See also* Heat recovery steam generators (HRSGs); Reboilers
 - circulating fluidized bed, 735
 - supercritical, 738–739
- Boiler feedwater heat exchangers, 382
- Boiling heat transfer, 234–237
 - film pool, 236
 - heat pipes, 239–244
 - nucleate boiling in forced convection, 236
 - nucleate pool, 235–236
 - simplified relations for boiling in water, 236–237
- Boiling limit, 240, 242–243, 422–423
- Boiling (bubble) point, 507, 508
- Boil-off losses, 1006

- Bomb wash method, 709
 - Booster pumps, 97
 - BOP (balance of plant) equipment, 974
 - Borohydride complexes, 1010
 - Bottom ash, 664
 - Bottoming-cycle cogeneration systems, 966–967, 1048, 1049
 - Boudouard reaction, 740
 - Boundary(-ies), 137
 - adiabatic, 138
 - conduction with convection on, 194, 197–198
 - diathermal, 139
 - flow between parallel, 76
 - Boundary conditions:
 - for Navier–Stokes equations, 74–75
 - for two- and three-dimensional flow, 63
 - Boundary layer:
 - flow about immersed objects at flat-plate, 116–117
 - impact of, on wind velocity, 961–962
 - Bourdon gauge, 53
 - BP, *see* Brake power
 - BQ-9000 program, 779
 - Brake engine efficiency, 1043
 - Brake horsepower (pump), 97
 - Brake power (BP), 863, 881, 885
 - Branca, Giovanni de, 1033, 1034
 - Brayton cycle, 737, 901, 926, 934
 - Brazed-plate condensers, 528
 - Brazoria, 846
 - “B” refrigerants, 507–510
 - Broad-crested weirs, 132
 - Brown, Boveri engine, 906–908
 - Broyden’s method, 604
 - Btu (unit), 319
 - Bubble point, 507, 508
 - Bubbling fluidized beds (BFBs), 733–735
 - Buckets, 903, 917–919
 - Bucket creep, 948
 - Buckingham Π theorem, 82
 - Building materials, thermal properties of, 190
 - Building thermal loads, 589–593
 - cooling, 592–593
 - heating, 589–591
 - Built-in volume ratio, 524
 - Bulk modulus, 44, 47, 1096–1097
 - Bulk temperature, 205
 - Buoyancy, 56–57
 - Burners:
 - circular, 660–662
 - duct, 972
 - furnace, 362–364
 - gaseous-fuel, 655–658
 - low-nitrogen oxide, 732–733
 - tangentially-fired, 661, 663
 - Burner ports, furnace, 364–365
 - Burner tiles, 653
 - Burning characteristics of coals, 711–713
 - Burnout point, 235
 - Butane, 510, 922
 - n*-Butane at atmospheric pressure, 26
 - Butanol, 799
 - Butler–Volmer equation, 1067
 - Bypass heat leak, 170
 - By-product fuels, 639–640
- ## C
- CAA (Clean Air Act of 1963), 724, 979–980
 - CAAA (Clean Air Act Amendments), 979–980
 - Caking, 708
 - Calibration:
 - of heat flux gauges, 298–299, 306–307
 - of temperature sensors, 249–250
 - Callendar–Van Dusen equation, 268, 269
 - Calorific properties of gaseous fuels, 678
 - Calorific value:
 - of coal, 709
 - of natural gas, 675–678
 - Calorimeters, 300–301
 - Cameras, infrared, 299, 303
 - Campbell–Stokes sunshine recorder, 817, 818, 828–829
 - Canada, CFCs banned in, 511
 - Capillarity, 50, 51
 - Capillary limit, 419–420
 - Capillary pressure, 418, 420
 - Capillary pumped loops (CPLs), 434–435
 - Capillary rise, 50, 51
 - Capillary tubes, 534–535
 - Capillary wicking limit, 240
 - Capital investment, in cogeneration, 965

- Carbonaceous materials, hydrogen storage in, 1005, 1011–1012
- Carbon dioxide (in general):
 - in DMFCs, 1076
 - emissions of, 792–793, 911–912
 - fuel-cell degradation by, 1070
 - GWP of, 511
 - as marker for human contaminants, 589
 - as refrigerant, 510
 - thermal radiation properties of, 229–231, 233
 - thermophysical properties of, 11–13
- Carbon dioxide capture, 755–759, 761–762
 - during combustion, 756–758
 - cost of, 759, 761–762
 - postcombustion, 758–759
 - precombustion, 755–756
- Carbon dioxide from coal conversion, 723–724, 754–762
 - capture of, 755–759, 761–762
 - cost implications with treating, 761–762
 - sequestration of, 760–762
 - transportation of, 759–760
 - utilization of, 761
- Carbon intensity, 724
- Carbon monoxide, 665, 911, 1070
- Carbon nanotubes, 1012
- Carbon resistors, 270
- Carbon sink management, 761
- Carbon-steam reaction (gasification), 740
- Cascade, fins in, 482
- Cascade cooling (refrigeration) systems, 502–503, 548–549
- Catalyst poisoning, 1070
- Catalytic combustion systems, 915
- CAV (constant air volume), 596
- Cavitation, 863
- Cavitation proof conduits, 95
- Cell-in-series SOFC design, 1078, 1080
- Celsius temperature scale, 247–248
- Center of pressure, 54, 55
- Centrifugal compressors:
 - characteristics of, 526–528
 - in closed-cycle systems, 502
 - gas compression in, 896
 - in gas turbines, 909
 - refrigerants in, 510
- Centrifugal fans, 358, 361, 881–887
 - affinity laws for, 883–884
 - controlling throughput of, 886–887
 - performance of, 884–886
 - vanes of, 881–883
- Centrifugal operation (in pumps), 858–861
- Centrifugal pumps, 858–871
 - centrifugal operation in, 858–861
 - flow control for, 865–869
 - generalized head loss with throughput for, 865, 866
 - performance curves for, 862–865
 - slurries in, 870–871
 - specific speed of, 861–862
 - and viscosity of liquid, 868–870
- Ceramic fiber filters, 367
- Cerro Prieto Fields (Mexico), 844
- Certificates for cogeneration, 982–983
- Cetane number (CN), 694–695
- CFBs, *see* Circulating fluidized beds
- CFCs, *see* Chlorofluorocarbons
- CFC-11, 511, 513
- CFD, *see* Computational fluid dynamics
- Channels, *see* Flow (in open channels)
- Charging heat-pipe working fluids, 432
- Chemical cleaning of coal, 728
- Chemical cycling, hydrogen fuel, 796
- Chemical exergy, 163
- Chemical hydrides, 1005, 1009, 1010
- Chemical hydrogen storage, 1011–1012
- Chemical looping combustion, 757–758
- Chevron plate heat exchangers, 618–623
 - CFD simulation of, 619, 620
 - offline approximation-assisted optimization of, 621–622
 - online approximation-assisted optimization of, 622, 623
- Chillers, absorption, 516–518, 972–974
- Chip module thermal resistances, 458–464
 - defined, 458–459
 - external resistance, 461–463
 - flow resistance, 463–464
 - internal thermal resistance, 459–460
 - substrate/PCB conduction, 460–461
 - total resistance–single chip packages, 464
- Chlorine, 710, 715
- Chlorodifluoromethane, 509, 512

- Chlorofluorocarbons (CFCs), 506–509, 511, 513
- Chlorotrifluoromethane, 509
- Chrysler, 908
- CIE (Commission Internationale de l'Éclairage), 830
- Circular burners, 660–662
- Circular cylinders:
 - in cross-flow, 208
 - flow around, 69
- Circular foil heat flux gauges, 296–297
- Circular tubes:
 - Navier–Stokes equations for flow through, 77–78
 - Nusselt numbers for, 205
 - turbulent flow in, 206–207
- Circulating fluidized beds (CFBs), 733, 735, 736
- Clapeyron relation, 150, 152
- Class I refrigerants, 511
- Class II refrigerants, 511
- Clathrates, 1015
- Clausius-Clapyeron relation, 423
- Clean Air Act Amendments (CAAA), 979–980
- Clean Air Act of 1956, Great Britain, 724
- Clean Air Act of 1963 (CAA), 724, 979–980
- Clean Air Mercury Rule, 724
- Cleaner coal technology, 719–763
 - carbon dioxide in, 754–762
 - defined, 720
 - motivation for, 724–725
 - postconversion clean-up, 745–754
 - preconversion, 726–729
 - in situ pollution control, 729–744
 - technologies for, 725–726
- Cleanliness, 429, 431, 432
- Clean Water Act of 1977, 981
- Closed-centered valves, 1108–1109
- Closed conduits, flow in, 82–108
 - and minor losses, 92–95
 - and pipe friction, 87–92
 - pipe network analysis of, 99–102
 - steady-state pipeline analysis of, 95–99
 - unsteady flow in pipe systems, 102–108
 - velocity distribution for, 83–86
- Closed-cycle engines, 902
- Closed-cycle refrigeration:
 - operation, 501–506
 - refrigerant selection for, 511, 513–514
- Closed systems:
 - defined, 137
 - first law of thermodynamics for, 138–139
 - second law of thermodynamics for, 140–142
- CLTDs (cooling-load temperature differences), 592
- Cluster, fins in, 482–483
- CN (cetane number), 694–695
- Coal(s), 703–718, 720–724. *See also* Cleaner coal technology
 - age of formation and properties of, 721
 - ash characteristics of, 713–715
 - burning characteristics of, 711–713
 - classifications of, 704–707
 - efficiency/exhaust of, 912
 - gasification of, 320–321
 - hydrogen/carbon ratios of, 674
 - as industrial fuel, 320
 - nature of, 703
 - and pollutants, 721–724
 - properties of, 709–711
 - quality of, 711
 - reserves of, 703–705
 - sampling of, 715–716
 - types of, 703, 707–709, 721
 - uses of, 707
- Coal cleaning, 716–718, 726–729
- Coal combustion, 730
- Coal conversion:
 - carbon dioxide from, 754–762
 - cleaning prior to, 726–729
 - clean-up technologies following, 745–754
 - potential pollutants from, 721–724
 - in situ pollution control for, 729–744
- Coal gasification, 320–321, 995
- Coalification, 703
- Coaxial parallel circular disks, 226
- Coaxial thermocouples, 300
- COE (cost of electricity), 955
- Coefficient of correlation, 833
- Coefficient of determination, 832–833
- Coefficient of drag, 115, 117, 118, 871
- Coefficient of flow (valve), 867

- Coefficient of lift, 115, 871
- Coefficient of performance (COP), 141, 517, 552
- Cogeneration, 963–965
 - constraints on, 965
 - history of, 964–965
- Cogeneration equipment, 968–974
 - absorption chillers, 972–974
 - balance of plant equipment, 974
 - electrical equipment, 971–972
 - fuel cells, 971
 - gas turbines, 969–970
 - heat recovery equipment, 972, 973
 - microturbines, 971
 - prime movers, 968–971
 - reciprocating engines, 970–971
 - regulations on, 980–982
 - steam turbines, 968–969
- Cogeneration regulations, 977–983
 - on air pollution, 979–980
 - American Recovery and Reinvestment Act of 2009, 979
 - Energy Improvement and Extension Act of 2008, 979
 - Energy Policy Act of 2005, 979
 - equipment-specific, 980–982
 - federal, 977–979
 - permits and certificates for cogeneration, 982–983
 - on water quality and solid waste disposal, 981, 982
- Cogeneration systems, 965–990
 - applications of, 967, 968
 - bottoming-cycle, 966–967
 - combined-cycle, 967, 968
 - economic evaluation of, 983–986
 - equipment in, 968–974
 - financing arrangements for, 986–989
 - ownership of, 986–989
 - packaged, 976–977
 - prime movers in, 968–971
 - regulations on, 977–983
 - steam turbines in, 1033, 1034, 1048–1049
 - technical design issues with, 974–977
 - topping-cycle, 965–966
- Coke, 320, 707
- Coke oven gas by-product, 320, 322, 324, 325
- Cold-plate heat exchangers, 483–486
- Color play bandwidth, 274
- Column separation, 104
- Combined-cycle cogeneration systems, 967, 968
- Combined-cycle power plants:
 - gas turbines in, 934–940
 - steam turbines in, 1033, 1034, 1048–1049
- Combustible wastes, 367
- Combustion, 635–671
 - air, 756
 - air–fuel ratios for, 635–639
 - carbon dioxide capture during, 756–758
 - chemical looping, 757–758
 - coal, 730
 - cyclone, 739
 - defined, 635
 - diffusion, 360
 - firing systems, 654–664
 - flame aerodynamics, 644–655
 - fluidized bed, 733–738
 - fuels used in, 639–640
 - and furnaces, 319–325
 - in gasification, 740
 - high-temperature, 709
 - of hydrogen, 992
 - oxy-fuel, 670–671, 756
 - and oxygen enrichment of combustion air, 325
 - pollutant emissions control, 665–666
 - pulverized coal, 731–733
 - requirements for, 730
 - safety considerations, 666–670
 - staged, 739
 - stoichiometric, 636
 - thermal aspects of, 640–644
- Combustion air, oxygen enrichment of, 325
- Combustion chambers, sizing resources for, 398
- Combustion characteristics of gaseous fuels, 678–679
- Combustion control equipment, furnace, 365–367
- Combustion products, ideal gas sensible enthalpies of, 37–38
- Combustors, gas turbine, 903, 910–911, 970
- Comfort zone, 587

- Commision Internationale de l'Éclairage (CIE), 830
- Compact heat exchangers, 382
- Compensation cables, 266–267
- Complex variables for irrotational flow, 65–66
- Composite tanks, pressurized hydrogen in, 795
- Composition, refrigerant, 515
- Compounds, phase transition data for, 6–7
- Compound refrigeration cycle, 501–504
- Compressibility, fluid, 44, 47–48
- Compressibility factor of Refrigerant 134a, 21
- Compression:
 - above-atmospheric, 894–897
 - adiabatic calculation for, 898
 - isothermal, 553
 - in liquids, 897
 - polytropic calculation for, 898–899
 - residual equations for vapor, 601–602
 - stages of, 900
 - thermodynamics of gas, 897–900
 - vapor compression refrigeration cycle, 500–501
 - vapor compression systems, 601–602
 - vapor recompression, 890–891
 - work of, 897–899
- Compression ratio, 879
- Compressors, 879, 892–897
 - for above-atmospheric compression, 894–897
 - axial-flow, 896, 908–909
 - centrifugal, 526–528, 896
 - configuration of, 522, 523
 - diaphragm, 894, 895
 - discharge pressures and throughputs for, 897
 - dynamic-type, 894
 - fans and blowers vs., 880
 - in gas turbines, 908–910
 - laws of thermodynamics applied to, 153
 - liquid ring, 893–894
 - piston, 894
 - reciprocating, 501–504, 522–523, 894, 895
 - refrigeration, 500, 522–528
 - rolling piston, 523–524
 - rotary, 523–524
 - rotary lobe, 892, 893
 - rotary sliding vane, 892, 893
 - rotary vane, 523, 524
 - screw, 524–526, 894, 895
 - scroll, 524, 525, 895
 - vacuum generation in, 892–894
- Compressor power:
 - field determination of, 900
 - total, 899
- Compressor stage, 903
- Computational fluid dynamics (CFD):
 - in airflow simulation programs, 594–595
 - chevron plate exchanger simulation with, 619, 620
 - parallel parameterized, 617–618
 - reducing aerodynamic losses in compressors with, 910
- Computer programs:
 - for indoor environmental control, 593–596
 - for thermal design of process heat exchangers, 403–410
- Concentrating tables, 727
- Concentric tube annuli, 207
- Condensate flow, 237
- Condensation heat transfer, 234, 237–239
 - effect of noncondensable gases, 239
 - film condensation, 237, 239
 - and saturated water properties, 238
- Condensation profiles, 389–390
- Condensed/saturated vapor carbon dioxide (200K to critical point), 11
- Condensers:
 - air-cooled, 529–530
 - brazed-plate, 528
 - considerations for, 528–530
 - geometry of, 609
 - in heat pipes, 239, 240, 244
 - refrigeration, 500
 - shell-and-coil, 528
 - shell-and-tube, 388–392, 528
 - tube-in-tube, 528
 - water-cooled, 528, 529
- Condensing (discharge) pressure, 513, 897
- Condensing steam turbines, 969, 1041
- Condensing units, 608, 610, 612–615

- Conditioning (of liquid fuel), 659, 660
- Conduction-dominated resources, 840
- Conduction heat transfer, 185–204
 - with convection heat transfer on
 - boundaries, 194, 197–198
 - defined, 185
 - at microscale, 199, 203, 204
 - with negligible load thermal resistance, 345
 - non-steady-state, 330, 341–344
 - one-dimensional, 187, 190, 193, 451–452
 - reducing, 555–556
 - shape factors in, 193–195
 - steady-state, 193–196, 330, 340–341
 - substrate, 460–461
 - thermal conductivity, 186–192
 - thermal modeling of, 451–454
 - transient, 198–204
 - two-dimensional steady-state, 193–196
- Conductivity, thermal, 326–328, 424–428
- Conduits:
 - cavitation proof, 95
 - flow in, *see* Flow (in closed conduits)
 - with noncircular cross sections, 91–92
- Cones, high-speed gas flow past, 211
- Configuration factor(s), 223–227
 - additive property, 227
 - for aligned parallel rectangles, 226
 - blackbody radiation exchange, 227
 - for coaxial parallel circular disks, 226
 - reciprocity relations, 224
 - for rectangles with common edge, 227
 - relation in enclosure, 227
 - for simple geometries, 225
- Configuration factor geometry, 224
- Confined jets, 647–649
- Confined spaces, natural convection in, 464–467
- Conformable tanks of hydrogen gas, 1006
- Conformal mapping, 66–68
- Conical diffusers, 95
- Conservation of mass:
 - equation for, 582, 583
 - in one-dimensional flow, 59–60
 - in two- and three-dimensional flow, 62
- Constant air volume (CAV), 596
- Constant heat flux experiments, 302–303
- Constant-pressure expansion valves, 534
- Constant surface temperature experiments, 303–305
- Constant temperature coefficient, 146
- Constructal theory, 143, 158, 173–182
 - and flow structures, 176–181
 - and geometric features, 174–177
 - and global constraints, 174
 - subscripts used in, 160
 - symbols/units used in, 158–160
 - thermodynamics vs., 181–182
- Contact angle, 417
- Contact resistance, 453–454, 470–473
- Contaminants, indoor, 588–589
- Continuity equation:
 - for one-dimensional flow, 59–60
 - for two- and three-dimensional flow, 62
 - for viscous flow, 75–76
- Continuous-type furnaces, 317
- Control(s):
 - centrifugal fan throughput, 886–887
 - combustion, 365–367
 - for gas turbines, 919–920
 - in refrigeration design, 541
- Control point, 596, 597
- Control scheduling, 945–946
- Control section, channel, 112, 113
- Control systems:
 - indoor-environmental, 596–597
 - for steam turbines, 1051
- Control valves, 1107–1110
- Control volume, 582
- Convection (convective heat transfer), 205–216, 455–457
 - from combustion, 641, 644
 - dimensionless parameters, 455
 - with external flow, 207–211
 - for finned surfaces, 457
 - flow resistance, 457
 - forced, 205–211, 456
 - free, 211–214
 - in furnaces, 350–353
 - heat conduction with, on boundaries, 194, 197–198
 - heat-transfer coefficient, 455
 - internal, 570, 571
 - with internal flow, 205–207

- log mean temperature difference, 214–216
- natural convection, 455–456
- phase change heat transfer, 456–457
- reducing, 556
- Convection heat-transfer coefficient, 194
- Convection resistance, 197
- Convective acceleration, 63
- Convective heat flux, measuring, 287–288
- Conventional (100%) ownership, of
 - cogeneration systems, 987–988
- Convention on Long-Range Transboundary Air Pollution, 724
- Convergence loops, 404–405
 - intermediate temperature loops, 404, 405
 - pressure balance loops, 404, 405
- Conversion factors, 4, 319
- Coolants, 518–522
 - alcohol-based, 519–521
 - comparison of, 520
 - considerations for, 519–520
 - glycol-based, 519–521
 - for low-temperature heat transfer, 519–521
 - salt-based, 519
- Coolers, 457
 - cryo-, 552–555
 - gas, 502
 - thermoelectric, 486–490
- Cooling. *See also* Electronic equipment cooling
 - with active devices, 435
 - air, 922
 - cascade cooling systems, 502–503, 548–549
 - expansion engine, 551–552
 - of gas turbines, 918–919, 922
 - inter-, 926–927, 970
 - Newton's law of, 194, 198
 - optimal, 166
 - pre-, 918
 - regenerative, 553
 - sensible, 582–583
 - spray, 490–494
 - steam, 919
 - sub-Kelvin, 574–575
 - viscous liquid, 401
 - water, 919, 922
- Cooling loads, 592–593
- Cooling-load temperature differences (CLTDs), 592
- Cooling towers, 528
- COP, *see* Coefficient of performance
- Core temperature, 839
- Co-rotating extruders, 876
- Correction factor, 214–216
- Correction for mixture effects, 392
- Correlation, coefficient of, 833
- Corrosion:
 - in fuel cells, 1070
 - in gas turbines, 947–94
 - and refrigerant selection, 515, 520
- Corrosive vapors, 389
- Cosine error, 819
- Cost estimation (for thermal systems optimization), 603, 604
- Cost of electricity (COE), 955
- Cotter approximation, 423
- Counterrotating devices, 876
- Coupled simulation tools, 595–596
- CPLs (capillary pumped loops), 434–435
- Crack tolerance, 948
- Crayons, heat-sensitive, 273
- Creep, 947–948
- Critical depth, 111
- Critical heat flux, 234, 402
- Critically lapped valves, 1108, 1109
- Critical pressure, 150, 514
- Critical Reynolds number, 207
- Critical slope, 112
- Critical-state properties, 150
- Critical temperature, 150, 514
- Cross-compound unit turbines, 1042
- Cross-flow:
 - circular cylinders in, 208
 - forced convection cylinders in, 474–475
 - forced convection noncircular cylinders in, 474, 475
 - liquid metals in, over tube banks, 210
 - noncircular cylinders in gas, 208–209
- Cross-sectional flow areas, 387
- Crude petroleum, 683
- Cryocompressed tanks of hydrogen gas, 1005–1006

- Cryocoolers, 552–555
 - pulse tube, 554, 555
 - regenerator materials in, 553, 554
 - Stirling cycle, 553, 554
 - Cryogenics:
 - defined, 499
 - and EGM, 165–166
 - Cryogenic distillation, 759
 - Cryogenic engineering, 543–575
 - air separation in, 565–567
 - cryocoolers, 552–555
 - cryostats, 555–561
 - flow measurement in, 562
 - fluid level measurement in, 564
 - helium(II) in, 570–574
 - instrumentation for, 561–565
 - materials suitable for, 544–548
 - pressure measurement in, 562
 - properties of cryogenic fluids, 544–547
 - refrigeration and liquefaction, 548–552
 - safety issues with, 568–570
 - sub-Kelvin cooling in, 574–575
 - temperature measurement in, 561–563
 - thermoacoustic oscillations in, 564–565
 - Cryogenic fluids:
 - maximum inversion temperatures of, 550
 - properties of, 544–547
 - Cryogenic heat pipes, 439
 - Cryogenic liquid hydrogen storage systems, 1004, 1006
 - Cryogenic liquid tanks of hydrogen, 796
 - Cryogenic materials:
 - emissivities of, 557
 - properties of, 548
 - thermal conductivity integrals of, 556
 - Cryostats, 555–561
 - design of, 555, 560–561
 - insulation for, 555–560
 - reducing conduction heat transfer in, 555–556
 - reducing convection heat transfer in, 556
 - reducing radiation heat transfer in, 556–561
 - Current meters, 122, 123
 - Curtis stage arrangements, 1036, 1038, 1039
 - Curved surfaces, fluid forces on, 54, 56
 - Cycles (term), 137
 - Cyclone combustion, 739
 - Cyclone-fired systems, 664
 - Cyclone gravity separators, 727
 - Cylinders. *See also* Noncircular cylinders
 - critical radius of insulation for, 197
 - in cross-flow, 208, 474–475
 - flow around, 69
 - in fluid power systems, 1091, 1094, 1113–1115, 1118–1120
 - free convection from, 212–213
 - heat conduction in hollow, 193
 - high-pressure gas, 1004–1006
 - hydraulic, 1113–1115, 1118–1120
 - transient heat conduction in, 199, 202–203
 - Cylindrical spine, 481
- ## D
- Damköler number, 1068
 - Darcy–Weisbach formula, 87, 89–92, 1099
 - Darrieus wind turbines, 957
 - Database for heat exchanger programs, 407
 - Data quality assessment, solar radiation study, 829–831
 - Dead-head condition, 858
 - Dead state, 161, 162
 - Dead zones, 1119, 1120
 - Deflector plate on fuel gun, 654
 - Defrost methods, 536–538
 - Degradation (in fuel cells), 1069–1070
 - Delayed-mixing burners, 657
 - Denmark, 955
 - Dense-media vessels, 727
 - Density:
 - defined, 42–44
 - liquid, 514
 - measuring, 118, 119
 - and specific gravity/API gravity, 685
 - vapor, 514
 - Department of Energy (DOE), 593, 918–919, 946, 1001, 1003, 1057, 1058, 1076
 - Depth, critical, 111
 - Depth filtration, 745
 - Design:
 - cogeneration system, 974–977
 - of experiment, 616

- heat-exchanger, 403–410
- SOFC, 1078–1080
- Detectors:
 - photo, 809, 810
 - resistance temperature, 267–270
 - thermal, 809
- Determination, coefficient of, 832–833
- Deutsch–Anderson equation, 747
- Dewars, 555. *See also* Cryostats
- Diaphragm compressors, 894, 895
- Diaphragm pumps, 877, 878
- Diathermal boundary, 139
- Dichlorodifluoromethane, 509, 512
- Dichlorotetrafluoroethane, 509
- Dichlorotrifluoroethane, 509, 512
- Diesel, Rudolf, 777
- Diesel cycle, 901, 951–952
- Diesel fuels, 694–697
 - cetane numbers for, 694–695
 - descriptions of, 695
 - properties of, 697
 - requirements for, 696
- Diesel index, 694–695
- Differential flame thermometers, 302
- Diffuse emitters, 216
- Diffuse-gray surfaces, 221, 228–229
- Diffuse radiation, 221
- Diffuse radiation data measurement errors, 821–825
- Diffusers, 156
 - minor losses in, 95
- Diffuse shadow-band correction models, 822–825
 - Battles et al. model, 823–826
 - Drummond model, 822, 824–826
 - LeBaron et al. model, 823–826
 - Muneer and Zhang model, 823–826
- Diffuse surfaces, 221
- Diffusion combustion, 360
- Diffusion flame burner systems, 657
- Diffusion media (DM) layer, 1060
- Diffusion-mixed turbulent flames, 650–651
- Diffusivity, 326
- Dilution refrigeration, 574
- Dimensional analysis:
 - with incompressible fluids, 81–82
- Dimensionless numbers, 455
- Diode thermometers, 271
- Direct air heaters, 443
- Direct-drive linear motor for electrohydraulic valve, 1111
- Direct-fired absorption chillers, 974
- Direct-fired air heaters, 443–445
- Direct-fired chillers, 516
- Direct gasification, 995, 996
- Direct methanol fuel cells (DMFCs), 1057, 1074–1076
- Direct steam conversion, 848–849
- Dirt carryover, 515
- Discharge coefficient, 1106
- Discharge (condensing) pressure, 513, 897
- Discs, 903
- Disjoining pressure (heat pipes), 418, 419
- Disks, 226, 917
- Disruption:
 - of insert heat flux gauges, 288–289
 - of surface-mounted heat flux gauges, 287–288
- Distillate oil, 674
- Distillation, cryogenic, 759
- Distribution:
 - of ethanol, 774–775
 - of hydrogen fuel, 793–795
- Dittus–Boelter equation, 206–207
- Divided flow exchanger, 377
- DMFCs (direct methanol fuel cells), 1057, 1074–1076
- DMF residual oil, 698
- DN5 pyrhelimeter, 814, 815
- DOE, *see* Department of Energy
- Doped germanium resistors, 270
- Double-pipe heat exchangers, 214, 215, 398
- Doublets, 68
- Drag:
 - at flat-plate boundary layer, 116–117
 - on immersed objects, 115, 117–118
 - total, 78–79, 117–118
- Drag coefficient, 115, 117, 118, 871
- Drainage, inadequate, 403
- Drawings (of flow systems), 174
- Drivetrains, wind-turbine, 959–960
- Dropwise condensation, 237
- Drummond model of diffuse shadow-band correction, 822, 824–826

- Dry air, 578
 - Dry bulb temperature, 579–582
 - Dry low NO_x combustors, 914–915
 - Dry scrubbing, 749–751
 - Dry sorbent injection, 751
 - Dry stack gas loss, 641
 - Dry steam, 844*n*.
 - Dual-flash systems, 849, 851
 - Ducts:
 - adiabatic, 153–155
 - forced convection in, 477–478
 - Duct burners, 972
 - Durability, 1074
 - Dusts, explosion characteristics of, 666, 669
 - Dynamic fluid movers, 857–858, 894
 - Dynamic power load (in cogeneration systems), 976
 - Dynamic pumps, 857–858
 - Dynamic-type compressors, 894
 - Dynamic (absolute) viscosity, 48, 49, 119, 870
- E**
- Earth's core temperature, 839
 - Economic evaluation of cogeneration systems, 983–986
 - economic merit of system, 985–986
 - operating costs of current system in, 983–984
 - operating costs of proposed system in, 984–985
 - Economic merit of cogeneration systems, 985–986
 - Economizers, 503–505
 - ECSA (electrochemical active surface area), 1070
 - Eductors:
 - ejectors vs., 879
 - operation of, 888, 889
 - performance of, 873, 874
 - EEVs (electronic expansion valves), 534
 - Effective thermal conductivity, 424–428
 - Efficiency:
 - adiabatic, 898, 1043
 - average, 1044, 1045
 - brake engine, 1043
 - fin, 198, 480
 - geothermal resource utilization, 849
 - internal, 1043
 - of jet pumps, 873
 - mechanical, 1043
 - overall, 1043, 1044
 - polytropic, 898
 - pumping, 860
 - PURPA standards for, 978
 - of steam turbines, 1034, 1036, 1043–1044
 - thermal, 1034, 1036, 1043, 1048, 1049
 - volumetric, 1043, 1104
 - EGM, *see* Entropy generation minimization
 - EGS (Enhanced Geothermal Systems), 844–845
 - Eilling, Aegidus, 1033
 - Ejectors, 888–892
 - eductors vs., 879
 - vacuum generation with, 891–892
 - vapor recompression in, 890–891
 - EKO M-S202 pyrgeometer, 814, 816
 - El, *see* Elenbaas number
 - Elastic forces, in dynamic similarity, 80
 - Elastic theory, 102, 106–108
 - Elbow meter, 127, 130
 - Elcogas/Puertollano IGCC plant (Puertoallano, Spain), 743
 - Electrical equipment, cogeneration system, 971–972
 - Electrical–hydraulic analogy, 1092, 1094
 - Electrical load:
 - in economic evaluation, 984–985
 - matching thermal load and, 975–976
 - and motivation of owners/investors in systems, 987
 - Electric defrost, 537
 - Electric generators, 972
 - Electricity costs, 965
 - Electricity sales, revenue from, 965
 - Electric power generation:
 - gas turbine applications in, 940–941
 - geothermal, 847–853
 - steam-based Rankine cycle facilities, 981
 - Electric utilities, steam turbine use by, 1049–1050
 - Electrochemical active surface area (ECSA), 1070

- Electrochemical combustors, 1016
- Electrolysis, 786, 787, 997–998
- Electrolytes, 1016, 1017
- Electrolyte loss, 1070
- Electrolyte poisoning, 1070
- Electrolyzers, alkaline water, 997
- Electromagnetic radiation spectrum, 217
- Electronic components, forced convection air flow over, 476–478
- Electronic equipment cooling, 451–494
 - heat-transfer correlations for, 464–478
 - thermal control techniques, 478–494
 - thermal modeling of, 451–464
- Electronic expansion valves (EEVs), 534
- Electrostatic filters, 367
- Electrostatic precipitators (ESPs), 666, 747–748
- Elements, phase transition data for, 4–6
- Elenbaas number (EI), 456, 465, 466
- Emissions:
 - from biodiesel, 780, 782, 783
 - carbon dioxide, 792–793, 911–912
 - from ethanol, 774
 - from gas turbines, 911–915
 - from hydrogen fuel, 792–793
 - hydrogen sulfide, 852
 - pollutant, 665–666
 - from prime movers, 983
- Emissivity(-ies), 218, 219, 276
 - of carbon dioxide, 229–230, 233
 - of cryogenic materials, 557
 - evaluation of, 338–339
 - of metallic surfaces, 221, 222
 - of nonmetallic surfaces, 222, 223
 - for solid-state radiation, 331–332
 - of water, 229–231, 233
- Enclosed spaces:
 - free convection in, 213
 - radiative exchange among diffuse-gray surfaces in, 228–229
- Enclosures:
 - black, 233
 - gas-turbine, 921
 - gray, 234
- Energy balance equation for zone air, 593–594
- Energy calculation programs, 593–594
- Energy cane, 769
- Energy change, 138
- Energy conservation, 593
- Energy correction factors, 85, 86
- Energy Improvement and Extension Act of 2008, 979
- Energy minimum principle, 143
- Energy Policy Act of 2005 (EPAAct), 979
- Energy profiles, constructing, 984
- Energy requirements of secondary coolants, 522
- Energy transfer equation, for turbine stages, 1036–1039
- Energy yield, wind-turbine, 957–959
- Engines:
 - closed-cycle, 902
 - gas-turbine, 941–947, 949, 951–953
 - heat, 140–142
 - Heinkel, 908
 - internal combustion, 788, 792, 970–971, 992, 1019–1020
 - open-cycle, 902
 - reciprocating, 970–971, 975, 980–981
- Engine efficiency, 1043
- Engineering-level system simulation, 600–602
- Engineering system component analysis, 153–156
- English units, 42–44, 316
- Enhanced Geothermal Systems (EGS), 844–845
- Enhanced oil recovery (EOR), 760
- Enthalpy, 145, 579, 581
- Enthalpy–log pressure diagram(s):
 - for carbon dioxide, 13
 - for mercury, 15
 - for Refrigerant 22, 18
 - for Refrigerant 134a, 22
- Entrained flow gasifiers, 740, 741
- Entrainment limit, 240, 242, 423
- Entrainment rate, 646
- Entropy change, 142
- Entropy generation, 142
- Entropy generation minimization (EGM), 157–158, 162, 164–173
 - approaches/applications of, 165
 - and cryogenics, 165–166

- Entropy generation minimization (EGM)
 - (*continued*)
 - and heat transfer, 166–168
 - and power plants, 170–173
 - and solar energy conversion, 169–170
 - and storage systems, 168–169
 - subscripts used in, 160
 - symbols/units used in, 158–160
- Entropy generation rate, 144
- Entropy maximum principle, 143
- Environment (term), 137
- Environmental control, indoor, *see* Indoor environmental control
- Environmental impact:
 - of cogeneration, 965
 - of natural gas, 674
 - of secondary coolants, 522
- Environmental Protection Agency (EPA), 588
- EOR (enhanced oil recovery), 760
- EPAct (Energy Policy Act of 2005), 979
- Eppley normal incidence pyrhelometer, 815
- Equation solvers (thermal systems optimization), 603, 604
- Equilibrium flow architecture, 176–181
- Equipment errors, solar radiation, 819
- Equipment-specific regulations, cogeneration, 980–982
- Equivalence ratio (ER), 637
- Equivalent furnace temperature profiles, 347–350
- Equivalent pipe technique, 104, 105
- ER (equivalence ratio), 637
- Erosion velocity, 407
- Errors:
 - diffuse radiation data measurement, 821–825
 - equipment, 819
 - furnace, 314
 - with heat flux gauge measurements, 307
 - mean bias, 833, 834
 - measurement, 249, 250
 - operational, 820–821
 - relative root-mean square, 630
 - root-mean-squared, 630, 833, 835
 - in solar radiation measurements, 819–826
- Eschka method, 709
- ESPs (electrostatic precipitators), 666, 747–748
- Ethane, 26, 510
- Ethanol, 768–777
 - biomass sources of, 769
 - current availability of, 775–776
 - emissions from, 774
 - manufacturing methods, 769–770
 - material compatibility with, 774
 - performance of, 773, 774
 - quality standards for, 770, 771
 - research and development on manufacturing, 770
 - resources on, 776
 - safety issues with, 775
 - storage of, 775
 - subsidies for, 775, 776
 - transportation and distribution of, 774–775
 - vehicle modifications for use of, 770–774
- Ethanol-in-glass thermometers, 252
- Ether, 499
- Ethylene, 26, 510
- Ethyl ether, 499
- E-type shell and tube heat exchangers, 376, 377, 389, 407, 408
- Euler's equation:
 - for one-dimensional flow, 60
 - for two- and three-dimensional flow, 62–63
- Evaporating pressure, 514
- Evaporators:
 - geometry of, 609
 - in heat pipes, 239, 244
 - performance of, 610
 - refrigeration, 501, 530–533
- Exergy analysis, 157–164
 - of heat transfer, 161
 - subscripts used in, 160
 - symbols/units used in, 158–160
 - wheel diagram, 162, 163
- Exhaust heat used in industrial gas turbines, 934–938
- Exhaust systems, gas-turbine, 921
- Expanders, 153
- Expansion devices, refrigeration, 532–536
 - capillary tube, 534–535
 - constant-pressure expansion valve, 534

electronic expansion valve, 534
 short-tube restrictor, 535–536
 thermostatic expansion valve, 532–534
 Expansion engine cooling, 551–552
 Expansion valves, 501, 532–534
 Explosions, 666–670
 Extended surface(s):
 heat transfer by, 197–198
 as thermal control technique, 478–483
 Extended surface analysis, 479
 Extension leads, thermocouple, 266–267
 Extensive properties (term), 137
 External flow (in forced convection),
 207–211
 average Nusselt number with transition,
 208
 circular cylinders in cross-flow, 208
 flow across banks of tubes, 209–210
 flow past sphere, 208
 high-speed flow over flat plate,
 210–211
 high-speed gas flow past cones, 211
 laminar flow on flat plate, 207
 liquid metals in cross-flow over tube
 banks, 210
 noncircular cylinders in cross-flow of
 gases, 208–209
 stagnation point heating for gases, 211
 turbulent flow on flat plate, 208
 External flow (of liquids):
 on plane surfaces, 473
 viscous fluid dynamics for, 73, 74
 External resistance, thermal modeling of,
 461–463
 Extruders, co-rotating, 876

F

Facultative autotrophs, 729
 Fahrenheit temperature scale, 247–248
 Falling-sphere viscometers, 119, 120
 Fans:
 affinity laws for, 883–885
 in air-cooled heat exchangers,
 397–398
 axial-flow, 887–889
 centrifugal, 358, 361, 881–887

 compression ratios for, 879
 general features of, 880–881
 model of, 610
 number of, 610
 Fan models, 610
 Faraday effect, 972
 Faraday's law, 1065
 Far outliers, 836
 Fast beds, 735
 Fatigue cracks, 948
 FDM (finite difference method), 194, 196
 Federal cogeneration regulations, 977–979
 Federal Water Pollution Control Act
 amendments of 1972, 981
 Federal Water Pollution Control Act of 1965,
 981
 Fermentation:
 acetone-butenol-ethanol, 799
 hydrogen production by, 787, 1001
 FGD (flue gas desulfurization), 749, 750
 FGR (flue gas recirculation), 665
 Figures of merit, 835, 944–946
 Films, thin, 199, 203, 204
 Film boiling, 234, 235
 Film condensation, 237
 inside horizontal tubes, 239
 on outside of horizontal tubes/tube banks,
 237
 on vertical plate, 237
 Film pool boiling, 236
 Filters:
 bag, 367, 745–747
 ceramic fiber, 367
 for diesel fuels, 695
 electrostatic, 367
 for indoor-air contaminants, 589
 Fins:
 in air-cooled heat exchangers, 381, 382
 algorithms for combining single, into
 arrays, 481–483
 examples of, 479
 heat transfer by, 197–198
 longitudinal, rectangular profile, 480
 radial, rectangular profile, 480–481
 thermal modeling of, 457
 Financing arrangements for cogeneration
 systems, 986–989

- Fin arrays, 468–470
 - algorithms for combining single fins into, 481–483
 - forced convection flow across pin, 476
- Fin effectiveness, 198
- Fin efficiency, 198, 480
- Finite difference method (FDM), 194, 196
- Fin spacing (FPI), 610
- Firing systems, 654–664
 - gaseous fuel, 654–658
 - liquid fuel, 658–660
 - oxy-fuel, 670–671
 - solid fuel, 659–664
- Firing temperatures, 903–904, 931–933
- First class pyrheliometers, 810, 811
- First law of thermodynamics, 135, 582
 - for closed systems, 138–139
 - for control volume, 582
 - engineering system component
 - applications of, 153–156
 - for human body, 585–586
 - for HVAC devices, 582
 - for open systems, 144
 - and reversibility, 144
- Fisher-Tropsch process, 800
- Fixed-bed gasifiers, 740, 741
- Fixed carbon test, 709
- Fixed-displacement pumps, 1100–1102
- Fixed-tube-sheet evaporators, 531
- Flame aerodynamics, 644–655
 - diffusion-mixed turbulent flames, 650–651
 - premixed flames, 644–650
 - turbulent diffusion flame types, 651–655
- Flame length, 364
- Flame luminosity, 336
- Flame radiation, 641
- Flame speed, 644–645
- Flame stability, 678, 679
- Flame stabilization, 652–655
 - by bluff bodies, 649–650
 - by burner tile, 653
 - by deflector plate on fuel gun, 654
 - by fuel rich, low-velocity pocket, 653, 654
 - by graded air entry, 653, 654
 - by target rod and plate, 653
 - on tubes, 645
- Flame temperature, 449, 678–679
- Flame types, turbulent diffusion, *see* Turbulent diffusion flame types
- Flammability limits:
 - for gaseous fuels, 666, 667, 679–681
 - for liquid fuels, 667, 668
 - for natural gas, 680–681
- Flammability rating system (for refrigerants), 507–510
- Flapper-nozzle servo valves, 1112–1113
- Flashback, 1020
- Flashed steam conversion, 849–850
- Flash intercoolers, 502
- Flash points, 521, 683
- Flash-type economizers, 503–505
- Flat plate(s):
 - free convection from, 212–213
 - high-speed flow over, 210–211
 - laminar flow on, 207
 - turbulent flow on, 208
- Flat plate boundary layer, immersed objects
 - at, 116–117
- “Float and sink” tests, 717
- Flooded refrigeration systems, 504
- Floors, heating load through, 591
- Flow (in general). *See also specific types*, *e.g.*: One-dimensional flow
 - around circular cylinders, 69
 - around spheres, 78–79
 - coefficient of, 867
 - between parallel boundaries, 76
 - through circular tubes, 77–78
- Flow (about immersed objects), 115–118
 - and drag on objects, 117–118
 - at flat-plate boundary layer, 116–117
 - and lift, 118
- Flow (in closed conduits), 82–108
 - and minor losses, 92–95
 - and pipe friction, 87–92
 - pipe network analysis of, 99–102
 - steady-state pipeline analysis of, 95–99
 - unsteady flow in pipe systems, 102–108
 - velocity distribution for, 83–86
- Flow (in furnaces), 354–361
 - centrifugal fan characteristics, 358, 361
 - laminar/turbulent flows, 360
 - preferred velocities, 355, 356, 358, 359

- Flow (in open channels), 108–115
 - measuring flow rate, 129, 131–133
 - steady, nonuniform, 112–113
 - uniform, 108–111
 - unsteady, nonuniform, 113–115
- Flow areas, cross-sectional, 387
- Flow availability, 162
- Flow control:
 - for axial fans, 888, 889
 - for centrifugal fans, 886–887
 - for centrifugal pumps, 865–869
- Flow exergy, 162
- Flowing-tube viscometers, 119, 120
- Flow maldistribution, 400–401
- Flow nozzle, 126, 128
- Flow rate measurements, 126–133
 - in cryogenic engineering, 562
 - with open-channel devices, 129, 131–133
 - pressure difference methods, 126–130
 - total quantity methods, 126
 - tracer transport methods, 127–129, 131
- Flow resistance, thermal modeling of, 457, 463–464
- Flow separation, 72, 73, 95
- Flow structures, 176–181
- Flow systems:
 - characteristics of, 174
 - configuration of, 158
- Flow velocities, 387
- Flue gas:
 - exit temperature of, 670–671
 - thermodynamic properties of, 328, 329
- Flue gas desulfurization (FGD), 749, 750
- Flue gas recirculation (FGR), 665
- Fluids. *See also* Mechanics of incompressible fluids
 - capillarity of, 50, 51
 - compressibility of, 44, 47–48
 - cryogenic, 544–547
 - defined, 42
 - density of, 42, 43
 - properties of, 42–51
 - specific gravity of, 43, 44
 - specific weight of, 43
 - surface tension of, 49–51
 - vapor pressure of, 50, 51
 - viscosity of, 48–50
- Fluid compressibility, 1096
- Fluid dynamics:
 - for external flows, 73, 74
 - ideal, 58–71
 - for internal flows, 72–73
 - Navier–Stokes equations in, 73–79
 - for one-dimensional flow, 59–61
 - for three-dimensional flow, 69–71
 - for two-dimensional flow, 62–69
 - viscous, 71–79
- Fluid flow (in furnaces), 354–361
 - centrifugal fan characteristics, 358, 361
 - laminar/turbulent flows, 360
 - preferred velocities, 355, 356, 358, 359
- Fluid forces:
 - on curved surfaces, 54, 56
 - on plane surfaces, 53–55
- Fluidized bed combustion, 733–738
 - with bubbling fluidized beds, 733–735
 - with circulating fluidized bed boilers, 735
 - with pressurized fluidized beds, 737–738
 - repowering with, 735–737
- Fluidized-bed gasifiers, 740, 741
- Fluidized-bed heat transfer, 351
- Fluidized bed systems, 663–664
- Fluid measurements, 118–133
 - in cryogenic engineering, 564
 - density, 118, 119
 - flow rate, 126–133
 - pressure, 121–122
 - specific weight, 118
 - velocity, 122–126
 - viscosity, 118–121
- Fluid movers, 857–900
 - axial-flow pumps, 871–872
 - axial-flows fans, 887–889
 - centrifugal fans, 881–887
 - centrifugal pumps, 858–871
 - classification of, 857
 - compressors, 892–897
 - ejectors, 888–892
 - of gases, 878–897
 - general features of fans and blowers, 880–881
 - jet pumps, 872–873
 - of liquids, 857–878
 - mixed-flow pumps, 871–872

- Fluid movers (*continued*)
 - positive-displacement pumps, 873–878
 - and thermodynamics of gas compression, 897–900
- Fluid power systems, 1089–1122
 - accumulators in, 1115–1116
 - advantages of, 1089
 - common nonlinearities in, 1119–1122
 - components of, 1095–1116
 - cylinders in, 1091, 1094, 1113–1115, 1118–1120
 - dynamic behavior of, 1116–1119
 - energy storage in, 1092
 - hydraulic hoses in, 1097–1099
 - hydraulic oils in, 1095–1097
 - hydraulic pumps in, 1099–1105
 - hydraulic valves in, 1105–1113
 - motors in, 1090, 1091, 1113–1115
 - pumps in, 1090, 1091
 - reservoirs in, 1092, 1116
 - schematic of, 1090
 - symbols/terminology used with, 1090–1094
 - valves/valve actuators in, 1091, 1093, 1094, 1105–1113
- Fluid statics, 51–58
 - acceleration of fluid masses without relative motion, 57–58
 - buoyancy and stability of objects, 56–57
 - forces on curved surfaces, 54, 56
 - forces on plane surfaces, 53–55
 - pressure-measuring devices, 52–53
 - pressure variation in fluids at rest, 51–52
- Flux:
 - heat, *see* Heat flux
 - solar radiation, 807–808
- Flyash, 664, 666
- Forced convection, 350, 351
 - cylinders in cross-flow, 474–475
 - external flow, 207–211
 - internal flow, 205–207
 - noncircular cylinders in cross-flow, 208–209, 474, 475
 - nucleate boiling in, 236
 - thermal modeling of, 456, 473–478
 - in tubes/pipes/ducts/annuli, 477–478
- Forced-convection boiling, 234, 236
- Forced-convection flow:
 - across arrays of pin fins, 476
 - across circular cylinders, 208
 - across noncircular cylinders, 208–209
 - across spheres, 208, 474, 475
 - across tube banks, 209–210, 475–476
 - of air over electronic components, 476–478
 - in circular tubes, 206–207
 - external, 207–211
 - on flat plates, 207, 208, 210–211
 - internal, 205–207
 - laminar fully developed flow, 205, 206
 - past cones, 211
 - for short tubes, 205, 206
- Ford, Henry, 769
- Ford Motor Company, 908
- Forward curved vanes, 882, 883
- Fossil fuels. *See also* Liquid fossil fuels from petroleum; *specific fuels*
 - consumption rate for, 319–320
 - hydrogen/carbon ratios of, 674
- Fouling, 713, 715
 - as factor in heat exchanger programs, 409–410
 - in heat exchangers, 398–399
- Fourier's law of heat conduction, 185–186, 194
- Four-way directional control valves, 1107–1109
- FPI (fin spacing), 610
- Free convection, 211–214
 - in cavities between horizontal walls, 213
 - in cavities between vertical walls, 214
 - in enclosed spaces, 213
 - from flat plates/cylinders, 212–213
 - from spheres, 213
- Free convection boiling, 234
- Free jets, 490, 646–647
- Free swelling index (D720), 710
- Freeze–thaw cycling, 1074
- Freezing temperatures, 514, 519, 520
- Friction, 1121–1122
- Frictional losses:
 - minor, 92–95
 - pipe, 87–92
- Frio Formation (Texas), 846

- Front heads, 408
- Froth flotation, 716–717, 727–728
- F-type shell and tube heat exchangers, 376, 377, 389, 408
- Fuels. *See also* Biofuels; Gaseous fuels
 - for combustion, 639–640
 - diesel, 694–697
 - for firing systems, 658–664
 - fossil, 319–320, 674. *See also specific types*
 - for furnaces, 319–325
 - granular, 661–664
 - liquid, 639, 658–660
 - pulverized, 660–663
 - solid, 639, 659–664
 - synthetic, 320, 674
 - waste, 639–640
- Fuel–air ratio:
 - for combustion, 635–639
 - controlling, 362–365
- Fuel cells, 1055–1084
 - advantages/limitations of, 1058, 1059
 - alkaline, 1081
 - applications of, 1056–1058
 - in cogeneration systems, 971
 - direct methanol, 1074–1076
 - gasification in, 744
 - Greek letters used with, 1084
 - historical background, 1055–1056
 - hydrogen in, 992, 1016–1019
 - hydrogen polymer electrolyte, 1070–1075
 - hydrogen vehicles with, 788–792
 - installations of, 1057
 - microbial, 1083
 - molten carbonate, 1018, 1081–1082
 - nomenclature used with, 1083–1084
 - operating principles, 1060–1070
 - phosphoric acid, 1018, 1019, 1082–1083
 - proton exchange membrane, 1018, 1019
 - schematic of generic, 1060
 - solid electrolyte, 1018, 1019
 - solid oxide, 1076–1080
 - subscripts used with, 1084
 - superscripts used with, 1084
 - types of, 789, 1061
 - worldwide patents in, 1056
- Fuel-cell stack, 1062–1063
- Fuel costs, with cogeneration, 965
- Fuel-directed burners, 657, 658
- Fuel gas industry, 320
- Fuel NO_x, 665
- Fuel oils, 684–698
 - applications by grade, 692
 - available heat for, 323
 - available heat from, 643
 - aviation turbine fuels, 693
 - classification of, 684–685
 - diesel fuels, 694–697
 - heating requirements for, 687
 - kerosene, 687, 692
 - properties of, 685, 686, 688
 - specifications, 689–691
- Fuel rich, low-velocity pocket, 653, 654
- Fuel saving(s):
 - investment in improvements for, 374
 - with preheated air use, 446, 448
- Fuel shutoff valves, 669–670
- Fuel storage, 670
- Fuel systems, gas-turbine, 921–922
- Full admission, turbines with, 1042
- Fully developed flow, 207
- Fully developed limit, 456
- Furnaces, 313–374
 - burner/control equipment for, 361–367
 - capacity of, 371–372
 - complex thermal process components, 371
 - construction of, 318–319
 - economics of, 374
 - fluid flow in, 354–361
 - fuels/combustion, 319–325
 - heat transfer in, 330–354
 - load handling in, 316–317
 - oxygen enrichment of combustion air, 325
 - probable errors with, 314
 - representative heating rates for, 372–373
 - selecting number of modules, 373
 - sizing resources for, 398
 - standard conditions for, 314, 316
 - symbols/abbreviations used with, 315
 - temperature profiles of, 346–347, 349, 372
 - thermal properties of materials for, 325–329
 - types of, 314, 316–318
 - and waste heat recovery systems, 367–371

- Furnace components in complex thermal processes, 371
- Furnace economics, 374
- Furnace temperature, 365
- Furnace temperature profiles, 346–347, 349, 372
- G**
- GAs, *see* Genetic algorithms
- Galileo Galilei, 806
- Gamma rays, 217
- Gardon, Robert, 296
- Gardon gauges, 296–297
- Gas(es):
 - characteristics of liquids vs., 878–879
 - CO₂, 229–231, 233
 - effect of noncondensable, 239
 - H₂O, 229–232
 - mean beam length, 230, 232
 - measuring temperature of, 251, 266, 275
 - participating, 230
 - physical properties of, 46
 - radiative exchange, 233
 - ratio of principal specific heats at atmospheric pressure, 32
 - stagnation point heating for, 211
 - temperature and compression in, 879
 - thermal conductivity of, 186, 188
 - thermal properties at atmospheric pressure, 192
 - thermal radiation properties of, 229–234
 - thermodynamics of compression in, 897–900
- Gas coolers, 502
- Gas diffusion layer (GDL), 1060, 1070
- Gaseous carbon dioxide at 1 bar pressure, 12
- Gaseous emissions, coal conversion, 748–753
- Gaseous fuels, 673–682
 - calorific properties of, 678
 - for combustion, 639
 - combustion characteristics of, 678–679
 - for firing systems, 654–658
 - flame stability of, 678, 679
 - flame temperature of, 678–679
 - flammability limits of, 679–681
 - gas gravity of, 677, 678
 - hydrogen/carbon ratios of fossil and synthetic fuels, 673, 674
 - liquefied petroleum gases, 680–682
 - minimum ignition temperature of, 679, 680
 - natural gas, 673, 675–680
 - properties of, 675–678
 - Wobbe index of, 678–679
- Gaseous-fuel applications, 656–658
 - aerodynamically staged or delayed-mixing burners, 655–658
 - diffusion flame or nozzle-mix burner systems, 657
 - fuel-directed burners, 657, 658
 - premix burner systems, 656, 657
- Gaseous-fuel burners, 655–658
 - open, natural draft-type, 655, 656
 - packaged, 656, 657
 - sealed-in, power, 655, 656
 - windbox, 656
- Gas-fuel lines, 669
- Gas gravity:
 - of gaseous fuels, 677, 678
 - of natural gas, 678
- Gasification, 740–744
 - coal, 320–321, 995
 - direct, 995, 996
 - in fuel cells, 744
 - hydrogen production by, 787–788
 - IGCC, 741–744, 912, 938–940
 - PGCC, 744
 - types of gasifiers, 740–741
- Gas movers, 878–897
 - axial-flow fans, 887–889
 - centrifugal fans, 881–887
 - compressors, 892–897
 - ejectors, 888–892
 - general features of fans and blowers, 880–881
 - and thermodynamics of gas compression, 897–900
- Gas power (GP), 899
- Gas radiation, 336, 338, 339, 641
- Gas-to-liquid (GTL) technologies, 800
- Gas turbines, 901–953, 969–970
 - combustors, 910–911
 - compressors used in, 908–910

- controls/accessories for, 919–922
- cooling of, 918–919
- design trends, 931–934
- emissions, 911–915
- engine/system selection for, 949, 951–953
- function, 915–918
- history of, 906–908
- maintenance intervals/availability/reliability of, 947–949
- operating principles of, 901–906
- operation of, 923–924
- performance of, 924–934
- regulations on, 981
- selection of, 947–953, 974–975
- steam vs., 1033
- subsystem characteristics/capabilities of, 908–919
- Gas turbine applications, 934–947
 - aircraft engines, 941–946
 - in electricity generation, 940–941
 - exhaust heat used in industrial gas turbines, 934–938
 - integrated gasification combined cycle, 938–940
 - surface-transportation engines, 946–947
- Gas turbine combustors, 910–911
- Gas turbine fuel oils, 693–694
- Gas volume radiative exchange, 233, 234
- GDL (gas diffusion layer), 1060, 1070
- GE 90, 945, 946
- Gear motors, 1114–1115
- Gear pumps, 858, 874–875, 1100
- Gemini space program, 1055
- General Electric, 903, 907, 908, 914, 1055
- Generalized head loss, with throughput, 865, 866
- Generators:
 - electric, 972
 - heat recovery steam, 934–936, 972, 973, 1033, 1048
- Genetic algorithms (GAs), 606–607
- Gen-sets, 972
- Geometry data (for heat exchanger programs), 407–409
- Geopressured resources, 845–846
- Geothermal brine, 851, 852
- Geothermal electric power generation, 847–853
 - binary cycle, 850–851
 - considerations, 852
 - direct steam, 848–849
 - flashed steam, 849–850
 - hybrid geothermal/fossil, 853
 - steam turbines used for, 1050
- Geothermal energy, 839–854
 - classification of, 840, 841
 - conversion of, 846–854
 - direct uses of, 847
 - electric power generation from, 847–853
 - in Enhanced Geothermal Systems, 844–845
 - geopressured, 845–846
 - and heat pumps, 853–854
 - from hot dry rock, 844–845
 - hydrothermal, 842–844
 - from magma, 845
 - resources for, 841–846
 - U.S. resource base, 841–842
 - worldwide power generation from, 840
- Geothermal heat pumps (GHPs), 853–854
- Geothermal resource utilization efficiency (GRUE), 849
- Germany, 955
- The Geysers (California), 842, 844, 848, 849
- GHPs (geothermal heat pumps), 853–854
- Gibbs–Dalton’s law for ideal gases, 578
- Gibbs free energy, 145
- Gland seals, 1051
- Glass load factor (GLF), 592
- Glass microspheres, hydrogen storage in, 796, 1012–1013
- Global warming potential (GWP), 511, 513
- Glycol-based coolants, 519–521
- Gouy–Stodola theorem, 144
- GP (gas power), 899
- Gr (Grashof number), 455
- Graded air entry, 653, 654
- Gradually varied channel flow, 112–113
- Granular fuels, 661–664
- Grashof number (Gr), 455
- Grashof Prandtl number product, 212
- Grate-fired systems, 661–663

Gravity-controlled flow, 391
 Gravity forces, in dynamic similarity, 80
 Gravity separation, 717, 718, 726–727
 Gray enclosures, 234
 Gray surfaces, 221
 “Greenhouse effect,” 911–912
 Grindability, 710
 Grooved wicks, 428–430
 Ground-loop GHP systems, 854
 GRUE (geothermal resource utilization efficiency), 849
 GTL (gas-to-liquid) technologies, 800
 G-type shell and tube heat exchangers, 378, 407, 408
 Gulf Coast (U.S.), 845, 846
 GWP (global warming potential), 511, 513

H

H₂ PEFCs, *see* Hydrogen PEFCs
 Hagen–Poiseuille law, 78, 1099
 Halocarbons, 507
 Hamaker constant, 419
 Hard coal, *see* Anthracite
 Hardgrove Grindability Index, 708
 Hardy Cross method, 99–100
 Harrison (pyrometric) cones, 271–272
 HAWT (horizontal axis wind turbine), 955–957
 Hazen–Williams formula, 87, 89
 HCFCs, *see* Hydrochlorofluorocarbons
 HDR resources, *see* Hot dry rock resources
 Head:
 compressor, 896
 of fluid, 860
 pump, 861, 865, 866
 types of, 408
 Health issues and requirements, indoor-air-quality, 588
 Healy coal bed, 708
 Hearth-type pusher furnaces, 317
 Heat conductivity, 572
 Heat diffusion equation, 186
 Heat dumping, 976
 Heat engines, 140–142
 Heat equation, 186

Heat exchangers, 375–412
 air-cooled, 381–382, 396–398
 blowdown, inadequate, 403
 boiler feedwater, 382
 compact, 382
 critical heat flux in vaporizers, 402
 drainage, inadequate, 403
 flow maldistribution, 400–401
 fouling of, 398–399
 geometric properties of original/optimized, 610
 inadequate venting/drainage/blowdown, 403
 instability, 402–403
 instability of, 402–403
 laws of thermodynamics applied to, 156
 nomenclature for, 410–412
 operational problems with, 398–403
 orientation of, 409
 plate-type, 380
 recuperators/regenerators, 382–383
 shell and tube, 375–380
 size/cost estimation for, 383–385
 spiral plate, 380, 381
 temperature pinch, 401–402
 temperature pinch for, 401–402
 thermal design of process, 403–410
 venting, inadequate, 403
 vibration in, 399–400
 Heat exchanger rating methods, 386–398
 air-cooled heat exchangers, 396–398
 shell and tube condensers, 388–392
 shell and tube reboilers/vaporizers, 392–396
 shell and tube single-phase exchangers, 386–388
 Heat flux:
 constant heat flux experiments, 302–303
 critical, 402
 hybrid, 293
 maximum, 395–396
 Heat flux gauges (in general), 285–307
 calibration of, 298–299, 306–307
 circular foil, 296–297
 disruption of, 287–289
 errors and uncertainty with measurements from, 307

- and heat sinks, 287
- insert, 288–289, 294–297
- one-dimensional planar, 289–294
- surface-mounted, 287–288
- thermophile, 290–294
- thin-film, 292, 298–299
- Heat flux gauges based on active heating
 - methods, 302–305
 - for constant heat flux experiments, 302–303
 - for constant surface temperature experiments, 303–305
- Heat flux gauges based on spatial temperature
 - difference, 289–297
 - insert gauges, 294–297
 - one-dimensional planar gauges, 289–294
 - radiometers, 297
- Heat flux gauges based on temperature
 - change with time, 297–302
 - coaxial thermocouples, 300
 - differential flame thermometers, 302
 - null-point calorimeters, 300–301
 - slug calorimeters, 301
 - thin-film gauges, 298–299
 - transient optical methods in, 299
- Heat flux microsensors (HFMs), 294
- Heat flux sensitivity, 291, 306
- Heating:
 - active, 302–305
 - air, 443–450
- Heating, ventilation, and air conditioning (HVAC) systems, 577
- Heating, ventilation, and air conditioning (HVAC) systems, 581–584. *See also*
 - Indoor environmental control
- Heating loads, 589–591
- Heating rates, furnace, 372–373
- Heating requirements, fuel-oil, 687
- Heating value, 1047
- Heat leak optimization, 165–166
- Heat losses, 328, 341
- Heat management:
 - in fuel cells, 1068–1069
 - in H₂ PEFCs, 1071–1074
- Heats of formation, 321, 322
- Heat pipes, 415–440
 - advantages/limitations of, 415, 416
 - boiling limit of, 422–423
 - capillary limit of, 419–420
 - capillary pressure in, 418
 - cleaning/charging, 429, 431, 432
 - and contact angle, 417
 - cryogenic, 439
 - defined, 415
 - disjoining pressure in, 418, 419
 - effective thermal conductivity of, 424–428
 - entrainment limit of, 423
 - fabrication processes for, 428–433
 - Greek symbols used with, 439–440
 - and heat transfer, 239–244
 - heat transport limitations of, 419–428
 - high-temperature, 439
 - and Laplace-Young equation, 417–419
 - LHP/CPL, 434–435
 - micro, 437–438
 - nomenclature for, 439–440
 - oscillating, 435–436
 - rotating, 438
 - schematic of, 416
 - sizing resources for, 398
 - sonic limit of, 424
 - subscripts used with, 440
 - and surface tension, 417
 - testing of, 432–433
 - thermosiphon, 433–434
 - vapor chambers, 436
 - variable-conductance, 438
 - viscous limit of, 424
 - wicks for, 428–430
 - working fluid selections for, 428–429, 431, 432
- Heat pipe thermal resistance, 243–244
- Heat pumps, geothermal, 853–854
- Heat rate, steam turbine, 1034, 1036, 1043, 1047
- Heat-recovery chillers, 516
- Heat recovery equipment, cogeneration
 - system, 972, 973
- Heat recovery steam generators (HRSGs):
 - in cogeneration systems, 972, 973, 1033, 1048
 - exhaust heat in, 934–936
- Heat rejection, 904, 905
- Heat-sensitive crayons, 273
- Heat-sensitive labels, 273

- Heat sinks, 287, 457
 - for cryogenic temperature sensors, 561, 563
 - natural convection, 467–470
 - thermal control with, 478–483
- Heat-to-power ratio, 968
- Heat transfer (in general), 183–244
 - boiling, 234–237
 - combined coefficients, 352–354
 - from combustion, 641, 644
 - condensation, 237–239
 - conduction, 185–204, 341–345
 - convection, 205–216, 350–353
 - and EGM, 166–168
 - equivalent temperature profiles, 347–350
 - exergy of, 161
 - and first law of thermodynamics, 138–139
 - fluidized-bed, 351
 - gas radiation, 336, 338, 339
 - Greek symbols used in, 184–185
 - heat pipes, 239–244
 - with negligible load thermal resistance, 345
 - Newman method, 345–348
 - non-steady-state conduction, 341–344
 - radiation, 214–234, 331–341
 - in slug calorimeters, 301
 - solid-state radiation, 331–338
 - steady-state conduction, 340–341
 - subscripts used in, 185
 - symbols/units used in, 183–184
 - temperature profiles, 346–347, 349
- Heat transfer (in furnaces), 330–354
 - combined coefficients, 352–354
 - combined radiation factors, 339–341
 - convection, 350–353
 - emissivity–absorptivity, 331–332
 - equivalent temperature profiles, 347–350
 - evaluation of mean emissivity–absorptivity, 338–339
 - fluidized-bed, 351
 - gas radiation, 336, 338, 339
 - with negligible load thermal resistance, 345
 - Newman method, 345–348
 - non-steady-state conduction, 341–344
 - radiation charts, 332, 333
 - solid-state radiation, 331–338
 - steady-state conduction, 340–341
 - temperature profiles, 346–347, 349
 - view factors for solid-state radiation, 332, 334–337
- Heat-transfer coefficient(s):
 - for air-cooled heat exchangers, 396–397
 - for convective heat transfer, 455
 - for radiative heat transfer, 458
 - for shell and tube condensers, 390–391
 - for shell and tube reboilers, 393–395
 - for shell and tube single-phase exchangers, 387–388
 - vapor-phase, 392
- Heat-transfer correlations for electronic equipment cooling, 464–478
 - forced convection, 473–478
 - natural convection heat sinks, 467–470
 - natural convection in confined spaces, 464–467
 - thermal interface resistance, 470–473
- Heat Transfer Research, Inc. (HTRI), 396, 399, 408
- Heat transport limitations of heat pipes, 240–243, 419–428
 - boiling limit, 422–423
 - capillary limit, 419–420
 - effective thermal conductivity, 424–428
 - entrainment limit, 423
 - sonic limit, 424
 - viscous limit, 424
- Heavy metals, from coal conversion, 723, 753–754
- Heinkel engine, 908
- Heisler charts, 199–204
- Helical baffles, 408
- Helium:
 - fluid properties of, 544–547
 - thermal acoustic oscillations in liquid, 564
- Helium(II), 545, 546, 570–574
- Helmholtz free energy, 145–146
- Hemispherical emissivity, 218, 219
- Hemispherical temperature, 710
- Hero, 1033, 1034
- Heterotrophs, 729
- HEVs (hybrid electric vehicles), 788
- HFCs, *see* Hydrofluorocarbons

- HFCIT (Hydrogen, Fuel Cells, and Infrastructure Technologies) Program, 1022
- HfMs (heat flux microsensors), 294
- HGMS (high gradient magnetic separation), 728
- Higher heating value (HHV):
 for hydrogen-containing fuels, 321
 for methane, 321
 for natural gas, 675–678
- High gradient magnetic separation (HGMS), 728
- High-power-density (HPD) SOFC design, 1078, 1079
- High-pressure gas cylinders, for hydrogen storage, 1004–1006
- High-pressure gas inspirators, 362–364
- High-pressure turbines, 1042
- High-speed flow:
 over flat plate, 210–211
 past cones, 211
- High surface area sorbents, 1015
- High-temperature combustion method, 709
- High-temperature heat flux gauges (HTHFS), 292–293
- High-temperature heat pipes, 439
- Horizontal acceleration of liquid with free surface, 57, 58
- Horizontal axis wind turbine (HAWT), 955–957
- Horizontal ground-loop GHP systems, 854
- Horizontal multitubepass, 376, 377
- Horizontal slope, channel with, 112
- Horizontal thermosiphons, 396
- Horizontal tubes/tube banks:
 film condensation inside, 239
 film condensation on, 237
 heat-transfer coefficients for, 391
- Horizontal walls, free convection in cavities between, 213
- Hoses, hydraulic, 1097–1099
- Hot dry rock (HDR) resources, 840, 841, 844–845
- Hot-film anemometer sensor, 124, 125
- Hot refrigerant gas defrost, 536–537
- Hot spot effect, 301
- Hot-wire anemometer sensor, 124
- HPD (high-power-density) SOFC design, 1078, 1079
- HRSs, *see* Heat recovery steam generators
- HTHFS (high-temperature heat flux gauges), 292–293
- HTRI, *see* Heat Transfer Research, Inc.
- H-type shell and tube heat exchangers, 378, 407
- Hub diameter, 931–932
- Human body, first law applied to, 585–586
- Human irritation responses, 588
- Humidification, adiabatic, 583–584
- Humidity ratio, 579–581
- HVAC (heating, ventilation, and air conditioning) systems, 577, 581–584.
See also Indoor environmental control
- H wind turbines, 957
- Hybrid electric vehicles (HEVs), 788
- Hybrid geothermal/fossil conversion, 853
- Hybrid heat flux, 293
- Hydraulic cylinders, 1113–1115, 1118–1120
- Hydraulic hoses, 1097–1099
- Hydraulic jump, 113
- Hydraulic motors, 1113–1115
- Hydraulic oils, 1095–1097
- Hydraulic pumps, 1099–1105
- Hydraulic systems, *see* Fluid power systems
- Hydraulic valves, 1105–1113, 1119, 1121
- Hydrocarbons, 513, 994
- Hydrochlorofluorocarbons (HCFCs), 506–513, 515
- Hydrofluorocarbons (HFCs), 506–509, 511, 513
- Hydrogen:
 fluid properties of, 544, 545
 nature of, 1021
 safety issues with liquid, 570
 storage of gaseous, 1004–1006
 storage of liquid, 1004, 1006
- Hydrogen (fuel), 785–799, 991–1023
 codes and standards on, 1022
 combustion of, 992
 current availability of, 797
 emissions from, 792–793
 in fuel cells, 1016–1019
 handling of, 1021–1022
 in hydrogen burner turbines, 1020

- Hydrogen (fuel) (*continued*)
- in internal combustion engines, 1019–1020
 - manufacturing methods, 786–788
 - production of, 992–1001
 - quality standards for, 788
 - research on, 798
 - resources on, 798–799
 - safety issues with, 797–798, 1021–1022
 - storage issues with, 794–797
 - storage of, 1001–1015
 - transmission and distribution of, 793–795
 - utilization of, 1015–1020
 - vehicles using, 788–792
- Hydrogen, Fuel Cells, and Infrastructure Technologies (HFCIT) Program, 1022
- n*-Hydrogen at atmospheric pressure, 26
- Hydrogen burner turbines, 1020
- Hydrogen/carbon ratios of fossil and synthetic fuels, 673, 674
- Hydrogen economy, 785, 1002
- Hydrogen (H₂) PEFCs, 1070–1075
- performance, 1070–1071
 - technical issues, 1071–1074
- Hydrogen production methods, 992–1001
- biological, 1000, 1001
 - biomass in, 995, 996
 - coal gasification, 995
 - electrolysis, 997–998
 - partial oxidation of heavy hydrocarbons, 994
 - photoelectrochemical, 1000
 - steam methane reformation, 992–994
 - thermochemical processes, 998, 999
- Hydrogen storage methods, 1001–1015
- for automotive applications, 1001, 1003
 - carbonaceous materials in, 1011–1012
 - chemical hydrogen storage, 1011–1012
 - clathrates in, 1015
 - comparison of, 1002
 - cryogenic liquid hydrogen storage systems, 1006
 - formation of metal–complex hydrides, 1006–1011
 - high-pressure gas cylinders, 1004–1006
 - high surface area sorbents in, 1015
 - and hydrogen economy, 1002
 - polymer nanostructures in, 1013–1015
- Hydrogen sulfide emissions, 852
- Hydrogen vehicles, 788–792
- emissions from, 792–793
 - with fuel cells, 788–792
 - with internal combustion engines, 792
 - specifications of, 790
- Hydrolysis reactions, 1011–1012
- Hydrothermal convection resources, 841–844
- liquid-dominated, 844
 - vapor-dominated, 842, 844
- Hysteresis, 1119, 1121
- ## I
- IAQ, *see* Indoor air quality
- Ice, 23, 515
- IC engines, *see* Internal combustion engines
- Ideal fluids, 58
- Ideal fluid dynamics, 58–71
- for one-dimensional flow, 59–61
 - for three-dimensional flow, 62–64, 69–71
 - for two-dimensional flow, 62–69
- Ideal gas(es):
- air, thermophysical properties of, 8–9
 - behavior of, 146–148
 - combustion products, sensible enthalpies of common, 37–38
 - equation of state, 149
 - mixture of, 149
- Ideal gas law, 253, 578
- IGCC, *see* Integrated gasification combined cycle
- Igneous resources, 840, 841
- Ignition qualities, 694–695
- Ignition sources, 666, 667
- Ignition temperature, minimum, 679, 680
- Imaging, thermal, 278–279
- Immersed objects, flow about, 115–118
- and drag on objects, 117–118
 - at flat-plate boundary layer, 116–117
 - and lift, 118
- Impellers, pump, 858, 859, 863–865
- Impulse turbines, 1034, 1036, 1037
- Incompressible flow, 211
- Incompressible substance model, 149–151
- Incremental area of heat transfer, 404

- Incremental heat curve, steam turbine, 1047
- Indirect air heaters, 443–445
- Indirect-fired absorption chillers, 974
- Indirect-fired chillers, 516
- Indirect refrigeration, 501, 518–522
 - coolants, 518–522
 - problems with, 520–522
- Indoor air quality (IAQ), 587–589
 - health issues/requirements, 588
 - problem mitigation, 589
- Indoor environmental control, 577–597
 - air-handling processes, 581–585
 - building thermal loads, 589–593
 - computer programs for, 593–596
 - equipment for, 596–597
 - indoor air quality, 587–589
 - parameters for, 578–581
 - psychometric chart for, 580–581
 - thermal comfort, 585–587
- Industrial furnaces, *see* Furnaces
- Industrial gas turbines, 934–938
- Industrial insulating materials, 191
- Industrial platinum resistance thermometers (IPRTs), 268, 269
- Industrial utilization, of carbon dioxide, 761
- Infiltration, heating load by, 591
- Infrared, 217
- Infrared cameras, 299, 303
- Infrared thermometry, 275–278
- Inlets, aircraft-gas-turbines, 944
- Inlet systems, gas-turbine, 920
- In-line centrifugal pumps, 871
- Inner swirl, 654, 655
- Input data (for heat exchanger programs), 407–410
 - fouling, 409–410
 - geometry data, 407–409
 - process data, 407
- Inserted materials, law of, 257
- Insert heat flux gauges, 294–297
 - circular foil gauges, 296–297
 - disruption of, 288–289
 - issues with, 286
 - with thin-film thermocouple sensors, 294–295
 - wire-wound gauges, 295
- In situ pollution control for coal conversion, 729–744
 - cyclone combustion, 739
 - fluidized bed combustion, 733–738
 - with gasification, 740–744
 - with magnetohydrodynamics, 739
 - pulverized coal combustion, 731–733
 - in supercritical boilers, 738–739
- In situ technologies, coal, 726
- Inspection, gas-turbine, 947–949
- Inspirators, 362–364
- Instability (in heat exchangers), 402–403
- Instrumentation, in refrigeration design, 541
- Insulation:
 - critical radius of, for cylinders, 197
 - for cryostats, 555–560
 - multilayer, 558, 559
 - thermal properties of materials for, 190, 191
- Integral fan burners, 656, 657
- Integrated gasification combined cycle (IGCC):
 - emissions from, 912
 - gas turbines in, 938–940
 - in situ pollution control with, 741–744
- Intensity measurements, 807–808
- Intensive properties (term), 137
- Interception factor, *see* Configuration factor
- Intercooling, 926–927, 970
- Interface resistance, 453–454
- Interior temperatures, law of, 257
- Intermediate materials, law of, 258
- Intermediate-pressure turbines, 1042
- Intermediate shields, cryostat, 558
- Intermediate systems, power plant, 976
- Intermediate temperature loops, 404, 405
- Intermetallic alloys, 1007
- Internal combustion (IC) engines:
 - fuel economy of gasoline, 788
 - hydrogen in, 992, 1019–1020
 - hydrogen vehicles with, 792
 - reciprocating, 970–971
- Internal constraints, 143
- Internal convection, 570, 571
- Internal efficiency, 1043

- Internal flow (in forced convection), 205–207
 - fully developed turbulent flow of liquid metals in circular tubes, 207
 - laminar flow for short tubes, 205, 206
 - laminar fully developed flow, 205, 206
 - turbulent flow in circular tubes, 206–207
 - Internal flow (in liquids), viscous fluid
 - dynamics for, 72–73
 - Internal thermal resistance, 459–460
 - International Classification of Brown Coals, 707
 - International Classification of Hard Coals, 707
 - International Fuel Cells, 1082
 - International Standards Organization (ISO), 880, 881
 - International System of Units (SI), 4
 - International Temperature Scale of 1990 (ITS-90), 248, 249
 - Invasive temperature measurement, 251–272
 - bimetallic thermometers for, 254–255
 - diode thermometers for, 271
 - liquid-in-glass thermometers for, 252–253
 - with manometric thermometry, 253–254
 - with noise thermometry, 271
 - pyrometric cones for, 271–272
 - RTDs for, 267–270
 - semiconductor sensors for, 270–271
 - thermocouples for, 255–267
 - Investors, cogeneration system, 986–987
 - Iodine–sulfur cycle, 999
 - IPRTs (industrial platinum resistance thermometers), 268, 269
 - Irradiation, spectral, 219
 - Irreversible operation, 140
 - Irrotational flow, complex variables for, 65–66
 - Irrotational flow-velocity potential, 63–64
 - Isentropic process, 148
 - ISO (International Standards Organization), 880, 881
 - Isochrome bandwidth, 274
 - Isoentropic process, 148
 - ISO firing temperatures, 903, 904
 - Isolated plate limit, 456
 - Isolated systems, 142–143
 - Isothermal compressibility, 146
 - Isothermal compression (Stirling cycle), 553
 - Isothermal expansion (Stirling cycle), 554
 - ISoTherM Research Consortium, 428
 - Italy, 840, 844
 - ITS-90 (International Temperature Scale of 1990), 248, 249
- ## J
- Japan Railway, 908
 - Jets:
 - confined, 647–649
 - free, 490, 646–647
 - liquid, 490, 493, 494
 - in spray cooling, 490–494
 - submerged, 490, 491, 493
 - Jet fuels, 693
 - Jet pumps, 858, 872–873
 - Johnson noise, 271
 - Joule–Thomson coefficient, 146
 - Joule–Thomson (JT) refrigeration, 549–551
 - J-type shell and tube heat exchangers, 377, 389, 407
- ## K
- Kapitza conductance, 573
 - Kcal, 319
 - Kelvin temperature scale, 247–248
 - Kendall radiometer, 297
 - Kerosene, 687, 692
 - Kettle, 396
 - Keystone Coal Industry Manual, 707
 - Kinematic viscosity, 120, 870
 - Kipp and Zonen CM11 pyranometer, 811–812, 819, 825, 827, 828
 - Kipp and Zonen CMA 6 albedometer, 818
 - Kirchhoff, Gustav, 809
 - Kirchhoff’s law, 809
 - Kirchhoff’s law of radiation, 221
 - Kriging method, 617
 - K thermocouples, 262
 - K-type shell and tube heat exchangers, 378–379, 408
 - Kyoto Protocol to the United Nations Framework Convention on Climate Change, 725

L

- Labels, heat-sensitive, 273
- LAER (lowest achievable emissions rate), 980
- Lagging, gas-turbine, 921
- Lake ground-loop GHP systems, 854
- Laminar flame speed:
 - of gaseous fuels, 679
 - premixed, 644–645
- Laminar flame stabilization on tubes, premixed, 645
- Laminar flow:
 - on flat plate, 207
 - fully-developed, 205, 206
 - in furnaces, 360
 - for short tubes, 205, 206
- Laminar sublayer, 85
- Laplace equation, 64, 193
- Laplace-Young equation, 417–419
- Lardarello (Italy), 840, 844
- Large Hadron Collider Project, 551–552
- Laser-Doppler velocimetry (LDV), 124, 126
- Latent heats, 325–326, 514
- Latent heat transfer, 383
- Law of inserted materials, 257
- Law of interior temperatures, 257
- Law of intermediate materials, 258
- Laws of thermodynamics, 138–144
 - for closed systems, 138–142
 - engineering system component applications of, 153–156
 - first, 138–139
 - open systems, 143–144
 - second, 140–142
- LDV (Laser-Doppler velocimetry), 124, 126
- Lean fuel mixtures, 1020
- LeBaron et al. model of diffuse shadow-band correction, 823–826
- Le Chatelier principle, 1064
- Levenberg Marquardt method, 604
- LHPs (loop heat pipes), 434–435
- LHV, *see* Lower heating value
- Life-cycle cost, 952–953
- Lift, 957
 - aerodynamic, 871, 872
 - and flow about immersed objects, 115, 118
 - Lift coefficient, 115, 871
- Lignites, 703, 705, 706, 708, 721
- Limestone, scrubbing with, 749
- Lindenfrost point, 235
- Linear momentum, 61–62
- Linear theory method of pipe network analysis, 100–101
- Liquefaction, 548
- Liquefied natural gas (LNG), 507, 570, 673
- Liquefied petroleum gases (LPGs), 680–682
 - consumption rate of, 681
 - physical properties of, 680, 681
 - refrigeration of, 504
 - storage of, 670
- Liquids:
 - characteristics of gases vs., 878–879
 - compression in, 897
 - measuring temperature of, 251, 265, 266
 - physical properties of, 45
 - ratio of principal specific heats at atmospheric pressure, 32
 - saturated, 31, 34, 35, 186, 188, 191
 - surface tension of, 33
 - temperature dependence of thermal conductivity of, 186, 188
- Liquid carryover, 515
- Liquid-cooled reciprocating engines, 971
- Liquid crystals:
 - in constant heat flux experiments, 303
 - measuring heat flux with, 299
 - thermochromic, 274–275
- Liquid density, 514
- Liquid-dominated resources, 844
- Liquid-flow eductors, 873
- Liquid fossil fuels from petroleum, 683–700
 - chemical analyses of crudes, 684
 - flash points of, 683
 - fuel oils, 684–698
 - oil–water emulsions, 700
 - properties of, 683
 - shale oils, 698–699
 - tar sands, oils from, 699–700
 - uses of, 683, 684
- Liquid fuels:
 - for combustion, 639
 - for firing systems, 658–660
- Liquid-fuel lines, 669

- Liquid hydrogen, storage of, 796–797, 1004, 1006
 - Liquid-in-glass thermometers, 252–253
 - Liquid jets, 490, 493, 494
 - Liquid metals:
 - in cross-flow over tube banks, 210
 - fully developed turbulent flow of, in circular tubes, 207
 - thermal properties of, 192
 - Liquid movers:
 - axial-flow pumps, 871–872
 - centrifugal pumps, 858–871
 - jet pumps, 872–873
 - mixed-flow pumps, 871–872
 - positive-displacement pumps, 873–878
 - Liquid pressure drop, 420, 421
 - Liquid recirculators, 504, 506
 - Liquid ring compressors, 893–894
 - Liquid–vapor interfaces, 417–419, 425–427
 - Lithium bromide absorption systems, 515–518
 - Lithium nitride, 1011
 - Ljungstrom (radial-outflow) turbine, 1039–1041
 - LMTD (log mean temperature difference), 214–216
 - LNG, *see* Liquefied natural gas
 - Load following, 976
 - Load handling, furnace, 316–317
 - Load sensing, 1103, 1104
 - Lobe pumps, 1100, 1101
 - Local acceleration, 63
 - Local Nusselt number, 207, 208
 - Log mean temperature difference (LMTD), 214–216
 - Longitudinal fin of rectangular profile, 480
 - Long-Range Transboundary Air Pollution Treaty, 724
 - Loop heat pipes (LHPs), 434–435
 - “Lord” value, 707
 - Los Alamos National Laboratory, 1056
 - Loss coefficients, for pipe
 - enlargements/contractions, 93
 - Lower heating value (LHV):
 - for hydrogen-containing fuels, 321
 - for methane, 322
 - for natural gas, 678
 - Lowest achievable emissions rate (LAER), 980
 - Low-nitrogen oxide burners, 732–733
 - Low NO_x combustors, 914–915
 - Low-pressure turbines, 1042
 - Low-temperature heat transfer coolants, 519–521
 - LPGs, *see* Liquefied petroleum gases
 - Lubricants, compressor, 523, 525
 - Lubricating systems, gas-turbine, 922
 - Lubrication, theory of, 76–77
 - Lumped heat-capacity method, 199
- ## M
- M1 Abrams Main Battle Tank, 947
 - MAD (mean of absolute deviations), 834
 - Magma, 845
 - Magnesium hydrides, 1008
 - Magnetohydrodynamics (MHD), 739
 - Manning formula, 87, 89, 90, 109–110
 - Manometer, 52, 53
 - Manometric thermometry, 253–254
 - Manufacturing methods:
 - biodiesel, 777, 779
 - ethanol, 769–770
 - hydrogen, 786–788
 - Marine industry, steam turbines in, 1050
 - Martinelli separated flow approach, 392
 - Mass balance, 594
 - Mass coefficient, 1044
 - Mass conservation, 143–144
 - Mass flow rate, 59, 1048
 - Mass velocities, 355, 356
 - Maximum heat flux, 395–396
 - Maximum inversion temperatures, cryogenic fluid, 550
 - MBE (mean bias error), 833, 834
 - MCFCs, *see* Molten carbonate fuel cells
 - Mean beam length, 230, 232
 - Mean bias error (MBE), 833, 834
 - Mean of absolute deviations (MAD), 834
 - Mean temperature difference (MTD):
 - for furnaces, 330–331
 - for heat exchangers, 383–384
 - in heat transfer rate calculations, 214
 - for reboilers, 393, 394

- Mechanical efficiency, 1043
- Mechanical servo valves, 1112–1113
- Mechanics of incompressible fluids, 41–133
 - definition of fluids, 42
 - dimensional analysis in, 81–82
 - flow about immersed objects, 115–118
 - flow in closed conduits, 82–108
 - flow in open channels, 108–115
 - fluid measurements, 118–133
 - fluid statics, 51–58
 - ideal fluid dynamics, 58–71
 - and properties of fluids, 42–51
 - similitude in, 79–81
 - units, 42–44
 - viscous fluid dynamics, 71–79
- Melting furnaces, 450
- Membrane separation, 759
- Mercaptan odorants, 673
- Mercury:
 - and coal conversion, 723, 753–754
 - enthalpy–log pressure diagram for, 15
 - saturated, 14
- Mercury-in-glass thermometers, 252, 253
- Metabolic heat production, 585–586
- Metals:
 - heavy, 723, 753–754
 - liquid, 192, 207, 210
- Metal–complex hydrides, 1005–1011
- Metallic solids, 189
- Metallic surfaces, 221, 222
- Metamodeling, 616–617
- Methane, 800
 - at atmospheric pressure, 16
 - available heat for, 323
 - available heat ratios for, 325
 - as gas turbine fuel, 922
 - heating values for, 321–322
 - as refrigerant, 510
 - thermodynamic properties of saturated, 16
- Methanol, 799, 1076
- Method of characteristics, 108
- Methods source (for heat exchanger programs), 407
- Metric conversion to English units, 316
- Mexico, 844
- MFCs (microbial fuel cells), 1083
- MHD (magnetohydrodynamics), 739
- Microbial fuel cells (MFCs), 1083
- Micro heat pipes, 437–438
- Micrositing, 961–962
- Microspheres, hydrogen storage in, 796, 1012–1013
- Microturbines, 971
- Microwave radiation, 217
- Mild slope, channel with, 112
- Mineral insulated metal sheathed (MIMS) thermocouples, 264, 265
- Mineral-matter-free basis, 704–707
- Minimum ignition temperature:
 - of gaseous fuels, 679, 680
 - of natural gas, 680
- Minor losses, in closed conduits, 92–95
- MixAlco process, 770, 799
- Mixed alcohols, 799
- Mixed-flow pumps, 858, 871–872
- Mixing-cup temperature, 205
- Mixture effects correction, 392
- MLI (multilayer insulation), 558, 559
- Moderately compressed liquid state, 153
- Moist air parameters, 578–580
- Molecular weight, 514
- Mollier diagrams, 1029–1032
- Molten carbonate fuel cells (MCFCs):
 - advantages of, 1062
 - applications of, 1055, 1056, 1061
 - characteristics of, 1018, 1061
 - degradation of, 1070
 - performance of, 1081–1082
 - polarization curves for, 1067
- Moment of momentum, 62
- Momentum, linear, 61–62
- Momentum correction factors, 85, 86
- Momentum equation, 61–62
- Monochromatic specific intensity, 807
- Monolithic cell-in-series design, 1078, 1080
- Montreal Protocol, 511
- Moody diagram, 87, 88
- Morey, Samuel, 768
- Motion, acceleration of fluid masses without, 57–58
- Motors:
 - direct-drive linear, 1111
 - in fluid power systems, 1090, 1091, 1113–1115

- Motors (*continued*)
 - gear, 1114–1115
 - hydraulic, 1113–1115
 - valve-driven, 1092
- MTD, *see* Mean temperature difference
- Multilayer insulation (MLI), 558, 559
- Multiscale heat exchanger simulation, 622, 624–630
 - assumptions in, 624
 - levels in, 622, 624
 - objective of, 626
 - offline approximation-assisted optimization for, 626–628
 - online approximation-assisted optimization for, 628–630
- Multistage valving, 1112, 1113
- Muneer and Fairouz quality control procedure, 830–831
- Muneer and Zhang model of diffuse shadow-band correction, 823–826

- N**
- NaAlH₄, hydrogen storage on, 1010
- NAAQS (National Ambient Air Quality Standards), 980
- Nacelle, 957
- Nafion conductivity, 1071–1074
- Nanofibers, 1013–1014
- Nanostructures, hydrogen storage in, 1013–1015
- Nanotubes, 1012
- NA (nonattainment) program, 980
- NASA, 1055
- National Ambient Air Quality Standards (NAAQS), 980
- National Energy Act, 977–978
- National Energy Policy Act of 1992, 988
- National Fire Protection Association (NFPA), 670
- National Hydrogen Association (NHA)
 - codes, 1022
- National Institute for Occupational Safety & Health (NIOSH), 589
- Natural convection, 350
 - in confined spaces, 464–467
 - optimal spacing for arrays using, 466–467
 - thermal modeling of, 455–456
- Natural convection heat sinks, 467–470
- Natural gas, 673, 675–680
 - available heat from, 642
 - calorific value/heating value, 675–678
 - cycle efficiency, 912
 - environmental impact, 674
 - flame stability, 678, 679
 - flame temperature, 679
 - flammability limits, 680–681
 - gas gravity, 678
 - hydrogen/carbon ratios of, 674
 - liquefied, 507, 570, 673
 - minimum ignition temperature, 680
 - net heating value, 678
 - properties, 675–678
 - sources/supply/storage, 674
 - types/composition, 674
 - uses/distribution, 673, 674
 - Wobbe index, 678–679
- Navier–Stokes equations, 73–79
 - boundary conditions for, 74–75
 - and continuity equation, 75–76
 - for flow around a sphere, 78–79
 - for flow through circular tubes, 77–78
 - and theory of lubrication, 76–77
- Near-equilibrium flow structures, 177
- Near outliers, 835, 836
- Net heating value (LHV), 678
- Net positive suction head–available (NPSH_A), 863
- Net positive suction head–required (NPSH_R), 863
- Net present value (NPV), 955
- Net pyrradiometers, 808
- Net thermoelectric emf, 259
- Newman method, 345–348
- Newtonian fluids, 42
- Newton–Raphson method, 101–102, 604
- Newton’s law(s):
 - of cooling, 194, 198
 - of viscosity, 78
- New Zealand, 844
- NFAN (number of fans), 610
- NFPA (National Fire Protection Association), 670
- NHA (National Hydrogen Association)
 - codes, 1022

- NIOSH (National Institute for Occupational Safety & Health), 589
- Nitric oxide, 722
- Nitrogen:
- from air separation, 565, 567
 - at atmospheric pressure, 26
 - and combustion, 636, 637
 - temperature–entropy diagram for, 546
- Nitrogen dioxide, 722
- Nitrogen oxides (NO_x):
- from biodiesel, 782
 - from coal conversion, 722
 - from gas turbines, 911–915
 - from internal combustion engines, 1020
 - low-nitrogen oxide burners, 732–733
 - reducing emission of, 665, 751–753
- Nitrogen oxide reburning, 733
- Nitrous oxide, 722, 753
- NO_x, *see* Nitrogen oxides
- Nodes, 194, 196
- Noise thermometry, 271
- Nonattainment (NA) program, 980
- Nonaviation gas turbine fuel, 695
- Noncircular cross sections, conduits with, 91–92
- Noncircular cylinders:
- in cross-flow, 208–209, 474, 475
 - forced convection with, 474, 475
 - gases in cross-flow of, 208–209
 - Nusselt numbers for, 205, 206
- Noncondensable gases, 239
- Noncondensing steam turbines, 969
- Noncondensing turbines, 1041
- Nondimensional MAD, 834
- Nondimensional MBE, 834
- Nondimensional RMSE, 835
- Nonequilibrium processes, 1032
- Nonflow availability, 161–162
- Noninvasive temperature measurement, 275–279
- with infrared thermometry, 275–278
 - with thermal imaging, 278–279
- Nonmetals, thermal properties of, 189
- Nonmetallic liquids, 188
- Nonmetallic surfaces, 222, 223
- Nonparticipating gases, 229
- Non-steady-state conduction, 330, 341–344
- Nonuniform flow:
- defined, 58
 - in open channels, 112–115
 - steady, 112–113
 - unsteady, 113–115
- No-slip condition, 63
- No-tube-in-window baffles, 408
- Nozzles:
- in aircraft engine gas turbines, 944
 - and condensate accumulation, 403
 - in diffusion-mixed burners, 650, 651
 - in gas turbines, 903, 916–917, 919, 949
 - for pulverized-fuel burners, 661
- Nozzle-mix burner systems, 657
- NPRC (Negishi, Japan), 743
- NPSH_A (net positive suction head–available), 863
- NPSH_R (net positive suction head–required), 863
- NPV (net present value), 955
- NREL (U.S. National Renewable Energy Laboratory), 829
- NTU method, 397
- Nu, *see* Nusselt number
- Nucleate boiling in forced convection, 236
- Nucleate pool boiling, 235–236
- Null-point calorimeters, 300–301
- Number of fans (NFAN), 610
- NUON/Demkolec/Willem Alexander IGCC plant (Buggenum, Netherlands), 743
- Nusselt number (Nu), 205–214, 455, 464–466
- O**
- Obligate autotrophs, 729
- Ocean thermal energy conversion (OTEC), 1050
- OD (tube diameter), 610
- ODHs (oxygen deficiency hazards), 568, 569
- Odorants, 673, 674
- ODP (ozone depletion potential), 511, 513
- Off-design operation (of refrigeration), 541
- Offline approximation-assisted optimization:
- for chevron plate heat exchanger, 621–622
 - for multiscale heat exchanger simulation, 626–628
- online vs., 618, 619

- OHPs (oscillating heat pipes), 435–436
- Oil(s):
 - atomization of, 364
 - as compressor lubricant, 523, 525
 - fuel, *see* Fuel oils
 - hydraulic, 1095–1097
 - residual, 674, 687
 - shale, 698–699
 - from tar sands, 699–700
- Oil heaters, 659
- Oil reservoirs, 1116
- Oil return, 530
- Oil–water emulsions, 700
- On-board reforming, of hydrogen fuel, 796–797
- One-dimensional flow:
 - Bernoulli equation for, 60–61
 - conservation of mass in, 59–60
 - Euler’s equations for, 60
 - ideal fluids in, 59–61
 - momentum equation for, 61–62
 - work–energy equation for, 61
- One-dimensional heat conduction, 193, 451–452
 - with internal heat generation, 452
 - steady-state, 187, 190, 193
- One-dimensional heat transfer with no internal heat generation, 186
- One-dimensional planar heat flux gauges, 289–294
 - surface-mounted gauges with RTD sensors, 290
 - surface-mounted gauges with thermocouple sensors, 290–293
 - surface-mounted wire-wound gauges, 293–294
- One-pass shell, 376, 377
- Online approximation-assisted optimization:
 - for chevron plate heat exchanger, 622, 623
 - for multiscale heat exchanger simulation, 628–630
 - offline vs., 618, 619
- Opaque surfaces, 221, 228
- Open-centered valves, 1108
- Open channels, flow in, 108–115
 - measuring flow rate, 129, 131–133
 - steady, nonuniform, 112–113
 - uniform, 108–111
 - unsteady, nonuniform, 113–115
- Open-cycle engines, 902
- Open-cycle refrigeration:
 - operation, 504
 - refrigerant selection for, 514–515
- Open-loop ground-loop GHP systems, 854
- Open natural draft-type burners, 655, 656
- Open systems:
 - defined, 137
 - exergy analysis of, 160
 - laws of thermodynamics for, 143–144
- Operating costs, cogeneration system, 983–985
- Operating schedules, furnace, 374
- Operational errors, with solar radiation measurements, 820–821
- Optical fiber-based infrared thermometers, 278
- Optical roughnesses, 221
- Optimization:
 - heat leak, 165–166
 - thermal system, 559–631
- Orifice meter, 126–130
- Orimulsion, 700
- ORR (oxidizer reduction reaction), 1062
- Orton (pyrometric) cones, 271–272
- Oscillating heat pipes (OHPs), 435–436
- Oscillations, thermoacoustic, 564–565
- OTEC (ocean thermal energy conversion), 1050
- Otto, Nikolaus, 769
- Otto cycle, 901, 951
- Outer swirl, 654, 655
- Outliers, 835–836
- Outlier analysis, 835–836
- Overall efficiency, steam turbine, 1043, 1044
- Overall heat-transfer coefficient, 197, 384–385
- Overlapped valves, 1108, 1109
- Overpressurization, cryogenic system, 568
- Owners, cogeneration system, 986–987
- Ownership of cogeneration systems, 986–989
 - characteristics of, 989
 - conventional (100%) ownership, 987–988
 - and motivations of owners/investors in systems, 986–987

- partnership arrangements, 988
- third-party ownership, 986*n.*, 988
- Oxidizer reduction reaction (ORR), 1062
- Oxy-fuel combustion, 670–671, 756
- Oxy-fuel firing, 670–671
- Oxygen:
 - from air separation, 565–567
 - at atmospheric pressure, 27
 - for combustion, 636, 637
 - safe cryogenic use of, 570
- Oxygen deficiency hazards (ODHs), 568, 569
- Oxygen enrichment of combustion air, 325
- Ozone depletion potential (ODP), 511, 513
- Ozone layer depletion, 511

- P**
- Packaged burners, 656, 657
- Packaged cogeneration systems, 976–977
- Packaging materials, 459, 460
- PAFCs, *see* Phosphoric acid fuel cells
- Page model, 830
- Paints:
 - pressure-sensitive, 122
 - temperature-sensitive, 273, 299
- Paraffinic crudes, 683
- Parallel boundaries, 76
- Parallel circuits, 610
- Parallel fins, 483
- Parallel parameterized CFD (PPCFD), 617–618
- Parallel pipelines, 105
- Pareto charts, 614–615
- Parker D1FH proportional valves, 1111, 1112
- Parker Hannifin, 1109–1112
- Parr formulas, 704, 705
- Parshall flumes, 131
- Parsons, Charles, 1033
- Parsons turbines, *see* Reaction turbines
- Partial admission, turbines with, 1042, 1047–1048
- Partial film boiling, 235
- Partial gasification combined cycle (PGCC), 744
- Partial oxidation (POX), 994
- Participating gases, 230
- Particle size effect on dryout heat flux, 428, 430
- Particulate matter (PM):
 - from coal conversion, 723, 745–748
 - emissions control of, 666
- Particulate radiation, 641
- Part-load operation, steam turbine, 1046–1048
- Partnership arrangements, 988
- Payback period, 985
- PCB conduction, 460–461, 466, 467
- Peak heat flux, 571
- Peaking systems, power plant, 976
- Peak shaving systems, 976
- Peak-temperature-indicating devices, 272–273
- Peat, 703, 708, 711
- PEC (photoelectrochemical) systems, 1000
- PEFCs, *see* Polymer electrolyte fuel cells
- Peltier effect, 486
- PEMFCs, PEM fuel cells, *see* Proton exchange membrane fuel cells
- Pentafluoroethane, 509, 512
- Pentane-in-glass thermometers, 252
- Percent ash test, 709
- Percent moisture test, 709
- Percent volatile matter test, 709
- Perch and Russell Ratio, 707
- Perfluorocarbon ion exchange membranes, 997, 998
- Performance:
 - alkaline fuel cell, 1081
 - of biodiesel, 779–782
 - centrifugal fan, 884–886
 - coefficient of, 141, 517, 552
 - eductor, 873, 874
 - of ethanol, 773, 774
 - evaporator, 610
 - gas turbine, 924–934
 - hydrogen PEFC, 1070–1071
 - jet pump, 873
 - molten carbonate fuel cell, 1081–1082
 - phosphoric acid fuel cell, 1082–1083
 - refrigerant, 512
 - solid oxide fuel cell, 1065, 1077–1080
 - steam turbine, 1043–1048
 - types of changes in, 181

- Performance curves, centrifugal pump, 862–865
- Peripheral pressure, in pumps, 858, 859
- Peristaltic pumps, 858, 877
- Perkins tube, 415
- Permeability, wick, 241
- Permits for cogeneration, 982–983
- Petroleos de Veneauels SA, 700
- Petroleumlike biofuels, 799
- PFBC (pressurized fluidized beds), 737–738
- PGCC (partial gasification combined cycle), 744
- Phases (term), 137
- Phase change heat transfer, 456–457
- Phase transition data:
 - for compounds, 6–7
 - for elements, 4–6
- Phosphors, thermographic, 273–274, 299
- Phosphoric acid fuel cells (PAFCs):
 - advantages of, 1058, 1062
 - applications of, 1056, 1061
 - characteristics of, 1018, 1019, 1061
 - degradation in, 1070
 - performance of, 1082–1083
- Phosphorus, 710
- Photo detectors, 809, 810
- Photoelectrochemical (PEC) systems, 1000
- Photoelectrolysis, 786
- Photolytic manufacturing of hydrogen, 786
- Photosynthesis, 787
- Physical cleaning of coal, 726–728
 - agglomeration, 727
 - froth flotation, 727–728
 - gravity separation, 726–727
 - high gradient magnetic separation, 728
- Physisorption, 1012
- PI (proportional plus integral) control, 597
- PID (proportional plus integral plus derivative) control, 597
- Piezoelectric effect, 820
- Piezoelectric transducers, 121
- Pinch point temperature difference, 972
- Pin fins, 476
- Pipes:
 - equivalent pipe technique, 104, 105
 - forced convection in, 477–478
 - heat, *see* Heat pipes
 - rough, 85, 86
 - smooth, 84, 85
- Pipe friction, 87–92
 - aging and, 90–91
 - in conduits with noncircular cross sections, 91–92
 - Darcy–Weisbach formula, 87, 89–92
 - Hazen–Williams formula, 87, 89
 - Manning formula, 87, 89, 90
- Pipeline transportation of carbon dioxide, 759–760
- Pipe network analysis, 99–102
 - Hardy Cross method, 99–100
 - linear theory method, 100–101
 - Newton–Raphson method, 101–102
- Pipe systems:
 - development of flow in, 83
 - with parallel pipelines, 105
 - with series pipelines, 97, 104, 105
 - single-pipeline, 96–99
 - unsteady flow in, 102–108
- Piston accumulators, 1115
- Piston compressors, 894
- Piston pumps, 877, 878, 1100–1105
- Pitch:
 - fan blade, 888
 - tube, 409
- Pitot-static tubes, 121–123
- Planck, Max, 808
- Planck's law, 217–220, 275–276, 808, 809
- Plane surfaces/walls:
 - fluid forces on, 53–55
 - forced convection external flow on, 473
 - heat conduction in, 193
 - transient heat conduction in, 199–201
- Plate-fin heat exchangers, 398
- Plate-type heat exchangers, 380, 398
- Platinum resistance thermometers, 267–269
- PM, *see* Particulate matter
- Polarization curve, 1066–1068
- Polk Power Station (Tampa, Florida), 743
- Pollutants. *See also specific compounds*
 - from coal conversion, 721–724
 - controlling emission of, 665–666
- Polyaniline, 1013–1015

- Polymer electrolyte fuel cells (PEFCs):
 - advantages of, 1058
 - applications of, 1056
 - degradation, 1069–1070
 - DMFCs, *see* Direct methanol fuel cells
 - H₂ PEFCs, *see* Hydrogen PEFCs
 - heat management, 1068–1069
 - operating principles of, 1060–1062
 - polarization curve, 1066–1067
- Polymerization, 515
- Polymer nanostructures, 1013–1015
- Polytropic compression calculation, 898–899
- Polytropic efficiency, 898
- Pond ground-loop GHP systems, 854
- Pool boiling, 234–236
- Poppet valves, 1106, 1107
- Positive-displacement fluid movers, 857, 858, 894
- Positive-displacement pumps, 858, 873–878
 - diaphragm, 877, 878
 - gear, 874–875
 - peristaltic, 877
 - piston, 877, 878
 - progressive cavity, 876, 877
 - screw, 875–876
- Postcombustion carbon dioxide capture, 758–759
- Postconversion clean-up technologies, 726, 745–754
 - for gaseous emissions, 748–753
 - for heavy metals, 753–754
 - for particulates, 745–748
 - for solid waste, 754
- Powell's dogleg method, 604
- Power. *See also* Fluid power systems
 - added to liquids by pumps, 97
 - brake, 863, 881, 885
 - of centrifugal pumps, 860, 863
 - compressor, 899, 900
 - gas, 899
 - heat-to-power ratio, 968
 - spectral emissive, 217
 - theoretical, 514
 - total emissive, 217
- Power coefficient, steam turbine, 1044
- Power equation, 957–958
- Power generation:
 - and EGM, 170–173
 - wind, 955–962
- Power ratings, reciprocating engine, 971
- POX (Partial oxidation), 994
- PPCFD (parallel parameterized CFD), 617–618
- Prandtl number (Pr), 455
- Prandtl–von Karman equation, 72
- Pratt & Whitney, 908
- Precombustion carbon dioxide capture, 755–756
- Preconversion technologies, 726–729
 - biological cleaning, 729
 - chemical cleaning, 728
 - physical cleaning, 726–728
- Precooling, 918
- Preheat coils, 585
- Preheating, 444–445, 447–450
- Premix burner systems, 656, 657
- Premixed flames:
 - aerodynamics of, 646–650
 - confined jets, 647–648
 - confined jets with swirl, 648–649
 - flame stabilization in bluff bodies, 649–650
 - free jets, 646–647
 - laminar flame speed, 644–645
 - laminar flame stabilization on tubes, 645
 - turbulent, 645–646
- Pressure:
 - absolute, 52
 - atmospheric, *see* Atmospheric pressure
 - barometric, 580–581
 - capillary, 418, 420
 - center of, 54, 55
 - condensing (discharge), 513, 897
 - critical, 150, 514
 - devices for measuring, 52–53
 - disjoining, 418, 419
 - and enthalpy, *see* Enthalpy–log pressure diagram(s)
 - evaporating (suction), 514
 - of fluids at rest, 51–52
 - measurement of, 121–122, 562
 - peripheral, 858, 859

- Pressure (*continued*)
 - and shear for viscous flow, 76
 - standby, 514
 - static, 121, 881
 - vapor, 50, 51, 522
- Pressure atomization, 658
- Pressure balance loops, 404, 405
- Pressure difference methods, 126–130
- Pressure drop:
 - in furnaces, 356–359
 - and heat exchanger programs, 407
 - in heat exchangers, 385
 - in heat pipes, 241
 - liquid, 420, 421
 - for shell and tube condensers, 392
 - for shell and tube single-phase exchangers, 388
 - vapor, 421–422
- Pressure forces, in dynamic similarity, 80
- Pressure ratio, 933–934, 1044
- Pressure ratio maps, 880
- Pressure-sensitive paint (PSP), 122
- Pressure transducers, 121
- Pressure waves, propagation of, 102–104
- Pressurized fluidized beds (PFBC), 737–738
- Pressurized hydrogen, storage of, 795, 796
- Prevention of significant deterioration (PSD) program, 980
- Prime movers (cogeneration system), 968–971
 - emissions from, 983
 - fuel cells, 971
 - gas turbines, 969–970
 - microturbines, 971
 - reciprocating engines, 970–971
 - selection and sizing of, 974–975
 - steam turbines, 968–969
- Principal specific heats for liquids/gases at atmospheric pressure, 32
- Printed circuits, 292
- Problem mitigation, indoor-air-quality, 589
- Process (term), 137
- Process data (heat exchanger programs), 407
- Process flow sheets, 541
- Producer gas, 320
- Production capacity, biodiesel, 783–784
- Programs, heat exchanger:
 - data base, 407
 - methods source, 407
 - quality/selection of, 406–407
 - suitability, 407
- Progressive cavity pumps, 858, 876, 877
- Prompt NO, 665
- Propane:
 - at atmospheric pressure, 27
 - available heat for, 323
 - as gas turbine fuel, 922
 - hydrogen/carbon ratios of, 674
 - as refrigerant, 510
- Propellers, 871
- Proportional plus integral (PI) control, 597
- Proportional plus integral plus derivative (PID) control, 597
- Proportional valves, 1111–1112
- Propylene, 27
- Protection tubes, thermocouple, 264
- Proton exchange membrane fuel cells (PEMFCs, PEM fuel cells):
 - advantages of, 1058
 - characteristics of, 1018, 1019
 - in hydrogen vehicles, 788–790
- Proximate analysis (D3172), 709
- PSD (prevention of significant deterioration) program, 980
- PSP (pressure-sensitive paint), 122
- Psychometric chart, 39, 580–581
- Public Utilities Regulatory Policies Act of 1978 (PURPA), 977–979
- Pulse tube cryocoolers, 554, 555
- Pulverized coal combustion, 731–733
 - low-nitrogen oxide burners for, 732–733
 - nitrogen oxide reburning in, 733
- Pulverized fuels, 660–663
- Pumps, 857–878
 - axial-flow, 858, 871–872
 - axial piston, 1103–1105
 - booster, 97
 - centrifugal, 858–871
 - diaphragm, 877, 878
 - dynamic, 857–858
 - fixed-displacement, 1100–1102

gear, 858, 874–875, 1100
 geothermal heat, 853–854
 hydraulic, 1099–1105
 jet, 858, 872–873
 laws of thermodynamics applied to, 153
 lobe, 1100, 1101
 mixed-flow, 858, 871–872
 peristaltic, 858, 877
 piston, 877, 878, 1100–1105
 positive-displacement, 858, 873–878
 progressive cavity, 858, 876, 877
 radial piston, 1102
 reciprocating, 858, 878
 recirculating, 504, 506
 screw, 858, 875–876
 source, 97
 steady-state analysis of single-pipeline
 systems with, 97–99
 twin-screw, 876
 vane, 1100–1102
 variable-displacement, 1100, 1103–1105
 vertical turbine, 98
 Pumping efficiency, 860
 Pumping systems, flow control and,
 865–869
 Pump outflow, 1104
 Pump performance description, 862–865
 Pump speed, 861–862
 Pure oxy-combustion, 756
 PURPA (Public Utilities Regulatory Policies
 Act of 1978), 977–979
 Pusher furnaces, 317
 Pyranometers, 811–814
 characteristics of, 813
 defined, 808
 shade ring correction factors for, 813,
 814
 with shading devices, 812–814
 Pyreometers, 808, 814, 816
 Pyrheliometers, 814–817
 characteristics of, 817
 classification of, 810–811
 defined, 808
 types of, 814–816
 Pyrolysis, 740, 787–788, 996
 Pyrometric cones, 271–272
 Pyrradiometers, 808

Q

QF (quality factor), 1044
 Quad (unit), 319
 Qualified facility status, for cogeneration
 facilities, 978–979
 Quality (property), 152
 Quality factor (QF), 1044
 Quality standards:
 for biodiesel, 779–781
 for ethanol, 770, 771
 for hydrogen as fuel, 788
 Quasistatistical process, 139, 148–149
 Quasistatic isothermal process, 149
 Quenching distance, 645

R

Ra, *see* Rayleigh number
 RACT (reasonable available control
 technology), 980
 Radial fin of rectangular profile, 480–481
 Radial-flow steam turbines, 1036, 1037,
 1039–1041
 Radial-inflow turbines, 1037, 1039
 Radially tipped vanes, 882, 883
 Radial-outflow turbines, 1039–1041
 Radial piston pumps, 1102
 Radial vanes, 881–883
 Radiant energy, 216
 Radiant tubes, 353
 Radiant tube recuperators, 370, 371
 Radiation. *See also* Radiation heat transfer
 blue flame, 641
 combined factors, 339–341
 from combustion, 641, 644
 gas, 336, 338, 339, 641
 solid-state, 331–338
 Radiation charts, 332, 333
 Radiation function, 220
 Radiation heat transfer, 214–234, 457–458
 and absorptivity for solar incident
 radiation, 222–224
 blackbody radiation, 216–220
 combined factors, 339–341
 configuration factor, 223–227
 diffuse-gray surfaces in enclosure,
 228–229

- Radiation heat transfer (*continued*)
 - electromagnetic spectrum of, 217
 - and emissivity of metallic surfaces, 221, 222
 - and emissivity of nonmetallic surfaces, 222, 223
 - gas, 336, 338, 339, 641
 - gas thermal radiation properties, 229–234
 - and Kirchhoff's law, 221
 - properties, 218–223
 - reducing, 556–561
 - solid-state, 331–338
- Radiation heat-transfer coefficient, 229
- Radiation laws, 808, 809
 - Kirchhoff's law, 809
 - Planck's law, 808, 809
 - Stefan–Boltzmann law, 809
 - Wien displacement law, 809
- Radiation shape factor, *see* Configuration factor(s)
- Radiation shields, 228, 229
- Radiative exchange, gas volume:
 - with black enclosure of uniform temperature, 233
 - with gray enclosure, 234
- Radioactive wastes, 367
- Radiocivity, 228
- Radiometers, 297
- Rankine cycle:
 - combined Brayton cycle and, 737, 934, 951
 - exergy wheel diagram of, 163
 - in gas turbines, 901, 951
 - solar Rankine cycle systems, 1050–1051
 - in steam turbines, 1029, 1030
- Rankine temperature scale, 247–248
- Rateau, August, 1033, 1034
- Rateau turbines, *see* Impulse turbines
- Rating methods, heat-exchanger, 386–398
 - air-cooled heat exchangers, 396–398
 - with computers, 405–406
 - shell and tube condensers, 388–392
 - shell and tube reboilers/vaporizers, 392–396
 - shell and tube single-phase exchangers, 386–388
- Ratio of principal specific heats for liquids/gases at atmospheric pressure, 32
- Rayleigh number (Ra), 212–214, 455–456, 465
- Re, *see* Reynolds number
- Reaction turbines, 1034, 1036, 1037
- Rear heads, 408
- Reasonable available control technology (RACT), 980
- Reboilers:
 - inadequate blowdown in, 403
 - shell and tube, 392–396
 - temperature pinch in, 401–402
- Reciprocating compressors:
 - above-atmospheric compression in, 894, 895
 - characteristics of, 522–523
 - closed-cycle operation of, 501–504
- Reciprocating engines:
 - in cogeneration systems, 970–971
 - regulations on, 980–981
 - selection of, 975
- Reciprocating pumps, 858, 878
- Reciprocity relations, 224
- Recirculating pumps, refrigerant, 504, 506
- Recirculation:
 - by bluff bodies, 649–650
 - flue gas, 665
 - primary, 648
 - secondary, 647–648
- Recompression, vapor, 890–891
- Re-compressors, *see* Ejectors
- Recovered waste heat, 443
- Recovery factor, 210
- Recovery temperature, 210
- Rectangles:
 - configuration factor for, with common edge, 227
 - configuration factor for aligned-parallel, 226
- Rectangular channels, 110
- Recuperators:
 - for air heating, 443, 449, 450
 - construction and operation of, 382–383
 - in furnace systems, 369–371
 - sizing resources for, 398
- Red-start temperature, 274

- Reentry stage arrangements, 1036, 1038, 1039
- Reflectivity, 219–221
- Reflux configuration, 389
- Reforming reaction, 796–797, 996
- Refractive index, 216
- Refractories, 318
- Refractory radiation, 644
- Refrigerants, 506–515
 - A1 group, 508–510
 - A3 group, 508, 510
 - B1 group, 508–510
 - B2 group, 508, 510
 - B3 group, 508, 510
 - classes of, 511
 - closed-cycle selection, 511, 513–514
 - comparative performance of, 512
 - numbering system, 507, 508
 - open-cycle selection, 514–515
 - physical properties of numbered, 27–30
 - regulations on production/use of, 511, 513
 - saturated, 17
 - secondary, 501
 - thermophysical properties of, 17, 27–30
 - toxicity/flammability rating system, 507–509
 - types of, 508–510
- Refrigerant 11, 507, 519–522
- Refrigerant 12, 509
- Refrigerant 13, 509
- Refrigerant 22, 509, 512
 - at atmospheric pressure, 17
 - enthalpy–log pressure diagram for, 18
 - in reciprocating compressors, 522
 - in rotary compressors, 522
 - saturated, 17
- Refrigerant 30, 519–521
- Refrigerant 50, 510
- Refrigerant 114, 509
- Refrigerant 115, 510, 512
- Refrigerant 123, 509, 510
- Refrigerant 125, 509, 511
- Refrigerant 134a, 509, 511
 - compressibility factor of, 21
 - enthalpy–log pressure diagram for, 22
 - interim properties, 20
 - thermodynamic properties of saturated, 19
- Refrigerant 143a, 511
- Refrigerant 170, 510
- Refrigerant 290, 510
- Refrigerant 407C, 509
- Refrigerant 410A, 509
- Refrigerant 502, 509
- Refrigerant 600, 510
- Refrigerant 744, 510
- Refrigerant 1120, 519–521
- Refrigerant 1150, 510
- Refrigerant cost, 514
- Refrigerant gas coolers, 502
- Refrigerating machines, 141
- Refrigeration, 499–541, 548–552
 - absorption systems, 515–518
 - adiabatic demagnetization, 575
 - cascade cooling systems, 548–549
 - closed-cycle, 501–506, 511, 513–514
 - compressors for, 522–528
 - condensers for, 528–530
 - cycles of, 501–506
 - defrost methods, 536–538
 - dilution, 574
 - evaporators for, 530–533
 - expansion devices for, 532–536
 - expansion engine cooling, 551–552
 - helium(II) for, 573, 574
 - history of, 499
 - indirect, 501, 518–522
 - Joule–Thomson, 549–551
 - open-cycle, 504, 514–515
 - principles of, 500–501
 - refrigerants, *see* Refrigerants
 - system components of, 522–536
 - system design considerations for, 538–539
 - system specifications for, 539–541
 - units of measure for, 501
- Refrigeration evaporators, 501, 530–533
 - oil return, 530
 - submergence effect, 531, 533
 - two-phase refrigeration distribution, 530
 - vapor–liquid separation, 530
- Regeneration, gas turbines with, 970
- Regenerative air preheating, 368–369
- Regenerative cooling (Stirling cycle), 553
- Regenerative gas turbine, 929–931
- Regenerative heating (Stirling cycle), 554

- Regenerators, 383
 - for air heating, 450
 - sizing resources for, 398
- Regenerator materials, cryocooler, 553, 554
- Regression, linear and nonlinear, 831
- Regulations:
 - cogeneration, 977–983
 - on refrigerant production/use, 511
- Reheat coils, 585
- Reheat factor, 1044
- Reheat (refired) gas turbines, 928, 929, 970
- Reinjection of geothermal fluids, 846,
 - 848–849, 851, 852
- Relative humidity, 579–581
- Relative motion, acceleration without, 57–58
- Relative root-mean square error (RRMSE), 630
- Relative roughness, 87
- Relative Seebeck coefficient, 259
- Reliability, gas-turbine, 949
- Relief valves, 1102, 1107, 1108
- Renewable Fuels Standard (RFS), 775
- Repowering, 735–737
- Required surface equations, 383
- Reserve base of U.S. coal, 704, 705
- Reservoirs:
 - fluid power system, 1092, 1116
 - hydraulic-oil, 1116
 - temperature, 140–142
- Residual equations for vapor compression system, 601–602
- Residual oils, 674, 687
- Resistance(s). *See also* Thermal resistance
 - contact, 453–454, 470–473
 - convection, 197
 - external, 461–463
 - flow, 457, 463–464
 - interface/contact, 453–454, 470–473
 - least, 176–177
 - single-chip package, 464
 - spreading, 452–453
 - and temperature, 268
 - total, 464
- Resistance temperature detectors (RTDs),
 - 267–270
 - carbon resistors, 270
 - in constant heat flux experiments, 303
 - doped germanium resistors, 270
 - platinum resistance thermometers, 267–269
 - rhodium iron resistors, 270
 - surface-mounted heat flux gauges with, 290
 - thermistors, 270
- Resistivity, 715, 747
- Resolution:
 - of cryogenic temperature sensors, 561, 563
 - spatial, 279
- Restricted dead state, 161
- Revenue from electricity sales, 965
- Reversibility, 144
- Reversible operation, 140
- Reynolds, Osbourne, 1033
- Reynolds number (Re):
 - defined, 354–355
 - for flow across tube banks, 359
 - for flow through tubes, 355, 359
 - formula for, 455
 - and pipe friction, 87
- RFS (Renewable Fuels Standard), 775
- Rhodium iron resistors, 270
- Rigid water column theory, 102, 104–106
- RMSE, *see* Root-mean-squared error
- Robitzch actinographs, 825, 826
- RoDbaffles, 408
- Rolling piston compressors, 523–524
- Rolls-Royce, 907, 908
- Root-mean-squared error (RMSE), 630, 833, 835
- Rotary compressors, 523–524
- Rotary-cup atomization, 659
- Rotary-hearth furnaces, 317
- Rotary kiln furnaces, 317
- Rotary lobe compressors, 892, 893
- Rotary sliding vane compressors, 892, 893
- Rotary vane compressors, 523, 524
- Rotating drum coal washing, 727
- Rotating heat pipes, 438
- Rotational angular velocity, for liquid, 58
- Rotational speed coefficient, steam turbine, 1044
- Rotational viscometers, 121
- Rotors, 957, 959–960

- Rotor speed, 931
- Roughness:
 - absolute and relative, 87
 - of commercial pipes, 88
 - optical, 221
- Rough pipes, velocity distribution for fluid in, 85, 86
- RRMSE (relative root-mean square error), 630
- RTDs, *see* Resistance temperature detectors

- S**
- Saccharification, 769, 770
- Safety considerations:
 - with biodiesel, 784, 785
 - with combustion, 666–670
 - with cryogenic engineering, 568–570
 - with ethanol, 775
 - with furnaces, 367
 - with hydrogen fuel, 797–798, 1021–1022
- Salt-based coolants, 519–521
- Sampling, coal, 715–716
- Sankey diagram, 640
- Saturated boiling, 234
- Saturated fluids, thermophysical properties of:
 - carbon dioxide, 11
 - liquids, 191
 - mercury, 14
 - methane, 16
 - Refrigerant 22, 17
 - Refrigerant 134a, 19
 - sodium, 23
 - specific heat at constant pressure, 31
 - steam, 24–25
 - thermal conductivity, 34
 - vapor air, 7–8
 - viscosity, 35
 - water, 24–25, 238
- Saturated liquids:
 - specific heat at constant pressure, 31
 - thermal conductivity, 34, 186, 188
 - thermal properties, 191
 - viscosity, 35
- Saturated solid state, 153
- Saturated vapor state, 150
- Saturation(s):
 - at ambient temperature, 514
 - in fluid power systems, 1119, 1120
 - of moist air, 578–579
- SBS (sick building syndrome), 588
- Scaling, 529
- scf (standard cubic feet), 641
- Schmidt–Boelter heat flux gauges, 295
- SCR (selective catalytic reduction), 751, 752
- Screening curve, 952
- Screen wicks, 428, 429
- Screw compressors, 524–526, 894, 895
- Screw pumps, 858, 875–876
- Scroll compressors, 524, 525, 895
- Scrubbing:
 - amine, 758–759
 - dry, 749–751
 - wet, 367, 748
- Seals, gland, 1051
- Sealed-in, power burners, 655, 656
- Sea level chart for standard barometric pressure, 580–581
- Seal-less tubular SOFC design, 1078, 1079
- SECA (Solid State Energy Conversion Alliance), 1076
- Seconds, Saybolt Universal (SSU), 685
- Secondary coolants, 518–522
- Secondary recirculation, 647–648
- Second class pyrheliometers, 810, 811
- Second-law efficiency, 162
- Second law of thermodynamics, 135, 140–142
 - engineering system component applications of, 153–156
 - for open systems, 144
 - and reversibility, 144
- Seebeck, Johann, 256
- Seebeck coefficients, 258–260
- Seebeck effect, 486, 487
- Seger (pyrometric) cones, 271–272
- Segmented cell-in-series design, 1078, 1080
- Segmented plate heaters, 303–304
- Selective catalytic reduction (SCR), 751, 752
- Selective noncatalytic reduction (SNCR), 751–753
- Semianthracites, 708
- Semiconductor temperature sensors, 270–271

- Semi-invasive temperature measurement,
 - 272–275
 - with peak-temperature-indicating devices, 272–273
 - temperature-sensitive paints for, 273
 - thermochromic liquid crystals for, 274–275
 - thermographic phosphors for, 273–274
- Sensible heat factor (SHF), 581, 583
- Sensible heating/cooling, 582–583
- Sensible-heat storage, 168–169
- Sensible heat transfer, 383
- Sensitivity:
 - of cryogenic temperature sensors, 561, 562
 - heat flux, 291, 306
 - thermal, 279
- Sensitivity analysis, 986
- Sensors:
 - heat flux microsensors, 294
 - hot-film anemometer, 124, 125
 - hot-wire anemometer, 124
 - semiconductor temperature, 270–271
 - solar radiation, 825–829
 - spectrally sensitive, 276
 - thin-film thermocouple, 294–295
- Separation:
 - air, 565–567
 - column, 104
 - flow, 72, 73, 95
 - gravity, 717, 718, 726–727
 - high gradient magnetic, 728
 - membrane, 759
 - with sorbents/solvents, 758–759
 - vapor–liquid, 530
- Separation proof, 95
- Sequestration, carbon dioxide, 760–762
- Series pipelines:
 - equivalent pipe technique for, 104, 105
 - steady-state analysis of, 97
- Servo valves, 1112–1113, 1117–1118
- Set point, 596–597
- SFC (specific fuel consumption), 941, 942
- sg (API gravity), 685, 686
- Shaft torque, 1046
- Shaft-type furnace, 317
- Shale oils, 698–699
- Shapes:
 - and conduction heat transfer, 193–195
 - and convection heat transfer, 209
- Shear-controlled flow, 390–391
- Shear-driven flow, 76
- Shear stress, in viscous fluids, 71, 72
- Shells:
 - diameter of, 386
 - and heat exchanger programs, 407–408
- Shell-and-coil condensers, 528
- Shell-and-tube condensers, 388–392, 528
 - correction for mixture effects, 392
 - gravity-controlled flow, 391
 - heat-transfer coefficients/pure components, 390–391
 - pressure drop, 392
 - selection of type, 388–389
 - shear-controlled flow, 390–391
 - temperature profiles, 389–390
- Shell and tube evaporators, 531, 532
- Shell and tube heat exchangers, 216, 375–380
 - baffle types, 379–380
 - condensers, 388–392
 - configurations of, 376–380
 - E-type, 376, 377
 - F-type, 376, 377
 - G-type, 378
 - H-type, 378
 - J-type, 377
 - K-type, 378–379
 - overall heat-transfer coefficient for, 384–385
 - rating methods for, 386–396
 - reboilers/vaporizers, 392–396
 - schematic of, 376
 - single-phase exchangers, 386–388
 - vibration in, 399–400
 - X-type, 377, 378
- Shell and tube reboilers, 392–396
 - heat-transfer coefficients, 393–395
 - maximum heat flux, 395–396
 - selection of type, 393
 - temperature profiles, 393, 394
- Shell and tube single-phase exchangers, 386–388
 - baffle spacing/cut, 387
 - cross-sectional flow areas/flow velocities, 387

- heat-transfer coefficients, 387–388
- pressure drop, 388
- tube length/shell diameter, 386
- Shell and tube vaporizers, 392–396
 - heat-transfer coefficients, 393–395
 - maximum heat flux, 395–396
 - selection of type, 393
 - temperature profiles, 393, 394
- Shellside flow, 387–388
 - maldistribution of, 400–401
 - temperature pinch in, 401–402
- Shellside reboilers, 395
- SHF (sensible heat factor), 581, 583
- Shift reaction (gasification), 740
- Ship propulsion, 947
- Short-tube restrictors, 535–536
- Sick building syndrome (SBS), 588
- Sieder–Tate equation, 205
- Sieve analyses, 716
- Sieve designations, 712, 713
- Similitude, 79–81
- Simple refrigeration cycle, 500, 501
- Simulation:
 - airflow, 594–595
 - computer use in thermal design of process
 - heat exchangers, 406
 - coupled building–environment, 595–596
 - engineering-level system, 600–602
 - multiscale heat exchanger, 622, 624–630
- Simultaneous linear equations, 603
- Simultaneous nonlinear equations, 603, 604
- Single-chip package resistance, 464
- Single-phase exchangers, 386–388
- Single-pipeline systems:
 - with pumps, 97–99
 - steady-state pipeline analysis of, 96–97
- Single-rod hydraulic cylinders, 1114
- Singular fins, 483
- Sintered metal wicks, 428, 429
- SI units, 4, 42–44
- Sky scanner MS-321LR, 816
- Slagging, 713–715
- Slightly superheated vapor state, 153
- Slope of best fit line, 832
- Slug calorimeters, 301
- Slurries, 870–871
- Smoke point, 687
- Smooth pipes, velocity distribution in, 84, 85
- SMR (steam methane reformation), 992–994
- SNCR (selective noncatalytic reduction), 751–753
- Society of Automotive Engineers, 1022
- Sodium:
 - in coal ash, 715
 - thermodynamic properties of saturated, 23
- Sodium hydroxide, 749
- SOFCs, *see* Solid oxide fuel cells
- Soft coal, *see* Bituminous coal
- Solar constant, 223
- Solar energy conversion, 169–170
- Solar incident radiation, 222–224
- Solar radiation instruments, 811–819
 - albedometers, 815–818
 - development of, 810
 - errors in, 819
 - with photo detectors, 809, 810
 - pyranometers, 811–814
 - pyrgeometers, 814, 816
 - pyrheliometers, 810–811, 814–817
 - sunshine recorders, 817–819
 - terminology for, 807–808
 - with thermal detectors, 809
- Solar radiation measurements, 805–829
 - defined, 811
 - equipment for making, 811–819
 - errors in, 819–826
 - history of, 805–806
 - of intensity and flux, 807–808
 - and radiation laws, 808, 809
 - sensors for making, 825–829
 - of solid angle, 806–807
 - uncertainty in, 819
 - units for, 808
- Solar radiation sensors, 825–829
 - of CM11 pyranometers vs. Robitzsch
 - actinographs, 825, 826
 - Delta-T BF3, 827–829
- Solar radiation studies, 829–836
 - data quality assessment for, 829–831
 - outlier analysis for, 835–836
 - statistical evaluation of models in, 831–835
- Solar Rankine cycle systems, 1050–1051
- Solenoids, 1110–1111

- Solenoid operated four-way directional control valves, 1110
- Solids:
 - measuring temperature of, 250–251, 265, 266
 - thermal conductivity of, 186–187
 - thermal properties of metallic, 190
- Solid angle, 806–807
- Solid fuels:
 - for combustion, 639
 - for firing systems, 659–664
- Solid oxide fuel cells (SOFCs), 744
 - advantages of, 1076–1077
 - applications of, 1055, 1056
 - characteristics of, 1018, 1019
 - degradation, 1069–1070
 - heat management, 1069
 - materials/performance of, 1077–1080
 - operating principles for, 1061, 1062
 - performance/efficiency of, 1065
 - performance of, 1065, 1077–1080
 - polarization curve, 1066–1067
 - technical issues, 1077
- Solid polymer electrolyte electrolyzer, 997, 998
- Solid State Energy Conversion Alliance (SECA), 1076
- Solid-state radiation, 331–338
 - emissivity–absorptivity, 331–332
 - radiation charts, 332, 333
- Solid-state storage of hydrogen, 797
- Solid waste, from coal conversion, 754
- Solid waste disposal, 982
- Solvents, separation of carbon dioxide with, 758–759
- Sonic atomization, 659
- Sonic limit, 240, 242, 424
- Soot blowing, 664
- Sorbents:
 - high surface area, 1015
 - separation of carbon dioxide with, 758–759
- Source pumps, 97
- “Sour” natural gas, 674
- Space shuttle orbiter, 1055, 1081
- Spain, 955
- Spatial resolution, 279
- Spatial temperature difference, 289–297
- Specific energy, 110–111
- Specific fuel consumption (SFC), 941, 942
- Specific gravity:
 - of fluids, 43, 44
 - of fuel oils, 685–687, 689–691
- Specific heat:
 - at constant pressure, 31, 146
 - at constant volume, 146
 - for liquids/gases at atmospheric pressure, 32
 - of secondary coolants, 521
- Specific intensity, 807
- Specific speed, 861–862, 884
- Specific volume of moist air, 579–580
- Specific weight, 43, 118
- Spectral emissive power, 217
- Spectral hemispherical absorptivity, 219
- Spectral hemispherical emissivity, 218, 219
- Spectral hemispherical reflectivity, 219
- Spectral hemispherical transmissivity, 219
- Spectral irradiation, 219
- Spectrally sensitive sensors, infrared, 276
- Spectral selectivity error, 819
- Specular radiation, 221
- Speed, specific, 861–862, 884
- Spheres:
 - forced convection flow across, 208, 474, 475
 - free convection from, 213
 - heat conduction in hollow, 193
 - Navier–Stokes equations for flow around, 78–79
 - three-dimensional flow around, 71
 - transient heat conduction in, 199, 203, 204
- Spines, cylindrical, 481
- Spiral plate heat exchangers, 380, 381
- Spool-in-sleeve valves, 1107
- Spray cooling, 490–494
- Spray dry scrubbing, 749–751
- Spray ponds, 528
- Spray-type evaporators, 531, 533
- Spreading resistance, 452–453
- SPRTs (standard platinum resistance thermometers), 268, 269
- SR (stoichiometric ratio), 637–639
- SSU (seconds, Saybolt Universal), 685

- St (Stanton number), 478
- Stability:
 - combustion, 639
 - flame, 678, 679
 - in heat exchangers, 402–403
 - of hydraulic oils, 1095–1096
 - of secondary coolants, 521
 - of submerged objects, 56–57
- Stacks, furnace, 356
- Stack draft, 358, 360
- Stack-type recuperators, 369, 370
- Stages, gas compression, 900
- Stage arrangements (steam turbine), 1036–1039
 - Curtis, 1036, 1038, 1039
 - reentry, 1036, 1038, 1039
 - velocity-compounded, 1036–1039
- Staged combustion, 739
- Staggered tubes, 209
- Staging of air, 665
- Stagnation point heating for gases, 211
- Stagnation temperature, 210
- Standard conditions, fan performance at, 885
- Standard cubic feet (scf), 641
- Standard platinum resistance thermometers (SPRTs), 268, 269
- Standard pyrheliometers, 810, 811
- Standby pressure, 514
- Stand-by rates, 965
- Stanton number (St), 478
- Starch saccharification, 769, 770
- Starnier and McManus fin arrays, 468
- Start-related wear-out mechanisms, 948, 950
- States (term), 137
- Static pressure, 121, 881
- Statistical evaluation of solar radiation models, 831–835
 - coefficient of correlation, 833
 - coefficient of determination, 832–833
 - figure of merit, 835
 - mean bias error, 833, 834
 - mean of absolute deviations, 834
 - nondimensional MAD, 834
 - nondimensional MBE, 834
 - nondimensional RMSE, 835
 - root-mean-squared error, 833
 - slope of best fit line, 832
 - Student's *t* distribution, 833, 834
- Steady flow:
 - defined, 58
 - nonuniform, 112–113
- Steady-state, one-dimensional heat transfer with no heat sink, 186
- Steady-state heat conduction:
 - in furnaces, 330, 340–341
 - two-dimensional, 193–196
- Steady-state pipeline analysis of flow in closed conduits, 95–99
 - for single-pipeline systems, 96–97
 - for single-pipeline systems with pumps, 97–99
- Steady-state with heat generation, 186
- Steam:
 - carbon-steam reaction, 740
 - direct steam conversion, 848–849
 - dry, 844*n*.
 - flashed steam conversion, 849–850
 - Mollier diagrams for, 1030–1032
 - saturated, 24–25
 - thermodynamic properties of, 1029–1030
- Steam atomization, 323
- Steam-based Rankine cycle electric power generation facilities, 981
- Steam cooling, 919
- Steam injection, 937–938
- Steam methane reformation (SMR), 992–994
- Steam rate, 1043
- Steam turbines, 951, 968–969, 974, 1029–1053
 - axial thrust in, 1052
 - blade erosion for, 1051
 - characteristics of, 1030–1033
 - classification of, 1039–1042
 - in cogeneration and combined-cycle plants, 1048–1049
 - control systems for, 1051
 - efficiencies of, 1043–1044
 - gas vs., 1033
 - gland seals for, 1051
 - Greek letters, 1053
 - historical evolution of, 1033–1036
 - industries using, 1049–1051

- Steam turbines (*continued*)
 - nondimensional parameters for, 1044–1045
 - performance of, 1043–1048
 - stage arrangements for, 1036–1039
 - subscripts, 1053
 - symbols, 1052
- Steepest decent method, 604
- Steep slope, channel with, 112
- Stefan–Boltzmann constant, 276, 809
- Stefan–Boltzmann law, 217, 331, 809
- Stirling cycle cryocoolers, 553, 554
- Stoichiometric combustion, 636
- Stoichiometric ratio (SR), 637–639
- Stokes’s law, 78–79
- Stokes’s stream function, 69
- Storage:
 - of biodiesel, 782, 783
 - and EGM, 168–169
 - of ethanol, 775
 - of hydrogen fuel, 794–797
 - of natural gas, 674
 - thermal, 976
- Stream function:
 - for three-dimensional flow, 69
 - for two-dimensional flow, 65
- Streamlines, 59, 64–65
- Student’s *t* distribution, 833, 834
- Subbituminous coal, 703, 705, 706, 708
- Subcooled boiling, 234
- Sub-Kelvin cooling, 574–575
- Submerged jets, 490, 491, 493
- Submerged objects, stability of, 56–57
- Submergence effect, 531, 533
- Subsidies:
 - for biodiesel, 784
 - for ethanol, 775, 776
- Substrate conduction, 460–461
- Suction (evaporating) pressure, 514
- Suction volume, 514
- Sugar extraction, 769, 770
- Suitability (of heat exchanger programs), 407
- Sulfur:
 - in coal, 709–710
 - emissions control of, 665–666
 - fuel-cell poisoning by, 1070
- Sulfur dioxide:
 - capture of, 734, 735
 - from coal conversion, 722
 - reducing emission of, 749–751
- Sulfur oxides, emissions control of, 665–666
- Sunshine recorders, 817–819
- Supercritical boilers, 738–739
- Supersaturation, 1032
- Supersonic flow, 211
- Surface(s):
 - equations for heat-exchanger, 383
 - as term, 383
- Surface disruption of temperature, 287–289
- Surface filtration, 745
- Surface heat balance, 287
- Surface-mounted heat flux gauges, 289–294
 - disruption of, 287–288
 - issues with, 286
 - with RTD sensors, 290
 - with thermocouple sensors, 290–293
 - wire-wound, 293–294
- Surface temperature:
 - adiabatic, 210
 - constant surface temperature experiments, 303–305
 - measuring, 250–251
- Surface tension, 49–51
 - in dynamic similarity, 80
 - and heat pipes, 417
 - of liquids, 33
- Surface-transportation engines, 946–947
- Surface-type economizers, 503
- Surge point, 527–528
- Surge theory, *see* Rigid water column theory
- Surging, 896
- Swashplate setting, 1103–1104
- Sweetening processes, 666
- “Sweet” natural gas, 674
- Swirl, effect of:
 - inner and outer swirl, 654, 655
 - turbulent diffusion flame types, 651–652
- Swirl number, 649
- Syngas, 740, 993
- Synthesis hydrocarbons, 800
- Synthetic fuels, 320, 674
- Synthetic natural gas, 320–321

T

- Tandem-compound unit turbines, 1042
- Tangential-flow turbines, 1040, 1041
- Tangentially-fired burners, 661, 663
- Tanks, 1116
- Target rod and plate, 653
- Tar sands, oils from, 699–700
- Technical design of cogeneration systems, 974–977
 - matching of dynamic power and thermal loads, 976
 - matching of electrical and thermal loads, 975–976
 - packaged systems, 976–977
 - selection and sizing of prime mover, 974–975
- TEMA, *see* Tubular Exchanger Manufacturers Association
- Temperature(s):
 - ash fusion, 710
 - bulk, 205
 - critical, 150, 514
 - dry bulb, 579–582
 - Earth's core, 839
 - firing, 903–904, 931–933
 - flame, 449, 678–679
 - freezing, 514, 519, 520
 - furnace, 365
 - and gas compression, 879
 - gauges based on temperature changes over time, 297–302
 - hemispherical, 710
 - ISO firing, 903, 904
 - law of interior, 257
 - maximum inversion, 550
 - minimum ignition, 679, 680
 - mixing-cup, 205
 - recovery, 210
 - red-start, 274
 - and resistance, 268
 - stagnation, 210
 - surface, 210, 250–251, 303–305
 - surface disruption of, 287–289
 - wet bulb, 579
- Temperature coefficients:
 - constant, 146
 - of resistance, 268
 - for thermistors, 270
- Temperature cross, 376, 378
- Temperature differences. *See also* Mean temperature difference (MTD)
 - cooling-load, 592
 - heat flux gauges based on spatial, 289–297
 - log mean, 214–216
 - pinch point, 972
 - spatial, 289–297
- Temperature disruption, by heat flux gauges, 287–289
- Temperature drops:
 - across liquid–vapor interface, 425–427
 - across shell and wick, 424–426
 - in vapor flow, 427–428
- Temperature–entropy diagrams, 544–546
- Temperature event range, 274
- Temperature glide, 507
- Temperature measurement, 247–280
 - calibration of sensors for, 249–250
 - in cryogenic engineering, 561–563
 - invasive, 251–272
 - nomenclature for, 279–280
 - noninvasive, 275–279
 - process, 248–249
 - range capabilities of methods, 252
 - selection of sensors/systems for, 250–251
 - semi-invasive, 272–275
- Temperature pinch, 376, 401–402
- Temperature profiles:
 - furnace, 346–347, 349, 372
 - for shell and tube condensers, 389–390
 - for shell and tube reboilers, 393, 394
- Temperature profiles, furnace, 346–347, 349, 372
- Temperature reservoirs, 140–142
- Temperature response error, 819
- Temperature scales, 247–249
 - Celsius, 247–248
 - Fahrenheit, 247–248
 - International Temperature Scale of 1990, 248, 249
 - Kelvin, 247–248

- Temperature scales (*continued*)
 - Rankine, 247–248
 - thermodynamic, 140, 247–248
- Temperature-sensitive paints (TSPs), 273, 299
- Tension wrapped fins, 381
- TESLA cryomodule, 558–560
- Testing of heat pipes, 432–433
- Tetrafluoroethane, 512
- 1,1,1,2-Tetrafluoroethane, 509
- Theoretical power, 514
- Thermal aspects of combustion, 640–644
- Thermal comfort, 585–587
- Thermal comfort indices, 586–587
- Thermal conductivity, 186–192
 - of cryogenic materials, 556
 - of furnace materials, 326–328
 - of gases, 186, 188
 - of heat pipes, 424–428
 - of liquids, 186, 188
 - of saturated liquids, 34
 - of solids, 186–187
 - temperature dependence of, 186–188
- Thermal control techniques, 478–494
 - cold plate, 483–486
 - extended surface/heat sinks, 478–483
 - spray cooling, 490–494
 - thermoelectric coolers, 486–490
- Thermal design of process heat exchangers
 - with computers, 403–410
 - incrementation, 403–404
 - input data, 407–410
 - main convergence loops, 404–405
 - program quality/selection, 406–407
 - rating/design/simulation, 405–406
- Thermal detectors, 809
- Thermal diffusivity, 326
- Thermal efficiency:
 - of cogeneration systems, 1048, 1049
 - of steam turbines, 1034, 1036, 1043
- Thermal expansion coefficient, 146, 328–329
- Thermal imaging, 278–279
- Thermal interface resistance, 470–473
- Thermal loads:
 - building, 589–593
 - in cogeneration systems, 975–976, 984–985, 987
- Thermal modeling of electronic equipment
 - cooling, 451–464
 - chip module thermal resistances, 458–464
 - conduction heat transfer, 451–454
 - convective heat transfer, 455–457
 - radiative heat transfer, 457–458
- Thermal modeling of forced convection, 456, 473–478
 - external flow on plane surface, 473
 - flow across arrays of pin fins, 476
 - flow across spheres, 474, 475
 - flow across tube banks, 475–476
 - flow of air over electronic components, 476–478
- Thermal NO_x, 665
- Thermal radiation, 216
- Thermal radiation properties of gases, 229–234
 - CO₂, 229–231, 233
 - H₂O, 229–232
 - mean beam length, 230, 232
 - radiative exchanges, 233
- Thermal resistance, 187, 190, 197
 - of chip modules, 458–464
 - of furnace materials, 327–328
 - heat pipe, 243–244
 - internal, 459–460
 - for packaging materials, 460
- Thermal resistance network, 458
- Thermal sensitivity, 279
- Thermal storage, 976
- Thermal system evaluation, 600–604
 - cost estimation, 603, 604
 - engineering-level system simulation, 600–602
 - equation solvers, 603, 604
- Thermal system optimization, 559–631
 - approximation-assisted, 614, 616–631
 - drivers of, 605–607
 - methodology, 607–615
 - symbols used for, 631
 - toolbox for, 600–607
- Thermal transmittance, 590–591
- Thermal vapor deposition, 292
- Thermistors, 270
- Thermoacoustic oscillations, 564–565
- Thermochemical cycles, 787

- Thermochemical hydrogen production, 998, 999
- Thermochemical properties at 1.013 bar, 298.15 K, 36–37
- Thermochromic liquid crystals, 274–275
- Thermocompressors, *see* Ejectors
- Thermocouples, 255–267
 - circuits of, 256
 - coaxial, 300
 - in constant heat flux experiments, 302–303
 - extension leads and compensation cables for, 266–267
 - installation of, 262–266
 - and law of inserted materials, 257
 - and law of interior temperatures, 257
 - and law of intermediate materials, 258
 - modeling fundamental thermoelectric phenomena with, 258–260
 - surface-mounted gauges with, 290–293
 - thin-film, 294–295
 - tolerances for, 261–262
 - types of, 260–263
- Thermodynamics, 135–156
 - analysis of engineering system components, 153–156
 - of closed systems, 138–142
 - constructal theory vs., 181–182
 - definitions used in, 137
 - energy minimum principle, 142–143
 - first law of, 135, 138–139
 - of gas compression, 897–900
 - of open systems, 143–144
 - relations among thermodynamic properties, 144–153
 - second law of, 135, 140–142
 - subscripts used in, 136–137
 - symbols/units used in, 135–136
- Thermodynamic charts, 899
- Thermodynamic properties:
 - of ice/water, 23
 - of liquid/saturated vapor air, 7–8
 - relations among, 144–153
 - of saturated methane, 16
 - of saturated Refrigerant 134a, 19
 - of saturated sodium, 23
 - of steam, 1029–1030
- Thermodynamic systems, 137
- Thermodynamic temperature scale, 140, 247–248
- Thermoelectric coolers:
 - analysis of, 489–490
 - design equations, 487–488
 - equations for thermoelectric effects, 487
 - optimization of, 488–489
- Thermoelectric emf, net, 259
- Thermographic phosphors, 273–274, 299
- Thermometers, 138
 - bimetallic, 254–255
 - differential flame, 302
 - diode, 271
 - liquid-in-glass, 252–253
 - platinum resistance, 267–269
- Thermometry:
 - infrared, 275–278
 - manometric, 253–254
 - noise, 271
- Thermophile heat flux gauges, 290–294
- Thermophysical properties of fluids, 3–39
 - at atmospheric pressure, 16, 17, 26, 27, 32
 - n*-butane, 26
 - carbon dioxide, 11–13
 - combustion products, 37–38
 - conversion factors, 4
 - on enthalpy–log pressure diagrams, 13, 15, 18, 22
 - ethane, 26
 - ethylene, 26
 - n*-hydrogen, 26
 - ideal gases, 8–9, 37–38
 - of liquid/saturated vapor air, 7–8
 - mercury, 14, 15
 - methane, 16
 - nitrogen, 26
 - oxygen, 27
 - and phase transition data, 4–7
 - propane, 27
 - propylene, 27
 - psychometric chart, 39
 - ratio of principal specific heats for liquids/gases, 32
 - refrigerants, 17, 27–30
 - Refrigerant 22, 17, 18
 - Refrigerant 134a, 19, 21–22

- Thermophysical properties of fluids
(*continued*)
of saturated liquids, 14, 16, 17, 19, 23, 31, 34, 35
of saturated steam/water, 24–25
surface tension, 33
and thermochemical properties at 1.013 bar, 298.15 K, 36–37
and thermodynamic properties, 7–8, 16, 19, 23
of U.S. Standard Atmosphere, 10
viscosity, 35
- Thermoscope bars, 272
- Thermostatic expansion valves (TXVs), 532–534
- Thermosyphons (thermosiphons), 240, 396, 433–434
- Thermowells, 265, 266
- Thin films, 199, 203, 204
- Thin-film evaporation, 425–427
- Thin-film heat flux gauges, 292, 298–299, 304, 305
- Thin-film thermocouple sensors, 294–295
- Third-party ownership of cogeneration systems, 986*n.*, 988
- Thomson effect, 486, 487
- Three-dimensional flow:
around a point source in uniform stream, 70–71
around a sphere, 71
boundary conditions for, 63
conservation of mass in, 62
Euler's equation for, 62–63
ideal fluids in, 62–64, 69–71
irrotational flow-velocity potential in, 63–64
Laplace equation for, 64
Stokes's stream function for, 69
- Three-way valves, 1108
- Threshold limit value–time weighted average (TLV-TWA), 507
- Throttles, 153–155
- Throttling, 1046
- Throughput:
of compressors, 897
control of, in centrifugal fans, 886–887
of gear pumps, 875
generalized head loss with, 865, 866
volumetric, 875
- Thrust, 941, 1052
- Thrust-specific fuel consumption (TSFC), 941
- Time-related wear-out mechanisms, 948, 950
- Tip diameter, 931
- TLV-TWA (threshold limit value–time weighted average), 507
- Toluene-in-glass thermometers, 253
- Topping-cycle cogeneration systems, 965–966, 1048, 1049
- Topping turbines, 1041
- Torque, shaft, 1046
- Torque coefficient, steam turbine, 1044
- Toshiba, 1057
- Total absorptivity, 221
- Total compressor power, 899
- Total drag, 78–79, 117–118
- Total emissive power, 217
- Total flow exergy, 164
- Total heat exchange, 583
- Total hemispherical absorptivity, 220
- Total hemispherical emissivity, 219
- Total hemispherical reflectivity, 220
- Total hemispherical transmissivity, 220
- Total nonflow exergy, 164
- Total quantity methods, 126
- Total reflectivity, 221
- Total transmissivity, 221
- Total volatile organic compound (TVOC) mixtures, 588
- Towers, wind, 957
- Town gas, 1016
- Toxicity:
of hydraulic fluids, 1097
and refrigerant selection, 520–521
- Toxicity rating system, refrigerant, 507–510
- Traceability, for temperature-measuring systems, 249
- Trains, gas turbines used in, 908
- Transesterification, 777, 779
- Transient heat conduction, 198–204
in cylinders, 199, 202–203
in plane walls, 199–201
in spheres, 199, 203, 204

- Transient optical methods for measuring heat flux, 299
- Transition boiling, 235
- Transmission, hydrogen fuel, 793, 794
- Transmissivity, 219–220
- Trapezoidal channel, most efficient, 110
- Triangles, constructal theory and, 176
- Triangular weirs, 132–133
- Trichlorofluoromethane, 507, 512
- TSFC (thrust-specific fuel consumption), 941
- TSPs (temperature-sensitive paints), 273, 299
- T thermocouples, 263
- Tubes:
 - diameter of, 408–409
 - film condensation inside horizontal, 239
 - film condensation outside horizontal, 239
 - forced convection in, 477–478
 - and heat exchanger programs, 408–409
 - laminar flow for short, 205, 206
 - layout of, 409
 - length of, 386, 408
 - material used in, 409
 - Navier–Stokes equations for flow through, 77–78
 - number of, 386
 - pitch of, 409
 - turbulent flow in circular, 206–207
 - types of, 408
 - vibration in, 399–400
- Tube-axial fans, 887, 888
- Tube banks:
 - in cross-flow, 210
 - film condensation outside horizontal, 239
 - forced convection flow across, 209–210, 475–476
 - staggered vs. aligned, 209
- Tube diameter (OD), 610
- Tube-in-tube condensers, 528
- Tubesheets, 375–376
- Tube-side flow, 387, 388, 401
- Tube-side forced circulation boiling, 396
- Tube-side reboilers, 395
- Tubular Exchanger Manufacturers Association (TEMA), 376, 399, 408, 409
- Tubular SOFC design, 1078, 1079
- Tunnel kiln furnaces, 317
- Turbines. *See also* Gas turbines; Steam turbines
 - hydrogen burner, 1020
 - laws of thermodynamics applied to, 153
 - micro, 971
 - wind, 955–962
- Turbine stage, 903
- Turbofans, 944–946
- Turbulent diffusion flame types, 651–655
 - effect of swirl, 651–652
 - stabilization methods, 652–655
- Turbulent flames:
 - diffusion-mixed, 650–651
 - premixed, 645–646
- Turbulent flow:
 - in circular tubes, 206–207
 - defined, 58
 - on flat plate, 208
 - in furnaces, 360
 - rational formulas for velocity of, 84–86
 - shear stress in, 72
- TVOC mixtures (total volatile organic compound mixtures), 588
- Twin-screw pumps, 876
- Two-dimensional flow:
 - boundary conditions for, 63
 - complex variables for irrotational flow, 65–66
 - conformal mapping for, 66–68
 - conservation of mass in, 62
 - doublets, 68
 - Euler’s equation for, 62–63
 - flow around circular cylinders, 69
 - ideal fluids in, 62–69
 - irrotational flow-velocity potential in, 63–64
 - Laplace equation for, 64
 - stream function for, 65
 - streamlines in, 64–65
- Two-dimensional steady-state heat conduction, 193–196
- Two-fluid atomization, 658–659
- Two-pass shell, 376, 377
- Two-phase refrigeration distribution, 530
- Two-phase thermosyphons, 240

- Two-way valves, 1108
- TXVs (thermostatic expansion valves), 532–534
- U**
- Ultimate analysis (D3176), 710
- Ultrasonic atomization, 659
- Ultraviolet, 217
- Uncertainty, measurement, 250, 307, 819
- Unconstrained equilibrium state, 143
- Underground sequestration, of carbon dioxide, 760
- Underlapped valves, 1108–1109
- Undersea sequestration, of carbon dioxide, 761
- Uniform flow:
 - critical depth in, 111
 - defined, 58
 - Manning formula for, 109–110
 - in open channels, 108–111
 - specific energy in, 110–111
- Uniform stream, point source in, 70–71
- Union Pacific railroad, 908
- United States:
 - CFCs banned in, 511
 - coal resources in, 704
 - coal uses in, 707
 - fuel demand in, 319
 - wind turbine installations in, 955, 956
- U.S. Bureau of Mines, 704
- U.S. Coal Reserves, 704
- U.S. Energy Information Administration, 577
- U.S. Geological Survey (USGS), 704, 841–842
- U.S. geothermal resource base, 841–843
- U.S. National Renewable Energy Laboratory (NREL), 829
- U.S. standard atmosphere, 10, 578
- U.S. Standard sieves, 713
- United Technologies Company (UTC), 1056, 1058, 1059, 1082
- Unsteady flow:
 - and column separation, 104
 - elastic theory of, 102, 106–108
 - in open channels, 113–115
 - in pipe systems, 102–108
 - rigid water column theory of, 102, 104–106
- Upwind, 955
- USGS (U.S. Geological Survey), 704, 841–842
- UT-3 cycle, 999
- UTC, *see* United Technologies Company
- U-tubes, 376
- V**
- Vacuum generation:
 - in compressors, 892–894
 - in ejectors, 891–892
- Valves:
 - ball, 1106, 1107
 - closed-centered, 1108–1109
 - control, 1107–1110
 - critically lapped, 1108, 1109
 - electronic expansion, 534
 - expansion, 501, 532–534
 - flow control with, 866–867, 869
 - fuel shutoff, 669–670
 - hydraulic, 1105–1113, 1119, 1121
 - laws of thermodynamics applied to, 153–155
 - minor losses in, 95
 - open-centered, 1108
 - overlapped, 1108, 1109
 - poppet, 1106, 1107
 - proportional, 1111–1112
 - relief, 1102, 1107, 1108
 - servo, 1112–1113, 1117–1118
 - spool-in-sleeve, 1107
 - three-way, 1108
 - two-way, 1108
 - underlapped, 1108–1109
- Valve-driven motors, 1092
- Vanadium, 687
- Vanes, centrifugal fan, 881–883
- Vane-axial fans, 887, 888
- Vane pumps, 1100–1102
- Van't Hoff equation, 1008
- Vapor air, 7–8
- Vapor chambers, 436

- Vapor compression refrigeration cycle, 500–501
- Vapor compression system:
 - network representation of, 601
 - residual equations for, 601–602
- Vapor density, 514
- Vapor-dominated resources, 842, 844
- Vapor flow, temperature drop in, 427–428
- Vaporizers:
 - critical heat flux in, 402
 - inadequate blowdown in, 403
 - shell and tube, 392–396
 - shell and tube heat exchangers, 392–396
- Vapor–liquid equilibrium (VLE), 389–390
- Vapor–liquid separation, 530
- Vapor-phase heat-transfer coefficient, 392
- Vapor pressure, 50, 51, 522
- Vapor pressure drop, 421–422
- Vapor recompression, 890–891
- Variable air volume (VAV), 596
- Variable-conductance heat pipes (VCHPs), 438
- Variable-displacement pumps, 1100, 1103–1105
- VAV (variable air volume), 596
- VAWT (vertical axis wind turbine), 957
- VCHPs (variable-conductance heat pipes), 438
- VEETC (Volumetric Ethanol Excise Tax Credit), 775
- Vegetable oil (as fuel), 777
 - availability of, 783
 - manufacturing method, 779
 - production capacity for, 783–784
 - research on production of, 785
 - vehicle modification for use of, 779
- Vehicles:
 - hybrid electric, 788
 - hydrogen, 788–792
- Vehicle modifications:
 - for biodiesel use, 779
 - for ethanol use, 770–774
- Velocity(-ies):
 - erosion, 407
 - of fluids, 58, 83–86, 122–126
 - and furnaces, 355, 356, 358, 359
 - rotational angular, 58
 - wind, 961–962
- Velocity-compounded stage arrangement, 1036–1039
- Velocity convergence loop, 404, 405
- Velocity distribution for flow in closed conduits, 83–86
 - and development of flow, 83–84
 - energy and momentum correction factors, 85, 86
 - rational formulas for turbulent flow, 84–86
- Velocity heads, 355–357, 359
- Venezuela, 700
- Ventilation, 592
- Venting, inadequate, 403
- Venturi flumes, 131
- Venturi meter, 126, 127
- Venturi mixers, 362
- Verification (approximation-assisted optimization), 617
- Vertical axis wind turbine (VAWT), 957
- Vertical ground-loop GHP systems, 854
- Vertical plate, 237
- Vertical single tubepass, 376, 377
- Vertical thermosiphons, 396
- Vertical tubes, 391
- Vertical turbine pumps, 98
- Vertical walls, 214
- Vibration, 399–400
- View factor, *see* Configuration factor(s)
- View factors for solid-state radiation, 332, 334–337
- Vinasse, 770
- Viscometers, 119–121
- Viscosity:
 - absolute (dynamic), 48, 49, 119, 870
 - and centrifugal pumps, 868–870
 - defined, 48–50
 - of diesel fuels, 695
 - of fuel oils, 659, 660
 - of hydraulic oils, 1095–1096
 - kinematic, 120, 870
 - measuring, 118–121
 - Newton’s law of, 78
 - of saturated liquids, 35
 - of secondary coolants, 521

- Viscous fluid dynamics, 71–79
 - for external flows, 73, 74
 - for internal flows, 72–73
 - Navier–Stokes equations in, 73–79
- Viscous forces, in dynamic similarity, 80
- Viscous limit, 240, 242, 424
- Viscous liquid cooling, 401
- Visible spectrum, 217
- VISPAR parameter, 869
- Vitiated air, 639
- VLE (vapor–liquid equilibrium), 389–390
- Volumetric efficiency, 1043, 1104
- Volumetric Ethanol Excise Tax Credit (VEETC), 775
- Volumetric throughput, 875

- W**
- Wabash River Generating Station (West Terra Haute, Indiana), 743
- Wairekei Fields (New Zealand), 844
- Washability data, 717, 718
- Waste(s):
 - combustible, 367
 - radioactive, 367
 - solid, 754, 982
- Waste fuels, 639–640
- Waste heat boiler, *see* Heat recovery steam generators (HRSGs)
- Waste heat recovery systems, 367–371, 443–445
 - recuperator combinations, 370–371
 - recuperator systems, 369–371
 - regenerative air preheating, 368–369
- Water:
 - splitting of, 998, 999
 - thermal radiation properties of, 229–232
 - thermodynamic properties of, 23
 - thermophysical properties of saturated, 24–25, 238
- Water-cooled condensers, 528, 529
- Water cooled heat flux gauges, 297
- Water cooling, 919, 922
- Water defrost, 538
- Water hammer, *see* Elastic theory
- Water–lithium bromide absorption chillers, 516–518
- Water management, 1071–1074
- Water Quality Act of 1965, 981
- Water quality regulations, 981, 982
- Water solubility, 521
- Water wash systems, 922
- Wave speed, in pipes, 106
- Wear-out mechanisms, 947–948
- Weight, specific, 43, 118
- Weirs, 131–133
- Welded plate exchangers, 380
- Well water, 529
- Westinghouse, 904, 915, 1078
- Wet bulb temperature, 579
- Wet flue gas desulfurization, 749, 750
- Wet scrubbing, 367, 748
- Wheels, 903
- Wicks:
 - capillary limits of, 240
 - effective thermal conductivities of, 425
 - fabrication of, 428–430
 - in heat pipes, 239–244
 - permeability of, 241
 - porosity of, 421
 - thermal conductivity for liquid-saturated, 243
- Wicking height, 418
- Wien displacement law, 218, 809
- Wilson, Robert, 1033
- Windbox burners, 656
- Windows, heating load through, 591
- Wind power generation, 955–962
 - market/economics, 955, 956
 - power production/energy yield, 957–959
 - turbine configurations, 955–957
 - turbine rotor/drivetrain design, 959–960
 - turbine site selection, 960–962
- Wind turbines, 955–962
 - configurations, 955–957
 - market/economics, 955, 956
 - rotor/drivetrain design, 959–960
 - site selection for, 960–962
 - turbine power production/energy yield, 957–959
- Wind velocity, boundary layer impact on, 961–962
- Wires, thin, 199, 203, 204
- Wire-wound heat flux gauges, 293–295

WMO, *see* World Meteorological Organization

Wobbe index, 320, 678–679

Work–energy equation:

 correction factors for flow in closed conduit, 85, 86

 for internal flows, 72

 for one-dimensional flow, 61

Working fluids for heat pipes:

 charging of, 429, 431, 432

 compatibility of, 432

 selection of, 428–429, 431, 432

 temperature ranges of, 431

Working standard pyrheliometers, 811

Work of compression, 897–899

Work transfer, 138–139

Work transfer rate, 161

World Coal Study, 703

World Meteorological Organization (WMO):

 pyranometer classification by, 813

 pyrheliometer classification by, 810, 811, 817

 radiation instrument classification by, 808

X

X rays, 217

X-type shell and tube heat exchangers, 377, 378, 389, 391, 407

Xylene-in-glass thermometers, 253

Z

Zeldovich mechanism, 912

Zeotropes, 507, 508, 513

Zinc borohydride, 1011

ZnO/Zn cycle, 999

WILEY END USER LICENSE AGREEMENT

Go to www.wiley.com/go/eula to access Wiley's ebook EULA.